ISBN: 978-3-95450-252-3 ISSN: 2673-5350 doi: 10.18429/JACoW-IPAC2026-MOI4M01

GANIL-SPIRAL2 FACILITY - RECENT ACHIEVEMENTS AND UPGRADES

R. Ferdinand, P. Anger, P-E. Bernaudin, F. Chautard, H. Franberg-Delahaye, M. Lewitowicz, X. Ledoux, F. Lutton, A. Orduz, H. Savajols, A. Savalle, J-C. Thomas
Grand Accélérateur National d'Ions Lourds, Caen, France

Abstract

The Grand Accélérateur National d'Ions Lourds (GANIL) is a multi-beam facility, unique in intensity, particle types and simultaneous production. The Système de Production d'Ions Radioactifs en Ligne de 2ème génération (SPIRAL2) facility covering an exceptionally broad intensity range, from nanoamperes to milliamperes further enhances the scientific opportunities of the laboratory. The first proton beams from the LINAC were produced in 2019 and is operational for physics experiments since 2022. The cyclotron operation and the initial operational challenges and lessons learned in the first years of operation of the LINAC and Neutrons For Science (NFS) facilities are presented. The physics program at GANIL-SPIRAL2 is briefly presented. The ongoing upgrades and developments essential to sustain increasingly ambitious pure and applied science programs are also presented.

INTRODUCTION

GANIL-SPIRAL2 [1, 2] is primarily focused on cutting-edge research in nuclear physics, nuclear astrophysics, nuclear data with complementary programmes in astrochemistry, material irradiation, nano-structuration, radiobiology and industrial and medical applications.

The field of low-energy nuclear physics is undergoing an important transformation based on results obtained at various facilities in Europe such as GANIL in France, GSI-FAIR in Germany, ISOLDE at CERN, JYFL in Finland and LNL & LNS in Italy and worldwide facilities in Canada, China, Japan, Korea, Russia, USA. These results have further motivated very ambitious efforts worldwide to produce and study nuclei far from stability using Radioactive Ion Beams. In the European roadmap, FAIR and GANIL-SPIRAL2 are classified as ESFRI landmark facilities, with complementary radioactive beams production methods. The FAIR facility will use high-stable energy beams (up to 1 GeV/u) of heavy-ions and will have an unrivalled potential to produce the heaviest exotic nuclei far from stability. The GANIL cyclotron facility delivers high-intensity stable beams up to uranium, as well as exotic nuclei produced via both in-flight fragmentation and the ISOL (Isotope Separation On-Line) technique through the SPIRAL1 facility. Radioactive beams from SPIRAL1 can be used directly or re-accelerated while preserving high optical quality. Together with facilities such as SPIRAL2, ISOLDE, and JYFL, and in the future SPES at LNL and ISOL@MYRRHA, GANIL will enable high-precision measurements at low energy that are complementary to those performed with the more energetic beams of FAIR.

GANIL has been operational since 1983, as a cyclotron-based facility. The SPIRAL2 LINAC commissioning started in July 2019 immediately after the authorization. The first test experiments started from Dec 2019 using proton beams and from Dec 2021 with deuteron beams. Three new experimental halls for exploiting stable, neutron and radioactive ion beams are available. The GANIL facility is a multi-beam facility, operating up to 5 simultaneous beams: IRRSUD, SME, CSS high energy, CIME, SPIRAL2, which renders GANIL unique in the world. Complementary atomic physic studies are also made in ARIBE.

The paper will briefly summarize the cyclotrons operation and discuss in more detail the LINAC operation. Some new results related to time optimized LINAC tuning and the projects currently underway at GANIL (S^3, DESIR NEWGAIN, CYREN, SAGA) will also be described.

GANIL-SPIRAL2 FACILITY

Figure 1 shows the cyclotrons and SPIRAL2 accelerators along with the associated experimental halls.

GANIL construction was decided in 1975 [3]. Between 1983 and 1990, the facility relied on a cascade of three warm cyclotrons ($K_{CO1,2}$=30, K_{CSS1}=400, K_{CSS2}=400). There is a rebuncher between the injectors and the first separate sectors cyclotron (CSS1) and a stripper between CSS1 and CSS2. A wide spectrum of stable and radioactive ion beams have been delivered since 1983.

The five cyclotrons of GANIL allow the acceleration of ions up to 95 MeV/u for "light" ions and up to 25 MeV/u for uranium.

Various techniques have been developed to enhance beam intensities, expand the range of available isotopes, and improve overall beam reliability. A major upgrade occurred in 2001 with the implementation of the "Cyclotron pour Ions de Moyenne Énergie" (CIME), enabling the post-acceleration of radioactive ions produced at the SPIRAL1 facility. In this scheme, the CSS cyclotrons serve as drivers for the production of radioactive species, using stable beams fragmented in a thick carbon target according to the ISOL technique.

These beams are delivered to different experimental areas hosting a large variety of detectors and spectrometers that allow detailed studies of nuclear structure and reactions, atomic and material science as well as applications. Among them, the charged particle FAZIA–INDRA array combines the large solid-angle coverage of the INDRA detector with the high isotopic resolution of the FAZIA detector. This unique combination makes FAZIA–INDRA a powerful instrument for studying reaction dynamics, fragment formation, and isospin-dependent properties of nuclear matter.

The GANIL ACTAR TPC detector is a next-generation

Content from this work may be used under the terms of the CC BY 4.0 licence (© 2026). Any distribution of this work must maintain attribution to the author(s), title of the work, publisher, and DOI.

ISBN: 978-3-95450-252-3 ISSN: 2673-5350 doi: 10.18429/JACoW-IPAC2026-MOI4M03

COMMISSIONING PROGRESS OF THE ESS LINEAR ACCELERATOR

N. Milas, on behalf of the commissioning team
European Spallation Source, Lund, Sweden

Abstract

The European Spallation Source (ESS) is in the final stages of commissioning its linear accelerator (linac), which will deliver a high-power proton beam for neutron production. The commissioning process involves progressive testing of subsystems, including the ion source, radio-frequency quadrupole (RFQ), and superconducting cavities, to ensure stable and reliable beam operation. Key challenges include beam dynamics optimization, machine protection, and high-power RF system integration. Within this presentation an overview of the commissioning status, key milestones achieved, and expectations for the first beam on target, marking a significant step toward full facility operation will be given.

THE ESS FACILITY

The European Spallation Source is a pan-European project with 13 European nations as members, including the host nations Sweden and Denmark. The ESS facility is under commissioning in Lund, while the ESS Data Management and Scientific Computing centre (DMSC) is located in Copenhagen. The construction of the facility began in the summer of 2014 and we expect to see the first neutrons at the start of 2027 (see Fig. 1). ESS is the fourth facility of its kind to be constructed, after the completion of the SNS in the United States, J-PARC in Japan, and CSNS in China. All three facilities have MW capabilities, but the design beam power of ESS will be the highest of the three [1]. The linac is designed to produce neutrons through spallation with an average flux comparable to that of the continuous ILL source, while maintaining a low pulse repetition rate that enables the production of high-flux, low-energy neutrons.

The ESS facility is a huge and highly complex jigsaw puzzle. The 13 ESS member states contributed to the construction of ESS via financial and in-kind contributions, exchanging knowledge and know-how. An in-kind contribution may cover technical components, design documentation, personnel needed to perform installation and testing, or other services.

The ESS linac

A schematic overview of the high-power linac currently being built [2] at ESS can be seen in Fig. 2. A proton beam at 75 keV is produced in the Ion Source (ISrc), focues in the Low Energy Beam Transport (LEBT) section and readily accelerated by a four-vane Radio-Frequency Quadrupole (RFQ), which is the first accelerating structure of the ESS LINAC. The 3.62 MeV bunched beam pulse matched in the Medium Energy Beam Transport (MEBT) to the Drift Tube LINAC (DTL) section, comprised of five DTL tanks accelerating the beam up to 90 MeV.



Figure 1: Photo of the ESS site from June 2022. Construction work is finished and it is possible to see the linac (orange), the Target building (yellow) and the long instruments hall (green).

Downstream of the DTL the accelerating structures are superconducting, and this part of the accelerator is referred to as the Superconducting LINAC (SCL). Three families of superconducting RF-cavities are used at ESS. The cavities are arranged in cryomodules with LINAC Warm units (LWUs) in between, each housing a quadrupole doublet and beam diagnostics. 26 Spoke-cavities (SPK) arranged two in each cryomodule, operating at 352.21 MHz, take the beam to 216 MeV. Both the 36 medium-β cavities (MBL) and 84 high-β cavities (HBL) are arranged four cavities per cryomodule and operate at a frequency of 704.42 MHz, twice the SPK frequency, and togehter bring the beam to a maximum energy of 877 MeV. Note that during the 2025 commissioning, only 5 cryomodules of HBL, were installed and operational. For the commissioning of 2026 one of the Spokes cavities tuning motor presented issues and the cavity could not be used for acceleration, reducing the final maximum achievable energy to 862 MeV. The High Energy Beam Transport (HEBT), is a contingency space for future upgrades, currently housing quadrupole doublets and beam diagnostics. After the HEBT section it is possible to send beam to the tuning beam dump, which accepts a maximum power of 12.5 kW, or to the ESS Target, the only destination that can take the full design power.

The ESS Target

The spallation process at ESS will take place when the accelerated protons beam hits the tungsten bricks of the 4.9 tonne target wheel, producing neutrons for scientific experiments across multiple disciplines [1]. The first step in this process is production of high-energy neutrons through a spallation process involving proton beam interaction with a tungsten target. The target is a 2.6 m diameter stainless steel disk containing bricks of tungsten. It weighs almost five tonnes. The wheel rotates at 23.3 RPMs, in time with

Content from this work may be used under the terms of the CC BY 4.0 licence (© 2026). Any distribution of this work must maintain attribution to the author(s), title of the work, publisher, and DOI.

ISBN: 978-3-95450-252-3 ISSN: 2673-5350 doi: 10.18429/JACoW-IPAC2026-MOI1T01

PROJECT STATUS AND R&D EFFORTS FOR SUPER TAU-CHARM FACILITY

Jingyu Tang* on behalf of the STCF team
University of Science and Technology of China, Hefei, China

Abstract

The Super Tau-Charm Facility (STCF) was proposed as a third-generation circular electron-positron collider in the energy range of 2-7 GeV (CoM) and with a luminosity greater than 5×10^{34} $cm^{-2}s^{-1}$ @4 GeV, aiming to explore charm physics and tau physics in the next decades. This paper introduces the facility design and ongoing R&D efforts for STCF, covering the design goal, accelerator and detector schemes, and key technological R&D efforts, with a particular focus on the accelerator. Supported by a key technology R&D project funded by the local governments and other national funding agencies, the STCF accelerator team including international collaborators has completed the conceptual design of the accelerator, and initiated the technical design. The accelerator comprises of a full-energy injector consisting of multi-section linacs and a positron accumulator ring and a double-ring collider with the crab-waist collision scheme. Key physics and technological challenges will be addressed. This paper also summarized ongoing R&D progresses and outlines future project planning.

INTRODUCTION

STCF was conceived around 2011 as the succesor to the currently operational BEPCII collider, aiming to explore rich physics in the tau-charm energy range over the next three decades [1]. As a circular electron-positron collider, it operates at a low but wide energy range of 2-7 GeV (center-of-mass energy), with a super high luminosity of 5×10^{34} $cm^{-2}s^{-1}$ @4 GeV or about two orders higher than that of BEPCII. STCF is being designed as a new-generation circular electron-positron collider employing the crab-waist collision scheme.

In 2023, a study team was formed to carry out the design and technological R&D of the STCF, hosted by University of Science and Technology of China (USTC) with broad participation from institutions across China. Major financial support has been provided by the local governments of Anhui Province and Hefei City, with additional support from the Chinese Academy of Sciences (CAS), National Natural Science Foundation of China (NSFC), Ministry of Science and Technology (MoST) and USTC. Currently, the project has been recommended by the CAS to the central government for starting the construction in the 15th Five-Year Plan period (2026-2030).

The collider will be built in Hefei, Anhui Province, adjacent to the four-generation light source - HALF (currently under construction). Both facilities are core components of the Hefei Comprehensive National Science Center.

* jytang@ustc.edu.cn

ACCELERATOR FRAME

As a new-generation or third-generation electron-positron collider, the STCF accelerator complex is required to deliver extremely high luminosity [2]. This goal is particularly challenging given the continuous and wide CoM energy range of 2-7 GeV. The accelerator consists of two major compenents: the two-ring collider and the injector. The collider rings, one electron ring and one positron ring, will operate in top-up injection mode to achieve high integral luminosity. Currently both conventional off-axia injection and the more advanced swap-out injection are under consideration. For the latter, each injection must provide as much as 8.5 nC for both electron and positron bunches. Considering the very short beam lifetime in the collider rings, in particular in the low beam energy region of 1-2 GeV, these requirements neccssitate that the injector provide full-energy electron and positron beams with high-repetitaion rate, with a variable beam energy of 1-3.5 GeV and a different bunch charge of 1-8.5 nC.

The acceleration of the electron beam is straightforward by using conventional S-band linacs at 2.998 GHz. The positron beam is generated by bombarding a high-energy and high-charge electron beam onto a tungsten target. After capture and initial acceleration, the positron beam of very large emittance and momentum spread will be sent to a damping ring for improving the beam quality. An injector scheme that is compatible with both off-axis injection and swap-out injection has been adopted, and further details are provided in the injector section. Figure 1 shows the general layout of the accelerator complex. Table 1 lists the key design goals of the STCF accelerator.

Table 1: Design Goals of the STCF Accelerator

Parameter	Value
Center-of-mass energy (GeV)	2-7
Luminosity @ 4 GeV ($cm^{-2}s^{-1}$)	5×10^{34}

DESIGN OF THE COLLIDER RINGS

Layout and Lattice Design

The collider rings adopt a hexagon-like layout, featuring four main arcs with 60° bending and four short arcs with 30° bending [3-4]. The Interaction Region (IR) is located in the middle of one pair of short arcs, while the crossing region of the two rings is situated on the opposite side. Four long straight sections serve the following functions:

injection/extraction, damping wigglers, RF stations and collimation; the two additional long straight sections near

Content from this work may be used under the terms of the CC BY 4.0 licence (© 2026). Any distribution of this work must maintain attribution to the author(s), title of the work, publisher, and DOI.

ISBN: 978-3-95450-252-3 ISSN: 2673-5350 doi: 10.18429/JACoW-IPAC2026-MOI1T02

LINEAR COLLIDER STUDIES AND PROSPECTS

S. Stapnes, University of Oslo, Norway

Abstract

Linear e^+e^- colliders can provide a broad physics programme spanning centre-of-mass energies from the Z pole to the TeV scale, enabling precision measurements of the Higgs boson, top quark, and the electroweak sector with polarised beams. Two mature accelerator technologies are under development for a possible linear collider facility (LCF) at CERN beyond the HL-LHC: the superconducting RF (SCRF) approach embodied by the ILC as developed for hosting in Japan, and the proposed normal-conducting high gradient RF (NCRF) two-beam scheme of CLIC. Both options are described in detailed documents contributed to the European Strategy for Particle Physics Update (ESPPU) process. Beyond an initial implementation in the 250-380 GeV range, upgrades in energy and/or luminosity enabled by R&D on cool copper structures, higher gradient SCRF, energy recovery and plasma wakefield options can be considered. This paper summarises the status of the studies and associated technology developments, potential long-term upgrade paths, and key implementation parameters including cost, power, and sustainability assessments.

1. INTRODUCTION

Linear e^+e^- colliders are the preferred technology for a precision lepton collider spanning a broad range of centre-of-mass energies up to one to a few TeV. Their defining advantages beyond the energy range include the availability of longitudinally polarised beams for both electrons and positrons, a clean experimental environment free of synchrotron radiation backgrounds at the interaction point, and inherent upgradability in energy and luminosity without or with limited additional civil construction. A linear collider is uniquely able to realise a true multi-stage Higgs factory while providing a natural path to the multi-TeV energy frontier.

At 250–380 GeV, $e^+e^- \rightarrow ZH$, also called Higgs-strahlung, yields model-independent Higgs coupling measurements to the percent level or better. An optional Z-pole run and W-mass threshold scan, both polarised, complement the programme with precision electroweak measurements.

While the top mass can be measured at the ttbar threshold (expected precision: 40 MeV), a centre of mass energy of 550 GeV enables measurements of the top Yukawa coupling (2.8%) and the trilinear Higgs self-coupling (11%). Beam polarisation aids the analyses at every stage [1]. The multi-stage design is a key asset: anomalies at one energy can be verified at the next, providing the robustness needed to establish genuine discoveries from precision measurements [1,2].

Two RF technologies have reached the level equivalent of a Technical Design Report (TDR). The International Linear Collider (ILC) is based on 1.3 GHz niobium SCRF cavities at 31.5 MV/m and has been studied for possible construction in Japan since 2012. The Compact Linear Collider (CLIC) uses a novel two-beam acceleration scheme with normal-conducting X-band cavities reaching 72-100 MV/m, targeting an initial stage at 380 GeV expanding to 1.5 TeV later. At CERN a 550 GeV version of an SCRF based collider has been studied, with a choice of higher luminosities and hence power consumption compared to parameters chosen for the ILC in Japan. Both are compatible with a civil-engineering footprint of approximately 30-34 km length near CERN. Advanced upgrade technologies - C^3, HELEN, Nb_3Sn coated or travelling wave SCRF, plasma wakefield acceleration, energy-recovery linac concepts, and more - are under active R&D as upgrade candidates towards higher energies and/or luminosities [1, 2].

2. SCRF TECHNOLOGY: LCF-SCRF AT CERN AND THE ITN

The ILC TDR, published in 2013, describes a 500 GeV linear collider based on 1.3 GHz nine-cell niobium SCRF cavities at 31.5 MV/m. The design has since been reviewed repeatedly by ICFA and Japanese government committees. A comprehensive cost update was completed in December 2024 by an international expert committee, confirming the technical maturity and establishing updated cost estimates consistent with the original TDR. Key technical advances since 2013 include the two-step baking surface treatment (sequential heat treatment at 75°C followed by 120°C), which reliably achieves $Q_0 \geq 1.0\times10^{10}$ at 35 MV/m. Large-scale SCRF-based free-electron laser facilities (Eu.XFEL, LCLS-II, SHINE) are in operation worldwide, demonstrating the full industrial maturity and reproducibility of the technology [3].

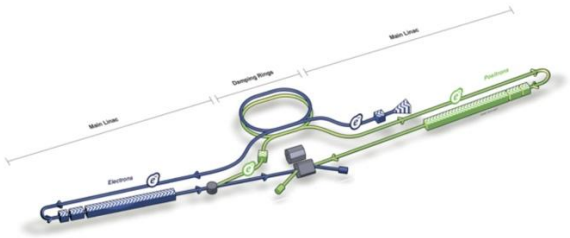

Figure 1: ILC in Japan. When adapted to a CERN facility two beam-delivery systems are foreseen providing two collision points.

The proposed Linear Collider Facility (LCF) at CERN adapts the ILC SCRF linac design for the CERN environment (Fig.1), combining it with the civil-engineering footprint and infrastructure standards developed over many years for CLIC. The baseline LCF configuration uses a 33.5 km tunnel that includes a 4-5 km beam-delivery region (BDS), with two interaction regions sharing the luminosity. The SCRF main linacs suggested for

Content from this work may be used under the terms of the CC BY 4.0 licence (© 2026). Any distribution of this work must maintain attribution to the author(s), title of the work, publisher, and DOI.

ISBN: 978-3-95450-252-3 ISSN: 2673-5350 doi: 10.18429/JACoW-IPAC2026-MOO1T01

OBTAINING A RECORD LUMINOSITY PRODUCTION IN THE LARGE HADRON COLLIDER IN 2025

J. Wenninger*, X. Buffat, A. Calia, J. Esteban Müller, S. Fartoukh, C. Hernalsteens, M. Hostettler, D. Jacquet, D. Mirarchi, M. Pojer, S. Redaelli, B. Salvant, M. Solfaroli, H. Timko, G. Trad, J. Wanczyk
European Organization for Nuclear Research (CERN), Geneva, Switzerland

Abstract

The Large Hadron Collider (LHC) run in 2025 was the last long production year of LHC Run 3 (2022 to 2026). To mitigate potential radiation damage to magnets installed in the low-beta sections due to the integrated radiation dose near the high luminosity experiments, a flat optics was used for the first time in beam operation, underlining the adaptability of the LHC. A record production of 125 fb^{-1} was achieved in 2025 despite vacuum component non-conformities leading to intensity limitations in one of the beams during part of the year. The integrated luminosity collected by each of the two high luminosity experiments since the startup of the LHC now exceeds 500 fb^{-1}. This paper presents the configuration, operational strategies and beam parameters of the LHC in 2025 which led to another record year.

INTRODUCTION

The LHC collider [1] serves four main experiments: the ATLAS and CMS high luminosity experiments located in interaction regions (IR) 1 and 5, the medium luminosity experiment LHCb in IR 8 and the low luminosity experiment ALICE in IR 2. ATLAS and CMS operate typically at peak luminosities above 2×10^{34} $cm^{-2}s^{-1}$, more than twice the design value, LHCb operates around 2×10^{33} $cm^{-2}s^{-1}$ and ALICE operates in the range 10^{31} $cm^{-2}s^{-1}$. Forward physics experiments FASER and SND installed around ATLAS complete the picture.

The fourth Run 3 operation year of the LHC in 2025 was the last long production year before a short run in 2026 and the 4 years long shutdown LS3 to install the equipment for the HL-LHC project [2].

OPTICS CONFIGURATION

Due to the very high rate of proton collisions, all equipment in and close to the LHC low-beta quadrupoles (inner triplets, ITs) in IR 1 and IR 5 is heavily irradiated. The recommended dose limit is 30 MGy for the IT magnets (superconducting main quadrupoles), and 75 MGy in the normal-conducting separation dipole magnets [3]. To preserve the magnet lifetime, the dose can be distributed over different coils using various optics and crossing angle configurations.

The target luminosity of 300 fb^{-1} in Run 3 can only be achieved by pushed beam parameters and crossing angle, and the dose projections for the nominal focusing-defocusing-focusing (FDF) inner triplet optics exceed the recommended limit. To spread the dose more evenly over different magnets, and to reduce the overall dose, a reverse-polarity (DFD) optics and a crossing angle change [4, 5] have been used in IR 1 for the 2024 run. This solution led however to an increased background at the forward physics experiments FASER and SND. For this reason, in 2025, the nominal polarity in IR 1 was restored and the reverse polarity was implemented in IR 5.

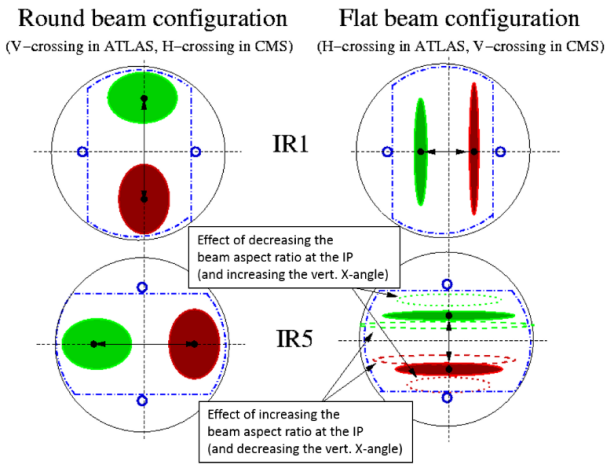

Figure 1: Beam envelopes in the low-beta quadrupoles around a high luminosity IP for round beam ($\beta_x^* = \beta_y^*$) and flat beam configuration ($\beta_x^* \neq \beta_y^*$).

At the same time the crossing angle planes were inverted, because the only change of triplet polarity in IR5 was not sufficient to mitigate appropriately the radiation dose expected in the IT of IR5 for the rest of Run 3. Due to the race-track shape of the beam-screens (see Fig. 1), this requires to flatten the optics ($\beta_x^* \neq \beta_y^*$) to preserve the machine performance, and actually even improve it in the end.

While in 2024 the LHC operated in physics conditions with round optics at a minimum β^* of 30 cm, in 2025 the lowest flat optics values were $\beta_x^* = 60$ cm and $\beta_y^* = 18$ cm in IR 1 with a horizontal crossing angle, the reverse configuration being used in IR 5 due to the orientation of the vacuum chamber beam screens and to the requirement of orthogonal crossing planes for long-range beam-beam compensation.

After being ramped to 6.8 TeV the beams are brought in collision with a round optics at β^* of 120 cm in ATLAS and CMS. The luminosity is leveled by β^* down to 60 cm with round optics. Then β^* in the plane of crossing is kept constant at 60 cm while β^* in the orthogonal plane is progressively lowered to 18 cm in flat optics configuration.

* jorg.wenninger@cern.ch

Content from this work may be used under the terms of the CC BY 4.0 licence (© 2026). Any distribution of this work must maintain attribution to the author(s), title of the work, publisher, and DOI.

ISBN: 978-3-95450-252-3 ISSN: 2673-5350 doi: 10.18429/JACoW-IPAC2026-MOO1T02

THE GHOST COLLIDER: AN INNOVATIVE HIGGS FACTORY*

A. Hutton[1], P. Williams[2], R. Apsimon[3], B. R. Gamage[1], M. K. Joshi[3], K. Yokoya[4]
[1]Jefferson Lab, Newport News, USA
[2]STFC, Accelerator Science and Technology Centre (ASTeC), Daresbury, UK
[3]Lancaster University, Lancaster, UK
[4]KEK, Tsukuba, Japan

Content from this work may be used under the terms of the CC BY 4.0 licence (© 2026). Any distribution of this work must maintain attribution to the author(s), title of the work, publisher, and DOI.

Abstract

The Ghost Collider is an innovative proposal for a 550 GeV centre-of-mass, 275 GeV per beam linear collider with four interaction regions, each with the design luminosity. The primary innovation is the use of "ghost bunches" containing equal numbers of electrons and positrons so they are electrically neutral. In the linacs, energy is transferred between electrons and positrons in the same bunch, decelerating one type of particle and using the energy to accelerate the other: a new class of Energy Recovery Linacs. At the interaction points, collisions between two neutral ghost bunches occurs with weakened electromagnetic interaction such as the beam-beam effect or disruption, ensuring that the particles and their energy can be recycled with minimal loss. Four "serial IPs" are incorporated, where chromatic errors produced in one IP are cancelled in the following IP. The neutral beam instability at the IP is also addressed. All interaction points have the nominal luminosity per IP of 2.8 x 10^{34} $cm^{-2}s^{-1}$ for a facility luminosity of 1.1 x10^{35} $cm^{-2}s^{-1}$ @ 100 MW electrical power for the RF systems. The result is a totally original concept for an electron-positron collider.

OVERVIEW

Two new bunch concepts are introduced and developed, both of which are electrically neutral, hence the name "Ghost Collider." Firstly, bunches within linacs contain an equal number of accelerating particles of one charge partnered with decelerating particles of the opposite charge. The bunches have no electromagnetic interaction with the linac cryomodules.

Secondly, bunches undergoing collision also have equal numbers of particles of both charges at the same energy. The bunches have little electromagnetic interaction with each other enabling recovery of both the particles and their energy.

BACKGROUND

The Ghost Collider concept grew out of two previous ideas. First, Valeri Telnov proposed a twin-axis energy recovery linac concept [1] consisting of two parallel superconducting linacs connected by RF couplers so that the fields are always equal. One linac is for acceleration, one for deceleration.

Erk Jensen suggested a different layout [2] and realized that if accelerating electrons and decelerating positrons (or vice versa) shared the same bucket, there would be no excitation of higher modes (HOMs) and no Multi-bunch Beam Break-Up (MBBU).

This differs from Telnov's proposal in that each of the four linacs is used for both acceleration and deceleration. For the same $E_{\max}$, the accelerating gradient is halved so dynamic losses are reduced by a factor 4, potentially allowing operation in CW mode. This comes at the expense of SR losses in the outer arcs at $E_{\max}/2$, which is still large, but only 1/16 of the synchrotron power at $E_{\max}$. A second variant of the Ghost Collider has been developed that eliminates these arcs, at the expense of additional length. This is described in an accompanying paper [3].

Accelerated electrons and decelerated positrons travel in the same linac and at the same phase location, so the total current is zero. Electrons are accelerated at the peak of the RF wave and positrons are decelerated. No energy is taken or added to the RF wave; the energy is transferred between the electrons and positrons – intra-bucket energy recovery – a new ERL mode.

GHOST COLLISIONS

Positrons and electrons in a single bunch can be brought into collision with positrons and electrons which are also in a single bunch; two neutral plasmas colliding so there will be little electromagnetic interaction (beam-beam effect or disruption).

This was first tried (unsuccessfully) at Orsay by the DCI Storage Ring Team [4]. This was followed by several papers showing that the plasmas are in an unstable equilibrium [5-8]. All of them considered a regime where the uncompensated disruption coefficient was high (between 5 and 10) as the beams would be dumped after collision. The Ghost Collider is aiming for a smaller uncompensated disruption coefficient because the beams will be recovered after collision. The previous work indicates that this regime should be stable, and this has been confirmed by simulation for the Ghost Collider conditions.

INTERACTION REGION DELAY CONCEPT

Electrons are injected into a bucket which accelerates the electrons; positrons are injected into the same bucket and are decelerated. Positrons are injected into a bucket $\lambda_{\mathrm{Linac}}/2$ behind the first bucket and are accelerated; electrons are injected into the same bucket and are decelerated.

A chicane delays the electrons between the Linac and the Interaction Region by $\lambda_{\mathrm{Linac}}/2$. The same layout is used for the other linac; collisions take place with zero crossing

* This material is based upon work supported by the U.S. Department of Energy, Office of Science, Office of Nuclear Physics under contract DE-AC05-06OR23177

ISBN: 978-3-95450-252-3 ISSN: 2673-5350 doi: 10.18429/JACoW-IPAC2026-MOO1T03

PROGRESS TOWARDS A MUON COLLIDER

P. B. Jurj*, Imperial College London, London, United Kingdom
C. Rogers, Science and Technology Facilities Council, Didcot, United Kingdom
on behalf of the International Muon Collider Collaboration

Content from this work may be used under the terms of the CC BY 4.0 licence (© 2026). Any distribution of this work must maintain attribution to the author(s), title of the work, publisher, and DOI.

Abstract

The muon collider concept promises a unique opportunity to push the energy frontier in particle physics. The large muon mass suppresses synchrotron radiation and allows the acceleration and collision of the beams in rings and the use of technology more similar to hadron colliders. Muons are point-like, in contrast to protons, and thus can achieve a similar physics reach with less energy, allowing for a more compact machine. However muons have a lifetime of only 2.2 microseconds at rest. The muon beam thus needs to be cooled and accelerated rapidly to maximise the luminosity, which creates several technology challenges. The International Muon Collider Collaboration is implementing an intense R&D programme to address these challenges and to develop the concept maturity. The paper will highlight the key challenges, summarise the progress of the work and the proposed R&D plan for the next decade.

INTRODUCTION

The muon collider is a unique, high-energy collider concept that combines the high-energy reach of a hadron collider with the precision of a lepton collider, opening the path to multi-TeV parton-parton collisions in a compact footprint. Two single-bunch muon beams of opposite charge are produced from a high-power proton driver, ionisation-cooled, accelerated rapidly, and brought to collision in a collider ring. The short muon lifetime of 2.2 µs at rest is the central technical challenge: the beams must be cooled and accelerated to multi-TeV energies on a timescale set by their own decay. The muon collider concept was developed by the U.S. Muon Accelerator Program (MAP) until 2017 [1]. It is now being progressed by the International Muon Collider Collaboration (IMCC) [2,3], formed following the previous European Strategy for Particle Physics Update (ESPPU), which recognised the importance of studying the muon collider as a potential path for the future of particle physics. This direction was subsequently reinforced by the U.S. Particle Physics Project Prioritisation Panel (P5), reflecting broad international support for the development of the concept. The scientific potential of the muon collider and the innovative research it demands have motivated a growing community, including many early career researchers, enabling the IMCC to pursue an active and innovative R&D programme to advance the muon collider design and underlying technologies. The collaboration provided a comprehensive input [4, 5] to the 2026 update of the European Strategy for Particle Physics, including an assessment of the concept and the technologies, a ten-year R&D plan, and implementation considerations. It also released the Consolidated Parameters Report [6] in October 2025, establishing a coherent baseline for the 10 TeV design across all subsystems. This paper summarises the current status of the design and the progress of the R&D programme. Detailed discussions of the latest developments are presented in dedicated contributions to this conference.

THE MUON COLLIDER CONCEPT

The baseline muon collider design targets a centre-of-mass energy of 10 TeV and an integrated luminosity of $10\,\mathrm{ab}^{-1}$ [2, 6]. An initial stage with implementation around 2050 is also under consideration. The schematic layout of the collider is shown in Fig. 1 and contains the following key areas (in colour-coded boxes, from left to right):

- The proton driver produces a short, high-intensity proton pulse.
- The pulse impinges on a target and produces pions. The decay channel guides the pions and forms a beam with the resulting muons via a buncher and phase rotator system.
- Several cooling stages reduce the longitudinal and transverse emittance of the beam through ionisation cooling, using a sequence of absorbers and RF cavities embedded in a high magnetic field.
- A linac and two recirculating linacs accelerate the beams to 63 GeV, followed by a chain of rapid-cycling synchrotrons reaching either 1.5 TeV or 5 TeV.
- The beams are injected at full energy into the collider ring, where they circulate and collide within the detectors until they decay.

Table 1 summarises the key target parameters for the muon collider, in two stages, for both a site-independent design and a specific implementation at CERN reusing existing infrastructure. The site-independent parameters at 3 TeV and 10 TeV centre-of-mass energy are set to probe the limits of each technology and design. If they can be fully met, the integrated luminosity goal is reached within five years of full operation, or 2.5 years with two detectors, leaving margin for further design and technology studies and for a realistic luminosity ramp-up.

Implementations at CERN and Fermilab are under consideration. At CERN, the existing SPS and LHC tunnels could host the high-energy muon acceleration chain, allowing a centre-of-mass collision energy of up to 7.6 TeV with a practical initial stage at up to 3.2 TeV, depending on the layout.

* paul.jurj13@imperial.ac.uk

ISBN: 978-3-95450-252-3 ISSN: 2673-5350 doi: 10.18429/JACoW-IPAC2026-MOI7M01

DEVELOPMENT OF LOW PERIOD CRYOGENIC PERMANENT MAGNET UNDULATORS

M. Valleau†, Synchrotron-SOLEIL, Gif-sur-Yvette, France

Abstract

Undulators are widely employed on accelerator-based light sources. The length of these devices is usually constrained by the length of the straight sections, and this will become even more critical for Diffraction Limited Storage Rings based on existing Synchrotrons, where the required number of magnets to store the electron beam is huge. Thus, to reach high brightness and flux, the total number of periods of undulators must remain large and the magnetic period values will be reduced. Cryogenic Permanent Magnets Undulators (CPMU) are a solution to keep a high peak field value while decreasing the magnetic period. Planar CPMUs have become widely adopted in Synchrotrons worldwide and some laboratories are developing equivalent devices providing also elliptical polarizations. A review of low period CPMU installed on accelerator-based light sources is presented.

INTRODUCTION

For 30 years, In-Vacuum Undulators (IVUs) are operated on accelerator-based light source, based on the pioneering work of SPring-8. Nowadays they are in use in nearly every Synchrotron Light Source. In 2005, SPring-8 developed the first prototype of CPMU, derived from a standard In-Vacuum Undulator (IVU) design. In 2008, the ESRF was the first to install on a storage ring a full scale CPMU. Presently 38 CPMUs are installed on 10 Synchrotron Radiation Facilities worldwide (see Table 1) and 14 prototypes have been developed, which highlights the strong interest for such a technology.

CONSTRUCTION OF SHORT CPMUS AT ROOM TEMPERATURE

Choice of the Permanent Magnet Grade

First IVUs were built using SmCo magnets due to their strong coercivity with hard resistance against demagnetization induced by electron beam irradiation. Then, to enhance the magnetic field, NdFeB magnet grades have been used. This magnet grade has also been used for the first CPMUs built by SPring-8, ESRF, DLS, SLS and SSRF [1-3]. When cooled down, the coercivity of this grade increases by at least a factor of 4, so as the remanence within 15%, which reaches a maximal value around 135 K before falling at 77 K due to the Spin Re-orientation Transition (SRT) [4-6]. Then Praseodymium has been chosen due to its properties more adapted with cryogenic temperatures. As the PrFeB magnets don't exhibit SRT between 50 K and 300 K [7], they can be cooled down directly at 77 K which simplifies a lot the thermal design and the operation with such undulators on storage rings. Before starting the magnetic design of an undulator, different magnet grades have been tested at low temperatures to be able to evaluate the magnetic field produced by the undulator under these conditions and select the appropriate period meeting the beamline requirements [4].

Mechanical and Magnetic Design

The mechanical design of CPMUs is generally derived from the one of the IVUs: magnets are clamped on holders, which are fixed on aluminium or Oxygen-Free Copper in-vacuum girders, connected to external ones thanks to several pairs of rods as shown in Fig 1. On an undulator, the magnetic forces increase exponentially while the gap decreases, which can imply some deformations on the in-vacuum girders, the global carriage itself and induce heavy load on the gap-drive system. This C-shape type carriage can usually handle magnetic forces up to 30 kN. NEOMAX Engineering developed spring modules installed on the carriage to reduce the magnetic efforts seen by the carriage and prevent from phase error variations at closed gap on a large range [8]. Some studies have also been held on the number and positioning of the rods and conclude that it is not necessary to implement a huge number of pairs uniformly positioned but sometimes, four pairs of rods is the optimal number and enable to reach lower phase error values [9]. At the ESRF, the rods between the top and bottom girders are shifted in longitudinal enabling a better control of the vertical magnetic field profiles.

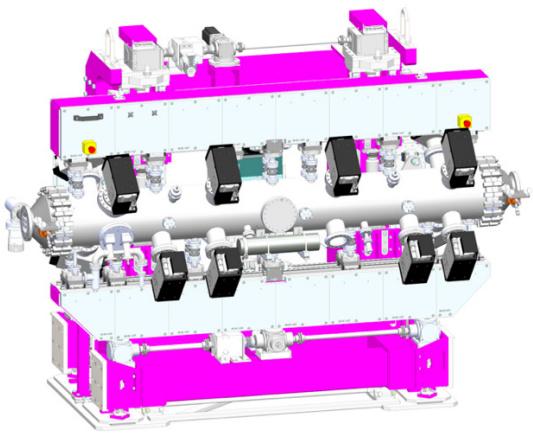

Figure 1: Mechanical design of CPMUs at ESRF.

†mathieu.valleau@synchrotron-soleil.fr

Content from this work may be used under the terms of the CC BY 4.0 licence (© 2026). Any distribution of this work must maintain attribution to the author(s), title of the work, publisher, and DOI.

ISBN: 978-3-95450-252-3 ISSN: 2673-5350 doi: 10.18429/JACoW-IPAC2026-MOI7M02

HTS TECHNOLOGY DEVELOPMENT FOR ENERGY EFFICIENT MAGNETS IN PSI LARGE RESEARCH FACILITIES

S. Sanfilippo[†,1], B. Auchmann[1], A. Brem[1], C. Calzolaio[1], M. Casciello[1,2], M. Duda[1], Q. Gorit[1], G. Montenero[1], J. Kosse[1], D. Martins[1], K. Puthran[1], R. Riccioli[1], D. Sotnikov[1], C. Zoller[1],
[1]PSI Center for Accelerator Science and Engineering, Villigen, Switzerland
[2]Politecnico di Torino, Torino, Italy

Abstract

Over the past decade, the Magnet Section at the Paul Scherrer Institute (PSI) has developed extensive expertise in superconducting magnet design, fabrication, assembly, and testing through PSI strategic projects and the CHART (Swiss Accelerator and Research Technology) MagDev program. This expertise provides a strong foundation for the energy transition of magnet systems in large research facilities. At PSI, this transition is supported by complementary initiatives: CHART, SMILE (Superconducting Magnets to Improve Large Research Facilities Efficiency), and the European project HTS4SRI. They enable the development of High-Temperature Superconductor (HTS) magnet technologies to improve performance while reducing electricity consumption and CO_2 emissions. This article outlines the proposed roadmap and presents the R&D directions. Key directions include HTS tape and cable technologies for DC and AC applications, conduction-cooled magnets, pulsating heat pipes for thermal management, efficient cryogenic powering, radiation-hard conductors for high-intensity target areas, and life-cycle assessment. An integrated framework for the design, manufacturing, and qualification of energy-efficient superconducting magnets is now being established. The long-term strategy is to progressively install efficient HTS magnets across PSI's large research facilities and supporting more sustainable accelerator technologies.

INTRODUCTION

Over the past decade, magnet technology for large research infrastructures at the Paul Scherrer Institute (PSI) has undergone a profound transformation. Initially focused on resistive magnets, developments have progressively shifted toward compact, energy-efficient solutions, and more recently toward approaches integrating sustainability considerations. This transition has been driven by major strategic projects such as the SLS 2.0 [1] and the IMPACT project, including the HIMB and TATTOOS beamlines [2] as well as by PSI's strong involvement in CHART (Swiss Accelerator Research and Technology consortium) and initiatives such as SMILE (Superconducting Magnets to Improve the Efficiency of Large research Facilities). This article presents the context and motivations behind the development, the key drivers enabling this transformation, and the outcomes in terms of infrastructure, coils, and magnets based on high-temperature superconducting technologies. Technologies related to the use of permanent magnets, as well as NbTi and Nb_3Sn superconductors, are addressed in separate articles [3, 4].

† stephane.sanfilippo@psi.ch

CONTEXT AND MOTIVATIONS

PSI Large Research Facilities

Large research infrastructures at the Paul Scherrer Institute are true engines of discovery, producing proton, neutron, muon, and photon beams that serve as probes of matter. Facilities such as the High Intensity of Proton Accelerator Complex (HIPA), the Swiss Light Source (SLS 2.0), and the two lines of the Free Electron Laser (SwissFEL) support fundamental research, materials science, and medical applications including proton therapy. These facilities are highly energy-intensive, with a large share of electricity consumed by accelerator magnets used to steer and control particle beams. At the Paul Scherrer Institute, the total annual energy consumption is approximately 140 GWh. The High-Intensity Proton Accelerator (HIPA) accounts for about 50% of this consumption, with around 26% attributed to magnets. Future projects such as the IMPACT project (HIMB and TATTOOS) will further intensify these needs, relying on more powerful magnets in demanding environments, which increases energy consumption with conventional technologies [5].

HTS Technology for PSI Magnets

PSI magnet section has progressively developed expertise in energy-efficient accelerator magnet technologies, particularly through high-temperature superconducting magnets. This evolution reflects a broader trend in which traditional requirements—performance, field quality, stability, and reliability—are now complemented by energy efficiency and sustainability, as illustrated in Fig. 1.

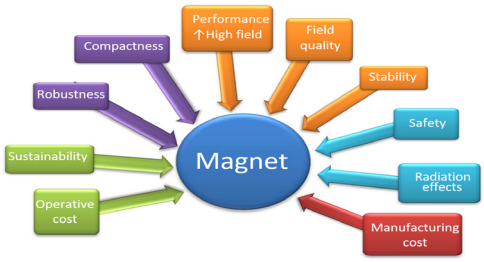

Figure 1: Accelerator magnet requirements combining core criteria—performance, field quality, stability, robustness—with emerging priorities such as energy efficiency, sustainability, operation cost, radiation tolerance.

Content from this work may be used under the terms of the CC BY 4.0 licence (© 2026). Any distribution of this work must maintain attribution to the author(s), title of the work, publisher, and DOI.

ISBN: 978-3-95450-252-3 ISSN: 2673-5350 doi: 10.18429/JACoW-IPAC2026-MOO7M01

COMMISSIONING OF THE RF SYSTEM FOR HIGH ENERGY PHOTON SOURCE

P. Zhang[1,2,*], T. Huang[1,2], D. Li[1], J. Li[1,2], H. Lin[1], Q. Ma[1,2], F. Meng[1], Z. Mi[1,2], Q. Wang[1,2], X. Zhang[1,2], F. Zhao[1], H. Zheng[1,2]
[1]Institute of High Energy Physics (IHEP), CAS, Beijing 100049, China
[2]University of Chinese Academy of Sciences (UCAS), CAS, Beijing 100049, China

Content from this work may be used under the terms of the CC BY 4.0 licence (© 2026). Any distribution of this work must maintain attribution to the author(s), title of the work, publisher, and DOI.

Abstract

The High Energy Photon Source (HEPS), recently commissioned in Beijing, is a 6 GeV diffraction-limited storage-ring light source. A double-frequency RF system was adopted, comprising five 166.6 MHz superconducting RF (SRF) cavities acting as the fundamental and two 499.8 MHz SRF cavities serving as the third harmonic for bunch lengthening. A β=1 quarter-wave SRF cavity was developed in-house to achieve the low RF frequency and high power within a compact longitudinal space, while also enabling heavy damping of higher order modes. Solid-state amplifiers provide a total installed RF power of 2.4 MW to drive the cavities in both the booster and the storage ring. A digital low-level RF system was also developed in-house and is currently in stable operation. A beam current of 100 mA was successfully achieved using the nominal SRF setup. The design, construction, and commissioning results of the HEPS RF system are presented.

INTRODUCTION

The High Energy Photon Source (HEPS) is a recently commissioned 6 GeV diffraction-limited synchrotron light source in Beijing [1–4]. The construction began in June 2019, and the facility passed its key performance tests in October 2025. The electron beam is first accelerated to 500 MeV by the linear accelerator, then injected into the 454 m booster ring to further ramp its energy to 6 GeV, and finally injected into the 1360.4 m storage ring, where a beam current of 200 mA can be stored. The main parameters of HEPS are listed in Table 1.

Table 1: Main Parameters of HEPS

Parameter	Value
Circumference [m]	1360.4
Beam energy [GeV]	6
Beam current [mA]	200
Energy loss (bare) [MeV]	2.64
Energy loss to 14 IDs [MeV]	1.5
Total energy loss [MeV]	4.14
Total beam power [kW]	850
Main RF freq. [MHz]	166.6
Total main RF voltage [MV]	5.16
Third-harmonic RF freq. [MHz]	499.8

* Email: zhangpei@ihep.ac.cn

A double-frequency RF system is employed for HEPS to achieve bunch lengthening [5] and to enable a novel on-axis accumulation injection scheme [6]. The main RF frequency was chosen to be 166.6 MHz, with a third harmonic frequency of 499.8 MHz [7]. The relatively low fundamental RF frequency yields longer bunches, lowering the bunch current density, thus reducing intra-beam scattering, raising impedance thresholds for coupled-bunch instabilities, and eventually improving the beam lifetime. Superconducting RF (SRF) technology was adopted for both cavities. The configuration consists of five 166.6 MHz SRF cavities serving for main acceleration [8, 9] and two 499.8 MHz SRF cavities for bunch lengthening, as shown in Fig. 1. To accommodate future HEPS upgrade requirements, six of the 48 straight sections have been allocated to the RF system. Furthermore, the booster ring utilizes six normal-conducting (NC) 5-cell cavities to ensure sufficient RF acceptance when receiving the high-energy electron bunches from the storage ring during charge accumulation [10].

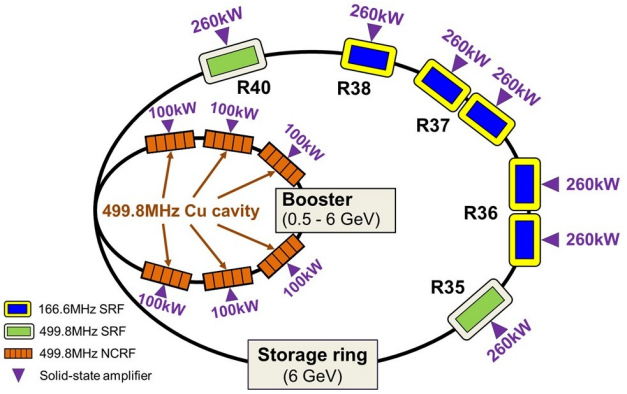

Figure 1: General layout of HEPS RF system.

The commissioning of the booster ring was conducted in 2023 with five NC cavities, providing an RF voltage of 6.2 MV to enable beam energy ramping from 500 MeV to 6 GeV [11]. The commissioning of the storage ring was performed in two stages. During the first stage (July 2024 to May 2025), two 500 MHz booster NC cavities and one 500 MHz SRF cavity were installed specifically for vacuum scrubbing. Large outgassing was expected from the newly installed vacuum chambers due to direct irradiation by synchrotron lights. The remaining SRF cavities were installed during the second stage in June 2025, after a sufficient beam dose had been accumulated. The nominal RF configuration was thus been restored preparing for the high-current operation. This scheme will lower the risk of SRF cavity

ISBN: 978-3-95450-252-3 ISSN: 2673-5350 doi: 10.18429/JACoW-IPAC2026-MOO7M03

MACHINE LEARNING TECHNIQUES FOR DESIGN OF COMPLEX ACCELERATOR MAGNETS*

S. Gresty[1†], T. Gallagher[1], A. Wolski[1], University of Liverpool, Liverpool, United Kingdom
B. Muratori[1], ASTeC STFC Daresbury Laboratory, Daresbury, Warrington, United Kingdom
[1]also at Cockroft Institute, Daresbury, United Kingdom

Abstract

The design of multipole and other magnets for accelerators is typically an iterative process in which the magnet geometry is optimised for the required beam dynamics properties. Modelling the field for a given geometry can be computationally expensive, so exploring the parameter space can be a time-consuming procedure. The task is particularly challenging when complex field properties are needed (for example, in magnets with several multipole components or with longitudinal field variation). Combined function magnets with several multipole components are particularly useful in accelerators with tight spatial constraints such as an X-ray Free Electron Laser (XFEL). Surrogate models using neural networks can provide a way of rapidly generating possible magnet geometries for given field or beam dynamics requirements. In this contribution, we discuss how machine learning tools may be used to improve the efficiency of the design process for complex accelerator magnets, and present results from a case study based on a combined function magnet for the beam spreader in a future XFEL.

INTRODUCTION

Accelerator magnets generally need to meet demanding field quality specifications if the accelerator is to achieve its performance goals; as a result, design studies for a new accelerator project will usually include a significant amount of magnet modelling work. The required beam properties, specified during the accelerator design process, are used to determine the field properties and field quality needed in each magnet or family of magnets. Modelling of the magnets is then commonly performed using computer codes based on finite element analysis (FEA), for example [1, 2] or boundary integral methods [3]: the design work proceeds iteratively until the desired field quality is achieved. Although numerical computer codes are capable of good accuracy in modelling the field from a given magnet design, calculation of the field is often computationally expensive, and if many design iterations are needed, achieving the required specifications can take a considerable amount of time.

In this paper, we present a technique to assist with accelerator magnet design based on the use of a machine learning (ML) surrogate model to predict the geometry of a magnet given a set of required multipole components. Surrogate models have been shown to be useful for optimisation problems in accelerator research, including for separate components (e.g. [4–6]) and for systems of many components (e.g. [7–11]). Machine learning has also been used to model hysteresis in magnets to assist accelerator tuning [12], but so far there has been little work on surrogate models for magnet design.

One previous study in this area [13] has demonstrated the ability to use machine learning for multipole magnet design in the case of "idealised" magnets in which the material in the core of the magnet is assumed to have infinite permeability and no field saturation limit. In this case, field calculations are simplified since the pole face lies on a surface of constant scalar potential. In these proceedings, we show that a similar machine learning approach can be applied to normal-conducting electromagnets with material in the core having realistic magnetic properties: we show an example based on permeability and field saturation limits typical of iron commonly used in accelerator magnets. The technique aims to increase the efficiency of magnet design work, especially in cases where field specifications may be complex (involving, for example, several multipole components) and where different parameter spaces need to be explored.

Although the use of machine learning tools means that some computational time is needed to generate training data for the surrogate model, generation of the training data is more readily automated than the iterative design process: once a surrogate model is established, it can be used to explore a wide range of design parameters without the need to recompute the field (using a numerical field solver) with each small change in the design. With further development of the technique, surrogate models could be trained to estimate magnet designs directly from beam dynamics specifications (e.g. in terms of required transfer functions). In principle, the techniques may be extended to other magnet technologies, e.g. permanent magnets.

The use of machine learning tools to improve the efficiency of magnet design could prove especially useful for magnets that are not simply conventional multipoles with essentially just a single multipole field component. Magnets with a single component are relatively straightforward, and design work for a magnet for a specific application can often be informed by existing devices. However, modern accelerators are increasingly using complex magnets, including magnets with several multipole field components and with strengths that vary along the length of a magnet: one example is the use of "longitudinal gradient dipoles" to help reduce the beam emittance in ultra-low emittance light sources [14–16]. Beam spreaders in high-power X-ray Free

* This work is supported by Science and Technology Facilities Council, UK, through a grant awarded to The Cockcroft Institute
† sophie.gresty@gmail.com

Content from this work may be used under the terms of the CC BY 4.0 licence (© 2026). Any distribution of this work must maintain attribution to the author(s), title of the work, publisher, and DOI.

ISBN: 978-3-95450-252-3 ISSN: 2673-5350 doi: 10.18429/JACoW-IPAC2026-MOP1001

STUDY OF QUENCH MARGINS FOR BETATRON HALO LOSSES WITH NEW HL-LHC COLLIMATION OPTICS

N. Duarte*, R. Bruce, L. S. Esposito, H. Guérin, A. Lechner, B. Lindstrom, S. Redaelli, V. Rodin
CERN, Geneva, Switzerland

Content from this work may be used under the terms of the CC BY 4.0 licence (© 2026). Any distribution of this work must maintain attribution to the author(s), title of the work, publisher, and DOI.

Abstract

The High-Luminosity Large Hadron Collider (HL-LHC) will mark a new phase of LHC operation, aiming to reach an integrated luminosity of 3000 fb^{-1} over 10 years of operation. A key element to achieve this target is the beam intensity increase, nearly doubling the number of protons per bunch compared to the initial LHC design. This increases the load on the collimators protecting against beam losses, particularly in the betatron cleaning insertion region (IR7), a multistage collimation system responsible for beam halo cleaning. Particles intercepted here may undergo diffractive scattering and propagate for hundreds of meters, reaching the adjacent dispersion suppressor (DS) sections.

To assess the impact of these losses, FLUKA simulations have been performed to predict the power deposition in the superconducting DS magnets on both sides of IR7. Accurate modeling of these losses is essential to ensure safe machine operation and to optimize beam loss monitor thresholds, minimizing unnecessary protective beam dumps.

In this contribution, we present shower simulation studies for the latest HL-LHC collimation optics (v1.6), with improved cleaning and impedance in IR7, and compare them to the previous one (v1.5).

INTRODUCTION

Run 4 of the LHC, scheduled to start in 2030 after the completion of Long Shutdown 3 (LS3), will mark the beginning of the High-Luminosity LHC (HL-LHC) proton-proton operation, and will already bring an increase of the levelled peak luminosity from 2.2×10^{34} cm^{-2} s^{-1} achieved during Runs 2 and 3 to about 5×10^{34} cm^{-2} s^{-1}, with a possible further increase in later years, ultimately reaching 7.5×10^{34} cm^{-2} s^{-1} [1]. This luminosity is intentionally limited through luminosity levelling to reduce event pile-up in the detectors, which in turn allows for longer fills [2].

The increase in luminosity is achieved through improvements on multiple fronts across the accelerator complex: the total number of protons circulating in each beam will be nearly doubled compared to the original design parameters, an upgrade of the inner triplet magnets at insertion regions IR1 (ATLAS) and IR5 (CMS) will provide reduced beam sizes by means of stronger focusing [3], and the installation of crab-cavities (also in IR1 and IR5) which rotate the proton bunches to maximize the overlap of the colliding beams [4].

To mitigate impedance-induced instabilities and accommodate higher luminosity and new experimental layouts, the HL-LHC upgrade includes the installation and replacement of multiple collimators [5]. Monte Carlo simulations are fundamental for optimizing collimation configurations [6] and assessing the quench margin with higher beam intensities in the HL-LHC era. Beam tracking simulations are used to model the dynamics of halo particles and to estimate where the most critical losses around the ring occur [7]. This information is then used as input for particle–matter interaction simulations, modelling the development of hadronic and electromagnetic showers in the accelerator components, allowing to predict localized energy depositions in sensitive elements, such as superconducting magnet coils [8, 9].

In this work, we study the impact of betatron halo losses, leaking out of the collimation system, on the dispersion suppressor (DS) magnets adjacent to the betatron cleaning insertion region IR7 using the latest HL-LHC collimation optics (v1.6), with increased beta functions in IR7 allowing for larger physical collimator gaps and reduced impedance [10]. The results are compared with those for the previous HL-LHC baseline optics version (v1.5).

HL-LHC COLLIMATION SYSTEM

The energy stored in each of the HL-LHC colliding beams, around 680 MJ, requires careful control of beam losses to prevent quenches of superconducting magnets. Of particular concern are the niobium-titanium (NbTi) coils of the LHC dipole magnets, operating at a temperature of 1.9 K, and in the immediate surrounding of the beam pipes. Local energy deposition from lost protons and secondary particles can induce a heating effect and increase the coil temperature beyond the critical value, resulting in a magnet quench, which may lead to several hours of downtime until proper cryogenic conditions are restored. To mitigate this, beam losses must be carefully monitored and controlled.

The LHC collimation system was designed to withstand beam lifetimes as low as 12 min, sustained for up to 10 s, at 7 TeV energy. This requirement is maintained for the HL-LHC, implying that collimators must be able to cope with higher power losses due to the higher beam intensity [11].

To achieve efficient cleaning, the LHC employs two complementary cleaning insertions: momentum cleaning in IR3 and betatron cleaning in IR7. Both regions use a multistage collimation hierarchy in which primary collimators are positioned closest to the beam, intercepting most of the halo particles with large transverse amplitudes. Particles scattered at the primary collimators (TCPs) generate particle showers that are subsequently intercepted by secondary collimators (TCSs) and active shower absorbers (TCLAs).

The main bottleneck of the LHC regarding collimation leakage are the dispersion suppressor (DS) sections on both

* Work supported by the High Luminosity LHC project.
Corresponding author: nuno.duarte@cern.ch

ISBN: 978-3-95450-252-3 ISSN: 2673-5350 doi: 10.18429/JACoW-IPAC2026-MOP1003

OBSERVATIONS OF 50 Hz HARMONICS IN THE LHC TRANSVERSE BEAM SPECTRA

A. Radoslavova*, H. Bartosik, I. Efthymiopoulos, S. Kostoglou, G. Sterbini
European Organization for Nuclear Research, Geneva, Switzerland
G. Franchetti†, GSI Helmholtz Centre for Heavy Ion Research, Darmstadt, Germany

Content from this work may be used under the terms of the CC BY 4.0 licence (© 2026). Any distribution of this work must maintain attribution to the author(s), title of the work, publisher, and DOI.

Abstract

In the Large Hadron Collider (LHC), several beam diagnostic systems provide turn-by-turn and bunch-by-bunch position, enabling a precise characterization of the transverse beam spectra up to high frequency. Using these instruments, the presence of external excitations at 50 Hz harmonics have been observed to affect the beam motion. In this work, we combine these measurements to study the evolution of the noise content in the LHC, with particular focus on the 50 Hz harmonics clustered around 8 kHz, which corresponds to an important range of the transverse beam spectrum. While the exact source of the excitation remains unknown, this study provides new insights into the mechanisms behind this excitation and the evolution of the harmonic lines along the LHC cycle based on statistics collected from operational physics fills in 2025.

INTRODUCTION

The Large Hadron Collider (LHC) is equipped with a variety of transverse beam diagnostics that provide turn-by-turn and bunch-by-bunch position measurements [1]. These systems enable detailed spectral analyses of transverse beam dynamics up to high frequency throughout the different phases of the LHC cycle, from injection to collision energy.

Among the spectral features observed in the transverse beam planes, a cluster of 50 Hz mains harmonics has been systematically observed in previous LHC runs, in particular around 8 kHz in close proximity to the lower betatron sideband of the revolution frequency. The spectral signature of this noise points to a dipolar excitation, rather than a tune modulation. In the current study, the focus is on the horizontal plane, since the amplitude of its harmonics is systematically larger than the harmonics in the vertical plane [2–4].

The 8 kHz cluster is of particular interest as it may be linked to the unexplained emittance growth observed in the LHC at injection and top energy. In fact, the measured emittance growth is not consistent with the expected emittance evolution considering Synchrotron Radiation (SR) and Intrabeam Scattering (IBS) effects. Furthermore, recent tracking simulations using a realistic 8 kHz harmonic excitation confirm a possible emittance growth contribution [5]. This motivates a deeper investigation into the nature and origin of the 8 kHz excitation and its role in emittance growth.

While these harmonics have been systematically observed at injection and top energy, their evolution during the energy ramp was not studied in the past. In addition, no mechanism responsible for changes in their amplitude had been found up to now that could help identify their underlying origin.

In the first part of this work, we study the evolution of the 8 kHz cluster throughout the energy ramp. A Fast Fourier Transform (FFT) is computed, showing the frequency content of the centroid motion of the bunches in the vicinity of the 8 kHz cluster as a function of time. An algorithm combining bunch-by-bunch and turn-by-turn position measurements, including a phase-advance correction between bunches, is used to extend the spectrum beyond the LHC turn-by-turn Nyquist frequency (≈5.5 kHz given the beam revolution frequency of ≈11 kHz) [2]. In the second part, we demonstrate a clear link between the Main Dipole Active Filters (AFs) and the enhancement of the 50 Hz harmonic amplitudes.

BEAM ENERGY DEPENDENCE

To highlight the dependence of the harmonic amplitudes on the beam energy, two representative fills are compared: a fill where the top energy was limited to 2.68 TeV and a physics fill at the nominal flat top energy of 6.8 TeV. Figure 1 shows the horizontal spectra in the range between 7400 Hz and 8700 Hz, from the start of the ramp to top energy, for the two cases. The different phases of the cycle are also indicated. Focusing on the nominal case (left), the amplitudes of the harmonics closest to the lower betatron sideband (blue) are strongly enhanced, which is consistent with the fact that the beam is more sensitive to external dipolar excitations close to the betatron tune. When the machine tune is changed from the injection working point to the collision one before the beams are brought into collision (ADJUST phase), the amplitudes of the harmonics above 8 kHz are attenuated while those below 8 kHz are enhanced, following the tune frequency evolution. This explains the change of the cluster location that is systematically observed at every fill.

However, an additional observation is that at 2.68 TeV, the 8 kHz cluster is either absent or just barely above the noise floor level (Fig. 1, right). Examining the evolution of the harmonic lines during the energy ramp in a nominal physics fill, a pronounced enhancement is observed at beam energies above approximately 5.5 TeV. Below this threshold the spectral content remains mostly unchanged, while the harmonic amplitudes increase rapidly above it during the

* also at Goethe University Frankfurt
† also at Goethe University Frankfurt, Frankfurt am Main, Germany; European Organization for Nuclear Research, Geneva, Switzerland

ISBN: 978-3-95450-252-3 ISSN: 2673-5350 doi: 10.18429/JACoW-IPAC2026-MOP1005

EMITTANCE GROWTH DUE TO POWER CONVERTER RIPPLE AND NOISE AT 50 Hz HARMONICS DURING LHC COLLISIONS

A. Radoslavova[1,2], H. Bartosik[1], I. Efthymiopoulos[1], S. Kostoglou[1], G. Sterbini[1], G. Franchetti[1,2,3]
[1]European Organization for Nuclear Research, Geneva, Switzerland
[2]also at Goethe University Frankfurt, Frankfurt am Main, Germany
[3]also at GSI Helmholtz Centre for Heavy Ion Research, Darmstadt, Germany

Content from this work may be used under the terms of the CC BY 4.0 licence (© 2026). Any distribution of this work must maintain attribution to the author(s), title of the work, publisher, and DOI.

Abstract

Transverse emittance growth can adversely affect the luminosity production performance of colliders such as the Large Hadron Collider (LHC) at CERN. While Intra-Beam Scattering (IBS) and Synchrotron Radiation (SR) effects represent important ingredients for the emittance evolution, measurements in the LHC do not match predictions from these two effects, suggesting the presence of additional emittance growth mechanisms. External excitations, such as power supply ripple and noise at 50 Hz harmonics, are additional sources of emittance growth especially in the presence of non-linearities as induced by beam-beam effects. In the LHC, the most prominent excitations during collisions are harmonics of 50 Hz clustered around 8 kHz. In this work, we quantify the expected contribution of these excitations to the emittance evolution and proton losses using single particle tracking simulations including a realistic excitation spectrum as observed in operation.

INTRODUCTION

In high-energy hadron colliders, such as the Large Hadron Collider (LHC), preserving low transverse emittances is essential to maximize the integrated luminosity. At the LHC top energy, Intra-Beam Scattering (IBS) and Synchrotron Radiation (SR) effects are expected to be the main contributors to the emittance evolution. However, measurements in the LHC indicate the presence of additional sources of emittance growth that are not captured by the present models.

One potential source of this extra emittance growth is power converter ripple, systematically observed on the transverse beam spectrum. It appears as dipolar excitations at harmonics of 50 Hz clustered around 8 kHz, close to the lower betatron sideband ($1 - Q_x$). The origin of this high-frequency cluster is still under investigation and is beyond the scope of this paper [1]. Here we focus on the impact of the 8 kHz cluster on the horizontal plane of the beam, since the measured amplitude of the harmonics in the horizontal plane is higher than the one in the vertical plane.

Analytical estimates suggest that power supply ripple can drive emittance growth, depending strongly on its proximity to the betatron tune [2]. In addition, beam-beam interactions generate a significant tune spread which, in the presence of external excitations, can enhance diffusion and ultimately lead to emittance growth.

In this paper, we use tracking simulations, including the measured excitation spectra [3], to quantify the contribution of the 8 kHz cluster to horizontal emittance growth during collisions. The analysis covers both nominal LHC operation and special runs, such as the Van der Meer (VdM) configuration, where beam and machine parameters deviate significantly from those of standard physics operation. In nominal operation, we observe a discrepancy between measured emittance growth and predictions based on IBS and SR alone. In contrast, in VdM configurations, simulations and measurements show good agreement, suggesting a reduced sensitivity to external excitations in this regime.

SIMULATION SETUP

This section describes the methodology used to evaluate horizontal emittance growth at top energy with $\beta^* = 120$ cm in Interaction Points 1 and 5 (IP1 and IP5). This is the first step of the luminosity levelling process in the LHC, where the optical β-functions at the IPs is dynamically changed during the fill to ensure constant luminosity. At this stage, the beams are colliding head-on with the maximum bunch intensity, which then decreases due to burn-off. All simulations are performed in this configuration as it corresponds to the case with the largest head-on tune spread, and thus it is expected to be most sensitive to the impact of power supply ripple.

The analysis workflow consists of three main steps:

- Extraction of calibrated spectrum of horizontal turn-by-turn beam oscillations from measurements.
- Including modulated dipolar kicks in the simulations to reproduce the measured spectrum.
- Element-by-element tracking simulations including beam-beam effects and noise.

Experimental Data

The data used to reproduce the noise in simulations were obtained from a calibrated beam position monitor, namely the ADTObsBox [3]. It consists of four high-sensitivity pickups measuring turn-by-turn, bunch-by-bunch transverse centroid beam motion.

The LHC revolution frequency is 11245.5 Hz. In order to resolve frequency components beyond the Nyquist limit of a single observation point, multiple observation points are required. This is achieved using a method previously introduced in [4], where individual bunches are treated as independent observation points. After correcting for the betatron phase advance between bunches, the signals can be combined, effectively extending the observable frequency range from ≈5.5 kHz up to ≈11.2 kHz (revolution frequency).

ISBN: 978-3-95450-252-3 ISSN: 2673-5350 doi: 10.18429/JACoW-IPAC2026-MOP1006

STUDY AND MITIGATION OF RADIATION EFFECTS IN THE LHCb UNDERGROUND AREAS

R. Calà*, C. Bertone, B. Bradu, F. Cerutti, J.-P. Corso, S. Fiore, G. Lerner, M. Pezzetti, M. Solfaroli Camillocci, CERN, Geneva, Switzerland

Abstract

During the 2024 and 2025 LHC proton-proton runs, the LHCb experiment, following its upgrade, achieved a substantial increase in delivered luminosity compared to previous years, exceeding the level of 10 fb^{-1} per year. While this enhancement greatly expands LHCb's physics reach, it also leads to a marked rise in radiation levels in the experimental insertion region, originally designed for a significantly lower luminosity target. Throughout the 2024 p-p operation, several failures of electronic racks and cryogenic sensors, mostly attributed to single-event effects (SEEs), were observed around the LHCb cavern and caused tens of hours of LHC downtime.

This work presents a benchmarking of dedicated FLUKA simulations, used to quantify the radiation levels and identify possible mitigation measures, against measurements by the Battery Radiation Monitors (BatMons). The study guided the relocation of sensitive equipment and the installation of additional shielding in specific underground areas hosting critical electronics, effectively reducing radiation exposure during the remainder of Run-3. Finally, possible improvements for shielding are also discussed in view of Run-4.

INTRODUCTION

The LHC beauty (LHCb) experiment is designed as a forward spectrometer, with a geometry specifically chosen to detect particles at small angles relative to the beam axis [1]. With respect to the general-purpose detectors at the LHC, which surround the interaction point with a enclosed structure, the open layout of LHCb allows collision debris to escape to a larger extent. This configuration leads to significant radiation streaming into the experimental cavern and adjacent service galleries, posing a challenge for the protection of nearby equipment. Coherently, while meeting its specific operational requirements, LHCb was originally designed to operate at luminosities substantially lower than those of the more hermetic ATLAS and CMS detectors.

However, during Long Shutdown 2 (LS2), the detector underwent a major upgrade (Upgrade I) to significantly increase its statistical reach [2]. This upgrade has enabled LHCb to operate at a leveled instantaneous luminosity of $2 \cdot 10^{33}$ $cm^{-2}s^{-1}$ during Run-3 (2022–2026), a factor of ∼5 higher than in the pre-upgrade era. The 2024 proton run marked a milestone in this new operational regime, delivering a record integrated luminosity of 10.9 fb^{-1} [3], more than four times the previous annual record achieved in 2018 [4].

This unprecedented increase in luminosity has led to a marked rise of radiation levels within the LHCb insertion region (IR8). In this environment, stochastic phenomena known as Single-Event Effects (SEEs) represent the primary threat to commercial electronic system functionality, causing operational downtime despite being mostly non-destructive to the hardware itself. Since the probability of a SEE is directly proportional to the hadron flux, High-Energy Hadron equivalent (HEH-eq) fluence is adopted as the critical metric for radiation environment assessment from the radiation to electronics (R2E) point of view [5, 6]. HEH-eq fluence accounts for all hadrons with energies above 20 MeV as well as 0.2–20 MeV neutrons weighted by their energy-dependent SEE-induction probability relative to a reference electronic device. For an area to be considered R2E-safe, the annual HEH-eq fluence must not exceed $3 \cdot 10^6$ $cm^{-2}yr^{-1}$ [7].

The impact of this luminosity upgrade became evident during the 2024 proton run and persisted throughout 2025, with a significant fraction of R2E events occurring in IR8 [8]. Many of these events involved pressure sensors located in the LHCb experimental cavern which were mitigated at software level. On the other hand, failures affecting the cryogenics system in the UL84 gallery, in particular the Active Magnetic Bearings (AMB) and PLC racks, led to tens of hours of LHC downtime [9]. This work details the estimation and validation of radiation levels through Monte Carlo simulations and *in-situ* measurements, and the mitigation strategies implemented to protect the critical infrastructures in UL84, including the relocation of sensitive equipment and the design of new shielding walls.

SIMULATION SETUP

Monte Carlo simulations are an essential tool for predicting the implications of particle shower propagation through complex geometries. In this study, radiation levels were evaluated using the FLUKA code, a multi-purpose simulation package providing accurate modeling of particle interactions with matter [10–13]. The comprehensive FLUKA model of IR8 incorporates a full three-dimensional description of the beamline, the LHC tunnel, the LHCb detector and the experimental cavern [14, 15].

The simulations presented here assume the proton-proton crossing schemes and optics for both Run-3 and Run-4, with colliding beam energies of 6.8 TeV and 7 TeV, respectively [16, 17]. To reflect operational reality, the simulations consider the total integrated luminosity as equally shared between the two polarity configurations of the LHCb spectrometer.

The HEH-eq fluence was evaluated using a 3D Cartesian mesh with $20 \times 20 \times 20$ cm^3 voxels. This resolution was chosen to provide a suitable representation of the spatial

* roberto.cala'@cern.ch

Content from this work may be used under the terms of the CC BY 4.0 licence (© 2026). Any distribution of this work must maintain attribution to the author(s), title of the work, publisher, and DOI.

ISBN: 978-3-95450-252-3 ISSN: 2673-5350 doi: 10.18429/JACoW-IPAC2026-MOP1014

FCC-ee RADIATION ENVIRONMENT AND SHIELDING

B. Humann*, A. Lechner, M. Ady, T.G. Banks, J. Bauche, D. Bozzato, J.P. Burnet, M. Calviani, F. Carra, R. Cowan, A. Frasca[1], R. Garcia Alia, C. Garion, D. Hajdu, K. Hanke, M. Jebramcik, G. Lavezzari, G. Lerner, I. Martin Melero, M. Morrone, D. Najdrowski, A. Perillo Marcone, A. Piccini, A. Romero Francia, K. Taylor, M. Timmins, M. Widorski, CERN, Geneva, Switzerland
F. Valchkova-Georgieva, CEGELEC SA, Carouge, Switzerland
[1]also at University of Liverpool, Liverpool, UK

Content from this work may be used under the terms of the CC BY 4.0 licence (© 2026). Any distribution of this work must maintain attribution to the author(s), title of the work, publisher, and DOI.

Abstract

In a high-energy lepton collider such as the Future Circular Collider (FCC-ee) at CERN, phenomena like synchrotron radiation (SR) create a challenging radiation environment for accelerator components and equipment including cables and electronics. This paper examines the radiation load in the collider arcs at the highest beam energies ($\mathrm{t\bar{t}}$) for two different optics schemes. Recent developments in the design of photon stoppers and dedicated radiation shielding are presented, highlighting progress towards a more realistic configuration while maintaining acceptable annual ionizing dose levels. The absorbed power in accelerator components and the surrounding tunnel environment is evaluated for various operation modes to ensure compliance with the thermal load limits of the ventilation system. Furthermore, neutron spectra due to photo-neutron production are quantified for the electronics bunkers located below the beamline, and the feasibility of employing radiation-tolerant, commercial-off-the-shelf electronics in these areas is assessed. Finally, a first evaluation of the radiation field in the alcoves, housing radiation-sensitive equipment, is presented.

INTRODUCTION

In an electron-positron collider like the Future Circular Collider (FCC-ee) at CERN, synchrotron radiation (SR) is one of the main contributors to the radiation load on the accelerator equipment and environment. FCC-ee will be operated at four energies, ranging from 45.6 GeV (Z pole) to 182.5 GeV ($\mathrm{t\bar{t}}$) [1]. The radiation field is characterised by the critical energy, $E_C \propto E^3$, which divides the photon spectrum into two equal-power halves. A higher critical energy implies a harder photon spectrum, leading to more penetrating secondary particles and an increased photo-neutron contribution. Two optics schemes are compared in this study focusing on the $\mathrm{t\bar{t}}$ operation mode, which produces the hardest SR spectrum. The GHC (global hybrid correction) optics [2] has been the baseline optics in the past years, while the LCC (local chromaticity correction) optics [3] is a newer design. The LCC lattice exhibits a higher dipole filling factor, which in turn yields a larger bending radius (ρ_{LCC} =10.91 km, ρ_{GHC} =10.04 km). This results in a mover favourable radiation environment, owing to the $1/\rho$ dependence of the SR energy loss and the critical photon energy. The corresponding values are listed in Table 1 for the Z pole and the $\mathrm{t\bar{t}}$ operation modes. For GHC, the SR power is assumed by design to be 50 MW/beam for all operation modes, corresponding to 11.3 MW for one arc (8.96 km) or 630 W/m/beam. Assuming the same beam current for LCC, the larger filling factor in LCC reduces the emitted power by 7% to 585 W/m/beam.

Table 1: Energy loss per turn ($\frac{\Delta E}{\mathrm{turn}}$), the critical energy ($E_C$), and the beam current (I_{Beam}) for the Z and $\mathrm{t\bar{t}}$ working points in both optics schemes.

	Z		tt	
	GHC	**LCC**	**GHC**	**LCC**
$\frac{\Delta E}{\mathrm{turn}}$	0.039 GeV	0.035 GeV	10.01 GeV	8.98 GeV
E_C	0.022 MeV	0.019 MeV	1.37 MeV	1.24 MeV
I_{Beam}	1285 mA		5 mA	

The radiation load is assessed with FLUKA Monte Carlo simulation [4–7] for one FODO cell of the $\mathrm{t\bar{t}}$ operation mode (Fig. 1). This paper builds upon previous radiation transport studies and shielding design iterations presented in [8–11], which is further developed in [12]. Recent updates to the design of the localized SR absorbers (SRA), the dipole, and the surrounding lead shielding are presented, targeting a reduction of the radiation load in the tunnel. The electronics bunker design presented in [10] is revisited, showing an increase in dimensions and a relocation to below the dipoles. Finally, a first assessment of the radiation field in the alcoves, located perpendicular to the accelerator tunnel, is presented.

SHIELDING ASSEMBLY DEVELOPMENTS

The 38 cm long SRAs intercepting the SR photons are made of a copper alloy (CuCrZr) and are placed in the winglets of the vacuum chamber (see Fig. 2) [13–15]. The vertical dimension of the SRAs has been increased to span the full available height within the dipole yoke, enhancing the shielding performance. A cooling plate is foreseen at

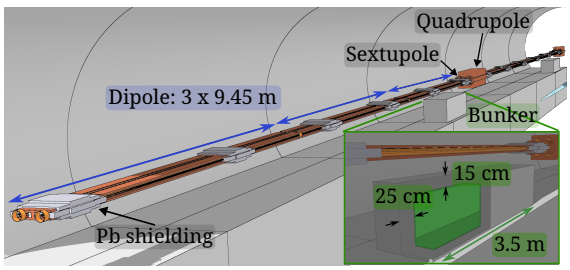

Figure 1: 63 m FODO cell (LCC) implemented in FLUKA.

* barbara.humann@cern.ch

ISBN: 978-3-95450-252-3 ISSN: 2673-5350 doi: 10.18429/JACoW-IPAC2026-MOP1015

OPTICS MODELLING CHALLENGES FOR THE HL-LHC

R. De Maria*, P. Bestmann, G. Dima, L. Fiscarelli, C. Petrone, V. Rude, K. Skoufaris,
European Organization for Nuclear Research, Geneva, Switzerland

Abstract

The HL-LHC will operate with very low β^* and tight alignment constraints around the upgraded ATLAS and CMS experiments. Minimizing the commissioning time required to reach the nominal will be key to achieving significant luminosity in the first years of operation. This contribution presents the status and perspectives of the solutions implemented to prepare machine models that allow us to predict, with the best possible accuracy, the orbit and optics of the machine at the start of commissioning in Run 4. In particular, it shows the status of modeling magnetic-axis deviations, the inclusion of measured magnetic transfer functions and quadrupole fringe fields in optics models, and their expected impact on residual orbit error and optics-correction convergence speed during commissioning.

INTRODUCTION

HL-LHC optics around the interaction regions at the end of luminosity leveling have large β-functions to produce a very small beam spot at the interaction point. The nominal β^* in the HL-LHC is 15 cm in both planes (achieved in one plane only in the LHC in 2026 [1]), with options to go down to 7.5 cm [2–4]. Compared with the LHC, even for the same β^*, the peak beta in the triplet is 45 % larger [5]. Nominal HL-LHC β-functions reach 22 km in the first quadrupoles close to the interaction point (in the inner triplets, MQXFA, MQXFB). Large β-functions increase the sensitivity to imperfections and nonlinear fields, making optics corrections more challenging. This paper describes the process of building an as-built operational model in Run 4 instead of a nominal one[1] and discusses the expected advantages.

MAGNETIC AXIS DEVIATIONS

Deviations of the magnetic axis generate 1) unwanted orbit errors proportional to the transverse offsets of the magnetic axis (the position at which the magnetic field is zero) relative to the ideal machine axis, and 2) coupling between the horizontal and vertical planes proportional to the roll of the magnetic field relative to the machine plane. Realignments (the HL-LHC has full remote alignment capabilities) can correct both transverse and roll offsets, but the available motion is limited by acceptable bellows deformation. Bellows also need to accommodate manufacturing imperfections, and production is not yet complete [7]. Here, we assume that transverse offsets can be up to 0.5 mm and roll offsets below 1 mrad. Orbit correctors can compensate for offset deviations to the extent that the errors are below 0.5 mm [8].

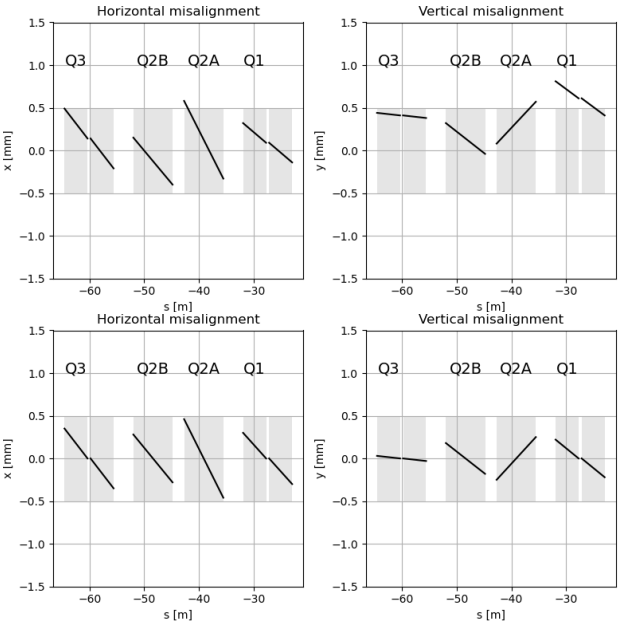

Figure 1: Expected magnetic-axis misalignment in the IT string before (top) and after correction (bottom). Grey boxes show the triplet-gradient locations used to identify the error sources.

Driving orbit correctors to their maximum strengths, however, is not desirable since their field quality deteriorates at large currents in both planes (orbit correctors are dual-plane nested correctors in the common-pipe region [9] and dual-plane 2-in-1 correctors in the two-pipe regions [10]). Roll deviations in the triplet can also be corrected with local and global coupling correctors; however, relying on global correctors implies either having coupling at the IP, which reduces luminosity, or coupling in the triplets, which enhances nonlinear coupling effects. In addition, starting commissioning with strong coupling inevitably increases commissioning time. Given these premises, the best strategy is to use the magnetic measurements to install the magnets with the best-aligned magnetic axes and to preset the orbit and coupling corrections during the first commissioning using the model.

As proof of principle, Figures 1 and 2 illustrate the strategy adopted to correct imperfections for the IT string installation [11]. The measured magnetic axis, transferred to the machine plane, results in a large orbit error and orbit-corrector usage. A complete correction of the axis, including the slopes, would result in excessive offsets in the bellows. A compromise solution [12], compensating only for the average axis correction, shows almost negligible orbit error and orbit-corrector usage while preserving the bellows range.

Measured roll deviations reached 2.5 mrad [7]. Uncompensated, they would require about half the available skew-

* riccardo.de.maria@cern.ch

[1] In the past, magnetic measurements could not be reconciled with optics measurements [6]

Content from this work may be used under the terms of the CC BY 4.0 licence (© 2026). Any distribution of this work must maintain attribution to the author(s), title of the work, publisher, and DOI.

ISBN: 978-3-95450-252-3 ISSN: 2673-5350 doi: 10.18429/JACoW-IPAC2026-MOP1016

SIMULATIONS AND MEASUREMENTS OF INJECTION BACKGROUNDS AT SuperKEKB*

G. Nigrelli[1,2,3†], M. Boscolo[2], G. Broggi[3], R. Bruce[3], Y. Funakoshi[4], N. Iida[4], H. Kaji[4], H. Koiso[4], M. Li[5,6], Q. Liu[7], H. Nakayama[4], T. Nemoto[8], Y. Ohnishi[4], K. Oide[3], S. Redaelli[3], J. P. T. Salvesen[3], T. Mori[4]
[1]Sapienza Univ. Rome, Italy, [2]INFN-LNF, Frascati, Italy, [3]CERN, Geneva, Switzerland
[4]KEK, Tsukuba, Japan, [5]CAS, China, [6]IJCLab, Orsay, France,
[7]Univ. Hawai'i at Mānoa, USA, [8]Univ. Tokyo, Japan

Abstract

SuperKEKB is an electron-positron collider, where the beams collide inside the Belle II detector. The design luminosity has not yet been achieved, partly due to limited injection efficiency in both rings, which limits the achievable beam current. The injection process also generates significant background in the Belle II detector, requiring vetoes during data taking that reduce the detector efficiency. To improve the understanding of these issues, the injection process at SuperKEKB has been simulated using the Xsuite simulation framework, including detailed multi-turn tracking and particle-matter interactions in the collimators. The results of these simulations have been used as input for a Belle II detector simulation to estimate the resulting background levels. This paper presents the simulation methodology and the comparison between simulation results and experimental data, collected during the 2025 run, as a prerequisite for future applications of the simulation framework including further optimization of the background at SuperKEKB as well as similar studies for future lepton colliders.

INTRODUCTION

The SuperKEKB collider, shown in Fig. 1, is an asymmetric electron–positron collider operating with a 4 GeV positron Low Energy Ring (LER) and a 7 GeV electron High Energy Ring (HER) [1–3]. It delivers high-luminosity collisions to the Belle II experiment for precision studies of B-meson decays and searches for physics beyond the standard model [4]. The accelerator complex also includes an injector linac and a positron damping ring. Due to beam lifetimes well below 30 minutes in collision, the machine operates in top-up injection mode to maintain stable luminosity. Although a record luminosity of $5.1 \times 10^{34}\,\mathrm{cm^{-2}\,s^{-1}}$ has been achieved, this remains well below the design value of $8 \times 10^{35}\,\mathrm{cm^{-2}\,s^{-1}}$ [5]. Several factors limit machine performance, such as injection inefficiency, generating beam losses and detector background at each injection [6, 7]. In 2024, achieved injection efficiencies were 80% in the LER and 60% in the HER. As injection losses and background increases with beam intensity, understanding and mitigating these losses is essential for future luminosity improvements.

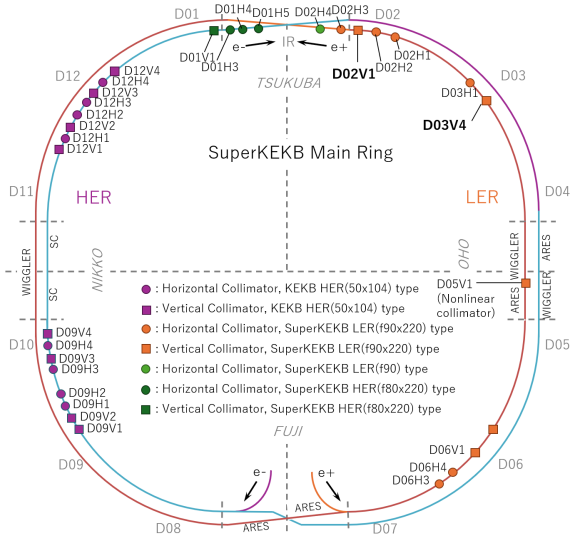

Figure 1: SuperKEKB collider layout with collimator location as of 2025. Courtesy of T. Ishibashi and S. Terui.

This paper presents a detailed simulation of LER injection losses and the resulting detector backgrounds, compared to measurements collected during the 2025 run.

SIMULATION SETUP

While Strategic Accelerator Design (SAD) [8] is commonly used for SuperKEKB studies, this work was performed using the Xsuite framework [9]. Xsuite, developed at CERN, combines accelerator-specific and Python-based tools for modeling complex effects such as collimation and beam-beam interactions. Collimation studies were carried out using the Xcoll module [10], including detailed aperture models and loss localization identification. Beam–matter interactions within the collimators were simulated through the Xsuite-BDSIM coupling [11, 12]. This work provides an important benchmark of the new tools. The full SuperKEKB lattice 2025c was converted from SAD to Xsuite using the SAD2XS converter [13], previously benchmarked [14], including a detailed interaction region (IR) aperture model and realistic collimator geometry. The distribution of the injected bunch is generated based on simulations of the beam transport between the injector and the main ring [15]. The distribution is rescaled to the measured emittances at the end of the transfer line ($\epsilon_y^n = 60\,\mathrm{mrad}$ $\epsilon_x^n = 170\,\mathrm{mrad}$) and

* Work partially funded by the EAJADE project.
† giulia.nigrelli@cern.ch

Content from this work may be used under the terms of the CC BY 4.0 licence (© 2026). Any distribution of this work must maintain attribution to the author(s), title of the work, publisher, and DOI.

ISBN: 978-3-95450-252-3 ISSN: 2673-5350 doi: 10.18429/JACoW-IPAC2026-MOP1017

EXPERIMENTAL STUDY OF LUMINOSITY CALIBRATION CORRECTIONS USING TUNE SCALING TO MIMIC MULTI-COLLISION CONFIGURATIONS

J. Wańczyk[1,*], V. Vlasenko[1], P. Collins[1], R. Matev[1], F. Pisani[1], V. Balagura[2], T. Pieloni[3], A. C. Piveteau[3], A. Villa[3], F. Ferrari[4], E. Franzoso[5], A. Shevelev[6], V. Zhovkovska[7]
[1] CERN, Geneva, Switzerland;
[2] Ecole Polytechnique, Palaiseau, France; [3] EPFL, Lausanne, Switzerland;
[4] INFN, Bologna, Italy; [5] INFN, Ferrara, Italy; [6] University of Maryland, College Park, USA;
[7] University of Warwick, Warwick, UK

Content from this work may be used under the terms of the CC BY 4.0 licence (© 2026). Any distribution of this work must maintain attribution to the author(s), title of the work, publisher, and DOI.

Abstract

Accurate luminosity calibration is essential for precise cross-section measurements and reliable machine performance optimization. In colliders with several interaction points, the cumulative beam–beam effects depend on the number of collision partners of individual bunches, which can bias luminosity calibration if not properly accounted for. To investigate this experimentally, a dedicated beam–beam experiment was performed at the LHC using tune scaling to mimic configurations with multiple collision partners within a single interaction region. By adjusting the fractional tunes, while preserving comparable beam–beam parameters, the dependence of luminosity calibration corrections on the effective number of collisions was systematically studied. The results are compared with expectations from numerical simulations, supporting the use of tune scaling as a valid strategy to reproduce multi-collision conditions for luminosity calibration corrections.

INTRODUCTION

The determination of luminosity from van der Meer (vdM) scans relies on the accurate modeling of beam–beam (BB) effects [1]. During a vdM scan, the two beams are separated transversely, and the presence of additional head-on collision partners at other interaction points (IPs) modifies the beam orbits and shapes throughout the scan, biasing the inferred luminosity calibration. The first-order effects of BB interactions include a tune shift, tune spread, and beta function change [2, 3]. A dedicated correction strategy to account for these multi-IP BB effects was derived in [1], and an initial experimental validation was performed in [4]. Building on this, the ATLAS and CMS experiments applied these corrections in their Run 2 luminosity analyses [5, 6], achieving the most precise luminosity measurements to date. The present work extends this validation to the multi-IP case, aiming to demonstrate experimentally that the effect of head-on collisions at multiple additional IPs on a vdM scan is equivalent, in first approximation, to applying a corresponding cumulative tune shift. We assess the consistency of this correction strategy across different IP configurations and evaluate its impact on the luminosity calibration.

* jwanczyk@cern.ch

EXPERIMENT DESCRIPTION AND BEAM PARAMETERS

The experiment was performed at the LHC at 6.8 TeV. The tune scaling approach exploits the fact that, in simulations, scaling the fractional tune reproduces the effective BB kick from a collision partner at a distant IP; this empirical rule was subsequently adopted as the basis for the multi-IP correction procedure [1]. The target beam–beam parameter was $\xi = 0.01$, with a sensitivity threshold of $\xi = 0.008$, below which the induced effect on the visible cross section would be too small to be reliably measured.

Since the tune shift had to be kept sufficiently large to remain above the sensitivity threshold, excessive intensity losses were anticipated as a potential risk, particularly for bunches colliding at IP8 with both beams, as these experience the largest total BB tune shift. To mitigate this, ATLAS was brought into collision only for the final scan pair, limiting the total BB tune shift on the most affected bunch families. The tests consisted of six pairs of horizontal and vertical separation scans. The filling pattern comprised four bunch families observed by ATLAS and CMS, with effective numbers of BB interactions ranging from 1 to 3. The BB collisions could occur at CMS, ATLAS and LHCb; due to the asymmetric location of LHCb, pairs of bunches colliding at CMS and ATLAS may have different numbers of collisions at LHCb. Additional interactions were introduced either via genuine changes to the LHC collision configuration or via tune changes applied to mimic the effect on tunes from the BB interaction at additional collisions at IP1, IP8, or both. The experimental scheme is illustrated in Fig. 1. The effective numbers of BB interactions shown in the scheme are estimated for $\xi = 0.01$; during the experiment, this parameter was expected to decrease over time due to bunch intensity losses and emittance growth.

FIRST RESULTS

Beam-Beam Parameter Evolution

The time evolution of the beam–beam parameter ξ for the colliding bunches is shown in Fig. 2. All families were expected to decay from $\xi = 0.01$ toward the sensitivity threshold of $\xi = 0.008$ over the course of the experiment. The IP1+IP5 family and the single-beam IP8 families evolved

ISBN: 978-3-95450-252-3 ISSN: 2673-5350 doi: 10.18429/JACoW-IPAC2026-MOP1019

LHC MAGNETIC MODEL REVISITED: BEAM-BASED MEASUREMENTS AND MACHINE REPRODUCIBILITY AT INJECTION

J. Wańczyk*, J. F. Esteban Müller, L. Fiscarelli, M. Hostettler, D. Jacquet, M. Solfaroli Camillocci, G. Trad, J. Wenninger, European Organization for Nuclear Research, Geneva, Switzerland

Content from this work may be used under the terms of the CC BY 4.0 licence (© 2026). Any distribution of this work must maintain attribution to the author(s), title of the work, publisher, and DOI.

Abstract

The harmonic components of the LHC superconducting magnets exhibit a characteristic decay at low field, primarily caused by current redistribution within the superconducting cables, inducing changes in the beam tune and chromaticity during the injection plateau. A feed-forward compensation system based on the FiDeL magnetic model counteracts these effects using parameterisations of the field harmonics as functions of time, current, and magnet history. In this work, dedicated beam-based measurements from the 2025 LHC run are used to update the FiDeL tune decay model parameters at 450 GeV. The fill-to-fill reproducibility of the machine at injection is assessed through the distribution of residual manual tune and chromaticity corrections, which yield σ_Q = 0.003–0.004 tune units and $\sigma_{Q'}$ = 2.0–2.7 chromaticity units respectively. For fills preceded by a high-energy flat top, the flat-bottom duration is identified as the dominant source of variability ($r > 0.5$), and a parametric correction model $H_{\mathrm{FB}}(t_{\mathrm{FB}})$ is derived and validated, reducing this correlation. A significant correlation between tune corrections and arc helium bath temperature is also reported as a candidate for future model improvement.

INTRODUCTION

In superconducting accelerators, current redistribution and changes in the local magnetization within the Rutherford cables of the main dipoles and quadrupoles cause characteristic drifts of the magnetic-field multipoles during the injection plateau. This field decay affects the allowed multipoles, such as the sextupole component (b3) in the dipoles, which drives chromaticity changes, and the main component (b2) in the quadrupoles, which drives tune changes. The phenomenon has been a known operational challenge since its discovery at the Tevatron in 1987, where chromaticity changes of up to 70 units were observed [1]. A further complication is that the decay amplitude depends on the magnet powering history prior to injection, making it non-reproducible from cycle to cycle. This motivated the development of FiDeL (Field Description for the LHC), a feed-forward prediction system whose mathematical framework is described in [2, 3]. A striking discrepancy emerged during early LHC operation: while single-magnet measurements predicted decay time constants of 200–300 s, beam-based measurements revealed time constants of 1000–4000 s and tune decay of ~0.04 units, far exceeding pre-operational expectations [4].

Since 2011, dynamic corrections for tune and chromaticity decay have been applied operationally using beam-based parameters; the most recent update prior to the 2025 run is documented in [3]. Despite these corrections, residual offsets persist fill-to-fill at injection, requiring frequent manual operator trims. This paper reports three related activities carried out on 2025 LHC data and applied in the 2026 run: an update of the FiDeL tune decay model parameters from dedicated beam measurements; a systematic characterisation of the residual manual corrections and their dominant drivers; and the derivation and validation of an improved flat-bottom correction term $H_{\mathrm{FB}}(t_{\mathrm{FB}})$ for the tune. Full details of the analysis are reported in [5].

UPDATED DECAY MODEL PARAMETERS

The FiDeL tune decay model parameters — decay amplitude δ_Q, mixing factor d, and time constant τ — were updated from dedicated beam measurements performed during 2025 commissioning at 450 GeV, for two fill categories: precycle fills (injection after a full precycle to recondition the magnets) and flat-top fills (injection after a high-energy flat top).

A key complication encountered in the measurements is that the observed decay is not fully reproducible across fills even under nominally identical powering conditions, as illustrated in Fig. 1: five PRE fills from early and mid-2025 commissioning span a visible spread, limiting the precision of any single-fill parameter extraction. To mitigate this, fits were performed simultaneously on all available fills.

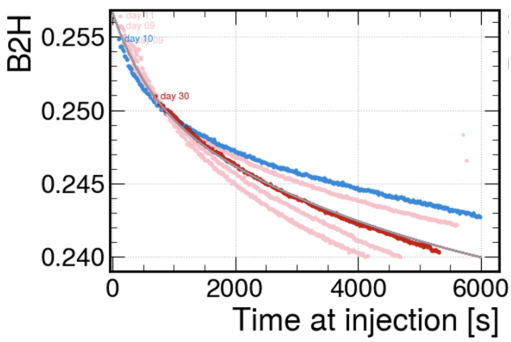

Figure 1: Fill-to-fill non-reproducibility of the tune decay on the injection plateau for five PRE fills. Three commissioning fills (pink) and two April 2025 fills (red, blue); grey line shows the simultaneous fit to all five.

For precycle fills, a free simultaneous fit to all five fills was adopted as the updated model. In the horizontal plane the new correction is larger than the Run 2 baseline by approximately 4–5 × 10^{-3} tune units after 4 h at injection; in the vertical plane it is smaller by 1–3 × 10^{-3}. For flat-top fills, only two dedicated fills were available, as measuring the full decay curve requires many hours at injection and

* joanna.wanczyk@cern.ch

ISBN: 978-3-95450-252-3 ISSN: 2673-5350 doi: 10.18429/JACoW-IPAC2026-MOP1020

STUDY OF THE IMPACT OF BFPP LOSSES IN THE LHCb INSERTION

R. Calà*, R. Bruce, R. Cai, F. Cerutti, CERN, Geneva, Switzerland

Abstract

Besides its proton–proton physics programme, the LHC operates with $^{208}Pb^{82+}$ ion beams colliding in its four experiments. At the interaction point, bound-free pair production (BFPP), occurring when an electron produced in an electromagnetic interaction is captured by one of the colliding nuclei, is one of the most critical processes in terms of beam losses. In fact, BFPP leads to the creation of a secondary beam with a well-defined change in magnetic rigidity, producing localized power deposition in the dispersion suppressors, possibly causing a magnet quench without proper mitigation measures.

Differently from the ALICE insertion, where two dedicated collimators were installed to protect the superconducting magnets, and the ATLAS and CMS ones, where BFPP losses can be displaced by an orbit bump into an empty cryostat, the LHCb insertion optics only allows for orbit bumps broadening the BFPP loss distribution, so as to reduce the peak power load on the concerned magnets.

This study investigates the resulting power density in the magnet coils and benchmarks the simulation framework against beam loss monitor (BLM) data recorded during Run-3, in order to set a safe luminosity limit.

INTRODUCTION

The Large Hadron Collider (LHC) physics programme includes heavy-ion operation as a fundamental component, typically scheduled for approximately one month per year [1]. During the 2023, 2024, and 2025 heavy-ion runs, fully-stripped $^{208}Pb^{82+}$ ions were accelerated in two counter-rotating beams (B1 and B2) to a top energy of 6.8 TeV per charge, colliding at the ALICE, ATLAS, CMS, and LHCb experiments [2]. Further heavy-ion runs are scheduled for 2026 and are expected to continue from Run-4 onwards [3,4]. Although beam intensity and luminosity are considerably lower than in proton-proton runs, heavy-ion operation introduces unique machine protection challenges arising from specific interaction processes.

A concern of primary importance for the four experimental insertions is the localized impact of secondary $^{208}Pb^{81+}$ beams. These are generated at the interaction point via Bound-Free Pair Production (BFPP) [5], an electromagnetic process in which an electron, created together with a positron, is captured into a bound state of a Pb ion:

$$^{208}Pb^{82+} + ^{208}Pb^{82+} \rightarrow ^{208}Pb^{82+} + ^{208}Pb^{81+} + e^{+} \quad (1)$$

BFPP generates a very small transverse momentum recoil but causes a well-defined change in magnetic rigidity. This gives rise to a narrow secondary beam, whose orbit exceeds the mechanical aperture in the dispersion suppressor (DS) of the four experimental insertions, leading to localized power deposition [6–9]. Due to the high cross-section of this process, the luminosity was limited to prevent magnet quenches [10].

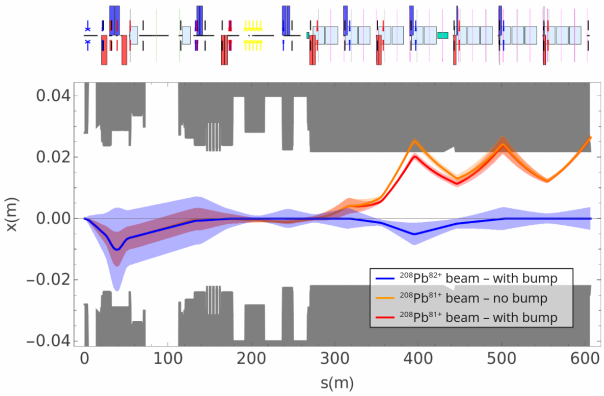

Figure 1: Horizontal trajectory of the BFPP secondary beam on the right side of LHCb in the 2025 configuration, computed with (red envelope) and without (orange envelope) a horizontal orbit bump. The horizontal trajectory of the primary beam is shown by the blue envelope for the orbit bump case. The machine aperture is shown in grey.

Since the optics differ across the four LHC experiments, ad-hoc interventions are required [3, 6, 9, 11]. For ATLAS and CMS, the risk of beam dumps was mitigated by shifting the BFPP beam impact from a superconducting dipole to an empty connection cryostat by means of a horizontal orbit bump around the impact location [6, 9, 11]. In contrast, the solution for ALICE involved the installation of a DS collimator (TCLD) in the connection cryostat to intercept the BFPP losses deflected by a horizontal orbit bump [3, 11].

To meet the requirement of increasing the integrated luminosity for LHCb, a mitigation strategy was implemented for the Interaction Region 8 (IR8) starting from Run-3 [12]. The solution consisted of a horizontal orbit bump applied to the outgoing beams. As shown in Fig. 1 for the right side of LHCb, this allows the BFPP impact to be shifted from half-cell 10 to half-cell 12, where the chromatic β-function seen by the BFPP beam is larger, thereby spreading out the power deposition. The effectiveness of this measure was preliminarily investigated at 6.37 Z TeV for various transverse emittances by means of a combined SixTrack and FLUKA simulations [12].

The present work focuses on the study of the orbit bump actually deployed in IR8 for the 2023–2025 Pb-Pb runs and is based on the combined use of the Xsuite and FLUKA codes. We present the expected loss distributions, benchmark the simulation model against BLM data, evaluate the peak power density resulting from BFPP losses in half-cell 12 and indicate a luminosity threshold to ensure safe LHC operation.

* roberto.cala'@cern.ch

Content from this work may be used under the terms of the CC BY 4.0 licence (© 2026). Any distribution of this work must maintain attribution to the author(s), title of the work, publisher, and DOI.

ISBN: 978-3-95450-252-3 ISSN: 2673-5350 doi: 10.18429/JACoW-IPAC2026-MOP1021

STUDY OF THE TOUSCHEK EFFECT IN THE FCC-ee

G. Broggi*[1,2,3], M. Boscolo[3], R. Bruce[2], G. Iadarola[2], L. Pauwels[2], S. Redaelli[2]
[1]Sapienza University of Rome, Rome, Italy
[2]CERN, Meyrin, Switzerland
[3]INFN-LNF, Frascati, Italy

Abstract

The Future Circular electron-positron Collider (FCC-ee) is a design study for a 90.7 km circumference high-luminosity and high-energy e^+e^- collider. In electron and positron machines, the Touschek effect can cause large transverse-to-longitudinal momentum exchange, leading to particle losses that can limit the beam lifetime and produce distinct beam loss patterns. A quantitative assessment of this mechanism is therefore essential to identify regions potentially exposed to Touschek-induced losses and to determine its impact on the beam lifetime relative to other lifetime-limiting processes. This paper presents a study of the Touschek effect in the FCC-ee, performed using a Monte Carlo Touschek-scattering simulation routine newly implemented in the Xsuite framework. The results include Touschek-lifetime estimates for the FCC-ee and an evaluation of the arising beam loss patterns. The performance of the FCC-ee beam collimation system to safely dispose of Touschek losses is also assessed.

INTRODUCTION

The FCC-ee [1,2] is a proposed 90.7 km circular e^+e^- collider designed for precision electroweak and Higgs physics. It will operate in four modes, with beam energies ranging from 45.6 GeV at the Z pole up to 182.5 GeV at the $t\bar{t}$ threshold. In electron and positron storage rings, the Touschek effect [3] arises from single Coulomb scattering events between two relativistic particles within the same bunch, which can convert transverse momentum into longitudinal momentum. If the resulting momentum deviation exceeds the momentum acceptance of the machine, or if the resulting closed-orbit or betatron oscillations exceed the physical or dynamic aperture, particles are lost from the beam. The Touschek effect is typically the primary beam lifetime limiting effect in low-emittance electron and positron storage rings. The Touschek scattering rate is strongly suppressed with increasing beam energy, so its impact is expected to be less severe in high-energy machines such as the FCC-ee. Nevertheless, a quantitative assessment of the Touschek effect remains important to verify this expectation, assess how the FCC-ee collimation system handles these losses, and evaluate the resulting beam loss patterns and their effect on the machine.

This paper introduces the Touschek scattering simulation routine recently implemented in the Xsuite framework (full details can be found in Ref. [4]), and presents the results of its application to the FCC-ee Z operation mode. This represents the most critical case for the Touschek effect, as it corresponds to the lowest beam energy and highest beam intensity among all FCC-ee operation modes.

SIMULATION METHODOLOGY

A Touschek scattering routine has been recently implemented in the Xsuite [5] framework, following the approach by Xiao and Borland [6], originally developed for ELEGANT [7]. This method uses a Monte Carlo sampling scheme combined with the Piwinski formalism [8] to evaluate the Touschek scattering rate and generate the kinematic parameters of the scattered particles. The Touschek scattering rate for particles with momentum deviation $|\delta| > \delta_m$ is evaluated via Monte Carlo integration as [6]:

$$R_{\mathrm{MC}} = \frac{V}{N}\sum_{i=1}^{M}\left[\frac{v^*}{\gamma^2}\frac{d\sigma^*}{d\Omega^*}\sin\Theta^*\,\rho(\vec{x}_1)\,\rho(\vec{x}_2)\right]_i = \sum_{i=1}^{M} r_i, \quad (1)$$

where V is the sampled phase-space volume, N the total number of simulated scattering events, and M the number of scattered particles with $|\delta| > \delta_m$. Quantities with asterisks refer to the center-of-mass frame: v^* is the particle velocity, Θ^* the scattering angle, and $d\sigma^*/d\Omega^*$ the Møller differential cross-section [6]. γ is the Lorentz factor, $\rho(\vec{x}_1)$ and $\rho(\vec{x}_2)$ the Gaussian phase-space densities of the two interacting particles, and r_i the rate contribution from the i-th scattered particle. Setting $\delta_m = \delta_a$ (the local momentum acceptance) gives the Touschek beam loss rate.

For each Monte Carlo event, the coordinates of the two scattering particles are sampled from a six-dimensional Gaussian phase-space distribution at the given lattice location, using the local optical functions. The polar and azimuthal scattering angles Θ^* and Ψ^* in the center-of-mass frame are also sampled, and the post-scattering momenta are obtained via a relativistic Lorentz boost.

A lumped-element approach is used to model scattering around the ring during tracking. `TouschekScattering` elements are placed at discrete longitudinal positions, with spacing chosen to resolve the local variation of the optical functions. Scattered particles emerging from these elements with $|\delta| > \delta_m$ are retained for tracking and assigned a weight [6]

$$R_i = \frac{r_i}{\sum r_i}\cdot\int R_P\,ds, \quad (2)$$

where R_P is the Piwinski scattering rate integrated between the current and the preceding `TouschekScattering` element. The Touschek lifetime is then

$$\tau_T = \frac{N_b}{\sum_{\mathrm{lost}} R_i}, \quad (3)$$

* giacomo.broggi@cern.ch

Content from this work may be used under the terms of the CC BY 4.0 licence (© 2026). Any distribution of this work must maintain attribution to the author(s), title of the work, publisher, and DOI.

ISBN: 978-3-95450-252-3 ISSN: 2673-5350 doi: 10.18429/JACoW-IPAC2026-MOP1022

AN EFFICIENT HIGGS FACTORY: THE LINEAR GHOST COLLIDER

Peter Williams*, STFC Daresbury Laboratory / Cockcroft Institute, Daresbury, UK
Andrew Hutton, B.R. Gamage, Jefferson Lab, Newport News, VA, USA
Robert Apsimon, Mohit Kumar Joshi, Lancaster University / Cockcroft Institute, Lancaster, UK
Kaoru Yokoya, KEK, Tsukuba, Japan

Content from this work may be used under the terms of the CC BY 4.0 licence (© 2026). Any distribution of this work must maintain attribution to the author(s), title of the work, publisher, and DOI.

Abstract

A 550 GeV centre-of-mass Higgs factory is presented, the Linear Ghost Collider (LGC). Acceleration and deceleration are performed within SRF linacs where the bunches transported are net neutral, comprising equal charges of electrons and positrons, termed ghost bunches. Within these, one charge partner accelerates, and the other decelerates. Energy is recovered after a collision, and all particles recycled. An accompanying paper - Ghost Collider (GC) - introduces this concept. LGC comprises an alternative configuration to GC that eliminates turn-around arcs. This enables a large reduction in energy lost to synchrotron radiation, and in bunch degradation, in comparison to GC. Two variants of LGC are presented: a pulsed version realisable with proven SRF technology with instantaneous luminosity 35×10^{34} cm^{-2} s^{-1} @ 100 MW electrical power; and a continuous-wave (CW) version based on expected parameters for thin-film Nb_3Sn-on-copper SRF technology, capable of 348×10^{34} cm^{-2} s^{-1} @ 160 MW electrical power.

DRIVE BUNCHES

In the original GC proposal [1] ghost bunches are formed by low-energy injected bunches of one charge partnered with collision energy spent bunches of the other. These then exchange energies as they pass through the linac, thus GC is a new type of energy recovery linac (ERL), one where energy recovery is intra-bunch. This eliminates to first order the generation of higher-order modes (HOM) within the cavities, thereby negating a key concern with high-current ERLs. A disadvantage of GC topology is that injection must be co-located with extraction from the interaction points (IPs), necessitating two turn-around arcs at half the collision energy, one at each end of the facility. This is expensive in terms of synchrotron radiation (SR) loss (which must be replaced), and concomitant beam quality degradation from emittance and energy spread increase (which must be damped before re-use of bunches).

The concept of intra-bunch energy recovery allows a reconfiguration to enable better performance through the elimination of turn-around arcs. To do this, one must first recognise that it is only necessary that each charge partner in a ghost bunch have matching velocities, not energies. For electrons and positrons, this is always the case provided their energies are more than a few GeV. Secondly, it is not necessary that both charge partners undergo collision, and therefore, only one partner needs to be accelerated to full collision energy. This allows each linac to be split into **n** stages, shown in Fig. 1. Over the **n** stages one charge partner, the *colliding bunch*, achieves collision energy E_{coll}, passes through multiple IPs in series, and is then decelerated to injection energy E_{inj}; whereas the set of **n** charge partners - termed *drive bunches* - are only decelerated and accelerated between E_{inj} and $E_{drive} \equiv (E_{coll} - E_{inj})/\mathbf{n} + E_{inj}$[1].

This process is illustrated sequentially in Fig. 2 for the arbitrary choice $\mathbf{n} = 4$. Only ghost bunches containing right-going colliding positrons are shown; simultaneously, there will also be ghost bunches containing right-going colliding electrons, one-half RF cycle separated from them. By default, counter-propagation of ghost bunches within each linac is allowed, leading to a further two sets of ghost bunches containing; left-going colliding electrons; and positrons. There are therefore another three equivalent illustrations of Fig. 2.

Drive bunches are transported in bypass lines parallel to the linac within the tunnel, being kicked into and out of partnership with their partner colliding bunch in turn. During acceleration of the colliding bunch, **n** drive bunches are decelerated from E_{drive} to E_{inj}, with the reverse occurring upon deceleration. Chicane delays to enable the formation, collision, and splitting of high-energy charge partner ghost bunches are reproduced from GC. Colliding bunches never experience an arc, thus LGC is a truly linear collider. The drive bunches must be recirculated at E_{drive}, enumerated for various values of **n** in Table 1.

SR SCALING WITH n

As power lost to SR when bending goes as the fourth power of the energy, and normalised emittance degradation as the fifth power, the decrease in energy loss of recirculating bunches more than compensates for the linearly increasing drive beam current as a function of **n**. In comparison to the half-collision-energy turn-around arcs of GC, the power lost to SR in **n** bunches at E_{drive} in an identical arc is $2^4/\mathbf{n}^3$, and the concomitant emittance degradation is $2^5/\mathbf{n}^5$. However, instead of keeping the large arc size of GC, it is chosen to sacrifice some of this gain in order to scale the drive beam recirculation arc radii in proportion to E^2; an accepted standard that balances cost with SR power [2], resulting in a smaller facility footprint. Including this, the loss per turn $\Delta E \propto E^4/R$ so $\Delta E_{LGC}/\Delta E_{GC} = 2^2/\mathbf{n}$. The drive beam emittance degradation $\Delta\epsilon \propto E^5/R^{3/2}$ so $\Delta\epsilon_{LGC}/\Delta\epsilon_{GC} = 2^2/\mathbf{n}^2$. The resulting arc radii and SR loss per turn are

* peter.williams@stfc.ac.uk

[1] E_{inj} for colliding bunches is not necessarily equal to E_{inj} for drive bunches, it is chosen to make them equal to minimise beam transport.

ISBN: 978-3-95450-252-3 ISSN: 2673-5350 doi: 10.18429/JACoW-IPAC2026-MOP1025

DEPENDENCE OF MUON COLLIDER LUMINOSITY ON IONIZATION COOLING PERFORMANCE*†

M. Vanwelde‡ [1], C. Carli[1], D. Schulte[1], B. Stechauner[1], R. Taylor[1]
[1]CERN, Geneva, Switzerland

Abstract

A 10 TeV center-of-mass muon collider is a high-energy lepton collider that has the potential to achieve physics reach comparable to significantly larger hadron colliders. The final luminosity depends on the performance of the entire complex, from muon beam production to the collider ring, including the rapid cooling and acceleration stages. Achieving the target luminosity imposes stringent constraints on the ionization cooling and the collider optics, such as extremely small betatron functions at the interaction points, which induce strong chromatic effects that ultimately limit the machine momentum acceptance. To meet the momentum acceptance requirements without significant luminosity loss, one possible strategy is to end the muon cooling stage earlier, since a reduction of the longitudinal emittance can be traded against larger transverse emittances with a shorter cooling system. A study of a common optimization of the ionization cooling and the collider ring design to maximize the luminosity is presented in this work.

INTRODUCTION

A 10 TeV center-of-mass muon collider is a high-energy lepton collider with the potential to deliver an integrated luminosity of approximately 10 ab^{-1} [1–4] with its nominal parameters, shown in Table 1 [5]. Muon beams, which originate from pion decay, have large transverse and longitudinal emittances, requiring fast ionization cooling due to their short lifetime [6]. The cooling system consists of two main stages. The rectilinear 6D cooling channel reduces both transverse and longitudinal emittances to near-equilibrium values. It is followed by the final cooling channel, which aims to reach the target parameters by further reducing the transverse emittance, at the cost of an increase in longitudinal emittance. The specific design of these cooling channels, along with the underlying assumptions and initial parameters, affects both the transmission and the transverse and longitudinal emittances at the end of the cooling system. Hence, the design and performance of the ionization cooling channel strongly influence the achievable luminosity.

In addition to beam characteristics determined by the cooling channels and fast acceleration, the luminosity also depends strongly on the optics of the collider itself. Specifically, the Twiss betatron functions at the interaction points (IPs) need to be as small as possible. The nominal collider parameters are based on the nominal longitudinal emittance and the assumption that an RMS momentum spread of $1 \cdot 10^{-3}$ is achievable, corresponding to an RMS bunch length of 1.5 mm. Setting $\beta^* = 1.5$ mm to the bunch length allows to keep a reasonable hourglass factor f_{hg}. However, such a small β^* makes the optics very challenging, with very large peak β-functions and strong chromatic aberrations that must be efficiently compensated to meet the dynamic aperture (DA) and momentum acceptance (MA) requirements (typically a DA of 3-4 times the RMS beam size over a momentum range of 2-3 times the RMS momentum spread). The current collider design satisfies these requirements for an imperfection-free machine only when β^* is relaxed from 1.5 mm to 3 mm, at the cost of reduced luminosity [7].

Table 1: Main Nominal Parameters of the 10 TeV Muon Collider Ring

Parameter	Symbol	Value
Beam energy [GeV]	E	5000
Luminosity per IP [$10^{34}\mathrm{cm}^{-2}\,\mathrm{s}^{-1}$]	$\mathscr{L}$	20
Bunch population [10^{12}]	N_p	1.8
Norm. transverse RMS emittance [µm]	$\varepsilon_{n,x} = \varepsilon_{n,y}$	25
Geom. transverse RMS emittance [nm]	$\varepsilon_{g,x} = \varepsilon_{g,y}$	0.528
Longitudinal emittance [mm]	ε_l	71
RMS bunch length [mm]	σ_z	1.5
Relative RMS momentum spread [%]	$\delta = \frac{\sigma_p}{p}$	0.1
Beta function at IP [mm]	$\beta_x^* = \beta_y^*$	1.5
Repetition rate [Hz]	f_r	5

As luminosity depends on all stages of the muon collider complex, a start-to-end simulation and optimization of the entire complex are required [8]. A first step in this overall optimization is to evaluate the impact of the ionization cooling performance on the luminosity. One strategy to increase the available luminosity is to end the muon cooling stage earlier, resulting in a significant reduction of the longitudinal emittance with only moderately larger transverse emittances. Reduced longitudinal emittance can facilitate meeting the MA requirements, potentially enabling a smaller optimized β^*. A shorter cooling system also achieves higher beam intensities, thus increasing the final luminosity, and has implications for hourglass effects and beam-beam strength.

This paper reports on a first common optimization of ionization cooling and collider ring design to maximize luminosity. In particular, this work evaluates the achievable luminosity when stopping the cooling channel at different stages (number of cooling cells). The performance of a specific design of the final cooling based on realistic assumptions is detailed.

* Work endorsed by the IMCC.
† Funded by the European Union (EU). Views and opinions expressed are however those of the author(s) only and do not necessarily reflect those of the EU or European Research Executive Agency (REA). Neither the EU nor the REA can be held responsible for them.
‡ marion.vanwelde@cern.ch

Content from this work may be used under the terms of the CC BY 4.0 licence (© 2026). Any distribution of this work must maintain attribution to the author(s), title of the work, publisher, and DOI.

ISBN: 978-3-95450-252-3 ISSN: 2673-5350 doi: 10.18429/JACoW-IPAC2026-MOP1029

STUDIES OF CRYSTAL AND AMORPHOUS COLLIMATION OF LEAD, OXYGEN AND NEON BEAMS AT LHC

M. K. Zielińska*[1], R. Bruce, R. Cai, A. Donadon Servelle, P. D. Hermes, B. Lindström, C. Maccani, D. Mirarchi, G. Nigrelli, M. Patecki[1], S. Redaelli, N. Triantafyllou, F. Van der Veken, A. Vella,
CERN, Geneva, Switzerland
[1]also at Warsaw University of Technology, Warsaw, Poland

Abstract

The Large Hadron Collider (LHC) at CERN operates with lead-ion beams for about one month each year, requiring a high-performance collimation system to protect the machine from beam losses. The baseline ion-collimation scheme includes crystal collimation. In 2025, additional ion runs were carried out using oxygen and neon beams, enabling the first experimental comparison of collimation performance between crystal-based and amorphous collimators for these lighter ions. This work presents a comparative review of measured collimation performance for lead, oxygen, and neon ions at the LHC using both amorphous and crystal collimation techniques. The results offer a valuable benchmark for the simulation typically used to predict collimation efficiency and provide key input for future LHC ion runs, for which ion species other than lead are being considered.

INTRODUCTION

The Large Hadron Collider (LHC) [1] at CERN typically operates with lead-lead (Pb-Pb) ion collisions for about one month each year. A highly efficient collimation system [2–5] is essential to protect the machine from beam losses, since the stored beam energy, so far reaching 27.5 MJ, is high enough that even small losses can cause magnet quenches or even damage. Compared to proton beams, ion beam collimation presents greater challenges because of nuclear fragmentation and electromagnetic processes occurring in the collimator materials, which enhance the leakage of losses to superconducting magnets [6–8].

In 2025, a special ion run was performed with proton-oxygen (p-O), oxygen-oxygen (OO), and neon-neon (Ne-Ne) collisions [9], during which the cleaning performance was studied experimentally with different collimation techniques (crystals and amorphous) for the first time at the LHC for these ion species. In this article, we present these results and compare them with the corresponding results for Pb ions. This offers very valuable inputs to studies of potential future LHC operation with other ions than Pb, which is particularly important for Run 5 (foreseen for 2036–2041), for which a range of ions is under consideration [10, 11].

LHC COLLIMATION

The LHC has a multi-stage collimation system for betatron losses in interaction region 7 (IR7), which was primarily designed for proton operation and consists of amorphous blocks of material with lengths up to 1 m. The carbon-based primary collimators (TCP) have the tightest apertures, and they scatter the primary beam halo particles onto the secondary collimators (TCS), complemented by a set of shower absorbers (TCLA). Tertiary collimators (TCT) provide local protection to the final focus system around the experiments [2–5]. We refer to this as the standard collimation system.

The standard system is much less efficient with ions than with protons, since ion fragments scattered out of the TCPs can bypass the TCSs and TCLAs and impact the dispersion suppressor (DS) downstream of the collimation insertion [6]. Therefore, as a part of the High-Luminoisty LHC upgrades [12], one horizontal and one vertical crystal collimator (TCPC) were installed in each beam to improve the performance. These are 4 mm long bent silicon crystals [13–16], which replace the TCPs as primary aperture restrictions during ion operation. The TCPs are then typically retracted to the position of TCS, while the rest of the collimator hierarchy is identical to the standard system.

Crystal collimation relies on the channeling (CH) process in bent crystals [17, 18]. Channeled halo particles acquire a large angular kick, steering them onto an amorphous absorber, where they hit at such a large impact depth that the leakage of out-scattered fragments is minimized. The performance of the LHC crystals is quantified experimentally through angular scans, linear scans, and loss maps.

The angular scans, where the crystal is rotated in the bending plane while provoking beam losses, allow to identify the optimal channeling (CH) orientation. In linear scans, the crystal is kept in CH, and the absorber is moved toward the beam starting from an open position while provoking beam losses. They are used to measure a crystal's deflection angle and its channeling efficiency [14–16].

Loss maps are performed to evaluate the collimation cleaning efficiency. Measured loss maps considered in this study are histograms of losses around the accelerator ring collected by BLMs [19], when beam losses are provoked. Three types of losses are distinguished: on collimators, on normal magnets (warm) and on superconducting magnets (cold). The loss maps are normalized by the beam loss rate [20].

LINEAR AND ANGULAR SCANS

Examples of measured beam losses during angular and linear scans with O at top energy (5.36 Z TeV) are shown in Figures 1 and 2, respectively.

* marta.katarzyna.monikowska@cern.ch,
marta.monikowska.dokt@pw.edu.pl

Content from this work may be used under the terms of the CC BY 4.0 licence (© 2026). Any distribution of this work must maintain attribution to the author(s), title of the work, publisher, and DOI.

ISBN: 978-3-95450-252-3 ISSN: 2673-5350 doi: 10.18429/JACoW-IPAC2026-MOP1030

MONTE CARLO STUDIES OF MUON BACKGROUND AT SND@LHC

A.-G. Şerban*, R. Bruce, F. Cerutti, A. Donadon Servelle, S. Ilieva, B. Lindström, R. Cala'
CERN, Geneva, Switzerland

Content from this work may be used under the terms of the CC BY 4.0 licence (© 2026). Any distribution of this work must maintain attribution to the author(s), title of the work, publisher, and DOI.

Abstract

The dominant background for neutrino signal at the SND@LHC experiment consists of muons reaching the detector after traversing several tens of meters of rock. Monte Carlo simulations were instrumental in the experiment design and the background study. For the latter, a two-step workflow was adopted, first simulating with FLUKA proton–proton collisions in ATLAS and recording secondary muons on a virtual interface plane in the rock, and then propagating them to SND@LHC with Geant4. Benchmarking of simulated integral fluxes against Run-3 measurements showed a level of agreement within 10–15% and enabled the interpretation of the significant variations that were observed as a function of the LHC optics and beam crossing plane. In particular, the role of diffractive proton losses in an accelerator cell upstream of the detector was highlighted. On this basis, effective mitigation strategies, such as orbit bumps displacing these losses to other cells, were explored. For the HL-LHC configuration of Run-4, first estimates indicate a significantly higher muon background than in Run-3, reflecting not only the planned luminosity increase but also the larger leakage due to the magnet aperture enlargement.

INTRODUCTION

The Scattering and Neutrino Detector at the LHC (SND@LHC) [1, 2] is a forward physics experiment located at 480 m from the ATLAS Interaction Point (IP1), in the TI18 tunnel. Designed to detect high-energy neutrinos (100 GeV–1 TeV) in the pseudo-rapidity region $7.2 < \eta < 8.4$ [3,4], the detector is shielded by roughly 70 m of rock and concrete along the ATLAS line-of-sight. In view of this shielding, long-range muons originating from proton–proton ($p-p$) collisions in IP1 constitute the primary background for neutrino interaction searches. These muons can escape the veto system and induce showers, mimicking neutrino signals. In addition, the sustained muon flux gradually saturates the emulsion target, necessitating periodic replacements during data-taking. A comprehensive characterization of the muon flux through measurements and Monte Carlo (MC) simulations is therefore essential. This work presents the evolution, interpretation, and mitigation of the muon background across the various LHC configurations during Run-3 (2022–2026), and provides an outlook for the High-Luminosity LHC (HL-LHC) era in Run-4 (2030–2033).

MC SIMULATION WORKFLOW

The SND@LHC muon background is simulated using a two-step approach. First, $p-p$ collisions at center-of-mass energies of $\sqrt{s} = 13.6$ TeV (Run-3) and 14 TeV (Run-4) are sampled with the DPMJET-III event generator [5, 6], embedded in FLUKA [7–9]. The resulting collision debris is transported through a detailed FLUKA geometry of the LHC tunnel, extending from the ATLAS cavern to a virtual interface plane 30 m upstream of SND@LHC. At this plane, the kinematics, statistical weight, and production history of each muon are recorded. Second, a Geant4 [10] simulation propagates these muons from the interface plane through the upstream rock and the SND@LHC detector, accounting for secondary particle production. Benchmarking of the MC simulated muon rate against experimental measurements at SND@LHC was performed for all Run-3 configurations, yielding a good agreement, as reported in the following section.

MUON BACKGROUND ACROSS RUN-3

The experimental muon rates, Φ_{exp}, at SND@LHC during Run-3, alongside their corresponding MC estimates, Φ_{MC}, are summarized in Table 1. Their level of agreement is quantified by the relative difference δ, defined as:

$$\delta = \frac{\Phi_{\text{MC}} - \Phi_{\text{exp}}}{\Phi_{\text{exp}}}, \tag{1}$$

where

$$\Phi_{\text{MC}} = \frac{\sum_{i=1}^{N_{\text{tracks}}} w_i}{N_{p-p}} \times \sigma_{\text{inel}} \times \mathscr{L}. \tag{2}$$

The number of simulated $p-p$ collisions (of the order of 50 to 100 million) is denoted by N_{p-p}, the number of muons reconstructed within the active volume of the detector is N_{tracks}, while w_i represents their statistical weight. The inelastic $p-p$ cross-section at $\sqrt{s} = 13.6$ TeV (including diffractive events) is $\sigma_{\text{inel}} \approx 80$ mb and the reference Run-3 instantaneous luminosity is $\mathscr{L} = 2 \times 10^{34}$ cm^{-2} s^{-1}. Despite the complexity of the multi-step simulation framework, the MC predictions are in good agreement with the measurements across all Run-3 configurations and reflect their significant variations.

These variations are driven by the machine optics and beam crossing scheme adopted in Insertion Region 1 (IR1), which hosts the ATLAS experiment. In 2022–2023, the LHC operated in IR1 with downward vertical crossing (VC, −160 µrad half-crossing angle) and nominal optics, employing a focusing-defocusing-focusing[1] (FDF) sequence for the Q1, Q2, and Q3 final-focus quadrupoles. This configuration yielded the lowest muon rate recorded during Run-3. To redistribute the impact of collision debris on the aforementioned quadrupoles, the 2024 run operated with upward VC

* alexandra.serban@cern.ch

[1] The focusing/defocusing effect applies to the outgoing proton beam in the horizontal plane.

ISBN: 978-3-95450-252-3 ISSN: 2673-5350 doi: 10.18429/JACoW-IPAC2026-MOP1032

USE OF DBSCAN FOR FULL-AUTOMATIC-DATA-BASED ANOMALY DETECTION METHOD ON TURN-BY-TURN BEAM POSITION MONITORS (TBT-BPMS) IN SuperKEKB

Q. Bruant*, B. Dalena†, V. Gautard, J. Potaczala
Commissariat à l'Énergie Atomique et aux Énergies Alternatives, Paris, France
M. Le Garrec, CNRS/IN2P3-LAPP, Annecy-le-Vieux, France
J. Keintzel, European Organization for Nuclear Research, Geneva, Switzerland
F. Bugiotti, E. Al Bouzidi, T. Tonin, A. Kahla, CentraleSupélec-LISN, Gif-sur-Yvette, France

Abstract

In order to operate a collider at a consistent peak luminosity, it is essential to possess a comprehensive understanding of the complete magnetic lattice of the colliding rings. This requires precise knowledge of the deviation of the actual lattice from the model used as the basis during the design phase. One of the methods available for the purpose of measuring the aforementioned deviation is Turn-by-Turn Beam Position Monitor (TbT-BPM) surveys. The n-BPM method, as developed at CERN, forms the basis of the spectral response of the TbT-BPMs around the rings. This enables the reconstruction of the full effective magnetic lattice. However, the reliability of this measurement depends on the status and precision of each TbT-BPM in the ring. This paper compares two methods for detecting and removing problematic BPMs from magnetic lattice reconstruction scripts, both using DBSCAN. It describes their assumptions and processes, and discusses the results obtained on the High Energy Ring of SuperKEKB.

INTRODUCTION

The SuperKEKB collider is characterized by its very nonlinear optic lattice and its very high current beams circulating both in a Low Energy Ring (LER) and a High Energy Ring (HER)(see Ref. [1]). This configuration happens to cause a high degree of sensitivity of the machine with respect to actual imperfections in the lattice, compared to the model lattice. In order to discern these variations and identify potential sources, it is possible to use a specific type of Beam Position Monitors (BPMs), designated as TbT-BPMs (which are capable of recording the passing beam for each turn), and employ their respective signal to reconstruct the actual optic lattice of SuperKEKB, such as in Ref. [2]. However, due to the challenging environment and modifications to the rings, some of these TbT-BPMs are prone to malfunction, sometimes only for a few measurements. Consequently, it is imperative to detect these defective BPMs and eliminate their signal from the lattice reconstruction algorithm. This study is motivated by the observation that standard quality cuts applied in the TbT-BPM pipeline (SuperKEKB Optics Measurement Analysis or SOMA (see Ref. [3, 4]) based on processes used for LHC, developed by the Optics Measurement and Correction group (OMC) available at Ref. [5], are not able to remove the entirety of the anomalous BPMs from the analysis. This paper presents two versions of an anomaly detection pipeline based on a clustering algorithm called DBSCAN (see Ref. [6]). The distinguishing factor between these pipelines is the computation of the characteristics of TbT-BPM signals. These characteristics constitute the hyperspace inside which the DBSCAN operates in order to differentiate anomalous BPMs from the functional ones.

* quentin.bruant@cern.ch
† barbara.dalena@cern.ch

METHOD

Datasets

In this paper, we use both simulated and experimental HER data from SuperKEKB. The simulated dataset is obtained by single-particle-SAD tracking with the model lattice parameters of June 2024, with $\beta^* = 0.9$ µm, and taking into account Synchrotron Radiation (SR). Gaussian noise is subsequently applied to all tracks and errors (random spikes in tracks, signal removal keeping noise, random zero-mask on part of tracks, ...) are added to randomly selected BPMs. The experimental dataset consists of several measurements performed in June 2024.

Pipeline Description

After the reading of the raw data, both pipelines (Time2Feat and Fixed Features) pre-process the TbT-BPM signals using a standard scaling method

$$\hat{x}_i^t = \frac{x_i^t - \mu_i}{\sigma_i}, \forall (i,t) \in 1, N_{BPM} \otimes 1, N_{turns} \qquad (1)$$

where $\hat{x}_i^t$ is the preprocessed value, x_i^t is the input, μ_i and σ_i are the mean and the standard deviation of the ith BPM signal over the full range of turns, respectively, N_{turn} is the number of turns recorded in the given measurement (i.e. 4096) and $N_{TbT-BPM}$ is the number of TbT-BPMs considered (i.e. 67 out of few hundred BPMs in total).

The two methods take different paths. The first method is data-centered. The signal of each TbT-BPM is passed to a library called Time2Feat (see Ref. [7]) which computes several statistical features related to these signals. The most meaningful features are then selected. This selection is based on a process called Principal Feature Analysis (PFA) (see Ref. [8]). The table of all the features computed and their respective values for all the TbT-BPMs is passed to this

Content from this work may be used under the terms of the CC BY 4.0 licence (© 2026). Any distribution of this work must maintain attribution to the author(s), title of the work, publisher, and DOI.

ISBN: 978-3-95450-252-3 ISSN: 2673-5350 doi: 10.18429/JACoW-IPAC2026-MOP1035

RADIATION AND POWER DEPOSITION STUDIES FOR THE FCC-ee HALO COLLIMATION SYSTEM

S. Marin*, G. Banks, G. Broggi, R. Bruce, R. Cowan, A. Frasca, B. Humann, A. Lechner, G. Lerner, G. Nigrelli, A. Perillo Marcone, K. Taylor
European Organization for Nuclear Research (CERN), Geneva, Switzerland

Abstract

The collimation system of the Future Circular Collider (FCC-ee) is essential to isolate losses away from the experiments and other machine elements, thus reducing the radiation background in the experiments, and avoiding damage to the machine in case of accidental beam losses. The primary and secondary collimators of the collimation hierarchy, employed to scatter halo particles from the beam and remove them, respectively, will be accommodated in one of the technical insertions of the collider ring (Point F). In this paper, FLUKA simulations are presented for the collimation straight section. The power deposition is determined for all elements in the section following beam impacts on the collimator jaws, including other collimators as well as dipole and quadrupole magnets. Finally, the paper discusses the radiation levels in the Point F tunnel resulting from beam losses on the collimation system, and the resulting radiation hardness requirements for machine equipment and infrastructure.

INTRODUCTION

The FCC-ee collimation system [1–3] is designed to protect machine equipment and detectors from beam losses and to reduce the experimental background in the 91 km electron-positron collider [4]. In a previous study [5], we assessed the power deposition induced by beam halo losses in the collimation insertion, using FLUKA Monte Carlo simulations [6–9]. That work demonstrated that, for the GHC (Global Hybrid Correction) optics v23 considered at the time, two strategically placed shower absorbers can intercept secondary radiation between primary and secondary collimators, reducing the power leaking to the environment from approximately 50 % to 15 % of the total halo-loss power.

This paper extends our earlier study in several directions. First, we present results for the LCC (Local Chromaticity Correction) optics v105 with a two-phase betatron collimation layout, now featuring four primary and six secondary collimators distributed over approximately 2 km of the straight section at Point F. Second, we investigate the radiation environment in the tunnel, quantifying the absorbed dose and equivalent particle fluences relevant for the radiation hardness requirement of machine equipment. Third, we briefly assess the contribution of synchrotron radiation to the overall radiation levels in the collimation insertion, comparing the photon spectra in Z-pole and $t\bar{t}$ operation modes.

* stefano.marin@cern.ch

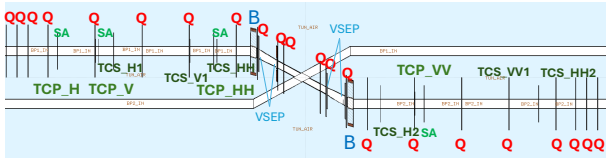

Figure 1: FLUKA geometry model of the betatron cleaning system including primary and secondary collimators, showing the location of optical and collimation system elements.

COLLIMATION SYSTEM AND SIMULATION MODEL

The simulation is performed with the FLUKA Monte Carlo code. The geometry model comprises a concrete tunnel of 5.5 m inner-bore diameter housing two 6 cm diameter copper vacuum chambers separated by 35 cm. The primary collimators (TCP) consist of a 25 cm-long graphite absorber with a TZM frame, while the secondary collimators (TCS) use a 30 cm-long TZM absorber. Both designs feature a double tapered jaw geometry at 9.5° on both upstream and downstream, with space to accommodate a beam position monitor. The jaws, including the tapers, measure 67 cm and 72 cm for primary and secondary collimators, respectively.

The full geometry of Point F is shown in Fig. 1, which illustrates the location of the magnets (Q for quadrupoles, B for bending, VSEP for vertical separators) and collimators (TCP for primary, TCS for secondary), as well as preliminary shower absorbers (SA), placed downstream of primary collimators to intercept radiation showers before they interact with the machine. Table 1 lists the half-gaps and positions for all collimators on the positron beamline. The two-phase collimation system features two primary collimators for each orientation, followed by secondary collimators. Due to limited space, only one secondary collimator for vertical betatron cleaning can be accommodated. We note that the LCC optics decouple the betatron and momentum collimation system, and Point-F will be dedicated to the former.

Table 1: Collimator Half-Gaps Δ and Positions s

	Δ (mm)	s (m)		Δ (mm)	s (m)
TCP.H	5.707	146.3	TCS.HH1	2.451	817.0
TCP.V	2.066	302.6	TCS.H2	5.023	1249.6
TCS.H1	4.999	362.8	TCP.VV	2.070	1364.3
TCS.V1	2.494	616.1	TCS.VV1	2.407	1677.8
TCP.HH	3.744	695.6	TCS.HH2	5.694	1775.5

The expected halo-loss power, listed in Table 2, is the source term considered in the FLUKA simulations of this

Content from this work may be used under the terms of the CC BY 4.0 licence (© 2026). Any distribution of this work must maintain attribution to the author(s), title of the work, publisher, and DOI.

ISBN: 978-3-95450-252-3 ISSN: 2673-5350 doi: 10.18429/JACoW-IPAC2026-MOP1036

BENCHMARKING FLUKA SIMULATIONS OF DOUBLE CHANNELING AND CRYSTAL ALIGNMENT AGAINST THE TWOCRYST EXPERIMENT

K. Taylor*, R. Cai, L. Esposito, P. Schoofs, CERN, Geneva, Switzerland

Content from this work may be used under the terms of the CC BY 4.0 licence (© 2026). Any distribution of this work must maintain attribution to the author(s), title of the work, publisher, and DOI.

Abstract

The TWOCRYST experiment at CERN is a as a proof-of-principle installation designed to demonstrate the feasibility of a crystal-based fixed target experiment, part of the Physics Beyond Colliders programme. The setup comprises two bent crystals installed in the LHC beamline at Insertion Region 3 (IR3), the same as the momentum collimation system. In the double channeling configuration explored in this set up, a splitting crystal (TCCS) extracts particles from the beam through channeling, directing them onto a long crystal (TCCP) inside which particles can be channeled again. This paper presents the FLUKA simulations performed to assess the crystals alignment procedures for various beam and crystal configurations. Since crystal alignment is achieved mainly by monitoring the Beam Loss Monitor (BLM) signals in the vicinity of both bent crystals, the main objective of the simulations is to evaluate the corresponding BLM responses at each step of the alignment. These simulations aim to confirm the validity of the alignment process by demonstrating that the BLM signals can be reliably used to gauge proper crystal alignment. The simulation outcomes are presented here and were found to be consistent with experimental observations.

INTRODUCTION

The use of bent crystals in high-energy accelerators allows precise manipulation of particle trajectories through channeling in the crystal lattice [1]. The proposed ALADDIN experiment is designed to employ this technique to measure the magnetic and electric dipole moments of charm baryons by inducing spin precession within bent crystals [2, 3].

As a precursor to this experiment, TWOCRYST [4, 5] serves as a proof-of-principle installation, testing the operational feasibility of double channeling, probing the crystal efficiency, and determining the particles on target, one of the main metrics of the experiment. One of the challenges in the operation of such a setup is the very precise angular alignment needed, and the high-precision, fast and sensitive controls needed for this. This study makes use of FLUKA [6–8] simulations to evaluate whether variations in Beam Loss Monitors (BLM) signals can be used to align the crystals during channeling and amorphous conditions across a range of beam energies (450 GeV, 1 TeV, 3 TeV and 6.8 TeV).

Charged particles can become confined within the electrostatic potential wells formed by the lattice planes of a crystal. When such a crystal is mechanically bent, the channeled particles follow the curvature of the planes, resulting in a controlled deflection of the particles [1, 9].

Channeling is possible only if the energy of the transverse motion of an incoming particle is less than the depth of the channel electrostatic potential well. This condition leads to the existence of a maximum incident angle for channeling, called *the critical angle*, defined as

$$\theta_c = \sqrt{\frac{2U_e}{pv}}, \tag{1}$$

where U_e represents the potential energy well, p the particle momentum, and v the particle velocity.

TWOCRYST exploits the channeling capabilities of two bent crystals: the TCCS (4 mm-long with a 50 μrad bending) extracts a beamlet from the LHC halo, while the TCCP (70 mm-long with a 700 μrad bending) performs further deflection of the particles [10–12]. Two Roman Pot stations house a pixel detector and a fibre tracker (TFT) which measure the deflected beam properties. The layout is shown in Fig. 1. This is done for one of the two counter-rotating beams of the LHC (beam 2).

The movement of the goniometer supporting each crystal is assisted by BLMs to ensure precise alignment. In the case of the TCCS, the BLM is located 1 m downstream and should see a signal reduction when the crystal is in channeling as fewer nuclear interactions occur, and thus fewer secondaries reach it. On the other hand, the TCCP BLM is positioned at the location where the channeled beam exits the vacuum chamber, such that when the TCCP is in channeling, deflected particles will directly impact the BLM, resulting in a sharp signal increase. The BLM responses were compared to beam halo losses on the primary collimator (TCPs) [13–18] for different beam energies.

FLUKA MODEL

To reproduce the geometry of the TWOCRYST setup in detail, dedicated FLUKA models were developed for both crystals and their vacuum tanks [19]. Figure 2 shows the resulting assemblies. Two BLMs were included in the model near the crystal locations corresponding to the integration in the LHC tunnel.

Each study case starts takes as input a set of six-dimensional coordinates representing particles impacting either the TCCS, TCCP, or the primary collimator (TCP). These are generated beforehand in dedicated combined tracking and particle-matter interaction simulations performed with MADX [20].

* ktaylor@cern.ch

ISBN: 978-3-95450-252-3 ISSN: 2673-5350 doi: 10.18429/JACoW-IPAC2026-MOP1037

FCC-ee ENERGY CALIBRATION AND POLARIZATION – TOWARDS THE REFERENCE DESIGN

J. Keintzel[1*], D.P. Barber[2], J. Bauche[1], J. Bendavid[1], A. Blondel[3], J. Burvill[1], C. Carli[1], J. Eysersman[12], A. Faus-Golfe[6], C. Goffing[1], E. Granados[1], K. Hock[8], W. Höfle[1], G. Iadarola[1], S. Keskar[1], A. Korsun[6], R. Kieffer[1], T. Lefevre[1], A. Martens[6], K. Oide[3], T. Pieloni[9], D. Sittard[1], J. Tamazirt[6], E. Torrence[11], M. Watson[1], J. Wenninger[1], G. Wilkinson[1], Y. Wu[9],
[1]CERN, Geneva, Switzerland, [2]DESY, Hamburg, Germany,
[3]DPNC, University of Geneva, Switzerland, [5]IHEP, Beijing, China; [6]IJCLab, Orsay, France;
[7]Jefferson Lab, Newport News, VA, USA, [8]BNL, Upton, USA, [9]EPFL, Lausanne, Switzerland,
[10]Cornell University, NY, USA, [11]University of Oregon, Eugene, USA
[12]MIT, Cambridge, MA, USA

Abstract

The FCC-ee aims at delivering high-precision particle-physics measurements over a wide beam-energy range, from the Z pole at 45.6 GeV up to 182.5 GeV, above the top-pair production threshold. Achieving the target physics precision requires an exceptionally accurate determination of the centre-of-mass energy and, consequently, of the beam energies. The baseline approach relies on resonant depolarization scan of dedicated, transversely polarized pilot bunches up to 80 GeV. By analysing the depolarization signatures with a 3D polarimeter, the spin tune can be extracted with a goal of reaching systematic uncertainties on the beam energy at the level of up to a few 10 keV. This contribution presents the latest progress of the FCC-ee Energy Calibration and Polarization Working Group, covering recent developments in polarization build-up studies, resonant-depolarization techniques, machine-optics optimization, and polarimetry concepts. The current status is summarized, and the roadmap of technical and conceptual milestones required for the reference design is outlined.

INTRODUCTION

The Future Circular electron-positron Collider (FCC-ee) is designed as an Higgs- and electroweak factory, with a centre-of-mass energy range, from the Z-pole at 45.6 GeV up to above the top-pair production threshold at 365 GeV. Achieving the target physics precision requires an exceptionally accurate determination of the centre-of-mass energy, $\sqrt{s}$, and, hence also of the beam energies, which is in the scope of the energy calibration, polarization and monochromatization working group (EPOL) [1, 2].

In the Feasibility Study Report [3–5], the baseline scenario to achieve polarized pilot bunches in the FCC-ee collider rings, relied on the build-up of transverse polarization via the Sokolov–Ternov effect [6]. However, the long natural polarization times ($\tau \approx 200$ h), even when reduced by the use of polarization wigglers, could significantly reduce achievable integrated luminosity [7]. This motivated to investigate the feasibility of injecting already transversely polarized pilot bunches. While this technique could improve availability, polarization transport and preservation must be ensured.

While the baseline method to determine the change of polarization when pilot bunches are depolarized with dedicated RF kickers is Resonant Depolarization (RDP), aimed to be applicable until 80 GeV [8], a novel technique, called Near Resonance Polarization Modulation (NRPM) [9], has recently been presented which could reduce the time required for one measurement.

Recently, studies have been performed for two FCC-ee optics designs, namely the Global Hybrid Correction (GHC) [10] and the Local Chromaticity Correction (LCC) [11]. After an extensive review, the LCC is recommended as the baseline lattice. Important findings which are associated with energy calibration and polarization are recalled here, while more information can be found in [12–14].

The FCC-ee is currently in the reference design phase, with the central objective to establish a coherent and robust machine design, including the energy calibration and polarization strategies under realistic conditions through detailed simulations. This paper summarises the current status of the FCC-ee EPOL team and outlines the key open challenges for the reference design phase.

PRECISION PHYSICS

Precision targets for physics observables are the most demanding at the lower energies for the Z and W-mass measurement, as also given in Table 1 [4, 8]. At higher energies, first estimates based on physics requirements indicate that a few MeV prevision at ZH and ttbar-energy are required [15].

The Sokolov–Ternov effect also leads to a polarization build-up of colliding bunches. Assuming a $\tau \approx 200$ h and a top-up of 10 % of the nominal bunch every 70 s, a vertical asymptotic polarization of close to 1×10^{-3} could be present. At the IP the longitudinal polarization must be controlled below 1×10^{-5}, and hence demanding a control of the axis of the invariant spin field, n_0, below 10 mrad.

* jacqueline.keintzel@cern.ch

Content from this work may be used under the terms of the CC BY 4.0 licence (© 2026). Any distribution of this work must maintain attribution to the author(s), title of the work, publisher, and DOI.

ISBN: 978-3-95450-252-3 ISSN: 2673-5350 doi: 10.18429/JACoW-IPAC2026-MOP1038

PROGRESS ON OPTICS MEASUREMENTS FOR THE FCC-ee

J. Keintzel*[1], D.B. Pio[2], R. Tomás[1]
[1]CERN, Geneva, Switzerland
[2]DTU, Lundtofte, Denmark

Abstract

Precise optics measurements will be crucial for commissioning and optimising the Future Circular electron-positron Collider, FCC-ee, across its full energy range. To prepare for this challenge, simulation studies have been performed to evaluate the accuracy and robustness of Turn-by-Turn (TbT) based optics diagnostics applied to the FCC-ee. A central element of this effort is the use of an AC-dipole to generate coherent, controlled beam oscillations suitable for high-quality TbT data analysis. This contribution presents the latest progress in simulated TbT optics measurements, including sensitivity to Beam Position Monitor (BPM) noise. Particular emphasis is placed on exploring the first specifications for BPMs and AC-dipoles for the FCC-ee, accounting for constraints related to synchrotron-radiation damping, excitation strength, and driving frequency. The results provide essential input for defining the optics-measurement strategy, hardware requirements, and correction schemes foreseen for the FCC-ee.

INTRODUCTION

The Future electron-positron Circular Collider (FCC-ee) [1, 2] has been recommended as the highest priority future collider succeeding the High-Luminosity LHC (HL-LHC) [3]. This lepton storage ring collider aims at an exceptionally high luminosity production at collision energies from 91.2 GeV to 365 GeV, corresponding to physics around the Z-pole up to above the $t\bar{t}$-threshold. Achieving its design performance requires an extremely precise beam optics control. In particular, accurate measurements of the β-functions, phase advances and linear coupling are fundamental to apply optics and emittance tuning techniques successfully [4].

Turn-by-Turn (TbT) Beam Position Monitor (BPM) data provide a powerful tool for optics measurements. Traditionally in lepton storage rings, such measurements rely on single kicks applied transversely to the beam. However, with a transverse damping time of 2600 turns to as low as 40 turns, respectively at 45.6 GeV to 182.5 GeV beam energy, the fast decay of free oscillations significantly limits the achievable measurement accuracy (see also Ref. [5]). An AC-dipole is, therefore, an attractive method to excite beams over a longer period at a constant amplitude and has been demonstrated reliable for various past and present machines, see e.g. [6, 7]. Due to strong Synchrotron Radiation (SR) damping for the FCC-ee this technique requires careful review.

In this paper, we investigate the use of AC-dipoles for global optics measurements in the FCC-ee. We study the performance versus excitation strength, and distance to the natural tune, including SR damping and amplitude detuning. Furthermore, we assess the impact of BPM resolution errors on the quality of optics measurements, aiming to set first tolerances. All studies are performed using Xsuite [8] and the LCC optics version 106.2.2, which has recently been selected as baseline [9, 10]. The overall goal is to contribute to define a global optics measurement strategy, tolerances, and to define the optimal parameter space for reliable and precise optics measurements.

THEORY

The transverse motion under AC-dipole excitation is well established in the absence of SR [11–13]. It can be written as

$$x(s,n) = \frac{B_m L}{4\pi B\rho\delta}\sqrt{\beta(s)\beta_0}\cos(2\pi Q_d n - \pi Q + \phi(s))\,, \tag{1}$$

where n is the turn number, β_0 is the β- function at the AC-dipole, Q_d is the driven tune, $\delta = Q_d - Q$ is the difference between the driven and natural tune, and $\beta(s)$ and $\phi(s)$ are the driven optics parameters. In contrast to free betatron oscillations, the AC-dipole generates a coherent driven motion that can be sustained over many turns. This is particularly advantageous in the FCC-ee, where SR leads to rapid damping of free oscillations.

The oscillation amplitude scales inversely with δ. Expressing the motion in units of the beam size, $x(s) = N_\sigma\sqrt{\varepsilon\beta(s)}$, the required kick angle without SR can be estimated as

$$\theta \approx N_\sigma\, 4\pi\delta\sqrt{\varepsilon/\beta_0}\,. \tag{2}$$

The transverse kick is generated by an AC dipole through an oscillating magnetic field which can be expressed in terms of the applied voltage. This scales with the desired excitation amplitude and can be expressed as

$$V \approx N_\sigma \frac{4\pi\delta\, p_0 c}{0.3}\sqrt{\varepsilon/\beta_0}\,. \tag{3}$$

In practice, however, various effects could modify this ideal excitation. Amplitude detuning introduces a dependence of the tune on the amplitude, effectively changing the detuning for large excitations. Additionally, SR damping leads to a time-dependent oscillation amplitude.

IMPLEMENTATION

In the FCC-ee AC-dipoles are already foreseen to be integrated in the dispersion suppressor, used for measurements of the beam energy via resonant depolarization (RDP), as part of the polarization and energy calibration effort [14–16].

* jacqueline.keintzel@cern.ch

Content from this work may be used under the terms of the CC BY 4.0 licence (© 2026). Any distribution of this work must maintain attribution to the author(s), title of the work, publisher, and DOI.

ISBN: 978-3-95450-252-3 ISSN: 2673-5350 doi: 10.18429/JACoW-IPAC2026-MOP1039

FCC-ee OPTICS TUNING – TOWARDS THE REFERENCE DESIGN

J. Keintzel[1*], R. Tomás[1], J. Bauche[1], C. Carli[1], R. De Maria[1], C.J. Eriksson[1], V. Gawas[1], C. Goffing[1], S.S. Jagabathuni[1], I. Garcia-Aguirrebeitia Sanchez[1], A. Kastrinellis[1], G. Katsanevakis[1], T. Lefevre[1], M. Liebsch[1], E.H. Maclean[1], H. Mainaud[1], Y. Papaphilippou[1], P. Raimondi[1], G. Roy[1], K. Skoufaris[1], L. Todorovic[1], F. Valchkova-Georgieva[1], W. Van Goethem[1], A. Vorozhtsov[1], F. Zimmermann[1], T.K. Charles[2], K. Andre[3], S. Liuzzo[3], S. White[3], E. Ahmadi[4], I. Agapov[5], E. Musa[5], A. Chance[6], B. Dalena[6], Q. Bruant[6], X. Huang[7], C. García-Jaimes[8], T. Pieloni[8], T. Prebibaj[8], L. van Riesen-Haupt[8], Y. Wu[8], H. Sugimoto[9], Y. Ohnishi[9], K. Oide[9], A. Hussain[10], M. Boland[11], P. Hunchak[11], M. Le Garrec[12],
[1]CERN, Geneva, Switzerland, [2]ANSTO - Australian Synchrotron, Australia,
[3]ESRF, Grenoble, France, [4]IPM, Tehran, Iran, [5]DESY, Hamburg, Germany, [6]CEA, Paris, France,
[7]SLAC, Stanford, USA, [8]EPFL, Lausanne, Switzerland, [9]KEK, Tsukuba, Japan,
[10]PAEC, Pakistan, [11]USASK, Canada, [12]LAPP, France.

Content from this work may be used under the terms of the CC BY 4.0 licence (© 2026). Any distribution of this work must maintain attribution to the author(s), title of the work, publisher, and DOI.

Abstract

The Future electron positron Circular Collider, FCC-ee, is a proposed next-generation facility designed to deliver very high luminosities across a broad beam-energy range, from the Z pole at 45.6 GeV up to 182.5 GeV. Achieving the target performance in the presence of realistic lattice imperfections represents a significant challenge. To address this, a comprehensive commissioning strategy is being developed, featuring dedicated optics configurations, robust beam-based alignment procedures, and advanced optics-correction techniques supported by refined beam-based measurements. In parallel, specifications for the main magnet families, corrector circuits, and required instrumentation are being explored to ensure compatibility with the expected tuning procedures. This contribution summarizes the current status of these developments and outlines the key steps and milestones envisioned on the path toward the reference design.

INTRODUCTION

Achieving the ambitious luminosity targets of the Future electron-positron Circular Collider, FCC-ee [1–3], requires precise control of the machine optics in the presence of realistic imperfections. Correcting linear optics distortions alone is not sufficient to fully restore dynamic aperture (DA) and momentum acceptance (MA), see e.g. [4–7]. In this context a staged tuning strategy is foreseen, starting from Beam-Based Alignment (BBA), orbit and global linear optics correction, followed by non-linear optimisation and dedicated local knobs to restore Interaction Point (IP) parameters. As part of the tuning strategy, novel optics, either with switched-off final focus or larger β^* have been developed, to ease start of commissioning.

Over the past years, optics design and tuning studies have been pursued for two versions of the FCC-ee, namely for the Global Hybrid Collider (GHC) [8] and the Local Chromaticity Correction (LCC) [9] lattices. At the end of 2025 a comprehensive comparison exercise has been carried out, including simulation studies which fall in the mandate of the FCC-ee optics tuning. These studies provide important insight into correction strategies and tolerances in the presence of realistic errors. Some findings of this are also given [10, 11] , with the full report being available in [12].

The FCC-ee project is currently in the reference design phase until roughly end of 2027. A central objective of this phase is to establish a coherent machine design. This includes, incorporating magnet and alignment errors, linear and non-linear corrections, optics measurement strategies and corrector circuit specifications. Furthermore, robust performance under realistic conditions should be demonstrated by comprehensive simulation studies and experiences from existing machines, such as SuperKEKB.

MACHINE IMPERFECTIONS

The definition of magnetic field tolerances relies on a strong interplay between magnet design and beam dynamics requirements. First estimates of achievable field quality are derived from magnet design studies and prototype measurements for the arc dipole, given at a reference radius of 10 mm [13], and summarised in Table 1 [14]. Effort for other magnet types is currently ongoing.

Sensitivity simulations provide complementary constraints to ensure that performance targets can be met in the presence of realistic errors. Multipole random error sensitivity studies at Z energy are performed including beam-beam effects, by determining the field error level at which the MA is reduced by 10 % using 40 seeds with Synchrotron Radiation (SR) and Quantum Fluctuation (QF), and are sum-

Table 1: Arc Dipole Manufacturing Field Errors, in 10^{-4} Relative Units at a Reference Radius of 10 mm

Component	Systematic	Random
b_1	–	10
b_2 / a_2	10 / 1	5 / 2
b_3 / a_3	0.5 / 0.5	0.5 / 0.5
b_4 / a_4	0.5 / 0.1	0.5 / 0.1
$b_{n>4}$ / $a_{n>4}$	0.1 / 0.1	0.1 / 0.1

* jacqueline.keintzel@cern.ch

ISBN: 978-3-95450-252-3 ISSN: 2673-5350 doi: 10.18429/JACoW-IPAC2026-MOP1040

SENSITIVITY OF FCC-EE BEAM PERFORMANCE TO RESONANCE DRIVING TERMS IN THE PRESENCE OF BEAM–BEAM INTERACTIONS

T. Prebibaj*[1], T. Pieloni[1], M. Seidel[1,2], X. Buffat[3], L. Van Riesen-Haupt[4]
[1]EPFL, Lausanne, Switzerland
[2]PSI, Villigen, Switzerland
[3]CERN, Geneva, Switzerland
[4]Old Dominion University, Norfolk, VA, USA

Abstract

The control of nonlinear beam dynamics is essential for achieving the luminosity targets of FCC-ee, particularly in the presence of strong beam–beam interactions and machine imperfections. Resonance Driving Terms (RDTs) provide a systematic framework to characterize nonlinear dynamics and quantify the strength of resonances excited by nonlinear magnetic elements in the lattice. This contribution presents a sensitivity study of individual RDTs and their impact on beam losses, vertical emittance, and luminosity in FCC-ee, evaluated using tracking simulations including beam–beam interactions. The results establish a ranking of the relative importance of individual RDTs on the performance, providing guidance for future RDT-based correction strategies.

INTRODUCTION

The Future Circular electron-positron Collider (FCC-ee) [1–3] is a proposed high-luminosity lepton collider designed to operate at multiple center-of-mass energies for precision studies of the Z, W, Higgs, and top quark. Achieving the demanding luminosity targets requires tight control of nonlinear beam dynamics in the presence of both machine imperfections and strong beam–beam interactions [4–6]. Lattice nonlinearities and magnetic field imperfections can degrade beam lifetime and luminosity through the reduction in Dynamic Aperture (DA) and Momentum Acceptance (MA). In addition, the strong beam-beam interactions at FCC-ee modify the linear and nonlinear properties of the lattice which can further reduce MA/DA as well as the effectiveness of standard optics corrections designed without beam-beam. Resonance Driving Terms (RDTs) provide a framework to characterize nonlinear dynamics and quantify the strength of resonances excited by magnetic errors and nonlinear elements in the lattice. Controlling the most harmful RDTs can therefore help mitigate the impact of nonlinearities on beam performance, especially in the presence of beam-beam effects. This paper presents a systematic sensitivity study to identify which RDTs most strongly affect beam performance in the presence of beam–beam interactions. Individual RDTs are varied in a controlled manner using a response-matrix and Singular-Value-Decomposition (SVD) approach, and tracking simulations are used to evaluate the impact on beam losses, emittance, and luminosity. The study focuses on the Local Chromaticity Correction (LCC) optics [7] at Z energy.

SIMULATION TOOLS

The studies are performed using the Xsuite simulation framework [8], which provides particle tracking, beam–beam modeling, and optics correction capabilities, as well as interfaces to external optics tools such as MAD-NG [9]. RDTs are evaluated using two methods. The first relies on analytical calculations in MAD-NG, allowing direct computation of RDTs from the lattice model. Figure 1 shows the third and fourth order normal RDTs around Interaction Point 2 (IP2) for the ideal lattice without beam–beam effects.

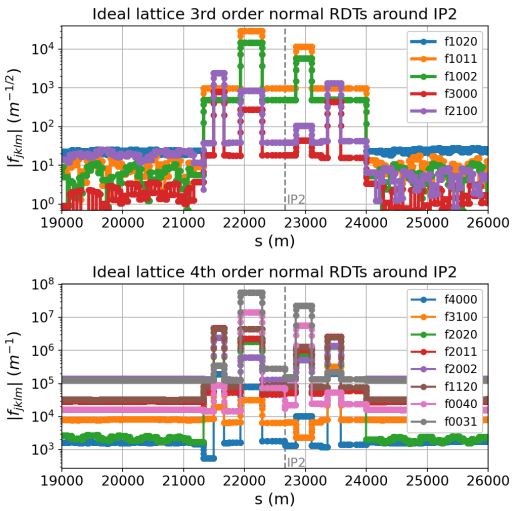

Figure 1: Calculation of third-order (top) and fourth-order (bottom) normal RDTs of the ideal lattice around IP2 using MAD-NG. f_{1020} (blue) overlays f_{1002} (green) around the IP.

The second method extracts RDTs from tracking simulations using Xsuite and OMC3 [10]. A single particle with an initial transverse offset is tracked for a few thousand turns (without synchrotron radiation), and turn-by-turn data at selected locations (e.g. BPMs) are analyzed in the frequency domain. The amplitudes of specific spectral lines are used to reconstruct the corresponding RDTs [11]. The advantage of this method is that it can incorporate the contribution of any lattice element (including beam-beam interactions) without requiring an explicit analytical model. The trade-off is that it is more computationally expensive as it requires

* tirsi.prebibaj@cern.ch

Content from this work may be used under the terms of the CC BY 4.0 licence (© 2026). Any distribution of this work must maintain attribution to the author(s), title of the work, publisher, and DOI.

ISBN: 978-3-95450-252-3 ISSN: 2673-5350 doi: 10.18429/JACoW-IPAC2026-MOP1041

BEAM-DELIVERY CHALLENGES FOR PLASMA-WAKEFIELD ACCELERATORS

L. Kennedy*[1,2], C. Caliari[2], R. Tomás[2], R. D'Arcy[1], P. N. Burrows[1]
[1]John Adams Institute, University of Oxford, Oxford, United Kingdom
[2]European Organization for Nuclear Research, Meyrin, Switzerland

Abstract

Plasma-wakefield acceleration offers a promising path towards a next-generation collider, but poses significant beam-delivery challenges. We present initial designs for final-focusing systems capable of transporting beams from the plasma-based-collider concepts, ALiVE and HALHF, each with distinct beam dynamics constraints. For ALiVE, where the beams are intrinsically round, we demonstrate an increase in $\mathcal{L}_{1\%}/\mathcal{L}_{tot}$ from 3.6% to 27%, and explore ultra-compact FFS configurations reflecting the potential for significantly reduced collider lengths. For HALHF, where the beams feature large horizontal emittance to alleviate the burden on the plasma linac, we show that a global chromaticity-correction scheme reduces aberrations to within 20% of the design beam size at 375 GeV, and identify synchrotron radiation as the dominant limitation at higher energies.

INTRODUCTION

ALiVE [1] aims to deliver low-emittance beams using a highly relativistic, short proton driver to generate wakefields in the strongly nonlinear blowout regime. The beams generated in this scheme, with parameters given in Table 1, feature an intrinsically round transverse profile, leading to enhanced disruption and relatively few collisions occuring within 1% of the nominal energy due to strong beamstrahlung radiation. HALHF [2] proposes an electron-driven plasma-wakefield arm for electron acceleration and an RF linac for positron acceleration, bypassing the inherent difficulties associated with plasma-based positron acceleration. The beams generated in this regime are flat, with the horizontal emittance much greater than the vertical, with parameters given in Table 1 [3], and are therefore not dominated by beamstrahlung effects. However, the HALHF beams exhibit a large emittance, leading to considerable beam size growth due to transport aberrations in the CLIC final focus system (FFS) [4, 5]. FFS configurations based on the CLIC and traditional FFS schemes [6] are presented, addressing the challenges associated with plasma-based acceleration.

ALIVE FINAL FOCUS SYSTEM

ALiVE beams were tracked in a CLIC FFS using PLACET, with the resulting beam distributions used to compute the luminosity using GUINEA-PIG [7–9]. Total and peak luminosities of $\mathcal{L}_{tot} = 14.1 \times 10^{34}\,\mathrm{cm^{-2}s^{-1}}$ and $\mathcal{L}_{1\%} = 0.37 \times 10^{34}\,\mathrm{cm^{-2}s^{-1}}$ were found, corresponding to a relative fraction of the luminosity within the 1% energy peak of $\mathcal{L}_{1\%}/\mathcal{L}_{tot} = 2.5\%$ due to beamstrahlung effects. For a typical collider, an $\mathcal{L}_{1\%}/\mathcal{L}_{tot}$ greater than 30% should be expected in order to minimize background radiation and maximize the signal-to-noise ratio at the detector. It is therefore necessary to flatten the round ALiVE beam via the optical beta functions β_x^* and β_y^* in the FFS to maximize the $\mathcal{L}_{1\%}/\mathcal{L}_{tot}$ ratio.

Table 1: Plasma Wakefield Beam Parameters For The Proton-Driven ALiVE And Electron-Driven HALHF Designs

Parameter	ALiVE	HALHF
Centre-of-mass energy [GeV]	250	250
Particles per bunch [$\times 10^{10}$]	2	1
e^- bunch length [μm]	105	150
e^+ bunch length [μm]	75	150
β_x^* at IP [mm]	13	3.3
β_y^* at IP [mm]	0.41	0.1
Norm. horizontal e^- emittance [nm]	100	90 000
Norm. vertical e^- emittance [nm]	100	320
Norm. horizontal e^+ emittance [nm]	400	10 000
Norm. vertical e^+ emittance [nm]	400	35
Bunch frequency [kHz]	7.2	16
Energy spread RMS [%]	0.10	0.15
Total luminosity [$10^{34}\,\mathrm{cm^{-2}s^{-1}}$]	9.3	1.2
Luminosity in top 1% [$10^{34}\,\mathrm{cm^{-2}s^{-1}}$]	0.34	0.76

The beta functions of a CLIC FFS were scanned by matching the FFS quadrupole strengths using MADX [10]. Figure 1 shows the total and peak luminosities as functions of β_x^* and β_y^*, demonstrating a linear reduction in beamstrahlung radiation due to beam flattening. A peak luminosity of $0.42{\times}10^{34}\,\mathrm{cm^{-2}s^{-1}}$ is found when $\beta_x^*/\beta_y^* = 80/0.11$ mm, corresponding to 27% of collisions within 1% of the nominal energy. However, the total luminosity is degraded due to large β_x^*, enhanced synchrotron radiation from the Oide effect, and vertical aberrations induced by β_y^* squeezing [11]. Figure 2 shows the layout and linear optics of the FFS, with length $L_{FFS} = 550$ m and final drift length $L^* = 6$ m.

Higher-order beam sizes were calculated semi-analytically using MAPCLASS [12–14], and were subsequently minimized using the higher-order multipoles in the FFS to reduce aberrations. Figure 3 shows good performance for the electron beam with RMS beam sizes of $\sigma_{x,e^-}/\sigma_{y,e^-} = 183/10$ nm at the interaction point (IP). However, due to a factor 4 larger positron emittance, the aberrations lead to enhanced beam size growth resulting in positron RMS beam sizes of $\sigma_{x,e^+}/\sigma_{y,e^+} = 428/71$ nm at the IP.

Exploratory studies assessed the performance of ultra-low β^*, ultra-short final focus systems for ALiVE, consistent

* lewis.kennedy@cern.ch

Content from this work may be used under the terms of the CC BY 4.0 licence (© 2026). Any distribution of this work must maintain attribution to the author(s), title of the work, publisher, and DOI.

ISBN: 978-3-95450-252-3 ISSN: 2673-5350 doi: 10.18429/JACoW-IPAC2026-MOP1043

DESIGN OF PION TRANSPORT FROM THE ESSnuSB+ TARGET TO THE LEnuSTORM RING*

M. Topp-Mugglestone†, I. Efthymiopoulos
CERN, Geneva, Switzerland

Abstract

Measurements of neutrino oscillations in low-energy regimes will require precise knowledge of neutrino-nucleus interaction cross sections for low-energy neutrinos. The ESSnuSB+ project aims to fill the gap in the interaction cross section data by creating a well-quantified neutrino beam from the circulation of stored muons in a low-energy racetrack decay ring, LEnuSTORM. To produce the circulating muon beam, a pion beam will be generated via the impingement of a 1.25 MW proton pulse on a target. The pions must then be focused, transported, and injected to the production straight of the decay ring wherein the pions will decay to muons. This contribution discusses the transport of the pions from the megawatt-class target station to their injection in the ring, and considerations for maximizing the muon yield – including momentum selection, maximization of acceptance, and designing a line with minimal path length to increase pion survival whilst accommodating optics matching and layout constraints.

INTRODUCTION

ESSnuSB [1] is a proposed long-baseline neutrino oscillation experiment making use of the 5 MW proton pulses at 2 GeV provided by the European Spallation Source (ESS) linac. Pulses from the linac are to be redirected to an accumulator ring before being sent onto a target assembly; the resulting secondary particles are focussed in the forwards direction by using an array of four magnetic horns; pions in the secondary particle shower will then decay to muons, producing a uniquely intense pulse of neutrinos for the neutrino oscillation measurements.

To support these physics studies, and as an intermediate stage to the construction of the full ESSnuSB experiment, the ESSnuSB+ project has been proposed [2]. This project will take only one in four pulses from the linac for an average beam power of 1.25 MW, directing these onto a single target/horn assembly. Forward-focussed pions will then be transported via a short beamline to a racetrack layout decay ring based on the nuSTORM concept [3]. This low-energy decay ring, termed LEnuSTORM, uses the stochastic injection principle [4] to inject this pion pulse, which passes along one of the ring's two straights (the so-called production straight), wherein the majority of the pion beam decays to muons. Muons at the desired momentum of 600 MeV/c then circulate for a number of turns; the decay of muons in the production straight produces a focussed beam of muon and electron neutrinos. This beam is then used to make precision measurements of neutrino-matter interaction cross-sections in the low-energy regime.

To facilitate the production of this precise neutrino beam, it is first necessary to transport the pions from the target station environment to the decay ring. This transfer line must satisfy a number of key requirements: firstly, it must be as short as possible to minimise premature pion decay; it must match the Courant-Snyder parameters (beta functions, alpha functions, and dispersion) of the pion distribution downstream of the horn to those demanded by the periodic Courant-Snyder parameters of the production straight; it must maximise its transverse and momentum acceptance to maximise pion yield; and finally, it must meet the geometric constraints established by the project's design.

LAYOUT

As shown in the schematic depicted in Fig. 1, the axis of the target station beam (and downstream decay tunnel) is directed towards the long baseline near detector, which is then shared with the neutrino beam produced by the LEnuSTORM production straight. The injection point of the LEnuSTORM ring must then be separated by sufficient distance from the target station to pass through the radiation shielding of the megawatt-class target station environment, as well as ensuring that the production straight does not intersect with the decay tunnel or its shielding. The requirement of a shared detector for the decay tunnel axis together with the separation requirement for the LEnuSTORM sets the constraints for the total bending angle required for the transfer line. The minimum angle α between the production straight and decay tunnel axes is given as $\tan\alpha = \frac{w}{s-T}$, in which w is the half-width of the decay tunnel and associated shielding, assumed to be 8 m, T is the length of the decay tunnel, and s is the position of the near detector with respect to the target station. Then, by computing the angle of the pion beam at injection with respect to the production straight, the total bending angle of the transfer line is determined.

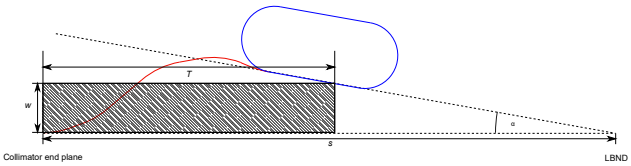

Figure 1: Geometry diagram showing the decay tunnel and shielding (shaded area), pion transfer line (red), and LEnuSTORM ring (blue). The elements are not depicted to scale.

The transfer line is based on a two-arc concept. The bending angle of the initial dipole is limited due to the low maximum field of the large-aperture target station dipole (LADM).

* EU Grant Agreement No 101094628
† max.emil.topp-mugglestone@cern.ch

Content from this work may be used under the terms of the CC BY 4.0 licence (© 2026). Any distribution of this work must maintain attribution to the author(s), title of the work, publisher, and DOI.

ISBN: 978-3-95450-252-3 ISSN: 2673-5350 doi: 10.18429/JACoW-IPAC2026-MOP1044

NEUTRINO FLUENCE ESTIMATES FOR FORWARD EXPERIMENTS AT A 10 TeV MUON COLLIDER

D. Calzolari, C. Ahdida, C. Carli, H. Guerin, A. Lechner, G. Lerner, J. Manczak, D. Schulte, M. Vanwelde, European Organization for Nuclear Research, Geneva, Switzerland
D. Lucchesi, Università di Padova and INFN - Sezione di Padova, Padua, Italy

Abstract

Intense and highly collimated neutrino beams are intrinsic by-products of muon decays in a high-energy muon collider. The large boost of the primary muons confines the emitted neutrinos within angular spreads of order of 10^{-5} rad, resulting in fluxes far exceeding those achievable in conventional neutrino facilities. Their unique properties also open opportunities for high-energy neutrino physics. In this work, the neutrino beams produced near the interaction point are characterised in terms of their spatial and energy distributions, with emphasis on their potential use for dedicated neutrino detectors. The neutrino fluence is evaluated as a function of distance from the interaction point for representative detector acceptances. At short distances, larger acceptances intercept nearly the entire neutrino core, leading to fluence saturation, while at kilometre scales the neutrino spot size becomes non negligible. These results demonstrate the strong collimation and intensity of muon-collider neutrino beams and support their potential use in high-precision, high-energy neutrino studies.

INTRODUCTION

The muon collider is a proposed next-generation particle physics facility aiming to reach centre-of-mass energies in the multi-TeV range within a compact footprint [1, 2]. By colliding muons rather than protons or electrons, it combines the high centre-of-mass energy of hadron machines with the cleaner initial state of a lepton collider. However, the short muon lifetime ($\tau_\mu \approx 2.2\,\mu s$) means that a significant fraction of muons decay before reaching the interaction point (IP), making both the machine and detector design particularly challenging. In particular, the muons decay in two neutrinos and an electron/positron:

$$\begin{cases} \mu^- \to e^- + \bar{\nu}_e + \nu_\mu \\ \mu^+ \to e^+ + \nu_e + \bar{\nu}_\mu \end{cases}$$

Therefore, a unique feature of a muon collider is the production of intense, collimated neutrino beams. Each muon decay produces a pair of neutrinos that, in the laboratory frame at multi-TeV energies, are boosted into extremely narrow cones along the beam direction. The resulting fluxes can reach values many orders of magnitude higher than those achievable at conventional neutrino facilities, opening up possibilities for precision cross-section measurements and searches for new interactions in the neutrino sector.

Many works in the literature describe the physics potential of muon collisions [3, 4]. In addition, the exploitation of neutrinos produced in muon decays is beginning to attract interest within the theory community [5]. This paper presents the neutrino fluences and spectra that could be available for a forward experiment at a 10 TeV center-of-mass energy muon collider.

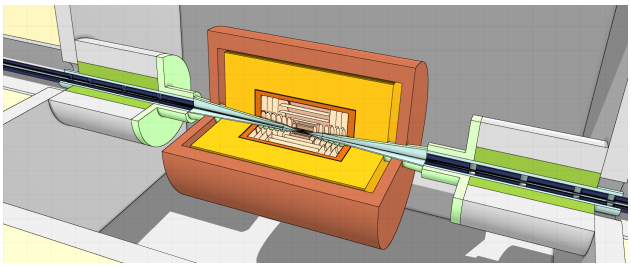

Figure 1: Machine-detector interface of a 10 TeV muon collider. In the picture, the final focus elements and the detector are shown.

The straight sections of the collider ring near the IP are particularly relevant in this context. Muon decays along these sections produce neutrinos that accumulate into intense, nearly collinear beams directed along the beam axis. These beams have two key consequences: they impose radiological constraints on the collider siting and optics design [6, 7], and they offer a remarkable opportunity for high-energy neutrino physics with a dedicated forward detector. In this paper, we focus on the latter, characterising the neutrino beams near the IP and evaluating the achievable fluence for representative detector configurations.

NEUTRINO BEAM GENERATION IN THE INTERACTION REGION

A critical aspect of the muon collider design is the Machine–Detector Interface (MDI), the region where the accelerator and detector systems must coexist. At a muon collider, the MDI faces a distinctive challenge: the decay products of the circulating muon beams (electrons and positrons) create a severe background environment for the detector [8, 9]. To suppress this background, two tungsten nozzles are placed inside the detector volume, shielding sensitive components from the secondary particles arising from muon decays [10, 11].

In Fig. 1, the main elements are shown. A large experimental cavern surrounds the detectors. The detector shown in the figure represents one of the options available in the literature [12, 13]. Immediately downstream of the detector and the nozzles, the final-focus elements are surrounded by several layers of shielding (tungsten, steel, concrete and borated polyethylene). All results presented correspond to

Content from this work may be used under the terms of the CC BY 4.0 licence (© 2026). Any distribution of this work must maintain attribution to the author(s), title of the work, publisher, and DOI.

ISBN: 978-3-95450-252-3 ISSN: 2673-5350 doi: 10.18429/JACoW-IPAC2026-MOP1045

VERTICAL DEFORMATION OF THE 10 TeV MUON COLLIDER RING FOR NEUTRINO FLUX MITIGATION*

M. Vanwelde†, C. Carli, K. Skoufaris
CERN, European Organization for Nuclear Research, Geneva, Switzerland

Abstract

Muons offer several advantages for circular colliders: as leptons, they allow for high-precision and similar physics reach as larger hadron colliders, while their higher mass suppresses the synchrotron radiation that limits circular electron colliders. The main challenge of muon colliders is the short lifetime of muons. Muon decay generates an intense neutrino flux emitted in a narrow cone tangential to the beam trajectory. To keep the resulting radiation at the Earth's surface negligible, dedicated mitigation strategies are required. Besides minimizing straight sections, the main mitigation measure under consideration is to periodically deform the beam trajectory and collider ring vertically to spread the neutrino flux over a larger area. This can be achieved by installing all ring magnets on a mechanical system allowing to move them regularly and adding horizontal magnetic field components. However, this affects the collider optics, especially since it introduces vertical dispersion that must be properly matched across the lattice. The present work presents the first studies on the impact of such vertical periodic deformation on beam dynamics and collider performance.

INTRODUCTION

A 10 TeV center-of-mass muon collider complex could serve as a high-energy lepton collider, allowing for high-precision and, at the same time, similar physics reach as larger hadron colliders [1–4]. One of the main challenges of a muon collider complex is the very short lifetime of muons (~ 2.2 µs at rest), which imposes unique challenges at every stage of the complex, from muon beam cooling, which requires the implementation of novel techniques, to the rapid cycling synchrotron chain, which must accelerate the beams within a few tens of turns. In the collider ring, this short lifetime leads to the inevitable decay of muons, significantly impacting the collider design.

First, muon decays lead to muon losses during operation, reducing the beam intensity and consequently the luminosity. The collider ring must therefore be as compact as possible to maximize the number of collisions at the two interaction points. Second, muon decays produce secondary particles that can reach the detectors or be lost in the collider structure. To mitigate these effects, careful design of the Interaction Regions (IR) is required to reduce the beam-induced background [5, 6], and radial tungsten shielding must be added inside the magnet aperture to mitigate the radiation damage and heat load [7]. Among the particles produced by muon decays are high-energy neutrinos emitted in a narrow cone tangential to the muon trajectory. The resulting intense neutrino flux can interact near the Earth's surface, generating hadronic showers and measurable radiation doses. The neutrino radiation dose strongly increases with the collider energy, since the angular distribution becomes narrower and the neutrino interaction cross section larger [8–11]. Radiation dose levels are particularly significant in the direction of straight sections, where neutrinos from successive muon decays accumulate. To keep the radiation at the Earth's surface negligible, dedicated mitigation strategies are required. In the collider IRs, long straight sections housing experiments are unavoidable. To manage the resulting intense neutrino flux, the collider placement is optimized by identifying where neutrinos from these long straight sections reach the surface and ensuring these locations lie in low-occupancy areas or in regions that could be purchased and fenced by the organization [12–14]. In the collider arcs, straight sections can be minimized by using only dipoles and combined-function magnets, with the remaining short straight sections limited to 30 cm-length interconnects between magnets [15].

Beyond minimizing straight sections, implementing additional mitigation strategies is required, as the radiation levels from the arcs straight sections and combined-function magnets are still too high [9, 10, 16]. The main mitigation measure under consideration is to periodically deform the beam trajectory and the collider ring vertically to spread the neutrino flux over a larger area [9, 11]. The so-called Vertical Incremental Periodic Excursion of the Ring (VIPER) scheme requires the addition of horizontal magnetic field components to all ring magnets and installing them on a mechanical system in order to move them regularly [17, 18]. While initial estimates indicate that peak radiation doses can be reduced by approximately two orders of magnitude using the VIPER scheme [9, 16], it also affects the collider optics by introducing vertical dispersion that must be properly matched throughout the ring, and may induce momentum-dependent coupling in strong sextupoles. In this context, it is essential to evaluate the impact of this mitigation scheme on beam dynamics and overall collider performance to assess its feasibility.

This work presents the first studies of the implementation of such vertical periodic deformations in the regular arc cells of the muon collider ring and their impact on the collider optics and performance. The basic VIPER scheme and its implementation in the Flexible Momentum Compaction (FMC) arc cells are described, and a specific VIPER configuration is proposed to address vertical dispersion matching across the FMC arcs. The collider performance is then evaluated

* Work endorsed by the IMCC
† marion.vanwelde@cern.ch

Content from this work may be used under the terms of the CC BY 4.0 licence (© 2026). Any distribution of this work must maintain attribution to the author(s), title of the work, publisher, and DOI.

ISBN: 978-3-95450-252-3 ISSN: 2673-5350 doi: 10.18429/JACoW-IPAC2026-MOP1048

SIMULATION AND STUDY OF THE MUON COOLING DEMONSTRATOR RECTILINEAR CHANNEL IN BDSIM

P. B. Jurj*, R. Kamath, J. Pasternak, K. Long, Imperial College London, London, United Kingdom
C. Rogers, STFC, Oxfordshire, United Kingdom
Endorsed by the International Muon Collider Collaboration

Abstract

The muon collider has great potential for enabling high-luminosity multi-TeV lepton–antilepton collisions provided low-emittance, high-intensity muon beams can be produced. Ionization cooling is the proposed technique to achieve the required muon beam emittance. The rectilinear cooling lattice used to compress the six-dimensional (6-D) phase-space volume of the beam comprises solenoids for strong focusing, dipoles to generate dispersion, wedge absorbers for differential energy loss, and RF cavities for longitudinal energy restoration. The International Muon Collider Collaboration aims to demonstrate the integration and reliable operation of a 6-D ionization cooling system, including RF acceleration in strong magnetic fields. This paper presents a full implementation of the Muon Cooling Demonstrator 6-D cooling lattice in BDSIM, together with an evaluation of its cooling performance.

INTRODUCTION

The muon collider is a promising candidate for a multi-TeV lepton collider, with the potential to reach centre-of-mass energies of up to 10 TeV at high luminosity. Realising such a machine requires beams with high brightness, and therefore low transverse and longitudinal emittances. In a proton-driven scheme, muons are produced as tertiary particles from pion decays, resulting in beams with large momentum and spatial spreads. Consequently, substantial beam cooling is required. As conventional techniques such as synchrotron radiation or stochastic cooling are ineffective for muons due to their short lifetime, ionisation cooling has been proposed as a novel and viable alternative.

Ionisation cooling involves passing the beam through an absorber, where muons lose momentum in all directions via ionisation energy loss. The longitudinal momentum is subsequently restored using RF cavities, leading to a net reduction in transverse emittance. In rectilinear (6-D) cooling channels, dipole magnets introduce dispersion, correlating particle momentum with transverse position. A wedge-shaped absorber then induces greater energy loss for higher-momentum particles, reducing energy spread at the expense of increased transverse emittance—effectively transferring emittance from the longitudinal to the transverse phase space and enabling net 6-D cooling. Performance is limited by multiple Coulomb scattering, which is mitigated by strong solenoidal focusing at the absorber and by using low-Z materials such as liquid hydrogen or lithium hydride to minimise scattering while maintaining sufficient energy loss.

MUON COOLING DEMONSTRATOR

The Muon Ionization Cooling Experiment (MICE) demonstrated transverse emittance reduction in high-emittance muon beams passing through a single, non-accelerating ionization cooling cell [1, 2]. Building on this proof-of-principle, the muon cooling demonstrator is an essential component of the muon collider R&D programme. Its aim is to demonstrate the successful integration of the cooling hardware (high-field solenoids, absorbers, dipoles, and high-gradient RF cavities), its operation with beam, and the achievement of the required beam-physics performance. To realise these objectives in a controlled and progressive manner, the programme follows a staged approach: starting with RF test stands to characterise the achievable gradients in high-field solenoids, then advancing to one-cell and multi-cell modules, and ultimately culminating in the operation of a complete cooling line with beam [3, 4].

A conceptual layout of the Muon Cooling Demonstrator is shown in Fig. 1. The muon beam is produced through the decay of pions resulting from the interaction of protons with a target. Pions emerging from the target are captured using a magnetic horn and transported through a quadrupole-based decay channel. A momentum-selecting chicane then delivers the resulting muons to a preparation system, where the beam emittance is tuned via collimation and the longitudinal phase space is rotated using RF cavities. The prepared muon beam is subsequently transported to and matched into the cooling channel.

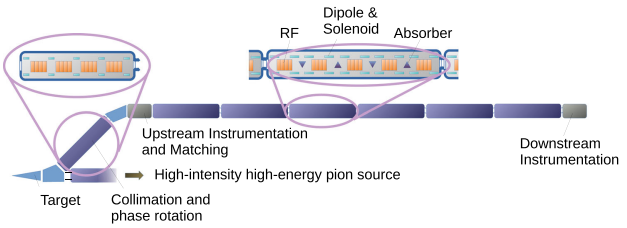

Figure 1: Conceptual layout of the Muon Cooling Demonstrator. [5]

BDSIM FOR MUON COOLING

BDSIM is a Geant4-based Monte Carlo particle-tracking code for modelling accelerators and particle–matter interactions [7]. It can be compiled and run across all major operating systems, and is also accessible through platforms such as Conda, Docker, and Apptainer. A dedicated BDSIM

* paul.jurj13@imperial.ac.uk

Content from this work may be used under the terms of the CC BY 4.0 licence (© 2026). Any distribution of this work must maintain attribution to the author(s), title of the work, publisher, and DOI.

ISBN: 978-3-95450-252-3 ISSN: 2673-5350 doi: 10.18429/JACoW-IPAC2026-MOP1050

INJECTION BACKGROUND STUDIES AT FCC-ee

G. Nigrelli[1,2,3*], M. Boscolo[2], G. Broggi[3], R. Bruce[3], Y. Dutheil[3], B. Francois[3], A. Frasca[3,4], T. Mori[5], A. Lechner[3], G. Lerner[3], F. Palla[6], S. Redaelli[3], K. Skoufaris[3], S. Yue[3]
[1]Sapienza Università di Roma, Rome, Italy, [2]INFN-LNF, Frascati, Italy,
[3]CERN, Geneva, Switzerland, [4]University of Liverpool, Liverpool, UK,
[5]KEK, Tsukuba, Japan, [6]INFN Pisa, Pisa, Italy

Abstract

The electron–positron Future Circular Collider (FCC-ee) is a proposed high-energy lepton collider designed to achieve unprecedented luminosity and precision in the study of fundamental particle physics. To fully exploit this potential, it is crucial to control beam-induced experimental backgrounds to ensure safe operation and optimal detector performance. This is particularly challenging due to the complex operational requirements; for example the top-up injection process that generates unavoidable losses at each injection while detectors are taking data. The present baseline scheme foresees a fast bump in the injection region that affects the full circulating beam, leading to additional beam-halo losses. In this paper, we study these losses, from their sources up to the detector using a multi-step simulation framework, employing multi-turn tracking followed by Monte-Carlo shower studies and detector occupancy analyses. The IDEA detector concept was used to evaluate their impact on vertex detector occupancy and compare them to the main luminosity background.

INTRODUCTION

FCC-ee is a proposed 90.7 km electron–positron collider that will operate at four center-of-mass energies: the Z pole (45.6 GeV), the WW threshold (80 GeV), the ZH production peak (120 GeV), and the $t\bar{t}$ threshold (182.5 GeV) [1]. Its design targets unprecedented luminosity through high beam currents and continuous top-up injection, required due to beam lifetimes well below one hour. This is possible thanks to a booster, compatible with all energies, so that energy ramps are not required in the collider. Injection is performed while the detectors are taking data, introducing a potential source of background. The Z pole is the most critical operating point for injection-induced backgrounds, featuring the highest beam currents (~ 1300 mA) and largest total stored beam energy (~ 18 MJ). Even a small fractional beam loss near the Interaction Regions (IRs) can deposit significant energy in the detectors. Experience at SuperKEKB has confirmed that backgrounds from injection losses can become a direct operational limitation [2, 3]. The injection scheme proposed for FCC-ee is even more challenging because it relies on a fast orbit bump that perturbs the circulating beam and enhances losses. The losses are mitigated by a global two-stage momentum and betatron collimation system in Point F (PF) [4], complemented by local tertiary collimators (TCT) upstream of the IRs.

* giulia.nigrelli@cern.ch

This paper evaluates injection-induced losses at the Z pole using a multi-step simulation framework to quantify their impact on the detector occupancies.

TOP-UP INJECTION SCHEME

At the Z pole, continuous top-up injection is performed every 3 s per beam, replenishing up to 10 % of the stored (1200) bunches with 10 % of the nominal bunch intensity (2×10^{10}), corresponding to approximately 1 % of the total stored beam energy per injection. The baseline scheme relies on full off-energy, on-axis injection [5]: the injected beam is placed onto the chromatic orbit and synchronously damps until it merges with the stored beam. With a longitudinal damping time of 1179 turns, more than 8 damping times are available between consecutive injections.

The transverse separation between the injected and circulating beams at the injection septum is determined by the local optics,

$$|D_x \cdot \delta| = 5\sigma_{\mathrm{circ}} + S + 5\sigma_{\mathrm{inj}}, \quad (1)$$

where D_x is the periodic ring horizontal dispersion, δ is the momentum offset of the injected beam, $\sigma_{\mathrm{circ}} = \sqrt{\beta\epsilon + (D\delta)^2}$ and $\sigma_{\mathrm{inj}} = \sqrt{\beta\epsilon}$ are the beam sizes of the circulating and injected beams respectively, δ is the relative energy spread of the circulating beam, and S is the septum thickness. For the injected beam, the dispersion contribution to the beam size is neglected to simplify the solution of Eq. 1 and to reduce the required separation. However, this introduces a dispersion mismatch between the two beams, which drives betatron oscillation of the injected beam around the chromatic orbit.

For lattice version GHC_V25.1 [6], $D_x = -1.5$ m and $\beta_x = 1000$ m, yielding an energy offset of $\delta_{\mathrm{offset}} = 0.95$ %, close to the momentum acceptance of ~ 1 %. To satisfy Eq. 1, the stored beam is displaced toward the septum by a one-turn π-orbit bump generated by two kicker magnets, such that the entire circulating beam passes at $5\sigma_{\mathrm{circ}}$ from the septum. An absorber, yet to be designed, upstream of the septum intercepts particles that would otherwise be scraped there, concentrating losses away from the septum itself.

SIMULATION FRAMEWORK

A three-step simulation workflow for beam-induced background (BIB) has been established, covering the full chain from tracking to detector occupancy estimates. In the first step, multi-turn beam tracking is performed using

Content from this work may be used under the terms of the CC BY 4.0 licence (© 2026). Any distribution of this work must maintain attribution to the author(s), title of the work, publisher, and DOI.

ISBN: 978-3-95450-252-3 ISSN: 2673-5350 doi: 10.18429/JACoW-IPAC2026-MOP1052

PROPOSED COLLIMATION LAYOUT FOR THE FCC-ee WITH LOCAL CHROMATICITY CORRECTION OPTICS

F.F. Van der Veken*[1], A. Bessenay[2], G. Broggi[1,3], R. Bruce[1], G. Iadarola[1], G. Nigrelli[1,3]
[1]CERN, Meyrin, Switzerland
[2]École Polytechnique Fédérale, Lausanne, Switzerland
[3]Sapienza University of Rome, Rome, Italy

Abstract

The Future Circular electron–positron Collider (FCC-ee), with a circumference of approximately 90 km, is designed to push both the luminosity and energy frontiers for high-brightness lepton beams. The unprecedented stored beam energy, reaching up to 17.7 MJ — around two orders of magnitude greater than in any previous lepton collider — poses major challenges for safe operation. Uncontrolled losses could result in high experimental backgrounds, downtime, or even damage to accelerator components, making an efficient and reliable collimation system essential.

Two layouts and optics configurations are currently under consideration for the FCC-ee: the Global Hybrid Correction (GHC) and the Local Chromaticity Correction (LCC) schemes. While a collimation concept has previously been proposed for the GHC optics, this paper presents a new collimation layout specifically designed for the LCC lattice. The collimation performance is then compared between the two optics and layout versions under representative loss scenarios to identify in which optics the collimation system works best.

INTRODUCTION

The FCC-ee [1–3] is a proposed circular e^+e^- accelerator with a circumference of about 90 km, intended to explore both extreme luminosities and the highest energies achievable for this type of machine. Its physics programme is based on four distinct operating modes, with beam energies of 45.6 GeV, 80 GeV, 120 GeV, and 182.5 GeV, each corresponding to optimal production conditions for the Z boson, W boson, Higgs boson, and top-quark pairs, respectively. The very large stored beam energy – reaching approximately 17.7 MJ with high local energy densities in the Z operating mode – implies a substantial potential for damage in the event of uncontrolled beam losses. For this reason, implementing an efficient collimation system is mandatory.

The Local Chromaticity Correction (LCC) optics [4], developed for the FCC-ee since 2022, represents an alternative lattice design that has become the new optics baseline, aimed at enhancing collider performance. The approach emphasises local compensation of chromaticity and non-linearities, ensuring high achromaticity, reduced sensitivity to errors, and improved control of beam dynamics. The LCC scheme facilitates very small β^* values and low emittances while maintaining flexibility through modular insertions that minimally perturb the overall lattice structure.

LAYOUT CONSIDERATIONS

In the design of a multi-stage collimation system, several key aspects must be carefully considered. Foremost, a robust collimation hierarchy is required to ensure continuous protection of the most restrictive apertures in the machine. At the same time, the primary collimator settings should avoid excessively small jaw openings, as overly tight gaps can adversely affect beam lifetime and increase impedance. This constraint naturally favours locations with large local β-functions for the primary devices.

Furthermore, the phase advance between primary and secondary collimators should be selected as close as possible to the optimal values,[1] to maximise the interception efficiency of halo particles scattered at the primary stage [5].

This dedicated cleaning insertion is complemented with local protection of sensitive aperture bottlenecks, which, for the considered FCC-ee layouts, are the final-focus doublets. These so-called tertiary collimators should, in turn, be positioned approximately at multiples of 180° in phase with respect to the critical aperture bottlenecks, thereby ensuring that these sensitive regions remain within their protected shadow. Finally, the impact of local dispersion must be carefully evaluated and controlled. Note that ensuring a suitable off-momentum cleaning insertion for the LCC lattice is still under discussion, as many factors must be taken into account (such as the induced dose on the sensitive devices in the booster ring, which is hosted in the same tunnel). For the current study, the off-momentum insertion has been preliminarily placed in the long straight section where the booster RF system is hosted, using the injection insertion optics.

An additional concern for the FCC-ee specifically arises from its large circumference, which may limit the effectiveness of relying solely on the betatron tune to clean the transverse halo over all betatron phase advances, especially for fast losses if the dynamic aperture is small. As mitigation, a double-phase collimation scheme can be deployed, with two primary collimators per transverse plane at both 0° and 90° betatron phase. Such a configuration can be integrated into the LCC lattice with relative ease and is adopted as a baseline, since it is significantly more effective than a single-phase scheme for fast losses, as discussed later.

* frederik@cern.ch

[1] These are given by $\pm\cos^{-1}\frac{n_1}{n_2}$ (with n_1 the normalised gap in σ of the primary collimator and n_2 of the two secondary collimators).

Content from this work may be used under the terms of the CC BY 4.0 licence (© 2026). Any distribution of this work must maintain attribution to the author(s), title of the work, publisher, and DOI.

ISBN: 978-3-95450-252-3 ISSN: 2673-5350 doi: 10.18429/JACoW-IPAC2026-MOP1054

LHC OPERATION WITH OXYGEN AND NEON IONS

R. Bruce*, R. Alemany-Fernandez, T. Argyropoulos, H. Bartosik, D. Butti, R. Cai, A. Donadon Servelle, Y. Dutheil, S. Fartoukh, P. Hermes, J. Jowett, S. Kostoglou, D. Kuchler, B. Lindstrom, E. Maclean, E. Mahner, E. Matheson, D. Mirarchi, G. Nigrelli, G. Papotti, S. Redaelli, R. Scrivens, M. Slupecki, M. Solfaroli, H. Timko, R. Tomas, N. Triantafyllou, J. Uythoven, D. Valuch, F. Van der Veken, J. Wenninger, D. Wollmann, C. Young, C. Zampolli,
European Organization for Nuclear Research, Geneva, Switzerland
C. E. Montanari, University of Manchester, Manchester, United Kingdom
E. Waagaard, École Polytechnique Fédérale de Lausanne, Lausanne, Switzerland
M. Zielińska, Warsaw University of Technology, Warsaw, Poland

Abstract

During the summer of 2025, the CERN Large Hadron Collider operated for the first time with oxygen and neon ion beams. Three different machine configurations—with collisions of p-O, O-O, and Ne-Ne and with varying beam energies and optics—were commissioned and exploited for physics operation during the eight days allocated. This short run was challenging because of its very tight schedule, the novel modes of operation, and new beam-physics effects such as transmutation of oxygen and neon nuclei into other nuclei with the similar magnetic rigidity. In spite of these challenges, the run was very successful with the luminosity targets set by the LHC experiments fully met and, in most cases, even exceeded by large factors. In addition, time was allocated for machine studies that provided the first LHC data on crystal channeling with O and Ne ions. In this article, we give a general overview of the LHC machine configuration, operational challenges, and experience during the run, as well as the achieved performance and the key contributors to the successful outcome. The results demonstrate the LHC's flexibility for mixed-species operation and give valuable input for future ion operation.

INTRODUCTION

The heavy-ion programme at the CERN Large Hadron Collider (LHC) [1] consists mainly of yearly one-month runs with collisions of fully stripped Pb ions with beam energies up to 6.8 Z TeV [1–5], but includes also asymmetric p-Pb collisions [6–8] and a short 2-day pilot run with Xe-Xe collisions in 2017 [9]. Following the success of the Xe-Xe run, the ion physics community requested a short LHC run with lighter nuclei [10]. Physics motivations included quark-gluon plasma studies and the emergence of collective phenomena in systems with lower mass, and the interactions of cosmic rays with Earth's atmosphere. The run was scheduled in summer 2025, relying on proton and fully stripped $^{16}O^{8+}$ and $^{20}Ne^{10+}$ beams from the CERN injector complex to provide proton–oxygen (p-O), oxygen–oxygen (O-O), and neon–neon (Ne-Ne) collision modes. Besides changing beams between these modes, the LHC optics and beam energy were changed to meet specific requirements from the experiments. A mere 8 days were assigned for p-O and O-O, with one additional day for Ne-Ne. Additional machine development time was allocated for studies of crystal collimation [11] with O and Ne beams [12].

This article presents first the constraints and requirements from the experiments for which the LHC machine configurations for each mode were devised. The commissioning, operational experience, and performance achieved in each mode are then reviewed. The production of the O and Ne beams in the CERN injector complex is described in [13].

CONSTRAINTS AND MACHINE CONFIGURATIONS

Ambitious luminosity targets for O-O and p-O were presented in the 2021 physics workshop [10] by the large LHC experiments (ATLAS at interaction point 1, called IP1, ALICE at IP2, CMS at IP5, and LHCb at IP8), and the LHCf experiment, which intercepts forward collision products from IP1. Early feasibility studies were based on the so-called "setup beam" limit at 3×10^{11} charges per ring (where interlocks can be masked to relax machine-protection requirements), and the re-use of an existing Pb-Pb configuration to shorten setup procedures. These indicated that the targets could be reached in about one week [14]. Subsequently, the experiments updated the final luminosity targets as summarised in Table 1, and also introduced further requirements on the configurations.

For p-O, LHCf, as one of the main requestors together with LHCb, demanded the highest possible beam energy of 6.8 Z TeV, a -145 μrad IP1 half crossing angle and a very low pileup at IP1 of $\mu = 0.01$ for the first 8 h followed by $\mu = 0.03$, as well as a large β^*. The other experiments favoured smaller β^* and $\beta^* = 1$ m was adopted as a compromise. LHCb, LHCf, and ALICE asked for p in the clockwise Beam 1 (B1) and O in the counter-clockwise Beam 2 (B2), while a beam reversal was not requested. Roman pot detectors for forward physics around IP1 (AFP) and IP5 (PPS) were to be inserted in p-O, while only AFP was to be inserted for O-O. ALICE also asked for $\mu \leq 0.2$ in all modes.

In addition to p-O and O-O operation, Ne-Ne collisions were also requested to study the effect of the different nuclear shapes between O and Ne. This was deemed technically

* roderik.bruce@cern.ch

Content from this work may be used under the terms of the CC BY 4.0 licence (© 2026). Any distribution of this work must maintain attribution to the author(s), title of the work, publisher, and DOI.

ISBN: 978-3-95450-252-3 ISSN: 2673-5350 doi: 10.18429/JACoW-IPAC2026-MOP1057

LHC MACHINE CONFIGURATION EVOLUTION OVER RUN 3 FOR MAXIMISED PERFORMANCE AND INNER TRIPLET LIFETIME

S. Fartoukh, F. Cerutti, M. Hostettler, S. Kostoglou
European Organization for Nuclear Research [CERN], Geneva, Switzerland

Abstract

Initially planned to start in 2021 and to end up in 2024, the third exploitation period of the LHC (Run 3) started in 2022 and was extended by two years to fit the adjusted schedule of the High Luminosity LHC (HL-LHC) project. Run 3 was not only marked by the exceptional performance of the machine (with 125 fb^{-1} delivered to the two high luminosity experiments ATLAS and CMS, both in 2024 and 2025). Run 3 was also used as a unique opportunity for the transition between the LHC and the HL-LHC, both in terms of optics and beam parameters, in particular with the smallest β^* of 15 cm put in operation so far, and the highest bunch charge of 1.8×10^{11} protons/bunch now routinely used for proton physics fills. In order to make this transition as adiabatic as possible, the machine configuration was modified year by year, not only to profit as much as possible from the incremental increase of the bunch charge available at the exit of the injector chain, but also to mitigate as much as possible the radiation dose deposited in the inner triplets of the ATLAS and CMS experiments. This paper describes the main changes applied to the machine configuration over this period, together with the motivations.

PERFORMANCE OVERVIEW IN RUN 3

The LHC machine was designed to deliver an instantaneous luminosity of 10^{34} $cm^{-2}s^{-1}$ in proton operation to the two multi-purpose ATLAS and CMS detectors [1]. The target integrated performance was set to 300 fb^{-1}, basically limited by the tolerance to radiation estimated at that time for the existing inner triplets (IT) equipping the experimental insertions (IR) of the ring. This performance target was based on a certain number of key beam and optics parameters which are recalled in Table 1 for the LHC, and compared to HL-LHC [2]. These parameters were then revisited before the start of Run 3 [3] in order to profit as much as possible from the beam quality improvement and intensity ramp up which was planned to be gradually offered by the upgrade project of the LHC injector chain (LIU [4]) during Run 3, pending the long shutdown 3 (LS3) for the complete installation of the HL-LHC and the full exploitation of the LIU beam. As shown in Table 1, the transverse beam emittances were basically twice smaller than initially targeted [6–8], essentially thanks to post-LHC-design RF beam manipulations in the injector chain (so-called BCMS beam [9]) and their preservation through the injector chain and LHC. These sensibly smaller emittance values could still be essentially maintained at higher bunch population, up to 1.8×10^{11} p/b, as targeted for Run 3 (due to limitations from existing LHC equipment [3]), to be compared with 2.2×10^{11} p/b for the HL-LHC operation planned after LS3. The maximum possible number of bunches colliding at IP1 and IP5 was however lower than initially planned ($\sim$ 2450 corresponding to the worst prediction in [3]), limited by heat-load from the electron cloud, and imposing shorter bunch trains (36 b or 48 b per train vs. 72 b per train for standard LHC beam production with 25 ns bunch spacing), or even hybrid beam production scheme (see [10] for more details). This limitation is planned to be lifted in LS3 thanks to an in-situ carbon-coating of the beam-screen surface, at least for a certain fraction of the LHC arc cells [11, 12]. The maximum possible instantaneous luminosity is about 2×10^{34} $cm^{-2}s^{-1}$ for the LHC, being limited by the cryo-cooling capacity of the existing ITs [13] (and, just in the shadow, by a maximum allowed average pile-up of $\mu \sim 60$ events per bunch crossing). In order to mitigate the impact on machine performance, additional levels of complexity were introduced for operating the LHC in Run 3, namely: (i) luminosity leveling with β^* [14] (discrete steps in β^*), (ii) later on (as of 2024), moving as well the beam separation at the IP for smoothing as much as possible the luminosity profile in stable beam and cope with slightly different requests from ATLAS and CMS, and (iii) finally reducing as well the crossing angle towards the end of leveling (in 2025 and 2026), when the bunch population is significantly smaller, in order to maximize the machine performance per fill. As of the beginning of Run 3, a 30 cm collision optics was targeted at the end of luminosity leveling, starting from a β^* calibrated to 1.2 m at the beginning of stable beams (only 60 cm in 2022) in order to avoid a luminosity excess at the start of the collisions, and then leveling the optics in purely telescopic mode [15] in order to gain experience for the HL-LHC but also to accommodate the requirements of forward physics experiment data taking (see detailed motivations in [3]). A deep change of configuration was however introduced in 2025/2026, passing from round to flat optics after rotation of the crossing plane in ATLAS and CMS (see below), with a final β^* of 15 cm achieved in 2026 in the plane perpendicular to the crossing plane.

Pushing the beam and optics parameters, and adapting consequently the machine configuration/operation clearly contributed to the outstanding performance of the LHC in Run 3, with an integrated luminosity of 41 fb^{-1} delivered in 2022 (recommissioning year) and about 125 fb^{-1} in both 2024 and 2025 [5], albeit only 32 fb^{-1} in 2023 due to an incident which severely truncated the proton run for this specific year [16]. A target of 30 fb^{-1} has been given for 2026, which will be a very short proton run (with in addition 50 % of the time allocated to a so-called low-μ run, i.e. at low luminosity). Together, the LHC should have delivered nearly 550 fb^{-1} to the ATLAS and CMS experiments, i.e.

Content from this work may be used under the terms of the CC BY 4.0 licence (© 2026). Any distribution of this work must maintain attribution to the author(s), title of the work, publisher, and DOI.

ISBN: 978-3-95450-252-3 ISSN: 2673-5350 doi: 10.18429/JACoW-IPAC2026-MOP1060

OPTIMISATION TECHNIQUES FOR INTEGRATED LUMINOSITY WITH AND WITHOUT β^* LEVELLING FOR A CIRCULAR COLLIDER WITH EXAMPLES FROM THE CERN LHC

M. Aquilina[1,2], A. Bazzani[3,4], F. Capoani[2], E. Mazzola[3], B. Giacobbe[4], M. Giovannozzi[2], G. Valentino[1,2]
[1]University of Malta, Msida, Malta
[2]CERN, Geneva, Switzerland
[3]Università di Bologna, Bologna, Italy
[4]INFN Sezione di Bologna, Bologna, Italy

Abstract

The main performance indicator of a particle collider is the integrated luminosity. It depends not only on operational efficiency, but also on a range of beam parameters to be optimised to enhance performance. It is common to operate a collider with decaying luminosity, due to beam burn-off. However, the planned luminosity upgrade of the LHC (HL-LHC) is based on luminosity levelling: a time variation of colliding-beam offset, crossing angle, and β^* is used to keep luminosity constant over a certain period of time. Operational experience with luminosity levelling is being acquired at the LHC using different levelling strategies. In this work, we investigate optimisation strategies to maximise integrated luminosity without and with β^* levelling. Monte Carlo simulations of years of physics runs have been performed with and without optimisation approaches. The key physical parameters are derived from a detailed analysis of the data collected at the LHC during the Run 2 and Run 3 periods. These findings provide valuable information for improving future LHC operational strategies and preparing for forthcoming collider configurations in the HL-LHC era.

INTRODUCTION

The performance of a particle collider is characterised by the luminosity, quantifying the rate of particle interactions delivered to experiments [1]. Instantaneous luminosity $L(t)$ relates the event rate to the total cross-section σ_{int} of particle interaction. The luminosity depends on various beam and optical parameters as given below:

$$L(t) = \frac{\Xi\, N_{\text{i}}^2}{(1+\sigma_{\text{int}}\, n_{\text{c}}\, \Xi\, N_{\text{i}}\, t)^2}\,, \quad \Xi = \frac{\gamma_{\text{r}} f_{\text{rev}} F(\theta_{\text{c}}, \sigma_z, \sigma^*)}{4\,\pi\epsilon^*\beta^*\, k_{\text{b}}}\,. \tag{1}$$

Here, N_{i} is the initial beam intensity, n_{c} is the number of collision points, γ_{r} is the Lorentz factor, f_{rev} is the revolution frequency, θ_{c} is the crossing angle, σ^* and σ_z are the transverse and longitudinal RMS bunch dimensions, respectively, ϵ^* is the normalised RMS emittance, and k_{b} is the number of bunches [2]. The primary quantity of interest is the integrated luminosity $\mathcal{L}_{\text{int}}$, defined as the time integral of $L(t)$ over a data collection period. This determines the recorded physics dataset. Maximising $\mathcal{L}_{\text{int}}$ requires balancing the duration of each collision phase with the interval between a beam dump and the start of the next data collection period. This time interval, known as the turnaround time, includes the operational overhead of preparing a new fill, such as the injection, ramp, and setup phases, as well as the recovery from faults and other inefficiencies until subsequent beams are brought into collision [3]. The duration of the fill has a random component: a fill may end with a programmed beam dump or a protection dump triggered by the machine protection system [4]. The probability that a fill survives up to a given time is described by the survival probability function $S(t)$ and must be considered in optimisation strategies [3,5]. Failures affect the expected integrated luminosity delivered over a run and must therefore be accounted for in any optimisation approach.

Whenever β^* and ϵ^* remain constant, the luminosity decreases during a collision phase due to beam burn-off and other beam dynamics effects [2,6]. This is the case for the CERN Large Hadron Collider (LHC) [7] during Run 2 [8,9]. Luminosity levelling was introduced in the LHC as early as Run 1 for the ALICE and LHCb experiments, by varying transverse beam separation [10]. From Run 3, it was also applied to the ATLAS and CMS high-luminosity experiments, due to constraints from the cryogenic system and pile-up level in the detectors. Levelling is then implemented by varying beam separation, β^*, and, more recently, the crossing angle to maintain approximately constant luminosity before natural decay resumes [11–14]. This operational mode changes how luminosity evolves during a collision phase and modifies the strategy to optimise integrated luminosity compared to head-on collisions at constant β^*. The High Luminosity (HL) LHC upgrade [15], scheduled to begin operation around 2030, anticipates levelling as the baseline scenario. In this study, we present optimisation approaches to maximise integrated luminosity in both scenarios, with and without β^* levelling, including or omitting the survival probability of the fill.

LUMINOSITY OPTIMISATION

Optimisation Without Levelling

In this work, the optimisation of the integrated luminosity over a period of time, such as the number of allocated physics days in a year, requires determining the optimal duration of

Content from this work may be used under the terms of the CC BY 4.0 licence (© 2026). Any distribution of this work must maintain attribution to the author(s), title of the work, publisher, and DOI.

ISBN: 978-3-95450-252-3 ISSN: 2673-5350 doi: 10.18429/JACoW-IPAC2026-MOP1061

OPTICS CYCLES FOR MAXIMUM INTEGRATED LUMINOSITY IN THE HL-LHC

R. De Maria*, B. Lindstrom, K. Skoufaris
European Organization for Nuclear Research [CERN], Geneva, Switzerland
Y. Angelis†, Aristotle University of Thessaloniki, Thessaloniki, Greece

Abstract

We present an update of the optics cycles foreseen during physics operation in the High-Luminosity LHC (HL-LHC) era. New optics around the upgraded ATLAS and CMS experiments are needed due to the new quadrupole layout and lower β^*. In addition, thanks to numerous studies and lessons learned during Run 3, the entire machine's optics will be modified to improve key aspects such as machine protection, beam-lifetime optimisation, and β^* minimisation. This is achieved by integrating the optimisation of octupole-induced resonances, phase advances between collimators and crab cavities, new collimation optics, control of dispersion, and flat-optics options. This paper presents a proposal for the β^* steps during Run 4 and Run 5 with the aim of maximising integrated luminosity. These new cycles will also be used in the Inner Triplet (IT) string operational validation programme and in future collimation studies.

INTRODUCTION

The HL-LHC upgrade baseline is documented in the technical design report [1]. The first LHC upgrade optics studies started in the 2004–2007 period, with an emphasis on the triplet design and a target of $\beta^* = 25$ cm at the high-luminosity experiments [2, 3]. Subsequently, an even lower $\beta^* = 15$ cm was chosen for the HL-LHC upgrade, exploiting the Achromatic Telescopic Scheme (ATS) [4]. Complete optics solutions based on the ATS scheme were developed, along with a flat optics options with and without crab cavities [5–8]. Recent studies motivated a review of the baseline optics based on the following reasons. Machine protection [9] and background studies [10] motivated the search for optimised phase advances at the flat top [11]. Incoherent effects from the electron cloud motivated a change in phase advances at injection [12,13]. Machine studies demonstrated that optimised flat-top optics for betatron collimation provide better cleaning and lower impedance [14]. An updated version of the machine layout is now being finalised for installation during the Long Shutdown 3 (LS3), starting in June 2026, in which the nominal magnetic lengths of the new Inner Triplet magnets have been refined and frozen to provide stable installation references. This requires small adjustments to the previous optics solutions. The most recent HL-LHC optics cycle incorporates new features derived from recent beam dynamics studies and will provide a comprehensive new baseline for HL-LHC studies and for operation in Run 4 [15, 16].

* riccardo.de.maria@cern.ch
† ioannis.angelis@cern.ch

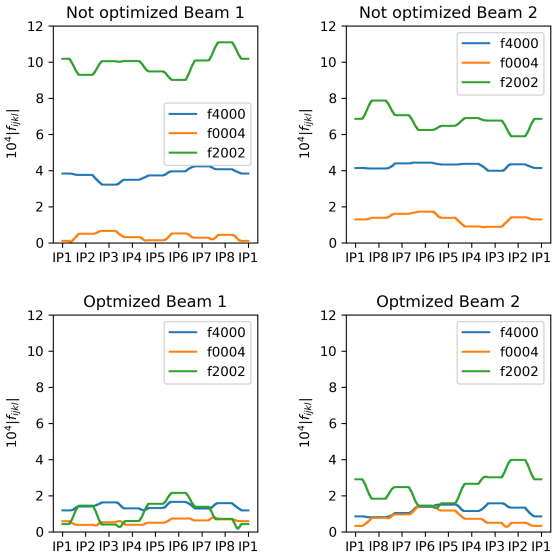

Figure 1: Optimisation of the octupolar resonance driving term at injection for Beam 1 and Beam 2. The plots show the amplitude of the first-order octupolar resonance driving terms (for the definition refer to [17]) in the lattice for the previous HL-LHC baseline injection optics and the newly proposed injection optics. The reduction of the perturbation is significant for both beams.

INJECTION OPTICS

Electron-cloud effects require operation with very large chromaticity ($Q' = 25$) and strong octupole currents ($I_{\mathrm{MO}} = 40$ A) to suppress coherent beam instabilities. The e-cloud octupolar nonlinearities are significant, especially the associated resonance $2Q_x - 2Q_y$ [12]. The phase advance can be adjusted arc by arc to reduce the resonance driving terms (RDTs) for the 3 main octupolar resonances ($2Q_x - 2Q_y$, $4Q_x$, and $4Q_y$), while preserving the existing amplitude detuning [13]. The phase advance modifications are implemented by rephasing the arcs and, unlike in the Run 3 optics, also by rematching the insertions; see Fig. 1. This strategy avoids introducing unnecessary beta-beating (up to 15% locally), which would reduce the available aperture. A change in the arc phase advances had to be implemented in 2025 to mitigate a collimator hierarchy breakage that appeared with the change of octupole polarity [16], which reduced the measured $4Q_x$ resonance. Incidentally, the new phase configuration also reduced the $3Q_y$ resonance [13] which is also beneficial for lifetime and for the choice of the working point.

Content from this work may be used under the terms of the CC BY 4.0 licence (© 2026). Any distribution of this work must maintain attribution to the author(s), title of the work, publisher, and DOI.

ISBN: 978-3-95450-252-3 ISSN: 2673-5350 doi: 10.18429/JACoW-IPAC2026-MOP1062

OPERATIONAL LOSS LIMIT IN THE OFF-MOMENTUM COLLIMATION SECTION OF THE LHC

S. Morales Vigo*, F. Carra, B. E. Karlsen-Baeck, A. Lechner, D. Mirarchi, L. Puddu, S. Redaelli, V. Rodin, B. Salvachua, K. Taylor, H. Timko
European Organization for Nuclear Research (CERN), Geneva, Switzerland

Abstract

At the Large Hadron Collider (LHC) at CERN, nearly 3 600 ionization chambers composing the Beam Loss Monitoring (BLM) system are distributed along the ring and at each collimator. They are responsible for protecting the machine against energy deposition originated from beam losses by requesting the beam extraction when the measured signals are above certain predetermined thresholds. The setup of these thresholds is complex and requires a combination of simulations and measurements. In preparation for the High Luminosity-LHC (HL-LHC) era, the bunch intensity has been pushed from 1.4×10^{11} to 1.8×10^{11} protons during the LHC Run 3. With this higher intensity, more power is required in the radio-frequency (RF) cavities to capture the beam and reduce beam losses due to off-momentum particles, in particular at the start of the energy ramp. The present limitation on maximum allowed beam losses on the off-momentum collimation region is around 60 kW and comes from the theoretical quench limit of the matching quadrupole magnets in cell 6 (Q6) which is based on the initial LHC magnet quench models. Supported by simulations, a dedicated machine development test took place in 2025 to assess in two steps if 200 kW and 500 kW beam losses from off-momentum particles could be sustained in the off-momentum collimation section without quenching the Q6 magnets. This paper describes the procedure of the test carried out and discusses the main findings in terms of the power loss reached and the recorded loss patterns.

INTRODUCTION

The LHC at CERN will finish its third period of operation, Run 3, at the end of June 2026. This will be followed by a period of shutdown that will extend until 2029 and will be mainly dedicated to the implementation of the upgrades required for the HL-LHC era [1]. In order to reach higher luminosities, one of the LHC parameters that will be pushed is the beam intensity, which has already been increased progressively during Run 3 to gain operational experience.

Higher beam intensities require higher RF power at capture and throughout the injection sequence [2]. Particles that are not captured by the RF fall outside the accelerating bucket and are lost at the start of the beam acceleration. These losses occur mainly in two locations. One is the off-momentum collimation section in the Interaction Region 3 (IR3), where the dispersion reaches a maximum by design. The other is the betatron collimation section in the Interaction Region 7 (IR7), where the dispersion is not null, thus intercepting also a fraction of these particles [3].

Both regions include a multi-stage collimation system for each counter-rotating beam with an arrangement of primary (TCP), secondary (TCS), and absorber (TCLA) collimators [4]. These regions also include warm and superconducting magnets. Each of these elements is equipped with BLM detectors that protect them from beam losses by requesting the immediate extraction of the beams if the signal of any of these detectors is above certain predetermined thresholds [5]. The thresholds depend on the protected element and the position of the detector.

These increasing beam intensities in the LHC have been causing higher losses at the start of the beam acceleration, with several BLM detectors reaching regularly signals above 30 % of their threshold in the IR3 region, even leading to the beam extraction in some cases. As an effort to mitigate this limitation, it was decided to investigate the possibility of increasing the BLM thresholds in the area.

This was followed by a series of studies that concluded in an experimental beam test to probe that the different elements in the IR3 area can sustain up to 500 kW beam losses impacting on the IR3 TCPs.

BEAM POWER LOSS LIMIT AT 450 GeV

The thresholds of the BLM detectors located at the collimators from the IR3 region of the LHC had been last reviewed in the shutdown period after Run 1, between 2013 and 2015 [6]. At the time, the sharing of beam losses between the IR3 and IR7 regions was not well known, so the BLM thresholds were set to a combined beam power loss in both regions of around 500 kW.

Thanks to a dedicated beam loss decomposition algorithm developed to study off-momentum losses using the signals from the BLM detectors at the collimators, today it is possible to obtain an estimate of the number of protons impacting on each TCP, providing a better understanding of the sharing of beam losses between both collimation sections [3].

Figure 1 shows an example of the estimates of second-by-second beam power lost on the beam 1 (B1) on the left, and beam 2 (B2) on the right, in the IR3 and IR7 sections during the first seconds of beam acceleration from a 2025 LHC fill. It is observed that for B1 the main peak of losses occurs mainly in IR7 collimators as opposed to B2, for which it occurs in IR3 collimators. This has been the case for most of the 2025 and 2026 LHC fills, and it appears to be caused by off-momentum particles that hit a resonance line and are lost betatronically.

* sara.morales.vigo@cern.ch

Content from this work may be used under the terms of the CC BY 4.0 licence (© 2026). Any distribution of this work must maintain attribution to the author(s), title of the work, publisher, and DOI.

ISBN: 978-3-95450-252-3 ISSN: 2673-5350 doi: 10.18429/JACoW-IPAC2026-MOP1063

A FIRST LOOK AT THE IMPACT OF BEAM-BEAM EFFECTS ON THE EMITTANCE SCAN OBSERVABLES IN THE LARGE HADRON COLLIDER

J. Wańczyk*, M. Hostettler, J. Wenninger, CERN, Geneva, Switzerland
T. Pieloni, EPFL, Lausanne, Switzerland

Abstract

During the operation of the Large Hadron Collider (LHC), regular beam separation (emittance) scans are essential for accurately determining beam emittance and give valuable observables for monitoring the stability of luminometers. These scans provide a critical insight into beam quality and detector performance. In this study, we investigate how beam-beam interactions influence emittance scan observables by combining numerical simulations and experimental data, and discuss the resulting implications for measurement accuracy.

INTRODUCTION

Beam separation scans, commonly referred to as emittance scans, are a standard tool in LHC operations serving two complementary purposes: on the machine side, they provide a direct measurement of the transverse beam emittance [1], while for the experiments they offer a means to monitor the stability of luminometers across fills [2]. The absolute luminosity calibration is performed during dedicated van der Meer (vdM) scans, where beam conditions are optimized for maximum measurement precision [3]. Emittance scans, conducted under nominal physics conditions, face a much more complex systematic landscape — in particular, the presence of long-range beam-beam interactions from 2460 circulating bunches introduces bunch-to-bunch variations entirely absent in the low-intensity vdM regime. Previous studies have already established that beam-beam effects introduce measurable biases to luminosity observables, including contributions to the apparent non-linearity and fill-to-fill stability of experimental luminometers [4]. However, those studies were limited to single-bunch or simplified multi-bunch models, motivating the full treatment presented here.

Quantifying these beam-beam contributions is a necessary step toward making emittance scans a more reliable tool for both purposes. However, a full treatment at realistic LHC conditions requires simultaneous modelling of head-on and long-range interactions across the entire bunch population with a realistic lattice description.

Recent developments in pyTRAIN [5] now allow this to be studied. In this paper we present a first look at how beam-beam interactions shape emittance scan observables, using a nominal Run 3 fill 10875 as a reference case. We find that while significant progress is possible, the current framework reveals important limitations, in particular the absence of full bunch distribution information, that will need to be addressed before beam-beam corrections to luminosity observables can be made practical.

SIMULATION SETUP

Simulations are performed using pyTRAIN [5], a multi-bunch beam-beam simulation code that tracks beam parameters turn by turn using a realistic LHC lattice model and filling patterns with bunch trains. The parameters used in this study are summarised in Table 1 and are based on fill 10875, with conditions corresponding to the third emittance scan of the fill, using the lattice model `R2025aRP_A18cmC18cmA10mL200cm_Flat.madx`.

Table 1: Simulation Parameters

Parameter	Value
Number of bunches	2460
Median intensity	1.1×10^{11}
Median emittance (x)	2.35 µm
Median emittance (y)	2.0 µm
β^* (crossing-angle plane)	0.6 m
β^* (non-crossing plane)	0.18 m
Tune (x)	62.315
Tune (y)	60.322
Chromaticity	15
Octupoles K	−12
ATLAS/CMS half crossing angle	160 µrad

Benchmark Against COMBI

The pyTRAIN simulation is benchmarked against COMBI [6], a strong-strong macro-particle tracking code which, by virtue of simulating the full particle distribution, captures non-Gaussian effects and beam shape distortions not accessible to pyTRAIN. The benchmark is performed using single-bunch separation scans at vdM-like parameters ($\xi = 3.24 \times 10^{-3}$). In pyTRAIN the real vdM lattice model is used, while COMBI applies linear phase advance transformations turn by turn. Results for the simulated β^* change at IP5 during the horizontal scan, expressed as $(\sigma_{BB}/\sigma_0)^2$ to allow direct comparison between the RMS beam size from COMBI and the β^* from pyTRAIN, are shown in Fig. 1. The two codes are in good agreement at larger separations where the linearised beam-beam approximation in pyTRAIN holds well; differences at small separation are expected, as the beams overlap more and a larger portion of the transverse distribution is exposed to the non-linear regime of the beam-beam force.

* jwanczyk@cern.ch

Content from this work may be used under the terms of the CC BY 4.0 licence (© 2026). Any distribution of this work must maintain attribution to the author(s), title of the work, publisher, and DOI.

ISBN: 978-3-95450-252-3 ISSN: 2673-5350 doi: 10.18429/JACoW-IPAC2026-MOP1064

LATEST MEASUREMENTS OF MAGNETIC NOISE IN THE LHC TUNNEL*

G. Sterbini†, H. Bartosik, M. J. Bednarek, M. Cerqueira Bastos, S. Cettour Cave, S. Kostoglou, M. Martino, M. Praznovsky, A. Radoslavova, G. Trad, D. Valuch, J. Wenninger
European Organization for Nuclear Research, Geneva, Switzerland

Abstract

The magnetic coupling between nearby accelerator rings can introduce unwanted perturbations to beam dynamics, representing a potential concern for future colliders such as the High-Luminosity Large Hadron Collider, or multi-ring facilities such as the Future Circular Collider or the Muon Collider complex. To explore and benchmark this effect, dedicated tests were performed to study the electromagnetic interplay between the SPS and the LHC. Controlled excitations in the SPS were applied while monitoring the response of the beams in the LHC using high-precision instrumentation. Clear signatures of coupling were observed, providing valuable input for the validation of simulation models and for improving the understanding of magnetic field propagation between accelerator infrastructures. In this paper, the results of these measurements are presented and discussed.

INTRODUCTION

The CERN Super Proton Synchrotron (SPS) [1] is a normal-conducting synchrotron with a circumference of approximately 6.9 km. It is located about 75 m above the lowest point of the Large Hadron Collider (LHC) [2, 3] tunnel (Fig. 1), which hosts a superconducting collider with a circumference of about 27 km. The 1.4% slope of the LHC tunnel is visible in Fig. 1.

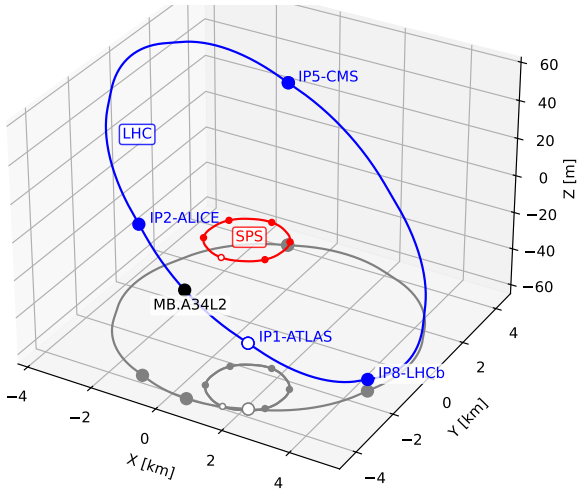

Figure 1: Relative position between SPS and LHC.

Before the LHC era, the tunnel hosted the Large Electron–Positron Collider (LEP) [4]. Several effects affecting LEP energy calibration were investigated in detail [5]. A magnetic coupling between SPS and LEP was already observed [6]: in general, when a current ΔI flows in the SPS ring, a magnetic field can be produced in the LHC tunnel through several mechanisms, for example:

1. a contribution related to the mutual induction voltage between SPS and LHC ($\propto \frac{d\Delta I}{dt}$, the dominant effect reported in [6]);
2. a contribution due to the SPS direct magnetic field ($\propto \Delta I$);
3. a coupling through ground loops [7].

In general, the situation may be further complicated by additional effects on the circuits (e.g., persistent currents in the superconducting cables) and the interplay of the external magnetic field with the active regulation of the involved power supplies (e.g., effect of the magnetic field on the DCCTs readings [8]).

A detailed understanding of the SPS–LHC magnetic coupling is beyond the scope of this study. In this paper we quantify the effect through magnetic measurements in the LHC tunnel and beam-based measurements using LHC beams at 450 GeV, the LHC injection energy.

MEASUREMENT SETUP

The powering and cabling of the SPS main dipoles are designed to cancel the overall SPS magnetic flux. This is not the case for the SPS arc quadrupoles, which belong to two families wired in opposite directions: focusing (QF) and defocusing (QD). Their induced magnetic flux thus cancels only if $I_{QF} = I_{QD}$. For this reason, and to avoid EMC issues with the LHC Quench Protection System [9], the operational currents of the QF and QD circuits are normally kept approximately equal. On 4 September 2025, an ad-hoc measurement was performed by deliberately unbalancing the SPS QF/QD currents up to $|I_{QF} - I_{QD}| = |\Delta I| = 1.7$ kA (Fig. 2) while beams were circulating in the LHC. The magnetic effect of the SPS in the LHC was measured using a

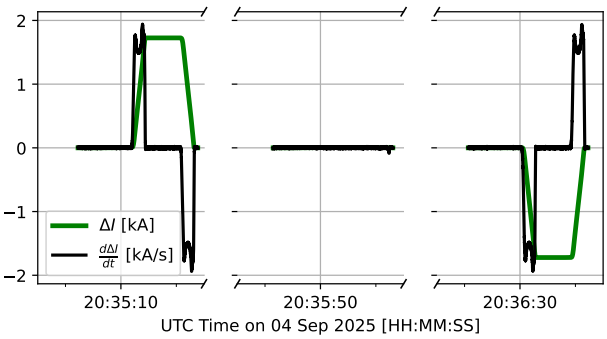

Figure 2: The SPS I_{QF} and I_{QD} powering cycle. The minor x-axis divisions represent 5-seconds intervals.

* Research supported by the HL-LHC project.
† guido.sterbini@cern.ch

This is a preprint - the final version is published with IOP

Content from this work may be used under the terms of the CC BY 4.0 licence (© 2026). Any distribution of this work must maintain attribution to the author(s), title of the work, publisher, and DOI.

ISBN: 978-3-95450-252-3 ISSN: 2673-5350 doi: 10.18429/JACoW-IPAC2026-MOP1066

PROBING THE ULTIMATE β^* REACH OF THE LHC

E.H. Maclean, S. Fartoukh, M. Stefanelli, R. Tomás, J. Dilly, J. Gray, W. Van Goethem, S. Horney, K. Sabin, K. Skoufaris, F. Soubelet, Y. Angelis
CERN, Geneva, Switzerland

Abstract

In 2026, the Large Hadron Collider concludes its final run, before being upgraded to the High-Luminosity Large Hadron Collider. Originally conceived with a nominal β^* of 0.55 m in both planes, its optics design has been steadily pushed beyond those initial goals, with round optics down to 0.25 m (2018), and flat optics down to 0.5 m/0.15 m (2026) used in operation. In 2025, dedicated beam-studies were performed to test the viability of controlling β^* waist errors at such low-β, and to explore the viability of squeezing and commissioning the optics even further. Possible operational scenarios down to 0.4 m/0.12 m were tested, and optics measurements down to a minimum β of 0.075 m achieved, the outcome of which are presented.

LOW-β COMMISSIONING

Collider operation at very low-β^* suffers from strong sensitivity to magnetic errors in the experimental IRs, leading in the LHC's case to large increases in β-beating through the squeeze unless dedicated beam-based corrections are applied [1–3]. In 2025 the LHC operational configuration was pushed to a flat $\beta^* = 0.6\,\text{m}/0.18\,\text{m}$ configuration [4, 5], with the low-β plane alternating between the ATLAS and CMS experiments. This led to a peak β-beat of 275 %. To successfully run the LHC in this configuration the optics quality must therefore be improved by about 2 orders-of-magnitude. This was successfully achieved during the 2025 LHC commissioning [6–8], as seen in Fig. 1.

Later in 2025, machine development tests were performed to try and squeeze further. The design β^* in the ATLAS and CMS insertions was reduced in two steps: to $\beta^* = 0.5\,\text{m}/0.15\,\text{m}$, then $\beta^* = 0.4\,\text{m}/0.12\,\text{m}$, with optics measurements performed at each step. The optics corrections commissioned previously for the operational 0.18 m configuration were maintained constant during the additional squeeze. Examples of the resulting optics quality at 0.15 and 0.12 m are shown in Figs. 2-3.

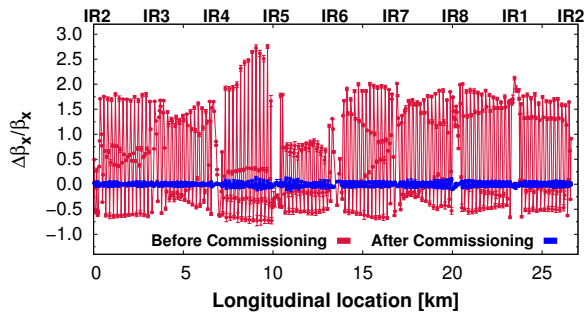

Figure 1: Example of measured β-beat (Beam 1) at $\beta^* = 0.18$ m in 2025, before/after optics commissioning.

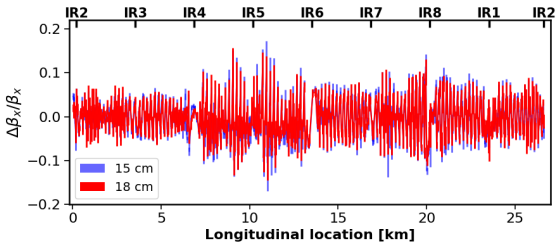

Figure 2: Example of measured β-beat (Beam 1 horizontal) at $\beta^* = 0.15$ m, compared to $\beta^* = 0.18$ m.

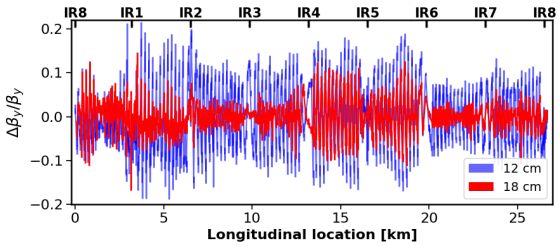

Figure 3: Example of measured β-beat (Beam 2 vertical) at $\beta^* = 0.12$ m, compared to $\beta^* = 0.18$ m.

The additional squeeze to $\beta^* = 0.15$ m was found to be approximately transparent in terms of optics quality, with negligible degradation compared to the operational scenario. Even when squeezing to a $\beta^* = 0.12$ m only a moderate degradation was found, reflecting the high-quality of local optics corrections in the experimental IR achieved over many years. It is also notable that even in this strongly pushed configuration, well beyond the LHC's original design, there was sufficient dynamic aperture and beam-lifetime to remain at low-β for many hours and perform extensive optics measurements via AC-dipole kicks, which further reflects the good control of nonlinear optics achieved in the LHC. Ultimately, the additional squeeze to $\beta^* = 0.15$ m was selected for inclusion in 2026 operation.

OPTICS STABILITY AT LOW-β

A particular issue for low-β collider operation is optics stability, since even small changes to magnetic errors and alignments in the IRs can result in large optics perturbations. This concern also holds true for future HL-LHC operation. While the LHC has generally exhibited good year-to-year stability at high-β^* [6], regular updates to the low-β operational scenario mean very limited year-to-year comparisons are available. During LHC commissioning in February 2026 however, the optics at $\beta^* = 0.15$ m could be directly compared with the $\beta^* = 0.15$ m machine development study in November 2025 [7, 9].

Between 2025 and 2026 a clear degradation to the optics quality was observed, growing through the squeeze. This

Content from this work may be used under the terms of the CC BY 4.0 licence (© 2026). Any distribution of this work must maintain attribution to the author(s), title of the work, publisher, and DOI.

ISBN: 978-3-95450-252-3 ISSN: 2673-5350 doi: 10.18429/JACoW-IPAC2026-MOP1067

DESIGN CHALLENGES AND SOLUTIONS FOR FLAT OPTICS IN HL-LHC

K. Skoufaris*, Y. Angelis, J. M. Gray, R. De Maria, R. Tomás García
CERN, Meyrin, Switzerland

Abstract

The High-Luminosity LHC (HL-LHC) upgrade imposes stringent requirements on optics design and correction to achieve its performance goals while maintaining beam stability, sufficient aperture margins, and controlled sensitivity to alignment and field imperfections. Among the explored configurations, flat optics—featuring asymmetric β-functions at the interaction points—has been proposed as an alternative to the conventional round-optics scheme, including scenarios where crab cavities (CC) are not fully deployed. This configuration can be implemented early in the squeeze cycle and offers several advantages, such as reduced impedance, a modified beam–beam interaction pattern, and potential performance improvements. Focusing on the optics at the end of luminosity leveling for the HL-LHC version 1.9, this paper discusses the phase-advance constraints for machine protection, one of the main design challenges, and presents the achieved flat-optics configurations. Research supported by the HL-LHC project.

INTRODUCTION

The High-Luminosity LHC (HL-LHC) project aims to deliver an integrated luminosity of at least 250 fb^{-1} [1–4] per year by upgrading interaction regions (IR1 and IR5) with Nb_3Sn triplet magnets and crab cavities (CC). While the baseline scenario focuses on "round" optics with equal β^* in both transverse planes, alternative configurations like "flat" optics are critical for performance optimization [5,7,8].

Flat optics, characterized by asymmetric β-functions at the Interaction Points (IPs), offer a strategic alternative when crab cavities are not fully deployed or to mitigate intensity limitations such as electron cloud and impedance. By using a larger β^* in the crossing plane and a smaller β^* in the orthogonal plane, the impact of the geometric luminosity reduction factor is minimized, potentially increasing virtual luminosity beyond what is achievable with round optics at comparable triplet apertures.

In the HL-LHC, an asynchronous beam dump occurs when the extraction kickers (MKD) fire out of sync with the "abort gap" in the beam. This causes the kicker field to rise while particles are still passing, resulting in bunches being deflected at intermediate angles rather than being safely sent down the extraction tunnel. To protect the machine during such a failure, the phase advance ($\Delta\mu$) between the extraction kickers (MKD) and the tertiary collimators (TCT) is a critical design parameter. As the HL-LHC uses much higher beam intensities and smaller "squeeze" factors (β^*) than the LHC, the TCT-MKD phase advance is among the most important restrictions that must be respected and well-controlled to push collider performance further. The optimization for a set of different flat optics is presented in this work.

HL-LHC OPTICS

The HL-LHC optics V1.9 was used for these studies; although the V2.0 is expected to be released soon, it remains a valid baseline for this analysis. For Run 4 and beyond, it is planned to reach $\beta^* = 0.15$ m for round beams at the end of luminosity leveling, and $\beta^*_{||/\times} = 0.075 - 0.09/0.18$ m if flat optics are used. Such strong focusing is made possible by the Achromatic Telescopic Squeezing (ATS) scheme [11] utilized for optics below 50 cm.

Flat Optics

Flat optics in the HL-LHC [6–8] are configurations where the horizontal and vertical beta functions at the IP are unequal ($\beta^*_x \neq \beta^*_y$). This leads to different beam sizes in the two transverse planes, providing an alternative to round optics for optimizing luminosity under aperture constraints. By using a larger β^* in the crossing plane and a smaller β^* in the parallel plane, flat optics can increase virtual luminosity compared to round optics with similar aperture limitations while reducing geometric reduction effects.

This scheme can be combined with crab cavities, which reduce the effective crossing angle and allow for stronger focusing. It can also help optimize optics conditions, such as lowering the β-function at the crab cavity locations to mitigate impedance issues. Specifically, it can compensate for luminosity loss in scenarios where crab cavities do not reach nominal performance and still provide an additional luminosity gain (on the order of a few percent) in nominal conditions. Additionally, with ideal phases for machine protection, the flat VH (vertical crossing in IP1 and horizontal in IP5) have better aperture than corresponding round also flat optics can contribute to reducing the head-on beam-beam interaction and also makes it easy to correct some resonances related to long-range interaction supporting performance goals for future upgrades.

LHC operated with flat optics for the first time in 2025, reaching $\beta^*_{||/\times} = 0.18/0.60$ m, increasing virtual luminosity and, hence, leveling time. In 2026 LHC reached $\beta^*_{||/\times} = 0.15/0.50$ m further improving performance [9, 10]. This optics could be a good target for the first year of Run 4 to reproduce achieved performances.

However, these advantages come with limitations: flat optics increase sensitivity to field imperfections in the triplets due to stronger focusing in the parallel plane, and require better control of beam size, orbit, coupling, and mechanical tolerances. Due to a lack of extensive tests with high telescopic indices and high intensity, the operational flexibility

* kyriacos .dot. skoufaris .at. cern .dot. ch

Content from this work may be used under the terms of the CC BY 4.0 licence (© 2026). Any distribution of this work must maintain attribution to the author(s), title of the work, publisher, and DOI.

ISBN: 978-3-95450-252-3 ISSN: 2673-5350 doi: 10.18429/JACoW-IPAC2026-MOP1069

IMPACT OF DIPOLE FIELD QUALITY ON THE EMITTANCE TUNING AND THE DYNAMIC APERTURE OF THE HIGH ENERGY BOOSTER OF THE FUTURE CIRCULAR COLLIDERS

M. Afif*, Q. Bruant†, A. Chance‡, B. Dalena§, V. Gautard
Commissariat à l'Énergie Atomique et aux Énergies Alternatives
and Université Paris-Saclay, Gif-sur-Yvette, France
F. Bugiotti, CentraleSupélec-LISN, Gif-sur-Yvette, France
A. Ghribi, Grand Accélérateur National d'Ions Lourds, Caen, France
A. Mashal, Institute for Research in Fundamental Sciences, Tehran, Iran

Abstract

We present the impact of the main dipole field quality on the dynamic aperture (DA) and the emittance tuning of the High Energy Booster (HEB) of the leptonic version of the Future Circular Collider (FCC-ee). Multipole field imperfections up to order six (normal: $b_2 - b_6$; skew: $a_2 - a_6$) are introduced into the main dipoles using measured values, interpolated at 8.8 mT (the HEB injection energy), and systematic errors of one unit. The study evaluates the degradation of the total DA as a function of the energy offset, computed for several angles in the transverse plane ($x - y$). The impact on the emittance achieved following optics correction and residual orbit are also evaluated. Key results show that even small multipolar errors can significantly impact optics stability, and further iterations with magnet experts are required to define tolerances of field quality and correctors specifications. The approach and scripts developed here (using the Xsuite modules) enable the rapid testing of various error configurations and can be adapted for future optimisation.

INTRODUCTION

The Future Circular Collider (FCC-ee) is a next-generation electron–positron collider [1], where the High Energy Booster (HEB) is used to accelerate beams up to the collision energy. Ensuring sufficient dynamic aperture (DA) is critical for efficient injection and beam stability.

The DA is defined as the region in the 6D phase space where particles remain stable over a given number of turns [1]. In this study, the DA is evaluated through tracking simulations and expressed in units of beam size (σ), as a function of the relative momentum deviation ($\Delta p/p$) and transverse angle. All the computations are done at the injection energy of 20 GeV, considering the normalized horizontal and vertical emittance of 20 µm and 2 µm, respectively.

In this study the impact of multipolar errors from the sextupole to the dodecapole order are discussed with respect to ideal lattice with no errors and correction of other imperfections, such as magnet displacement or main field errors. Transverse tunes and linear chromaticity are simply corrected using all available quadrupoles and sextupoles in the magnetic lattice, respectively. The reference DA corresponds to the ideal lattice without magnetic field errors. It provides the baseline against which the impact of multipolar errors is assessed.

The impact of the low field harmonics components of the main dipole and of the main quadrupole is also assessed on the residual emittance obtained after orbit and optics correction, together with the alignment errors of the lattice elements.

We present results for the HEB ring optics designed to be compatible with the collider baseline optics described in [1].

ERRORS

Magnetic field imperfections in the main dipoles are modelled as multipole errors up to order six, including both normal (b_n) and skew (a_n) components. Two types of errors are considered:

- Measured multipole components, provided at two magnetic field values and linearly interpolated to 8.8 mT, corresponding to the HEB injection energy, as reported in Table 1. These values contain the effect of hysteresis at injection.
- Systematic errors of one unit, used as a reference to evaluate sensitivity to each multipole order.

Table 1: Measured Magnetic Field Errors of a Short Prototype of the FCC High Energy Booster ring [2]

n	b_n**[unit]**	a_n **[unit]**
2	0.27	0.17
3	−0.14	−0.11
4	0.01	−0.02
5	−0.06	0.002
6	0.004	0.0001

The multipole coefficients are converted into integrated strengths (k_nL, $k_{sn}L$) and injected into the main dipoles of the lattice using the Xsuite [3] framework.

In order to evaluate the impact of the systematic normal and the skew quadrupolar errors (b_2 and a_2) of the main dipole on the transverse emittance and orbit, these errors are added to the alignment and main field errors reported in Table 2.

* manal.afif@universite-paris-saclay.fr
† quentin.bruant@cern.ch
‡ antoine.chance@cea.fr
§ barbara.dalena@cern.ch

Content from this work may be used under the terms of the CC BY 4.0 licence (© 2026). Any distribution of this work must maintain attribution to the author(s), title of the work, publisher, and DOI.

ISBN: 978-3-95450-252-3 ISSN: 2673-5350 doi: 10.18429/JACoW-IPAC2026-MOP1070

INVERSE MODELING OF SPATIALLY COHERENT RANDOM VIBRATIONS FOR ASSESSING IMPACT ON PARTICLE BEAM DYNAMICS IN CIRCULAR ACCELERATORS

P. Lersnimitthum*[1], B. Dalena†[1]
Commissariat à l'Énergie Atomique et aux Énergies Alternatives, Saint-Aubin, France
[1]also at Université Paris-Saclay, Gif-sur-Yvette, France

Abstract

Vibrations cause emittance growth, beam misalignment at the interaction point, and particle loss, limiting accelerator performance. Ground motion and technical noise are characterized by absolute power spectral density (PSD) and spatial correlation. Mechanical support resonances, which amplify these effects, are determined via transfer functions. A method to generate random displacements from these vibration characterisations is developed using one- and two-dimensional inverse Fourier transforms. The generated displacements accurately reproduced the input PSD spectra and spatial correlation, as verified by Welch's estimation.

INTRODUCTION

Vibrations have a significant effect on the performance of the particle accelerator as they can cause the two beams to miss each other at the interaction point (IP), and emittance growth [1]. They contribute to the offset of the beam from the ideal orbit. If the beam offset is too large or there is a sudden change, the beam will be lost [2]. Having a numerical model to accurately describe the motions of each magnet in the lattice will benefit in the assessment of accelerator designs. The characteristics of vibration are described by the Power Spectral Density (PSD) and spatial correlation. These two characteristics can be modelled by the Seryi and Napoly two-dimensional Power Spectral Density (2D-PSD) [3]:

$$P_\alpha^{\mathrm{GM}}(\omega,k)=\frac{A}{\omega^2k^2}[1-\cos(l_0k)]+\sum_i E_i(\omega,k), \quad (1)$$

$$\text{where } l_0=\frac{B}{A\omega^2},\ E_i(\omega,k)=D_i(\omega)U_i(\omega,k),$$

$$U_i(\omega,k)=\begin{cases}\frac{2}{\sqrt{k_{i,max}^2-k^2}},\ \forall k_{i,max}>k\\ 0,\ \forall k_{i,max}\le k\end{cases},$$

$$D_i(\omega)=\frac{a_i}{1+[d_i(\omega-\omega_i)/\omega_i]^4},$$

$\omega=2\pi f$ is an angular frequency, $k=2\pi\tilde{\nu}=2\pi/\lambda$ is a wavenumber corresponding to wavelength λ. A and B are parameters related to the geological condition of the site, $\omega_i, a_i, d_i, v_i, k_{i,max}=\omega/v_i$ are parameters related to the contribution of elastic waves. The 2D-PSD was used to analytically compute the beam offset and beam size at the interaction point of linear colliders. Collette *et al.* [4] updated the model parameters by measurements in the LHC tunnel. A method was established to take into account technical noise and resonances of the mechanical support.

Instead of computing analytically, the method proposed reconstructs the misalignments of circular accelerator elements, which can then be used as input to beam dynamics simulation tools such as XSuite [5], enabling consolidation with other effects such as synchrotron radiation and particle loss, thereby providing more realistic simulation conditions.

The following section outlines how the horizontal and vertical displacements $\alpha\in\{x,y\}$ are obtained from a given PSD, along with methods to account for technical noise and mechanical support.

METHODOLOGY

One-Dimensional Inverse Fourier Transform

Given that $\hat{\alpha}(f)$ is the Fourier transform of the displacements $\alpha(t)$, where t is time and f is frequency, the inverse Fourier transform and its discrete form can be expressed as:

$$\alpha(t)=\int_{-\infty}^{+\infty}\hat{\alpha}(f)e^{j2\pi ft}df, \quad (2)$$

$$\alpha_p=\frac{1}{N}\sum_{n=0}^{N-1}C_{\alpha;n}e^{j2\pi np/N},\forall p=0,...,N-1 \quad (3)$$

Preumont [6] (section 12.11) demonstrated the method to obtain time series α_p, corresponding to time $t=p/(Nf_0)$, with given absolute PSD $\Phi_{\alpha\alpha}(2\pi nf_0)$. Assuming α is a stationary centred ergodic stochastic process, the Fourier coefficients are defined as:

$$|C_{\alpha;n}(\Phi_{\alpha\alpha})|=N[\Phi_{\alpha\alpha}(2\pi nf_0)f_0]^{1/2}, \quad (4)$$

where $\forall n = 1,...,N/2$ and N is an even number, $C_{\alpha,0}(\Phi_{\alpha\alpha})=0$ (the zero frequency) gives centred α_p over the period, and $C_{\alpha;(N/2)}(\Phi_{\alpha\alpha})$ must be a real number. The other coefficients are allowed to be complex numbers $C_{\alpha;n}(\Phi_{\alpha\alpha})=|C_{\alpha;n}(\Phi_{\alpha\alpha})|e^{j\theta_n}$. For simplicity, the phases $\theta_n\in[0,2\pi[$ were chosen from the uniform distribution.

Two-Dimensional Inverse Fourier Transform

A field $x(t,s)$ depending on time t and space s (the longitudinal coordinate of an accelerator) can be reconstructed from 2D-PSD by the two dimensional inverse discrete Fourier transform, which reads:

$$\alpha_{p,q}=\frac{1}{NM}\sum_{n=0,m=0}^{N-1,M-1}C_{\alpha;n,m}e^{j2\pi np/N}e^{j2\pi mq/M}. \quad (5)$$

* purinutlers@gmail.com
† barbara.dalena@cea.fr

Content from this work may be used under the terms of the CC BY 4.0 licence (© 2026). Any distribution of this work must maintain attribution to the author(s), title of the work, publisher, and DOI.

ISBN: 978-3-95450-252-3 ISSN: 2673-5350 doi: 10.18429/JACoW-IPAC2026-MOP1071

LUMINOSITY LOSS FROM GROUND MOTION IN THE FCC-ee: MDI AND ARC QUADRUPOLE VIBRATION STUDIES

M. Le Garrec*, G. Balik, L. Brunetti, G. Lamanna, M. Marchand, F. Poirier
Laboratoire d'Annecy de Physique des Particules (LAPP), CNRS/IN2P3, Annecy-le-Vieux, France

Abstract

Ground motion can significantly impact beam stability in the FCC-ee, potentially degrading luminosity at the interaction point (IP). The study models vibrations of accelerator components, including the interaction region cryostats at the Machine Detector Interface (MDI) and the quadrupole girders in the arcs. Using measured power spectral densities (PSDs) and component specific transfer functions, realistic time dependent displacement signals are generated and applied in Xsuite particle tracking simulations. Analysis of beam centroid motion at the IP and the relative transverse offset between colliding beams quantifies the resulting luminosity degradation. These results indicate that ground-induced motion may necessitate dedicated feedback systems for both orbit correction and luminosity stabilization. Findings inform the design of vibration mitigation strategies and feedback strategies for the FCC-ee.

INTRODUCTION

FCC-ee luminosity at the Z pole relies on tight control of the relative transverse beam position at the interaction point (IP) [1]. Ground vibrations, amplified by mechanical structures, can perturb trajectories and reduce collision overlap. Quantifying this chain informs required mechanical tolerances and orbit stabilization.

While previous work [2, 3] focused on fixed and sinusoidal excitations, this study incorporates realistic ground motion spectra and mechanical responses. Two sources are considered: MDI cryostat motion and arc quadrupoles motion through girders. With the current Z-mode optics and several vibration scenarios, turn-by-turn IP offsets are tracked and the resulting luminosity loss is estimated. The study is based on the 106.2 version of the LCC lattice.

SIMULATION FRAMEWORK

Mechanical Modelling & Ground Motion

The MDI cryostat [4, 5] in Fig. 1 is modelled after the current engineering design and simplified to match the experimentally measured resonant frequency of the MDI at SuperKEKB [6, 7]. From these measurements, one main flexion mode at 15.6 Hz, in the vertical plane, is considered. Additional scenarios explore asymmetric frequencies, such as 15.2 Hz, to evaluate the impact of manufacturing or installation tolerances. Girders supporting arc quadrupoles are also modelled with resonances at 14 Hz (horizontal) and 73 Hz (vertical) based on measurements at CERN [8].

* mael.legarrec@lapp.in2p3.fr

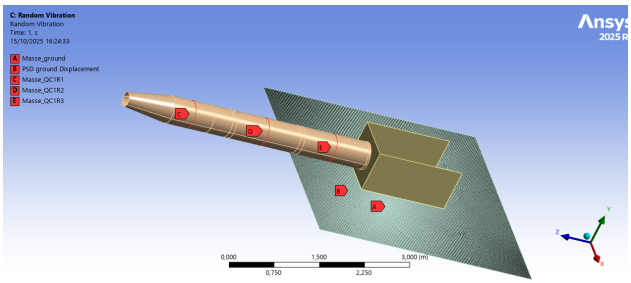

Figure 1: Simplified mechanical model of the MDI cryostat with magnets labelled. Its main vertical flexion mode is set after measurements performed at SuperKEKB.

The amplification is described with transfer functions from finite element analysis [9]. Transfer function $H(f)$ shown in Fig. 2 is defined below, where f is frequency, f_n is resonance frequency, and ζ is damping ratio:

$$H(f) = \frac{1}{\left(1 - \left(\frac{f}{f_n}\right)^2\right) + j\left(2\zeta\frac{f}{f_n}\right)} \tag{1}$$

Applying the transfer function to the input ground motion spectra yields the effective magnet vibration spectra.

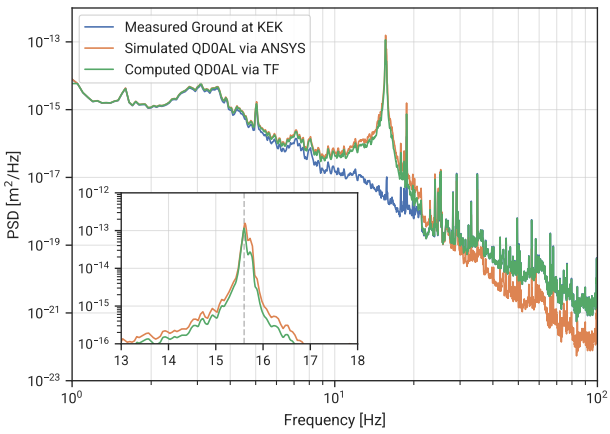

Figure 2: PSD of ground vibrations measured at SuperKEKB at the cryostat, amplified by the MDI structure modelled in ANSYS from empirical measurements and the corresponding fitted transfer function H.

LHC tunnel measurements [10–12] provide representative input pending FCC-ee site data. The measured envelope defines *low* and *high* ground motion cases in Fig. 3, restricted to 1–100 Hz.

Content from this work may be used under the terms of the CC BY 4.0 licence (© 2026). Any distribution of this work must maintain attribution to the author(s), title of the work, publisher, and DOI.

ISBN: 978-3-95450-252-3 ISSN: 2673-5350 doi: 10.18429/JACoW-IPAC2026-MOP1072

UPDATES ON IMPEDANCE STUDIES FOR THE FCC-ee HIGH ENERGY BOOSTER

K. H. Kim*, A. Ghribi†[1], S. Martinez[2], GANIL, Caen, France
Q. Bruant, A. Chance, B. Dalena, CEA, Gif-sur-Yvette, France
C. Antuono, D. Gibellieri[1], C. Zannini, F. Zimmermann, CERN, Geneva, Switzerland
A. Mashal, IPM, Tehran, Iran
M. Migliorati, University of Rome La Sapienza and INFN - Roma1, Rome, Italy
M. Zobov, INFN - LNF, Frascati, Rome, Italy
[1]also at University of Caen Normandy, Caen, France
[2]also at Paris-Saclay University, Orsay, France

Abstract

Following the Future Circular Collider (FCC) Feasibility Study completion, the impedance model for the FCC-ee High-Energy Booster (HEB) has been significantly expanded beyond the initial copper vacuum pipe resistive wall analysis. This paper presents a comprehensive impedance and wake budget incorporating RF cavities, bellows, and beam position monitors, evaluated through 3D electromagnetic simulations and analytical methods.

The updated model provides the basis for future beam dynamics studies, including transverse coupled bunch instability analyses and single bunch tracking simulations. The present work focuses on the construction and comparison of the main impedance and wake contributions, identifying the dominant sources and the components requiring further investigation. These results will be used to refine the HEB collective effects studies and to support future assessments of instability margins and mitigation requirements.

INTRODUCTION

The FCC-ee HEB is an essential part of the FCC-ee injector complex. It accelerates the beams from the injection energy to the collider injection energy. Therefore, its collective effects must be carefully assessed over the relevant operating range. In particular, the impedance and wake model of the HEB provides the input for single bunch tracking studies, transverse mode coupling instability scans, and coupled bunch instability analyses.

Previous studies of the HEB mainly focused on the resistive wall contribution of the vacuum chamber [1]. In the present work, the impedance model is extended to include additional geometric impedance sources: bellows, beam position monitors (BPMs), and RF cavities. The resistive wall contribution is evaluated analytically using ImpedanceWake2D (IW2D) [2], while the geometric contributions are obtained from 3D electromagnetic simulations performed with CST Studio Suite [3].

The present study focuses on the Z operation mode, with an injection energy of 20 GeV and an extraction energy of 45.6 GeV. This configuration is particularly useful for impedance studies because of its small emittance and sensitivity to collective effects. This paper presents the updated longitudinal and transverse impedance budgets and the corresponding wake potentials for a short bunch.

Table 1: Machine Parameters of the HEB for Z Operation

Parameter	Value
Circumference (km)	90.644836
Injection beam energy (GeV)	20
Extraction beam energy (GeV)	45.6
Bunch population, filling (10^{11})	0.25
Bunch population, top-up (10^{11})	0.216
RF frequency (MHz)	800
Injection RF voltage (MV)	64.25
Extraction RF voltage (MV)	60.98
Injection energy loss per turn (MeV/turn)	1.31
Extraction energy loss per turn (MeV/turn)	35.45
Longitudinal damping time at injection (s)	4.61
Longitudinal damping time at extraction (s)	0.389
Momentum compaction factor (10^{-6})	9.24
Horizontal tune	368.225
Vertical tune	283.29
Injection normalized emittance, Hor/Vert (μm)	20/2
Injection RMS bunch length (mm)	4
Injection RMS energy spread (%)	0.1
Extraction RMS bunch length (mm)	2.62
Extraction RMS energy spread (%)	0.0386

HEB MACHINE PARAMETERS

The main machine parameters used in this study are summarized in Table 1. The parameters correspond to the Z operation mode.

IMPEDANCE AND WAKE MODEL

The impedance and wake model considered in this work is summarized in Table 2. The model includes the resistive wall contribution of the beam pipe and the geometric contributions from bellows, BPMs, and RF cavities.

The HEB beam pipe is modeled as a circular multilayer chamber with a radius of 30 mm, including a 150 nm NEG

* keon-hee.kim@ganil.fr
† adnan.ghribi@cern.ch

Content from this work may be used under the terms of the CC BY 4.0 licence (© 2026). Any distribution of this work must maintain attribution to the author(s), title of the work, publisher, and DOI.

ISBN: 978-3-95450-252-3 ISSN: 2673-5350 doi: 10.18429/JACoW-IPAC2026-MOP1074

MONOCHROMATIZATION OPTICS FOR FCC-ee OPTIMIZED PERFORMANCE STUDY AND FIRST ATTEMPT FOR IR OPTICS DESIGN FOR FCC-ee LCC LATTICE

A. Korsun*, A. Faus-Golfe, Université Paris-Saclay, CNRS/IN2P3, IJCLab, Orsay, France

Abstract

Monochromatization is one of the most intriguing proposed operation modes of the FCC-ee, enabling a significant reduction of the centre-of-mass (CM) energy spread to a level comparable to the Higgs boson's natural width produced through the s-mode direct channel at 125 GeV. Previous studies demonstrated its feasibility using earlier versions of the FCC-ee Global Hybrid Correction (GHC) optics. A first draft implementation of the scheme on the Local Chromaticity Correction (LCC) lattice is explored in this paper. The performances of the new optics types are presented in terms of luminosity and energy spread, supported by the simulation results. This provides an early outlook on the potential operational flexibility of future FCC-ee configurations operating in monochromatization mode.

INTRODUCTION

While a significant body of previous work successfully demonstrated the feasibility of the monocromatization [1–10] scheme using various versions of the GHC lattice [11–16], this paper presents an updated implementation built upon the LCC lattice configuration with 4 IPs as the primary baseline [17]. Parametric optimization is conducted using a multi-objective optimization algorithm adapted from [18], integrating self-consistent beamstrahlung-induced emittance growth via the formulations for the beamstrahlung (BS) effect in the condition of monochromatization [19–24]. This paper is focused on implementing non-zero vertical dispersion in the interaction point (IP) D_y^*. Future studies will include performance analysis of horizontal dispersion in the IP D_x^* implementation and the hybrid mode.

ANALYTICAL OPTIMIZATION FRAMEWORK

To identify the optimal IP parameters for the monochromatization mode of the LCC lattice at 62.5 GeV, a self-consistent multi-objective optimization framework was developed. This framework relies on a numerical solver structured around the Non-dominated Sorting Genetic Algorithm II (NSGA-II) provided by the `pymoo` Python library, expanding upon the analytical methodologies for high-energy lepton colliders design [18].

The primary objective of this framework is to navigate a highly constrained, non-linear parameter space to minimize the CM energy spread (σ_w) and maximize the machine's instantaneous luminosity (L).

Decision Variables and Physical Boundaries

The optimization framework explores a four-dimensional parameter space defined by the key adjustable variables of the IP configuration. These parameters include D_y^*, the number of bunches per beam (N_b), and the horizontal and vertical betatron functions at the IP (β_x^* and β_y^*). To ensure baseline design compatibility, these variables are scanned within the following predefined physical boundaries:

$$\vec{x} = \begin{bmatrix} D_y^* \\ N_b \\ \beta_x^* \\ \beta_y^* \end{bmatrix} = \begin{cases} 0.0 \le D_y^* \le 2.0\,\text{mm} \\ 2000 \le N_b \le 12\,000 \\ 0.09\,\text{m} \le \beta_x^* \le 10.0\,\text{m} \\ 0.7\,\text{mm} \le \beta_y^* \le 5.0\,\text{mm} \end{cases} \quad (1)$$

To maintain baseline compatibility with the overall LCC lattice design, certain parameters remain fixed during the optimization loops. The horizontal equilibrium emittance (ϵ_x) is kept constant at its purely synchrotron radiation (SR)-dominated baseline value. The vertical emittance (ϵ_y) is not parameterized independently; instead, it is calculated dynamically using a defined betatron coupling factor coupled with the localized BS blow-up. Similarly, the synchrotron tune (Q_s) is held fixed.

The design enforces a maximum allowable beam-beam parameter ceiling of $\xi_{x,y}^{\max} = 0.15$ for both planes to prevent premature beam disruption. The physical constraints are further regularized by defining a lower-bound luminosity threshold $L_{\text{target}} = 1 \times 10^{34}\,\text{cm}^{-2}\,\text{s}^{-1}$.

Self-Consistent BS Modeling and Equilibrium Parameters

A key feature of the optimization loop is the calculation of self-consistent equilibrium parameters at each genetic iteration. At 62.5 GeV, intense electromagnetic fields at the collision point trigger strong BS emissions, modifying the global bunch distributions. The underlying physics model calculates the final total energy spread σ_δ and the subsequent emittance values by iterating the self-consistent analytical formulations [19].

Because the vertical beam size in this setup is heavily dominated by the dispersive component ($\sigma_y^* \approx D_y^* \sigma_\delta$), any BS-induced increase in the energy spread creates a coupled feedback loop that directly impacts the vertical beam dimension and total luminosity. The framework evaluates these loops analytically for every generated parameter set, verifying that the resultant Pareto-optimal entries reflect true steady-state conditions.

In this model, the quantum excitation from BS during a single collision $\{n_\gamma \langle u^2 \rangle\}_{\text{BS}}$ increases both the nominal

* anna.korsun@ijclab.in2p3.fr

Content from this work may be used under the terms of the CC BY 4.0 licence (© 2026). Any distribution of this work must maintain attribution to the author(s), title of the work, publisher, and DOI.

ISBN: 978-3-95450-252-3 ISSN: 2673-5350 doi: 10.18429/JACoW-IPAC2026-MOP1075

EXPERIMENTAL STUDY OF CHARGING AND MOBILISATION OF DUST GRAINS ON BEAM SCREEN SURFACES

P. Ziegler*,[1,2], M. Himmerlich[2], P. Krkotić[2], M. Horanyi[4], X. Wang[4], C. Wiesner[2], D. Wollmann[2], R. Schmidt[3], H. Podlech[1,5]
[1]Goethe-Universität Frankfurt am Main, Frankfurt am Main, Germany
[2]CERN, Geneva, Switzerland
[4]LASP, University of Colorado Boulder, Boulder, CO, USA
[3]Technische Universität Darmstadt, Darmstadt, Germany
[5]Helmholtz Research Academy Hesse for FAIR (HFHF), GSI Helmholtzzentrum für Schwerionenforschung, Campus Frankfurt, Germany

Abstract

Beam losses caused by interactions between the circulating beam and dust grains have been observed at many particle accelerators, leading to premature beam dumps, quenches of superconducting magnets, and vacuum pressure bursts. At some facilities, these events have a significant impact on the overall accelerator performance. The mechanisms by which dust grains detach from vacuum-chamber surfaces and enter the beam are not yet fully understood; one possible process is charge build-up on the grain followed by lofting due to the beam potential. We present an experimental study of the charging and mobilisation of silica dust on accelerator-relevant surfaces: Cu, co-laminated Cu, laser-treated Cu, NEG-coated substrates and samples treated with VacSeal, a silicone-based resin widely used to seal vacuum leaks. The observations provide input for dust-dynamics simulations and studies of beam losses.

INTRODUCTION

Dust particles mobilised from vacuum-chamber surfaces have caused beam losses at numerous particle accelerators, including the LHC [1–3] and SuperKEKB [4–7]. Such events can trigger premature beam dumps, quench superconducting magnets, and cause vacuum pressure bursts, significantly impacting accelerator performance.

The mechanisms leading to dust detachment and subsequent beam interaction remain poorly understood. One proposed process involves negative charging of dust grains due to interaction with synchrotron radiation or electron clouds and subsequent electrostatic lofting. This process was demonstrated in Refs. [8–10] using UV light to mimic the effects of synchrotron radiation.

This study presents experimental results on dust charging and mobilisation from accelerator-relevant surfaces. Dust is deposited onto grounded substrates in a vacuum chamber and exposed to a homogeneous electric field. Grains were charged using UV light and their motion was recorded with a high-speed camera. The trajectories are reconstructed to extract charge-to-mass ratios and launch velocities. Different behaviours were observed on conductive and insulating surfaces. In addition, the insulating VacSeal layer exhibited discharge events. VacSeal is of interest because it was found inside the SuperKEKB beam pipe and is believed to be correlated with sudden beam losses [6].

EXPERIMENTAL SETUP

The experiments were performed in a cylindrical vacuum chamber 30 cm high and 30 cm in diameter at a pressure of $\sim 1.2\times10^{-5}$ mbar (see Fig. 1). The electric field was oriented toward the substrate to mimic positively charged beams, and reversed (toward the mesh) to represent negatively charged beams.

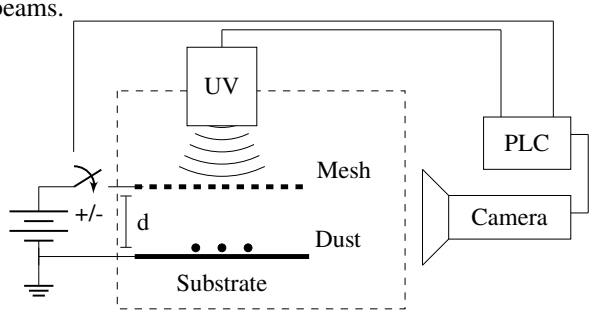

Figure 1: Schematics of the experimental setup. Dust grains are deposited on the grounded substrate. A Programmable Logic Controller (PLC) allows control of the high voltage (HV), the UV source [11] and of the triggering of the high-speed camera.

A conductive mesh with radius $R_{mesh} = 5$ cm was placed at a distance $d = 1.7$ cm above an electrically grounded sample (substrate). A bias voltage $\Phi = \pm 2$ kV was applied.

All substrates used oxygen-free (OFE) copper [12] as base material. The surface properties and the dust-lofting results are summarised in Table 1. They include bare Cu-, co-laminated Cu (75 µm) on stainless steel (representative of the LHC beam screen [13]) and laser-treated Cu in cleaned (LESS 1) and non-cleaned (LESS 2) states, both with groove depths of [15 – 25] µm [14]. Additionally, 70 nm Ti, 250 nm non-evaporable getter (NEG), and 50 nm amorphous carbon (a-C.) [15] coating as well as an insulating 71 µm-thick Kapton tape [16] and a thin film of VacSeal (VS), a silicone-resin-based vacuum sealant [17], were used.

For LESS 1 and LESS 2, the values in Table 1 are effective conductivities derived from measured surface resistances. They describe the laser-treated surface rather than

* philipp.ziegler@cern.ch

Content from this work may be used under the terms of the CC BY 4.0 licence (© 2026). Any distribution of this work must maintain attribution to the author(s), title of the work, publisher, and DOI.

ISBN: 978-3-95450-252-3 ISSN: 2673-5350 doi: 10.18429/JACoW-IPAC2026-MOP1076

INTEGRATED SIMULATION OF COMPTON BACKSCATTERING AND BEAM–BEAM EFFECTS FOR BUNCH INTENSITY CONTROL IN FCC-ee

I. Drebot*, INFN, Milano, Italy
S. Gessner, P. Kicsiny, SLAC National Accelerator Laboratory, Menlo Park, CA, USA
G. Broggi, S. Redaelli, F. Zimmermann, CERN, Geneva, Switzerland

Abstract

Precise regulation of the bunch population in FCC-ee is required to maintain the charge imbalance between collision bunches within the 3–5% tolerance that preserves beamstrahlung limits, bunch-length stability, and avoids flip–flop behavior. Laser-driven Compton backscattering (CBS) has been proposed as an active actuator for bunch-by-bunch intensity control. An Xsuite-based simulation framework is employed to track the beam over many turns, while the bunch population is continuously updated according to the CBS-induced particle removal. The modified bunch intensity is then propagated in the presence of the beam–beam interaction model, allowing the resulting impact on beam parameters and overall stability margins to be quantified.

INTRODUCTION

The Future Circular Collider (FCC-ee) project [1, 2] aims to provide unprecedented luminosity for high-energy physics experiments. However, operating at these intensities introduces significant beam dynamics challenges, the among the most critical being beamstrahlung [3, 4]. In collision mode, beamstrahlung strongly influences bunch length and energy spread, creating conditions for the "flip-flop" instability [5]. In this work we focus in the Z operation mode.

This instability occurs in an asymmetric scenario: a "strong" beam (with higher charge) induces more intense beamstrahlung in its "weak" (with low charge) partner bunch, leading to an increase in the latter's vertical emittance and a subsequent loss of luminosity [6]. To mitigate this, the charge imbalance between colliding bunches must be strictly maintained within a tolerance of less than 5% for the Z-pole and less than 3% for higher collision energies [7, 8]. While the standard top-up injection scheme balances intensities, the growth rate of the instability (approximately 10 000 turns) [5] can exceed the injection system's reaction time.

As a solution, Laser Compton Backscattering (CBS) has been proposed as a fast, non-invasive actuator for bunch-by-bunch intensity control [3, 9, 10]. The physics involves colliding high-power laser photons with relativistic electrons or positrons. At a beam energy of 45.6 GeV (Z operation mode), a scattered particle loses nearly 50 % of its energy, while at 182.5 GeV ($t\bar{t}$ operation mode), the loss reaches 80 % [10]. Since the momentum acceptance of the FCC-ee ring is only approximately few %, these scattered particles are immediately extracted from the stable orbit and removed by the collimation system by the smart choice of the laser IP.

Recent progress in high-average-power laser technology has made CBS-based bunch intensity control increasingly realistic for FCC-ee operation. Modern multi-kHz laser systems are capable of delivering pulse energies ranging from hundreds of millijoules up to the joule-class regime [11–13], compatible with the effective FCC-ee bunch circulation frequency of approximately 3.7 kHz. Such systems enable turn-by-turn bunch-by-bunch intensity regulation through CBS.controlled particle removal.

This paper presents the next stage in the design of the intensity control system: the transition from analytical estimates to Integrated Simulation. Using a framework combining Xsuite [14] and CAIN [15] (via the Xcain [16] interface), we track particle distributions through a realistic magnetic lattice including the effects of synchrotron radiation. We quantitatively analyze how the modified bunch intensities evolve in particle tracking in presence of beam-beam effects, evaluating the resulting impact on emittance evolution and the overall stability margins of the collider.

COMPTON BACK SCATTERING

Compton Back Scattering is an interaction in which a photon collides with a relativistic charged particle, such as an electron or positron, and is scattered with altered energy and direction. During this process, energy and momentum are exchanged between the photon and the charged particle, leading to corresponding changes in the kinematic properties of both particles.

The energy E_{ph} of the scattered photons can be calculated using the following formula:

$$E_{\mathrm{ph}} = \frac{4\gamma^2 E_L \cos^2\left(\frac{\alpha_0}{2}\right)}{1 + X\cos^2\left(\frac{\alpha_0}{2}\right)} \tag{1}$$

where E_L is the laser photon energy, γ is the Lorentz factor of the electron at the beam energy E_0, α_0 is the collision angle, mc^2 is the rest energy of the electron, and $X = 4\gamma E_L/mc^2$ is the recoil factor.

Given that the FCC-ee ring has a momentum acceptance of about 1% in the Z operation mode, nearly all electrons or positrons undergoing CBS with such energy loss are expected to be removed from the circulating bunch.

The actual number of scattered particles and their energy distribution depend on several factors, including the beam energy, beam emittance, laser parameters, and the interaction geometry. Therefore, realistic Monte Carlo simulations are

* illya.drebot@mi.infn.it

Content from this work may be used under the terms of the CC BY 4.0 licence (© 2026). Any distribution of this work must maintain attribution to the author(s), title of the work, publisher, and DOI.

ISBN: 978-3-95450-252-3 ISSN: 2673-5350 doi: 10.18429/JACoW-IPAC2026-MOP1078

ON-AXIS INJECTION WITH MULTIPOLE INJECTION KICKER IN FCC-ee

S. Yue*, Y. Dutheil, G. Favia, T. Kramer, J. Ruf
European Organization for Nuclear Research, Geneva, Switzerland
M. Aiba, PSI Center for Accelerator Science and Engineering, Villigen, Switzerland

Content from this work may be used under the terms of the CC BY 4.0 licence (© 2026). Any distribution of this work must maintain attribution to the author(s), title of the work, publisher, and DOI.

Abstract

To reach and maintain its target luminosity despite a beam lifetime well below 1 h, the Future Circular Collider for electrons and positrons (FCC-ee) relies on top-up injection. The present baseline uses on-axis injection with a conventional one-turn orbit bump because of its robustness and its expected low impact on detector background. As an alternative, a multipole injection kicker (MIK) can provide on-axis injection without an orbit bump and can therefore reduce perturbations to the circulating beam.

This paper presents a first assessment of a pulsed conductor MIK for the FCC-ee injection scheme, with emphasis on the Z operation mode. The field requirements for an FCC-ee MIK are first established, and a preliminary pulsed conductor design is then presented. The beam-dynamics impact of the residual field is evaluated for both beams: a local compensation scheme based on a compensation MIK (CMIK) is studied for the circulating beam, while transfer-line optics correction is used for the injected beam. Other operation modes and alternative MIK topologies are beyond the scope of this work and remain to be studied in the future.

INTRODUCTION

The present Future Circular Collider for electrons and positrons (FCC-ee) baseline relies on on-axis, off-energy injection. The injected beam is placed on a chromatic orbit and separated from the circulating beam by the combined effect of the dispersion at the injection point and the injected beam energy offset. Since the dispersion at the interaction points (IP) is null, the injected beam overlaps with the circulating beam, thereby minimising additional synchrotron radiation photons near the experiment. The successful operation of on-axis injection in LEP also demonstrated reduced detector background and high injection efficiency [1].

A conventional local orbit bump is widely used in both light sources and colliders because of its maturity and robustness. Accordingly, the present FCC-ee baseline adopts on-axis injection with a conventional orbit bump, following the scheme successfully implemented in LEP [2]. However, a local bump is difficult to close perfectly, and residual orbit oscillations after injection have been observed in several light sources [3, 4]. In addition, a thin septum is required to minimize the separation between the circulating and injected beams.

To overcome these limitations, the multipole injection kicker (MIK) has been proposed as a bump free alternative. It was first demonstrated at the KEK Photon Factory in 2007 [3]. A MIK provides an approximately field free region around the beam pipe center, so that the circulating beam remains nearly unperturbed during injection, while a sufficiently strong field is generated at a transverse offset to deflect the injected beam into the ring. This concept can therefore relax the requirements on septum technology while reducing the impact of injection on the stored beam.

Among the possible MIK implementations, the pulsed conductor concept proposed at BESSY II [4] offers a particularly favourable field distribution and has since been adopted in several light sources either in operation or planned, including MAX IV [5], ALS-U [6], SOLEIL [7], ESRF-EBS [8], and ALBA [9].

In this contribution, the pulsed conductor concept is used as the reference MIK topology to evaluate the feasibility of on-axis top-up injection in FCC-ee. Two main points are addressed: first, the field requirements for an FCC-ee MIK are established; second, a local compensation scheme is studied for the circulating beam, while transfer-line optics optimization is used for the injected beam. This first study is restricted to the Z operation mode, which is used as the reference case for evaluating the feasibility of the scheme.

FIELD REQUIREMENTS FOR ON-AXIS INJECTION

For on-axis injection, the dispersion at the injection point and the injected beam energy offset must satisfy:

$$|D_x \times \Delta| = 5\sigma_{cir} + S + 5\sigma_{inj} \quad (1)$$

where D_x is the horizontal dispersion at the injection point, Δ is the energy offset of the injected beam, and S is the separation between the circulating and injected beams.

For this study, the 5σ envelopes of the circulating and injected beams are used to define the required apertures and the separation is chosen as $S = 2.8$ mm to maintain the comparison with the conventional scheme which uses a septum of that thickness. The magnetic field in the field free region should be as small as possible, whereas the field in the injection region should provide sufficient strength. In the FCC-ee Z operation mode, the beam sizes at the MIK are $5\sigma_{cir} = 8.8$ mm and $5\sigma_{inj} = 1.7$ mm [10].

The required MIK deflection angle is 100 rad, which is the same angle provided by the thin septum in the conventional injection scheme. The corresponding integrated magnetic-field strength is comparable to that used in light sources, even at the highest beam-energy mode (182.5 GeV). In general, the combination of a large field free region, a finite injection region, and a narrow separation zone, each varying across operation modes, makes the MIK topology for FCC-ee particularly demanding.

* sen.yue@cern.ch

ISBN: 978-3-95450-252-3 ISSN: 2673-5350 doi: 10.18429/JACoW-IPAC2026-MOP1080

SUPERKEKB BEAM TRANSPORT TRACKING AND DYNAMIC APERTURE COMPARISON AS AN APPROXIMATION FOR INJECTION EFFICIENCY*

N. Z. van Gils†[1], J. Salvesen[2], European Organization for Nuclear Research, Geneva, Switzerland
A. Gerbershagen[2], Particle Therapy Research Center, Groningen, Netherlands
N. Iida, T. Mori, High Energy Accelerator Research Organization, Tsukuba, Japan
[1] also at Particle Therapy Research Center, Groningen, Netherlands,
[2] also at John Adams Institute for Accelerator Science, University of Oxford, Oxford, UK

Abstract

A new Energy Compression System (ECS), consisting of four RF cavities, was installed in the SuperKEKB electron transfer line (BTe) during the 2025 summer shutdown. Optimising BTe performance using full multi-turn injection simulations is computationally demanding. To accelerate this process, we compare the beam tracked through BTe, including the ECS, to the dynamic aperture of the High-Energy Ring lattice obtained from Xsuite simulations. The SAD lattices were converted to Xsuite and benchmarked to ensure consistency between the two frameworks. A fast, first order-estimate of the injection efficiency is obtained by comparing the action amplitudes of particles tracked through BTe with computed main ring dynamic apertures and septum positions. The injection efficiency is then optimised by varying ECS parameters. Radiation effects and a tapering can be optionally included. Different injection schemes are supported within the same framework. Together, these elements enable rapid optimisation of the ECS parameters with significantly reduced computational cost.

INTRODUCTION

SuperKEKB is an asymmetric, double ring electron-positron collider located at KEK, Japan [1, 2]. Electrons at 7 GeV are stored in the High Energy Ring (HER) for collision with 4 GeV positrons stored in the Low Energy Ring (LER). SuperKEKB holds the record for instantaneous luminosity at 5.24×10^{34} cm^{-2}s^{-1}, achieved in March 2026 [3]. To achieve high luminosity, SuperKEKB employs the nano-beam collision scheme [4], the crab-waist scheme [5] with a large full crossing angle of 83 mrad, and high operational beam currents exceeding 1 A. To facilitate such high current operation, top up injection [6] is required with high injection frequency and efficiency.

Beam generation and preparation are provided by KEK's injector complex [7, 8]. Positrons are injected into the LER from the beam transport line BTp while electrons are injected into the HER from the beam transport line BTe. These transport lines feature complex geometries, descending by ~7 m over their 500 m extent.

BTe Upgrade

In the summer of 2025, the BTe was upgraded to include a new Energy Compression System (ECS), which was first implemented during the 2025c operation period. The ECS is composed of four Radio Frequency (RF) cavities operating with a single frequency, voltage and lag. The RF frequency is nominally 2.856 GHz with a maximum voltage of 25 MV per cavity.

The ECS operates by combining RF cavities with dispersive optics to remove correlated energy spread and rotate the longitudinal phase space, thereby minimising the energy spread σ_δ. This not only allows the transported beam to better satisfy the stringent energy acceptance and matching requirements for injection into HER but also enables maximising of both injection efficiency and beam quality.

MODELLING KEK'S BT TRANSPORT LINES

The design and operation of SuperKEKB's BT lines are performed using SAD (Strategic Accelerator Design) [9], a FORTRAN based tool developed at KEK since 1986. For the studies presented here it was chosen to use Xsuite [10], a set of python packages for modelling particle accelerators developed at CERN since 2021. Following recent successful modelling of the LER and HER with Xsuite [11] it was a natural choice to expand to modelling the BT lines with Xsuite as well. Furthermore, the same strong synergies between SuperKEKB studies and Future Circular Lepton Collider (FCC-ee) [12, 13] studies extend to their respective transport lines and allows for crucial benchmarking of these tools on existing lepton colliders. The conversion of the BT lattices from SAD to Xsuite was performed using the SAD to Xsuite converter (SAD2XS) [14].

Apertures were not included in the SAD models of the BT lines but have been incorporated for all elements in the Xsuite model, with the following specifications: 47 mm diameter round cross-section at drifts and quadrupoles and 30 mm height and 50 mm width rectangular cross-section at dipoles.

Benchmarking

Prior to performing any ECS studies, the Xsuite lattice models were benchmarked against the SAD models. The first aspects benchmarked were the orbits and linear optics, computed in both 4D and 6D configurations. Excel-

* This work was partially supported by the European Union's Horizon Europe Marie Sklodowska-Curie Staff Exchanges programme under grant agreement no. 101086276.

† nikita.zena.van.gils@cern.ch

Content from this work may be used under the terms of the CC BY 4.0 licence (© 2026). Any distribution of this work must maintain attribution to the author(s), title of the work, publisher, and DOI.

ISBN: 978-3-95450-252-3 ISSN: 2673-5350 doi: 10.18429/JACoW-IPAC2026-MOP1083

EFFECT OF FCC-ee* COLLIMATOR IMPEDANCE ON BEAM STABILITY: DESIGN AND OPTIMIZATION STRATEGY

D. Gibellieri†[1,2], C. Antuono[1], A. Ghribi[2], L. Giacomel[1], M. Migliorati[3], G. Rumolo[1], C. Zannini[1], F. Zimmermann[1], M. Zobov[3]
[1]European Organization for Nuclear Research, Meyrin, Switzerland
[2]University of Caen Normandy and GANIL, Caen, France
[3]University of Rome La Sapienza and INFN - Roma1, Rome, Italy

Content from this work may be used under the terms of the CC BY 4.0 licence (© 2026). Any distribution of this work must maintain attribution to the author(s), title of the work, publisher, and DOI.

Abstract

Operating at 45.6 GeV with high beam current, low emittances, and long damping times, the FCC-ee low-energy collider configuration is particularly sensitive to collective effects and impedance-induced beam instabilities. Controlling these effects requires a continuously refined impedance model to guide design choices and to establish reliable instability thresholds. Recent studies identify the collimation system as a dominant contributor to the total machine impedance, with geometric effects playing a key role in beam stability. Within this framework, a flexible, modular, and comprehensive impedance model enables targeted optimization and systematic stability assessments. The total impedance model includes the beam pipe, collimators, RF cavities, bellows, tapers, and beam position monitors. This work presents the latest FCC-ee impedance model with a full evaluation of collimator impedance, addressing current limitations related to the challenging simulation regime. It provides an in-depth analysis of the contribution of collimators to beam stability, comparing different optics configurations, novel materials, and advanced design solutions, as well as highlighting ongoing progress in impedance modelling, intensity threshold evaluation, and instability mitigation.

INTRODUCTION

In the FCC-ee Z operation mode (45.6 GeV), the combination of high beam current, low emittances, and long damping times makes the machine particularly sensitive to impedance-driven collective effects [1]. In this regime, an accurate impedance model is essential to predict instability thresholds and guide design choices. Relevant prior work is presented in [2–8].

Recent studies identify the collimation system as a dominant contributor to the total impedance [2, 3]. While resistive wall effects are well understood [9, 10], the geometric impedance of realistic collimators remains challenging to accurately quantify.

In this work, the FCC-ee impedance model is extended to include a comprehensive set of collimator impedances derived from full 3D electromagnetic simulations, providing a comprehensive framework to capture both geometric and resistive effects, as well as additional features such as surface roughness. This enables a realistic evaluation of their impact on beam stability.

Several mitigation strategies are investigated, including taper optimization, collimator length reduction, and material improvements, providing guidance for the design of the FCC-ee collimation system.

IMPEDANCE MODEL FRAMEWORK

The impedance model describes the cumulative electromagnetic interaction between the beam and the surrounding accelerator structures, including vacuum chambers, RF systems, diagnostics, and protection devices such as collimators [11]. Each element contributes to the overall impedance spectrum and can drive beam instabilities.

The analysis focuses on the FCC-ee Z operation mode using the latest Local Chromaticity Correction (LCC) optics [12]. The main parameters are listed in Table 1.

Table 1: FCC-ee Parameters of the FCC-ee Z Configuration for the Version 106 of the LCC Optics [12]

Parameter	Value
Beam energy E (GeV)	45.6
Circumference C (m)	90644.816
Arc-cell setup	52°/45°
Momentum compaction factor α_c (10^{-6})	28.6
Energy Loss per turn W_0 (GeV)	0.035
Beam Intensity N (10^{12} particles)	2424
Bunch Intensity N_b (10^{11} particles)	2.02
Number of Bunches	12000
Horiz. β-function at IP β_x^* (cm)	9
Vert. β-function at IP β_y^* (mm)	0.7
Hor. emittance ε_x (nm)	0.70
Target vert. emittance in collision ε_y (pm)	1.40
Transverse tune Q_x / Q_y	194.16 / 170.20
Chromaticity Q'_x/Q'_y	5 / 5
Harmonic number h at 400 MHz	121200
Total RF voltage of 400/800 MHz (GV)	0.09/0
Synchrotron tune Q_s	0.031
RF momentum acceptance (%)	1.3
Bunch length σ_z (non coll./coll.) (mm)	5.1 / 16.7
Rel. mom. spr. σ_p (non coll./coll.) (10^{-3})	0.39 / 1.34
Long. damping time τ_z (turns)	1297
Beam-beam parameter ξ_x/ξ_y (10^{-3})	1.4 / 80
Luminosity $\mathscr{L}$ (1×10^{34} s^{-1}/cm^2)	150

The model is implemented in a modular framework based on `PyWIT/Xwakes`, integrated in `Xsuite` [13, 14], allowing

* Part of FCCIS – Future Circular Collider Innovation Study. Funded by the EU Horizon 2020 programme under grant No. 951754.

† dora.gibellieri@cern.ch

ISBN: 978-3-95450-252-3 ISSN: 2673-5350 doi: 10.18429/JACoW-IPAC2026-MOP1089

PULSE STRETCHER FOR THE PADME-X17 EXPERIMENT

A. De Santis*, A. Ciarma, S. Bilanishvili, M. Boscolo, A. Gallo, G. Franzini,
D. Quartullo, M. Zobov, Laboratori nazionali di Frascati - INFN, Frascati, Italy
P. Valente, INFN - Sez. Roma, Roma, Italy

Abstract

The PADME-X17 experiment is searching for a light dark matter candidate. The experiment would greatly benefit from the availability of a dedicated beam with long pulse duration and minimal instantaneous current. In this contribution, a third-order resonant slow-extraction scheme is considered, starting from the present lattice of the DAFNE damping ring. This solution, already integrated with the DAFNE complex, could provide the necessary positron-beam improvements within the existing facility. This study, currently aimed at improving the sensitivity of fixed-target experiments with positrons, could open new possibilities for beamlines based on the beam extracted from the damping ring.

INTRODUCTION

The PADME-X17 experiment [1] aims at searching for a light dark-sector candidate using positron interactions on a fixed target. The experimental sensitivity would benefit from a dedicated positron beam with a pulse duration significantly longer than that presently available at the BTF facility, namely 1–2 ms instead of about 250 ns, and with a reduced instantaneous current, about 0.1 instead of 13 e^+/ns [2]. This would mitigate event pile-up in the detector and improve the control of beam-induced background. Depending on the effective spill duration and on the total integrated statistics, such an improved beam is expected to reduce the total uncertainty by a factor between two and ten.

The DAΦNE complex offers a possible route to provide such a beam by using the damping ring as a pulse stretcher. In this scheme, the beam is injected in the ring and is then slowly extracted by means of a third-order resonant process. The concept is motivated by the possibility of exploiting an accelerator infrastructure already available at LNF, while extending the use of the complex to extracted-beam applications. This activity is therefore part of a broader effort to assess the flexibility of the DAΦNE complex beyond collider operation, including the use of the damping ring for dedicated experimental programs and accelerator studies [3].

Similar studies were previously performed using the DAΦNE positron ring [4] and the same damping ring [5], with the aim of providing a longer pulse for the original PADME experiment at higher energy [6].

Beam Requirements for PADME-X17

The main beam requirements are driven by the need to reduce the instantaneous particle rate on the target while preserving a sufficient integrated positron flux. The relevant quantities, summarized in the Table 1 are the beam energy, the average particle flux, the spill duration, the instantaneous rate, the transverse beam size and divergence at the target, and the energy spread.

Table 1: Indicative Beam Requirements for PADME-X17

Parameter	Target value
Beam species	e^+
Beam energy	280 ± 30 MeV
Energy tunability	1 MeV step
Average particle flux	$\gtrsim 4 \times 10^6$ e^+/s
Instantaneous rate	$\lesssim 0.1$ POT/ns
Spill duration	> 1 ms
Repetition rate	50 Hz
Beam spot at target	1×1 mm^2
Divergence at target	< 1 mrad
Energy spread	< 0.3 %

SLOW-EXTRACTION CONCEPT FROM THE DAΦNE DAMPING RING

The proposed scheme is based on third-order resonant slow extraction from the DAΦNE damping ring. The horizontal tune is moved close to a third-integer resonance,

$$Q_x = n + \frac{1}{3} + \Delta Q_x,$$

where ΔQ_x is the distance from the exact resonance. Sextupole magnets excite the resonance and generate a triangular separatrix in the horizontal phase space. Particles outside the stable triangular region move along the separatrix and can be extracted by means of a septum.

The resonant dynamics can be described, in normalized phase-space coordinates, by a Hamiltonian of the form

$$H = 3\pi\Delta Q_x \left(X^2 + X'^2\right) + S\left(3XX'^2 - X^3\right),$$

where S is the third-order resonance driving term generated by the sextupole configuration. The extraction efficiency depends on the separatrix size, the step size at the septum, the septum thickness, the available aperture, and the stability of the mechanism used to drive the particles toward the resonance. A detailed discussion of slow-extraction theory can be found in Ref. [7].

Two possible extraction approaches are under study. In the first one, the RF is switched off and the resonance condition is reached naturally through the combination of synchrotron-radiation energy loss and chromaticity. This "free extraction" scenario has the advantage of requiring limited additional hardware, but the spill duration is essentially determined

* antonio.desantis@lnf.infn.it

Content from this work may be used under the terms of the CC BY 4.0 licence (© 2026). Any distribution of this work must maintain attribution to the author(s), title of the work, publisher, and DOI.

ISBN: 978-3-95450-252-3 ISSN: 2673-5350 doi: 10.18429/JACoW-IPAC2026-MOP1090

ENERGY RAMPS FOR THE HIGH-ENERGY BOOSTER OF THE FCC-ee COLLIDER

L. Valle*[1], A. Chance[2], I. Karpov[1]
[1]CERN, Geneva, Switzerland
[2]Université Paris-Saclay - CEA, Gif-Sur-Yvette, France

Abstract

The FCC-ee full-size booster synchrotron prepares electron and positron bunch trains alternately for all foreseen beam energies from 45.6 GeV to 182.5 GeV and operation modes such as filling the collider from scratch or top-up. Polarized bunches could furthermore be supplied for the beam energy calibration. The first two operation modes require optimizing the energy ramps and RF voltage programs to achieve the small transverse beam sizes for injection in the collider while maintaining longitudinal beam stability. Specifically, the ramp for the ZZ operating point has an energy overshoot to boost the synchrotron radiation damping effect. Beam stability issues at low energy can be mitigated by damping wigglers at the cost of a higher energy spread at extraction. Further optimizations reduce the RF power requirements for all cycles.

INTRODUCTION

The booster accumulates, then accelerates alternatively electron and positron beams before injection into the Future Circular Collider (FCC-ee), for the four foreseen beam energies, 45.6 GeV (ZZ), 80 GeV (WW), 120 GeV (ZH) and 182.5 GeV ($t\bar{t}$), with 112 800 MHz superconducting cavities. An extra 336 cavities will be installed for the $t\bar{t}$ mode. There are two main operation modes of the booster [1]: filling the collider from scratch with shorter booster cycle and maximum bunch charge, and the top-up mode with adaptable bunch charges. The present contribution focuses on the filling mode which combines highest bunch charges and shorter cycles.

The energy and voltage ramps for acceleration are optimized to ensure the beam meets the extraction requirements while minimizing peak and average RF power and homogenize dynamic power losses between all booster cycles. Semi-analytical tools to compute the energy and voltage ramps of the high-energy booster were developed for that purpose [2]. Once the energy ramp and filling factor are defined, the voltage ramp is matched to the evolution of the longitudinal emittance and energy spread turn by turn. This contribution proposes energy ramps for all operation modes, shows the impact of injection errors on the longitudinal beam sizes at extraction and evaluates the dynamic power losses and RF power requirements of all booster cycles.

* lina.valle@cern.ch

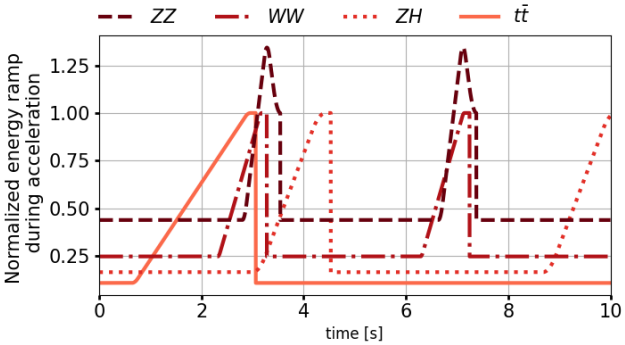

Figure 1: Energy ramps normalized to the extraction energy for all beam energies, displayed on a 10 s $t\bar{t}$ cycle.

ENERGY RAMPS FOR ALL BOOSTER CYCLES

Parabolic ramp round-offs are foreseen for the booster accelerating ramps for all operation modes. Figure 1 illustrates the foreseen energy ramps on the time scale of a $t\bar{t}$ 10 s booster cycle. The parabolae conserve the adiabaticity of the start and end of the accelerating ramp, by preserving the continuity of the energy gain. In all but ZZ mode, the energy gain is rapidly defined by the compensation of synchrotron radiation losses. The beam sizes then reach their natural values, defined by the equilibrium between radiation damping and quantum excitation [3, 4].

Turn by turn, the expected evolution of the longitudinal emittance following radiation damping and quantum excitation is calculated. The RF voltage is then matched to the longitudinal emittance. The voltage at flat top is adjusted to match the bunch length required for extraction. All voltage per cavity V_{cav} programs are displayed in Fig. 2. Further iterations will be needed depending on the location of the injection points of both the electron and the positron beams, which will change the desired energy of the injected bunches.

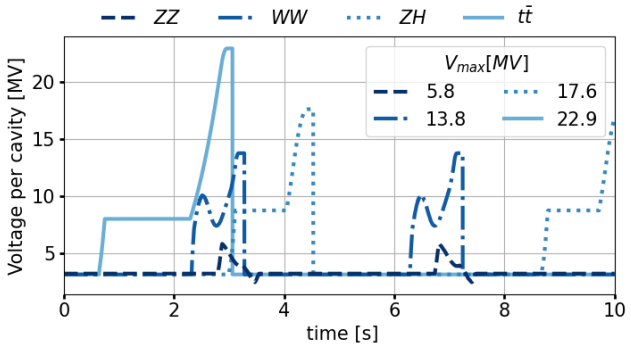

Figure 2: Example of the foreseen voltage per cavity V_{cav} programs for all beam energies, stacked on a 10 s $t\bar{t}$ booster cycle. ZZ mode includes an overshoot energy ramp [3, 4].

Content from this work may be used under the terms of the CC BY 4.0 licence (© 2026). Any distribution of this work must maintain attribution to the author(s), title of the work, publisher, and DOI.

ISBN: 978-3-95450-252-3 ISSN: 2673-5350 doi: 10.18429/JACoW-IPAC2026-MOP1091

CHALLENGES OF LONG SHUTDOWN 3 FOR THE LHC: FROM PREPARATION TO EXECUTION

M. Loffredo*, M. Barberan Marin, M. Bernardini, B. Di Girolamo, D. Nisbet, G. Papotti, D. P. Slimings, J.-Ph. Tock, E. Vergara Fernandez
CERN, Geneva, Switzerland

Abstract

The Long Shutdown 3 (LS3) of the Large Hadron Collider (LHC) represents a pivotal phase in the lifecycle of CERN's accelerator complex. The unprecedented complexity of LS3 arises from the challenge of integrating the High-Luminosity LHC (HL-LHC) upgrade, together with multiple key projects, extensive maintenance and consolidation activities, into a single coherent schedule with a fixed duration of 47 months. Achieving this goal requires precise orchestration of interventions and effective management of resources shared across different facilities. This paper first outlines the LS3 preparation framework for the LHC, with an emphasis on the adopted methodology to accomplish the LS3 objectives and the preparation of the LHC schedule. It also investigates the main challenges associated with LS3 execution and presents the strategies and tools used to address them. A unifying environment for monitoring and reporting is introduced, a platform that integrates interactive dashboards designed to streamline the progress visualisation and ensure a reliable reporting throughout the LS3 period.

INTRODUCTION

Between 2026 and 2030, the CERN accelerator complex will undergo its third long shutdown, LS3 [1], following LS1 (2013–2015) [2] and LS2 (2018–2021) [3].

The goal of LS3 is to ensure a reliable long-term operation and an increased luminosity target for the next physics run (Run4), while fulfilling safety and regulatory requirements. These objectives are addressed through a comprehensive programme of extended maintenance, consolidation activities, and upgrades across the accelerator chain.

A key element of the LS3 in the LHC is the implementation of the High-Luminosity LHC, which aims to increase the integrated luminosity delivered over the lifetime of the accelerator by approximately one order of magnitude [4]. The HL-LHC project consists in replacing full portions of the machine (1.2 km of the 26.7 km ring) and related infrastructures with entirely new equipment, primarily in the long straight sections around two of the four main experiments, ATLAS and CMS [4], resulting in the most extensive upgrade of the LHC since its construction. The detectors of these two experiments will be also upgraded during LS3 to fully exploit the significantly increased number of collisions [5, 6].

CHALLENGES FACED IN LS3 PREPARATION

The main challenge in the preparation of LS3 within the LHC is to ensure that the HL-LHC installation scope, accounting for ~50% of the total LS3 activities duration, fit within the fixed 47-month shutdown period defined by the CERN long-term schedule [1], thereby defining the critical path of LS3.

In addition, resource and personnel limitations play a critical role. As CERN service groups work per technical domain and not per facility (e.g., electrical engineering), resources allocated to activities in the LHC are also shared across the wider CERN accelerator complex. This means that delays affecting other machines can propagate to the overall LHC schedule, and viceversa, generating domino effects that must be anticipated in the preparation phase, when possible.

Preparation and execution are conditioned by the interdependence between the LHC and adjacent facilities, including accelerators, experimental areas, and LHC experiments. Transport spans multiple infrastructures, requiring detailed scheduling to coordinate interface openings, access conditions, and operational sequencing to minimise bottlenecks.

LS3 Preparation Framework

The preparation of LS3 is orchestrated by the Accelerator Coordination and Engineering group (EN-ACE) and pivots around a well-established methodology developed by the group successfully validated during LS1 and LS2 [7–9]. This methodology consists of combining expertise in safety, integration, configuration and layout, site coordination and scheduling to prepare and coordinate programmed stops of the CERN accelerator complex [7–9]. This is complemented by Electrical Safety and Lock-out (ESL), and Support, Strategy and Projects (SSP), tackling the criticality of electrical safety and tools management during LS3.

A significant part in LS3 preparation is the role of the HL-LHC project. Its installation planning was initiated well in advance of the LS3 preparation (started in 2021), driving the overall shutdown duration and the boundary conditions for the other activities. Its broad scope also required the involvement of a vast number of CERN groups. This setting differs from LS2, whose time interval was driven by consolidation needs coming from the injectors chain: on the LHC side indeed, the main project Diode Insulation and Superconducting Magnets Consolidation (DISMAC), was initiated

* michele.loffredo@cern.ch

Content from this work may be used under the terms of the CC BY 4.0 licence (© 2026). Any distribution of this work must maintain attribution to the author(s), title of the work, publisher, and DOI.

ISBN: 978-3-95450-252-3 ISSN: 2673-5350 doi: 10.18429/JACoW-IPAC2026-MOP1092

FERMI LINAC UPGRADE: COMMISSIONING EXPERIENCE OF THE FIRST S-BAND HIGH-GRADIENT MODULE

N. Shafqat*, F. Gelmetti, C. Maschiovecchio, M. Milloch, A. Milocco, M. Trovo
Elettra Sincrotrone Trieste S.C.p.A., Trieste, Italy

Abstract

The FERMI seeded free-electron laser (FEL), located at the Elettra laboratory in Trieste, is a 4th-generation light source operating in the vacuum ultraviolet to soft X-rays range. In order to extend the FEL spectral range to shorter wavelengths, an increase in the linear accelerator (linac) energy from 1.5 to 2.0 GeV is required. S-band HG module is designed to fulfill the upgrade requirement of 30 MV/m accelerating gradient with the breakdown rate (BDR) in the range of low 10^{-8} bpp/m. One HG module consists of two HG structures, 3.0 m in length, and one Spherical Pulse Compressor (SPC). The 1st HG module is successfully commissioned at the FERMI linac up to an accelerating gradient of 27 MV/m with the BDR of around 5×10^{-8} bpp/m. In this paper, we share the commissioning experience of the HG module from installation, conditioning, high power operation, and commissioning with the beam.

INTRODUCTION

FERMI FEL, located at Elettra Sincrotrone, Trieste, Italy, is a 4th-generation light source operating in Extreme-Ultraviolet (EUV) to soft X-rays. FERMI is driven by a 1.5 GeV normal-conducting S-band linac outlined in Fig. 1. An upgrade plan to reach the shorter wavelength of 4 nm to

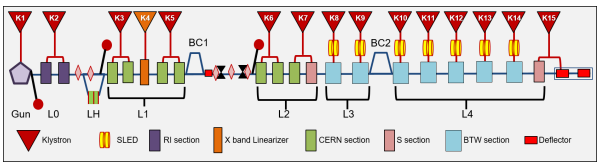

Figure 1: The layout of the existing FERMI linac.

cover the whole water window is underway [1]. One component of this upgrade plan aims to increase the linac energy from the present 1.5 GeV to 2.0 GeV and improve the beam quality. This goal will be achieved by replacing the existing Backward Traveling Wave (BTW) accelerating structures and SLEDs pulse compressors with the newly designed HG accelerating structures and spherical pulse compressors, as shown in Fig. 2.

COMMISSIONING OF HG MODULE

HG modules are designed to fulfill the FERMI requirement of 30 MV/m accelerating gradient with the breakdown rate (BDR) in the range of low 10^{-8} bpp/m [**?**]. One HG module consists of two HG accelerating structures, each 3.0 m long, and one SPC. RF parameters of the HG structures are listed in Table 1.

* nuaman.shafqat@elettra.eu

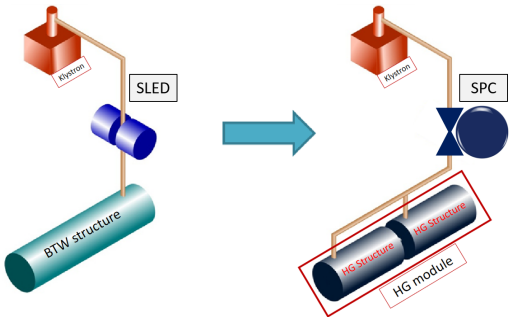

Figure 2: FERMI linac upgrade plan to replace BTWs and SLEDs with the HG modules and SPC.

Table 1: RF Parameters of the HG Structure

Parameter	Value	Unit
f_0	2998.01	MHz
Mode	$2\pi/3$	–
$L_{\text{prototype}}$	353.332	mm
L_{cell}	33.332	mm
N_{cell}	84	–
N_{coupler}	2	–
Iris radius a	11.382–8.801	mm
Cell radius b	41.610–41.076	mm
R_{shunt}	72–81	MΩ/m
Q_0	≈ 15850	–
v_g/c	2.07–0.97	–
t_f	≈ 645	ns
τ	0.385	Neper

Installation of HG Module

After successful testing and conditioning of the first HG structure (HG1) at the Elettra high-power test facility, the 2nd HG structure (HG2) was directly installed in the FERMI linac at K15 in place of one accelerating section and one deflector, as shown in the Figures. 3 and 4. The goal was to condition the HG2 structure on the FERMI linac in the available time slots between the user beam operation. The HG module was installed with the Barrel Open Cavity (BOC) type pulse compressor due to the delay in the delivery of SPC.

Conditioning of HG Module

The first problem encountered at the start of conditioning was the bad vacuum in the re-combiner region. As shown in Fig. 5, a re-combiner is installed at the output of a two-armed klystron used to feed the HG module, 4th port of which is terminated with a small ferrite-based RF terminator. Initially, the bad vacuum in this region was attributed to degassing but when it persisted, and further investigations were performed,

Content from this work may be used under the terms of the CC BY 4.0 licence (© 2026). Any distribution of this work must maintain attribution to the author(s), title of the work, publisher, and DOI.

ISBN: 978-3-95450-252-3 ISSN: 2673-5350 doi: 10.18429/JACoW-IPAC2026-MOP1094

IMPACT OF RAPID ACCELERATION ON BEAM DYNAMICS IN THE RAPID-CYCLING SYNCHROTRONS OF A MUON COLLIDER *

L. Soubirou[†,1], A. Chance[‡,1], D. Amorim[2], H. Damerau[3], E. Lamb[3], E. Metral[3], L. Thiele[3,4]
[1]Université Paris-Saclay - CEA, France
[2]École Polytechnique Fédérale de Lausanne, Lausanne, Switzerland
[3]CERN, Geneva, Switzerland
[4]University of Rostock, Rostock, Germany

Abstract

Circular muon colliders offer a promising route to multi-TeV center-of-mass energies with high luminosity. The baseline design for the high-energy complex includes a chain of pulsed synchrotrons covering energies from 63 GeV to 5 TeV. This chain combines normal and hybrid synchrotrons, using both fixed-field superconducting and pulsed normal-conducting magnets. The short muon lifetime (2.2 µs in the rest frame) constitutes a major challenge for the accelerator complex: attaining high luminosity requires a muon survival rate of up to 70 % throughout the acceleration chain, which implies acceleration within a few milliseconds. Such rapid acceleration causes a mismatch between the beam energy in the arcs and the linearly ramped fields of the dipoles and quadrupoles. The corresponding field errors affect both the beam trajectory and optical functions. Preliminary tracking studies have been conducted to assess the emittance growth arising from these effects.

INTRODUCTION

Circular muon colliders provide a promising path to reach multi-TeV centre-of-mass energies with high luminosity. A baseline design for a muon collider was developed by the US Muon Accelerator Program (MAP) [1]. Within the framework of the International Muon Collider Collaboration (IMCC) and the MuCol program, an updated design is currently under investigation [2]. After production, the muon beam is cooled to reduce its transverse and longitudinal emittance. It is then accelerated to 63 GeV, using a linear accelerator followed by two recirculating linacs. Subsequently, a chain of Rapid-Cycling Synchrotrons (RCS) accelerates the beam to collision energy. Finally, the muons are injected into the collider ring. The layout of the muon collider is presented in Fig. 1.

The fast decay of the muon beam (with a lifetime of 2.2 µs in the rest frame) represents the principal challenge for the muon collider facility, since production, cooling, acceleration, and collision must all occur within the relativistically dilated muon lifetime. Reaching high luminosity requires a total survival rate of up to 70 % throughout the acceleration chain, which demands for acceleration through the entire chain of RCS in about ten milliseconds. Four RCSs accelerate the beam from 63 GeV to 5 TeV with energy stages at 314 GeV, 750 GeV and 1.5 TeV. The first RCS is a conventional synchrotron, whereas the following are hybrid RCS. The hybrid RCS consists of fixed-field superconducting dipoles interleaved with normal-conducting dipoles that pulse from negative to positive saturation. These pulsed dipoles provide rapid cycling and fast acceleration, while fixed-field strong dipoles help achieve a high average bending field for a compact ring. Due to the extremely fast acceleration, the pulsed magnets must be ramped at rates of up to 4.2 kT/s for RCS1. Such ramps create a mismatch between the discretely increased beam energy and the continuously ramped fields of the pulsed magnets, which include dipoles and quadrupoles. For RCS1, with a distribution of radiofrequency (RF) cavities over 8 stations, it represents a dipolar error of up to 3 % in the first arc. The consequences of this error on the beam dynamics are carefully studied for RCS1, the accelerator with the fastest acceleration of the chain. The first RCS of the chain covers an energy range from 63 GeV to 314 GeV in 0.34 ms. The beam circulates for 17 turns in a 5990 m long ring, providing an energy gain of 14.8 GeV per turn. A lattice design with 8 arcs is considered, featuring 90° FODO cells and a dispersion suppressor at entrance and exit of the RF insertions. The transverse and longitudinal emittances, $\varepsilon_{x,y}$ and ε_s, are set at 25 µm and 0.025 eV s, respectively.

ANALYTICAL MODEL

We consider a dipole of length L with its entry face placed at s_0, with the reference $s = 0$ at the beginning of the arc. Following the ramp, the strength of an infinitesimal slice of dipole at s is a function of the longitudinal position along the arc:

$$k_0(s) = k_0^* + k_0' \, (s - s^*) \tag{1}$$

where k_0^* is the strength at the reference energy, s^* the position where the magnetic field crosses the reference field, $k_0' \equiv \dot{B}/(B\rho c)$, with $\dot{B}$ the dipole ramp, $(B\rho)$ the magnetic rigidity, and c the light velocity.

In the following, we will note $M_{a\to b}$ and $T_{a\to b}$ the reference 1st order and 2nd order matrices from $s = a$ to $s = b$, $M = M_{s_0\to s_0+L}$, $\delta X(s)$, $\delta M(s)$, and $\delta T(s)$ the infinitesimal offset, matrix, and T-matrix perturbation in s, and ΔX and

* Endorsed by the IMCC. Funded by the European Union (EU). Views and opinions expressed are however those of the author(s) only and do not necessarily reflect those of the EU or European Research Executive Agency (REA). Neither the EU nor the REA can be held responsible for them.

† lisa.soubirou@cea.fr
‡ antoine.chance@cea.fr

Content from this work may be used under the terms of the CC BY 4.0 licence (© 2026). Any distribution of this work must maintain attribution to the author(s), title of the work, publisher, and DOI.

ISBN: 978-3-95450-252-3 ISSN: 2673-5350 doi: 10.18429/JACoW-IPAC2026-MOP1095

ESSNUSB+: TARGET STATION STUDIES

J. Hiegel*, E. Baussan, Institut Pluridisciplinaire Hubert Curien, Strasbourg, France
On behalf of the ESSνSB+ collaboration

Abstract

The ESSnuSB+ project aims to accurately measure the neutrino cross-sections for ESSnuSB leptonic CP violation measurements and to perform sterile neutrino searches and astroparticle physics. The implementation of the whole project depends on the time evolution of the European Spallation Source (ESS) beam power. Three phases are under consideration: 300 kW (Stage 1), 1.25 MW (Stage 2) and the full power at 5 MW (Stage 3).

This article will focus on the status of the 1.25 MW target station (phase 2). The full chain from particle production to energy deposition across major components of this target station has been estimated thanks to a Monte Carlo simulation. The design of all these components, which are exposed to high levels of radioactivity, is essential for validating the feasibility of the target station facility, assessing the lifetime of the components, and guiding the design of the cooling and shielding systems.

THE ESSNUSB+ TARGET STATION

The next generation of neutrino experiments, such DUNE [1] in USA or HK [2] in Japan, aims at addressing fundamental open questions in particle physics, such as the determination of the neutrino mass ordering and the search for CP violation in the leptonic sector. Accelerator-based facilities rely on high-intensity neutrino beams produced from the decay of secondary particles, primarily pions, generated by the interaction of a high-power proton beam impinging a solid target. In this context, the ESSnuSB collaboration [3] proposes to exploit the high-power proton linac of the European Spallation Source (ESS) to produce an intense neutrino superbeam.

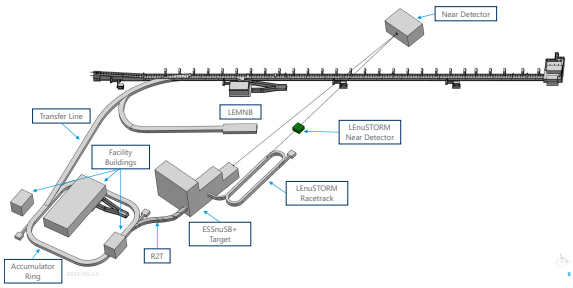

Figure 1: Facilities implementation in the ESSnuSB+ project.

A 2.5 GeV proton beam impinges on a target station, where secondary pions are produced, focused by a magnetic horn into a decay tunnel (Stage 3) or deviated by a magnetic dipole located downstream of the horn to feed a muon racetrack ring in the case of ESSnuSB+ (Stage 2) as shown in Fig 1. The target station constitutes a critical component of the facility, as it must withstand high power deposition and intense radiation fields while ensuring efficient secondary particle production and collection. The optimisation of this system involves a trade-off between maximising the useful π^+ (or π^-) flux and limiting energy deposition in sensitive components, such as the target, horn, and downstream elements. In this work, the simulations are performed to describe the full chain of interactions within the target station. The results provide quantitative estimates of power deposition, as well as updated predictions of pion production, supporting the design and optimisation of the ESSnuSB+ facility.

SIMULATION SETUP

The simulations were performed using the FLUKA Monte Carlo code [4, 5] to model the interaction of a 2.5 GeV proton beam with the target station, as shown in Fig 2. The geometry implemented in the simulations includes the main components of the ESSnuSB+ target station, described below.

Target and Canister The granular target consists of a 78 cm long cylinder with 3 cm diameter filled with 3 mm titanium spheres. The cylinder is surrounded by a titanium canister equipped with slits on top and bottom to allow a pressurized helium gas circulation for an efficient transverse cooling. In the simulation, the uniform titanium cylinder with a density of $\rho = 2.57\,\mathrm{g/cm^3}$ to take in account the sphere arrangement.

Magnetic Horn The target system is enclosed within a MiniBooNE like horn made of aluminium. The magnetic field is generated by a 350 kA pulse (100 microseconds half-sinusoid width) circulating in the conductor. Theses pulses are synchronized with the proton pulse frequency at 14 Hz. A specific power supply based on modular approach has been developed to work under these specific conditions.

Shielding - Collimator A shielding element, referred to as the collimator, is placed between $z = 300\,\mathrm{cm}$ and $z = 450\,\mathrm{cm}$. It is primarily made of iron and includes a tungsten ring to enhance radiation absorption (see Fig 3). The aperture of the tungsten insert is 30 cm, which imposes constraints on the horn focusing performance to ensure efficient transmission of useful pions selected by the physics objectives (700 MeV $\pm$10%).

Bending Dipole A bending dipole magnet is located between $z = 450\,\mathrm{cm}$ and $z = 600\,\mathrm{cm}$. This component is one of the most critical elements of the target station due to the

* julien.hiegel@iphc.cnrs.fr

Content from this work may be used under the terms of the CC BY 4.0 licence (© 2026). Any distribution of this work must maintain attribution to the author(s), title of the work, publisher, and DOI.

ISBN: 978-3-95450-252-3 ISSN: 2673-5350 doi: 10.18429/JACoW-IPAC2026-MOP1098

LEnuSTORM: A LOW-ENERGY MUON STORAGE RING FOR NEUTRINO CROSS-SECTION MEASUREMENTS

T. W. Choi*, M. Olvegård, Uppsala University, Uppsala, Sweden
M. Topp-Mugglestone, CERN, Geneva, Switzerland

Abstract

The LEnuSTORM (Low-Energy neutrinos from STORed Muons) is a proposed facility that enhances the performance of the ESSnuSB (European Spallation Source Neutrino Super Beam) project by measuring neutrino cross sections in the energy range 200–600 MeV, where data is largely missing. The facility utilizes a 1.25 MW proton beam from the European Spallation Source linac, which is compressed in an accumulator into 1.2 µs pulses and directed at a granular titanium target embedded in a horn. Pions collected by the horn are transferred and injected into a racetrack-shaped storage ring, where they decay and emit muons that will be stored in the ring for a few tens of turns. The neutrinos emitted in the muon decay in one of the straight sections will travel to a water Cherenkov detector, where the interactions are monitored.

At LEnuSTORM, the beam is large and very divergent, and thus difficult to contain. The ring design presented in this paper uses iron-dominated magnets to reduce complexity, and a compact FODO lattice to maximise neutrino production by allowing a large transverse acceptance. However, the design pushes fringe-field effects beyond the linear regime and requires a paraxial expansion with higher-order terms, introducing resonances and reduced dynamic aperture. We present here a design that aims at balancing the transverse and momentum acceptance with the dynamic aperture, to maximise neutrino production.

INTRODUCTION

The neutrino beam for the ESSnuSB (European Spallation Source Neutrino Super Beam) long baseline experiment to measure the leptonic charge-parity violation will be produced using the ESS proton linear accelerator. The ESS 5 W, 2.5 GeV, 2.86 ms proton beam will be sent to an accumulator ring and compressed into four sub-pulses, each of 1.2 µs duration before hitting a target [1].

As an extended project of ESSnuSB, the main goal of the LEnuSTORM (Low-Energy neutrinos from STORed Muons) facility is to study precisely the neutrino interaction cross-section for electron and muon neutrinos and their antiparticles. In LEnuSTORM, one of the 1.2 µs compressed proton pulses from the accumulator was extracted to hit a target to produce pions. They are then focused with a magnetic horn and transported to a muon storage ring through a pion transfer line. The transfer line includes a magnetic chicane to separate the pions from the other charged particles emerging from the target, including remaining protons, and will also serve as a momentum selection stage. The pions are injected into the storage ring at the end of one of the arc sections. The pions will decay into muons while traveling in the straight section. Muons within the acceptance will be stored in the ring for a few tens of turns until they eventually decay. Muons outside the acceptance will be dumped or lost, together with any remaining pions. At 30 m from the end of the first straight section, labeled the production straight, a detector named LEMMOND is placed to detect neutrinos produced in the muon decay.

To fulfill the physics goals of the ESSnuSB project, the muon momentum should exceed 400 MeV/c to produce a neutrino energy spectrum covering 200–400 MeV. We have chosen 600 MeV/c muons as the reference circulating particle and 1000 MeV/c pions for the injection. When these pions decay, they will produce 600 MeV/c muons at angles small enough to fall within the ring acceptance.

LATTICE DESIGN

Due to the short lifetime of pions and muons, the geometry of the racetrack ring and the particle momenta influence the neutrino flux. A production straight section of approximately 80 m is sufficient to allow the majority of the pions to decay before they reach the arc. Furthermore, the arc length should be no more than half of the length of the straight section, to enhance the amount of usable muon decays, those occurring within the straight section.

In this design, we aim at favoring a so-called stochastic injection method, which relies on a distinct separation in pion and muon momentum, and the merging of the beams in a dispersive region [2]. The arc must thus offer sufficient dispersion for the physical separation of the beams before the merge.

Since the muons to be stored in the ring have an unusually large transverse emittance and a large momentum spread, our primary goal is to maximise both the transverse and the momentum acceptance. For simplicity, this study only considers normal-conducting magnets, with the magnetic field strength limited to below 2 T. We aim at an aperture radius of 20 cm to reduce cost. These parameters and aspects constrain the storage ring design.

Previous studies of higher-energy nuSTORM facilities have demonstrated the feasibility of a racetrack ring composed of focusing-defocusing (FODO) cells [3]. Other designs use a fixed-field alternating gradient lattice only [4] or in combination with FODO cells [5]. In this design, we explore the use of FODO cells exclusively.

To maximize the number of stored muons, the transverse acceptance of the FODO-cell should be maximized, which implies that the cell length is minimized. We employ a fairly

* ting.choi@physics.uu.se

Content from this work may be used under the terms of the CC BY 4.0 licence (© 2026). Any distribution of this work must maintain attribution to the author(s), title of the work, publisher, and DOI.

ISBN: 978-3-95450-252-3 ISSN: 2673-5350 doi: 10.18429/JACoW-IPAC2026-MOP1099

POWERING CONCEPTS FOR RESISTIVE MAGNETS IN THE MUON COLLIDER RAPID CYCLING SYNCHROTRON*

F. Boattini†, D. Aguglia, L. Bottura
European Organization for Nuclear Research, Geneva, Switzerland
D. Fazioli‡, M. Breschi, University of Bologna, Bologna, Italy
M. Gast§, Karlsruhe Institute of Technology, Karlsruhe, Germany

Abstract

The development of a power converter for the resistive magnets of the Muon Collider Rapid Cycling Synchrotron (RCS) represents one of the most critical challenges of the muon accelerator system, given the required peak power levels in the 50–100 GW range. To address this, a modular resonant converter is proposed, consisting of several hundred identical series-connected cells interleaved with the magnets. This configuration distributes the total system voltage — on the order of tens of megavolts — evenly across the cells, while limiting the insulation voltage to ground. A key design requirement is a highly repeatable current ramp across successive pulses, with deviations at or below 100 ppm. Given the very short acceleration times, a pulse-to-pulse Iterative Learning Control (ILC) strategy is proposed to progressively meet this target. The paper presents the main converter topologies, repeatability studies, simulation results, and the proposed control approaches.

INTRODUCTION

The short muon lifetime necessitates extremely rapid acceleration across multiple Rapid Cycling Synchrotron (RCS) stages, with acceleration times of 0.5–6 ms and magnetic field ramp rates of 800–2000 T/s. To maximize muon survival and constrain RF peak power, acceleration must proceed in an approximately linear regime. The RCS geometry and magnet specifications [1] result in very large magnetic stored energy that must be delivered over very short intervals, implying peak power levels of 100 GW and operating voltages of 10 MV. Despite these extreme requirements, the low repetition rate of 5 Hz keeps the duty cycle very small, with current flowing for at most 6 ms per 200 ms cycle.

SWITCHED RESONANCE

In a previous paper [2], a resonant powering principle based on superimposed harmonics was proposed, where a main capacitor bank and an auxiliary series LC branch, connected in parallel, were simultaneously switched onto the magnet string to generate an approximately linear current ramp. This paper introduces a new concept, denoted as a switched resonant powering system, in which the converter is subdivided into hundreds of smaller series-connected power cells. Figure 1 shows the two possible single-cell topologies: unipolar (two-quadrant, allowing positive current and bipolar voltage) and bipolar (four-quadrant, allowing both current and voltage reversal). The bipolar configuration is required for the hybrid RCS (HCS), where part of the ring operates with a fixed dipole field and the remainder with a time-varying field. Tab. 1 lists the accelerator chains considered in the CERN (C) and GREENFIELD (GF) scenarios; simulation results presented here focus on the RCS1-C case.

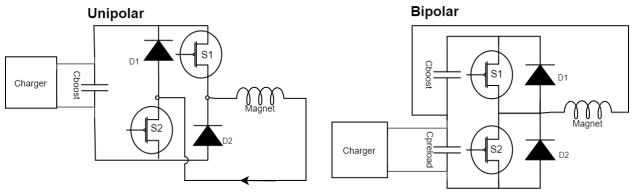

Figure 1: Unipolar and Bipolar switched resonance power cells.

Table 1: Accelerator Scenarios (U = Unipolar, B = Bipolar)

Scenario	E_{inj} [GeV]	E_{ext} [GeV]	Type	t_{ramp} [ms]	L_{tot} [m]
RCS1-C	63	350	U	0.45	4 103
RCS2-C	350	1 600	U	2.60	18 650
HCS3-C	1 600	3 800	B	4.42	12 940
RCS1-GF	63	314	U	0.35	3 654
HCS2-GF	314	750	B	1.10	2 539
HCS3-GF	750	1 500	B	2.37	4 366
HCS4-GF	1 500	5 000	B	6.37	20 376

In both power-cell topologies, the underlying operating principle is the same. A resonant interaction between the cell capacitor and the magnet string is established and terminated by periodically switching S_1 and S_2 between their ON and OFF states. A large number of such cells, potentially several hundred, can be connected in series and interleaved with the magnets, thereby forming a single series circuit, as schematically illustrated in Fig. 2. In this arrangement, the magnets do not require individual return-path extensions, except for the first and last units of the RCS. Since all magnet coils are connected in series and interleave with the power cells, the overall system behaves as a single electrical circuit, which avoids the need for independent current control of separate sectors.

RCS1 CERN Case Study

As a representative design exercise, the switched-resonance converter is dimensioned for the RCS1 CERN

* This work was supported by the European Union grant agreement 101094300 and is endorsed by the IMCC.
† fulvio.boattini@cern.ch
‡ davide.fazioli@studio.unibo.it
§ marco.gast15@gmail.com

Content from this work may be used under the terms of the CC BY 4.0 licence (© 2026). Any distribution of this work must maintain attribution to the author(s), title of the work, publisher, and DOI.

ISBN: 978-3-95450-252-3 ISSN: 2673-5350 doi: 10.18429/JACoW-IPAC2026-MOP1100

IMPACT OF INTRABEAM SCATTERING AND SPACE-CHARGE IN THE FIRST THREE CELLS OF THE MUON COLLIDER FINAL COOLING CHANNEL*,†

P. Desiré‡,1,2, A. Latina[1], A. Gerbershagen[2]
[1]CERN, Geneva, Switzerland
[2]University of Groningen, Groningen, Netherlands

Abstract

The cooling process is one of the most critical challenges for the future Muon Collider, as muons are initially produced with a very large emittance that must be significantly reduced before acceleration. This cooling must occur rapidly, well within the muon lifetime. At low energies, collective effects such as space charge and intrabeam scattering can strongly influence emittance growth and must therefore be considered in the lattice design, which is currently under development. This work presents studies of space charge and intrabeam scattering effects within the first three cells of the latest Muon Collider final cooling lattice design, evaluating their impact on emittance growth using the tracking code RF-Track.

INTRODUCTION

The Muon Collider is a leading candidate for a future high-energy lepton collider [1]. Owing to the large muon mass, synchrotron radiation is strongly suppressed, enabling a compact multi-TeV circular design. However, the short muon lifetime imposes strict constraints on beam manipulation and acceleration.

Muons are produced as tertiary particles from proton–target interactions, followed by pion decay, resulting in beams with large emittances. Therefore, emittance reduction is required to achieve the target luminosity. Since most of the conventional cooling techniques are incompatible with the muon lifetime, ionization cooling is adopted [2]. In this method, muons loose momentum in low-Z absorbers (in this specific design, liquid hydrogen), while RF cavities restore the longitudinal component. High-field solenoids provide strong transverse focusing to mitigate multiple Coulomb scattering and enable net transverse cooling. The present work addresses the first three cells of the final cooling stage.

In the final cooling stage, the muon kinetic energy decreases from approximately 120 MeV to about 10 MeV in the last cells. Under these conditions, space charge (SC) and intrabeam scattering (IBS) are expected to play a significant role along the entire channel, with increasing impact at lower energies. These collective effects can drive emittance growth and may ultimately limit the achievable cooling performance. A quantitative evaluation of their impact is therefore required and constitutes the main objective of this study.

Collective effects may induce modifications of the beam phase space, including transverse emittance growth, bunch lengthening, and an increase in energy spread. Since the lattice was originally designed without accounting for these effects, a re-matching of the optical parameters may be required to preserve the intended cooling performance. In this context, the present study focuses on the first three cells of the channel, where the onset of such effects is expected and where early deviations from the nominal matching conditions can already be identified.

Simulations have been performed using RF-Track [3], a tracking code developed at CERN. The code allows self-consistent modeling of SC, multiple Coulomb scattering in matter (important for the absorbers), wakefields, beam loading, modeling of non-ultrarelativistic muons and muon decay within a time-integration framework that supports overlapping elements, such as absorbers embedded in solenoids. In addition, it was recenly equipped with a novel methodology to simulate IBS [4], making RF-Track a very suitable tool for the simulation of the final cooling channel.

The lattice considered in this study corresponds to one of the latest baseline design [5], which is described in detail in the next section. Alternative final cooling concepts have also been proposed at CERN, including machine-learning-optimized lattices [6, 7].

More recently, within the framework of the European Strategy for Particle Physics Update [1], an alternative design for the final cooling channel has been introduced [8]. Preliminary investigations of space charge (SC) effects for this scheme have been performed using Geant4Beamline [9],

Table 1: Muon Beam Characterization at the Entrance of the Final Cooling Section

Particle	μ^+
Number of muons	$5.3 \cdot 10^{12}$
Kinetic energy (MeV)	123.61
Norm. trans. emittance $\epsilon_\perp$ (mm· mrad)	299.48
Long. emittance $\epsilon_\parallel$ (eV· ms)	0.5244
Bunch length σ_t (mm/c)	29.14
Energy spread σ_E (MeV)	5.3948
Number of macroparticles	10000
Number of cells (SC and IBS algorithms)	$32 \times 32 \times 32$

* Funded by the European Union (EU). Views and opinions expressed are however those of the author(s) only and do not necessarily reflect those of the EU or European Research Executive Agency (REA). Neither the EU nor the REA can be held responsible for them
† Work endorsed by IMCC
‡ pdesirev@cern.ch

Content from this work may be used under the terms of the CC BY 4.0 licence (© 2026). Any distribution of this work must maintain attribution to the author(s), title of the work, publisher, and DOI.

ISBN: 978-3-95450-252-3 ISSN: 2673-5350 doi: 10.18429/JACoW-IPAC2026-MOP1105

REFINED DESIGN OF THE FRONT-END COMPLEX FOR A MUON COOLING DEMONSTRATOR AT CERN

P. B. Jurj*, R. Kamath, J. Pasternak, Imperial College London, London, United Kingdom
C. Rogers, Science and Technology Facilities Council, Didcot, United Kingdom
C. Ahdida, D. Calzolari, S. Candido, A. Lechner, R. Losito,
J. Manczak, J. F. Roncal, R. F. Ximenes, CERN, Geneva, Switzerland
Endorsed by the International Muon Collider Collaboration

Abstract

The muon collider has great potential for enabling high-luminosity multi-TeV lepton–antilepton collisions provided low-emittance, high-intensity muon beams can be produced. Ionization cooling is the proposed technique to achieve the required muon beam emittance. The International Muon Collider Collaboration aims to demonstrate the integration and reliable operation of a 6D ionization cooling system, including RF acceleration in strong magnetic fields. This study advances the design of the muon production and transport systems for a Muon Cooling Demonstrator implemented in the CERN CTF3 building. Building on previous work, the design is extended to the beam-preparation section and the matching of the transport line into the cooling channel. The target–horn model has been further developed and now incorporates a forced-convection helium cooling system, providing a more mature and realistic representation. An extended FLUKA model of the target area is used to assess and optimise shielding requirements.

MUON COOLING DEMONSTRATOR

A central challenge on the path towards a muon collider is the production of low-emittance, high-intensity muon beams, which requires efficient and compact 6D ionization cooling systems. The Muon Ionization Cooling Experiment (MICE) demonstrated transverse emittance reduction in high-emittance muon beams passing through a single, non-accelerating ionization cooling cell [1, 2]. Building on this proof-of-principle, the muon cooling demonstrator is an essential component of the muon collider R&D programme. Its aim is to demonstrate the successful integration of the cooling hardware (high-field solenoids, absorbers, dipoles, and high-gradient radiofrequency (RF) cavities), its operation with beam, and the achieement of the required beam-physics performance. To realise these objectives in a controlled and progressive manner, the programme follows a staged approach: starting with RF test stands to characterise the achievable gradients in high-field solenoids, then advancing to one-cell and multi-cell modules, and ultimately culminating in the operation of a complete cooling line with beam [3, 4].

A conceptual layout of the Muon Cooling Demonstrator is shown in Fig. 1. The muon beam is produced through the decay of pions resulting from the interaction of protons with a target. The pions emerging from the target are captured using a magnetic horn and collected into a quadrupole-based decay channel. At the end of this channel, a momentum-selecting chicane delivers the resulting muon beam into a beam preparation system (BPS), where the beam emittance is tuned through collimation and the beam is rotated and bunched in the longitudinal phase space using RF cavities. The prepared beam is then matched into the cooling channel.

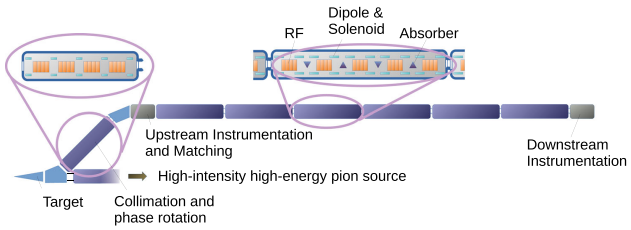

Figure 1: Conceptual schematic of the Muon Cooling Demonstrator [5].

Candidate sites at CERN, Fermilab, and other laboratories have been identified. At CERN, two siting options making use of existing infrastructure—the TT7 tunnel and the CTF3 building—have been studied in detail, including lattice design, engineering integration, and cost estimation. Both configurations would operate with a low-power proton beam (≤ 10 kW) from the CERN PS. The CTF3 option (Fig. 2) requires substantially less civil engineering, making it a cost-effective solution that can support all stages of the programme. A similar site study has also been approved at Fermilab. This paper presents recent progress on the front-end design, with particular emphasis on the target system, the beam preparation and matching sections of the muon transport line, and a preliminary radiation protection study for the CTF3 target area layout.

TARGET SYSTEM

The pion production system is based on a cylindrical graphite rod placed within a magnetic horn, a configuration motivated by the maturity and widespread use of such systems in proton-driven meson production. To further develop the target system and assess the pion capture yield with a more realistic design, a target cooling system based on forced helium convection has been added to the existing baseline FLUKA [6] model [7]. The cooling system is based on a double-walled titanium vessel, similar to that proposed for the Muon Collider target [8]. A schematic and a view of

* paul.jurj13@imperial.ac.uk

Content from this work may be used under the terms of the CC BY 4.0 licence (© 2026). Any distribution of this work must maintain attribution to the author(s), title of the work, publisher, and DOI.

ISBN: 978-3-95450-252-3 ISSN: 2673-5350 doi: 10.18429/JACoW-IPAC2026-MOP1106

STUDY OF THE IMPEDANCE-RELATED INSTABILITIES IN THE FCC-ee DAMPING RING*

S. Bilanishvili†[1], A. De Santis[1], M. Migliorati[2,3], C. Milardi[1], M. Zobov[1]
[1]INFN Laboratori Nazionali di Frascati, Frascati, Italy
[2]Sapienza University of Rome, Rome, Italy
[3]INFN Sezione di Roma 1, Rome, Italy

Abstract

The design of the Future Circular Collider-ee damping ring is progressing, with ongoing optimisation of beam parameters and key accelerator systems. Accordingly, the coupling impedance model is updated to reflect the latest vacuum chamber and hardware layouts. In parallel, the estimates of collective effects and impedance-related instabilities are being refined. This paper presents the current wakefield and impedance models for the FCC-ee damping ring and reports the results of the respective instability studies, including possible mitigation strategies.

INTRODUCTION

The Future Circular Collider (FCC) is an ambitious project proposed at CERN to host, in a common tunnel, both a hadron collider (FCC-hh) and an electron–positron collider (FCC-ee) [1, 2]. The FCC-ee is foreseen to operate at four main energy stages, corresponding to the Z, W, Higgs, and top-quark pair production regimes [3]. These operation modes require high beam quality and therefore place demanding requirements on the injector complex.

The FCC-ee injector complex includes a damping ring designed to reduce the transverse emittance before beam injection into the collider [4]. Since the damping-ring design is still evolving, the beam and machine parameters used in this study are those presented at FCC Week 2025 and are summarised in Table 1 [5]. This parameter set corresponds to a 2.86 GeV ring with a circumference of about 373 m, a natural bunch length of approximately 5 mm, and up to 40 stored bunches. The parameters listed in Table 1 define the reference working point used for the present beam-stability studies. In particular, they are used to evaluate the impact of wakefields and coupling impedance on single-bunch and multi-bunch collective effects [6, 7]. The impedance model of the FCC-ee damping ring is being developed together with the optimisation of the vacuum chamber and accelerator hardware. Contributions from the resistive wall and from selected vacuum chamber components are included in order to estimate their impact on the beam dynamics. In the following paragraphs the current status of the wakefield model for the FCC-ee damping ring is presented and the corresponding impedance related instabilities are analyzed.

Table 1: FCC-ee damping ring parameters used in the simulations.

Parameter	Value
Energy [GeV]	2.86
Circumference [m]	373.46
Natural emittance [nm rad] (WGL on/off)	1.3 / 2.3
Bunch length [mm]	5.1
Damping time $\tau_{x,y}$ [ms] (WGL on/off)	16.9 / 29.4
Natural chromaticity (x/y)	−38.2/ − 28.3
Natural energy spread (WGL on/off) [10^{-4}]	7.1 / 5.2
Betatron amplitude max. (x/y) [m]	9.66 / 6.49
Betatron amplitude min. (x/y) [m]	0.5 / 1.1
Tune (Q_x, Q_y)	27.8707 / 22.3728
Momentum compaction (WGL on/off) [10^{-3}]	1.55 / 1.57
Revolution period [μs]	1.2457
Max. number of stored bunches / bunch current [mA]	40 / 4
Energy loss per turn (WGL on/off) [keV]	422.2 / 246.7
SR power loss in wigglers [kW]	27.83
Bunch population, N_{part}	$3.120\,75 \times 10^{10}$
Bunch current, I_{bunch} [A]	0.003 964 02

IMPEDANCE MODEL

The impedance model of the FCC-ee damping ring includes the resistive wall of the vacuum chamber and a first set of representative vacuum hardware components. Since the damping-ring layout is still evolving, the model is based on preliminary geometries and component counts estimated from modern storage-ring examples. In particular, the number of BPMs, bellows, flange joints and vacuum transitions was evaluated by comparison with several reference machines [8–15]. The studied component designs follow low-impedance concepts already used or proposed in existing storage rings and can be adapted to the FCC-ee damping-ring vacuum system.

The longitudinal and transverse wake potentials for a 5 mm Gaussian bunch, obtained from electromagnetic simulations with CST Studio Suite, are shown in Figs. 1 and 2, respectively [16]. These wake potentials are used to compare the relative importance of the different impedance sources and to define a preliminary impedance budget.

The resistive-wall contribution was evaluated with IW2D for stainless-steel vacuum chambers coated with a 100 nm NEG layer [17–21]. This material choice is motivated by electron-cloud studies for FCC-ee damping-ring vacuum-chamber options, where NEG-coated chambers were con-

* This work was done in the framework of the ADDENDUM FCC-GOV-CC0205(KE 4907), between INFN-LNF and CERN.
† shalva.bilanishvili@lnf.infn.it

Content from this work may be used under the terms of the CC BY 4.0 licence (© 2026). Any distribution of this work must maintain attribution to the author(s), title of the work, publisher, and DOI.

ISBN: 978-3-95450-252-3 ISSN: 2673-5350 doi: 10.18429/JACoW-IPAC2026-MOP1108

FIRST RESULTS ON FAST ION INSTABILITY IN THE FCC-ee INJECTOR COMPLEX DAMPING RING

C. Bayar*, Roketsan Inc., Ankara, Türkiye
O. Etisken, Kırıkkale University, Kırıkkale, Türkiye
H. Bartosik, F. Groenvold, L. Mether, F. Zimmermann, CERN, Geneva, Switzerland
C. Milardi, INFN Laboratori Nazionali di Frascati, Frascati, Italy

Abstract

The FCC-ee injector complex design includes a dedicated damping ring (DR) to significantly reduce the transverse beam emittance of the incoming positron beam at 2.86 GeV prior to injection into the high-energy linac, where it is accelerated up to 20 GeV for the main booster ring. The DR is also foreseen for the electron beam to mitigate possible emittance growth due to alignment errors and collective effects in the electron linac. Ionization of residual gas molecules due to interactions with the circulating bunches can lead to ion trapping in the beam's potential well. These ions may accumulate over many turns and oscillate around the bunch train centroid, potentially causing fast ion instabilities (FII) and degrading beam quality in the damping ring. This study investigates the impact of FII on the two considered FCC-ee DR options: the six-fold symmetry (baseline) and the three-fold symmetry (alternative). A range of vacuum conditions, gas compositions, and bunch parameters are explored to identify the operational regimes in which fast ion instabilities may become significant. In this context, we evaluate the trapping mechanism and its impact on each lattice option based on analytical estimates and tracking simulations performed with the PyHEADTAIL code.

INTRODUCTION

The Future Circular Collider e^+e^- (FCC-ee) is a proposed high-luminosity precision frontier accelerator aimed at comprehensively investigating the Higgs, W and Z bosons, and the top quark. The FCC-ee injector complex relies on a 2.86 GeV damping ring (DR) to achieve low beam emittance prior to subsequent acceleration in the high-energy linac and the booster synchrotron to meet the stringent luminosity requirements of the collider ring [1–8]. The fast ion instability (FII) is one of the effects that must be evaluated before finalizing the DR design. The interaction of the dense circulating electron beam with residual gas molecules such as H_2, He, CH_4, N_2, CO, O_2, and CO_2 leads to collisional ionization in low-emittance rings. The resulting positively charged ions are attracted towards the center of the beam by the electromagnetic fields of the electron bunches and can become trapped in the potential well of the beam. As the bunch train passes, these trapped ions accumulate turn-by-turn, forming an increasingly dense ion cloud. The coupled interaction between the ion cloud and the subsequent bunches in the train can induce instabilities [9–11]. A detailed analysis of the specific lattice design is needed to understand the dynamics of ion accumulation, as variations in optical functions, beam sizes, and magnetic fields along the ring strongly influence the ion trapping conditions. Accurate estimates of the critical mass, instability rise times, the resulting beam offset and emittance evolution are necessary to define the design specifications for the vacuum and feedback systems. Ionization cross section (σ_{ion}) is one of the crucial parameters required for the analytical estimates and simulations. Thus, these cross sections for common ions that can be present in the vacuum pipe for the working energy of DR are calculated based on Bethe theory by using the following expression [12, 13]:

$$\sigma = 4\pi Z^2 \left(\frac{\hbar}{mc}\right)^2 \frac{1}{\beta^2}(M^2 x + C). \quad (1)$$

where M^2 and C are experimental constants depending on the gas species, $x = 2\ln(\gamma) - \beta^2$, c is the speed of light, m is the mass of the electron. The calculated values for several ions together with their mass numbers (A) are listed in Table 1.

Table 1: Ionization cross sections at 2.86 GeV

Gas species	Mass number (A)	σ_{ion} [Mbarn]
H_2	2	0.436
He	4	0.445
CH_4	16	3.109
N_2	28	2.688
CO	28	2.678
O_2	32	3.011
CO_2	44	4.199

ION EFFECT CALCULATIONS

Beam Parameters

The purpose of the DR design is to accept the 2.86 GeV positron beam from the positron linac, damp the beam emittance, and provide the required beam parameters for injection into the high-energy linac where both positron and electron beams are accelerated up to 20 GeV. The DR is primarily required to reduce the geometrical emittance of the incoming positron beam from 2.36×10^{-6} m·rad to about 1.8×10^{-9} m·rad. In addition, the DR is also foreseen for electron beam emittance cooling to mitigate possible growth due to alignment errors and collective effects in the electron linac. Two alternative DR designs are considered: six-fold

* cafer.bayar@roketsan.com.tr

Content from this work may be used under the terms of the CC BY 4.0 licence (© 2026). Any distribution of this work must maintain attribution to the author(s), title of the work, publisher, and DOI.

ISBN: 978-3-95450-252-3 ISSN: 2673-5350 doi: 10.18429/JACoW-IPAC2026-MOP1109

FIRST OBSERVATION OF CONTROLLED BEAM-HALO POPULATION AND CLEANING AT THE LHC BY AN AC DIPOLE

D. Veres*, D. Butti, F. Capoani, J. Dilly, M. Giovannozzi, S. Kostoglou, B. Lindstrom, E. Maclean, D. Valuch, European Organization for Nuclear Research, Geneva, Switzerland
G. Franchetti, GSI Helmholtz Centre for Heavy Ion Research, Darmstadt, Germany

Abstract

Experimental observations indicate that a significant fraction of the stored beam energy in the CERN Large Hadron Collider (LHC) is contained in the transverse beam halo. Combined with the anticipated increase in beam brightness in the High-Luminosity LHC (HL-LHC) and new expected fast failure scenarios resulting in a loss of large-amplitude particles, an overpopulated beam halo poses risk to the safe operation of the machine. Following removal from the HL-LHC baseline of the Hollow Electron Lens, which was studied as the preferred method for active halo control, alternative halo-cleaning methods need to be investigated. A novel method being explored is the use of an AC multipole operated in resonance with the betatron tune to create a stable island in phase space in which halo particles are adiabatically trapped and transported to the collimators in a controlled manner. This paper presents the results of the first successful proof-of-principle measurement of both controlled beam-halo population and cleaning using an AC dipole at the LHC.

INTRODUCTION

Non-linear beam manipulations, including the CERN Proton Synchrotron Multi-Turn Extraction (MTE) [1–6], have emerged as promising means of novel beam manipulations. Recently, exciter devices have been considered [7] and have found promising applications, among others, as beam-halo cleaners [8].

In June 2025, an eight-hour proof-of-principle test of halo cleaning with stable islands at the LHC [9] was performed. The transverse feedback (ADT) was used for the custom AC dipolar excitation during the measurement. The study was carried out at the injection energy of 450 GeV, which allowed efficient re-injection of bunches when needed and scanning parameters. Ten low-intensity bunches with approximately 4.5×10^{10} protons per bunch were injected each time, with a normalised beam emittance of 2 µm in both planes, and only Beam 1 (clockwise beam) was used.

EXCITATION PROTOCOLS

Several excitation protocols were tested: the bunches were first blown up using the ADT to create different normalised emittance bunches in the 2 µm to 4.5 µm range; halo cleaning was applied directly after the bunches were injected relying on the natural population of the tails; the excitation was adapted to populate the tails first before cleaning. Finding the optimal excitation protocol took longer than expected, resulting in insufficient time to perform a chromaticity scan, and therefore measurements were only performed at $Q'_x = Q'_y = 3$.

Furthermore, measurements were hindered by the observation that despite the excellent correction of the linear coupling ($|c_-| = 0.001$), the excitation applied in the horizontal plane was strongly felt by the vertical plane as well, and vice versa, as evidenced by a very clear peak observed in the tune spectrum measured by the Band-Based Tune (BBQ) pickup. Hence, it was decided to proceed with only vertical excitations that left the horizontal plane undisturbed because of the lower fractional tune in the horizontal plane ($Q_x = 62.28$, $Q_y = 60.30$ at injection into the LHC).

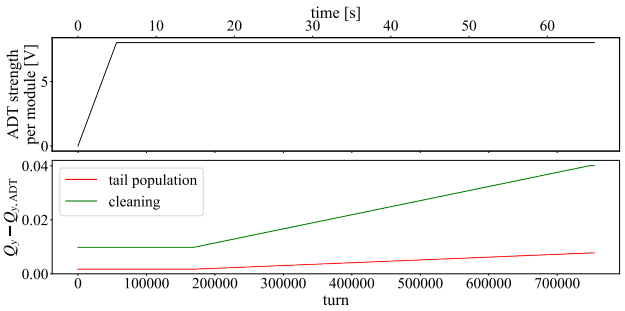

Figure 1: Excitation protocol used during the measurement.

Halo cleaning could be best observed when the tails were intentionally populated first. Hence, the same excitation protocol was applied as for cleaning, but the starting and end frequencies were adjusted to be much closer to the vertical tune. This resulted in the trapping of a significant number of particles in the beam core (approximately 15%) that were then displaced to larger amplitudes (still below that of the collimators) to form the halo. The excitation protocols applied during the population and the cleaning of the tail are shown in Fig. 1. To measure the tail population, a single excitation, as shown in Fig. 1, was sufficient, whereas effectively depleting the halo required applying this function at least five times in succession.

DATA ANALYSIS AND RESULTS

The transverse beam profile was recorded using both the Wire Scanners (WS) and the Beam Synchrotron Radiation Telescope (BSRT), which uses synchrotron light emitted by the protons. Due to the invasive nature of wire scans, they cannot be performed continuously, but the BSRT records and logs the beam profile approximately every second. However, the BSRT has a finite line-spread function that limits the resolution as well as the signal-to-noise ratio. Therefore,

* dora.erzsebet.veres@cern.ch

Content from this work may be used under the terms of the CC BY 4.0 licence (© 2026). Any distribution of this work must maintain attribution to the author(s), title of the work, publisher, and DOI.

ISBN: 978-3-95450-252-3 ISSN: 2673-5350 doi: 10.18429/JACoW-IPAC2026-MOP1110

LINEAR IMPERFECTION AND ORBIT CORRECTION SCHEME FOR THE PERLE ACCELERATOR *

R. Abukeshek[1†], H. Abualrob[2], A. Fomin[1], W. Kaabi[1], J. Michaud[1], L. Perrot[1], A. Stocchi[1]
[1] Université Paris-Saclay, CNRS/IN2P3, IJCLab, Orsay, 91405, France
[2] An-Najah National University, Nablus, Palestinian Territories
On behalf of the PERLE collaboration[‡]

Abstract

PERLE is a multi-turn Energy Recovery LINAC, currently under construction at IJCLab in Orsay (France). It is designed to accelerate electrons of 20 mA beam current to an energy of 250 MeV through three accelerating passes followed by three decelerating passes to dump the beam at injection energy (7 MeV). The first order lattice design has emerged. Therefore, assessing the sensitivity of the optics to linear imperfections is a crucial step toward stable operation. This work investigates the impact of quadrupole misalignments on the beam orbit in both planes, accounting for the presence of horizontal and vertical dispersive sections in PERLE. The resulting orbit distortions are used to identify the most critical locations for diagnostics and correction elements. A correction strategy based on BPM–corrector pairs is implemented using the BMAD framework, and the achievable orbit restoration is evaluated with adequate correction strengths.

INTRODUCTION

Energy Recovery Linacs (ERLs) impose stringent requirements on beam stability, as the beam should be efficiently transported and decelerated to recover its energy. In such machines, even small trajectory deviations can degrade the energy recovery efficiency and potentially lead to beam losses.

PERLE [1] is a multi-turn high-current ERL, in which the same beam is transported through multiple accelerating and decelerating passes. This multi-pass configuration increases the sensitivity to lattice imperfections, as their effects accumulate over successive turns.

In this work [2], the impact of quadrupole misalignments on the PERLE single-turn lattice is investigated using BMAD [3] simulations. The resulting orbit distortions are analyzed to identify optimal locations for beam position monitors (BPMs) and corrector magnets. An orbit correction scheme is then implemented, and its performance is evaluated in terms of orbit and optics restoration.

* This work received government funding managed by the Agence Nationale de la Recheche (ANR) in the France 2030 framework - reference ANR-24-RRII-0001
Work supported by funding from European Union's program EU HORIZON-INFRA-2023-TECH-01-01 under GA n°101131435
† rasha.abukeshek@ijclab.in2p3.fr
‡ https://perle-web.ijclab.in2p3.fr/instituts/

ORBIT DISTORTION FROM QUADRUPOLE MISALIGNMENTS

In linear beam optics, a transverse displacement of a quadrupole magnet introduces an effective dipole component, resulting in a localized kick to the beam trajectory. For a quadrupole of normalized strength $k_1 = G/(B\rho)$ and magnetic length L, a transverse offset Δx generates an angular deviation given by

$$\Delta x' = k_1 \, \Delta x \cdot L. \tag{1}$$

This kick propagates along the lattice according to the linear transport, leading to orbit distortions whose amplitude scales with the lattice β-function. As a result, regions of high β are particularly sensitive to misalignments.

IMPACT OF QUADRUPOLE MISALIGNMENTS ON PERLE OPTICS

Figure 1 shows the nominal optics of the first turn [4]. The lattice is designed to be achromatic, with vanishing dispersion at the entrance and exit of each section [5, 6].

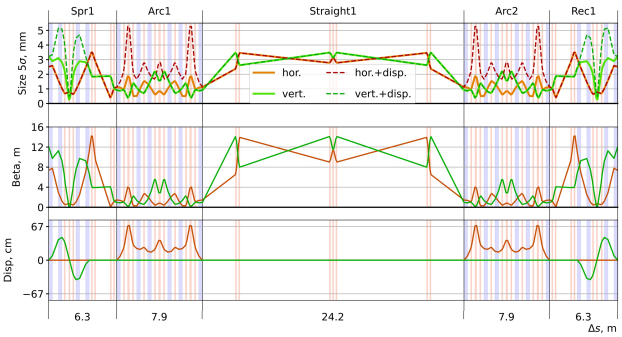

Figure 1: The 5σ beam size, the horizontal and vertical beta functions (β_x, β_y) and dispersion (D_x, D_y) along the first-turn lattice. Quadrupoles are indicated in red, while dipoles are marked in blue.

Random transverse offsets are assigned to all quadrupoles. The offsets are drawn from a Gaussian distribution with zero mean and a standard deviation of $\sigma = 0.1$ mm, consistent with typical installation tolerances. For each configuration, the transverse orbit, dispersion, and optics functions are computed and compared to the nominal design in order to quantify the effect of misalignments.

Orbit Distortion

Figure 2 shows the particle orbit along the PERLE first-turn lattice with random quadrupole transverse misalign-

Content from this work may be used under the terms of the CC BY 4.0 licence (© 2026). Any distribution of this work must maintain attribution to the author(s), title of the work, publisher, and DOI.

ISBN: 978-3-95450-252-3 ISSN: 2673-5350 doi: 10.18429/JACoW-IPAC2026-MOP1111

MEASURED AND SIMULATED CHANNELED-HALO DISTRIBUTIONS FOR THE TWOCRYST EXPERIMENT AT THE LHC

C. Maccani* on behalf of the TWOCRYST collaboration,
CERN, Geneva, Switzerland and University of Padova, Italy

Abstract

The TWOCRYST experiment at the CERN Large Hadron Collider provides a unique setup to study the behaviour of high-energy beam particles channelled by bent crystals. Two two-dimensional detectors in Roman Pots enable direct observation of channelled protons at energies from 0.45 TeV to 6.8 TeV. We present measured channelled-beam distributions for two bent silicon crystals with 50 µrad and 7000 µrad bending and compare them to combined beam-dynamics and particle–crystal interaction simulations including the full LHC lattice. The measured positions of the channelled beam is compared with beam-position-monitor data of the main beam to assess the sensitivity of the channelled-beam trajectory to realistic orbit drifts, providing key input for the requirements of future bent-crystal-based fixed-target experiments.

INTRODUCTION

The TWOCRYST experiment [1, 2] was installed at the Large Hadron Collider (LHC) [3] in 2025 to demonstrate the feasibility of spin-precession fixed-target experiments within CERN's Physics Beyond Colliders initiative [4]. The ultimate physics goal of such experiments is the first direct measurement of the electromagnetic dipole moments of short-lived charm baryons by exploiting the channeling phenomenon of positively charged particles in bent crystals [5] — an idea first proposed for the LHC in 2016 [6, 7] and since developed into a concrete experimental design that could be implemented in the HL-LHC era [8].

In a bent crystal, the intense electric fields between atomic planes act on a relativistic particle as an effective magnetic field orders of magnitude stronger than conventional magnets, simultaneously deflecting the trajectory and inducing a measurable spin precession before decay [9].

TWOCRYST is designed as a proof-of-principle test of this experimental concept — first demonstrated by the E761 collaboration at the Tevatron in 1992 [10] — applied to the new LHC setup. Initially considered for integration in the LHCb experiment [6], the focus shifted to a dedicated setup in the LHC collimation insertion IR3 [11] for improved performance. Installed on LHC Beam 2, the experiment consists of two silicon crystals bent in the vertical plane [12], a tungsten fixed-target, and two tracking detectors housed in Roman Pots [13] (RP). All devices can be independently moved, allowing for a broad variety of test conditions.

The first crystal — the Target Collimator Crystal for Splitting (TCCS) — deflects particles by 50 µrad. 120 m downstream of the TCCS, the target and the 7 mrad precession crystal (TCCP) are installed, followed by two Roman Pots that house the two different detectors: a silicon pixel detector [14] and the TWOCRYST Fiber Tracker (TFT) [15]. A downstream vertical collimator (TCLA) absorbs the channeled halo. Figure 1 shows the experiment layouts and illustrates the propagation of a channeled beamlet from its source at the TCCS to its absorption in the TCLA.

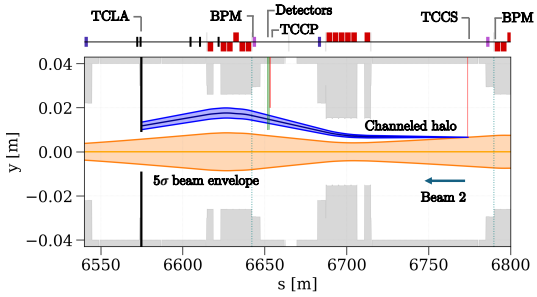

Figure 1: Vertical dynamics of the TWOCRYST setup at 450 GeV for channeling measurements as a function of the longitudinal position s. The 5σ main beam envelope is shown in orange, and channeled particles are shown in blue. Vertical dashed lines indicate the two Beam Position Monitors (BPMs) closest to the setup.

Beyond its role in validating the fixed-target physics concept, the two-dimensional imaging in TWOCRYST offers unprecedented insight into channeling physics and multi-turn beam dynamics. This work presents a comparison between measurements and simulations to characterize the channeling profiles at the LHC energy and study their multi-turn dynamics.

MEASURED BEAMLET PROFILE

Four measurements of the channeled halo profile from the TCCS were recorded across three separate sessions in 2025 (June 21, 22, and October 9) at injection energy of 450 GeV. The TCCS was aligned to the $5\sigma_y$ main envelope, where σ denotes the RMS beam size assuming a normalized emittance of 3.5 µm rad. The four sets of 2-dimensional hit distributions at the pixel detector are displayed in Figure 2. Except for the second measurement, the data was collected while utilizing the LHC Transverse Damper [16] (ADT) to induce white noise and excite the beam in the vertical plane.

The outgoing angular distribution of particles channeled by a crystal is determined by its critical angle, which for a crystal with the specifications of the TCCS at 450 GeV is $\theta_c = 9.12$ µrad. In Figure 1, this is represented by the blue envelope: the central line represents the trajectory of a particle that has received a kick of $\theta_{\text{bend}} = 50$ µrad from the TCCS, while the upper and lower lines correspond to

* chiara.maccani@cern.ch

Content from this work may be used under the terms of the CC BY 4.0 licence (© 2026). Any distribution of this work must maintain attribution to the author(s), title of the work, publisher, and DOI.

ISBN: 978-3-95450-252-3 ISSN: 2673-5350 doi: 10.18429/JACoW-IPAC2026-MOP1114

BEAM TRANSFER CONCEPT AT THE FCC-EE INJECTOR COMPLEX

Y. Dutheil*, S. Yue, European Organization for Nuclear Research, Geneva, Switzerland

Abstract

The FCC-ee collider complex relies on continuous top-up injection to maintain the bunch charge and luminosity required for its physics goals. The injector complex must generate and accelerate electron and positron beams up to 20 GeV, while a damping ring is foreseen to reach the emittance required by the high-energy booster.

This contribution presents a first concept for the damping-ring injection and extraction systems, including the layout, optics design, and main hardware constraints. A possible implementation of the newly introduced polariser ring and its associated beam-transfer scheme is also outlined. The beam dynamics and operational constraints of these transfer systems are discussed, together with the next steps towards a baseline layout for the injector complex.

INTRODUCTION

The present FCC-ee injector concept uses a linac-based chain to deliver the intensity and emittance needed for top-up operation. In the current baseline, the complex produces electron and positron beams at up to 100 Hz, with four bunches per RF pulse and 25 ns spacing, and accelerates them to 20 GeV before transfer to the booster [1]. Recent studies also consider a polariser ring [2], which may affect the transfer layout discussed below. Other options, such as an SRF linac [3] or different bunch spacing [4], are still being discussed and are therefore not addressed in the present contribution.

The injector complex is located at the edge of the CERN Prévessin site. This location offers favourable topography, available space, and good availability of services for the planned technical infrastructure [5]. As shown in Fig. 1, the complex includes several linacs and transfer lines.

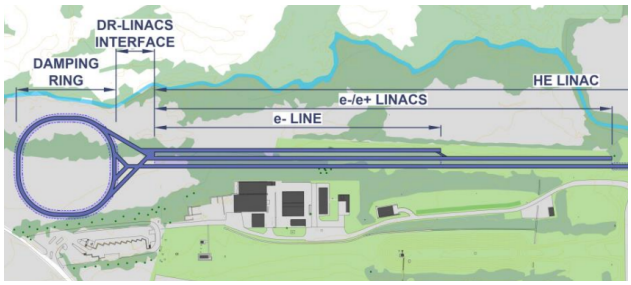

Figure 1: Layout of FCC-ee injector-complex baseline option [5].

In the current concept, an electron source on the right-hand side of Fig. 1 produces bunches of up to about 5 nC, which are accelerated to 2.86 GeV by the electron linac. Electrons are then transported through the electron line to the damping ring. Positrons are produced from the 2.86 GeV electron beam upstream of that line, captured at 185 MeV, and re-accelerated in the positron linac before being sent to the damping ring. This brings both species to the damping-ring–linac interface region shown in Fig. 1.

This interface region is one of the most constrained parts of the injector layout. It must combine injection and extraction, transport of both electrons and positrons, and beam transfer to and from the damping ring within the same compact area. It must also accommodate equipment such as kickers and septa while remaining compatible with a polariser ring. The symbolic layout in Fig. 2 shows a non exhaustive list of the possible beam transfer in the region. The exact role of the polariser ring remains to be established as it may not only polarise positrons but could also be used as pre-damping ring, which would constrain further the region.

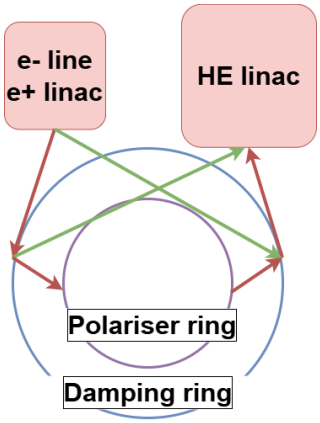

Figure 2: Schematic representation of the interface region, with an arbitrary placement of a polariser ring inside a damping ring. Electron beam lines are shown in green and positron beam lines in red.

DAMPING RING BEAM TRANSFER

The initial concept for the beam-transfer system was established for an earlier 1.54 GeV damping-ring design [6], whereas the present concept operates at 2.86 GeV. The longitudinal beam structure remained unchanged: the injection and extraction schemes still require rise and fall times within 82.5 ns, with a short flat-top of 80 ns. That first concept relied on terminated stripline kickers providing a deflection of about 1.5 mrad over a length of 0.3 m.

Since then, the damping-ring design has evolved with the change in beam energy and with several lattice studies. No final lattice was available at the time of this contribution, so we consider the latest design, which uses a hexagonal layout fitting within the footprint discussed earlier [7]. This design features a long insertion straight section with a 2 m drift available for injection devices. The FODO structure uses realistic quadrupole lengths of 0.3 m, separated by drifts between 0.3 m and 0.8 m.

* ydutheil@cern.ch

Content from this work may be used under the terms of the CC BY 4.0 licence (© 2026). Any distribution of this work must maintain attribution to the author(s), title of the work, publisher, and DOI.

ISBN: 978-3-95450-252-3 ISSN: 2673-5350 doi: 10.18429/JACoW-IPAC2026-MOP1116

DESIGN AND MANUFACTURING OF THE NEXT GENERATION OF CERN'S NORTH AREA SPLITTER COLLIMATORS (TCSC)

J. Braken*, J.L. Grenard†, N. Solieri‡, P.R. Menachilis, A. Romero Francia, M. Timmins, P. Schneider, T. Coiffet, G. Mazzola, D. Wasik, L.S. Esposito, D. Grenier, B. Pittet, M. Fraser, A. Gorn, I. Prieto Rivero, T. Parmentier, A. Perillo Marcone, M. Calviani
CERN, Geneva, Switzerland

Abstract

CERN's Transfer Tunnel 20 (TT20) connects the Super Proton Synchrotron (SPS) to three primary targets in the North Area which provide secondary particles to experiments further downstream. Two splitter collimators (TCSC) are installed along this line, each protecting their respective downstream Lambertson septum magnets, which distribute the slow-extracted 400 GeV/c proton beams among the targets. During Long Shutdown 3 (LS3, 2026–2029), two redesigned TCSCs will be installed to improve cooling efficiency, mechanical robustness, and maintainability in the context of the North Area Consolidation (NA CONS) project. The new design also incorporates additional radiation shielding to reduce dose rates in the surrounding area and minimise personnel exposure during tunnel interventions. This contribution presents the main design improvements, thermo-mechanical analyses, and manufacturing developments implemented to enhance the reliability, radiation safety, and thermal performance of the TT20 splitter collimators.

INTRODUCTION

CERN's North Area beamlines use slow extraction from the Super Proton Synchrotron (SPS) to deliver 400 GeV/c proton beams to multiple targets, providing secondary beams for downstream experiments [1]. Two sets of Lamberton septum magnets (MSSB) split the vertically blown up beam over the branched primary beam lines. A TCSC (Target Collimator Splitter version C) installed upstream of each MSSB, intercepts part of the beam to protect the septum from direct beam impact [2]. Each currently installed TCSC consists of two CuCr1Zr absorber blocks enclosed in a vacuum tank. When clamped together, the absorber blocks form two internal beam apertures that replicate the shape of the splitter magnet yoke located downstream. The separation between both TCSC apertures is formed by a pair of symmetrical wedges, which absorb the portion of the beam that would otherwise strike the MSSB septum, see Fig.1. The energy deposited by this intercepted beam fraction is converted into heat within the TCSC core. The absorber blocks are water-cooled to dissipate heat caused by the absorbed beam energy.

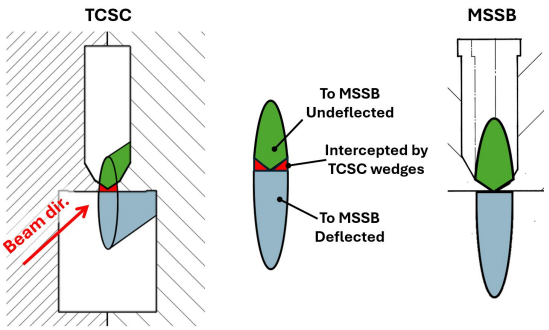

Figure 1: Left: Diagram of beam position with respect to the TCSC cross section. Right: Diagram of nominal beam position with respect to the MSSB septum.

History

The first pair of TCSCs was built and installed in the late 1970s during the construction of the North Area. Since their installation, one of the devices has been subject to significant corrosion because of a corrosive liquid leak onto its vacuum tank, leading to its replacement by a spare device. As a result of high radiation levels generated by beam impact onto the absorber coupled with its unshielded vacuum tank, water connections have aged and failed during the operation of these devices, leading to high radiation doses received by personnel during replacement interventions.

DESIGN IMPROVEMENTS

Two redesigned TCSCs will be installed during Long Shutdown 3 (2026–2029) [3]. Their design aims to improve the device robustness and reliability while limiting potential downtime and minimising radiation dose to personnel during interventions. The upgraded CuCr1Zr core retains the initial design idea, consisting of two water-cooled absorber blocks that are bolted together, each maintaining their wedge profile capable of intercepting a portion of the high energy beam, see Fig.2.

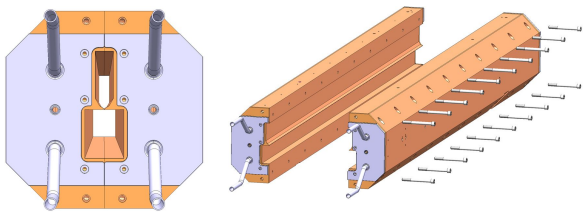

Figure 2: Left: Front view of the TCSC core assembly. Right: The two water-cooled CuCr1Zr blocks are bolted together to form the TCSC core.

* Jules.Johannes.Braken@cern.ch
† Jean-Louis.Grenard@cern.ch
‡ Nicola.Solieri@cern.ch

Content from this work may be used under the terms of the CC BY 4.0 licence (© 2026). Any distribution of this work must maintain attribution to the author(s), title of the work, publisher, and DOI.

ISBN: 978-3-95450-252-3 ISSN: 2673-5350 doi: 10.18429/JACoW-IPAC2026-MOP1117

CURRENT STATUS AND RECENT DEVELOPMENT OF THE XCOLL-FLUKA INTERFACE

A. Donadon Servelle*, R. Bruce, F. Cerutti, G. Hugo, B. Lindström, S. Redaelli, L.S. Esposito, F. Van der Veken, V. Vlachoudis, CERN, Geneva, Switzerland

Abstract

The Xsuite framework offers a modern environment for high-performance accelerator physics simulations. Its Xcoll module handles particle-collimator interactions using dedicated scattering routines, both built-in and external. FLUKA, a well-established Monte Carlo code, can be linked to Xcoll, enabling detailed modelling of particle-matter interactions and support for complex geometries. This paper presents the status of the Xcoll-FLUKA interface, which provides a consistent and efficient link between deterministic beam tracking and Monte Carlo simulations. The new setup builds upon the experience gained with the previous SixTrack-FLUKA coupling, introducing a more user-friendly design and significant improvements in data exchange, modularity, and extensibility within the Xsuite architecture. Recent developments include a new filtering algorithm with memory optimisation that improves simulation speed, a versatile definition of bent crystals, support for simplified collimator geometries represented as plain blocks of material, and an enhanced beam-beam interaction routine. These advancements represent an important step toward a flexible and performant framework for collimation and background studies in present and future accelerators.

INTRODUCTION

Simulations of beam collimation processes are regularly performed in accelerator complexes to assess cleaning performance and minimise particle losses around the ring. These simulations combine accelerator physics for element-by-element symplectic tracking of high-energy particles through a lattice, and particle-matter interactions at collimators.

Historically, Sixtrack [1] with its internal K2 scattering routine [2] served as the reference tracking code [3]. Since 2010 [4], Sixtrack could be coupled to the Monte Carlo code FLUKA [5–7], enabling more accurate results and support for ion beams, which K2 did not support. Sixtrack is being phase out and replaced by Xtrack. This is one of the various packages included in the Xsuite [8, 9] ecosystem, a modern collection of Python packages for beam dynamics simulations. Among these packages, Xcoll [10] handles particle-collimator interactions via its native engine *Everest* [11], the successor of K2, or through the interface with external codes like aforementioned FLUKA and Geant4 [12–14] via BDSIM [15].

This paper announces the public release of the Xcoll-FLUKA interface, to summarise its current status and the most relevant developments available.

* andre.donadon.servelle@cern.ch

SIMULATION WORKFLOW

Using the Xcoll-FLUKA interface requires a sequence of setup and runtime steps that are largely shared between the Sixtrack and Xsuite codes. The workflow proceeds as follows:

- Insert extraction/insertion markers (defined as `FlukaCollimator/FlukaCrystal` elements) into the lattice.
- Generate the FLUKA input file using *FLUKABuilder*, a sub-branch of Linebuilder code (see next section). This file defines, among other simulation features, the detailed geometry of all collimators included in the simulation.
- Launch `flukaserver` and initialise the TCP/IP network through `FLUKAIO` [16].
- During Xtrack tracking, whenever a particle reaches a collimator marker, Xcoll redirects the particles to FLUKA for interaction with matter (Fig. 1).
- Surviving particles, including energy losses and scattering products, are returned to Xsuite.
- Tracking continues until the target number of turns is reached or all particles are lost.

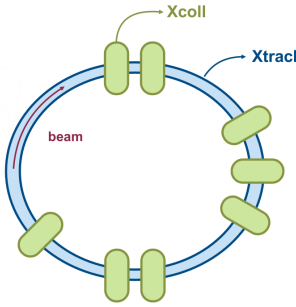

Figure 1: Schematic of Xtrack and Xcoll domains during particle tracking.

While these steps are conceptually equivalent between the two codes, Xcoll introduces a key architectural improvement: the `FlukaEngine` class encapsulates and automates the entire workflow. It launches both FLUKA and the `flukaserver` as background processes from within Xcoll, and interfaces Xsuite tracking with `FLUKAIO` through a lightweight Fortran wrapper. This design eliminates the manual, multi-step setup previously required from users and reduces the risk of configuration errors.

FLUKA INPUT GENERATION

A central task of the Xcoll-FLUKA interface is the automated generation of the FLUKA input file. The

Content from this work may be used under the terms of the CC BY 4.0 licence (© 2026). Any distribution of this work must maintain attribution to the author(s), title of the work, publisher, and DOI.

ISBN: 978-3-95450-252-3 ISSN: 2673-5350 doi: 10.18429/JACoW-IPAC2026-MOP1119

PREPARATIONS FOR THE EXECUTION PHASE OF BDF/SHIP AT THE HI-ECN3 FACILITY IN CERN'S NORTH AREA

I. Angulo*, F. Pedrosa†, M. Fraser‡ European Organization for Nuclear Research, Geneva, Switzerland

Abstract

The High-Intensity ECN3 (HI-ECN3) Project [1] will upgrade the ECN3 underground experimental area in CERN's North Area (NA) [2], to host the Beam Dump Facility (BDF) [3, 4] and the Search for Hidden Particles (SHiP) experiment [5–8]. The required refurbishment of underground infrastructure and associated surface facilities is scheduled for Long Shutdown 3 (LS3) [9], while installation of BDF and SHiP is foreseen in 2030 and beam commissioning of the BDF is planned in 2031 [10]. HI-ECN3 must share specialised resources during LS3 with other activities in the SPS [11] and the NA, without having priority over them. This makes the coordination and scheduling of limited resources a challenge, particularly during LS3 when the workload will be at its maximum. To reduce these risks, a set of preparatory measures have been implemented ahead of LS3. This contribution details the key preparatory activities and efforts to smooth the demand on resources during LS3 and enhance the readiness of the ECN3 facility for the subsequent installation phase.

INTRODUCTION

The HI-ECN3 project aims to upgrade CERN's NA for the Beam Dump Facility (BDF) and SHiP experiment by dismantling the NA62 experiment during LS3. This paper presents the preparation strategy to execute this phase under resource, radiological, and logistical constraints, using a procedure-driven, resource-aware planning approach based on Work Package Analyses (WPAs) [12, 13] applied to LS3 Baseline 0 [14]. The results demonstrate early identification of critical operations, resource conflicts, and execution constraints, enabling a realistic dismantling sequence and improved readiness for the installation phases.

HI-ECN3 FACILITY AND INFRASTRUCTURE UPGRADE

To enable the installation of the Beam Dump Facility (BDF) and the SHiP experiment, the ECN3 and TCC8 facilities, located at the end of the P42 beamline in the North Area (Fig. 1), [15], must undergo substantial infrastructure modifications. The North Area is the largest experimental area and extracts its beam from the SPS complex [16, 17].

These modifications include the dismantling of the current experimental setup (Fig. 2a), the installation of the SHiP configuration (Fig. 2b), upgrades to beam transport systems, radiation shielding, machine protection, and cavern layout.

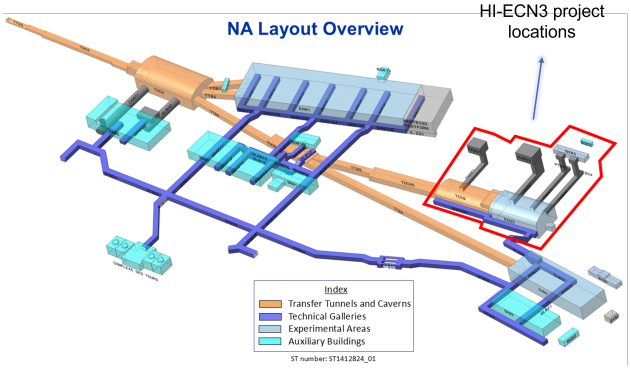

Figure 1: TCC8 and ECN3 location in CERN's North Area

In addition to underground works, significant surface infrastructure modifications are required. A new service building will be constructed next to building 911 to host systems supporting the BDF target complex [18], including cooling, electrical distribution and control systems. The design also foresees provisions for remote handling and dismantling of activated components, driven by the expected high-radiation environment.

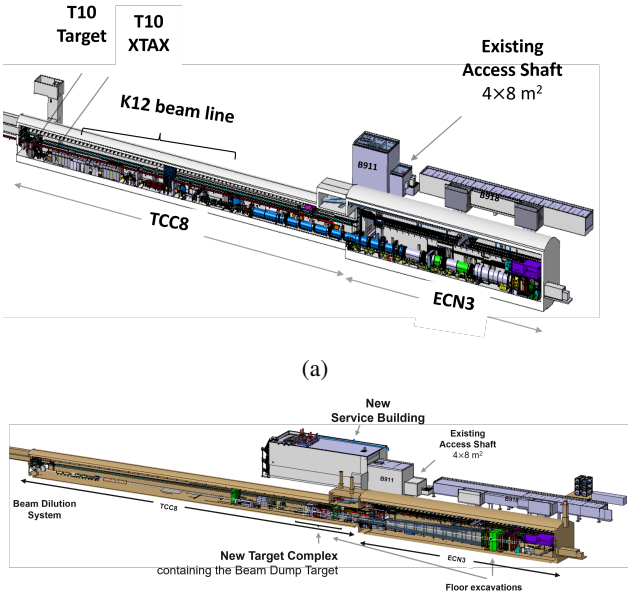

Figure 2: TCC8 and ECN3 cavern integration: (a) current configuration, (b) configuration after the installation of the BDF and SHiP experiment

* ixone.angulo.vaquero@cern.ch
† fernando.pedrosa@cern.ch
‡ matthew.fraser@cern.ch

Content from this work may be used under the terms of the CC BY 4.0 licence (© 2026). Any distribution of this work must maintain attribution to the author(s), title of the work, publisher, and DOI.

ISBN: 978-3-95450-252-3 ISSN: 2673-5350 doi: 10.18429/JACoW-IPAC2026-MOP1301

RCS POLARIZATION CORRECTION USING INFORMATION THEORETIC AND MACHINE LEARNING TOOLS

V. Ranjbar*, W. Bergan, V. Schoefer,
M. Signorelli, E. Gianfelice-Wendt, Brookhaven National Laboratory, Upton, United States

Abstract

One of the main challenges for the EIC Rapid Cycling Synchrotron is to maintain high polarization transmission during acceleration to 18 GeV. While SVD-based orbit smoothing is sufficient below 10 GeV, the stronger residual imperfection spin resonances at higher energy make performance increasingly sensitive to vertical quadrupole misalignments and dipole rolls. A promising approach is therefore to infer the underlying magnet errors from BPM-based orbit-response measurements and use those fitted errors in the resonance-correction workflow. Here we present a direct lattice-fitting method based on simultaneous K_1 dithering and backpropagation through the full accelerator model. In idealized synthetic studies without BPM noise, the method recovers quadrupole offsets and dipole rolls at essentially the numerical precision limit of the model. These results establish a best-case baseline for future studies that will incorporate BPM noise, finite resolution, and Fisher-information-guided optics perturbations to improve conditioning in more realistic scenarios.

INTRODUCTION

High polarization transmission in the EIC Rapid Cycling Synchrotron (RCS) requires control of the imperfection spin resonances driven by vertical closed-orbit errors. Previous tracking studies showed that standard SVD orbit correction is sufficient to maintain more than 99% transmission up to 10 GeV, but that acceleration to 18 GeV becomes sensitive to vertical quadrupole offsets at the 100 µm scale and to dipole rolls at the 100 µrad scale. In that regime, estimating the underlying magnet errors and correcting the corresponding resonance harmonics is more effective than orbit smoothing alone.

The natural starting point is beam-based alignment (BBA), in which small quadrupole-strength variations are used to infer magnetic center offsets from BPM data [1, 2]. For the RCS, the measured vertical orbit can be written as

$$\mathbf{y}_{\mathrm{orb}} = \mathbf{M}_{rQm}\,\mathbf{q}_{\mathrm{mis}}, \tag{1}$$

where $\mathbf{M}_{rQm}$ is the orbit response matrix and $\mathbf{q}_{\mathrm{mis}}$ is the vector of vertical quadrupole misalignments. Once these offsets are estimated, the corresponding imperfection resonance strengths can be computed with DEPOL [3] and reduced with vertical correctors through a second response matrix,

$$\mathbf{w}_{\mathrm{imp}} = \mathbf{M}_{rCW}\,\mathbf{c}. \tag{2}$$

Figure 1 shows that this approach already gives a useful reconstruction of the quadrupole offsets and supports high-transmission correction in synthetic RCS error ensembles.

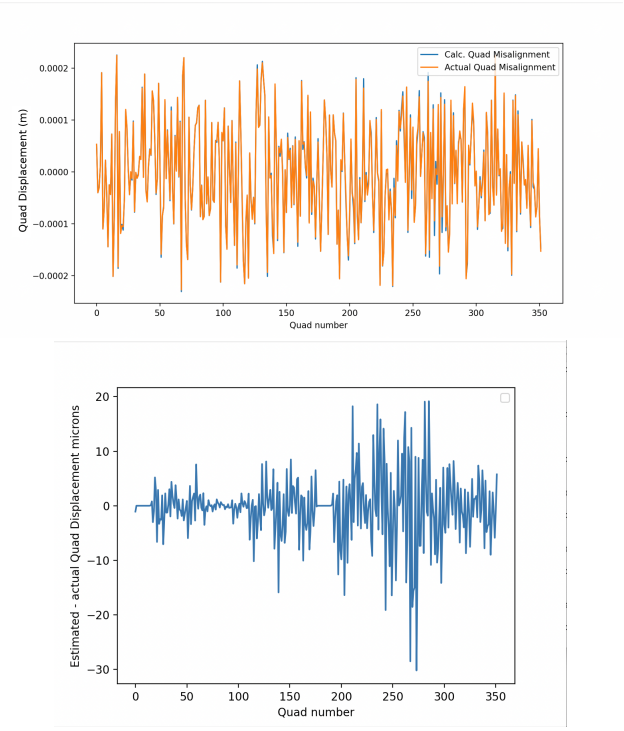

Figure 1: Quadrupole-misalignment reconstruction from a vertical orbit response fit in a misaligned and rolled RCS lattice. Top: fitted and true offsets for a 100 µm RMS quadrupole misalignment ensemble. Bottom: residual difference between the true and reconstructed misalignments.

However, the inversion is not unique: dipole rolls create orbit signatures that can closely resemble those produced by quadrupole vertical offsets. This is closely related issues in BBA [1,2] which is widely used to find the bpm measurement offset with respect to the quadrupole's magnetic center. It is also similar to problems facing LOCO-style optics fits [2], where an orbit response matrix is used to help fit optics and errors.

The problem can be understood as a tomographic reconstruction of the error sources. Each optics configuration produces a different set of response-matrix columns, or "views," of the same underlying misalignments. The goal is to choose optics perturbations that make those views as independent as possible. For a stack of response matrices $\hat{\mathbf{J}}$, this can be quantified by the weighted Fisher matrix

$$\mathbf{F} = \hat{\mathbf{J}}^{T-1}\hat{\mathbf{J}}, \tag{3}$$

* vranjbar@bnl.gov

Content from this work may be used under the terms of the CC BY 4.0 licence (© 2026). Any distribution of this work must maintain attribution to the author(s), title of the work, publisher, and DOI.

ISBN: 978-3-95450-252-3 ISSN: 2673-5350 doi: 10.18429/JACoW-IPAC2026-MOP1302

STATUS OF THE RAPID CYCLING SYNCHROTRON OPTICS*

W. Bergan†[1], B. Bhandari[1], M. Blaskiewicz[1], A. Blednykh[1], E. Gianfelice-Wendt[1], Y. Li[1], C. Montag[1], S. Nagaitsev[1], V. Ranjbar[1], V. Schoefer[1], K. Smith‡[1], Q. Wu[1], K. Deitrick[2], B. R. Gamage[2], I. Neththikumara[2], T. Satogata[2], N. Sereno[2], S. Setiniyaz[2]
[1]Brookhaven National Laboratory, Upton, NY, United States
[2]Thomas Jefferson National Accelerator Facility, Newport News, VA, United States

Abstract

The spin-preserving Rapid Cycling Synchrotron (RCS) is an integral component of the Electron-Ion Collider (EIC) complex. It will accelerate 750 MeV electrons from the Beam Accumulator Ring (BAR) to 5, 9, or 18 GeV, as required by the Electron Storage Ring (ESR), all while preserving the polarization. We discuss here the design considerations and the current optics solution, including considerations related to dynamic aperture and spin preservation as well as a reduced-cost RCS for operations to 9 GeV.

INTRODUCTION

The Electron-Ion Collider (EIC) is a new collider to be constructed at Brookhaven National Laboratory within the coming decade which will collide electrons with protons or ions in order to probe proton and nuclear structure [1]. In order to meet its science goals, the EIC requires polarized electron beams of 5, 9 and 18 GeV with charges of up to 28 nC. This necessitates the construction of an electron injector chain consisting of a linac, which produces 1.2 nC electron bunches and accelerates them to 750 MeV; the Beam Accumulator Ring (BAR), which combines the electrons from several linac pulses into a bunch of up to 28 nC; and the spin-preserving Rapid Cycling Synchrotron (RCS), which ramps this bunch to the desired collision energy and injects it into the EIC's Electron Storage Ring (ESR) once per second. A schematic of the electron injector as part of the total EIC complex is shown in Fig. 1. In order to save on project costs, the RCS will initially be constructed to only accelerate to 9 GeV, with full 18 GeV capability being added during operations. We discuss here the design considerations for both the full 18 GeV RCS and the upgradable 9 GeV version.

RCS LAYOUT

The RCS will be built as a 1507 m racetrack with two straight sections connected by arcs, as can be seen in Fig. 1. One straight section will include injection from the BAR, while the second will house the RF cavities and extraction elements. Intrinsic spin resonances occur when $G\gamma = nP \pm \nu_y$ where G is the electron's anomalous magnetic moment, γ is the relativistic gamma factor, n is an arbitrary integer, P is the lattice periodicity, and ν_y is the vertical tune [2]. If ν_y and $P - \nu_y$ are both larger than $G\gamma$ during the entirety of the ramp, we can guarantee that we will not cross any intrinsic resonances. The racetrack design for the RCS would normally result in a periodicity of 2, which is not sufficient to handle acceleration to 18 GeV, where $G\gamma \approx 40.8$. However, if the straights have a vertical phase advance equal to an integer multiple of 2π, they are invisible from a spin perspective, and so we can recover the desired periodicity condition by having sufficient FODO cells in the arcs [3]. We choose to have 4π phase advance across each straight, a vertical tune of 56.21, and 80 FODO cells per arc. This gives us a periodicity of 160 and an effective arc tune of 52.21 (since we ignore the straights), avoiding all intrinsic resonances which we would encounter on the ramp to 18 GeV. This also avoids the strongest imperfection resonances, which occur when $G\gamma$ is an integer near $nP \pm \nu_y$. However, we still cross weaker imperfection resonances whenever $G\gamma$ takes on an integer value. Strategies for reducing their impact will be discussed in [4]. The bending radius of the RCS dipoles is chosen as 92 m in order to minimize costs; a larger bending radius would increase tunnel length, while making it shorter would increase synchrotron radiation and increase the RF costs. We have chosen to make the horizontal phase advance across each arc an integer multiple of 2π. This automatically results in zero dispersion in the straights, reducing complications with the RF system. In order to provide space for the eight 591 MHz 5-cell RF cavities required to recover

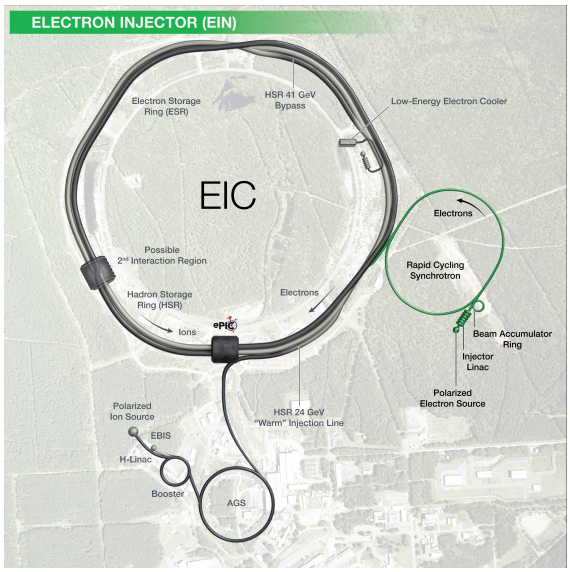

Figure 1: The EIC, with the RCS and electron injection chain highlighted.

* This work was supported by Brookhaven Science Associates, LLC under U.S. DOE Contract No. DE-SC0012704 and by Jefferson Science Associates, LLC under U.S. DOE Contract No. DE-AC05-06OR23177.
† wbergan@bnl.gov
‡ Currently at xLight, Palo Alto, CA, United States

Content from this work may be used under the terms of the CC BY 4.0 licence (© 2026). Any distribution of this work must maintain attribution to the author(s), title of the work, publisher, and DOI.

ISBN: 978-3-95450-252-3 ISSN: 2673-5350 doi: 10.18429/JACoW-IPAC2026-MOP1303

UPDATE ON INJECTION OPTICS INTO THE ELECTRON ION COLLIDER HADRON STORAGE RING*

H. Lovelace III†, V. Schoefer‡, J. S. Berg, E. Link, Ch. Liu, H. Oh, V. Ptitsyn, N. Tsoupas
Brookhaven National Laboratory, Upton, NY, United States

Abstract

The Electron Ion Collider Hadron Storage Ring (HSR) will be built on the campus of Brookhaven National Laboratory. The injection into the HSR will be vastly different from what is currently performed in the Relativistic Heavy Ion Collider. This paper will highlight the differences from RHIC, present the injection optics, and layout of the current design.

INTRODUCTION

The Electron Ion Collider (EIC) [1, 2] is currently being built on the campus of Brookhaven National Laboratory in the existing Relativistic Heavy Ion Collider (RHIC) [3] tunnel. The proton and heavy ion beams will circulate counterclockwise through the former RHIC yellow ring. The arcs of the RHIC lattice will be reused as the Hadron Storage Ring (HSR) arcs. The straight sections, with the exception of the experimental interaction region and the electron cooling section as a future upgrade, will keep the standard RHIC layout with the triplet optics of RHIC. The only changes to the the lattice geometry within the straight sections are the removal of the DX magnets which were the final bend into collisions for RHIC. The experimental hall, which houses the electron-Proton/Ion Collider (ePIC) detector, is upstream of the injection region in the denominated 6 o'clock region [4]. Upstream of the ePIC experimental hall is the 8 o'clock region where the Superconducting Radio Frequency (SRF) 591 MeV cavities reside. The 10 o'clock region is the dump location. The 12 o'clock region is designed with the ambition of a second detector possibly placed in the region as a future upgrade. The 2 o'clock region is the location of the hadron cooling system future upgrade where the injected beam will be pre-cooled prior to acceleration and cooled again, during the store.

INJECTION REGION LAYOUT

The layout of the injection region is shown in Fig. 2. The beam enters the HSR from the newly designed Alternating Gradient Synchrotron (AGS) to HSR (AtH) transfer line [5], through the two split DC current septa and an induction septum with a 15 mrad bend and a wall thickness of 4.9 mm. The beam is accelerated through the four 24.6 MHz normal conducting cavities. The eight 197 MHz normal conducting cavities are used at store. The 49.2 MHz cavities are split with two cavities immediately downstream of the 197 MHz system and the third cavity downstream of the triplet. The pair of warm dipoles follow with the 98.4 MHz system composed of 4 normal conducting cavities placed immediately after. The 49.2 MHz and the 98.4 MHz system are used for bunch splitting.

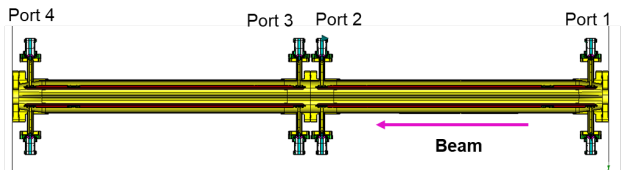

Figure 1: A simplified schematic of the two cell stripline injection kicker design

The 20 injection kickers, which have been updated from the previous discussions [6, 7] for a more compact design, are located ~65 m away from the from the induction septum. Figure 1 is a simplified schematic of the stripline kicker where each kicker module has two cells. A set of legacy triplet quadrupole magnets follows the injection kickers. The polarimetry instrumentation-proton-carbon (pC) coulomb nuclear interference (CNI) polarimeters [8], the helium-3 polarimeter [9, 10], and the hydrogen jet polarimeter (H-jet) [11]-is located directly downstream. The two plane pC polarimeter measures the instantaneous hadron beam polarization in the vertical and horizontal plane by rotating a thin carbon ribbon target through the accelerated beam. The jets measure the absolute polarization of the stored beam. Forward taggers are needed to reject the breakup products produced by the collision of the $^3He^{+2}$ with the jet beam. The dipoles downstream of the jets are then used to separate the protons, deuterons, and neutrons.

Between the warm dipoles used to separate the particles from the byproducts of the beam/jet collisions and the taggers is a longitudinal stochastic cooling pickup and the transverse stochastic cooling kickers. The stochastic cooling transversely cools the hadron beam by applying a RF kick to the off momentum particles based on the pickup signal amplified and processed [12, 13]. Downstream of the taggers is a helical dipole snake [14], which is used to rotate the spin vector of the particles 180° vertically.

LATTICE OPTICS

Injection

Figure 3 shows a comparison between the injection optics and the pre-ramp optics of the injection region. The asymmetric injection optics are driven by the placement of the kicker in comparison to the septum and the asymmetry of dipole placement in comparison to the triplet magnets. The

* Work supported by Brookhaven Science Associates, LLC under Contract No. DE-SC0012704 with the U.S. Department of Energy.
† hlovelace@bnl.gov
‡ schoefer@bnl.gov

Content from this work may be used under the terms of the CC BY 4.0 licence (© 2026). Any distribution of this work must maintain attribution to the author(s), title of the work, publisher, and DOI.

ISBN: 978-3-95450-252-3 ISSN: 2673-5350 doi: 10.18429/JACoW-IPAC2026-MOP6001

ELIMINATING MAINS NOISE EFFECTS IN ACCELERATORS WITH MACHINE LEARNING

V. Kain*, [1], P. A. Arrutia Sota[1], H. Bartosik[1], F. F. Ferber[2], F. Follin[1], C.-M. Genton[1], Q. King[1], B. Rodriguez Mateos[1], O. Michels[1], M. Schenk[1]
[1]CERN, Geneva, Switzerland
[2]University of Salzburg, Salzburg, Austria

Abstract

Power supply ripple at various frequencies — characteristic to the magnet circuits or from the electrical network — has always been an issue for accelerator operation. In the CERN Super Proton Synchrotron (SPS) this is particularly detrimental at low energy for LHC-type beams and at top energy for slowly extracted beams. This contribution summarises the efforts in the CERN SPS over the last years to compensate the ripple at 50 Hz and its harmonics in the main quadrupole circuits using Machine Learning methods. The implementation required hardware modifications on the power converter electronics side, additions to the controls infrastructure and the development of adaptive algorithms that can deal with changes in the electrical distribution network throughout the day. Continuous control with tailored adaptive Bayesian Optimisation has been implemented for slow extracted spill control throughout 2024 and 2025. The improved spill quality obtained over the years is discussed, while results from R&D towards one-shot correction algorithms for beams that are only played on-demand are also briefly summarised.

INTRODUCTION

The CERN Super Proton Synchrotron (SPS) is a 7 km circumference synchrotron that serves as injector to the Large Hadron Collider (LHC) and provides beams for fixed-target physics in the North Area (NA) via chromatic slow extraction (SX) in the horizontal plane, exploiting the 2/3 resonance. Mains power supply ripple at 50 Hz and its harmonics is a significant source of perturbation in both operational modes.

For SX beams, spill quality can be degraded by several mechanisms such as macro-spill shape distortions from magnetic hysteresis or very high-frequency intensity ripple arising from slow RF debunching. The focus of this work is the time-varying ripple at $n \times 50$ Hz originating from the SPS power supplies, whose phase and amplitude drift on timescales of minutes to hours due to changes in the electrical distribution network. The operational goal is to keep normalised spill modulation amplitudes below 0.15 for more than 85% of the spill duration. For LHC-type beams, experiments with single-bunch proton beams in 2017–2018 established that 50 Hz tune ripple from the quadrupole power converters causes emittance blow-up and particle losses [1]. This effect was confirmed to persist for multi-bunch beams in dedicated Machine Development sessions in 2024, making 50 Hz compensation a priority also for LHC beams.

CORRECTION SCHEME

Hardware

The correction scheme, conceived in 2018, derives a reference signal from the 50 Hz mains voltage and injects sinusoidal corrections at 50 Hz and its harmonics into the voltage reference of the quadrupole and main dipole power converters. The gain and phase of each harmonic component are free parameters to be optimised. The FGC Class 63 digital controller provides the infrastructure for harmonic injection. One sinusoidal generator per harmonic order runs phase-locked to the 50 Hz network reference. Their outputs, scaled and shifted by the gain and phase parameters, are added to the current loop voltage reference. This superposes a time-varying correction onto the nominal magnet excitation without affecting the main regulation loop.

Measurement

The primary feedback signal in case of fixed target physics is the SPS beam intensity spill monitor (BSI), a high-bandwidth (~100 kHz) detector measuring the extracted particle flux. Its time-domain signal is Fourier-transformed in real time to extract the normalised amplitudes at 50 Hz and its harmonics, which serve as the objective for the optimisation algorithm. DC current transformers (DCCTs) on the QF, QD and main dipole magnet bus bars provide measurements of the current ripple in the corresponding circuit, enabling model-based and direct DCCT-feedback approaches for all SPS beam types, i.e. also in the case of LHC beams.

CONTROL ALGORITHM

Adaptive Bayesian Optimisation

Since 2023, Adaptive Bayesian Optimisation (ABO) provides 24/7 continuous spill quality control [2] in the SPS. Inspired by work on Gaussian Process (GP) kernels for pattern discovery and extrapolation [3,4], the algorithm builds a GP surrogate model that incorporates time t as an additional input dimension. This allows the model to predict the objective at the next time step $t + 1$ given observations up to time t, enabling continuous closed-loop control. The objective for ABO and continuous spill control was to minimise the normalised amplitude at $n \times 50$ Hz measured by the BSI.

Initially, only the Upper Confidence Bound (UCB) acquisition function was used with fixed hyperparameters tuned

* verena.kain@cern.ch

Content from this work may be used under the terms of the CC BY 4.0 licence (© 2026). Any distribution of this work must maintain attribution to the author(s), title of the work, publisher, and DOI.

ISBN: 978-3-95450-252-3 ISSN: 2673-5350 doi: 10.18429/JACoW-IPAC2026-MOP6302

APS-RAG: A DOMAIN-AWARE HYBRID RETRIEVAL AUGMENTED GENERATION SYSTEM FOR ACCELERATOR OPERATIONS AND KNOWLEDGE SYNTHESIS*

R. Sainju†, J. Dariusz, H. Shang, M. Prince, R. Aydelott, M. Cherukara, Y. Sun, M. Borland
Advanced Photon Source, Argonne National Laboratory, Lemont, IL, USA

Abstract

Effective knowledge management is essential for minimizing downtime and maintaining institutional memory in large-scale accelerator facilities. We present APS-RAG, a domain-aware Retrieval-Augmented Generation (RAG) system currently deployed at the Advanced Photon Source (APS), designed to synthesize operational intelligence and facilitate semantic retrieval from dispersed databases. The system consolidates over 10,000 unique documents from four live databases: the Best Electronic Logbook Yet (BELY) scientific electronic logbook, operational Microsoft Teams chat history, the Integrated Content Management System (ICMS), and the Work Request system - under a single retrieval interface. By leveraging the latest frontier LLMs via Argonne's ARGO platform, APS-RAG integrates a specialized query-preprocessing pipeline that performs temporal parsing, domain-acronym resolution, multi-query expansion, and final response generation.

To ensure high precision, a hybrid retrieval architecture is utilized, combining dense vector and keyword searches. Results are aggregated using Reciprocal Rank Fusion (RRF) and refined with cross-encoder reranking to maximize relevance. A 100-question evaluation dataset was built using the InPars methodology, supplemented with qualitative user feedback. Final responses from APS-RAG include inline citations embedded which display the source document chunk and a web-accessible link to the original document. Future developments include multimodal integration and agentic knowledge-graph-aware retrieval.

INTRODUCTION

The Advanced Photon Source (APS), like any large scientific facility, generates an enormous amount of operational data every day. Operating a facility of this scale for stable user operations exercises every part of the operational record: shift entries, logbook entries, trouble shooting and control procedures, equipment replacement and maintenance work orders, and the operations chat messages (e.g., Microsoft Teams). All of these sources contain critical institutional knowledge. Each of these sources is searchable on its own, but no single interface lets APS staff pose a free-form question – e.g., " How to calibrate the new digital cameras in BTS and what's the last study that used those cameras?" -- and receive a synthesized, source-grounded answer.

* Work supported by the U. S. Department of Energy, Office of Science, under Contract No. DE-AC02-06CH11357.
† rsainju@anl.gov

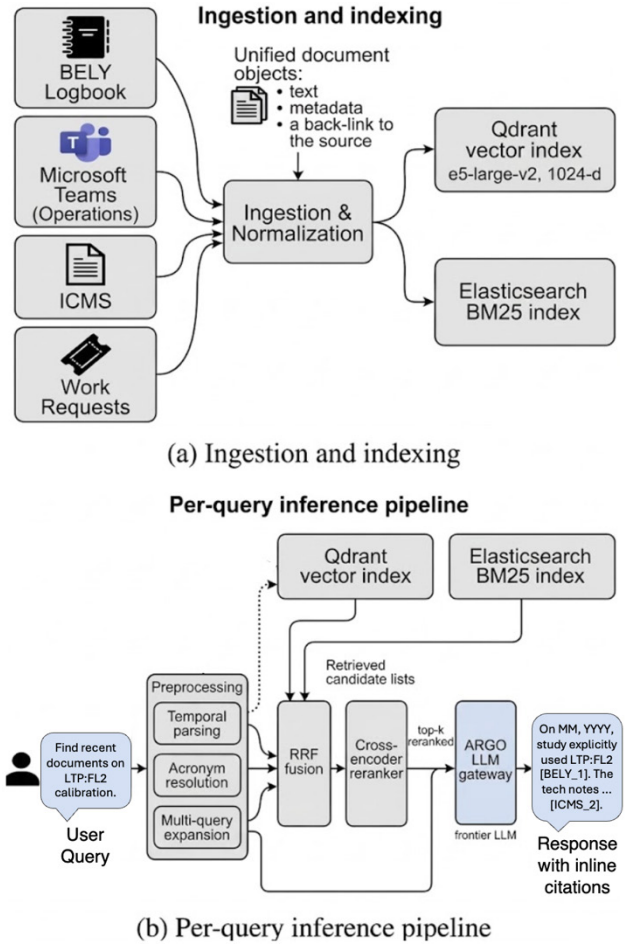

Figure 1: APS-RAG end-to-end architecture. (a) Ingestion and indexing: records from the four operational sources: BELY logbook [1], Microsoft Teams (Operations), ICMS, and the work-request system are normalized into a unified JSON document representation and indexed (b) Per-query inference: the user query passes through temporal parsing, acronym resolution, and multi-query expansion, fans out to the two indices in parallel, and the returned candidate lists are merged by RRF fusion and re-scored by a cross-encoder reranker before the top-k context is passed to a frontier LLM through the ARGO (Argonne National Labs AI platform) gateway, which emits a response with inline, clickable citations.

Several accelerator laboratories have begun closing this gap with LLMs. GAIA [2], developed at DESY, couples an open-weights LLM with logbook and control-system tools through the ReAct prompting paradigm [3]. A multi-

Content from this work may be used under the terms of the CC BY 4.0 licence (© 2026). Any distribution of this work must maintain attribution to the author(s), title of the work, publisher, and DOI.

ISBN: 978-3-95450-252-3 ISSN: 2673-5350 doi: 10.18429/JACoW-IPAC2026-MOP6303

LEVERAGING LOW-COST SENSORS AND MACHINE LEARNING FOR PUMP ANOMALY DETECTION IN ACCELERATOR FACILITIES*

R. Sainju†, O. Mohsen, J. Ackley, J. Fuerst, R. Wright, Y. Sun, M. Borland
Advanced Photon Source, Argonne National Laboratory, Lemont, IL, USA

Abstract

The reliability of cooling systems is critical for removing substantial amounts (in megawatts) of waste heat from numerous high-power accelerator components (e.g., magnets, RF structures, power supplies) and beamline components. Reliance on manual inspection of hundreds of pumps is inefficient and increases the risk of costly component damage and unplanned downtime. This study introduces a real-time method for automated vibration-based pump anomaly detection that is designed to help transition facility operations from reactive to predictive maintenance. Our approach integrates (i) affordable vibration sensors and (ii) machine learning models for anomaly detection. We have deployed vibration sensors on Bunch Lengthening System (BLS) helium pump, and a set of deionized water-cooling pumps, where Linux edge nodes aggregate and preprocess the hourly collected data. To support operational decision-making, a web-based diagnostic platform provides real-time visualization of vibration trends against a rolling weekly baseline, together with Short-Time Fourier Transform (STFT) spectrograms and integrated Power Spectral Density (PSD) plots for frequency and time-domain analysis. Additionally, the web platform will display hourly inferences from the machine learning models such as autoencoder on the data stream, autonomously detecting spectral anomalies indicative of mechanical faults. The integration of scalable edge data collection, advanced visualization, and unsupervised machine learning will provide a vital safeguard for maintaining operational readiness in particle accelerators.

INTRODUCTION

Cooling water systems are an unglamorous but indispensable part of any modern accelerator. At APS, deionized water removes heat from magnets, radio-frequency structures, power supplies, and beamline components through a primary distribution system that operates at flow rates approaching 10,000 gallons per minute, together with dozens of smaller closed-loop secondary systems [1]. Pumps are the active elements that keep this network running, and an unexpected pump failure can cascade quickly: components interlock on flow and temperature, downtime is expensive, and damage to high-power loads is difficult to repair on a user-driven schedule.

Today, pump health at APS is assessed primarily through walk-down inspections, supplemented by reactive trips after the fact. Across hundreds of pumps this is labor-intensive, occurs periodically, and makes it difficult to catch the slow drifts that precede a hard failure. This bottleneck can be addressed through vibration-based condition monitoring [2], and by applying machine learning methods that learn the normal operations signature of a machine from unlabeled operating data [3, 4]. Recent work has shown that autoencoder-style reconstruction analysis transfers well to the accelerator setting: it has been applied to magnet fault prediction in the APS storage ring [5, 6] and to errant-beam and pressure anomalies at other facilities [7, 8]. Pumps, however, have received comparatively little attention in the accelerator literature. This work extends our earlier proof-of-concept on cooling water pumps [9] and adds the BLS helium pump and an web-based diagnostic platform.

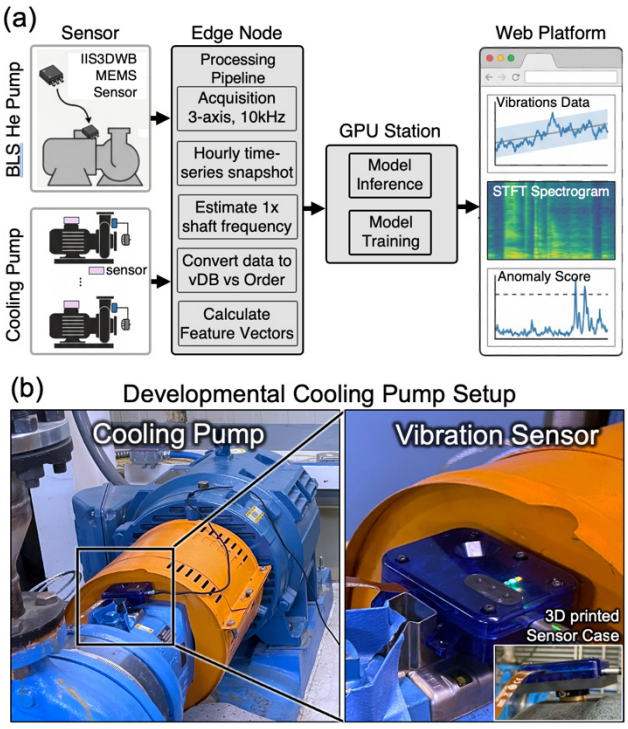

Figure 1: Developmental pump-monitoring system at APS. (a) End-to-end data flow: 3-axis MEMS vibration sensors mounted on accelerator pumps stream data to Linux edge nodes, which perform hourly aggregation, preprocessing, and feature vector calculations; the data is then sent to a GPU workstation for inference; outputs are served through a web-based diagnostic platform to engineers. (b) Representative sensor installation on the cooling pump, showing sensor mounting location, cable run to the local edge node, and 3D printed sensor case.

* Work supported by the U. S. Department of Energy, Office of Science, under Contract No. DE-AC02-06CH11357.
† rsainju@anl.gov

Content from this work may be used under the terms of the CC BY 4.0 licence (© 2026). Any distribution of this work must maintain attribution to the author(s), title of the work, publisher, and DOI.

ISBN: 978-3-95450-252-3 ISSN: 2673-5350 doi: 10.18429/JACoW-IPAC2026-MOP6307

ONLINE TUNING OF THE NSLS-II INJECTOR USING BAYESIAN OPTIMIZATION WITH DIFFERENT PACKAGES

M. Song*, Y. Hidaka, G. Wang, Xi Yang, Brookhaven National Laboratory, Upton, NY, USA

Content from this work may be used under the terms of the CC BY 4.0 licence (© 2026). Any distribution of this work must maintain attribution to the author(s), title of the work, publisher, and DOI.

Abstract

The injector of the NSLS-II consists of a linear accelerator (LINAC) that accelerates the electron beam to 170 MeV, followed by a linac-to-booster (LTB) transport line and a booster synchrotron that further increases the beam energy to 3 GeV. The performance of LINAC and LTB is critical to achieve efficient and stable beam injection. Automated online tuning is an effective method to improve injector performance. In this paper, we present an automated tuning approach based on Bayesian optimization, using different software packages to optimize the LINAC and LTB. We evaluate and compare these packages based on their ability to improve injection efficiency. Our results demonstrate that Bayesian optimization can significantly enhance injector performance and show differences in performance between different packages.

INTRODUCTION

The injector of a storage ring light source typically consists of an electron gun, a linear accelerator (LINAC), a LINAC-to-booster (LTB) transport line, a booster synchrotron, and a booster-to-storage ring (BTS) transport line. It is the upstream accelerator system that generates, accelerates, and transports electrons to the storage ring, where they are stored to produce synchrotron radiation. The injector directly determines the quality of the injected beam, including emittance, energy spread, and injection efficiency. In practice, even if the same machine settings are reloaded after a shutdown, the system does not behave exactly the same. Small changes in magnet calibration, temperature variations, and slow drifts over time introduce deviations. These effects accumulate and lead to suboptimal beam conditions. Because the injector is a complex and nonlinear system, existing physics models cannot fully capture all real-world variations and coupling between components. As a result, model-based prediction alone is not sufficient to achieve optimal performance. Therefore, online tuning is necessary to restore and optimize injector performance.

Online tuning is an effective approach to recover and improve machine performance by iteratively adjusting machine parameters based on real-time beam measurements. To reduce the need for manual effort, automated online tuning has emerged as a powerful method to efficiently optimize accelerator performance. It has been successfully applied using traditional optimization algorithms [1, 2]. However, these algorithms are often inefficient, as they typically require a large number of objective function evaluations to reach a global optimum. Given the limited machine study time available, this becomes a practical limitation. To address this, machine learning–based optimization methods have been introduced to improve efficiency. These approaches have been successfully applied in storage ring light sources [3], free-electron lasers [4].

The goal of this work is to deploy a Python-based Bayesian optimization framework to the control room input/output controller (IOC) for routine NSLS-II injector tuning. To support this effort, we also implemented a MATLAB-based version as a benchmark and compared optimization performance across platforms. Because these packages implement Bayesian optimization with different configurations and settings, their performance can vary. Therefore, a systematic comparison is necessary to provide practical guidance for automated online tuning of the NSLS-II injector [5]. This paper presents optimization results for the LINAC and LTB using both Python- and MATLAB-based Bayesian optimization packages. The results demonstrate that injector performance can be significantly improved through automated online tuning.

BAYESIAN OPTIMIZATION PACKAGES

There are many Bayesian optimization packages available in different programming languages, with varying features and implementations. In this work, we used both Python- and MATLAB-based packages for NSLS-II injector online tuning.

For the Python-based package, we employed `Xopt` [6], which is specifically developed for accelerator optimization applications. It provides flexible interfaces for defining optimization problems, supports Gaussian process–based surrogate models, and allows easy integration with control systems, making it well suited for online real-time tuning.

For the MATLAB-based package, we used the built-in Bayesian optimization function (`bayesopt`) from the MATLAB Machine Learning Toolbox [7]. This implementation offers a well-documented and standardized framework with robust default settings, making it convenient for quick testing and benchmarking.

Using both packages, we compared their performance in terms of convergence behavior, robustness, and optimization efficiency, and assessed their suitability for practical deployment in the NSLS-II injector tuning workflow.

BAYESIAN OPTIMIZATION SETTINGS

In this work, we used the default settings for `Xopt` and `bayesopt`. For both implementations, a Gaussian process (GP) model [8] was used as a surrogate to approximate the objective function.

For Bayesian optimization using `Xopt`, the GP used a radial basis function (RBF) kernel [8], which assumes the

* msong1@bnl.gov

ISBN: 978-3-95450-252-3 ISSN: 2673-5350 doi: 10.18429/JACoW-IPAC2026-MOP6310

MACHINE-LEARNING–ASSISTED BAYESIAN UNCERTAINTY QUANTIFICATION FOR ACCELERATOR DIGITAL TWIN MODELING AND CONTROL*

W. Lin†[1], K. Brown[1], J. Edelen[2], E. Hamwi[1], G. Hoffstaetter[1,3], C. Kelly[1], N. Urban[1]
[1]Brookhaven National Laboratory, Upton, NY, United States
[2]RadiaSoft, Boulder, CO, United States
[3]Cornell University (CLASSE), Ithaca, NY, United States

Abstract

Digital twins of particle accelerators are increasingly used for experiment planning, machine studies, and model-based control. Achieving high-fidelity predictions requires knowledge of machine properties that are difficult to measure directly, such as magnet alignments, transfer function variations, nonlinearities, and stray fields. In this work, we introduce parameterizations to capture these effects and employ Bayesian inference to estimate their values and uncertainties by calibrating a digital twin to orbit response measurements from the AGS Booster at Brookhaven National Laboratory. A machine-learning emulator trained on a perturbed ensemble of Bmad simulations enables computationally efficient sampling of the high-dimensional posterior. The resulting joint parameter distribution incorporates BPM uncertainties and provides data-constrained variations that, when inserted back into the digital twin, significantly improve agreement with measured beam orbits while yielding uncertainty estimates on both parameters and predictions.

INTRODUCTION

Digital twins provide a powerful framework for predictive control, online optimization, and machine studies planning in particle accelerators. Their accuracy, however, is limited by uncertainties in component properties such as magnet alignments, saturation effects, current-to-field transfer functions, and stray fields. In the AGS Booster, comparisons between measured and simulated orbit response matrices (ORMs) show systematic discrepancies larger than the beam position monitor (BPM) noise level, pointing toward deficiencies in the magnetic model and motivating a formal uncertainty quantification (UQ) approach. Bayesian UQ is particularly well suited to accelerator modeling because it provides a principled way to quantify correlated parameter uncertainties and propagate them through a physics-based model, yielding interpretable corrections and uncertainty-aware predictions.

In this work, we introduce a Bayesian UQ framework that infers magnet-specific variations to quadrupole strengths using ORM data. To make the inference tractable, we employ a machine-learning surrogate model of the Bmad [1] digital twin capable of fast and differentiable predictions, enabling efficient Hamiltonian Monte Carlo (HMC) sampling in a 48-dimensional parameter space. The resulting posterior distributions provide both parameter estimates and uncertainty bounds, while the inferred variations yield substantial improvements when integrated into the digital twin.

METHODS

Orbit Response Data

ORM data were collected by stepping each of the Booster's corrector magnets sequentially through 22 A, 0 A, and −22 A. Each setting included multiple (2–5) repeated BPM measurements at the 92 ms flat-top of the magnet cycle. After automated outlier removal, the dataset consisted of 23 horizontal and 14 vertical perturbed ORM measurements using 15 and 18 valid BPMs, respectively. Orbit differences (perturbed minus baseline) were used to suppress static orbit offsets and reduce sensitivity to unrelated systematic errors, allowing the inference to isolate the effect of each corrector more cleanly.

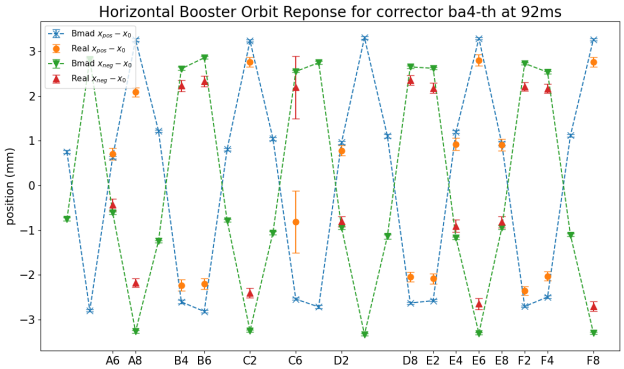

Figure 1: Comparison between measured and simulated horizontal orbit responses with corrector A4 set to ±22 A, data taken at 92 ms in the Booster cycle. The larger error on BPM C6 is due to a known hardware problem.

A comparison of the orbit differences between positive, zero, and negative corrector settings for corrector A4 is shown in Fig. 1. The error bars are estimated based on the fluctuations over the repeated measurements. We observe that the difference between measured and simulated differential orbits are mostly within 1 mm, but still much larger than the error bars of the measurements. This discrepancy implies there are sources of error in the real machine that

* Work supported by Brookhaven Science Associates, LLC under Contract No. DE-SC0012704, No. DE-SC0024287, and No. DE-SC0025351 with the U.S. Department of Energy.
† wlin1@bnl.gov

Content from this work may be used under the terms of the CC BY 4.0 licence (© 2026). Any distribution of this work must maintain attribution to the author(s), title of the work, publisher, and DOI.

ISBN: 978-3-95450-252-3 ISSN: 2673-5350 doi: 10.18429/JACoW-IPAC2026-MOP6311

AI-READY LATTICE REPRESENTATION AND ML OPTIMIZATION FOR THE BNL BOOSTER-TO-AGS TRANSFER LINE*

W. Lin†[1], A. Kasparian[2], K. Brown[1], L. Hajdu[1], E. Hamwi[1],
G. Hoffstaetter[1,3], T. Satogata[2], M. Schram[4]
[1]Brookhaven National Laboratory, Upton, NY, United States
[2]Thomas Jefferson National Accelerator Facility, Newport News, VA, United States
[3]Cornell University (CLASSE), Ithaca, NY, United States
[4]Pacific Northwest National Laboratory, Richland, WA, United States

Abstract

As part of the Nuclear Physics AI-Ready Accelerator Data (NARAD) project, Brookhaven National Laboratory is developing a demonstration use case based on the Booster-to-AGS (BtA) transfer line. We establish an AI-ready representation of the BtA lattice using the Particle Accelerator Language Standard (PALS), extended with semantic metadata linking lattice elements to control system signals and device capabilities. This NARAD-PALS model enables direct mapping between simulation, operational devices, and machine data. We implement this framework for the BtA line and demonstrate semantic device queries and control-channel resolution within the BNL Accelerator Device Objects (ADO) system. This unified representation supports integration of streaming and archived data and provides a foundation for ML-based optimization of AGS injection and cross-facility interoperability.

INTRODUCTION

Modern accelerator facilities increasingly rely on machine learning (ML) techniques for applications such as online optimization, anomaly detection, and digital-twin development. However, these efforts are often limited by heterogeneous, facility-specific data structures and control system representations. Existing infrastructures, including Brookhaven National Laboratory's Accelerator Device Objects (ADO) [1] and EPICS [2], provide essential operational interfaces but lack the semantic structure needed for scalable interoperability, automated reasoning, and reusable ML workflows across facilities.

The DOE Nuclear Physics AI-Ready Accelerator Data (NARAD) initiative addresses these challenges by developing standardized, AI-ready schemas for accelerator data and lattice models. Within this effort, the Booster-to-AGS (BtA) transfer line at Brookhaven National Laboratory serves as a demonstration use case. The BtA line contains a diverse set of magnets and diagnostics integrated into a legacy ADO-based control system, making it a representative testbed for challenges related to device modeling, signal consistency, and control system semantics. Figure 1 illustrates the high-level NARAD architecture, showing how facility-specific models are represented using Particle Accelerator Language Standard (PALS) and integrated into a knowledge graph and data services layer to support downstream applications.

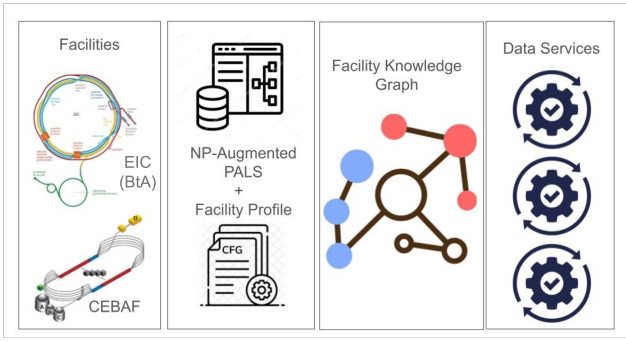

Figure 1: High-level architecture of the NARAD framework, illustrating the integration of facility models, PALS representations, knowledge graph infrastructure, and data services for AI-ready accelerator workflows.

Building on this architecture, we extend PALS with NARAD semantic metadata that unifies physics-based lattice descriptions with machine-queryable control system information. The resulting framework links lattice elements, control signals, device capabilities, and operational constraints within a single structured representation. Building on this representation, we develop methods for semantic device queries, control-signal mapping, and integration of streaming and archived machine data from the BNL accelerator database. The framework also enables higher-level orchestration workflows using large language model (LLM)-based tools.

Using these components, we aim to construct an AI-ready BtA model suitable for simulation-driven ML optimization studies, including optimization of AGS injection quality. This work demonstrates how standardized semantics and shared data representations can accelerate AI applications in accelerator facilities while providing a prototype for cross-facility interoperability within the emerging NARAD ecosystem.

BTA TRANSFER LINE OVERVIEW

The Booster-to-AGS (BtA) transfer line transports beam from the Booster extraction point at F6 to the AGS injection

* Work supported by the U.S. Department of Energy, Office of Science, Office of Nuclear Physics, under the Nuclear Physics AI-Ready Accelerator Data (NARAD) project, Award No. DE-SCL0000127, and under Contract Nos. DE-SC0012704, DE-AC05-06OR23177, and DE-AC05-76RL01830.
† wlin1@bnl.gov

Content from this work may be used under the terms of the CC BY 4.0 licence (© 2026). Any distribution of this work must maintain attribution to the author(s), title of the work, publisher, and DOI.

ISBN: 978-3-95450-252-3 ISSN: 2673-5350 doi: 10.18429/JACoW-IPAC2026-MOP6312

OPTIMIZATION OF THE FERMILAB BOOSTER USING A HYBRID BAYESIAN AND RL FRAMEWORK*

N. Kuklev†, J. Eldred, M. Balcewicz, R. Sharankova, J. St. John
Fermi National Accelerator Laboratory, Batavia, IL, USA

Abstract

The PIP-II project will raise the Fermilab Booster intensity and ramp rate. Beam losses will limit the maximum power and are hard to simulate. Presently, the Booster uses operator-guided empirical tuning - a challenging task due to high dimensionality, multiple objectives, critical safety constraints, and drifts. We developed a synergistic suite of Bayesian optimization (BO) and reinforcement learning (RL) tools to optimize and stabilize beam losses, including novel techniques for fast risk-aware Bayesian optimization and exploration. For the initial tune-up, we performed single and multi-objective tuning using scalarized objectives comprised of critical beam loss locations, achieving significant rebalancing of losses as well as an overall improvement in transmission efficiency. To build a data-driven surrogate, active learning was used to collect data while relying on risk-aware constraints to successfully avoid beam trips. A few thousand points were collected, and a GP surrogate validated for uncertainty-aware predictions. Several off-policy RL agent architectures were trained for long-term stabilization. In surrogate-based testing, SAC with BPM context and history embedding had the best performance with fast and robust convergence when subjected to energy and trajectory perturbations. Experimental testing is ongoing to enable operational use.

INTRODUCTION

The Fermilab Booster is a key component of the Fermilab accelerator complex providing 8 GeV protons to various users directly, as well as sending beam to the Recycler/Main Injector. For the future LBNF/DUNE program, the PIP-II linac upgrade will increase the power on target to 1.2 MW. It includes a new superconducting linac, a new BTL transfer line, and various improvements to the complex including the Booster. Key changes for the Booster are the increase of injection energy to 800 MeV, higher beam intensity (from 4.8×10^{12} to 6.7×10^{12}), a new painting scheme, new collimation and RF systems, and a faster ramp rate of 20 Hz. Given that the Booster is a 50-year-old machine with aging hardware, areas of concern have been identified in terms of machine reliability and capability to operate at PIP-II parameters. Significant beam dynamics challenges are expected due to extreme levels of space charge at injection, as well as new instabilities at transition crossing.

The maximum Booster power is determined primarily by administrative beam loss limits, with PIP-II requiring a two-fold reduction in relative losses as compared to the current levels. An extensive simulation campaign is ongoing to better understand and control beam dynamics, but so far it has proven difficult to obtain quantitative agreement with experimental data, especially for the local loss distribution. Thus, it is expected that an extensive experimental tune-up will be necessary to commission the Booster for PIP-II.

Driven by PIP-II requirements as well as challenges in the DOE GARD roadmap [1, 2], several AI/ML projects were started at Fermilab, focusing on the development of advanced optimization algorithms, fast differentiable simulations [3], and integrated facility-scale virtual accelerators (digital twins) [4]. Together, they enable both direct optimization using Bayesian methods, and a transition to more data-intensive but scalable methods like reinforcement learning (RL). In this paper, we describe our results in applying Bayesian and RL methods to experimentally control optics and injection properties for Booster loss reduction.

FERMILAB BOOSTER

The Fermilab Booster is a rapid cycling synchrotron with 24 sectors (short (S) and long (L) subsections). The main combined function magnets are connected to a shared resonant power supply. In addition, there are 48 independently powered correction elements with dipole, quadrupole, skew quadrupole, sextupole, and skew sextupole components [5]. The Booster diagram is shown in Fig. 1.

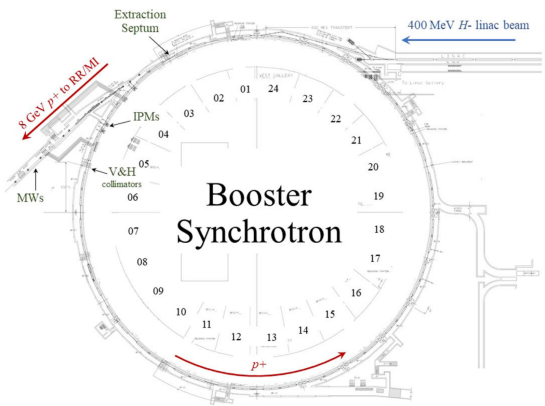

Figure 1: Booster synchrotron.

Time-dependent current ramps with up to 64 points can be set, forming thousands of potential knobs. Such high dimensionality is infeasible so we identified two smaller scenarios. First, for Bayesian loss minimization, we chose a set of quadrupole ramp offsets either in 24D (short or long) or

* This manuscript has been authored by FermiForward Discovery Group, LLC under Contract No. 89243024CSC000002 with the U.S. Department of Energy, Office of Science, Office of High Energy Physics.
† nkuklev@fnal.gov

Content from this work may be used under the terms of the CC BY 4.0 licence (© 2026). Any distribution of this work must maintain attribution to the author(s), title of the work, publisher, and DOI.

ISBN: 978-3-95450-252-3 ISSN: 2673-5350 doi: 10.18429/JACoW-IPAC2026-MOP6316

HARDWARE AWARE ARTIFICIAL INTELLIGENCE (HAAI): PROGRESS ON REALTIME BEAM TOMOGRAPHY RECONSTRUCTION FOR THE FERMILAB RECYCLER USING MACHINE LEARNING AND EDGE PROCESSING

K. Hazelwood*, R. Ainsworth, J. Berlioz, K. Danison-Fieldhouse,
C. Gonzalez-Ortiz, W. Leinonen†, Li Xiang, M.-J. Yang
Fermi National Accelerator Laboratory, Batavia‡, United States
N. Isenberg, M. Jain, J. Strube
Pacific Northwest National Laboratory, Richland, United States

Abstract

The resistive wall current monitor (RWCM) data from the Fermilab Recycler Ring (RR) is used to reconstruct the longitudinal profile of proton beams circulating in the machine. This procedure, commonly referred to as tomography, has proved to be invaluable in tuning the machine. In 2013 Recycler was re-purposed as a proton stacker and charged with implementing slip-stacking to double the intensity for the Main Injector (MI). With two slipping beams, the RWCM data from Recycler is difficult to differentiate and the tomography procedure is slow to compute using traditional means. Building upon past efforts, the Hardware Aware Artificial Intelligence (HAAI) project aims to develop a Machine Learning (ML) model to reconstruct the Recycler beam tomography in real-time and deploy this model on edge hardware. Once developed, this new streaming virtual diagnostic would be used to better track the beam parameters over larger time spans, attribute settings to beam effects, tune the machine, and provide an input into other future automatons of the machines.

INTRODUCTION

Longitudinal tomography is the process of reconstructing the longitudinal phase space profile of bunch(es) of beam using successive turn measurements from a resistive wall current monitor (RWCM).

TARDIS

In 2013 a software client affectionately named TARDIS (Tomography And Related Diagnostics In Synchrotrons) was developed to reconstruct the beam tomography in both Main Injector and Recycler [1]. TARDIS has become an invaluable tool for tuning the machines, giving relatively quick insight into important beam measurements such as injection phase offset, injection energy offset, and overall bunch size and distribution (Fig. 1). While TARDIS has greatly improved our monitoring of the beam longitudinal profile, it does leave some things to be desired. TARDIS relies on RWCM data collected by an oscilloscope. This can take up to a minute, while typical Recycler beam cycles only last a fraction of a second. Furthermore, while pre-made configuration files exist for most beam scenarios, their values often need to be checked against the current running state of the machine, otherwise incorrect measurements occur.

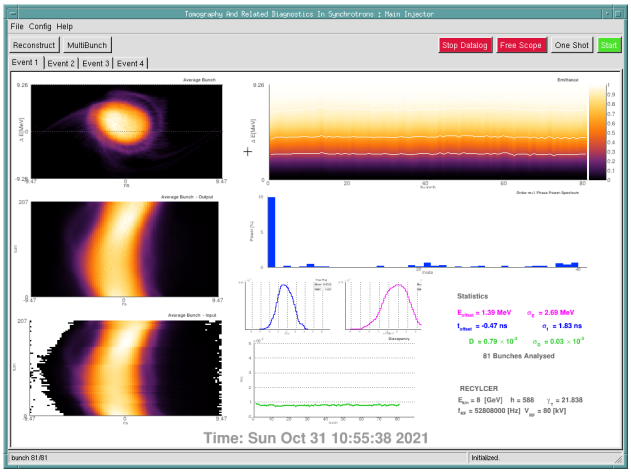

Figure 1: Example of TARDIS output. Left-Center shows the processed averaged bunch RWCM data, Left-Top shows the longitudinal tomography reconstruction.

Recycler Slip-Stacking

The most problematic deficiency of TARDIS is its inability to distinguish between the two slipping beams from the RWCM data. Recycler is now used as a proton stacker for injection into Main Injector and ultimately extraction to the NuMI experiments. Recycler utilizes slip-stacking [2], a process in which batches of beam are injected, decelerated, and then more batches are injected. At the end of slip-stacking, the two momentum beams are quickly accelerated to form double intense batches for extraction to Main Injector. This means that the RWCM at the ideal Recycler frequency samples the in-bucket motion of the on momentum bunch, as well as the streak of decelerated bunches, as the on momentum beam slips past them (Fig. 2).

* kjh@fnal.gov
† Also at University of Glasgow, Glasgow, United Kingdom
‡ This work was supported in part by the U.S. DOE Office of Science, Office of High Energy Physics, under award 84399: "Hardware-aware Artificial Intelligence". Fermi National Accelerator Laboratory is managed by Fermi Forward Discovery Group, LLC, for the U.S. Department of Energy under under Contract No. 89243024CSC000002. Pacific Northwest National Laboratory is operated by Battelle Memorial Institute for the U.S. Department of Energy under Contract No. DE-AC05-76RL01830.

Content from this work may be used under the terms of the CC BY 4.0 licence (© 2026). Any distribution of this work must maintain attribution to the author(s), title of the work, publisher, and DOI.

ISBN: 978-3-95450-252-3 ISSN: 2673-5350 doi: 10.18429/JACoW-IPAC2026-MOP6317

ACCELERATOR PERFORMANCE DRIFT COMPENSATION WITH A MODIFIED MG-GPO ALGORITHM*

R. W.-Y. Yeung†, Michigan State University, East Lansing, MI, USA
X. Huang, SLAC National Accelerator Laboratory, Menlo Park, CA, USA
Y. Hao, Facility for Rare Isotope Beams, East Lansing, MI, USA

Content from this work may be used under the terms of the CC BY 4.0 licence (© 2026). Any distribution of this work must maintain attribution to the author(s), title of the work, publisher, and DOI.

Abstract

Performance drift has been a longstanding problem for accelerators. A desirable solution is to tune the machine slowly and gently to compensate for such drift. Previously, we presented a version of the Multi-Generation Gaussian Process Optimizer which tunes accelerator settings during operation to maintain optimal performance. In this paper, we present an improved version of the algorithm and its application test examples, in which it corrects deviations from the ideal orbit caused by a drifting orbit corrector magnet and a drifting injection kicker magnet respectively. The modified algorithm takes measures to ensure the accuracy of the Gaussian process regression models and to improve the validity of the new trial solutions. We demonstrate that this is a promising development toward using safe, real-time tuning algorithms during accelerator programs to compensate for performance drift.

INTRODUCTION

Accelerator operation and commissioning benefit from online optimization algorithms that can be used to compensate for the differences between the accelerator design and the physical machine. Popular choices of optimization algorithms include the Nelder-Mead simplex method [1], the robust conjugate direction search [2], particle swarm optimization [3], and Bayesian optimization [4], which can efficiently provide optimal accelerator settings. However, during the optimization process, these algorithms may sample accelerator settings with unacceptably poor performances, making their use during the accelerator's normal operation ill-advised. This precludes their use in compensating for the deterioration of performance in particle accelerators, often caused by environmental factors.

The typical solution is to insert dedicated tuning periods in the schedule to re-optimize the accelerator after its performance deviates too much from the optimum, leading to undesired interruptions to the user program. Therefore, developing online optimization algorithms that can be used to tune for optimal accelerator performance while keeping the performance within an acceptable threshold during the tuning process would be an profitable direction of research.

In a previous study, a modified version of the Multi-Generation Gaussian Process Optimizer (MG-GPO) algorithm [5] was presented, in which it was applied to the kicker-bump matching problem [6]. This version has had its candidate point generation and selection mechanisms modified to provide a more accurate picture of the changing objective function landscape for the Gaussian process, which brings it closer to the original MG-GPO algorithm.

IMPROVEMENTS

Between the version of the code presented in [6] and the current version, several changes have been made in order to improve the performance, including the modification of the candidate proposal mechanisms, the reintroduction of an exploration term in the objective function selection, and some bug fixes.

Reintroducing the candidate proposal mechanisms of MG-GPO, which involve particle swarm optimization (PSO) and simulated binary crossover (SBX), albeit in a modified form, has improved the performance of the algorithm. The primary difference involves the time-dependence of the PSO portion of the algorithm. MG-GPO implicitly assumes a static optimum which can be approached. Thus the search range of PSO is, in addition to the distance between the optima of two generations, also a decreasing function of time. As the assumption no longer holds, that is, the optimum of the objective function changes over time, the search range decreasing over time would simply impair the performance of the algorithm. Therefore, the time dependence has been removed, allowing the algorithm to propose candidate points in a larger region to compensate for the drifting optimum.

Similarly, the re-addition of an exploration term aids in providing a more thorough picture of the objective function landscape to the GP, leading to more accurate predictions. Similarly to the candidate generation, the original MG-GPO algorithm has an exploration term which decreases over time. This is preferable for a static optimum, as the overall trend of the optimizer would be to approach that optimum, but with a drifting optimum, it would be questionable as the optimum may not approach a static value over time. Thus having a constant-value exploration term would allow the algorithm to have a better picture of the changing objective function landscape.

The two changes mentioned above are spiritually continuations of one of the modifications in [6], which involve changing the record of optimal points such that only the best points in the last two generations are included, i.e. optima using settings from too long ago are not considered, as the knob settings represented therein are not guaranteed to be optimal or even near-optimal at later times.

One change which proved to not be as successful as desired was the attempt to maintain safe evaluations based

* Work supported under DOE Contract No. DE-AC02-76SF00515
† yeung@frib.msu.edu

ISBN: 978-3-95450-252-3 ISSN: 2673-5350 doi: 10.18429/JACoW-IPAC2026-MOP6318

DETERMINISTIC METHODS AND BAYESIAN OPTIMIZATION ALGORITHMS APPLIED TO THE UH MĀNOA LINAC

N. Bidault*, S.H.P. Chan, C. Komo, S. Li, E. Valetov†, University of Hawai'i at Mānoa, HI, USA

Abstract

The University of Hawai'I at Mānoa (UHM) linac delivers up to 45 MeV electron beams to a Free-Electron Laser (FEL) oscillator. As the linac is being recommissioned for renewed FEL operation, we are developing simulation and optimization tools to recover operational settings and to explore the landscape of beam-manipulation techniques for future experimental apparatus. This paper benchmarks classical deterministic methods and Bayesian optimization (BO) algorithms on three representative beam-optics tuning scenarios using a beam dynamics simulation model developed in-house. For problems with only a few free parameters, classical methods converge reliably, while finite-difference derivative information improves the performance of constrained gradient-based solvers. For the higher-dimensional case, BO with a Gaussian Process (GP) surrogate and Sobol initialization provides a more robust path toward convergence. The emphasis is on the number of optimization iterations required for each scenario, in order to anticipate the computational cost of applying the same workflow to higher-fidelity models.

INTRODUCTION

The University of Hawai'i Free Electron Laser (UH FEL) facility, previously led by Prof. John Madey, comprises a compact S-band linear accelerator and an infrared FEL system originally developed as the Mark-III FEL undulator. The facility entered recommissioning in 2024 after a nearly decade-long standby period. A description of the recommissioning activities is reported in Ref. [1]. Additional research plans for the UHM accelerator and FEL laboratory were presented in Ref. [2].

The present work aims to benchmark optimization algorithms to determine the optimal beam transport parameters at the entrance to the FEL undulator and at an upstream Interaction Point (IP) used for the Inverse-Compton Scattering (ICS) experiment. This is a typical scenario where the Diagnostic Chicane beamline is used to shape the beam between the linac and the FEL. The Diagnostic Chicane beamline consists of a Chasman-Green Double Bend Achromat (DBA) configuration adapted to linear geometry; it offers several focusing doublet and triplet sections, allowing for the minimization of the transverse envelopes at the IP and a specific focusing of the beam at the FEL undulator entrance.

The optimization algorithms were implemented within a more general beam-dynamics simulation framework, FELsim [3]. The framework includes several widely used beam-dynamics codes (RF-Track [4], XSuite [5], COSY INFINITY [6]) and a fast linear beam-matrix-theory code developed in-house. We run the optimization algorithms on the fast linear beam-matrix-theory code as a proof of concept, before scaling the optimizers to other, more complex codes in future studies. We therefore do not aim to measure the code's ultimate execution time. Instead, we use it to estimate the number of iterations required to solve various beam-matching scenarios.

The simulation model includes quadrupoles with fringe fields, dipoles with wedge angles, and uses quadrupole currents as the optimization variables. The code returns the 6D beam parameters, and, in the context of the studies, the parameters of interest are the transverse Courant-Snyder (β_x, β_y, α_x, α_y), dispersion functions, and beam envelopes at selected locations along the transport line. The practical questions addressed here are which optimization algorithms are reliable for beam matching, how many evaluations they require, and how their performance changes with the number of free quadrupole settings. Three tuning scenarios of increasing complexity are considered. *Scenario A* uses a two-quadrupole doublet and adjusts the currents to meet the conditions $\alpha_x = 0$ and $\alpha_y = 0$ at a downstream observation point, representative of the transfer line between the linac and the first dipole of the DBA lattice. *Scenario B* extends the study to the entire Diagnostic Chicane beamline up to the undulator entrance (UE), covering the interaction point (IP). The problem is decomposed into 12 sequential stages; each stage optimizes the relevant subset of quadrupoles and passes the beam state to the following section. *Scenario C* is tested to optimize a high-dimensional parameter space by controlling 16 quadrupoles simultaneously over the IP–UE region. It combines the IP focusing constraints, an intermediate dispersion target, and the undulator Courant-Snyder matching into a single objective.

For all scenarios, the objective is the weighted mean-squared error between simulated observables and target values:

$$\mathrm{MSE} = \frac{\sum_i w_i \left(\frac{o_i - g_i}{s_i} \right)^2}{\sum_i w_i}, \tag{1}$$

where o_i is the simulated observable, g_i the target observable, s_i a normalization scale, and w_i is a weight for each observable.

* nbidault@hawaii.edu
† Department of Physics and Astronomy, Michigan State University, East Lansing, MI 48824, USA

Content from this work may be used under the terms of the CC BY 4.0 licence (© 2026). Any distribution of this work must maintain attribution to the author(s), title of the work, publisher, and DOI.

ISBN: 978-3-95450-252-3 ISSN: 2673-5350 doi: 10.18429/JACoW-IPAC2026-MOP6320

MACHINE LEARNING-ASSISTED CALIBRATION OF THE ACCELERATOR SIMULATOR HPSim

C. Leon, A. Scheinker, P. M. Anisimov
Los Alamos National Laboratory, Los Alamos, United States

Abstract

Manually calibrating the HPSim simulator to the LANSCE accelerator is time-intensive and demands substantial domain expertise. In this work, we investigate the use of machine learning (ML) to automate much of the calibration process and substantially reduce tuning time. Specifically, our focus is the calibration of the front-end of the accelerator, which involves obtaining the amplitudes and phases of the pre-buncher, main buncher and tank 1 of the drift tube linac (DTL). To get empirical data of the accelerator, we use current-phase curves obtained from absorber/collectors, both with the pre-buncher on and off. We derived features from the curves (e.g., standard deviation of each signal and average distance between them) and used these features to train the ML models. By combining classical ML methods—gradient-boosted decision trees and Random Forests—with a state-of-the-art transformer model, we achieve a significant speed-up of the calibration process, from about a month of human expert labor to 2–3 days of mostly computational processing.

INTRODUCTION

The LANSCE (Los Alamos Neutron Science Center) facility accelerates both positive and negative hydrogen ions, H^+ and H^-, respectively. Due to the enormous complexity of the machine, the intricate physics (e.g. space charge effects), and the limited amount of non-invasive diagnostics available, much of the analysis is done on the accelerator simulator HPSim [1]. Over time, the state of the accelerator drifts with normal wear-and-tear, age of the facility, equipment replacement, etc. As a result, HPSim periodically needs to be re-calibrated to reflect the current state of the machine.

Specifically, the amplitudes and phases of different components need to be tuned. For the front-end, we are concerned with three components: the pre-buncher (PB), the main buncher (MB) and Tank 1 of the DTL (T1) (see Fig. 1). An absorber/collector was placed behind tank 2, which was shut off. This produces a current vs. phase plot. The phase is with regard to the DTL nominal frequency of 201.25 MHz. Using the measurements from there, HPSim can be calibrated for the front-end of the accelerator. Specifically, we aim to determine five physical variables: the amplitude of T1 (T1Amp), the MB amplitude (MBAmp), main buncher phase (MBPhs), pre-buncher amplitude (PBAmp) and the pre-buncher phase (PBPhs). By convention, all phase variables are taken relative to tank 1.

There are many difficulties tuning PB, MB and T1 [2]. Manually calibrating HPSim is a laborious process and requires significant expertise. A brute-force approach is infeasible. To see this, based on the required resolution (see Table 1), approximately 5×10^{13} states would need to be evaluated. Using a high performance computing platform, we can currently run $\sim 5 \times 10^3$ simulations per day. Thus, an exhaustive search would require roughly 27 million years to complete.

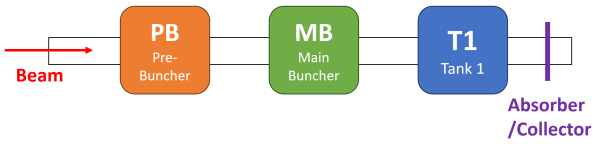

Figure 1: Simplified schematic showing the front-end of LANSCE and the relevant components.

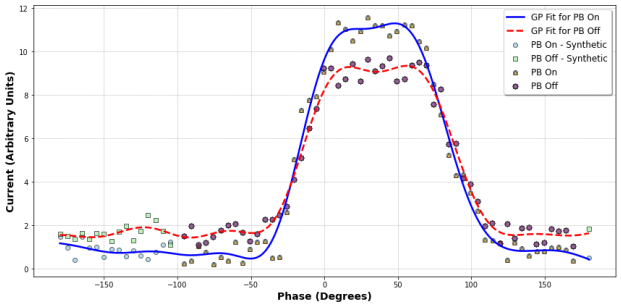

Figure 2: An example showing the raw data from the absorber/collector, the synthetic data created for the tails and mean functions from the Gaussian Process fits.

Hence, we turned to machine learning (ML) to speed the process up while making much of it automated. Specifically, we are interested in the inverse task of given experimental parameters, determine the physical variables of the accelerator components.

DATA

Table 1: Parameter Ranges and Resolution Requirements

Parameter	Range	Accuracy	Points
MBAmp	10–12	0.01	200
MBPhs	−180° to 180°	0.1 °	3600
PBAmp	3–5	0.01	200
PBPhs	−180° to 180°	0.1 °	3600
T1Amp	25–26	0.01	100

LANSCE Data The real world data from LANSCE. Two current vs. phase signals are obtained from an absorber/collector pair, one with the PB on and one with the PB off. For all that follows, only the H^+ beam will be used.

Using the raw signal comes with many issues. First, not all signals are sampled at the exact same phases. For exam-

Content from this work may be used under the terms of the CC BY 4.0 licence (© 2026). Any distribution of this work must maintain attribution to the author(s), title of the work, publisher, and DOI.

ISBN: 978-3-95450-252-3 ISSN: 2673-5350 doi: 10.18429/JACoW-IPAC2026-MOP6321

EVALUATING IN-CONTEXT LEARNING FOR ADVANCED LIGHT SOURCE EPICS PROCESS VARIABLE PREDICTION

A. Wu*, J. De Chant, T. Hellert, S.C. Leemann, G. Martino, A. Sulc
Lawrence Berkeley National Laboratory, Berkeley, CA, USA

Abstract

Large language models are becoming increasingly relevant for accelerator operations, where they assist with common tasks like retrieving historical data, preparing analysis scripts, and coordinating multi-step procedures. At the Advanced Light Source (ALS), these operators use their personal jargon (e.g. "sector 4 beam current") to search for the correct PV name from numerous channels, resulting in countless variations of naming conventions. Strong scores on general-purpose benchmarks do not indicate how well a model maps operator jargon to facility-specific EPICS process variable (PV) identifiers. Building on the semantic channel-finding benchmark, we evaluate chat-based large language models on two tasks using 101 ALS expert query–PV pairs. The first probes query-level grounding via single-item testing. The assessment is executed with varying inference-time cues, scored by character-wise correspondence (Levenshstein ratio). The second probes structural understanding by requiring the model to infer character-sequence mapping from the global naming-token vocabulary under prescribed edge-count budgets. We report precision, recall, combined retrieval score (F1), and token overlap (Jaccard similarity). Applied to 27 models, these evaluations split PV retrieval from structural understanding of hierarchical naming patterns, and offer strong dependency of end-to-end PV identification on the ALS control system's naming conventions.

INTRODUCTION

Large-scale experimental facilities, particle accelerators, synchrotron light sources, and free-electron lasers depend on the EPICS control system [1] to orchestrate tens of thousands of hardware channels. Each channel is identified by a Process Variable (PV) name: a structured string that encodes subsystem, location, device, and signal information based on facility-specific naming conventions. Operators routinely translate informal, jargon-rich requests, e.g., "sector 4 ion gauge values", into the correct PV names; automating or assisting this translation with large language models (LLMs) is an active research area [2, 3]. Facility interest in operational LLMs (assistants, log mining, scripted workflows) assumes models are grounded to the correct channels, but LLMs are not trained to "speak EPICS" or a given site's naming rules. A confident wrong PV is significant; it can point monitoring, alarms, or control at an unintended signal.

This paper explores how far current LLMs get on *non-trivial*, facility-grounded tasks: jargon-heavy EPICS-style identifiers and realistic operator queries that stress retrieval and plausible-but-wrong channel suggestions. Hellert *et al.* [2] lay out the conceptual and engineering path for production-ready, LLM-based semantic channel finding; reinforcing that proposal, our work measures that LLM capability via hard benchmark scores on an ALS instantiation of that program, not a deployed control-room integration. Despite rapid progress on general-purpose LLM benchmarks (*e.g.*, MMLU [4] and HumanEval [5]), none specifically target the mapping between operational language and EPICS identifiers. This matters because: (i) PV names follow domain-specific hierarchical conventions that do not appear in public training corpora; (ii) queries use facility shorthand and spoken abbreviations; (iii) correct answers are often sets of correlated channels rather than a single string. Following that framework [2], we instantiate semantic channel finding at the ALS [6] with two tasks: **Task 1** (*PV Name Prediction*) and **Task 2** (*Token Graph Reconstruction*).

Together they yield a reproducible audit of query-level PV retrieval and of naming token graph's structural knowledge, diagnosing hallucination-prone behavior on challenging inputs. Both tasks are fully automated with deterministic scoring, use leave-one-out protocol to avoid train–test leakage, and are evaluated on 27 chat-mode models from eight providers.

BENCHMARK DATASET

The dataset has 101 items, each pairing a natural-language operator request with at least one gold-standard EPICS PV name identified by ALS domain experts, reinforcing facility-grounded query-to-channel supervision in the framework described in [2]. Queries range from terse directives ("beam current") to multi-PV enumerations, e.g., "list the sector 11 ion pump pressures" → 6 PVs, and span beam diagnostics, RF systems, vacuum instrumentation, magnets, radiation monitors, and facility infrastructure.

The target PV names have many ALS conventions (e.g., `BRL2:Gamma:Dose:1Hour`, `SR04C___SHD2___AM00`); see Fig. 1. To expose these names' internal syntax, we tokenize each PV by splitting each non-alphabetic character (digits, underscores, colons, etc.). The alphabetic tokens are in this hierarchy: *System/Ring* → *Section/Type* → *Device/Attribute* → *Signal* → *Qualifier*, shown in Fig. 2. The full token vocabulary has 139 unique tokens connected by 178 gold undirected adjacency edges across 226 PV token sequences.

TASK 1: PV NAME PREDICTION

Task 1 tests the semantic channel-finding capability as seen in [2]: picking operators' correct EPICS PV identifiers.

* wua@lbl.gov; github.com/amyawu/als-language-model-evaluation.git

Content from this work may be used under the terms of the CC BY 4.0 licence (© 2026). Any distribution of this work must maintain attribution to the author(s), title of the work, publisher, and DOI.

ISBN: 978-3-95450-252-3 ISSN: 2673-5350 doi: 10.18429/JACoW-IPAC2026-MOP6322

STATUS OF OSPREY: A FRAMEWORK FOR AGENTIC AI IN CONTROL SYSTEMS

T. Hellert*[1], G. Martino[1], R. Lehe[1], A. Huebl[1], K. Iliev[1], S. C. Leemann[1], A. Sulc[1], J.-L. Vay[1], A. Wu[1], E. Zoni[1], Z. Zhang[2], N. Kuklev[3], M. Smith[4], H. Shang[4], C. Xu[4], A. Carpenter[5], N. Wang[6], and the Multi-Office Accelerator Team
[1]Lawrence Berkeley National Laboratory, Berkeley, CA, USA
[2]SLAC National Accelerator Laboratory, Menlo Park, CA, USA
[3]Fermi National Accelerator Laboratory, Batavia, IL, USA
[4]Argonne National Laboratory, Lemont, IL, USA
[5]Thomas Jefferson National Accelerator Facility, Newport News, VA, USA
[6]Cornell University, Ithaca, NY, USA

Abstract

Operating large-scale scientific facilities requires coordinating diverse subsystems, translating operator intent into precise hardware actions, and maintaining strict safety oversight. Language-model agents offer a natural interface for these tasks, but most existing approaches are not yet reliable or safe enough for production use. We introduce Osprey, a framework that wraps a coding agent in a control-room operator interface, a tool surface that reaches hardware through pluggable connectors for the control system used in our community, and a first-class component for natural-language search of facility electronic logbooks. The agent itself is treated as a replaceable component: operator interface, safety policy, tool servers, and connectors stay under facility control, while the agent backend can be swapped as the AI ecosystem evolves. A declarative build-profile mechanism lets each facility maintain its own configuration without forking the shared framework, keeping deployments reproducible across updates. Osprey has been deployed at several DOE accelerator facilities through the MOAT seed effort within the Genesis Mission. This paper presents the current framework architecture and reports on the substantial evolution Osprey has undergone over the past year.

INTRODUCTION

Operating an accelerator means coordinating many heterogeneous subsystems, translating operator intent into precise hardware actions, and maintaining strict safety oversight. Today, that work depends on graphical control interfaces and on tacit expert knowledge held by a small team. Reasoning across subsystems, finding the right control variable, recalling a past procedure, or assembling context during a fault still falls largely on individual operators.

Language-model coding agents have matured rapidly outside our community and are an attractive interface for this kind of work. Commercial agent products, however, do not come with the connectors, safety policy, facility knowledge, or operator workflows required for a control-room deployment. Closing that gap in a way that is reproducible across various facilities is the architectural problem this paper addresses.

Osprey's prior incarnation [1] was a self-maintained orchestrator with task extraction, capability classification, and planning implemented in-house on top of a fixed agent backend. A recent DOE workshop on agentic AI for user facilities [3] since recommended the opposite approach: domain-specific integration layers built atop general-purpose agent frameworks rather than competing ones, and a "co-pilot" pattern with default read-only access and human-approved writes. The architecture reported here is a substantial evolution in line with both findings — the in-house orchestrator has been retired in favor of a general-purpose coding agent, the periphery (operator interface, safety chain, tool servers, connectors) has been redesigned to stay under facility control while the agent itself becomes a replaceable component, and a declarative build profile lets each facility deploy and re-deploy its own configuration reproducibly. The framework has been deployed at seven DOE accelerator facilities under the MOAT seed effort within the Genesis Mission [4], with the Ariel logbook component presented separately in MOP6326 [5].

ARCHITECTURE

Figure 1 shows the resulting layout: a stable periphery, comprising the operator interface, the safety chain, the MCP tool surface, and the hardware connectors, wrapped around an externally-sourced coding agent, with the subsections below taking each layer in turn.

External Coding Agent

The coding agent at the center of Osprey — the software that turns a language model into a working assistant with tool access, conversation memory, and execution control — is the part of the AI stack moving fastest, with commercial and open-source projects releasing significant changes on a timescale of weeks. A small facility team cannot keep pace by maintaining its own, so Osprey treats this layer as an external dependency, swapped when the surrounding ecosystem makes a different choice attractive. The current reference is Claude Code, with the language model behind it

* thellert@lbl.gov

Content from this work may be used under the terms of the CC BY 4.0 licence (© 2026). Any distribution of this work must maintain attribution to the author(s), title of the work, publisher, and DOI.

ISBN: 978-3-95450-252-3 ISSN: 2673-5350 doi: 10.18429/JACoW-IPAC2026-MOP6330

HYBRID ONLINE OPTIMIZATION FOR HANDS-OFF TUNING OF THE ALS INJECTOR

G. Martino*, T. Hellert, S. C. Leemann, A. Sulc
Lawrence Berkeley National Laboratory, Berkeley, United States

Abstract

Reliable hands-off injector operation calls for fast, sample-efficient tuning under drift and competing goals (e.g., capture efficiency, energy spread, transmitted charge). We present an autotuning framework for the ALS injector combining complementary online optimizers for robust performance under strict machine-protection/operability constraints. The controller alternates methods based on objective structure and information gain, fusing diagnostics across longitudinal and transverse systems. The framework itself is generic: optimization procedures layer on top, and an operator or expert selects the appropriate one for the task—including a cold-start bring-up that recovers beam through staged charge gates, and a close-bounds optimization that refines around a known working point with narrowed search bounds. Both enforce safety via bounded steps and surrogate constraints. Initial studies on the ALS injector show that the automated procedures reach comparable working points faster than operator-driven tuning and with better run-to-run repeatability, while preserving capture within the booster's tight longitudinal acceptance.

INTRODUCTION

The Advanced Light Source (ALS) [1] at Lawrence Berkeley National Laboratory is a DOE user facility, and uninterrupted user delivery during topoff operation requires the injector to feed the booster reliably. Maintaining high performance day to day requires regular tuning across the injector's RF, focusing, steering, and timing systems. Today, this tuning is performed primarily by operators: the process is time-consuming, its results can vary from shift to shift, and it draws on the experience of a small group of experts.

Several method families have proven effective for online accelerator tuning, including Bayesian [2, 3], model-free descent (RCDS) [4], and extremum seeking [5]. On the injector's drifting landscape, where capture efficiency, energy spread, and transmitted charge compete, no single method dominates, and free-running any of them under strict machine-protection bounds wastes time on infeasible proposals. Our goal is hands-off, sample-efficient tuning that is robust under drift and safe by construction. We pursue this through hybrid orchestration of these complementary optimizers, diagnostic fusion across longitudinal and transverse subsystems, and a layered safety envelope that constrains every proposal regardless of which optimizer produced it.

HYBRID OPTIMIZATION FRAMEWORK

Architecture

The framework, `tuning_scripts` shown in Fig. 1, is a modular monorepo built around a FastAPI [6] + CLI core with a Dash [7] web UI and an EPICS hardware plugin. A plugin layer isolates hardware specifics (live ALS, ALS read-only, and simulator), keeping the optimization core environment-agnostic and portable to other facilities. Redis [8]-backed job tracking lets the web UI, scripts, and agents drive runs over a shared Representational State Transfer (REST) API; the API in turn communicates with Redis via the Redis Serialization Protocol (RESP). The framework is generic by design: predefined optimization procedures—cold-start bring-up, close-bounds refinement, and others—layer on top of the same core, with the operator or expert selecting the appropriate procedure for the task at hand.

Optimizers and Surrogates

The optimizer pool is built primarily on Xopt [9] and spans several method families. Local deterministic descent uses RCDS [4] and Nelder-Mead. Model-based search relies on Bayesian optimization with upper-confidence-bound (UCB) and expected-improvement (EI) acquisitions, complemented by BAxUS [10] for high-dimensional problems on adaptive nested subspaces. Multi-objective and evolutionary search are covered by NSGA-II [11] and its constrained variant CNSGA, with hypervolume-improvement acquisitions [12] for the Bayesian counterpart. Continuous-control tuning uses extremum seeking (ES) [5], which is robust on noisy landscapes. Random sampling and Latin-hypercube sampling (LHS) supply broad exploration. Surrogate models are configurable: a BoTorch [13] Gaussian process is the default for sample-efficient continuous tuning, while tree-based ensembles—random forests [14] and extra trees [15]—scale to larger evaluation budgets and natively handle mixed continuous, categorical, and conditional parameter spaces.

Safety and Operability

Safety is enforced as a layered envelope that is optimizer-agnostic: the same bounds and step-size constraints apply to every optimizer in the pool, so BO, RCDS, ES, and LHS all share the same operability guarantees. Every proposal is constrained to bounded knob ranges and a bounded step size ($\|\Delta x\| \leq \delta$), an approach with prior precedent for safe Bayesian optimization on production accelerators [16]. These constraints are enforced server-side: the API validates each request against the active bounds before actuation,

Content from this work may be used under the terms of the CC BY 4.0 licence (© 2026). Any distribution of this work must maintain attribution to the author(s), title of the work, publisher, and DOI.

* gmartino@lbl.gov

ISBN: 978-3-95450-252-3 ISSN: 2673-5350 doi: 10.18429/JACoW-IPAC2026-MOP6336

ACTIVE SUPERVISION FOR AGS BUNCH-MERGING WITH LLM-BASED REINFORCEMENT LEARNING*

Y. Zhao†[1], K. Brown[2], A. Edelen[3], Y. Gao[2], E. Hamwi[4], G. H. Hoffstaetter[4], A. Kasparian[5], D. Kuzovkova[4], W. Lin[2], T. Miceli[6], J. Morris[2], M. Schram[5], V. Schoefer[2], A. Sukhanov[2], S. Tajne[2], J. Unger[4], K. Zeno[2], Y. Wang‡[1]
[1]Industrial and Systems Engineering Department, Rensselaer Polytechnic Institute, Troy, NY, USA
[2]Collider-Accelerator Department, Brookhaven National Laboratory, Upton, NY, USA
[3]SLAC National Accelerator Laboratory, Menlo Park, CA, USA
[4]CLASSE, Cornell University, Ithaca, NY, USA
[5]Thomas Jefferson National Accelerator Facility, Newport News, VA, USA
[6]Fermi National Accelerator Laboratory, Batavia, IL, USA

Abstract

Radio-frequency (RF) bunch-merging gymnastics is used in the RHIC heavy-ion program to combine individual source pulses into single bunches with suitable intensity. Preserving intensity and emittance during these gymnastics requires careful coordination of the voltages and phases of RF cavities at several harmonic numbers, which is labor-intensive and fragile against machine drift. Recent work using a physics-based simulator of the Brookhaven Alternating Gradient Synchrotron (AGS) has shown that reinforcement learning (RL) can learn effective merge configurations. RL is data-intensive and requires many training interactions with the environment. Large language models (LLMs) have recently demonstrated the ability to extract patterns from large, noisy data and to integrate domain knowledge into the control loop, making them an attractive aid for tuning complex accelerator systems. However, domain adaptation (i.e., prompt engineering, finetuning, etc.) is always required for deploying LLM in the target domain and has not been investigated in particle accelerators. To fill this gap, we propose an active supervision framework in which the LLM-based teacher first transfers general control principles from human operators to the student agent. Then, the student agent further finetunes the control policy by interacting with the simulator/experiments with improved sample efficiency.

INTRODUCTION

The Relativistic Heavy Ion Collider (RHIC) at Brookhaven National Laboratory (BNL) provides the world's only high-energy polarized proton beam and is therefore in a unique position to study the spin structure of the nucleon [1, 2]. The polarized proton beam is generated by an Optically Pumped Polarized Ion Source (OPPIS) and then accelerated through the Linac, Booster, and Alternating Gradient Synchrotron (AGS) before injection into RHIC [3, 4].

Preserving polarization along this chain is a difficult task because the spin of each particle evolves slightly differently as it samples different fields along its trajectory, leading to depolarization at numerous spin resonances [5,6]. To reduce space charge effects and improve the beam polarization, the beam bunches are split in the Booster into two or four smaller bunches. The smaller bunches with reduced space charge will limit polarization loss during particle acceleration [7,8].

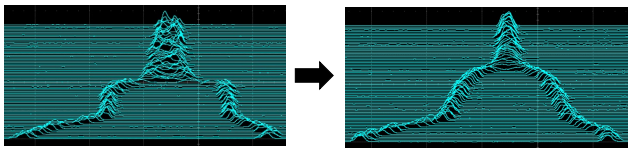

Figure 1: Mountain-range wall-current-monitor (WCM) signal before (left) and after (right) RF bunch-merging gymnastics in the AGS [9].

Before transfer to RHIC, the lower-intensity, smaller bunches are recombined into a single high-intensity bunch with suitable intensity near the extraction energy of AGS. This step is known as radio-frequency (RF) bunch-merging gymnastics. It is essential for preserving both intensity and emittance. As shown in Fig. 1, the mountain-range wall-current-monitor (WCM) signal evolves from multiple separated bunches into a single merged bunch after correction.

At present, the AGS bunch-merging process relies heavily on expert interpretation of mountain range WCM measurements. Experts evaluate the evolution of bunch widths and center-of-charge oscillations, and then iteratively adjust the RF voltage and phase programs. While this procedure can produce acceptable merges, it is labor-intensive, difficult to reproduce, and fragile against machine drift. Maintaining high merge quality requires constant monitoring and retuning, which motivates machine learning methods that can learn robust RF settings and sustain consistent performance during the AGS bunch-merging process.

Recent work has shown that reinforcement learning (RL) can provide an effective framework for the AGS bunch-merging process. Gao *et al.* [10] used an inverse-reinforcement-learning (IRL) approach on a Bmad-based simulator and showed that expert merge behavior can be learned as an RF control policy. In addition, Gao *et al.* [9] de-

* This work was supported in part by the grants DE-SC0024287 and DE-SC0025351.
† zhaoy23@rpi.edu
‡ wangy88@rpi.edu

Content from this work may be used under the terms of the CC BY 4.0 licence (© 2026). Any distribution of this work must maintain attribution to the author(s), title of the work, publisher, and DOI.

ISBN: 978-3-95450-252-3 ISSN: 2673-5350 doi: 10.18429/JACoW-IPAC2026-MOP6338

BEAM-BASED CHARACTERISATION OF BPM ELECTRONICS THERMAL SENSITIVITY AFTER TWO DECADES OF OPERATION*

D. J. Scott †, SLAC, Menlo Park, CA, USA

Abstract

Beam-based measurements of the thermal sensitivity of beam position monitor (BPM) electronics were performed in SPEAR a third-generation storage ring after more than twenty years of routine user operations. Controlled building-temperature excursions were applied to two equipment buildings containing key BPM front-end and digitiser racks. Using orbit- and charge-normalised BPM signals and independent temperature logging, we performed lag-aware regression to estimate effective position-versus-temperature coefficients for each BPM, and compared several alternative temperature-driver models (global, per-building and hybrid). The method was applied to two measurement campaigns, months apart, with different ambient conditions. The results show clearly distinguishable building-level responses and reproducible patterns within subsets of BPMs, but also highlight strong correlations between temperature, beam conditions and slowly varying lattice effects.

INTRODUCTION

SPEAR BPM pickup buttons are installed in the accelerator tunnel, while the associated front-end and digitiser electronics are housed in surface equipment buildings, mainly Building 132 and Building 116. Building 132 was deliberately temperature-cycled using the HVAC system. Building 116 was not deliberately cycled and provides a comparison population. In this paper, thermal sensitivity is used in a beam-based sense, denoting an effective fitted coefficient between an electronics-building temperature driver and the BPM orbit in μm/°C. It should not be interpreted as a unique intrinsic electronics constant for each BPM, since it depends on the selected temperature driver, fitted lag, beam conditions and any remaining correlated orbit motion. Two fast orbit feedback (FOFB) off measurements are used for the primary analysis. Experiment 1 is the clean controlled measurement. Experiment 2 is a repeat measurement under different ambient and machine conditions, but with stronger coherent beam motion.

MEASUREMENTS

For each measurement, rack-temperature readbacks from the BPM electronics buildings were reduced to mean-centred temperature drivers (shown in Fig. 1). Experiment 1 gave the cleanest Building 132 excitation and the lowest apparent background structure. Experiment 2 repeated the measurement under different ambient and machine conditions, but showed larger coherent orbit structure.

* Work supported by DoE Contract DE-AC02-76SF00515

† dscott@slac.stanford.edu

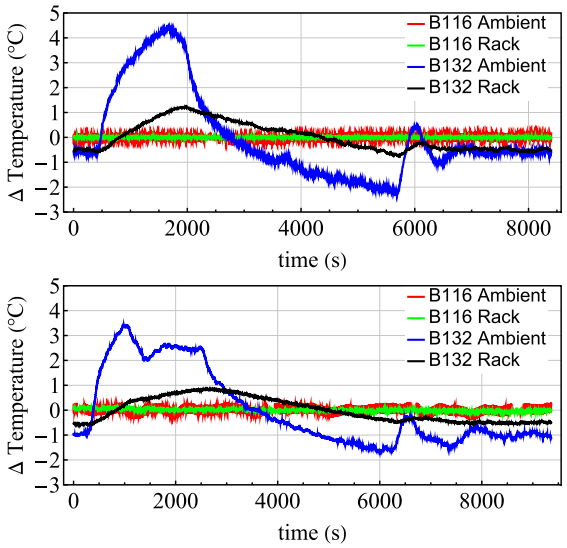

Figure 1: Mean-centred rack-temperature driver for Experiments 1 (top) and 2 (bottom).

ANALYSIS METHOD

For each BPM and plane, lag scans were used to allow for delayed electronics response to the building-temperature change. The reported coefficient was obtained from a current-adjusted linear model:

$$x_i(t) = a_i + \beta_{T,i} T_b(t - \tau_b) + \beta_{I,i} I(t) + \epsilon_i(t)$$

where x_i is the measured BPM position for BPM i in the selected plane, T_b is the rack-temperature driver for the relevant electronics building, I is the stored beam current, and τ_b is the fitted building-temperature lag. The reported coefficient is $\beta_{T,i}$, in μm/°C. The current term reduces false attribution of current-dependent BPM response to temperature. The regression was tested using both ordinary least squares (OLS) and robust Huber fitting. Huber fitting reduces the influence of transient outliers and poorly modelled points, and was used as a robustness check. The Huber fits gave the same qualitative building-level conclusions as OLS. OLS is used for the reported coefficients because the fitted slopes, residuals, confidence intervals and R^2 values are simpler to interpret. The R^2 value is the fraction of variance in the fitted BPM position trace explained by the selected regression model. It is used as a fit-quality indicator, not as proof that all explained motion is purely thermal. Error bars on individual BPM coefficient plots show the 95% confidence interval for the fitted temperature coefficient. They do not include model dependence or repeatability between measurements.

Content from this work may be used under the terms of the CC BY 4.0 licence (© 2026). Any distribution of this work must maintain attribution to the author(s), title of the work, publisher, and DOI.

ISBN: 978-3-95450-252-3 ISSN: 2673-5350 doi: 10.18429/JACoW-IPAC2026-MOP6344

XBPM CALIBRATION AND SIMULATIONS AT SIRIUS

A. G. Oliveira-Filho*, G. Ascenção, S. Luiz, J. Vieira
Brazilian Synchrotron Light Laboratory, Campinas, Brazil

Abstract

X-ray Beam Position Monitors (XBPMs) at SIRIUS/LNLS employ a blade-type design [1] and are not yet fully operational due to ongoing calibration challenges. Minor asymmetries in construction and variations in blade gains can distort the calculated beam position. We applied standard linear-transformation corrections and extended them using a simulated annealing algorithm to optimise the suppression matrix. We also developed a simulation tool that models blade response to radiation for various configurations of blade angles, inter-blade distances, electronic gains, and input beam profiles.

INTRODUCTION

Beam position monitors (BPMs) are an important tool for beam tracking and diagnostics. A common type of device has four sensors that are used to determine the beam position by measuring the field effects on them and then calculating the position using the standard equations for the ratios x_R and y_R,

$$x_R = \frac{(A+D)-(B+C)}{A+B+C+D}, \qquad y_R = \frac{(A+B)-(C+D)}{A+B+C+D}, \tag{1}$$

where A, B, C, and D represent the signals from the sensors (arranged clockwise in a square). The scaled positions, x and y, are then calculated by

$$x = k_x x_R + \delta_x, \qquad y = k_y y_R + \delta_y, \tag{2}$$

where k_x and k_y are the dimensional calibration constants and δ_x and δ_y are the respective offsets. This determination of the beam position is possible in the central region of the device, where the sensors' response is approximately linear.

In the case of an electron beam, which may be considered point-like in a transversal cross-section, Eq. (1) are usually valid in the central region of the BPM. However, in the case of the X-ray beam, the measurement of the beam position may be distorted by its profile, which is relatively large and has a non-uniform intensity distribution. Moreover, minor differences in the construction of the X-ray BPM (XBPM) and variations in the electronic gains of its sensors can amplify these distortions, making the calculated beam position inaccurate.

* arnaldo.filho@lnls.br

XBPM CALIBRATION

We used standard calibration methods to determine the XBPM response, as described by Yang [2] and Chuang *et al.* [3], and then extended these methods by optimizing the transformation matrix using simulated annealing. We also developed a simulation algorithm to model the response of the blades to the incident X-ray radiation, which allows us to calculate the apparent beam position for different configurations of blade angles, inter-blade distances and electronic gains. The simulation accepts a range of input beam profiles, including two-dimensional Gaussian distributions or outputs from radiation transport simulators, and can apply transformations such as stretching and rotation to these profiles.

Standard Calibration Methods

As a calibration method, the XBPM may be displaced to generate a grid of points whose positions are known from the displacement. Beamlines at SIRIUS do not yet have a displacement system for the XBPMs themselves. Alternatively, the calibration was performed by applying orbit bumps to the electron beam at each sector of beamlines with XBPMs, generating such grids [4]. These positions are verified against the beam angles calculated from BPM measurements propagated to the XBPM locations. There are some issues with this approach, however: the bumping process depends on machine study availability, since bumps may interfere with the beam orbit; it is time-consuming for all the XBPMs (the calibration with this method is performed one at a time), and there may be uncertainties associated with wakefields, background noise, and a non-linear trajectory of the electron beam at the source. Nevertheless, the results obtained look consistent with simulations and previous results from the literature [2, 3]. Figure 1 shows the grid of points generated for the Manaca beamline (SIRIUS) as an example. The grid obtained from the XBPM measurements (blue circles in Fig. 1), using Eq. (1), can be compared to the nominal positions (red crosses).

To address these issues, we performed measurements in four SIRIUS beamlines by bumping the electron beam at each corresponding sector and calculating the beam positions with the XBPMs. We followed the procedures described by Chuang *et al.* [3] to apply corrections to the calculated beam position. They consist of applying a linear transformation directly to the signals (A, B, C and D), replacing Eq. (1), before calculating the beam position with Eq. (2). The transformation is calibrated by analyzing the blade behavior along central-symmetry lines, which are the lines where the response of pairs of blades is expected to be equal. Along the central horizontal line, blades A and D are expected to have the same response, as well as blades B and C; along the central vertical line, blades A and B are

Content from this work may be used under the terms of the CC BY 4.0 licence (© 2026). Any distribution of this work must maintain attribution to the author(s), title of the work, publisher, and DOI.

ISBN: 978-3-95450-252-3 ISSN: 2673-5350 doi: 10.18429/JACoW-IPAC2026-MOP6348

BEAM-INDUCED HEATING AND THERMAL ANALYSIS FOR THE EIC HSR CRYOGENIC HELICAL MAGNET AND BPM ASSEMBLY*

M. Sangroula†, M. Anerella, B. Brenton, D. Gassner, K. Hock, C. Liu, F. Micolon, V. Ptitsyn
Brookhaven National Laboratory, Upton, NY, USA

Abstract

The EIC Hadron Storage Ring (HSR) reuses the RHIC yellow ring with substantial reconfiguration. A major challenge is mitigating beam-induced heating of cryogenic components caused by the shorter hadron bunches and an average beam current three times that of RHIC. In addition, large transverse beam offsets at injection due to helical magnet itself generate asymmetric resistive-wall losses in the cryogenic BPM region. To limit these losses, the HSR helical magnet assembly uses a new copper-plated stainless-steel beam pipe with an amorphous-carbon coating. This paper presents heating and thermal analysis of the EIC HSR cryogenic helical magnet and BPM assembly. Thermal simulations show narrow thermal margin for the helical magnet unit, and adequate margin for the BPM assembly.

INTRODUCTION

The Electron-Ion Collider (EIC) [1–4] leverages the existing yellow ring of the Relativistic Heavy Ion Collider (RHIC) as the Hadron Storage Ring (HSR), with substantial upgrades. The HSR accumulates an average beam current of 0.69 A from 290 bunches with a 60 mm rms bunch length in the highest charge-per-bunch scenario, which produces the maximum resistive wall (RW) heating. In addition, the hadron beam undergoes a large horizontal offset of up to ± 20 mm [5] to synchronize bunch collisions with the electron beam. This large radial offset significantly enhances RW heating [6, 7].

In this paper, we investigate beam-induced heating and perform thermal analysis of the HSR cryogenic helical dipole magnet and BPM assembly. Our earlier papers on beam-induced heating and thermal analysis for other EIC components can be found in [8–12]. To perform the thermal analysis, we compute heat loads arising from beam-induced RW losses and electron cloud effects. We then incorporate these heat loads into ANSYS simulations with appropriate boundary conditions to determine the steady state temperature distribution within the helical dipole magnet and BPM assembly.

HSR CRYOGENIC HELICAL MAGNET AND BPM ASSEMBLY GEOMETRY

The HSR helical magnet assembly consists of four superconducting dipole magnet units and a centrally located BPM. All these components reside inside a cryostat (gray tank with a blue helical stripe) as shown in Fig. 1. The total assembly length is ~12.2 m, with each helical dipole unit measuring ~2.4 m. There are two types of helical dipole magnet assemblies; snakes and rotators. The snakes rotate the spin 180° across all energies and the rotators are used at store energies to rotate the spin into the horizontal plane. The EIC HSR will have total of 6-snakes and 2-rotators [13, 14].

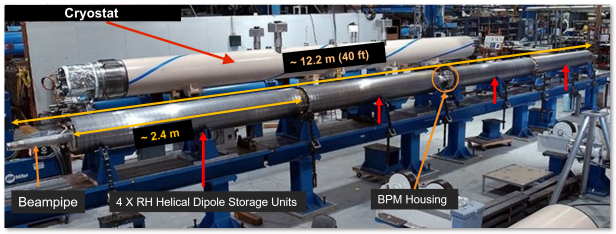

Figure 1: Geometry of the HSR cryogenic helical magnet assembly.

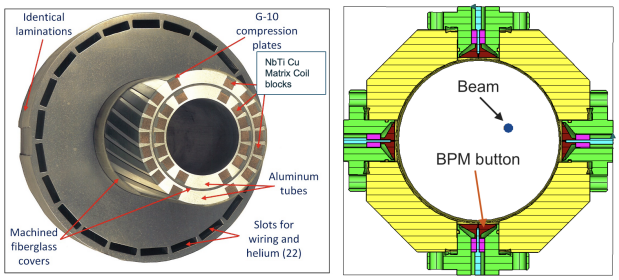

(a) Helical dipole unit (b) Cryogenic BPM

Figure 2: Helical magnet assembly, cross-sectional view.

Fig. 2 shows cross-sectional views of the two sections of the helical magnet assembly. The existing RHIC helical dipole, Fig. 2(a), inner beam pipe is made of stainless steel 316L. It also includes two concentric aluminum cylinders of specified thickness that house the helical Nb–Ti coil windings. These aluminum cylinders are externally wrapped with Kelvar and fiberglass (epoxy) to provide electrical insulation and to contain electromagnetic forces from the coil windings [15]. The iron yoke consists of laminated extra-low-carbon steel to enhance magnetic performance. The outer cold mass shell is fabricated from stainless steel 304L.

To adapt the helical dipole for the HSR, we replace the existing (inner) beam pipe with a new stainless steel 316L pipe coated with a 25 μm copper layer, followed by a nanometer-scale (~300-500 nm) amorphous carbon film. The copper layer reduces beam-induced heating, while the amorphous carbon suppresses secondary electron yield (SEY).

Fig. 2(b) depicts the cross-sectional view of the cryogenic BPM showing BPM-buttons and dielectric materials (magenta color). We adopt our original orthogonal button

* Work supported by Brookhaven Science Associates, LLC under Contract No. DE-SC0012704 with the U.S. Department of Energy.
† corresponding author

Content from this work may be used under the terms of the CC BY 4.0 licence (© 2026). Any distribution of this work must maintain attribution to the author(s), title of the work, publisher, and DOI.

ISBN: 978-3-95450-252-3 ISSN: 2673-5350 doi: 10.18429/JACoW-IPAC2026-MOP6352

DIGITAL TWIN DEVELOPMENT FOR THE NASA SPACE RADIATION LABORATORY*

W. Lin†,[1], P. Adams[1], K. Brown[1,2], T. D'Ottavio[1], L. Hajdu[1], E. Hamwi[1], K. Hock[1], G. Hoffstaetter[1,3], M. McCarthy[1], J. Morris[1], S. Nemesure[1], T. Olsen[1]
[1]Brookhaven National Laboratory, Upton, NY, United States
[2]Stony Brook University (ECE), Stony Brook, NY, United States
[3]Cornell University (CLASSE), Ithaca, NY, United States

Abstract

The NASA Space Radiation Laboratory (NSRL) at Brookhaven National Laboratory simulates the galactic cosmic ray space radiation environment by delivering high energy heavy ions and protons to the NSRL Target Room for radiobiology studies and microelectronics testing. The AGS Booster synchrotron delivers beams to the NSRL beamline via resonant slow extraction. NSRL tuning is difficult due to the non-linearity from slow extraction and octupoles, and the beam shape is optimized empirically by operators. To streamline and improve NSRL operations, we develop a real-time digital twin for the beam line, starting from the extraction bumps in the Booster and extending all the way to the targets. This digital twin allows users to both load live settings from the real system to the online model, and to send model suggested settings to the real machine. We demonstrate that an accurate digital twin can improve operations at the NSRL beam line.

INTRODUCTION

The NASA Space Radiation Laboratory (NSRL) facility at Brookhaven National Laboratory (BNL) is designed to study the radiation effects of a wide variety of heavy ion species over different beam intensities and energies. Figure 1 shows the NSRL acceleration chain. The beam is first injected into the AGS Booster synchrotron via one of three transfer lines: LINAC to Booster (LtB), EBIS to Booster (EtB), or TVdG to Booster (TtB). In the Booster, the beam is accelerated to kinetic energies ranging from 50 to 2500 MeV/n (MeV per nucleon) and then extracted to the NSRL beam line using resonant slow extraction [1].

In this work, we present the development and operational application of a digital twin (DT) framework for the NASA Space Radiation Laboratory (NSRL) facility at Brookhaven National Laboratory. The framework combines physics-based accelerator models with live machine data to support beam diagnostics, interpretation, and tuning. The implementation centers on three principal elements: the Booster extraction system, the NSRL beam line optics, and the integration of these models within a control-oriented DT architecture that enables virtual diagnostics and model-guided operation.

* Work supported by Brookhaven Science Associates, LLC under Contract No. DE-SC0012704, No. DE-SC0024287, and No. DE-SC0025351 with the U.S. Department of Energy and by NASA (Contract No. T570X).
† wlin1@bnl.gov

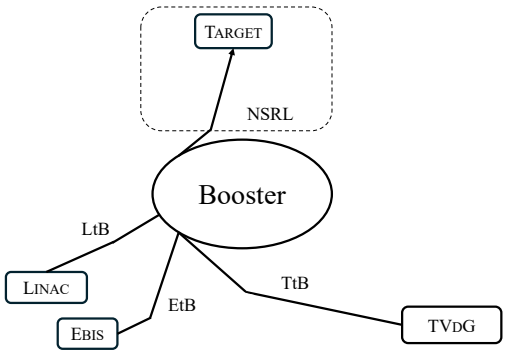

Figure 1: Schematic layout of the NSRL line, the AGS Booster, and the three injector lines (LINAC, EBIS, and TVdG). Adapted from [1].

DIGITAL TWIN ARCHITECTURE

A digital twin is defined as "a set of virtual information constructs that mimics the structure, context, and behavior of a natural, engineered, or social system (or system-of-systems), is dynamically updated with data from its physical twin, has a predictive capability, and informs decisions that realize value" [2]. Two-way interaction between virtual and physical systems is widely regarded as a defining characteristic of a digital twin framework.

In accelerator applications, we adopt the following definitions:

- Virtual Accelerator (VA): A model-based representation of a physical accelerator constructed from simulations, surrogate models, or appropriate simplifications suitable for describing the machine state [3].
- Digital Shadow: A VA that remains continuously synchronized with the physical accelerator, but does not control machine settings.
- Digital Twin: A VA that is continuously synchronized with the physical system with bidirectional interaction.

Figure 2 illustrates how a VA-based digital twin framework integrates into the operational workflow of a particle accelerator. In this work, the virtual accelerator underlying the DT is based on nonlinear, multi-particle tracking implemented in Bmad [4] and SciBmad [5]. The DT systems described in this paper operate in two modes, as shown in Fig. 3. In monitor mode, the system functions as a Digital Shadow, providing continuous virtual diagnostics without altering machine settings. In control mode, the DT supports model-based evaluation of machine configurations, control studies, and software validation workflows. This frame-

Content from this work may be used under the terms of the CC BY 4.0 licence (© 2026). Any distribution of this work must maintain attribution to the author(s), title of the work, publisher, and DOI.

ISBN: 978-3-95450-252-3 ISSN: 2673-5350 doi: 10.18429/JACoW-IPAC2026-MOP6355

SELECTION OF TRANSVERSE DIAGNOSTICS TO MEASURE FEW-MICRON BEAM MODULATIONS IN THE NANOPATTERNED MICROBUNCHING EXPERIMENT*

R. Margraf-O'Neal†, A. Ody, J. Power, Argonne National Laboratory, Lemont, United States
J. Maxson, Cornell University, Ithaca, United States
R. Ryne, Lawrence Berkeley National Laboratory, Berkeley, United States
H. Xu, N. Yampolsky, Los Alamos National Laboratory, Los Alamos, United States
G. Ha, B. N. Temizel Ozdemir, Northern Illinois University, DeKalb, United States
A. Halavanau, N. Majernik, SLAC National Accelerator Laboratory, Menlo Park, United States
G. Andonian, J. Phillips, J. Rosenzweig, University of California, Los Angeles, United States
D. Abell, University of Maryland, College Park, College Park, United States

Abstract

A nanopatterned microbunching collaboration has been formed to test the production of electron microbunches by rotating transverse beamlets into the longitudinal plane using the emittance exchange (EEX) beamline of the Argonne Wakefield Accelerator (AWA). This mechanism has been suggested, such as by the Compact X-ray Free-Electron Laser (CXFEL) group at Arizona State University, to hold the potential to make short-wavelength free-electron lasers (FELs) more compact. Our collaboration will pattern AWA's 44 MeV electron beam with a TEM grid to produce micro-scale beamlets that will become mico-to-nano scale microbunches in the longitudinal plane. Characterizing an array of beamlets with a modulation period at the few micron scale and a low, single pC scale total charge presents challenges in achieving the necessary transverse resolution and signal strength. These proceedings will detail the diagnostics explored to characterize these transverse modulations. We will discuss the merits and challenges of each approach in relation to our application, and progress towards demonstrating these desired diagnostics.

INTRODUCTION

The nanopatterned microbunching experiment [1, 2] is sketched in Fig. 1. 44 MeV electrons are scattered by a 12.5 µm TEM grid, creating transverse beamlets that are then demagnified with quadrupoles [3] to 3 µm, and converted through emittance exchange to 800 nm microbunching.

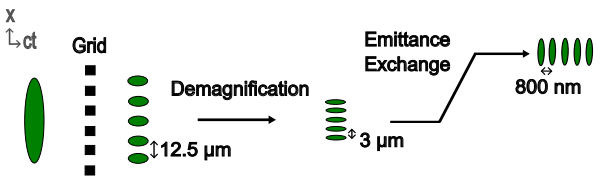

Figure 1: Nanopatterned microbunching experiment.

To tune the quadrupole demagnifier, we need to characterize the micron-scale transverse beamlet pattern after demagnification. However, resolving a single or sub-micron patterned electron beam at 44 MeV is non-trivial. Figure 2 shows a focused 44 MeV electron beam at AWA on a 100 µm thick YAG:Ce screen. The imaging system (BFLY-PGE-23S6M-C Blackfly camera and Nikon AF FX 200mm f/4D IF-ED Lens, with a 381 mm extension between the lens and camera) had 1.3 µm/pixel, and 6.2 µm resolution as measured on a USAF target. However, the smallest RMS beam size measured was $\sigma = 40$ µm. This large size may be due to a blurring of the beam from the YAG:Ce screen, YAG saturation from high charge intensity, an inability to focus the beam to a smaller spot, or a combination of effects.

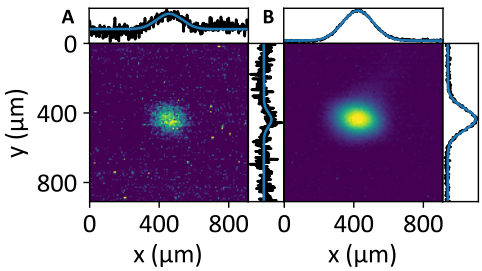

Figure 2: Electron beam measurements at AWA on a 100 µm thick YAG:Ce screen. A) 0.3 pC beam charge, $\sigma_x = 74$ µm, $\sigma_y = 40$ µm, B) 3 pC beam charge, $\sigma_x = 88$ µm, $\sigma_y = 62$ µm.

To better understand this system, we reviewed the literature for high-resolution transverse electron beam diagnostics measuring beams similar to our 44 MeV, ≈1 pC beam. This proceedings will summarize our investigation of transverse diagnostic methods and their applicability to the nanopatterned microbunching experiment.

RESOLVING MEV-SCALE BEAMS

Table 1 presents several examples of high-resolution transverse diagnostics catered towards our goal of measuring a 3 µm modulation at 44 MeV and 1 pC. Since our goal is to measure a patterned beam, not a single beam, resonant cavity beam position monitors have been excluded.

Screen Methods

Screen-based diagnostics provide single-shot 2D profiles.

* This work is supported by the U. S. Department of Energy, under contract No. DE-AC02-06CH11357.
† rmargrafoneal@anl.gov

Content from this work may be used under the terms of the CC BY 4.0 licence (© 2026). Any distribution of this work must maintain attribution to the author(s), title of the work, publisher, and DOI.

ISBN: 978-3-95450-252-3 ISSN: 2673-5350 doi: 10.18429/JACoW-IPAC2026-MOP6357

DESIGN OF IONIZATION PROFILE MONITORS AT THE INTEGRABLE OPTICS TEST ACCELERATOR (IOTA) FACILITY AT FERMILAB

M. Mwaniki*, P. Snopok, Illinois Institute of Technology, Chicago, United States
R. Ainsworth, N. Banerjee, M. Bressler, K. Carlson, D. Edstrom,
B. Fellenz, H. Piekarz, A. Romanov, A. Semenov, R. Thurman-Keup,
Fermi National Accelerator Laboratory, Batavia, United States

Abstract

The Integrable Optics Test Accelerator (IOTA) at Fermilab is transitioning from an electron-beam facility to a proton-beam facility for studies of nonlinear accelerator optics and space-charge-dominated proton beams. This project involves commissioning and fabricating Ionization Profile Monitors (IPMs) to enable beam-profile measurements at IOTA. In general, IPMs operate on the principle of residual-gas ionization by the beam to generate a beam profile. This work focuses on a mechanical design that leverages a controlled injection of noble gases, primarily Argon, as the ultra-high vacuum of the IOTA ring provides insufficient residual gas for ionization. Efforts to understand vacuum integration to ensure compatibility with the storage ring environment, to integrate real-time data acquisition systems, and to commission the IPMs will be discussed. This project provides a versatile diagnostic tool that supports IOTA's role as a testbed for larger-scale accelerator facilities and contributes to the broader understanding of beam physics in high-intensity, high-space-charge regimes.

INTRODUCTION

The Integrable Optics Test Accelerator (IOTA) is a 40 m storage ring at Fermilab designed as a testbed for advanced beam physics research. IOTA is currently transitioning from electron operation to a proton program. The proton program [1] will use 2.5 MeV protons to study incoherent tune shifts from space charge and coherent instabilities that would lead to uncontrolled beam losses by transverse emittance measurements similar to the Fermilab Booster.

Ionization Profile Monitors (IPMs) are being designed for non-destructive transverse profile measurements at IOTA [2]. Table 1 shows the design parameters of the IPMs to meet these needs. IPMs are widely used in accelerators, and their operating principle is well established. A primary beam, in this case at 2.5 MeV, passes through the IPM chamber and ionizes the residual gas therein. This makes the IOTA IPMs one of the lowest-energy IPM applications to date, comparable to the 4.2 MeV/u measurements performed at LEIR [3, 4].

The baseline IOTA residual gas level currently consists of H_2, H_2O, NH_3, CO and CO_2 at 1×10^{-10} Torr. This level is too low to generate sufficient ionization for reliable profile reconstruction. To increase the signal, the vacuum in the IPM region will be locally raised via a controlled injection of 1×10^{-9} Torr of a noble gas and maintained at that pressure in the IPM chamber. Four ion pumps [5] at both boundaries of the IPM region will confine the elevated pressure to the IPM region as seen in Fig. 1. The IPM chamber, as seen in Fig. 2, is supplied with a 16 kV high voltage that creates an electric field to guide ions generated during the ionization, toward the two stacked micro-channel plates (MCPs). The MCPs amplify the ion signal by liberating electrons each time an ion enters a channel, and this process cascades, releasing additional electrons. The amplified charge is then collected on a strip detector that is aligned parallel to the proton direction. The strips enable the signal to be digitized for profile reconstruction.

Table 1: IOTA IPMs Design Parameters

Parameter	Design	Range
Number of IPMs	2	
Total insertion length	0.808 m	
HV gap, D	57 mm	
HV cage length	93 mm	
Strips per IPM	60	
Strip width	0.35 mm	
Pitch, Δ	0.5 mm	
IPM Voltage, V_0	16 kV	4–30
Interg. Time	1 turn	1–100
Vacuum, P_{IPM}	1×10^{-9} Torr	$10^{-9\ldots-7}$

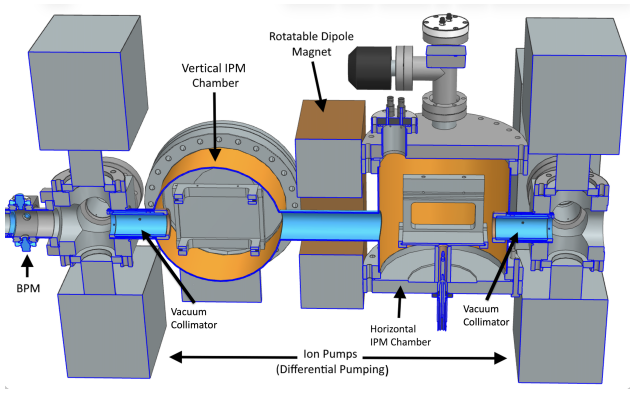

Figure 1: The IOTA IPM region (0.808 m) with a horizontal and a vertical IPM chamber, a rotatable dipole trim in the middle, and four end-mounted ion pumps connected using vacuum collimators.

Motivation

The objective of this work is to optimize the spatial and temporal resolution of the IPMs for beam intensities between

* mmwaniki@hawk.iit.edu

Content from this work may be used under the terms of the CC BY 4.0 licence (© 2026). Any distribution of this work must maintain attribution to the author(s), title of the work, publisher, and DOI.

ISBN: 978-3-95450-252-3 ISSN: 2673-5350 doi: 10.18429/JACoW-IPAC2026-MOP6370

DIAGNOSING GHOST BUNCHES WITH THE UPSTREAM EXTINCTION MONITOR IN THE Mu2e EXPERIMENT * †

R. Hensley‡, E. Prebys, University of California, Davis, Davis, United States
A. Gaponenko, Fermi National Accelerator Laboratory, Batavia, United States

Abstract

The Mu2e experiment has a stringent requirement for extinction of the pulsed proton beam, referring to the elimination of particles between proton bunches to a relative level of 10^{-10}, which means a single out-of-time particle in the inter-pulse gaps for every 250 complete proton pulses. As the construction of the Mu2e experiment nears completion, it is crucially important to make an early measurement of the beam extinction in its current condition. Hence the upstream extinction monitor was constructed and operated to probe for problems in the proton pulse structure or a higher than expected incidence rate of out-of-time particles.

The analysis in this work comes from data taken in March 2026. The long data run showed a significant presence of out-of-time particles from ghost bunches in the Delivery Ring approximately 388 ns after the centers of the main proton pulses. These are hypothesized to be the result of a combination of a RF frequency mismatch, particle space charge, and machine impedance during the rebunching sequence in the Recycler Ring, which can lead to particles leaking into adjacent buckets, but further studies and simulations are needed to confirm this.

INTRODUCTION AND MONITOR

The Muon-to-Electron Conversion Experiment (Mu2e) at Fermilab [1] searches for the neutrinoless conversion of a muon into an electron in the field of a nucleus, which would be a clear sign of physics beyond the Standard Model. The experiment uses a pulsed proton beam to produce muons, and has a stringent requirement for beam extinction, which refers to the elimination of out-of-time particles between the proton bunches. Basic extinction is defined as the ratio of out-of-time particles to in-time particles, and must be at a level of 10^{-10}, which means a single out-of-time particle in the inter-pulse gaps for every 250 complete proton pulses.

The beam extinction is crucial for the experiment, as out-of-time particles can produce background events that mimic the signal of muon-to-electron conversion, and therefore must be minimized to achieve the desired sensitivity. The Mu2e proton-pulse timing and a representative Upstream Extinction Monitor detector element are shown in Figs. 1 and 2.

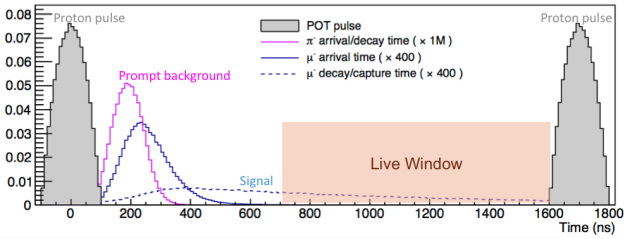

Figure 1: Mu2e proton-pulse timing and the live search window between pulses.



Figure 2: A quartz Cherenkov radiator with PMT assembly used in the Upstream Extinction Monitor.

Beam Extinction

Proton delivery to the Delivery Ring starts with RF manipulations in the Recycler Ring. The 53 MHz RF system quickly turns off, after which the 2.5 MHz RF system adiabatically ramps up, reshaping batches from the Booster Ring in preparation for transfers of individual bunches of protons into the Delivery Ring (note the frequency mismatch between the 53 MHz buckets and the 2.5 MHz buckets). Once one bunch is orbiting the Delivery Ring, resonant extraction starts wherein one small pulse of protons is transferred into the M4 Beamline each time the proton bunch completes a revolution. Resonant extraction completes after approximately 25,440 revolutions of the bunch around the Delivery Ring. Given the 1695 ns Delivery Ring revolution period, this establishes the basic time structure for the pulsed proton beam at an estimated preliminary extinction level of 10^{-4}.

The remaining portion of the 10^{-10} extinction requirement is achieved via the operation of a system known collectively as the AC Dipole, a series of collimators and dipole magnets synchronized in phase to the transfers of the proton pulses. The dipole magnets give transverse kicks to any out-of-time beam while allowing in-time particles to pass through unaffected.

Upstream Extinction Monitor Setup

Previous work has been done to install and commission an Upstream Extinction Monitor [2, 3] in the M4 beamline.

* This work was supported by the U.S. Department of Energy, Office of Science, Office of High Energy Physics under Award Number DE-SC0009999.
† Fermilab Report Number: FERMILAB-CONF-26-0327-PPD
‡ rshensley@ucdavis.edu

Content from this work may be used under the terms of the CC BY 4.0 licence (© 2026). Any distribution of this work must maintain attribution to the author(s), title of the work, publisher, and DOI.

ISBN: 978-3-95450-252-3 ISSN: 2673-5350 doi: 10.18429/JACoW-IPAC2026-MOP6371

REAL TIME LONGITUDINAL BEAM MEASUREMENTS IN THE CROCKER NUCLEAR LABORATORY ISOCHRONOUS CYCLOTRON*

L. Knudson†, Crocker Nuclear Lab., Davis, United States
M. Backfish, E. Prebys, University of California, Davis, Davis, United States

Abstract

The UC Davis Crocker Nuclear Laboratory (CNL) operates a 76-inch isochronous cyclotron dating to the 1960s, with limited internal beam diagnostic instrumentation. Direct measurements of the Cyclotron beam are challenging due to the harsh environment, including high radiation, strong magnetic fields, RF interference, and spatial constraints. A novel beam probe has been developed for transverse bunch structure and longitudinal phase measurements in a 15 mm square transverse profile with 16 independent pixels. The probe consists of a segmented fast plastic scintillator array coupled via fiber optics to external Silicon Photomultipliers (SiPMs), mounted on a radially translating probe. Bunch and phase information are measured and analyzed in real time, with continuously updating visualizations available to operators with sub nano second time resolution. Additionally, offline analysis is performed to support the development of simulations and improve understanding of beam dynamics in the CNL Cyclotron. The Fast Beam Probe opens the door to improved beam stability, more accurate modeling, and future integration with automated control systems at CNL.

MOTIVATION

The CNL Cyclotron is currently commissioning a production process for the medical isotope astatine-211 [1]. It was determined that an internal target location within the machine would be used for isotope production. To characterize the beam at this location, a stack of Type HD-V2 Gafchromic film was mounted on a radially translating probe and exposed under the proposed production conditions. A large 12.7 mm square transverse beam spot was observed, indicating significant radial and vertical beam oscillations that were not expected by CNL personnel. As no existing diagnostic hardware is capable of directly resolving these distributions, the Fast Beam Probe has been commissioned to provide direct measurements of beam dynamics inside the Cyclotron.

FAST BEAM PROBE

The Fast Beam Probe is capable of measuring longitudinal phase and several sequential buckets across 16 independent channels arranged in a 4 × 4 grid spanning 15 mm square. The detector consists of a 4 × 4 array of fast plastic scintillators (Eljen EJ-232Q 0.5% benzophenone) coupled to UV-VIS fused silica fibers, seen in Fig. 1, which transmit

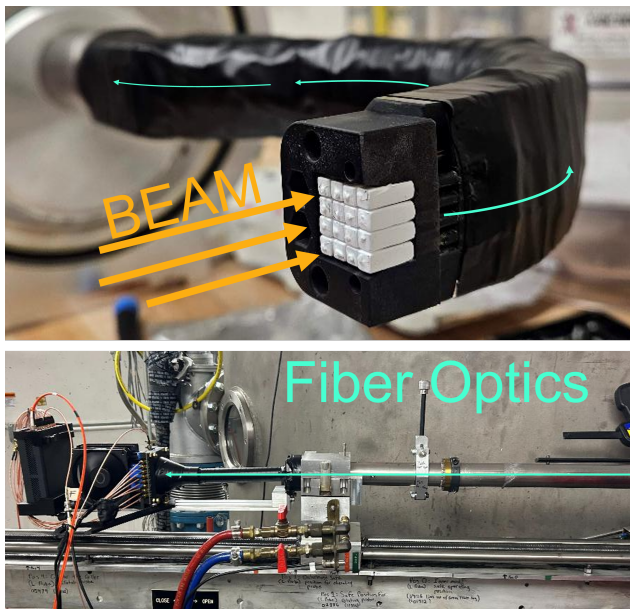

Figure 1: Fast Beam Probe setup showing the in cyclotron detector head (top) and the air side readout with fiber optics and SiPM coupling (bottom).

light to an Onsemi 16-channel SiPM array (Array-J) outside the Cyclotron [2–4]. All SiPM channels and the Cyclotron RF are digitized by a 16+1 channel, 12-bit, 5 GS/s CAEN digitizer (DT5742) [5].

The digitizer was operated in continuous trigger mode at an approximate 1700 Hz acquisition rate with a 400 ns acquisition window, capturing 9 RF buckets[1] per event at a sampling rate of 2.5 GS/s. A peak finding algorithm is used to identify the leading edge of each SiPM pulse, establishing beam arrival time relative to RF with a constant but arbitrary phase offset. From this analysis, both the longitudinal beam phase and transverse bunch profile are extracted. Further details regarding the Fast Beam Probe construction and signal analysis can be found in [6, 7]

All digitized events are processed in real time using a parallelized Python framework and C++ modules to perform peak detection and RF timing determination. The system provides live visualization of beam phase evolution to operators, displaying a primary phase plot as a two dimensional histogram of beam phase over time and a secondary plot with mean phase and intensity of all channels. Channels can be dynamically selected as the primary display without loss of historical information. In addition to the live analysis, all raw waveforms are saved for offline analysis.

* Work supported by US Department of Energy Grant DE-NA0003996 and University Office of the President (UCoP) grant LF-20-653232
† lsknudson@ucdavis.edu

[1] For an RF frequency of 22.5 MHz and the largest digitizer window at 2.5 GS/s, 9 buckets are contained within each acquisition.

Content from this work may be used under the terms of the CC BY 4.0 licence (© 2026). Any distribution of this work must maintain attribution to the author(s), title of the work, publisher, and DOI.

ISBN: 978-3-95450-252-3 ISSN: 2673-5350 doi: 10.18429/JACoW-IPAC2026-MOP6372

PARALLEL BEAM-BASED ALIGNMENT AT THE SIRIUS STORAGE RING

V. D. de Souza*[1], F. H. de Sá, L. Liu, M. M. S. Velloso[1], X. R. Resende
Brazilian Synchrotron Light Laboratory, Campinas, Brazil
[1]also at Gleb Wataghin Institute of Physics, University of Campinas, Campinas, Brazil

Content from this work may be used under the terms of the CC BY 4.0 licence (© 2026). Any distribution of this work must maintain attribution to the author(s), title of the work, publisher, and DOI.

Abstract

In fourth-generation light sources such as SIRIUS, tight orbit tolerances require accurate knowledge of BPM offsets with respect to the magnetic center of nearby quadrupoles. This work presents the implementation and experimental validation, at the SIRIUS storage ring, of the Parallel Beam-Based Alignment (PBBA) method proposed by X. Huang. This method allows the simultaneous calibration of many BPMs. Simulations and machine experiments demonstrate that the method reduces the overall BBA time from several hours to a few minutes while preserving accuracy at the level of a few micrometers, making it practical for routine accelerator operation.

INTRODUCTION

Fourth-generation synchrotron light sources, such as SIRIUS, are designed to achieve ultra-low emittances and extremely high brightness, imposing stringent requirements on beam orbit stability. SIRIUS is the Brazilian fourth-generation synchrotron light source operated by the Brazilian Synchrotron Light Laboratory (LNLS) [1]. Its storage ring operates with a 3 GeV electron beam with a natural emittance of 250 pm·rad and a circumference of 518.4 m [2].

At SIRIUS, the transverse position of the beam is monitored by 160 Beam Position Monitors (BPMs). While BPMs offer sub-micrometer precision in measuring orbit variations, their absolute accuracy is limited to the order of hundreds of micrometers – larger than the typical magnet misalignment errors. Accurate BPM offset calibration is therefore essential for orbit-based feedbacks and corrections, to keep the optics close to the nominal, preserve dynamic aperture, coupling control, beam lifetime and the overall machine performance.

Beam-Based Alignment (BBA) is the standard experimental method to determine these offsets by using the beam as a probe to locate the quadrupole magnetic centers [3–6]. In the traditional serial BBA, the beam is steered near each BPM-quadrupole pair using orbit bumps, the quadrupole gradient is modulated by $\pm\Delta K$, and a linear or quadratic regression of the orbit distortion versus beam position identifies the BPM offset. This procedure is inherently serial: the calibration of all 160 BPMs at SIRIUS usually takes 6–8 hours [7], making it a bottleneck for routine operation.

This paper describes simulation studies and experimental validation of the Parallel BBA (PBBA) method proposed by X. Huang [8], which allows the simultaneous calibration of many BPMs. Simulations using the SIRIUS storage ring model and machine experiments are presented to validate the approach and assess its accuracy relative to the traditional serial BBA method.

* vitor.souza@lnls.br

PARALLEL BBA

In the PBBA method [8], BPM-quadrupole pairs are separated in several groups. The strengths of all the quadrupoles associated with the BPMs of a given group are then modulated simultaneously in two steps ($\vec{K}^+$ and $\vec{K}^-$). The resulting orbit distortion, called the Induced Orbit Shift (IOS), is defined as

$$\vec{\xi}(\vec{\theta}) = \vec{u}(\vec{\theta}, \vec{K}^+) - \vec{u}(\vec{\theta}, \vec{K}^-), \tag{1}$$

where $\vec{u}(\vec{\theta}, \vec{K}^\pm)$ is the closed orbit read on all BPMs for corrector kicks $\vec{\theta}$ and quadrupole strengths $\vec{K}^\pm$. When the orbit passes through the magnetic center of all modulated quadrupoles, the IOS must vanish. PBBA therefore seeks the corrector kick changes $\Delta\vec{\theta}$ that minimize – or ideally null – the measured IOS via

$$\Delta\vec{\theta} = -\mathbf{R}^\dagger\,\vec{\xi}, \tag{2}$$

where $\mathbf{R}$ is the IOS response matrix and $\mathbf{R}^\dagger$ its pseudo-inverse. Once the IOS is driven to its minimum, the readings of the BPMs in the set yield their offsets directly. The procedure is applied iteratively until convergence. We refer to the original paper for further details [8].

The definition of the sets of BPMs whose offset can be determined simultaneously is accelerator dependent. One important rule to be satisfied is that orbit correctors and BPMs must be interleaved between consecutive BPM-quadrupole pairs of the group in order to properly correct the IOS. Additional constraints arise from tune shift and coupling: simultaneous modulation of many quadrupoles and skew quadrupoles can shift the betatron tunes and increase transverse coupling, perturbing the optics away from nominal. Groups are therefore selected to keep the tune shift and coupling small while maximizing the number of BPMs processed at once.

SIMULATIONS

Before machine tests, the PBBA algorithm was validated using the SIRIUS storage ring model. Simulations were carried out with the FAC/LNLS simulation suite, which comprises *Trackcpp* [9] for particle tracking, *pyAccel* [10] and *APSuite* [11] for orbit and optics calculations, and *pyModels* [12] for the accelerator models. BPM offsets were randomly assigned according to Gaussian distributions with rms ~1 mm – more than 10 times larger than the typical offset drifts observed at the machine.

ISBN: 978-3-95450-252-3 ISSN: 2673-5350 doi: 10.18429/JACoW-IPAC2026-MOP6374

SPEAR3 BOOSTER RESPONSE MATRIX MEASUREMENT*

D. Khan†, J. Safranek, D. Scott
SLAC National Accelerator Laboratory, Menlo Park, CA, USA

Content from this work may be used under the terms of the CC BY 4.0 licence (© 2026). Any distribution of this work must maintain attribution to the author(s), title of the work, publisher, and DOI.

Abstract

In this paper, we present the orbit response matrix (ORM) measurements for the SPEAR3 booster obtained using a set of Libera Spark ERXR beam-position processors. The turn-by-turn acquisition capability of these processors enables continuous tracking of the beam trajectory throughout the full energy ramp prior to injection into SPEAR3. This dataset provides sufficient resolution to extract the booster's optical functions and measure the orbit response matrix. The resulting refinements to the booster machine model have contributed to improved understanding of beam-loss mechanisms, thereby enabling future development of algorithms to improve beam capture from the linac-to-booster (LTB) transport line and injection efficiency into SPEAR3.

INTRODUCTION

The SPEAR3 injector complex consists of a 120 MeV linac, a 3 GeV booster synchrotron, and the associated transport lines used to deliver beam into the SPEAR3 storage ring [1]. The booster synchrotron operates at a 10 Hz repetition rate with a resonant-driven White circuit that accelerates the beam from 120 MeV to 3 GeV in approximately 37 ms. During each top-up cycle, approximately 50 single-bunch injections are transferred through the injector chain and accumulated in the storage ring.

Accurate diagnostics of the booster orbit are essential for understanding injection efficiency, beam capture dynamics, and beam losses during the acceleration cycle. The original booster beam-position monitor (BPM) system at SPEAR3 was based on a multiplexed analog architecture developed in the early 1990s [2]. While adequate for routine operations, the system provided limited temporal resolution and was capable of orbit measurements only every 1.5 ms during the ramp cycle.

To address these limitations, Libera Spark-ERXR BPM processors were installed and evaluated in the SPEAR3 booster [3, 4]. The processors provide high-resolution turn-by-turn acquisition throughout the full energy ramp and allow continuous monitoring of the beam orbit from injection through extraction (~ 85k turns). In addition to operational diagnostics, the improved BPM performance enables detailed accelerator physics studies, including optics characterization and orbit response matrix analysis.

The work presented here builds upon previous studies demonstrating the suitability of Libera Spark systems for booster diagnostics [5–8]. By measuring the dispersion at injection energy, the tune evolution along the acceleration cycle, and finally, the ORM we are able to more comprehensively characterize the booster, enabling the future development of advanced optics and correction algorithms for operation.

BOOSTER BPM SYSTEM

The SPEAR3 booster synchrotron uses stripline BPMs distributed around the ring. In the current configuration, several booster BPMs were connected directly to Libera Spark-ERXR processors through RG223 coaxial cables though a future upgrade to LM240, or even LM400, is planned. The Spark processors were configured for the booster RF frequency near 358 MHz. Signals from the stripline pickups were filtered and sampled using PLL-controlled analog-to-digital converters operating at 109.8 MHz.

The Libera Spark processors sampled the beam signals 49 times per revolution during the 446 ns booster revolution period. This configuration enables turn-by-turn measurements throughout the entire acceleration cycle, including the beam capture process immediately following injection, longitudinal damping during acceleration, and the extraction phase. The processors demonstrated sufficient sensitivity to resolve single-bunch motion during the full ramp even when operated using the existing lossy coaxial infrastructure [2].

TURN-BY-TURN BOOSTER MEASUREMENTS

Orbit And Sum Signal

The upgraded BPM system provides detailed observation of beam dynamics during the booster cycle. Figure 1 shows representative turn-by-turn beam motion measured from a booster BPM immediately following injection.

Continuous acquisition over the 37 ms acceleration ramp revealed modulation structures in both beam position and beam intensity during the low-energy portion of the cycle. These oscillations are associated with the longitudinal capture dynamics of the injected beam. Approximately five to seven S-band bunches from the linac are injected into a single booster RF bucket, and the bunches subsequently damp into a single equilibrium bunch through synchrotron radiation and longitudinal phase-space evolution. The measurements indicate that the damping process is largely complete after approximately 17 ms into the acceleration cycle. Prior to this point, the observed orbit oscillations reflect complex synchrotron motion and capture dynamics.

There exists a vertical orbit distortion near the top of the energy ramp associated with the extraction septum magnet pulse. Measurements show an approximately 1 mm vertical orbit shift during extraction magnet excitation and can provide important information for minimizing beam loss during transfer into the Booster-to-SPEAR3 (BTS) transport line.

* Work supported by the U.S. DOE Contract DE-AC02-76SF00515.
† donish@slac.stanford.edu

ISBN: 978-3-95450-252-3 ISSN: 2673-5350 doi: 10.18429/JACoW-IPAC2026-MOP6375

INTEGRATION OF X-RAY DIAGNOSTICS INTO FAST ORBIT FEEDBACK FOR LOCAL SOURCE STABILIZATION AT NSLS-II

S. Kongtawong[1,2], M. Capotosto[1], K. Ha[1], Y. Hidaka[1], J. Mead[1], D. Padrazo[1], T. Shaftan[1], Y. Tian[1], G. Wang[1], H. Yan[1]
[1]NSLS-II, Brookhaven National Laboratory, Upton, NY, USA
[2]Synchrotron Light Research Institute, Nakhon Ratchasima, Thailand

Content from this work may be used under the terms of the CC BY 4.0 licence (© 2026). Any distribution of this work must maintain attribution to the author(s), title of the work, publisher, and DOI.

Abstract

We present an accelerator-based X-ray beam stabilization approach that integrates X-ray beam position monitor (XBPM) signals into the fast orbit feedback (FOFB) system at NSLS-II. A high-speed electrometer and fiber-optic data link were developed to transmit XBPM position data to the storage-ring feedback controller at a 10 kHz rate. On the accelerator side, the XBPM signal is incorporated into the FOFB infrastructure as a virtual beam position monitor, allowing photon beam motion to be corrected through the electron beam orbit using fast corrector magnets. Experimental tests demonstrate suppression of dominant beamline vibration peaks near 27 Hz and 120 Hz when the feedback is enabled. These results demonstrate the feasibility of integrating photon diagnostics into accelerator feedback systems for improved X-ray beam stability and motivate the development of unified photon–electron feedback architectures for routine operation.

INTRODUCTION

Modern synchrotron experiments increasingly require high stability of the delivered X-ray beam, particularly for techniques that rely on precise beam positioning. Storage rings typically employ fast orbit feedback systems to stabilize the electron beam orbit using signals from electron beam position monitors (BPMs). While this approach effectively suppresses electron orbit motion, it does not directly measure the photon beam delivered to beamlines. As a result, residual X-ray beam motion may occur when disturbances originate from beamline optics rather than from the electron beam itself.

To address this limitation, we developed a system that integrates X-ray beam position monitor signals into the existing FOFB infrastructure at the Hard X-ray Nanoprobe (HXN) beamline of the National Synchrotron Light Source II.

In this approach, the X-ray beam position is used as the feedback signal while the electron beam orbit acts as the actuator through fast corrector magnets. This paper describes the architecture of the system and demonstrates its operation for source stabilization using X-ray diagnostics.

SYSTEM ARCHITECTURE

The X-ray feedback system integrates photon beam diagnostics with the accelerator FOFB infrastructure, as illustrated in Fig. 1. X-ray beam position is measured using diamond X-ray beam position monitors installed along the Hard X-ray Nanoprobe beamline of the National Synchrotron Light Source II. The XBPM electrodes generate photocurrent proportional to the incident X-ray beam intensity, and beam position is computed using the difference-over-sum method. The resulting beam position signals serve as the input to the feedback system.

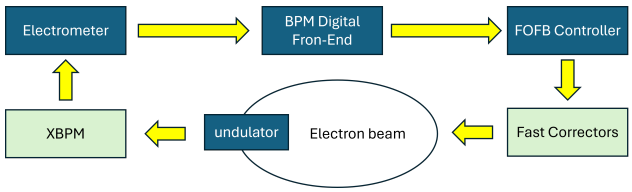

Figure 1: Conceptual architecture of the X-ray feedback system. X-ray beam position measured by the XBPM is digitized by a high-speed electrometer and transmitted to the accelerator feedback system through the BPM digital front-end. The fast orbit feedback controller drives fast corrector magnets to adjust the electron beam orbit near the insertion device, forming a closed-loop X-ray feedback system.

The XBPM currents are read out using a four-channel high-speed electrometer developed at NSLS-II. The electrometer digitizes the detector currents using high-resolution analog-to-digital converters and performs real-time signal processing in FPGA logic to calculate beam position and intensity [1]. The FPGA processes the electrode signals and generates beam position data streams at approximately 10 kHz, providing a data rate suitable for integration into the existing feedback system [2].

The processed XBPM position data are transmitted from the beamline electronics to the accelerator feedback system through a high-speed optical fiber link. This fiber-optic connection provides a low-latency communication path between the beamline instrumentation and the storage-ring control system. At the accelerator side, a digital front-end module receives the transmitted data and converts them into a format compatible with the BPM data stream used by the FOFB system [3]. In this configuration, the X-ray beam position signal can be treated as an additional virtual BPM input by the controller without modification of the core feedback algorithm.

The feedback system calculates the required orbit correction and drives fast corrector magnets distributed around the storage ring. To confine the feedback action near the beamline insertion device, a local orbit bump was implemented using multiple fast corrector magnets to control the electron beam position and angle at the insertion device source point.

ISBN: 978-3-95450-252-3 ISSN: 2673-5350 doi: 10.18429/JACoW-IPAC2026-MOP6376

TEST-BENCH MEASUREMENT OF POWER-SUPPLY, MAGNET, AND VACUUM-CHAMBER BANDWIDTH AT NSLS-II

S. Kongtawong[1,2,*], Y. Hidaka[1], K. Ha[1], G. Wang[1], D. Bergman[1], M. Capotosto[1], J. Escallier[1], M. Charumaneeroj[1], Y. Tian[1], R. Todd[1], H. Dave[1], L. Doom[1], D. Padrazo[1], T. Shaftan[1]
[1]Brookhaven National Laboratory, Upton, NY, USA
[2]Synchrotron Light Research Institute, Nakhon Ratchasima, Thailand

Abstract

In 2019, the NSLS-II fast orbit feedback (FOFB) system was upgraded by reducing BPM and Cell Controller latency, increasing the closed-loop bandwidth from about 250 Hz to 400 Hz. The dynamic behavior of the power supply, magnet, and vacuum chamber, however, had not been directly measured and was treated as a lumped delay. To provide baseline parameters for the NSLS-IIU upgrade, we developed a dedicated test bench and remeasured these components. The existing fast-corrector power supplies show bandwidths of about 4.5 kHz horizontally and 1.5 kHz vertically, while the magnet and chamber responses are near 10–15 kHz with an overall response time of about 10 μs. We also characterized a newer power-supply regulator design and tuned it to achieve a 6 kHz bandwidth in both planes for use in the upgraded FOFB system. Incorporating these measurements into a physics-based model yields good agreement with observed system behavior. These results provide the first full experimental characterization of the fast-corrector chain at NSLS-II and establish the baseline for designing next-generation hardware for NSLS-IIU.

INTRODUCTION

Fast orbit feedback (FOFB) systems require high closed-loop bandwidth to suppress beam motion. At NSLS-II, the FOFB system was upgraded in 2019 by reducing latency in the BPM and cell controller, increasing the closed-loop bandwidth from approximately 250 Hz to 400 Hz in the horizontal plane [1]. Despite this improvement, the dynamic behavior of key components, including the power supply, fast corrector magnet, and vacuum chamber, was not directly measured and was instead treated as a lumped response. This limits the ability to accurately model the system and to identify bandwidth bottlenecks for further upgrades. To address this, a dedicated test bench was developed to measure the transfer function and latency of these components and to provide baseline parameters for the NSLS-IIU upgrade. The system response is described using a physics-based model that relates the transfer function to the power-supply and vacuum-chamber dynamics, digital processing effects, and total system latency,

$$G(s) = \frac{1}{(s+p_{\mathrm{ps}})(s+p_{\mathrm{chamber}})}\left(\frac{1-e^{-sT_{\mathrm{avg}}}}{s}\right) \times \left(\frac{1-e^{-sT_{\mathrm{zoh}}}}{s}\right) e^{-sT_{\mathrm{latency}}} H_{\mathrm{PID}}, \quad (1)$$

where p_{ps} and p_{chamber} represent the power-supply and vacuum-chamber poles, T_{avg} is the averaging time, T_{zoh} is the zero-order hold, T_{latency} is the total system latency, and H_{PID} is the controller response. The measured parameters are incorporated into this model to predict closed-loop performance and to evaluate upgrade scenarios for the FOFB system [2].

TEST-BENCH SETUP AND MEASUREMENT METHOD

A dedicated test bench was developed to characterize the dynamic response of key components in the fast orbit feedback system. The setup consists of a function generator used to excite the system over a range of frequencies and an oscilloscope to measure the input and output signals. A spare fast corrector magnet and vacuum chamber were used to represent the system under realistic conditions, as shown in Fig. 1.

Pickup coils were designed to measure the magnetic field response of the magnet and chamber. Different coil geometries and numbers of turns were evaluated to optimize signal sensitivity and bandwidth. The coils were mounted using a custom 3D-printed holder to ensure repeatable positioning during measurements. The transfer function of each component was obtained by applying a sinusoidal excitation over a range of frequencies and measuring the corresponding response. The amplitude and phase were extracted from the input and output signals to construct the frequency response. Latency was determined from time-domain measurements by applying a step-like input signal and measuring the delay between the input and output responses. This procedure was applied consistently to the power supply, vacuum chamber, and fast corrector magnet to enable direct comparison.

RESULTS

The latency of the fast-corrector power supply was measured using time-domain step excitation, as shown in Fig. 2. The delay between the input signal and the magnetic field response is approximately 10 μs. The transfer function of the power supply was then measured, as shown in Fig. 3.

* skongtawong@bnl.gov

Content from this work may be used under the terms of the CC BY 4.0 licence (© 2026). Any distribution of this work must maintain attribution to the author(s), title of the work, publisher, and DOI.

ISBN: 978-3-95450-252-3 ISSN: 2673-5350 doi: 10.18429/JACoW-IPAC2026-MOP6379

IMPLEMENTATION AND DESIGN OF A LASER NEUTRALIZER IN THE LANSCE LEBT

C. Rohde†, H. Andrews, E.-C. Huang, M. Kay, D. Kleinjan, A. Poudel, N. Regis,
Los Alamos National Laboratory, Los Alamos, NM, United States

Abstract

We present the design and installation of a laser wire scanner for H- bunches at the Los Alamos Neutron Science Center (LANSCE) in the low energy beam transport section of the LANSCE beam line. The presented design is modular and supports a variety of input laser options, including diameters, powers and wavelengths. A custom-built laser interaction point, and drift chamber were added to the current beam line to photo-ionize the H- secondary electrons and collect the freed electrons in a custom-built, high-speed Faraday cup detector. Our chamber design is modular and constructed to minimally impact LANSCE production, while also allowing for in-run cycle reconfigurations. This setup will allow testing of a variety of laser system diagnostics configurations at the LANSCE facility.

INTRODUCTION

The LANSCE facility uses a combination of invasive and non-invasive diagnostics to characterize the beam position. While the invasive wire and slit scanners and emittance measurement devices can supply highly accurate data, they cannot be operated during full beam operations. Wire- and slit-scanners for particle beams generate too much radiation spill to be used during production mode in the LANSCE accelerator. The remaining non-invasive diagnostics such as inductive beam position monitors, current monitors, and beam loss monitors cannot provide transverse beam profile or emittance data. We are examining the feasibility of implementing laser wire scanners to mitigate this challenge.

DESIGN

Customized rotating mirror mounts, and COTS optical hardware elements, based on 2" lens tube compatible elements are assembled to provide an enclosed laser transport path to the interaction point (IP) along two orthogonal scanning directions with position monitoring, as illustrated in Fig. 1. The laser wire scanner is built around a standard 6-way cross with 2.75" CF flanges. Thorlabs DDR25 rotating mirror mounts with 60 µrad rotation repeatability were implemented to control the laser scan angle. The path selection mirror is located at the bottom right corner, as shown in Fig. 1, and is a 45º mounted metallic elliptical mirror (Thorlabs PFE10-G01). Front surface coated, high damage threshold, dual wavelength (532 nm and 1064 nm) prisms (Thorlabs MRA25-K13) are mounted with the front surface centered on the mount rotation center with custom 3D printed mounts (Formlabs Form 4, Tough 2000 resin). Position monitors (Thorlabs S440C/S442C) are mounted before/after the interaction point to calibrate scan motion. Beams are terminated into Thorlabs LB2 beam blocks. Mechanical alignment irises are used at the front and back of the cross ports for initial beam centering, and alignment.

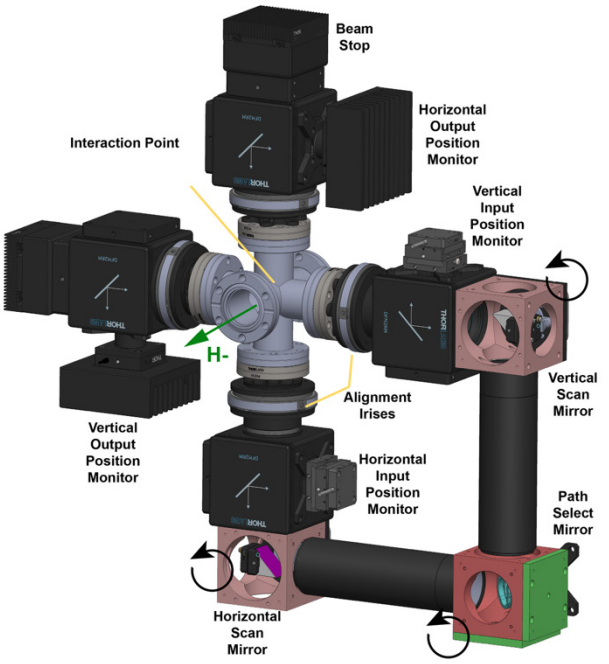

Figure 1: Implemented dual path selector and beam scanner. Rotating mirror mounts at the cube corners allow for the scanning and path selection of the laser beam. Beam sampling positions and motion monitors, and H- bunch flight path is indicated.

EXPERIMENTAL SETUP

LANSCE LEBT Layout

Shown in Fig. 2, the LANCSE Low Energy Beam Transport (LEBT) line turns the post Cockcroft-Walton injector 750keV H- beam 81º before combining with the H+ beam near the drift tube linear accelerator (DTL) entrance. The new test stand is positioned downstream of both the H- beam chopper and the 81º bending magnet. When the bending magnet is off, the beam bypasses the bend and is sent to the test stand. An original Faraday cup (FC) monitor diagnostic was displaced to the end of the new test line. The beam chopper was turned off for our initial experiments and deflector set to generate a 300 µs, 2Hz pulse. Instantaneous current is estimated to be on the order of 10 mA.

†crohde@lanl.gov

Content from this work may be used under the terms of the CC BY 4.0 licence (© 2026). Any distribution of this work must maintain attribution to the author(s), title of the work, publisher, and DOI.

ISBN: 978-3-95450-252-3 ISSN: 2673-5350 doi: 10.18429/JACoW-IPAC2026-MOP6380

FACILITY-WIDE MONITORING AND EARLY DETECTION OF FAILURES AT LANSCE*

N. Yampolsky†, A. Garcia, En-Ch. Huang, J. Quemuel, M. Rautela, A. Scheinker,
Los Alamos National Laboratory, Los Alamos, NM, USA

Content from this work may be used under the terms of the CC BY 4.0 licence (© 2026). Any distribution of this work must maintain attribution to the author(s), title of the work, publisher, and DOI.

Abstract

Accelerator complexes contain tens of thousands of interdependent components, and aging infrastructure amplifies the risk of equipment faults and costly, unscheduled shutdowns. At the Los Alamos Neutron Science Center (LANSCE), we are developing a data-driven framework that flags developing problems early enough to address them during scheduled maintenance, thereby improving reliability and increasing beam availability for users. Our approach analyzes all available signals within a subsystem to learn the facility's "normal" operating envelope and to detect subtle deviations that precede failures. Unlike the current warning scheme, it captures hidden correlations among parameters and generates interpretable indicators of abnormal behavior. Predictions are validated against historical control-room log records. We report progress on three fronts: (i) extending anomaly prediction from a single beamline to all major LANSCE subsystems; (ii) expanding data archiving capacity by an order of magnitude to support broader coverage and longer look-back windows; and (iii) developing operator-facing algorithms that both warn of emerging anomalies and localize likely problem elements along the beamline. Together, these advances are designed to shift maintenance from emergency response to planned intervention, reducing downtime and enhancing overall facility performance.

INTRODUCTION

The Los Alamos Neutron Science Center (LANSCE) is a multi-user accelerator facility that accelerates both H+ and H− beams and delivers them to several experimental areas with different energy and timing requirements [1]. The accelerator must therefore operate in multiple beam modes, and many diagnostics characterize only a subset of those modes. This makes automated assessment of machine status more difficult than monitoring a single-purpose industrial system. At the same time, LANSCE is a mature facility whose reliability is affected by aging equipment, intermittent subsystem degradation, and complex operational history. The need for early identification and localization of equipment problems is therefore directly connected to beam availability.

Traditional alarm systems are based primarily on threshold checks: an alarm is generated when a selected process variable exceeds a predefined range. Such systems are useful, but they have two limitations for predictive maintenance. First, only a small fraction of the available process variables can be manually curated by operators and subject matter experts. Second, threshold alarms usually treat variables independently and therefore miss correlated deviations in which every individual variable remains within its allowed range. Accelerator operation is highly correlated: magnet setpoints and readbacks, beam current, losses, vacuum, radio-frequency parameters, cooling, and environmental variables all evolve together. A physically abnormal state may therefore appear not as a single out-of-range value, but as an unusual combination of otherwise acceptable readings.

Another difficulty is accelerator redundancy. A failing element may be compensated by retuning other components, allowing acceptable beam delivery to continue while the underlying machine state drifts away from its historical norm [2]. Such compensation is useful operationally, but it hides the early stages of degradation. A predictive maintenance system must therefore separate harmless retuning and environmental drift from signatures associated with equipment degradation.

This work develops and evaluates an unsupervised anomaly-detection framework for accelerator data, extending recent efforts to apply machine-learning anomaly detection to accelerator facilities [3]. It does not require a complete labelled database of failures, which is important because equipment failures are rare and historical records are incomplete. Instead, the method learns the distribution of normal operation from archived process variables, assigns an anomaly score to new states, and identifies the channels most responsible for the deviation. The approach was first tested on Line D, the high-energy beam transport line from the linear accelerator to the Proton Storage Ring (PSR), and was later observed during 2024 front-end operation. The method is intended to complement operator judgment rather than replace it: high anomaly scores and high-impact channels provide a ranked list of machine states requiring attention.

MATHEMATICAL FORMALISM

At each archived time step, the accelerator state is represented by an n-dimensional vector

$$x(t) = \{x_1(t), x_2(t), \ldots, x_n(t)\}^T, \quad (1)$$

where each coordinate is a readout from an accelerator diagnostic or controls process variable. These variables include beam currents, magnet currents and voltages, vacuum signals, RF parameters, cooling-system parameters, beam losses, status readbacks, *etc*. During normal operation, $x(t)$ does not remain fixed. It changes because of

*Research presented in this paper was supported by the Laboratory Directed Research and Development program of Los Alamos National Laboratory under project number 20240474MFR.
†nyampols@lanl.gov

ISBN: 978-3-95450-252-3 ISSN: 2673-5350 doi: 10.18429/JACoW-IPAC2026-MOP6381

EXPLORING CAUSES OF BEAM LOSS AT CEBAF

C. Matthews*[1], J. Benesch[2], R.M. Bodenstein[2,1], B. Freeman[2], D. Moser[2],
D. Turner[2], K. Price[2], J. Samari[2], B. Terzić[1]
[1]Old Dominion University, Norfolk, VA, USA
[2]Thomas Jefferson National Accelerator Facility, Newport News, VA, USA

Content from this work may be used under the terms of the CC BY 4.0 licence (© 2026). Any distribution of this work must maintain attribution to the author(s), title of the work, publisher, and DOI.

Abstract

At Jefferson Lab, the Continuous Electron Beam Accelerator (CEBAF) features a unique design with two linear accelerators and two arc sections allowing for multiple turns of the electron beam, as well as four experimental end stations. This topology leads to increased beam losses, especially in the spreader and recombiner regions connecting the arcs to the linacs and in the extraction regions connecting the experimental end stations to the accelerator. These losses result in equipment activation and operational interruptions. Recent upgrades to the facility's diagnostic systems, including the addition of xenon ion chambers, have provided higher-resolution data regarding these loss events. Building on this improved observational capability, we are developing a simulation framework using optics codes and the Geant4-based BDSIM to model beam extinction and halo formation in these regions. This work aims to correlate simulation results with experimental data to isolate the causes of beam loss and inform future machine tuning strategies. We present a summary of conclusions drawn from recent operational studies and outline a plan to model the beam loss and validate the simulations.

INTRODUCTION

Beam loss is a persistent concern for accelerator operations. It presents an operational and environmental hazard through the creation of activated materials. Beam loss damages the accelerator components and nearby equipment, necessitating repairs. Significant beam loss results in accelerator "trips" that force a shutdown, complicating ongoing operations and experiments. Therefore, the minimization of beam loss is a high priority for all accelerator facilities, including the Continuous Electron Beam Accelerator (CEBAF) [1]. In this paper, the success of recent improvements in monitoring beam loss will first be reported. Then, persisting issues in beam loss monitoring will be highlighted. Finally, potential improvements to beam loss monitoring at CEBAF will be proposed.

SUCCESSES

One source of improvement in beam loss monitoring (BLM) is in the addition of xenon ion chambers (IDX). Similar to the neutron dose rate meters (NDX) installed in CEBAF, IDX instead monitor ionizing radiation [2]. In the 2022-2023 run, there were just under 40 000 BLM fast shut down (FSD) trips across the 278 days of operation located in the extractor region [3, 4]. With the addition of 4 IDX in the region where beam is deflected for extraction to a hall rather than continued recirculation, the 2023-2024 run reported around 9000 BLM FSD trips instead, conservatively reducing the number of BLM FSD trips by a factor of four after accounting for the different beam energies between each run [3, 4]. This reduction was largely driven by the IDX monitors allowing operators to distinguish exactly which pass needed steering attention. Table 1 provides a comparison between the trips before the addition of the IDX monitors and after at three specific locations [4].

Table 1: Change in Trip Number Before and After IDX Installation

BLM Monitor	2022–2023	2023–2024
ILM7S01	2885	1283
ILM4E02	1140	270
ILM4E08	12305	963

While this is not a rigorous comparison, as there are a multitude of confounding factors that would appear in the comparison between two runs a year apart, there is a clear significant improvement. Moreover, in the 2024 scheduled accelerator maintenance (SAM), an additional 4 IDX units were installed in the northeast spreader region, which unveiled more causes of beam trips and revealed orbit drift in low-current runs [3, 4].

Additionally, beamline monitors and beam cavity monitors (BCMs) have been used successfully to perform both real-time and offline diagnostics. First, specific beamline monitors are more useful in minimizing beam loss due to monitor degradation [5]. Unlike legacy photomultiplier tubes (PMTs) whose glass darkens over time with high exposure, the IDX monitors provide a much more stable baseline. Moreover, some legacy monitors have high baseline noise during beam off operations [5], and therefore can be misleading during diagnostics without prior knowledge. For instance, legacy spreader BLMs often see field emission background from the C100 cryomodules [1], whereas the xenon-filled IDXs are largely immune to this. Figure 1 shows how different BLM monitors have different inherent noises.

With the increasing familiarity and notation of troublesome monitors, more accurate diagnostics have been made [5]. BCMs have also been used to correct beam currents in experimental halls [6]. With Gaussian fits and linear regressions, successive analyses of recorded loss signals to Hall A and C currents were able to reduce the average instantaneous loss to 24 nA with a standard deviation of around 250 nA [6].

* cmatt025@odu.edu
Authored in part by Jefferson Science Associates, LLC under U.S. DOE Contract No. DE-AC05-06OR23177.

ISBN: 978-3-95450-252-3 ISSN: 2673-5350 doi: 10.18429/JACoW-IPAC2026-MOP6385

DEVELOPMENT OF A LOW LEVEL RF SYSTEM FOR THE SIRIUS PASSIVE 3rd-HARMONIC CAVITY BASED ON MTCA.4 PLATFORM

D. Daminelli*, G. Ricioli†, A. F. Giachero, L. S. Perissinotto
A. P. B. Lima, P. H. Nallin, D. O. Tavares, Brazilian Synchrotron Light Laboratory, Campinas, Brazil
H. Hou, Y. Zhao, Shanghai Advanced Research Institute, Pudong, China

Abstract

The SIRIUS storage ring RF system currently operates with two 500 MHz superconducting cavities, each powered by a 130 kW RF plant composed of two solid-state amplifiers (SSA) and a 200 mA stored beam current. A passive 2-cell superconducting 3rd-harmonic cavity (3HC) is planned for installation in 2027 to increase beam lifetime through bunch lengthening and and increase the stored beam current to the nominal value of 350 mA. This paper presents the current status of the development of a Low Level RF (LLRF) system for the 3HC based on MTCA.4 platform. The system includes a dedicated analog front-end for RF signal acquisition and conditioning, as well as clock and local oscillator (LO) generation. The digital hardware is based on Struck MTCA modules and an additional digital front-end for external signal isolation and interface with the FPGA GPIOs. Finally, the proposed DSP chain for the cavity signal processing and control is presented and discussed.

INTRODUCTION

The SIRIUS storage ring RF system currently operates with two 500 MHz CESR-B type superconducting cavities, each powered by a 130 kW RF plant composed of two solid-state amplifiers (SSA) and a 200 mA stored beam current. A passive 2-cell superconducting 3rd-harmonic cavity designed by SARI (Shanghai Advanced Research Institute) is scheduled for installation in 2027. The objective of this upgrade is to increase beam lifetime by reducing the bunch length [1–3] and increase the stored beam current to the nominal value of 350 mA.

This report presents the current status of the development of a Low Level RF (LLRF) system for the passive 2-cell superconducting 3rd-harmonic cavity, based on a commercial off-the-shelf (COTS) MTCA.4 platform. The final design of the analog front-end, including clock and local oscillator (LO) generation, is described, as well as the digital front-end for signal conditioning and interface with Struck MTCA modules. The intended DSP chain is also discussed.

GOALS AND REQUIREMENTS

The main parameters and stability requirements for the SIRIUS 3rd-harmonic cavity are presented in Table 1.

The voltage in a passive harmonic cavity can be expressed as [4]:

Table 1: Main Parameters of the 3rd-harmonic Cavity

Parameters	Value	Unit
n	3	-
f_{rf}	499.687	MHz
f_{hrf}	1499.001	MHz
R/Q (π mode)	<90	Ω
R/Q (0 mode)	<0.2	Ω
Q (π mode)	$> 2 \cdot 10^8$	-
Nominal Beam Current	350	mA
Harmonic Voltage Stability	$< \pm 0.2$	%
Nominal Harmonic Voltage	1	MV

$$V_b \approx -I_{dc} \frac{R_s}{Q} \frac{f_{hrf}}{\Delta f} \cos\left(n \cdot 2\pi f_{rf} \cdot \tau - \psi_h\right), \quad (1)$$

where I_{dc} is the beam current, R_s and Q are respectively the shunt impedance and quality factor of the cavity π-mode, f_{hrf} is the harmonic cavity resonance frequency, f_{rf} is the fundamental RF frequency, ψ_h is the harmonic cavity detuning angle, n is the harmonic number, and $\Delta f = f_{hrf} - n f_{rf}$ is the harmonic cavity detuning frequency. The relationship between the detuning angle ψ_h and the detuning frequency is given by:

$$\tan \psi_h = 2Q \frac{\Delta f}{f_{hrf}}. \quad (2)$$

The control system aims to keep the harmonic voltage amplitude constant ($|V_b| \approx I_{dc} \frac{R_s}{Q} \frac{f_{hrf}}{|\Delta f|}$). As shown in Eq. (1), the voltage fundamentally depends on the cavity detuning, allowing V_b to be controlled by adjusting its resonance.

According to the data in Table 1 and Eq. (1), the operational detuning is determined to be $\Delta f \approx 45$kHz. To meet the voltage stability requirement, the tuning stability must achieve a minimum of 90 Hz.

LLRF MAIN MODULES

The tuning system consists of an analog front-end for conditioning the cavity and its control signals; a digital front-end responsible for conditioning and interfacing digital signals with the FPGA hardware; an MTCA Rear Transition Module (RTM) for downconversion; and an MTCA Advanced Mezzanine Card (AMC) for digitization and FPGA-based digital signal processing (DSP). The mechanical actuators for the cavity tuner are composed of a stepper motor for coarse tuning and a piezoelectric for fine tuning. Figure 1 presents the general block diagram of the system. The details of these

* david.daminelli@cnpem.br
† guilherme.ricioli@lnls.br

Content from this work may be used under the terms of the CC BY 4.0 licence (© 2026). Any distribution of this work must maintain attribution to the author(s), title of the work, publisher, and DOI.

ISBN: 978-3-95450-252-3 ISSN: 2673-5350 doi: 10.18429/JACoW-IPAC2026-MOP6388

PYTHON-EPICS RF CONDITIONING AUTOMATIC CONTROL SYSTEM AT THE SPALLATION NEUTRON SOURCE *

Sung-Woo Lee†, George Toby, Timothy Miner, Mark Crofford,
Kay Kasemir, Haitao Ren, John Moss
Oak Ridge National Laboratory (ORNL), Oak Ridge, TN, USA

Abstract

The RF Test Facility (RFTF) at the Spallation Neutron Source (SNS) is used for the conditioning of RF components such as ceramic vacuum windows and power couplers prior to their installation in the H^- ion linear accelerator. This process exposes components to high-power RF fields and thermal cycling to improve performance and remove surface impurities. To automate and optimize this process, a Python-based EPICS control system was developed alongside targeted hardware upgrades. The system enables real-time monitoring and control of RF power levels, temperature, and vacuum pressure. A user-friendly graphical interface was implemented using CS-Studio (Phoebus), allowing operators to adjust parameters and collect data efficiently. The system integrates a High-Power Protection Module (HPM) for interlocks based on vacuum and arc detection, ensuring safe operation. These upgrades have significantly improved the efficiency, accuracy, and safety of RF conditioning at the SNS RFTF. This paper describes the updated RF conditioning system, highlighting the software and hardware developments and their application in support of the Proton Power Upgrade (PPU) project.

INTRODUCTION

The Spallation Neutron Source (SNS) at Oak Ridge National Laboratory is a pulsed proton driver facility whose linear accelerator delivers beam to a liquid-mercury target for neutron production. High-power RF components, including ceramic vacuum windows, waveguide couplers, and klystron amplifiers are conditioned off-line to their full operational duty cycle and power levels at the RFTF before accelerator installation. This conditioning progressively exposes components to increasing RF fields and temperatures which aids in the outgassing of surface contaminants and suppresses multipacting [1].

The nearly completed Proton Power Upgrade (PPU) aims to increase the SNS beam power capability from 1.4 MW to 2.8 MW by raising the beam energy by 30% and the beam current by 50% [2]. Meeting the PPU schedule required conditioning substantially more RF components and spares, including new PPU superconducting couplers and klystrons which placed significant demands on RFTF. To address these requirements, the RFTF control system was modernized from a legacy EPICS sequencer program to a Python-based EPICS state machine; the operator interface was updated to CSS-Phoebus; and coordinated hardware upgrades were implemented for the High-Power RF (HPRF) and Low-Level RF (LLRF) systems. This paper describes the updated system architecture, the end-to-end conditioning workflow, and the upgrades and conditioning results achieved in support of the PPU project.

RFTF SYSTEM OVERVIEW

The RFTF at the SNS consists of two independent HPRF test stands that operate at 402.5 MHz and 805 MHz. The 402.5 MHz test stand utilizes a WR2100 waveguide system and supports klystrons rated for up to 3 MW of RF peak power. The 805 MHz test stand uses WR1150 and WR975 waveguide sections and incorporates klystrons capable of providing 5 MW of RF peak power. Both test stands are powered by High-Voltage Converter Modulators (HVCM) with a maximum output of 11 MW at an 8% duty cycle and 60 Hz.

Each stand integrates three subsystems: An HPRF transmitter, which includes the klystron, circulator, waveguide system, and associated components; a LLRF system, which provides precise control of the RF power; and vacuum diagnostics, which include cold cathode gauges, roughing and turbo pumps and a residual gas analyzer. Fast protection against vacuum faults, arcing, and RF faults is provided by the LLRF system through a VXI-based LLRF High-Power Protection Module (HPM). Directional couplers at the input and output of the test assembly provide forward and reflected power measurements to the HPM and RF power meters used by the conditioning program. Fig. 1 shows a schematic of the system during RF vacuum window conditioning.

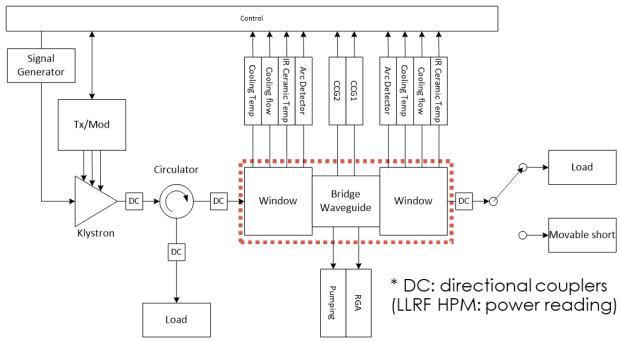

Figure 1: Schematic of the SNS RFTF test stand showing the back-to-back bridge waveguide (BWG) assembly, directional couplers, vacuum instrumentation, and HPM interlock signal path. The water load is replaced by a movable short for standing-wave conditioning.

* ORNL/SNS is managed by UT-Battelle, LLC, for the U.S. Department of Energy under contract DE-AC05-00OR22725
† lees1@ornl.gov.

Content from this work may be used under the terms of the CC BY 4.0 licence (© 2026). Any distribution of this work must maintain attribution to the author(s), title of the work, publisher, and DOI.

ISBN: 978-3-95450-252-3 ISSN: 2673-5350 doi: 10.18429/JACoW-IPAC2026-MOP6389

HIGH-POWER TEST AND SYSTEM INTEGRATION OF DIRECT RF SAMPLING BASED LLRF CONTROL AND MONITORING SYSTEM FOR S-BAND ACCELERATING STRUCTURES*

C. Liu†, A. Dhar, M. Hoganson, J. Olszewski, E. Snively, W. H. Tan, S. Morton, T. Le, E. Nanni
SLAC National Accelerator Laboratory, Menlo Park, United States

Abstract

High precision Low-level RF (LLRF) control and monitoring systems for future particle accelerators will be a significant technical challenge as the requirements in performance, flexibility and affordability become increasingly stringent. We have developed an RF system-on-chip (RFSoC) based next-generation LLRF (NG-LLRF) for S-band accelerating structures, which samples and synthesizes the RF pulses directly without the analog mixers used for traditional LLRF systems. The platform delivered considerably better performance than the requirements of the targeted applications, such as the upgrades for Next Linear Collider Test Accelerator (NLCTA) and test facilities at SLAC. As part of the upgrade program, we also developed a custom solid-state amplifier (SSA) to deliver RF pulses at the desired power level of the klystron. Integration of the LLRF with the SSA and the high-power test facility could be challenging. The power levels and RF pulse stability at each stage of the high-power RF drive system must be optimized to deliver the desired RF performance. In this paper, the integration procedure and the test and characterization results at each stage of integration will be summarized, analyzed and discussed. This integration is an essential step for the full deployment of the NG-LLRF system to test facilities and accelerators in different frequency bands.

INTRODUCTION

Direct RF sampling technology has been applied to a range of astrophysics [1–5]and high energy physics experiments and projects [6–10] at SLAC and the wider community. In [11], the results of a high-power test of NG-LLRF with a prototype C-band accelerator were summarized, remarking the successful integration of an NG-LLRF and a high-power test stand. Based on research and development for C-band accelerators, we adapt the operating frequency of the NG-LLRF system to S-band and the RF stability demonstrated with a loop back test setup is considerably better than the requirements of LCLS [12]. We began to integrate S-band NG-LLRF and a new SSA with test facilities at SLAC, starting from NLCTA S-band test station. with synergy of the research in Artificial Intelligence (AI) and Machine Learning (ML) based autonomous control for particle accelerator, we design and implement the S-band NG-LLRF as a base platform for AI/ML ready dataset accumulation and edge deployment of real-time control algorithms. The NG-LLRF has distinctive advantages compared with conventional heterodyne based LLRF that are essential for AI/ML based control, including wider RF bandwidth coverage, higher flexibility, higher data streaming throughput, and larger integrated computation resources. In this paper, the initial integration stages between NG-LLRF and NLCTA are described, summarized, and discussed.

SYSTEM INTEGRATION

Integration of the NG-LLRF and the custom SSA with the S-band station has been performed stage by stage. In this section, the key components will be described and the characterization results will be summarized.

S-band NG-LLRF

The NG-LLRF chassis for S-band has been built based on the ZCU208 evaluation board. Figure 1 shows the front panel of the chassis. The chassis has 8 RF input channels with sampling rate up to 5 giga samples per second (GSPS), which has a maximum RF input frequency of 6 GHz, and 8 RF output channels with sampling rate up to 7 GSPS with current system configuration. The NG-LLRF can be triggered by an external trigger signal or be used as a master trigger source for other components, such SSA, klystron and etc. The NG-LLRF can be clocked from an internal oscillator or locked to an external reference using the ”REF IN” port on the front panel. The control and data streaming interfaces are on the back plane, including GbE for remote update of the firmware and software images, control, configuration and low speed data streaming, and two SFP connectors for timing and high-speed data streaming.

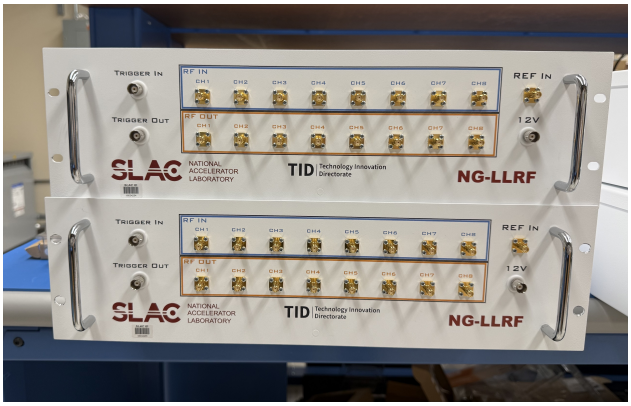

Figure 1: The front panel of the NG-LLRF chassis with 8 RF inputs and 8 RF outputs.

* This work was supported by the U.S. DOE, Office of Science contract DE-AC02-76SF00515.

† chaoliu@slac.stanford.edu

Content from this work may be used under the terms of the CC BY 4.0 licence (© 2026). Any distribution of this work must maintain attribution to the author(s), title of the work, publisher, and DOI.

ISBN: 978-3-95450-252-3 ISSN: 2673-5350 doi: 10.18429/JACoW-IPAC2026-MOP6390

AUTOMATED TUNING TECHNIQUES AT TRIUMF FOR THE ARIEL ERA

O. Hassan*, O. Shelbaya, P. Jung, T. Planche, O. Kester, W. Fedorko, TRIUMF, Vancouver, Canada

Abstract

Implementing automated tuning techniques has been a priority at TRIUMF, driven by the need to support the significant increase in RIB availability expected with the new Advanced Rare Isotope Laboratory (ARIEL). This efficiency boost will facilitate a broad spectrum of research in nuclear, particle, and astrophysics. This work outlines the shift from manual tuning to an automated approach for optimizing beamline transport. We utilize the predictive digital twin, Model Coupled Accelerator Tuning (MCAT), to compute transport and accelerated beam tunes, while Bayesian Optimization for Ion Steering (BOIS) handles beam orbit correction. BOIS treats steering as a black-box optimization problem, maximizing beam current based solely on direct measurement. By combining MCAT and BOIS, this method offers a more efficient, physics-grounded tuning process, with potential applications for facilities beyond TRIUMF.

INTRODUCTION

Rare Isotope Beam (RIB) facilities are highly complex systems that require frequent retuning for different beam species, energies, and charge-to-mass ratios. At TRIUMF's Isotope Separator and ACcelerator (ISAC) facility [1] which serves about 16 experiments with radioactive beam, beam tuning involves repeated adjustment of beamline optics, corrective steerers, and linear accelerator (linac) parameters. This tuning process places a significant burden on operators, who may be responsible for beam delivery to multiple experiments or, in some cases, may be the only operator on shift. The complexity of the tuning process also makes it more difficult to train new operators and to ensure reproducible and efficient beam delivery.

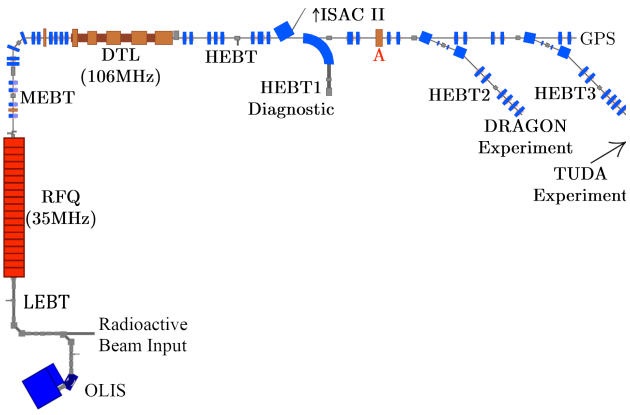

Figure 1: Overview of the ISAC-I RIB postaccelerator, showing major components.

* ohassan@triumf.ca

ISAC-I

The Isotope Separator and ACcelerator (ISAC) facility is capable of providing both stable and rare isotope beam to experiments. This facility produces rare isotope beams using proton beam from TRIUMF's 520 MeV cyclotron to bombard production targets, where the resulting isotopes are ionized, extracted, separated [2, 3] and delivered to experiments. Stable beam is provided by the Off-Line Ion Source (OLIS) [4]. The post-accelerator, shown in Fig. 1, is comprised of a Radio-Frequency Quadrupole and a Drift Tube Linac (DTL), the latter of which is a separated function layout [5], where the cavities and bunchers are individually tunable. The post-accelerator is divided into low, medium, and high energy sections by these two linacs: electrostatic ion optics (before the RFQ) define the low energy section, while magnetic optics (after the RFQ) are used in the medium and high energy sections.

ARIEL

The commissioning of the Advanced Rare Isotope Laboratory (ARIEL) [6, 7] will allow for the simultaneous delivery of three RIBs and one stable beam. This expansion includes a new proton beamline from the cyclotron, a superconducting electron linear accelerator (e-linac), and two new target stations, enabling greater coverage of the nuclear chart. With these developments comes a significantly increased operational load and tunable parameters.

To mitigate the future operational load, a change of the tuning paradigm is required, which relies on more automation in the beam delivery process. In this paper, we present an automated tuning approach that decouples the optimization of beamline optics from corrective steering. Optical elements are determined using the digital twin Model Coupled Accelerator Tuning (MCAT) [8], which computes optics (and linac) settings from user-defined constraints. Corrective steerers are then optimized using a previously developed Bayesian optimizer [9].

By combining model-based optics tuning with steering correction, this approach reduces the dimensionality of the tuning problem while providing an easily trainable approach to beam delivery. This technique is compared with a fully Bayesian approach, where both the optics and steerers are tuned using the Bayesian optimizer. Tests were carried out on real beam for several beam species and energies, demonstrating the advantages of the decoupled approach.

AUTOMATED TUNING TECHNIQUES

Driven by the expected completion fo the ARIEL project in 2027, automated tuning techniques have been developed and significantly expanded upon [9–13]. A key aspect of the technique employed at TRIUMF is the decoupling of optics and corrective steerers, which is different from several

Content from this work may be used under the terms of the CC BY 4.0 licence (© 2026). Any distribution of this work must maintain attribution to the author(s), title of the work, publisher, and DOI.

ISBN: 978-3-95450-252-3 ISSN: 2673-5350 doi: 10.18429/JACoW-IPAC2026-MOP6393

LONGITUDINAL PHASE SPACE DIAGNOSTICS FOR THE AGS*

Y. Gao[1,†], K. Brown[1,2], M. Costanzo[1], K. Hock[1], G. H. Hoffstaetter[1,3], J. Morris[1], V. Schoefer[1], A. Sukhanov[1], S. Tajne[1], K. Zeno[1]
[1]Collider-Accelerator Department, Brookhaven National Laboratory, Upton, NY, USA
[2]Electrical and Computer Engineering Department, Stony Brook University, Stony Brook, NY, USA
[3]CLASSE, Cornell University, Ithaca, NY, USA

Abstract

The Collider-Accelerator Department (C-AD) maintains and operates an injector complex that provides beams for the Relativistic Heavy Ion Collider (RHIC) and the future Electron-Ion Collider (EIC). Beams traveling in accelerator rings are grouped in bunches, where their profiles can be measured and displayed by a Wall Current Monitor (WCM). By analyzing those WCM signals, conclusions can be made about the beam quality, and necessary tuning can be performed accordingly. Meanwhile, it will be very helpful to have the beam property parameters available while doing beam experiments, such as the longitudinal emittance, momentum spread, bunch length, etc. In this work, we present such a newly developed software tool that will process and publish those parameters in real time, based on live machine data and WCM signals. Those parameters will also be logged to the system and will be available for later retrieval and analysis.

INTRODUCTION

The Collider-Accelerator Department (C-AD) at Brookhaven National Laboratory (BNL) maintains the pre-injector complex, including Tandem, EBIS, Linac, Booster, AGS, etc. The performance of the pre-injector complex is critical to the functionality and efficiency of the Relativistic Heavy Ion Collider (RHIC), the NASA Space Radiation Laboratory (NSRL), and the future Electron-Ion Collider (EIC).

Beams can generally come from three sources. The Tandem Van de Graaff Facility [1] consists of two 15-megavolt electrostatic accelerators which generate various heavy ions. The Electron Beam Ion Source (EBIS), has been used as a pre-injector system for RHIC and NASA Space Radiation Laboratory (NSRL), beginning with the 2012 run [2]. The EBIS can provide stable highly charged ion species. With EBIS, the ion species will be able to be switched on a time scale of one second. The Linac [3] is a drift tube linear accelerator which injects polarized or high intensity H- into the Booster (via LTB) at 200 MeV. It also injects H- into Brookhaven Linac Isotope Producer (BLIP) at energies ranging from 66 to 200 MeV. The Booster receives heavy ions from EBIS or protons from the Linac. It accelerates them and then feeds them to the AGS for further acceleration and delivery to RHIC. It can also send the beam to the NSRL target area.

A Wall Current Monitor (WCM) is a very important diagnostic tool during beam operations, especially during injection. A WCM is a passive, non-destructive device measuring current flowing lengthwise along the surface of a beam pipe. While beams traveling in the beam pipe, they will induce an image current on the beam pipe, since the beam pipe can be seen as a conductor. The image current is same in magnitude and opposite in charge. However, the wall current monitor does not "see" the DC component of the beam current, since a constant charge flow does not induce image current. Thus, the WCM becomes more useful after the beam are bunched by RF. The WCM signals can be displayed by a scope. WCMs can measure several properties of the beam. They measure the beam intensity and charge, transverse position, longitudinal size and shape without affecting the beam. The WCM bunch intensity can be calculated [4] as in Eq. (1):

$$N_{bunch} = \left[\int \frac{V_{bunch}(t)}{R} dt\right] (6.24 \times 10^{18} \frac{charges}{Coulomb}) \quad (1)$$

A WCM measures local beam current at a single location in the accelerator ring, but the signal acquired at that single point during one revolution of beam in the accelerator can be visualized as an image of the beam around the entire ring. Data acquisition of each new scope trace is triggered at intervals in synchronize with the beam revolution. The mountain range therefore displays an evolution of this image of beam around the ring as time advances within the accelerator cycle. Figure 1 is a good example showing such beam profile evolution during a bunch merge process.

There are several other fundamental concepts that will be used in the proposed tool:

Accelerator Device Object (ADO)

It abstracts features from the underlying devices into a collection of control points (also known as parameters), and provide those parameters to the users of the control systems. ADO designers determine the number and names of parameters based on the needs of the system. ADO parameters can be viewed or edited by the Parameter Editing Tool (PET). ADOs provide the *set()* and *get()* methods as the controls interface to the accelerator devices. The accelerator complex is controlled by users or applications which set() and get() parameter values in instances of the ADO classes.

* Work supported by Brookhaven Science Associates, LLC under Contract No. DE-SC0012704 with the U.S. Department of Energy. This work was supported in part by the grants DE-SC0024287 and DE-SC0025351.
† ygao@bnl.gov

Content from this work may be used under the terms of the CC BY 4.0 licence (© 2026). Any distribution of this work must maintain attribution to the author(s), title of the work, publisher, and DOI.

ISBN: 978-3-95450-252-3 ISSN: 2673-5350 doi: 10.18429/JACoW-IPAC2026-MOP6394

PROGRESS IN THE DEVELOPMENT OF THE COMMUNITY PARTICLE ACCELERATOR LANGUAGE STANDARD (PALS)

D. Sagan[1], Z. Brencic[2], A. Edelen[3], R. Roussel[3], T. Hellert[4], A. Huebl[4], C. Mitchell[4], J. Qiang[4], E. Zoni[4], J.-L. Vay[4], D. Kallendorf[5], D. Winklehner[6], D.L. Bruhwiler[7], E. Valetov[8,16], T. Satogata[9], C. Tennant[9], H. Zhang[9], K. Brown[10], W. Lin[10], L. Deniau[11], N. Kuklev[12], Y. El Hayek[13], Y. Hao[14], A. Brynes[15]
[1]Cornell University (CLASSE), Ithaca, NY, USA
[2]Jožef Stefan Institute, Ljubljana, Slovenia
[3]SLAC National Accelerator Laboratory, Menlo Park, CA, USA
[4]Lawrence Berkeley National Laboratory, Berkeley, CA, USA
[5]Technical University of Darmstadt, Darmstadt, Germany
[6]Massachusetts Institute of Technology, Cambridge, MA, USA
[7]RadiaSoft LLC, Boulder, CO, USA
[8]Michigan State University, East Lansing, MI, USA
[9]Thomas Jefferson National Accelerator Facility, Newport News, VA, USA
[10]Brookhaven National Laboratory, Upton, NY, USA
[11]European Organization for Nuclear Research, Geneva, Switzerland
[12]Fermi National Accelerator Laboratory, Batavia, IL, USA
[13]GSI Helmholtz Center for Heavy Ion Research, Darmstadt, Germany
[14]Facility for Rare Isotope Beams, East Lansing, MI, USA
[15]Science and Technology Facilities Council, UK
[16]University of Hawai'i at Mānoa, Honolulu, HI, USA

Abstract

The Particle Accelerator Language Standard (PALS), originally named the Particle Accelerator Lattice Standard, is a community effort to create an open standard to promote lattice and other information exchange for particle accelerators. PALS development is a community-wide international effort involving accelerator physicists from multiple institutions. While it started primarily as a lattice standard for beam dynamics simulations, PALS is now being extended to support other particle accelerator activities, in particular, accelerator operation.

With new accelerators that are becoming more complex, and with larger collaborations and the increasing imprint of artificial intelligence in all accelerator activities (from design to operation to workforce development), the imperative for a common, standardized accelerator ontology has been transitioning from "nice-to-have" to "must-have".

Presented here is the status of PALS and its relationship to other projects. This includes two particle accelerator related projects within the US DOE Genesis Mission: the Multi-Office Accelerator Team (MOAT) project and the Nuclear Physics AI-Ready Accelerator Data (NARAD) project.

INTRODUCTION

Modern accelerator facilities depend on shared software for design, simulation, commissioning, operations, optimization, and analysis. As machines grow more complex, collaborations more distributed, and AI tools become more relevant, a persistent interoperability problem has become more urgent: accelerator information is often encoded in facility-specific lattice files, databases, controls middle layers, process-variable names, archivers, and operational conventions. Consequently, tools developed for one machine are difficult to reuse at another without substantial translation and local expertise.

The Particle Accelerator Language Standard (PALS) is a community effort to develop a common, open representation for accelerator information. PALS began as the Particle Accelerator Lattice Standard, focused on lattice exchange for beam-dynamics simulation and analysis. That scope remains essential, but cross-facility workflows now require a broader language describing accelerator objects, hierarchy, roles, parameters, capabilities, signals, constraints, and links to facility-specific controls and data systems. This expanded scope aligns with Nuclear Physics AI-Ready Accelerator Data (NARAD) development and Multi-Office Accelerator Team (MOAT) [1] needs for portable, machine-readable accelerator context for AI-ready data products and reusable agentic workflows.

FROM "LATTICE" TO "LANGUAGE": AN EXPANDING SCOPE

PALS began primarily as a lattice standard [2]: a common way to describe beamline elements, their parameters, and their organization into lines and machine complexes for simulation, exchange, and analysis. That scope remains

Content from this work may be used under the terms of the CC BY 4.0 licence (© 2026). Any distribution of this work must maintain attribution to the author(s), title of the work, publisher, and DOI.

ISBN: 978-3-95450-252-3 ISSN: 2673-5350 doi: 10.18429/JACoW-IPAC2026-MOP6395

GENETIC OPTIMIZATIONS OF RF CELL PROFILE USING SUPERFISH*

M. Kaemingk†, P. M. Anisimov, L. Duffy, J. W. Lewellen, K. Shipman, B. Sims, H. Xu
Los Alamos National Laboratory, Los Alamos, NM, United States

Abstract

Important radio-frequency (RF) cell parameters such as the shunt impedance R_s, the quality factor Q, and the ratio of accelerating to peak field, depend on the cell geometry. Thus, it is desirable to optimize the cell profile to maximize the performance of the cell. The use of B-splines to optimize cell profiles with an evolutionary algorithm has previously been demonstrated. The RF field solver Superfish, however, does not support defining cell geometries using B-splines. Here we discuss a similar approach using only linear and elliptical segments supported by Superfish to define the cell geometry, making it possible to carry out genetic optimizations with Superfish.

INTRODUCTION

The effectiveness of radio-frequency (RF) cells in accelerating and bunching particle beams depends on parameters such as the shunt impedance R_s, the unloaded quality factor Q, and the maximum achievable accelerating gradient, which is limited by the peak field the cell can sustain. These parameters are in turn dependent on the cell geometry. Optimizing the cell profile for any particular application is therefore necessary to maximize the cell performance. Evolutionary optimizations have been used for this purpose, as described in Ref. [1]. Evolutionary optimizations require performing large numbers of simulations, making light-weight RF field solver codes like Superfish [2] well suited to carry them out.

In the work described in Ref. [1], the cell profile was defined as a B-spline. The positions of the points defining the B-splines could then be varied to optimize the cell profile. Superfish does not support the use of B-splines. In Superfish, the cell profile can be defined by a series of elliptical and linear segments. The parameters defining these segments can be varied to perform the optimization.

In this work, we describe a system developed for performing genetic optimizations of cell profiles using Superfish. This system has been implemented in Python which allows the use of packages such as PySuperfish [3] and Xopt [4]. These packages and the flexibility offered by Python enable the use of a variety of optimization approaches beyond genetic algorithms, and make it easy to optimize for many different possible objectives. In the last section we show a basic example of a genetic optimization performed using this system.

* Work supported by U. S. Department of Energy through the Laboratory Directed Research and Development program of Los Alamos National Laboratory, under project number 20260114ER.

† kaemingk@lanl.gov

SYSTEM DESCRIPTION

In this section we describe the optimization approach. In general, the workflow can be described as an iterative procedure consisting of the following steps:

1. Generate parameters for defining the cell profile
2. Validate the cell profile
3. Perform simulations with Superfish
4. Evaluate results

Each of these steps is described in greater detail in the following subsections.

Cell Profile Parameters

As discussed in the introduction, we define the cell profile using a series of elliptical and linear segments. Each segment is defined by the segment endpoints as well as the slopes of the tangent lines at each endpoint. Defining the segments in this way makes it easy to ensure that the segments define a continuous curve with a continuous derivative. Therefore, the optimization variables are the endpoint coordinates of the segments and the endpoint tangent slopes. The number of segments is determined from the number of endpoints and endpoint slopes given.

Superfish only allows segments from axis-aligned ellipses, which can be described by the equation $\frac{(z-h)^2}{a^2} + \frac{(r-k)^2}{b^2} = 1$. This can be rewritten as

$$(z-h)^2 + c(r-k)^2 = a^2. \tag{1}$$

This can be differentiated to obtain expressions for the tangent slopes. Substituting in endpoint coordinates (z_n, r_n) and (z_{n+1}, r_{n+1}) and endpoint slopes s_n, s_{n+1}, conveniently yields a set of linear equations which can be expressed in matrix form as follows

$$\begin{pmatrix} h \\ ck \\ c \end{pmatrix} = M \begin{pmatrix} z_n^2 - z_{n+1}^2 \\ z_n \\ z_{n+1} \end{pmatrix}, \tag{2}$$

where

$$M = \begin{pmatrix} 2(z_n - z_{n+1}) & 2(r_n - r_{n+1}) & -(r_n^2 - r_{n+1}^2) \\ 1 & s_n & -s_n r_n \\ 1 & s_{n+1} & -s_{n+1} r_{n+1} \end{pmatrix}.$$

Together with Eq. (1) and $c = a^2/b^2$, Eq. (2) can then be used to find h, k, a, b, which are the parameters used by Superfish to define ellipse segments. Thus the optimizer (e.g. Xopt) generates a set of coordinates $(z_1, r_1), (z_2, r_2), ..., (z_{N+1}, r_{N+1})$ and slopes $s_1, s_2, ..., s_{N+1}$. The ellipse parameters are then obtained using Eqs. (1) and (2). Figure 1 shows an example of a cell profile defined in this way.

Content from this work may be used under the terms of the CC BY 4.0 licence (© 2026). Any distribution of this work must maintain attribution to the author(s), title of the work, publisher, and DOI.

ISBN: 978-3-95450-252-3 ISSN: 2673-5350 doi: 10.18429/JACoW-IPAC2026-MOP6605

REAL-TIME TOMOGRAPHY OF SYNCHROTRON LONGITUDINAL PHASE SPACE BASED ON SPATIO-TEMPORAL NEURAL NETWORKS

Yixuan Luo, Peizhi Fang, Yihao Huang, Hongjuan Yao, Shuxin Zheng*
Department of Engineering Physics, Tsinghua University, Beijing, China

Abstract

Accurate acquisition of the longitudinal phase space distribution is crucial for synchrotron optimization, but traditional tomography is time-consuming and difficult to meet the needs of real-time diagnostics. This paper proposes a novel spatio-temporal network model integrating Convolutional Neural Networks (CNN) and Transformers to achieve end-to-end continuous reconstruction from one-dimensional beam projections to two-dimensional phase space dynamic evolution. Based on a high-fidelity simulation dataset incorporating nonlinear effects such as space charge, test results show that this model can accurately restore complex phase space topological structures. Meanwhile, the model achieves fast reconstruction at the sub-millisecond level. This non-intrusive diagnostic tool provides a new paradigm for high-intensity accelerators to achieve high-fidelity online real-time beam measurement and automated feedback.

INTRODUCTION

The longitudinal phase space of a synchrotron is a core dynamic parameter characterizing the longitudinal motion state of the beam. Accurate diagnosis of it is important for improving accelerator performance and ensuring stable beam operation. Traditional tomographic methods couple particle tracking with iterative corrections, which heavily rely on complex physical calculations. [1–3] This heavy computational overhead leads to long single-reconstruction times (typically several minutes), making it difficult to meet the demands of real-time diagnostics. When handling nonlinear dynamic effects in high-intensity scenarios, it will also face a dual challenge of efficiency and accuracy.

In recent years, end-to-end tomographic techniques based on deep learning have been introduced. Convolutional Neural Networks (CNN) successfully reduced the single-reconstruction time to second level by establishing a direct mapping from 1D projections to 2D phase spaces. [4–7] However, early network designs were mostly limited to the reconstruction of static single-frame images. The newly developed Transformer architecture, featuring a multi-head attention mechanism, is highly powerful in processing complex temporal dependencies and dynamic modeling. This paper proposes a novel spatio-temporal neural network integrating the CNN and Transformer to continuously reconstruct the dynamic evolution process of the phase space. The training dataset is optimized using the BLonD code, introducing collective effects to make the data more closely resemble real beam conditions and enhance the network's generalization capability.

* zhengsx@mail.tsinghua.edu.cn

MODELING AND DATASET GENERATION

To enable the model to learn the real physical evolution laws and possess the capability to handle high-intensity beams, this study constructs a high-fidelity spatio-temporal evolution dataset using Beam Longitudinal Dynamics (`BLonD`), developed by the European Organization for Nuclear Research (CERN). This simulation is based on the machine parameters of the Xi'an 200MeV Proton Application Facility (XiPAF) project. This study focuses on introducing the space charge effect into the simulation, which is slowly applied via an adiabatic process to ensure the stability of the simulated beam.

To enhance the generalization capability of the spatio-temporal neural network, the simulation conducts extensive random sampling on multiple physical parameters. For example, parameters such as beam intensity, bunch length, RF voltage amplitude stabilization error, and the initial phase space distribution profile are randomly varied within specific ranges. More importantly, mismatch factors are applied to excite longitudinal dipole and quadrupole oscillations, thereby enriching the network's learning features during dynamic evolution. During tracking, 1280 synchronous turns are discretely sampled to obtain the current projection data, while the corresponding 2D phase space distribution is mapped into a 128×128 pixel image.

SPATIO-TEMPORAL NETWORK

To achieve reconstruction of the multi-turn continuously evolving longitudinal phase space, this study designs a hybrid model combining CNN and Transformer. This network possesses the advantages of both CNN in high-precision spatial image processing and Transformer in highly continuous global temporal perception. The input to the network is 1D projection sequences, and output is the corresponding 2D phase space dynamic evolution video. As shown in Fig. 1, the network architecture is divided into three core modules:

1D CNN Tokenizer: To extract spatial features and compress dimensions, the front end of network employs a tokenizer composed of multi-layer 1D convolutions paired with BatchNorm and GELU activation functions. This module maps the single-frame 1D projection data into feature vectors (Tokens) with a dimension of 256, retaining the local features of the beam line density.

Transformer Encoder: The extracted feature sequence is first injected with sine- and cosine-driven absolute positional encoding, and subsequently fed into the Transformer encoder. Transformer encoder contains 4 encoding layers, each utilizing a multi-head attention mechanism with

Content from this work may be used under the terms of the CC BY 4.0 licence (© 2026). Any distribution of this work must maintain attribution to the author(s), title of the work, publisher, and DOI.

ISBN: 978-3-95450-252-3 ISSN: 2673-5350 doi: 10.18429/JACoW-IPAC2026-MOP6612

WAVEFORM PATTERN CONTROL OF THE PAINT BUMP POWER SUPPLY FOR THE J-PARC RCS USING NEURAL NETWORKS*

M. Sugita†, T. Ueno, K. Horino, Y. Kuriyama, S. Shinozaki, T. Takayanagi,
Japan Atomic Energy Agency, Tōkai Mura, Japan

Abstract

The J-PARC RCS uses four horizontal and two vertical painting magnets to generate a high-intensity beam through painting injection. Their IGBT-chopper power supplies can reproduce current waveforms with an accuracy better than 1%. By combining automatic generation of command voltage waveform with manual finetuning keeps the current deviation of the painting pattern within ±1.0% of the required accuracy. There are 90 waveform patterns in total, including two types: trapezoidal waveforms for low-beam-loss studies and decay waveforms for high-intensity beam production. As these patterns have different current demands and impose different loads on the power supplies, the tuning process becomes increasingly complex. Adjusting a single painting pattern takes approximately one hour and optimizing all 90 patterns takes several days; therefore, reducing the adjustment time is essential. To address this issue, we applied a neural network approach to generate optimized command voltage waveforms. After training the neural network using painting patterns generated by the actual machine, we achieved predictions with a deviation within ±0.2%. Furthermore, we were able to significantly reduce the time required for prediction to just a few seconds.

INTRODUCTION

The J-PARC [1] RCS [2] uses four horizontal and two vertical painting magnets to generate a high-intensity beam through painting injection [3]. The painting magnet power supplies [4] consist of rectifiers that uses an IGBT unit to generate currents with arbitrary waveforms, and an indirect conversion device comprising a chopper. These systems can generate and output trapezoidal or decay waveforms as required. In current operation, it achieves high-precision control, with the difference between the set-point and the output value falling within the required accuracy of ±1.0%. However, because the load impedance of the electromagnets exhibits nonlinearity with input waveforms, it takes about an hour to adjust a single waveform pattern. Furthermore, since 15 waveform patterns are used per unit during accelerator beam studies at the RCS, a total of 90 waveform patterns are required for the six painting magnets. As a result, it takes several days to adjust all the waveform patterns required for operation, and in the limited beam studies time available, there is a need to reduce the time required to adjust the waveform patterns for the painting magnets.

In this study, we used a neural network (NN) to model the nonlinear relationship between the command voltage waveforms and the output current waveforms, enabling the rapid determination of the appropriate command voltage waveform for a given output current waveform. The predictions for trapezoidal waveforms are as reported in IPAC'25[5]. This paper presents decay waveforms, the configuration of the NN, the waveform data employed for training, and the obtained results.

PAINTING MAGNET POWER SUPPLIES

The painting magnet power supplies require excitation waveforms of various shapes, such as trapezoidal waveforms used for low-beam-loss studies and decay waveforms used in painting injection. These waveforms are shown in Fig. 1. To generate these arbitrary waveforms, the painting magnet power supplies multiplex twelve IGBT unit assemblies operating at 54 kHz and outputs the required excitation waveforms through wave-form synthesis using high-speed switching at 648 kHz [6]. Figure 2 shows the basic configuration of the painting magnet power supplies. The output current of these is analog-controlled by an IGBT control signal converted from the command voltage waveform. This control signal is generated through current feedback and voltage feedforward. The response time constant of the current feedback is approximately 20 μs. Therefore, when the current value changes significantly and continuously over a short beam injection time of 500 μs, the command voltage waveform adjusted for voltage feedforward is directly applied. This ensures that the output current does not deviate from the reference current waveform. Furthermore, for the injection schemes in different paint areas required for the MLF [7] and MR [8], the command voltage waveforms for the respective excitation waveforms are applied.

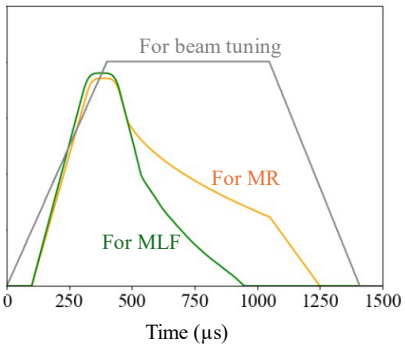

Figure 1: Examples of decay-type and trapezoidal waveforms for MLF and MR.

* Yes
†moe.sugita@j-parc.jp

Content from this work may be used under the terms of the CC BY 4.0 licence (© 2026). Any distribution of this work must maintain attribution to the author(s), title of the work, publisher, and DOI.

ISBN: 978-3-95450-252-3 ISSN: 2673-5350 doi: 10.18429/JACoW-IPAC2026-MOP6613

IN-AIR OPTICAL TECHNIQUES FOR TEMPORAL DIAGNOSTICS AT PICOSECOND RESOLUTION

P. Pushkarna*[1], R. Dowd[2], P. Giansiracusa[1], V. Lu[1], R. Rassool[1], S. Sheehy[1,3], E. Tan[2], G. N. Taylor[1], J. Valerian[1], M. Volpi[1]
[1]The University of Melbourne, Melbourne, Australia
[2]Australian Synchrotron, ANSTO, Clayton, Victoria, Australia
[3]ANSTO, Lucas Heights, New South Wales, Australia

Abstract

Radiative temporal diagnostics like Cherenkov diffraction radiation easily offer ps-resolution but require in-vacuum operation. For detectors in air, prompt Cherenkov radiation (ChR) provides ps-resolution while greatly reducing deployment complexity. We investigate such in-air ChR diagnostics to resolve sub-ns bunch structure at the Australian Synchrotron's injector linac. Existing monitors can resolve 2 ns bunch spacing but cannot detect possible 330 ps satellite bunches induced by 3 GHz travelling-wave structures. A mirrored silica crystal is considered for generating and guiding ChR towards a photodetector. Impacts of path-length dispersion in the crystal are assessed, alongside optimisation of photodetector placement relative to the crystal. Ability of existing diagnostics (such as a Fast Current Transformer) to resolve sub-ns bunch structure is assessed. Existing diagnostics serve to benchmark the performance of novel monitors exploiting the mirrored crystal. These techniques support improved longitudinal phase-space measurement, thus increasing injection efficiency, improving bunch purity, and optimising RF-phasing in a dual-RF system.

IN-AIR LONGITUDINAL DIAGNOSTICS

Design of in-air picosecond diagnostics is needed for resolution of 3 GHz satellite bunches at the 100 MeV injector LINAC of the Australian Synchrotron (AS). This is necessary for assessment of bunch purity to optimise routine top-up operation, as well as operation of the PEER (Pulsed Energetic Electrons for Research) beamline, which leverages the injector LINAC for detector physics [1], dosimetry [2, 3], and fundamental accelerator science [4, 5]. While the 2 ns interbunch spacing can be resolved, bandwidth limitations in existing monitors make detection of sub-nanosecond bunch profiles challenging.

In this proceeding, we outline ongoing efforts to develop in-air longitudinal diagnostics for resolving sub-nanosecond bunch structure at picosecond resolution. We first detail measurements to characterise an existing Fast Current Transformer attached to the injector LINAC. Then, we outline 2D ray-tracing simulations of a mirrored, polished silica crystal, which can be used to generate and guide large intensities of Cherenkov light toward a photodetector. Difficulties encountered during testing of the mirrored crystal under beam are explained, with electron incidence on the photodetector being the primary obstacle.

More broadly, radiative, non-invasive bunch profile monitors are challenging to realise for compact electron machines operating between 10 MeV to 100 MeV [6, 7], because the impact parameter required to generate diagnostic radiation is $O(0.1\,\mu\text{m})$. Invasive, in-air optical methods leveraging Cherenkov Radiation (ChR) provide a simple and flexible alternative [8], as conventional ChR is prompt. This is especially useful for compact Infra-Red and Terahertz Free Electron Lasers (IR-FELS) such as the Fritz-Haber-Institut (FHI) FEL [9], Delhi Light Source (DLS) [10], and the proposed Waterloo Free Electron Laser (WaterFEL).

Injector Overview

The injector LINAC is a turn-key system closely modelled after the Swiss Light Source injector prior to it's upgrade [11–13]. Electrons are generated by a dc triode gun, and accelerated by it's 90 kV anode potential toward a 500 MHz standing wave pre-buncher cavity, operated in $\pi/2$ mode. The 4-cell 3 GHz Primary Bunching Unit (PBU) boosts electrons to 300 keV, after which the 3 GHz Final Bunching Unit (FBU) β-matches bunches with two travelling wave S-band accelerating structures. Electrons then enter the LINAC-to-booster transfer line at their nominal energy of 100 MeV [14]. This dual RF system induces complex sub-nanosecond microstructure on each 500 MHz macrobunch.

FAST CURRENT TRANSFORMER

To determine if proposed diagnostics have performance advantages over those currently accessible, we need to assess whether existing diagnostics can resolve sub-nanosecond bunch structure. One such instrument is the Bergoz Fast Current Transformer (FCT) [15], installed immediately after the final S-band accelerating cavities of the injector LINAC. The in-flange FCT has a generates 1.25 V A^{-1} with its 20-turn primary winding, and has an upper cutoff frequency at −3 dB of 1.5 GHz to 1.75 GHz. The resulting nominal rise time is 200 ps to 230 ps. To confirm these properties, we characterise the FCT with beam-based testing, using single bunches contained within a ∼1 ns envelope to probe the upper limit of FCT frequency response. Bunch length is varied by changing the grid voltage of the 90 keV triode gun. This is because the grid voltage opposes the 90 kV potential difference between the anode flange and gun cathode, limiting extracted charge. The resulting current profiles generated by

* pushkarnap@student.unimelb.edu.au

Content from this work may be used under the terms of the CC BY 4.0 licence (© 2026). Any distribution of this work must maintain attribution to the author(s), title of the work, publisher, and DOI.

ISBN: 978-3-95450-252-3 ISSN: 2673-5350 doi: 10.18429/JACoW-IPAC2026-MOP6614

THE DEVELOPMENT OF NOVEL BEAM DIAGNOSTICS FOR LOW-MEV PROTONS

J.A. Bellesini*[1], J.S.L. Yap[1,2], A.F. Steinberg[1], S. Barg[1], S.L. Sheehy[1,3]
[1]The University of Melbourne, Melbourne, Australia
[2]Peter MacCallum Cancer Centre, Melbourne, Australia
[3]Australian Nuclear Science and Technology Organisation, Sydney, Australia

Abstract

A low-energy (0.5–3 MeV) demonstrator beamline for proton therapy is under development as part of the TURBO (Technology for Ultra-Rapid Beam Operation) project [1, 2]. In charged particle therapy, high energy layer switching times prolong beam delivery times, where beamlines with a large momentum acceptance (±42%) could alleviate this bottleneck and increase treatment efficiency. This beamline is being constructed for the University of Melbourne's Pelletron accelerator which operates at low energies and high current densities, requiring novel beam diagnostic instrumentation to monitor key parameters. We develop a pepper-pot mask method to measure the beam phase space distribution and quantify the emittance, and a multi-layer Faraday cup (MLFC) to measure the beam energy distribution, providing the adaptations required to operate under our experimental conditions. This work contributes to the development of a beam shaping section, and integration of a fixed-field, closed-dispersion beam transport section, toward demonstration of a proton beamline with the potential to shorten beam delivery times.

INTRODUCTION

A beam shaping section is required upstream of the large momentum acceptance beam transport section to modify the transverse distribution of the beam and to rapidly change the mean energy. This necessitates instrumentation and methods to be able to accurately measure and monitor fundamental parameters of the beam, including the transverse beam phase space and energy distribution. Pepper-pot masks are diagnostic devices used to measure the 4D transverse beam phase-space, commonly used for high-intensity particle beams at low-energies [3–6]. The operating principle of this technique is that a metal mask (e.g. steel, copper, tungsten) with a grid of holes of known size and spacing, intercepts the beam, splitting the incident beam into an array of smaller beamlets. These beamlets then travel over a known drift length to a scintillator screen or detector, where the pattern of beamlet spots is captured. This array of beamlets represent samples of the initial beam distribution, such that the analysis of the diverged beamlet pattern over this drift allows for an estimation of the beam position-angle phase space. From this, a statistical estimation of the emittance and Twiss (Courant-Snyder) parameters [7] to describe this elliptical distribution can then be acquired. While this technique is well established, only few studies have performed this method for low-MeV proton applications [8, 9].

A MLFC is a highly accurate diagnostic device which can measure the energy distribution of the proton beam [10–14]. The MLFC is constructed using conductive media segmented into multiple electrically isolated layers along the beam axis. When the beam is intercepted, charge is deposited and accumulates within each layer, where it can be measured independently to acquire a composite range distribution. Proton ranges are monotonic and strongly correlated with incident proton energy, thereby allowing direct beam energy determination from the measured charge distribution. This device provides benefits of minimal calibration requirements, compact form factor and robustness to high currents, compared to alternate methods of energy determination such as scintillation detectors or magnetic spectrometry [15, 16]. However, MLFCs available off-the-shelf are built for clinical energy ranges (70–250 MeV) and therefore are unsuitable for our experimental conditions with low-MeV protons. The adaptation to lower energies poses challenges on component design and construction, requiring the conductive material to be of lower stopping power or comprised of significantly thinner layers to achieve an energy resolution comparable to clinical systems. Due to this, MLFCs have not previously been implemented for this energy range.

PEPPER-POT MASK-BASED METHOD FOR MEASURING BEAM EMITTANCE

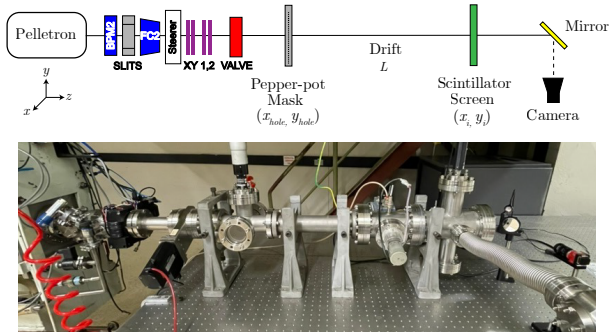

Figure 1: Pepper-pot experimental measurement. Diagram of apparatus (top), image of beamline (bottom).

Initial experimental work involving a pepper-pot based emittance measurement has been performed, showing the reconstruction of the full 4D transverse phase space of the proton beam generated by the University of Melbourne Pelletron accelerator (x, x' phase space is shown in Fig 2). We used a

* joel.bellesini@student.unimelb.edu.au

Content from this work may be used under the terms of the CC BY 4.0 licence (© 2026). Any distribution of this work must maintain attribution to the author(s), title of the work, publisher, and DOI.

ISBN: 978-3-95450-252-3 ISSN: 2673-5350 doi: 10.18429/JACoW-IPAC2026-MOP6620

DESIGN OF A LASER-BASED EMITTANCE METER AT CSNS LINAC*

B. Zhang, C. Chen, M. Li, S. Yan, R. Liu, Z. Xu, M. A. Rehman, J. Peng, R. Yang† and X. Li
Institute of High Energy Physics, Beijing, China
also at Spallation Neutron Source Science Center, Dongguan, China

Abstract

Following the successful profile measurement of an 80 MeV negative hydrogen (H^-) beam using a laser wire monitor at the China Spallation Neutron Source(CSNS), an emittance measurement system with a Low-Gain Avalanche Diode (LGAD) sensor has been developed and is currently under commissioning this year. This system utilizes the LGAD to reconstruct the spatial distribution of neutral hydrogen atoms (H^0) generated through laser photodetachment. By combining this distribution with laser wire position, it enables complete phase-space reconstruction and accurate emittance measurement of the H^- beam. This paper focuses on the design and characterization of the LGAD-based H^0 distribution measurement system, including H^0 energy deposition simulation, LGAD sensor performance characterization, the design of a ceramic PCB readout board, and local signal response tests. The proposed system offers a promising non-interceptive, high-precision solution for negative hydrogen beam emittance measurement.

INTRODUCTION

The China Spallation Neutron Source (CSNS) linear accelerator (linac) will be upgraded with a superconducting section, boosting the beam energy from 80 MeV to 300 MeV and increasing the Rapid Cycling Synchrotron (RCS) beam power from 100 kW to 500 kW [1–3]. To prevent contamination of the superconducting cavities from broken physical wires, a non-destructive diagnostic method was developed [4, 5]. This method uses a 1064 nm laser to ionize H^- ions into electrons and neutral hydrogen,(binding energy 0.75 eV), with the resulting electrons, proportional to the local ion density, collected to reconstruct the beam profile as the laser scans the beam [6–9]. By detecting the neutral hydrogen distribution 5 m downstream of the laser–beam interaction point, the angular distribution of the beam at the stripping location can be inferred, enabling reconstruction of the transverse phase space of the beam. The Low-Gain Avalanche Diode (LGAD) is a high precision silicon-based timing detector with a typical gain of 10-50. This paper presents test results of an LGAD sensor for H^0 detection.Besides, a fluorescent screen is also designed to detect the two dimension distribution of the detached H^0 for phase space reconstruction.

* Work supported by National Natural Science Foundation of China (No. 12305166) and the Natural Science Foundation of Guangdong Province, China (No. 2024A1515010016).

† yangrenjun@ihep.ac.cn

LASER WIRE SYSTEM

Figure 1 provides a schematic overview of the entire laser wire system [10]. The CSNS linac comprises a radio-frequency quadrupole (RFQ) that accelerates the negative hydrogen beam to 3 MeV and four drift tube linacs (DTLs) that further accelerate the beam to 80 MeV. For the upgrade of the emittance monitor [11, 12], the laser wire station is allocated in the linac transport beam line (about 150 m downstream of the DTL), where the beam energy is 80 MeV. The time structure of the pulsed beam in the linac, shaped by an RF chopper cavity for RCS injection, is depicted in Fig. 2. The beam pulse consists of 324 MHz micro-bunches, 550 ns intermediate bunches, and a 750 µs (max.) macro-pulse with a repetition rate of 25 Hz.

A high-power Q-switched Nd:YAG laser, operating at 1064 nm, serves as the light source for efficient photodetachment. This laser has a full width at half maximum (FWHM) of approximately 10 ns and a repetition rate of 1-10 Hz. By synchronizing the timing between the beam and the laser, the laser can precisely interact with a specific intermediate bunch, detaching approximately six micro-bunches per laser pulse. The demonstrated synchronization timing jitter is about 1 ns.

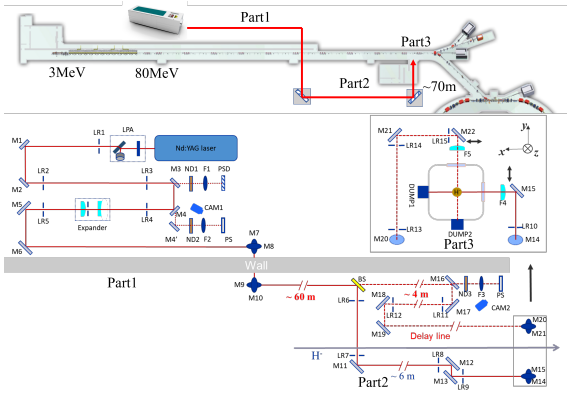

Figure 1: Outline of the laser wire system installed in the CSNS linac.

The number of stripped electrons is related to the laser energy and is assessed by

$$-\mathrm{d}n = \sigma(E_{\mathrm{cm}}) \times \Phi(x, y, z, t) \times n(t)dt \qquad (1)$$

where $n(t)$ is the number of negative hydrogen beam in an elementary volume element, $\sigma(E_{\mathrm{cm}})$ is the photodetachment cross-section [13], and Φ is the photo flux. The laser beam is kept at a fixed position and focused into the vacuum vessel with a diameter of approximately 100 µm. Due to the beam quality factor $M^2 = 4$, the laser beam diameter remains nearly constant when interacting with the millimeter-

Content from this work may be used under the terms of the CC BY 4.0 licence (© 2026). Any distribution of this work must maintain attribution to the author(s), title of the work, publisher, and DOI.

ISBN: 978-3-95450-252-3 ISSN: 2673-5350 doi: 10.18429/JACoW-IPAC2026-MOP6621

INVESTIGATION OF DIAGONAL CUT–PLANE BPM PERFORMANCE IN THE CSNS RCS*

M. A. Rehman, L. Fang, X. Li, M. Liu, R. Liu, X. Nie, R. Qiu, S. Wang, C. Xie, Z. Xu, R. Yang†
Institute of High Energy Physics, Chinese Academy of Sciences (CAS), Beijing, China
also at Spallation Neutron Source Science Center, Dongguan, China

Abstract

Diagonal-cut plane Beam Position Monitors (BPMs) are used to measure the transverse position of the proton beam in the Rapid Cycling Synchrotron (RCS) at the China Spallation Neutron Source (CSNS). Significant transverse beam position offsets were observed at several locations along the RCS. These offsets are potentially attributable to abrupt changes in the cross-section of the upstream and downstream vacuum ducts, BPM calibration constants determined at a single frequency on the calibration system, and limitations in the position calculation algorithm. To assess the impact of the sudden changes in beam duct aperture, numerical simulations were performed. Additionally, BPMs were re-calibrated on a test bench to evaluate the influence of abrupt cross-sectional changes in the BPM and vacuum ducts on the observed offsets at different frequencies.

INTRODUCTION

The China Spallation Neutron Source (CSNS) [1, 2] is a high-intensity pulsed neutron facility designed to support a broad range of scientific research and industrial applications. Its accelerator system consists of three main components, an 80 MeV H^- beam linac, a 1.6 GeV Rapid Cycling Synchrotron (RCS), and a solid tungsten target station. The 80 MeV H^- beam is injected into the RCS by multi-turn charge-exchange process. The RCS subsequently accelerates the proton beam to 1.6 GeV, achieving a beam intensity of 1.56×10^{13} ppb and a nominal beam power of 100 kW. Recent upgrades, including the installation of harmonic cavities and an improved injection painting scheme, have successfully increased the beam power to 185 kW [3].

The diagonal cut–plane beam position monitor (BPM) has been used in CSNS RCS to accurately measure the transverse beam position of the proton beam during the injection painting and beam energy ramping. During beam studies and routine operation, unphysical transverse position offsets have been observed at several locations along the RCS. It was found that when the beam passes through sections where the beam duct and BPM have different diameters or shapes, the electromagnetic (EM) field of the beam is significantly distorted near the edges of the BPM, this distortion of beam EM field results in unphysical and know as edge effect [4]. A similar issue also has been reported for the in J-PARC MR [5].

To investigate and compensate for these unwanted transverse position offsets, four BPMs in the RCS were removed during the 2025 summer maintenance period. The BPMs were re-calibrated using realistic upstream and downstream dummy pipes to accurately incorporate the edge effects into the calibration equations. In addition, CST Wakefield simulations were performed for four different combinations of upstream and downstream beam pipe cross-sections in the BPM region. The wire calibration results and simulation are in good agreement with each other.

DIAGONAL CUT–PLANE BPM

The 32 diagonal cut–plane BPMs in the RCS are installed to provide transverse position measurements for the injection painting and circulating beam as well for the tune measurement. The diagonal cut–plane BPMs consist of two electrodes separated by a slanted cut, where the induced charge on each plate varies linearly with the beam's transverse position. This design is advantageous for an RCS because it provides a highly linear response over a large region of the vacuum duct's aperture [6, 7]. Given the rapid ramping of magnetic fields and the significant beam excursions during the injection and acceleration phases in an RCS, this linearity ensures accurate beam position measurement. The BPM inner diameter is 220 mm. A 3D schematic view of the RCS diagonal cut–plane BPM is shown in Fig. 1.

Table 1: RCS Diagonal Cut-plane BPM Parameters

Parameters	Values
Inner diameter	220 mm
Electrode Length	84 mm
Material	Ti-6Al-4V
Capacitance	300 pF
Electrode Isolation	−40 dB
Position Accuracy	1 % half of Aperture

Due to the stringent space constraints in the RCS, the BPM must be installed inside the AC corrector magnet. To minimize power dissipation in the BPM body due to eddy currents, a ribbed structure is incorporated on its grounded housing. The BPM is made of Ti-Alloy (Ti-6Al-4V), which has a low electrical conductivity of 5.8×10^5 S/m, which further suppresses eddy-current heating [8].

Two adjacent electrodes are separated by a 3 mm gap, which provides the required electrode isolation (S_{21}). The cross-talk between two adjacent electrodes in the frequency range (1.02–2.44 MHz) is approximately −40 dB. Long alu-

* Work supported by the National Science Foundation for Young Scientists of China (12305166).

† yangrenjun@ihep.ac.cn

Content from this work may be used under the terms of the CC BY 4.0 licence (© 2026). Any distribution of this work must maintain attribution to the author(s), title of the work, publisher, and DOI.

ISBN: 978-3-95450-252-3 ISSN: 2673-5350 doi: 10.18429/JACoW-IPAC2026-MOP6623

SOFTWARE DEVELOPMENT OF BEAM DIAGNOSTICS READOUT SYSTEM BASED ON A MULTI-CHANNEL HIGH-SPEED DIGITIZER*

Z. H. Xu[1,2], L. Zeng[1,2], F. Li[1,2],M. Y. Liu[1,2], M. A. Rehman[1,2], R. Y. Qiu[1,2],W. L. Huang[1,2], Z. J. Lu[1,2], C. J. Xie[1,2], R. Yang[1,2], R. J. Yang†,[1,2]
[1]Institute of High Energy Physics, Chinese Academy of Sciences, Beijing, China
[2]Spallation Neutron Source Science Center, Dongguan, China

Abstract

In the upgraded accelerator of the China Spallation Neutron Source Phase II project, several multi-channel beam diagnostic detectors are installed, including a Ionization Profile Monitor for measuring the injection beam profile and a Multi-Wire Profile Monitor for measuring the target beam profile. In the China Spallation Neutron Source, similar multi-channel detectors typically utilize multiple PXIe acquisition cards to construct a PXIe-based signal acquisition system, which suffers from high cost and limited flexibility. This paper presents an alternative signal readout solution using a multi-channel high-speed digitizer to replace the PXIe system. The digitizer incorporates built-in front-end amplification functionality, eliminating the need for separate analog electronics for signal amplification. With a maximum sampling rate of 125 MS/s, it fully meets the sampling requirements for the beam pulse width in the CSNS-II Rapid Cycling Synchrotron, which ranges from 500 ns to 80 ns. Moreover, the multi-channel signal acquisition system implemented with this digitizer offers high integration and reduced cost compared to the PXIe system, making it an ideal choice for beam diagnostics systems.

INTRODUCTION

In the upgraded accelerator complex of the China Spallation Neutron Source Phase II project, the beam diagnostics system employs various multi-channel detectors, such as the Ionization Profile Monitor and the Multi-Wire Profile Monitor. Traditionally at CSNS, signal acquisition for such detectors relies on systems built with multiple PXIe cards. While functional, this approach presents challenges in terms of high cost and system integration complexity. This paper presents the development of a new readout solution centered on a CAEN DT2745B multi-channel high-speed digitizer. The digitizer integrates front-end amplification, eliminating the need for separate analog electronics. Its maximum sampling rate of 125 MS/s is sufficient for the beam pulse widths (80 ns to 500 ns) in the CSNS-II Rapid Cycling Synchrotron. The associated data acquisition and control software, developed in C on the Linux platform and integrated with the Experimental Physics and Industrial Control System, offers a more open, stable, and cost-effective alternative to the previous LabVIEW and PXIe-based system[1].

* Work Supported by National Natural Science Foundation of China (NO. 12305166) and the Natural Science Foundation of Guangdong Province, China, (NO. 2024A1515010016)
† yangrenjun@ihep.ac.cn

HARDWARE ARCHITECTURE

PXIe-Based Acquisition System

The conventional signal acquisition system for multi-channel beam diagnostics detectors at CSNS is built upon a PXIe platform. This architecture typically consists of a PXIe chassis housing a system controller and multiple high-speed multifunction data acquisition cards. Each card provides a limited number of analog input channels . To achieve the required channel count for detectors like the Multi-Wire Profile Monitor, multiple such cards are installed within the same chassis[2]. Separate rack-mounted or custom-designed front-end analog electronics are required for signal conditioning and amplification before feeding signals to the DAQ cards. The system offers high performance and precise synchronization between channels on the same card via the PXIe backplane. However, it results in a system composed of multiple discrete components: chassis, multiple DAQ cards, and external analog electronics, leading to increased system footprint, cabling complexity, and overall cost.PXIe hardware architecture diagram is shown in Fig. 1.

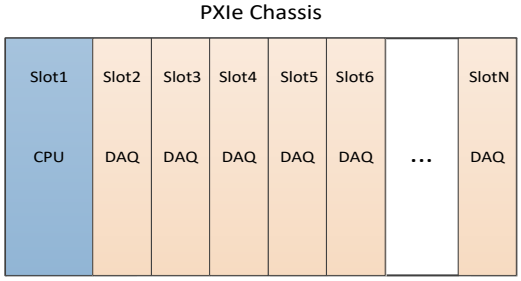

Figure 1: PXIe hardware architecture diagram.

Multi-Channel Digitizer System

The core hardware of the new proposed system is the CAEN DT2745B digitizer. Its key specifications include 64 analog input channels, a 16-bit ADC, a maximum sampling rate of 125 MS/s, and integrated programmable-gain front-end amplifiers (gain range: 0 to 40 dB, adjustable in 0.5 dB steps per 16-channel group). The device features both USB and Gigabit Ethernet interfaces for control and data transfer, and runs a Debian-based embedded operating system on its internal ZYNQ UltraScale+ SoC, allowing for standalone or networked operation. A single DT2745B unit integrates the functions of multiple PXIe cards into one compact device[3][4]. The multi-channel digitizer system diagram is shown in the Fig. 2.

Content from this work may be used under the terms of the CC BY 4.0 licence (© 2026). Any distribution of this work must maintain attribution to the author(s), title of the work, publisher, and DOI.

ISBN: 978-3-95450-252-3 ISSN: 2673-5350 doi: 10.18429/JACoW-IPAC2026-MOP6624

OPTIMIZATION OF DCCT MAGNETIC CORE MATCHING USING UNSUPERVISED MACHINE LEARNING TECHNIQUES FOR HIGH-PRECISION BEAM CURRENT MEASUREMENT*

W.L. Huang†, R. Yang, F. Li, R.Y. Qiu, L. Zeng, M.Y. Liu, X. Qi, R.J. Yang
Institute of High Energy Physics, Beijing, China

Abstract

DC Current Transformers (DCCTs) are essential instruments for non-interceptive beam current measurement in particle accelerators. The zero-flux modulation principle demands exceptional symmetry between paired magnetic cores to achieve sub-μA offset stability. Conventional core matching based on static magnetic parameters provides only an engineering approximation, as it neglects the dynamic magnetization behavior under AC modulation. This paper presents a novel approach employing unsupervised machine learning techniques applied to 6 dynamic magnetic parameters ($\mu_{\mathbf{a}}$, δ, $B_{\mathbf{r}}$, $B_{\mathbf{m}}$, $H_{\mathbf{c}}$, $H_{\mathbf{m}}$) measured at 50 kHz sinusoidal excitation for 19 Fe-based nanocrystalline cores. Principal Component Analysis (PCA) reduces the feature space while preserving 89.64% of total variance. An adaptive multi-objective K-Means strategy successfully isolates anomalous specimens ($K = 2$), while a density-based evaluation framework partitions the remaining operational cores into 5 highly homogeneous sub-groups. This two-tier matching scheme enables a physically rigorous core pairing that accounts for real-world dynamic magnetization and domain wall losses under actual DCCT operating conditions.

INTRODUCTION

Based on the zero-flux principle, Direct Current Current Transformers (DCCTs) are the standard for non-interceptive absolute beam current measurement in accelerators [1, 2]. In a dual-core DCCT, an AC modulation signal drives two identical toroidal cores into deep saturation. Ideally, their symmetric dynamic B–H loops cancel out even harmonics when no beam is present. However, residual magnetic asymmetry between the paired cores generates a parasitic second-harmonic signal, manifesting as zero drift [3]. For high-precision applications like the China Spallation Neutron Source Phase-II (CSNS-II) beam instrumentation, achieving sub-μA stability imposes strict requirements on core matching.

Traditional matching relies on quasi-static DC parameters (remanence $B_{\mathbf{r}}$, coercivity $H_{\mathbf{c}}$). However, this approach fails for Fe-based nanocrystalline alloys under dynamic AC modulation, as it ignores frequency-dependent eddy current losses, domain wall dynamics, and amplitude permeability $\mu_{\mathbf{a}}$ variations that directly govern waveform symmetry.

To address these limitations, this work proposes an unsupervised machine learning approach to cluster and pair nanocrystalline cores based on their high-dimensional dynamic magnetic responses. By applying an adaptive K-Means strategy and density-sensitive analysis to a 6-dimensional dynamic feature space, we establish a physically rigorous framework for high-precision core pairing.

EXPERIMENTAL METHODOLOGY

Core Specimens and Measurement

Nineteen toroidal core specimens wound from Fe-based nanocrystalline ribbon (nominal dimensions: OD 260 mm, ID 245 mm, H 8 mm) were fabricated by Guangzhou Jinchaina Co. for the CSNS-II DCCT R&D phase. The dynamic magnetic properties of these 19 samples were fully characterized using an automated AC magnetic measurement system(LINKJOIN CX-3110AW) under a 50 kHz sinusoidal excitation condition.

Feature Selection

Based on the zero-flux modulation principle and electrical symmetry demands, 6 dynamic parameters were selected as the high-dimensional feature vector for clustering analysis: Amplitude Permeability $\mu_{\mathbf{a}}$, Loss Angle δ (deg), Remanence $B_{\mathbf{r}}$ (mT), Maximum Induction $B_{\mathbf{m}}$ (mT), Coercivity $H_{\mathbf{c}}$ (A/m) and Maximum Field Strength $H_{\mathbf{m}}$ (A/m). The statistical distributions of these extracted dynamic features across all 19 fabricated nanocrystalline specimens are summarized in Table 1.

As indicated by the data, the maximum induction $B_{\mathbf{m}}$ exhibits an extremely narrow standard deviation (0.06 mT), which confirms that all cores reached a highly consistent, predefined deep saturation level under the 50 kHz sinusoidal voltage control. Conversely, key structural-sensitive parameters such as the amplitude permeability $\mu_{\mathbf{a}}$ and dynamic coercivity $H_{\mathbf{c}}$ demonstrate profound operational variance, with the maximum $\mu_{\mathbf{a}}$ value exceeding its minimum counterpart by a factor of four. This remarkable intra-batch discrepancy highlights the inadequacy of traditional single-point matching methods and underscores the crucial necessity of implementing a high-dimensional clustering framework to ensure dynamic magnetic symmetry.

Data Preprocessing and Dimensionality Reduction

To eliminate scaling discrepancies among different physical units, the 6-dimensional feature space was standardized to zero mean and unit variance. Principal Component Anal-

* † huangwei@ihep.ac.cn

† Work supported by China Spallation Neutron Source Phase-II (CSNS-II) project and National Natural Science Fund (No. 12275294)

Content from this work may be used under the terms of the CC BY 4.0 licence (© 2026). Any distribution of this work must maintain attribution to the author(s), title of the work, publisher, and DOI.

ISBN: 978-3-95450-252-3 ISSN: 2673-5350 doi: 10.18429/JACoW-IPAC2026-MOP6627

DEVELOPMENT OF ANALOG ELECTRONICS FOR THE BEAM LOSS MONITOR IN THE SUPERCONDUCTING SECTION OF THE CSNS II LINAC *

L. Zeng[1, 2], Z.J. Lu[1, 2], R.Y. Qiu[1, 2], F. Li[1, 2], Z. H. Xu[1, 2], W.L. Huang[1, 2]
M.Y. Liu[1, 2], C.J. Xie[1, 2], R.J. Yang[†, 1, 2]
[1]Institute of High Energy Physics, Chinese Academy of Sciences (CAS), Beijing, China
[2]Spallation Neutron Source Science Center, Dongguan, China

Abstract

The China Spallation Neutron Source (CSNS) upgrade project has been launched on 2024, and aims to increase the beam power on the neutron target to 500 kW. A superconducting accelerating section will be constructed to boost the negative hydrogen beam energy from 80 MeV to 300 MeV. For the beam loss control and fast machine protection of the superconducting accelerator, the parallel-plate ionization chamber, which has been massively implemented to the Large Hadron Collider (LHC), will be employed. The beam loss monitor electronics is designed with an extremely wide measurement range (200 pA to 20uA) and requires a machine protection response time of less than 10 μs for major beam loss events. In this paper, two electronics schemes, current-to-voltage (IV) and current-to-frequency (IF) conversion analog circuits are designed and compared in detail. The beam test at the CSNS Linac is also reported.

INTRODUCTION

The power upgrade of the CSNS-II linear accelerator will adopt a superconducting acceleration structure, and the beam pipe will be located inside the cryogenic module, so the detection of beam loss can only be performed on the outer surface of the cryogenic module. The overall layout of the CSNS-II linac [1] is presented in Fig. 1. Due to the thick cavity, it has a significant shielding effect on the secondary radiation generated by beam loss. On the other hand, the need for superconducting quench protection requires a beam loss monitor (BLM) with faster response speed.

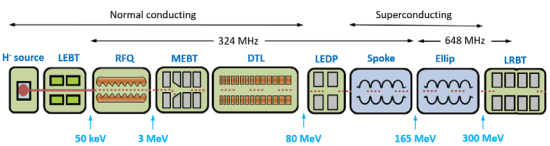

Figure 1: CSNS-II Linac layout.

CSNS-II accelerator plans to use parallel-plate multi-electrode ionization chambers as BLMs for its superconducting section, drawing on LHC BLM design in Fig. 2. This parallel-plate electrode BLM, critical for LHC [2], enhances sensitive volume and time response, and is widely used in ESS, GSI and other labs. A total of 45 such BLMs will be installed in the CSNS-II linac superconducting section.

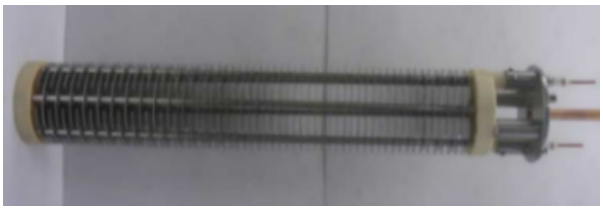

Figure 2: Parallel-plate ionization chamber.

The CSNS-II superconducting section BLM analog electronics conditions BLM detector output signals and provides interlock signals for machine protection, with detector, current range and electronics bandwidth similar to other mainstream international accelerators [3].

A comparison of BLM indicators of CSNS, ESS, SNS, LHC and FRIB shows none fully meet CSNS' needs: FRIB/LHC BLM beam abort response times are inadequate, other systems' hardware is incompatible with CSNS' planned platform, but their ionization chamber beam loss signal ranges are similar.

To measure such small pulse current signals, current amplification is needed to convert them into high-amplitude voltage/frequency signals. Mainstream international BLM front-end analog electronics fall into two types: ESS/SNS/FRIB's "current-to-voltage" (IV) conversion and LHC's "current-to-frequency" (IF) conversion.

IF CONVERSION

The IF conversion front-end analog circuit is designed with reference to LHC's beam loss electronics [4], consisting of an integrating amplifier, threshold comparison circuit, monostable circuit, and constant current discharge loop in Fig. 3. Its working principle: the detector's output current charges the integrating capacitor; during charging, the operational amplifier's output voltage decreases continuously. When it drops to the comparator's threshold voltage Vtr, the comparator triggers the monostable circuit, which outputs a fixed-width pulse to control the reference current source to discharge the capacitor. The total beam loss charge detected by the ionization chamber is accumulated as Qt at intervals T. The Machine Protection System (MPS) is generated by comparing the pulse counter's count with the calibrated unit-time count.

* Work Supported by National Natural Science Foundation of China (NO. 12305166) and the Natural Science Foundation of Guangdong Province, China, (NO. 2024A1515010016), Xie jialin's Grant (NO. E65461U2).
† yangrenjun@ihep.ac.cn

Content from this work may be used under the terms of the CC BY 4.0 licence (© 2026). Any distribution of this work must maintain attribution to the author(s), title of the work, publisher, and DOI.

ISBN: 978-3-95450-252-3 ISSN: 2673-5350 doi: 10.18429/JACoW-IPAC2026-MOP6629

APPLICATION OF WALL CURRENT MONITOR AT CSNS RAPID CYCLING SYNCHROTRON*

F. Li[1,2], T. G. Xu[1,2], J. L. Sun[3], W. L. Huang[1,2], Z. J. Lu[1,2], R. Y. Qiu[1,2], M. A. Rehman[1,2], W. W. Chen[4], Z. H. Xu[1,2], R. J. Yang†[,1,2], L. Zeng[1,2], C. J. Xie[1,2]
[1]Institute of High Energy Physics, Chinese Academy of Sciences (CAS), Beijing, China
[2]Spallation Neutron Source Science Center, Dongguan, China
[3]PSI Center for Accelerator Science and Engineering, Villigen, Switzerland
[4]University of Chinese Academy of Sciences, Beijing, China

Abstract

Two sets of Wall Current Monitors (WCMs) have been installed in the Rapid Cycling Synchrotron (RCS) of the China Spallation Neutron Source (CSNS) for longitudinal bunch shape measurement, longitudinal emittance calculation, and beam instability diagnosis. This paper presents the WCM system design (probe and DAQ) and recent beam measurement results, including bunch shape evolution, bunch length measurement, and RF frequency tracking during the acceleration cycle.

INTRODUCTION

The China Spallation Neutron Source (CSNS) is a large-scale scientific facility located in Dongguan, China [1]. Its accelerator complex consists of an 80 MeV H^- linac, a 1.6 GeV Rapid Cycling Synchrotron (RCS), and beam transport lines. The RCS operates at 25 Hz with harmonic number $h = 2$ (double bunches) and a design beam power of 100 kW. The beam is accelerated from 80 MeV to 1.6 GeV in approximately 20 ms.

The Wall Current Monitor (WCM) is a broadband, non-destructive diagnostic device that measures the image current on the vacuum chamber wall with nanosecond-scale time resolution, making it indispensable for longitudinal dynamics studies. Unlike current transformers that only provide slowly varying beam current, the WCM captures the high-frequency bunch structure directly.

Two sets of WCMs are installed in the CSNS-RCS: one dedicated to beam diagnostics and another serving the RF control system. This paper presents the WCM system design, the custom data acquisition system, and recent measurement results.

WCM SYSTEM OVERVIEW

Working Principle

When a charged particle beam travels through the vacuum chamber, it induces an image current (wall current) on the inner surface of the chamber wall. By introducing a ceramic gap to interrupt the wall current path and placing a matched resistor across the gap, the wall current generates a measurable voltage signal proportional to the beam current:

$$V_{\mathrm{WCM}}(t) = R \cdot I_{\mathrm{wall}}(t) \approx R \cdot I_{\mathrm{beam}}(t) \tag{1}$$

where R is the matching resistance. Ferrite and nanocrystalline magnetic rings are placed around the gap to extend the low-frequency response by increasing the inductance.

Probe Design

The CSNS-RCS WCM probe consists of the following key components [2]:

- **Ceramic gap:** 97-porcelain ring (ID 225 mm, OD 251 mm, thickness 12 mm), $\varepsilon_r = 9.5$, $C_{\mathrm{gap}} \approx 68.1$ pF, $Z_0 = 1.96\,\Omega$.
- **Matching resistors:** Two configurations have been tested: 25 parallel thick-film resistors of 50 Ω each, or 150 parallel metal-film resistors of 300 Ω each. Both yield ~2 Ω matched to the gap impedance.
- **Magnetic rings:** Four rings symmetrically placed around the gap: two iron-based amorphous rings (1K101, effective from 1 kHz to 100 MHz) and two nanocrystalline rings (1K107B, effective from 1 kHz to 500 kHz). Each ring has dimensions of $\phi275\times\phi330\times25$ mm.
- **Signal pickup:** Four symmetric cables combined through a power combiner to cancel position dependence.

The cutoff frequencies are:

$$f_h = \frac{1}{2\pi R C_{\mathrm{gap}}}, \quad f_l = \frac{R}{2\pi L} \tag{2}$$

Laboratory S21 tests confirmed ±1 dB flatness from 300 kHz to 50 MHz with the upper −3 dB cutoff at ~500 MHz [2].

Data Acquisition System

A custom NI-PXIe oscilloscope system has been developed for WCM data acquisition [3]. Key specifications are in Table 1.

The 12-bit resolution provides significantly better sensitivity than typical 8-bit oscilloscopes for weak beam signals.

* Work supported by the National Natural Science Foundation of China (No. 12275294) and the National Science Foundation for Young Scientists of China (No. 12305166).

† yangrenjun@ihep.ac.cn

Content from this work may be used under the terms of the CC BY 4.0 licence (© 2026). Any distribution of this work must maintain attribution to the author(s), title of the work, publisher, and DOI.

ISBN: 978-3-95450-252-3 ISSN: 2673-5350 doi: 10.18429/JACoW-IPAC2026-MOP6631

OBSERVATION OF INTRA-MACROPULSE POSITION MONITOR OF H⁻ BEAM OF CSNS LINAC*

C. Xie, Z. Xu, R. Qiu, C. Chen, M. A. Rehman, B. Zhang, R. Yang†
Institute of High Energy Physics, Beijing, China
also at Spallation Neutron Source Science Center, Dongguan, China

Abstract

The China Spallation Neutron Source (CSNS) accelerator, consisting of a H⁻ linac and a rapid cycling synchrotron (RCS), is undergoing an upgrade to increase the average beam power to 500 kW. At the CSNS linac, shorted-stripline beam position monitor (BPM) determines beam position by averaging over the entire macro-pulse. However, significant intra-macropulse beam position fluctuations have been observed in recent commissioning, which may cause undesired beam loss and degrade the injection efficiency. In this work, an intramacropulse beam position is reconstructed based on the signal integral algorithm. During 2025 autumn and 2026 spring operation, the intra-macropulse beam position behaviors have been uncovered at the MEBT and LRBT sections. Although beam conditions vary between two different experiments, a significant beam position drift during the first 100 μs, with a maximum amplitude of more than 5 mm, has been revealed.

POSITION RECONSTRUCTION ALGORITHM

The intra-macropulse beam position is reconstructed using a multi-step digital signal processing procedure. First, the raw BPM signals are digitally filtered to suppress noise and remove undesired frequency components. The processed signals are then segmented according to the chopper timing structure, where each segment corresponds to an individual chopped beam pulse with a repetition frequency of 1.02 MHz or 0.51 MHz. The normalized beam positions are subsequently calculated using the difference-over-sum method, followed by a third-order polynomial calibration derived from prior measurements to correct the position nonlinearity. By processing each segmented chopper window individually, the evolution of the intra-macropulse beam position within the macro-pulse can be reconstructed.

To investigate the influence of the sampling rate and filter bandwidth on the intra-macropulse beam position reconstruction, we using an R&S RTO2044 oscilloscope with a sampling rate of 6.25 GSPS and a vertical resolution of 16 bits to record data. In addition, a 20 kHz high-pass filter was applied to each electrode channel to suppress low-frequency interference from power supplies or magnet systems. In the upper plot of Fig. 1, the red markers represent the intra-macropulse beam positions reconstructed from BPM signals

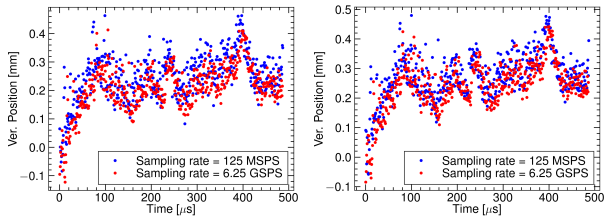

Figure 1: Comparison of intra-pulse beam position calculation results at different sampling rates with filter bandwidths of 50 MHz (upper) and 2 MHz (bottom).

sampled at 6.25 GSPS after applying a digital band-pass filter with a center frequency of 324 MHz and a bandwidth of 50 MHz. The blue markers correspond to the reconstruction results obtained by first applying the same filter to the original waveform, followed by down-sampling by a factor of 50 before the beam position calculation, corresponding to an effective sampling rate of 125 MSPS. In the lower plot of Fig. 1, the red markers show the intra-macropulse beam positions reconstructed using a digital band-pass filter centered at 324 MHz with a bandwidth of 2 MHz. The blue markers represent the reconstruction results obtained from the down-sampled waveform using a digital band-pass filter centered at 51 MHz with the same bandwidth of 2 MHz. These figures show that a sampling rate of 125 MSPS is sufficient for accurate intra-macropulse beam position measurement, while the reconstruction accuracy is not significantly affected by the selected filter bandwidth within the present measurement conditions.

EXPERIMENTAL RESULTS

The proposed method was applied to reconstruct the intra-macropulse beam position evolution using BPMs installed along the MEBT and LRBT sections of the CSNS LINAC. To reduce the impact of shot-to-shot jitter, measurements from more than 10 shots were analyzed, and the mean value together with the standard deviation was calculated for some BPMs. And all the measurements were performed using the same oscilloscope operated at a sampling rate of 1 GSPS with 16-bit vertical resolution. During the signal processing procedure, no down-sampling was applied, and the intra-macropulse beam positions were reconstructed using a digital band-pass filter with a center frequency of 324 MHz and a bandwidth of 2 MHz.The reconstructed intra-macropulse beam position evolution is shown in Fig. 2 for the LRBT section with a chopping frequency of 1.02 MHz measured in November 2025, Fig. 3 for the MEBT section with a chopping frequency of 0.51 MHz measured in April 2026, and

* Work supported by National Natural Science Foundation of China (No. 12305166) and the Natural Science Foundation of Guangdong Province, China (No. 2024A1515010016), Xie Jialin's Grant (No. E65461U2).
† yangrenjun@ihep.ac.cn

Content from this work may be used under the terms of the CC BY 4.0 licence (© 2026). Any distribution of this work must maintain attribution to the author(s), title of the work, publisher, and DOI.

ISBN: 978-3-95450-252-3 ISSN: 2673-5350 doi: 10.18429/JACoW-IPAC2026-MOP6635

DESIGN OF THE HIGH-SPEED, HIGH-PRECISION AVERAGE BEAM CURRENT AND LIFETIME MEASUREMENT SYSTEM

An Wang[1,2], X. Yang[1], Y. Deng[1], Y. Leng[†,1]
[1]University of Science and Technology of China, Hefei, China
[2]Suzhou Laboratory, Suzhou, China

Abstract

This paper presents a high-speed, high-precision system for measuring average beam current and lifetime, addressing the low data refresh rates of existing systems that fail to capture rapid beam dynamics. A comprehensive performance analysis identifies key error sources, including the beam probe, data acquisition card, electromagnetic interference, and quantization noise. Experimental validation at the HLS shows that with a 0.5 μA resolution probe, the system achieves measurement accuracy better than 1 μA at a 1 Hz update rate and 2 μA at 100 Hz. This high-speed, high-precision current measurement enables rapid and accurate lifetime determination. The system provides a critical tool for real-time monitoring of injection efficiency and beam stability, and offers essential data support for analyzing beam loss mechanisms and beam dynamics.

INTRODUCTION

The development of advanced light sources and colliders demands higher accuracy and data rates for beam current and lifetime measurement to support diagnosis and control of dynamic processes[1, 2]. Beam current and lifetime are core parameters reflecting storage ring operation, directly serving operation control and injection optimization[3].

Beam lifetime is determined by mechanisms including the Touschek effect, residual gas scattering, and quantum diffusion[4]. In routine operation, beam lifetime measurement is typically limited to the decay cycle, with a blind spot during injection due to high frequency and short intervals. Touschek lifetime extraction relies on dedicated machine studies using long-duration current decay data. High-speed, high-precision measurement enables continuous monitoring during injection. Continuou beam lifetime data can support Touschek lifetime calculation[5].

This paper presents a new average current measurement system based on a high-speed, high-precision ADC and an FPGA board. A coordinated real-time processing architecture enables a full pipeline from signal acquisition to data output, achieving a maximum effective output rate of 2 MHz and μA-level accuracy at a 1 Hz output rate. System performance has been verified through beam experiments at HLS-II.

MEASUREMENT SYSTEM SETUP

HLS-II is a second-generation synchrotron radiation (SR) light source dedicated to VUV and soft X-ray production, consisting of an 800 MeV linear accelerator injector and an 800 MeV electron storage ring. After undergoing major upgrades, its performance now approaches the level of third-generation SR sources. HLS-II routinely operates in top-up filling with a stored beam current of 500 mA.

The current average beam current measurement system at HLS-II is based on a digital multimeter (DMM) scheme with a data rate of 1 Hz[6]. By implementing a high-speed, high-precision measurement approach, rapid measurement of both the beam current and beam lifetime can be achieved.

System Architecture

The overall hardware architecture of the beam current measurement system is shown in Fig. 1. A voltage signal induced by the beam is acquired using an NPCT sensor and conditioned by front-end electronics. The ADC board then samples and digitizes the signal. The resulting digital data enters the FPGA for real-time processing. The processed results are transmitted to an EPICS IOC running on the processor core.

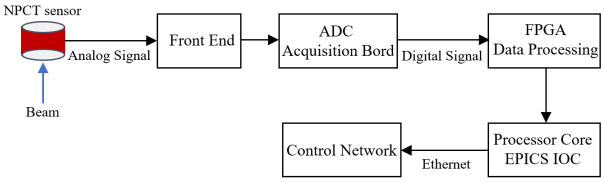

Figure 1: Architecture of the measurement system.

Signal acquisition processor

The signal acquisition and processing system is shown in Fig. 2. The ADC board connects to the FPGA board via an FMC interface, enabling high-speed data transfer. The FPGA evaluation board employs an XCZU19EG chip. Its programmable logic receives the high-speed data stream, executes processing algorithms, computes the beam lifetime. An EPICS IOC, running on the ARM processor under Linux.

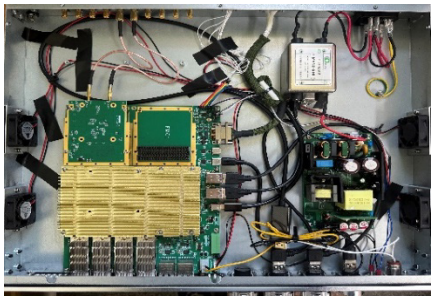

Figure 2: Signal acquisition processor.

* Work supported by Large-Scale Scientific Facility Renovation and Upgrade Project of the Chinese Academy of Sciences -"Universal Signal-Processing Platform for Accelerator Beam Measurement and Control"
† email address: lengyb@ustc.edu.cn

Content from this work may be used under the terms of the CC BY 4.0 licence (© 2026). Any distribution of this work must maintain attribution to the author(s), title of the work, publisher, and DOI.

ISBN: 978-3-95450-252-3 ISSN: 2673-5350 doi: 10.18429/JACoW-IPAC2026-MOP6636

OSCILLOSCOPE-BASED TCSPC LONGITUDINAL BEAM DIAGNOSTICS AT HLS-II*

Mingdong Ma, Xing Yang, Yongbin Leng†
National Synchrotron Radiation Laboratory,
University of Science and Technology of China, Hefei, China

Abstract

The longitudinal density distribution of electron bunches is a critical parameter for evaluating the performance of storage rings. To meet the requirements for real-time, cost-effective, and flexible longitudinal diagnostics for the Hefei Advanced Light Facility (HALF), we have developed a Time-Correlated Single Photon Counting (TCSPC) measurement system based on a general-purpose high-speed oscilloscope at the Hefei Light Source II (HLS-II). Unlike traditional setups relying on dedicated TCSPC modules, this system utilizes an oscilloscope to directly acquire single-photon pulses from a Photomultiplier Tube (PMT). Experiments conducted at the HLS-II beamline successfully recovered the bunch fill pattern and reconstructed the photon arrival time distribution. To address the measurement errors caused by amplitude fluctuations, a post-processing algorithm incorporating Software Constant Fraction Discrimination (CFD) and time folding was developed. This approach effectively suppressed the time walk effect and enabled high-resolution reconstruction of the bunch profile. The results demonstrate that this oscilloscope-based scheme possesses excellent online monitoring capabilities, providing a cost-effective technical solution for HALF and similar facilities.

INTRODUCTION

The longitudinal density distribution of electron bunches is a parameter of paramount importance for evaluating beam dynamics in storage rings [1]. For longitudinal diagnostics, dual-sweep streak cameras are traditionally favored due to their sub-picosecond time resolution [2, 3]. However, their inherent deflection scanning mechanisms and limited readout speeds often preclude continuous, real-time online monitoring at the high repetition rates typical of modern accelerators. Furthermore, streak cameras entail prohibitive costs and complex maintenance [4, 5].

As a robust alternative, Time-Correlated Single Photon Counting (TCSPC) offers superior dynamic range, excellent statistical precision, and continuous real-time monitoring capabilities [6-9]. Conventional TCSPC setups rely on photodetectors paired with dedicated Time-to-Digital Converter (TDC) or Time-to-Amplitude Converter (TAC) modules [10]. While these hardware-centric systems process timestamps rapidly, they fundamentally discard the raw analog waveforms. This reliance on fixed, hardware-level signal discrimination restricts the adaptability of the system when confronted with complex and fluctuating beam conditions in accelerator environments.

† Corresponding author (email: mmd@mail.ustc.edu.cn).

To overcome these hardware limitations and fulfill the stringent diagnostic requirements of the future Hefei Advanced Light Facility (HALF) [11], this paper proposes a highly flexible, oscilloscope-based TCSPC system experimentally validated at the Hefei Light Source II (HLS-II). By leveraging a general-purpose, high-bandwidth oscilloscope for direct raw waveform acquisition, the proposed scheme shifts critical signal processing into the software domain. This "software-defined" architecture allows core algorithms, such as Constant Fraction Discrimination (CFD), to be executed dynamically, thereby circumventing the rigid constraints of traditional hardware and providing a cost-effective, adaptable solution for longitudinal beam monitoring.

EXPERIMENTAL SETUP

The experimental apparatus was deployed at the diagnostic beamline of HLS-II, which operates with a revolution frequency of 4.534 MHz. The system architecture is divided into the optical front-end, the detector auxiliary path, and the integrated acquisition and control system.

Optical Front-end

As shown in Fig. 1, synchrotron radiation is generated by the electron beam passing through the B8 bending magnet. The extracted light is directed to an optical table via a series of high-reflectivity mirrors. To ensure high-fidelity imaging, two achromatic doublets with focal lengths of 1000 mm and 400 mm are employed to achieve 1:1 imaging of the radiation source point at a distance of 2800 mm. The use of achromatic lenses effectively sup-presses chromatic aberration from the broadband synchrotron radiation, ensuring the quality of the image spot.

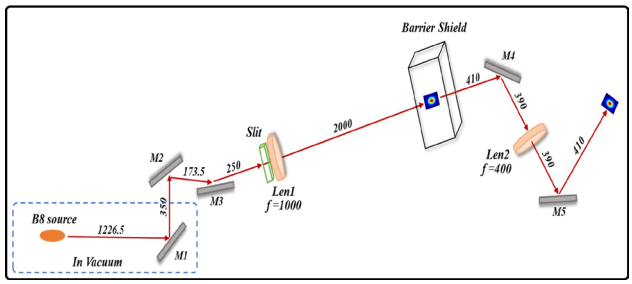

Figure 1: Front-end optical path of the detector.

Detector and Optical Path Conditioning

The layout of the optical table is illustrated in Fig. 2. A high-performance photomultiplier tube (Hamamatsu H10721-110) serves as the photon detector, with its photocathode precisely positioned at the 1:1 imaging point. To ensure the system operates within the single-photon

Content from this work may be used under the terms of the CC BY 4.0 licence (© 2026). Any distribution of this work must maintain attribution to the author(s), title of the work, publisher, and DOI.

ISBN: 978-3-95450-252-3 ISSN: 2673-5350 doi: 10.18429/JACoW-IPAC2026-MOP6637

DEVELOPMENT OF A SIMULATOR FOR RING ACCELERATOR ELECTRON BEAM SIGNALS

H. Liu, Y. Deng, X. Gao, Y. Leng†, X. Yang, University of Science and Technology of China, Hefei, China
D. Wang, National Synchrotron Radiation Laboratory, Hefei, China

Abstract

Beam diagnostic systems are crucial for the Hefei Advanced Light Facility (HALF), a fourth-generation light source under construction. However, the testing of its key devices—such as Digital Beam Position Monitors (DBPMs), the Fast Orbit Feedback (FOFB) system, and Bunch-by-Bunch (BbB) processors—is limited by the lack of a laboratory signal generator capable of simulating accelerator physics, which hinders comprehensive closed-loop testing prior to installation. To address this, we have developed an FPGA-based hardware simulator featuring two input ports for feedback signals and four output ports with independently adjustable signal amplitudes and synchronous triggers. It integrates a simplified physics model to generate realistic, wideband beam signals with a pulse width of approximately 5 ns, enabling low-cost, repeatable testing without an actual beam. The system quantizes real bunch signals, simulates transverse/longitudinal oscillations in an FPGA, and outputs specific waveforms upon a set trigger. By modelling beam dynamics, it also produces signals closely resembling those expected during actual operation in Hefei Light Source (HLS). This simulator assists in designing and optimizing beam feedback algorithms while reducing development difficulty for DBPM and BbB systems. Crucially, it fulfills application needs by enabling previously impossible lab tests—such as evaluating BbB algorithms and measuring FOFB latency/bandwidth—before the beam is ready.

INTRODUCTION

As a fourth-generation diffraction-limited storage ring synchrotron light source, HALF is currently under construction [1]. The associated beam diagnostic devices are being developed to ensure the facility can produce bunches with low emittance, small size, and high brightness.

Under laboratory conditions, only simple single-item tests can be conducted on these systems and algorithms, such as single-frequency verification of DBPM performance, ADC sampling accuracy of feedback systems, and validity of data transmission logic [2-4]. Tests involving beam pattern dependence of measuring instruments and closed-loop characteristics of feedback systems require on-beam measurements inside the storage ring, together with specific bunch filling modes provided by accelerator facilities, which is extremely inefficient and inconvenient.

† lengyb@ustc.edu.cn

To address this issue, a beam simulation algorithm is developed based on a four-output-port FPGA+DA hardware platform, supporting adjustable signal amplitude and synchronous triggering. As illustrated in Fig. 1, the designed system can generate realistic beam signals, enabling low-cost, repeatable device testing without actual beams, and facilitating offline optimization of feedback algorithms.

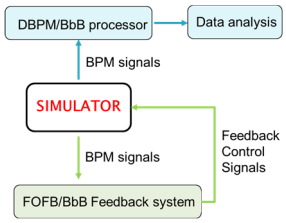

Figure 1: Schematic diagram of simulator application.

PHYSICAL PRINCIPLE

Generation of BPM Signals

Assuming a Gaussian charge distribution in the electron bunch, the induced voltage on button electrodes can be expressed as [5]:

$$V_B(t) = \frac{\pi a^2}{2\pi b}\frac{1}{\beta c}\cdot Z\cdot\frac{t-t_0}{\sigma^2}\cdot I(t)\cdot\frac{a^2-\delta^2}{a^2+\delta^2-2a\delta cos\theta}, \quad (1)$$

$$I(t) = \frac{Q}{\sqrt{2\pi}\sigma}e^{-\frac{(t-t_0)^2}{2\sigma^2}}. \quad (2)$$

Figure 2 shows the parameters involved, and Q is the bunch charge, σ is the bunch length, βc is the beam velocity, t_0 is the phase offset, and Z is the transfer impedance (mainly the equivalent impedance of the coupling capacitance between the electrode and the beam pipe wall as well as external cable impedance), and $I(t)$ represents instantaneous current of the bunch.

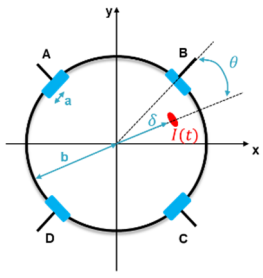

Figure 2: Beam parameters in the storage ring.

Transverse and Longitudinal Oscillations

In practical accelerator storage rings, the transverse and longitudinal positions of particle beams deviate from the

Content from this work may be used under the terms of the CC BY 4.0 licence (© 2026). Any distribution of this work must maintain attribution to the author(s), title of the work, publisher, and DOI.

ISBN: 978-3-95450-252-3 ISSN: 2673-5350 doi: 10.18429/JACoW-IPAC2026-MOP6641

DEVELOPMENT OF A BUNCH-BY-BUNCH BPM MEASUREMENT SYSTEM AT SSRF BASED ON MACHINE LEARNING

J. L. Pan[1,2], L. W. Lai[†,3], Y. M. Zhou[3], Y. B. Yan[3], C. L. Wang[1,2], Y. X. Han[1,2]
[1]Shanghai Institute of Applied Physics, Chinese Academy of Sciences, Shanghai, China
[2]University of Chinese Academy of Sciences, Beijing, China
[3]Shanghai Advanced Research Institute, Chinese Academy of Sciences, Shanghai, China

Abstract

Real-time bunch-by-bunch monitoring of transverse position and longitudinal phase has become increasingly important for the stable operation of storage ring light sources and for accelerator physics studies. This paper presents a real-time three-dimensional bunch-by-bunch position measurement system based on machine learning. The system eliminates the need for sampling delay adjustment and avoids complex front-end circuitry by directly digitizing BPM electrode signals with high-speed ADCs at a sampling rate of five times the storage ring RF frequency. By deploying neural network models within the FPGA, the system simultaneously achieves real-time measurement of the transverse position and longitudinal phase with low latency. Beam experiments were conducted at Shanghai Synchrotron Radiation Facility (SSRF) to validate the system's phase measurement capability. The results demonstrate a bunch-by-bunch phase resolution of 0.4ps while maintaining a measurement latency within 1μs.

INTRODUCTION

The SSRF is a third-generation medium-energy synchrotron radiation light source. It operates with a beam energy of 3.5 GeV, a storage ring circumference of 432 meters, a harmonic number of 720, and an RF frequency of 499.654 MHz. To improve the operational stability of the facility, implement bunch-by-bunch beam feedback, high-precision online real-time measurements of the storage ring's bunch-by-bunch transverse position and longitudinal phase are required.

Current mainstream online real-time measurement systems are primarily based on digital boards. Data acquired by ADCs, with sampling clocks synchronized to the accelerator machine clock, is directly transmitted to the FPGA to calculate the transverse position. In this scheme, the ADC sampling rate is typically identical to the RF frequency of the electron storage ring. By precisely adjusting the sampling clock delay, the ADC sampling points are aligned with the peak moments of the beam signal. The single-point sample value is then used to represent the signal amplitude[1], which is processed via a difference-over-sum calculation to derive the beam transverse position. Current bunch-by-bunch transverse feedback systems, such as the iGp-12 and Libera Bunch-by-Bunch, all adopt this scheme [2]. The issue with this scheme lies in the need for precise adjustment of the sampling delay, which hinders its application in large-scale engineering projects. Furthermore, beam longitudinal oscillations and clock jitter can cause the sampling points to deviate from the peak, thereby introducing measurement errors.

This paper proposes a bunch-by-bunch transverse position and longitudinal phase measurement system based on machine learning. The system performs RF direct sampling of BPM electrode signals via a high-performance ADC. A fully connected neural network (FCNN) is trained for each BPM electrode channel and the four-electrode sum signal, respectively. The weights and biases are then deployed on the Programmable Logic (PL) side of the processor FPGA.

The input layer consists of N consecutive sampling points belonging to the same bunch. The network undergoes offline training using a large dataset of real beam signals to learn the complex mapping from a sequence of sampling points at arbitrary phases to the true signal peaks and zero-crossings, thereby accurately reconstructing the signal amplitude and zero-crossing time. The zero-crossing points of the four-electrode sum signal serve directly as the longitudinal phase, while the transverse position is obtained by performing a difference-over-sum calculation on the amplitudes of each BPM electrode channel. The phase measurement function has been tested at SSRF. Experimental results demonstrate that the system achieves a bunch-by-bunch phase resolution of 0.4 ps.

THEORETICAL BASIS

When a bunch passes through a BPM, signals correlated with the bunch parameters are induced on the button electrodes. The signal on the BPM electrode is given by:

$$V(t)=\frac{ZSQ(t-t_0)}{\sqrt{2\pi}L\beta c\sigma^3}\exp\left[-\frac{(t-t_0)^2}{2\sigma^2}\right]F(\delta,\theta) \quad (1)$$

Where S is the area of the button electrode, L is the circumference of the vacuum pipe at the BPM, βc is the velocity of the beam, σ is the bunch length, t_0 is the longitudinal phase, Q is the bunch charge, and F is the transverse position factor. Equation (2) represents the sum signal of the four BPM electrodes, where the zero-crossing time is the longitudinal phase.

$$V_S=\frac{4ZSQ(t-t_0)}{\sqrt{2\pi}L\beta c\sigma^3}\exp\left[-\frac{(t-t_0)^2}{2\sigma^2}\right] \quad (2)$$

And the transverse position is obtained by performing a difference-over-sum calculation on the amplitudes of the four electrode signals:

* Work supported by The National Science Foundation of China (Grant No.12175239). Youth Innovation Promotion Association, CAS (Grant No.2019290). Outstanding member of the Youth Innovation Promotion Association, CAS(Gant No.Y2023079).
† Corresponding author: lailw@sari.ac.cn

Content from this work may be used under the terms of the CC BY 4.0 licence (© 2026). Any distribution of this work must maintain attribution to the author(s), title of the work, publisher, and DOI.

ISBN: 978-3-95450-252-3 ISSN: 2673-5350 doi: 10.18429/JACoW-IPAC2026-MOP6643

BEAM DIAGNOSTICS SYSTEM FOR HALF STORAGE RING

Y. Leng†, B. Sun, X. Yang, Y. Deng, C. Wang, D. Wang, J. Wang, Q. Wang, X. Ma, T. Zhou, Q. Luo, A. Wang, L. Tang, University of Science and Technology of China, Hefei, China

Abstract

The Hefei Advanced Light Facility (HALF) is a fourth-generation, low-energy diffraction-limited synchrotron light source currently under construction. Its storage ring has an energy of 2.2 GeV, a circumference of 480 meters, and an emittance of 86 pm·rad. To ensure the smooth commissioning of HALF to meet its design specifications and to fully exploit the operational potential of this facility, it is necessary to develop a comprehensive beam diagnostic system with high temporal and spatial resolution. This paper will introduce the overall structure and design of the HALF storage ring beam diagnostics system, focusing on the latest development progress of the high-resolution, high-stability beam orbit measurement and feedback system, and the bunch-by-bunch multi-parameter diagnostic system.

SYSTEM OVERVIEW

The Beam Instrumentation system is one of the critical subsystems of the Hefei Advanced Light Facility (HALF) storage ring. It will play a pivotal role during the key stages of the facility, including commissioning, acceptance testing, and user operation. The system is required to provide precise and comprehensive beam parameter information for evaluating machine operational performance, while also offering real-time data and diagnostic tools for accelerator physicists, thereby comprehensively ensuring the stable and efficient operation of the accelerator. To meet these requirements, the BI system must be capable of real-time measurement of key parameters, including beam position, beam current, lifetime, filling pattern, tune, beam profile/emittance, bunch length, and beam loss. Furthermore, to effectively guarantee the stability of the orbit and the beam, the system must incorporate bunch-by-bunch feedback and fast orbit feedback subsystems, laying a solid foundation for the high-quality operation of the HALF storage ring.

Table 1: Specification for HALF Ring BI system

Measurement	Specification	Quantity
Beam position	50 nm @ 10Hz 200 nm @ 20 kHz 1 μm @ TBT	240
Average current	2 μA @ 1 Hz	2
Bunch charge	0.05 % @ 1 kHz	1
Beam profile	2 μm / 10 μm	3
Bunch length	2 ps	1
Tune monitor	0.0001	1
FOFB	BW 500 Hz	1
MBFB	BW 250 MHz	1

†lengyb@ustc.edu.cn

Table 1 shows the primary specification of the all subsystems. Figure 1 shows the layout of all diagnostics sensors around the entire ring.

The layout of beam instrumentation probes around the entire ring is shown in the figure below:

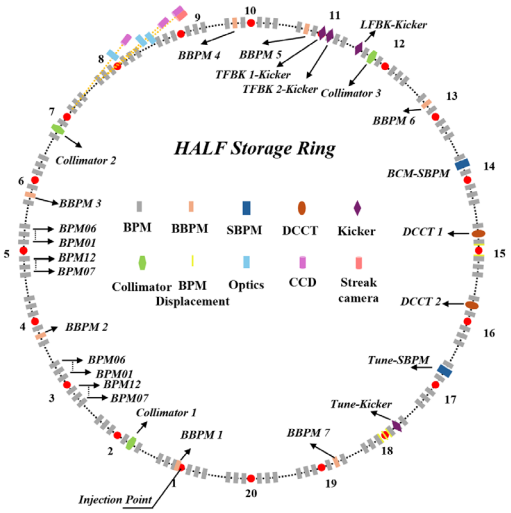

Figure 1: The layout of beam instrumentation probes around the entire ring.

BEAM POSITION MONITOR

Beam orbit measurement will be done at a total of 240 monitoring points across 20 units around the ring. It uses small-diameter (6 mm) button electrodes as beam probes and is equipped with a digital beam signal processor. Under the condition of a beam current higher than 100 mA, the resolution of the closed-orbit data (with a sampling frequency of 10 Hz) must be better than 50 nm; the resolution of the fast feedback data (with a sampling frequency of 20 kHz) must be better than 200 nm; and the resolution of the turn-by-turn data must be better than 1 μm [1].

To meet the above requirements, a custom designed DBPM processor using dual pilot tones and high oversampling ratio technologies have been developed tested in the SSRF ring. Figure 2 shows the photo of prototype.



Figure 2: Prototype of DBPM processor for HALF storage ring.

The beam experimental results demonstrate that the resolution of this prototype is better than 10 nm for SA, better than 80 nm for FA, and better than 400 nm for TBT. Figure 3 shows the TBT data (left) and coresponding FFT

Content from this work may be used under the terms of the CC BY 4.0 licence (© 2026). Any distribution of this work must maintain attribution to the author(s), title of the work, publisher, and DOI.

ISBN: 978-3-95450-252-3 ISSN: 2673-5350 doi: 10.18429/JACoW-IPAC2026-MOP6644

THZ-DRIVEN DEFLECTION OF ULTRASHORT ELECTRON BUNCH

Li Sun*, Chengzhe Wang, Zhicheng Huang, Yelong Wei
National Synchrotron Radiation Laboratory,
University of Science and Technology of China, Hefei, China

Abstract

Accurate characterization of longitudinal properties in ultrashort electron bunches constitutes a fundamental prerequisite for advancing scientific applications of compact particle accelerators. Here, we present an on-chip integrated terahertz (THz)-driven dielectric particle deflector based on the inverse Cherenkov effect: by coherently illuminating a high-breakdown-threshold right-angle prism with two linearly polarized lasers featuring a 180° phase difference, synchronized evanescent waves are excited on the prism's hypotenuse surface, enabling phase matching between particle velocity and wave velocity to generate sustained transverse deflection forces. This method successfully reconciles the inherent constraints of optical laser bunch length and radio-frequency input power, while achieving scalable temporal resolution from 10 femtoseconds to the attosecond regime. Simulation results validate that the proposed scheme provides a robust technical platform for on-chip longitudinal bunch diagnostics and particle manipulation, holding significant application prospects in electron bunch-based scientific facilities.

INTRODUCTION

Transverse deflection structures (TDS) have been widely used as diagnostics and optimization devices to characterize longitudinal properties of electron bunchs in many electron bunch-based scientific facilities such as ultrafast electron diffraction (UED) and microscopy (UEM), free electron laser (FEL), dielectric laser accelerator (DLA), laser-driven (LWFA) and bunch-driven plasma wakefield accelerator (PWFA) [1–6]. The X-band (11.4 GHz) TDS with compact design have demonstrated its ability to achieve femtosecond and sub-femtosecond longitudinal resolution , the recent experiments even show that sub-femtosecond resolution can be achieved at the C-band (5.7 GHz) range. However, emerging applications like femtosecond and attosecond pulses demand bunch diagnostics shorter than femtoseconds, a regime where conventional RF deflectors face two intrinsic limitations: (i) the low breakdown threshold of metallic cavities , and (ii) the lack of high-power sources at frequencies beyond the X-band.

In this work, we propose a THz-driven dielectric particle deflector that allows one to record the complete longitudinal information of an ultrashort electron bunch which can be integrated on chip. Though accurate control of two incident THz laser pulses' phase shift to 180 degree, the bunch channel constructed by symmetric dual prisms can generate a continuous synchronized deflecting force. In a two-dimensional model, the fields can be decomposed into TE (with E_y, H_x, and H_z nonzero) and TM (with E_x, E_z, and H_y nonzero) polarization. The deflecting strength can be adjusted via THz field intensity, enabling deflecting voltages from MV/m to GV/m over micron-to-millimeter scales. Here, a simulation is presented to demonstrate the deflecting capability of dielectric prisms structure with a MV/m scale via inverse Cherenkov effect. Such a THz-driven dielectric particle deflector should have wide applications in many electron bunch-based facilities.

STRUCTURE DESIGN

The schematic diagram of the proposed THz-driven electron bunch deflecting scheme is shown in Fig. 1. The design leverages the unique advantages of the THz regime, which bridges radio frequency and optical domains, to achieve both extended linear interaction lengths and higher than femtosecond-level temporal resolution. The perpendicularly incident single-cycle parallel-polarized THz pulses, generated via narrow band emission or optical rectification in lithium niobate (LN) crystals or other nonlinear organic materials, are used as driven laser pulses in prism micro structures. The electron bunch traverses a gap between prisms, interacting with evanescent waves generated via total internal reflection at the prism hypotenuse surfaces. The phase difference between two incident lasers is set as 180°, which causes the longitudinal acceleration electric fields (E_z) along the axis to cancel each other out, while the transverse deflection electric fields (E_x) are superimposed. Phase-matching between the electron velocity β_b and surface wave phase velocity β_p is achieved by optimizing the prism refractive index n and THz incidence angle θ, satisfying $\beta_b = \beta_p = (n \sin\theta)^{-1}$. Here, the longitudinal center of the electron bunch remains aligned with the zero phase position of the surface wave, which can achieve the maximum deflecting gradient.

In order to fully understand the interaction between particles and deflection fields, we first define the input optical source. The incident THz pulses are modeled as single-cycle Gaussian waveform:

$$E(t) = E_0 exp(-0.5((t-t_0)/\sigma)^2) sin[\omega_0(t-t_0)]. \quad (1)$$

where E_0 is the peak field, σ is the rms pulse duration, t_0 the time delay, and ω_0 the central angular frequency. Figure. 2(a) shows the temporal profile of the THz pulse, with a pulse duration of 2 ps, while Fig. 2b shows its frequency spectrum centered at 0.25 THz (bandwidth: 0.22 THz).

The electron bunch with Gaussian distributions in both transverse and longitudinal directions is employed as the

* sunli27@ustc.edu.cn

Content from this work may be used under the terms of the CC BY 4.0 licence (© 2026). Any distribution of this work must maintain attribution to the author(s), title of the work, publisher, and DOI.

ISBN: 978-3-95450-252-3 ISSN: 2673-5350 doi: 10.18429/JACoW-IPAC2026-MOP6648

STRETCHED WIRE CALIBRATION FOR BEAM POSITION MONITORS WITH 2X THRU DE-EMBEDDING

T. Toyama*, High Energy Accelerator Research Organization, Tsukuba, Japan

Abstract

Calibration with stretched wire on a test bench is widely used for beam position monitors. Addressing impedance mismatches at both ends of the system is difficult, especially at high frequencies exceeding 100 MHz. Tapered pipes are sometimes utilized for better impedance matches which is difficult for applying to the BPMs, because the wire position moves in horizontal and vertical directions. To eliminate mismatch effects more efficiently in this system, we propose applying 2x Thru de-embedding and demonstrate its effectiveness through electromagnetic simulation using CST Studio Suite.

INTRODUCTION

Stretched wire calibration on a test bench is important in quality verification of manufactured devices, and in determining the actual beam position sensitivity coefficient. Conventional methods make it difficult to address the effects of impedance mismatches between the cables from/to a network analyzer and the wire. This problem can be solved by the 2x Thru de-embedding method using the proposed configuration. We explain this problem with the stretched wire calibration bench for the J-PARC MR BPMs. Next, the 2x Thru de-embedding method is introduced for a 4-port system having two wire input/output ports and two signal pickup ports. The method is simulated using the electromagnetic simulator CST studio suite, with a rectangular diagonal-cut BPM and a rectangular beam pipe. The position responses in the frequency domain were obtained, demonstrating favorable behavior at lower frequencies and degraded behavior at higher frequencies.

STRETCHED WIRE CALIBRATION TEST BENCH FOR J-PARC MR

As an example of stretched wire calibration test bench, we explain the system for J-PARC MR (Fig. 1) [1, 2].

In Fig. 2 the configuration of measurement and the responses from the wire input to the signal output (S parameters) are plotted, in the case with outer matching loads. Frequencies below 10 MHz seem usable.

In Fig. 3 the configuration of measurement and the responses from the wire input to the signal output (S parameters) are plotted, in the case with series matching loads at the wire. This matching method was proposed by F. Caspers [3]. The RF finger contacts are installed at the pipe ends to contact the end-plates, allowing the DUT to slide on the end-plates. Frequencies below 100 MHz seem usable. This approach was successfully applied to the BPMs for the RIKEN superconducting LINAC [4].

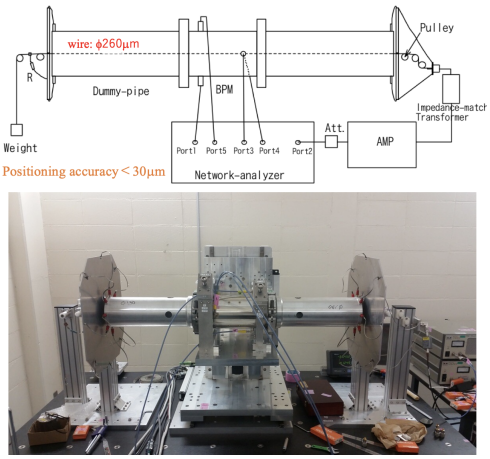

Figure 1: Stretched wire calibration system for J-PARC MR.

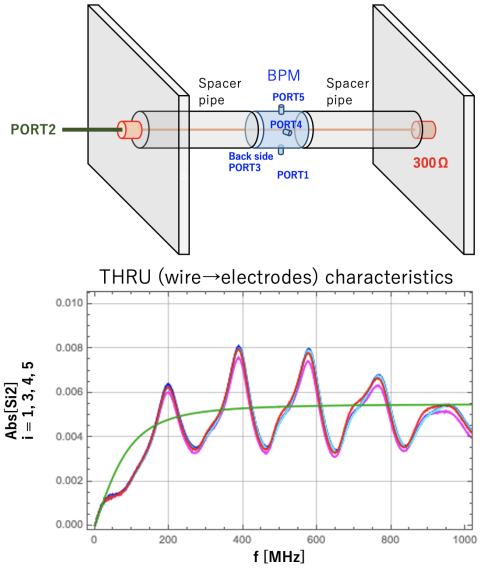

Figure 2: Frequency response with outer matching loads.

To access frequencies higher than those mentioned above, further solutions are required. The 2x Thru de-embedding method appears to be a promising candidate.

2X THRU DE-EMBEDDING METHOD FOR BPMs

The 2x Thru de-embedding method evaluates the S-parameters of each adapter by measuring the S-parameters of two adapters connected in series, and removes those effects from the full S-parameters of the DUT [5, 6].

* takeshi.toyama@kek.jp

Content from this work may be used under the terms of the CC BY 4.0 licence (© 2026). Any distribution of this work must maintain attribution to the author(s), title of the work, publisher, and DOI.

ISBN: 978-3-95450-252-3 ISSN: 2673-5350 doi: 10.18429/JACoW-IPAC2026-MOP6650

EXPERIMENTAL VERIFICATION OF ENERGY DEPENDENCE IN A CNT WIRE MONITOR FOR BEAM PROFILE MEASUREMENTS IN THE J-PARC LINAC*

T. Miyao, KEK Accelerator Laboratory, Tsukuba, Japan
A. Miura, K. Moriya, Japan Proton Accelerator Research Complex, Tōkai Mura, Japan
Y. Liu†, High Energy Accelerator Research Organization, Tsukuba, Japan

Content from this work may be used under the terms of the CC BY 4.0 licence (© 2026). Any distribution of this work must maintain attribution to the author(s), title of the work, publisher, and DOI.

Abstract

The J-PARC linac accelerates a 50 mA H^- beam up to 400 MeV for user operation. To mitigate emittance growth caused by space-charge effects, transverse beam profiles are measured using wire scanner monitors (WSMs) for routine beam tuning. Tungsten is generally used as the wire material. However, the WSMs employ carbon nanotube (CNT) wires in the low-energy region between the RFQ and DTL, because the beam energy is low as 3 MeV and the thermal load is substantial. CNT wires were introduced in 2017 as a more heat-resistant alternative, and since then they have operated without replacement due to beam-induced damage, demonstrating excellent durability. In this study, we report beam profile measurements obtained with the CNT WSM at various beam energies.

INTRODUCTION

The J-PARC consists of three accelerators (Linac, 3-GeV Synchrotron (RCS), and 50-GeV Synchrotron (MR)) and three experimental facilities (MLF, NU, and HD) [1]. The beam accelerated up to 400 MeV by the J-PARC Linac is further accelerated to 3 GeV in the RCS and then delivered to the MLF and MR. Their design beam powers are 1 MW and 1.3 MW, respectively, and part of these goals has already been achieved.

The J-PARC Linac accelerates a negative hydrogen ion (H^-) beam up to 400 MeV. In user operation, a maximum of beam pulse width is 500 μs, and a peak beam current reaches 50 mA. Beam tuning is indispensable for realizing high-intensity beam operation with minimal beam loss. A wire scanner monitor (WSM) is one of the most important diagnostic devices because it is used to determine a current settings of quadrupole magnets (QMs) for optimizing a transverse beam profile. A WSM signal is obtained by measuring current induced when the wire intercepts the H^- beam, using a preamplifier that converts the current into a voltage signal. However, when a beam current increased to 50 mA, the carbon fiber wire previously used in the WSM could no longer withstand the thermal load induced by the 3 MeV H^- beam. Therefore, a carbon nanotube (CNT) wire manufactured by Hitachi Zosen Corporation [2] was adopted, and performance evaluations have been carried out since 2017 at the 3 MeV H^- beam test stand [3]. In this study, we report the beam-energy dependence of H^- beam measurements using the CNT wire in the J-PARC Linac.

* miyao@post.j-parc.jp

WSMS FOR PERFORMANCE EVALUATION

In the J-PARC Linac, three beam dumps, shown in Figure 1, are used for high-intensity beam tuning. The 0-degree dump has a limited beam power capacity of 0.6 kW; however, because it is installed on the straight beamline section, it can accept beams with energies ranging from 3 MeV to 400 MeV. The 30-degree dump has a larger beam power capacity of 5.8 kW compared with the 0-degree dump, but because the beam must pass through a bending magnet, it is generally used only for 400 MeV beam operation. The 100-degree dump has a beam power capacity of 2.0 kW and is used to receive the 400 MeV beam immediately upstream of injection into the RCS. For beam monitor studies, we have installed one WSM in the 0-degree dump beamline and has been investigating its energy dependence. However, because the accelerator is primarily used for user operation, it is difficult to secure sufficient beam time for dedicated beam tests.

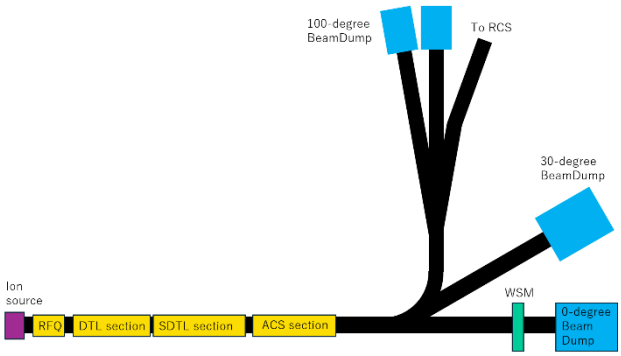

Figure 1: Layout of the J-PARC Linac.

For the development of beam diagnostic devices for high-intensity hadron beam facilities, we constructed a test stand consisting of an ion source and a radio-frequency quadrupole linac (RFQ) cavity [4]. The maximum beam parameters of a test stand (RFQ-TS) are a beam energy of 3 MeV, a peak beam current of 50 mA, a pulse width of 500 μs, and a repetition rate of 25 Hz. Figure 2 shows a layout of beamline connected to the RFQ. Three quadrupole magnets (QMs), a bending magnet, a test chamber, and a beam dump are installed. Between the

ISBN: 978-3-95450-252-3 ISSN: 2673-5350 doi: 10.18429/JACoW-IPAC2026-MOP6653

DEVELOPMENT OF NON-DESTRUCTIVE EMITTANCE TUNING SYSTEM UTILIZING SYNCHROTRON RADIATION MONITORS

Y. Seimiya*, N. Iida, T. Mori, High Energy Accelerator Research Organization, Tsukuba, Japan

Abstract

In SuperKEKB, the emittance of the injected beam is an essential parameter that significantly affects the injection rate. In the LINAC, the beam tail can be kicked depending on the orbit through the accelerating structures, which leads to a degradation of the emittance. Fortunately, these effects can be minimized by appropriately optimizing the beam oribt. On the other hand, the KEKB LINAC uses pulse steering to supply beams to four different rings. However, the number of pulse steering is limited in the upstream part of the LINAC, and orbit drift in the upstream part often leads to emittance drift, deteriorating injection rate. To address this issue, we have developed a non-destructive emittance tuning system utilizing Synchrotron Radiation Monitors.

INTRODUCTION

SuperKEKB is e-/e+ collider for high energy particle physics in KEK. Recent operation is as described in the following report [1, 2]. Required beam parameters for injection beam are shown in Fig. 1. These emittance values are slightly large since that is included during troubles and studies. Double bunches are delivered at 96 ns intervals in the LINAC. The current bunch charge is lower than the target especially for HER. This reason is that low emittance transport is not successful at high bunch charge, and the impact of the emittance growth to the background of Belle II detector also cannot be ignored. We have to convey this high quality beam to the main ring without emittance degradation as far as possible. Otherwise, the injection rate would be worse and the luminosity would not be able to reach the target value.

	Beam	Bunch Charge (nC)	Norm. Emit. (Hor./Ver.) (μm)	Energy Spread (%)
Target	e^-	4	40/20	0.07
	e^+	4	100/15	0.16
Actual (April 2026) (BT1)	e^- (1st)	1.9	94/71	0.075
	e^- (2nd)	1.8	136/103	
	e^+ (1st)	3.1	111/3.5	0.068
	e^+ (2nd)	2.9	115/3.9	

Figure 1: Required and averaged measured beam parameters at BT1 in April 2026 for SuperKEKB injector LINAC. The energy spread value is the value of 1σ when the total width is assumed to be 3σ.

A layout of the LINAC and the beam transport line (BT) is shown in Fig. 2. The LINAC is composed of Sector A, B, J-ARC, C, and 1-5. The LINAC has two kinds of electron gun; a thermionic gun to obtain high-current beam used for positron production and a photocathode RF gun for low emittance electron beam. The large emittance of the positron beam emittance for LER is reduced by a damping ring (DR), which is placed beside the end of Sector 2. The beam is extracted from the end of Sector 2 to the LTR line at 1.1 GeV and injected to the DR. After two cycles of the LINAC pulse, the damped beam is, through the RTL line, resumed to the start of Sector 3 in the LINAC. Positron beam is accelerated up to 4 GeV and transported through the positron BT line and finally reaches the low energy ring (LER). Low emittance electron beam is accelerated up to 7 GeV and transported through the electron BT line and finally reaches the high energy ring (HER). We mainly discuss injection beam for HER in this report.

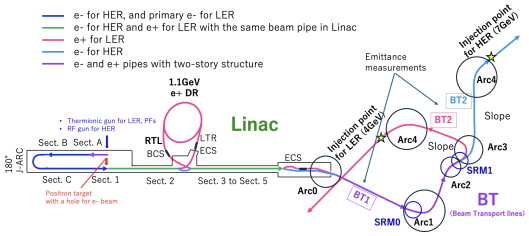

Figure 2: A layout of SuperKEKB injector LINAC and the beam transport line.

EMITTANCE FLUCTUATION

Emittance fluctuation has been observed in the LINAC. One of the reason is orbit fluctuation. In the LINAC, the beam tail is kicked depending on the orbit through the accelerating structures, which leads to a degradation of the emittance. The emittance growth in the LINAC cause a reduction of injection efficiency. Since beam lifetime of SuperKEKB ring is much shorter than KEKB, injection efficiency affects total beam current of the ring. Therefore, emittance fluctuation sometimes causes reduction of the SuperKEKB performance, luminosity. Main orbit fluctuations are correlated with temperature fluctuations in the upstream of the LINAC. Despite ongoing mitigation efforts, the impact remains significant.

The LINAC performs continuous injection into four different rings, HER, LER, PF, and PF-AR. The orbit for each ring is controlled by pulsed steering magnet. Unfortunately, the number of the pulsed steering magnet is limited at the LINAC upstream, Sector A, B, J-ARC, and C. We cannot fix the orbit at the region completely.

As an example, orbit drifts of two nearby BPMs was found at the entrance of J-ARC. The orbital difference shifted by about 0.1 mm to 0.2 mm over a few days. To verify the effect of this orbital difference on emittance, we reproduced this orbital difference by changing the upstream steering magnet during LINAC's standalone operation and performed emittance measurements. As a result, it was confirmed that

* seimiya@post.kek.jp

Content from this work may be used under the terms of the CC BY 4.0 licence (© 2026). Any distribution of this work must maintain attribution to the author(s), title of the work, publisher, and DOI.

ISBN: 978-3-95450-252-3 ISSN: 2673-5350 doi: 10.18429/JACoW-IPAC2026-MOP6658

REFINEMENT OF TUNE MONITOR IN TPS BOOSTER

P.-Ch. Chiu†, K.-T. Hsu, J.-Ch. Huang, S.-H. Lee, C.-Y. Wu,
National Synchrotron Radiation Research Center, Hsinchu, Taiwan

Abstract

The Taiwan Photon Source (TPS) is a high-brightness, 3-GeV third-generation synchrotron light source characterized by its ultra-low emittance [1]. Its booster synchrotron, featuring a 496.8-meter circumference composed of six FODO cells, is housed concentrically within the same tunnel as the storage ring. A precise tune measurement system is critical for monitoring and correcting tune variations during energy ramping, ensuring the beam avoids resonance lines that would otherwise lead to significant beam loss. While this system was instrumental during the initial commissioning of the TPS booster, over a decade of operation has surfaced various reliability and performance issues. To improve injection efficiency and enhance diagnostic capabilities, the booster tune measurement system has been upgraded to provide more reliable and streamlined measurements. This report summarizes the design and performance of the refined monitor system.

INTRODUCTION

The installation of the TPS booster synchrotron is illustrated in Fig. 1. It is housed concentrically within the same tunnel as the storage ring. The booster magnets are fastened on the wall. During the initial commissioning in September 2014, magnetic shakers—consisting of two multi-turn coils mounted on the vacuum chamber—were used to excite the beam. These shakers, driven by 50W amplifiers with 50Ω terminated loads, provided a calibration factor of 3 mG/A. It features vertical and horizontal pairs of 300 mm long stripline electrodes, enabling both single and continuous measurements during the 150 ms ramping period. Subsequently, the stripline electrodes replaced the magnetic shakers to provide higher excitation strength [2].

Initially, R3BPM8 was equipped with a pre-amplifier for tune measurement, using bandpass-limited white noise for beam excitation. While this setup provided tune values, the results were not entirely satisfactory as the spectrum peaks were occasionally too faint to identify. Although increasing the excitation strength could clarify the peaks, it often led to significant beam loss. To address this, the system was upgraded to include more suitable BPMs respectively for the horizontal and vertical planes, enhancing both accuracy and reliability. Furthermore, the excitation method was transitioned to a swept-sine waveform. This approach requires less power to excite the beam, effectively preventing beam loss while maintaining injection efficiency and minimizing interference with normal operations.



Figure 1: TPS installation. The left arc is storage ring; the right arc is booster synchrotron.

TUNE MONITOR

Turn-by-turn (TBT) data provided by the BPM electronics is acquired to extract the tune via Fast Fourier Transform (FFT). The Libera Brilliance Plus platform is utilized for both storage ring and booster BPMs, providing two types of TBT data: Digital Down Converter (DDC) and Time Domain Processing (TDP). The resolution can reach approximately 150 um at a beam current of 0.5 mA. To utilize TDP effectively, the phase offset and mask window must be correctly configured. While both data chains can be used for tune extraction, TDP is superior for resolving beam loss and extracting tunes—especially at lower currents or with smaller beam motions. This is due to the clear, 'non-smeared' nature of TDP TBT data. Consequently, TDP is the preferred choice for the tune monitor system. Furthermore, an Agilent arbitrary signal generator provides adjustable swept-sine excitation signals. The functional block diagram of this upgraded system is illustrated in Fig. 2. Additionally, the injection trigger of the timing system has been modified for operational flexibility, allowing it to be enabled for single-bunch, multi-bunch, or combined mode.

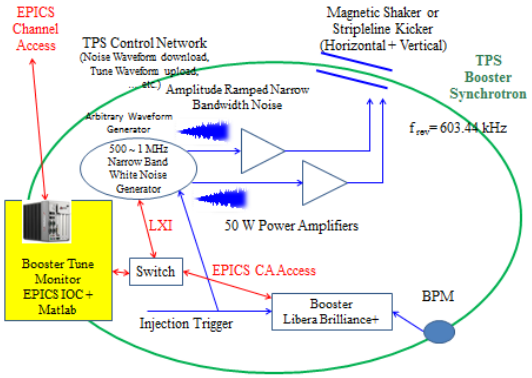

Figure 2: Functional block diagram of the tune monitor for TPS booster.

†peichenchiu@nsrrc.org.tw

Content from this work may be used under the terms of the CC BY 4.0 licence (© 2026). Any distribution of this work must maintain attribution to the author(s), title of the work, publisher, and DOI.

ISBN: 978-3-95450-252-3 ISSN: 2673-5350 doi: 10.18429/JACoW-IPAC2026-MOP6660

DESIGN AND INTEGRATION OF MOTION CONTROL FOR THE IUT24 IN-VACUUM UNDULATOR AT TPS

C. Y. Wu*, C. Y. Liao, Z. Q. Wu, J. Chen, Y. S. Cheng
National Synchrotron Radiation Research Center, Hsinchu, Taiwan, R.O.C.

Abstract

The In-Vacuum Tapered Undulator (IUT24) was developed for the Phase-III beamline project at the Taiwan Photon Source (TPS). To counteract strong, non-linear magnetic attraction forces while maintaining precise synchronization between magnet arrays, a robust motion control architecture was implemented. This system integrates an EPICS-based supervisory layer with EtherCAT field I/O and BiSS-C absolute linear encoders (50 nm resolution) in a closed-loop pulse-command configuration. Experimental results demonstrate that during dynamic gap transitions, the tracking error is strictly maintained within ± 2.5 μm, and inter-axial synchronization remains within 0.5 μm. Furthermore, long-term position stability was measured at ±150 nm over 200 minutes. This paper details the hardware integration, advanced motion control strategies, and comprehensive performance evaluations that confirm the system's readiness for high-precision beamline operations.

INTRODUCTION

The Taiwan Photon Source (TPS) is adding new beamlines through the Phase-III project [1]. One of the devices introduced in this program is the IUT24 in-vacuum undulator, which was integrated into the storage ring in 2026. Its magnetic field is set by adjusting the gap between two opposing magnet arrays over a range of 5–25 mm. Compared with a conventional out-of-vacuum device, an in-vacuum undulator places tighter demands on the motion system because vacuum loading and magnetic force both act directly on the mechanism. The controller must therefore provide fine positioning and keep the two drive axes synchronized during gap tuning and tapering. This paper describes the hardware layout, the control scheme, and the test results obtained on the IUT24 platform before routine operation.

SYSTEM HARDWARE ARCHITECTURE

The control system for the IUT24 in-vacuum undulator is constructed around a distributed heterogeneous network architecture designed to balance high-precision motion execution with robust peripheral monitoring. A Linux-based industrial PC, specifically the ADLINK MXC-6300 series, functions as the EPICS Input/Output Controller (IOC) [2] to manage high-level process variables and interface with the broader beamline control network via an EPICS gateway. For real-time operations, a Galil DMC-4040 multi-axis controller handles trajectory generation and high-speed close loop regulation [3], communicating with the IOC through a private UDP link that supports state updates at rates up to 100 Hz. Complementing this, peripheral instrumentation such as vacuum gauges and corrector power supplies are integrated using the EtherCAT protocol (IEC 61158), which reduces wiring complexity and provides the deterministic communication required for synchronized operation. [4]

The systemic integration of the IUT24 control framework is illustrated in the hardware architecture diagram (see Fig. 1), which emphasizes a modular, three-tier topology consisting of the supervisory EPICS layer, the real-time motion control core, and the distributed fieldbus. At the supervisory level, an industrial PC acts as the EPICS Input/Output Controller (IOC), orchestrating data exchange between the beamline control Ethernet and the underlying motion hardware. The real-time layer centers on a multi-axis motion controller that receives feedback from BiSS-C (Bidirectional/Serial/Synchronous-Continuous) absolute linear encoders through specialized wiring adapters to ensure nanometer-scale positioning resolution. Simultaneously, an EtherCAT-based fieldbus manages auxiliary subsystems, including vacuum gauges and temperature-monitoring RTD sensors, ensuring that environmental parameters are digitized and synchronized with the motion state.

The physical implementation of this architecture is realized through a dual-rack configuration, as shown in the installed hardware assembly (see Fig. 2), which is designed to isolate sensitive control signals from high-power vacuum and magnet electronics. The primary Motion Control Rack consolidates the EPICS IOC, the trajectory-generation controller, and high-performance motor drivers, utilizing custom hardware protection boards to handle limit-switch and emergency-stop interlocks. In contrast, the Vacuum and Power Supply Rack houses the ion-pump controllers, Bayard-Alpert (BA) gauge controllers, and correction-magnet power supplies. This spatial decoupling serves a dual purpose: it significantly reduces electromagnetic interference (EMI) across the feedback loop and streamlines maintenance protocols by separating the core drive mechanics from the vacuum support infrastructure.

Protection of the vacuum chamber and magnet arrays is implemented at several levels. Software limits in the EPICS motor record block invalid user commands, while the Galil controller monitors the following error and aborts motion when it exceeds 0.05 mm. Hardware interlocks, including limit switches and torque-limit sensors, are wired directly to the motor-driver inhibit pins to prevent collision even if network communication is lost.

* chunyiwu@nsrrc.org.tw

Content from this work may be used under the terms of the CC BY 4.0 licence (© 2026). Any distribution of this work must maintain attribution to the author(s), title of the work, publisher, and DOI.

ISBN: 978-3-95450-252-3 ISSN: 2673-5350 doi: 10.18429/JACoW-IPAC2026-MOP6662

DEVELOPMENT OF AN MTCA.4-BASED DIGITAL LOW-LEVEL RF CONTROL SOLUTION FOR THE TLS LINAC SYSTEM

Y. S. Cheng*, K. T. Hsu, S. H. Lee, C. Y. Wu, C. Y. Liao
National Synchrotron Radiation Research Center, Hsinchu, Taiwan

Abstract

The Linac of Taiwan Light Source (TLS) has operated for over thirty years, necessitating modernization to ensure sustainability operation. A new digital low-level RF (DLLRF) control system has been developed to replace aging components and address the situation of having only a single backup unit. The MTCA.4 platform was adopted for its scalability and high-performance throughput. The system integrates the DACs module for arbitrary waveform generation with external triggering, and a direct-sampling down-converter with the ADCs module for waveform acquisition and advanced real-time diagnostics. The DLLRF interface has been fully integrated into the EPICS framework for seamless compatibility with existing controls. The new system supports I/Q waveform downloads with online amplitude and phase adjustments, and it provides waveform digitization capabilities for monitoring RF signals associated with the klystron modulator. Dedicated graphical applications have been designed and integrated into the current operator interfaces. The MTCA.4-based DLLRF system has been successfully deployed and validated during routine operations. This paper presents the development, implementation, and operational results of the upgraded control system.

INTRODUCTION

TLS is a third-generation synchrotron at the NSRRC and has been operational since 1993. Its injection chain comprises a 50 MeV Linac, a 1.5 GeV booster, and a storage ring supporting 360 mA top-up injection. Originally based on a proprietary VMEbus architecture, the control system utilized Intelligent Local Controllers (ILCs) for subsystem interfacing. Driven by rapid computing advancements, the system has undergone multiple hardware upgrades and a seamless migration to the Linux platform to ensure long-term operational sustainability.

Following the successful implementation of the EPICS framework at the Taiwan Photon Source (TPS) [1,2], EPICS was adopted for the TLS control system's modernization. This strategy leverages established expertise to ensure long-term maintainability. Currently, newly installed and refurbished subsystems operate within the EPICS environment, coexisting effectively with the legacy architecture. This hybrid integration has proven highly reliable, significantly enhancing operational performance without encountering major technical conflicts.

The beam quality of a 50 MeV Linac is primarily determined by the stability and flatness of the RF field amplitude and phase. These parameters are highly dependent on the performance of the klystron modulator and beam-loading effects. While a well-tuned pulse-forming network (PFN) is essential for generating effective microwave pulses, achieving optimal tuning is often a complex and labor-intensive process. To circumvent the challenges of manual PFN tuning, an RF feed-forward system serves as a viable alternative for performance enhancement. This control mechanism not only compensates for beam-loading effects but also mitigates slow drifts caused by environmental or systemic variations. The feasibility studies on RF feed-forward control have been conducted at the TLS Linac in recent years [3,4]. Ongoing R&D efforts will focus on refining control algorithms and developing advanced RF control hardware to further optimize injector performance in support of top-up operations.

TLS pre-injector comprises a 140 kV thermionic gun and a 50 MeV traveling-wave Linac; its schematic layout is illustrated in Fig. 1. The microwave system incorporates a frequency multiplier that converts 499.654 MHz to 2.998 GHz, a 1 kW GaAs solid-state RF amplifier (SSA), and a high-power klystron amplifier. Specifically, the klystron is driven by an 80 MW PFN-based modulator, which is charged by a switching power supply. To regulate the RF field injected into the linac, a vector modulator (VM) output from the DLLRF control unit is positioned upstream of the GaAs amplifier.

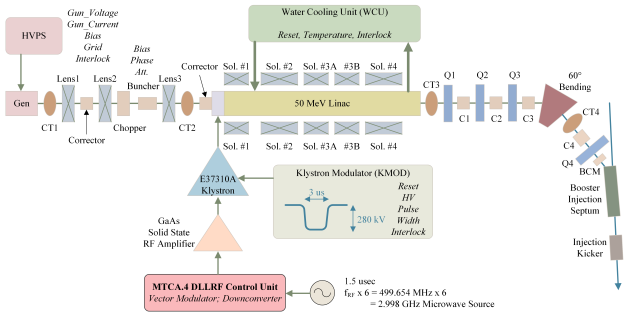

Figure 1: Schematic layout of the 50 MeV TLS linac system, illustrating the pre-injector, klystron, and RF power chain.

Following the migration of the TLS Linac klystron to the E37310A model [5], the DLLRF control system was concurrently upgraded. This transition effectively addressed long-standing challenges regarding the availability of legacy spare parts. The upgrade incorporates mainstream technologies, specifically the MTCA.4 architecture [6], which significantly enhances operational performance, streamlines maintenance procedures, and introduces advanced signal diagnostic capabilities. Central to this MTCA.4-based platform is the integration of a VM output module and a multi-channel downconverter. This configuration enables real-time monitoring and precise regulation of RF signals across all stages

* cheng.ys@nsrrc.org.tw

Content from this work may be used under the terms of the CC BY 4.0 licence (© 2026). Any distribution of this work must maintain attribution to the author(s), title of the work, publisher, and DOI.

ISBN: 978-3-95450-252-3 ISSN: 2673-5350 doi: 10.18429/JACoW-IPAC2026-MOP6663

PRELIMINARY STUDY OF A BUNCH-BY-BUNCH MONITORING SYSTEM FOR THE TPS BOOSTER SYNCHROTRON

Y. S. Cheng*, K. T. Hsu, P. C. Chiu, C. Y. Wu, J. C. Huang
National Synchrotron Radiation Research Center, Hsinchu, Taiwan

Content from this work may be used under the terms of the CC BY 4.0 licence (© 2026). Any distribution of this work must maintain attribution to the author(s), title of the work, publisher, and DOI.

Abstract

The Taiwan Photon Source (TPS) booster synchrotron has been in routine operation since 2015, accelerating electron beams from 150 MeV to 3 GeV at a 3 Hz repetition rate. Ensuring beam stability during the energy ramp is essential, particularly through tune correction to mitigate particle loss associated with betatron resonances. Tune variations primarily arise from magnetic field imperfections, space-charge effects, and injection-related errors. Effective tune control is therefore required to maintain the beam on its intended trajectory and to achieve high acceleration efficiency. To support this objective, a bunch-by-bunch feedback processor has been adapted as a diagnostic toolkit capable of measuring and tracking the booster tune throughout the energy ramp, enabling real-time correction. The system acquires waveform data using configurable multi-bunch or single-bunch triggers, and advanced signal-processing techniques are applied to suppress background noise for improved spectral clarity. Ultimately, the developed system aims to perform tune compensation to reduce tune fluctuations and enhance injection efficiency. This report summarizes the development and performance evaluation of the proposed efforts.

INTRODUCTION

The TPS booster synchrotron accelerates electron beams from 150 MeV to 3 GeV with a repetition rate of 3 Hz. The beam is injected at 150 MeV and ramped up to 3 GeV within 155 msec before extraction [1]. During this rapid acceleration process, beam losses are strongly influenced by orbit distortion, beam instability, and tune evolution.

To further investigate booster performance, a spare bunch-by-bunch feedback processor was installed in the booster for detailed studies. Uncontrolled tune shifts can lead to resonance crossing, resulting in beam loss and reduced injection efficiency into the storage ring.

The primary sources of tune variation include magnet tracking errors, residual field nonlinearities, space-charge effects at low energy, and injection mismatches. Although global tune correction schemes have been implemented, real-time and high-resolution diagnostics remain essential for fully characterizing beam dynamics during ramping process.

In this study, a bunch-by-bunch feedback processor (iGp12) is used in the TPS storage ring for bunch-by-bunch feedback [2]. A spare unit has recently been installed in the booster synchrotron for various diagnostic tests. The system enables turn-by-turn and bunch-resolved measurements of beam motion, providing additional insights into both longitudinal and transverse beam dynamics. The goal is to establish a reliable measurement framework for a better understanding of ramping behavior and to explore the possibility of further performance improvements.

SYSTEM SETUP FOR IGP12

The iGp12 system is based on a digital bunch-by-bunch feedback architecture with high-speed ADCs and FPGA-based signal processing [3]. It was deployed for the TPS storage ring to suppress beam instability since 2015. In the booster application, the initial step is used for diagnostic purposes without feedback functionality, and the system operates in acquisition mode. The booster synchrotron operates in multi-bunch and single-bunch modes. The bunch train length is selectable from several tens to several hundred bunches. The iGp12 can capture multi-bunch beam signals for all 828 buckets (harmonic number of the booster synchrotron) on a turn-by-turn basis with approximately 25 msec. Longer recording durations are achievable using decimation; down-sampling by a factor of seven is applied to record the full ramping process. Single-bunch acquisition supports a recording time of up to 160 msec.

The beam signal is obtained from BPM pickups and processed through an analog front-end to adjust phase and attenuation, thereby determining whether the detector operates in quasi-position or quasi-phase mode. Since the booster synchrotron low-level RF system includes amplitude and phase loops, the synchronous phase decreases as energy increases to ensure sufficient acceleration. Consequently, the detector cannot operate in pure position or pure phase mode throughout the entire ramp cycle. The digitized signals are synchronized with the RF frequency and revolution clock to ensure accurate bunch indexing.

The low-level RF system of the booster synchrotron regulates amplitude according to a predefined amplitude program to optimize RF acceptance. The phase is not actively controlled; however, the synchronous phase decreases by approximately 35 degrees during the ramp from 150 MeV to 3 GeV to compensate for synchrotron radiation losses, with most of the phase shift occurring near 2 GeV. This 35 degrees phase shift causes the demodulated signal to contain mixed amplitude and phase components with crosstalk; therefore, a quasi-phase representation is used to describe position and phase information. Nevertheless, this approach remains acceptable for test purposes.

Two kinds of iGp12 data memory are available to record all bunch beam data (up to 828 bunch locations) for 25 msec (~15,000 turns) and single-bunch data for 160 msec. It can be decimated from the all bunch data according to requirements to extend the recording time. To record data for the

* cheng.ys@nsrrc.org.tw

ISBN: 978-3-95450-252-3 ISSN: 2673-5350 doi: 10.18429/JACoW-IPAC2026-MOP6665

IMPLEMENTATION AND PERFORMANCE EVALUATION OF A HIGH-RESOLUTION BUNCH-BY-BUNCH PHASE DETECTION SYSTEM WITH GEOMETRIC CALIBRATION

J.K. Liao*, L.P. Hsu, Z.Q. Wu, C.H. Huang, S.H. Lee, C.Y. Liao, C.Y. Wu, J.C. Huang
National Synchrotron Radiation Research Center, Hsinchu, Taiwan

Abstract

A high-resolution, real-time bunch-by-bunch phase detection system has been developed and deployed at the Taiwan Photon Source (TPS) to monitor and analyze synchronous phase behavior. The system is integrated with the control system to implement the remote phase adjustment function. The detector architecture utilizes an analog I/Q demodulation scheme operating at the 1.5 GHz third harmonic of the RF frequency to achieve precise phase extraction. Limited by hardware non-idealities, DC offsets and quadrature phase imbalances distort the I/Q signal trajectory into an elliptical profile, leading to periodic measurement errors. To address these issues, a digital calibration strategy based on ellipse-fitting is implemented to eliminate offsets and quadrature errors within the I/Q channels. After calibration, the phase error of this system at 1.5 GHz is within 1.5°, therefore, when used to measure a 500 MHz signal, the corresponding phase error is within ±0.5°. The extracted phase data is integrated into the accelerator control system with a 3 Hz update rate, enabling real-time visualization of transient beam loading effects. Furthermore, the system's capability to record 700 turns of bunch motion for phase variation analysis.

INTRODUCTION

The Taiwan Photon Source (TPS) is a 3 GeV synchrotron light source located at the National Synchrotron Radiation Research Center (NSRRC), requiring exceptional beam stability to support high-brightness research applications. To improve beam lifetime by increasing the bunch length, a 1.5 GHz superconducting harmonic cavity (HC) has been installed. However, due to the transient beam loading effects, this configuration introduces significant synchronous phase shifts along the bunch train [1, 2]. As a result, a bunch-by-bunch (BbB) phase detection system is required to monitor these effects and allow a variety of applications during daily operations.

A common method for measuring the BbB phase is using high-sampling-rate oscilloscopes or analog-to-digital converters (ADCs) [3–5] to capture raw waveforms, followed by zero-crossing detection to extract phase information. However, this method requires powerful computing capabilities. Another technique utilizes gated circuits to detect the phase of specific bunches, often integrated into turn-by-turn beam position monitor (BPM) systems [6, 7]. Additionally, streak cameras can provide exceptional phase resolution, but they are typically constrained by high equipment costs and lower data refresh rates [8].

To fulfill the requirements for real-time monitoring within the control system, a detection scheme employing an analog in-phase and quadrature (I/Q) demodulator is proposed. In this approach, the sampling rate is synchronized with the RF clock, allowing phase calculation via simple trigonometric functions. This effectively reduces the computational resources required for the real-time monitoring of long bunch trains.

This paper describes the implementation of the TPS bunch-by-bunch phase detection system, including its hardware component layout and control software development. To overcome hardware non-idealities, a geometric calibration approach based on an ellipse-fitting algorithm is used to digitally compensate for signal distortions. Finally, the system was utilized to detect beam phase shifts and variations during routine storage ring operations.

SYSTEM ARCHITECTURE

The essential method for extracting the bunch-by-bunch (BbB) phase relative to the accelerator's master clock is analog I/Q demodulation. The architecture of the system is shown in Fig. 1. The system synchronizes with the TPS master RF clock at about 500 MHz, which serves as the input reference for a phase-locked loop (PLL) synthesizer with an integrated voltage-controlled oscillator (ADF4372), generating a 1.5 GHz third-harmonic signal. This reference signal is divided into two local oscillator (LO) paths, where a 90° quadrature phase shift is achieved by adjusting the physical path lengths. Phase trimmers are integrated into both paths for precise calibration of the effective electrical length.

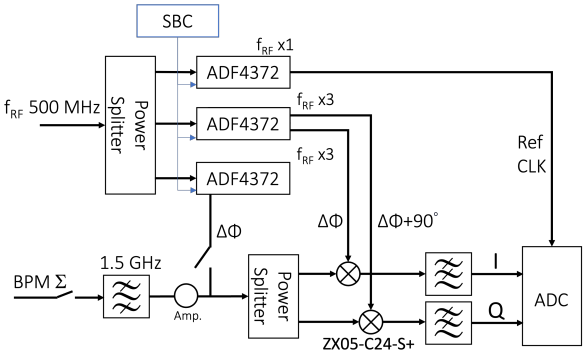

Figure 1: The infrastructure of the bunch-by-bunch phase detector.

* liao.jinkun@nsrrc.org.tw

Content from this work may be used under the terms of the CC BY 4.0 licence (© 2026). Any distribution of this work must maintain attribution to the author(s), title of the work, publisher, and DOI.

ISBN: 978-3-95450-252-3 ISSN: 2673-5350 doi: 10.18429/JACoW-IPAC2026-MOP6667

IMPLEMENTATION OF FAST BEAM-BASED ALIGNMENT AT THE TAIWAN PHOTON SOURCE

Ch.-H. Huang*, P.-Ch. Chiu, K.-T. Hsu, K. H. Hu, F.-H. Tseng, Ch. Wu
National Synchrotron Radiation Research Center, Hsinchu, Taiwan

Abstract

A fast beam-based alignment (BBA) method has been implemented at the Taiwan Photon Source to significantly enhance the efficiency of aligning beam position monitors with quadrupole magnet centers. By utilizing sinusoidal excitation of correctors and employing synchronous detection algorithms, alignment offsets are efficiently extracted across the entire storage ring. Experimental results demonstrate that the total measurement time is reduced from 8 hours to under 40 minutes, while maintaining precision comparable to conventional BBA methods. The primary sources of measurement uncertainty are attributed to betatron tune and orbit variations induced by magnetic hysteresis and ocean-induced ground motion. This approach provides a robust and time-efficient solution for routine orbit characterization in modern synchrotron light sources.

INTRODUCTION

The Taiwan Photon Source (TPS) operates at an electron energy of 3 GeV with a 500 mA nominal beam current [1]. During startup after long shutdowns, beam-based alignment (BBA) is performed to calibrate offsets between the 173 BPMs and 240 quadrupole magnets. The standard BBA procedure [2] at the TPS utilizes slow correctors and slow-acquisition data, requiring approximately 8 hours for full-ring measurements.

To improve efficiency, a fast BBA (FBBA) method has been developed using fast correctors [3,4] to excite the beam at distinct frequencies. This system records 30 kHz fast-acquisition data for real-time signal processing. This paper describes the FBBA methodology, hardware configuration, and discusses measurement uncertainties along with optimization strategies.

MEASUREMENT PRINCIPLE AND SETUP

Each cell at the TPS is equipped with four horizontal and four vertical fast correctors to perform fast orbit feedback, with a corrector bandwidth exceeding 5 kHz. These eight fast correctors are managed by a corrector power supply controller (CPSC) in each cell. The CPSC is capable of delivering arbitrary waveforms to each individual power supply. To calibrate the l-th BPM, the nearest quadrupole magnet is selected and its current is modulated by 1 A. The most effective i-th fast corrector is determined using the response matrix $\boldsymbol{R}$. A sinusoidal current $C_i(t)$ is applied to the corrector to excite the beam, and the resulting beam

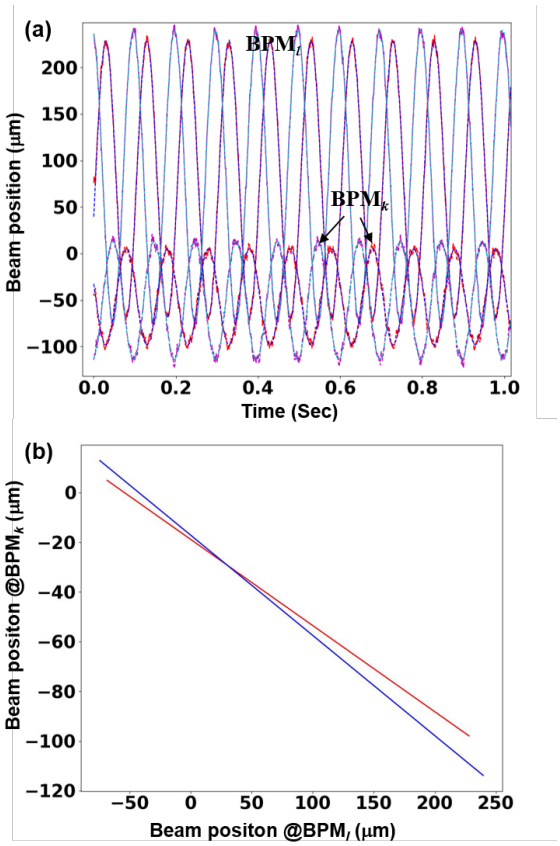

Figure 1: (a) Beam motion at BPM$_l$ and BPM$_k$ resulting from an increase and decrease in the current of the quadrupole magnet near BPM$_l$, and (b) the relationship between beam positions at these two BPMs under two different quadrupole current settings.

position at the k-th BPM (BPM$_k$) is denoted as X_{k1}, as illustrated in Fig. 1(a).

A dedicated computer is used to record the beam positions from all BPMs at a 30 kHz sampling rate. The data is transmitted from the BPM electronics, which aggregate the synchronized data from all monitors, to the computer via Gigabit Ethernet. The relationship between the corrector currents and the beam positions at the BPMs is given by [5]:

$$X_{l1}(t) - X^0_{l1} = R_{li1}(C_i - C_0), \quad (1)$$

$$X_{k1}(t) - X^0_{k1} = R_{ki1}(C_i - C_0), \quad (2)$$

where C_0 and X^0_{k1} in Eqs. (1) and (2) represent the initial corrector current and the beam position at the k-th BPM, respectively, prior to the application of the excitation waveform. The indices l and k denote the target BPM undergoing FBBA and the other observation BPMs in the storage ring.

* huang.james@nsrrc.org.tw

Content from this work may be used under the terms of the CC BY 4.0 licence (© 2026). Any distribution of this work must maintain attribution to the author(s), title of the work, publisher, and DOI.

ISBN: 978-3-95450-252-3 ISSN: 2673-5350 doi: 10.18429/JACoW-IPAC2026-MOP6669

DISTRIBUTED CONTROL OF LARGE-SCALE MAGNET POWER SUPPLIES IN THE HALF*

Fang Li[1], Ke Xuan[†,1], Chuan Li[1], Liuguo Chen[1], Qun Liu[1], Gongfa Liu[1]
[1]National Synchrotron Radiation Laboratory, University of Science and Technology of China, Hefei, China

Abstract

The fourth-generation synchrotron radiation source, with its ultra-high brightness and nanometer-level spatial resolution, has become a core facility supporting cutting-edge scientific research. The Hefei Advanced Light Source comprises nearly 2,000 magnet power supplies, requiring remote online adjustment and synchronized current settings to meet the physical requirements of the electron beam. This paper proposes a distributed control system architecture to address the control requirements of large-scale magnet power supplies. At the hardware level, build server clusters and leverage virtualization technology to deliver highly available system services. At the network level, a star-topology Ethernet network and a synchronized timing network are constructed. At the software level, a customized communication protocol enables remote monitoring of the magnet power supply. Additionally, data security and efficient deployment were also taken into consideration. This distributed control system provides a scalable solution for batch magnet management in fourth-generation light sources.

INTRODUCTION

The Hefei Advanced Light Source (HALF) is a fourth-generation synchrotron radiation light source operating in the low-energy regime, based on a diffraction-limited storage ring (DLSR) [1, 2]. The HALF accelerator complex comprises an injector and an electron storage ring. The injector, composed of a full-energy linear accelerator (Linac) and a beam transport line, serves as the source for generating high-energy electron beams. The electron storage ring operates at an energy of 2.2 GeV, achieving a horizontal natural emittance of 86 pm·rad for the circulating beam. This diffraction-limited storage ring, characterized by its ultra-low emittance, is pivotal for realizing high-performance synchrotron radiation. The storage ring utilizes a modified hybrid 6-Bend Achromat (6BA) lattice structure, which incorporates a multitude of dipole, quadrupole, sextupole, and octupole magnets, as well as fast orbit correctors [3]. Consequently, a corresponding array of power supplies is indispensable to energize these various magnets and coils.

Magnet power supplies modulate the magnetic field strength by regulating the output current, thereby controlling the particle beam trajectories. Remote control of the power supplies for the injector and storage ring encompasses current setting and readback, operational status acquisition, as well as fault monitoring and alarm handling. Effective control of these magnet power supplies is closely correlated with the stability and quality of the synchrotron radiation. Specifically, HALF employs 1,998 power supply units to provide stable power output for magnets distributed across the 366-meter-long injector and the storage ring, which has a circumference of 480 meters. Given the large quantity and extensive spatial distribution of these devices, the adoption of distributed control technology is imperative to ensure reliable online adjustment and monitoring [4, 5].

This paper presents a magnet power supply control system tailored for the HALF. By designing the system architecture, implementing custom communication protocols, and developing control software supporting batch configuration, the distributed control of large-scale power supplies is realized.

DESIGNE AND IMPLEMENTATION

Architecture

The architecture of the power supply control system is illustrated in Fig. 1. The distributed control is implemented via a network infrastructure, providing Ethernet communication as the channel for data exchange between the power supplies and the upper-level control software. To achieve effective monitoring and control of the power supplies, which are distributed across various equipment rooms, dedicated network switches are deployed to provide network access. The control system network is logically divided into multiple Virtual Local Area Networks (VLANs) to improve network efficiency and enhance security.

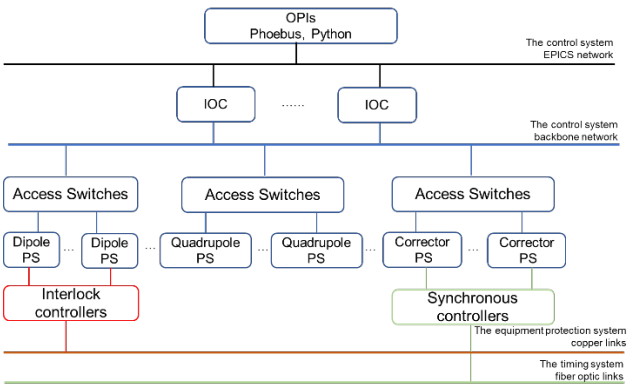

Figure 1: The system architecture.

The control network adopts a standard hierarchical structure, comprising the access layer, the aggregation layer, and the core layer. Access switches are installed in the

* Work supported by the University of Science and Technology of China under Grant No. KY2310000064
† xuanke@ustc.edu.cn

Content from this work may be used under the terms of the CC BY 4.0 licence (© 2026). Any distribution of this work must maintain attribution to the author(s), title of the work, publisher, and DOI.

ISBN: 978-3-95450-252-3 ISSN: 2673-5350 doi: 10.18429/JACoW-IPAC2026-MOP6670

DEVELOPMENT OF THE BEAM PERMIT SYSTEM FOR THE RAON ACCELERATOR

E. Kwon*† [1,2], Y. Ahn† [1], E. Im[1], H. M. Jang[1], J. Kwon[1], M. Park[1], H. Yoo[2]
[1]Institute for Rare Isotope Science (IRIS), Institute for Basic Science (IBS), Daejeon, Korea
[2]Department of Electronics Engineering, Chungnam National University, Daejeon, Korea

Abstract

The Beam Permit System (BPS) has been implemented as a software-level permit and verification layer for the Rare isotope Accelerator complex for ON-line experiments (RAON), a heavy-ion accelerator being commissioned at the Institute for Basic Science (IBS) in Korea. While the Machine Protection System (MPS) provides fast hardware signal-based protection against beam-induced equipment damage, the BPS complements it by checking software-level conditions such as EPICS Input/Output Controller (IOC) availability, Process Variable (PV) consistency, and operating-mode correctness. By combining IOC monitoring, configuration checks, and mode-based permit logic, the BPS ensures that beam delivery is allowed only when all required operating conditions are satisfied. Commissioning tests in the currently operational RAON section (up to SCL3) confirm that the BPS reliably identifies hardware or software inconsistencies and inhibits beam extraction when necessary, demonstrating the effectiveness of this combined hardware–software protection approach.

INTRODUCTION

The RAON [1] is a heavy-ion accelerator being developed at IBS in Korea. Initial beam commissioning has begun with the low-energy superconducting linac (SCL3), and accelerator operation now involves cryogenic plants, magnets, RF systems, vacuum equipment, diagnostics, and thousands of controllers coordinated through an EPICS-based control system handling nearly 400,000 signals.

Safe and validated beam delivery in this environment requires not only fast hardware protection but also verification of software-layer readiness. The Machine Protection System (MPS) [2] provides microsecond-scale shutdown based on hardware fault triggers such as beam loss, magnet trips, RF failures, and vacuum faults. However, hardware interlocks alone cannot detect software anomalies, including IOC downtime, invalid PV states, or inconsistent operating-mode configurations. Furthermore, the increasing number of operational modes and beam paths necessitates a supervisory mechanism that verifies that only the required subsystems for the selected configuration are enabled. The Beam Permit System (BPS) was developed as a supervisory software-permit layer that evaluates these conditions before beam extraction and feeds the resulting permit state back into the MPS. It integrates EPICS PV–based verification with hardware interlocks, providing a protection framework that is easier to maintain and scalable to complex mode-based structures.

This paper presents the design, implementation, and commissioning-phase validation of the RAON BPS, demonstrating a combined hardware–software protection architecture for safe and consistent beam operation.

BPS ARCHITECTURE

Overview

The BPS structure is shown in Fig. 1. To the MPS inputs, the BPS adds two subsystem inputs: IOC Monitor (IOCM) and Readiness Manager (RM). These subsystems, including the MPS, are coordinated by mode-based configurations. RAON operates with three mode definitions: Beam Mode, Machine Mode, and Source Mode. For the BPS, Machine Mode is the key operating context because it defines the intended beam path and destination, and therefore determines which software and hardware conditions must be included in the permit decision. Each subsystem covers a different software-state domain: the IOCM monitors network connectivity and IOC error PVs, while the RM evaluates section-based device readiness (setpoint consistency and PV ranges).

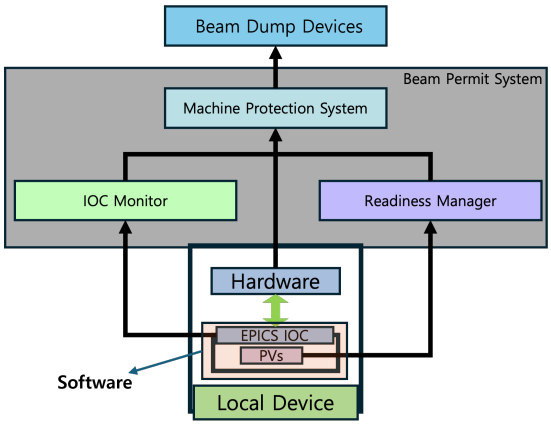

Figure 1: BPS architecture linking EPICS software-state checks with the MPS beam-dump chain.

IOCM

The IOCM uses EPICS “Alive” and “iocmon” as its main modules. These modules evaluate heartbeat PVs and IOC error PVs. The state is evaluated every 1 s; a 15 s heartbeat timeout or unreadable permit PV forces `IOC_OK = 0`.

* eunsang.kwon@ibs.re.kr
† These authors contributed equally to this work.

Content from this work may be used under the terms of the CC BY 4.0 licence (© 2026). Any distribution of this work must maintain attribution to the author(s), title of the work, publisher, and DOI.

ISBN: 978-3-95450-252-3 ISSN: 2673-5350 doi: 10.18429/JACoW-IPAC2026-MOP6673

A SLIDING MODE CONTROL APPROACH FOR PHOTON BEAM STABILITY AT THE SIAM PHOTON SOURCE

S. Klinkhieo†, S. Chunjarean, N. Suradet, T. Pulampong, T. Chanwattana
Synchrotron Light Research Institute, Nakhorn Ratchasima, Thailand

Content from this work may be used under the terms of the CC BY 4.0 licence (© 2026). Any distribution of this work must maintain attribution to the author(s), title of the work, publisher, and DOI.

Abstract

This paper presents the enhancement of photon beam position stability at the Siam Photon Source (SPS) through a real-time feedback control system based on a Sliding Mode Control (SMC) algorithm. The proposed system employs Photon Beam Position Monitor (pBPM) measurements within a global orbit feedback loop to minimize beam position fluctuations. The SMC-based Fault-Tolerant Control (FTC) algorithm enhances system robustness by effectively compensating for disturbances, and actuator faults, thereby maintaining stable beam conditions under various operational scenarios. Experimental results demonstrate that the integration of SMC significantly reduces photon orbit deviations and improves synchrotron radiation quality. By strengthening reliability and adaptability, the developed control system ensures precise beam positioning, making the SPS more dependable for scientific and industrial applications that demand high beam stability.

INTRODUCTION

The Siam Photon Source (SPS), a 1.2 GeV synchrotron radiation facility operated by the Synchrotron Light Research Institute (SLRI) in Nakhon Ratchasima, Thailand, has served as a national research platform for over two decades. Originally built using components from the former SORTEC synchrotron and continuously upgraded, the SPS supports a wide range of scientific applications in materials science, chemistry, biology, and applied physics. With growing user demand, achieving and maintaining excellent beam stability has become critical for experimental accuracy and reproducibility [1-3].

While electron beam orbit stability has been significantly improved through existing feedback systems, photon beam position stability remains a major challenge, especially in beamlines lacking dedicated photon Beam Position Monitors (pBPMs). Photon beam position is highly sensitive to electron orbit variations, insertion device settings, thermal drifts, mechanical vibrations, and other disturbances. Even small fluctuations can degrade beamline performance and limit experimental capabilities. Conventional hardware solutions, such as installing additional pBPMs, are often limited by space, cost, and integration constraints [4, 5].

To overcome these limitations, this work implements a real-time global orbit feedback system based on Sliding Mode Control (SMC) integrated with Fault-Tolerant Control (FTC). Leveraging the inherent robustness of SMC against uncertainties and disturbances, the proposed controller effectively minimizes photon beam position deviations and compensates for actuator faults using available pBPM measurements.

The remainder of this paper first presents the theoretical foundation of the Fault-Tolerant Sliding Mode Control strategy, followed by the experimental setup, results and discussion, and finally the conclusion.

FAULT-TOLERANT SLIDING MODE CONTROL

FTC maintains acceptable system performance despite faults and disturbances. At the SPS, actuator faults, sensor degradation, thermal variations, and modeling uncertainties can seriously degrade orbit correction. Traditional controllers often lack the necessary robustness, resulting in beam position drift and reduced reliability [6, 7].

To overcome these issues, this work implements a Sliding Mode Control (SMC)-based FTC strategy. SMC is inherently robust as it drives system states onto a sliding surface and keeps the motion there despite bounded uncertainties and disturbances. Combining SMC with FTC enables both disturbance rejection and real-time actuator fault estimation/compensation without needing an exact fault model [6, 7]. This makes it well-suited for the complex, time-varying environment of a synchrotron storage ring.

The proposed framework augments the conventional orbit feedback loop with an online fault estimation scheme. It uses pBPM measurements as feedback signals and generates corrective commands for the corrector magnets via the SMC law. When faults occur, the fault-tolerant component adjusts the control effort to maintain stability and minimize photon beam position deviations.

The next section presents the theoretical foundation of Sliding Mode Control and its extension to the fault-tolerant architecture.

SLIDING MODE CONTROL THEORY

The SMC is a robust nonlinear control technique that has gained significant attention in engineering applications due to its remarkable insensitivity to parameter variations, external disturbances, and model uncertainties. The fundamental concept of SMC is to drive the system states onto a predefined sliding surface and maintain the system motion along this surface through high-frequency switching control action. Once the sliding mode is achieved, the system dynamics become governed by the sliding surface equation, which is independent of matched uncertainties and disturbances, thereby providing strong robustness [8, 9].

This property makes SMC particularly suitable for complex systems such as synchrotron storage rings, where precise beam orbit control must be maintained despite actuator

* Work supported by SLRI
† supat@slri.or.th

ISBN: 978-3-95450-252-3 ISSN: 2673-5350 doi: 10.18429/JACoW-IPAC2026-MOP6677

PRELIMINARY DESIGN OF BEAM FEEDBACK SYSTEMS FOR THE SHENZHEN SUPERCONDUCTING SOFT X-RAY FREE ELECTRON LASER*

Y. Li[1], J. Zhu[†1], Z. Zhang[1], J. Han[1], H. Ding[‡2], J. Yang[2], W. Zhang[2]
[1]Institute of Advanced Light Source Facilities Shenzhen, Shenzhen, China
[2]Dalian Institute of Chemical Physics, Dalian, China

Abstract

The Shenzhen Superconducting Soft X-ray Free Electron Laser (S^{3}FEL) requires a high-quality electron beam with stable energy, bunch length, and arrival time to ensure efficient lasing. To maintain stringent beam quality, a comprehensive beam feedback system has been preliminarily designed, incorporating five dedicated feedback loops:

1. Gun Feedback: Monitors bunch charge and arrival time after the electron gun, controlling the input laser power and delay to stabilize charge and timing.
2. Laser Heater Feedback: Measures beam energy at the laser heater and adjusts the RF amplitude of small module CM00 and large module CM01 accordingly.
3. Bunch Compressor 1 (BC1) Feedback: Monitors beam energy, energy spread, and bunch length in BC1, regulating RF amplitude and phase of large modules CM02, CM03 and harmonic cavities CMH01, CMH02.
4. Bunch Compressor 2 (BC2) Feedback: Similarly monitors beam parameters in BC2 and controls RF amplitude and phase of large modules CM04–CM09.
5. Linac End Feedback: Measures final beam energy and adjusts RF amplitude and phase of large modules CM10–CM20 to ensure energy stability before transport to the undulator.

This integrated feedback design aims to suppress slow drifts, enhance beam stability, and provide the reliable beam quality required for high-performance soft X-ray FEL operation at S^{3}FEL.

INTRODUCTION

Free-electron lasers (FELs) have become indispensable tools in frontier research areas such as condensed matter physics, materials science, chemistry, and life sciences due to their exceptional properties, including ultra-high brightness, ultrashort pulse duration, and wide wavelength tunability [1]. The Shenzhen Superconducting Soft X-ray Free-Electron Laser (S^{3}FEL) requires extremely stable electron beam parameters to ensure efficient and stable laser generation [2]. In particular, beam energy stability, bunch length stability, and arrival-time stability directly affect FEL output quality.

During long-term accelerator operation, beam parameters are inevitably affected by external disturbances such as temperature fluctuations, humidity variations, RF system drift, and mechanical vibrations. These perturbations can lead to slow drifts in beam intensity, beam position, energy spread, ultimately degrading FEL performance [3]. Therefore, an effective beam feedback system is essential for maintaining accelerator stability and ensuring reliable FEL operation.

This paper presents the preliminary design of the S^{3}FEL beam feedback system. The system integrates five dedicated fast-feedback loops distributed across key accelerator sections. Through coordinated multi-loop control, high-speed optical-fiber communication, and FPGA-based real-time signal processing, the proposed system achieves precise closed-loop stabilization of critical beam parameters.

OVERALL ARCHITECTURE OF THE BEAM FEEDBACK SYSTEM

The electron beam in S^{3}FEL passes through multiple accelerator subsystems, including the electron gun, buncher, accelerating cryomodules, harmonic cavities, and bunch compressors. The primary objective of the beam feedback system is to suppress slow beam parameter drifts and improve the long-term stability of beam energy, bunch length, and arrival time.

Figure 1 illustrates the conceptual architecture of the beam feedback system. Beam diagnostics installed at critical accelerator locations continuously monitor beam parameters in real time. The measured values are compared with predefined reference values, and the resulting errors are processed by dedicated fast-feedback controllers. The controllers then adjust RF amplitudes, RF phases, laser delay, and laser power to compensate for beam fluctuations.

Benefiting from high-bandwidth optical-fiber interconnections and low-latency FPGA-based processing, the feedback system is capable of rapidly responding to external disturbances while maintaining high control precision and operational reliability.

FEEDBACK LOOP DESIGN

Gun Feedback

The topology of the electron gun feedback loop is shown in Fig. 2. The electron gun feedback loop is designed to stabilize bunch charge and bunch arrival time. An integrated current transformer (Turbo ICT) is employed to measure bunch charge, while a bunch arrival-time monitor (BAM) is used for timing diagnostics downstream of the electron gun.

* Work supported by the National Natural Science Foundation of China (Grant No. 12405221).
† zhujinfu@mail.iasf.ac.cn
‡ dinghongli@dicp.ac.cn

Content from this work may be used under the terms of the CC BY 4.0 licence (© 2026). Any distribution of this work must maintain attribution to the author(s), title of the work, publisher, and DOI.

ISBN: 978-3-95450-252-3 ISSN: 2673-5350 doi: 10.18429/JACoW-IPAC2026-MOP6678

DEVELOPMENT OF AN MTCA.4-BASED HIGH-SPEED DATA ACQUISITION SYSTEM FOR GAS MONITOR DETECTORS AT S^{3}FEL*

J. Zhu†, Y. Li, L. Huang, Z. Zhang, Q. Li, Institute of Advanced Light Source Facilities, Shenzhen, China
H. Ding‡, W. Zhang, Dalian Institute of Chemical Physics, Chinese Academy of Sciences, Dalian, China

Content from this work may be used under the terms of the CC BY 4.0 licence (© 2026). Any distribution of this work must maintain attribution to the author(s), title of the work, publisher, and DOI.

Abstract

This paper presents the prototype design of a high-speed data acquisition (DAQ) system for Gas Monitor Detectors (GMDs) at the Shenzhen Superconducting Soft X-ray Free-Electron Laser (S^{3}FEL), China's first high-repetition-rate soft X-ray FEL facility operating at up to 1 MHz. Six S^{3}FEL beamlines are each equipped with two orthogonal GMDs (horizontal and vertical configurations) to monitor pulse-by-pulse intensity (0.1 μJ–1 mJ range) and beam position in real time. Building upon custom front-end electronics (including a self-designed low-noise preamplifier and an adapter board with high-voltage filtering), the proposed MTCA.4-based DAQ system integrates AMC digitizer boards with a four-channel 1 GSPS sampling rate and 16-bit resolution ADCs. Key features include dual SFP fiber interfaces (primary for 1 MHz timing synchronization and secondary redundancy), PCIe-based backplane communication for per-pulse intensity data streaming, and EPICS-based slow control via dedicated CPU modules. This work details the DAQ system architecture, signal processing chain, and performance validation strategies for the GMD monitoring platform.

INTRODUCTION

Accurate measurement of absolute photon flux in Free Electron Lasers (FELs) remains a critical challenge for accelerator facilities, as its precision directly determines the reliability of experimental results across ultrafast sciences [1-3]. While conventional radiation detectors (e.g., semiconductor photodiodes, microchannel plates (MCPs), and photomultiplier tubes (PMTs)) have been widely adopted, Gas Monitor Detectors (GMDs) exhibit unique advantages in MHz-repetition-rate FEL environments, particularly for facilities like the Shenzhen Superconducting Soft X-ray FEL (S^{3}FEL) [4]. As China's first MHz-class superconducting soft X-ray FEL, S^{3}FEL requires six parallel GMD systems to deliver pulse intensity measurements spanning 0.1 μJ–1 mJ with sub-1% accuracy, sub-micrometer spatial resolution, and MHz-rate detection capability across its beamlines. To address these requirements, we have developed an MTCA.4-based data acquisition (DAQ) system building upon our custom front-end electronics [5], which integrates a self-designed low-noise preamplifier and a high-voltage filtered adapter board. The Advanced Mezzanine Card (AMC) digitizer module features four synchronized channels with 1 GSPS sampling rate and 16-bit vertical resolution. Dual SFP fiber interfaces ensure robust 1 MHz hardware timestamp synchronization from the event timing system [6], while the MTCA.4 backplane enables real-time pulse-by-pulse intensity data streaming via PCIe Gen3. A dedicated CPU blade running the Experimental Physics and Industrial Control System (EPICS) provides comprehensive slow control functionalities, including gain calibration, threshold adjustment, and system monitoring.

This paper is organized as follows: Section 2 details the design of the GMD detector and its front-end signal conditioning chain. Section 3 elaborates on the MTCA.4 DAQ architecture, encompassing both hardware implementation and software integration strategies. Preliminary test results are presented in Section 4, including ADC linearity, event timing jitter analysis, and PCIe throughput test. Finally, Section 5 discusses the roadmap for full-scale beamline deployment and potential applications in other FEL facilities.

DETECTORS

The GMDs at S^{3}FEL employ a dual-chamber ionization design with high-purity xenon or nitrogen monoxide as the detection medium. Each beamline integrates two orthogonal detector pairs (horizontal and vertical orientations) to enable simultaneous intensity and position monitoring. As illustrated in Fig. 1 and Fig. 2, each detector assembly contains four parallel copper electrodes (two electron-collection plates and two ion-collection plates) housed within a vacuum-sealed ceramic chamber with 30 mm inter-electrode spacing.

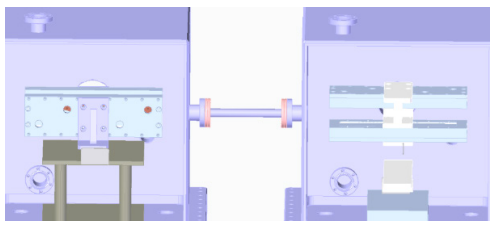

Figure 1: The model of two orthogonal detector pairs.

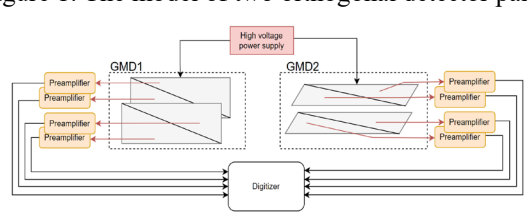

Figure 2: Four parallel copper electrodes and signal readout structure.

* Work supported by the National Natural Science Foundation of China (Grant No. 12405221).
† zhujinfu@mail.iasf.ac.cn
‡ dinghongli@dicp.ac.cn

ISBN: 978-3-95450-252-3 ISSN: 2673-5350 doi: 10.18429/JACoW-IPAC2026-MOP6682

R&D OF THE BUNCH-BY-BUNCH FEEDBACK PROCESSOR PROTOTYPE FOR HALF*

X. Yang, Y. Leng†, Y. Deng
University of Science and Technology of China, Anhui, China

Abstract

The Hefei Advanced Light Facility (HALF) is designed to generate and operate with a beam current of up to 350 mA while maintaining the beam emittance at the diffraction-limited level. The bunch-by-bunch feedback system serves as a critical tool for suppressing beam instabilities, requiring feedback control targeting the position oscillations of each bunch. To meet this demand, the engineering team has independently developed a bunch-by-bunch feedback system, fabricated a prototype, and conducted relevant tests. Through high-precision phase alignment, the analog front-end conditions the original signals into high-precision and wide-dynamic-range sum-and-difference signals. Utilizing the phase-splitting and time-delaying method, the processor can measure the high-precision three-dimensional (3D) position of each bunch and implement feedback control accordingly. This paper presents the design of the system as well as the details of the prototype development and testing.

MANUSCRIPTS

During the construction of HALF, we made the decision to independently develop the bunch-by-bunch feedback processor [1]. Based on the team's previous technical accumulation in bunch-by-bunch parameter measurement [2, 3], we decided to adopt a FPGA-based direct radio frequency (RF) sampling processor scheme for data acquisition. Compared with the bunch-by-bunch parameter diagnostic system, the bunch-by-bunch feedback system needs to acquire 3D position information in the shortest possible time and generate feedback signals, which are then amplified to drive the kickers for trajectory control of the bunches. Meanwhile, the bunch-by-bunch feedback process does not focus on the absolute position of the beam, but only on the relative position change of the beam within a certain time period, and it is necessary to maximize the resolution of relative changes.

Integrating the above basic requirements with mature bunch-by-bunch feedback schemes from other facilities [4], we designed a complete set of analog front-ends for the bunch-by-bunch feedback system. It can realize closed orbit subtraction in the analog circuit and provide amplitude-matched synthesized signals for the processor. In this way, the processor can directly obtain the 3D position changes of the bunches through the variation of signal amplitudes without performing the delta-over-sum operation. Compared with conventional schemes, this front-end eliminates frequency mixing, which simplifies the front-end structure, reduces interference, and correspondingly improves the 3D position resolution of the feedback processor.

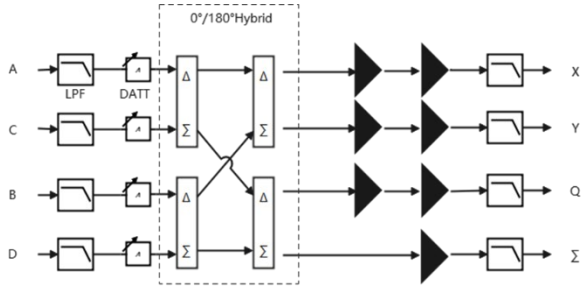

Figure 1: The layout of Front-End.

After prototype fabrication and testing, our current scheme, as shown in Fig. 1, implements filtering, phase shifting, delta-over-sum calculation, and amplitude matching of the input signals. This paper details the research and development of this front-end prototype, including the key issues encountered during the design process and the signal transformations within the system.

SCHEME DESIGN

In the direct RF sampling scheme, to obtain the synthesized signals that accurately reflect the bunch position changes, careful conditioning of the beam position monitor (BPM) signals is required before performing analog sum-and-difference calculations. In practice, even the four signals derived from the same BPM exhibit subtle differences. Direct synthesis would lead to severe signal distortion and degraded resolution, and even result in erroneous measurement results. We plan to solve this problem in two parts.

The first issue is the difference in response functions. Ideally, when the same bunch passes through a perfectly symmetric BPM probe, only signals with different amplitudes induced by the transverse position difference are generated on the probe. Other properties of the signals, especially the response functions, should be consistent. However, in practice, due to factors such as process precision, slight inconsistencies exist among different channels. For example, the gaps between the BPM electrodes and the vacuum chamber introduce different beam impedances, which cause unexpected changes in the bunch signal waveforms. Figure 2 shows a typical set of response functions and their original spectra, where slight differences can be observed among the four channels.

* Work supported by the Fundamental Research Funds for the Central Universities (WK2310250133)
† lengyb@ustc.edu.cn

Content from this work may be used under the terms of the CC BY 4.0 licence (© 2026). Any distribution of this work must maintain attribution to the author(s), title of the work, publisher, and DOI.

ISBN: 978-3-95450-252-3 ISSN: 2673-5350 doi: 10.18429/JACoW-IPAC2026-MOP6684

DEVELOPMENT OF A MICROTCA.4-BASED FEEDBACK SYSTEM FOR ENVIRONMENTAL PHASE COMPENSATION OF THE BEAM-MONITOR REFERENCE AT J-PARC LINAC

E. Cicek*, Z. Fang, Y. Fukui, K. Futatsukawa, Y. Liu, T. Miyao, S. Mizobata,
High Energy Accelerator Research Organization, Tsukuba, Japan
J. Kamiya, K. Moriya, H. Nakano, Japan Proton Accelerator Research Complex, Tōkai Mura, Japan
Y. Sato, NAT Corporation, Hitachinaka, Japan
O. E. Delialioglu, The Graduate University for Advanced Studies, SOKENDAI, Hayama, Japan

Abstract

In the J-PARC LINAC, the beam monitor and LLRF systems operate with independent RF references. The LLRF system at 312 MHz and 960 MHz incorporates active environmental compensation to enhance stability. However, the 324 MHz beam-monitor RF reference lacks such functionality, resulting in humidity-dependent phase drift. To improve environmental long-term stability, we have developed a feedback-based reference compensation system implemented on a MicroTCA.4 platform. The system takes the 324 MHz beam-monitor reference from the SSA output and down-converts it to 12 MHz on the MicroRTM, enabling IF-phase measurement in the ADCs and fast feedback computation in the FPGA. The feedback-corrected I/Q signals drive the IQ modulator on the MicroRTM to regenerate a stabilized 324 MHz reference, which drives SSA and is redistributed to monitor stations, enabling real-time compensation of environmental phase drift with minimal additional hardware. The system is integrated into the existing LLRF infrastructure at MEBT1, achieving full synchronization, compact installation and cost-effective operation. Long-term studies demonstrated suppression of humidity-induced phase fluctuations and improved reference stability, contributing to enhanced beam-monitor reliability and supporting future high-power beam upgrades at J-PARC. This paper presents the system design, FPGA implementation, and long-term measurements characterizing humidity-induced drift and the stabilized performance with feedback.

INTRODUCTION

The linear accelerator (LINAC) at the Japan Proton Accelerator Research Complex (J-PARC) accelerates a 50 mA H^- beam to a final energy of 400 MeV for injection into the rapid cycling synchrotron (RCS), as illustrated in Fig. 1 [1,2]. The LINAC is equipped with various beam diagnostics devices, among which fast current transformers (FCTs) play a key role in beam phase measurements [3] used for phase scans during commissioning [4–6].

The LINAC employs separate RF reference systems for low-level RF (LLRF) control and beam diagnostics. The LLRF system operates at 312 MHz and 960 MHz, based on a down-conversion and intermediate-frequency (IF) sampling scheme [7], and uses a phase-stabilized optical distribution scheme maintained in a temperature- and humidity-controlled environment to ensure high phase stability as part of the original LLRF design [8, 9]. In the legacy cPCI system, the beam diagnostics reference is derived from the LLRF RF&CLK board (324 MHz) and fed to a semiconductor amplifier (SSA), then distributed via coaxial cables to the LINAC monitor systems through directional couplers. This configuration provides synchronization with the LLRF system but was not designed with active environmental compensation, and has been successfully used for commissioning measurements over long-term LINAC operation (Fig. 2a).

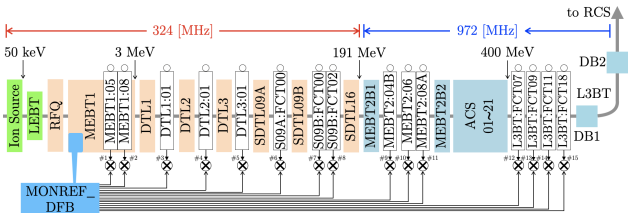

Figure 1: Layout of the J-PARC LINAC highlighting relevant sections and FCT locations used for phase measurements. The symbols ⊗ denote analog phase detectors.

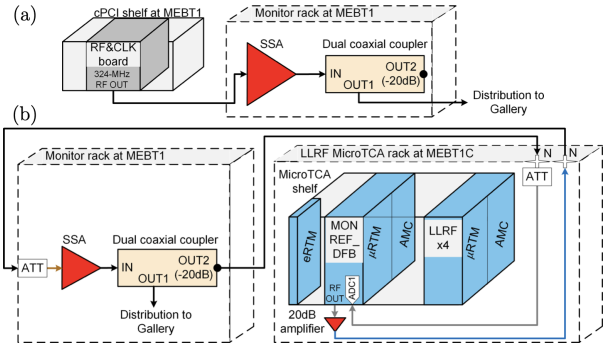

Figure 2: Schematic of the monitor RF reference generation system: (a) conventional configuration without feedback; (b) upgraded MicroTCA.4-based configuration with feedback.

Recent observations have revealed that the Monitor RF reference signal is susceptible to environmental effects, particularly humidity-induced phase drift in the klystron gallery, leading to degradation of long-term phase measurement stability. To address this issue, we leverage existing LLRF infrastructure by implementing a feedback-based RF reference compensation system, referred to as MONREF_DFB, within same MicroTCA.4 shelf using a µRTM and an AMC-based digitizer, replacing the legacy cPCI-based platform. The

* ecicek@post.kek.jp

Content from this work may be used under the terms of the CC BY 4.0 licence (© 2026). Any distribution of this work must maintain attribution to the author(s), title of the work, publisher, and DOI.

ISBN: 978-3-95450-252-3 ISSN: 2673-5350 doi: 10.18429/JACoW-IPAC2026-MOP6685

INTEGRATING FPGA INTO EPICS FOR ON-THE-FLY SCAN CONTROL AT THE TPS 35A BEAMLINE

C.-Y. Lin†, C.-Y. Lee, H.-S. Fung, L-Y. Chang, C-C. Yang, S.-C. Haw
National Synchrotron Radiation Research Center, Hsinchu, Taiwan

Abstract

On-the-fly scanning is an effective technique for improving data-collection efficiency in X-ray Absorption Spectroscopy (XAS). Its application at undulator beamlines requires deterministic synchronization among undulator motion, beamline energy scanning, and data acquisition. To address these requirements, a hardware-integrated on-the-fly scan control system has been developed for the TPS 35A beamline, which is currently under construction.

The proposed system integrates a Field-Programmable Gate Array (FPGA) based hardware backend with the Experimental Physics and Industrial Control System (EPICS) control framework. EPICS provides supervisory beamline control, including scan configuration, operation flow management, and system monitoring, while all time-critical synchronization and processing are executed in FPGA hardware. In a fixed master–follower scheme, the EPU66S undulator gap motion is treated as the master trajectory and the AM-PGM grating is controlled as the follower axis to maintain time-consistent tracking during continuous scans. The FPGA performs real-time control to dynamically drive the Active Mirror–Plane Grating Monochromator (AM-PGM) grating so that it continuously tracks the EPU66S undulator gap during energy scans. A system-on-chip (SoC) FPGA based backend with an FMC ADC module is employed as the beamline-local deterministic data-acquisition backend. System functionality has been validated through hardware-in-the-loop testing using simulated motion trajectories. This EPICS-integrated architecture provides a scalable, beamline-independent solution prepared for future commissioning of undulator-based on-the-fly scanning systems.

INTRODUCTION

On-the-fly scanning [1] eliminates the repetitive start–stop motion inherent in point-to-point acquisition, improving data acquisition efficiency while reducing radiation dose. This approach is widely adopted in synchrotron spectroscopy experiments requiring fast and continuous measurements.

At undulator beamlines, accurate implementation is challenging because photon flux depends on the coupled nonlinear relationship between insertion-device gap motion and monochromator energy. During long continuous scans, network latency and software-trigger jitter can degrade synchronization accuracy. Therefore, deterministic master–follower coordination between the undulator gap and the grating motion is required for stable on-the-fly scans.

To address these challenges, a hybrid architecture combining Experimental Physics and Industrial Control System (EPICS) [2] and Field-Programmable Gate Array (FPGA) is developed. EPICS handles supervisory control and user operation, while deterministic timing, synchronized triggering, and real-time motion tracking are implemented in FPGA hardware. The system is validated through hardware-in-the-loop testing without synchrotron radiation.

BEAMLINE DESIGN

The 35A Soft X-ray Absorption Spectroscopy beamline at the Taiwan Photon Source (TPS) is a soft X-ray beamline driven by an elliptically polarized undulator, EPU66S (period 66 mm, magnetic length 0.8 m) [3], supporting 100–3000 eV via continuous gap tuning. The beamline optical layout and key components are summarized in Fig. 1, highlighting the locations of the two key on-the-fly scan elements: the EPU66S undulator and the Active Mirror–Plane Grating Monochromator (AM-PGM) grating section downstream along the optical path.

For on-the-fly scans, maintaining high photon throughput requires time-consistent coordination between the EPU66S gap trajectory and the AM-PGM grating trajectory during continuous motion. The AM-PGM grating is actuated by a sine-drive mechanism and driven by a stepper motor. The FPGA generates the grating target accordingly so that the grating follows the undulator gap as a follower axis. In the proposed scheme, the EPU66S gap motion is treated as the master trajectory, and the FPGA backend performs real-time control to drive the AM-PGM grating so that it continuously tracks the EPU66S undulator gap over the full scan range, enabling hardware-synchronized on-the-fly scanning (Fig. 1).

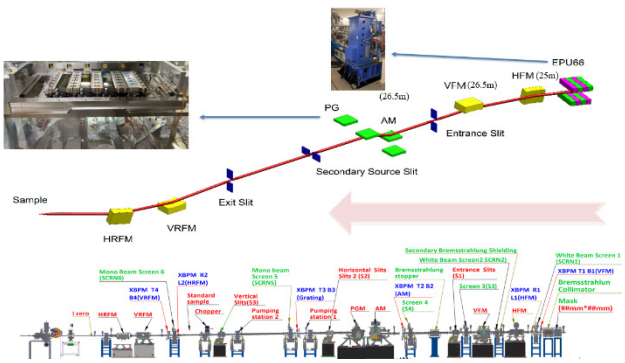

Figure 1: TPS 35A beamline layout highlighting the two key on-the-fly scan elements, the EPU66S undulator and the AM-PGM grating section downstream along the optical path. The undulator gap motion provides the master trajectory, while the grating position is tracked as the follower motion during continuous scans.

Content from this work may be used under the terms of the CC BY 4.0 licence (© 2026). Any distribution of this work must maintain attribution to the author(s), title of the work, publisher, and DOI.

ISBN: 978-3-95450-252-3 ISSN: 2673-5350 doi: 10.18429/JACoW-IPAC2026-MOP6687

OVERVIEW OF THE ACCELERATOR OPERATION AT CHINA SPALLATION NEUTRON SOURCE SINCE ITS OFFICIAL OPENING

Y. Yuan†,1,2, J. Zeng1,2, Y. An1,2, Y. Chen1,2, M. Liu1,2, Y. Zhang1,2

[1]Institute of High Energy Physics Chines Academy Sciences, Beijing, China
[2]Spallation Neutron Source Science Center, Dongguan, China

Abstract

The China Spallation Neutron Source（CSNS） is the first large-scale pulsed spallation neutron source in China and the fourth of its kind in the world. It is a large multi-disciplinary user facility. The facility passed national acceptance and officially opened for operation in 2018. It has been in operation for seven years. During this period, the beam power has continually increased, and both the beam runtime and availability have gradually improved. In the 2023-2024 period, it achieved a maximum beam on target time of 5,433 hours and the highest beam availability of 97.4%, which are the best among similar international facilities. This article will comprehensively introduce the operational performance of the accelerator over the past seven years, including annual beam runtime, beam availability, and statistics on hardware system downtime. Additionally, it will briefly discuss some measures taken to enhance operational reliability.

INTRODUCTION

The China Spallation Neutron Source (CSNS) is a large-scale, multidisciplinary experimental facility that generates neutrons by bombarding a target with a high-intensity proton beam. Phase I was designed for a beam–target power of 100 kW and includes three neutron spectrometers. The proton beam energy at the target is 1.6 GeV, and the pulse repetition rate is 25 Hz. After passing national acceptance in 2018, the facility was officially opened to external users. The schematic layout of the facility is shown in Fig. 1[1].

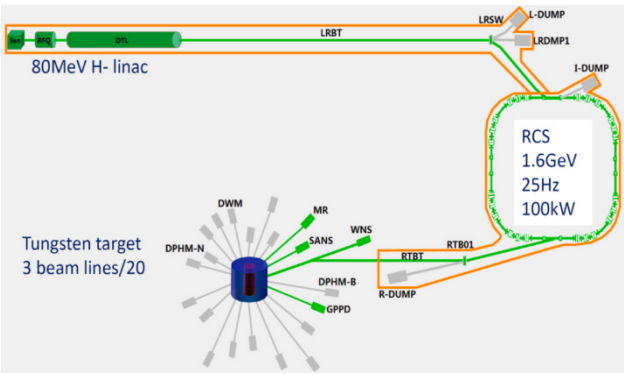

Figure 1: Schematic layout of CSNS.

At acceptance the beam-on-target power was 25 kW; through machine studies and hardware upgrades it was raised to 100 kW in February 2020 and to 170 kW in October 2024, with stable operation thereafter. Figure 2 shows the operational progression of the accelerator's beam-on-target power.

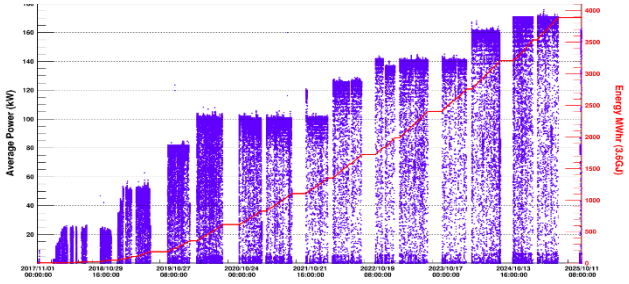

Figure 2: The operational progression of the accelerator's beam-on-target power.

Beam Delivery Time and Beam Availability

Since CSNS officially began operation in 2018, it has increased the proton beam power delivered to the target while gradually extending delivered beam time and improving beam availability. In the 2021–2022 operational year, delivered beam time first exceeded 5,000 hours and beam availability first exceeded 95%. In 2023–2024 the facility achieved its highest values to date—5,433 hours of delivered beam time and 97.4% availability. These operational metrics are also the highest among comparable facilities worldwide.

Beam availability is defined as delivered beam time divided by the sum of delivered beam time and fault-induced downtime, i.e. the scheduled (planned) beam time:

Availability = Delivered beam time / (Delivered beam time + Downtime).

In early 2024 CSNS formally began Phase II construction, requiring a balance between ongoing operation and upgrade works; together with an unexpected failure in the target station, this caused the summer maintenance shutdown in the 2024–2025 operational year to be roughly one month longer than usual, resulting in a noticeable reduction in delivered beam hours that year. Figure 3 summarizes the accelerator operating data from 2018 to 2025.

Content from this work may be used under the terms of the CC BY 4.0 licence (© 2026). Any distribution of this work must maintain attribution to the author(s), title of the work, publisher, and DOI.

† yuanyue@ihep.ac.cn

ISBN: 978-3-95450-252-3 ISSN: 2673-5350 doi: 10.18429/JACoW-IPAC2026-MOP6689

RECENT UPGRADE AND OPERATIONAL EXPERIENCE OF THE VIBRATION MONITORING SYSTEM AT TPS

K.-H. Hsu†, Ch.-K. Kuan, T.-Ch. Tseng, H.-S. Wang, National Synchrotron Radiation Research Center, Hsinchu, Taiwan

Abstract

In late 2024, the vibration monitoring system at the Taiwan Photon Source (TPS) was upgraded to enhance stability and usability. The system now includes beamline-floor measurement points and a central measurement center for station management, data export, automated reporting, and web-based access to real-time vibration levels and spectra. During more than a year of routine operation, issues such as abnormal sensor signals, DAQ faults, and station instability were encountered and resolved. The upgrade improves monitoring reliability and enhances the capability to record vibration behavior during events such as earthquakes and typhoons. This paper presents the upgraded system architecture, new analysis functions, operational experience, and examples of post-event vibration analysis.

INTRODUCTION

For the low-emittance and high-stability Taiwan Photon Source (TPS), vibration effects on the electron beam have been studied for many years. Ground vibration measurements were performed at the NSRRC site before the construction of TPS [1]. However, the vibration characteristics may change with environmental variations and the installation of utility systems such as cooling water systems and air handling units.

A vibration monitoring system was previously developed to continuously observe the vibration status of the TPS storage ring [2]. However, the previous system stored data independently at each station, provided only integrated vibration levels, and did not preserve raw data completely. These limitations made cross-station comparison and event tracing inefficient.

In late 2024, the system was upgraded to improve stability and usability. This paper presents the upgraded architecture, new analysis functions, and operational experience during more than a year of routine operation.

SYSTEM UPGRADE AND CONFIGURATION

System Overview

The key upgrade is the implementation of a central measurement center and the addition of beamline-floor measurement points. The upgraded system, shown in Fig. 1, consists of sensors, data acquisition (DAQ) sites, and a central measurement center for control, data processing, and web services.

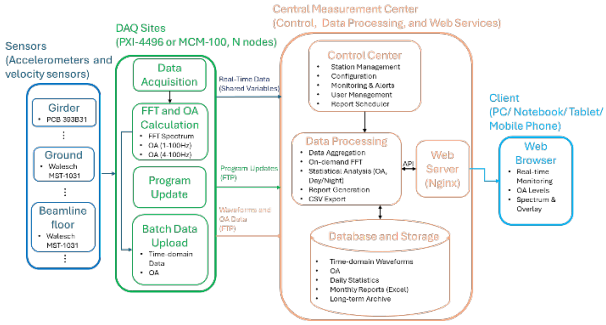

Figure 1: Architecture of the upgraded vibration monitoring system at TPS.

Vibration signals are acquired at the DAQ sites and processed in real time. The real-time data are transmitted within the vibration monitoring system by shared variables, while time-domain waveforms and overall vibration level (OA) values are uploaded to the central measurement center through FTP.

Sensors and Measurement Points

The system uses PCB 393B31 accelerometers on girders and Walesch MST-1031 tri-axial velocity sensors on the ground and beamline floor. Figure 2 shows one of the newly added beamline-floor measurement points.



Figure 2: Beamline-floor measurement point with a Walesch MST-1031 tri-axial velocity sensor.

The measurement points are categorized as girder, ground, and beamline floor. The X, Y, and Z directions correspond to horizontal transverse, vertical, and longitudinal directions, respectively.

DAQ Sites and Data Processing

Each DAQ site is based on either a PXI-4496 or an MCM-100 system. At each DAQ site, fast Fourier transform (FFT) spectra and OA values are calculated in real time. In this work, OA is defined as the root-mean-square displacement obtained by integrating the displacement

†khhsu@nsrrc.org.tw

Content from this work may be used under the terms of the CC BY 4.0 licence (© 2026). Any distribution of this work must maintain attribution to the author(s), title of the work, publisher, and DOI.

ISBN: 978-3-95450-252-3 ISSN: 2673-5350 doi: 10.18429/JACoW-IPAC2026-MOP6690

LOW-ENERGY INJECTION STUDY FOR TPS BOOSTER RING DURING LINAC MODULATOR DEGRADATION

W. Y. Lin*, H. J. Tsai, T. W. Hsu, T. Y. Lee, C. Y. Hung, B. Y. Huang,
National Synchrotron Radiation Research Center (NSRRC), Hsinchu, Taiwan

Abstract

In early 2025, Linac modulator 3 at the Taiwan Photon Source (TPS) exhibited signs of performance degradation. To reduce electrical stress and prevent an unplanned failure during user operations, BR injection feasibility was evaluated at 130 MeV, 140 MeV, and the nominal 150 MeV. Two compounding mechanisms limit low-energy injection efficiency: increased geometric emittance from the Linac, and degraded BR power supply waveform reproducibility at the earlier injection point on the ramp, which reduces the dynamic aperture. At 130 MeV, the mean BR current of 0.168 mA cannot satisfy the 5-second top-up window. At 140 MeV, a mean of 0.342 mA meets the >0.3 mA operational criterion, and this 140 MeV rescue mode maintained uninterrupted user service throughout the modulator degradation period.

INTRODUCTION

The Taiwan Photon Source (TPS) is a 3 GeV third-generation synchrotron light source. Its injector chain consists of a 150 MeV Linac followed by a booster ring (BR) that ramps beam from the injection energy to 3 GeV at 3 Hz, injecting into the storage ring (SR) in top-up mode to maintain 505 mA [1].

Each top-up cycle must complete within 5 seconds to minimise disruption to user experiments, requiring each BR pulse to deliver >0.3 mA to the SR. In early 2025, modulator 3 showed signs of imminent failure. To mitigate the risk of a catastrophic fault during user time, the modulator voltage was reduced, lowering the Linac output energy below 150 MeV. This paper analyses the two dominant physical mechanisms responsible for the observed performance degradation and reports the operational results of the 140 MeV rescue mode.

EFFECT OF LINAC ENERGY ON BEAM EMITTANCE

The TPS Linac is specified with a normalised emittance of $\varepsilon_n = 50\,\pi$ mm·mrad. The geometric emittance at the BR injection point scales inversely with Linac energy:

$$\varepsilon(E) = \frac{\varepsilon_n \times 0.511\,\text{MeV}}{E}, \qquad (1)$$

so reducing the energy from 150 MeV to 140 MeV (−9.3%) and 130 MeV (−13.3%) increases the geometric emittance by approximately 10.2% and 15.4%, respectively. The resulting enlargement of the transverse beam size raises particle losses at the injection septum and during the early ramp phase. The theoretical emittance curve is shown in Fig. 1, and the measured beam profiles during the BR energy ramp (Fig. 2) and the corresponding beam sizes as a function of ramp energy (Fig. 3) are both consistent with this scaling behaviour.

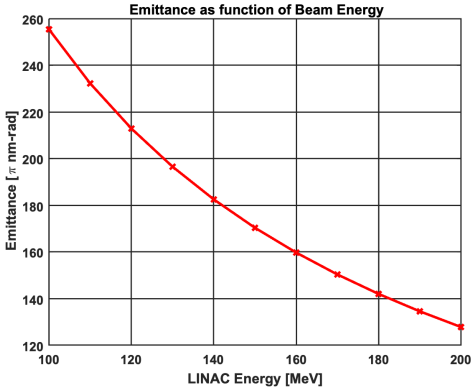

Figure 1: Theoretical geometric emittance vs. Linac energy from Eq. (1) with $\varepsilon_n = 50\,\pi$ mm·mrad.

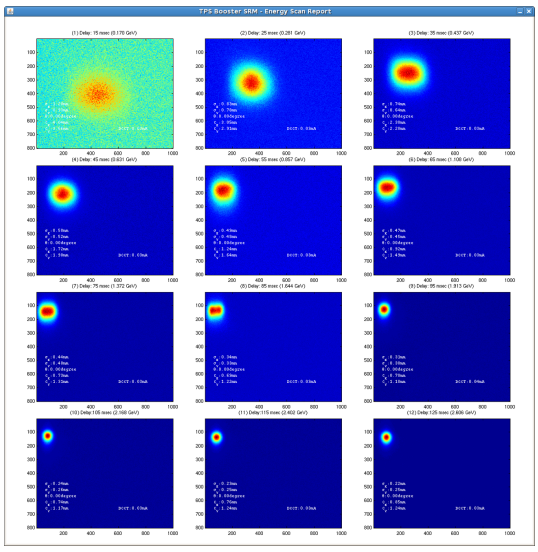

Figure 2: Measured transverse beam profiles at the BR during the energy ramp, recorded at selected delay times from 75 ms to 125 ms (corresponding to beam energies of approximately 1.37–2.60 GeV). The beam size decreases as the beam is accelerated, consistent with the $\varepsilon \propto 1/E$ scaling of Eq. (1).

* lin.lucien@nsrrc.org.tw

Content from this work may be used under the terms of the CC BY 4.0 licence (© 2026). Any distribution of this work must maintain attribution to the author(s), title of the work, publisher, and DOI.

ISBN: 978-3-95450-252-3 ISSN: 2673-5350 doi: 10.18429/JACoW-IPAC2026-MOP6691

DEVELOPMENT OF A REAL-TIME WAVEFORM MONITORING SYSTEM FOR PULSED POWER SUPPLIES AT TAIWAN PHOTON SOURCE

W. Y. Lin*, H. J. Tsai, T. W. Hsu, T. Y. Lee, C. Y. Hung, B. Y. Huang
National Synchrotron Radiation Research Center, NSRRC, Hsinchu, Taiwan

Abstract

A real-time waveform monitoring system has been developed for the pulsed power supplies in the injection chain of the Taiwan Photon Source (TPS). The system covers eight kicker and septum magnets spanning the Booster Ring and Storage Ring injection path. Two operational incidents involving SR Injection Septum 1 motivated its development: in both cases, waveform anomalies that were imperceptible by visual inspection led to severe injection efficiency degradation or complete injection failure. The system acquires waveforms via EPICS Channel Access, computes shot-averaged deviations from a stored reference, and compares them against physics-motivated alarm thresholds derived from dedicated machine study experiments. The thresholds are expressed as time-resolved curves that directly map waveform error to injection efficiency degradation. The system has been deployed and is currently in operation at TPS.

INTRODUCTION

The Taiwan Photon Source (TPS) is a 3 GeV third-generation synchrotron light source operated by the National Synchrotron Radiation Research Center (NSRRC) in top-up mode to maintain a stable stored current [1]. The injection chain consists of a Booster Ring (BR) and a Storage Ring (SR) connected in series, and the waveform quality of pulsed power supplies — kicker and septum magnets — directly determines injection efficiency and beam stability.

Two separate incidents involving SR Injection Septum 1 motivated this work. The first occurred on June 25, 2025: injection into the storage ring was completely lost despite normal BTS transport, and post-incident investigation revealed a waveform deviation so subtle that it was virtually indistinguishable by visual inspection (Fig. 1b) — a peak amplitude deviation of only a few percent was sufficient to cause complete injection failure. The second occurred on July 17, 2025, when unstable septum output caused injection efficiency to fluctuate severely and repeatedly drop toward zero (Fig. 1a). Both incidents highlighted a fundamental limitation of conventional operator monitoring, motivating the development of an automated system capable of detecting subtle waveform deviations quantitatively before injection performance degrades.

MONITORING SYSTEM DESIGN

Monitored Devices

The system monitors eight pulsed power supply devices covering the complete injection path from the BR injection point to the SR injection point. All eight devices operate at a nominal injection efficiency of approximately 84%, measured independently for each device during the machine study experiments.

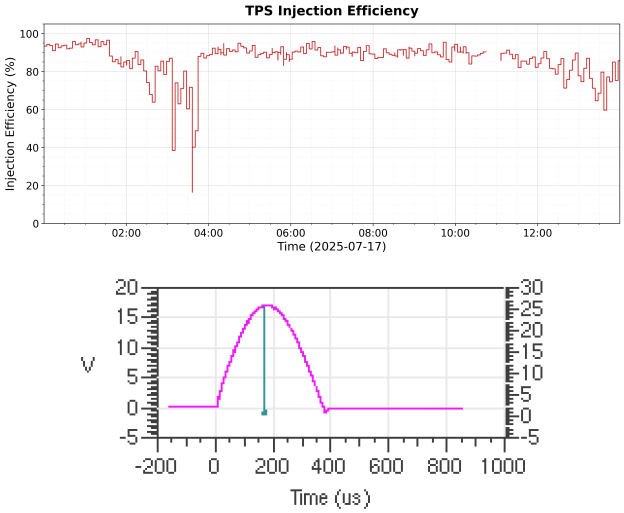

Figure 1: Operational incidents motivating this work. (a) Injection efficiency recorded on July 17, 2025, showing severe fluctuation due to unstable SR Injection Septum 1 output. (b) SR Injection Septum 1 waveform as displayed on the operator console. A peak amplitude deviation of only a few percent — imperceptible at this display scale — is sufficient to cause complete injection failure, as experienced on June 25, 2025.

Software Architecture

The system is implemented in Python and acquires waveform data via EPICS Channel Access [2]. After each injection trigger, a background thread accumulates 30 consecutive waveforms and computes their average for comparison against a stored reference. The graphical interface is built with Qt and provides three views: a *Status Overview* showing real-time Mean Diff, Max Diff, and alarm status for all eight devices (Fig. 2, top); a *Waveform View* displaying the averaged waveform overlaid with the reference and the difference curve with three threshold lines (Fig. 2, bottom); and an *Alarm Log* with timestamped records exportable as CSV.

Reference Waveform and Monitor Window

At startup or on operator request, the system presents a dialog allowing the operator to either capture 30 consecutive shots as a fresh reference or load a previously saved reference from file. The monitor window and difference metrics are defined according to device type.

* lin.lucien@nsrrc.org.tw

Content from this work may be used under the terms of the CC BY 4.0 licence (© 2026). Any distribution of this work must maintain attribution to the author(s), title of the work, publisher, and DOI.

ISBN: 978-3-95450-252-3 ISSN: 2673-5350 doi: 10.18429/JACoW-IPAC2026-MOP6697

NEURAL NETWORK-BASED AMPLITUDE FEEDFORWARD CONTROL ALGORITHM FOR LLRF SYSTEMS*

Yuchen Wang, Xiaofang Hu†, Shenghua Yang, Jian Pang,
Fangfang Wu, Kai Zhang, Shancai Zhang
National Synchrotron Radiation Laboratory, University of Science and Technology of China,
Hefei, Anhui, 230029, China

Abstract

In free-electron laser facilities, the amplitude-phase stability of the microwave pulses driving the electron beam is a key factor determining beam energy spread. Aiming at the long bunch train operation mode, this paper proposes a neural network-based amplitude feedforward control for low-level radio frequency (LLRF) systems to suppress intra-pulse amplitude fluctuations. The algorithm has been validated at the output of a solid-state amplifier (SSA): under four randomly selected vector modulator (VM) output configurations, the average intra-pulse amplitude flatness (RMS) was reduced from 1.208 % to 0.398 %, and the average peak-to-peak variation was reduced from 4.683 % to 1.353 %, demonstrating a significant compensation effect.

INTRODUCTION

For linear accelerators with relatively high average beam currents, the beam loading effect within the accelerating tubes is significant, leading to inconsistent energy gains for particles at different times within the pulse, thereby substantially degrading the uniformity of particle acceleration [1, 2]. Furthermore, as critical components of the accelerator's microwave high-frequency system, the nonlinear characteristics of solid-state amplifiers (SSA) and klystrons introduce significant waveform distortion. This results in issues such as non-flat tops and rising edge distortions in the ideally flat-top pulses generated by the low-level radio frequency (LLRF) vector modulator (VM) after transmission and amplification, upon reaching the entrance of the accelerating tube, also impacting beam quality. To ensure uniformity in the accelerating fields experienced by each bunch, the LLRF control system and the microwave high-frequency system must provide RF power with stable intra-pulse and pulse-to-pulse amplitude and phase characteristics to the accelerating structure. In engineering practice, feedback control is often employed to enhance pulse-to-pulse amplitude and phase stability [3–5]. However, due to inherent delays in the feedback loop, achieving rapid, point-by-point intra-pulse amplitude and phase flattening control is challenging. Consequently, precise and fast waveform control is typically addressed using feedforward compensation. For compensating this nonlinear distortion, traditional fixed-model-based feedforward methods often prove complex to implement under conditions where amplitude settings vary over a wide range and pulse widths and delays are adjusted [6, 7]. U-Net is a deep learning architecture that is data-efficient and excels at capturing local details within complex data and performing nonlinear fitting, making it widely applied in the field of image processing [8, 9]. This paper proposes a data-driven deep learning method by introducing U-Net into the LLRF controller domain. By constructing a one-dimensional U-Net neural network, the inverse response characteristic from the distorted amplitude output of the microwave high-frequency system to the ideal amplitude input is directly learned, serving as a pre-distortion model to implement feedforward control.

MODEL AND DATASET DESIGN

The core objective of this study is to construct a deep neural network model capable of accurately learning the nonlinear inverse response of an RF power system, thereby achieving waveform pre-distortion compensation based on feedforward control. The overall application framework comprises two phases: offline training and online application. In the offline phase, we first need to acquire a large-scale dataset consisting of measured VM output waveforms and the corresponding waveforms at the controlled location of the RF power system. Subsequently, using this dataset, we employ the waveforms from the controlled location as the network input and the measured VM output waveforms as the target output. This training process yields a deep neural network that learns the mapping from the distorted output of the RF power system to the ideal low-level input (i.e., the inverse model of the power chain). During the online application phase, this deep neural network module, serving as a pre-distortion module, is deployed on a computer equipped with a GPU. The desired waveform for the controlled location is fed into the neural network, which generates the corresponding pre-distorted low-level excitation waveform data. This data is then written directly into the memory of the LLRF system's DAC via Direct Memory Access (DMA) and output through the VM, thereby enabling real-time compensation at any controlled location within the RF power system.

Network Architecture: 1D U-Net Convolutional Neural Network

To effectively process long-sequence time-domain waveforms and capture their local features along with global context, we adopted a one-dimensional U-Net architecture. This network adopts an encoder-decoder structure as its

* Supported by National Natural Science Foundation of China (12505182)
Supported by National Key Research and Development Program of China (2024YFA1612200)

† Corresponding author, email: huxiaofang@ustc.edu.cn

Content from this work may be used under the terms of the CC BY 4.0 licence (© 2026). Any distribution of this work must maintain attribution to the author(s), title of the work, publisher, and DOI.

ISBN: 978-3-95450-252-3 ISSN: 2673-5350 doi: 10.18429/JACoW-IPAC2026-MOP6698

DESIGN AND TESTING OF A UNIVERSAL EMBEDDED FEEDBACK CONTROLLER FOR RF CAVITIES

A. Sharma*,[1,2], S. Kar[1], Y. Dabas[2], B. K. Sahu[2], P. Singh[2],
Y. Mathur[2], V. V. V. Satyanarayana[2], S. Venkatramanan[2]
[1]Indian Institute of Technology Delhi, New Delhi, India
[2]Inter-University Accelerator Centre, New Delhi, India

Content from this work may be used under the terms of the CC BY 4.0 licence (© 2026). Any distribution of this work must maintain attribution to the author(s), title of the work, publisher, and DOI.

Abstract

The design of low-level feedback (LLRF) controllers used to stabilize the amplitude and phase of the field within the RF cavities is typically customized to the frequency and mode of operation. IUAC, New Delhi, India, operates accelerators with RF structures in the range of 12.125-97 MHz, in both normal and superconducting modes. Currently, all the LLRF controllers are structure-specific and designed in the analog electronics domain. Component aging and obsolescence have made it challenging to maintain them due to frequent failures. To overcome this, a universal digital controller has been developed whose design is based on the philosophy of using the same hardware for all the RF structures at IUAC. It is a compact, frequency-reconfigurable, standalone device controlled by an EPICS IOC. With an aim to cater to the requirements of multi-accelerator facilities, this controller has been tested as a Sawtooth Waveform Generator for the Multi-Harmonic Buncher (MHB), as a generator-driven (GDR), and as a self-excited loop (SEL)-based LLRF for various RF cavities at IUAC. Long-term RMS stability of ~1% in amplitude and a $< \pm 0.4^\circ$ in phase locks have been obtained. Design details and test results are discussed in this paper.

INTRODUCTION

RF resonant cavities are the heart of an RF accelerator, which energizes incoming ion beams. These structures use extremely high axial electric fields inside them and transfer their energy to the incoming beam particles. For effective energy transfer, the stability of this field, in terms of amplitude and phase, is paramount. This stability is achieved using the Low-Level RF (LLRF) controllers. A small fraction of the cavity field is picked up and fed into this controller as feedback, which then performs feedback control algorithms to ensure the required stability. At IUAC, there are multiple RF structures, including the Superconducting Linear Accelerator (SC-LINAC), the High Current Injector (HCI), a Multi-Harmonic Buncher (MHB) for the Pelletron DC Accelerator, and a Table-Top (TT) Cyclotron. The operating frequency of RF cavities ranges from 12.125 MHz to 97 MHz. The LLRF electronics for all these RF structures are in the analog domain and have been in use for many years [1–3]. The SC-LINAC has SEL-based LLRF [2, 4, 5], whereas HCI, MHB, and TT cyclotron use GDR-based electronics [1, 3]. While the current solutions have performed satisfactorily, maintenance cycles have recently grown due to component-level issues. These controllers are rigid in their designs with limited modification capabilities. Maintaining spares inventory is also a challenging task amid component obsolescence. Analog techniques used here for cavity field stabilization were first proposed in [4, 5]. Since then, many advancements, especially the introduction of high-speed A/D and D/A converters and specialized signal-processing hardware, have led to the widespread development of digital LLRF electronics [6–11]. Several implementations invoke backplane-based methods, such as VME, cPCI, and microTCA. These solutions are often costly, bulky, and difficult to adopt due to a customized design goal. Standalone, non-crate-based systems provide a more versatile, fast, and cost-effective alternative. The use of a SoC-FPGA makes this a complete system implementation, as the same chip can host both the signal-processing logic and the remote-control server logic. This paper builds-up from the findings of [10, 11] to devise an universal digital LLRF design that can be used as a sawtooth waveform generator for MHB, GDR-based RF controller for HCI, and TT cyclotron, and SEL-based RF controller for SC-LINAC. The main feature of our design is the hardware configuration, which remains the same regardless of the cavity type, without the need for FPGA reprogramming. In addition to the LLRF algorithm, the same FPGA contains logic for the motorized Frequency Tuner Control, considerably lowering the system's cost. Besides that, a set of EPICS device drivers has also been written for generic record types (AI, AO, BI, BO, MBBI, MBBO) in the processor part of the SoC-FPGA [12]. EPICS Qt-based code-free GUI is used for remote control. Further sections detail its construction and test results with various facilities at IUAC.

DESIGN AND CONSTRUCTION

The major blocks of the system as shown in the overall physical block diagram (Fig. 1a) are a wideband Analog Front-End (AFE), microcontroller programmed PLL Multiplier, and a SoC-FPGA-based digital board. Different blocks of the finished prototype (Fig. 1b) are explained in the following subsections.

Analog Front–End (AFE)

This module (Fig. 2) is responsible for the down- and up-conversion of RF signals entering or leaving the digital board. Since the design philosophy is universal, it features wideband components to convert all incoming RF signals to the low-frequency domain and vice versa. In addition, it

* idz208685@iitd.ac.in

ISBN: 978-3-95450-252-3 ISSN: 2673-5350 doi: 10.18429/JACoW-IPAC2026-MOP6700

COMPREHENSIVE INTEGRATION AND INNOVATION ON THE 1.5 GHz SRF HARMONIC CAVITY CONTROL SYSTEM AT NSRRC

Fu-T. Chung†, M.-Ch. Lin, Ch.-H. Huang, Z.-K. Liu, Ch.-H. Lo, L.-J. Chen, M.-H. Chang, S. W. Chang, Yi-Ta Li, M.-S. Yeh, Tao Wang, National Synchrotron Radiation Research Center, Hsinchu, Taiwan
Fu-Yu Chang, National United University, Miaoli, Taiwan

Abstract

This paper presents a self-developed, comprehensive electronic control system for the Superconducting Radio-Frequency passive Harmonic Cavity (SRF HC) at the Taiwan Photon Source (TPS) in Hsinchu, Taiwan. The system integrates the Break Out Box (BOB) interfaces for the cavity, Valve Box (VB), cooling water signals, and interlock systems. Additionally, it includes an intuitive correction module and updates for the discontinued or unmaintainable dial gauge module, ensuring that the system operates safely and transparently with clear status display.

INTRODUCTION

The TPS is a third-generation 3 GeV synchrotron light source. To meet the increasing demand for high-brightness, the National Synchrotron Radiation Research Center (NSRRC) has deployed various high-performance insertion devices (IDs) [1] to enhance beam brightness and experimental capability. However, although bunch shortening is beneficial for increasing peak brightness, it is often accompanied by an increase in bunch charge density, which intensifies the Touschek scattering effect and consequently reduces beam lifetime. This not only requires more frequent top-up injections, but also increases the power consumption of Radio-Frequency (RF) systems and the thermal load on the magnet systems.

To effectively address these challenges, NSRRC conducted a preliminary technical evaluation and officially launched the TPS 5-year Upgrade Project in 2020 to build up a 1.5 GHz double-cell SRF HC system [2-7]. Upon completion, this system is expected to significantly extend beam lifetime, reduce thermal loading, and improve overall operational efficiency.

The core design is based on the proven KEKB-type SRF HC technology. The niobium (Nb) cavity and the higher-order-mode (HOM) damping structures were fabricated by Mitsubishi Heavy Industries (MHI) and RI Research Instruments GmbH (RI), whereas the cryostat was independently designed and assembled by NSRRC. Similar SRF HC technologies have already been implemented and validated at international light source facilities such as the Shanghai Synchrotron Radiation Facility (SSRF) [8], demonstrating excellent operational stability.

ARCHITECTURE AND DESIGN OF THE SRF HC ELECTRONIC CONTROL SYSTEM

Based on experience gained from the installation of three KEKB-type SRF systems, NSRRC has developed an in-house electronic control architecture (Fig. 1) for TPS. The design addresses critical constraints, including limited installation space, power distribution limits, and component obsolescence. The system consists of four main sections: signal integration, control logic, upgrade modules, and infrastructure optimization. Details of each section are given below.

Signal Interface and Conditioning

To ensure effective signal isolation and transmission under the susceptible on-site conditions of the TPS, the system integrates four Break Out Boxes (BOBs) and hardware-level buffer modules:

SRF HC BOB

Two BOBs (Fig. 2) [9] dedicated to the SRF HC are housed beneath the support structure. To enhance environmental resilience in this specific location, a dual-layer physical protection scheme was implemented: externally, a 10 mm acrylic cover safeguards against potential cooling-water leaks, while internally, a 3 mm lead plate mitigates the effects of ionizing radiation.

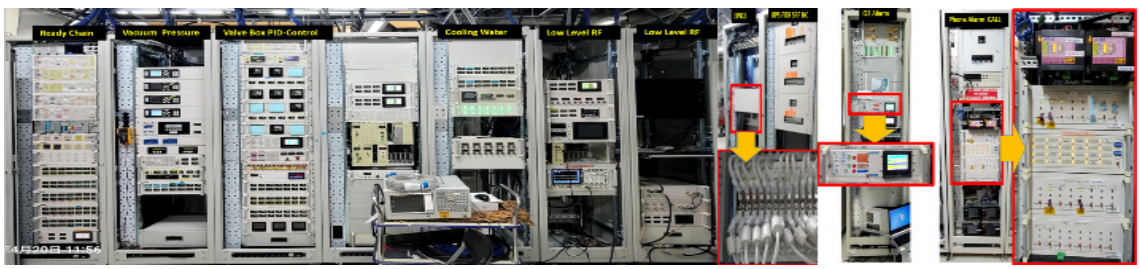

Figure 1: SRF harmonic cavity electronic-control system rack.

† gofor@nsrrc.org.tw

Content from this work may be used under the terms of the CC BY 4.0 licence (© 2026). Any distribution of this work must maintain attribution to the author(s), title of the work, publisher, and DOI.

ISBN: 978-3-95450-252-3 ISSN: 2673-5350 doi: 10.18429/JACoW-IPAC2026-MOP6701

APPLICATION OF PYAPAS IN PWFA BEAM COMMISSIONING

Y. Zhao, X. Lu, H. Ji, N. Li, C. Shen, C. Meng, Y. Wang, Z. Ming, H. Xu
Accelerator Physics Group, Accelerator Center, IHEP, CAS, China

Content from this work may be used under the terms of the CC BY 4.0 licence (© 2026). Any distribution of this work must maintain attribution to the author(s), title of the work, publisher, and DOI.

Abstract

The Plasma Acceleration is an important development direction for future accelerators for its high acceleration gradient. The PWFA experimental platform in IHEP consists of two beamlines. Beamline 1 (BL1) transports the electron-positron beams from the BEPCII linear accelerator, with a beam energy of about 2 GeV. At present, BL1 has achieved the penetration of electrons and positrons, as well as the parameter measurement of electron beams. Beamline 2 (BL2) is a new linear accelerator featuring an energy of 150 MeV and a bunch charge exceeding 5 nC. The hardware installation of BL2 is drawing to a close, and the beam commissioning will start very soon. Together, these two beamlines support a range of plasma acceleration experiments, including positron acceleration, electron-cascade acceleration, high transformer-ratio electron acceleration, and external-injection electron acceleration. Pyapas, an independently developed High-Level Application (HLA) by the Institute of High Energy Physics (IHEP), has been successfully applied on beam commissioning of High-Energy Photon Sources(HEPS). We have achieved the successful porting and application of Pyapas in the beam commissioning of the PWFA linear accelerators.

INTRODUCTION

Plasma wakefield acceleration (PWA) achieves gradients up to 100 GV/m, two orders of magnitude higher than conventional RF accelerators [1], enabling compact high-energy accelerators. IHEP has constructed a dual-beamline PWFA platform: BL1 transports 2 GeV electron/positron beams from BEPCII for positron and cascade acceleration studies. The critical challenge is matching the three-dimensional beam sizes produced by conventional radio-frequency (RF) accelerators to the plasma accelerating structures. With innovative design concept, the beam from BEPCII achieves a tenfold compression of the three-dimensional beam sizes. BL2 is a newly constructed 150 MeV, > 5 nC linac and a peak current above 10 kA. The layout of BL1 and BL2 is shown in Fig. 2.

Efficient commissioning and precise diagnostics are essential for PWFA. PYAPAS a pure Python-based Accelerator Physics Application Set [2], features modular design, physical-quantity-based control, and dual-layer physical modeling. It has been sucessfully used in the commissioning of HEPS LINAC [4], Booster [5] and Storage Ring.

PORTING AND EXTENSION OF PYAPAS

PYAPAS is selected as the commissioning tools of PWFA. To meet the requirements of PWFA beam commissioning, a series of Pyapas-based applications have been developed and ported, including the PWFA controller for machine control with physical values, model manager for optics parameters saving and restoring, online simulator to displays physical parameters in real time and facilitate beam commissioning, beam-based alignment (BBA), emittance measurement, energy and energy spread measurement, response matrix measurement and orbit correction, and so on. These applications provide a unified software environment for daily beam tuning and diagnostic measurements. Some program interfaces are shown in Fig. 1.



Figure 1: Some applications of Pyapas for PWFA.

Due to the unique characteristics of the PWFA beamlines, especially the ultra-wide energy range of AM4 (0.05-25 GeV) and the requirement for flexible emittance measurement with solenoid scanning method, further functional extensions are implemented in Pyapas.

Emittance Measurement via Solenoid Scanning

The emittance and Twiss parameters are critical indicators of beam quality and key parameters for plasma wakefield acceleration. The quadrupole-scanning algorithm in Pyapas has been implemented and used in HEPS. Now, it was extended to measure with solenoids. The solenoid transfer matrix including coupling effect was implemented first, and a solenoid-scanning option was added to the GUI (Fig. 3). Based on the beam envelope theory, the squared beam size measured at profile monitors has a linear relation with Twiss parameters and emittance. For the case of measure with scanning solenoid method it is expressed in matrix form as Eq. (1):

where σ_{xi}^2, σ_{yi}^2 are squared horizontal/vertical beam sizes at the i-th monitor, $m_{ij,k}$ denotes the (i, j) element of transfer matrix at the k-th solenoid setting, $\beta_{x,y}$, $\alpha_{x,y}$, $\gamma_{x,y}$ are Twiss parameters, and $\varepsilon_{x,y}$ are horizontal/vertical emittances.

We tested the code with virtual accelerator based on BL2 lattice. The beam spot sizes under different solenoid settings are shown in Fig.3. The results yielded horizontal/vertical emittances of 0.17 µm and 0.24 µm, which means the fitting error is < 4%, as shown in Table 1 and Fig. 3(Lower).

Energy and Energy Spread Measurement Using 2D Interpolation

There are several bending magnets and PR targets used for energy and energy spread measurement, such as AM4 and PR03 in BL1, BL2BC02 and BL2PR02, BL2BC04 and

ISBN: 978-3-95450-252-3 ISSN: 2673-5350 doi: 10.18429/JACoW-IPAC2026-MOP6703

MACHINE-LEARNING SURROGATE MODELING OF THE RAON LEBT BEAMLINE

C. S. Park*[1]
[1]Korea University, Sejong, Republic of Korea

Abstract

We present a machine-learning surrogate model for the RAON Low Energy Beam Transport (LEBT) beamline that enables fast prediction of beam centroids at multiple diagnostics. A dataset of TRACK simulations spanning steering-magnet and electrostatic-quadrupole settings is used to train fully connected neural networks (FCNNs). The surrogate model reproduces the underlying beam dynamics with high accuracy while providing orders-of-magnitude faster evaluation than conventional beam dynamics simulations. This approach supports rapid orbit studies, optimization, and future data-driven beam control applications in the RAON front-end transport system.

INTRODUCTION

The Rare isotope Accelerator complex for ON-line experiments (RAON) is a heavy-ion accelerator facility in Korea for stable and rare isotope beams [1]. The Low Energy Beam Transport (LEBT) section transports ion beams from the Electron Cyclotron Resonance Ion Source (ECR-IS) to the Radio Frequency Quadrupole (RFQ), as shown schematically in Fig. 1. This front-end section determines the injection quality for downstream acceleration. Reliable control of the transverse beam centroid in this region is essential for minimizing beam loss and preserving beam quality.

Orbit control in the LEBT is challenging because the beam energy is low and the dynamics are affected by space charge, nonlinear focusing fields, alignment errors, and uncertainties in machine settings [2, 3]. Conventional correction based on linear response matrices is useful for routine tuning but can become inaccurate when nonlinearities and space-charge effects are important. High-fidelity particle tracking can model these effects, but repeated TRACK calculations are too expensive for fast parameter scans or online optimization.

Machine-learning (ML) surrogate models offer a practical approach for accelerating beam dynamics studies by learning nonlinear mappings between machine settings and beam responses [4–6]. In this work, fully connected neural networks (FCNNs) are trained on TRACK simulation data to predict beam centroids at multiple RAON LEBT diagnostics. The resulting model is implemented in the Python-based `synapticTrack` framework and provides a fast model for orbit studies and future data-driven beam control.

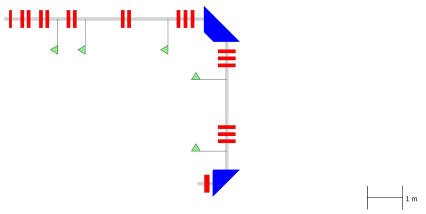

Figure 1: Schematic layout of the RAON LEBT beamline from ECRIS to RFQ. Red elements indicate focusing elements, and green symbols indicate diagnostic locations.

SIMULATION AND CALIBRATION FRAMEWORK

The TRACK code [7] was used to generate beam dynamics data for the RAON LEBT. The simulation model includes steering magnets, electrostatic quadrupoles (EQuads), drift sections, and diagnostic locations corresponding to four wire scanners (WSs), one Allison scanner (AS), and the LEBT exit. Ar^{8+} operating conditions were considered, and the simulations recorded horizontal and vertical beam centroids for each machine configuration.

Simulation, calibration, and ML workflows were managed using `synapticTrack`, a modular Python framework developed for this study. The framework handles TRACK data conversion, scanner analysis, feature normalization, visualization, and PyTorch-based surrogate model training. This common workflow allows measured and simulated data to be treated consistently during calibration and dataset generation [8].

To improve agreement with measurements, the TRACK model was calibrated using scanner data, as summarized in Fig. 2. Steering magnet kicks were adjusted to minimize differences between measured and simulated beam centroids, while EQuad voltages were calibrated using RMS beam-size information. The EQuads were grouped into three scaling families to reduce dimensionality and improve optimization stability. The calibrated model was then used as the reference simulation model for training-data generation.

SURROGATE MODEL DEVELOPMENT

The surrogate model was trained on a large TRACK dataset generated with Latin Hypercube Sampling (LHS) [9]. The 13-dimensional input vector consisted of five horizontal steering kicks, five vertical steering kicks, and three grouped EQuad scaling factors. The 12-dimensional output vector consisted of horizontal and vertical centroids at WS1–WS4, AS1, and the LEBT exit. Approximately 50,000 simulation

* kuphy@korea.ac.kr

Content from this work may be used under the terms of the CC BY 4.0 licence (© 2026). Any distribution of this work must maintain attribution to the author(s), title of the work, publisher, and DOI.

ISBN: 978-3-95450-252-3 ISSN: 2673-5350 doi: 10.18429/JACoW-IPAC2026-MOP7001

UPGRADE OF THE ARCING SUPPRESSION SYSTEM FOR THE WAVEGUIDES IN THE EUROPEAN XFEL

M. Bousonville†, F. Mantas, S. Wiesenberg, P. Hülsmann, C. Christou
Deutsches Elektronen-Synchrotron DESY, Hamburg, Germany

Content from this work may be used under the terms of the CC BY 4.0 licence (© 2026). Any distribution of this work must maintain attribution to the author(s), title of the work, publisher, and DOI.

Abstract

When planning the European XFEL, the decision was made to avoid using SF_6 in the waveguide systems. Instead, air was used at slight to high overpressure. When slight overpressure is used, the air is also in motion. The air flow travels from the RF source towards the cavities and is released again before the coupler. This ensures that, in our non-gas-tight waveguide system, the air quality in the waveguides corresponds to the air quality supplied by the compressor. Particles and ionised air that could promote arcing are blown out. Originally, the air pressure was generated by local compressors and the air used came from the ambient atmosphere. Now, the accelerator's central compressed air system is utilised. Locally, only the newly developed controls for air pressure and flow remain. The advantage of the central compressed air supply lies in the significantly better air quality and greater operational reliability.

INTRODUCTION

In the past, SF_6 was used in the FLASH accelerator for the 1.3 GHz systems to prevent arcing. However, the use of SF_6 presents a number of problems. It is an inert asphyxiant that can decay into toxic products, difficult to handle and a highly environmentally harmful gas. For this reason, it was decided as part of the planning for the European XFEL that the new RF stations would be operated without SF_6 [1].

The XFEL operates using very long RF pulses (1.4 ms / 10 Hz). The klystrons used can deliver up to 10 MW of RF power. To prevent the RF power in the output windows from becoming too high, the output power is split between two RF windows, so that a maximum of 5 MW is present in each window. The power from both outputs is recombined only at the gun, so that in operation a maximum of 6.5 MW occurs in a single waveguide. For all the other 25 klystrons of the XFEL, which drive the superconducting accelerator modules, the power is not recombined. Each klystron feeds 4 accelerator modules with a total of 32 cavities (Fig. 1). Two of these accelerator modules are connected to each of the klystrons' two RF outputs. The klystrons deliver a maximum of 6.6 MW during operation. Consequently, a maximum of 3.3 MW is present in the waveguides here.

The waveguides are filled with air. To supply the gun with the high RF power of 6.5 MW via one waveguide, an overpressure of 2 bar was originally used [2]. According to Paschen's law [3], this measure significantly increases the breakdown strength. The gun waveguide distribution has since been modified, and the RF power is now fed to the gun via two air-vacuum windows, so that each window only has to transmit half the RF power and the overpressure could be reduced.

Higher internal pressure is one way of decreasing the probability of breakdown in air-filled waveguides. In this case, however, special waveguide components are required that can withstand these pressures and are sufficiently gas-tight. This is a very complex process and has therefore only been envisaged for the end of the gun waveguide distribution system.

AIRFLOW IN THE WAVEGUIDES

Another way of decreasing the probability of breakdown in air-filled waveguides is to use air of a high degree of purity. Generally speaking, impurities in the air promote breakdown in waveguides. The air should therefore be as pure as possible. We achieve this by injecting air of a known quality (Fig. 1). The air is fed into both klystron waveguide arms. The tree-like structure of the waveguide distribution allows the air to follow the same path as the RF wave and to split symmetrically towards the cavity couplers. At the end of each waveguide branch, just before the coupler, there is an outlet valve through which the compressed air can escape. The air is typically injected at 0.05 bar overpressure, resulting in an air flow of 10 to 30 l/min. These varying air flow rates result from the waveguide distribution being more or less airtight, as standard air waveguides are used which are not gas-tight. This system ensures that the air quality in the waveguides is identical to that of the injected air. This allows control over the air quality in the waveguides. If the air were to stagnate rather than flow, ionised air resulting from arcing would not be dissipated and would cause subsequent problems – namely, the promotion of further arcing.

AIR QUALITY UPGRADE

Originally, the air used was simply drawn from the ambient atmosphere in the accelerator tunnel. One compressor per station drew in air from the surrounding environment and blew it into the waveguide arms. It should be noted, however, that air – or compressed air – always contains particles of dirt. These include, above all, solid particles, water and oil [4]. As there is a significant level of dust in the XFEL's accelerator tunnel, the air being blown in was obviously contaminated with particles.

†michael.bousonville@desy.de

ISBN: 978-3-95450-252-3 ISSN: 2673-5350 doi: 10.18429/JACoW-IPAC2026-MOP7002

EXPERIMENT DESIGN FOR BEAM-BASED CHARACTERIZATION OF A SUB-THZ DOUBLE BEND MODE CONVERTER

M. Kellermeier*[1], Z. Tibai[2], T. Vinatier[1], C. Bruni[3], G. Martinet[3], F. Burkart[1]
[1]Deutsches Elektronen-Synchrotron DESY, Hamburg, Germany
[2]University of Pécs, Pécs, Hungary
[3]IJCLab, Université Paris Saclay, Orsay, France

Content from this work may be used under the terms of the CC BY 4.0 licence (© 2026). Any distribution of this work must maintain attribution to the author(s), title of the work, publisher, and DOI.

Abstract

Laser-based high power THz generation advances rapidly, enabling THz-driven electron acceleration beyond the breakdown limits of conventional RF-driven structures. For this purpose the polarization of the externally coupled THz pulse has to match the required TM_{01} mode. Vice versa, beam-driven high power THz generation also relies on the TM_{01} mode and requires efficient out-coupling and transport. A crucial step in both applications is the conversion between the fundamental mode, and the TM_{01} in a compact manner, which can be achieved efficiently in a double bend geometry.

However, the double bend mode converter is fully integrated with the chained neighbouring devices. The embedding imposes challenges on the independent characterization of the converter, especially due to the strict tolerances. Utilising the wake field excited by an externally injected electron beam reduces the de-embedding complexity due to the requirements for THz in-coupling. Following tolerance studies, a beam-based experiment at ARES at DESY is proposed to study the conversion quality of the mode converter at 165 GHz, the design frequency envisioned for the TWAC project. The wake-driven excitation enables a wideband characterization around the design frequency.

A gently compressed (≈1 ps rms) high charge (≈50 pC) electron bunch is passed through a dielectric loaded waveguide, thereby exciting the TM_{01} mode. The out-coupled, sub-µJ THz pulse will be polarization filtered to determine the relative mode content between the residual unconverted TM_{01} and the expected TE_{11}.

INTRODUCTION

Cylindrical dielectric loaded waveguides (DLW) are of major interest for both externally driven THz structures for acceleration and manipulation of electron bunches, as well as for beam-driven THz generation for external applications [1]. While the fundamental TE_{11}-like hybrid mode enables transverse deflecting structures for current profile characterization [2], the TM_{01} mode is utilized for acceleration and compression, and predominantly excited by the wake. In both cases coupling of the THz pulse between freespace and waveguide is preferably done with a fundamental linearly polarized Gaussian to lower the requirements for the THz radiation transport in comparison to higher order Gaussians. An integrated mode converter has been proposed [3] which converts the TE_{11} mode to the TM_{01} by curvature of the waveguide. However, the mechanical tolerances require a detailed characterization of the mode conversion performance to potentially correct or compensate for design mismatches.

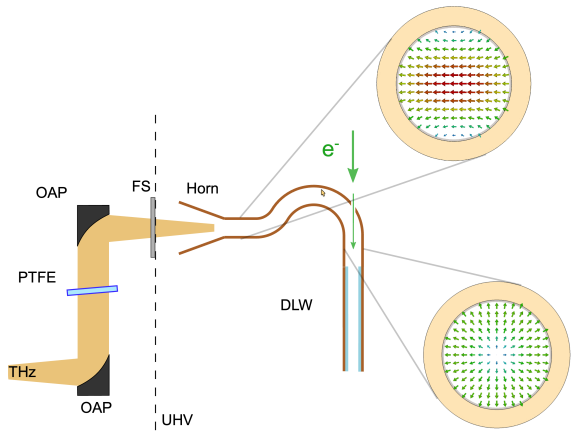

(a)

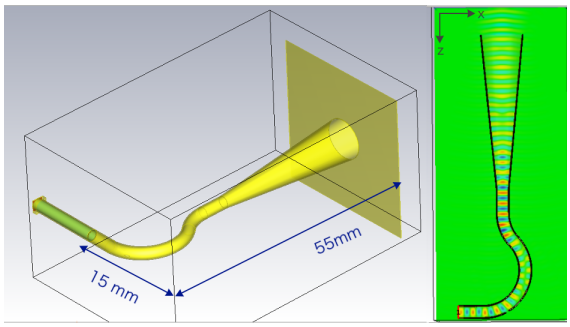

(b)

Figure 1: (a) Schematic of in-coupling from a free space THz beam into a metallic waveguide, followed by the mode converter and finally the dielectric loaded waveguide for THz acceleration. (b) Corresponding CAD representation for time-domain electromagnetic simulations in CST Studio Suite, and in-plane field pattern E_x at 165 GHz.

Here, the double bend mode converter is scaled to 165 GHz [4] to match the expected frequency for the TWAC project [5], and embedded with the horn antenna for free-space coupling and the dielectric loaded waveguide as linac, as shown in Fig. 1a. To study the mode conversion a beam-driven experiment is proposed at ARES [6] which is based on the excitation, out-coupling and detection of the THz wake. A preliminary working point has been set up to estimate the detectable THz pulse energy.

* max.kellermeier@desy.de, orcid:0000-0002-8840-782X

ISBN: 978-3-95450-252-3 ISSN: 2673-5350 doi: 10.18429/JACoW-IPAC2026-MOP7003

PROGRESS ON LOW-LEVEL RF QUALIFICATION OF A 3D-PRINTED 704.4 MHz CH CAVITY

E. Boos*[1], R. Böhm, R. Cherif, A. Japs, S. Wunderlich[1], C. Zhang[1,2]
GSI Helmholtz Centre for Heavy Ion Research, Darmstadt, Germany
[1]also at Goethe University Frankfurt, Frankfurt am Main, Germany
[2]also at Helmholtz International Center for FAIR, Frankfurt am Main, Germany

Abstract

Additive manufacturing enables compact accelerating structures with complex internal features such as integrated cooling channels. Within the Resonators Additively Constructed for Experiments project at GSI, a 3D-printed 704.4 MHz CH cavity was developed as a compact high-frequency H-mode prototype. This paper reports on the progress from the first low-level radio-frequency (RF) characterization to the modified, copper-plated and retuned cavity configuration. Initial measurements showed a resonance frequency below the target value and an asymmetric field distribution, attributed to the initial cavity geometry, preliminary contact conditions and the capacitive coupling scheme.

Based on these findings, the cavity configuration was refined by replacing the capacitive coupling with an inductive loop and adding four static tuners. After these modifications, the field asymmetry was reduced and the cavity frequency could be adjusted to the design value of 704.4 MHz. The dynamic tuners provided a measured tuning range from 701.9 MHz to 706.3 MHz. Together with the quality-factor evaluation and computed-tomography inspection of the integrated cooling channels, these results confirm the successful low-level RF and manufacturing qualification toward future high-power operation.

INTRODUCTION

Metal additive manufacturing (MAM) is a promising route for normal-conducting accelerator components because it enables compact geometries and internal cooling structures that cannot easily be realized by conventional manufacturing. For high-frequency H-mode cavities, this design freedom is particularly attractive, since small cavity dimensions, high radio-frequency (RF) power density and tight mechanical tolerances have to be combined. The increased RF power density makes the removal of local thermal losses more challenging and motivates cooling channels placed close to the thermally loaded regions. At the same time, the RF performance remains sensitive to dimensional accuracy, electrical contact conditions and surface quality.

The present work builds on an earlier study of a compact 704.4 MHz CH-cavity concept with seven accelerating gaps and integrated cooling channels [1], which forms the basis of the current Resonators Additively Constructed for Experiments (RACE) test-cavity development at GSI. The broader RACERS initiative, Research on Additive Construction for Efficient Resonating Structures, provides the framework for several MAM-based accelerator and storage-ring R&D activities at GSI and was recently summarized in Ref. [2]. Following this prototype stage, the present contribution reports on the subsequent development and low-level RF qualification of the updated modular test cavity, see Fig. 1. The work includes retuning of the RF structure, improvement of the coupling scheme and inspection of the integrated cooling channels.

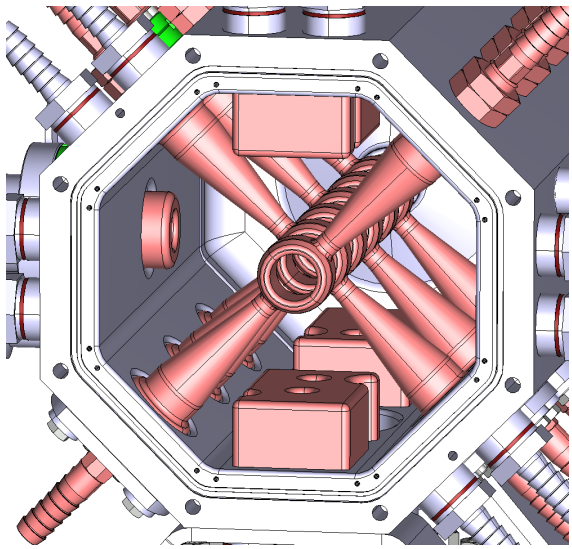

Figure 1: Additively manufactured 704.4 MHz CH cavity after the final mechanical modifications.

INITIAL RF CHARACTERIZATION

The first low-level RF characterization was performed before copper plating and before the final mechanical modifications of the cavity. In this diagnostic configuration, the cavity was excited by capacitive input and pickup antennas, while the mountable electrodes were installed with preliminary contact conditions. The dynamic tuners were already available and were used to investigate the frequency response of the cavity.

The measured resonance frequency was significantly below the design value of 704.4 MHz. Depending on the dynamic tuner positions, the resonance frequency was found between approximately 676 MHz and 680.5 MHz. At a nominal dynamic tuner position of 12 mm, a frequency of 678.8 MHz was measured. The dominant contribution to this frequency offset was identified as the larger inner tank radius used in the initial cavity geometry. An additional

* e.boos@gsi.de

Content from this work may be used under the terms of the CC BY 4.0 licence (© 2026). Any distribution of this work must maintain attribution to the author(s), title of the work, publisher, and DOI.

ISBN: 978-3-95450-252-3 ISSN: 2673-5350 doi: 10.18429/JACoW-IPAC2026-MOP7007

ELETTRA CAVITY HOM AND DEDICATED DAMPERS DESIGN

N. Shafqat *, C. Pasotti
Elettra-Sincrotrone Trieste S.C.p.A., Trieste, Italy

Abstract

The 500 MHz Elettra type cavities have been implemented in the 3rd-generation light source Elettra Sincrotrone Light Source since the beginning of its operation. These are normal conducting, single cell cavities with no High-Order-Modes (HOMs) dedicated dampers. The very same cavities will be used for the new low-emittance Elettra 2.0 (E2.0) project. E2.0 will host four independent RF accelerating cavities, each fed with its own amplifier. A complete investigation of the possible coupled bunch longitudinal instabilities has been carried out due to the most demanding beam quality requirement, together with the installation constraints given by the new vacuum chamber of the E2.0 layout with respect to the Elettra storage ring. Results in the time domain and frequency domain up to 7.0 GHz have been double-checked. Some high impedance high frequency longitudinal HOMs have been identified thanks to this analysis. The feasibility to realize a dedicated damper for the most dangerous modes that could also fit the available space is also investigated.

INTRODUCTION

The Elettra 2.0 project significantly enhances beam brilliance and reduces emittance through a high-density magnetic lattice featuring combined-function elements (3 dipoles and 4 quadrupoles) [1]. For the radio-frequency system, the new low-emittance machine will retain the Elettra-type 500 MHz single-cell normal conducting (NC) copper cavities (see Fig. 1) [2]. These cavities lack dedicated Higher Order Mode (HOM) dampers; instead, longitudinal and transverse coupled-bunch instabilities (CBIs) are mitigated by precisely shifting the HOM frequencies through an active cavity body temperature control system.

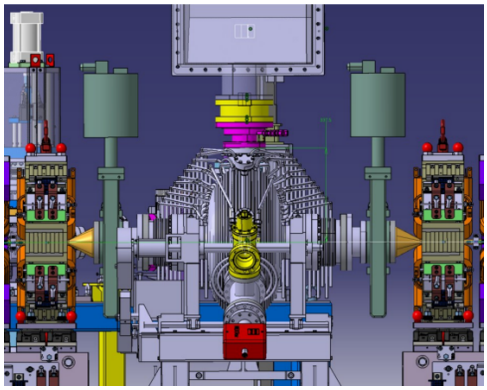

Figure 1: Elettra-type RF cavity. Rendering of Elettra 2.0 installation.

The available space for cavity installation in E2.0 is limited to 1260 mm, including tapers, and is shorter than in the present Elettra ring. This reduces the attenuation volume for evanescent modes. In addition, the E2.0 vacuum chamber cross-section is 8.8 times smaller, increasing the beam pipe cut-off frequency from 2.2 GHz to 6.5 GHz. The combined effect of reduced length and smaller aperture requires steeper tapers. A comparison of the two vacuum chamber geometries is shown in Fig. 2.

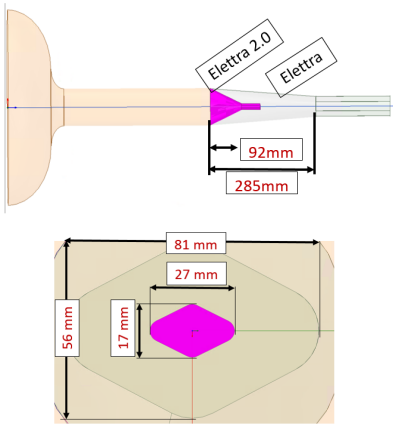

Figure 2: Comparison of the vacuum chamber of E2.0 (pink shapes) with Elettra. Top: Side view. Bottom: Cross-section.

SIMULATION SETUP

A detailed study of Elettra cavity HOMs up to 6.5 GHz was performed to assess potential multibunch instabilities. Numerical simulations were carried out in both time (CST Wakefield Solver) and frequency domains (CST Eigenmode Solver and HFSS), using a simplified model omitting the three equatorial ports for Input Power Coupler (IPC), the ultra-high vacuum (UHV) pump, and the Higher Order Mode Frequency Shift (HOMFS) plunger, whose impact on on-axis impedance is negligible while including the full beam path up to the Elettra 2.0 vacuum chamber (cavity, bellows, valves, and tapers, as shown in Fig. 3. The wakefield solver of CST is used for the time domain simulations, which are benchmarked using the frequency domain solver (Eigen solver) of both CST and HFSS.

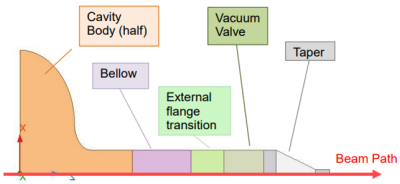

Figure 3: All beam path inclusive cavity model profile as implemented for the EM simulations (CST and HFSS).

* nuaman.shafqat@elettra.eu

Content from this work may be used under the terms of the CC BY 4.0 licence (© 2026). Any distribution of this work must maintain attribution to the author(s), title of the work, publisher, and DOI.

ISBN: 978-3-95450-252-3 ISSN: 2673-5350 doi: 10.18429/JACoW-IPAC2026-MOP7009

CHARACTERIZATION OF THE FOUR-QUADRANT X-BAND CAVITY PROTOTYPE FOR THE ASTERIX PROJECT.

L. Faillace[1,†], D. Alesini[1], M. Bellaveglia[1], S. Bini[1], F. Cardelli[1], M. Carillo[1], A. Falone[1], A. Gallo[1], A. Giribono[1], A. Liedl[1], L. Piersanti[1], S. Pioli[1], G. Silvi[3], B. Spataro[1], C. Vaccarezza[1], L. Ficcadenti[2], E. Chiadroni[3,1], L. Giuliano[3,2], M. Migliorati[3,2], L. Palumbo[3,2], G. Mauro[4], M. Mostajeran[9], G. Sorbello[5], G. Torrisi[4], Z. Huang[6], Y. Wei[6], V. Dolgashev[7], T. Abe[8], Y. Higashi[8]

[1]Istituto Nazionale di Fisica Nucleare – Laboratori Nazionali di Frascati, Frascati, Italy
[2]Istituto Nazionale di Fisica Nucleare – Roma1, Roma, Italy
[3]Sapienza Università di Roma, Roma, Italy
[4]Istituto Nazionale di Fisica Nucleare – Laboratori Nazionali del Sud, Catania, Italy
[5]Università degli Studi di Catania, Catania, Italy
[6]University of Science and Technology of China, Hefei, China
[7]SLAC National Accelerator Laboratory, Menlo Park, California, USA
[8]High Energy Accelerator Research Organization KEK, Tsukuba, Japan
[9]Faculty of Physics, Yazd University, Yazd, Iran

Content from this work may be used under the terms of the CC BY 4.0 licence (© 2026). Any distribution of this work must maintain attribution to the author(s), title of the work, publisher, and DOI.

Abstract

The ASTERIX project, hosted by the INFN–LNF, seeks to achieve the first demonstration of a practical, meter-scale X-band RF accelerating structure suitable for operational linear accelerators (>100 MV/m accelerating gradient). The goal is to produce innovative RF structures to qualify as part of the world-wide scientific collaboration (SLAC/CERN/INFN-LNF/KEK/Tsinghua) for R&D in the accelerator development and high-power testing of innovative cavities with high gradients. The structure is composed of four-quadrants ("open-type"), made of hard copper, joined and vacuum sealed by using TIG welding ("braze-free" technique) through a cost-effective and robust manufacturing. The full-structure RF design, in single-bunch operation mode, was carried out with the 3D numerical simulation codes Ansys HFSS and CST Microwave Studio. In this paper, we report on the engineering of the full-structure prototype optimized for low RF power measurements and initial mechanical tests in order to validate the quadrant straightness and alignment, the TIG welding process, the vacuum tightness; etc. The prototype was fabricated with lower precision of geometric dimensions and more relaxed mechanical tolerances.

INTRODUCTION

This research is conducted within an international collaboration involving SLAC National Accelerator Laboratory, CERN, INFN-LNF, KEK, and Tsinghua University, focused on the development of advanced X-band (11–12 GHz) accelerating structures for next-generation particle accelerators [1-8]. The study investigates hard-copper accelerating structures, which demonstrate improved high-gradient performance compared with conventional soft-copper designs [9], and explores innovative geometries such as open-type cavities together with braze-free assembly techniques, including TIG welding. The main goal is the realization of compact accelerating structures capable of operating above 100 MV/m for applications in research facilities [10-13], industrial systems, and medical accelerators, including EuPRAXIA@SPARC_LAB [14,15].

This paper presents the initial results obtained for the fabrication of the braze-free cavity in single-bunch operating mode to be TIG welded.

ACCELERATING STRUCTURE DESIGN

The RF design was developed for the single-bunch operating case with a gap of 1 mm, while the iris aperture was fixed at 3.5 mm throughout the structure, as shown in Figure 1 (design details can be found in [16-18]). To ensure high efficiency for the full 1-meter-long accelerating structure, composed of 120 cells, the disk thickness was set to 2 mm, resulting in an RF pulse length of 123 ns and a required input power of 77 MW.

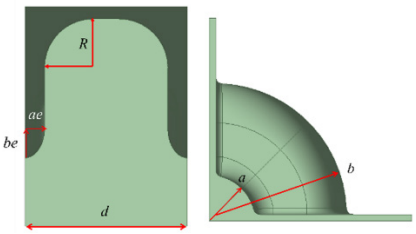

Figure 1. The geometry of the quadrant cell with gap size of 1mm.

The cavity geometry was carefully optimized in order to improve RF performance and mitigate surface field effects. In particular, the rounding applied on the cavity top increases both the shunt impedance and the quality factor by approximately 10%, while the elliptical chamfer introduced at the iris was optimized to minimize the peak surface electric fields. In addition, a 0.5 mm rounding at the

† luigi.faillace@lnf.infn.it

ISBN: 978-3-95450-252-3 ISSN: 2673-5350 doi: 10.18429/JACoW-IPAC2026-MOP7010

STUDY AND MITIGATION OF TRANSIENT BEAM LOADING IN THE DOUBLE RF SYSTEM OF ALBA II

I. Bellafont*, J. Ocampo, F. Perez, I. Serrano, S. H. Shaker, P. Solans
ALBA Synchrotron, Cerdanyola del Vallès, Spain
J. González-de-Regàs, Universitat de Barcelona, Barcelona, Spain

Abstract

ALBA, a 3rd generation synchrotron light source in Barcelona, Spain, is currently preparing its upgrade to the 4th generation low emittance machine ALBA II. As part of this upgrade, an active normal conducting harmonic RF system will be installed to improve beam lifetime. However, discontinuities in the filling pattern, such as ion clearing gaps, induce RF cavity voltage variations along the revolution period. This effect, known as transient beam loading (TBL), severely degrades the bunch lengthening performance of the double RF system. In this contribution, we present a semianalytical study of the TBL effect in ALBA II as a function of gap size, together with a mitigation strategy. The results show that, by modulating the power delivered to the main and harmonic RF cavities at the revolution frequency, the impact of TBL can be effectively mitigated, limiting the degradation of the bunch lengthening performance to 2–18% for gap lengths ranging from 2–11%.

INTRODUCTION

ALBA is currently designing an upgrade of its storage ring that will transform the facility into a 4th generation light source, ALBA II. The new storage ring aims to achieve an emittance of 205.6 pm·rad, around 22 times lower than that of the current machine, with a beam current of 300 mA [1,2]. The Touschek lifetime is expected to be approximately 4.1 h for a 50% emittance coupling. To increase this value to more operationally acceptable levels, the installation of a 3rd harmonic RF system was considered necessary.

The new ring is expected to operate with ion clearing gaps in its filling pattern to avoid ion trapping, especially during early commissioning. Between 8 and 48 empty buckets out of 448 are foreseen, corresponding to 2-11% of the storage ring circumference (see Table 1). Gaps, however, interrupt the homogeneous beam loading build-up in the RF cavities, causing them to deliver different voltage values along the revolution period. This phenomenon, known as transient beam loading (TBL), leads to a severe degradation of the bunch lengthening performance of the double RF system [3, 4], since even very small phase or amplitude variations of the RF voltage break the flatness of the voltage slope around the synchronous particle [5].

In this context, we present a study of the impact of transient beam loading on the lengthening performance of the double RF system of ALBA II, together with a mitigation strategy based on existing literature on the topic [6, 7].

* ibellafont@cells.es

Table 1: Main bare lattice parameters of the ALBA II storage ring vA2L006C considered in this study

Parameter	Symbol	Value
Energy	E_0	3 GeV
Beam current	I_{sr}	300 mA
Circumference	C	268.8 m
Harmonic number	h_b	448
RF frequency	f_{rf}	499.65 MHz
Revolution frequency	f_{rev}	1.12 MHz
Energy loss per turn (w/ IDs)	U_0	1.07 MeV
Momentum compaction	α_c	1.04×10^{-4}
Energy spread	σ_e	1.27×10^{-3}
Longitudinal damping time	τ_e	7.0 ms
Touschek lifetime w/o HC	τ_T	4.1 h

ALBA II DOUBLE RF SYSTEM

The double RF system of ALBA II will consist of six EU higher order mode (HOM) damped normal conducting (NC) main cavities (MCs) [8] and four active 3rd harmonic NC cavities (HCs) [9–11]. Their main parameters and operating settings are shown in Table 2. Active technology was chosen for the HCs owing to the following advantages:

- Optimal bunch lengthening can be obtained over the full beam current range, including single bunch operation, with a higher voltage stability.
- Direct RF feedback [12, 13] can be applied to increase the HC voltage threshold for double RF system intrinsic instabilities [14–19], thereby improving the otherwise limited lengthening performance.
- TBL mitigation by modulating the power delivered to the cavities, as explained in this contribution.

Table 2: Main parameters of the double RF system of the ALBA II storage ring vA2L006C considered in this study

Parameter	Symbol	MC	HC
Harmonic order	n	1	3
Total voltage	V_t	2.4 MV	0.68 MV
Shunt impedance	R_s	3.3 MΩ	1.1 MΩ
Unloaded Q factor	Q_0	29500	13000
Coupling factor	β	3.5	0.7
Synchronous phase	ϕ_s	149.9º	-11.0º
Tuning angle	ψ_d	-43.6º	66.0º
Number of cavities	N	6	4

Content from this work may be used under the terms of the CC BY 4.0 licence (© 2026). Any distribution of this work must maintain attribution to the author(s), title of the work, publisher, and DOI.

ISBN: 978-3-95450-252-3 ISSN: 2673-5350 doi: 10.18429/JACoW-IPAC2026-MOP7011

SSPA EFFICIENCY IMPROVEMENT STUDIES AT ALBA IN THE FRAMEWORK OF THE RF2.0 PROJECT

I. Serrano*, I. Bellafont, J. Ocampo, F. Perez, P. Solans,
ALBA Synchrotron (Spain), Cerdanyola del Vallès, Spain
R. Casals, A. Soler, A. Torrent, COMMTIA SYSTEMS S.A., La Garriga, Spain

Abstract

ALBA is a 3rd generation synchrotron light source and member of the RF2.0 project, which aims to reduce the carbon footprint of this kind of large research facilities by improving its efficiency, reliability and operational sustainability. In this contribution, we present the work done together with our partner COMMTIA, that has developed an Active Parametrization Digital Control (APDC) for a 5 kW 1.5 GHz SSPA, which enables a real-time efficiency optimization by changing dynamically the drain voltage of the transistors while delivering RF power.

This is done in two different ways: either the SSPA user sets the desired voltage as function of the output power or the Digital Low Level RF (DLLRF) system sets the voltage automatically to the SSPA by means of a digital signal as a function of the input reference value. This maximizes the efficiency at each point of operation, ensuring stable performance under the varying load and thermal environments common on accelerator facilities.

The laboratory measurements indicate substantial improvements in efficiency, that comes with the cost of the SSPA linearity gain reduction. These developments show how flexible solid-state RF systems can fulfil demanding high-performance requirements while lowering the energy consumption and carbon footprint of accelerator infrastructures.

This project has received funding from the European Union's Horizon Europe research and innovation program under grant agreement No. 101131850.

INTRODUCTION

Synchrotron light sources are large scale scientific infrastructures with significant power consumption, where Radiofrequency systems constitute a significant fraction of the total energy demand. In recent years, increasing emphasis has been placed on improving the energy efficiency and sustainability of these facilities. In this context, the RF2.0 project aims to reduce the carbon footprint of accelerator facilities and one of the strategies is to promote the development of more energy efficient RF sources.

Conventional SSPA typically operate with fixed drain voltages, which results in suboptimal efficiency when the output power deviates from the nominal design point. It is in this context that ALBA together with its partner COMMTIA have developed and tested the APDC that adjust the transistor's drain voltage to maximize the efficiency in the whole power range of the amplifier. This is done even when the amplifier is under operation.

Taking advantage of the SSPA prototype developed by COMMTIA for the ALBA 3rd harmonic system [1], the equipment has been retrofitted and the APDC has been implemented in it. This SSPA is a GaN transistor based high power amplifier. This technology offers higher power density, higher drain efficiency and improved thermal capability due to their wide bandgap characteristics, making them particularly suitable for high-power CW accelerator applications [2, 3].

The SSPA provides up to 5 kW continuous wave (CW) at 1.5 GHz. The SSPA is based on a modular architecture with two identical power amplifier (PA) units, each one is able to deliver up to 2.5 kW. The output of each of this modules is then combined in an hybrid coupler to achieve the required output power.

Each PA integrates multiple transistor-based amplification stages, including LDMOS based driver stages with a final stage of parallel GaN based power transistors. Power combination inside each PA is performed by multi-stage combiners after an individual circulator for each transistor, providing robustness and protection against reflected power due to amplitude or phase mismatches in the combiners. The baseline design achieves an overall AC to RF efficiency of approximately 50 % at maximum power.

The APDC enables real time adjustment of drain voltage during operation as a function of the output power, thus providing the SSPA the capability to maintain high efficiency in a wider range of output power level. This is particularly beneficial during power ramps, such as full range current injection or cavities conditioning.

APDC IMPLEMENTATION

Overall scheme of the APDC can be seen in Fig. 1.

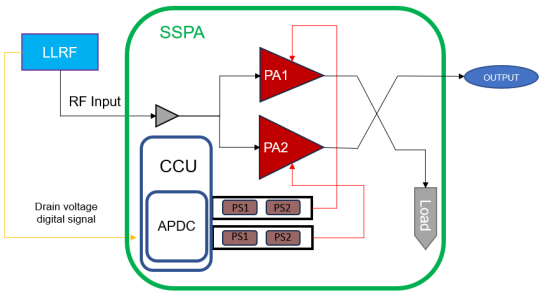

Figure 1: APDC and SSPA block diagram.

There are two operation modes for the APDC:

* iserrano@cells.es

Content from this work may be used under the terms of the CC BY 4.0 licence (© 2026). Any distribution of this work must maintain attribution to the author(s), title of the work, publisher, and DOI.

ISBN: 978-3-95450-252-3 ISSN: 2673-5350 doi: 10.18429/JACoW-IPAC2026-MOP7012

POWER COUPLERS CONDITIONING AND MULTIPACTING SIMULATIONS FOR THE ESS-BILBAO ARGITU RFQ

J. L. Muñoz*, I. Bustinduy, N. Garmendia, P. González
ESS-Bilbao, Zamudio, Spain

Abstract

The ARGITU RFQ at ESS-Bilbao is a 352.2 MHz, 4-vane RFQ that will accelerate protons from 45 keV to 3.0 MeV. The RF power comes from a modulator/klystron power chain by rectangular waveguides adapted to coaxial lines that are finished by the two loop power couplers. The couplers are made of copper and no brazing has been used in their production. For this reason, the vacuum/air window is made of PEEK material attached by mechanical pressure to the copper structure. For the initial stages of the ARGITU RFQ, the duty cycle will not rise above 1%, so these couplers were designed without active cooling. This paper summarizes the conditioning setup and focuses on the RF, thermal and multipacting simulations used to define safe high-power conditioning limits.

INTRODUCTION

The HiCANS Platform [1] will demonstrate the feasibility of a full high current accelerator driven neutron source in Europe. This platform will use the high current proton accelerator system (3 MeV) from ESS-Bilbao linac together with the target-moderator-reflector unit built and tested at JCNS [2] and the HERMES time-of-flight reflectometer instrument from LLB [3]. The proton accelerator consists of an ion source and a Low Energy Beam Transport (LEBT), which will inject the beam into an RFQ (Radio Frequency Quadrupole) linear accelerator. The RFQ will accelerate the 45 keV proton beam extracted from the source to the required 3 MeV.

The RFQ fabrication, tuning and low power testing are finished. Next steps are the conditioning of the power couplers and the RFQ itself. The RFQ [4–7] is a 4-vane RFQ that will accelerate protons from 45 keV to 3.0 MeV, in a 3.1-m long copper structure. The RFQ is powered by two power couplers. A set of two prototypes of the coupler design were built, tested at low power (at ESS-Bilbao facilities), and at high power connected to the FETS RFQ at RAL, as previously reported [8]. The dielectric window that separates the vacuum and air sections of the coaxial line is made of PEEK polymer, and it is fixed to the copper inner and outer conductors without using brazing or other welding technique. Therefore, the couplers could be disassembled and assembled again if some component needs replacement. Two new units of the same design were manufactured and will be used for RFQ operation.

Each power coupler connects a 4-1/2 inch EIA coaxial waveguide that comes from the RF power chain to a loop that is inserted into the RFQ body through the RFQ coupler/tuners ports (close to DN40). The coupler has a taper transition from the coaxial diameters of 45 mm (inner) and 103 mm (outer), to a coaxial section with diameters of 9.2 mm (inner) and 21.6 mm (outer). The small size of the final section makes it difficult to design and fabricate a loop and coaxial section that include channels for cooling water, so these couplers are a first iteration of the design procedure that therefore cannot operate at high duty cycles. The estimated RF power losses and the required beam power in the RFQ amount to a total power input close to 500 kW, so both couplers and the RFQ will be conditioned to a total peak power of 600 kW. This means that each coupler needs to stand a peak power of 300 kW at a maximum duty cycle of 1% without cooling. Operation at these power levels was already demonstrated in the tests at FETS-RAL RFQ [8]. This duty cycle will be used for the first stages of the HiCANS Platform project to demonstrate the production of neutrons in the facility. For latter stages, a new set of power couplers, with active cooling, will be used.

COUPLER CONDITIONING SETUP

Coupler conditioning will be performed in the copper-plated stainless-steel test box shown in Fig. 1. The re-entrant pillbox has ports for the two couplers, plunger tuners, vacuum diagnostics and sensors. The same RF chain foreseen for RFQ operation is used: the klystron feeds one coupler through the circulator, waveguide and coaxial transition, while the second coupler extracts the power to a waveguide load. The target is 300 kW peak power per coupler at up to 1 % duty cycle, reached by increasing RF power and pulse length up to about 1.5 ms at 7 Hz. Vacuum, arcs, RF power and coupler temperatures are interlocked and logged. Since the campaign is ongoing, the following sections focus on simulations defining safe conditioning limits.

COUPLER AND TESTBOX SIMULATIONS

Electromagnetic simulations of the couplers and test box system have been already reported [8]. These simulations are described here in connection to the thermal simulations and the temperature limits to be set in the conditioning control. Figure 2 shows the electric-field map for 300 kW of RF peak power injected through one coaxial port. The metallic surfaces are modeled with an impedance boundary condition using an effective copper surface resistance of 0.0052 Ω, including roughness, adjusted to reproduce the measured $Q_0 = 10757$.

* jlmunoz@essbilbao.org

Content from this work may be used under the terms of the CC BY 4.0 licence (© 2026). Any distribution of this work must maintain attribution to the author(s), title of the work, publisher, and DOI.

ISBN: 978-3-95450-252-3 ISSN: 2673-5350 doi: 10.18429/JACoW-IPAC2026-MOP7015

MULTIPACTING IN THE 150 MHz FLAT-TOP CAVITY OF HIPA: SIMULATION, VERIFICATION, AND MITIGATION STRATEGIES

T. G. Lucas*, J-Y. Raguin, M. Pedrozzi, M. Schneider, P. Craievich
PSI Center for Accelerator Science and Engineering, Villigen, Switzerland

Abstract

Local X-ray production, beam losses, and surface discolouration in colloidal graphite coated regions of the cavity indicate that multipacting continues to affect the operation of the 150 MHz flat-top cavity of the HIPA Ring Cyclotron. Particle-in-cell simulations were performed to confirm the phenomenon driving the issues and identify the specific operational conditions where it is driven. Simulations at the nominal cavity voltage show resonant electron trajectories between the electrodes and cavity wall, producing stable multipacting patterns consistent with observed surface discolouration. Guided by these results, the cavity geometry was modified to flatten the field minimum near the backplane, which demonstrated effective mitigation of multipacting under various operational conditions.

INTRODUCTION

The 150 MHz flat-top cavity of the PSI Ring Cyclotron at the Paul Scherrer Institute is being redesigned to support operation at an increased beam current of up to 3 mA, as the existing cavity is limited by its RF power capability [1]. The upgraded design targets a peak voltage of 700 kV with approximately 140 kW of average dissipated power, while maintaining compatibility with the current mechanical layout and integration constraints.

The present cavity has long been suspected to exhibit multipacting, with indications such as localised X-ray production, elevated power consumption, and beam losses reported over more than a decade of operation [2, 3]. These phenomena suggest the presence of a resonant electron multiplication process that limits achievable performance and operational stability.

This work presents a detailed numerical investigation of multipacting in the existing flat-top cavity using particle-in-cell (PIC) simulations. The study aims to confirm that the observed operational limitations are the result of multipacting, and to identify the regions and conditions under which it occurs. In addition, potential mitigation strategies will be explored in the context of the upgraded cavity design to ensure reliable operation at higher beam currents.

FLAT-TOP CAVITY OF HIPA AND HISTORY OF MULTIPACTING

The flat-top cavity is a normal-conducting aluminium resonant structure operating at 150 MHz, corresponding to the third harmonic of the Ring cyclotron RF frequency (Fig. 1). Multipacting in the cavity has long been suspected due to observations of anomalous power absorption, beam losses, and localised heating, which motivated this study. Over the operation of the machine, several attempts to mitigate the multipacting have been attempted including removing the cavity for observation and the application of colloidal graphite to reduce the secondary emission yield (SEY) of the surface expected to be involved. Later in its operational history the cavities in wall was photographed and was used as a motivation for this study.

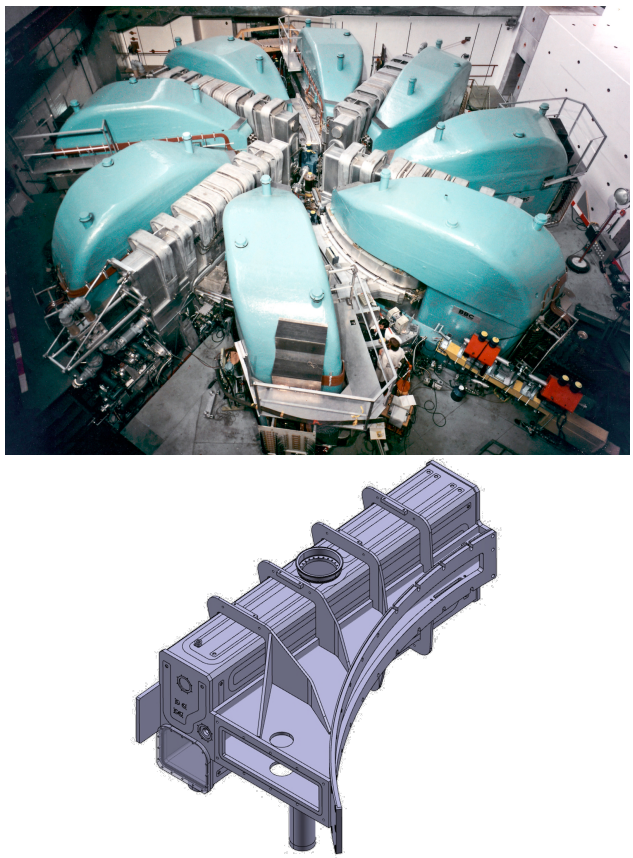

Figure 1: HIPA Ring Cyclotron (top) and flat-top cavity (bottom).

PARTICLE-IN-CELL SIMULATIONS

To investigate multipacting in the flat-top cavity, simulations were performed using CST Studio Suite, combining the eigenmode solver and the particle-in-cell (PIC) module [4]. First, the eigenmode solver was used to compute the electromagnetic field distribution within the cavity at the operating frequency. These simulations included the adjacent vacuum chamber which is integrated into the cavity's design [1]. These fieldmaps serve as the basis for subsequent PIC simulations.

* thomas.lucas@psi.ch

Content from this work may be used under the terms of the CC BY 4.0 licence (© 2026). Any distribution of this work must maintain attribution to the author(s), title of the work, publisher, and DOI.

ISBN: 978-3-95450-252-3 ISSN: 2673-5350 doi: 10.18429/JACoW-IPAC2026-MOP7016

AN ALTERNATIVE HOM LOAD DESIGN FOR THE EU HOM DAMPED CAVITY

M. Dehler*, R. Fortunati, T. Kleeb, L. Stingelin, R. Zennaro
PSI Center for Accelerator Science and Engineering, Villigen, Switzerland

Abstract

For the 500 MHz cavities in the main storage ring of SLS 2.0, we plan to manufacture additional spares of the higher order mode (HOM) loads. We saw the current design using ferrite tiles as too risky for us to produce, so we did a redesign using silicon carbide (SiC) blocks, used already with good results for HOM damping in the SLS 2.0 stripline kickers. For good performance specially near cutoff, a prolonged load geometry allows the SiC blocks to taper in smoothly. Up to 1200 W HOM power can be accepted by the load. SiC being quite tolerant to heat up, we rely on black body radiation for cooling resulting in a more homogeneous heat load distribution of the containing waveguide. The load is cooled by water circuits integrated into the waveguide ridges. Two dedicated pumping ports and an optical view port complete the technical design. Even taking into account possible large variations in the RF properties of SiC, we expect a quite satisfactory performance with a RF match better than 10 dB near the waveguide cutoff and even better than 20 dB for frequencies above 1 GHz. A prototype is currently under production and will undergo lab tests under nominal conditions this summer.

INTRODUCTION

The European HOM damped cavity [1] has evolved into a very popular device used in lots of synchrotron radiation facilities. Its special features are its three higher order mode (HOM) couplers allowing stable operation at elevated currents without having to resort to techniques like HOM tuning. Also the recent upgrade of the Swiss Light Source [2] uses four of these cavities for the main RF system, which were produced by RI Research Instruments GmbH.

In order to stay compact and to minimize the interference with the main acceleration mode, the damper couple via ridged waveguides with cutoffs slightly above the fundamental, which connect to a waveguide load. A secondary advantage of the double ridged geometry is its enlarged operating bandwidth compared to standard rectangular waveguide. The standard design [3] of the load uses ferrite tiles brazed to a strongly tapered part of the ridged waveguide. The heat is absorbed via water cooling channels in the backing ridges.

This combination of ferrite with copper makes fabrication a complicated process. The brazing needs to take account of strongly differing thermal expansion of the two materials. In normal operation, all the power absorbed the ferrite tiles need to propagate homogeneously into the copper bulk. Any imperfections in the brazing may lead to localized heat-up and thermal stress. In extreme case, this may cause individual tiles to fall off. In the case of a vertical load, this is a catastrophic event, the tile falls into the cavity itself and may cause discharges and damage on the cavity wall. This led some accelerator facilities to opt for a different strategy. Accepting higher HOM impedances and deteriorated thresholds for coupled bunch instabilities, they use only the two lower dampers, the vertical load is replaced with a metallic short.

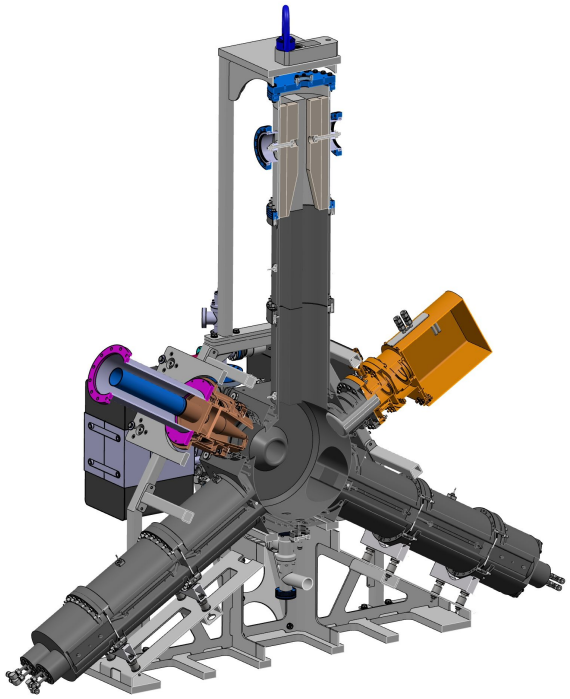

Figure 1: Full cavity layout with the new load design on top. Also visible the lifting device for the full assembly, which was responsible for some mechanical limitations to be observed in the design.

While SLS currently uses all three loads, this risk assessment led to the current development project. The goal is to have a plug in replacement of the ferrite load with similar RF characteristics (Fig. 1), simultaneously avoiding these weaknesses. Cooling should not rely on a defined thermal contacts between damping material and the casing, but be possible even purely via black body radiation. Nonuniform temperature distributions should not cause undue thermal stress. Given previous experiences, we decided to use silicon carbide (SiC), a ceramic able to stand up to 2000 °C heat, as a damping material. Where ferrites have magnetic losses, SiC introduces a dielectric loss, so this required a completely new design.

* micha.dehler@psi.ch

Content from this work may be used under the terms of the CC BY 4.0 licence (© 2026). Any distribution of this work must maintain attribution to the author(s), title of the work, publisher, and DOI.

ISBN: 978-3-95450-252-3 ISSN: 2673-5350 doi: 10.18429/JACoW-IPAC2026-MOP7017

RF PROPERTIES OF NON EVAPORABLE GETTER COATINGS IN THE SUB THz RANGE

M. Dehler*, A. Citterio, R. Ganter, Paul Scherrer Institute, Villigen, Switzerland
X. Liu, Institute of High Energy Physics, Beijing, China
C. Hauser, Hamburg University, Hamburg, Germany
S. Alberti, J. Genoud, École Polytechnique Fédérale de Lausanne, Lausanne, Switzerland

Abstract

We report on the measurement of the surface impedance of thin sub-micron non-evaporable getter (NEG) coatings on a copper substrate, as used for distributed pumping in the vacuum system of the Swiss Light Source upgrade (SLS 2.0). Given the low electrical conductivity of NEG, a sub micron thickness with well known properties is required to avoid heat up and beam instabilities. Measurement frequencies of 100 GHz and above are required to obtain a good measurement sensitivity for these ultra-thin coatings. Two quasi-optical test stands were designed for frequencies around 100 and 170 GHz, based on an asymmetric Fabry Perot with spherical feed mirrors coupling to standard waveguides and planar probe mirrors whose surface is to be characterized. 3D printing allowed to produce the feed mirrors together with the RF coupler and waveguide flanges in one integral part, which required only minimal additional processing. The surface impedance of a NEG coated probe is computed by comparing the Q factor of the resonance with that obtained from reference probes fabricated from bulk stainless steel and copper.

INTRODUCTION

Non-evaporable getter (NEG) coatings, typically ternary alloys composed of titanium, zirconium and vanadium, have several attractive properties [1–3]:

A strongly reduced secondary electron yield helps suppressing multipactor effects in RF cavities and other devices. After heat activation, NEG surfaces absorb and store gas molecules, which results in a distributed pumping effect for vacuum devices and obviating the need for external vacuum pumps. For geometries with small apertures and a corresponding low conductance, these are actually the only option to reach ultra low pressures.

We also see a strong reduction of electron (ESD) and photon stimulated (PSD) gas desorption effects. While the ESD properties are attractive for vacuum electronic devices like klystrons to maintain low vacuum pressures, reduced photon stimulated desorption is an important for ring type electron accelerators, where we have high levels of X-ray synchrotron radiation.

The interest in NEG stems from the upgrade of the Swiss Light Source, SLS 2.0 [4–6]. It features a factor 40 improvement of the emittance by a state of the art design using small aperture magnets. The required small diameter vacuum chambers (18-21 mm) pose two interrelated challenges. The first is the vacuum pressure. Scattering between the electrons of the beam and the rest gas affects the beam lifetime and can create instabilities. Pressures below 10^{-9} mbar are required in the presence of the PSD effects, the low pumping conductance of the chamber makes the use of NEG coatings mandatory.

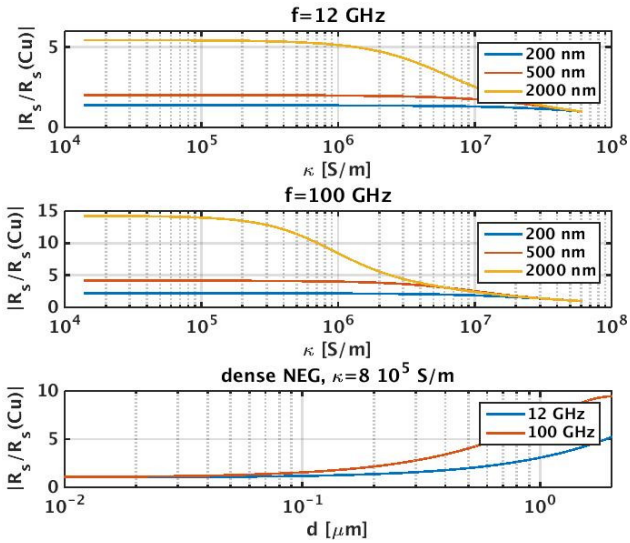

Figure 1: Surface resistance versus coating thickness and frequency. Coatings in the sub micron range require frequencies of 100 GHz and above to be detectable.

The rather high beam current of 400 mA and the wide beam spectrum up to 10 GHz (extending even further for certain kinds of instabilities) makes the surface conductivity of the chamber wall a critical parameter. Depending on the morphology, columnar or dense, bulk type NEG has conductivities between $1.4 \cdot 10^4$ and $8 \cdot 10^5$ S/m [7], very low compared to copper (the bulk material of the chamber) of $5.8 \cdot 10^7$ S/m. Due to the skin effect, the NEG coating dominates the surface impedance at high frequencies with the transition frequency given by the layer thickness. Therefore, to avoid any beam degradation due to resistive wall effects, we use ultra-thin coatings of 500 nm assuming a dense morphology.

Generic measurements of the conductivity of NEG and NEG coatings have already been performed at 7.8 GHz [7] and between 220 and 750 GHz [8]. Both types of measurement require specially prepared samples, an approach not suitable in our case, since we want to be able to use process samples from the actual fabrication.

* micha.dehler@psi.ch

Content from this work may be used under the terms of the CC BY 4.0 licence (© 2026). Any distribution of this work must maintain attribution to the author(s), title of the work, publisher, and DOI.

ISBN: 978-3-95450-252-3 ISSN: 2673-5350 doi: 10.18429/JACoW-IPAC2026-MOP7018

X BAND LINAC MACHINE DESIGN FOR VERY HIGH ENERGY ELECTRON THERAPY

E. Smith[1,2], A. Wheelhouse[1], R.M. Jones[1,2]
[1]The Cockcroft Institute of Accelerator Science and Technology, Warrington, UK
[2]University of Manchester, Oxford Road, Manchester, UK

Abstract

Very high energy electrons (VHEE) are a potential future modality in the field of radiotherapy. They have garnered considerable interest because they possess a unique combination of several properties including: being capable of deep tissue penetration (>30 cm), relative insensitivity to tissue inhomogeneities and being well suited to FLASH therapy. FLASH is the use of ultra-high dose rates which have been shown to reduce cell death in healthy tissue whilst maintaining toxicity to tumours. This paper provides a design for a 250 MeV linac with dose rates exceeding 100 Gy s^{-1} in a 5 cm diameter field. The design is centred on a bi-periodic, $\pi/2$ mode, normal conducting, standing wave, accelerating cavity with a gradient of 80 MV m^{-1} to achieve the compactness required to fit the accelerator in a hospital setting. To this end, 11.9942 GHz X-band technology has been selected which, along with extensive cell geometry optimisation, has produced a shunt impedance of >100 MΩ m^{-1} whilst minimising surface electric and magnetic fields.

INTRODUCTION

Very High Energy Electron (VHEE) beams with energies typically ranging from 100 MeV to 250 MeV are an emerging modality in the field of radiotherapy, driven by the following potential benefits. VHEE beams can reach deep seated tumors more effectively than X-rays, the most commonly used modality [1]. VHEE beams are also relatively insensitive to tissue inhomogeneities in the body [2] allowing for more robust treatment planning.

X-ray beams are in general produced by colliding low energy electrons with a tungsten target in a process that converts only 1 % to 2 % of the electrons' energy into usable photons making high dose rates difficult to reach. Ultra High Dose Rates (UHDR), usually defined as >40 Gy s^{-1} have been empirically shown to reduce damage to healthy tissue whilst maintaining toxicity to cancerous cells [3]. This "FLASH" therapy widens the therapeutic window and could be used to reduce required dose fractionation. VHEE beams can also be steered readily by magnetic fields.

One of the primary challenges of delivering VHEE FLASH therapy to patients is the development of an electron linac capable of the required energy and dose rate with a form factor compact enough to fit easily within a hospital setting. Recent advances in high gradient accelerator cavities designed for linear colliders [4] could be used to realize this requirement. The following paper outlines a high level design for an X-band 250 MeV linac operating at a gradient of 80 MV m^{-1} whilst targeting a dose rate of 100 Gy s^{-1} in a circular field 5 cm in diameter.

ACCELERATING CAVITY

The main accelerating cavities of the linac are 25 normal conducting copper structures operating at the X band frequency of 11.9942 GHz. This frequency was chosen over the lower S and C bands more common in radiotherapy to allow for high shunt impedance which becomes particularly important at the high gradients required for compact VHEE machines. For this project a shunt impedance of 100 MΩ m^{-1} was targeted. The cavities are designed to operate in the $\pi/2$ coupling mode of acceleration because of its inherent stability which is particularly important in medical applications. As is standard for a $\pi/2$ mode accelerator, the cell structure is bi-periodic to reduce the space used by coupling cells however the cells are left on axis to ease the manufacturing cost and complexity of an X-band system. Standing wave fields will be used to prevent fields entering the coupling cells. The electric field distribution for one of the 13.76 cm long optimized 19 cell (10 accelerating and 9 coupling) structures can be seen in Fig. 1. The optimization is detailed below.

The geometry of the cavities was initially designed and tested as a half unit cell which can be seen in Fig. 2. Each accelerating cell is defined by four elliptical arc segments joined by straight line segments which were optimized by a

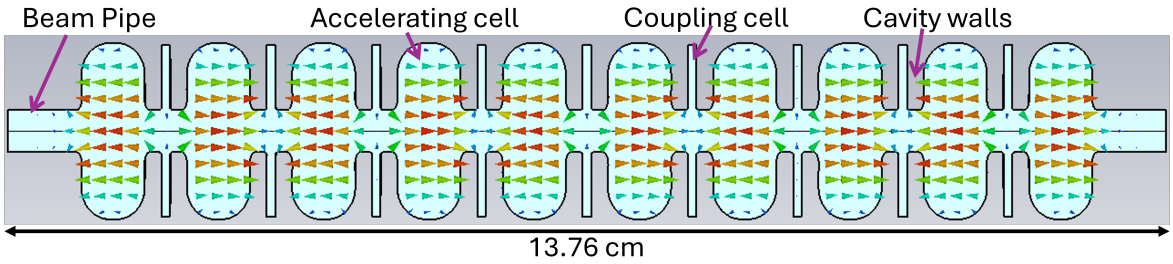

Figure 1: Electric field distribution for the 19 cell $\pi/2$ coupling mode main accelerating cavity simulated in CST.

Content from this work may be used under the terms of the CC BY 4.0 licence (© 2026). Any distribution of this work must maintain attribution to the author(s), title of the work, publisher, and DOI.

ISBN: 978-3-95450-252-3 ISSN: 2673-5350 doi: 10.18429/JACoW-IPAC2026-MOP7019

OPTIMIZED LOW-COST, HIGH-EFFICIENCY CAVITY DESIGN FOR 90-500 MEV PROTON LINACS

S. Ahmadiannamin*, J.-B. Lagrange
ISIS Neutron and Moun Source, RAL, Harwell, Didcot, UK

Abstract

Over the past four decades, the accelerator community has made substantial progress in advancing both normal-conducting and superconducting RF cavity design and fabrication technologies. As the global demand for new accelerator facilities continues to increase, the development of low-cost, high-efficiency RF cavities has become essential for ensuring the long-term sustainability of accelerator science.

In this work, we introduce a new RF cavity concept, designated ALANSA-PL, developed by the ISIS Linac R&D Group. This design provides a simpler and more efficient alternative to conventional coupled-cavity structures. Preliminary studies indicate that the ALANSA-PL cavity exhibits enhanced performance for proton accelerators in the 90–500 MeV energy range. The conceptual design and electromagnetic modelling of the cavity, operating at 972 MHz with $\beta = 0.5$, are presented and discussed in this paper.

INTRODUCTION

RF cavities for high-intensity proton accelerators must ensure power efficient, stable, and reliable operation under high beam currents while minimising losses and activation [1]. A key requirement is high accelerating efficiency, typically achieved through a high effective shunt impedance to maximise energy transfer and reduce RF power consumption [2]. Cavities must also maintain stable electromagnetic fields and control higher-order modes (HOMs) to prevent beam instabilities [3].

Beam dynamics compatibility is critical, as β increases continuously along proton linacs, requiring varying cell lengths and careful optimisation to maintain synchronism and minimise emittance growth. This contrasts with electron accelerators, where β rapidly approaches 1, allowing constant cell lengths ($\approx \beta\lambda$) and simpler designs [4].

Conventional normal-conducting structures such as side coupled cavity (CCL), annular ring cavities (ACS), and cutting-disk cavities rely on intermediate coupling cells between accelerating gaps, increasing complexity, size, and length [5-7]. In contrast, parallel-coupled cavities eliminate these coupling cells, enabling more compact structures, reduced losses, and simpler fabrication [8]. However, their application to proton accelerators is more challenging due to the continuous change in β, which disrupts periodicity and complicates field distribution, coupling, and frequency control [9].

Thermal, mechanical, and practical constraints remain essential, including efficient cooling, structural stability, manufacturability, and ease of tuning [10, 11].

If parallel-coupled structures demonstrate robust performance after prototyping, low and high-power measurements, they could enable the use of a single cavity type and design concept across a wide β range (≈0.41 to 0.758, corresponding to 90–500 MeV). While the geometry would still scale with β, the electromagnetic configuration, power feed scheme, and mechanical layout would remain consistent, reducing the need for multiple cavity families and simplifying system integration.

This unified approach improves scalability and engineering efficiency. It also supports the development of brazeless cavity technologies, as the design can reduce or eliminate brazing and electron beam welding [12, 13]. This is critical for accelerator sustainability, significantly lowering production costs, reducing manufacturing complexity, minimising failure points, and simplifying tuning and maintenance.

Although some performance variation (e.g. transit-time factor) is expected across the β range, the overall concept offers a strong balance between RF efficiency, cost-effectiveness, and operational simplicity for high-intensity proton linacs.

To address these challenges, we introduce the ALANSA-PL cavity, a novel parallel-coupled cavity concept developed by the ISIS Accelerator Physics Group. The design targets proton accelerators in the 100–500 MeV energy range. Initial simulation studies are based on operation at 972 MHz with $\beta = 0.5$. The ALANSA-PL structure aims to provide a simpler and more efficient alternative to conventional coupled-cavity systems.

500 MEV INJECTOR RF CAVITIES AND ALANSA-PL FEATURES

Two normal-conducting linac configurations are considered for the 3–500 MeV injector linac of ISIS-II. In both options, a 324 MHz drift tube linac (DTL) is used up to 90 MeV, followed by a 972 MHz annular coupled structure (ACS) from 180 to 500 MeV. The difference lies in the intermediate energy range (90–180 MeV): either a 972 MHz coupled-cavity linac (CCL) is used (Option A: 324/972/972 MHz), or a 324 MHz PIMS structure (Option B: 324/324/972 MHz). The RF frequency scheme is based on 324 MHz and its third harmonic (972 MHz), enabling simultaneous H^+ and H^- acceleration by shaping the RF waveform to create two stable phase regions within a single RF period.

* Sasan.Ahmadiananmin@stfc.ac.uk

Content from this work may be used under the terms of the CC BY 4.0 licence (© 2026). Any distribution of this work must maintain attribution to the author(s), title of the work, publisher, and DOI.

ISBN: 978-3-95450-252-3 ISSN: 2673-5350 doi: 10.18429/JACoW-IPAC2026-MOP7020

AI-BASED DIAGNOSTICS FOR THE CRYOGENIC AND RF SYSTEMS OF THE SPIRAL2 SUPERCONDUCTING LINAC

C. Lassalle[1,2], A. Ghribi[1], M. Di Giacomo[1], F. Bouly[2], P. Bonnay[3]
[1]GANIL, Caen, France
[2]Univ. Grenoble Alpes, CNRS/IN2P3, Grenoble INP, LPSC, Grenoble, France
[3]CEA/IRIG/DSBT/LEA, Grenoble, France

Abstract

The SPIRAL2 superconducting LINAC at GANIL operates 26 quarter-wave resonator cavities whose online diagnostics currently rely on physics-based models limited to single operating points. This paper presents two complementary AI-based diagnostic tools: (i) neural network heat-load virtual observers that estimate the cavity thermal dissipation — a proxy for the intrinsic quality factor Q_0 — from cryogenic process signals, with prediction errors predominantly in $[-2, +1]$ W@4.2 K for loads up to 20 W@4.2 K; and (ii) a machine-learning pipeline meant to detecting anomalies in LLRF data, predicting alarms before they fire, and classifying fault subtypes within the cavity-quench category ($F_1 = 92\%$). This paper presents a state of progress on these two applications.

INTRODUCTION

SPIRAL2 (Système de Production d'Ions Radioactifs Accélérés en Ligne, 2nd generation) is a multi-beam LINAC at GANIL (Caen, France) designed to accelerate protons, deuterons, and heavy ions for nuclear-physics experiments. Its superconducting section comprises 26 quarter-wave resonator (QWR) cavities at 88.05 MHz arranged in two families: 12 type-A cavities ($\beta_{opt} = 0.07$, cryomodules CMA01–CMA12) and 12 type-B cavities ($\beta_{opt} = 0.12$, cryomodules CMB01–CMB07). Each cryomodule houses one or two cavities immersed in a liquid helium bath at 4.2 K; the naming convention is `CMA`*`XX`*`-CAV`*`Y`* and `CMB`*`XX`*`-CAV`*`Y`*, where *XX* is the module index and *Y* the cavity index within the module.

Reliable operation requires continuous monitoring of both cryogenic and radio-frequency (RF) systems. Operational cryogenic diagnostics currently rely on physics-based state observers that are limited to a single linearization point and would require frequent recalibration. On the RF side, fault events are recorded as post-mortem files by the Low-Level RF (LLRF) control system; identifying and anticipating these faults manually is time-consuming. This paper describes two complementary AI applications developed for SPIRAL2. (i) neural network heat-load observers that estimate, in real time, the thermal dissipation in the helium bath as a *virtual* quality-factor Q_0 observable; and (ii) a machine-learning pipeline for the detection, early prediction, and subtype classification of the LLRF anomalies.

Table 1: Input Observable Selections Evaluated for Heat-load Estimation.

Selection	P	L	V_{in}	V_{out}	T_{in}	T_{out}
1	✓	✓	✓	✓	✓	✓
2	✓			✓		
3					✓	✓
4						
5			✓	✓		
6				✓		

HEAT LOAD VIRTUAL OBSERVER

Motivation and Problem Formulation

The dynamic heat load $\dot{Q}$ dissipated by the cavity walls into the helium bath is a key indicator of cavity performance and a proxy for the intrinsic quality factor Q_0. The intrinsic quality factor is defined as

$$Q_0 = \omega_0 \frac{W}{P_{dis}}, \qquad \dot{Q} \equiv P_{dis}, \tag{1}$$

where $\omega_0 = 2\pi \times 88.05$ MHz is the resonant angular frequency, W the stored electromagnetic energy, and $P_{dis} = \dot{Q}$ the power dissipated in the cavity walls and extracted by the helium bath. A continuous, real-time estimate of $\dot{Q}$ is therefore equivalent to a virtual Q_0 observer. Existing state observers (Luenberger, extended Kalman filter) provide estimates but are valid only near a linearisation point and are sensitive to sensor calibration drift. The extended Kalman filter is, in addition, too large to run on industrial PLCs used at GANIL [1]. Neural networks are trained in a supervised fashion using cryogenic process signals as inputs, with the regression target derived from dedicated heat load variation campaigns thanks to embedded resistive heaters in the cryomodules.

Dataset and Observable Selection

Measurements were taken during dedicated heat-load campaigns on cryomodules in 2022 and 2023. Six cryogenic observables are considered (Table 1): helium pressure (P), inlet/outlet temperatures (T_{in}, T_{out}), liquid helium level in the cryostat (L), and inlet/outlet valve positions (V_{in}, V_{out}). Six input configurations (selections 1–6, from all six signals down to T_{out} alone) are evaluated to assess model robustness to missing or unreliable sensors.

Content from this work may be used under the terms of the CC BY 4.0 licence (© 2026). Any distribution of this work must maintain attribution to the author(s), title of the work, publisher, and DOI.

ISBN: 978-3-95450-252-3 ISSN: 2673-5350 doi: 10.18429/JACoW-IPAC2026-MOP7022

DIELECTRIC CHARACTERIZATION OF BEAM LINE ABSORBER SAMPLES FOR NEXT-GENERATION HIGH INTENSITY ELECTRON BEAM SRF ACCELERATORS*

A. Perez Ruiz†,1,2,3, A. Miyazaki[1,2], P. Martinez Reviriego[4], S. Gorgi Zadeh[4], N. Catalan-Lasheras[4], A. Grudiev[4], A. Iziquel[3]
[1]Université Paris-Saclay, CNRS/IN2P3, IJCLab, Orsay, France
[2]On behalf of the PERLE collaboration
[3]Accelerators & Cryogenic Systems, Orsay, France
[4]CERN, Geneva, Switzerland

Abstract

PERLE, under construction at IJCLab, is designed for high intensity electron beams of 5 MW peak power (20 mA, 250 MeV). Simulations of its SRF cryomodule predict more than 100 W of higher-order-mode (HOM) power per cavity induced by the short bunches, indicating that Beam Line Absorbers (BLAs) at 40 K may be required between cavities to dissipate the HOM power and protect the 2 K stage. However, the lack of complete properties of dielectric materials for candidate absorbers limits accurate BLA design. To address this, we are conducting dedicated studies of BLA materials at IJCLab. We measured the broadband dielectric properties of Kyocera SC1000 samples from BNL at room temperature using a setup at CERN developed for CLIC study and cross-validated the results with independent measurements from JLab. In parallel, we designed and simulated two cryogenic coaxial test stands, one operating up to 18 GHz and another extending coverage to 40 GHz. These warm measurements provide baseline data for upcoming cryogenic studies and validated input for the design of BLAs in next-generation accelerators such as the EIC at BNL, FCC-ee at CERN, and in particular PERLE at IJCLab.

INTRODUCTION

Kyocera SC1000 [1] has been primarily investigated for HOM absorbers in EIC and FCC-ee applications at warm, and here it also serves as a benchmark for cryogenic absorbers such as those required for PERLE [2] (see Fig. 1) and other ERLs or FEL facilities. Although dielectric measurements at cryogenic temperatures have been reported for various materials [3–5], only a limited number have been demonstrated to be compatible with cryogenic operation. In this work, we propose a systematic dielectric characterization approach for candidate absorber materials at cryogenic conditions using a coaxial-based setup, and in parallel, we perform simulations of BLA radio frequency (RF) absorption performance, enabling reliable prediction of their behaviour.

* Work supported by funding from European Union's program EU HORIZON-INFRA-2023-TECH-01-01 under GA n°101131435.
† axel.perez-ruiz@ijclab.in2p3.fr

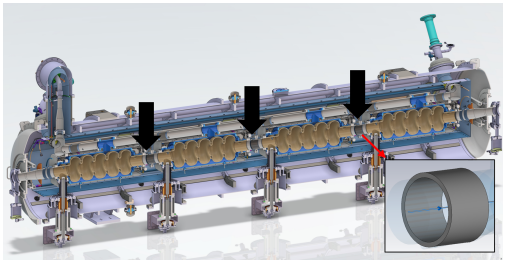

Figure 1: BLAs for the PERLE Cryomodule.

DIELECTRIC PROPERTIES OF MATERIALS

The RF absorption performance of BLAs is primarily determined by the dielectric properties of the material [6], which is described by the complex permittivity,

$$\varepsilon = \varepsilon' - j\varepsilon'', \tag{1}$$

where the real part ε' accounts for energy storage in the material and the imaginary part ε'' represents dielectric losses. Another relevant derived quantity is the loss tangent,

$$\tan\delta = \frac{\varepsilon''}{\varepsilon'} + \frac{\sigma}{\omega\varepsilon'}, \tag{2}$$

where ω is the angular frequency, and σ the electrical conductivity. Since most BLA candidate materials are ceramics, they behave as electrical insulators; therefore, the contribution of σ to the losses can be neglected [6–8]. However, low conductivity is not a strict requirement for BLA materials, as slightly conductive ceramics have also been used as HOM absorbers [3]. Ideally, candidate materials should exhibit a high loss tangent $\tan\delta > 0.3$ over a broad frequency range.

Another relevant parameter is the complex permeability,

$$\mu = \mu' - j\mu'', \tag{3}$$

which, for non-magnetic materials, can be treated as $\mu = \mu_0$. Nevertheless, it has been reported that under cryogenic conditions some materials may exhibit apparent magnetic losses, as observed in [5], although these effects were ultimately attributed to calibration artifacts.

Throughout this work, the relative quantities are used, such that $\varepsilon_r = \varepsilon/\varepsilon_0$ and $\mu_r = \mu/\mu_0$.

Content from this work may be used under the terms of the CC BY 4.0 licence (© 2026). Any distribution of this work must maintain attribution to the author(s), title of the work, publisher, and DOI.

ISBN: 978-3-95450-252-3 ISSN: 2673-5350 doi: 10.18429/JACoW-IPAC2026-MOP7023

CURRENT STATUS AND PROGRESS OF DESIGN AND COMMISSIONING OF HELIAC CAVITIES

Alexey Gunya*[,1], Florian Dirk Dziuba[1,2], Holger Podlech[3,4,5], Maksym Miski-Oglu[1,2], Stepan Yaramyshev[1], Uwe Scheeler[1], Viktor Gettmann[1], Julian List[1]
[1]GSI Helmholtz Centre for Heavy Ion Research, Darmstadt, Germany
[2]Helmholtz Institute Mainz (HIM), Mainz, Germany.
[3]Institute of Applied Physics, Goethe University, Frankfurt am Main, Germany
[4]Helmholtz Research Academy Hesse for FAIR (HFHF),
[5]GSI Helmholtz Centre for Heavy Ion Research, Campus Frankfurt

Content from this work may be used under the terms of the CC BY 4.0 licence (© 2026). Any distribution of this work must maintain attribution to the author(s), title of the work, publisher, and DOI.

Abstract

The GSI Helmholtzzentrum für Schwerionenforschung is developing various particle accelerators, with the superconducting Helmholtz Linear Accelerator (HELIAC) as a key project, complementing the existing UNILAC. The project of HELIAC targets beam energies exceeding 7 MeV per nucleon via a four-cryomodule structure, optimised for heavy-ion acceleration at around 217 MHz resonant frequency. The first cryomodule, incorporating Crossbar-H (CH) cavities, has been successfully constructed and is currently undergoing vacuum, cryogenic, and RF tests, validating the design for subsequent modules.

This contribution overviews HELIAC's general aspects, focusing on CH resonators. It details the current project status, including design, fabrication, and testing of SRF components, optimised via simulations to target resonance frequency, with tolerances managed through assembly adjustments, buffered chemical polishing (BCP), and tuning. Plans and expected performance are discussed.

INTRODUCTION

The GSI Helmholtzzentrum für Schwerionenforschung has operated the Universal Linear Accelerator (UNILAC) for five decades as its primary heavy-ion driver. While UNILAC remains an excellent pulsed machine delivering high beam energies (up to ~11.4 MeV/u) with excellent beam quality, its pulsed nature (duty factor typically below a few percent) and normal-conducting technology limit the average beam intensity and continuous operation required by many modern experiments.

To overcome these limitations and to complement the upgraded UNILAC within the FAIR facility, the superconducting HElmholtz LInear ACcelerator (HELIAC) was proposed about ten years ago. In contrast to UNILAC, which is pulsed based accelerator, HELIAC is designed as a fully superconducting continuous-wave (CW) LINAC operating at 217 MHz. This fundamental difference enables high duty factor, significantly higher average beam currents (up to 1 mA), lower operating costs, and excellent energy stability — features that are essential for superheavy element (SHE) discovery, nuclear structure studies, material science under extreme conditions, and high-precision atomic physics.

* a.gunya@gsi.de

HELIAC DESIGN

The HELIAC is a project of a superconducting continuous-wave heavy-ion linear accelerator dedicated to complement the existing UNILAC, providing high-duty-factor beams for experiments. The normal-conducting pre-accelerator section, driven by a 108 MHz RF source, delivers ions with a mass-to-charge ratio of up to 6 at an injection energy of 1.4 MeV/u to the superconducting section. The primary design plan (see Fig. 1) implies that the superconducting part must consist of four sequentially connected cryomodules, accelerating the beam to a final energy of up to 7.3 MeV/u, with a maximum beam current up to 1 mA.

Each cryomodule contains three Crossbar-H (CH) cavities, two superconducting solenoids for transverse focusing, and a dedicated rebuncher. It receives ions with $A/q \leq 6$ at 1.4 MeV/u from the High Charge State Injector (HLI) and accelerates them to a final energy of 7.3 MeV/u with beam currents up to 1 mA in CW mode with acceleration of ions up to ^{238}U and similar species.

The cryomodule CM1 (see Cryomodule 1 on Fig. 1) [1], which is currently in operation, comprises cavity CH0, which primarily handles initial acceleration of the incoming ion beam after pre-acceleration section, which is then focused by the first solenoid S1 before entering a dedicated buncher B1 section—a single-gap or low-cell cavity optimized for longitudinal beam compression to ensure synchronous operation with the subsequent accelerating cavities CH1 and CH2. The beam then undergoes further acceleration in the remaining two CH cavities before passing through the final solenoid S2 for transverse beam focusing. Each subsequent cryomodule will work according to the afore-described algorithm, ensuring continuous ion-beam acceleration up to the projected output energy.

CAVITY DESIGN

The most important component of the cryomodule is the SRF cavity. Its design, fabrication, and commissioning represent one of the most complex parts of HELIAC design [2].

The Crossbar H-mode (CH) cavity is a specialised superconducting radio-frequency (SRF) resonator optimised for the acceleration of low- to medium-energy heavy ions ($\beta = v/c \approx 0.05$–0.08) in continuous-wave (CW) linear accelerators. Unlike conventional TM-mode structures (e.g.,

ISBN: 978-3-95450-252-3 ISSN: 2673-5350 doi: 10.18429/JACoW-IPAC2026-MOP7024

VERTICAL TESTING OF THE WAVEGUIDE-HOM-DAMPED 1.5 GHz 4-CELL PROTOTYPE CAVITIES FOR THE VSR-DEMO PROJECT*

H.-W. Glock† [1], F. Glöckner[1], J. Knobloch[1,2], R. Schöder[1], A. Tsakanian[1], A. Velez[1,3]
[1] Helmholtz-Zentrum Berlin für Materialien und Energie, Berlin, Germany
[2] University of Siegen, Siegen, Germany
[3] Technical University Dortmund, Dortmund, Germany

Abstract

The VSR Demo project aims for the validation of a cavity design suitable for the application in electron storage rings, characterized by currents of several hundreds of mA and a dense wakefield spectrum caused by inhomogeneous fill patterns. The cavities are equipped with five waveguides plus a coaxial fundamental power coupler, forming two groups of three radial extensions at either cavity end. Recently two prototypes were manufactured and are in the process of vertical testing at HZB's Large Vertical Test Stand. First tests completed with Prototype 1, covering all modes of the fundamental passband and different temperature levels, did not match the Q(E)-performance expectations, but indicate a yet unknown loss mechanism in the cavity's periphery, i.e. waveguide endgroups, beam pipe extensions, blind flanges or the coupling feedthrough. Further insights are expected from the ongoing testing program with modified coupling and with Prototype 2.

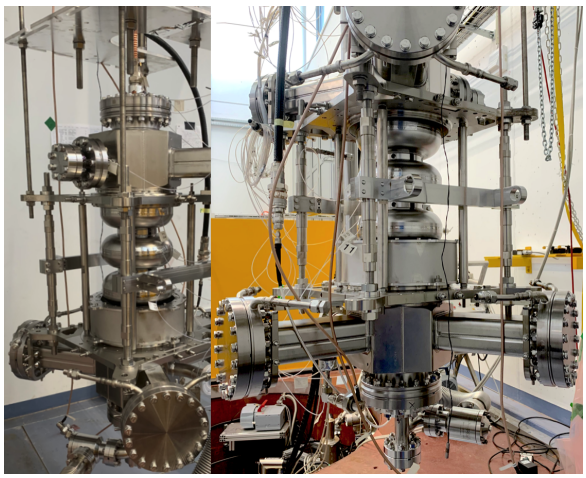

Figure 1: Second prototype of the VSR 1.5 GHz 4-cell SRF cavity in preparation of it's first vertical test in HZB's Large Vertical Test Stand, March 2026, in two opposing perspectives.

INTRODUCTION

Even though elliptical superconducting rf (SRF) cavities found a broad range of applications in a variety of accelerator designs, partially reaching large industry-scale volumes, the domain of *waveguide-damped*, elliptical multicell cavities still remains widely uncharted, once the sole proven path following from the "Original CEBAF" waveguide-damped 5-cell 1497 MHz cavity ended in HOM damping designs with filtering couplers [1].

A comprehensive summary from 2017 (cf. [2], Table 1) about high-current SRF cavity projects, partially looking back into the early 2000's, reveals only 4 (of 16, not all of them multicell) cavity designs providing a waveguide higher-order-mode- (HOM-)damping. To the best of author's knowledge, none of those four, nor any other, got into regular operation ever since and only one, JLAB's 5-cell 1497 MHz so called "high current" cavity successfully proved vertical testing with two prototypes [3]. This is a remarkably poor progress in view of the, at least conceptional, intrinsic simplicity and elegance of just hollow pipes providing both accelerating mode rejection – by the pipe's cutoff – and capable HOM power guiding, but it may indicate a severe risk of unexpected complications of the concept. This is unfortunate, since it seems to be ideally suite if high amounts (say $\geq 100\ W$) of average wake power need to be drained and/or if high duty cycles need to be managed, both uncomfortable for most HOM-coupler designs. Compared with dielectric beam pipe absorbers, the other alternative HOM-damping concept, waveguides excel by their modest requirements of real-estate length; a decisive property when hard length limits are given.

At HZB, two projects studied waveguide-damped multicell SRF cavities. The energy-recovery-linac project bERLinPro, later renamed to SeaLab [4], which recently received the notification of an imminent final shutdown, developed an rf design for a 7-cell 1300 MHz cavity with 5 waveguides and a coaxial FPC port, but did not enter into deep engineering. It nevertheless helped in the development of the so-called Variable-Storage-Ring (VSR) 1.5 GHz cavity, which followed the same concept, but needed to reduce the planned number of cells from 5 to 4, dictated by the available length found in between the magnet lattice of HZB's synchrotron light source BESSY-II. This cavity type was developed [5, 6] to act as a (primarily) passive 3rd harmonic cavity that, by lengthening the accelerating voltage's flat top and thus reducing the phase space density of bunches, should increase the synchrotron's beam's life-time in the trade off to the accessible bunch charge.

Whilst the VSR project first was de-scoped to present and test a 2-cavity demonstrator module, this endeavor now also is stopped. We are still aiming for the completion of both prototypes, which have been build and processed by Research Instruments, Bergisch-Gladbach, Germany with

* Work supported by the Helmholtz Association.
† hans.glock@helmholtz-berlin.de

Content from this work may be used under the terms of the CC BY 4.0 licence (© 2026). Any distribution of this work must maintain attribution to the author(s), title of the work, publisher, and DOI.

ISBN: 978-3-95450-252-3 ISSN: 2673-5350 doi: 10.18429/JACoW-IPAC2026-MOP7025

MID-T-BAKING OF SRF CAVITIES DRIVEN BY RF POWER*

R. Schöder†,1, H.-W. Glock, J.[1], Knobloch[1,2], A. Velez[1,3]
[1]Helmholtz-Zentrum Berlin für Materialien und Energie, Berlin, Germany
[2]University of Siegen, Siegen, Germany
[3]Technical University Dortmund, Dortmund, Germany

Abstract

Mid-T (ca. 220 to 350 °C) heat treatment is known to improve the dissipation of superconducting Nb cavities by dissolving the surface oxide and diffusing oxygen into the near-surface bulk. HZB explores the use of RF power coupled into the cavity as a technique to perform the heat treatment directly in the cryostat, thereby also avoiding venting and re-oxidation following the treatment. Such an RF-driven heating may be an attractive option for in-situ processing of an operation-ready accelerator module. We have demonstrated effective RF heating both with a TESLA-9-cell and a 1.5 GHz single-cell cavity reaching temperatures of 207 °C (TESLA cavity) and 260 °C (VSR single cell). Whilst the TESLA-cavity was driven via the fundamental power coupler using various modes of the fundamental passband, the single cell was heated using a higher-order mode at 4.263 GHz. The later was selected because of both its strong coupling and acceptable homogeneity of RF power dissipation. Experiments took place in two cryostats, HZB's HoBiCaT and the Large Vertical Test Stand (LVTS), operated under elevated temperatures. In this paper, details of the experimental setup and process, heating performance and, in case of the single cell, a subsequent cold test are reported.

INTRODUCTION

Recent investigations [1–3] indicated the potential to improve the performance of superconducting cavities by a thermal cavity treatment in a moderate temperature range of ca. 220 to 350°C whilst evacuated. Originally vacuum ovens are used [2], but also heating set-ups with ohmic heaters placed on the outer surface of cavities feasibility [4]. In this study we omit the use of external heaters and investigate whether rf fields in the cavity may be utilized to heat the cavity walls accordingly. Under most favourable conditions, rf installations like transmitter, rf power lines and couplers that already exist for the regular cavity operation may be utilized with only minor modifications to provide heating power. The feasibility of performing rf mid-T bake is further studied and described in this paper (in parts already in [5, 6]) by testing the thermal reaction of cavities to the excitation with different modes (fundamental passband and HOMs) with the goal to obtain the necessary temperatures for sufficiently long periods of time.

EXPERIMENTAL

Two rf heating experiments are presented here. The first one investigates heating of a multi-cell TESLA 9-cell cavity making use of the fundamental passband mode and the limited coupling ranges provided by standard FPC components (TTF III). The second focuses on the use of higher-order modes (HOMs) as an alternative way to provide both larger coupling values and homogeneous energy deposition. To this end a 1.5 GHz VSR single-cell cavity [7] undergone a heating test with the intention to demonstrate a proper rf heating performance and, if possible, apply a full mid-T bake-out recipe as described in [4]. As it is later described a cold Q_0 vs. E_{acc} characterization of the the cavity was finally carried out. Figure 1 shows a schematic of the first experimental setup at the Horizontal Bi-Cavity Test Stand (HoBiCaT) [8]. A Rohde & Schwarz ZNB20 vector network analyzer (VNA) was used to drive a Cryoelectra CRE-350F 1.3 GHz, 15 kW CW solid-state power amplifier. The rf power was fed by a TTF-III coupler and into the TESLA cavity, such fully utilizing rf installations primarily intended for cold cavity operations. The cavity under test is an undressed 1.3 GHz 9-cell (RRR300, fine grain). Its field profile is not flat, as verified by bead-pull measurements [6]. Due to open beam pipes, the cavity volume and the test vessel shared the same insulation vacuum. The cavity pickup signal was looped back to the VNA, such providing a full S_{21} measurement during amplifier operation in any required frequency range. This was used both for mode selection, frequency fine tun-

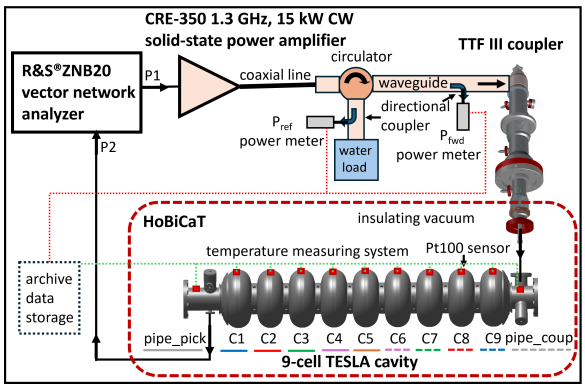

Figure 1: Schematic overview of the experimental setup at [8]. The rf heating system is driven by a vector network analyzer (VNA) and a solid-state power amplifier. The temperature measurement system comprises sensors mounted on each cell of the TESLA 9-cell cavity as well as on the beam pipes. The waveguide is connected to the cavity via a TTF-III coupler.

* Work supported by the Helmholtz Association.
† rene.schoeder@helmholtz-berlin.de

Content from this work may be used under the terms of the CC BY 4.0 licence (© 2026). Any distribution of this work must maintain attribution to the author(s), title of the work, publisher, and DOI.

ISBN: 978-3-95450-252-3 ISSN: 2673-5350 doi: 10.18429/JACoW-IPAC2026-MOP7031

DESIGN AND MULTIPHYSICS ANALYSIS OF β=0.18 HALF-WAVE RESONATOR FOR IFMIF-DONES ACCELERATOR

F. Grespan†, M. D'Andrea, A. Facco, L. Ferrari, A. Palmieri, C. Pira, A. Pisent,
INFN-LNL, Legnaro, Italy
P. Mereu, C. Mingioni, M. Nenni, E. Nicoletti, INFN-Torino, Torino, Italy

Abstract

The IFMIF-DONES facility will irradiate and characterize materials to be used in fusion reactors using a neutron flux produced by the interaction of a deuteron beam with a liquid lithium target. A superconducting RF linac will accelerate the beam to the final energy of 40 MeV through two series of superconducting half-wave resonators operating at 175 MHz. The study of a new design for the second family of 27 cavities (optimized for β = 0.18) has been recently presented by INFN, to optimize it from the point of view of production, while maintaining its performance close to what was observed at the first CEA prototype. This paper describes the electromagnetic and mechanical design of the β = 0.18 HWR, conducted in a Multiphysics approach of the cavity optimization. The contributions of pressure, tuners, Lorentz's force, thermal expansion, construction techniques are analysed up to meet physical and mechanical requirements.

INTRODUCTION

The International Fusion Materials Irradiation Facility – DEMO Oriented Neutron Source (IFMIF-DONES) [1-3], currently under construction in Granada (Spain), is a state-of-the-art facility whose main goal will be the testing of materials to be used in the DEMO fusion reactor [4]. Material specimens will be exposed to a neutron flux of 10^{14} $cm^{-2}s^{-1}$ produced by the interaction of a deuteron beam of unprecedented intensity with a liquid lithium target. A complex accelerator system was designed to achieve the required deuteron beam parameters of 40 MeV energy and 125 mA CW current (for a total power of 5 MW) [3, 5]. A superconducting radiofrequency (SRF) linac composed of 46 half-wave resonators (HWRs) acts as the final acceleration stage. The resonators, made of Niobium and operating at 175 MHz, are organized in two families optimized for different deuteron velocities: the first two cryomodules house 19 "low-β" cavities (optimized for $\beta = 0.115$), while the remaining three cryomodules house 27 "high-β" cavities (optimized for $\beta = 0.18$).

Italy has recently joined the IFMIF-DONES project in official capacity and, as part of the in-kind agreement, the Italian National Institute for Nuclear Physics (INFN) will procure the high-β family of resonators. Starting from the prototype designed by the French Alternative Energies and Atomic Energy Commission (CEA) [6] and incorporating the experience collected at the Facility for Rare Isotope Beams (FRIB) with similar devices [7-9], a new design was developed by the Legnaro National Laboratories (LNL) and the Torino section of INFN.

† francesco.grespan@lnl.infn.it

ELECTROMAGNETIC DESIGN

The IFMIF-DONES high-β HWRs are required operate at 4 K and reach a nominal accelerating field of 4.2 MV/m and a quality factor higher than 10^9. Furthermore, considering the high current of the accelerated beam, each cavity operates with an RF input power of up to 200 kW. The required beam aperture diameter is 50 mm. An extensive study, described in [10], was carried out at INFN-LNL to define an electromagnetic design which satisfies all requirements, while keeping the surface electric and magnetic fields under control to avoid field emission and quenching. A 3D model of the final design is shown in Fig. 1 and its electromagnetic properties, simulated with CST Studio Suite [11] are listed in Table 1. The quality factor is estimated assuming a surface resistance of 30 nΩ for Nb in superconducting regime. Multipacting simulation studies were also conducted, revealing two barriers (one for very low accelerating field and one for medium-high accelerating field). This is consistent with experimental tests of the CEA protype, which showed that both barriers can be overcome either by adequate conditioning or by shaping appropriately the input power pulse. An advantage of this design is that its geometry allows it to be almost entirely built from formed metal sheets (as described in the next section), reducing the cost and simplifying the manufacturing process.

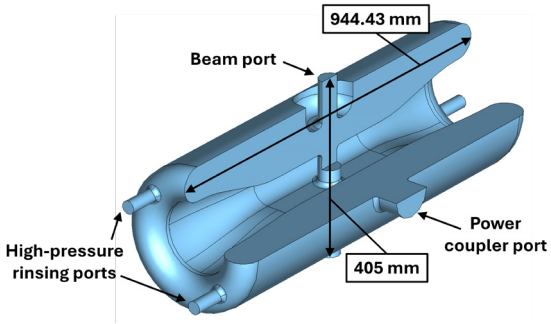

Figure 1: Cross-section view of the inner volume of the cavity. The relevant dimensions are also shown.

Table 1: Simulated electromagnetic properties of the LNL HWR design.

Frequency [MHz]	175
β_{opt}	0.18
E_{peak}/E_{acc}	4.91
B_{peak}/E_{acc} [mT/(MV/m)]	8.59
R/Q [Ω]	224.4
G [Ω]	51
Q (assuming $R_s = 30$ nΩ)	$1.7 \cdot 10^9$

Content from this work may be used under the terms of the CC BY 4.0 licence (© 2026). Any distribution of this work must maintain attribution to the author(s), title of the work, publisher, and DOI.

ISBN: 978-3-95450-252-3 ISSN: 2673-5350 doi: 10.18429/JACoW-IPAC2026-MOP7032

ADVANCES IN PLASMA PROCESSING FOR MEDIUM- AND HIGH-BETA CAVITIES OF THE ESS LINAC*

E. Del Core†, A. Bosotti, R. Paparella, D. Sertore, INFN - LASA, Segrate, Italy
P. Pierini, ESS, Lund, Sweden
E. Cenni, CEA, Paris-Saclay, France

Abstract

Plasma processing is increasingly recognized as an effective technique for mitigating field emission and restoring the performance of superconducting radiofrequency (SRF) cavities. A collaboration among CEA, ESS, and INFN is currently working to adapt and optimize this method for the medium- and high-beta elliptical cavities installed in the ESS linac. This contribution summarizes the ongoing efforts toward implementing plasma processing both in fully assembled cryomodules and in cavities prepared for vertical testing. Here, we present the first experimental results obtained on a medium-beta 704 MHz cavity equipped with different couplers, along with preliminary investigations carried out on the high-beta 704 MHz cavity.

INTRODUCTION

One of the main factors limiting the performance of superconducting radio-frequency (SRF) cavities is field emission. To address this issue, plasma processing has attracted increasing attention as an effective technique for removing hydrocarbon contaminants from cavity surfaces, which are known to trigger electron emission. By improving the niobium work function [1], this method contributes to the reduction of field emission.

Recent studies [2, 3] have demonstrated that low-pressure reactive plasma discharges generated using a mixture of a noble gas and oxygen are effective in cleaning surface impurities. Consequently, the mitigation of field emission can lead to a significant improvement in SRF cavity performance. Within this framework CEA, ESS and INFN are jointly developing a plasma processing procedure specifically designed for medium-beta MB (β = 0.67) 704.42 MHz 6-cell and high-beta HB (β = 0.86) 704.42 MHz 5-cell ESS cavities. Two different application scenarios are currently under investigation. The first consists of plasma treatment of the cavity in a vertical test stand (VTS) before cold RF measurements. The second, more advanced approach, involves performing in-situ plasma processing directly inside the cryomodule. This latter solution is particularly promising, as it enables field emission mitigation without removing the cavities from the cryomodule, significantly reducing downtime, manpower, and operational costs. In addition, a reduction in field emission directly translates into lower RF power dissipation within the cryomodule.

The plasma processing technique is based on the generation of a room-temperature plasma sustained by an RF-induced glow discharge. During the procedure, a noble gas—typically argon or neon—with a small oxygen admixture is injected into the cavity. Free electrons in the plasma, with kinetic energies of the order of 10 eV, dissociate molecular oxygen into highly reactive atomic species. These reactive species interact with hydrocarbon contaminants deposited on the niobium surface, converting them into volatile compounds such as CO_2, CO, and H_2O. The gas flow then removes these reaction products, while their evolution is continuously monitored by a residual gas analyzer (RGA). Besides increasing the niobium work function, this cleaning process also lowers the secondary electron emission coefficient, both effects contributing to the mitigation of field emission.

In this work, we present simulations and preliminary results obtained on the *MBLG002* ESS cavity (Q_0 of about 10^4 at room temperature), using either a unity coupler ($Q_{ext} \approx 6 \cdot 10^9$) or a custom, more coupled antenna (Q_{ext} of approximately 10^5), emulating the coupling of the power coupler. In addition, S_{21} and S_{11} measurements have been performed on a HB cryomodule, and preliminary simulations have been started.

RF AND VACUUM SETUP

Unlikely 1.3 GHz cavities, where Higher Order Mode (HOM) couplers are commonly used for plasma ignition, these ESS cavities lack such couplers; therefore, RF power is injected through the main coupler (MC) port. Initial measurements were carried out using the unity coupler in order to investigate the possibility of igniting plasma and performing plasma processing in the VT configuration. However, at room temperature this antenna is only weakly coupled to the cavity, resulting in non-optimal operating condition for plasma ignition and stable operation.

Figure 1 presents the latest schematic layout of the RF and vacuum setup adopted for the experimental tests. The RF system includes a Vector Network Analyzer (VNA), power meters, bidirectional couplers, two frequency synthesizers, amplifiers, a spectrum analyzer, and power splitter/combiners. In addition, the cavity is equipped with viewports on the beam tube flanges that allow direct plasma observation through a dedicated camera system. From the vacuum perspective, the current configuration operates under static vacuum conditions, with the pumping system connected on the MC side and gas injection line located on the pickup (PU) side.

* This work was partially supported by the European Union's Horizon Europe Marie Sklodowska-Curie Staff Exchanges programme under EAJADE grant agreement no. 101086276

† elisa.delcore@mi.infn.it

Content from this work may be used under the terms of the CC BY 4.0 licence (© 2026). Any distribution of this work must maintain attribution to the author(s), title of the work, publisher, and DOI.

ISBN: 978-3-95450-252-3 ISSN: 2673-5350 doi: 10.18429/JACoW-IPAC2026-MOP7034

STATUS OF THE HIGH Q-HIGH G R&D ACTIVITIES ON SRF CAVITIES AT INFN LASA*

L. Monaco†, M. Bertucci, A. Bosotti, E. Del Core, F. Fiorina, C. Pagani‡,
R. Paparella, D. Sertore, P. Spruzzola, B. Vitali,
Istituto Nazionale di Fisica Nucleare, Laboratori Acceleratori e Superconduttività Applicata,
Segrate, Italy

Content from this work may be used under the terms of the CC BY 4.0 licence (© 2026). Any distribution of this work must maintain attribution to the author(s), title of the work, publisher, and DOI.

Abstract

INFN LASA started an R&D activity dedicated to the development of the knowledge needed to understand how to improve SRF cavity performances to reach High Q and High G values to accomplish the sustainability and cost reduction requests, as needed for the future large particle accelerators. This R&D activity, funded by INFN, is also enriched by synergies with other LASA activities like the PIP-II low beta cavity production, the participation to ILC Technology Network, and by the LASA experience in SRF cavity industrialization developed during the large-scale production of the Eu-XFEL and the ESS SRF cavities. The first results obtained on 1.3 GHz single and multi-cell cavities, and the status of the upgraded LASA infrastructures for Vertical Test are here presented.

INTRODUCTION

Next-generation facilities, such as lepton colliders and advanced light sources, require accelerator technologies that surpass current limits in energy and beam quality. Achieving these goals also demands improved sustainability and reduced costs.

A major contribution to these improvements comes from advancements in accelerating components, in particular Superconducting Radio Frequency (SRF) cavities, as emphasized in the 2020 European Strategy for Particle Physics (ESPP) [1]. Targeted R&D on cavity surface preparation and thermal treatments is therefore crucial to achieve both high-quality factors (Q) and high accelerating gradients (G).

The INFN Milano–LASA SRF group has extensive expertise in the design, prototyping, and industrial production of bulk niobium based superconducting cavities and related components, with strong efforts toward technology transfer. This approach has been successfully validated through in-kind contributions to major international projects such as the European XFEL, ESS, and PIP-II [2-5].

To sustain and expand this expertise, INFN launched in 2023 a multi-year program focused on future large-scale projects including ILC, Muon Collider, and FCC. Similar initiatives are pursued worldwide within international collaborations we are participating to, such as the ILC Technology Network (ITN), which targets high gradients (31.5 MV/m) while maintaining high Q_0 ($\geq 1\ 10^{10}$) in line with its pulsed operation design goals [6].

OUR R&D STRATEGY

To address these challenges, the strategy we have developed is structured in two main phases. The first focuses on R&D using 1.3 GHz single-cell cavities—the reference frequency for these studies—with the goal of developing surface and thermal treatments that extend high-Q performance into the high-gradient regime. Once these processes are consolidated, the second phase aims to transfer them to multicell cavities and, critically, to make them compatible with industrial production in view of future large-scale applications. This approach is fully synergic with our ongoing programs dedicated to future collider projects (ILC, Muon Collider, FCC, etc.), as previously outlined.

Moreover, the R&D activities described here - particularly those focused on High-Q performance - will strongly benefit from ongoing studies carried out in the framework of optimizing the treatments of PIP-II low-beta cavities, operating at 650 MHz which is the first subharmonic of 1.3 GHz [7]. These efforts are especially relevant given the very high Q requirements of the project, despite the relatively modest accelerating gradients associated with their continuous-wave (CW) operation.

Over a 3–4 years horizon, we will deliver a focused, results-driven program built on 1.3 GHz technology:

- **High-Q / High-Gradient process development:** We will optimize two single-cell cavities starting from a proven European XFEL-like baseline treatment (150 µm bulk EP, 900 °C annealing, 10–20 µm final EP, 120 °C 48h baking), and advance performance through innovative methods such as mid-temperature and two-step baking. Rigorous validation at LASA and partner laboratories (e.g., CEA) will ensure robust cross-comparison and rapid process qualification.
- **Scalable technology transfer:** We will extend the validated process to two 9-cell cavities, demonstrating reliable performance at the multicell level while establishing industrialization workflows, including integrated quality assurance and control (QA/QC) protocols, to support future large-scale production.
- **Targeted R&D on enabling systems:** In parallel, we will strengthen key ancillary technologies—such as tuners and magnetic shielding—to guarantee full

* This work was partially supported by the European Union's Horizon Europe Marie Sklodowska-Curie Staff Exchanges programme under EAJADE (Europe-America-Japan Accelerator Development Exchange) grant agreement no. 101086276.
†laura.monaco@mi.infn.it
‡Also at University of Milan, Milan, Italy

ISBN: 978-3-95450-252-3 ISSN: 2673-5350 doi: 10.18429/JACoW-IPAC2026-MOP7035

R&D ACTIVITIES IN VIEW OF PIP-II LB650 CAVITY PRODUCTION

M. Bertucci*, R. Paparella, A. Bosotti, E. Del Core, L. Monaco, C. Pagani, D. Sertore, B. Vitali
Istituto Nazionale di Fisica Nucleare, Laboratori Acceleratori e Superconduttività Applicata, Segrate, Italy
J. Bernardini, V. Chouhan, L. Grassellino, K. McGee, J. Ozelis, D. Passarelli
Fermi National Accelerator Laboratory, Batavia, United States
A. Tsymbaliuk Zanon Research & innovation, Schio, Italy

Content from this work may be used under the terms of the CC BY 4.0 licence (© 2026). Any distribution of this work must maintain attribution to the author(s), title of the work, publisher, and DOI.

Abstract

A joint LASA–Fermilab activity is in progress to study the impact of key surface processing steps on the performance of LB650 superconducting cavities in view of future series production. Among the several cavity preparation steps, electropolishing (EP) and mid-temperature heat treatment are considered the most critical and require specific optimization for the LB650 geometry. Single-cell and 5-cell cavities are used as test prototypes to investigate the effects of EP and mid-temperature bake. Vertical RF tests are performed at Fermilab after EP and after the mid-T bake under identical conditions. The ongoing program aims to provide insight into the evolution of Q_0 and accelerating gradient along the processing sequence. Preliminary observations and results are here presented.

INTRODUCTION

LASA-INFN is responsible for the production and qualification of the low-beta cavities for the PIP-II Project. The low-beta section is a key part of the PIP-II superconducting linac, accelerating the H^- beam from approximately 177 MeV up to 516 MeV before injection into the downstream high-beta section. It consists of 36 five-cell elliptical superconducting cavities (labeled in the following as LB650), operating at a frequency of $f = 650$ MHz and designed for a geometric beta factor of $\beta_g = 0.61$ [1]. The project specifications for the LB650 cavity operation in the linac are an accelerating gradient of $E_{acc} = 16.9\,\mathrm{MV\,m^{-1}}$ and an intrinsic quality factor of $Q_0 = 2.4 \times 10^{10}$. To ensure an adequate performance margin, the acceptance criterion in the vertical test of the naked cavity is set to a higher value, corresponding to at least $Q_0 = 2.9 \times 10^{10}$ at nominal field. This vertical test performance therefore represents the effective qualification target for cavity acceptance and subsequent cryomodule integration. Given the demanding quality-factor requirement, the choice of an appropriate surface treatment is crucial [2]. Following an extensive R&D campaign carried out on single-cell and multi-cell cavity prototypes, a recipe based on medium-temperature furnace baking was selected. Compared to other high-Q_0 treatments, such as nitrogen doping, mid-temperature baking offers a simpler and more robust process chain for the LB650 cavity geometry, as it does not require an additional electropolishing step to optimize the impurity diffusion profile in the RF penetration layer. Among the various temperature-time combinations investigated by the SRF community, a treatment at 350 °C for 3 h was selected as the baseline recipe. This choice results from the favorable balance between BCS resistance reduction and magnetic flux sensitivity, while preserving compatibility with the cavity geometry and industrial processing workflow. Studies on 650 MHz cavities have shown that medium-temperature baking in this temperature range can provide quality factors comparable to nitrogen-doped cavities, while significantly simplifying the final surface preparation procedure [3].

SURFACE PROCESSING OPTIMIZATION

To support the industrial implementation of the medium-temperature baking treatment for the PIP-II LB650 cavity production, a dedicated investigation was established to assess the reproducibility and consistency of the surface preparation workflow implemented by the qualified vendor. This activity was conceived as a process verification strategy aimed at consolidating the treatment recipe under production-relevant conditions, with particular focus on the electropolishing (EP) and furnace baking stages. The objective of the campaign was to verify that both the EP infrastructure and the furnace treatment could reproduce performance levels consistent with those previously observed during the R&D phase on prototype cavities. To this end, historical vertical test data collected on comparable cavities under similar operating conditions were used as reference guidelines to frame the expected performance and support the interpretation of the experimental results. To this purpose, two configurations were selected. The first one was the INFN single-cell prototype cavity EZ-SCCFG004, developed within the PIP-II R&D program and fully representative of the reference cavity geometry. The second was the five-cell 644 MHz elliptical cavity S65-001, owned by Michigan State University and designed for the FRIB energy upgrade [4], which was selected as a multicell benchmark. Although not a nominal PIP-II LB650 cavity, S65-001 features comparable geometrical and RF characteristics, thus providing a structure of similar complexity and dimensions for validating the industrial workflow. Both cavities were tested in two different surface conditions: after the *Baseline EP* process and after the application of the *Medium-Temperature Baking* treatment at 350 °C for 3 h. This approach enables a direct comparison of the RF performance before and after the furnace treatment, allowing the assessment of both the treatment effectiveness and the reproducibility of the complete industrial process. The main performance indicator considered in this campaign was the intrinsic quality factor, Q_0, measured

* michele.bertucci@mi.infn.it

ISBN: 978-3-95450-252-3 ISSN: 2673-5350 doi: 10.18429/JACoW-IPAC2026-MOP7036

SRF CAVITY DETUNING CHARACTERIZATION BY CONTINUOUS WAVELET TRANSFORM: A TIME-FREQUENCY ANALYSIS*

J. S. Romero[2], P. Echevarria[1], A. Neumann[1], A. Ushakov[1], C. M. Cuesta[2], J. Knobloch[1,3]
[1]Helmholtz-Zentrum Berlin für Materialien und Energie, Berlin, Germany
[2]University of the Basque Country, Leioa, Spain
[3]University of Siegen, Siegen, Germany

Abstract

Sustainability is a key issue for both current and future particle accelerators. Superconducting RF cavities with high loaded quality factors play an important role in not only lowering the energy demands of particle accelerators but also the initial investment in RF amplifiers. But the narrow bandwidth associated with this high loaded quality, makes the need to minimize cavity detuning critical to maintain stable and efficient operation. In this context, characterization of microphonics detuning is essential, as it is a major error source, for implementation of effective mitigation schemes to reduce peak and rms RF power requirements.

Here we analyze SRF cavity detuning using the Continuous Wavelet Transform (CWT). Unlike conventional Fourier-based approaches, the CWT enables localized time-frequency decomposition, making it well-suited for identifying transient features that influence cavity behavior. Applying the CWT to measured detuning signals from a TESLA cavity at HoBiCaT testing facility at Helmholtz-Zentrum Berlin allows us to identify dominant detuning frequencies and track their evolution over time. The resulting time-frequency maps offer a more comprehensive understanding of the underlying mechanical environment and can support the development of more robust detuning mitigation and compensation strategies for SRF systems.

INTRODUCTION

Particle accelerators are not immune to the current political, social, and economic situation. In this regard, both climate change and rising energy costs make sustainability a key consideration in both existing accelerators and future projects, [1]. Different research projects funded by the European Union [2, 3] are studying different strategies to tackle this issue. One of the tasks in [2] is trying to find paths to save energy from the RF power. More specifically in the case of low beam loading applications, as it is also stated in the European Roadmap for Particle Physics, [4], one major challenge due to the very small intrinsic cavity bandwidth, are small mechanical vibrations known as microphonics.

While active compensation via the cavity tuner is an open field of research, [5–10], passive measures like cryoplant operation optimization, vacuum pumps isolation, etc., should always be considered in the first place, [11]. And for these measures to be effective, a proper characterization of the microphonics is fundamental.

The analysis of detuning signals requires tools capable of capturing time-dependent spectral variations. Classical Fourier analysis provides a global description that does not retain temporal information. To address this limitation, extensions such as the short-time Fourier transform (STFT) introduce time localization by applying the transform over sliding windows. However, the STFT uses a fixed window length, leading to a trade-off between time and frequency resolution that remains constant across all frequencies. This can be limiting for cavity detuning signals, where slow drifts and fast transient events may coexist.

For this reason, the continuous wavelet transform (CWT) is used in this work, as it provides a time-frequency representation with adaptive resolution, [12].The wavelet transform of a continuous time signal, $x(t)$, is defined as

$$T(a,b) = \frac{1}{\sqrt{a}} \int_{-\infty}^{\infty} x(t) \psi^* \left(\frac{t-b}{a} \right) \mathrm{d}t, \tag{1}$$

where $\psi(t)^*$ is the complex conjugate of the wavelet function $\psi(t)$, a is the scale parameter (inversely related to frequency), and b is the time-shift parameter of the wavelet. This formulation represents the signal as a superposition of time-localized contributions at different scales and positions.

Different choices of the wavelet function $\psi(t)$ emphasize specific signal features; for instance, commonly used wavelets such as Morlet or Mexican hat offer different compromise between time and frequency localization.

In this work, the complex Morlet wavelet is used and is given by the following equation

$$\psi(t) = \frac{1}{\sqrt{\pi B}} e^{2\pi i F t} e^{-t^2/B} \tag{2}$$

as it offers a well-defined central frequency and is particularly suitable for analyzing oscillatory signals. The specific parameters used are $F = 1.5$ and $B = 2.5$, where F is the center frequency and B is the bandwidth parameter.

The results shown in this paper were obtained in the HoBiCaT facility at HZB, [13, 14], using a TESLA cavity but also briefly during the first beam commissioning of SEALab's photoinjector, [15, 16].

EXPERIMENT SETUP AND RESULTS

In order to measure the detuning of a cavity, the equation $\Delta f(t) = \frac{f_0}{2Q_L} \tan(\Delta\Phi(t))$ can be used, where $\Delta f(t)$ is the detuning, f_0 the cavity's fundamental mode's frequency,

* Funded by the EU Horizon Europe program grant N. 101131435 and partly funded by the Global Training Program, an initiative of Basque Trade and Investment, SPRI and Basque Government (Spain).

Content from this work may be used under the terms of the CC BY 4.0 licence (© 2026). Any distribution of this work must maintain attribution to the author(s), title of the work, publisher, and DOI.

ISBN: 978-3-95450-252-3 ISSN: 2673-5350 doi: 10.18429/JACoW-IPAC2026-MOP7037

ADDITIONAL INSTALLATION EFFORT FOR THE 3MW READINESS AT ESS

H. Przybilski*, Ph. Arnold, E. Asensi, W. Borg, N. Elias, A. Gevorgyan, A. Krawczyk, C. Maiano, D. Nicosia, P. Nilsson, P. Pierini, M. Skiba, E. Trachanas, J. Zhang, A. Zwozniak,
European Spallation Source ERIC (ESS), Lund, Sweden

Abstract

Since the last installation campaign, additional High-Beta (HB) cryomodules (CM) have been tested and qualified Ready-for-Installation (RFI) at the ESS Test Stand. Their installation was planned for the summer'25, right after the first Beam On Dump (BOD) commissioning phase and a complete warm-up of the accelerator. The number of HB CM has raised to 11 out of 21 allowing for a potential maximum power of the Linac of 3 MW. This paper will present the lessons learned from the previous phase, as well as the necessary measures taken in order to install 6 cryomodules in an RP controlled area in only 3 months.

INTRODUCTION

The European Spallation Source (ESS) in Lund, Sweden [1] has begun its transition towards an operating facility. A major milestone of the first Beam On Dump (BOD) phase was reached in May 2025, when the probe proton beam successfully traversed the superconducting linac and was measured at an energy exceeding 800 MeV. Cryomodule preparation readiness and commissioning activities were previously reported at SRF2025 [2] and an update is given at this conference [3]. This paper focuses on the summer 2025 installation campaign (shown in dark blue in Fig. 1, as well as on improvements implemented to the existing infrastructure.

ADDITIONAL CRYOMODULES INSTALLATION

Motivations

At the beginning of 2025, the ESS P6 plan identified a gap of several months between the end of BOD commissioning and the start of Beam On Target (BOT) commissioning. This period was identified as an opportunity for the installation of additional cryomodules. Installing CMs at this stage provides increased flexibility for future machine shutdown planning, allowing greater focus on the needs of the ESS Neutron Scattering Systems (NSS). Furthermore, the ongoing qualification campaign of elliptical cryomodules [5] enabled the installation of six additional High Beta (HB) cryomodules. It is important to note that these cryomodules will not initially be powered. The RF gallery upgrade from 2 MW to 3 MW was scheduled to start after summer 2025. Once powered, the additional energy margin will provide much needed operational flexibility on the path towards reliable 2 MW operation. Finally, as the main cryomodule installation campaign (27 CMs) had just been completed, the installation teams were still present at ESS. This represented a strong asset for carrying out the installation swiftly and efficiently.

Lessons Learned

As noted in the previous section, the main cryomodule installation had recently concluded [6], and lessons learned were documented to ensure an equivalent or faster installation pace for the six additional HB cryomodules. During the BOD phase, one machine-off day per week was allocated. These periods were used to prepare the infrastructure for the summer installation. It was identified that water cooling piping constitutes a resource-intensive task in the installation schedule. Pre-fabrication of the piping, together with pre-installation of the lower part of the water distribution system, proved to be highly efficient. The risk of equipment damage was significantly reduced, and the working conditions for the fitters were correspondingly improved. Once BOD commissioning was completed and the accelerator was warmed back to room temperature, the main differences compared to the previous installation were the presence of an RP controlled area and the re-use of already installed equipment (Linac Warm Units (LWUs), water cooling manifolds, etc.). As the accelerator had operated for several weeks up to the Tuning Beam Dump (TBD), a total of seven LWUs and six dummy beam pipes had been exposed to beam and had to be removed, temporarily for the LWUs and permanently for the dummy pipes, to allow installation of the additional HB cryomodules.

The LWUs were removed using mobile cleanrooms after the RP group had surveyed and cleared the work area. Activation levels remained very low (<5 µSv/h), even on the flanges connecting the dummy pipes to the LWUs. The preparation of the cryogenic piping followed a similar approach to the previous installation. The CM piping was prepared in advance in the klystron gallery, reusing the existing set of jigs. The preparation of the valve boxes (VBs) was performed after completing the cleanroom work and, in this campaign, with stricter dust containment measures during cutting and grinding operations. A dedicated booth (Fig. 2) was installed for each valve box, ensuring no potential contamination of surrounding areas and including an RP check at the end of the work. A total of four weeks was required to prepare the six positions. Another improvement in the installation sequence concerned the water cooling manifolds, which previously had to be fully disconnected. In this campaign, the manifolds were tilted towards the ceiling, allowing

* henry.przybilski@ess.eu

Content from this work may be used under the terms of the CC BY 4.0 licence (© 2026). Any distribution of this work must maintain attribution to the author(s), title of the work, publisher, and DOI.

ISBN: 978-3-95450-252-3 ISSN: 2673-5350 doi: 10.18429/JACoW-IPAC2026-MOP7038

OPERATIONAL EXPERIENCE WITH THE COLD TUNING SYSTEM FOR ESS SUPERCONDUCTING CAVITIES

M. Skiba†, N. Elias, A. Krawczyk, C. Maiano, P. Pierini, H. Przybilski, M. Wang, A. Zwozniak,
European Spallation Source, Lund, Sweden

Abstract

The European Spallation Source (ESS) is undergoing its next technical commissioning run, with the goal of achieving first Beam On Target (BOT). This milestone requires the full superconducting linac—27 cryomodules consisting of 26 Spoke, 36 Medium-Beta, and 20 High-Beta cavities—to achieve nominal parameters. This paper presents a statistical study of the Cold Tuning System (CTS) based on data from repeated tuning and detuning operations. The analysis focuses on tuning methodology and key parameters, assessing its repeatability and stability. The results provide a detailed characterisation of each CTS, ensuring stable cavity fields.

INTRODUCTION

The European Spallation Source (ESS) [1] is constructing a 5 MW superconducting proton linac that will comprise in future 43 cryomodules to accelerate the beam to 2.0 GeV. Between December 2024 and June 2025, ESS completed a major commissioning run that delivered the first beam on dump (BOD) at energies above 800 MeV. This campaign demonstrated stable operation of the cryogenic plant, RF systems, and superconducting cavities under integrated conditions [2] [3].

The next commissioning phase (BOD2) begins in November 2025 and will focus on achieving nominal RF pulse parameters (14 Hz, 3.2 ms). This phase will prepare the facility for the first beam on target (BOT), planned for January 2027, marking the transition toward high-power operations [3].

COLD TUNING SYSTEM

The cold tuning system (CTS) for the ESS superconducting cavities is based on proven CEA tuner design. For slow mechanical tuning, it uses a stepper motor, gearbox, and main screw assembly to drive lever arms and eccentric shafts to alter the cavity frequency. Additionally, two piezo actuators provide fast tuning to actively counteract dynamic Lorentz force detuning - essential for pulsed operations (Fig. 1) [4].

A key mechanical difference in CTS design exists between the Spoke and Elliptical cavities. The MBL and HBL cavities are pre-tuned and operate with all mechanical play removed. In this configuration, the tuner must apply a positive frequency shift of 120–220 kHz to bring the cavity to its nominal operating frequency.

In contrast, the CTS Spoke cavities operate from a mechanically free state, without initial pre-tensioning or closed mechanical play.

† marek.skiba@ess.eu

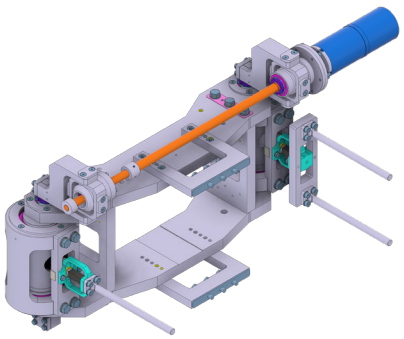

Figure 1: CTS CAD model of elliptical cavities with coloured stepper motor (blue), drive screw (orange) and piezo actuator (turquoise).

The CTS works under vacuum at cryogenic temperature, thermalizing near 18 K for MBL/HBL and 60 K for the Spoke cavities. The system converts motor rotation into cavity elongation through a sequence of reduction stages - gearbox, drive screw, and lever mechanism - which together define the tuning resolution, as listed in Table 1.

Table 1: Cold Tuning System Parameters

Parameters	Spk	MBL	HBL
CTS sensitivity [kHz/mm]	135	217	197
Motor steps per turn	200	200	200
Gearbox ratio	256	100	100
Leverage ratio	20	17	17
Screw pitch [mm]	2	1.5	1.5
Resolution [Hz/step]	0.26	0.96	0.87

TUNING METHODOLOGY

ESS uses an FFT-based tuning method that analyses transmitted-power signals from the LLRF system, integrated into the EPICS control system. The procedure has three stages [5]:

- Far Tuning

  FFT identifies the detuned cavity as a distinct peak, and initial motor steps confirm the tuning direction.
- Signal Beating

  As the cavity approaches the drive frequency, the peak merges with the carrier, and time-domain beating provides a visual measure of the remaining detuning.

Content from this work may be used under the terms of the CC BY 4.0 licence (© 2026). Any distribution of this work must maintain attribution to the author(s), title of the work, publisher, and DOI.

ISBN: 978-3-95450-252-3 ISSN: 2673-5350 doi: 10.18429/JACoW-IPAC2026-MOP7039

ESS SRF CAVITY PREPARATION FOR BEAM ON DUMP 2/BEAM ON TARGET PHASE

A. Zwozniak†, N. Elias, A. Krawczyk, C. Maiano, M. Nabywaniec, P. Pierini, H. Przybilski, M. Skiba, M. Wang, European Spallation Source, Lund, Sweden

Abstract

The ESS (European Spallation Source) is presently configured as a 1.3 GeV linac, with three superconducting cavity sections starting from 90 MeV. For the moment in operation, we have 82 superconducting cavities: 26 double spoke resonators (β=0.5), 36 medium and 20 high beta elliptical cavities (respectively β=0.67 and 0.86). In this paper we would like to present the restart of the Linac after 4 months of summer break and further cryomodule installations. During this time all data from previous Beam on Dump (BOD) run at 870 MeV was collected to have a better overview before BOD2/BOT (Beam on Dump 2/ Beam on Target). The Warm Coupler Conditioning (WCC) started in the middle of October 2025. In November 2025 the first cryomodule was tuned and restored to the nominal gradient, after the off-resonant Cold Coupler Conditioning (CCC). During this process the key performance indicators are compared to those obtained during the Site Acceptance Test (SAT) and the 2025 BOD.

GENERAL OVERVIEW

During the first phase of the ESS project for beam operation on the temporary dump (BOD) at 800 MeV, 27 cryomodules were installed and commissioned (13 spoke containing two cavities each, 9 medium and 5 high beta elliptical, containing 4 cavities each). This configuration can provide 2 MW beam power capability at the nominal energy of 870 MeV and 62.5 mA of current. The first cooldown was performed in late November 2024 and cavity preparation, conditioning and testing for beam operation occurred in the period between January and April 2025. Beam operation on the dump was carried until July 2025 [1, 2].

To move to the second phase of the project additional 6 high beta elliptical cryomodules were installed during summer 2025 [3], pushing the energy reach to 1.3 GeV and the beam power capability to 3 MW. No RF power sources are however presently available for these cryomodules, so their tuning and RF operation is postponed to a later stage, after the completion of the RF infrastructure. In November 2025 the linac was cooled down again and a further "Beam on Dump 2" (BOD2) operation phase was started.

For each cavity the crucial parameters of their RF performances were followed from the first measurement in vertical test, up to the last beam commissioning phases – an example for MBL-010 S1 (CM08 cavity M021) can be found in Table 1.

† agnieszka.zwozniak@ess.eu

Table 1: Cavity Calibration and Performance Tracking

	Qt	Ql	Eacc [MV/m]
Vertical test	3.63E11	-	12.8
TS2	2.39E11	7.7E5	11.1
Linac BOD	2.21E11	7.14E5	
Linac BOD2	2.25E11	7.1E5	11.1

Warm and Cold Coupler Conditioning

For the Linac we followed the standard cavity test procedure usually performed at the test stands where the performances are verified prior to installation. The preparation starts from the warm coupler conditioning (WCC) at room temperature, followed by a second round of non-resonant cold coupler conditioning (CCC) after the linac cooldown. For both coupler conditionings the total time was compared with the times spent at the test facilities. Comparison between the Lund Test-Stand 2 (TS2), BOD and BOD2 conditioning times can be found in Fig. 1 (WCC) and Fig. 2 (CCC). Generally a shorter conditioning time was needed after the TS2 initial operation, but for some systems the time needed for coupler conditioning in the linac was substantially longer, as a possible hint of particulate redistribution during the installation or handling operation.

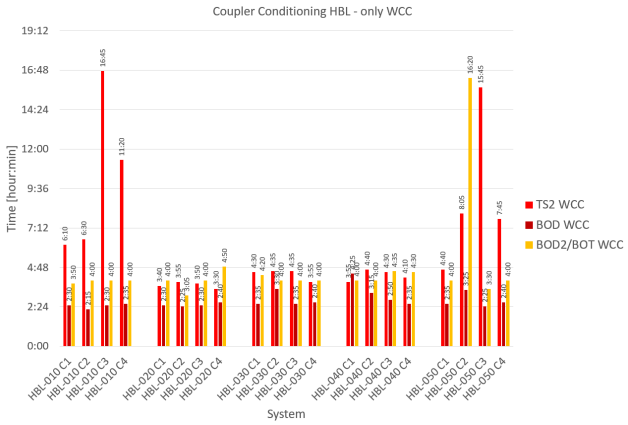

Figure 1: Comparison of the time needed for WCC between TS2, BOD and BOD2 (HB Section).

Cryogenic Operation

The cool down for the BOD2 started in November 2025 following an identical strategy to the one used during the first commissioning run [4, 5] where a distributed control architecture was used for the automated sequential process control, however this time with 6 additional cryomodules we integrated into the accelerator cryogenic system.

Content from this work may be used under the terms of the CC BY 4.0 licence (© 2026). Any distribution of this work must maintain attribution to the author(s), title of the work, publisher, and DOI.

ISBN: 978-3-95450-252-3 ISSN: 2673-5350 doi: 10.18429/JACoW-IPAC2026-MOP7040

ESS SCL FAST TUNING SYSTEM CHARACTERIZATION DURING LINAC COMMISSIONING

A. Zwozniak†, A. Krawczyk, C. Maiano, M. Nabywaniec, P. Pierini, M. Skiba
European Spallation Source, Lund, Sweden
W. Cichalewski, G. Jablonski, W. Jalmuzna, R. Kielbik, K. Klys, W. Tylman
Lodz University of Technology, Lodz, Poland

Abstract

In this paper we present the results of European Spallation Source (ESS) Superconducting Linac (SCL) cavities measurements which allowed us to determine crucial parameters for future SCL operation and Low-Level Radio Frequency (LLRF) systems tuning. The campaign of measurements was performed during the SCL commissioning for the second beam on dump campaign and prior to beam on target. All the measurements taken involved the usage of the cavity fast tuning system – the piezo tuner. Additionally, measurements of mechanical modes were done for all cavity types, which allowed to determine their longitudinal natural frequencies and prepare accordingly for optimal piezo tuners usage in the presence of the Lorentz Force Detuning (LFD). To confirm the frequency range of possible LFD, the LFD coefficient has been determined, and to ensure the piezo tuners are able to compensate for it, their characterisation has been carried out. SCL cavities passband modes were measured, in order to fine tune notch filter frequency position for all cavity types (expected π-mode neighbour position shows, as expected, a natural spread due to small variation in the cavity geometries). Piezo capacitance as function of temperature was measured, which can be used as a fault tuning tool in case of piezo aging effects, causing unexpected cavity detuning at high gradient. The described tools and measurement outcome are presented with their future implementation in the ESS Linac environment.

GENERAL OVERVIEW

For the current ESS operation phase at 2 MW on the beam dump (BOD2) 27 cryomodules can be powered with RF in the linac, 13 spoke cryomodules containing 26 spoke cavities, 9 medium beta cryomodules containing 36 medium beta cavities and 5 high beta cryomodules containing 20 high beta elliptical cavities, for a total of 82 RF systems. Additional 6 high beta cryomodules with another 24 high beta cavities have been installed in the tunnel but will be kept detuned in this phase while the RF systems installation is being completed for the next commissioning stages. During the first ESS linac commissioning on the beam dump in 2024/2025 the piezo tuners were not used, as the RF pulse length was only limited to 1 ms and the Lorentz Force Detuning (LFD) at the nominal field could be compensated with the LLRF feedback operation. For BOD2 the RF pulse length was increased to the nominal value 3.2 ms and to compensate for the LFD piezo tuners were applied.

For a complete characterization of the piezo action the following tests were done:

- Capacitance measurements during cool down and warm up (carried out also during BOD)
- Characterization of the cavity mechanical modes
- LFD compensation
- Piezo tuner identification
- Cavity bandpass-modes identification

Capacitance Versus Temperature

Electrical properties of the piezo components can change over time and are connected to possible degradation phenomena. This allows the possibility to detect degradation of the piezo components by continuous monitoring the capacitance of the piezoelectric stacks. The capacitance at room temperature (300K) is usually 3-4 times higher than the value in operating conditions at 2K [1, 2].

Table 1 lists the capacitance values for 300K for the piezo stacks chosen for the different cavity sections.

Table 1: Capacitance Value Versus Temperature for Spoke and MB/HB Elliptical Cavities

	Piezo	**Capacitance at 300K [nF]**
SPOKE	Noliac NAC2022-H72	13860
MB/HB	Noliac NAC2022-H30	5540

Figure 1 shows the variation of the piezo capacitance for a specific MBL system during the cool down transients, as a function of the temperature. Data is shown for both cooldown campaigns in March 2025 (BOD) and November 2025 (BOD2), showing a reproducible behaviour. The nominal room temperature capacitance as specified by the piezo stack vendor is shown in the plot with a star. Each tuner contains two piezo actuators stacks (indicated with A and B) for fault redundancy and voltage derating.

A full statistical analysis of the capacitance measurement of all the cold tuning piezo systems is being performed, in order to implement a continuous monitoring system allowing to monitor component degradation and plan maintenance intervention to exchange them when needed.

† agnieszka.zwozniak@ess.eu

Content from this work may be used under the terms of the CC BY 4.0 licence (© 2026). Any distribution of this work must maintain attribution to the author(s), title of the work, publisher, and DOI.

ISBN: 978-3-95450-252-3 ISSN: 2673-5350 doi: 10.18429/JACoW-IPAC2026-MOP7043

DETAILED DESIGN OF A TWIN-AXIAL TYPE FE-FRT FOR SASE

H. Jiang*, M. Dissanayake, G. Burt, Lancaster University, Lancaster, UK
I. Ben-Zvi, Stony Brook University, Stony Brook, New York, USA

Abstract

A Twin-axial type Ferro-Electric Fast Reactive Tuner (FE-FRT) is under development for UK-XFEL, aiming to provide fast and efficient microphonics suppression. The tuner consists of two magnetically coupled cylindrical resonators operating in opposing phases. In a high-frequency FE-FRT, the temperature rise may limit the tuning range. The twin-axial configuration doubles the tuning range for the same temperature rise in the ferroelectric wafers. A key innovation of this work is the use of CST eigenmodes to rapidly optimize the figure of merit (FoM) of the FRT tuner, with some approximations, by sweeping the parameter space, including the FE wafer dimensions and cavity geometry. The thermal analysis has also been performed to assess the temperature rise during operation.

INTRODUCTION

In modern particle accelerators, the frequency tuning system is a cornerstone for the stable operation of Radio Frequency (RF) cavities. It is imperative to tune these cavities to their design resonance and maintain this state amidst operational perturbations. Superconducting Radio Frequency (SRF) cavities, characterized by their extremely high-quality factors and narrow bandwidths, are particularly susceptible to resonance frequency shifts caused by mechanical vibrations, a phenomenon known as microphonics. Consequently, both ”slow” and ”fast” tuners have become indispensable components of SRF systems [1]. Fast Reactive Tuners are proposed as a method of changing the frequency in timescales that are sub microsecond, where an external reactance is coupled in parallel to the cavity reactance. In Ferroelectric-Fast Reactive Tuners (FE-FRT) an external capacitance is varied by applying a voltage across a ferroelectric [2].

The performance of an FE-FRT is primarily governed by its Figure of Merit (FoM) which is the ratio of the change in reactive power to the resistive power dissipated in the device. This paper presents a new FoM fast optimization method by CST eigenmode, and a novel FE-FRT structure specifically optimized for the 1.3 GHz superconducting cavities. We introduce a configuration that integrates an increased number of ferroelectric wafers to simplify the cooling requirements and propose an efficient optimization methodology for the FoM applicable to arbitrary geometries using electromagnetic simulation.

THE NEW TWIN-AXIAL TYPE FE-FRT

An FE-FRT typically is a coaxial resonator with ferroelectric wafers placed in capacitive gaps in series along its length. The more gaps the more efficient the device is but cooling on the central conductors becomes an issue if using two or more wafers. At L-band frequencies, and above, the FE-FRT becomes very compact and access to cool the central conductor becomes a major limitation. With two wafers it may be possible to only cool from the outside and cool the central conductor via conduction through the wafers but the temperature rise could be excessive if the power loss is too high. We propose two use two coaxial resonators in parallel, operating in a dipole mode, to share the heat load across 4 wafers rather than two, which will allow cooling only fom the outside. The new type of Twin-axial FRT structure is shown below in Fig. 1, in this type there are two sub-FRTs coupled together by the magnetic field.

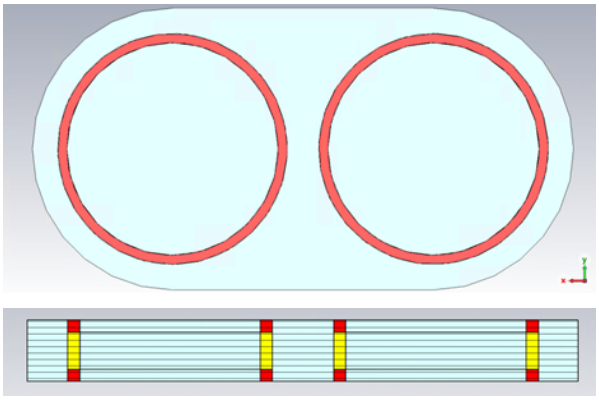

Figure 1: The geometry of the Twin-axial type FE-FRT

SRF Cavities and Microphonics

The energy stored (U_c) in an SRF cavity is a function of its accelerating gradient (E_{acc}) and the R/Q ratio. For a TESLA 9-cell cavity operating at nominal gradients, for example the UK-XFEL is about 19 MV/m, U_c typically reaches approximately 100 J [1].

Microphonics Compensation: Operational experience with TESLA cavities indicates that microphonics-induced detuning typically spans a range of ±30 Hz [3]. To provide a sufficient safety margin, the FE-FRT in this work is designed with a tuning range of ±50 Hz. Reactive Power Requirement:The required reactive RF power (P_{reactive}) is proportional to the stored energy and the detuning bandwidth $\Delta\omega$:

$$P_{\mathrm{reactive}} = \Delta\omega U_c. \quad (1)$$

Given the 100 J stored energy and the ±50 Hz tuning requirement, the FE-FRT must handle a reactive power of approximately 3.14 kVAR.

Equivalent Circuit and Perturbation Theory

The FE-FRT tuning system can be modeled as a coupled system consisting of the main power coupler, the SRF cavity,

* h.jiang6@lancaster.ac.uk

Content from this work may be used under the terms of the CC BY 4.0 licence (© 2026). Any distribution of this work must maintain attribution to the author(s), title of the work, publisher, and DOI.

ISBN: 978-3-95450-252-3 ISSN: 2673-5350 doi: 10.18429/JACoW-IPAC2026-MOP7048

UNCERTAINTY ANALYSIS OF TIME CONSTANT MEASUREMENTS IN SRF CAVITY TESTING

M. Jones*, A. Baig, C. Jenkins, P. Smith
ASTeC, STFC Daresbury Laboratory, Warrington, United Kingdom

Abstract

At the start of superconducting radio frequency (SRF) cavity testing, cavity time constant measurements are made. From the measured time constant the field probe external quality factor is calculated. This value is then used for the calculation of unloaded quality factor and accelerating gradient for the remainder of the testing process. In previous work the uncertainty of the time constant measurement has been given as 3%, but this is dependent on the measurement equipment and method used to estimate the time constant from the measured cavity decay curve. In the vertical test facility (VTF) at STFC's Daresbury Laboratory the decay curve is measured using different hardware to other facilities. We present efforts to estimate the uncertainty of time constant measurements at our VTF to compare our measurement method with those used elsewhere.

INTRODUCTION

Superconducting radio frequency (SRF) cavities are a well established technology and have been deployed in many large-scale accelerator facilities. A key stage in the production of these cavities is a test to ascertain the 2K performance of the cavity at Vertical Test Facilities (VTFs). The testing, known as "Q vs E" testing, generates a plot of the unloaded quality factor (Q_0) against accelerating gradient (E_{acc}) for a range of gradients. These values are not directly measured, and instead calculated from measurements of power incident to the cavity (forward power, P_f), reflected from the cavity (reflected power, P_r) and coupled out of the cavity via the field probe (transmitted power, P_t). Throughout most of the process in the Superconducting Radio Frequency Lab (SuRF Lab) at STFC's Daresbury Laboratory the following calculations are used:

$$Q_0 = \frac{Q_t P_t}{P_c}$$

$$E_{acc} = \sqrt{Q_t P_t \frac{r/Q}{L}}$$

Where L is the cavity length, and r/Q is the design ratio of shunt impedance to quality factor.

The field probe quality factor, Q_t, is a measure of the ratio of stored energy in the cavity to the energy dissipated externally to the cavity through the field probe in an RF period. This Q_t value is calculated early in the process from measurements of power decay, and is used in the above calculations for the remainder of the testing. The decay measurement process initially requires capturing the forward, reflected and transmitted power in steady state operation, and then switching off forward power to the SRF cavity. The stored energy is then dissipated through loss mechanisms in the cavity walls and the two couplers. With no forward power to the cavity, the total power lost (P_{tot}) over time (t) is given via:

$$P_{tot} \propto e^{\frac{-t}{\tau_L}}$$

This relationship allows for the estimation of the power decay constant of the cavity, τ_L, by tracking the field probe power following incident power switch off and using calculations to estimate the value of τ_L. The derivations required to calculate Q_t, Q_o and E_{acc} following these measurements can be found in [1]. The work discussed here focuses on the calculation of standard uncertainty that can be applied to each decay constant measurement in the SuRF Lab. The motivation of the work was to understand if the measurement method used in the SuRF Lab provides a different uncertainty than the 3-4% cited by other facilites [1–3].

DECAY CONSTANT MEASUREMENT AT DARESBURY LABORATORY

The decay measurement in the SuRF Lab is performed in a different way to other SRF cavity test facilities. The decay is measured via the envelope output of the Analog Devices ADL5511 Envelope and TruPwr RMS Detector [4], rather than a power detector [3, 5], spectrum analyser [2], or oscilloscope [6]. Between the cavity output and envelope detector there is a signal chain of switches, digital step attenuators and amplifiers that give the operator control over the power level at the input of the detector. This ensures the full dynamic range of the envelope detection system can be used at as much as practicable. The ADL5511 outputs a voltage that is proportional to the voltage envelope of the original signal. The minimum voltage output is ~1.15V, which is taken to be the noise floor.

The envelope output voltage is then digitised via a National Instruments CompactRIO with the sample rate set by the operator. A regression analysis is performed on the data by a LabVIEW program to determine the time constant of the cavity. The digitised voltage still contains the ~1.15V DC offset, so the curve never decays to zero. This necessitates the use of non-linear least squares regression methods. The testing software makes use of the LabVIEW Exponential Fit Virtual Instrument (VI), which implements the Levenburg-Marquardt algorithm [7].

Note that the envelope output of the detector is proportional to the voltage envelope of the cavity, so any calculations give the voltage time constant, which is double the power time constant used in the calculations of Q_0 and E_{acc}.

* matt.jones@stfc.ac.uk

Content from this work may be used under the terms of the CC BY 4.0 licence (© 2026). Any distribution of this work must maintain attribution to the author(s), title of the work, publisher, and DOI.

ISBN: 978-3-95450-252-3 ISSN: 2673-5350 doi: 10.18429/JACoW-IPAC2026-MOP7049

1.6 MW, 144 MHz SOLID STATE POWER AMPLIFIER FOR ELSA ELECTRON LINAC

A.-S. Chauchat[†,1,2], M. Collet[1,2], V. Le Flanchec[1,2], B. Fritsche[3]
[1]CEA DAM Île-de-France, Bruyères-le-Châtel, France
[2]Université Paris-Saclay, CEA, Laboratoire Matière en Conditions Extrêmes, Bruyères-le-Châtel, France
[3]Ampegon, Baden, Switzerland

Abstract

The 19 MeV electron linear accelerator ELSA at CEA DAM has been in operation for 30 years. A renovation of the RF system was necessary to improve the reliability of the system. The second part of the renovation addresses the 144 MHz RF amplifier that supplies power to the photo-injector. The former tetrode-based amplifier has been replaced by a 1.6 MW Solid State Power Amplifier delivered by Ampegon company. One of the challenges was to design a compact amplifier to keep the same footprint. This paper presents the amplifier, the tests and the commissioning.

INTRODUCTION

The ELSA facility was commissioned in the early 90's as a high efficiency IR FEL [1]. For this purpose, the electron linac was designed to meet FEL requirements such as low emittance beam and high repetition rate. Thus, the photo-injector was designed at 144 MHz in order to have a large homogeneous accelerating field on the photo-cathode and to minimize energy dispersion at emission. The second accelerator stage consists of 3 cavities at 433 MHz, powered by a 6 MW klystron. The original RF system was designed to deliver high repetition rate RF pulses up to 150 Hz.

Since the beginning of the 2000's, ELSA facility has been used as a high-brightness electron source or as a picosecond X-ray source either by bremsstrahlung radiation in high-Z materials or by inverse Compton scattering. Several upgrades of the facility have been made during the two last decades such as adding a third accelerating stage at 1300 MHz, adding a new beam line, improving the inverse Compton source. But the original RF sources were still in operation until recently. The main failures occurring during beam delivery were actually due to RF amplifier faults and resulted in a decrease of the mean time between failures (MTBF) because of component obsolescence. This was not acceptable for users. In 2022, the 433 MHz klystron modulator has been replaced by a new one delivered by JEMA company. In 2024, the original 2.5 MW tetrode-based amplifier was replaced by a Solid State Power Amplifier (SSPA) (Fig. 1).

SPECIFICATIONS & DESIGN

Main specifications of the RF amplifier are given in Table 1. With a maximum of 4 kW mean power, either pulse duration or repetition rate must be decreased to maximize the other parameter.



Figure 1: Picture of the new SSPA on ELSA Facility.

Whereas the pulse droop can be balanced by the low-level RF (LLRF) signal at the input, the pulse-to-pulse reproducibility specification is a parameter of uttermost importance to guarantee the stability of the electron beam, since this fluctuation is purely random.

Table 1: RF Amplifier Specifications

Parameter	Value
Frequency	144.44 MHz
Maximum power	1.6 MWp
Pulse duration	500 µs max.
Repetition rate	1-10 Hz
Mean power	4 kW max.
Pulse droop	< 2%
Pulse to pulse reproducibility	< ± 0.1%

Another important specification in this kind of equipment was the footprint available for the amplifier. It had to be fitted in a 8300 mm × 1200 mm footprint.

To meet those requirements, Ampegon Company proposed a design based on the combination of 80 × 22 kWp RF power modules with splitters and combining structures. Each module is composed of a splitter, 16 amplifier pallets fixed on a water-cooled plate, a control board and an

†anne-sophie.chauchat@cea.fr

Content from this work may be used under the terms of the CC BY 4.0 licence (© 2026). Any distribution of this work must maintain attribution to the author(s), title of the work, publisher, and DOI.

ISBN: 978-3-95450-252-3 ISSN: 2673-5350 doi: 10.18429/JACoW-IPAC2026-MOP7050

CONCEPTUAL DESIGN OF A 0.2 MW PULSED 140 GHZ GYROKLYSTRON AMPLIFIER AND STUDIES TOWARDS 1 MW OPERATION FOR ACCELERATOR APPLICATION

A. Malygin, L. Feuerstein, M. Fuchs, S. Illy, J. Jelonnek, M. Thumm, A.-S. Müller
Karlsruhe Institute of Technology, Karlsruhe, Germany

Content from this work may be used under the terms of the CC BY 4.0 licence (© 2026). Any distribution of this work must maintain attribution to the author(s), title of the work, publisher, and DOI.

Abstract

We present the conceptual design of two pulsed 140 GHz gyroklystron amplifiers intended as RF power sources for millimeter-wave accelerator systems. The interaction circuit in each design adopts a two-cavity configuration comprising an input cavity, a drift section, and an output cavity. The electron beam is generated by a triode-type magnetron injection gun (MIG), providing operational flexibility and stable performance across a broad operating range. Two gyroklystron configurations targeting output powers of 0.2 MW and 1 MW are investigated. Design details of the MIG and the interaction structures for both gyroklystron versions are presented.

INTRODUCTION

Exploration of accelerator technologies in the millimeter-wave regime offers a promising route toward extremely high accelerating gradients [1]. Owing to the high shunt impedance and short filling times of mm-wave accelerating structures relative to conventional S- and C-band systems, accelerating gradients at the GV/m level become attainable. Consequently, mm-wave accelerator concepts are of strong interest for applications such as future linear colliders, charged-particle therapy, compact X-ray free-electron lasers (XFELs), and ultrafast electron diffraction (UED) [2-4]. High-power RF sources operating in the mm-wave frequency range are therefore of considerable interest for advanced accelerator applications. This paper presents the design and simulation of two pulsed 140 GHz gyroklystrons [5-8] with target output powers of 0.2 MW and 1 MW. The 0.2 MW version is designed to operate together with a downstream pulse compressor to achieve the peak RF power levels required for high-gradient accelerator systems. In contrast, the 1 MW gyroklystron is intended to power accelerating structures directly, eliminating the need for additional pulse compression. The following sections describe the design methodology, interaction structures, and simulation results for both gyroklystron configurations.

CONCEPTUAL DESING OF A 0.2 MW PULSED 140 GHZ GYROKLYSTRON

Figure 1 illustrates a potential configuration for the 0.2 MW pulsed 140 GHz gyroklystron system. In this scheme, the input RF signal is generated by a pulsed extended interaction klystron (EIK) driven by a solid-state power amplifier (SSPA). The output RF power from the gyroklystron is subsequently compressed using a pulse compressor before being coupled into an accelerating structure for high-gradient applications.

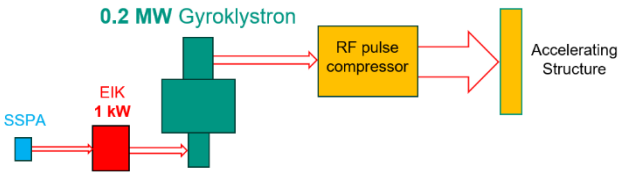

Figure 1: Layout of the 0.2 MW gyroklystron system including the SSPA, 1 kW EIK, and downstream RF pulse compressor.

The operating mode $TE_{7,3}$ in the output cavity was selected to minimize ohmic losses while providing sufficient beam–wave interaction to achieve 200 kW of output power. Simultaneously, the guiding center radius was chosen to be large enough to accommodate a 10 A electron beam while maintaining the required magnetic compression, emitter current density and guiding center spread. The design utilizes the following beam parameters: beam voltage $U = 60$ kV, beam current $I = 10$ A, pitch factor = 1.3, and a guiding center radius of 2.55 mm. A triode magnetron injection gun configuration (Fig. 2) was selected to provide enhanced flexibility in adjusting the electron beam parameters.

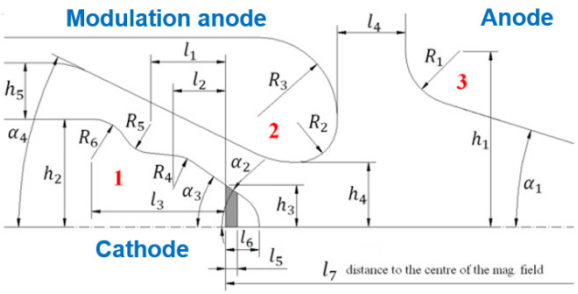

Figure 2: Configuration of the triode magnetron injection gun (MIG) with the key optimization parameters indicated.

The achieved electron beam parameters are summarized in Table 1; all values meet the specified requirements. The electron beam trajectories and the electric field distribution within the triode MIG are displayed in the top and bottom panels of Fig. 3, respectively. The two-cavity configuration, shown in Fig. 4, consists of an input cavity, a drift section, and an output section. Multimode simulations were performed using simpleRICK [5], an in-house code developed at the Institute for Pulsed Power and Microwave Technology (IHM) at the Karlsruhe Institute of Technology (KIT).

ISBN: 978-3-95450-252-3 ISSN: 2673-5350 doi: 10.18429/JACoW-IPAC2026-MOP7052

OPERATIONAL EXPERIENCE ON A COMMERCIAL SOLID STATE POWER AMPLIFIER WITH INTEGRATED LLRF UNIT

D. Giove, M. Bertucci, A. Bosotti, R. Paparella, Istituto Nazionale di Fisica Nucleare, Laboratori Acceleratori e Superconduttività Applicata, Segrate, Italy
F. Corvo, M. Villa, M. Corvino, R. Cavallanti SyES, Lissone, Italy

Content from this work may be used under the terms of the CC BY 4.0 licence (© 2026). Any distribution of this work must maintain attribution to the author(s), title of the work, publisher, and DOI.

Abstract

In this contribution we report on the operational experience gained with a commercial off-the-shelf solid-state RF power amplifier equipped with an embedded low-level RF (LLRF) control system, in use for the sub-harmonic buncher cavity of the HB²TF project at INFN LASA. We summarize the motivations behind adopting a turnkey solution, highlighting expected benefits in terms of reliability, maintainability, and integration effort. The paper presents the main results of our testing campaign, including performance stability, response under varying operating conditions, and preliminary assessments of control accuracy. Finally, we provide notes on the synchronization strategy implemented to interface the RF control system with the laser-driven photo-cathode used as beam source.

INTRODUCTION

The electron bunches generated by the DC Gun of the HB2TF Test Facility currently being installed at INFN LASA [1] have a long longitudinal profile to avoid emittance dilution. After the gun, to minimize nonlinear energy spreading due to RF waveform in the foreseen SC booster, bunches need to be compressed to shorter length. As the beam is still non-relativistic, the simplest method of bunch compression is the velocity bunching. To this purpose a sub-harmonic bunching stage has been designed making use of two 650 MHz, spherical re-entrant shape, copper cavities. The first of these two buncher cavities (Buncher #1) has been machined and will be installed and tested in June 2026 on the first version of the beam line. The cavity will operate using a power amplifier internally specified and commissioned to the Italian Company SyES srl [2]. In this paper we will describe the main features of the amplifier and the first experience gained during its development.

THE BUNCHER CAVITIES

The two bunchers designed for the HB²TF test-stand took inspiration from the structure used in cERL and scaled down in frequency. The E.M. studies have been carried out using as a first tool the Superfish code and the detailed behavior has been optimized using Ansys HFSS commercial simulator.

The cavities have been machined from bulk copper pieces using a high-precision lathe and the resulting two main halves have been brazed. The cooling channels have been inserted in the outer shell of the cavities, and they are able to remove all the thermal power dissipated in the wall. The cooling circuit comprises an external thermos-chiller (model HRS 150-WF-40 from SMC) for each cavity.

A compact coaxial power coupler, able to withstand the full incident RF power, has been designed and is now in the machining phase. Further details about the buncher cavities, the coaxial power coupler and their current status are in the paper THP2107 [3] also at this conference.

The beam loading of the buncher cavities is minor, as the RF power is almost all dissipated in the cavity walls. The power budget to feed both buncher cavities is reported in Table 1.

Table 1: Nominal Requirements for the RF Power Chain of the Two Bunchers

	$E_{z\ max}$ = 2.7 [MV/m] Buncher #1	$E_{z\ max}$ = 2.7 [MV/m] Buncher #2
Beam power [kW]	2	2
Cavity power [kW]	11	14
Total power [kW]	13	16
+15% margin	15	18
Target forward power – [kW]	16-18	18-20

POWER AMPLIFIER REQUIREMENTS

The use of RF power amplifier with resonating cavities introduces specific operational aspects that in turn result in few uncommon requirements for the amplification unit. These may be summarized as in the following:

- Fast response time for RF shutdown: the electric fields excited in the resonant cavity can occasionally generate discharges. Since a discharge causes a large mismatch in the load, the reflected power will increase significantly. The implemented protection system will shut down the RF power (zeroing the small signal) in a time interval suitable to prevent damage to the amplifier.
- Robustness to multipacting: multipacting is a resonant permanent discharge phenomenon that may occur when operating a resonator under vacuum. It causes a mismatch in the load, which results in an increase in the VSWR (Voltage Standing Wave Ratio).
- Compliancy to pulsed operation at least for cavity conditioning: cavity conditioning requires rapid pulsing of the RF signal while steadily increasing both amplitude and duration until target operating conditions are achieved. Typical pulses in use could be:
    - Forward power rise time: < 1 μs
    - Pulse duration: 20 – 100 μs

ISBN: 978-3-95450-252-3 ISSN: 2673-5350 doi: 10.18429/JACoW-IPAC2026-MOP7054

LIPAC RF SYSTEM: ON THE VERSATILE USE OF PHOTOMULTIPLIERS*

J.-P. Adam†, CEA, DAM, CEA-Gramat, F-46500, Gramat, France
L. Maurice, CEA Paris-Saclay - Etablissement de Saclay, Saclay, France
F. Scantamburlo, Fusion for Energy, Rokkasho, Japan
K. Hirosawa, National Institutes for Quantum Science and Technology, Rokkasho, Japan

Abstract

As part of the Linear IFMIF Prototype Accelerator (LIPAc) and its Radio Frequency (RF) system protection, three applications of PhotoMultipliers (PMs) are presented.

INTRODUCTION

LIPAc (Linear IFMIF Prototype Accelerator) in Rokkasho, Japan, an accelerator designed to provide a 125 mA deuteron beam up to 9 MeV in CW (Continuous Wave), is an important step to study materials that will withstand the intense neutron flux coming from the fusion plasma of future Tokamaks [1].

Modern photomultipliers (PMs) are affordable, highly sensitive, easy to operate, compact with convenient form factors, and sufficiently robust for demanding accelerator environments. For LIPAc Radio Frequency (RF) subsystem which delivers over 2 MW of RF power distributed among all the accelerating cavities (Fig. 1), these characteristics make PMs particularly effective for monitoring components prone to multipacting and micro-discharge. The light produced by these phenomena is detected even at very low levels, enabling detailed investigation and fast triggering of interlocks.

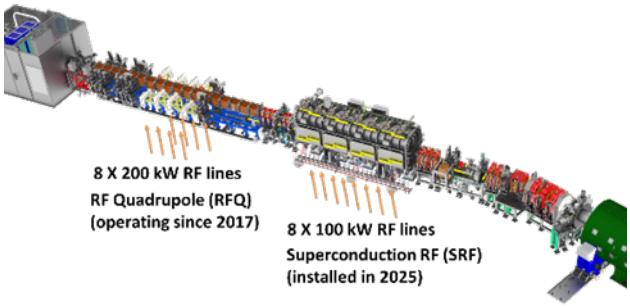

Figure 1: Overview of LIPAc.

APPLICATION 1: SRF LINAC COUPLERS

At LIPAc, the Superconducting RF (SRF) accelerator currently being commissioned is fully equipped with PMs for early arc detection, enabling a fast RF power shutdown and thus avoiding severe damage caused by arcs. As shown in Fig. 2, the detectors are located at a T-shaped transition and at the RF window. This latter part separates the vacuum section from the air section of the power coupler, and it can be a weak point as well as a location where multipacting occurs on its vacuum side.

This is the standard setup for power couplers designed by CEA/Saclay [2]. This fact made a specific PM easily available on-site (Hamamatsu photomultiplier tube module H10721) and made the other applications presented here possible.

Small sized PMs can be installed very close to the power coupler to significantly reduce the fiber length. Short optic fibers have significant advantages: reduced attenuation due to fiber aging (see part 3 of this document) and no false trigger due to the Cherenkov effect in fiber as reported in [3]. However, some drawbacks need to be considered: the PMs are not specifically designed as radiation-resistant and their driver circuit needs bulky control cable bundles with 5 lines and sufficient EMC shielding.

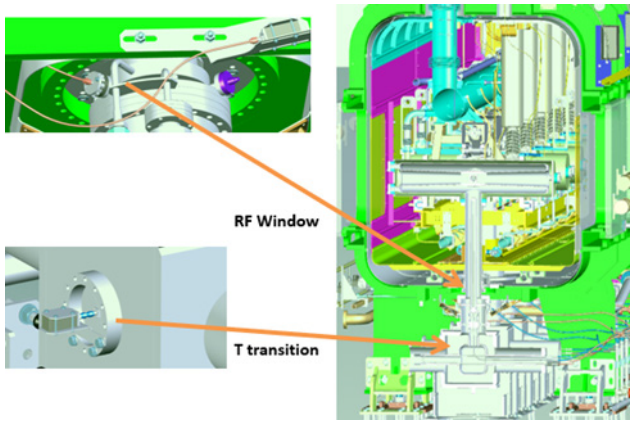

Figure 2: Locations of the PMs installed in the SRF of LIPAc. The 8 SRF cavities have the same setup. For the RF window, the PM is not directly on the viewport (short orange fiber) for accessibility.

APPLICATION 2: HIGH POWER TEST BENCH

PMs have also been successfully used in a temporary test bench for the conditioning of RF Quadrupole (RFQ) couplers. The setup is described in detail in [4]. Since power couplers are involved, this application is naturally derived from part 1 of this document. The first version of the protection system was based on commercially available arc detectors; however, their sensitivity was not suitable for multipacting analysis. The setup was easily converted to a

*This work was undertaken under the Broader Approach Agreement between the European Atomic Energy Community and the Government of Japan.
†jean-pierre.adam@cea.fr

Content from this work may be used under the terms of the CC BY 4.0 licence (© 2026). Any distribution of this work must maintain attribution to the author(s), title of the work, publisher, and DOI.

ISBN: 978-3-95450-252-3 ISSN: 2673-5350 doi: 10.18429/JACoW-IPAC2026-MOP7055

RF POWER TRANSIENTS AT INJECTION ENERGY IN THE FCC-ee HIGH-ENERGY BOOSTER

L. Valle*, I. Karpov
CERN, Geneva, Switzerland

Abstract

The FCC high-energy booster RF system consists of 112 superconducting cavities at 800 MHz for the operation modes at ZZ, WW, and ZH energies, with an additional 408 cavities for the $\bar{t}t$ stage. The first three working points require a wide total voltage range from 50 MV to 2 GV. To cover this huge range, Reverse Phase Operation (RPO) will be employed. It groups the cavities into focusing and defocusing families, according to their phase. To provide beam for the relevant operation modes with the booster and provide sufficient voltage per cavity, the RF power requirements are estimated and minimized analytically assuming a defined detuning program. This includes Lorentz force detuning compensation. Additionally, transient power requirements of the RF system in the RPO operation are dynamically computed using the BLonD tracking code. The simulations are performed with sparse profiles, to limit the beam observation to the filled buckets. An LHC-like cavity feedback is adapted to the booster characteristics and allocated to both RPO families. Mitigation measures to reduce the power transients are discussed in this contribution.

INTRODUCTION

The FCC high-energy booster alternatively prepares electrons and positrons for injection into the collider. Each booster cycle includes an accumulation period at flat bottom with parameters listed in Table 1. Then, an acceleration part brings the bunches to the design extraction energy for injection into the collider. The energy ramp of the ZZ mode includes an overshoot in energy to boost radiation damping and achieve smaller beam sizes at extraction [1]. Finally, a flat top for extraction followed by a 'deceleration' mode restore the booster parameters before the following cycle. This contribution focuses on the accumulation part of the booster cycles for all foreseen operation modes.

Table 1: Parameters of the Booster Cycles for all Four Operation Modes

Mode	ZZ	WW	ZH	$\bar{t}t$
Number of bunches	1120	928	292	60
Bunch intensity [10^{10}]	2.725	1.268	1.268	1.268
Accumulation time [s]	2.8	2.32	1.92	0.6
Number of trains	40	8	2	2
Number of batches per train	7	29	146	30
Number of bunches per batch	4	4	2	2
Injection rate [Hz]	100	100	100	50

* lina.valle@cern.ch

SIMULATION FRAMEWORK

Macroparticle tracking simulations of the full accumulation period of each booster cycle has been conducted using the code Beam LONgitudinal Dynamics (BLonD) [2]. Particles are represented via macroparticles. The beam profile is obtained as a time projection of the bunch distribution in the longitudinal phase space. The time resolution is defined by slices. In the case of the FCC-ee booster, the bunches are about 60 ps-long in a 1.25 ns bucket and distributed along the 242400 buckets. Consequently, the profile object requires a large number of slices to properly resolve the FCC bunches along the 90 km high-energy booster.

Sparse Profiles and Multi-Turn Injection

Optimizing simulations for memory usage required the development of so-called sparse profiles. A sparse profile holds a finite number of continuous sub-profiles. Each sub-profile covers one or multiple buckets, defined through a filling pattern. Previous implementations defined a continuous profile per bucket for beam monitoring. An update extended the sparse profiles to create a profile per bucket or batch, respectively. For instance, for 1024 slices per bucket, a significant reduction of a factor 112 and 5.6 is achieved with a sparse profiles per bucket and per batch respectively, for the initial two batches of the ZZ booster cycle. The sparse profiles only hold slices at the supposed location of the bunches, alleviating their memory allocation.

Implementation of the cavity feedback in the booster BLonD simulation called for a continuous profile over one batch, as the charge counting of the RF beam current calculation needs a profile length longer than a bucket. As such, a sparse profile per batch was implementing for accurate charge counting. Additionally, the input file of BLonD was reworked towards minimization of memory: the tracking map is prepared outside the main file, results and beam files saved at each turn for post-processing.

Cavity Loop Parameters

Each cavity must be equipped with its own feedback system. For the simulations, the LHC direct RF feedback was adapted to the FCC-ee booster characteristics [3, 4]. The gain G_a of the feedback is adjusted for each booster cycle to ensure that the RF power required for compensation of transient beam loading does not exceed the power source limit of 60 kW [5]. This contribution refers to the ratio $a = G_\mathrm{a}/G_\mathrm{a}^\mathrm{max}$, with $G_a^\mathrm{max} = 1/2/(R/Q\omega_\mathrm{RF}\tau_{loop})$ as the maximum gain which ensures the loop stability [6]. The ratio R/Q is the normalized shunt impedance, ω_RF the angular RF frequency and the overall loop delay $\tau_\mathrm{loop} = 700$ ns. The

Content from this work may be used under the terms of the CC BY 4.0 licence (© 2026). Any distribution of this work must maintain attribution to the author(s), title of the work, publisher, and DOI.

ISBN: 978-3-95450-252-3 ISSN: 2673-5350 doi: 10.18429/JACoW-IPAC2026-MOP7056

INTEGRATION OF A GaN HEMT SOLID-STATE DRIVER AMPLIFIER FOR THE 10 MHz RF SYSTEM OF THE CERN PS

M. Taquet*, G. Gnemmi†, H. Damerau, S. Energico, M. Morvillo, S.Ramberger
CERN, Geneva, Switzerland

Abstract

The progressive obsolescence and the discontinuation of vacuum tube production are driving the transition towards solid-state alternatives in RF acceleration systems. In the 10 MHz RF system of the Proton Synchrotron (PS) at CERN, the discontinuation of a specific tetrode model used in the amplifier chain has motivated the evaluation of solid-state technology as a potential replacement. In particular, amplifiers based on Gallium Nitride High Electron Mobility Transistors (GaN HEMTs) are being considered due to their inherent radiation tolerance. For this purpose, a prototype driver amplifier based on the GaN technology has been built. This contribution presents the different development steps of this prototype, as well as its integration into the 10 MHz RF system. This includes a system-level description of the RF system and of the constraints associated to the integration of such a prototype, followed by its hardware description and qualification process. This qualification was carried out in two steps: firstly through RF measurements without beam, and secondly with a characterization of the system with high-intensity proton beams, under normal operating conditions.

THE 10 MHz RF SYSTEM IN THE PS

The Proton Synchrotron (PS) at CERN accelerates high-intensity protons up to an energy of 26 GeV. The longitudinal beam structure and energy is obtained through the cumulative action of several RF systems [1]. Among those, the main RF system can operate at multiple harmonics of the revolution frequency. It consists of 11 cavities distributed over the entire PS circumference. Each cavity comprises two $\lambda/4$ resonators loaded with ferrite rings. A bias field in these ferrite rings allows tuning of the cavity from 2.8 MHz to 10 MHz [2]. The accelerating field develops across capacitive gaps.

The amplifier chain feeding the power to the cavity relies on tetrode amplifiers. It is composed of a driver stage with three YL1056 tubes and a final stage based on a single RS1084CJ tetrode. While this technology has historically provided robust performance in the high-radiation environment of the PS, it now faces progressive phase-out of key components. The discontinuation of the YL1056 tetrode in 2022 highlights a broader trend of obsolescence in RF vacuum tube technology, raising concerns regarding the long-term availability and maintainability of vacuum tube-based RF systems at CERN. Consequently, alternative solutions, such as the solid-state technology, must be investigated to ensure continued operation.

While Metal–Oxide–Semiconductor Field-Effect Transistors (MOSFETs) are already used in low-radiation areas at CERN [3], higher radiation levels in the 10 MHz cavity locations limit their application. A promising alternative is the Gallium Nitride High Electron Mobility Transistor (GaN HEMT), which offers significantly higher radiation resistance [4,5]. Multiple irradiation campaigns are ongoing to assess the suitability of GaN devices in the PS environment [6–8].

This paper is focused on the integration of an internally developed GaN-based amplifier in the 10 MHz RF system, with the objective of demonstrating the feasibility of replacing the tetrode-based driver stage with a solid-state alternative. For this purpose, an overview of the RF system and the constraints associated with integrating such a prototype amplifier into the existing RF system is first provided. The two main stages of its qualification within the amplifier chain are then discussed: RF measurements without beam, followed by a characterization of the system with high-intensity proton beams, under operational conditions.

THE SOLID-STATE DRIVER

The integration of a solid-state driver amplifier into the existing 10 MHz RF system imposes constraints beyond those associated with driving the final stage to achieve 10 kV at the cavity gaps. These constraints have guided the hardware choices for the amplifier design. As illustrated in the block diagram with the new driver amplifier (Fig. 1), the RF system comprises several feedback control loops designed to reduce beam loading.

A wideband feedback loop around the driver and final amplifiers, as well as the cavity reduces the beam-induced voltage. As the system operates across a large bandwidth over which the phase changes significantly, a tunable element is required to maintain negative feedback in the entire frequency range. This is achieved by means of a tunable grid resonator, installed between the driver and final stages. As a result, the driver amplifier must maintain stable operation over the frequency range while driving a varying load. The grid resonator contributes mainly to the overall group delay of the wideband feedback loop [2], which must be minimized to maximize the achievable stable gain. To mitigate this effect without reducing the real part of the resonator impedance, thereby avoiding an increase in the power required to the driver amplifier, the latter is equipped with a local feedback loop based on the same principle as

* mathieu.florent.taquet@cern.ch
† giulia.gnemmi@cern.ch

Content from this work may be used under the terms of the CC BY 4.0 licence (© 2026). Any distribution of this work must maintain attribution to the author(s), title of the work, publisher, and DOI.

ISBN: 978-3-95450-252-3 ISSN: 2673-5350 doi: 10.18429/JACoW-IPAC2026-MOP7058

MAGNETS DEVELOPMENT FOR THE ESRF-EBS INJECTION UPGRADE

C. Benabderrahmane†, D. Baboulin, T. Brochard, N. Carmignani, G. Le Bec, B. Ogier, S. White
European Synchrotron Radiation Facility, Grenoble, France

Abstract

Projects to improve the injection performance of the storage ring and to reduce the equilibrium emittance of the booster are currently in progress at the ESRF. The booster light upgrade involves replacing 18 existing quadrupoles with 3 families (6 magnets per family) of quadrupoles featuring different yoke lengths. An upgrade of the injection zone includes the installation of a Non-Linear Kicker and the replacement or modification of several electromagnets, as well as the septum S3. In this paper, we present the magnetic design of the booster electromagnet quadrupoles and the TL2 transfer-line permanent-magnet quadrupoles. A preliminary design of a permanent magnet septum S3 is also presented.

INTRODUCTION

The ESRF booster was constructed over 30 years ago as the injector for the original ESRF storage ring and remains in use today for injection into the Extremely Brilliant Source (EBS). While several of its components have been upgraded over time, and it is now operated off-energy with emittance exchange at extraction, the lattice itself has not been modified since the 1990s. A proposed upgrade aims to reduce both the equilibrium emittance and the bunch length by replacing 18 quadrupole magnets [1]. The booster is based on a FODO lattice with three straight sections featuring dispersion suppression. It currently includes 39 focusing quadrupoles, 39 defocusing quadrupoles, and 66 dipoles, all powered in series by independent channels of the Ramped Injector Power Supply (RIPS). This upgrade is relatively cost-effective, as it reuses the existing ramped power supply and requires only the replacement of 18 quadrupole magnets. The new lattice design achieves lower horizontal emittance and shorter bunch length (Table 1). An additional benefit of replacing these magnets is the recovery of 18 old quadrupoles that can be kept as spares, addressing the current limitation of having only two spare units available.

Table 1: Main Booster Parameters

	Present Booster	Light Upgrade
εx (nm rad)	83.1	59.6
BL (mm)	22.6	19.9
Quad families	2	5
Sext families	2	2

The ESRF-EBS injection scheme currently relies on a conventional off-axis injection using four kickers. In user service mode (USM), this approach achieves an injection efficiency of up to 80%. However, during injection, some beamlines are perturbed and data acquisition must be temporarily halted. The existing system is now reaching its limits in meeting the objective of fully transparent injection, making it necessary to explore alternative schemes.

A new approach based on non-linear kickers (NLK) has therefore been considered. Preliminary studies indicate that this scheme could enable fully transparent injection while preserving high injection efficiency [2]. To implement this solution, modifications to both the storage ring and transfer line optics, as well as to the lattice layout, were required. These changes ensure the integration of the non-linear kickers within the injection cells and the replacement or modification of several electromagnets, as well as the septum S3.

DESIGN OF BOOSTER QUADRUPOLE MAGNETS

The magnets will be laminated to limit the eddy currents generated by the energy ramp. Table 2 presents the main parameters of the booster quadrupole magnets. The magnetic design of the 18 booster quadrupoles magnet has been done using Radia Software [3] (Fig.1).

Table 2: Booster Quadrupole Parameters

Description	Parameter	Unit
Gradient	15	T/m
Bore radius	30	mm
Current	481	A
Magnet length	500-575	mm
Ramping rate	4	Hz

The design of the new quadrupole is based on the existing magnet geometry, with a limited number of targeted modifications. In particular, the previously implemented multi-step chamfer with a specific contour has been removed in favour of a simplified pole profile. This change reduces manufacturing complexity while maintaining the required magnetic performance. The 18 quadrupoles are divided into three families, with six magnets in each family. All magnets share the same two-dimensional cross-section; the only difference lies in their length along the longitudinal (beam) axis. The integrated multipoles are reduced to few units for all the current range from 15 A to 481 A.

Figure 2 shows the mechanical design of the booster quadrupole. The main differences from the current design lie in the pole profile, as well as in the electrical and hydraulic connections.

† bchams@esrf.fr

Content from this work may be used under the terms of the CC BY 4.0 licence (© 2026). Any distribution of this work must maintain attribution to the author(s), title of the work, publisher, and DOI.

ISBN: 978-3-95450-252-3 ISSN: 2673-5350 doi: 10.18429/JACoW-IPAC2026-MOP7059

THE SOLEIL II MAGNETS

A. Ouazib*, F. Marteau, R. Bailler, Y. Benyakhlef, A. Berlioux, M.-E. Couprie, A. Esper, Ch. Kitegi, A. Loulergue, T. Mutin, V. Pinty, K. Tavakoli, C. Tournier
Synchrotron SOLEIL, Saint-Aubin, France

Abstract

The SOLEIL II upgrade relies on a lattice combining 7BA and 4BA High-Order Achromat (HOA) cells. Strict compactness constraints and energy efficiency objectives have driven the adoption of permanent magnet based technology for the main bending and focusing elements, while quadrupole correctors, sextupoles, and octupoles remain resistive to preserve operational flexibility. This paper presents the latest progress in the design, optimization, and prototyping of the SOLEIL II magnet system.

INTRODUCTION

SOLEIL II, the upgrade project of the SOLEIL booster and storage ring, aims at reducing the horizontal emittance of the electron beam to 85 pm·rad. To achieve this goal, the lattice combines 7BA and 4BA HOA cells [1–3]. This performance requires an exceptionally dense magnet system, with approximately 1300 magnets integrated into the existing storage ring tunnel, which currently accommodates 312 magnets, imposing severe constraints on compactness and integration. This was addressed by designing more compact magnets with improved performance. This paper summarizes the current status of the magnet development program for SOLEIL II at the launch of the construction phase [4, 5].

PERMANENT MAGNET BASED DIPOLES AND QUADRUPOLES

Dipoles, quadrupoles and reverse bends of SOLEIL II are iron dominated magnets, using low-carbon steels combined with Samarium Cobalt (Sm_2Co_{17}) permanent magnet blocks. The list of all permanent magnets designed for SOLEIL II is presented in table 1.

Dipoles

Based on the initial design [6], two dipole prototypes, a short dipole and a three region 3T long dipole (figure 1) were produced to validate the design. Measurements on these prototypes were conducted using a single stretched wire (SSW) system [7] and Hall probe measurements. Good agreement was observed between both measurements and the calculated fields, with less than 0.5% error in the integrated field and less than 1% error in the integrated gradient. All magnetic calculations are performed using OPERA software suite [8]. Due to the compactness of the machine, magnetic crosstalk induces additional multipole components [6]. To mitigate these effects, magnetic shielding was tested on the prototypes and subsequently adopted for all dipoles.

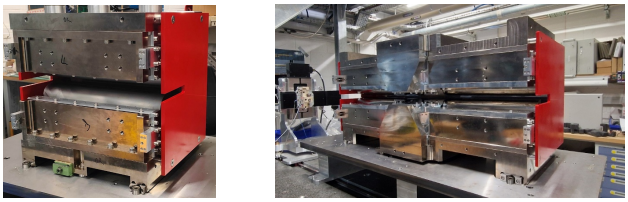

Figure 1: Dipole prototypes with shielding plates. short dipole (left), 3 region 3T long dipole (right).

Several modifications to the initial design were introduced for the final configuration. The short dipoles length was reduced while maintaining the same magnetic field strength. Single region long dipoles were introduced and replaced all the 1.2 T three region dipoles, with only 12 higher-field three-region dipoles (1.7 T and 3 T) retained. In addition, the three regions were physically separated, resulting in three-part dipoles. These modifications reduced design complexity while increasing overall compactness. Figure 2 shows 3D models of the final dipole configuration.

In addition to the standard 7BA/4BA cells, the lattice contains one special 7BA cell with 3 special permanent magnet chicane dipoles designed in order to accommodate two canted undulators on the same straight section.

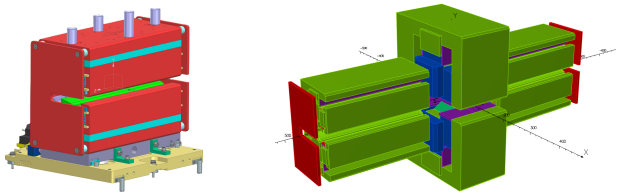

Figure 2: 3D models of the dipoles with shielding plates. short dipole (left), 3 part long 3T dipole (right).

Quadrupoles and Reverse Bends

The quadrupole and reverse bend designs remain unchanged and follow the geometry proposed by ESRF [9]. Fourteen mechanical families are designed to produce 24 magnetic families by adjusting the thickness of magnetic



Figure 3: Quadrupole prototype 2.

* abderraouf.ouazib@synchrotron-soleil.fr

Content from this work may be used under the terms of the CC BY 4.0 licence (© 2026). Any distribution of this work must maintain attribution to the author(s), title of the work, publisher, and DOI.

ISBN: 978-3-95450-252-3 ISSN: 2673-5350 doi: 10.18429/JACoW-IPAC2026-MOP7060

CONCEPTUAL ELECTROMAGNETIC DESIGN OF A MAGNETISED HADRON STOPPER FOR THE BDF/SHIP EXPERIMENT AT CERN

V. Ferrentino*, M. Liebsch, D. Schoerling, P. Schwarz
CERN, Meyrin, Switzerland

Abstract

The discovery of the Higgs boson marked a major milestone for the Standard Model of particle physics. Nevertheless, several open questions remain, including the nature of dark matter, neutrino oscillations and baryon asymmetry of the universe. Many theoretical models predict new, yet undiscovered particles; however, their detection remains highly challenging due to their weak interactions with ordinary matter. In this context, the SHiP experiment at CERN aims to explore feebly interacting long-lived particles. This paper presents the electromagnetic design of a magnetised hadron stopper for SHiP, required to absorb residual secondary particles from the hadronic shower and providing dipole strength to deflect muons trajectories. The design is particularly challenging due to the high-radiation environment, stringent spatial constraints, and demanding magnetic field requirements. The magnetic design is developed and validated using finite-element models. The results prove that the proposed design meets the magnetic requirements while ensuring flexibility for manufacturing and maintenance, and support the development of a reduced-scale prototype.

INTRODUCTION

The Magnetised Hadron Stopper (MHS) is part of the Beam Dump Facility (BDF) upgrade [1, 2] within the High Intensity upgrade for the ECN3 North Experimental Area (HI-ECN3) of the Super Proton Synchrotron (SPS) at CERN [3,4]. It is a key element of the Muon Shield (MS) [5] for the Search for Hidden Particles (SHiP) experiment foreseen to be installed there. Figure 1 shows the layout of the BDF target station, with the MHS highlighted by the orange rectangle. It fulfills two primary functions: it absorbs residual secondary particles from the hadronic shower induced by the proton beam interaction with the target and initiates the deflection of the muon flux away from the SHiP detector acceptance. The MHS electromagnetic design poses significant challenges. A compact geometry is required to facilitate manufacturing, installation and maintenance. To sufficiently deflect muons with momenta up to 350 GeV/c, a magnetic flux density of 1.9 T is needed. In addition, the proximity to the target vessel exposes the MHS to high radiation levels, demanding a challenging coil design to enable reliable operation over the 15 years of data taking foreseen for the experiment. This paper presents the electromagnetic design of the MHS, optimised to achieve the target magnetic flux density while meeting spatial constraints and limiting manufacturing and operational costs. The 2D cross-section and the coil design are presented and validated through 2D and 3D Finite-Element (FE) simulations. To enable intervention on the coil in case of failure, a careful optimisation of the magnetic circuit to limit residual magnetization and the associated magnetic forces is also performed.

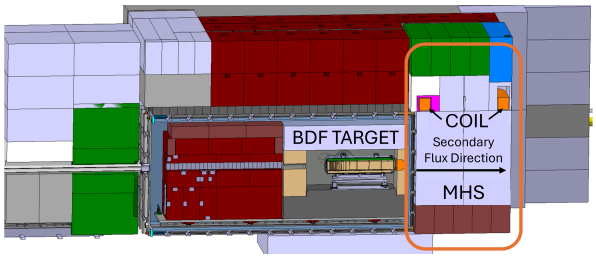

Figure 1: MS complex layout [5].

MHS GEOMETRY

The MHS is an unconventional magnet as it does not require a central aperture. The design follows an install-and-forget philosophy, with coil failure representing the only potential intervention (a part from disposal). The MHS is manufactured with adjacent blocks to facilitate manufacturing, transport and installation. The 2D cross-section of the magnet is shown in Fig. 2. The core (dark blue) is made of high-purity ultra-low-carbon steel (XC06) [6], with transverse dimensions of 0.8 m × 0.8 m ($w_0 \times h_0$). Its centre corresponds to the beam axis. This material and its geometry are selected to concentrate the magnetic flux in the core, enabling the 1.9 T target field to be achieved. To reduce manufacturing costs, the return yoke (light blue) is assembled from 1010 steel, which still provides adequate permeability. The coil region (red) includes conductors, inter-turn and ground insulation. To limit ionizing radiation damage, the coil is positioned at 1.7 m from the beam axis. The iron block between the coil windings is also made of XC06 to mitigate local saturation. Green areas consist of non-magnetic steel.

While the yoke is normally demagnetised before intervention, this may not be possible in the event of a complete failure of the coil. Thus, non-magnetic sheets (black) are placed between the coil insert and the uppermost block to enable removal of the upper yoke block under residual magnetisation. To control the residual field and ensure manageable magnetic forces during lifting, the thickness of the non-magnetic sheet is $g_{a,m} = 6$ mm. 1 mm air gaps (g_a) are also included to account for contact imperfections between adjacent iron blocks, increasing the reluctance of the magnetic circuit. The return yoke block widths (ω_1, ω_2 and ω_3),

* email: vittorio.ferrentino@cern.ch

Content from this work may be used under the terms of the CC BY 4.0 licence (© 2026). Any distribution of this work must maintain attribution to the author(s), title of the work, publisher, and DOI.

ISBN: 978-3-95450-252-3 ISSN: 2673-5350 doi: 10.18429/JACoW-IPAC2026-MOP7061

ELETTRA 2.0 MAGNETS AND MAGNETIC MEASUREMENTS RESULTS

D.Castronovo†, D.Caiazza, A.Gubertini
Elettra Sincrotrone Trieste, Basovizza, Italy

Abstract

The Elettra 2.0 project involves the installation of 648 new electromagnets for the upgrade of the existing light source [1]. Following the design and prototyping phase, the magnet series are currently being manufactured and delivered to Elettra to be suitably characterized before the installation. To this aim, a new magnetic measurement laboratory has been built and equipped during last year.

The measurements currently being performed at Elettra consists of the magnetic field quality measurement (for acceptance tests), magnetic field excitation curves, the alignment of multipole magnet, and the 3D magnetic field mapping. This article presents the results of the magnetic measurements performed until now.

MAGNETS

As previously reported [2], the magnet layout of Elettra 2.0 consists of 552 iron-dominated magnets, comprising 72 dipoles, 24 correctors, 168 quadrupoles, 240 sextupoles, 48 octupoles, and 72 fast correctors made from air coils. The magnets were procured through two interna-tional tenders: one comprising two lots of solid-iron quadrupoles and laminated-core sextupoles and octupoles; the other comprising a single lot of all solid-iron dipoles. The former and latter tenders were awarded to Danfysik A/S (DK) and SigmaPhi Electronics (FR), respectively. The contracts for the quadrupole and multipolar magnets tender were countersigned by Danfysik in August 2023, and the relevant deliveries were completed in March 2026. The contract for the dipole magnets tender was counter-signed by SigmaPhi in December 2023, and the relevant deliveries will be completed by August 2026. As stipulated in the aforementioned contracts, magnetic measurements are not included in the scope of supply and are performed at Elettra [2]. Until April 2026, 120 multipolar magnets were measured, including 36 Q24RB, 12 Q24RBs, 14 Sx20, 48 Sx16 and 9 Sx16s.

Measurement results are presented and discussed in the following paragraphs.

QUADRUPOLES

Unlike all other magnets, in the case of quadrupoles, the production of the First of the Serie (FoS) revealed an effect that had not been predicted in the simulations. The high quality of the magnetic field (achieved through the optimisation of the pole profiles and the precision of the assembly of the pole roots) has, in fact, emphasized a constant sextupole component stemming solely from the Earth's magnetic field. After some investigations, it be-came clear that the reason for this anomaly was due to the fact that the yoke of the quadrupoles consisted mainly of two magnetic halves separated by non-magnetic aluminum spacers. By manufacturing the spacers from iron too, it was possible to close the magnetic circuit around the poles and thus cancel out the magnetic potential (and the associated sextupole component) of the Earth's magnetic field.

Figures and table below report the results of the magnetic measurements carried out using the rotating coil technique [3]. Table 1 and Figure 1 report the Q24RB results.

Table 1: Q24RB Magnetic Measurement Avarage Values

Current [A]	-∫B2 [T]	∫c3 [units]	∫c4 [units]	∫c6 [units]
50	6.65	1.34	0.24	0.06
70	9.23	1.40	0.25	0.06
90	11.71	1.29	0.26	0.06
100	12.71	1.25	0.25	0.07

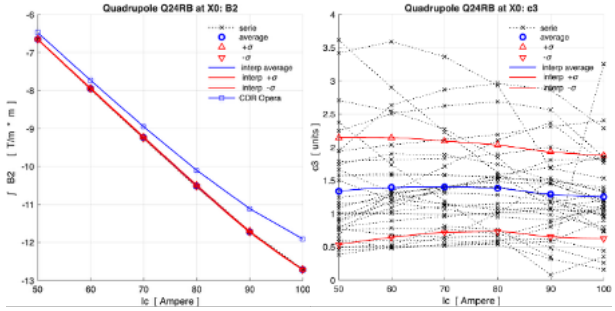

Figure 1: Q24RB magnetic measurement results.

Table 2 and Figure 2 report the Q24RBs results.

Table 2: Q24RBs Magnetic Measurement Average Values

Current [A]	-∫B2 [T]	∫c3 [units]	∫c4 [units]	∫c6 [units]
50	6.65	1.39	0.17	0.04
70	9.26	1.33	0.17	0.03
90	11.71	1.46	0.21	0.04
100	12.66	1.28	0.25	0.07

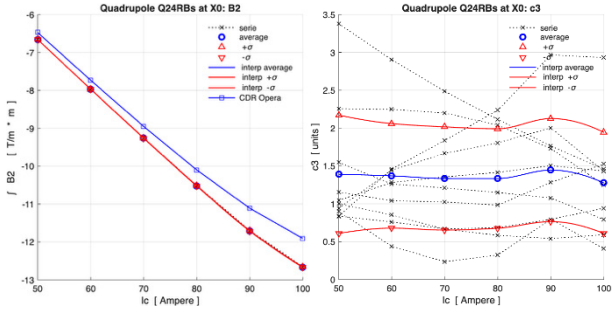

Figure 2: Q24RBs magnetic measurement results.

Content from this work may be used under the terms of the CC BY 4.0 licence (© 2026). Any distribution of this work must maintain attribution to the author(s), title of the work, publisher, and DOI.

ISBN: 978-3-95450-252-3 ISSN: 2673-5350 doi: 10.18429/JACoW-IPAC2026-MOP7063

THE NEW CALIBRATION SYSTEM FOR MAGNETIC FIELD PROBES AT THE LNF-INFN MAGNETIC MEASUREMENT LABORATORY

A. Trigilio*[1], M. Del Franco[1], L. Sabbatini[1], A. Vannozzi[1],
L. Bernot[2], R. Boucher[2], C. Germain[2], M. Rollo†[2], S. Travel[2]
[1]National Institute for Nuclear Physics, National Laboratories of Frascati, Frascati, Italy
[2]CAYLAR Scientific Instrumentation, Villebon-sur-Yvette, France

Abstract

Accurate calibration of probes is essential for high-quality magnetic-field measurements. Within the PNRR IRIS project, the Magnetic Measurement Facility (MMF) at LNF-INFN has implemented a new dedicated calibration system designed and manufactured by CAYLAR. The setup includes a 2.23 T dipole magnet with a 35 mm gap, a 5 ppm four-quadrant power supply for low-field operation, and three NMR probes with associated electronics, covering the 20 mT to 2.2 T range. The probes are mounted on a dedicated holder positioned in a highly uniform field region, ensuring that all sensors experience the same magnetic environment. Achieving excellent homogeneity over a large volume and wide field range was a key challenge; this was addressed through a genetic-algorithm-optimized magnet design complemented by active shimming coils. This contribution presents the design, construction, and factory acceptance tests of the system, along with the first calibration results obtained at MMF. Future improvements include thermostating the probe holder, potentially using cryogenic liquids, to extend the temperature range for calibrations, an important capability for probes used in superconducting magnets.

INTRODUCTION

The INFN Frascati Laboratories have a long-standing tradition in magnetic measurements, supported by instrumentation that has enabled, over the years, the testing of magnets for particle accelerators (DAFNE, SPARC, CNAO, ELI, STAR, etc.) as well as for experimental applications. In recent years, a major upgrade of both the existing instrumentation and the facility infrastructure has been carried out, including civil engineering and technical systems. The LATINO project, funded by the Regione Lazio, enabled the installation of a rotating coil bench and a stretched-wire bench, as well as the refurbishment of existing infrastructure (cooling system, flooring, main gate) [1].

More recently, the IRIS project (Innovative Research Infrastructure for applied Superconductivity), funded by Next Generation EU (PNRR), has extended the capabilities of the laboratory toward superconductivity, particularly in the context of room-temperature measurements of superconducting magnets [2]. The instrumentation has been further enhanced through upgrades to the Hall probe positioning system, the acquisition of three-axis probes, a vibrating wire bench, a laser tracker and precision alignment accessories, power converters of various ranges, and additional ancillary equipment for laboratory activities. A mezzanine has also been constructed within the existing building to improve the organization of space and equipment [3,4]. The flexibility of the instruments will allow to cover a large range of magnetic measurements, from point maps to integrated fields, from multipolar analysis to fiducialization.

Within this framework, the laboratory has been equipped with a new calibration system developed by CAYLAR[1], described in this contribution. The study and implementation of this system have led to a strong collaboration between CAYLAR and the INFN research group, driven by evolving requirements in magnetic field intensity and homogeneity. This joint effort focuses on performance optimization, improved space efficiency through precise probe positioning and reduced pole gap, and continuous system enhancement.

THE CALIBRATION SYSTEM

The system is based on a reference dipole electromagnet powered by a dedicated four-quadrant power converter. The objective is to achieve high magnetic field intensity and homogeneity. A larger homogeneous volume allows simultaneous calibration of multiple Hall sensors, improving throughput, while precise probe positioning ensures measurement repeatability and accuracy.

The electromagnet features a 35 mm gap and elliptical pole faces of 140 mm diameter, optimized using a genetic algorithm to balance field intensity and homogeneity. The central field reaches up to 2.23 T, with a homogeneity better than 0.02 % within a $15 \times 15 \times 15$ mm^3 volume across the full operating range.

The power supply operates in four quadrants, enabling smooth polarity reversal and accurate low-field operation. It delivers up to 70 V and 150 A (10.5 kW), with a long-term stability of 5 ppm over 8 hours, a thermal drift of 2 ppm/°C, and low ripple (2 mV). Field stability is ensured through NMR-based feedback regulation, allowing sub-ppm stability by actively controlling the current based on real-time magnetic field measurements.

Absolute field measurements rely on three NMR probes covering the range from 20 mT to 2.2 T, with overlapping regions for cross-calibration. A high-precision gaussmeter provides measurements with 10 nT resolution and better than 0.5 µT accuracy.

* antonio.trigilio@lnf.infn.it
† maxime.rollo@caylar.net

[1] https://www.caylar.net

Content from this work may be used under the terms of the CC BY 4.0 licence (© 2026). Any distribution of this work must maintain attribution to the author(s), title of the work, publisher, and DOI.

ISBN: 978-3-95450-252-3 ISSN: 2673-5350 doi: 10.18429/JACoW-IPAC2026-MOP7065

STATUS OF MAGNETS FOR ALBA II PROJECT: DESIGN, PROTOTYPING AND PRODUCTION PLANS

J. Marcos*, A. Fontanet, A. Girón, V. Massana, M. Ning, P. Salmerón, B. Zhang
ALBA Synchrotron, Cerdanyola del Vallès, Spain

Abstract

The upgrade project of the ALBA Synchrotron Light Source is gaining momentum following the official approval of the required funds at the end of 2025. The design of the magnets for the new ALBA II storage ring began in 2021 with the launch of a comprehensive prototyping program aimed at developing and validating the various magnet types required by the new multi-bend achromat (MBA) lattice. The first prototype magnets became available at the end of 2025 and are currently being characterized at ALBA's magnetic measurements laboratory to assess their performance against the design specifications, as well as to investigate critical aspects such as magnetic cross-talk and mechanical integration between neighboring magnets. In parallel with prototype fabrication, the magnet designs have continued to evolve to keep pace with the successive refinements of the ALBA II lattice over the past years. The lattice is now approaching its final configuration, and together with the lessons learned from the prototyping campaign, this will enable the completion of the magnet designs during 2026.

INTRODUCTION

The ALBA II project will transform the existing ALBA storage ring, in operation since 2012, into a fourth-generation synchrotron light source by implementing an ultra-low emittance multi-bend achromat (MBA) lattice [1]. A key element of this upgrade is the development of a new set of storage ring magnets capable of meeting the stringent optical and integration requirements imposed by the compact MBA layout, while maintaining compatibility with the existing tunnel and beamline infrastructure.

An initial set of design studies and conceptual solutions for the ALBA II magnets was reported previously [2], focusing on the definition of magnet requirements and the development of first resistive and permanent-magnet-based prototypes. Since then, the project has entered a new phase in which detailed engineering, prototyping, and experimental validation are being carried out in parallel with the convergence of the ALBA II lattice toward its final 5BA configuration. The present paper provides a comprehensive status update of this program, covering design evolution, prototyping results, magnetic measurements, and production planning.

EVOLUTION OF LATTICE AND MAGNET REQUIREMENTS

The reference lattice for ALBA II has evolved in recent years from the initial 6BA concepts toward a more flexible 5BA solution [3]. This evolution has led to updated requirements for all magnet families (dipoles, reverse bends, quadrupoles, sextupoles, and correctors). In addition, octupoles were introduced at the end of 2024 as a necessary element to improve the dynamic aperture [4].

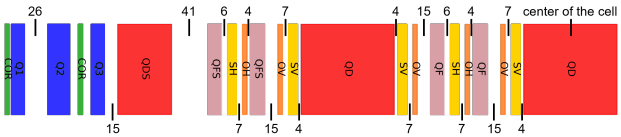

Figure 1: Schematic view of half a cell of the 5BA lattice designed for ALBA II. The quadrupole triplet on the left side is facing a straight section, and the dipole on the right side sits in the middle of the cell. Numbers indicate distances in [cm] between the effective lengths of each pair of magnets.

The current set of magnet requirements is summarized in Table 1, while Fig. 1 shows the magnet distribution within one cell [5]. The lattice remains extremely compact, with magnet-to-magnet distances as small as 40 mm. This imposes significant challenges in terms of both mechanical integration and magnetic cross-talk between neighboring elements.

At present, most magnets are foreseen to use resistive technology, i.e. iron-dominated yokes with water-cooled copper coils. This choice is driven by the high degree of tunability required across the different magnet families. Two notable exceptions are identified:

- The QDS dipoles (outer dipoles of each 5BA cell), for which tunability is less critical and which will therefore be based on permanent magnet (PM) technology.
- The QD superbend magnets, designed for beamlines requiring higher photon critical energy. These will combine a PM-powered high-field (> 3 T) central pole with coil-powered side poles to preserve tunability.

Compared to the initial design described in [2], one important modification is that each sextupole will now include both horizontal and vertical dipolar correctors. As a counterpart, skew quadrupole correctors will be relocated from sextupoles to octupoles.

OVERVIEW OF THE PROTOTYPING PROGRAM

To address the main design challenges, ALBA launched a comprehensive prototyping program in 2021 covering all critical magnet families foreseen for ALBA II. These prototypes are being procured through industrial contracts.

Due to the continuous evolution of the accelerator lattice, each prototype has been designed according to the lattice version available at the time of contract definition. As a

* jmarcos@cells.es

Content from this work may be used under the terms of the CC BY 4.0 licence (© 2026). Any distribution of this work must maintain attribution to the author(s), title of the work, publisher, and DOI.

ISBN: 978-3-95450-252-3 ISSN: 2673-5350 doi: 10.18429/JACoW-IPAC2026-MOP7066

PROTOTYPING OF A TUNABLE PERMANENT MAGNET QUADRUPOLE*

J. Voelker†, I. Asparuhov, V. Dürr, F. Pflocksch
Helmholtz-Zentrum Berlin für Materialien und Energie, Berlin, Germany
J. Marcos, F. Perez, Bo Zhang, ALBA Synchrotron, Cerdanyola del Vallès, Spain
A. Costa, J. Lucas, Elytt Energy, Madrid, Spain

Content from this work may be used under the terms of the CC BY 4.0 licence (© 2026). Any distribution of this work must maintain attribution to the author(s), title of the work, publisher, and DOI.

Abstract

Within the Research Facility 2.0 (RF2.0) project, one of the objectives is the development of novel permanent magnet technologies and refurbishment strategies aimed at reducing energy consumption in accelerator facilities. In this context, ALBA, ELYTT, and HZB are jointly developing a tunable quadrupole prototype based on permanent magnets, conceived as a demonstrator for next-generation, energy-efficient magnet systems. The prototype is designed to achieve high-gradient focusing while drastically reducing power consumption relative to conventional electromagnets, eliminating the need for large coils and water cooling. Its compact architecture also eases integration into densely packed storage-ring lattices. Tunability is provided through a hybrid approach combining movable soft-iron elements and small auxiliary coils, offering a wide operational range with minimal energy demand. This contribution presents the electromagnetic and mechanical design of the prototype, the assembly strategy, and the current status of the manufacturing and testing.

MAGNETIC CONCEPT

As part of the European funded RF2.0 [1] project, the three partners ALBA, ELYTT and HZB are developing a tunable permanent-magnet (PM)-based quadrupole (QP) magnet[1] to explore the feasibility of high-gradient focusing magnets in upcoming particle accelerators like ALBA II [2–4] or BESSY III [5–8] with extremely low power consumptions, but large operational ranges similar to existing electromagnets. The main advantage of this new design is an expected power consumption of less than 100W (during tuning) instead of up to 2 kW for a similar electromagnet design, maintaining a tuning range of up to ±20 %. In addition, no direct water-cooling system for the magnet is necessary, which further reduces the overall power consumption of the system, as well as the sources of vibrations. This magnet concept has the potential to reduce the overall CO2 footprint of highly stable future particle accelerators, without the loss of flexibility. The elimination of the large driving coils for an electro-quadrupole enables a more compact design, leading to more space between magnets in storage ring lattices. The initial magnet concept can be seen in Fig. 1. It is based on a PM-QP magnet where NdFeB PM blocks (yellow) are installed in the magnet yoke (grey), guiding the magnetic flux to the inner pole tip region with a small aperture diameter of ≈ 25 mm. Hereby, magnetic gradients of up to 110 T/m are possible. Additional tuning plates (purple) next to the PM blocks can be moved via motors into and out of the yoke gaps. This changes the amount of magnetic flux that goes through the magnet pole fingers and by this the magnetic gradient. A reduction by more than 40 % with respect to the maximum gradient can be achieved. For faster, but less efficient corrections, compact electric coils (orange) can be installed, to vary the gradient by a few percent.

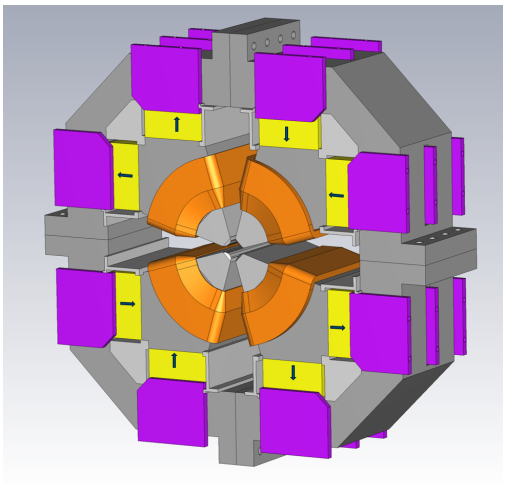

Figure 1: Tunable QP-PM concept, based on mechanical (purple) and electrical (orange) tuner techniques.

MAGNETIC MODEL AND OPTIMIZATION

Based on the magnet concept, we started an optimization of the magnet pole tip design with an aperture diameter of 23 mm to stabilize the main quadrupolar component and to reduce the higher order multipoles. The magnetic field $\mathfrak{B}$ in the central plane next to the geometric axis of the magnet can be described by Fourier components

$$\mathfrak{B} = \sum_n (A_n + iB_n)(x + iy)^{(n-1)} \quad (1)$$

with A_n and B_n as the real (skew) and imaginary (normal) amplitudes of the multipole-components of order n, at transverse distance from the magnetic axis given by x and y. These amplitudes will be measured along a reference circle with radius r_{ref}.

Because of symmetry and boundary conditions, for quadrupole magnets only the amplitudes B_2, B_6,B_{10}, B_{14}, etc. are non-zero. Here, B_2 describes the main quadrupolar

* This project has received funding from the European Union's Horizon Europe research and innovation programme under grant agreement No. 101131850 and from the Swiss State Secretariat for Education, Research and Innovation (SERI).

† jens.voelker@helmholtz-berlin.de

[1] Grant of patent: DE 10 2023 004 594 B4 2025.05.22

ISBN: 978-3-95450-252-3 ISSN: 2673-5350 doi: 10.18429/JACoW-IPAC2026-MOP7068

CONCEPTUAL MAGNET DESIGNS FOR MAX 4^{U}

H. O. C. Duarte*, K. Åhnberg, L. Roslund, MAX IV Laboratory, Lund, Sweden
A. Vorozhtsov†, European Organization for Nuclear Research, Geneva, Switzerland

Abstract

The MAX 4^{U} project aims to reduce the natural horizontal emittance of the MAX IV 3 GeV storage ring from 328 pm rad to less than 75 pm rad. A key constraint for the new lattice design is the preservation of the 7-bend achromat structure layout. Each cell is implemented as a single magnet block, which includes an integrated dipole, removable quadrupole pole tips, and stand-alone sextupoles and octupoles. This configuration imposes strict limitations on the level of intervention possible within each block. This contribution presents conceptual magnetic designs and initial crosstalk studies.

INTRODUCTION

The MAX IV 3 GeV storage ring lattice (hereafter referred to as the *standard lattice*), through the MAX 4^{U} project [1,2], is undergoing an upgrade to reduce the natural horizontal emittance from the present 328 pm rad to less than 75 pm rad. The project is currently in the TDR phase [3], and the most recent lattice design (TDR_1) delivers 65 pm · rad emittance.

In order to keep the upgrade intervention cost-effective and fast, several constraints were put in place: keep the vacuum chamber profile and therefore the magnet aperture of ϕ25 mm; use magnet blocks [4], and preserve their height and layout. Each cell is realised as two halves of a magnet block. Their machining includes complete dipoles and correctors, quadrupole pole roots, and grooves for their coils. Additional grooves are milled for stand-alone sextupoles and octupoles [4]. Quadrupole pole tips, sextupole and octupoles are removable. This integrated design ensures mechanical stability and tight alignment tolerances and streamlines installation.

This paper presents conceptual magnet designs for the TDR_1 lattice with emphasis on magnetic performance, integration constraints, and cross-talk effects.

DESIGN METHODOLOGY

The magnet strengths required for the MAX 4^{U} lattice exceed the capabilities of some of the standard-lattice magnets (SLM). However, the reduced dynamic aperture of the MAX 4^{U} lattices (compared to that of the existing MAX IV 3 GeV ring) allows for a smaller good field region (GFR), whose radius was reduced from 10 mm to 7 mm. The improved field quality in this reduced GFR [5] allows to pursue narrower pole tips while still achieving about ±1 unit field quality inside the GFR.

We increase the magnet strength limits by: i) narrowing the pole tips; ii) widening of the pole roots, to the potential detriment of coil size and heat load; iii) employing Permendur as the pole tips material instead of low-carbon steel . As an example of (i) and (ii), Fig. 1 compares the 2D pole tip profiles of a quadrupole magnet. Solution (iii) has so far been kept as a last resort, and ARMCO is considered for the designs presented here. Electromagnetic (resistive) magnets are considered in this paper, while permanent-magnet-based solutions are being explored within the RF 2.0 project [6].

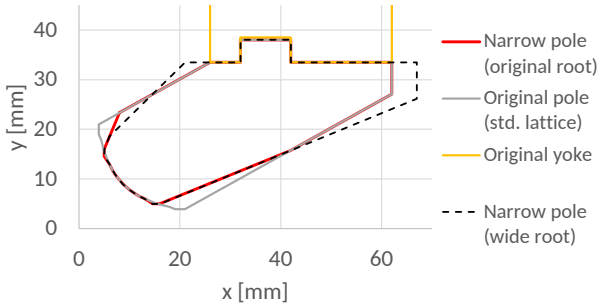

Figure 1: 2D sketch (quarter symmetry) of quadrupole pole tips: original (solid grey); narrow but keeping original root width (solid red) and widening the root (dashed black). Part of the original yoke (solid yellow) is shown as reference.

The electromagnetic designs were performed using OPERA-2D and 3D [7] and CST Studio Suite [8]. To improve mesh homogeneity, an arc or toroidal surface (for the 2D or 3D simulations) was created on the GFR boundary surrounding the ideal orbit point or path, respectively. Field maps were exported for post processing, where multipolar expansion was performed on the polar basis [5] neglecting the longitudinal fields in 3D analysis.

ELECTROMAGNETIC DESIGN

The SLM correctors and octupoles can be used for the TDR_1 lattice. 3D stand-alone EM designs have been developed for the dipoles (D2), quadrupoles (Q1 and Q2), reverse bends (R2) and sextupoles (S1, S2, S3 and S4) of the TDR_1 lattice. The most stringent families for each of these designs are shown in Table 1. No challenges are expected in designing the remaining families, D1 and R1. They are excited at a level below their SLM counterparts.

The results indicate that the required field strengths can be achieved by the proposed models, with R2 being the most constricted design. It is asymmetric, so some R2 parameters in the table refer to the halves on the inner and outer sides of the ring circumference. Not shown here, The Q1 and Q2 designs employ the narrow pole geometry (wide root), as depicted by Fig. 1.

* henrique.caiafa_duarte@maxiv.lu.se
† formerly at MAX IV Laboratory

Content from this work may be used under the terms of the CC BY 4.0 licence (© 2026). Any distribution of this work must maintain attribution to the author(s), title of the work, publisher, and DOI.

ISBN: 978-3-95450-252-3 ISSN: 2673-5350 doi: 10.18429/JACoW-IPAC2026-MOP7069

ABSOLUTE PULSED-MODE, LONG-DURATION INTEGRAL FIELD INSTRUMENTATION USING A MULTI-SENSOR APPROACH

A. Ganesh*[1], A. Bellelli[1], M. Bonora-Tam[1], M. Buzio[1], C. Petrone[1]
[1]European Organization for Nuclear Research (CERN), Geneva, Switzerland

Abstract

A recent upgrade of the CERN Super Proton Synchrotron (SPS) quadrupole magnet measuring system enables high relative accuracy on the order of 10^{-5} over cycle sequences up to 800 seconds long, as needed for machine-learning based modeling and control of hysteresis effects in the frame of the Efficient Particle Accelerator (EPA) initiative. A new fluxmeter assembly integrates multiple arrays of PCB induction coils with Hall probes and local coils for in-situ cross-calibration, while new FFMM (Flexible Framework for Magnetic Measurements) C++ classes provide automation of complex excitation current cycles, data reduction and database storage. A Python data processing pipeline uses Kalman filters to fuse multiple sensors, correcting for integrator drift. This enables absolute measurements even without traditional Nuclear Magnetic Resonance (NMR) probes, which operate only in uniform fields.

INTRODUCTION

The SPS is a fast-ramped machine with iron-dominated magnets affected by strong (~ 6%) non-linear eddy currents and magnetic hysteresis effects [1]. The bending dipole field is measured in real time by a so-called B-train system [2, 3] combining integral induction coils with NMR probes, used as a ppm-level absolute reference, installed in reference magnets in series with the ring dipole magnets. A similar system ("G-train") was attempted in the past for the main focusing (QF) and defocusing (QD) quadrupole magnets, but since NMR probes do not work at all in field gradients [1, 4], the accuracy was too low. Alternative, recent approaches shift the burden from real-time setups onto neural-network field-prediction models trained on data obtained from extensive measurement campaigns, carried out in the laboratory under more favourable, controlled conditions [5–7]. Hysteresis model training relies crucially on the ability to measure the integral field at a 10^{-5} relative accuracy level over many, several minutes-long sequences of cycles in different combinations, without interruption. The legacy integral induction coils were designed to compare magnets against reference units in differential mode over current pulses lasting only a few seconds, and are inadequate for longer durations. This paper presents the new multi-sensor quadrupole fluxmeter developed to meet this demand. We describe in detail the instrumentation setup and compare classic piecewise linear integrator drift correction with a novel sensor fusion method, providing result examples and conclusions.

* abhishek.ganesh@cern.ch

MEASUREMENT SETUP

Magnet and Operational Cycles The 3050 mm-long SPS QF/QD quadrupole magnets reach 21.7 T/m at 2110 A, well into the saturated regime of the iron. Their 1260 A RMS rating caps the current that can be sustained continuously, and with it the upper bound of any DC field characterization. Classical instruments such as rotating coils or stretched wires deliver the highest absolute accuracy but require steady-state excitation. Excitation current is supplied by a 6 kA peak / 3.2 kA RMS Holec power converter, voltage-driven by a 24-bit DAC source providing a nominal 7.775 mA resolution and read by a DCCT with 1.3 A accuracy. The two supercycles (series of consecutive acceleration cycles) used for the tests reported here are the LHC2/SFTPRO/MD1 (Q20 beam optics) and LHCPILOT/SFTPRO/MD1 (Q26 beam optics) cycles. The tests included 70 consecutive cycles lasting up to 800 s, with plateaus at flat-bottom (55 A), injection (200 A) and extraction (2110 A).

Fluxmeter Assembly The fluxmeter (Fig. 1(a)) is comprised of 7 × (600.0 ± 0.2) mm-long, 136.0 ± 0.2 mm wide 12-layer coil array PCBs, covering the whole extension of the magnet's field and mounted on a 3D-printed Poly-lactic Acid (PLA) support structure shaped to fit the quadrupole bore with or without vacuum chamber. One array of hybrid Hall-probe/induction coil sensors (Fig. 1(b)) is installed on the PCB at the centre of the magnet.

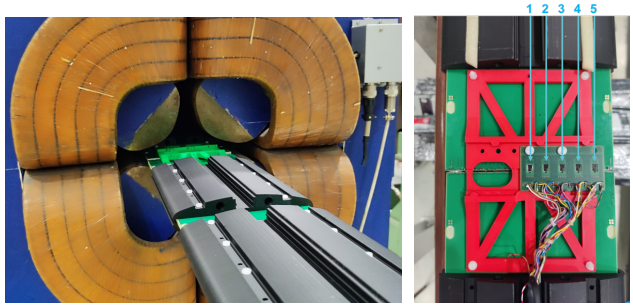

(a) Multi-sensor fluxmeter assembly inside the SPS quadrupole bore.

(b) Hall probe array with short coils.

Figure 1: Fluxmeter assembly.

Induction coil array Each PCB carries 21 parallel 596.0 mm-long, 4.92 mm wide, 84-turn induction coils, spaced $\Delta x = 6.4$ mm apart, with surfaces individually calibrated against NMR in a reference dipole averaging $A = 0.1086\,\mathrm{m}^2$ with $\sigma_A/A = 1.0 \times 10^{-5}$. Any pair of coils can in principle be connected in series opposition (known as *bucking*) to directly provide the field gradient G suppressing the dipole component and common-mode pickup [8].

Content from this work may be used under the terms of the CC BY 4.0 licence (© 2026). Any distribution of this work must maintain attribution to the author(s), title of the work, publisher, and DOI.

ISBN: 978-3-95450-252-3 ISSN: 2673-5350 doi: 10.18429/JACoW-IPAC2026-MOP7070

STATIC AND DYNAMIC FIELD CHARACTERISATION OF THE SUPER PROTON SYNCHROTRON BENDING MAGNETS

A. Bellelli*[1,2], A. Ganesh[1], C. Petrone[1], M. Buzio[1], M. Bonora–Tam[1], A. Huschauer[1], S. Russenschuck[2]
[1]European Organization for Nuclear Research (CERN), Geneva, Switzerland
[2] Technische Universität Wien, Vienna, Austria

Abstract

To ensure precise control of field quality in normal-conducting accelerator magnets, it is essential to develop models that accurately represent magnetic hysteresis during operational cycles. This study focuses on the dipole magnets of the CERN Super Proton Synchrotron (SPS) and investigates how variations in operational cycles produce different hysteresis and dynamic patterns in the integrated main magnetic and higher-order field multipoles. A combination of various magnetic field measurement systems was employed to evaluate the magnetic field quality, enabling direct observation of history dependence and reproducibility. Three regimes are identified: a history-dependent reversal curve along the ramp, eddy-current settling during end-of-ramp transients, and a rate-independent transfer function at the plateau. The analysis covers the integrated dipole and sextupole components, distinguishing rate-dependent eddy current effects from quasi-static hysteretic contributions. Two pre-cycle patterns currently used in operation are compared: a 200 GeV cycle and a 26 GeV cycle introduced in 2026 within the CERN Efficient Particle Accelerator (EPA) initiative. The aim is to provide a quantitative single-magnet assessment of this change of operation.

INTRODUCTION

The Super Proton Synchrotron (SPS) at CERN relies on 744 main dipole magnets, of two types (MBA and MBB), to bend protons along its 6.9 km circumference. Besides serving as Large Hadron Collider (LHC) injector, the SPS delivers proton beams to the North Area fixed targets [1], where the dipolar B_1 and sextupolar B_3 field components directly drive orbit stability and beam quality at slow extraction. In normal-conducting magnets with time-varying magnetic field, two phenomena complicate the field description: (i) iron hysteresis, which introduces history-dependent static contributions, and (ii) eddy currents in the laminated yoke, end plates, and vacuum chamber, which produce rate-dependent dynamic effects. A real-time monitoring system (B-train) measures the magnetic fields of two reference dipoles, powered in series with the ring. Integrating over time the induced voltages from several pickup coils and periodically correcting the resulting flux measurement with a Nuclear Magnetic Resonance (NMR) field marker [2, 3], the system measures the integrated magnetic field, which serves as input to low-level radio-frequency (RF) and feed-forward correction [4, 5].

* alberto.bellelli@cern.ch

MOTIVATION

Current SPS operation uses a pre-cycle magnet excitation function, named MD1, before each SPS Fixed-Target PROton (SFTPRO) cycle for North Area experiments. The MD1 cycle was originally introduced to improve magnetic reproducibility and historically reached the equivalent of 200 GeV beam energy during the early LHC beam-scheduling era [6, 7]. In 2024, the presence of this cycle accounted for about 5 GWh of electrical energy consumption and 18 % of SPS operational time [4]. Following studies within the CERN Efficient Particle Accelerator (EPA) framework [1], the MD1 function was flattened at the beginning of 2026 to a 26 GeV plateau. This operational change motivates a quantitative assessment of how different magnetic histories affect the reproducibility and dynamic response of the SPS dipole magnets.

This work describes how the hysteretic response of the SPS dipole magnets has changed following the flattening of the MD1 cycle, and analyses their dynamic behaviour. To obtain this characterisation of the magnetic field response, a systematic measurement campaign was initiated in 2024, new instrumentation was developed, and a dedicated magnetic measurement procedure was implemented. This paper details the procedure, metrological characterisation, and measurement results.

MEASUREMENT METHODS

Measurement Setup

The measurements were performed on an MBA magnet, connected in series with an MBB laboratory reference dipole and driven by a voltage-controlled converter, with a reproducibility of 0.03 % of the set point. A seven-metre-long coil array, with transverse positions at x_i = 0, ±19.5, ±39.0, ±58.5 mm, and two 470-mm-long rotating coil segments are employed.

The measurements used to compare the legacy and the current operational MD1 cycles are the following: A = legacy 200 GeV MD1 (peak 2340 A), B = flattened 26 GeV MD1 (peak 300 A), each consisting of twenty identical MD1 cycles.Ten standardisation pre-cycles to 5780 A (LHC cycles) precede each supercycle, and after the MD1 cycle, an SFTPRO cycle (peak 4820 A) is executed.

Figure 1 shows the two supercycles compared in this work.

Eddy-Current Characterisation

The post-ramp settling of the magnetic field measured by the long search coil is fitted as [8] $B(t) = B_\infty +$

Content from this work may be used under the terms of the CC BY 4.0 licence (© 2026). Any distribution of this work must maintain attribution to the author(s), title of the work, publisher, and DOI.

ISBN: 978-3-95450-252-3 ISSN: 2673-5350 doi: 10.18429/JACoW-IPAC2026-MOP7071

PROTOTYPE DEVELOPMENT OF A COMPACT HTS WIGGLER FOR SYNCHROTRON LIGHT SOURCES

L. Bortot*, C. Benabderrahmane, F. Cianciosi, G. Le Bec, F. Perratone, Z. Qiu
European Synchrotron Radiation Facility, Grenoble, France

Abstract

The European Synchrotron Radiation Facility is developing a novel, compact, superconducting wiggler for beamline BM18. The design features three pole pairs delivering up to 1.58 T at 60 K using high-temperature superconducting tapes and a no-insulation winding technique. A current-controlled continuous field variation ensures field-tunability requirements for low-photon energy applications within tight space constraints. Completed milestones include magnetic and thermal design, HTS tape procurement, and winding prototype testing. A production winding machine will be delivered in May 2026, followed by the wiggler assembly. Upcoming 77 K testing will validate the wiggler before final installation.

INTRODUCTION

The European Synchrotron Radiation Facility (ESRF) is pursuing the development of short-period, high-field, high-temperature superconducting (HTS) undulators for future synchrotron radiation sources [8]. In this framework, a field-tunable HTS wiggler is currently being developed for beamline BM18 upgrade to enable low-photon energy applications. In conventional permanent-magnet wigglers, such tunability relies on mechanical gap variation, which is impractical within the severe spatial constraints. This HTS wiggler serves dual purposes: as a demonstrator for BM18 and as a technological development platform for future HTS undulators.

This paper presents the wiggler design, manufacturing progress, and preparations for prototype validation. Design criteria emphasize simplicity and robustness to minimize technical risk while ensuring reliable operation for user experiments. The project builds on ESRF's 30-year legacy [5] and serves as a technological development platform for future short-period, high-field HTS undulators.

MAGNET DESIGN

The magnet assembly has dimensions of 200 mm in length, 90 mm in width, and 120 mm in height. The magnet features an iron-dominated configuration with rectangular-like coils wound on magnetic poles made of pure iron, producing a peak field of 1.58 T in a magnetic gap of 24 mm at 60 K. The magnet vacuum is separated from that of the storage ring. The complete wiggler is shown in Fig. 1. The iron yoke serves both as magnetic flux circuit and structural support for the windings and the titanium brackets that withstand the electromagnetic vertical forces during operation, up to 5 kN. The main design parameters of the magnet are summarized in Table 1.

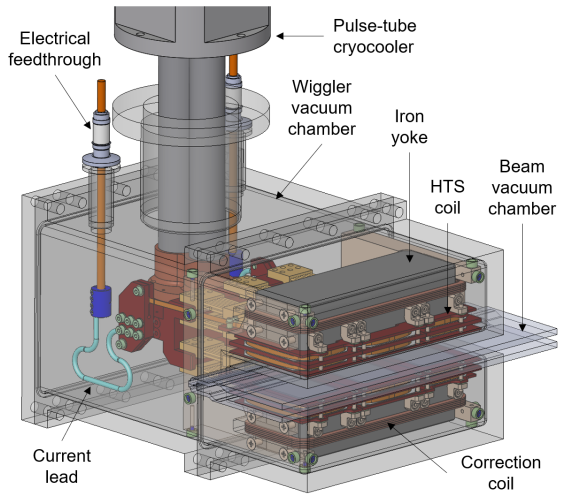

Figure 1: HTS superconducting wiggler including the magnet assembly, the cryocooler cold head, and the vacuum chamber.

Table 1: Specifications of the Superconducting Wiggler

Parameter	Unit	Value
Magnetic gap	mm	24
Maximum field strength	T	1.58
Peak field at conductor	T	1.5
Operating temperature	K	60
Field integral target	T mm	<0.1
Field integral tunability	T mm	± 0.5
Operating current	A	80
Quench margin	%	35
Inductance	mH	38
Stored energy	kJ	0.125

The superconducting coil consists of three pole pairs. The coil is wound using rare-earth barium-copper-oxide (ReBCO) HTS tapes. The tapes feature a critical current of 120 A at 77 K in self field conditions. The coil comprises six double-pancake windings: the central pole pair features 113 turns per pancake, while each side pole pair contains 53 turns. At nominal current of 80 A, this configuration provides a total excitation of 72 kA t, for a stored magnetic energy of 0.125 kJ and an inductance of 38 mH. The magnetic field profile and the residual of the first field integral are shown in Fig. 2. The latter is kept below 0.1 T mm across the operating current range. To address residual field errors, the magnet assembly is equipped with a correction coil made

* lorenzo.bortot@esrf.fr

Content from this work may be used under the terms of the CC BY 4.0 licence (© 2026). Any distribution of this work must maintain attribution to the author(s), title of the work, publisher, and DOI.

ISBN: 978-3-95450-252-3 ISSN: 2673-5350 doi: 10.18429/JACoW-IPAC2026-MOP7073

REPAIR AND IMPROVEMENT OF THE SUPERCONDUCTING MAGNETS OF THE S^3 SPECTROMETER AT GANIL

A. Wagret-Quatromme[†,1,2], G. Brunet[1,2], M. Cloitre[1,2], M. Faye[1,2], M. Lecluze[1,2], T. Lefrou[1,2], F. Lutton[1,2], L. Rossard[1,2], G. Peschard[1,3], M.-H. Stodel[1,2], L. Quettier[1,3]
[1]Grand Accélérateur National d'Ions Lourds, Caen, France
[2]Institut National de Physique Nucléaire et Particule (CNRS), Gif-sur-Yvette, France
[3]Institut de Recherche sur les Lois Fondamentales de l'Univers (CEA), Gif-sur-Yvette, France

Content from this work may be used under the terms of the CC BY 4.0 licence (© 2026). Any distribution of this work must maintain attribution to the author(s), title of the work, publisher, and DOI.

Abstract

In order to achieve optimal performance in terms of transmission and separation for the S^3 spectrometer, the project chose to design superconducting magnets integrating 11 magnetic functions in a single cryostat. There are seven of these magnets, called Superconducting Multipole Triplets, in the spectrometer. The compactness of these magnets makes them remarkable and unique, but has led to significant commissioning difficulties. As the design was very close to the acceptable operating limits, we experienced several breakages and leaks, as well as limitations in terms of nominal current. In this presentation, we will show the important work we carried out to repair the main conductor, improve the robustness of the current leads and feedthrough, and repair the various leaks.

SUPER SEPARATOR SPECTROMETER

S^3 spectrometer sorts elements by mass/energy and deliver a high intensity beam of highly curated heavy ions. To achieve this great feat, it uses seven Superconductor Magnetic Triplet to drive the particles beam through hot magnet, beam dumps, electrostatic dipole and beam characterization devices.

SUPERCONDUCTING MAGNETIC TRIPLET

SMT Characteristics

SMT (Fig. 1) are cryogenically cooled magnet divided in three sections:

- Twelve magnetic fields in total. Each singlet embedding bipolar, quadripolar, sextupolar and octupolar coils.
- 16 Current lines to feed up to 450 Amps coils / 48 current feedthrough.
- Use liquid Nitrogen to cool and shield the liquid Helium tank.
- Cold mass is suspended around an Ø360mm beam chamber.
- Weight 3 metric tons, measure 1.8 m high, 1.8 m long.
- Superconductor coils protected by high sensitivity voltage monitors.

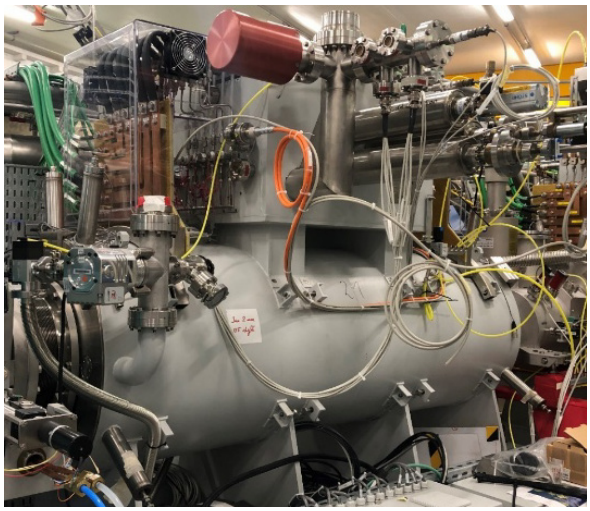

Figure 1: SMT set-up on beam line.

HTS CURRENT LEAD REPAIR

The High temperature Superconductor current lead (Fig. 2) feed electrical current from the « warm » side (liquid Nitrogen) to the « cold » part (liquid Helium). This constructor development is made of two part. the top section transfer current from copper lead (80 K), through a DI-BSCCO type G tape (Tc 108 K) and the lower part is an addition of YBCO flexible tapes (Tc 93 K). We mostly had to deal with delamination on the YBCO part, likely due to ripping effect of mechanical stress and sudden high current flux. Since 2022, we practiced more than 80 HTS current lead changes, refining tools and methods. We mostly use IN/SN soft solder with Tixflux but also pure Indium sheet strongly clamped. It is important to limit HTS current lead heat exposure and we cool them abundantly after soldering with compressed air and isopropanol. IRFU of DACM helped us in defining a new generation of ReBCO current lead in order to achieve high degree of reliability and manage spare parts availability.



Figure 2: HTS lead assembly. YBCO tapes on the left, BiSCCO rod on the right.

ISBN: 978-3-95450-252-3 ISSN: 2673-5350 doi: 10.18429/JACoW-IPAC2026-MOP7074

INTEGRATED HTS CCT MAGNET AND BEAM PIPE : A PROPOSAL FOR THE FCC-ee FINAL FOCUS QUADRUPOLE QC1L/R1

M. Marchand*, L. Brunetti, G. Lamanna, M. Le Garrec, CNRS/IN2P3-LAPP, Annecy, France
F. Bardi, M. Koratzinos, CERN, Geneva, Switzerland
F. Toussaint, SYMME-USMB, Annecy, France
M. Duda, PSI Center for Accelerator Science and Engineering, Villigen, Switzerland

Abstract

High Temperature Superconductors (HTS) and Canted Cosine Theta (CCT) technologies have been extensively studied in recent years, particularly for high-field accelerator magnets. Their application to next-generation particle accelerators is especially promising. This article presents the combination of these two technologies for the FCC-ee Final Focus (FF) quadrupole QC1L/R1, including its integration within the Machine-Detector Interface (MDI).

We detail the specific design, mechanical specifications, and manufacturing process—driven by the coil's significant curvature angle—as well as the cryogenic test strategy and results. Additionally, we describe the design of a cooled beam pipe adapted to the magnet and cryostat constraints.

INTRODUCTION

The Future Circular Collider (FCC) will operate as a Higgs and electroweak factory, colliding positron and electron beams at high energy (FCC-ee) [1]. The particles are guided and focused by magnets throughout the collider, particularly near the Interaction Point (IP) within the MDI. The design of these FF quadrupole magnets is a critical challenge for the feasibility of FCC-ee.

The current baseline magnet technology for the FCC-ee MDI [2,3] uses conventional NbTi superconducting magnets. However, to address the demands of next-generation particle accelerators [4], several research teams have explored advanced technologies, such as direct-winded magnets [5–8] and other alternative solutions [9–12]. This work focuses on the FF quadrupoles for the MDI, with particular emphasis on QC1L/R1[1], the optical element closest to the IP, where the stakes are highest [13]. Our proposed solution combines two promising approaches: HTS tapes [14, 15] and CCT winding [16–18]. This combination optimizes the high-precision magnetic field, stress distribution in the coils, compactness, sustainability, and design flexibility.

This article outlines the demonstrator strategy, focusing on the development of the first prototype. We detail the magnetic field design, magnet specifications, and the manufacturing process for machining highly specific parts, including the complex groove design within a confined space and the stringent tolerances required. We also present cryogenic test results to evaluate the superconducting properties of various HTS tapes under severe bending and symmetrical angle constraints. The goal is to select the most suitable supplier based on critical current performance, manufacturability, and cost.

Furthermore, we describe the beam pipe design, adapted for integration within the cryostat, along with numerical simulations and prototype manufacturing in preparation for preliminary tests.

THE FINAL FOCUS HTS CCT QUADRUPOLE

Before developing a full-scale HTS CCT QC1L/R1 prototype and measuring its magnetic field, we must validate the mechanical feasibility and superconducting efficiency of the conductor, despite the stringent magnetic and mechanical specifications. Selecting the appropriate conductor is paramount.

Design and Manufacturing

The primary objective of the FCC-ee QC1L/R1 quadrupole is to generate a highly precise magnetic field to focus the particle beams at the IP, ensuring the desired luminosity. Magnetic simulations define the quadrupole field, which in turn determines the CCT coil shape (Fig. 1a). The mechanical specifications are then derived from this design.

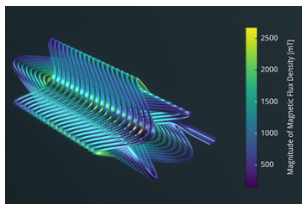

(a) QC1L/R1 Magnetic design and shape of CCT coil.

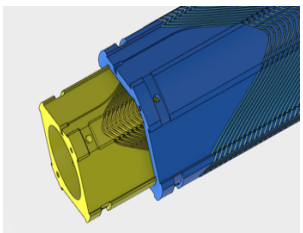

(b) QC1L/R1 design : a 2-layer magnet.

Figure 1: Overview of QC1L/R1 magnetic and mechanical design.

The final magnet will consist of two CCT layers, each with an opposed and canted groove carved into an aluminum body (Fig. 1b). To achieve a 3.2 T field, the HTS coil, shaped as a 4 mm square tape is inserted into the tortuous groove.

The 700 mm-long magnet with a 40 mm aperture presents a major mechanical challenge: ensuring the spatial precision of the coil. The 123 turns of the 4 mm-deep groove must

* matthieu.marchand@lapp.in2p3.fr

[1] QC1L/R1 is the designation of the last quadrupole before IP in the z Lattice. QD0A is its designation in the LCC Lattice

Content from this work may be used under the terms of the CC BY 4.0 licence (© 2026). Any distribution of this work must maintain attribution to the author(s), title of the work, publisher, and DOI.

ISBN: 978-3-95450-252-3 ISSN: 2673-5350 doi: 10.18429/JACoW-IPAC2026-MOP7079

SUPERBENDS FOR DIFFRACTION-LIMITED LIGHT SOURCES: REVIEW AND RECENT ADVANCES

M. Modica, D.Castronovo, D.Caiazza, S. Di Mitri, A. Fabris, S.Krecic, E.Karantzoulis
Elettra – Sincrotrone Trieste, Trieste, Italy

Abstract

All third-generation synchrotron radiation sources are currently planning upgrades toward diffraction-limited storage rings with brightness close to the theoretical limit and higher hard-x-ray production. In these new photon sources superconducting bending (superbend) magnets may play an important role to extend the useful photon energy range. The radiation produced by a superbend magnet is an order of magnitude higher in photon brightness and flux than that produced by a normal conducting bending magnet, making it a superior source of very hard x-rays. As an example, in the framework of the Elettra 2.0 project, a new superbend magnet is under development to provide photons up to 140 keV with an innovative compact design integrated with quadrupole side magnets. The 6T superbend will replace a B80 normal conducting with combined transverse and longitudinal gradient (1.4T central field) magnet. The magnetic design reflects the philosophy of the B80 design combined with innovative cryogenic solutions aimed at achieving a liquid helium-free system. This approach enables a simpler and more reliable design while avoiding the operational costs and uncertainties associated with liquid helium.

INTRODUCTION

The superbend, in the framework of the Elettra 2.0 project [1] will be conduction-cooled by two Sumitomo cryocoolers, ensuring stable operation without the use of liquid helium while maintaining a simple and robust system design [3].

The NbTi superconducting magnet will operate at approximately 3.5 K in conduction-cooled mode, using an integrated system of heat exchangers thermally coupled to the second cooling stage, thereby eliminating the need for a liquid helium bath [2, 4, 5].

A novel C-shaped configuration will allow the magnet to be easily installed and removed from its position on the storage ring vacuum chamber [7, 8, 9].

The procurement process has been completed, and according to the contract, the magnet will be delivered and fully tested by February 2028.

MAGNETIC DESIGN

The superbend design must comply with the constraints imposed by beam dynamics and the ring geometry, including a total bending angle of 6.5° and a magnetic length of 800 mm. Figure 1 presents the target magnetic field profile for the Elettra light source (blue line). This profile features a high-field central region extending over 80 mm with a non he superbend is cooled and maintained at cryogenic temperature using two Sumitomo 4 K cryocoolers operating in conduction -gradient bending angle of 3.44°. On either side, two lateral sections of 360 mm each provide an additional 1.53° per side, reaching a field level of 0.594 T with a nominal gradient (k) of −2.02, adjustable within ±20%.

The design requires a peak magnetic field of 6 T, while the gradient region must extend over at least 720 mm without exceeding 0.8 T at any point. To accurately reproduce the target field profile shown in Fig.1, the solution combines a dipole with two quadrupoles (Fig. 2), as reflected by the calculated magnetic field of the complete system (red curve). The quadrupole field is achieved by introducing a current imbalance between the left and right windings. In this configuration, the four windings are not connected in series; instead, the left and right sides are powered independently.

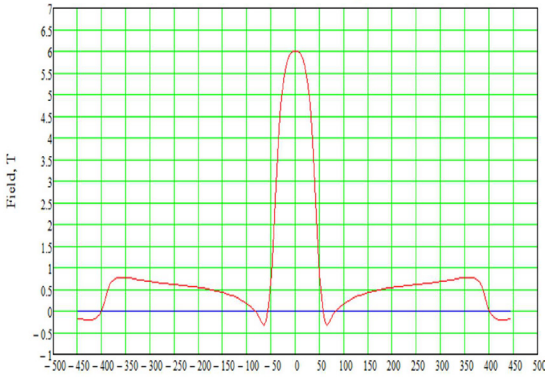

Figure 1: Superbend magnetic field profile.

This approach simplifies both the mechanical layout and the magnetic tuning, enabl ing remote optimization through adjustment of the power supply settings.

Simulation results indicate that a superbend with an increased total magnetic length of 880 mm induces only minor distortions in the linear beam optics.

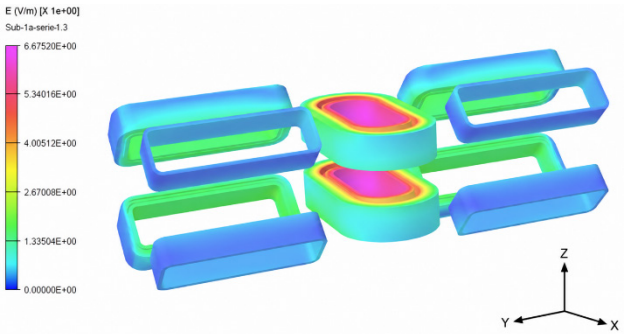

Figure 2: Magnetic field distribution on cold mass.

Content from this work may be used under the terms of the CC BY 4.0 licence (© 2026). Any distribution of this work must maintain attribution to the author(s), title of the work, publisher, and DOI.

ISBN: 978-3-95450-252-3 ISSN: 2673-5350 doi: 10.18429/JACoW-IPAC2026-MOP7081

THE CANTED COSINE THETA HTS SEXTUPOLE DEMONSTRATOR OF FCC-EE

M. Koratzinos*, F. Bardi, V. Batsari, I. Dimoulios, O. Kuhlmann, A. Thabuis
European Organization for Nuclear Research, Geneva, Switzerland
M. Duda, Paul Scherrer Institute, Villigen, Switzerland

Content from this work may be used under the terms of the CC BY 4.0 licence (© 2026). Any distribution of this work must maintain attribution to the author(s), title of the work, publisher, and DOI.

Abstract

A single-aperture, two-layer Canted-Cosine-Theta (CCT) sextupole magnet using high-temperature superconducting (HTS) ReBCO tape has been developed for the short straight sections (SSS) of FCC through the FCCee-HTS4 project. The magnet was designed, manufactured and tested under cryogenic conditions. Two HTS tapes from two manufacturers have been qualified for this specific application. Design and manufacturing details and cryogenic temperature measurements are presented. This demonstrator represents the first HTS CCT magnet ever constructed.

INTRODUCTION

The design of the Future Circular Collider (FCC-ee) aims to increase luminosity while reducing operational costs and environmental impact. In the current baseline [1], arc magnets are based on normal-conducting technology, resulting in significant power consumption. Sextupoles contribute a substantial fraction of this load and are therefore a key target for innovation.

The FCCee-HTS4 project investigates the use of high-temperature superconducting (HTS) magnets in the collider arcs. By reducing electrical losses and enabling more compact nested magnet layouts, this approach can improve machine performance and reduce RF requirements [2].

A 240 mm long HTS canted cosine theta (CCT) sextupole demonstrator was designed and constructed using insulated HTS tape conductors. The CCT design was selected for its excellent stress management, high field quality, and simple manufacturing. Aluminium formers with CNC-machined grooves accommodate the tape stacks, and the coils are wound manually without tape pre-tensioning.

MATERIALS AND METHODS

Design and Manufacturing

The target magnetic field parameters are summarized in Table 1. The maximum operating current is kept low to reduce heating losses through the current leads. The canted cosine theta (CCT) sextupole geometry follows a Frenet-Serret trajectory which ensures no hard-way bending [3]. It has been computed using the RAT suite of programs [4]. Computed field quality is excellent, helped by the large aperture. The optimized conductor path features a minimum bending radius of 4.85 mm and a groove width of 1.6 mm, corresponding to the accommodation of a stack of 10 HTS tapes. In total, approximately 300 m of HTS conductor is needed for the winding of the demonstrator. The selected groove geometry represents a compromise between electromagnetic performance and manufacturability (in particular it follows a binormal Frenet-serret geometry), while remaining compatible with the mechanical limits of the conductor and the practical constraints of winding. The conductor path, coloured by magnetic the magnitude of the flux density at the operating current of 260 A, is shown in Fig. 1. The magnet was tested without iron shielding. Iron shielding, according to simulations, can increase the field gradient by up to 20 %, depending on its distance from the coil.

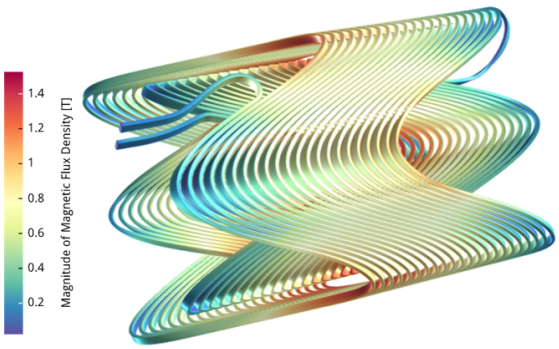

Figure 1: Conductor trajectory colored by the magnitude of the magnetic flux density (T).

Table 1: Main design parameters of the HTS CCT sextupole demonstrator using the double-sided 4 mm wide HTS tape from Faraday Factory Japan.

Specifications	Value
Magnet type	CCT
Aperture	90 mm
Operating current	260 A
Operating temperature	40 K
Field gradient	1000 T/m^2
Max. field at conductor	1.5 T
Inductance	12.6 mH
Critical current fraction	23 %
Temperature margin	27 K

Because the grooves are not perpendicular to the former axis and follow a continuously varying three-dimensional trajectory, the winding former was manufactured using 5-axis CNC machining. Al 6082-T6 was selected as the former material owing to its favorable cryogenic properties, including good mechanical strength, dimensional stability, and thermal conductivity at low temperature. X-ray computed tomography (CT) was used to verify the geometric conformity of the machined former. This non-destructive technique enabled

* michael.koratzinos@cern.ch

ISBN: 978-3-95450-252-3 ISSN: 2673-5350 doi: 10.18429/JACoW-IPAC2026-MOP7082

THE FIRST FULLY AUTOMATED ANALYSIS OF THE HARDWARE COMMISSIONING TESTS FOR SUPERCONDUCTING CIRCUITS AT THE LHC

A. Chmielińska*, A. Barba, M. Cerqueira Bastos, S. Mazenoux, A. Mnich, A. Murariu, M. Medeiros Pereira, A. Verweij, CERN, Geneva, Switzerland

Abstract

The superconducting magnet circuits of the Large Hadron Collider (LHC) at CERN undergo a commissioning campaign at regular intervals, referred to as Hardware Commissioning (HWC), to validate magnet powering and protection functions. During each campaign, more than 1,500 circuits must be commissioned, requiring the execution and analysis of several thousand powering tests. Historically, this process relied on legacy or manual tools, resulting in high workload and sometimes inconsistent results.

To streamline the validation process, a Python-based automated analysis framework has been developed within the Signal Monitoring (SigMon) project over the past two years. The 2026 HWC campaign marked the first time this automated analysis was applied to all powering tests across the superconducting magnet circuits of the LHC. This paper describes the SigMon analysis framework, reports on the 2026 HWC campaign, evaluates the impact of automation, and presents key circuit performance findings.

INTRODUCTION

The LHC superconducting magnet circuits operate under cryogenic conditions and store significant energy, which can reach 1.3 GJ in the case of the Main Dipole circuits. Their reliable operation — including power converters, superconducting magnets and all connected components (current leads, busbars, diodes, instrumentation), as well as associated protection systems such as quench heaters, Quench Detection System (QDS), Energy Extraction (EE) and related interlocks — is critical. Undetected faults may lead to equipment damage and accelerator downtime.

The LHC comprises approximately 8,000 superconducting magnets along its circumference of 26.7 km, divided into eight sectors and independently powered sub-sectors [1]. The superconducting circuits are grouped into eight families: low-current circuits (60 A, 80–120 A, and 600 A) and high-current circuits — Individually Powered Dipoles (IPDs), Individually Powered Quadrupoles (IPQs), Inner Triplets (ITs), Main Quadrupoles and Main Dipoles — with nominal currents for the latter ranging from 4 kA to 11.6 kA. Before each LHC restart, after the annual Year-End Technical Stop (YETS) or after a Long Shutdown (LS), all circuits must be qualified for safe operation. This is performed during the HWC campaign. The number of circuits commissioned during the 2026 HWC is shown in Table 1.

Table 1: Superconducting Circuits Commissioned during the 2026 HWC Campaign and the Maximum Test Current

Family Name	Number of Circuits	Max. Test Current (A)
Main Dipole	8	11 600
Main Quadrupole	16	11 300
IT	8	6850
IPQ	76	2900
IPD	16	6050
600 A	389	590
80-120 A	279	105
60 A	749	55
Total	**1541**	—

During powering tests, the circuit current is increased in steps to its nominal value in strict sequential order — a test may only commence once all preceding tests have been validated. Figure 1 shows the post-LS test program, consisting of Power Converter Configuration (PCC) and Powering Interlock Controller (PIC) tests at minimum operating current, followed by intermediate current (PLI1–3) and nominal current tests (PNO). Suffixes denote test variations, e.g. a – current cycling, b – EE discharge triggered by the QPS, d – power converter failure, e – Slow Power Abort (SPA) via PIC. Following a YETS, only a subset of these tests is required. The total number of tests ranges from approximately 5,000 (YETS) to 9,000 (LS). Tests are scheduled and tracked via the Accelerator Test Tracking framework (AccTesting) [2] and executed by the HWC Sequencer [3]. Test analysis must be signed off by experts from different domains, namely MP3 (LHC Magnet Circuits, Powering and Performance Panel), MI (Machine Interlocks), and PO (Power Converters), with responsibilities shown in Fig. 1.

Historically, powering test analysis relied on a fragmented ecosystem of tools [4]: MP3 used legacy automated tools (LabVIEW and eDSL [5]) or manual analyses executed via the Service for Web-based Analysis (SWAN), while other teams maintained their independent tool-chains. Validation required signatures across two platforms — AccTesting and the Post Mortem Event Analyser (PMEA) [6]. This fragmentation led to inconsistent acceptance criteria and reduced traceability of the validation process. Legacy tools were difficult to maintain and evolve, while manual analyses and multi-party sign-offs imposed a significant workload on experts and prolonged campaign durations. These limitations motivated the automation effort described in this paper.

* agnieszka.chmielinska@cern.ch

Content from this work may be used under the terms of the CC BY 4.0 licence (© 2026). Any distribution of this work must maintain attribution to the author(s), title of the work, publisher, and DOI.

ISBN: 978-3-95450-252-3 ISSN: 2673-5350 doi: 10.18429/JACoW-IPAC2026-MOP7083

FIELD QUALITY OF MQXFB QUADRUPOLES FOR HL-LHC*

M. Bonora-Tam†, G. Deferne, G. Dima, L. Fiscarelli, S. Izquierdo Bermudez, M. Pentella, C. Petrone, CERN, Meyrin, Switzerland

Abstract

This paper presents the main results of the magnetic measurements performed on the Nb_3Sn MQXFB quadrupole magnets for the High Luminosity LHC (HL-LHC) upgrade at both room and cryogenic temperature. The measurement program, carried out during the different stages of the magnet assembly and by using different instruments such as rotating-coil and stretched-wire systems, allows an early identification of the field errors and a comprehensive characterization of the field quality. A fine tuning of the low-order multipoles is achieved by magnetic shims using iron inserts, which provides a means for improving the field quality of some magnets. The transfer function, the field harmonics, and the effects of superconductor magnetization and iron saturation are reported. In addition, a warm-to-cold extrapolation method is developed for the prediction of the integrated gradient at 1.9 K and nominal current, with a target accuracy of 5×10^{-4}, allowing an appropriate sorting of the magnets at an early stage and before the final cold test. In conclusion, all the MQXFB magnets tested so far meet the field-quality requirements for the HL-LHC, and the adopted measurement and correction strategy has proven to be effective for the series production.

INTRODUCTION

The high luminosity upgrade for the LHC (HL-LHC) foresees the replacement of the inner triplet quadrupole magnets in the main experimental insertions housing the ATLAS and CMS experiments, with wider bore, stronger focusing quadrupoles [1]. The new magnets are based on Nb_3Sn cables, and operate at a nominal current of 16.23 kA, corresponding to a gradient of 132.2 T m^{-1} and peak fields of 11.3 T. Including spares, a total of 30 magnets will be produced, in two different length configurations: MQXFA (4.3 m, 20 in total), and MQXFB [2] (7.3 m, 10 in total). The MQXFA will be assembled in the Q1/Q3 cryo-assemblies (2 magnets per assembly), while the MQXFB will be combined with the MCBXFB dipole orbit corrector, see Fig. 1, with two such assemblies (Q2a/Q2b) installed per side of each interaction point. The main design parameters of the MQXFB quadrupoles [3] are reported in Table 1.

A dedicated magnetic measurement program has been implemented for the different stages of magnet assembly with a final test at 1.9 K (cold) [4]. Measurements at ambient temperature (warm) provide early information on geometric field errors, while measurements at cold, and up to nominal current, allow the characterization of all relevant field contributions, including effects of superconductor magnetization and iron saturation.

This paper summarizes the results obtained on the MQXFB series magnets, with emphasis on the transfer function, field harmonics, magnetic shimming, and warm-to-cold extrapolation of the integrated gradient.

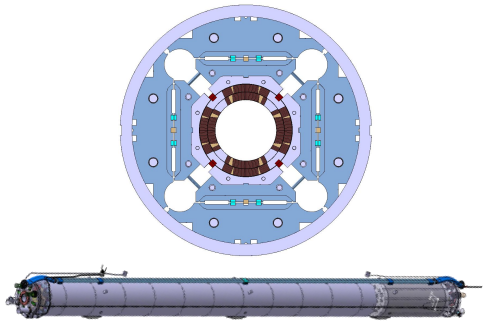

Figure 1: The cross-section of the MQXFB quadrupole (top), and the Q2 cryo-assembly (bottom), integrating the MQXFB quadrupole magnet (left) and the MCBXFB dipole orbit corrector (right).

Table 1: Main Design Parameters of the MQXFB

Parameter	Unit	Value
Aperture diameter	mm	150
Operational temperature	K	1.9
Nominal current I_{nom}	A	16230
Nominal gradient	Tm^{-1}	132.2
Integrated nominal gradient	T	948.1
Magnetic length	m	7.17

MAGNETIC MEASUREMENT STRATEGY

Ambient temperature measurements are carried out at low current (10 A) during several stages of the assembly, including after coil-pack assembly, centering, loading, pre-alignment during cold-mass assembly, and final alignment with respect to reference points.

At 1.9 K, the magnets are measured up to the nominal current of 16.23 kA. The powering program includes stair-step cycles, machine cycles, and variable ramp-rate cycles, optimized to characterize the field within the available test time. In particular, the machine cycles emulate the main features of the operational powering profiles such as the reset current, the injection plateau, the acceleration ramp, and the flattop plateau at nominal current.

Instrumentation includes rotating coils for field harmonics both at warm (rotating coil scanner [5]) and cold (chain of rotating coil shafts [6]), and a stretched-wire system [7, 8] for the transfer function measurement and magnetic axis alignment at warm and cold.

* Work supported by the HL-LHC project

† matthias.bonora@cern.ch

Content from this work may be used under the terms of the CC BY 4.0 licence (© 2026). Any distribution of this work must maintain attribution to the author(s), title of the work, publisher, and DOI.

ISBN: 978-3-95450-252-3 ISSN: 2673-5350 doi: 10.18429/JACoW-IPAC2026-MOP7086

IMPROVING HELIUM SUSTAINABILITY: CURRENT PERFORMANCE AND UPGRADE OF THE ALBA HELIUM LIQUEFACTION FACILITY

M. Quispe†, J. Casas, C. Colldelram, G. Peña Calurano, M. Sánchez Hidalgo
B. de Abreu Francisco, ALBA Synchrotron, Cerdanyola del Vallès, Spain

Abstract

Efficient use of gaseous and liquid helium, a non-renewable resource essential for accelerator-based experiments, is a key priority at ALBA Synchrotron Light Source. This work presents the operational status of ALBA's helium liquefaction plant and the liquid-helium production achieved in recent years, based on recovery from its use in the BOREAS, LOREA, CLAESS and MSPD beamlines. The helium liquefaction plant's operating mode is discussed, with emphasis on its main limitation: the system can only process recovered gas with an average helium purity of 99.5%. To overcome this constraint, the plant was upgraded during 2025–2026 with the installation of a gas purifier capable of treating gas helium with purities as low as 90%. The first operational results and performance of the helium liquefaction plant with the integrated purifier are presented.

BACKGROUND

Helium, in both its liquid and gaseous states, plays a fundamental role in the operation of the ALBA Synchrotron owing to its cryogenic properties and chemically inert nature. Currently, four of ALBA's experimental beamlines – BOREAS, LOREA, MSPD, and CLAESS – use liquid helium in the execution of their experiments.

In the case of BOREAS, a beamline specialized in advanced X-ray spectroscopy techniques for studying materials, liquid helium is used to cool superconducting magnets (enabling magnetic field generation) and to maintain samples at cryogenic temperatures, thereby allowing the investigation of magnetic and quantum materials using advanced X-ray techniques. For LOREA, primarily dedicated to photoemission spectroscopy using VUV and soft X-ray radiation, helium is used to reach cryogenic temperatures to study low temperature phase transitions, to have better ultra-high vacuum conditions, and get (a factor 10) better spectroscopic resolution.

At CLAESS (Core Level Absorption and Emission Spectroscopies), helium gas at room temperature is used for routine operations in the ionization chambers, as it allows data collection, and in experiments both as an inert gas to purge the line and test for leaks, and in mixtures to dilute reactive gases (this is related, for example, to heterogeneous catalysis and CO_2 conversion). Liquid helium is also used for the Dynaflow cryostat to access low temperatures, enabling two main functions: exploring the temperature range from approximately 10 K to 300 K, also allowing transferring samples from cold storage (80 K) to the cold data collection environment. In addition to enabling temperature-dependent experiments (typically, but not exclusively, on superconductors, magnetoelectronic, spintronic, multiferroic, and strongly electron-correlated systems), it helps to reduce the risk of radiation damage in sensitive samples (typically soft matter).

In the case of MSPD (Materials Science Powder Diffraction), beside marginal need of helium in gas form for specific scientific applications (chemical reactions under pure or mixed helium), it is essentially helium in liquid form which is required by so called Dynaflow LHe cryostat to collect data down to 5K. Such studies generally relate to highly correlated electron system for which transport properties, magnetic and crystal structures interplay.

Table 1 summarizes the liquid helium purchases made by ALBA during the last three years for the operation of these beamlines, together with the associated costs. In terms of consumption distribution in 2025, liquid helium usage was allocated as follows: BOREAS (74%), LOREA (22%), MSPD (2%), and CLAESS (2%). The cost data also illustrate the progressive increase in the price of liquid helium, from €38/L in 2023 to €41.7/L in 2024 and €43.5/L in 2025.

Table 1: Liquid Helium Purchases at ALBA

Year	Liquid Helium purchased [L]	Cost [k€]
2023	5220	198
2024	9060	376
2025	10050	437

At present, the use of helium presents a structural challenge, as it is a non-renewable resource on a human timescale and its global availability is limited, with a supply chain subject to geopolitical and economic volatility [1]. In this context, helium recovery and reuse have become a strategic priority for the international scientific community.

During operation in cryostats and superconducting systems, liquid helium inevitably evaporates due to thermal loads, transitioning into the gaseous phase. Traditionally, this gas was vented to the atmosphere, resulting in the irreversible loss of a critical resource. However, advances in recovery infrastructure have demonstrated that evaporated helium can be effectively captured, purified, and reliquefied. At synchrotron facilities such as ALBA, these systems comprise low-pressure piping networks that convey helium gas to compressors, purification units, and liquefaction plants, thereby closing the helium usage cycle [2]. Table 2 summarizes the amount of liquid helium recovered at the ALBA facility over the past three years, as well as the corresponding market value of the recovered helium.

Content from this work may be used under the terms of the CC BY 4.0 licence (© 2026). Any distribution of this work must maintain attribution to the author(s), title of the work, publisher, and DOI.

†mquispe@cells.es

ISBN: 978-3-95450-252-3 ISSN: 2673-5350 doi: 10.18429/JACoW-IPAC2026-MOP7087

LARGE-SCALE HELIUM REFRIGERATION CRYOGENIC SYSTEMS COSTING FOR SUPERCONDUCTING PARTICLE ACCELERATORS SUCH AS THE FCC-ee

B. Bradu, D. Delikaris, L. Delprat†, B. Naydenov
European Organization for Nuclear Research (CERN), Geneva, Switzerland

Content from this work may be used under the terms of the CC BY 4.0 licence (© 2026). Any distribution of this work must maintain attribution to the author(s), title of the work, publisher, and DOI.

Abstract

Large-scale helium refrigeration cryogenic systems are a key element, essential to the safe and reliable operation of particle accelerators using superconducting devices such as radio-frequency cavities or magnets. The long-term success of the LHC operation with an outstanding physics production to date paves the way towards the High-Luminosity LHC (HL-LHC) upgrade to be operated until the early 2040s, after which it could be followed by the Future Circular Collider (FCC). Such large-scale projects, requiring a significant amount of cryogenic cooling capacity to be installed, pose the question of the cost estimation methodology to be employed, as the cryogenic system represents a non-negligible fraction of the total capital, operation & maintenance cost of the facility. Capitalizing on the experience of the LHC project, then on its recent HL-LHC upgrade, the existing CERN methodology was updated with the latest available industrial indexation, thus allowing the cost of the FCC cryogenic system to be assessed. This paper reports on the approach used to estimate the cost of the FCC cryogenics, refining the method adopted at the time of the LHC project. It considers the evolution of material and labour costs over the past two decades, studies the updated economics of 4.5 K and 1.8 K helium refrigeration, and presents the strong impact of the cryogenic distribution system. It also identifies and proposes ways for improving the capital, operation & maintenance expenditure.

INTRODUCTION

The design maturity of the Future Circular Collider (FCC) cryogenic system has progressed significantly from the initial 2018 concept to the 2025 feasibility report, triggering the need for an update of the cost estimate for the FCC-ee machine. The first exercise was performed along with the release of the FCC Conceptual Design Report (CDR) in 2018, with the feasibility report of 2025 the opportunity to update and complete the methodology that was proposed by S. Claudet et al in July 1999 in their Economics of large helium cryogenic systems publication in the context of the LHC project [1].

CRYOGENICS FOR FCC-ee

The latest FCC baseline layout (PA31-3.0) is a 91-km long circular tunnel consisting of eight sectors, each of which is 11.35-km in length. It hosts four experimental points, and four technical points, out of which two (points PH for the collider and PL for the booster) are associated with the superconducting radiofrequency (SRF) system. These need to be operated at both 2 K (800 MHz cavities) and 4.5 K (400 MHz cavities) to accelerate the particles to the required energies. Detailed information about the cryogenic architecture associated with the FCC-ee machine and its SRF system at its ttbar stage are to be found in the FCC Feasibility Report [2] published in March 2025. Figure 1 gives a general overview of the cryogenic system associated with the FCC-ee machine in its ttbar stage.

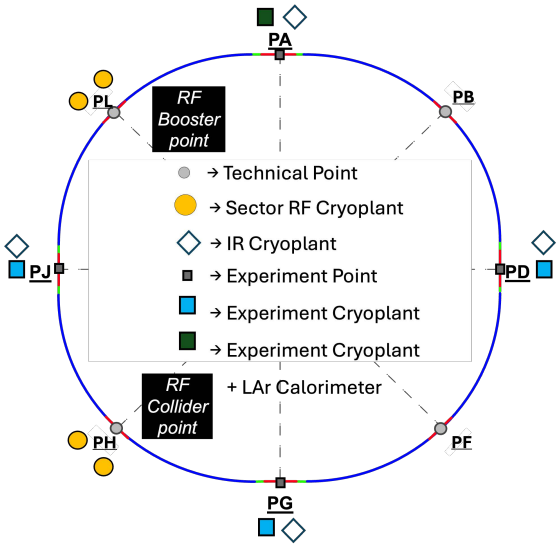

Figure 1: FCC-ee cryogenic system layout for ttbar operation.

METHODOLOGY

The cryogenic system for particle accelerators is usually composed of five main types of components: the cryoplants, the cryogenic distribution, the cryogen inventory and storage, the control and instrumentation, and the warm piping. Those items are used as high-level categories to create the Product Breakdown Structure (PBS) necessary to evaluate the cost of FCC-ee cryogenics.

EVALUATING THE COST: THE INDEX

The costing methodology is mainly based on an analogous technique, where LHC and HL-LHC data are used as a main reference to create a scaling law and to verify its accuracy. Extensive cost data is available from 1998 when the LHC project was being finalised [1]. To scale this data to 2023 figures, the date at which this exercise was performed, an index was compiled and used with the support of the CERN Procurement Group.

† laurent.delprat@cern.ch

ISBN: 978-3-95450-252-3 ISSN: 2673-5350 doi: 10.18429/JACoW-IPAC2026-MOP7088

NUMERICAL-EXPERIMENTAL COMPARATIVE RESEARCH OF TITANIUM FOIL GRADES FOR ACCELERATOR OUTPUT WINDOWS*

V. V. Yepremyan†, A. H. Davtyan, H. A. Isunts, A. A. Hovhannisyan
CANDLE Synchrotron Research Institute, Yerevan, Armenia

Abstract

The stress-strain state of titanium foils used for accelerator output windows was investigated with various foil thicknesses and titanium grades. Initial material data included deformation diagrams, densities, Young's moduli, and Poisson's ratios for each grade. Experimental studies were performed to validate the central displacements of Titanium Grade 2 foils. Measurements were conducted using a Hexagon precision measurement machine to determine the effective friction coefficients between titanium and two contacting materials: stainless steel 304L and oxygen-free copper. The latter was obtained via fitting the displacement curves of the initial simulations and experimental measurements conducted. These coefficients were subsequently incorporated into refined numerical simulations to obtain a more accurate representation of the stress–strain state within the sealing region of the output window assembly. Comparative analyses of the simulation results were carried out for all selected titanium grades. The advantages and limitations of each grade were evaluated in terms of mechanical performance, deformation behavior, and suitability for use in accelerator output window applications.

INTRODUCTION

Accelerator output windows serve as transition units for the generated beam when it passes from a vacuum environment to an atmospheric-pressure environment. During this transition, the metal foil absorbs a certain portion of the beam, thereby altering its characteristics.

The AREAL linear electron accelerator at the CANDLE Synchrotron Research Institute [1-6] is equipped with two output windows, each consisting of two flanges, a 50 μm thick Grade 2 titanium foil, and a copper gasket (see Fig. 1). This assembly is sealed using bolts, nuts, and washers, forming a detachable joint.

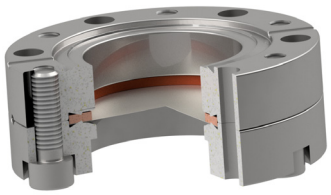

Figure 1: Accelerator output window assembly.

The output window assembly can be realized using detachable and non-detachable joints. In detachable joints, the gasket is plastically deformed to ensure sealing. These joints can be configured in two ways, depending on the foil position: above-gasket and beneath-gasket. In non-detachable joints, vacuum brazing or welding is applied. These can also be classified into two types: brazing using molten filler material and diffusion bonding using specially designed foil-type filler materials. A summary of these approaches is illustrated in Fig. 2.

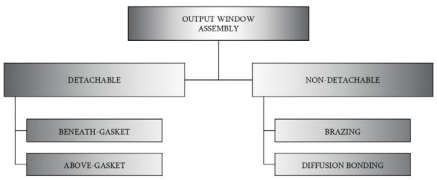

Figure 2: Methods of output window fabrication.

Various foil materials are used in accelerators [7-9], but titanium foils are the most commonly applied. However, selecting the appropriate titanium grade remains a challenge. In accelerator technology, Grade 2 and Grade 5 titanium foils are widely used. Grade 1 titanium (Ti Gr-1) foils are generally not suitable for the AREAL linear electron accelerator, since the required stable thickness is too high, making the foil act as a barrier rather than a window for the beam [10, 11]. Therefore, it is essential to investigate not only Grade 2 but also Grade 5 titanium foils.

The stability of the foil in the assembly depends on its diameter. In the AREAL linear electron accelerator, one side of the output window uses a DN35CF–DN40CF flange [12], while the other side uses an ATLAS flange [13]. In both cases, the foil is fixed along a circular line passing through the tip of the knife edge. This circle defines the effective diameter of the foil.

Table 1: Properties of Ti Gr-2 and Gr-5

Properties	Gr-2	Gr-5
Density (g/cc)	4.51	4.43
Tensile Strength, Ultimate (MPa)	430	950
Tensile Strength, Yield (MPa)	340	880
Poisson's Ratio	0.34	0.342
Modulus of Elasticity (GPa)	102	113.8

Before thermal effects become significant, the foil in accelerator output windows is primarily subjected to atmospheric pressure. As a result, it experiences deformation during each vacuum pumping cycle. Under identical thickness conditions, Grade 2 and Grade 5 titanium foils exhibit different mechanical behaviors [14-15]. Table 1 a comparison of these materials shows that although Ti Gr-5 has superior mechanical properties, it is less economically advantageous.

* Work supported by Higher Education and Science Committee of RA (Research project № 23AA-2D015).
† epremyan@asls.candle.am

Content from this work may be used under the terms of the CC BY 4.0 licence (© 2026). Any distribution of this work must maintain attribution to the author(s), title of the work, publisher, and DOI.

ISBN: 978-3-95450-252-3 ISSN: 2673-5350 doi: 10.18429/JACoW-IPAC2026-MOP7089

SEY REDUCTION USING ULTRATHIN TiN/NbN MULTILAYERS FOR ACCELERATOR APPLICATIONS

G. Sattonnay‡, Y. Pisi†, D. Longuevergne, Université Paris-Saclay, CNRS/IN2P3, IJCLab, Orsay, France
E. Blanquet, A. Mantoux, Science et Ingénierie des Matériaux et Procédés, Saint-Martin-d'Hères, France

Abstract

Multipacting and electron cloud formation remain major limitations for the performance of modern particle accelerators. In superconducting radio-frequency (SRF) cavities, multipacting can prevent stable cavity operation and restrict achievable accelerating gradients. In positively charged particle machines such as the LHC, the build-up of electron clouds results in beam instabilities, vacuum degradation, and additional heat loads on the cryogenic systems. Reducing the secondary electron yield (SEY) of vacuum-facing surfaces is therefore a key strategy to mitigate these effects. To mitigate these effects, several strategies have been proposed, in particular the deposition of thin films designed to reduce the secondary electron yield (SEY) of the relevant surfaces. We investigated the SEY behaviour of ultrathin TiN/NbN multilayers, with particular attention to the influence of both the number of layers and the TiN/NbN stacking sequence. Multilayers composed of individual 3 nm films were deposited by PVD to probe interfacial effects and possible electronic confinement phenomena. SEY measurements performed before and after electron conditioning reveal a dependence on the multilayer architecture. One particular multilayer configuration achieves a significantly reduced SEY, reaching 0.98 after conditioning.

INTRODUCTION

Particle accelerators such as the Large Hadron Collider (LHC) are limited by secondary electron emission, which can trigger electron cloud formation through multipacting (secondary electron yield (SEY) > 1), leading to beam instabilities. SEY originates from electrons produced by residual gas ionization or synchrotron radiation interacting with beam pipe walls. Mitigation strategies include increasing surface roughness to enhance electron trapping, but these are not always compatible with component constraints. An alternative is the deposition of intrinsically low-SEY coatings. In this work, we investigate TiN/NbN multilayer thin films, combining low intrinsic SEY with interface-engineered electron trapping. These multilayers create potential barriers (~0.2 eV) that reduce electron transmission and promote confinement, especially for low-energy secondary electrons. Increasing the number of interfaces enhances energy dissipation and lowers effective SEY.

TiN and NbN are particularly suitable due to their low SEY, structural compatibility, and ease of deposition. This approach offers a promising route for next-generation anti-multipacting coatings in accelerator environments.

EXPERIMENTAL

Thin films were deposited by PVD using a Plassys MP500S system equipped with DC/RF cathodes, enabling co-sputtering and reactive deposition under argon plasma. Films were grown on mirror-polished Si (110) substrates under high vacuum (~10^{-7} mbar) to minimize contamination. TiN/NbN multilayers were fabricated by alternating sputtering from TiN and Nb targets, with optimized conditions (0.3 Pa, 40 sccm Ar, 200 mA) to ensure slow, uniform growth. Individual layer thicknesses (~2–3 nm) were controlled via deposition time (1 min 30 s per layer), and various architectures were explored by adjusting the number of layers and the top layer composition. The substrate temperature (300 °C) was chosen to obtain dense, slightly rough films (Thornton transition zone), while avoiding excessive roughness effects on SEY. Characterization was performed using XRR, XRD, XPS, TEM, along with SEY measurements.

RESULTS

Structural and Chemical Characterization

To investigate the chemical structure of the multilayer, X-ray photoelectron spectroscopy (XPS) depth profiling was performed. The depth profile was acquired using a 500 eV argon ion beam with an abrasion spot size of 400 µm. A total of 200 sputtering steps were carried out, each lasting 5 s. After each step, a survey spectrum was recorded, along with high-resolution spectra for the elements of interest (C, N, Nb, and Ti). The XPS depth profile (Fig. 1) shows the elemental distribution across the alternating NbN and TiN layers. The oxygen concentration remains approximately constant at ~8 at.% throughout the multilayer, while nitrogen is stable at ~35 at.%. The Nb 3d and Ti 2p core-level spectra confirm the presence of Nb–N (binding energy ~203.6 eV) and Ti–N (~455 eV) bonds, respectively. As shown in Fig. 2, titanium appears to be present within Nb-rich layers and, conversely, niobium within Ti-rich layers. This may result from partial interdiffusion during deposition. It may also reflect an intrinsic limitation of XPS: its information depth (~5–10 nm) exceeds the individual layer thickness (~3 nm), leading to signal contributions from adjacent layers.

Content from this work may be used under the terms of the CC BY 4.0 licence (© 2026). Any distribution of this work must maintain attribution to the author(s), title of the work, publisher, and DOI.

† Also at Science et Ingénierie des Matériaux et Procédés, Saint-Martin-d'Hères, France
‡ gael.sattonnay@ijclab.in2p3.fr

ISBN: 978-3-95450-252-3 ISSN: 2673-5350 doi: 10.18429/JACoW-IPAC2026-MOP7091

BEAM MEASUREMENTS WITH CRYOINSERTS IN SIS18

L.H.J. Bozyk*[1], P.J. Spiller[1]
[1]GSI Helmholtzzentrum für Schwerionenforschung, Darmstadt, Germany

Abstract

In oder to increase the maximum achievable intensity of medium charge state heavy ion beams in SIS18 at GSI for FAIR-operation, the installation of cryoinserts is foreseen. These cryogenic surfaces with high sticking probability provide high pumping speed around the ion-catcher, where most of the beam-loss induced gas desorption takes place. Such, gas particles get quickly removed, minimizing beam loss by charge exchange from interaction with the residual gas.

A prototype cryoinsert was designed, manufactured and tested, showing the clear reduction of artificial gas pulses. Most recently, the prototype was installed into SIS18. There, a reduction of the static pressure extending several meters after cooldown was observed.

In 2025 the first beam experiments with medium charged Uranium beams and the cryoinserts took place to observe their influence. The charge exchange could be measured, showing a significant decrease due to the cryoinserts and also a slight influence on the transmission in an acceleration cycle was measurable. In the meantime, a series production of cryoinserts is prepared, including improvements and simplifications of the design.

MOTIVATION AND INTRODUCTION

Serving as a booster synchrotron for FAIR, SIS18 will have to provide $1.5 \cdot 10^{11}$ particles per pulse to reach $5 \cdot 10^{11}$ particles in SIS100. To reach these intensities, medium charge state heavy ions like U^{28+} have to be used which avoid stripping losses in the transfer channel and shift the space charge limit to higher number of particles. Unfortunately the probability of charge exchange in collisions with residual gas particles for such ions is much higher, than for higher charge states like U^{73+}. As charge exchanged ions have a different magnetic rigidity than the reference ion, they get separated from the circulating beam. When they are lost at a grazing incidence on the vacuum chamber wall, they release a huge amount of gas via ion impact induced gas desorption. This local increase of residual gas density in turn increases the probability for further charge exchange and gives rise to a self-amplification up to complete beam loss. In this case, the residual gas density is no longer constant during operation, but a *dynamic vacuum* develops. It limits the maximum achievable intensity of heavy ion beams.

There are several technical measures to shift this limit, like lowering the static gas density or the installation of low desorbing surfaces, which is applied in the ion catchers, see [1]. The intensity of SIS18 could be increased significantly [1,2], but the FAIR-intensities are not yet reached. However, simulations using cryogenic surfaces hint, that they would help to increase the maximum intensity [3]. The sticking probability on cryogenic surfaces is close to one and such much higher than on NEG surfaces.

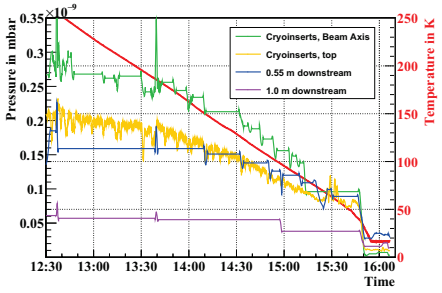

Figure 1: Temperature (red) and pressure evolution at the cryoinserts and at neighboring positions downstream.

A prototype with cryogenic inserts has been set up and tested. It is described in [4,5]. It contains gold-coated copper surfaces, which are cooled by a commercially available cold head. This cold head can be removed without breaking the beam vacuum for the vacuum-bakeout. It has been installed in SIS18 and could be successfully tested without beam, showing significant decrease of the residual gas density [6].

MEASUREMENTS IN SIS18

In July 2025 the cryoinserts could be tested for the first time with medium charged Uranium beams, U^{28+}. The tests were performed within three different cooldowns, each lasting for almost 8 hours. During two of these cooldowns, the lifetime was measured continuously by repetitive storing of low intensity beams for 10 s at injection energy. Alternating to these cycles, high intensity beams with $2-3 \cdot 10^{10}$ injected particles were stored to measure collimator currents. Before and after cooldown respectively, the intensity dependent transmission for different ramping rates was measured.

Figure 1 shows pressure evolution during a cooldown in Section 01, where the cryoinserts are located. The cryoinsert's temperature is shown as well. The continuous decrease of pressure is followed by a sudden drop, when the Hydrogen pumping emerges below 40 K [5].

MEASUREMENT RESULTS

Lifetime Measurements

An increase of lifetime indicating vacuum relaxation after high loss operation during beam setup could be observed. Apart from this effect, no clear signs of lifetime improvement can be seen. The alternating high intensity cycles spoiled the beam life time. Nevertheless, moving the gate valve next to the cryoinserts induces a pressure bump, whose decrease can be investigated by lifetime measurements. Figure 2 shows lifetime evolution at three different temperatures. The lower

* L.Bozyk@gsi.de

Content from this work may be used under the terms of the CC BY 4.0 licence (© 2026). Any distribution of this work must maintain attribution to the author(s), title of the work, publisher, and DOI.

ISBN: 978-3-95450-252-3 ISSN: 2673-5350 doi: 10.18429/JACoW-IPAC2026-MOP7095

PARTICULATE STUDY OF NEG PUMPS IRRADIATED IN THE CEBAF TUNNEL*

G. Ciovati†, D. Hamlette, D. Heck, J. Jordan, A. Wildeson,
Thomas Jefferson National Accelerator Facility, Newport News, United States
B. Busetto, L. Caruso, E. Maccallini, P. Manini, D. Nicolosi, F. Siviero,
SAES Getters S.p.A., Lainate, Italy
S. Wulfsberg, SAES Getters/U.S.A., Inc., Colorado Springs, United States

Abstract

Non-evaporable getter (NEG) pumps are being used to maintain ultra-high vacuum in the beamline of superconducting radio-frequency (SRF) accelerators, such as the Continuous Electron Beam Accelerator Facility (CEBAF) at Jefferson Lab. Because of the sensitivity of the performance of SRF cavities to particulate contamination, it is important to evaluate the integrity of the NEG material after exposure to high radiation during beam operation. The particulate count from two NEG pumps based on ZAO® getter alloy was measured with a particle counter in a clean-room. The pumps were assembled onto a hermetically sealed setup which was placed in the CEBAF tunnel. The setup was exposed to 24 h beam operation for ~ 230 days. The total gamma-rays dose measured on the test setup was ~ 1.6 Mrad. The total neutron dose measured at ~ 75 cm of the test setup was ~ 11 krad. The particulate count from the two pumps was measured again in the clean-room after irradiation. Whereas an increase of particulate counts was measured, compared to before irradiation, subsequent measurements indicate the absence of systematically loose particulate. The pumping speed of one of the irradiated pumps was also measured to be consistent with that of a non-irradiated one, corroborating the absence of significant damage to the ZAO® NEG material due to irradiation.

INTRODUCTION

Non-evaporable getter (NEG) pumps are being installed in the pump drops of both the warm girders and the cryomodules that are installed in the Continuous Electron Beam Accelerator Facility (CEBAF) after refurbishment [1]. The NEG pumps being used are made of a sintered alloy of zirconium, vanadium, titanium and aluminum, referred to as ZAO®. This type of pump offers high pumping speed and pumping capacity for hydrogen, which is the main residual gas of clean ultra-high vacuum systems, with a smaller size and weight compared to ion pumps. Residual hydrogen gas adsorbed on the surface of SRF cavities at 2 K may enhance or trigger field emission from particulates present on the surface [2–4]. The NEG pumps from SAES Getters have low particulate emission and they have been qualified for use in the vacuum system of SRF cavities [5–7]. They have also been used to pump the cavity string for LCLS-II and LCLS-II HE cryomodules [8]. This manuscript presents the results of a study to evaluate any significant change with respect to emission of particulate after the NEG pump was exposed to gamma and neutron radiation produced during beam operation in the CEBAF tunnel.

EXPERIMENTAL SETUP

Preparation for Installation in CEBAF Tunnel

Two NEG pumps, a CapaciTorr® Z 400 [9] and a CapaciTorr® HV 200 [10] were loaned by SAES Getters for this study. Both pumps are made of the ZAO® alloy. The CapaciTorr HV 200 is the same model as the one used in the pump-drops of refurbished cryomodules and warm girders. The HV 200 and Z 400 pumps have a nominal hydrogen pumping speed of 200 l/s and 400 l/s, respectively.

The NEG cartridges were cleaned in isopropyl alcohol with ultrasonic agitation for 5 min, followed by blow-down with filtered nitrogen and placed in a sealed nylon bag. Figure 1 shows a picture of the pumps inside the clean room (CR). A four way cross was cleaned using ultra-high vacuum (UHV) cleaning protocols, consisting of ultrasonic cleaning with a detergent, solvent rinses and blow down with filtered nitrogen. The parts were transferred to the clean-room in a sealed nylon bag, then assembled with the NEG pumps as shown in Fig 2.

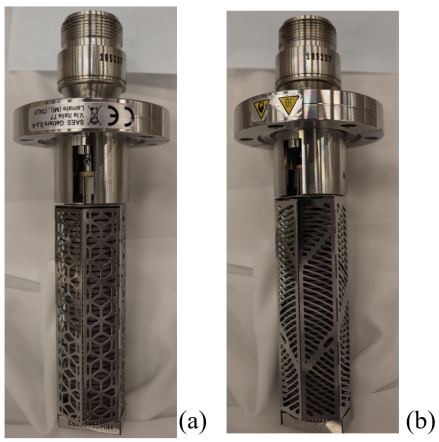
(a) (b)

Figure 1: NEG pumps CapaciTorr HV 200 (a) and Z 400 (b) in the clean room.

Each NEG pump was cleaned with ionized nitrogen on above a particle counter (Lighthouse Solair 3100) inside the

* This material is based upon work supported by the U.S. Department of Energy, Office of Science, Office of Nuclear Physics under contract DE-AC05-06OR23177.

† gciovati@jlab.org

Content from this work may be used under the terms of the CC BY 4.0 licence (© 2026). Any distribution of this work must maintain attribution to the author(s), title of the work, publisher, and DOI.

ISBN: 978-3-95450-252-3 ISSN: 2673-5350 doi: 10.18429/JACoW-IPAC2026-MOP7096

ALBAII VACUUM SYSTEM: DESIGN EVOLUTION AND PROTOTYPING*

R. Parise†,1, B. Francisco[1], L. Carvajal[1], J. Álvarez[1], O. Traver[1], G. Peña[1], L. Ribo[1], P. Salmerón[1], M. Llonch[1], M. Quispe[1], N. Gonzalez[1], J. Casas[1], F. Perez[1], K. Blümer[2], R. Schwertfeger[2], H. Henninger[2], C. Colldelram[1]
[1]ALBA Synchrotron, Cerdanyola del Vallès, Spain
[2]FMB Feinwerk- und Messtechnik, Berlin, Germany

Abstract

ALBA is upgrading its storage ring into a 4th-generation diffraction-limited facility, which demands redesigned vacuum chambers. Most of the 268.8 m ring, divided into 16 arcs, will use OFHC-Cu or CuCrZr to dissipate synchrotron radiation and minimize resistive-wall impedance. To meet the injection-efficiency requirements, former 16 mm circular cross-section has been replaced by a rhombic geometry providing a 22 mm horizontal aperture, 1.25 mm wall thickness and clearances of 1 mm to the magnet poles. Its structural response shows 13 MPa maximum stress with deformations of 3 µm. A short bellows is foreseen between each pair of BPM blocks to absorb chamber displacements from alignment tolerances and thermal expansions while keeping BPM positions fixed. At dipole positions, antechambers with crotch absorbers manage the radiation heat load, with each arc receiving 20.5 kW of power. The entire ring will be NEG-coated to accelerate conditioning and reach the required pressure of 1×10^{-9} mbar at 100 Ah. This contribution presents the vacuum system status and the design, fabrication progress of the prototypes.

INTRODUCTION

ALBA is upgrading its storage ring into ALBA II, a 4th-generation diffraction-limited synchrotron light source [1]. The compact lattice imposes strong constraints on the vacuum system, including magnet aperture, synchrotron radiation power, conductance, impedance, and injection-efficiency requirements. To satisfy these constraints, the chamber design has evolved from the previously planned 16 mm circular cross-section to a rhombic profile with increased horizontal aperture. This paper presents the vacuum concept, the chamber geometry optimization, and the status of the prototype fabrication program.

ALBAII VACUUM SYSTEM CONCEPT

The ALBA II vacuum system follows a modular arc concept combining compact integration, distributed NEG pumping, and synchrotron radiation power management. Each arc forms one vacuum section delimited by two gate valves, with NEG-coated chambers activated ex-situ before installation.

A typical arc includes five copper-alloy dipole chambers, five pumping locations, and five crotch absorbers, while part of the synchrotron radiation is distributed directly onto the chamber walls. Eleven BPMs are foreseen per arc: seven as standalone BPM/bellows assemblies and four integrated into dipole chambers. Short bellows are foreseen between BPM blocks to absorb alignment tolerances and thermal expansion while preserving the BPM positions.

The dipole chambers use OFS/OFHC copper or CuCrZr depending on thermal and mechanical requirements. They combine a rhombic beam aperture, integrated cooling, antechambers for synchrotron radiation extraction, pumping blocks, and crotch absorbers at selected locations. Compact MO-type flanges are used where space is critical, while adapted CF ones are kept where required.

DESIGN EVOLUTION

The initial vacuum chamber concept was based on a 16 mm circular internal cross-section. Further lattice and injection studies showed that this aperture was too restrictive to meet the required injection efficiency [2]. As a result, alternative chamber profiles were investigated to increase the horizontal aperture while preserving compatibility with the existing magnet geometry [3], as adopted in other compact storage rings [4,5]. A rhombic cross-section, similar to Elettra 2.0 [4], was selected as the most promising option.

Since the magnet poles were kept fixed, and a minimum clearance of 1 mm to the chamber wall had to be maintained, the available external envelope imposed a strong geometrical constraint. Figure 1 shows the resulting available area obtained from the superposition of the surrounding magnet pole profiles. The boundary corresponds to a 1 mm offset from the nearest magnet pole, and the previously 16 mm circular cross-section is shown for reference.

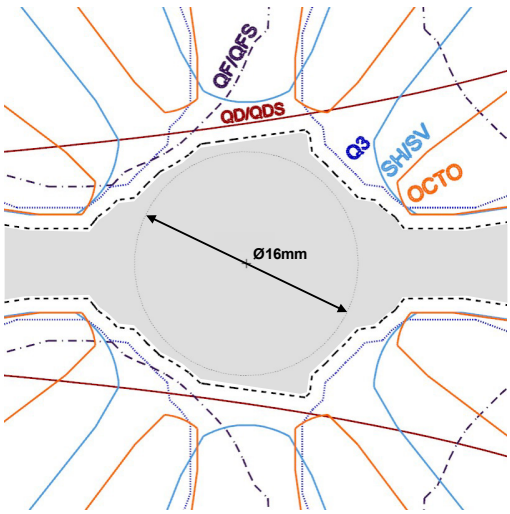

Figure 1: Available chamber envelope.

* Work supported by Spanish MCIN and the European Union – NextGenerationEU project 28.50.460D.74903 from the Recovery and Resilience Mechanism.
† rparise@cells.es

Content from this work may be used under the terms of the CC BY 4.0 licence (© 2026). Any distribution of this work must maintain attribution to the author(s), title of the work, publisher, and DOI.

ISBN: 978-3-95450-252-3 ISSN: 2673-5350 doi: 10.18429/JACoW-IPAC2026-MOP7098

THE BEAM STOPS FOR THE ESS SUPERCONDUCTING LINAC

Elena Donegani*, Artur Gevorgyan, Anders Olsson
European Spallation Source (ESS), Lund, Sweden

Abstract

For the ESS superconducting linac in Sweden, two types of insertable beam stops were manufactured instead of bulky beam dumps. The beam stops dump protons either up to 100 MeV or 250 MeV; the most demanding beam modes have an average beam power of 700 or 1140 W, respectively. The beam stops are water-cooled and moved by pneumatic actuators. The beam stops were designed at the ESS in Sweden and manufactured by Proactive R&D in Spain, supported by the ESS workshop and many companies from all around Europe. The assembly, acceptance tests and metrology measurements were performed in ISO5 cleanrooms, before the installations in the particle-free environment next to the superconducting cavities of the ESS linac.

This contribution summarizes the assembly, test and commissioning experience.

INTRODUCTION

The commissioning of the proton accelerator for the European Spallation Source (ESS) started in Lund (Sweden) during 2018, with the ultimate goal of delivering 2.86 ms long pulses at 14 Hz and the nominal current of 62.5 mA on the ESS spallation target [1]. The compact ESS beam stops were designed in place of bulky beam dumps to safely dump the proton beam within two superconducting linac sections: the SPoKe (SPK) and Medium Beta Line (MBL) sections (see Tab. 1 with the key beam parameters and impact). The most demanding beam modes have an average beam power of 700 W and 1140 W for the SPK and MBL IBS, respectively. In the most demanding beam modes, the beam-interceptive cores reach a temperature of 685 °C in the SPK beam stop and 280 °C in the MBL beam stop.

Table 1: Key Beam Parameters and Impact on the Insertable Beam Stops (IBS) for the ESS Superconducting Proton Linac

	SPK IBS	MBL IBS
Nominal Energy	92 MeV	216 MeV
Energy Range	[21, 100] MeV	[21, 250] MeV
Peak Power	700 W	1140 W
Peak Power Density	4 GW/cm^3	30 MW/cm^3
Peak Temperature	685 °C	280 °C

The design of the ESS beam stops required a careful selection of the materials, geometry and cooling system, informed by neutronics and thermo-mechanical calculations [2]. The Insertable Beam Stops (IBS) were designed to fit in the limited space inside as well outside the vacuum vessel (see for instance the fully packed SPK1 section in Fig. 1). Moreover, they must fulfill the ISO5 requirements. In particular, during the operation with beam the outgassing must remain below 10^{-7} mbar·L/s. In this paper, the assembly and tests are summarized, with emphasis on the rigorous control of particulate contamination which is mandatory to sustain the high accelerating gradients in the ESS superconducting linac [4]. The very first commissioning results are presented.

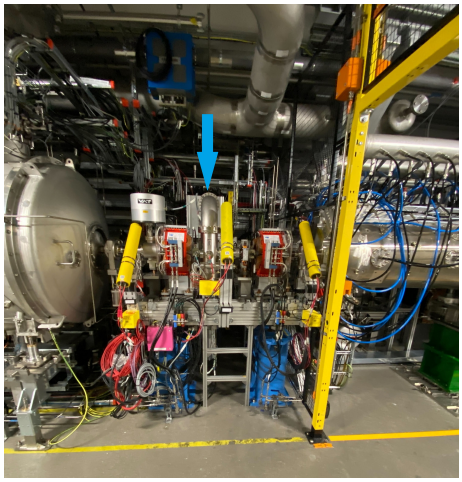

Figure 1: Installation location of the SPK IBS [3] between the first cryomodule of the ESS superconducting linac (on the left), and the end of the DTL5 section in the ESS normal conducting linac (on the right).

ASSEMBLY IN ISO5 CLEANROOMS

The beam stops were designed at the ESS; the detailed design and assembly was performed in collaboration with the company Proactive R&D (in Spain). The manufacturing of all the components was supported by the ESS workshop and many companies from all around Europe. All the ESS beam stops have a graphite core to fully stop the proton beam; the core is enclosed in a TZM shell. The graphite cores required thermal treatment in order to minimize the outgassing prior to installation in the ESS superconducting linac. This is evident from the results of the RGA measurements in Fig. 2, which compares the RGA scans before and after after vacuum firing at 950 °C and pumping for 24 h of the MBL IBS graphite core. The final RGA confirmed the absence of heavy hydrocarbons.

The beam stops are water-coooled and movable in/out of the beam axis by means of a pneumatic actuator operated at 6 bar. The welding of the cooling pipes was performed by Allectra Ltd (in UK). The brazing of the cooling pipes on the TZM bulk was performed by the company Reuter Technologie GmbH (in Germany) for the SPK beam stops, and by TWI (in the UK) for the MBL beam stops, requiring in both cases multiple furnace runs above 950 °C.

* elena.donegani@ess.eu

Content from this work may be used under the terms of the CC BY 4.0 licence (© 2026). Any distribution of this work must maintain attribution to the author(s), title of the work, publisher, and DOI.

ISBN: 978-3-95450-252-3 ISSN: 2673-5350 doi: 10.18429/JACoW-IPAC2026-MOP7099

VACUUM DESIGN AND PRESSURE MODELLING OF THE AWAKE Run 2c BEAMLINES

M.C. Giordano*, J.A. Ferreira Somoza, A. Gutierrez, C. Capelli, N.S. Chritin, F. Galleazzi
CERN, Geneva, Switzerland

Abstract

The Run 2c upgrade of the Advanced Proton Driven Plasma Wakefield Acceleration (AWAKE) Experiment at CERN introduces complex integration requirements for its vacuum infrastructure due to the coexistence of multiple new beamlines. This contribution presents the proposed vacuum architecture, detailing tailored pumping strategies, hardware choices, and the remote-control system, collectively designed to ensure operational reliability and minimize maintenance across diverse pressure regimes (down to 10^{-10} mbar). The baseline layout, established with analytical dimensioning, is validated through Molflow+ 3D simulations to guarantee meeting the pressure requirements in critical interaction regions.

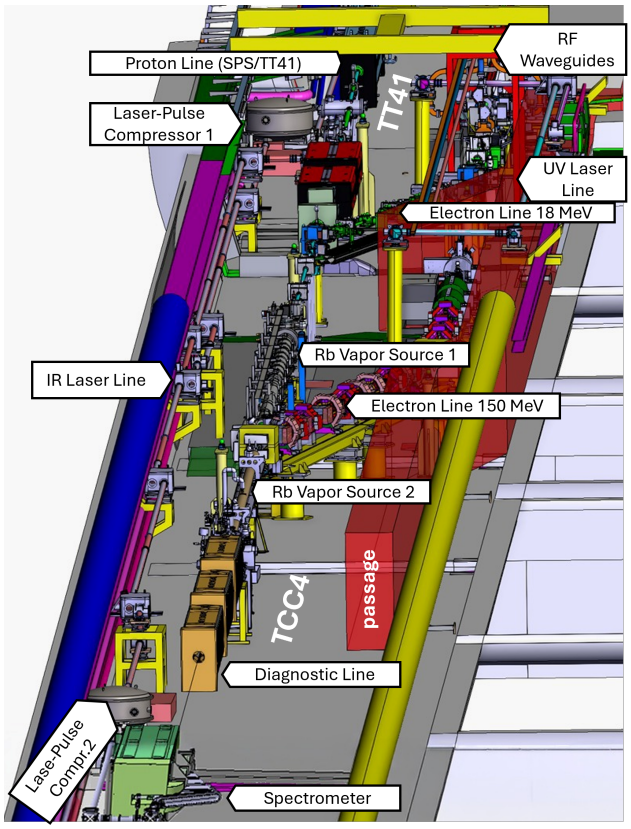

Figure 1: 3D CAD model illustrating the high-density integration of the AWAKE Run 2c experimental area.

INTRODUCTION

The Advanced WAKE-field Experiment (AWAKE) at CERN investigates proton-driven plasma wakefields to achieve gigavolt-per-meter accelerating gradients [1]. The Run 2c phase (from 2029) aims to achieve 10 GeV electron acceleration by physically decoupling the proton self-modulation and electron acceleration stages using a two-plasma-source configuration [2]. Integrating these systems in the experimental area significantly increases vacuum complexity and demands a high-density layout. The upgrade introduces a 150 MeV electron beamline alongside the existing, relocated 18 MeV system. Optical transport requirements expand with ~150 m of in-vacuum infrared (IR) laser lines for the Rb vapor ionization and an ultraviolet (UV) laser driving two electron guns. Furthermore, the electron source RF waveguides transition from sulfur hexafluoride insulation to vacuum operation. Integrating these diverse systems—spanning primary to ultra-high vacuum regimes—within the spatial constraints of the experimental area dictates a new architecture. This contribution outlines the resulting vacuum design and operational choices.

VACUUM ARCHITECTURE

Strict spatial constraints (Fig. 1) and coexisting beamlines dictate a modular vacuum architecture covering a range from 10^{-3} to 10^{-10} mbar, organized by operational needs, gas loads, and restricted accessibility in a radiation environment (Table 1). Proton, diagnostic, and electron beamlines rely entirely on robust, low-maintenance, Sputter Ion Pumps (VPI). To manage periodic venting, each sector includes a fixed Turbomolecular Pumping Group (VPG) repurposed from Run 2b. To maximize lifespan, VPGs remain unpowered during beam operation, activated remotely only for pump-downs or dealing with unexpected transient gas loads. Electron sources and RF waveguides foresee minimal venting, hence they are initially evacuated to 10^{-5}–10^{-6} mbar via mobile groups before NEG cartridge activation and ion pump flashing. The ultra-high vacuum required for the e-guns is provided by a space-optimized mix of legacy and new pumps consisting of NEG cartridges, VPIs, combined NEG-ion pumps (VPN), and Titanium Sublimation Pumps (VPS). RF Waveguides rely exclusively on VPIs. UV and IR laser transport lines rely on a single permanent pump per line and require strict vibration mitigation. The IR laser line ($>$ 150 m, 10^{-2} mbar) traverses a radioactive zone where standard dry scroll pumps could degrade, therefore it utilizes a single vibration-damped VPG, relying on the turbomolecular stage to block hydrocarbon backstreaming from its rotary vane backing pump. The UV line uses a single dry scroll pump (VPP) housed in an adjacent gallery to protect the tip seals from radiation and decouple vibrations. High-vacuum laser lines connecting pulse compressors to merging chambers do not share this vibration sensitivity. In-

* maria.carmen.giordano@cern.ch

Content from this work may be used under the terms of the CC BY 4.0 licence (© 2026). Any distribution of this work must maintain attribution to the author(s), title of the work, publisher, and DOI.

ISBN: 978-3-95450-252-3 ISSN: 2673-5350 doi: 10.18429/JACoW-IPAC2026-MOP7100

VACUUM SIMULATIONS FOR HL-LHC LONG STRAIGHT SECTIONS*

A. Galloro†, G. Bregliozzi, V. Baglin, J. Sestak
European Organization for Nuclear Research (CERN), Meyrin, Switzerland

Abstract

The High Luminosity Large Hadron Collider (HL-LHC) is entering its final development phase, requiring the optimisation of its vacuum layout to ensure reliable operation. The main upgrades with respect to the current LHC involve the Long Straight Sections next to the two large, general-purpose experiments (ATLAS and CMS), including new final focusing magnets and a full crab crossing implementation using superconducting crab cavities. Since residual gas critically affects collider performance, extensive vacuum simulations have been conducted to evaluate and minimise pressure levels. These include steady-state studies accounting for phenomena, like photon, electron and ion-induced desorption, to determine pressure. The simulations employ several complementary tools: Molflow+ for Monte Carlo particle tracking in ultra-high vacuum conditions, Synrad+ for synchrotron radiation effects, and MATLAB-based VASCO code for pressure stability analysis.

INTRODUCTION

The Large Hadron Collider (LHC) is the largest particle collider in the world [1]. With its roughly 27km of circumference, it hosts one of the largest vacuum systems. This includes ~55km of beam vacuum, which must ensure a low enough pressure to preserve beam lifetime and emittance.

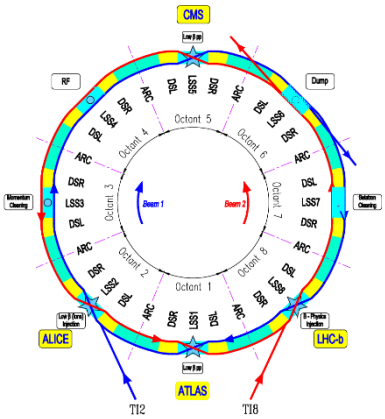

Figure 1: LHC schematic layout [1].

The beam vacuum system of the LHC, schematized in Fig.1, can be conceptually divided into two types:

- The 8 ARC vacuum sectors, each ~2.8 km long, in which the beam is bent by the cryogenic, superconducting LHC dipole magnets. Each beam travels in a separate pipe equipped with a beam screen to intercept the heat load and provide lower dynamic pressure and vacuum stability.
- The 8 Long Straight Sections (LSS), each roughly 500m in length, where the beam mostly travels in NEG coated warm beam pipes. Each LSS has a specific function (acceleration, injection, collimation, dump, collision) and is composed of multiple vacuum sectors. In the sectors closest to the four main LHC experiments the two beams share the same beampipe.

With the upcoming High Luminosity LHC upgrade [2], the whole of LSS1 and LSS5, hosting the ATLAS and CMS experiments respectively, will be completely renovated to improve the performance of the LHC machine. The goal of the High Luminosity LHC (HL-LHC) project is to increase the integrated luminosity by a factor of 10 compared to the LHC, to increase statistics on rare particle interactions.

The increase in luminosity is achieved through three major changes:

- Increase of the bunch intensity up to $2.3 \times 10^{11} p^+/bunch$
- New high-field, large-aperture, final-focusing triplet quadrupole magnets, to lower the β* at the interaction points to 0.15m.
- Implementation of a crab crossing scheme, to increase the effective interaction cross section.

The higher intensity, as well as the completely new layout, requires a careful study from the vacuum point of view to ensure good performance of the vacuum system. Multiple tools are used to simulate UHV conditions at CERN, providing a powerful method to predict the behavior of complex vacuum systems.

The following sections describe the specific use of the different tools employed to perform the simulations of the entire LSS of the HL-LHC.

MOLFLOW+ AND SYNRAD+, MONTE-CARLO SIMULATIONS OF VACUUM SYSTEMS AND SYNCHROTRON LIGHT

Molflow+ is a Test Particle Monte-Carlo (TPMC) simulator for vacuum simulations, developed at CERN [3]. The software can estimate the molecular flow of molecules in a vacuum system by tracking the trajectory of a subset of molecules and then scaling the results.

In the context of HL-LHC simulations, Molflow+ has been extensively used to estimate the conductance of non-cylindrical components and the effective pumping speed of vacuum pumps behind RF screens.

The Synrad+ code was also developed at CERN [3]. It shares the GUI and the TPMC algorithm with Molflow+ and allows calculation of the photon flux on surfaces due to synchrotron radiation (SR) emitted by particle beams.

† alessio.galloro@cern.ch

* Research supported by the HL-LHC Project

Content from this work may be used under the terms of the CC BY 4.0 licence (© 2026). Any distribution of this work must maintain attribution to the author(s), title of the work, publisher, and DOI.

ISBN: 978-3-95450-252-3 ISSN: 2673-5350 doi: 10.18429/JACoW-IPAC2026-MOP7102

FUNCTIONALISED a-C COATINGS TO REDUCE SEY AND CONTROL SURFACE RESISTANCE FOR THE HL-LHC INJECTION KICKER BEAM-PIPE CERAMIC SUPPORTS

P. Costa Pinto, G. Favia, C. Kouzios, M. Himmerlich, L. Mourier, W. Vollenberg
European Organization for Nuclear Research, Geneva, Switzerland
N. Bundaleski, I. Ferreira, D. Galhano, Universidade Nova de Lisboa, Lisbon, Portugal
P. Guerreiro, Centro de Física e Investigação Tecnológica, Caparica, Portugal
A. Costa, Centro de Ciências e Tecnologias Nucleares, Bobadela, Portugal

Abstract

Functionalized amorphous carbon (a-C) coatings are being developed to reduce the secondary electron emission yield (SEY) and to control the surface resistance of ceramic supports for the new generation of HL-LHC injection kicker magnets. Pressure spikes observed during high-voltage pulsing of the new injection kicker magnets are attributed to flashovers caused by high electron emission and insufficient draining of surface charge on the alumina supports of the beam-pipe. To address this issue, the alumina supports for the next generation of injection kicker magnets are coated with an a-C film, providing suitable surface resistivity to prevent charge accumulation whilst preserving the insulating function of the supports, together with a low SEY.

This contribution reports on the R&D programme aimed at tuning the resistivity of the a-C films through hydrogen doping while maintaining acceptable SEY performance. Results from the production of a series of 25 coated supports are presented, along with complementary studies carried out to optimise the coating pro-cess for future large-scale production. The potential of these resistive a-C films as alternatives to Ti and TiN coatings for insulating components is also discussed.

MANUSCRIPTS

The first units of HL-LHC MKI Cool injection kicker magnets, which have already been installed during the third operational run of the LHC, have demonstrated effective mitigation of beam-induced heat loads and improved vacuum performance [1]. However, pressure spikes during high-voltage pulsing have raised concerns about electron emission from alumina supports due to their high SEY. To address this issue, alumina supports are coated with amorphous carbon (a-C), which must simultaneously provide an SEY significantly lower than alumina (SEY ≈ 4–8) [2], and a surface resistance in the range 0.1–10 MΩ. Very thin a-C films (~5 nm) already exhibit a surface resistance of around 1 MΩ. However, two limitations arise: (i) the minimum thickness required to effectively screen substrate emission is ~10 nm [3], and (ii) at low thickness, surface resistance is highly sensitive to rough-ness and nucleation effects. To decouple thickness and resistance constraints, hydrogen doping is introduced, increasing resistivity and enabling the target surface resistance (~1 MΩ) at thicknesses of ~100 nm. The drawback is that the SEY increases with hydrogen content [4]. This work investigates the resistivity and SEY dependence on hydrogen concentration and thickness, the control via discharge power and the thermal stability under bakeout conditions.

FILM DEPOSITION AND CHARACTERIZATION

Films are deposited by DC magnetron sputtering using graphite targets. The system is baked at 120 °C for 8 hours prior to deposition, reaching ~1×10^{-7} mbar base pressure after cooling. Target–substrate distance is 200 mm and discharge pressure is 8×10^{-3} mbar. Reference films are deposited in pure Ar (60 grade), while doped films use Ar/D_2 mixtures (98.7%/1.3%). Deuterium distinguishes intentional doping from residual hydrogen contamination [4]. Unless stated otherwise, discharge power is 100 W.

Thickness is measured by profilometry, resistivity by four-point probe. The composition of the film is analysed using ion beam analysis combining Rutherford Back Scattering, Elastic Recoil Detection Analysis, and Nuclear Reaction Analysis, Taug gap obtained via optical absorption spectroscopy, and SEY is measured in a dedicated setup (instrumentation and methodologies are described in [4]).

RESISTIVITY AND H DOPING

Figure 1 shows the dependence of surface resistance on thickness for reference and doped films. Reference films reach 1 MΩ at ~5 nm, while doped films require ~70 nm. A sharp decrease in resistance occurs within the first 15–20 nm, attributed to nucleation and surface roughness effects, strongly affecting reproducibility. Figure 2 shows resistivity versus discharge power. Lower discharge power increases hydrogen incorporation, promoting sp^3 bonding and increasing resistivity [5, 6]. Alumina substrates yield 2–5 times higher resistivity than glass due to surface roughness effects.

Content from this work may be used under the terms of the CC BY 4.0 licence (© 2026). Any distribution of this work must maintain attribution to the author(s), title of the work, publisher, and DOI.

ISBN: 978-3-95450-252-3 ISSN: 2673-5350 doi: 10.18429/JACoW-IPAC2026-MOP7103

TOWARDS LASER ROUGHENING OF INNER BEAM SCREEN SURFACES FOR ELECTRON CLOUD MITIGATION IN STANDALONE MAGNETS AROUND IP1 AND IP5 OF THE LHC*

M. Himmerlich†, L. Guenther, A. K. Reascos Portilla, E. Bez, A. Lechner, H. Neupert, P. Krkotić,
European Organization for Nuclear Research, Geneva, Switzerland

Abstract

Laser-induced surface roughening facilitates secondary electron yield reduction of materials. The first demonstration on small scale in 2014 motivated an initiative to scale-up the technology for processing of long vacuum components with inner surfaces to be treated in apertures < 50 mm, which is challenging. To address this, we have developed a technique that enables the selective transformation of the inner beam screen (BS) surfaces in LHC standalone magnets for electron cloud mitigation. This requires scanning the light generated by a pulsed laser across the surface of ~10 m long beam screens. The developed system consists of an IR laser and a 17 m long optical fiber that transmits the light to an inchworm mole that houses an optical focusing unit and allows the laser spot to be scanned across the surface. Here we present our solutions to the challenges that emerged: *i)* mitigate surface oxidation, *ii)* avoid the contamination of cryosorbers, *iii)* integrate a synchronized fiber management system, *iv)* assure an acceptable treatment speed, *v)* find a compromise to match all material requirements, *vi)* extract ablated particulates, *vii)* monitor the process for quality control, and *viii)* perform a post-processing cleaning. By combining these steps, the influence on the beam impedance was minimized, and the compatibility with LHC operation was demonstrated.

INTRODUCTION

Laser-induced surface roughening to reduce the secondary electron emission from materials was reported on laboratory-scale samples in 2014 [1]. The first tests, that included detailed material studies, were performed with scanning laser systems that allowed direct exposure of the beam to the surface [2–6] and then characterizing the secondary electron yield (SEY). A first accelerator test was performed using the electron cloud monitors installed in the SPS [7]. However, to realize such a surface technology in particle accelerator vacuum systems, several technological hurdles had to be overcome to succeed in processing of inner surfaces in long tubes with small diameter. The basic principle of coupling ultra-short pulsed laser light into a hollow-core optical fiber and transmitting it to a crawling robot with scanning and focusing optics was successfully demonstrated in 2023 for LHC beam screens [8]. Since then we have continued upscaling the process and the infrastructure to a production system that will enable the BS treatment of four LHC standalone Q5 magnets [9] during the long shutdown 3 (LS3 2026-2030) of the LHC. This included development of a control system [10] and the definition of the processing strategy for the central quadrupole region of the magnet [11].

One main consideration for approval of this surface technology was to prove the compatibility with the ultra-high vacuum and beam operation conditions of the LHC. The process is based on ablation of surface material and ~ 90 % of the generated particulates are typically ejected, while the rest are re-adsorbed and bound to the surface, forming a rough, nanostructured, surface layer that is a key parameter for the SEY reduction [5, 12]. If these particulates are released during the laser treatment to a confined space such as in the BS, they will naturally settle on its inner surface and so a mechanism has to be applied to remove all these loose particulates. The main concern is a potential critical scenario in which particulates would detach from the BS and get attracted to the beam, potentially inducing large beam losses or even a beam dump [13, 14]. A simple qualification by applying forces to the surface in a centrifuge [11, 15] gave first insights on the size distribution and quantity of such particulates. Nonetheless a final qualification of the surface during LHC beam operation was mandatory. A demonstrator vacuum chamber with a laser-treated inner surface was therefore installed in the LHC to study possible dust-beam-interaction events. This manuscript summaries the results of this qualification test and the solution developed for the laser treatment and the post-processing cleaning of the vacuum components.

LASER PROCESSING SOLUTIONS AND POST-PROCESSING CLEANING

To demonstrate the readiness for treating the BS of Q5 magnets, a mock-up was constructed with an 11 m long BS where the full length was laser-treated. A photograph of the installation is shown in Fig. 1. It comprises an actuation system that enables the movement of the robot via a cable chain that houses the optical fiber, all the signal cabling, and the nitrogen supply lines. The chain movement inside the BS is supported by full-metal trolleys, and performed via a servomotor driven gear with rotational encoder (bottom left). This is synchronized to the robot motion to avoid any external forces and friction on the treatment system. Originally, ablated dust was extracted from the BS during processing by a vacuum suction unit attached at one end of the setup. It turned out that this was ineffective, since the ablated partic-

* We are grateful for the support from J. Tagg, L. Cordier-Temple, T. M. Hedstrand for the development of the control system, from B. M. Salvachua Ferrando for the installation of additional BLMs around the demonstrator setup in the LHC, as well as from the members of TE-VSC at CERN for the diverse support of the project.

† marcel.himmerlich@cern.ch

Content from this work may be used under the terms of the CC BY 4.0 licence (© 2026). Any distribution of this work must maintain attribution to the author(s), title of the work, publisher, and DOI.

ISBN: 978-3-95450-252-3 ISSN: 2673-5350 doi: 10.18429/JACoW-IPAC2026-MOP7104

NEW WARM VACUUM INTERCONNECTION DESIGN FOR HL-LHC*

T. Silva†, V. Baglin, G. Bregliozzi, C. Garion, J. Hansen,
European Organization for Nuclear Research, Geneva, Switzerland

Abstract

Warm vacuum interconnections are critical components used to couple adjacent vacuum chambers in the warm sectors of the LHC. Their primary functions are to ensure vacuum tightness, to accommodate small radial misalignments between chamber flanges, to ensure electrical continuity via RF fingers, and to compensate for longitudinal thermal expansion and contraction of the Long Straight Sections during bakeout operations. Within the framework of the High Luminosity LHC (HL-LHC) upgrade, a new generation of warm vacuum interconnections has been developed. This design introduces a novel concept of RF contacts utilising a deformable radio-frequency contact bridge.

This contribution outlines the main design, manufacturing strategies and qualification of these new warm modules for the HL-LHC operation.

INTRODUCTION

Design Requirements

Warm vacuum interconnections couple adjacent vacuum chambers in the warm sectors of the Large Hadron Collider (LHC), providing vacuum tightness, radial misalignment compensation, and longitudinal thermal stroke accommodation during bakeout. Beyond mechanical compliance, they must also ensure reliable electrical continuity between beamline elements while maintaining low beam coupling impedance. The current standard design, based on RF fingers, accommodates radial misalignments of up to ±2 mm.

The High-Luminosity LHC project (HL-LHC) imposes more demanding geometric tolerances, driving the development of a new generation of interconnections built around a deformable radio frequency (DRF) contact bridge [1, 2]. This concept extends the misalignment compensation range to ±5 mm while enhancing mechanical robustness, avoiding buckling of RF bridges and reducing the probability of electrical contact loss under operational conditions. The design is presented in Fig. 1.

Components

These vacuum interconnections differ in aperture size according to their functional position within the LHC, while maintaining a common design philosophy. Each interconnection is composed of four primary elements.

The body is in stainless steel, constructed from welded assemblies of flanges, bellows, and tube sections, as can be seen in Fig. 2. It defines the structural envelope of the module and provides axial flexibility determined by the stroke of the bellows. Depending on requirements, modules may be manufactured with zero, one, or two auxiliary ports. When the tube section serves as a support interface for additional components, a base plate is integrated into the design.

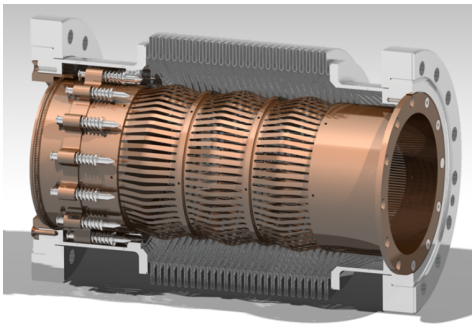

Figure 1: DRF Design of Vacuum Interconnections.

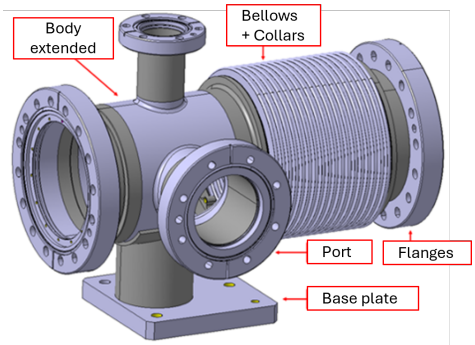

Figure 2: DRF Body.

The DRF insert is composed of a welded assembly integrating the DRF contact bridge, the flange, and a strip of RF contacts, as presented in Fig. 3. The flange is made of OFE copper, but the RF contacts and RF bridge are made of copper-beryllium (CuBe) because they need to withstand considerable mechanical stresses during installation and operation, even after bakeout at 250°C, while keeping excellent electrical continuity. The RF bridge has 3 convolutions, a length of 137.75 mm and a thickness of 0.1 mm.

The functional principle is based on the elastic deformation of the contact fingers, which compensates for the relative displacements arising during installation, nominal beam operation, and transient phases (e.g. thermal cycles or mechanical realignments). In the operational configuration, the convolutions are elongated, reaching an angle of 11° and forming a nearly linear profile. This straightened geometry minimises the contribution of the contact assembly to the longitudinal beam coupling impedance, thereby ensuring compatibility with HL-LHC impedance requirements [3].

The transition tube is made of OFE copper and has a thickness of 5 mm. To ensure low-resistance current transfer and long-term stability, the contact interface on the tube is rhodium-coated (see Fig. 4). Depending on the installa-

* Research supported by the HL-LHC project
† tomas.h.silva@cern.ch

Content from this work may be used under the terms of the CC BY 4.0 licence (© 2026). Any distribution of this work must maintain attribution to the author(s), title of the work, publisher, and DOI.

ISBN: 978-3-95450-252-3 ISSN: 2673-5350 doi: 10.18429/JACoW-IPAC2026-MOP7105

LATEST ADVANCEMENTS OF THE TEST-PARTICLE MONTE CARLO CODE MOLFLOW

P. Trifunović*, M. Ady, R. Kersevan
European Organization for Nuclear Research, Geneva, Switzerland

Abstract

MolFlow is a test-particle Monte Carlo code for ultra-high vacuum simulations, primarily intended for use in the field of particle accelerators. This contribution gives an overview of updates made to the code in recent years. The graphical user interface has been improved and a new feature has been added for extracting simulation results along user-defined 3D paths. Additionally, the code can now count the number of particles present on a surface at a specified time. Furthermore, the calculation of particle residence time (sojourn time) has been updated to allow for temperature variations during a particle's residence on a surface. This enables simulations of surface decontamination through heating (bake-out). Finally, MolFlow can now simulate particle collisions with static background gases using the hard-sphere collision model.

INTRODUCTION

MolFlow is a simulation tool for ultra-high vacuum, originally developed in the 1990s. In 2007 it was modernized and rewritten in C++, preserving the original algorithm [1]. Using the test-particle Monte Carlo method, it traces virtual particles in 3D geometries from gas sources to absorption points such as vacuum pumps. The geometry is defined as a set of planar polygons, which represent the boundaries of the vacuum space. Together with their physical properties, such as the outgassing rate, sojourn time, temperature, sticking factor etc., these polygons are referred to as *facets*. As the simulation runs, MolFlow keeps track of the number of virtual particles hitting each facet, which enables calculation of physical properties of the system, such as pressure, impingement rate and density. These properties can be visualized in the form of plots or color-coded cells on facets called textures. With time, the simulation converges to a more precise state and the user can decide when the precision is satisfactory. A more detailed description of this simulation tool and its internal workings can be found in the official documentation [2], in the introduction to MolFlow's algorithm [1], and in previous IPAC contributions [3, 4].

This article presents an overview of the most important updates of MolFlow in recent years, with reference to version 2.11.0 of the MolFlow code [5], the latest release at the time of writing.

NEW TOOL FOR DATA EXTRACTION ALONG A PATH

Until recently, extracting results and values at different points in the geometry at once was not possible out-of-the-box and required workarounds such as creating transparent sampling facets that stretch along the geometry and record particle hits. In the case of curved geometry shapes, these workarounds were cumbersome and not straightforward for users to configure manually.

A new tool has been added to facilitate result extraction. It enables users to define paths in the geometry and extract results along them. Each path is defined as a set of points with two consecutive points defining a vector as one path segment. Paths are split into a number of equal-sized bins specified by the user. The users can select a set of facets with textures and extract simulation results from them along a path. Each texture cell's result are assigned to the closest bin. The distance from a texture cell to a bin is the length of the orthogonal projection vector from the cell's center to the bin. If a cell cannot be orthogonally projected to the path, it is not included in the extraction. The extraction can be visualized as a plot of either the sum of texture cell results per bin (useful for number of hits) or as an average per bin (useful for pressure, impingement rate, or density).

Figure 1 shows a curved geometry, with a path visualized with red dots and blue arrows. Simulation results can be extracted from the line of textured facets. Figure 2 shows the new tool with a plot of average pressure extracted along the defined path.

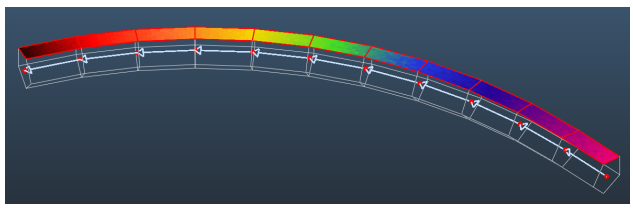

Figure 1: Curved shape for texture extraction.

REFLECTION COUNTER AND PARTICLE BALANCE CALCULATION

In previous versions, facet counters recorded three quantities—desorptions (number of particles created and outgassed from the facet), absorptions (number of particles stuck to (pumped by) the facet), and incident hits (sum of absorbed and bounced particles). *Bouncing*, or *reflection*, denotes particles that hit a facet and reflect from it without being absorbed. In time-dependent mode, such a counter is maintained for each defined time moment.

* petar.trifunovic@cern.ch

Content from this work may be used under the terms of the CC BY 4.0 licence (© 2026). Any distribution of this work must maintain attribution to the author(s), title of the work, publisher, and DOI.

ISBN: 978-3-95450-252-3 ISSN: 2673-5350 doi: 10.18429/JACoW-IPAC2026-MOP7107

SMAUG EXPERIMENTS AT CERN'S HIRADMAT FACILITY FOR THE STUDY OF MATERIALS USED FOR PARTICLE BEAM WINDOWS

A. Harrison†, P. Alexaki, G. Calchi, N. Charitonidis, V. Clerc, B. Descargues, L. S. Esposito, A. T. P. Fontenla, V. Giovinco, A. M. Goillot, A. Gutierrez, A. Lund, D. Manousou, M. Morrone, C. Pasquino, A. E. Rahmoun, X. Sax, P. Simon, N. Solieri, J. A. F. Somoza, A. Stoeltzel, F. M. Velotti.
CERN, Geneva, Switzerland

Abstract

The SMAUG experimental campaign was conducted at CERN's HiRadMat facility to investigate the performance and limits of particle beam window materials to intense pulsed proton irradiation. Samples of glassy carbon, beryllium (grades I-220-H, S-200-FH, and PF-60), and silicon nitride (Si_3N_4) were exposed to 440 GeV/c proton beams with total intensities of up to 2.8×10^{15} protons per pulse and beam spot sizes ranging from $\sigma_{x,y} = 0.5$ mm to 0.25 mm. Three experimental configurations (SMAUG-1, -1.5, and -2) were used to reproduce operational beam conditions relevant to existing CERN accelerators and future facilities. Post-irradiation analyses included vacuum leak testing, optical microscopy, scanning electron microscopy, and three-dimensional surface topography measurements. FLUKA Monte Carlo simulations were performed to evaluate energy deposition in the irradiated materials. The results provide comparative performance data for beam window materials and support the selection of suitable solutions for high-intensity accelerator applications.

INTRODUCTION

Beam windows are essential components in high-intensity accelerators, providing vacuum separation while exposed to intense particle beams. Increasing beam brightness in future upgrades imposes stringent demands on window materials to endure extreme thermal and mechanical stresses while preserving vacuum integrity.

Past operational experience at CERN has shown that beam-induced damage or failure of window components can lead to significant downtime, increased radiation exposure risks for personnel and potential exposure to beryllium dust. Notably, two consecutive failures of PF-60 diffusion-bonded beryllium windows occurred at the TT66 HiRadMat facility [1] during experimental runs in 2021, when subjected to beam brightnesses of 5×10^{13} p^+/mm^2 (Fig. 1). These incidents led to the establishment of a dedicated working group tasked with investigating the failure mechanisms and defining operational limits relevant to high-intensity proton beam applications.

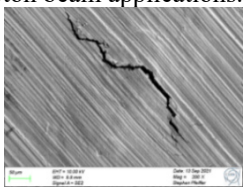

Figure 1: Microcrack on TT66 HiRadMat facility window, Beryllium PF-60 0.254mm.

The SMAUG experimental programme was initiated to evaluate candidate beam window materials under controlled, high-intensity proton beam conditions at the HiRadMat facility. In addition to benchmarking materials currently used in the CERN accelerator complex, the programme also investigated new applications, including the use of ultra-thin silicon nitride membranes as isolation barriers between hydrogen absorbers and vacuum in the final cooling section of a muon collider [2].

Throughout this paper, beam "brightness" refers to the peak intensity for a gaussian beam Eq. (1), expressed in protons per square millimetre.

$$Power_{Density(x,y)} = \frac{Protons\ Per\ Pulse}{2\pi\sigma_x\sigma_y} \quad (1)$$

EXPERIMENTAL SETUP

Configuration

The SMAUG-1 and SMAUG-2 experiments employed a common configuration consisting of eight window samples mounted in hermetically sealed flanges and arranged between alternating vacuum and air chambers (HELIOX for SMAUG-2), as shown schematically in Fig. 2. The assemblies were designed to allow independent leak testing of each window before, during and after the experiment.

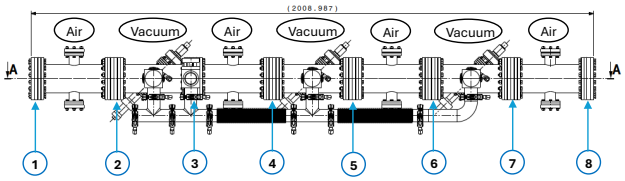

Figure 2: SMAUG 1 and SMAUG 2 experiment layout drawing indicating window positions.

SMAUG-1.5 was a parasitic experiment operated in parallel with another HiRadMat experiment. It consisted of a single vacuum chamber equipped with a 1 µm-thick Si_3N_4 membrane providing a beam aperture of 6 mm × 6 mm upstream. A downstream window made of a 3 mm-thick glassy carbon disc with a Ø60 mm aperture was used as a secondary window.

Sample Mounting and Alignment

All experiments were assembled, tested, and pre-aligned on the experimental TABLE 1 in the dedicated HiRadMat surface laboratory before installation in Station 2 (FP2) of the HiRadMat facility (CERN TNC). The table features a horizontal motor-driven baseplate that allows translation of

Content from this work may be used under the terms of the CC BY 4.0 licence (© 2026). Any distribution of this work must maintain attribution to the author(s), title of the work, publisher, and DOI.

ISBN: 978-3-95450-252-3 ISSN: 2673-5350 doi: 10.18429/JACoW-IPAC2026-MOP7108

VACUUM TOLERANCE LIMITS FOR LSS7: BALANCING PERFORMANCE AND RADIATION EXPOSURE FOR HL-LHC

M. Kyprianidis*, V. Baglin, G. Bregliozzi, G. Cattenoz
European Organization for Nuclear Research, Geneva, Switzerland

Abstract

The High Luminosity LHC project requires a flexible approach to collimator vacuum conditioning that addresses both operational vacuum performance and the maintenance constraints associated with highly radioactive equipment. This work combines outgassing studies and LHC pressure profile analyses to optimize the vacuum conditioning procedure for collimators used for betatron cleaning installed in the Long Straight Section of Point 7 (LSS7) of the LHC. The proposed approach simplifies the bake-out procedure aligning with As Low As Reasonably Achievable (ALARA) principles [1], reducing intervention complexity and personnel radiation exposure without compromising vacuum quality. This study was supported by the HL-LHC project.

INTRODUCTION

Over the past three years, there have been an increasing number of critical failures of the edge-welded bellows of LHC collimators [2] which required interventions during operation for leak detection and inspection. Following identification of the main stress factors of the bellows, a detailed risk assessment of the existing collimators identified 6 critical units and 51 at high risk of failure. These failures are likely to cause leaks throughout the first Run of the high luminosity LHC era (foreseen to start in 2030) requiring machine interventions for the replacement of collimator units.

As nearly 40 % of the collimators are installed for betatron cleaning in the Long Straight Section of Point 7 (LSS7), a number of interventions are expected in this area. LSS7 is amongst the most radioactive regions of the LHC, with ionizing radiation levels above 2 mSv/h, measured 40 cm away from the beam path, which could further increase during HL-LHC operation. To minimize radiation exposure to personnel, the vacuum conditioning procedure for LSS7 sectors must be simplified by lowering the bakeout temperature and excluding selected components from the bakeout cycle.

Following the replacement of a collimator (TCSG) in the A6R7 sector of LSS7 (TCSG.A6R7.R), a systematic study was performed to assess the effects of the different vacuum conditioning procedures on the collimator and of a partial bakeout on the A6R7.R sector: a) A test was carried out during LHC operation by increasing the sector pressure to determine the maximum tolerable residual gas density with minimal operational impact, b) A series of outgassing studies were performed on a spare secondary collimator (TCS), along with pressure-profile simulations of the sector under different scenarios, c) A new procedure was applied for the reconditioning of the sector after the replacement of the TCSG during the Year End Technical Stop (YETS) of 2025-2026.

Table 1: EoF Test Beam Parameters

Beam Intensity [p^+/b]	Number of Bunches [b]	Beam Energy [TeV]
1.6×10^{11}	2400	6.8

END OF FILL TEST

During LHC proton operation, an End-of-Fill (EoF) test was performed to locally increase the A6R7.R sector pressure in LSS7 to assess the impact on machine operation. This determined the maximum acceptable pressure during operation. The LHC parameters used during this test are listed in Table 1.

For triggering a pressure increase, the 8 NEG cartridges (CapaciTorr Z 400) along the 70 m long vacuum sector were remotely heated for a few minutes, releasing mostly chemisorbed H_2 gas from the bulk of the NEG sinterized disks. As shown in Fig. 1, the nitrogen-equivalent maximum pressure reached 1×10^{-6} mbar, during which the beam lifetime reduced from 47 h to 45 h. This reduction remains acceptable as LHC proton fills last no more than 24 h. No impact was observed on any LHC detector backgrounds and no unusual beam losses were detected along the entire LHC ring.

ULTIMATE PRESSURE STUDIES

The positive EoF test results prompted a series of outgassing studies on a spare secondary (TCS) collimator.

Experimental Setup

The setup used is illustrated in Fig. 2; it consists of a real LHC collimator fitted with its upstream and downstream pumping modules, fully instrumented. The collimator jaws are made of C-C composites; an orifice with a known conductance of 9.6 l/s for N_2 separates the testbench domes. After bakeout at 250 °C for 48 h, the testbench ultimate pressure

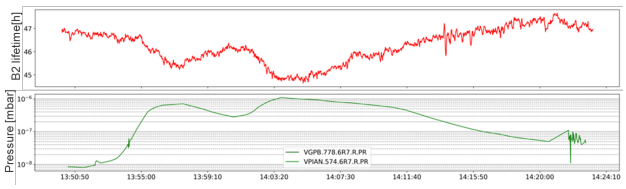

Figure 1: EoF test results, showing the beam lifetime (red) and nitrogen equivalent pressure (green)

* marios.kyprianidis@cern.ch

Content from this work may be used under the terms of the CC BY 4.0 licence (© 2026). Any distribution of this work must maintain attribution to the author(s), title of the work, publisher, and DOI.

ISBN: 978-3-95450-252-3 ISSN: 2673-5350 doi: 10.18429/JACoW-IPAC2026-MOP7109

QUALITY ASSURANCE FOR THE HL-LHC BEAM SCREEN PRODUCTION

D. Sadowska†, C. Garion, M. Seremeti
European Organization for Nuclear Research, Geneva, Switzerland

Abstract

The HL-LHC project is currently in the fabrication and assembly phase for numerous components and systems, in particular the new beam-screen assemblies to be installed inside the upgraded final-focusing superconducting magnets operating at 1.9 K. These complex beam screens integrate tungsten absorbers and exist in two variants: the Q1 and Q2 types, with absorber thicknesses of 16 mm and 6 mm, respectively. In total, 24 assemblies will be installed. Their successful implementation requires complex design work, non-standard and demanding manufacturing processes, and stringent quality assurance. Fabrication has proven to be very challenging in terms of welding and assembly and requires close follow-up and dedicated qualification processes throughout the manufacturing phase. To maintain a high standard of manufacturing, a Quality Management approach derived from industrial standards and based on ISO 9001 principles, has been implemented. This paper presents how the quality-management framework is deployed throughout the project phases and how it ensures traceability, smooth process execution, and compliance with the required workflows and technical specifications.

INTRODUCTION

The HL-LHC project aims to upgrade the current LHC infrastructure, in particular in the regions close to the two large, general-purpose experiments, ATLAS and CMS. The primary objective is the increase of luminosity which leads to a high heat load reaching the beam screen cryogenic vacuum system operating at 60 to 80 K installed in the 1.9 K superconducting magnets. [1]. One of the key internal components of the new final focusing magnets is the design and production of new beam screens. To protect the superconducting coils from premature radiation-induced damage caused by particle beam collision debris and to intercept heat load created by the collision debris to preserve cryogenic cooling capacity, it is necessary to add external shielding to the beam screen [2]. Each side of interaction points 1 (ATLAS) and 5 (CMS) includes six magnets: four quadrupoles (Q1, Q2a, Q2b and Q3), one corrector package (CP) and one dipole magnet (D1), leading to 24 shielded beam screens to install in the machine. The design of the shielded beam screen is shown in Fig. 1. It relies on a co-laminated and perforated octagonal beam screen tube, actively cooled by four spot welded cooling tubes. Tungsten absorbers are positioned in both vertical and horizontal planes. Thermal links brazed on the absorbers are welded to the cooling tubes to ensure efficient heat transfer to the cryogenic cooling system [2].

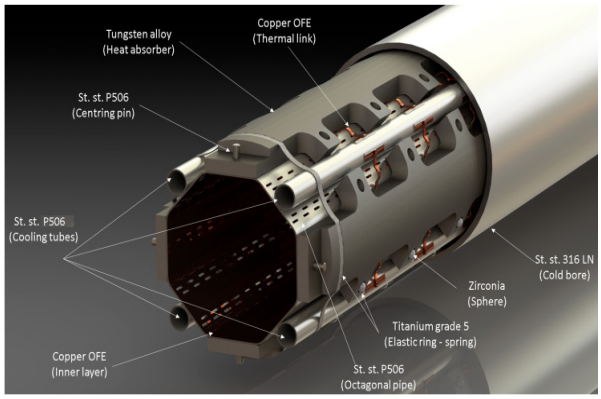

Figure 1: Beam screen design [3].

QUALITY ASSURANCE AND QUALITY CONTROL STRATEGY FROM MATERIAL SELECTION TO INTEGRATION IN THE MAGNETS

During the manufacturing and integration phases, all critical parameters must be verified and validated to eliminate the risk of chemical contamination, as well as mechanical defects and ensure full compliance with all specifications. Due to the high criticality and precision requirements specified in the technical documentation, the processes of component sourcing, preparation, and installation require exceptionally tight tolerances and specialised verification methods that differ significantly from those used in standard manufacturing. To maintain the manufacturing quality, a series of interrelated activities are carried out depending on the progress of each installation stage. These stages are divided into three phases:

Phase 1 – Material Preparation

During the first phase, components are chemically cleaned to eliminate any possible contamination within the vacuum system. The first quality checkpoint is a vacuum acceptance test that includes a Residual Gas Analysis (RGA) [4]. During this procedure, the mass spectrum is measured using a quadrupole mass spectrometer at room temperature. Analysis of the mass spectrum, presented in the form of diagrams, confirms the absence of unwanted molecules or contaminants as shown in Fig. 2. The test for the standard beam screen components such as titanium compression rings, titanium springs, ceramic balls, and pumping slot shields is carried out once on 100% of the parts, or twice for the parts that undergo additional thermal treatment processes such as the tungsten absorbers (Fig. 3). In the latter case, only 20% of the batch is tested as a final

Content from this work may be used under the terms of the CC BY 4.0 licence (© 2026). Any distribution of this work must maintain attribution to the author(s), title of the work, publisher, and DOI.

ISBN: 978-3-95450-252-3 ISSN: 2673-5350 doi: 10.18429/JACoW-IPAC2026-MOP7110

PRODUCTION OF THE HL-LHC EXPERIMENTAL BEAM VACUUM CHAMBERS*

J. Sestak†, G. Bregliozzi, A. Galloro, M. Kukkola, F. Prizio, T. Raska, O. Santos, V. Baglin
European Organization for Nuclear Research, Geneva, Switzerland

Abstract

For the High-Luminosity LHC (HL-LHC) era following the third long shutdown (LS3 2026-2030), new generations of experimental vacuum chambers will be installed in the ATLAS, ALICE, CMS, and LHCb experiments. These chambers, located at the interaction points, ensure the required beam vacuum conditions while minimizing the impact of chamber materials on detector performance. The HL-LHC upgrade imposes tighter demands on mechanical precision, radiation tolerance, and surface quality to sustain higher beam currents, luminosity and radiation dose levels. Building on the experience gained during the LS2 exchange of the ALICE and CMS chambers, the LS3 designs introduce optimized materials, geometry, and production methods to meet these challenges. This contribution outlines the main design principles, manufacturing strategies, and qualification steps guiding the development of the LS3 experimental vacuum chambers for HL-LHC operation.

INTRODUCTION

During LS3 the experimental beam vacuum systems of ATLAS, ALICE, and CMS will undergo major upgrades to meet HL-LHC requirements. The baseline HL-LHC layout introduces new inner triplet assemblies at Points 1 and 5, absorbers for secondary particles produced in the collisions (TAXS) and upgraded vacuum assemblies for experiments (VAX) connecting the experimental beam vacuum sector via a gas injection system (GIS) to its ancillaries for pump-down, venting and diagnostics [1]. Furthermore, detector-specific upgrades dictate additional structural changes: ATLAS requires new beam vacuum chambers spanning ± 4 m from the interaction point (IP) to accommodate the new Inner Tracker (ITk) [2] and High Granularity Timing Detector (HGTD) [3], while ALICE's integration of their new Inner Tracking System (ITS3) [4] and a new Forward Calorimeter (FOCAL) [5] alters the vacuum layout from –9 m to +1 m from the IP.

DESIGN CONSIDERATIONS

The design of the particle accelerator beam vacuum chamber within the experimental areas shall follow requirements from both the experiment and the accelerator. Over the last two decades, a multi-domain design approach has been developed and implemented allowing a more comprehensive understanding of global design constraints and limitations.

Detector Requirements

Physics-motivated requirements for coverage and acceptance, together with general detector geometry, drive the main design parameters of the beam vacuum system. Tracker detectors, which form the innermost layer of the experiment, require chambers made of high-purity beryllium metal (> 98.5% Be) to minimize their impact on track reconstruction. Figure 1 shows a simplified integration of the ATLAS central chamber.

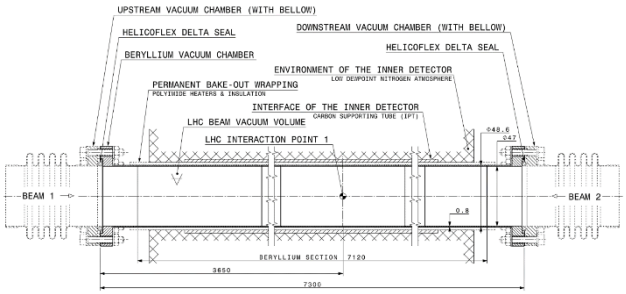

Figure 1: Integration of ATLAS central chamber.

Material budget presented to the detector within its spatial coverage, defined by the polar angle (pseudorapidity) η and the azimuthal angle φ directly contributes to its performance. The transparency of the vacuum system is a function of its geometry and the material of the chambers and expressed using the radiation length X_0 [6].

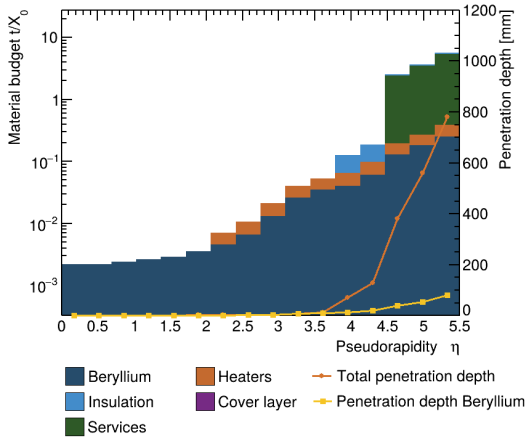

Figure 2: Contribution of ATLAS central chamber to material budget.

The contribution of the vacuum system to the material budget of the detector is shown by Fig. 2. It is defined as the ratio of penetration length during which the primary particle interacts with the chamber and its services. Permanent services present a non-negligible part of the material

* Work supported by the High Luminosity LHC Project
† josef.sestak@cern.ch

Content from this work may be used under the terms of the CC BY 4.0 licence (© 2026). Any distribution of this work must maintain attribution to the author(s), title of the work, publisher, and DOI.

ISBN: 978-3-95450-252-3 ISSN: 2673-5350 doi: 10.18429/JACoW-IPAC2026-MOP7111

TOWARDS A LOW IMPEDANCE VACUUM SYSTEM FOR THE FCC-ee

P. Krkotić *, M. Ady, V. Baglin, P. Chiggiato, C. Garion, V. Giovinco,
G. de Gois Saretti, M. Morrone, CERN, 1217 Geneva, Switzerland

Abstract

The design of the Future electron–positron Circular Collider (FCC-ee) vacuum system integrates vacuum engineering, impedance mitigation, and surface functionalisation to achieve compatibility with high beam currents and sustained operational stability. Based on these design principles, this contribution presents an overview of the principal vacuum components and outlines the studies conducted to evaluate and optimise their electromagnetic and vacuum performance. Particular emphasis is placed on the interplay between material properties, surface treatments, and component geometry, as well as on the distribution and integration of vacuum elements and transitions within the accelerator. Impedance studies were performed to evaluate the electromagnetic impact of representative vacuum components. The main findings are summarised, highlighting the achieved performance and outlining directions for further optimisation.

INTRODUCTION

The FCC-ee is a proposed high-luminosity lepton collider operating in the energy range from the Z pole (45.6 GeV) to the $t\bar{t}$ threshold (182.5 GeV) [1]. High beam currents up to 1.2 A, short bunch lengths of 2–15 mm, and intense synchrotron radiation (SR) power (45 MW/beam) impose stringent constraints on the vacuum system, particularly with regard to beam-coupling impedance and trapped electromagnetic (EM) fields that can limit beam stability and generate significant parasitic power deposition.

The adoption of the local chromatic correction (LCC) optics scheme [2, 3] introduces a novel arc-cell structure shown in Fig. 1, defining the vacuum component integration strategy. In this configuration, each arc half-cell consists of a periodic sequence of sextupole and quadrupole magnets (or vice versa) together with a beam position monitor installed on girders, followed by three dipole magnets. The arc sections account for approximately 77 % of the collider circumference (~70 km of vacuum system). At this scale, even small impedance contributions from individual components can accumulate to a significant fraction of the machine impedance budget, making impedance reduction a central design requirement.

The FCC-ee vacuum system is based on an integrated design approach, in which vacuum, thermal, mechanical, and impedance-related constraints are considered simultaneously from the earliest design stage. Material selection, surface treatment, and component geometry are optimised alongside impedance-aware assembly solutions to minimise both broadband and narrowband contributions. Particular attention is devoted to identifying and mitigating resonances and radio-frequency (RF) discontinuities.

In this paper, the dominant impedance sources of the principal vacuum elements are analysed together with optimisation guidelines for their design.

FCC-EE ARC VACUUM COMPONENTS

Vacuum Chamber

The vacuum chamber (VC) constitutes a dominant broadband impedance source through the resistive wall impedance (RWI), arising from the finite surface impedance of the chamber material, coating, and surface finish, and scaling linearly with the machine length.

The baseline VC section shown in Fig. 2 consists of an extruded oxygen-free silver-bearing (OFS) copper (≥99 % IACS[1]) profile, coated with a 150-200 nm thick non-evaporable getter (NEG) layer. The horizontally symmetric antechamber geometry separates the 60 mm diameter beam aperture from the SR fan, while providing space for localised SR absorbers and preserving a nearly circular cross-section to minimise geometric impedance contributions.

The NEG coating provides distributed pumping and reduces photon-stimulated desorption and secondary electron yield [4, 5]. Its thickness is optimised to minimise the additional RWI contribution while maintaining adequate vacuum performance and acceptable single-bunch instability thresholds [6, 7]. In this thin-film regime, the RWI is dominated by the coating thickness and remains predominantly inductive, as shown in Fig. 3, where the dashed green curve indicates the increase in surface reactance relative to smooth copper.

Surface roughness also contributes to the impedance due to the broad beam-frequency spectrum extending to tens of GHz and the resulting small skin depths. Using the multi-

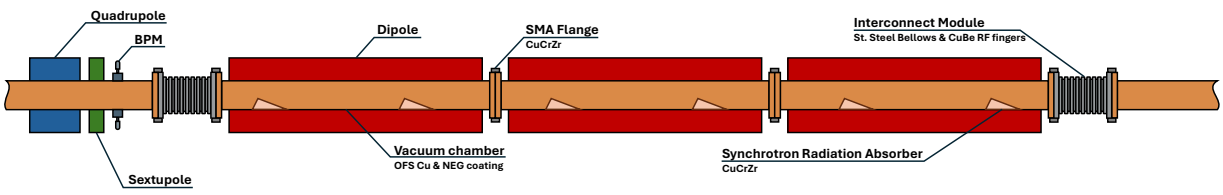

Figure 1: Schematic of a representative arc cell configuration for the FCC-ee LCC optics layout.

* patrick.krkotic@cern.ch

[1] IACS: conductivity relative to annealed pure copper (100%).

Content from this work may be used under the terms of the CC BY 4.0 licence (© 2026). Any distribution of this work must maintain attribution to the author(s), title of the work, publisher, and DOI.

ISBN: 978-3-95450-252-3 ISSN: 2673-5350 doi: 10.18429/JACoW-IPAC2026-MOP7112

ELECTROMAGNETIC RESONANCE BEHAVIOUR OF LHC VACUUM INTERCONNECT MODULES

H. R. Gobakken*, G. Bregliozzi, S. Calatroni, P. Chiggiato, P. Krkotić, I. Wevers
CERN, Geneva, Switzerland

Abstract

Beam-induced heating has become increasingly relevant for vacuum interconnect modules (VIMs) in the Large Hadron Collider (LHC) with the continuing rise in the beam intensity heightening their sensitivity to electromagnetic resonances. While the heating itself is not the primary subject of this work, the associated failures have motivated a broader examination of how the different geometries of the VIMs respond to strong beam-induced electromagnetic fields. Circular and elliptical interconnect RF-finger modules were studied using the standard coaxial stretched-wire method. The intrinsic resonances of the modules were identified as a function of the variation of module length and controlled misalignment by means of a new testbench that enables wide geometry variations while keeping the coaxial wire under constant tension.

The measurements reveal clear differences in the resonant spectra of the various designs and show that small geometric deviations can strongly influence mode frequencies and field localisation. Understanding these behaviours is essential, as the High Luminosity upgrade of the LHC (HL-LHC) foreseen to start operation in 2030 will run with even higher bunch intensities, increasing the likelihood that unfavourable resonant conditions could lead to excessive local power deposition. The results contribute to improved assessment and qualification of VIMs for future high-luminosity operation and support the design and development of novel VIMs for next-generation machines.

INTRODUCTION

With the increase in bunch intensity in the Large Hadron Collider (LHC), beam-induced electromagnetic fields in warm vacuum components have become increasingly significant [1]. In particular, VIMs equipped with RF fingers have shown sensitivity to beam-induced heating, and several cases of mechanical degradation and component failure have been reported [2–4]. Of particular concern are fields in regions behind the RF shielding, where unwanted heating has occurred due to field leakage, leading to failures.

VIMs are mechanically flexible structures designed to accommodate installation tolerances, alignment offsets, and thermal expansion. As a result, the modules may operate under varying installation lengths and transverse misalignments [5]. Since electromagnetic resonances are strongly dependent on geometry, such geometric variations may shift resonant frequencies, alter field localisation, and potentially increase local power deposition [1, 2]. Understanding the dependence of resonance behaviour on module geometry is therefore important for assessing operational risks and for the qualification of VIMs.

The electromagnetic behaviour of the modules was investigated experimentally using the coaxial stretched-wire method, a well-established technique for impedance measurements in accelerator components [6, 7]. This study demonstrates its suitability for resonance measurements to identify hidden or unexpected resonances that are computationally intensive to detect, while verifying the functionality of a vacuum component design. A dedicated test bench was developed to maintain constant wire tension while allowing controlled elongation, compression, transverse misalignment, and variation of antenna coupling. This enables systematic and repeatable characterisation of resonances in LHC VIMs without disassembling the measurement setup between configurations.

The approach is demonstrated on an elliptical and a circular interconnect module, for which preliminary results are reported. Resonance behaviour is characterised with respect to module geometry and measurement configuration, including variations in module length, transverse displacement, and antenna coupling, with emphasis on physical interpretation. The impact of degraded electrical shielding is addressed separately to isolate its influence on the measured response.

EXPERIMENTAL SETUP

Measurement Principle

A thin copper wire stretched along the beam axis forms a coaxial transmission line — wire as inner conductor, module body as outer — supporting beam-like electromagnetic excitation, as shown in Fig. 1.

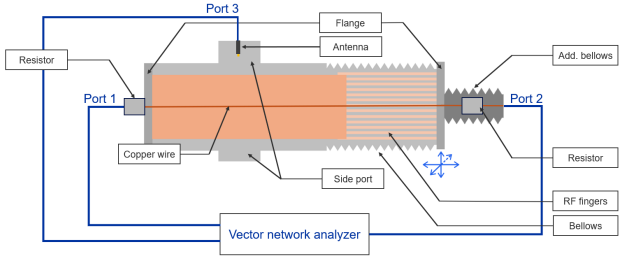

Figure 1: Schematic of the experimental setup. The Blue arrows indicate the adjustable segment.

The stretched wire is connected to a vector network analyzer (VNA) through impedance matching fixtures at both ends of the module. Coupling to the resonances is achieved through the side of the VIM.

* Henrik.ross.gobakken@gmail.com

Content from this work may be used under the terms of the CC BY 4.0 licence (© 2026). Any distribution of this work must maintain attribution to the author(s), title of the work, publisher, and DOI.

ISBN: 978-3-95450-252-3 ISSN: 2673-5350 doi: 10.18429/JACoW-IPAC2026-MOP7113

SWISS LIGHT SOURCE 2.0 VACUUM SYSTEM CONDITIONING AND FIRST YEAR OF OPERATION

N. Kirchgeorg*, H.-H. Braun, N. Gaiffi, R. Ganter†, C. Rosenberg, D. Stephan, X. Wang
Paul Scherrer Institut, Villigen, Switzerland

Abstract

After more than two decades of user operation, the Swiss Light Source (SLS) entered a major upgrade phase in October 2023, targeting a 40-fold reduction of electron-beam emittance via a new 7-bend achromat lattice at 2.7 GeV. The vacuum system, central to machine performance, was completely rebuilt to meet the stringent requirements imposed by the compact lattice. The new storage ring vacuum consists of an 18 mm aperture, 288 m long system assembled from over 500 chambers. Following 14 months of installation, first beam was achieved in January 2025. Vacuum conditioning represented a critical milestone, enabling delivery of light, with nominal beam current, to the first experiments in April. This contribution presents the vacuum conditioning of the SLS 2.0 storage ring during this first year of operation, from initial commissioning to user operation.

INTRODUCTION

The SLS at the Paul Scherrer Institut (PSI) started user operation in June 2001 and delivered ≈5000 h of user beam time per year at 98.5% availability [1]. The emergence of diffraction-limited storage rings (DLSRs) based on multi-bend achromat (MBA) lattices motivated the SLS 2.0 upgrade project. The new ring replaces the 12-fold triple-bend-achromat (3BA) with a 12-fold 7BA lattice achieving a natural horizontal emittance of 150 pm rad at 2.7 GeV – within the existing 288 m tunnel [2, 3]. Vacuum system undergone complete re-design to match the new magnetic array.

The 14-month dark period began in October 2023. The beam commissioning started in January 2025; the first stored beam was obtained four weeks later; 400 mA was first achieved in April 2025 [4].

VACUUM SYSTEM DESIGN

The twelve 7BA arcs each span ≈18 m and contain continuous vacuum chamber strings with the following key parameters [5,6]: (i) 18 mm inner diameter electron channel – four times smaller cross-sectional area than SLS 1.0; (ii) OFE-Cu walls (steel for chambers located in Fast-Steering magnets) of minimum 1 mm thickness; (iii) 500 nm Ti-Zr-V NEG coating, baked and activated ex-situ to $\approx 10^{-11}$ mbar before installation; (iv) seven active pumping blocks per arc containing ion pump (Diode, 55 l/s); NEG cartridge pump (Capacitorr Z400); and (v) glidcop (Cu - Al) crotch absorbers handling up to 3.7 kW per standard bend [5].

Straight sections contain a mix of new and old vacuum components connected to the arc strings via tapered transitions.

VACUUM CONDITIONING (JANUARY–AUGUST 2025)

Arc Conditioning Curve

The normalised average dynamic pressure rise $\mathrm{d}P/I$ [mbar/mA] was computed from stable beam periods of minimum 2 h after subtracting static base pressure. Figure 1 shows the conditioning curve versus accumulated beam dose. The initial scrubbing phase was interrupted by frequent beam dumps; nevertheless, a clear downward trend became apparent as commissioning progressed. After 100 Ah, the design target $\mathrm{d}P/I = 2 \times 10^{-12}$ mbar/mA was reached in April 2025, demonstrating the effectiveness of NEG coating and its ex-situ activation.

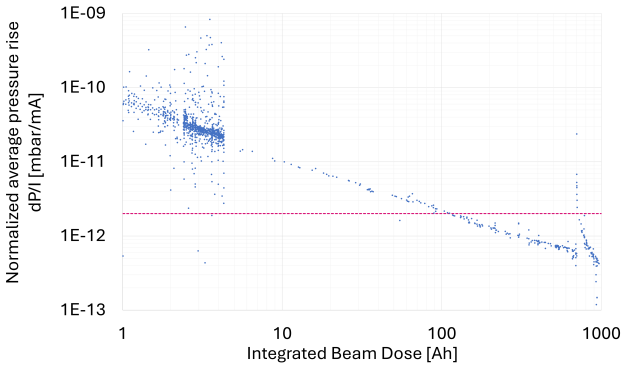

Figure 1: Normalised average pressure rise $\mathrm{d}P/I$ [mbar/mA] vs. accumulated beam dose [Ah] for SLS 2.0. Design target 2×10^{-12} mbar/mA (pink line) reached at ≈100 Ah. The September 2025 ID installation and subsequent recovery are visible above 500 Ah.

Residual Gas Analysis

The ring is equipped with four RGAs, located above crotch absorbers. Figure 2 shows spectra from four representative sectors. In the best-conditioned sectors (e.g. Sector 11), H_2 is the dominant species, confirming effective NEG pumping of reactive gases. Sector 1 exhibits anomalous CH_4 and Argon peaks attributed to residuals of an abrasive cleaning brush found inside the crotch absorbers. It can also indicate a small air leak. Sector 8 shows elevated H_2O and CO/N_2 from less-conditioned straight-section components.

* natalia.kirchgeorg@psi.ch
† romain.ganter@psi.ch

Content from this work may be used under the terms of the CC BY 4.0 licence (© 2026). Any distribution of this work must maintain attribution to the author(s), title of the work, publisher, and DOI.

ISBN: 978-3-95450-252-3 ISSN: 2673-5350 doi: 10.18429/JACoW-IPAC2026-MOP7120

KIT SUPERCONDUCTING UNDULATOR AND MAGNET DEVELOPMENTS - OVERVIEW AND STATE OF THE ART R&D ON HTS TECHNOLOGY

B. Krasch*, A. Bernhard, S. Fatehi, N. Glamann, A. Grau, A.-S. Müller, D. Saez de Jauregui,
Karlsruhe Institute of Technology (KIT), Karlsruhe, Germany
A. Hobl, W. Walter, Bilfinger Nuclear & Energy Transition (Bilfinger) GmbH, Würzburg, Germany

Content from this work may be used under the terms of the CC BY 4.0 licence (© 2026). Any distribution of this work must maintain attribution to the author(s), title of the work, publisher, and DOI.

Abstract

Undulators are widely used in synchrotron storage rings and free-electron laser facilities. With the advent of low-temperature superconductors (LTS), a new generation of superconducting undulators (SCUs) emerged, including the recent new THz LTS undulator for FLUTE. At KIT, state-of-the-art magnetic and cryogenic measurement capabilities — provided by the Magnet and Cryogenics Facilities (MCF) and the Accelerator Technology Platform (ATP) — form a foundation for the development and characterization of these systems.

Building on this experience, KIT is now advancing magnets and undulators based on high-temperature superconductors (HTS), aiming for compact, sustainable, energy- and resource-efficient solutions. These activities are driven by in-house research and providing the full value chain of HTS technology from tape development via structuring to prototypes and tests in real-world environments at KIT.

In this contribution, we provide an overview of our current developments and the supporting experimental infrastructure.

INTRODUCTION

Undulators are key components in modern synchrotron storage rings and free-electron laser facilities, enabling the generation of highly brilliant and tunable radiation for a wide range of applications. While permanent magnet undulators are widely used, SCUs enable significantly higher magnetic fields on the symmetry axis for comparable geometric constraints, allowing for shorter period lengths and enhanced photon energies [1]. With the commercial availability of LTS, SCU technology has matured and demonstrated its potential in various accelerator facilities [2–5]. At the Institute for Beam Physics and Technology (KIT-IBPT), extensive expertise in the development and operation of conduction-cooled LTS undulators has been established over the past decades [6], including recent developments such as a THz undulator for FLUTE (Ferninfrarot Linac- und Test-Experiment) [7, 8]. A key stone for this development are the MCF which allow a precise measurement of the magnetic properties and therefore a direct approach to the quality of the undulator. In close collaboration with our industrial partner Bilfinger, this work has also led to the successful industrialization of SCU technology [6]. Building on this experience, current research at KIT-IBPT focuses on the development of magnets and undulators based on HTS, aiming at compact, sustainable, and energy- and resource-efficient solutions.

In the following sections, a short motivation for HTS is given, followed by the HTS undulator research and is concluded by the HTS magnets. Lastly, the MCF and its possibilities are outlined.

FROM LTS TO HTS: MOTIVATION AND OPPORTUNITIES

LTS materials such as NbTi and Nb_3Sn have enabled the successful development of SCUs with high magnetic performance and reliable operation [9]. However, their operation at temperatures around 4 K requires complex and energy-intensive cryogenic systems. While conduction cooling has significantly simplified operation by eliminating the need for liquid helium, the overall cooling effort remains substantial. In addition, intrinsic geometric limitations arise from the finite cross-section and mechanical properties of LTS wires, restricting the minimum achievable bending radius and thus limiting undulator period lengths to approximately 8 mm and above. These constraints hinder further miniaturization and performance scaling of SC IDs. HTS conductors, often available as tapes, allow for novel design approaches that can overcome these geometric limitations and enable shorter period lengths. Their higher critical temperatures enable operation at elevated temperatures or, alternatively, significantly higher current densities and magnetic fields at 4 K. This opens up new possibilities for more compact designs, enhanced field strengths, and improved energy efficiency, contributing to more sustainable and resource-saving accelerator technologies. Beyond accelerator applications, HTS materials are widely regarded as a key enabling technology for next-generation high-field systems.

HTS UNDULATOR R&D AT KIT

The use of HTS enables fundamentally new approaches to undulator design, see Fig. 1, particularly when employing **structured HTS tapes**. At KIT, high-intensity laser pulses are used to define a meander-shaped current path within the SC layer, resulting in a quasi-sinusoidal magnetic field distribution along the beam axis [10]. Based on this concept, two main design approaches are currently pursued [11, 12]. In a first concept, a single 15 m long HTS tape is structured and wound around a stainless-steel yoke to form a continuous, jointless current path. In a second approach, 25 cm short

* bennet.krasch@kit.edu

ISBN: 978-3-95450-252-3 ISSN: 2673-5350 doi: 10.18429/JACoW-IPAC2026-MOP7121

IN-VACUUM UNDULATORS FOR BESSY II

A. Meseck*[1], S. Grimmer, K. Karimi, C. Kuhn, C. Lorey, O. Reichel, E. Rial, S. Schäfer, N. Vogt, P. Volz, E. Wiesel, Helmholtz-Zentrum Berlin für Materialien und Energie, Berlin, Germany
[1] also at Johannes Gutenberg University Mainz, Mainz, Germany

Abstract

Since 2018, the BESSY II storage ring has operated a cryogenic permanent magnet undulator (CPMU), which was developed and constructed in-house. CPMU17, with a period of 17 mm, was the first in-vacuum undulator to be installed at BESSY II. Another CPMU (CPMU20) and the world's first in-vacuum APPLE II undulator (IVUE32) are currently under construction and will be installed at BESSY II within the next few years. To meet the needs of its diverse and ever-evolving user community, BESSY II has pioneered innovative operating modes, such as low-alpha and TRIBS, in addition to the hybrid mode. These special operating modes are based on phase space manipulation, which is enabled by the accelerator lattice's great flexibility and tight tolerances for the insertion devices. Consequently, there are also tight tolerances for in-vacuum IDs. This paper discusses some of the main challenges as well as the key developments and strategies involved in meeting tolerance requirements.

INTRODUCTION

The CPMU17, a cryogenic permanent-magnet undulator with a period of 17 mm, was installed in 2018 as the first in-vacuum insertion device (ID) at BESSY II. It serves as a source of hard X-rays in the canted double-undulator system of the Energy Materials In-situ Laboratory EMIL [1, 2]. Based on the CPMU17 design, another CPMU with a period length of 20 mm, CPMU20, is currently under construction. CPMU20 is dedicated to battery research [3]. It covers an energy range from 500 eV to 5000 eV by adjusting the undulator gap from 6 mm to 22 mm. It is due to be installed in BESSY II and become operational in 2029 [4]. A third in-vacuum undulator currently under construction for BESSY II is an APPLE II Type insertion device with a period of 32 mm (IVUE32). It is the world's first variable polarisation in-vacuum insertion device [5–7].

CPMUs take advantage of the enhanced field of rare earth magnets at low temperatures. In addition to the higher fields, the cooling down leads to higher radiation stability of the magnets. Furthermore, the issue of RF and synchrotron radiation heating is significantly reduced compared to conventional in-vacuum devices due to the substantial cooling capacity of the magnet structure. Thus, CPMUs are particularly well-suited to serving as short-period, small-gap insertion devices [8]. Although most of the technology developed for conventional in-vacuum devices can be used for a CPMU, several key components needed to be adapted for the realisation of CPMU17, including Dy-hardened PrFeB-magnets, a low permeability stainless steel in-vacuum-girder without keepers, direct liquid Nitrogen cooling, gap measurements and feedback loop based on an optical micrometer [1]. The cooling concept utilising liquid nitrogen was optimised empirically based on the undulators team's existing experimental knowledge.

The taper sections at entrance and exit of the CPMU17 form the connection between the variable aperture of the magnet structure, i.e. undulator gap, and the fixed aperture of the storage ring's vacuum chamber. They have been designed to compensate for changes in the gap during operation and to reduce the effects of the RF field generated by the electron beam as it passes through the devices. The magnets are covered by a RF-shields made of a 50 μm Copper layer coated on a 50 μm thick Nickel foil. Extensive measurements have been carried out during the commissioning phase in order to study the impact of CPMU17 on the impedance budget of BESSY II on the one hand and to investigate the heating up the taper sections due to their impedance on the other hand [9, 10]. While no hint of coupled bunch impedance due to CPMU17 was found, the heating of the taper sections exceeded the expected value. This was counteracted by improving the water cooling of the taper structure [2]. For the CPMU20, however, improved taper sections with significantly reduced impedance are designed.

The taper section design is more complex for the IVUE32 because it has to accommodate both shift and gap motion. For the taper structure to handle gap motion similarly to a CPMU, shift motion must be compensated for. The corresponding design is detailed in [11, 12].

This paper presents the improved flexible taper section design of the CPMU20, including simulation studies showing the impedance of the taper structure for different gap settings. Additionally, simulation studies of the liquid nitrogen-based cooling system are presented. They show the effectiveness of the cooling concept and support the empirically found optimisations.

CPMU20 TAPER SECTION

The flexible taper sections at the entrance and exit of the CPMU20 connect the movable ID-gap to the fixed aperture of the storage ring's vacuum chamber. The vacuum pipe has a vertical size of 11 mm at the entrance and exit of the CPMU, whereas the undulator's movable gap can be varied from approximately 5 mm up to 40 mm. Although a gap motion of 6 mm to 22 mm is needed to deliver the requested energy range of 500 eV to 5 keV, the wider motion range is necessary for maintenance and commissioning reasons. With the smallest gap the ID mimics a collimator configuration whereas the gaps larger than 11 mm lead to a cavity configuration. Both configurations can cause the

* ameseck@uni-mainz.de

Content from this work may be used under the terms of the CC BY 4.0 licence (© 2026). Any distribution of this work must maintain attribution to the author(s), title of the work, publisher, and DOI.

ISBN: 978-3-95450-252-3 ISSN: 2673-5350 doi: 10.18429/JACoW-IPAC2026-MOP7123

A HALL-PROBE CALIBRATION SETUP IN THE TEMPERATURE RANGE FROM 300 K TO 4 K AT EUROPEAN XFEL

M. Yakopov†, S. Abeghyan, D. Carias, S. Casalbuoni, U. Englisch
European XFEL, Schenefeld, Germany

Abstract

Precise magnetic-field measurements are essential for the characterization of both superconducting (SC) and permanent-magnet (PM) undulators. Since the accurate characterization of these devices relies directly on precisely calibrated Hall probes, a dedicated Hall-probe calibration setup for magnetic fields from – 2 T to + 2 T has been developed, produced, and is under commissioning at European XFEL, capable of operating over a broad temperature range from 300 K down to 4 K. This contribution presents the setup and first results.

INTRODUCTION

Undulators are used in light sources to generate highly brilliant photon beams. European XFEL has three undulator lines based on permanent magnet technology: two for hard and one for soft X-rays [1]. Moreover, in order to access photon energies above 30 keV and to overcome the limitations of permanent-magnet undulators (PMUs), up to six superconducting undulator (SCU) modules are planned to be installed downstream with respect to the PMUs of one of the hard X-ray lines [2]. Undulator quality assurance is carried out through magnetic field measurements. Hall probes are widely used for magnetic field mapping due to their compact size and wide dynamic range.

An accurate calibration of the Hall probes is at the basis of the precise magnetic field profile measurements required for undulator characterization prior to their installation in the accelerator. For PMUs, the Hall probes are calibrated at 21 ± 0.1 °C, which is the same temperature at which the measurements take place. SCU coils are characterized at 4.2 K in the liquid helium bath test stand SUNDAE1[3], and then in the SUNDAE2 setup while installed in the final cryostat [4]. The SUNDAE2 setup foresees Hall probes scanning the magnetic field while moving in the electron beam chamber. Their temperature will be measured, and it is foreseen to range between 30 K and 200 K. We therefore developed a Hall probes calibration system operating from 300 K down to 4 K.

SETUP DESCRIPTION

The calibration setup has been designed with the goal of combining magnetic field quality, thermal control, and mechanical precision in a single integrated system. The magnetic field is generated by a GMW 3474 dipole electromagnet with a pole diameter of 250 mm. The magnet provides a sufficiently homogeneous field < 0.1 mT in a region of the order of 16 mm^2 and has a magnetic field ranging from – 2 T to + 2 T. This area is defined as a good field region (GFR) and will be used for the calibration routine.

The magnet is powered by a precision current-regulated power supply of the Danfysik System 8500 series, which is a 0.1ppm stability class device. This type of supply is specifically designed for applications requiring high current stability and low noise.

To access the cryogenic regime, the setup employs a closed-cycle cryostat produced by ARS, Inc. The cryostat is equipped with the Cernox temperature sensors, allowing precise monitoring and control of the Hall probe sample temperature from 300 K to 4 K.

To precisely position both the Hall probe samples and the reference NMR probes within the GFR, a dedicated mechatronic positioning system was developed and manufactured by LabVECTOR GmbH. The system is based on three motorized xHUBER linear stages combined with two high-precision goniometers, enabling full three-dimensional translational positioning as well as angular alignment of the probe.

The angular alignment is realized using goniometers with a high angular resolution. This allows fine alignment of the Hall probe with respect to the magnetic field, minimizing systematic errors due to angular misalignment. The parameters of the mechatronic positioning system are listed in Table 1.

Table 1: Positioning resolution of the five-axis Hall probe positioning system.

Axis	Spindle pitch	Gear box	Microstep-ping	Resoluti on
X	2 mm	No	20	0.5 µm
Y	2 mm	No	20	0.5 µm
Z	2 mm	20:1	2	0.25 µm
Pitch	1°	20:1	2	0.45″
Yaw	1°	20:1	2	0.45″

Particular attention was paid to the mechanical stability of the system. By lowering the center of gravity and simplifying the structural design, a rigid and compact configuration was achieved. The motion system is controlled via a multi-axis stepper motor controller, enabling operation of all degrees of freedom and reproducible automated scan sequences.

† mikhail.yakopov@xfel.eu

Content from this work may be used under the terms of the CC BY 4.0 licence (© 2026). Any distribution of this work must maintain attribution to the author(s), title of the work, publisher, and DOI.

ISBN: 978-3-95450-252-3 ISSN: 2673-5350 doi: 10.18429/JACoW-IPAC2026-MOP7124

OVERVIEW OF SUPERCONDUCTING UNDULATOR DEVELOPMENT AT THE EUROPEAN XFEL

S. Casalbuoni*, S. Abeghyan, L. Biasia, U. Englisch, A. Doosti,
A. Elghandour, E. Fioresi, G. Geloni, S. Karabekyan, A. Nandawadekar, G. Perosa,
A. Rajabi, M. Ronniger, T. Schmidt, H. Sinn, M. Yakopov, P. Ziolkowski,
European XFEL, Schenefeld, Germany
S. Barbanotti, W. Decking. A. Hauberg, C. Helwich, K. Jensch, S. Liu, L. Müller, E. Schneidmiller,
R. Wichmann, T. Wohlenberg, J. Wu,
Deutsches Elektronen-Synchrotron, Hamburg, Germany
A. Hobl, A. Vatagin, W. Walter,
Bilfinger Nuclear & Energy Transition GmbH, Würzburg, Germany

Content from this work may be used under the terms of the CC BY 4.0 licence (© 2026). Any distribution of this work must maintain attribution to the author(s), title of the work, publisher, and DOI.

Abstract

This contribution describes the recent progress of the European XFEL superconducting undulators (SCUs) program. This includes: an industrially-produced NbTi-based SCU afterburner foreseen for one of the two hard X-ray lines; a prototype SCU module (S-PRESSO) in production by Bilfinger; two magnetic measurement test stands to perform quality assurance; and further development of SCU technology to reach even larger magnetic fields, by leveraging recent developments in High Temperature Superconducting (HTS) tapes for future upgrades.

INTRODUCTION

We report here about the latest achievements of the Superconducting Undulator (SCU) program at Euroepean XFEL. The program, described in Refs. [1, 2] aims to maintain the European XFEL (EuXFEL) at the forefront of XFELs even as new competing facilities mature. The primary goals of the program are:

- As the first XFEL to implement SCUs, establish a long-term world-leading capability in production of high intensity ultrashort x-rays above 30 keV and enable flexibility for other potential upgrades of EuXFEL (i.e. High Duty Cycle).
- Demonstrate the ability of the EuXFEL team to develop SCU technology. As the first major milestone of the SCU program, install an industrially-produced NbTi-based SCU afterburner in SASE2.
- Gain experience in the installation, commissioning and operation of SCUs in a XFEL environment.
- Further development of SCU technology to reach even larger magnetic fields, by leveraging recent developments in High Temperature Superconducting (HTS) tapes for future upgrades. This could revolutionize all light sources, including the EuXFEL, with increases in undulator magnetic fields by factors of about five.

* sara.casalbuoni@xfel.eu

The program will proceed through two major phases culminating in the installation of up to six SCU modules in the SASE2 tunnel downstream with respect to the presently installed permanent magnet undulators by 2033. These will provide photon with energies > 30 keV and unprecedented pulse energies in the few hundreds μJ range which will be delivered to the three instruments served by the SASE2 undulator line. The six SCU modules consist of a Superconducting undulator PRre-SerieS mOdule (S-PRESSO) and five small series FESTA (Free Electron laser SuperconducTing undulator Afterburner) SCU modules. They plan to be installed downstream with respect to the permanent magnet undulator (PMU) SASE2 line. Phase 1 focuses on developing an industrial partner, further development of SCU technology including HTS tape undulators, test infrastructure, and measuring and installing S-PRESSO delivered by the industrial partner; and Phase 2 on the industrial production and installation of up to five FESTA modules.

In this paper we present FESTA, as well as the dedicated measurement test stands developed for quality assurance of superconducting undulator (SCU) coils, and report on the current status of the S-PRESSO project. We emphasize magnetic measurements on one of S-PRESSO's two 2-m SCU magnets — to our knowledge the longest SCU coil yet manufactured and the longest length at which magnetic characterization of such a coil has been successfully performed. These results demonstrate the capability of the FESTA stands and constitute an important step toward scaling SCU production.

FESTA

The FESTA and S-PRESSO SCU modules will be 5 m long and will contain two 2 m long undulator coils, horizontal and vertical correctors at the exit of the first set of SCU coils and at the entrance of the second set of SCU coils, as well as a phase shifter. The main parameters of the SCU modules are listed in Table 1 [3].

Different operation schemes have been investigated. Amplification of the fundamental radiation from the PMUs using the fundamental of the SCUs is feasible for photon en-

ISBN: 978-3-95450-252-3 ISSN: 2673-5350 doi: 10.18429/JACoW-IPAC2026-MOP7125

FIRST RESULTS FROM THE SUNDAE1 TEST STAND AT EUROPEAN XFEL

A. Elghandour, S. Abeghyan, S. Casalbuoni, A. Doosti, E. Fioresi,
A. Nandawadekar, A. Rajabi, M. Ronniger, M. Yakopov, P. Ziolkowski
European XFEL, Schenefeld, Germany
A. Hobl, A. Vatagin
Bilfinger Nuclear & Energy Transition GmbH, Würzburg, Germany
S. Barbanotti, A. Hauberg, C. Helwich, K. Jensch
Deutsches Elektronen-Synchrotron DESY, Hamburg, Germany

Content from this work may be used under the terms of the CC BY 4.0 licence (© 2026). Any distribution of this work must maintain attribution to the author(s), title of the work, publisher, and DOI.

Abstract

European XFEL is planning the installation of superconducting undulators as afterburners downstream with respect to SASE2, one of the hard X-ray undulator lines, to provide even harder X-ray photon energies and a larger tuning range. The Superconducting undulator PRE-SerieS mOdule (S-PRESSO) consisting of two pair of coils, a phase shifter, and correction coils is in production by Bilfinger Nuclear & Energy Transition GmbH. In order to perform quality assurance of the superconducting coils a vertical test stand SUNDAE1 (Superconducting UNDulAtor Experiment) has been developed. SUNDAE1 allows to train the superconducting coils, as well as to measure the magnetic peak field profile by means of Hall probes. We report here on first results.

INTRODUCTION

Superconducting undulator (SCU) technology is strategically important for the future development of the European XFEL, as it would extend the accessible photon energy range and better exploit the accelerator capability [1].

Because of the strategic relevance of superconducting undulators to the European XFEL facility, a project to develop an SCU afterburner for the SASE2 line has been initiated. The main parameters of its pre-series prototype module, Superconducting undulator PRE-SerieS mOdule (S-PRESSO), have been reported in Ref. [2].

With the main goal of training and measuring the magnetic field profile of superconducting undulator coils with Hall probes, SUNDAE1 is a Liquid helium bath vertical test stand developed at European XFEL [3]. In this contribution, we report on the commissioning of SUNDAE1, as well as the first results obtained for one of the two 2 m-long SCU magnets of S-PRESSO, which is, to the best of our knowledge, the first 2 m-long superconducting magnet ever to be characterized.

EXPERIMENTAL SETUP

SUNDAE1 has been described in more detail in Refs. [1] and [3]. The system includes an insert to lead the current from the power supplies down to the magnet which is vertically attached. The insert with the attached magnet is hosted in a liquid helium bath vertical cryostat with operation capability at 4 K (~1 bar) and at 2 K (~30 mbar).

Two bipolar power supplies rated ± 1500 A and six 20 A power supplies, each fitted with its own quench detector, are available for use. It is possible to power coils with a maximum current of 3000 A. To locate possible quenches, five Cronosflex HISO-8 units are used. The SUNDAE1 insert consists of a main top flange carrying all sensor connectors, current flanges, and cryogen inlets/outlets. Current leads and LN_2 and LHe heat exchangers (HEs) are mounted below the flange. The cryogenic sections are vertically separated by super-insulated baffles.

Copper parts of the high-current (500 A and 1000 A) and low-current (20 A) leads are cooled by LN_2 heat exchangers. The HTS sections of the 20 A leads are also connected to LN_2 heat exchangers, while their HTS and LTS (NbTi wire-in-channel) ends are thermally anchored to the LHe bath using copper braids. For the 500 A and 1000 A leads, the HTS sections are cooled by dedicated LHe heat exchangers, and their HTS and LTS ends are similarly thermally anchored to the LHe bath.

Temperatures at the end of the LN_2-cooled copper section and before the HTS section are monitored with PT100 sensors, while the top of the NbTi wire-in-channel section is monitored using Cernox sensors.

The tested magnet consists of a main coil powered with 1000 A, and two auxiliary coils, as described in Ref. [3], which can be tuned to minimize the second field integral.

SUNDAE1 is equipped with a quench detection system and data acquisition system for the quench events diagnostics. Further, the system is capable of measuring local magnetic field using Hall probes, which are mounted on a 4 mm-thick sledge driven by a linear motion system (LMS). The LMS can scan over 2.4 m between coils with gaps as small as 6.5 mm with a resolution of 1 μm. This allows characterization of coils up to 2 m long. The Hall probe used for the characterizations reported below has been calibrated at the Karlsruhe Institute of Technology and has a calibration error of ± 0.1 mT. In the future, Hall probes are planned to be calibrated at European XFEL [4].

BENCHMARKING SUNDAE1 WITH CASPER1

The magnetic field profile, as well as the magnetic field quality in terms of $(\frac{\Delta K_{\mathrm{half}}}{K_{\mathrm{half}}})$ rms, as defined below, are measured and compared in the test stands SUNDAE1 and CASPER1 for the same magnet: the S-PRESSO mock-up [5].

ISBN: 978-3-95450-252-3 ISSN: 2673-5350 doi: 10.18429/JACoW-IPAC2026-MOP7128

DEVELOPMENT AND CHARACTERIZATION OF THE DOUBLE DIPOLE KICKER PROTOTYPE AT ALBA*

R. Muñoz Horta†, G. Benedetti, M. Carlà, F. Perez, O. Traver
ALBA Synchrotron, Cerdanyola del Vallès, Spain

Abstract

The Double Dipole Kicker (DDK) topology has been designed to perform off-axis injection into the ALBA II storage ring, currently under design. The DDK creates a multipole magnetic field by summing two opposite dipolar fields generated by four inner and four outer conductor rods. The two dipolar fields are powered by two independent pulsed power supplies that deliver identical pulses of up to 3 kA and 1.75 µs. The rods are precisely positioned along in-air ceramic grooves, to maximize the kick of the injected beam coming from the booster synchrotron and, to minimize the field at the stored beam position during top-up injections. A pure dipolar mode is also available when the inner rods are not powered, which it will be used during ALBA II commissioning. The in-vacuum ceramic chamber is coated with a titanium layer of a variable thickness with the aim of minimizing the effect of induced eddy currents on the stored beam. A DDK prototype has been built and installed alongside the four kickers that generate the injection bump at the ALBA storage ring. First injection tests with the DDK are presented.

INTRODUCTION

Low-emittance storage rings require injection schemes capable of preserving orbit stability and beam quality during top-up operation. Pulsed multipole kickers are a promising solution for transparent injection [1]. For the ALBA II upgrade, a compact injection magnet combining nonlinear kicker functionality with a dipole operational mode for commissioning has been designed, the so-called Double Dipole Kicker (DDK) [2]. A prototype program was initiated to validate the DDK concept and to demonstrate its feasibility under realistic operating conditions in the existing ALBA storage ring.

THE DDK CONCEPT AND DESIGN

The DDK consists of eight straight copper conductor rods of 2 mm diameter arranged symmetrically around the beam axis: four inner rods and four outer rods. The rods are positioned around a 300 mm long in-vacuum alumina ceramic chamber by in-air ceramic grooves. The grooves were manufactured with a machining accuracy better than 50 microns. The precise positioning of the rods with respect to the ceramic aperture is essential to guarantee cancellation of the magnetic field at the stored beam position and to achieve the required nonlinear field profile at the injected beam trajectory. Independent pulsing of the inner and outer rods compensates mechanical tolerances and mitigates transient field errors. An horizontal orbit distortion of less than 10% of the beam size requires the two current

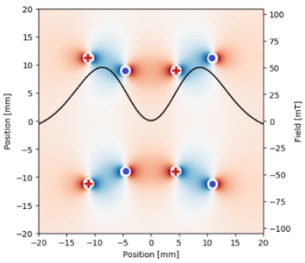

Figure 1: Transversal magnetic field profile of the DDK generated by powering the eight rods.

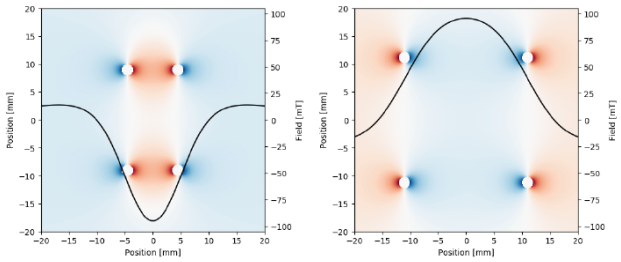

Figure 2: Transversal magnetic field profile generated by powering only the 4 inner rods (left) and only the 4 outer rods (right). The dipolar field of the outer rods will be used for on-axis injection during ALBA II commissioning.

pulses to be identical, with a relative difference below 0.12% of the pulse amplitude.

Figure 1 and Fig. 2 show the resulting magnetic field from the superposition of the inner and outer rods, as well as the dipole fields generated independently when each set of rods is powered separately. The magnetic field peak is located at the injected beam trajectory, at x=8.7 mm.

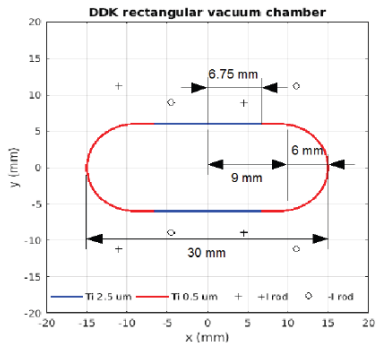

Figure 3: Aperture of the DDK ceramic chamber and the two different titanium coating thicknesses.

* Work supported by the Spanish and Catalan Governments, and co-funded by the European Union – NextGenerationEU project Ref. ICTS-MRR-2021-02-CELLS from the Recovery and Resilience Mechanism.
† rmuñoz@cells.es

Content from this work may be used under the terms of the CC BY 4.0 licence (© 2026). Any distribution of this work must maintain attribution to the author(s), title of the work, publisher, and DOI.

ISBN: 978-3-95450-252-3 ISSN: 2673-5350 doi: 10.18429/JACoW-IPAC2026-MOP7129

INITIAL DESIGN OF A LUMPED INDUCTANCE KICKER FOR THE FCC-EE

G. Sergentanis*, L. Ducimetière, Y. Dutheil, S. Dylan, G. Favia, T. Kramer, J. Ruf, S. Yue
European Organization for Nuclear Research, Geneva, Switzerland

Abstract

CERN is working towards a new, larger circular collider complex, the Future Circular Collider (FCC-ee), with a perimeter of 90.7 km. This paper addresses some of the challenges associated with beam-transfer equipment. The FCC-ee requires numerous kicker systems for beam disposal and transfers from injectors to the main collider ring. To standardise hardware parameters across machines and reduce the variety of beam-line components, this work proposes a lumped-inductance kicker magnet for multiple systems. To adapt the design for different purposes within the FCC complex, only the number of modules is adjusted to achieve the required deflection, while maintaining a low voltage for each module to enable operation outside the vacuum. This common design offers significant advantages for spares, maintenance, production, and machine protection. Initial design-study results from numerical simulations of the beam-line element are presented, along with system-level options for integration with the FCC-ee accelerator.

INTRODUCTION

The FCC-ee, a proposal for CERN's next flagship accelerator, will enable higher precision measurements of the Higgs particle with collision energies up to 365 GeV in the $t\bar{t}$ mode [1].

Key accelerator systems are currently being developed as part of the project's reference design phase. These include the injection and extraction systems, which comprise kicker magnets to steer the beam. Established kicker technologies comprise lumped inductance, transmission line, and stripline kickers, with the selection depending on required beam timings, desired deflection angles, and available beamline length [2].

Lumped Inductance (LI) kickers offer strong beam deflection capabilities and are cost-effective due to their simplicity and robustness. A primary limitation is that achieving field rise and fall times considerably below the 1 µs range is challenging, given their lumped-element nature and the travelling wave phenomena in cable connections [2]. The injection and extraction kicker systems for the FCC-ee and their requirements have been outlined in [3]. Table 1 details the systems for which an LI kicker magnet topology has been chosen, along with their key specifications. This paper presents the design of a common LI kicker magnet module suitable for all these systems. While the requirements for the magnetic field homogeneity are identical for these systems, the necessary deflection angle (kick strength) varies. These differing requirements can be accommodated by using a variable number of identical modules based on a single LI kicker design, as well as by varying their generator characteristic impedance.

Table 1: FCC-ee LI Kicker System Requirements

	Booster extraction	**Booster dump**	**Collider injection**	**Collider dump**
Energy [GeV]	45–182.5	45–182.5	45–182.5	45–182.5
Kick angle [mrad]	0.196	0.396	0.08	0.396
Rise/fall times [ns]	600	600	600	600
Flat top length [µs]	304	304	304	304
Flat top quality [%]	±0.6	±20	±1.5	±20
Maximum repetition rate [Hz]	0.3	1	0.3	0.1
Magnetic field homogeneity [%]	0.5	0.5	0.5	0.5

MAGNET DESIGN

The design of an appropriate LI kicker must satisfy several key requirements. The magnetic field quality must meet the specifications set by beam optics considerations. Additionally, the inductance must be sufficiently low to enable the required magnetic field rise and fall times. Other important considerations include the beam-coupling impedance and its impact on beam stability.

Field Quality

One of the challenges in the magnet design is the required magnetic field homogeneity of ±0.5%. The field homogeneity is defined as the maximum deviation of the vertical magnetic field within the good field region (GFR) compared to its centre point value. For this design, the GFR is preliminary defined to coincide with the required beam stay-clear area (BSC). This deviation is calculated as shown in Eq. (1), with the y-axis being the vertical axis of the magnet cross section.

$$\Delta B_y = \left| \frac{B_y - B_{y,\text{centre}}}{B_{y,\text{centre}}} \right| \cdot 100\% \tag{1}$$

An initial design choice is the shape of the magnetic yoke, with options including a C-core and a window-frame topology. A window-frame magnet fully encloses the busbars with ferrite material, splitting the magnetic flux between two return paths and allowing the use of a thinner yoke for the same magnetic field strength and aperture. Furthermore, its symmetric field distribution, makes the window-frame design more suitable for meeting the stringent field homogeneity requirements.

* grigorios.sergentanis@cern.ch

Content from this work may be used under the terms of the CC BY 4.0 licence (© 2026). Any distribution of this work must maintain attribution to the author(s), title of the work, publisher, and DOI.

ISBN: 978-3-95450-252-3 ISSN: 2673-5350 doi: 10.18429/JACoW-IPAC2026-MOP7130

HIGH-VOLTAGE COILS OPTIMIZATION FOR THE LHC BEAM DUMP DILUTOR KICKER MAGNETS

V. Namora†, Ch. Bracco, L. Ducimetière, G. Favia, S. Huon, V. Senaj
European Organization for Nuclear Research (CERN), Geneva, Switzerland

Abstract

Two sets of 6 fast-pulsed vertical and two sets of 4 fast-pulsed horizontal dilutor kicker magnets form part of the so-called LHC beam dumping system, which removes the counter-rotating beams safely from the collider onto an absorber block. Each vertical and horizontal diluter magnet is powered by a pulse generator via a low-impedance transmission line resulting in maximum damped sinusoidal voltage of 16 kV and a maximum damped sinusoidal current pulse of 30 kA. The fast-pulsed dilutor kickers magnets, MKBV and MKBH, consist of a steel yoke with excitation coils, which are immersed in the accelerator vacuum. As part of a consolidation program, high-voltage insulated coil spares will be manufactured. The coils are composed of conductor bars of quasi-rectangular cross-section, junction pieces, and conductor contact pieces. The coils are completely insulated for the 16 kV and 10 kV peak voltages. The surface of the insulation is coated with a resistive layer and connected to earth. The connector contact terminals are moulded sockets, surrounded by stress rings. This paper describes the design of the MKBV and MKBH kicker magnets, focusing on the fabrication processes and validation tests for both types of coils.

INTRODUCTION

During a HL-LHC beam dump, energies up to 700 MJ per beam at 7 TeV must be absorbed in the dump block. To perform a safe beam dump the dilution kicker magnets sweep the beam, in a spiral pattern (see Fig. 1), reducing the peak energy density and avoiding damage to the dump block [1].

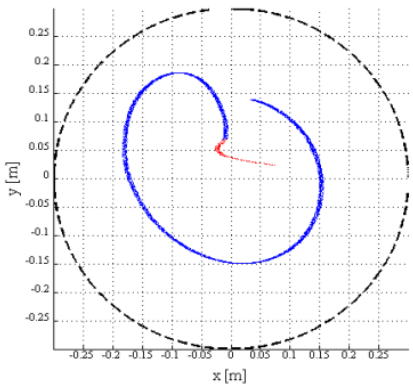

Figure 1: Diluted beam sweep on the dump block. Blue: nominal particles, red: particles in filled abort gap.

To perform the sweep the MKBV magnets are first energised with a damped sinusoidal voltage of 13,2 kV peak, producing a damped sinusoidal current pulse with a maximum amplitude of 24 kA and a period of 87 µs. Fifteen microseconds later, the MKBH magnets are energised with a similar sinusoidal voltage of 24,5 kV, resulting in a damped sinusoidal current pulse with a maximum amplitude of 25,3 kA with a period of 73 µs [2].

All the dilution magnets are located outside the circulating beam line and installed in vacuum tanks, typically at a pressure of ~10^{-8} mbar. Dilution kicker magnets parameters are show in Table 1.

Table 1: Dilution Kicker Magnets Parameters

	MKBV	MKBH
Number of magnets per system	6	4
Number of magnets per tank	2	2
Maximum Deflection angle per system [mrad]	0.277	0.278
Kick strength per magnet [T.m]	1.077	1.624
Operating Voltage (peak) [kV]	13.2	24.5
Operating Current (peak) [kA]	24.0	25.3
Coil turns per magnet	2	1
Magnet horizontal beam aperture [mm]	70	63
Magnet vertical beam aperture [mm]	43.5	36
Magnetic effective length [mm]	1267	1936
Mechanical yoke length [mm]	1196	1899
Vacuum length (flange to flange) [mm]	4076	4582

MKBV KICKER MAGNET COIL

The MKBV is a window-frame magnet that consists of a steel yoke with a two-turn excitation winding. The yoke is composed of tape-wound cores made from 50 µm thick Si-steel, into which a gap is cut, as shown in Fig. 2.

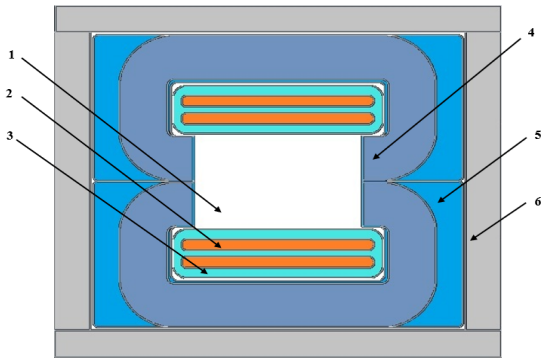

1. Magnet gap
2. Conductor of high-voltage coil
3. Insulation of high-voltage coil
4. Tape-wound core
5. Epoxy C-core moulding
6. Frame

Figure 2: Cross-section of the MKBV magnet.

Three cores are moulded using a charged epoxy into a unit which form a triple pack.

During the assembly of a magnet, these triple packs are stacked up longitudinally to the required yoke length.

†vasco.namora@cern.ch

Content from this work may be used under the terms of the CC BY 4.0 licence (© 2026). Any distribution of this work must maintain attribution to the author(s), title of the work, publisher, and DOI.

ISBN: 978-3-95450-252-3 ISSN: 2673-5350 doi: 10.18429/JACoW-IPAC2026-MOP7131

DESIGN AND OPERATION OF SLS2 THIN SEPTUM

S. Dordevic†, M. Paraliev, M. Aiba
PSI Center for Accelerator Science and Engineering, Villigen, Switzerland

Abstract

In the SLS2.0 upgrade project at the Paul Scherrer Institute (PSI) the injector complex remained mostly unchanged, but we had to design three new storage ring injection elements: the thick septum, the thin septum and beam dump system. Because of the limited dynamic aperture of the upgraded machine, 1 mm septum wall thickness was necessary. To limit stored beam disturbance to 10% of the beam sigma, extremely low (< 8 μT) leakage field was required. To achieved this, we used a "sandwich" septum consisting of a copper sheet and a layer of soft magnetic material. In this way we achieved very good screening of the main field.

To power the thin septum, we designed a pulse generator based on a two-stage fast thyristors switch and a matrix capacitor. The latter was built using multiple commercially available ceramic SMD capacitors to avoid the risk of catastrophic failure of the oil filled foil capacitors. We successfully built and commissioned the thin septum and, it works reliably.

In this paper, we present design and operational results of the pulsed thin septum, including simulations and measured results of the main and leakage field. Beam based leakage field evaluation is described as well.

INTRODUCTION

The upgraded machine with limited dynamic aperture requires the septum magnet wall thickness of 1 mm [1, 2]. Very thin eddy current septum (Fig. 1) should ensure inserting the injected beam very close (~3 mm) to the stored beam. Powder cores are chosen for the magnetic circuit to cover the frequency and the field strength requirements. Septum should provide the required field and at the same time extremely low leakage field to limit stored beam disturbance. 3D electromagnetic numerical simulator CST® Studio Suite [3] was used to optimize the screening of the thin septum. A "sandwich" configuration (Fig. 2, top left) from a cooper sheet and a layer of soft magnetic material was chosen for the screening.

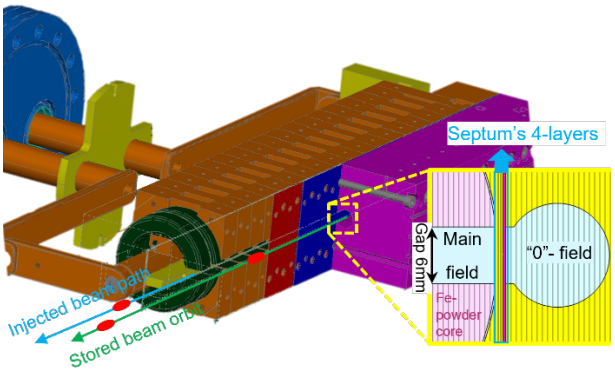

Figure 1: Septum magnet 3D drawing and cross-section of the simulated model. The blue line indicates injected beam path and the green line stored beam orbit.

THIN SEPTUM SIMULATION

Having in mind small thickness of metal sheets that were used, fine meshing was necessary to provide reliable results. Local meshing gives the minimal number of mesh cells for geometry with thin layers. Tetrahedral mesh for the septum model is based on usage of different local meshing (Fig. 2, top right).

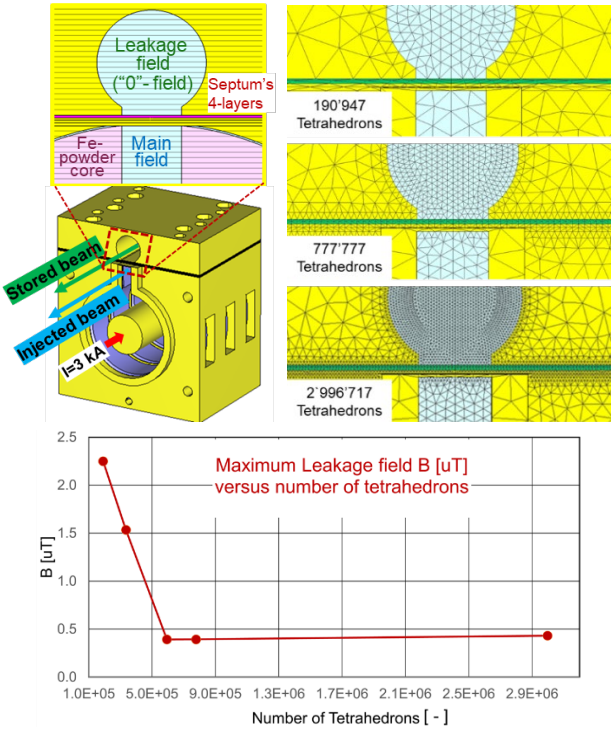

Figure 2: 3D CST® model and cross-section of a "sandwich" configuration with 4 layers used in parametric study (top left). Different mesh density based on different local meshing (top right). Influence of mesh size (number of tetrahedrons) on CST leakage field results (bottom plot) for thin septum excitation pulse of 3 kA amplitude.

Proper meshing is crucial to get consistent results. Diagram at Fig. 2 (bottom plot) shows that number of mesh cells up to 600'000 tetrahedrons significantly influences the result, but further increase (using smaller mesh size) has negligible influence.

For practical excitation pulse (sin wave with T=12.5 μs) one mm of copper does not provide the required screening (Fig. 3, top plot). No other engineering material (at room temperature) could provide significantly larger conductivity, respectively better screening. Eq. (1) shows steady state solution of skin depth (δ) for sine wave field. It can be easily seen that for a given frequency (f) skin depth (δ)

† sladana.dordevic@psi.ch

Content from this work may be used under the terms of the CC BY 4.0 licence (© 2026). Any distribution of this work must maintain attribution to the author(s), title of the work, publisher, and DOI.

ISBN: 978-3-95450-252-3 ISSN: 2673-5350 doi: 10.18429/JACoW-IPAC2026-MOP7132

EVALUATION OF ERROR PROPAGATION IN THE FIRST-ORDER GEODETIC NETWORK OF THE FCC TUNNEL USING TOPOGRAPHICAL TECHNIQUES

V. Gerligand[1], D. Mergelkuhl, L. Watrelot, CERN, Geneva, Switzerland
S. Durand, Laboratoire Géomatique et Foncier, Cnam, Le Mans, France
[1]also at Laboratoire Géomatique et Foncier, Cnam, Le Mans, France

Abstract

The Future Circular Collider (FCC-ee) is a next-generation electron-positron collider under design at CERN to advance particle physics beyond the Large Hadron Collider (LHC) era. This 91 km-long accelerator, located at a depth of about 200 m underground, raises significant challenges for the alignment of its components. Thousands of elements must be positioned within a few tens of micrometers precision relative to each other to ensure optimal machine performance. To achieve this, a first-order alignment network transferred from surface references must be established along the entire tunnel. This network should provide the basis for tracing, installation and absolute alignment of components prior to the relative alignment phase.

A dedicated simulation tool has been developed to model the FCC-ee tunnel, including shafts and bypasses. Then, different network configurations can be generated to simulate polar, gyroscopic, and leveling measurements. This paper presents the methodology used to build these simulations, and studies the resulting error propagation and expected precision for each measurement configuration.

INTRODUCTION

The Future Circular Collider (FCC-ee) is a 91 km-long electron–positron collider under development at CERN, which requires high-precision alignment to maintain the beam on a smooth trajectory, with expected tolerances around 150 µm for certain components to be aligned in arc sections [1]. To achieve these requirements, a First-Order Geodetic Network must be installed and measured along the entire tunnel to provide the reference for installation and absolute alignment of components, prior to the relative alignment phase. Based on LHC absolute alignment tolerances of approximately ±3 mm (1σ) [2] and considering that component positioning must not interfere with tunnel integration or exceed adjustment support limits, the FCC absolute alignment tolerances are expected to remain within ±5 mm (1σ), which is larger than for the LHC due to the size of the FCC. Given these tolerances, the 11.3 km between adjacent FCC shafts, which also corresponds to the spacing of network reference points transferred from the surface, makes error propagation along the tunnel a critical issue that needs to be studied. This paper presents a preanalysis-based approach to evaluate error propagation and assess whether the alignment tolerances can be achieved using polar, gyroscopic, and leveling measurements.

REALISTIC FCC GEOMETRY MODEL

Before simulations can be performed, a complete representation of the FCC alignment network must be generated. This requires a detailed geometric model of the entire accelerator infrastructure, serving as the basis for the definition of network points and measurements. This step already constitutes a major challenge due to the scale of the project and the complexity of the tunnel geometry, particularly in experimental and technical Long Straight Sections (LSS), as well as in shafts and associated bypasses. A dedicated Python software tool has been developed, to create a geometry as realistic as possible with respect to the expected final design of the machine infrastructure. It uses two different inputs: the integration design derived from CAD models and the optics design obtained from MAD-X files. From the integration data, two-dimensional cross sections of the tunnel are extracted. The longitudinal dimension of the model is introduced by assigning these cross sections to cumulative distance intervals. The resulting geometry is a linear tunnel. To account for the machine curvature, the current model is segmented into 1-m slices which are then successively positioned along the MAD-X reference trajectory. In parallel, shafts, bypasses, and other specific areas are loaded from the integration data using the same approach as for tunnel cross sections, with the two dimensions describing a top view rather than a transverse profile. These elements can then be inserted and positioned at their nominal locations by the software user.

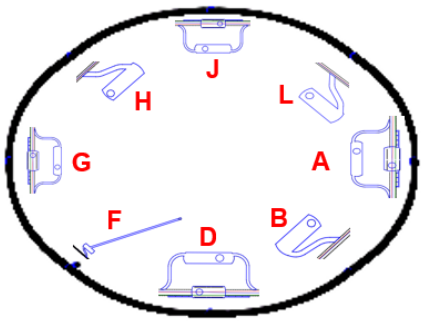

Figure 1: Generated FCC infrastructure.

While developed and employed to model a finely detailed FCC geometry with the most up-to-date known information available (see Fig. 1), this software and its workflow could be applied to any other accelerator facilities where both tunnel data and a MAD-X beamline trajectory exist (usually available from the authors upon request).

This is a preprint - the final version is published with IOP

Content from this work may be used under the terms of the CC BY 4.0 licence (© 2026). Any distribution of this work must maintain attribution to the author(s), title of the work, publisher, and DOI.

ISBN: 978-3-95450-252-3 ISSN: 2673-5350 doi: 10.18429/JACoW-IPAC2026-MOP7135

DESIGN AND DEVELOPMENT OF THE NEW ISOLDE BEAM DUMPS AT CERN

I. Z. Johansen*, E. Grenier-Boley†, A. P. Bernardes‡, I. R. Boff, T. F. Calvet, C. Cipriani, T. Coiffet, L. S. Esposito, M. A. Fraser, P.R. Menachilis, J.D.J. Pegg, A. Perillo Marcone, F. Pozzi, S. Sgobba, M. Simoes, M. Timmins, A.N. Osthus, M. Calviani, CERN, Geneva, Switzerland

Abstract

New beam dumps have been developed for the Isotope mass Separator On-Line facility (ISOLDE) at CERN, as part of the ISOLDE Beam Dump Replacement and Sustainability (IBDRS) project. The new design is engineered to ensure an operational lifetime of 30 years, additionally, to accommodate the planned quadrupling of beam power. The absorber assembly consists of water-cooled plates of cladded CuCr1Zr as well as pure copper. The cladding consists of an encapsulation of 316LN stainless steel, diffusion bonded to the cuprous core by means of Hot Isostatic Pressing (HIP). The cladded blocks are enclosed within a 316LN stainless steel vessel, which allows the use of pressurised water to cool the dump.

Extensive Monte Carlo and thermomechanical studies were conducted to evaluate temperature and stress distributions under nominal and accidental beam conditions, as well as the fatigue lifetime and cooling requirements. Prototyping of the cladded blocks has been carried out successfully. This contribution presents the final design, which employs advanced manufacturing methods to provide a sustainable and robust solution for the future ISOLDE beam dumps.

INTRODUCTION

The Isotope mass Separator On-Line (ISOLDE) facility at CERN produces a variety of Radioactive Ion Beams (RIB) for a comprehensive nuclear, medical and solid state physics program [1]. The ISOLDE Beam Dump Replacement and Sustainability (IBDRS) project aims to facilitate the increase of beam power (2.8 kW to 13 kW) at ISOLDE whilst mitigating existing concerns for radiation protection, with an improved life-cycle management [2, 3]. This is done by replacing the current beam dumps and increasing the surrounding shielding during CERN's Long Shutdown 3 (LS3, 2026-2028). Compared to the existing dumps installed in 1991, which consist of stacked steel blocks with no active cooling, the new beam dumps deploy Copper-Chromium-Zirconium (CuCr1Zr) and local water cooling for efficient heat extraction. To avoid corrosion-related issues like the observed corrosion at the n_TOF facility [4], erosion of copper in demineralised water [5], and radiolytic corrosion [6], the copper alloy is cladded with 316LN stainless steel.

* ida.zarei.johansen@cern.ch
† edouard.grenier-boley@cern.ch
‡ ana-paula.bernardes@cern.ch

Facility

Figure 1 depicts the overview of the two beam dumps for the General Purpose Separator (GPS), and the High Resolution Separator (HRS), in the post-LS3 configuration. The beam is supplied by the Proton Synchrotron Booster (PSB) through the PSB-to-ISOLDE (BTY) transfer line. The beam dumps are positioned 3 meters downstream from the RIB producing target. As opposed to the former beam dumps which had concrete shielding buried in soil, the new beam dumps will be surrounded by a steel shielding, with access from the top for interventions and endoscopy inspection.

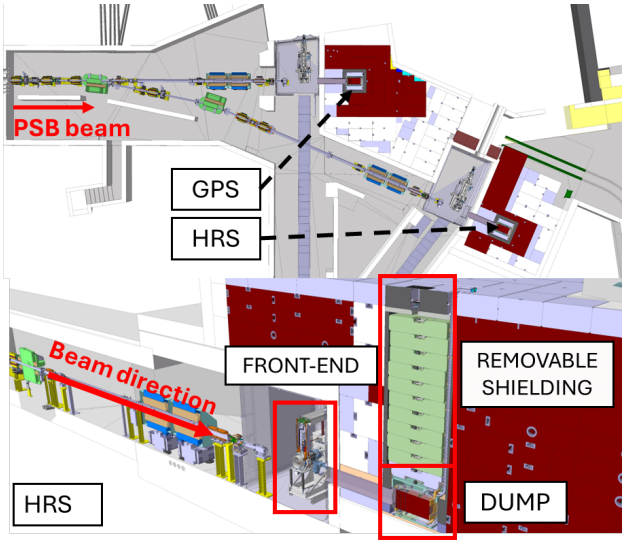

Figure 1: Overview of the ISOLDE complex depicting the HRS and GPS beam dump area and integration.

WATER-COOLED CUCR1ZR DUMP

The beam dump absorbers consist of 4 CuCr1Zr plates, of variables thicknesses, where the deposited energy density is highest, followed by a pure copper block. The cross section of the blocks is 420×420 mm^2 to sufficiently absorb the beam within its "stay-clear" region (+/-135 mm), with margin for initial alignment in the difficult to access area and no realignment until the end of the device's life. The combined length of the absorber blocks is limited to the material that needs active cooling (800 mm).

The dump core is enclosed within a 5 mm thick 316LN pressure vessel and is supported by stainless steel supports within the tank, designed to allow for thermal expansion. The material of the vessel is chosen due to its strength and

Content from this work may be used under the terms of the CC BY 4.0 licence (© 2026). Any distribution of this work must maintain attribution to the author(s), title of the work, publisher, and DOI.

ISBN: 978-3-95450-252-3 ISSN: 2673-5350 doi: 10.18429/JACoW-IPAC2026-MOP7136

UPGRADE OF THE SPS TARGET EXTERNAL DUMP FOR HIGH INTENSITY OPERATION IN CERN'S NORTH AREA

P. R. Menachilis†, N. Solieri, A. L. Lund, D. Grenier, M. Calviani, T. Coiffet, L.S. Esposito, M. A. Fraser, G. Garlaschelli, J-L. Grenard, A. P. Marcone, G. Mazzola, T. Parmentier, B. Pittet, F. Sanda, C. Sharp, M. Timmins, H. Vincke,
European Organization for Nuclear Research, Geneva, Switzerland

Abstract

As part of the consolidation of CERN's North Experimental Area (NA-CONS project), a dump located in the TT20 transfer line has been redesigned to comply with the higher beam intensities required for the future BDF/SHiP facility, and to improve its operational reliability. The new dump must be capable of dissipating up to 45 kW of steady-state power generated by the slow extraction of 400 GeV/c protons from the SPS under various operational scenarios. In addition, it shall also be able to withstand short, high-intensity pulses during machine development phases. Building upon proven design concepts implemented in the previous generation of SPS dumps [1,2], the dump core consists of graphite blocks clamped by actively cooled CuCr1Zr plates, and is enclosed by two shielding layers, steel and marble, for radiological protection. The design has been validated by performing beam-matter and thermo-mechanical simulations. A dedicated testbench was used to estimate the thermal contact conductance between materials and provide realistic values for the simulations. This contribution presents the main stages of this upgrade, from definition of updated beam parameters to conceptual design and validation.

INTRODUCTION

The Target External Dump (TED) is a movable dump/beam stopper located in the TT20 transfer line connecting the Super Proton Synchrotron (SPS) to the experimental areas of CERN's North Area. This device absorbs high-energy proton and ion beams during accesses, commissioning and machine development (MD) phases, when the slow extraction system is set up and optimized. The TED, mounted on rails transverse to the beam direction, is moved to the in-beam position during those phases, while remaining out of beam during normal beam operation. In view of the increased beam intensities foreseen for the Search for Hidden Particles (SHiP) experiment after Long Shutdown 3 (LS3), the existing TED approaches its thermo-mechanical limits [3]. While the commissioning scenarios are within the current TED's capabilities, the MD cases significantly exceed the allowed pulsed intensity. In addition to these thermomechanical limitations, the age of the existing device, installed in 1975, poses a challenge for its long-term reliability. A joint consolidation and upgrade was therefore required to maintain reliable absorption of steady-state power and to withstand short, intense pulses, while maintaining structural integrity and adequate radiation shielding [4]. The redesigned TED is based on updated beam requirements [5] and validated through analyses and dedicated thermal contact conductance measurements.

BEAM PARAMETERS

The beam parameters of the design-driving scenarios during post-LS3 operation are summarized in Table 1. Up to 45 kW of average power will be deposited on the TED during commissioning and MD phases. Higher intensity pulses are foreseen during MD, with intensities of up to 7×10^{13} protons per pulse for possible future operational modes. This increase in intensity will be compensated by increasing the duty cycle, thereby limiting the average power on the TED.

Table 1: Design Driving Beam Parameters [5]

Parameter	Commissioning [BDF/SHiP]	MD [Ultimate]
Energy per proton [GeV]	400	400
Pulse intensity [$\times10^{13}$]	0.5	7.0
Beam size sigma H [mm]	3.9	> 3.9
Beam size sigma V [mm]	1.5	> 1.5
Spill length [s]	1.0	1.0 – 9.6
Cycle length [s]	7.2	7.2
Repetition period [s]	7.2	~ 120
Average power [kW]	44	~ 40

UPGRADED TED

The new TED consists of a core assembly which is made of graphite and CuCr1Zr, encapsulated by two layers of radiation shielding, made of steel and marble respectively (Fig. 1). The overall design aims to combine efficient beam absorption with efficient heat extraction and adequate shielding of secondary radiation, while respecting the dimensional and integration constraints of the existing TT20 installation. Particular attention was given to preserving the external envelope and support interfaces of the current device, to limit modifications to the surrounding infrastructure.

† panagiotis.romanos.menachilis@cern.ch

Content from this work may be used under the terms of the CC BY 4.0 licence (© 2026). Any distribution of this work must maintain attribution to the author(s), title of the work, publisher, and DOI.

ISBN: 978-3-95450-252-3 ISSN: 2673-5350 doi: 10.18429/JACoW-IPAC2026-MOP7137

CONCEPTUAL COMPARISON OF LIQUID LEAD FLOW CONFIGURATIONS FOR A MUON COLLIDER TARGET

S. Candido *[1], R. F. Ximenes[1], M. Calviani [1], D. Calzolari[1],
J. Manczak[1], G. Lerner[1], A. Lechner[1], M. Tarantino[2],
C. Carrelli[2], L. Tricarico[2], G. Banks[1]
[1]CERN—European Laboratory for Particle Physics, CH-1211 Geneva, Switzerland
[2]ENEA – Agenzia nazionale per le nuove tecnologie, Brasimone, Italy

Abstract

Liquid lead is under investigation at CERN as a candidate material for a multi-MW class production target for a future Muon Collider. A free-surface curtain was initially proposed to decouple structural walls from beam-driven shock waves resulting from the high instantaneous energy deposition on the target material. However, later studies revealed that the large vertical extent required for this configuration limits the particle production efficiency, which motivated the development of a jet concept proposed in this work. Because the target operates within a 20 T solenoidal magnetic field, magnetohydrodynamic (MHD) effects are expected to influence the liquid-metal flow. Estimates indicate operation at low magnetic Reynolds numbers (between 0.2 and 0.3), where electromagnetic induction is weak but Lorentz forces can significantly affect flow stability and hydraulic performance. Both configurations are analysed using coupled multiphase computational fluid dynamics-magnetohydrodynamics (CFD-MHD) simulations in the quasi-static approximation to investigate current distribution, electromagnetic damping, and free-surface deformation. The comparison highlights the main physical trade-offs between the two concepts and defines the next optimisation steps for nozzle geometry and hydraulic load.

INTRODUCTION

A production target for a future Muon Collider facility must withstand high average power and extremely intense proton beams while operating in a harsh radiation and magnetic environment. In particular, the target system must dissipate multi-megawatt beam power while being located inside a strong solenoidal magnetic field used for the capture of secondary pions and muons. These conditions pose severe challenges for conventional solid targets in terms of thermal shock resistance, radiation damage, and heat removal [1].

Liquid metal targets offer an attractive alternative, as the flowing medium continuously removes the heat, can tolerate large instantaneous power densities and is not subjected to long-term fatigue nor radiation damage. Liquid lead (Pb) is a promising candidate due to its heat capacity and relatively low melting temperature. Similar concepts have previously been explored in high-power target experiments, notably the MERIT experiment, which demonstrated the feasibility of liquid mercury jets interacting with intense proton beams [2].

For the Muon Collider target currently under development at CERN, the baseline solution consists of an 80 cm long isostatic graphite rod, originally studied for a proton beam power of 1.5 MW [3]. An upgrade of the proton driver to 10 GeV and 4 MW is under consideration to improve collider performance [4]. Furthermore, the proton driver is expected to deliver proton pulses at 5 Hz, with bunch lengths of approximately 2 ns. At these beam parameters, the limitations of solid materials become increasingly critical, motivating the investigation of liquid metal target concepts.

Previous studies investigated the feasibility of a free-falling liquid lead curtain operating inside the strong magnetic field of approximately 20 T required for particle capture [5]. Multiphase MHD simulations showed that the interaction between the conductive liquid and the magnetic field can significantly alter the flow behaviour and induce instabilities [6].

Particle-matter interaction studies showed that a rod-like configuration increases the pion and positive muon yield by approximately 10%, and the negative muon yield by up to 40%, compared with the baseline graphite target, while curtain-like geometries tend to reduce the yield due to the larger material interception of secondary particles [7].

Building on these studies, the present work investigates two liquid lead flow configurations for a Muon Collider target: a free-falling curtain and a jet-like concept aimed at approaching the ideal rod interaction geometry. A schematic representation of the two concepts inside the Muon Collider target region is shown in Fig. 1.

PROBLEM DEFINITION

For the present conceptual analysis, the ideal pion production interaction region is approximated as a cylindrical rod of length and radius $(L_t, R_t) = (50.9, 1.5)$ cm, where L_t corresponds to approximately three nuclear interaction lengths [7]. The objective is to assess how two different flowing liquid-metal configurations can occupy this region while remaining hydraulically and magnetohydrodynamically stable. In both cases, argon is used as the cover gas due to its chemical compatibility with liquid lead and inert behavior at high temperature.

The first configuration corresponds to the free-falling curtain concept previously investigated in [6]. Liquid lead is injected through a rectangular inlet with a thickness of $W_i = 4$ cm and length $L_i = 50.9$ cm, with an inlet height of 4 cm to allow the flow to develop before reaching the

* silvio.candido@cern.ch

Content from this work may be used under the terms of the CC BY 4.0 licence (© 2026). Any distribution of this work must maintain attribution to the author(s), title of the work, publisher, and DOI.

ISBN: 978-3-95450-252-3 ISSN: 2673-5350 doi: 10.18429/JACoW-IPAC2026-MOP7138

TARGET COMPLEX DESIGN FOR A HIGH INTENSITY BEAM DUMP FACILITY IN THE NORTH EXPERIMENTAL AREA AT CERN

G. Humphreys*, J-L. Grenard†, C. Ahdida, G. Banks, T. Brouwer, M. Calviani, G. Dumont, C. D. Gutierrez, L. Esposito, M. Fraser, R. Jacobsson, L. Jorat, M. Liebsch, B. M. Sutil, C. Mucher, M. Parkin, A. P. Marcone, P. R. Menachilis, O. Pinto, R. Rinaldesi, D. Wasik, R.F. Ximenes,
European Organization for Nuclear Research (CERN), Geneva, Switzerland

Abstract

The Search for Hidden Particles (SHiP) is a new high-intensity fixed-target experiment to be located within the Experimental Cavern North 3 (ECN3) at CERN's North Area, utilising a 400 GeV proton beam from the SPS. The construction of a Beam Dump Facility (BDF) Target Complex is required for the successful operation of SHiP. It comprises an underground Target Station within the Tunnel Target Cave 8 (TCC8) cavern, upstream of ECN3, which will house a 1.5 m-long, 0.25 m-diameter HE-cooled tungsten target, and an above-ground service building that includes the target cooling systems, associated services, and waste package infrastructure. The required infrastructure to investigate target failures, including the cutting of spent targets and other CERN legacy waste in view of their packaging for disposal, has been studied. This contribution presents the current design status of the Target Complex, including radiation protection, remote handling, utilities and cooling/ventilation systems, installation and operation procedures, maintenance and decommissioning plans, and sustainability aspects.

INTRODUCTION

High-Intensity Experimental Cavern North 3 (HI-ECN3) is a project required for the operation of the new Search for Hidden Particles (SHiP) experiment looking for particles within the hidden sector [1]. The construction of the Beam Dump Facility (BDF) Target Complex is required as part of the HI-ECN3 project [2]. The new facility and experiment will be located in CERN's North Area and will receive a 400 GeV/c proton beam from the Super Proton Synchrotron (SPS) [3]. The beam will be fully absorbed by the BDF Target which has a 1.5 m-long, 0.25 m-diameter HE-cooled tungsten core [4]. A major part of the facility is the Target Complex, the development of this is detailed in this paper. An overview of the facility can be seen in Figure 1, with the red labels indicating what makes up the Target Complex.

TARGET COMPLEX

The Target Complex consists of the underground Target Station and Target Area, the access shaft, and Building 911 (B911). Additionally, a new surface-level service building will be constructed to support the operation of the Target Station. TCC8, ECN3, B911 and the access shaft are all existing infrastructure and will be used to bring all components for BDF and SHiP underground for installation. A more detailed view of the Target Complex can be seen in Figure 2.

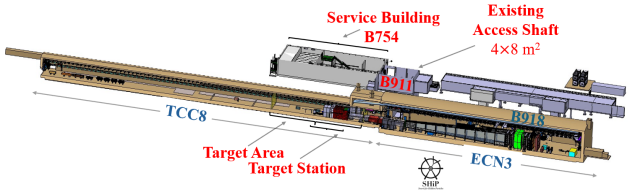

Figure 1: Overview of BDF/ SHiP Facility.

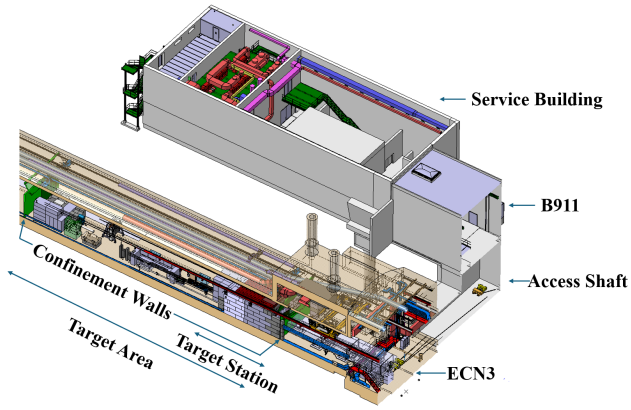

Figure 2: BDF Target Complex.

Target Area

Within the Target Complex is the Target Area, located 10 m underground in TCC8. The Target Area is defined by the surface between two ventilation confinement walls (Fig 2) and contains the Target Station, equipment for the first helium-cooling heat exchanger, the filter for the target helium-cooling, water-cooling cartridges of the proximity shielding, and the vacuum system for the vacuum vessel. Additionally, there is a space of around 400 m^2 upstream of the target, which will be used for the immediate storage of faulty components or during maintenance operations and target exchanges to place components of the Target Station to gain access within the system.

Target Station

The Target Station (Fig. 3) is located within the Target Area. It contains the BDF target alongside all relevant cooling, instrumentation, shielding, the magnetised hadron stop-

* gemma.stacey.humphreys@cern.ch
† jean-louis.grenard@cern.ch

Content from this work may be used under the terms of the CC BY 4.0 licence (© 2026). Any distribution of this work must maintain attribution to the author(s), title of the work, publisher, and DOI.

ISBN: 978-3-95450-252-3 ISSN: 2673-5350 doi: 10.18429/JACoW-IPAC2026-MOP7139

COMPARATIVE CONCEPTUAL DESIGNS OF LIQUID LEAD ABSORBERS FOR THE FCC-ee BEAMSTRAHLUNG DUMP

S. Candido *, [1], R. F. Ximenes[1], M. Calviani [1], R. Seidenbinder[1],
A. Perillo-Marcone[1], G. Lerner[1], A. Frasca[1], A. Lechner[1]
M. Tarantino[2], C. Carrelli[2], L. Tricarico[2], Louise Jorat[1], G. Banks[1]
[1]CERN - European Laboratory for Particle Physics, CH-1211 Geneva, Switzerland
[2]ENEA - Agenzia nazionale per le nuove tecnologie, Brasimone, Italy

Abstract

At CERN's Future Circular Collider (FCC-ee), the beamstrahlung photon beams produced at each interaction point carry several hundred kilowatts of power, requiring a reliable and thermally efficient absorber. Building upon an initial slope-based liquid-lead concept, this work investigates two improved configurations: 1) a double-slope geometry, designed to mitigate photon backscattering observed in earlier designs; and 2) an inclined slope section with an accumulation pool at the back, intended to maximize photon absorption, reduce system size, and ensure thermal and flow stability. Both concepts operate under an inert argon atmosphere and target an effective absorption thickness of 10–20 cm, with a liquid-lead mass flow rate of approximately 300 kg/s. Monte Carlo simulations are employed to compute photon energy deposition, while multiphase computational fluid dynamics (CFD) analyses characterize the coupled thermal and hydrodynamic behavior. The results compare the performance of the two configurations and identify key parameters for further optimization of the FCC-ee liquid-lead photon dump system.

INTRODUCTION

The proposed CERN Future Circular Collider (FCC) will initially operate as a high-luminosity electron–positron collider (FCC-ee) [1, 2]. During each bunch crossing, strong electromagnetic beam–beam interactions generate beamstrahlung (BS) radiation, producing two intense photon beams at every interaction point. At the Z pole, each beam carries an average power of approximately 370 kW [3], creating a significant power load that must be safely absorbed downstream of the collision region. Dedicated photon absorbers are required to dissipate this radiation while protecting accelerator components and ensuring stable collider operation.

Solid absorbers based on materials such as graphite face important limitations under these operating conditions due to temperature limitations, thermally-induced fatigue and radiation damage. Circulating heavy liquid metals offers an attractive alternative, as the flowing medium continuously renews the interaction region thus efficiently transporting heat away from the beam interaction zone, besides mitigating potential radiation damage and structural limitations of the absorber. Among candidate materials, liquid lead is particularly suitable due to its high density and atomic number, which provide efficient photon absorption, combined with a melting temperature compatible with operation at around 400 °C and high heat capacity [4, 5]. Furthermore, a flowing liquid absorber can tolerate temporary power excursions that may occur due to beam misalignments at the interaction point [6].

The beamstrahlung photons propagate in a narrow forward cone along the outgoing beam direction and are intercepted by the dump located approximately 500 m from the interaction point in order to maintain adequate separation from the circulating beams. Monte Carlo simulations using the FLUKA radiation transport code [7–10] indicate that a Pb absorber volume of approximately 70 cm×70 cm with an effective lead thickness of about $d_{\text{eff}} \approx 20$ cm is required to absorb most of the incident beamstrahlung power [11].

To achieve this effective interaction thickness while remaining within the hydraulic constraints of a circulating liquid-lead loop, different absorber geometries can be considered. Two candidate concepts investigated in this work are illustrated in Fig. 1.

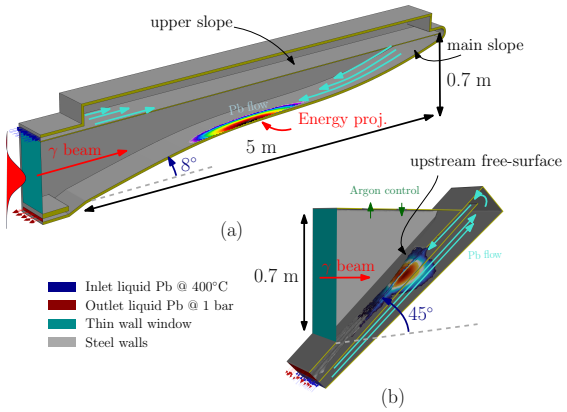

Figure 1: Conceptual layouts of the two liquid-lead absorber configurations considered for the FCC-ee beamstrahlung dump: (a) Double-Slope (DSlope) concept and (b) Compact Upstream Slope plus Pool (CUSP).

The first concept uses a sloped flowing lead layer to increase the effective photon path length inside the liquid without increasing the mass flow rate. A refined double-slope configuration is introduced to mitigate photon backscattering [12]. The second concept, referred to as the Compact Upstream Slope plus Pool (CUSP) [13], divides the absorption into two stages: a thin free-surface lead upstream flow

* silvio.candido@cern.ch

Content from this work may be used under the terms of the CC BY 4.0 licence (© 2026). Any distribution of this work must maintain attribution to the author(s), title of the work, publisher, and DOI.

ISBN: 978-3-95450-252-3 ISSN: 2673-5350 doi: 10.18429/JACoW-IPAC2026-MOP7140

TARGET DESIGN CONSIDERATIONS FOR LINAC-BASED ASTATINE-211 PRODUCTION

T. M. Mendonca[†,1], E. Benedetto[1], G. Dellepiane[1], P. Haas[2], A. Adilji[2], U. Amaldi[1]
[1]Tera-Care Foundation, Geneva, Switzerland
[2]Haute École du Paysage, d'Ingénierie et d'Architecture, Geneva, Switzerland

Abstract

Astatine-211 (^{211}At) is a highly promising radionuclide for targeted alpha therapy (TAT), yet its clinical adoption is limited by production constraints. ^{211}At is predominantly produced using cyclotrons, where beam currents rarely exceed a few hundred μA, thereby limiting achievable production yields. Linear accelerators (LINACs) offer an attractive alternative due to their potential for substantially higher beam currents, reduced irradiation times, and improved overall efficiency. To enable a reliable ^{211}At supply, the Tera-Care Foundation is developing a target system specifically engineered to withstand the power levels of the planned LINAC, which will directly irradiate bismuth targets. The initial analyses focus on estimating thermal loads, energy deposition, and temperature profiles to determine safe operating limits and prevent material degradation. This work establishes the foundational design framework needed to implement a reliable, high-power ^{211}At production system.

INTRODUCTION

Targeted alpha therapy (TAT) has emerged as a promising approach for cancer treatment, supported by encouraging clinical results [1, 2]. It combines α-emitting radionuclides with suitable targeting agents, such as antibodies or peptides, to deliver highly localized radiation over a range of only a few cell diameters. This localized dose deposition, resulting from the short path length and high linear energy transfer of the α-particles, makes TAT particularly attractive for treating small and disseminated tumours while limiting damage to healthy tissues.

Among the α-emitters considered for TAT, astatine-211 (^{211}At) is of particular interest because of its favourable decay properties, including a 7.2-hour half-life and α-particle emission suitable for therapeutic applications. ^{211}At is commonly produced through the ^{209}Bi(α,2n)^{211}At reaction by irradiating natural bismuth targets with α-particles. This route is typically implemented using cyclotrons; however, achievable yields are often constrained by the available beam currents, which commonly range from a few μA to a few hundred μA [3]. This limitation restricts the total activity produced per irradiation and remains a barrier to routine regional and large-scale clinical supply.

Linear accelerators (LINACs) offer a potential pathway toward increased ^{211}At production capacity, as they can operate at substantially higher beam currents than conventional cyclotrons. Higher beam currents may reduce irradiation time and improve production efficiency, but they also increase the deposited beam power in the target. Efficient heat removal and control of peak temperatures are therefore critical to maintaining target integrity and preventing material degradation during irradiation.

To address this challenge, the Tera-Care Foundation [4], a not-for-profit research organization based in Geneva, Switzerland, is developing a dedicated target system for high-power ^{211}At production using a LINAC, such as the one recently designed at CERN [5]. This activity is part of the CHeFS (Clinical Helium Facility for Switzerland) project that Tera-Care is promoting, based on the technologies developed by the NIMMS activities, led by CERN [5], which includes a LINAC-based infrastructure for medical applications and therapeutic radionuclide production. Within this project, high-current α-particle beams will directly irradiate bismuth targets, with the aim of improving the availability of ^{211}At for TAT. The target system must therefore be designed to withstand elevated beam power densities while maintaining acceptable operating temperatures.

This paper presents the initial design analysis of the proposed high-power ^{211}At production target. The study focuses on beam-induced energy deposition, thermal loading, and temperature profiles in the target assembly, providing a basis for defining safe operating conditions and guiding the future target design, cooling-system development, and experimental validation.

^{211}AT PRODUCTION TARGET SYSTEM CONCEPT

The production of ^{211}At from natural bismuth is based on the ^{209}Bi(α,2n)^{211}At reaction. The α-particle beam energy must be selected within a restricted energy window that favours ^{211}At production while limiting the competing ^{209}Bi(α,3n)^{210}At reaction, which produces ^{210}At and subsequently the long-lived radiotoxic ^{210}Po.

Production targets for ^{211}At commonly consist of a thin metallic bismuth layer deposited on a thermally conductive backing material, which provides mechanical support and the main heat-removal path during irradiation. For high-current pulsed LINAC operation, the target must withstand elevated volumetric power densities while maintaining the bismuth below its melting point of approximately 546 K. The design must also limit thermal gradients and cyclic stresses that may cause deformation, fatigue, or degradation of the thermal contact between the bismuth layer and the backing material.

† tania.melo.mendonca@gmail.com

Content from this work may be used under the terms of the CC BY 4.0 licence (© 2026). Any distribution of this work must maintain attribution to the author(s), title of the work, publisher, and DOI.

ISBN: 978-3-95450-252-3 ISSN: 2673-5350 doi: 10.18429/JACoW-IPAC2026-MOP7141

DEVELOPMENT OF A HIGH-TEMPERATURE ELECTRON BEAM TEST STAND FOR THERMAL STUDIES OF THE TATTOOS TARGET AT PSI

R. Martinie, R. Eichler, A. Ivanov, S. Jollet, D. Kiselev, M. Mostamand,
D. Reggiani, M. Sapinski, J. Snuverink, R. Sobbia, Ph. Spätig, S. Warren
Paul Scherrer Institute, Villigen, Switzerland

Abstract

The Targeted Alpha Tumor Therapy and Other Oncological Solutions (TATTOOS) facility at the Paul Scherrer Institute (PSI) will address the growing demand for medically relevant radionuclides using proton-induced spallation at the PSI High Intensity Proton Accelerator (HIPA). The target is designed to operate with a 100 µA - 590 MeV proton beam up to 2400 °C for 2 to 5 weeks. To study the thermal mechanisms critical for the target performance, a high-temperature test stand was developed based on a 60 keV, 100 mA electron beam welding machine. This setup allows heating tantalum foils in vacuum while investigating temperature distributions using a Gaussian beam profile with a rotating frequency up to 1000 Hz. We present here the static and rotating beam profile measurements using a 50 µm tungsten wire scanner moving up to 70 mm/s, with thermionic emission suppressed by voltage biasing. The differences in penetration and energy deposition between 590 MeV protons and 60 keV electrons are discussed to justify the use of electron beam heating as a surrogate for proton irradiation. Finally, preliminary temperature measurements under rotating beam conditions are presented, as well as a preliminary comparison with FEM simulations. Pyrometric measurements show that temperature oscillations remain below 10 °C at 100 Hz for an average temperature of 1715 °C, and preliminary FEM simulations show reasonable agreement with the measurements.

INTRODUCTION

The Targeted Alpha Tumor Therapy and Other Oncological Solutions (TATTOOS) facility [1] at the Paul Scherrer Institute (PSI) aims to produce radionuclides via proton-induced spallation using the PSI High Intensity Proton Accelerator (HIPA). The production scheme relies on the Isotope Separation On-Line (ISOL) technique [2]: a 100 µA, 590 MeV proton beam [3] impinges on a target heated to temperatures above 2000 °C through both beam power deposition and resistive heating. Neutral spallation products diffuse out of the target material, undergo molecular flow until they reach an ion source, where they are ionized, then accelerated to up to 65 keV, transported as a radioactive ion beam (RIB) and finally mass-separated. ISOL targets have been developed and operated at several facilities, including ISOLDE at CERN [4] and ISAC at TRIUMF [5]. Thermal management is a well-known challenge: temperature homogeneity, cold spots, and heat dissipation capacity directly impact isotope release and target lifetime. Building on this experience, the TATTOOS target baseline consists of thin tantalum foils (25-100 µm) stacked in a 20 cm long cylindrical tantalum container, with a total equivalent tantalum thickness of up to 10 cm.

Sustained operation at high temperatures induces thermal ageing mechanisms, such as grain growth, thermal grooving, sintering and creep, that degrade target performance over time. Since the target becomes highly activated during irradiation and requires costly heavy-handling procedures for exchange, extending the target lifetime is a key design objective. This demands a thorough understanding of the thermal environment and its long-term effects on the target materials. To study these thermal mechanisms under controlled conditions, a high-temperature test stand was developed based on the PSI electron beam welding machine. This setup allows heating tantalum samples in vacuum to the relevant temperatures. This article presents the beam characterization using a tungsten wire scanner, preliminary pyrometric temperature measurements under rotating beam conditions, and preliminary FEM validation.

PROTON VS ELECTRON BEAM DIFFERENCES

Differences between the operational (590 MeV protons) and experimental (60 keV electrons) beam-matter interactions require careful consideration. At 590 MeV, protons penetrate deep into tantalum with a Bragg peak at approximately 17 cm, well beyond the 10 cm equivalent tantalum thickness of the target. MCNP simulations yield between 200 and 300 W/mm in the TATTOOS target, depending on the geometry [6]. In contrast, 60 keV electrons penetrate only a few micrometers into tantalum: according to the ESTAR [7] CSDA (Continuous Slowing Down Approximation) range of 1.29×10^{-2} g/cm^2, electrons penetrate 7.75 µm in tantalum. The electron backscattering coefficient η_{BSE} at this energy is 50 % [8]. Therefore, the total electron beam power of 6 kW, reduces to approximately 3 kW after backscattering, delivers orders of magnitude more power to a single foil than under proton irradiation.

EXPERIMENTAL SETUP

Electron Beam Welding Machine

The electron beam welding machine at PSI operates at an energy E_{beam} of 60 keV with a maximum current I_{beam} of 100 mA. A magnetic focusing lens, controlled by the coil current I_{focus}, sets the beam size and a deflection coil steers the beam, enabling circular rotation patterns at frequencies up to 1 kHz. The work table can be displaced horizontally at speeds up to 70 mm/s.

This is a preprint - the final version is published with IOP

Content from this work may be used under the terms of the CC BY 4.0 licence (© 2026). Any distribution of this work must maintain attribution to the author(s), title of the work, publisher, and DOI.

ISBN: 978-3-95450-252-3 ISSN: 2673-5350 doi: 10.18429/JACoW-IPAC2026-MOP7142

THE CYREN PROJECT: REFURBISHMENT OF THE GANIL CYCLOTRONS FACILITY

P. Anger †, F. De Oliveira Santos
Grand Accélérateur National d'Ions Lourds, CEA-DRF/CNRS-IN2P3, Caen, France

Abstract

For over 40 years, the GANIL facility has been supplying stable beams (carbon to uranium, 60 keV/A to 95 MeV/A) and low- and high-energy radioactive ion beams for fundamental, applied and industrial research from a set of 5 cyclotrons.

Since 2010, the maintenance and refurbishment of the cyclotrons has been reduced to a bare minimum due to the SPIRAL2 construction and compliance work following the mandatory safety review from French safety authorities. Consequently, the failure rate has increased over the years.

The outlined exceptional scientific and industrial program presented by the users of the facility is requesting GANIL to guarantee its operation over the next 20 years or more. Therefore an ambitious renovation program, the CYREN (CYclotrons RENovation) project, was launched in 2024.

This article covers the progress of the project. It details the challenges encountered, which are partly due to the diversity of the different installations and their unique equipment. The project encompasses the five cyclotrons, beam lines, associated experimental caves, building infrastructure, technical utilities, and safety, security, and radiation protection systems.

INTRODUCTION

The GANIL cyclotron facility [1] delivers high-intensity stable beams up to uranium, as well as exotic nuclei produced via both in-flight fragmentation through the LISE separator and the ISOL (Isotope Separation On-Line) technique through the SPIRAL1 facility. Radioactive beams from SPIRAL1 can be used directly or re-accelerated while preserving high optical quality. The GANIL cyclotron facility, without SPIRAL2, is a multi-beam facility, capable of operating up to 4 simultaneous beams: IRRSUD, SME (medium energie), CSS high energy and CIME [2]. Figure 1 shows the cyclotrons facility with the associated experimental halls.

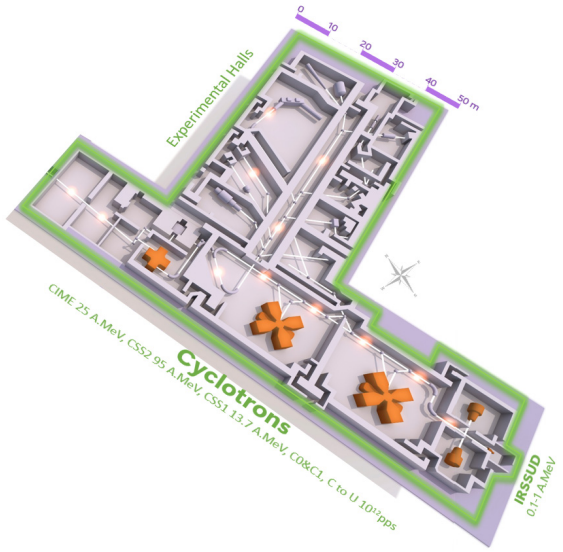

Figure 1: GANIL cyclotron facility.

CURRENT CONTEXT AND SCIENTIFIC OBJECTIVES

Since the start of its operation in 1983, GANIL has carried out regular refurbishment works on its equipment, enabling this research infrastructure to remain operational to this day. Since 2010, renovation work has been significantly reduced due to the redeployment of human and financial resources towards the construction of the SPIRAL2 facility and the implementation of the action plan resulting from the first safety review [3].

This minimal renovation and the aging of the facility, GANIL is now facing difficulties. It includes ther obsolescence of an ageing stock of equipment (some datesback to its construction), and difficulties to maintain and operate. The human resources required to handle the volume and complexity of repairs are becoming difficult to manage, posing a threat to the smooth operation of the cyclotrons. Figure 2 illustrates beam downtime trend. User satisfaction follows the same trend.

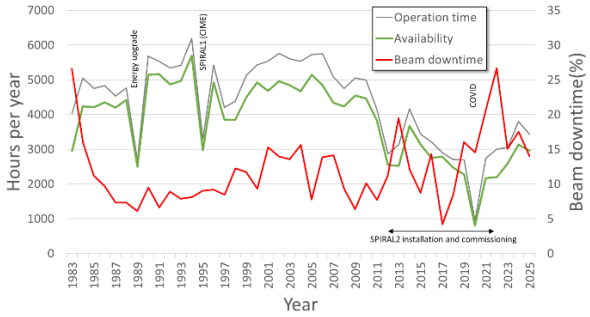

Figure 1: Cyclotrons beam availability and failure rate.

† pascal.anger@ganil.fr

Content from this work may be used under the terms of the CC BY 4.0 licence (© 2026). Any distribution of this work must maintain attribution to the author(s), title of the work, publisher, and DOI.

ISBN: 978-3-95450-252-3 ISSN: 2673-5350 doi: 10.18429/JACoW-IPAC2026-MOP7143

UPDATES ON THE SUSTAINABILITY IMPROVEMENTS OF THE KARLSRUHE RESEARCH ACCELERATOR

J. Gethmann*, E. Bruendermann, W. Mexner, T. Mexner, A.-S. Mueller, R. Ruprecht, B. Shen,
Karlsruhe Institute of Technology, Karlsruhe, Germany

Abstract

The thermal well system supporting the cooling plant of the Karlsruhe Research Accelerator (KARA) accelerator test facility at the Karlsruhe Institute of Technology (KIT) is in test operation after about one year of commissioning. To avoid any impact on the environment, follow the governmental regulations, and document different aspects and operation statistics, KIT developed a special robust and reliable data handling pipeline.

We describe the implementation of the data archiving strategy, as well as the experiences gained and statistics on, e. g. power reduction from the first year of commissioning of the thermal wells. Furthermore, our plans for improvement and extension of KARA efforts towards sustainable operation are presented.

INTRODUCTION

The Karlsruhe Research Accelerator (KARA) is operated by the Institute for Beam Physics and Technology (IBPT) at the Karlsruhe Institute of Technology (KIT). KARA is a 2.5 GeV electron synchrotron operated as a light source for up to 100 days a year in recent years and up to 50 days as a test facility for accelerator physics experiments. The latter are often carried out at energies of 1.3 GeV or 0.5 GeV.

Since last year, a new thermal well cooling plant is under commissioning which is described in more detail in [1]. The operation of the thermal well system must comply with legal regulations requiring continuous monitoring as well as monthly, annual, and multi-annual reports. To reduce operational complexity, all relevant limits, thresholds, and monitoring functionalities are integrated into a dedicated monitoring system. This allows cooling domain experts to document disturbances directly within the monitor interface, while automatically generated reports provide comprehensive documentation of the thermal well system's operation. On the other hand, the raw data is also interesting for accelerator physicists trying to optimize the energy efficiency of the overall system, so it should be accessible to them as well from within the internal machine networks. From an IT security perspective, it is desirable to segregate different domains and security-critical areas from one another in such a way that data can only flow out of security-critical areas, but no access to these areas is permitted. Finally, from an operational point of view, one wants to maintain as few additional systems as possible and make use of existing infrastructure.

After going into details of the data flow and archiving workflow, we present some results of the thermal well system with respect to our sustainability approaches and mention our ideas for future improvements therein.

EXISTING INFRASTRUCTURE AT KIT

KIT operates a central long-term data archiving service for research data [2]. This service stores data for at least ten years and is accessible from within the whole KIT via FTP. We use this service to store our reports we are obliged to create every month and year.

We obtain additional data from a campus-wide network of monitoring wells used for groundwater monitoring. These data are used to see the temperature changes in groundwater beyond the thermal well system's monitoring.

Existing Infrastructure at IBPT

Our accelerator control systems are based on EPICS [3]. Data of selected process variables are saved in a Cassandra database via a dedicated input output controller (IOC) as described in [4]. These controls are running in our machine internal networks and are only directly accessible from within the same networks. Data from our internal networks are published towards our institute network in read-only mode via an HTTP file service to obtain a minimal attack surface. Besides the general machine networks, there are further dedicated networks for IoT devices, like for Programmable Logic Controllers (PLCs), technical process and building controls. From there data can only flow outwards to one EPICS server, which is collecting the data.

DEVELOPMENT OF THE DATA FLOW

The data flows are depicted in Fig. 1. Here, the darker KIT green represents services that were operated before the commissioning of the thermal wells, light blue are the services developed for the thermal wells, and light green that were developed for the reporting tasks. The boxes match the different network locations quite well, except for the service node which is also running in the EPICS network.

The EPICS IOC pulls its data from the PLC based thermal well control system via OPC-UA. Another IOC polls the first IOC and writes the minutely averaged data to the file server. The first IOC is also polled by our archiving system which writes the raw data to a Cassandra database that is also accessible from the institute network via a gateway providing an REST-API. The extra storage of the data on the file server/data store is done to provide the data in the already aggregated way — minutely data as requested by regulations and in a simple CSV format following the KISS principle of software development.

* julian.gethmann@kit.edu

Content from this work may be used under the terms of the CC BY 4.0 licence (© 2026). Any distribution of this work must maintain attribution to the author(s), title of the work, publisher, and DOI.

ISBN: 978-3-95450-252-3 ISSN: 2673-5350 doi: 10.18429/JACoW-IPAC2026-MOP7144

ELETTRA 2.0 – STATUS OF THE REMOVAL & INSTALLATION ACTIVITIES

R. Visintini†, F. Barbo, A. Buonanno, B. Mazzucco, A. Savron, G. Simonetti
Elettra-Sincrotrone Trieste S.C.p.A., Trieste, Italy

Abstract

On July 2, 2025, at Elettra, we began the "Dark Period" (DP): the definitive shutdown of Elettra's Storage Ring (SR) with its auxiliary equipment and most of its beamlines. During the first phase of the DP, we removed the entire SR lattice structure with its associated cabling, piping, and supports. At the same time, the Service Area (SA), where most of the equipment for operating the SR was and will be located, was emptied to allow for infrastructure work and the subsequent installation of new racks and equipment. "On the other side of the wall," most of the photon beam lines are being reconfigured, upgraded, or installed, which involves several changes to the configuration of the SR tunnel's outer shielding wall. The paper describes the status of DP activities, the difficulties encountered, and the mitigation strategies adopted. Logistics plays an important role in this scenario, organizing the handling, transport, storage, and arrival times of materials, equipment, and instrumentation racks. This flow is bidirectional and includes both what is removed and disposed of and the parts to be installed, with a significant coexistence of old and new material.

INTRODUCTION

After the first "stored e-beam" occurred in October 1993, over the years, Elettra received several improvements, the most relevant of all was the installation of the booster-based full energy injector in 2008 and the subsequent start of Top-up operations in 2010 [1].

Elettra 2.0 is the upgrade project of the existing Elettra synchrotron light source (see, e. g. [2]) with the complete replacement of the Storage Ring (SR) with a new low-emittance ring and the enhancement of the beamlines either with the upgrade of existing ones or the installation of new ones.

"The Final Beam Dump" on July 2, 2025 ended the 31-year long career of Elettra, starting the removal phase of the old accelerator from SR and its ancillary systems in the Service Area (SA). The decommissioning of the SR, including the removal of the concrete supports of the magnets, was completed on December 5, 2025.

The installation phase of the accelerator will begin as soon as the construction company has completed the first two sections and handed them over to Elettra's teams (as of end of May 2026 at the time of writing).

The activities on the beamlines in the Experimental Hall (EH) of Elettra comprise the removal of some obsolete beamlines, including their shielding hutches, the upgrade of some beamlines that keep the same position in Elettra 2.0 and the installation of three new beamlines and associated hutches.

During the previous years we anticipated many activities on the beamlines and on the shielding wall of the Storage Ring [3, 4]. We also addressed several logistics aspects with focus on the handling and storing of the old parts from Elettra and the new ones for Elettra 2.0 [5]. The so-called "Main Building" houses the SA, the SR, and the EH, and is also undergoing significant plant engineering work.

STORAGE RING AND SERVICE AREA

Following the LOTO of the plants and systems and the radioprotection initial checks, we started to remove the ~ 400, 5-ton each, concrete slabs covering the SR tunnel (Fig. 1), exposing the ring for its removal (Fig. 2).



Figure 1: Slabs removal from SR roof.

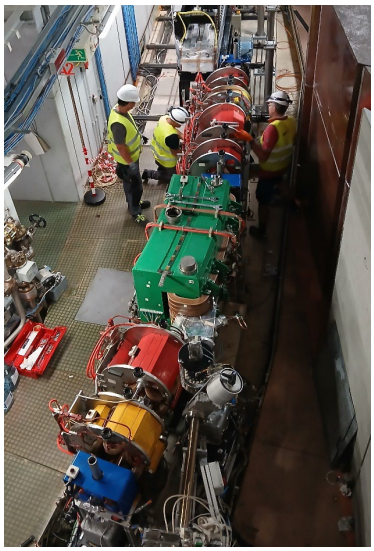

Figure 2: View of the SR (roof removed).

In parallel, in SA, after protecting the equipment to reuse and that had to stay *in situ*, with the support of an industrial demolition company, we completely removed all racks,

† roberto.visintini@elettra.eu

Content from this work may be used under the terms of the CC BY 4.0 licence (© 2026). Any distribution of this work must maintain attribution to the author(s), title of the work, publisher, and DOI.

ISBN: 978-3-95450-252-3 ISSN: 2673-5350 doi: 10.18429/JACoW-IPAC2026-MOP7145

EURO-LABS: INTEGRATING EUROPEAN RESEARCH INFRASTRUCTURES FOR PHYSICAL SCIENCES*

I. Efthymiopoulos†, CERN, Geneva, Switzerland; M. Colonna, P. Giacomelli, INFN, Italy;
M.J. Garcia Borje, CIEMAT, Spain; A. Maj, IFJ-PAN, Poland;
M. Mikuz, JSI, Slovenia; A. Navin, GANIL, France

Abstract

The European Laboratories for Accelerator Based Sciences (EURO-LABS) advances research frontiers by providing unified **Transnational Access (TNA)** to leading European Research Infrastructures (RIs) in the Physical Sciences. It brings together the nuclear physics, accelerator, and HEP detector R&D communities to foster collaboration and stimulate synergies. With 33 partners across Europe, EURO-LABS forms an integrated network of RIs ranging from small-scale test facilities to large European Strategy Forum on Research Infrastructures (ESFRI). The access provided enables research at the technological frontiers of accelerator and detector development, supporting the exploration of new physics concepts and opening new avenues in both fundamental and applied research — from optimizing reactor operation to mimicking stellar reactions. EURO-LABS actively promotes diversity and inclusion, offering broad and open access to researchers across nationalities, genders, ages, and career stages, while strengthening Europe's collaborative scientific landscape.

This contribution gives an overview of the project structure, the participating research infrastructures and access activities, together with highlights of the outcomes.

INTRODUCTION

EURO-LABS [1] is a pioneering European project aimed at building synergies and collaborations between the Research Infrastructures (RIs) of the Nuclear Physics (NP) and High-Energy Physics (HEP) communities. The project was established in response to a challenge of the Horizon Europe Programme [2], to bring together communities in the Physical Sciences domain, with the objective of providing wider, simplified, and more efficient access to leading research infrastructures across Europe. By offering transnational access free of charge, EURO-LABS enables researchers to conduct curiosity-driven research independently of their geographical location.

A central goal of the programme is to support breakthrough and frontier research by making advanced RI services available for access to a broader scientific community. For the first time, the Nuclear Physics and High-Energy Physics RI communities are brought together within a common framework, promoting harmonised services and a more efficient use of resources through the exploitation of complementarities and synergies. Additional objectives include fostering cross-disciplinary collaborations, enhancing the exchange of knowledge and technologies, and training a new generation of researchers to fully exploit advanced research infrastructures and equipment. The project also addresses the efficient management of transnational access procedures, including the implementation of FAIR data principles for the large volumes of data produced by the participating facilities.

RIS LANDSCAPE

EURO-LABS started in September 2022 and will run until August 2026. It brings together 33 partner institutions from 18 European and non-European countries, involving 45 leading RI facilities (Fig. 1).

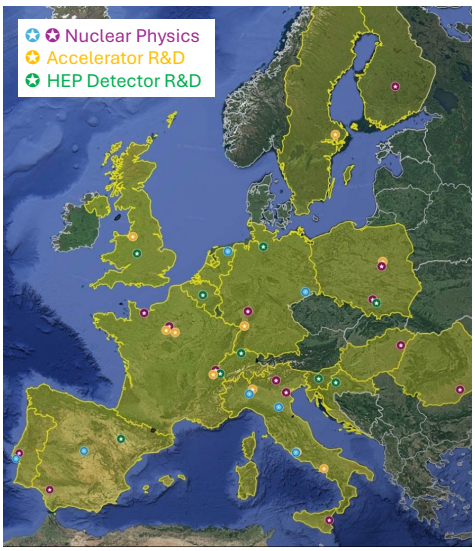

Figure 1: Map of EURO-LABS partner institutions and participating RIs across Europe. Associated-partner facilities in the US and Japan, are not shown here.

Nuclear Physics RIs

The Nuclear Physics RIs within EURO-LABS provide European and international users with TNA access to world-leading facilities delivering high-intensity stable ion beams, in some cases reaching the pμA range, covering isotopes from hydrogen to uranium. The broad EURO-LABS portofolio extends to facilities producing high-energy radioactive ion beams, nuclei not existing on Earth, using in-flight fragmentation techniques (of nano-sec lifetime). Post-accelerated radioactive ion beams (of msec half-time) using ISOL (Isotope Separation On-Line) methods offered for TNA access, as well as to neutron-beam facilities.

For the first time, EURO-LABS also introduced a **Virtual Access (VA)** scheme offering access to the European Centre

* EU Grant Agreement No 101057511
† Ilias.Efthymiopoulos@cern.ch

Content from this work may be used under the terms of the CC BY 4.0 licence (© 2026). Any distribution of this work must maintain attribution to the author(s), title of the work, publisher, and DOI.

ISBN: 978-3-95450-252-3 ISSN: 2673-5350 doi: 10.18429/JACoW-IPAC2026-MOP7146

UNIFYING EFFORTS IN ELECTRICAL SAFETY FOR AN ACCELERATOR COMPLEX

C. M. Schmitt†, A-L. Perrot, D. Ribiollet, G. Podoleanu, K. Zielinski, K. Papastergiou
CERN, Geneva, Switzerland

Content from this work may be used under the terms of the CC BY 4.0 licence (© 2026). Any distribution of this work must maintain attribution to the author(s), title of the work, publisher, and DOI.

Abstract

Large research facilities with continuously evolving electrical installations and many stakeholders often face unique challenges in implementing electrical safety. The Electrical Safety Project at CERN aims to standardize methods and processes to improve electrical risk management during maintenance and operation of the CERN accelerator complex. The project focuses on several axes for improvement. Two of these are to clearly define the limits of responsibility along the powering supply chain among different teams that provide equipment for accelerators, and to build the electrical dependencies between equipment from the source to the load. The paper will report on the progress made by the Electrical Safety Project in these fields and on the proposed methodology towards their long-term implementation.

INTRODUCTION

Effective electrical risk management relies on technical measures and on clearly defined organizational responsibilities. Ambiguity in equipment responsibility increases the risk of missed safety actions and unauthorized interventions. Both unclear responsibilities and misidentification due to inconsistent on-site labelling can lead to personnel performing interventions that they are not authorised to perform.

The need for improvement is highlighted by previously reported electrical incidents. In 2025, five incidents involving operational equipment related to accelerator systems were recorded: two were caused by unauthorized interventions (dismantling equipment belonging to another unit, intervening in electrical racks without authorization), and one resulted from incorrect equipment identification (disconnection of cables in the wrong rack). Implementing mitigation actions at CERN is challenging due to the scale of the accelerator complex, legacy infrastructure and operational coactivity: The CERN accelerator complex comprises a geographically distributed and highly interconnected network of accelerator rings, transfer lines, and experimental areas, resulting in a very large number of electrical equipment with complex dependency chains. These installations were designed and commissioned over several decades, meaning documentation standards vary significantly, and inherent information decay leads to gaps especially on older installations. CERN operates in a context of strong coactivity between different internal organisational units and external stakeholders – organisational complexity being a known risk factor for accidents [1]. The Electrical Distribution Network work package of the Electrical Safety Project aims to put in place the methodology for defining clear responsibilities along the different powering scenarios, ensuring on-site identification, and to develop and implement a system to keep up to date the electrical dependencies between equipment within CERN's electrical distribution network.

This paper presents the methodology, the outcome of pilot tests carried out in field and the path towards implementation for these goals.

METHODOLOGY

Context within CERN

The scope covers equipment of the Accelerator Technology Sector (ATS) with potential electrical risk to people, excluding the power distribution grid. Extra low voltage (<50 V RMS AC or 120 V DC) connections are thus only considered when additional safety risks are present.

For achieving its goals, the work package closely collaborates with stakeholders across the organisation: Notably, Health and Safety experts provide input in defining roles and ensuring compatibility with internal and external safety practices. Specialists in the CERN digital infrastructure facilitate data storage in the electronic asset management (EAM) database and implement user interfaces to visualize and let users interact with the data. These relations are shown in the Fig. 1 below.

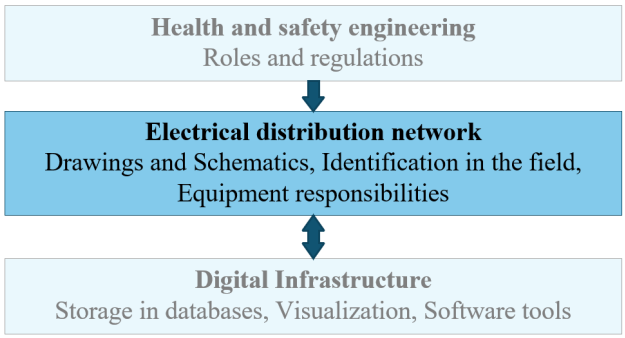

Figure 1: Context within the CERN.

Terminology

Two key roles were identified as critical for the clear identification of responsibility along the powering chain.

The Equipment Owner (EOw) is defined as the organisational unit responsible for the overall safety of their electrical equipment.

The Equipment Operator (EOp) is defined as the person (typically from within the Equipment Owner unit) trained on the equipment and its operation in the machine, who serves as a contact-person for facility coordinators, electrical safety teams, works and services supervisors (WSS) and other stakeholders, for matters related to electrical safety of their equipment. They maintain the relevant

ISBN: 978-3-95450-252-3 ISSN: 2673-5350 doi: 10.18429/JACoW-IPAC2026-MOP7147

INFRASTRUCTURE WORKSITE COORDINATION LESSONS LEARNED FROM THE HL-LHC CASE STUDY

T. Bauler, M. Bonnet, H. de Maynard
CERN, Geneva, Switzerland

Abstract

The High-Luminosity Large Hadron Collider (HL-LHC) project at CERN is a major upgrade LHC's today instantaneous luminosity by a factor of five and today total integrated luminosity by ten. This involves extensive new infrastructure, including underground galleries, access shafts, and surface facilities, pushing accelerator technology beyond current limits. Managing this complexity requires centralized coordination through a worksite hub that enables real-time communication, adaptive planning, and stakeholder support from conception to commissioning. A combined top-down and bottom-up planning approach ensures alignment with long-term objectives while addressing operational challenges. Dedicated planning tools support milestone tracking, resource management, and coordination of activities. Operational efficiency relies on safety, schedule adherence, and rapid response to technical issues. This paper highlights the importance of flexible on-site coordination, integrated planning, and advanced monitoring tools for large-scale projects. The approach demonstrates strong adaptability, reactivity, and collaborative problem-solving.

INTRODUCTION

The Large Hadron Collider (LHC), one of the most complex scientific instruments ever constructed, requires a major upgrade to sustain and enhance its discovery potential. This upgrade aims to increase the LHC's instantaneous luminosity by a factor of five and its integrated luminosity by a factor of ten beyond original specifications. Given the LHC's high complexity, the upgrade demands meticulous planning and spans over a decade. The High-Luminosity LHC (HL-LHC) represents a significant advancement in accelerator technology. Its technical infrastructure includes civil engineering, electrical distribution, cooling and ventilation, access and alarm systems, technical monitoring, transport and logistics, storage, and operational safety. Key civil engineering elements include access shafts, underground galleries (distinct from the LHC tunnel), and surface buildings for compressors, ventilation equipment, electrical systems, and storage tanks for helium and nitrogen. Construction is divided between two experimental sites: Point 1 (for the ATLAS experiment) and Point 5 (for the CMS experiment). At each site, the underground work comprises a shaft, a cavern, a power converter gallery, service galleries, safety galleries, and vertical cores connecting the new infrastructure to the existing LHC (see Fig. 1) [1].

At CERN, accelerator coordination is managed by the Accelerator Coordination and Engineering group. For the case studies presented here, coordination involved two Facility Coordinators and one Safety Coordinator (*Coordination Sécurité et Protection de la Santé*, CSPS). The Facility Coordinators oversee co-activity management, short- and long-term scheduling, and serve as primary liaisons for stakeholders. Due to the high volume of working hours (Category 1), a Safety Coordinator is required to manage risks arising from interactions between tunnel maintenance and HL-LHC activities. The CSPS ensures compliance with safety best practices, reports on new activities, and provides expert guidance. All activities require approval from both coordinators before initiation.

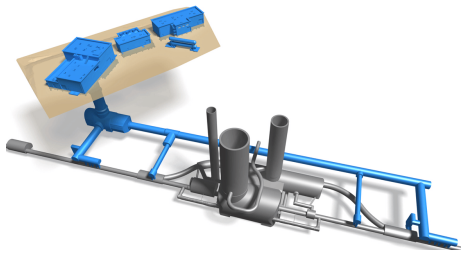

Figure 1: Overview of the HL-LHC infrastructure shown in blue. The existing LHC facility is shown in gray.

COORDINATION CHALLENGES OF THE VERTICAL SHAFTS

Two case studies illustrate the coordination challenges encountered during the HL-LHC infrastructure phase. The project involves constructing surface buildings, along with new underground galleries located approximately 75 meters below. The shaft, serving as the sole access point to the underground, is a critical component of the project's infrastructure. Its central role in the critical path necessitated dedicated coordination efforts to address the challenges its installation posed.

Non-Conformity Within Shaft Commissioning

The first case study examines a non-conformity during the commissioning of the shaft at Point 1. After completing the civil engineering work, the lift installation began. However, concrete debris falling during commissioning disrupted the process, threatening to delay infrastructure installation in the galleries. Given the shaft's critical role, both as a worker access point and a material delivery route, the initial plan to complete lift installation at Point 1 before moving to Point 5 would have caused cascading delays. The coordination team proposed a revised schedule to prioritize Point 5 despite the delay at Point 1, minimizing the overall project delay from 9 months to 3.5 months. A dedicated coordination team was subsequently established to supervise on-site activities and

Content from this work may be used under the terms of the CC BY 4.0 licence (© 2026). Any distribution of this work must maintain attribution to the author(s), title of the work, publisher, and DOI.

ISBN: 978-3-95450-252-3 ISSN: 2673-5350 doi: 10.18429/JACoW-IPAC2026-MOP7148

DEGASSING OF DISTILLED WATER-COOLING CIRCUITS AND AFFECTED COPPER-WALLED STRUCTURES

R.P. Kan*[1], R. Eichler[1,2] and A. Weber[1]
[1] PSI Center for Accelerator Science and Engineering, Villigen, Switzerland
[2]University of Bern, Bern, Switzerland

Abstract

Cooling circuits running with distilled water to cool copper structures like magnets or cooling plates are vulnerable to air leaking in. The leaked-in air contains carbon dioxide that lowers the pH from 7 to quite acidic distilled water and makes it possible for the intruded oxygen to react with the surface of the copper tubing, forming copper oxides that can grow and mechanically be displaced to clog in locations where the flowrate is low. The process also reduces the wall thickness of the tubing, eventually followed by water leakage. Regular unclogging causes the circuit to be opened more often and therefore accelerating the destructive process. A good solution to this problem comes with a steep price: Degassing by reverse osmosis in every copper cooling circuit.

PURE WATER TURNING ACIDIC

A Troublesome Copper Cooling Circuit at the Paul Scherrer Institute

Between 2000 and 2005, several water-cooled magnets like in Figure 5 overheated. A muddy residue caused the cooling water not to flow properly. Flushing the lines resulted in even faster interruptions and more residues as can be seen Fig. 1. An investigation, by the responsible beamline scientist and the leader of the magnet group, resulted in a report[1] on the influence of the dissolution of oxygen and carbon dioxide in distilled water, causing acidic conditions (regime 5 of Fig. 6 due to CO_2) and the steady ablation of the interior of copper coils / tubes (due to O_2).

Ongoing Chemistry at the Surface

The corrosion mechanism is illustrated in Figure 4. Oxygen (O_2) and carbon dioxide (CO_2) are always present in water due to interaction with the atmosphere. No water-cooling system stays vacuum tight. Atmospheric gases can enter the cooling system through tiny leaks and diffusion through non-metallic tubing. The presence of CO_2 in the water results in the formation of carbonic acid (H_2CO_3), which dissociates into HCO_3^- and H+-ions. This acidity fixes the pH of the coolant between 5 and 6. Oxygen dissolves in water increasing the redox potential. The cuprous oxide Cu_2O (reddish in colour like in Fig. 2) is initially formed at the surface. Upon further oxidation by dissolved oxygen CuO (blackish in colour as in Fig. 3) forms. In the absence of other influences this stable surface, non-soluble in water at these pH-levels, would render this surface stable to further corrosion. However, the mechanical stress from the coolant flow removes this oxide layer as a solid, leaving the metal surface unprotected again to the oxygen-rich acidic water. This leads to further dissolution of the metal (eventually leaks) and macroscopic slug formation.

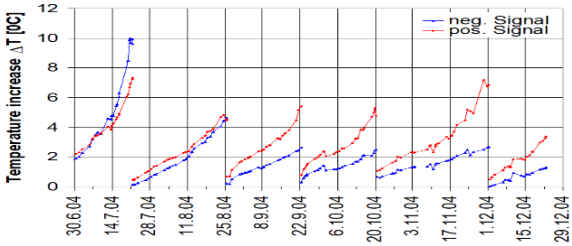

Figure 1: The measured temperatures of a quadrupole magnet in a regular pattern of temperature increases ΔT due two parallel cooling circuits clogging, then recovering after flushing the deposition products out of the magnet [1].



Figure 2: Accumulations of corrosion sludge (ø6 mm), consisting of CuO and/or Cu_2O, from behind a flow restrictor. A Swiss 50 centime coin is shown in the background [1].

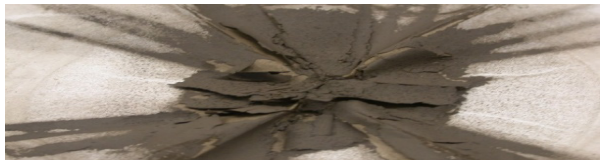

Figure 3: Filtrated deposits of various copper oxides. The pore size of the filter is 12 µm. The dry weight of the residue is 0.72 g [1].

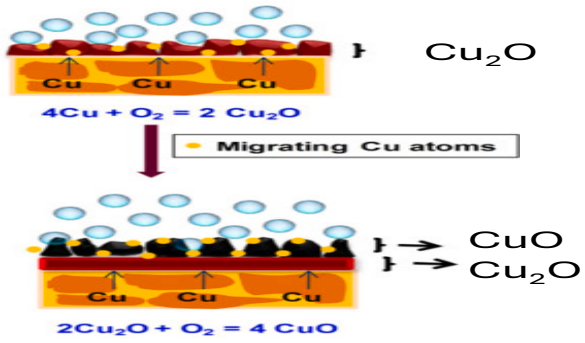

Figure 4: Corrosion mechanism at a copper surface due to dissolved O_2 and CO_2 in distilled water [2]. Even small air leaks promote water leakage and obstructive corrosion.

*Richard.Kan@psi.ch

Content from this work may be used under the terms of the CC BY 4.0 licence (© 2026). Any distribution of this work must maintain attribution to the author(s), title of the work, publisher, and DOI.

ISBN: 978-3-95450-252-3 ISSN: 2673-5350 doi: 10.18429/JACoW-IPAC2026-MOP7150

MODELLING AND EXPERIMENTAL STUDIES OF A X-BAND WINDOW FOR MOBILE LINACS*

Y. Rozier†, Epsyl, Pertuis, France
M. Boucard, AVELION, Peynier, France

Abstract

Radio-frequency (RF) windows are sensitive components that ensure both RF power transmission and vacuum integrity in linear accelerators (LINACs). In the X-band frequency, improving reliability is critical for compact LINAC systems, including application in non-destructive testing and medical technologies.

This study presents an RF window designed for operation at 9.3 GHz with a 2.0 MW peak-power design target. This window is optimised to reduce peak electric field at the ceramic–metal brazed interface while preserving low insertion loss and broad bandwidth. Coupled RF–fluidic–thermal simulations guided an extended cylindrical pillbox design exploiting the TE_{112} mode.

A prototype has been fabricated, and low-power RF measurements have been carried out to validate both the design and manufacturing process. RF simulations and low-power tests show insertion losses below 0.1 dB and a standing-wave ratio lower than 1.05 at 9.3 GHz. High-power endurance tests carried out on the prototype demonstrated stable behaviour.

Results of the engineering design will be compared with tests and discussed.

INTRODUCTION

High-gradient X-band LINACs require robust and low-loss RF windows that reliably transmit high peak power while ensuring vacuum integrity. The main design objectives are therefore to suppress unwanted mode conversion, avoid resonant ghost modes and, minimize peak electric field in the designed component. Achieving these goals demands solutions that go beyond a simple pill-box design [1] for field considerations. Integration of iris in waveguide [2], progressive taper [3] or over-sized dimensions [4] approaches leads to dimensional constraints on the final system. Mixed-mode designs [5, 6] have also been reported in the literature.

The RF window presented in this study is designed to operate at a peak power level of 2.0 MW with a pulse duration of 5 µs. The technical requirements are further constrained by the need to minimize heating of the component and running in an ultra-high vacuum ($P < 5 \times 10^{-9}$ mbar). The full set of specifications for this window developed for our new accelerator section [7] is provided in Table 1.

The simultaneous requirements of mechanical compactness and ultra-high vacuum operation in the LINAC impose significant design constraints. In particular, the reduction of the RF field must be achieved without compromising insertion loss or bandwidth performance. Given the limited availability of commercial devices operating near the target frequency of $f_C = 9.3$ GHz, the development of a dedicated solution is therefore required to meet these specifications.

Table 1: RF window specification

Item	Value	Unit
Central frequency f_C	9.3	GHz
RF peak power	2.0	MW
RF average power	1.6	kW
RF bandwidth	> 50	MHz
Reflection S_{ii}	< −19.1	dB
Transmission S_{ij}	< 0.2	dB
Pressure withstanding	3.0	bar abs.

ENGINEERING DESIGN

Process Considerations

The RF window includes a customised choke with a DN40CF vacuum flange on the LINAC side and a WR90 square cover flange on the external side. The component is manufactured using a two-stage brazed approach. A 97.6 % vacuum grade Al_2O_3 (AL300®, Morgan Advanced Ceramics) has been used for this purpose. Its relative permittivity is 9.04 at 8.5 GHz, which is consistent with the operating frequency range. During assembly, particular attention is given to the alignment of both flanges (< 1.0 ° deviation) to minimise the contribution of a ghost mode at 8.895 GHz. The manufacturing drawing of the RF window is shown in Fig. 1. Cooling pipes (not shown here) are subsequently integrated with tailored orientations and terminations to comply with the environmental and operational constraints of the complete system.

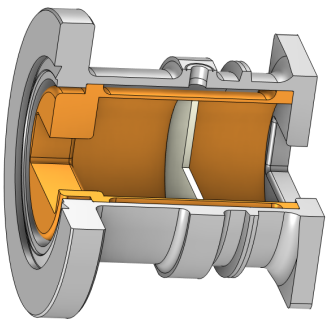

Figure 1: Mechanical design of the RF window.

* This work was supported by a grant from the French Public Investment Bank (Bpifrance) as part of the France 2030 program.

† yrozier@avelion-alcen.com

Content from this work may be used under the terms of the CC BY 4.0 licence (© 2026). Any distribution of this work must maintain attribution to the author(s), title of the work, publisher, and DOI.

ISBN: 978-3-95450-252-3 ISSN: 2673-5350 doi: 10.18429/JACoW-IPAC2026-MOP7151

CHALLENGES IN THE DEVELOPMENT OF THE SIS100 ELECTROSTATIC EXTRACTION SYSTEM

M. Petryk†, GSI Helmholtz Centre for Heavy Ion Research, Darmstadt, Germany

Abstract

The "Facility for Antiproton and Ion Research" (FAIR) is a new international accelerator complex, which is currently built in Darmstadt, Germany. Part of this complex is the SIS100 heavy ion synchrotron with a circumference of ~1086 m. One of the extraction systems is the electrostatic septum. This septum was built by Danfysik. It is operating with voltages up to 180 kV. The requirements on the vacuum quality (low 10e-11 mbar region) combined with voluminous chambers (in total ~6m long), the reproducibility and precision of the applied voltage as well the mechanical stability and exact positioning even after bakeout cycles up to 300 °C have been the biggest challenges on this project. Specifications on rise and fall times for the high voltage implies the need of a bleeder resistor, used for improved voltage accuracy, too. During this project numerous problems had to been solved to end up with a stable system. The results of the tests and lessons learned are presented.

SYSTEM OVERVIEW

The electrostatic septum (Fig. 1) is a device for so called slow extraction of the ion beam from the ring accelerator.

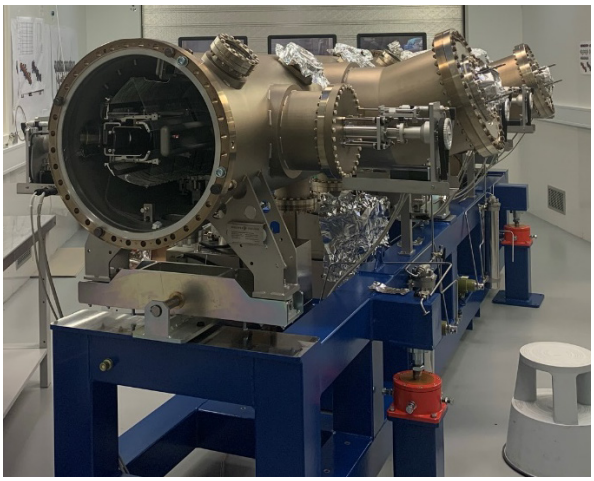

Figure 1: The SIS100 Extraction Septum currently build at DanFysik [1] in Denmark

During extraction most of the particle beam circulates undisturbed through the septum, a small fraction of the beam reaches the region between anode wires and cathode.

The high electric field leads to a deflection (Fig. 2), magnified by following quadrupole magnets and can be extracted out of the ring by a magnetic septum.

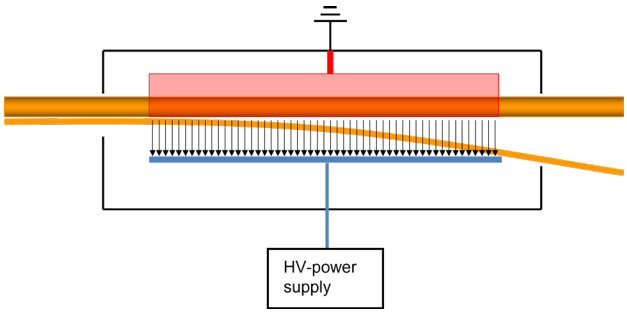

Figure 2: Deflection of part of the beam.

To achieve the required deflection angle, a high voltage between -5 kV and -180 kV is used. Due to the required length, two electrode systems of 2.5 m length each are used in this septum. Protection resistors (Fig. 3) are used to absorb the energy stored in the cables in case of a flashover. This prevents severe damage of the electrodes. Both electrode systems are supplied with the same voltage, a T-shaped resistor is used to absorb the power of the long cable between HV power supply and the device in the ring tunnel.

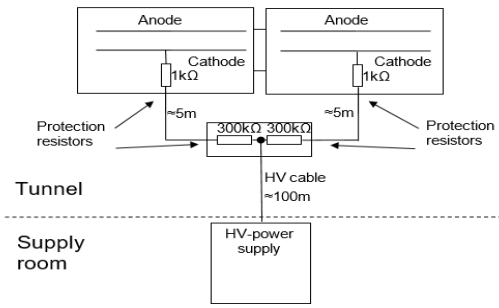

Figure 3: Protection resistor system for electrode and wires.

The high precession positioning of the electrodes is realized by eight stepper motors.

The intensity of the beam can destroy the anode wires if the beam parameters are chosen wrong. To reduce the damage, broken wire detection in multiple independent sections rises an alarm and switch of the accelerator immediately.

NEG-Modules have to build into the chambers to reach the required vacuum quality. The area between the electrodes is protected by a screen from the dust of the NEG modules mounted above.

† m.petryk@gsi.de

Content from this work may be used under the terms of the CC BY 4.0 licence (© 2026). Any distribution of this work must maintain attribution to the author(s), title of the work, publisher, and DOI.

ISBN: 978-3-95450-252-3 ISSN: 2673-5350 doi: 10.18429/JACoW-IPAC2026-MOP7152

DEVELOPMENT OF A GUANELLA-TYPE 4:1 IMPEDANCE TRANSFORMER FOR THE FUTURE SIS100 BROADBAND CAVITY SYSTEMS

C. J. Wegmann*,[1], H. Klingbeil[1,2], R. Balß[2], M. Frey[2], U. Laier[2], S. Orth[2]
[1]Technical University Darmstadt, Darmstadt, Germany
[2]GSI Helmholtzzentrum für Schwerionenforschung GmbH, Darmstadt, Germany

Abstract

The SIS100 heavy-ion synchrotron under construction at GSI/FAIR will contain a total of 4 broadband cavities for barrier bucket and longitudinal feedback operation. These need to generate non-harmonic gap voltages with relevant spectral components in a range from 100 kHz to 15 MHz. Previous analyses showed that the input capacitance of the tetrode amplifier limits the cavity's upper cutoff frequency. To counteract this effect, the load impedance at the input of the tetrode amplifier shall be reduced from 50 Ω to 12.5 Ω at the expense of more driver amplifier power. In this case, achieving an impedance matching to the driver amplifier necessitates the inclusion of a transformer generating a broadband 4:1 impedance transformation over the entire relevant frequency range. A Guanella-type 4:1 ferrite transmission line transformer meeting these requirements was developed, built, and verified by measurement.

INTRODUCTION

The SIS100 heavy-ion synchrotron currently under construction at GSI/FAIR will contain 4 broadband RF cavities for barrier bucket and longitudinal feedback operation [1–3]. These are magnetic alloy / MA-loaded RF cavities (see e.g., Ref. [4]) excited by high-power RF tetrode amplifiers. For the considered types of operation, non-harmonic gap signals with relevant frequency components between 100 kHz and 15 MHz need to be induced.

The tetrode's control grid input, fed by a DC-bias and an RF driver amplifier [5] connected via a LCF12 line [6] of about 100 m length, represents a capacitance of about 800 pF to 1000 pF in parallel to the resistive load. While techniques directly improving the signal quality of the gap voltage are planned – e.g. predistortion [2, 7] – a bottleneck due to impedance mismatching needs to be prevented. One possibility is the inclusion of a transformer allowing for the reduction of the load impedance at the cost of increased driver power as shown in Fig. 1. A secondary-side transmission line with characteristic impedance $Z_L = 25\,\Omega$ and length $l = 1$ m is used to further improve impedance matching. This paper discusses the design of a 4:1 Guanella-type impedance transformer [8] suitable for the considered frequency range and power level (2 kW to 3 kW).

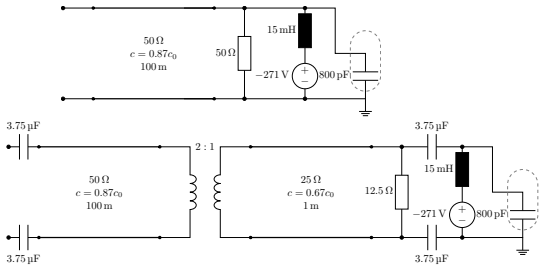

Figure 1: Control grid circuit without (upper diagram) and with 4:1 impedance transformer (lower diagram, voltage ratio 2:1).

BASIC OPERATING PRINCIPLE

Figure 2 shows the circuit diagram of the Guanella-type 4:1 impedance transformer. It features two transmission lines connected in series on the input side and in parallel on the output side [8]. Hence, the input voltage is split over the

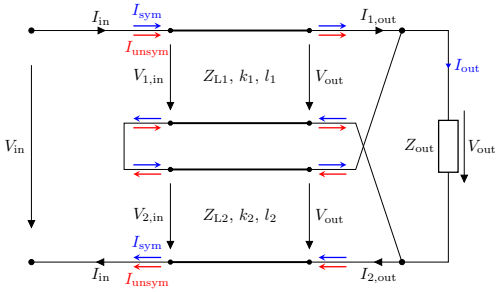

Figure 2: Equivalent circuit of the 4:1 Guanella-type transmission line transformer with symmetrical and unsymmetrical current components [8, 9].

two lines on the primary side while on the secondary side the currents carried by the two lines are added. Since all terminals are connected with each other by DC short circuits, capacitive DC blocks are included in Fig. 1. Assuming exactly equal and opposite (symmetrical) currents carried by the conductors of each line and identical transmission lines with $Z_{L1} = Z_{L2} = Z_L$, $k_1 = k_2 = k$ and $l_1 = l_2 = l$, circuit analysis using standard transmission line equations [10–12] leads to an impedance transformation according to

$$Z_{in} = 4Z_{out}\frac{1 + jt\frac{Z_L}{2Z_{out}}}{1 + jt\frac{2Z_{out}}{Z_L}}, \quad t = \tan(kl)\ . \tag{1}$$

With the matching condition $Z_L = 2Z_{out}$, Eq. (1) yields an ideal impedance transformation

$$Z_{in} = 4Z_{out}. \tag{2}$$

* julien.wegmann@tu-darmstadt.de

This is a preprint - the final version is published with IOP

Content from this work may be used under the terms of the CC BY 4.0 licence (© 2026). Any distribution of this work must maintain attribution to the author(s), title of the work, publisher, and DOI.

ISBN: 978-3-95450-252-3 ISSN: 2673-5350 doi: 10.18429/JACoW-IPAC2026-MOP7153

RF WINDOW Ti COATING CHARACTERIZATION

M. Campostrini[†,1], L. Bellan[1], F. Grespan[1], C. Roncolato[1], M. Taborelli[2], W. Vollenberg[2],
[1]Istituto Nazionale di Fisica Nucleare, Laboratori Nazionali di Legnaro, Legnaro, Italy
[2]CERN, Geneva, Switzerland

Abstract

Thin titanium coatings were deposited on alumina RF windows at CERN to reduce the secondary electron emission yield. The deposition process was optimized to ensure uniform coverage of the components used in high-power RF systems. Witness samples were characterized to assess their suitability for accelerator applications. Surface resistivity was measured under controlled conditions, while the Secondary Electron Yield was evaluated to determine the effectiveness of the coating in reducing electron emission. Thickness uniformity was characterized through detailed mapping using Rutherford Backscattering Spectrometry at the Laboratori Nazionali di Legnaro, providing spatially resolved information on deposition homogeneity and confirming process reproducibility. These results provide a comprehensive overview of the properties of the titanium coatings and serve as a useful reference for optimizing surface treatments of RF windows in accelerator facilities.

INTRODUCTION

Alumina radio-frequency (RF) windows are a key component in high-power accelerator systems, owing to their excellent dielectric properties, compatibility with ultra-high vacuum (UHV) environments, and robust thermo-mechanical stability. Despite these advantages, their performance can be adversely affected under high electromagnetic field intensities, where ceramic surfaces may trigger electron multiplication phenomena such as multipactor discharge and electron loading. These effects can lead to significant limitations in RF performance and long-term component reliability [1, 2].

The occurrence of such phenomena is strongly dependent on the Secondary Electron Yield (SEY) of the material surface. Alumina is known to exhibit relatively high SEY values, making it particularly susceptible to multipactor effects. The development of effective surface treatments aimed at reducing secondary electron emission is therefore of primary importance for accelerator applications. Among the various mitigation strategies explored, the deposition of thin conductive coatings with intrinsically low SEY has emerged as a viable and effective solution, capable of mitigating multipactor while preserving acceptable RF transparency and performance [1, 3].

Titanium is considered a promising candidate for this purpose, as it combines moderate electrical conductivity, relatively low SEY, good compatibility with UHV conditions, and high chemical stability. The use of thin-film coatings also allows for the reduction of surface charging effects without significantly compromising the electromagnetic properties of the RF window [3].

Thin-film coatings have demonstrated effectiveness in reducing SEY and suppressing multipactor on ceramic substrates, with sputter-deposited films providing significant improvements on alumina surfaces. Conductive coatings have also been employed to mitigate electron cloud effects and secondary emission phenomena in RF structures [4].

In this context, the present work investigates the thickness uniformity and compositional consistency of thin titanium coatings deposited on alumina RF windows at CERN. Witness samples were characterized by means of surface resistivity measurements, Secondary Electron Yield (SEY) analysis, and Rutherford Backscattering Spectrometry (RBS) mapping at the Laboratori Nazionali di Legnaro. The objective is to assess coating uniformity, reproducibility, and overall suitability for RF accelerator applications.

COATING DEPOSITION SYSTEM

The titanium deposition on alumina (Al_2O_3) RF windows, developed at CERN, is carried out in a dedicated coating facility consisting of a cylindrical vacuum chamber with a diameter of 1.5 m and a height of 1 m. The deposition process is performed by means of DC magnetron sputtering, employing a 10-inch cathode mounted at the bottom of the chamber in a sputter-up configuration and laterally offset by approximately 300 mm with respect to the chamber axis.

The substrate, either the RF window itself or, for qualification purposes, a dedicated sample holder equipped with witness samples, is positioned along the chamber axis at a distance of approximately 350 mm from the sputtering source. A rotation system for the sample holder is integrated into the setup to enhance the uniformity of the deposited film thickness across the entire exposed surface.

For the validation of the deposition process, different substrate materials were selected (Fig. 1), depending on the specific characterization technique to be employed. Glassy carbon substrates, Structure Probe Inc. (GC_X) were used for Rutherford Backscattering Spectrometry (RBS) measurements, owing to their suitability for quantitative compositional analysis and accurate determination of thin film thickness.

For the characterization of secondary electron emission properties, sintered alumina samples (Ce_Y) were utilized, featuring a composition and surface roughness comparable to those of the operational RF windows (Ra ≈ 1.6 μm), in order to ensure a representative assessment of the SEY behaviour of the coated system.

Content from this work may be used under the terms of the CC BY 4.0 licence (© 2026). Any distribution of this work must maintain attribution to the author(s), title of the work, publisher, and DOI.

ISBN: 978-3-95450-252-3 ISSN: 2673-5350 doi: 10.18429/JACoW-IPAC2026-MOP7155

STATUS OF THE CRYOMODULE TESTS AS A PART OF POLISH IN-KIND CONTRIBUTION TO THE EUROPEAN SPALLATION SOURCE (ESS) REALIZED BY IFJ PAN

M. Wartak, D. Bocian, W. Gaj, P. Halczynski, J. Jaros, S. Kubaj, A. Lipka, K. Markulis, K. Sowicki, P. Straczek, J. Swierblewski, K. Wartak
Institute of Nuclear Physics Polish Academy of Sciences, Krakow, Poland

Abstract

The European Spallation Source (ESS) is next-generation neutron source, that require testing, installation and commissioning of various systems and components. In this paper, the current status of cryomodule (CM) testing is presented including the Scope of Work (SoW), assigned to group of engineers and technicians from the Henryk Niewodniczanski Institute of Nuclear Physics Polish Academy of Science (IFJ PAN).

INTRODUCTION

The ESS is one of the Europe's largest research infrastructure. Superconducting linac at ESS is designed to provide 5 MW of average proton beam power with an energy of 2 GeV. The main acceleration of the proton beam is achieved by use of the superconducting part of linear accelerator (SCL). The SCL part of the linac consists of 13 spoke, 9 medium beta (MB) and 21 high beta (HB) cryomodules [1].

IFJ PAN, as an in-kind partner for ESS, has provided resources for testing of the accelerator components, building the infrastructure and developing different systems. The Polish institute was involved i.e. in the installation of Low Level RF (LLRF) and Local Protection System (LPS), testing and installation of RF Distribution Systems (RFDS), testing and installation of RF Power Stations (RFPS) [2-4] as well as commissioning and development of the cryogenic control system [5-9]. Apart from these works, the IFJ PAN team was also involved in reception check, testing, troubleshooting and support with installation of the cryomodules in the tunnel [10]. Nevertheless, the largest resources provided by the IFJ PAN was assigned to the work package related to Site Acceptance Tests (SAT) of the MB and HB elliptical cryomodules (Fig. 1). These tests took place at ESS in Test Stand 2 (TS2) and were realized jointly with team of ESS SRF Section [11-13].

IFJ PAN CONTRIBUTION TO SAT

The SAT has been foreseen at ESS for testing of the elliptical cryomodules at TS2. The facility in TS2 includes an RP bunker, a test stand, a dedicated cryoplant and RF power sources that allow for testing both types of the cryomodules (MB and HB) at nominal temperatures. Both cryogenic and RF operability were evaluated at the time of testing. Since the arrival of the cryomodule to ESS, the processes were jointly controlled by IFJ PAN and ESS SRF crews until the cryomodule was approved for further installation in the tunnel. IFJ PAN provided specialists in electrical, mechanical, cryogenic and vacuum fields for that purpose. The scope of work for the cryomodule testing contains various operations that can be divided into different phases. Depending on the type of activity, it is performed in different areas of TS2 (Fig. 2). Below, the main activities supported by the crew from the Polish institute for cryomodule testing at TS2 are described.

Initial Inspection of the Cryomodule

At the early stage, after the cryomodule arrives at ESS two types of the inspections are carried out: electrical and mechanical incoming inspections. This is the first stage of the cryomodule check before any further activities. During the electrical inspection, various measurements are performed. The goal is to confirm that electrical instrumentation of the cryomodule shows no signs of damage and can be approved for further use during cold tests in the bunker. The electrical measurements include checking temperature sensors, liquid helium level gauges, electrical heaters, stepper motors and piezo actuators. Mechanical inspection allows verification of whether any obvious defects of the cryomodule are present. Mainly a visual inspection is performed at that time. External components are verified such as: the cryomodule's vacuum vessel, cryogenic valves, vacuum valves, beam equipment in the bells section, auxiliary line ports, instrumentation flanges etc.

Preparation of the Cryomodule for the Cold Tests

Preparation of the cryomodule for further cold tests consists of installation of the instrumentation and cryomodule equipment. In parallel, vacuum tests of the cryomodule are performed. The work is carried out in the TS2 area, which has two slots available for these activities (Fig. 3).

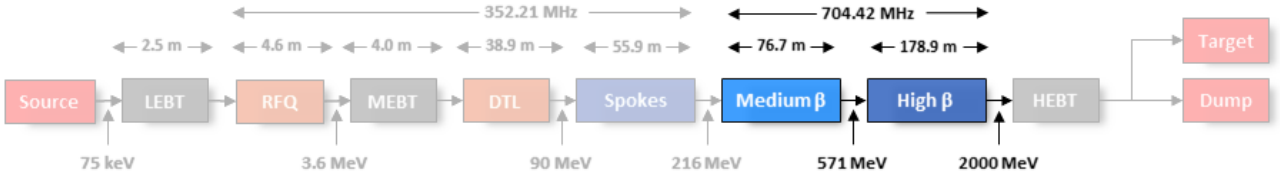

Figure 1: Block diagram of the ESS accelerator with the medium and high beta cryomodule sections highlighted, being tested during SAT at ESS TS2.

Content from this work may be used under the terms of the CC BY 4.0 licence (© 2026). Any distribution of this work must maintain attribution to the author(s), title of the work, publisher, and DOI.

ISBN: 978-3-95450-252-3 ISSN: 2673-5350 doi: 10.18429/JACoW-IPAC2026-MOP7156

FEA–CFD NUMERICAL APPROACHES IN THE DESIGN OF THE FAST PERIODIC SHUTTER FOR FAXTOR-BL31 AT ALBA

A. Cano Navarro*, A. Carballedo Costa, A. Patera, M. Quispe, B. de Abreu Francisco
ALBA Synchrotron, Cerdanyola del Vallès, Spain

Abstract

In the context of the experiments to be carried out at the fast X-ray tomography and radioscopy beamline (FAXTOR-BL31) of the ALBA synchrotron, a Fast Periodic Shutter (FPS) is being designed. Its purpose is to prevent a high dose rate on the sample and to provide synchronization with the acquisition protocol. This FPS is based on the combination of tungsten blades driven by a servomotor. This work details the FEA-CFD numerical simulations (ANSYS) developed for the FPS's thermo-mechanical design. Models considered steady-state and transient (periodic) conditions. Initial steady-state analysis (under vacuum) quantified baseline mechanical stress. Subsequently, a coupled CFD approach modeled the cooling gas and forced convection effects. The thermal modeling incorporated combined synchrotron radiation and Stefan-Boltzmann radiation modeling. The main objective of these simulations is to quantify the resulting thermo-mechanical stress and temperature distribution to ensure the structural integrity of the blades. Complementarily, the influence of air resistivity on rotor performance and the temperature dynamic considering air cooling and periodic radiation were examined.

BACKGROUND

FAXTOR (FAst X-ray TOmography and Radioscopy) is the first hard X-ray imaging beamline constructed at ALBA Synchrotron. It is a versatile beamline designed for quasi-real-time three-dimensional computed tomography. Beyond conventional 3D tomography, FAXTOR provides the user community with a powerful tool for investigating the dynamics of processes occurring at the micrometric scale by means of X-ray imaging [1].

As part of its projects, a Fast Periodic Shutter (FPS) is being designed, with the aim of preventing high dose rates on the sample and providing synchronization with the acquisition protocol. This work presents the results of FEA–CFD simulations of this design, carried out using ANSYS® [2].

GEOMETRICAL MODEL

The FPS consists of a titanium rotor integrating four TRIAMET tubes ($\phi_{ext} = 18\,mm$, $L = 60\,mm$) through which the beam passes. The rotor is supported by lateral aluminium mounts, which are themselves fixed to a granite base (Fig. 1). All components are housed within an aluminium enclosure. Table 1 summarizes the main FPS material properties: Poisson ratio ν, thermal conductivity λ, Young's modulus E, emissivity ε, density ρ, and specific heat capacity C_p [3].

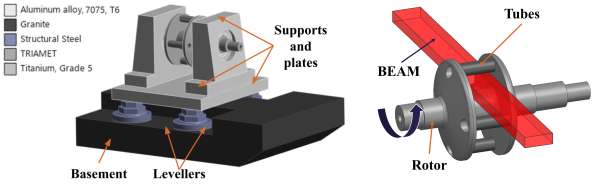

(a) Full assembly geometry (b) Reduced geometry

Figure 1: Parts & materials of the FPS system.

Table 1: Properties of FPS Materials

Material	ν [-]	λ [W/mK]	E [MPa]	ε [-]	ρ [kg/m^3]	C_p [J/kgK]
TRIAMET	0.27	96	3.1×10^5	0.45	17 000	150
Ti Gr. 5	0.34	7.00	1.05×10^5	0.40	4470	580

SIMULATION SETUP

Simulation Cases

Table 2 presents the cases simulated in this work. M1 and M2 are static structural vacuum simulations, while M3 is a mechanical computational fluid dynamics (CFD) case. MS1, SS1, SS2 and SS3 are steady-state thermal simulations, whereas TR1 is a FEM transient thermal case and TR2 is its lumped-parameter counterpart implemented in Simulink [4]. Finally, TM-CFD1 is the thermal CFD study.

Table 2: Simulation Cases Summary

Type	Codes	Geometry
Mechanical	M1, M2 & M3	Reduced
Map simplification	MS1	Prism benchmark
Steady-state thermal	SS1, SS2 & SS3	Full assembly
Transient thermal	TR1 & TR2	Reduced & lumped model
Thermal CFD	TM-CFD1	Full assembly

Mesh Generation

Unstructured meshes were used, with refinement concentrated in the tubes, where thermal gradients are highest (Fig. 2). A mesh convergence study was performed for all cases, ensuring that variations in the output variables remained below <5%.

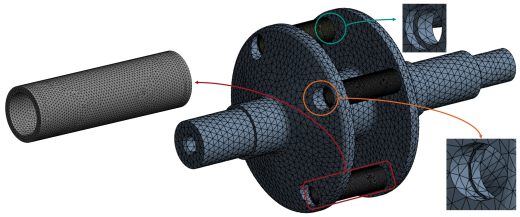

Figure 2: Example of refined mesh near beam footprint.

* adrian.cano.nav@gmail.com

Content from this work may be used under the terms of the CC BY 4.0 licence (© 2026). Any distribution of this work must maintain attribution to the author(s), title of the work, publisher, and DOI.

ISBN: 978-3-95450-252-3 ISSN: 2673-5350 doi: 10.18429/JACoW-IPAC2026-MOP7158

EVALUATION OF LOW-COST, MULTIMODAL-SENSOR, DATA ACQUISITION SYSTEMS FOR AD-HOC APPLICATIONS IN PARTICLE ACCELERATORS

P. Ellison*, R. Gauthier, K. Papastergiou, F. Velotti, CERN, Geneva, Switzerland

Abstract

With more than 30 km of beam lines and over 10,000 devices, CERN's particle accelerators are rich sources of data, providing real opportunities for developing new equipment monitoring and automation tools using data analysis and machine learning.

The ready availability of low-cost computers and microcontrollers, such as Raspberry Pi and ESP32 devices, could enable a flexible data acquisition system for short-term applications that do not require, or cannot justify, the development and installation of permanent acquisition infrastructure.

This paper presents the initial work from a pilot project to develop such a system and assesses its use for several applications, including speculative investigations of environmental conditions, such as temperature and high-energy hadron flux, as well as assessing the feasibility of detecting arc faults in power converters and gathering datasets for training machine learning models.

Key considerations for the implementation of this system are also discussed, including concerns around network security, data quality, data availability, hardware configurations, deployment conditions, and avoiding control system dependency, with initial recommendations given for each.

INTRODUCTION

Reaching the higher targeted collision energies and beam intensities of future particle accelerators requires a significant increase in the size of the facilities and the quantity of equipment within them. Within the existing accelerator complex at CERN, a large amount of operational time is already spent diagnosing, repairing and recovering from equipment and system failures [1]. With the planned increase in complexity, the widespread integration of equipment and process automation will be required to avoid unsustainable downtime and ensure high machine availability. The Efficient Particle Accelerators (EPA) project is a CERN initiative to improve the operational efficiency of the accelerator complex in terms of equipment automation, beam operation and data analysis. For equipment automation, a key focus is leveraging recent developments in machine learning (ML), artificial intelligence (AI) and continual learning to enable automated fault and anomaly detection [2]. Developing automation is a data-driven process and potentially requires measurements that are not currently acquired, or are not required permanently. Accelerator commissioning, for example, can last up to several months, and standard tests such as magnet polarity checks and heat run tests could be automated using temporary acquisition devices. The existing data acquisition system at CERN is directly integrated with the controls system, meaning it is highly reliable, but as a consequence has a high per-unit cost and a long development time, and requires control system experts to deploy. Due to the speculative nature of automation pilots, they typically cannot justify this high initial investment, and if they could, the lengthy development time would significantly delay the wider adoption of automation across the accelerator complex. To support automation development, this paper presents the initial work to develop a low-cost, non-controls-based data acquisition system designed for short-term, ad-hoc deployments with flexible hardware configurations.

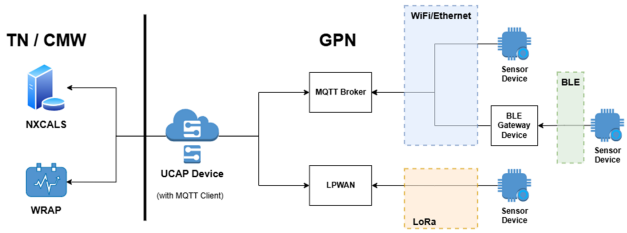

Figure 1: Diagram of the different network topologies and their connection in the wider data acquisition pipeline.

INITIAL PILOT

The aim of this pilot project is to evaluate the feasibility of using a low-cost, multimodal-sensor data acquisition system for ad-hoc applications in the CERN accelerator complex. The objectives are to assess the hardware, software and network configurations required for its use, the suitability of existing CERN infrastructure for supporting it, as well as the data quality and development-to-deployment times that are possible. For this pilot's scope, 'short-term' deployments are defined as having a duration that is less than one machine run (~3 years), and 'ad-hoc' applications refer to applications with differing deployment environments, durations, sensor configurations and sample rates. The initial requirements for the pilot acquisition system are: the use of existing CERN systems, or industry-standard tools where possible, central data logging in Next CERN Accelerator Logging System (NXCALS), real-time data publishing on Controls Middleware (CMW), and the support of flexible deployment locations, sensor configurations and sample rates.

Identified Network Topologies

For this pilot project, three main network communication methods were identified for further testing (Fig. 1), to evaluate the communication range, data bandwidth and power consumption required for the target deployment use cases.

* patrick.ellison@cern.ch

Content from this work may be used under the terms of the CC BY 4.0 licence (© 2026). Any distribution of this work must maintain attribution to the author(s), title of the work, publisher, and DOI.

ISBN: 978-3-95450-252-3 ISSN: 2673-5350 doi: 10.18429/JACoW-IPAC2026-MOP7159

ETHERNET-ENABLED DATA ACQUISITION AND SUPERVISION SYSTEMS FOR THE HL-LHC QUENCH PROTECTION SYSTEM

P. J. Oliveras Cejas*, T. Podzorny†, M. Christensen, D. del Castillo, R. Denz,
L. Flores Sanz De Acedo, M.-A. Galilée, J. Steckert, J. Uythoven
European Organization for Nuclear Research, Geneva, Switzerland

Abstract

Ethernet-enabled Data Acquisition and Supervision (EDAQ) systems have become the standard platform for commissioning, controlling, and supervising the next generation of Quench Protection Systems (QPS) for superconducting magnets at CERN. EDAQ-equipped QPS devices have been installed in recent upgrades to magnet test facilities, most notably in the Inner Triplet String (IT String) test facility for the high luminosity LHC (HL-LHC) upgrade. This contribution summarizes the operational experience gained during these installations and highlights the key advancements that have enabled the EDAQ ecosystem to mature into a production-ready solution. Notable developments include a configuration validation system, improved error-recovery strategies, remote firmware update, and seamless integration with the full range of QPS equipment that will be installed for the HL-LHC upgrade. The results of a comprehensive set of performance tests are presented and discussed, confirming that the EDAQ system is ready for deployment as part of the HL-LHC upgrade, for which installation will start in summer 2026.

INTRODUCTION

The superconducting magnets on each side of Interaction Regions IR1 (housing the ATLAS experiment) and IR5 (housing the CMS experiment) in the LHC accelerator are to be replaced as part of the the High Luminosity Upgrade of the LHC project (HL-LHC). The collection of magnets at either side of these interaction regions form what is known as the inner-triplet magnet chain. Their replacement is one of the core activities of the HL-LHC project, allowing the significant increase in the overall luminosity to be delivered to the experiments [1].

The elements to be replaced include the superconducting magnets, superconducting links, current leads and bus-bars. They must be protected to avoid serious damage and downtime in case of a quench. This function is achieved by the Quench Protection Systems (QPS) which include the detection of the quench by the Quench Detection Systems (QDS) and triggering the systems which actively protect the circuit (e.g. Quench heaters or the new CLIQ system, bypass diodes, energy extraction systems and others).

The safe powering of the inner triplet circuit requires all these protection systems to function reliably, with Supervisory Control And Data Acquisition (SCADA) systems providing accurate data representing the circuit and protection status. This is crucial for all phases of machine operation, including testing, commissioning and beam operation. To this end, the QPS is designed with data acquisition in mind, with communication interfaces allowing nformation to be transmitted to CERN's SCADA infrastructure.

In the QPS of the presently operational LHC this is achieved by interfacing QPS equipment with radiation-tolerant WorldFip communication cards. The WorldFip field-bus connects a number of devices to a Front-End Computer (FEC), which aggregates and relays data to the supervision and control infrastructure, while providing timing to devices and delivering control commands.

For the future HL-LHC, Ethernet-enabled Data Acquisition and Supervision (EDAQ) will be used as the communication interface between multiple kinds of QPS equipment and the SCADA. QPS devices which support EDAQ usually include a MCU-based communication card (EDAQ Controller) which is also connected to a FEC. In this case connections are made using Ethernet cables through a network switch in a star network topology. Timing is distributed to devices via Precision Time Protocol (PTP), while data acquisition and control traffic is sent by UDP [2].

Since its introduction in 2021, EDAQ has been used for the QPS in magnet test facilities at CERN, including in SM18, FRESCA and the Super-FRS Magnet Test Facility testing magnets for the Facility for Antiproton and Ion Research (FAIR) at GSI. QPS devices with EDAQ support have also recently been installed in the Inner Triplet String (IT String) facility, a testbed for HL-LHC. These installations provided the necessary experience to transition from a development project to the present production solution.

EDAQ IN HL-LHC

Integration with QPS

Five different EDAQ Controllers have been developed to supervise six types of QPS equipment to be installed as part of the HL-LHC upgrade. The EDAQ firmware modules and core components are identical for all systems, while the hardware design of the PCBs and application-specific firmware modules are adapted to each system. EDAQ integration with all these systems is complete up to the SCADA level. From left to right in Fig. 1:

- Universal Quench Detection System (UQDS) [3]: The same EDAQ Controller is used for the five different UQDS configurations in use to protect different elements. EDAQ controller instances are likewise configured for the different number of signals according

* pau.oliveras@cern.ch
† tomasz.podzorny@cern.ch

Content from this work may be used under the terms of the CC BY 4.0 licence (© 2026). Any distribution of this work must maintain attribution to the author(s), title of the work, publisher, and DOI.

ISBN: 978-3-95450-252-3 ISSN: 2673-5350 doi: 10.18429/JACoW-IPAC2026-MOP7160

ELECTRO-MAGNETIC SEPARATOR TOPOLOGY CONCEPT FOR FCC-ee

L. Porta*, A. Potet, B. Balhan, C. Bracco, I. Valencia Ruiz, J. Borburgh, Y. Dutheil
European Organization for Nuclear Research, Geneva, Switzerland

Abstract

The layout of the FCC-ee collider requires the separation of the electron and positron beams, which are circulating in opposite directions, on either side of the RF system. Only one of the two beams must be deflected, while the other one (the beam circulating in the direction of the RF) shall remain untouched to avoid synchrotron radiation being emitted toward the RF section. This functionality is achieved using a combination of an electric field and a perpendicular magnetic field, which must be matched to each other along the entire length of the separator to avoid synchrotron radiation (SR) emission toward the superconducting RF cavities. In order to satisfy the matching condition $B = E/c$ for relativistic particles, an extremely weak magnetic field (5 mT) is required for a given achievable static electric field (1.5 MV/m). This article presents a concept that combines an under-vacuum electrostatic system with a low-field large-aperture outside-vacuum dipole magnet to achieve the main separation functionality while providing excellent field matching and low SR production. In addition to the concept development, three critical aspects have been identified and are the subject of ongoing studies to assess feasibility by end of 2027: high-voltage (HV) breakdown, beam coupling impedance and machine protection.

INTRODUCTION

The Future Circular Collider electron-positron (FCC-ee) [1] is a high-luminosity lepton collider proposed at CERN, designed to operate at four centre-of-mass energies: the Z (45.6 GeV), WW (80 GeV), H (120 GeV) and $t\bar{t}$ (182.5 GeV) modes. At the two highest energy modes, the collider RF system, located in the long straight section at Point PH, is shared between both counter-rotating beams. In this common-RF scheme, the electron and positron beams traverse the RF cavities on a common trajectory, but at different times. This arrangement avoids the need for two dedicated RF systems and maximises the use of the RF infrastructure. This configuration requires a specific beam separation system at each end of the RF section and involves a new type of equipment: the Electro-Magnetic Separator (EMS) [2]. Downstream of the EMS, septa magnets will support beam separation and add to the integration challenge at Point PH, where space is constrained despite the kilometer-scale straight section. The EMS must deflect the beam leaving the RF section toward the arc (outgoing beam), while leaving the beam circulating in the direction of the RF system (incoming beam) entirely unperturbed. This constraint is critical since any deflection of the incoming beam would produce synchrotron radiation (SR) toward the superconducting RF cryomodules, risking thermal perturbation.

The EMS concept is currently developed by CERN's Beam Transfer group (SY-ABT). The present article introduces the electromagnetic topology concept, the preliminary specifications, and the key technical challenges under investigation in the framework of the Reference Design Phase.

OPERATING PRINCIPLE

The EMS separates the beams trajectories by exploiting (i) the Lorentz-force contributions from the electric and magnetic fields and (ii) the reversal of both charge sign and propagation direction between the two counter-rotating beams. Given the Lorentz force $F_x = q\,(E_x - v_z\,B_y)$ and considering the left side EMS in Fig. 1, the transverse horizontal forces on the electron beam (charge $-e$, incoming with velocity c_z) and on the positron beam (charge $+e$, outgoing with velocity $-c_z$) are respectively:

$$F_{x,e^-} = (-e)\,(E_x - c_z\,B_y) = -e\,E_x + e\,c_z\,B_y, \quad (1)$$

$$F_{x,e^+} = (+e)\,(E_x + c_z\,B_y) = e\,E_x + e\,c_z\,B_y. \quad (2)$$

When the fields amplitudes satisfy the matching condition in Eq. (3), the contributions of E_x and B_y cancel for the electron beam (incoming), which sees a zero net force, while they add up for the positron beam (outgoing), which experiences a net deflection. Following similar principle, the same but opposite situation occurs in the right-side EMS of Fig. 1.

$$B_y = E_x/c \quad (3)$$

Satisfying condition in Eq. (3) pointwise along the full device length, including in fringing regions, is the central design challenge addressed in the following section.

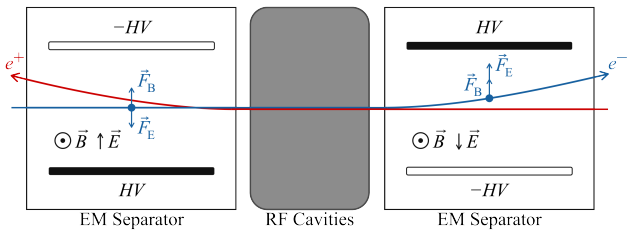

Figure 1: Lorentz force vectors acting on the e^- beam at two locations: as the incoming beam (zero net force) and as the outgoing beam (superimposed deflecting force).

ELECTROMAGNETIC TOPOLOGY CONCEPT

Topology and Design Choices

The EMS topology combines two co-axial static devices: an *under-vacuum electrostatic separator* providing the electric field, and an *outside-vacuum dipole magnet* surrounding

* lucien.porta@cern.ch

Content from this work may be used under the terms of the CC BY 4.0 licence (© 2026). Any distribution of this work must maintain attribution to the author(s), title of the work, publisher, and DOI.

ISBN: 978-3-95450-252-3 ISSN: 2673-5350 doi: 10.18429/JACoW-IPAC2026-MOP7162

CURRENT STATUS OF BESSY III MAGNET DESIGN

J. Voelker*, I. Asparuhov, V. Dürr, P. Goslawski, F. Pflocksch,
Helmholtz-Zentrum Berlin für Materialien und Energie, Berlin, Germany

Abstract

HZB is developing BESSY III, a future 4th-generation low-emittance diffraction-limited soft-to-tender X-ray synchrotron light source, as a green-field facility in 2035 on the premises of the Adlershof technological campus in Berlin, Germany. We are in the design phase of magnet concepts for all permanent-magnet (PM-)based linear and resistive multipole magnets. Exposition is given to the optimization of the magnetic design and resulting technical considerations for solutions of field tunability and correction, thermal operational stability, and follow-up mechanical realization for the energy-efficient linear optics and ring performance of BESSY III, stepping on lessons so-far learned from the BESSY II+ [1] upgrade and RF2.0 [2] projects. In this paper, we give an overview of the design progress on the PM-based magnets and of considered options for the required higher-order magnet families such as resistive sextupoles and octupoles.

MAGNETIC DESIGN CONCEPT OF PM-BASED MAGNETS FOR BESSY III

As part of the BESSY III [3–6] project - a 4th-generation low-emittance diffraction-limited light source in Berlin - HZB is currently developing the lattice design of the storage ring for a Higher-Order Achromat Multi-Bend Achromat (HOA-MBA). In parallel, the developing of a concept for a sustainable magnet system has been started based mostly on permanent-Magnet (PM-)based magnets for the linear lattice components and electromagnets (EM) for adjustable QPs in the straight, sextupoles (SP) and octupoles (OP). This concept reduces the overall amount of energy per year for the storage ring magnetic system from ≈ 8 GWh to ≈ 2 GWh. Table 1 summarizes the different main types of the latest lattice magnets from a field-generation perspective. Also given are corresponding numbers of sub-types differing by certain physical parameters (length).

All magnets have a minimal aperture radius of 12.5 mm. In a general-purpose approach, PM-based magnets shall use identical PM blocks in terms of dimensions (35 × 35 × 50 mm^3) and material properties (high-remanence N42-grade rare-earth NdFeB) for more robust performance. This approach simplifies the mechanical PM installation tooling for all magnets and the mechanical and magnetic control of the individual PM blocks. The final size of the PM blocks was determined by ensuring that the minimal field requirements of all magnets can be fulfilled. The different magnet designs must be able to handle subsequent field adjustment options, such as mechanical tuners with steel shimming plates. Additionally, Thermoflux plates (based on a NiFe alloy) [7] will be installed next to the PM blocks to compensate NdFeB temperature dependence and stabilize the magnetic field around the beam trajectory over a wide temperature range [8]. A similar approach is adopted for the magnet design itself: using an identical transverse design for all bending magnets (only their lengths differ) as well as for the quadrupole (QP) and reverse-bend (RB) return yokes. The latter are high-gradient combined-function magnets with a weak additional dipole contribution (see Tab. 1) which can be built as 3- or 4-mm horizontally displaced quadrupole magnets. The horizontal offset requires a slightly larger aperture diameter, but the same outer design as the QP. This approach seeks a reduction in individual-unit fabrication processes with higher reproducibility of individual components.

Magnetic Optimization

All 2D and 3D magnet model field calculations are done with the CST suite [9]. For field optimization, the magnetic multipole contributions are obtained via Fast Fourier Transform (FFT) computation on a 10-mm reference radius. The elimination of unwanted multipole components was performed in two steps: Local 2D optimization followed by a fringe-field optimization for the integrated 3D field. For this, the complex Fourier definition of the 2D magnetic field distribution is used:

$$B = \sum_{\mathrm{n}} \left(\mathrm{A}_n + \mathrm{iB}_n\right) (x+iy)^{n-1},$$

with normal longitudinally integrated multipole components given in "units" derived according to

$$b_n^{\mathrm{int}} = \frac{\int B_n dz}{\int B_2 dz} 10^4. \quad (1)$$

The particular procedure applied in the case of the quadrupole magnets can be found in [10], which exemplifies a strong PM-based quadrupole magnet with motorized tuning plates and electrical-coil correctors for magnetic-gradient variation over a range of >30 % with respect to a nominal 100-T/m gradient.

Magnet Field Tunability and Correction

For tuning the magnetic field of a PM-based DP or QP magnet, thick steel tuning plates (shims) can be moved manually or in a motorized manner vis-a-vis the PM-block channel. They work as an additional magnetic load in the magnetic circuit of the magnet and reduce the magnetic flux in its pole shoe as a function of the shim position/insertion depth. While such manually positioned mechanical tuners serve to fine-tune the magnetic field, as per compensating small PM or material parameter variations, the motorized option is reserved for large on-the-spot field adjustments up to some tens

* jens.voelker@helmholtz-berlin.de

Content from this work may be used under the terms of the CC BY 4.0 licence (© 2026). Any distribution of this work must maintain attribution to the author(s), title of the work, publisher, and DOI.

ISBN: 978-3-95450-252-3 ISSN: 2673-5350 doi: 10.18429/JACoW-IPAC2026-MOP7164

DESIGN OVERVIEW AND PROJECT STATUS OF THE PM GRADIENT DIPOLE AT MAX IV*

A. Sharma†, A. Andersson, , K. Åhnberg, L. Roslund, P.F. Tavares
MAX IV Laboratory, Lund, Sweden
A. Vorozhtsov‡, European Organization for Nuclear Research, Geneva, Switzerland

Abstract

As part of the RF2.0 project*, a permanent-magnet (PM) gradient dipole has been designed at MAX IV Laboratory to replicate the performance of a conventional electromagnet gradient dipole in Unit Cell-1 of the MAX IV 3.0 GeV storage ring. The new PM gradient dipole follows a modular design and utilises NdFeB permanent-magnet blocks. The main advantage of this design is the expected reduction of up to 42% in the power consumption of the ring's magnet system, assuming replacement of all dipoles. Moreover, the use of PMs enables a more compact dipole magnet, potentially freeing space within the existing Unit Cell footprints for the integration of higher-performance multipole magnets anticipated for the MAX 4^U upgrade. This report summarises the electromagnetic and mechanical design, installation planning, and the overall project status.

INTRODUCTION

The magnet system of the MAX IV 3 GeV storage ring consists of 20 multi-bend achromats, each containing seven unit cells (MC1, UC1, UC2, UC3, UC4, UC5, and MC2). Each unit cell is a precision-machined iron block designed to accommodate different types of magnet elements [1].

A permanent-magnet (PM) gradient dipole, shown in Fig. 1, has been designed for the UC1 unit cell to match the footprint and performance of the existing UC1 conventional electromagnet gradient dipole while reducing power consumption and cooling requirements. This work is aligned with the RF2.0 project's vision of developing energy-efficient accelerator technologies. The concept is also relevant for future upgrades of MAX IV, as a more compact dipole could free space for higher-performance multipole magnets within the current cell footprint. This PM solution is being developed as a demonstrator and will be qualified under realistic operating conditions.

PM GRADIENT DIPOLE DESIGN

The primary magnetic design objective was to retain the magnetic behaviour of the installed UC1 gradient dipole

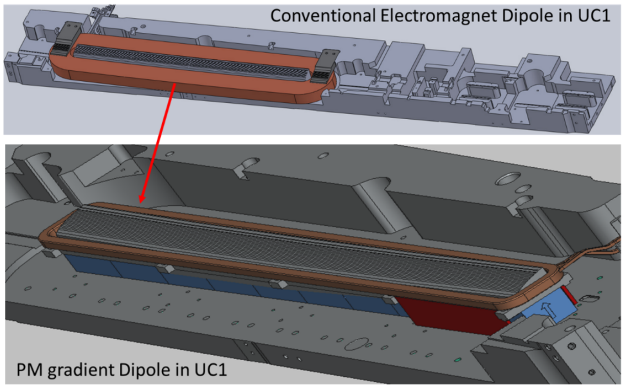

Figure 1: PM gradient dipole in UC1.

while replacing the main excitation source with permanent-magnet material. The magnetic material used for the PM gradient dipole is NdFeB. The various sub-components of the PM dipole are shown in Fig. 2.

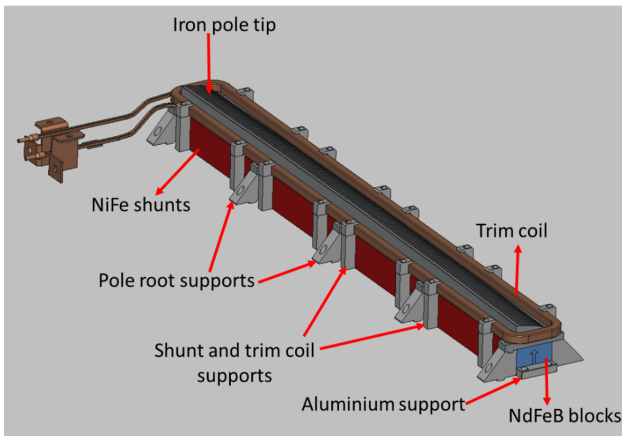

Figure 2: Key components of PM dipole.

As shown, the PM blocks will be installed below the removable pole tip. A common aluminium support structure has been designed to support both the trim coils and the pole tips. Thin strips of NiFe are placed around the PM blocks to compensate for the temperature-induced variation in the remanence of NdFeB. The aluminium support design allows for the change in the overall thickness of the NiFe strips, so that it can be changed during the experimental validation of the performance of this magnet. The main design parameters of the PM dipole are given in Table 1.

MAGNETIC DESIGN OF PM DIPOLE

The PM dipole design was optimised using Opera 3D. The simulation results were compared with experimental

* This work is part of the Research Facility 2.0 project that has received funding from the European Union's Horizon Europe research and innovation programme under grant agreement No. 101131850 and from the Swiss State Secretariat for Education, Research and Innovation (SERI). Views and opinions expressed are however those of the author(s) only and do not necessarily reflect those of the European Union or SERI. Neither the European Union nor SERI can be held responsible for them.
† aashoo.sharma@maxiv.lu.se
‡ formerly at MAX IV Laboratory

Content from this work may be used under the terms of the CC BY 4.0 licence (© 2026). Any distribution of this work must maintain attribution to the author(s), title of the work, publisher, and DOI.

ISBN: 978-3-95450-252-3 ISSN: 2673-5350 doi: 10.18429/JACoW-IPAC2026-MOP7165

RESULTS FROM THE HEPTO COMBINED FUNCTION PERMANENT MAGNET*

A.G. Hinton†,1,2, B.J.A. Shepherd[1,2], A. Shahveh[3], D. Topalović[4]
[1]ASTeC, STFC Daresbury Laboratory, Sci-Tech, Daresbury, Warrington, UK
[2]Cockcroft Institute, Sci-Tech Daresbury, Warrington, UK
[3]Diamond Light Source, Didcot, UK
[4]Kyma S.p.A., Trieste, Italy

Content from this work may be used under the terms of the CC BY 4.0 licence (© 2026). Any distribution of this work must maintain attribution to the author(s), title of the work, publisher, and DOI.

Abstract

The Hybrid Electromagnet-Permanent Magnet Tuneable Optics (HEPTO) magnet has been designed and built as part of the I.FAST collaboration as an energy saving alternative to traditional resistive electromagnets. The prototype magnet has been designed to meet the magnetic field requirements of the combined function dipole-quadrupole (DQ) magnets required for the Diamond-II upgrade. The prototype contains several design features for maintaining and tuning the field strength and quality, including a novel mechanical shimming method, trim coils and passive temperature compensation. We present here the results of the magnetic measurements of the built prototype magnet and demonstrate the ability to tune the field using the design features. We demonstrate that the nominal integrated field strength and homogeneity can be achieved with the permanent magnet solution, representing a 2.3 kW reduction in nominal power consumption compared to the equivalent electromagnet.

INTRODUCTION

Fourth generation synchrotron light sources make use of multi-bend achromat (MBA) lattices to enable a reduction in beam emittance and hence order of magnitude increase in brightness relative to third generation sources [1]. These MBA lattices contain large numbers of magnets, and complex magnet designs, including combined function magnets [2]. The increase in number of lattice magnets results in an increase in the electrical power requirements and corresponding carbon footprint of the facilities.

Permanent magnets provide an attractive alternative to traditional resistive electromagnets to reduce both the operating costs and environmental impact of accelerator facilities [2].

As part of the I.FAST collaboration [3], the Hybrid Electromagnet-Permanent magnet Tuneable Optics (HEPTO) prototype has been built as a technology demonstrator of a permanent magnet based combined function dipole-quadrupole magnet with application for fourth generation light sources.

MAGNET DESIGN

The HEPTO magnet (Fig. 1) has been designed to meet the same integrated field strength and homogeneity requirements as the dipole-quadrupole (DQ) electromagnets designed for the Diamond-II storage ring upgrade [4]. The nominal integrated dipole and gradient of the HEPTO magnet are -0.6047 T.m ±0.1 % and 28.1857 T ±0.1 % respectively. The specified field homogeneity ΔB/B in the 7 mm radius good field region was 5E-4. These values are the same as those defined for the equivalent electromagnet in order to give the same performance. [5].



Figure 1: Photograph of the HEPTO prototype magnet.

The HEPTO design is based on a single-sided quadrupole [6]. The main source of the field is provided by grade 45M6 NdFeB permanent magnet blocks with a remanent field of 1.3 T ±1 %. Nickel-iron thermal shunts [7] located parallel to the permanent magnet blocks to the sides of the main poles provide passive temperature compensation. Small air cooled coils provide the ability to scan the quadrupole field independent of the dipole field for emittance measurements.

Material, machining and assembly tolerances all contribute to errors being introduced in the field profile produced by the built magnet. In traditional electromagnets, the current can be varied to achieve the target integrated field strength. Permanent magnets are fixed field devices, making adjustment of the field strength more challenging. With this in mind, the HEPTO magnet has been designed with a comprehensive mechanical shimming method to allow for adjustment of the field strength and homogeneity of the built magnet. This shimming method primarily relies on the use of brass shims placed between spacers to finely adjust the mechanical separation between the main and auxiliary poles.

* Work supported by funding from the I.FAST collaboration
† alex.hinton@stfc.ac.uk

ISBN: 978-3-95450-252-3 ISSN: 2673-5350 doi: 10.18429/JACoW-IPAC2026-MOP7166

ADVANCES IN MAGNETIC FIELD QUALITY FOR ZEPTO TUNABLE PERMANENT MAGNET QUADRUPOLE

A. R. Bainbridge*, C. Hill, A. G. Hinton, P. O'Donnell, B. J. A. Shepherd.
ASTeC, STFC Daresbury Laboratory, Warrington, UK
and The Cockcroft Institute, Sci-Tech Daresbury, Warrington, UK

Abstract

The Zero Power Tunable Optics (ZEPTO) project has developed tunable permanent magnets for accelerators as an alternative to resistive electromagnets, with a focus on quadrupoles. The project has previously produced three quadrupole prototypes, with the 3rd spending two years installed on Diamond Light Source. A 4th prototype has been designed and is under construction for installation on the CLARA electron accelerator at Daresbury Laboratory. This prototype features two novel improvements over previous iterations to offset the risk of the complex manufacturing and assembly procedures resulting in poor field homogeneity and magnetic axis displacement as a function of strength. We discuss the design of this prototype and show how these new features can correct the unique challenges in designing and building a permanent magnet with very high tuning range.

INTRODUCTION

The Zero Power Tunable Optics (ZEPTO) project at STFC Daresbury Laboratory has developed several prototype Permanent Magnet (PM) quadrupoles with tunable magnetic field gradient [1–5]. This area has attracted much attention globally, with several institutes working on tunable PM systems of varying designs and tuning ranges [6–12]. However, the ZEPTO design retains the largest tuning range so far demonstrated for PM quadrupoles. While other designs tend to focus on rotating magnetic rods [9–12] or Halbach rings [7, 8], ZEPTO magnets move PM blocks relative to fixed steel structures that define the flux path, allowing gradient to be adjusted while homogeneity remains defined by the steel shape. This arrangement is mechanically complex, however, maintaining stable field homogeneity and magnetic axis position during adjustment remains a challenge that requires extremely high precision during manufacture and assembly to achieve.

Based on learnings from the 3rd ZEPTO prototype [3–5], which operated for 2 years installed on Diamond Light Source, we have designed a 4th prototype which is currently under construction. This will be installed on CLARA [13], the 250 MeV electron linear accelerator at Daresbury Laboratory, replacing an equivalent electromagnetic quadrupole. This new prototype improves over predecessors to overcome the difficulties in manufacturing and assembly precision. If measurements reveal poor field harmonics, or magnetic axis shift as a function of gradient adjustment, the new prototype can correct these errors without re-assembling the magnet or re-machining components. We show here an overview of this magnet and that by adding magnetic steel shims in defined patterns we can correct excessive higher order field components, and that by removing rods of material from the yoke in predefined patterns we can tune the level of field saturation in one half of the magnet to correct horizontal magnetic axis movement as a function of strength. We propose that, once demonstrated by measurement, these will be key steps to bringing the ZEPTO tunable PM concept into direct competition with resistive electromagnets in terms of quality, convenience and reliability.

MAGNET OVERVIEW

The general concept of ZEPTO tuning has previously been explained in multiple publications [1–5], we refer the reader to these rather than explaining the principle in detail here. This 4th prototype has a specified strength range of ≥ 3 T integrated gradient at maximum and ≤ 0.18 T integrated gradient at minimum. The aperture diameter is 42 mm and magnetic length is 178 mm. The target for integrated field homogeneity is $\leq 1 \times 10^{-3}$ to a radius of 17 mm.

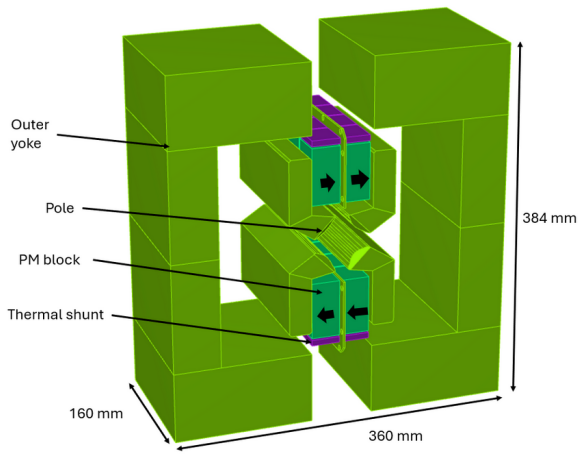

Figure 1: Simplified OPERA model of the new ZEPTO prototype, without the button shims and tuning rods described below.

A simplified 3D FEA model, produced in OPERA [14], is shown in Fig. 1. There are 16 PM blocks of grade N52 NdFeB, each measuring $30 \times 60 \times 36$ mm^3. The yokes are AISI grade 1010 low carbon steel. The magnet carriages each move by up to 70 mm. The simulated integrated gradient as a function of magnet carriage position is shown in Fig. 2. Unlike previous iterations of ZEPTO there are passive thermal shunts in a 6 mm layer on each magnet carriage which, in simulation, provide temperature stability in the

* alex.bainbridge@stfc.ac.uk

Content from this work may be used under the terms of the CC BY 4.0 licence (© 2026). Any distribution of this work must maintain attribution to the author(s), title of the work, publisher, and DOI.

ISBN: 978-3-95450-252-3 ISSN: 2673-5350 doi: 10.18429/JACoW-IPAC2026-MOP7167

MATERIAL-EXTRUSION ADDITIVE MANUFACTURING OF PURE COPPER COMPONENTS FOR ACCELERATOR VACUUM SYSTEMS

A. Hovhannisyan†, A. Davtyan, H. Isunts, V. Yepremyan
Center for the Advancement of Natural Discoveries using Light Emission, Yerevan, Armenia

Content from this work may be used under the terms of the CC BY 4.0 licence (© 2026). Any distribution of this work must maintain attribution to the author(s), title of the work, publisher, and DOI.

Abstract

This report presents a carried out study of the technology and performance of three-dimensional printing for the production of parts intended for ultra-high-vacuum assemblies. The simple part geometry was taken as the reference sample. Computer-aided design and finite element method (FEM) analysis are employed to predict thermomechanical stresses and deformations at the sintering stage. Experiments were conducted, and a comparative analysis was carried out to fit the initial FEM results with the experimental ones to obtain actual mathematical models for further simulations. During the printing process, the influence of layer thickness, nozzle temperature, and printing speed on the final density, dimensional accuracy, and surface quality is systematically investigated. Using the given essential parameters new printing setup was developed to ensure the highest density. New samples were printed with the different hole diameters to assess the actual properties using different accuracy printheads. The above-mentioned research was conducted to obtain the highest density of the printed parts, which will be used to evaluate the probability of the accelerator vacuum systems' fabrication.

INTRODUCTION

Additive manufacturing (AM) has become an increasingly relevant approach for the fabrication of complex engineering components, offering advantages in design flexibility, reduced material waste, and shortened production cycles [1, 2]. In accelerator technology, these capabilities are particularly important, as many components require precise geometries, high structural integrity, and efficient thermal management [3]. Conventional manufacturing methods often limit the realization of such features, especially for parts with complex internal structures [2, 3].

AM enables the production of geometries that are difficult or impractical to achieve using traditional machining, including conformal channels and integrated structures [2, 3]. This is of particular interest for accelerator applications such as vacuum components, beamline elements, and thermally loaded structures [3, 4]. However, the implementation of AM in accelerator systems requires careful evaluation of material properties, dimensional accuracy, and process-induced defects [3, 5].

* The work was carried out within the framework of the scientific research topics of the "Vacuum Technologies" basic research laboratory at CANDLE SRI.

† hovhannisyan@asls.candle.am

Among the available AM technologies, Bound Metal Deposition (BMD) represents a material-extrusion approach in which a metal–polymer feedstock is extruded layer-by-layer, followed by debinding and sintering [5, 6]. Systems such as the Studio System™ developed by Desktop Metal allow the fabrication of metal parts without handling loose powders, simplifying operation and improving safety in laboratory environments [6, 7]. At the same time, the sintering stage introduces challenges related to shrinkage, residual stresses, and deformation, which are critical for functional components [5, 8, 9]. Vacuum components are essential elements in accelerator systems, where mechanical stability, material homogeneity, and dimensional precision directly influence performance [10]. The application of AM to such components requires not only geometric feasibility but also a detailed understanding of material behavior during thermal processing and the resulting microstructure [5, 8, 10].

In this work, a copper vacuum pipe with a KF flange [11] on one end and a closed opposite side was fabricated using BMD technology. The sintering process was analyzed using finite element simulations performed in SIMULIA ABAQUS to evaluate stress evolution and thermal deformation during heating and cooling [12]. In addition, microstructural investigations were carried out using a metallographic microscope to assess grain morphology, inter-layer bonding, and porosity for samples produced with different printing parameters [13].

The objective of this study is to assess the applicability of BMD-fabricated copper components for accelerator vacuum applications by combining numerical simulation and experimental characterization. The results provide insight into the influence of process parameters on structural integrity and support further integration of AM technologies into accelerator engineering practice.

INITIAL DATA OF SIMULATION

The simulation was conducted in SIMULIA ABAQUS 2019 software environment using following physicomechanical and thermal properties Table 1.

- Table 1: Physicomechanical and Thermal Properties

Properties	Copper
Density before sintering [g/cc]	5.2
Density after sintering [g/cc]	8.75
Modulus of Elasticity [GPa]	128
Poisson's Ratio	0.35
Expansion Coeff. [1/°C]	17.24E-06
Thermal Conductivity [W/m×K]	401

The plastic properties are also crucial to include in the model for the simulation of its sintering process. Thus, in

ISBN: 978-3-95450-252-3 ISSN: 2673-5350 doi: 10.18429/JACoW-IPAC2026-MOP7168

HIGHT VOLTAGE ELECTRIC DIPOLE CONDITIONING FOR THE SUPER SPECTROMETER SEPARATOR AT GANIL/SPIRAL2

F. Carville[1,2], F. Esnault[1,2], M. Faye[1,3], C. Joly[3,4], T. Lefrou[1,3], R. Levallois[1,3], F. Lutton[1,3], A. Madeline[1,3], G. Olivier[3,4], J. Piot[1,3], A. Wagret-Quatromme[1, 3], J.F. Yaniche[4]

[1] Grand Accélérateur National d'Ions Lourds (GANIL), Cean, France
[2] Commissariat à l'énergie atomique et aux énergies alternatives (CEA-IRFU), Gif-sur-Yvette, France
[3] Centre National de la Recherche Scientifique (CNRS-IN2P3), Paris, France
[4] Laboratoire de Physique des 2 Infinis Irène Joliot-Curie (IJCLab), Orsay, France

Abstract

The "Super Separator Spectrometer" project S^3 is under technical commissioning at the GANIL facility (Caen-France). It is a new research installation designed for fundamental physics experiments with high intensity heavy ions beams produced from the SPIRAL2 linear accelerator. This spectrometer will open new horizons for nuclear physics. The S^3 spectrometer is made of 77 Superconducting magnets, 12 room temperature magnets and one electric dipole to guide and focalize the beam and select the particles of interest.

This paper presents technology of the Electric Dipole and the first operation of its conditioning before the commissioning of S^3 project.

S^3 SUPER SEPARATOR SPECTROMETER

S^3 Project [1] [2] aims to push the boundaries of nuclear physics by enabling the study of unstable nuclei and super heavy elements, particularly those beyond 104 in the periodic table (Fig.1). The design of the primary target is optimized for fusion-evaporation production. S^3 is a two-stage optical structure combining a large acceptance momentum achromat and a high-resolution mass separator. Each stage includes 2 dipoles and 4 multipoles triplets. 77 superconducting magnets, 3 room temperature dipoles, 3 open quadrupoles and 1 electric field dipole will allow S^3 to achieve high transmission and high resolution in mass to charge ratio for scientists [3].

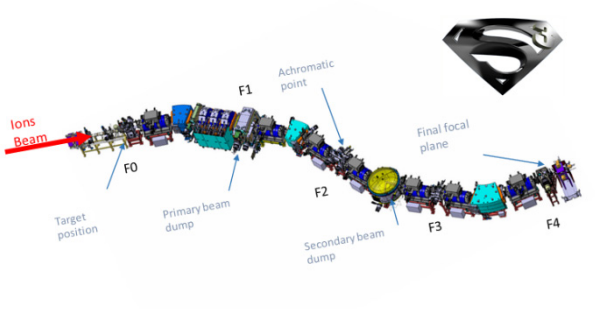

Figure 1: S3 spectrometer.

An electric dipole and a magnetic dipole are used in concert to provide an achromatic image at the final focal plane that is dispersive in m/q (Fig.2). The electric dipole separates the particles based on their kinetic energy so they exiting this dipole with the same mass but different charge states. In second stage, the magnetic dipole does a charge states separation to perform a mass resolution power about 500.

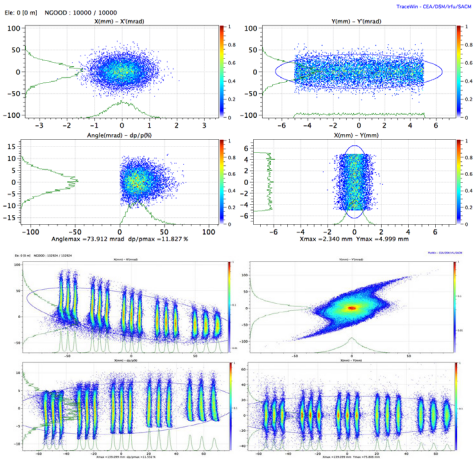

Figure 2: Input and final focal point emittance for different mass SN like distribution with 22+ to 26+ charge state.

ELECTRIC DIPOLE

The electric dipole consists of two titanium electrodes placed in a vacuum chamber (Table 1). Titanium was chosen for its good dielectric rigidity.

Table 1: Electric Dipole Dimensions

Vessel diameter [m]	Total height [m]	Total weight [kg]	Bending angle [°]	Bending radius [m]	Beam axis height [m]
1.9	2.4	2500	22	4	1.5

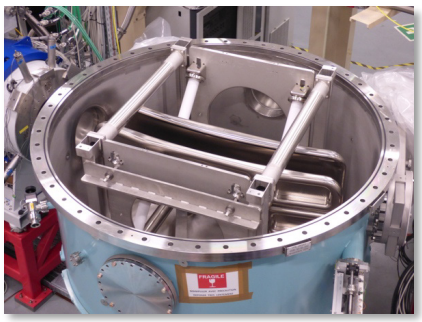

Figure 3: Electric dipole (IJClab).

The electrodes are held in place by a frame and ceramic insulators sized for the high voltages (Fig.3). Two ceramic insulated feedthroughs equipped with anti-corona protection are designed for connecting the 300kVcables.

Content from this work may be used under the terms of the CC BY 4.0 licence (© 2026). Any distribution of this work must maintain attribution to the author(s), title of the work, publisher, and DOI.

ISBN: 978-3-95450-252-3 ISSN: 2673-5350 doi: 10.18429/JACoW-IPAC2026-MOP7169

ADVANCING ULTRA-HIGH-FREQUENCY ACCELERATORS THROUGH METAL ADDITIVE MANUFACTURING

C. Zhang †,1,2,3, R. Böhm[1], E. Boos[1,2], R. Cherif[1], A. Japs[1], S. Wunderlich[1,2]
[1] GSI Helmholtzzentrum für Schwerionenforschung, Planckstr. 1, 64291 Darmstadt, Germany
[2] Institute for Applied Physics, Goethe-University Frankfurt, 60438 Frankfurt am Main, Germany
[3] Helmholtz Research Academy Hesse for FAIR (HFHF), 60438 Frankfurt am Main, German

Abstract

To minimize the footprint and costs of RF accelerators, R&D is evolving toward ultra-high frequencies (0.3–3 GHz). However, miniaturization imposes severe fabrication constraints and thermal challenges. We address these issues by leveraging metal additive manufacturing (MAM), enabling intricate geometries and design flexibility for enhanced performance. This paper highlights key advancements from GSI's ongoing UHF-MAM projects, demonstrating its role in the development of next-generation UHF accelerator structures.

INTRODUCTION

A key R&D focus of the Research on Additive Construction for Efficient Resonating Structures (RACERS) team at GSI is the development of efficient Ultra-High Frequency (UHF, 0.3–3 GHz) accelerators for low-to-medium beam energy ranges. As indicated by the scaling laws in Table 1, increasing the resonant frequency allows for a reduced footprint, lower power consumption, and enhanced sparking resistance, significantly cutting construction and operation costs.

Table 1: Scaling of Normal Conducting Resonator Parameters With Frequency

Parameter	Scaling
Linear dimensions	f^{-1}
Power consumption per length	$f^{-1/2}$
Quality factor Q_0	$f^{-1/2}$
Shunt impedance per length @ same E_{acc}	$f^{1/2}$
Kilpatrick limit	$\approx f^{1/2}$

However, operating at such high frequencies results in RF structures with highly compact dimensions, posing significant cooling challenges for room-temperature operations due to increased power density. To address this, the RACERS team has spent years investigating Metal Additive Manufacturing (MAM) as a smart solution for future accelerators and storage rings [1-4]. By bypassing conventional manufacturing constraints, MAM offers numerous advantages, including unprecedented design freedom that enables novel and more efficient cooling schemes. While the RACERS team's earlier R&D, including evaluations of surface roughness, vacuum compatibility, and low-level RF performance of MAM-fabricated components, has been summarized in [4], this paper presents the RACERS team's most recent progress across several key projects within the UHF-MAM domain. These efforts contribute to an emerging global community dedicated to additive manufacturing for particle accelerators [4-8].

†c.zhang@gsi.de; ORCID: 0000-0002-6108-7942

704.4 MHz CH-DTLs

As a flagship project of the RACERS team, the 704.4 MHz RACE (Resonators Additively Constructed for Experiments) cavity represents both the highest-frequency Crossbar H-mode (CH) resonator achieved to date and the first realization of such a structure via MAM. This fully additively manufactured Drift-Tube Linac (DTL) cavity comprises pure copper electrodes and a 316L stainless-steel cavity wall, with the latter intended for copper plating. A key highlight is the unique, slim lotus-root-inspired curved channels ($Ø_{min}$ = 3 mm), as shown in the CT scan in Fig. 1 and more clearly in Fig. 2. This novel cooling architecture, enabled by MAM, provides exceptionally efficient thermal management [3, 4].



Figure 1: Realization of the fully additively manufactured 704.4 MHz RACE CH cavity.

Following further mechanical modifications, copper plating of the cavity wall, and a change in the coupling scheme from the original capacitive configuration to an inductive loop, a second low-level RF measurement campaign was conducted on the MAM-fabricated RACE cavity [9]. The dynamic tuners demonstrated a tuning range from 701.9 MHz to 706.3 MHz. A representative S-parameter measurement at 704.43 MHz yielded a loaded quality factor of about 2.48×10^3. Accounting for the measured coupling levels, the unloaded quality factor was estimated at 5.5×10^3. Furthermore, updated bead-pull measurements revealed a marked improvement in field symmetry compared to the initial capacitive-coupling configuration [4]. More precise characterizations will be performed on the final assembly of the RACE cavity, ensuring optimized contact and integration with the final RF coupler (also MAM-fabricated). Meanwhile, the

Content from this work may be used under the terms of the CC BY 4.0 licence (© 2026). Any distribution of this work must maintain attribution to the author(s), title of the work, publisher, and DOI.

ISBN: 978-3-95450-252-3 ISSN: 2673-5350 doi: 10.18429/JACoW-IPAC2026-MOP7170

MEASUREMENT OF DIELECTRIC PROPERTIES OF 3D PRINTED POLYMER-BASED MATERIALS FOR RF APPLICATIONS AT 500 MHz

P. Müller*, H. Hähnel
Institute of Applied Physics, Goethe University Frankfurt, Frankfurt am Main, Germany

Abstract

To include 3D printed polymer-based materials in accelerator parts, the relative permittivity and the dielectric loss tangent of these materials have to be well known. A quarter wave cavity was built to measure these properties at a resonance frequency of 500 MHz by inserting a cylinder of the material under test, resulting in a frequency and quality factor shift of the cavity. By fitting the measured data to detailed CST simulations, the values of the relative permittivity and the dielectric loss tangent can be obtained. These results provide the necessary material parameters for further investigations into their use in RF accelerator components such as power couplers.

INTRODUCTION

Metal 3D printing is already under investigation in linear accelerator components, enabling complex geometries that are almost impossible to manufacture conventionally [1–4]. In addition, consumer desktop 3D printers are widely used for fast prototyping, using polymer-based thermoplastic materials.The wide variety of polymer-based materials could also allow the use of these materials in linear accelerator components, such as RF power couplers, RF windows or in vacuum isolators. Therefore, it is important to estimate the dielectric properties of these materials, especially the relative permittivity ε_r and the dielectric loss tangent $\tan(\delta)$ are crucial parameters.For the common 3D printing materials such as PLA, PETG, and ABS, measurements of the relative permittivity were already performed at different frequencies [5–9]. Unfortunately, these materials have relatively low heat resistance compared to conventionally used materials such as ceramics (Al_2O_3) for this type of application, which motivates the investigation of advanced polymer-based materials.To estimate the values of the relative permittivity and the dielectric loss tangent a dedicated quarter-wave ($\lambda/4$) test cavity (see Fig. 1) was built from aluminum to achieve a high quality factor. The test cavity consists of three parts (inner conductor, tank, lid). A cylindrical test object made of the material under test induces a shift in frequency and quality factor of the test cavity. A comparison with detailed CST simulations yields the values of the relative permittivity ε_r and dielectric loss tangent $\tan(\delta)$ of the material under test.

SIMULATIONS

The dedicated quarter-wave test cavity in Fig. 1 was designed in CST Microwave Studio for a resonant frequency of 500 MHz. Due to tolerances in the manufacturing process, a corresponding simulation using the final dimensions was performed, yielding a resonance frequency of $f_0 = 499.627$ MHz and an unloaded quality factor of $Q_0 \approx 9746$.In CST, the contact resistance between the three parts was not taken into account, which is why the simulated quality factor is too optimistic. The real quality factor was measured and the CST simulation was adjusted to match this real quality factor of $Q_0 = 6127$. The measured resonance frequency $f_{0,\text{measured}} = 499.628$ MHz of the test cavity agrees with the simulated value within 1 kHz, indicating a good match between measurement and simulation.

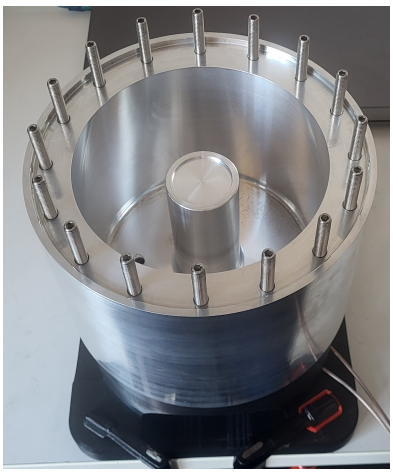

Figure 1: Final setup of the dedicated test cavity with removed top lid.

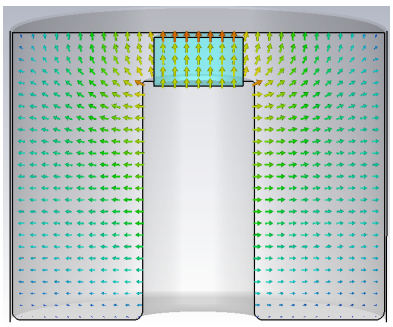

Figure 2: Cross-section of the CST model with a test object placed on the inner conductor. The arrows visualize the electric field inside the cavity.

Due to the quarter-wave ($\lambda/4$) structure of the test cavity, the electric field between the top of the inner conductor and the lid is approximately uniform; this region also exhibits the maximum field amplitude. A field disturbance caused by insertion of dielectric material in this region leads to a shift in resonance frequency and quality factor of the test cavity.A

* mueller@iap.uni-frankfurt.de

Content from this work may be used under the terms of the CC BY 4.0 licence (© 2026). Any distribution of this work must maintain attribution to the author(s), title of the work, publisher, and DOI.

ISBN: 978-3-95450-252-3 ISSN: 2673-5350 doi: 10.18429/JACoW-IPAC2026-MOP7171

EXPERIMENTAL VALIDATION OF AN ADDITIVELY MANUFACTURED 1.3 GHz RADIO FREQUENCY CAVITY

H. Winter*,†,1, V. Schuster*,1, G. Dollinger[1], S. Brenner[1], V. Nedeljkovic-Groha[1], B. Reinarz[2], M. Mayerhofer[1]
[1]University of the Bundeswehr Munich, Neubiberg, Germany
[2]EOS GmbH Electro Optical Systems, Düsseldorf, Germany

Abstract

A compact continuous-wave (CW) 1.3 GHz linear particle accelerator (linac) is currently under development as the core component of a high energy positron annihilation lifetime spectroscopy setup. The associated thermal load imposes stringent requirements on the design and manufacturing of the underlying multi-cell radio-frequency (RF) cavity. Metal-based laser powder bed fusion (PBF-LB/M) has recently demonstrated the capability to fabricate pure copper RF cavities as monolithic components with integrated complex geometries, such as cooling channels. In this work, we present and evaluate a first 1.3 GHz single-cell RF cavity as a prototype for the intended multi-cell structure, manufactured from pure copper using PBF-LB/M. Helium leak rate and low-level RF measurements meet the linac expectations. While the dimensional accuracy is reduced compared to conventional manufacturing methods, it can be compensated by an iterative design approach. These results demonstrate, for the first time, the feasibility of PBF-LB/M as a manufacturing route for monolithic 1.3 GHz RF cavities.

INTRODUCTION

A 1.3 GHz linear particle accelerator (linac) is currently under development at the *University of the Bundeswehr Munich* for a novel material characterization setup based on pulsed positron annihilation lifetime spectroscopy [1]. The linac will accelerate positrons from a few keV up to 1 MeV in continuous-wave (CW) operation. To achieve a high shunt impedance and a compact layout, the linac design is based on a side-coupled radio-frequency (RF) cavity [2]. However, enabling CW operation and thus high positron count rates requires an advanced and highly integrated cooling system. Metal-based laser powder bed fusion (PBF-LB/M) enables the fabrication of highly complex normal-conducting RF cavities as monolithic components, allowing, in particular, enhanced cooling performance and reduced fabrication effort [3–9]. To date, the applicability of pure copper-based laser powder bed fusion (PBF-LB/Cu) to side-coupled RF cavities at 1.3 GHz has not yet been experimentally demonstrated. Therefore, in this work, we present and evaluate a PBF-LB/Cu-fabricated 1.3 GHz single-cell RF cavity (hereafter referred to as *cavity prototype*), representing the first accelerating cell of the planned side-coupled structure.

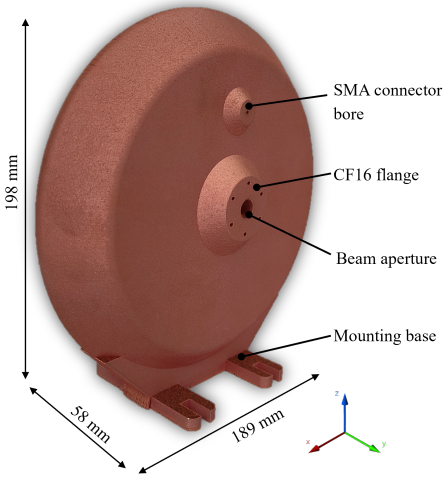

Figure 1: PBF-LB/Cu manufactured 1.3 GHz single-cell cavity structure with features.

MATERIALS AND METHODS

Figure 1 shows a picture of the manufactured cavity prototype, while Fig. 2(a) presents the corresponding CAD model. The cavity prototype was fabricated from pure copper (*EOS Copper CuCP* [10]) using an *EOS M290* [11] with a layer thickness of 40 µm and standard process parameters.

Each side of the cavity features a bore for mounting a *SubMiniature version A* (SMA) RF connector and a *ConFlat* (CF) 16 flange. The helium leak rate of the cavity prototype was evaluated using a *Pfeiffer ASM 340* helium leak detector [12] (Fig. 3). The CF16 flanges were CNC-machined to ensure proper sealing surfaces for elastomer O-rings. A plastic enclosure around the cavity ensured a saturated helium atmosphere during the measurement.

The resonance frequency f_R and unloaded quality factor Q_0 were measured using a *Siglent SNA5012A* vector network analyzer (VNA) [13] with capacitive input and output couplers, as shown in Fig. 4.

Dimensional accuracy was assessed using two complementary approaches. The deviation Δf_R between the simulated (*CST Studio Suite* [14]) and measured resonance frequency was used to evaluate the global geometric deviations [15]. Local geometric deviations were measured directly using a structured-light 3D scanner (*KEYENCE VL550* [16]) with a specified accuracy of 10 µm. The evaluated features are shown in Fig. 2(a).

In addition, metallographic microsections were analyzed at twelve locations across the cavity geometry to assess

* These authors contributed equally to this work.
† Corresponding author: hermann.winter@unibw.de

Content from this work may be used under the terms of the CC BY 4.0 licence (© 2026). Any distribution of this work must maintain attribution to the author(s), title of the work, publisher, and DOI.

This is a preprint - the final version is published with IOP

ISBN: 978-3-95450-252-3 ISSN: 2673-5350 doi: 10.18429/JACoW-IPAC2026-MOP7172

POST-PROCESSING OF ADDITIVELY MANUFACTURED PURE COPPER RFQ ELEMENTS*

T. Romano†, M. Vedani, Politecnico di Milano, Milan, Italy
T. Torims, M. Vretenar, CERN, Geneva, Switzerland
C. A. Bloem Irazabal, L. Portolés Griñán, T. M. Zanello Rial, AIDIMME, Valencia, Spain
G. Pikurs, A. Ratkus, Riga Technical University, Riga, Latvia
M. Pozzi, Rösler Italiana S.R.L., Concorezzo, Italy

Content from this work may be used under the terms of the CC BY 4.0 licence (© 2026). Any distribution of this work must maintain attribution to the author(s), title of the work, publisher, and DOI.

Abstract

The utmost design freedom of additive manufacturing (AM) can be leveraged to fabricate complex particle accelerator components, such as radiofrequency quadrupoles (RFQs). However, the high surface roughness typical of as-printed parts represents a major barrier to the integration of AM technologies into established fabrication workflows. This work investigates finishing processes aimed at improving the surface quality of additively manufactured RFQ components, with a focus on the hard-to-access vane tip region. A dedicated mock-up was developed, consisting of a copper vane representing a one-quarter RFQ section, mounted in a plastic holder to replicate the full part. This setup allows the copper part to be removed after each treatment step to measure material removal and assess effects on vane modulation and surface roughness. Both mechanical mass finishing with abrasive media and chemical polishing were examined, applying each treatment in multiple intermediate steps. Comprehensive surface characterization was conducted by means of profilometry and roughness measurements, showing that both treatments reduce the roughness primarily through the removal of surface asperities. The mechanical treatment approached a plateau after two cycles, achieving a final Ra of ~4.9 µm, while the chemical process reached a slightly higher Ra (~7.7 µm) due to material oxidation and partial exhaustion of the solution. Localized peak flattening and deviations in the vane modulation profile indicate the need for further optimization of both design compensation strategies and post-processing conditions.

INTRODUCTION

AM, particularly laser powder bed fusion (LPBF), offers great potential for the fabrication of complex accelerator components, such as RFQs [1], owing to its high design flexibility and its ability to guarantee properties comparable to those of conventionally processed materials [2]. However, the relatively high surface roughness of LPBF-fabricated parts remains a major limitation, as surface irregularities may compromise the breakdown performance and vacuum compatibility of components [3]. For RFQ applications, a Ra of ~0.4 µm is typically required [4], making post-processing an essential step.

* This work was carried out as part of the I.FAST project within the framework of the European Union's Horizon 2020 Research and Innovation programme under Grant Agreement No. 101004730 and was supported by the Latvian Council of Science under Grant Agreement VPP-IZM-CERN-2022/1-0001.
†tobia.romano@cern.ch

In this study, mechanical mass finishing and chemical polishing were investigated as post-processing techniques to improve the surface quality of pure copper RFQ elements manufactured via LPBF, with particular attention to the hard-to-access vane tip region.

MATERIALS AND METHODS

The RFQ samples were fabricated using a TruPrint1000 Green Edition LPBF system equipped with a disk green laser (λ =515 nm). A linear energy density of 0.625 J/mm was employed to process a 99.95% Cu powder with 15–45 µm particle size, deposited in layers of 40 µm thickness. After printing, the samples were subjected to light blasting using AMACAST 10 stainless steel media. The sample geometry was designed to reproduce one quarter of the CERN 750 MHz RFQ module, as described in [4]. Based on previous measurements conducted on a full RFQ prototype made by LPBF [5], a 250 µm thick allowance was added to the nominal model to compensate for material removal during post-processing. A plastic holder made of polyamide-12 was produced by fused filament fabrication to replicate the full RFQ structure (120 mm in diameter and 150 mm in length) when inserting the copper vane, as shown in Fig. 1.

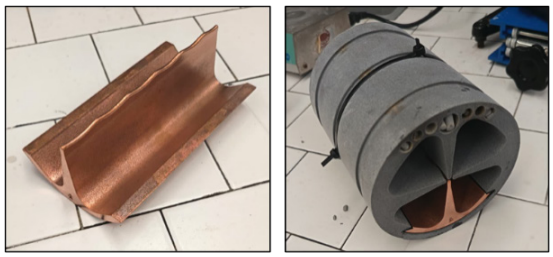

Figure 1: RFQ ¼ vane fabricated by LPBF and inserted in plastic holder for post-processing experiments.

Mechanical mass finishing and chemical polishing post-processing routes were investigated. The mechanical treatment consisted of four cycles of 1 h each, performed in a BRS 22 vibratory tumbler with R.Ecoshape 06/10 ZS abrasive media and water. The chemical treatment also included four cycles, each comprising 30 min of immersion in a chemical solution followed by 30 min rinsing. After these steps, two additional vibrofinishing cycles of 4 h were carried out using a R 150 DL tumbler, with the samples in fixed position, and R.Ecoshape 10/20 DZS abrasive media. All equipment and media were developed and supplied by Rösler Italiana. After each step, the samples were extracted from the holder, rinsed with water, and subjected to comprehensive surface characterization by means of

ISBN: 978-3-95450-252-3 ISSN: 2673-5350 doi: 10.18429/JACoW-IPAC2026-MOP7173

OPTIMIZED PLASMA ELECTROLYTIC POLISHING FOR CU 1.3 GHz SRF CAVITIES

T. E. Ezeaba*,[1,2], E. Chyhyrynets[1], C. Pira[1], O. Azzolini[1], G. Cassarà[1], D. Ford[1], M. Lazzari[1], F. Stivanello[1], G.J. Rosaz[3], H. Araki[3,4], M. Yamanaka[4]
[1]INFN - Laboratori Nazionali di Legnaro, Legnaro, Italy
[2]University of Padua, Padua, Italy
[3]CERN, Geneva, Switzerland
[4]KEK, Tsukuba, Japan

Abstract

The performance of Superconducting Radio Frequency (SRF) cavities is critically dependent on surface quality. While Electropolishing (EP) has traditionally been the standard for achieving low-roughness surfaces on Niobium (Nb) and Copper (Cu) substrates, it relies on hazardous and corrosive acids. Since 2019, Legnaro National Laboratories (LNL) has developed an eco-friendly alternative: Plasma Electrolytic Polishing (PEP). Utilizing only diluted salt solutions, PEP offers significant advantages over EP, including superior removal rates (2-8 μm/min for Nb and 3-30 μm/min for Cu) and surface roughness (R_a) below tens of nanometers. Furthermore, the setup has been optimized to use external cathodes, eliminating the need for complex internal cathode insertion in elliptical cavities. Following the establishment of patented recipes in 2022, PEP was successfully applied to Cu 6 GHz elliptical cavities, QPRs, and 3D-printed devices. A major milestone was achieved in August 2024 with the successful scaling of the process to a 1.3 GHz Cu elliptical cavity. In collaboration with CERN and KEK, the RF performance of PEP was validated on a hydroformed seamless cavity (coated with Nb thin film), demonstrating compatibility and slight performance improvements over standard EP. Further RF validation of PEP on differently produced Cu 1.3 GHz cavities will be presented.

INTRODUCTION

Surface quality of accelerating structures plays a critical role in determining the efficiency and operational reliability of particle accelerators. Surface roughness, often regarded as a persistent challenge in accelerator technology, introduces resistive effects that can impede particle motion, promote unwanted field emission, and degrade overall system performance. These effects ultimately lead to reduced operational efficiency and increased running costs. Consequently, the demand for accelerator components with minimal surface roughness has become increasingly important across the particle accelerator community, particularly within Superconducting Radio Frequency community (SRF) and other related research communities [1].

To address this challenge, INFN-LNL initiated a research program on surface treatment technologies and engineering in 2019 [2]. This effort focused both on the development of novel treatment methods and on the optimization of existing polishing technologies to achieve improved surface quality and process reproducibility. These years of research and development led to the adoption of Plasma Electrolytic Polishing (PEP) as a promising alternative surface treatment method due to its superior surface finish quality, versatility, and economic and environmental advantages over conventional techniques [3].

PEP is an advanced electrochemical surface finishing technique that utilizes the plasma and vapor–gas envelope (VGE) formed around the anodic workpiece to uniformly remove material from surface peaks, thereby reducing roughness and improving surface finish [4]. The advantages of PEP extend beyond its ability to relatively achieve significant roughness reduction and mirror-like surface quality compared with conventional techniques such as electropolishing (EP), buffered chemical polishing (BCP), and mechanical polishing methods. Unlike EP and BCP, which rely on hazardous acid mixtures such as hydrofluoric acid (HF), PEP employs predominantly aqueous electrolytes consisting mainly of water with low concentrations of benign salts, making the process safer for both operators and the environment.

At INFN-LNL, PEP has been successfully applied to a wide range of components, including 6 GHz and 1.3 GHz SRF cavities, one example of which is presented below.

PEP METHODOLOGY AND EXPERIMENTAL PROCEDURE

Figure 1 shows the INFN-LNL Plasma Electrolytic Polishing (PEP) setups used for polishing 6 GHz and 1.3 GHz cavities, respectively. The optimized polishing procedure adopted for both cavity types is identical; the only significant difference lies in the dimensions of the electrolyte bath, which are adjusted according to the cavity size. The standard PEP procedure developed at INFN-LNL consists of the following stages:

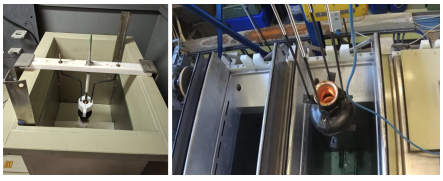

Figure 1: Left: PEP setup for 6 GHz cavity. Right: PEP setup for 1.3 GHz cavity.

* tochukwuemmanuel.ezeaba@studenti.unipd.it

Content from this work may be used under the terms of the CC BY 4.0 licence (© 2026). Any distribution of this work must maintain attribution to the author(s), title of the work, publisher, and DOI.

ISBN: 978-3-95450-252-3 ISSN: 2673-5350 doi: 10.18429/JACoW-IPAC2026-MOP7175

LARGE SCALE PRODUCTION OF AMORPHOUS CARBON COATINGS FOR THE NEW BEAM SCREENS OF THE HL-LHC PROJECT

B. Henrist†, P. Costa Pinto, S. Fiotakis, M. Himmerlich, C. Kouzios
European Organization for Nuclear Research, Geneva, Switzerland

Abstract

The new beam screens for the High Luminosity LHC (HL-LHC) will be coated with a low Secondary Electron Yield (SEY) amorphous carbon (a-C) thin film to suppress electron multipacting and reduce heat loads to the cryogenic system. The production will cover 40 beam screens for the new superconducting magnets of the inner triplets in LHC interaction region 1 (hosting the ATLAS experiment) and 5 (hosting the CMS experiment), as well as 24 beam screens for the drift line of the cryomodules housing the radio frequency CRAB cavities. This contribution presents the implementation of a large-scale coating facility dedicated to the deposition of a-C films on the various HL-LHC beam screens, adaptable to different geometries and lengths up to 14 meters. The rationale behind the chosen coating technology and process parameters is discussed, with emphasis on adhesion optimization, SEY minimization, and production throughput to meet the HL-LHC schedule. We report on the current status of the production campaign, including quality assurance statistics, and highlight the main challenges encountered together with the solutions adopted.

INTRODUCTION

The emission of secondary electrons from carbon thin films depends strongly on their microstructure. Films with a higher fraction of carbon atoms bonded with sp^2 hybridization exhibit lower secondary electron emission, reaching SEY values below 1, while higher fractions of sp^3 bonding may lead to SEY values above 2 [1,2]. Low-SEY amorphous carbon (a-C) coatings have been produced on a large scale by sputtering from graphite targets, usually using Ar as the discharge gas [3]. However, hydrogen contamination, originating from impurities in the discharge gas and outgassing of the coating system, promotes the formation of the sp^3 phase and consequently increases SEY values.

To overcome this issue, particularly when the coating system cannot be baked, two approaches have been investigated: the addition of a small percentage of N_2 to the Ar discharge gas [4], and the co-deposition of a getter material [5]. The latter solution was adopted to coat the new beam screens for the HL-LHC project. In addition to the gettering effect, the deposition of a titanium pre-layer enhances the adhesion of the carbon coating to the copper surface of the beam screens [5].

The beam screens are made of stainless-steel sheets, providing structural strength, with a copper cladding to reduce the resistive wall impedance [6]. Details and dimensions are given in Table 1, and Fig. 1 shows beam screens installed in the coating bench. The beam screens for the CRAB cavity cryomodules are relatively short and are coated in pairs inside a vacuum vessel. The longer beam screens for the new magnets in IR1 (ATLAS) and IR5 (CMS) are coated individually inside a vacuum chamber. They will equip the new inner triplet region magnets, composed of quadrupoles Q1, Q2a, Q2b, and Q3, a corrector package (CP), and the separation dipole magnet D1. The beam screens in the D2 dipole magnet, with two separate beam pipes, will also be coated. These beam screens, except those in D2, are shielded with tungsten blocks to protect the magnet coils from secondary particle showers originating at the interaction point and can weigh up to 300 kg.

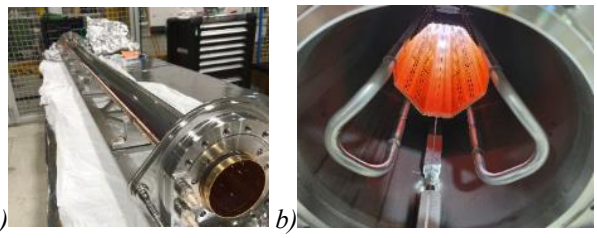

a) b)

Figure 1: a) set of 2 crab cavity beam screens before coating. b) Triplet magnet beam screen before coating.

Table 1: Beamscreen Number, Dimensions and Status (4/26)

Magnet	BS type	Nb	Shape	Dim (mm)	L (mm)	aCC Status
CRAB	DQW	12	Circular	ID 70.1	800	done (2024)
	RFD	12			1 019	done (2024)
ITL	Q1	5	Octogonal	99.7 x 99.7	10 723	2/5
	Q2a	5		119.7 x 110.7	10 292	6/10
	Q2b	5				
	Q3	5			10 607	1/5
	CP	5			7 461	3/5
	D1	5			8 499	1/5
	D2	10		86 x 77	14 083	6/10

COATING PROCESS AND TECHNOLOGY

The coating is performed by magnetron sputtering and involves three main steps: surface preparation by argon ion etching, deposition of a titanium pre-layer, and deposition of the functional amorphous carbon layer. After coating, the beam screens are pumped and stored under a nitrogen atmosphere.

Coating Technology

The sputtering device is a mobile trolley, known as a "train", composed of two targets (Fig. 2a): one graphite and one titanium. The assembly is mounted on rolling supports to keep it centred within the beam screen and to allow smooth axial displacement.

The targets are biased independently via two coaxial Kapton-insulated wires and incorporate encapsulated

† Bernard.Henrist@CERN.CH

Content from this work may be used under the terms of the CC BY 4.0 licence (© 2026). Any distribution of this work must maintain attribution to the author(s), title of the work, publisher, and DOI.

ISBN: 978-3-95450-252-3 ISSN: 2673-5350 doi: 10.18429/JACoW-IPAC2026-MOP7176

ADVANCING ACCELERATOR COMPONENTS DESIGN THROUGH ADDITIVE MANUFACTURING

S. R. Rajendran†, J. Speed, ISIS Neutron and Muon Source, Didcot, United Kingdom
B. Vaidhyanathan, Loughborough University, Loughborough, United Kingdom

Abstract

Additive manufacturing (AM) enables new design approaches for accelerator components by allowing internal features, such as conformal cooling channels, to be integrated directly into parts. At the ISIS Neutron and Muon Source, development began with a polycarbonate cooling jacket for an RF plasma chamber, later replaced with glass-filled nylon due to sealing limitations. The work was extended to metal AM, including a stainless-steel beam dump produced by direct metal laser sintering (DMLS), demonstrating the need for selective post-machining of sealing surfaces. These lessons informed the design of an ion source main flange with internal cooling channels, successfully prototyped, machined, and validated using neutron imaging at the IMAT instrument. Current research focuses on ceramic AM for plasma chambers, integrating cooling channels within the ceramic wall to allow closer RF coil placement. A digital-light-processing (DLP) printed alumina green-body chamber has been produced as a proof of concept, supporting future development in aluminium nitride (AlN) and multi-material ceramic–copper systems for improved thermal management.

INTRODUCTION

Mechanical engineering for particle accelerators frequently demands components with complex internal features - conformal cooling channels, lightweight structures and integrated assemblies - that are difficult or impossible to produce by subtractive methods. AM offers a route to such geometries across polymer, metal and ceramic feedstocks [1]. This paper summarises three streams of development at ISIS that progressively extend AM into vacuum- and thermally-critical accelerator hardware: (i) a polymer cooling jacket for an RF plasma chamber, (ii) a DMLS stainless-steel beam dump and a main flange with internal cooling channels validated by neutron imaging, and (iii) a DLP-printed alumina plasma chamber as a stepping stone towards AlN ceramics.

POLYMER AM

A 3D-printed (selective laser sintering, SLS), epoxy-impregnated polycarbonate cooling jacket was developed and tested as a first iteration to cool an RF plasma chamber under realistic pressure and thermal loads. Experimental testing up to ~2.7 kW demonstrated cooling performance consistent with simulation, validating the overall concept; however, after thermal cycling, leaks developed at the O-ring interface, driven primarily by the limited print resolution and surface finish on the sealing face (Fig. 1). The test campaign also revealed thermal expansion mismatch in the rig, polymer degradation, and galvanic corrosion within the cooling loop. While the cooling principle was proven, these limitations made clear that the polycarbonate route could not deliver the sealing reliability required.

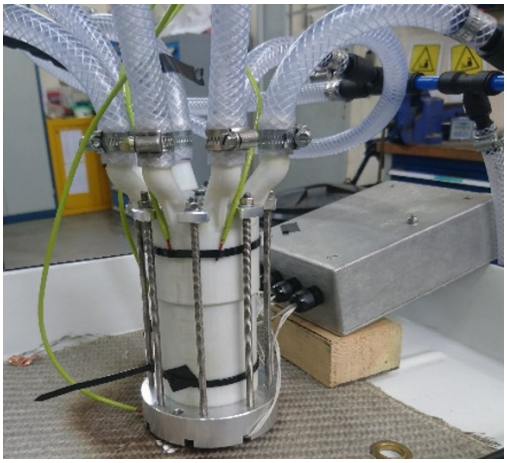

Figure 1: Epoxy-impregnated polycarbonate cooling jacket on the test rig.

The design was therefore transitioned to glass-filled nylon (SLS), which offers higher temperature resistance, improved mechanical robustness, greater dimensional stability under thermal cycling, and a superior as-printed surface finish for reliable O-ring sealing (Fig. 2). Compared with the epoxy-impregnated polycarbonate prototype, the glass-filled nylon material is less susceptible to thermal deformation and degradation, making it better suited for sustained operation under realistic pressure and thermal loads.



Figure 2: Glass-filled nylon cooling jacket assembled over the plasma chamber.

The outer housing used in ion source insertion was manufactured from Stainless Steel primarily to accommodate and support internal components. However, because of its proximity to the RF coil, the metallic housing was

Content from this work may be used under the terms of the CC BY 4.0 licence (© 2026). Any distribution of this work must maintain attribution to the author(s), title of the work, publisher, and DOI.

† sankar.rajendran@stfc.ac.uk

ISBN: 978-3-95450-252-3 ISSN: 2673-5350 doi: 10.18429/JACoW-IPAC2026-MOP7177

DESIGN AND INTEGRATION OF A PASSIVE CAESIUM DELIVERY SYSTEM FOR THE ISIS RF H⁻ ION SOURCE

S. Rajendran†, J. Speed, O. Tarvainen
ISIS Neutron and Muon Source, STFC, Rutherford Appleton Laboratory, Didcot, UK
R. Welton, Oak Ridge National Laboratory, Oak Ridge, TN, USA

Abstract

The ISIS Neutron and Muon Source has developed a new RF-driven H⁻ ion source to replace the caesiated Penning source in use since the 1980s. The new source operates without caesium and has achieved extracted beam currents of up to 18 mA. To increase the beam current further toward operational requirements, a passive caesium delivery system using Cs_2CrO_4 dispensers has been designed and integrated into the RF ion source. The system releases caesium by heating a Cs collar with the plasma, while forced-air cooling and thermocouples provide temperature control. This paper describes the design, materials, cooling approach, and manufacturing process used to convert the source to a caesiated configuration. Important design features include caesium distribution, thermal isolation between components, and cooling of the main flange. Future work will focus on commissioning the system and optimising caesium delivery for stable, high-current operation.

INTRODUCTION

The ISIS H⁻ ion source has used a caesiated Penning surface-plasma source since the 1980s [1]. To improve the ion source reliability and lifetime, an RF-driven volume-mode H⁻ ion source has been developed at ISIS [2] and currently produces extracted beam currents of up to 18 mA without caesium [3]. To reach the operational target current of 45mA (after the installation of a beam chopper), a passive caesium delivery system based on Cs_2CrO_4 dispensers has been designed and integrated into the source, following the approach used routinely at the Spallation Neutron Source (SNS) [4, 5]. This paper describes the system architecture, materials, thermal design, and the two manufacturing routes investigated for the main flange.

CAESIUM DELIVERY SYSTEM DESIGN

System Architecture

The caesium delivery system uses Cs_2CrO_4 dispensers housed in a slotted collar, with forced-air cooling regulating the operating temperature (Fig. 1). A spacer between the collar and the converter acts as a thermal break, allowing the two components to operate at different temperatures. The converter is isolated from the plasma electrode by ceramic balls, which provide both mechanical support and thermal insulation.

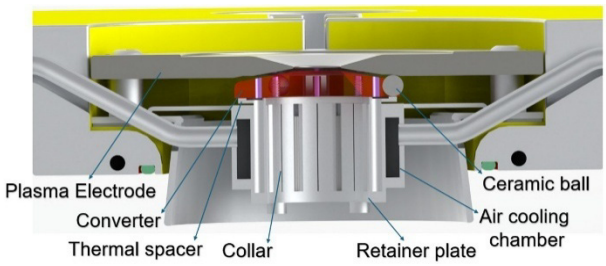

Figure 1: Caesium delivery system — cross section.

Materials and Instrumentation

The converter and plasma electrode are made from molybdenum because of its favourable interaction with caesium for efficient H⁻ production. The remaining components of the caesium system are manufactured from stainless steel 304. Four type-K thermocouples - two in the collar and two in the converter for operational redundancy - are integrated into the assembly to provide temperature monitoring and closed-loop control of caesium delivery.

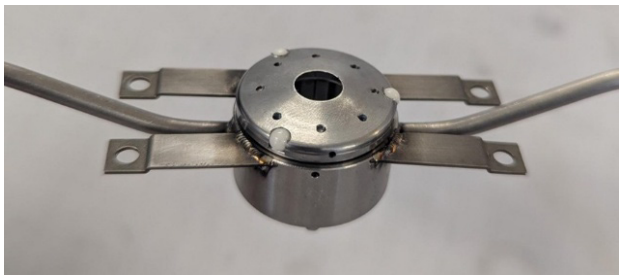

Figure 2: Collar and converter assembly.

Thermal Design

The thermal design is based on calculations for airflow rate, spacer contact area, and O-ring protection. During operation mode the airflow cools the collar from its 550 °C caesiation temperature down to approximately 200 °C, while a thermal-break spacer (25 % contact area) limits heat transfer from the plasma-heated converter and allows it to sit at its 350 °C operating set-point. O-rings located near the heated region are protected by a heat shield and a layered stainless-steel sleeve, which together extend the heat-conduction path and keep elastomer temperatures within safe operating limits.

The airflow rate was sized from a steady-state sensible-heat balance, $\dot{Q} = \dot{m}\, c_p\, \Delta T$, where $\dot{Q}$ is the plasma-deposited heat load on the collar (50kW at 2% duty factor), c_p is the specific heat capacity of air at the film temperature, and ΔT is the permissible air temperature rise across the cooling chamber. The convective heat-transfer coefficient between the collar and the cooling air was evaluated from the Dittus–Boelter correlation, $Nu = 0.023\, Re^{0.8}\, Pr^{0.4}$,

† sankar.rajendran@stfc.ac.uk

Content from this work may be used under the terms of the CC BY 4.0 licence (© 2026). Any distribution of this work must maintain attribution to the author(s), title of the work, publisher, and DOI.

ISBN: 978-3-95450-252-3 ISSN: 2673-5350 doi: 10.18429/JACoW-IPAC2026-MOP7178

A FRAMEWORK FOR ENVIRONMENTALLY CONSCIOUS DESIGN OF PARTICLE ACCELERATORS

A. T. Herrod*, Y. Claereboudt, E. Gravier, F. Stichelbaut
Ion Beam Applications (Belgium), Louvain-la-Neuve, Belgium

Abstract

Particle accelerators typically use multiple times more electrical energy than the kinetic energy of the accelerated particles, resulting in low plug to beam efficiencies. The resources required for such machines are also substantial. Considering these points, we present a multifaceted approach with which we can calculate both the carbon emission impact for production and operation of particle accelerators, as well as the relative scarcities of materials used and their possible radioactivation during a lifecycle. To demonstrate a comprehensive use case, we apply these methods to the EcoCyclone permanent magnet cyclotron concept and compare to a normal-conducting coil powered cyclotron with the same output particle energy: the IBA Cyclone®Kiube. We find the two machines produce similar lifetime carbon emissions where the electricity supply is more carbonised, but caveats such as differing impacts of different material sourcing apply. We discuss how the calculated impacts may change over time, noting increasing electricity cost with decarbonisation, and argue these analyses should be performed during the design phase of all new accelerators.

INTRODUCTION

Particle accelerators typically use many different components often containing scarce materials in their construction, from copper in normal-conducting radiofrequency cavities to rare-earth metals in permanent magnets and HTS conductors. In addition to this, the electrical wall-plug efficiency of particle accelerators is regularly poor due to both RF plug-to-beam efficiency and magnets required for beam manipulation [1].

As different electricity grids have different contributions of high/low/zero-carbon energy sources, and so any electricity saved is beneficial, energy efficiency is a good first indicator of environmentally conscious design.

Cyclotrons typically consume between 10 and 100 kW of electrical power solely for the main coils [2], providing the main magnetic dipole field. While reducing the electricity consumption (and related carbon emissions) of a cyclotron by this amount would be a substantial prize, we must consider the cost in terms of the scarcity of materials required with the carbon emissions for production (and the increased financial cost).

In the work presented here, we develop a method to evaluate and compare the full carbon impact of production and use of particle accelerator components and the scarcity of materials used, applying these as an example to two cyclotron magnet designs from IBA: the Cyclone(R) Kiube [3] and the EcoCyclone concept [4]. We then discuss material sourcing, machine manufacture and use in different countries, and how this affects the overall impact of the machine.

We then briefly discuss water usage and conclude that the framework presented here is suitable for any accelerator component. For the example of magnets presented here, we conclude some rare minerals/materials used in pursuit of lower operation emissions cause high production emissions. In some cases, we find this completely counterbalances what these changes would otherwise save over the lifetime of a device, though this is found to depend on the country of manufacture and country of installation.

STUDY CASES

To best illustrate the framework, we present its application to two designs of cyclotron magnet, with the same methods applicable to any device in a particle accelerator. The properties of each design are given in Table 1.

Table 1: Magnet Properties

Magnet:	**Kiube**	**EcoCyclone**	
		NdFeB	SmCo
Steel Mass[t]	14	35	39
Copper Mass[t]	2	0	0
NdFeB Mass[t]	0	8.4	0
SmCo Mass[t]	0	0	12
Total Power[kW]	19	0	0

The IBA Cyclone(R) Kiube represents a compact cyclotron already on the market, consisting of a square yoke and normal-conducting copper coil. The "total power" we consider for this case is the sum of the coil and the coil-cooling system (water pump and heat exchangers) of 19 kW.

The IBA EcoCyclone represents a possible solution to implementing permanent-magnet cyclotron magnets, providing a field equivalent to that of the Kiube. Two options exist for this design: neodymium (NdFeB) or samarium-cobalt (SmCo) permanent magnets, with the latter requiring more steel to compensate for the typically weaker magnetic strength at room temperature [5]. We shall examine both options for the study here.

We consider a 25-year magnet lifetime, with possible extension to 30 years, with an average of 8 hours per day magnet up-time.

CARBON EMISSIONS

To obtain the carbon emissions from production and electricity consumption during use, we use the Ecoinvent Database [6, 7]. Particularly, carbon emissions values in

* alexander.herrod@iba-group.com

Content from this work may be used under the terms of the CC BY 4.0 licence (© 2026). Any distribution of this work must maintain attribution to the author(s), title of the work, publisher, and DOI.

ISBN: 978-3-95450-252-3 ISSN: 2673-5350 doi: 10.18429/JACoW-IPAC2026-MOP7179

PRELIMINARY POWER BALANCE ASSESSMENT OF THE PERLE ENERGY RECOVERY LINAC*

F. Bouly†, M. Baylac, Univ. Grenoble Alpes, CNRS/IN2P3, Grenoble INP, LPSC, Grenoble, France
R. Abukeshek, M. Ben Abdillah, S. Blivet, S. Chance, P. Duchesne, P. Duthil,A. Fomin, W. Kaabi, A. Lermitage, B. Mercier, J. Michaud, G. Olivier, G. Olry, L. Perrot, D. Reynet, R. Roux, H. Saugnac, A. Stocchi, D. Till, Université Paris-Saclay, CNRS/IN2P3, IJCLab, Orsay, France
H. Abualrob, An-Najah National University, Nablus, Palestinian Territories
On behalf of the PERLE collaboration

Abstract

The PERLE project aims to build a high-power electron Energy Recovery Linac (ERL) demonstrator (5 MW) to develop and apply the energy recovery technique in a multi-turn configuration. In an initial intermediate phase, PERLE will operate in a single-turn mode with a 5 mA beam at 89 MeV. In its final layout, the machine will run in a three-turn mode, delivering a 20 mA electron beam at 250 MeV. These challenging parameters make PERLE a unique multi-turn ERL facility operating in an unexplored power regime, enabling the study and validation of a broad range of accelerator phenomena and paving the way for future, larger-scale ERLs. The principal advantage of ERLs lies in their ability to return the power of a spent beam to the RF system. This recovered power can then be used for acceleration with practically no losses, thereby improving the sustainability of high-power machines. One of PERLE's goals is to assess the overall sustainability of a multi-megawatt ERL. In this work, we present the current status of the studies carried out to evaluate the total electrical power consumption ("plug-to-grid") of the accelerator and relate this consumption to the average beam power delivered at the interaction point. The power balance of a high-power multi-turn ERL is discussed and its efficiency is compared with that of conventional accelerator types (e.g. linacs). The impact of configuration (single-turn and multi-turn) is also briefly discussed.

CONTEXT

Efficiency and Power Consumption

The sustainability of research infrastructures is a multi-dimensional challenge. It is not limited to electrical energy consumption alone, but also encompasses issues related to the management of cooling and cryogenic systems, including water and helium consumption, as well as the use of critical materials and component lifecycle management. Nevertheless, for many accelerator-based facilities, reducing electrical power consumption has become a primary concern and an important factor to optimise operation.As a first example, one could consider CERN. Its annual electricity consumption is approximately ∼1.3 TWh. During accelerator shutdown periods, this consumption decreases by about ∼60 % [1, 2]. These figures highlight the sustainability challenges for future large-scale facilities, such as high-power superconducting (SC) linacs like ESS (European Spallation Source) or SNS (Spallation Neutron Source). For the latter, the overall efficiency (see Eq. 1) has been measured to be around 10 % [3] : the linac requires more than 16 MW of electrical power to deliver an average beam power of 1.4 MW. Nearly half of this consumption originates from the RF power systems (high-voltage modulators + klystrons), which are also one of the most failure-sensitive subsystems [4]. To reduce these risks and improve efficiency, several approaches can be considered. One option is the modernisation of existing facilities using more efficient technologies. For example, the Swiss Light Source aims to reduce its energy consumption by ∼30 % through the use of permanent magnets, upgraded cooling pump systems, and more efficient RF amplifiers (solid-state based) [5]. Efficiency also depends on beam availability and, consequently, on subsystem reliability. In some cases, fast fault-compensation strategies and retuning procedures [6–8] can help ensure sustainable operation and maximise beam availability. For applications that are non-destructive or only minimally perturb the beam, alternative accelerator concepts have been developed. Energy Recovery Linacs (ERLs), based on well-established technologies, enable the recovery of beam power and thereby allow a substantial reduction in overall energy consumption [9].

ERL POWER CONSUMPTION

PERLE & Linac

The aim of this study was to provide a first estimate of the overall power consumption of the PERLE facility and to assess the efficiency gain of an ERL relative to a conventional SC linac. In this context, a first comparison was performed between the PERLE ERL configuration and a SC linac delivering the same electron beam at the interaction point: 20 mA at 250 MeV (i.e. 5 MW) in continuous wave (CW) mode (cf. Fig. 1). The metric used to quantify efficiency is the ratio between the beam power at the interaction point (i.e. the power transferred to the beam, ΔP_b) and the electrical power drawn from the grid (P_{grid}):

$$\eta = \frac{\Delta P_b}{P_{\text{grid}}}. \quad (1)$$

* Work supported by the Agence Nationale de la Recherche via its program ANR-24-RRII-0001 and by the European Union's program EU HORIZON-INFRA-2023-TECH-01-01 under GA n°101131435.

† frederic.bouly@lpsc.in2p3.fr

Content from this work may be used under the terms of the CC BY 4.0 licence (© 2026). Any distribution of this work must maintain attribution to the author(s), title of the work, publisher, and DOI.

ISBN: 978-3-95450-252-3 ISSN: 2673-5350 doi: 10.18429/JACoW-IPAC2026-MOP7180

COOLING-TOWER TECHNOLOGIES FOR THE IFMIF-DONES HEAT REJECTION SYSTEM: TECHNICAL AND ENVIRONMENTAL CONSIDERATIONS

I. Sampedro†,[1], C. Caballero[1], J. Cantero[1], P. Cara[2,4], R. Folgoso[3], M. Luque[1], A. Moreno[1], I. Podadera[1], C. Torregrosa-Martin[1], M. Weber[1]
[1]Consorcio IFMIF-DONES España, Granada, Spain
[2]Fusion for Energy, Garching, Germany
[3]ATG Science and Engineering S.L., Barcelona, Spain
[4]DONES Programme Team, Granada, Spain

Abstract

The International Fusion Materials Irradiation Facility-DONES (IFMIF-DONES) is a scientific infrastructure intended to test and qualify materials for fusion reactors by exposing them to intense neutron fluxes. Several auxiliary systems will ensure its continuous operation, among which the Heat Rejection System (HRS) is designed to remove and discharge to the environment the heat mainly generated by the Accelerator's primary cooling loops and the Test Cell. While open evaporative cooling towers are widely used for industrial heat rejection, alternative technologies may be more suitable depending on site-specific conditions and project priorities. Environmental factors—particularly local weather patterns and their expected evolution under climate change—play a decisive role in overall system performance. Their proper assessment is therefore essential for selecting the most appropriate cooling-tower technology. This work presents a comparative evaluation of candidate heat-rejection solutions to identify the technology that best fits the site conditions, optimises performance over the system's life cycle, and supports the project's commitment to minimising its environmental footprint.

INTRODUCTION

Water is considered a high-value resource, particularly in regions with potential future water scarcity, such as some areas of southern Spain. Despite Granada's area is nowadays out of those areas, minimizing water consumption has been identified as a key objective in both the design and operational phases of the IFMIF-DONES project.

As part of the plant systems, Heat Rejection System (HRS) is a critical auxiliary system that ensures continuous and reliable operation by removing heat mainly from the accelerator primary cooling loops, test systems and lithium systems [1].

Although open evaporative cooling towers constitute the reference design for the HRS, their water consumption raises justified the assessment of alternatives which could reduce the demand. This paper summarises a comprehensive technical assessment of water demand, optimisation opportunities and alternative cooling-tower technologies, supporting the selection of the most appropriate solution for the IFMIF-DONES site.

IFMIF-DONES INFRASTRUCTURE LOCATION AND WATER AVAILABILITY

Location

IFMIF-DONES infrastructure is located at Metropolitan, Industrial and Technological Park of Escúzar [2], 18 km southwest of Granada city, Spain (Fig. 1).

It is an industrial area where there are several companies from different sectors already running.



Figure 1: IFMIF-DONES infrastructure location.

Water availability

The water available is provided to the industrial area by underground natural sources linked to Sierra Nevada snowmelt (Fig. 2). Currently, two of the five sources available are in operation, with a combined capacity of 100 l/s (50 l/s per source), while the three remaining sources are available for future use when needed.

The total officially assigned capacity to the industrial area is 31.95 l/s (998,000 m³/year), of which current industrial consumption represents approximately 20%. There is no specific consumption cap defined per consumer, and capacity upgrades can be managed if required.

Based on the first assessment of the project, make-up water for cooling towers represents about 95% of the total water demand and, therefore, dominates any optimisation strategy [2]. The assessed demand confirms the feasibility of operating the HRS within the existing water-supply framework.

This work has been partially carried out in the framework of the European Regional Development Fund (ERDF) 2021-2027, through the DONES-TOPS project, co-funded by the Government of Spain and the European Union, and the DONES-BASE project, co-funded by the Regional Andalusian Government and the European Union.
†ignacio.sampedro@ifmif-dones.es

Content from this work may be used under the terms of the CC BY 4.0 licence (© 2026). Any distribution of this work must maintain attribution to the author(s), title of the work, publisher, and DOI.

ISBN: 978-3-95450-252-3 ISSN: 2673-5350 doi: 10.18429/JACoW-IPAC2026-MOP7181

ENERGY EFFICIENCY IN THE NORTH EXPERIMENTAL AREA AT CERN

T. Zickler, M. Brugger, N. Charitonidis, S. Deleval, Y. Gaillard, X. Genillon, A. Huschauer, Y. Kadi, N. Kahn, J. Ridewood, Ph. Schwarz, M. Wolf
European Organization for Nuclear Research, Geneva, Switzerland

Abstract

The North Experimental Area at CERN is a versatile experimental facility that provides proton, hadron, electron, muon, and ion beams to over 2000 users annually for detector R&D and fixed-target experiments. Currently, this facility, which is more than 45 years old, is undergoing a consolidation program to enhance availability and reliability and to prepare for new experiments and test beams in the coming decades. In this context, and within the framework of ISO 50001, energy efficiency was assessed, potential energy-saving opportunities were identified, and various strategies for sustainable operation were evaluated. This contribution summarizes the results and outlines planned measures for future implementation.

CERN EXPERIMENTAL AREA NORTH

The North Experimental Area at CERN, commonly known as the "North Area", was constructed in the 1970s at the CERN Prévessin site. It features a complex of three experimental halls, service buildings, and underground tunnels, comprising approximately 7 km of beamlines. The total surface area of the North Area facilities is 60 000 m^2. With a primary beam provided by the Super Proton Synchrotron (SPS), the North Area offers particle beams across a broad energy spectrum and various particle types for fixed-target experiments and R&D test-beam programs for collaborations. Over the last fifty years, the North Area has been one of the most frequently utilized experimental areas at CERN. Figure 1 illustrates the range of beamlines, experiments, and test facilities available. Due to its unique characteristics, the North Area remains the only place in the world where such physics studies can be performed.

To secure the availability of this facility for the physics community in the future, the North Area Consolidation (NACONS) project was approved in 2021. This project aims to enhance the North Area's reliability, safety, and scientific capabilities in the next decade through infrastructure renovation, beamline upgrades, safety improvements, and the modernization of scientific equipment.

Energy Consumption in the North Area

The North Area has an average annual electricity consumption of 104 GWh during a Run year[1], representing approximately 8 % of CERN's total electrical energy use. In Shutdown years, the electricity consumption of the North Area drops to less than 20 % of that in a Run year. Magnets account for a large share of the North Area's total power consumption. In 2024, a typical Run year, they used 57.6 GWh: The 154 DC beamline magnets consumed 19.8 GWh, while the 396 cycled beamline magnets used 22.9 GWh. Additionally, the five large experimental magnets, all operated in DC, used 14.9 GWh of electricity. Figure 2 illustrates the distribution of electrical energy consumption for the North Area magnets in 2024.

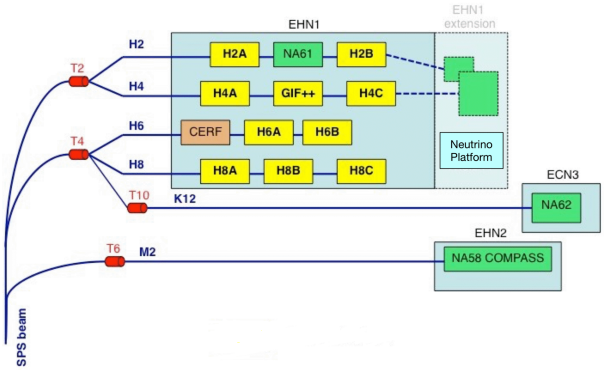

Figure 1: North Area beamlines, with targets (red), experiments (green), and test-beam areas (yellow).

Power Metering

For a reliable assessment of present and future power consumption, a sensible power metering system is key. Today, CERN manages around 500 energy meters across its electrical distribution network, organized by load type and zone via *WebEnergy* [1]. However, the metering in the North Area has a limited monitoring granularity. Planned upgrades to the North Area electrical distribution system will introduce finer metering, fostering a more accurate evaluation of future power consumption. Despite these improvements,

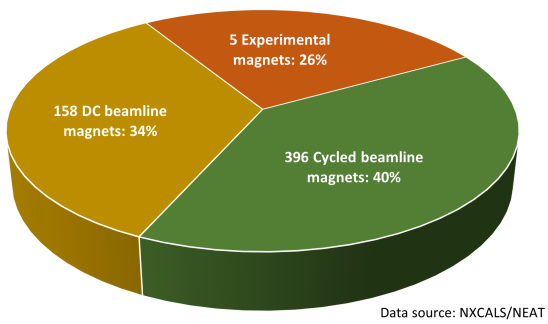

Figure 2: Distribution of electrical energy consumption amongst the North Area magnets in 2024.

[1] During a **Run** year at CERN, machines operate and physics data is collected, with magnets and power converters fully active, resulting in the highest energy consumption. During a **Shutdown** year, most machines are offline for maintenance and consolidation, leading to significantly lower energy use.

Content from this work may be used under the terms of the CC BY 4.0 licence (© 2026). Any distribution of this work must maintain attribution to the author(s), title of the work, publisher, and DOI.

ISBN: 978-3-95450-252-3 ISSN: 2673-5350 doi: 10.18429/JACoW-IPAC2026-MOP7182

METAL ADDITIVE MANUFACTURING FOR ACCELERATOR TECHNOLOGIES (MAAT PROJECT AT INFN)

O. Azzolini[1,†], L. Angioletti[1], [2]M. Cannavó, E. Chyhyrynets[1], F. Grespan[1], G. Keppel[1], C. Pira[1], [3]P. Rebesan, F. Stivanello[1]

[1]INFN Laboratori Nazionali di Legnaro, viale dell'Università 2, 35020, Legnaro (PD), Italy
[2]INFN Sezione di Milano, Via Celoria,16, 20133 Milano, Italy
[3]INFN Sezione di Padova, Via Marzolo 8, 35131 Padova - Italy

Abstract

The MAAT (Metal Additive Manufacturing for Accelerator Technologies) project is a three-year INFN research programme launched in 2026, aimed at establishing Additive Manufacturing (AM) as a validated production route for high-performance accelerator components. MAAT brings together three INFN units: Legnaro (LNL), Padova (PD), and Milano LASA, combining complementary expertise in superconducting RF, materials science, and advanced manufacturing. This paper reports on the activities and preliminary results during the first year of the project, in particular covering:

1. the Design for Additive Manufacturing (DfAM) of 6 GHz cavities produced by Laser Powder Bed Fusion (LPBF).
2. the preliminary tests of the Wire Laser Additive Manufacturing (WLAM) combined with CNC machining for the fabrication of a 1.3 GHz RF cavity prototype in CuCrZr.

INTRODUCTION

The design of next-generation particle accelerators including the Future Circular Collider (FCC-ee) and the Muon Collider imposes unprecedented requirements on critical components such as accelerating cavities, current leads, and cryogenic magnet end spacers. These facilities will demand thousands of highly integrated, geometrically complex, and thermally stable components that conventional manufacturing methods, based on spinning [1], hydroforming, or electron-beam welding, struggle to supply at the required scale, cost, and performance. Additive Manufacturing (AM) has emerged as a transformative technology capable of addressing these challenges. In particular, Laser Powder Bed Fusion (LPBF) enables the direct fabrication of complex internal geometries such as conformal cooling channels, while Wire Laser Additive Manufacturing (WLAM), combined with CNC machining of internal surfaces, offers a hybrid route for large, near net shape components. However, the application of AM to accelerator components remains technologically immature. Critical open issues include high as-built surface roughness incompatible with RF quality factor (Q_0) requirements, residual porosity and powder contamination in internal channels, and the absence of validated end to end manufacturing workflows.

†oscar.azzolini@lnl.infn.it;

The MAAT project directly addresses these gaps through a coordinated three-year programme structured in three Work Packages (WPs): WP1 Materials Research and Development, WP2 Process Engineering and Design for AM, and WP3 Characterisation and Post-Processing Treatments. This paper presents the status of first year activities (January - May 2026).

PROJECT STRUCTURE

MAAT is organised in three Work Packages, each led by a different INFN unit and addressing a specific technological layer of the AM workflow for accelerator components.

WP1 - Materials Research and Development (Leader: MI-LASA)

WP1 targets the development and optimisation of novel copper-based alloys for AM processes. The key objective is to identify materials that offer superior performance compared to the baseline Oxygen-Free Electronic (OFE) copper, currently the reference material for normal-conducting RF cavities, by improving mechanical strength and high temperature resistance while preserving thermal and electrical conductivity. The alloys of primary interest for MAAT are Cu-Ag, Cu-W, and, as an established reference, Cu-Cr-Zr. Table 1 summarises selected properties compared to OFE copper.

Table 1: Key Properties of Copper Alloys Under Investigation in MAAT

Material	Thermal Cond. (W/m·K)	Tens. Strength (MPa)	High-T Resistance
OFE Cu	~398	220–250	Limited
Cu-Cr-Zr	~320-340	400–550	Good
Cu-W	140-250	200–850	Excellent
Cu-Ag	330-390	200–600	Improved

The first-year activities focus on Task 1.1 (powder blend formulation and characterisation): copper-based alloy

Content from this work may be used under the terms of the CC BY 4.0 licence (© 2026). Any distribution of this work must maintain attribution to the author(s), title of the work, publisher, and DOI.

ISBN: 978-3-95450-252-3 ISSN: 2673-5350 doi: 10.18429/JACoW-IPAC2026-MOP7183

OPERATIONAL SEQUENCER FOR ESS FACILITY

M. Celary*[1], A. Gorzawski[2], D. Spruce[2]
[1]S2Innovation, Kraków, Poland
[2]European Spallation Source, Lund, Sweden

Abstract

The Operational Sequencer is a software framework developed to automate complex and frequently executed high-level procedures that are essential to the operation of accelerator systems at the European Spallation Source (ESS). By transforming manual control room tasks into predefined sequences, the tool enhances process repeatability, reliability, and safety by reducing human error.

Designed within the ESS Integrated Control System Software group, the sequencer provides a unified architecture for defining, executing, and monitoring operational tasks. It supports multiple task execution types, scalable system design, and an intuitive graphical interface to facilitate operator oversight.

This paper presents the architectural concepts, implementation challenges, and scalability strategies of the Operational Sequencer, as well as lessons learned from its deployment during ESS commissioning. The framework represents a significant step toward efficient and reproducible operations, reducing both operator workload and time-to-beam for scientific experiments.

RATIONALE

The concept of an operational sequencer for ESS has been discussed for several years. In the earlier stages of beam production, only a limited part of the accelerator was in operation. As a result, the overall complexity remained manageable and many activities could be carried out manually. In this context, existing tools such as Save and Restore were sufficient for tracking configuration settings and machine states.

As the scope of operation expands, there is a growing need to organize higher-level procedures composed of actions typically performed by operators. These actions may include setting process variables (PVs), executing sequences available within the EPICS control system, or incorporating steps that require manual intervention. The Operational Sequencer is intended to support this type of structured workflow.

Experience from other facilities shows clear advantages of applying automated sequencing to common accelerator operations. Previously, procedures were often documented as detailed written instructions describing how to interact with GUI interfaces and which parameters to set in a specific order. Such an approach is susceptible to human error, as individual executions may deviate from the intended procedure, making reproducibility difficult to ensure. The Operational Sequencer provides a way to address these issues.

* mateusz.celary@gmail.com, linkedin.com/in/mateusz-celary/

TECHNICAL DESIGN AND IMPLEMENTATION

Existing Alternative Solutions

Numerous discussions during the design phase considered several alternative approaches. Among them were the "classic" EPICS sequencer [1] and the more recently introduced oac-tree developed at ITER [2]. The EPICS sequencer operates at the IOC level, with state transitions driven by changes in process variables. While effective for local control logic, this model is less suitable for procedures spanning multiple IOCs and large numbers of PVs. Its reliance on the State Notation Language (SNL), which must be compiled and deployed to IOCs, also makes it less convenient in environments where operational procedures evolve frequently. In addition, it does not support pvAccess, the preferred protocol at ESS.

Another commonly used alternative is to implement procedures as custom Python scripts or Jupyter notebooks. Although such solutions are flexible and can be developed quickly, they are generally more difficult to review, validate, and maintain in an operational setting. In practice, their logic is often primarily understood by the original author, which can introduce an unnecessary divide between technically specialized operators and regular users. This also makes it more difficult to assess whether a given implementation correctly reflects the intended operational procedure.

The oac-tree [2] represents a recent addition to the EPICS software ecosystem. Although it is not currently used in ESS operations, it may still offer value as an intermediate orchestration layer for coordinating sequences across multiple systems.

The ESS Operational Sequencer was therefore designed as a higher-level solution operating across multiple applications and beyond the strict EPICS layer. This makes it possible to integrate different sequencing approaches within a single operational framework and to combine their advantages in a manner better suited to the needs of ESS.

Architecture

The software architecture was intentionally kept simple and minimalistic, designed to satisfy the minimum known requirements without over-engineering. Sequence definitions are written in YAML with optional Jinja2 templates. This is a well-established format used by tools such as GitHub Actions, GitLab CI/CD, and Ansible. It is readable, parameterizable, and widely recognizable, which made it a natural design choice and allowed us to avoid creating a dedicated sequence definition language.

Content from this work may be used under the terms of the CC BY 4.0 licence (© 2026). Any distribution of this work must maintain attribution to the author(s), title of the work, publisher, and DOI.

ISBN: 978-3-95450-252-3 ISSN: 2673-5350 doi: 10.18429/JACoW-IPAC2026-MOP7185

TECHNOLOGICAL INNOVATION FOR NEXT-GENERATION PARTICLE ACCELERATORS: KEY OUTCOMES OF THE I.FAST PROJECT*

M. Vretenar†, T. Torims, F. Carra, F. Zimmermann, CERN, Geneva, Switzerland
C. Antoine, S. Leray, L. Quettier, CEA-IRFU, Gif-sur-Yvette, France
R. Bartolini, DESY, Hamburg, Germany
P. Forck, G. Franchetti, C. Roux, GSI, Darmstadt, Germany
E. De Matteis, M. Ferrario, M. Morandin, N. Pastrone, INFN, Italy
P. N. Burrows, University of Oxford, Oxford, United Kingdom
M. Seidel, PSI, Villigen, Switzerland
A. Ratkus, Riga Technical University, Riga, Latvia
O. Malyshev, STFC, Swindon, United Kingdom
R. Edgecock, University of Huddersfield, United Kingdom
T. Romano, Politecnico di Milano, Milan, Italy

Content from this work may be used under the terms of the CC BY 4.0 licence (© 2026). Any distribution of this work must maintain attribution to the author(s), title of the work, publisher, and DOI.

Abstract

Next-generation particle accelerators demand innovative technologies able to meet the performance and sustainability requirements of particle physics and applied science, while ensuring high efficiency and reduced costs for industrial and societal applications. The I.FAST (Innovation Fostering in Accelerator Science and Technology) Project, supported by the European Commission under the Horizon 2020 program, has fostered progress in the accelerator community by developing a portfolio of breakthrough technologies and strategic roadmaps for future research infrastructures, such as energy-frontier hadron and lepton colliders, and for medical and environmental applications. The project contributed to the development of novel accelerator designs – including multi-TeV muon colliders, plasma-based accelerators, and high-brightness synchrotron light sources – as well as advanced materials, high-performance components, and cutting-edge manufacturing and diagnostic tools. These efforts collectively aim to improve the energy efficiency, sustainability, affordability, and compactness of future facilities. Key outcomes include novel radiation-resistant beam window and absorber materials, stabilization tools for laser accelerators, C- and X-band RF devices for free electron lasers, low-loss LTS and high-temperature superconducting CCT magnets, innovative SRF cavity fabrication and coating methods, additively manufactured linac structures, and high-efficiency klystrons and permanent magnets.

INTRODUCTION

Next-generation particle accelerator facilities face increasingly stringent requirements in terms of performance, energy efficiency, and cost to serve both fundamental research and a wide range of applied sciences and societal applications. Meeting these expectations demands new technologies, materials, and design approaches that enable more compact, energy-efficient, and cost-effective infrastructures. In parallel, the growing market demand for accelerator-based solutions, including medical, industrial, and environmental applications, highlights the need for an innovation ecosystem capable of rapidly translating R&D advances into practical, deployable systems.

The I.FAST project was implemented in continuation with previous EU projects on accelerator technologies [1-3] to address these strategic needs within the accelerator domain. Through extensive networking initiatives involving a broad community of academic, research, and industrial partners – which included four Challenge-Based Innovation events [4], the Accelerator Industry Permanent Forum [5], and a dedicated industry exchange program [6] – the project has expanded and structured the accelerator innovation ecosystem and reinforced long-term collaboration between research and industry, promoting the rapid transfer of emerging technologies to applied science and societal applications. Partly through its Innovation Fund [7], the project has also supported the development of a diverse portfolio of high-level prototypes, demonstrating novel solutions for magnet technologies, RF systems, and compact components suitable for a wide range of accelerator platforms and applications [8].

This paper provides an overview of the main achievements of the I.FAST project and their impact on accelerator technology. Detailed technical methodologies and results are documented in the project's technological delivery reports, available in [8].

FUTURE CONCEPTUAL DESIGNS AND TECHNICAL SOLUTIONS

I.FAST contributed to new design concepts and key technologies for future high-energy facilities. The project participated in the design of the multi-TeV muon collider based on a proton driver source, and to its structured technological R&D plan [9]. In laser-plasma acceleration, both ultrashort targets for high repetition-rate operation and long targets for high-energy electron beams at low

* This project has received funding from the European Union's Horizon 2020 Research and Innovation programme under Grant Agreement No. 101004730.

† maurizio.vretenar@cern.ch

ISBN: 978-3-95450-252-3 ISSN: 2673-5350 doi: 10.18429/JACoW-IPAC2026-MOP7186

CAD INTEGRATION FOR THE PETRA IV PROJECT

B. List*, M. Diercks, L. Hagge, M. Huening, C. Kula, P.-O. Petersen,
Deutsches Elektronen-Synchrotron DESY, Hamburg, Germany

Abstract

The PETRA IV project at DESY in Hamburg aims for a new, 4th generation light source with first light in 2032. It comprises the installation of a completely new, 2.3 km long 6 GeV electron storage ring and a new injection chain, installation and refurbishment of 31 photon beam lines with 60 end stations, and the construction and refurbishment of 49 buildings including a new 600 m long underground experimental hall.

The project will reuse existing tunnels and halls of the PETRA III light source, and targets a dark time without beam of only 30 months, which is a challenging task that requires thorough planning. To meet this challenge, a comprehensive CAD model has been set up that integrates the data of all participants: construction, photon science, accelerator, campus and logistics.

The model comprises representations of all systems and subsystems in different abstraction levels. A strict structure aligned with the project's WBS and PBS, extensive use of interfaces, and a focus on review and change management processes ensure that the model is complete, consistent and correct and will remain so throughout the entire life cycle of the project.

INTRODUCTION

Large scale accelerator projects pose exceptional challenges on design coordination and the design process. PETRA IV is representative of these challenges in several respects: the project comprises a new, 2.3 km long accelerator with more than 4000 components, 49 buildings including a 600 m long underground experimental hall, and 31 photon beamlines. The disposal of the existing PETRA III accelerator, demolition of three existing experimental halls, construction of the new hall and installation of the new accelerator need to fit into a 30 month dark time, conducted by teams drawn from multiple DESY departments and groups, and external contractors.

The diversity of stakeholder needs constitutes a first challenge to the integrated design model. Project leadership requires a reliable overview of project structure, design status, and consistency across work packages. Accelerator physicists, beamline scientists, civil engineers and infrastructure specialists ask fundamentally different questions, and the integrated model must serve all of them to be useful to the project.

Responsibilities and ownership pose the challenge that the work packages conducting the design work need to be responsible and accountable for their work, without altering or the need to duplicate work outside their remit, to ensure consistency across the project.

This leads to the third, and in practice often most critical, challenge of interfaces. Large projects rarely fail within the domain of single responsible group, but more likely at the boundaries between groups. Requirements and design decisions need to be communicated clearly and reliably, avoiding unnecessary repetition or delay of design work due to incomplete or changing interfaces, and preventing that items fall between the cracks due to unclear responsibilities and scope definition.

Finally, the model must remain useful across all project phases – from conceptual layout through detailed engineering, tendering, installation, and into operation and maintenance. The type of information required, and the precision with which it must be represented, changes substantially across these phases. A model architecture that is not designed for this evolution will either be abandoned as requirements change or will require costly reconstruction.

METHODS

The integrated design model of PETRA IV has been planned from the outset to address the organisational and technical challenges described above. Several principles guide its architecture.

Comprehensive Design Model

A comprehensive Computer Aided Deign (CAD) integration has been established at DESY as part of the PETRA IV project. This model includes all project relevant buildings and tunnel systems as well as the entire machine equipment along the storage ring and its pre-accelerator complex, represented in different configurations (current state and target design). In addition, the model incorporates user systems, experimental installations and technical infrastructure, including supply routes, escape paths and transport routes. It serves as a single source of truth and provides all stakeholders involved in construction and design processes with a complete and reliable geometric context.

Structure

The model hierarchy – complex, facility, area, unit, component – is explicitly aligned with the project's Product Breakdown Structure, as managed in the PLM system. It has been adapted from the physical hierarchy of the ISA-106 standard [1]. This alignment is not merely organisational convenience: it ensures that each work package owns and is accountable for a well-defined portion of the model, and that design review processes can be conducted within the boundaries of individual work packages or work package groups. The linkage to the PBS also provides the foundation

* benno.list@desy.de

Content from this work may be used under the terms of the CC BY 4.0 licence (© 2026). Any distribution of this work must maintain attribution to the author(s), title of the work, publisher, and DOI.

ISBN: 978-3-95450-252-3 ISSN: 2673-5350 doi: 10.18429/JACoW-IPAC2026-MOP7187

FROM LATTICE TO ENGINEERING DESIGN: A RAPID, RELIABLE DEVELOPMENT CYCLE

B. List*, M. Diercks, L. Hagge, M. Huening, C. Kula,
Deutsches Elektronen-Synchrotron DESY, Hamburg, Germany

Abstract

The future PETRA IV synchrotron radiation facility at DESY, Hamburg will be a 4th generation light source in the 2.3 km long PETRA tunnel, with first light in 2032. It comprises 8 straight sections and 8 arcs with 288 girders and space for 72 insertions.

The hybrid 6 bend achromat accelerator lattice aims for as much periodicity as possible to maximise symmetry, which is beneficial for beam dynamics, and minimise cell design variants. However, straight sections each fulfilling differing functions such as injection, rf acceleration or photon generation, more than a dozen variants of insertion devices, and differing tunnel cross sections introduce substantial variability of girders, cells, and arcs, increasing the engineering effort.

We have set up an engineering process, supported by a set of automated tools, that establishes a rapid, reliable translation of the lattice to the positions of all components that act on the beam. More than 4000 individual beamline elements are positioned in this way. As part of the process, we analyse girder variants to minimise the number of different mechanical designs for magnets, vacuum, and other systems, and to facilitate logistics processes. A managed change process ensures that lattice updates are systematically propagated to the engineering design.

INTRODUCTION

The design of a particle accelerator requires two complementary representations of the same machine: the lattice, and the full engineering model. The lattice, as the physicist's model, is the result of beam optics calculations and is the authoritative specification of how the accelerator works. The engineering model, must also account for the concrete physical shape of components, power cables and cooling pipes, vacuum bellows, radiation absorbers, maintenance access envelopes or mechanical supports [1].

As detailed design proceeds, physical realities feed back into the lattice. The lattice and the engineering model therefore co-evolve through an iterative process, and maintaining consistency between them is a central challenge of the design. This consistency requirement has a precise meaning: every beam-influencing element in the lattice must have a corresponding physical component in the engineering model, positioned exactly according to the lattice specification. This correspondence must be traceable and verifiable at any point in the project. For PETRA IV, with more than 4000 individual beamline elements placed along 2.3 km of storage ring, maintaining this traceability by hand is not feasible.

A further complication arises from the hierarchical, repetitive structure of the ring. Components are grouped onto girders, girders into cells, cells into arcs. Identical physical assemblies appear at multiple locations, and the same physical device may correspond to different lattice elements, and conversely, what appears as an identical lattice element at two locations may require physically distinct designs due to local constraints. Mapping correctly between the logical structure of the lattice and the physical variant structure of the engineering model, and doing so consistently across hundreds of assemblies, requires a systematic approach.

Finally, the lattice is not static. It evolves as engineering constraints are identified and fed back into the optics design, and it will continue to evolve throughout the project. Each new lattice version must be propagated into the engineering model rapidly and reliably, without introducing errors or inadvertently disturbing parts of the model that were unaffected by the change. This is particularly important as detailed engineering matures: girder designs that have been finalised and released for manufacturing must not be invalidated by a lattice update that affects a different part of the ring entirely.

Systems whose design depends on the lattice only indirectly need also be taken into account. The lattice directly governs the positions of beam-influencing elements – magnets and beam position monitors. But the vacuum system, the mechanical support structure, and the routing of services such as cooling water and electrical cabling must all fit around these components, and therefore have to be adapted whenever the components themselves change. Managing this dependency chain – from lattice update, through revised positioning data, to updated beamline component assembly, updated vacuum assembly, and revised girder assembly – requires an explicit versioning discipline.

The work described here addresses these four challenges: establishing a direct, automated derivation of component positions from the lattice; providing a rapid and reliable process for translating a new lattice version into an updated engineering model; ensuring that changes propagate only where they are genuinely needed, preserving the stability of released designs elsewhere; and maintaining the integrity of the full assembly hierarchy as both the lattice and the engineering design evolve.

METHODS

To address the challenges outlined above, a number of methods are applied to implement a managed, iterative design process (Fig. 1) that is reproducible, reliable, fast end efficient:

* benno.list@desy.de

Content from this work may be used under the terms of the CC BY 4.0 licence (© 2026). Any distribution of this work must maintain attribution to the author(s), title of the work, publisher, and DOI.

ISBN: 978-3-95450-252-3 ISSN: 2673-5350 doi: 10.18429/JACoW-IPAC2026-MOP7188

MOVING TONS OF FRAGILE CRYSTALS WITH CARE: THE CMS ECAL ENFOURNEUR2 PROJECT

R. Bianco On behalf of the CMS ECAL Group*, Istituto Nazionale di Fisica Nucleare, Rome, Italy

Abstract

The CMS experiment at the CERN Large Hadron Collider features a high-precision electromagnetic calorimeter (ECAL) made of 61,200 lead tungstate crystals in its central (barrel) part. The crystals are both heavy and fragile, requiring extreme care during handling. As part of the HL-LHC upgrade, the ECAL barrel front-end electronics will be replaced, requiring the extraction, refurbishment, and re-insertion of all 36 supermodules (SM), each weighing about 3 tons, within a strict schedule of the technical operations inside the CMS cavern during Long Shutdown 3. A specialized machine, the Enfourneur, will be used for SM extraction. To accelerate operations, a second Enfourneur has been developed, replacing hydraulic actuators with electrical motors and controls. The new system manages three movements: rotation to the insertion angle, forward-backward motion, and controlled SM push-pull. Safety of SMs handling is ensured by numerous sensors and an advanced control system. A touchpad interface provides real-time control of SMs positioning with extreme accuracy, thanks to the implementation of electric motors and related controls, and operational safety, offering to the machine operator predefined movements, fine adjustments, and a continuous monitoring of the forces applied by the machine and ongoing deformations on the most critical metallic carpentry structures. This paper details the Enfourneur2 design, commissioning and operational performance after an intensive testing campaign carried out at CERN.

INTRODUCTION

ECAL is the high-precision electromagnetic calorimeter in CMS experiment at CERN [1, 2]. Its barrel is made of 61,200 lead tungstate crystals, distributed in 36 supermodules (SM), each weighing about 3 tons. During Long Shutdown 3 (LS3), the SMs need to be extracted and re-inserted to allow the replacement of the front-end electronic as part of the HL-LHC upgrade.

The handling of the ECAL SMs requires stringent constraints imposed on the design of the extraction and insertion system [1]. The machine that handles the ECAL supermodules (called the Enfourneur) must reach millimetre-level precision in positioning of these multi-ton elements, avoid mechanical stress on the crystals and on the supporting structures, and be compatible with the confined geometry of the CMS cavern. Safety is a primary concern, both for the protection of the ECAL detector elements and for personnel. The system must provide continuous monitoring of applied forces, structural deformations and positions, and include multiple interlocks to prevent operations under unsafe conditions. In addition, reliability and ease of operation are essential, as the extraction and re-installation of the 36 SMs must be performed within a limited time window.

These requirements motivated the production of a second machine (Enfourneur2 or E2), that will help increase the flexibility and reduce the time required by the ECAL SM insertion/extraction activities. The design changes, with respect to the first machine, aim at improving precision, reducing the activity time and ensuring the highest possible level of safety - for people and objects - guaranteed by the certification of the machine in accordance with the latest regulations in force, issued by the manufacturer. E2 design and construction were entirely coordinated by INFN Roma, as a core contribution to the CMS upgrade.

ENFOURNEUR2 DESIGN

Enfourneur2 is a dedicated 20-tons handling machine designed to interface directly with the ECAL barrel SMs (Fig. 1). It will be placed in front of the CMS detector allowing operators to access the internal layer of the ECAL barrel. It consists of four main mechanical subsystems, derived from the geometry of the Enfourneur1 but individually optimized to meet the requirements of the new machine [3]: Bati, Cradle, Cage and Yellow Beam (Fig. 2).

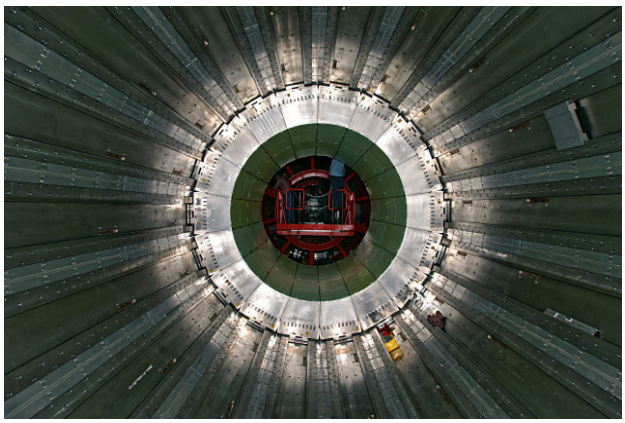

Figure 1: one side along the beam axis of ECAL barrel SMs installed in 2007.

The Bati is the metal carpentry structure that supports the other components during the operations, offers walkways and harnesses connections to allow operators to safely work on the machine, also at height, allows first

* Copyright 2026 CERN for the benefit of the CMS Collaboration. Reproduction of this article or parts of it is allowed as specified in the CC-BY-4.0 license.

Content from this work may be used under the terms of the CC BY 4.0 licence (© 2026). Any distribution of this work must maintain attribution to the author(s), title of the work, publisher, and DOI.

ISBN: 978-3-95450-252-3 ISSN: 2673-5350 doi: 10.18429/JACoW-IPAC2026-MOP7191

DEVELOPMENT OF A HARMONISED FRAMEWORK FOR ELECTRICAL SAFETY COMPLIANCE AT CERN

R. Simpson, L. Scibile, CERN, Geneva, Switzerland

Abstract

Electrical safety has been identified as one of the main risks in large research infrastructures. At CERN, new regulations for electrical safety are being reviewed to align with current best practices and harmonise the approach. Among other aspects, it covers the compliance of electrical equipment and installations before they are put into operation, to further reduce the risk of accidents, to save time and cost by simplifying design processes, and to standardise the application of the legal requirements.

While the new regulations were developed for CERN, they offer a model that can be applied to other research infrastructures. This paper describes the harmonised framework that was implemented to provide a practical guide for applying electrical compliance in the context of a research infrastructure. It was developed based on an analysis of best practices, validated through application to current CERN installations, and verified by industry experts. The framework optimises organisational efficiency by promoting 'right-first-time' compliance through a guided quality process.

This work is part of the CERN Electrical Safety Project, an initiative established within CERN's Accelerator and Technologies sector to take proactive steps to further mitigate electrical risks, prevent recurrence, and build an even stronger safety culture.

INTRODUCTION

Large research infrastructures, such as CERN, rely on extensive and complex electrical systems, and as such electrical safety is regarded as one of the main risks [1]. Since the late 19th century, the inherent risks associated with electrical power have necessitated the development of rigorous safety frameworks, evolving into a sophisticated legal landscape. In Europe, this is characterised by EU Directives for Electrical Equipment [2], and national laws for Electrical Installations [3, 4].

This paper describes the translation of this complex legal landscape into a practical framework termed 'Compliance' within the specific context of research infrastructures. While the framework was conceived and implemented within CERN's Accelerator and Technologies sector, it offers a scalable model that can be applied to other organisations.

In the context of designing and implementing electrical equipment and installations, compliance represents a systematic, guided approach that empowers engineers to produce inherently safe systems. This methodology was developed for three key objectives: to reduce the risk of accidents, to save time and cost by simplifying design processes, and to standardise the application of the legal requirements.

The framework distinguishes between two primary subcategories: Electrical Equipment Compliance and Electrical Installation Compliance, addressed through two distinct processes.

This paper is organised as follows: first, definitions and classifications for electrical systems are established; second, the equipment compliance methodology is described; third, the installation compliance methodology is described; fourth, the resources developed to facilitate the application of the framework are outlined.

DEFINITION AND CLASSIFICATION FOR COMPLIANCE

From a regulatory perspective, the framework is classified into two domains: Electrical Equipment and Electrical Installations.

1. **Electrical Equipment** is defined as an *item used for the generation, conversion, transmission, distribution, or utilization of electrical energy*, [5]. Equipment compliance is modelled through European Directives and Standards.
2. **Electrical Installations** are defined as an *assembly of electrical equipment to fulfil specific purposes*, [5]. Installation compliance is modelled through IEC standards and national laws for electrical installations.

The distinction between these two domains is fundamental: while the legal framework for equipment focuses on the internal design, installation compliance addresses the permanent external wiring and connections between multiple pieces of equipment installed in a specific location.

Classification Model of a Research Infrastructure

To define the roles of installations and equipment within a complex research environment, a simple top-down model was developed. This model is based on how systems are electrically connected, starting with the concept of a 'Facility', a widespread area housing multiple electrical installations.

As shown in Fig. 1, each facility is composed of several installations. These installations are further broken down into equipment, which includes off-the-shelf equipment alongside equipment that could be designed in-house or by an in-kind contributor.

ELECTRICAL EQUIPMENT COMPLIANCE

Since the legal responsibility for compliance rests with the manufacturer (as defined in [6]), commercial off-the-shelf equipment is presumed compliant for its intended use upon purchase. Consequently, the following

Content from this work may be used under the terms of the CC BY 4.0 licence (© 2026). Any distribution of this work must maintain attribution to the author(s), title of the work, publisher, and DOI.

ISBN: 978-3-95450-252-3 ISSN: 2673-5350 doi: 10.18429/JACoW-IPAC2026-MOP7192

DESIGN OF AN RF-GRIDDED GUN FOR A HIGH-EFFICIENCY TRISTRON

A. S. Thakur†, W. L. Millar, I. Syratchev, European Organization for Nuclear Research, Geneva, Switzerland
G. Burt, Z. Un Nisa, Lancaster University, Lancaster, United Kingdom

Abstract

The RF gridded gun is a key component of the RF power sources chosen for the FCC-ee tristron. It enables the generation of bunched electron beams via the application of an RF voltage across the cathode-grid gap. The tristron allows a compact tube architecture and provides high RF power production efficiency. The emitted, grid intercepted, and transmitted beam currents are governed by the applied RF grid voltage and DC cathode voltage, providing additional degrees of freedom for controlling the bunch formation. For continuous wave tristron operation at an RF power level of 0.5 MW in the UHF band, particular attention must be paid to several critical design aspects, including beam grid interception, beam optics design, thermomechanical effects, and stress. These factors strongly influence the operational stability, device lifetime, and overall performance. The current status of the RF gridded gun design for the tristron is reported.

INTRODUCTION

Gridded vacuum electron devices, such as the Inductive Output Tube (IOT) [1], are well known for their high efficiency in high-power RF applications. However, their efficiency is fundamentally limited by the quality of electron bunching. To overcome this limitation, the tristron concept was proposed as an extended IOT configuration incorporating an additional idler cavity to improve bunching and achieve significantly higher RF conversion efficiency [2]. Therefore, the multibeam (MB) tristron has emerged recently as a promising RF power source for FCC-ee [3]. In this work, the conceptual design and numerical investigation of a gridded gun for an MB tristron are presented, with emphasis on beam formation, beam-grid interception, and current modulation.

GRIDDED GUN NUMERICAL STUDIES

The MB tristron is currently selected as the baseline 400 MHz, 0.5 MW continuous wave RF power source for the FCC-ee. It offers a high operational efficiency, compact and cost-efficient solution [4]. The gridded gun is one of the most critical components of the tristron. We designed this device starting with common recommendations for the grid cathode spacing 0.3 mm and the grid's wire cross-section 0.15 mm × 0.15 mm. The hexagonal (HEX) grid topology (Fig. 1, right) was selected based on a comparative analysis with other grid configurations, where the HEX grid appeared to be superior in terms of heat evacuation. Contrary to the spherical cathodes with electrostatic focusing (beam area compression) normally used in conventional IOTs [1, 5], we selected a flat cathode-grid assembly without beam compression. This choice simplifies the beam optics (Fig. 1, left) as the cathode itself is embedded in the constant magnetic field of 0.08 T provided by the external solenoid.

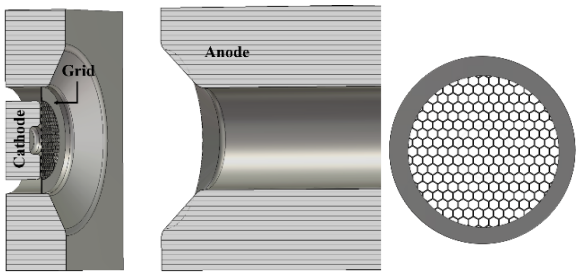

Figure 1: The gridded gun setup (left) and the hexagonal grid (right) used in the CST simulations.

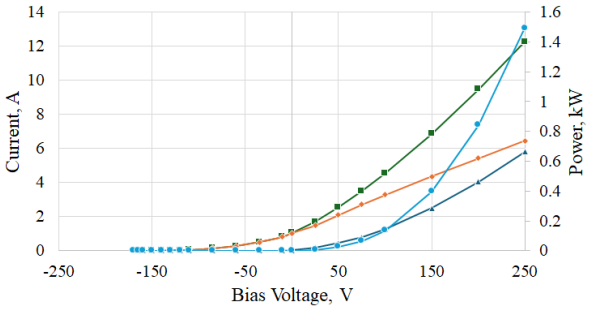

Figure 2: Emitted (rectangles), grid-intercepted (triangles), and transmitted (diamonds) currents, together with the power intercepted on grid (circles) versus bias voltage.

To avoid current emission from the cathode when the input RF signal is inhibited, the grid is operated at DC bias with respect to the cathode voltage [5]. The optimum value of this bias voltage depends on the ratio between the cathode-grid gap and the grid-anode gap lengths, the cathode voltage, as well as the grid opacity to the electric field.

In the proposed gridded gun configuration, a 46 kV voltage is applied to the cathode-anode gap. Using the CST 3D beam tracking (TRK) software, we simulated DC parameters in the system like emitted current, current intercepted on the grid, power intercepted on the grid, and transmitted current as functions of the grid bias voltage (Fig. 2). Here a -165 V DC voltage should be applied to block the current emission. It shall be noted that, following the standard approach applied in CST user community, the cathode in simulations is assigned to a ground potential and anode is set to a positive potential.

In an approximation of very short cathode-grid gap, the bunched beam current envelopes and transient intercepted

†aditya.singh.thakur@cern.ch

Content from this work may be used under the terms of the CC BY 4.0 licence (© 2026). Any distribution of this work must maintain attribution to the author(s), title of the work, publisher, and DOI.

ISBN: 978-3-95450-252-3 ISSN: 2673-5350 doi: 10.18429/JACoW-IPAC2026-MOP7301

REPRESENTATION OF MECHANICAL MODES SPECTRUM

S. Koscielniak*, TRIUMF, Vancouver, Canada

Abstract

The static and dynamic Lorentz force detuning (LFD) derive from the sum of many mechanical modes and their interplay with EM radiation pressure. The LFD may give rise to instabilities in which the EM resonance frequency moves away from the "set point" value. The usual analytic theory for the oscillatory instability, and its threshold, are for a single, isolated mechanical mode; not a sum. We want a mathematical representation of the LFD spectrum that is compatible with an "isolated resonance" style of stability analysis, but nevertheless captures the phase-advance properties of a sum of many modes.

INTRODUCTION

We wish to emphasize four aspects of the mechanical modes spectra responsible for ponderomotive instability encountered in superconducting radio frequency (SRF) cavity resonators.

1. The absence of super-harmonic generation.
2. The collective behaviour of mechanical modes (MMs).
3. The crucial importance of mechanical breathing modes.
4. The representation of many interacting mechanical resonances. Provided that isolation criteria are satisfied, each mode can be replaced by a single resonance plus a complex number that is the collective effect of the other modes. Let K_k be the kth mode coupling.

Absence of RF Harmonics

The best known, and probably most studied, nonlinear resonator is the driven Duffing oscillator [1] encountered in mechanical systems; it has a cubic nonlinearity of the restoring force versus amplitude that introduces a shift of the resonance frequency. If this frequency falls with amplitude of oscillation, the system is called a softening resonator. An important feature in the response of the classical cubic oscillator is the appearance of harmonics of the drive frequency. The cubic term triples the drive frequency. Sum and difference frequencies between the fundamental and third harmonic introduce second and fourth harmonic, and so on.

In contrast to that behaviour, the SRF resonator (with a cubic dependence of resonance frequency on amplitude due to the Lorentz-force detuning) does not display super-harmonic response. The nonlinearity enters through the agency of mechanical modes, whose spectrum extends into the kHz but not into MHz or GHz. The slow response of these modes results in averaging of very many RF cycles, and so there is no frequency multiplication of the RF fundamental. Thus the SRF resonator behaves as a driven mean-square oscillator [2]. This prediction is not widely known; and the absence of RF harmonics needs to be confirmed by measurement.

Ponderomotive Instability

The Lorentz-force detuning (LFD) may give rise to a so-called ponderomotive instability in which the EM resonance frequency moves away from the desired or "set point" value. There is an analytic theory of this instability: due to Schulze [3] for the generator driven case, and to Delayen [4] for the self-excited resonator. Usually it is stated that there are two types of instability: a monotonic variation that occurs near DC; and an oscillatory variation that occurs in the neighbourhood of a strong mechanical mode (one having large quality factor and coupling constant). Schulze treats these individually: a sum of modes at DC for the monotonic, and a single mode for the oscillatory. Delayen uses the DC and AC response of the same, single mode for both types of instability. In essence, these theories for the oscillatory instability, and its threshold, are for a single, isolated mechanical mode. Of course, there may be several such strong modes. This raises the question of how to represent the effect of many interacting mechanical modes.

COLLECTIVE BEHAVIOUR OF MODES

The RF cavity resonator is supposed to have some idealised shape, which is considered a thin shell. Any deformations of that shape are described by a superposition of mechanical eigenmodes each of which has a shape function and a damped sinusoidal time dependence. In principle, there is an infinite set of these modes. The cavity shape in the steady state is a superposition of modes, each excited at zero frequency. For example, an external mechanical tuner that deforms the cavity relies on a superposition of modes.

The mechanical modes always act collectively. At DC, the modes cooperate to produce exactly the steady state deformation of the shell. If the cavity shell is excited mechanically at "low frequency", the modes act coherently to follow the time-dependent deformation. The response of a single mode when excited at its resonance frequency is Q_m times larger than the DC response of that mode. If the modes have large mechanical quality factors Q_m, then "low frequency" means below the first mechanical resonance. If the modes have small quality factors, then "low frequency" can extend well above the first resonance. When the quality factors are large, we may think of the response (of the modes) as being described by either of two simplified models: (i) when the excitation frequency is between the individual resonances, the collective response is coherent; and (ii) when the excitation frequency lies within the bandwidth of a single high-Q mode, the response ceases to be collective and is almost entirely the response of the individual mode j if $K_j Q_j \gg \sum_k K_k$. In this second model, the residual response of all the other modes contributes a very small amplitude and phase shift. This way of thinking about the collective response and its mathematical description is elaborated in Ref. [5].

* shane@triumf.ca

Content from this work may be used under the terms of the CC BY 4.0 licence (© 2026). Any distribution of this work must maintain attribution to the author(s), title of the work, publisher, and DOI.

ISBN: 978-3-95450-252-3 ISSN: 2673-5350 doi: 10.18429/JACoW-IPAC2026-MOP7302

MUELLER, SLATER & CASIMIR VERSUS KAHAN & PAPAS TIME TO SET THE RECORD STRAIGHT

S. Koscielniak*, TRIUMF, Vancouver, Canada

Abstract

The relative fractional change of resonance frequency equals the fractional change in stored energy. This relation predicts the change of EM frequency when the walls of a metallic cavity are deformed or small objects inserted. J.M. Müller derived this formula in 1939 by conceptual and mathematical errors. Casimir corrected those errors in 1949. The formula is also associated with J.C. Slater, published in 1946. Similar formulae were derived by Kahan in 1946 and by Papas in 1954. The Kahan version was reported, influentially, by Borgnis & Papas in the 1958 Handbook of Physics. Nevertheless, the relation is often called Slater's theorem. The Müller, Slater and Casimir versions rely only on the properties of eigenfunctions, and electromagnetic boundary conditions at a metallic surface. The Kahan and Papas short cut to the formula relies on thermodynamics, the adiabatic theorem, perfect thermal isolation and infinite time, and that the cavity contains EM oscillations in quadrature. The latter derivation (K-S) relies on assumptions that are artificial and unnecessary, and fails completely if there is no EM field present while the cavity is deformed. The situation of multiple derivations and attributions has led to some confusion. The time to set the record straight is overdue!

INTRODUCTION

The theory of electromagnetic (EM) waves in resonant cavities is not a modern subject. It was a short step, made by Lord Rayleigh pre-1900, from Maxwell's equations to studying trapped waves in closed cavities. And shortly afterward to the realization of the ultra-violet catastrophe (for cavity radiation) that spurred the early quantum-mechanics revolution post-1900. However, the modern understanding of EM cavity resonators in terms of eigenmodes each of which can be represented by an equivalent lumped-element (parallel) LCR-circuit stems from the period immediately proceeding and, in particular, during World War II. The importance of radio-communications, and RADAR, spurred many developments; including the theoretical basis for cavity resonance tuning and methods for measuring the EM field profile.

Frequency Tuning

The relative fractional change of resonance frequency (f) equals the fractional change in stored energy (W):

$$\delta f/f \;=\; \delta W/W\,. \tag{1}$$

Equation (1) is a consequence of Slater's theorem. Slater never wrote the relation in precisely this form. Equation (1) predicts the change of EM frequency when the walls of a metallic cavity are deformed (δV) or small objects (beads) inserted. The formulae for δV or beads are similar but distinct. This article concerns five separate versions of the derivation of Eq. (1). Three start from Maxwell's curl equations, use the vector identity

$$\nabla\cdot(\mathbf{E}\times\mathbf{H}) = \mathbf{H}\cdot(\nabla\times\mathbf{E}) - \mathbf{E}\cdot(\nabla\times\mathbf{H})\,, \tag{2}$$

and stipulate *perturbation at constant* electric and magnetic field $\mathbf{E}$, $\mathbf{H}$. A fourth/fifth derivation is loosely based on the adiabatic theorem for slow variations performed on a lossless Hamiltonian system. We shall take them in historical order.

IN ESSENCE

With hindsight, the Müller and Casimir derivations can be reduced to their essence. Take time-harmonic fields $e^{+i\omega t}$ with spatial parts $\mathbf{E}(\mathbf{x}), \mathbf{H}(\mathbf{x})$. Maxwell's curl equations:

$$A:\quad \nabla\times\mathbf{E} + i\omega\mu\mathbf{H} = 0, \quad B:\quad \nabla\times\mathbf{H} - i\omega\epsilon\mathbf{E} = 0\,. \tag{3}$$

For Müller take $\mathbf{H}^*A \;+ \mathbf{E}^*B$ thus:

$$i\omega[\mu\mathbf{H}\mathbf{H}^* - \epsilon\mathbf{E}\mathbf{E}^*] + \mathbf{H}^*(\nabla\times\mathbf{E}) + \mathbf{E}^*(\nabla\times\mathbf{H}) = 0\,. \tag{4}$$

For Casimir take $\mathbf{H}^*A \;- \mathbf{E}^*B$ thus:

$$i\omega[\mu\mathbf{H}\mathbf{H}^* + \epsilon\mathbf{E}\mathbf{E}^*] + \mathbf{H}^*(\nabla\times\mathbf{E}) - \mathbf{E}^*(\nabla\times\mathbf{H}) = 0\,. \tag{5}$$

Here * denotes complex conjugate. For a lossless cavity resonator, EM fields are in quadrature. Hence $\mathbf{E}$ is real, and $\mathbf{H} \to -i\mathbf{H}$ with $\mathbf{H}$ real. We substitute Eq. (2) in Eq. (4). Let $\chi \equiv [\mathbf{H}(\nabla\times\mathbf{E}) + \mathbf{E}(\nabla\times\mathbf{H})]$. Let W_E and W_H be the electric and magnetic stored energy, respectively. We form the integrals of Eqs. (4, 5) over the cavity volume:

$$\omega[W_H - W_E] - \int_S(\mathbf{E}\times\mathbf{H})dS \;=\; 0\,, \tag{6}$$

$$\omega[W_H + W_E] - \int_V \chi(\mathbf{E},\mathbf{H})dV \;=\; 0\,. \tag{7}$$

Equation (6), Poynting's theorem [1] for a cavity, was used by Müller. In the unperturbed state, both terms in Eq. (6) are zero. Equation (7) was used by Casimir. Note that Eq. (7)+Eq. (6), and Eq. (7)-Eq. (6), gives expressions for W_H and W_E, respectively.

The next step is to form the total derivative of Eqs. (6) or (7) including variation of the surface and volume, while holding $\mathbf{E}$, $\mathbf{H}$ constant inside the volume (but not necessarily on the surface). Starting from Eq. (7) take plus sign in Eq. (8). Starting from Eq. (6) take the minus sign in Eq. (8).

$$\delta\omega[W_H \pm W_E] + \omega\int_{\Delta V}[H^2\delta\mu \pm E^2\delta\epsilon]dV \;+\; \omega\int_{\delta V}[\mu H^2 \pm \epsilon E^2]dV \;=\; J_\pm \tag{8}$$

* shane@triumf.ca

Content from this work may be used under the terms of the CC BY 4.0 licence (© 2026). Any distribution of this work must maintain attribution to the author(s), title of the work, publisher, and DOI.

ISBN: 978-3-95450-252-3 ISSN: 2673-5350 doi: 10.18429/JACoW-IPAC2026-MOP7303

RF DESIGN PROGRESS OF THE 197 MHz CRAB CAVITY FOR EIC*

B. Xiao†,[1], J. C. Brutus[1], A. Blednykh[1], Z. Conway[2], J. Cox[2], J. R. Delayen[2,3], S. U. De Silva[3], R. Fernandes[2], J. Guo[2], D. Holmes[1], N. Huque[2], G. Li[1], Z. Li[4], J. B. Mandel[2], S. Verdú-Andrés[1], G. Wang[1], Q. Wu[1], W. Xu[1]
[1]Brookhaven National Laboratory, Upton, New York, USA
[2]Thomas Jefferson National Accelerator Facility, Newport News, VA, USA
[3]Center for Accelerator Science, Old Dominion University, Norfolk, VA, USA
[4]SLAC National Accelerator Laboratory, Menlo Park, CA, USA

Abstract

The interaction region (IR) crab cavity system is a special RF system designed to recover head-on collision since there will be luminosity loss caused by the 25 mrad crossing angle at the interaction point (IP) of the Electron-Ion collider (EIC). The configuration includes six crab cavities in the Hadron (proton or ion) Storage Ring (HSR) installed on each side of the IP, four operating at 197 MHz and two at 394 MHz, along with one (or two) 394 MHz crab cavity on each side of the IP in the Electron Storage Ring (ESR). This paper presents the recent progress in the RF design of the 197 MHz crab cavity, addressing the geometrical constraints, required crabbing voltages, multipole components, and the Higher Order Mode (HOM) power and impedance thresholds.

INTRODUCTION

The EIC crab cavities are designed to provide local crabbing scheme in the horizontal plane for two possible interaction points (IPs), with 197 MHz and 394 MHz for hadron storage ring (HSR) and 394 MHz for electron storage ring (ESR). Challenges include large cavity size, longitudinal and transverse space constraints in both IPs, tight impedance budget, and beyond the state-of-art low level RF (LLRF) control specs [1, 2]. In this paper, we focus on the design of the 197 MHz crab cavity RF components, including the Fundamental Power Coupler (FPC), Higher Order Mode (HOM) dampers, pickup couplers and beamline bellows.

197 MHz HSR CRAB CAVITY

Both Double Quarter Wave (DQW) and RF-dipole (RFD) designs were adopted in High Luminosity Large Hadron Collider (HL-LHC) at 400 MHz. For the 197 MHz crab cavity for EIC HSR, both DQW and RFD were considered, and the RFD was chosen majorly due to the stiffeners and components added to the cavity system are more complex in the DQW [3]. RFD design is simpler and closer to the HL-LHC version while comparing with DQW. Two designs were proposed for the RFD HOM damper, one with waveguide absorbers, and the other with coaxial absorbers. Coaxial design was chosen over the waveguide design due to its simplicity on design and mechanical integration [3-5]. Recent progress of the cavity design and fabrication has been covered in [6], in which the cavity optimization includes changing the capacitive poles from flat surface for the prototype cavity [7] to curved surface for the production cavity [8] to meet the requirement on multipole components [9, 10]. Due to this change, the number of coaxial dampers for each cavity has increased from 3 to 4 [8]. In this paper, the RF design progress of the 197 MHz crab cavity RF components for EIC will be covered. Figure 1 shows the RF components of this cavity, including one FPC, two HOM dampers on VHOM waveguide, two HOM dampers on HHOM waveguide, two pickup couplers on HHOM waveguide per cavity, as well as two warm-cold bellows and one cold-cold bellows per cryomodule, with two cavities per cryomodule.

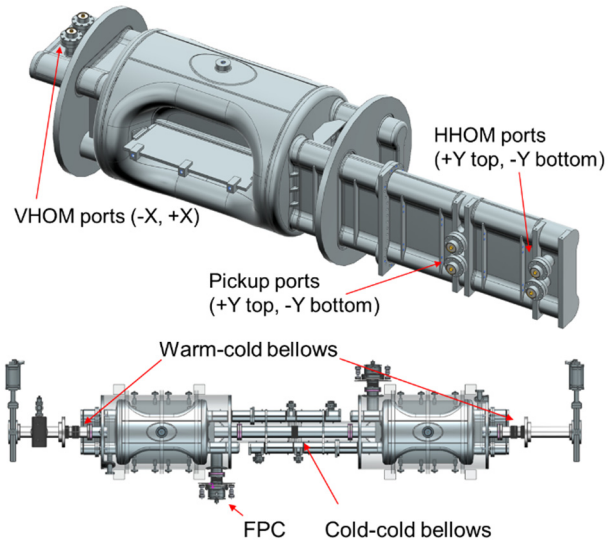

Figure 1: EIC HSR 197 MHz crab cavity with RF components.

FUNDAMENTAL POWER COUPLER

With a beam offset of $\Delta x = 0.6$ mm and microphonic detuning of $\delta f = 50$ Hz for a beam current of 1.0 A and cavity $[R/Q]_t = 1034\ \Omega$, FPC's external quality factor should be $Q_{ext} = 1.75\times10^6$ for optimal power requirement. With this the maximum power required at the cavity is 50 kW, it is

* Work supported by Brookhaven Science Associates, LLC under Contract No. DE-SC0012704 with the U.S. Department of Energy, and by DOE Contract No. DE-AC02-76SF00515. This work used computer resources at the National Energy Research Scientific Computing Center.
† binping@bnl.gov

Content from this work may be used under the terms of the CC BY 4.0 licence (© 2026). Any distribution of this work must maintain attribution to the author(s), title of the work, publisher, and DOI.

ISBN: 978-3-95450-252-3 ISSN: 2673-5350 doi: 10.18429/JACoW-IPAC2026-MOP7602

DESIGN OF A C-BAND COMPACT PHASE SHIFTER FOR PARTICLE ACCELERATORS

Z. Zhang*, Z. Huang, Y. Wei, G. Feng
University of Science and Technology of China, USTC, Hefei, China

Abstract

A phase shifter is a key component to tune the phase of RF power for accelerating or deflecting structures in linear accelerators (linacs). This paper presents the design of a compact C-band variable phase shifter for our high-power test platform. It consists of a dual-polarization mode coupler and a movable short-circuited piston for adjusting RF phases. In order to isolate the coaxial port formed by the movable piston and the pipe a choke is introduced inside the piston. Through optimizations, the RF phase variation is simulated to be 10.1233 °/mm of piston moving distance.

INTRODUCTION

For accelerating structures in linear accelerators (linacs), it is of great importance to satisfy the requirement for precise adjustment of radio frequency (RF) power. The variable RF power splitter is a typical multiport component in high RF power tests, which is used to divide input power proportionally into several branches. In order to distribute RF power among all the output ports not only with arbitrary ratio, but also in high precision, it is necessary to attach a phase shifter to the power splitter to manipulate output RF power [1–4]. There is already a variable phase shifter for X-band implemented in Compact Linear Collider (CLIC) in CERN [5]. To meet the demand for application in C-band linacs, the design of a compact phase shifter at center frequency 5.712 GHz is established on Ansys HFSS [6]. In this work, the 2-port variable phase shifter realizes the RF phase variation of about 10.12 °/mm of piston moving distance, with the reflection coefficient S_{11} reduced below −55 dB and the transmission coefficient S_{12} achieving nearly 0 dB.

DESIGN AND OPTIMIZATION

The C-band variable phase shifter consists of two components – the E-rotator with dual-polarized modes and the movable short-circuited piston. The input RF power is transmitted through the E-rotator, and excites dual circular-polarized TE_{11} modes in the circular waveguide. Then the RF power enters into the movable piston to be reflected at the terminal short-circuited plane. By adjusting position of the piston, one can alter phase of S_{12} linearly with little power loss through the phase shifter. These two components should be designed and optimized independently from each other.

E-rotator with Dual-Polarized Modes

The E-rotator is introduced as the power feeding section for the whole phase shifter. The prototype of E-rotator comes from the E-bend 3dB-hybrid, as shown in Fig. 1. The hybrid outputs RF power through port 3 and 4 and the amplitude of each branch is equal to half of the total input power while port 2 is isolated from the other ports. If port 3 and 4 merge into one single circular port on the top of the hybrid, the E-rotator with dual-polarized modes based on the 3dB-hybrid is formed, as shown in Fig. 2.

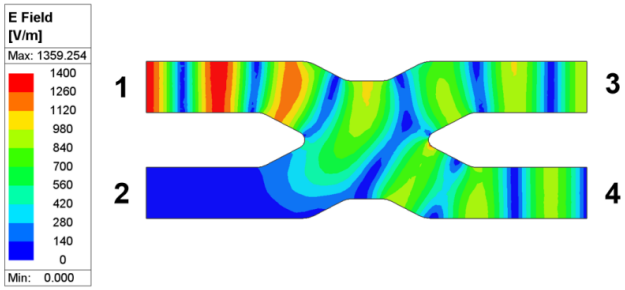

Figure 1: The electric field distribution for an E-hybrid.

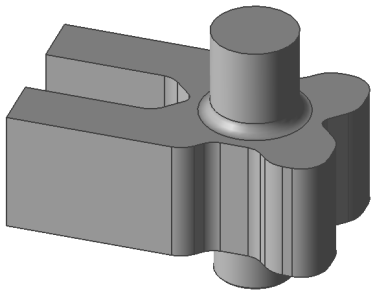

Figure 2: Geometry of the E-rotator with dual-polarized modes.

For the E-rotator, port 3 and 4 of the 3dB-hybrid are short-circuited, and RF power can only be output through the circular waveport, where the movable piston is linked to the rotator. In this case, the original 4-port structure is modified to 3-port structure. It is expected that the input RF power should be transmitted to the circular waveport to be fully adjusted later by the movable piston. As for geometrical dimensions of the component, the model BJ-48 are selected for rectangular waveguide to transmit TE_{10}. The radius of the circular waveguide is also determined to make sure there are only TE_{11} modes. The bend part near the input rectangular waveguide causes reflection due to the nonconformity of transmission structure. Therefore, the bend functions as an impedance matching section. As for the circular waveguide added on the bottom as well as the terminal short-circuited structure at the far side from the input port, the fields distribution of microwave is optimized to a more symmetric situation, which puts a substantial effect on transmission

* zhangzs24231@mail.ustc.edu.cn

Content from this work may be used under the terms of the CC BY 4.0 licence (© 2026). Any distribution of this work must maintain attribution to the author(s), title of the work, publisher, and DOI.

ISBN: 978-3-95450-252-3 ISSN: 2673-5350 doi: 10.18429/JACoW-IPAC2026-MOP8301

DEVELOPMENT AND FABRICATION OF A CW COPPER INJECTOR FOR SRF INDUSTRIAL CRYOMODULES

C. Jing†, R. Kostin&, E. Gomez, P. Avrakhov, Euclid Techlabs LLC, Bolingbrook, USA
S I. Gonin, V. Yakovlev, N. Solyak, T. Khabiboulline, C.Edwards, J. Thangaraj
Fermilab, Batavia, IL, USA

Abstract

Compact SRF industrial linacs enabled by conduction cooling provide high-power (>100 kW) electron beams within a compact footprint. However, the limited cryogenic cooling capacity imposes strict requirements on beam quality, particularly near-zero beam loss in the SRF cavity. We report on the development and fabrication of a CW normal-conducting RF injector consisting of a gridded RF gun integrated with a multi-cell copper booster cavity. Compared to previous designs, beam dynamics optimization has reduced injector beam losses from several percent to ~0.1% while maintaining full transmission through the SRF cryomodule. The design incorporates RF, thermal, multipacting, and engineering optimizations. A full injector structure has been fabricated, and initial bench RF measurements of the pre-brazed assembly are presented. These results demonstrate readiness toward integration with conduction-cooled Nb_3Sn SRF cryomodules.

INTRODUCTION

Compact SRF linacs have emerged as a promising solution for industrial applications such as irradiation, sterilization, and environmental processing, where beam energies around 10 MeV and power levels up to hundreds of kW are required. Conduction-cooled Nb_3Sn SRF technology enables standalone systems without liquid helium infrastructure, significantly reducing system complexity and footprint. However, the limited cryocooling capacity and vulnerability of Nb_3Sn layer impose stringent constraints on beam losses, requiring essentially zero beam interception on SRF cavity walls.

To meet these requirements, an external injector capable of producing well-bunched, low-loss beam is essential. In earlier work [1], a CW normal-conducting injector based on a gridded RF gun integrated with a multi-cell copper booster cavity was proposed and demonstrated in simulation. While initial designs achieved acceptable performance, injector losses remained at a few percent level, which is incompatible with long term SRF cryomodule operation.

This paper reports significant progress in injector optimization, engineering design, fabrication, and initial RF characterization. Beam dynamics improvements have reduced injector losses to near-zero levels, and a full injector structure has been fabricated and bench-tested, waiting for the final brazing.

INJECTOR RF OPTIMIZATION

The injector consists of six independently powered RF cells operating at 1.3 GHz, with the first cell integrated with a gridded RF gun. Independent solid-state amplifiers (SSA) provide flexibility in phase and amplitude control for each cell, enabling optimization of beam dynamics and RF efficiency.

Each cell was optimized to balance accelerating gradient, shunt impedance, and thermal load under CW operation. Compared to earlier designs, the updated geometry increases shunt impedance while maintaining acceptable surface fields and power dissipation (Fig. 1). Typical RF parameters include ~800 W total power per cell, with ~500–700 W wall losses and the remainder beam loading, as shown previously.

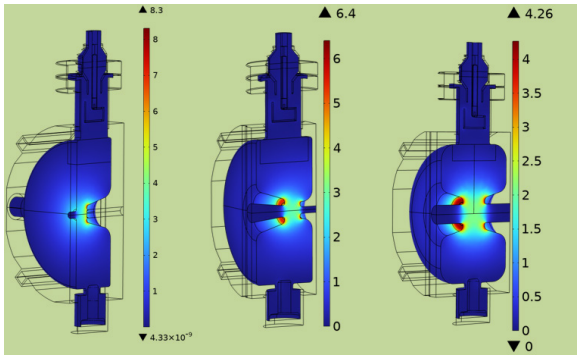

Figure 1: E-field of linac: (from left to right) Cell 0, Cell 2 and Cell2-5. Cells were optimized to provide uniform power dissipation along the injector to maximize the voltage gain and to provide optimum beam dynamics.

Table 1: Main RF Parameters of The Cavity Cells.

Parameter	C0	C1	C2-5
Gap, mm	13.5	16.2	25
V, kV	43.6	53	57
R/Q, ohm	193	254	318
Q	13850	15600	17000
Wall Losses, W	715	694	684
Beamloading, W	87	106	114
Total power, W	800	800	800
Emax_axis, MV/m	4.5	3.0	2.0

Each cell has its own tuning plunger and RF pickup. Multipacting was carefully evaluated and mitigated through geometry optimization of RF couplers and tuning plungers. As shown in the previous study [1],

† c.jing@euclidtechlabs.com
& now with Lam Research Co.

Content from this work may be used under the terms of the CC BY 4.0 licence (© 2026). Any distribution of this work must maintain attribution to the author(s), title of the work, publisher, and DOI.

ISBN: 978-3-95450-252-3 ISSN: 2673-5350 doi: 10.18429/JACoW-IPAC2026-MOP8303

STANDARD AND MICROBEAM LINATRONS BY VAREX IMAGING CORPORATION

A. Amoroso, A. Anderton, J. Cloud, M. Hu, R. LaFave, J. Merkley, A. Mishin†, C. Patterson, S. Proskin, S. Sheaffer, D. Shedlock, Y. Toombes, Varex Imaging Corporation, Salt Lake City, United States

Abstract

At Varex Imaging Corporation, High Energy Systems (HES) Department staff with help and support of our Production and Imaging groups continue adding new features to our LINATRON™ linear accelerator (LINAC) systems and transitioning new developments to our products. HES is at the final stages of productizing our usual LINATRONs, equipped with our new, in-house developed and built Accelerator Beam Centerlines (ABC). The products we offer today match or exceed the older products specifications, which were offered before we established our own ABC development and production line. In addition, we are making good progress on our new Microbeam LINATRON™ (MBL) systems, and we present the latest results on our MBL production prototypes. Our 6 MeV MBL6 prototype has been packaged, and it is under extensive testing and qualification process, getting ready for demonstration to our customers and for delivery. The similar packaging of our 3 MeV LINATRON systems offers option of Ultra Low Leakage (ULL) shielding and an option of integrated X-Ray Head packaging for both 3 MeV and 9 MeV, for our security LINACs and for NDT LINACs under development.

VAREX LINATRON™ FAMILY

Introduction

Our standard line of products, which includes LINATRON™ systems for NDT and security screening is well-known in the industry [1]. All the systems installed worldwide are operating in energy range from 1 MeV to 9 MeV (many more than 1000 units) and use the predecessor Beam Centerlines (BCL), which were equipped and operated exclusively with a diode electron gun. Compared to a triode electron gun, a diode version has its advantages and disadvantages, and the industry mostly prefer triode e-gun configuration for a better control of such e-gun and LINAC performance. In addition, the BCL operates at high electron gun voltage at approximately 30 kV while a proprietary electron gun design is used. Hence, designing and building Accelerator Beam Centerline (ABC) drop-in replacements for such BCLs presented a special challenge for High Energy System team. It was important to ensure that we have ABC for field replacements with a different, commercially available and lower voltage electron gun and having a newly developed to Varex ABC RF structure design, which meets or exceeds the parameters of the predecessor units. We selected a commercially available triode electron gun operating at less than 15 kV and modified its design to a diode configuration with intent of using both versions - a diode version for the drop-in replacements and a triode version for most of the new LINACs, which may provide the new models with many new capabilities [2].

Traditional LINATRON Linear Accelerators



Figure 1: "Standard" LINATRON packaging for NDT and Security, used with separate blocks - modulator and chiller, BCL equipped with diode e-gun.



Figure 2: LINATRON "Tower" packaging with Solid State Modulator (SSM) used on a 6 MeV Mi6SSM (diode e-gun), but now the similar packaging is used for Mi6SSM-T (triode e-gun), both are subsystems for security screening systems.

Before we introduced new designs, two primary configurations were used in Varex LINATRONS. A "standard" classic configuration of the X-ray head shown in Fig. 1 operated with a line modulator block, chiller block, and control console. The other, newer "tower" design (Fig. 2) utilized a Solid-State Modulator (SSM) incorporated in the tower, but it still used BCL with a diode electron gun, for which a diode electron gun driver (DEGD) was used, also built in the tower.

†andrey.mishin@vareximaging.com

Content from this work may be used under the terms of the CC BY 4.0 licence (© 2026). Any distribution of this work must maintain attribution to the author(s), title of the work, publisher, and DOI.

ISBN: 978-3-95450-252-3 ISSN: 2673-5350 doi: 10.18429/JACoW-IPAC2026-MOP8304

MEASURING AND CHARACTERIZING BEAM ENERGY OF A COMPACT MEDICAL LINEAR ACCELERATOR*

T. Chen*, RefleXion Medical (United States), Hayward, United States
L. Huo, T. Li, H. Tao, Z. Feng, L. Hu, L. Zhou, Y. Liu*, Chengdu Elekom Vacuum Electron Technology Co. Ltd (China), Chengdu, China

Content from this work may be used under the terms of the CC BY 4.0 licence (© 2026). Any distribution of this work must maintain attribution to the author(s), title of the work, publisher, and DOI.

Abstract

Beam energy is an important parameter of linear accelerator. Compact linacs for medical and industrial applications are usually not equipped with beam monitors. The commonly used methods are "half value layer" (HVL) in industrial and "Percentage Depth Dose" (PDD) in medical to evaluate the beam energy of linac. However, these methods are not easily and accurately carried out, the HVL method needs big and heavy steel plates to prevent scattering x ray beams and PDD method need standard beam position and expensive 3D water tank to measure the beam energy. Most importantly, those methods cannot measure electron beam energy, but the photon distribution generated through Bremsstrahlung. This article introduced a method to measure and characterize the average electron beam energy when hitting the target by combining the external measurements and simulation beam profile results under different deflection magnetic field generated by steering coils. This method not only gives confidence in developing and operating the medical equipment but also reveals relation between beam energy and RF power settings. In addition, this paper provides energy and dose output variation across the RF pulse. This data provides guidance for proper setting of gun pulse width and timing.

INTRODUCTION

Unlike accelerators in physics laboratories which are facilitated with various kinds of beam monitors, medical and industrial linacs are sealed with permanent target and RF cavities together directly without monitors[1-3]. While these monitors are not necessary during typical operation for those applications, it is very difficult to characterize the beam performance during research and development. The measurable output from the linacs is typically the photons generated by Bremsstrahlung, which has a broad spectrum and strongly depending on target structure. In case of troubleshooting, it is difficult to find out if the linac is delivering electron beam properly. This article introduced a method for measuring electron beam energy of compact linac that has no internal monitors. In addition, because the medical and industrial linacs are operating with pulsed RF power and e-gun pulse, the relative timing between the pulses affects the output energy and dose rate as well. This article also presented these variations using short gun emission pulse with different injection timing.

METHOD

As typical accelerator beam energy measurement, steering magnetic field is applied to the beam line after acceleration, and the beam energy can be found from the displacement. However, in the compact linac case, there is not room between linac output and target for such measurement. The steering field can only be applied in the upstream part of the linac during beams acceleration. The electrons after the steering are subject to strong RF fields, that changes electrons' energy and transverse momentum significantly. The displacement cannot be simply calculated. In this paper, we combine linac beam simulation and beam spot centre shifting measurement to determine the electron beam energy.

A pair of steering coils are installed on the linac, close to the e-gun. The beam spot profile is measured with a scanning slit device[4-5]. The measured profiles with different steering current settings are shown in Fig. 1.

The profile data is fitted with dual-Gaussian function which is typically observed in this kind of linac[4]. To determine the beam center, we take the center of the narrow Gaussian. (More discussions regarding the two Gaussians, please refer to another paper in this conference.) The beam center shift vs steering current is obtained, and the steering rate is calculated, as plotted in Fig. 2(a).

Above procedure is repeated with varying RF power (HV applied to magnetron), which changes e-beam energy. The steering rate with various RF power is shown in Fig. 3(a).

The same process is applied to simulation data. The beam spot center shift with various steering current is plotted in Fig. 2(b), which is used to obtain steering rate with various average electron beam energies. Therefore, we obtained the relation of steering rate vs e-beam energy, as plotted in Fig. 4. The data are fitted with a quadratic curve. The measurement data points are overlaid on the curve with equal steering rate. This yields the relationship between beam energy and RF power setting (Mod_HV). Figure 5 shows the relation. From this plot, one can find out the electron beam energy once RF power is set.

ISBN: 978-3-95450-252-3 ISSN: 2673-5350 doi: 10.18429/JACoW-IPAC2026-MOP8306

CONCEPTUAL DESIGN OF A NOVEL DEUTERON ACCELERATOR DRIVEN NEUTRON SOURCE FOR NUCLEAR WASTE TRANSMUTATION

Y. Jiang† and J.L. Hirshfield, Omega-P R&D, Inc., New Haven, USA
M. Gai, University of Connecticut, Groton, CT, USA

Abstract

A novel deuteron cyclotron auto-resonance accelerator (dCARA) is under development to produce neutrons via breakup of high current 40-MeV deuterons on a low-Z target. Compared to the proton-based Accelerator-Driven Systems (ADS), a dCARA system can be much more compact and cost effective, with notable features including continuous acceleration without bunching for good beam stability, high efficiency, wide beam aperture, and an exceptionally short length of few meters. The applications of dCARA include transmutation of used nuclear fuel, medical isotope production system, or material test for a future fusion power reactor. The R&D progress and the conceptual design of dCARA are reported here.

INTRODUCTION

Accelerator-Driven Systems (ADS) technologies have been widely studied as a means to reduce the lifetime and toxicity of nuclear waste through neutron-induced transmutation [1, 2]. In conventional ADS designs, high-energy (GeV scale) proton beams generate neutrons via spallation reactions in targets of high-Z materials. While technically feasible, such systems require a rf quadrupole structure (RFQ) and long superconducting radio-frequency (SRF) linacs, leading to high capital costs, complex operation, and stringent reliability requirements. Another approach is to use a conventional proton cyclotron, but increasing beam current and beam power is quite challenging.

This work explores an alternative ADS architecture [3-5] based on accelerating moderate-energy deuteron beams (~ 40 MeV) to produce neutrons through deuteron breakup reactions [6]. In this approach, a novel compact deuteron cyclotron auto-resonance accelerator (dCARA) supports high-current operation with simplified structure and potentially lower cost, enabling the possibility of using multiple small-scale neutron sources collectively to achieve transmutation performance comparable to a single large facility while improving reliability and scalability.

DESCRIPTION OF DCARA

The dCARA concept builds upon the mechanism of cyclotron auto-resonance acceleration (CARA) [7], in which charged particles maintain phase synchronism with transverse electromagnetic fields while gyrating in a uniform static magnetic field. Unlike conventional accelerators where bunched particles gain energy in discrete gaps or cavities during a narrow rf phase, dCARA allows continuous energy gain without bunching throughout the acceleration. The absence of bunching mitigates space charge instability and allows accelerating beams of high currents.

A key innovation in dCARA is the use of a transverse electromagnetic mode (TEM) cavity which has a much smaller transverse dimension to allow accelerator cavities at tens of MHz frequency range fit inside a strong superconducting magnet similar to a whole-body MRI magnet. This configuration opens up a new parameter space suitable for ion acceleration, bringing a paradigm shift in the application of CARA from limited electron acceleration [7] into ion acceleration [3-5].

Fig. 1 shows the schematics of a compact dCARA-driven neutron source. A low-energy deuteron beam at tens of keV is transported from an ion source by a low energy beam transport (LEBT) to a dCARA cavity. The cavity is submerged within a strong axial magnetic field (~6–10 T) generated by a superconducting solenoid. The cavity is driven by external rf sources at different rf phases through multiple ports, to support a rotating dipole mode at tens of MHz frequency range [3-5]. The large cavity aperture enhances tolerance to misalignment and beam losses, contributing to improved operational reliability. With continuous acceleration through phase synchronization governed by the CARA mechanism, the deuteron beam is accelerated to tens of MeV energy, transported by a high energy beam transport (HEBT) and injected into a neutron production target, where a high flux of neutrons is generated via deuteron breakup.

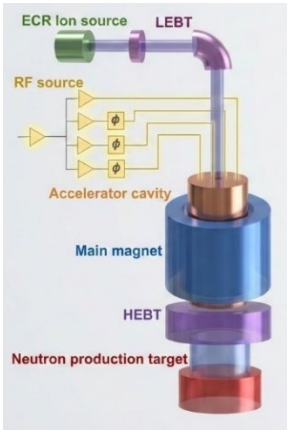

Figure 1: Schematics of a compact dCARA-driven neutron source.

As shown in Fig. 2, inside a dCARA cavity, deuterons follow helical trajectories. Because particles can be injected at arbitrary rf phases (with different rf field polarization), the output beam produces a circular sweeping pattern on the target surface, effectively achieving beam

† email: yong.jinag@aya.yale.edu

Content from this work may be used under the terms of the CC BY 4.0 licence (© 2026). Any distribution of this work must maintain attribution to the author(s), title of the work, publisher, and DOI.

ISBN: 978-3-95450-252-3 ISSN: 2673-5350 doi: 10.18429/JACoW-IPAC2026-MOP8604

PROOF-OF-PRINCIPLE EXPERIMENTAL DESIGN OF SOLENOID-BASED RELATIVISTIC ELECTRON BEAM PULSE COMPRESSION

Ch. Shi, H. Zha*, H. Chen, J. Shi, An Li, W. Huang, Tsinghua University, Beijing, China

Abstract

Relativistic electron beam pulse compression can enhance the beam current intensity within the pulse and generate higher peak current, showing significant potential for applications such as FLASH radiotherapy and wakefield acceleration. This paper proposes a proof-of-principle experimental design for a solenoid-based electron beam pulse compression scheme. The core device of the experiment, namely the magnetic compressor, has an approximately cylindrical structure with a diameter of 42 cm and a height of 47 cm. By utilizing the uniform magnetic field generated by the solenoids, the compressor converts the energy difference of the injected beam bunch into a path-length difference to achieve pulse compression. Simulation studies show that, under a transverse geometric emittance of 10 mm · mrad, the beam loss remains below 10 %, while the output current waveform exhibits a peak-to-peak ratio of approximately 5, demonstrating an obvious pulse compression effect.

INTRODUCTION

In accelerator physics, high-current high-energy electron beams are not only important subjects of research but also key tools for a wide range of applications. For example, in FLASH radiotherapy [1], they have the potential to achieve efficient tumor irradiation while providing better protection for normal tissues. In two-beam acceleration schemes [2], they can be used to enhance the wakefield gradient generated by the drive beam. However, due to the pronounced relativistic effects of high-energy electron beams, whose particle velocities approach the speed of light, it is difficult to achieve effective bunch compression solely through energy modulation and the resulting velocity modulation. Consequently, realizing short pulse durations and high peak beam currents remains a significant challenge.

In contrast, exploiting the dispersive properties of electron beams in magnetic fields to manipulate particle trajectories, thereby directly converting energy modulation into path-length modulation for bunch compression, provides a more effective approach. GELINA [3] is a representative facility that achieves electron bunch compression based on this principle. However, the compression magnet in GELINA relies on a relatively large energy chirp, resulting in a bulky system and limited compression scalability, which restricts its broader application and further development.

In this work, a proof-of-principle experimental scheme for electron bunch compression based on a solenoidal magnetic field is proposed. In this scheme, the electron beam propagates along helical trajectories generated by the solenoidal field, with the beam path tightly confined and folded within a finite cylindrical volume. Compared with conventional compression structures, the proposed scheme requires only a compact cylindrical device while still providing a sufficiently long propagation path for beam compression, thereby significantly improving space utilization efficiency.

PRINCIPLE AND EXPERIMENTAL DESIGN

Magnetic Compression Principle

Assume that there exists a uniform magnetic field B_0 along the axial z direction. When the electron velocity is neither perpendicular nor parallel to the magnetic field, the electron performs helical motion around the magnetic field direction, as shown in Fig. 1.

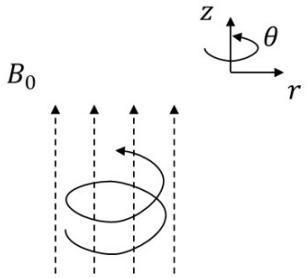

Figure 1: Helical motion of electrons in a solenoid magnetic field.

The equations of motion can be written as

$$\frac{dz}{dt} = v_z \tag{1}$$

$$\frac{d\theta}{dt} = \frac{eB_0}{\gamma m_e} \tag{2}$$

where e is the electron charge, $\gamma = E/(m_e c^2)$ is the Lorentz factor, m_e is the electron rest mass, and E is the electron energy.

When two electrons have the same propagation direction but different energies, Eq. (2) indicates that their angular velocities in the helical motion become different. Consequently, the path-length difference in the θ direction between electrons with different energies continuously accumulates during propagation. When the axial velocity component v_z is much smaller than the azimuthal velocity component v_θ, the path-length difference in the θ direction can be approximately regarded as the effective compression distance, thereby enabling longitudinal compression of the electron beam.

However, when the condition $v_z \ll v_\theta$ is no longer satisfied, or when the propagation distance becomes excessively

* zha_hao@mail.tsinghua.edu.cn

Content from this work may be used under the terms of the CC BY 4.0 licence (© 2026). Any distribution of this work must maintain attribution to the author(s), title of the work, publisher, and DOI.

ISBN: 978-3-95450-252-3 ISSN: 2673-5350 doi: 10.18429/JACoW-IPAC2026-MOP8615

A COMPUTATIONAL METHODOLOGY FOR THE EFFICIENT AC-225 PRODUCTION VIA PROTON IRRADIATION OF RA-226

Xinya Sun[1,2,3], Chen Xia*[1,2], Ming Lv[1,2], Xiaobin Tang[3], Wencheng Fang†[1,2], Zhentang Zhao[1,2]
[1]Shanghai Synchrotron Radiation Facility, Shanghai, China
[2]Shanghai Advanced Research Institute, Chinese Academy of Sciences, Shanghai, China
[3]Department of Nuclear Science and Technology
Nanjing University of Aeronautics and Astronautics, Nanjing, China

Abstract

^{225}Ac is a crucial isotope for targeted alpha therapy, yet its clinical application is severely constrained by supply shortages. The use of high-intensity proton beams to irradiate ^{226}Ra targets offers a viable approach to significantly enhance ^{225}Ac production, as it enables higher yields and greater scalability. However, the process is also accompanied by the generation of other isotopes of actinium, especially the long-lived ^{227}Ac, which challenges the purification process. This work establishes a parameterized model that combines beam energy, target thickness, and cooling time for optimizing ^{225}Ac production while minimizing ^{227}Ac impurity levels and target material consumption. We determine the optimal parameters, which effectively maximize ^{225}Ac yield while controlling impurity levels and target material consumption. This method provides a valuable reference for the efficient production of ^{225}Ac.

INTRODUCTION

Actinium-225 (^{225}Ac) is a highly promising radionuclide that has attracted considerable interest in Targeted Alpha Therapy (TAT) [1]. However, its relatively short half-life of $T_{1/2}$ = 9.92 days poses a severe challenge to the stability of its supply chain. Currently, the accelerator-based production methods including proton irradiation of thorium or radium targets and photonuclear reactions induced by gamma irradiation, have been developed to increase the yield of ^{225}Ac. However, these methods are accompanied by the production of other impurity isotopes of actinium, especially the long-lived actinium-227 (^{227}Ac, $T_{1/2} \approx 21.8$ years). The radiation toxicity of ^{227}Ac, lasting for decades, may offset therapeutic benefits and pose serious safety hazards. Therefore, the stringent control of ^{227}Ac and other actinide impurities is of paramount importance.

The method of proton irradiation of ^{226}Ra achieves a balance between product yield and impurity ratios. Given the high cost of ^{226}Ra target material, optimizing target thickness to maximize yield while minimizing target consumption is crucial. Although previous studies generally consider an energy around 16 MeV as the optimal incident energy for producing ^{225}Ac via proton irradiation of radium targets [2, 3], this conclusion is largely based on yield alone as the criterion. To address this issue, this work proposes an optimization methodology. By systematically regulating the target thickness d, incident proton energy E, and cooling time t_c after irradiation, the optimization process aims to achieve the dual objectives of maximizing ^{225}Ac yield while minimizing the impurity ratio and target consumption. The optimal combination of process parameters determined in this work provides theoretical basis and reference for the actual production and quality control of ^{225}Ac.

METHOD

The Monte Carlo (MC) method is widely used for simulating proton irradiation. However, its high computational cost and long processing times make it less suitable for a systematic optimization algorithm. Therefore, we employed ISOTOPIA [4] to calculate nuclide generation from proton bombardment of radium targets. The ISOTOPIA code is designed for predicting isotope production using an analytical method, by calculating the energy loss and isotope production rate, which is much faster than MC methods.

To validate the reliability of the analytical calculation, we compared the ^{225}Ac production cross section obtained from MC simulations with ISOTOPIA and experimental data [5]. We adopt PHITS [6] and Geant4 [7] tools for MC simulation. PHITS version 3.28, coupled with the INCL 4.6 intranuclear cascade model and the GEM evaporation model [8], is employed to simulate proton irradiation of radium targets. The GEANT4 toolkit with the `QBBC` physics list [9] is used for comparison. The simulation geometries are shown in Fig. 1. Using the simulated results, the corresponding cross sections can be calculated as follows [8]:

$$\sigma = \frac{-\ln\left(1 - \frac{N_{\text{prod}}}{N_{\text{in}}}\right)}{nd} \tag{1}$$

where N_{prod} is the number of product nuclei, N_{in} is the number of incident particles, n is the number density of target nuclei, and d is the target thickness.

A comparison of the ^{225}Ac production cross sections is shown in Fig. 2. The ISOTOPIA calculations, Monte Carlo simulation results, and experimental data demonstrate good agreement, with all curves peaking located in the 15–18 MeV energy range. This consistency confirms the reliability of the activity data calculated by ISOTOPIA.

Using ISOTOPIA, the yields for four nuclides ^{224}Ac, ^{225}Ac, ^{226}Ac, and ^{227}Ac were calculated on a two-dimensional grid covering a proton energy E range of

* xiac@sari.ac.cn
† fangwc@sari.ac.cn

Content from this work may be used under the terms of the CC BY 4.0 licence (© 2026). Any distribution of this work must maintain attribution to the author(s), title of the work, publisher, and DOI.

ISBN: 978-3-95450-252-3 ISSN: 2673-5350 doi: 10.18429/JACoW-IPAC2026-MOP8617

ACCELERATOR-DRIVEN RADIATION STUDIES OF YSZ-MgO COMPOSITES FOR NUCLEAR APPLICATIONS

Rishvana Parveen[1], Parswajit Kalita[1], Devesh Kumar Avasthi[2]
[1]Department of Physics, Applied Science Cluster, UPES, Dehradun, India
[2]Centre for Interdisciplinary Research and Innovation, UPES, Dehradun, India

Content from this work may be used under the terms of the CC BY 4.0 licence (© 2026). Any distribution of this work must maintain attribution to the author(s), title of the work, publisher, and DOI.

Abstract

YSZ and YSZ-MgO thin films were deposited on Si (100) substrates using RF sputtering and RF-DC co-sputtering techniques and studied under low-energy heavy-ion irradiation. Two sets of films were prepared: YSZ sputtered in argon environment and YSZ and Mg co-sputtered in argon and oxygen environment. Irradiation studies show enhanced crystallinity in single-component YSZ and significant degradation of YSZ crystallinity in YSZ-MgO films. These results indicate a strong dependence of radiation response on composition of the material.

INTRODUCTION

Materials employed in radiation environments, including nuclear reactors, outer space, and accelerator laboratories, are subjected to extreme radiation conditions. Such exposure results in radiation-induced damage, which severely affects the structural integrity of the materials and shortens their operational lifespan. Therefore, the development of materials with superior radiation tolerance has become critically important. In this context, a thorough understanding of the behaviour of materials under irradiation is essential for designing advanced materials with enhanced resistance to radiation-induced degradation.

Composite materials have recently attracted attention as they are expected to exhibit enhanced radiation tolerance compared to their single-component counterparts due to the presence of heterointerfaces. It has been reported that heterointerfaces in composites serve as more efficient defect sinks than the grain boundaries present in single-component materials [1].

A major challenge in the nuclear industry is the safe management of waste containing plutonium and minor actinides, which contribute to long-term radiotoxicity [2,3]. The inert matrix fuel (IMF) concept addresses this issue by incorporating PuO_2 and MAs into UO_2-free inert matrices to enable their transmutation [4]. IMF materials must possess high radiation resistance, thermal conductivity, chemical and thermal stability, low neutron absorption cross-section, and compatibility with fuel components [5]. YSZ and MgO are well-studied radiation-resistant materials, with YSZ considered a promising IMF candidate. However, YSZ has lower thermal conductivity, limiting its application. To overcome this, MgO can be combined with YSZ to form composites with improved thermal conductivity and potentially enhanced radiation tolerance [6]

Radiation damage in materials can be studied using various approaches, such as in-pile irradiation in nuclear reactors, investigation of natural analogues through actinide doping, computer simulations, and ion irradiation using particle accelerators [7]. Among these methods, accelerator-based ion irradiation is considered one of the most efficient techniques for examining radiation-induced damage. By carefully selecting the ion species and energy, ion beams can effectively mimic the radiation damage produced in materials under extreme environments [7].

This work investigates the radiation response of YSZ and YSZ-MgO thin films under low-energy heavy-ion irradiation at room temperature. The study aims to understand how the radiation response of a composite material differs from that of a single-component material.

EXPERIMENTAL TECHNIQUES

YSZ and YSZ-MgO thin films were deposited on Si (100) substrates using RF and DC sputtering techniques. Prior to deposition, substrates were cleaned using a standard procedure to avoid contamination. In Set 1, YSZ thin films were prepared by RF sputtering of a ZrO_2 (8 mol% Y_2O_3) target at 3×10^{-2} mbar and 573 K, using 100 W RF power for 2 h in an argon atmosphere (30 sccm). In Set 2, YSZ-MgO films were grown by RF co-sputtering of YSZ and DC sputtering of Mg in an argon and oxygen atmosphere (15 sccm each), at 1×10^2 mbar and 673 K, using 120 W RF and 50 W DC power for 2 h. The deposited films were characterized using GIXRD for phase identification and composition analysis. For irradiation studies, Set 1 film were irradiated with 200 keV Kr ions at 5×10^{16} ions/cm^2, while Set 2 films were irradiated with 100 keV Kr ions at 1×10^{16} ions/cm^2 using the LEIBF facility at IUAC, New Delhi. Low-energy heavy ions are selected because they can effectively simulate the damage caused by alpha-recoil nuclei present in nuclear reactor environments. Post-irradiation characterization was carried out using GIXRD.

RESULTS AND DISCUSSIONS

Figure 1 shows the GIXRD patterns of the synthesized thin films. The YSZ thin film exhibits a fluorite-type cubic phase. The thin film synthesized using YSZ and Mg targets in an oxygen and argon environment (Set 2) exhibits the formation of a distinct crystalline MgO phase along with a significant reduction in the crystallinity of the YSZ phase.

The YSZ thin films were irradiated with low energy 200 keV Kr ions. The nuclear energy loss (S_n), electronic energy loss (S_e), and projected range of 200 keV krypton ions in YSZ are 2.24 keV/nm, 0.37 keV/nm and 62±24 nm respectively. From the GIXRD patterns of pristine and irradiated YSZ thin films (Set 1) shown in Figure 2, it is observed that irradiation leads to grain growth or an improvement in crystallinity.

ISBN: 978-3-95450-252-3 ISSN: 2673-5350 doi: 10.18429/JACoW-IPAC2026-MOP8619

A REPORT FROM ISBA25, ACCELERATOR SCHOOL IN SHANGHAI, CHINA

M. Kuriki*, Hiroshima University, Hiroshima, Japan
Y. Kim, Korea Atomic Energy Research Institute, Daejeon, South Korea
Z. Zhao, Shanghai Advanced Research Institute, Shanghai, China

Abstract

ISBA25 (The 8th International School on Beam dynamics and Accelerator technology) was held from September 1st to 10th 2025 in Shanghai, China. This is the 8th school of the ISBA series, which is an international accelerator school for graduate students and young researchers who are new to the accelerator field. The school curriculum is composed of fundamental topics (e.g., beam dynamics and RF theory), applications (e.g., medical accelerators), and the latest topics (e.g,. AI for accelerators). More than 90 students from around the world participated and spent meaningful days, including hands-on training for accelerator design, student presentations, a laboratory tour of SARI, and an excursion. The school is reported.

INTRODUCTION

The 8th International School on Beam Dynamics and Accelerator Technology (ISBA25) was held over 10 days from September 1 to 10, 2025, at the Shanghai Advanced Research Institute (SARI) of Chinese Academy of Sciences in Shanghai, China. This school series has been held as a part of the IINAS-NX project since 2018, and ISBA25 was co-hosted by Hiroshima University and SARI. Participants included 91 individuals, primarily graduate students and young researchers from around the world. With 135 applicants, the competition rate was 1.5, making it highly selective. Participants came from: China (57), Japan (13), South Korea (10), Thailand (5), India (3), Turkey (2), and France (1). A group Photo is shown in Photo 1.

Shanghai is China's largest city, located at the mouth of the Yangtze River in eastern China. It is now the central city of the Yangtze River Delta economic zone, accounting for 10% of China's total population and 22.3% of its GDP. The total population within the basin reaches about 450 million. Historically, it has served as a central transportation route in Central China, where waterborne trade has long flourished.

CURRICULUM OF ISBA25

The diverse range of accelerator uses from the fundamental science to many applications has led to a growing demand for accelerator physicists and engineers from both academia and industry. However, opportunities to learn the fundamentals of accelerators—such as beam dynamics, accelerator design, and key technologies—remain extremely limited. ISBA25 was planned to address this need, aiming to serve as an entry point for graduate students and young researchers worldwide, particularly from the Asian region, to advance into more sophisticated accelerator research.

For this purpose, the ISBA25 curriculum offered a comprehensive, well-balanced, and forward-looking education in beam dynamics and accelerator technology. By integrating rigorous theoretical lectures, extensive hands-on training, exposure to real facilities, and emerging topics such as AI, the school successfully equipped participants with both fundamental understanding and practical skills. ISBA25 thus made a significant contribution to the training of the next generation of accelerator scientists and engineers in an international and collaborative environment. Detailed information, including lecture materials, is available on the ISBA25 website [1].

Hands-on Training

Hands-on training was held in ISBA25. Students selected one of three themes (ELEGANT, ASTRA, and GENESIS). Starting with software installation, they practiced with basic examples before forming teams to tackle a theme assigned by the tutors. Students gained hands-on experience in accelerator design using the software. Teams of 4-5 students tackled this practical exercise. In such exercises, significant differences in student achievement typically arise due to computer skills and prior simulation study experience. However, by having them work in teams, peer learning among students helps level the outcomes. Interestingly, the skills of the tutors also improved. Photo 2 shows a snapshot in the hands-on training session. The students concentrated on the discussion. Another major benefit of the session is the promotion of communication among students. Communication between students is not only crucial for the school's operation, but also an essential quality students should cultivate as future researchers. This is because accelerator research and operation require organizational efforts, and demonstrating individuality within an organization is a necessary condition for success as a future researcher. The outcomes of this training were presented by each group on the final day. The lecturers evaluated these presentations, and the top five groups were awarded. The awarded groups and members are as follows. We extend our heartfelt congratulations. Photo 3 is a snapshot of the presentation in the summary session.

Student Session

In the evening, student sessions were held over four nights. In this session, the students presented their studies in their home institute. The purpose of this student session is for students to gain mutual understanding of the research conducted

* mkuriki@hiroshima-u.ac.jp

Content from this work may be used under the terms of the CC BY 4.0 licence (© 2026). Any distribution of this work must maintain attribution to the author(s), title of the work, publisher, and DOI.

ISBN: 978-3-95450-252-3 ISSN: 2673-5350 doi: 10.18429/JACoW-IPAC2026-MOP8620

IPAC'25 PRE SESSION-REPORT: FOSTERING A PRODUCTIVE RESEARCH ENVIRONMENT IN THE ACCELERATOR COMMUNITY

Y. Sato†, M. Masuzawa, High Energy Accelerator Research Organization, Tsukuba, Japan
S. Chunjarean, Synchrotron Light Research Institute, Nakhon Ratchasima, Thailand
A. Faus-Golfe, Université Paris-Saclay, CNRS/IN2P3, IJCLab, Orsay, France
R. Geometrante, Kyma S.p.A., Trieste, Italy
R. Hajima, National Institutes for Quantum Science and Technology, Kyoto, Japan
F. Perez, ALBA Synchrotron, Barcelona, Spain

Abstract

The Productive Research Environment (PRE) session at IPAC'25 examined key practices and challenges in fostering sustainable and motivating research environments within the accelerator community. A preliminary survey of 51 managers and leaders indicated generally high levels of satisfaction and motivation during their own early career stages. However, the results also revealed systematic structural concerns, particularly related to staffing limitations, administrative burden, and uncertain career prospects for early-career researchers. The session combined personal perspectives, institutional studies, and survey-based insights. The subsequent panel discussion highlighted critical issues including human resource development, diversity, leadership training, mentorship practices, and intergenerational collaboration. The findings emphasize that productive research environments require clear goals, adequate resources, inclusive and collaborative cultures, and structured leadership and mentoring frameworks. At the same time, the results point to a tension between strong intrinsic motivation and structural constraints. Continued dialogue and expanded surveys are essential to strengthen human resource capacity and sustain the accelerator community.

INTRODUCTION

The PRE session at IPAC'25 was designed as an interactive forum to exchange perspectives on building sustainable, inclusive, and effective research environments in the accelerator community. The session aimed to promote dialogue across career stages, regions, and institutional contexts, fostering engagement between senior leaders and early-career researchers. To support open discussion, the session was held in an informal setting, encouraging active participation and exchange of experiences. PRE was established as a complementary initiative, building on ongoing efforts such as the Women in Science and Engineering (WISE) and Equal Opportunity (EqO) sessions at previous IPAC conferences, including the EqO session at IPAC'23 [1] and the WISE session at IPAC'24 [2], with a more direct focus on the practical conditions and organizational practices that shape research productivity across diverse cultural and institutional settings. A preliminary survey was conducted in advance among members of the IPAC Organizing Committee (OC), Scientific Program Committee (SPC), and Scientific Advisory Board (SAB) from IPAC'22 through IPAC'25. The survey results provided a common framework for the session and enabled speakers to align their contributions with shared themes.

PRE-SURVEY AND ITS RESULTS

The survey was designed to capture both early-career experiences and current working conditions within the accelerator community. The questionnaire included the following key questions:

- Q1: To what extent were you satisfied with your working environment?
- Q2: Have you ever wondered whether you should continue with your job?
- Q3: To what extent were you motivated to take on a managerial role?
- Q4: To what extent are you satisfied with the adequacy of staffing levels in your group?
- Q5: What is the level of interest among early-career researchers in building their careers in your group?

Responses were recorded on a five-point scale, with question-specific interpretations. Questions Q1–Q3 refer to early-career experience, while Q4–Q5 address the current situation.

Fig. 1 summarizes the survey responses, separated by gender to highlight differences between male and female researchers. Both groups report high satisfaction with early-career working environments (Q1) and strong career commitment (Q2). In contrast, responses to staffing levels (Q4) and the perceived interest of early-career researchers (Q5) are more widely distributed, with some variation between male and female respondents, indicating differing perceptions of current working conditions and career attractiveness. While no statistical comparison is performed, these differences suggest that perceptions of the research environment may vary across respondent groups, highlighting the importance of inclusive policies.

Fig. 2 presents the distribution of respondents by gender and geographic region. It should be noted that the survey targeted members of the IPAC OC, SPC and SAB. As such, the sample may not fully reflect the gender or regional distribution of the broader accelerator community.

† yoichi.sato@j-parc.jp

Content from this work may be used under the terms of the CC BY 4.0 licence (© 2026). Any distribution of this work must maintain attribution to the author(s), title of the work, publisher, and DOI.

ISBN: 978-3-95450-252-3 ISSN: 2673-5350 doi: 10.18429/JACoW-IPAC2026-MOP8621

HIGH-POWER TEST OF A 40kW INDUSTRIAL ELECTRONIC LINEAR ACCELERATOR

H. Deng, H. Zha, J. Shi*, H. Chen, Y. Zhao, Tsinghua University, Beijing, China
H. Shi, Nuctech (China), Beijing, China

Abstract

Electron accelerators with high average power output are widely used in radiation processing fields such as material modification, food sterilization, and environmental pollutant treatment. This paper presents a comprehensive high-power test of a 40kW electron accelerator. Key parameters including electron beam energy, average beam current, output power, and pulse characteristics were measured. The results show that the accelerator's electron beam energy, the average beam current, and the effective output power all meet the design specifications. The energy test was performed via the aluminum foil stacking method, ensuring high measurement accuracy. This study validates the reliability and stability of the accelerator, providing technical support for its industrial application.

INTRODUCTION

With the rapid development of advanced manufacturing, new materials, food safety, and environmental protection industries, high-power industrial electron linear accelerators have become core equipment for efficient, clean, and controllable radiation processing [1, 2]. Compared with traditional irradiation sources, MeV-level electron accelerators feature high energy utilization, adjustable beam parameters, good safety, and no radioactive waste, making them widely applied in polymer cross-linking, composite material curing, surface functionalization, food sterilization, medical device disinfection, and industrial wastewater/waste gas treatment.

In recent decades, standing-wave (SW) and traveling-wave (TW) accelerating structures have been the mainstream choices for industrial electron linacs. SW structures offer high shunt impedance and compact size but suffer from poor power efficiency at high repetition rates. TW structures provide high power efficiency and beam stability but require complex focusing systems, increasing equipment complexity and operating costs. These limitations restrict the further improvement of average power, stability, and reliability in high-power industrial irradiation scenarios. The backward-traveling-wave (BTW) accelerating structure, as a magnetically coupled traveling-wave configuration, combines the advantages of both TW and SW structures [3]. It features low power reflection, short filling time, high shunt impedance, and compact structural length, making it highly suitable for high-average-power industrial accelerators. Based on decades of research on BTW structures, Tsinghua University and its industrial partners have developed a 10 MeV 40 kW S-band BTW linear accelerator for industry application.

* shij@tsinghua.edu.cn

This paper reports the high-power test of this 40 kW BTW electron accelerator, including RF conditioning, beam energy measurement, average/pulse beam current test, output power verification, and beam scanning uniformity. All tests follow national standards and industrial specifications in China, providing a practical and high-performance solution for high-power industrial irradiation applications.

DESIGN OF THE ACCELERATING STRUCTURE

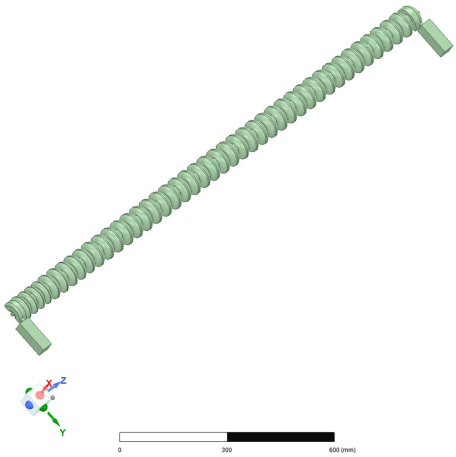

Figure 1: 3D model of the accelerating structure.

First, we briefly introduce the design of the BTW structure. Optimized from the previous design [**?**], it operates stably in the $3\pi/4$ phase advance mode, which is favorable for efficient particle acceleration and transverse beam confinement. As shown in Fig. 1, with a total of 42 accelerating cells and an overall axial length controlled within 1.6 m, the structure realizes a compact accelerator design, enabling an energy gain up to approximately 10 MeV and a peak pulse beam current exceeding 300 mA. To improve beam capture efficiency and initial acceleration stability, a dedicated buncher section is integrated at the front end of the accelerating structure. The main accelerating part adopts a tappered structure to provide stable acceleration field for electrons and boost their energy to the target level continuously. The key radio-frequency (RF) parameters of the BTW accelerating structure are summarized in Table 1. High-power operation of the 40 kW BTW structure causes severe RF power deposition, thermal accumulation, deformation, and frequency detuning. To address this issue, structural and water cooling optimizations are adopted. The coupling aperture and adjacent disks of cells near input coupler were modified: the disk thickness was increased, the aperture opening angle was re-

Content from this work may be used under the terms of the CC BY 4.0 licence (© 2026). Any distribution of this work must maintain attribution to the author(s), title of the work, publisher, and DOI.

ISBN: 978-3-95450-252-3 ISSN: 2673-5350 doi: 10.18429/JACoW-IPAC2026-MOV1001

HIGH-INTENSITY LHC TESTS IN 2025 FOR TRANSVERSE BEAM DYNAMICS STUDIES

S. Kostoglou*, H. Bartosik, I. Efthymiopoulos, B. E. Karlsen-Baeck, M. Hostettler, N. Mounet, A. Radoslavova, G. Sterbini, H. Timko, R. Tomás, CERN, Geneva, Switzerland

Abstract

During dedicated machine development periods in 2025, the LHC operated with High-Luminosity LHC (HL-LHC) beam parameters to study transverse beam dynamics in a high-intensity and high pile-up regime. For the first time, collisions with trains of 2.3×10^{11} ppb were achieved, reaching a pile-up of 150 and reproducing operational conditions close to those foreseen for the HL-LHC. These experimental tests allowed for detailed measurements of emittance growth and proton losses. In particular, a fill with bunches having different transverse distributions was performed to assess the impact of non-Gaussian tails on beam lifetime and losses beyond the burn-off limit when the two beams are brought into collisions. Furthermore, the evolution of the beam quality throughout the cycle was studied for different HL-LHC beam types. These results represent a key milestone towards the demonstration of the HL-LHC operational conditions.

INTRODUCTION

The High-Luminosity LHC (HL-LHC) performance relies on operation with high bunch intensity, low transverse emittances, long trains for fast filling and a high number of bunches, high pile-up and very small β^* at the two high-luminosity experiments, ATLAS and CMS [1, 2]. Reaching these conditions will push the machine into a beam-beam regime that is significantly more demanding than what is routinely explored in the LHC today. Although the present LHC already operates in a highly optimized configuration, several observations of beam degradation, such as emittance growth and intensity losses, are still not fully understood and are only partially captured by existing models. A series of Machine Development (MD) studies was therefore carried out in 2025 to investigate how these effects scale under HL-LHC beam conditions and study the beam-beam effects of the HL-LHC era, marking important milestones such as the first collisions with HL-LHC beams at high pile-up.

Reproducing the fully nominal HL-LHC conditions is, however, not possible in the present LHC configuration [3], as several systems will only be upgraded during Long Shutdown 3 (LS3) and additional mitigation measures are required to enable operation with nominal HL-LHC beams [4, 5]. The HL-LHC MD program therefore relied on a range of baseline and alternative beam configurations to probe HL-LHC regimes while remaining within present machine constraints. The studies followed a progressive approach, starting with HL-LHC individual bunches, then HL-LHC baseline beams at injection and finally 8b4e beams or short 25 ns trains with reduced bunch intensity compared to the HL-LHC target at top energy. The information collected will help refine and strengthen confidence in the HL-LHC operational scenario.

LOSSES AT THE START OF COLLISIONS AND TRANSVERSE TAILS

When the beams are brought into collision during nominal LHC operation, a significant increase in losses is systematically observed, well above what is expected from luminosity burn-off alone. Luminosity simulations indicate that, in the most critical cases, this effect can lead to a reduction in integrated luminosity of up to 4%. Improvements in beam preparation in the injectors led to a reduced tail population in the transverse bunch distributions and the LHC consequently started receiving bunches with transverse profiles closer to a Gaussian distribution [6–8]. No significant tail re-population was observed in the LHC cycle and the losses at the start of collisions were reduced, already pointing to a direct link between tail population and losses [9].

To demonstrate this correlation more clearly, dedicated MD studies were performed with bunches having similar emittances but different transverse tail populations, prepared already in the injectors. Two classes of bunches were compared, with q-values from q-Gaussian fits [10] equal to 1 (Gaussian) and 1.4 (heavy tails), respectively. The test configurations consisted of six bunches with 2.3×10^{11} ppb and one bunch at 1.5×10^{11} ppb.

Figure 1 shows the evolution of the effective cross section, defined as the loss rate normalized by the luminosity, for Gaussian bunches (green) and for bunches with a q-value of 1.4 as obtained by a q-Gaussian fit (heavily populated tails) at HL-LHC bunch intensity (red) or at lower bunch intensity (black). The inelastic cross section, around 81 mb, is indicated by the horizontal black line. The graph clearly shows that bunches with enhanced transverse tails suffer systematically larger losses beyond burn-off at the start of collisions compared to the Gaussian bunches. The measured loss of performance for the non-Gaussian bunches corresponds to about 3% in integrated luminosity, in very good agreement with simulated predictions. These additional losses beyond burn-off are therefore strongly mitigated for Gaussian bunches.

The underlying mechanism is consistent with a reduction of Dynamic Aperture (DA) when entering the head-on beam-

* sofia.kostoglou@cern.ch

Content from this work may be used under the terms of the CC BY 4.0 licence (© 2026). Any distribution of this work must maintain attribution to the author(s), title of the work, publisher, and DOI.

ISBN: 978-3-95450-252-3 ISSN: 2673-5350 doi: 10.18429/JACoW-IPAC2026-MOV1003

FCC-ee INJECTOR COMPLEX: STATUS, HIGHLIGHTS AND OUTLOOK

P. Craievich, PSI, Villigen PSI, Switzerland
A. Grudiev, CERN, Geneva, Switzerland
I. Chaikovska, CNRS/IN2P3, IJCLab, Orsay, France
C. Milardi, INFN-LNF, Frascati, Roma
on behalf of the CHART/FCC-ee Injector collaboration

Abstract

The FCC-ee demands an injector complex capable of delivering high-current, high-brightness electron and positron beams with exceptional efficiency. Within the CHART/FCC-ee Injector Study collaboration, a revised injector layout has been developed to optimize performance, cost, and power consumption. A central pillar of this effort is the tuning-free, high-gradient normal-conducting RF structure technology pioneered at PSI for SwissFEL and since extended across S-, C-, and X-band systems. This scalable approach underpins future developments in the FCC-ee linacs, enabling reliable acceleration. In parallel, the P³ program at PSI is advancing the positron source, with commissioning foreseen in 2026, while upcoming work will enhance the electron source and refine RF requirements for the positron linac. This contribution presents the current injector complex status, key design highlights, and the outlook toward the FCC-ee injector technical design report.

INTRODUCTION

Following the conclusion of the Feasibility Study (FS) phase of the Future Circular Collider project, culminating in the publication of the Feasibility Study Report (FSR) in April 2025 [1], the project will enter the next phase focused on the preparation of the Reference Design Report (RDR) and the development of functional specifications for the subsystems of the FCC-ee injector complex. The main objective of the injector RDR is to finalise the physics design of the injector complex, including linacs, particle sources, damping ring (DR) and polarisation schemes. The RDR will also address the integration of the injector complex within the CERN site, including civil engineering requirements, siting constraints, surface integration, and technical infrastructure needs.

Figure 1 illustrates the baseline layout of the injector complex as presented in the FSR. The injector architecture has been developed to support operation at repetition rates of up to 100 Hz with trains of four bunches separated by 25 ns, thereby satisfying the demanding filling requirements of the Z running mode [1]. Table 1 summarizes the main collider and booster parameters that define the injector requirements. The injector is also designed to deliver high-brightness electron and positron beams for both filling-from-scratch and continuous top-up operation of the collider. Owing to the relatively short beam lifetime and stringent luminosity requirements, the injector must sustain frequent alternating injections of electrons and positrons while maintaining a controlled charge balance between the two beams in the collider ring. The baseline configuration comprises dedicated electron and positron linacs operating up to 2.86 GeV, followed by a damping ring for emittance reduction and a high-energy linac that boosts the beam energy to 20 GeV prior to injection into the booster ring. The positron source baseline is based on a conventional target-driven production scheme in which electrons from the electron linac impinge on a tungsten target. In this context, high-temperature superconducting (HTS) solenoids surrounding the target region play a key role in maximizing positron capture efficiency.

The present injector design also reflects a broader optimization effort focused on operational reliability, efficiency, cost, and power consumption. In particular, the RF systems are being reconsidered toward commercially available S-band technologies while preserving compatibility with the operational flexibility required by the collider complex. Special attention is devoted to the reliability of the RF systems under continuous top-up operation, where injector interruptions caused by RF breakdowns could directly impact collider performance. Consequently, experimentally validated low-breakdown-rate accelerating structures constitute a key requirement for the injector design.

A major contribution to this effort comes from the PSI-developed tuning-free, high-gradient normal-conducting RF technology initially developed for SwissFEL and subsequently extended to S-, C-, and X-band accelerating systems [2]. This tuning-free and scalable approach provides an attractive solution for the FCC-ee injector linacs, offering both operational robustness and reduced maintenance.

The injector complex will be constructed primarily within the existing CERN Prévessin site. The civil engineering infrastructure foreseen for the injector complex includes dedicated tunnels for the high-energy, electron and positron linacs, the damping ring, and the transfer lines connecting the injector systems to the booster. The underground structures will extend over approximately 1.2 km and will mainly rely on cut-and-cover construction techniques using reinforced concrete tunnels buried up to 15 m below ground level.

Switzerland and the Paul Scherrer Institute (PSI) continue to play a central role in supporting the FCC-ee injector activities through the *CHART collaboration*. The injector design presented in the Feasibility Study Report (FSR) was developed within the framework of the FCC-ee injector studies conducted under the CHART 2020–2024 programme, while the next stage of development toward the Reference Design Report (RDR) and Technical Design will be carried

Content from this work may be used under the terms of the CC BY 4.0 licence (© 2026). Any distribution of this work must maintain attribution to the author(s), title of the work, publisher, and DOI.

ISBN: 978-3-95450-252-3 ISSN: 2673-5350 doi: 10.18429/JACoW-IPAC2026-MOV6603

DEVELOPMENT AND FIRST BEAM OBSERVATIONS OF AN ULTRA-FAST BUNCH-BY-BUNCH X-RAY BEAM SIZE MONITOR AT SuperKEKB

R. Nomaru[†,1,2], G. Mitsuka[2], M. Andrew[3], K. Yoshihara[3], C. Driver[3]
[1]The University of Tokyo, Tokyo, Japan
[2]High Energy Accelerator Research Organization, Ibaraki, Japan
[3]University of Hawaii, HI, USA

Abstract

We have developed a new ultra-fast bunch-by-bunch beam size monitor for SuperKEKB and initiated beam observations in the electron ring (HER) starting in November 2025. Using this system, we successfully acquired data and achieved, for the first time at SuperKEKB, bunch-by-bunch measurements of the beam size. The measured beam sizes show good agreement with those obtained using the conventional, slower beam size monitor, demonstrating the reliability of the new system. The high temporal resolution of the monitor enables detailed investigation of beam size variations along the bunch train. Furthermore, the measurements reveal that the bunch-to-bunch beam size variation increases during collision operation compared to single-beam conditions, suggesting a significant contribution from beam–beam effects.

INTRODUCTION

The SuperKEKB accelerator [1] is a high-luminosity electron–positron collider operating with 7 GeV electrons and 4 GeV positrons. In March 2026, it achieved a peak luminosity of 5.2×10^{34} $\mathrm{cm}^{-2}\mathrm{s}^{-1}$ surpassing its previous world record. Commissioning efforts are ongoing toward even higher luminosity. In such high-luminosity colliders, it is crucial to stably store a large number of high-current bunches in the storage rings. Under these conditions, various beam instabilities—such as electron cloud effects, ion trapping, and beam–beam interactions—can degrade machine performance. Understanding these effects requires diagnostics with high temporal resolution capable of resolving individual bunches.

To address this need, we have developed a new bunch-by-bunch beam size monitor for SuperKEKB. This system combines synchrotron radiation X-rays with a silicon strip detector, enabling fast sampling of beam images. During the 2025–2026 operation periods, we successfully performed the first bunch-by-bunch beam size measurements using this system. In this paper, we describe the detector system, measurement methodology, data analysis procedures, and present initial beam measurement results.

BUNCH-BY-BUNCH X-RAY BEAM SIZE MONITOR

At SuperKEKB, the beam size is measured using synchrotron radiation X-rays emitted from bending magnets. The X-rays pass through a coded aperture mask, and the resulting image is reconstructed and fitted to extract the beam size [2]. In routine operation, a CMOS camera is used as the imaging device. While this system has been extensively used during commissioning, its exposure time (typically tens of microseconds or longer) and limited frame rate (<100 Hz) prevent bunch-by-bunch measurements. To overcome this limitation, we developed a new detector system, referred to as the Silicon X-ray Radiation Monitor (SiXRM), which employs a silicon strip sensor instead of a CMOS camera for high-speed sampling, thereby enabling bunch-resolved measurements. This system is designed to complement the conventional CMOS-based monitor, providing time-resolved information that is not accessible with the existing system.

Figure 1 shows the SiXRM system. It consists of a silicon sensor board, a preamplifier board, and a data acquisition (DAQ) board. The system was developed in collaboration between KEK, the University of Hawaii, and SLAC National Accelerator Laboratory, and the DAQ is based on the system used in the Belle II TOP detector [3]. The silicon strip sensor has 128 strips in the vertical direction, making the system sensitive to the vertical beam size. Due to wire-bonding issues between the sensor and readout electronics, currently only 42 channels are used. The DAQ system uses waveform sampling ASICs and FPGAs, enabling analog waveform sampling at 2.7 GSa/s followed by subsequent digitization. Given the minimum bunch spacing of 4 ns in the SuperKEKB main ring, this sampling rate is sufficient for bunch-by-bunch measurements. A more detailed description of the system design and its commissioning can be found in Ref. [4]. The waveform length per acquisition is limited to approximately 12 RF buckets (~24 ns). A full-turn measurement (~10 μs, 5120 buckets) is therefore obtained by repeatedly acquiring short waveform windows while shifting the acquisition timing. The full waveform is reconstructed by concatenating these segments. Each window acquisition takes about 50 ms, and a full-turn measurement requires approximately 20 seconds.

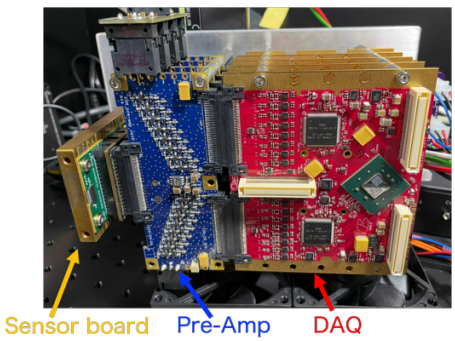

Figure 1: Photograph of the SiXRM system.

† nomaru@post.kek.jp

Content from this work may be used under the terms of the CC BY 4.0 licence (© 2026). Any distribution of this work must maintain attribution to the author(s), title of the work, publisher, and DOI.

ISBN: 978-3-95450-252-3 ISSN: 2673-5350 doi: 10.18429/JACoW-IPAC2026-MOV7001

QUALIFICATION AND COMMISSIONING OF SUPERCONDUCTING MAGNETS FOR THE S3 SPECTROMETER AT GANIL

M.-H. Stodel†, M. Aburas, B. Haize, F. Esnault, T. Lefrou, R. Levallois, F. Lutton, A. Wagret-Quatromme, Grand Accélérateur National d'Ions Lourds, Caen, France
G. Dilasser, C. Génot, T. Lécrevisse, Commissariat à l'Énergie Atomique et aux Énergies Alternatives, Paris, France
G. Tocabens, Université Paris-Saclay, CNRS/IN2P3, IJCLab, Orsay, France

Content from this work may be used under the terms of the CC BY 4.0 licence (© 2026). Any distribution of this work must maintain attribution to the author(s), title of the work, publisher, and DOI.

Abstract

In order to achieve optimal performance in terms of transmission and separation for the S3 spectrometer, the project team decided to design superconducting magnets integrating 11 magnetic functions in a single cryostat. There are seven of these magnets, called Superconducting Multipole Triplets, in the spectrometer, and they operate at liquid helium temperature. These are unique objects with no equivalent anywhere else in the world, offering a very high degree of integration. This complexity has resulted in a significant commissioning delay and the need for a dedicated team to operate this set of magnets. This presentation will show the progress made in qualifying the various functions associated with these magnets: the qualification of cryogenic, electrical, and magnetic functions.

GANIL / SPIRAL2

GANIL (Fig. 1) is one of the world's leading laboratories for research with heavy ion beams covering areas such as nuclear and atomic physics, condensed matter physics astrophysics and radiobiology. Since the year 80s, the installation comprising five cyclotrons, two ion sources and ten experimental rooms make it possible to offer scientists a large variety of stable or radioactive beams.

Complementary to these installation, **SPIRAL2** is a superconducting linear accelerator which deliver one of the most intense heavy ion beam at this energy. Two experimental rooms, NFS (*Neutrons For Science)* and **S^3** (*Super Spectrometer Separator*) are specifically designed to carry out experiments with beams from the LINAC [1].

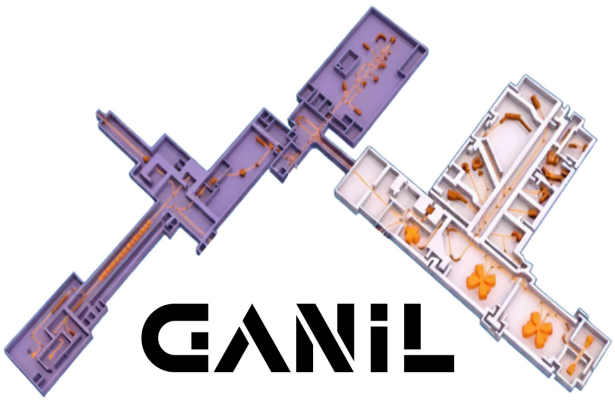

Figure 1: SPIRAL2 and GANIL.

S^3 SUPER SEPARATOR SPECTROMETER

S^3 Project (Fig. 2) aims to push the boundaries of nuclear physics by enabling the study of unstable nuclei and super heavy elements, particularly those beyond 104 in the periodic table [2]. The design of the primary target is optimized for fusion-evaporation production. S^3 is a two-stage optical structure combining a large acceptance momentum achromat and a "high-resolution" mass separator. This high-resolution is obtained by cancelling high order aberrations thanks to sextupoles and octupoles placed along the spectrometer.

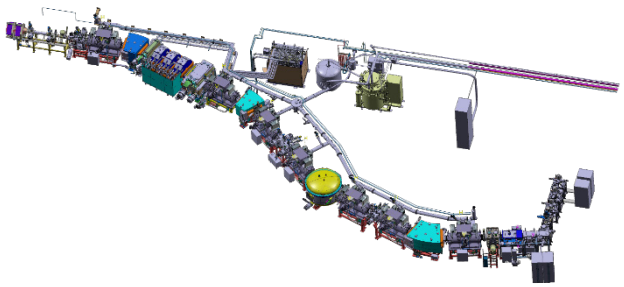

Figure 2: S^3 Spectrometer with 7 SMT.

Each stage includes 2 dipoles and 4 multipoles triplets. These multipoles are quadrupoles superimposed with sextupoles and most of the time, octupoles and steerers. Next to the target station is the beam dump region, where the radiation environment is intense. At that place, the multipoles are resistive magnets. The remaining part of the spectrometer takes advantage of a compact design using 7 Superconducting Multipoles Triplets (Fig. 3). The expected performances of the spectrometer are a mass resolution up to 450, and a transmission of 50% (+/-10%).

SMT

The **SMTs** (Fig. 3) are superconducting iron-free magnets designed to generate multipolar magnetic fields [3]. Each triplet is composed of three singlets, and each singlet is an assembly of independent functions: quadrupoles, sextupoles, octupoles and steerers, allowing precise control of the magnetic field. A SMT has the following characteristics (Table 1):

Table 1: SMT Characteristics

Long [cm]	Width [cm]	Height [cm]	Total mass [t]	Cold mass [kg]	Volume [L]
170	165	188	2.7	365	45 LHe 31 LN2

ISBN: 978-3-95450-252-3 ISSN: 2673-5350 doi: 10.18429/JACoW-IPAC2026-MOV7004

THE POTENTIAL OF MULTI-MATERIAL LASER POWDER BED FUSION ILLUSTRATED BY AN RFQ PROTOTYPE

M. Mayerhofer*[1], S. Brenner[1], G. Dollinger[1], C. Jugert[2],
M. Lehmann[2], V. Nedeljkovic-Groha[1], G. Schlick[2]
[1]University of the Bundeswehr Munich, Neubiberg, Germany
[2]Fraunhofer Institute for Casting, Composite and Processing Technology, Augsburg, Germany

Content from this work may be used under the terms of the CC BY 4.0 licence (© 2026). Any distribution of this work must maintain attribution to the author(s), title of the work, publisher, and DOI.

Abstract

A variety of studies have shown that additive manufacturing (AM) of particle-accelerator components using laser powder bed fusion (PBF-LB/M) offers significant potential to reduce investment costs while simultaneously improving figures of merit. However, the classical PBF-LB/M process does not support the combination of different materials within a single part. Conventional manufacturing routines are therefore still required, for example, to join steel flanges with knife-edge sealing interfaces to copper cavities. Novel multi-material (MM) PBF-LB/M processes enable the fabrication of high-quality, e.g., high-density, geometries by combining different materials such as Cu, CuCr1Zr, Ta, W, aluminium alloys, or stainless steel. Highly functional parts tailored to the diverse requirements of particle-accelerator components can thus be additively manufactured within a single process step. To demonstrate this potential, we fabricated a monolithic radio-frequency quadrupole (RFQ) prototype from two materials using MM PBF-LB/M. The RFQ inner cavity was manufactured from CuCr1Zr, while the co-printed outer shell was made of tool steel to integrate two DNCF63 and four DNCF16 flanges. The inner cavity surface was electropolished and subsequently copper plated to increase the cavity quality factor. Low-level RF measurements showed good agreement with CST simulations when the remaining surface roughness was taken into account. Helium leak-rate measurements demonstrated vacuum performance compatible with conventional RFQ applications. For the first time, these results demonstrate the feasibility of MM PBF-LB/M for manufacturing functional multi-material particle-accelerator components.

POTENTIAL OF MULTI-MATERIAL LASER POWDER BED FUSION

Laser powder bed fusion of metals (PBF-LB/M) is an additive manufacturing process in which thin metal powder layers are selectively melted by a laser to build components layer by layer. This enables complex monolithic geometries that are difficult or impossible to realize conventionally. For particle-accelerator components, such as radio-frequency (RF) cavities, PBF-LB/M is therefore of increasing interest to reduce manufacturing effort and cost while improving performance, for example through integrated cooling channels or topology-optimized structures [1–5].

* michael.mayerhofer@unibw.de

However, conventional mono-material PBF-LB/M remains limited when different material properties are required within one component. In normal conducting RF cavities, for instance, the cavity body is typically made from highly conductive copper or copper alloys, whereas vacuum interfaces often require stainless-steel knife-edge flanges. Such assemblies still rely on conventional joining processes, which increase manufacturing complexity, restrict design freedom, and may introduce additional cost and failure risks. Multi-material PBF-LB/M addresses this limitation by enabling the layer-wise fabrication of components composed of different metals within a single process [6, 7]. Functional requirements such as high electrical conductivity, mechanical robustness, thermal management, and vacuum compatibility can thus be combined directly in one additively manufactured structure. MM PBF-LB/M can therefore reduce or even eliminate conventional joining steps and further expand the design freedom for particle-accelerator components composed of different materials. Several MM PBF-LB/M processes are currently under development, and for selected material combinations the technology has reached a maturity level that allows the fabrication of functional prototypes. For example, at Fraunhofer IGCV a MM PBF-LB/M process for producing high-quality multi-material components was developed [8].

Figure 1 summarizes material combinations already processed by MM PBF-LB/M that may be relevant for particle-accelerator applications. Given the rapidly growing research activity in this field, the overview is not exhaustive. The numbers in the fields refer to the corresponding literature references. The color code distinguishes material combinations investigated in initial studies, qualified at laboratory scale, and demonstrated in application-specific prototypes. One such prototype is the RFQ demonstrator first presented in Brenner et al. [9]. It combines a CuCr1Zr inner RF cavity with a co-printed tool-steel outer structure containing integrated CF knife-edge flanges (see Fig. 2).

RFQ PROTOTYPE

Design and MM PBF-LB/M Process

The potential of single-material PBF-LB/M for manufacturing RF cavities from pure copper has already been demonstrated [1–5]. However, pure copper is challenging for realizing vacuum-tight knife-edge sealing interfaces. Therefore, most PBF-LB/M-manufactured RF cavities

ISBN: 978-3-95450-252-3 ISSN: 2673-5350 doi: 10.18429/JACoW-IPAC2026-MOV7005

EXPERIMENTAL STUDY OF BEAM-INDUCED DAMAGE IN Nb_3Sn SAMPLE COILS PRE-IRRADIATED UP TO 30 MGy*

D. Domange†[1,3], D. Gancarcik[1], C. Hernalsteens[1], C. Lannoy[1],
D. Wollmann[1], R. Babouche[2], M. Bonura[2], C. Senatore[2], N. Pauly[3]
[1]CERN, Geneva, Switzerland
[2]University of Geneva, Geneva, Switzerland
[3]Université libre de Bruxelles, Brussels, Belgium

Content from this work may be used under the terms of the CC BY 4.0 licence (© 2026). Any distribution of this work must maintain attribution to the author(s), title of the work, publisher, and DOI.

Abstract

Superconducting magnets of high-energy accelerators are vulnerable to beam-induced damage and previous experiments have characterized the damage limits of Nb_3Sn sample coils under proton-beam impact. This paper presents a follow-up experiment at CERN's HiRadMat facility investigating the combined effect of radiation ageing and beam impact on superconducting sample coils. The coils were pre-irradiated to simulate the integral dose anticipated for the final-focusing triplet quadrupole magnets of the High Luminosity LHC (HL-LHC) at the end of their lifetime. Following a review of the experimental motivation and preparation of the samples, the final experimental setup is described, including sample positioning and expected temperature profiles under beam impact. Metrology measurements, survey operations, and beam-based alignment, used to ensure adequate beam impact parameters, are detailed together with the proton beam parameters used to irradiate the samples. FLUKA simulations constrained by measured beam size, intensity, and position provide estimates for the local temperature rises and gradients. The timeline of the successfully completed experiment is reviewed. The ongoing post-irradiation analysis, including the assessment of beam-spot characteristics using radiation-sensitive film and the critical-current measurement campaign, is discussed in detail.

INTRODUCTION

The High-Luminosity Large Hadron Collider (HL-LHC) final-focusing triplet quadrupole magnets, the first high-energy accelerator magnets based on Nb_3Sn technology, will be exposed to mixed radiation fields produced at the interaction points of the ATLAS and CMS experiments [1, 2]. Throughout their operational lifetime, they will accumulate a total dose of 20 to 30 MGy, which will degrade the mechanical strength of the CTD101k epoxy impregnating the coils [3–5]. In addition, ultra-fast failure events, such as kicker misfires, can deflect the beam onto an unintended trajectory, generating particle showers that could deposit considerable amounts of energy in the superconducting coils and cause localised heating and mechanical stress [6–12]. The HRMT-61 experiment at the HiRadMat facility of the CERN Super Proton Synchrotron (SPS) characterised the damage limits of non-aged Nb_3Sn racetrack sample coils under 440 GeV/c proton-beam impact, finding no degradation up to hot-spot temperatures of 670 K and peak strains of 0.5 % [13, 14]. Whether radiation ageing lowers these limits remained unknown. The HRMT-70 experiment was designed to address this question by combining γ-ray pre-irradiation to doses of 25 and 30 MGy with subsequent proton-beam impact at cryogenic temperature [15].

EXPERIMENT DESIGN

The goal of the experiment is to assess the potential impact of radiation ageing on the damage limits by comparing the results to the non-aged results from HRMT-61 [14]. Similar hot-spot temperatures and temperature gradients were therefore targeted for the aged samples, while higher values — above 700 K and 200 K/mm — were sought for non-aged samples to probe the onset of damage. FLUKA [16] simulations were performed to optimise the coil layout and the number of copper shower blocks required. The final plate design is shown in Fig. 1. The most radiation-aged samples (30 MGy) are placed at the lowest hot-spot temperature position, followed by the 25 MGy samples, and finally the non-aged samples (green) at the highest energy deposition positions. There are two batches of four coils with identical spacing and shower-block configuration. One 10 mm thick copper block is placed upstream of the first coil and two additional 9 mm thick blocks are positioned upstream of the last coil of each batch. Simulations were carried out for beam sizes between σ = 1.0 and 1.3 mm and bunch intensities between 1.2×10^{11} and 1.8×10^{11} protons per bunch (ppb), all of which could be produced at the HiRadMat facility [17,18].

The optimal parameters — σ = 1.2 mm and 1.65×10^{11} ppb with 24 bunches — were selected to simultaneously match the four target temperature windows while achieving a gradient above 200 K/mm in the last sample of each batch.

Three complementary systems were integrated into the experimental setup to fully characterise the beam position relative to the samples throughout the experiment. A dedicated beam-based alignment (BBA) window is placed between the two coil batches. It consists of three copper blocks (Fig. 2): two side blocks (W1 and W2), each 9 mm thick and 30 mm tall, forming a horizontal aperture of 16 mm, with one 9 mm thick block (W3) placed on top. The precise dimensions allow the beam centre to be reconstructed relative to the metrology reference frame before the high-intensity shots. Tin foils, to be used for post-irradiation beam-trajectory

* Supported by the HL-LHC project
† delphine.domange@cern.ch

ISBN: 978-3-95450-252-3 ISSN: 2673-5350 doi: 10.18429/JACoW-IPAC2026-TUP7368

ALS-U SR MODULES PRESTAGING PLANNING TOOL AND METHODOLOGY

J. Shaw, R. Bloemhard, C. Espino Devine, D. Gudkov, M. Holmes, M. F. Khalid, K. Mccombs, H. Singhal, A. Talon, Lawrence Berkeley National Laboratory, Berkeley, United States

Content from this work may be used under the terms of the CC BY 4.0 licence (© 2026). Any distribution of this work must maintain attribution to the author(s), title of the work, publisher, and DOI.

Abstract

The Advanced Light Source Upgrade (ALS-U) project faces strict schedule requirements demanding rigorous planning of manufacturing assembly activities well in advance of assembly and installation. Delays of module components, and changes to the module tunnel installation sequence may significantly impact the module assembly (Prestaging) schedule for all 48 Storage Ring (SR) modules and therefore the installation of those modules during the 9-month SR removal and darktime installation period. To assess the adherence to schedule requirements, Prestaging developed a Visual Basic for Application coded planning tool to automate estimation of SR module assembly duration and resource needs. The tool methodology is based on bottom-up task sequencing where individual assembly tasks are laid out in succession with adjustments made for resource constraints and equipment conflicts. The model processes schedule and resource needs across 5 resource types for approximately 35 assembly tasks per module, generating duration estimates and resource profiles for SR module production. Functional testing has demonstrated the tool's capability to reduce planning time from approximately 4 hours of manual work per scenario-to-scenario processing to minutes while reducing inherent human error. With the model, Prestaging can quickly react to module component delays ensuring assembly planning is optimized within the constraints of the project. This contribution describes the model development methodology, functional testing results, and applications for future use during the ALS-U module assembly phase.

INTRODUCTION

During the 9-month darktime installation period, the existing ALS storage ring will be replaced with the new ALS-U storage ring [1]. To expedite the installation of the ALS-U SR, the 48 discrete modules that comprise the ring will be preassembled outside the tunnel by the Prestaging group [2]. Each module is comprised of magnets, vacuum chambers, LCW lines, support features, compressed air lines, electronics, and cabling [3]. It's the role of Prestaging to streamline the module assembly procedure, optimize the module assembly space within preexisting facility constraints, and perform functional tests on the module prior to installation.

The Prestaging assembly plan faces various challenges;

- Assembly spaces are limited to the existing LBNL facilities.
- Investment into the facility or assembly equipment must be justified by resource and assembly time schedule improvements.
- Module component delays were expected based on experience from previous assembly phases and tight procurement timelines.

The planning tool is a macro which generates a Gantt chart of assembly steps for each module in the production schedule with adjustments made for resource overallocation. Another output is a resource chart which sums personnel resource groups needed by week. The macro's outputs had to be considered along with a qualitative assessment of material storage, logistics, and risks to determine the most efficient assembly strategy that meets schedule constraints.

The macro was developed in support of two planning phases; the first to determine what facility equipment investment and resource allocation minimizes production duration, the second to optimize the assembly sequence within the equipment and facility constraints as determined in the first phase.

MACRO DEVELOPMENT PHASE 1 : FACILITY AND EQUIPMENT CONSTRAINT DETERMINATION

Tool development began with a breakdown of the assembly sequence for one module. Prestaging stakeholders (Prestaging, subsystem engineers, and technical support groups including mechanical and electrical tech teams, and Survey & Alignment) reviewed the module assembly design documentation and developed a baseline assembly process. The baseline assembly process identified 35 assembly steps, established assembly component sequence dependencies, equipment and personnel resources, and the estimated working duration for each assembly step.

Adjustable variables were built into the macro so the number of shared resources could be modified each time the macro was run. The Prestaging team toggled these production variables and iterated running the macro to produce unique outputs for each variable configuration. A comparison of the iterated Gantt charts provided insights into which features had the greatest impact on the production schedule.

Case Study 1: Crane Investment Optimization

Figure 1 graphs the overall production duration against 2 variables, the number of cranes and the number of Prestaging assembly stations. Multiple cranes mean assembly steps that require a crane can be performed on different modules in parallel.

The maximum number of stations that could fit in the Prestaging areas (High Bay 1 & High Bay 2) is limited to 10.

ISBN: 978-3-95450-252-3 ISSN: 2673-5350 doi: 10.18429/JACoW-IPAC2026-TUO2M01

SOLEIL II: THE FRENCH 4GLS PROJECT - FIRST YEAR OF THE CONSTRUCTION PROGRAM

L. S. Nadolski* and A. Nadji† Synchrotron SOLEIL, Saint-Aubin, France

Abstract

SOLEIL II [1] is the French upgrade project of SOLEIL delivering next-generation synchrotron light source through a full renewal of the accelerator complex, the upgrade of 29 beamlines and six laboratories, and a major IT transformation. The compact 2.75 GeV, 354 m Storage Ring (SR) will reach 50 pm rad round-beam emittance using an atypical 7BA–4BA HOA (Higher Order Achromat) lattice, extensive use of permanent-magnet technologies, nearly 100% NEG coating, 12 mm diameter vacuum chambers, a new in-vacuum nonlinear kicker for transparent top-up operation, new 4th-harmonic cavities, and 10 µm magnet alignment. The new 5 nm rad emittance Booster adopts a 14-HOA lattice. Both lattices are frozen, enabling construction. SOLEIL II will provide up to a 100-fold coherent-flux gain, a nine-decade energy range, nanoscale resolution, and fully multimodal in-operando capability. This contribution highlights how the prototype phase builds confidence in these targets, with progress in accelerator technology, in collimation, risk mitigation, and major prototypes. Building refurbishments have started, and the first major equipment tenders are being launched. The project optimizes cost and ensures environmental compliance, targeting 50% electricity savings. The SR commissioning is scheduled early 2030.

THE SOLEIL FACILITY

The 2.75 GeV SOLEIL facility [2, 3] was commissioned in 2006 as a multidisciplinary large-scale French research infrastructure and characterization platform serving scientific communities and industry. With a natural emittance of 4 nm rad and a circumference of 354 m, the facility delivers high-brilliance photon beams with exceptional stability to 29 beamlines (BLs). The photon energy spectrum spans 8 orders of magnitude, from THz to hard X-rays up to 100 keV.

THE SOLEIL II UPGRADE PROJECT

To maintain competitiveness and deliver best-in-class performance to the scientific community and industry, the SOLEIL II upgrade project [1, 4] was initiated with a Conceptual Design Report published in 2021 [5], followed by an intensive Technical Design Report phase including extensive prototype R&D. The Construction stage was officially launched in January 2025 [6]. This transformation into a fourth-generation synchrotron light source will enhance performance up to 100 times in brilliance and coherent photon flux, enabling experiments up to 10 000 times faster and 1000 times more sensitive, with nanoscale spatial resolution and the ability to study complex systems under real operating conditions. These advances are underpinned by a unique light source spanning from infrared to hard X-rays, complemented by a versatile BL portfolio and specialized techniques. The project spans 11 years and is organized in two stages: *Construction (2025–2030)*, covering the upgrade of the accelerator complex, encompassing the new storage ring, the injection accelerator complex, and infrastructure, the overhaul of the information system, and the modernization of support laboratories and the adaptation of the beamlines. *Toward full performance (2031–2035),* bringing all beamlines to full exploitation of the ultralow-emittance beam through upgrades of photon sources, optics, and detectors, completion of accelerator performance, and the progressive development of innovative techniques.

INJECTOR COMPLEX

LINAC Upgrade to 150 MeV

The existing LINAC, currently operating at 110 MeV, is being upgraded to 150 MeV to ease the injection energy of Booster II. This upgrade constitutes the first spearhead subproject of SOLEIL II. All required equipment — including a direct beam stopper, SOLEIL II-standard power supplies, upgraded PLC and Pandabox control platforms for radiation safety, diagnostics and vacuum systems — is either ready to install or in manufacture, with no expected delay. The energy upgrade is planned during the 2026 summer shutdown.

A 5 nm rad *new Booster Ring*

The Booster is an entirely new synchrotron designed in collaboration with NSRL [7–12], replacing the existing one. It accelerates electrons from 150 MeV to 2.75 GeV. Its lattice is based on a two-superperiod 14BA structure combining three High Order Achromat-type 5BA cells, with horizontal and vertical phase advances of $(0.40, 0.10) \times 2\pi$ per cell. The resulting natural emittance is 5.2 nm rad at 2.75 GeV, representing a 27-fold reduction compared to the present booster. Key-parameters are summarized in Table 1.

Table 1: Present and Upgrade Booster at 2.75 GeV

Parameter	Present	Booster II
Energy range (GeV)	0.11–2.75	0.15–2.75
Circumference (m)	156.6	156.569
Nat. emittance (nm rad)	140	5.2
Betatron tunes Q_x/Q_z	6.65/4.58	13.18/4.195
Mom. compaction factor	2.8×10^{-2}	3.3×10^{-3}
Energy loss/turn (keV)	409	554
RMS bunch length (ps)	50 @ 3.6 MV	25 @ 3 MV

The magnet lattice consists of 210 ramped magnets in total, including 4 normal dipoles (D1), 28 combined-function

* laurent.nadolski@synchrotron-soleil.fr
† amor.nadji@synchrotron-soleil.fr

Content from this work may be used under the terms of the CC BY 4.0 licence (© 2026). Any distribution of this work must maintain attribution to the author(s), title of the work, publisher, and DOI.

ISBN: 978-3-95450-252-3 ISSN: 2673-5350 doi: 10.18429/JACoW-IPAC2026-TUO2M02

EUPRAXIA AT ELI ERIC: DEVELOPMENT OF A COMPACT LPA FEL AND PLASMA SOURCES FOR ULTRAFAST SCIENCE

A. Molodozhentsev†, Extreme Light Infrastructure Beamlines, Dolní Břežany, Czech

Content from this work may be used under the terms of the CC BY 4.0 licence (© 2026). Any distribution of this work must maintain attribution to the author(s), title of the work, publisher, and DOI.

Abstract

The ELI Beamlines Centre (part of the European Light Infrastructure), located near Prague in the Czech Republic, has been selected as the second pillar of the EuPRAXIA distributed user facility. It utilises a novel laser–plasma accelerator (LPA) to generate a high-quality electron beam for a range of applications. A key initiative is to develop an LPA-driven free-electron laser (FEL) spanning the soft X-ray water-window range, as the main objective of EuPRAXIA Phase 1. A two-phase development strategy is adopted, with an EUV-FEL prototype at around 400 MeV electron beam energy serving as the first step to validate the full system chain before the Phase 1 upgrade to 1 GeV. The soft X-ray LPA-based FEL will use 1 GeV electrons at 100 Hz, supporting research in biology, ultrafast chemistry, and nanoscale materials. The project leverages unique features of LPA-based FELs compared with LINAC-based facilities: naturally few-femtosecond electron bunches, high peak currents without compression, inherent sub-femtosecond synchronisation with the drive laser, and a significantly smaller accelerator footprint. These features enable experimental regimes that are challenging for existing large-scale FELs, particularly in ultrafast pump–probe and attoscience applications. Complementary developments at ELI Beamlines within the EuPRAXIA project include a betatron X-ray source and a low-energy positron source, broadening user access to advanced plasma-driven radiation and particle beams.

INTRODUCTION

Modern X-ray FELs are well-established, user-oriented facilities with broad applications across biology, chemistry, and imaging. Conventional radio-frequency linear accelerator (LINAC)-based FEL facilities, such as the European XFEL and the Linac Coherent Light Source (LCLS), deliver world-leading performance in photon flux, coherence, and pulse energy. However, these facilities impose major constraints on footprint (kilometre-scale), construction cost, operational cost, and user accessibility. The performance of compact designs such as SwissFEL [1], which achieved low emittance and a smaller footprint, demonstrates that more affordable FEL facilities can broaden access to ultrafast science. Reducing size and cost would fundamentally change the current paradigm of limited access to XFEL science, enabling university-scale installations [2]. Laser–plasma acceleration (LPA) technology offers a revolutionary route to compact free-electron lasers (FELs) by utilising the extremely high electric fields produced when a powerful laser pulse propagates through an underdense plasma. LPA can sustain acceleration gradients exceeding 100 GV/m, enabling electrons to reach GeV energies within a few centimetres [3]. Moreover, the electron beams generated by LPA can achieve six-dimensional brightness comparable to that of traditional LINAC-based sources [4]. Beyond their compactness, LPA beams offer inherent advantages for FEL applications: the acceleration process naturally produces electron bunches lasting a few femtoseconds with high peak currents. These bunches are intrinsically synchronised with the drive laser on a sub-femtosecond timescale, enabling pump–probe experiments with unmatched timing accuracy. Recently, several teams worldwide have demonstrated proof-of-principle free-electron lasing at different wavelengths [5-8], confirming that LPA technology has matured to the point where compact, plasma-based FELs are both scientifically and technically feasible. EuPRAXIA (European Plasma Research Accelerator with eXcellence In Applications) is the pan-European initiative to translate plasma-accelerator science into a user-facility platform and to build the first international plasma-accelerator-based research infrastructure. Its inclusion in the European Strategy Forum on Research Infrastructures (ESFRI) roadmap reflects broad recognition of the transformative potential of plasma-based accelerators for photon science, high-energy physics, and medical applications. EuPRAXIA's conceptual design [9] incorporates both laser-wakefield acceleration (LWFA) and particle-beam-driven plasma wakefield acceleration (PWFA). As an ESFRI project, EuPRAXIA aims to have two facilities operational by 2031, located at INFN-LFN (Frascati, Italy) and ELI Beamlines (Czech Republic), each hosting dedicated user zones for FEL pilots and complementary applications in materials science, structural biology, and high-field physics.

This paper presents the current development status of EuPRAXIA at ELI ERIC, focusing on the compact LPA-driven FEL and complementary plasma-based secondary sources for ultrafast science.

ELI ERIC AND EUPRAXIA

ELI Beamlines (the ELI ERIC user-oriented facility in the Czech Republic) will host the LWFA-focused second pillar of the EuPRAXIA distributed European infrastructure. Its world-leading laser capabilities [10] and established experimental infrastructure for laser-plasma interactions and secondary-source generation underpin this role. Multiple beamlines based on high-harmonic generation (HHG), betatron radiation, and plasma-generated X-ray sources are currently operational at ELI Beamlines, supporting ultrafast XUV and X-ray user experiments [11]. This infrastructure and operational experience enable ELI Beamlines to rapidly integrate LPA-based electron beams and FEL testbeds into its user program.

† alexander.molodozhentsev@eli-beams.eu

ISBN: 978-3-95450-252-3 ISSN: 2673-5350 doi: 10.18429/JACoW-IPAC2026-TUO8T01

FIRST MIXED HE/C ION BEAMS IN A CLINICAL FACILITY: TWO YEARS FROM CONCEPT TO FIRST ION IMAGING EXPERIMENTS

E. Renner*, K. Holzfeind, F. Ulrich-Pur, TU Wien, Vienna, Austria
N. Gambino, L. Grevillot, M. Kausel, L. Kelleter, D. Prokopovich,
C. Schmitzer, MedAustron, Wiener Neustadt, Austria
H. Fuchs, Medical University of Vienna, Vienna, Austria

Abstract

Patient irradiation with mixed $^{4}He^{2+}$ and $^{12}C^{6+}$ ion beams is a promising proposal for online monitoring in carbon ion therapy. Over the past years, major developments have enabled the generation of such beams at MedAustron, where they are now used in accelerator, detector, and medical physics research projects.

This contribution summarizes the key innovations that made this achievement possible. Among these are a new double multiturn injection scheme for merging helium and carbon ion beams in the synchrotron, concepts for simultaneous slow extraction of both ion species, and dedicated diagnostic tools for mixed beam characterization in the accelerator and experimental room. Together, these advances pave the way for continued progress in the field of mixed ion beam acceleration and application.

INTRODUCTION

In recent years, patient irradiation with mixed helium ($^{4}He^{2+}$) and carbon ion ($^{12}C^{6+}$) beams has been proposed as a new concept for online monitoring in carbon ion therapy [1,2]. Given their similar mass-to-charge ratio, with a relative difference of $\frac{\Delta(m/q)}{(m/q)} = 6.5 \times 10^{-4}$, both ions can be simultaneously accelerated and delivered to the patient. Extracted at the same energy-per-mass $\frac{E}{m}$, $^{4}He^{2+}$ has an approximately three times larger range in matter than $^{12}C^{6+}$. This means that the carbon Bragg peak can be used to deliver the treatment dose to the tumor (blue in Fig. 1), while helium can be detected behind the patient to indicate, for example, anatomical changes or patient setup errors (orange in Fig. 1).

The development and application of mixed helium and carbon ion beams is still in an early research phase. In 2023, such beams were delivered for the first time to medical physics researchers at GSI using the SIS18 synchrotron [3,4]. In the same year, a concept study was launched to explore how such beams could be delivered for research users at MedAustron, a synchrotron-based center for ion beam therapy and research in Austria. A key requirement from the project outset was to deliver such beams using the existing infrastructure, without requiring any hardware upgrades. The first milestone was reached in summer 2024 when the first mixed beam was extracted to the research irradiation room (IR1) at MedAustron [5], which is to the knowledge of the authors the first mixed He/C beam delivery at a clinical synchrotron facility. Since summer 2025, we have been able to reliably deliver such beams with suitable beam properties for first research applications. First range probing experiments have been performed since late 2025 (Fig. 1).

This paper summarizes the accelerator developments undertaken to enable mixed-beam delivery at MedAustron.

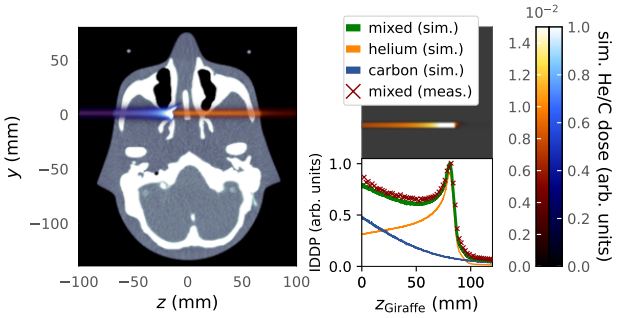

Figure 1: Preliminary results from first mixed beam irradiation experiments at MedAustron. Analysis and benchmarking with OpenGate [6] simulations are ongoing.

MIXED BEAM DELIVERY

Mixed Beam Generation

The starting point of the project was to identify a scheme for mixed-beam generation compatible with the existing infrastructure. The straightforward approach would be to extract the ion mixture directly from an ion source and transport it through the accelerator chain. This method was used for the mixed beam studies at GSI, using a mixture of $^{4}He^{1+}$ and $^{12}C^{4+}$ with $\frac{m}{q} \approx 4$ [3]. However, this is not possible with the existing infrastructure at MedAustron (or comparable clinical facilities), as no possible helium-carbon isotope combination simultaneously meets the requirements of the 14.5 GHz ECR ion source, the LINAC ($\frac{m}{q} < 3$) and the synchrotron [5, Sec. II.B].

We therefore implemented an alternative scheme in which helium and carbon ions are generated in separate ion sources, as in standard operation, and mixed during a sequential multiturn injection into the synchrotron [5, 7] (Fig. 2). In the first step, helium is injected. The injector is subsequently reconfigured for carbon injection from the second ion source. When ramping the injection bump in preparation for the carbon multiturn injection (hereafter referred to as *bump 2* for brevity), most of the previously injected helium beam is

* elisabeth.renner@tuwien.ac.at

Content from this work may be used under the terms of the CC BY 4.0 licence (© 2026). Any distribution of this work must maintain attribution to the author(s), title of the work, publisher, and DOI.

ISBN: 978-3-95450-252-3 ISSN: 2673-5350 doi: 10.18429/JACoW-IPAC2026-TUO8T02

ACCELERATORS ACTIVITIES AT ENEA FOR AEROSPACE

G. Bazzano†[1], A. Ampollini[1], M. D. Astorino[1], A. Doria[1], F. Fortini[1], P. Nenzi[1], E. Pavoni[1]
G. Picardi[1], C. Poggi[2], C. Ronsivalle[2], V. Surrenti[2], E. Nichelatti[2], E. Trinca[2]
[1]ENEA Frascati Research Centre, Rome, Italy
[2]ENEA Casaccia Research Centre, Rome, Italy

Abstract

The ENEA Frascati Particle Accelerators Laboratory operates a set of S-band electron and proton linear accelerators providing beams relevant for radiation-effects studies in the aerospace sector. The TOP-IMPLART proton LINAC delivers low-energy (1–6 MeV) and high-energy (up to 71 MeV) beams, while the REX and TECHEA facilities supply 3.5–5 MeV and 1–3 MeV electron beams, respectively; both can also operate as X-ray sources via removable bremsstrahlung converters. The contribution reviews ENEA activities in aerospace applications, including irradiation of electronic components, material and shielding studies, and radiobiology and astrobiology experiments. ENEA is involved in several national and European projects— such as Cryptomars, Space It Up!, Space-EBC, and Thread — addressing key topics for space exploration. In parallel, ENEA provides irradiation services within infrastructures such as DIANA and ASIF supporting component testing and material qualification. This work highlights ENEA's role in supporting the aerospace community through advanced accelerator capabilities, coordinated research initiatives, and a broad portfolio of irradiation services aimed at enhancing the robustness and space-readiness of technologies for future missions.

INTRODUCTION

The increasing demand for reliable technologies for space missions requires ground-based infrastructures capable of providing controlled, reproducible and well-characterized irradiation conditions. This need is closely related to radiation hardness assurance activities, which address the main radiation effects relevant to space systems, including total ionizing dose, displacement damage and single-event effects [1]. Accelerator-based facilities are particularly relevant in this framework, since they allow the investigation of radiation effects on materials, electronic components and biological systems under selected particle, energy, flux and dose-rate conditions [2,3].

Since ground-based tests cannot reproduce the full complexity of the orbital radiation environment in a single exposure, complementary irradiation facilities are often required to cover different particle species, energies and dose-rate regimes. In this context, multi-source and mixed-field irradiation infrastructures represent an important approach for testing components and systems under controlled yet representative radiation conditions.

This paper presents an overview of ENEA activities for aerospace applications, with emphasis on the accelerator facilities operated at the Frascati Research Centre, their integration with complementary irradiation infrastructures, and selected research programs exploiting these capabilities.

†giulia.bazzano@enea.it

ENEA FRASCATI PARTICLE ACCELERATORS LABORATORY

The ENEA Frascati Particle Accelerators Laboratory (ACP) has developed and operated compact RF linacs since the 1980s, along two main technological lines: electron radiation sources for research and industrial processes, and accelerator prototypes for medical applications. Accelerators currently in operation are one proton linac, TOP-IMPLART, and two S-band electron linacs, REX and TECHEA. Although different in layout, energy range and original purpose, the three machines share a common emphasis on compact RF technology, pulsed operation, and flexible beam delivery.

TOP-IMPLART is a pulsed proton linear accelerator developed as a full-linear prototype for proton therapy, with the original objective of reducing the complexity and cost of proton-therapy systems. The machine is based on a commercial 7 MeV injector, including a duoplasmatron source followed by a 425 MHz RFQ and DTL section, and on an ENEA-designed booster composed of eight S-band Side Coupled Drift Tube Linac modules operating at 2997.92 MHz [4]. The booster modules are grouped in two RF sections each one powered by a 10 MW peak-power klystron. The accelerator provides two lines: a low-energy vertical line in the 1–6 MeV range and a high-energy horizontal line up to 71 MeV [5, 6]. A summary of the beam parameters for the vertical (V) and horizontal (H) lines is reported in Table 1.

Table 1: Beam Parameters of TOP-IMPLART Extraction Lines

Parameter	Line	Value
Pulse length	V	20 - 100 μs
Peak current	V	100 μA
Energy on target	V	1 – 6 MeV
Beam spot size on target (diameter)	V	10 mm
Pulse length	H	2.4 μs
Peak current	H	15 μA
Max energy on target	H	70 MeV
Pencil beam size on target (FWHM)	H	25 mm
Rep. rate	H&V	25 Hz

Content from this work may be used under the terms of the CC BY 4.0 licence (© 2026). Any distribution of this work must maintain attribution to the author(s), title of the work, publisher, and DOI.

ISBN: 978-3-95450-252-3 ISSN: 2673-5350 doi: 10.18429/JACoW-IPAC2026-TUV8002

MAPPING GLOBAL COLLABORATION IN ACCELERATOR RESEARCH

A. Zamora*, University of Lausanne, Lausanne, Switzerland

Content from this work may be used under the terms of the CC BY 4.0 licence (© 2026). Any distribution of this work must maintain attribution to the author(s), title of the work, publisher, and DOI.

Abstract

This contribution examines particle accelerator research through a sociological lens. It combines a database of accelerator counts per country with a large corpus of accelerator-related publications from Web of Science to analyse how infrastructure distribution shapes scientific collaboration across regions and disciplines. The results reveal marked geographical asymmetries: some regions sustain dense internal publication networks while others participate primarily through cross-regional partnerships. The analysis also identifies clear disciplinary differences in how fields such as astronomy, materials science, and chemistry mobilise accelerator infrastructure through distinct collaboration configurations. Together, these patterns illustrate how scientific collaboration crystallises around shared infrastructures, how expertise circulates unevenly between regions, and how accelerators support the emergence of differentiated epistemic communities. The study offers an empirical perspective on the social dynamics underpinning global accelerator research and raises questions for future qualitative and longitudinal investigation.

INTRODUCTION

Particle accelerators occupy a distinctive position in the landscape of contemporary science, especially in science and technology studies [1–4]. Attention has extended to synchrotron light sources and other mid-range facilities serving materials science, chemistry, medical imaging, and environmental research [5–7]. Yet the relationship between infrastructure and knowledge production remains underexplored at a global scale. Existing analyses focus on specific facilities [8–10] or established communities [11, 12], rather than offering a comparative multi-regional perspective. Three questions guide this study: How are infrastructure and publication production distributed ? How are collaboration networks organised across regions? And do disciplinary communities mobilise accelerator infrastructure through distinct collaboration configurations?

METHODOLOGY

Data Sources

The accelerator database was constructed from the IAEA Accelerators Database[1] (578 facilities), expanded via the NEC World Pelletron Census,[2] the HVEE Tandetron database,[3] and scientific publications such as [13], reaching 809 facilities across 68 countries. Each entry records location, type, energy range, and commissioning year. As ~97% of the world's 30,000 accelerators serve industrial or medical purposes [14], this sample targets research-relevant facilities. Publication data were retrieved from Web of Science (1928–2022) using keyword searches for accelerator types and components (*linac, synchrotron, pelletron, van de graaff, RFQ*, and others), translated into 12 languages to mitigate language bias. The corpus does not distinguish between facility operators and user communities.

Analytical Approach

The analysis proceeds in three steps: comparing regional infrastructure and publication shares using proportional ratios; characterising collaboration profiles by distinguishing intraregional publications (all co-authors within the same region) from extraregional ones (at least one external partner), examined both in aggregate and longitudinally; and disaggregating profiles by WOS subject category to identify disciplinary collaboration patterns. Data processing was carried out in Excel and RStudio.

Classifications & Limitations

Countries were assigned to six world regions (UN M49) and to Global North or Global South (NORRAG),[4]. These categories are used as analytical tools; their limitations are acknowledged [15]. Regional affiliation reflects institutional address at time of publication, not researcher nationality or mobility. Of the 256,227 publications, 2.63% could not be regionally classified due to missing affiliation data and are excluded from regional analyses.

Three further limitations bear noting. The accelerator database remains incomplete and would benefit from broader surveying. WOS is biased toward English-language output, likely undercounting activity in underrepresented regions. The keyword-based search captures publications that explicitly mention instrument types, and user communities that do not name the facility in their output will be undercounted. This study is exploratory: the patterns documented are observations warranting interpretation, not measures of regional performance.

ACCELERATOR INFRASTRUCTURES & RELATED PUBLICATIONS

The following results examine whether and how infrastructure presence shapes scientific participation, and where other factors intervene.

Figure 1 presents the global and regional distribution of the 809 research accelerator facilities alongside 249,476 accelerator-related publications. At the global level the two distributions are nearly identical: the Global North hosts 81.21% of facilities and accounts for 82.24% of publications;

* annabella.zamora@unil.ch

[1] IAEA Accelerators Database, accessed 13 May 2026.

[2] National Electrostatics Corp., accessed 13 May 2026.

[3] High Voltage Engineering Europa B.V., accessed 13 May 2026.

[4] Network for International Policies and Cooperation in Education and Training.

ISBN: 978-3-95450-252-3 ISSN: 2673-5350 doi: 10.18429/JACoW-IPAC2026-TUI3T01

HIGH QUALITY ELECTRON BEAMS WITH TUNABLE ENERGY PRODUCED BY LASER-PLASMA ACCELERATION

B. Cros†, Ch. Ballage, P. Désesquelles, O. Khomyshyn, M. Masckala, F. Massimo, I. Moulanier, T. L. Steyn, O. Vasilovici, Laboratoire de Physique des Gaz et des Plasmas, CNRS, Université Paris Saclay, Orsay, France
Y.-Yu Chang, F. M. Herrmann[1], A. Irman, M. Laberge, M. Samir, S. Schöbel, U. Schramm[1], P. Ufer[1], Helmholtz-Zentrum Dresden-Rossendorf, Dresden, Germany,
S. Dobosz Dufrénoy, A. Panchal, Laboratoire Interactions, Dynamiques et Lasers, CEA, Université Paris Saclay, Gif-sur-Yvette, France
[1] also at Technische Universität Dresden, Dresden, Germany

Abstract

Laser wakefield acceleration (LWFA) of electrons occurs when an intense short laser pulse focused in an underdense plasma drives in its wake a plasma wave with an amplitude large enough to trap and accelerate electrons. Relativistic electron bunches are easily obtained through this mechanism and have given rise to a large number of studies and publications. Despite these efforts, the achievement of a high quality reliable electron source, ready for use in applications, still needs some developments. Electron beams with high quality, and tunable electron energy, have been achieved by the authors using the DRACO facility (HZDR Dresden), showing that the injection and acceleration processes can be controlled consistently in a gas cell. Dark current free, relativistic electron bunches with energy peaked at tunable values between 60 MeV, and 200 MeV, 40 pC charge in the peak and sub-mrad rms divergence, reaching up to 14pC/MeV/mrad, have been achieved experimentally and reproduced in Particle in Cell (PIC) simulations using measured input parameters. On going work is aimed at increasing the charge in the peak beyond 100pC through new gas cell development.

INTRODUCTION

Laser driven WakeField Acceleration (LWFA) [1] is a concept providing high gradient (> 1 GV/m) electron acceleration through the interaction of intense, short laser pulses with plasmas. In this process, 10 micron-scale plasma cavities, with radial accelerating and focusing fields, are created in the wake of intense laser pulses, providing opportunities for compact accelerator developments. Most of the studies using LWFA include the developments of electron sources, as plasma electrons can be trapped and accelerated in the plasma cavity, generating electron bunches of a few femtosecond (fs) duration at relativistic energy over a few millimeters of plasma.

The so-called mechanism of ionization injection [2] of electrons in a laser driven plasma cavity is a way to create locally a large number of electrons, which can be trapped and accelerated to hundreds of MeVs over millimeter scales. Without additional mechanisms, ionization injection cannot generate high charge density electron beams, and the charge in the beam is proportional to the spatial volume in the plasma over which injection occurs, resulting in energy spectra with large energy spread (100%).

In order to control this process, and achieve electron beams with smaller energy spread, efforts from several groups [3] are aiming at structuring the plasma density profile which contributes to control laser intensity along the propagation and separate the regions of the plasma where electron injection and acceleration take place. In addition, plasma ramps can be used as lenses and dechirpers to further improve beam quality [4].

Coupling laser beams to structured plasmas provides a large number of parameters to tune the electron beam quality and is the main topic of the presented work. Experimental results obtained at the HZDR using the LPGP gas cell are presented and discussed. Analysis of electron dynamics was performed using PIC simulations with the code SMILEI [5].

EXPERIMENT

Experiments were performed at the HZDR centrum using the DRACO laser as a driver for the laser wakefield electron source [6, 7]. A sketch of the experimental set-up is shown in Fig. 1. The laser beam, with a centre wavelength of λ_0 = 0.8 μm, and an energy on target of maximum 3 J, is focused inside the gas cell to a 24 μm FWHM spot size. The duration of each laser pulse is 30 fs FWHM, and a repetition rate of 0.1 Hz is used. The laser distribution in the focal volume is characterized by an almost constant peak intensity on the propagation axis and the transverse distribution is close to a focused flattened gaussian function (order N=8, w_0=14 μm). Measurements of the input laser in vacuum were performed, showing that the laser distribution is characterized by a good symmetry around the propagation axis, with a rotational symmetry parameter [8] larger than 0.8 over a distance of 4 mm in the focal volume. On line diagnostics at focus, and at 2 mm away on each side of the focus were implemented to monitor the transverse and longitudinal focus fluctuations on each shot [9].

† brigitte.cros@universite-paris-saclay.fr

Content from this work may be used under the terms of the CC BY 4.0 licence (© 2026). Any distribution of this work must maintain attribution to the author(s), title of the work, publisher, and DOI.

ISBN: 978-3-95450-252-3 ISSN: 2673-5350 doi: 10.18429/JACoW-IPAC2026-TUI3T02

FIRST DIRECT OBSERVATION OF A WAKEFIELD GENERATED WITH STRUCTURED LIGHT

A. Liberman*, A. Golovanov, A.-M. Talposi, S. Tata, and V. Malka
Weizmann Institute of Science, Rehovot, Israel
S. Smartsev
Laboratoire de Physique des 2 Infinis Irène Joliot-Curie, Orsay, France

Abstract

Since their inception, laser-wakefield accelerators (LWFAs) have shown their capability to produce high-quality, monoenergetic electron beams. Yet, the push toward higher electron energies and more efficient accelerators is constrained by several limitations. Foremost among these are the dephasing and diffraction limits. A promising strategy to address these issues involves using structured light to modulate the on-axis propagation velocity in LWFAs. By pairing the diffraction-resistant properties of Bessel beams with spatio-temporal pulse shaping, this approach offers an unprecedented combination of extended acceleration lengths and strong acceleration gradients.

Here we present the first experimental observation of wakefields driven by such structured, flying-focus beams. Spatio-temporally tailored pulses are directed through a specialized focusing mirror to form a quasi-Bessel beam, and the resulting wakefield is directly probed using femtosecond relativistic electron microscopy. Simulations corroborate the experimental data, offering novel insights into this underexplored regime. We show an experimental demonstration of the ability to modify the on-axis propagation velocity of the wakefield. We track the wakefield's evolution throughout the focal region and examine how specific spatio-temporal manipulations influence both its structure and propagation velocity. Finally, we present the first results using such wakefields to accelerate electrons. These findings establish a foundation for harnessing flying-focus-based strategies to overcome dephasing in LWFA.

INTRODUCTION

Since their inception [1], laser wakefield accelerators (LWFAs) have attracted considerable attention due to their capability to produce accelerating gradients far exceeding those of conventional radio-frequency accelerators [2, 3]. Over the past decades, LWFAs have successfully generated high-quality, quasi-monoenergetic electron beams [4–6], reaching energies as high as 10 GeV [7]. These systems have opened pathways toward a range of applications, including compact light sources [8, 9], advanced radiotherapy techniques [10], and experimental studies of strong-field quantum electrodynamics [11, 12]. Nevertheless, many envisioned applications require even higher electron energies. A key factor limiting further energy gain is dephasing—the mismatch between the velocity of the plasma wave and that of the electrons—which ultimately halts efficient acceleration [2, 13].

Various strategies have been proposed to alleviate dephasing. These include density-transition-based rephasing schemes [14, 15] and staged acceleration using multiple LWFA modules [16]. To date, the most effective approach has been to operate at reduced plasma density [7, 17], which decreases the velocity mismatch between the laser pulse and the electron bunch. While this method has enabled electron energies approaching 10 GeV [7], it comes at the cost of a reduced accelerating gradient [1]. Consequently, the laser must be guided over extended distances to counteract diffraction [13, 17]. Both the diminished gradient and the increased propagation length become more restrictive at higher target energies, as the acceleration length grows nonlinearly while the gradient continues to decrease [13].

An alternative approach to overcoming dephasing involves tailoring the structure of the driving laser field to control the effective on-axis velocity of the intensity peak, thereby synchronizing the wakefield with the electron bunch [18–22]. This concept is realized through the "flying focus," in which the focal region is extended over multiple Rayleigh lengths and different portions of the beam focus at distinct longitudinal positions with adjustable timing. Several implementations of this concept have been investigated, such as the interference of tilted laser pulses [20] and the combination of longitudinal chromatism with group-delay dispersion [18, 19]. However, these methods are challenging to implement at the high intensities required for LWFA operation.

A more experimentally viable realization of the flying focus for LWFAs employs spatio-temporal pulse shaping in conjunction with focusing optics designed to produce quasi-Bessel beams [21, 22]. In particular, the axiparabola [23, 24] introduces both focusing and controlled spherical aberrations. This engineered aberration extends the focal region [23] and modifies the temporal evolution of the on-axis intensity [21, 22]. Additional control can be achieved by imposing a radially dependent pulse-front delay through spatio-temporal shaping prior to focusing [21]. Numerical studies indicate that this could enable electron acceleration beyond 100 GeV in existing facilities [21, 22].

Here we report the experimental observation of wakefields driven by flying-focus pulses of this kind, conducted on the HIGGINS 2 × 100 TW laser system at the Weizmann Institute of Science. Spatio-temporally engineered laser pulses are focused with an axiparabola and the resulting

* aaronrafael.liberman@weizmann.ac.il

Content from this work may be used under the terms of the CC BY 4.0 licence (© 2026). Any distribution of this work must maintain attribution to the author(s), title of the work, publisher, and DOI.

ISBN: 978-3-95450-252-3 ISSN: 2673-5350 doi: 10.18429/JACoW-IPAC2026-TUI4M01

STATUS AND COMPARISON OF WORLD-WIDE IN-FLIGHT FRAGMENT SEPARATORS

H. Simon*, M. Winkler, H. Weick
GSI Helmholtz Centre for Heavy Ion Research, Darmstadt, Germany

Abstract

Generation of rare isotope beams by means of in-flight separation of nuclear fragments and fission products requires complex optical structures usually comprising multiple separator stages. Large apertur magnets providing maximum acceptance, radiation hard and superconducting are used to separate the reference isotope from the bulk of the primary and secondary heayv ion beam. The pre-separator stages are designed to dump a majority of the secondary beam in a controlled way and are therefore often a challenge for radioprotection, shielding and beam catchers. The complex optics of fragment separators makes use of energy degraders, intermediate focal- and image planes to minimie contamination of the desired isotopes. A comparison of optical designs and magnet technologies will be presented.

SECONDARY EXOTIC ISOTOPES

Since the pioneering experiments at the BEVALAC in Berkeley in order to study nuclei far form stability lines in the 1980ies, there has been developments all over the world in order to come up with different methods in order to get a handle on secondary beam production. The most common methods have been identified and described in Ref. [1] where production in targets and their extraction via the ISOL method is explained together with the at that time upcoming in-flight separation method being explored e. g. at the Lise spectrometer at GANIL in the Normandy, France, the A1200 at NSCL in Michigan, USA, the RIPS facility at RIKEN, Saitama, Japan, or at the FRS at GSI, Germany. Especially the latter, being coupled to a synchrotron driver are favorable when trying to perform experiments [2] at coupled storage rings. The current paper will capitalize on the upcoming instruments for in-flight production with energetic secondary beams. These are routinely explored at the aforementioned FRS and at second generation facilities where FRS will be extended to the Super-FRS [3] and the comparison with several similar upcoming or already running facilities will be performed.

USE CASE FOR SECONDARY BEAMS

Leaving the stability lines leads to sizable changes in nuclear structure. The Nuclear Physics Astrophysics and Reactions community formed and defining the requirement via viable physics program at the Super-FRS project developments at GSI/FAIR represents the current driving force for several secondary beam facilities. Astrophysics scenarios require precise data especially for unstable nuclei which also needs to be predicted and interpreted with modern theory approaches. Reference [4] shows as an example that meanwhile computational power seconded with suitable methods in many-body theory and modeling based on realistic nucleon-nucleon forces reaches also heavy nuclei. Their production and separation are demanding, and require suitable methods for unambiguous identification for these heavier systems.

SEPARATION TECHNIQUES

A separation in-flight at sizeable primary beam energies of 0.1 GeV/nucleon to 1 GeV/nucleon is dominated by an interaction with the target leading to breakup reactions through fission and fragmentation. Energy loss and straggling in the target will be reduced with higher energies, allowing for the use of thick targets (i. e. thicknesses larger than 1 g/cm²). This is also the domain where the internal Fermi momentum of nuclei in the nucleus become smaller than the momentum of the incoming beam particles. This leads to kinematical focusing along the beam direction, so that higher beam energy leads to increased transmission of secondary beam products. The basic principle is a combination of magnetic separation via magnetic rigidity Bρ which depends on the beam particle momentum over charge ratio. Different charge states (i.e. incomplete ionization of the ions) will lead to a different bending of the magnets and, thus, possible contaminants by unwanted sid products that cannot be spatially separated. The charge can be identified by measurement of the specific energy loss in dedicated transmission detectors. Also here the different appearing charge states lead to tails in the energy loss distributions towards lower energy loss in the detectors. The magnetic separation system can be extended (as described in Ref. [3]) at dispersive planes with wedge-shaped degrader plates, that allow to make use of energy loss in the material depending on the squared ratio charge (state) over beta (the relative velocity to the velocity of light) of the particles. The dependence allows refocusing of beam particles in the next stages of the separator that come with certain charge states. At areas of the separator system where intensities are low enough to perform event-wise measurements with all beam particles detectors for energy loss measurements (ΔE, with a few percent relative resolution), time-of-flight (TOF - at a level of a few 10 ps resolution) and position with mm resolution, with particle rates of up to a few million particles-per-second (pps). The discussion of the dedicated instrumentation is outside the scope of this paper.

Typically, several magnet stages with degrader wedges at dispersive planes are combined into the full separator.

* h.simon@gsi.de

Content from this work may be used under the terms of the CC BY 4.0 licence (© 2026). Any distribution of this work must maintain attribution to the author(s), title of the work, publisher, and DOI.

ISBN: 978-3-95450-252-3 ISSN: 2673-5350 doi: 10.18429/JACoW-IPAC2026-TUI4M02

ACCELERATOR COMPLEX EVOLUTION AT FERMILAB

M. Convery†, Fermi National Accelerator Laboratory, Batavia, United States

Abstract

The largest hadron accelerator facility in the US is undergoing radical changes and the undertaking of new HEP-driven neutrino research. This talk will discuss the wide-ranging projects and impacts to the accelerator community taking place at Fermi National Accelerator Laboratory.

INTRODUCTION

For roughly the last decade, the Fermi National Accelerator Laboratory (Fermilab) accelerator complex has been supporting world-class short- and long-baseline neutrino, muon, and test-beam programs.

As Fermilab's main focus shifts to the Deep Underground Neutrino Experiment (DUNE), the accelerator complex must modernize to improve reliability and maximize beam power. The 1970s Linac will be replaced by a new superconducting-RF (SRF) linac, Linac2, already under construction. The Booster will be upgraded to cycle at 20 Hz and to optimize for beam from the new linac. The Main Injector must reliably provide 1.2-2.4 MW proton beams to the new Long Baseline Neutrino Facility (LBNF) to produce neutrinos for DUNE.

STATUS OF THE FERMILAB COMPLEX

The Booster Neutrino Beam has delivered $3x10^{21}$ protons on target (POT) at 8 GeV to the short-baseline neutrino experiments over the last ten years including the requested $6.6x10^{20}$ POT to the Short Baseline Near Detector, yielding the largest neutrino-argon dataset in the world. Two additional runs are planned prior to the Linac2 era.

The Main Injector, which delivers 120-GeV proton beam for the long-baseline neutrino experiments, has been executing a campaign to increase beam power by shortening the cycle time rather than by increasing beam intensity. The ramp was shortened from an initial 1.33s to 1.067s, and a record beam power of 1.02 MW was demonstrated in 2024 [1].

The Muon Campus has been commissioning resonant extraction for the Mu2e experiment in preparation for a physics run which is planned for late 2027.

Infrastructure failures in 2024, the most notable of which was an electrical transformer needed to power the Main Injector, brought to the forefront the need to invest in reliable infrastructure for the DUNE era. In spite of recent challenges, we have delivered $4.6x10^{21}$ POT to the NOvA experiment since 2014. The Accelerator and NuMI Upgrades portion of the NOvA project was designed to deliver 3.6×10^{21} POT.

†convery@fnal.gov

TRANSITION TO THE LINAC2, LBNF/DUNE ERA

The Fermilab Accelerator Complex in 2026 is shown in Figure 1 in comparison with the complex in 2031 in Figure 2.

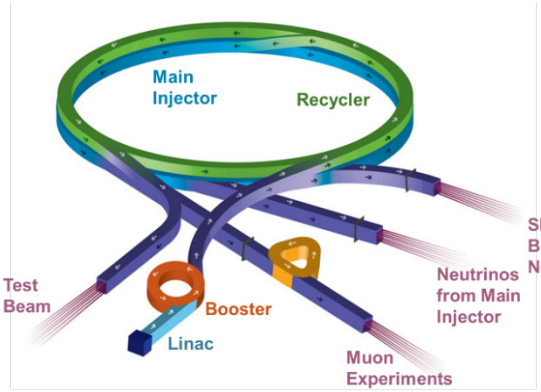

Figure 1: Fermilab Accelerator Complex in 2026.

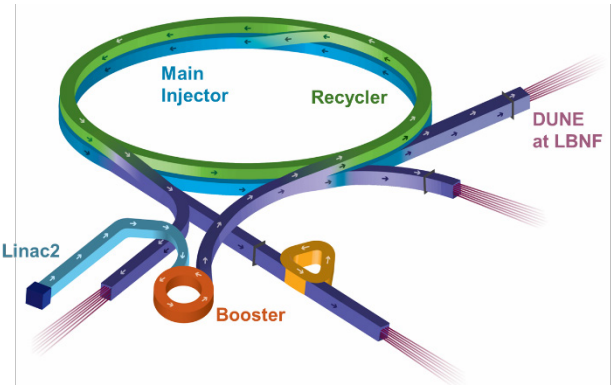

Figure 2: Fermilab Accelerator Complex in 2031.

The Proton Improvement Plan II (PIP-II) project is building a state-of-the-art superconducting-RF linac, Linac2, that will accelerate H- ions to 800 MeV [2]. A new Beam Transfer Line (BTL) will connect to the existing Booster, which will be upgraded to deliver the 8-GeV proton beam at a rate of 20 Hz, compared to the current 15 Hz. Together with other upgrades of the Booster and Main Injector, this will provide a beam power of 1.2 MW to LBNF/DUNE.

The LBNF/DUNE-US project provides a beamline to deliver a 1.2-2.4 MW proton beam, a target station to produce neutrinos, a "near detector" facility on the Fermilab site in Illinois, and excavated and outfitted detector caverns 1.5 km underground at the Sanford Underground Research Facility in South Dakota for the "far detector". The international DUNE collaboration provides the detectors with support from the US project.

Content from this work may be used under the terms of the CC BY 4.0 licence (© 2026). Any distribution of this work must maintain attribution to the author(s), title of the work, publisher, and DOI.

ISBN: 978-3-95450-252-3 ISSN: 2673-5350 doi: 10.18429/JACoW-IPAC2026-TUO2M04

HIGH CHARGE OPERATION AND FUTURE UPGRADES OF THE APS-U INJECTOR CHAIN*

J. Calvey†, T. Berenc, M. Borland, R. Hong, O. Mohsen, Y. Sun, K.P. Wootton
Argonne National Laboratory, Lemont, IL, United States

Abstract

For swap-out operation in the APS-Upgrade storage ring, the injector must supply a full charge bunch in one shot. For 200 mA operation in 48 bunch timing mode, the required charge per bunch is 16 nC, which is challenging for the injector chain. In this paper we report on the present status of high charge operation and discuss upcoming improvements to increase the charge limit. We also propose two future upgrades to the APS-U injector chain: a high charge photoinjector for direct injection into the booster, and a high energy accumulator ring in the booster tunnel.

INTRODUCTION

The APS-Upgrade (APS-U) is a 4th generation electron storage ring (SR) light source, which has a natural emittance of 42 pm at 6 GeV [1]. Achieving this ultralow emittance requires strong focusing and nonlinearities, which results in a small dynamic aperture, precluding accumulation. Instead, the APS-U uses swap-out injection [2, 3]: a depleted bunch in the SR is replaced by a full charge bunch from the injector.

For 216 bunch brightness mode, the injector chain can easily deliver the required charge (up to 5 nC), and the full SR current of 200 mA has been achieved. In 48 bunch timing mode, the injector must deliver at least 16 nC to the SR, which is very challenging.

For the APS-Upgrade, it was decided to leave the old APS injector chain in place, and make individual improvements when needed. The injector chain consists of 3 machines (Fig. 1), which operate on a 1 Hz cycle: a linac, Particle Accumulator Ring (PAR), and booster. The PAR accumulates 1 nC pulses from the linac (up to 20 nC), and compresses the bunch with a 12th harmonic cavity (RF12) before injection into the booster. The booster must capture this bunch with high efficiency, accelerate it to 6 GeV, and maintain a reasonably low emittance.

Challenges of the APS-U injector upgrade included aging and obsolete accelerator components, operating the booster and SR at different frequencies [4], and stricter requirements for charge stability [5]. This paper will describe recent progress on the key requirement: delivering a high charge bunch to the storage ring. It will also describe two potential long term upgrades of the injector chain, which would further improve on high charge performance.

* Work supported by the U.S. Department of Energy, Office of Science, Office of Basic Energy Sciences, as well as Laboratory Directed Research and Development (LDRD) funding from Argonne National Laboratory, provided by the Director, Office of Science, of the U.S. D.O.E., both under Contract No. DE-AC02-06CH11357.

† jcalvey@aps.anl.gov

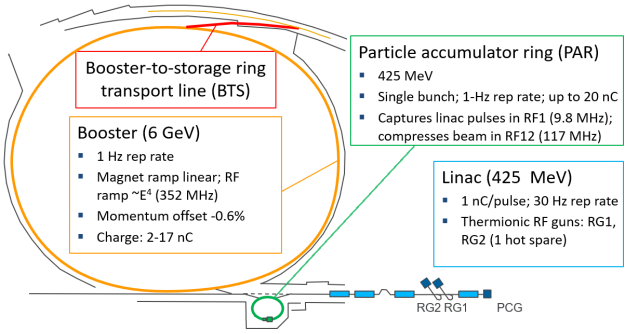

Figure 1: APS-U injector complex.

Other accelerator projects have taken different approaches to the challenge of high charge swap-out injection. ALS-U will use a full energy accumulator ring in the storage ring tunnel [6]. In the HEPS, the booster doubles as an accumulator ring by maintaining a flat top at full energy [7]. These schemes avoid the problem of high charge transport at low energy, at the cost of requiring a complex and high performance machine in the injector chain.

BOOSTER INJECTION

The main bottleneck to high charge transport through the APS-U injector is booster injection efficiency. The efficiency is good at low charge, but quickly drops above ~10 nC. Extensive simulations [8] indicated two main reasons for the reduced efficiency: PAR bunch lengthening and beam loading in the booster cavities.

PAR Bunch Length

As previously reported [9, 10], the PAR bunch length increased from 350 ps to more than 700 ps between low and high charge, due to a combination of potential well distortion and microwave instability. One of the largest sources of impedance was the kicker chambers. During the APS-U dark time, new chambers were installed with a patterned Ti coating, which both reduced the impedance (Fig. 2) and limited eddy currents.

In addition, a high power amplifier for the 12th harmonic cavity was installed, to provide increased bunch compression. The amplifier was recently tested up to full power, which provides 30 kV RF12 voltage. Figure 3 plots the measured bunch length vs charge for different RF12 voltages. At 30 kV, the bunch length is kept below 500 ps up to 18 nC.

A method of further reducing the extracted bunch length, by modulating the 12th harmonic rf voltage, is also under investigation, and has recently been demonstrated at low charge.

Content from this work may be used under the terms of the CC BY 4.0 licence (© 2026). Any distribution of this work must maintain attribution to the author(s), title of the work, publisher, and DOI.

ISBN: 978-3-95450-252-3 ISSN: 2673-5350 doi: 10.18429/JACoW-IPAC2026-TUO2M05

CLARA COMMISSIONING AND FIRST FRIENDLY USER EXPERIMENTS

D. Angal-Kalinin*[1,2], M.A. Johnson[1,2], J.K. Jones[1,2], and T. Pacey[1,2], on behalf of the CLARA Team
[1]ASTeC, STFC Daresbury Laboratory, Sci-Tech Daresbury, Warrington, UK
[2]The Cockcroft Institute, Sci-Tech Daresbury, Warrington, UK

Abstract

The CLARA facility at Daresbury Laboratory is a medium energy facility for R&D into a wide range of applications such as novel acceleration, cancer-therapy, and advanced diagnostics. CLARA is currently finalizing beam commissioning after an upgrade to 250 MeV followed by technical systems commissioning. During this period CLARA hosted its first set of friendly user experiments in its dedicated full energy beam exploitation (FEBE) beamline. Five different experiments were selected, covering a range of applications including: advanced diagnostics measurements using coherent transition radiation (CTR) and optical transition radiation (OTR) stations; Very High Energy Electron (VHEE) cancer-therapy studies; beam-driven plasma wakefield acceleration studies related to next generation colliders. These experiments exploited the full capabilities of the CLARA facility, including up to 250 MeV bunches with up to 250 pC per bunch at 100 Hz repetition rate, and with variable longitudinal compression. The experiments chosen will help develop and prepare CLARA for user experiments in the future. The installation and commissioning of the 120 TW laser transport system into the FEBE hutch is planned for 2026, which will expand the range of experiments to include those combining electron beams and high-power lasers.

INTRODUCTION

The Compact Linear Accelerator for Research and Applications (CLARA) is a high-brightness electron beam test facility at STFC Daresbury Laboratory. The layout of the accelerator facility is shown in Fig. 1. The CLARA front end, comprising a 2.5-cell S-band 10 Hz gun followed by a 2 m S-band linac, was made available for users in two dedicated experimental runs from 2018 until 2022 [1]. The installation of new components to upgrade the facility from the previously-installed front end at 50 MeV to 250 MeV was completed in 2024, including replacement of the 10 Hz S-band gun with a 1.5-cell S-band 100 Hz gun. This was followed by RF conditioning of the gun, four S-band accelerating structures and one S-band Transverse Deflecting Cavity (TDC). The first full energy CLARA beam was transported to the straight-on beam dump in April 2025, and threaded through the FEBE beam line to the final beam dump in October 2025. Beam commissioning progressed alongside technical systems commissioning, and included the testing and deployment of many high-level software applications for setting and characterising the beam parameters. Table 1 summarises design beam parameters of CLARA at the Interaction Point (IP) in FEBE.

Table 1: Design CLARA Beam Parameters at the FEBE IP Following Initial Commissioning of the Accelerator [2]

Parameter	Low Charge	High Charge
Repetition rate [Hz]	1 – 100	
Bunch charge [pC]	5	250
Bunch length [fs]	50	100
Energy spread [%]	< 1	< 5
RMS spot size [μm]	20	100
Norm. emittance [μm]	2	5

The first friendly user experiments were chosen in November 2025 to cover a wide range of disciplines with the aim to prepare the facility to commission these experiments in collaboration with users. Beam was successfully delivered to multiple experiments from January to April 2026. This paper describes the upgrade of CLARA, highlights from beam commissioning, and a brief description of beam delivery to the five user experiments.

CLARA UPGRADE

The swap of photoinjector gun; installation of three additional 4 m S-band linacs; a chicane-type Variable Bunch Compressor (VBC); an X-band linearizing cavity for harmonic correction; and a dedicated diagnostics section including an S-band TDC and a dielectric dechirper were completed in early 2025. The upgraded beamline is capable of accelerating electron bunches to the facility's design energy of 250 MeV.

A four-dipole arc, located at the end of the full-energy diagnostics section, transports beam to the FEBE user area, a separately-shielded enclosure where the majority of user experiments take place [2]. Installation of the FEBE beamline was completed in parallel with beam commissioning activities in the main accelerator hall. The installation and Site Acceptance Test (SAT) of the 120 TW laser were completed in November 2025 with the laser beam transport planned to be installed and commissioned later in 2026.

Conditioning of the RF structures began in March 2024 using a proprietary automated RF conditioning application, NO-ARC (No Operator Automated RF Conditioner). Details of the RF conditioning strategy, controls framework and procedure automations are described in [3–5].

Technical systems commissioning with beam followed RF commissioning. The first 250 MeV beam was generated using a Cu photocathode and transported to the straight-on beam dump in April 2025; further transport through FEBE to the final beam dump followed in October 2025. The existing

* deepa.angal-kalinin@stfc.ac.uk

Content from this work may be used under the terms of the CC BY 4.0 licence (© 2026). Any distribution of this work must maintain attribution to the author(s), title of the work, publisher, and DOI.

ISBN: 978-3-95450-252-3 ISSN: 2673-5350 doi: 10.18429/JACoW-IPAC2026-TUO2M06

SLS 2.0 COMMISSIONING PROGRESS

M. Aiba, PSI Center for Accelerator Science and Engineering, Villigen, Switzerland
on behalf of SLS 2.0 Team

Abstract

Commissioning of SLS 2.0, the first light-source storage ring employing a substantial number of permanent magnets, began in January 2025. The nominal beam current of 400 mA was achieved within the first three months of accelerator-dedicated commissioning. Since then, significant progress has been made. The Swiss Light Source facility upgraded to fourth-generation has reached a level of availability sufficient to begin user operation, delivering high-brightness photon beams to operational beamlines. First user operations have been carried out with internal and external users. We present the commissioning results, lessons learned, and experience gained during the initial user operation.

INTRODUCTION

The new storage ring at the Swiss Light Source (SLS), known as SLS 2.0, was successfully commissioned in 2025. It is the first light-source storage ring to employ a substantial number of permanent magnets to realize a compact multi-bend achromat lattice: the beam orbit and linear optics along the achromat arc are realized entirely with permanent magnets [1, 2]. The nominal beam current of 400 mA was achieved within the first three months of accelerator-dedicated commissioning [3]. Subsequently, the SLS facility upgraded to fourth-generation has reached a level of availability sufficient to begin user operation, delivering high-brightness photon beams to operational beamlines. First user operations have been carried out with both internal and external users. This paper highlights major commissioning progress achieved after the first three months, together with early user operation experience. The key parameters of SLS 2.0 are summarized in Table 1 for reference.

Table 1: Key Parameters of the New SLS Storage Ring

Parameters	Values
Beam energy	2.7 GeV
Circumference	288 m
Natural emittance	150 pm w/o IDs, w/o SC superbends
Lattice	7-BA, 12 sectors
Beam current	400 mA
Beam lifetime	9 hours w/o IDs

BEAMLINE COMMISSIONING AND ID INSTALLATION

Beamline commissioning followed the initial three months of accelerator commissioning. We began with dipole beamlines, which do not require additional machine-side preparation. For insertion-device (ID) beamlines, orbit feed-forward tables were established based on beam measurements and implemented in the control system. Characterization of the installed IDs is ongoing [4], and additional feed-forward tables are being developed to mitigate optics distortions.

The *first light* at each beamline was typically achieved within one day, allowing the subsequent mandatory radiation survey in the optical and/or experimental hutch to be completed the following day(s). As soon as the first set of beamlines was commissioned, it became apparent that orbit bumps of up to hundred µm at each photon source were required, indicating a misalignment between the photon beam directions and the reference axes of the beamlines. A realignment campaign was therefore scheduled to reduce these mismatches, as described later.

Undulators are currently installed in eight straight sections, while installation in three additional straight sections is planned. We encountered a serious vacuum pressure issue with a 2-meter-long APPLE-type undulator with a 9-mm inner-diameter vacuum chamber. Due to the proximity of the undulator permanent magnets, the NEG coating of the chamber could not be activated in-situ, and we relied only on beam vacuum conditioning for this short chamber. Vacuum conditioning with beam, however, was not effective, and hence high vacuum pressure along the chamber resulted in a significant reduction of beam lifetime. This problem was partially resolved by an unconventional in-situ activation method, in which pressurized hot water (about 140°C) was circulated through the chamber cooling-water channel. Technical details of the vacuum system can be found in Ref. [5].

BEAM STABILITY AND FEEDBACK

In parallel with the beamline commissioning, the fast orbit feedback system [6] was taken into operation. The feedback is implemented in the FPGA (programmable logic) part of a Multiprocessor System-On-Chip (MPSoC) that receives beam position monitor (BPM) data via dedicated multi-gigabit fiber optic links, using an in-house low-latency protocol. The same protocol and fiber links are used by the MPSoC to update the orbit corrector magnet power supply currents, combined with a beam momentum correction via the ring main RF frequency. With the present conservative settings, orbit stability on the order of 100 nm has been achieved in both transverse planes at 40 kHz correction rate (Fig. 1). The corresponding 0 dB points were 400 Hz and 500 Hz in the horizontal and vertical planes, respectively. With a future firmware upgrade, we expect to achieve >1 kHz 0 dB point at >80 kHz correction rate.

Regarding beam stability, stabilization of the RF voltage and phase is also essential, and the digital low-level RF system [7] plays a key role. The parameters of the internal feedback loops were optimized to minimize RF voltage and

Content from this work may be used under the terms of the CC BY 4.0 licence (© 2026). Any distribution of this work must maintain attribution to the author(s), title of the work, publisher, and DOI.

ISBN: 978-3-95450-252-3 ISSN: 2673-5350 doi: 10.18429/JACoW-IPAC2026-TUO7T02

A Compact Ultra-High Brightness Cryogenic C-Band RF Gun for Ultra-Fast Electron Diffraction Applications

C. Pennington[1], G. Lawler[1], F. Bosco[1], A. Bartnik[2], J. Jimenez-Zepeda[1], S. Tantawi [3], J. Maxson[2], J. Rosenzweig[1]
[1]University of California, Los Angeles, Los Angeles, CA 90095, USA
[2]Cornell University, Ithaca, NY 14853, USA
[3]Arizona State University, Tempe, AZ 85281, USA

Content from this work may be used under the terms of the CC BY 4.0 licence (© 2026). Any distribution of this work must maintain attribution to the author(s), title of the work, publisher, and DOI.

Abstract

We present the current status of the Cryogenic Brightness-Optimized Radiofrequency Gun (CYBORG), a compact high-field cryogenic C-band photoinjector beamline for ultrafast electron diffraction applications. Using General Particle Tracer (GPT) simulations together with multi-objective optimizations, we investigate the performance of the beamline as a high brightness source for MeV ultrafast electron diffraction (UED). The optimization targets were minimization of the electron bunch length and normalized 4D transverse emittance at the sample plane, with emphasis on high-brightness single-shot UED operation. For practical cathode source sizes of 40 µm, optimized solutions achieved brightness values approaching 10^{14} A/m^2 with bunch durations near 50 fs. Simulations using micron-scale source sizes demonstrated brightness exceeding 10^{16} A/m^2 with a bunch length of less than 20 fs at the sample, illustrating the performance potential of high-field cryogenic photoinjectors combined with low mean transverse energy photocathodes. Diffraction simulations further indicate that, despite post-sample space-charge broadening, the essential diffraction features remain intact in the low-charge operating regime considered here. These results demonstrate the potential of normal-conducting cryogenic photoinjectors for compact high-brightness MeV UED operation.

INTRODUCTION

Photocathode-based ultrafast electron diffraction (UED) systems require electron beams with high brightness, femtosecond-scale duration, and sufficient charge for single-shot or high signal-to-noise measurements. Existing UED beamlines are primarily based on DC and room-temperature normal-conducting RF (NCRF) photoinjectors, each offering distinct advantages in beam quality, coherence, and achievable energy [1, 2]. Recent advances in cryogenic NCRF photoinjectors have opened a promising path toward significantly enhanced beam brightness through operation at substantially higher accelerating fields and reduced intrinsic emittance [3–5].

Cryogenic copper RF cavities operated at temperatures of ~27–77 K exhibit reduced RF losses, increased conductivity, and improved mechanical hardness, enabling operation at electric fields substantially exceeding those achievable in room-temperature copper structures [6, 7]. In parallel, low-temperature photocathode operation can suppress excess momentum during photoemission, reducing intrinsic emittance and improving beam quality. Together, these effects make cryogenic RF photoinjectors attractive candidates for next-generation high-brightness UED sources.

The CrYogenic Brightness Optimized Radio-frequency Gun (CYBORG) beamline at UCLA was recently commissioned as a high-field cryogenic RF photoinjector platform compatible with insertable cathode plugs [8]. In this work, we investigate the expected UED performance of the CYBORG beamline using beam dynamics simulations based on the present and near-term machine configuration. The study focuses on optimization of ultrafast, high-brightness operating points relevant to MeV-UED applications.

To quantify beamline performance, we employ the five-dimensional brightness

$$B_{5D} = \frac{Q}{\epsilon_{nx}\epsilon_{ny}\sigma_t}, \tag{1}$$

where Q is the bunch charge, ϵ_{nx} and ϵ_{ny} are the normalized transverse emittances, and σ_t is the rms bunch duration. Assuming radial symmetry, we define the normalized four-dimensional transverse emittance as

$$\epsilon_{4D} = \sqrt{\epsilon_{nx}\epsilon_{ny}}, \tag{2}$$

allowing the brightness expression to be recast as

$$B = \frac{Q}{(\epsilon_{4D})^2\sigma_t}. \tag{3}$$

THE CYBORG BEAMLINE

The CYBORG beamline at UCLA is a compact cryogenic C-band photoinjector platform designed for high-brightness beam studies and ultrafast electron diffraction applications. The present beamline configuration is shown in Fig. 2. The injector consists of a 5712 MHz half-cell cryogenic copper cavity with re-entrant nose cones designed to enhance the on-axis accelerating field and maximize shunt impedance [8, 9]. The high shunt impedance achievable in cryogenic copper cavities is particularly advantageous for compact accelerator systems, as large accelerating fields can be obtained with comparatively modest RF power. This operating regime enables relativistic beam generation in a substantially reduced footprint relative to conventional MeV-UED facilities while maintaining the high brightness required for ultrafast diffraction applications. Electromagnetic field maps used in the beam dynamics simulations were obtained from COMSOL calculations.

ISBN: 978-3-95450-252-3 ISSN: 2673-5350 doi: 10.18429/JACoW-IPAC2026-TUO7T03

ANALYSIS OF LCLS-SC COMMISSIONING AND OPERATIONAL QUENCHES*

N. R. Neveu†, S. Aderhold, L. E. Alsberg, L. Alston, D. Gonnella, J. T. Maniscalco, H. A. Marts, J. Nelson, R. D. Porter, L. Zacarias
SLAC National Accelerator Laboratory, Menlo Park, CA, United States

Abstract

LCLS-SC achieved first light in 2023 and continues to ramp up performance. The linac consists of 35 cryomodules at 1.3 GHz, plus two cryomodules operating at the 3rd harmonic (3.9 GHz). The high repetition rate linac has been operating at 3.8 GeV regularly since 2024. As with any SRF machine, quenches occurred both during commissioning (as a part of normal processing) and during normal operations (tuning and beam delivery). After several years of operation, there are now thousands of quench events that can be analyzed and mapped to machine performance. In this work, quench rates in all cavities in the linac are identified and compared to operational quench rates and gradient limits.

INTRODUCTION

The Linac Coherent Light Source facility consists of two linear electron linacs, one normal conducting (NC) and one superconducting (SC) both installed in the existing SLAC 3 km tunnel. The NC linac, now called LCLS-NC, has been operating as a Free Electron Laser (FEL) since 2009. An upgrade of the facility (LCLS-II) installed an SC linac in the first third of the tunnel. The SC linac, now called LCLS-SC, is the first superconducting accelerator operated at SLAC. LCLS-SC has been commissioned and operated from 2022 to 2025. First light was accomplished in August 2023, and through 2025 regular user delivery and machine development took place. Simultaneous delivery to both hard and soft x-ray hutches was demonstrated in preparation for the increase in beam energy from the LCLS-II-HE project. Starting in December 2025, LCLS-SC was shut down for planned construction of LCLS-II-HE, another upgrade project that will add an additional 23 cryomodules to the LCLS-SC linac (L4). This will increase the operational energy from 4 GeV to 8 GeV starting in 2027. After the new cryomodules are commiossitoned, the repetition rate will ramp-up to 1 MHz. See Fig. 1 for the full LCLS-SC layout that includes both LCLS-II and LCLS-II-HE.

Currently, LCLS-SC contains four main accelerating sections: L0, L1, L2, and L3 with a total of 35 cryomodules operating at 1.3 GHz. Each cryomodule contains eight superconducting TESLA-style RF cavities [1] made of niobium. This type of cavity and variations on the cryomodule design are installed in several facilities, including Eu-XFEL and Fermilab. In this work, we review all commissioning and operational quenches during the 2022-2025 run of LCLS-SC. In Section , we review the current quench classification method at SLAC and typical SRF cavity decay and quench waveforms. In Section , we then use the classification method to analyze all historical quenches for LCLS-SC, including false quenches, multipacting processing events, and normal operations.

QUENCH CLASSIFICATIONS

SRF cavity quenches occur when an SC cavity loses SC properties and becomes normal conducting. This can occur due to impurities in the cavity surface during fabrication, installation and/or migration of particles during operation [2]. Once a small spot on the cavity surface becomes normal conducting, heat is dissipated throughout the cavity and it is no longer able to hold the operating gradient. These quenches are not as violent as SC magnet quenches, and once the cavity cools down again, it can resume operation. Typically, if caught fast enough, turning off the cavity prevents serious impact to the accelerator, and the cavity can be returned to operation within minutes or less. The quench, cool down and reset pattern is the reason a robust interlock system is needed. If the power supplied to a quenched cavity is not stopped, the cavity will continue to remain normal conducting and cause a disturbance in the helium bath (i.e. becoming a high heat load on the cryogenics system). The LCLS-SC interlock system compares the forward and reverse power supplied to the cavity. Although the heat load issue is a transient problem solved by robust interlocking, there is also the potential for trapped magnetic flux in the cavity after a quench. This is a persistent negative effect of quenches, which reduces the quality factor of the cavity (Q) [2]. Trapped magnetic flux can be purged with a fast cool down of the cavity, but that is not a routine operation. All attempts are made to reduce the number of warm up and cool down cycles necessary for maintenance and operations. Each warm and cool cycle takes 2-3 days, which impacts operational up time and delivery to users.

With high heat load being the high impact effect of quenches, the interlock detection is intentionally conservative. It often results in 'false' quenches: events flagged as a quench, but in which the cavity turns off for another reason. During normal operations, an SRF cavity might shut off for a variety of reasons, including tunnel access, equipment health, or beam tuning in targeted areas. When the interlock sees this drop in power, it is logged as a quench. To reduce the number of quench waveforms flagged for human review, a classification function and watcher process were written to reset LCLS-SC cavities when the quench is false. This is

* Work supported by the U.S. Department of Energy under contract DE-AC02-76SF00515.

† nneveu@slac.stanford.edu

Content from this work may be used under the terms of the CC BY 4.0 licence (© 2026). Any distribution of this work must maintain attribution to the author(s), title of the work, publisher, and DOI.

ISBN: 978-3-95450-252-3 ISSN: 2673-5350 doi: 10.18429/JACoW-IPAC2026-TUP2001

STATISTICAL PROPERTIES OF ATTOSECOND SASE FELs

J. Ribbing*, V. Goryashko, Uppsala University, Uppsala, Sweden

Abstract

Free electron lasers can now generate xray pulses with durations in the attosecond regime. Optimal utilization of the short pulses for attosecond science necessitates precise measurement of the pulse durations which there are promising methods to achieve. However, these are developing experimental techniques, not yet routine procedure. Until they mature, there is a wealth of information in the measured pulse energies and xray spectra, which are easily obtained. We show that while this information is insufficient to draw any conclusions about a single shot, with a large enough dataset, the statistics can determine length of the electron bunches, on average. FEL theory then predicts the distribution of the xray pulse durations. To achieve this, we extend the classical theory put in place by Saldin and Bonifacio to include short bunches with arbitrary current profiles, deriving integral expressions for some key statistical observables. The analytical is approach compared to 1D nonlinear simulations, showing good agreement until saturation sets in.

INTRODUCTION

The behavior of most of the matter we interact with on earth depends strongly on the distributions of bound electrons and the correlations between them [1–3]. These electrons move and redistribute on time scales of femtoseconds and attoseconds. Being able to access these scales directly with radiation opens up completely new avenues of physics [4]. One important tool for this purpose is the free electron laser (FEL) [5], an instrument that can produce attosecond xray pulses with extreme peak power. [6–11] At this moment, the only way to achieve attosecond hard x-ray pulses at an FEL is in the SASE [12, 13] mode (Self Amplified Spontaneuous Emission) which works by exponentially amplifying incoherent undulator radiation. [14] SASE is an inherently random process and thus the properties of the xray pulses vary significantly between shots. In particular, the duration of the pulses can fluctuate dramatically. [15] In addition to the natural randomness from SASE, the duration of the electron bunches themselves also fluctuates due to jitter in the LINAC and the strong bunch compression required. [16] To use the FEL to its fullest potential, ultra-fast experiments ideally require shot by shot direct measurement of the pulse durations. The leading method is currently angular streaking, which has been successful in characterizing attosecond UV sources based on high-harmonic generation and has been demonstrated for FELs. [3, 17, 18] For attosecond xray FELs it is still practically complicated and requires significant computation. Direct measurements of the electron bunch durations is also non-trivial because the resolution is usually limited by RF frequency in transverse deflecting cavities. [19, 20] What is readily available at most xray FEL facilities is the xray spectrum and pulse energy. The statistics of those measurements carry information about the electron bunches and there are succesful demonstrations of reconstructing relatively long bunch lengths at FLASH and LCLS. As seen in Refs. [15, 21, 22], one can for example use the variance of the pulse energy or spectral intensity correlations. Bunch lengths have also been diagnosed with the spectrum of spontaneous undulator radiation. [23] In a heuristic sense, xray spectra are also commonly used when tuning FEls – seeing wide, smooth spectra indicates that the (lasing part of) electron bunches are sufficiently short. For long uniform bunches, there is a complete analytical description of the statistics [24, 25], but for short bunches only numerical results are available. [15] Our contribution is generalizing the analytical picture, providing a wide description of the statistics of short bunches with an arbitrary current profile. Based on analytical calculations and numerical data, we draw these conclusions: 1) The average bunch length can be estimated from the mean and variance of the mean bandwidth. 2) While the estimate from energy statistics is most sensitive at long bunch lengths, the estimate from bandwidths is sensitive at short bunch lengths. 3) There exists a specific bunch length such that the pulse duration is very stable. 4) A single spectrum gives no information about the pulse duration or bunch length, even when there is no chirp in the bunch.

Analytical Model and Statistics

As a basis for analytical development we use the linearized, dimensionless 1D collective variables equations from Ref. [26]:

$$\begin{cases} \partial_\zeta^2 b = ia, \\ (\partial_\zeta + \partial_\tau)a = q(\tau)b, \\ b(\zeta = 0, \tau) = b_0(\tau), \end{cases} \tag{1}$$

with the remaining boundary conditions being homogeneous at $\zeta = 0$ and $\tau = 0$. Here a, b are the field envelope and bunching factor and ζ, τ are the distances along the undulator and along the bunch, scaled by the gain length $l_g = \lambda_u/(4\pi\varrho)$ and cooperation time $\ell_c = \lambda_r/(4\pi\varrho)$ respectively. ϱ is the usual Pierce parameter [26] with 3D corrections included and λ_u, λ_r are the spatial periods of the undulator and the radiation. q is the current profile, normalized to a peak value of 1 and we take it to be an arbitrary continuous function with support on $(0, \tau_b)$, so that τ_b is dimensionless full-length of the bunch. Since we are interested in SASE, the initial bunching factor b_0 is a random variable modeling shot noise. The dimensionless power is related to real units through the Pierce parameter: $P_{\text{real}} = \varrho|a|^2 P_b$, where P_b is the peak power of the electron beam. We derive

* johan.ribbing@physics.uu.se

Content from this work may be used under the terms of the CC BY 4.0 licence (© 2026). Any distribution of this work must maintain attribution to the author(s), title of the work, publisher, and DOI.

ISBN: 978-3-95450-252-3 ISSN: 2673-5350 doi: 10.18429/JACoW-IPAC2026-TUP2002

OPERATIONAL ASPECTS OF CRAB CAVITIES AT THE ELETTRA 2.0 STORAGE RING LIGHT SOURCE

S. Di Mitri[1,2,*], S. Cleva[1], S. Dastan[1], A. Fabris[1], E. Karantzoulis[1], K. Manukyan[1], C. Masciovecchio[1], M. Modica[1], N. Shafqat[1]
[1] Elettra Sincrotrone Trieste, I-34149 Basovizza, Trieste
[2] University of Trieste, Dept. Physics, V. A. Valerio I-34100 Trieste

Content from this work may be used under the terms of the CC BY 4.0 licence (© 2026). Any distribution of this work must maintain attribution to the author(s), title of the work, publisher, and DOI.

Abstract

We investigate the upgrade of the Elettra 2.0 diffraction-limited storage ring light source with radiofrequency transverse deflecting cavities generating picosecond-long X-ray pulses of moderate intensity and high repetition rate. Based on a preliminary RF design, operational aspects, challenges and solutions to make the crab cavity scheme simultaneous to the standard operation of the facility, are presented and discussed, also in view of the users' community wish list.

INTRODUCTION

Elettra 2.0 is a cutting-edge upgrade of the existing Elettra synchrotron light source facility positioned to be one of the most advanced research infrastructures worldwide and devoted to supporting a wide range of scientific fields [1]. From advanced materials science to biology and medical applications, the new facility will provide researchers with access to vastly enhanced high-resolution imaging and spectroscopic capabilities. This project aims to significantly enhance the scientific output of the facility by upgrading the accelerator and beamline systems to the production of X-ray pulses of picosecond-scale duration, at MHz repetition rate, and simultaneous to the standard multi-bunch operation of the light source, to meet the growing demands of scientific and industrial users.

WORKING PRINCIPLE

Three superconducting (SC) RF cavities, a.k.a. crab cavities (CC), connected in series, resonant respectively at a 6-fold (3 GHz for the two outer cavities) and 6.5-fold frequency (3.25 GHz for the single inner cavity) of the main RF, determine a steady-state configuration of vertically tilted bunches, with varying inclination along the ring circumference [2]. The charge distribution reaches the equilibrium in the 6-dimensional phase space [3,4]. The photon beam emitted by tilted bunches exhibits a longitudinal-vertical correlation (t,y). A vertical slit at some distance from the ID samples the central portion of the stretched photon pulse, thus selecting a short portion in time, though at some reduced flux. The vertical plane of deflection is chosen because the ratio of radiation flux over pulse duration is maximized by a smaller electron beam emittance. Indeed, Elettra 2.0 adopts a flat-beam configuration, with the vertical emittance controlled to be less than 5% of the horizontal one. The CC are installed in a non-dispersive straight section to avoid synchro-betatron coupling and beam instability [5]. The short pulse performance is tightly related to the design of the front-end and optical elements of the photon beamlines. Indeed, the short light pulse can be produced either through physical cut of the emitted radiation in the front-end area (drift mode) or, after a gentle angular selection in the front-end, at the location of light beam's waist, for example generated by vertical pre-focusing optics at the entrance of a monochromator (hybrid mode).

†simone.dimitri@eletra.eu

DISTRIBUTIONS AT EQULIBRIUM

The reach of equilibrium duration by three bunch modes is shown in Fig.1. The different longitudinal emittances reflect the different focusing to which the three bunches are subject in the longitudinal plane. The horizontal emittance at equilibrium is the same, which confirms a linearized motion of the vertically-tilted particles and weak coupling. The vertical emittance of the tilted bunch is dominated by the correlation in the vertical phase space. The vertical emittance of the standard bunch is approximately doubled by the residual (unbalanced) kick from the CC (not shown).

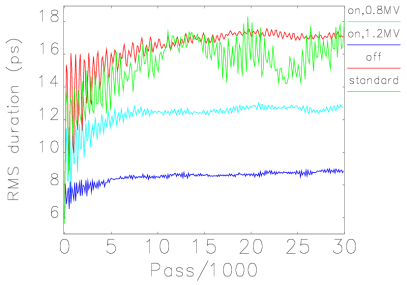

Figure 1: RMS bunch duration from zero-current parameters to the equilibrium in the presence of 3HC, for the tilted bunch ("on", blue and light blue), the same camshaft bunch with CC turned off ("off", red), and for the standard bunch in the middle of the train with CC turned on ("standard", green). The tilted bunch's duration is shown for two maximum deflecting voltages of 0.8 MV and 1.2 MV at 3 GHz (respectively, 1.5 and 2.3 MV total voltages).

LIGHT PULSES

Figure 2 shows the theoretical minimum pulse duration at each beamline in the limit of diffraction and electron-light matching condition. The impact of the energy spread is evaluated (solid lines) and compared to the case of a monochromatic electron beam (dotted lines). As expected, the elongation of the pulse duration due to the electron

ISBN: 978-3-95450-252-3 ISSN: 2673-5350 doi: 10.18429/JACoW-IPAC2026-TUP2301

OPTIMIZING THE NSLS-IIU ENERGY FOR MAXIMUM BRIGHTNESS AT OPERATIONAL BEAM INTENSITY

V. Smaluk*, Brookhaven National Laboratory, Upton, United States

Abstract

The most updated complex bend achromat lattice for the high-brightness upgrade of NSLSII provides a record-low electron beam emittance of 23 pm at 3 GeV. However, collective effects of beam dynamics, especially intra-beam scattering, are the main limiting factors of emittance and brightness at operational beam Intensity. Since the emittance and collective effects are strongly dependent on the beam energy, we estimated the lowest possible emittance scaled with energy and intensity, taking into account intrabeam scattering, vacuum chamber impedance, and bunch lengthening by higher-harmonic RF cavities.

INTRODUCTION

The high-brightness upgrade of NSLS-II is one of the top priorities of Brookhaven National Laboratory. Since reducing the electron beam emittance is an efficient way to increase the brightness, the low-emittance lattice based on the complex bend approach is being developed for the NSLS-II upgrade (NSLS-IIU) [1]. However, a common feature of low-emittance synchrotrons is short and intense electron bunches. The high particle density leads to strong collective effects that significantly increase the emittance with the beam current.

So, the relevant machine design problem is not simply to minimize the natural emittance determined by the lattice only but to find optimal beam parameters for maximum brightness at operational beam intensity [2,3]. To solve this problem for NSLS-IIU, we use the following approach: 1) learn from the experience of other low-emittance rings; 2) set up a reliable technique to estimate emittance at operational intensities, including collective effects; 3) scale the operational emittance with energy, intensity, and lattice-determined emittance; 4) optimize the lattice design to achieve the minimum operational emittance.

BEAM INTENSITY LIMITATIONS

The most direct limit of the beam energy E and current I_b in a storage ring results from the synchrotron radiation power rapidly increasing with the beam energy:

$$P_{\mathrm{rad}} = I_b U_0 = I_b \frac{C_\gamma}{2\pi} E^4 \int \frac{1}{\rho^2} ds \,, \qquad (1)$$

where $C_\gamma = 8.846 \cdot 10^{-5}$ m/GeV^3, U_0 is the radiation energy loss per turn, ρ is the bending radius. This strong E^4 dependence explains why higher-energy light sources are generally operated at lower current; there are no light sources with the beam current exceeding 500 mA. Fig. 1 shows the operational beam current as a function of energy for several synchrotrons; all the data were found in published materials. The dashed line represents an empirical rule $I_b(E)$.

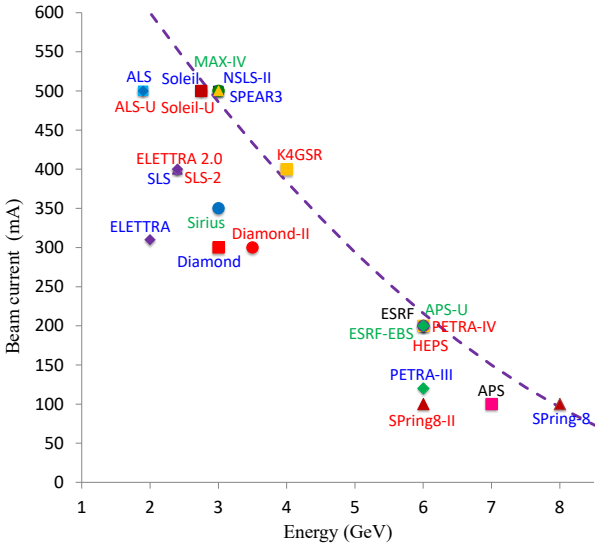

Figure 1: Operational beam current as a function of energy.

Vacuum-chamber heating provides a second practical constraint. The beam-induced power resulting from the interaction with resistive-wall impedance scales with the square of the beam current and increases when the chamber aperture is reduced.

$$P_{\mathrm{rw}} = \frac{k_{\|} I_\Sigma^2}{N_b f_0} \,, \qquad (2)$$

where I_Σ is the average beam current, N_b is the number of bunches, f_0 is the revolution frequency, and $k_{\|}$ is the longitudinal loss factor. That point matters particularly for low-emittance rings, including NSLS-IIU, where strong quadrupole magnets and advanced insertion devices require small-aperture chambers. The same small apertures also raise the impedance, which can drive collective instabilities.

INTRABEAM SCATTERING

Small-angle intrabeam scattering (IBS) results in an intensity-dependent 3D emittance growth. Although it does not lead to loss of particles, the emittance growth is significant in low-emittance rings, and this is a common problem for modern synchrotron light sources. Several IBS theories were developed: Piwinski theory for proton beams (two-particle collision kinematics, Rutherford cross-section) [4]; completely integrated modified Piwinski approximation (high energy beams) [5]; Bjorken&Mtingwa general solution (Gaussian bunch, variation of lattice parameters along the ring, no coupling) [6]; Bane's high-energy approximation with average lattice parameters [7]. We cross-checked

* smaluk@bnl.gov

Content from this work may be used under the terms of the CC BY 4.0 licence (© 2026). Any distribution of this work must maintain attribution to the author(s), title of the work, publisher, and DOI.

ISBN: 978-3-95450-252-3 ISSN: 2673-5350 doi: 10.18429/JACoW-IPAC2026-TUP2302

LIMITATIONS OF INTRABEAM SCATTERING THEORIES FOR HIGH-DENSITY BEAMS

A. Khan*[1], G. Stupakov[2], V. Smaluk[1], T. Shaftan[1]
[1]NSLS-II, BNL, Upton, NY, USA
[2]xLight Inc., Palo Alto, CA, USA

Abstract

We examine the regime of validity of classical intrabeam scattering (IBS) formalisms for ultra-low-emittance storage rings. These theories share foundational assumptions—Gaussian beam distributions, weak binary perturbations, and uncorrelated two-body encounters—that break down progressively as emittance decreases. We clarify the hierarchy among these formalisms, identifying the specific approximations that connect them and that become less accurate in the parameter range of modern machines. Using a parametric FODO lattice scan spanning two orders of magnitude in horizontal emittance, we identify quantitative boundaries where each assumption fails: below a critical emittance the IBS-to-damping ratio exceeds unity, the large-angle collision time collapses by several orders of magnitude, and the plasma response time approaches the scattering time scale.

INTRODUCTION

Intrabeam scattering is one of the key factors limiting the performance of modern high-brightness synchrotron light sources at high beam intensity [1]. The foundational theories of IBS were developed by Piwinski [2] and Bjorken and Mtingwa [3] in the 1970s and 1980s, when typical beam emittances were on the order of a few to tens of nm·rad. Since then, storage ring emittances have been reduced by up to two orders of magnitude in multi-bend achromat (MBA) lattices now being deployed at fourth-generation light sources [1], reaching the sub-nm·rad regime. The assumptions underlying the classical IBS formalisms—Gaussian beam distributions, weak binary perturbations, and uncorrelated two-body encounters—were never designed for this regime, yet they continue to be used as the primary prediction tools.

In this study, we examine where those assumptions break down. We first clarify the hierarchy among the classical formalisms, identifying the approximations that connect them. We then use a parametric FODO lattice scan to identify quantitative boundaries where each foundational assumption fails.

CLASSICAL IBS FORMALISMS AND THEIR ASSUMPTIONS

Piwinski and Bjorken-Mtingwa

The first comprehensive IBS theory was developed by Piwinski [2], who computed momentum-transfer rates from two-body Coulomb collisions using classical kinematics with the Rutherford cross section for a smooth-lattice Gaussian beam. He later extended the theory to include linear coupling and arbitrary beam sizes [4]. Bjorken and Mtingwa (B-M) independently derived IBS growth rates from relativistic quantum field theory [3], evaluating the rates through a phase-space integral at each lattice point with a cubic-polynomial denominator in the integration variable λ. Extensions with vertical dispersion and non-ultrarelativistic corrections exist for MAD-X [5], and coupled generalizations require the Lebedev-Nagaitsev-Mais-Ripken formalism [6]. Nagaitsev [7] reformulated the B-M integrals using Carlson's symmetric elliptic integrals, producing results strictly identical to B-M but roughly 20 times faster to evaluate. The same growth rates follow independently from the Landau kinetic equation [8] applied to the beam-frame velocity distribution [9]. In the ultrarelativistic limit $\gamma^2 \gg \beta_{x,y}/\epsilon_{x,y}$ the λ^3 term in the B-M denominator is negligible and the full B-M result reduces exactly to the Nagaitsev-Lebedev expressions.

Revised Bane's High-Energy Approximation

Bane's high-energy approximation [10] introduces simplifications to B-M but makes approximations some of which are only valid when dispersion is relatively small. We would like to point out that a more accurate and still relatively simple approximation can be found in Ref. [9], p. 199. This approximation is also obtained for high-energy taking into account that in practice the longitudinal temperature in the beam frame is much smaller than the transverse one. For the rate of the relative energy spread σ_δ, this approximation, after some transformations, can be written as:

$$\frac{d\sigma_\delta^2}{dt} = \frac{N r_0^2 c}{4\sqrt{2}\gamma^3 \sigma_z} \left\langle \frac{\Lambda}{\tilde{\sigma}_x \sigma_y} \tilde{\Upsilon}(\theta_x, \theta_y) \right\rangle_s , \qquad (1)$$

where N is the number of particles in the bunch, $\tilde{\sigma}_x^2 = \epsilon_x \beta_x + \sigma_\delta^2 D_x^2$,

$$\theta_x^2 = \frac{\epsilon_x}{\beta_x}\left(1 + \frac{\sigma_\delta^2}{\sigma_x^2}(\beta_x D_x' + \alpha_x D_x)^2\right), \qquad \theta_y^2 = \frac{\epsilon_y}{\beta_y}, \quad (2)$$

and

$$\tilde{\Upsilon}(x,y) = \frac{2^{1/2}}{\pi} \int_0^\infty \frac{d\lambda}{\sqrt{(1+x^2\lambda^2)(1+y^2\lambda^2)}}. \qquad (3)$$

Here Λ is the Coulomb logarithm and we use the standard notations for the lattice functions and the beam parameters. The angular brackets in Eq. (1) indicate averaging over the circumference of the ring.

* akhan1@bnl.gov

Content from this work may be used under the terms of the CC BY 4.0 licence (© 2026). Any distribution of this work must maintain attribution to the author(s), title of the work, publisher, and DOI.

ISBN: 978-3-95450-252-3 ISSN: 2673-5350 doi: 10.18429/JACoW-IPAC2026-TUP2304

RECENT DEVELOPMENTS TOWARDS THE SDLS*

D. Khan†, X. Huang, P. Liu, Y. Nosochkov, J. Safranek,
SLAC National Accelerator Laboratory, Menlo Park, United States

Abstract

We report on the development of an advanced storage ring lattice, the Stanford Diffraction-Limited Light Source, tailored for installation in the existing PEP-II tunnel at SLAC, which consists of six arcs and six long straight sections. The SDLS cell is based on the hybrid 6-bend achromat optics optimized for ultra-low emittance and maximum dynamic aperture, essential for diffraction-limited synchrotron radiation production. The long straight sections, which will house the insertion devices and injection systems, are designed to satisfy the transparency conditions that mitigate periodicity-breaking effects affecting the dynamic aperture and momentum acceptance. The latest designs advances the SDLS concept by replacing the H6BA cell with a non-achromatic cell or combining a new compact (insertion device-less) cell in three arcs and the H6BA in the other arcs.

INTRODUCTION

The Stanford Synchrotron Radiation Lightsource (SSRL) is a third-generation synchrotron light source facility currently operating the Stanford Positron–Electron Asymmetric Ring-III (SPEAR3) [1]. It has served as a major facility for photon science and accelerator research, but recent advances in accelerator physics and magnet technology have driven the global development of next-generation diffraction-limited storage rings. To maintain SSRL's competitiveness among modern synchrotron facilities, multiple upgrade strategies have been investigated. One such upgrade, the Stanford Diffraction Limited Synchrotron (SDLS), involves the construction of a storage ring equipped with Hybrid Six-Bend Achromat cells (H6BA) [2] within the existing Positron Electron Project (PEP) tunnel. The PEP tunnel features a six-fold symmetric geometry consisting of six arcs, each 243.2 m, and six long straight sections (SS), each 123.35 m, giving a total ring circumference of 2199.3 m.

The H6BA cell (Fig. 1, left), recently proposed as a promising architecture for diffraction-limited storage rings [3], serves as the foundation of the upgrade discussed here. The design prioritizes maximizing the photon beam brightness while simultaneously ensuring operational performance through large dynamic aperture (DA), high momentum acceptance (MA), off-axis injection capability, and long beam lifetime. These performance goals are intended to reduce the demands on the injector system while maintaining robust long-term beam storage. Additionally, transparency conditions are also implemented in the long SS optics to preserve favorable nonlinear beam dynamics (Fig. 2, left).

Since the PEP tunnel is underground, excavation is required to create space for photon beamlines. On-site surveying has determined that three arcs are suitable for excavation and beamline construction while the other three arcs will be deemed vacant [4]. Under these constraints, at least 33 insertion device (ID) beamlines can be accommodated in short-ID SS, with six additional beamlines possible in adjacent long SS. The vacant arcs give flexibility in optics design and an opportunity to further push the limits of performance.

In this paper, we present two non-achromatic variations of the SDLS's nominal H6BA cell, currently under development. The first is the H6BN cell, retaining much of the nominal H6BA's characteristics but with reduced emittance. The second is an emittance-minimized, compact cell, the CH6B, that is intended only for the three vacant arcs while the H6BA will be used in the other arcs. In the next sections, the methodology for these alternative designs is outlined, and the overall performance is compared with that of the SDLS's nominal H6BA at 5 GeV electron energy.

ALTERNATIVE LATTICE DESIGNS

All designs assumed the use of experimentally demonstrated technologies, including conventional magnet and vacuum system [5]. Combined-function dipoles with longitudinal field gradients are utilized to improve emittance performance and increase lattice compactness. The dipoles include integrated quadrupole field to provide distributed focusing while maintaining the required bending profile. Quadrupole gradients were limited to 110 T/m, consistent with state-of-the-art magnet technology. A summary of the cell optical parameters is listed in Table 1.

Table 1: Parameters of H6BA, H6BN, and CH6B cells

Parameter	Units	H6BA	H6BN	C6HB
ϵ_x	pm rad	28	18	13
Q_x	–	1.77	1.77	1.41
Q_y	–	0.91	0.91	0.61
Nat. ξ_x	–	-2.6	-2.5	-2.5
Nat. ξ_y	–	-2.9	-2.9	-4.7
σ_E/E_0	10^{-4}	6.4	8.0	6.1
$U_0/Cell$	keV	9.5	11.9	5.7
J_x	–	1.67	1.60	1.96
α_c	10^{-5}	3.93	3.73	4.03

H6BN

The H6BN cell was developed as a direct replacement for the H6BA cell across all arcs, hence twelve H6BN cells can be included per arc. This cell (Fig. 1, middle) is designed to reduce the H6BA's emittance by optimizing the

* Work supported by the U.S. DOE Contract DE-AC02-76SF00515.
† donish@slac.stanford.edu

Content from this work may be used under the terms of the CC BY 4.0 licence (© 2026). Any distribution of this work must maintain attribution to the author(s), title of the work, publisher, and DOI.

ISBN: 978-3-95450-252-3 ISSN: 2673-5350 doi: 10.18429/JACoW-IPAC2026-TUP2306

CLS: RETURN TO OPERATION

F. Le Pimpec*, Canadian Light Source, Saskatoon, Canada

Abstract

After approximately 60 years of service in 2024, the 2856 MHz CLS LINAC injector was removed and exchanged with a newer, more compact injector capable of 10 Hz operation and producing an electron beam of 250 MeV at a frequency of 3000.24 MHz. Unfortunately, the commissioning of this injector did not go as planned, and the facility stayed dark 1 year longer than scheduled. Below, we are summarizing the effort taken by the facility to provide beam to our users since the start of the injector commissioning, and a plan to remediate the existing deficiencies with the risk and/or impact associated to it.

INTRODUCTION

On 27 May 2024, the 2856 MHz injector LINAC was dismantled to make room for a new turn-key injector LINAC. Purchased from Research Instruments GmbH (RI), the new injector for the CLS storage ring operates at 1 Hz for beam operation and is capable of 10 Hz for RF conditioning. It is comprised of a 90 keV DC thermionic gun, pulsed with a 500.04 MHz modulated grid, a 500.04 MHz Subharmonic Pre-Buncher (SPB), a Pre-Bunching Unit (PBU) and a traveling wave Final Bunching Unit (FBU) both operating at a frequency of 3000.24 MHz to match the 6th harmonic of the CLS storage ring frequency [1]. The core acceleration is provided by three 5.26 m long S-band traveling wave accelerating structures (ACC1,2 & 3), with two of them being powered through one SLED [2]. The layout of the machine is shown in Fig. 1. The design of the RI injector is based on the original design made for the Paul Scherrer Institute (PSI) for the Swiss Light Source project [3]. The installation of the RI injector was completed on time in early August 2024; commissioning followed. The commissioning, however, did not go as planned and stable operation was not achieved until October 2025, hence the 1 year past the original schedule. A comprehensive report on our commissioning, RF conditioning and beam commissioning has been published [4].

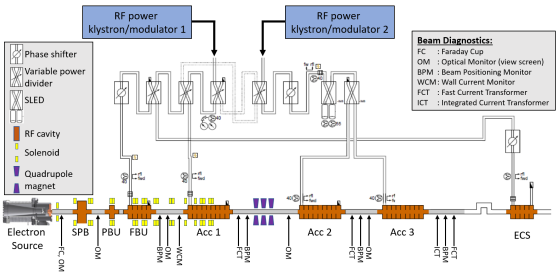

Figure 1: General layout of the new CLS LINAC injector, bought from Research Instruments (RI GmbH) [4].

COMMISSIONING RESULTS

The following figures, Figs. 2, 3 and 4, summarize the effort taken to commission the new LINAC in our search of a stable point for operation. By stable point, we were targeting the production of an electron beam which could be reliably captured and accelerated by our booster synchrotron, before injection, in the CLS storage ring at 2.9 GeV, and ensuring top-up mode operation. In October 2025 a stable point was found, and the beam characteristic, compared to our initial technical specification, is provided in Table 1. As one can see, the performances reached are below the requirements. Yet, the beam production by the injector is reliable, and the question on reaching the technical specification will be treated later.

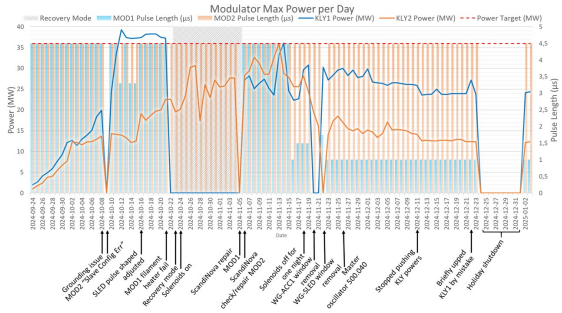

Figure 2: Klystron power output into the RF structures (FBU, ACC1, ACC2 and ACC3, with or without SLED until December 2024 [4].

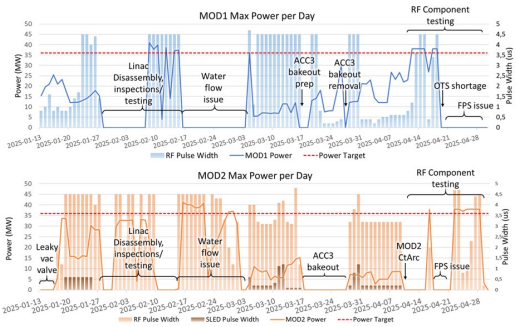

Figure 3: Klystron power output into the RF structures (FBU, ACC1, ACC2 and ACC3, with or without SLED until April 2025 [4].

RETURN TO OPERATION

Around July 2025, a stable beam was produced and the ring was filled in top-up. Following this success, and a bit too hastily, user operation was requested despite a lack of confidence in the long term stability of the beam. An RF arc occurred that necessitated an RF conditioning of the Accelerating structure that had arced. The month of August

* frederic.le.pimpec@lightsource.ca

Content from this work may be used under the terms of the CC BY 4.0 licence (© 2026). Any distribution of this work must maintain attribution to the author(s), title of the work, publisher, and DOI.

ISBN: 978-3-95450-252-3 ISSN: 2673-5350 doi: 10.18429/JACoW-IPAC2026-TUP2308

ACCURACY AND STABILITY OF LATTICE CORRECTION FOR THE UPGRADED APS*

V. Sajaev†, A.J. Dick, L. Emery
Argonne National Laboratory, Argonne, IL, USA

Abstract

A well-corrected lattice is essential for the performance of any modern synchrotron light source. Beyond the standard motivations – such as preserving optimized nonlinear dynamics and maintaining sufficient dynamic and momentum acceptance – accurate lattice correction is particularly important in Advanced Photon Source Upgrade (APS-U) for achieving the predicted emittance reduction associated with insertion device radiation. In APS-U, lattice characterization relies on response matrix fitting. Simulations performed during the design phase indicated that the achievable accuracy of such measurements would be limited to the few-percent level, thereby constraining the ultimate lattice correction precision. This paper presents the typical results of the APS-U lattice correction, examines approaches to improving lattice measurement accuracy, and discusses the long-term stability of the corrected lattice.

INTRODUCTION

The Advanced Photon Source (APS) currently operates with a design natural emittance of 42 pm · rad and routinely provides an electron beam with a measured emittance of 30 pm · rad in full coupling mode [1]. With insertion devices (IDs) set to typical user gaps, the emittance is further reduced to about 25 pm · rad. This paper aims to document how routine operational activities – such as adjusting ID gaps, orbit steering for beamline optimization, and magnet conditioning following maintenance – affect the lattice of a fourth-generation light source.

LATTICE DETERMINATION ACCURACY

Before analyzing the lattice changes over time, we first examine the accuracy of lattice determination. In storage rings, the lattice is typically reconstructed using either response matrix (RM) fitting [2] or turn-by-turn betatron motion analysis [3]. RM fitting is generally considered the more reliable approach, and it is therefore adopted in this work.

There is no direct method to quantify the accuracy of lattice determination obtained from an RM fit. Instead, commissioning simulations provide a practical benchmark. In these simulations, realistic machine errors are introduced and subsequently corrected, after which the lattice is reconstructed using a simulated RM fit [4]. Because both the "true" lattice and the reconstructed lattice are known, the accuracy of the RM-based determination can be evaluated directly. By repeating this process over many error realizations, one obtains a statistical estimate – typically expressed as an rms deviation – of the lattice determination accuracy. The accuracy achieved in real operation is unlikely to exceed that observed in simulation.

Commissioning studies [4, 5] indicate that RM fitting typically achieves lattice determination accuracy at the level of a few percent rms. The origin of this limitation is not fully understood. Since resolving lattice drift in routine operation requires the highest possible accuracy, this motivates a closer examination of the RM fitting procedure and potential strategies for improvement. One possible contributing factor is the residual error in the RM fit itself.

Modification of RM Fit to Include Sextupole Effects

It is expected that the dominant contribution to lattice distortion arises from non-zero orbit offsets in sextupoles, rather than from intrinsic quadrupole strength errors. However, the RM fitting program used at APS (`SRLOCOFitting`) has traditionally relied only on quadrupole strength errors and tilts to reproduce the measured response matrix. This approach is based on experience with the pre-upgrade APS, where the number and distribution of quadrupoles were sufficient to effectively represent all focusing errors – including those originating from orbit offsets in sextupoles – using quadrupole variations alone. This assumption has also been applied in APS-U lattice correction until recently. Here, we examine whether explicitly including sextupole-induced focusing improves lattice determination accuracy.

The most direct way to incorporate focusing from orbit offsets in sextupoles within `SRLOCOFitting` is through the "special variables" option, which allows arbitrary parameters to be varied with user-defined rules. This option allows to directly include the horizontal and vertical offsets of sextupoles as fit variables. However, varying these offsets during the fit alters the closed orbit at each iteration, thereby modifying the response matrix itself and complicating convergence.

To avoid this issue, we instead introduce zero-length multipole elements adjacent to each sextupole and vary their strengths in the fit. The multipole components model the quadrupole and skew-quadrupole components arising from horizontal and vertical orbit offsets, respectively. This follows the existing treatment of focusing dipole tilts in `SRLOCOFitting`, where multipole elements are used to represent quadrupole tilts without generating vertical orbit.

Including these sextupole-related focusing multipoles resulted in a modest improvement in the response matrix fit, reducing the residual error by approximately 20%. How-

* Work supported by US DOE Office of Science under contract DE-AC02-06CH11357
† sajaev@anl.gov

Content from this work may be used under the terms of the CC BY 4.0 licence (© 2026). Any distribution of this work must maintain attribution to the author(s), title of the work, publisher, and DOI.

ISBN: 978-3-95450-252-3 ISSN: 2673-5350 doi: 10.18429/JACoW-IPAC2026-TUP2316

MACHINE LEARNING BASED PREVENTIVE MAINTENANCE AND AUTONOMOUS POWER CONTROL FOR RF CAVITIES IN A FREE-ELECTRON LASER

T. Yuvaraj*, Columbia University, New York, United States
A. Sharma, Indian Institute of Technology Delhi, New Delhi, India
B. K. Sahu, Inter-University Accelerator Centre, New Delhi, India

Abstract

This paper presents a machine learning system for automated RF power control during high-power conditioning of the RF photocathode gun at the Free Electron laser based Delhi Light Source (DLS) facility, IUAC. A hybrid model combining K-means clustering, linear regression, and a decision tree classifier categorizes ion-pump current ranges, predicts baseline behavior, and detects anomalies in real time. Integrated with the EPICS control system, the algorithm adjusts power every 50 ms to prevent trips and recover from faults, enabling effective automated conditioning with reduced operator workload.

INTRODUCTION

The Delhi Light Source (DLS) at IUAC, New Delhi, is a compact, pre-bunched Free Electron Laser facility designed to produce electron beams up to 8 MeV using a 2.6-cell normal-conducting RF photocathode gun at 2860 MHz [1,2]. The RF gun is powered by a high-power klystron modulator based RF system from M/S Scandinova Systems [3] (Fig. 1), delivering peak RF power of several megawatts [4, 5]. RF conditioning is required to reach the target accelerating gradient while minimizing breakdown and dark current and keeping stable ultra-high vacuum conditions ($< 10^{-9}$ mbar) for reliable operation, particularly when using semiconductor photocathodes.

Before beam production, the gun must undergo RF conditioning, gradually increasing power while maintaining stable vacuum. Breakdowns and multipacting cause pressure rises that trip the system. This manual process requires continuous monitoring, with nighttime operation at IUAC making sustained oversight impractical. A predictive ML system to automate RF conditioning, reducing operator workload and trip frequency, was developed. In order to protect the source against high reflected power during conditioning, an SF_6-based isolator was installed [6], enabling conditioning to higher field gradients up to 100 MV/m.

Conditioning Challenges

High-power RF conditioning of metallic cavities is inherently challenging due to the risk of RF breakdowns, multipacting, and vacuum degradation. The process requires:

- Starting from low power and gradually increasing, with careful monitoring of vacuum levels.
- Continuous tracking of the gun resonance frequency with the signal generator to minimize reflected power.
- Optimization of the photocathode plug position for impedance matching.
- Maintaining VSWR interlock conditions within the klystron's specified limits.

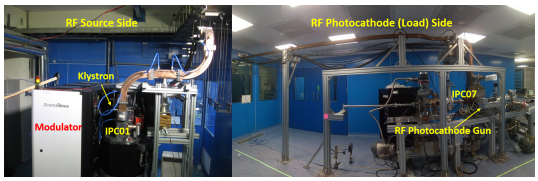

Figure 1: RF system for the photocathode gun.

DATA COLLECTION AND EXPLORATION

A Python client interfacing with the EPICS (Experimental Physics and Industrial Control System) framework logs process variables to CSV files every 2 s, with accelerated sampling during periods of high-current fluctuation. The key process variables monitored include: machine operating state (integer-encoded as 13=Trigger, 9=High Voltage, 5=Standby, 1=Off), high-voltage reading, pulse width, ion-pump pressures and currents at three locations (IPC01—klystron, IPC03—circulator, IPC07—cavity), forward and reflected RF output power, driver amplifier forward power, and the commanded set power and frequency.

Among these, the IPC07 current (directly proportional to cavity pressure) and the set power are the most critical variables. The entire control algorithm operates by adjusting the set power in response to IPC07 current fluctuations, while the RF Forward power (RFOutFwd) dropping to zero serves as the definitive indicator of a system trip, which is what the algorithm aims to prevent.

Several analyses guided model development. A correlation matrix computed across all process variables using Pandas showed limited inter-variable correlation for anomalous events, partly because the 2 s sampling interval is too slow to capture the fast rising edge of current surges during RF breakdowns.

Data exploration during manual conditioning revealed that the t-distributed Stochastic Neighbor Embedding (t-SNE) algorithm, applied for dimensionality reduction, produced clear clustering by set power level (Fig. 2), confirming RF input power as the dominant organizing parameter of the

* tushnim.yuvaraj@columbia.edu

Content from this work may be used under the terms of the CC BY 4.0 licence (© 2026). Any distribution of this work must maintain attribution to the author(s), title of the work, publisher, and DOI.

ISBN: 978-3-95450-252-3 ISSN: 2673-5350 doi: 10.18429/JACoW-IPAC2026-TUP2329

HIGH-CHARGE AND HIGH-BRIGHTNESS BEAM GENERATION AT THE ADVANCED PHOTON SOURCE PHOTOINJECTOR*

Y. Sun†, T. Berenc, W. Berg, J. Calvey, J. Dooling, T. Fors, R. Hong, O. Mohsen, P. Piot, O. Ramachandran, K. P. Wootton, Y. Yang, Argonne National Laboratory, Lemont, IL, USA
T. Suzuki, Michigan State University, East Lansing, MI, USA

Abstract

The recent installation of a new photocathode drive laser has significantly improved the reliability of photoinjector operations at the Advanced Photon Source (APS), Argonne National Laboratory. The photoinjector can operate in either high-charge or high-brightness mode. The high-charge mode is ultimately intended to support direct injection from the linac into the booster ring, eliminating the need for charge accumulation performed in the Particle Accumulator Ring (PAR). In contrast, the high-brightness mode optimizes the photoemission source to produce bright, compressed electron bunches that can be delivered to the Linac Extension Area (LEA) for accelerator R&D. This paper discusses the design considerations and initial commissioning results of the photoinjector with the new laser system.

INTRODUCTION

In its current configuration, the electron beams injected into the Advanced Photon Source (APS) storage ring are generated by a thermionic RF gun, owing to its reliability. Trains of ~15–30 bunches separated by 350 ps are accelerated to 425 MeV in the S-band linear accelerator and injected into the PAR, where the bunches are merged and accumulated up to ~20 nC single bunch for the injection to booster; see Fig. 1. In the booster, the bunch is accelerated to 6 GeV prior to injection into the APS storage ring [1, 2].

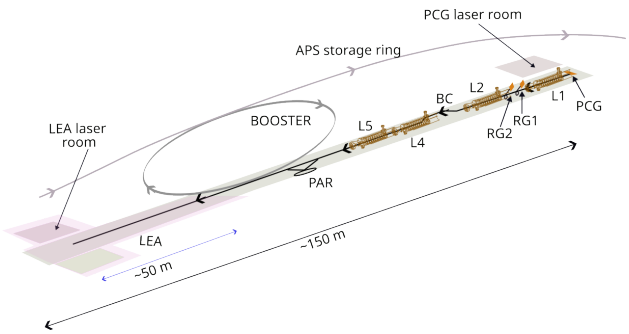

Figure 1: Overview of the APS injection complex chain. The labels "PCG", "RG", "L", and "BC" refer to the photocathode rf gun, thermionic rf gun, linac sections, and bunch compressor chicane, respectively.

In addition to the nominal and spare thermionic radiofrequency (rf) guns (RG1 and RG2), the APS linac also houses a rf photoemission source (PCG) of similar design to the LCLS rf gun [3, 4]. The photoinjector's operation has been limited over the years by the performance of the photocathode laser system. In 2025, a new commercial laser system was commissioned, enabling the generation of electron bunches with charges $Q \in [0.1, 2]$ nC for R&D purposes and possibly for direct injection into the PAR. In the longer term, further upgrades to the laser and/or photocathode could support the generation of ~20 nC bunches – potentially arranged as a multi-bunch train from the linac – enabling direct injection from the linac into the booster and storage rings while bypassing the PAR, which represents a current bottleneck in the APS injection chain due to bunch length blowup at higher single bunch charge [2]. Additionally, the photoinjector can be optimized to produce high-brightness electron bunches with sub-micrometer normalized emittances at $Q = 100$ pC.

NEW PHOTOCATHODE-LASER SYSTEM

The laser system was upgraded to an Ytterbium-doped Potassium Gadolinium Tungstate (Yb:KGW) PHAROS laser from LIGHTCONVERSION capable of producing amplified infrared (IR) pulses with energies up to 4 mJ at $\lambda = 1030$ nm. The laser is comprised of an integrated oscillator operating at 68 MHz (42nd subharmonic of 2856 MHz reference signal) and a regenerative amplifier. The oscillator cavity is phase-locked to the reference signal using a commercial synchronization system (PHASELOCK module from TEM Messtechnik). Initial in-loop synchronization measurements indicate ~ 300 fs (rms) timing jitter; see Fig. 2. The regenerative amplifier is operated at 1.2 kHz and a pulse picker extracts laser pulses at 30 Hz timed to coincide with the linac RF macropulses. In its short-pulse settings the system produces ~450-fs (FWHM) amplified IR pulses. Following frequency quadrupling via two cascaded second-harmonic

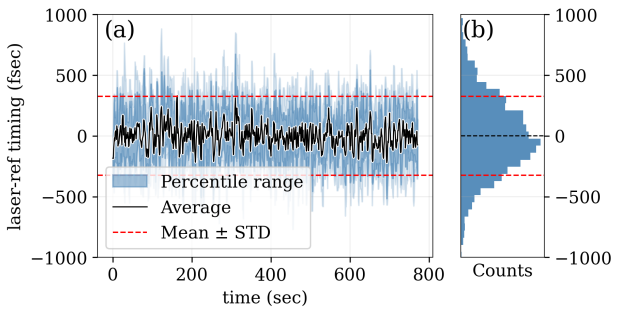

Figure 2: Example of timing jitter between the laser oscillator and the 2856-MHz reference signal, measured using an in-loop comparative phase detector.

* This material is based upon work supported by Laboratory Directed Research and Development (LDRD) funding from Argonne National Laboratory, provided by the Director, Office of Science, of the U.S. Department of Energy under Contract No. DE-AC02-06CH11357.

† yinesun@anl.gov

Content from this work may be used under the terms of the CC BY 4.0 licence (© 2026). Any distribution of this work must maintain attribution to the author(s), title of the work, publisher, and DOI.

ISBN: 978-3-95450-252-3 ISSN: 2673-5350 doi: 10.18429/JACoW-IPAC2026-TUP2330

RF CONDITIONING AND MICROWAVE GUN SIMULATIONS FOR THE UNIVERSITY OF HAWAI'I LINAC AND FEL

N. Bidault*, S. Li
University of Hawai'i at Mānoa, Honolulu, HI, USA

Content from this work may be used under the terms of the CC BY 4.0 licence (© 2026). Any distribution of this work must maintain attribution to the author(s), title of the work, publisher, and DOI.

Abstract

The S-band electron linac and free-electron-laser facility at the University of Hawai'i at Mānoa is being recommissioned after an extended period of inactivity. Following the restoration of vacuum and thermionic cathode systems, recent work focused on the high-power RF chain and on conditioning of the linac and microwave electron gun. We report RF conditioning measurements obtained during progressive power-up sessions at 1–4 Hz, including forward power delivered to the linac and forward and reflected power at the microwave gun. The linac RF response is stable and consistent with legacy calibrations, while the gun exhibits strong multipacting signatures. To guide the next conditioning campaign, we also present the developing RF-Track model of the thermionic TM_{010} gun, incorporating field maps, space charge, and beam loading.

INTRODUCTION

The University of Hawai'i Free Electron Laser (UH FEL) facility is based on a compact S-band injector and traveling-wave linac originally developed as part of the Mark-III/Mark-V FEL program. The accelerator produces electron beams for a mid-infrared FEL oscillator and for inverse Compton scattering x-ray experiments [1]. The previous recommissioning activities included the restoration of the vacuum, the installation of a thermionic cathode, and the upgrade of a low-level RF preamplifier, after the facility had remained inactive for several years [2]. The present paper reports the next step in that effort: reconditioning the RF systems for beam operation and improving the injector model used to prepare for and interpret the next runs. The injector consists of a LaB_6 thermionic cathode installed in a single-cell 2856 MHz microwave gun operating in a TM_{010}-like mode. The gun is followed by an Enge alpha-magnet that serves as a compressor and momentum filter before the beam is injected into a 10-ft SLAC-type traveling-wave linac, which typically accelerates the beam to 35–45 MeV. The same high-power klystron chain feeds the linac and the microwave gun through separate RF distribution branches. The RF conditioning, therefore, provides information not only on the available linac accelerating power, but also on the state of the gun cavity and its waveguide section, which are critical for stable beam emission and injection.

RF SYSTEM UPGRADES

The renewed low-level RF (LLRF) system was designed to provide a clean and reproducible S-band drive for the klystron. The 2856 MHz drive is generated by a new signal generator locked to a 10 MHz reference via a GPS disciplined oscillator. A frequency counter measures the quality of the generated signal, using an independent 10 MHz reference from a rubidium frequency standard. The timing signal generation was also upgraded to support reproducible pulsed operation during RF conditioning. The RF drive chain includes a new solid-state preamplifier that drives the high-power klystron. Stand-alone tests of the preamplifier showed an output power of approximately 58.4 dBm (about 700 W), with a measured pulse stability of 5×10^{-3} dBm and rise and fall times of about 11 ns. These measurements provide a baseline for the reproducibility expected from the LLRF and driver chain. High-voltage conditioning of the pulse-forming network and thyratron modulator was completed before RF conditioning, and the klystron perveance was measured near the nominal value of 1.7 μA $V^{-3/2}$ at 36.5 kV.

RF CONDITIONING RESULTS

RF conditioning was performed in several sessions, each lasting a few hours. The procedure consisted of progressive increases of RF pulse duration, input drive, and repetition rate, with operation between 1 and 4 Hz. The klystron and modulator behaved as expected throughout the conditioning runs, with no indication of sparking of abnormal high-voltage behavior during the power scans. Before increasing the RF power in the gun branch, frequency scans were performed to determine the microwave gun's effective resonant frequency at the current cooling-water temperature. The cavity response indicated a resonance at $f = 2859.85$ MHz. The RF drive was then increased progressively while recording the linac forward power (P_{LFP}) and gun forward power (P_{GFP}). The signals were acquired in the control room with a 6 GHz oscilloscope after propagation through the attenuation chains connected to the linac and gun RF couplers. Although the measured control-room signals are only at the level of a few dBm, Fig. 1 reports the inferred powers delivered to the linac and gun after applying the corresponding calibration and attenuation factors.

The measurements were performed at 1 Hz and repeated across several data sets to quantify shot-to-shot stability. The power levels are close to the historical operating regime, with P_{GFP} near 1 MW and P_{LFP} near 33 MW [3]. Figure 1 shows three input-power settings, corresponding to 0, +1, and +2 dBm from the 2856 MHz signal generator before amplification by the klystron driver. The linac forward power increases consistently with the applied RF drive and remains comparatively stable over the pulse. This behavior confirms

* nbidault@hawaii.edu

ISBN: 978-3-95450-252-3 ISSN: 2673-5350 doi: 10.18429/JACoW-IPAC2026-TUP2331

FIRST DEGRADED BEAMS IN THE CEBAF INJECTOR*

A. Sy, M. Bruker, J. Grames, S. Ogur, Y. Roblin, M. Stutzman, D. Turner,
Thomas Jefferson National Accelerator Facility, Newport News, United States
C. Valerio, Universidad Autónoma de Sinaloa, Culiacán, Sinaloa, México
V. Lizárraga-Rubio, Universidad de Guanajuato, Guanajuato City, México

Abstract

The electron beam degrader in the Continuous Electron Beam Accelerator Facility (CEBAF) injector at Jefferson Lab serves to generate electron beams with transverse emittance over 10x the nominal values, with the ultimate goal of using degraded electron beams to measure machine acceptance. Electron beams are degraded through multiple scattering in thin carbon foils, and maximum transverse emittance is defined through two collimating apertures. The degrader device was installed in late 2024, with commissioning and first beams on degrader targets during the 2025 physics run. We report on first operation of the degrader device.

INTRODUCTION

The transport of large emittance beams in CEBAF is of interest for optimizing beam properties near the limits of the machine acceptance. This is especially important for the Ce^+BAF positron project [1]; the polarized positron source generates beam emittances that are 1-2 orders of magnitude larger than nominal electron beam emittances in CEBAF, and understanding large emittance beam transport will help to establish limits on positron beam intensity available for the Ce^+BAF physics program.

The electron beam degrader [2, 3] generates large emittance beams through multiple scattering in thin targets. The targets are sufficiently thin, a fraction of the material radiation length, yielding transverse emittance degradation with immaterial effects on the longitudinal emittance. This allows for independent characterization of transport of large emittance transverse and longitudinal beams.

The degrader device was designed, fabricated, and installed under a Jefferson Lab Laboratory Directed Research and Development (LDRD) project. The device was installed in the CEBAF injector in late 2024 and is shown in Fig. 1. Degrader commissioning began in March 2025, and first degraded beams were generated in June 2025.

DEGRADER COMMISSIONING

Degrader commissioning focused on exercising the various components to demonstrate functionality while ensuring that degrader operation would not be detrimental to normal CEBAF operations. During the commissioning period, vacuum and radiation signals were monitored for degrader operations with beam on target. Radiation monitors in the area are sensitive to gamma and neutron radiation. Vacuum signals were monitored both upstream and downstream of the degrader device. Beam loss monitors for machine protection also exist upstream and downstream of the degrader. Figure 2 shows radiation signals nearest to the degrader device over a 12 hour period during which beam was first incident on each of the three degrader targets (carbon foils with thicknesses of 1, 5, and 10 µm). Degrader operation is administratively limited to 160 nA of average current; most tests were performed with 8 µA of low duty factor, "tune mode" beam, where beam current is pulsed on for 150 µs at 60 Hz. In the commissioning test, electron beams were incident on degrader targets for about 48 total minutes, and the activity generated during this period is within the range of normal activity during routine physics operation for both vacuum and radiation signals. We note that beam loss monitors nearest to the degrader did not register increased activity during the commissioning tests.

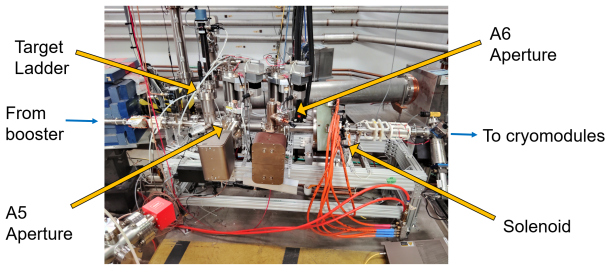

Figure 1: The degrader device as installed in the CEBAF injector.

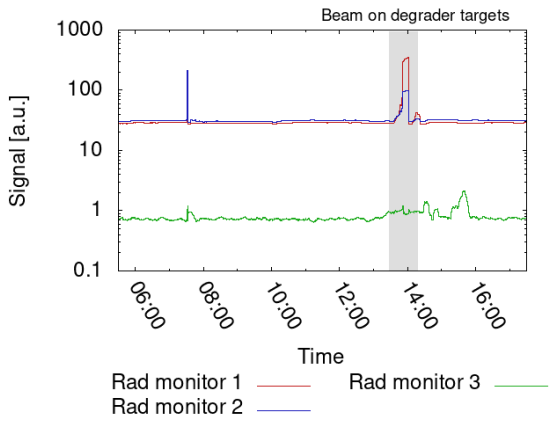

Figure 2: Signals from radiation monitors near the degrader during degrader commissioning. The shaded region indicates time for which beams were incident on degrader targets.

* amysy@jlab.org

Content from this work may be used under the terms of the CC BY 4.0 licence (© 2026). Any distribution of this work must maintain attribution to the author(s), title of the work, publisher, and DOI.

ISBN: 978-3-95450-252-3 ISSN: 2673-5350 doi: 10.18429/JACoW-IPAC2026-TUP2332

RF KICKS IN THE SUPER CONDUCTING LINAC OF LCLS-II*

F.-J. Decker†, C. E. Adolphsen, D. B. Cesar, M. P. Ehrlichman, A. Halavanau,
SLAC, Menlo Park, CA, U.S.A.

Abstract

RF kicks are produced by misalignments between an electron beam in the acceleration structure. By analyzing these kicks, produced by the super conducting standing wave accelerator for the Linac Coherent Light Source (LCLS-II), a few unexpected observations were recognized. Initially, an out-of-phase (90 deg away from the accelerating phase) component was observed, which is similar in size to the expected by theory in-phase component. Then other observations like modeling errors (e.g.: not closed three-corrector bumps) led to a deeper analysis of the currently used model.

INTRODUCTION

Oscillation data along the LCLS-II beam path revealed quite some coupling terms from the Super Conduction (SC) RF Cryo-Modules (CM). In the example in Fig. 1 the coupled oscillation is closed in CM03 (BPM #28) after tuning for best FEL performance.

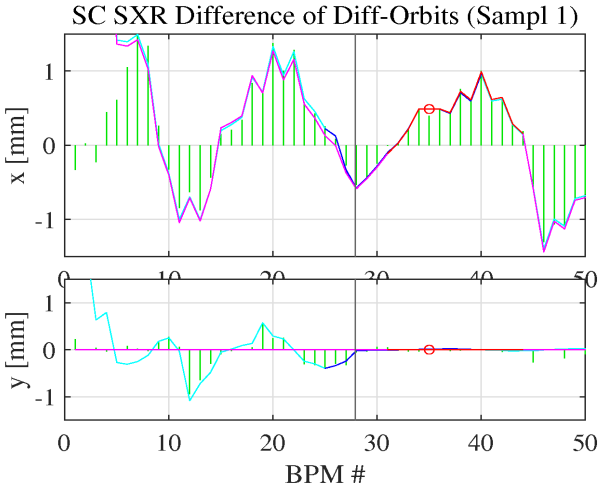

Figure 1: Oscillation data analysis. Trajectory oscillations are combined so that there is only an x offset, but no x' or y or y' at a certain location (red circle). The vertical black line is chosen where an unexpected kick occurs which corresponds to a skew quad of -0.25 kG. The start of the coupled part originates between BPM # 8 and 9 in the heater chicane and is a skew term of -0.21 kG [1].

During phasing the CM cavities, it was recognized that they kick the beam quite a bit transversely. Fitting the angle the kicks were quantified for most of the 8 cavities of all working cryogenic modules. Figure 2 shows the results of a part of L2B from CM04 to CM10. A focussing strength of -0.3 kG is quite reasonable (see below), but the out-of-phase component lags a good explanation.

* Work supported by U.S. Department of Energy, Contract DE-AC02-76SF00515.
† Decker@SLAC.Stanford.edu

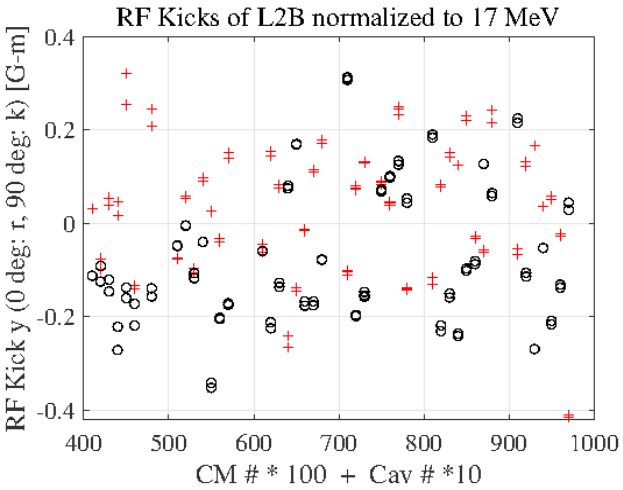

Figure 2: RF kicks measurements from two data sets. They are of the order of 0.3 kG-mm. Besides the expected in-phase (with the energy gain) component (red crosses) there is quite some out-of-phase part (black circles).

Measurement Accuracy

The accuracy of the measurements is very precise as see in Fig. 3 at around 0.01 G-m rms.

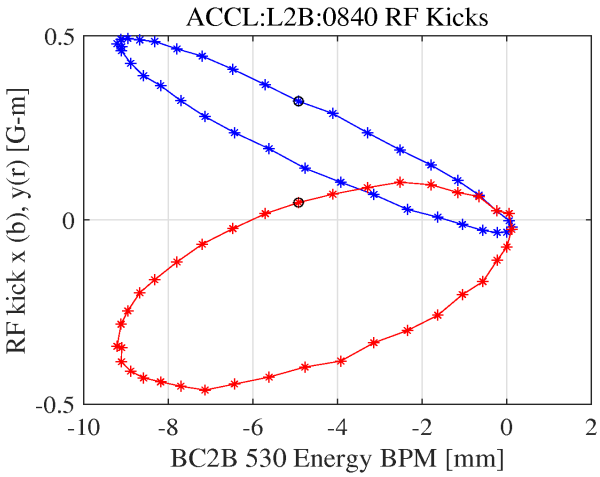

Figure 3: The fitted kick strength in x and y is plotted against the energy BPM (Beam Position Monitor) in BC2B (Bunch Compressor 2). [The reference orbit is subtracted therefore the on-crest phase is close to zero, while typically the range is centered around zero (±5 mm)].

THEORY AND CODES

After going through lots of theoretical papers [2-4] searching for an out-of-phase component one of us (CEA) pointed out his small simulation code which integrates motion along an accelerator structure. Fig. 4. shows an output of a standing wave 9 cell cavity with 18 MeV/m at 900 MeV beam energy.

Content from this work may be used under the terms of the CC BY 4.0 licence (© 2026). Any distribution of this work must maintain attribution to the author(s), title of the work, publisher, and DOI.

ISBN: 978-3-95450-252-3 ISSN: 2673-5350 doi: 10.18429/JACoW-IPAC2026-TUP2333

DUAL BEAM DYNAMIC MODES IN A COMPACT STANDING WAVE LINEAR ACCELERATOR

T. Chen, RefleXion Medical (United States), Hayward, CA, USA
H. Tao, L. Huo, T. Li, Z. Feng, L. Zhou, Y. Liu
Chengdu Elekom Vacuum Electron Technology Co. Ltd (China), Chengdu, China

Abstract

It has been commonly observed that the beam spot profile of compact standing wave linacs have a dual Gaussian distribution. Further study of this paper shows that the two Gaussian distributions are generated by different acceleration processes and beam dynamics. Simulation data analysis concludes that the particles in the two Gaussian distributions are strongly dependent on their initial phases. Experiment results have demonstrated the two Gaussian distributions responded differently to steering magnetic field.

INTRODUCTION

Compact standing wave linac is widely used in radiation therapy equipment. In this industry, it has been common knowledge that the beam spot is typically showing a dual-Gaussian distribution [1-2], rather than a single Gaussian type that most accelerator beam features. It is desire to have a further understanding how the dual Gaussian profile is generated, which is potentially helpful to optimize beam dynamics design, improving characteristics such as spot size and energy spread.

OBSERVATION

A 6 MeV standing wave linac is designed and developed by Chengdu Elekom Vacuum Electron Technology Co. Ltd for RefleXion Medical Inc. The beam spot profile on the target is measured at RefleXion with scanning-slit apparatus. The measured results can be fitted fairly well of summation of two Gaussian functions – one narrow and one wide. In addition, we observed that the two Gaussian distributions respond to steering field, which is generated by a pair of coils mounted on the gun side of the linac, differently!

Figure 1 shows the measured beam profiles with various steering currents. Each profile is fitted with sum of two independent Gauss functions. It is quite visible as the steering current increases; the two Gaussian distribution centres no longer have the same displacements. The narrow Gauss moves more than the wider Gauss. In addition, the size of the two distributions also varies, with the wider Gauss shrinks.

Figure 2 plots the center shifting of the two distributions, versus steering current. The narrow Gauss tends to respond linearly with steering current, while the wider Gauss responds rather nonlinear.

This observation indicates that the electrons in these two Gaussians possess different beam dynamics.

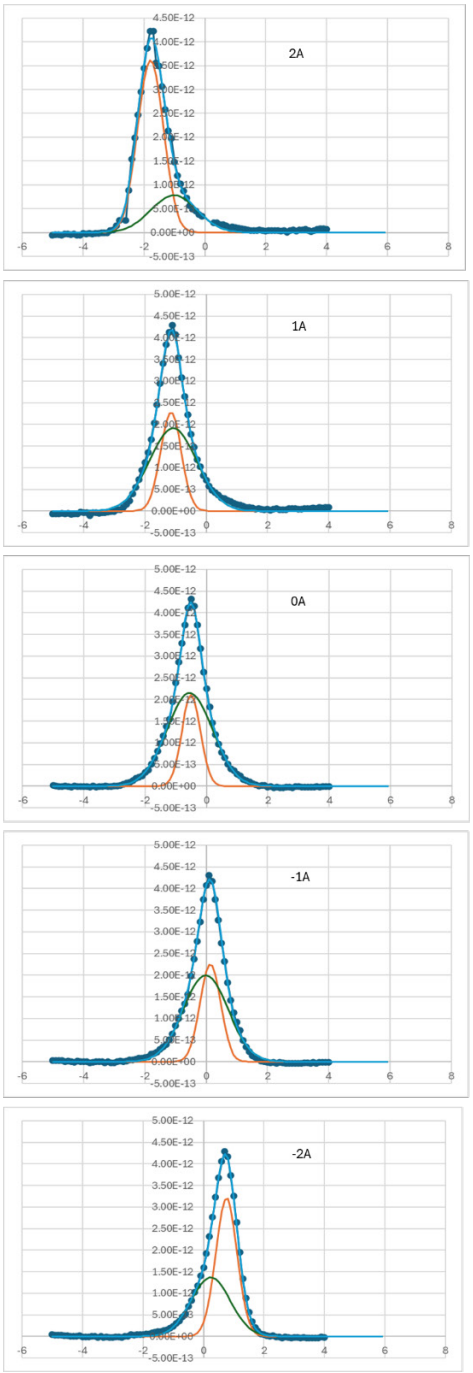

Figure 1: Measured beam profiles and Gauss fittings with varying steering currents.

Content from this work may be used under the terms of the CC BY 4.0 licence (© 2026). Any distribution of this work must maintain attribution to the author(s), title of the work, publisher, and DOI.

ISBN: 978-3-95450-252-3 ISSN: 2673-5350 doi: 10.18429/JACoW-IPAC2026-TUP2335

ULTRAVIOLET TRANSVERSE SHAPING WITH STRUCTURED-STOCHASTIC PHASE-PLATES FOR PHOTOCATHODE APPLICATIONS*

T. Jogand-Coulomb† [1], R. Margraf-O'Neal[2], N. Burdet[4], D. Czaplezski[2], R. Divan[2], J. Xu[3], A. Osman[4], J. Power[2], A. Halavanau[4], P. Piot[2], Y.K. Kim[1,5]
[1]University of Chicago, Chicago, USA
[2]Argonne National Laboratory, Lemont, USA
[3]University of Wisconsin-Madison, Madison, USA
[4]SLAC National Accelerator Laboratory, Menlo Park, USA
[5]Fermi National Accelerator Laboratory, Batavia, USA

Content from this work may be used under the terms of the CC BY 4.0 licence (© 2026). Any distribution of this work must maintain attribution to the author(s), title of the work, publisher, and DOI.

Abstract

Transverse shaping of the photocathode drive laser can improve beam quality in high-brightness photoinjectors. We present progress on UV-compatible fused-silica phase plates for passive laser shaping at the Argonne Wakefield Accelerator. A first-generation binary phase plate, designed using an iterative Fourier transform algorithm, was fabricated and optically characterized. The measured Fourier-plane profile demonstrates transverse redistribution of the incident UV beam, while residual central intensity indicates sensitivity to binary phase quantization and etch-depth error. To address these limitations, we introduce an improved genetic algorithm workflow in which structured initial phase seeds are optimized with an NSGA-II assisted IFTA. The resulting simulated four-level phase plates are selected using target-profile fidelity and zeroth-order diffraction intensity, providing a fabrication-aware path for next-generation devices.

INTRODUCTION

The performance and cost of electron accelerators depend critically on the transverse emittance of the electron beam [1–6]. This emittance depends partially on the initial conditions set by the photoinjector. There are three major areas of improvement for photoinjectors: (i) refining the transverse profile, (ii) reducing transverse jitter, (iii) reducing charge jitter. Addressing these challenges would reduce tune-up time and allow for more stable beam delivery and experimental uptime.

Despite advances in existing shaping techniques such as spatial light modulators [7, 8] and digital mirror devices [9], these techniques still incur significant power losses or lack compatibility with UV drive wavelengths. To overcome these limitations, recent work [10] has demonstrated that custom fused-silica phase plates, designed using an optical Iterative Fourier Transform (IFTA) [11], can generate high-precision transverse UV profiles while maintaining greater than 99% transmission at 253 nm. These phase plates provide a passive solution for tailoring laser distributions without sacrificing energy at the cathode. This project aims to adapt and extend phase-plate technology specifically for the Argonne Wakefield Accelerator (AWA) photoinjector.

BINARY PHASE PLATE

A binary phase plate was designed to transversely shape an incident UV beam into a truncated, flat-top transverse profile at the Fourier plane. This 2-level phase mask, with discrete phase levels of 0 and π, was designed using an Optical-IFTA workflow (Fig. 1) from previous work [10]. This phase plate serves as a proof-of-principle that the simulation could be applied to fabricate a phase plate for AWA while also identifying the limitations that motivate the optimized multi-objective designs discussed in the following section.

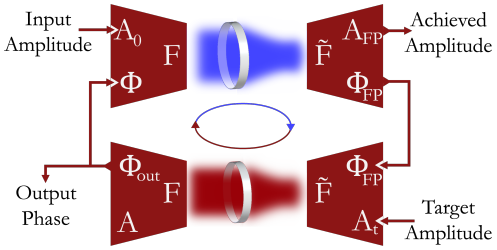

Figure 1: Schematics of the Optical IFTA implemented to generate the phase masks.

The binary plate was fabricated at the Center for Nanoscale Materials on a UV fused-silica substrate using a single lithography and etch step. The etched depth d sets the phase delay according to

$$\Delta\phi = \frac{2\pi}{\lambda}\,(n_{\mathrm{fs}} - n_{\mathrm{air}})\,d, \tag{1}$$

where λ is the operating wavelength and n_{fs} and n_{air} are the refractive indices of fused silica and air. Optical microscopy was used to verify the transverse pattern fidelity, while atomic force microscopy (AFM) measured the etched step height, as shown in Figs. 2 and 3. From this metrology, the transverse feature size area agreed with the design, with $A_{\mathrm{etch}} = 38 \pm 2\ \mu\mathrm{m}^2$ compared with $A_{\mathrm{design}} = 38.4\ \mu\mathrm{m}^2$. However, AFM showed a significant etch-depth error of $\delta h = 78.0 \pm 0.1$ nm relative to the target π-phase depth. This depth error changes the intended phase step and contributed residual zeroth-order diffraction in the Fourier plane.

* Work supported by DOE Award DE-SC0024907
† coulomb@uchicago.edu

ISBN: 978-3-95450-252-3 ISSN: 2673-5350 doi: 10.18429/JACoW-IPAC2026-TUP2337

SIRIUS STORAGE RING EMITTANCE MEASUREMENT USING UNDULATOR RADIATION

J. B. Vieira[2*], G. R. Ascenção[2], S. A. L. Luiz
Brazilian Synchrotron Light Laboratory - LNLS, Campinas - SP, Brazil
[2]also at Gleb Wataghin Institute of Physics, University of Campinas, Campinas - SP, Brazil

Abstract

This work presents a measurement the SIRIUS electron-beam emittance from undulator radiation at EMA and MANACA beamlines. Two observables are used: the peak-to-valley ratio of the projected even-harmonic profile and the direct minimization of the 2D spatial distribution intensity versus radiation energy. The two beamlines provide distinct beta functions, which helps separate emittance from optics. Turn-by-turn (TbT) beta-beating sets the beta uncertainty, and the undulator field maps are corrected to align measured and simulated resonances. The extracted emittances are consistent with the expected ~ 250 pm.rad value.

INTRODUCTION

Low-emittance storage rings demand beam diagnostics that remain sensitive in the picometer-radian regime. At SIRIUS, standard imaging becomes less robust when the photon-beam size approaches detector resolution and the diffraction limit [1].

This work uses undulator radiation from two beamlines with different optics: EMA, a low beta straight section [2], and MANACA, a high beta straight section [3]. The analysis combines SPECTRA-based simulations, field-map calibration, and spatial-profile fitting [4, 5].

The paper is organized as follows: first, the model and objective functions are defined, then a brief introduction of the beamlines and methods is given, and finally, the fitted parameters and extracted emittance values are shown.

Table 1: SIRIUS storage ring and insertion-device parameters used in the emittance study.

Storage ring parameters	Value		Symbols [units]
Nominal energy	3.0		E_0 [GeV]
Natural emittance	250		ϵ_0 [pm rad]
Coupling (emittance ratio)	1		κ [%]
Energy spread	0.084		σ_E [%]
	EMA	MNC	
Hor. beta function @ ID SS center	1.499	17.22	β_x [m]
Ver. beta function @ ID SS center	1.435	3.60	β_y [m]
Undulators parameters	IVU	APU	
Period	18.5	22.0	λ_u [mm]
ID length	2.0	1.2	L [m]
No. periods	108	51	
Máx. deflection parameter	2.14	1.47	

The adopted strategy combines simulations performed with SPECTRA and measured two-dimensional photon images. The analysis focuses on two observables only: the peak-to-valley ratio of the projected even-harmonic profile, and the direct minimization of the spatial distribution as a function of radiation energy.

THEORETICAL APPROACH

The size of the electron beam propagated at a distance d [5] follows:

$$\sigma_e^2 = \underbrace{\epsilon\beta_0 + \epsilon\left(-2\alpha_0 d + \frac{1+\alpha_0^2}{\beta_0}d^2\right)}_{\approx 10^{-8}} + \underbrace{\sigma_\delta^2\eta_0^2}_{\approx 10^{-16}} + \underbrace{\sigma_\delta^2\eta_0'^2 d^2}_{\approx 10^{-18}}, \quad (1)$$

where ϵ is the emittance, d is the propagation distance, and η_0, η_0' are the dispersion terms in the SIRIUS straight sections.

The source-point dispersion is negligible in both beamlines, so the energy-spread term is much smaller than the emittance term for the propagation distances used here. The orders of magnitude of the terms involved are expressed in equation 1. The dispersive term within the undulator was calculated using the symplectic integrator [6]. This reduces the fit to ϵ and $\beta_{x,y}$, with the remaining degeneracy handled by combining fits from EMA and MANACA. So the fit is dominated by the emittance–beta dependence.

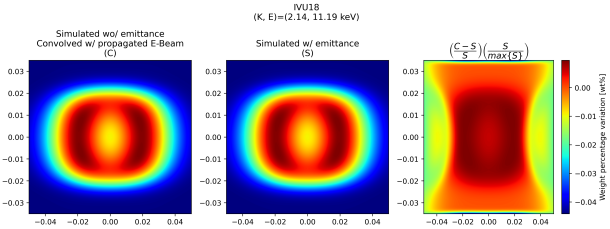

Figure 1: Comparison between direct emittance-dependent flux calculation and FFT-based convolution. The small difference validates our approach.

The photon distribution from a single electron is convolved with the propagated electron distribution using FFT-based numerical convolution [7]. This keeps the SPECTRA [8] calculation fast while preserving the flux distribution, as one can see in Figure 1.

BEAMLINE SETUP

EMA uses the In-Vacumm Undulator (IVU18) source (Table 1), with Photon Beam Visualization (DVF) at 33.35 m, DVF is a scintillator-based imaging system of Yttrium Aluminum Garnet (YAG) material. The Double-Crystal Monochromator (DCM) was scanned in ~10 eV steps across

* jefferson.vieira@lnls.br

Content from this work may be used under the terms of the CC BY 4.0 licence (© 2026). Any distribution of this work must maintain attribution to the author(s), title of the work, publisher, and DOI.

ISBN: 978-3-95450-252-3 ISSN: 2673-5350 doi: 10.18429/JACoW-IPAC2026-TUP2338

IMPACT OF THE VPU UNDULATOR ON THE SIRIUS STORAGE RING BEAM DYNAMICS

J. B. Vieira[1*], G. R. Ascenção[1], S. A. L. Luiz
Brazilian Synchrotron Light Laboratory, LNLS, Campinas, SP, Brazil
[1]also at Gleb Wataghin Institute of Physics, University of Campinas, Campinas, SP, Brazil

Abstract

This work evaluates the effects of the two vertical polarization undulators (VPUs) installed at the SIRIUS storage ring electron beam dynamics. These insertion devices (IDs) are light sources for the CARNAÚBA and CATERETÊ beamlines at the SIRIUS. The analysis combines numerical simulations and beam-based measurements to quantify static and dynamic orbit distortions, optics perturbations (tune shifts), effects on injection efficiency, and changes in equilibrium beam parameters, and also on beam lifetime. The effectiveness of ID feedforward compensation in mitigating orbit distortion is assessed.

INTRODUCTION

The CARNAÚBA (CNB) [1] and CATERETÊ (CAT) [2] beamlines were modernized with the installation of the first vertically polarized undulators (VPUs) at SIRIUS. Previously, CNB and CAT had Adjustable Phase Undulator (APU) type insertion devices (IDs); the VPUs increased brightness compared to the APU for user experiments. Figure 1 shows a comparison between the brilliance of both sources.

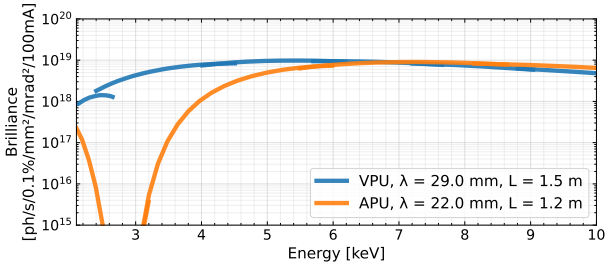

Figure 1: Brilliance comparison of the old APUs and the new VPUs.

A key factor was the matching between the undulator polarization and the vertical plane of incidence in the four-crystal monochromator. The VPUs were installed in low-beta straight section. The section parameters are presented in Table 1 and the VPU parameters in Table 2.

When these devices are installed, they can generate orbit distortions, tune deviations, and alterations in the nonlinear response of the ring. In the case of SIRIUS, this point is particularly relevant because the injection is done off-axis [3], which makes it important not to impact the dynamic aperture. Therefore, the experimental characterization of VPUs is not limited to evaluating photon emission, but also includes the effect on beam behavior in the ring.

Table 1: SIRIUS Storage Ring Parameters

Storage ring parameters		Symbols [units]
Nominal energy	3.0	E_0[GeV]
Natural emittance	250	ϵ_0[pm rad]
Coupling (emittance ratio)	1	κ[%]
Energy spread	0.084	σ_E[%]
Hor. beta function @ ID SS center	1.49	β_x[m]
Ver. beta function @ ID SS center	1.43	β_y[m]

Table 2: VPUs Parameters

ID parameters	CAT	CNB	Symbol [units]
No. periods	51	51	N
Period length	29	29	λ_u[mm]
ID length	1.5	1.5	L_u[m]
Max. gap	80	80	g_{max}[mm]
Min. gap	9.7	9.7	g_{min}[mm]
Peak field @ min. gap	0.83	0.85	B_{max}[T]
Deflec. par. @ min. gap	2.24	2.31	K_{max}
Spectrum range	0.8 – 24	0.8 – 20	[keV]

This work focuses on the effects observed during commissioning with the new VPUs and the strategies used to minimize these impacts. This report is organized to connect the different aspects of the machine: first the orbit, the optics, followed by injection efficiency, and finally, the impact on beam lifetime.

EFFECTS ON ORBIT

The presence of residual field integrals in insertion devices typically leads to closed-orbit distortions (CODs) [4]. In the case of VPUs, this effect was evaluated as a function of the gap in order to measure the dynamic response of the distortion during gap movement.

Figure 2 should present the measured CODs as a function of the VPU gap with the slow orbit feedback (SOFB) and fast orbit feedback (FOFB) correction systems turned off.

To mitigate this effect, an orbit feedforward (FF) system was implemented using dedicated correctors installed close to the devices. The correction tables were constructed from measurements at different gaps and adjusted to reproduce the local contribution of the VPU, separating it from more global variations in the ring [5]. The central idea of this approach is to anticipate the necessary correction before the

* jefferson.vieira@lnls.br

Content from this work may be used under the terms of the CC BY 4.0 licence (© 2026). Any distribution of this work must maintain attribution to the author(s), title of the work, publisher, and DOI.

ISBN: 978-3-95450-252-3 ISSN: 2673-5350 doi: 10.18429/JACoW-IPAC2026-TUP2339

APS STORAGE RING SOLID STATE AMPLIFIER UPGRADE CURRENT STATUS*

Y. Luo†, T. Berenc, A. Goel, D. Horan, T. Madden, A. Nassiri, B. Popovic, J. Schultz, K. Suthar, G. Trento, G. Waldschmidt, Argonne National Laboratory, Lemont, IL, USA

Abstract

Radiofrequency (RF) power for the Argonne Advanced Photon Source (APS) storage ring (SR) and Booster cavities is currently supplied by multiple klystrons. APS is in the process of transitioning to 160 kW solid state amplifier (SSA) system per SR cavity [1]. Several SSA systems have already been delivered, and site acceptance testing (SAT) has been completed on four units. New 200 kW circulators have also been tested. A typical SAT waveguide setup is shown. Improvements have been implemented, including modifications to RF cable lengths to increase access clearance and reduce environmental power dissipation. During the initial tests, 60 Hz noise was observed on the monitoring spectrum. This issue was investigated, and a successful mitigation solution has been implemented. To minimize the risks and to validate both the new hardware and control software, one SSA system will be placed into operational service around January 2026. For this deployment, the SR RF system will be in a hybrid configuration, with the SSA powering one cavity while the remaining eleven cavities continuously being powered by klystrons. Several intermediate interfaces are required to bridge the existing infrastructure with the new SSA system. After the hybrid operation, RF power for the remaining three cavities in the same sector will be transitioned to SSAs too. The remaining two SR sectors, are planned for SSA conversion within the following few years, completing the multi-year APS SR RF system upgrade.

INTRODUCTION

As mentioned before, 1 MW klystrons operating at 352 MHz are no longer available for the APS [1]. SSAs offer multiple advantages over klystrons such as lower supply voltage, reduced RF noise levels, and redundancy through combining multiple individual kW amplifier units. Furthermore, by leveraging from the APS-upgrade (APS-U) digital low-level RF (dLLRF) systems, the SR can now transition from the analog LLRF to full digital LLRF control. At the end of 2025, one 160 kW SSA system was installed to provide RF power to one SR cavity (S36 C1). Since Jan. 2026, APS SR RF power is on a hybrid mode. RF power to other 11 SR cavities are provided by two active 1 MW klystrons except that S36 C1 is on SSA. Tuning and some improvements are made to the hardware and control software for actual routine beam operation. Experience and knowledge from routine operations are accumulated for next step of SSA upgrade project in APS.

WAVEGUIDE RECONFIGURATION AND SAT SETUP

The storage-ring (SR) RF systems consist of multiple normal conducting cavities. Backup klystrons were installed as hot spares. As part of the APS-U the number of cavities was reduced from 16 to 12. After the SSA sector 36 C1 cutover, one klystron is used to power 7 cavities now instead of 8, while the second klystron powers 4 cavities. Conversion of the remaining 3 cavities in S36 are planned for the April/May 2026 maintenance period. The remaining two SR sectors conversion are planned to take place in subsequent years.

The waveguide reconfiguration is shown in Fig. 1 for S36 C1 SSA cutover. A blanking plate is attached to the specific 3 dB hybrid port that allowed the SSA to drive the S36 C1 cavity. A new waveguide was installed to connect the SSA and a new 200-kW circulator to the existing waveguide section leading to the cavity.

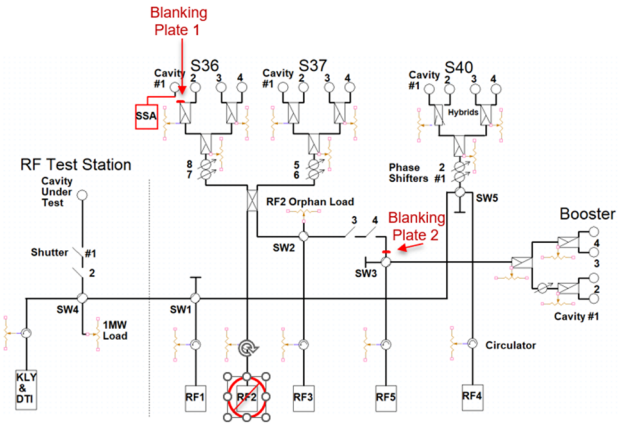

Figure 1: Waveguide and RF power system after S36 C1 SSA cutover.

The delivered SSA units and 200kW circulators are tested on-site as part of SAT. A typical SAT setup is shown in Fig. 2. Improvements have been implemented, including modifications to RF cable length to increase access clearance and reduce environmental power dissipation. The first 200 kW circulator was tested using a different setup to verify its performance. The other circulators were used in SSA SAT.

* Work supported by US Department of Energy, Office of Science, under contract number DE-AC02-06CH11357.
† yluo@anl.gov

Content from this work may be used under the terms of the CC BY 4.0 licence (© 2026). Any distribution of this work must maintain attribution to the author(s), title of the work, publisher, and DOI.

ISBN: 978-3-95450-252-3 ISSN: 2673-5350 doi: 10.18429/JACoW-IPAC2026-TUP2340

APPLICATION OF LSTM AUTOENCODER TO THE 10 KHZ STORAGE RING ORBIT DATA*

J. Choi†, I. Lobach, Brookhaven National Laboratory, Upton, United States

Abstract

In NSLS-II storage ring, the 10 kHz orbit data are always available and can be collected at any time interval. At this moment, they are being collected every 10 minutes to review the machine stability status or investigate orbit related issues impacting user satisfaction. To improve the machine performance, we are studying the machine learning techniques with which we can detect any orbit stability issue as early as possible. As one of the strong candidates, we are testing models constructed by the long short-term memory (LSTM) autoencoder from the orbit data. In this paper, we present the optimized LSTM autoencoder parameters and test results.

INTRODUCTION

The NSLS-II storage ring is the 3 GeV electron storage ring of the National Synchrotron Light Source II (NSLS-II) at Brookhaven National Laboratory. For the monitoring of the machine performance as well as to prepare the case of investigation, we continually collect the 10 kHz fast acquisition (FA) orbit data. They are very useful to review the machine stability status or investigate orbit related issues impacting user satisfaction. The available spectrum of the 10 kHz orbit data is from DC to 5 kHz, which is much higher than the typical spectrum of the slow orbit data (10 Hz) but we can also identify the low frequency information very clearly.

Many methods are available and applicable to analyze the 10 kHz orbit data in reviewing the past operation, but the traditional methods has limitations in detecting the orbit stability issue in real time. To overcome the limitations of the traditional methods, we are studying the machine learning techniques with which we can detect any orbit stability issue as early as possible with the trained model. As one of the strong candidates, we are testing models constructed by the long short-term memory (LSTM) autoencoder from the orbit data.

LSTM is a type of recurrent neural network (RNN) that is designed to handle sequential data and capture long-term dependencies. An autoencoder is a type of neural network that learns to encode input data into a lower-dimensional representation and then decode it back to the original input. By training an LSTM autoencoder on the 10 kHz orbit data, we can learn the normal patterns of the orbit and detect any deviations from the trained patterns, which may indicate stability issues.

* Work supported by the U.S. Department of Energy (DOE) under contract No. DE-SC0012704.

† jchoi@bnl.gov

Data Collection

The 2026 user operation of NSLS-II started on January 20 and the schedule until the April shutdown is shown in Table 1.

Table 1: NSLS-II User Operation Schedule Until the April Shutdown.

01	2026-01-20 08:00:00	2026-01-27 06:00:00
02	2026-01-29 08:00:00	2026-02-06 08:00:00
03	2026-02-09 08:00:00	2026-02-17 06:00:00
04	2026-02-19 08:00:00	2026-02-27 08:00:00
05	2026-03-02 08:00:00	2026-03-10 06:00:00
06	2026-03-12 08:00:00	2026-03-20 08:00:00
07	2026-03-23 08:00:00	2026-03-31 06:00:00
08	2026-04-02 08:00:00	2026-04-10 08:00:00

During the 8 periods of the 2026 user operation, we collected FA orbit data every 10 minutes. The total file number of the collected data is 7344, and each file contains 2000 points for all the beam position monitors (BPM). Even though insertion device (ID) BPMs are also included in the collection, they are not used in the general analysis and used when specific investigation is needed. Therefore, the total number of BPMs in the analysis is 360, 180 for horizontal motion and 180 for vertical motion.

Data Analysis

As the usually review of the machine performance, we analyze the FA data with the singular value decomposition (SVD). Detailed analysis of singular vectors, spectrum analysis or pattern analysis are reserved for the specific investigation, but, instead, we focus on the variation analysis using singular values. The advantage is the method is very simple and fast while providing suitable information about the orbit stability.

Figure 1 shows the variation of the variation of SVD analysis parameters together with the beam properties collected together with FA data. The lifetime and injection efficiency, in the beam properties compared to the SVD analysis parameters are, usually considered as the most important indicators of the machine performance. And the beam size and emittance are also important indicators which impact the user satisfaction.

The total energy of the SVD analysis is the sum of the squares of the singular values, which represents the total variance in the orbit data. There are various ways to define the rank of the matrix using the singular values and three of them are shown in the figure, which are the number of singular values above 95 % of the total energy (Energy95), the hard threshold based on well-known algorithm

Content from this work may be used under the terms of the CC BY 4.0 licence (© 2026). Any distribution of this work must maintain attribution to the author(s), title of the work, publisher, and DOI.

ISBN: 978-3-95450-252-3 ISSN: 2673-5350 doi: 10.18429/JACoW-IPAC2026-TUP2341

REAL-TIME STORAGE RING OPTICS MONITORING AND CORRECTION FEEDBACK SYSTEM*

J. Choi†, I. Lobach, Brookhaven National Laboratory, Upton, NY, USA

Abstract

Recently, an EPICS IOC server was installed in NSLS-II storage ring which provides real-time optics information during the user service periods. The server calculates the storage ring optics using the turn-by-turn (TBT) BPM data triggered by the disturbance from the injection kickers. The data are verified to be reliable, and the efforts are being invested to implement optics feedback system which will continually restore the storage ring optics to the desired status during the user service. This paper presents how the reliable optics information is obtained from the injection TBT data as well as how the data will be used in the optics correction feedback system.

INTRODUCTION

The NSLS-II storage ring is a 3rd generation light source with a 3 GeV electron storage ring which provides high brightness and high flux beams to the users. The storage ring is carefully designed and optimized to provide the best beam quality to the users, and the quality can be easily affected by the deviation in the storage ring optics. Therefore, monitoring the storage ring optics with proper correction when needed is important to maintain the user satisfaction with high quality synchrotron beam. However, it should not give any disturbance to the user service, and the available tools are quite limited during the user service periods.

To maintain the user satisfaction with high quality synchrotron beam, the electron bunches are, as the top-off injection, continually injected into the storage ring to compensate the beam loss due to the Touschek scattering and the gas scattering. The storage ring injection system is meticulously designed not to disturb the stored beam and, so that, minimize the impact on the user experiments. However, the injection system is not perfect, and even when the disturbance does not affect user performance, it still produces a very small turn-by-turn (TBT) signal in the beam position monitor (BPM) data that can be used to calculate the storage-ring optics.

Of course, the injection TBT data are not ideal for optics calculation, and the data processing is required to obtain reliable optics information. As can be easily expected, the injection TBT data are very noisy and the signal is very small, and the disadvantages can be listed as follows:

- Generated by leakage field.
- Damped very fast due to the bunch-by-bunch (BxB) feedback system. (Decoherence info. is not available.)
- Signal is weak and, accordingly, has low signal to noise ratio (SNR).
- Vertical signal is coming from coupling –- further weaker.
- Dispersion can be obtained from injection energy mismatch. (Dispersion info. is not available.)

That means we need to use strict thresholds to select the reliable data and many data sets are filtered out. However, the frequent top-off injection guarantees the real-time monitoring of the storage ring optics during the user service periods.

Furthermore, because our analysis focuses on the linear optics only, the data quality is not as critical as the nonlinear optics analysis, and the reliable optics information can be obtained from the injection TBT data with proper data processing.

DATA PROCESSING

The main tool of the analysis is the model independent analysis (MIA) method, which allows us to extract the linear optics parameters from the TBT data without relying on a detailed model of the storage ring. MIA includes the singular value decomposition (SVD), and it is used to filter out the noise and extract the dominant modes of the TBT data, which are related to the storage ring optics. In addition, the phase advance is very robust against the BPM gain errors,

Expected Tune Values

The bunch by bunch feedback system of NSLS-II storage ring provides the tune information in real-time, and the expected tune values can be obtained from the feedback system. Not frequently, but sometimes, the tune values from the feedback system apparently unreasonable, we set the expected tune values to the nominal values from the design model.

Apply Mean Substraction to the TBT Data

Following the standard principal component analysis (PCA) procedure , the mean value of the TBT data is subtracted from the data to center the data around zero, which allows us to focus on the variations in the data rather than the absolute values. In fact, because we are interested in the linear optics parameters, skipping the mean value subtraction hardly affect the results. The difference is that, when the raw TBT data are decomposed, the horizontal closed orbit mode becomes the most dominant mode having significantly larger singular value than the other modes. The betatron and dispersion modes properties can be still available.

* Work supported by the U.S. Department of Energy (DOE) under contract No. DE-SC0012704.

† jchoi@bnl.gov

Content from this work may be used under the terms of the CC BY 4.0 licence (© 2026). Any distribution of this work must maintain attribution to the author(s), title of the work, publisher, and DOI.

ISBN: 978-3-95450-252-3 ISSN: 2673-5350 doi: 10.18429/JACoW-IPAC2026-TUP2343

DESIGN AND INTEGRATION OF ALS-U STORAGE RING MODULES

D. Gudkov, F. Matichard, A. Talon, C. Espino Devine, C. J. Valdez, E. Newman,
J. Shaw, J. Osborn, M. Holmes, M. F. Khalid, S. Myers, T. Peev
Lawrence Berkeley National Laboratory, Berkeley, CA, United States

Content from this work may be used under the terms of the CC BY 4.0 licence (© 2026). Any distribution of this work must maintain attribution to the author(s), title of the work, publisher, and DOI.

Abstract

The Advanced Light Source Upgrade (ALS-U) is an ongoing project at Berkeley Lab to transform the ALS into a fourth-generation synchrotron light source. To minimize the ALS users facility down time, the ALS-U Storage Ring (SR) is composed of 48 unique, highly integrated modules, each split into approximately 11 subsystems. Thousands of unique physical interfaces are distributed across the modules and between modules, facilities and beamlines.

This contribution presents how the complex interfaces have been managed using interface control documentation and tailored interface verification methods based on a combination of Computer-Aided Design (CAD) assemblies and dedicated prototypes. These tools were adopted to manage both module-level integration and external interfaces with facility infrastructure and beamlines to mitigate integration risks. To validate the design solutions a physical 1:1 mockup has been developed alongside the CAD models.

The combined CAD-mockup validation approach revealed critical issues not detectable through CAD only, including cables' installation feasibility problems that would have caused redesign work and significant delays. The physical mockup also enabled more accurate analysis of maintenance access, assembly process and electrical safety. The practical experience from SR modules design in facility/beamlines integration context, methodology evolution during the design process, and recommendations for similar accelerator upgrade projects are also presented.

INTRODUCTION

Reducing the beam emittance for ALS-U to improve the coherent flux requires a complete replacement of the existing storage ring (SR) by introducing a multi-bend achromat (MBA) lattice [1]. The new SR lattice is a nine bend achromat with reverse bends and features 384 magnets divided across 12 sectors.

These sectors comprise a total of 48 unique modules, each housing between 6 and 10 magnets. A general view of a module is shown in Fig. 1. In addition to magnets (3 in Fig. 1), the modules include other components such as support structures (1), alignment systems (2), vacuum systems (4), beam diagnostics (9), water cooling (5) using low-conductivity water (LCW), and compressed air (8) systems. Control electronics (7) are located near the controlled devices. The modules house survey and alignment (S&A) target nests (10) and approximately 200 short-haul cables with an associated cable management system (6).

The available design volume and external interfaces are defined by the existing tunnel configuration, the multitude of ALS beamline front-ends [2], and the proximity of the new transfer lines. The compactness of the systems, combined with limited available volume and a complex operational contextrequires a rigorous interface management process using CAD models, design structure matrices (DSM), interface control checklists (ICC), and physical mockups.

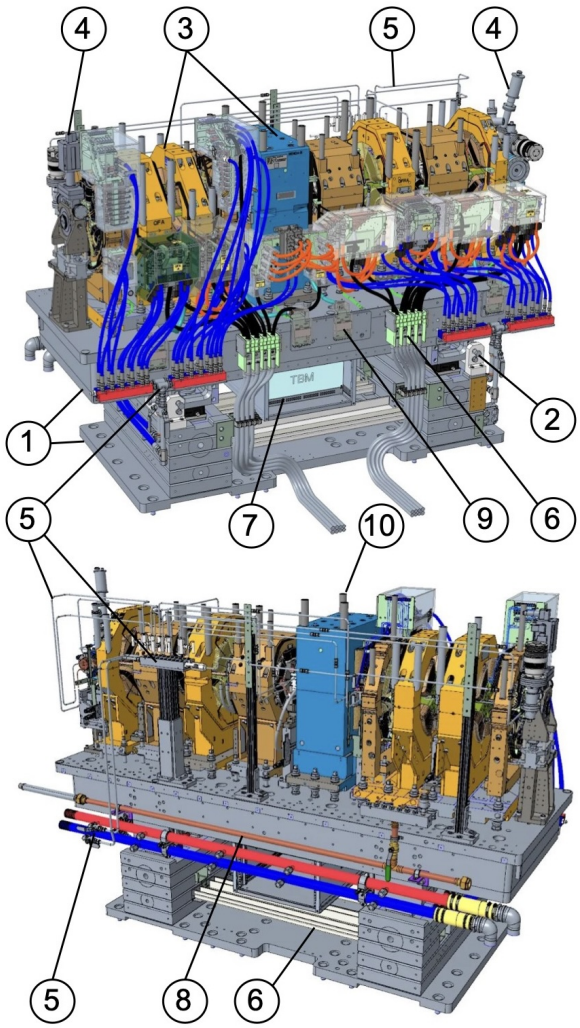

Figure 1: SR Module General View.

SR MODULES DESIGN OVERVIEW

Design Data Management

The Parametric CAD system, paired with the Product Lifecycle Management (PLM) system, are used for designing the SR and managing documentation. Figure 2 illustrates the interrelationships of design data as defined in the PLM system for the SR modules. An Item is the data entity that

ISBN: 978-3-95450-252-3 ISSN: 2673-5350 doi: 10.18429/JACoW-IPAC2026-TUP2344

ELECTRICAL INTEGRATION OF THE ALS-U STORAGE RING MODULES

A. Talon, R. Bloemhard, A. Can Atmaca, M. Castillo Sosa, Ch. De La Jolla, M. Erdmann, D. Gudkov, P. Gupta, M. Holmes, M. Leitner, D. Leitner, D. Li, F. Matichard, S. Myers, E. Newman, S. Omolayo, A. Ratti, D. Rice, J. Shaw, H. Singhal, C. Steier, A. Stewart, Ch. Sun, Ch. Swenson, Lawrence Berkeley National Laboratory, Berkeley, USA

Abstract

The ALS-U (Advanced Light Source Upgrade) project is an upgrade to the ALS at the Lawrence Berkeley National Laboratory.

The new multibend achromat SR (Storage Ring) will be installed during Dark Time when the ring is not used by the scientists due to installation work. Dark Time is currently scheduled to start in the middle of 2027 and will last at least 2 years. To meet the tight schedule and space constraints, the 48 modules of magnets are prestaged and aligned in advance.

Prestaging is the phase when the module is built in advance before it is transported to the tunnel. All local electrical wiring is prestaged to reduce the installation time in the tunnel.

Electrical work includes cabling for grounding, thermocouples, MPS (Machine Protection System), magnet power and correctors, vacuum, beamline feedback (diagnostics) and AC cables, all arranged to minimize heat buildup. Key challenges include module transport requirements and managing the overall routing as well as future upgrades in the tightly packed lattice arrangement.

This paper describes the electrical integration on the module during prestaging in detail. It further outlines the testing activities and the prototype modules developed to validate and optimize installation procedures. It details the schematics, cable and material management for the 48 modules, as well as the ALS-U configuration management system and databases used for electrical routing.

INTRODUCTION

The ALS-U Project is an ongoing upgrade of the Advanced Light Source (ALS) at Berkeley Lab that will provide a soft X-ray source that is up to 1,000 times brighter than today's capabilities, whilst generating a significantly higher fraction of coherent light in the soft X-ray region than currently available at the ALS [1].

To achieve this performance, the ALS-U Project will replace the existing SR with a new nine bend-achromat ring that delivers ultra-low-emittance electron beams to generate fully diffraction-limited X-ray light. A full energy Accumulator Ring (AR) is also added (see Fig. 1). Transfer lines from the AR to the SR are added to deliver a high-quality beam to the new SR [2].

These 2 new rings and transfer lines significantly increase the number of magnets, vacuum and control equipment.

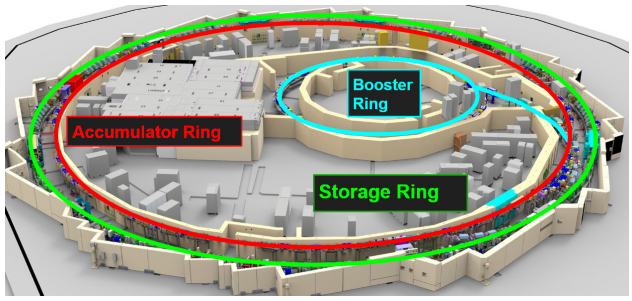

Figure 1: The rings that comprise the ALS complex: Booster Ring, Accumulator Ring (AR) and Storage Ring (SR).

Consequently, it also increases the number of cables, in a space that was originally designed to house only one ring. To facilitate the SR installation and reduce the Dark Time, the modules are prestaged. The ring is composed of 12 sectors. Every sector is made of 4 modules.

Prestaging the modules reduces the Dark Time duration [3]. The work is performed in a designated assembly space outside the ALS, to maximize beam time for users. All SR cables are separated in 2 categories:

- Short-haul cables are cables of various sizes in which both cable ends terminate on module mounted components. Short-haul cables will be prestaged. Having short-haul cables saves installation time. Furthermore, some short-haul cables would be difficult to install in the tunnel.
- Long-haul cables will be pulled in the tunnel once the modules are installed. These cables are pulled from the equipment racks (in the pit, which is the area circled by the ring that stores all of the racks, as well as the booster ring and the linear accelerator) to termination points on the modules in the tunnel.

The goal of this electrical integration activity is to plan and document all the cable routing to ensure a smooth installation during prestaging and in the tunnel.

This paper first describes the prototyping phase used to detect design issues early and solve them accordingly.

Secondly, it presents the documentation, testing procedures and work instructions that will be used during installation.

Finally, it describes the integration of electrical tasks within the overall project logistics.

Content from this work may be used under the terms of the CC BY 4.0 licence (© 2026). Any distribution of this work must maintain attribution to the author(s), title of the work, publisher, and DOI.

ISBN: 978-3-95450-252-3 ISSN: 2673-5350 doi: 10.18429/JACoW-IPAC2026-TUP2345

CONSIDERATION OF AN UNBUNCHED HIGH ENERGY ELECTRON STORAGE RING

M. Ehrlichman*, M. Bai, K. Bane, S. Littleton, A. Young,
SLAC National Accelerator Laboratory, Menlo Park, United States
D. Ratner, Thomas Jefferson National Accelerator Facility, Newport News, United States

Content from this work may be used under the terms of the CC BY 4.0 licence (© 2026). Any distribution of this work must maintain attribution to the author(s), title of the work, publisher, and DOI.

Abstract

Electron storage ring light sources rely exclusively on RF cavities to restore energy to the beam that is lost to photon emission. A limitation of RF is that it can store particles in only a small region of the RF waveform, yielding a bunched beam. Only a few percent of the ring circumference actually contains charge. Thus, high average current entails high peak current. While high average current and low emittance are the target parameters of the light source, the limitations come from peak current effects.

With recent advances, induction cells are potential replacements for RF cavities. The cells are compact, and a small number of them could be orchestrated to provide DC, or nearly DC, restoring voltage, yielding a continuous, unbunched beam.

SLAC is investigating the physics of continuous beam induction storage rings. Potential applications include continuous beam light sources with smaller emittances and higher currents, and also coherent emission light sources utilizing steady state microbunching (SSMB). For applications including SSMB, we are investigating isochronous rings based on anti-bend cell acromats.

INTRODUCTION

Recent experiments have demonstrated that induction cells can be reset on time scales nearing one-tenth of a storage ring revolution period. This raises the possibility of using them as a replacement for RF cavities to restore energy lost by a stored beam due to photon emission. Historically, induction cells have been used in induction linacs to generate several meter long, kV-level beams of a few 100 MeV energy.

Induction linacs are typically single-shot accelerators, and conventionally they are reset slowly after every experiment. Active-reset induction cells, developed in the BiRX experiment as a potential upgrade for FXR to facilitate cinematographic radiography, use a bipolar pulsed power supply to shorten the reset time [1]. Following a ramp where an induction cell delivers a voltage V_{set} to the beam for t_{set} seconds, a reverse resetting current is applied such that $V_{reset} \cdot s_{reset} = -V_{set} \cdot s_{set}$, whereupon the induction cell can again be ramped. $-V_{reset}$ is decelerating and necessitates a gap in the beam. The BiRX experiment demonstrated 25 kV per cell delivered to a 1.6 to 1.8 kA beam and the times scales of 10s of nanoseconds. In a storage ring, beams are typically less than 1 amp. It is expected that the reduced beam loading could be exploited to engineer cells for a storage ring with shorter time scales and higher voltages.

An induction cell occupies about 20 cm of longitudinal space and a typical storage ring straight is a few meters long. A sequence of several induction cells could be installed, with the sum of the voltage provided equaling the energy loss per turn. For example, a 100 m circumference storage ring at 1 GeV radiates between 25 and 50 kV per turn, well within the reach of a few induction cells. If the induction cells can be reset in 20 ns, then a constant ΔV could be applied to the beam for about 90% of the circumference. The beam would be gapped during the 20 ns reset.

An additional new induction cell technology worth mentioning is *masked-reset*, where diodes or transistors are used to modify the cell topology between set and reset to mask the beam from the decelerating reset voltage [2]. This would negate the necessity of a gap during the reset, enabling a truly continuous stored beam. Additionally, is would no longer be necessary to reset the cells on time scales $<< T_{rev}$, simplifying the cell and power supply engineering. However, this technology has a lower technological readiness level (TRL) than active reset cells, and one proposed design has recently been shown to be incompatible with beams stored much longer than a few 1000 turns [3].

During the ramp, the voltage applied by an induction cell has no time dependence. A passing beam sees a constant ΔV and experiences no longitudinal focusing. By setting ΔV equal to the energy loss per turn a beam is maintained at constant energy without being bunched. An important aspect of our work is to explore the beam dynamics of such a stored unbunched beam.

In an RF storage ring, most of the ring circumference is devoid of charge. Charge can be stored only in about 3% of the RF wave form. Harmonic cavities can be used to lengthen the bunch and increase this somewhat, to perhaps 5%.

The benefits of an induction ring and an unbunched beam are a significantly reduced peak current. Most of the driving concerns in the latest generation of storage ring light sources stem from high peak current. Intrabeam scattering spoils the emittance. Touschek scattering shortens lifetime necessitating sophisticated nonlinear optics optimizations and top-off injection schemes. Heating caused by peak current makes for difficult vacuum chamber engineering. Collective instabilities limit beam current and necessitate aggressive feedback systems. For the same average beam current, the peak current in an unbunched beam is about 25 times lower

* mpe@slac.stanford.edu

ISBN: 978-3-95450-252-3 ISSN: 2673-5350 doi: 10.18429/JACoW-IPAC2026-TUP2349

FINITE ELEMENT STUDIES OF THE CANREB ELECTRON GUN FOR A TEST STAND SETUP

M. Hartmann*, F. Ames, J. Cardona, C.R.J. Charles, M. Dehghan, M. Good, S. Ismagilova, O. Kester, A. Kwiatkowski, B. Schultz, TRIUMF, Vancouver, Canada

Abstract

The CANadian Rare isotope facility with Electron Beam ion source (CANREB) is an important component of the Advanced Rare IsotopE Laboratory (ARIEL) at TRIUMF. CANREB will deliver highly charged radioactive ion (HCI) beams for post-acceleration to nuclear physics experiments. Ion beams injected into CANREB are bunched using a radiofrequency quadrupole (RFQ) cooler-buncher and energy adjusted using a pulsed drift tube for injection into an electron beam ion source (EBIS) charge state breeder. Charge breeding occurs by collisions with an electron beam (up to 15 keV, 500 mA) produced by an electron gun. During EBIS commissioning, the electron gun became unstable at currents above 40 mA, with a large fraction of the beam intercepted by the anode. To address this issue, an electron gun with an updated design is planned to be fabricated and installed in CANREB. In order to characterise the new electron gun, a test-stand will be built allowing for systematic testing. This paper describes a full simulation model of the test-stand using Finite Element Analysis (FEA) software TRAK.

INTRODUCTION

The TRIUMF cyclotron delivers a 500 MeV CW (23 MHz) proton beam with currents up to 120 µA to spallation and meson production targets for particle, nuclear, and solid-state physics research [1]. Rare isotope beams (RIBs) are produced by irradiating solid U, Ta, Si, Th, Nb, or C targets with 480 MeV protons at currents up to 100 µA [2]. The resulting ions are extracted at energies up to 60 keV and delivered either to low-energy experimental stations at the ISAC facility or to a multi-stage linac for further acceleration and high-energy experiments. TRIUMF's ARIEL facility [3] will add two new target stations for RIB production as well as integrating the CANadian Rare isotope facility with Electron Beam ion source (CANREB) for charge breeding of ions [2] (Fig. 1). CANREB uses an electron beam ion source (EBIS) to produce highly charged ions (HCI). The EBIS accepts ions with energies up to 14 keV and confines them electrostatically within the center of a split-bore superconducting Helmholtz magnet operating at fields up to 6 T. An electron gun generates an electron beam that is compressed in the trapping region before being collected by an electron collector. During EBIS commisisoning, the electron gun became unstable at currents above 40 mA, with a large fraction of beam intercepted by the anode [2]. To overcome these limitations, an upgraded design is being developed for installation in CANREB. A dedicated test-stand will be constructed to facilitate detailed and reproducible performance studies of the new electron gun. This paper presents a complete simulation model of the test-stand using FEA software TRAK (Field Precision) [5] as well as benchmarking with ion optics code, IGUN [6]. In the following section the electron gun model (design and simulation) is described.

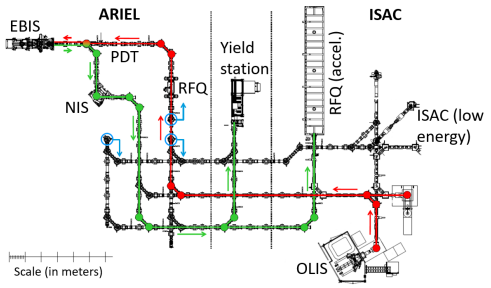

Figure 1: The CANREB facility at ARIEL [4]. Beam is injected from the ISAC RIB targets or the off-line ion source (OLIS) along the red path. The charge-bred beam is extracted via the green path and directed either to the yield station or the ISAC linac. In the future, beams from the ARIEL RIB targets (blue circles) will also be injected into CANREB.

ELECTRON GUN AND TEST-STAND MODEL

Electron Gun Components

Figure. 2 shows an axial cross-section of the new CANREB electron gun. It is a Brillouin-type gun [7] comprising a 6.35 mm, spherically shaped barium dispenser cathode producing an electron beam of energy up to 15 keV (500 mA). Downstream of the cathode, a high purity copper anode accelerates the emitted electrons. Between the cathode and anode, a focusing electrode (Wehnelt Electrode) shapes the electric field around the cathode, providing efficient control over the electron beam emission [8]. The potential applied to the Wehnelt Electrode can be used to rapidly switch the emission current on and off (a higher negative potential compared to the cathode will suppress

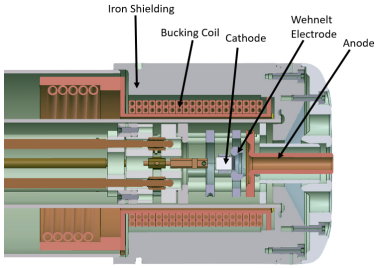

Figure 2: Cross section of the new CANREB electron gun.

* mhartmann@triumf.ca

Content from this work may be used under the terms of the CC BY 4.0 licence (© 2026). Any distribution of this work must maintain attribution to the author(s), title of the work, publisher, and DOI.

ISBN: 978-3-95450-252-3 ISSN: 2673-5350 doi: 10.18429/JACoW-IPAC2026-TUP2350

EXPERIMENTAL RECONSTRUCTION OF SOURCE 4D PHASE SPACE WITHOUT PRIOR KNOWLEDGE OF TRANSFER MATRIX

C. Zhang*, E. Echeverria, A. Flint, C. Pennington,
I. Bazarov, A. Bartnik, J. Maxson, Cornell University (CLASSE), Ithaca, NY, United States
C. Pierce, University of Chicago, Chicago, IL, United States
A. Galdi, University of Salerno, Fisciano, Italy
W. Li, Brookhaven National Laboratory, Upton, NY, United States

Abstract

We use the PHOEBE test beamline at Cornell to experimentally demonstrate a simple method for reconstructing the transverse 4D phase space of an electron beam at the source from downstream aperture scans of the beam. This method does not rely on detailed knowledge of the beamline transport, besides assuming that linearity and symplecticity are satisfied. We apply this method to measure the source 4D phase space of electrons emitted from a spatially-structured alkali-antimonide cathode with periodic quantum efficiency modulations. The reconstructed 4D phase space is checked for fidelity, and we observe that the source spatial distribution matches the spatial structure of the cathode, and the source momentum distribution produces a mean transverse energy that is consistent with 4D beam emittance measurements.

INTRODUCTION

Understanding the physics of photoemission is important for engineering photocathodes that produce high-quality beams. However, much of the experimental work currently done in accelerators only focuses on ensemble beam quantities such as quantum efficiency (QE) and mean transverse energy (MTE) [1–3], instead of probing the full position and momentum distribution of the emitted electrons at the source. A method for measuring the phase space of the beam at the source, in particular, would provide insight into the local correlations between momentum and position induced by surface deformities (physical and chemical) at the high surface fields [4, 5] necessary for accelerator applications.

In this paper, we demonstrate a method where 4D transverse phase space measurements performed with a downstream aperture scan diagnostic can be used to reconstruct the 4D transverse phase space at the source. The reconstruction relies on experimentally determining the transfer matrix by measuring the beam moments, the centroids and covariances, at the aperture scan diagnostic and their dependence on experimentally accessible beam moments at the source, which is the beam position centroid in our setup. Once the transfer matrix is known, the source phase space can be calculated by applying the inverse transfer matrix to a measured downstream phase space.

We first discuss the theory behind this source reconstruction method, our experimental setup, and then discuss the practical implementation of this method for a spatially structured photocathode.

4D RECONSTRUCTION THEORY

A linear transfer matrix, $\mathbf{M}$, is often a good approximation for relating the source position and momentum of a particle to its final position and momentum downstream near the design trajectory of a beamline. Here, we only consider the transverse positions and momentums $\{x, p_x, y, p_y\}$, but many of our results can be generalized to 6D provided a means to measure some of the longitudinal transfer matrix elements.

In principle, the elements of the transfer matrix between the source and the downstream beamline diagnostic can be measured by linearly fitting the final position and momentum of a particle measured at the beamline diagnostic to its source position and momentum. In practice, instead of measuring individual particle positions and momentums, we measure the beam centroid in 4D phase space since it transforms with the transfer matrix like a single particle. In addition, we often only have control over the source position centroid. In the case of a photocathode, this can be inferred from the position of the laser spot driving photoemission. As a result, we cannot directly measure the entire 4D transfer matrix, but we will shortly discuss additional constraints derived from the symplectic condition and beam covariances that will yield the full 4D transfer matrix.

For each laser position, the 4D phase space of the beam is measured, and the beam centroid is calculated. For phase space centroids $(x_1, p_{x,1}, y_1, p_{y,1})$ and $(x_2, p_{x,2}, y_2, p_{y,2})$ measured when the laser is at positions $(y_L, 0)$ and $(x_L, 0)$, respectively, we can directly measure the first and third columns of the transfer matrix,

$$\begin{pmatrix} m_{11} & m_{13} \\ m_{21} & m_{23} \\ m_{31} & m_{33} \\ m_{41} & m_{43} \end{pmatrix} = \begin{pmatrix} x_2/x_L & x_1/y_L \\ p_{x,2}/x_L & p_{x,1}/y_L \\ y_2/x_L & y_1/y_L \\ p_{y,2}/x_L & p_{y,1}/y_L \end{pmatrix}. \quad (1)$$

For convenience, we refer to this as the partial transfer matrix. In practice, the partial transfer matrix will be determined by linearly fitting the measured phase space centroids to the measured laser positions.

With the partial transfer matrix and a few additional assumptions, we can solve for the full 4D transfer matrix. A system of 5 independent non-linear equations can be obtained from the symplectic condition, $\mathbf{M}\Omega\mathbf{M}^T = \Omega$, where

* cz266@cornell.edu

Content from this work may be used under the terms of the CC BY 4.0 licence (© 2026). Any distribution of this work must maintain attribution to the author(s), title of the work, publisher, and DOI.

ISBN: 978-3-95450-252-3 ISSN: 2673-5350 doi: 10.18429/JACoW-IPAC2026-TUP2353

LCLS-II INJECTOR OPERATIONAL CHALLENGES AND DEVELOPMENTS*

F. Zhou†, A. Brachmann, D. Cesar, W. Colocho, Y. Ding, D. Dowell, G. Just, A. Osman, N. Sudar, T. Vecchione, Z. Zhang, and C. Zimmer
SLAC National Accelerator Laboratory, Menlo Park, United States

Abstract

The Linac Coherent Light Source II (LCLS-II) has been in user operations since 2023 and has successfully ramped up the beam repetition rate to 93 kHz. The LCLS-II photoinjector has demonstrated the ability to deliver a high-brightness, low-emittance electron beam at high repetition rates, meeting key performance targets. However, several operational challenges have emerged during commissioning and user operation. These include substantial gun dark current, degradation of cathode quantum efficiency (QE) uniformity, unexpected electron beam breakup, significant emittance growth through the laser heater chicane, the presence of beam halos, and cathode QE dependence on e-beam rate. This paper provides an overview of these challenges and highlights recent efforts to address these outstanding issues and discusses plans for further improvement of the performance.

INTRODUCTION

Continuous-wave (CW) free-electron laser (FEL) facilities such as LCLS-II impose stringent requirements on the photoinjector to deliver high-brightness, low-emittance, and reliable electron beams. The LCLS-II 1 MeV electron source was successfully commissioned between 2018 and 2020, following the resolution of several significant technical challenges [1]. In 2022, the full-scale >70 MeV injector was commissioned, and its beam performance was then characterized and optimized. Figure 1 presents a schematic layout of the complete injector.

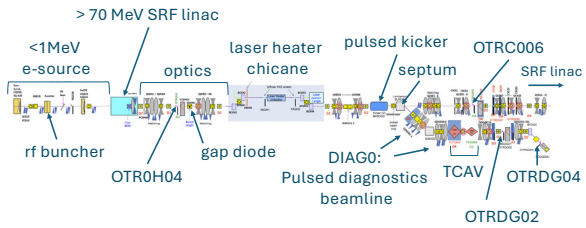

Figure 1: Schematic of the LCLS-II injector layout.

The injector consists of the 1 MeV electron source, a >70 MeV standard cryomodule (CM01), a laser heater chicane, and multiple diagnostic stations. These include the first emittance station (OTR0H04) and a gap diode for relative bunch length measurements, both located before the laser heater chicane; a second emittance station (OTRC006) located downstream of the chicane; and a dedicated off-axis diagnostics station equipped with a transverse deflecting cavity (TCAV) for absolute bunch length measurement, along with an additional emittance measurement station.

Since the start of FEL user operations in 2023, a variety of operational challenges have been encountered in the injector system. This paper discusses the key issues and the corresponding efforts toward their resolutions, including:

- Improvement of gun vacuum 10-fold after processing major low energy multipacting barriers.
- Mitigation of large gun dark current, significantly reducing dark current loss downstream in high energy area.
- Observation of the formation of QE crater/bump on the photocathode within weeks of operation, resulting in spatial and charge instability in the beam and emittance dilution, and QE dependence of the beam rate.
- Correction of stray magnetic fields in the laser heater chicane, mitigating emittance growth.
- Observation of beam halos and mitigation with new bunching scheme.
- Maintaining low beam emittance.
- Observation of harmonic laser energy modulation through laser heater chicane.

PERFORMANCE AND OPERATIONAL CHALLENGES

The following sub-sections present an overview of major operational challenges and the systematic efforts undertaken to diagnose and resolve them.

CW Gun Operational Improvements

The gun vacuum gradually degraded over time, increasing from 8×10^{-10} Torr in 2023 to 2×10^{-9} Torr by December 2024. In October 2024, a small step-like increase in vacuum pressure was observed; however, the source of this change remained unidentified until December 2024, when a vacuum leak was discovered on one of two RF windows. Following the identification of the leak, the faulty window was replaced, and the entire gun assembly was baked at 150–170 °C. During following RF power processing of the gun, we processed through all major multipacting barriers this time rather than jumping over these barriers for rapidly increasing the RF power to nominal in the past, resulting in a significant improvement in vacuum conditions. The base pressure with CW RF on was improved by 10-fold. The gun vacuum has remained stable at 2.4×10^{-10} Torr over the five months of operation following the RF processing.

*Work supported by US DOE Contract
†zhoufeng@slac.stanford.edu

Content from this work may be used under the terms of the CC BY 4.0 licence (© 2026). Any distribution of this work must maintain attribution to the author(s), title of the work, publisher, and DOI.

ISBN: 978-3-95450-252-3 ISSN: 2673-5350 doi: 10.18429/JACoW-IPAC2026-TUP2355

EXPERIENCE ADJUSTING BEAM TRANSPORT AND BOOSTER SYNCHROTRON SYSTEMS FOR DIFFERENT LINAC OUTPUT ENERGIES AT THE CANADIAN LIGHT SOURCE

W. A. Wurtz*, C. Baribeau, T. Batten, M. A. Bree, C.-L. Randall, X. Shen, T. Sové, J. M. Vogt
Canadian Light Source, Saskatoon, Saskatchewan, Canada

Abstract

Due to linac operational issues, the Canadian Light Source has recently reduced the injection energy of its booster synchrotron from 250 MeV to 152 MeV. We found that we needed to be increasingly careful with the booster ring transverse tunes as we decreased the injection energy. We needed to make fine adjustments of the tunes during the low energy part of the ramp, requiring new software. Adjusting the energy compression system (ECS) and transfer line was mostly a linear process. Recent improvements in diagnostics and software have greatly simplified ECS and transfer line setup.

INTRODUCTION

The Canadian Light Source (CLS) injector is a collection of systems from various past decades. The original linac for the Saskatchewan Accelerator Laboratory (SAL) dates from 1964 [1, 2]. In the 1980s, an energy compression system (ECS) was added that includes a three-magnet chicane to chirp the beam, followed by an S-band rf cavity operated at the zero crossing [3]. Later, SAL stopped operations and its building and accelerator systems were incorporated into the newly funded CLS, with the booster ring commissioned in 2002 [4]. The SAL linac saw many changes and upgrades over the years, and was recently replaced by a new linac from Research Instruments GmbH (RI) [5].

Figure 1 shows the conceptual layout of the injection system as the electrons are produced at the source, accelerated in the linac, and then transported from the sub-basement to the booster ring. As both the SAL linac location, and the location of the green field CLS was built on, were fixed by the original SAL building, the CLS designers built a 78 m long transfer line [6], using mostly parts scavenged from SAL. The linac-to-booster (LTB) transfer line moves the electrons from the linac and ECS to booster injection without any longitudinal acceleration.

PROCESS OVERVIEW

The booster ring was designed to capture electrons at 250 MeV, which was an energy that the SAL linac could easily achieve. There were a number of instances through the years where, usually due to modulator problems, the SAL linac needed to be operated at lower energies. At these times, booster capture efficiency and stability suffered. It ran as low as 158 MeV in 2011. While we had planned to operate the replacement linac at 250 MeV, we settled on 152 MeV to ensure reliable operation of the accelerating sections [7].

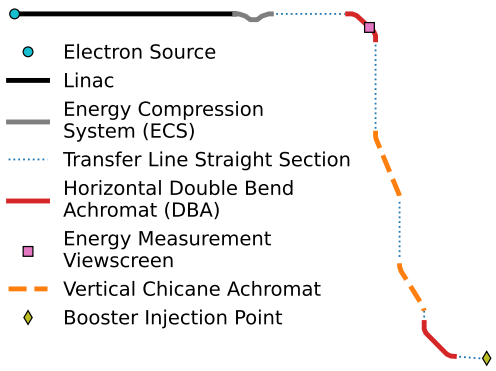

Figure 1: A conceptual layout of the accelerators and transfer line showing both horizontal and vertical bends. The electrons begin at the source, are accelerated to 152 MeV by the linac, and are transported to the booster ring through the LTB transfer line. The LTB uses two vertical chicanes to move the beam from the linac in the sub-basement to the ground floor, at ring height.

Scaling the energy of the ECS, LTB and booster injection is not conceptually hard, as it is mostly linear. In practice, there were some interesting challenges along the way.

After setting the linac to a specific energy, we linearly scaled the LTB and booster ring. To start, we turned off and degaussed the ECS chicane magnets and sent zero power to the ECS cavity, rendering the ECS a drift section. With the ECS turned off, we made measurements of the linac beam properties, such as emittance and energy spread, using diagnostics in the first part of the LTB. Our goal in this configuration was to make 1000 turns around the booster ring with the booster rf off. If we achieved 1000 turns, we knew the trajectory was okay and it was time to turn on the ECS chicane.

We turned on the three ECS chicane magnets one-at-a-time, adjusting them slightly as we went along. They were almost, but not entirely, linear. With all three magnets on, we recovered the 1000 turns around the booster by carefully adjusting the final ECS chicane magnet, plus some vertical steering to compensate for a small vertical kick from the chicane magnets.

The beam coming out of the ECS was chirped, but not compressed. Using a viewscreen in a region with horizontal dispersion, we set the power and phase of the ECS rf cavity to compress the energy spread of the beam and to operate at the zero crossing, where there is no net acceleration. We

* ward.wurtz@lightsource.ca

Content from this work may be used under the terms of the CC BY 4.0 licence (© 2026). Any distribution of this work must maintain attribution to the author(s), title of the work, publisher, and DOI.

ISBN: 978-3-95450-252-3 ISSN: 2673-5350 doi: 10.18429/JACoW-IPAC2026-TUP2602

PROGRESS OF PHYSICS STUDIES AND BEAM COMMISSIONING OF THE HIGH ENERGY PHOTON SOURCE*

Y. Jiao†, W. Bao, J.S. Cao, S.Y. Chen, X.H. Cui, Y.H. Dong, Z. Duan, Y.Y. Guo, P. He, X.Y. Huang, Y.S. Huang, D.H. Ji, H.F. Ji, W. Kang, D.B. Li, J. Li, J.Y. Li, N. Li, X.Y. Li, Y. Li, Z.Q. Li, S.Y. Lin, Y.Z. Liu, X.H. Lu[1], Y.H. Lu, C. Meng, W.M. Pan, Y.M. Peng, L.Y. Qin, H.M. Qu, M.Y. Su, S.K. Tian, J.Q. Wang, N. Wang, Z.H. Wang, Y.Y. Wei, Y.F. Wu, G. Xu, H.S. Xu, F. Yan, Y.C. Yang, C.H. Yu, F.C. Zeng, J. Zhang, F.C. Zhao, Y.L. Zhao, Z.H. Zhao, H.J. Zheng, Institute of High Energy Physics, Beijing, China
[1]also at Spallation Neutron Source Science Center, Dongguan, China

Abstract

The High Energy Photon Source (HEPS) is a 35-pm, 1360-m storage ring light source built in the suburb of Beijing, China. The HEPS construction started in 2019, with the main civil construction finished at the end of 2021. Beam commissioning of the storage ring began in July 2024. In about 14 months of commissioning interleaved with equipment installation, all key performance parameters have met or exceeded the acceptance targets. In this paper, we will briefly introduce commissioning of the HEPS storage ring, and relevant physics studies.

INTRODUCTION

The High Energy Photon Source (HEPS) is a 6-GeV, 1360.4-m storage ring light source built in Beijing, China. It adopts a hybrid seven-bend achromat (7BA) lattice and achieves a natural emittance of 34.8 pm·rad, making it the first fourth-generation synchrotron radiation facility in Asia [1, 2]. The main parameters are listed in Table 1.

Table 1: HEPS Main Performance Parameters

Parameter	Value	Unit
Beam energy	6	GeV
Beam current	200	mA
Circumference	1360.4	M
Natural emittance	34.8	pm·rad
Momentum compaction	1.83	10^{-5}
Energy loss per turn (w/o ID)	2.64	MeV

After more than ten years' R&D, including the HEPS test facility project (2016-2018), construction of the HEPS project began in mid-2019 [3], and multiple milestones have been achieved since then (see, e.g., [4, 5]). The main civil construction was largely completed in July 2021, followed by equipment installation and beam commissioning of the injector in 2023. Equipment Installation of the storage ring was largely finished in July 2024, and beam commissioning commenced shortly afterward. Joint commissioning of the accelerator and beamlines was completed in October 2025, at which point HEPS passed its performance acceptance review.

From the perspective of accelerator physics, following the completion of the preliminary design report in 2018, modification of the accelerator's overall design was performed and frozen by the end of 2019 to address emerging challenges in the hardware and engineering design. By the end of 2021, design and studies on relevant physics issues were basically completed based on the final design. From 2020 to the end of 2022, pre-commissioning preparations were preformed, where we programmed the commissioning plan, implemented the commissioning simulation for specific commissioning process, and especially developed a set of commissioning software (that for storage ring finally finished in 2024). In 2023, we finished the commissioning of the injector (including Linac and booster). In July 23, 2024, the storage ring beam commissioning commenced. Over the past year and a half, the HEPS accelerator team has completed eight rounds of commissioning, interspersed with shutdowns for equipment installation and conditioning. All key performance parameters passed the acceptance review in October 2025. In the following we will introduce reports the detailed progress on equipment installation, beam stability, orbit and optics correction, high-current commissioning, and insertion device (ID) commissioning. Details of previous physics design, related studies and commissioning progress can be found in Ref. [6-13].

EQUIPMENT INSTALLATION AND CONDITIONING

Not all hardware systems were ready at the start of ring commissioning. As shown in Fig. 1, two major shutdowns in 2025, totally about 130 days, were used for equipment installation and conditioning. The first shutdown (February–March 2025) focused on installing most insertion devices, performing fine global alignment, and installing the beam dump kicker. The second shutdown (May–August 2025) focused on installing the 166 MHz and 500 MHz superconducting RF cavities, the fourth collimator, and the remaining insertion devices.

By August 2025, tunnel installation and conditioning of nearly all equipment were completed. Theoretical-position alignment of all 288 magnet units was completed during the first shutdown, reducing RMS absolute position

* Work supported by High Energy Photon Source (HEPS), a major national science and technology infrastructure and NSFC (12275284, 11922512).
† jiaoyi@ihep.ac.cn

Content from this work may be used under the terms of the CC BY 4.0 licence (© 2026). Any distribution of this work must maintain attribution to the author(s), title of the work, publisher, and DOI.

ISBN: 978-3-95450-252-3 ISSN: 2673-5350 doi: 10.18429/JACoW-IPAC2026-TUP2606

FEASIBILITY OF A COMPACT X-RAY FREE-ELECTRON LASER OSCILLATOR BASED ON DIFFRACTION LIMITED STORAGE RING*

W. Qin†,1,2, W. Liu1,2, Y. Zhao1,2, J. Wei1,2, M. Li1, X. Li1,2, Y. Jiao1, S. Wang1,2
[1]Institute of High Energy Physics, Chinese Academy of Sciences, Beijing, China
[2]Spallation Neutron Source Science Center, Dongguan, China

Abstract

X-ray Free-Electron Laser Oscillators (XFELOs) utilize Bragg crystal-based x-ray cavities to generate high-brightness x-ray pulses with ultra-fine bandwidth. The successful realization of XFELOs would greatly benefit high-resolution photon-hungry experiments, such as nuclear resonant scattering and inelastic x-ray scattering. Existing XFELO proposals, constrained by either the electron beam repetition rate or limited single-pass gain in the undulator, typically require long undulators and long cavities. In this work, we investigate the feasibility of a compact XFELO design, utilizing the 6-meter straight sections of a Diffraction Limited Storage Ring (DLSR) and a cavity path length well below 100 meters. We show that sufficient single-pass gain can be achieved by optimizing the undulator and electron beam parameters. We present the projected performance of the proposed scheme based on the parameters of the High Energy Photon Source (HEPS) and discuss the practical challenges associated with its implementation.

INTRODUCTION

High-spectral-brightness is crucial for high-resolution experiments using synchrotron or free-electron laser-generated hard x-ray pulses. So far, the diffraction-limited storage ring (DLSR) [1] and the hard x-ray self-seeding (HXRSS) [2] represent the state-of-the-art sources generating the highest spectral density in circular and linear accelerators. Cavity-based x-ray free-electron lasers (CBXFELs) are attracting increasing interest for the possibility of pushing the spectral brightness one big step forward and enabling new frontiers in material sciences and x-ray quantum optics. The CBXFELs utilize high-reflectivity Bragg crystals as mirrors to form x-ray cavities, which can be categorized into x-ray free-electron laser oscillators (XFELOs) when the gain inside the cavity is low and x-ray regenerative amplification free-electron lasers (XRAFELs) when the gain is high. After more than 40 years of development, the CBXFEL was recently experimentally demonstrated [3] for the first time with a pulse-mode superconducting linac at DESY, opening a new era for the x-ray sciences.

Despite new projects established aiming at demonstrating CBXFELs among the high-repetition-rate XFEL facilities around the world [4–7], the idea of realizing CBXFELs using the storage ring electron beam is still limited to feasibility and performance studies [8–10]. The DLSR enabled ultra-low transverse emittance down to the diffraction limit, while its energy spread is still one order of magnitude higher than linac-based sources. A combination of a transverse gradient undulator (TGU) and a local vertical dispersion is proposed to compensate the energy spread. Another aspect is that the storage ring beam usually has a beam current of a few tens of Amperes, making it difficult to obtain sufficient gain in a typical straight section of only a few meters long in storage rings. A recent study of XFELO [10] using the PETRA-IV [11] long straight section required 30 meters of TGU and the cavity length of around 150 meters.

In this paper, we propose a more compact layout for realizing the XFELO using DLSR electron beams and present a preliminary feasibility study. In the following, we first introduce the proposed setup, then show the optimization of the small signal gain in a short TGU. Using parameters of the High Energy Photon Source (HEPS) [12], we show the projected performance obtained through numerical simulations. Finally, we discuss the challenges of actual implementation and discuss the road map for further development.

LAYOUT

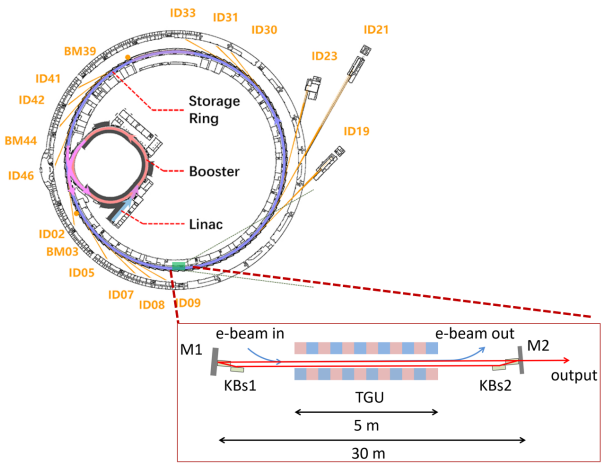

Figure 1: Schematic layout of the compact DLSR-XFELO.

Figure 1 gives the schematic layout of the proposed XFELO based on DLSR. The crystal cavity is composed of two high-reflectivity crystals with the working angles slightly off normal incidence. A closed loop is formed by adding two pairs of KB mirrors as retro-reflectors. The distance between the two crystals is about 30 meters, allowing the electron beam repetition rate of about 5 MHz. The forward and return optical paths are separated by a few millimeters.

* This work was supported by Guangdong Basic and Applied Basic Research Foundation (No.2026A1515030037), the Department of Science and Technology of Guangdong Province (No.2024QN11X220).
† qinwl@ihep.ac.cn

Content from this work may be used under the terms of the CC BY 4.0 licence (© 2026). Any distribution of this work must maintain attribution to the author(s), title of the work, publisher, and DOI.

ISBN: 978-3-95450-252-3 ISSN: 2673-5350 doi: 10.18429/JACoW-IPAC2026-TUP2607

BEAM BASED ALIGNMENT OF QUADRUPOLES AT HEPS

Xiaohao Cui†, Yi Jiao, Key Laboratory of Particle Acceleration Physics and Technology, Institute of High Energy Physics, CAS, Beijing, China

Abstract

In modern storage ring light source, large offset of quadrupoles will degrade the beam quality in the ring. Beam based alignment (BBA) methods have been used widely in storage rings, to correct the orbit of the beam to the magnetic center of quadrupoles. The BBA algorithm and commissioning procedure at HEPS is described in this paper. Two measurement algorithms were implemented: a fast BBA method using AC excitation and turn-by-turn BPM data, and a traditional BBA method based on closed orbit distortion optimization. The commissioning campaign spanned 16 months from September 2024 to January 2026, during which several key technical challenges were identified and resolved, including 50 Hz power line interference, quadrupole corrector coil effects, and low-frequency beam orbit jitter. Through systematic optimization of slow corrector power supplies and iterative measurement procedures, all 578 BPMs in the HEPS storage ring were successfully calibrated with RMS precision better than 30 μm, meeting the design requirements for high-performance accelerator operation.

INTRODUCTION

In modern synchrotron light sources, even small offsets of the beam relative to the magnetic center of quadrupoles can significantly impact accelerator performance. Due to the high field gradient of quadrupole magnets, micrometer-level position deviations can cause beam position instability, emittance growth, and reduced dynamic aperture. Beam Based Alignment (BBA) is a precision calibration technique that actively steers particle beams through the exact magnetic center of quadrupole magnets, thereby determining the offset between the Beam Position Monitor (BPM) electrical center and the quadrupole magnetic center [1]. BBA technology has been adopted by leading synchrotron facilities worldwide as a critical commissioning procedure for achieving design specifications [2, 3].

The High Energy Photon Source (HEPS) is a fourth-generation synchrotron light source in Beijing, China. The storage ring features a 48-period hybrid multi-bend achromat (HMBA) lattice, with each period containing 12 BPMs strategically positioned for comprehensive orbit measurement. Including two additional BPMs in the injection and extraction regions, a total of 578 BPMs require precise offset calibration [4]. Pre-commissioning simulations established the requirement that BBA precision must achieve better than 30 μm RMS to meet orbit correction and optics analysis specifications. This paper summarizes the complete BBA commissioning campaign at HEPS from September 2024 to January 2026, describing the measurement algorithms, key technical challenges encountered, and the solutions that enabled successful calibration of all BPMs.

METHODOLOGY

Fast BBA Algorithm

The Fast BBA (FBBA) method follows the approach described in reference [2]. A sinusoidal excitation at 10 Hz is applied to a fast corrector magnet, creating controlled beam oscillation. Turn-by-turn (TBT) BPM data is then acquired across the storage ring. Under this excitation, the readings of any two BPMs in the ring exhibit a linear relationship. Subsequently, the strength of the quadrupole near the target BPM is adjusted, and a new set of TBT data is acquired, yielding a modified linear relationship. Linear fitting is performed on both datasets, and the intersection point of the two fitted lines reveals the BPM offset relative to the quadrupole magnetic center.

The primary advantage of the FBBA method is its speed, with a typical measurement time of approximately 1–2 minutes per BPM. The small-amplitude AC excitation from the fast corrector has minimal impact on the stored beam. However, the method is susceptible to various noise sources in the ring, and the precision of TBT data is generally lower than that of SA BPM data. The HEPS team developed an automated FBBA measurement program using the Pyapas high-level application framework [5], which integrates control system APIs for magnet control, BPM readout, and real-time data analysis.

Traditional BBA Algorithm

The traditional BBA method, also referred to as Slow BBA (SBBA), is based on the principle that in an ideal linear optics system, when the beam passes exactly through the magnetic center of a quadrupole, a small perturbation of the quadrupole strength produces no change in the beam orbit. Conversely, the sensitivity of the orbit to quadrupole strength variations directly reflects the degree of beam offset from the magnetic center [3].

The measurement procedure consists of the following steps. First, a strength perturbation of $\pm\Delta k$ is applied to the target quadrupole. The orbit change function $f = \Sigma[x_i(+\Delta k) - x_i(-\Delta k)]^2$ is defined using readings from all BPMs in the ring, where x_i represents the orbit position at BPM i. Next, nearby correctors are adjusted to change the beam position through the quadrupole, and an optimization algorithm is employed to find the orbit state that minimizes f. When f reaches its minimum value, the beam is judged to pass through the quadrupole magnetic center. The BPM reading at this condition is recorded as the offset. This process is repeated for all BPMs in the ring. The SBBA method offers

† cuixh@ihep.ac.cn

Content from this work may be used under the terms of the CC BY 4.0 licence (© 2026). Any distribution of this work must maintain attribution to the author(s), title of the work, publisher, and DOI.

ISBN: 978-3-95450-252-3 ISSN: 2673-5350 doi: 10.18429/JACoW-IPAC2026-TUP2608

STATUS OF HEPS BOOSTER OPERATION

Yuemei Peng†, Jinhui Chen, Haiyi Dong, Zhe Duan, Daheng Ji, Fang Liu, Fengli Long, Haisheng Xu, Pei Zhang, Yi Jiao, Jingyi Li
Institute of High Energy Physics, CAS, Beijing, China

Abstract

The High Energy Photon Source is the first fourth-generation synchrotron light source in Asia. As a greenfield facility, HEPS began construction in 2019 and now the commissioning of the storage ring has been basically finished. The booster synchrotron, serving as the second-stage accelerator, completed its initial beam commissioning between July and November 2023 and was officially put into operation in July 2024 to support the storage ring commissioning. This paper presents the beam performance of the booster since the start of operation, key upgrades and optimizations implemented, major operational challenges encountered, and the ongoing plans for further performance enhancement.

INTRODUCTION

Asia's first fourth-generation synchrotron radiation light source—the High Energy Photon Source (HEPS)—is being built in China [1]. HEPS successfully passed its process acceptance in October 2025. This marks the successful completion of its construction phase and the transition from the construction stage to the preparation phase for trial operation and open access.

HEPS complex consists of a 500 MeV Linac [2], a low energy transport line (named LB) [3], a 454 m booster synchrotron with a max repetition rate of 1 Hz [4], two high energy transport lines (named BR and RB) [5], a 6 GeV storage ring with an emittance lower than 60 pm.rad [6], and multiple beam line experimental stations. The layout of HEPS complex is shown as Fig. 1.

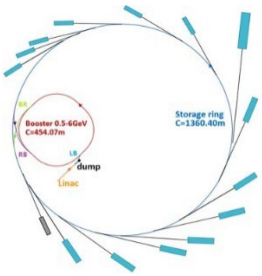

Figure 1: Layout diagram of the HEPS complex.

As a full energy injector, the HEPS booster increases the energy of the electron beam from 500 MeV to a design energy of 6 GeV and provides a sufficiently high-quality electron beam for injection into the storage ring. The installation and conditioning of the equipment were completed in January 2023, beam commissioning of the booster began in July of the same year, and process acceptance was finalized in November [7] —all while the storage ring and its subsystems were still under installation. The beam commissioning of the HEPS storage ring began in July 2024. The stable operation of the injector has laid the foundation for this process.

DESIGN AND RAMPING CONTROL

The HEPS booster lattice features four-fold symmetry. Each super-period comprises 14 standard FODO cells with matching sections at both ends, housing 32 dipoles, 37 quadrupoles, and 17 sextupoles. Such a period also delivers a dispersion-free straight section of roughly 8.8 meters to accommodate the injection/extraction systems and RF cavities. The quarter-lattice optics are presented in Fig. 2 and the main parameters are listed in Table 1.

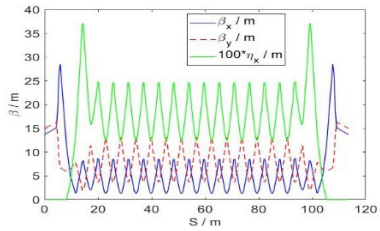

Figure 2: Optics of a super-period in the booster.

The HEPS booster is designed to support both single-bunch and multi-bunch operation. Bunches are injected and extracted one by one using a set of kickers operating at 50 Hz. Due to the pulse width limitation of the current kickers, the minimum achievable bunch spacing restricts the maximum number of stored bunches in the booster to five.

Full-energy bunches can either be injected directly into the storage ring or be merged with bunches reinjected from the storage ring using a "high-energy accumulation" injection scheme. To realize this scheme, the HEPS booster is operated as an accumulator ring at its extraction energy. By combining the charge replaced from the storage ring with the bunches accelerated to 6 GeV in the booster, the single-bunch charge is increased, meeting the requirements of the storage ring's high-charge mode. Consequently, in addition to a high-energy transport line for extracting the beam from the storage ring back to the booster, an off-axis injection system has also been installed in the booster to facilitate beam accumulation.

To accommodate both multi-bunch filling patterns and the high-energy accumulation injection scheme, the booster's energy ramping profile features extended flattops at the injection energy (500 MeV) and the extraction energy (6 GeV). A schematic diagram of the energy ramping cycle is shown in Fig. 3.

† pengym@ihep.ac.cn

Content from this work may be used under the terms of the CC BY 4.0 licence (© 2026). Any distribution of this work must maintain attribution to the author(s), title of the work, publisher, and DOI.

ISBN: 978-3-95450-252-3 ISSN: 2673-5350 doi: 10.18429/JACoW-IPAC2026-TUP2612

PRELIMINARY LATTICE DESIGN TO THE 1 PM-LEVEL EMITTANCE FOR THE SOUTHERN ADVANCED PHOTON SOURCE*

Y. Zhao† [1,2], W. H. Liu[1,2], W. L. Qin[1,2], J. L. Chen[1,2], Y. Jiao‡ [1]
[1]Institute of High Energy Physics, Chinese Academy of Sciences, Beijing, China
[2]Spallation Neutron Source Science Center, Dongguan, China

Abstract

The pursuit of diffraction-limited storage rings has driven emittance targets into the picometer regime. This paper presents a novel Single Hybrid Multi-Bend Achromat (SH-MBA) lattice design for the Southern Advanced Photon Source (SAPS), targeting an emittance at the 1 pm level. The compact SH-16BA design, operating at 3.5 GeV with 36 periods and a 945 m circumference, employs high-gradient quadrupoles, reverse bends, and longitudinal gradient bends. While collective effects such as intra-beam scattering allow the equilibrium emittance to reach the diffraction limit for hard X-rays, the most critical challenge lies in nonlinear dynamics optimization. The required sextupole strengths are extremely high, generating nonlinear driving terms three orders of magnitude larger than in typical 4th-generation sources and restricting the dynamic aperture to about 1 mm. This work demonstrates that achieving a reliable 1 pm-level design will require novel methods to suppress these severe nonlinearities.

INTRODUCTION

The pursuit of higher brightness and improved transverse coherence has long driven the evolution of synchrotron radiation sources. Fourth-generation storage rings, built on multi-bend achromat (MBA) lattices, have reduced natural emittance by two to three orders of magnitude and enhanced brightness by one to two orders of magnitude compared with third-generation facilities [1]. This advance has accelerated the global development of fourth-generation light sources. Among these, sources such as APS-U [2], HEPS [3], and NSLS-II-U [4] have achieved natural emittances in the range of several tens of pm·rad, effectively reaching the diffraction limit for soft X-rays. For hard X-rays at a wavelength of 0.1 nm, however, the diffraction-limited emittance of approximately 8 pm·rad remains unattained. Reducing the emittance to the 1 pm level would yield substantial brightness gains, with transverse coherence approaching unity for soft X-rays and improving significantly for hard X-rays, thereby enabling new classes of coherent scattering and imaging experiments.

Achieving such ultra-low emittance typically requires increasing the number of bending magnets and employing high-gradient quadrupoles for stronger focusing. Scaling studies based on existing designs, such as HEPS, indicate that pushing the emittance down to 3-5 pm·rad would necessitate a ring circumference exceeding 2500 m. Consequently, the central challenge in pm·rad-level lattice design is to realize 1 pm·rad emittance within a compact, practically feasible circumference.

This work builds on the conceptual design of the Southern Advanced Photon Source (SAPS) [5], a 3.5 GeV facility planned for Guangdong, China, adjacent to the China Spallation Neutron Source. Guided by the SAPS baseline parameters, we propose a novel lattice to allow more bends within a reasonable circumference. Finally, we developed a 16BA lattice with a natural emittance of 5.5 pm·rad and conducted a preliminary analysis of its nonlinear dynamics. This paper details the linear optics design, outlines the principal challenges encountered during nonlinear optimization, and discusses the limitations of current nonlinear correction methods in pm-level lattice design.

LINEAR LATTICE DESIGN

To achieve lower beam emittance within a limited storage ring circumference, increasing the number of dipoles or incorporating additional ultra-low emittance unit cells is essential. The hybrid multi-bend achromat(H-MBA) lattice widely adopted in modern light source design typically comprises two modified DBA cells and $M-4$ modified TME cells [6]. In this configuration, the modified TME cells are primarily responsible for emittance suppression, while the modified DBA cells generate a pair of high-dispersion bumps that reduce the required strength of sextupoles housed within them for chromaticity correction. However, taking the H-7BA lattice as an example, the modified DBA cells occupy approximately 60% of the longitudinal space in the arcs, yet their contribution to emittance reduction is significantly smaller than that of the modified TME cells. For a fixed arc length, minimizing the fraction of modified DBA cells and increasing the proportion of ultra-low emittance cells can effectively shorten the circumference required to reach pm-level emittance. To address this, we propose a novel lattice, as shown in Fig. 1. Using the H-7BA as a reference, removing one modified DBA cell allows three additional modified TME cells to be accommodated within the same period. Since this conceptual design features only a single dispersion bump per period, in contrast to the double dispersion bump arrangement of the conventional hybrid MBA, we term it the single dispersion bump hybrid MBA (SH-MBA). As a proof of concept, applying this configuration to the HEPS lattice reduces the emittance from 34 pm·rad to 15 pm·rad.

* Work supported by National Natural Science Foundation of China (No.12505165 and No.12275284)
† email address
‡ jiaoyi@ihep.ac.cn

Content from this work may be used under the terms of the CC BY 4.0 licence (© 2026). Any distribution of this work must maintain attribution to the author(s), title of the work, publisher, and DOI.

ISBN: 978-3-95450-252-3 ISSN: 2673-5350 doi: 10.18429/JACoW-IPAC2026-TUP2614

PERFORMANCE COMPARISON OF VARIABLE BENDING MAGNETS AND SANDWICH MAGNETS FOR THE SOUTHERN ADVANCED PHOTON SOURCE*

Y. Zhao† [1,2], W.H. Liu[1,2], W.L. Qin[1,2], J.L. Chen[1,2], Y. Jiao‡ [1]
[1]Institute of High Energy Physics, Chinese Academy of Sciences, Beijing, China
[2]Spallation Neutron Source Science Center, Dongguan, China

Abstract

The Southern Advanced Photon Source (SAPS) is a planned 3.5 GeV ultra-low emittance storage ring based on a modified hybrid 7-bend achromat (H-7BA) lattice, located in Dongguan, China. To achieve an extremely low natural emittance, the lattice incorporates a novel unit cell consisting of a 'Sandwich' bending magnet combined with reverse bends. This design has resulted in a remarkable natural emittance of 26.3 pm·rad. Although variable bending magnets with a trapezoidal bending radius and gradient are also recognized for their effectiveness in emittance reduction, their performance relative to the compact thin-center 'Sandwich' design remains unclear. This paper presents a comprehensive comparison of these two magnets, along with the performance differences of the SAPS lattice employing each of them, detailing the nonlinear optimization process and evaluating their respective performance.

INTRODUCTION

The storage ring emittance of the fourth-generation synchrotron light source approaches or even reaches the diffraction limit of X-rays. Compared with third-generation sources, the brightness is increased by one to two orders of magnitude. In addition, it intersects with cutting-edge fields such as quantum information, coherent imaging, and in-situ characterization, becoming a key facility driving multidisciplinary breakthroughs [1]. As the main part of the storage ring lattice, the unit cell is central to achieving ultra-low emittance in the storage ring. Over the past decades, researchers have devoted considerable efforts to exploring different unit cells, aiming to minimize the beam emittance under reasonable nonlinearities and cell lengths. Concretely, to reach the theoretical minimum emittance within a practical cell length, the positions of the two quadrupoles in the standard TME cell [2] were swapped [3]. Subsequently, the modified TME cell, which integrates the horizontally defocusing quadrupoles on both sides of the bending magnet into the dipole itself, was developed and widely used in multi-bend achromat lattices, further reducing the cell length [4].

However, although the modified TME cell compresses emittance over a short cell length, its emittance compression capability is inferior to that of the standard TME cell. Under reasonable nonlinearities, the lowest achievable emittance is about twice the TME limit. To further lower the emittance, a cell composed of a longitudinal gradient bend (LGB) and two reverse bends (RBs) has been proposed. This cell requires a longer length than the modified TME cell, but it can attain an emittance close to or even below the TME limit under reasonable nonlinearities [5, 6]. The LGB/RB cell was first proposed and applied in the storage ring design of SLS-2.0 [7], and has since been widely adopted in fourth-generation light source storage rings [8, 9]. Nevertheless, using too many LGB/RB cells drastically reduces the momentum compaction factor, potentially making it negative, which leads to short bunch lengths and a low instability threshold.

To address this issue, a "sandwich" magnet, termed the transverse-longitudinal gradient combined dipole (TLGB) in this paper, is proposed to replace the LGB magnet in the LGB/RB cell. This combination preserves the emittance compression capability while minimizing the reduction of the momentum compaction factor. Previous work [10] has shown that a thin-center TLGB/RB cell can achieve an emittance comparable to that of an LGB/RB cell with a shorter cell length and reasonable nonlinearities. The Southern Advanced Photon Source (SAPS) [11], a medium-energy (3.5 GeV) diffraction-limited storage ring light source planned for construction in Guangdong Province, China, adopts this thin-center TLGB/RB cell in its storage ring design and reaches an ultra-low emittance of approximately 26.3 pm·rad.

Recently, it has been noted that when the bending radius of the dipole field in a combined-function dipole follows a trapezoidal distribution, the beam emittance can also be effectively reduced. Such variable bending magnets (VB) were demonstrated in the CLIC DR [12, 13] and applied to the design of ELETTRA 2.0 [14]. However, the performance difference between the thin-center TLGB/RB cell and this VB/RB cell under the same bending angle remains unclear. Hence, in this paper we compare the performance of the two types of unit cells, as shown in Fig.1, and replace the thin-center TLGB/RB cell in the SAPS baseline lattice with a VB/RB cell to evaluate the performance differences.

UNIT CELL COMPARISON

To ensure a fair comparison between the two different unit cells, the optimization of their linear performance is carried out using a multi-objective particle swarm algorithm. The optimization objectives are the natural emittance and the sum

* Work supported by National Natural Science Foundation of China (No.12505165 and No.12275284)
† zhaoyu@ihep.ac.cn
‡ jiaoyi@ihep.ac.cn

Content from this work may be used under the terms of the CC BY 4.0 licence (© 2026). Any distribution of this work must maintain attribution to the author(s), title of the work, publisher, and DOI.

ISBN: 978-3-95450-252-3 ISSN: 2673-5350 doi: 10.18429/JACoW-IPAC2026-TUP2616

OPTIMIZATION OF THE RESPONSE MATRIX MEASUREMENT APPLICATION IN PYAPAS

Y. Zhao*, H. Ji, D. Ji, Y. Wei, H. Xu, Institute of High Energy Physics, Beijing, China

Abstract

Measurement of the response matrix serves as the foundation for orbit correction and optics correction. To obtain more accurate response matrix (RM) data while minimizing the measurement time in storage ring of High Energy Photon Source (HEPS), we have meticulously optimized parameters such as the number of data points collected by Beam Position Monitors (BPMs) and the waiting time. Additionally, due to the long overall measurement duration for the entire ring, factors including orbit drift and hysteresis effects during the process can introduce deviations to the measurement results. Therefore, we integrate RM measurement with orbit correction and radio frequency (RF) adjustment to further ensure the consistency of the beam state throughout the entire measurement process. This paper will elaborate on the relevant work in detail.

INTRODUCTION

HEPS is a fourth-generation synchrotron radiation light source [1]. It comprises a 500 MeV S-band linac, a 454 m full-energy booster synchrotron, a 1.36 km storage ring, and three beam transport lines. Designed as a high-energy DLSR operating at 6 GeV, HEPS utilizes a modified hybrid seven-bend achromat (7BA) lattice to achieve an ultra-low natural emittance of approximately 35 pm·rad. With rigorous on-site testing on October 29, 2025, it is confirmed that all Key Performance Parameters were (KPPs) met or exceeded specifications, validating the robustness of the accelerator design and the precision of its engineering. HEPS is currently in the trial operation phase.

Pyapas (Python-based Accelerator Physics Application Set) is a pure Python framework developed at IHEP for accelerator online commissioning and simulation [2]. The program architecture is shown in Fig. 1. It adopts a modular and model-based design, built on physical quantities rather than raw device values. Pyapas provides integrated GUI tools for orbit correction, response matrix measurement, optics analysis, and machine parameter control. It has been successfully deployed at HEPS and extended to other accelerator projects.

The response matrix serves as the fundamental basis for orbit correction, optics correction, and orbit feedback. Accordingly, we developed an upper-level application based on Pyapas, which integrates functions of response matrix measurement and orbit correction. This application has been successfully implemented in the beam commissioning of the Linac [3] and booster [4] of HEPS. As a diffraction-limited storage ring (DLSR), the HEPS storage ring comprises 575 beam-position monitors (BPMs) and 1152 corrector magnets, leading to considerable time consumption for full-ring response matrix measurement. Slow orbit drifts during measurement are non-negligible. In addition, closed-orbit distortions accumulate throughout the measurement due to hysteresis effects and other factors, degrading the measurement precision of the response matrix. In preliminary work, we systematically optimized measurement parameters, including program logic, data acquisition counts per BPM, and hardware settling waiting time, aiming to minimize measurement duration while ensuring measurement validity. Under the current network environment of HEPS, the full-ring response matrix measurement takes 3–4.5 hours. To further improve measurement precision, we incorporated orbit correction and RF frequency correction into the response matrix measurement procedure.

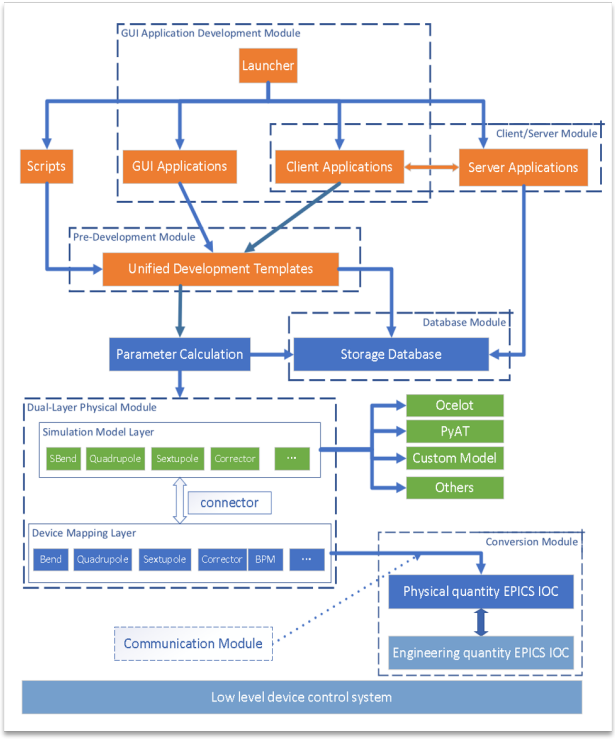

Figure 1: Architecture of Pyapas.

EXTENSION OF RESPONSE MATRIX MEASUREMENT PROCEDURE

Response matrix measurement in a large storage ring requires sequentially exciting individual correctors and reading BPM responses. For HEPS, the full-ring measurement involves a large number of correctors and BPMs, leading to long measurement durations. During this process, slow orbit drift, power supply hysteresis, and RF frequency variations

* zhaoyl@ihep.ac.cn

Content from this work may be used under the terms of the CC BY 4.0 licence (© 2026). Any distribution of this work must maintain attribution to the author(s), title of the work, publisher, and DOI.

ISBN: 978-3-95450-252-3 ISSN: 2673-5350 doi: 10.18429/JACoW-IPAC2026-TUP2617

STUDY OF GAS SCATTERING–INDUCED BEAM LOSSES AND COLLIMATION FOR THE SOLEIL II STORAGE RING

Y. Huang*[1,2], Z. Bai[1], B. Wei[1], P. Brunelle†[2], L. S. Nadolski‡[2]
[1]National Synchrotron Radiation Laboratory, USTC, Hefei, China
[2]Synchrotron SOLEIL, L'Orme des Merisiers, Saint-Aubin, France

Abstract

The SOLEIL II storage ring will be equipped with many in-vacuum undulators (IVUs) and superbends, which are vulnerable to gas scattering–induced beam losses due to their small vertical gaps. In this paper, gas scattering–induced beam losses in SOLEIL II are studied with tracking simulations. The results show that, without vertical scrapers, 53% of elastic scattering–induced losses happen at IVUs with 4 mm vertical gaps, posing a risk of damage to their magnets over 15 years of operation. Detailed tracking finds that most of these losses originate from scattering events in short range, e.g., within half a turn. This suggests that one vertical scraper located upstream of each IVU group could provide optimal collimation, protecting the IVUs while maintaining the beam lifetime. However, this scheme is not allowed due to space constraints. A second optimal vertical collimation scheme is proposed with 2 scrapers, which reduces the beam losses at IVUs by 40% while maintaining an elastic scattering lifetime of 40 hours. In contrast to elastic scattering, inelastic scattering leads to only minor beam losses and remains acceptable.

INTRODUCTION

The SOLEIL II project aims to upgrade the French 3rd-generation synchrotron light source to a 4th-generation machine [1, 2]. Operating at an energy of 2.75 GeV with a maximum beam current of 500 mA, the upgraded storage ring lattice is designed to be highly compact and achieve an ultra-low natural horizontal of 85 pm·rad [3]. The SOLEIL II storage ring will utilize numerous insertion devices, predominantly in-vacuum undulators (IVUs), and superbends. These IVUs have very small gaps, with a minimum vertical physical aperture of ±2 mm [4]. Consequently, electrons undergoing scattering with residual gas molecules have large betatron oscillation amplitudes and are eventually lost on the walls of vacuum chamber and IVUs [5]. The steady flux of the scattered electrons striking the narrow IVU gaps, mostly from elastic gas scattering, poses a serious risk, as the cumulative radiation damage can lead to the demagnetization of IVU magnets over the expected 15-year operation of the machine. To protect the IVUs, the spatial distributions of the losses of scattered electrons are evaluated and an optimized collimation scheme is designed, which is critical to the safe and continuous operation of the SOLEIL II storage ring.

* pb188560@mail.ustc.edu.cn
† pascale.brunelle@synchrotron-soleil.fr
‡ laurent.nadolski@synchrotron-soleil.fr

BEAM LOSSES WITHOUT COLLIMATION

To study the detailed distribution of lost electrons, tracking simulations were carried out using the code ELEGANT [6]. For elastic gas scattering, particles were tracked for 1026 turns with a grid of 24 in polar and 19 in azimuthal. The local dynamic acceptance in angle was set in the range of 0.0001 ~ 0.005 rad. Initial tracking was performed for the SOLEIL II storage ring lattice V3631 [2] with physical apertures and systematic multipole errors, but without other errors or vertical scrapers. An equivalent two-step gas pressure profile of N_2 was assumed to be 10^{-10} mbar in straight sections and 10^{-9} mbar in arc sections. The linear optics, vertical physical apertures, and distribution of electron loss rate from elastic gas scattering are shown in Fig. 1. The calculated lifetime for elastic gas scattering is 62.7 hours. As for inelastic (bremsstrahlung) gas scattering, simulation yields a lifetime of 123.4 hours. Since inelastic gas scattering induced beam losses are not significant and do not distribute on the vertical surfaces of IVUs in the uncoupled lattice, the remainder of this paper focuses only on elastic gas scattering.

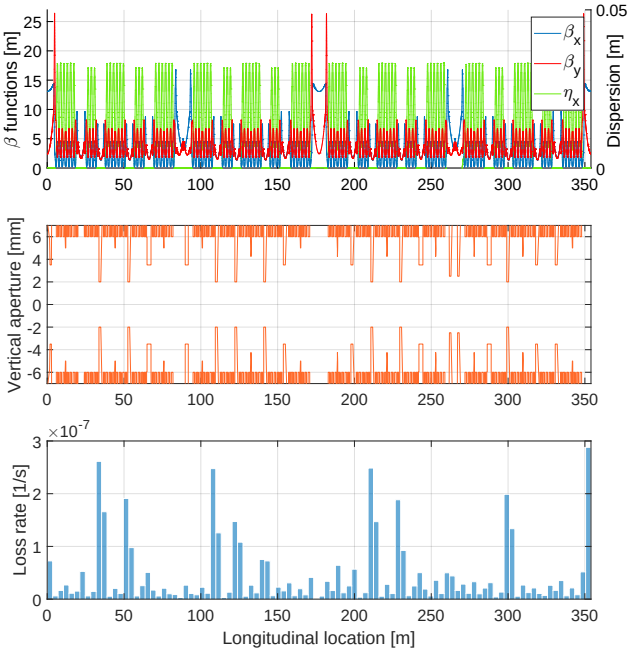

Figure 1: Linear optics (top), vertical physical apertures (middle), and distribution of electron loss rate from elastic gas scattering (bottom) of the SOLEIL II storage ring.

It is seen in Fig. 1 that most of the beam losses due to gas scattering are distributed in the positions with small vertical apertures, corresponding to the narrow gaps of IVUs. Specif-

Content from this work may be used under the terms of the CC BY 4.0 licence (© 2026). Any distribution of this work must maintain attribution to the author(s), title of the work, publisher, and DOI.

ISBN: 978-3-95450-252-3 ISSN: 2673-5350 doi: 10.18429/JACoW-IPAC2026-TUP2618

COUPLED-BUNCH INSTABILITY STUDY FOR UTEF STORAGE RING

Y. L. Chen[1], S. W. Wang*[1], Y. Zhang[1] J. C. Xiao[2], B. C. Jiang[1],
[1]Chongqing University, Chongqing, China
[2]University of Science and Technology of China, Hefei, Anhui, China

Abstract

The Ultra-fast Transient Experimental Facility (UTEF) at Chongqing University is currently constructing a 500 MeV storage ring. This paper investigates the transverse coupled-bunch instabilities (TCBI) critical to its high-current operation. Building on a method previously developed at Diamond Light Source—which enables the calculation of all coupled-bunch instability modes within a single simulation—this work extends the approach to non-zero chromaticity cases using a multi-particle-per-bunch model. Results for the UTEF ring demonstrate that non-zero chromaticity and synchrotron radiation damping have a negligible impact on the grow-damp curve. On the other hand, the inclusion of short-range impedance brings an obvious shift of the grow-damp curve. This paper provides a detailed account of the simulation and results.

INTRODUCTION

The Ultra-fast Transient Experimental Facility (UTEF) at Chongqing University is constructing a 500 MeV synchrotron light source designed for advanced material analysis, targeting a high beam current of 1000 mA [1]. Achieving this design current presents challenges due to collective effects, particularly the transverse coupled-bunch instability (TCBI) driven by long-range wakefields. The storage ring features a compact four-fold DDBA lattice (Table 1 and Fig. 1). In this paper, we investigate the TCBI for the UTEF ring using a method originally developed at Diamond Light Source [2] to evaluate the grow-damp rates of all coupled-bunch modes across various scenarios.

Table 1: Main Parameters of the UTEF Storage Ring

Parameters	
Circumference	76.78 m
Emittance	4.74 nm
Momentum compaction factor	3.144×10^{-3}
Harmonic number	128
Energy spread	3.8×10^{-4}
Tune	7.161/3.178
Synchrotron tune	0.00716
Natural chromaticity	-13.42/-17.30
Corrected chromaticity	0.0/0.0
Damping time $\tau_x/\tau_y/\tau_s$	58.2/59.0/29.7 ms
Natural bunch length w/o HC	2.0 mm
Natural bunch length with HC	10.7 mm

* wsw290@cqu.edu.cn

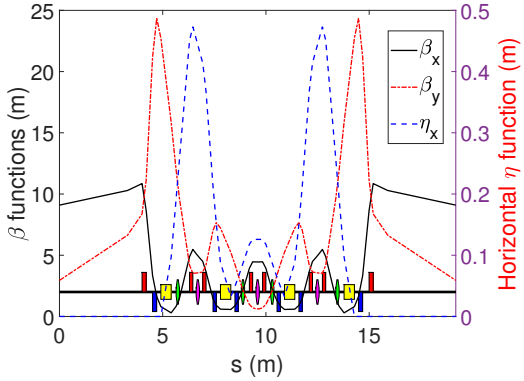

Figure 1: Optics and lattice layout of the UTEF storage ring.

COUPLED-BUNCH INSTABILITY MODES

The transverse coupled-bunch motion of the bunch centroids in a uniformly filled beam is characterised by coupled-bunch modes. The analytical complex frequency shift is given by [3]:

$$\Delta\Omega_\mu = \frac{ecI_0}{4\pi E_0 \nu_\beta} \sum_p Z_\perp(\omega_p) \exp\left(-\left(\omega_p + \frac{\xi\omega_0}{\alpha_c}\right)^2 \sigma_t^2\right), \quad (1)$$

where c is the speed of light, I_0 is the total beam current, and E_0/e denotes the beam energy in eV. $Z_\perp$ represents the lumped impedance following the `ELEGANT` convention [4]. For one-turn map tracking, ν_β is evaluated as $\nu_\beta = C/(2\pi\bar{\beta})$, where $\bar{\beta}$ is integrated into the impedance via normalisation by the local beta function. The exponential term accounts for the effect of chromaticity, where ξ is the chromaticity, ω_0 is the angular revolution frequency, and α_c is the momentum compaction factor. The impedance is sampled at the following frequencies:

$$\omega_p = (\mu + Mp + \nu_\beta)\omega_0, \quad (2)$$

where μ is the mode index ($0 \le \mu \le M-1$) and ν_β is the betatron tune. The summation is performed over the integer index p to obtain the total contribution to mode μ. The real and imaginary parts of the complex frequency shift yield the tune shift and the growth rate of the mode, respectively.

COUPLED-BUNCH INSTABILITY FROM RESISTIVE-WALL WAKE

The transverse resistive-wall (RW) long-range wake for the UTEF storage ring is generated for each element using `IW2D` [5]. A lumped wake element is then calculated by summing the wakes, normalised by the local beta functions:

$$W_{\perp,x,y}(t) = \frac{1}{\beta_{0x,y}} \sum_i \beta_{x,y,i} W_{i,\perp}(t), \quad (3)$$

Content from this work may be used under the terms of the CC BY 4.0 licence (© 2026). Any distribution of this work must maintain attribution to the author(s), title of the work, publisher, and DOI.

ISBN: 978-3-95450-252-3 ISSN: 2673-5350 doi: 10.18429/JACoW-IPAC2026-TUP2620

DESIGN AND MAGNETIC MEASUREMENT RESULTS OF THE HALF STORAGE RING MAGNETS*

T. H. Sun, H.-L. Xu†, B. Liu, G. Feng
University of Science and Technology of China, Hefei, China

Abstract

The Hefei Advanced Light Facility (HALF) is a fourth generation synchrotron light source under construction, centered on a 2.2 GeV diffraction limited storage ring (DLSR) with a design natural emittance below 86 pm·rad. The storage ring has a circumference of nearly 480 m and contains 880 magnets in 20 lattice cells, including longitudinal gradient bends (LGB), reverse bends (RB), quadrupoles (Q), sextupoles (S), octupoles (O), and all corrector magnets (CR). As of early 2026, all magnet types except the octupoles had completed series production and factory magnetic measurements. This paper presents the physical design methodology and key magnetic measurement results of the HALF storage ring magnets, and also outlines ongoing studies on Preisach hysteresis modeling and on magnetic crosstalk in selected compact magnet assemblies through three dimensional simulations and stretched wire measurements.

INTRODUCTION

HALF adopts a compact hybrid multi-bend achromat lattice to achieve ultralow emittance within a limited ring circumference [1], as shown in Fig. 1. Under this constraint, the storage ring magnets are densely packed, leading to short magnetic lengths for the multipole magnets. Meanwhile, to provide a relatively large good field region (13 mm) while maintaining high field quality (<0.05%), relatively large apertures are required [2]. The combination of short magnetic lengths and large apertures results in small aspect ratios, which enhance fringe field effects and make magnetic crosstalk between adjacent magnets non-negligible. These constraints increase the difficulty of magnet design and fabrication.

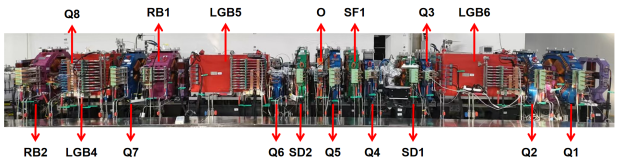

Figure 1: The lower half-cell of the HALF storage ring mockup, showing the compact arrangement of the main magnets. Corrector magnets are omitted for clarity.

To address these challenges, we established a magnet optimization workflow based on Gauss Newton algorithm (GNA) and Non-dominated Sorting Genetic Algorithm II (NSGA-II) and completed the physical design of the HALF storage ring multipole magnets [2]. Within the good field region, the designed multipole components of all magnets are better than 0.01%. Magnetic measurements obtained so far show that all magnets satisfy the physics requirements over their specified field or gradient tuning ranges.

The closed orbit of the storage ring is jointly provided by the longitudinal gradient bends and the reverse bends. By longitudinally redistributing the bending field, longitudinal gradient bends can suppress quantum excitation and reduce the beam equilibrium emittance. To accommodate a future energy upgrade of HALF to 2.5 GeV, an electromagnetic variable-gap concept was adopted for these magnets, offering more accurate and reproducible field tuning over a wide operating range than permanent magnets commonly used in fourth generation light sources [3]. Based on a design code based on the actual beam trajectory, all 123 longitudinal gradient bends in the storage ring, including three prototypes, have been fabricated and measured. The results confirm that the field homogeneity, trajectory control, and series consistency satisfy the design requirements.

The latter part of this paper also briefly discusses ongoing studies, including further investigations of magnetic crosstalk and hysteresis effects in magnets.

DESIGN AND MEASUREMENT RESULTS FOR HALF MAGNETS

Multipole Magnets

We developed a magnet optimization workflow based on the GNA and NSGA-II, as shown in Fig. 2. The workflow was implemented in MATLAB and coupled with OPERA for field evaluation during the optimization process [4,5]. GNA was used for magnets with relatively simple optimization objectives, whereas NSGA-II was introduced for cases requiring more stringent field quality optimization. To remain consistent with rotation coil measurements, the objective function was defined directly from the weighted multipole components normalized to the main field. For a quadrupole magnet, the objective function for pole shape optimization can be written as

$$F_Q = \sum_{m=1}^{4} W_m \, b_{2(2m+1)}^2, \qquad m = 1, 2, 3, 4.$$

In the geometric model, the initial pole shape was placed symmetrically on the positive semiaxis of the Y axis in a Cartesian coordinate system, and the profile perturbation was parameterized using a Legendre series. This parameterization helps preserve contour smoothness and suppress field quality degradation caused by local saturation. The

* This Work is supported by the National Nature Science Foundation of China under Grant No. 12075239.
† hlxu@ustc.edu.cn

Content from this work may be used under the terms of the CC BY 4.0 licence (© 2026). Any distribution of this work must maintain attribution to the author(s), title of the work, publisher, and DOI.

ISBN: 978-3-95450-252-3 ISSN: 2673-5350 doi: 10.18429/JACoW-IPAC2026-TUP2623

A MODULAR OPTIMIZATION FRAMEWORK FOR 4TH GENERATION LIGHT SOURCE LATTICE DESIGN: SYNERGIZING PHYSICS PRIORS AND STATISTICAL LEARNING

L. L. Mao*, Shanghai Institute of Applied Physics, CAS, Shanghai, China
S. Q. Tian, X. Z. Liu, L. Y. Tan, Shanghai Advanced Research Institute, CAS, Shanghai, China
Y. H. Gong, Shanghai Synchrotron Radiation Facility, Shanghai, China

Abstract

The design of fourth-generation synchrotron light sources based on Hybrid Multi-Bend Achromat (H-MBA) structures faces significant challenges due to the high dimensionality of design variables and the strong nonlinear effects induced by strong focusing forces. The traditional paradigm of "manual matching followed by stepwise fine-tuning" encounters bottlenecks in optimization efficiency and physical interpretability. This paper proposes a modular optimization framework that fuses physics priors with statistical learning to achieve synergistic optimization of linear optics and nonlinear dynamics. The framework uses Twiss parameter evolution as an intermediate physical representation, and a physics-prior screening mechanism driven by linear transport is combined with the Covariance Matrix Adaptation Evolution Strategy (CMA-ES). This approach identifies stable periodic solutions with reduced natural emittance within minutes and shows reproducible efficiency gains over manual initializations. Machine-learning classifiers trained on the generated dataset perform high-confidence pruning of the solution space and retain high-quality solutions. A local trust region constructed around these "promising solutions" introduces the Sequential Model-based Algorithm Configuration (SMAC) strategy based on Random Forests for refined iteration. This method provides an efficient and intelligent pathway for complex, high-dimensional lattice design.

INTRODUCTION

Fourth-generation synchrotron light sources based on hybrid multi-bend achromat (H-MBA) lattices require joint control of low natural emittance, periodic linear optics, chromatic correction, dynamic aperture (DA), and energy acceptance (EA) [1]. The lattice considered in this paper is a 3.5 GeV ring with a circumference of 406.6 m. Strong focusing and compact dispersion bumps in an H7BA cell produce a constrained search space. Nonlinear tracking can reject a candidate with excellent linear emittance.

The present work treats lattice design as a staged physics-and-data workflow rather than as a single black-box minimization. Twiss parameter evolution through the cell is used as an intermediate physical representation. The optimizer searches for periodic and interpretable linear optics and passes selected candidates to statistical screening, local acquisition, and final DA/EA validation [2].

* maolinglong@sinap.ac.cn

MODULAR OPTIMIZATION METHOD

Physics-prior CMA-ES

The physics-prior module uses linear transport and Twiss evolution to reject candidates that do not return to the desired cell boundary. The boundary conditions include $\beta_x \simeq 5$ m, $\beta_y \simeq 3$ m, $\alpha_{x,y} \simeq 0$, and dispersion close to zero. These quantities give the search a direct optical meaning prior to expensive nonlinear calculations.

CMA-ES acts on the physics-filtered magnet-strength variables, namely the K-value vector used by the lattice model [3]. Parallel runs on 24 cores identify stable low-emittance periodic optics within minutes. Figure 1 shows the adaptation of the sampled search distribution.

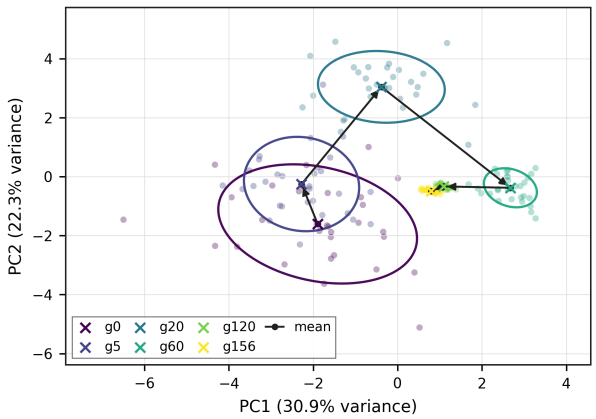

Figure 1: CMA-ES Gaussian search distributions projected onto the first two principal components. The coloured contours show 1.5σ covariance envelopes for selected generations, and the black curve follows the sampled mean path.

RF Pruning and SMAC-style Acquisition

The generated candidate pool is converted into a labelled data set for Random-Forest (RF) screening [4], as summarized in Fig. 2. The aggregated data set contains 11928 unique lattice-candidate rows from 35 computation batches, covering CMA-ES branches, trust-region DA scans, GPU-SMAC trials, and ML trust-region proposals. Labels are assigned from the corresponding optics checks, EA scans, quality criteria, and DA tracking outputs.

Four RF classifiers were trained for physics evaluability, EA acceptance, high-quality retention, and DA-promising identification. Figure 3 summarizes their ROC-AUC values. The physics, EA, and high-quality classifiers provide robust

Content from this work may be used under the terms of the CC BY 4.0 licence (© 2026). Any distribution of this work must maintain attribution to the author(s), title of the work, publisher, and DOI.

ISBN: 978-3-95450-252-3 ISSN: 2673-5350 doi: 10.18429/JACoW-IPAC2026-TUP2626

DYNAMIC APERTURE PREDICTION BASED ON MACHINE LEARNING

J. Xu*, J. Xia, University of Science and Technology of China, Hefei, China

Content from this work may be used under the terms of the CC BY 4.0 licence (© 2026). Any distribution of this work must maintain attribution to the author(s), title of the work, publisher, and DOI.

Abstract

The dynamic aperture (DA) is one of the most important parameters of nonlinear beam dynamics in storage rings. It describes the transverse phase space region where the motion of a particle can remain stable. In the design and optimization of storage rings, long-term particle tracking is usually required to ensure an sufficient DA. However this process is very time consuming. This study explores the possibility of using machine learning methods for DA prediction. Firstly, several regression models from magnet strengths to resonance driving terms are constructed using different machine learning methods, showing that the use of machine learning can be applied to the nonlinear performance analysis of storage ring lattice. Then predictive regression models from magnet strength to DA are constructed, and the results show that artificial neural network have better prediction accuracy. The method will be further developed for nonlinear analysis and optimization of storage ring.

INTRODUCTION

The Hefei Advanced Light Facility (HALF) is a diffraction-limited storage ring designed to deliver high-brightness synchrotron radiation [1]. Its ultra-low emittance is achieved through a hybrid multi-bend achromat lattice, which inherently introduces strong nonlinearities. The dynamic aperture (DA), a key metric of lattice nonlinear performance, must be sufficiently large to ensure stable beam injection and long beam lifetime. Conventionally, DA evaluation requires extensive particle tracking, which is computationally expensive and limits the scope of lattice optimization.

Machine learning (ML) has emerged as a powerful tool in accelerator physics, with applications in beam diagnostics, control, and lattice design. In this work, we propose an ML-based surrogate model to directly predict resonance driving terms and DA from magnet strengths, bypassing the need for time-consuming analytical calculations or particle tracking. We generate a large dataset of HALF lattice solutions using a localization method combined with multi-objective optimization, then train several regression models to map magnet settings to key nonlinear performance indicators. The results demonstrate that ML can effectively capture the complex relationship between lattice parameters and nonlinear behavior, providing a fast and reliable evaluation tool for lattice design and optimization.

DATASET GENERATION AND FEATURE ANALYSIS

The HALF storage ring lattice consists of 11 variable magnets: 8 quadrupoles and 3 sextupoles. To generate a diverse and representative dataset, we employed a localization method based on NSGA-II, which iteratively optimizes the upper and lower bounds of the variables to cover the feasible solution space. Constraints included:

- Natural emittance $\varepsilon_{\mathrm{nat}}$ <90 pm · rad,
- Tune fractional parts in $[0.1, 0.4]$,
- Dispersion at straight sections $|\eta|$ <0.002 m,
- Corrected chromaticity in $[2, 6]$.

A total of 90,000 feasible lattice solutions were obtained. For each solution, we recorded the 11 magnet strengths (features), and computed resonance driving terms: second- and third-order chromaticities ($\partial\nu_{x,y}/\partial\delta^2$, $\partial\nu_{x,y}/\partial\delta^3$) and amplitude-dependent tune shifts (ADTS), as well as the DA area via particle tracking using. To reduce redundant data for DA tracking, DBSCAN clustering was applied to the feature space, yielding 3,081 representative lattice configurations. Tracking these configurations took approximately one week on a personal computer.

A Spearman correlation analysis reveals several insights into the HALF lattice shown in Fig. 1. Strong negative correlation ($\rho < -0.8$) is observed between Q4 and Q5 in the high-dispersion region, consistent with their opposing roles in dispersion control. Horizontal second-order chromaticity shows strong negative correlation with dispersion at straight sections and with optical functions at sextupole SD2, suggesting that controlling these parameters is beneficial for managing chromatic aberrations. The three ADTS terms exhibit weak linear correlation with individual magnet strengths, reflecting the complexity of their underlying formulas. These correlation patterns provide valuable guidance for linear lattice design and inform the feature selection for ML models.

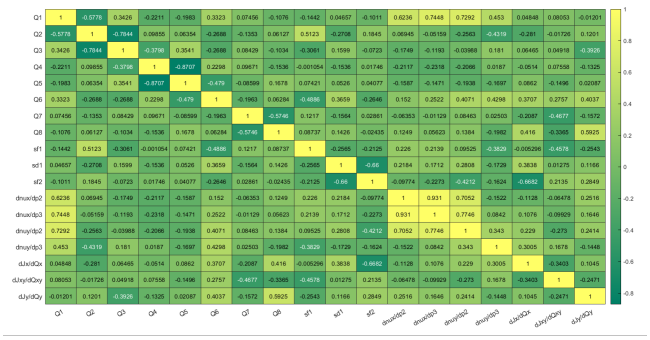

Figure 1: Correlations between single variables.

MACHINE LEARNING METHODS

Problem Formulation and Model Selecting

We formulate two distinct prediction tasks:

Task 1: Prediction of Resonance Driving Terms Predict seven nonlinear parameters (second- and third-order chromaticities, three ADTS terms) from 11 magnet strengths. This represents a multi-output regression problem where the

* xujianhao@ustc.edu.cn

ISBN: 978-3-95450-252-3 ISSN: 2673-5350 doi: 10.18429/JACoW-IPAC2026-TUP2627

OPTIMIZATION AND UPDATE OF THE HALF STORAGE RING PHYSICS DESIGN

Z. H. Bai*, G. Y. Feng, T. L. He, W. W Li, G. W. Liu, X. Y. Liu, J. Y. Tang,
B. F. Wei, J. H. Xu, P. H. Yang
National Synchrotron Radiation Laboratory, USTC, Hefei, China

Abstract

The Hefei Advanced Light Facility (HALF), a soft X-ray diffraction-limited storage ring light source at NSRL, began construction in 2023. This paper presents the optimization and update of the physics design for the HALF storage ring in the past two years.

INTRODUCTION

The Hefei Advanced Light Facility (HALF), shown in Fig. 1, is a soft X-ray diffraction-limited storage ring light source currently under construction in Hefei, China, with construction started in 2023 and scheduled for completion in 2028. The HALF storage ring, with a full-energy linac as its injector, consists of 20 identical cells, which employ a modified hybrid six-bend achromat (H6BA) lattice with both long and short straight sections [1, 2]. The natural emittance of the HALF storage ring is 85 pm·rad at an energy of 2.2 GeV, with the capability to be increased to 2.5 GeV. HALF will have approximately 35 beamlines in total, the vast majority of which are insertion device (ID) beamlines, and 10 ID beamlines will be constructed in the present Phase I. HALF has now entered the equipment installation phase. In the past two years, some optimizations and updates have been made to the physics design of the HALF storage ring, which will be presented in this paper.



Figure 1: Hefei Advanced Light Facility (HALF) currently under construction in Hefei, China.

LATTICE AND ERROR EFFECTS

All magnets of the HALF storage ring are electromagnets, with energy increase taken into account. For the combined-function reverse bends, before their installation, we slightly adjusted their quadrupole fields while keeping their dipole fields unchanged, which reduced the magnetic field saturation of one RB family and also helped increase the dynamic aperture (DA). Considering the adjustment of the RBs, through linear and nonlinear lattice optimization [3], the DA with RF cavity included was increased, and the amplitude-dependent tune shifts (ADTSs) were better controlled for beam injection in the full-coupling beam mode. This resulted in a new version (Version 2025) of the HALF storage ring lattice, shown in Fig. 2. Table 1 presents the main storage ring parameters, including the parameters with two damping wigglers (DWs), for both the 2.2 GeV and 2.5 GeV energies. To provide a safety margin for off-axis injection, we also designed an alternative lattice solution with a larger DA by moving the integer parts of betatron tunes from (48, 17) to (47, 18) [3].

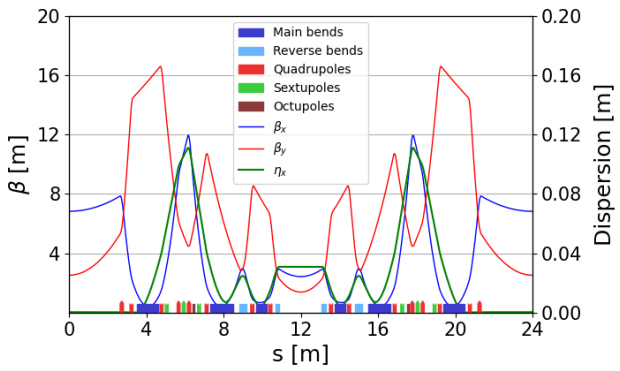

Figure 2: Modified H6BA lattice (Version 2025) of one cell of the HALF storage ring.

Table 1: Main Parameters of the HALF Storage Ring

Parameter	**2.2 GeV**	**2.5 GeV**
Circumference	479.86 m	
Straight sections	20 × 5.3 m + 20 × 2.2 m	
Natural emittance	85.4 pm·rad	110.3 pm·rad
Natural emittance w/DWs	71.9 pm·rad	92.8 pm·rad
Betatron tunes	48.21/17.21	
Natural chromaticities	-82.5/-59.6	
Momentum compaction	0.94×10^{-4}	
Natural damping times	28/39/24 ms	19/26/16 ms
Damping times w/DWs	22/27/16 ms	16/20/12 ms

For this new lattice version, with error effects considered, the DA with RF cavity included, as shown in the left plot of Fig. 3, is about 7 mm in the positive horizontal direction, from which the beam is injected. The 6D local momentum aperture (LMA) with error effects is shown in the right plot of Fig. 3. With a beam current of 400 mA and the bunch

* baizhe@ustc.edu.cn

Content from this work may be used under the terms of the CC BY 4.0 licence (© 2026). Any distribution of this work must maintain attribution to the author(s), title of the work, publisher, and DOI.

ISBN: 978-3-95450-252-3 ISSN: 2673-5350 doi: 10.18429/JACoW-IPAC2026-TUP2629

GENERATION AND DIAGNOSTICS OF NANOSECOND-INTERVAL LASER PULSE TRAINS WITH FEMTOSECOND-LEVEL TIMING CONTROL FOR THE KOREA-4GSR PHOTOCATHODE RF GUN

N. Go†, W. J. Byeon, S.-H. Kwon, Ch.-Ki Min
Pohang Accelerator Laboratory, Pohang, South Korea

Abstract

The Korea-4GSR (4th Generation Storage Ring) requires a highly stable and precisely synchronized laser pulse train to drive its photocathode RF gun in multi-bunch mode. To meet this requirement, we developed a laser system capable of generating nanosecond-interval pulse trains with femtosecond-level timing control. The pulse train is formed using a beam-split/delay-and-combine method, producing a 64-pulse sequence with 2 ns separation, synchronized to a 500 MHz RF reference. To further enhance synchronization accuracy and diagnose timing jitter at the femtosecond scale, a 500 MHz femtosecond oscillator is being developed and integrated into the system. This fs-oscillator enables precise timing diagnostics, long-term drift monitoring, and improved stability for multi-bunch operation. The combined system is designed to provide low-emittance, low-energy-spread electron bunches required for Korea-4GSR's high-brightness injector and ensures reliable operation in both single-shot and multi-bunch modes.

Introduction

The Korea-4GSR injector is designed to generate high-brightness electron beams for stable multi-bunch operation. The injector consists of a photocathode RF gun and a linear accelerator system, where precise control of the initial beam conditions is critical for achieving low emittance and low energy spread. As shown in Fig. 1, the overall injector system includes the RF gun, accelerating structures, and beam transport line. In such a system, the performance of the electron beam is strongly influenced by the laser-driven photocathode, requiring a highly stable and precisely synchronized laser pulse train.



Figure 1: Korea-4GSR injector system including the photocathode RF gun, accelerating structure, and beamline components.

Laser System

A laser system has been developed to generate a multi-pulse train suitable for driving the Korea-4GSR photocathode RF gun in multi-bunch mode. The system is designed to produce a sequence of 64 laser pulses with a temporal separation of 2 ns, corresponding to a repetition rate of 500 MHz, synchronized to the RF reference signal. As shown in Fig. 2, the pulse train is generated using a beam splitting, delay, and recombination scheme, in which a single input pulse is divided into multiple paths with carefully controlled optical delays. These delayed pulses are then recombined to form a temporally structured pulse train. The entire system is designed to maintain high temporal precision and stability while ensuring uniform beam characteristics across all pulses. This configuration enables flexible generation of multi-bunch laser patterns while maintaining compatibility with the RF synchronization requirements.

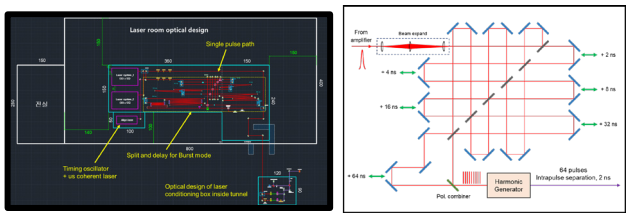

Figure 2: 4GSR laser room optical design and Split and delay for burst mode schematic.

Timing Synchronization Diagnostic Setup

This diagnostic system (Fig.3) is designed to synchronize the pulse spacing with a reference frequency (~500 MHz). The multi-pulse laser train is cross-correlated with quasi-CW pulses from a timing reference laser oscillator synchronized to the RF reference. By scanning the relative time delay on the reference oscillator side, the cross-correlation signals of individual pulses within the 64-pulse train can be resolved. This enables direct measurement of the relative timing offsets among the pulses. With sufficient signal averaging, the pulse train can be temporally aligned with an accuracy better than 200 fs.

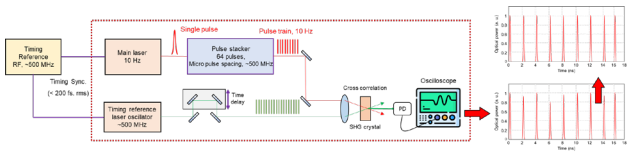

Figure 3: Timing synchronization diagnostic setup, The pulse train with a repetition rate of 500 MHz, corresponding to a pulse spacing of 2 ns.

500 MHz Femtosecond Laser Oscillator

As shown in Fig. 4, the pump source is a single-mode, fiber-coupled, linearly polarized laser diode delivering 1000 mW at 980 nm. The laser cavity has a Z-shaped configuration with a length of 30 cm to achieve a repetition rate of 500 MHz, and the pulse duration is expected to be

Content from this work may be used under the terms of the CC BY 4.0 licence (© 2026). Any distribution of this work must maintain attribution to the author(s), title of the work, publisher, and DOI.

ISBN: 978-3-95450-252-3 ISSN: 2673-5350 doi: 10.18429/JACoW-IPAC2026-TUP2630

UPDATED ORBIT STABILITY EVALUATION FOR THE KOREA-4GSR INCOPORATING NEW MECHANICAL AND BEAM DISTURBANCE MEASUREMENTS

Gyeongsu Jang[1, †], Hyunchang Jin[2], Jaehyun Kim[1], Jaeyu Lee[1], Jimin Seok[1], Junha Kim[1]
[1]Pohang Accelerator Laboratory, Pohang, Republic of Korea
[2]Korea Basic Science Institute, Cheongju, Republic of Korea

Abstract

Beam orbit stability is a critical requirement for fourth-generation synchrotron radiation facilities. An initial evaluation for the Korea-4GSR quantified expected orbit disturbances from ground vibration, magnet current ripple, and energy oscillations. Since that baseline study, additional measurements and refined models have enabled a more accurate assessment. Newly acquired ground-motion data provide updated vibration spectra affecting magnet and girder motion. Orbit fluctuations induced by the EPU and the canted-ID configuration have been characterized and incorporated into the analysis. Vacuum-chamber vibration, previously unaccounted for, has also been measured to assess mechanical coupling to the beam. Using these updated disturbance sources, revised orbit-stability predictions have been obtained through beam-dynamics simulations. The study identifies the dominant contributors under current design conditions and discusses implications for orbit-feedback performance and mechanical design optimization.

INTRODUCTION

Beam orbit stability is a critical requirement for fourth-generation storage rings (4GSRs). The defining feature of these 4GSRs is a low emittance achieved through advanced multi-bend achromat (MBA) lattice designs. While this drastically increases photon brightness, it also makes the beam exceptionally sensitive to minuscule mechanical and electromagnetic perturbations. Even sub-micron displacements can degrade the effective emittance, causing beam spot movement and intensity fluctuations at user beamlines. Therefore, maintaining orbit stability for the requirement of the beamline user is imperative.

To address these stabilization challenges, global research regularly characterizes and mitigates dominant perturbation sources [1-5]. These typically include ground vibrations [1-3], power supply current ripples [2-3], and RF-driven longitudinal energy oscillations [2-5]. Standard mitigation strategies involve mechanical optimization of magnet girders, stable power supplies, and high-performance orbit feedback systems [6]. Furthermore, recent efforts emphasize feedforward compensation schemes to combat localized, deterministic orbit distortions induced by insertion devices (IDs), such as elliptically polarizing undulators (EPUs) [7].

In line with these stringent stability demands, the Korea-4GSR project [8] is currently under development utilizing a MBA concept lattice. A primary baseline evaluation was previously conducted to quantify expected orbit disturbances from initial ground motion, magnet current ripples, and energy oscillations [9]. However, that baseline study was influenced by nearby construction activities and omitted secondary mechanical effects. This paper presents a comprehensive update to the primary estimation, incorporating refined operational measurements and sophisticated modelling frameworks to establish a more rigorous orbit stability prediction.

This paper systematically outlines the updated disturbance inputs and their impacts on the Korea-4GSR orbit stability. First, the integration of newly acquired day-time and night-time ground-motion data alongside a modelled girder amplification factor is detailed. Next, the newly incorporated coupling of vacuum-chamber vibrations to the electron beam inside quadrupole magnets is evaluated. This is followed by a description of an EPU kick compensation scheme comparing advanced nonlinear kick maps with machine learning position-dependent models. Finally, combining all updated error source are presented and benchmarked against the facility's stability requirements.

GROUND VIBRATION AND GIRDER AMPLIFICATION

To achieve an updated, realistic assessment of mechanical disturbances for the Korea-4GSR, new ground vibration measurements were conducted. While the primary baseline study was severely impacted by transient ambient noise from nearby construction activity [9], this updated study evaluates ground motion under day-time and night-time conditions to isolate and characterize these noise level.

The raw ground motion power spectral densities (PSDs) were translated into electron beam orbit distortions at the ID source points by evaluating the mechanical response of the magnet support structures. The girder amplification factor across the frequency spectrum, illustrated in Fig. 3, was incorporated using a simplified approximation model [10]. By comparing the day-time and night-time spectra shown in Fig. 1 (horizontal) and Fig. 2 (vertical), a clear divergence in the integrated vibration amplitude is observed at lower frequencies, directly quantifying the impact of localized civil engineering works during operational hours.

The resulting integrated electron beam motion at the ID locations was evaluated over a frequency range of 1 Hz to 100 Hz. Incorporating the girder amplification factor, the horizontal root-mean-square (RMS) orbit distortion was determined to be 150.8 nm during the day and dropped 87.5 nm at night (Fig. 1). Vertically, the integrated orbit

Content from this work may be used under the terms of the CC BY 4.0 licence (© 2026). Any distribution of this work must maintain attribution to the author(s), title of the work, publisher, and DOI.

ISBN: 978-3-95450-252-3 ISSN: 2673-5350 doi: 10.18429/JACoW-IPAC2026-TUP2632

RECENT PROGRESS ON THE INFRARED FREE-ELECTRON LASER FACILITY OF ANHUI UNIVERSITY

M. Wu, Anhui University, Hefei, China

Abstract

Since May 2022, the researchers at Anhui University, Hefei, China have been constructing an internationally advanced infrared free-electron laser (IR-FEL) facility. The project mainly includes one FEL light source device, six experimental stations, and other supporting systems. The tunable IR-FEL system covers the mid-infrared to far-infrared bands. Its linear accelerators provide an electron beam energy of 12-55 MeV, adopting an oscillator-type FEL scheme to generate ultrashort laser pulses (maximum 100 mJ/pulse) with continuously tunable wavelengths (2.5-200 μm), quasi-monochromaticity, and high peak power. The system includes linear accelerators, oscillators, and an optical transmission system, along with electron beam diagnostics, synchronization control, and laser parameter measurement systems. The six experimental stations focus on high temporal, spatial, and energy resolution to realize the characterization and measurement of light-matter interactions, constructing an internationally advanced materials science research platform for light-matter interaction studies.

INTRODUCTION

The concept of the free-electron laser was first proposed by J. M. J. Madey at Stanford in 1971 [1]. Then in 1976, Elias and Madey at Stanford achieved the first successful amplified output from a free-electron laser amplifier experiment at the infrared wavelength of 10.6 μm [2]. In 1986, the University of Science and Technology of China and the Chinese Academy of Sciences conducted China's first accelerator-based free-electron laser research, and successfully obtained infrared spontaneous emission at a wavelength of 10 μm from an undulator [3]. Nowadays, there are various free-electron laser facilities around the world, with radiation wavelengths from millimeter waves to X-rays.

The infrared free-electron laser facility under construction at Anhui University includes a thermionic electron gun, two linear accelerators, one mid-infrared oscillator and one far-infrared oscillator. The whole 3D diagram of the IR-FEL facility is shown in Fig. 1.

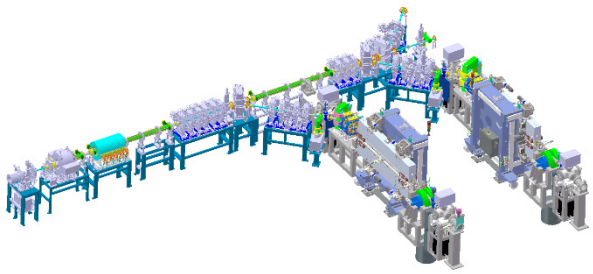

Figure 1: The infrared FEL facility at Anhui University.

There are six experimental stations in this IR-FEL facility. They are: ultrafast spectroscopy station under strong magnetic fields, scanning probe microscopy station under strong magnetic fields, magneto-optical station under strong magnetic fields, multi-field regulation station under strong magnetic fields, comprehensive characterization station, and laser diagnostics and energy materials station.

The year 2025 was a critical year for the construction of the Anhui University Free-Electron Laser Facility. During this year, breakthrough progress was made in key aspects such as the processing, commissioning, integration, and performance testing of core components for the infrared free-electron laser system, laying a solid foundation for subsequent system commissioning and stable operation. All six experimental stations have been fully constructed and commissioned, with some achieving high-level scientific research output and beginning to provide external services.

PROGRESS ON THE IR-FEL SYSTEM

At present, the IR-FEL project at Anhui University have fully entered the stages of component precision machining, system integration and commissioning, and performance verification. The project team carried out technical breakthroughs on key subsystems such as the linear accelerators, undulators, and microwave power sources, achieving landmark results in each area. The core specifications have all met or exceeded design standards, providing a solid foundation for achieving the goal of system integration and first lasing. The FEL hall under construction is shown in Fig. 2.



Figure 2: The IR-FEL hall under construction.

The details are as follows:

Electron Gun

The grid controlled thermionic high voltage electron gun passed the 100 kV withstand voltage test and was then concentrically aligned and welded with the cone tube supporting the cathode. All components, including the anode and the cathode focusing cup, were fabricated and processed through mechanical polishing followed by manual polishing, achieving a surface roughness of less than Ra 0.1 for

Content from this work may be used under the terms of the CC BY 4.0 licence (© 2026). Any distribution of this work must maintain attribution to the author(s), title of the work, publisher, and DOI.

ISBN: 978-3-95450-252-3 ISSN: 2673-5350 doi: 10.18429/JACoW-IPAC2026-TUP2635

MULTI-OBJECTIVE BAYESIAN OPTIMIZATION OF MULTI-STAGE OK-SASE FOR EFFICIENT HIGH-ENERGY XFEL OPERATION

X. Liu[1,2], H. Yang[2], N. Huang[2], J. Cai[1], H. Wen[1], J. Yu*[1], H. Deng†[2]
[1]Hunan University, School of Physics and Electronics, Hunan University, Changsha, China
[2]Shanghai Advanced Research Institute, Chinese Academy of Sciences, Shanghai, China

Abstract

Femtosecond hard X-ray radiation beyond 12.4 keV enables unprecedented opportunities for probing matter at atomic scales, however, its generation remains challenging for self-amplified spontaneous emission (SASE)-based XFELs due to reduced FEL gain, leading to extended undulator requirements and limited radiation efficiency. To address this issue, we investigate a multi-stage optical-klystron SASE (OK-SASE) scheme that enhances microbunching through dispersive sections and shortens the gain length. A multi-objective Bayesian optimization (MOBO) framework is introduced to systematically optimize the configuration. Using SHINE as a representative case, steady-state simulations at 15 keV show that the optimized setup reduces the required undulator length relative to conventional SASE by about 7% to 22%, depending on the electron-beam energy spread. The optimization indicates that several chicanes can remain effectively inactive, enabling a more compact beamline layout. Time-dependent simulations also demonstrate the feasibility of multi-stage OK-SASE for efficient high-energy XFEL operation.

INTRODUCTION

The generation of femtosecond hard X-ray free-electron laser pulses at very high photon energies is highly desirable for probing matter with atomic-scale spatial and temporal resolution [1]. However, as the photon energy approaches 25 keV (corresponding to a wavelength of 0.5 Å), the FEL gain decreases significantly, leading to substantially increased saturation lengths of up to ∼200 m in the self-amplified spontaneous emission (SASE) mode and posing significant challenges for the design of compact hard X-ray beamlines. This issue is particularly relevant to high-energy XFEL beamlines, such as FEL-III of SHINE, which covers the photon-energy range of 10-25 keV using superconducting undulators [2]. Multi-stage optical-klystron [3–5] (OK) configurations can enhance the FEL gain and shorten the saturation length, but their performance depends on the coordinated tuning of multiple dispersive sections. In this work, we combine the multi-stage OK-SASE scheme with multi-objective Bayesian optimization (MOBO) framework to optimize FEL configurations, using FEL-III as a representative case study. Chicane delays are optimized with saturation length and output performance as two objectives, and a shorter saturation length is preferred when selecting the representative solution. Optimization also reveals an efficient distribution of dispersive chicanes, indicating that several chicanes can remain inactive, enabling a more compact FEL configuration. Both steady-state and time-dependent simulations confirm the effectiveness of the proposed optimized scheme.

METHODS

As shown in Fig. 1, the multi-stage OK-SASE layout consists of a series of undulators, with one dispersive chicane inserted between every two neighboring undulators. In this configuration, the energy modulation generated in an upstream undulator is converted by the following chicane into density modulation before the electron beam enters the next undulator. As a result, the microbunching is strengthened from stage to stage, leading to enhanced FEL gain. According to the one-dimensional theory of OK [3], the maximum gain is obtained when $2\pi R_{56}\sigma_\delta/\lambda_r \sim 1$, where λ_r is the radiation wavelength, R_{56} is the momentum compaction of the dispersive chicane, and σ_δ is the rms relative energy spread of the electron beam. The optical-klystron effect becomes more pronounced when $\sigma_\delta \ll \rho$, where ρ is the FEL Pierce parameter.

Based on the proposed layout described above, Bayesian optimization (BO) is employed to determine the operating configuration, as illustrated in Fig. 2. The chicane delays in the FEL-III beamline are taken as the optimization variables, denoted by $\mathbf{x} = (d_1, d_2, \ldots, d_N)$, where d_i is the delay of the ith chicane. Each delay is bounded within $d_i \in [0, d_i^{\max}]$, where the upper bound $d_i^{\max}$ is determined from the OK condition, while the lower bound is set to zero so that a given chicane can remain inactive. These variables define an N-dimensional search space for BO. The optimization is formulated as a bi-objective problem,

$$\mathbf{y}(\mathbf{x}) = \left(-z_{\text{sat}}(\mathbf{x}),\, Q_{\text{sat}}(\mathbf{x})\right),$$

where z_{sat} is the saturation length and Q_{sat} denotes the FEL output at saturation. In the steady-state simulations, $Q_{\text{sat}} = P_{\text{sat}}$, while in the time-dependent simulations, $Q_{\text{sat}} = E_{\text{sat}}$, with $E(z) = \int P(t,z)\,dt$, where $P(t,z)$ is the temporal power profile at the longitudinal position z. The minus sign converts the minimization of z_{sat} into a maximization form. Each BO trial starts from an initial set of valid training samples. When no predefined initial dataset is available, the initial points are generated by Sobol sampling to provide a more uniform coverage of the search space. Based on these samples, separate Gaussian-process surrogate models are trained for the two objectives [6], and new candidate points are selected through the qLogEHVI acquisition

* jinqing.yu@hnu.edu.cn
† denghx@sari.ac.cn

Content from this work may be used under the terms of the CC BY 4.0 licence (© 2026). Any distribution of this work must maintain attribution to the author(s), title of the work, publisher, and DOI.

ISBN: 978-3-95450-252-3 ISSN: 2673-5350 doi: 10.18429/JACoW-IPAC2026-TUP2636

MODELING OF CSR AND ITS CANCELLATION IN DBA/CHICANE TYPE COMPRESSORS *

F. Zeng[1,2], Y. Jiao[† 1,2], W. Liu[1,3], C.-Y. Tsai[4]
[1]Institute of High Energy Physics, Chinese Academy of Sciences, Beijing, China
[2]University of Chinese Academy of Sciences, Beijing, China
[3]Spallation Neutron Source Science Center, Dongguan, China
[4]School of Electrical and Electronic Engineering, Huazhong University of Science and Technology, Wuhan, China

Content from this work may be used under the terms of the CC BY 4.0 licence (© 2026). Any distribution of this work must maintain attribution to the author(s), title of the work, publisher, and DOI.

Abstract

The most significant advances in accelerator-based light sources (i.e., x-ray free electron lasers) are driven by the production of a kiloampere-level peak current. As a prerequisite to achieve the desired high peak current, bunch compressors, like arc-type (DBA) and linear-type (chicane), are widely used to generate high-quality electron beams with several peak currents. However, a serious problem in increasing the peak current even higher is the significant degradation of beam quality caused by the coherent synchrotron radiation (CSR) effect. To tackle this, we develop a new analytical model for CSR that can describe beam transport with varying bunch lengths, establish a practical framework for analyzing CSR in both DBA and chicane-type compressors. General analytical conditions for CSR cancellation are derived for these designs. This work provides important guidance for enhancing the performance of existing accelerator facilities, as well as for the development of next-generation accelerator-based light sources.

INTRODUCTION

In modern accelerators, electron bunch compressors play a pivotal role, with wide applications in linear colliders, linacs, beam driven plasma-wakefield accelerators, and significant roles in x-ray free electron lasers (FELs) [1]. Combined with the position-energy correlation provided by the rf cavity, the following dispersive element converts the energy difference into a difference in the time of flight of the particles. This effect causes the particles at the head and tail to become closer, enabling beam compression [2].

Currently, symmetric C-chicanes and DBA-based compressors are the most commonly used bunch compressors in linac-based systems and arc systems, respectively. However, due to the high peak current required for FELs, the ability to compress an electron bunch with minimal degradation of beam quality becomes challenging because of the effects of coherent synchrotron radiation (CSR). CSR is emitted for wavelengths longer than or comparable to the length of the electron bunch, and leads to detrimental tail-head interactions in the bends [3]. The emission of CSR results in projected transverse emittance growth [4]. In the past decades, various efforts have been stimulated to suppress CSR-induced emittance growth in chicane and DBA compressors, including analytical, numerical, and experimental studies [5–8]. Among them, the approach of manipulating beam optics has sparked continuing research interest.

The optical balance method was first proposed by Douglas [9] and was further developed by Courant-Snyder (C-S) formalism analysis [6]. Subsequently, the point-kick model was proposed and works well in transport systems where the bunch length remains constant or changes very little (hereafter referred to as the constant-σ_z point-kick model) [7, 8]. However, for magnetic bunch compressors, this model lacks self-consistency due to significant variations in bunch length within the bends.

To address this issue, in this study, we propose a self-consistent modified CSR point-kick model that accounts for variations in bunch length. Based on this model, we establish a practical framework for analyzing CSR in both DBA and chicane-type compressors, envisaging the potential designs for a CSR-immune DBA and chicane compressors.

MODIFIED CSR POINT-KICK MODEL

When considering only the steady state case and assuming the beam distribution in the dipole is Gaussian, The influence due to CSR along the bending angle can be derived based on the 1D CSR model [7].

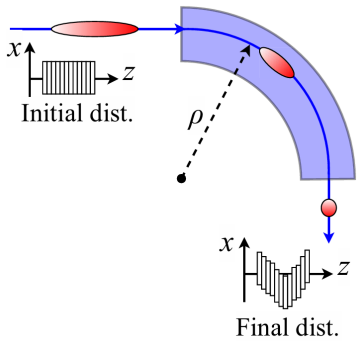

Figure 1: Schematic of the compression process after a bunch passes through a dipole, within sets of the initial beam distribution and final one affected by CSR in the $x - z$ phase plane.

* Work supported by National Natural Science Foundation of China (No.12275284 and No. 12275094), the Fundamental Research Funds for the Central Universities (HUST) under Project No. 2021GCRC006, and National Key Research and Development Program of China (No.2022YFA1603402).

† jiaoyi@ihep.ac.cn

ISBN: 978-3-95450-252-3 ISSN: 2673-5350 doi: 10.18429/JACoW-IPAC2026-TUP2637

SIMULATION STUDY OF THE FULL WAVEGUIDE DESIGN FOR HIFEL*

Guanzheng Wu, Zhouyu Zhao, Yuanfang Xu†, Heting Li‡
National Synchrotron Radiation Laboratory,
University of Science and Technology of China, Hefei, Anhui, China

Abstract

Hefei infrared Free Electron Laser (HiFEL) facility aims to provide high-quality lasers with wavelengths covering the mid to far infrared range. However, there is an obvious decrease in the output power at long wavelengths. The mode field mismatch and truncation loss at the waveguide to free space region are the main reasons for low output power. We propose a full waveguide design and simulation results suggest that compared to partial waveguide configurations, the full waveguide structure improves the saturated output power in the long wavelength range.

INTRODUCTION

Free Electron Lasers (FELs) are high-power, high-beam-quality, and widely tunable sources of coherent radiation that cover a wide spectral range from microwaves to hard X-rays and have broad application prospects [1]. In the infrared (IR) range, one of the main operation modes named FEL Oscillator (FELO) has attracted considerable attention because of its capability to produce narrow linewidth, high-intensity coherent radiation with a relatively compact configuration. Accordingly, various FELO facilities have been developed worldwide.

The Hefei infrared Free Electron Laser (HiFEL), also known as FELiChEM, is China's first FEL user facility covering the mid- to far-IR range. This facility is dedicated for energy chemistry research, providing laser radiation for applications in condensed matter physics, materials science, and surface chemistry [2]. It consists of two FEL oscillators driven by a 60 MeV linac, capable of generating mid-IR (2-50 μm) and far-IR (20-200 μm) laser radiation independently. As a cavity-based FEL facility, HiFEL relies on the multi-pass interaction between the electron beam and the radiation field within the resonant cavity to achieve exponential amplification and saturation. As the radiation wavelength increases, diffraction effects become sharply pronounced, leading to rapid expansion of the optical beam's transverse size within the cavity. The diffracted optical beam tends to undergo losses in the undulator vacuum chamber, greatly reducing the FEL gain and efficiency, which may make lasing impossible.

For suppression of the diffraction effects, HiFEL uses the partial rectangular waveguide configuration to confine the transverse size of the optical beam. However, during the actual operation, there is an obvious decrease in output power at long wavelengths, particularly in the far-IR range. This is probably because when the long-wavelength radiation field enters the waveguide from the free space region between the undulator and the cavity mirrors, its transverse profile changes rapidly. This abrupt geometric transition induces severe mode field mismatch and truncation loss. Such high intra-cavity losses greatly decrease the single-pass gain, ultimately resulting in the obvious decrease in output power.

Several ways are proposed including using a full waveguide cavity, which has been applied in experiments [3]. Consequently, to overcome this power decrease, we propose a full waveguide cavity design for HiFEL and analyze its impact on FEL performance through simulations, so as to improve the saturated output power in the long wavelength regime.

WAVEGUIDE DESIGN

The existing partial waveguide structure of HiFEL is engineered to confine the optical mode solely within the undulator section, as Fig. 1(a) shows. While this configuration effectively suppresses diffraction loss within the undulator region, it introduces an unavoidable abrupt transition of transverse boundary at the waveguide entrance and exit. This discontinuity triggers two dominant loss mechanisms, one is the severe mode field mismatch between the guided mode and the free-space diverging mode, which breaks the multi-pass coherent resonance condition; the other one is obvious truncation loss at the waveguide edge, where the expanded optical field is partially blocked and absorbed by the cavity. These losses increase with wavelength, directly causing the observed power drop in the far-IR regime.

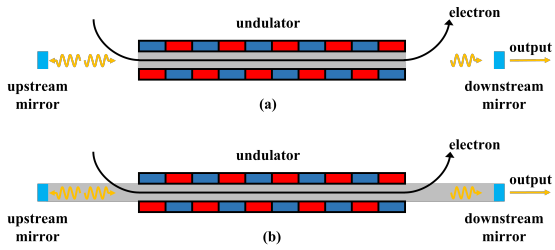

Figure 1: Side views of the two distinct waveguide configurations, where (a) partial waveguide design and (b) full waveguide design.

In order to avoid the existence of interfaces between the waveguide and free space, we propose a full waveguide design by extending the waveguide structure throughout the entire resonant cavity, which can establish a continuous, closed optical path from the upstream cavity mirror to the downstream cavity mirror, as illustrated in Fig. 1(b). It fully encloses the entire resonant cavity, including the undulator

* Work supported by the National Natural Science Foundation of China under Grants (No. 12241501 and No. 12305361)
† xyf1224@ustc.edu.cn
‡ liheting@ustc.edu.cn

Content from this work may be used under the terms of the CC BY 4.0 licence (© 2026). Any distribution of this work must maintain attribution to the author(s), title of the work, publisher, and DOI.

ISBN: 978-3-95450-252-3 ISSN: 2673-5350 doi: 10.18429/JACoW-IPAC2026-TUP2639

THEORETICAL ANALYSIS OF A NOVEL SEEDED FREE-ELECTRON LASER SCHEME WITH THE SAME LAYOUT AS EEHG

Z. Wang, Z. Bai*, Q. Jia, Y. Huang, Z. Zhao, G. Feng†
National Synchrotron Radiation Laboratory,
University of Science and Technology of China (USTC), Hefei, China

Abstract

Seeded free-electron lasers (FELs) are advanced, accelerator-based light sources characterized by high coherence and stability. In our previous research, we proposed an intelligent optimization framework for studying the micro-bunching process in seeded FELs. Using this framework for exploratory optimization, we identified a novel seeded FEL scheme. This scheme employs an optical layout identical to echo-enabled harmonic generation (EEHG), but by adjusting the parameters of the seed lasers and chicanes, it achieves bunching factors exceeding the theoretical limit of conventional EEHG. In this paper, using a representative set of realistic beam parameters, we demonstrate how this novel scheme induces a high harmonic density modulation in the electron beam. Then, we theoretically analyze this novel seeded FEL, presenting its underlying principles.

INTRODUCTION

In a high-gain single-pass free-electron laser (FEL), the radiation field grows exponentially from spontaneous emission as the electron beam develops density modulation at the radiation wavelength, ultimately reaching saturation within a single undulator pass and yielding gigawatt-level coherent output in the extreme ultraviolet and X-ray regimes [1]. The most commonly used mode, self-amplified spontaneous emission (SASE) [2], typically starts from shot noise, resulting in limited temporal coherence [3]. Seeded FELs introduce stable external seed lasers to interact with the electron beam. After density modulation, the electron beam forms micro-bunching, which generates harmonic radiation that undergoes coherent amplification. Since the quality of the output radiation is similar to that of the seed lasers, seeded FELs offer advantages over the SASE mode, such as narrow bandwidth and a stable central wavelength.

An intelligent optimization framework for studying the micro-bunching process in seeded FELs was developed in our earlier work [4]. By pre-defining feasible components and their parameter ranges, this framework can automatically generate optimized seeded FEL configurations for specific performance objectives. Using it, we have successfully reproduced previously proposed seeded FEL schemes. Furthermore, we have identified a novel seeded FEL scheme with the same layout as that of echo-enabled harmonic generation (EEHG) [5, 6], as shown in Fig. 1. The longitudinal phase space evolution of the novel scheme differs from that of EEHG, which results in its ability to achieve a larger bunching factor. In this paper, we will present the characteristics of this novel scheme and compare it with EEHG. We will also explain the underlying physical principles governing the micro-bunching process with theoretical analysis.

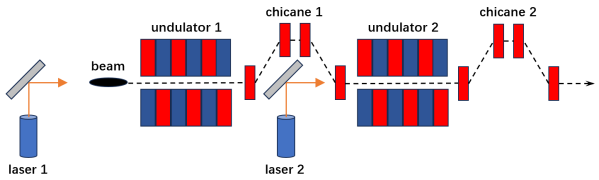

Figure 1: Schematic layout of the novel scheme, with same layout as EEHG. The dashed line represents the path of the beam.

CHARACTERISTICS OF THE NOVEL SCHEME

To intuitively illustrate the characteristics of the novel scheme, we first present a specific example. We adopt standard FEL parameters for the initial electron beam, with a beam energy of 1.2 GeV and an rms energy spread of 150 keV. The seed lasers shown in Fig. 1 have the same wavelength of 260 nm. It is known that in EEHG, the energy modulation induced by the first seed laser is typically significantly stronger than that of the second. In contrast, the novel scheme relies on a strong energy modulation induced by the second seed laser as the key to generating micro-bunching, where undulator 1 provides an amplitude of 532.5 keV and undulator 2 provides an amplitude of 1.29 MeV. The dispersive strengths of the two chicanes are 0.50 mm and 0.05 mm, respectively, which are much smaller than those in EEHG.

The longitudinal phase space of the beam after passing through undulator 1 and chicane 1 is shown in the left plot of Fig. 2, where no separated energy bands are formed, unlike in EEHG. Then, after passing through undulator 2 and chicane 2, shown in the middle and right plots of Fig. 2, the final phase space distribution in the novel scheme approximates a non-uniform multi-peak distribution. The bunching factors for the novel scheme at different harmonic numbers are shown in Fig. 3, together with those for the EEHG scheme optimized at the 15th harmonic for ease of comparison. In EEHG, the bunching factors are typically optimized for some specific harmonic numbers, with most of the other harmonic components being strongly suppressed. However, the novel scheme not only achieves larger bunching factors at the targeted harmonic numbers but also generates significant

* baizhe@ustc.edu.cn
† fenggy@ustc.edu.cn

Content from this work may be used under the terms of the CC BY 4.0 licence (© 2026). Any distribution of this work must maintain attribution to the author(s), title of the work, publisher, and DOI.

ISBN: 978-3-95450-252-3 ISSN: 2673-5350 doi: 10.18429/JACoW-IPAC2026-TUP2640

RECENT PROGRESS IN INTENSE VORTEX RADIATION SOURCES AT SXFEL

X. R. Zhu[1,2], C. L. Li[3], Y. Kang*[,3], C. Feng†[,3], Z. T. Zhao[3]
[1]Shanghai Institute of Applied Physics, Chinese Academy of Sciences, Shanghai, China
[2]University of Chinese Academy of Sciences, Beijing, China
[3]Shanghai Advanced Research Institute, Chinese Academy of Sciences, Shanghai, China

Abstract

Vortex radiation carries orbital angular momentum (OAM) and is attractive for applications including chiral characterization, magnetic imaging, and ultrafast light–matter interaction studies. A scheme for vortex radiation generation and diagnostics at the Shanghai Soft X-ray Free-Electron Laser facility (SXFEL) based on wavefront shaping of a 266 nm external seed laser is studied. Three-dimensional simulations with realistic SXFEL parameters show clear annular intensity and helical phase distributions, with peak power reaching the sub-gigawatt level at a representative working point. The proposed diagnostics further enable clear identification and characterization of the generated OAM radiation. The results support the feasibility of controlled vortex radiation generation at SXFEL and its future extension to shorter wavelengths.

INTRODUCTION

Radiation carrying OAM, or vortex radiation, has a helical wavefront, an on-axis phase singularity, and a hollow transverse intensity profile. These features enable coupling to angular-momentum degrees of freedom and make vortex radiation useful for chiral-structure identification, magnetic-order imaging, nanoscale angular-momentum transport, and ultrafast nonequilibrium studies [1–4].

Free-electron lasers (FELs) provide high brightness, ultrashort, and tunable coherent radiation, making them promising sources of intense vortex beams. Proposed FEL-based OAM schemes include seeded FELs, FEL oscillators, and self-seeding configurations [5–9]. Seeded FELs are especially attractive because an external seed laser allows flexible phase control and harmonic up-conversion. Motivated by the wavefront-shaping method for high-gain FEL vortex generation [10], this paper studies its implementation at SXFEL using a 266 nm seed laser, with emphasis on realistic simulations and experimentally accessible diagnostic signatures.

The remainder of this paper is organized as follows. In Section 2, the basic principle of the proposed technique is introduced. Section 3 presents the simulation results. Section 4 presents the diagnostic method and criterion. Finally, concluding remarks are given in Section 5.

* kangy@sari.ac.cn
† fengc@sari.ac.cn

SCHEME

A wavefront shaping unit is introduced into the seeded FEL platform at SXFEL so that the 266 nm seed laser obtains the required transverse phase before entering the modulator, as shown in Fig. 1. The shaped seed imprints an azimuth-dependent energy modulation on the electron beam; the dispersive section converts it into helical density modulation; and the radiator amplifies the corresponding vortex microbunching. The shaping concept uses two planar mirrors with a small relative angle.

Following the wavefront-tilt scheme, the seed field at the modulator entrance is [10]

$$E_s(x,y) = E_{\mathrm{G}}(x,y)\exp\left[ik_s\alpha x\ \mathrm{sgn}(y)\right], \tag{1}$$

where E_{G} is the Gaussian envelope, $k_s = 2\pi/\lambda_s$, and α is the effective wavefront tilt. In the beam–laser overlap region, $k_s\alpha x\,\mathrm{sgn}(y)$ can approximate the target azimuthal phase $l\theta$.

In the modulator, the seed induces an energy modulation [5, 11, 12]

$$\Delta\gamma(r,\theta,s) = \frac{eK_mJJL_m}{2\gamma mc^2}E_s(r)\sin(k_s s + l\theta + \phi_0), \tag{2}$$

where K_m and L_m are the dimensionless undulator parameter and effective length of the modulator, respectively, JJ is the planar undulator coupling factor, γ is the relativistic Lorentz factor of the electron beam, s is the longitudinal coordinate, and ϕ_0 is the initial phase. After the dispersive section, the density modulation becomes

$$\rho = \rho_0\left[1 + 2\sum_{n=1}^{\infty}|b_n|\cos(nk_s s + nl\theta + \psi_n)\right], \tag{3}$$

with average charge density ρ_0, harmonic bunching factor b_n, and phase ψ_n. For HGHG, the helical bunching at the nth harmonic is [5, 11]

$$b_n(r,\theta) = e^{-B^2n^2/2}J_n(-nAB)\,e^{inl\theta}, \tag{4}$$

where $A = \Delta E/\sigma_E$ and $B = k_sR_{56}\sigma_E/E_b$. Thus the radiator tuned to the selected harmonic amplifies microbunching carrying the seed-imposed azimuthal phase.

SIMULATION RESULTS OF THE PRESENT SCHEME

The feasibility of the present SXFEL scheme was evaluated with three-dimensional GENESIS 1.3 simulations [13]. A representative fundamental working point was selected,

Content from this work may be used under the terms of the CC BY 4.0 licence (© 2026). Any distribution of this work must maintain attribution to the author(s), title of the work, publisher, and DOI.

ISBN: 978-3-95450-252-3 ISSN: 2673-5350 doi: 10.18429/JACoW-IPAC2026-TUP2641

SymCSR: TRACKING 6D PHASE SPACE DYNAMICS OF ELECTRON BEAM WITH COHERENT SYNCHROTRON RADIATION

Z. Liu*, X. Deng†, T. Li, L. Yan‡, Tsinghua University, Beijing, China

Abstract

Coherent synchrotron radiation (CSR) is a critical effect in the design and operation of high-brightness electron accelerators, as it can lead to significant energy loss and emittance growth. In this paper, we present SymCSR, a first-principle tracking program for simulating the 6D phase space dynamics of electron beams under the influence of CSR. SymCSR computes the radiation reaction field of electrons based on its retarded and instantaneous trajectory, which efficiently reduces the requirement on macroparticle numbers. The dynamics of electron beam in various dimensions are calculated using SymCSR and are compared with theoretical models.

INTRODUCTION

Generating ultrashort electron beam to produce coherent radiation has attracted substantial interest in accelerator physics community in recent years [1, 2]. Advanced phase space manipulation methods and lattice designs have been proposed to achieve ultrashort bunch length in linear accelerators and storage rings [3, 4]. Due to the high peak current of the ultrashort electron beam, when the beam traverses bending magnet or radiator, the coherent synchrotron radiation (CSR) produced by the beam itself could have significant impact on the dynamics. Meanwhile, in these scenarios the bunch length could be comparable to the transverse beam size and the 6D phase space distribution of the beam could evolve notably in the radiator. To accurately model the CSR effect, it should go beyond the 1D approximation and simulate the full 6D phase space dynamics with CSR effect.

Here, we demonstrate a first-principle tracking program, SymCSR, for calculating the 6D beam dynamics with CSR effect. The program utilizes radiation reaction (RR) field formalisim to eliminate the space-charge singularity in calculation of CSR effect, therefore largely reduce the requirement on macroparticle number for a convergent result.

RADIATION REACTION FIELD

In the simulation of CSR effect, the Lienard-Wiechert solution is frequently applied to calculate the electromagnetic field of a moving charge. However, the two terms in the Lienard-Wiechert solution both contain space-charge singularity which complicates the analysis of CSR effect.

In the previous work, we have shown that the solution of Maxwell equations can also be decomposed into three terms, namely, space-charge field, compression field and RR field [5]. It is shown that the CSR effect is induced by the RR field, and the space-charge related effects are included in the first two terms which are instantaneous. For the electric field, the decomposition can be written as

$$E = E_{\mathrm{sc}} + E_{\mathrm{comp}} + E_{\mathrm{rr}}, \tag{1}$$

with

$$\begin{aligned} E_{\mathrm{sc}} =& \frac{e}{4\pi\epsilon_0}\frac{\hat{R}}{R^2}\frac{1-\beta^2}{(1-(\beta\times\hat{R})^2)^{3/2}}, \\ E_{\mathrm{comp}} =& -\frac{e}{4\pi\epsilon_0}\frac{1}{cR}\frac{\dot{\beta}+\left(\dot{\beta}\cdot\hat{R}\right)\hat{R}}{2(1-(\beta\times\hat{R})^2)^{3/2}} \\ &+\frac{e}{4\pi\epsilon_0}\frac{1}{cR}\frac{3(\beta\cdot\hat{R})^2\left(\dot{\beta}\cdot\hat{R}\right)\hat{R}}{2(1-(\beta\times\hat{R})^2)^{5/2}}. \end{aligned} \tag{2}$$

where $\hat{R} = R/R$, $\dot{\beta} = \mathrm{d}\beta/\mathrm{d}t$, $R = r_i - r_j$ is the distance between the source particle (j) and the test particle (i), βc is the velocity of the source particle.

The magnetic field can also be decomposed accordingly. To simulate the CSR effect, the Lorentz force from the RR field is calculated at every time step. Since the RR force does not include space-charge singularity, numerical convergence can be achieved with fewer macroparticles.

SYMPLECTIC INTEGRATOR

During each field evaluation time step, a symmetric second-order symplectic integrator is employed to update the 6D phasespace coordinates of the particles. The use of symplectic integrator instead of Runge-Kutta integrator preserves the phase space volume and at the same time reduces the computation time which is essential for simulating CSR effects in storage rings.

For simplicity, assuming only the x component of the vector potential of the external field is non-zero, the Hamiltonian of an electron under the external field can be written as [6]

$$\begin{aligned} &\mathscr{H}(x,p_x,y,p_y,s,p_s,-l,\delta;\sigma) = K_1 + K_2 \\ =&\frac{(p_x-a_x)^2}{2D} + \frac{p_y^2+p_s^2-(1+\delta)^2}{2D} \end{aligned} \tag{3}$$

where $p = (p_x, p_y, p_s)$ is the electron momentum, $r = (x, y, s)$ is the electron position, δ is the momentum deviation, l is the electron path length and

$$D = \sqrt{(1+\delta)^2 + \frac{1}{\beta_0^2\gamma_0^2}} \tag{4}$$

where β_0, γ_0 is the velocity and Lorentz factor of the reference particle.

The independent variable of this Hamiltonian is σ, satisfying $\mathrm{d}\sigma = c\,\mathrm{d}t$. Since the Hamiltonian does not contain σ

* liu-zy20@mails.tsinghua.edu.cn
† dengxiujie@mail.tsinghua.edu.cn
‡ yanlx@mail.tsinghua.edu.cn

Content from this work may be used under the terms of the CC BY 4.0 licence (© 2026). Any distribution of this work must maintain attribution to the author(s), title of the work, publisher, and DOI.

ISBN: 978-3-95450-252-3 ISSN: 2673-5350 doi: 10.18429/JACoW-IPAC2026-TUP2646

ANALYSIS OF SLICE ENERGY SPREAD INCREASED BY INTRA-BEAM SCATTERING AT THE SHINE INJECTOR AND LINAC

W. C. Cheng, D. Gu, M. Zhang, H. X. Deng*
Shanghai Advanced Research Institute, Chinese Academy of Sciences, Shanghai, China

Content from this work may be used under the terms of the CC BY 4.0 licence (© 2026). Any distribution of this work must maintain attribution to the author(s), title of the work, publisher, and DOI.

Abstract

Intra-beam scattering (IBS) can substantially enhance the slice energy spread of high-brightness electron beams, thereby degrading the performance of free-electron laser (FEL) facilities. This effect is particularly detrimental for advanced operation modes such as self-seeding, which impose stringent requirements on beam longitudinal coherence. Consequently, an accurate evaluation of IBS growth in both the injector and the main linac is essential. SHINE, the first superconducting-linac–based FEL facility in China, has recently completed beam commissioning up to the first bunch compressor (BC1). In this work, we present a theoretical and numerical analysis of IBS-induced slice energy spread growth throughout the SHINE injector and linac. The analytical estimates show good agreement with start-to-end simulations, confirming that IBS leads to 0.5 keV increase in slice energy spread at the injector stage. In the linac section, the accu- mulated IBS-induced energy spread growth before the first bunch compressor (BC1) reaches 1.48 keV. These results highlight the necessity of incorporating IBS considerations into the beam dynamics design and optimization of high-repetition-rate FEL facilities such as SHINE.

INTRODUCTION

X-ray free-electron lasers (XFELs) have become indispensable tools for ultrafast science, enabling studies of matter with unprecedented spatial and temporal resolution [1–3]. The performance of an XFEL critically depends on the quality of the driving electron beam, especially its slice properties, such as slice emittance and slice energy spread (SES). In particular, the SES plays a crucial role in determining the FEL gain process, since it directly affects the Pierce parameter and the longitudinal coherence of the emitted radiation. For advanced FEL operation modes, including self-seeding and external seeding, the requirements on SES are even more stringent. Therefore, understanding and controlling the mechanisms responsible for SES growth is of great importance for modern high-brightness FEL facilities.

Recent experimental studies at facilities such as European XFEL [4], PITF at DESY [5] and SwissFEL [6, 7] have reported measured slice energy spreads significantly larger than the values predicted from conventional injector simulations. These discrepancies were attributed mainly to intra-beam scattering (IBS), which can increase the uncorrelated energy spread during beam transport, particularly in low-energy and high-brightness regimes. Such observations indicate that IBS is an important collective effect that cannot be neglected in superconducting-linac–based XFEL facilities operating with high repetition rates and ultra-high beam brightness.

Shanghai High Repetition Rate XFEL and Extreme Light Facility (SHINE) is the first superconducting-linac–based XFEL facility in China [3]. The facility is designed to deliver high-brightness electron beams for multi-user hard X-ray FEL applications. Due to the relatively long transport distance from the injector to the first accelerating sections, together with the extremely small intrinsic energy spread of the beam, IBS is expected to induce non-negligible SES growth along both the injector and the early linac sections.

In this paper, we present a theoretical and numerical investigation of IBS-induced slice energy spread growth throughout the SHINE injector and linac. The IBS analytical models are first introduced and applied to the SHINE beam parameters. Start-to-end simulations based on RF-Track [8] are then performed to benchmark the theoretical predictions. For the injector section, good agreement is obtained between the analytical calculations and the numerical simulations, showing that IBS leads to an SES increase of approximately 0.5 keV at the injector exit. In the linac section, the accumulated IBS-induced energy spread growth before the first bunch compressor (BC1) reaches 1.48 keV. The results demonstrate that IBS constitutes an important collective effect for SHINE and should be carefully considered in the beam dynamics design and optimization of high-brightness, high-repetition-rate XFEL facilities.

IBS ANALYTICAL MODEL

Intra-beam scattering (IBS) is a multiple small-angle Coulomb scattering process among particles within an electron bunch, which can lead to emittance dilution and energy spread growth during beam transport. For high-brightness electron beams in XFEL facilities, IBS may significantly increase the slice energy spread (SES), especially in low-energy and high-density regions such as the injector and bunch compression sections.

In this work, the IBS analytical model is based on the modified Piwinski formalism developed for low-energy injector and linac applications. Since synchrotron oscillations are negligible in a linear accelerator, the conventional storage-ring treatment can be simplified [9]. For a three-dimensional Gaussian bunch, the SES growth over a transport distance Δs can be expressed as

$$\sigma_\gamma^2 = \sigma_{\gamma,0}^2 + \frac{r_e^2 N_b \Lambda_c}{4\sigma_x \epsilon_n \sigma_z} \Delta s, \quad (1)$$

* denghx@sari.ac.cn

ISBN: 978-3-95450-252-3 ISSN: 2673-5350 doi: 10.18429/JACoW-IPAC2026-TUP2657

OFF-AXIS HOLLOW-CHANNEL PLASMA TAILORING FOR GENERATING TWO-COLOR X-RAY FREE-ELECTRON LASERS*

H. Li[1,2], Y. Kang[3], T. Liu†[3], B. Liu[3]
[1]Shanghai Institute of Applied Physics, Shanghai, China
[2]University of Chinese Academy of Sciences, Beijing, China
[3]Shanghai Advanced Research Institute, Shanghai, China

Abstract

Plasma-wakefield-based acceleration offers a route to realize compact X-ray free-electron lasers, but its application is currently limited by beam quality. Two-color X-ray FEL pulses provide a powerful tool for probing ultrafast dynamics. Here we propose a scheme for generating such pulses by using an off-axis elliptical hollow-channel plasma to tailor the electron-beam phase space while preserving its quality. In this approach, the plasma wakefield imprints a time-dependent transverse tilt along the bunch, while the elliptical channel geometry effectively suppresses the quadrupole wakefield and minimizes the induced mismatch. This enables fresh-slice lasing control at different wavelengths in two undulator sections. Simulations show the feasibility of generating femtosecond-scale, high-power two-color pulses with tunable temporal separation at the Shanghai Soft X-ray Free Electron Laser facility.

INTRODUCTION

X-ray free-electron lasers (FELs), which produce ultrashort, high-brightness X-ray pulses, play a critical role in a wide range of fundamental research and applications in medicine, chemistry, biology, and so on [1, 2]. Two-color FELs, delivering two consecutive pulses with adjustable time and wavelength separation, are particularly valuable for pump-probe experiments at atomic and molecular scales. Traditional approaches, such as using two electron bunches or split undulator schemes, provide limited flexibility in controlling the time or wavelength separation between pulses.

Recently, the fresh-slice method has been demonstrated to generate two-color pulses from a single electron bunch [3]. By introducing a time-dependent transverse offset, i.e., tilt or focusing mismatch, selected temporal slices lase in one undulator segment while other slices remain "fresh" for subsequent lasing. This method enables independent control of pulse delay and duration while preserving beam emittance, as shown in simulations at LCLS and SwissFEL [4, 5].

Plasma wakefield acceleration (PWFA) has been introduced to the FEL community as a promising route toward compact X-ray FELs due to its ultra-high accelerating gradients [6]. However, the extreme longitudinal and transverse fields intrinsic to PWFA—specifically, the extremely strong, non-uniform accelerating fields and the nonlinear transverse focusing fields—pose significant challenges for preserving the high brightness and low emittance required for X-ray FEL operation.

Hollow plasma channels (HPCs) have been proposed to mitigate these issues. Unlike uniform plasmas, the HPC is devoid of plasma electrons along its axis, effectively suppressing nonlinear focusing forces and providing an emittance-preserving environment for high-brightness electron beam modulation [7–9]. By maintaining beam quality within the plasma, HPCs allow the generation of controlled transverse tilts when the beam propagates off-axis.

In this work, we propose a novel PWFA based technique to produce tilt beam suitable for two-color FELs with an off-axis hollow plasma channel. Particle-in-Cell (PIC) simulations show that an elliptical channel design can naturally suppress quadrupole wakefield, ensuring high-quality tilted beams. Full simulations confirm that our approach can generate femtosecond-scale, high-power two-color pulses.

LAYOUT

The layout of the proposed two-color FEL operation is illustrated in Fig. 1, including the elliptical HPC modulation section, the match and orbit control beamline, the undulator sections, and the magnetic chicane used to separate and delay the lasing slices. The electron bunch is first injected off-axis into an elliptical hollow plasma channel, which imparts a transverse dipole wakefield along the bunch, generating a tilt in the off-axis direction.

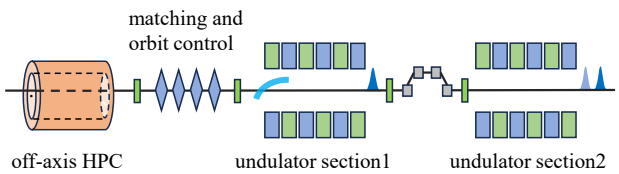

Figure 1: Schematic layout of the two-color FEL operation. Both undulator sections contain several undulator modules, the FODOs between undulators are not shown for clarity.

The subsequent beamline provides matching and orbit control. It matches the electron beam to the designed Twiss parameters at the undulator entrance position while steering specific temporal slices onto the beamline axis, enabling the fresh-slice lasing scheme: only the on-axis slice interacts efficiently with the radiation field, while the other slices oscillate near the undulator axis, and remain "fresh" for subsequent lasing.

* Work supported by the National Natural Science Foundation of China (12475322), Young Scientists in Basic Research CAS (YSBR-060), the Youth Innovation Promotion Association CAS (2023302), and the Oriental Talent Young Scientist Program (QNZH2024036).
† liut@sari.ac.cn

Content from this work may be used under the terms of the CC BY 4.0 licence (© 2026). Any distribution of this work must maintain attribution to the author(s), title of the work, publisher, and DOI.

ISBN: 978-3-95450-252-3 ISSN: 2673-5350 doi: 10.18429/JACoW-IPAC2026-TUP2661

DESIGN STUDY OF INJECTOR SYSTEM USING RF ELECTRON GUN WITH GRIDDED THERMIONIC CATHODE TOWARDS SOFT X-RAY FREE-ELECTRON LASER*

T. Asaka†, A. Agui, Y. Hosaka, K. Inaba, K. Kan, N. Nishimori, S. Obara, C. Saji, K. Ueshima,
NanoTerasu center/National Institutes for Quantum Science and Technology, Sendai, Miyagi, Japan

Abstract

The high-brightness synchrotron radiation facility NanoTerasu provides users with extremely stable synchrotron radiation by employing top-up injection of an electron beam from a 3-GeV linear accelerator into a diffraction-limited storage ring. NanoTerasu plans to develop a soft X-ray free-electron laser (SX-FEL) using this linear accelerator. To achieve an SX-FEL with a practical gain length, the linear accelerator must generate an electron beam with a peak current of 2.5 kA and a normalized emittance of 2 mm mrad or less. We have already developed a low-emittance electron gun system based on a gridded thermionic cathode and have begun designing a low-emittance pre-injector using this system. The linear accelerator based on the electron gun system is planned to serve both as the injector for the storage ring and as the driver for the SX-FEL. This presentation describes the configuration of a compact SX-FEL linear accelerator that can be installed within existing facilities. It also presents a bunch compression scheme that preserves slice emittance, together with particle tracking simulation results for the newly designed pre-injector.

INTRODUCTION

The high-brightness synchrotron radiation facility NanoTerasu employs a 3 GeV low-emittance storage ring based on a multi-bend achromat (MBA) lattice [1]. Synchrotron radiation generated by undulators achieves a brilliance exceeding 10^{21} photons/s/mm²/mrad²/0.1% b.w. in the soft X-ray to tender X-ray region, with a coherence ratio of approximately 10% [2]. A 3 GeV electron beam with an emittance of 2 nm rad and a bunch charge of 0.36 nC, generated by a 3 GeV linear accelerator, is injected into the storage ring through an 80 m-long beam transport line. The linear accelerator has a total length of 110 m and consists of a 40-MeV pre-injector equipped with a low-emittance electron gun system and a high-gradient C-band accelerator [3].

One of NanoTerasu's future plans is to repurpose the linear accelerator currently used as the injector for the 3 GeV storage ring as the drive system for a soft X-ray free-electron laser (SX-FEL). The required beam performance for the SX-FEL includes a beam energy of 2.5 GeV, an energy spread of 0.01% or less, a peak beam current of 2.5 kA or higher, and a normalized emittance of 1.5 mm mrad or less. To generate such a high-density electron beam, a low-emittance pre-injector and two magnetic bunch compression systems are essential.

CONFIGURATION OF LINEAR ACCELERATOR FOR SX-FEL

Table 1 summarizes the radiation and beam parameters for the SX-FEL, and Fig. 1 shows the layout of the NanoTerasu accelerator complex**.** The SX-FEL undulator section and the experimental hall are planned to be located downstream of the 3-GeV linear accelerator. A magnetic chicane for beam energy filter is installed between the exit of the linear accelerator and the undulator section. Downstream of the undulator section, a beam diagnostic system capable of measuring the bunch length and beam charge is installed to evaluate the peak beam current. The 2.5 GeV electron beam is then guided to a bending magnet and finally to the beam dump.

Table 1: Radiation and Beam Parameters for SX-FEL

Parameter	Value
Wavelength	1.2 nm
Beam energy	2.5 GeV
Energy spread	0.01 %
Normalized emittance	< 2 mm mrad
Beam charge	0.3 nC
Peak beam current	2.5 kA
Bunch length	< 80 fs
Repetition rate	> 10 pps
Saturation length	25 m
Peak power	2 GW

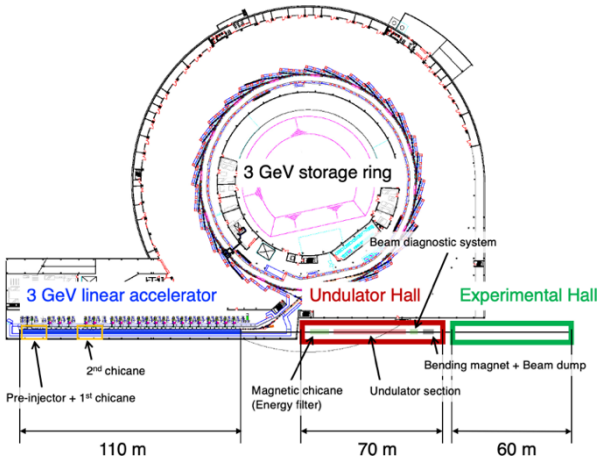

Figure 1: Layout of NanoTerasu accelerator complex, which consist of 3 GeV linear accelerator, 80 m long beam transport line and 3-GeV storage ring. Experimental hall and undulator hall of SX-FEL site is placed after the 3-GeV linear accelerator building.

Content from this work may be used under the terms of the CC BY 4.0 licence (© 2026). Any distribution of this work must maintain attribution to the author(s), title of the work, publisher, and DOI.

ISBN: 978-3-95450-252-3 ISSN: 2673-5350 doi: 10.18429/JACoW-IPAC2026-TUP2664

OPTIMIZATION OF A STORAGE RING PRE-INJECTOR FOR HIGH TRANSMISSION EFFICIENCY AND LOW ENERGY SPREAD*

W. Xu[1], F. Zhang[1], Z. Dong[1], Z. Shao[2], T. Zhang[†2], L. Wang[‡1,2], Y. Lu[1,2]
[1]University of Science and Technology of China, Hefei, China
[2]Hefei National Laboratory, Hefei, China

Abstract

In this paper, the Non-dominated Sorting Genetic Algorithm II (NSGA-II), combined with the beam dynamics code ASTRA, was employed for the multi-objective optimization of the output performance of an electron linear accelerator (linac). Taking the pre-injector of a storage ring light source as an example, the electron linac consists of a thermionic cathode high-voltage electron gun, a sub-harmonic buncher (SHB), a buncher, and a traveling-wave accelerator tube. Maximizing the transmission efficiency and minimizing the energy spread were defined as the core objectives of the optimization. The optimization results indicate that the beam energy at the linac exit reaches approximately 65 MeV, with the transmission efficiency exceeding 70% and the energy spread maintained below 0.35 %.

INTRODUCTION

Linacs are widely used in medical treatment, industry and scientific research. In the scientific research field, serving as an injector/pre-injector for storage-ring lightsources, free-electron lasers(FELs) and colliders, electron linacs provide electron beams to generate high-quality light sources, supporting cutting-edge research in physics, chemistry, biology, materials science and medicine [1].

For storage-ring light sources, electron linacs are most commonly used as pre-injectors. In this role, the pre-injector forms the low-energy front end of the accelerator chain and conditions the beam emerging from the electron gun by performing longitudinal phase-space manipulation, bunch compression, and initial acceleration. These processes establish the beam parameters required for efficient booster capture, making high transmission efficiency and low energy spread the primary design objectives.

The pre-injector configuration used in this work is shown in Fig. 1. It includes a high-voltage thermionic cathode electron gun, a six-harmonic sub-harmonic buncher (SHB), a buncher, and a traveling-wave accelerating structure. Multiple solenoids placed in the low-energy region suppress space-charge–induced emittance growth, allowing high-quality beam formation within a compact layout.

Given the strong space-charge effects and nonlinear RF dynamics involved, numerical optimization is widely used in pre-injector design, with MOGA and MOPSO being common approaches [2–6]. In this study, the NSGA-II [7] was used to simultaneously optimize RF phases, RF voltages, and solenoid magnetic fields, with the aim of maximizing transmission efficiency while minimizing energy spread. The optimization procedure and resulting beam performance are presented in the following sections.

BEAM DYNAMICS SIMULATION

Start-to-End Simulation Setup

To evaluate the beam dynamics performance of the proposed pre-injector scheme, Start-to-End simulations were carried out using the ASTRA code [8], covering the entire process from electron emission to the exit of the accelerating cavity. An initial simulation with 1×10^4 macro-particles was performed to obtain a reasonable starting working point. The number of macro-particles was then increased to 5×10^4 to improve statistical accuracy and numerical stability. Electrons are emitted from a high-voltage thermionic cathode electron gun, whose output parameters are listed in Table 1. Four solenoid magnets are placed in the low-energy section to mitigate strong space-charge effects and suppress emittance growth, ensuring effective beam focusing.

Table 1: Beam Parameters at the Electron Gun Exit

Parameter	Value
Energy [keV]	100
Charge [nC]	1
Full bunch length [ns]	1

The electron beam sequentially passes through a 0.499654 GHz standing-wave sub-harmonic buncher (SHB), an S-band buncher, and a main accelerating structure operating at 2.997924 GHz. The buncher is a $2\pi/3$ traveling-wave structure composed of six phase-velocity-tapered cells and forty-eight constant-velocity cells (54 cells in total). The main accelerating structure is a 2.997924 GHz S-band $2\pi/3$ traveling-wave cavity with 90 cells, accelerating the beam to approximately 65 MeV.

In the initial simulation stage, key operating parameters were manually tuned based on physical intuition to establish a stable working point. Subsequently, the NSGA-II was employed to perform multi-objective global optimization based on the Pareto optimality principle. The optimization aims to maximize the transmission efficiency and minimize the energy spread, with solenoid magnetic fields, SHB phase, buncher phase, and accelerating cavity phase selected as optimization variables. The parameter ranges were determined

* Work supported by the National Natural Science Foundation of China (No. 12405173) and the Anhui Provincial Natural Science Foundation (No. 2508085QA013, Youth Project, Category C)
† zhangtong@hfnl.cn
‡ wanglin@ustc.edu.cn

Content from this work may be used under the terms of the CC BY 4.0 licence (© 2026). Any distribution of this work must maintain attribution to the author(s), title of the work, publisher, and DOI.

ISBN: 978-3-95450-252-3 ISSN: 2673-5350 doi: 10.18429/JACoW-IPAC2026-TUP2665

BEAM DYNAMICS ANALYSIS OF AN ELECTRON MICROTRON USING GENERAL PARTICLE TRACER*

W. Xu[1], F. Zhang[1], Z. Dong[1], Z. Shao[2], T. Zhang[†2], L. Wang[‡1,2], Y. Lu[1,2]
[1]University of Science and Technology of China, Hefei, China
[2]Hefei National Laboratory, Hefei, China

Abstract

Electron microtrons are extensively employed as injectors for tabletop light source facilities. In this paper, a 5 MeV electron microtron is designed, and an external injection scheme is adopted to achieve a large stable longitudinal phase region. We investigated the beam dynamics of this microtron using General Particle Tracer (GPT). After optimization, the width of stable longitudinal phase region is approximately 40 degrees, which is about four times larger than that of conventional internal-injection microtrons.

INTRODUCTION

The concept of resonant acceleration of relativistic charged particles was first proposed by V. I. Veksler in 1944, which led to the development of two major classes of circular accelerators: synchrotrons and microtrons [1]. While synchrotrons employ time-varying magnetic fields to maintain a constant orbit radius during acceleration, classical microtrons operate in a uniform, time-invariant magnetic field, where particles gain a fixed amount of energy each time they traverse a radio-frequency (RF) accelerating cavity.

In a classical microtron, the resonance condition ensures that electrons return to the RF cavity with a constant phase after each revolution, forming a sequence of circular equilibrium orbits with increasing radii [2]. This resonant mechanism enables stable multi-turn acceleration and the generation of electron beams with relatively small energy spread [3]. Owing to their compact structure and reliable operation, classical microtrons have been widely used in scientific research, industrial irradiation, and medical applications, and are particularly suitable as injectors for synchrotron and free-electron laser facilities [4, 5].

According to the injection scheme, classical microtrons can be divided into internal-injection and external-injection configurations. In internal-injection microtrons, electrons are emitted directly within the accelerating cavity and captured into the synchronous acceleration process from the first turn. Although this configuration enables a compact design, the longitudinal capture process is strongly constrained by the RF phase at emission, resulting in a narrow stable phase region and limited capture efficiency [6, 7].

In contrast, external-injection microtrons employ an independent electron gun to generate and pre-accelerate the beam before injection into the microtron cavity. This scheme allows more flexible matching of longitudinal and transverse beam parameters and provides the potential to enlarge the stable longitudinal phase region, thereby improving capture efficiency and operational stability.

Motivated by the demand for compact and reliable injectors for tabletop light source facilities, this work presents the design and beam dynamics analysis of a 5 MeV external-injection classical electron microtron. The beam dynamics are investigated using the GPT code, with particular emphasis on longitudinal phase stability [8]. By optimizing the injection parameters and RF phase, a stable longitudinal phase region with a width of approximately 40 degrees is achieved, representing an improvement by a factor of about four compared with typical internal-injection microtron configurations.

BEAM DYNAMICS SIMULATION

Resonance Conditions

Let the total energy and rest mass energy of an electron in the microtron be U and $U_0 = m_0c^2$, respectively. The corresponding Lorentz factor is defined as $\gamma = U/U_0$. In a uniform magnetic field B, relativistic electrons follow circular orbits with an orbital period given by [3]:

$$T = \frac{2\pi\gamma m_0}{eB} = \frac{2\pi U}{eBc^2}. \tag{1}$$

Each time the electron passes through the RF cavity, it gains an energy increment:

$$\Delta U = eV_{\mathrm{acc}} \cos\phi_s, \tag{2}$$

where V_{acc} is the effective accelerating voltage and ϕ_s is the synchronous phase.

As the electron energy increases turn by turn, the increase in the orbital period must remain synchronized with the RF field. The resonance condition of a classical microtron requires that the period difference between successive orbits equals an integer multiple of the RF period T_{rf}:

$$\Delta T = T_{n+1} - T_n = \frac{2\pi\Delta U}{eBc^2} = nT_{\mathrm{rf}}, \tag{3}$$

where n is the harmonic number.

Under this synchronization condition, the total energy of the electron at the n-th orbit increases linearly and can be written as:

$$U_n = n\Delta U + U_0. \tag{4}$$

* Work supported by the National Natural Science Foundation of China (No. 12405173) and the Anhui Provincial Natural Science Foundation (No. 2508085QA013, Youth Project, Category C)

† zhangtong@hfnl.cn
‡ wanglin@ustc.edu.cn

Content from this work may be used under the terms of the CC BY 4.0 licence (© 2026). Any distribution of this work must maintain attribution to the author(s), title of the work, publisher, and DOI.

ISBN: 978-3-95450-252-3 ISSN: 2673-5350 doi: 10.18429/JACoW-IPAC2026-TUP2666

RF COMMISSIONING RESULTS IN THE SHINE

Y.B.Zhao *, X.Zheng, K.Xu, Z.G.Zhang, Q.Chang, S.J.Zhao
X.F.Huang, X.Y.Li, D.Gu, M.Zhang†, J.F.Chen, B.Liu ‡, Z.T.Zhao
Shanghai Advanced Research Institute, Chinese Academy of Sciences, Shanghai, China

Abstract

SHINE is an 8 GeV continuous-wave (CW) free-electron laser (FEL) facility, mainly composed of an injector, LINAC, an undulator segment, and experimental beamlines. Currently, for the accelerator section, the commissioning of the injector and the L1 segment of the LINAC has been completed. The RF structures in these two segments include a VHF electron gun, an L-band buncher, a dual-feed superconducting cavity, an injection eight-cavity module, two standard 1.3 GHz cryo-modules, and two 3.9 GHz cryo-modules. The RF specification of these accelerating structures have all met the design requirements. This paper will introduce the final parameters achieved through the commissioning of these accelerating structures and some problems encountered during the commissioning process.

INTRODUCTION

Currently, there are three hard X-ray free-electron laser facilities based on superconducting acceleration structures: the European XFEL [1], LCLS-II [2] in the United States, and the Shanghai HIgh repetition rate XFEL aNd Extreme light facility (SHINE) [3]. The first two are already in operation, while SHINE is under construction.

The LINAC of SHINE has a maximum design energy of 8 GeV and operates in continuous-wave (CW) mode. It consists of an injector and four linac sections (L1–L4), as shown in Figure 1. The injector includes a VHF electron gun, an S-band deflecting cavity, a 1.3 GHz buncher cavity, a single-cavity cryomodule, and an ABBA-type 8-cavities cryomodule. Section L1 comprises two standard 1.3 GHz 8-cavities cryomodules and two 3.9 GHz harmonic cryomodules, totaling 16 harmonic cavities. Section L2 has 18 standard 1.3 GHz 8-cavities cryomodules, L3 has 10, and L4 has 24. The total length of the accelerator is approximately 1.4 km. Commissioning of the injector and L1 segment has been completed. The injector output energy is 100 MeV, and the L1 output energy is 270 MeV with normalized emittances of 0.5/0.5 μm in the x/y directions.

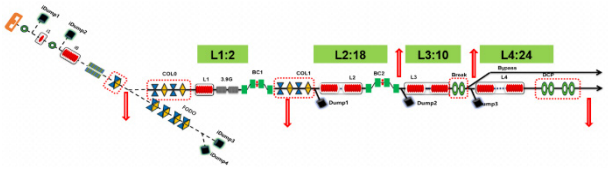

Figure 1: Layout of SHINE Facility

INJECTOR

The main parameters of the injector are listed in Table 1. Figure 2 shows a photograph of the injector front-end. The injector mainly includes a VHF electron gun, a buncher cavity, a single-cavity cryomodule, and an 8-cavities cryomodule.

Table 1: Main Parameters of the Injector

Parameter	Value	Unit
Bunch charge	100	pC
Beam energy	100	MeV
Normalized slice Emittance	≤0.45	μm
Peak current	≥10	A
Bunch repetition rate	0–1	MHz



Figure 2: SHINE injector front-end

VHF Gun

The injector electron gun adopts a VHF gun [4] which operates at 216 MHz, powered by two 60 kW solid-state amplifiers, the gun output voltage is 750kV. The low-level RF (LLRF) system features two up-conversion channels driving the two amplifiers independently. Amplitude and phase balance between the two sources are adjusted online via FPGA algorithms. Since the VHF gun is made of copper and requires high power, significant frequency shifts occur between cold and warm states, leading to a long thermal settling time. An automatic power-up procedure is implemented: first, find resonance at low power in DDS mode with 1% duty

*zhaoyubin@sari.ac.cn, †bo.liu@ari.ac.cn, ‡zhangmeng@sari.ac.cn

Content from this work may be used under the terms of the CC BY 4.0 licence (© 2026). Any distribution of this work must maintain attribution to the author(s), title of the work, publisher, and DOI.

ISBN: 978-3-95450-252-3 ISSN: 2673-5350 doi: 10.18429/JACoW-IPAC2026-TUP2668

PREPARATION AND RESEARCH OF CSBR-COATED CS3SB PHOTOCATHODES

T. hou*, Q. Gu†, X. Li,Y. Cheng, Shanghai Institute of Applied Physics, Pudong, China
Z. Jiang‡, H. Meng, Shanghai Advanced Research Institute, Pudong, China
Ch. Wang, Helmholtz-Zentrum Berlin für Materialien und Energie, Berlin, Germany
Q. Zhou, Zhangjiang Laboratory, Shanghai, China
Z. tong, University of Chinese Academy of Sciences, Beijing, China
N. Delerue, Université Paris-Saclay, CNRS/IN2P3, IJCLab, Orsay, France

Abstract

Abstract Cs_3Sb photocathodes are promising electron sources for accelerators because of their high quantum efficiency (QE) under visible light, but the low robustness under low vacuum limits practical operation. In this work, Cs_3Sb photocathodes coated with CsBr were prepared and characterized. The experimental results indicate that the coating improved the pressure adaptability of the photocathodes by approximately two orders of magnitude, although it inevitably reduced the initial QE. After exposure, the QE of the coated photocathode can be recovered by annealing to its original value.

INTRODUCTION

Advanced accelerator facilities such as free electron lasers (FELs) and energy recovery linacs (ERLs) require high brightness electron beams and therefore impose stringent requirements on photocathodes with respect to quantum efficiency (QE), intrinsic emittance, visible light operation, and operational stability [1,2]. Semiconductor alkali antimonide photocathodes are attractive because of their high QE together with low intrinsic emittance under visible light [1,3]. Among them, Cs_3Sb is a promising candidate for accelerator electron sources [4,5].

However, Cs_3Sb photocathodes are chemically reactive and highly sensitive to residual gases, which can lead to rapid QE degradation and limited 1/e lifetime. Coating photocathodes with thin protective films has been considered a promising route to improve their robustness. Among the candidate materials, CsBr is a representative material for protective films on alkali antimonide photocathodes [6–8]. Such protective films can improve the robustness, but usually unavoidably leading to the QE loss associated with electron transport through the interface and in the coating film [7,8]. In the present work, a CsBr film was deposited on Cs_3Sb photocathode, and the coated photocathodes were evaluated by vacuum adaptability tests and post annealing experiments. Particular attention was paid to the vacuum pressure at which rapid QE degradation began and to the recovery of QE by annealing after exposure.

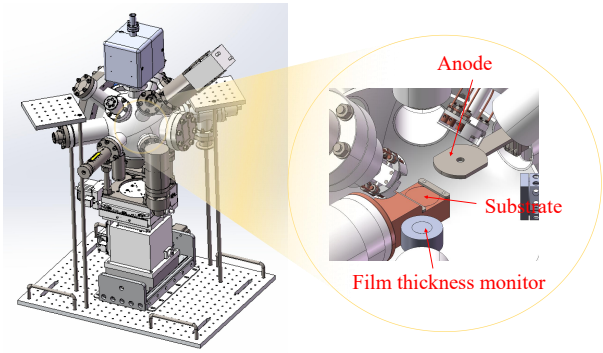

Figure 1: Schematic of the ultra-high-vacuum photocathode preparation apparatus.

EXPERIMENTS

Experimental Setup and Preparations

A dedicated ultra-high-vacuum (UHV) in-situ characterization and preparation equipment, as shown in Fig. 1, was used in this work. At room temperature, the vacuum pressure of the chamber can be maintained at approximately 1×10^{-8} Pa. Two evaporator source holders are mounted, and each holder can equipped with three types of evaporation sources-Cs, Sb and CsBr. A quartz crystal microbalance (QCM) is installed besides the substrate for in situ monitoring of deposition rate. Substrate temperature is monitored by a thermocouple mounted in the substrate holder. The anode is placed above the substrate for photocurrent collection.

Before assembly to the equipment, the Mo substrates were cleaned in ethanol in ultrasonic bath. Prior to photocathode preparation, the Mo substrate was degassed at 500 °C for 6 h, and the chamber was pumped down to 1×10^{-8} Pa.

Following the substrate preparation, Cs_3Sb photocathodes were prepared on Mo substrates by sequential deposition of Sb and Cs layers in a manner similar to the yo-yo process [9]. During the deposition, the pressure was kept below 1×10^{-7} Pa to minimize the interference of rest gases. The growth was started by depositing an initial thin 1 nm Sb layer on the substrate at substrate temperature of 75 °C. Then Cs layer was deposited, while the QE was monitored under 405 nm laser. While Sb and Cs deposition were repeated several times for best QE, in most cases, the peak QE (~3%) was already achieved after the first round, as presented in Fig. 2.

* also at University of Chinese Academy of Sciences, Beijing, China
† Corresponding author: guq@sari.ac.cn
‡ Corresponding author: jiangzg@sari.ac.cn

Content from this work may be used under the terms of the CC BY 4.0 licence (© 2026). Any distribution of this work must maintain attribution to the author(s), title of the work, publisher, and DOI.

ISBN: 978-3-95450-252-3 ISSN: 2673-5350 doi: 10.18429/JACoW-IPAC2026-TUP2670

THE COLLIMATOR SYSTEM FOR REDUCING THE DARK CURRENT IN NSRRC PHOTOINJECTOR

An-Ping Lee, Ming-Chang Chou, Yi-Chieh Chang, Wei-Yuan Chiang, Hsin-Pai Hsueh
National Synchrotron Radiation Research Center, Hsinchu, Taiwan
Shan-You Teng, Department of Physics, National Central University, Taoyuan, Taiwan

Abstract

The NSRRC photo-injector generates ultrashort electron beams to produce superradiant radiation in the 100–500 μm range using a gap-tunable U100 planar undulator. The system comprises an S-band, laser-driven photocathode RF gun equipped with a compensation solenoid and a 5-meter-long linear accelerator (linac) that employs velocity bunching to create sub-picosecond electron beams. Under certain conditions, electrons emitted from the cathode surface can be accelerated to higher energies, while the main beam continues to gain energy in the linac. These stray electrons may strike the vacuum chamber, generating unwanted radiation that poses risks to accelerator components and radiation safety. To mitigate dark current, a collimator was installed between the photocathode gun and the linac to intercept these electrons before transport. This report presents experimental results alongside simulations, demonstrating the effectiveness of the collimator.

INTRODUCTION

The coherent terahertz (THz) facility at NSRRC is a superradiant THz source powered by a relativistic, sub-picosecond, high-brightness electron beam generated by a photoinjector [1,2]. The facility is designed to deliver MW-level superradiant THz radiation for scientific users, covering wavelengths from 100 to 500 μm. As illustrated in Fig. 1, the photocathode injector primarily consists of a 2998 MHz photocathode RF gun driven by a high-pulse-energy, 266 nm ultraviolet laser with a few-picosecond pulse width, and a 5.2 m long 2998 MHz booster linac. A gun solenoid is installed to control the transverse emittance of the electron beam. In operation, a high charge density photoelectron beam is emitted from a copper cathode and accelerated to 2.5 MeV by the RF field at 60 MV/m at the gun exit, thereby reducing the detrimental effects of space-charge forces on beam quality. To further mitigate space-charge effects, the downstream booster linac increases the beam energy to approximately 25 MeV.

However, the strong accelerating field in the gun cavity can induce field emission from the copper surface. These field-emitted electrons are the primary source of background current, commonly referred to as dark current. Some electrons emitted under conditions similar to those of the main beam can be further accelerated by the RF structures to high energies. These uncontrolled electrons then strike the metallic walls of the accelerator vacuum chamber, becoming a major source of excessive ionizing radiation. Effective mitigation of radiation dose induced by dark current can be achieved by removing unwanted particles in the low-energy region of the accelerator. This is best accomplished by introducing a collimator system between the electron gun and the first linac. Positioning the collimator upstream of the linac, where the beam energy is low, minimizes radiological activation, since particle losses at low energy are far less detrimental than those occurring at higher energies later in the accelerator. In this work, we conduct simulations to evaluate the collimator's effectiveness in suppressing dark current and subsequently install the collimator on the photoinjector system to measure the dark current under operational conditions. The experimental measurements are then compared with the simulation results to verify the collimator's blocking performance.

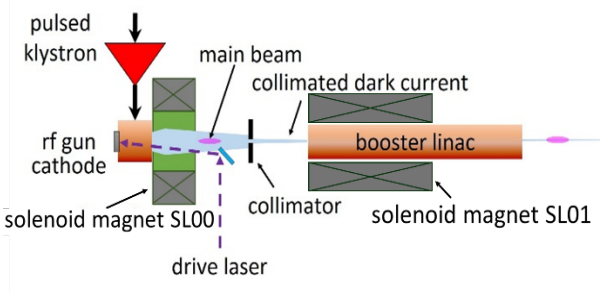

Figure 1: Schematic layout of the NSRRC photoinjector with a collimator installed to mitigate the entry of field-emitted electrons from the rf gun into the booster linac.[3]

DARK CURRENT SIMULATION

In earlier studies [3], a photoinjector system model was constructed by integrating a two-dimensional field map of the photocathode RF gun with the three-dimensional space-charge tracking code IMPACT-T, thereby enabling simulations of both the primary electron beam and the accompanying dark current. Building upon this established framework, the present work applies the same model while adopting the system parameters corresponding to actual operating conditions used for the generation of ultra-short electron beams. This approach allows us to investigate, under realistic circumstances, the effectiveness of a collimator in suppressing dark current.

In the IMPACT-T simulations, the main beam is modeled as a 250-pC electron bunch represented by 100,000 macroparticles, with both space-charge and image-charge effects included. A zero-momentum spread is assumed. The initial transverse distribution of field-emission electrons is calculated using the Fowler–Nordheim equation, which depends on the RF gun cavity field distribution at the cathode surface. Electrons are assumed to be uniformly distributed over an initial longitudinal interval, such that the RF phase experienced by the first emitted particle differs by 90° from that of the last particle.

Content from this work may be used under the terms of the CC BY 4.0 licence (© 2026). Any distribution of this work must maintain attribution to the author(s), title of the work, publisher, and DOI.

ISBN: 978-3-95450-252-3 ISSN: 2673-5350 doi: 10.18429/JACoW-IPAC2026-TUP2672

DESIGN OF A 10-MHz HIGH-ENERGY-RESOLUTION LIGHT SOURCE

J. Liu, C. Feng*, Z. Wang, Z. Zhao, Shanghai Advanced Research Institute, Shanghai, China
Q. Liu, Shanghaitech University, Shanghai, China

Abstract

High energy resolution is essential for advanced spectroscopic studies of quantum materials, especially for resolving low-energy electronic features in angle-resolved photoemission spectroscopy (ARPES). However, existing light sources for ARPES still face difficulties in simultaneously providing narrow bandwidth and high photon flux. We are developing a 10-MHz coherent light source based on angular-dispersion-induced microbunching (ADM), aiming to generate narrow-band radiation with sub-meV-level energy resolution. Start-to-end simulations from the injector to the radiator have been performed to evaluate the beam dynamics and radiation performance. The simulation results show that the proposed source can provide sub-meV-level energy resolution and a photon flux above 10^{12} photons/s over a broad photon-energy range.

INTRODUCTION

Angle-resolved photoemission spectroscopy (ARPES) is a central technique for resolving the electronic band structure of quantum materials [1]. Recent studies of subtle electronic features, such as superconducting gaps and Dirac-cone dispersions, require higher spectral resolution and better photon statistics. Since photons in the 10–100 eV range are particularly useful for valence-band and Fermi-surface measurements, a source providing sub-meV-level bandwidth and sufficient photon flux over this range is highly desirable. Moreover, for a given average photon flux, a higher repetition rate reduces the photons per pulse, helping to mitigate space-charge effects and improve measurement stability.

Although existing light sources used for ARPES have achieved impressive performance, they still involve trade-offs among energy resolution, photon flux, and spectral coverage. Laser-based systems provide excellent energy resolution at low photon energies but have limited photon-energy tunability, whereas synchrotron beamlines offer broad spectral coverage but cannot easily reach sub-meV-level bandwidth without a substantial loss of photon flux.

In this work, we propose a 10-MHz coherent light source based on angular-dispersion-induced microbunching (ADM) [2], using a 550-MeV electron beam. In this scheme, the electron-beam energy is correlated with the transverse divergence before the modulator, which mitigates the impact of initial energy spread on high-harmonic microbunching. As a result, ADM can reduce the required seed-laser power by two to three orders of magnitude compared with conventional coherent harmonic generation (CHG) [3]. The proposed source aims to provide narrow-band radiation with sub-meV energy resolution, high photon flux, and broad photon-energy coverage.

LAYOUT

The layout of the proposed scheme is shown in Fig. 1. This facility consists of an injector, a linac, and a downstream ADM section. The electron gun design follows the SHINE injector scheme [4]. A VHF gun generates 10 MHz, 10 pC electron bunches with a pulse duration of 20 ps, corresponding to an average current of 0.1 mA. The beam is focused by solenoids and accelerated by a single 9-cell superconducting cavity followed by an injector 8-cavity cryomodule (i8CM), reaching an injector exit energy of 130 MeV.

The main linac consists of one 3.9 GHz cryomodule and three 1.3 GHz accelerating cryomodules, boosting the beam energy from 130 MeV to 550 MeV. At the linac exit, the normalized emittance and relative energy spread are about 0.15 mm·mrad and 0.01%, respectively. Three-dimensional start-to-end (S2E) simulations have been carried out using *ASTRA* and *ELEGANT* for injection and acceleration [5,6].

* fengc@sari.ac.cn

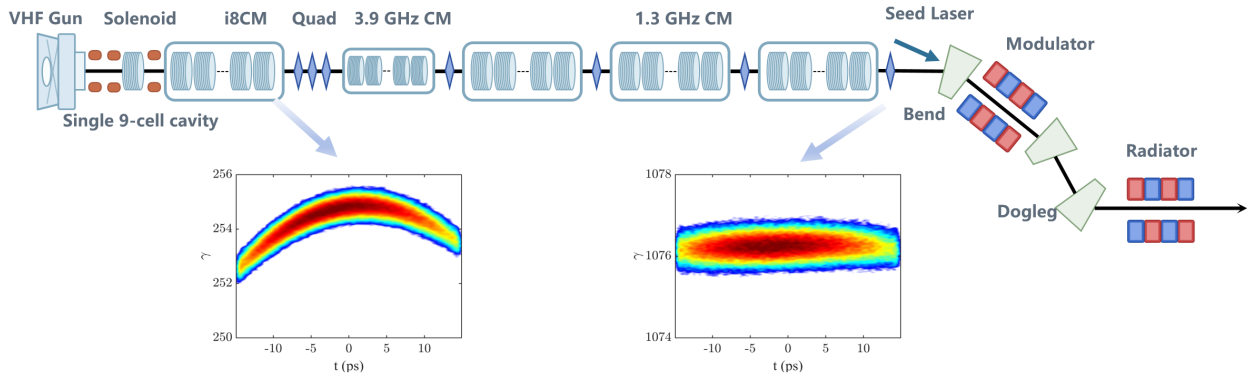

Figure 1: Layout of the proposed source, together with the longitudinal phase-space distributions after the injector and after the main linac.

Content from this work may be used under the terms of the CC BY 4.0 licence (© 2026). Any distribution of this work must maintain attribution to the author(s), title of the work, publisher, and DOI.

ISBN: 978-3-95450-252-3 ISSN: 2673-5350 doi: 10.18429/JACoW-IPAC2026-TUP2673

COMMISSIONING EXPERIENCES OF ACTIVE DOUBLE-RF SYSTEM IN HEPS STORAGE RING*

H. Xu† [1], N. Wang [1], Q. Wang [1], X. Huang [1], D. Ji [1], S. Tian [1], Z. Zhao [1], L. Qin [1], P. Zhang [1], Y. Jiao [1]
Institute of High Energy Physics, Beijing, China
[1]also at University of the Chinese Academy of Sciences, Beijing, China

Abstract

The High Energy Photon Source (HEPS) is the first fourth-generation synchrotron light source in Asia. In HEPS storage ring, there are five 166.6 MHz superconducting cavities serving as fundamental cavities and two 499.8 MHz superconducting cavities as active third harmonic cavities. The employment of active harmonic cavities enables 'ideal bunch lengthening' at any beam current, laying a foundation for flexible beam operation. Beam commissioning of the HEPS storage ring started on July 23, 2024. Due to the presence of delays in the 166.6 MHz cavities, the 499.8 MHz cavities were temporarily utilized as fundamental cavities to provide the required beam acceleration for the first-year commissioning. Starting from August 2025, we initiated the commissioning of an active double-RF system composed of the 166.6 MHz and 499.8 MHz cavities, successfully realizing ideal bunch lengthening under different beam current. Since August 2025, we have commissioned the active double-RF system, successfully achieving ideal bunch lengthening under various beam current conditions. During the ring commissioning process, some beam phenomena associated with the operation of the double-RF system were observed, and experiences in commissioning active double-RF systems was accumulated. This paper reports the key experiences gained from the commissioning and operation of the active double-RF system in the HEPS storage ring, aiming to provide references for similar accelerator projects.

INTRODUCTION

The High Energy Photon Source (HEPS) [1,2], as China's first fourth-generation synchrotron light source, is under the trial operation stage in Beijing, China. HEPS aims to provide ultra-bright hard X-rays for frontier scientific research in various fields. Its accelerator complex is composed of three key parts: a 500 MeV linear accelerator (Linac), a 6 GeV full energy booster for beam energy ramping, and a 6 GeV ultra-low emittance storage ring. The beam commissioning of the HEPS storage ring was officially initiated on July 23, 2024. The first beam storage was achieved in two weeks [3]. Notably, HEPS passed the process acceptance on October 29, 2025, marking that HEPS fulfilled the construction contents and tasks approved by the National Development and Reform Commission, which was a critical step towards the formal operation of HEPS.

* Work supported by National Natural Science Foundation of China (No. 12375149), and the High Energy Photon Source (HEPS) project, a major national science and technology infrastructure in China.
† xuhs@ihep.ac.cn

The HEPS storage ring is designed with the on-axis swap-out injection scheme as its baseline injection strategy, which ensures efficient beam replenishment while maintaining beam quality. One of its core baseline operation modes is the so-called 'high-bunch charge mode', featuring 63 bunches with a total beam current of 200 mA and a single-bunch charge of approximately 14.4 nC. To meet the strict requirements for beam stability, long lifetime, and operational flexibility in this mode, the storage ring is equipped with an double radio-frequency (RF) system. For keeping the flexibility to test the longitudinal injection scheme based on RF gymnastics proposed by ourselves, the higher-harmonic cavities was selected to be active. This system consists of five 166.6 MHz superconducting cavities serving as the fundamental RF system and two 499.8 MHz superconducting cavities acting as active third harmonic cavities [4], shown in Fig. 1. By implementing active harmonic cavities, the HEPS storage ring has the flexibility of achiving arbitrary bunch lengthening at any beam current, for instance, enabling the 'ideal bunch lengthening' condition at any beam current, which is crucial for suppressing collective beam instabilities and supporting stable high-performance operation for users.

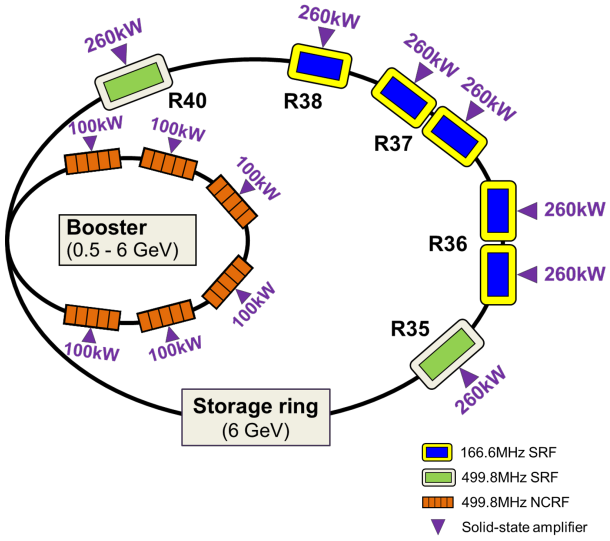

Figure 1: Schetch of the HEPS RF system (Courtesy of Pei Zhang).

During the initial phase of storage ring commissioning, due to delivery delays of the 166.6 MHz fundamental cavities, the 499.8 MHz cavities were temporarily repurposed as fundamental cavities to provide the necessary RF voltage and beam acceleration for initial beam commissioning. Starting from August 2025, the formal commissioning of the

Content from this work may be used under the terms of the CC BY 4.0 licence (© 2026). Any distribution of this work must maintain attribution to the author(s), title of the work, publisher, and DOI.

ISBN: 978-3-95450-252-3 ISSN: 2673-5350 doi: 10.18429/JACoW-IPAC2026-TUP2675

OPTIMIZING A LOW-GAIN FEL OSCILLATOR FOR THE SAPS STORAGE RING: A PARAMETER STUDY*

Weihang Liu[1,2,3†], Fancong Zeng[1,3], Weilun Qin[1,2,3], Yu Zhao[1,2], Jianliang Chen[1,2]
[1]Institute of High Energy Physics, Chinese Academy of Sciences, Beijing, China
[2]Spallation Neutron Source Science Center, Dongguan, China
[3]University of Chinese Academy of Sciences, Beijing, China

Abstract

Achieving higher spectral brightness in fourth-generation light sources like the Southern Advanced Photon Source (SAPS) through integrated free-electron laser (FEL) oscillators presents significant challenges. In response, we present a systematic optimization of the parameters for a low-gain FEL oscillator on the SAPS storage ring. Our work quantitatively evaluates how a transverse gradient undulator (TGU) modifies the ring's equilibrium beam parameters and analyzes the effects of harmonic operation and undulator length on FEL gain. These findings offer essential design guidance for implementing such FEL oscillators in storage rings.

INTRODUCTION

Fourth-generation storage-ring light sources provide high-brightness synchrotron radiation with excellent stability and high repetition rate. However, further improving the spectral brightness, especially in the hard x-ray range, remains an important goal for future light-source development. One possible approach is to integrate a low-gain x-ray FEL oscillator into a storage ring, where coherent radiation can be built up in an optical cavity while preserving the high-repetition-rate nature of the ring-based source [1]. For storage-ring-based FEL oscillators, the relatively large equilibrium energy spread and transverse beam size can strongly limit the single-pass FEL gain. A transverse gradient undulator (TGU), combined with a local dispersion, provides a possible way to improve the transverse overlap between electrons with different energies and the radiation field, thereby enhancing the gain. This concept is particularly attractive for storage rings, but it also introduces additional constraints. When the TGU is installed directly in a storage-ring straight section, the local dispersion and the TGU field can modify the equilibrium beam parameters, especially the vertical emittance. Therefore, the FEL gain optimization must be performed together with an evaluation of the resulting storage-ring equilibrium parameters. In this work, we study a low-gain FEL oscillator based on the SAPS storage ring parameters. Because the SAPS beam energy is 3.5 GeV, harmonic radiation is considered to reach the hard x-ray photon-energy range compatible with high-reflectivity Bragg crystal cavities. We first evaluate the effect of a vertically oriented TGU on the storage-ring equilibrium parameters. We then optimize the main FEL oscillator parameters, including the vertical dispersion, TGU gradient, Rayleigh length, and undulator length. The study identifies the parameter range required to obtain a practical single-pass gain and clarifies the main physics and technical challenges for implementing such an FEL oscillator in SAPS.

IMPACT OF THE TGU ON THE STORAGE-RING EQUILIBRIUM PARAMETERS

We consider installing the TGU directly in a storage-ring straight section, avoiding the frequent extraction and reinjection required in a bypass configuration. Although operationally simpler, this layout can modify the ring equilibrium parameters, especially the emittance, through the combined effect of the TGU and local dispersion. An analytical treatment, to be reported elsewhere, shows that a vertically oriented TGU in a section with vertical dispersion D modifies the vertical dispersion as

$$\varepsilon_y = C_q \gamma^2 \frac{I_{5,\mathrm{TGU}}}{j_{y,\mathrm{TGU}} \left(I_{2,0} + I_{2,\mathrm{TGU}}\right)}. \tag{1}$$

Here $j_{y,\mathrm{TGU}}$ is given by

$$j_{y,\mathrm{TGU}} = 1 - \frac{I_{4,\mathrm{TGU}}}{I_{2,0} + I_{2,\mathrm{TGU}}}. \tag{2}$$

The TGU contributions to the radiation integrals are

$$I_{2,\mathrm{TGU}} = \frac{B_0^2 L_u}{2(B\rho)^2}, \tag{3}$$

$$I_{4,\mathrm{TGU}} = \frac{B_0^2 L_u}{(B\rho)^2} \left[\alpha \left(D + \eta_0\right) - \frac{3}{8} \frac{B_0 \eta_0}{B\rho} \right], \tag{4}$$

and

$$I_{5,\mathrm{TGU}} = \frac{B_0^3 L_u}{(B\rho)^3} \Big[\frac{4}{3\pi} \frac{\left(D + \eta_0\right)^2}{\beta_{y0}} - \frac{3}{4} \frac{\eta_0 \left(D + \eta_0\right)}{\beta_{y0}} + \frac{4}{15\pi} \left(\frac{4}{\beta_{y0}} + \beta_{y0} k_u^2 \right) \eta_0^2 \Big]. \tag{5}$$

The parameter η_0 is defined as

$$\eta_0 = \frac{eB_0(\alpha D - 1)}{mc\gamma^2 k_u^2}. \tag{6}$$

This expression allows us to evaluate the contribution of the TGU to the equilibrium emittance. Using the SAPS storage-ring parameters, we then scan the vertical dispersion D and the TGU gradient α to quantify their impact on the beam emittance. Figure 1 shows the resulting dependence of the vertical emittance on D and α.

* Work supported by National Natural Science Foundation of China (No. 12405176)

† liuwh@ihep.ac.cn

Content from this work may be used under the terms of the CC BY 4.0 licence (© 2026). Any distribution of this work must maintain attribution to the author(s), title of the work, publisher, and DOI.

ISBN: 978-3-95450-252-3 ISSN: 2673-5350 doi: 10.18429/JACoW-IPAC2026-TUP2676

BEAM BASED ALIGNMENT FOR BENDING MAGNETS WITH TRANSVERSE GRADIENT*

Kemin Chen, Zhe Wang, Tao He, Zhonghan Wang, Wei Xu†
NSRL, University of Science and Technology of China, Hefei, Anhui, China

Abstract

For storage rings, bending magnets with transverse gradient are commonly adopted to reduce the natural emittance. These magnets are typically offset quadrupoles, which generate combined dipole and quadrupole fields. Therefore, it is crucial to ensure that the beam travels at the designed off-axis position within the target magnets. Otherwise, particles would experience an additional dipole field due to the magnetic field feed-down effect, which could influence the beam dynamics. To determine the beam position in the bending magnets with transverse gradient, a beam-based alignment method is presented in this paper.

INTRODUCTION

Due to the superior performance of synchrotron radiation-based light sources, they play an important role in modern scientific research on quantum materials, catalytic science, bioscience, and other fields. As synchrotron radiation facilities, storage ring-based light sources are in operation, under construction, or in design around the world. The brightness of the light sources is the key parameter for end-users. Therefore, achieving low emittance is crucial.

To achieve low emittance, storage rings usually adopt the multi-bend achromat (MBA) lattice structure and some combined-function magnets. Bending magnets with transverse gradient are a common type of combined-function magnets, which can be realized using an off-axis quadrupole design [1, 2]. It is crucial to ensure that the beam position is corrected in these magnets in order to provide the designed bending angle and quadrupole field. Otherwise, the dynamic performance could be degraded due to the magnetic field feed-down effect. A beam-based alignment (BBA) method can be employed to determine the beam position in transverse gradient dipoles.

The remaining content is organized as follows. First, the beam-based alignment method for dipoles with transverse gradient is introduced. Subsequently, the simulation using the BBA method is presented. Finally, a concise summary is provided.

METHOD

The bending magnet with transverse gradient is an off-axis quadrupole. The beam position $X(s_0)$ of the particles at the location of the quadrupole s_0 can be described by

$$X(s_0) = x\hat{x} + y\hat{y}, \tag{1}$$

where x and y are the particle offsets relative to the magnetic center in the horizontal and vertical planes, respectively. The magnetic field strength can be expressed as

$$B_x = B_0\rho_0 K y, \tag{2}$$

$$B_y = B_0\rho_0 K x_0 + B_0\rho_0 K(x - x_0), \tag{3}$$

where x_0 is the designed offset of the beam in the combined-function magnets, $B_0\rho_0$ is the magnetic rigidity, and K is the normalized quadrupole strength.

Due to the magnetic field feed-down effect, the electron beam experiences an additional kick when it travels away from the design offset of the combined-function magnets, which has a significant influence on the ring dynamics. To suppress this effect, the beam should pass through the design offsets of the bending magnet with transverse gradient. The BBA technique is used to determine the current offset by using the dipole coils combined to the target magnets.

By changing the quadrupole strength by ΔK, the variation of the dipole field is given by

$$\Delta B_x = B_0\rho_0 \Delta K y, \quad \Delta B_y = B_0\rho_0 \Delta K x, \tag{4}$$

which causes a perturbation to the beam orbit.

To perform the beam-based alignment technique, the magnets are equipped with horizontal and vertical dipole corrector coils. During the measurement, the strengths of these corrector coils are adjusted, yielding

$$\Delta B_x = B_x^{\mathrm{VCM}} + B_0\rho_0 \Delta K y, \tag{5}$$

$$\Delta B_y = B_y^{\mathrm{HCM}} + B_0\rho_0 \Delta K x, \tag{6}$$

where B_y^{HCM} and B_x^{VCM} are the strengths of the horizontal and vertical dipole corrector coils, respectively. The variation of dipole field strength results in an orbit change at location s [3],

$$\Delta X(s) = \frac{\Delta B}{B_0\rho_0} \frac{\sqrt{\beta(s)\beta(s_0)}}{2\sin(\pi\nu)} \cos\left(|\phi(s) - \phi(s_0)| - \pi\nu\right), \tag{7}$$

where $\beta(s_0)$ and $\beta(s)$ are the beta functions at the location of the quadrupole and the observation points respectively, $\phi(s_0)$ and $\phi(s)$ are the betatron phases, and ν is the betatron tune.

Assuming that the Courant-Snyder parameters are constant when the change of quadrupole field strength ΔK is small, the orbit change $\Delta X(s)$ is proportional to ΔB. If the beam orbit is minimally affected by changing the quadrupole

* Work supported by the National Natural Science Foundation of China (No. 11975227)

† wxu@ustc.edu.cn

Content from this work may be used under the terms of the CC BY 4.0 licence (© 2026). Any distribution of this work must maintain attribution to the author(s), title of the work, publisher, and DOI.

ISBN: 978-3-95450-252-3 ISSN: 2673-5350 doi: 10.18429/JACoW-IPAC2026-TUP2678

ANALYSIS AND COMPENSATION OF THE INSERTION DEVICE EFFECTS IN THE HALF STORAGE RING*

Gangwen Liu, Penghui Yang†, Zhouyu Zhao††, Zhenghe Bai
National Synchrotron Radiation Laboratory,
University of Science and Technology of China, Hefei, Anhui, China

Abstract

The Hefei Advanced Light Facility (HALF) is a diffraction-limited storage ring light source with a beam energy of 2.2 GeV. Thirteen insertion devices (IDs) will be installed in the storage ring, which will have a substantial impact on the low-energy beam. Particularly for the long-period EPU, the nonlinear effects significantly reduce the dynamic aperture of the storage ring. In this paper, the effects of the IDs are analyzed in detail with kick-map models for the HALF storage ring. Each ID is compensated using a local quadrupole feedforward method. For some EPUs with significant impacts, additional compensation is provided through the shimming of current strips. The analysis and compensation results will be presented in this paper.

INTRODUCTION

The Hefei Advanced Light Facility (HALF) [1], a new VUV and soft X-ray diffraction-limited storage ring-based light source, is currently under construction and is expected to be in operation in 2028. The design aims to achieve a natural emittance below 100 pm·rad at an electron beam energy of 2.2 GeV with 20 long straight section and 20 short straight section available for installing insertion devices. In the first construction phase, 13 insertion devices will be installed for 10 beam lines, including 2 wigglers for beam damping. The parameters of these IDs are listed in Table 1. These IDs will introduce additional focusing effects that alter the linear optics parameters such as betatron tune and beta functions, and their field errors and misalignments can distort the closed orbit. Moreover, their nonlinear magnetic fields can reduce the dynamic aperture, impacting beam injection efficiency and lifetime [2]. These effects caused by insertion devices must be compensated to ensure the stable operation of the storage ring.

Local compensation using pairs of quadrupoles placed adjacent to an insertion device is an effective method to locally correct the induced linear optics distortions without affecting the rest of the storage ring. Nevertheless, this method still has difficulty dealing with the higher-order nonlinear effects induced by these insertion devices. As a widely and maturely applied method, Current strip shimming has the ability to correct higher-order nonlinear effects by compensating the field integrals and multipole errors with current-carrying strips placed near the magnetic poles [3, 4].

Table 1: Main Parameters of the Insertion Devices in the HALF Storage Ring

ID	Period /mm	Period number	Min. Gap/mm	Max. K
IVU21	20.7	54	6	2.1
IVU21	20.7	182	6	2.1
LPU38	38.2	108	12	3.39
LPU38	38.2	108	12	3.39
Wiggler	100	41	12	16
EPU42	41.5	99	14	2.65
EPU44	43.5	33*2	14	2.94
EPU46	46	90	14	3.24
EPU63	63	65	14	5.65
HU115	115	35	14	8.89
EPU120	120	33	20	11.26

KICK-MAP THEORY

Kick-map theory is a powerful analytical framework to model the integrated effects of insertion devices on the dynamics of charged particle beams. The kick-map approach condenses the net effect into a set of transverse momentum kicks imparted to the beam as a function of its initial position and angle. The kicks are derived from the integrated magnetic field, which can be expressed using the following formula [5]:

$$\frac{dx}{ds}(\infty) = -\frac{1}{2}\left(\frac{e}{\gamma mc}\right)^2 \frac{\partial \Psi}{\partial x} \quad \frac{dy}{ds}(\infty) = -\frac{1}{2}\left(\frac{e}{\gamma mc}\right)^2 \frac{\partial \Psi}{\partial y} \quad (1)$$

$$\Psi(x,y,s) = \int_{-\infty}^{\infty}[(\int_{-\infty}^{s} B_x(x,y,s)ds)^2+(\int_{-\infty}^{s} B_y(x,y,s)ds)^2]ds \quad (2)$$

Where *Bx*, *By* are the magnetic field components along the insertion device. By performing Fourier transform on the magnetic field and applying a first-order approximation, Eq. (1) can be simplified to the following equation.

$$\frac{dx}{ds}(\infty) = -\left(\frac{e}{\gamma mc}\right)^2 \frac{N\lambda_0^3}{16\pi^2}\frac{\partial (B_{x,1}^2+B_{y,1}^2)}{\partial x} \quad (3)$$

$$\frac{dy}{ds}(\infty) = -\left(\frac{e}{\gamma mc}\right)^2 \frac{N\lambda_0^3}{16\pi^2}\frac{\partial (B_{x,1}^2+B_{y,1}^2)}{\partial y} \quad (4)$$

Where λ_0 is the period length of the inseriton device, and *N* is the period number. From the Eq. (3) and Eq. (4), it can be seen that the dynamic integrated field effect of the insertion device is inversely proportional to the square of

* This work was supported by the Fundamental Research Funds for the Central Universities (No. WK2310000107) and the National Natural Science Foundation of China (No.12205299).

† penghui1@ustc.edu.cn
†† yuzz@ustc.edu.cn

Content from this work may be used under the terms of the CC BY 4.0 licence (© 2026). Any distribution of this work must maintain attribution to the author(s), title of the work, publisher, and DOI.

ISBN: 978-3-95450-252-3 ISSN: 2673-5350 doi: 10.18429/JACoW-IPAC2026-TUP2679

SYMPLECTIC TRACKING OF DAMPING WIGGLERS USING GENERALIZED GRADIENT REPRESENTATIONS*

W. Fan, J. Li†, R. Li, Y. Lu, Zhangjiang Laboratory, Shanghai, China
Y. Ding, Q. Zhang‡, C. Feng§, Shanghai Advanced Research Institute, Shanghai, China

Abstract

Strong wigglers are installed in the storage ring to provide a strong damping effect and thus can make the particle beam reach an equilibrium state quickly. Nevertheless, particle tracking of damping wigglers with strong peak field strengths typically uses the field map analysis approach, which does not account for radiation effects and quantum excitations in ELEGANT. To address this, the Generalized Gradient Expansion (GGExp) method is employed to describe the strong magnetic fields of damping wigglers in storage rings. The GGExp method provides an alternative approach to define the wiggler field, incorporating synchrotron radiation effects with symplectic tracking, and offers benefits for both linear and nonlinear analysis.

INTRODUCTION

Light sources are one of the most powerful tools for scientific research. Although both the synchrotron light source and free electron laser (FEL) have been developed for decades, the poor coherence of the synchrotron radiation and the low repetition rate of the FEL radiation are the main constraints for the high average power. Hence, a Storage-Ring-based Coherent Light Source (SRCLS) [1] is proposed, which combines relatively high coherence with an ultra-high repetition rate and can overcome the disadvantages of these two types of light sources. The SRCLS consists of a photoinjector to produce electron beams with small emittance and a full-energy linac to accelerate them to 1400 MeV. This electron beam then is transported into a storage ring with 12 damping wigglers. The coherent radiation can be generated when the electron beam in the storage ring is extracted to the bypass line, where the electron beam will work in the angular dispersion-induced modulation (ADM) scheme [2]. The degraded electron beam will be reinjected back to the storage ring and damped to the new equilibrium state. To achieve high-repetition-rate FEL radiation, the damping rate should be high. Therefore, a large number of superconducting damping wigglers with high peak field strength are deployed. These wigglers cannot be accurately modeled in the particle tracking code ELEGANT [3] using the CWIGGLER or FTABLE elements. Therefore, the Generalized Gradient Expansion (GGExp) [4, 5] is adopted to reconstruct the real wiggler field to get precise results related to dispersion, emittance, and so on.

* Work supported by Shanghai Municipal Science and Technology Major Project
† liji@zjlab.ac.cn
‡ zhangql@sari.ac.cn
§ fengc@sari.ac.cn

NUMERICAL IMPLEMENTATIONS FOR AN ELLIPTICAL CYLINDRICAL BOUNDARY

Previous simulations show that the dynamic aperture of a light source with damping rings is highly sensitive to the nonlinear characteristics of wiggler transfer maps. In many cases, the computation of single-particle transfer maps for wigglers has relied on idealized wiggler models. However, wiggler transfer maps are generally influenced by fringe-field and high-order multipole effects, which can significantly impact their accuracy. Accounting for these effects requires a detailed and realistic representation of both the interior and fringe magnetic fields, including precise knowledge of higher-order spatial derivatives. In this section, we examine the benefits of calculating these transfer maps using data defined on the surface of a cylinder with an elliptical cross-section.

We have obtained a detailed model of a wiggler field with an elliptical cross-section using data exported from OPERA. Specifically, OPERA provided the three-dimensional magnetic field (**B**) along the entire length of the wiggler, including both the central region and the fringe-field regions. These data were represented on a rectangular mesh, covering the complete magnetic field distribution of the wiggler. By applying polynomial spline interpolation, we extracted the normal magnetic field component (**B**) on the surface of the elliptical cross-section. Subsequently, using these normal components on the surface and employing the scalar potential as an intermediate step, we computed the expansion of the vector potential (**A**) inside the wiggler. This process provides a precise foundation for describing the nonlinear characteristics of the wiggler and its dynamic behavior in damping rings.

In a current-free region, we use a scalar potential ψ that satisfies $\mathbf{B} = \nabla\psi$. To describe the system, we adopt elliptic cylindrical coordinates, which are defined by the intersection of confocal ellipses and confocal hyperbolas. These coordinates are expressed as follows [6]

$$\begin{aligned} x &= f\cosh(u)\cos(v), \\ y &= f\sinh(u)\sin(v), \\ z &= z, \end{aligned} \tag{1}$$

where f is the distance from the origin to the two foci, and u,v are the radial and angular coordinates. Additionally, the scalar potential must satisfy $\nabla^2\psi = 0$. To account for the longitudinal variation, we apply a Fourier transform in z:

$$\tilde{\psi}(r,\phi,k) = \frac{1}{\sqrt{2\pi}}\int_{-\infty}^{\infty}\psi(r,\phi,k)e^{-ikz}dz, \tag{2}$$

Content from this work may be used under the terms of the CC BY 4.0 licence (© 2026). Any distribution of this work must maintain attribution to the author(s), title of the work, publisher, and DOI.

ISBN: 978-3-95450-252-3 ISSN: 2673-5350 doi: 10.18429/JACoW-IPAC2026-TUP2680

INVESTIGATION OF THE COMPENSATION SCHEME USING THE BROADBAND KICKER CAVITY TO MITIGATE THE TRANSIENT BEAM-LOADING EFFECT IN SYNCHROTRON LIGHT SOURCES*

D. Naito†, A. Motomura, S. Sakanaka, T. Takahashi, N. Yamamoto
Accelerator Laboratory, High Energy Accelerator Research Organization (KEK), Tsukuba, Japan

Abstract

The bunch lengthening technique is the most reliable method to mitigate the intrabeam scattering in synchrotron light sources. However, the performance of the bunch lengthening can be degraded by the transient beam-loading (TBL) effect, which increases when long gaps are introduced in the bunch filling pattern. To mitigate the TBL effect, we have proposed a compensation method using a broadband kicker cavity, and carried out the performance tests of the low-power model cavity. In this presentation, the performance of the TBL compensation using the kicker cavity is discussed in detail, based on the results of these tests. As an example, the TBL compensation at the KEK PF 2.5 GeV ring is investigated using semianalytical calculations.

INTRODUCTION

At storage-ring light sources, the bunch-lengthening technique using a combination of fundamental and harmonic cavities is useful to mitigate the harmful effects of intrabeam scattering [1]. When large gaps are introduced in the fill pattern of the bunch train, the performance of the bunch-lengthening can be degraded by the transient beam loading (TBL) effect [2]. To mitigate the TBL effect, we have proposed a compensation method using a broadband cavity [3]. We have also investigated the conceptual design of the kicker cavity, and carried out performance tests of a low-power model cavity that can be used to compensate for the TBL effect [4]. In this paper, as an example of the TBL compensation, we investigate the performance of the TBL compensation at the KEK Photon Factory (PF) 2.5 GeV ring [5] based on semianalytical calculations. At first, we evaluate the performance of the bunch lengthening using a double RF system, which is under consideration at the PF ring. Second, the strategy of the TBL compensation at the PF ring is discussed. Finaly, the performance of the TBL compensation using the kicker cavity is investigated.

BUNCH LENGTHENING AT THE PF RING

Table 1 shows the beam parameters assumed in this paper. In the PF ring, there are two operation modes: multi-bunch mode and hybrid mode. The fill pattern of the hybrid mode consists of 129 bunches, 91 gaps, a single bunch and 91 gaps. The beam current of the multi bunches and the single bunch are 0.4 A and 0.05 A, respectively. Table 2 shows the RF parameters of the fundamental and harmonic cavities. At present, the harmonic cavities are not installed in the PF ring, and they are under consideration for the bunch lengthening. In this paper, we investigate the bunch lengthening using two or three harmonic cavities, which are defined as Cases A and B, respectively. In Table 2, the values allocated to Cases A and B are denoted by two values separated by ''/''. The operation of the harmonic cavities are assumed to be the passive. The parameters of the fundamental and harmonic cavities are based on those of the cavity installed in the PF ring and the TM020 cavity developed by our group, respectively [6].

Table 1: Beam Parameters of Hybrid Mode

Parameter	Value
Total beam current	0.45 A
Number of multi bunch	129
Number of gaps	91 × 2
Harmonics	312
Bucket interval	2 ns
Beam energy	2.5 GeV
Momentum compaction	0.0064
Energy loss per turn	399 KeV
Energy spread	7.28e-4

Table 2: RF Parameters for the Bunch Lengthening at the PF Ring

Parameter	Fundamental	Harmonic
Number of cavity	4	2 / 3
Frequency	500.1 MHz	1500.3 MHz
Total R/Q[1]	697.4 Ω	136 / 204Ω
Unloaded Q	39000	31400
Coupling factor	3.5	0.5
Total cavity voltage	1.7 MV	320 / 480 kV
Synchronous phase	1.29 / 1.26 radian	−1.82 radian
Tunning angle	−0.99 radain	1.32 radian

The performance of the bunch lengthening at the PF ring is evaluated using a semianalytical calculation, the details of which are described in reference [3]. In this calculation, we assumed that the bunch charge in multi bunches is uniform and that the bunch shape is gaussian. Figures 1 shows the bunch length calculated by semianalytical calculations. In Fig. 1, the horizontal and vertical axises show the bucket index and the longitudinal bunch length for each bunch,

* Work supported by JSPS KAKENHI Grant Numbers JP24K03210 and JP24K15601

† daichi.naito@kek.jp

[1] $R = V_c^2/P_c$

Content from this work may be used under the terms of the CC BY 4.0 licence (© 2026). Any distribution of this work must maintain attribution to the author(s), title of the work, publisher, and DOI.

ISBN: 978-3-95450-252-3 ISSN: 2673-5350 doi: 10.18429/JACoW-IPAC2026-TUP2681

SUPPRESSION OF LONGITUDINAL INSTABILITY AT NanoTerasu

K. Ueshima*, A. Agui, T. Asaka, Y. Hosaka, K. Inaba, K. Kan, N. Nishimori, S. Obara, C. Saji
NanoTerasu Center, QST, Sendai, Miyagi, Japan
R. Saida, K. Moriya, T. Tsuchiyama, R. Yoshioka
NAT Corporation, Hitachinaka, Ibaraki, Japan

Content from this work may be used under the terms of the CC BY 4.0 licence (© 2026). Any distribution of this work must maintain attribution to the author(s), title of the work, publisher, and DOI.

Abstract

NanoTerasu is a newly constructed 3 GeV synchrotron radiation light source located in Sendai, Japan. The compact normal-conducting RF cavity operating in the TM020 mode with higher-order mode (HOM) dampers is employed for beam acceleration. However, a longitudinal coupled-bunch instability was observed during the storage ring commissioning in 2023 at a beam current of approximately 150 mA. The energy spread was continuously monitored using the stored beam profile monitor to detect the longitudinal coupled-bunch instability. Although partial suppression was achieved by adjusting the RF cavity temperature, the stored beam current during user operation remained limited to 200 mA in 2024. To overcome this limitation, a compact waveguide-overloaded kicker cavity and longitudinal bunch-by-bunch feedback (LBBF) system were developed and installed. The commissioning of the LBBF system in July 2025 enabled stable beam storage at the design current of 400 mA. The longitudinal coupled-bunch instability was perfectly suppressed. The stored beam current for user operation was subsequently increased, and routine user operation at 400 mA with high reliability began in November 2025. The longitudinal instability suppression at NanoTerasu was reported.

INTRODUCTION

The NanoTerasu is a compact 3 GeV synchrotron radiation light source newly constructed in Sendai, Japan [1, 2]. The circumference of storage ring (SR) is 349 m and the natural emittance is 1.14 nm rad, which is realized by a double-double-bend achromat lattice. The designed stored beam current is 400 mA.

The normal-conducting accelerating cavity adopts the world's first compact cavity that accelerates the stored beam in the TM020 mode [3]. The ferrite-based RF absorbers are installed inside the slot which is placed at the magnetic field node of the axially symmetric TM020 mode. This structure is designed to attenuate higher-order mode (HOM) components that can induce coupled-bunch beam instabilities. To reduce the HOM components, the superconducting or normal-conducting HOM free cavities were widely used in various synchrotron radiation facilities. At NanoTerasu normal-conducting TM020 HOM-damped cavity with a higher unloaded quality factor (Q_0) and accelerating gradient was employed. In contrast to the conventional HOM-damped cavities employed at European light sources such as BESSY [4] and ESRF [5], which operate in the TM010 accelerating mode and rely on strong broadband HOM absorbers, the TM020 cavity utilizes a higher-order accelerating mode with intrinsically lower R/Q_0, where R is the shunt impedance. Consequently, the beam-cavity interaction is significantly reduced. This feature reduces beam loading and longitudinal coupling impedance, while allowing efficient HOM damping by absorbers placed at field nodes without degrading the fundamental mode performance.

The commissioning of the storage ring started in June 2023 [6]. Although HOM-damped cavity was employed, the longitudinal coupled-bunch instability was observed when the stored beam current exceeded 150 mA in August 2023. As a result of investigating the accelerating cavity, this instability was attributed to the growth of a 1.9 GHz component of HOM.

To suppress the longitudinal instability, the temperature of TM020 HOM-damped cavity was adjusted. However, the stored beam current was limited to 200 mA due to the longitudinal instability in 2024. To increase the stored beam current, we started to develop the waveguide-overloaded kicker cavity and the LBBF system. The waveguide-overload kicker cavity was developed at DAΦNE in 1990s [7]. This type of kicker cavity was used in the various facilities to suppress the longitudinal coupled-bunch instability. We also developed a compact kicker cavity with low quality factor and wide bandwidth.

The kicker cavity was installed in the storage ring in May 2025. The commissioning of LBBF system was carried out in July 2025. We achieved the designed 400 mA stable beam accumulation using TM020 HOM-damped cavity and LBBF system in July 2025. The suppression of longitudinal coupled-bunch instability using TM020 HOM-damped cavity and LBBF system was reported.

LONGITUDINAL INSTABILITY

The some HOM field components exhibit nodal points of the HOM damper in the TM020 cavity, which limits the effectiveness of the damper and leads to residual unabsorbed HOM power. Among the residual HOM components, the 1.9 GHz component caused significant longitudinal coupled-bunch instability and limited the stored beam current to 200 mA.

Figure 1 shows the spectrum of the 1.9 GHz HOM from the pickup of the accelerating cavity, as well as the frequency spectrum of the beam position monitor (BPM), during the occurrence of longitudinal beam instability. In the BPM signal spectrum, sideband frequency components shifted by

* ueshima.kouta@qst.go.jp

ISBN: 978-3-95450-252-3 ISSN: 2673-5350 doi: 10.18429/JACoW-IPAC2026-TUP2682

EVALUATION AND MITIGATION OF MAGNETIC CROSS-TALK IN THE KOREA-4GSR STORAGE RING

S. An, Y. G. Choi, G. Hahn, D. E. Kim*
Pohang Accelerator Laboratory, POSTECH, Pohang, Republic of Korea

Content from this work may be used under the terms of the CC BY 4.0 licence (© 2026). Any distribution of this work must maintain attribution to the author(s), title of the work, publisher, and DOI.

Abstract

Korea-4GSR is a new 4-GeV synchrotron light source under construction since 2021, targeting ultralow emittance performance of 60 pm rad. To reach this regime, the lattice uses a hybrid multi-bend achromat (HMBA) configuration, which increases the number of magnets per cell and raises concerns about magnetic cross-talk. The short magnet spacing may degrade field quality, perturbing particle orbits and enhancing nonlinear effects in beam dynamics. 3D finite-element simulations were performed for all magnet pairs in the ring, and no meaningful cross-talk was identified in most configurations. Magnet pairs involving dipoles, however, can alter the bending strength and thus directly impact the beam trajectory, necessitating focused evaluation. For these dipole pairs, we performed both simulations and magnetic measurements and demonstrated that a field-clamp effectively suppresses the cross-talk. This paper highlights the mitigation capability of the field-clamp approach.

INTRODUCTION

Korea-4GSR is a new 4-th generation storage ring under construction in Ochang, Korea, designed to achieve an ultralow emittance of 60 pm rad via a hybrid multi-bend achromat (HMBA) lattice [1]. To realize this lattice within the available cell length, the HMBA design packs standard multipoles together with combined-function magnets such as dipole-quadrupole to their physical limits [2]. The resulting narrow magnet-to-magnet separation makes magnetic cross-talk one of the principal challenges of the design: it alters the multipole components and the integrated bending strength, consuming the correction margin reserved for manufacturing tolerance and misalignments, and – in dipole-bearing pairs – can directly steer the beam trajectory.

Similar cross-talk issues have been reported across modern low-emittance storage rings, with mitigation strategies ranging from passive shielding (TPS [3]) and software-based current compensation (APS-U [4]) to lattice-integrated correction informed by 3D finite-element (FEM) simulations (ESRF-EBS [5]); PETRA IV [6] and SLS-2.0 [7] have more recently reported nonlinear cross-talk behaviors and tailored compensation schemes. The specific combinations of longitudinal-gradient bending magnet (LGBM) and center bending magnet (CBM) in the Korea-4GSR HMBA cell, however, have not yet been characterized in this context.

In this work, we evaluate cross-talk on multipole components and beam trajectory through 3D FEM simulations of every magnet pair in the storage ring. Most pairs exhibit negligible cross-talk, and the present analysis therefore focuses on dipole-quadrupole combinations, which dominate the effect. We then demonstrate mitigation via field clamps and apply feed-forward pre-tuning to compensate for the combined field deficit that remains after clamp installation.

EVALUATION

Cross-talk in the Korea-4GSR storage ring was evaluated by 3D FEM simulations in Opera-3D. Because the effect is short-range and geometry-sensitive, the full ring was decomposed into magnet pairs comprising one main magnet and one neighbor with longitudinal separation. This pair-wise approach, adopted in most prior studies [3–7], keeps the simulation tractable while preserving the dominant interactions. Non-dipole pairs were retained only when their longitudinal separation did not exceed 110 mm, beyond which neighbor effects become negligible. Dipole-bearing pairs were evaluated at all longitudinal separations, because even a small decrease in their integrated field directly perturbs the beam trajectory. Each pair was modeled in its actual lattice geometry; whenever a pair contained a dipole, the dipole's bending introduces a small longitudinal angle between two magnets, and this geometry was preserved in the simulation. Each LGBM consists of five modules; only the edge modules facing the neighbor were retained, while the central modules are too far away to contribute to the cross-talk. An initial survey of all such pairs identified no meaningful cross-talk in configurations not involving a dipole; only dipole-bearing pairs are therefore retained for detailed analysis.

Two scope decisions further narrow the analysis. First, dipole-bearing pairs are retained at all longitudinal separations, including those exceeding 110 mm, because even a small reduction in their integrated field directly perturbs the beam trajectory. Second, the leakage of the DQ32 quadrupole field into the neighboring octupole (about 2.0 % of the octupole's design field) is absorbed at the source by adjusting the DQ32 operating current, an approach distinct from the lattice rematching adopted for the same cross-talk channel at ESRF-EBS [5], and is therefore not discussed further here. The five dipole-quadrupole combinations retained for the detailed analysis are listed in Table 1, and a representative pair as modeled in Opera-3D is shown in Fig. 1.

Each pair was simulated in three configurations: both magnets fully powered (*paired*), and each magnet powered in isolation with its neighbor replaced by a non-magnetic block of identical geometry but vacuum permeability (*main isolated* and *neighbor isolated*, respectively). The block removes both the neighbor's yoke material and its excitation,

* dekim@postech.ac.kr

ISBN: 978-3-95450-252-3 ISSN: 2673-5350 doi: 10.18429/JACoW-IPAC2026-TUP2686

INVESTIGATION AND DIAGNOSTIC POTENTIAL OF OFF-AXIS RESONANCE IN THz FREE-ELECTRON LASERS

Tong Li†, Zhuoyuan Liu, Xiujie Deng‡, Lixin Yan*
Tsinghua University, Beijing, China

Content from this work may be used under the terms of the CC BY 4.0 licence (© 2026). Any distribution of this work must maintain attribution to the author(s), title of the work, publisher, and DOI.

Abstract

We study undulator radiation observed away from the beam axis for terahertz (THz) free-electron laser (FEL) beams. Earlier work on a *single* short bunch relates the *continuous* off-axis spectrum to the longitudinal bunch profile without a discrete angular 'resonance' tied to micro-bunch harmonics. For a pre-bunched pulse-train beam, the bunching factor develops narrow spectral lines at the fundamental frequency and its integer harmonics. Off-axis phase matching selects a specific resonant polar angle for each line, producing pronounced, spatially separated ring-like intensity patterns in the coherent far field. We utilize the non-averaged 3D FEL code PUFFIN to simulate single-bunch radiation—reproducing non-integer harmonic patterns consistent with analytical Liénard-Wiechert (LW) results—and to demonstrate the expected off-axis resonance for pulse-train beams.

INTRODUCTION

Compact terahertz (THz) free-electron laser (FEL) sources driven by pre-bunched pulse-train electron beams are increasingly important for high-field spectroscopy and pump-probe experiments [1]. The reliable operation of these facilities necessitates accurate, preferably non-intercepting, longitudinal beam diagnostics. Conventional methods, such as coherent transition or diffraction radiation, are typically destructive or limited by the spectral response of the detection systems in the THz range.

Earlier studies by Neuman *et al.* [2] proposed that for a single short bunch, the continuous off-axis undulator spectrum encodes the longitudinal bunch profile. While providing a useful non-intercepting diagnostic, this single-bunch regime lacks the discrete phase-matching required for a sharp angular "resonance". In contrast, a pulse-train beam introduces discrete micro-bunching frequencies. When these frequencies lock with the undulator harmonics at specific observation angles, they produce distinct, ring-like intensity patterns in the far field—a phenomenon we define here as off-axis resonance.

In this work, we employ the three-dimensional, non-averaged FEL code PUFFIN [3] to investigate these off-axis dynamics. We first validate our simulation approach by reproducing single-bunch radiation patterns, including non-integer harmonics, showing excellent agreement with analytical Liénard-Wiechert (LW) formulations. Subsequently, we demonstrate the emergence of the predicted off-axis resonance for pulse-train beams. These resonant rings provide a clear spatial signature of the beam's temporal micro-structure, offering a potential candidate for future online, non-destructive THz FEL diagnostics.

† lit22@mails.tsinghua.edu.cn
‡dengxiujie@mail.tsinghua.edu.cn
* yanlx@mail.tsinghua.edu.cn

OFF-AXIS PHASE MATCHING AND PULSE-TRAIN RESONANCE

Undulator Tuning at Finite Angle

For an electron of Lorentz factor γ emitting at polar angle θ from the undulator axis, the fundamental resonance wavelength is

$$\lambda_r = \left(1 + \frac{K^2}{2} + \gamma^2\theta^2\right)/2\gamma^2 \cdot \lambda_u \quad (1)$$

The angular position at which the fundamental radiation frequency is red-shifted to $1/n$ of its on-axis value is therefore

$$\theta_{1/n} = \sqrt{[(n-1)(1 + K^2/2)]}\,/\,\gamma \quad (2)$$

Equations (1) and (2) describe standard undulator kinematics, defining the specific frequency emitted along a given ray. For a single short bunch, the radiated power versus frequency is weighted by a broad longitudinal form factor [1]; varying θ scans this continuous spectrum but does not create the sharp, ring-like resonant images that emerge when discrete micro-bunch lines must simultaneously satisfy Eq. (2).

Pulse-Train Micro-Bunching and Off-Axis Resonance

For a pre-bunched pulse-train beam, the longitudinal bunching factor $b(\omega)$ develops sharp peaks centered at the fundamental micro-bunching frequency and its integer harmonics. Each peak corresponds to a specific spatial harmonic of the beam's longitudinal density. When one of these bunching peaks matches the red-shifted undulator frequency at a specific off-axis angle—as governed by the kinematic relation in Eq. (2)—the emission becomes phase-matched. Consequently, rather than a smooth filled cone of emission, the coherent far-field radiation intensity is significantly enhanced around this specific angle, manifesting as a pronounced ring. This spatial intensity contrast is the direct signature of off-axis resonance, a phenomenon intrinsically absent for an isolated single bunch lacking such periodic density modulation.

Away from axis one must retain the full three-dimensional bunching factor. When the particle beam is transverse-longitudinally uncoupled, it factorises according to

$$\rho(\theta,\varphi,\omega) = \rho_\perp(\theta,\varphi,\omega) \cdot \rho_z(\omega) \quad (3)$$

where $\rho_z(\omega)$ is the usual longitudinal form factor and the transverse bunching factor is the two-dimensional Fourier transform of the transverse density $\rho(x,y)$:

ISBN: 978-3-95450-252-3 ISSN: 2673-5350 doi: 10.18429/JACoW-IPAC2026-TUP2687

ELLIPTICAL BEAM SHAPING IN A STANDARD BOW-TIE PLANAR FOUR-MIRROR OPTICAL ENHANCEMENT CAVITY USING A CYLINDRICAL LENS

G. Zhang†, Y. Du, X. Liu, L. Yan, Tsinghua University, Beijing, China

Content from this work may be used under the terms of the CC BY 4.0 licence (© 2026). Any distribution of this work must maintain attribution to the author(s), title of the work, publisher, and DOI.

Abstract

The standard bow-tie (SBT) planar four-mirror optical enhancement cavity (OEC) can amplify laser power, circulate laser pulses, and adjust the laser beam waist. It is widely applied in fields such as steady-state micro-bunching light sources, inverse Compton scattering light sources and fusion energy. However, the different effective radii of curvature in the sagittal and tangential directions vary with the incidence angle, which in turn leads to an elliptical cavity mode. Conventional approaches suppress this effect by restricting the transverse dimensions of the cavity, but this sacrifices the transverse design freedom of the optical enhancement cavity.

This paper proposes an elliptical cavity mode correction method using a cylindrical lens, enabling the fundamental mode at the beam waist to recover a circular shape. The method utilizes a cylindrical lens to differentially compensate the wavefront curvatures in sagittal and tangential directions, eliminating elliptical spot distortion without compressing the transverse dimensions of the cavity. Consequently, it overcomes the de-sign constraints on the transverse size of the optical enhancement cavity and provides a new approach for designing large-volume, high-power optical enhancement cavities.

Introduction

The application of OECs in many fields imposes requirements on their transverse dimensions. For example, in inverse Compton scattering (ICS), a certain transverse spatial size is needed to support the collision between electrons and photons [1]. In steady-state micro-bunching (SSMB), multiple OECs are used as laser modulators, which also requires that these OECs be scalable in transverse dimensions [2].

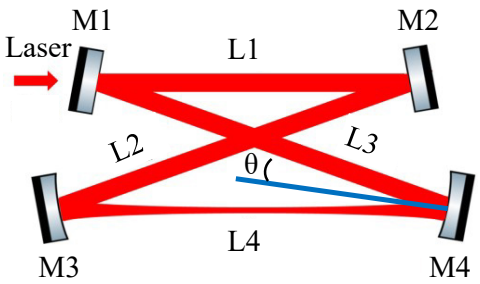

Figure 1: SBT cavity. M3 & M4: spherical mirrors with an effective radius of curvature R.

†zgj22@mails.tsinghua.edu.cn

However, increasing the transverse dimensions leads to a larger laser incidence angle θ. For a spherical mirror with radius of curvature R, the effective radii of curvature in the sagittal and Tangential directions are $R_{e,s} = R/\cos\theta$ and $R_{e,t} = R\cos\theta$, respectively. Consequently, the radial direction reaches the stability edge first, resulting in a smaller beam waist and larger divergence angle in that direction (Fig. 2), which manifests as the major axis of the elliptical spot on the cavity mirror, and will increase the instability of the cavity mode and affect the gain of the OEC [3]. Therefore, in the applications such as SSMB and ICS, elliptical cavity modes also need to be avoided.

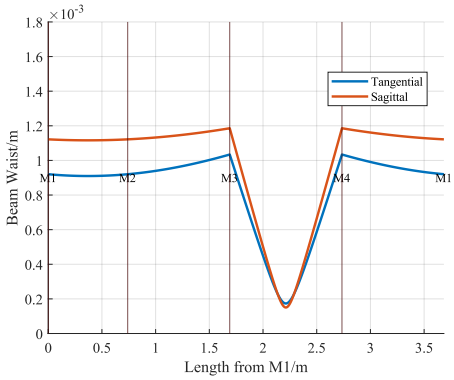

Figure 2: Simulation of gaussian beam radius evolution

Beam Shaping With a Cylindrical Lens

To suppress the elliptical cavity modes, the conventional approach is to reduce the transverse dimension of the OEC in order to decrease the incidence angle θ. However, as mentioned earlier, practical applications require a larger transverse dimension of the OEC. This paper proposes a method to correct the elliptical cavity mode using a cylindrical lens, enabling the fundamental mode at the beam waist to recover a circular shape. The cylindrical lens *CL* is inserted at the center of *L1*, adding focusing in the sagittal direction without affecting the tangential direction.

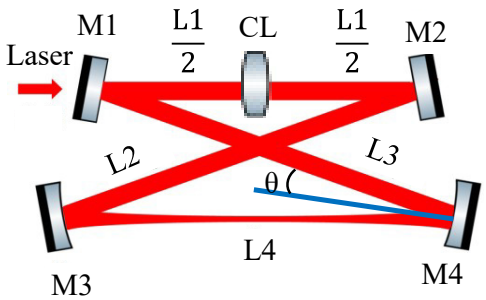

Figure 3: SBT cavity with a cylindrical lens *CL*

ISBN: 978-3-95450-252-3 ISSN: 2673-5350 doi: 10.18429/JACoW-IPAC2026-TUP2688

A NOVEL METHOD FOR MEASURING THE ENERGY SPECTRUM OF AN INVERSE COMPTON SCATTERING SOURCE BASED ON NUCLEAR RESONANCE FLUORESCENCE

J. Lin*, H. Ding, Y. Du, J. Sun, C. Tang, H. Zhang, Z. Zhang
Tsinghua University, Beijing, China

Abstract

We proposed a novel method of using nuclear resonance fluorescence (NRF) as a probe for spectrum measurements. By utilizing the continuous tunability of an ICS source, NRF photons can be excited at different points across the spectrum. The shape of the energy spectrum can then be effectively scanned and reconstructed by recording the relative NRF yields at different energy points. The feasibility of the proposed method was validated by Geant4 simulations of measuring NRF photon emission from ^{56}Fe irradiated by an ICS source. The simulation results showed high precision for quasi-monochromatic gamma ray spectrum measurements, with a normalized root mean square error (NRMSE) of less than 5 %. To maintain a sufficient signal-to-noise ratio (SNR) during the measurement, the energy resolution of detectors is suggested to be less than 1 % of the energy being measured. Given an energy tuning precision of ΔE, the minimum measurable width of the energy spectrum, in terms of standard deviation, can reach $0.85 \cdot \Delta E$.

INTRODUCTION

ICS sources have emerged as an advanced light source for generating high-energy gamma rays by colliding relativistic electrons with a laser beam, during which the electrons transfer energy to the photons. The characteristics of the gamma ray pulses generated by ICS sources are quasi-monochromatic, continuously tunable over a wide energy range and ultrashort, allowing a broad range of applications. Before employing an ICS source in gamma ray applications, measuring its energy spectrum is crucial for both produced beam analysis and subsequent experimental use. Traditional direct energy spectrum measurement methods, which rely on energy-sensitive detectors, are highly susceptible to severe pulse pile-up problems due to the short pulses and high brightness of ICS sources. Indirect measurement methods include the Compton scattering method [1], the Bragg crystal diffraction method [2] and the transmission method [3]. The Compton scattering method required placing collimators in front of detectors to achieve higher accuracy, which substantially reduced detection efficiency. The Bragg crystal diffraction method faced challenges in measuring an scattering angle of less than 0.01 degree when the energy reach the MeV level. The reconstruction of the energy spectrum from transmission data was a highly ill-conditioned problem for energy above 100 keV because the attenuation coefficient exhibited an increasingly smooth variation. In summary, current energy spectrum measurement methods face challenges in achieving high-precision and efficient measurements of high-energy and quasi-monochromatic ICS spectra. In this work, we proposed a novel method to measure the spectrum of an ICS gamma ray source based on NRF. By leveraging the continuous energy tunability of the ICS source, the NRF process can be excited at distinct energy points across the spectrum. The spectral shape can then be reconstructed by scanning the energy range and recording the relative NRF yields at different energy points. Simulation work was performed to validate the feasibility of the proposed method using Geant4.

* linj21@mails.tsinghua.edu.cn

THEORY AND METHOD

^{56}Fe was chosen as the target in this work. The abundance of ^{56}Fe is 91.75 % in nature with less isotopic interference. ^{56}Fe has two nuclear levels at approximately 845 keV and 3449 keV, which provide a larger measurable energy range. The NRF cross section of ^{56}Fe is also relatively higher. Geant4 was used to simulate the measurements of NRF photons from ^{56}Fe. The layout of the simulation was depicted in Fig.1. The gamma ray source was a cone beam with an energy spectrum following a Gaussian distribution or a segmented Gaussian distribution. Incident gamma rays propagated along the Z axis, and the linear polarization was along the X axis. Four HPGe detectors were positioned around the target at an angle of 135 degrees (α in Fig.1) relative to the direction of incident photons. The total number of incident gamma ray events was 10^{11}.

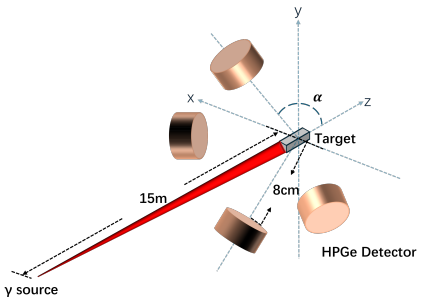

Figure 1: The schematic diagram of the layout.

The normalized root mean squared deviation (NRMSE) was employed to evaluate the accuracy of energy spectrum measurements, which was defined as:

$$NRMSE = \frac{\sqrt{\sum_{i=1}^{M} (S_{m,i} - S_{t,i})^2 / M}}{max(S_t) - min(S_t)}. \quad (1)$$

Content from this work may be used under the terms of the CC BY 4.0 licence (© 2026). Any distribution of this work must maintain attribution to the author(s), title of the work, publisher, and DOI.

ISBN: 978-3-95450-252-3 ISSN: 2673-5350 doi: 10.18429/JACoW-IPAC2026-TUP2691

USING STRETCHING-MODULATION-COMPRESSION EFFECT TO GENERATE ISOLATED FEW-FEMTOSECOND MeV ELECTRON BUNCHES*

Q. Luo[1], W. Qin[†2,3], C.-Y. Tsai[‡1]
[1]Huazhong University of Science and Technology, Wuhan, China
[2]Institute of High Energy Physics, Chinese Academy of Sciences, Beijing, China
[3]Spallation Neutron Source Science Center, Dongguan, China

Abstract

Femtosecond (fs) electron beams serve as effective tools for investigating ultrafast dynamic processes in matter, providing complementary capabilities to femtosecond laser beams. We propose a scheme combining an undulator with THz modulation to generate isolated few-fs electron bunches. We have developed a theoretical method that incorporates the transport dynamics of low-energy relativistic electrons interacting with the THz modulation field in the undulator and the space charge effects within the bunch itself. The results indicate that the proposed scheme can generate single isolated ultrafast electron bunches with kinetic energy 3 MeV, bunch length about 9 fs (rms) with core charge about 8 fC. We have also evaluated the influence of several relevant physical quantities on the final bunch length and arrival time. The proposed scheme and the developed theoretical model presented may provide useful insights for generating few-fs electron bunches in accelerator-based ultrafast electron diffraction (UED) facilities.

INTRODUCTION

The mechanism of our proposed scheme is conceptually similar to high-gain harmonic generation (HGHG) [1]. First we use a chicane to stretch the bunch, and then generate a shorter bunch by modulating a local portion of the beam core, thereby mitigating space-charge effects at the cost of losing some particles in the head and tail regions. Broadly speaking, these schemes share the common feature of using external electromagnetic field and undulator to modulate the electron beam. The key difference is that our proposed scheme is intended for the single-MeV energy regime relevant to UED applications. At these low electron energies, space charge effects become important during beam transport, and such dynamics have not yet been studied in detail using currently available simulation tools.

THEORETICAL MODEL

Our proposed scheme includes two chicanes and one short undulator with THz modulation. In the two chicanes, AS-

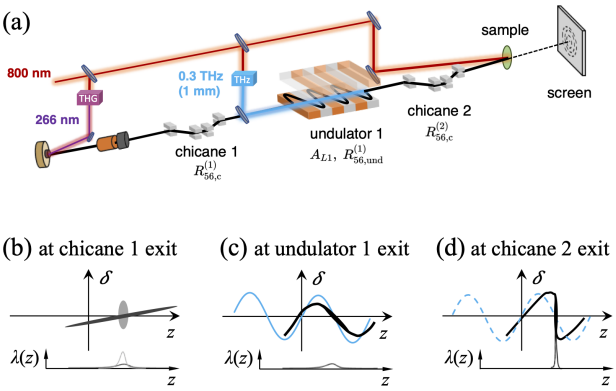

Figure 1: (a) Schematic layout of a MeV UED facility incorporating the bunch compression scheme proposed in this paper. In the figure, the 800-nm laser serves three purposes: exciting the sample, generating 266-nm UV laser through third-harmonic generation (THG) to strike the photocathode and produce photoelectrons, and generating the THz modulation wave. After acceleration by the RF cavity and focusing by the solenoid, the electron beam first passes through chicane 1 to be stretched, then modulated by the THz wave, and finally appropriately compressed in chicane 2 to achieve the possible minimum bunch length before probing the sample. (b), (c) and (d) show the bunch phase space distribution and line density at the exit of the chicane 1, the undulator 1, and the chicane 2, respectively. In the panel (b), the gray represents the initial phase space and line density distributions. The distance from the photocathode to chicane 1 is roughly 0.3 m, the length of chicane 1 itself is approximately 3.92 m, the undulator length is approximately 0.1 m and the length of chicane 2 is about 0.88 m.

TRA [2] is used to simulate beam dynamics, including 3D space charge effects. In the undulator we construct a period-by-period tracking algorithm that includes both the external THz modulation and the longitudinal and transverse space charge effects. Below we briefly summarize the period-by-period tracking equations and space charge models.

Period-by-period Tracking Equations

Assume the phase space coordinates can be written as $[x\ x'\ y\ y'\ z\ \delta]$, where x and x' are the transverse horizontal position and divergence coordinates, y and y' are the transverse vertical counterparts, z is the bunch coordinate ($z > 0$ for bunch head and $z < 0$ for bunch tail) and $\delta = (E - E_0)/E_0$

* This work is supported by the Fundamental Research Funds for the Central Universities (HUST) under Project No. 2021GCRC006 and National Natural Science Foundation of China under Project No. 12275094. WQ's work is supported by the Department of Science and Technology of Guangdong Province (No.2024QN11X220).
† qinwl@ihep.ac.cn
‡ jcytsai@hust.edu.cn

Content from this work may be used under the terms of the CC BY 4.0 licence (© 2026). Any distribution of this work must maintain attribution to the author(s), title of the work, publisher, and DOI.

ISBN: 978-3-95450-252-3 ISSN: 2673-5350 doi: 10.18429/JACoW-IPAC2026-TUP2695

COMMISSIONING OF THE INJECTOR SYSTEM FOR THE X-BAND ELECTRON LINEAR ACCELERATOR IN MELBOURNE

J. Valerian*, M. Volpi, P. Pushkarna, P. Giansiracusa[1], R. Rassool, S. L. Sheehy[2], V. Lu
University of Melbourne, Melbourne, Australia
R. Dowd, Y.-R. E. Tan, Australian Synchrotron - ANSTO, Melbourne, Australia
[1]also at Australian Synchrotron - ANSTO, Melbourne, Australia
[2]also at ANSTO, Sydney, Australia

Abstract

The University of Melbourne's X-band Laboratory for Accelerators and Beams (X-LAB) is developing a compact electron linear accelerator. The injector system will consist of a 100-keV DC photogun, a pulsed UV laser, an S-band (2.9985 GHz) RF buncher, and magnetic elements for beam transport. This paper reports on the commissioning of the injector system. We present the characterisation of the test laser and buncher, as well as initial electron beam measurements with Faraday cup. Particle tracking simulations using General Particle Tracer (GPT) code were used to obtain approximate optimal solenoid currents. We also report on the conditioning of the photogun, including photocathode inspection, vacuum performance, dark current, and stray radiation.

INTRODUCTION

The University of Melbourne's X-band Laboratory for Accelerators and Beams (X-LAB) hosts the Mel-BOX, which is one half of XBox-3, a high-power RF test stand previously at CERN built to evaluate X-band (11.994 GHz) accelerators for the Compact Linear Collider (CLIC) collaboration [1, 2]. It was relocated and reassembled in Melbourne and is now fully operational [3]. Following reassembly, high-power conditioning has progressed well [4], and several studies on accelerator structure diagnostics have been carried out [5, 6]. In parallel, X-LAB has been developing an injector that may be used in conjunction with such high-power high-gradient X-band technology. In this paper, we present its current progress.

The injection system uses a 100 kV DC photogun where a laser generates the initial electrons which are then accelerated to 100 keV. The beam is then collimated and focused using solenoids before entering an S-band (2.9985 GHz) RF buncher. Upstream of the buncher, steering coils provide beam control, while correction coils compensate for the Earth's magnetic field. During commissioning, either a Faraday cup or the sample chamber is installed directly downstream of the buncher to characterise the photogun output as shown in Fig. 1. A nanosecond test laser is used in place of a picosecond laser, and the buncher is turned off. The commissioning setup is shown schematically in Fig. 2.

First, we discuss the photogun conditioning and issues encountered. The test laser characterisation is then presented, followed by General Particle Tracer (GPT) simulations to determine approximate optimal solenoid currents. Preliminary beam measurements are then reported, along with vector network analyser (VNA) measurements of the buncher S-parameters.

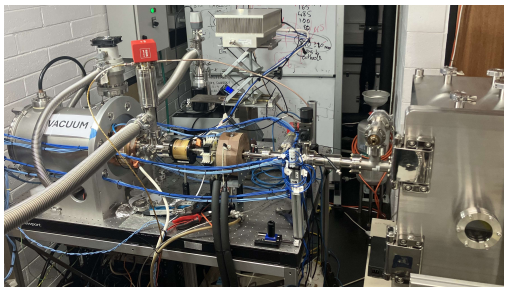

Figure 1: The injector status after reassembly. The laser enclosure is not shown.

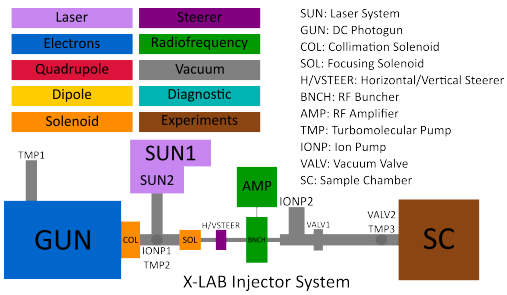

Figure 2: Schematic of the injector system during commissioning. Correction coils are omitted for clarity.

CONDITIONING

The photogun was conditioned to minimise dark current and suppress electric breakdown by first pumping the system down to high vacuum over approximately one week using turbomolecular pumps and ion pumps, followed by high-voltage training to 105 kV using the manufacturer's conditioning algorithm. A non-evaporable getter was occasionally activated to improve vacuum quality. Ideally, the pressure inside the photogun should be stable below 10^{-6} mbar, but we could only reach a few 10^{-6} mbar.

During high-voltage training, a faint blue spot was observed on the phosphor screen (Blue RE 800 Speed) in the sample chamber (Fig. 3). As the laser was disabled, this was attributed to dark current, estimated to be in the nanoampere range, while a few microamperes were measured at the pho-

* joel.valerian@student.unimelb.edu.au

Content from this work may be used under the terms of the CC BY 4.0 licence (© 2026). Any distribution of this work must maintain attribution to the author(s), title of the work, publisher, and DOI.

ISBN: 978-3-95450-252-3 ISSN: 2673-5350 doi: 10.18429/JACoW-IPAC2026-TUP2697

THE ANALYSIS OF BEAM LOADING EFFECT OF DARK CURRENT IN C-BAND PHOTOCATHODE ELECTRON GUN*

S. Jiang[1,2], S. Liu[1,2], X. Liu[†,1,2], X. Li[1,2], W. Qin[1,2]
[1] Institute of High Energy Physics, Chinese Academy of Sciences, Beijing, China
[2] Spallation Neutron Source Science Center, Dongguan, China

Abstract

In the research on the C-band high-gradient photocathode electron gun, the existence of dark current not only introduces measurement errors in photocurrent and damage to the cavity, but also leads to deviations between results of high-power testing and the cold test. In this paper, based on the parameters of C-band photocathode electron gun designed for the Southern Advanced Photon Source, the time structure of dark current and beam evolution under a high-gradient acceleration field are analysed through theoretical numerical calculations and beam simulations, and the beam load field characteristics introduced by dark current under single-pulse and multi-pulse conditions are further discussed. The results show that when the maximum macro-pulse current of dark current exceeds 50 mA, the cavity voltage of the beam load field will exceed 0.5 MV and introduce non-negligible influence to the acceleration field. This research provides guidance for the testing of the C-band electron gun and a reference for the dark current analysis of RF guns.

INTRODUCTION

In recent years, the C-band photocathode radio frequency (RF) electron gun operating in the 5.712 GHz band has become a research hotspot in the field of advanced high-performance electron beam sources due to its advantage of high-gradient acceleration structure, and has shown important application potential in cutting-edge fields such as compact free-electron lasers (FEL), ultrafast electron diffraction (UED), and Terahertz technology [1-3]. At present, a field with a gradient of 160 MV/m has also been established in the cavity power test at the European INFN laboratory [4], which represents a significant improvement compared with the accelerating field (~100 MV/m) of the commonly used S-band photocathode electron gun.

However, this core advantage of high gradient also brings a severe challenge—dark current, which refers to the field emission current induced by a strong RF field when the photocathode is not excited by laser. According to the Fowler-Nordheim (FN) theory, the current density increases exponentially with the electric field gradient, and it will rise sharply when the C-band electron gun operates at an ultra-high gradient. It not only affects the beam measurement of the photocurrent but also is lost on the cavity wall, causing vacuum breakdown and secondary electron multiplication, and damaging the structure of the electron gun. In addition, since the excitation of dark current occurs simultaneously with the establishment of the cavity acceleration field, its micro pulse repetition frequency resonates with the cavity, which further amplifies the beam loading field, reduce the accelerating gradient, and results in a discrepancy between the cavity's parameters from high-power testing and cold testing. Therefore, discussing the evolution of dark current and beam loading effect in RF gun is of great significance for judging the cavity performance and preventing the impact of dark current.

In this paper, based on the parameters of the C-band photocathode electron gun designed for the Southern Advanced Photon Source [5], we investigate the temporal structure of dark current and the beam evolution process under different field gradients. We also compare the differences in beam load field induced by dark current single pulse and multi-pulses, and study the dark current threshold that can significantly affect the accelerating field, which will provide a reference for subsequent design and test work.

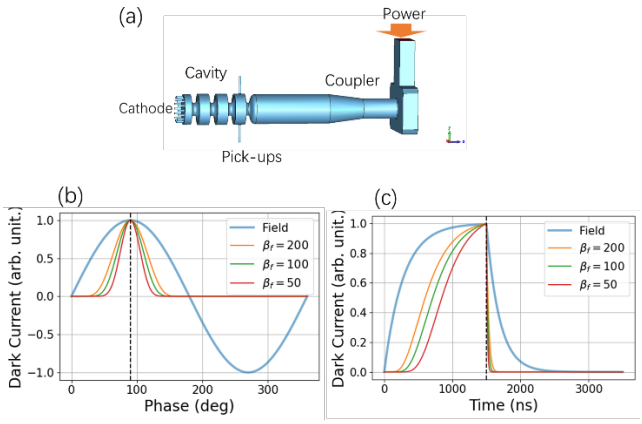

Figure 1: (a) The model of C-band photocthode electron gun, (b) the normalized dark current micro pulse intensity distribution for different enhanced factor, (c) the normalized dark current macro-pulse intensity distribution for different enhanced factor.

THEORY

In 1928, Fowler and Nordheim derived the relationship between field emission current I_{FN} and electric field gradient E by solving the Schrödinger equation as follows [6],

$$I_{FN} = A(\beta_f E)^2 \exp\left(-\frac{6.32 \times 10^9 \phi^{1.5}}{\beta_f E}\right), \quad (1)$$

where $A = 1.54 \times 10^{-6} \frac{A_e}{\phi}$, A_e is the effective area of field emission in m², ϕ is the work function (in eV) of the emitting surface, β_f is the empirical field enhancement

* Work supported by the Department of Science and Technology of Guangdong Province (No.2024QN11X220)
† liuxg@ihep.ac.cn

Content from this work may be used under the terms of the CC BY 4.0 licence (© 2026). Any distribution of this work must maintain attribution to the author(s), title of the work, publisher, and DOI.

ISBN: 978-3-95450-252-3 ISSN: 2673-5350 doi: 10.18429/JACoW-IPAC2026-TUP2702

SIMULATION STUDY OF HEPS BOOSTER OPERATION AT LOWER INJECTION ENERGY

A. Wang*, J. Wang, Institute of High Energy Physics, Beijing, China
C. Meng, Y. Peng, Chinese Academy of Sciences, Beijing, China

Content from this work may be used under the terms of the CC BY 4.0 licence (© 2026). Any distribution of this work must maintain attribution to the author(s), title of the work, publisher, and DOI.

Abstract

This study investigates the feasibility of high-charge, low-energy 300 MeV linac-to-booster injection for the High Energy Photon Source (HEPS) injector. The primary aim is to enable a klystron hot-standby for the HEPS linac, thereby enhancing its operational reliability. Energy ramping simulations for the booster were conducted using elegant, both Gaussian and non-Gaussian bunches were tracked. Simulations and analysis indicate that, with a suitable initial RF voltage, Transverse Mode-Coupling Instability (TMCI) is the limiting factor for the beam transmission rate in the booster. By optimizing the chromaticity to enhance Landau damping, TMCI can be effectively suppressed, significantly improving beam transmission rate. A further reduction in the injected bunch energy spread leads to additional gains in beam transmission rate. Through this synergistic optimization of multiple parameters, it looks feasible to achieve stable transport of beam with bunch charge exceeding 5 nC in the booster at the lower injection energy mode for the HEPS injector.

INTRODUCTION

The HEPS injector consists of a 500 MeV linac and a 6 GeV full-energy booster synchrotron [1]. Currently, the linac is equipped with five klystrons, which cannot provide a single-klystron hot-standby capability while still delivering a beam energy of 500 MeV. For the purpose to enable a klystron hot-standby for the HEPS linac, thereby improving the operational reliability of HEPS linac and reducing power consumption of HEPS, while also meeting the design requirement of at least 5 nC per bunch, this study investigates the feasibility of high-charge, low-energy linac-to-booster injection when the beam energy from the linac is reduced to 300 MeV [2].

Many synchrotron light sources worldwide have gained valuable experience in low-energy linac-to-booster injection under the condition that the beam energy from the linac is reduced. For example, ALBA achieved low-energy linac-to-booster injection when the injection energy was reduced from 110 MeV to 67 MeV through a fine quadrupole calibration and tuning of the quadrupoles at low excitation current and the compensation of the dipole eddy currents effect during booster ramping [3]. NSLS-II also successfully achieved low-energy linac-to-booster injection when the injection energy was reduced from 200 MeV to 115 MeV using beam-based online optimizations on the booster [4,5]. Beam dynamics simulations of TPS booster synchrotron showed the significant impact of magnet field errors and space charge effects on beam transmission rate when the injection energy was lowered from 150 MeV to 100 MeV [6].

However, due to the requirement to achieve low natural emittances together with high charge in the HEPS booster [1], new challenges arise in the HEPS injector during low-energy 300 MeV linac-to-booster injection, beyond those reported in the aforementioned experiments. In our study, we found that the main factors limiting the beam transmission rate for the booster can be attributed to two aspects. First, the high-charge requirement makes the TMCI highly prone to being triggered, leading to a significant degradation in beam transmission rate. Second, ignoring the effect of charge, when the linac operates at 300 MeV, the emittances and energy spread of the output beam increase by approximately 60% compared to operation at 500 MeV [2]. The larger energy spread and larger emittances may cause some particles to more easily trigger an integer resonance at $\nu_x = 21$, resulting in particle loss, further reducing the beam transmission rate.

The key parameters used in this study are shown in Table 1.

Table 1: Key Parameters of the HEPS Booster Used in This Study

Parameter	Symbol	Value and Unit
Circumference	C	454.07 m
Beam energy	E_0	300 MeV / 6 GeV
Betatron tunes	ν_x/ν_y	21.15 / 11.21
Momentum compaction factor	α_c	2.26×10^{-3}
Horizontal radiation damping time	τ_x	37.46 s / 4.68 ms
Vertical radiation damping time	τ_y	37.46 s / 4.68 ms
Longitudinal radiation damping time	τ_δ	18.73 s / 2.34 ms
Radiation energy loss per turn	U_0	24.26 eV / 3.88 MeV
Repetition rate	f_{rep}	1 Hz
RF frequency	f_{RF}	499.8 MHz
Harmonic number	h	757

SIMULATION SETUPS

In our study, the Gaussian and non-Gaussian bunches were used as the initial beam distributions at the low-energy injection point of the booster for tracking. The Gaussian bunch features a Gaussian distribution with a 3σ cut-off in six-dimensional phase space. The non-Gaussian bunch is

* gywan@ihep.ac.cn

ISBN: 978-3-95450-252-3 ISSN: 2673-5350 doi: 10.18429/JACoW-IPAC2026-TUP2703

COMMISSIONING STATUS OF BOOSTER-BASED BEAM-RECYCLING SWAP-OUT INJECTION AT HEPS

Z. Duan*, J. H. Chen, Y. Y. Du, J. He, X. Y. Huang, D. H. Ji, Y. Jiao, J. Y. Li, F. Liu, P. Liu, Z. Liu, X. H. Lu, Y. H. Lu, C. Meng, Y. M. Peng, S. K. Tian, G. W. Wang, G. Xu, H. S. Xu, Y. Zhao
Institute of High Energy Physics, Chinese Academy of Sciences, Beijing, China

Abstract

The High Energy Photon Source (HEPS) adopts on-axis swap-out injection to relax the dynamic-aperture requirement of its ultralow-emittance storage ring. To provide high-charge bunches for swap-out operation, a booster-based beam-recycling scheme has been developed, in which a depleted storage-ring bunch is extracted, transported to the booster, combined with a newly accelerated bunch at high energy, damped, and reinjected into the original storage-ring bucket. This paper summarizes the commissioning status of this scheme. Closed-loop beam recycling has been demonstrated, paving the way for user operation toward high bunch charge. The results validate the basic beam-recycling architecture and identify the main directions for further optimization toward routine high-charge operation.

INTRODUCTION

Fourth-generation synchrotron light sources [1, 2] pursue ultralow emittance and high brightness, but the resulting small dynamic aperture makes conventional off-axis accumulation increasingly difficult. On-axis swap-out injection [3], in which a stored bunch is replaced by a fresh bunch with higher charge, can be accommodated with the most relaxed dynamic aperture and releases the full potential of performance optimization. The main challenge is then transferred from storage-ring acceptance to the preparation and high-efficiency transport of high-charge bunches. As a 6 GeV, 1.3 km-scale light source [4–6], the HEPS storage ring features an ultralow natural emittance of 34.8 pm, and therefore adopts swap-out injection. The high-charge filling mode, as required by timing experiments, with 63 bunches and a design bunch charge of 14.4 nC at 200 mA, is the most demanding case for the full-charge injector. For HEPS, this challenge is addressed by using the full-energy booster as a recycling and accumulation stage [7]. The bunch extracted from the storage ring is not discarded. Instead, it is transported back to the booster, combined with a newly accelerated bunch, damped at high energy, and then re-injected into the same storage-ring RF bucket. This approach avoids a dedicated accumulator ring [8, 9] and reduces the demand on high-charge bunch production at the low-energy end of the injector [10, 11]. This paper focuses on the system layout, staged commissioning path, representative diagnostics, and early performance indicators of the booster-based beam-recycling swap-out injection scheme.

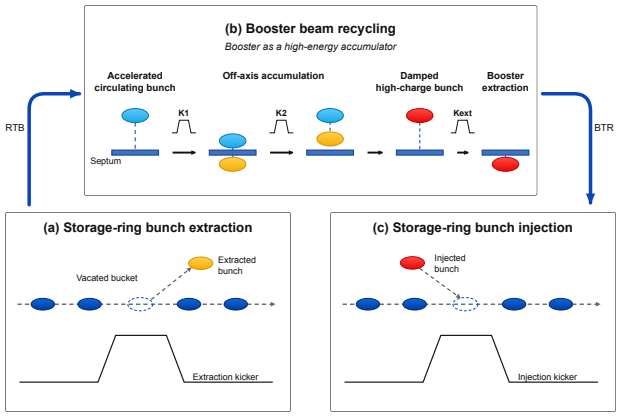

Figure 1: Schematic of on-axis swap-out injection with booster beam recycling. Blue, yellow, and red bunches denote stored/circulating bunches, recycled/injected bunches, and damped high-charge bunches, respectively. In panel (b), K1 first deflects the circulating booster bunch toward the septum, while K2 closes the local bump and brings both the circulating and reinjected bunches into the booster dynamic acceptance. The accumulated high-charge bunch is then extracted by Kext.

BEAM-RECYCLING SWAP-OUT SCHEME

Figure 1 shows the basic scheme. The two high-energy transport directions are denoted as RTB, from the storage ring back to the booster, and BTR, from the booster to the storage ring. In each recycling cycle, a moderate charge bunch is first injected into the booster and accelerated to the extraction energy, then a selected storage-ring bunch is extracted through RTB and injected off-axis into the booster, where it is combined with this circulating booster bunch. The two bunches are captured within the booster dynamic acceptance and merge after radiation damping, forming a higher-charge bunch. This bunch is then extracted through BTR and injected into the vacated storage-ring bucket. Repeating this recycling cycle for a selected RF bucket can progressively build up the stored bunch charge. In multi-bunch operation, the same procedure is applied sequentially to the selected filling buckets. This approach requires only a moderate bunch charge of a few nC to be captured in the booster and accelerated to full energy, but high transmission efficiencies in both directions between the storage ring and the booster are still essential for building up high bunch charge in the storage ring. Combinations of Lambertson septa [12] and vertical deflecting kickers are used for injection into and extraction from both the HEPS storage ring and booster. The bucket spacing is 6 ns in the storage ring [13,14].

* duanz@ihep.ac.cn

Content from this work may be used under the terms of the CC BY 4.0 licence (© 2026). Any distribution of this work must maintain attribution to the author(s), title of the work, publisher, and DOI.

ISBN: 978-3-95450-252-3 ISSN: 2673-5350 doi: 10.18429/JACoW-IPAC2026-TUP2706

DESIGN AND SIMULATION OF THIN EDDY-CURRENT SEPTUM FOR INJECTION OF THE TPS

Ch.-K. Yang†, Y.-L. Chu, Fu-Y. Lin, Ch.-S. Yang,
National Synchrotron Radiation Research Center, Hsinchu, Taiwan

Abstract

The eddy current type septum is the development trend for next generation storage ring. To reduce the impact of leakage magnetic fields on the stored beam during injection and develop our technology for the Taiwan Photon Source (TPS), we propose a conceptual design of an eddy current type septum as a replacement.

Theoretical analyses and transient field simulations have been performed using OPERA software to evaluate magnetic behavior under pulsed excitation. Due to the thin septum structure, several optimization strategies have been applied—such as shielding with strongly paramagnetic materials and excitation with a full-cycle driving pulse—to ensure the leakage field remains below 0.1% of the main field.

This paper presents the design approach, analyzes the influence of eddy currents on field distribution, and investigates compensation methods to enhance magnetic field quality and injection performance.

INTRODUCTION

Modern light sources pursuit higher brilliance through diffraction-limited lattices, resulting in a significantly smaller dynamic aperture. This trend requires thinner septum magnets to accommodate the narrower injection acceptance. While direct-drive septa offer precise field control, their complex cooling systems lead to bulkier structures. In contrast, eddy-current septum magnets eliminate internal current loops, allowing for a much thinner and simpler design with easier thermal management. The thin profile and mechanical simplicity of eddy-current septa make them the preferred choice for next-generation storage rings.

For these reasons, although the TPS is currently using direct drive type septum [1], we are going to upgrade an eddy-current septum magnets for its storage ring injection system. This new magnet provides a reliable way to deflect the beam while fitting into tight spaces. More importantly, it meets the strict requirements for low leak-age fields in the storage ring.

As shown in Fig. 1, the bumper height is set at 16.2 mm. This value balances two needs: it must be high enough to avoid hitting the septum wall, yet low enough to reduce kicker power. Because the beams are so close, space for the vacuum chambers is very limited. After leaving 1 mm of clearance on each side for tuning, only 3.0 mm remains for the septum wall. This is why a thin eddy-current septum is essential. It allows both beams to stay in their own spaces without interference, even during early commissioning.

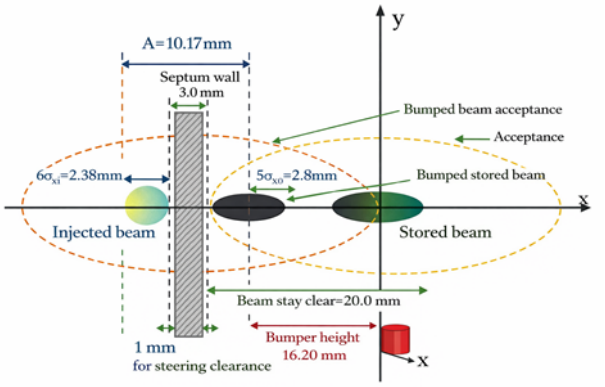

Figure 1: Phase space at the injection point.

Table 1 summarizes the design specifications for the septum magnet. The septum's thickness depends on the limited space at the injection point, where it must fit alongside the vacuum chambers. For the current direct-drive design, the system uses a 300 μs half-sine current pulse to drive the magnet. To achieve the required deflection, we use a 0.8-meter magnet with a core made of 0.3 mm CSC1300 silicon steel. Using thin laminations is important to stop eddy currents, which can cause heat and field distortion. The magnet provides a peak field of 0.694 T. To keep the stored beam stable, the leakage field must be less than 0.1% of the main field. This strict limit prevents unwanted kicks to the electrons, ensuring the storage ring stays stable during the injection process.

Table 1: Target Specifications of the Septum

Parameters	Value
Deflection Angle (mrad)	55.5
Core length (mm)	800
Peak field (T)	0.694
Magnet gap (mm)	15
Septum thickness (mm)[a]	<3
Nominal current (A)	8231
Pulse width (μs)	100~300
Pulse shape	Full sine or half sine
Leakage field (%)	<0.1

[a]At the beam injection point into the storage ring

†yang.ck@nsrrc.org.tw

Content from this work may be used under the terms of the CC BY 4.0 licence (© 2026). Any distribution of this work must maintain attribution to the author(s), title of the work, publisher, and DOI.

ISBN: 978-3-95450-252-3 ISSN: 2673-5350 doi: 10.18429/JACoW-IPAC2026-TUP2707

STUDY ON POLARIZATION CONTROL OF PLANAR UNDULATOR SYSTEM BASED ON MAGNETIC FIELD MODULATION*

Nanrui Yang† Zhouyu Zhao, Yuanfang Xu, Heting Li‡
National Synchrotron Radiation Laboratory,
University of Science and Technology of China, Hefei, China

Abstract

The fast polarization switching of undulator radiation has attracted more and more attention in recent years. Recently, a new method has been proposed for fast polarization switching up to kilohertz of undulator radiation by using magnetic field modulation generated from low-current electromagnetic coils. Through fast switching the power of coils, the radiation spectra of two undulators can be rapidly shifted into and out of the bandpass of a monochromator, enabling fast polarization switching for the user beamline. In this paper, we have studied the scheme using planar undulators, focusing on the required magnetic field of coils. The performance of the modulated spectrum will also be reported.

INTRODUCTION

In recent years, various types of undulators have been developed to enable controlling of radiation characteristics, including polarization degree, flux distribution, and photon energy. Examples include variable-polarization undulators such as APPLE-II [1] and APPLE-X [2, 3], harmonic-suppressing quasi-periodic undulators, and figure-8 undulators. Fast polarization switching has become increasingly important for experimental techniques like X-ray magnetic circular dichroism and X-ray magnetic linear dichroism, which are used to investigate orbital and spin moments in materials.

To achieve fast polarization switching, some strategies have been taken into consideration. The first involves direct control of the magnetic source. Mechanically adjustable undulators, such as APPLE-type undulators, control polarization by shifting magnetic arrays. Permanent magnet-electromagnet designs, implemented at facilities like SOLEIL [4, 5], enable fast switching of circular polarization by reversing coil currents. When the magnetic source cannot be altered quickly enough, a second strategy, is typically realized using twin-undulator systems and separating the two radiation beams, where two undulators generate radiation with different polarization states .

An innovative third strategy is based on spectral modulation. Instead of physically separate the photon beams with different polarization, this method uses phase shifters between undulators to split the spectrum [6, 7] or applies a modulating magnetic field to slightly detune the undulator harmonics [8, 9]. Cross-undulator schemes also achieve fast polarization switching with the help of phase shifters.

In previous work, we proposed a novel polarization switching scheme based on magnetic field modulation [10]. This scheme has significant advantages, including collinear emission of two photon beams with different polarization states and high stability of the electron beam trajectory. It also ensures high-quality radiation with both high polarization and high photon flux, while maintaining strong engineering feasibility.

The Hefei Advance Light Facility (HALF) [11, 12] is a 2.2 GeV diffraction-limited storage ring developed by the National Synchrotron Radiation Laboratory in China. It features 20 long and 20 middle straight sections. A specialized undulator system has been designed to realize fast polarization switching, where two EPU41 undulators will be installed sequentially and connected by a phase shifter in one straight section.

In this paper, we further investigate the proposed polarization switching scheme. Based on the HALF parameters we studied the performances of this scheme using planar undulators. The paper is organized as follows: First, a theoretical analysis on the required coil field of the proposed scheme is presented using planar undulators. Then, the distribution of the modulated spectrum is studied in detail. Finally, a summary is provided.

POLARIZATION SWITCHING

To illustrate the basic principle of the proposed scheme, in the following we introduce an electron radiation model to accurately calculate the photon energy shift.

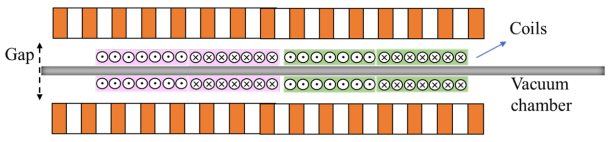

Figure 1: The schematic of the setup of the field modulation linear undulator.

Because the magnetic field of the coils only affects the vertical magnetic field, first we only consider the vertical magnetic field, corresponding to the movement of electrons in the horizontal direction. When an electron beam passes through the system above, the magnet field B_y that it experiences can be expressed as the superposition of the undulator field and the weak field generated by the coils.

* Work supported by the National Natural Science Foundation of China under Grants (No. 12575343 and No. 12241501
† larry17@mail.ustc.edu.cn
‡ liheting@ustc.edu.cn

Content from this work may be used under the terms of the CC BY 4.0 licence (© 2026). Any distribution of this work must maintain attribution to the author(s), title of the work, publisher, and DOI.

ISBN: 978-3-95450-252-3 ISSN: 2673-5350 doi: 10.18429/JACoW-IPAC2026-TUP2708

THE ESSENCE FACTOR TO DETERIORATE THE CIRCULAR POLARIZATION RADIATION PERFORMANCE IN APPLE-KNOT UNDULATOR*

B. Zhang, N. Yang, Y. Xu, C. Chen, Q. Jia, Z. Zhao†, H. Li‡
National Synchrotron Radiation Laboratory, University of Science and Technology of China, Hefei, China

Abstract

The APPLE-KNOT undulator forms composite magnetic fields by superimposing APPLE and KNOT fields with different period lengths. In this configuration, in which the APPLE field serves as the dominant component to approximate the target photon energy, while the KNOT field acts as an additional component to transversely deflect the electron beam off-axis. Although variable polarization modes can be realized with a low on-axis heat load, previous studies have observed a sharp reduction in flux and significant degradation of the polarization degree in the circular polarization (CP) mode. This paper discusses this phenomenon in detail from a theoretical perspective. The analysis reveals that the presence of an additional field with a longer period is the essence factor that inherently suppresses the radiation performance of CP mode. Theoretical findings are highly consistent with simulation results, demonstrating that selecting the KNOT field as the dominant component can effectively improve CP characteristics without significantly compromising the linear polarization performance.

INTRODUCTION

Various types of undulators have been developed to meet different experimental requirements. The APPLE-type undulator is well known as the light source for generating variable polarization. The most conventional polarization-tunable undulator is the APPLE-II undulator [1]. However, low photon energy applications in high-energy storage rings lead to substantial on-axis heat load in linear polarization modes. To address this issue, the APPLE-KNOT(AK) undulator combines APPLE and KNOT arrays with a period ratio of 2:3 to achieve variable polarization while maintaining low on-axis heat load [2]. Subsequent developments including four-row merged configurations have been implemented at various facilities [3, 4]. Despite these advances, a common observation across AK undulator designs is that the circular polarization (CP) mode exhibits lower photon flux and polarization degree compared to linear modes. This phenomenon has been noted in both simulation studies and practical implementations [5], yet the underlying mechanism has not been systematically analyzed. Understanding this degradation is essential for optimizing future undulator designs for beamline requiring high-performance circularly polarized radiation.

This paper theoretically investigates the essence factor that deteriorates CP mode radiation performance in AK undulators. Analysis of the composite magnetic field structure reveals that the presence of an additional field with a longer period is the fundamental cause. Theoretical findings are validated through numerical simulations based on Hefei Advanced Light Facility (HALF) parameters [6] and further verified using High Energy Photon Source (HEPS) parameters [7]. The end magnet design and field integral analysis for a novel APPLE-KNOT undulator developed for HALF are also presented to demonstrate its engineering feasibility. The detailed design has been reported elsewhere [8].

PRINCIPLES

In theory, the composite magnetic field of AK undulator at circular polarization mode can be simplified as

$$\begin{aligned} B_y &= -B_{strong}\sin\frac{2\pi}{\lambda_1}z - B_{weak}\cos\frac{2\pi}{\lambda_2}z \\ B_x &= B_{strong}\cos\frac{2\pi}{\lambda_1}z - B_{weak}\sin\frac{2\pi}{\lambda_2}z \end{aligned} \tag{1}$$

where B_{strong} and B_{weak} are the peak fields corresponding to the period lengths of λ_1 and λ_2, respectively. With $B_{strong} = \alpha B_{weak} = \alpha B_0$, and $\lambda_1 = m\lambda_2 = m\lambda_0(\alpha > 1, m > 0$, and $m \neq 1)$, we have

$$\begin{aligned} B_y &= -B_0\left(\alpha\sin\frac{2\pi}{m\lambda_0}z + \cos\frac{2\pi}{\lambda_0}z\right) \\ B_x &= -B_0\left(-\alpha\cos\frac{2\pi}{m\lambda_0}z + \sin\frac{2\pi}{\lambda_0}z\right). \end{aligned} \tag{2}$$

In the traditional AK undulator (Case A), the APPLE array (shorter period) serves as the strong field and the KNOT array (longer period) as the weak field, corresponding to $m = 2/3$. In contrast, the new proposed configuration (Case B) selects the KNOT array as the strong field, yielding $m = 3/2$. The following analysis compares two cases in HALF. Using parameters listed in Table 1, with the same period and field strength ratio, to identify the origin of CP mode degradation using far-field approximation:

$$\frac{d^2I}{d\omega d\Omega} = \frac{N^2e^2\omega_u^2}{(4\pi\varepsilon_0)4\pi^2c}\times \left|\int_{-\frac{\lambda_u}{2\bar{\beta}c}}^{\frac{\lambda_u}{2\bar{\beta}c}}\left[n\times(n\times\beta)\right]e^{i\omega(t-\frac{n\cdot r}{c})}dt\right|^2 L(N\Delta\omega/\omega_1(\theta)) \tag{3}$$

* Work supported by National Natural Science Foundation of China under Grants No. 12575343.

† yuzz@ustc.edu.cn
‡ liheting@ustc.edu.cn

Content from this work may be used under the terms of the CC BY 4.0 licence (© 2026). Any distribution of this work must maintain attribution to the author(s), title of the work, publisher, and DOI.

ISBN: 978-3-95450-252-3 ISSN: 2673-5350 doi: 10.18429/JACoW-IPAC2026-TUP2709

APPLICATION OF DEEP LEARNING METHODS FOR INSERTION DEVICE EFFECTS IN THE SSRF

X. Z Liu[1], S. Q Tian[1,2], L. Y Tan[1], Y. H Gong[1,2,3], L. L Mao[2,3]
[1]Shanghai Advanced Research Institute, Chinese Academy of Sciences, Shanghai, China
[2]University of Chinese Academy of Sciences, Beijing, China
[3]Shanghai Institute of Applied Physics, Chinese Academy of Sciences, Shanghai, China

Abstract

A deep-learning-based feedforward scheme has been developed to compensate insertion-device (ID) effects in the Shanghai Synchrotron Radiation Facility (SSRF). Neural networks predict orbit and betatron-coupling perturbations caused by ID gap and phase changes. The orbit model reduces residual closed-orbit distortion (COD) to below 2 um and shortens preparation time by about a factor of 50 compared with conventional feedforward-table measurements. A coupling model trained with turn-by-turn (TBT) beam-position-monitor (BPM) data reaches an R^2 value above 0.95. These results show that deep learning can support fast and reproducible ID compensation during light-source operation.

INTRODUCTION AND ID COMPENSATION CHALLENGES

Insertion devices are essential to synchrotron radiation facilities because they provide tunable photon energy, polarization, and brightness. Their gap, phase, and polarization changes also modify magnetic field integrals and local focusing, which can drive COD, tune drift, beta-beating, coupling, and beam-size variation. These effects directly appear as photon-beam position, angle, flux, and brightness fluctuations.

SSRF is a 3.5 GeV third-generation light source with a 432 m storage ring, a nominal emittance of about 3.9 nm rad, and 27 operational IDs, including IVUs, CPMUs, EPUs, wigglers, and a Superconducting wiggler (SCW). Representative measurements show the scale of the compensation problem: 20EPU60 gap changes produce COD up to about +/-80 um horizontally and +/-60 um vertically, while 09EPU58 gap changes alter the horizontal and vertical beam sizes by about 3 um and 28 um, respectively. Thus, ID compensation must address both orbit and coupling.

The conventional SSRF feedforward system uses correction coils, quadrupoles, skew quadrupoles, response matrices, and look-up tables. It is robust but time-consuming: a planar-ID gap table typically takes about 0.5 h per ID, while a two-dimensional EPU gap-phase table can take about 4 h for one mode. A full measurement campaign for 27 IDs can exceed 60 h and must be repeated after lattice changes, ID maintenance, or BPM recalibration. Deep learning is introduced to learn the mapping from ID states to beam response from a compact data set, while the measured response matrix remains the basis for bounded and interpretable correction.

Previous SSRF feedforward and ID beam-dynamics studies provide the operational baseline [1-3]. Related machine-learning correction and stabilization studies at MAX IV and ALS are reported in Refs. [4-6]. Broader ML-based optics correction, BPM fault detection, magnet-error reconstruction, physics-informed modeling, surrogate optimization, and accelerator-ML roadmaps are discussed in Refs. [7-8].

NEURAL NETWORK FOR ID ORBIT FEEDFORWARD

The orbit feedforward model is formulated as a supervised learning problem. The input vector contains the gap settings of 19 IDs. The output vector contains beam-position responses measured by 138 BPMs in both transverse planes, giving 276 output targets. Instead of measuring dense tables for each device independently, the training data are obtained by changing several ID gaps and recording the resulting global orbit response. Data are recorded every 0.2 s, so about 3000 data sets can be collected in 10 min. The model structure and training workflow are shown in Fig. 1.

The neural-network architecture contains three hidden layers. Hyperparameters were scanned for activation function, batch size, hidden-layer width, and learning rate. The best orbit model uses ReLU activation, hidden layers of [64, 128, 256], a batch size of 16, and a learning rate of 0.001. The training, test, and validation losses are 0.00692, 0.00869, and 0.00097, respectively. The model reaches an R^2 value above 0.98 over the sampled operating range.

The model was tested with randomized ID gap settings over a range of 6-30 mm. Figure 2 shows a representative testing result for ID orbit correction, where the predicted BPM responses closely follow the measured values across both transverse output ranges. The predicted perturbation is then converted into correction currents using the existing response matrix and feedforward coils. After correction, the residual COD is reduced to less than 2 um. The complete model-based preparation takes about 3.5 min, which is about 50 times faster than traditional feedforward-table measurements.

This workflow has two operational strengths. First, it sharply reduces the time required to prepare ID feedforward data. Second, it represents the combined effect of several IDs, which is closer to real operation than treating each

Content from this work may be used under the terms of the CC BY 4.0 licence (© 2026). Any distribution of this work must maintain attribution to the author(s), title of the work, publisher, and DOI.

ISBN: 978-3-95450-252-3 ISSN: 2673-5350 doi: 10.18429/JACoW-IPAC2026-TUP2714

GPU-ACCELERATED SIMULATION FRAMEWORK FOR PARTIALLY COHERENT EUV LIGHT TRANSPORT IN TSINGHUA SSMB BEAMLINE OPTICS*

H. Hu†, Y. Li, X. Song, J. Sun, C. Tang, Y. Zhang, Tsinghua University, Beijing, China

Abstract

Accurate simulation of partially coherent beam transport and coherence evolution is critical for next-generation accelerator-based light sources. In this work, we develop a dedicated numerical approach for partially coherent EUV beamline propagation to support the optical design and optimization of Steady-State Microbunching (SSMB) beamlines under development at Tsinghua University.* A GPU-accelerated mutual optical intensity framework is developed for two-dimensional propagation of partially coherent radiation. Using spatially partitioned diffraction-integral kernels with locally reconstructed paraxial approximation, the method achieves substantial speedup over conventional mutual-intensity and wavefront-based propagation methods while maintaining high accuracy. Complex optical components, including arbitrary curved and rough reflective surfaces, are fully supported for efficient simulation of realistic EUV systems. In summary, the proposed framework provides a practical tool for optical design and end-to-end simulation of EUV beamlines, enabling coherence analysis and accurate light propagation modeling of partially coherent radiation.

INTRODUCTION

With the development of advanced lithography technologies and high-brightness accelerator-based light sources, accurate simulation of EUV radiation propagation and coherence evolution has become increasingly important [1, 2]. Tsinghua University is currently developing a Steady-State Microbunching (SSMB) accelerator light source aiming to generate high-brightness narrow-bandwidth EUV radiation in a storage ring [3].

The Mutual Optical Intensity (MOI) formalism provides a rigorous theoretical framework for describing the propagation of partially coherent radiation [4,5]. However, its numerical implementation involves four-dimensional propagation calculations, resulting in high computational complexity and limiting its practical application in complex optical systems.

To address this challenge, we develop a GPU-accelerated numerical framework for partially coherent radiation propagation optimized for SSMB EUV beamline optics. The proposed method preserves full two-dimensional propagation coupling and supports efficient simulation of complex curved optical components and rough surfaces.

* Work supported by the National Natural Science Foundation of China (No.124B2109)

† huhw22@mails.tsinghua.edu.cn

MUTUAL OPTICAL INTENSITY FORMALISM

In the analysis of partially coherent radiation, the MOI formalism provides a rigorous theoretical framework for describing statistical coherence properties [4, 5]. Unlike scalar field descriptions that characterize instantaneous field distributions, MOI describes the second-order spatial correlation of the optical field through statistical averaging, making it suitable for modeling partially coherent radiation.

For monochromatic partially coherent radiation in free space, the optical field can be described by the mutual optical intensity function [4]

$$J(\mathbf{r}_1, \mathbf{r}_2) = \langle E(\mathbf{r}_1) E^*(\mathbf{r}_2) \rangle$$

where $\langle \cdot \rangle$ denotes statistical averaging.

Assuming that the radiation propagates from a source surface Σ_0 to an observation surface Σ_1, the propagation of the mutual optical intensity can be written as

$$J_1(\mathbf{P}_1, \mathbf{P}_2) = \iint_{\Sigma_0} \iint_{\Sigma_0} J_0(\mathbf{Q}_1, \mathbf{Q}_2)\, h(\mathbf{P}_1, \mathbf{Q}_1)\, h^*(\mathbf{P}_2, \mathbf{Q}_2)\, dS_{\mathbf{Q}_1} dS_{\mathbf{Q}_2}.$$

Here $h(\mathbf{P}, \mathbf{Q})$ denotes the scalar diffraction propagation kernel. To support propagation between arbitrary curved surfaces, a general formulation based on the free-space Green's function is adopted:

$$h(\mathbf{P}, \mathbf{Q}) = \frac{1}{i\lambda} \frac{e^{ik\rho}}{\rho} \cos(\hat{\mathbf{n}}(\mathbf{Q}), \mathbf{P} - \mathbf{Q}), \qquad \rho = |\mathbf{P} - \mathbf{Q}|.$$

This expression is applicable to propagation between arbitrary surfaces and provides a unified theoretical basis for partially coherent propagation simulations involving complex optical components such as curved mirrors and rough surfaces.

For two-dimensional transverse coordinates, the mutual optical intensity depends on four spatial variables (x_1, y_1, x_2, y_2). If each transverse direction is discretized using N sampling points, the direct numerical evaluation leads to a computational complexity of $\mathcal{O}(N^4)$, resulting in substantial computational and memory requirements in practical beamline simulations. Therefore, efficient numerical methods are required to enable fast simulation of partially coherent radiation propagation in complex EUV optical systems.

Content from this work may be used under the terms of the CC BY 4.0 licence (© 2026). Any distribution of this work must maintain attribution to the author(s), title of the work, publisher, and DOI.

ISBN: 978-3-95450-252-3 ISSN: 2673-5350 doi: 10.18429/JACoW-IPAC2026-TUP2716

DEVELOPMENT OF IN-SITU FIELD MEASUREMENT SYSTEM FOR KOREA-4GSR IN-VACUUM UNDULATORS

G. Choi†, Korea Basic Science Institute, Daejeon, South Korea
Y. G. Choi, B. J. Kim, G. Hahn, Y. Jung, D. E. Kim, W. Lee
Pohang Accelerator Laboratory, Pohang, South Korea

Content from this work may be used under the terms of the CC BY 4.0 licence (© 2026). Any distribution of this work must maintain attribution to the author(s), title of the work, publisher, and DOI.

Abstract

Precise magnetic-field characterization of in-vacuum undulators is essential for achieving stable beam dynamics in synchrotron light sources. This work presents an in-situ measurement platform that integrates a SAFALI-based Hall probe scanner with a stretched-wire measurement system. The Hall probe unit measures the local magnetic-field distribution along the undulator, achieving micrometer-level positioning accuracy through laser interferometry and optical feedback. In parallel, the stretched-wire system enables reliable determination of the first and second magnetic-field integrals. To minimize magnetic distortion, most mechanical structures are fabricated from low-permeability materials. The system is designed to characterize in-vacuum undulators with magnetic lengths of up to 3 m, allowing comprehensive field mapping without removing the vacuum chamber. The integrated platform is currently under construction for application to in-vacuum undulators at the Korea-4GSR Facility and is expected to improve phase-error reproducibility while providing direct verification of undulator magnetic performance.

INTRODUCTION

Several advanced accelerator laboratories worldwide have developed and successfully operated in-situ magnetic field measurement systems for undulators. However, no equivalent system has yet been established in Korea. In the framework of the Korea 4th Generation Synchrotron Radiation Facility (Korea-4GSR) project, an in-situ magnetic field measurement system for in-vacuum undulators (IVUs) is being developed at Pohang Accelerator Laboratory (PAL). The fundamental design concept draws reference from the SAFALI (Self-Aligned Field Analyzer with Laser Instrumentation) system at SPring-8, Japan [1], and the in-situ measurement system at the National Synchrotron Radiation Research Center (NSRRC), Taiwan [2].

Given that the measurement system operates in close proximity to magnetic structures, minimization of magnetic interference is a primary design consideration. Low magnetic permeability materials were therefore adopted for all major structural and fastening components. The mechanical and optical subsystems were further designed to ensure stable alignment and motion accuracy over the full measurement range.

Prior to full-scale fabrication, prototype assemblies — comprising the carriage, rail, optical alignment subsystem, and wire tension control mechanism — were manufactured and experimentally evaluated. The prototype aimed at identifying potential mechanical instabilities, bearing contact issues, optical alignment limitations, and structural constraints relevant to 4 m translation performance.

Based on the outcomes of prototype evaluation, a series of design improvements are currently being implemented, targeting enhanced carriage stability, improved optical alignment reproducibility, refined wire tension control, and overall system reliability in view of future deployment on Korea-4GSR IVUs.

CONCEPT AND DESIGN

Figure 1 shows the overall schematic layout of the in-situ magnetic field measurement system developed for Korea-4GSR IVUs. The fundamental design concept follows that of the in-vacuum cryogenic undulator measurement system at NSRRC, incorporating a wire-driven Hall probe carriage, an optical alignment subsystem, and a stretched-wire measurement configuration within a unified measurement platform [2, 3].

Hall Sensor Actuating System

The Hall probe carriage is driven along a 4 m rail structure with high positional repeatability. The translation mechanism comprises a stepper motor and pulley assemblies, with stainless-steel wire connected to both ends of the carriage; bidirectional motion is achieved through rotational actuation of the stepper motor.

The carriage and rail assembly form the primary mechanical guide structure of the system. The carriage accommodates the Hall probe sensor, retroreflector, optical pinholes, and associated mechanical fixtures. To minimize magnetic interference during measurements, all major fastening components on the carriage were fabricated from 316L stainless steel.

As the current measurements are planned under out-vacuum conditions, vacuum-compatible treatment procedures — such as lubricant removal from stepper motor assemblies and carriage bearings — were not applied at the present prototype stage. Nevertheless, the overall mechanical structure was designed with future applicability to in-vacuum measurement environments in mind.

To improve translation stability, a dedicated wire tensioner mechanism (Fig. 2) was developed to maintain approximately constant wire tension throughout carriage motion. In the absence of adequate tension stabilization, fluctuations in wire tension can induce longitudinal oscillation and vibration during measurements. The tension control mechanism therefore plays a critical role in suppressing

†ghee1107@kbsi.re.kr

ISBN: 978-3-95450-252-3 ISSN: 2673-5350 doi: 10.18429/JACoW-IPAC2026-TUP3001

ANALYTICAL SOLENOID MATCHING ROUTINES WITH COOLPY* †

B. Stechauner‡, P. Desiré[1], D. Schulte, R. Taylor, CERN, Geneva, Switzerland
C. Rogers, Rutherford Appleton Laboratory, Didcot, UK
[1] also at University of Groningen, Groningen, Netherlands

Abstract

Muon colliders require strong beam cooling to reduce the large phase space of muon beams produced from pion decay. The final stage of ionization cooling employs high-field solenoids, absorbers, and RF cavities, where precise beam matching is essential to avoid emittance growth. In this work, we present a beam-parameter–based approach to design and optimize solenoid lattices for the final cooling channel. The method models realistic solenoid fields and solves the coupled beam envelope equation while accounting for momentum changes in absorbers and RF systems. To implement this approach efficiently, we developed the Python package coolpy, which computes the evolution of Twiss parameters and optimizes matching coil settings. Two case studies demonstrate matched beam transport in solenoid-based beamlines.

INTRODUCTION

The concept of a muon collider was first proposed in the late 1960s [1] and has the potential to represent a paradigm shift in accelerator and particle physics [2]. One of the main challenges arises from the short lifetime of the muon, 2.2 µs, in its rest frame. As a result, substantial effort has been invested in creating new accelerator technologies that can generate intense muon beams. These technologies must quickly accelerate the muons to TeV-scale energies before a large portion of them decay. A muon collider would provide a powerful probe for physics beyond the Standard Model (SM). It would simultaneously enable high-precision studies within the SM itself, like the investigations of the Higgs self coupling [3] and of lepton-parton distribution functions [4].

Muon Ionization Cooling

This paper focuses on the technological developments required for a muon collider, in particular muon ionization cooling [5]. Muon ionization cooling is a rapid method used to reduce the beam emittance of muons that were originally produced in proton-target interactions.

The resulting muon beam initially spans a large phase space, which must be substantially compressed to reach the high luminosities required for a collider. Ionization cooling decreases the emittance of a muon beam by passing the muons through an energy-absorbing medium, where their momentum is reduced by ionization losses. The longitudinal momentum is subsequently restored using radio-frequency (RF) acceleration. Repetition of these stages multiple times can progressively reduce the phase space of the muon beam.

In this paper, we discuss the final cooling channel [6, 7], which is the last part of the ionization cooling complex [8] of the proposed muon collider. The final cooling channel consists of a sequence of low- and high-field transport solenoids, absorbers, and RF cavity systems. Its purpose is to reduce the transverse emittance while keeping the growth of longitudinal emittance under control. The principal challenge is to optimize this final cooling system so that the optical beam parameters are correctly matched. If this condition is not met, an increase in emittance will arise and must be carefully prevented.

When designing such a final cooling system, four main aspects must be considered:

- a precise representation of the solenoid's magnetic field, taking its fringe regions into account,
- the dynamical evolution of the muon beam momentum in the absorber and RF cavities,
- a proper description of the beam parameters in a transversely coupled system, and
- an appropriate optimization procedure.

Coolpy: A Solenoid Based Lattice Design Solution

In principle, it is possible to optimize such an ionization cooling system using macro-particle tracking codes. However, these methods are computationally expensive. A faster approach is to solve the beam parameters for one or a few reference particles and tune the solenoid settings once specific targets are met. This multi-reference particle optimization is especially useful for bunches with large relative momentum spread, as in ionization cooling. After an optimized configuration is obtained, the same solenoid setup can then be applied in full multi-particle tracking simulations.

We have developed a code that follows this beam-parameter–based optimization approach and named it coolpy, which we introduce here for the first time. In the following, we provide a brief discussion of the evolution of beam parameters within a solenoid and the corresponding description of the solenoidal magnetic field. We next present two beam case studies using coolpy and conclude with a summary.

BEAM PHYSICS IN SOLENOIDS

Transverse Coupled Motions

The uncoupled motion of single or multiple charged particles in accelerators is described using the Courant–Snyder [9] or Twiss [10] formalism. In the presence of a solenoid, a

* Funded by the European Union (EU). Views and opinions expressed are however those of the author(s) only and do not necessarily reflect those of the EU or European Research Executive Agency (REA). Neither the EU nor the REA can be held responsible for them.
† Work endorsed by IMCC.
‡ bernd.stechauner@cern.ch

Content from this work may be used under the terms of the CC BY 4.0 licence (© 2026). Any distribution of this work must maintain attribution to the author(s), title of the work, publisher, and DOI.

ISBN: 978-3-95450-252-3 ISSN: 2673-5350 doi: 10.18429/JACoW-IPAC2026-TUP3008

RESEARCH STATUS ON THE ECRIPAC ACCELERATOR CONCEPT

A. Cernuschi*[1], T. Thuillier[1], L. Garrigues[2], A. Beck[3]
[1]Laboratoire de Physique Subatomique et de Cosmologie, Grenoble, France
[2]Laboratoire Plasma et Conversion d'Energie, Toulouse, France
[3]Laboratoire Leprince-Ringuet, Palaiseau, France

Abstract

This study presents the current advancement on our investigation of the Electron Cyclotron Resonance Ion Plasma Accelerator (ECRIPAC), revisiting and expanding this original accelerator concept initially developed in the ninties. ECRIPAC is an innovative compact plasma device able to generate energetic pulsed ion beams using robust and well mastered electron cyclotron resonance ion source technologies, without requirements for axial RF cavities or powerful laser beams. It relies on the gyromagnetic auto-resonance of plasma electrons in a time growing magnetic field, followed by the axial acceleration of ions through the plasma space-charge field inside a magnetic field gradient, up to energies close to 100 MeV/A. The theoretical behaviour of ECRIPAC is summarized. Some preliminary results of kinetic plasma simulations inside a preliminary design of an ECRIPAC machine able to accelerate He^{2+} ions up to ≈ 10 MeV/A are presented. Two sets of simulations are considered, one working with a cylindrical geometry and azimuthal mode decomposition in the open-source code Smilei and the other using a 3D geometry in the open-source code WarpX, providing interesting insights on the plasma behaviour inside the accelerator.

INTRODUCTION

The Electron Cyclotron Resonance Ion Plasma Accelerator (ECRIPAC) [1] is an original concept proposed by R. Geller, consisting in a plasma-based particle accelerator able to generate very energetic pulsed ion beams. Owing to its compact dimensions and the well-mastered technologies used in its design, the ECRIPAC is suitable for a wide array of applications, with a particular focus in the medical field as a possible instrument for ion cancer therapy. In our recent publications [2, 3], we reviewed and corrected the physical theory behind the ECRIPAC, and a short resume of its working principles and operating cycle is proposed in the the rest of this section.

An ECRIPAC device, which is schematically represented in Fig. 1, is composed of three main section. The first one is an injector of a highly ionized low-pressure plasma, with a possible candidate being an ECR ion source [4]. The second one is called the GYRAC section, which is characterized by the presence of a microwave injector and a reverse pulsed field coil acting on a small part of the accelerating cavity, generating a transient magnetic mirror trap which is slowly restored over time (red curve in Fig. 1). The third one is the PLEIADE section, composed by the rest of the accelerating cavity. Some static coils encompass the whole device, generating a static field represented with a blue curve in Fig. 1. The ECRIPAC working cycle is composed by three main phases: the gyromagnetic autoresonance (GA) phase, the plasma compression (PC) phase and the PLEIADE (PL) phase. The GA phase starts with the injection of both the plasma and the microwave when the pulsed coil reaches its maximum power, generating a magnetic mirror trap with an intensity equal to $B_{\min}$ at its center, which must be close to the magnetic field value satisfying the ECR condition for the injected microwave with frequency ω_{HF} ($B_{ECR} = m\omega_{HF}/e$ where m and e are the mass and the charge of the electron). The interaction of the plasma with the injected microwave inside a magnetic field growing over time onsets a physical phenomena called gyromagnetic autoresonance [5, 6] (GA), which determines a synchronous increase of the electron energy with the magnetic field

$$\gamma(t) = \frac{B(t)}{B_{\min}}\,, \tag{1}$$

where γ is the electron Lorentz factor. The PC phase starts when the microwave injection is halted, while the magnetic field is still increasing. During this phase, the plasma bunch is compressed under the action of the electric field induced by the variation of the magnetic field over time, which also further increases the electron energy. The plasma compression lasts until the restoration of the static field, which determines the start of the PL phase, where the ions are accelerated by the electrons through ion entrainment [7].

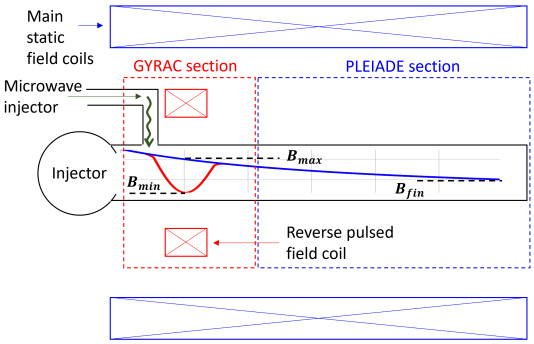

Figure 1: Schematic representation of an ECRIPAC device and the magnetic field generated inside the cavity. The blue curve represents the magnetic field profile when the pulsed coil is turned off (with $B_{\max}$ and B_{fin} being the maximum and final field intensities respectively), while the red curve is the magnetic field profile in the GYRAC section when the pulsed coil is working at its maximum power ($B_{\min}$ is the minimum field intensity inside the mirror trap).

* cernuschi@lpsc.in2p3.fr

Content from this work may be used under the terms of the CC BY 4.0 licence (© 2026). Any distribution of this work must maintain attribution to the author(s), title of the work, publisher, and DOI.

ISBN: 978-3-95450-252-3 ISSN: 2673-5350 doi: 10.18429/JACoW-IPAC2026-TUP3009

BEAMLINE OPTIMIZATION FOR LASER-ACCELERATED IONS

D. Dewitt*, O. Boine-Frankenheim, Technical University of Darmstadt, Darmstadt, Germany

Content from this work may be used under the terms of the CC BY 4.0 licence (© 2026). Any distribution of this work must maintain attribution to the author(s), title of the work, publisher, and DOI.

Abstract

Laser-plasma acceleration produces ultrashort, high-brightness ion beams reaching tens of MeV, yet their large divergence and broad energy spread require dedicated capture elements for beam transport. Using laser-accelerated protons from the GSI PHELIX laser to the LIGHT beamline as a reference, we developed a framework to optimize and assess such combined capture and transport systems, with emphasis on injection into conventional accelerators. In addition to our numerical analysis we derive scaling laws linking transmission and chromatic emittance growth to the initial half-opening angle, showing that the present performance is primarily divergence-limited. We also estimate and predict the longitudinal bunch quality and quantify the divergence reduction needed to approach injector-relevant intensities.

INTRODUCTION

Target normal sheath acceleration (TNSA) can produce ion beams with more than 10^{12} particles per shot and very low intrinsic source emittance [1], making it attractive for applications such as conventional accelerator injection [2] and medical applications [3]. Its practical use is nevertheless limited by the large initial divergence and broad energy spread, which make efficient capture and transport challenging. Within the LIGHT project at GSI [2], we numerically optimize a reference beamline consisting of a capture solenoid, a debunching cavity, and a second solenoid to determine the maximum delivered ion number per shot compatible with transverse and longitudinal acceptance constraints. Despite the low intrinsic source emittance, we find that the large divergence and broad energy spread drive strong emittance growth in both the transverse and longitudinal planes.

OPTIMIZATION OF THE LIGHT SETUP FOR MAXIMUM TRANSMISSION

The optimization was performed using a genetic algorithm (GA) [4] coupled to ASTRA [5] through the Python wrapper `lume-astra` [6], followed by a Nelder–Mead refinement step [7]. Space-charge effects were neglected in the present results and are discussed in more detail in [8]. The source was described by a simplified TNSA model with an exponential energy spectrum and an energy-dependent half-opening angle.

Figure 1 shows the transverse envelope and transmission (top) as well as the transverse emittance (bottom) of an optimized beamline for a reference energy of 11.4 MeV.

The transverse emittance initially follows the intrinsic drift growth and then rises sharply at the solenoid entrance. This

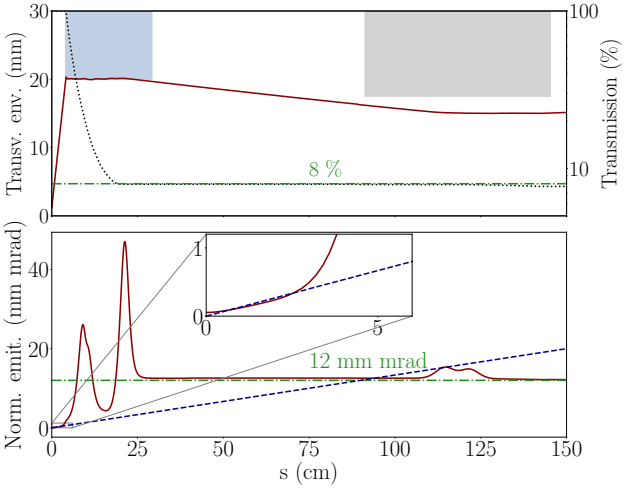

Figure 1: **Top:** Transverse envelope **(red, solid)** and transmission **(black, dotted)** for an optimized beamline. Solenoid and cavity apertures are indicated in blue and gray; the analytical transmission estimate is shown in **(green, dash-dotted)**. **Bottom:** Transverse emittance **(red, solid)** compared with the intrinsic drift growth **(blue, dashed)** and the analytical estimate **(green, dash-dotted)**. All values are 2σ-equivalent.

transient spike is an evaluation artifact of ASTRA's time-based tracking for beams with large energy and temporal spread [9]; after the solenoid, the emittance is dominated by chromatic growth [10]:

$$\varepsilon_{\mathrm{n}} = \gamma_0\beta_0\alpha f\frac{\Delta E}{E_{\mathrm{k}}}\theta^2 . \tag{1}$$

Both emittance and transmission are largely dictated by the first capture solenoid acting on the highly divergent TNSA beam. While the emittance is virtually zero at the source, it increases strongly after the capture element, which can be attributed to the beam divergence and energy spread combined with the chromatic aberrations of the magnetic lens.

Figure 2 shows the longitudinal beam evolution. Before the debunching cavity, the energy spread remains nearly constant and the bunch length increases linearly. The longitudinal emittance growth is approximated by

$$\varepsilon_z = \left(\frac{1}{\beta_0^2\gamma_0^2}\frac{\Delta E}{E_0}\right) d_1 E_{\mathrm{k}}\theta^2\frac{d_0}{d_1} = \frac{\Delta E}{\gamma_0(\gamma_0+1)} d_0\theta^2 \tag{2}$$

and remains nearly constant after capture, apart from local evaluation artifacts near the cavity.

The beam parameters at the end of the LIGHT beamline can be compared with the acceptances of the transfer channel (TK) and SIS18 to estimate the number of particles viable for injection. For typical LIGHT TNSA parameters, the interval 11.4 MeV ± 5% contains about 10^{10} protons at the

* daniel.dewitt@tu-darmstadt.de

ISBN: 978-3-95450-252-3 ISSN: 2673-5350 doi: 10.18429/JACoW-IPAC2026-TUP3010

SMART – A SMALL PARTICLE ACCELERATOR ON CHIP

A. Marcia *[1], E. Corte, R. H.Wilton, A. Picciotto
Fondazione Bruno Kessler (Sensor and Devices, NEXT unit), Trento, Italy
[1]also at University of Trento, Trento, Italy

Abstract

The miniaturization of particle accelerators via Dielectric Laser Acceleration (DLA)offers a route to ultra-compact, cost-effective devices powered by commercial laser systems. This work explores the extension of DLA technology—historically focused on electrons—to protons, aiming to enable "on-chip" sources of high energy hadrons. We present the design and simulation of a novel microstructure optimized for the acceleration of non-relativistic protons. Key challenges addressed include the management of phase slippage and the requirement for strong transverse confinement of heavy particles at low β. This study aims to demonstrate the potential for stable acceleration and focusing, validating the pDLA(proton-DLA) concept as a viable candidate for future compact accelerator architectures.

INTRODUCTION

Dielectric laser-driven accelerators (DLAs) [1] are currently the subject of extensive research as a cornerstone for the next generation of compact particle sources. The fundamental advantage of DLAs over conventional radio-frequency (RF) metallic accelerators lies in the superior Laser-Induced Damage Threshold (LIDT) of dielectric materials at optical and near-infrared frequencies. While traditional metallic cavities are strictly limited by surface breakdown and vacuum discharge typically constraining accelerating gradients to below 100 MV/m dielectric structures can sustain electromagnetic fields in the GV/m regime when driven by ultra-short laser pulses. This high-gradient capability allows for a radical miniaturization of the accelerating distance, potentially reducing kilometer-scale infrastructures to millimetric chip-scale devices. Leveraging these unique characteristics, recent investigations have moved beyond the ultra-relativistic electron regime to explore the application of DLA technology for proton acceleration [2]. The transition to hadrons presents significant opportunities for developing portable ion sources for nuclear physics and cost-effective, chair-side proton therapy systems. However, this extension requires sophisticated structural designs to maintain phase synchronicity in the non-relativistic regime ($\beta \ll 1$), where the grating periodicity Λ must be precisely tapered to match the evolving velocity of the heavier particles. These advancements underscore the versatility of DLAs as a transformative platform for both fundamental research and medical applications. This paper investigates the acceleration of protons in a double-grating structure [3], performing a comprehensive parameter study to maximize both fabrication feasibility and the achievable accelerating gradient. By optimizing the structural geometry and laser-matter interaction, we aim to bridge the gap between theoretical high-gradient performance and the practical constraints of modern nano-fabrication. To achieve this, numerical optimizations are performed using the CST Studio Suite [4]. The structural geometry is primarily optimized through Finite-Difference Time-Domain (FDTD) simulations to characterize the electromagnetic field distribution and maximize the synchronous accelerating components within the vacuum channel. This approach ensures that the design maintains phase synchronicity for non-relativistic particles ($\beta < 1$) while preserving beam quality and stability during the high-gradient acceleration process.

OPTIMIZATIONS FOR ACCELERATION OF NON RELATIVISTIC PROTONS

Upon dual-sided illumination of a double-grating structure by counter-propagating laser beams, the coherent diffraction of the optical fields facilitates the excitation of multiple spatial harmonics. In the regime of non-relativistic proton acceleration, achieving efficient energy gain is strictly dependent on the synchronicity condition, formulated as $\lambda_p = n\lambda_0\beta$ where λ_p denotes the grating period (as illustrated in Fig. 1), β represents the relativistic velocity factor of the particle, and the integer n defines the harmonic order, characterizing the number of optical cycles elapsed per grating period.

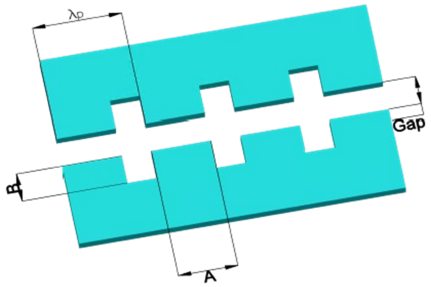

Figure 1: CAD schematic of the double-grating dielectric structure. The labels indicate the geometric dimensions required to satisfy the phase-matching conditions.

As expressed by the synchronicity condition, the non-relativistic nature of the protons imposes rigorous constraints on the geometric fabrication parameters of the dielectric structure. Numerical simulations were performed using a monochromatic plane wave with a central wavelength of $\lambda_0 = 2\,\mu$m. The structure was modeled using Fused Silica (SiO_2, refractive index $n = 1.53$), selected for its high optical transparency and superior laser-induced damage threshold

* amarcia@fbk.eu

Content from this work may be used under the terms of the CC BY 4.0 licence (© 2026). Any distribution of this work must maintain attribution to the author(s), title of the work, publisher, and DOI.

ISBN: 978-3-95450-252-3 ISSN: 2673-5350 doi: 10.18429/JACoW-IPAC2026-TUP3014

INTERACTION OF HIGH-INTENSITY LASER BEAM WITH STRUCTURED SOLID SURFACE PLASMA FOR WAKEFIELD ACCELERATION

B. Lei*, C. Welsch[1], H. Zhang[1], University of Liverpool, Liverpool, United Kingdom
G. Xia[1], University of Manchester, Manchester, United Kingdom
J. Resta-Lopez, Universidad Europea de Valencia, Valencia, Spain
A. Bonatto, Universidade Federal de Ciências da Saúde de Porto Alegre, Porto Alegre, Brazil
[1]also at Cockcroft Institute, Daresbury, United Kingdom

Abstract

Recent research into the interaction between high-intensity beams and surface plasmas has revealed the significant potential for generating extremely strong (TV/m) fields for particle acceleration and radiation production. By overcoming several longstanding challenges in beam–solid interactions, this emerging approach opens new opportunities to extend the energy frontier of particle physics while enabling the development of next-generation micro-scale accelerator facilities with unprecedented flexibility. At the same time, it provides new insights into the highly complex nonlinear dynamics of surface plasmons (SPs) under strong-field conditions and establishes a previously unexplored regime of plasma-based particle acceleration. In this study, we theoretically and numerically investigate high-intensity laser-driven excitation of relativistic surface plasmons (RSPs) on micro-scale smooth surfaces for high-gradient wakefield generation by using particle-in-cell (PIC) simulations. Sub-TeV/m-level leaky and bubble wakefields are shown to be driven by a TW laser with high energy efficiency, enabling the acceleration of both electrons and positrons. These results provide a new pathway toward the development of ultrahigh-gradient, ultra-compact particle accelerators for a broad range of scientific and technological applications.

INTRODUCTION

The current state-of-the-art laser-driven gaseous plasma-based accelerators practically work with a low-density classical plasma in the range of $n_e \sim 10^{14-18}\mathrm{cm}^{-3}$ [1, 2]. This density can, in principle, support an acceleration gradient of approximately $G \sim 1 - 100$ GeV/m. While the recent progress of laser-driven plasma wakefield acceleration (LWFA) mainly benefits from the rapid development of high-power lasers, it is still very challenging to further increase the beam energy. A higher-power laser pulse can introduce very strong nonlinear instabilities during the laser-plasma interaction that degrade the qualities of the plasma wakefield [3]. Although a higher-density plasma n_p can sustain a higher acceleration gradient G_z as $G_z \propto \sqrt{n_p}$, the total energy gain is decreased due to the limited laser penetration, which depends on the laser wavelength λ_0 via the critical density $n_c = m_e c^2/4\pi e^2 \lambda_0^2$ and scales the maximum energy gain as

$$\Delta\mathscr{E}_{\max}[\mathrm{GeV}] \simeq 1.7 \left(\frac{P[\mathrm{TW}]}{100}\right)^{1/3} \left(\frac{10^{18}}{n_p[\mathrm{cm}^{-3}]}\right)^{2/3} \cdot \left(\frac{0.8}{\lambda_0[\mu m]}\right)^{4/3},$$

where P denotes the laser power. m_e and e denote the rest mass and charge of an electron, respectively. c is the speed of light in vacuum. Another major challenge in applying LWFA toward high-energy colliders is the efficient acceleration of positrons, which experience transverse defocusing inside the plasma cavity formed in a uniform plasma [4].

Beyond gaseous plasma-based accelerators, the solid-state plasma accelerator is a promising direction to provide both an extremely high acceleration gradient and a stable field structure for particle acceleration. Recent progress in high-power laser-driven, grating-free RSPs on a metallic surface has opened a new route toward ultra-high gradient, ultra-compact plasma-based particle acceleration and radiation generation [5]. In these schemes, as the laser propagates in the vacuum while interacting with the high-density surface plasma, it then enables stable laser propagation, ultrahigh wakefield, high energy efficiency and flexible structures for field control and beam modulation. Particularly, in this approach, RSPs are excited on the smooth surface instead of the grating surface typically used for conventional SP excitation. Therefore, these methods are intrinsically suitable for high-intensity laser-driven SPs excitation. In the grating-free scheme, RSPs are excited when an intense laser pulse interacts with a finite or curved solid surface, with the coupling efficiency determined primarily by the modal overlap between the incident laser field and the SP eigenmode. As the surface geometry intrinsically governs the SP eigenmodes, this approach enables precise mode selection and controlled manipulation of the excitation dynamics.

The nanostructured low-density vertically-aligned carbon nanotube (VCNT) is proposed to be the platform to support these strong RSP [6–10]. These materials can provide excellent thermal and electronic properties, large-area uniformity, high damage thresholds and well-tailorable geometry as shown in Fig. 1 (b)-(f). More importantly, they can provide a flexible effective surface plasma density down to 10^{19} cm^{-3} that is critical for efficiently supporting the resonance RSP excitation.

* bifeng.lei@liverpool.ac.uk

Content from this work may be used under the terms of the CC BY 4.0 licence (© 2026). Any distribution of this work must maintain attribution to the author(s), title of the work, publisher, and DOI.

ISBN: 978-3-95450-252-3 ISSN: 2673-5350 doi: 10.18429/JACoW-IPAC2026-TUP3016

cSTART – A COMPACT ELECTRON STORAGE RING FOR NON-EQUILIBRIUM ACCELERATOR RESEARCH AND TECHNOLOGY

R. Ruprecht*, A. Bernhard, E. Blomley, T. Borkowski, E. Bründermann, D. El Khechen, S. Fatehi, M. Fuchs, J. Gethmann, A. Grau, B. Härer, H. Hoteit, B. Krasch, A. Malygin, A. Mochihashi, M. J. Nasse, J. Natal, H. Nordmeyer, A. Papash, N. Ray, D. Saez de Jauregui, A. Y. Saw, J. Schäfer, T. Schmelzer, S. Schott, P. Schreiber, M. Schuh, M. Schwarz, B. Shen, N. Smale, D. Squires, J. L. Steinmann, C. Weiss, P. Wesolowski, C. Widmann, A.-S. Müller
Karlsruhe Institute of Technology, Karlsruhe, Germany

Content from this work may be used under the terms of the CC BY 4.0 licence (© 2026). Any distribution of this work must maintain attribution to the author(s), title of the work, publisher, and DOI.

Abstract

The goals of the compact STorage ring for Accelerator Research and Technology (cSTART) at Karlsruhe Institute of Technology (KIT), are to demonstrate the storage of ultra-short electron bunches and to investigate their non-equilibrium dynamics. Furthermore, it aims to study the application of laser-plasma accelerators (LPAs) as injectors for storage rings.

To achieve these goals, cSTART has a specifically designed flexible magnetic lattice with large momentum acceptance that can be tuned to ultra-low momentum compaction factor operation. cSTART will have two independent injectors: FLUTE (Ferninfrarot Linac und Test Experiment) and an LPA.

In 2024, the collaboration between KIT, RI Research Instruments GmbH, and its subcontractors completed the Technical Design Report (TDR), followed by the Final Design Report (FDR) until mid-2026. Most magnets and power supplies for the injection line (IL), which will connect FLUTE to the storage ring, are already available at KIT. Some of the diagnostics were delivered and are being tested at KIT, the others are in production. Magnets, power supplies, and vacuum chambers for the storage ring are currently in production. This article provides an overview of the current status and outlines the next steps of the cSTART project.

MOTIVATION FOR cSTART

The scientific objectives of the compact STorage ring for Accelerator Research and Technology (cSTART) project [1] are the proof of concept for the injection and circulation of ultra-short electron bunches in a storage ring and the demonstration of laser-plasma accelerators (LPAs) as injectors for storage rings, i.e.:

(i) the injection of ultra-short electron bunches and their circulation,

(ii) studies of injection of electron beams that are generated by novel LPAs, and

(iii) research program to investigate nonlinear non-equilibrium dynamics, ultimately the phase-space manipulation, and control of ultra-short bunches in a storage ring.

The experiments performed at cSTART have the potential to have a paradigm-shifting impact on future accelerator complexes. To achieve this objective, Karlsruhe Institute of Technology (KIT) plans to initially inject ultra-short electron bunches from the linac-based FLUTE accelerator. One technological objective of the cSTART project is to build a very large momentum acceptance compact electron storage ring (VLA-cSR) at KIT. The VLA-cSR has a flexible magnetic lattice and vacuum design that supports different optics: one with a momentum acceptance of up to 4 % suitable for straight injection of LPA-generated beams [2] and one that allows circulation of ultra-short electron bunches with a duration of femtoseconds to a few picoseconds [3].

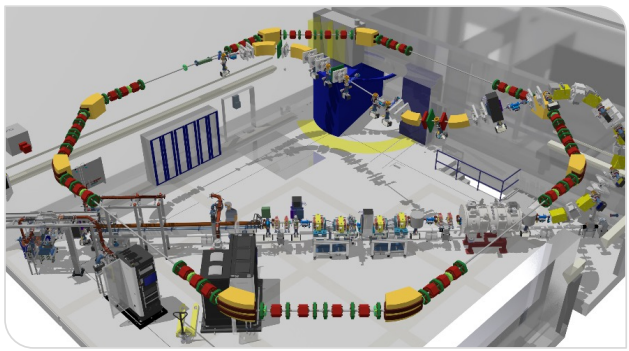

Figure 1: Artistic view of the cSTART project. The VLA-cSR at a height of about 4.5 m is connected to the FLUTE injector (1.2 m above ground floor) by a complex 3D injection line.

With a circumference of less than 45 m and an energy operation range of 40 MeV to 90 MeV, the design of the VLA-cSR is also focused on compact size and energy efficiency as part of KIT's portfolio to develop technologies for compact and energy-efficient accelerators. Figure 1 gives an artistic overview of the accelerator complex.

FLUTE [4], [5] will be used as one of the injectors for the VLA-cSR. FLUTE was upgraded to produce a wide range of electron pulses with a charge of 1 pC to 1 nC, bunch length of a few fs to 300 fs, and energy between 40 and 90 MeV. Using the FLUTE bunch compressor (BC) and the injection line (IL) the operators will tune the electron beam to ultra-short bunches just before the septum. The ultra-short duration of the electron bunches that circulate in the storage ring causes the emission of coherent synchrotron radiation with frequencies of up to tens of THz, leading to substantial energy loss and results in rapid, very rich and highly nonlinear dynamics [6]. As mentioned previously, part of the scientific program of the VLA-cSR is to study this non-equilibrium

* robert.ruprecht@kit.edu

ISBN: 978-3-95450-252-3 ISSN: 2673-5350 doi: 10.18429/JACoW-IPAC2026-TUP3017

TOWARDS INTEGRATED DIAGNOSTICS FOR MULTI-STAGE DIELECTRIC LASER ACCELERATION: A CONCEPTUAL STUDY

T. Egenolf*, O. Boine-Frankenheim†, Technical University of Darmstadt, Darmstadt, Germany

Content from this work may be used under the terms of the CC BY 4.0 licence (© 2026). Any distribution of this work must maintain attribution to the author(s), title of the work, publisher, and DOI.

Abstract

Dielectric laser acceleration (DLA) enables compact, chip-scale accelerators. Recent demonstrations of multi-stage acceleration, alternating-phase focusing and interaction length in the millimeter range in dielectric nanostructures have verified the scalability of DLA concepts but the compactness places extreme demands on beam diagnostics due to submicron apertures, sub-fs bunch lengths and strong non-linear dynamics. To support the development of multi-stage structures and precise matching between stages, we explore diagnostic concepts that use the dielectric structures themselves. Tailored gratings can encode beam properties—such as bunch length—into emitted radiation, providing compact, high-resolution, on-chip diagnostics. Additionally to these hardware approaches, we propose to apply a machine-learning–based virtual diagnostic for DLA experiments. A neural network trained on 6D tracking simulations reconstructs key interaction parameters from the post-DLA electron beam and intermediate diagnostics and enables real-time optimization even in strongly non-linear regimes. Combining integrated dielectric diagnostics with ML-based reconstruction provides a scalable strategy for precise characterization and control of next-generation dielectric laser accelerators.

INTRODUCTION

Dielectric laser acceleration (DLA) has emerged as a promising route to compact, chip-scale electron accelerators by exploiting optical near-fields in dielectric nanostructures to reach gradients in the GV/m regime [1–3]. Recent experimental advances have demonstrated beam confinement by alternating-phase focusing, laser pulse shaping, and interaction lengths in the millimeter range, confirming the scalability of DLA concepts beyond single-stage proof-of-principle experiments [4–6]. However, the extreme compactness and submicron apertures of DLA structures impose stringent demands on the electron beam, including sub-femtosecond bunch durations, submicron-level transverse beam sizes, and tight tolerances on arrival time and phase stability [7, 8].

In this regime, conventional accelerator diagnostics, such as transverse deflecting cavities [9] or bunch compressor monitors [10] to measure the bunch length, reach their limits. Direct access to the interaction region is restricted by nanometer-scale vacuum gaps, and inserting invasive diagnostics between closely spaced stages risks disrupting the beam or breaking the compact integration that makes DLA attractive. Moreover, the strong non-linear dynamics in the optical near-field coupling and in the mapping from interaction region to downstream spectrometers complicate straightforward reconstruction of beam and laser parameters. To support the development of multi-stage DLAs and precise matching between stages, there is a need for diagnostics that are both integrated into the dielectric structures and capable of resolving the ultrafast, non-linear beam dynamics.

This contribution outlines a strategy "towards integrated diagnostics for multi-stage dielectric laser acceleration" by combining two complementary approaches. First, tailored dielectric structures are used as compact sources of radiation in the THz to optical range, encoding beam properties such as bunch length or arrival time into the emitted spectrum and angular distribution. Second, a machine-learning–based virtual diagnostic, previously developed for laser pulse shape reconstruction [11], is extended conceptually to multi-stage configurations and electron beam diagnostics, using a digital twin of the interaction to reconstruct key parameters from the post-DLA electron beam. Together, these approaches provide a scalable path towards precise, on-chip characterization and control of future multi-stage DLA setups.

DIAGNOSTIC REQUIREMENTS

Multi-stage DLA structures impose tight constraints on both beam quality and diagnostics. Submicron vacuum channels and high-gradient optical modes require transverse beam sizes well below the aperture in the submicron to few-micron range and trajectory alignment at the tens-of-nanometers level to avoid beam scraping and to maintain high transmission. At the same time, efficient energy gain over many optical periods demands synchronization between the laser field and the electron beam at the level of a small fraction of the optical cycle, corresponding to sub-femtosecond arrival time jitter and tight control of the DLA phase (see Table 1).

Diagnostics must therefore resolve longitudinal properties such as arrival time, phase relative to the drive laser, and bunch length at sub-femtosecond down to tens-of-attoseconds scales, while being compatible with the limited space available between stages. Conventional RF deflecting structures and large spectrometers are difficult to integrate into a chip-scale environment and often require large drift lengths or macroscopic components that break the compactness of DLA-based systems. Furthermore, strong non-linearities in the interaction — arising from the optical near-field, phase slippage, and transverse–longitudinal coupling — mean that simple linear reconstruction methods based on a few projections are insufficient, especially when aiming for single-shot, shot-to-shot–resolved diagnostics in the presence of fluctuations.

* thilo.egenolf@tu-darmstadt.de
† also at GSI Helmholtz Centre for Heavy Ion Research, Darmstadt, Germany

ISBN: 978-3-95450-252-3 ISSN: 2673-5350 doi: 10.18429/JACoW-IPAC2026-TUP3019

BETATRON RADIATION STUDIES AS A PATH TO PLASMA UNDULATORS

E. Chiadroni*, A. Curcio, A. Mostacci, Sapienza University of Rome, Rome, Italy
A. Cianchi, University of Rome Tor Vergata, Rome, Italy
A. Biagioni, C. Buitrago, G. Costa, L. Crincoli, A. Del Dotto, R. Demitra, M. Ferrario, M. Galletti, A. Giribono, R. Pompili, G. J. Silvi, L. Verra, Istituto Nazionale di Fisica Nucleare, Laboratori Nazionali di Frascati, Frascati, Italy
A. R. Rossi, Istituto Nazionale di Fisica Nucleare, Milan, Italy

Content from this work may be used under the terms of the CC BY 4.0 licence (© 2026). Any distribution of this work must maintain attribution to the author(s), title of the work, publisher, and DOI.

Abstract

There is strong interest in developing compact user facilities, with plasma technology emerging as a promising solution not only for acceleration modules but also for ancillary components such as free-electron lasers. While substantial progress has been achieved in miniaturizing diagnostics, detectors, and transfer lines, conventional undulators remain bulky and costly. This has motivated the exploration of advanced undulator concepts, including plasma ion-channel undulators based on electron betatron motion. We present a feasibility study for plasma-based undulators at SPARC_LAB within the EuPRAXIA@SPARC_LAB project, providing quantitative predictions of gain and radiation performance under realistic experimental conditions.

INTRODUCTION

The manuscript investigates the feasibility of plasma-based undulators at the SPARC_LAB facility [1] within the EuPRAXIA [2] and EuPRAXIA@SPARC_LAB [3] projects, aimed at developing compact plasma-based user facilities for free-electron lasers (FELs). Since conventional magnetic undulators remain bulky and expensive, the study explores advanced concepts based on the betatron motion of electrons in plasma ion channels to emulate undulator behavior. In particular, the work focuses on a wakeless ion-column configuration, which enables compact FEL amplification with larger energy-spread tolerance and shorter gain lengths compared to conventional undulators. Using realistic electron beam parameters from SPARC_LAB and numerical simulations, the formation of a stable ion channel is described and the onset of FEL radiation is shown in a 10 cm plasma undulator, providing a proof-of-principle framework for future compact X-ray sources.

THEORETICAL BACKGROUND

Ion Channel Formation

Ion column (IC) formation requires that the thin cylindrical volume, after ionization, is depleted of all electrons for a length much longer than the plasma wavelength. In this paper, we will consider depletion by use of an electron bunch (driver) preceding the bunch intended to emit radiation (witness). The ionization technique might rely on the propagation of ultrashort, high-intensity laser pulses in gases that is governed by the interplay between Kerr self-focusing and plasma-induced defocusing arising from multi-photon or tunnel ionization. This dynamic balance leads to intensity clamping and the formation of extended plasma channels, known as filaments [4,5]. This technique enables the generation of plasma channels with tunable transverse dimensions and density profiles. In particular, plasma channels can be produced with radii comparable with the transverse size of the driving bunch, creating the conditions for the formation of a fully evacuated ion channel . In this regime, the strong space-charge fields of the driver expel nearly all plasma electrons from the channel volume, leaving behind a stationary column of ions. Because the expelled electrons cannot return quickly enough to restore charge neutrality, the ion column persists over the interaction length and provides a stable linear focusing force for the propagating beam.

Such a configuration is especially attractive for plasma-undulator applications, where the controlled betatron oscillations of relativistic electrons inside the ion channel can emulate the behavior of a conventional magnetic undulator in a much more compact setup. Figure 1 shows an example of well-formed ion channel, as considered in the simulations. The plasma is assumed to be ionized through laser filamentation.

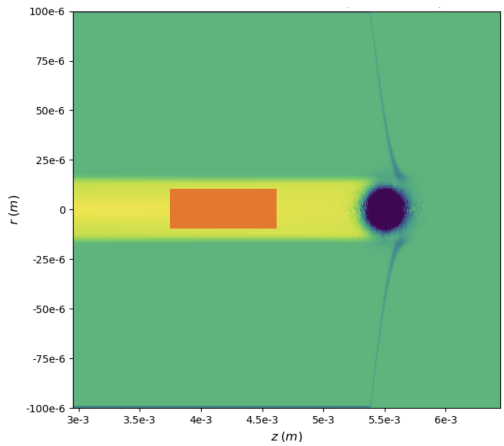

Figure 1: Example of a well-formed ion channel, assuming the following parameters: $n_0 = 5 \cdot 10^{15}$ cm^{-3}, $R_{ch} = 15$ μm, $Q_b = 600$ pC, $\sigma_z = 90$ μm.

* enrica.chiadroni@uniroma1.it

ISBN: 978-3-95450-252-3 ISSN: 2673-5350 doi: 10.18429/JACoW-IPAC2026-TUP3021

SUB-10 FS SYNCHRONIZATION IN LASER-PLASMA ACCELERATORS WITH TERAHERTZ FREQUENCY BUNCH MANIPULATION*

A. Amini†[1], L. R. Reid[2], J. K. Jones[2], M. T. Hibberd[1], L. Corner[3], D. M. Graham[1], S. P. Jamison[4], G. Burt[4], R. B. Appleby[1]
Cockcroft Institute, Sci-Tech Daresbury, Keckwick Lane, Warrington, United Kingdom
[1]also at University of Manchester, Oxford Road, Manchester, United Kingdom
[2]also at ASTeC, STFC Daresbury Laboratory, Warrington, United Kingdom
[3]also at University of Liverpool, Brownlow Hill, Liverpool, United Kingdom
[4]also at Lancaster University, Bailrigg, Lancaster, United Kingdom

Abstract

External injection offers a pathway to high-quality electron bunches in laser-plasma accelerators, yet precise synchronization between the drive laser and the injected electron bunch remains a major challenge. We investigate a temporal-locking mechanism using THz-driven waveguides to overcome these synchronization limits. Start-to-end simulations based on the CLARA/FEBE facility show that sub-10 fs synchronization is achievable, corresponding to an eight-fold reduction in arrival time jitter compared to conventional Radio Frequency systems and resulting in an order-of-magnitude improvement in laser-plasma final beam energy stability.

INTRODUCTION

Laser-driven acceleration methods [1–4] offer a promising route toward compact, high-gradient accelerators. In particular, laser-plasma wakefield acceleration (LWFA) has attracted significant attention [5, 6] for producing GeV-class electron beams with gradients of several GV/m. However, the inherently nonlinear laser–plasma interaction limits the generation of stable, high-quality bunches with narrow energy spread and consistent shot-to-shot performance. Such beam quality and stability are essential for applications in high-energy physics (HEP) [7] and free-electron lasers (FEL) [8, 9].

LWFA beams are typically generated via internal (self-) injection, where electrons originate from the background plasma [10–12], offering limited control over the bunch properties. External injection [13–15] provides an alternative by introducing pre-formed electron bunches into the wakefield, enabling improved control of beam quality. Significant efforts [16, 17] have therefore focused on developing reliable external sources, often based on conventional Radio Frequency (RF) injectors.

High-quality electron bunches by LWFA with external injection require femtosecond electron bunches with the precise synchronization of laser and electron beam [18]. Conventional RF injectors typically rely on a magnetic compression system to provide ultrashort electron bunches [19–21] and numerical studies [16] suggest that such systems have critical challenges to produce stable ultrashort electron bunches suitable for LWFA applications, primarily due to nonlinearities and jitter introduced by the RF cavities coming from their mutual independence and asynchronization with the drive laser.

In this paper, we explore a recent temporal-locking concept based on THz-driven waveguides for generating sub-femtosecond electron bunches with precise synchronization for external injection [22], and discuss its advantages over conventional approaches. THz-driven acceleration is a promising approach for next-generation laser-driven accelerators [23], enabled by recent GV/m-level THz sources [24]. THz waveguides have attracted interest for beam manipulation, particularly femtosecond-scale compression [25]. Our recent results [26] show intrinsic temporal locking and reduced timing jitter in high-energy beams, enabling stable high-quality bunch generation and supporting applications such as multi-stage LWFA and storage ring injection.

THz-FREQUENCY CONTROL OF ELECTRON BUNCHES

The concept of THz-controlled electron bunches for external injection into an LWFA takes advantage of the intrinsic synchronization between THz pulse generation and plasma wakefield excitation enabled by using a common laser system to drive both processes, enabling the delivery of stable, high-quality ultrashort bunches. The concept is illustrated schematically in Fig.1(a), where electron bunches (a) from an external RF source (injector and linac) interact with laser-generated THz pulses inside a dielectric-lined waveguide (DLW). The THz-driven DLW (b) acts as a linear energy chirper, imprinting a time-energy correlation on the bunch that intentionally increases its energy spread. This is followed by a magnetic chicane for longitudinal phase-space rotation, compression, and transverse matching into the final stage of laser-plasma acceleration (c).

The THz-driven beam control can be analysed analogously to conventional RF injectors by considering the single-particle dynamics within a theoretical framework. In a rectangular DLW, a set of orthonormal modes known as longitudinal section magnetic (LSM_{mn}) modes are supported, where m and n represent the number of half-wavelength variations along the horizontal and vertical directions. These modes are characterised by the absence of transverse mag-

* Work supported by the Cockcroft Institute and STFC.
† aras.amini@manchester.ac.uk

Content from this work may be used under the terms of the CC BY 4.0 licence (© 2026). Any distribution of this work must maintain attribution to the author(s), title of the work, publisher, and DOI.

ISBN: 978-3-95450-252-3 ISSN: 2673-5350 doi: 10.18429/JACoW-IPAC2026-TUP3022

NEWGAIN PROJECT AT GANIL: CONSTRUCTION OF THE NEW HEAVY ION INJECTOR FOR SPIRAL2*

F. Chautard[1,†], D. Ackermann[1], O. Cakir[1], O. Delahaye[1], J. Dumas[5], V. Gérard[3], M. Di Giacomo[1], F. Hanchin[1], C. Haquin[1], C. Jamet[1], G. Jevelot[2], C. Lesigne[1], M. Michel[1], G. Normand[1], A. Outreman[1], C. Peaucelle[3], O. Piquet[5], Ph. Robillard[1], D. Simon[5], I.Stephan[4], Y.Trehudic[1], Q. Tura[1]

[1]GANIL, Caen, France
[2]Université de Bordeaux, CNRS-LP2I, Bordeaux, France
[3]Université Grenoble Alpes, CNRS-LPSC, Grenoble, France
[4]Université Paris-Saclay, CNRS-IJCLAB, Orsay, France
[5]CEA/IRFU, Saclay, France

Abstract

The NEWGAIN (NEW GAnil INjector) project is now in the construction phase at GANIL. It aims to install a second injector for the SPIRAL2 facility. It is designed to accelerate heavy ions with a mass-to-charge ratio (A/q) of up to 7. With this upgrade, SPIRAL2 will provide high-intensity beams, from protons to uranium, strengthening GANIL international competitiveness, both in fundamental sciences and related applications. The paper will provide an update on the progress of the construction phase and the main milestones achieved and to come. The layout and the main technical components of the new injector, based on 2 ECR ion sources (one of them existing), two Low Energy Beam Transport (LEBT) line, one RFQ and a Medium Energy Beam Transport (MEBT) line to transport the beam into the present MEBT connected to the SPIRAL2 LINAC are presented.

INTRODUCTION

The NEWGAIN project aims to build a second injector designed for A/q = 3 to 7 ions, to produce and accelerate very intense heavy ion beams using a new RFQ (RFQ2) up to uranium, far exceeding the performance of the existing injector. Thus, a new superconducting source will be developed to complement the existing sources and achieve high-intensity uranium beams.

Thanks to this improvement, the Système de Production d'Ions Radioactifs en Ligne de 2ème génération (SPIRAL2) LINAC [1] will deliver, within the limits of its operating energy, the most intense beams in the world (Table 1) on a wide variety of ions ranging from protons to uranium, and will strengthen GANIL's international competitiveness, both in fundamental sciences and in associated applications.

The project is organized within a large technical collaboration framework, composed of the following French accelerator laboratories of CEA/DRF/IRFU and CNRS/IN2P3: GANIL, IRFU/DACM and DIS, LPSC, LPCCaen, IPHC, LP2iB, IJCLab. These different partners have already collaborated in different projects with GANIL, the latest example to date being the construction of the SPIRAL2 facility. The NEWGAIN project is coordinated by GANIL.

Table 1: Ion Beam Intensities SPIRAL2 vs NEWGAIN

Ions	Intensity [pμA]		
	SPIRAL2	NEWGAIN	
	Phoenix V3 A/Q≤3	Phoenix V3 A/Q≤6	Superconducting Ion Source A/Q≤7
18O	80*	-	375
19F	>15	>40	>40
36Ar	16*	70	45
40Ar	3.6	70	45
36S	2.3	-	-
40Ca	2.9*	10	20
48Ca	1.2	10	20
58Ni	1.1*	4	8
84Kr	0.1	10	20
139Xe	0.001	7	>10
238U	<<0.001	0.1	10

*Measured, Foreseen

GENERAL LAYOUT

This second injector is designed to be fully compatible with the existing facility (Fig. 1) and to further enhance its 'multi-user' capabilities. It is composed of the following (Fig. 2):

- A high-performance superconducting ion source (the Source 1/7) called ASTERICS [2]
- Low energy beam transport lines connecting the ion sources (superconducting ion source and existing room temperature ion source) to the RFQ (LBE3). The mass separation at the exit of the ion sources can be tuned up to 150, depending on the ion choices and the experiment needs,
- A RFQ that will accelerate heavy ions with minimal beam losses up to the injection energy for the superconducting LINAC (RFQ2),

*This work benefited from state aid managed by the French National Research Agency under the Future Investment Program bearing the reference ANR-21-ESRE-0018
†chautard@ganil.fr

Content from this work may be used under the terms of the CC BY 4.0 licence (© 2026). Any distribution of this work must maintain attribution to the author(s), title of the work, publisher, and DOI.

ISBN: 978-3-95450-252-3 ISSN: 2673-5350 doi: 10.18429/JACoW-IPAC2026-TUP3033

SIMULATION OF PLASMA DECHIRPER AND LENS FOR LASER WAKEFIELD ACCELERATION*

T. L. Steyn†, C. Ballage, B. Cros, P. Désesquelles, O. Khomyshyn, M. Masckala,
F. Massimo, I. Moulanier, O. Vasilovici, LPGP, CNRS, Université Paris Saclay, Orsay, France
S. Dobosz Dufrénoy, A. Panchal, LIDYL, CEA, Université Paris Saclay, Gif-sur-Yvette, France
Y.-Yu Chang, A. Irman, M. Laberge, S. Schöbel, F. M. Herrmann[1], M. Samir[1], U. Schramm[1], P. Ufer[1]
Helmholtz-Zentrum Dresden-Rossendorf, Dresden, Germany
[1] also at Technische Universität Dresden, Dresden, Germany

Abstract

Laser wakefield accelerators can produce compact, high-gradient electron sources, but typically generate chirped beams with significant energy spread and divergence. We present a simulation study of a tailored plasma density profile that performs post-acceleration phase-space manipulation within a single gas-cell target: a plasma down-ramp providing transverse lensing and a long, low-density plasma tail acting as a beam-driven dechirper and lens. Using OpenFOAM fluid simulations to generate the density profile and Particle-in-Cell simulations to resolve the wakefields, we analyze the longitudinal and transverse fields responsible for chirp generation, dechirping, and collimation.

INTRODUCTION

Laser wakefield acceleration (LWFA) produces relativistic electron beams over mm-scale distances using the large longitudinal electric fields sustained by plasma waves [1–3]. In the laser-driven blowout-regime configuration considered here, the accelerated bunch spans a finite fraction of the accelerating phase, so the longitudinal field varies along the bunch length; different longitudinal slices therefore accumulate different energy gains, imprinting a head–tail energy–position correlation (chirp). In particular, situations where the rear of the bunch experiences a higher accelerating field lead to a positive chirp. Although optimal beam loading [4, 5] can mitigate these effects, it imposes strict requirements on the longitudinal charge distribution [6, 7]. In addition, the beam must be extracted and transported with minimal transverse momentum spread.

Here we give a fuller description of how the wakefields in the accelerating phase lead to chirped beams and how the post-acceleration fields remove this imposed chirp, as first described in [8, 9] and elsewhere in this conference as [10]. We model a compact plasma structure including: (i) a plasma density down-ramp that behaves as a lens, reducing transverse momentum spread via the transverse wake focusing forces generated by the wakefield driven by the laser [11, 12]; and (ii) a long, low-density plasma tail (LPT) where the electron bunch drives its own wakefield, providing simultaneous focusing and dechirping.

SIMULATION MODELS

The longitudinal plasma density distribution is obtained from computational fluid dynamics simulations of a two-compartment gas cell and a downstream channel using OpenFOAM [13, 14]. The simulated neutral density distribution (hydrogen and nitrogen) is converted to an electron density profile for the PIC input. The density profile of a simulation where the pressure is equal between the two compartments is shown in Fig. 1. The mesh lines are coloured based on the local concentration of nitrogen in the gas. Black lines indicates parts where the nitrogen concentration is high (close to 15%), which is the concentration of gas in the reservoir providing nitrogen to the first compartment (C1) in this simulation. White lines indicate the absence of nitrogen. Thus having the pressures equal in both compartments leads to proper confinement of the nitrogen in the first compartment. The gradient of the nitrogen concentration between the two compartments leads to an electron density down-ramp which is where the ionisation injection occurs.

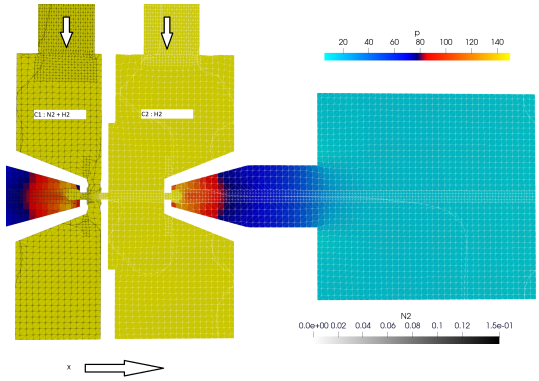

Figure 1: OpenFOAM simulation of the gas-cell exit and low-density tail. The horizontal arrow denotes the laser propagation direction. The first compartment (C1) is filled with a mixture of hydrogen and nitrogen. The fraction nitrogen is indicated by the colour of the mesh lines. The second compartment (C2) is filled with pure hydrogen. The pressure here is shown as the color map of the background in units of Pa.

The maximum value the pressure scale of the profile is intentionally saturated to show the low density structure that forms in the outlet of the gas cell (C2). This structure is particularly important as it forms the plasma lens and

* arXiv:2604.26486
† theunis-lodewyk.steyn@universite-paris-saclay.fr

Content from this work may be used under the terms of the CC BY 4.0 licence (© 2026). Any distribution of this work must maintain attribution to the author(s), title of the work, publisher, and DOI.

ISBN: 978-3-95450-252-3 ISSN: 2673-5350 doi: 10.18429/JACoW-IPAC2026-TUP3034

ANALYTICAL CALCULATION OF TRANSVERSE EMITTANCE AND TWISS PARAMETERS

S. Marini, L. Batista, N. Chauvin, A. Chancé, D. Uriot, P. A. P. Nghiem
CEA, Université Paris-Saclay, Gif-sur-Yvette, France

Content from this work may be used under the terms of the CC BY 4.0 licence (© 2026). Any distribution of this work must maintain attribution to the author(s), title of the work, publisher, and DOI.

Abstract

Achieving plasma-based accelerators for users demands careful control not only of the beam energy and energy spread, but also of transverse beam properties such as emittance, size, and divergence. Since plasma-based accelerators typically produce beams with significantly larger energy spread and emittance than conventional RF accelerators, several questions remain to be addressed, particularly, the transverse beam dynamics. In this article, it is presented an analytical description of the transverse beam properties evolution in a constant-focusing channel representing a plasma density plateau assuming a finite energy spread. The resulting expressions provide qualitative and quantitative guide to understand the transverse beam dynamics under these conditions.

INTRODUCTION

Laser-plasma accelerators are moving from proof-of-principle experiments to a realistic option for compact accelerator facilities [1, 2]. Their main advantage is the accelerating gradient, which can reach 10–100 GV/m, making it possible to reduce typical machine length by orders of magnitude. Recent laser-plasma accelerator studies report strong beam quality at the plasma exit [3–8]. The main challenge is now make stable and repeatable the beam delivery at the user point, where transverse beam quality is critical.

Achieving operational plasma-based accelerators requires integrated studies to control not only the beam energy and energy spread, but also of transverse beam properties such as emittance, size, and divergence. The transverse beam dynamics is governed by the focusing gradient K. In a plasma density plateau, K is typically of order 10^6 m^{-2}, whereas in the surrounding magnetic transport lines the effective focusing is only a few m^{-2}. In presence of energy spread, such large variations of K across interfaces are the main reason of beam Twiss mismatch and consequent emittance growth [9–11].

To qualify and quantify the transverse beam properties evolution, particularly the emittance, we present a fully analytical description for a constant-focusing channel representing a plasma density plateau acting over an electron beam with finite energy spread.

The work described in this article expands the model presented in Ref. [11] in contrast to earlier works [10] (semi-analytical) calculation, the energy spread is here kept up to second order. Then, an analytical expression of emittance growth in a constant-K channel with finite energy spread is derived, from which the Twiss-parameter evolution, the decoherence length, and the saturated emittance are obtained.

THE KEY PARAMETER K

The plasma wakefield focuses particles in all the transverse planes. It can be considered as a cylindrically symmetric focusing channel, characterized by the focusing gradient K (in m^{-2}) expressed as

$$K = \frac{e}{\gamma_{\mathrm{rel}} m_e c^2} \left(\frac{\partial E_r}{\partial r} - \beta_{\mathrm{rel}} c \frac{\partial B_\theta}{\partial r} \right)\Big|_{r=0}, \tag{1}$$

where e and m_e are the electron charge and mass, c is the speed of light in vacuum, β_{rel} and γ_{rel} are the relativistic speed and Lorentz factor, r the transverse coordinate and E_r, B_θ the radial electric and azimutal magnetic field components.

Because K depends explicitly on the beam energy through γ_{rel}, the focusing is chromatic. For a particle with momentum deviation $\delta = \Delta p/p_0$, the effective focusing gradient becomes

$$K^* \equiv \frac{K}{1+\delta}, \tag{2}$$

where K is the focusing gradient defined in Eq. (1) for the reference particle, which has $\delta = 0$ and Lorentz factor γ_{rel}. Particles with different energies are focused differently, inducing oscillations on the beta functions, which in turn induce emittance growth by the phase mixing mechanism. All these will be explicitly derived in the following.

EVOLUTION OF THE TWISS PARAMETERS

To model the plasma-density plateau, we assume that the focusing gradient K remains constant along the propagation direction. The transverse coordinate u ($u = x$ or y) of a particle then follows Hill's equation

$$u'' + K^* u = 0, \tag{3}$$

whose general solution is given by

$$u = u_0 \cos[z\sqrt{K^*}] + \frac{u_0'}{\sqrt{K^*}} \sin[z\sqrt{K^*}], \tag{4}$$

$$u' = -u_0\sqrt{K^*} \sin[z\sqrt{K^*}] + u_0' \cos[z\sqrt{K^*}]. \tag{5}$$

The projected transverse emittance of the beam is defined from the second-order moments as

$$\varepsilon^2 = \langle u^2 \rangle \langle u'^2 \rangle - \langle uu' \rangle^2. \tag{6}$$

These moments can be written in terms of the Twiss parameters according to

$$\langle u^2 \rangle = \beta\,\varepsilon, \qquad \langle u'^2 \rangle = \gamma\,\varepsilon, \qquad \langle uu' \rangle = -\alpha\,\varepsilon, \tag{7}$$

ISBN: 978-3-95450-252-3 ISSN: 2673-5350 doi: 10.18429/JACoW-IPAC2026-TUP3035

NONLINEAR TRANSVERSE BEAM DYNAMICS IN AWAKE RUN 2C

J. P. Farmer*, Max Planck Institute for Physics, Garching, Germany,
T. Wilson, A. Pukhov, Heinrich-Heine-Universität Düsseldorf, Germany,
M. Moreira, M. Turner, E. Gswendtner, CERN, Meyrin, Switzerland,
C. Amoedo, Instituto Superior Técnico, Lisboa, Portugal, and CERN, Meyrin, Switzerland,
(the AWAKE collaboration)

Content from this work may be used under the terms of the CC BY 4.0 licence (© 2026). Any distribution of this work must maintain attribution to the author(s), title of the work, publisher, and DOI.

Abstract

The AWAKE experiment harnesses the 400 GeV proton beam from the CERN SPS to drive plasma wakefields, which in turn accelerate a witness bunch of electrons to high energy. Upgrades are currently being carried out to facilitate the experimental programme of Run 2c, which includes control of the witness bunch quality during acceleration. In this work, particle-in-cell simulations are used to investigate the wakefields excited by the proton driver. We find that nonlinearities in the plasma response result in "wakefield tearing", a shift in the relative phase of the focusing and accelerating regions of the wakefield. We demonstrate that tearing can have a significant impact on the witness energy gain which can be achieved while simultaneously maintaining witness quality, with shorter drive bunches offering a path to mitigate the effect. These simulations inform the choice of parameters for the experiment.

INTRODUCTION

Plasma wakefield acceleration has attracted considerable attention due to the high fields which plasma can support, potentially leading to a significant reduction in the length, and hence the cost, of linear accelerators [1]. A plasma wave is excited by a driver, with the plasma acting as a transformer to couple energy from the driver to a co-propagating witness bunch. Currently available electron and laser drivers have limited energy, and so multiple acceleration stages would be required to reach high energies. Proton-driven wakefield acceleration offers the potential to accelerate a witness bunch of electrons to the energy frontier in a single stage [2].

To effectively excite a large amplitude wakefield, the drive bunch should be short, on the scale of the plasma skin depth $1/k_p$, with $k_p = (ne^2/\varepsilon_0 mc^2)^{1/2}$ the plasma wavenumber. Here, n is the plasma number density, $-e$ and m the electron charge and mass, c the vacuum speed of light and ε_0 the vacuum permittivity. Currently available proton beams have a typical length of a few centimetres, too long to drive high-amplitude wakefields. One solution is to develop methods for generating short proton bunches at high repetition rates [3], as pursued by the ALiVE project, which would open the path towards the high luminosities required collider applications [4]. Alternatively, plasma instabilities can be harnessed to modulate currently available proton beams, as in the AWAKE experiment at CERN [5].

Figure 1a shows the longitudinal profile (in terms of the effective current, I_{eff} [6]) of a proton drive beam with $\sigma_z \gg 1/k_p$. The associated longitudinal wakefields are shown in Fig. 1b in terms of the characteristic field amplitude $E_c = mc^2 k_p/e$. The initial wakefields are small, but the plasma response also generates transverse fields which are sufficient to "self-modulate" the long drive bunch into a train of microbunches over a distance of a few metres [7, 8]. The beam profile and associated wakefields after 10 m of plasma propagation are also shown. At this point, the proton beam is fully modulated and the wakefields are much larger and increase along the length of the beam.

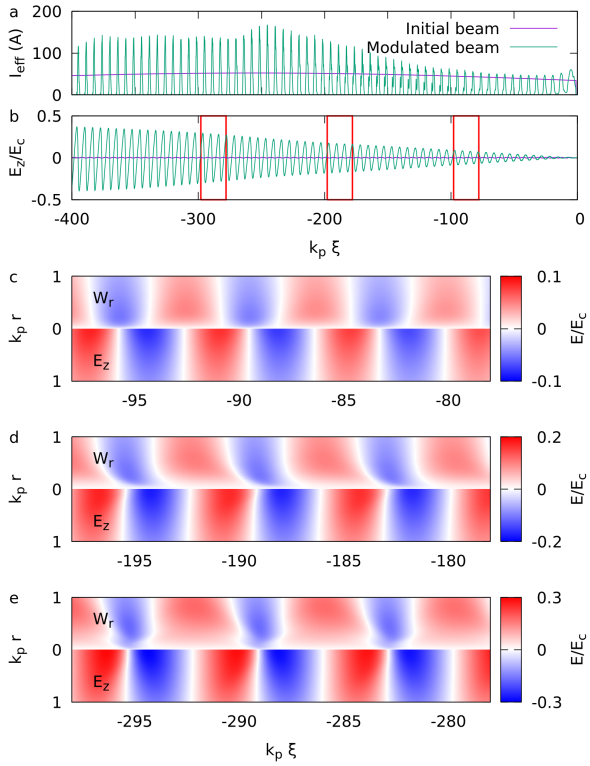

Figure 1: a) Effective current of the proton drive beam (propagating right) and b) the associated on-axis longitudinal wakefield, for the initial beam and for the modulated beam after 10 m of plasma propagation. c-e) the radial dependence of $W_r = E_r - cB_\theta$ and E_z after 10 m propagation at different positions along the beam, indicated by red boxes in (b).

The use of a train of microbunches requires that the wakefields persist over many plasma periods. Small changes in the local plasma frequency, which can arise due to the relativistic shift in the mass of plasma electrons and the influence of the driver charge, can then lead to significant phase shifts, which ultimately lead to the destruction of the microbunch

* j.farmer@cern.ch

ISBN: 978-3-95450-252-3 ISSN: 2673-5350 doi: 10.18429/JACoW-IPAC2026-TUP3039

CHARACTERIZATION OF SELF-MODULATION IN A PLASMA WAKEFIELD ACCELERATOR

J. Mezger*,[1], G. Demeter[2], L. Ranc[1], M. Bergamaschi[3], P. Muggli[1,3]
[1]Max Planck Institute for Physics, Munich, Germany
[2] Wigner Research Centre for Physics, Budapest, Hungary
[3]CERN, Geneva, Switzerland

Abstract

AWAKE uses a long relativistic proton bunch to drive wakefields in plasma. The amplitude of the wakefields increases along the plasma as the bunch undergoes self-modulation (SM). Wakefields are energy deposited in the plasma that must dissipate, a fraction of which is emitted as light. Light diagnostics measuring the amount of light emitted can be used to study the development of the wakefield amplitude along the plasma. A finite radius plasma column may influence wakefields, their energy balance and possibly the self-modulation process. To study these effects, the evolving plasma column radius has to be measured. Here we report on the use of light diagnostics in the absence of wakefields for this purpose.

INTRODUCTION

Charged particle bunches propagating through plasma drive wakefields by displacing plasma electrons [1]. Wakefields can be used for particle acceleration. The accelerating gradients sustained by wakefields can be several orders of magnitude higher than in RF-cavities. AWAKE uses a long relativistic proton bunch (400 GeV, 48 nC) as driver. To reach accelerating gradients on the order of 1 GeV/m, the proton bunch must undergo self-modulation [2]. For this purpose, a 10.3 m rubidium vapor plasma source is used [3]. The plasma is created by a laser pulse ($I_0 \sim 10\,\mathrm{TW/cm^2}$, $t_{pulse} = 120\,\mathrm{fs}$ (FWHM), $\lambda = 780\,\mathrm{nm}$, $\Delta\lambda \gtrsim 5\,\mathrm{nm}$ [4]) ionizing the rubidium atoms with an ionization fraction of 100 % [5]. This ensures density uniformity within 0.2 % [3] and enables control over the plasma density by means of controlling the vapor density. A characteristic of a laser ionized plasma is that the radius of the plasma column changes along the pulse propagation due to the evolution of the laser beam energy, radius and thus intensity. We show here that the time integrated light recorded by ten CMOS cameras placed along the 10.3 m plasma column is consistent with the amount of ionized Rb atoms calculated by a simple model for laser ionization through which the radius of the plasma column can be extrapolated. The setup for the experiment and details on the light diagnostic can be found in Ref. [6]. Measurements presented in this work are taken in the absence of wakefields.

LASER IONIZATION MODEL

We introduce the laser ionization model that is used to interpret the light measurements of the laser ionized plasma column. Figure 1 illustrates the influence of each component in the model. We use the same approach as in Ref. [6] with some modifications, mainly the inclusion of ionization in the sheath layer and self-focusing of the laser pulse. The model assumes a Gaussian transverse beam profile. The beam is described by the two sigma beam width $w(z) = w_0\sqrt{1 + M^4\left(\frac{z-z_0}{z_R}\right)^2}$, which is measured in vacuum at five locations within the Rayleigh length $z_R = \frac{\pi w_0^2}{\lambda}$. The beam quality factor is M = 1.33, the waist size is $w_0 = 1.6\,\mathrm{mm}$ and its location $z_0 = 5.42\,\mathrm{m}$ from the entrance of the Rb vapor column. Field ionization occurs above an intensity threshold I_{th} and produces a plasma of 100 % singly ionized Rb atoms. In vacuum, the radius where intensity $I(r) = I_0(z)e^{-\frac{2r^2}{w(z)^2}} \geq I_{th}$ is $r_0(z) = \sqrt{\frac{w(z)^2}{2}\ln\left(\frac{I_0(z)}{I_{th}}\right)}$ (red solid line Fig. 1). When propagating through rubidium vapor, $r_0(z)$ changes as the laser pulse looses energy to ionization and its intensity decreases.

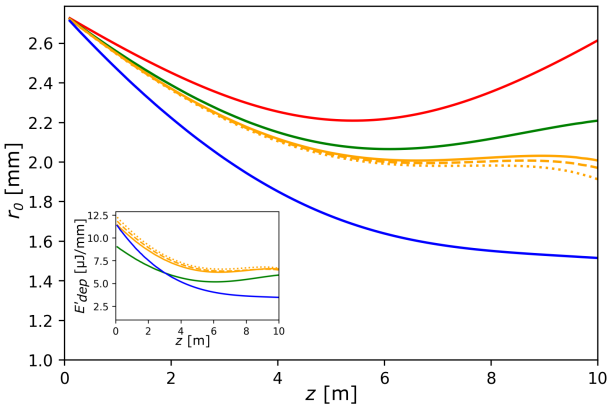

Figure 1: Plasma radius $r_0(z)$ (where $I(z,r) = I_{th}$) plotted against propagation distance of laser pulse z. Inset: Energy deposited in the vapor/plasma by the laser pulse per unit length. Red line: in vacuum. Green line: field ionization. Orange line: ionization in sheath layer. Orange dotted line: excitations in sheath layer. Orange dashed line: ponderomotive potential. Blue line: self-focusing.

First, we consider energy loss due to field ionization only. Over a distance Δz, the number of Rb atoms ionized through field ionization is $N_{ion,fi} = \pi r_0^2(z)\cdot\Delta z\cdot n_{rb}$, which requires energy $\Delta E_{fi}(z) = N_{ion,fi}\cdot e\phi_1$, where $e\phi_1 = 4.18\,\mathrm{eV}$ is the ionization potential and n_{rb} is the vapor density. We subtract the energy lost over a small step ($\Delta z = 1\,\mathrm{cm}$, $\Delta E_{fi} \ll E_{pulse}$) from the total energy of the pulse E_{pulse} and recalculate

* jan.mezger@cern.ch

Content from this work may be used under the terms of the CC BY 4.0 licence (© 2026). Any distribution of this work must maintain attribution to the author(s), title of the work, publisher, and DOI.

ISBN: 978-3-95450-252-3 ISSN: 2673-5350 doi: 10.18429/JACoW-IPAC2026-TUP3041

DENSITY DOWNRAMP INJECTION INTO A DISCHARGE-BASED PLASMA ACCELERATION STAGE

L. Boulton[1*], J. C. Wood, J. Beinortaitė[2], J. Björklund Svensson, S. Bohlen, G. Boyle, J. M. Garland, P. Gonzalez Caminal[3], C. A. Lindstrøm, G. Loisch, S. M. Mewes[3], T. Parikh, F. Peña[3], K. Põder, S. Schröder, M. Thévenet, S. Wesch, M. Wing[2], J. Osterhoff, R. D'Arcy
Deutsches Elektronen-Synchrotron DESY, Hamburg, Germany
[1]also at SUPA, Department of Physics, University of Strathclyde, Glasgow, United Kingdom
[2]also at University College London, London, United Kingdom
[3]also at Institute of Experimental Physics, Universität Hamburg, Hamburg, Germany

Abstract

Electron bunches internally injected into plasma accelerators reach relativistic energies in giga-volt-per-metre-level fields, reducing emittance growth due to space charge and ultimately yielding high-brightness beams. Density downramps with steep gradients have provided an effective method of controllable injection into beam-driven plasma-wakefield accelerators, but previously have relied on the fields of an intense particle beam or laser to preionise the acceleration stage. Here, injection using downramps formed via optical ionisation is experimentally shown to be compatible with discharge-based-acceleration stages, producing bunches with up to six times higher energy than with laser-only preionisation. Results demonstrating injection of charge using a purely discharge-preionised acceleration stage and a low-energy injection laser suggest the feasibility of a scalable, high-repetition-rate injection stage—potentially attractive for high-average-power applications.

INTRODUCTION

Plasma accelerators driven by intense laser [1] or particle beams [2, 3] can generate giga-volt-per-metre level accelerating gradients, making them a promising technology for future compact light sources and particle colliders [4]. However, plasma accelerators can also be a source of high-quality particle bunches, where the rapid acceleration of injected particles to relativistic energies can drastically mitigate emittance growth due to space-charge forces. Although several schemes exist for the injection of particles into a plasma wake, Density Downramp Injection (DDRI) [5–7] has been identified as a particularly robust option that can yield transverse normalised emittances of order 100 nm [8, 9]. In this scheme, as the driver traverses a negative plasma density gradient, the plasma wake elongates. Plasma electrons at the back of the wake that have a high enough longitudinal velocity sample the accelerating phase of the wakefield long enough to reach the same velocity as the driver, which in beam-driven plasma wakefield acceleration (PWFA) propagates at approximately the speed of light. This enables controlled, dark-current-free injection [10], but also necessitates either the use of steep downramps [11] or high-current drivers that can generate the accelerating gradients necessary to successfully trap injected electrons.

Several experimental demonstrations of DDRI in PWFA have been performed, using beam drivers from both conventional [12–14] and laser-wakefield [15–17] accelerators. In particular, Ref. [18] details a PWFA experiment in which electron bunches were injected via steep density downramps generated by optical ionisation [19]. A high injection success rate allowed for a thorough, multi-shot characterisation of the injected bunches which simultaneously displayed low horizontal emittances and high spectral densities, resulting in a high 3D brightness. The injected bunches, however, achieved relatively low energy gains of 30 MeV, primarily attributed to ionisation defocusing of the laser beam that generated the plasma channel used for acceleration [20].

Here we expand upon results presented in Ref. [18] with preliminary measurements of density-downramp-injected electron beams accelerated in a discharge-preionised plasma stage. Energy gains that were multiple times higher than the laser-only-preionised case were demonstrated, albeit at the expense of the charge of the injected bunches. This paper describes the setup and results from two experimental campaigns. In the first, injection and acceleration of charge up to energies of (176 ± 4) MeV was observed, but only in the presence of the discharge plus both the preionisation and injection lasers. In the second, the intermittent production of 90 MeV electron bunches is shown using only the discharge and injection laser. We discuss the advantages of such discharge-based plasma stages for internal injection in PWFA, as well as future work.

EXPERIMENTAL SETUP

The experiment was performed at the FLASHForward facility at DESY [21]. The experimental setup is shown in Fig. 1, with more details provided in Ref. [18]. To summarise, drive electron bunches were delivered by the FLASH linac [22]. At the optimal injection working point found in Ref. [18], the bunches had an energy of 689 MeV and charge of (304 ± 2) pC and were compressed to a duration of (96 ± 6) fs rms, with peak currents reaching (1.9 ± 0.2) kA. The beam was focused at the entrance of the plasma stage by a collection of final-focusing quadrupoles. The hori-

* lewis.boulton@desy.de

Content from this work may be used under the terms of the CC BY 4.0 licence (© 2026). Any distribution of this work must maintain attribution to the author(s), title of the work, publisher, and DOI.

This is a preprint - the final version is published with IOP

ISBN: 978-3-95450-252-3 ISSN: 2673-5350 doi: 10.18429/JACoW-IPAC2026-TUP3043

A FULL-ENERGY ELECTRON INJECTOR FOR THE EIC BASED ON PROTON-DRIVEN PLASMA-WAKEFIELD ACCELERATION

H. Jaworska*[1], A. Pukhov[1], A. Caldwell[2], J. P. Farmer†[2], N. Lopes[3], F. Willeke[4], M. Wing[5,6]
[1]Heinrich-Heine-Universität Düsseldorf, Düsseldorf, Germany
[2]Max Planck Institute for Physics, Garching, Germany
[3]Instituto Superior Técnico, Lisbon, Portugal
[4]Brookhaven National Laboratory, Upton, NY, USA
[5]University College London, London, UK
[6]DESY, Hamburg, Germany

Abstract

The Electron-Ion Collider (EIC) is presently under construction at Brookhaven National Laboratory, and will collide electrons with an energy of up to 18 GeV with hadrons of up to 275 GeV. In this work we evaluate the feasibility of using proton-driven plasma wakefield acceleration (PWFA) to accelerate electron bunches to full energy for injection into the EIC Electron Storage Ring. Particle-in-cell simulations are used to identify a scheme which allows the acceleration of electron bunches with high charge and low energy spread, building on previous studies which investigated the potential energy gain.

The RHIC "BLUE RING", which accelerates hadrons in the same direction as the electrons of the EIC, can be exploited to drive the plasma wakefields, offering the potential to significantly reduce the capital cost of the EIC facility. We show that by increasing bunch population to 3×10^{11}, and moderate compression of the drive bunch to 2.5 cm, high accelerating fields can be achieved by exploiting the self-modulation of the proton beam, as harnessed by the Advanced Wakefield Experiment (AWAKE) project at CERN. To facilitate the use of a plasma discharge, we consider the possibility of using different ions, instead of rubidium.

INTRODUCTION

The Electron-Ion Collider (EIC) is a new collider which is planned to be built at Brookhaven National Laboratory, and will re-use some infrastructure of the existing Relativistic Heavy Ion Collider (RHIC) [1]. Currently, RHIC is composed of two ion accelerator/storage rings. The construction of the EIC would involve adding an electron accelerator ring, which would allow collisions between electrons with energy up to 18 GeV and protons with energy up to 275 GeV. This addition would involve significant changes to the layout of the collider, which will be expensive to complete. To offer a lower-cost alternative, this work investigates the feasibility of proton-driven plasma wakefield accelerator for injection of electron bunches into the EIC electron storage ring. The scheme is based on technology developed at the AWAKE experiment at CERN [2], and investigated using LCODE particle-in-cell simulations [3].

* helena.jaworska@hhu.de
† j.farmer@cern.ch

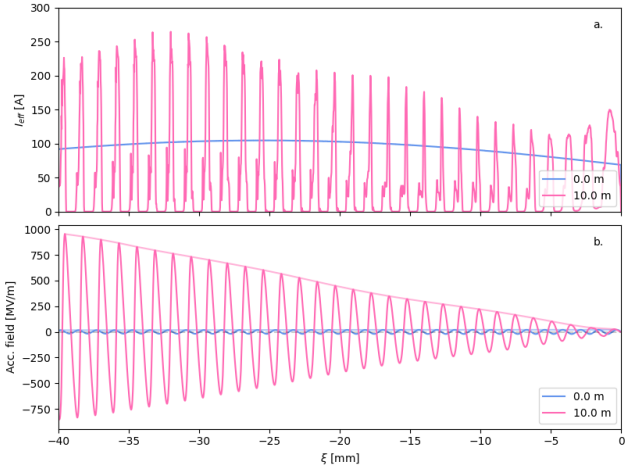

Figure 1: a) Effective current of the drive beam, b) the associated longitudinal wakefields, with the envelopes of the field shown. Both are pictured as the beam first enters the plasma (blue) and after 10 m after the start of the plasma (red).

PROTON-DRIVEN PWFA

This scheme is based on the planned design for Run 2c of AWAKE at CERN [4]. AWAKE is a proof-of-concept accelerator facility, which uses a proton bunch from the CERN Super Proton Synchrotron (SPS) to drive wakefields in plasma. Plasma can support high fields, and therefore has the potential to significantly reduce the length of linear accelerators [5, 6]. Using a proton driver has the significant advantage of higher driver energy compared to electron or laser drivers [7].

Most often, the bunch used as the driver in a plasma wakefield accelerator is shorter than the plasma wavelength. Using a short bunch is preferable, and other studies have investigated the use of a short proton bunch as a driver [8]. For injection into a storage ring, considered in the present work, high average current from the injector is not required, and so it may be possible to avoid significant compression of the proton bunch, greatly reducing the cost. While it is possible to increase the plasma wavelength, such that the length of the bunch is comparable to it, it is undesirable, as it decreases the maximum fields the plasma can sustain [9].

Content from this work may be used under the terms of the CC BY 4.0 licence (© 2026). Any distribution of this work must maintain attribution to the author(s), title of the work, publisher, and DOI.

ISBN: 978-3-95450-252-3 ISSN: 2673-5350 doi: 10.18429/JACoW-IPAC2026-TUP3044

GAUSSIAN PROCESS REGRESSION AND BAYESIAN OPTIMIZATION FOR A 40-90 MeV LASER-PLASMA INJECTOR FOR THE dSTART STORAGE RING

D. Squires, E. Sailer, J. Natal, A. Saw, N. Ray, T. Schmeltzer, M. Fuchs
Karlsruhe Institute of Technology, Karlsruhe, Germany

Content from this work may be used under the terms of the CC BY 4.0 licence (© 2026). Any distribution of this work must maintain attribution to the author(s), title of the work, publisher, and DOI.

Abstract

Laser-plasma accelerators (LPAs) generate ultrashort high intensity electron bunches from a compact source size. At the Karlsruhe Institute of Technology (KIT), we will use an LPA as one of the injectors for the compact, high-momentum acceptance, non-equilibrium storage ring cSTART.

The LPA injector with a length of only a few millimeters will be optimized to match the cSTART operation beam energy of 40–90 MeV. It will be based on an ionization trapping scheme in combination with a tailored plasma density profile to produce an electron beam with small energy spread that maximizes the spectral charge density at our target energy, which is (for LPAs) comparably low. Moreover, the LPA injector must produce controlled electron beams with high shot-to-shot stability and avoid high-energy tails. These goals can be achieved largely by the detailed design of the plasma density profile and the laser pulse parameters.

In an LPA, small changes across the high-dimensional parameter space can have a disproportional influence on overall performance. To find parameters for stable high-quality LPA beams, we perform particle-in-cell (PIC) simulations and implement a machine-learning driven approach by using Bayesian Optimization (BO) based on Gaussian Process Regression (GPR). This procedure allows us to both optimize our gas target design and characterize the effects of the interaction parameters, giving us a functional LPA with a simple tuning mechanism.

INTRODUCTION

KIT is in the process of building a compact electron storage ring cSTART [1], which will be able to accept femtosecond bunches with large momentum spread for accelerator research into the storage of ultrashort bunches as well as non-equilibrium beam dynamics, beam stabilization, future compact light sources, and next-generation accelerator technologies. [2]

As part of the project, we plan to use LPAs (see Table 1) to inject femtosecond electron bunches into the compact storage ring [3]. LPAs have long been considered a promising technology for this purpose [4], and the high accelerating gradients produced in a plasma wakefield allow us to accelerate beams to our target energies over millimeter-scale acceleration distances, allowing the LPA injectors themselves to be orders of magnitude smaller than traditional RF-based approaches.

However, one persistent challenge associated with LPAs as stable electron sources is the shot-to-shot fluctuations of LPA generated electron beams [5]. This variability is currently substantially higher in LPAs than that of RF-based accelerators due to the nonlinearity of the laser plasma interaction coupled with a high accelerating gradient, which imply that small variations in the input parameters of an LPA system lead to disproportionately large changes in the properties of the generated beam.

Table 1: LPA Target Parameters

Parameter	Value
Energy Range	40 - 90 MeV
Momentum Spread	<4 %
Bunch Duration	femtosecond

We intend to mitigate this weakness through a careful choice of laser and plasma input parameters, selecting not just for suitable beam parameters, but for reproducible generation of such beams even when those carefully selected parameters vary from shot to shot.

PARAMETER SPACE

Our first strategy to mitigate LPA variability is our selection of an ionization trapping scheme, which adds a gas dopant with a higher atomic Z-number than the typical LPA background gas target in order to control when and where electrons begin to accelerate. [6] This scheme has been shown to substantially improve the stability of LPA beams [7].

In our simulations, this is implemented into the gas targets via a density up-ramp followed by a density plateau of a background atom species (hydrogen in our case), which forms the accelerating structure of the LPA. A small, localized dopant species (nitrogen in our case) is introduced close to the up-ramp. The simulated gas target ends with a gradual density downramp which increases energy stability by forcing the LPA to reach the dephasing length at the target energy (see Figure 1).

Similar density profiles can be generated experimentally, both with paired gas jets [8] and with gas capillaries at equilibrium [9]. We identified several relevant parameters which may randomly vary from shot to shot in an experimental LPA setup and affect beam stability. These parameters include the densities of both the background and dopant species, the laser focus position, as well as the overall gas density profile. Limiting ourselves to parameters that may affect beam stability, while also being simple to alter and simulate, left us with an 6-dimensional parameter space.

ISBN: 978-3-95450-252-3 ISSN: 2673-5350 doi: 10.18429/JACoW-IPAC2026-TUP3045

FIXED-FIELD ALTERNATING GRADIENT TRANSPORT LINE FOR LASER-PLASMA ACCELERATED ELECTRONS

S. Fatehi[1]*, D. J. Kelliher[2], A. Bernhard[1], S. Machida[2]
[1]Karlsruhe Institute of Technology (KIT), Karlsruhe, Germany
[2]Science and Technology Facilities Council (STFC), Rutherford Appleton Laboratory, Didcot, UK

Abstract

A transport line for laser-plasma accelerated electrons is proposed based on the Fixed Field Alternating Gradient (FFA) concept. To accommodate the large LPA energy spread and match the beam to a transverse gradient undulator (TGU), the lattice incorporates matching cells with high-temperature superconducting quadrupoles providing gradients of up to 220 T/m, along with a compact FFA dispersion creator. This configuration allows strong focusing and dispersion tailoring within a compact geometry. The study represents an initial step toward demonstrating the feasibility of FFA-based dispersion management for LPA-driven light sources, while outlining the requirements of further optimization.

INTRODUCTION

Accelerators, with dimensions ranging from meters to kilometers, are essential tools for fundamental research as well as for applications in medicine and industry. In recent years, significant effort has been devoted to developing compact accelerator concepts. Laser plasma acceleration (LPA) is one of the most promising approaches, in which an ionized plasma medium sustains electric field gradients up to 100 GeV m^{-1}, far exceeding those of conventional radio-frequency (RF) accelerators.

In LPAs, a high-power terawatt (TW) laser pulse excites a plasma wave, generating a strong longitudinal electric field that accelerates electrons to GeV energies over cm-scale distances, as illustrated in Fig. 1. Moreover, LPAs naturally produce ultra-short electron bunches with micrometer-scale lengths, making them attractive for compact radiation sources and free-electron lasers (FELs) [1].

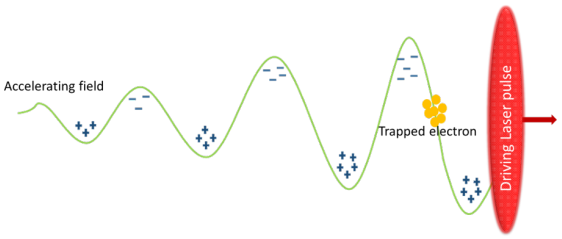

Figure 1: Schematic sketch of an LPA acceleration process.

Despite these advantages, LPA beams exhibit intrinsic limitations, in particular percent-level energy spread and milliradian divergence, which make beam transport and matching challenging. To efficiently utilize such beams, advanced transport lines are required.

* samira.fatehi@kit.edu

A promising approach combines an optimized transport line with a transverse gradient undulator (TGU). In a TGU, the magnetic field varies transversely, allowing electrons with different energies to emit radiation at the same wavelength by traversing different transverse positions. The resonance condition is given by

$$\lambda = \frac{\lambda_u}{2\gamma^2(x)}\left(1 + \frac{K_u^2(x)}{2}\right), \tag{1}$$

with λ the radiation wavelength, λ_u the undulator period, γ the electron's Lorentz factor, and K_u the undulator parameter, the latter two being matched as a function of transverse position x, which enables narrow-bandwidth radiation even for beams with large energy spread [2, 3]. At KIT, several compact transport lines have been developed for LPA applications at energies between 120 MeV and 700 MeV, using both normal-conducting and high-temperature superconducting (HTS) magnets [4–6]. These studies demonstrate the feasibility of compact transport systems, while highlighting the need for improved solutions capable of handling large energy spread with high acceptance.

Fixed Field Alternating Gradient (FFA) concepts offer a promising approach for high-acceptance beam transport. Originally developed for hadron accelerators [7–9], FFA optics have more recently been extended to transport lines [10, 11]. FFA lattices combine static magnetic fields with alternating-gradient focusing, providing stable transport over a wide momentum range. The magnetic field, in the case of a circular accelerator, is characterized by a geometrical field index K and defined as

$$B(r,\theta) = B_0\left(\frac{r}{r_0}\right)^K F(\theta). \tag{2}$$

where B_0 is the vertical field at reference radius r_0 and $F(\theta)$ is a periodic variation with azimuthal angle θ. In transport lines, in the limit of large reference radius r_0, one can write

$$B_y(x,\theta) \approx B_{y0}\exp(mx)\,F(\theta), \tag{3}$$

where $m = K/r_0$ is the normalised field index. FFAs provides controlled orbit separation and large momentum acceptance [10].

In this work, an FFA-based transport line is proposed for LPA electron beams at a reference energy of 300 MeV. By combining a compact FFA dispersion creator with strong focusing provided by HTS quadrupoles, the design aims to generate the required dispersion and match the beam to a TGU within a compact geometry.

Content from this work may be used under the terms of the CC BY 4.0 licence (© 2026). Any distribution of this work must maintain attribution to the author(s), title of the work, publisher, and DOI.

ISBN: 978-3-95450-252-3 ISSN: 2673-5350 doi: 10.18429/JACoW-IPAC2026-TUP3046

LASER-PLASMA ELECTRON INJECTOR DEVELOPMENT FOR THE cSTART STORAGE RING

A.Y. Saw*, D. Squires, J. Natal, N. Ray, T. Schmelzer, M. Fuchs
Karlsruhe Institute of Technology, Karlsruhe, Germany
P. Winkler, S. Jalas, M. Kirchen, A.R. Maier
Deutsches Elektronen-Synchrotron DESY, Hamburg, Germany

Abstract

Laser-plasma accelerators (LPAs) generate ultrashort, high-intensity electron bunches in a compact form factor. At Karlsruhe Institute of Technology (KIT), we are developing an LPA for direct injection into a specifically built storage ring with high momentum acceptance. The compact storage ring for accelerator research and technology (cSTART) can be tuned to energies between 40 – 90 MeV and its lattice is designed to accept electron beams with ±4 % energy spread. Furthermore, the ring lattice can be set up for the storage of ultrashort electron bunches. The LPA electron injector must be readily tunable to match the storage ring parameters. This contribution reports proof-of-concept experiments that demonstrate the generation of high-quality LPA electron beams with parameters that fulfill the cSTART requirements.

INTRODUCTION

The Karlsruhe Institute of Technology is developing cSTART, which will soon enter the construction phase [1]. cSTART is a compact storage ring, which will be able to accept femtosecond electron bunches for investigation of non-equilibrium dynamics, storage of ultrashort electron bunches, compact light sources, and next-generation accelerator technologies [2, 3].

A laser-plasma accelerator will be used as one of the injectors for high-brightness femtosecond electron bunches into cSTART [4]. An LPA is a promising technology for this purpose because the high accelerating gradients produced in a plasma wakefield allow electrons to be accelerated to the target energies over millimeter-scale acceleration distances, which is orders of magnitude smaller than traditional RF-based machines can achieve [5]. The target parameters for the LPA injector for cSTART are listed in Table 1.

Table 1: Target Parameters for cSTART LPA Injector

Parameter (Unit)	Value
Charge	1 - 100 pC
Energy Range	40 - 90 MeV
Energy Spread	< 4 %
Bunch Duration	< 30 fs

One challenge of LPAs is designing them to make stable high-quality electron beams at (for LPAs) relatively low energies of < 100 MeV. To test if this can be done for our application, we performed a proof-of-concept experiment at the Deutsches Elektronen-Synchrotron LUX LPA setup [6].

EXPERIMENT

To achieve the required electron energy range for cSTART (40 – 90 MeV), we significantly detuned the LUX LPA system away from the system's standard operating range. The laser parameters were 1.56 J energy, 30 fs pulse width at full-width at half-maximum (FWHM), 22 µm spot size, 1 Hz repetition rate, 800 nm wavelength, resulting in an a_0 of 2.53. From there, we explored the densities and mixtures of gases in the plasma-cell target. A schematic of the LUX electron beamline is shown in Fig. 1 [7].

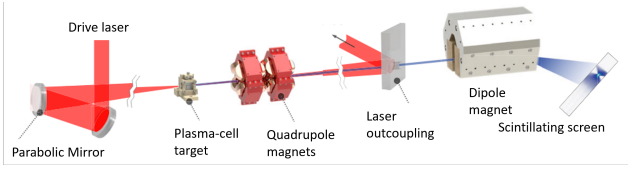

Figure 1: Simplified schematic of the LUX LPA experiment adapted from [7]. The driver laser (red) is focused into a plasma-cell target, where it ionizes argon-doped hydrogen gas creating the laser-plasma electron-accelerating structure. After the plasma-cell target, the electrons (blue) are focused with electromagnetic quadrupoles and the laser is out-coupled leaving the electron beam to travel through a spectrometer comprised of a permanent dipole magnet and a scintillating screen.

The plasma target was a gas-capillary of approximately 500 µm x 5 mm as shown in Fig. 2 [8]. The LPA is based on localized ionization trapping using Ar and H_2 as background gas.

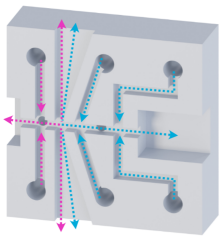

Figure 2: Schematic of the LUX plasma-cell target adapted from [8]. Gas is supplied to the central gas-capillary. A mixture of H_2 and Ar is shown in magenta, and pure H_2 is shown in blue. The laser propagates from left to right.

* alexander.saw@kit.edu

Content from this work may be used under the terms of the CC BY 4.0 licence (© 2026). Any distribution of this work must maintain attribution to the author(s), title of the work, publisher, and DOI.

ISBN: 978-3-95450-252-3 ISSN: 2673-5350 doi: 10.18429/JACoW-IPAC2026-TUP3049

AWAKE: PREPARING FOR PHYSICS BEYOND LS3

E. Gschwendtner†, CERN, Geneva, Switzerland
on behalf of the AWAKE Collaboration

Abstract

The AWAKE programme at CERN has evolved from its initial proof-of-principle phase to a comprehensive facility dedicated to advancing proton-driven plasma wakefield acceleration towards first particle-physics applications. In preparation for this next stage, AWAKE will undergo a major upgrade during CERN's Long Shutdown 3 enabling the demonstration of electron acceleration to 4–10 GeV in a 10 m plasma source with controlled beam quality and validated scalability. Meeting the targets of 5-8% energy spread, 100 pC of accelerated charge and controlled emittance requires strong beam loading. This will be provided by a new RF photo-injector system equipped with two X-band structures and an optimized transfer line, delivering 150 MeV electrons with 5.75 μm beam size at injection and 2 mm mrad normalized emittance. In parallel, the 400 GeV SPS proton bunch must reach full self-modulation in the first plasma source ('self-modulator') before the electrons are injected into the second plasma source ('accelerator'). Extensive infrastructure modifications are already in progress, including the dismantling of the CNGS target area in order to create the space required for the upgraded AWAKE facility. We present the consolidated roadmap, the scientific goals, upgrade status and the key challenges associated with both the facility design and the experimental programme starting in 2029.

INTRODUCTION

Proton-driven plasma wakefield acceleration was proposed as a route to very high particle energies by exploiting the large energy stored in the proton beams of existing high-energy accelerators such as the CERN SPS or LHC [1]. Using proton bunches as drivers allows electron acceleration in a single plasma stage, circumventing the need for multiple accelerating stages required when using laser or electron drivers. The AWAKE experiment at CERN is the world's first realisation of this concept, using a 400 GeV SPS proton bunch to drive plasma wakefields in a rubidium vapour source. The driver bunch length must however be comparable to the plasma wavelength ($\lambda_p \sim 1$ mm at AWAKE), whereas the SPS proton bunch is ∼6 cm long. As the long bunch traverses the plasma, it splits into a micro-bunch train through the self-modulation instability (SMI) [2] that then resonantly drives strong wakefields in which externally injected electrons can be accelerated to high energies. This unique approach leverages infrastructure already in place at CERN and offers a compelling path towards compact, high-energy particle accelerators for both fundamental physics research and future applications.

The AWAKE experiment has successfully achieved all objectives to date. AWAKE Run 1 (2016–2018) demonstrated, for the first time, the proton-driven plasma wake-field acceleration concept: in particular, the controlled self-modulation of a long proton bunch in plasma [3–5] and the subsequent acceleration of externally injected electrons to 2 GeV in a 10 m plasma source [6]. Building on these results, AWAKE entered Run 2 in 2021 with a programme extending through Long Shutdown 3 (LS3) up to LS4, aiming at electron acceleration to 4–10 GeV in a 10 m plasma, control of beam quality (normalised emittance in the range 2–30 mm mrad), and demonstration of scalability of the acceleration process [7].

Run 2 consists of four phases: seeding of the proton bunch self-modulation with an electron bunch (Run 2a); use of a plasma density step to freeze the evolution of the modulation and sustain high wakefield amplitudes over the full plasma length (Run 2b). Both phases were successfully completed in 2025 with all milestones achieved [8].

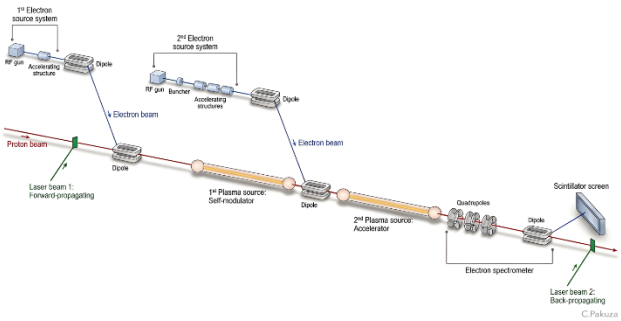

Figure 1: AWAKE Run 2c layout.

To address the goals of the remaining two phases substantial area extensions and facility upgrades are foreseen during LS3: Run 2c will demonstrate electron acceleration with con-trolled bunch emittance using two plasma sources: a first plasma dedicated to optimising the self-modulation of the proton bunch, and a second plasma for controlled electron acceleration in the resulting wakefields. A second photo-injector and electron beamline providing 150 MeV for injection into the accelerating plasma source, is a key element of this upgrade [9]. Figure 1 shows the AWAKE Run 2c layout. During Run 2d, scalable plasma source technologies extending plasma lengths to the tens-of-metres scale will be implemented. The timeline of the preparation programme for the AWAKE post-LS3 run is shown in Fig. 2. After completing the CNGS target area dismantling in end 2026, Run 2c service and equipment installation takes place in 2027–2028, with commissioning completing before LS3 ends in Q2 2029. Run 2c physics operation with protons begins thereafter.

CNGS TARGET AREA DISMANTLING

Run 2b concluded its proton beam measurement program on 2 June 2025. Subsequently the AWAKE facility

†edda.gschwendtner@cern.ch

Content from this work may be used under the terms of the CC BY 4.0 licence (© 2026). Any distribution of this work must maintain attribution to the author(s), title of the work, publisher, and DOI.

ISBN: 978-3-95450-252-3 ISSN: 2673-5350 doi: 10.18429/JACoW-IPAC2026-TUP3060

BREAKTHROUGHS IN EUPRAXIA-DN ON THE PATH TO NEXT-GENERATION PLASMA ACCELERATORS*

C.P. Welsch†, [1], Cockcroft Institute, Warrington, UK
[1]also at INFN, Frascati, Italy

Abstract

The EuPRAXIA Doctoral Network (EuPRAXIA-DN) has delivered major advances over the past year in laser–plasma physics, beam diagnostics, and compact radiation-source concepts. Experiments demonstrated superradiant nonlinear Thomson scattering, showing collective enhancement of radiation from relativistic electron bunches interacting with azimuthally polarized laser pulses. Diagnostics developments include new methods to retrieve femtosecond longitudinal bunch profiles from coherent THz transition-radiation images, as well as preliminary shot-to-shot charge measurements in high-EMP environments using diamond detectors, supported by high-precision characterization of the detector.

This contribution presents these important results in the context of the broader EuPRAXIA-DN project. It highlights how coordinated R&D, structured training, cross-sector international secondments, EuPRAXIA Schools and Camps, as well as hands-on training at world-class research facilities accelerate the technological progress and talent pipeline required for compact, user-ready plasma accelerators.

INTRODUCTION

Plasma-based accelerators show excellent potential to reduce the size and cost of research infrastructures while offering new opportunities for scientific discovery, industry, and medicine. EuPRAXIA, the European Plasma Research Accelerator with eXcellence in Applications [1], is the first European project to develop a compact multi-GeV accelerator with reliable beam quality. The project was added to the European Strategy Forum on Research Infrastructures (ESFRI) roadmap in 2021.

The 3.2 M€ EuPRAXIA-DN was launched in 2023, funded by the European Union and the UKRI Guarantee Fund. It contributes directly to the preparation and delivery of the EuPRAXIA infrastructure [2] and trains 12 Doctoral Candidates that are based at institutions across Europe and supports a coordinated research program. The network features three scientific Work Packages (WPs) on Laser and Plasma science, Facility Design and Optimization, and Applications.

This paper gives an overview of the research outcomes from three Fellows and puts their results into the wider context of the network. In addition, key results from the network's training, communication, and outreach activities are also described.

* Work supported by the European Union´s Horizon Europe research and innovation programme under grant agreement no. 101073480 and the UKRI Guarantee Funds.
† carsten.welsch@cockcroft.ac.uk

RESEARCH

The following section presents results from the interdisciplinary research within EuPRAXIA-DN. This includes advanced beam diagnostic and sensor development, as well as a key application in the generation of superradiant single-cycle light pulses.

Ultra-short Bunch Length Measurements with fs Resolution

Ultrashort electron bunches produced in the femtosecond (fs)) range in plasma accelerators require high-resolution longitudinal diagnostics, with the added challenge of making them cost-effective while maintaining a compact size compatible with the reduced footprint of future plasma accelerator facilities. Polarization radiation such as transition, diffraction or Smith-Purcell radiation is a suitable source of information for recovering the particle distribution from its longitudinal form factor. By analyzing its coherent spectral components across frequencies from the THz to the optical region, bunch lengths ranging from a few hundred fs to sub-fs can be measured.

EuPRAXIA-DN Fellow Ana Maria Guisao Betancur at the Cockcroft Institute/University of Liverpool in the UK develops a diagnostic that is based on imaging the source of transition radiation by placing a broadband camera at the image plane to capture the point-to-point spatial distribution of the coherent transition radiation (CTR). A monitor prototype has been designed, installed, and is currently being tested at the MAX IV facility in Sweden, in the THz to near infrared range, to study bunch lengths down to their operating limit of $\tau_{FWHM} \approx 10$ fs [3]. The spatial features of the broadband image contain information about the original profile that generated the radiation. Image analysis allows for the determination of an apparent bunch length, the description of some particle distribution features [4], and, with deep learning, even the reconstruction of the full bunch profile [5].

Data taken at the MAX IV Short Pulse Facility have shown promising results. Two acquisitions are taken at each datapoint: (a) bunch profile reference data from a Transverse Deflecting Structure (TDS) and (b) corresponding CTR images. A sample parameter scan is shown in Fig. 1, varying the current at the sextupoles (SX01) at the bunch compressor (BC1). Using the second moment to estimate an apparent length metric, it is shown how the size of the CTR image follows the equivalent change in the bunch length for this particular operation on the bunch compressor.

Content from this work may be used under the terms of the CC BY 4.0 licence (© 2026). Any distribution of this work must maintain attribution to the author(s), title of the work, publisher, and DOI.

ISBN: 978-3-95450-252-3 ISSN: 2673-5350 doi: 10.18429/JACoW-IPAC2026-TUP3061

CHALLENGES OF MODERATE ENERGY EXTERNAL INJECTION INTO LASER-DRIVEN WAKEFIELD ACCELERATORS

J. Byrne*[1,2], O. Apsimon[1,2]
[1]University of Manchester, Manchester, United Kingdom
[2]Cockcroft Institute, Daresbury, United Kingdom

Abstract

Laser Wakefield Acceleration (LWFA) enables GV/m acceleration gradients, promising compact accelerator designs with advantages in cost, environmental impact and portability. Standard LWFA schemes can suffer from poor shot-to-shot stability and beam quality, resulting in broad energy spectrums, beam current variations, high emittance and limited intensity. External injection schemes attempt to overcome such challenges by treating the LWFA stage as purely an accelerating structure and not as a source. Motivated by the pursuit of compactness, external injection of moderate-energy (< 60 MeV) electron beams into plasma will be explored using the Fourier-Bessel Particle-In-Cell (FBPIC) code. The sensitivity of the final beam quality to sub-optimal injection parameters will be explored. Bayesian optimisation is employed to assess whether sub-optimal injection parameters can be compensated for with laser and plasma parameters. This investigation presents working points from which future compact external injection designs can be optimised.

INTRODUCTION

Laser Wakefield Acceleration (LWFA) offers accelerating gradients orders of magnitude higher than those achieved with conventional radiofrequency technology [1, 2]. Gradients of order GV/m could enable more compact accelerator facilities and help widen the accessibility of accelerator-based applications. There is a growing demand for stable, high-quality LWFA for various applications such as next-generation light sources and biological applications [3]. However, in the absence of controlled injection, LWFA typically produces beams with large energy spread, high emittance and poor shot-to-shot stability [4]. External injection into LWFA decouples beam generation from acceleration: a particle beam is externally injected and the plasma acts as a pure accelerating structure. The challenge with external injection is preserving the witness beam quality whilst exploiting the large accelerating fields.

External injection is typically performed within the linear or quasi-linear regime, with the normalised laser strength parameter $a_0 \lesssim 2$. For an on-axis plasma density 1×10^{23} m^{-3}, the accelerating and focusing region corresponds to a temporal window of ~ 88 fs. To minimise the final energy spread, the witness bunch length should be a fraction of this interval imposing the bunch to be ultra-short. Assuming a linear focusing, there exists a matched beam size, σ_m, which satisfies

$$\sigma_m = \sqrt[4]{\frac{2}{\gamma}}\sqrt{\frac{\epsilon_n}{k_p}}, \quad (1)$$

where γ is the relativistic Lorentz factor, ϵ_n is the projected normalised transverse emittance and k_p is the plasma wave number [1]. Transversely matching the beam into the plasma reduces betatron oscillations and therefore transverse phase space distortion. Consider a 40 MeV, 400 nm rad witness bunch in a $n_e = 1 \times 10^{23}$ m^{-3} plasma density, the matched beam size is ~ 1 µm, according to Eq. (1). The simultaneous combination of longitudinal and transverse size places constraints on the beam generation and transport system, especially for moderate energy beams. Nevertheless, it is important to understand the sensitivity of final beam quality to sub-optimal witness beam injection. Compact external injection into LWFA therefore requires trade-offs between witness beam preparation and post-plasma beam quality. The Fourier-Bessel Particle-In-Cell (FBPIC) code is employed to first study the sensitivity of beam quality preservation to the injected beam parameters. Secondly, Bayesian optimisation is employed to investigate the external injection of a more realistic beam and explore optimal trade-offs.

BEAM QUALITY SENSITIVITY

Parameter scans were conducted to assess contributing factors to beam quality preservation. Unless stated otherwise, these parameter scans use a 10 pC bunch with 400 nm rad projected normalised transverse emittance, 1 % RMS energy spread and 10 fs bunch length. Assuming a typical driving laser with a 800 nm wavelength, 25 fs FWHM pulse length, 30 µm spot size and a normalised strength parameter of 0.8. A 2 cm flat-top plasma density of 1×10^{23} m^{-3} with a transverse parabolic channel matched to the laser spot size is used. The laser centroid is initialised 20 µm before the plasma entrance, while the bunch centroid is initialised at waist 35 µm behind the laser centroid.

As indicated in Eq. (1), injection of higher energy beams reduces the optimal injection spot size. This arises from the change in balance between the beam divergence and the plasma focusing. The optimal spot sizes for emittance preservation, shown in Fig. 1a, display the correct trend, although the optimal beam sizes remain larger than those predicted with Eq. (1). Furthermore, the minimum emittance increase ranged from 10 nm rad to 15 nm rad suggesting that other factors are contributing to the observed emittance growth. Injection energy indirectly influences the wakefield structure through beam loading, modifying both longitudinal and

* jordan.byrne@manchester.ac.uk

Content from this work may be used under the terms of the CC BY 4.0 licence (© 2026). Any distribution of this work must maintain attribution to the author(s), title of the work, publisher, and DOI.

ISBN: 978-3-95450-252-3 ISSN: 2673-5350 doi: 10.18429/JACoW-IPAC2026-TUP3063

PERFORMANCE ANALYSIS OF A MACH–ZEHNDER INTERFEROMETER USING SYNTHETIC INTERFEROGRAMS

F. Alharthi *[1,2,3], D. Graham[1,3], M. Hibberd[1,3], and Ö. Apsimon[1,3]
[1]The University of Manchester, Manchester, United Kingdom
[2]University of Bisha, Bisha, Saudi Arabia
[3]Cockcroft Institute of Accelerator Science and Technology, Daresbury, United Kingdom

Abstract

In this work, we assess the performance and limitations of Mach–Zehnder interferometry for plasma diagnostics using a fully synthetic, numerically generated dataset. We explore regions of parameter space that are difficult to access experimentally, including fringe behaviour, the dynamic range of measurable phase shifts, and the resolution limits for low-density plasmas. By introducing controlled phase errors, we quantify the robustness of common phase retrieval and phase unwrapping algorithms and identify the conditions under which these methods succeed or fail. Our results provide practical design guidelines for optimising interferometric measurements across a wide range of plasma conditions.

INTRODUCTION

In 1979, Tajima and Dawson proposed using plasma waves to accelerate charged particles [1], demonstrating that plasma could generate electric fields thousands of times stronger than those used in conventional accelerators. This remained theoretical until 1988, when Rosenzweig and his team experimentally proved it for the first time [2], paving the way for a new generation of accelerators.

The field then advanced significantly through pioneering experiments at the Berkeley Lab Laser Accelerator (BELLA) facility, which demonstrated the use of plasma channels for laser-driven wakefield acceleration. The first GeV-class electron beam was achieved in 2006 using a capillary discharge plasma channel [3], and subsequent improvements led to the acceleration of electrons up to 7.8 GeV in a 20-cm-long channel [4]. A key advancement was the development of laser-heated capillary channels, in which an auxiliary laser is used to shape the radial plasma density profile, enabling efficient guiding of the drive laser over long distances distances [4]. In all these experiments, precise measurement of plasma density plays a crucial role, and the Mach–Zehnder interferometer (MZI) is one of the most common instruments used for this purpose. However, its accuracy depends on phase-recovery algorithms and is affected by physical limitations such as phase wrapping at high densities. In this work, we evaluate the performance and limitations of the MZI using a fully synthetic dataset, and we investigate the effect of plasma density, spectral window selection and width, and probe beam wavelength on retrieval accuracy.

* fatimah.alharthi@postgrad.manchester.ac.uk

METHODOLOGY

Synthetic Interferograms

A fully synthetic dataset of Mach–Zehnder interferograms was generated so that the plasma phase is known exactly (see Fig. 1), allowing the retrieval algorithm to be tested independently of experimental noise. Each interferogram was simulated on a 1024×1024 grid with pixel size $\Delta x = 1.75\,\mu\text{m}$ (field of view $L \approx 1.79$ mm). The plasma was modelled as a cylinder of radius $R = 400\,\mu\text{m}$ with axis along y (parallel to the carrier fringes) and perpendicular to the probe direction z, with a parabolic radial profile $n_e(r) = n_{e0}(1-r^2/R^2)$, where $r = \sqrt{x^2 + z^2}$. Translational invariance along y implies that the line-integrated density $N_e(x) = \int n_e\, dz$ depends only on x.

In the regime $n_e \ll n_c$, where $n_c = \varepsilon_0 m_e \omega^2/e^2$ is the critical density at which the plasma frequency ω_{pe} equals the probe angular frequency ω, the phase shift reduces to

$$\Delta\varphi(x) = -r_e \lambda\, N_e(x), \tag{1}$$

with $r_e = 2.818 \times 10^{-15}$ m the classical electron radius and $\lambda = 532$ nm the probe wavelength (frequency-doubled Nd:YAG). Interferograms were constructed as $I = \frac{1}{2}[1 + \cos(2\pi f_0 x + \Delta\varphi)]$, with $\Delta\varphi = 0$ for the reference, and n_{e0} was scanned over 10^{15}–10^{20} cm^{-3}.

Phase Retrieval and Density Extraction

The plasma-induced phase was recovered using the Fourier-Transform Method (FTM) [5]. Since $\Delta\varphi$ is invariant along y, the 2D interferograms were averaged column-wise into 1D traces $g_{\text{pl}}(x)$ and $g_{\text{ref}}(x)$. An FFT of each trace yields a DC peak and two sidebands at $\pm f_0$ (Fig. 2); the positive sideband is isolated with a spectral window centred on $+f_0$. Four window types (Hann, Gaussian, Tukey, super-Gaussian) and a range of widths were tested. After shifting the filtered sideband to the origin and applying an inverse FFT, the wrapped phase is obtained from the argument of the complex ratio, which cancels the carrier and any residual phase. The unwrapped phase (Fig. 3) is inverted using Eq. (1) to obtain $N_e(x)$, and a three-point Abel transform [6] recovers $n_e(r)$. The relative error between retrieved and input peak densities is used as the performance metric, with a 5% threshold defining the failure point.

RESULTS AND DISCUSSION

Interferograms were generated across an electron density range from 10^{15} to 10^{20} cm^{-3} using an 800 nm probe. The

Content from this work may be used under the terms of the CC BY 4.0 licence (© 2026). Any distribution of this work must maintain attribution to the author(s), title of the work, publisher, and DOI.

ISBN: 978-3-95450-252-3 ISSN: 2673-5350 doi: 10.18429/JACoW-IPAC2026-TUP3067

INSTALLATION AND STARTUP OF AN 18 GHz ECRIS FOR HIGHLY CHARGED METALLIC IONS AND GASES

A. Morana*, V. Bertrand, D. Zanuttini, Pantechnik, Bayeux, France

Abstract

This paper presents the technical improvements and experimental characterisation of a hybrid superconducting 18 GHZ Electron Cyclotron Resonance Ion Source (ECRIS) manufactured by Pantechnik. Since the last one manufactured in 2011, the source has undergone significant upgrades to enhance its performance and reliability for heavy ion beam production. Key improvements include optimisation of the magnetic confinement system, aiming to increase the production of highly charged ions while maintaining stable operation at high RF power levels. An extensive experimental campaign is currently underway at Pantechnik's facilities to characterise the source performance on a selection of ions (N, Al, Ar, Au, Pb) and the goal of demonstrating stable Xe^{28+} and Ta^{36+} beams.

INTRODUCTION

Electron Cyclotron Resonance Ion Sources (ECRIS) are among the essential components of modern heavy-ion accelerator facilities, providing intense beams of highly charged ions for both fundamental research and industrial applications [1]. Operating at microwave frequencies matched to the electron cyclotron resonance condition, these devices sustain a magnetically confined plasma in which successive electron-impact ionisation events produce ions in progressively higher charge states. The trend towards higher operating frequencies—driven by the well-known frequency scaling laws predicting higher ion currents and charge states with increasing RF frequency—has motivated the development of third-generation, 18 GHz class machines [2]. Pantechnik has developed in the past and is currently commissioning again an 18 GHz source specifically designed for the production of highly charged metallic and gaseous ions required by accelerator injectors. This contribution describes the technical design improvements implemented in the source and reports on the ongoing experimental commissioning campaign on a range of ion species, including argon (Ar) and helium (He). The ultimate objectives of the campaign are the demonstration of stable Xe^{28+} and Ta^{36+} beams, representative of the demanding requirements of modern heavy-ion physics.

SOURCE DESCRIPTION

The source under test is the second commissioned at Pantechnik and is described in detail in Ref. [3]. The source is designed to achieve optimum performance at 18 GHz RF frequency and was conceived to operate on a high-voltage platform with minor power consumption. The present campaign is conducted without the high-voltage platform used in the original installation.

* ambra.morana@pantechnik.fr

Mechanical Layout

The source body, shown in Fig. 1, is approximately 1 m in length (including the injection system) with an external diameter of 0.7 m, for a total weight of approximately 1600 kg. The iron yoke incorporates the permanent magnet hexapole, the plasma chamber, and the cryostat. The plasma chamber is an aluminium cylinder of 82 mm inner diameter and 450 mm length. The outer diameter of the yoke is 680 mm with a length of 730 mm.

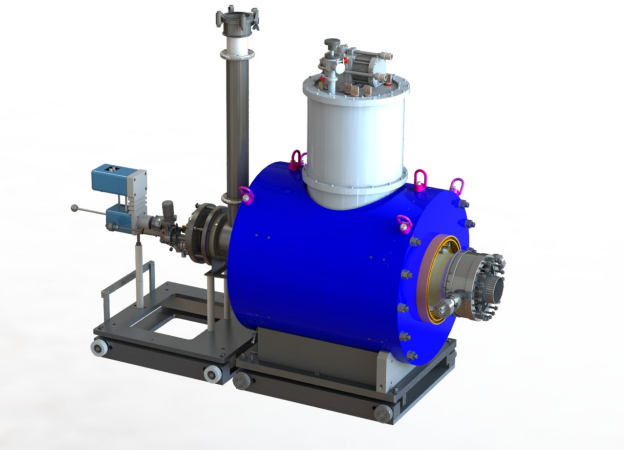

Figure 1: Schematic of the 18 GHz ECRIS ensemble.

Magnetic Confinement System

The magnetic confinement of the ion source relies on a hybrid configuration combining superconducting axial coils with a multi-layer, multi-grade permanent magnet hexapole for the radial field [3].

Axial field The axial mirror field is generated by three independent NbTi/Cu superconducting coils (INJECTION, CENTRE, EXTRACTION) wound on a single-piece aluminium former and epoxy-impregnated, each powered by an independent bipolar supply (100 A, 5 V). The nominal operating current is ≈86 A with a total stored energy of ≈143 kJ. The field is tuned to the 18 GHz resonance condition (B_{ECR} = 0.648 T), with injection and extraction field variable up to 2.1 T and 1.5 T respectively, and B_{min} independently adjustable between 0.4 T and 0.6 T. The axial magnetic field measurements were performed with the HIRST Magnetic Instrument Gaussmeter (GM08). The Gaussmeter was connected to a cylindrically shaped triaxial Hall probe. Results of the measurement, shown in Fig. 2 point out a really good agreement with the simulated value.

Radial field The radial confinement is provided by a multi-layer, multi-grade permanent magnet hexapole assembly, achieving a maximum radial field of 1.32 T at the wall

Content from this work may be used under the terms of the CC BY 4.0 licence (© 2026). Any distribution of this work must maintain attribution to the author(s), title of the work, publisher, and DOI.

ISBN: 978-3-95450-252-3 ISSN: 2673-5350 doi: 10.18429/JACoW-IPAC2026-TUP3068

WARPX SIMULATION OF THE PLASMA MENISCUS EFFECT IN A NEUTRAL BEAM INJECTION SYSTEM

B. Nguyen*[1,2], K. Shih[1], R. Lehe[3], O. Shapoval[3], J. Eickman[1], A. Formenti[3], C. M. Jacobson[1], A. Latrille[1], A. Persaud[3], D. A. Sutherland[1], J.-L. Vay[3]
[1]Realta Fusion, Madison, Wisconsin, United States
[2]Imperial College London, London, United Kingdom
[3]Lawrence Berkeley National Laboratory, Berkeley, United States

Abstract

The US Department of Energy INFUSE collaboration between Realta Fusion and Lawrence Berkeley National Laboratory (LBNL) aims to extend WarpX towards high fidelity modeling of neutral beam injection (NBI) systems. WarpX is a parallel, open source, and portable particle-in-cell (PIC) code with an active developer community and demonstrated scalability. In this work, we implement and validate the plasma meniscus modeling for a positive ion source using first principle PIC simulations. These simulations are performed in the electrostatic mode with extraction electrodes represented as embedded boundaries. The upstream plasma reservoir is modeled using a thermal injection scheme with real electron mass to capture the correct sheath physics. These results and validations form a crucial basis for future extensions to negative ion sources and photoneutralization, enabling start to end NBI modeling within WarpX.

INTRODUCTION

Realta Fusion is a startup based in Madison, Wisconsin, working on the magnetic mirror fusion concept [1, 2]. The Wisconsin High-temperature superconductor Axisymmetric Mirror (WHAM) is a high-field platform for prototyping this technology, where plasma heating is achieved through neutral beam injection (NBI) and electron cyclotron heating (ECH) [3]. Among different NBI approaches, positive-ion beam systems are the most mature and well-studied [4, 5]: ions are extracted from a plasma source, accelerated through a multi-electrode structure, and neutralized by a background gas to form a high-energy neutral beam. Reliable modeling of such systems is therefore crucial for optimizing plasma power balance and overall machine performance.

Traditionally, ion-optics codes such as PBGUNS and IBSimu are used to model NBI devices [6,7]. These approaches assume steady-state beam transport and treat space-charge compensation using ad hoc neutralization factors, which is generally sufficient for engineering studies of conventional positive- and negative-ion NBI systems. However, more advanced concepts such as photoneutralization require self-consistent treatment of space-charge effects and transient particle dynamics [8]. The particle-in-cell (PIC) method provides a natural framework to capture these effects [9].

Under funding by the US Department of Energy INFUSE program, Realta Fusion and LBNL are extending the capabilities of the WarpX PIC code for high-fidelity modeling of NBI systems [10]. WarpX is an open-source, massively parallel PIC code designed to run efficiently on both GPU and CPU architectures [11, 12]. It has demonstrated strong scalability on modern high-performance computing platforms and has been applied to a wide range of problems, including laser–plasma interactions, accelerator, and beam physics [13–15].

In this paper, we implement and validate plasma meniscus modeling in WarpX for a positive-ion NBI system, benchmarking against published PBGUNS results for the WHAM-relevant NBI settings [16]. This work establishes a foundation for future studies of more advanced NBI designs and their coupling to mirror plasma simulations.

SIMULATION SET-UP

Simulations are performed using the WarpX PIC code in the electrostatic mode with the default energy-conserving option. The set-up follows the extraction of a single 40 keV H^+ beamlet from the WHAM-relevant NBI system as described by Sorokin *et al.* [16].

The electrodes are implemented through the embedded boundary capabilities in WarpX. As shown in Fig. 1, the simulation domain is fully three-dimensional with the longitudinal direction along z, with dimensions $L_x = L_y = 0.8$ cm and $L_z = 2.7$ cm. Through a convergence study, the resolution parameters are chosen to be $(n_x, n_y, n_z) = 128 \times 128 \times 256$ with $\Delta t = 1.8\omega_{pe}^{-1}$, where ω_{pe} is the electron plasma frequency. Note that ω_{pe} does not need to be explicitly resolved when using the energy-conserving option. However, if the chosen timestep is too large, significant current oscillations can occur during the transient phase of the simulation.

Particles are subject to absorbing boundary conditions at the domain boundaries and embedded electrode surfaces. For the field solver, Neumann boundary conditions are applied on all boundaries except at the negative z boundary, where a Dirichlet condition $\phi = 0$ kV is imposed. The electrode potentials are specified such that the second electrode is at −41 kV and the final electrode at −40 kV.

The upstream plasma reservoir occupies the region -0.2 cm $\leq z \leq 0$ cm and consists of H^+ ions and electrons with density n_p and temperature T_p. Here, real electron mass is used in order to capture the correct sheath physics of

* william.nguyen21@imperial.ac.uk

Content from this work may be used under the terms of the CC BY 4.0 licence (© 2026). Any distribution of this work must maintain attribution to the author(s), title of the work, publisher, and DOI.

ISBN: 978-3-95450-252-3 ISSN: 2673-5350 doi: 10.18429/JACoW-IPAC2026-TUP3069

MULTI-OBJECTIVE BAYESIAN OPTIMISATION (MOBO) FOR HIGH-QUALITY PHOTOINJECTOR OPTIMISATION

E. J. Brookes*, T. Kamps, Helmholtz-Zentrum Berlin für Materialien und Energie, Berlin, Germany
S. Zeeshan, Deutsches Elektronen-Synchrotron DESY, Zeuthen, Germany

Content from this work may be used under the terms of the CC BY 4.0 licence (© 2026). Any distribution of this work must maintain attribution to the author(s), title of the work, publisher, and DOI.

Abstract

Optimising SRF photoinjector parameter space is a challenging task due to the high-dimensional, non-linearly coupled parameters and competing objectives such as transverse emittance and bunch length. Conventional methods such as manual tuning or MOGA require thousands of evaluations and are impractical for routine operation or computationally expensive simulations. This work presents a multi-objective Bayesian optimisation approach that uses Gaussian-process surrogate models and tunable, uncertainty-aware acquisition functions to identify Pareto-optimal solutions in an order of magnitude fewer evaluations. When applied to the 1.4-cell SRF photoinjector at SEALab, and the 1.6-cell SRF gun and 20 m injector beamline for EuXFEL, this optimisation outperforms MOGA in solution-efficiency and provides interpretable sensitivity information for injector tuning. These results demonstrate the potential of MOBO as an efficient, machine-ready strategy for SRF photoinjector optimisation.

INTRODUCTION

High-brightness SRF photoinjectors are required to provide electron beams with stringent longitudinal and transverse properties. Since the quality of the beam delivered to downstream sections is strongly influenced by the beam generated at the source, efficient injector tuning is essential for reliable accelerator operation. The optimisation of photoinjector settings is a coupled and multi-objective problem. High-brightness photoinjector performance is critically reliant on the simultaneous minimisation of bunch length and transverse emittance, two competing objectives. The machine controls for these problems form a multi-dimensional parameter space in which manual tuning can be slow and incomplete. Population-based methods such as Multi-Objective Genetic Algorithms (MOGA) have been successfully used to identify high-quality Pareto fronts in accelerator physics [1], but they often require many thousands of evaluations, and can therefore be inefficient for expensive evaluations. Rather than densely sampling the full parameter space, Multi-Objective Bayesian Optimisation (MOBO) builds probabilistic surrogate models of the accelerator response and uses the uncertainty of these models to select informative new samples.

This paper applies the same MOBO framework to the simultaneous minimisation of bunch length and transverse emittance on two SRF photoinjector optimisation problems: a 1.74 m SEALab beamline [2] and a 20 m EuXFEL injector beamline [3].

* brookesemily17@yahoo.com

MULTI-OBJECTIVE BAYESIAN OPTIMISATION

MOBO aims to solve for the vector, x, which optimises the objectives, $[\sigma_z(\mathbf{x}), \epsilon_n(\mathbf{x})]$, subject to $Q_{\text{transported}}/Q_0 > Q_{\text{min}}$ [4]. Here, σ_z and ϵ_n are the bunch length and normalised transverse emittance measured at the observation point, and $Q_{\text{min}} = 0.95$ characterises the minimum acceptable transport efficiency.

The MOBO workflow is represented by Fig 1. MOBO is an iterative procedure, in which the parameter space is sampled based on the previous iteration results. In this work, for each iteration, five new samples are identified and evaluated in parallel. These measured points are used to train the Gaussian process surrogate models for both objectives, and a third model for the constraint parameter (here, Q_{min}). The models provide both a prediction and uncertainly for each point in the input space which are then used by the acquisition function to determine the next most useful location to sample in by balancing the improvement of the identified optima or by exploring in regions of high uncertainty [4]. This intelligent approach to sampling allows for efficient navigation in high-dimensional spaces and thus reduces the total number of evaluations necessary. Throughout optimisation, the algorithm attempts to increase the hypervolume score (HV). This determines how much of the output space is being dominated by the Pareto front, relative to a user-defined reference point.

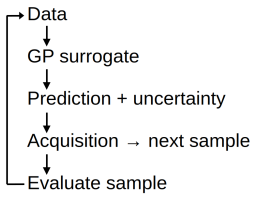

Figure 1: MOBO workflow used for photoinjector tuning.

BEAMLINE SETUPS

First, the SEALab case is discussed which represents a transverse Gaussian electron bunch through 1.4-cell SRF gun cavity followed by a 1.74 m beamline including an emittance compensation solenoid, two steerer magnets and a compact set of diagnostics. More details on this setup can be found in [2]. This study is designed to simulate the commissioning stage of operation, with bunch charges from 5-9 pC, and beam energies limited to ~2 MeV from the gun. The low charges limit the effect of space charge, but low energies decrease the adiabatic damping. The SEALab gun aims to produce beams with transverse emittance <1mm mrad, with

ISBN: 978-3-95450-252-3 ISSN: 2673-5350 doi: 10.18429/JACoW-IPAC2026-TUP3071

OPTIMIZED DESIGN OF A C-BAND 100 MeV ELECTRON LINAC FOR FLASH RADIOTHERAPY

S. Farina*, S. Akbar, R. Boldrini, E. Chiadroni, M. Coppola, A. Curcio, G. Francosioni, L. Frassi, L. Giuliano, M. Magi, M. Migliorati, A. Mostacci, L. Palumbo, V. Patera, A. Sarti
Sapienza University of Rome, Rome, Italy
D. Alesini, F. Cardelli, L. Faillace, Istituto Nazionale di Fisica Nucleare, LNF, Italy
L. Ficcadenti, Istituto Nazionale di Fisica Nucleare, Sezione di Roma I, Rome, Italy
G. Mauro, G. Torrisi, Istituto Nazionale di Fisica Nucleare, LNS, Italy

Content from this work may be used under the terms of the CC BY 4.0 licence (© 2026). Any distribution of this work must maintain attribution to the author(s), title of the work, publisher, and DOI.

Abstract

Electron LINACs are key tools for radiotherapy. Conventional low energy ones can treat only superficial tumors. Achieving Very High Energy Electrons (VHEE, >100 MeV) enables treatment of deep-seated tumors. Furthermore, electrons are well-suited for delivering Ultra-High Dose Rates (UHDR) required for FLASH therapy, which improves healthy-tissue sparing. Combining VHEE and FLASH in a hospital environment represents an important step forward for Radiotherapy. In the context of the SAFEST project at Sapienza, this work presents a compact and cost-effective accelerator layout capable of delivering hundreds of nC at 100 MeV within tens of pulses over 1 ms of irradiation. The design emphasizes efficient RF power usage through high-efficiency C-band structures and a pulse compressor. Beam dynamics simulations and low-power RF tests validate the approach. A strong focus is placed on flattening the compressor signal, which must remain stable over 1 µs to accommodate electrons from a triode thermionic gun, a compact and economical source for this accelerator. The resulting 3 m LINAC, powered by a single 20 MW klystron, shows strong potential for future hospital based FLASH VHEE treatments.

INTRODUCTION

Medical accelerators must be compact, cost-effective, and simple for hospital integration. VHEE (E > 100 MeV) and UHDR operation can improve the treatment of deep-seated tumors and enhance tissue sparing [1,2] through the FLASH effect. Radio Frequency (RF) accelerators currently represent the most reliable technology for this purpose [3,4]. Standard S-band structures lead to excessive footprints for a clinical accelerator with E > 100 MeV, while X-band systems require strict tolerances and expensive components. The C-band (5.712 GHz, $E_{acc} \approx 50\,\mathrm{MV\,m^{-1}}$) offers an optimal compromise between efficiency and cost-effectiveness [5]. At present, no cost-effective and compact VHEE accelerators are available in clinical environments. It is therefore crucial to investigate the feasibility of developing such accelerator, ensuring a step forward in research for cancer treatment.

A 24 MeV FLASH LINAC [6], currently under construction at Sapienza University, will serve as a testbed for this technology. This work presents the design of a VHEE and UHDR accelerator tailored for deep-seated tumors as a future extension of the Sapienza LINAC, using a genetic algorithm for working point optimization, ASTRA for beam transport, and FLUKA for dose mapping.

100 MeV COMPACT ACCELERATOR LAYOUT

A commercial 14 kV thermionic triode gun [7] generates the beam, delivering a continuous 100 mA with a 35 % capture efficiency when installed directly onto the first structure. The selected model can emit up to 1.5 A, ensuring reliable operation at 100 mA within the LINAC.

After electrostatic acceleration, the continuous electron beam is captured, bunched, and accelerated to 4 MeV in a 22 cm standing-wave (SW) C-band injector [8], derived from the SAFEST prototype [6]. Two subsequent constant-gradient traveling-wave (TW) structures (1.2 m total length) operate at 40 $\mathrm{MV\,m^{-1}}$ to reach 100 MeV. The TW cells are derived from the 24 MeV prototype.

A 20 MW klystron (5 µs pulse, 200 Hz repetition rate), combined with a BOC-type pulse compressor, feeds the accelerating structures. The compressor design is based on the system implemented in the Sapienza prototype [9]. To deliver sufficient dose, the beam duration must be on the order of 1 µs. High-intensity beams (100 mA) of this duration induce strong beam loading [10], requiring dedicated RF pulse shaping. It reduces the accelerating field along the bunch train, requiring increasing RF compensation for later bunches, which in turn increases energy spread and reduces average energy. More details can be found at [10]. Additionally, the pulse compressor response is not flat in the amplified region, further complicating the optimization. The required klystron modulation is therefore obtained via a multi-variable genetic algorithm. Table 1 and Fig. 1 summarize the main parameters.

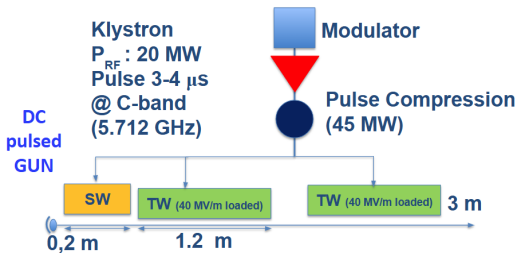

Figure 1: Accelerator layout scheme.

* stefano.farina@uniroma1.it

ISBN: 978-3-95450-252-3 ISSN: 2673-5350 doi: 10.18429/JACoW-IPAC2026-TUP3073

STUDY AND TEST OF A TRIODE GUN FOR THE FLASH ELECTRON LINAC AT SAPIENZA

S. Akbar†, R. Boldrini, E. Chiadroni, A. Curcio, M. Coppola, S. Farina, G. Francosioni, L. Giuliano, M. Migliorati, E. Montanucci, M. Magi, A. Mostacci1, L. Palumbo
Sapienza University of Rome, Rome, Italy
L. Ficcadenti, Istituto Nazionale di Fisica Nucleare, Sezione di Roma I, Rome, Italy
L. Faillace, Istituto Nazionale di Fisica Nucleare, LNF, Frascati, Italy.

Content from this work may be used under the terms of the CC BY 4.0 licence (© 2026). Any distribution of this work must maintain attribution to the author(s), title of the work, publisher, and DOI.

Abstract

A 24 MeV prototype LINAC is under development at Sapienza University of Rome for FLASH radiobiological studies. The injector is a 12 keV triode thermionic electron gun from HeatWave Labs, providing grid-controlled current modulation for high current, low perveance, and short-pulse operation. To optimize its integration with the 24 MeV C-band hybrid standing- and travelling-wave structure, extensive particle tracking simulations of the electron gun were performed using CST Particle Studio. Parametric scans of the anode voltage and grid potential were used to evaluate beam current, perveance, and emittance, identifying operating points that balance beam stability and charge for FLASH applications. As the modern dispenser cathode requires stringent vacuum conditions below 1×10^{-6} mbar, the LINAC was also modeled in Molflow+ to predict pressure profiles under realistic gas-load scenarios. Simulations revealed a potential vacuum limitation near the gun, leading to the design and implementation of an additional pumping port for better evacuation of gas molecules. These results are benchmarked with initial experimental tests performed on an electron gun test bench at Sordina IORT Technologies. The combined simulation and experimental validation provide key design requirements for compact FLASH LINAC injectors.

INTRODUCTION

FLASH radiotherapy requires the delivery of ultra-high dose rates in microsecond-scale pulses, imposing stringent constraints on the electron injector in terms of peak current, beam stability, and temporal control [1]. In the framework of the SAFEST project, a 24 MeV prototype C-band hybrid standing- and travelling-wave LINAC is under development at Sapienza University of Rome for FLASH radiobiological studies [2-4].

The design of the injector presents several critical challenges. From a beam dynamics perspective, achieving high current while maintaining low emittance and stable transport requires accurate modelling of the emission process in thermionic triode electron guns. Parametric studies are particularly important during the initial commissioning phase of the LINAC, therefore requiring detailed particle tracking simulations.

In addition, vacuum conditions play a crucial role in the performance of modern dispenser cathodes, which require pressures below 10^{-6} mbar for proper activation and homogeneous emission. Due to limited vacuum conductance, cathode degassing at elevated temperature leads to gas accumulation near the gun region resulting in degraded emission performance and non-uniform cathode activation, thus limiting the achievable operating voltage and beam current [5].

Another key aspect is the control and operation of the electron gun. The dispenser cathode is activated by gradually increasing the heater voltage until stable electron emission is achieved [6]. This requires an automatic control logic which gradually increases the heater voltage in discrete steps while respecting the permissible vacuum limits. FLASH applications also require precise timing and reproducibility of beam for irradiation time of less than 100 ms, motivating the development of a dedicated control scheme capable of single-shot operation by generating a finite burst of pulses within a 100 ms irradiation window. This involves synchronization between the modulator trigger and grid pulses, with appropriate timing logic to ensure stable beam extraction [7].

This work addresses these challenges through a combined numerical and experimental approach. A detailed 3D model of a thermionic triode electron gun is simulated in CST Particle Studio to study emission and beam dynamics. Vacuum performance is analyzed using Molflow+ to identify and mitigate pressure limitations. Experimental measurements are performed to validate the model, and a dedicated control system is implemented to enable reliable activation of cathode and single-shot operation. The results provide key insights for the design of compact FLASH LINAC injectors.

DESIGN OF ELECTRON GUN

The injector is based on a 12 keV pierce-convergent type thermionic triode electron gun (HeatWave Labs), enabling grid-controlled emission as shown in (Fig. 1). The gun consists of a dispenser cathode, control grid, focusing electrode and anode, allowing precise modulation of the emitted current. A realistic control grid structure was implemented in the simulations using a honeycomb geometry with 0.5 mm apertures and 0.25 mm thickness, corresponding to an estimated beam blockage of 10–15%.

The gun is designed for short-pulse operation in the microsecond range, supporting high peak current and low perveance conditions. The integration of this gun into a LINAC for FLASH applications requires careful matching of beam parameters at injection.

† shoaib.akbar@uniroma1.it

ISBN: 978-3-95450-252-3 ISSN: 2673-5350 doi: 10.18429/JACoW-IPAC2026-TUP3074

RF DESIGN OF THE 1 kHz PHOTOINJECTOR FOR THE RUEDI ELECTRON DIFFRACTION FACILITY

L. S. Cowie*, A. J. Gilfellon, B. R. Hounsell, B. L. Militsyn, J. W. McKenzie,
T.C.Q. Noakes, S. S. Percival, UKRI STFC Daresbury Laboratory, Warrington, UK
G. Burt, Lancaster University, Lancaster UK

Content from this work may be used under the terms of the CC BY 4.0 licence (© 2026). Any distribution of this work must maintain attribution to the author(s), title of the work, publisher, and DOI.

Abstract

The RUEDI RF photoinjector will have a 2.45 cell S-band gun producing electrons at 4 MeV. The gun is designed to operate at 1 kHz repetition rate. This will be achieved by a combination of RF over-coupling to reduce the RF pulse length, and an advanced water cooling system based on that of the CLARA 400 Hz photoinjector. The shorter pulse length is also intended to limit the dark current, along with operation at 70 MV/m, and the use of a flat back plate cathode. The cell lengths are optimised to improve jitter cancellation performance, as well as to limit surface electric fields on the irises. The cavity is dual side-coupled into the middle cell with a racetrack coupling cell to reduce the quadrupole component of the RF field, and has an RF probe on the final cell.

INTRODUCTION

RUEDI (Relativistic Ultrafast Electron Diffraction & Imaging) is a proposed user facility to be based at Daresbury Laboratory [1, 2], with a diffraction line that will deliver ultrafast electron diffraction down to 10 fs timescales and an imaging line for single-shot, time-resolved imaging with MeV electrons. The diffraction line will consist of a 2.45 cell S-band RF photoinjector with a magnetic compression arc and variable diffraction optics [3]. The interaction region will have a large variety of pumps and sample environments and electron bunch diagnostics. The RF design of the RUEDI photoinjector for the diffraction line is presented here.

CAVITY GEOMETRY DESIGN

The photoinjector is a 2.45 cell S-band (2998.5 MHz RF gun, with a Ti:sapphire laser producing UV pulses at the third-harmonic wavelength 266 nm. It will have a focusing solenoid after the cavity, 0.22 m from the cathode. S-band was chosen due to it being a well-developed technology with easily available power sources and transport. It also allows high enough RF fields to operate in the beam-blowout regime [4]. The bunches will be long (188 fs RMS) at the exit of the gun but will be compressed to under 10 fs at the sample in a magnetic compression stage. The magnetic compressor will also suppress the time of flight jitter to the sample to below 10 fs [5]. The fields, however, will be low enough to minimise dark current whilst still reaching the full RUEDI kinetic energy of 4 MeV in a single RF cavity. Operation at 70 MV/m reduces the theoretical dark current by 92% compared to 100 MV/m [6]. In the 2.45 cell CLARA photoinjector, which operates at a similar cathode field, it was found that the most problematic dark current was mostly from the edge of the vacuum-interchangeable cathode plug, and from the rim around the plug opening [7]. For this reason for RUEDI the copper back plate will serve as the cathode; it will be exchangeable, but not under vacuum.

The gun design, including a racetrack coupling cell, is shown in Fig. 1. Side power coupling was chosen to allow both a large aperture for the photoinjector laser transport at near-normal incidence and optimal solenoid placement. Z-coupling with rounded slots will reduce the fields on the coupler opening. Elliptical irises between the cells minimise the surface fields. The shortest major radius (iris thickness) that would allow the same cooling design as the CLARA 400 Hz photoinjector is 8 mm [8], and was chosen to maximise shunt impedance. The iris radius (from the beam axis) is 14.5 mm to give a mode separation of greater than 15 MHz, with the final iris radius 15 mm to allow photoinjector laser transport.

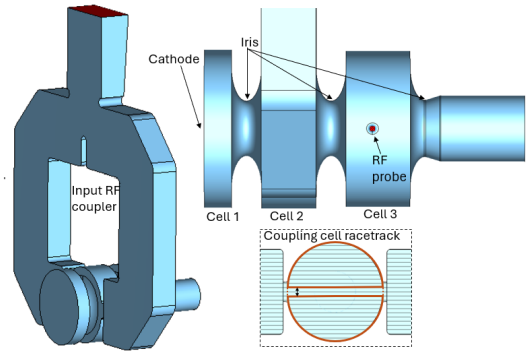

Figure 1: Final RF design geometry.

A racetrack shaped coupling cell minimises the quadrupole component from the dual waveguide coupler. This can be seen in Fig. 2, which shows the electric field E_z in the z direction around a 3 mm radius circle around the z axis in the coupling cell for three racetrack lengths. A 4 mm straight on the cell equator reduces the quadrupole component to below the simulation noise level. GPT [9] simulations show that a 4 mm racetrack decreases the difference in vertical and horizontal normalised RMS emittance (transverse emittance asymmetry) from 13.7 to 1.7 nm · rad compared to a round cell for a bunch with approximate total transverse emittance 40 nm · rad. The gun design also includes a probe on the third cell; it has −67.2 dB coupling and is symmetrised by using a dummy probe port opposite.

* louise.cowie@stfc.ac.uk

ISBN: 978-3-95450-252-3 ISSN: 2673-5350 doi: 10.18429/JACoW-IPAC2026-TUP3075

EVIDENCE FOR RF BREAKDOWNS CAUSING SURFACE ANOMALIES ON CAESIUM TELLURIDE CATHODES AT CLARA

A. Pollard*, J. Jones, L. Jones, H. Owen, D. Walsh
Accelerator Science and Technology Centre, Warrington, UK
STFC Daresbury Laboratory, Warrington, UK
Cockcroft Institute, Warrington, UK

Content from this work may be used under the terms of the CC BY 4.0 licence (© 2026). Any distribution of this work must maintain attribution to the author(s), title of the work, publisher, and DOI.

Abstract

The Compact Linear Accelerator for Research and Applications (CLARA) at Daresbury Laboratory has recently undertaken an upgrade of its photocathodes from using a copper emission surface to using caesium telluride (Cs_2Te). During the conditioning of the first Cs_2Te cathode a significant number of RF breakdowns were detected, and so that cathode was replaced; subsequent inspection of the cathode identified a number of surface defects. To better study the second cathode, a diagnostic camera was used to collect images of the surface *in situ* during RF conditioning; the frequent formation over time of surface defects was observed. In this paper we present a statistical analysis of the breakdown events and surface image data, utilizing cross-correlation of the signal derivatives to account for cumulative trends. The analysis reveals a correlation between the rate of defect formation and the incidence of RF breakdowns, with a Pearson coefficient of $r = 0.59$ at zero time lag. These results provide quantitative evidence that RF breakdown events are the likely driver of surface morphology changes on Cs_2Te cathodes.

INTRODUCTION

Caesium Telluride Cathodes at CLARA

Copper is a simple yet robust photocathode with limited quantum efficiency (QE) of approximately 2×10^{-4} under illumination at 266 nm, while Cs_2Te is somewhat less robust but offers QE typically in the region of 10 – 20 % at 266 nm; Cs_2Te is therefore commonly used in high-brightness electron sources to deliver electron bunch charges in the nC range, for example in photoinjectors for free-electron lasers (FELs). The CLARA [1] photoinjector [2] is a test-bed for novel high-brightness applications, and its electron source was recently upgraded from using a Cu emitting surface [3,4] to using Cs_2Te. The Cs_2Te photocathodes developed for CLARA were manufactured by sequential Cs and Te deposition onto polished molybdenum (Mo) substrates (INFN-style photocathode plugs), carried out at room temperature using our dedicated offline Alkali metal Photocathode Preparation Facility (APPF) deposition system [5]. Early photocathode plugs obtained QE around 5 %, increasing to typically ~15 % as the deposition process was refined [6]. Transitioning CLARA to regular use of Cs_2Te allows the drive laser power to be reduced, due to the much-increased QE of Cs_2Te compared to Cu. Prior to the use of Cs_2Te, CLARA operated for 2 years using a similar Cu-tipped hybrid Mo/Cu photocathode plug (reference # 020 in our series of production). Upon its removal it was noted that the Cu cathode surface was significantly marked and pitted as shown in Fig. 1 (when photographed under white light with the cathode located in the gun load-lock storage chamber), with additional marking and discolouration evident on the edge of the plug between the tip and RF spring contact area. This morphology is somewhat similar to cathodes examined elsewhere, and is perhaps caused by breakdowns occurring on the cathode surface over extended periods of operation.

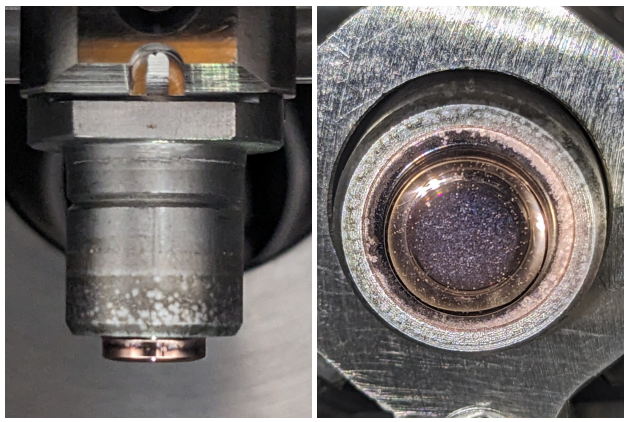

Figure 1: Photocathode # 020 (Cu) on removal from the CLARA photoinjector.

For Cs_2Te deposition, nine Mo plugs were manufactured by Abelco GmbH from a variety of sintered Mo stock material, then polished with the assistance of DESY (Hamburg) to attain surface finishes with measured reflectivity of > 57 % at 532 nm. All plugs met this surface finish criteria, though several plugs retained very-small visible surface feature, believed to be pits associated with the sintered nature of

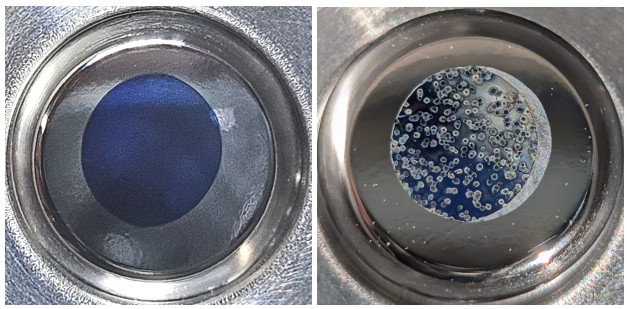

Figure 2: Photocathode # 036 (Cs_2Te) as-deposited (left) and on removal from the CLARA photoinjector after 3 days of RF conditioning (right).

* amelia.pollard@stfc.ac.uk

ISBN: 978-3-95450-252-3 ISSN: 2673-5350 doi: 10.18429/JACoW-IPAC2026-TUP3076

RECENT DARK CURRENT MEASUREMENTS ON THE CLARA S-BAND RF ELECTRON GUNS

F. Jackson*,[1], L. Cowie[1], M. Furmaniak[1], L.B. Jones[1], J. K. Jones[1], S. Mathisen[1], J. W. McKenzie[1], B. L. Militsyn[1], T.C.Q. Noakes[1], ASTeC, STFC Daresbury Laboratory, Warrington, UK
P. Goudket, ESS, Lund, Sweden
[1]also at the Cockcroft Institute, Sci-Tech Daresbury, Warrington, UK

Abstract

The CLARA accelerator at Daresbury Laboratory has recently commissioned a new electron gun as part of a larger upgrade to the facility. The new gun ('HRRG') is a high repetition rate (400 Hz) 1.5 cell S-band cavity (3 GHz fundamental frequency) designed to produce low emittance beams with momenta up to 5 MeV/c, with field gradients at the cathode surface up to 120 MV/m and RF pulse lengths of up to 3 μs. The previous CLARA gun ('LRRG') was a similar 2.5 cell device but of low repetition rate (10 Hz). Dark current emitted from the gun is an important issue for several reasons, so is monitored and managed throughout CLARA commissioning and user operation. We present dark current measurements from the new HRRG gun through its commissioning phase and early stage operation, and make a comparison to those taken from previous LRRG gun.

INTRODUCTION

The CLARA (Compact Linear Accelerator for Research and Applications) accelerator, operating since 2013 at Daresbury Laboratory, is a medium energy electron accelerator providing low emittance, moderate charge beams of high quality for various applications [1]. The original CLARA design was intended to generate a beam with short bunches for free electron laser development, but this has evolved more general range of exploitation. The CLARA electron sources were designed to generate an electron beam with energies up to 5 MeV using a photocathode in an S-band RF gun with up to 400 Hz single-bunch repetition rate. As is the case with many guns of this type, field emission from the gun, or dark current, is of interest and concern. Dark current has negative effects such as the irradiation and damage of machine components, but may also serve as an indication of gun and cathode performance. Dark current behaviour and characteristics are complex due to many convolved factors including its very large temporal and energy spread in comparison to the core electron beam, macroscopic surface geometry and microscopic surface details, and has been the subject of several studies in similar electron guns [2, 3].The LRRG (Low Rep Rate Gun) CLARA gun was a 2.5 cell copper RF cavity operated at a maximum rate of 10 Hz in which the cavity backplane served as photocathode. This was later upgraded with a new backplane which facilitated photocathode exchange supported by a 'load-lock' system. This enabled beam operation with cathodes of different preparation and composition. More recently, a new HRRG (High Rep Rate Gun) 1.5 cell RF cavity gun with capability to run up to 400 Hz was commissioned and used at CLARA, which again uses a load-lock system, and for the first time Cs_2Te cathodes are being used in CLARA.

CLARA GUN, INJECTOR, AND DARK CURRENT DIAGNOSTICS

For the work in this paper we examined the dark current near to the gun exit, using the first diagnostic screen after the gun and the wall current monitor located immediately upstream of this screen. The injector beamline (gun and beamline with diagnostics upstream of the first main linac) is shown in Fig. 1. A beam focussing solenoid surrounds the gun and a bucking solenoid exists so that the magnetic field at the cathode surface can be set to zero. There are apertures which may affect the transport of the dark current from the source including the gun RF coupler and the light box.

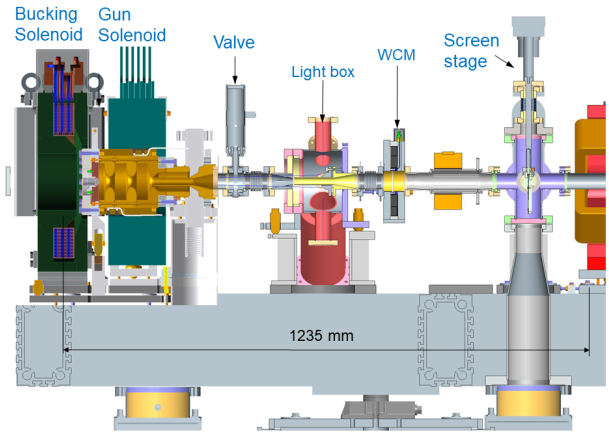

Figure 1: CLARA injector schematic.

The cathode region of the gun is illustrated in Fig. 2 which strongly influences certain features of the dark current, as described below. Based on a design elsewhere [4] the cathode insert or 'plug' incorporates a rounded elliptical edge profile or 'rim' and is positioned in an opening in the gun backplate, which itself has deeper elliptical rim. These rounded rim profiles are designed to optimise the shape the gun electric field in the cathode region, and to limit the electric field strength in certain locations and thus suppress generation of dark current.

* frank.jackson@stfc.ac.uk

Content from this work may be used under the terms of the CC BY 4.0 licence (© 2026). Any distribution of this work must maintain attribution to the author(s), title of the work, publisher, and DOI.

ISBN: 978-3-95450-252-3 ISSN: 2673-5350 doi: 10.18429/JACoW-IPAC2026-TUP3078

LASER WAKEFIELD ACCELERATION IN CARBON NANOTUBE BUNDLES*

J. Zhang†, H. Saberi, S. Wen, G. Xia, University of Manchester, Manchester, United Kingdom
J. Resta-Lopez, Instituto Universitario de Ciencia de los Materiales, Paterna, Spain
A. Bonatto, Universidade Federal de Ciências da Saúde de Porto Alegre, Porto Alegre, Brazil
C. Bontoiu, B. Lei, University of Liverpool, Liverpool, United Kingdom

Content from this work may be used under the terms of the CC BY 4.0 licence (© 2026). Any distribution of this work must maintain attribution to the author(s), title of the work, publisher, and DOI.

Abstract

Laser wakefield acceleration (LWFA) can produce accelerating fields of several hundred GV/m, greatly reducing accelerator size and cost. Carbon nanotube (CNT) bundle-based targets, featuring high plasma density ($>10^{19}$ cm^{-3}), tunable effective density, excellent thermal properties, and hollow channels that enable laser propagation in overcritical-density targets, have attracted interest as solid-state plasma sources. Previous studies suggested that CNT-based structures can increase the acceleration field to the TV/m range, making them promising for compact radiation sources and radiotherapy. However, the insufficient beam quality still limits their broad application. In this work, we model a hollow solid-state plasma channel composed of CNT bundles. A 2 PW laser pulse based on the parameters of the ELI-ALPS High-Field Laser facility is injected into the channel, generating self-injected electron bunches that are trapped and accelerated by a TV/m-scale accelerating field, as demonstrated by WarpX particle-in-cell simulations. Compared with previous LWFA results using solid-state targets, this work produces a quasi-monoenergetic electron bunch with a charge of 2.8 nC, a mean energy of 198 MeV, and an energy spread of 2.8% over an acceleration length of 104 μm, demonstrating the potential of CNT bundle-based targets for compact TV/m-scale acceleration.

INTRODUCTION

Laser wakefield acceleration (LWFA) was first proposed by Tajima and Dawson in 1979 [1]. Since then, LWFA has developed from proof-of-principle demonstrations to GeV-scale electron acceleration. An early proof-of-principle experiment demonstrated an accelerating field of ∼1.7 GV/m [2], while later experiments at Berkeley Lab using capillary-discharge-guided gaseous plasmas achieved multi-GeV electron beams with an average accelerating field of ∼47 GV/m [3]. Since the plasma wave breaking field increases with plasma density, crystals and solid-state plasmas have been proposed as potential media for ultra-high-gradient acceleration [4, 5]. Among these solid-state plasma candidates, carbon-based nanostructures such as graphene and carbon nanotubes (CNTs) have attracted particular interest because of their high electron density, structural tunability, and potential to guide intense laser pulses through hollow channels. Recently, graphene structures have been reported to support an acceleration field up to 4.79 TV/m in simulations [6], while ultrahigh-density carbon nanotubes (CNTs) have been predicted to achieve fields on the order of 100 – 400 TV/m [7]. In addition, a new acceleration mechanism has been identified in CNT-based structures, where sub-TeV/m acceleration is achieved in the leaky surface plasmon polariton (SPP) regime [8]. These advances suggest that nanostructured carbon-based plasmas provide a promising route toward compact, ultra-high-gradient laser-driven accelerators.

However, previous studies of CNT targets at plasma densities of 10^{21}–10^{22} cm^{-3} have reported relatively low beam quality, particularly with large energy spread [9]. One critical reason is the laser–plasma instabilities caused by the mismatch between the laser pulse duration, τ, and the plasma wavelength, λ_p, when $c\tau > \lambda_p$ [10–12], where c denotes the speed of light.

In full three-dimensional particle-in-cell (PIC) simulations, the spatial resolution must be sufficiently high to resolve the nanostructured CNT units accurately, making such simulations computationally expensive. To reduce this cost, the effective density approach (EDA), which represents nanostructured CNT targets using a volume-averaged plasma density, was proposed in Ref. [13]. This approach enables analytical expressions originally derived for uniform plasmas to estimate the wakefield properties.

In this work, we investigate LWFA in CNT-bundle targets at relatively low plasma densities of 10^{19}–10^{20} cm^{-3}, where the laser pulse length can be better matched to the plasma wavelength than in ultrahigh-density CNT regimes. We first perform parameter scans over the effective plasma density, laser waist, and inner radius of uniform CNT targets to optimise the beam quality. The optimal parameter set is then applied to CNT-bundle targets, where the geometry is further optimised to reduce the energy spread.

TARGET GEOMETRY

Figure 1 shows a schematic of the CNT bundle-based target, which consists of several tens of concentric shells of CNT bundles surrounding a central hollow channel. Each bundle is composed of nanoscale single-walled CNTs. Applying the effective density approach, the periodically non-uniform CNT bundle distribution is approximated as an equivalent homogeneous plasma, defined as [7]:

$$n_{\mathrm{eff}} = n_{\mathrm{b}} \frac{Nf}{1 + (N-1)(1+\kappa)}. \quad (1)$$

* Cockcroft Institute Core Grant No. ST/V001612/1 and STFC SCARF cluster.

† jiaqi.zhang@manchester.ac.uk

ISBN: 978-3-95450-252-3 ISSN: 2673-5350 doi: 10.18429/JACoW-IPAC2026-TUP3079

HIGH CURRENT ACCELERATOR-DRIVEN NEUTRON SOURCE PLATFORM OVERVIEW

I. Bustinduy*, J. L. Muñoz, F. J. Villacorta, M. Pérez, ESS Bilbao, Zamudio, Spain
P. Zakalek, J. Baggemann, U. Rücker, T. Gutberlet, Forschungszentrum Jülich, Germany
A. Menelle, F. Ott, CEA, France
M. A. Paulin, CNRS, France

Abstract

ESS-Bilbao, JCNS, and LLB have joined forces to develop Europe's first HICANS Platform (HiCANS stands for "High Current Accelerator-driven Neutron Source"). This project aims to integrate the high current proton accelerator system, currently under construction at ESS Bilbao, with the target-moderator-reflector unit that has been successfully built and operated at Forschungszentrum Jülich, and a diffractometer and a reflectometer to be installed and operated by LLB, plus additional neutron instrumentation provided by the three partners. This facility intends to validate and demonstrate the technological developments that will take part of these medium-flux neutron sources.

In this demonstrator, the first stage of the ARGITU source will be used to produce a pulsed proton beam with an energy of 3 MeV and a repetition rate of 30 Hz hitting a lithium target, generating neutrons that are then moderated at the desired thermal and cold energy ranges for the operation of a diffractometer and a reflectometer.

INTRODUCTION

High-current accelerator-driven neutron sources (HiCANS) are being developed to complement the decreasing availability of reactor-based neutron beam time in Europe. The HiCANS platform at ESS-Bilbao (Fig. 1) is conceived as an integrated demonstrator for a compact pulsed proton driver, a dedicated target–moderator station, and neutron scattering instrumentation. It brings together the ARGITU accelerator development in Spain, the Jülich target station experience, and LLB instruments formerly operated at reactor and CANS facilities. The main objective is to demonstrate reliable production, moderation and transport of useful thermal and cold neutron beams at moderate accelerator power, while preparing the route towards future higher-power HiCANS facilities.

ACCELERATOR

The accelerator will deliver a pulsed high-current proton beam of 3 MeV, with pulses up to 1.5 ms at 30 Hz and a peak current of up to 30 mA. The front end consists of a proton ion source, a Low Energy Beam Transport (LEBT) section and a Radio-Frequency Quadrupole (RFQ). The ion source provides an approximately 45 keV beam, which is matched by the LEBT into the RFQ [1]. Solenoidal focusing in the LEBT controls the transverse envelope and mitigates space-charge effects, with the objective of preserving emittance and maximizing RFQ capture. The RFQ (Fig. 2) is the main accelerating structure of the linac. Operating at 352.21 MHz, it bunches, focuses and accelerates the incoming proton beam to about 3 MeV. Simulations using the manufactured field-map geometry predict high transmission over the expected current range, providing beam parameters compatible with transport to the neutron-production line.

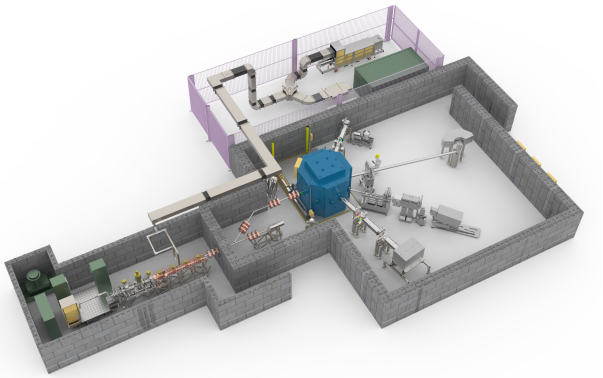

Figure 1: HiCANS platform to be installed at ESS-Bilbao, Zamudio, Spain: accelerator, transfer line, target station and neutron instruments.

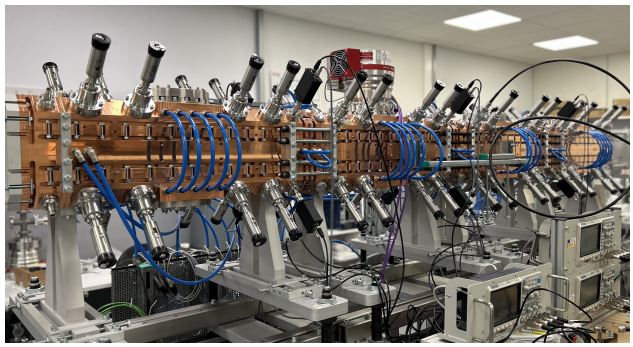

Figure 2: RFQ during the bead-pull campaign in the integration laboratory.

Downstream of the RFQ, a dogleg-type transfer line [2] transports the 3 MeV beam towards the lithium target while providing diagnostics, steering and beam-size control. The main branch uses a dipole deflection to direct the beam to the target and reduce direct exposure to ionizing radiation produced at the target. A secondary, undeflected branch terminates in a beam stop for commissioning, tuning and safe disposal during start-up or transient operating conditions. Beam position, profile, current and emittance diagnostics

* ibustinduy@essbilbao.org

Content from this work may be used under the terms of the CC BY 4.0 licence (© 2026). Any distribution of this work must maintain attribution to the author(s), title of the work, publisher, and DOI.

ISBN: 978-3-95450-252-3 ISSN: 2673-5350 doi: 10.18429/JACoW-IPAC2026-TUP3081

SHIELDING CALCULATIONS AND ACTIVATION STUDIES FOR THE PSI POSITRON PRODUCTION EXPERIMENT

M. I. Besana*, P. Craievich, J. Snuverink, R. Zennaro
PSI Center for Accelerator Science and Engineering, Villigen, Switzerland
N. Vallis, European Organization for Nuclear Research (CERN), Geneva, Switzerland

Abstract

The Future Circular Electron-Positron Collider (FCC-ee) is a proposed next-generation particle accelerator, planned as the first stage of the larger Future Circular Collider project at CERN. It is an electron-positron collider designed to be a precision instrument for studying fundamental physics.

The PSI Positron Production (P^3) is the planned proof-of-principle experiment for the FCC-ee positron source. The main goal of this experiment is to test new technology and validate the envisioned positron production scheme. To this end, a prototype of the FCC-ee positron source will be hosted at the SwissFEL facility at the Paul Scherrer Institute in Switzerland.

A dedicated bunker has been built inside the SwissFEL tunnel, and the experimental components are installed. Simulations have been performed with the FLUKA.CERN Monte Carlo code to dimension the P^3 bunker and local shielding elements. Calculations have been repeated for various target models since different target options will be tested.

This contribution briefly describes the ingredients of the P^3 experiment and details the dedicated bunker and the local shielding. It shows the expected dose rate distribution outside the P^3 bunker. The foreseen activation is also discussed.

GEOMETRY MODEL

The P^3 experiment is installed in the SwissFEL linac at the Paul Scherrer Institute (PSI) inside a dedicated bunker. A brief description of the different components is reported in the following. Additional details can be found in Refs. [1, 2].

The geometry implemented in the FLUKA.CERN Monte Carlo code [3–6] is shown in Fig. 1.

During operation, the SwissFEL 6 GeV electron beam will be deflected towards a target. A charge of 200 pC will be delivered at a frequency of 1 Hz. The goal is to estimate the rate of positron production for different targets. Three target models were considered in the calculations. Two targets are made of tungsten. The first has a cylindrical shape, while the second is conical [7]. The third is a tantalum cylinder.

The target is surrounded by a high-temperature superconducting (HTS) solenoid [8]. Its magnetic field is taken into account in the simulations.

The produced electrons and positrons are subsequently accelerated using two radio-frequency (RF) cavities, each of which is surrounded by eight solenoids.

The electron and positron beams are then separated by a bending magnet and directed toward two Faraday cups,

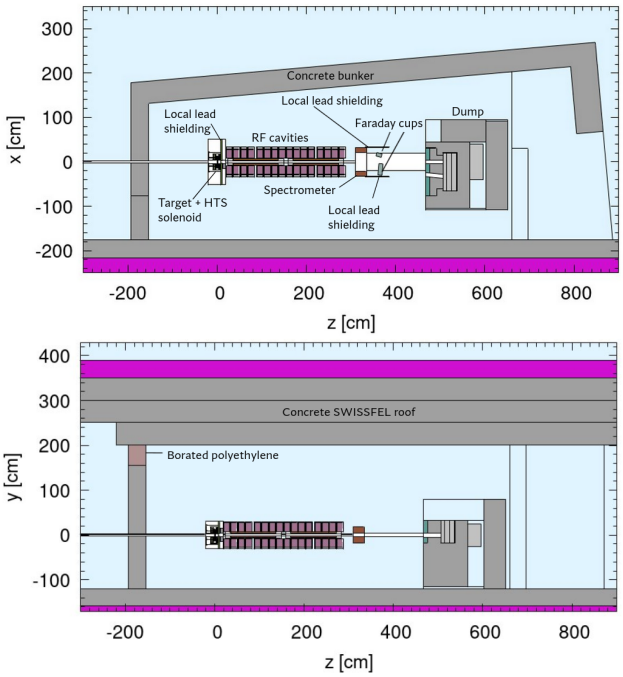

Figure 1: P^3 experiment geometry implemented in the FLUKA.CERN code: top view at beam height (top) and side view at beam position (bottom). The beam is moving along the z-axis. The x-axis is the horizontal axis, oriented towards the SwissFEL tunnel. The y-axis is opposite to gravity. The main components are indicated in the picture. Iron is shown in brown, the representative mixture of copper and water in orchid, tungsten in turquoise, steel in light grey, polyethylene in green, normal concrete in grey, borated polyethylene in light-red and soil in violet. The figure is obtained using the Flair graphical interface [9].

which are used to measure the generated charge. The magnetic field is assumed to be constant inside the magnet opening and multiple values have been studied.

Lastly, a beam dump is incorporated at the end of the beamline. This is made up of various blocks of different materials: steel, concrete, and polyethylene. An existing beam dump will be used, but it has been reinforced to comply with the P^3 experiment and the radioprotection requirements.

Two local shielding components have been designed to reduce the prompt dose. A 6 cm long lead plate is placed at the exit of the HTS magnet to absorb the radiation generated at the target.

Two identical lead plates are located at the side of each Faraday cup to intercept low energy charged particles, which have a high deflection angle and are deviated by the dipole

* ilaria.besana@psi.ch

Content from this work may be used under the terms of the CC BY 4.0 licence (© 2026). Any distribution of this work must maintain attribution to the author(s), title of the work, publisher, and DOI.

ISBN: 978-3-95450-252-3 ISSN: 2673-5350 doi: 10.18429/JACoW-IPAC2026-TUP5301

BEAM PERFORMANCE OF THE POSITRON TRANSPORT LINE FOR THE CEBAF POSITRON UPGRADE*

S. Ogur†, J. Benesch, J. Grames, Y. Roblin, A. Ushakov
Thomas Jefferson National Accelerator Facility, Newport News, VA, USA

Abstract

The Low Energy Recirculator Facility (LERF), formerly used for the Free Electron Laser program, has been proposed as the injector site for the planned 12 GeV CEBAF positron upgrade (Ce^+BAF). The 123 MeV positron transport line from LERF to the North Linac spans 872.5 m and is designed using a combination of FODO cells and Double-Bend Achromat (DBA) arcs, keeping transverse beta functions below 130 m and horizontal dispersion within ±0.3 m. Multi-particle tracking with Elegant demonstrates nearly complete transmission (>99%) to the North Linac for nominal beam parameters, while spin tracking with Bmad confirms a total spin rotation of approximately 100° in good agreement with analytical predictions. A systematic 6D acceptance study for Ce^+BAF shows that transmission above 70% requires a normalized transverse emittance $\epsilon^n_{x,y} < 100$ mm·mrad, an rms bunch length $\sigma_z < 1$ mm, and an rms momentum spread $\Delta p/p < 0.5\%$.

INTRODUCTION

The CEBAF 12 GeV positron upgrade (Ce^+BAF) plans to reuse the Low Energy Recirculator Facility (LERF) building, formerly hosting the JLab FEL program, as the host for a positron source and pre-accelerator. Positrons generated on a high-Z target by an electron driver are captured and accelerated in LERF to 123 MeV [1–3]. They must then be transported from the LERF to CEBAF and injected into the final chicane dipole of the existing electron injector.

The transport line that connects LERF to CEBAF must meet two main constraints, first: it must fit within the existing CEBAF tunnel, leaving sufficient egress for personnel and maintenance, and second: it must accept a positron beam whose transverse and longitudinal emittances are roughly two orders of magnitude larger than those of the CEBAF electron beam. The same transport line is also considered to deliver 650 MeV electrons from the LERF to CEBAF for the 22 GeV FFA@CEBAF upgrade [4, 5], requiring common beamline components and demands bipolar power supplies for transporting either electrons or positrons. This contribution summarizes the optics solution adopted for this transport line, the multi-particle and spin-tracking performance, and the resulting six-dimensional acceptance limits for Ce^+BAF.

LAYOUT AND OPTICS

The 872.5 m transport line is suspended from the tunnel ceiling along the inner tunnel wall of the CEBAF ring, opposite the existing CEBAF accelerator located on the outer radius of the ring. It merges into the CEBAF accelerator at the entrance to the North Linac by mirroring the last two dipoles of the present electron injector chicane (Fig. 1). Bipolar power supplies on every dipole and quadrupole make it usable for both 123 MeV positrons and for 650 MeV electrons. The beamline consists of four functional blocks: (i) a vertical and horizontal LERF-to-South matching section that closes both transverse dispersions; (ii) a 14-cell horizontal FODO South straight optimized to minimize the quadrupole count while keeping the $|\mathrm{Tr}(M_{\mathrm{cell}})| < 2$; (iii) a 180° West arc built from Double-Bend Achromat (DBA) cells; and (iv) a NL merger that suppresses both transverse dispersions and simultaneously matches the Twiss parameters at the injector chicane for either 123 MeV positron or 650 MeV electron operation.

For the DBA cell the horizontal phase advance between the two dipole centers is set to $\mu_x = \pi$, which is the standard DBA achromat condition that simultaneously closes the horizontal dispersion and its derivative. Elegant [6] returns $\mu_x \approx 3.135$ rad for the cell, i.e. within 0.2% of π, confirming that the cell is achromatic to numerical precision. The full optics is shown in Fig. 2: the beta functions remain less than 130 m through the entire 872.5 m line, and the horizontal dispersion is maintained within ±0.3 m.

The dipoles are 1-m-long sector bends and the quadrupoles are 15-cm normal-conducting magnets, scaled from standard CEBAF designs [7] perform at both 123 MeV and 650 MeV. The bend apertures are 104 mm gap arc-zero dipoles with pole width of 20 cm to accommodate the sagittas for all applications in the arc, including the final vertical dipole which deflects beam to the North Linac injection point.

MULTI-PARTICLE TRACKING

Multi-particle tracking has been performed in Elegant with 10^4 macroparticles drawn from a non-truncated Gaussian distribution using the nominal Ce^+BAF capture parameters. The transmission from the LERF exit to the NL is 99.7%; the rms bunch length grows from 0.5 mm to 1.7 mm and the normalized transverse emittances from 31/31 to 50/34 mm·mrad in the horizontal/vertical planes. The bunch-length elongation follows from the unchirped longitudinal transfer

$$\sigma_{z,\mathrm{out}} = \sqrt{(1 + R_{56}\, h)^2 \sigma_z^2 + (R_{56}\sigma_{\delta_0})^2}, \qquad (1)$$

with $R_{56} = 0.284$ m at the NL injection point. An alternative optics solution with a smaller (and even negative) R_{56} is also

* This material is based upon work supported by the U.S. DOE, Office of Science, Office of Nuclear Physics contract DE-AC05-06OR23177.

† ogur@jlab.org

Content from this work may be used under the terms of the CC BY 4.0 licence (© 2026). Any distribution of this work must maintain attribution to the author(s), title of the work, publisher, and DOI.

ISBN: 978-3-95450-252-3 ISSN: 2673-5350 doi: 10.18429/JACoW-IPAC2026-TUP7009

OPERATION OF THE KARA BOOSTER IN STORAGE-RING MODE FOR ACCELERATOR STUDIES AND SYSTEM DEVELOPMENT

H. Hoteit*, E. Blomley, A. Malygin, A. Mochihashi, A.-S. Mueller, M. Schuh, J. Steinmann,
Karlsruhe Institute of Technology, Karlsruhe, Germany

Abstract

The Karlsruhe Research Accelerator (KARA) booster synchrotron, normally used to accelerate electrons from 53 MeV to 500 MeV for injection into the KARA storage ring, has recently been successfully operated in a stand-alone storage ring mode. This capability was enabled by the modernization of its magnet power supplies and their integration into an EPICS-based control system. Operating the booster in this mode provides a flexible platform for accelerator physics studies, including the development of energy-ramping procedures, characterization of magnet hysteresis effects, and verification of control strategies under low-energy storage conditions. Initial commissioning demonstrated stable beam storage at several energies up to 500 MeV.

The future compact storage ring cSTART, designed for energies of 50-90 MeV, is currently being constructed at KIT. The new power supplies allow preliminary experiments to be conducted across this energy level in the KARA Booster, enabling studies of beam and machine characterizations under realistic conditions. Additionally, the ability to store beam up to 500 MeV supports tests relevant for the KARA storage ring. This mode establishes the booster as a compact and flexible experimental platform prior to deployment in cSTART and the main KARA storage ring. Future work will focus on beam dynamics and diagnostics in the lower energy region with reduced radiation damping, as well as optimization of ramping cycles for stable injector operation.

INTRODUCTION

The KARA booster synchrotron provides electron beams up to 500 MeV for injection into the 2.5 GeV storage ring and is primarily designed for acceleration cycles at 1 Hz [1].The lattice is optimized for booster operation and consists of a single quadrupole family without dedicated sextupoles, limiting flexibility in optics control and chromaticity correction. A detailed description of the machine design can be found in [2]. In its original configuration, continuous beam storage was not feasible due to limited stability and controllability of the legacy magnet power supplies, which were based on a resonant circuit and could not provide sufficiently constant current to maintain high-field operation; additionally, the associated cabling required upgrades.

A recent upgrade replaced these power supplies with high-stability units equipped with embedded EPICS support, enabling direct integration into the existing EPICS-based control system [3]. This enables steady-state operation at fixed energies, allowing the booster to operate as a storage ring over an energy range of approximately 50 MeV to 500 MeV.

In this energy range, radiation damping is weaker compared to operation at higher energies, such as in the 2.5 GeV KARA storage ring, while space charge, wakefield effects, magnet hysteresis, and longitudinal beam dynamics have a stronger impact. Since this range overlaps with the design energies of future compact storage rings like cSTART [4], the booster serves as a convenient test platform.

This work represents the first demonstration of stable beam storage and controlled energy ramping in a booster synchrotron originally designed for cycling at 1 Hz operation. This significantly extends the operational capabilities of the KARA booster and establishes it as a flexible platform for accelerator studies in a low-energy regime relevant to future compact storage rings.

COMMISSIONING AND STORAGE TESTS

A dedicated measurement campaign was conducted to evaluate storage-ring operation.

Stable beam storage was first achieved at 500 MeV following injection at 53 MeV and acceleration to top energy (see Fig. 1). During flat-top operation, magnet currents and RF voltage were held constant, resulting in reproducible beam conditions with no abrupt beam losses observed

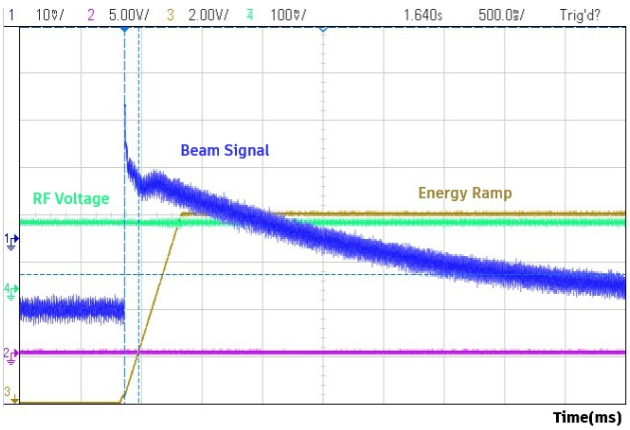

Figure 1: Beam signal during acceleration to 500 MeV and subsequent flat-top operation at 23 kV RF voltage.

Subsequently, beam storage was demonstrated at 53 MeV, 250 MeV,(see Fig. 2), and 500 MeV by operating the magnet currents at fixed values and adjusting the RF voltage for stable beam capture. These measurements confirmed that the booster optics can be reproducibly set over a wide energy range.

At 250 MeV with 10 kV RF voltage, the beam intensity remained approximately constant over the observation window, indicating stable beam storage under these conditions. In contrast, a faster beam decay was observed at 500 MeV with

* houssameddine.hoteit@kit.edu

Content from this work may be used under the terms of the CC BY 4.0 licence (© 2026). Any distribution of this work must maintain attribution to the author(s), title of the work, publisher, and DOI.

ISBN: 978-3-95450-252-3 ISSN: 2673-5350 doi: 10.18429/JACoW-IPAC2026-TUP7010

PROGRESS OF THE MAGNETIC MEASUREMENT BENCH FOR PULSED MAGNETS BASED ON A MODIFIED VIBRATING WIRE TECHNIQUE

M. Carlà, O. Blanco-García, A. Rodriguez
ALBA-CELLS Synchrotron, Cerdanyola del Vallès, Barcelona, Spain

Abstract

A measurement bench, dedicated to the characterization of pulsed magnets such as injection kickers, is under development at ALBA. The bench employs a modified vibrating wire technique allowing to measure high frequency magnetic fields in the range of hundreds of kHz. In the traditional vibrating wire technique an AC current carrying wire is stretched through the bore of the magnet and the force acting on the wire is proportional to the product of the wire current and the magnet field. A vibration of the wire is observed when the frequency of the wire current happens to be equal to the natural resonant frequency of the wire, typically a few hundreds of Hz. To characterize the high frequency behavior of the magnet, the measurement is modified by offsetting the frequency of the wire current by an amount equal to the magnet excitation frequency. This condition results in a resonant excitation of the wire vibration independently of the magnet field frequency. A feedback system based on the continuous excitation of multiple frequencies allows to track the resonant frequency of the wire, drastically increasing the measurement accuracy.

INTRODUCTION

An attempt at pulsed magnetic measurements by means of a vibrating wire setup was previously presented in [1] In a first experiment the traditional vibrating wire technique was applied to sample the field of a small bore kicker magnet powered with a constant current source. A thin metallic wire under tension was stretched through the bore and an alternating current tuned to the mechanical resonant frequency of the wire was applied to the wire. The wire vibration resulting from the interaction between the magnetic field and the current was sampled using an optical pickup allowing to determine the vibration amplitude and from this the magnetic field strength. Furthermore it was shown how the same technique could be modified in order to measure a field oscillating in the range of hundreds of kHz, well above the mechanical resonant frequency of the wire. For this purpose the wire was excited with a high frequency current tuned to the frequency of the magnetic field plus the mechanical resonant frequency of the wire, this condition allows in fact to produce a resonant excitation of the wire similarly to what was obtained in the constant field case. While the experimental test shown how the proposed technique can indeed be applied to sample an alternating field at high frequency, the overall results had a limited precision, and therefore were not suitable for an accurate characterization of a magnet.

In the following sections we proceed to illustrate further optimizations to the already described technique along with the experimental results.

FREQUENCIES COMB EXCITATION AND FEEDBACK

As shown in [2–4] the magnetic field strength is determined by fitting the wire frequency response. In the previous work a total of 25 frequencies were used to sample the wire response resulting in an overall acquisition time of roughly 20 minutes. This long acquisition time makes the measurement sensitive to any drift in the wire parameters. For instance a temperature drift during the measurement can easily change the wire resonance enough to result in a distortion of the measured resonant curve.

In the new setup to cut off the measurement time, the single frequency excitation of the magnet is changed changed in favor of multiple frequencies, allowing to measure several points of the response curve at the same time (Fig. 1). For

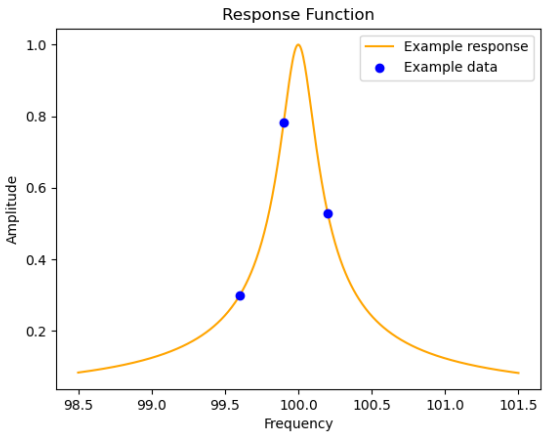

Figure 1: The simultaneous excitation of 3 frequencies provides the minimum required information to carry out the fit of the wire frequency response (solid line).

simplicity only 3 frequencies were used, a central frequency that is tuned to the resonant frequency of the wire and two equally spaced side frequencies. The signal is generated by applying an amplitude modulation to the magnet current with frequency equal to the required frequency spacing. The frequency spacing was set to 100 mHz such that the two side frequencies result in an excitation amplitude of roughly half the peak amplitude. To be able to resolve the contribution of each spectral line the acquisition time is set to a multiple of the period of the frequency spacing. It was found that

Content from this work may be used under the terms of the CC BY 4.0 licence (© 2026). Any distribution of this work must maintain attribution to the author(s), title of the work, publisher, and DOI.

ISBN: 978-3-95450-252-3 ISSN: 2673-5350 doi: 10.18429/JACoW-IPAC2026-TUP7011

THE TEX FACILITY UPGRADE AT INFN-LNF

F. Cardelli*, D. Alesini, M. Bellaveglia, C. Buitrago, B. Buonomo, S. Cantarella, M. Cianfrini, G. Catuscelli, G. Costa, C. Di Giulio, E. Di Pasquale, V. Dompè, X. Fang, A. Giribono, G. Latini, A. Liedl, G. Luminati, L. Piersanti, S. Pioli, B. Serenellini, L. Spallino, A. Vannozzi
INFN - Laboratori Nazionali di Frascati (LNF), Frascati, Italy

Abstract

The TEX (TEst stand for X band) facility at INFN-LNF is a high-power RF test stand dedicated to the qualification of X-band components and accelerating structures for the EuPRAXIA@SPARC_LAB linac and related projects. An upgrade program is underway to extend its capabilities by increasing the available peak and average power, repetition rate and operational flexibility for both X-band (11.994 GHz) and C-band (5.712 GHz) operation. The major intervention includes the installation of two new high-repetition rate RF sources, one X-band and one C-band, together with dedicated waveguide distribution networks and improved diagnostics for breakdown detection, pulse shaping and long-term stability studies. Moreover, the C-band station, with the integration in the bunker of a C-band RF photo-gun developed within the IFAST project, will serve as the first testbed for a full C-band high-brightness photo-injector, enabling experimental validation of compact injector schemes. These enhancements will allow parallel conditioning stations, advanced high-gradient tests of accelerating structures and accelerated validation of RF components under realistic operating conditions for next-generation accelerators. The contribution will describe in detail the upgrade of the TEX facility and its future perspectives.

INTRODUCTION

INFN-LNF has developed a dedicated high-power RF test stand to validate the reliability and performance of the X-band technology in view of the realization of the EuPRAXIA@SPARC_LAB linac [1]. Commissioned in 2022, the TEX (TEst stand for X-band) facility was conceived to reproduce, as closely as possible, the operating conditions of the X-band RF module, enabling systematic testing of accelerating structures and RF components. The infrastructure has been co-funded by the Lazio Region within the LATINO project and is designed to operate as an open user facility for both industry and research institutions.

The availability of a test environment representative of the final accelerator configuration has made it possible not only to assess system performance and reliability, but also to identify critical aspects at both component and subsystem level, including vacuum, controls, safety, diagnostics and LLRF systems. In parallel, the facility has provided a valuable platform for training personnel and consolidating operational expertise in high-power RF systems.

The initial configuration, developed in collaboration with CERN, was based on an X-band 50 MW RF source driven by a solid-state pulsed modulator capable of delivering high-voltage pulses up to 430 kV, with pulse lengths up to 3 µs at repetition rates up to 100 Hz [2, 3]. Following the commissioning phase, an extensive experimental program was carried out, including the testing of several X-band RF components and accelerating structures [4, 5].

Over the past year and a half, a major upgrade program of the facility has been carried out to significantly expand its testing capabilities. The upgrade has been implemented within Spoke 5 of the PNRR Rome Technopole project and focuses on increasing peak and average RF power, extending the repetition rate and improving the overall flexibility of the facility for both X-band and C-band operation. This upgrade is described in detail in the following sections of this paper.

FACILITY UPGRADE

The main upgrade activities, designed to extend the performance and operational flexibility of the facility, can be summarized as follows:

- Installation of an X-band pulse compressor of the Barrel Open Cavity (BOC) type, developed at PSI, on the existing 50 MW RF line. This system enables temporal compression of the RF pulse, increasing the peak power beyond the klystron output level and allowing high-gradient testing of accelerating structures and RF components.
- Integration of a new X-band (11.994 GHz) RF power station based on a Canon E37119 klystron driven by a solid-state modulator, capable of delivering up to 25 MW peak power at repetition rates up to 400 Hz, enabling high average power operation.
- Integration of a C-band (5.712 GHz) RF power station based on a Canon E37217 klystron and solid-state modulator, capable of providing up to 22 MW peak power at repetition rates up to 400 Hz.
- Implementation of two new RF distribution lines (X-band and C-band), including X-band low-loss waveguide systems, directional couplers, high-power loads, and BOC type pulse compressors, to transport RF power into the bunker for both the two new sources.
- Upgrade of a new C-band Low Level Radiofrequency (LLRF) system, based on Libera LLRF and an enhanced Machine Protection System (MPS) for the

* fabio.cardelli@lnf.infn.it

Content from this work may be used under the terms of the CC BY 4.0 licence (© 2026). Any distribution of this work must maintain attribution to the author(s), title of the work, publisher, and DOI.

ISBN: 978-3-95450-252-3 ISSN: 2673-5350 doi: 10.18429/JACoW-IPAC2026-TUP7012

CHARACTERIZATION AND ALIGNMENT OF LINAC MAGNETS FOR ELI-GBS FACILITY*

C. D. Cirdei[1,2], C. Matei[1,2], H. Schubert[1], P. Tracz[1], G. Chen[1], A. Ionescu[1,2], E. Udup[1], C. Bratu[1]
[1]Extreme Light Infrastructure - Nuclear Physics,
Horia Hulubei National Institute for R and D in Physics and Nuclear Engineering, Măgurele, Romania
[2]Faculty of Applied Sciences,
National University of Science and Technology POLITEHNICA Bucharest, Bucharest, Romania

Abstract

This paper presents an overview of the magnet system used in the ELI-GBS linear accelerator (LINAC), including the configuration of quadrupole and dipole magnets, their placement along the accelerator, and the results of magnetic field characterization performed at factory and in laboratory conditions. The alignment methodology used to position the magnetic centers relative to the mechanical axes is also summarized. The results confirm that the Q2041i quadrupoles and D2018i dipoles meet the required field specifications and that the alignment procedures ensure the tolerances necessary for stable beam transport.

INTRODUCTION

The Extreme Light – Gamma Beam System (ELI-GBS) LINAC incorporates 23 quadrupole magnets (Q2041i) and 2 dipole magnets (D2018i), distributed along six accelerating modules [1] and are presented in Fig. 1. Quadrupoles provide transverse focusing and beam steering through main and trimming coils, while dipoles deflect the beam toward diagnostic lines. All magnets were characterized at factory and in specialized laboratory conditions to verify compliance with the design requirements. This paper summarizes the magnet layout, the main results of magnetic measurements, and the alignment procedures applied to ensure proper beam transport.

MAGNET TYPES AND FUNCTIONS

Quadrupoles are arranged in groups of two to four units. Each quadrupole includes a main focusing coil and a trimming coil for horizontal (H) or vertical (V) steering. The last two quadrupoles in each group are equipped with trimming coils to provide fine steering corrections. Dipoles are installed at the end of modules 2 and 6, providing an 18° deflection toward diagnostic stations.

Main Magnets Characteristics

D2018i Dipole:

- 2 pc, 20 mm gap, 18° bend, $l_{\text{eff}} = 0.524$ m.
- Field: −1.60 T; Coils: 2 × 132 turns.
- $I = 103$ A; $R = 0.364$ Ω.

Q2041i Quadrupole:

- 23 pcs, 20 mm gap, $l_{\text{eff}} = 0.052$ m.
- Gradient: −50 T/m (±0.02 T).
- Coils: 4 focus + 4 trim; Turns: 170 (focus), 15 (trim).
- $I = 13$ A (±12 A trim); $R = 0.939$ Ω (0.105 Ω trim).

Quadrupole and dipole models are shown in Fig. 1.

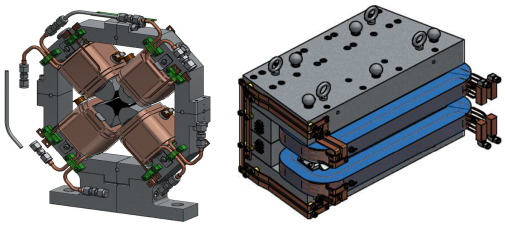

Figure 1: Views of the LINAC quadrupole and dipole.

MAGNET LAYOUT

The magnet layout follows the design of the ELI-GBS LINAC shown in Fig. 2. Quadrupoles alternate between focusing (QF) and defocusing (QD) configurations, while trimming coils provide local steering corrections. The dipoles provide an 18° deflection toward diagnostic lines. Electrical polarity determines whether a quadrupole acts as QF or QD. Trim coils are wired so that:

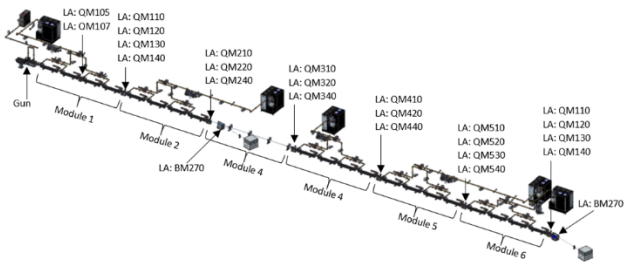

Figure 2: Placement of magnets along the ELI-GBS LINAC.

- Positive current → $+x$ steering (horizontal corrector).
- Positive current → $+y$ steering (vertical corrector).

This ensures consistent steering behavior across all modules.

* This work is carried out under the contract PN 23 21 01 06 sponsored by the Romanian Ministry of Research, Innovation and Digitalization.

Content from this work may be used under the terms of the CC BY 4.0 licence (© 2026). Any distribution of this work must maintain attribution to the author(s), title of the work, publisher, and DOI.

ISBN: 978-3-95450-252-3 ISSN: 2673-5350 doi: 10.18429/JACoW-IPAC2026-TUP7302

THEORY OF CAVITY TUNING WITH PERPENDICULAR BIASED FERRITE

S. Koscielniak*, TRIUMF, Vancouver, BC, Canada

Abstract

Yttrium-Iron-Garnet (YIG) ferrites have one-to-two orders of magnitude smaller magnetic permeability than Ni-Zn ferrites. In the frequency range above 10 MHz, Ni-Zn ferrites are too lossy to be useful. However in the frequency range roughly 30-120 MHz, YIG has high magnetic (and electrical) quality factor. Further, ferrites perpendicular-biased near saturation, have large incremental permeability due to the ferro-magnetic resonance (FMR). These properties presented an opportunity for effective wide-range RF cavity tuning, with low losses. Although high-Q narrow-range tuning was achieved, the promise of both wide tuning range and high Q was not achieved (despite more than a decade of development).This has never been explained, even prompting Shapiro to suggest the magnetic Q (material property) varies quickly with frequency. Here we present a simple theory of cavity tuning with perpendicular biased ferrite (and FMR) that predicts tuning range and effective quality factor; and explains why the high Q cannot be maintained across a large range, and instead Q falls at low frequency.

INTRODUCTION

The quasi-DC, large amplitude magnetic bias H-field sweeps out a *major loop* hysteresis curve. The radio frequency, small amplitude RF H-field sweeps out a *minor loop* starting from a location on the major loop. The RF incremental permeability $\mu_\Delta = \Delta B/(\mu_0 \Delta H)$ differs greatly from the DC value μ. μ_Δ has many dependencies: location on the B-H curve, frequency of the RF wave, polarization, temperature, etc, and has to be measured for every point on the main B-H curve.

The cavity drive frequency must be perfectly matched to an integer multiple of the charged particle revolution frequency around the synchrotron. If the particles accelerate, there will be a program of values drive-frequency versus time called a *frequency law.* The magnetic bias field must track a corresponding program of values. Thus we wish to find the bias field (law) that makes the cavity resonance frequency $\omega_{\rm res}$ and drive frequency equal. Now $\omega_{\rm res}$ is a function of the incremental permeability, which in turn is a function of the resonance frequency and DC bias. This recursive relationship has to be found/solved self-consistently. We shall illustrate by a crude example. Suppose ω_c is the RF cavity resonance frequency without ferrite. If filled with ferrite, the frequency becomes:

$$\omega_{\rm res} = \omega_c/\sqrt{\mu_\Delta[H, B(H), \omega_{\rm res}]} \qquad (1)$$

This is a nonlinear equation that is solved iteratively for bias as a function of frequency, $H(\omega_{\rm res})$.

Symbols

- Let H_z be the applied bias magnetic field, M_z the induced magnetization.
- Let h_y be the applied RF magnetic field, and m_y the induced RF magnetization.
- Let $\rho \equiv M_z/M$ be the ratio of magnetization in the bias direction to the total magnetization M modulus.
- Let $\delta \equiv \alpha\rho$ where α is the LLG relaxation parameter.
- Let $g \equiv \mu_0\gamma_e$ where μ_0 is the permeability of free space and γ_e is the gyromagnetic ratio of the electron.
- We drop the subscript "res": $\omega_{\rm res} \to \omega$.

PERPENDICULAR BIAS

In the particular regime of perpendicular bias, we may appeal to the Landau-Lifshitz-Gilbert (LLG) equation to give the frequency dependence of $\mu_\Delta = 1 + \Re[m_y/h_y]$. The LLG equation and the form of the effective field $H_{\rm eff}$ used here assumes that the material is near saturation (M almost independent of H) and that the static values H_z and M_z are mutually self-consistent.

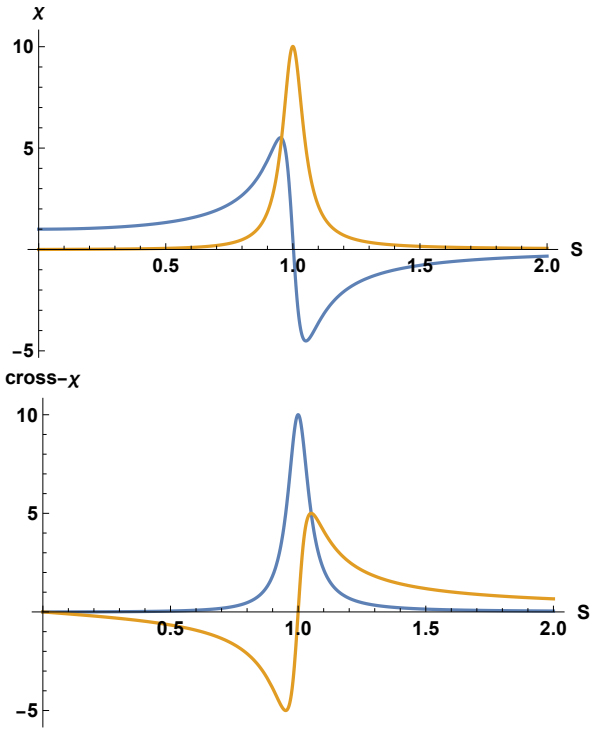

Figure 1: Complex susceptibility components of m_y (left graph) and m_x (right graph). $\delta = 0.05$ The in-phase (real) component χ' shown blue; the quadrature (imaginary, lossy) component χ'' shown gold. The bias field is fixed, as is the scale parameter between angular frequency ω and S.

* shane@triumf.ca

Content from this work may be used under the terms of the CC BY 4.0 licence (© 2026). Any distribution of this work must maintain attribution to the author(s), title of the work, publisher, and DOI.

ISBN: 978-3-95450-252-3 ISSN: 2673-5350 doi: 10.18429/JACoW-IPAC2026-TUP7304

NONLINEAR SOLUTION OF THE LANDAU-LIFSCHITZ-GILBERT EQUATION

S. Koscielniak*, TRIUMF, Vancouver, Canada

Abstract

Ferrites may be used to shrink cavity resonator size. If a variable magnetic bias field is applied, the resonance frequency may be varied to follow proton/ion revolution frequency. The RF magnetic field can be applied either parallel or perpendicular to the bias. If the ferrite is near saturation, the incremental permeability is dominated by the electron spins - which are described by the Landau-Lifschitz-Gilbert (LLG) equation. Here (for the first time) the LLG equation is solved analytically in the strong nonlinear regime to give dependence of permeability on RF amplitude. For RF parallel to bias, a constant magnetization emerges. For RF perpendicular to bias, the resonance frequency rises with amplitude leading to the hardening oscillator "jump" instability.

SPIN-MAGNETIZATION EQUATION

The Landau-Lifshitz [1] and Gilbert [2] versions of the spin relaxation equation of motion are mathematically equivalent, although they differ in the interpretation of the relaxation parameter α. $\mathbf{H}$ will be the effective magnetic field, and $\mathbf{M}$ the magnetization. We write the time derivative $d\mathbf{M}/dt \equiv \dot{\mathbf{M}}$. Here $g \equiv \mu_0 \gamma_e$. The LLG equation is:

$$\dot{\mathbf{M}} = g\mathbf{H} \times \mathbf{M} + g\frac{\alpha}{M}\,\mathbf{M} \times (\mathbf{H} \times \mathbf{M}). \qquad (1)$$

The LLG equation admits steady-state solutions, but does not generate them. For the steady-state, we must apply the equations of magneto-statics. We assume the bias field is sufficiently strong to align all the magnetic domains into a single domain; so the material is near/at saturation. Because of the demagnetizing field, both the DC and RF fields inside the material differ from the outside applied values. We denote static values by upper case letters, and dynamic values by lower case.

The demagnetizing field is $\mathbf{H}_d = \bar{\mathbf{N}}\mathbf{M}$ with magnetization $\mathbf{M}$ and tensor $\bar{\mathbf{N}}$. However, $\mathbf{M}$ depends on the prior history of the external applied $\mathbf{H}_2$ which penetrates into the interior. The DC internal field is $\mathbf{H} = \mathbf{H}_2 + \mathbf{H}_d = \mathbf{H}_2 - \bar{\mathbf{N}}\mathbf{M}$.

In order to find the dynamics, we add an AC/RF term $\mathbf{h}_2$ to the external H-field. This will apply an alternating torque to the spins, causing them to precess. Summing over all the spins leads to a gyrating magnetic moment $\mathbf{m}$. The AC internal field is $\mathbf{h} = \mathbf{h}_2 - \bar{\mathbf{n}}\mathbf{m}$, where $\bar{\mathbf{n}}$ is the AC/RF demagnetization tensor. Hence, with respect to the LLG equation, we make the substitutions:

$$\mathbf{M} \to \mathbf{M} + \mathbf{m} \quad \text{and} \quad \mathbf{H} \to (\mathbf{H}_2 - \bar{\mathbf{N}}\mathbf{M}) + (\mathbf{h}_2 - \bar{\mathbf{n}}\mathbf{m})\ . \qquad (2)$$

The resulting equation contains a large number of terms; and nonlinearity up to cubic terms. This complexity is dealt with by taking single-component forms for $\mathbf{H}_2$ and $\mathbf{h}_2$; and assuming that the coordinate axes are taken parallel with the symmetry axes of the magnetized object, in which case, the matrices $\bar{\mathbf{N}}$ and $\bar{\mathbf{n}}$ take diagonal form. Thus we take a Cartesian system and the DC bias aligned with the z-axis such that $\mathbf{H}_2 = [0, 0, H_z]$. We assume the bias field is strong, so the magnetic material is near saturation with domains aligned. The static magnetization is $\mathbf{M} = [0, 0, M_z]$. For brevity, we define $\tilde{\mathbf{H}} \equiv \mathbf{H}_2 - \bar{\mathbf{N}}\mathbf{M} - \bar{\mathbf{n}}\mathbf{m}$.

RF PARALLEL TO BIAS

We consider the case that an external RF magnetic field is applied parallel to an external DC magnetic bias field. The angular frequency of the RF field is ω. $\mathbf{h} = [0, 0, h_z \cos(\omega t)]$ and $\mathbf{m} = [m_x(t), m_y(t), m_z(t)]$. The combination $g \times H$ has the dimensions of angular frequency.

A simplification is needed to make the system of equations tractable. We take the case of a sphere or cube with equal demagnetizing factors $N_1 = N_2 = N_3$ and $n_1 = n_2 = n_3$. However, we admit the possibility that AC and DC factors are not identical; and that $n_1 \neq N_3$. $\mathbf{H}$ and $\mathbf{M}$ are substituted in the Landau Eq. (1), leading to equations of motion for the three components of magnetization:

$$\begin{aligned}
\dot{m}_x &= -g(\tilde{H}_z + h_z \cos\omega t)[Mm_y + \alpha m_x(M_z + m_z)]/M \\
\dot{m}_y &= +g(\tilde{H}_z + h_z \cos\omega t)[Mm_x - \alpha m_y(M_z + m_z)]/M \\
\dot{m}_z &= +g\alpha(\tilde{H}_z + h_z \cos\omega t)(m_x^2 + m_y^2)/M. \qquad (3)
\end{aligned}$$

We make the definitions $(\omega/g)R \equiv \tilde{H}_z$ and $(\omega/g)r \equiv h_z$; and $s = \omega t$ and $m' \equiv dm/ds$. When $R = 1$, the drive frequency becomes $\omega = gH_z$ which can be considered the resonance frequency. The ratio $r/R = h_z/\tilde{H}_z$. This is the most economical notation; but if we wish to keep the fields H_z, h_z fixed while the drive frequency is varied, then R and r must be updated.

The magnitude of the magnetization is preserved by the LLG equations, and so we may replace $(m_y^2 + m_x^2)$ by $M^2 - m_z^2$ in the equation for $\dot{m}_z$. Equation (3) is solved for the time-varying magnetizations:

$$\begin{aligned}
m_x(s) &= \operatorname{sech}[Mc_1 + \alpha\chi][c_2 \cos\chi - c_3 \sin\chi] \\
m_y(s) &= \operatorname{sech}[Mc_1 + \alpha\chi)][c_3 \cos\chi + c_2 \sin\chi] \\
m_z(s) &= M \tanh[Mc_1 + \alpha\chi] - M_z. \qquad (4)
\end{aligned}$$

Here $\chi(s) = Rs + r \sin s$. The constant of integration c_1 is chosen to yield the initial value of m_z. Thus $\tanh(Mc_1) = m_z(0)/M$. At large times $m_z \to (M - M_z)$ and $m_x, m_y \to 0$. The reader may recognize that $\cos(r \sin s)$ and $\sin(r \sin s)$ are representations of the Bessel functions, and may be Fourier analysed into a spectrum with frequency components at multiples of ω (the drive frequency). The form of

* shane@triumf.ca

Content from this work may be used under the terms of the CC BY 4.0 licence (© 2026). Any distribution of this work must maintain attribution to the author(s), title of the work, publisher, and DOI.

ISBN: 978-3-95450-252-3 ISSN: 2673-5350 doi: 10.18429/JACoW-IPAC2026-TUP7305

RF DESIGN AND COMMISSIONING OF A NOVEL MULTI-HARMONIC BUNCHER FOR THE TRIUMF 500 MeV CYCLOTRON

V. Zvyagintsev†, T. Au, Y. Bylinskii, X. Fu, J. Keir, O. Law, R. Laxdal, M. Marchetto, K. Piletskiy, S. Saminathan, TRIUMF, Vancouver, Canada

Abstract

The horizontal injection section of the TRIUMF 500 MeV cyclotron has been replaced after 50 years of operation and the historic buncher configuration which consists of two separated double-gap bunchers for the 1st and 2nd harmonics of the cyclotron RF frequency of 23.06 MHz were successfully replaced with a multi-harmonic buncher operating on three harmonics. The novel multi-harmonic buncher structure has two electrodes and three gaps: one electrode driven with 1st and 3rd harmonics and the second electrode – with the 2nd harmonic. It is a combination of two double-gap structures having one common gap inside the cavity. The device is now installed and operational. The RF design, fabrication and commissioning results are presented and discussed in the article.

INTRODUCTION

The new horizontal injection section design for the TRIUMF 520 MeV cyclotron necessitated the development of a three-harmonic buncher. A new concept of the three-harmonic buncher was developed and studied with respect to beam dynamics [1]. Finally, the new three-harmonic buncher has been installed and successfully commissioned [2].

NOVEL THREE-HARMONIC BUNCHER

Concept

Originally, we considered for the design a well-known multi-harmonic single gap buncher with two drift tubes driven with coaxial RF resonators [3]. However, to suppress the effect of parasitic tails outside the drift tubes, a one-gap structure required more longitudinal space than was available in the new injection section design. On the other hand, a one-gap structure also required relatively high RF voltage due to its low TTF (transit time factor). Another approach is to employ two double-gap structures, as was implemented for the PIAVE project at LNL INFN [4]. This is very efficient due to the high TTF but is not compact enough longitudinally.

To reduce the longitudinal footprint, we decided to use a combination of two double-gap structures sharing one common gap, as shown in Fig. 1. There are two drift tubes and three gaps. The first drift tube has a gap-to-gap distance of $\beta\lambda/2$ for the 1st harmonic and $3\beta\lambda/2$ for the 3rd harmonic. It must be driven with a 2nd-harmonic resonator, which can be represented as a QWR (quarter-wave resonator) for the 1st harmonic and 3QWR/2 for 3rd harmonic. The second drift tube has a gap-to-gap distance of $\beta\lambda/2$ for the 2nd harmonic and is driven with a QWR for the 2nd harmonic.

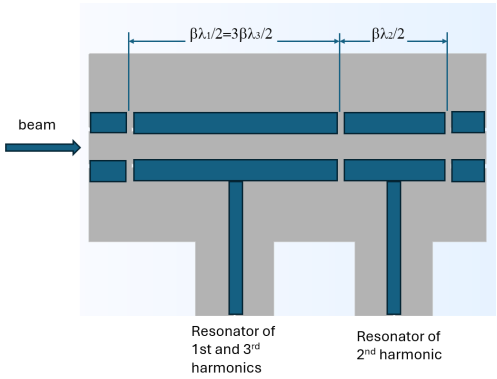

Figure 1: Novel multi-harmonic buncher RF structure concept.

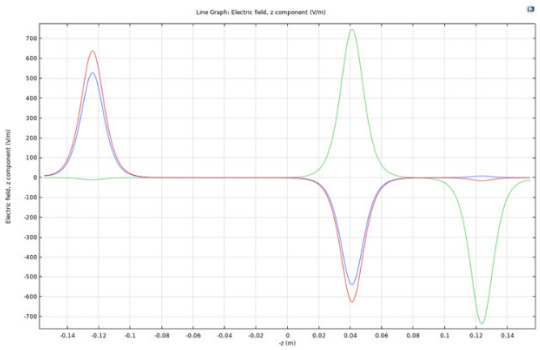

Figure 2: Distribution of longitudinal component of electric field along the structure for three harmonics (1st – red, 2nd – green, 3rd – blue).

Figure 2 shows the distribution of the longitudinal component of the electric field along the structure for three harmonics (1st – red, 2nd – green, 3rd – blue). This distribution shows the relative values from COMSOL RF module [5] solutions (computed independently for each harmonic) for the RF structure, and is used for beam dynamics simulations [1] to determine the required RF amplitudes to be applied to the drift tubes; TTF and R_{sh}/Q_o presented on Table 1. The buncher structure has quite high TTF (efficiency) and moderate required RF amplitudes Vo.

RF Design

The buncher RF structure consists of a chamber with drift tubes separated with RF feedthroughs and outside resonators with couplers, pickups, and tuning elements (Fig. 3). Initially, we considered spiral (coil) resonators but opted for coaxial lines (3-1/8") due to the complexity of the

†zvyagint@triumf.ca

Content from this work may be used under the terms of the CC BY 4.0 licence (© 2026). Any distribution of this work must maintain attribution to the author(s), title of the work, publisher, and DOI.

ISBN: 978-3-95450-252-3 ISSN: 2673-5350 doi: 10.18429/JACoW-IPAC2026-TUP7307

NORMAL CONDUCTING RF CAVITIES FOR ELECTRON ION COLLIDER HADRON STORAGE RING*

B. Xiao†[1], P. Berrutti[1], Z. Conway[2], M. Esposito[1], X. Gu[1], J. Guo[2], L. Guo[1], D. Holmes[1], V. Kaye[1]
G. Li[1], D. Lukach[1], P-D Malendele[1], L. Panjoj[1], E. Polanco[1], R. Rimmer[2], F. Severino[1]
K. S. Smith[1], B. Vassallo[1], S. Verdú-Andrés[1], S. Wang[2], Q. Wu[1], W. Xu[1], A. Zaltsman[1]
[1]Brookhaven National Laboratory, Upton, New York, USA
[2]Thomas Jefferson National Accelerator Facility, Newport News, VA, USA

Abstract

The Normal-Conducting Radiofrequency (NCRF) systems for the Electron-Ion Collider Hadron Storage Ring (EIC HSR) comprise four unique cavity systems. These systems include a 24.6 MHz capture and acceleration system, a combined 49.2 MHz and 98.4 MHz bunch splitting system, and a 197 MHz storage system for collider operations. All systems have successfully passed their final design reviews, and the detailed drawings are currently being completed for procurement. This paper reports on the recent progress achieved across these NCRF cavity systems.

INTRODUCTION

The Relativistic Heavy Ion Collider (RHIC) operating at Brookhaven National Lab (BNL) is comprised of 2 ion rings (referred to as blue that circulate clockwise, and yellow counterclockwise). Split evenly between the 2 rings there are four 28 MHz Quarter Wave Resonator (QWR) NCRF cavities to accelerate and capture the beam, and ten 197 MHz NCRF cavities to store the beam [1-4]. The EIC will reuse the modified 28 MHz system for the HSR 24.6 MHz. The 49.2 MHz and 98.4 MHz QWR for bunch splitting will be new QWR cavities. The HSR 197 MHz storage NCRF system will reuse the RHIC 197 MHz cavities and will operate with a superconducting RF (SRF) 591 MHz system to both store the ion beam and provide bunch compression [5-7].

Converting RHIC to the EIC HSR is nontrivial. The EIC HSR will have 3 times greater stored beam current, shorter bunch length (6 cm RMS, relative to RHIC's 60 cm), and more bunches (290 or 1160, relative to RHIC's 110). The EIC HSR has the same challenging requirements for energy ramp and transition crossing of heavy ions. The designs of the EIC HSR NCRF systems are significantly more challenging than those present in RHIC operations today. There are more RF systems in EIC HSR, two new systems with two modified systems from RHIC. It needs to deal with higher beam induced fundamental mode damper (FMD) and higher order mode (HOM) power, as well as broader fast tuning range and higher beam loading. It has tighter HOM impedance threshold. Combining all these together, the Multiphysics of these designs will be challenging. In this paper we show the design of the EIC HSR NCRF systems and our solutions for the challenges of the EIC HSR.

REQUIREMENTS

The typical RHIC collision store bunch pattern is currently 111 bunches in an h=120 bunch pattern. Bunches at store are compressed longitudinally to approximately a 1 ns (30 cm) RMS bunch length, using a non-adiabatic "rebucket" gymnastic [8]. For the EIC, 290 bunches in an h=315 bunch pattern will be injected, captured and accelerated using the upgraded 24.6 MHz NCRF cavity system. Several store scenarios are planned, involving 290 (h=315), 580 (h=630) or 1160 (h=1260) bunches. The 580 and 1160 bunch patterns will be produced via adiabatic bunch splitting using the new 49.2 MHz and 98.4 MHz NCRF QWR bunch splitting cavity systems, and the bunches will then be adiabatically compressed to their store length at 6 cm RMS using the upgraded 197 MHz NCRF cavity system, together with the new 591 MHz SRF cavity system that is not covered in this paper.

To deal with higher current and thus higher beam loading, and to regulate the voltage fluctuation, all QWRs are designed with relative low R/Q (circuit definition is used throughout the paper) and loaded Q Q_L. RHIC 28 MHz cavity has an R/Q of 67.6 Ω, the EIC 24.6 MHz cavity is designed to have a lower R/Q at 41.7 Ω, while for the new 49.2 and 98.4 MHz cavities, the R/Q are 26.3 and 21.0 Ω, respectively. The FPCs of the QWRs are set to have β at around 2 to lower the Q_L.

During energy ramp, the 49.2, 98.4 and 197 MHz RF cavities will be kept at zero voltage and should be transparent to the accelerating and transition crossing beam. FMDs will be used to lower the fundamental shunt impedance during ramp, and the FMD of each cavity will be extracted out of the cavity when voltage needs to be built up. The 24.6 MHz RF system is used to accelerate and capture the beam during energy ramp or during transition crossing of heavy ions, so needs fast tuners, while it does not need an FMD.

All these cavities need mechanical tuners. Each cavity needs a minimum of 78 kHz tuning range to cover +/- half of the revolution frequency. For 24.6 MHz cavities, an additional 120 kHz tuning range is needed to cover the frequency shift due to energy ramp, thus a total 200 kHz (- 160 to +40 kHz) tuning range. For 49.2 MHz cavities, it is needed for pre cooler for bunch lengthening, cavity voltage starts to ramp up right after transition crossing, an

* Work supported by Brookhaven Science Associates, LLC under Contract No. DE-SC0012704 with the U.S. Department of Energy.
† binping@bnl.gov

Content from this work may be used under the terms of the CC BY 4.0 licence (© 2026). Any distribution of this work must maintain attribution to the author(s), title of the work, publisher, and DOI.

ISBN: 978-3-95450-252-3 ISSN: 2673-5350 doi: 10.18429/JACoW-IPAC2026-TUP7309

CONVERSION OF 28 MHZ CAVITIES TO 24.6 MHZ CAVITIES FOR THE EIC HADRON STORAGE RING

Guangjiang Li†, John Butler, Helena Belzer, Marco Esposito, Lin Guo, Douglas Holmes, Prince-David Malendele, Luis Panjoj, Silvia Verdú-Andrés, Binping Xiao, Alexander Zaltsman
Brookhaven National Laboratory, Upton, United States

Abstract

The Hadron Storage Ring of the Electron-Ion Collider (EIC) will require 600 kV of 24.6 MHz RF voltage for capture and acceleration. Four 28 MHz normal-conducting Quarter Wave Resonator (QWR) cavities from the Relativistic Heavy Ion Collider (RHIC) will be modified for this purpose. We present the main requirements for the EIC HSR 24.6 MHz cavities, along with the RF design and multiphysics validation. The design is mature and meets all the requirements.

INTRODUCTION

The EIC Project plans to start operation in 2034 [1][2]. The normal conducting RF (NCRF) systems for the EIC hadron storage ring (HSR) consist of 4 types of unique cavity resonators: a 24.6 MHz capture and acceleration, a combined 49.2 MHz and 98.4 MHz bunch splitting system [3], and a 197 MHz storage system. Four 28 MHz cavities, two installed in the yellow ring and two in the blue ring, have operated in Relativistic Hadron Ion Collider (RHIC) for more than twenty years [4]. The RHIC 28 MHz cavities are quarter-wave resonators made of ASTM A36 carbon steel with a copper-plated finish. To reduce cost, we will reuse their large outer conductor, vacuum pump, fundamental power coupler (FPC) for the EIC HSR 24.6 MHz system. We designed new long inner conductors, short inner conductor, short outer conductor, h-HOM dampers, e-HOM dampers, mechanical tuners and increased the number of ferrite fast tuners to four. Standard 25 Ohm HOM windows are used across the 98, 49, and 24.6 MHz cavity systems to minimize the design effort and cost.

DESIGN AND SIMULAITOINS

The 24.6 MHz cavities are designed to provide an accelerating voltage of 150 kV per cavity (Fig. 1). The system requires 60-kW input power from a tetrode power amplifier. The new EIC 24.6 MHz cavity parameters are summarized in Table 1 with a comparison with the RHIC 28 MHz cavity. The total RF longitudinal impedance (circuit definition) of the 24.6 MHz NCRF cavity system shall not exceed 90 kΩ·GHz. The total RF transverse impedance (horizontal and vertical, circuit definition) of the 24.6 MHz NCRF cavity system shall not exceed 2.5 MΩ/m. The cavity geometry and the HOM damper design are optimized via electromagnetic simulation in CST Studio to meet the beamline impedance thresholds [5].

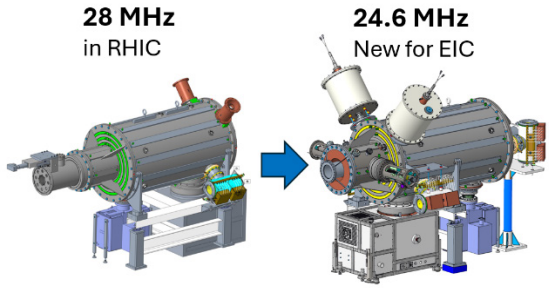

Figure 1: Conversion from RHIC 28 MHz cavity system to new EIC 24.6 MHz cavity system.

Table 1: Cavity Parameters Comparison

Cavity Parameters	28 MHz in RHIC	24.6 MHz for EIC
Frequency (MHz)	28.175	24.631
V_{acc} per cavity (kV)	300	150
E_{peak} (MV/m)	15	5.3
H_{peak} (A/m)	8e3	6e3
Q	15400	14000
R/Q cir. [Ω]	64.3	42

Tuning

The nominal frequency of 24.631 MHz corresponds to harmonic number 315 of the 78 kHz revolution frequency of the storage ring. The cavity shall provide a tuning range sufficient to cover at least one revolution frequency (−40 kHz to +40 kHz relative to 24.631 MHz). To accommodate different species energy ramping, an additional 120 kHz tuning margin shall be included, resulting in minimum required a total tuning range of 200 kHz (−160 kHz to +40 kHz relative to 24.631 MHz).

Two mechanical tuners are symmetrically mounted on the short outer conductor of the cavity, with their locations optimized to satisfy impedance requirements. The tuner mechanical design is shared with the 49 MHz and 98 MHz cavity systems [3]. The cavity has a nominal frequency of 24.631 MHz and provides a tuning range from −202 kHz to +58 kHz for the tuner insertion from 0 to −2 inches, as shown in Figure 2. A negative insertion value indicates that

*Work supported by Brookhaven Science Associates, LLC under Contract No. DE-SC0012704 with the U.S. DOE.
† Email: gli3@bnl.gov

Content from this work may be used under the terms of the CC BY 4.0 licence (© 2026). Any distribution of this work must maintain attribution to the author(s), title of the work, publisher, and DOI.

ISBN: 978-3-95450-252-3 ISSN: 2673-5350 doi: 10.18429/JACoW-IPAC2026-TUP7310

RF DESIGN OF THE 49 AND 98 MHZ NORMAL-CONDUCTING CAVITIES FOR BUNCH SPLITTING IN THE EIC HSR*

L. Guo†, B. Xiao, D. Holmes, M. Esposito, B. Vassallo, E. Polanco, P. Malendele, E. Link, S. Verdú-Andrés, Brookhaven National Laboratory, Upton, NY, USA

Abstract

Two normal-conducting RF cavities at 49 MHz and 98 MHz have been developed for the bunch-splitting system in the Hadron Storage Ring of the Electron-Ion Collider. Both cavities use compact quarter-wave-resonator structures to satisfy RF, mechanical, and tunnel-integration constraints. Key components, including the fundamental power coupler (FPC), fundamental mode damper (FMD), higher-order-mode (HOM) dampers, mechanical tuners, and pickup couplers, were optimized to meet all design performance requirements. HOM impedances and powers satisfy their limits across the full tuning range. Frequency shifts due to mechanical tolerances can be compensated by trim tuning to adjust the cavity gap. Multipacting studies were carried out using SPARK3D. The designs of both cavities fulfill the performance and interface requirements and are ready to proceed to the procurement phase.

INTRODUCTION

The Electron–Ion Collider (EIC) [1, 2] is being constructed on the existing Relativistic Heavy Ion Collider (RHIC) complex to provide high-luminosity collisions between polarized electron and hadron beams. The Hadron Storage Ring (HSR) will reuse the upgraded RHIC Yellow ring, and requires substantially higher beam current, shorter bunch length, and a much larger number of bunches than RHIC operation.

The HSR RF system [2, 3] combines refurbished RHIC cavities with newly developed RF systems for beam capture, acceleration, bunch splitting, and bunch compression. The bunch-splitting process is performed in two stages: three 49 MHz normal-conducting RF (NCRF) cavities provide 500 kV total voltage to split 290 bunches into 580, followed by four 98 MHz NCRF cavities providing 600 kV total voltage to further split the beam into 1160 bunches.

The 49 MHz and 98 MHz cavities are designed as quarter-wave resonators (QWR), following the general concept of the existing RHIC 28 MHz cavities [4]. To reduce technical risk and simplify fabrication, installation, and operation, common or similar solutions are adopted for key RF components wherever practical. Compared with RHIC operation, the EIC HSR beam conditions impose more stringent higher-order-mode (HOM) damping requirements [3]. This paper summarizes the cavity design requirements, cavity and key component RF designs, HOM impedance results, fabrication-error compensation, and multipacting studies for the two cavities. The main RF design requirements for the cavity systems are summarized in Table 1. All impedance values and R/Q in this paper are given in the circuit definition.

Table 1: RF design requirements for the 49 and 98 MHz cavity systems. E-HOM/H-HOM denote electrical/magnetical coupled HOM dampers.

Parameter	49 MHz	98 MHz
Number of cavities	3	4
Nominal frequency (MHz)	49.263	98.525
Total RF voltage (kV)	500	600
Voltage per cavity (kV)	167	150
Manufactured Q_0	≥ 10000	≥ 7650
FPC Q_{ext}	(4.6±0.2)e3	(3.9±0.2)e3
FPC window rating (kW)	120	120
Pickup Q_{ext}	(5.3±1.0)e7	(5.4±1.0)e7
Tuner range (kHz)	-280→+40	-120→+120
FMD Q_{ext} fully inserted	≤ 250	≤ 150
Min FMD power handling (kW)	5	5
H-HOM damper power (kW)	≤ 5 each	
E-HOM damper power (kW)	≤ 0.5 each	
Fund. leakage from damper (kW)	≤ 0.2 each	
Longitudinal impedance	≤ 90 kΩ · GHz	
Transverse impedance	≤ 2.5 MΩ/m	

CAVITY AND COMPONENT RF DESIGN

Figure 1 (a) and (b) show the two cavities and their ancillaries, including the fundamental power coupler (FPC), quarter-wave stub (QWS) necessary to enable FPC water cooling and DC biasing, fundamental mode damper (FMD), two H-HOM dampers, two E-HOM dampers, two pickup couplers, two mechanical tuners, and a vacuum port for each cavity. The components use the same design concepts with dimensions adjusted for the different cavity frequencies and geometries. Port orientations accommodate the tunnel layout and maintain sufficient clearance for installation and maintenance.

CST Studio Suite was used for the electromagnetic simulations. The main simulated RF parameters are summarized in Table 2. The higher operating frequency of the 98 MHz cavity leads to a more compact geometry and a reduced beam-pipe diameter, half of the other NCRF cavities in HSR. The long inner conductor of the 98 MHz cavity is flared in the high magnetic field region to reduce the local RF power density, unlike the straight conductor in the 49 MHz design, as shown in Fig. 1 (c). Port blending radii were optimized to reduce peak fields, with the resulting maxima located on the nose of the long inner conductor for the electric field and on the H-HOM damper loop for the magnetic field.

* Work supported by Brookhaven Science Associates, LLC under U.S. DOE contract No. DE-SC0012704.

† lguo1@bnl.gov

Content from this work may be used under the terms of the CC BY 4.0 licence (© 2026). Any distribution of this work must maintain attribution to the author(s), title of the work, publisher, and DOI.

ISBN: 978-3-95450-252-3 ISSN: 2673-5350 doi: 10.18429/JACoW-IPAC2026-TUP7312

PROGRESS TOWARDS RF CONDITIONING OF LOW-LOSS COUPLERS FOR A CONDUCTION-COOLED CRYOMODULE*

N. Stilin†, G. Ciovati, J. Gubeli, K. Jordan, J. Vennekate, H. Wang, C. Wilson
Thomas Jefferson National Accelerator Facility, Newport News, United States

Abstract

This work presents current progress on the conditioning of two new 25 kW couplers optimized for use in a compact, conduction-cooled SRF cryomodule. A connecting waveguide, previously used for conditioning the 805 MHz SNS couplers, was altered for use at 915 MHz. The necessary modifications were determined via RF modeling, while thermal analysis results identified additional cooling requirements during RF conditioning and provided insight about potential higher-power operation. Initial low-power conditioning will be performed with a 2.5 kW solid-state amplifier, with plans to use an industrial magnetron for RF conditioning at 25 kW in the near future.

INTRODUCTION

Studies by the U.S. DOE and national labs have found many critical applications which could be served by small-scale accelerators producing beams of a few MeV. These applications exist in a wide range of fields such as medicine, environmental sustainability, food processing, national security and more [1, 2]. Utilizing SRF cavities would offer more efficient handling of high-power beams, translating to increased throughput in many applications. However, the cooling requirements of SRF cavities have historically been cost prohibitive when considering MeV-scale machines.

Fortunately, recent improvements in both the RF performance of Nb_3Sn-coated cavities and the 4 K cooling capacities of multi-stage cryocoolers have made small-scale SRF accelerators feasible, with many new designs proposed for various industrial applications [3 - 5]. One of the designs currently pursued at Jefferson Lab also aims to take advantage of industrial magnetrons as a power source, greatly increasing the power efficiency of the system [6]. As part of this project, new fundamental power couplers (FPCs) were needed which could deliver high power to the SRF cavity while minimizing the heat load at the cold mass. The design and fabrication of these FPCs were completed by our collaborators at RadiaBeam [7]; the FPCs were then delivered to Jefferson Lab for RF conditioning.

COUPLER TEST STAND

A new coupler test stand is based on a setup previously used for the SNS 805 MHz couplers [8]. This design features a test cart with a removable connecting waveguide to which two couplers are mounted for RF conditioning. This section will discuss the primary modifications made for use with the new 915 MHz couplers.

Connecting Waveguide Modification

One of the connecting waveguides used for the conditioning of the SNS PPU 805 MHz couplers was sent to Jefferson Lab, which required modification for 915 MHz operation. The necessary length reduction would have caused machining interference with the various ports on the waveguide. To avoid this, the waveguide length was instead increased while its operational mode was changed from TE102 to TE103. In addition, small ports for IR windows were added to the bottom side of the waveguide, such that an IR camera could monitor the ceramic RF window temperatures during bakeout and RF conditioning. RF simulations of the coupler-waveguide system in traveling wave mode (performed in CST Microwave Studio) were used to optimize the parameters of these modifications; the model is shown in Figure 1. The optimized geometry resulted in an S11 of -40.14 dB at 915 MHz.

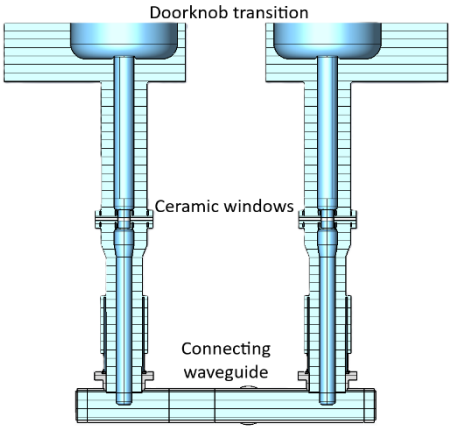

Figure 1: RF model of the couplers and connecting waveguide used in CST simulations.

Thermal Modelling of RF Conditioning

Thermal modelling was also performed in CST using coupled electromagnetic (EM) - thermal simulations. The EM portion used the same setup as the RF simulations described previously, while the thermal portion used a more detailed model to better represent the thermal response. Temperature-dependent thermal conductivities were applied for all materials, including a special material defined to model 316L stainless steel plated with 10 μm of copper. The coupled EM solver provided surface and volume loss densities as the primary heat loads in the system. A fixed temperature of 303 K was applied to represent water cooling where it was already included in the coupler design:

* Work supported by the Accelerator Stewardship and the Accelerate Innovations in Emerging Technologies programs from the U.S. Department of Energy under contract DE-AC05-06OR23177.
† stilin@jlab.org

Content from this work may be used under the terms of the CC BY 4.0 licence (© 2026). Any distribution of this work must maintain attribution to the author(s), title of the work, publisher, and DOI.

ISBN: 978-3-95450-252-3 ISSN: 2673-5350 doi: 10.18429/JACoW-IPAC2026-TUP7313

HIGH GRADIENT TESTING OF A TWO-CELL C-BAND ACCELERATOR CAVITY WITH NICR HIGHER-ORDER MODE ABSORBERS*

E. I. Simakov†, W. B. Haynes, D. Kim, D. Rai, H. Xu
Los Alamos National Laboratory, Los Alamos, NM, USA
M. D. Zuboraj, Air Force Research Laboratory, Albuquerque, NM, USA
Z. Li, E. Nanni, SLAC National Accelerator Laboratory, Menlo Park, CA, USA

Abstract

This paper reports on the status of fabrication, tuning, and high gradient testing of a two-cell accelerator cavity with distributed coupling and higher-order-mode (HOM) damping slots covered with nickel-chromium (NiCr) absorbing material. The cavity is designed with a specific purpose to demonstrate applicability of NiCr material for damping HOMs in a C-band distributed-coupling accelerating structure, such as may be used in a C^3 linear collider. We are performing this simple high-power test to understand fabrication challenges for the cavity with NiCr HOM absorbers and examine behavior of the NiCr coating during high power conditioning. This paper provides details on electromagnetic and engineering design of the cavity, fabrication, cold testing, tuning, and reports the current status of high gradient testing at the CERF-NM C-band high gradient test facility at Los Alamos National Laboratory.

INTRODUCTION

At Los Alamos National Laboratory (LANL), we conduct high gradient C-band accelerator studies for multiple applications. In particular, LANL is a part of collaboration to develop cryo-cooled normal conducting radiofrequency (NCRF) C-band accelerating structures for the future Cool Copper Collider (C^3) and for compact high-repetition rates X-ray free electron lasers (FELs) [1-3].

The achieved luminosity for Higgs production in C^3 as well as the number of photons produced by the FEL source are highly dependent on the quality (low emittance and high brightness) of the electron beam. Among the sources of emittance growth in the long linac are the short and long-range higher-order-mode (HOM) wakefield effects in accelerating structures. Hence, wakefield damping by means of inserting damping materials into the accelerating structure is essential to decrease the quality and kick factors of excited wakefields. The accelerating structure that is proposed for construction of the cryo-cooled linac was designed with distributed-coupling to achieve high shunt impedance and reduce power requirements for high gradient acceleration [4]. Calculations of the long-range wakefields were performed numerically using the CST Studio Wakefield solver and ACE3P suite and was previously published in Ref. [5]. A new HOM damping design with longitudinal damping slots coated with nickel-chromium (NiCr) absorbing material was proposed for its compatibility with the proposed fabrication methods for distributed-coupling structures when the accelerating structure was fabricated in four quadrants which were then brazed together.

In order to test high-gradient performance of the distributed-coupling accelerator structure with a novel HOM damping configuration, LANL designed a simple two-cell standing-wave accelerator cavity for the high-power testing at LANL's C-band Engineering Research Facility in New Mexico (CERF-NM) [6]. This paper describes the design, fabrication, low-power testing, tuning, and the current status of the high-power tests for the two-cell C-band (5.712 GHz) accelerator cavity with NiCr absorbers.

DESIGN OF THE TWO-CELL TEST CAVITY

The CST Microwave Studio model of the two-cell C-band accelerator test cavity is shown in Fig. 1. The input power from a standard WR187 waveguide is divided equally into two cells. The four HOM damping slots were designed to be plated with NiCr and were supposed to be exposed to relatively low electromagnetic fields during the high gradient conditioning process apart from during the breakdown events when electromagnetic power coupled into the cavity would convert into HOMs.

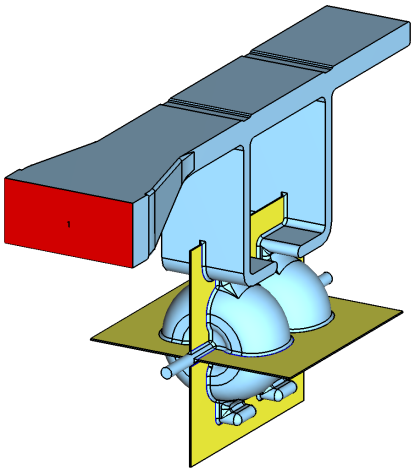

Figure 1: A CST Microwave Studio model for the test cavity with NiCr absorbers: blue color shows the vacuum volume, and yellow color highlights the surfaces of the HOM coupling slots covered with NiCr.

The details of the electromagnetic and engineering designs for the two-cell test cavity are presented in Ref. [7]. The design characteristics of the cavity are summarized in Table 1. During design, a particular attention was paid to minimizing the pulse heating temperature rise due to high surface magnetic fields at the location of the absorbing

* Work supported by the U.S. Department of Energy, under Contract No. 89233218CNA000001 and DE-AC02-76SF00515.
† smirnova@lanl.gov

Content from this work may be used under the terms of the CC BY 4.0 licence (© 2026). Any distribution of this work must maintain attribution to the author(s), title of the work, publisher, and DOI.

ISBN: 978-3-95450-252-3 ISSN: 2673-5350 doi: 10.18429/JACoW-IPAC2026-TUP7314

STATUS OF THE CARIE HIGH GRADIENT PHOTOCATHODE TEST FACILITY AT LANL*

E. I. Simakov†, W. Choi, W. B. Haynes, S. S. Kurennoy, V. Pavlenko, D. Rai, T. Tajima, H. Xu
Los Alamos National Laboratory, Los Alamos, NM, United States

Abstract

This paper reports on the status of assembling and commissioning of the Cathodes And Radio-frequency Interactions in Extremes (CARIE) C-band high gradient photoinjector test facility and the status of high gradient testing of a 1.6 cell C-band RF photoinjector at Los Alamos National Laboratory (LANL). The construction of CARIE began in October of 2022. CARIE will house a high gradient copper RF photoinjector and other high gradient C-band accelerating structures (e.g., multi-cell cryo-cooled accelerating structures). The 50 MW 5.712 GHz Canon klystron powers the facility. The klystron was installed and conditioned in 2023. The output of the klystron is connected to a circulator that was conditioned to operate for up to 12 MW of power. The WR187 waveguide line brings the power from the circulator into a concrete vault that is rated to provide radiation protection for electron beam powers up to 20 kW. The first RF injector that was fabricated is made of copper and does not have cathode plugs. This injector is installed at the end of the waveguide line and is awaiting high gradient conditioning, which will validate operation of the CARIE facility. This paper provides the update on the status of the facility, the designs of the photoinjector and the beamline, and the status of the high-power testing of the injector.

INTRODUCTION

At Los Alamos National Laboratory (LANL), we conduct high gradient C-band accelerator studies motivated by multiple LANL projects and future mission needs. For example, LANL proposed a high gradient C-band upgrade to Los Alamos Neutron Science Center's (LANSCE) proton linac to enable higher energy proton radiography [1, 2]. There is also an identified need for a powerful directional high-repetition-rate narrow-bandwidth complementary X-ray Inverse Compton Scattering (ICS) light source at LANSCE [3]. The accelerator structures delivering beams for these proposed facilities must operate at high accelerating gradients because of the space limitations. For applications such as the LANSCE proton booster linac, testing of longer, multi-cell accelerating structures is also desired [4], which would result in production of energetic dark current that prevents testing these structures in a test stand with limited radiation protection such as LANL's C-band Engineering Research Facility in New Mexico (CERF-NM) [5].

The construction of Cathodes And Radio-frequency Interactions in Extremes (CARIE) [5, 6] test facility started in October of 2022. We prepared a new radiation protection vault rated for electron beam energy up to 20 MeV and electron beam power up to 20 kW. We procured and commissioned a new C-band klystron from Scandinova, designed, installed, and conditioned the waveguide line that includes a high-power circulator and brings the RF power from the klystron into the vault, and designed and installed the all-copper RF photoinjector structure at the end of the waveguide line. The photoinjector that is currently installed at the end of the line has a non-removable copper photocathode. Commissioning the photoinjector to its full operational parameters will verify the operational functionality of the constructed CARIE facility for testing of the high gradient structures. This paper describes the current status of CARIE and photoinjector commissioning work.

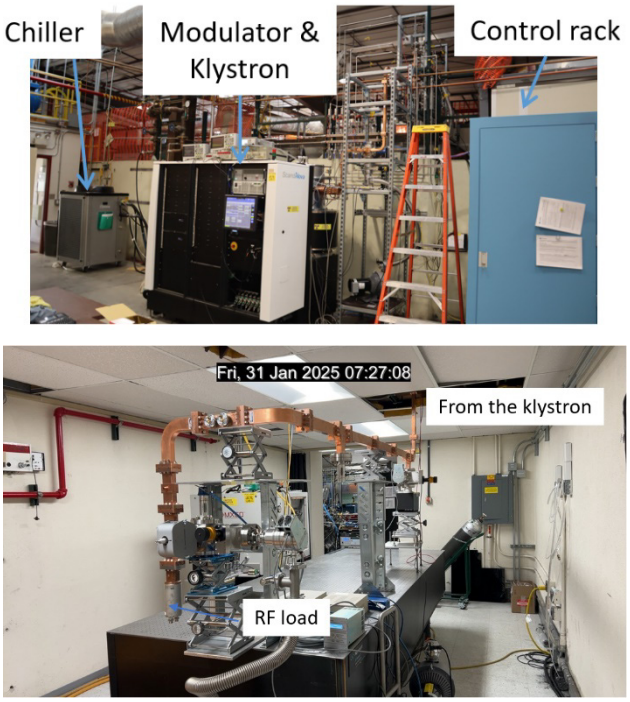

Figure 1: A photograph of the CARIE klystron (top); a photograph of the waveguide line inside of the CARIE vault before installation of the RF photoinjector (bottom).

STATUS OF THE INSTALLATION AND COMISSIONING OF THE WAVEGUIDE LINE

The RF power to the CARIE facility is provided by the 50 MW C-band klystron received from Scandinova Systems and installed in 2023 [Fig. 1 (top)] [7]. The klystron was fully conditioned to the peak output power of approximately 30 MW with 30 Hz repetition rate limited by the

* This work was supported by Los Alamos National Laboratory's Laboratory Directed Research and Development (LDRD) Program.
† smirnova@lanl.gov

Content from this work may be used under the terms of the CC BY 4.0 licence (© 2026). Any distribution of this work must maintain attribution to the author(s), title of the work, publisher, and DOI.

ISBN: 978-3-95450-252-3 ISSN: 2673-5350 doi: 10.18429/JACoW-IPAC2026-TUP7315

PROGRESS ON UPGRADES TO CCL RESONANCE CONTROL AT LANSCE

W. Hall†, M. Rodriguez, J. Valladares, J. Vega, Los Alamos National Laboratory, Los Alamos, United States

Abstract

The resonance control system for the cavity-coupled linear accelerator (CCL) portion of the Los Alamos Neutron Science Center (LANSCE) has been a consistent source of operational downtime. The present system has been used since installation with only minor upgrades, so a system is being developed to replace it with modern components to reduce maintenance and downtime. The present control algorithm maintains water temperature at a set point based on the average RF power, and other parameters that are direct indications of resonance such as the cavity field phase or its ratio to forward power should be implemented to improve issues inherent to the present control system. These relevant data have been collected for several RF modules and analyzed. Additionally, the control of the valve used to maintain water temperature is antiquated, and a commercially available off-the-shelf stepper motor driver is required as other parts are upgraded. A prototype of a new system is discussed.

INTRODUCTION

The Los Alamos Neutron Science Center (LANSCE) accelerates H^+ and H^- through a drift tube linear accelerator (DTL) to 100 MeV, and the H^- beam continues acceleration up to 800 Mev through 44 cavity coupled linear accelerator (CCL) modules. This facility has delivered beam at this energy since 1972, and many systems have undergone few changes in the subsequent decades. One such system in the resonance control used for the CCL.

The CCL operates at a frequency of 805 MHz with a peak power between 500 and 1200 kW, and with a pulse repetition rate of 120 Hz and a pulse width of about 1ms, there is about 50 to 140 kW average power that must be dissipated in the cooling system. The cooling system is also the method for maintaining resonance at 805 MHz and consists of a tank that mixes the water in the cooling loop with a variable amount of chilled water. The flow of chilled water that is input into the mix tank is varied by a stepper motor-controlled valve, and the electronic control is automated based upon average RF measurements. A schematic of the system is shown in Fig. 1.

The control method of the water temperature has several flaws that have resulted in beam downtime and extensive labor throughout the life of the CCL. The control system has four temperatures readings of the inlet and outlet going in two directions across the length of the CCL module, and the average of these readings is maintained at a temperature that is set by the measurement of average RF. The proper operation requires the temperature near zero average RF power and at high average RF power to be set individually by adjusting two potentiometers until the reflected power is minimized for each condition. The desired water temperature is then determined by a linear interpolation based on those two points.

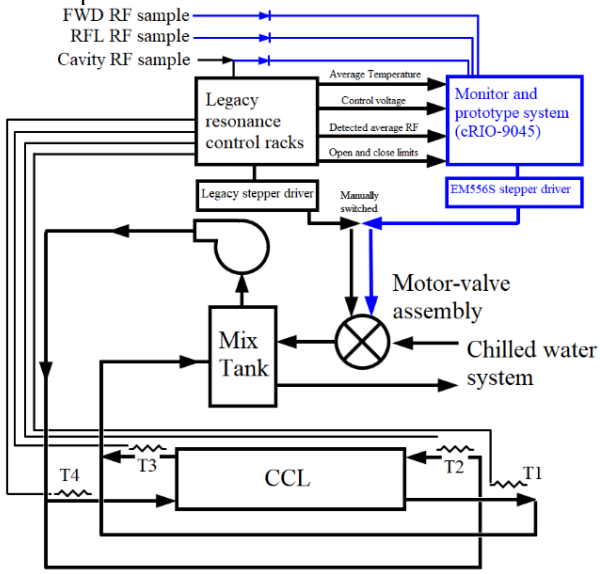

Figure 1: Block diagram of resonance control system. The present system is in black and the monitor and prototype system is in blue.

This process is performed each year, and some of the issues that have occurred in the past several years include: bad thermistor contacts, improper RF attenuation due to changes in tuning, and shifts in required temperature or poor initial settings. These issues necessitate an upgrade to the system.

A monitor and prototype system has been developed using a cRIO-9045 to both log key data and to demonstrate methods of control. The cRIO uses the FPGA module for signal collection, and the real-time application runs with UI output to a monitor. Several temperature control methods based on those signals were then developed to progressively build toward an autonomous system. The interaction of this system to the present resonance control is also shown in blue in Fig 1.

LEGACY SYSTEM MONITORING

The FPGA is used to read both pulsed RF signals and DC signals that are output from the original resonance control system. These signals have been used in the past to

†twh@lanl.gov

*Work was performed under the auspices of the US Department of Energy by Triad National Security, LLC, under contract 89233218CNA000001.

Content from this work may be used under the terms of the CC BY 4.0 licence (© 2026). Any distribution of this work must maintain attribution to the author(s), title of the work, publisher, and DOI.

ISBN: 978-3-95450-252-3 ISSN: 2673-5350 doi: 10.18429/JACoW-IPAC2026-TUP7317

CAVITY OPTIMIZATIONS AND BEAM DYNAMICS SIMULATIONS FOR LANSCE UPGRADES*

M. Kaemingk†, P. M. Anisimov, L. Duffy, J. W. Lewellen, K. Shipman, B. Sims, H. Xu
Los Alamos National Laboratory, Los Alamos, NM, United States

Abstract

The Distributed Drive Linear accelerators (DDLs), in which each accelerating cell is independently powered, offer the flexibility to set the phase and amplitude of the RF fields in each cavity individually. In the limiting case of a linac composed entirely of independently-driven single-cell cavities, the RF power required per individual cavity can be a good match to the capabilities of solid-state amplifiers. For these reasons, the possibility of upgrading the current Coupled-Cavity Linac (CCL) in the LANSCE accelerator at Los Alamos National Laboratory to a DDL architecture is being investigated. Here we report results from cell profile optimizations and beam dynamics simulations carried out to study the potential advantages of a DDL architecture in the LANSCE accelerator.

INTRODUCTION

The Los Alamos Neutron Science Center (LANSCE) accelerator complex supports a wide variety of applications. These include applications for national security, medical, and scientific research. In an effort to explore possible upgrades to LANSCE, the replacement of a Coupled-Cavity Linac (CCL) section with a Distributed Drive Linac (DDL), where each cell is individually powered by solid state amplifiers, is being investigated. Previous studies of the CCL can be found in Ref. [1]. One aspect of the upgrade investigation consists of optimizing the cell profile using the approach described in Ref. [2]. Here we report results of these optimizations as well as some preliminary beam dynamics simulations.

CELL PROFILE OPTIMIZATION

The desired resonant frequency of the cell is $f_0 = 805$ MHz. The cell length is 8.0274 cm and the bore radius is 1.5875 cm, matching the cell design described in Ref. [1]. This cell design is used in the CCL Module 5 Tank 1 (M5T1) in LANSCE. The cell was assumed to have ideal copper walls with a resistivity of 1.7241 μΩ cm. The optimization used Superfish [3] to perform the radiofrequency field simulations, and the results were verified using CST Studio Suite [4].

The objectives in this optimization were to maximize the time-dependent shunt impedance per unit length and to minimize the ratio of peak surface field, E_{peak}, to accelerating gradient E_{acc}. We define the time-dependent shunt impedance as $R_s = V_{\text{acc}}^2/P_{\text{diss}}$, where P_{diss} is the dissipated power, and $V_{\text{acc}} = \int_{-L/2}^{L/2} E_z(z)\cos\left(\frac{2\pi f_0 z}{\beta c}\right) dz$. E_z is the on-axis longitudinal electric field, L is the cavity length, and β is equal to 0.4311 [1], corresponding to the velocity of a 101.6 MeV proton beam. We can express E_{acc} in terms of these quantities as V_{acc}/L. The resonant frequency was constrained to be within 1 MHz of the target frequency. As described in Ref. [2], the optimization is performed by varying the endpoint coordinate and tangent slope values of elliptical and linear segments that define the cell profile. Let the endpoint coordinates of a given point be (r_i, z_i) and let the slope of the tangent at that point be s_i. The values for these parameters are given by

$$z_i = u_i Z,$$

$$r_i = v_i(R - r) + r,$$

$$s_i = t_i R/Z,$$

with R, r, Z defined as shown in Fig. 1 and the set of parameters u_i, v_i, t_i being the optimization variables. The ranges of optimization variables are shown in Table 1.

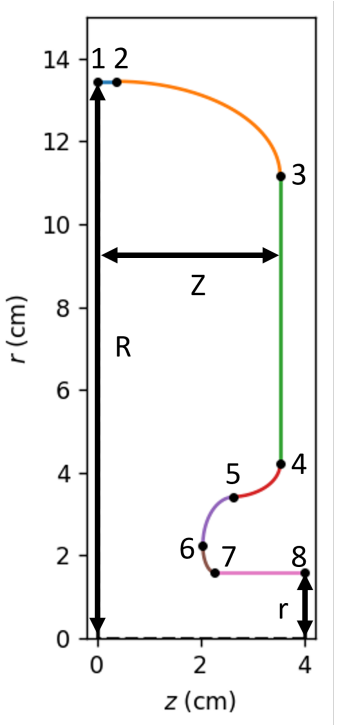

Figure 1: Reference figure for cell optimization parameters. R was allowed to vary in the range 12 cm–13.5 cm and Z was allowed to vary in the range 3 cm–3.537 45 cm. The bore radius r was fixed at 1.5875 cm.

* Work supported by U. S. Department of Energy through the Laboratory Directed Research and Development program of Los Alamos National Laboratory, under project number 20260114ER.

† kaemingk@lanl.gov

Content from this work may be used under the terms of the CC BY 4.0 licence (© 2026). Any distribution of this work must maintain attribution to the author(s), title of the work, publisher, and DOI.

ISBN: 978-3-95450-252-3 ISSN: 2673-5350 doi: 10.18429/JACoW-IPAC2026-TUP7318

CERAMIC ENHANCED ACCELERATING STRUCTURE (CEAS) OPTIMIZATION FOR IMPROVED SHUNT IMPEDANCE*

B. Sims†, H. Xu, J. W. Lewellen, L. Duffy
Los Alamos National Laboratory, Los Alamos, United States

Abstract

We present a COMSOL Multiphysics®–based workflow, using the Optimization Module, to increase RF cavity shunt impedance (R_{sh}) by systematically reshaping the nose cones. The cavity being optimized is utilizing the Ceramic Enhanced Accelerating Structure (CEAS) approach with a ceramic tube insert at the inner electric field zero of the TM020 mode, which increases the efficiency by reducing power dissipation. The CEAS concept, combined with the improved shunt impedance from nose cone optimization, yields a particularly efficient cavity. The cavity is parameterized with smooth geometric variables (nose tip radius, cone angle, gap, fillets). This optimization maximizes R_{sh} subject to frequency locking and engineering limits based on the cavity geometry. Eigen-frequency studies are used as the primary optimization tool producing a field map of the desired TM020 mode as well as the power dissipated on the walls and within the ceramic material. Post processing optimization computes R_{sh} and peak nose cone field from the electric field profile and losses. Single cell studies show higher R_{sh} without degrading cavity performance; optimal profiles provide moderating curvature to control local field enhancement.

CERAMIC ENHANCED ACCELERATING CAVITIES

Ceramic Enhanced Accelerating Cavities are single-cell standing-wave accelerator structures using a typical copper accelerating cell design with a ceramic tube inserted parallel to the beam axis [1–3]. CEAS Cavities operate in a TM020 mode, creating a TM010-like field pattern in the paraxial region. In a typical metallic TM010 cavity, RF currents in the metal are the dominant cause of ohmic losses. This is alleviated in a CEAS cavity as the ceramic insert is an insulator which leads to minimized ohmic losses, dielectric losses are also low due to the loss tangent of the ceramic. The low source of losses in a CEAS cavity leads to higher efficiency than a conventional metallic accelerator cavity.

Distributed Drive Cavities

The CEAS concept can utilize modern RF sources, such as a distributed RF drive, to remove the need for a fixed RF phase advance per cell. We modeled a distributed RF drive case, where each CEAS cell would powered by its own solid-state amplifier [4] with independent phase and power control. In Fig. 1, the CEAS cavity length (L_{cav} = 40.27 mm) is not set by a constant phase advance; instead, it is chosen to maximize energy gain, i.e. beta-matching [5]. In addition, because the RF power to each cavity can also be controlled separately, the accelerator's output beam energy can modified, which allows for many different operational modes.

Optimizer Parameters

COMSOL was used for simulation and optimization [6] of a 5.1 GHz CEAS cavity nose cone geometry, shown in Fig. 1. The figure shows the 2D axially symmetric cross section of with labeled parameters. Dimensions in black were kept constant, while those in red were optimized. The COMSOL simulations used Trans-Tech D3500 ceramic. The design also uses the nose cone gap to beta match the transit time of an ultra-relativistic beam.

Table 1: Trans-Tech D3500 Material Properties

Material	ε_r	$tan(\delta)$
D3500	35.5	1.06×10^{-4}

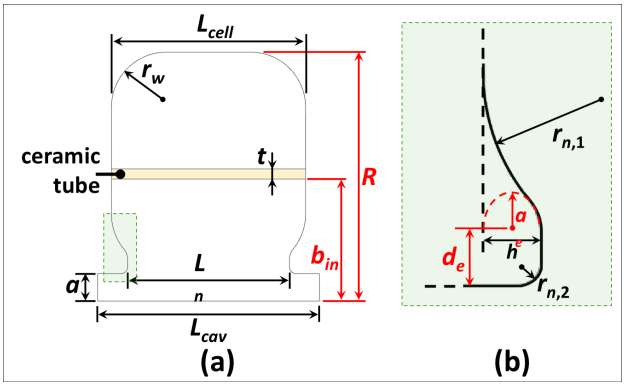

Figure 1: Optimizer parameters, black indicate fixed parameters, red indicates parameters being optimized.

RESULTS

Electric Fields

The COMSOL figure of merit (FOM) was defined as shown in Eq. 1.

$$\mathrm{FOM} = \frac{R_{sh}}{(\frac{E_{pk}}{E_{acc}})}. \quad (1)$$

R_{sh} is the time-dependent shunt impedance, E_{pk} is the peak electric field inside the cavity, and E_{acc} is the accelerating gradient. This optimization target was chosen as it works to

* Work supported by U.S. Department of Energy through the Laboratory Directed Research and Development program of Los Alamos National Laboratory, under project numbers 20210083ER and 20240136ER.
† sims@lanl.gov

Content from this work may be used under the terms of the CC BY 4.0 licence (© 2026). Any distribution of this work must maintain attribution to the author(s), title of the work, publisher, and DOI.

ISBN: 978-3-95450-252-3 ISSN: 2673-5350 doi: 10.18429/JACoW-IPAC2026-TUP7319

DESIGN AND TEST OF AN *X*-BAND CAVITY FOR SHORT-PULSE RF BREAKDOWN STUDIES

G. Rijal*, M. Shapiro, X. Lu†
Northern Illinois University, DeKalb, IL 60115, United States
G. Chen, S. Doran, J. Hlavenka, W. Liu,
R. Margraf-O'Neal, A. Ody, P. Piot, J. Power, E. Wisniewski
Argonne National Laboratory, Lemont, IL 60439, United States

Abstract

High-gradient operation of normal-conducting radiofrequency (RF) cavities is fundamentally limited by RF breakdown, a phenomenon driven by processes including field emission, surface heating, multipacting, and plasma formation. Recent studies have indicated that operating *X*-band RF cavities in a short-pulse regime, with RF pulses only a few nanoseconds long, can modify the onset and dynamics of RF breakdown. In particular, short pulses can limit multipactor-driven electron growth and reduce field-emission-induced Joule heating on cavity surfaces. However, systematic experimental investigations of these effects remain limited. We present the design of a dedicated experiment using a single-cell high-gradient *X*-band cavity to be tested at the Argonne Wakefield Accelerator (AWA) for studies of RF breakdown under short-pulse operation. The experiment will employ short, adjustable RF pulses in the few-nanosecond range. We describe the cavity design optimized for short-pulse operation, the planned operating parameter space, and the diagnostics for time-resolved dark current and RF measurements, with the goal of revealing breakdown behavior in the short-pulse regime.

INTRODUCTION

The maximum achievable accelerating gradient in normal-conducting radiofrequency (RF) structures is fundamentally limited by RF breakdown, which remains a critical constraint in the development of compact accelerators. Breakdown processes are governed by a combination of field emission, multipacting, surface heating, and plasma formation, among other phenomena. Their onset depends on the complex interplay of multiple factors, including local field conditions, surface materials, and structure geometry [1, 2].

Recent experiments at the Argonne Wakefield Accelerator (AWA) have demonstrated that operating *X*-band cavities with nanosecond-scale RF pulses can significantly modify breakdown behavior, enabling accelerating gradients approaching the sub-GV/m regime [3–6]. At AWA, these short high-power RF pulses are produced using an *X*-band power-extraction system driven by a high-charge multi-bunch train [5]. In this regime, the RF pulse duration becomes comparable to or shorter than the characteristic development time of breakdown-related processes, potentially suppressing electron multiplication and limiting surface heating. Recent analytical and numerical studies have further highlighted the importance of dark current and multipacting dynamics in short-pulse high-gradient RF structures [4, 7–9]. Understanding how the breakdown-related processes evolve in the short-pulse regime is therefore important for the development of future high-gradient normal-conducting accelerators.

While these results are promising, systematic experimental studies of RF breakdown in the short-pulse regime remain limited. In particular, fabrication and surface continuity may also influence dark current emission and breakdown onset. Here, we present the design and planned experimental study of a single-cell *X*-band cavity at 11.7 GHz, fabricated in two configurations: a mechanically clamped structure and a brazed structure. Both configurations share the same electromagnetic design. This enables a detail study of RF performance, dark current generation, and breakdown response under short-pulse excitation.

CAVITY DESIGN

A single-cell cavity operating at 11.7 GHz has been designed for studies of RF breakdown and dark current in the short-pulse regime at AWA. The structure employs a symmetric re-entrant geometry optimized for high-gradient operation under nanosecond-scale RF excitation. The cavity geometry is shown in Fig. 1(a), while Fig. 2 summarizes the

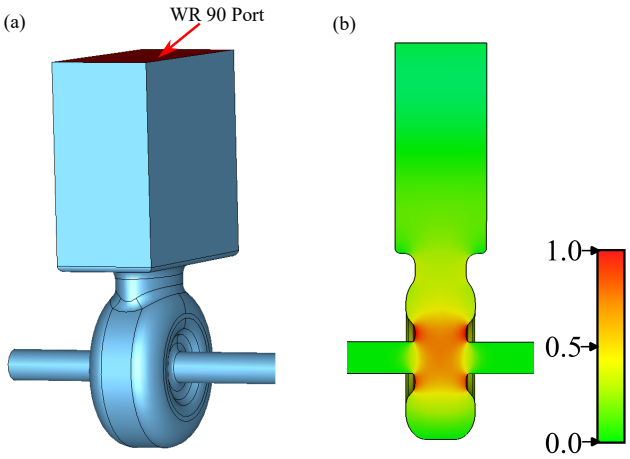

Figure 1: Geometry of the single-cell *X*-band cavity operating at 11.7 GHz. (a) Vacuum model of the cavity with the WR90 waveguide coupler. (b) Normalized E_z field distribution on the cavity midplane.

* grijal1@niu.edu
† Also at Argonne National Laboratory, Lemont, IL 60439, United States

Content from this work may be used under the terms of the CC BY 4.0 licence (© 2026). Any distribution of this work must maintain attribution to the author(s), title of the work, publisher, and DOI.

ISBN: 978-3-95450-252-3 ISSN: 2673-5350 doi: 10.18429/JACoW-IPAC2026-TUP7320

A NOVEL APPROACH TO RF POWER COUPLING IN RADIO-FREQUENCY QUADRUPOLE (RFQ) STRUCTURES: BUILT-IN COAXIAL DOUBLE-LOOP COUPLING PORT*

Sung-Woo Lee†, Haitao Ren, George Toby, Timothy Miner, John Moss,
Charles Peters, Sang-ho Kim, Yoon W. Kang
Oak Ridge National Laboratory (ORNL), Oak Ridge, TN, USA

Abstract

Efficient and reliable RF power coupling in accelerating cavities requires precise impedance matching and mechanical stability to ensure optimal beam energy transfer. In radio-frequency quadrupole (RFQ) accelerators, RF power is commonly delivered using waveguide iris couplers or coaxial loop couplers. Iris couplers can handle high RF power but present challenges in tuning, while coaxial loop couplers offer tuning flexibility but are limited in power handling and thermal performance. This paper proposes a novel RFQ power coupling concept: a single-input coaxial center-fed double-loop antenna built directly into the vane structure of an RFQ. The design integrates back-to-back loops into the RFQ vanes, fed by a TEM coaxial transmission line with a standard 50-Ω characteristic impedance. The configuration enables straightforward ceramic window replacement without retuning, and coupling strength can be adjusted with protruding tuning rods. Numerical simulations using a simplified RFQ model have demonstrated that the coaxial double-loop coupler is a practical alternative for high-power RFQ coupling.

INTRODUCTION

The SNS front end accelerates H^- ions to 2.5 MeV using a 402.5 MHz RFQ fed with two balanced coaxial couplers up to 700 kW peak RF power at 8% duty cycle. RF couplers must transfer power into the RFQ resonant structure with minimal reflection and thermal stress while maintaining vacuum integrity and field symmetry. Waveguide iris couplers accommodate high average power but have fixed geometry that limits retuning. Coaxial loop couplers provide tunability but require a tapered coaxial transition when the port area is small, constraining power handling and thermal performance. Loop coupler replacement is labor-intensive, requiring rotational realignment, vacuum reassembly, and rebalancing when multiple couplers are used in parallel [1].

Operational and maintenance experience with SNS RFQ couplers has motivated a study of coupling alternatives, with improvements sought in thermal management, RF tuning flexibility, multipacting mitigation, and window maintenance [2]. This paper proposes the coaxial double-loop coupler built-in to the cavity structure to address these issues. The design integrates the coupler directly into the RFQ vane body, enabling a larger coaxial conductor cross-section, direct thermal coupling to the RFQ cooling infrastructure, and improved mechanical stability delivering simplified window maintenance. The larger port geometry also opens the possibility of a single-coupler configuration, which would eliminate the magic-tee power splitter and associated balancing requirements. The concept is evaluated through electromagnetic simulations on a short benchmark RFQ model.

* ORNL/SNS is managed by UT-Battelle, LLC, for the U.S. Department of Energy under contract DE-AC05-00OR22725
† lees1@ornl.gov.

RF COUPLING PHYSICS IN THE RFQ

The RFQ operates in the quadrupole transverse-electric (TE_{210}) mode, in which the magnetic field runs longitudinally along the vane faces with the H-field in adjacent quadrants oriented in antiparallel directions. For efficient coupling, the driven magnetic flux must align longitudinally along the vane faces and alternate in sign between adjacent quadrants. Both conventional coaxial loop couplers and iris couplers achieve this by penetrating the quadrant wall, but introduce local cavity field perturbations that shift the resonant frequency and can excite dipole modes (TE_{110}-family), which distort the transverse focusing fields and degrade beam quality (Fig. 1). The proposed coupling scheme may also introduce some field perturbations in the cavity. Its effect and compensations are considered later in this paper.

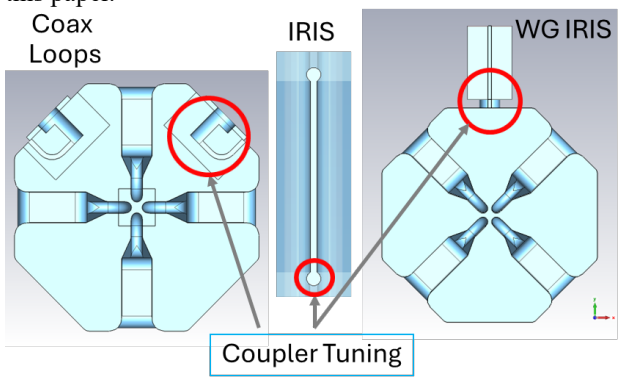

Figure 1: Conventional RFQ power coupling methods: coaxial loop coupler (left) and waveguide iris coupler (right) shown in cross-section. Red circles indicate the coupling loop and iris aperture locations. Both configurations penetrate may introduce geometric perturbations that can affect the cavity fields.

PROPOSED CONCEPT: BUILT-IN COAXIAL DOUBLE-LOOP COUPLER

As shown in Fig. 2, a single coaxial feed enters the RFQ through the top vane. The center conductor is electrically

Content from this work may be used under the terms of the CC BY 4.0 licence (© 2026). Any distribution of this work must maintain attribution to the author(s), title of the work, publisher, and DOI.

ISBN: 978-3-95450-252-3 ISSN: 2673-5350 doi: 10.18429/JACoW-IPAC2026-TUP7321

TEST CAVITY AND IRIS-TO-COAX TRANSITION FOR TUNING AND HIGH-POWER VERIFICATION OF SNS DTL IRIS COUPLERS *

Sung-Woo Lee†, Austin Wheat, Stephen Stewart, Haitao Ren
George Toby, Timothy Miner, John Moss
Oak Ridge National Laboratory (ORNL), Oak Ridge, TN

Content from this work may be used under the terms of the CC BY 4.0 licence (© 2026). Any distribution of this work must maintain attribution to the author(s), title of the work, publisher, and DOI.

Abstract

The Spallation Neutron Source (SNS) Drift Tube Linac (DTL) employs iris couplers to efficiently deliver RF power into the accelerating structure. To support the development, tuning, and high-power conditioning of these couplers prior to installation in the actual DTLs, a dedicated test cavity and an iris-to-coaxial transition structure have been designed. This work presents the electromagnetic design, simulation, and optimization of the test setup, enabling precise characterization of the iris coupler's performance. The transition structure allows for tuning of the iris opening dimensions without requiring a waveguide taper or full-size waveguide transitions, while maintaining impedance matching between the coaxial feed and the iris geometry to minimize reflection and power loss. During low-power tests, the iris opening dimensions can be evaluated using the iris-to-coax transition attached to the test cavity. For high-power conditioning, full-size waveguides with ceramic vacuum windows are connected to the test cavity to replicate operational conditions. Key design parameters were optimized using computer-aided simulation, and sensitivity studies were conducted to assess the impact of mechanical tolerances on RF performance. The resulting test platform provides a reliable and efficient means for tuning and validating iris couplers, contributing to improved operational stability in the SNS DTL.

INTRODUCTION

The SNS DTL comprises six normal-conducting tanks operating at 402.5 MHz, each fed by a tapered double-ridge waveguide iris coupler through a ceramic vacuum window [1]. As hardware ages and availability requirements grow, the facility must maintain spare iris couplers conditioned off-line to reduce installation risk and shorten commissioning time. This is challenging since pre-tuning and conditioning require connection to the actual DTL tanks, or identical cavities, to quantify coupling and transfer RF power through the coupler.

To address this, a single-cell test cavity and iris-to-coax transition were developed for low-power iris coupling characterization and tuning. A cold-model iris coupler was fabricated in two sections: an iris section and a waveguide taper section. The iris-to-coax transition decouples low-power bench measurements from bulky waveguide hardware by providing a traveling-wave passband near the operating frequency and high measurement fidelity to small changes in iris opening dimensions. The test cavity incorporates inductive and capacitive tuners for frequency tunability across the range of iris opening dimensions under characterization.

The same RF design concept, extended with cooling and vacuum system integration, is intended to support high-power RF conditioning without requiring full-scale DTL tanks. The regular copper iris coupler will be connected to a waveguide ceramic window and to the high-power RF system via WR2100 waveguide, providing an input match and transmitting most of the power with modest dissipation without enlarging the iris opening solely to achieve single-port match during testing. Electromagnetic design studies validated the RF design and established allowable iris geometry ranges. The resulting workflow demonstrates a path toward practical off-line pre-conditioning of SNS DTL iris couplers.

IRIS-TO-COAX TRANSITION

The test platform enables low-power characterization and tuning of the iris using standard coaxial instrumentation through a compact transition, such that iris geometry changes are directly reflected in the measured coupling factor.

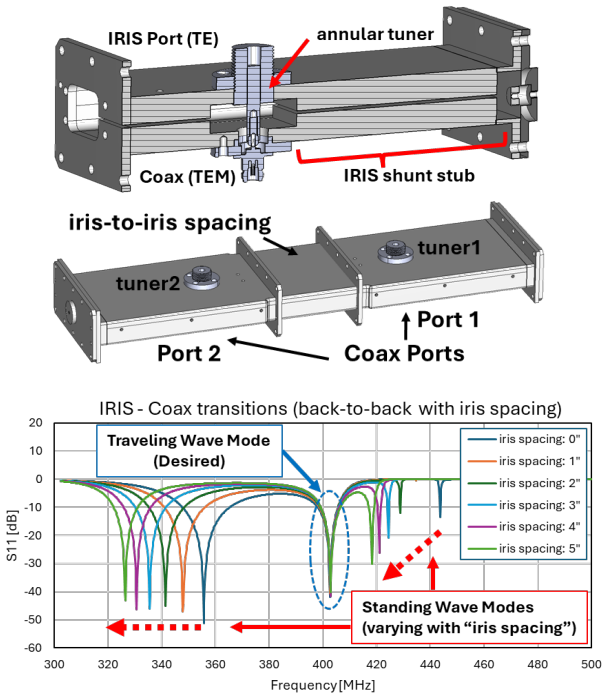

Figure 1: Iris-to-coax transition with annular tuner and iris shunt stub (top), back-to-back through fixture with varying iris-to-iris spacing (middle), and simulated S-parameter responses confirming traveling-wave operation (bottom).

* ORNL/SNS is managed by UT-Battelle, LLC, for the U.S. Department of Energy under contract DE-AC05-00OR22725
† lees1@ornl.gov.

ISBN: 978-3-95450-252-3 ISSN: 2673-5350 doi: 10.18429/JACoW-IPAC2026-TUP7326

INVESTIGATION OF RF SURFACE RESISTANCE IN SUB-GHz SUPERCONDUCTING ELLIPTICAL CAVITIES PROCESSED WITH VARIOUS NITROGEN-DOPING SURFACE TREATMENTS*

S. M. Moskaitis, S.-H. Kim, B. Barker, Y.-L. Cheon, K. Elliott, A. Ganshyn, W. Hartung, E. Metzgar, P. N. Ostroumov, T. Xu
Facility for Rare Isotope Beams, Michigan State University, East Lansing, MI, USA

Content from this work may be used under the terms of the CC BY 4.0 licence (© 2026). Any distribution of this work must maintain attribution to the author(s), title of the work, publisher, and DOI.

Abstract

Superconducting radio-frequency (SRF) cavity surface treatment with nitrogen-doping (N-doping) was a breakthrough in cavity processing which was found capable of increasing the cavity quality factor (Q_0) by more than a factor of 2 compared to standard electropolish (EP) surface treatments, as well as achieving a highly desirable anti-Q slope behavior, an increase of Q_0 with increasing accelerating field, in 1.3 GHz superconducting niobium cavities. N-doping has been extensively studied in 1.3 GHz cavities; however, a similarly significant increase in performance had not yet been observed in sub-GHz cavities. In this study, field-dependent BCS and residual resistances were measured in 644 MHz cavities for the FRIB energy upgrade with various surface treatments. The frequency dependence of the Q-slope was investigated by measuring BCS and residual resistances in the fundamental mode (FM) and a 1.45 GHz higher-order mode (HOM) in the same cavity. We will report effects of various N-doping surface treatments on the FM and HOM performance, including the achievement of Q_0 as high as 4.9×10^{10} at 17.5 MV/m in this class of SRF cavities.

INTRODUCTION

Maximizing the intrinsic quality factor (Q_0) is critical for superconducting radio-frequency (SRF) accelerators to minimize the cryogenic load and operating cost. Past studies of GHz-range SRF nitrogen-doped niobium cavities have shown both improved Q_0 and an "anti-Q slope"—an increase in Q_0 with accelerating gradient (E_{acc}) in the medium-field range ($E_{acc} \sim 2$ to 20 MV/m) [1].

Higher Q_0 and a possible anti-Q slope are of particular interest for the FRIB energy upgrade (FRIB400) project, which will make use of 5-cell elliptical niobium cavities operating at 644 MHz in CW at 2 K, with a goal of $Q_0 = 2 \times 10^{10}$ at an E_{acc} of 17.5 MV/m [2]. For cavities near 644 MHz, studies on the effects of mid-temperature baking (MTB) with 900 °C annealing have been found to increase Q_0 significantly [3]. Additionally, pioneering studies on 5-cell cavities were done using 800 °C N-doping, finding an increase Q_0, but by a lesser margin than for 1.3 GHz cavities [4]. However, the optimization of N-doping parameters has not yet been well-studied in this frequency range.

* This material is based upon work supported by the U.S. Department of Energy, Office of Science, Office of Nuclear Physics and used resources of the Facility for Rare Isotope Beams (FRIB) Operations, which is a DOE Office of Science User Facility under Award Number DE-SC0023633.

Additionally, studying the frequency dependence of the BCS resistance (R_{BCS}) and residual resistance (R_{res}) via measurements of different monopole modes in the same cavity, thus removing the dependence of cavity-to-cavity surface treatment variations, could provide guidance towards reducing Q-slope at 644 MHz.

CAVITY PROCESSING

Two FRIB energy upgrade single-cell cavities were used for this study (S65-901, S65-903). These cavities underwent N-doping of 800 °C and 900 °C, respectively. The process consisted of heat treatment at 800 °C or 900 °C for 3 hours in an ultra-high vacuum furnace (UHV) to reduce hydrogen concentration in the niobium bulk. For the last 2 minutes of the heat treatment, nitrogen was introduced at a pressure of 25 mTorr to promote diffusion of nitrogen into the cavity inner surface. After these 2 minutes, the nitrogen was pumped out, and the cavity was cooled back down to room temperature. This process is referred to as 800 °C or 900 °C 2N0-doping. The temperature and pressure for the 900 °C treatment of S65-903 are shown in Fig. 1. The N-doping treatment was preceded by bulk electropolishing (EP) and followed by light EP (5 µm). The post-treatment EP removes the harmful niobium nitride layer formed during N-doping, as the NbN layer significantly degrades Q_0 [1]. The cavities were then ultrasonic cleaned (USC), high-pressure rinsed (HPR), and clean-assembled for cold testing.

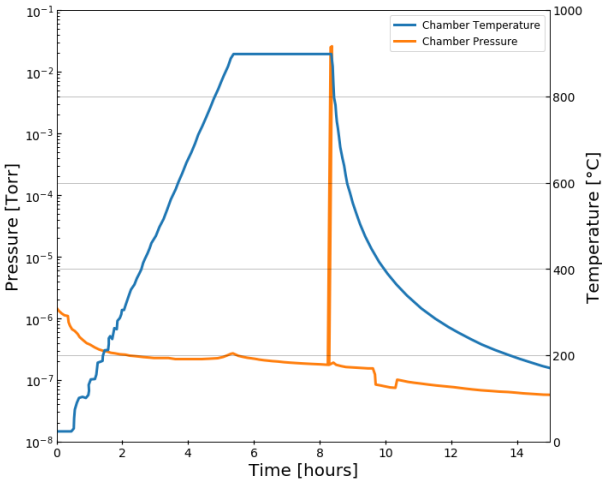

Figure 1: Chamber temperature and pressure during the 900 °C 2N0-doping procedure.

To measure Q_0 as a function E_{acc}, a "Q-curve", at cryogenic temperatures for both the TM_{010} FM (644 MHz) and

ISBN: 978-3-95450-252-3 ISSN: 2673-5350 doi: 10.18429/JACoW-IPAC2026-TUP7340

UNDERSTANDING THE CONNECTIONS BETWEEN GRAIN GROWTH AND FLUX EXPULSION IN LOW RRR NIOBIUM SRF CAVITIES*

K. Howard†, Y.-K. Kim, University of Chicago, Chicago, IL, USA
D. Bafia, W. Dziedzic-Misiewicz, Z. Sung, Fermi National Accelerator Laboratory, Batavia, IL, USA

Abstract

The SRF community has shown that high temperature annealing can improve the flux expulsion of niobium cavities during cooldown. The required temperature will vary between cavities and different batches of material, typically around 800 °C and up to 1000 °C. However, for niobium with a low residual resistance ratio (RRR), even 1000 °C is not enough to improve its poor flux expulsion. The purpose of this study is to observe the grain growth behavior of low RRR niobium coupons subjected to high temperature annealing to identify the mechanism for improving flux expulsion in low RRR cavities. We anneal the low RRR material up to 1200 °C to understand the limits of flux expulsion performance. We observe that low RRR material experiences less grain growth than high RRR when annealed at the same temperature. We search for the limitations to grain growth in low RRR material and develop a diagnostic based on grain structure to determine the appropriate recipe for good flux expulsion. The results of this study have the potential to unlock a new understanding on SRF materials and enable the next generation of high Q_0/high gradient surface treatments.

INTRODUCTION

As we approach the theoretical limits of niobium for superconducting radio-frequency (SRF) cavities, immense improvements in quality factor (Q_0) and accelerating gradients have been possible though intentionally added impurities into the niobium surface [1]. Many SRF studies follow a "clean bulk dirty surface" technique by adding impurities to the surface layer of high purity niobium such as nitrogen through N-doping [2]. N-doped cavities are found to have a high sensitivity to trapped flux, so efficient flux expulsion has been critical for their implementation in accelerators [2–8].

During cavity testing, a fast cooldown is typically performed to prevent trapped magnetic flux [5–10]. In this process, there is a large thermal gradient across the cavity as it crosses through the superconducting transition temperature T_c. This allows for a sweeping phase transition to the Meissner state, where the depinning force is stronger than the attraction of the vortices to the pinning sites, and the flux is effectively expelled [7, 8]. As the cavity transitions to superconducting, the expulsion of flux from the cavity walls increases the magnetic field outside the cavity [8]. We observe a step change in the magnetic field, like in Fig. 1, which corresponds to the amount of flux expelled in this phase transition [8, 9].

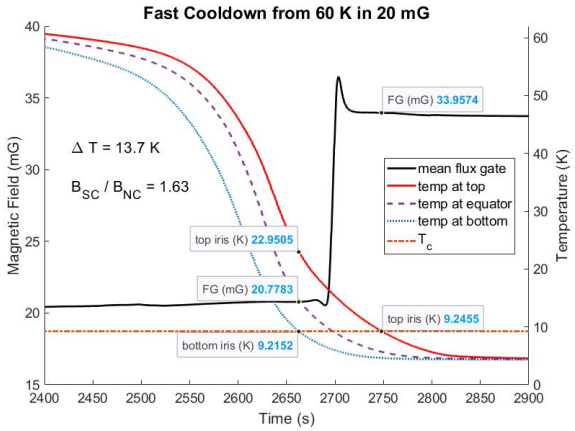

Figure 1: Fast cooldown with gradient $\Delta T = 13.7$ K in 20 mG external magnetic field expels flux at $B_{SC}/B_{NC} = 1.63$.

By not following the fast cooldown procedure, normal conducting vortices may get trapped within the superconducting lattice. Oscillation of vortices during RF operation introduces significant dissipation [11, 12]. If all regions reach T_c simultaneously, the superconducting phase nucleates in multiple locations [7, 8]. If attraction between vortices and pinning sites is more energetically favorable than the onset of superconductivity, flux becomes trapped, and we observe minimal change in the magnetic field [9], like in Fig. 2.

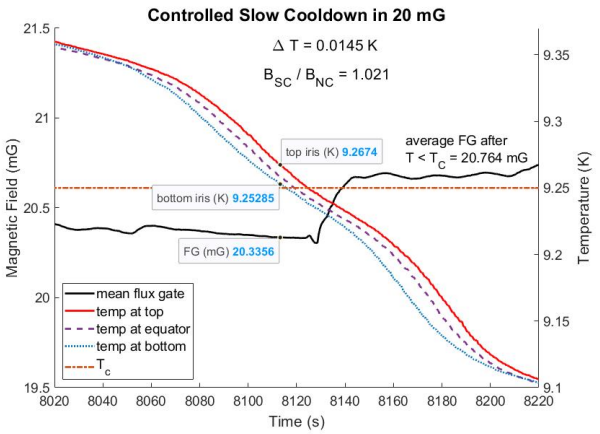

Figure 2: Slow cooldown with gradient $\Delta T = 0.0145$ K in 20 mG external magnetic field traps flux at $B_{SC}/B_{NC} = 1.021$.

For accelerator application, we need SRF cavities to be robust against small magnetic fields, as creating a large thermal gradient across many cryomodules is difficult. For cavities with poor flux expulsion, we must fix this issue in order to reach high Q_0. A high temperature anneal of 900 °C or 1000 °C is known to improve flux expulsion [6, 9, 13–17]. Alongside this improvement, sample studies observe grain

* FERMILAB-CONF-26-0331-TD
† khoward99@uchicago.edu

Content from this work may be used under the terms of the CC BY 4.0 licence (© 2026). Any distribution of this work must maintain attribution to the author(s), title of the work, publisher, and DOI.

ISBN: 978-3-95450-252-3 ISSN: 2673-5350 doi: 10.18429/JACoW-IPAC2026-TUP7342

DIGITAL SIGNAL COMPONENT SEPARATOR FOR THE LANL SOLID-STATE POWER AMPLIFIER*

Sungil Kwon†, M. Brown, W. Hall, J. T. M. Lyles, S. J. Russell, P. Torrez
Los Alamos National Laboratory, Los Alamos, NM, USA

Content from this work may be used under the terms of the CC BY 4.0 licence (© 2026). Any distribution of this work must maintain attribution to the author(s), title of the work, publisher, and DOI.

Abstract

Because of aging, and product discontinuity, LANSCE is investigating the replacement of high power RF amplifiers. A promising candidate is the GaN solid-state power amplifier (SSPA). The outphasing technique provides high efficiency operation of the SSPA. A key element of the outphasing technique is the signal component separator(SCS), which converts an Amplitude Modulation-Phase Modulation(AM-PM) signal to two PM only signals. In this paper, a design of a digital signal component separator (DSCS) in In-phase/Quadrature(I/Q) coordinate is addressed. In addition, the feedback linearizers are proposed to suppress the input disturbances to the SSPA. The DSCS is implemented on the present Field Programmable Gate Array(FPGA) based LANSCE digital low level RF (DLLRF) control system. The performance of the DSCS on the cavity field control system is verified on a low power teststand and the results are reported.

INTRODUCTION

The high power RF amplifiers, klystrons, of LANSCE 805 MHz CCLs have been operating for more than 5 decades. Because of aging, and product discontinuity, LANSCE is investigating the replacement of high power RF amplifiers. One of the highly promising amplifiers are the GaN amplifiers[1]. Currently, an available GaN amplifier can produce 5kW pulsed RF power. Hence, in order to produce the equivalent or better performance than a LANSCE klystron of which peak power is 1.25 MW, a multitude of Solid-State Power Amplifiers are to be combined together. For a high drain voltage, the drain power dissipation is increased as the operating efficiency becomes low[1]. In order to operate a SSPA at high efficiency, the amplifier is operated as close as possible to the 1 dB compression zone or even at the saturation region. The outphasing technique can provide this requirement of the SSPA operation[2]. In the outphasing amplifier, the Amplitude Modulation-Phase Modulation(AM-PM) input signal is converted to constant envelope PM signals, so that each amplifier of the forward signal path linearly amplifies constant envelope PM input signals[3,4]. The combiner sums the amplified PM signals, yielding the signal of linear amplification of the outphasing amplifier input signal.

The core part of the outphasing amplifier is the signal component separator(SCS), which converts the AM-PM input signal to constant envelope PM signals. Most SCS techniques are implemented on the analog circuits[3]. In this paper, a digital signal component separator (DSCS) design in the In-phase/Quadrature(I/Q) coordinate is addressed.

In addition to the DSCS, compensators for the slowly varying amplitude and phase disturbances that may exist on the RF forward paths are addressed. The sources of these disturbances may be the parameter drifts of the amplifiers themselves, droops of DC power source, or temperature variation of the component. In this outphasing amplifier design, digital feedback linearizers are implemented to compensate for these disturbances.

The proposed techniques of DSCS, feedback linearizers are to provide the stable RF power to a plant, accelerator cavity. In this paper, they are designed, implemented and their performances are verified on the low power cavity field control system testbench experiment.

OUTPHASING AMPLIFIER AND DIGITAL SIGNAL COMPONENT SEPARATOR

The phase modulated components are generated using vector decomposition of the baseband signal in I/Q coordinate.

Consider the phasor diagram shown in Figure 1. The input vector $\vec{s}$ can be expressed as the complex form in I/Q coordinate as

$$\vec{s} = re^{j\alpha} = I + jQ \qquad (1)$$
$$|\vec{s}| = r \le r_{max}, \quad \alpha = atan\left({}^{Q}/_{I}\right)$$

When the vector $\vec{s}$ is projected to the circle of the radius of r_{max} the projecting vector is defined by

$$\vec{e} = e_I + je_Q \qquad (2)$$
$$e_I = -\sin(\alpha)\sqrt{r_{max}^2 - r^2}$$
$$e_Q = +\cos(\alpha)\sqrt{r_{max}^2 - r^2}$$

and the two signals of two-port SCS are given by

$$\vec{d}_0 = r_d\, e^{j(\alpha+\theta)} = I_{d0} + jQ_{d0} \qquad (3)$$
$$\vec{d}_1 = r_d\, e^{j(\alpha-\theta)} = I_{d1} + jQ_{d1} \qquad (4)$$

where

$$\theta = \text{atan}\left(\frac{\sqrt{r_{max}^2 - r^2}}{r}\right)$$
$$I_{d0} = I + e_I, \quad Q_{d0} = Q + e_Q$$
$$I_{d1} = I - e_I, \quad Q_{d1} = Q - e_Q$$

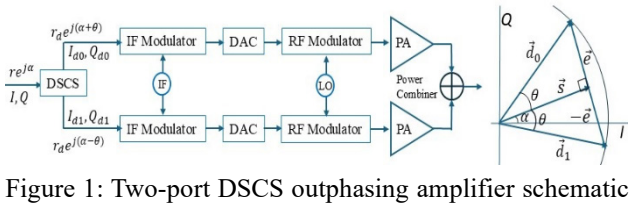

Figure 1: Two-port DSCS outphasing amplifier schematic and vector diagram.

* Work supported by LANL LDRD DI
† email address :skwon@lanl.gov

ISBN: 978-3-95450-252-3 ISSN: 2673-5350 doi: 10.18429/JACoW-IPAC2026-TUP7346

HIGH-POWER AMPLIFIER CONSIDERATIONS FOR TESTING THE LAMP RFQ AND FIRST DTL CAVITY*

M. Sanchez Barrueta†, W. Hall, J. Lyles, R. Bratton, J. Lewellen, Los Alamos National Laboratory, Los Alamos, United States

Abstract

As part of the LANSCE Accelerator Modernization Project (LAMP), critical portions of the proposed accelerator will be tested as proof of concept and aid in planning the installation of LAMP at Los Alamos Neutron Science Center. As part of this demonstration, the radio frequency quadrupole (RFQ) and the first drift-tube linac (DTL) cavity will be tested with beam. For this purpose, high-power RF amplifiers are being designed to meet the testing demands. This is a description of the requirements of these amplifiers and how the design is intended to meet them.

INTRODUCTION

The LAMP project endeavours to replace the ion sources, low-energy beam transport and the entire drift-tube linac (DTL) section of the LANSCE accelerator [1]. The largely unchanged 1972 structures have increasingly shown signs of obsolescence and aging that has manifested in production beam down-time. LAMP intends to address this major area of concern while reusing a large portion of the recently updated radio-frequency (RF) power plant.

Currently, the beam is accelerated to 750 keV with a Cockcroft-Walton (C-W) DC accelerator, prebunched, and injected into the LANSCE drift-tube linac. Four DTL tanks (or cavities), driven by high-power 201.25 MHz amplifiers, accelerate the beam to 100 MeV. The first cavity uses a solid-state driven TH781 tetrode amplifier and the remaining three use the combined output of two TH628L Diacrodes (double ended tetrodes for high power RF) amplifiers driven by a single tetrode amplifier.

The current LAMP design uses a DC accelerator to achieve the first 65 keV of energy, an RFQ cavity to accelerate the beam to 2.1 MeV, and six DTL cavities to accelerate the beam to 100 MeV. The current high-power RF design incorporates either a dual tetrode or a single Diacrode amplifier feeding the RFQ, and separation of the existing three dual-Diacrode amplifier stations into six individual Diacrode amplifiers. Other changes to the system include the installation of separate 90 kW solid-state power amplifier (SSPA) drivers feeding each Diacrode amplifier, as well as circulators as reflected power protection, and small changes to the existing high-voltage power supplies and capacitor banks. Additional low-level radio-frequency (LLRF) controls and cRIO-based controllers will be required to independently monitor and regulate cavity resonance and low-voltage controls.

To demonstrate the performance of the key design features, a test with a subset of components, namely the ion-sources, low-energy beam transport, RFQ, medium-energy beam transport and first DTL cavity are expected to be performed [2] in an existing accelerator building originally used to test the Low-Energy Demonstration Accelerator (LEDA) [3]. The building in question is called Accelerator Development and Experimental Facility (ADEF) and the reduced test is named LAMP in ADEF Tunnel (LAT). The description of the estimated RF power plant used to provide power to these RF cavities follows.

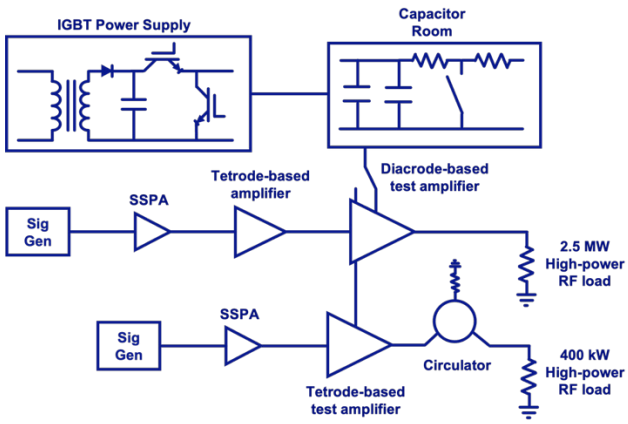

Figure 1: Block-diagram for the existing 201.25 MHz high-power amplifier test stand at LANSCE.

EXISTING TEST STAND

The original 1968 triode-based RF amplifiers for the DTL cavities experienced shortened lifetimes and adversely impacted beam availability in 2006. From 2014 until 2021, during individual maintenance periods, single RF amplifiers were upgraded to the current tetrode-driven dual-Diacrode version [3]. The expected power delivered for a single DTL cavity at LANSCE is 2.7 MW, with a 1.35 MW peak power delivered per Diacrode amplifier. All amplifier components used during the upgrades were tested under operational conditions in a test stand [4] located in the LEDA building, a block-diagram for which can be found in Fig. 1. In 2017-2020, an addition was made to the test stand to allow testing of the first drift tube linac RF amplifier [5], which due to lower power requirements, only uses a single tetrode.

The test stand is composed of an IGBT power supply providing charging current to a 225 µF capacitor bank (crowbar protection device included). A signal generator

*Work was performed under the auspices of the US Department of Energy by Triad National Security, LLC, under contract 89233218CNA000001.

†msb@lanl.gov

Content from this work may be used under the terms of the CC BY 4.0 licence (© 2026). Any distribution of this work must maintain attribution to the author(s), title of the work, publisher, and DOI.

ISBN: 978-3-95450-252-3 ISSN: 2673-5350 doi: 10.18429/JACoW-IPAC2026-TUP7347

HIGH POWER GaN AMPLIFIER DEVELOPMENT FOR COUPLED-CAVITY LINAC AT LANSCE*

J. T. M. Lyles †, M. Sanchez Barrueta, J. T. Bradley III, M. C. Brown, T. W. Hall, S. I. Kwon, S. A. Mano, C. G. Miera, E. R. Olivas, J. D. Alvarez Prieto, S. Rocha, S. J. Russell, P. J. Van Rooy, T. R. V. Roybal, B. Singh, P. A. Torrez, J. A. Vega, J. Zhang
Los Alamos National Laboratory, Los Alamos, NM, USA

Abstract

The Los Alamos Neutron Science Center (LANSCE) uses a coupled-cavity linac (CCL) to accelerate H- ions from 100 to 800 MeV. It is powered by forty-four 1.25 MW 805 MHz klystrons, each capable of 150 kW of average power. A prototype solid-state amplifier (SSA) that meets these requirements is in development. Commercial silicon LDMOS transistors have reduced power above 600 MHz and are also limited by the maximum drain to source breakdown voltage. We are using high voltage Gallium Nitride (GaN) on Silicon Carbide (SiC) high electron mobility transistors (HEMT) to reduce the number of active devices and the complexity of power combining smaller amplifiers. These wide bandgap semiconductors can operate at high channel temperatures around 200 degrees Celsius without shortened life. We are testing new devices up to 5 kW of peak power at 100 volts. Operating in saturation mode, outphasing modulation is used to maintain high device efficiency to reduce thermal dissipation, compared to conventional class AB linear amplifiers. The power supply requires stored energy with a capacitor bank. Power combining uses a combination of 2-way Gysel, 40-way radial and magic tee combiners in waveguide.

INTRODUCTION

The LANSCE facility uses a room-temperature copper CCL to accelerate H^- ion beam from 100 to 800 MeV. This structure is powered by forty-four 1.25 MW 805 MHz klystrons, which all together provide approximately 44 MW of peak RF power and 5.3 MW of average power. These klystrons have been manufactured essentially unchanged since their introduction in 1968. LANSCE is expected to provide beams beyond 2050, which has raised concerns about relying solely on this vacuum electron tube technology for 24 years or more.

The LANSCE klystrons require 86 kV beam voltage supplied from conventional AC mains charging power supplies and capacitor banks, which present their own set of difficulties. The magnetic components (transformer and regulator) are no longer available from the original source. Seven capacitor banks, each feeding 6-7 klystrons, rely on a large number of oil-paper insulated series/parallel capacitor strings. It is common for component failures to result in collateral damage in the bank due to the 230 kJ of stored energy. These high voltage equipment challenges are exacerbated as we add a younger engineering team less familiar with high voltage engineering than the designers who built the systems 54 years ago.

This institutionally funded R&D has been underway since 2024, to develop a replacement RF power amplifier that can fit in the space of one klystron and its modulator tank [1, 2]. Three-hundred and twenty solid-state amplifier (SSA) pallets are to be combined to produce equivalent or better performance than that of a klystron. This can replace the legacy high voltage vacuum electron tube technology with state-of-the art low voltage RF amplifiers. As an added benefit, this development has attracted and hired early-career engineers to help us form a strong R&D team.

SSA DESIGN CONSIDERATIONS

Applicable Transistor Technologies

Peak power capability has been a hallmark for vacuum tubes, where the thermal mass is large and the peak to average power ratio is very high. For a SSA, the most reliable approach is operating in continuous mode, and this has enabled silicon laterally diffused metal-oxide semiconductor (LDMOS) transistors to be combined to replace klystrons or inductive output tubes at dozens of synchrotrons and storage rings worldwide. Pulsed operation at the LANSCE CCL requires understanding the intrinsic peak capability of the individual junctions or channels inside the devices, their packaging for thermal design, and using energy storage with capacitors at one thousandth of the voltage of klystrons. Lessons learned from published SSA developments and discussions with staff from other accelerators using LDMOS were reviewed for this project.

LDMOS has been a mature technology from multiple manufacturers since 1990s, used for wireless communication, military, industrial and broadcast transmission. Transistors are made from large wafers in conventional silicon foundries so the price per watt is attractive. Rated at a maximum operating V_{ds} (drain to source) voltage of 50-65 volts these field-effect transistors generate up to 1.9 kW of saturated peak power below 400 MHz. A recent exception is a 4 kW peak LDMOS device operating at 75 Volts up to 450 MHz. At 805 MHz the peak power capability is reduced significantly. The drain to source capacitance of large LDMOS devices limit their maximum frequency-times-power product. Conventional linear amplification

* Work supported by the U.S. Department of Energy through the Los Alamos National Laboratory, operated by Triad National Security, LLC, for the National Nuclear Security Administration of U.S. Department of Energy (Contract No. 89233218CNA000001). Research presented in this article was supported by the Laboratory Directed Research and Development program of Los Alamos National Laboratory under project number 20240723DI.
† jtml@lanl.gov

Content from this work may be used under the terms of the CC BY 4.0 licence (© 2026). Any distribution of this work must maintain attribution to the author(s), title of the work, publisher, and DOI.

ISBN: 978-3-95450-252-3 ISSN: 2673-5350 doi: 10.18429/JACoW-IPAC2026-TUP7356

ARIEL RADIOACTIVE GAS MANAGEMENT SYSTEM

F. Rahimi, D. Yosifov, N. Mathur
TRIUMF, Vancouver, BC, Canada

Abstract

The Advanced Rare Isotope Laboratory (ARIEL) facility expands TRIUMF's isotope production by adding two new target stations operating in parallel with the existing infrastructure, enabling high-intensity Radioactive Ion Beam (RIB) production. At the core of this facility, a complex vacuum system is designed to maintain the conditions required for RIB production while safely managing radioactive gases generated during beam-material interactions. The activated gases from the target and RIB modules are continuously evacuated and transferred via a radioactive gas management system to storage tanks for controlled decay. The radioactive gas management system is designed to support parallel and independent target station operation, prevent cross-contamination between exhaust streams, enable future scalability, and provide fault tolerance to ensure uninterrupted operation in the event of equipment failure. This system incorporates controlled gas recirculation and sampling capabilities to ensure the collection of a uniform sample for radiological assessment prior to release to the nuclear ventilation system. In addition, this system is operated and controlled remotely, enabling remote control of devices, data archiving, and implementation of interlocks for machine protection. This work presents the key design features and operational principles of the ARIEL radioactive gas management system.

INTRODUCTION

The vacuum system for the ARIEL electron and proton stations is designed to maintain a high-vacuum environment while managing radioactive gases released during operation. These highly radioactive gases are continuously evacuated at a rate that ensures the required vacuum level during operation and are transferred to decay storage tanks via the ARIEL radioactive gas management system. This system allows operators to direct gases to designated storage volumes for controlled decay [1]. Turbo-molecular pumps handle the continuous evacuation of the released gases during operation, while hermetically sealed and oil-lubricated backing pumps manage their exhaust. The exhaust from these backing pumps is routed to the ARIEL radioactive gas management manifold via the vacuum pump manifold, which will then be directed into pre-evacuated storage tanks.

Once stored, the gases undergo radioactive decay. After a designated period, a sample is drawn from the decay tanks through the sampling system for radioactivity assessment [2]. If the sample meets regulatory safety requirements, then the radioactive gas management system evacuates the decay tank and releases the gases into the Nuclear Ventilation System (NVS) for controlled atmospheric discharge [3]. A schematic representation of the ARIEL radioactive gas management system and its interfaces with other systems is provided in Fig. 1.

The design challenge is multidisciplinary. The system must maintain leak-tight vacuum service, be compatible with a radiation environment, support remote operation, minimize contamination spread, and remain maintainable in a constrained installation envelope. It must also support operational modes such as tank selection, pre-evacuation, gas transfer, sampling, tank evacuation, and discharge to NVS after verification that stored gases meet release requirements.

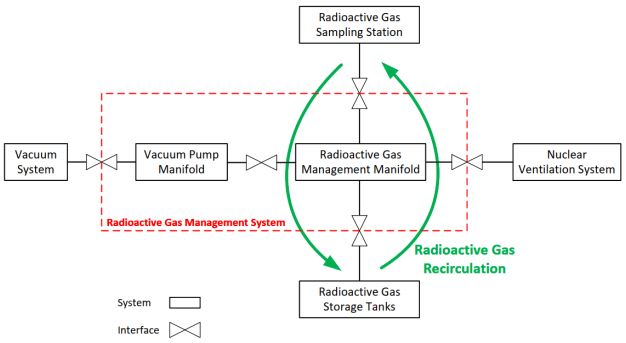

Figure 1. Schematic illustration of the radioactive gas management system interfacing and interacting with other systems.

CONCEPTUAL DESIGN

ARIEL Radioactive Gas Management P&ID

The conceptual design of the ARIEL radioactive gas management system is built around two major assemblies: i) the radioactive gas management manifold and ii) the pump manifold. This system is designed to safely and efficiently control the storage, monitoring, and release of radioactive gases. Figure 2 presents a high-level P&ID, showing the main equipment layout, process connections, and control interfaces. The system can be operated remotely and is connected to multiple decay storage tanks, which provide dedicated storage volume for radioactive gas decay.

A key function of the system is the ability to select a specific decay tank for gas storage. The system also allows operators to collect gas samples for radioactivity assessment, confirming that each stored gas batch satisfies safety and regulatory requirements before release to the environment.

Content from this work may be used under the terms of the CC BY 4.0 licence (© 2026). Any distribution of this work must maintain attribution to the author(s), title of the work, publisher, and DOI.

ISBN: 978-3-95450-252-3 ISSN: 2673-5350 doi: 10.18429/JACoW-IPAC2026-TUP7358

RECONFIGURATION OPTIONS FOR REUSING A PERMANENT MAGNET UNDULATOR AS A LOW-FIELD WIGGLER SOURCE*

M. J. Sigrist†
Canadian Light Source .Inc, Saskatoon, Canada

Abstract

The Canadian Light Source (CLS) currently operates a 1.9 T super conducting wiggler (SCW) that has been in service since 2005. As the risk of failure and maintenance requirements for this aging device increase, and funding for a permanent replacement remains pending, an interim solution is needed to ensure continued beamline operation. Reconfiguring a decommissioned permanent magnet undulator offers a cost-effective alternative that could minimize downtime. Several approaches to modifying the magnetic layout to enhance wiggler performance are under consideration, with the goal of reusing existing mechanical supports, permanent magnets, and vacuum chambers. Proposed modifications include reducing the gap and halving the magnetic period to achieve the desired field characteristics.

BACKGROUND

The CLS has operated a 1.9 T SCW as a photon source on the HXMA (Hard X-ray Micro-Analysis) beam line since January 2005. Maintenance needs are increasing for this aging device. High numbers of past quenches [1] also raise concerns regarding the risk of failure. Funding for a new wiggler has not yet been successful driving a need for a low cost option with minimal effort which could be implemented and restore beamline operations quickly if needed.

UNDULATOR RECONFIGURATION

This work explores the feasibility of reconfiguring a decommissioned permanent magnet undulator, U185 [2], as a low-field wiggler. This approach leverages additional decommissioned equipment made available from the previous beamline upgrades to minimize cost and design effort. U185 has a 185 mm magnetic period (λ), a peak field of 0.72 T and could generate photons as low as 5.5 eV with the first harmonic on the 2.9 GeV storage ring at the CLS.

U185 - Design

The U185 device has an eight block per period design, see Fig. 1a, that offers some additional design options for building a replacement wiggler with better field characteristics. The U185 magnet block shape is a square cross-section with sides 23.1 mm, $\sim \lambda/8$. A pair of magnets with aligned magnetization was installed so that the polarization changed by 90° every $\lambda/4$. This cost saving design only required a single block type for full sized magnets. Additionally the device only operated with a minimum gap of 25 mm but the vacuum chamber had an outer thickness of 10 mm. Decreasing the magnetic gap would further increase the peak magnetic fields and improve the performance of the device as a wiggler source.

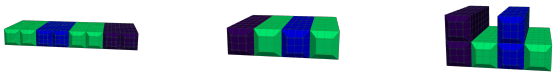

(a) U185 (b) U93A (c) U93B

Figure 1: Magnet blocks in a single period.

Reconfiguration Approaches

Several strategies for modifying the U185 were considered to achieve the required wiggler field and photon energy range with minimal cost and design effort. The main approaches include:

- Reducing the magnetic gap to increase the peak field.
- Halving the magnetic period to increase field strength and number of periods.
- Reusing existing mechanical supports, vacuum chambers, and permanent magnets to minimize engineering changes.

Magnetic modeling and field calculations were performed for each configuration to assess feasibility and performance trade-offs.

Table 1: Summary of Key Parameters for U185 Reconfiguration

Config.	Period mm	Gap mm	Poles #	Length m
SCW	35.3	13.5	61	1.06
U185 (orig)	185	25	17	1.635
U93 A	92.5	11-25	33	1.612
U93 B	92.5	11-25	21	1.057

The two reconfigurations U93A and U93B use four and six blocks per period as seen in Fig. 1. While U93B generates higher fields needed for a higher critical energy (ϵ_c), the additional blocks per period reduces the total length of the device that is possible while reusing existing magnet blocks. This tradeoff of ϵ_c versus total length changes with different minimum gaps and will be constrained by the maximum magnetic forces possible with the existing support structure.

* The Canadian Light Source receives funding from CFI, NSERC, the University of Saskatchewan, CIHR, and the Government of Saskatchewan.
† michael.sigrist@lightsource.ca

Content from this work may be used under the terms of the CC BY 4.0 licence (© 2026). Any distribution of this work must maintain attribution to the author(s), title of the work, publisher, and DOI.

ISBN: 978-3-95450-252-3 ISSN: 2673-5350 doi: 10.18429/JACoW-IPAC2026-TUP7360

A NOVEL MAGNETIC MEASUREMENT SYSTEM FOR CRYOGENIC PERMANENT MAGNET UNDULATOR

Toshiya Tanabe*, Brian Eipper, Marco Musardo, Thomas Brookbank, James Rank, Dean Hidas, Bryan Holland, Daniel Migliorino
Energy & Photon Science Directorate, National Synchrotron Light Source-II, Brookhaven National Laboratory, Upton, NY, USA

Abstract

A standardized magnetic measurement system exists for evaluating the field characteristics of conventional insertion devices, including in-vacuum undulators designed for NSLS-II, which utilize a rectangular measurement window. However, in the case of cryogenic permanent magnet undulators (CPMUs), each facility employs a distinct design, and no commercially available measurement system currently exists. At NSLS-II, we intend to retain a side-mounted rectangular window for room-temperature characterization. An in-vacuum magnetic measurement system (IVMMS) suitable for 1.5 m long CPMUs was developed during the NSLS-II project. A newly developed in-vacuum Hall probe system, capable of accommodating devices longer than 1.5 m, has been designed to interface with this window. This paper presents a preliminary design of the in-vacuum Hall probe measurement bench, designated IVMMS-II, developed to characterize a 3 m long CPMU planned for the NEXT-III (NSLS-II Experimental Tools III) project beamline, High Resolution Powder Diffraction (HRD).

INTRODUCTION

For the characterization of insertion devices, two categories of magnetic field measurement systems are required. One is a field mapping apparatus, typically employing a three-dimensional Hall probe. The other is a field integral measurement system, commonly utilizing either a single-wire configuration or a multi-turn coil. Our group has previously developed a field integral measurement system based on an in-vacuum flip coil [1] which is applicable to CPMUs. During the NSLS-II project, an in-vacuum Hall mapping system, referred to as In-Vacuum Magnetic Measurement System (IVMMS), was developed and optimized for 1.5 m long CPMUs. This measurement system was validated using a 20 cm long Prefab CPMU at the vendor's facility, as illustrated in Fig. 1. The new beamline for the NEXT-III (NSLS-II Experimental Tools III) project, designated as High Resolution Powder Diffraction (HRD) [2], requires a radiation source incorporating a 3.0 m long CPMU. A concise summary of the device specifications is provided in Table 1.

Table 1: HRD-CPMU Parameters

Item	Specification
Magnet Core length (including magic fingers)	3.0 m
Period Length	18.0 mm
Min. Vertical Physical Aperture	4.50 mm
Min. Operational Vertical Physical Aperture	5.97 mm
Max. Operational Magnetic Gap	25.0 mm
Min. Fully Open Gap (with vacuum chamber, with transitions)	40.0 mm
K_{eff} at 5.97 mm vertical aperture@77 K*	> 1.795

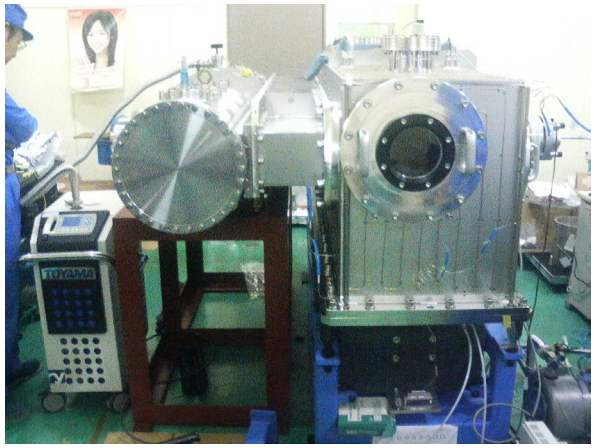

Figure 1: IVMMS measuring a 20 cm long prefab undulator with liquid Nitrogen cooling.

DESIGN CONCEPT

The IVMMS employed the concept of incorporating a compact granite bench within the vacuum environment. However, extending this approach to accommodate longer devices has proven to be prohibitively expensive. The existing IVMMS allows adjustment only in the X, Y, and Z directions, as well as roll (rotation about the X-axis). A newly developed system should provide full six-degree-of-freedom adjustment, encompassing X, Y, Z translations and pitch (T_x), yaw (θ_y), and roll (θ_z) rotations. Figure 2 illustrates the definitions of these parameters. The Z-direction corresponds to the longitudinal axis, extending up to 4000 mm.

* tanabe@bnl.gov

Content from this work may be used under the terms of the CC BY 4.0 licence (© 2026). Any distribution of this work must maintain attribution to the author(s), title of the work, publisher, and DOI.

ISBN: 978-3-95450-252-3 ISSN: 2673-5350 doi: 10.18429/JACoW-IPAC2026-TUP7364

BUILDING A MOPA LASER FOR H- BEAM SHAPING

C. Rohde‡ and K. Bishofberger†, LANL, Los Alamos, USA

Abstract

We present the design and initial amplification stages of a seeded Master Oscillator Power Amplifier (MOPA) laser for H- beam shaping applications. Customizable modulation of the input (seed) laser pulse shape will be shown at the nanosecond level, allowing for high speed 'notching' or 'trimming' of photo-ionized H- bunch shapes after sufficient optical amplification. By matching the laser pulse train shape to the inverse of the desired H- bunch shape, the design of our laser system could be applied to the selective longitudinal neutralization of low energy (1 MeV) H- beams. Theoretically needed pulse energies for high percentage photo-ionizations above 99.9% will be presented and challenges for reaching the required laser pulse energies and repetition rates will be discussed.

INTRODUCTION

RFQ Bunching Output

In simulations of the LAMP RFQ output it has been noted that significant satellite pulses will likely be generated. This concept is qualitatively shown in Figure 1. The satellite bunches will have an approximate 1.5 ns duration and 5 ns spacing. We are mainly concerned with the first three pairs of satellite bunches, and will concentrate on removing only those bunches, without effecting the centeral signal bunch.

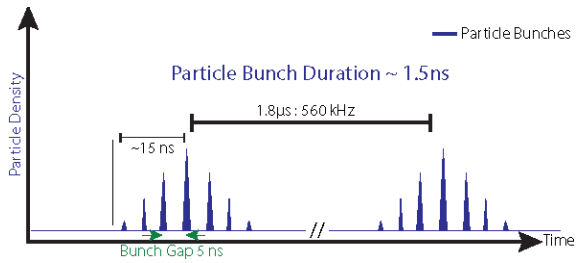

Figure 1: Notional structure of RFQ output illustrating satellite structure formation with ~1.5 ns micro-spacing and 1.8 µs macro-spacing.

Laser / Bunch Overlap

The question we are staring to ask in this work is, is it possible to accurately overlap laser pulses with bunch satellites without affecting the center (signal) bunch. In Figure 2 we are illustrating the concept of overlapping tailored, high power laser pulses to photo-detach the secondary electron in the H- anion. Tailoring the pulse shapes becomes important when estimating the amount of laser energy needed to neutralize the H- density by 99%. Even with only 50 µJ/pulse energy in a continuous pulse train of 2ns bunches at a 600 MHz (1.6 ns spacing) the average output power of such a laser system is 30 kW. A laser power that becomes challenging to manage due thermal and nonlinear losses. As shown below pulse energies much greater than 50 µJ will be needed to efficiently neutralize all satellite bunches with an efficiency > 99%.

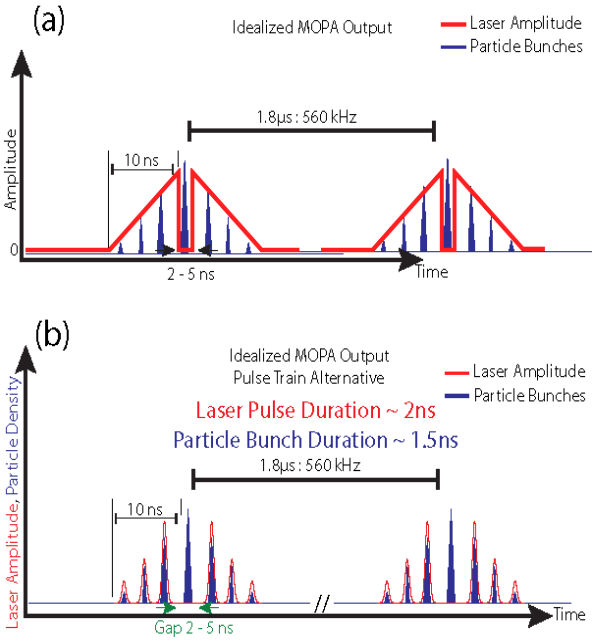

Figure 2: laser pulse overlap concept. (a) Double triangle pulse train with a center gap. (b) Exact pulse to bunch matching.

THEORY OF LASER STRIPPING

Laser-based Neutralization

A strong laser beam intersecting an H- bunch can neutralize a fraction, F_{H^-}, of the hydrogen anions. The neutralization fraction can be calculated using [1]:

$$\frac{\mathbf{dn_{H^0}}}{\mathbf{dt}} = -\boldsymbol{\sigma_N}\ \mathbf{n_{ph}}\ \mathbf{n_{H^0}v}$$

$$F_{H^{-1}} = \frac{N_{H^0}}{N_{H^-}} = 1 - e^{-\frac{4\,\sigma_N\,E_{cm}\,(1-\beta\cos\theta)}{\pi\,d\,\beta\,c\sin\theta}}$$

and the laser bunch intersection geometry shown in Figure 3. Where σ_N is the photo-detachment cross section [2], n_{ph} is the photon flux density, n_{H^0} is the density of generated neutrals, and v is the speed of the particles. F_{H^-} is the fraction of remaining negative hydrogen anions, N_{H^0} is the number of generated neutral hydrogens, N_{H^-} is the number of negative hydrogen anions, and E_{cm} is the center of mass energy of the photons in the particle rest frame.

‡ crohde@lanl.gov, †kbish@lanl.gov

Content from this work may be used under the terms of the CC BY 4.0 licence (© 2026). Any distribution of this work must maintain attribution to the author(s), title of the work, publisher, and DOI.

ISBN: 978-3-95450-252-3 ISSN: 2673-5350 doi: 10.18429/JACoW-IPAC2026-TUP7370

STATUS UPDATE OF PERMANENT MAGNET RADIATION RESILIENCY STUDIES AT CEBAF*

R. M. Bodenstein†, C. Decker, K. E. Deitrick, B. R. Gamage, J. F. Gubeli, D. Hamlette, M. Janak, K. Jordan, S. Lee, C. Matthews, M. X. Mason, J. Meyers, B. Mosbrucker, I. Neththikumara, E. Nissen, V. Okey-Ejiowhor, J. Samari, S. Shriner, M. Smith, A. Ramirez, D. Thomas, N. Wilson
Thomas Jefferson National Accelerator Facility, Newport News, VA, USA
S. J. Brooks, Brookhaven National Lab, Upton, NY, USA
S. Boogert, Cockcroft Institute, Daresbury, UK
W. Shields, Royal Holloway University London, Egham, UK
B. Shepherd, STFC, Daresbury, UK

Abstract

The proposed CEBAF energy upgrade incorporates Fixed-Field Alternating-gradient (FFA) arcs utilizing permanent magnets. Validating their long-term stability in the tunnel's radiation environment is critical for technical feasibility. We present an overview of Jefferson Lab's permanent magnet radiation resiliency program, reviewing the in-situ demagnetization monitoring methodology and initial operational results. We also discuss upgrades for the ongoing second exposure campaign, which target refined dose correlations and reduced systematic uncertainties. Finally, we outline the roadmap for certifying permanent magnet optics for the upgrade energies.

INTRODUCTION

The FFA@CEBAF energy upgrade study proposes increasing the beam energy beyond 20 GeV by replacing conventional electromagnetic arcs with permanent-magnet FFA arcs [1]. Understanding the long-term radiation stability of these magnets in the CEBAF tunnel is critical for the project's technical feasibility. Radiation-induced demagnetization is a well-studied phenomenon in accelerator contexts, particularly for undulator magnets at light sources [2]. The established damage hierarchy ranks protons as most damaging, followed by neutrons, electrons, and gammas [3, 4]. However, prior studies typically relied on small sample sets ($N \leq 12$), doses far exceeding the CEBAF environment, or single material families. This LDRD project addresses all three limitations by deploying 60 sample plates carrying 540 individual magnets (spanning two NdFeB and two SmCo grades) in the operational tunnel for 12 months. An additional 57 plates serve as unexposed laboratory controls. Co-locating radiation-sensitive NdFeB with radiation-hard SmCo on each plate enables a gain-immune intra-plate differential measurement that cancels instrumental drift and isolates radiation-induced changes. This paper reports preliminary results from the first data-taking campaign and preparations for the second. Prior publications [5–7] detail the experimental design, dosimetry, simulations, and measurement apparatus.

EXPERIMENTAL OVERVIEW

Sample Design

Thirty Y-plates, each carrying four randomized permanent magnet samples (two NdFeB grades: N42EH and N52SH; two SmCo grades: SmCo33H and SmCo35), were deployed at eight tunnel regions (four recirculating arcs, two linacs, and two labyrinths) for approximately 12 months. Nine identical Y-plates remained in the laboratory as unexposed controls. The randomized co-location of all four materials on each plate is central to the analysis: the intra-plate differential between the radiation-sensitive NdFeB and radiation-hard SmCo cancels the dominant Helmholtz coil gain drift (± 0.124 %) by construction, enabling sub-percent detection sensitivity.

Additionally, pair assemblies (H-plates) with controlled magnetic configurations (aligned, antiparallel, and perpendicular) approximate different field orientations within a Halbach array [8, 9], providing data relevant to multifunction FFA magnet design.

Measurement and Dosimetry

Magnetic moments are measured with a precision Helmholtz coil system [10] and point fields with a Senis 3MH6 Teslameter [11], both mounted on mobile carts for in-situ tunnel access during accelerator downtime [12, 13]. Each plate is tracked with co-located dosimetry: optically stimulated luminescence (OSL) area monitors for photon and neutron dose, and FWT-70 optichromic rods for high-dose gamma fields [5]. Gamma doses span five orders of magnitude, from 0.3 Gy (labyrinths) to 23,000 Gy (linac positions).

FIRST CAMPAIGN RESULTS

Headline Result

Table 1 and Fig. 1 show the per-material results. Both NdFeB grades exhibit negative shifts (demagnetization), while both SmCo grades are consistent with zero, as the thermal

* Authored by Jefferson Science Associates, LLC under U.S. DOE Contract No. DE-AC05-06OR23177. The research described in this work was conducted under the Laboratory Directed Research and Development Program at Thomas Jefferson National Accelerator Facility for the U.S. Department of Energy.

† ryanmb@jlab.org

Content from this work may be used under the terms of the CC BY 4.0 licence (© 2026). Any distribution of this work must maintain attribution to the author(s), title of the work, publisher, and DOI.

ISBN: 978-3-95450-252-3 ISSN: 2673-5350 doi: 10.18429/JACoW-IPAC2026-TUP7602

HIGH-POWER TESTING OF X-BAND HIGH-GRADIENT STRUCTURES AND RF COMPONENTS AT THE MEL-BOX FACILITY

M. Volpi*, P. Giansiracusa, P. Pushkarna, R. Rassool, J. Valerian, V. Lu, M. Sun
The University of Melbourne, Melbourne, Australia
R. Dowd, S. Sheehy, Y.-R. E. Tan
Australian Nuclear Science and Technology Organisation, Sydney, Australia

Abstract

Mel-BOX, the reinstallation of half of CERN's XBOX3 test stand, has been operating at the University of Melbourne's X-LAB for several years. The facility provides 12 GHz high-power pulsed RF for the testing of X-band high-gradient accelerating structures and associated components relevant to the CLIC baseline. Two TD24 structures, previously conditioned at CERN and stored for approximately five years, were successfully reconditioned and tested at Mel-BOX, demonstrating that long-term storage does not significantly degrade high-gradient performance. SLED-I pulse compressors were also reconditioned as high-gradient RF subsystems in standalone operation. One unit was subsequently upgraded with newly designed removable copper tuning plates (cups), enabling improved matching control. High-power loads, installed at the end of the line throughout all campaigns, were exposed to the full RF conditions. They sustained peak power levels of up to 50 MW delivered by the upgraded pulse compressors, demonstrating reliable operation under nominal high-power conditions. These results establish Mel-BOX as a mature X-band platform for high-gradient testing and subsystem integration, supporting the development of compact accelerator systems for medical, industrial, and scientific applications.

INTRODUCTION

The realisation of the CLIC [1] concept requires normal-conducting X-band accelerating structures capable of operating at gradients of 100 MV/m with breakdown rates below 3×10^{-7} per pulse per metre, in order to limit luminosity degradation. Achieving these conditions relies on systematic high-power RF testing to characterise breakdown behaviour and optimise performance.

Mel-BOX [2–6], installed at the University of Melbourne, provides a dedicated high-gradient test platform derived from CERN's XBOX3 infrastructure. The facility delivers 12 GHz pulsed RF using two klystrons combined through SLED Type I pulse compression [7], enabling peak powers of several tens of MW with sub-microsecond pulse lengths at high repetition rates.

The present work extends the experimental programme towards system-level validation, including the reconditioning of stored accelerating structures, standalone operation and optimisation of pulse compressors (PC), and high-power testing of RF loads under nominal conditions.

* mvolpi@unimelb.edu.au

THE TEST STAND FACILITY

A layout of the final RF network of Mel-BOX configuration is shown in Fig. 1.

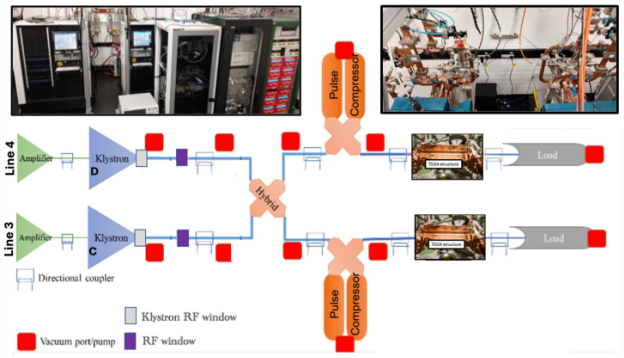

Figure 1: Last Layout of the Test Stand: Two Lines with Two Structures and Pulse Compressors.

Two RF windows (E42170 Canon Electron Tubes & Devices) have been installed between the kylstrons and the rest of the waveguide network [8], Fig. 1, where they provide an extra layer of protection for the klystrons which have a long lead time for replacement, particularly so in Australia.

Klystron RF power is guided into two high-Q cavities after in-phase combination at a hybrid coupler. The cavities then discharge RF power in the forward direction upon a 180° phase reversal, producing a compressed pulse with higher peak power and shorter duration. The cavities are tuned via a removable copper piston. An improved design, developed at CERN, was implemented on Line 3 to mitigate dipole mode effects and reduce breakdown rates. During conditioning of this pulse compressor, each cavity was controlled by a separate chiller, rather than using a single chiller to keep both cavities at the same temperature. Both lines are terminated with ~1m stainless steel RF loads, with directional couplers, pumping ports, and vacuum gates completing the network.

HIGH POWER CONDITIONING

A key advancement in this campaign is the upgrade of the pulse compressors through a new copper cup design applied to the cavity end plates. While the pulse compressors had previously been tested at CERN, the final tuning elements were replaced at Mel-BOX. The upgraded pulse compressor was reconditioned to withstand 50 MW peak power for the first time in Line 3 of Mel-BOX (Fig. 2), which was operated without a structure and terminated with a stainless steel load. The 50 MW milestone highlights that both the modified

Content from this work may be used under the terms of the CC BY 4.0 licence (© 2026). Any distribution of this work must maintain attribution to the author(s), title of the work, publisher, and DOI.

ISBN: 978-3-95450-252-3 ISSN: 2673-5350 doi: 10.18429/JACoW-IPAC2026-TUP7603

THE DESIGN OF THE QUASI-TRAVELING WAVE PARALLEL-COUPLED STRUCTURE

W. Gu*, Y. Zhao†, H. Chen, J. Shi, H. Zha, Tsinghua University, Beijing, China

Abstract

A quasi-traveling-wave parallel-coupled (TWPC) accelerating structure is proposed for compact linacs requiring both high RF efficiency and improved frequency tolerance. In contrast to conventional standing-wave parallel-coupled structures, the proposed topology enables partial reflected power generated under detuned conditions to be redistributed through the feeding manifold and reabsorbed by downstream cavities. A 12-cell X-band TWPC structure operating in the $5\pi/6$ mode was designed using a cascaded waveguide feeding network. The structure achieves approximately 95% unloaded RF power utilization with a 1.8 MW input power level. Beam dynamics simulations predict a 5 MeV energy gain with a 95%-bandwidth (the frequency range corresponding to a 5% drop in accelerating voltage) of 1.4 MHz.

INTRODUCTION

High-gradient and compact electron linacs are widely required in medical irradiation, industrial processing, and compact radiation-source applications. In these systems, both RF efficiency and operational stability are critical considerations. Conventional traveling-wave accelerating structures generally provide relatively broad operating bandwidth because the microwave power propagates continuously through the structure. However, a considerable fraction of the incident RF power must be dissipated in the output load, which limits the achievable RF utilization efficiency. In contrast, standing-wave accelerating structures can operate with significantly higher efficiency by storing microwave energy inside resonant cavities, but their performance is strongly affected by frequency detuning and fabrication errors.

Parallel-coupled accelerating structures have attracted increasing attention because they distribute microwave power to each cavity through an external feeding manifold rather than through beam-aperture coupling [1]. This configuration provides additional flexibility for cavity optimization and has been investigated in several high-gradient accelerator studies. Nevertheless, conventional standing-wave parallel-coupled structures still operate as resonant systems, where reflected microwave power generated under detuned conditions mainly returns to the input port and contributes little to the accelerating process.

To address this limitation, a quasi-traveling-wave parallel-coupled (TWPC) accelerating structure is proposed in this work. The proposed topology introduces a different microwave power reuse mechanism inside the feeding manifold. Under off-resonance conditions, reflected signals from upstream cavities are redirected through the waveguide network and partially absorbed by downstream cells. Consequently, the reduction of accelerating voltage caused by frequency deviation can be mitigated while maintaining high RF utilization efficiency. The present study mainly focuses on the RF design and dynamics simulation of the TWPC concept. A 12-cell X-band TWPC accelerating structure operating in the $5\pi/6$ mode was designed and optimized.

THEORETICAL ANALYSIS

The TWPC structure can be modeled as a cascaded microwave network composed of multiple waveguide T-junctions and cavity-coupling units, as shown in Fig. 1. Each cavity is independently fed through the external manifold, and the microwave interaction between adjacent cavities mainly occurs through the feeding network rather than through the beam aperture.

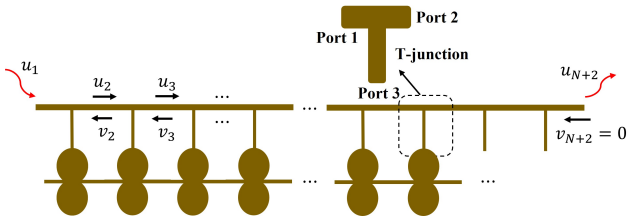

Figure 1: The quasi-traveling wave parallel-coupled structure with one manifold feeding cavities.

Assuming that each T-junction behaves as a lossless and reciprocal three-port microwave network, the electromagnetic response of the TWPC structure can be described by a cascaded scattering-matrix formalism. The relationship between adjacent cavity-coupling units can therefore be expressed as [2]:

$$\frac{1}{2}\begin{bmatrix} s_n - e^{j\theta} & s_n + e^{j\theta} & w_n \\ s_n + e^{j\theta} & s_n - e^{j\theta} & w_n \\ w_n & w_n & -2s_n^*\frac{w_n}{w_n^*} \end{bmatrix} \cdot \begin{bmatrix} u_n \\ v_{n+1} \\ \Gamma x_n \end{bmatrix} = \begin{bmatrix} v_n \\ u_{n+1} \\ x_n \end{bmatrix} \quad (1)$$

where s_n and w_n are undetermined complex numbers in the n-th three-port network, with s_n^* and w_n^* denoting their respective complex conjugates, and $|s_n|^2 + |v_n|^2/2 = 1$. θ is an undetermined degree number. Γ is the reflection coefficient in a resonant-cavity system [3].

When the operating frequency deviates from resonance, reflected signals are generated at each cavity-coupling port. In conventional standing-wave systems, these reflected signals mainly propagate back toward the source. However, when the matrix element S_{33} of the three-port junction is designed as a negative real value, the reflected microwave signals generated by frequency detuning can propagate constructively through the external feeding network and be partially reused by other cavities. As a result, part of the mi-

* gwh5784@163.com
† zhaoyan23@mails.tsinghua.edu.cn

Content from this work may be used under the terms of the CC BY 4.0 licence (© 2026). Any distribution of this work must maintain attribution to the author(s), title of the work, publisher, and DOI.

ISBN: 978-3-95450-252-3 ISSN: 2673-5350 doi: 10.18429/JACoW-IPAC2026-TUP7610

STUDY OF A DUAL-FEED TM020-MODE CAVITY FOR THE SUPER TAU-CHARM FACILITY*

Li Sun, Yelong Wei†, Zhicheng Huang, Yihao Zhang, Zexin Cao, Chengzhe Wang
National Synchrotron Radiation Laboratory,
University of Science and Technology of China, Hefei, China

Abstract

Radio frequency (RF) cavities play an important role in the ring RF systems of accelerator facilities by replenishing the beam energy lost to synchrotron radiation. Compared to the TM_{010}-mode RF cavity, the TM_{020}-mode cavity exhibits a high quality factor and low characteristic impedance, which can effectively mitigate coupled-bunch instabilities. However, the leakage of the operating mode and input coupler power capacity under high beam current remain critical issues for the TM_{020}-mode cavity. This paper proposes elliptical choke geometry for coaxial slot and dual-feed input couplers to reduce field asymmetry and thermal load for a normal-conducting TM_{020}-mode cavity. Electromagnetic simulations confirm excellent RF performance, demonstrating a cavity voltage of > 500 kV, an unloaded quality factor of > 60000, and operating-mode leakage suppressed to < 1%. Overall, the proposed dual-feed cavity with elliptical choke meets the demanding power, stability, and reliability requirements of next-generation high-current ring RF systems.

INTRODUCTION

As a key platform for next-generation frontier particle physics research, the Super Tau-Charm Facility (STCF) imposes unprecedented demands on beam performance, particularly in terms of ultrahigh luminosity and operation under high-current conditions [1]. In such facilities, the RF system serves not merely as an energy-replenishing unit but as a core subsystem that critically determines beam stability, lifetime, and ultimate luminosity. Due to its intrinsic R/Q, the TM_{020}-mode cavity would be helpful to suppress coupled-bunch instability (CBI) under the high-current scenarios envisioned for STCF. Therefore, a TM020-mode normal-conducting (NC) cavity has been selected as a candidate for the RF system of STCF [2–6].

This study aims to develop a high-performance and highly reliable TM_{020}-mode cavity suitable for the STCF project. An innovative design integrating an elliptical coaxial-slot cavity with a symmetrical dual-feed waveguide-type strongly rounded input coupler is proposed. This design incorporates a waveguide-type input coupler with large rounded corners to mitigate localized heating at the coupling iris under high power, and integrates a symmetric configuration with elliptical coaxial slots to suppress field leakage.

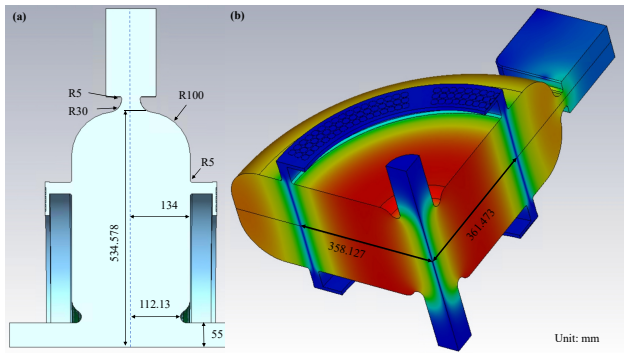

Figure 1: (a) Corresponding geometric structure and parameters with strongly rounded coupling iris, input coupler and elliptical choke-type coaxial-slot. (b) Magnetic field distribution of operation mode.

CAVITY DESIGN

Based on the physics design goals of the STCF project, such as its wide energy range (2–7 GeV) and high peak luminosity ($> 0.5 \times 10^{35}\mathrm{cm}^{-2}\mathrm{s}^{-1}$), the key parameters of the electron storage ring relevant to the RF system are summarized in the Table. 1. Under the requirement of a 2 A high beam current, a single ring rf system must provide at least 6 MV of accelerating cavity voltage and 3 MW of beam power.

The vacuum model of the main structure, which consists of one main cavity, two waveguide-type input couplers, two parasitic mode absorber structures, and four frequency tuners (temporarily excluding vacuum ports and pick-up ports). The cavity frequency is primarily determined by the equatorial radius of the main cavity body, while the R/Q, E_p/E_{acc}, and H_p/E_{acc} are mainly governed by the nose-cone curvature. The unloaded quality factor Q_0 is largely influenced by the chamfer design on both sides of the main cavity body and the geometry of the coaxial-slot structure. Additionally, the beam-pipe diameter significantly affects both R/Q and Q_0, which a smaller diameter leads to higher values of these parameters. To balance the requirements for R/Q and Q_0 while mitigating coupled-bunch instability (which favors a lower R/Q), the beam-pipe radius has been set to 55 mm. The nose cone incorporates optimized top and bottom chamfers to reduce the surface peak electric field, thereby preventing breakdown. The nose-cone design adopts a 30° angle complemented by a 30 mm top chamfer. The corresponding geometric parameters are illustrated in Fig .2.

* This work is supported in part by the "Hundred Talents Program" of Chinese Academy of Sciences (Grant No. KJ2310007003); in part by the Fundamental Research Funds for the Central Universities (Grant No. WK2310000114); in part by Chinese Academy of Sciences President's International Fellowship Initiative (Grant No. 2025PD0102); in part by the Super Tau Charm Facility Key Technology Research Project

† wylong@ustc.edu.cn

Content from this work may be used under the terms of the CC BY 4.0 licence (© 2026). Any distribution of this work must maintain attribution to the author(s), title of the work, publisher, and DOI.

ISBN: 978-3-95450-252-3 ISSN: 2673-5350 doi: 10.18429/JACoW-IPAC2026-TUP7611

HIGH-POWER EXPERIMENTAL STUDY ON A COMPACT C-BAND SPHERICAL PULSE COMPRESSOR

Y. Wei*[1], D. Alesini[4], Z. Cao[1], L. Faillace[4], G. Feng[1], P. Huang[1],
Z. Huang[1], S. Jiang[2,3], X. Liu[2,3], L. Sun[1], H. Zhang[2,3], Y. Zhang[1]
[1]University of Science and Technology of China, Hefei, China
[2]Institute of High Energy Physics, Chinese Academy of Sciences, Beijing, China
[3]Spallation Neutron Source Science Center, Dongguan, China
[4]INFN Frascati National Laboratories, Frascati, Rome, Italy

Abstract

In order to enhance the accelerating gradient of the 1-meter C-band Traveling-wave accelerating structure, as well as meet the physics requirements on the linear injector of the proposed Jinhua light source (JHLS) project, a compact C-band spherical pulse compressor was developed to boost the output power from klystron. This pulse compressor excites TE_{114} modes inside the spherical cavity by coupling power via a compact polarized coupler. In the preliminary high-power tests, an input pulse of 8.7 MW, 2.6 µs was compressed to 53.9 MW,400 ns output pulse through this pulse compressor, thereby enabling an average power gain of 4.2. Amplitude modulation (AM) was utilized to generate a flat-top output pulse. After modulation, an average power gain of 3.78 with a full-width at half-maximum (FWHM) pulse duration of 280 ns was achieved.

INTRODUCTION

The proposed Jinhua Light Source (JHLS) project is being developed by the National Synchrotron Radiation Laboratory (NSRL) at University of Science and Technology of China (USTC). Its linear injector consists of a C-band unit and a S-band unit. In the C-band unit, a C-band klystron is utilized to deliver 2.5-µs duration pulses with a peak power of 40 MW to two C-band accelerating structures, achieving an average gradient of 40 MV/m.

To date, a 1-meter C-band accelerating structure with a filling time of 253 ns has been developed [1]. In order to satisfy the requirements of the JHLS physics and high-power tests on our C-band accelerating structure, a compact C-band spherical pulse compressor based on dual-mode polarized coupler and the TE_{114} mode storage cavity has been developed, as reported in [2]. Firstly, this pulse compressor should be sufficient for filling up the whole C-band accelerating structure. Additionally, it exhibits a trade-off between the power gain and the compression efficiency. The basic parameters of this C-band unit are listed in Table 1.

The rest of this paper is organized as follows. Section II briefly describes the RF design of this C-band pulse compressor, Section III presents the cold-test results after tuning, Section IV presents the high-power tests as well as the flattop pulse experiment. Section V summarizes this paper.

* wylong@ustc.edu.cn

Table 1: Basic Parameters of the C-Band RF Unit

Parameter	Value	Unit
Operating frequency /f	5.712	GHz
Klystron power /P_{in}	40	MW
Repetition rate	60	Hz
Pulse width (uncompressed)/t_1	2.5	µs
Pulse width (compressed) /$t_2 - t_1$	300	ns
Output power /P_{out}	≥150	MW

RF DESIGN

In this C-band pulse compressor, the sphere cavity is chosen to operate at TE_{114} modes because of the higher quality factor and the available cavity size. The dual-mode polarized coupler is designed to convert TE_{10} mode at the rectangular waveguide into orthogonally polarized TE_{11} modes at the circular waveguide. This coupler is optimized to achieve the impedance matching so that the RF power can be transmitted smoothly into the storage cavity with negligible reflections. Meanwhile, the emitted power will flow to the other waveguide port instead of returning back to klystron. For more detailed information, see [2].

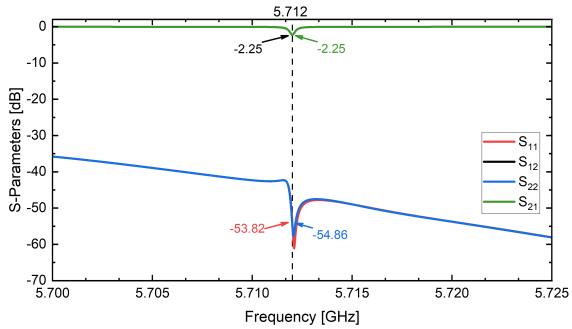

Figure 1: S-parameters of the whole C-band spherical pulse compressor.

In summary, this C-band spherical pulse compressor is designed to realize an optimized average power gain of 4.49 with a high coupling coefficient of 8. The corresponding efficiency is 54.2%. The simulated S-parameters of the whole C-band spherical pulse compressor are shown in Fig. 1.

Figure 2 shows the simulated electric field, magnetic field, and modified Poynting vector S_c [3] on the surface of the pulse compressor at an input power of 1 W from port

Content from this work may be used under the terms of the CC BY 4.0 licence (© 2026). Any distribution of this work must maintain attribution to the author(s), title of the work, publisher, and DOI.

ISBN: 978-3-95450-252-3 ISSN: 2673-5350 doi: 10.18429/JACoW-IPAC2026-TUP7613

RF DESIGN OF A COMPACT X-BAND TWO-STAGE PULSE COMPRESSION SYSTEM

Y. Zhang*, Z. Cao, G. Feng, Z. Huang, Y. Wei,
University of Science and Technology of China, Hefei, China
D. Alesini, L. Faillace,
Istituto Nazionale di Fisica Nucleare, Rome, Italy

Abstract

This paper presents the design of a compact X-band two-stage pulse compression system featuring bowl-shaped open cavities, developed for a newly acquired 6-MW X-band klystron. The system consists of a correction cavity chain, a first-stage and a second-stage storage cavity. By employing bowl-shaped geometries, which have an unloaded quality factor (Q_0) higher than those of spherical cavities, the system significantly enhances both power gain and compression efficiency. With an input pulse of 5-μs from the klystron, the first-stage pulse can be flattened, generating a two-stage compressed pulse of 200 ns with exponentially decaying waveforms, thereby achieving a total peak power gain of ≥ 10.

INTRODUCTION

To meet the demanding power requirements of modern linear accelerators (linacs), advanced pulse compression techniques have become increasingly vital. The pulse compressor is a RF component that converts a long input pulse into a shorter, higher-amplitude pulse, reducing dependence on high-power klystrons [1, 2]. Due to inherent physical limitations, the peak power gain of a single-stage pulse compressor is typically capped at a threshold of 9 [3].

To achieve a higher power gain, this paper proposes the design of a two-stage pulse compression system, which incorporates a correction cavity chain (CC), a first-stage storage cavity (SC1), and a second-stage storage cavity (SC2). Due to the energy discharge process within the resonant cavity, the waveform generated by a single-stage pulse compressor exhibits a characteristic exponential decay. However, a flattop output is preferable, as it facilitates the acceleration of multiple bunches while effectively reducing the maximum surface fields of the structure. The correction cavity chain is an efficient method to compensate for the exponentially decaying output pulse from the first-stage pulse compressor [4]. The correction cavity consists of 6 resonant cavities, which are designed to create periodically spaced resonant peaks centered around the operating frequency of the storage cavities. The input pulse is modulated by the correction cavity chain into a rising-edge pulse. This shaped waveform compensates for the decaying pulse released by the first-stage storage cavity, ultimately resulting in a flattop output pulse. This output pulse is imperfectly flat because of the limited number of correction cavities and has some ripples at the top. Both the correction cavities and storage cavities employ the bowl-shaped geometry proposed in Ref. [5]. This specific cavity has a high unloaded quality factor (Q_0) while maintaining a compact physical size. After optimization, the proposed two-stage pulse compression system achieves a theoretical peak power gain of 16.95. Table 1 summarizes the main parameters of the two-stage pulse compression system.

Table 1: Parameters of the Two-stage Pulse Compression System

Parameters	Value
Input pulse length	5 μs
Output pulse length	200 ns
Number of correction cavities	6
Peak Power Gain	16.95
Unloaded quality factor of CC	1.7×10^5
Unloaded quality factor of SC1	2.5×10^5
Unloaded quality factor of SC2	2.4×10^5
Coupling factor of CC	2.0
Coupling factor of SC1	2.8
Coupling factor of SC2	28.4

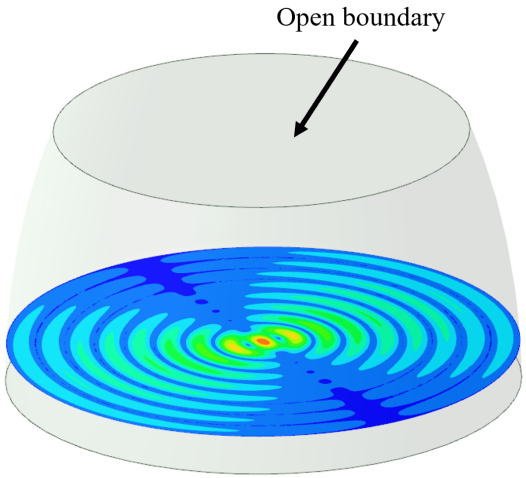

Figure 1: The electric field distributions of the working mode of $TE_{1,2,9}$.

* zhyh123@mail.ustc.edu.cn

Content from this work may be used under the terms of the CC BY 4.0 licence (© 2026). Any distribution of this work must maintain attribution to the author(s), title of the work, publisher, and DOI.

ISBN: 978-3-95450-252-3 ISSN: 2673-5350 doi: 10.18429/JACoW-IPAC2026-TUP7615

DESIGN, FABRICATION AND LOW-POWER MEASUREMENTS OF AN X-BAND PARALLEL-COUPLED ACCELERATING STRUCTURE

Z. Huang, P. Huang, Y. Zhang, Y. Wei*, G. Feng
University of Science and Technology of China, Hefei, China

Abstract

This paper presents the design, fabrication and low-power measurements of an X-band parallel-coupled accelerating structure for short-pulse high-gradient applications. The structure, consisting of 16 cells fed in parallel by a smooth-waveguide network, is designed to operate under an input pulse length of 50 ns. Aluminum and copper prototypes were fabricated and cold-tested. The frequency deviation for each cell is tuned using bead-pull method, showing good agreement with the simulations.

INTRODUCTION

High-gradient RF accelerating structures are essential for compact accelerator systems such as X-ray FELs and future linear colliders. X-band technology enables gradients above 100 MV/m, but the breakdown rate strongly depends on both gradient and RF pulse length [1]. Reducing the pulse length is therefore critical for high-gradient operation [2].

Parallel-coupled accelerating structures provide an effective solution by distributing RF power directly to each cavity instead of relying on inter-cell coupling [3–5], allowing short filling time and flexible cavity design. In this paper, an X-band parallel-coupled structure based on a SLAC-type feeding topology is developed and experimentally tuned using the bead-pull method.

RF DESIGN

The structure consists of a feeding network and 16 accelerating cells, as shown in Fig. 1. The feeding network is formed by cascading 3-port smooth-waveguide T-junctions, which distribute RF power with a π phase difference between adjacent ports to match the π-mode operation.

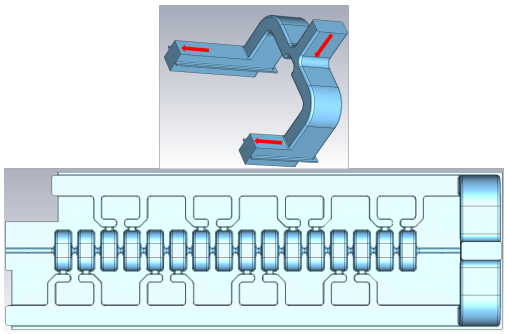

Figure 1: The geometry of the parallel-coupled structure with the coupler.

The regular cells adopt a racetrack-like geometry with a small iris aperture of 1.3 mm to achieve weak power coupling, as shown in Fig. 2. The electromagnetic field distributions of the regular cell is shown in Fig. 3. The parameters of the structure is shown in Table 1. The overall coupling coefficient is designed to be 4.8, corresponding to a filling time of approximately 40 ns.

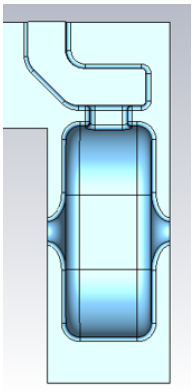

Figure 2: The geometry of the regular accelerating cell.

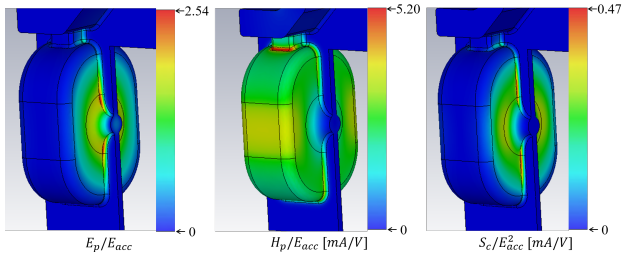

Figure 3: The normalized electric (a), magnetic (b) fields and modified poynting vector S_c (c) of the regular cell.

Under this condition, the transient accelerating field can be approximately expressed as:

$$E_{acc} \propto \frac{2\sqrt{\beta'}}{1+\beta'}(1-e^{-t/t_f}) \tag{1}$$

where $t_f = 2Q_0/\omega(1+\beta')$ is the filling time determined by the coupling coefficient β' of the full parallel-coupled structure, which is defined by:

$$\beta' = 2N\frac{1-|s_{33}|}{1+|s_{33}|}\beta \tag{2}$$

where β, N are the coupling coefficient and number of the regular cells.

The simulated on-axis field distribution is shown in Fig. 4. It can be observed that the 1# and 16# cells should be tuned a little due to the power coupling.

* wylong@ustc.edu.cn

Content from this work may be used under the terms of the CC BY 4.0 licence (© 2026). Any distribution of this work must maintain attribution to the author(s), title of the work, publisher, and DOI.

ISBN: 978-3-95450-252-3 ISSN: 2673-5350 doi: 10.18429/JACoW-IPAC2026-TUP7617

DESIGN OF AN IMPROVED S-BAND SLED PULSE COMPRESSOR

Pengbin Huang, Yelong Wei†, Yihao Zhang, Zexin Cao, Zhicheng Huang, Guangyao Feng,
University of Science and Technology of China, Hefei, China

Abstract

This paper presents the design of an improved SLED pulse compressor for our beam test platform at National Synchrotron Radiation Laboratory (NSRL). It consists of a 3 dB hybrid, a TE_{10}-TE_{01} mode converter, and a resonator storage cavity. Through geometrical optimizations, the resonator is designed to operate in the $TE_{0,1,10}$ mode, which offers a high intrinsic quality factor while maintaining cost-effectiveness. Additionally, the conventional cylindrical configuration has been modified to a double-ended conical structure, which facilitates better mode isolation.

INTRODUCTION

RF pulse compression is widely used to increase peak RF power when the klystron pulse length is long compared with the pulse required by an accelerating structure. In a SLED-I system two identical storage cavities are filled through a 3 dB hybrid coupler and, near the end of the drive pulse, the incident phase is reversed by 180 degrees to release the stored energy into a shorter, higher power pulse [1]. Compact high-power systems require high intrinsic quality factor and stable mode operation. TE01-like cylindrical modes are attractive because the magnetic field in the wall is small, enabling high Q_o, while adiabatic tapers transitions can suppress excitation of unwanted modes and reduce the size of the mode converters [2],[3].

DESIGN REQUIREMENTS

The compressor comprises (i) a four-port 3 dB hybrid for power splitting/combining and source isolation, (ii) two identical $TE_{0,1,10}$ storage cavities, and (iii) a compact TE_{10}-TE_{01} mode converter to connect a rectangular waveguide input to the circular cavity. Fig. 1 demonstrates the prototype pulse compressor of the CERN BOX2 SLED. Figure 2 shows a block diagram of the proposed configuration. The intended operating point is 2.9982 GHz with 4 us input pulses at 50 Hz repetition. Low-power acceptance is specified by input intrinsic quality factor, while pulse-compression performance is expressed by peak and average power gains at the required compressed pulse length.

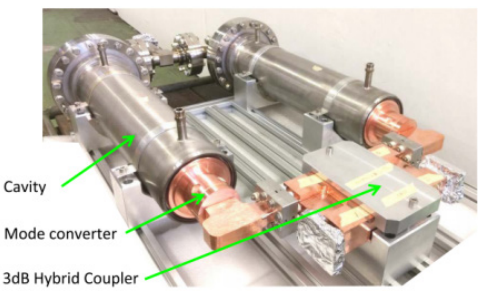

Figure 1: CERN BOX2 SLED.

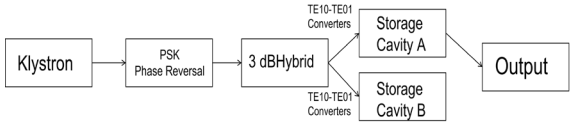

Figure 2: Block diagram of the improved SLED-I pulse compressor with two storage cavities and a 3 dB hybrid [4].

Table 1: Main Design Targets of the S-band Pulse Compressor

Parameter	Target	Unit
Operating frequency	2.9982	GHz
Repetition	50	Hz
Input pulse width /	4	us
Output pulse width	0.8	μs
Input power	45	MW
Cavity mode	$TE_{0,1,10}$	-
Q_o	>=95,000	-
Peak	>= 5	-
Average power gain	>= 3	-

$TE_{0,1,10}$ STORAGE CAVITY WITH PARAMETRIC ADIABATIC TAPERS

The time - domain method [1] directly characterizes the pulse compression process through the analysis of the transient behavior of resonant cavities. This approach can be integrated with frequency - domain analysis for verification. By utilizing rectangular pulses as ideal input pulses, any pulse compressor can be assessed based on the following key parameters:

$$M = \frac{1}{t_2 - t_1} \frac{\int_{t_1}^{t_2} P_{out}(t)\,\mathrm{d}t}{\int_{t_1}^{t_2} P_{in}(t)\,\mathrm{d}t} = \frac{\int_{t_1}^{t_2} P_{out}(t)\,\mathrm{d}t}{\int_{t_1}^{t_2} P_{in}(t)\,\mathrm{d}t} \,. \qquad (1)$$

Where t_1 denotes the phase inversion time, t_2 represents the input pulse width, M indicates the equivalent power amplification factor within the duration of a radio frequency pulse. The parameter analysis of the mode converter is shown in Fig. 3.

†wylong@ustc.edu.cn

Content from this work may be used under the terms of the CC BY 4.0 licence (© 2026). Any distribution of this work must maintain attribution to the author(s), title of the work, publisher, and DOI.

ISBN: 978-3-95450-252-3 ISSN: 2673-5350 doi: 10.18429/JACoW-IPAC2026-TUP7618

DESIGN OF AN X-BAND COMPACT MODE CONVERTER FOR CONVERTING TE_{10} MODE TO TE_{01} MODE*

W. Zhang, P. Huang, Z. Huang, Ch. Wang, Y. Wei†, Y. Zhang
University of Science and Technology of China, Hefei, China

Abstract

This paper presents the design of a compact and efficient rectangular waveguide TE_{10} to circular waveguide TE_{01} mode converter operating in the X-band. By incorporating two choke slots, the design achieves a high-purity circular waveguide TE_{01} mode. The optimized results show that at the operating frequency of 11.424 GHz, the conversion efficiency for the circular waveguide TE_{01} mode is calculated to be approximately 100%, while the reflection coefficient is better than -50 dB. The bandwidth reaches more than 260 MHz for the transmission coefficient while the bandwidth is approximately 210 MHz for the reflection coefficient better than -20 dB.

INTRODUCTION

With the rapid development of microwave technology in accelerator systems, high-power pulse compressors have been utilized to double the energy of the Klystron. The pulse compressor is mainly based on the theory of SLAC energy doubler (SLED) [1]. The initial mode converter of the SLED directly coupled a TE_{10} rectangular waveguide into the resonant cavity, which led to mode mixing in the cavity. Therefore, by additionally designing a multi-stage mode converter, we can achieve a larger bandwidth and isolation between adjacent degenerate modes. The TE_{01n} mode in a cylindrical cavity achieves a high quality factor because its surface current has no axial component, leading to minimal wall loss [2, 3]. In addition, since the electric field vanishes at the waveguide wall, the mode can sustain higher power levels without surface breakdown[4]. Thus, The TE_{01n} mode was chosen as the operating mode of the SLED system. To ensure the purity of the storage mode, the design of an X-band compact and efficient rectangular waveguide TE_{10} to circular waveguide TE_{01} mode converter is presented in this paper.

RF DESIGN

The rectangular waveguide TE_{10}-circular waveguide TE_{01} mode converter described in this paper has a center frequency of 11.424 GHz. And it is composed of two parts: the rectangular waveguide TE_{10}-TE_{20} mode converter and the rectangular waveguide TE_{20}-circular waveguide TE_{01} mode converter, as shown in Fig 1.

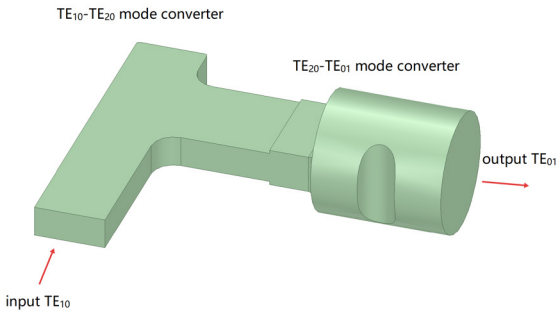

Figure 1: The rectangular waveguide TE_{10}-circular waveguide TE_{01} mode converter.

TE_{10}-TE_{20} Mode Converter

The rectangular waveguide TE_{10}-TE_{20} mode converter structure is relatively simple, it consists of a standard rectangular waveguide WR90 and a widened rectangular waveguide, with a smooth connection between the widened waveguide and the standard waveguide section. The input power is fed into Port 1, while the TE_{10} mode is converted to TE_{20} mode in the converter at Port 2. The two TE_{10} modes at Port 2 have opposite phases, resulting in the excitation of the TE_{20} mode and the suppression of the TE_{10} mode. Figure 2 shows the electric field distribution of the rectangular waveguide TE_{10}–TE_{20} mode converter after optimization. Figure 3 shows the S-parameters of the rectangular waveguide TE_{10}-TE_{20} mode converter. The TE_{10} mode is suppressed, with a transmission coefficient lower than -30 dB.

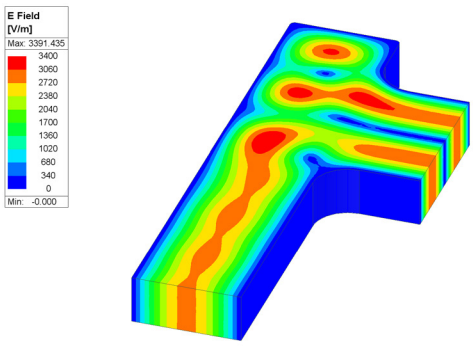

Figure 2: Electric field distribution of the rectangular waveguide TE_{10}-TE_{20} mode converter.

†wylong@ustc.edu.cn

Content from this work may be used under the terms of the CC BY 4.0 licence (© 2026). Any distribution of this work must maintain attribution to the author(s), title of the work, publisher, and DOI.

ISBN: 978-3-95450-252-3 ISSN: 2673-5350 doi: 10.18429/JACoW-IPAC2026-TUP7621

DESIGN AND THEORETICAL ANALYSIS OF A HIGHLY COMPACT TRIPLE-FOLDED 20 MHZ QUARTER-WAVE CAVITY FOR SSMB

Peizhi Fang, Shuxin Zheng*, Lianmin Zheng, Xiujie Deng, Zhilong Pan, Chuanxiang Tang, Hongjuan Yao
Department of Engineering Physics, Tsinghua University, Beijing, China

Abstract

To meet the energy compensation requirements of Steady-State Micro-Bunching (SSMB), a 20 MHz RF cavity with extreme axial compactness is essential. This paper presents an innovative triple-folded quarter-wave cavity design that overcomes the size limitations of conventional structures. Based on cascaded transmission line theory, we established an analytical model to optimize the cavity's shunt impedance and tuning range. A triple-folded 20 MHz prototype was designed and validated via CST simulations, showing that the axial length is compressed to 1.25 m (approximately 1/3 the length of a standard QWC) while achieving a high shunt impedance of 558 kΩ with excellent thermal stability. This compact design offers a high-efficiency solution for low-frequency RF systems.

INTRODUCTION

The Steady-State Micro-Bunching (SSMB) mechanism [1] offers a promising path toward high-power, high-repetition-rate coherent radiation, particularly for extreme ultraviolet (EUV) lithography. Unlike traditional storage rings, SSMB requires a specialized RF system to compensate for the energy loss of long electron bunches without introducing unwanted longitudinal modulation. For the General Longitudinal Strong Fousing (GLSF) SSMB design, an auxiliary RF system operating at a fundamental frequency of 20 MHz is required.

Designing an efficient RF cavity at such a low frequency presents significant challenges. A standard $\beta = 1$ quarter-wave cavity (QWC) at 20 MHz would exceed 3.7 meters in length, which is impractical for compact lattice integration. While magnetic-alloy loaded cavities or high-capacitive loading cavity can reduce the physical footprint, they often suffer from substantial power dissipation or high risk of multipacting [2–4]. Previous developments, such as the folded QWCs at RHIC, have demonstrated improved compactness [5], but further reduction in axial length is necessary for GLSF SSMB light sources.

In this paper, an innovative multi-folded cavity scheme is proposed, with a specific focus on the triple-folded configuration. A theoretical model based on cascaded transmission line theory is developed to analytical characterize the electromagnetic properties of the structure. Utilizing this model, a comprehensive parametric sweep is performed to evaluate the shunt impedance and frequency sensitivity, leading to the determination of optimized geometric parameters. Finally, the analytical results are validated against CST eigenmode simulations, demonstrating excellent agreement and confirming the effectiveness of the proposed design methodology.

EVOLUTION OF THE CAVITY CONFIGURATION

The multi-folded quarter-wave cavity is evolved from a standard coaxial quarter-wave structure. As shown in Fig. 1(a), a conventional QWC consists of a simple coaxial line that is shorted at one end and open at the accelerating gap, requiring a physical length of $\lambda/4$. By folding the outer conductor back towards the gap, a single-folded QWC (Fig. 1(b)) reduces the axial length by approximately half.

The proposed multi-folded design (Fig. 1(c)) further extends this concept by using several nested coaxial cylinders. This creates multiple "folds" where the electromagnetic wave propagates back and forth within the nested layers (indicated by the red arrows in Fig. 1). This technique effectively compresses the axial footprint to approximately $1/n$ of the original QWC length, where n is the fold number which represents the number of nested coaxial sections between the accelerating gap and the shorted end.

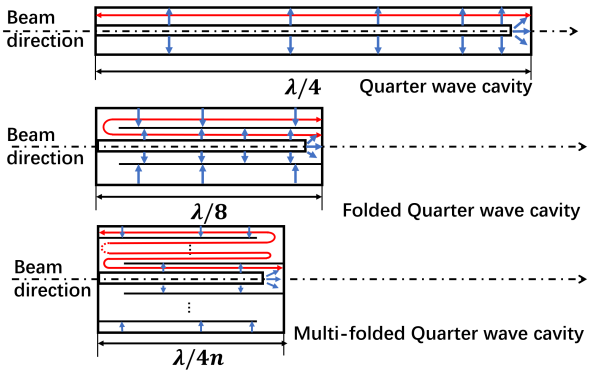

Figure 1: Schematics of a conventional coaxial cavity(a), a folded quarter-wave cavity(b), and the proposed multi-folded quarter-wave cavity(c). Blue arrows indicate the electric field distribution, while red arrows represent the propagation paths of the electromagnetic fields within the cavities.

THEORETICAL SCALING AND FOLD-NUMBER ANALYSIS

To evaluate the fundamental advantages and trade-offs of the multi-folded geometry, an analytical study was conducted focusing on the impact of the fold number n.

To establish a baseline for spatial compression, we first consider an idealized case where the characteristic impedances of all n sections are identical ($Z_1 = Z_2 = \cdots =$

* zhengsx@tsinghua.edu.cn

Content from this work may be used under the terms of the CC BY 4.0 licence (© 2026). Any distribution of this work must maintain attribution to the author(s), title of the work, publisher, and DOI.

This is a preprint - the final version is published with IOP

ISBN: 978-3-95450-252-3 ISSN: 2673-5350 doi: 10.18429/JACoW-IPAC2026-TUP7622

DESIGN OF A COMPACT ENERGY-TUNABLE X-band LINAC FOR FLASH RADIOTHERAPY*

Z. H. Gao, P. Wang†, J. H. Tan‡, C. Wang, D. H. Su, Y. F. Lan, X. X. Huang
Y. X. Lu, Y. S. Guo, C. Xia, R. C. Qin, H. L. Wan, X. Y. Sun, W. C Fang
Shanghai Advanced Research Institute, Chinese Academy of Sciences, Shanghai, China

Content from this work may be used under the terms of the CC BY 4.0 licence (© 2026). Any distribution of this work must maintain attribution to the author(s), title of the work, publisher, and DOI.

Abstract

FLASH radiotherapy (FLASH-RT) demonstrates the potential to maintain tumor control while reducing normal tissue toxicity through ultra-high dose rates. This paper presents a novel compact X-band (9.3 GHz) accelerating system designed for FLASH-RT applications. The core innovation is a dual-structure common-source architecture: the first structure provides a fixed 6 MeV energy gain, while the second enables independent continuous energy adjustment from 0 to 6 MeV via a tunable microwave network. This design allows a single klystron to drive both structures without mutual interference during energy adjustment. The system length is only approximately 1 meter. The design process integrates radio frequency (RF) simulation and beam dynamics simulation in a coupled manner, with particular focus on the bunching section optimization. This compact system provides a high-performance accelerator solution for next-generation FLASH radiotherapy, especially for intraoperative applications requiring rapid energy adjustment.

INTRODUCTION

FLASH Radiation Therapy (FLASH-RT) employs ultra-high dose rates to reduce normal tissue toxicity while maintaining tumor control compared to conventional radiotherapy [1, 2]. This novel approach has attracted significant interest from the accelerator community, with exploration of various radiation modalities including X-rays, protons, very-high-energy electrons (VHEE), and low-energy electrons for FLASH dose delivery.

X-ray-based systems require high beam currents due to the inefficiency of bremsstrahlung conversion. VHEE offers improved efficiency but still requires high beam power. Intra-operative electron radiation therapy (IOeRT) represents another approach, combining surgical resection with targeted electron irradiation. Clinically applied for decades in cancers such as soft tissue sarcoma, pancreatic, rectal, and breast malignancies, IOeRT can deliver electron beams at dose rates compatible with the FLASH regime [3, 4].

Standing-wave linear accelerators are key enabling technologies for FLASH-RT. X-band accelerators are particularly attractive due to their high accelerating gradients supporting rapid dose delivery and compact, lightweight design enhancing clinical versatility. This work presents a novel X-band microwave system operating at 9.3 GHz, engineered specifically for FLASH-RT applications. The system comprises two accelerating structures integrated into a compact assembly with a total length of only 1 meter. Its key innovation is a dual-tube architecture: the first tube provides fixed acceleration to 6 MeV, while the second enables real-time energy tunability from 0 MeV to 6 MeV. Both tubes are powered by a same klystron, yet the energy adjustment operates independently without interference.

SYSTEM DESIGN

The accelerator system employs a dual-structure common-source architecture to achieve energy tunability from 6–12 MeV. High-energy electron beams are used for deeper tissue penetration, while low-energy beams are suited for superficial treatments. The energy must be adjusted based on tumor thickness and location.

Overall System Architecture

As shown in Fig. 1, microwave power from a single klystron passes through a circulator and a 3 dB power divider, equally distributing power to both acceleration structures. Half the power enters the first structure directly, while the other half passes through a phase shifter and a tunable power divider before entering the second structure. The power divider uses a movable short-circuit plane to continuously adjust output power from 0% to 100%. The 3 dB power divider ensures independence: reflected power from one port cannot enter the other, making the two channels mutually independent.

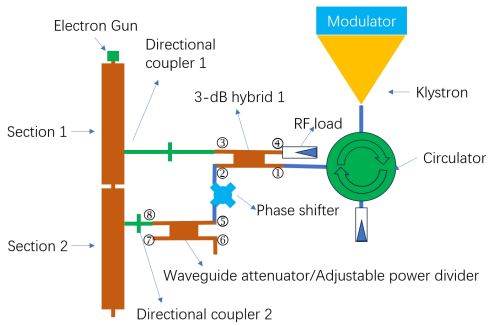

Figure 1: Schematic diagram of the microwave system with dual-structure common-source architecture.

ACCELERATING STRUCTURE DESIGN

This system uses a hot cathode electron gun. Since the electron source produces a DC beam, a bunching section

* Work was supported by the National Natural Science Foundation of China (No. 12405178) and (No. 12505171).
† wangping@sari.ac.cn
‡ tanjh@sari.ac.cn

ISBN: 978-3-95450-252-3 ISSN: 2673-5350 doi: 10.18429/JACoW-IPAC2026-TUP7623

DESIGN AND IMPLEMENTATION OF RIDGE WAVEGUIDES FOR DUAL-MODE MICROWAVE STRUCTURE*

X.X. Huang†,1, A. Grudiev[2], J.H. Tan[1], W.C. Fang[1]
[1]Shanghai Advanced Research Institute, Chinese Academy of Sciences, Shanghai, China
[2]European Organization for Nuclear Research, Geneva, Switzerland

Abstract

The dual-mode microwave structure is receiving increasing attention and research. In the application of dual-mode structures, it is necessary to solve the problem feeding microwave power at different frequencies. One method is to use complex waveguide components, such as first and second harmonic photocathode bimodal gun, which consists of the assembly of the directional coupler and the mode launcher. The structure combines the S-band and C-band power into a waveguide and feeds them into the dual-mode electronic gun. Another method is to use ridge waveguide to achieve selectable transmission or blocking of specific frequency. Currently, the ridge waveguide has been applied to dual-mode deflecting structure. This paper presents a X-band bandpass filter has been engineered to achieve a power reflection level of less than -30 dB at 12 GHz and a power transmission level of less than -40 dB at 24 GHz.

INTRODUCTION

In modern accelerator and radio frequency (RF) structures, dual-mode and dual-frequency operation has attracted considerable attention due to its ability to integrate multiple functions and improve beam performance. Examples include photoinjector operating with fundamental and second harmonics [1], variable-polarization deflection realized by a dual-mode transverse deflecting structure (TDS) [2], and bunch length manipulation based on a double-RF system [3]. All these schemes superimpose different frequencies or modes within a single cavity to achieve longitudinal bunch shaping, transverse deflection control, and suppression of emittance and energy spread. Such designs typically require simultaneous handling of multiple resonant modes, placing high demands on frequency isolation, power coupling, and higher-order mode (HOM) suppression.

To achieve frequency selection and directional power transmission, various waveguide structures have been introduced. A directional coupler, through its multi-branch design, shown in Fig. 1, enables dual-frequency combining and high-directivity transmission, ensuring that microwave power is delivered along a prescribed direction while providing bandpass/band-stop functionality. However, its structure including multiple branches and matching sections is relatively complex, making fabrication and tuning more difficult. In contrast, a ridge waveguide, shown in Fig. 1, owing to its simple structure and controllable bandwidth, can effectively realize transmission or band-stop or bandpass filtering at specific frequencies. It has been used, for example, as a bandpass filter in a dual-mode TDS to effectively isolate reverse leakage of high-frequency signals. Furthermore, in a dual-mode (TM_{010}/TM_{020}) harmonic cavity, a ridge waveguide is employed as an HOM extraction structure, and its band-stop property is utilized to precisely suppress the third-harmonic power. By adjusting the length of the short-circuited stub and the position of the tuning vane in the band-stop waveguide, an isolation bandwidth of approximately 15 MHz with –20 dB rejection can be achieved around 1.5 GHz, effectively blocking harmonic power leakage while introducing only minor loss to the operating modes.

In summary, ridge waveguides are increasingly used in dual-mode and dual-frequency RF structures, meeting diverse requirements such as compact filtering, suppression of reverse power transmission, and high-power harmonic rejection. It will provide important support for the integrated design of advanced accelerator and light source systems.

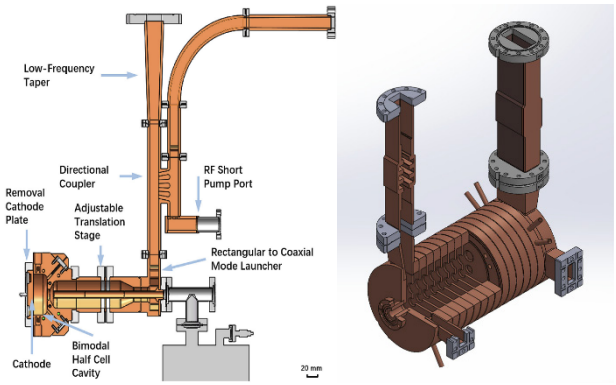

Figure 1: Engineering drawing of the first and second harmonic photocathode bimodal gun (left) and two-mode transverse deflecting structure (right).

SCHEME DESIGN FOR THE RIDGE WAVEGUIDE

The Compact Linear Collider (CLIC) is a proposed high-energy electron-positron collider based on normal-conducting accelerating structures operating at high frequencies, typically in the X-band (12 GHz) and above [4]. In such high-frequency accelerators, the feeding waveguide for the accelerating structure is conventionally a standard rectangular waveguide. However, a significant drawback of a conventional rectangular waveguide is that it supports not only the fundamental TE_{10} mode but also a large number of higher-order modes (HOMs) at the operating

* Work supported by the National Natural Science Foundation of China (No. 12505171).
† huangxx@sari.ac.cn

Content from this work may be used under the terms of the CC BY 4.0 licence (© 2026). Any distribution of this work must maintain attribution to the author(s), title of the work, publisher, and DOI.

ISBN: 978-3-95450-252-3 ISSN: 2673-5350 doi: 10.18429/JACoW-IPAC2026-TUP7624

DESIGN OF 166 MHz AND 500 MHz BIMODAL RF CAVITIES BASED ON COAXIAL COUPLING

D. Su[1,2], C. Wang*[3], Z. Gao[3], J. Tan[3], W. Fang†[3], Z. Zhao[3]
[1]Shanghai Institute of Applied Physics, Shanghai, China
[2]University of Chinese Academy of Sciences, Beijing, China
[3]Shanghai Advanced Research Institute, Shanghai, China

Abstract

Ultra-low emittance is one of the primary directions for the development of synchrotron radiation facilities. To mitigate coupled-bunch instabilities and meet beam-lifetime requirements, higher-harmonic cavities are commonly required in diffraction-limited storage rings. Bimodal cavities are considered multifunctional and compact accelerating structures capable of integrating the functions of a fundamental RF cavity and a higher-harmonic cavity. To support the application of active bimodal RF cavities in low-energy storage-ring light sources, this paper investigates a coaxial coupling and mode-isolation scheme for bimodal cavity operation at 166 and 500 MHz.

INTRODUCTION

Advanced storage rings are core platforms for delivering high-brightness synchrotron radiation. Driven by the concept of diffraction-limited storage rings, fourth-generation light sources are evolving from high-flux facilities toward radiation sources with higher brightness and enhanced transverse coherence [1]. Today, approximately five fourth-generation storage rings worldwide are in operation or user operation, while more than ten others are under construction, being upgraded, or in the design stage. Among these facilities, MAX IV, ESRF-EBS, Diamond-II, Elettra 2.0, and other advanced light sources have adopted or plan to adopt a double-RF system consisting of a normal-conducting fundamental RF cavity and a higher-harmonic cavity. Considering operational reliability, construction cost, and maintenance cost, normal-conducting RF cavities remain a practical and preferred option for many storage-ring light sources. This indicates that the advantages of normal-conducting RF systems are receiving increasing attention in the development of next-generation storage rings.

The bimodal normal-conducting RF cavity is a recently proposed concept for storage-ring applications. By supporting two electromagnetic eigenmodes within a single cavity, this structure can simultaneously provide accelerating voltage and higher-harmonic voltage for bunch lengthening, thereby offering a potential alternative to conventional double-RF systems based on separate fundamental and harmonic cavities. In addition, the compact configuration of the bimodal cavity can reduce the overall footprint of the storage-ring RF system and alleviate the limited space available in the straight sections. Therefore, this concept is of practical significance for compact lattice design and miniaturized storage-ring light-source applications [2].

In the design of a bimodal cavity, a suitable pair of operating modes must first be selected, and their resonant frequencies must be tuned to satisfy the required harmonic relationship. Employing the TM_{010} mode as the fundamental accelerating mode and the TM_{020} mode as the third-harmonic mode can provide favorable RF characteristics for bimodal operation [3]. To optimize the performance of the TM_{020} mode, its field should be confined within the cavity volume. Therefore, suppressing the leakage of the TM_{020} mode through the fundamental power coupler is a key issue in bimodal cavity design. In this work, a coaxial fundamental-power-coupler scheme for a bimodal cavity is investigated, enabling efficient fundamental-mode power coupling while providing effective isolation of the TM_{020} mode.

MAIN CAVITY DESIGN

The cavity adopts a nose-cone-loaded pillbox-type cylindrical geometry, which is commonly used in normal-conducting RF cavities. The electromagnetic performance of the bimodal cavity was analyzed using the frequency-domain solver in CST Studio Suite, and the corresponding simulation model is shown in Fig. 1. To achieve frequency matching between the two operating modes, the nose-cone gap and the main cavity dimensions were carefully optimized. The cavity radius is r = 502.38 mm, and the nose-cone gap is g = 620.19 mm.

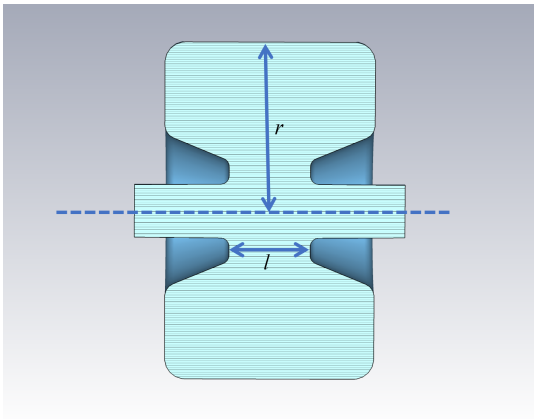

Figure 1: Cavity model.

The optimized design parameters of the bimodal cavity are summarized in Table 1. The shunt impedances of the TM_{010} and TM_{020} modes are 11.82 MΩ and 0.98 MΩ, re-

* wangc@sari.ac.cn
† fangwc@sari.ac.cn

Content from this work may be used under the terms of the CC BY 4.0 licence (© 2026). Any distribution of this work must maintain attribution to the author(s), title of the work, publisher, and DOI.

ISBN: 978-3-95450-252-3 ISSN: 2673-5350 doi: 10.18429/JACoW-IPAC2026-TUP7625

APPLICATION OF MAGNETIC-ALLOY-LOADED CAVITIES BEYOND 10 MHz

C. Ohmori*[1,2], K. Adachi[1,3], K. Hasegawa[1,2], K. Hara[1,2], R. Muto[1,2], M. Nomura[1,3], H. Okita[1,3], Y. Sato[1,2], K. Seiya[1,2], Y. Sugiyama[1,2], T. Shimada[1,3], F. Tamura[1,3], M. Yoshii[1,2]
[1]Japan Proton Accelerator Research Complex, Tōkai, Japan
[2]High Energy Accelerator Research Organization, Tsukuba, Japan
[3]Japan Atomic Energy Agency, Tōkai, Japan

Content from this work may be used under the terms of the CC BY 4.0 licence (© 2026). Any distribution of this work must maintain attribution to the author(s), title of the work, publisher, and DOI.

Abstract

Magnetic-Alloy-loaded cavities have been used for many applications; beam accelerations of high-intensity proton and heavy ion beams, beam manipulations, medical accelerators and anti-proton decelerations. The material has a large permeability and the cavities have bandwidth below approximately 10 MHz. Using an external inductor for reducing the effective inductance of a cavity system, the cavity bandwidth can be moved beyond 10 MHz. The higher harmonic cavity is required in J-PARC Main Ring to enlarge the longitudinal beam emittance before reaching the flat-top energy. For the slow extraction, the emittance growth will be inevitable to suppress the beam instability. For Hyper-Kamiokande neutrino experiment, high-intensity beam with lower peak current will be required to avoid the event-pile-up at a new intermediate detector (IWCD). In this paper, we present the emittance control scenario with the cavity, beam effects on it, and design of a new VHF RF system.

INTRODUCTION

The construction of Hyper-Kamiokande, a next-generation neutrino observatory in Japan, is currently underway. Once completed, Hyper-Kamiokande will be one of the world's largest and most sensitive detector for studying neutrinos, proton decays and astrophysical phenomena. The present long-baseline neutrino, T2K, experiment, will continues in an upgraded form, often referred to as "T2HK" (Tōkai to Hyper-Kamiokande) after the start of Hyper-Kamiokande. In this experiment, a high-intensity neutrino beam is produced by the extracted proton beam with world's largest numbers of the J-PARC facility in Tōkai-mura. The beam is then directed over a distance of about 295 km toward Hyper-Kamiokande. Compared to the original design, the beam power will be significantly increased to 1.3 MW [1]. In the Hyper-Kamiokande experiment, the Intermediated Water Cherenkov Detector (IWCD) plays a crucial role as a near detector. The IWCD is located relatively close to the neutrino source at J-PARC. It primary function is to measure the properties of the neutrino beam before oscillation occurs. The IWCD detects the cherenkov light of the charged particle produced by a neutrino reaction. When the peak intensity of neutrino beam becomes to high, unwanted pile-up of neutrino reaction will be increased in short beam pulses. The pile-up may disturb to identify the properties of neutrino beam.

To reduce the peak intensity of the neutrino beam, a task force was organized within J-PARC Main Ring group in 2020 to investigate the time structure of proton beam bunch. Several beam manipulation techniques were investigated using a simulation code to extend the beam bunch widths at the flat top energy of 30 GeV [2, 3]. Beam instability during the de-bunching process was also evaluated. An advantage of these manipulations was to extend bunch length with less cost. The disadvantages were long manipulation time to extend beam bunch and existing risk of beam instabilities. The additional time period causes the extension of cycle time and reduction of beam power to produce the neutrino beam. As an alternative idea, we proposed a higher harmonic RF to expand the longitudinal beam emittance [4–6]. This scheme can be applied during acceleration [7]. It requires wideband VHF cavities to excite a parametric resonance on the beam bunch, continuously. The resonance will be excited by a phase modulation of the VHF voltage. The previous studies have determined the VHF voltage of 40 kV to reduce the peak proton intensity by half [8] as shown in Fig. 1. The VHF scheme is also beneficial for slow extraction, since the larger momentum spread associated with increased emittance helps suppress beam instability during de-bunching [9, 10]. In this paper, we discuss a realistic scenario using the minimum required hardware for a proof-of-concept demonstration in J-PARC accelerator.

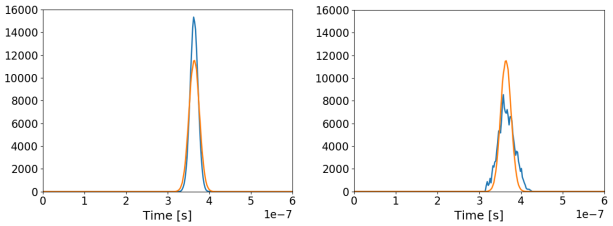

Figure 1: Effects of VHF RF. Left: without VHF, Right: 40 kV VHF voltage. Red and blue lines are bunch shapes before and after applying VHF voltage.

EMITTANCE GROWTH BY LOWER VHF VOLTAGE

In previous studies, phase modulation of the VHF voltage was applied in the second half of the acceleration, when the RF bucket area becomes much larger than the initial emittance. The total RF voltage during the modulation is

* chihiro.ohmori@kek.jp

ISBN: 978-3-95450-252-3 ISSN: 2673-5350 doi: 10.18429/JACoW-IPAC2026-TUP7626

DESIGN AND CONSTRUCTION OF A HOM-DAMPED TM_{020} TYPE HARMONIC CAVITY FOR LUMINOSITY ENHANCEMENT IN RI-ELECTRON SCATTERING

M. Wakasugi, R. Ohtake, H. Tongu
Kyoto University, Kyoto, Japan
D. Hasegawa, T. Kurihara, A. Kurosawa, A. Morishige
Metal Technology Co. Ltd., Kanagawa, Japan
M. Yamamoto, Omega Solutions, Inc., Tokyo, Japan
R. Ogawara, T. Ohnishi, RIKEN Nishina Center, Wako, Saitama, Japan

Content from this work may be used under the terms of the CC BY 4.0 licence (© 2026). Any distribution of this work must maintain attribution to the author(s), title of the work, publisher, and DOI.

Abstract

The RIKEN SCRIT facility that involves an electron storage ring (SR2) is a dedicated RI-electron scattering experiment. In the SCRIT system, the target RI ions are confined at high density on the beam axis by the focusing force provided by the electron beam itself. Therefore, electron beam stability is essential to increase the luminosity and maintain it for a sufficient time during scattering experiments. Since the current RF cavity induces beam instabilities due to higher order modes (HOM), a new HOM damped cavity is being designed and constructed and will soon be replaced. Here, we adopted the TM_{020} type harmonic cavity, which has recently been developed and first practically used at the NanoTerasu synchrotron light source. The cavity has coaxial slots at both the front and rear ends with ferrite absorbers inside. It is a very simple and compact design, yet it efficiently damps most resonant modes except for the TM_{020} mode. The design frequency of the TM_{020} is 956.220 MHz, which is the fifth harmonic of the current drive frequency 191.244 MHz, and accordingly the harmonic number in SR2 is changed from 14 to 70. As revealing from simulation studies, an increase in the harmonic number makes the trapping lifetime of the target RI ions longer, and this effect, coupled with the stabilization due to the disappearance of HOMs, is expected to significantly improve the luminosity performance in RI electron scattering.

INTRODUCTION

Electron scattering from atomic nuclei is one of the most important and reliable tools for precise nuclear structure studies and has long been awaited in the study of unstable nuclei. The key issue was how to make a small number of unstable nuclei with finite lifetime into sufficiently thick targets for electron scattering. SCRIT is a target formation technique that utilizes ion trapping, a well-known phenomenon that occurs within electron storage rings. The strong focusing force generated by an electron beam confines RI ions and forms a high-density RI ion cloud along the electron beam axis. [1] The first electron scattering for online produced RI has been successfully performed in recent year [2]. At that time, the target thickness was 10^8 cm^{-2} and the achieved luminosity was 10^{26} cm^{-2}s^{-1} with 10^7 target RI ions, and they were unfortunately maintained only for a few seconds. One of the main reasons for the short lifetime and relatively low luminosity is the instability of the electron beam caused by HOMs excited in the currently operating RF cavity. Therefore, HOM damped cavity is now necessary to improve SCRIT's performance in terms of target thickness, luminosity, and target lifetime.

HOM DAMPED CAVITY

A compact and simple HOM damping cavity, with the TM_{202} mode selected as the acceleration mode, was proposed more than 10 years ago [3, 4] and has recently been put into practical use at KEK [5] and NanoTerasu [6]. In a normal reentrant-type cavity with the radius of R_c, TM_{020} mode has a magnetic field node at a_2 in radius, where the differential of Bessel function is $J_0'(j_{02}a_2/R_c) = 0$. Figure 1 shows a schematic diagram of the cavity structure designed in this time. The cavity has two circumferential slots along the magnetic field nodes in the front and rear ends, and ferrite absorbers are put deep within the slots. While the TM_{020} mode remains unaffected, the magnetic fields for most other modes are significantly absorbed by the ferrite absorber, resulting in a drastic decrease in the Q values.

Electromagnetic Design

Acceleration frequency required in this cavity is f_0 =956.220 MHz which is the fifth harmonic of the currently operating frequency of 191.244 MHz, and it was chosen to ensure a reasonable cavity size. After optimizing characteristics such as resonant frequency, Q value, gap distance,

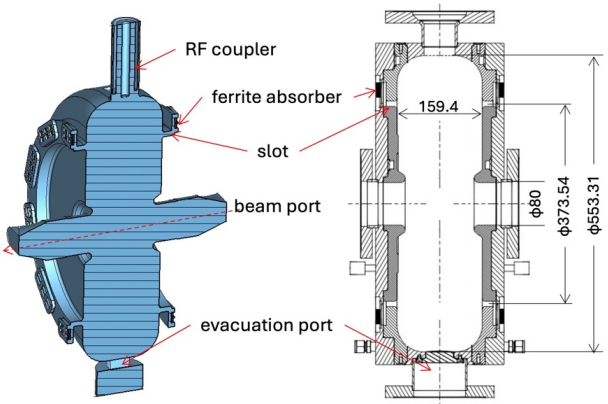

Figure 1: Conceptual structure of the HOM damped cavity.

ISBN: 978-3-95450-252-3 ISSN: 2673-5350 doi: 10.18429/JACoW-IPAC2026-TUP7627

BEAM TEST OF C-BAND COMPACT ACCELERATING STRUCTURE MADE OF LONGITUDINALLY-SPLIT TWO HALVES

M. Kimura†, H. Hara, K. Higa, N. Shigeoka, T. Sugano, S. Takagi
Mitsubishi Heavy Industries Machinery System, Ltd., Kobe, Japan
T. Abe, High Energy Accelerator Research Organization, Tsukuba, Ibaraki, Japan

Abstract

Our 6 MeV medical C-band accelerating structure uses a disk-stacked method, in which multiple oxygen-free copper components are stacked along the beam axis. Because the side-coupled (SC) re-entrant structure has a complex shape and many components, manufacturing efficiency is limited. In contrast, the longitudinally-split method divides the structure along a plane including the beam axis, typically into two halves or four quadrants, thereby reducing the number of components. Based on development experience of the quadrant-type X-band accelerating structures in the CLIC project, we have been developing a compact, high-gradient, high-shunt impedance SC-type C-band accelerating structure using this concept. In previous work, we reported fabrication of the full-scale structure, low-power RF test result, and preliminary first beam acceleration test limited by the available test facility. This paper reports recent progress, including RF conditioning and a high-power beam test under actual operating conditions.

INTRODUCTION

Background and Objectives

Compactness, high accelerating gradient, and improved manufacturability are increasingly required for medical and industrial electron accelerators. Our conventional 6 MeV SC-type C-band accelerating structure uses a disk-stacked method, which requires many parts and a complex brazing process.

A longitudinally-split concept, also called horizontal split, has been studied for high-gradient accelerating structures [1,2]. In this approach, the cavity is divided along a plane including the beam axis and machined as integrated halves, reducing part count and simplifying fabrication and assembly.

Based on this concept, we developed a longitudinally-split SC-type C-band accelerating structure to simplify fabrication and assembly while maintaining performance comparable to that of the conventional structure.

Overview of the SC-Type C-band Structure

Table 1 summarizes the main specifications, and Fig. 1 compares the conventional and longitudinally-split configurations.

The developed structure consists of a buncher section, accelerating cells, coupling cells, waveguide, and vacuum piping, with a total length of approximately 300 mm. To improve manufacturability while maintaining RF performance, the accelerating cells adopt a nose-cone geometry under a pending patent application (PCT/JP2023/023388). In addition, the coupling cells are arranged on one side of the beam axis to improve material utilization efficiency, compared with a layout in which they are placed on both sides.

The number of components was reduced from 59 in the conventional structure to 25 in the longitudinally-split structure, and the brazing process was simplified from a two-step to a one-step procedure.

Table 1: Outline of the SC-Type C-Band Structure

Item	Value
Frequency	5714±0.5 MHz
Coupling β	1.4 ~ 2.0
Beam energy	6 MeV
Beam current	> 75 mA
Beam Transmittance	> 40 %
Beam diameter	1.5 ~ 2.0 mm

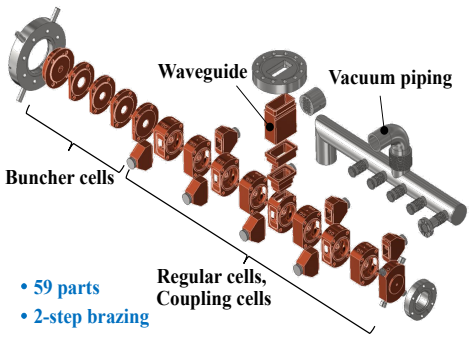

(a) Disk-stacked structure (conventional structure)

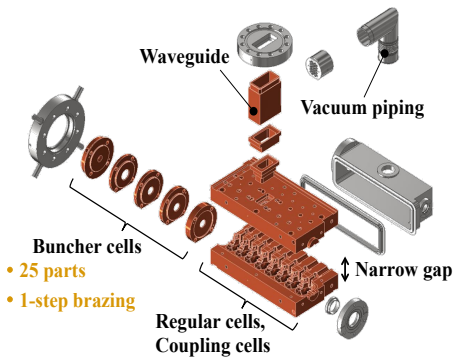

(b) Longitudinally-split method

Figure 1: Structural comparison of SC-type C-band accelerating structures.

† masashi.kimura.ck@mhi.com

Content from this work may be used under the terms of the CC BY 4.0 licence (© 2026). Any distribution of this work must maintain attribution to the author(s), title of the work, publisher, and DOI.

ISBN: 978-3-95450-252-3 ISSN: 2673-5350 doi: 10.18429/JACoW-IPAC2026-TUP7628

PRECISE FREQUENCY TUNING OF S-BAND PULSE COMPRESSORS AT HIGH-POWER OPERATION IN THE ELECTRON AND POSITRON INJECTOR LINAC OF KEK

H. Ego†,1, S. Ushimoto2
[1]KEK, Ibaraki, Tsukuba, Japan
[2] Mitsubishi Electric System & Service Co., Ltd, Ibaraki, Tsukuba, Japan

Abstract

The KEK electron-positron injector linac employs pulse compressors to amplify high-power radio frequency waves generated by S-band 40-MW klystrons. Accurate tuning of these compressors during high-power operation is essential to minimize their voltage standing wave ratio and maximize output power. We developed a real-time, labor-saving tuning system that consists of a waveform analyzer and a removable remote-controlled tuner driver. The analyzer calculates frequency deviations and waveform distortions in real-time by comparing the compressor's output waveform to an optimal waveform derived from fourth-order Runge–Kutta calculations. The tuner eliminates frequency deviations, whereas the analyzer monitors pulse-to-pulse adjustments. Consequently, all compressors were tuned efficiently and precisely.

INTRODUCTION

The KEK electron-positron injector linac currently operates 60 S-band, i.e., 2856 MHz, acceleration units at a frequency of 50 Hz. Figure 1 illustrates the typical configuration of the unit where the radio frequency (RF) output from the klystron compressed and amplified by a pulse compressor before being fed into four accelerating structures. SLAC energy doublers (SLEDs) [1] serve as pulse compressors and are installed in 56 units. Figure 2 shows a photo of the SLED. It consists of a 3-dB hybrid coupler and two cylindrical high-Q cavities; its RF properties are listed in Table 1. From 2022, single-cavity pulse compressors were introduced to replace SLEDs and are currently in stable operation [2].

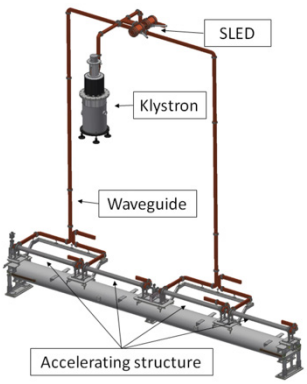

Figure 1: S-band acceleration unit

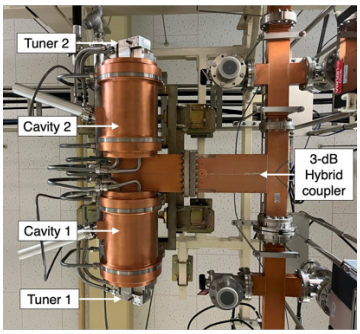

Figure 2: SLED in the KEK injector linac

This study presents improvements to the SLED tuning method and the latest results. Tuning the cavities to the operating frequency during rated high-power operation is necessary to ensure the SLED achieves optimal output. Conventional tuning methods have involved measuring RF waveforms with an oscilloscope and manually adjusting tuners attached to the cavities, relying heavily on the operator's visual judgment to maximize peak output and minimize reflections. This approach was unclear about whether the SLED was accurately tuned to the operating frequency. To address this, we developed a waveform analyzer and a removable remote tuning controller to enable easy and precise tuning of the SLED at the operating frequency.

Table 1: SLED's RF Characteristics

Operating frequency [MHz]	2,856
Resonant mode	TE_{015}
Unloaded Q (Q_0)	100,000
Coupling coefficient β	6.4
Peak voltage compression ratio	6.2
Input pulse length [μs]	4.0
Phase-reversed duration [μs]	1.0
Input power [MW]	40

PRECISE TUNING TOOLS

Waveform Analyzer

The control system was significantly improved as part of the injector upgrade to facilitate simultaneous top-up injection into the downstream storage rings [3]. A new precise timing system enabled synchronization of all pulse-driven accelerator components at 50 Hz [4]. Synchronous RF waveform monitors were introduced, and

† ego@post.kek.jp

Content from this work may be used under the terms of the CC BY 4.0 licence (© 2026). Any distribution of this work must maintain attribution to the author(s), title of the work, publisher, and DOI.

ISBN: 978-3-95450-252-3 ISSN: 2673-5350 doi: 10.18429/JACoW-IPAC2026-TUP7629

ASSESSMENT OF RF SYSTEM CAPABILITY IN THE J-PARC MAIN RING TOWARD 1.3 MW OPERATION

K. Seiya*, K. Adachi, K. Hara,, K. Hasegawa, C. Ohmori, H. Okita,
T. Shimada, Y. Sugiyama, F. Tamura, M. Yamamoto, M. Yoshii
Japan Proton Accelerator Research Complex, Tōkai Mura, Japan

Abstract

The J-PARC Main Ring plans to increase its beam power from 830 kW to 1.3 MW for the Hyper-Kamiokande neutrino experiment by 2028. To enable this high-power operation, the RF system has been upgraded by increasing both the number of RF cavities and the anode current of the tetrode amplifiers. However, the required anode current is approaching the operational limits of the RF tubes, and several associated power-supply systems are also close to their design limits.

Traditionally, the anode current has been estimated using a phasor diagram model. In this study, we instead evaluate the anode current using LTspice simulations, which allow detailed modeling of the vacuum tubes, cavity impedance, and beam loading. An LTspice model of the Main Ring RF system has been developed, including a magnetic-alloy-loaded cavity, two 600 kW tetrode tubes, and an eight bunch beam with a total intensity of 3.3×10^{14} protons per pulse. This model enables estimation of anode and screen grid currents, and the results are compared with measurements.

This paper presents LTspice-based RF system calculations for the Main Ring and evaluates the RF power requirements for 1.3 MW beam operation.

INTRODUCTION

The J-PARC Main Ring plans to increase its beam power from 830 kW to 1.3 MW for the Hyper-Kamiokande neutrino experiment by 2028 [1]. To enable this higher power operation, the RF system has been upgraded by increasing both the number of cavities and the anode current of the tetrode tubes. However, the required anode current is now approaching the maximum capability of the tubes, and several associated power supply systems are also nearing their operational limits [2].

Traditionally, the anode current has been estimated using a phasor diagram approach [3–5]. As an alternative, we evaluate the current using LTspice simulations, which can incorporate the vacuum tube characteristics, cavity impedance, and beam loading [6, 7]. We have constructed an LTspice model of the Main Ring RF system that includes the impedance of the magnetic alloy loaded RF cavity, two 600 kW tetrode tubes, and the beam current corresponding to eight bunches with a total intensity of 3.3×10^{14} protons. This allows us to estimate not only the anode current but also the screen grid currents, and the simulation results have been compared with measurements.

In this paper, we present LTspice-based RF system calculations for the Main Ring and evaluate the RF power requirements necessary to achieve 1.3 MW beam operation.

MR RF SYSTEM AND OPERATION

Eight bunches are injected from the Rapid Cycling Synchrotron (RCS) and accelerated while the RF frequency is ramped from 1.67 MHz to 1.72 MHz. The total injection voltage is 160 kV, which is increased linearly to 450 kV after completion of injection. Since the harmonic number is 9, the beam consists of a train of eight filled buckets and one empty bucket.

Figure 1 (left) shows a typical wall current monitor (WCM) signal at extraction energy, measured using a 2 GHz sampling oscilloscope over 5 μs. The signal is extended to the revolution frequency by repeating the recorded waveform.

To provide 450 kV, nine RF cavities are used at the fundamental frequency. Each cavity consists of three or four cells, each containing a ceramic gap and magnetic alloy cores. A single final amplifier feeds multiple gaps in parallel, resulting in a gap voltage of 13.45 kV and a total of 33 accelerating gaps.

The shunt impedance of the four-gap cavity is approximately 400 Ω, with a quality factor of about 21.

Figure 1 (right) shows the FFT spectrum of the WCM signal at extraction, overlaid with the cavity impedance. The low-level RF (LLRF) system controls not only the fundamental harmonic $h = 9$ but also neighboring harmonics ($h = 6, 7, 8, 10, 11, 12$) to achieve the desired gap voltage using I/Q feedback [8].

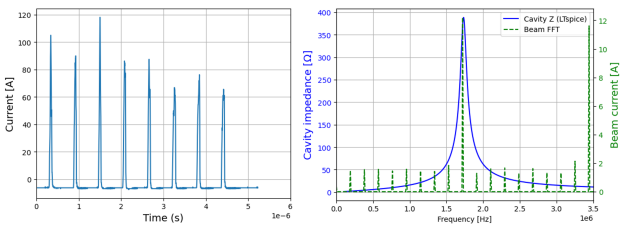

Figure 1: (left) WCM signal was extended to the revolution frequency by repeating the last oscilloscope data, (right) shows the FFT result of the WCM signal at extraction, overlaid with the cavity impedance.

* kiyomis@post.kek.jp

Content from this work may be used under the terms of the CC BY 4.0 licence (© 2026). Any distribution of this work must maintain attribution to the author(s), title of the work, publisher, and DOI.

ISBN: 978-3-95450-252-3 ISSN: 2673-5350 doi: 10.18429/JACoW-IPAC2026-TUP7630

FABRICATION AND RADIO-FREQUENCY TESTS OF A 1.3 GHz 9-CELL COPPER CAVITY AT ROOM TEMPERATURE AS A PROCESS QUALIFICATION STEP FOR NIOBIUM SUPERCONDUCTING CAVITY PRODUCTION

S. Choi and E. Kim, Korea University Sejong Campus, Sejong, South Korea
J. Han and H. Park, Kiswire Advanced Technology Ltd., Daejeon, South Korea
E. Kako, High Energy Accelerator Research Organization, Tsukuba, Japan

Abstract

The KU–KEK–KAT collaboration produced a 1.3 GHz copper 9-cell cavity with the goal of establishing a domestic Nb cavity fabrication flow in Korea and performed preprocess verification under the same conditions as the Nb fabrication procedure. Prior to fabrication, the reliability of the actual manufacturing was enhanced through EM simulations and engineering simulations using CST, and the fabricated copper 9-cell cavity was evaluated by measuring the resonance frequency with a network analyser and tuning the frequency using a tuner. For this purpose, we construct new antenna by redesigning and simulating 1-cell measurement antenna to 9-cell antenna for room temperature RF measurement, and all measurements were conducted with this antenna. In the initial measurement after fabrication, the resonance frequency of TM_{010} π-mode was measured to be 1.2978 GHz, and the field flatness was around 34%.

INTRODUCTION

In this study, a 1.3 GHz Tesla-type copper 9-cell cavity was designed [1], fabricated, and experimentally evaluated to support participation in the International Linear Collider (ILC) project [2] and to establish domestic superconducting accelerator fabrication capability. The cavity geometry was based on the superconducting Tesla-type 9-cell structure [3]. Based on the paper design, three copper 9-cell cavities were fabricated at KAT.

The fabricated cavity was evaluated through RF measurements and bead-pull tests to examine key parameters such as resonant frequency, field flatness, and coupling characteristics. The measured results were compared with simulation results and previous studies. The overall design, fabrication, and measurement results are expected to provide an important basis for securing domestic superconducting accelerator fabrication technology and supporting future participation in large-scale international accelerator projects, including the ILC.

ELECTROMAGNETIC SIMULATION

Electromagnetic analysis was carried out by first constructing the cavity using parameters shown in Fig. 1 and Table 1, then performing resonant frequency analysis using the Eigenmode solver. The electric field distribution as shown in Fig. 2 was examined, and the bead size for the bead-pull test was optimized through bead-pull simulations.

Resonance Frequency and E-field Simulation

The electromagnetic (EM) simulation was performed to define the design and evaluate fabrication stability. In particular, the differences between Nb and Cu cavities were compared key parameters (e.g., Q_0 and resonant frequency) of the copper prototype against the reference design.

The electromagnetic design was compared with the superconducting radio frequency (SRF) Tesla-type 9-cell cavity [3]. The target was to keep the error within 0.5% relative to the reference data, while the geometric parameters followed the DESY design.

Table 2 shows the main RF parameters of the 9-cell cavity by EM simulation. The simulation results showed that the resonant frequency difference from the target value was within about 0.1 %. In addition, a high R/Q value was maintained, indicating good accelerating efficiency. The shunt impedance and quality factor also satisfied the target values, while the B_p/E_{acc} value showed an error within about 5% of the target.

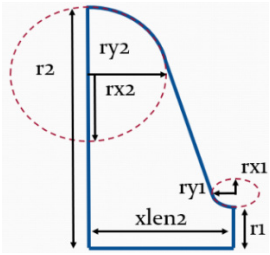

Figure 1: Cavity Parameter Naming.

Table 1: Parameters of 9-Cell Copper Cavity

Parameter	Center-cell [mm]	End-cell 1 [mm]	End-cell 2 [mm]
r1	35.00	39.00	39.00
r2	103.45	103.45	103.45
rx1	9.00	10.00	19.00
rx2	42.00	40.34	42.00
ry1	12.80	13.50	12.00
ry2	42.00	40.34	42.00
xlen2	57.00	56.00	57.7

Content from this work may be used under the terms of the CC BY 4.0 licence (© 2026). Any distribution of this work must maintain attribution to the author(s), title of the work, publisher, and DOI.

ISBN: 978-3-95450-252-3 ISSN: 2673-5350 doi: 10.18429/JACoW-IPAC2026-TUP7632

DEVELOPMENT AND OPERATION OF 166.6 MHZ SRF MODULES AT HEPS

X. Zhang[1,2*], P. Zhang[1,2], Q. Ma[1,2], J. Dai[1], T. Huang[1,2], H. Zheng[1,2], F. Meng[1], Z. Mi[1,2], H. Lin[1], Q. Wang[1,2], D. Li[1], F. Zhao[1], S. Jin[1,2], J. Li[1,2]

[1]Institute of High Energy Physics, Chinese Academy of Sciences, Beijing 100049, China

[2]University of Chinese Academy of Sciences, Beijing 100049, China

Abstract

The storage ring of the High Energy Photon Source (HEPS) is driven by 166.6 MHz β=1 quarter-wave superconducting cavities. Five higher-order-mode-damped 166.6 MHz cavities were designed to provide a total of 850 kW beam power and to accelerate the electron beam to 200 mA. The beamline elements of the module were designed to meet the compact requirements. Given the large beam aperture of 505 mm to realize HOM damping, an exquisite clean assembly procedure was developed and demonstrated with excellent rf performance preserved from vertical tests to horizontal tests. Five cryomodules have been successfully assembled and horizontally tested. The cavity's Q0 at the design voltage of 1.2 MV reached 1.5e9~2.1e9 at 4 K corresponding to 5~7 W dynamic heat loads in the horizontal tests, comfortably exceeding the design goal. Field emission was less than 0.13 mSv/h during the entire test up to a rf voltage of 1.6 MV, equivalent to a peak electric field of 43 MV/m. Subsequently, five modules were installed in the HEPS tunnel. A beam current of 100 mA was successfully achieved in September 2025. This work represents the first successful implementation of superconducting QWRs as the main accelerating system for a high-current storage ring, thereby extending their application limits from the conventional use in low-beta accelerators to high-current electron storage rings, and establishing them as a proven technology for future high-performance light sources.

INTRODUCTION

The High Energy Photon Source (HEPS) is China's first fourth-generation synchrotron light source with ultra-low beam emittance [1–4]. Located in Huairou, Beijing, HEPS commenced construction in June 2019 and successfully passed its key performance acceptance test in October 2025.

A dual radio-frequency (rf) system was employed for the storage ring to achieve bunch lengthening, thereby enabling the novel on-axis accumulation beam injection scheme [5]. Due to the low frequency of 166 MHz, the ellipsoidal cavity typically used for electron acceleration was no longer feasible because of its excessive size. Instead, a quarter-wave superconducting cavity featuring a novel acceleration path [6] was adopted. This active cavity offers a practically realizable size while being capable of accelerating relativistic electrons. Under an operating current of 200 mA, the higher-order modes (HOMs) of the cavity must be effectively damped by dedicated HOM absorbers. The high continuous-wave input power of 170 kW per cavity presented another challenge for both cavity design and stable operation. Two cryomodules were required to be accommodated within a 6-meter straight section, necessitating a compact cavity string design that met multiple requirements, including low beam impedance, proper collimation, reasonable cryogenic heat loads, mechanical robustness, and maintainability. Furthermore, a sufficiently large margin in rf performance is essential to ensure the stable operation of HEPS as a user facility.

SRF MODULE DESIGN

SRF cavity and string

The electromagnetic field optimization and favorable performance of the PoP cavity [7–9] were retained in the design of the 166 MHz HOM-damped cavity. At an operating voltage of 1.2 MV, a margin of 25% on the peak fields was reserved. Increasing the large beam pipe diameter from 170 mm to 505 mm was selected as the baseline among various HOM suppression schemes for its simplicity, reliability, and compliance with the stringent damping requirements [10]. The 166.6 MHz jacketed cavity model and its electromagnetic field distributions are shown in Fig. 1.

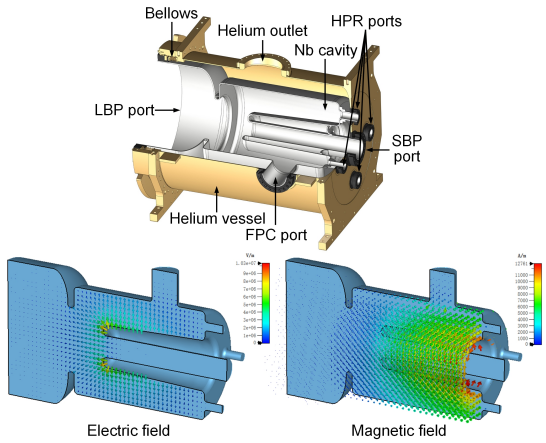

Figure 1: The 166.6 MHz cavity model and its electromagnetic field distributions.

Increasing the LBP diameter to three times its original size introduced numerous challenges to the cavity's mechanical design. Stresses at multiple locations on the cavity, such as the high-pressure rinsing (HPR) ports, the short-end plate, the iris, and connecting fillets, exceeded allowable limits.

* Email: zhangxinying@ihep.ac.cn

Content from this work may be used under the terms of the CC BY 4.0 licence (© 2026). Any distribution of this work must maintain attribution to the author(s), title of the work, publisher, and DOI.

ISBN: 978-3-95450-252-3 ISSN: 2673-5350 doi: 10.18429/JACoW-IPAC2026-TUP7633

PRELIMINARY DESIGN OF MOTOR DRIVERS FOR THE SHENZHEN SUPERCONDUCTING SOFT X-RAY FREE ELECTRON*

X. Dai, Z. Zhang, J. Zhu†, Institute of Advanced Light Source Facilities, Shenzhen, China
H. Ding‡, J. Yang, W. Zhang, Dalian Institute of Chemical Physics, Chinese, Dalian, China

Abstract

This paper presents the preliminary design of two motor drivers developed for the S^{3}FEL(Shenzhen Superconducting Soft X-ray FEL) project: one for cavity tuning and the other for coupler adjustment. Both drivers control stepper motors to regulate the resonant frequency and coupling degree of the 1.3GHz superconducting cavities, respectively. Each driver comprises two functional modules: a motor driver board and a limit signal conditioning circuit. The driver board translates low-power control signals (enable, direction, speed) into high-power outputs to drive the motor. Key design features include optocoupler-based isolation between control and power stages to prevent interference, subdivided stepping for improved positioning accuracy and motion smoothness, and real-time current monitoring to ensure correct output. The limit signal conditioning circuit provides excitation to the limit switches, samples their status, and returns the signals to the controller. Both drivers also supply a holding current to maintain motor position when stationary. Experimental validation confirms that the designed drivers satisfy the operational requirements for precise tuning and coupling control in the S^{3}FEL system.

INTRODUCTION

Stepper motors are widely used in various precision positioning systems owing to their simple open-loop control and high positioning accuracy [1]. In an accelerator, the tuner is driven by a stepper motor mounted external to the cryomodule that transfers torque through two rotary feedthroughs and the coupler is also driven by a stepper motor to control the coupling strength between the superconducting cavity and the external RF line by varying the depth of the coupling probe. However, in applications requiring high reliability, such as superconducting cavity tuning in particle accelerators, present several challenges for traditional stepper motor drivers:

1. Electromagnetic interference (EMI) generated by high-voltage, high-power drive circuits [2].
2. Low-frequency oscillation [3] and step loss [4] are prone to occur at low speeds.
3. The inability to retain motor position memory and automatically return to a safe position poses a significant risk of damaging expensive superconducting cavities.

SYSTEM ARCHITECTURE

A standard 1.3GHz cryomodule at S^{3}FEL contains eight superconducting RF cavities with eight coupler motors and sixteen tuner motors [5, 6]. Coupler motors are used to adjust the coupling coefficient of the superconducting cavity and tuner motors are used to tune the resonant frequency of the superconducting cavities. S^{3}FEL includes 222 coupler motors and 219 tuner motors. Each motor needs a motor driver, the driver for two types of motors are quite different because of the different rated operating parameters. Two types of motor are shown in Fig. 1 and Fig. 2.



Figure 1: Coupler motor.

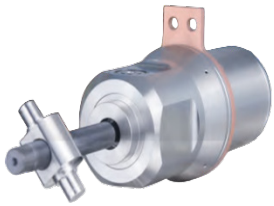

Figure 2: Tuner motor.

The operating parameters of the motors are shown in Table 1.

Table 1: Motor Parameters

Parameter	Coupler Motor	Tuner Motor
Rated Voltage	5V	24V
Rated Current	1.3A	1.2A
Phase	2	2
Step Angle	1.8°	1.8°
Step	0.003175mm	0.0001mm

MOTOR DRIVER DESIGN

Optocoupler-isolated Signal Transmission

To prevent electromagnetic interference (EMI) and ground potential drift from the rear-stage high-power circuit (strong-current side) to the front-stage controller (low-

* Work supported by the National Natural Science Foundation of China (Grant No. 12405221).
† zhujinfu@mail.iasf.ac.cn
‡ dinghongli@dicp.ac.cn

Content from this work may be used under the terms of the CC BY 4.0 licence (© 2026). Any distribution of this work must maintain attribution to the author(s), title of the work, publisher, and DOI.

ISBN: 978-3-95450-252-3 ISSN: 2673-5350 doi: 10.18429/JACoW-IPAC2026-TUP7636

PERFORMANCE AND PRODUCTION STATUS OF HIGH-Q CRYOMODULES FOR THE SHINE PROJECT

Jinfang Chen, Yue Zong, Xiaoyun Pu, Shuai Xing, Zheng Li, Xuming Liu, Shengwang Xiang, Yongzhou He, Lingling Gong, Shanshan Cao, Yanfei Zhai, Hongtao Hou, Lijun Lu, Zhenyu Ma, Yeliang Zhao, Xiang Zheng, Yubin Zhao, Meng Zhang†, Shenjie Zhao, Sen Sun, Zhiqiang Jiang, Yingbing Yan, Yiyong Liu, Qiang Gu, Lixin Yin, Bo Liu‡ and Zhentang Zhao
Shanghai Advanced Research Institute, Chinese Academy of Sciences, Shanghai, China
Yawei Huang, ShanghaiTech University, Shanghai, China
Xiaowei Wu, Zhangjiang Lab, Shanghai, China

Abstract

The SHINE Linac was optimized to accelerate the beam to 8 GeV with 54 high-Q cryomodules (CMs), benefiting from the higher performance of the cavities and CMs. Currently, the mass production of SHINE cavities and CMs is ongoing. Up to now, around 350 high-Q cavities with mid-T baking or N-doping recipes have been fabricated and tested. Most of them have been assembled in CMs. More than 30 CMs have been tested. In this paper, we report the performance of high-Q CMs and lessons learned during the production.

INTRODUCTION

SHINE accelerator consists of an injector, and a Linac separated into four sections by three bunch compressors, designated as BC1 to BC3 [1, 2]. Due to performance improvements in SHINE 1.3 GHz high-Q cavities, the specifications for high-Q cavities and CMs were updated with the Q_0 of 3.0×10^{10} at a higher average gradient of 20 MV/m since 2024 [3]. Hence, the number of CMs can be reduced from the original 75 sets to reach the designed energy of 8 GeV. The distribution of the CMs in the four Linac sections is illustrated in Figure 1.

Similar to the CM designs for E-XFEL and LCLS-II projects [4, 5], each regular 1.3 GHz CM for SHINE includes 8 high-Q cavities, 8 fundamental power couplers (FPCs), 8 tuners, 8 cavity magnetic shields, 1 superconducting magnet, 1 cold beam position monitor (BPM), 1 set of cryostat and cold mass, several vacuum tubes and valves, supports and other accessories. Some components are procured from mature international or domestic vendors, while many others are developed, verified and adopted for SHINE CMs.

As key components in CM, totally five vendors are involved for SHINE cavity production, including two European companies for both mechanical fabrication and surface treatment, and three domestic ones for mechanical fabrication [6]. All the surface treatment of domestic cavities is conducted by SHINE facilities in Wuxi [7]. The international cavities are treated with a modified 3/60 N-doping recipe, while almost all the domestic cavities are treated with mid-T baking [8-10].

Acceptance check of the main components is done before starting the assembly of each CM, which assures the quality for CMs. In principle, only qualified components are accepted, except a few ones with slight concession considering the tight time schedule.

All the CM assembly and horizontal tests are carried on the platforms dedicatedly built for SHINE project in SARI campus. Two cavity-string lines in ISO4 clean room enable the assembly of two CMs in quasi-parallel. Three horizontal test benches are used for CM tests.

Currently, 2~3 CMs per month can be guaranteed, considering the delivery of CM components, the capacity of CM assembly and horizontal test.

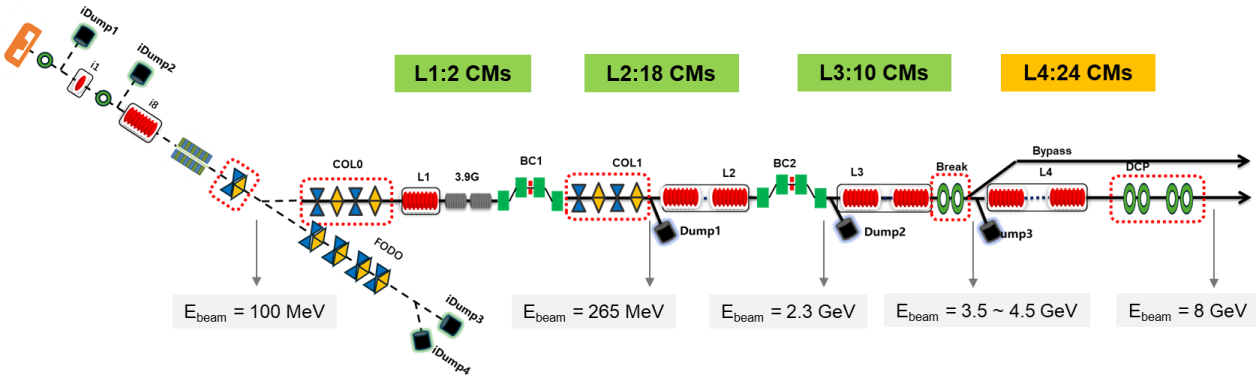

Figure 1: Layout of SHINE accelerator. High-Q CMs for L1-L3 have been installed tunnel, including HOM absorbers.

† zhangmeng@sari.ac.cn
‡ bo.liu@sari.ac.cn

Content from this work may be used under the terms of the CC BY 4.0 licence (© 2026). Any distribution of this work must maintain attribution to the author(s), title of the work, publisher, and DOI.

ISBN: 978-3-95450-252-3 ISSN: 2673-5350 doi: 10.18429/JACoW-IPAC2026-TUP7638

RF DESIGN OF A WAVEGUIDE HOM-DAMPING 1.3 GHz SUPERCONDUCTING CAVITY PROTOTYPE

W. Z. Chen[1,2], X. W. Wu*[,2], Z. T. Zhao†[,3], X. H. Guo[1]
[1]ShanghaiTech University, Shanghai, China
[2]Zhangjiang Laboratory, Shanghai China
[3]Shanghai Institute of Applied Physics, Chinese Academy of Sciences, Shanghai China

Abstract

Superconducting radio-frequency (SRF) cavities represent a key technology for modern particle accelerators. In high-current energy recovery linac (ERL) facilities, suppressing higher-order modes (HOMs) is critical to ensure beam stability and minimize additional cryogenic heat loads. This work introduces a waveguide-based scheme to extract and damp harmful HOMs excited by intense beams. A systematic RF design and optimization procedure for this waveguide damping method is presented. By implementing the damping scheme into a single-cell cavity geometry, consistent HOM suppression is achieved while maintaining good properties for the fundamental accelerating mode. The single-cell waveguide HOM-damping cavity, adopting the TESLA shape with an enlarged beam pipe, is currently under fabrication and will be tested in cryogenic experiments.

INTRODUCTION

Energy recovery linac (ERLs) have become a promising solution for modern high-brightness, high-effciency accelerator applications. For high-current ERL operation, the higher-order modes (HOMs) excited by intense beam loads in superconducting radio-frequency (SRF) cavities can lead to beam breakup instability, additional cryogenic heat load, and degraded beam stability [1]. Therefore, effective HOM damping is essential to ensure reliable and stable machine operation.

Various HOM damping concepts have been investigated, such as coaxial couplers, beampipe absorbers, and waveguide dampers. Among these solutions, waveguide-based HOM damping offers broadband damping performance, high power handling capability, and a compact layout, making it a preferred choice for high-current SRF cavities [2, 3].

This paper presents the design and fabrication of a 1.3 GHz single-cell SRF cavity prototype with waveguide HOM damping. The cavity is developed for high-current ERL applications with a nominal beam current of 10 mA. The design focuses on the waveguide HOM damping optimization, fundamental mode leakage, multipacting analysis, and mechanical design. The prototype will be used to validate the waveguide fabrication techniques and support the development of a multi-cell waveguide-damped SRF cavity in the future.

* wuxw@zjlab.ac.cn
† zhaozt@sinap.ac.cn

RF CAVITY DESIGN

For high-current ERL applications, the HOM damping performance is evaluated according to the longitudinal and transverse impedance thresholds derived from beam stability constraints. The longitudinal threshold for monopole modes is determined based on the beam-induced HOM power [4], as expressed in Eq. (1):

$$P = 2 \times I^2 Q_e (R/Q)_{\parallel}. \tag{1}$$

Given the design beam current $I = 10$ mA and a allowable cavity HOM power of 3.6 kW [5], the longitudinal shunt impedance $Q_e(R/Q)_{\parallel}$ should be lower than $3.6 \times 10^7\ \Omega$.

The transverse threshold for dipole modes is obtained from the beam breakup (BBU) threshold current [6] given by Eq. (2):

$$I_{th} \approx \frac{2}{e} \frac{E_0}{Q_e (R/Q)_{\perp} k}, \tag{2}$$

where k denotes the wave number of the dipole mode, and E_0 is the beam energy. For a beam energy of 10 MeV [7], the transverse impedance limit can be deduced from Eq. (2), yielding $Q_e(R/Q)_{\perp} k < 2 \times 10^9\ \Omega/\mathrm{m}$.

Waveguide optimization focuses on four parameters: cross-section, edge blend radius, length, and position. In stage 1, the cross-section and blend radius are optimized by using a 3-cell cavity model, as shown in Fig. 1a, to meet HOM damping and impedance thresholds. The 3-cell model is used because the designed HOM-damping waveguide will be applied to a multi-cell cavity in the future. In stage 2, waveguide length and position are optimized with a single-cell model, as shown in Fig. 1b, to ensure sufficient fundamental-mode attenuation and avoid cavity quench in cryogenic tests. This two-stage optimization achieves strong HOM damping while maintaining stable fundamental-mode performance.

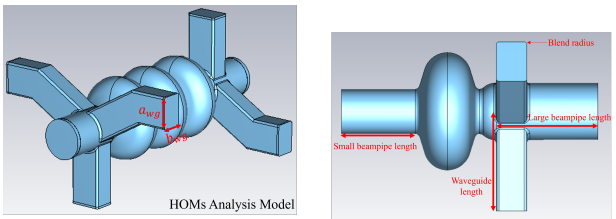

(a) (b)

Figure 1: (a) Model of the 3-cell cavity; (b) Model of the single-cell cavity.

Content from this work may be used under the terms of the CC BY 4.0 licence (© 2026). Any distribution of this work must maintain attribution to the author(s), title of the work, publisher, and DOI.

ISBN: 978-3-95450-252-3 ISSN: 2673-5350 doi: 10.18429/JACoW-IPAC2026-TUP7640

DESIGN AND VERTICAL TEST OF A PASSIVE 3RD HARMONIC SUPERCONDUCTING CAVITY FOR HALF STORAGE RING

Y. Wei†[1], Z. Huang[1], F. Xu[1], K. Zhang[1], G. Feng[1]
Z. Mi†[2], F. He[2], H. Zheng[2], S. Jin[2], R. Ge[2], W. Pan[2]
[1]University of Science and Technology of China, Hefei, China
[2]Institute of High Energy Physics, Chinese Academy of Sciences, Beijing, China

Abstract

A 3rd harmonic superconducting (SC) cavity is being developed for lengthening bunch and improving beam lifetime in the Hefei Advanced Light Facility (HALF) storage ring. This SC cavity is excited by an electron beam with 350 mA current, 1 nC charge, and ~6.7 ps length and requires strong damping of higher-order-modes (HOMs) in order to meet beam instability requirements. This paper presents design and vertical test of this passive 3rd harmonic SC cavity in detail. The vertical test results indicate that the cavity accelerating voltage reaches as high as 1.5 MV with the quality factor better than 3.4E8 and there is no multipacting or field emission.

INTRODUCTIONS

Hefei Advanced Light Facility (HALF) [1] is a soft X-ray and Vacuum Ultra-Violet fourth-generation diffraction-limited light source which is being constructed by National Synchrotron Radiation Laboratory (NSRL), University of Science and Technology of China. HALF consists of an injector, a storage ring, a few optical beamlines, and many experimental end-stations. The total length of the linac is 192 m. Electron beam is generated from a thermionic high voltage DC gun and the beam energy can be increased to 2.2 GeV at the exit of the linac. After passing through a 138 m long transport-line, the electron beam is injected into the storage ring. Synchrotron radiation will be generated by the insertion devices and the dipole magnets. The overall layout of HALF is shown in Figure 1. The HALF storage ring employs modified hybrid 6BA lattice as the baseline lattice to generate a beam with 85 pm·rad emittance, 350 mA current and 2.2 GeV energy.

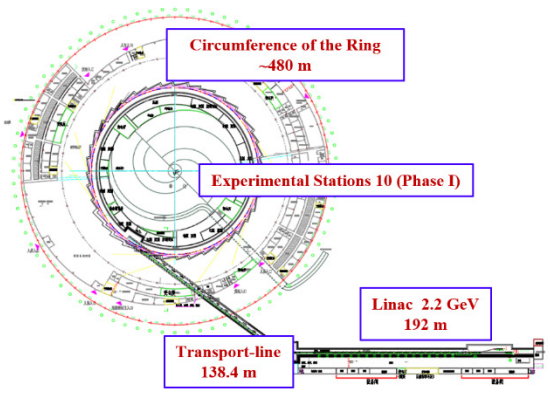

Figure 1: Layout of HALF.

†wylong@ustc.edu.cn, mizh@ihep.ac.cn

RF DESIGN ON HARMONIC SC CAVITY

The RF system consists of a main 500 MHz superconducting (SC) cavity and a passive 3rd-harmonic 1.5 GHz SC cavity for the HALF storage ring. The beam lifetime is one of the most important parameters that synchronous radiation users are concerned about, and it directly determines the performance of the electron storage ring. A 3rd-harmonic SC cavity is utilized to lengthen bunch and to improve beam lifetime in the HALF storage ring [2]. The RF system parameters have been calculated for HALF storage ring, as shown in Ref. [3]. The required voltage in 3rd harmonic SC cavity is calculated to be <0.5 MV. The bunch lengthening factor is calculated to be about 6, thereby increasing a Tousheck life time by a factor of 6.

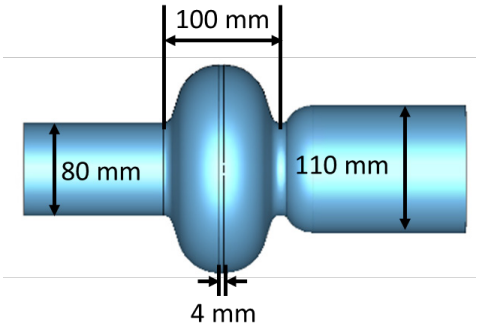

Figure 2: Geometry of a 3rd harmonic SC cavity.

Table 1: RF Parameters of a Harmonic Cavity

RF parameters	
Working mode	TM_{010}-π
frequency f [MHz]	1499.4
Cavity length [mm]	360
Geometry factor G [Ω]	291.6
Design voltage [MV]	0.5
R/Q [Ω]	81.8
E_p/E_{acc}	2.05
B_p/E_{acc} [mT/(MV/m)]	4.72

Considering its straightforward fabrication process, proven technological maturity, and reliable operational performance, such a 3rd harmonic SC cavity utilizes the TESLA shape with different beam pipes. Through optimizations by CST [4], the small beam pipe has a diameter of 80 mm while the large beam pipe has a diameter of 110 mm,

Content from this work may be used under the terms of the CC BY 4.0 licence (© 2026). Any distribution of this work must maintain attribution to the author(s), title of the work, publisher, and DOI.

ISBN: 978-3-95450-252-3 ISSN: 2673-5350 doi: 10.18429/JACoW-IPAC2026-TUP7641

GROUND-STATE AND RF-FREQUENCY SCALING FOR SUPERCONDUCTING QUANTUM SYSTEMS*

Heetae Kim†, Juwan Kim

Institute for Rare Isotope Science, Institute for Basic Science, Daejeon, Republic of Korea

Abstract

A fixed-volume comparison of three-dimensional hard-wall quantum confinement is extended to a volume-dependent frequency model for superconducting quantum systems. The equivalent confinement-frequency scale is obtained from the lowest Dirichlet eigenvalue and compared with radio-frequency (RF) scales used in superconducting radio-frequency (SRF) cavities. The calculation separates the Schrödinger confinement scale from the electromagnetic wavelength scale: the quantum frequency follows an inverse two-thirds volume law, whereas a dimensional RF half-wave scale based on $L = V^{1/3}$ follows an inverse one-third volume law. Equating the two frequency scales maps MHz-to-GHz SRF operation to submicron-to-micron local confinement lengths, supporting applications to superconducting islands, surface defects, quasiparticle traps, and cavity-integrated quantum devices.

INTRODUCTION

Geometry-dependent quantum confinement provides a compact way to connect boundary shape to the lowest allowed kinetic energy. A fixed-volume comparison of rectangular, cylindrical, spherical, and prolate ellipsoidal hard-wall domains shows that the sphere gives the lowest eigenvalue among the representative compact shapes considered [1]. This result follows the standard quantum-mechanical connection between the Dirichlet Laplacian eigenvalue and the particle-in-a-box ground state [2, 3].

This paper reformulates that result for accelerator and superconducting-quantum-system applications. A superconducting cavity has an RF resonant frequency fRF, whereas the quantum confinement model gives a ground-state energy-equivalent frequency scale $f_q = E_1/h$. These frequencies have different physical origins: f_{RF} is an electromagnetic eigenfrequency, whereas f_q is a Schrödinger/Laplacian kinetic-energy benchmark. The comparison is therefore a scale map rather than a replacement for an electromagnetic cavity eigenmode calculation.

The present model does not describe the electromagnetic eigenmodes of SRF cavities themselves, but instead provides a local confinement-scale estimate for microscopic superconducting regions interacting with RF fields. The useful comparison is therefore not to treat the full cavity as an infinite potential well. Instead, the model identifies the local volume scale at which a confined electron-like or Cooper-pair-like degree of freedom would have a frequency comparable to the applied RF field. This scale is relevant to superconducting surface oxides, hydride or impurity inclusions, weak links, quasiparticle traps, nanoscale islands, and engineered quantum-computing structures.

FIXED-VOLUME SCALING MODEL

Inside a hard-wall domain the non-relativistic ground state is obtained from the Dirichlet Laplacian eigenvalue problem [2, 3]. The hard-wall boundary condition imposes zero wave function on the boundary of the domain, so the first eigenvalue sets the kinetic-energy scale.

$$-\frac{\hbar^2}{2m_{\mathrm{eff}}}\nabla^2\psi = E\psi \tag{1}$$

$$-\nabla^2\psi = \lambda\psi, \qquad E_1 = \frac{\hbar^2}{2m_{\mathrm{eff}}}\lambda_1 \tag{2}$$

For geometrically similar domains, scaling all lengths by a factor s changes the volume as s^3 and the eigenvalue as s^{-2}. Therefore, the lowest eigenvalue can be written with a unit-volume shape factor, separating pure size dependence from shape dependence.

The different scaling exponents arise because the Schrödinger kinetic-energy operator scales as L^{-2}, whereas electromagnetic wavelength scales as L^{-1}.

$$\lambda_1(g, V) = C_g V^{-2/3} \tag{3}$$

$$f_q(g, V, m_{\mathrm{eff}}) = \frac{E_1}{h} = \frac{h}{8\pi^2 m_{\mathrm{eff}}} C_g V^{-2/3} \tag{4}$$

For an electron-like particle, the effective mass is the electron mass. For a simple Cooper-pair estimate, the effective mass is twice the electron mass, so all quantum frequencies are reduced by one half. With $h = 6.62607015 \times 10^{-34}$ J s and $m_e = 9.1093837 \times 10^{-31}$ kg, the electron-mass constant is

$$K_e = \frac{h}{8\pi^2 m_e} = 9.2125 \times 10^{-6}\ \mathrm{m^2/s} \tag{5}$$

GEOMETRY FACTORS

For a cube of side L, the ground-state eigenvalue is obtained by adding the three equal Cartesian contributions. Since the volume is L^3, the cube shape factor is 29.6088. For a sphere of radius R, the lowest eigenvalue is obtained from the first spherical Bessel root. This gives the spherical factor 25.6463, used as the reference minimum.

$$C_{\mathrm{sph}} = \pi^2 \left(\frac{4\pi}{3}\right)^{2/3} = 25.6463 \tag{6}$$

For a cylindrical infinite well, the ground-state eigenvalue contains the first zero of the Bessel function

* This work was supported by the National Research Foundation of Korea (NRF) funded by the Ministry of Science and ICT (RS-2022-00214790).

† kimht7@ibs.re.kr

Content from this work may be used under the terms of the CC BY 4.0 licence (© 2026). Any distribution of this work must maintain attribution to the author(s), title of the work, publisher, and DOI.

ISBN: 978-3-95450-252-3 ISSN: 2673-5350 doi: 10.18429/JACoW-IPAC2026-TUP7642

ENTROPY GENERATION ANALYSIS OF HEAT LOADS IN AN SSR2 SUPERCONDUCTING CRYOMODULE*

Heetae Kim†, Juwan Kim
Institute for Rare Isotope Science, Institute for Basic Science, Daejeon, Republic of Korea

Content from this work may be used under the terms of the CC BY 4.0 licence (© 2026). Any distribution of this work must maintain attribution to the author(s), title of the work, publisher, and DOI.

Abstract

The SSR2 superconducting cryomodule is analyzed in terms of static and dynamic heat loads and the associated entropy rates at the 2 K stage. The reference cryomodule contains six superconducting single-spoke resonator cavities. Static heat loads arise from conduction through cryomodule supports, couplers, cables, and beam-pipe interfaces, and from radiation through the insulation vacuum. Dynamic heat load is produced by radio-frequency surface dissipation. At 2 K, static and dynamic heat loads of 20 W and 80 W correspond to entropy rates of 10 W/K and 40 W/K, respectively, for a total cold-stage entropy rate of 50 W/K. The dynamic contribution accounts for 80% of the total entropy rate and scales inversely with the intrinsic quality factor Q_0. A coefficient-of-performance analysis shows that 100 W at 2 K requires at least 14.9 kW in the Carnot limit and about 100 kW for a representative real COP of 0.001. The results show that reducing radio-frequency loss, increasing Q_0, minimizing static heat leakage, and improving refrigerator performance directly reduce entropy generation and improve cryomodule efficiency.

INTRODUCTION

Superconducting radio-frequency (SRF) cavities are operated at cryogenic temperatures to achieve high accelerating fields with low RF surface resistance [1]. Although the surface resistance of a superconducting cavity is extremely small, it remains finite. As a result, part of the stored electromagnetic energy is dissipated on the cavity wall and converted into heat. This RF wall loss appears as a dynamic heat load in the helium cooling system. Related studies on zero-temperature phenomena [2], quality-factor conservation under relativistic motion [3], generalized effective temperature [4], unified analysis of quantum and relativistic effects in superconducting cavities [5], and SSR cavity performance [6] have been reported previously.

In addition to dynamic RF losses, the cryomodule receives static heat loads through mechanical supports, couplers, instrumentation cables, beam-pipe interfaces, residual-gas effects, and thermal radiation across the insulation vacuum. A conventional heat-load budget lists these contributions in watts at each temperature stage. From a thermodynamic viewpoint, however, a watt deposited at 2 K is much more severe than a watt deposited at a higher temperature because the entropy associated with heat transfer increases as the heat load is deposited at lower temperature [7]. This penalty is also evident in practical SRF cryogenic systems, where wall-plug conversion factors of approximately 800 W/W at 2 K [8] and 720.3 W/W near 1.8 K [9] have been reported.

This paper converts the SSR2 cryomodule heat-load budget into an entropy-rate budget. The objective is to connect SRF cavity quality factor, RF surface dissipation, static heat leakage, coefficient of performance (COP), and refrigerator irreversibility within a common thermodynamic framework. This approach provides a direct method for evaluating how RF-loss reduction, improved cryomodule thermal design, and higher cryogenic efficiency reduce entropy generation and improve overall accelerator performance [10].

SSR2 CRYOMODULE HEAT-LOAD BASIS

The reference cryomodule considered here contains six SSR2 superconducting single-spoke resonator cavities operated in a 2 K class helium system. The parameters used for the entropy analysis are summarized in Table 1. The reference 2 K heat-load basis consists of 20 W static heat load and 80 W dynamic RF heat load, for a total of 100 W at the cold stage.

Table 1: Representative SSR2 Parameters used in the Entropy Analysis

Parameter	Value
T_c	2 K
f	325 MHz
V_{acc}	4.1 MV
E_{acc}	>8.7 MV/m
$Q_{0,ref}$	5×10^9
R/Q	252 Ω
G	123 Ω
N_{cav}	6
Static heat load	20 W
Dynamic RF heat load	80 W

The static load is controlled mainly by cryomodule hardware and thermal shielding. The dynamic load is controlled mainly by RF surface resistance and cavity operating field. For the reference case, the dynamic RF load is the dominant contribution and therefore strongly determines the entropy burden during powered operation.

THERMODYNAMIC FORMULATION

Cold-Stage Entropy Rate

For a heat load deposited at a cold stage, the cold-stage entropy rate is approximated by

$$\dot{S}_c = \frac{\dot{Q}_c}{T_c}, \quad (1)$$

* This work was supported by the National Research Foundation of Korea (NRF) funded by the Ministry of Science and ICT (RS-2022-00214790).
† kimht7@ibs.re.kr

ISBN: 978-3-95450-252-3 ISSN: 2673-5350 doi: 10.18429/JACoW-IPAC2026-TUP7644

DEVELOPMENT OF A NOVEL SOLID-STATE MODULATOR AND ITS APPLICATION IN HIGH-POWER KLYSTRONS*

X. Chen, C. Liu†, F. Shang, L. Shang, W. Song, J. Pang, Z. He Z. Zhong
University of Science and Technology of China, Hefei, China

Abstract

This paper presents a highly integrated solid-state modulator designed to drive high-power klystrons in linear accelerators. The modulator employs a vertically integrated architecture in which the solid-state module array is directly combined with the high-voltage pulse transformer. This configuration eliminates long high-voltage cable connections, reduces parasitic inductance, and improves compactness and maintainability. The proposed modulator has been experimentally validated in high-power tests with an 80 MW S-band klystron at the Hefei Advanced Light Facility (HALF), achieving the required pulse waveform quality and stability. In addition, with limited modification, the same architecture can be adapted to higher repetition-rate applications such as the Super Tau-Charm Facility (STCF) injector, demonstrating its scalability for future large-scale accelerator facilities.

INTRODUCTION

High-power pulse modulators are essential for driving klystrons and other high-power microwave sources in linear accelerators [1]. The quality and stability of the modulator output directly affect beam performance and operational reliability in large-scale accelerator facilities. Owing to the lifetime limitations and maintenance burden of conventional thyratron-based systems, solid-state modulators based on insulated gate bipolar transistors (IGBTs) have become the mainstream solution in modern accelerator applications [2]. Their adoption in recent light-source facilities, including APS-U, MAX IV, and HEPS, has demonstrated the advantages of solid-state technology in reliability, controllability, and long-term operation [3–5].

Despite this progress, important engineering challenges remain in the practical deployment of high-power solid-state modulators. In conventional separated architectures, the power module array and the pulse transformer are often connected through long high-voltage transmission paths [6]. This arrangement increases parasitic inductance, which may aggravate voltage overshoot and transient waveform distortion. In addition, complex interconnections and enclosed modular layouts can reduce maintenance accessibility and prolong the mean time to repair, which is undesirable for accelerator facilities requiring high availability and efficient operation.

To overcome these challenges, this paper presents a novel solid-state modulator featuring a vertically integrated architecture that directly combines the power module array with the high-voltage pulse transformer. By eliminating long-distance high-voltage cabling and shortening the main current path, the proposed configuration reduces parasitic inductance and improves compactness and maintainability. The modulator has been experimentally validated in high-power operation with an 80 MW S-band klystron at the Hefei Advanced Light Facility (HALF). In addition, the adaptability of the same topology to higher repetition-rate applications, such as the STCF injector, is briefly discussed.

SYSTEM ARCHITECTURE AND DESIGN

To meet the stability, reliability, and maintainability requirements for driving high-power S-band klystrons, the proposed solid-state modulator adopts a highly integrated system architecture. As shown in Fig. 1, the system consists of four main parts: a primary high-voltage charging power supply, a modular solid-state power array, an integrated pulse transformer, and a central control and health management unit.

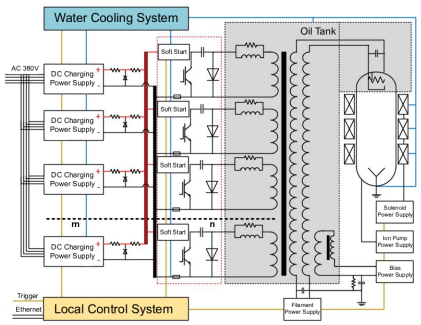

Figure 1: Block diagram of the proposed solid-state modulator system, including the primary charging supply, modular solid-state power array, integrated pulse transformer, and central control unit.

In operation, the primary charging supply provides a stable and adjustable DC input to the solid-state module array. When a synchronous trigger is applied, the active modules conduct simultaneously and generate a high-current primary pulse, which is delivered to the primary winding of the pulse transformer. The transformer then steps up the pulse to the required high-voltage level for driving the klystron cathode. Auxiliary power supplies are also included for the filament, focusing coils, and ion pump.

The proposed modulator features a vertically integrated architecture. Instead of using a conventional separated layout,

* This work was supported in part by the Fundamental Research Funds for the Central Universities (No. KY2310000050), in part by the Hefei Advanced Light Facility Project, and in part by the Super Tau-Charm Facility Key Technology Research Project.
† chaoliu@ustc.edu.cn

Content from this work may be used under the terms of the CC BY 4.0 licence (© 2026). Any distribution of this work must maintain attribution to the author(s), title of the work, publisher, and DOI.

ISBN: 978-3-95450-252-3 ISSN: 2673-5350 doi: 10.18429/JACoW-IPAC2026-TUP7647

CURRENT STATUS OF THE UPGRADE AND OPERATION OF THE NSRRC TPS LINAC PULSE HIGH-POWER RF SYSTEM

W. Y. Chiang, Y. C. Chang, A. P. Lee, K. L. Tsai, C. L. Chen, H. P. Chang, M. C. Chou, H. P. Hsueh,
NSRRC, Hsinchu, Taiwan
H. Matsumoto, KEK, Ibaraki, Japan

Abstract

The NSRRC Taiwan Photon Source (TSP) pre-injector system includes a DC thermionic electron gun, a Sub-Harmonic Pre-Buncher, a Primary Buncher, a Final Buncher, three S-band LINAC sections, and three 35-MW S-band-Klystrons. While the original klystrons were Thales TH2100A, recent instability and shorter tube lifetimes led NSRRC to upgrade to the E37310A klystron from CETD. This work analyses the RI-designed pre-injector system, implements modifications to ensure compatibility with the CETD E37310A, and ensures the supply of the required RF power. In August 2023, using the THz FEL pulse RF system, NSRRC upgraded the TLS pre-injector pulse RF system. Following six months of stable operation, upgrades to all three TPS pre-injector pulse RF systems began in 2024. This paper presents installation, modulator modifications, testing, and operational status of the first two TPS systems, completed in September 2025 and February 2026.

INTRODUCTION

The TPS pre-injector system is designed and manufactured by Research Instruments (RI) as a turnkey system, as shown in Figure 1. It consists of five major components:

1. Direct current (DC) thermionic electron gun: supports single-bunch mode (pulse width 1 ns, output charge 2 nC) and multi-bunch mode (pulse width 200 ~1000 ns, output charge 5 nC). The maximum repetition rate for both modes is 5 Hz. After acceleration in the electron gun, the beam energy reaches 90 keV.
2. Sub-harmonic pre-buncher: a single-cavity resonator operating at 499.654 MHz that compresses the electron beam pulse width to below 1 ns.
3. Primary buncher: consists of four resonant cavities operating in the 2π/3 mode at 2997.912 MHz (40 °C). It accelerates the electron beam from 90 keV to 300 keV and requires 2 MW of radio-frequency (RF) input power.
4. Final buncher: consists of 16 resonant cavities operating in the 8π/9 mode at 2997.912 MHz (40 °C). It further accelerates the beam from 300 keV to 3 MeV and requires 3.5 MW of RF input power.
5. S-band linear accelerator: includes 156-cell traveling-wave structure operating in the 2π/3 mode at 2997.912 ± 0.03 MHz and maintained at 38 ~ 42 ± 0.1 °C. This final stage consists of three S-band accelerator sections, which raise the beam energy to 150 MeV. Each section requires roughly 16 MW of RF power.

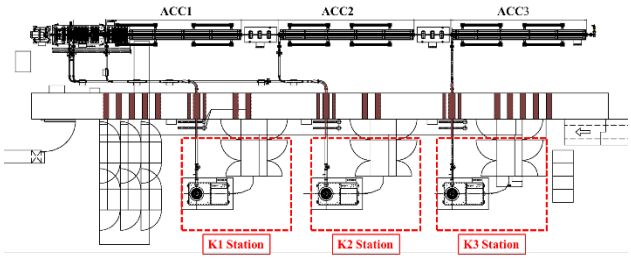

Figure 1: TPS pre-injector system [1].

KLYSTRON UPGRADE

The TPS pre-injector system uses three high-power RF stations in pulsed mode: K1 supplies RF power to the Primary Buncher, Final Buncher, and LINAC-ACC1, while K2 and K3 supply RF power to LINAC-ACC-2 and ACC-3. All stations use the Thales TH2100A Klystron (Fig. 2(a)), whose electron gun has a high arcing rate, leading to failures. Additionally, manufacturing quality has declined in recent years, shortening operational lifetimes and reducing TPS reliability. To address these issues and improve reliability, a Klystron Upgrade Program was launched in 2024 to replace the TH2100A with the E37310A Klystron (Fig. 2(b)) from Canon Electron Tubes & Devices (CETD). Table 1 shows that the E37310A's performance and operating parameters are similar to those of the TH2100A, fully meeting TPS LINAC requirements. Experience from the Taiwan Light Source (TLS) LINAC upgrade demonstrates that the E37310A enhances operational stability and light-source performance. The upgrade also requires modifications to the high-voltage insulating oil tank and the pulsed modulator system to ensure long-term reliability.

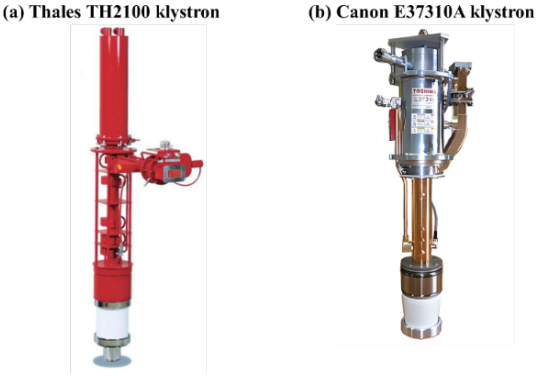

Figure 2: (a) Thales TH2100 Klystron [2] and (b) CETD E37310A Klystron [3].

Content from this work may be used under the terms of the CC BY 4.0 licence (© 2026). Any distribution of this work must maintain attribution to the author(s), title of the work, publisher, and DOI.

ISBN: 978-3-95450-252-3 ISSN: 2673-5350 doi: 10.18429/JACoW-IPAC2026-TUP7651

MAGNET MEASUREMENTS OF THE HALF MAGNETS

Y. Lu*, C. Zhang, Z. Ren, B. Liu, G. Feng
University of Science and Technology of China, Hefei, China

Abstract

The Hefei Advanced Light Facility (HALF), a fourth-generation light source based on a multi-bend achromat (MBA) lattice, is currently under construction. The storage ring consists of 20 cells and requires over 800 magnets. To assess the magnetic field quality and perform magnet fiducialization, several dedicated measurement systems have been developed. These include rotating-coil, stretched-wire, and Hall-probe systems. The field quality of multipole magnets is characterized using the rotating-coil system, while their magnetic centers are determined through single stretched-wire measurements. This paper presents the design of the measurement benches, outlines the corresponding measurement procedures, and reports the current measurement progress.

INTRODUCTION

The Hefei Advanced Light Facility (HALF) is a fourth-generation synchrotron radiation light source based on a diffraction limited storage ring in the low-energy region [1]. The overall layout of HALF is shown in Fig. 1. Electron beam is generated from a thermionic high voltage DC gun and the beam energy can be accelerated to 2.2 GeV at the exit of the linac. The HALF storage ring uses a hybrid six-bend-achromat (H6BA) lattice, which replaces the three combined-function bend unit cells of the original H7BA lattice with two longitudinal gradient bend (LGB) and reverse bend (RB) unit cells and a mid-straight section. The storage ring consists of 20 cells and requires over 800 magnets. All multipole magnets and LGB magnet are fiducialized and measured before the installation to confirm that alignment and field quality satisfy the requirement.

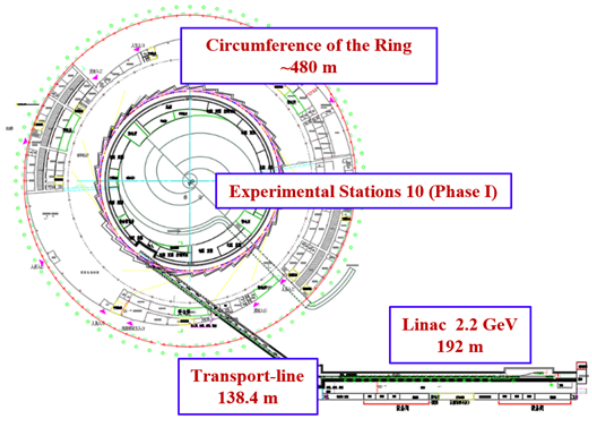

Figure 1: Layout of the HALF accelerator system.

Three types of measurement systems—the rotating coil measurement system, the single stretched wire measurement system, and the Hall probe measurement system—have been designed and established in the testing hall. To enable the measurement of all magnets prior to installation, each system has two measurement platforms. The rotating coil is used for measuring magnetic field harmonic components and integrated field gradient, and the single stretched wire system measures the magnetic center for magnet fiducialization. The measurement benches are installed in an air-conditioned room with constant temperature and humidity. The detail of the measurement systems are explained in the following sections.

ROTATING COIL MEASUREMENT SYSTEM

The rotating coil measurement system mainly consists of two Newport XY stages, a fast digital integrator (FDI), a rotatory encoder, a stepper motor and a marble platform support. The photo of the rotating coil measurement system is shown in Fig. 2. The coil is embedded within a ceramic structure, offering enhanced mechanical strength and extended service life. There are two different rotating coils for quadrupole and sextupole bucking. Before the measurement of magnetic flux, the magnets must be precisely aligned to ensure that the central axis of the ceramic coil coincides with the mechanical center axis of the magnet.

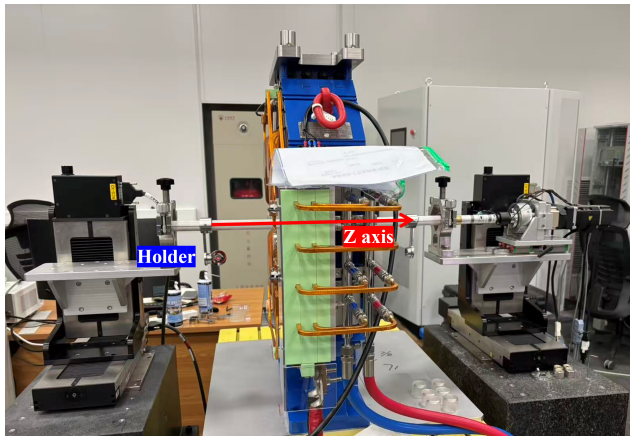

Figure 2: Photo of the rotating coil measurement system.

To accomplish the fiducialization of the magnets, the positions of the fiducial targets in the magnet mechanical coordinate system are first determined at the fabrication facility using a Coordinate Measuring Machine (CMM). In the testing hall, two target holders are mounted at both ends of the ceramic coil. By rotating the coil and recording the positions of the target spheres with a laser tracker, circles are fitted to the measured trajectories at both ends. The Newport stage is used to adjust the height difference between the upstream and downstream ends to less than 5 µm. The

* yaolu131@ustc.edu.cn

Content from this work may be used under the terms of the CC BY 4.0 licence (© 2026). Any distribution of this work must maintain attribution to the author(s), title of the work, publisher, and DOI.

ISBN: 978-3-95450-252-3 ISSN: 2673-5350 doi: 10.18429/JACoW-IPAC2026-TUP7653

PROGRESS IN THE PM BASED LGBM MAGNETS FOR K-4GSR

Y. G. Jung, B. J. Kim, S. H. Ahn, G. Hahn, I. Chun , W. W. Lee, Y. G. Choi, D. E. Kim*
Pohang Accelerator Laboratory, POSTECH, Pohang, KyungBuk, Republic of Korea

Content from this work may be used under the terms of the CC BY 4.0 licence (© 2026). Any distribution of this work must maintain attribution to the author(s), title of the work, publisher, and DOI.

Abstract

A 4th generation storage ring based light source is being developed in Korea since 2021. It features <60 pm rad intrinsic beam emittance, about 800 m circumference, 4 GeV e-beam energy, full energy booster injection, and more than 40 beamlines which includes more than 24 insertion device (ID) beamlines. To optimize the beam emittances, longitudinal gradient bending magnet is applied in the storage ring design. To minimize the operation costs, and to save the lattice space, Sm_2Co_{17} based Longitudinal Gradient Bending Magnet (LGBM) is being developed following ESRF-EBS, and HEPS. It has 5 steps of field level ranging from 0.73 T ~ 0.15 T with approximately 2 m total length. In this report, the compensation scheme of temperature dependence, and field tuning to meet the bending angle, and apex points will be described.

INTRODUCTION

Third generation storage ring based light sources have been used as a bright light source for many years. Recently multi-bend achromat (MBA) lattice presents a further decrease in the electron beam emittances and becoming a new standard for next generation light source like MAX-IV in Sweden, ESRF-EBS in France, SIRIUS in Brazil. Many other laboratories are also preparing their own version of 4th generation light sources. In this context, Korea is trying to build a 4th generation light source (K-4GSR) based on modified hybrid multi-bend achromat lattice (MHMBA). The Korea fourth-generation storage ring (K-4GSR) adopt H7BA considering better nonlinear beam dynamics compared to the conventional 7BA and lower emittance compared to MH6BA [1–3].

K-4GSR consists of total 28 periodic sectors. As shown in Fig. 1, each sector is equipped with 1 center bending (CB) magnet, 4 longitudinal gradient bending (LGBM) magnets, 2 transverse gradient bending (DQ51) magnets, 6 reverse-bending combined quadruple magnets (RDQ), 12 quadrupole magnets, 6 sextupole magnets (S), 2 octupole magnets, and 4 fast correctors, totaling 37 main electromagnets.

In most types of 4GSR based light sources, longitudinal gradient magnet (LGBM) is routinely used to achieve low bending field in high dispersion area. APS-U [4] tried current excited 5 step longitudinal gradient magnet. ESRF-EBS [5], and HEPS [6] are using permanent magnet (PM) excitation to reduce operating costs. PM excitation has an advantage of compact magnet size, and nearly zero operating energy costs. However, there is a possibility of long term degradation (although small) due to the radiation damage, and lack of tunability. ESRF-EBS and HEPS are adopting Sm_2Co_{17} for their magnet material which shows minimal radiation damage compared to NdFeB based magnet.

* dekim@postech.ac.kr

K-4GSR LGBM DESIGN

K-4GSR LGBM magnet has also 5 step field profile ranging from 0.15 T to 0.734 T with varying magnetic length. The magnetic geometry is similar to ESRF-EBS and HEPS although the field strength and file profile is different. Sm_2Co_{17} rare earth magnet is adopted for magnetic material for stronger resistance to the radiation damage. Permanent magnet version has additional advantage of small longitudinal space since there is no excitation coil. The field shape has a 5-step profile which is not easy to match precisely. The magnet is designed to have the design value of the 1st integral (bend angle) and the 2nd integral (apex points). The beam dynamics study confirmed that exact profile is not important for beam emitances. It should be also noted that the upstream and downstream version of LGBM has mirror symmetric field profile. The LGBMs are composed of 5 modules depending on the required field level. A central pole is surrounded by PM magnets to produce magnetic field. The field level is adjusted by controlling the number of full size blocks, and quarter sized blocks, with longitudinal spacing. After assembling each module, field uniformity is measured, and temperature compensation experiment is carried out using FeNi plates at two temperatures with Δ T = 3.0 K. The major parameters of the LGBMs are listed in the Table 1.

Table 1: Major Parameters of LGBM1, LGBM2 Magnet

Parameter	LGBM1	LGBM2
Magnet Type	LGBM1U/D	LGBM2U/D
PM type	Sm_2Co_{17}	-
B_r	1.08 ~ 1.12 T	-
Required Num.	28/28	28/28
B range	0.734 T-0.150 T	0.312 T-0.153 T
Uni. |x| < 10 mm	< 1.0E-3	< 1.0E-3
Min. Pole gap.	24.4 mm	24.4 mm
Total Bend	41.69 mrad	33.56 mrad
Apex point	0.7425 m	0.8500 m
B_1 /L_1	0.7342 T/0.1649 m	0.3121 T/ 0.5397 m
B_2 /L_2	0.4302 T/0.2061 m	0.2396 T/ 0.3076 m
B_3 /L_3	0.2870 T/0.4662 m	0.2026 T/ 0.4869 m
B_4 /L_4	0.1972 T/0.6441 m	0.1732 T/ 0.3586 m
B_5 /L_5	0.1504 T/0.5690 m	0.1535 T/ 0.2912 m
Total Len.	2.0505 m	1.9847 m

NMR Calibration of the Hall Probe

Before any serious measurement, the existing Hall probe system is calibrated using NMR system. Precise fixtures are designed to place the NMR teslameter at the center of each

ISBN: 978-3-95450-252-3 ISSN: 2673-5350 doi: 10.18429/JACoW-IPAC2026-TUP7654

MEASUREMENTS OF MAGNET PROTOTYPES FOR STORAGE RING OF SIAM PHOTON SOURCE II

P. Sunwong†, P. Chaithaweep, A. Kwankasem, T. Leetha, P. Numanoy, S. Prawanta
P. Pruekthaisong, M. Sroison, N. Thiabsi, T. Yan
Synchrotron Light Research Institute, Nakhon Ratchasima, Thailand

Abstract

A series of magnet prototypes has been developed for the storage ring of Siam Photon Source II (SPS-II), the second synchrotron light source in Thailand. The prototypes include dipole, combined dipole, quadrupole, sextupole and octupole magnets designed for half of the Double Triple Bend Achromat lattice. To validate the performance of magnet prototype, magnetic field characterization was carried out using stretched wire and Hall probe measurement systems. Following some mechanical improvements, 10 out of 15 magnets met the specified field quality requirements, while possible sources of field errors in the remaining magnets were identified. This work represents a critical milestone toward SPS-II construction, as the storage ring magnets are planned to be manufactured domestically.

INTRODUCTION

Siam Photon Source II (SPS-II), Thailand's next-generation synchrotron light source, has been designed to support the country's advanced manufacturing industry [1]. As one of the key components of the machine, magnet prototype for the SPS-II storage ring has been developed. A total of 15 magnets, corresponding to half of a Double Triple Bend Achromat (DTBA) lattice cell, were designed and fabricated through a collaboration between the Synchrotron Light Research Institute (SLRI) and a local manufacturer. These magnets comprise two dipole magnets (BM1, BM2), one combined dipole magnet (DQ1), eight quadrupole magnets (QF1, QD2, QD3, QF4, QF5, QD6, QF7, QF9), three sextupole magnets (SD1, SF2, SD3) and one octupole magnet (OF1) [2, 3]. To validate the prototype performance prior to finalizing the design and proceeding to mass production, comprehensive measurements including mechanical, electrical, hydraulic and magnetic field characterization were carried out. This paper presents the results of the magnetic field measurements. In addition, results from other measurements and the potential sources of magnetic field errors are discussed.

MAGNET REQUIREMENTS

The magnetic field strength and required field quality of magnet prototype for SPS-II storage ring are summarized in Table 1. For the combined dipole magnet (DQ1), the design is based on the offset quadrupole concept as implemented in some facilities [4, 5]. In this approach, the required dipole field of 0.6 T is achieved by transversely offsetting a quadrupole magnet with a field gradient of 26.4 T/m by 22.5 mm. The quadrupole magnets are divided into two groups with bore radii of 16 mm and 18 mm, corresponding to the Good Field Region (GFR) requirements of 10 mm and 15 mm, respectively. The normalized field errors listed in the table are defined differently depending on the magnet type. For dipole and combined dipole magnets, the values represent the normalized integrated field error evaluated at the mid-plane (y = 0). For quadrupole, sextupole and octupole magnets, the values correspond to the normalized integrated multipole components obtained from Fourier analysis.

Table 1: Magnet Requirements for SPS-II Storage Ring

Magnet	Field Strength	GFR (mm)	Normalized Field Error
BM1 BM2	0.87 T	12	1×10^{-4}
DQ1	0.6 T 26.4 T/m	8	5×10^{-3}
QF1	45 T/m	10	5×10^{-4}
QD2 QD3 QD6	51 T/m	10	5×10^{-4}
QF4 QF5	44 T/m	15	5×10^{-4}
QF7	60 T/m	10	5×10^{-4}
QF9	50 T/m	10	5×10^{-4}
SD1 SF2 SD3	1,800 T/m^2	15	1×10^{-3}
OF1	72,000 T/m^3	13	5×10^{-3}

DIPOLE MAGNETS

The magnetic field homogeneity of the dipole magnets and combined dipole magnet was evaluated using a Hall probe measurement technique. The Hall sensor was scanned in the XZ plane along a curved trajectory within the magnet bending angle and along a straight trajectory outside the magnet. The magnetic field was then integrated along these trajectories at various horizontal (X) positions. The resulting normalized integrated field errors for the dipole and combined dipole magnets are presented in Fig. 1 and Fig.2, respectively. Within the GFR, the normalized field error is below 1×10^{-4} in the dipole magnets and below 5×10^{-3} in the combined dipole magnet. These values satisfy the tolerance requirements specified in Table 1. Multipole analysis of the measured fields indicates that the dominant error component in both magnet types is the sextupole term, with the normalized amplitudes of 7×10^{-5} for the dipole magnets and 2×10^{-3} for the combined dipole magnet.

†prapaiwan@slri.or.th

Content from this work may be used under the terms of the CC BY 4.0 licence (© 2026). Any distribution of this work must maintain attribution to the author(s), title of the work, publisher, and DOI.

ISBN: 978-3-95450-252-3 ISSN: 2673-5350 doi: 10.18429/JACoW-IPAC2026-TUP7655

VALIDATION OF AN IMPROVED QUADRUPOLE DESIGN FOR THE 3 GeV SPS-II STORAGE RING

T. Leetha†, P. Numanoy, T. Phimsen, S. Prawanta, P. Sunwong
Synchrotron Light Research Institute (Public Organization), Nakhon Ratchasima, Thailand

Abstract

Achieving high beam stability in the 3 GeV SPS-II storage ring critically depends on the precision of its quadrupole magnets. This work presents a crucial phase of the magnet prototype development, which is central to fostering domestic high-technology manufacturing with Thai industry partners field measurements on the initial quadrupole design featuring removable poles revealed a critical engineering issue of significant multipole errors caused by mechanical pole rotation. This error was traced to the stresses and assembly error that occurred during pole removal and re-assembly for coil installation to solve this specific problem, an improved quadrupole design was employed. The new symmetrical geometry eliminates the pole-removal step, thus intrinsically preventing the assembly error and significantly increasing structural stability and field quality. Coupled mechanical-magnetic analysis using ANSYS Workbench and Opera-3D confirms this approach. The simulations demonstrate that the improved design provides the required mechanical stability to minimize multipole field errors. The data presented validates this successful design change. The strict production tolerances were defined, and it is demonstrated precisely how the new design resolves the pole rotation issue. The presentation will feature a direct comparison of magnetic field measurements from both the initial and the improved prototypes, definitively verifying the enhanced performance necessary for SPS-II commissioning.

INTRODUCTION

The Siam Photon Source II (SPS II), Thailand's second synchrotron light source, is a 3.0 GeV fourth generation facility based on a Double Triple Bend Achromat (DTBA) lattice, delivering ultra bright photon beams with intensities up to one million times higher than the existing source. SPS II supports advanced research across multiple scientific and industrial fields and enhances regional scientific capacity within Southeast Asia through its location in the Eastern Economic Corridor of Innovation (EECi).

Quadrupole magnets are essential to the performance of DTBA storage rings, providing strong focusing required for ultralow emittance and precise control of functions and dispersion in compact lattices. [1, 2] Their field quality is critical for nonlinear cancellation, dynamic aperture, and beam lifetime, while the compact layout increases sensitivity to magnetic crosstalk, necessitating accurate modelling and multipole control.

This study compares two quadrupole magnet core designs to assess the impact of geometry, manufacturing precision, and assembly alignment on magnetic field quality. All processes adhere to the Terms of Reference (TOR) with dimensional tolerances within 20 μm, enabling reliable validation of measured fields against simulations and confirming the effectiveness of the improved design.

MAGNET DESIGN

The mechanical design of the quadrupole magnet was developed using SOLIDWORKS, where the iron-core geometry and mounting interfaces were refined following the prescribed pole-profile specifications. Structural integrity and natural frequencies were subsequently evaluated using ANSYS Workbench through finite element analysis ensure that the deformation conformed to Table 1.

Table 1. Parameter tolerance criteria for quadrupole design

Item	Tolerance
Pole rotation	≤ 250μrad
Pole positioning	≤ ±20 μm
Yoke deformation	≤ ±5 μm
Assembly reproducibility	≤ ±10 μm

Magnet type A demonstrated that pole rotation is the dominant source of sextupled and higher-order multipole errors in the initial quadrupole configuration. Even small angular deviations of the pole pieces lead to substantial, non-correctable multipole components, particularly problematic in the compact DTBA environment. [3, 4]

In this study, Magnet Type A was designed and fabricated; magnetic-field measurements revealed assembly-related errors, as illustrated in Fig. 1. Consequently, Magnet Type B was developed with fully symmetric components to minimize manufacturing and assembly deviations, thereby improving structural stability and magnetic-field quality.

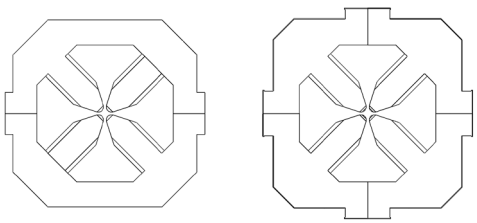

Figure 1: Quadrupole magnet type A and B.

Content from this work may be used under the terms of the CC BY 4.0 licence (© 2026). Any distribution of this work must maintain attribution to the author(s), title of the work, publisher, and DOI.

ISBN: 978-3-95450-252-3 ISSN: 2673-5350 doi: 10.18429/JACoW-IPAC2026-TUP7656

INFLUENCE OF CURRENT EXCITATION PROFILES ON SCREENING-CURRENT EFFECTS IN REBCO BENDING MAGNETS FOR THE HEFEI ADVANCED LIGHT FACILITY

J. Xia*, Z. Bai, C. Chen, J. Xu, Z. Zhu, J. Zhao
University of Science and Technology of China, Hefei, China

Abstract

ReBCO coated conductors are promising for compact high-field bending magnets and are being considered for use in the Hefei Advanced Light Facility (HALF) to enhance the photon energy from bending-magnet radiation. However, screening-current effects induced during excitation remain an important issue for such magnets. In this work, these effects are investigated in the proposed bending magnet using the H-formulation. Several current excitation profiles with different ramping and holding stages are compared. The results show that the charging history strongly affects screening-current relaxation and the induced-field distribution. Under the present conditions, final holding at the operating current is more effective than a slow final ramp or distributed intermediate holding, providing guidance for optimizing charging schemes for future ReBCO bending magnets.

INTRODUCTION

ReBCO coated conductors are promising for compact high-field bending magnets because of their high current-carrying capability and excellent performance under strong magnetic fields. In the Hefei Advanced Light Facility (HALF), selected conventional dipole magnets are planned to be replaced by ReBCO high-temperature superconducting (HTS) bending magnets to enhance the photon energy from bending-magnet radiation [1].

However, screening currents are induced in ReBCO tapes during magnet excitation because of the large aspect ratio of coated conductors [2, 3]. The resulting screening-current-induced field (SCIF) can affect the magnetic-field behavior of the magnet and may lead to excitation-history-dependent field deviations. This effect needs to be carefully considered for storage-ring applications, where field stability and reproducibility are important.

In this study, screening-current effects in a HALF ReBCO bending magnet are simulated using the H-formulation. Several current excitation profiles with different ramping and holding stages are compared, including uniform ramping, fast ramping with final holding, fast-to-slow ramping, and stepwise excitation with intermediate holding. Their effects on screening-current relaxation and the resulting induced-field distribution are analyzed, providing guidance for optimizing charging schemes for future HTS bending magnets.

* waterx09@gmail.com

MAGNET CONFIGURATION AND SIMULATION SETUP

Magnet Configuration and Numerical Model

Figure 1 shows the two-dimensional cross-sectional model of the HTS bending magnet, which consists of an iron core, HTS coil regions, and an air domain. To reduce the computational cost, only one quarter of the cross section is modeled using geometric symmetry, and the multilayer ReBCO coated conductors are represented by equivalent homogeneous HTS domains [4]. The main operating parameters are summarized in Table 1.

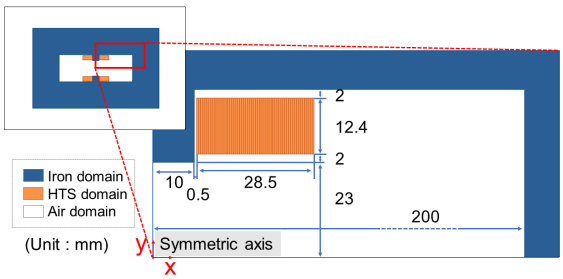

Figure 1: Two-dimensional cross-sectional model and geometric parameters of the HTS bending magnet.

Table 1: Main Operating Parameters of the Investigated ReBCO HTS Bending Magnet

Item	Unit	Value
Operating temperature, T_{op}	K	4.2
Operating current, I_{op}	A	270
Estimated critical current, I_c	A	385
Perpendicular field on conductor, $B_\perp$	T	5
Peak on-axis magnetic field, B_{peak}	T	6
On-axis field integral, $\int B_y dz$	T·m	0.368

The electromagnetic behavior of the HTS magnet is calculated using the H-formulation. The governing equation is written as

$$\nabla \times (\rho \nabla \times \mathbf{H}) + \mathbf{M}\frac{\partial \mathbf{H}}{\partial t} = 0, \quad (1)$$

where $\mathbf{H}$ is the magnetic field intensity, ρ is the electrical resistivity, and $\mathbf{M}$ represents the material-dependent magnetic constitutive relation [5]. The nonlinear magnetization of the iron core is included through the measured B–H curve. The ReBCO conductor is described by an E–J power-law relation, and the magnetic-field dependence of the critical current density J_{cB} is represented by a Kim-type

Content from this work may be used under the terms of the CC BY 4.0 licence (© 2026). Any distribution of this work must maintain attribution to the author(s), title of the work, publisher, and DOI.

ISBN: 978-3-95450-252-3 ISSN: 2673-5350 doi: 10.18429/JACoW-IPAC2026-TUP7657

DESIGN AND CONSTRUCTION OF THE TWIN-APERTURE SUPERCONDUCTING QUADRUPOLE FULL-SIZE PROTOTYPE FOR THE STCF IRSM*

W. Ma †,1, S. Wei[2], L. Gao[2], M. Liu[1], J. Zhang[3], Y. Zhu[3], X. Wu[1], J. Tang†,4
[1]High Magnetic Field Laboratory, Chinese Academy of Sciences, Hefei, China
[2]Institute of Plasma Physics, Chinese Academy of Sciences, Hefei, China
[3]Shanghai Advanced Research Institute, Chinese Academy of Sciences, Shanghai, China
[4]University of Science and Technology of China, Hefei, China

Abstract

The first Super Tau Charm Facility (STCF) final focus quadrupole prototype (named as QD1) has been designed, manufactured, assembled and tested at cold. The prototype is a full-size twin-aperture quadrupole magnet of the CCT type. The prototype reached the design field with no training quench and exhibit good field quality. In this paper, details of QD1 design, construction and test are reported.

INTRODUCTION

The super tau-charm facility (STCF) is a symmetric, third-generation electron-positron collider under design which is proposed by the University of Science and Technology of China. It has a design goal of center-of-mass-energy ($\sqrt{s}$) range from 2 to 7 GeV with a peak luminosity above 0.5 × 10^{35} $cm^{-2}s^{-1}$ at $\sqrt{s}$ = 2 GeV CoM energy. To achieve STCF accelerator requirements, it is required to place symmetrically two high gradient and high field quality twin-aperture interaction region superconducting magnets (IRSM) at each side of the interaction point (IP) [1]. Twin-aperture IRSM is considered as one of the top technical challenging systems for the STCF accelerator, therefore, it is decided that the first stage of key technology R&D activity is to prototype a full-size QD1 coil, as the QD1 has the highest field gradient and is closest to the IP (thus, it has the least allowable design space).

IRSM QD1 MAGNET DESIGN

IRSM General Requirements

Figure 1 shows IRSM sketch layout. In each IRSM system, there are two sets of twin-aperture quadrupoles, QD1 and QF2, two sets of orbit corrector coils, Orbit Corrector Positron (OCP) and Orbit Corrector Electron (OCE), and a set of series connected anti-solenoid coils (AS). The magnetic front of QD1 and QF2 are positioned at 0.9 m (L*) and 1.8 m away from IP, respectively, and both focus quadrupoles are distributed at beam crossing angle of 60 mrad (2θ). Orbit corrector coils, such as a1, b1, a2, a3, b4, etc., are required to compensate for field errors and improve beam optics dynamics. The whole IRSMs are operated inside the solenoid field of the detector magnet with a central field of 1.0 Tesla [2].

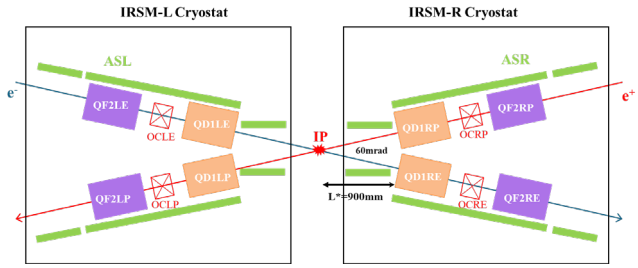

Figure 1: IRSM schematic layout (QD1RP - QD1 quadrupole at Right Positron beam; OCRP - Orbit Corrector at Right Positron beam; ASR - Anti-Solenoid Right; others are similar named.).

Table 1: Main Parameters of Final Focus Quadrupoles

Parameters	units	QD1	QF2	QD1_P
Gradient	T/m	50	40	50
Magnetic length	mm	400	300	400
Harmonics @ r_{ref}		≤0.2‰	≤0.2‰	≤1.0‰
Ref. radius, r_{ref}	mm	10	15	10
Beam pipe diameter, Ø	mm	30	50	Na
Coil front to IP distance	mm	900	1800	na

The key parameters of QD1 and QF2 are listed in Table 1. The beam pipe is designed to be room temperature and as a component of the cryostat. The beam pipe has an inner diameter of 30 mm and 50 mm for QD1 and QF2, respectively. Given the L* of 900 mm and beam crossing angle of 60 mrad, this gives the minimum distance between two apertures of QD1 quadrupole about 54 mm. Iron-free CCT (Canted Cosine Theta) was selected over cos2θ and serpentine as technique route for further R&D and prototype at this stage.

QD1 Quadrupole Design

Figure 2 shows twin-aperture CCT QD1 windings and its magnetic field strength contour, and Table 2 lists its main parameters. The QD1 design uses 4 wires co-wind method, the wires are directly wound on to CNC machined aluminium alloy formers and jointed in series at

* Work supported in part by the National Key Research and Development Program of China (Grant No. 2023YFA1607302), in part by the National Natural Science Foundation of China (Grant No. 12341501). We thank the Hefei Comprehensive National Science Center for their strong support on the STCF key technology research project.
† wbma@hmfl.ac.cn, jytang@ustc.edu.cn

Content from this work may be used under the terms of the CC BY 4.0 licence (© 2026). Any distribution of this work must maintain attribution to the author(s), title of the work, publisher, and DOI.

ISBN: 978-3-95450-252-3 ISSN: 2673-5350 doi: 10.18429/JACoW-IPAC2026-TUP7660

STRAIN GAUGE IMPLEMENTATION FOR A Nb_3Sn SUPERCONDUCTING MULTIPOLE WIGGLER DEVELOPED IN KEK PHOTON FACTORY

S. Nishi*
The Graduate University for Advanced Studies, SOKENDAI, Hayama, Japan
C. Mitsuda, K. Suzuki, H. Saito, S. Shinohara, T. Nogami, T. Ogitsu, K. Tsuchiya, S. Eguchi
High Energy Accelerator Research Organization (KEK), Tsukuba, Japan
K. Saito, M. Yoshikawa, S. Ito, S. Yokoyama
Japan Superconductor Technology, Inc. (JASTEC), Hyogo, Japan

Abstract

KEK Photon Factory is developing a Nb_3Sn superconducting multipole wiggler for a next generation light source ring. Following the Unit 1 [1], we conducted an excitation test of the Unit 2 at the current density of 378 A/mm^2. In this test, one of the purposes is to evaluate a new strain measurement system that was first introduced into the Unit 2. Multiple strain gauges were attached at positions determined by FEM simulation. We also compared simulation and measured results to assess the FEM model. In the future, we plan to conduct excitation tests at the target current density of 1000 A/mm^2. In the test, a strain-monitoring system will be implemented to the quench detection. We report the Unit 2 test results and progress toward the next excitation test.

INTRODUCTION

In KEK Photon Factory, Nb_3Sn superconducting multipole wiggler (SC-MPW) units are being developed as part of the technology development toward next generation light source ring. The main design parameters of the SC-MPW test-coil unit are listed in Table 1.The full-length device is designed to have 14 poles, corresponding to 7 wiggler periods. At present, two short-model SC-MPW units with 3 poles and 1.5 wiggler periods are being fabricated in order to identify fabrication issues prior to the construction of the full-length device. In this paper, the test-coil unit refers to a single unit, whereas the complete device consists of two facing units. The 300 A excitation test is the first test after heat treatment and impregnation. The test was launched as a validation program whose goal is to check conformity of the coils as well as commissioning of the quench protection, DAQ, strain-monitoring and temperature-monitoring system. Because the SC-MPW uses strain-sensitive Nb_3Sn conductor, strain monitoring during cool-down and excitation is a central issue at this stage. In this paper, we present the results of the excitation test of the second test-coil unit and the strain measurements, and discuss future prospects.

DETERMINATION OF STRAIN MONITORING POINTS

The strain to be monitored is the coil strain, $\varepsilon_{\mathrm{coil}}$, which includes thermal strain during cool-down and Lorentz-force-induced strain during excitation. During cool-down, an apparent strain, $\varepsilon_{\mathrm{apparent},T}$, arises from the temperature dependence of the gauge resistance and the differential thermal contraction between the strain gauge and the coil. During excitation, an additional apparent strain, $\varepsilon_{\mathrm{apparent},B}$, arises from magnetoresistance. Taking tensile strain as positive, the strain-gauge reading attached to the coil is written as $\varepsilon_{\mathrm{SG}} = \varepsilon_{\mathrm{coil}} + \varepsilon_{\mathrm{apparent},T} + \varepsilon_{\mathrm{apparent},B}$. Here, $\varepsilon_{\mathrm{coil}}$ is decomposed into the free thermal strain, $\varepsilon_{\mathrm{free}}$, and the mechanical strain, $\varepsilon_{\mathrm{mech}}$. In the present analysis, $\varepsilon_{\mathrm{mech}}$ is treated separately for cool-down and excitation. The free thermal strain is the strain integrated as the coil cools from room temperature to the operating temperature (4.2 K), based on the linear thermal expansion coefficient of the coil, α_{coil}. The $\varepsilon_{\mathrm{mech(cooldown)}}$ denotes the mechanical strain induced during cool-down by coil constraints and by differential thermal contraction between the coil and the support structure, whereas $\Delta\varepsilon_{\mathrm{mech(excitation)}}$ denotes the mechanical strain increment during excitation, including the contributions of Lorentz forces and the coil support structure. Accordingly, during cool-down, $\varepsilon_{\mathrm{SG(cooldown)}}$ is given by the sum of $\varepsilon_{\mathrm{free}}$, $\varepsilon_{\mathrm{mech(cooldown)}}$, and $\varepsilon_{\mathrm{apparent},T}$. Thus, the coil strain during cool-down is obtained by correcting the measured value for $\varepsilon_{\mathrm{apparent},T}$. For excitation, the strain increment is evaluated with respect to the state after cool-down and before excitation. The strain-gauge reading increment during excitation, $\Delta\varepsilon_{\mathrm{SG(excitation)}}$, is then given by the sum of $\Delta\varepsilon_{\mathrm{mech(excitation)}}$ and $\Delta\varepsilon_{\mathrm{apparent},B}$. The mechanical strain increment during excitation is obtained by correcting the measured increment for $\Delta\varepsilon_{\mathrm{apparent},B}$. Based on this formulation, compensation

Table 1: Main Design Parameter of the SC-MPW Test Coil Unit

Item	Specification
operating temperature	4.2 K
superconducting wire	Nb_3Sn
fabrication process	bronze process
Wire dia. (insulation)	1.2 mm (1.36 mm)
Copper ratio (Cu/Cu+Non-Cu)	0.3 ±0.1
current	792 A (1000 A/mm^2)
number of turns	493 turns
magnetic field on the beam axis	> 2 T
magnetic period length	80 mm
pole gap	> 30 mm

* snishi@post.kek.jp

Content from this work may be used under the terms of the CC BY 4.0 licence (© 2026). Any distribution of this work must maintain attribution to the author(s), title of the work, publisher, and DOI.

ISBN: 978-3-95450-252-3 ISSN: 2673-5350 doi: 10.18429/JACoW-IPAC2026-TUP7661

CHARACTERIZATION OF WET-WOUND INSULATED 2G-HTS TAPE IN A DEWAR*

J. C. Jan†, C. C. Tsai, F. Y. Lin, C. K. Yang and T. Y. Chung
National Synchrotron Radiation Research Center, Hsinchu, Taiwan.

Abstract

The second-generation high-temperature superconductor is under consideration for accelerator applications because its operating temperature, which is higher than 4.2 K, eliminates the need for liquid helium. However, the relatively low engineering critical current, inter-layer insulation challenges, welding reliability and quench protection remain key technical issues. In this work, an insulated high-temperature superconducting tape was wet-wound using a low-temperature adhesive. The winding method, charging behavior, as well as quench protection were experimentally investigated. A simple liquid-helium-free test dewar is also presented.

INTRODUCTION

Second-generation high-temperature superconducting tape (2G-HTS tape) is a promising option for winding accelerator magnets, offering high current density and excellent performance under strong magnetic fields. In addition, HTS materials can operate at higher temperatures, thereby reducing reliance on liquid helium. However, compared with low-temperature superconductors such as NbTi wire, 2G-HTS tape presents greater challenges in winding and electrical characteristics. These include constraints on minimum bending radius, the need to avoid twisting, and difficulties in quench detection. No-insulated (NI), metal-insulated (MI), and insulated (INS) windings have been studied to understand HTS behavior after winding. NI winding suffers from charging delays and shielding current effects; however, its excellent thermal stability enables self-protection during a quench [1, 2]. MI winding has disadvantages including low packing factor, charging delay, contact resistance instability, and complex winding, but its metallic insulation provides a more efficient heat dissipation path during a quench compared to INS winding [2]. INS winding has disadvantages such as a low packing factor, slow quench propagation, thermal mismatch, and insulation delamination. However, it also offers advantages, including predictable electrical paths, no charging delay, and simple current control [1-3]. The final goal of this project is to generate a 3.5 T magnetic field using 12 mm 2G-HTS tape operating at 20 K in a cryogen-free dewar [4]. Considering the relatively low magnetic field requirement and operating current, the insulated (INS) winding method was selected to fabricate a prototype, referred to as HTS-P1-5t. In this study, insulated 2G-HTS tape was wound and fixed using cryogenic epoxy, and then installed in a cryogen-free dewar to evaluate its thermal and charging characteristics.

*Work supported by NSTC
† janjc@nsrrc.org.tw

2G-HTS TAPE WINDING

The HTS-P1-5t was wound using insulated SCS12050-AP-i HTS tape supplied by SuperPower Inc. (Furukawa), with the joints formed by PbSn soldering. The HTS tape is insulated with a 0.025 mm thick layer consisting of polyimide film and silicone adhesive, applied with a 30% overlap. The final average width and thickness of the insulated 2G-HTS tape are 12.04 mm and 0.169 mm, respectively.

Figure 1(a) shows the HTS-P1-5t and the return yoke, with a magnified view of the joint (red box) presented in Fig. 1 (b). The pole and return yoke are fabricated from DT4E pure iron, and a 1 mm thick copper spacer (Cu-spacer) is inserted between the pole and the 2G-HTS tape to prevent the peak magnetic field from concentrating on the tape surface. The Cu-spacer must provide good contact with the pole while maintaining effective heat conduction. Therefore, ten turns of 0.1 mm thick copper sheets are wet-wound directly onto the pole, as shown in Fig. 1(b). A 0.4 mm groove is subsequently machined to solider the 2G-HTS extended leads. After curing of the Cu-spacer, the 2G-HTS tape was wet-wound onto the Cu-spacer. The 2G-HTS tape layers were bonded together using a cryogenic epoxy prepared from GY285 and HY5922. The tension applied during 2G-HTS winding is approximately 2 kgf. In addition, each 2G-HTS extended lead is overlapped with three 2G-HTS tapes to improve mechanical robustness and reliability, as shown in Fig. 1(a). Figure 1(c) shows the HTS-P1-5t installed in a copper cooling housing. The HTS-P1-5t is enclosed by copper on three sides, while one side is intentionally left open to simulate the electron-beam pass-through region, which experiences relatively poor cooling conditions. Cryogenic grease or Indium sheets is applied to all contact surfaces to enhance thermal transfer efficiency. The composition materials of the HTS-P1-5t include DT4E, copper, polyimide film, Hastelloy and cryogenic epoxy. Figure 2 illustrates the material contact arrangement and corresponding thickness within the HTS-P1-5t winding. Table 1 lists the integrated thermal contraction ($\Delta L/L$) of these materials [5-8]. The thermal contraction of the Hastelloy was approximated using the cryogenic contraction data of Inconel 718. The polyimide and cryogenic epoxy are relative soft compared to DT4E or copper. Therefore, these thin soft layers can maintain good thermal contact and buffering small deformations between the metal layers.

Content from this work may be used under the terms of the CC BY 4.0 licence (© 2026). Any distribution of this work must maintain attribution to the author(s), title of the work, publisher, and DOI.

ISBN: 978-3-95450-252-3 ISSN: 2673-5350 doi: 10.18429/JACoW-IPAC2026-TUP7665

A CONTROL SCHEME FOR HIGH POWER DENSITY MULTI-UNIT POWER SUPPLIES

Yucheng Shang, Zhouyu Zhao
National Synchrotron Radiation Laboratory
University of Science and Technology of China, Hefei, China

Abstract

A control scheme for high-power density multi-unit constant current power supplies based on compact high-speed PLC is proposed. The scheme adopts a hybrid analog-digital dual-loop control approach. The power supplies utilize mature commercial customized modules with internal analog voltage control loop, while a single PLC constructs the current feedback loop for multiple power modules. This scheme has been successfully applied to multi-unit klystron solenoid power supplies and industrial Linac power supplies, achieving very high power density, simple interlocking and communication interfaces, and high operational reliability.

INTRODUCTION

In particle accelerators, microwave tubes, and other beam devices, multi-unit solenoid constant current power supplies are widely used. Typically, each coil of the focusing magnet is powered by an independent power supply. When the number of coils is large, the number of power supplies increases accordingly, leading to larger overall volume and weight, as well as more complex communication interfaces and interlocking circuit. This is unfavorable for achieving miniaturization of the entire accelerator system and improving its simplicity and reliability.

We adopt a hybrid analog-digital dual-loop control method [1], where power units use mature and commercially customized modules as internal analog voltage control loops. In [1], the stability of the outer current loop is provided by a Proportional-Integral compensation circuit, while in our scheme, a compact high-speed PLC is used to construct the current feedback loops for multiple power modules.

The internal analog loop of the power modules offers high bandwidth and fast response speed, effectively suppressing fast disturbances such as power grid fluctuations. The outer loop utilizes a digital controller to form a digital feedback current loop, which compensates for slow variations caused by temperature changes and load variations. The combination of both loops enables excellent dynamic performance and high static stability.

Unlike the dedicated digital controller solutions in [2] or the large-scale system designs in [3–5], our scheme prioritizes compactness and convenience by leveraging commercial modules, following a design similar to [6] but extended to multi-unit PLC-based control.

This scheme has been successfully applied to multi-unit klystron solenoid power supplies and industrial Linac power supplies. It achieves a very high power density, along with simplified interlocking and communication interfaces, greatly simplifying the design of the upper-level control network. The entire power supply system exhibits very high operational reliability.

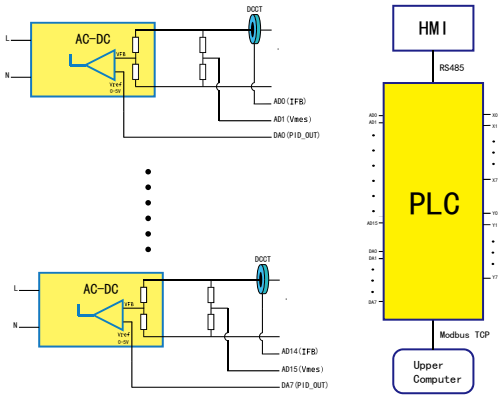

Figure 1: Overall Control Scheme.

DESIGN ARCHITECTURE

Overall Control Scheme

As shown in Fig. 1, the left side shows a group consisting of 8 commercial regulated power modules (each with a rated power of 1000 W), all uniformly installed within the same chassis. All of the eight modules are controlled by a single compact high-speed PLC. Current and voltage signals from the load side of each power supply are sampled and input through ADC channels (A0–A15, totaling 16 channels) of the analog input module GL20-8AD.

Inside the PLC, a closed-loop compensation control program based on the PID algorithm is executed, with a digital control sampling period of 1 ms for the system. The deviation between the current setpoint and the actual feedback value is processed by PID calculation to generate 8 channels of control voltage signals (0–5 V). These signals are sent to the regulation ports of each module via channels DA0–DA7 of the GL20-8DA analog output module, thus achieving stable control of load currents.

Power Module

The commercialized industrial power module is UHP-1000-48, made by MEAN WELL ENTERPRISES CO.,LTD. The principle of the power module is illustrated in Fig. 2. The main circuit of the power module adopts a two-phase interleaved forward converter topology. Its front stage consists of a dual interleaved Booster-type PFC circuit, achieving a

Content from this work may be used under the terms of the CC BY 4.0 licence (© 2026). Any distribution of this work must maintain attribution to the author(s), title of the work, publisher, and DOI.

ISBN: 978-3-95450-252-3 ISSN: 2673-5350 doi: 10.18429/JACoW-IPAC2026-TUP7666

DEVELOPMENT OF A FAST-FEEDBACK DEFLECTOR MAGNET POWER SUPPLY FOR THE NEXT GENERATION HEAVY ION THERAPY*

K. Okamura†, K. Takayama, High Energy Accelerator Research Organization, Tsukuba, Japan
H. Kamezaki, Pulsed Power Japan Laboratory Ltd., Kusatsu, Shiga, Japan

Content from this work may be used under the terms of the CC BY 4.0 licence (© 2026). Any distribution of this work must maintain attribution to the author(s), title of the work, publisher, and DOI.

Abstract

Application of a 10 Hz fast-cycling induction synchrotron (IS) to the next generation of heavy ion therapy called Energy Sweep Compact Rapid Cycling Hadron Therapy (ESCORT), where the ion beam with energy sweeping is delivered tracking a tumor target in a deformed and moving organ and monitoring the irradiation dose profile in a real-time during irradiation, is under investigation in the collaboration of KEK, SAMEER in India, and Subatech in France. To enable precise targeting, the final deflector magnet must adjust the beam on its irradiation position accurately by varying the polarity and peak current value for each pulse with the excitation pattern of the main magnet system. The developed power supply for the final deflector magnet makes this possible. This paper describes the initial experimental results obtained by combining a prototype power supply with a steering magnet.

INTRODUCTION

In the next-generation of particle therapy, the beam must be delivered tracking a cancer target in a deformed and moving organ and monitoring the irradiation dose profile in a real-time during irradiation. We have proposed and investigated Energy Sweep Compact Rapid Cycling Hadron Therapy (ESCORT) based on the acceleration principle of induction synchrotron (IS) [1, 2] with these features. Its driver is the rapid-cycling IS that is operated at 10 Hz. In the ESCORT system, the beam extracted from the accelerator ring is scanned not only across the entire 2D cross-section of the irradiation target, but is also swept in depth; for this purpose, the two sets of deflector electromagnet shown in Fig. 1 are used in combination. The first set is a deflector that kicks the beam following the pre-programmed settings corresponding to the target irradiation position; it is called the program-operated deflector. The second set requires the maximum excitation value to be varied for each shot in response to signals from a real-time feedback computer while tracking the movement of the cancer target; we refer to this as the fast feedback deflector system (FFDS). This paper describes the magnet power supply in the FFDS that can provide the peak current amplitude and polarity in response to the command values varying each acceleration cycle.

EXPERIMENT WITH A PROTOTYPE POWER SUPPLY

Circuit Diagram

The proto type power supply was developed modifying the pattern waveform high-voltage dc power supply [3], which has the H bridge dc-dc converter scheme (Fig. 2). The key difference is that while the previous power supply used voltage control based on output voltage feedback, this power supply uses current control based on output current feedback.

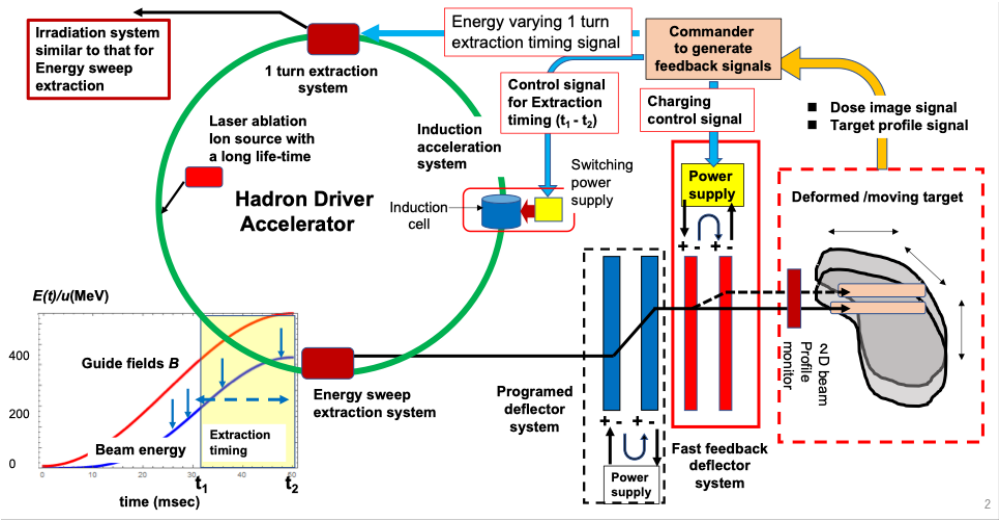

Figure 1: Conceptual diagram of the ESCORT.

* This study is supported by by Grant-In-Aid for Scientific Research (B) (KAKENHI No. 23H03666
†katsuya.okamura@j-parc.jp

ISBN: 978-3-95450-252-3 ISSN: 2673-5350 doi: 10.18429/JACoW-IPAC2026-TUP7668

DEVELOPMENT AND EXPERIMENTAL VALIDATION OF A MODULAR MAGNET POWER SUPPLY FOR THE KOREA-4GSR STORAGE RING

Hyeonjun Jang, Wi-Min Kim, Min-Kyu Choi, Yoon Geol Choi, Garam Hahn, Min-Jae Kim
Pohang Accelerator Laboratory, Pohang, South Korea

Content from this work may be used under the terms of the CC BY 4.0 licence (© 2026). Any distribution of this work must maintain attribution to the author(s), title of the work, publisher, and DOI.

Abstract

The Korea 4th Generation Synchrotron Radiation (Korea-4GSR) storage ring comprises 1,184 magnets, 792 of which require rated currents of 140 A or 280 A. To drive these magnets, a magnet power supply (MPS) supporting parallel operation was developed to minimize the number of MPS types, thereby improving maintenance efficiency and reducing manufacturing costs. To ensure beam stability and low-emittance operation, current accuracy below 100 ppm and stability below 10 ppm are required. This paper presents a storage ring modular MPS (SR Modular MPS) rated at 140 A, designed with master–slave parallel operation capability to expand the rated output current to 280 A through two-unit parallel configuration. Operating-condition-dependent calibration methods are applied to satisfy the performance requirements over the entire operating range. Experimental results demonstrate that the developed SR Modular MPS achieves an accuracy of 45.79 ppm and a stability of 2.28 ppm in single-unit operation, and 45.88 ppm and 5.1 ppm, respectively, in parallel operation.

INTRODUCTION

The Korea-4GSR storage ring comprises 28 cells, each containing Center-bend, Quad-bend, Reverse-bend, Quadrupole, Sextupole, and Corrector magnets, as shown in Fig. 1 [1]. Among the 1,184 magnets, 792 require rated currents of 140 A or 280 A with a current accuracy below 100 ppm and stability below 10 ppm to ensure beam stability and low-emittance operation. A modular 140 A-rated unit featuring master–slave parallel operation was developed to cover both current ratings with a single MPS type, enabling expansion to 280 A through two-unit parallel configuration. This approach reduces manufacturing costs and simplifies maintenance. This paper describes the power stage configuration, calibration methodology, and experimental validation of the developed SR Modular MPS.

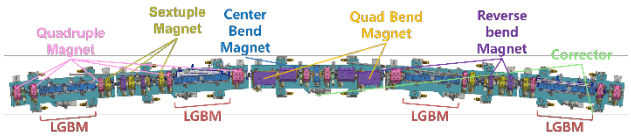

Figure 1: Layout of one cell in the Korea-4GSR storage ring.

POWER STAGE AND PARALLEL OPERATION

Figure 2 illustrates the power stage of the SR Modular MPS. At the input stage, the AC power is isolated by a switched-mode power supply (SMPS) and converted to DC to form the DC-link voltage. This DC-link voltage is supplied to a full-bridge inverter based on SiC MOSFETs operating at a switching frequency of 100 kHz. The high-frequency ripples generated by the inverter are attenuated via an LC–LC–RC output filter, delivering a stable, low-ripple DC output current to the magnet load.

In parallel operation, synchronization between the digital signal processor (DSP) Pulse Width Modulation (PWM) loop and Small Form-factor Pluggable (SFP) frame transmission is critical. The SFP frame aligns with the 33.3 kHz DSP interrupt loop (PWM: 100 kHz), while Programmable logic (PL) internal sync is managed via AXI. Header–Payload–CRC packets exchange master duty commands and slave feedback (current, status, and faults).

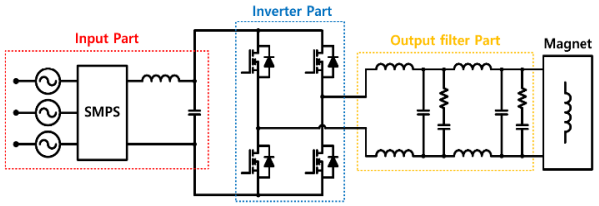

Figure 2: Power stage of the SR Modular MPS.

ACCURACY IMPROVEMENT VIA CALIBRATION

Offset Calibration

Offset calibration is implemented to reduce the fixed deviation between the command current and the measured output current. The rated current range (1–140 A) is swept at 1 A intervals, and the stabilized mean current is measured at each point to construct an offset calibration table. During operation, the DSP references this table and applies the corresponding correction to the command value in real time, thereby minimizing the offset error across the entire operating range.

Temperature Calibration

Temperature calibration compensates for current drift caused by ambient temperature changes and internal heat generation, thereby ensuring output precision during long-term operation. A thermocouple is mounted on the sensor board housing the analog-to-digital converter (ADC) to acquire real-time temperature data. The MPS is operated at the rated current of 140 A over an extended period, and the resulting temperature–current correlation is used to derive temperature-dependent correction coefficients. These coefficients are applied in the DSP firmware to compensate for thermal drift in real time.

As shown in Fig. 3, both calibration methods effectively reduce the current error over the entire operating range.

ISBN: 978-3-95450-252-3 ISSN: 2673-5350 doi: 10.18429/JACoW-IPAC2026-TUP7669

DEVELOPMENT OF A GaN-FET-BASED FAST CORRECTOR MAGNET POWER SUPPLY FOR THE TPS

B. S. Wang, K. B. Liu, and Y. S. Wong
NSRRC, Hsinchu, Taiwan

Abstract

A modular GaN-FET-based fast corrector magnet power supply has been developed for the Taiwan Photon Source (TPS). The high switching speed of GaN devices enables a significant increase in the output current bandwidth, which improves the response of the fast orbit feedback (FOFB) system and enhances the overall beam stability and photon beam quality of TPS. In the existing FOFB system, the operating current of the corrector magnet power supply is within ±5 A. The developed power supply provides a maximum output current of ±5 A and achieves improved current resolution by optimizing the internal turn ratio of the DC current transformer (DCCT). A digital control architecture is implemented, integrating an ADC interface, interlock protection, and a PI controller, and is fully compatible with the TPS control system. With a switching frequency of 250 kHz, the proposed power supply achieves a current control bandwidth of approximately 9 kHz, providing a significant improvement over the existing system.

INTRODUCTION

The Taiwan Photon Source (TPS) has achieved excellent beam quality and stable operation over the past decade. To further enhance beam stability and meet increasing demands for high-precision experiments, upgrades of accelerator subsystems are necessary, particularly to improve the bandwidth of the fast orbit feedback (FOFB) system for suppressing rapid orbit disturbances.

The TPS storage ring consists of 24 sectors, each equipped with bending, quadrupole, and sextupole magnets, as well as seven beam position monitors (BPMs) as shown in Fig. 1 [1].

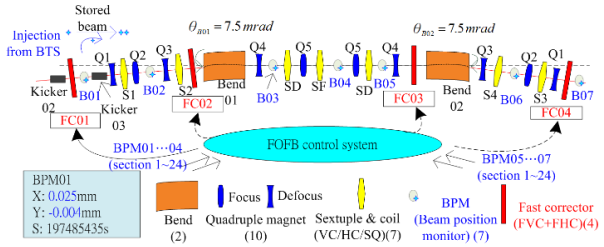

Figure 1: Distribution of BPMs and fast CMPS.

The FOFB system relies on fast corrector magnets driven by power supplies with limited bandwidth (≈1.6 kHz small-signal at 40 kHz switching) [2]. To improve FOFB performance, a higher-bandwidth, higher-resolution fast corrector magnet power supply (DFCMPS) was developed. The design employs a digital control architecture, GaN FETs in a modular full-bridge topology (250 kHz switching), and LEM ITN-12-P DCCT current feedback, achieving ±5 A full-scale resolution while maintaining compatibility with existing TPS infrastructure. Experimental results demonstrate enhanced bandwidth and current stability, validating the proposed system.

DESIGN OF THE DFCMPS

To increase the control bandwidth of the FOFB system at TPS, a DFCMPS has been developed based on the architecture of the existing TPS Corrector Magnet Power Supply (CMPS). The overall system configuration is shown in Fig. 2. The power stage adopts a modular half-bridge topology, where two half-bridge modules form a full-bridge (H-bridge) structure to generate bipolar output current for the fast corrector magnets. A digital control architecture based on a Texas Instruments DSP is implemented together with analog signals conditioning circuits. The feedback current signal is digitized and processed by the DSP, where a proportional–integral (PI) compensator is used to achieve closed-loop current regulation [3].

For current feedback measurement, a high-precision DCCT is used. A LEM ITN-12-P DCCT operates in a shunt-type configuration. By modifying the primary winding turns ratio, the current measurement range is reduced from 12.5 A to 6.25 A, thereby improving the current measurement resolution and regulation accuracy.

Compared with the existing CMPS, the switching frequency of the power stage is increased from 40 kHz to 250 kHz. To support high-frequency operation, the PI control algorithm and DSP firmware are optimized to ensure that compensation calculations can be completed within each PWM interrupt cycle. In addition, conventional MOSFET devices are replaced with GaN FETs to reduce switching losses and improve high-frequency performance. The modular half-bridge design also simplifies system debugging and facilitates future upgrades of the power devices.

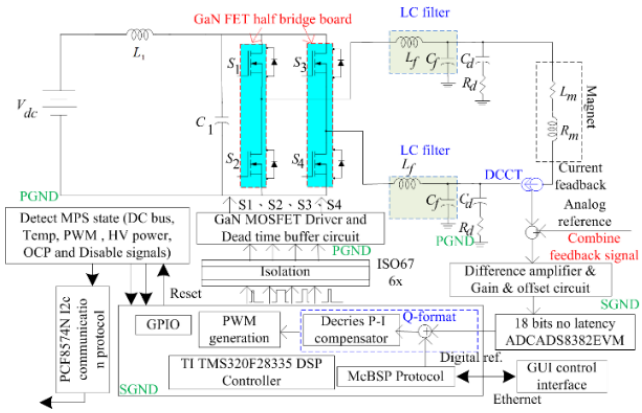

Figure 2: Architecture of DFCMPS.

Content from this work may be used under the terms of the CC BY 4.0 licence (© 2026). Any distribution of this work must maintain attribution to the author(s), title of the work, publisher, and DOI.

ISBN: 978-3-95450-252-3 ISSN: 2673-5350 doi: 10.18429/JACoW-IPAC2026-TUP7673

SUSTAIN THERMAL INSULATION VACUUM OF A LIQUID NITROGEN COOLING SYSTEM FOR TPS CRYOGENIC PERMANENT UNDULATOR

F.-Z. Hsiao†, P.-S. Chuang, H.-H. Tsai, H.-Ch. Li, W.-R. Liao, Ch.-K. Yang, Ch. Shueh
National Synchrotron Radiation Research Center, Hsinchu, Taiwan

Abstract

At the Taiwan Photon Source (TPS) a cryogenic permanent magnet undulator, CUT18, utilizes the latent heat of vaporization of liquid nitrogen for magnet cooling. After a period of operation, some condensed water, which caused rust at the structure of CUT18, appeared at the flange connecting the cooling system and the vacuum beam chamber of CUT 18. This condensed water was mainly due to deterioration of the thermal insulation vacuum of the liquid nitrogen cooling system. Moreover, the period became much shorter after the maintenance to recover a proper vacuum under cold conditions. This paper presents the efforts to extend the period of sustaining a proper thermal insulation vacuum without the appearance of condensed water. A residual gas analyzer was used to study outgases from the insulation vacuum of the liquid nitrogen cooling system at warm and cold conditions. These efforts succeed to extend the period longer than three months, thus greatly reduced the burden from insulation vacuum maintenance.

INTRODUCTION

A cryogenic permanent magnet undulator CUT18 was installed at the accelerator of Taiwan Photon Source (TPS) to provide a photon source for the highly brilliance micro-focus X-ray beamline TPS 15A. The coolant of CUT18 is liquid nitrogen where its latent heat of vaporization is used for cooling the terbium (Tb)-diffused neodymium-iron-boron (NdFeB) permanent magnets of CUT18 [1].

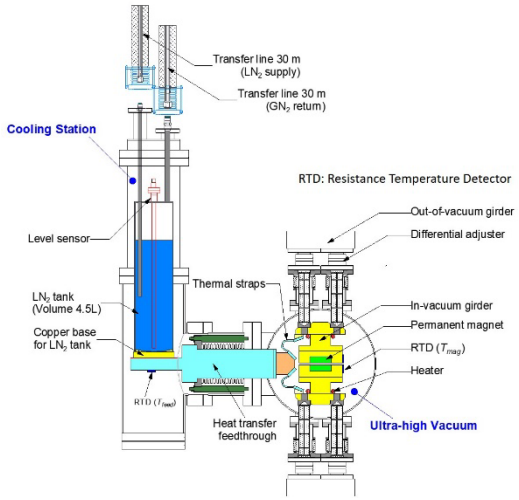

Figure 1: Cooling station with a LN2 tank.

†fzh@nsrrc.org.tw

Liquid nitrogen does not directly cool the NdFeB permanent magnet. Instead, the heat conduction mechanism is implemented via a copper bar with one end contacting a cooling station with a 4.5-liter nitrogen tank close to 77.3 K and the other end connecting to the permanent magnets through several flexible copper thermal straps, as shown in Fig. 1 [1]. Using adopted heater loads combined with the thermal load induced from the beam current 500 mA in TPS electron storage ring, the NdFeB magnets keep at 160 K to provide superior magnet properties.

Liquid nitrogen comes from the main streams of rigid cryogenic transfer pipe for TPS photon beamlines, as shown in Fig. 2 [2]. The transfer length from the source tank of volume 60 m^3 to the cooling station tank is more than 300 m. The pressure at the source tank varies in between 2.5 to 3.5 bar, and a valve at the exhaust line for gas nitrogen regulates the pressure at the cooling station tank in the range 1.05 to 1.1 bar.

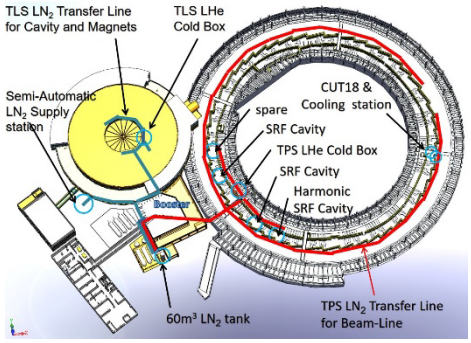

Figure 2: Infrastructure of liquid nitrogen system.

After operation a period, some condensed water appeared at the flange connecting to the vacuum beam chamber of CUT 18, dropped at the frame and caused rust. This condensed water was mainly due to deterioration of the thermal insulation vacuum of the liquid nitrogen cooling system. The period became much shorter after the maintenance to recover a proper vacuum under cold conditions. This paper presents the efforts to extend the period of sustaining a proper thermal insulation vacuum without appearance of condensed water.

COOLING SYSTEM DETAIL

The nitrogen cooling system of CUT18 includes a valve box and a controller for the liquid level and gas pressure control, two 4.5-liter tanks as the cooling stations, and flexible cryogenic pipes for the transfer of liquid and gas nitrogen between the valve box and the cooling station, as indicated in Fig. 1. The valve box and controller are located

Content from this work may be used under the terms of the CC BY 4.0 licence (© 2026). Any distribution of this work must maintain attribution to the author(s), title of the work, publisher, and DOI.

ISBN: 978-3-95450-252-3 ISSN: 2673-5350 doi: 10.18429/JACoW-IPAC2026-TUP7674

EFFECT OF FILLING MODES ON BOILING HEAT TRANSFER MECHANISMS IN LIQUID NITROGEN COOLING SYSTEM

H.-Ch. Li†, W.-R. Liao, H.-H. Tsai, F.-Z. Hsiao, P.-S. Chuang, S.-H Chang
National Synchrotron Radiation Research Center, Hsinchu, Taiwan

Content from this work may be used under the terms of the CC BY 4.0 licence (© 2026). Any distribution of this work must maintain attribution to the author(s), title of the work, publisher, and DOI.

Abstract

Liquid nitrogen (LN_2) cooling is widely utilized in the cooling systems of superconducting devices and scientific instruments. During the cooling process, the boiling heat transfer mechanism plays a decisive role. When the solid surface temperature significantly exceeds the saturation temperature of the liquid nitrogen, the Leidenfrost effect occurs, forming a vapor film at the solid-liquid interface that drastically reduces heat transfer efficiency. Previous research has primarily focused on altering the boiling curve and enhancing the Critical Heat Flux (CHF) through surface roughness, micro-nano structures, or various material properties. Few studies have explored the impact of filling modes within the cooling system on disrupting the vapor film and improving boiling heat transfer. This study utilizes a self-developed liquid nitrogen cooling experimental platform to investigate four distinct filling and cooling modes designed for an Oxygen-Free High Conductivity (OFHC) copper test block. By examining the boiling curves under various filling modes, this thesis analyzes the underlying mechanisms influencing the wall superheat at the Leidenfrost point (ΔT_{LP}) and the Critical Heat Flux (ΔT_{CHF}). The results indicate that the bottom-filling method, characterized by impingement kinetic energy, effectively increases fluid disturbance and disrupts the vapor film encapsulation. This significantly reduces the duration of the Leidenfrost effect and facilitates an earlier transition into the high-efficiency nucleate boiling stage.

INTRODUCTION

Cryogenic cooling technologies are increasingly utilized in modern industry and advanced scientific research. However, when cryogenic liquids contact solid surfaces at room temperature, the extreme temperature gradient typically triggers vigorous boiling. In the initial cooling stage, the system inevitably enters the film boiling regime. During this phase, due to the Leidenfrost effect, the solid surface becomes entirely encapsulated by a continuous vapor film. The vapor layer, characterized by extremely low thermal conductivity, acts as a thermal insulator, leading to a significant reduction in the heat transfer coefficient and overall cooling efficiency. To enhance the efficiency and safety of cooling systems, effectively shortening the duration of film boiling and elevating both the Leidenfrost Point (LP) and Critical Heat Flux (CHF) have become primary challenges in the field of cryogenic heat transfer. The boiling curve is standardly used to characterize the relationship between surface heat flux (q) and wall superheat ($\Delta T = T_{wall} - T_{sat}$). This curve encompasses four primary regimes: single-phase natural convection, nucleate boiling, transition boiling, and film boiling. When liquid nitrogen contacts a high-temperature surface, it immediately enters the film boiling regime. As the surface temperature decreases to the Leidenfrost Point temperature (T_{LP}), the vapor film becomes unstable and collapses, allowing intermittent contact between the liquid and the solid surface; at this point, the system enters the transition boiling regime. Subsequently, as the temperature further drops to the Critical Heat Flux point (T_{CHF}), the system enters the nucleate boiling regime. In this stage, heat transfer efficiency peaks as bubbles rapidly form and detach from the surface, removing a substantial amount of thermal energy. In practical cooling applications, the system must successfully transition from film boiling to nucleate boiling to achieve stable and efficient thermal management. Figure 1 presents the typical boiling heat transfer curve.

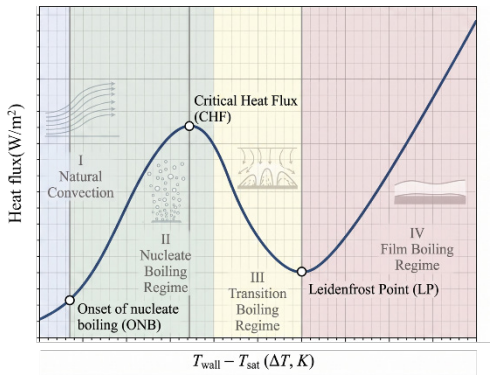

Figure 1: Typical boiling heat transfer curve.

Extensive prior research has focused on enhancing boiling heat transfer performance by modifying the physical or chemical properties of solid surfaces. Increasing surface roughness provides more micro-cavities to serve as bubble nucleation sites, thereby significantly improving the heat transfer coefficient during the nucleate boiling stage [1]. Nano-porous structures, fabricated via techniques such as Micro-arc Oxidation or femtosecond laser processing, can substantially increase surface capillary forces and hydrophilicity. Such superhydrophilic surfaces facilitate liquid penetration through the vapor film to contact the wall, leading to extraordinary shifts in the Leidenfrost temperature—in some cases exceeding 175°C [2]. In liquid nitrogen pool boiling experiments, CHF performance varies across materials such as copper, aluminum, and stainless steel, with copper surfaces typically exhibiting the highest CHF [3]. While surface treatments and roughening effectively improve boiling heat transfer, large-scale implementation is

†shingjay@nsrrc.org.tw

ISBN: 978-3-95450-252-3 ISSN: 2673-5350 doi: 10.18429/JACoW-IPAC2026-TUP7675

OPERATIONAL STATUS AND FAULT ANALYSIS OF THE CSNS VACUUM SYSTEM AND DEVELOPMENT PROGRESS OF THE CSNS-II VACUUM SYSTEM

Pengcheng Wang* [1,2,3], Jiaming Liu[1,2,3], Shunming Liu[1,2,3], Biao Tan[1,2,3], Xiaoyang Sun[1,2,3], Yigang Wang[1,2,3], Bangle Zhu[1,2,3]
[1]Spallation Neutron Source Science Center, Dongguan 523000, China
[2]Institute of High Energy Physics, Chinese Academy of Sciences, Beijing 100049, China
[3]Guangdong Provincial Key Laboratory of Extreme Conditions, Dongguan, 523803, China

Abstract

Since the China Spallation Neutron Source (CSNS) was officially commissioned in 2018, its operational performance has been continuously improved. To date, the beam power has reached 185 kW, which is 85% higher than the design value, with a stable annual beam delivery time of more than 5000 hours and good overall operational reliability. The vacuum system serves as the core support for stable beam transport, mainly consisting of the Linear Accelerator (LINAC), Rapid Cycling Synchrotron (RCS), Low Energy Beam Transfer Line (LRBT), and High Energy Beam Transfer Line (RTBT). In addition, supporting vacuum systems for application beamlines such as APEP and Back n have been developed, with operating vacuum pressures ranging from 10^{-3} Pa to 10^{-7} Pa.The first phase vacuum system is equipped with 294 ion pumps, 64 cold cathode gauges, 12 turbo molecular pumps, and more than 600 vacuum pipelines. After nearly ten years of operation, the vacuum system has remained stable overall; however, typical faults such as DTL leakage, bellows corrosion, vacuum gauge fluctuation, and vacuum chain fracture have occurred. Based on practical operational experience, this paper systematically summarizes fault characteristics, analyzes fault mechanisms, and proposes corresponding countermeasures, providing a reference for the stable operation of vacuum systems in similar accelerators.The CSNS II project was officially launched in 2024 to meet the 500 kW high power requirement, with a five year construction plan focusing on superconducting cavities, high energy proton beamlines, and a muon beamline. The vacuum system has been comprehensively upgraded based on the first phase configuration. Meanwhile, this paper presents the latest development progress of the CSNS II vacuum system.

1. INTRODUCTION

The China Spallation Neutron Source (CSNS) is a major national scientific and technological infrastructure in China. Since its commissioning in 2018, key indicators including beam power, operational stability, and beam delivery duration have been continuously improved, providing a high level research platform for materials science, new energy, life sciences, and other fields. For accelerators, vacuum is essential for stable operation. Poor vacuum conditions cause beam loss, high voltage arcing, and equipment contamination, directly affecting operational efficiency and safety. The first phase CSNS vacuum system covers the entire beam path from the ion source to the front of the target station, featuring a wide range of vacuum levels, a large number of components, and complex operating conditions. Over nearly ten years of operation, typical vacuum faults have occurred due to equipment aging, high radiation, high power operation, and material outgassing, affecting vacuum stability and beam continuity. To further increase beam power and expand research capabilities, the CSNS II project was officially launched in 2024 with a five year construction plan. The core upgrades include introducing superconducting cavities, constructing new spectrometers, and adding high energy proton beamlines and a muon beamline. The vacuum system requires comprehensive upgrades based on the first phase design to meet higher vacuum requirements and enhanced stability. High radiation induced corrosion and seal failure are common challenges for high power accelerator vacuum systems. This paper systematically summarizes typical faults, analyzes mechanisms, proposes mitigation strategies, and presents the latest CSNS II upgrade progress, providing a valuable reference for peer institutions.

2. OVERVIEW OF THE CSNS VACUUM SYSTEM

2.1 System Composition and Vacuum Specifications

The first-phase vacuum system comprises four core sections:The vacuum system of the Linear Accelerator (LINAC), LINAC to RCS Beam Transfer Line (LRBT), Rapid Cycling Synchrotron (RCS), and RCS to Target Beam Transfer Line (RTBT), along with supporting vacuum systems for application beamlines such as the Associated Proton Experimental Platform (APEP) and the Back streaming White Neutron Source (Back-n), which together form a complete gradient vacuum network. Strict vacuum specifications are defined for each section: the ion source and low energy beam transport section (IS&LEBT) requires a pressure below 5×10^{-3} Pa, the radio frequency quadrupole to drift tube linac section (RFQ–DTL), LRBT and RTBT demand a pressure less than 1×10^{-5} Pa, the Rapid Cycling Synchrotron (RCS) requires a vacuum pressure below 5×10^{-6} Pa, and the proton

* email address wangpc@ihep.ac.cn

Content from this work may be used under the terms of the CC BY 4.0 licence (© 2026). Any distribution of this work must maintain attribution to the author(s), title of the work, publisher, and DOI.

ISBN: 978-3-95450-252-3 ISSN: 2673-5350 doi: 10.18429/JACoW-IPAC2026-TUP7680

INVESTIGATION ON THE VACUUM PROPERTIES OF Al-TiZrV Bi-layer FILMS*

X. Y. Jin, T. Guo, X. P. Xu, W. J. Ma, X. S. Zhou, L. Fan, Y. Z. Hong, S. H. Wang†
National Synchrotron Radiation Laboratory, University of Science and Technology of China, Hefei, China

Abstract

Maintaining an ultra-high vacuum (UHV) environment is essential for the Hefei Advanced Light Facility (HALF) to achieve its design performance. Owing to the dimensional limitations imposed by small-aperture vacuum chambers, non-evaporable getter (NEG) films are commonly applied to the inner walls to enhance vacuum performance. However, conventional NEG films increase the resistive-wall impedance of the vacuum pipes, thereby exacerbating the wakefield effects. To address this problem, a novel composite film, Al-TiZrV, has been developed. By covering the TiZrV film surface with a highly conductive film, it can reduce the resistivity of the composite film. The results show that while the addition of the Al layer reduces the resistivity significantly, it increases the secondary electron yield (SEY), exacerbating the electron cloud effect. This study provides insights into the complex properties of similar bilayer films for future research on accelerator-related materials.

INTRODUCTION

In modern particle accelerators, the performance of the vacuum system is critical for maintaining the stability of particle beams. Traditional NEG films, such as TiZrV, are widely used to achieve ultra-high vacuum due to their excellent gas absorption capability [1]. They play a critical role in adsorbing residual gases, and ensuring a stable vacuum environment, all of which are vital for the efficient operation of particle accelerators. However, the TiZrV film has a relatively high resistivity, which may significantly aggravate the resistive-wall impedance of the vacuum chamber. This effect is particularly pronounced in vacuum chambers with small apertures, such as those used in the HALF, where it can lead to beam instabilities. The resistive-wall effects can cause beam emittance growth, energy dispersion, and other undesirable effects, thereby limiting the performance of the accelerator [2].

To address this issue, this research has explored adding an Al layer to the surface of the TiZrV film to suppress the adverse impacts caused by high resistivity [3]. Therefore, a comprehensive investigation of the properties of Al-TiZrV composite films is essential for evaluating their potential in improving the performance of accelerator vacuum systems.

* Work supported by the National Natural Science Foundation of China (Grant No. 12175225), the National Key Research and Development Program of China (No. 2023YFA1608602), and the Youth Innovation Promotion Association CAS, China (No. 2023478).

† sihui@ustc.edu.cn

EXPERIMENTAL PROCEDURES

Film Deposition

The Al-TiZrV composite films were deposited via a direct-current magnetron sputtering system. High-purity TiZrV alloy target (99.9% purity, atomic ratio 1:1:1) and Al target (99.9% purity) were utilized. Prior to deposition, oxygen-free copper (OFC) substrates were cleaned using RSB-117 solution, passivated in ammonium citrate solution, and dried with high-purity nitrogen. Silicon wafers were ultrasonically cleaned in acetone solution and dried similarly.

The composite film was commenced with the deposition of the TiZrV film onto the substrates, employing a direct current (DC) magnetron sputtering technique. This initial layer was followed by the sequential deposition of an Al layer. The detailed parameters are shown in Table 1. To systematically vary the thickness of the Al layer, deposition time was precisely controlled at 10, 20, and 30 minutes. To ensure comparability, standalone TiZrV film was also deposited under identical conditions, facilitating a direct assessment of the influence exerted by the Al layer on the characteristics of the composite film.

Table 1: Deposition Parameters

Film	Deposition Time[min]	Current[A]	Working Pressure[Pa]	Gas
TiZrV	180	0.6	1	Ar
Al	10/20/30	0.1	1	Ar

Microstructural Characterization

A scanning electron microscope (SEM) coupled with an energy dispersive X-ray spectrometer (EDS) was utilized to assess the surface morphology and cross-sectional structure of the film. The cross-sections were prepared by cleaving the silicon wafers. The EDS analysis was used to map the elemental distribution within the films, providing insights into the composition and structure of the deposited film.

Secondary Electron Yield Measurement

The secondary electron yield (SEY) measurement setup consists of a sample chamber, an electron gun, a test chamber, and a pumping system, as shown in Fig. 1. The test chamber was pumped to 5×10^{-7} Pa using a 300 L/s turbo-molecular pump and a 200 L/s sputter ion pump. The sample was placed in the sample chamber, pumped to 5×10^{-5} Pa, then transferred to the test chamber by the transfer arm and the pressure of the test chamber should be pumped below 5×10^{-7} Pa for measurement.

Content from this work may be used under the terms of the CC BY 4.0 licence (© 2026). Any distribution of this work must maintain attribution to the author(s), title of the work, publisher, and DOI.

Content from this work may be used under the terms of the CC BY 4.0 licence (© 2025). Any distribution of this work must maintain attribution to the author(s), title of the work, publisher, and DOI.

ADVANCES IN LARGE-SCALE NON-EVAPORABLE GETTER COATING TECHNIQUES FOR THE HEFEI ADVANCED LIGHT FACILITY*

X.P. Xu, T. Guo, X.Y. Jin, C.T. Gao, T. Huang, S.H. Wang†
National Synchrotron Radiation Laboratory
University of Science and Technology of China, Hefei, P.R. China
J.H. Wang, Z.B. Li, Zhejiang Institute of Photoelectronics, Jinhua, P.R. China
P.Y. Liang, X.L. Lu
SKY Technology Development Co., Ltd. Chinese Academy of Sciences, Shenyang, P.R. China

Abstract

The Hefei Advanced Light Facility (HALF), currently under construction, is a fourth-generation synchrotron radiation source operating in the low-energy region (2.2 GeV) and based on diffraction-limited storage ring technology. The storage ring employs a modified hybrid 6BA lattice with a beam emittance of 86.3 pm·rad and consists of 20 achromat cells with a total circumference of approximately 480 meters. To meet the ultra-high vacuum environment of the storage ring, non-evaporable getter (NEG) films are applied to the inner surfaces of the vacuum chambers to provide distributed pumping capability and to reduce surface outgassing and photon-stimulated desorption. Large-scale NEG coating of the HALF storage ring vacuum chambers has been officially initiated. This paper presents an overview of the HALF storage ring vacuum system and provides a systematic description of the large-scale NEG coating system, including the equipment configuration and control system. In addition, a storage system for coated vacuum chambers is described to ensure film quality prior to installation, which provides technical support for subsequent assembly and commissioning.

INTRODUCTION

The Hefei Advanced Light Facility (HALF) is a fourth-generation synchrotron radiation source operating in the low-energy region and based on diffraction-limited storage ring (DLSR) technology. As illustrated in Fig. 1, the HALF project consists of a 192 m linear accelerator, a transport line with a length of 138.4 meters, and a storage ring with a circumference of 480 meters, with ten beamlines planned for construction in phase I. The storage ring comprises 20 achromat cells, and the total length of the straight sections is 5.3 m × 20 + 2.2 m × 20, accounting for approximately 31% of the ring circumference. HALF is designed to achieve one of the lowest beam emittances among fourth-generation synchrotron radiation storage rings operating in the low-energy region [1].

* Work supported by the project of Hefei Advanced Light Facility, a major national science and technology infrastructure in China. This work is also supported by the National Key Research and Development Program of China (No. 2023YFA1608602), and the Youth Innovation Promotion Association CAS, China (No. 2023478). The authors acknowledge SKY Technology Development Co., Ltd., Chinese Academy of Sciences, for its assistance in the design, construction, and assembly of the coating system.
† email address: sihui@ustc.edu.cn

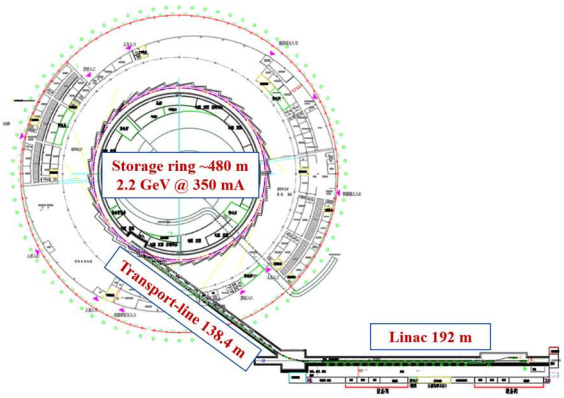

Figure 1: Schematic layout of the HALF.

STORAGE RING VACUUM SYSTEM

The vacuum layout of a standard achromat cell is shown in Fig. 2. In addition to the vacuum chambers, each cell consists of four gate valves, eleven beam position monitors (BPMs), four photon absorbers, four NEG pumps and one NEG strip, etc. Except for certain stainless-steel components, all remaining vacuum chambers (including Inconel structures) are fabricated from copper–zirconium alloy. This material exhibits high electrical conductivity and a low outgassing rate, which are beneficial for reducing impedance and improving vacuum performance [2]. The inner diameter of most beam pipes is 26 mm, with a wall thickness of 1 mm, the gap between the magnetic poles and the vacuum chamber is 1 mm (minimum 0.5 mm). The small aperture and the extremely compact magnet–chamber spacing impose stringent requirements on the design and fabrication of the vacuum system.

The vacuum system provides and maintains an ultra-high vacuum environment for the stable operation of high-intensity beams. The design specifications require a static vacuum better than 2×10^{-8} Pa and a dynamic vacuum better than 2×10^{-7} Pa for HALF. Due to the limited conductance of the small-aperture chambers and the compact spatial constraints, conventional lumped pumping schemes cannot satisfy the vacuum requirements of a diffraction-limited storage ring. Therefore, the Ti–Zr–V non-evaporable getter (NEG) coatings are deposited on the inner surfaces of the storage ring vacuum chambers to address the aforementioned challenges. The activated NEG coatings provide distributed pumping capability, improving the vacuum performance and reducing the pressure gradient along

ISBN: 978-3-95450-252-3 ISSN: 2673-5350 doi: 10.18429/JACoW-IPAC2026-TUP7683

STUDY ON THE VACUUM PROPERTIES OF Pd/Ti BILAYER THIN FILM*

T. Guo, X. P. Xu, X. Y. Jin, X. S. Zhou, C. T. Gao, S. H. Wang†
National Synchrotron Radiation Lab., University of Science and Technology of China, Hefei, China

Abstract

Non-evaporable getter (NEG) thin films are essential for achieving ultra-high vacuum in the narrow-bore chambers. Pd/Ti bilayer NEG thin films were deposited on oxygen-free copper and silicon substrates by DC magnetron sputtering. The microstructure and elemental distribution were characterized by scanning electron microscopy (SEM) and energy-dispersive X-ray spectroscopy (EDS). The films exhibit a cauliflower-like surface morphology and a columnar cross-sectional structure, providing a high specific surface area and effective pathways for gas diffusion. The pumping speed for H_2 was evaluated using the constant-pressure dynamic flow method after activation at 150 °C for 12 h. The pumping speed decreases from 0.13 to 0.02 L s^{-1} within a pumped quantity range of 1×10^{-5} - 6.5×10^{-3} Pa L. A non-monotonic variation in pumping speed was observed, which is attributed to hydrogen adsorption, dissociation on the Pd surface, and subsequent diffusion into the Ti layer for hydride formation. The results demonstrate that the Pd overlayer effectively enables low-temperature activation and enhances hydrogen sorption behavior, indicating that Pd/Ti NEG thin films are promising candidates for ultra-high vacuum applications in accelerator systems.

INTRODUCTION

The fourth-generation synchrotron radiation storage rings employ a Multi-Bend Achromat (MBA) lattice to achieve ultra-low emittance and ultra-high brightness, which are commonly referred to as diffraction-limited storage rings (DLSRs) [1]. This design necessitates small magnetic apertures and narrow-bore vacuum chambers integrated within the magnets. Conventional lumped pumping schemes are insufficient to provide the ultra-high vacuum (UHV) required for stable beam operation. To meet these UHV requirements, non-evaporable getter (NEG) thin films are typically deposited on the inner surfaces of the vacuum chambers [2]. NEG films can effectively suppress thermal outgassing from the chamber walls while simultaneously pumping residual gases without occupying additional space. Furthermore, NEG films exhibit low photon-stimulated desorption (PSD), low electron-stimulated desorption (ESD), and low secondary electron yield (SEY) [3, 4]. Since its development at CERN [5], NEG thin film technology has been widely adopted in particle accelerators, including LHC, ESRF, MAX IV, Diamond, and HEPS.

Activated NEG films exhibit strong physical and chemical sorption capabilities, effectively capturing reactive gases such as H_2, CO, CO_2, and H_2O. However, upon exposure to air, the film surface readily oxidizes to form a passivation layer, resulting in the loss of pumping capacity. Activation is essential for restoring the sorption performance of NEG thin films and is typically achieved by annealing under high vacuum (HV) or UHV. This thermal treatment promotes the desorption of surface oxides and their diffusion into the bulk, thereby removing the passivation layer and regenerating active metallic surfaces [6].

Due to its excellent oxidation resistance, a palladium (Pd) overlayer can be deposited on titanium (Ti) films to suppress oxidation of the underlying layer, thereby enabling a reduced activation temperature for Pd/Ti NEG thin films. Pd/Ti films were deposited on copper and silicon substrates by magnetron sputtering. The microstructure of the films was characterized, and the H_2 pumping speed was evaluated after activation by baking at 150 °C.

EXPERIMENTAL PROCEDURES

Sample Preparation

Pd/Ti films were deposited on oxygen-free copper (OFC) substrates (20 mm × 20 mm × 1 mm) and silicon substrates (10 mm × 10 mm × 1 mm) by DC magnetron sputtering in an argon atmosphere. Prior to deposition, the OFC substrates were subjected to acid cleaning followed by ammonium citrate passivation, while the silicon substrates were ultrasonically cleaned in acetone. After cleaning, all substrates were dried with high-purity nitrogen gas. High-purity Ti (99.99%) and Pd (99.95%) targets were used. The Ti target was sputtered at a current of 0.6 A for 4 h under a working pressure of 2 Pa, followed by Pd deposition at a current of 0.15 A for 5 min under the same pressure. During deposition, the Ti target was replaced by the Pd target in situ without breaking vacuum. The thicknesses of the Ti and Pd layers were approximately 433 nm and 56 nm, respectively. The main characteristics of the Ti and Pd/Ti films are summarized in Table 1.

Table 1: Deposition parameters for Pd/Ti thin films

Film	Working pressure [Pa]	Working current [A]	Working gas	Thickness [nm]
Ti	2	0.6	Ar	433
Pd	2	0.15	Ar	56

Microstructure Characterization

The surface morphology and cross-sectional thickness of the films were characterized using a Gemini 500 scanning

* Work supported by the National Key Research and Development Program of China 196 (No. 2023YFA1608602)
† sihui@ustc.edu.cn

Content from this work may be used under the terms of the CC BY 4.0 licence (© 2026). Any distribution of this work must maintain attribution to the author(s), title of the work, publisher, and DOI.

ISBN: 978-3-95450-252-3 ISSN: 2673-5350 doi: 10.18429/JACoW-IPAC2026-TUP7684

DESIGN OF DISTRIBUTED PUMPING SYSTEM USING NEG STRIPS FOR HALF*

L. Fan, B. W. Yao, T. Huang, W. L. Zhang†, T. L. He, Y. Z. Hong, X. Q. Ge††
National Synchrotron Radiation Laboratory, University of Science and Technology of China, Hefei, China

Abstract

The design of a distributed pumping system using NEG (Non-Evaporable Getter) strips for the slender beam pipes of the Hefei Advanced Light Facility (HALF) is presented. To achieve a high pumping speed and pumping capacity in a limited pumping space, a NEG strip with distributed pumping capacity was considered. A prototype of HALF vacuum chamber, which can be inserted into NEG strip and matched with magnet system, is designed. The activation temperature of NEG strip and the ultimate vacuum after activation are tested, and the results are in good agreement with those obtained from the simulation.

INTRODUCTION

Typically, in order to effectively evacuate the beam pipes of particle accelerators, a distributed pumping system is adopted because the beam pipe usually has a limited conductance. The commonly used pumps are distributed sputter-ion pumps (DIP) [1-3] or NEG (Non-Evaporable Getter) pumps [4-7]. A DIP is an integrated sputter-ion pump, and it utilizes a magnetic field of bending or quadrupole magnets. DIPs have been widely used in various accelerators. In addition, a NEG-coated beam pipe, which provides pumping action to the inner surface, is applied to various accelerators. However, the small capacity and high activation temperature of the film become unavoidable problems. Normally, the film can be activated at 180°C, but the activation temperature is gradually increased as the number of activations increases. The low gas desorption rate of the NEG coating, furthermore, may not be as effective because a uniform coating all over the pipe is impossible owing to the complicated structure, such as in the case of a beam pipe with antechambers [7]. A strip-type NEG, on the other hand, can be used anywhere, irrespective of the presence of magnetic fields, and they have been used widely since they were adopted on a large scale in LEP [8, 9].

Presented in this paper is the design study of a distributed pumping system using NEG strips in a narrow pumping space, where a beam pipe with antechambers for Hefei Advanced Light Facility (HALF) has been considered as an example. The activation temperature of NEG strip and the ultimate vacuum after activation are tested.

EXPERIMENT

Experimental Setup

- The storage ring is responsible for accelerating the beam injected by the intensifier to the energy required by the storage ring, providing a high-quality electron beam for the high energy beam line to extract synchrotron radiation. As an important part of the storage ring vacuum system, its main task is to maintain a reasonable vacuum degree and ensure the stable operation of the beam. A typical stainless-steel antechamber for HALF storage ring vacuum system is shown in Figure 1. It can be inserted into NEG strip. After the vacuum chamber assembly is welded, a 20 μm thick copper film needs to be electroplated on the inner wall of the beam channel.

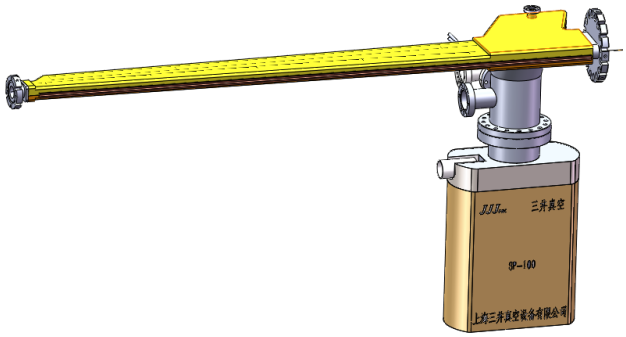

Figure 1: A typical stainless-steel antechamber for HALF storage ring vacuum system.

- According to the overall size requirements, in order to ensure the feasibility of getter integrated assembly, getter pills with a diameter of 13 mm were designed as getter units. TiZrV is a widely used low-temperature activated inspiratory material, and does not contain magnetic elements such as Fe, Co, Ni, etc. Therefore, the inspiratory material based on TiZrV system is selected to prepare NEG strips. According to the installation space requirements, the dimensions of the NEG bar are 930 mm long, 20 mm wide, and 20 mm high. The number of getter pills is 288, and the length of the external electrode of the NEG strip is 300 mm ~ 400 mm, as shown in Figure 2.

* Work supported by "the National Natural Science Foundation of China" (Grant No. GG2310000442) and "the Fundamental Research Funds for the Central Universities" (Grant No. WK2310250132)
† wenlizhang@ustc.edu.cn
†† xqge@ustc.edu.cn

Content from this work may be used under the terms of the CC BY 4.0 licence (© 2026). Any distribution of this work must maintain attribution to the author(s), title of the work, publisher, and DOI.

ISBN: 978-3-95450-252-3 ISSN: 2673-5350 doi: 10.18429/JACoW-IPAC2026-TUP7687

INVESTIGATION OF OUTGASSING PROPERTIES OF CuZr AND CuCrZr VACUUM PIPES*

T. Huang, B. W. Yao, L. Fan, W. L. Zhang†, T. L. He, Y. Z. Hong, X. Q. Ge††, National Synchrotron Radiation Laboratory, University of Science and Technology of China, Hefei, China

Abstract

The Hefei Advanced Light Facility (HALF) is the fourth-generation synchrotron radiation light source based on Diffraction-limited Storage Ring (DLSR) with low beam emittance, high brightness and coherent photon flux. According to the physical design requirements of the HALF, the vacuum chamber structural materials should have low outgassing rate, good electrical and thermal conductivity, high strength, and non-magnetic. CuZr and CuCrZr were selected as structural materials for the HALF storage ring vacuum chamber structural materials, taking into account material properties and manufacturing process. In this paper, thermal outgassing performances of CuZr and CuCrZr alloy pipes under temperature rise was investigated for the design and calculation of HALF vacuum systems.

INTRODUCTION

The accelerator develops toward high energy, high beam current, high luminosity, and long beam lifetime. The corresponding requirements for the vacuum environment change from ultra-high vacuum (UHV) to extreme conditions, such as extreme-high vacuum and extreme-low temperature. The fourth-generation light source based on the diffraction-limited storage ring (DLSR) has a huge improvement in brightness and coherence compared to the third-generation light source [1], which also places higher demands on structural materials. Copper is used as the preferred structural material for DLSR due to the low outgassing rate, good electrical and thermal conductivity, high strength, and non-magnetic [2]. Considering the properties and processing technology, CuZr and CuCrZr were selected as the storage ring structure materials of Hefei Advanced Light Facility (HALF) [3,4]. Vacuum material outgassing is the primary source of residual gases in accelerator, among which thermal outgassing mainly affects the static vacuum pressure. The outgassing properties of CuZr and CuCrZr vacuum pipes at different temperatures were tested in this paper to evaluate the reliability of the design for HALF vacuum system and the corresponding calculation of the vacuum pressure.

EXPERIMENT

Experimental Setup

The testing setup used for outgassing properties is shown in Fig. 1. The sputter ion pump (SIP) with nominal pumping speed of 200 L/s was used as the main pump. The turbomolecular pump (TMP) unit served as the roughing pump of the system. The DN40 all-metal angle valves were used to connect the pumping chamber to the TMP unit (MAV1) and to the vacuum pipe (MAV2). The B-A gauges were used as the measuring gauges, and the data measured by the B-A gauge at the pumping chamber (BAG1) were set as P_1, and the data measured by the B-A gauge at the end of the pipe (BAG2) were set as P_2.

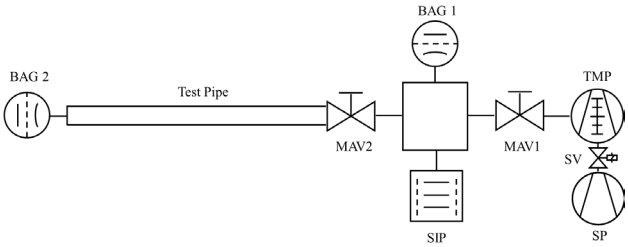

Figure 1: Schematic illustration of pipe outgassing property testing setup.

Experimental Procedures

- System cleaning, installation and leak detection: The rest of the testing setup was cleaned and installed first, followed by the cleaning and installation of the copper pipe. The system leakage rates of CuZr (Φ26 mm × 500 mm) and CuCrZr (Φ22 mm × 500 mm) pipes were below 3×10^{-12} mbar·L/s.
- System bakeout and ultimate vacuum testing: Stainless steel pumping chamber and gauge pipes were baked at 230°C for 48 h, and copper pipes were baked at 180°C for 48 h. The baking curves were set as shown in Fig. 2. After the baking and cooling of the system were completed, the system was left to stand at room temperature for 36 h, while the BAG2 was read as the first ultimate vacuum data.

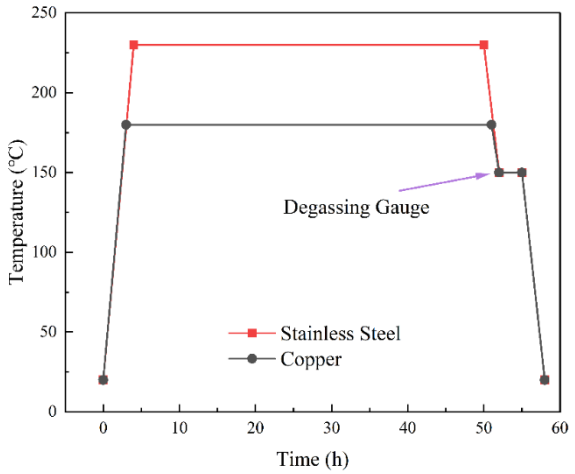

Figure 2: Bakeout procedure for testing setup.

† wenlihzhang@ustc.edu.cn, †† xqge@ustc.edu.cn

Content from this work may be used under the terms of the CC BY 4.0 licence (© 2026). Any distribution of this work must maintain attribution to the author(s), title of the work, publisher, and DOI.

ISBN: 978-3-95450-252-3 ISSN: 2673-5350 doi: 10.18429/JACoW-IPAC2026-TUP7689

DESIGN OF PHOTON ABSORBERS FOR THE SPring-8-II VACUUM SYSTEM

H. Dewa†, K. Tamura[1], Y. Ueda, S. Takahashi, T. Itoga[1], M. Oishi[1], M. Shoji[1], H. Ota, Y. Taniuchi, M. Masaki, T. Masuda, S. Takano[1], T. Watanabe[1]
Japan Synchrotron Radiation Research Institute (JASRI), Sayo, Hyogo, Japan
[1]also at RIKEN SPring-8 Center (RSC), Sayo, Hyogo, Japan

Abstract

SPring-8-II, the forthcoming fourth-generation light source upgrade of SPring-8, aims to achieve X-ray brilliance approximately two orders of magnitude higher than that of the current facility by reducing the electron beam emittance to 100 pm·rad or less. To fit with the narrow-bore five-bend lattice, the vacuum system features discrete photon absorbers with dedicated pumps along with compact thin-walled stainless steel chambers. Two types of absorbers were developed: a horizontal-insertion type capable of handling a maximum total power of 2.25 kW, and a vertical-insertion type designed for a maximum peak power density of 224 W/mm². The absorber design incorporates a grazing incidence angle on the incident surface to reduce power density, a shielding structure designed to confine scattered radiation, and a flange integrated without brazing or welding to eliminate the risk of vacuum leaks. Copper-chromium-zirconium (CuCrZr) was chosen as the material for its superior thermal conductivity and high yield strength. Finite-element analysis using ANSYS was employed to optimize the cooling-channel layout and to ensure compliance with maximum allowable temperature and stress limits.

INTRODUCTION

SPring-8 is Japan's flagship third-generation synchrotron radiation source that commenced user operation in October 1997. Its upgrade, SPring-8-II, has three primary objectives: enhancing light source performance, refurbishing aging systems, and reducing overall power consumption [1]. To achieve an increase of approximately two orders of magnitude in X-ray brilliance compared to the current facility, SPring-8-II targets an ultra-low emittance of 100 pm·rad or less by employing a five-bend lattice comprising densely packed high-gradient magnets, which necessitates reduced vacuum chamber apertures.

To protect these narrow chambers from bending magnet radiation, discrete photon absorbers with grazing-incidence surfaces are deployed to manage the high incident power density. These absorbers utilize materials with high thermal conductivity and resilience to thermal stress, supplemented by water cooling to maintain temperatures within operational limits. This paper presents the design of SPring-8-II photon absorbers validated through thermal-structural analysis.

†dewa@spring8.or.jp

DESIGN OF PHOTON ABSORBERS

The five-bend lattice was designed to reuse the existing tunnel and beamline layout, maintaining the same 48-cell configuration as SPring-8. Within these spatial constraints [2], a total of 14 absorbers are installed per cell [3] to protect the compact vacuum chambers from synchrotron radiation. Table 1 summarizes the total radiation power and peak power density for each absorber. Embedded (Emb) types are integrated into the bending section chambers, whereas discrete horizontal (Hor) and vertical (Ver) insertion absorbers are installed between vacuum chambers. Because the Emb types are subjected to sufficiently low radiation power and power density, they present no significant thermal design issues. The two discrete types are selected based on radiation power and installation constraints. High-power absorbers, as significant sources of photo-stimulated desorption (PSD) gas, are evacuated using an integrated pumping system consisting of a non-evaporable getter pump and a sputter ion pump [3].

Table 1: Total Power and Peak Power Density of the Radiation at the Absorbers for SPring-8-II

Absorber	IDD	AB1	AB2	CR1	BCA 2	AB3
Power [kW]	0.67	0.029	1.30	0.22	0.22	0.88
Power density [W/mm2]	17.5	13.5	99.2	27.8	11.6	224
Type	Hor	Hor	Hor	Hor	Emb	Ver

AB4	AB5	AB6	AB7	CR2	AB8	BCA S	AB9
0.99	0.85	1.98	1.18	2.25	0.31	0.28	0.68
185	28.4	182	40.4	164	38.7	13.0	129
Ver	Hor	Hor	Hor	Hor	Ver	Emb	Hor

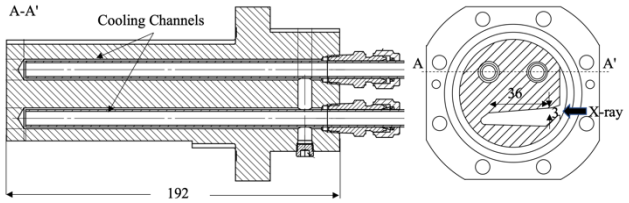

Figure 1: Schematic views of the horizontal-insertion absorber. The cross section (left) is cut along A-A' in the right view.

Among the horizontal-insertion absorbers, AB6 exhibits the highest power density at 182 W/mm², while CR2 receives the highest total power of 2.25 kW. As shown in Fig. 1 (right), the shape is cylindrical, and the incident

Content from this work may be used under the terms of the CC BY 4.0 licence (© 2026). Any distribution of this work must maintain attribution to the author(s), title of the work, publisher, and DOI.

ISBN: 978-3-95450-252-3 ISSN: 2673-5350 doi: 10.18429/JACoW-IPAC2026-TUP7690

BEAM LIFETIME EVALUATION BASED ON SIMULATION OF A VACUUM PRESSURE DISTRIBUTION FOR THE SPring-8-II COMMISSIONING STRATEGY THROUGH VACUUM CONDITIONING

Y. Ueda†, K. Tamura[1], H. Dewa, M. Masaki, T. Masuda, M. Oishi[1], H. Ota, M. Shoji[1], S. Takano[1], Y. Taniuchi, T. Watanabe[1]
Japan Synchrotron Radiation Research Institute (JASRI), Sayo, Hyogo, Japan
[1]also at RIKEN SPring-8 Center (RSC), Sayo, Hyogo, Japan

Content from this work may be used under the terms of the CC BY 4.0 licence (© 2026). Any distribution of this work must maintain attribution to the author(s), title of the work, publisher, and DOI.

Abstract

SPring-8-II, a major upgrade of the third-generation light source SPring-8, aims to achieve low emittance below 100 pm·rad and to reduce the power consumption of the light source machine. The magnets in SPring-8-II feature narrow bore diameters for high magnetic fields, and are arranged with high packing factors. As a result, vacuum chambers along the entire storage ring are designed with narrow apertures, leading to low conductance, and space for vacuum components is limited. To overcome these constraints, we employ small-diameter stainless steel chambers and discrete compact photon absorbers. Non-Evaporable Getter (NEG) pumps are placed near photon absorbers to effectively evacuate photon stimulated desorption gas. We simulated the pressure distribution of the representative normal unit cell in SPring-8-II as a function of integrated beam dose considering the degradation of the pumping speed of the NEG pump due to gas sorption. On the basis of these results, we evaluated the beam lifetime evolution and formulated a preliminary commissioning strategy for increasing a stored current through systematic vacuum conditioning.

INTRODUCTION

The SPring-8-II project, a major upgrade of the third-generation light source SPring-8, has started in FY2024 [1, 2]. SPring-8-II is designed to achieve a beam emittance of less than 100 pm · rad and a stored beam current of 200 mA at an electron energy of 6 GeV. Simultaneously, the project aims for green facility operations by reducing power consumption to half that of the current SPring-8.

In SPring-8-II, multipole magnets for the high magnetic field gradients result in narrow bore diameters. To install vacuum chambers without the mechanical interference, we have adopted small-diameter, thin-walled stainless steel vacuum chambers. Furthermore, the magnets are arranged with high packing factors. Compact discrete photon absorbers [3] have been employed to protect the chamber walls from synchrotron radiation within the limited space. The small-diameter vacuum chambers result in the low conductance. Vacuum pumps are placed near the photon absorbers, which are the primary sources of photon-stimulated desorption (PSD) gas, thereby enhancing evacuation efficiency.

The pumping speed of the Non-Evaporable Getter (NEG) pumps, which are the main pump in SPring-8-II, saturates as gas sorption proceeds. Since this saturation leads to a stagnation of pressure improvement as operation progresses, restoring the pumping speed through NEG reactivation at appropriate intervals is essential for stable operation. In this study, we calculated the pressure distribution of the representative normal unit cell via Monte Carlo simulations and evaluated the beam lifetime before and after NEG reactivation at various integrated beam doses to provide a baseline for the commissioning strategy.

VACUUM SYSTEM

The storage ring of SPring-8-II consists of 48 unit cells. The normal cell accounts for 34 of 48 cells. Each normal cell, approximately 26 m long, comprises five bending sections (BSs) and six straight sections (SSs). Between the lowermost straight section (SS6) on the upstream cell and the uppermost straight section (SS1) on the downstream cell, a straight section is provided for the installation of insertion devices (IDs). The conceptual layout of a normal cell omitting the ID section is shown in Fig. 1.

Thirteen photon absorbers are installed in each normal cell. These include nine absorbers (ABs), two crotch absorbers (CRs) that have the extraction aperture of synchrotron radiation to the beamlines, and two bending chamber absorbers (BCAs) located at the downstream parts of BS2 and BS5. The photon absorber (AB/CR) features a radiation shielding structure that confines synchrotron radiation within itself to reduce scattered light toward the chamber walls [3, 4]. In contrast, the BCA adopts a simple geometry designed to reflect scattered light from its inclined plane toward the chamber walls. In straight sections where an ID is not initially installed, ID dummy chambers (IDDs) are placed. An AB (IDD_AB) is installed at the downstream end of the IDD. ABs, CRs, and IDD_AB are made of chromium-zirconium copper (CuCrZr) alloy. BCAs are made of oxygen-free copper (OFC).

Since photon absorbers are the primary sources of PSD gas, vacuum pumps are strategically located in their vicinity for the evacuation efficiency. Furthermore, vacuum pumps are installed at all five BS locations regardless of the presence of a BCA. The IDD, which is approximately 4 m long, has the evacuation chamber (IDD_Pump) equipped with a vacuum pump at the upstream end. The pumping system is a combination of NEG pump for evacuating active gases such as hydrogen (H_2) and carbon monoxide (CO), with sputter ion pump (SIP) of the noble diode (ND) type for evacuating gases not sorbed by the NEG, such as methane (CH_4) and noble gases.

† yueda@spring8.or.jp

ISBN: 978-3-95450-252-3 ISSN: 2673-5350 doi: 10.18429/JACoW-IPAC2026-TUP7693

CURRENT STATUS OF TPS VACUUM SYSTEM

Yi-Ch. Yang†, Ch.-K. Chan, Ch.-Ch. Chang, Bo-Y. Chen, Ch.-Mu Cheng, T.-W. Hsu, J.-H. Kang,
National Synchrotron Radiation Research Center, Hsinchu, Taiwan

Abstract

The TPS is currently operating at a beam current of 500 mA for users. Until now, 17 insertion devices have been installed in the straight vacuum sections, and the associated vacuum components have been upgraded. The average vacuum pressure of the storage ring is 8.5 nPa, and the beam lifetime under 500 mA operation is approximately 8 hours. The behavior of vacuum readings, the pressure distribution and the related interlock will be discussed in this paper.

INTRODUCTION

The Taiwan Photon Source (TPS) began operation for users in 2016 with a beam current 300mA. The beam current was raised to 400mA in December 2017, and regularly reached 450mA by the end of 2020. In 2021, the target storage beam current of 500mA was successfully archived. Until the end of 2025, a total accumulated beam dose of 24525Ah has been reached, with a beam lifetime of approximately 8 hours during 500 mA operation. Two operation modes, uniform filling and hybrid mode, are utilized periodically to meet the needs of user experiments.

The vacuum pressure distribution of the storage ring under 500mA operation is illustrate in Fig. 1, which shows a higher pressure spike in the SR24 section resulting from the machine upgrade in 2026. The dynamic average pressure is 8.9 nPa, compared to a static pressure of 6.8 nPa without beam. To date, 17 insertion devices (IDs), two superconductivity cavities, and one harmonic cavity (HC) have been installed in the straight sections of the storage ring. Corresponding vacuum components, including bending magnet chambers and front-end (FE) vacuum system, have also been upgraded [1, 2]. The lumped NEG-ion combination pumps used in EPU ID vacuum chamber was developed to improve and increase the effective pumping speed [3]. A vacuum gauge was installed at the center of each EPU chamber to measure local pressure accurately. The average pressure rise normalized to the beam current dP / I (Pa / mA), follows a downward trend proportional to $D^{-0.791}$, was shown as Fig. 2.

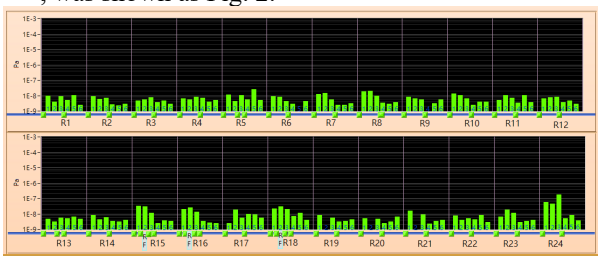

Figure 1: The vacuum pressure distribution of the storage ring.

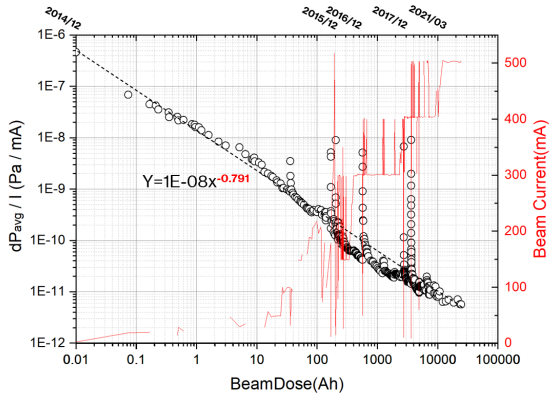

Figure 2: The average pressure rise normalized to the beam current.

BEAM TRIP EVENT

Over the past several years, seven beam trip events occurred during user time. The specific incidents and their causes are summarized.

- In 2017, two trip events were recorded. The first was caused by the temperature of the SR02S1 bellows exceeding its set-point. The second involved an ambiguous vacuum signal in the SR16 SRF section. It was difficult to determine whether the pressure spike originated from the storage ring or the SRF vacuum system. Consequently, Post-Mortem system was developed by I&C group to better identify abnormal signals across TPS subsystem.
- In 2018, a noisy signal from the cooling water flow meter triggered the machine protection system (MPS). The signal recovered immediately after the flow meter was reset.
- In 2019, An unready vacuum signal from FE07 vacuum system, combined with a burst signal (>1E-6 Pa) near the FE07, triggered a trip. This was classified as an unexpected incident.
- In 2020, a copper plate from the strip-line kicker in the SR14 section detached. While the vacuum remained stable, but the electron beam could not be stored, and high beam lose signal was detected in this section during injection. A dummy chamber and an additional NEG pump were installed to enhance pumping efficiency. The total downtime was 23.83 hours.
- In 2022, a cooling water interlock of the crotch absorber in SR21 section was triggered. The root cause was a failed of the DC power supply unit for flow meter, rather than an actual water flow issue.
- In 2024, an unexpected outage of vacuum gauges and pumps occurred in Control Instrument Area 24

† jolas@nsrrc.org.tw

Content from this work may be used under the terms of the CC BY 4.0 licence (© 2026). Any distribution of this work must maintain attribution to the author(s), title of the work, publisher, and DOI.

ISBN: 978-3-95450-252-3 ISSN: 2673-5350 doi: 10.18429/JACoW-IPAC2026-TUP7694

STUDY OF THE EMISSIVITY OF COPPER OXIDE THIN FILMS BY CYLINDRICAL MAGNETRON SPUTTERING

Bo-Y. Chen†, Ch. Shueh, J.-H. Kang, Ch.-K. Chan, Ch.-Ch. Chang, Yi-Ch. Yang, Ch.-Mu Cheng
National Synchrotron Radiation Research Center, Hsinchu, Taiwan

Abstract

High-energy electron beams operating in accelerator vacuum chambers can easily cause heat accumulation on the surfaces of in-vacuum components. When convective cooling and effective conductive heat dissipation are limited, the thermal radiation capability of material surfaces becomes an important heat dissipation mechanism. In this study, copper oxide (CuO) thin films were deposited on Oxygen-Free Copper (OFC) substrates to investigate their enhancement of surface thermal radiation characteristics. Experimental results show that the prepared CuO films exhibit dense columnar grain structures with a monoclinic CuO (002) preferred orientation. Emissivity measurements indicate that the average high-temperature emissivity of bare OFC substrates is approximately 0.1, while CuO-coated samples can achieve values up to 0.52, demonstrating improved infrared thermal radiation performance. The coating system setup, experimental procedures, and emissivity measurement methods will be further described in this paper.

INTRODUCTION

High-energy electron beams operating in accelerator vacuum chambers can easily cause heat accumulation on the surfaces of in-vacuum components due to beam-induced heating effects [1]. If the generated heat cannot be effectively dissipated, it may lead to degradation of mechanical properties and increased vacuum outgassing, thereby affecting beam stability. When in-vacuum components cannot effectively dissipate heat through water-cooling convection and the materials themselves possess limited thermal conductivity, thermal radiation from the material surface becomes an important heat dissipation mechanism. In recent years, high-emissivity coatings have gradually been applied in the thermal management of optoelectronic and high-heat-load components [2].

Among these materials, copper oxide (CuO), owing to its excellent high-temperature stability and infrared optical properties, has been widely utilized in thermal control coatings and infrared-related applications [3]. Therefore, in this study, copper oxide (CuO) thin films were deposited on Oxygen-Free Copper (OFC) substrates to investigate their film structures and high-temperature emissivity characteristics, with the aim of evaluating their feasibility as thermal dissipation coatings for in-vacuum components in accelerator vacuum chambers.

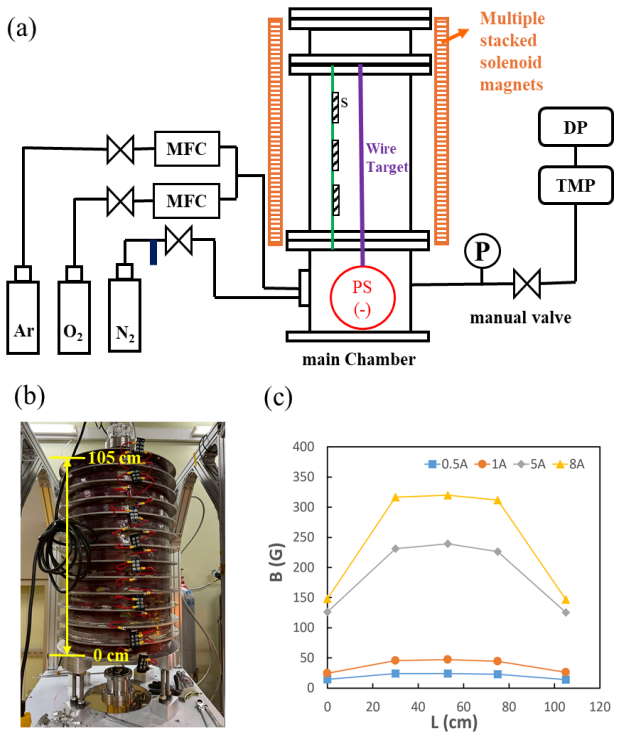

Figure 1: Cylindrical magnetron sputtering system. (a) Schematic diagram, (b) photograph of the sputtering system, and (c) magnetic field strength measurement.

COATING SYSTEM AND EXPERIMENT

The thin films in this study were prepared using cylindrical magnetron sputtering [4], and the sputtering system is shown in Fig. 1(a) and Fig. 1(b). A 99.99% purity bare copper twisted wire was used as the target material. The sputtering power was supplied by a DC power supply (PS), and 99.999% (5N) argon or oxygen gas was introduced as the reaction gas. The base pressure was 2×10^{-6} torr. Stacked solenoid magnets connected in series were used to generate the magnetic field. Under an operating current of 8 A, a relatively uniform magnetic field could be obtained in the center region (30–75 cm), with a magnetic field strength of approximately 320 Gauss, as shown in Fig. 1(c). Corning glass and Oxygen-Free Copper Substrates (OFC) were used depending on the requirements for electrical, thickness, structural, and emissivity measurements. The target-to-substrate distance was fixed at 30 mm.

Before deposition, the glass substrates were ultrasonically cleaned using acetone, isopropyl alcohol (IPA), and alcohol, followed by drying. The OFC substrates were ultrasonically cleaned using soap water, 5% Citranox solution, and deionized water, followed by dry air blowing and

†chen.bob@nsrrc.org

Content from this work may be used under the terms of the CC BY 4.0 licence (© 2026). Any distribution of this work must maintain attribution to the author(s), title of the work, publisher, and DOI.

ISBN: 978-3-95450-252-3 ISSN: 2673-5350 doi: 10.18429/JACoW-IPAC2026-TUP7695

DEVELOPMENT AND GEOMETRIC VALIDATION OF ALUMINUM VACUUM CHAMBER PROTOTYPES FOR THE SPS-II STORAGE RING*

T. Phimsen[1,†], S. Boonsuya[1], S. Chitthaisong[1], W. Woranut[1], K. Trongklang[1], A. Kwankasem[1], S. Sumklang[1], O. Seegauncha[1], J. Sukain[1],
[1] Synchrotron Light Research Institute, Nakhon Ratchasima, Thailand

Abstract

The development of the Siam Photon Source II (SPS-II), a fourth-generation light source, represents a significant leap in Thailand's synchrotron infrastructure. A primary objective of the project is the establishment of domestic technical expertise and industrial capability for producing high-precision vacuum components. This paper details the manufacturing and geometric validation of two critical aluminum alloy prototypes: a straight-section chamber and a bending chamber.

Key technological advancements include the optimization of domestic aluminum extrusion processes to achieve ultra-high vacuum (UHV) surface requirements and the implementation of oil-less, ethanol-cooled CNC machining to eliminate hydrocarbon contamination while maintaining high precision. A comprehensive metrology framework, utilizing laser trackers and high-resolution profiling, was employed to characterize manufacturing-induced distortions. Results confirm that the integrated fabrication workflow, which combines specialized internal fixturing and multi-pass TIG welding, successfully maintains the stringent geometric tolerances required for the storage ring. This work validates the technical readiness of Thailand's industrial sector for the full-scale production of the SPS-II vacuum system.

INTRODUCTION

The Siam Photon Source II (SPS-II) is a 3.0 GeV fourth-generation synchrotron light source currently under development at the Synchrotron Light Research Institute (SLRI) in Thailand. Formally approved in January 2025, the machine adopts a Double Triple Bend Achromat (DTBA) lattice with a total circumference of 327.6 m, distributed across 14 identical unit cells, and is designed to achieve a natural emittance of 0.96 nm·rad [1, 2]. Meeting the high-brightness performance goals of this lattice imposes exceptionally stringent requirements on the vacuum system, as the ultra-low emittance necessitates high-gradient quadrupole and sextupole magnets with small bore radii that reduce the available clearance between the chamber exterior and the magnet poles to the sub-millimeter level at the most constrained locations [2].

The SPS-II vacuum system design philosophy concentrates high-capacity pumping near photon absorbers, which are the dominant outgassing sources under synchrotron radiation [2, 3]. Three-dimensional Molflow+ simulations predict an operational average pressure of 1.1 $\times 10^{-9}$ mbar after 100 Ah of beam conditioning, satisfying the vacuum lifetime requirements of the storage ring [2]. The vacuum chambers are fabricated from aluminum alloys, A6061-T6 for arc section bending chambers and A6063-T5 for straight section extrusion profiles, selected for their favorable combination of low outgassing rate, high thermal conductivity, and machinability [2, 3].

DESIGN SPECIFICATIONS AND ACCEPTANCE CRITERIA

The prototyping program addresses two components: the middle straight section and the VCB-4 bending chamber. The geometric tolerance criteria governing these chambers are derived from the magnet aperture constraints detailed in the lattice design. Specifically, a manufacturing tolerance of 0.3 mm per meter of functional length is specified for transverse deformations, while a limit of 1.0 mm per meter is set for longitudinal deformation. These criteria, along with vacuum integrity requirements, are summarized in Table 1.

Table 1: Prototype Deformation Acceptance Criteria

Parameter	Specification
Transverse deformation	< 0.3 mm/m
Longitudinal deformation	< 1.0 mm/m
Magnet interface clearance	≥ 0.5 mm

STRAIGHT CHAMBER FABRICATION AND VALIDATION

The final dummy chamber design, shown in Fig. 1, adopts a circular main body profile (62.71 mm ID) with integrated cooling channels. This geometry achieved an as-extruded internal surface roughness of R_a 0.162–0.529 µm without requiring additional polishing, confirming that the domestic manufacturer had successfully internalized prior process improvements. To ensure the absence of surface contaminants that could compromise the ultimate pressure, all components underwent a standardized multi-stage chemical cleaning protocol prior to assembly. This process included alkaline etching to remove the native oxide layer, followed by deionized water rinsing, mixed acid passivation, and a final stage of ultrasonic cleaning. Welding was subsequently performed using a second-generation optimized fixture, developed through the iterative prototyping program [4], in a five-stage sequence designed to minimize accumulated thermal distortion: starting with taper-to-flange sub-assemblies and concluding with the final

† thanapong@slri.or.th

Content from this work may be used under the terms of the CC BY 4.0 licence (© 2026). Any distribution of this work must maintain attribution to the author(s), title of the work, publisher, and DOI.

ISBN: 978-3-95450-252-3 ISSN: 2673-5350 doi: 10.18429/JACoW-IPAC2026-TUP7698

ANALYSIS AND REFURBISHMENT OF A RADIATION-DAMAGED UNDULATOR*

Jinya Chen, Shudong Zhou, Ya Zhu, Yongzhou He, Cheng Yu, Jie Yang, Jun Wang, Jidong Zhang, Wei Zhang†,
Shanghai Advanced Research Institute, Chinese Academy of Sciences, Shanghai, China

Abstract

Synchrotron radiation facilities impose stringent requirements on the magnetic field quality, stability, and lifetime of undulators. During long-term operation of a beamline at the Shanghai Synchrotron Radiation Facility (SSRF), a gradual degradation of photon-beam performance was observed. To identify the cause, the cryogenic permanent magnet undulator of this beamline was warmed up and re-measured at room temperature during the summer shutdown. The on-axis field was found to be most strongly attenuated in the upstream region, with a maximum reduction of about 20% that gradually relaxed towards the downstream end. In addition, several sharp local drops of the magnetic field were detected in the central section. Visual inspection revealed pronounced melting holes in the copper foil in this area, indicating localized electron-beam impacts that likely damaged the underlying magnets and led to the abnormal field reduction. This paper presents the magnetic measurement results and the longitudinal attenuation pattern of the radiation-damaged undulator, and describes how local magnet replacement, re-shimming, and re-measurement were used to refurbish the device, providing a reference for future operation, maintenance, and radiation-protection design of similar undulators.

INTRODUCTION

Insertion devices, such as undulators, are core components of synchrotron radiation facilities and free-electron lasers. By generating periodic magnetic fields, they deflect high-energy electron beams and emit synchrotron radiation with high brightness and high coherence. Cryogenic permanent magnet undulators (CPMU), which have advanced rapidly in recent years, enable higher peak fields and smaller magnetic gaps, making them a key technology for enhancing light source performance. They have been successfully implemented at numerous synchrotron radiation facilities [1-4]. However, these devices face severe radiation environment challenges during long-term operation. In storage rings, lost electrons interact with vacuum chambers and surrounding components, generating complex mixed radiation fields comprising high-energy electrons, gamma rays, neutrons, and other particles. The interaction of this radiation with permanent magnets can cause irreversible demagnetization, leading to reduced magnetic field strength and degraded field quality in undulators, ultimately affecting the flux, brightness, and spectral stability of the output photon beams [5, 6].

* This work was Sponsored by Shanghai Rising-Star Program (Grant No. 24YF2752400).

† zhangwei@sari.ac.cn

During long-term operation at SSRF, a gradual decline in photon beam performance was observed from a cryogenic permanent magnet undulator installed at the fast X-ray imaging beamline BL16U2. To identify the cause and restore its performance, comprehensive off-line diagnostics and refurbishment were conducted on this undulator. This work provides important references for the operation and maintenance of similar equipment at SSRF and offers a valuable engineering case study for addressing comparable issues at other light source facilities worldwide.

UNDULATOR STATUS AND PRELIMINARY DIAGNOSIS

Basic Information of the Damaged Undulator

The undulator refurbished in this study is a cryogenic permanent magnet undulator (CPMU) installed at the fast X-ray imaging beamline BL16U2 of the Shanghai Synchrotron Radiation Facility (SSRF). Since its commissioning, this device has been in operation for many years, providing high-quality synchrotron radiation to beamline users. Its main design parameters are listed in Table 1. The undulator employs PrFeB permanent magnet material, which takes advantage of its significantly increased coercivity and remanence at low temperatures to achieve a higher peak magnetic field at a small magnetic gap.

Table 1: Main Design Parameters of the Damaged CPMU

Parameter	Value
Period length	18 mm
Number of periods	170
Minimum gap	6 mm
B_{eff}	0.86 T

Inspection and Preliminary Assessment

Figure 1 shows a photograph of the undulator placed in the magnetic measurement laboratory after warm-up.

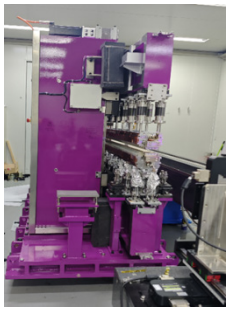

Figure 1: Photograph of the undulator in the magnetic measurement laboratory after warm-up.

Content from this work may be used under the terms of the CC BY 4.0 licence (© 2026). Any distribution of this work must maintain attribution to the author(s), title of the work, publisher, and DOI.

ISBN: 978-3-95450-252-3 ISSN: 2673-5350 doi: 10.18429/JACoW-IPAC2026-TUP7699

DESIGN OF A COMPACT HYBRID PLANAR UNDULATOR*

Jun Wang, Shudong Zhou†,
Shanghai Advanced Research Institute, Chinese Academy of Sciences, Shanghai, China

Content from this work may be used under the terms of the CC BY 4.0 licence (© 2026). Any distribution of this work must maintain attribution to the author(s), title of the work, publisher, and DOI.

Abstract

Undulators are key insertion devices in synchrotron radiation and free-electron laser facilities, where reducing the period length is an effective approach to achieving shorter radiation wavelengths and more compact systems. For short-period operation, the magnetic field of conventional hybrid planar undulators is limited by the efficiency of magnetic flux utilization, while highly closed magnetic structures, although capable of providing higher fields, often suffer from increased structural complexity and limited tunability. In this work, a compact hybrid planar undulator scheme is proposed based on a high-field magnetic structure. By removing part of the side magnets, the proposed design significantly reduces structural complexity while retaining the capability of field tuning via gap variation. Three-dimensional finite element simulations are performed to systematically investigate the influence of key structural parameters on the effective field and field quality. In addition, a combination of NdFeB magnets with different grades is adopted to mitigate demagnetization in critical regions. The results demonstrate that the proposed compact hybrid structure can achieve relatively high magnetic field levels under short-period conditions, while maintaining good engineering feasibility and operational reliability. This design provides a promising approach for next-generation compact high-performance undulators.

INTRODUCTION

Undulators generate high-brightness synchrotron radiation and free-electron laser radiation by inducing small-amplitude oscillations of an electron beam through a periodic magnetic field. For a given electron beam energy, the radiation wavelength is primarily determined by the undulator period length and the deflection parameter. Therefore, reducing the period length is an effective approach to achieving shorter wavelengths and improving the compactness of the facility. In recent years, short-period undulators have attracted significant attention in next-generation synchrotron light sources and free-electron laser facilities.

At present, several technical approaches have been developed for short-period undulators, including in-vacuum undulators, cryogenic permanent magnet undulators, and superconducting undulators. In-vacuum undulators are technologically mature; however, further reduction of the gap is constrained by beam lifetime and radiation damage. Cryogenic permanent magnet undulators can provide enhanced magnetic fields, but at the cost of increased system complexity [1]. Superconducting undulators offer even higher field potential, yet challenges remain in terms of operational stability and engineering implementation [2]. Therefore, within the framework of room-temperature permanent magnet technology, improving the performance of short-period undulators through magnetic structure optimization remains an important and practical approach.

DIFFERENT MAGNETIC STRUCTURE CONFIGURATIONS

To enhance the magnetic field performance of short-period planar undulators, various novel magnetic structures have been developed in recent years. These designs mainly aim to improve the magnetic field by optimizing the magnetic flux distribution, increasing the degree of magnetic circuit closure, or modifying the arrangement of magnets. From the perspective of magnetic circuit topology, these structures can be understood as an evolution from conventional open magnetic circuits toward highly closed configurations. Figure 1 shows schematic diagrams of different magnetic structures.

The conventional hybrid planar undulator, consisting of alternating permanent magnets and ferromagnetic poles, features a simple structure, mature fabrication technology, and good field tunability, and has been widely adopted in synchrotron radiation facilities. However, under short-period conditions, its magnetic field strength is limited by the relatively low efficiency of magnetic flux utilization in the gap region. To address this limitation, additional magnets can be introduced at the sides and above the poles (Type-a), which enhances the magnetic flux concentration near the beam channel. This type of structure can improve the magnetic field while maintaining good engineering feasibility, although the improvement remains moderate due to the partially open magnetic circuit [3].

Further enhancement can be achieved by increasing the degree of magnetic circuit closure. For example, quasi-ring or quasi-circular magnetic structures can be formed around the beam channel (Type-b and Type-c), significantly reducing magnetic flux leakage and improving flux concentration, thereby enabling higher magnetic field strength. However, such configurations are typically associated with fixed apertures and limited field tunability. To overcome this limitation, more complex configurations, such as dual-ring structures (Type-d) or designs with increased numbers of magnetic blocks (Type-e), can be introduced to enable field adjustment through changes in magnetization orientation or structural parameters. Nevertheless, these approaches generally lead to increased structural complexity, a larger number of magnetic components, and greater challenges in fabrication, assembly, and magnetic error control. In addition, their operational flexibility may still be constrained in practical applications.

* This work was supported by the National Natural Science Foundation of China (No. 12505370) and the Shanghai Rising-Star Program, China (No. 24YF2752400).
†zhousd@sari.ac.cn

ISBN: 978-3-95450-252-3 ISSN: 2673-5350 doi: 10.18429/JACoW-IPAC2026-TUP7704

IMPROVEMENT AND OPTIMIZATION OF A PERMANENT-MAGNET PHASE SHIFTER

Ch.-S. Yang‡, Ch.-K. Yang†, H. Chen and Ti.-Y. Chung
National Synchrotron Radiation Research Center, Hsinchu, Taiwan

Abstract

A permanent-magnet (PM) phase shifter for phase matching between tandem elliptically polarizing undulators (EPUs) at the Taiwan Photon Source (TPS) has been developed, and its initial version has already been installed in the storage ring. Current efforts focus on improving the device by enhancing the mechanical precision of the gap-adjustment system, maintaining magnetic-field quality, and minimizing beam-orbit perturbations within the limited installation space. Magnet sorting and shimming techniques were used to refine the magnetic performance of the first version. At small operating gaps, strong magnetic forces introduce substantial mechanical loading and can affect the field directionality. To overcome this limitation, an upgraded design incorporating a spring-assisted compensation mechanism is under development. This work presents the optimization approach and the resulting improvements achieved through integration of the spring system, demonstrating enhanced structural stability and improved repeatability under high-force operating conditions.

INTRODUCTION

Segmented undulator systems are widely adopted in modern synchrotron light sources and free-electron lasers to provide installation space for focusing elements, beam diagnostics, vacuum components, and correction magnets between insertion-device segments. To preserve radiation coherence and maximize photon flux between adjacent undulator segments, phase shifters are required to provide controllable phase delays between the electron beam and the emitted radiation.

At the Taiwan Photon Source (TPS), a tandem elliptically polarizing undulator (EPU) system has been installed to support variable-polarization photon-beam operation. A permanent-magnet phase shifter was previously developed and installed between the tandem EPUs for phase matching. The initial PM phase shifter design, including the mechanical structure, magnet sorting process, and magnetic-field optimization methods, has been reported previously[1]. Compared with electromagnetic phase shifters, the PM design offers several advantages, including compact size, reduced fringe fields, lower power consumption, and minimal impact on the nearby storage-ring lattice. Magnetic-field optimization of the initial version was achieved through magnet sorting and shimming techniques, resulting in satisfactory field-integral performance and negligible beam-orbit perturbation.

To further improve the phase-shifting capability and operational flexibility, the minimum operating gap of the upgraded phase shifter was reduced from 20 mm to 16 mm. However, reducing the magnetic gap significantly increases the magnetic attraction force between the upper and lower magnetic assemblies. Under small-gap operation, the increased magnetic loading introduces structural deformation, backlash effects, and degradation of gap-motion repeatability. These mechanical effects become increasingly critical because stable magnetic-field quality and precise mechanical positioning are required to maintain reliable phase matching and beam stability.

The primary operating range of the phase shifter is between 16 mm and 30 mm, where the magnetic force varies rapidly with gap size. To improve mechanical stability within this region, a spring-assisted compensation mechanism was developed to reduce the variation of magnetic-force-induced loading acting on the transmission structure. Multiple compression springs were symmetrically integrated into the magnet support frame to provide balanced preload forces and suppress asymmetric deformation during gap operation.

This paper presents the upgraded mechanical design and evaluates the effectiveness of the spring-assisted compensation mechanism. Mechanical measurements, including parallelism and repeated gap-motion tests, were performed to investigate the structural stability and repeatability of the upgraded system under high-force operating conditions.

SPRING COMPENSATION DESIGN

Figure 1 shows a schematic view of the upgraded PM phase shifter with the spring-assisted compensation mechanism integrated into the magnet support frame and transmission structure. The movable magnetic assemblies are driven by a vertical screw mechanism and guided by linear guide rails to maintain stable gap motion during operation. Multiple compression springs are symmetrically distributed on both sides of the magnet support frame to provide balanced preload forces and minimize asymmetric deformation.

The preload force of each spring can be individually adjusted through threaded support structures, allowing optimization of the compensation-force distribution. Compared with a single compensation element, the distributed spring arrangement provides more uniform loading conditions and improves the mechanical stability of the transmission structure. The passive spring-assisted design allows stable compensation without additional actuators or active control systems.

†yangzs@nsrrc.org.tw

Content from this work may be used under the terms of the CC BY 4.0 licence (© 2026). Any distribution of this work must maintain attribution to the author(s), title of the work, publisher, and DOI.

ISBN: 978-3-95450-252-3 ISSN: 2673-5350 doi: 10.18429/JACoW-IPAC2026-TUP7705

SUSTAINABILITY-ORIENTED CRYOGENIC PERMANENT MAGNET UNDULATOR (LN_2-ENABLED C^3-CPMU)*

J.-C. Huang†, C.-S. Yang, P.-S. Chuang
National Synchrotron Radiation Research Center, HsinChu, Taiwan
H. Kitamura, RIKEN SPring-8 Center, Sayo, Hyogo, Japan

Abstract

A sustainability-oriented cryogenic permanent magnet undulator, the LN_2-enabled C^3-CPMU, has been successfully demonstrated at the Taiwan Photon Source (TPS). The system is designed to address cryogenic performance, thermal stability, and cost efficiency for high-current storage ring operation (up to 500 mA). The undulator employs a conduction-cooled architecture combined with an LN_2 reservoir-based cooling scheme with simplified flow and pressure control, eliminating the need for dedicated cryogenic units. Operating at an intermediate temperature of 150–160 K, the system consumes approximately 8 L/h of LN_2. Active temperature control maintains the magnet temperature within ± 0.08 K under varying beam conditions, ensuring stable magnetic field performance. The enhanced magnetic properties at cryogenic temperatures enable shorter undulator periods, while integration with existing facility LN_2 infrastructure significantly reduces system complexity and operational overhead. These results demonstrate a scalable and energy-efficient solution for next-generation synchrotron and XFEL light sources.

INTROUDCTION

As synchrotron radiation facilities pursue higher X-ray spectral brightness, cryogenic permanent magnet undulators (CPMUs) have become one of the keys enabling technologies [1]. At cryogenic temperatures, permanent magnets exhibit higher remanence and coercivity, enabling stronger magnetic fields and improved photon performance. This allows shorter undulator periods and more compact device configurations.

In modern accelerator facilities, energy efficiency and sustainability have become important considerations. As a result, undulator design is constrained not only by device performance but also by facility-level requirements such as space, energy consumption, and infrastructure. In X-ray free-electron lasers (XFELs), long undulator lines significantly increase facility size and infrastructure demand. In ultra-low-emittance sources (ULESs), limited straight-section length requires compact and short-period undulators. The challenge is to achieve high performance under constraints of space and energy use. Although CPMUs improve magnetic performance, their implementation often relies on dedicated cryogenic systems that require continuous electrical power and maintenance. This limits their practicality for large-scale deployment. To address this, we have proposed a conduction-cooled, constant-temperature CPMU (C^3-CPMU) based on LN_2 reservoir-based cooling [2]. The system maintains stable magnet temperature under varying beam conditions with existing facility LN_2 infrastructure, eliminating standalone cryogenic systems and their power consumption. The concept has been validated with the TPS CUT18 undulator under realistic operating conditions [1].

*Work supported by National Science and Technology Council, Taiwa
† huang.juiche@nsrrc.org.tw

DESIGN CONCEPT AND STRUCTURE OF LN_2-ENABLED C^3-CPMU

Facility-Integrated LN_2 Cooling

The LN_2-enabled C^3-CPMU utilizes evaporative liquid nitrogen (LN_2) as the primary cooling source, stored in a reservoir [3] and directly supplied from the existing beamline cryogenic infrastructure (Fig. 1). Compared with recently developed CPMUs, including cryocooler-based CPMU or LN_2-cooled CPMUs employing standalone cryogenic flow control and pressure regulation unit, the LN_2-enabled C^3-CPMU adopts a simplified flow-control strategy based on standard industrial components. As a result, the initial capital cost is significantly reduced, requiring only cryogenic valves and piping infrastructure. In addition, operational costs are minimized due to the absence of continuous electrical power consumption and reduced maintenance requirements associated with cryocoolers. A typical LN_2 consumption of approximately 8 L/h (corresponding to 4 ~ 5 kW of electric power) has been demonstrated (e.g., CUT18 [2]), whereas cryocooler-based CPMUs may require continuous electrical power on the order of ~16 kW (e.g., CU15 [3]).

Conduction-Cooled and Dual-Source Operation

The C^3-CPMU adopts a conduction-cooled architecture in which heat is transferred from the magnet array through high-conductivity copper feedthrough before reaching the cooling system. In this indirect cooling scheme, the thermal resistance and thermal mass of the conduction path act as a natural low-pass filter, suppressing rapid temperature fluctuations and smoothing transient disturbances. The design also ensures a "zero-leakage" configuration by isolating the cryogenic fluid from the UHV environment, thereby improving reliability and simplifying maintenance. In addition, the conduction-cooled design supports a dual-source cooling configuration [3], which enhances operational flexibility and sustainability across different

Content from this work may be used under the terms of the CC BY 4.0 licence (© 2026). Any distribution of this work must maintain attribution to the author(s), title of the work, publisher, and DOI.

ISBN: 978-3-95450-252-3 ISSN: 2673-5350 doi: 10.18429/JACoW-IPAC2026-TUP7707

EFFICIENT DESIGN OF AN 8-CONDUCTOR NONLINEAR KICKER FOR HALF USING A PYTHON-BASED TOOLCHAIN*

Weibo Hu[1], Xiao Ding[1], Wenbin Song†,[1], Lei Shang[1], Feng-lei Shang[1]
[1]University of Science and Technology of China, Hefei, China

Abstract

An 8-conductor nonlinear kicker (NLK) is proposed for the Hefei Advanced Light Facility (HALF) injection system. Its design is highly sensitive to conductor positions and must accommodate a vacuum chamber. This study develops an automated toolchain combining Opera-2D and Python with Bayesian optimization (Optuna) to search for feasible conductor configurations under strict magnetic and spatial constraints. A feasible design was obtained within 40 iterations, greatly improving R&D efficiency and offering a generalized approach for nonlinear magnet optimization in fourth-generation light sources.

INTRODUCTION

The Hefei Advanced Light Facility (HALF) is a fourth-generation diffraction-limited storage ring (DLSR) designed to achieve ultra-low emittance for providing high-brightness synchrotron radiation [1]. Such low emittance typically results in a narrow dynamic aperture, posing significant challenges to traditional off-axis injection schemes [2]. To achieve transparent top-up injection, a nonlinear kicker (NLK) is required to provide a specific magnetic field profile: a zero-field region at the center for the stored beam and a high-field region with a flat-topped peak for the injected beam.

The 8-conductor NLK is an ideal choice for HALF due to its structural simplicity and flexibility in field shaping. However, its design process faces two major obstacles. First, the field quality is extremely sensitive to the spatial coordinates of the conductors; sub-millimeter deviations can significantly shift the peak position, alter the magnetic flux density at the injection point, and degrade the central zero-field region. Second, a vacuum chamber with a substantial cross-section must be accommodated within the 8-conductor support structure to allow beam passage. This requires the NLK to not only produce the target field distribution but also ensure that the conductors are positioned sufficiently far from the origin to provide adequate clearance for the chamber [3, 4].

Traditionally, the design of such magnets relies on manual iterations using simulation software. This process is time-consuming and must be restarted from scratch whenever design specifications change, making targeted optimization of magnetic performance difficult. To enhance design efficiency and reliability, this paper proposes an automated design framework. By integrating the Opera-2D simulation engine with a Python-based optimization environment, a toolchain capable of automating modeling, field extraction, and performance evaluation was developed. This approach enables rapid exploration of the design space and has successfully yielded feasible configuration schemes for the HALF NLK.

* Work supported by the Fundamental Research Funds for the Central Universities (WK2310250134) and National Natural Science Foundation of China (No. 12205293)

† songwb@ustc.edu.cn

SYSTEM ARCHITECTURE AND MODELING

Design Objectives of the Nonlinear Kicker

The NLK for HALF employs a symmetric 8-conductor configuration to generate the required multipole magnetic field. The conductors are arranged around the axis of the stored beam, with their cross-sectional coordinates serving as the primary design variables. Due to the structural symmetry, the degrees of freedom are reduced to the position coordinates of two conductors in the first quadrant. Let Conductor A be the one closer to the origin and Conductor B be the other, with their coordinates denoted as (AX, AY) and (BX, BY), respectively. The design objective is to create a field-free region at the center for the stored beam, while providing a deflection field for the injected beam at an injection point of $x = 7\,\mathrm{mm}$, with the magnetic field peak located near this position. Accordingly, several critical points are defined: the vertical magnetic field component (B_y) at $x = 0\,\mathrm{mm}$ is denoted as By_0, at $x = 1\,\mathrm{mm}$ as By_1, and at $x = 7\,\mathrm{mm}$ as By_7. The simulation was configured with a half-sine pulsed current featuring a pulse width of 1.6 µs and a peak of 3 kA. The design constraints require By_0 to be 0 Gauss, $By_1 \leq 25$ Gauss, and $By_7 \geq 800$ Gauss.

Automated Modeling based on Opera-2D and Python

To achieve automated modeling, a closed-loop workflow was implemented using the operapy interface, encompassing geometric parameter definition, mesh generation, time-varying current drive settings, finite element method (FEM) solving, and data extraction. This integration allows the solver to be invoked as a "black-box" function within the optimization loop, where the input is a set of coordinates and the output is the magnetic field data from the completed simulation.

Spatial Constraints of the Vacuum Chamber

A critical constraint in the NLK design is the integration of the vacuum chamber. To ensure mechanical feasibility, an elliptical region centered at the origin is defined as a "forbidden zone", as shown in Fig. 1. This forbidden zone is dimen-

Content from this work may be used under the terms of the CC BY 4.0 licence (© 2026). Any distribution of this work must maintain attribution to the author(s), title of the work, publisher, and DOI.

ISBN: 978-3-95450-252-3 ISSN: 2673-5350 doi: 10.18429/JACoW-IPAC2026-TUP7709

DESIGN AND EXPERIMENT OF ENERGY FEEDBACK UNIT FOR 15 kV/15 kA AMD EXCITATION PULSE SOURCE*

Z. Zhong, F.-L. Shang†,Ch. liu‡, L. Shang, W. Hu
University of Science and Technology of China, Hefei, China

Abstract

Abstract: The Super Tau-Charm Facility (STCF), a next-generation electron-positron collider led by the University of Science and Technology of China, necessitates a high-quality positron source to sustain continuous operation with high luminosity. The Adiabatic Matching Device (AMD) serves as a critical component for focusing positrons produced by electron bombardment, requiring its excitation pulse source to deliver a peak current of ≥ 15 kA and a pulse rise time of ≤ 3.5 µs. To mitigate the significant power dissipation of the pulse discharge system, an energy feedback circuit was designed. According to the simulation results, the optimized system achieved a dramatic reduction in losses, with the input power reduced by 75% under the condition of the same output power, while enhancing long-term operational stability. This paper elaborates on the power loss simulation of the AMD excitation pulse source, as well as the design and simulation of the energy feedback circuit.

Key words: excitation pulse power for AMD; power loss; energy feedback; photoconductive semiconductor switch

INTRODUCTION

Electron-positron colliders are vital tools for high energy physics research, A high-quality positron source is critical for the high luminosity of the STCF [1]. The STCF plans to use a 2.5 GeV electron beam to bombard a 15 mm tungsten target to generate positrons [2]. This approach generates a positron beam with small transverse dimensions and high current but suffers from significant divergence, making direct acceleration challenging [3]. Positrons produced by electron-tungsten target collisions require focusing by a high-pulse magnet, commonly referred to as Adiabatic Matching Device (AMD), to match the aperture of the capture structure [4]. As shown in Fig. 1, the AMD is a copper pulsed solenoid featuring a tapered inner bore and constant outer diameter, which requires a fast kA-level high-current pulse for operation. The AMD generates a strong magnetic field at the magnet entrance to enable positron focusing. consequently, the AMD and its excitation source are indispensable components of the positron source.

Excitation pulse sources, a branch of pulse power technology, rapidly release energy stored in capacitive and inductive components to generate a specific current waveform across the load, thereby achieving energy compression and power amplification [5]. These sources are primarily utilized to provide driving currents for various high-pulse magnet systems in accelerators to enable the focusing, deflection, or confinement of particle beams.

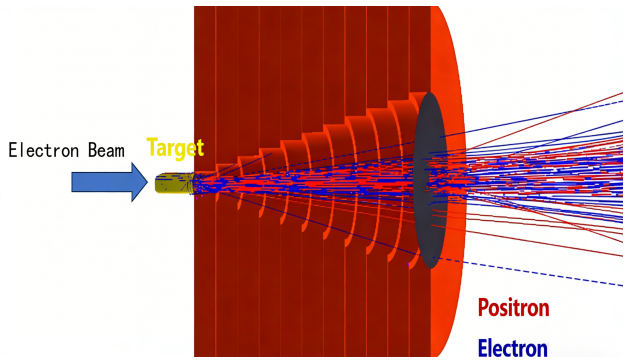

Figure 1: Schematic of the AMD Structure.

In this study, the RLC series configuration was selected for discharge to generate the current. To suppress the post-pulse oscillation, an energy feedback circuit is proposed in this paper, which reduces power loss and enhances the long-term operational stability of the excitation pulse source.

EXCITATION PULSE SOURCE SCHEME

Two primary discharge method are employed in excitation pulse sources: the RLC series discharge configuration, which generates a half-sine wave; and the Pulse Forming Line (PFN) or Pulse Forming Network (PFL), which produce square-wave pulse currents. Although PFN and PFL schemes are also applicable in some high-voltage conditions, their circuit structures are relatively more complex, and they are usually only adopted in applications that require a long flat-top pulse [6]. So we select RLC series discharge configuration of this excitation pulse source, the parameters are shown in Table 1.

Table 1: Technical Parameters of Excitation Pulse Source

Technical Index	Parameter Requirement
Pulse Current Waveform	Half-Sine Wave
Peak Pulse Current	≥ 15 kA
Pulse Width	5 ± 0.5 µs
Pulse Rise Time	≤ 3.5 µs
Repetition Frequency	50 Hz
Pulse Amplitude Stability	± 0.5%
Peak Charging Voltage	≤ 15 kV
Time Jitter	± 20 ns

* We thank the Hefei Comprehensive National Science Center for their strong support on the STCF key technology research project. This work is supported by the National Key R&D Program of China under Contract No. 2022YFA1602200 and the international partnership program of the Chinese Academy of Sciences Grant No. 211134KYSB20200057.

† shangfl@ustc.edu.cn
‡ chaoliu@ustc.edu.cn

Content from this work may be used under the terms of the CC BY 4.0 licence (© 2026). Any distribution of this work must maintain attribution to the author(s), title of the work, publisher, and DOI.

ISBN: 978-3-95450-252-3 ISSN: 2673-5350 doi: 10.18429/JACoW-IPAC2026-TUP7711

EVALUATION AND MITIGATION OF RESIDUAL MAGNETIC FIELD FROM THE HIGH-VOLTAGE PULSE POWER SUPPLY FOR THE BEAM KICKER IN THE MUON G-2/EDM EXPERIMENT

Y. Kawase*, S. Narita, R. Hosokawa, Iwate University, Japan
H. Iinuma, H. Sato, Ibaraki University, Japan
S. Ogawa, T. Mibe, High Energy Accelerator Research Organization, Tsukuba, Japan
T. Takayanagi, Japan Atomic Energy Agency, Tokai, Japan
R. Matsushita, T. Mibe, The University of Tokyo, Tokyo, Japan
T. Yamanaka, Kyushu University, Fukuoka, Japan

Abstract

In the J-PARC muon $g-2$/EDM experiment, precise control of the muon beam is essential to achieve the required measurement accuracy. For this purpose, the development of a new high-voltage and high-current pulse power supply (kicker power supply) is indispensable. Because the accuracy of the $g-2$ measurement strongly depends on the uniformity of the magnetic field, and the muon beam must remain confined within a region of ± 5 cm in height and a radius of 33.3 cm, any residual magnetic field leads to a degradation of the precision. While the design of the static magnetic field is being developed to meet the experimental requirements, the residual dynamic magnetic field remains a challenge. In this study, aiming to develop a power supply that satisfies the required precision, we evaluated the impact of the residual magnetic field caused by the kicker power supply on the measurement accuracy. This paper reports the evaluation results and our future plans to reduce the residual magnetic fields.

INTRODUCTION

The Standard Model describes elementary particle interactions with high precision, but phenomena such as dark matter and baryon asymmetry remain unexplained, motivating searches for physics beyond the Standard Model (BSM).

The anomalous magnetic moment of the muon $(g-2)$ is a powerful probe of BSM physics due to its high theoretical and experimental precision. Previous measurements at BNL [1] and FNAL [2] employed similar techniques, leaving the possibility of common systematic uncertainties.

The J-PARC muon $g-2$/EDM experiment adopts a different approach, using a compact storage ring with an ultra-low emittance beam and no electric field focusing [3]. By employing a three-dimensional spiral injection, it provides an independent measurement with a distinct systematic uncertainty [4], aiming at 0.45 ppm (stat.) with < 0.1 ppm (syst.).

THREE-DIMENSIONAL SPIRAL INJECTION AND KICKER SYSTEM

A μ^+ beam with a momentum of 300 MeV/c is injected obliquely downward from the upper edge of the storage magnet and follows a spiral trajectory while moving downward, wrapping around the main magnetic field of approximately 3 T applied inside the storage magnet (Fig. 1). After injection, the beam is guided by the kicker magnetic field and the weak focusing magnetic field, and subsequently oscillates within a limited region around a certain plane in the storage magnet (the storage plane). The muons then circulate stably in a nearly circular orbit until they decay.

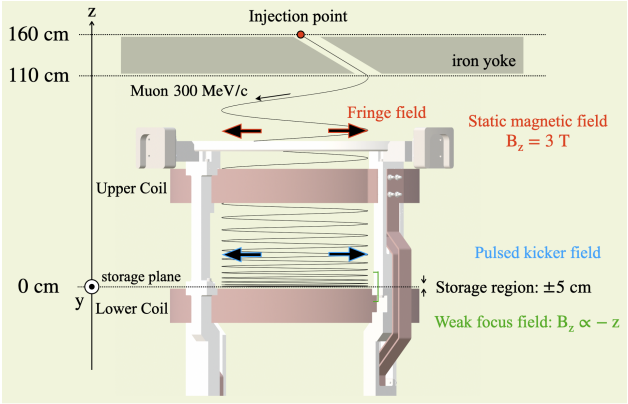

Figure 1: Concept of three-dimensional beam injection.

The weak focusing magnetic field [4, 5] is described by

$$B_r = -n\frac{B_0}{r_0}z, \quad B_z = B_0\left[1 - n\frac{r-r_0}{r_0} + \frac{n}{2}\left(\frac{z}{r_0}\right)^2\right],$$

where B_r and B_z are the radial and axial magnetic field components, respectively, r and z denote the radial and vertical positions, and $B_0 = 3$ T and $r_0 = 33.3$ cm. The field was implemented using the field index n $(= 1.5 \times 10^{-4})$. This weak focusing field induces vertical betatron oscillations (VBO), causing the stored muon beam to oscillate vertically around the storage plane with a period of approximately 600 ns.

The kicker magnetic field is generated by applying a pulsed current from pulse power supplies (kicker power supplies) to single-turn coils (kicker coils) placed above and below the storage region. As shown in Fig. 2, the current waveform delivered from the kicker power supply to the kicker coil can be categorized according to the kick timing and detector operation timing into three regions: the main pulse, the pulse-end region, and the fit range.

To achieve the target physics measurement precision and to confine the muon beam within the storage acceptance of

* s3125003@iwate-u.ac.jp

Content from this work may be used under the terms of the CC BY 4.0 licence (© 2026). Any distribution of this work must maintain attribution to the author(s), title of the work, publisher, and DOI.

ISBN: 978-3-95450-252-3 ISSN: 2673-5350 doi: 10.18429/JACoW-IPAC2026-TUP7714

PULSED MAGNETS DEVELOPMENT FOR THAILAND'S SPS-II

T. Yan*, S. Boonsuya, S. Jummunt, P. Klysubun,
A. Kwankasem, T. Leetha, W. Phacheerak, T. Phimsen,
S. Prawanta, T. Pulampong, P. Sudmuang, P. Sunwong
Synchrotron Light Research Institute, Nakhon Ratchasima, Thailand
N. Chaijaroenmaitree, K. Phochanasombut
Chulalongkorn University, Bangkok, Thailand

Content from this work may be used under the terms of the CC BY 4.0 licence (© 2026). Any distribution of this work must maintain attribution to the author(s), title of the work, publisher, and DOI.

Abstract

Thailand's upcoming 3 GeV light source (SPS-II), based on compact fourth-generation storage ring design, requires precise and reliable operation of pulsed magnet systems for successful beam injection and extraction. The requirements exceed our experience from operations of Thailand's current synchrotron, and also poses significant technical challenge beyond the currently demonstrated capability of local manufacturing. We present our latest progress in developing the pulsed magnets and power supplies domestically.

INTRODUCTION

The Siam Photon Source II (SPS-II), planned for operation in 2034, will be Thailand's new 3 GeV fourth-generation light source based on DTBA (double triple bend achromat) lattice with designed emittance of 0.96 nm · rad [1]. A key goal to the development of Thailand's new synchrotron light source is developing the necessary industrial capabilities to produce at least 50% of all components domestically. Currently, all the vacuum chambers [2] and storage ring magnets [3] are being developed in-house to near completion, satisfying the requirements of a fourth-generation light source. The injection and extraction system poses another set of challenges, as the institutional knowledge to develop and operate pulsed power systems do not currently exist domestically. By self-developing the pulsed magnets and power supplies for SPS-II, we ensure full understanding of the systems and the capability to fix any issues that may arise during commissioning and operation. With the economical savings of self-developed systems compared to turn-key systems, we can also stock replacement parts of the magnets and power supplies, ensuring maximum up-time independent of external parties.

MAGNET DESIGNS

Septum

The storage ring injection septum is the most challenging to design as leak field minimization is crucial in reducing perturbation to the stored beam. The in-air design of the magnet has a maximum allowed septum sheet thickness of 3 mm including the vacuum chambers, due to the small beam offset of 15 mm. Simulations indicate that a 1 mm sheet of copper and a 0.5 mm sheet of NiFe shielding material is enough to minimize the leak field.

* taylor@slri.or.th

Table 1: Key Parameters for the Storage Ring Injection Septum Magnet

Parameters	Septum
Field Strength	0.87 T
Effective Length	1200 mm
Deflecting Angle	6°
Aperture	9 × 20 mm
Beam Offset	15 mm
Septum Thickness	3 mm
Pulse Width	100 µs
Current	9 kA
Voltage	2.5 kV

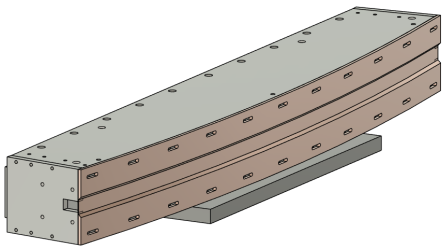

Figure 1: CAD of the prototype septum currently being built. Note that vacuum chambers are not included in the picture.

The septum magnets (booster injection, booster extraction, storage ring injection) are based on the septum of SLS (Swiss Light Source) [4] which has demonstrated reliable operation for over two decades, and the new thick septum of SLS2.0. Figure 1 shows the design, with the structural casing assembled from several pieces of machined 304 stainless steel, with slots for alignment of the silicon steel laminates. The silicon steel laminates are laser-cut with thickness of 0.2 mm, and can be assembled into the structural casing sheet-by-sheet without needing to be bonded together into a solid core. The conductor coil is made from a round copper bar, held in place with fiber-filled composite insulator. The septum sheet is made from a long piece of machined copper, installed onto the magnet after the magnet is positioned onto the prior-installed vacuum chambers at the injection/extraction points. This allows for independent installation and baking of the vacuum systems. The vacuum chamber inside the septum magnet gap is made from seamless 316L stainless steel racetrack tube, with wall thickness of 0.5 mm to minimize field attenuation. The design pa-

ISBN: 978-3-95450-252-3 ISSN: 2673-5350 doi: 10.18429/JACoW-IPAC2026-TUP7715

MECHANICAL DESIGN AND STRUCTURAL ANALYSIS OF SEPTUM MAGNET FOR THAILAND NEW SYNCHROTRON LIGHT SOURCE (SPS-II)

K. Phochanasombut*[1], N. Chaijaroenmaitree[1], S. Morakul[1]
T. Leetha[2], T. Phimsen[2], P. Sunwong[2], T. Yan[2]
[1]Chulalongkorn University, Bangkok, Thailand
[2]Synchrotron Light Research Institute, Nakhon Ratchasima, Thailand

Abstract

The Synchrotron Light Research Institute of Thailand is developing a new eddy-current septum magnet as part of the pulsed magnet systems for its next-generation synchrotron light source, the Siam Photon Source II (SPS-II). This work focuses on mechanical design and structural analysis of the septum magnet to improve the prediction of anomalies and potential failures over the machine's operational lifetime. The finite element method is used to evaluate both the static deformation of the in-air magnet yoke and the transient vibration response of the septum blade under pulsed magnetic force, which can induce fatigue damage through cumulative stress cycles. Static analysis indicates that the proposed design satisfies the structural integrity and magnetic field uniformity requirements. The impulse vibration fatigue assessment of the septum blade falls within the ultra-high-cycle fatigue (UHCF) regime, with established S–N data for copper alloys providing design guidance for extending the magnet's operational life.

INTRODUCTION

The development of the Siam Photon Source II (SPS-II) represents a major advancement in scientific infrastructure in Southeast Asia, with the potential to significantly enhance research and innovation capabilities across the region. As a next-generation synchrotron facility, SPS-II will offer higher energy and higher intensity photon beams with improved beam characteristics compared to the existing Siam Photon Source (SPS). It will play a significant role in supporting Thailand, as well as other ASEAN countries, in the transition to a research and innovation-driven economy [1].

SPS-II will consist of three accelerating structures: the linear accelerator (LINAC), the booster synchrotron, and the storage ring synchrotron. Beam transfer between accelerators requires injection and extraction systems designed to minimize beam loss; a combination of septa and kicker magnets is frequently used for these applications.

A septum separates two field regions: one with a homogeneous field for deflecting the beam, and the other with a low fringe field so as not to affect the circulating beam, providing spatial separation of the circulating and injected/extracted beams [2]. This research focuses on the eddy-current septum, powered with a half or full sine wave current pulse to create a fast-rising magnetic field. When pulsed, eddy currents induced in the septum counteract the fringe field. The operational magnet is subjected to static and dynamic forces that can cause deformation and alter its electromagnetic properties, motivating mechanical stress–strain and impulse vibration analysis using the finite element method (FEM).

LITERATURE REVIEW

Eddy-current septum magnets maintain very thin effective septa of 1 mm to 3 mm with unconstrained coil dimensions [2]. They have been developed in many accelerators, such as the SOLEIL synchrotron [3], the SSRF storage ring [4], the CERN SPS [5], and J-PARC [6, 7]. Studies on the MSe1 septum magnet [8] showed that finite element optimization with reinforcement plates significantly reduced stress concentrations at the coil–conductor interface. At CERN, high-fidelity modelling and vibration monitoring of pulsed septa demonstrated the importance of modal and transient response simulations in predicting fatigue life [9].

Various methods exist to characterise vibration fatigue in both the time and frequency domains [10–12]. The rainflow counting method is widely regarded as the most accurate cycle-counting algorithm for variable amplitude and random loadings, extracting cycles based on material memory mechanisms introduced through the "pagoda-roof" method. Several formulations have been developed, including the ASTM "3-points" algorithm [13], the "4-points" algorithm [14], and Rychlik's non-recursive formulation [15]. Identified cycle amplitudes are used with the Palmgren–Miner linear damage rule [16].

Ultra-high-cycle fatigue (UHCF) [17–19], defined as the regime beyond 10^8 cycles and extending to 10^{10} or more, is crucial for copper alloys in accelerator applications. Investigations for CLIC structures with a design lifetime of 2.33×10^{10} cycles [20, 21] established that pure copper (C10100) in a 50 % cold-worked state exhibits only 110 MPa fatigue strength at 10^{10} cycles, while precipitation-hardened CuZr (C15000) achieved 180 MPa and GlidCop Al-15 (C15715) reached 160 MPa.

METHODOLOGY

Static Structural Analysis

A static structural analysis was conducted in ANSYS using the plane-strain assumption, which is valid here because the yoke length along z greatly exceeds the in-plane dimensions,

* kantanat.pho@gmail.com

Content from this work may be used under the terms of the CC BY 4.0 licence (© 2026). Any distribution of this work must maintain attribution to the author(s), title of the work, publisher, and DOI.

ISBN: 978-3-95450-252-3 ISSN: 2673-5350 doi: 10.18429/JACoW-IPAC2026-TUP7719

BEAM DUMP DESIGN AND SIMULATION FOR A 280-MeV ELECTRON LINEAR ACCELERATOR

K. Kittimanapun*, P. Aim-O, P. Boonpornprasert, T. Chanwattana, S. Chunjarean, N. Juntong
Synchrotron Light Research Institute, Nakhon Ratchasima, Thailand

Abstract

A 280-MeV electron linear accelerator has been designed to expand the research capabilities and applications of high-energy electron beams in Thailand. For commissioning and energy verification, two dedicated beam dumps are positioned downstream of the bending magnet. This work presents the simulation-based design and optimization of these beam dumps using the PHITS Monte Carlo radiation transport code. Different material configurations and geometries were evaluated to reduce prompt radiation and suppress secondary particle leakage. A multilayer structure combining high-Z and low-Z materials was found to provide effective energy absorption while confining photon and neutron secondaries within the shielding volume. The resulting radiation field in the tunnel meets all applicable safety criteria and regulatory limits. These results establish the validated baseline design for the beam dumps and support their transition to detailed engineering and fabrication.

INTRODUCTION

Synchrotron Light Research Institute has developed a high-energy electron beam accelerator intended to provide 280-MeV electron beam to various applications and serve as a prototype of the pre-injector for the future light source. The pre-injector primarily consists of a thermionic electron gun, two sub-harmonic bunchers, and four accelerating structures. To facilitate machine commissioning, two beam dumps will be installed: one at 0° to absorb the beam from the linac and another at 45° following the bending magnet to measure the beam energy. Since both beam dumps are intentionally used to collect the electron beam of equivalent energy, a single design is sufficient. The main purpose of the design is to develop a compact beam dump built with simple materials and structure, while ensuring the radiation leakage dose remains below the Thai regulatory limit.

COMPUTATIONAL SETUP

The beam dump design has been evaluated using PHITS, a Monte Carlo particle transport simulation code [1]. The simulation used the EGS5 library package for electromagnetic interaction; JENDL-4, JENDL-5, INCL4.6, and GEM library packages for nuclear interaction; and DCHAIN for a decay chain analysis and activation study.

Figure 1 illustrates the geometry of the pre-injector vault containing two beam dumps. The vault is shielded by the 1.2-m thick concrete wall, floor, and ceiling to prevent radiation leakage to the controlled area dedicated to a linac klystron gallery, and by the 1.5-m thick wall that separates the vault from the main tunnel. Two entrance doors were designed to allow access to the vault: the concrete door positioned opposite the beam dump and a composite door—comprising iron, lead, and polyethylene layers with a total thickness of 13 cm—located at the beginning of the maze. To monitor radiation leakage around the vault, six NaI detectors with a radius of 15 cm are placed virtually outside the shielding wall in the area of expected high radiation or where personnel exposure is most likely.

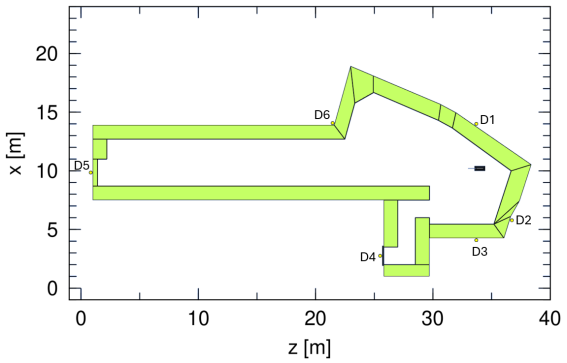

Figure 1: Pre-injector vault geometry where a beam dump is located, together with six detectors outside shielding walls.

The beam dump is designed to absorb the electron beam from a linear accelerator and attenuate the radiation field in the vault, ensuring that the external dose rate remains below the Thai regulatory limit of 3 μSv h^{-1}. Accounting for uncertainties in Monte-Carlo simulation and nuclear data, a safety factor of 10 was applied, resulting in a conservative target dose of 0.3 μSv h^{-1}. Figure 2 depicts the beam dump design, featuring a central core surrounded by three shielding layers:

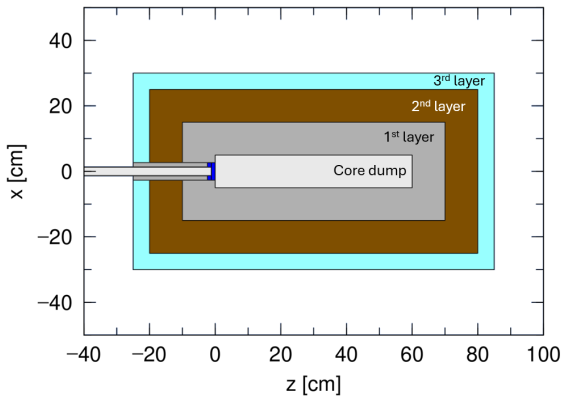

Figure 2: Design of a beam dump with an aluminum core dump and three layers of lead, steel, and borated polyethylene.

* kritsadak@slri.or.th

Content from this work may be used under the terms of the CC BY 4.0 licence (© 2026). Any distribution of this work must maintain attribution to the author(s), title of the work, publisher, and DOI.

ISBN: 978-3-95450-252-3 ISSN: 2673-5350 doi: 10.18429/JACoW-IPAC2026-TUP7720

LASER PHASE NOISE MEASUREMENTS AND ANALYSIS IN A HIGH-POWER OPTICAL ENHANCEMENT CAVITY

Z. Yang*[1], Y. Zhao[1], Y. Huang[1], X. Liu†[1], X. Lu[1], Q. Tian[1], W. Huang[1], C. Tang[1], L. Yan‡[1], A. Renaux[2,3,4], R. Chiche[2,3,4], K. Dupraz[2,3,4], A. Martens[2,3,4], F. Zomer[2,3,4]
[1]Department of Engineering Physics, Tsinghua University, Beijing, China
[2]Université Paris-Saclay, Orsay, France
[3]CNRS/IN2P3, Paris, France
[4]IJCLab, Orsay, France

Abstract

Optical resonators serve as excellent spatiotemporal filters and are widely used for stabilizing laser frequency. They can also function as passive optical enhancement cavities (OECs), providing power gains of thousands to tens of thousands. High-power OECs hold promise for applications such as steady-state microbunching (SSMB) advanced light sources and laser interferometer gravitational-wave observatory (LIGO). However, systematic studies on the phase noise characteristics of high-power OECs remain lacking. In this paper, based on a high-power OEC platform, we measure the phase noise of both the injected laser and the transmitted laser, and investigate the influence of key cavity-locking parameters on the phase noise performance, thereby providing valuable references for the application of high-power OECs.

INTRODUCTION

Optical resonators, leveraging coherent superposition of light fields, enable resonant enhancement of laser power while simultaneously acting as spatiotemporal filters for optical fields. The intracavity field exhibits excellent transverse mode quality and frequency stability, leading to a wide range of applications. Carefully designed ultrastable cavities can be used as optical frequency references, achieving laser outputs with ultra-low linewidths [1, 2]. The phase-sensitive characteristic of optical cavities has also been exploited in laser interferometer gravitational-wave observatory (LIGO) [3]. Moreover, advances in coating techniques for ultrahigh-reflectivity mirrors have facilitated the development of optical enhancement cavities (OECs), where power gains of more than ten thousand can produce megawatt-level intracavity circulating power [4–6]. Such high-power cavities offer new potential solutions for fields such as inertial confinement fusion and ion neutralization [7, 8]. OECs are also widely used in accelerator-based advanced light source research, for example, in the ThomX project, the Gamma Factory, and the steady-state microbunching (SSMB) advanced light source [4, 5, 9–11]. Current research on high-power OECs has focused primarily on stored intracavity power, mirror thermal effects, and damage thresholds [4–6], with few studies addressing the phase noise characteristics of high-power OECs. Nevertheless, phase noise performance is critically important for applications such as SSMB and LIGO [3, 11, 12]. Taking SSMB as an example, it not only requires megawatt-level intracavity power but also stable phase locking among several high-power cavities, which imposes stringent demands on cavity design. Based on a megawatt-level OEC platform, we employ the heterodyne self-beat technique to measure the phase noise properties of both the injected laser and the transmitted laser. We analyze the possible underlying mechanisms and compare the influence of different cavity-locking parameters on phase noise performance, thereby providing a new perspective for cavity optimization.

EXPERIMENTAL SETUP AND MEASUREMENT METHOD

We have constructed a four-mirror OEC platform consisting of high-reflectivity mirrors, a vacuum system, a low-noise continuous-wave laser, an optical transmission line, and a cavity locking electronics system, as shown in Fig. 1. The cavity itself is composed of four high-reflectivity mirrors: two flat mirrors (M1, M2) and two concave mirrors (M3, M4), where M1 serves as the input coupling mirror. Due to minor contamination from environmental dust and imperfections in coating smoothness, the experimentally measured finesse of the cavity is 26,000, lower than the theoretical value of 32,000, corresponding to an actual cavity linewidth of approximately 3.1 kHz. The low-noise continuous-wave laser can deliver an incident laser power of up to approximately 130 W. The optical transmission line consists of lenses, waveplates, and motorized mirrors, enabling mode matching, polarization matching, and alignment of the incident laser to the cavity resonance mode. The Pound-Drever-Hall (PDH) locking technique is utilized to lock the laser frequency to the cavity resonance. It features a dual-loop structure: a digital slow loop using a piezoelectric transducer (PZT) as the actuator and an analog fast loop using an acousto-optic modulator (AOM) as the actuator. Based on this platform, we measured the phase noise of both the injected laser and the transmitted laser using a heterodyne self-beat technique, as illustrated in Fig. 1. The laser under test was coupled into an optical fiber and split into two paths. One path was frequency-shifted by 110 MHz using an AOM, while the other path propagated through a 1 km

* yang-z23@mails.tsinghua.edu.cn
† liuxing09thu@gmail.com
‡ yanlx@mail.tsinghua.edu.cn

Content from this work may be used under the terms of the CC BY 4.0 licence (© 2026). Any distribution of this work must maintain attribution to the author(s), title of the work, publisher, and DOI.

ISBN: 978-3-95450-252-3 ISSN: 2673-5350 doi: 10.18429/JACoW-IPAC2026-TUP7722

HIGH-PRECISION PCB-BASED ROTATING COIL SYSTEM FOR MULTIPOLE MAGNET MEASUREMENTS IN THE 4GSR STORAGE RING

Y. G. Choi, D. E. Kim, G. Hahn, Y. Jung, B. J. Kim, W. Lee, M.-J. Kim, Pohang Accelerator Laboratory, Pohang, South Korea

Abstract

For the reduction of beam emittance in a Korea-4GSR project, the storage ring will be equipped with 344 quadrupole, 168 sextupole, and 56 octupole magnets. These multipole magnets require precise magnetic measurements to verify not only the field strength but also harmonic components within the specified tolerances over a good field region with a diameter of 30 mm. To meet this requirement, a PCB-based rotating coil measurement system has been developed. The PCB consists of a 14-layer multilayer structure incorporating both main and bucking coils, enabling high-precision measurement of allowed and higher-order harmonic components. The PCB length was designed to be 660 mm, considering to the effective magnetic length of the 4GSR multipole magnets. To minimize mechanical sag, the rotating shaft was fabricated from ceramic material and positioned at the magnetic field center using a high-precision XY stage with 0.1 μm resolution. The developed rotating coil system achieves a measurement precision better than 5×10^{-4}, demonstrating its suitability for high-accuracy characterization of small-aperture multipole magnets in the 4GSR project.

INTRODUCTION

The Korea-4GSR (Fourth-Generation Synchrotron Radiation Source) is currently under construction in Ochang, Korea, with facility completion scheduled for 2028, followed by accelerator installation and beam commissioning in 2029, and user operation beginning in 2030. Unlike conventional third-generation synchrotron light sources based on Double-Bend Achromat (DBA) lattices with nanometer-scale emittance, the 4GSR storage ring adopts a Hybrid 7-Bend Achromat (H7BA) lattice based on the Multi-Bend Achromat (MBA) concept. By employing multiple bending magnets with reduced bending angles within a single lattice cell, the MBA lattice achieves ultralow emittance at the picometer scale, enabling significantly enhanced brightness and transverse coherence compared with previous-generation light sources [1].

The MBA lattice substantially increases the magnet density within each cell and consequently amplifies the influence of magnetic field errors on beam dynamics. In addition, the magnet aperture is reduced to approximately 30 mm, resulting in a limited Good Field Region (GFR) and requiring highly precise magnetic field characterization for quality assurance. A total of approximately 420 quadrupole magnets, including 344 storage-ring and 76 booster-ring magnets, are planned for the 4GSR accelerator complex (Fig. 1). Quadrupole magnets play a critical role in beam focusing and in controlling the beta and dispersion functions. Therefore, accurate evaluation of both the integrated gradient and higher-order harmonic components is essential. However, in conventional non-bucking single-coil measurements, the dominant quadrupole fundamental component occupies most of the signal amplitude, limiting the sensitivities of higher-order harmonics [2]. This degrades measurement repeatability and long-term stability and limits the consistency of large-scale magnet quality control.

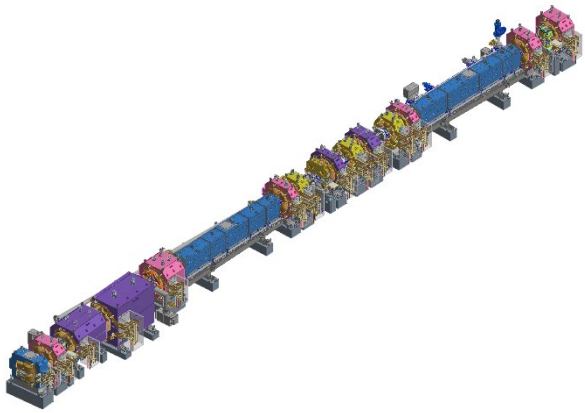

Figure 1: Half-cell layout of the 4th Generation Synchrotron Radiation Accelerator (4GSR) storage ring.

DEVELOPED ROTATING BUCKING COIL SYSTEM

To overcome the limited sensitivity to higher-order harmonics in conventional non-bucking measurements, a PCB-based bucking rotating coil system was developed for high-precision harmonic measurements of small-aperture quadrupole magnets for the Korea-4GSR (Fig. 2). The proposed system employs a multilayer PCB structure to realize a highly reproducible coil geometry and electrically suppresses the dominant quadrupole fundamental component in bucking mode, thereby significantly enhancing sensitivity to higher-order harmonics. The effective coil length was designed to be 660 mm, sufficient to cover the longest quadrupole magnets used in both the storage ring and booster ring. In addition, a high-resolution digital integrator and a precision motion-control system were implemented to achieve a repeatability better than 3×10^{-4} and an absolute accuracy below 5×10^{-4}. Consequently, the developed system provides a standardized measurement infrastructure suitable for full inspection of 4GSR quadrupole magnets.

The developed sensor consists of a 14-layer multilayer PCB structure with 84-turn main coils and 126-turn compensated coils. The coil radii were designed as $r_1 = 12$ mm,

Content from this work may be used under the terms of the CC BY 4.0 licence (© 2026). Any distribution of this work must maintain attribution to the author(s), title of the work, publisher, and DOI.

ISBN: 978-3-95450-252-3 ISSN: 2673-5350 doi: 10.18429/JACoW-IPAC2026-TUP7723

CONSTRUCTION OF PERMANENT MAGNET ARRAYS WITHOUT CUSTOM MATERIALS

A. F. Steinberg*[1], S. Barg[1], J. A. Bellesini[1], S. L. Sheehy[1,2], J. S.L. Yap[1,3]
[1]The University of Melbourne, Melbourne, Australia
[2]Australian Nuclear Science and Technology Organisation, Sydney, Australia
[3]Peter MacCallum Cancer Centre, Melbourne, Australia

Content from this work may be used under the terms of the CC BY 4.0 licence (© 2026). Any distribution of this work must maintain attribution to the author(s), title of the work, publisher, and DOI.

Abstract

Permanent magnet Halbach arrays can be used for beam steering and focusing for synchrotron light sources, Fixed Field Accelerators, and plasma accelerators. Conventional implementations require many custom wedge-shaped magnets with tailored geometries and magnetisation angles, preventing material reuse. We present a method for constructing Halbach arrays from many identical rectangular magnets, each rotated in the transverse plane to approximate the optimal configuration. Although this introduces gaps and reduces magnetic efficiency compared with custom-wedge designs, it simplifies fabrication, lowers costs, and enables the magnets to be redeployed for future applications. A prototype array based on this approach has been built for Project TURBO at the University of Melbourne, and measurements confirm that the magnetic field quality meets the requirements of the planned beamline. Construction of the full arrays for TURBO will soon commence, and the reusability of the magnets is expected to provide long term flexibility for subsequent accelerator projects.

INTRODUCTION

Permanent magnets for particle accelerators offer potential advantages over conventional electromagnets in cases where the magnetic field does not need to vary over time. The design of these magnet arrays was proposed by Halbach, taking advantage of the high fields achievable by oriented rare earth materials, in excess of 1.3 T [1]. An ideal 'Halbach array' uses material with a continuously varying magnetisation axis, however realistic constraints instead require many individual pieces, each with a singular orientation. To reduce costs and improve prospects of material reuse, we propose to use magnets arrays comprising many identical bar magnets, which do not necessarily approximate the Halbach solution. This has proven successful in the context of compact NMR machines [2], where the requirements on field uniformity are more stringent than for particle accelerators, and has also been proposed for accelerator facilities [3]. At The University of Melbourne, we are working towards the construction of permanent magnet arrays with large nonlinear multipolar components. The first-order design of these magnets, which will be used in a large momentum acceptance closed-dispersion arc for 'Project TURBO', has already been completed [4]. As a first step towards the construction of these arrays, we have built a prototype dipole magnet and measured the magnetic field it produces, finding that magnetisation errors degrade the field quality, and that the results can be accurately replicated by our simulations.

MAGNET DESIGN AND OPTIMISATION

To demonstrate the viability of TURBO's magnet arrays, a prototype dipole has been designed. To facilitate the design of the magnet array, a wrapper for the Python library Magpylib [5] has been developed. This wrapper provides convenience classes for the definition of accelerator magnets, the calculation of multipole coefficients, and visualisation of the arrays and B-fields produced. It also provides tools to automate the production of the magnet mounts, using CadQuery [6] to build the geometry. The Python wrapper also enables optimisation of the multipole content of a given magnet array. Each magnet block has three degrees of freedom: its position in the transverse plane (x, y), and its rotation angle about the longitudinal axis (θ_y), measured relative to the y-axis. The symmetry requirements of accelerator multipole magnets simplifies the optimisation problem, as the position and orientation of magnets beneath the horizontal midplane can be inferred by mirroring and flipping the sign on the rotation of magnets above the midplane, via the transformation $(x, y, \theta_y) \rightarrow (x, -y, -\theta_y)$. If we also constrain magnets on the midplane such that they must remain on the midplane and are not rotated during optimisation, this reduces the number of degrees of freedom for an n-magnet array from $3n$ to $(3n-2)/2$. For the purpose of magnet prototyping, 35 identical permanent magnet blocks have been procured from Chinese supplier Kingsun Magnetics. Each individual magnet is $10 \times 10 \times 100$ mm^3, magnetised along one of the short axes. They are made of NdFeB material, nominally N42H grade with a remanent field of 1.3 T. In practice, the large length/diameter ratio of these magnets will reduce the actual magnetic polarisation, requiring experimental determination of the field strength. It was decided that eight magnet blocks would be used to create the first prototype array. Using a small number of magnets allowed us to ensure that our magnet construction techniques were safe with a reduced risk of injury from the magnets, at the expense of reduced field uniformity and a lower maximum field strength. Beginning with the Halbach solution, Nelder-Mead simplex optimisation was performed to improve the field quality at the magnet centre and increase the field strength in the magnet bore, without changing the number of magnets. The good field radius was set to 15 mm, however a totally uniform field could not be achieved out to this distance due

* a.steinberg@unimelb.edu.au

ISBN: 978-3-95450-252-3 ISSN: 2673-5350 doi: 10.18429/JACoW-IPAC2026-TUP7724

DESIGN OF HIGH-FIELD PERMANENT DIPOLE MAGNET WITH ULTRA LOW LEAKAGE FIELD

Zihan Wang, Zhenghe Bai*, Guangyao Feng†
National Synchrotron Radiation Laboratory, USTC, Hefei, China

Abstract

In the fourth-generation light sources, storage ring lattices are typically compact, potentially leading to serious cross-talk effects. Reducing the leakage field of a magnet offers an effective solution. In this paper, a novel permanent dipole magnet structure is proposed to address the magnetic flux leakage in conventional designs. Compared to traditional steel sheet shielding, this structure demonstrates superior performance in reducing leakage fields. Based on this structure, a protective permanent dipole magnet for the front end of a beamline of the Hefei Advanced Light Facility is developed and simulated using the 3D finite element method. The dipole achieves a peak field of 1.49 T with a leakage field significantly reduced to under 10 Gauss at 30 mm. This work offers a viable method to developing future permanent magnets with low magnetic cross-talk.

INTRODUCTION

The use of permanent magnets (PMs) is one of the new features of the fourth-generation synchrotron light sources [1, 2]. This PM technology has been extensively studied and adopted in some light source facilities, such as ESRF-EBS [3], Sirius [4] and SLS 2.0 [5]. Compared to conventional electromagnets, PMs offer advantages in saving space in the magnetic system, ensuring stable beam operation, and reducing power consumption. However, PM technology is also subject to several limitations. For example, PMs typically lack tunability in their magnetic fields and can suffer from gradual magnetic field degradation when exposed to radiation environments.

Furthermore, in conventional PM designs, an increase in the center field often results in stronger leakage fields, which can lead to serious cross-talk effects and compromise the stability of a light source. To address this issue, this paper proposes a novel PM-based dipole structure designed to effectively reduce leakage fields. By incorporating auxiliary PM blocks, the proposed design generates a counter magnetic flux that opposes the primary leakage flux, thereby reducing leakage fields to very low values. As an application example, a protective dipole based on the proposed structure is designed for the front end of a beamline of the Hefei Advanced Light Facility (HALF) [6]. Simulation results of the magnetic field demonstrate the effectiveness of this new design.

* baizhe@ustc.edu.cn
† fenggy@ustc.edu.cn

PM SHIELDING STRUCTURE

Figure 1(a) shows the cross section of a conventional H-shaped PM-based dipole design, where the blue and green areas denote the soft iron and the PMs, respectively. The symmetry of the yoke geometry can compensate the magnetic forces and cancel even-order harmonics. The required dipole field in the gap is established by the magnetic flux generated from the PM blocks. While the designed primary path for this flux is through the adjacent yokes and poles, a portion inevitably leaks into the air around the dipole. Taking the upper half of the dipole as an example, the magnetization directions of all three PM blocks are oriented toward the center. As a result, the combined leakage flux on the front and rear surfaces of the upper half points outward. Similarly, the combined leakage flux on the front and rear surfaces of the lower half points inward, as illustrated in Fig. 1(b). The leakage fields scale with the central field strength, making their control a critical challenge in designing high-field PM-based dipoles.

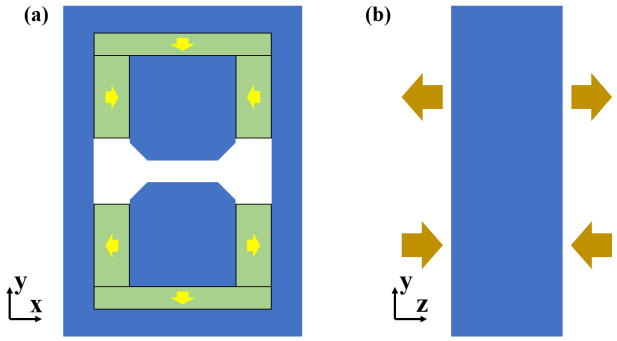

Figure 1: Cross-sectional view of a conventional H-shaped PM-based dipole design (a), and the schematic of its magnetic flux leakage in the longitudinal direction (b). The yellow arrows in the left plot indicate the magnetization directions of the PM blocks.

To address this challenge, this paper proposes a novel magnetic shielding design with auxiliary PM blocks. The design

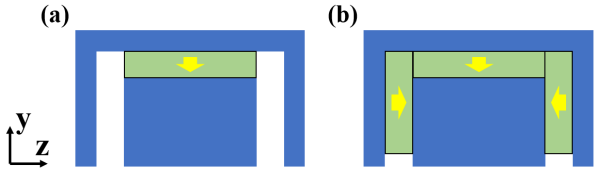

Figure 2: Cross-sectional views in the longitudinal plane for the PM-based dipoles with different magnetic shielding methods: (a) steel sheet shielding and (b) proposed PM shielding. The yellow arrows indicate the magnetization directions of the PM blocks.

Content from this work may be used under the terms of the CC BY 4.0 licence (© 2026). Any distribution of this work must maintain attribution to the author(s), title of the work, publisher, and DOI.

ISBN: 978-3-95450-252-3 ISSN: 2673-5350 doi: 10.18429/JACoW-IPAC2026-TUP7726

HIGH-EFFICIENCY NEUTRON TRANSPORT USING MAGNETIC GRADIENT WITH PERMANENT MAGNETS*

Y. Iwashita†[1], S. Matsui[1], Y. Kuriyama[2], Y. Fuwa[2], M. Yamada[3], K. Hirota[4], Z. Wang[5], M. Kitaguchi[5], H.M. Shimizu[5]
[1]The University of Osaka, Ibaraki, Osaka, Japan
[2]JAEA, Tokai, Ibaraki, Japan
[3]KEK, Tokai, Ibaraki, Japan
[4]KEK, Tsukuba, Ibaraki, Japan
[5]Nagoya University, Nagoya, Aichi, Japan

Abstract

Neutron guide tubes, which utilize reflection at material surfaces, are used for neutron transport. In many cases, neutron guide tubes with small divergence angles are sufficient. By arranging thin guide tubes radially according to the size of the sample, the overall efficiency of the system can be improved. We are developing a new type of neutron mirror that utilizes the orbital refraction of neutrons in a gradient magnetic field. Six prototype magnet plates were fabricated and tested at BL16. We report on the current status of research and development regarding this mirror.

INTRODUCTION

Slow neutron beams are widely used not only in fundamental physics and materials research but also in industrial applications. The cost of generating neutron beams is high compared to other imaging methods, such as X-rays. Because experimental areas are located far from the source due to radiation shielding, it is important to establish a mechanism for efficiently transporting neutrons between these areas. To address this issue, neutron guide tubes are used to reflect neutrons off the surface of materials. By employing multilayer mirror coatings for neutrons within the guide tube, it is possible to transport neutron beams with a wide range of divergence angles downstream (see Fig. 1).

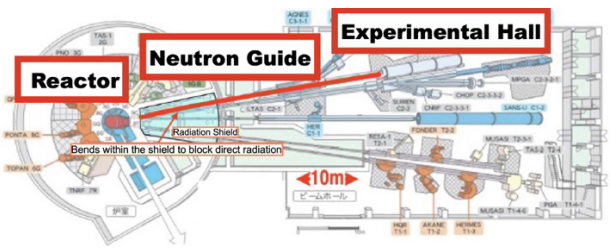

Figure 1: Layout of JRR3. The experimental area is far from the source due to radiation shielding. Neutron guide tubes that utilize reflections at the surface of materials are used to transport neutrons.

* Work supported by partially supported by JSPS KAKENHI Grant Number JP23H03659. The neutron experiment at the Materials and Life Science Experimental Facility of the J-PARC was performed under a user program 2024B0198.
† iwashita.yoshihisa.4x@kyoto-u.jp

However, in many experiments, such as small-angle neutron scattering, the divergence angle of the incident beam must be sufficiently small to obtain measurements with good q-resolution. Although guide tubes transport beams with large divergence angles, most of the neutrons are removed by collimators. This can lead to an increase in radioactive waste and background radiation. In fact, in many small-angle scattering measurements, only beams with a divergence angle corresponding to m=1 in a supermirror, are used. Furthermore, in modern neutron facilities, a single experimental apparatus is installed directly at the end of a single guide tube. The beam does not branch during transport. In such cases, guide tubes capable of accommodating large divergence angles are unnecessary. Arranging thin guide tubes radially to match the size of the sample would likely improve the overall efficiency of the facility. (see Fig.2).

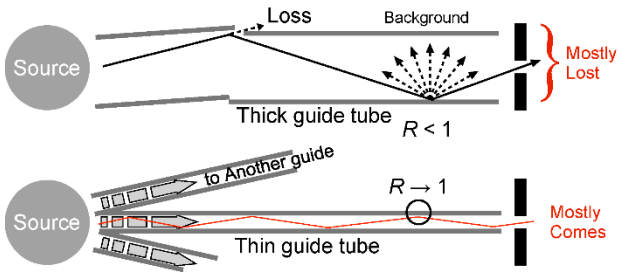

Figure 2: Top: Conventional guide tube with loss and background. Bottom: New concept of guide tube for modern neutron facilities. This will increase the number of beamlines. Fuzzy mirror surface eases alignment tolerances and reduce collisions with tiny dust particles on the mirror surface. Most transported neutrons will be used.

MAGNETIC NEUTRON DEFLECTION

We are developing a new type of neutron mirror that utilizes the orbital refraction of neutrons in a gradient magnetic field (see Figure 3). In a magnetic field, the neutron orbits are deflected according to the following equation:

$$\frac{d^2\boldsymbol{r}}{dt^2} = \pm\left|\frac{\mu_n}{m_n}\right| \cdot \nabla|\boldsymbol{B}|$$

where $\boldsymbol{r}$ and t are position of a neutron and time, μ_n and m_n are the magnetic dipole moment and mass of the neutron, respectively [1]. $\nabla|\boldsymbol{B}|$ is gradient of magnetic field

Content from this work may be used under the terms of the CC BY 4.0 licence (© 2026). Any distribution of this work must maintain attribution to the author(s), title of the work, publisher, and DOI.

ISBN: 978-3-95450-252-3 ISSN: 2673-5350 doi: 10.18429/JACoW-IPAC2026-TUP7731

ENHANCED SUPERCONDUCTING PROPERTIES OF Nb FILMS VIA A HIGH-POWER IMPULSE MAGNETRON RE-SPUTTERING/SPUTTERING APPROACH FOR Nb–Cu 1.3 GHz RF CAVITIES

J. Xiao[1,2], P. Dong[1,2], Y. Wang[1,2], Z. Chen[†,3], J. Chen[3], D. Wang[3], Y. Chen[1,2], Z. Liu[2,3], J.Li[,1,2]
[1]State Key Laboratory of Quantum Functional Materials, School of Physical Science and Technology, ShanghaiTech University, Shanghai, China
[2]ShanghaiTech Laboratory for Topological Physics, School of Physical Science and Technology, ShanghaiTech University, Shanghai, China
[3]Center for Transformative Science (CTS), Shanghai, China

Abstract

Conformal deposition of high-performance superconducting films on complex cavity geometries, particularly ensuring robust film-substrate adhesion, remains a fundamental challenge. We address this by introducing a novel high-power impulse magnetron re-sputtering and sputtering (HiPIMRS) system designed for uniform niobium (Nb) film deposition on the interior surfaces of 1.3 GHz copper cavities. A key innovation is an in-situ copper substrate re-sputtering step prior to Nb deposition, which eliminates interfacial oxides and degradation, ensuring atomic-scale interfacial integrity. Through in-situ re-sputtering prior to deposition, we achieve oxide-free Nb/Cu interfaces with atomic-scale integrity. Crucially, electrical transport measurements demonstrate a significant enhancement in the superconducting transition temperature (T_c) from 8.5 K to 9.3 K for HiPIMRS films, along with smooth surfaces (R_a < 20 nm) and a preferred (110) orientation. This work establishes HiPIMRS as a viable pathway for next-generation superconducting radiofrequency (SRF) cavity production, with its interfacial engineering protocols offering significant advancements in film conformity and superconducting properties.

INTRODUCTION

Superconducting radio frequency (SRF) cavities are critical components in particle accelerators and quantum computing infrastructures [1-5]. While bulk niobium has been the traditional material of choice, copper-based niobium film cavities provide significant advantages including reduced material costs, enhanced thermal conductivity, and superior mechanical properties [6-9].

Depositing high-quality Nb films on Cu cavities requires uniform coverage in complex geometries and strong adhesion. High power impulse magnetron sputtering (HiPIMS), pioneered at CERN [5, 8], has achieved accelerating gradients up to 21 MV/m for 1.3 GHz Nb-Cu cavities [10]. However, Nb films often exhibit residual resistance and Q-slope issues [11, 12]. Preventing Cu substrate oxidation is acknowledged as pivotal for enhancing performance [13-15], necessitating in-situ surface cleaning techniques [16].

In this work, we present a high-power impulse magnetron re-sputtering/sputtering (HiPIMRS) system for fabricating 1.3 GHz Nb-Cu SRF cavities. The system integrates translational target positioning, dynamic power control, and optimized magnetic fields for conformal Nb deposition under ultra-high vacuum (<10^{-7} Pa). In situ substrate re-sputtering enables oxide-free, atomic-scale interfacial preparation. The superconducting Nb films are observed with a high critical temperature of 9.3 K, flat surface roughness (R_a < 20 nm for 4 μm films). The Nb films exhibit a strong (110) preferred orientation, accompanied by a minor (211) peak. This work demonstrates exceptional film uniformity and interface integrity, establishing HiPIMRS as a scalable pathway for next-generation SRF cavities.

EXPERIMENTAL SETUP AND METHODS

Instrument Design

Fig. 1(a) illustrates the HiPIMRS apparatus used for conformal Nb deposition on 1.3 GHz Cu cavities. The system integrates an adaptable magnetron target system and a water-cooled magnetron target containing a high-purity Nb cylindrical tube cathode and ring-shaped NdFeB magnets, all housed within a 316 stainless steel ultra-high vacuum (UHV) chamber with a base pressure below 10^{-7} Pa. A precision translation stage (±0.1 mm) enables axial positioning of the target over a 1.0 m range, allowing full coverage of the single-cell cavity (length ~50 cm) in Fig. 1(b).

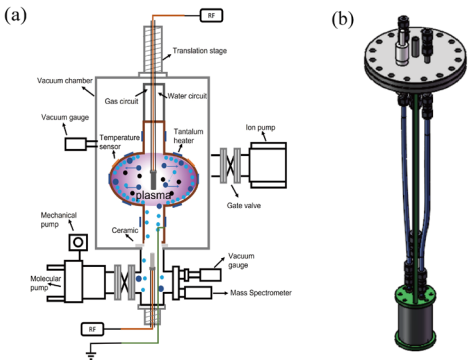

Figure 1: (a) Schematic diagrams of the modular apparatus for high-energy pulsed magnetron re-sputtering/sputtering (HiPIMRS); (b) The sputtering module of the HiPIMRS apparatus.

Content from this work may be used under the terms of the CC BY 4.0 licence (© 2026). Any distribution of this work must maintain attribution to the author(s), title of the work, publisher, and DOI.

ISBN: 978-3-95450-252-3 ISSN: 2673-5350 doi: 10.18429/JACoW-IPAC2026-TUP7733

MAGNETIC DESIGN OF A PROTOTYPE HYBRID IN-VACUUM UNDULATOR AND PASSIVE FORCE CANCELLATION SYSTEM FOR SPS-II

"N. Sutthimon†, H. Nakajima, Ch. Pasatcha, S. Rugmai, R. Satasasawat, S. Soontaranon, N. Wasanbongngem, Synchrotron Light Research Institute, Nakhon Ratchasima, Thailand

Abstract

This paper presents the comprehensive magnetic design and simulation-based optimization of a prototype hybrid in-vacuum undulator (IVU), developed as a proof-of-concept for the 4th-generation synchrotron light source (SPS-II) at the Synchrotron Light Research Institute (SLRI). A configuration featuring a 20 mm period length and a 5 mm minimum gap was simulated at a 3 GeV electron beam energy for Small-Angle and Wide-Angle X-ray Scattering (SAXS/WAXS) techniques. The magnetic structure was subsequently modeled in 3D using the RADIA code, employing NdFeB permanent magnets and FeCo-V poles. To counteract the massive magnetic attraction force at the minimum gap, a passive force cancellation system was integrated and optimized. Simulations demonstrate that this system successfully reduces the total mechanical load by 99%, enabling a highly compact and lightweight IVU design.

INTRODUCTION

The Synchrotron Light Research Institute (SLRI) is developing a prototype hybrid in-vacuum undulator (IVU) for the 3 GeV Siam Photon Source II (SPS-II) [1]. A precise main magnetic design is essential to achieve the high-brightness hard X-ray beams required for Small-Angle and Wide-Angle X-ray Scattering (SAXS/WAXS) techniques. Although beam dynamics restrict the nominal operational gap to 5.0 mm to satisfy vertical stay-clear requirements [2], the prototype's mechanical framework must safely accommodate the storage ring's physical minimum gap of 4.2 mm. Evaluating the system at this absolute limit is critical, as the NdFeB magnets and FeCo-V poles generate a massive 17.64 kN vertical attraction force. Maintaining micrometer-level gap precision under this immense load traditionally requires bulky and costly mechanical support, posing severe installation challenges within the constrained accelerator tunnel.

To address this mechanical bottleneck, this paper presents the 3D magnetic design and RADIA-based optimization [3] of a passive force cancellation system using a secondary Pure Permanent Magnet (PPM) array [4].

MAIN MAGNETIC DESIGN AND OPTIMIZATION

Analytical Parameters and Spectra Simulations

The conceptual design of the IVU was initially driven by the photon beam requirements of the SAXS/WAXS beamline at the SPS-II storage ring. To determine the fundamental magnetic parameters, numerical simulations of the synchrotron radiation spectra were performed using the SPECTRA code [5]. The optimization targeted a high photon flux at an energy of 9.1 keV at the 7th harmonic, corresponding to a deflection parameter (K) of 2.14 for the 3 GeV electron beam energy of the low-emittance lattice of the SPS-II. Based on these analytical calculations, a periodic magnetic length (λ_u) of 20 mm and a nominal minimum operational magnetic gap of 5 mm were selected. The prototype consists of 51 full periods, generating a peak magnetic field (B_{peak}) ranging from 1.32 T at the nominal minimum gap of 5.0 mm to 0.47 T at a 10.0 mm gap. This corresponds to a maximum K of 2.28, which provides the ample tuning margin necessary to ensure the continuous, high-brightness harmonic spectrum required for the 8-20 keV SAXS/WAXS beamline. The main parameters of the IVU prototype are summarized in Table 1.

Table 1: Main Parameters of the IVU Prototype

Parameter	Value	Unit
Electron beam energy	3.0	GeV
Number of periods	51	-
Period length	20	mm
Main magnet size	56 × 7 × 31	mm
Pole size	46 × 3 × 23	mm
Minimum magnetic gap	5	mm
Peak magnetic field range	0.47 – 1.32	T

3D Magnetic Modeling and Material Selection

The structure utilizes high-remanence NdFeB grade 38UH permanent magnets with a remanence (B_r) of 1.24 T and an intrinsic coercivity (H_{cj}) exceeding 1990 kA/m to prevent radiation-induced demagnetization. The

†nonthaphat@slri.or.th

MC7: Accelerator technology and sustainability
MC7.T15: Technology: Undulators and Wigglers

Content from this work may be used under the terms of the CC BY 4.0 licence (© 2026). Any distribution of this work must maintain attribution to the author(s), title of the work, publisher, and DOI.

ISBN: 978-3-95450-252-3 ISSN: 2673-5350 doi: 10.18429/JACoW-IPAC2026-TUP7734

DEVELOPMENT AND MAGNETIC CHARACTERIZATION OF THAILAND'S FIRST IN-VACUUM WIGGLER PROTOTYPE

N. Wasanbongngem†, H. Nakajima, Ch. Pasatcha, S. Rugmai, R. Satasasawat, S. Soontaranon, N. Sutthimon, Synchrotron Light Research Institute, Nakhon Ratchasima, Thailand

Abstract

This paper details the development of Thailand's first prototype in-vacuum wiggler (IVW). The project began with 3D magnetic field simulations using the RADIA package to define the optimal magnetic configuration. To verify their magnetic properties and ensure field quality, individual magnet blocks are characterized using a Helmholtz coil system. The magnet arrays are assembled onto an in-vacuum girder utilizing a custom workstation and specialized keeper tools to maintain strict mechanical tolerances and ensure safety against strong magnetic forces. Optical alignment using a leveling camera verifies girder planarity and gap consistency prior to final metrology. Furthermore, this work details a custom-built Hall probe measurement bench—also driven by newly developed control and data acquisition software—which is employed for the inaugural field mapping of the assembled IVW. A preliminary comparison between the experimental field data and RADIA simulations, prior to the application of shimming or magic finger end-field corrections, is presented. This study establishes a critical technical framework for future high-performance ID development in Thailand.

INTRODUCTION

Synchrotron light sources depend on insertion devices (IDs), such as wigglers and undulators, to enhance photon flux and brightness [1]. Transitioning toward high-performance in-vacuum IDs is essential for expanding experimental capabilities. However, in-vacuum wigglers (IVWs) present significant engineering challenges, particularly regarding complex mechanical structures and precise magnetic field control within ultra-high vacuum environments [2-4].

This paper details the development of Thailand's first domestically fabricated prototype IVW. The design phase utilized 3D magnetic simulations via the RADIA package [5-8]. To manage the strong attractive forces of high-remanence magnets, specialized assembly workstations and custom keeper tools were developed to ensure both precision and safety.

To validate the simulations, a robust characterization framework was established [9]. Individual magnet blocks were characterized using a Helmholtz coil system from Kyma company with in-house developed software. Furthermore, this work describes a custom-built Hall probe measurement bench featuring a Metrolab sensor and in-house developed mechanics and control software. Initial comparisons between experimental data and RADIA simulations, conducted prior to field corrections, provide a technical framework for future ID development in Thailand.

†noppharit@slri.or.th

MAGNETIC DESIGN AND SIMULATION

Magnetic Design

The 3D magnetic geometry of the wiggler was modeled and optimized using the RADIA package integrated within the Mathematica environment. Individual permanent magnet blocks were designed with physical dimensions of 79 × 79 × 50 mm. To satisfy the stringent coercivity requirement (> 2000 kA/m). The Neodymium-Iron-Boron (NdFeB) was selected as the permanent magnet material. Correspondingly, The Vanadium Permendur was chosen for the pole structures due to its exceptionally high saturation polarization characteristics. The final magnetic configuration features 5 main poles and 2 end poles, establishing a stable magnetic period (λ_u) of 230 mm capable of providing a peak magnetic field of 2.0 T at the minimum working gap of 15 mm [5]. The detailed engineering design and clamping assembly layout of these magnet blocks and poles are illustrated in Fig. 1.

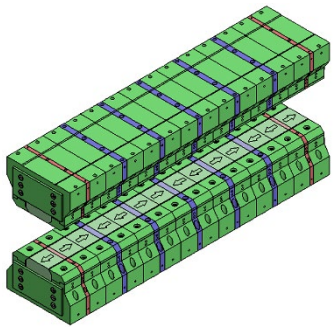

Figure 1: Mechanical design and clamping assembly layout of the wiggler magnet arrays and pole pieces.

Simulation Results and Comparative Analysis

Magnetostatic simulations were carried out across various magnetic gaps, with primary focus on 15 mm, 20 mm, and 25 mm. These simulated configurations established the theoretical baseline for the subsequent experimental magnetic characterization phases. The peak magnetic field demonstrates a clear inverse relationship with the gap size, yielding values of 2.0 T, 1.6 T, and 1.4 T at operational gaps of 15 mm, 20 mm, and 25 mm, respectively (while a maximum of 2.4 T is obtained at a tight gap of 10 mm).

The first field integral (I_1) and second field integral (I_2) profiles across the operational gaps show consistent symmetric alternating wave patterns along the beam axis.

Content from this work may be used under the terms of the CC BY 4.0 licence (© 2026). Any distribution of this work must maintain attribution to the author(s), title of the work, publisher, and DOI.

ISBN: 978-3-95450-252-3 ISSN: 2673-5350 doi: 10.18429/JACoW-IPAC2026-TUP7901

R&D ON EFFICIENT ULTRA-HIGH FREQUENCY RFQ STRUCTURES

S. Wunderlich* [1,2], E. Boos[1,2], C. Zhang[1,2,3]
[1]GSI Helmholtzzentrum für Schwerionenforschung, Darmstadt, Germany
[2]Institute for Applied Physics, Goethe University Frankfurt, Frankfurt am Main, Germany
[3]Helmholtz Research Academy Hesse for FAIR (HFHF), Frankfurt am Main, Germany

Abstract

RFQ (radio-frequency quadrupole) accelerating structures for frequencies below 400 MHz have been extensively investigated for decades. To realize modern medical accelerators with more compact layouts, there is growing interest in using ultra-high frequencies (UHF: 0.3–3 GHz). At high frequencies, 4-vane RFQs tend to surpass 4-rod RFQs in terms of efficiency and beam parameters. However, 4-rod RFQs offer lower cost per meter, reduced mechanical complexity, and a simpler tuning process, making them particularly attractive for low-cost applications. This study presents R&D toward efficient UHF 4-rod RFQ structures, with a focus on dipole effect mitigation.

THEORY

Dipole field effects are an intrinsic problem that degrades the performance of 4-rod RFQ accelerators due to the asymmetry of their internal structures. Various techniques have been developed to mitigate these effects by balancing the length differences of the current paths from the ground plate to the electrodes at different heights. Solutions that modify the stem geometry in the plane perpendicular to the beam axis (xy-plane) are common practice and have been extensively studied [1]. A new technique has been developed that modifies the stem geometry along the beam axis (longitudinally in yz-plane), called "bending the lower-electrode supporters along the accelerating channel" (BLESAC) [2]. Additionally, a new modified perpendicular compensation technique was developed, based on an already available design [1]. This new technique uses a lateral displacement and widening of the stem cut, while also shifting the outer border of the arm to the upper electrodes by the same amount. Advantages of this new method are:

- equal width of all stems—no width differences for even-odd stems. Therefore, tuner plates can employ the full width of the structure.
- Higher mechanical stability of the upper electrodes—lower vibration susceptibility.
- More space for water cooling channels—especially useful when used in combination with additive manufacturing [2].
- Possibility of lower parasitic inductance of the upper electrode stem arms—higher reluctance due to increased magnetic path lengths and therefore lower dipole field effects (this has not yet been confirmed).

Dipole field effects in 4-rod RFQs are detrimental because they introduce an unwanted transverse field component that displaces/focuses the beam from its ideal central axis. This leads to beam deflection, reduces the effective aperture, and thereby lowers the transmission efficiency. In addition, the dipole field can deteriorate the symmetry of the focusing forces (see Fig. 1).

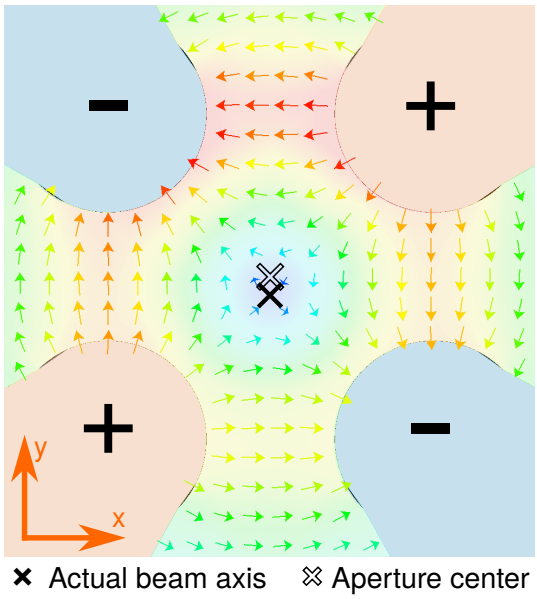

Figure 1: Strongly deflected beam axis by an unwanted dipole field.

The dipole factor D of a 4-rod RFQ arises from the different heights $\sim L$ of the electrodes above the ground plate. This creates two current paths of unequal length, resulting in different inter-rod voltages. Equivalently—considering that upper and lower electrodes form part of the same resonating structure— the upper electrodes are slightly farther from the resonator's feeding point (the ground plane). Therefore, the resonator's standing wave produces a slightly higher voltage at the upper electrodes (see Fig. 2). The dipole factor D is defined as follows:

$$D \equiv 1 + \frac{V_{uir} - V_{lir}}{V_{lir}}\,, \tag{1}$$

where V_{uir} is the upper inter-rod voltage and V_{lir} is the lower inter-rod voltage. For this study, the specific shunt impedance R_p is defined as follows:

$$R_p = \frac{V^2}{P/l}\,, \tag{2}$$

where V is the average inter-electrode (inter-rod) voltage, and P is the RF power loss within the resonator, and l is the

* s.wunderlich@gsi.de

Content from this work may be used under the terms of the CC BY 4.0 licence (© 2026). Any distribution of this work must maintain attribution to the author(s), title of the work, publisher, and DOI.

ISBN: 978-3-95450-252-3 ISSN: 2673-5350 doi: 10.18429/JACoW-IPAC2026-TUP8002

COMPACT X-BAND LINEAR ACCELERATORS DESIGN FOR ON-SITE INDUSTRIAL APPLICATIONS*

M. Boucard†, AVELION, Peynier, France
Y. Rozier, Epsyl, Pertuis, France

Abstract

The progressive replacement of radioactive sources is stimulating growing interest in compact linear accelerators, which are better suited for field deployment. Such systems must emphasize modularity, transportability, and, above all, reliable performance under operational conditions.

This work introduces a family of compact X-band linear accelerators designed to produce electron beams in the low-MeV energy. The engineering design focuses on the key component: the accelerating structure. A biperiodic on-axis coupled standing-wave structure was selected, operating in $\pi/2$ mode.

Simulation results demonstrate that the proposed configurations achieve the targeted energy levels with controlled beam transmission, while providing a focal spot size (FWHM) below 1 mm, significantly outperforming conventional radioactive sources ($\approx$ 5 mm).

This paper summarizes the overall design approach, highlights the main simulation results, and outlines the current progress of development activities.

INTRODUCTION

Among the various methods of non-destructive testing (NDT), X-ray imaging plays a key role, particularly for the inspection of thick materials. Currently, on-site NDT applications rely mainly on radioactive sources such as ^{60}Co and ^{192}Ir. However, these sources present several limitations, including their relatively low dose rates, stringent regulatory constraints associated with their handling and storage, and the fact that they continuously emit radiation even when not in operation [1].

Linear accelerators offer a promising alternative as they can generate X-rays with sufficiently high energy to penetrate thick materials structures, along with dose rates that enable rapid radiographic [2].

Despite these advantages, their use in NDT is usually reserved for controlled environments such as bunkers. The purpose of the system under development is to replace radioactive sources for on-site industrial applications [3]. The system must combine several key requirements, including transportability, modularity, simplicity, and reliability.

NDT linear accelerators typically work in S-band (3 GHz). Increasing the resonant frequency of the accelerating structure offers the possibility to scale down overall dimension of the system. An answer to this requirement could be found at upper frequencies in the X-band.

Operation in the X-band is advantageous not only for reducing the system dimensions but also for improving the nominal performance. For the same radio-frequency (RF) power, for example, higher beam energies can be achieved. In addition, the filling time is reduced, the shunt impedance is increased, and a higher maximum electrical field strength can be obtained [4].

The purpose of this work is to design an X-band accelerating structure that satisfies the associated space constraints. This paper outlines the main design choices along with the results obtained from RF modeling and beam dynamics simulations.

ACCELERATING STRUCTURE DESIGN

Product Specifications

To achieve the objective of modularity and transportability, the accelerating structure should fulfill specific requirements, especially in terms of length and accelerating gradient. However, these constraints should not compromise the beam quality in term of current, transmission, energy, and spot size. The chosen frequency band is the X-band, around 9.3 GHz, with a magnetron pass band ranging between 9.275 GHz and 9.315 GHz. The resulting specifications are summarized in Table 1. The target energy of 1.8 MeV has been selected as the most effective level for replacing the radioactive sources.

Table 1: Specifications of the X-band Accelerator

Item	Value	Unit
Energy	1.8	MeV
Transmission	> 30 %	
Quality factor	> 8000	
Shunt impedance	> 150	MΩ
Frequency	9.275 to 9.315	GHz
Beam spot size (FWHM)	< 1	mm
On-axis peak gradient	> 40	MV

Design

The selected design is a bi-periodic on-axis coupled standing wave structure.

The mode $\pi/2$ is chosen due to its favorable characteristics on the dispersion curve. The coupling cells are located on the axis, which helps reduce the overall diameter and has a minimal effect on the total length of the system. Moreover, this kind of design builds upon previous accelerators developed by AVELION.

The accelerating structure consists of a 4-cavity buncher, followed by a series of relativistic cavities depending on the target energy. For a beam energy of 1.8 MeV, 7 accelerating

* This work was supported by a grant from the French Public Investment Bank (Bpifrance) as part of the France 2030 program.
† mboucard@avelion-alcen.com

Content from this work may be used under the terms of the CC BY 4.0 licence (© 2026). Any distribution of this work must maintain attribution to the author(s), title of the work, publisher, and DOI.

ISBN: 978-3-95450-252-3 ISSN: 2673-5350 doi: 10.18429/JACoW-IPAC2026-TUP8004

MEASURED PROPERTIES OF THE MIXED HELIUM AND CARBON ION BEAM AT MEDAUSTRON

M. Kausel*,1,2, C. Schmitzer[1], [1]EBG MedAustron GmbH, Wiener Neustadt, Austria
K. Holzfeind[2], E. Renner[2], [2]TU Wien, Vienna, Austria

Abstract

The implementation of a sequential injection scheme for mixing helium and carbon ions from different ion sources at the MedAustron accelerator facility enabled the first successful delivery of a mixed helium and carbon ion beam in a synchrotron therapy facility. Precise knowledge of both the helium and the carbon properties is an essential input for designing treatment monitoring experiments, however, it is not trivial to distinguish the helium and carbon beam properties within the mixed beam.

This contribution discusses the acquired beam properties delivered to the first treatment monitoring research experiments at MedAustron since late 2025. Most notably, the measurements demonstrate that beam compositions with 0-100 % helium content can be achieved. The mixed beam generation at MedAustron is still in an early stage, which is reflected in significant shot-to-shot fluctuations in the beam intensity and composition as well as differences in the transverse beam sizes of the extracted helium and carbon ions.

INTRODUCTION

A sequential injection scheme has been developed at the MedAustron ion therapy and research center to generate mixed helium ($^4He^{2+}$) and carbon ($^{12}C^{6+}$) ion beams for research on treatment monitoring [1–3]. The presence of both helium and carbon ions in the beam introduces additional degrees of freedom that need to be understood and controlled to guarantee the desired beam properties.

Although still in an early stage, mixed beams generated using the sequential injection scheme are already being employed in first treatment monitoring experiments conducted at MedAustron since late 2025. A detailed characterization of these beams is therefore required to provide input to the experimental programs. In this contribution, we present and discuss the results of ongoing characterization measurements, focusing on key beam parameters such as intensity, beam composition and extracted beam spot sizes. Further, we outline aspects related to the sequential injection scheme that offer potential for further optimization. Please note that the measurement procedures presented in this proceeding are still experimental and, as such, subject to systematic and statistical errors that have not yet been fully quantified. The presented data is only intended as input to the research users, to illustrate general trends, and highlight potential for optimization in the future.

MIXED BEAM GENERATION AT MEDAUSTRON

The generation of mixed helium and carbon ion beams via sequential injection at MedAustron [1, 2] consists of three stages: (i) multiturn injection of the helium ions from one ion source, (ii) deceleration of the stored helium beam to the carbon injection energy while the injector is reconfigured for carbon injection, and (iii) multiturn injection of carbon ions from a separate ion source using a lower injection bump amplitude. Following the sequential injection, the mixed beam is captured, accelerated, and extracted to the research irradiation room [4].

A key control parameter in this sequential injection scheme is the strength of the second (carbon) injection bump. By varying the carbon injection bump amplitude, helium contents from 0-100 % can be achieved. The sequential injection produces a distinct horizontal phase space distribution [1] which directly correlates to the beam composition. In very simple terms, the situation can be understood as follows: For lower carbon orbit bump amplitudes, more helium survives in the core of the distribution, while predominantly carbon ions from the annulus are lost at the horizontal beam pipe apertures. Hence, we expect the helium content to increase and the carbon content to steadily decrease with lower injection kicker strengths. For details on the sequential injection scheme, please refer to references [1, 2].

BEAM COMPOSITION

One key characteristic of mixed beams is the beam composition, i.e. the number of helium and carbon ions in the beam (N_{He}, N_C). We quantified the beam composition using current measurements together with a novel RF-based quantification method in the synchrotron, as well as measurements with a range-separated ionization chamber array in the irradiation room. Both measurement procedures are described in reference [5]. Figure 1 shows the measured intensities for both ion species at flat-bottom (left), flat-top (middle), and after extraction in the irradiation room (right), each for various amplitudes of the carbon injection bump and hence different helium fractions. The underlying data corresponds to the 262.3 MeV/u measurement at a radial loop position of 27.5 mm reported in reference [5].

As expected, at flat-bottom after capture but before acceleration[1], lower orbit bump amplitudes lead to an increase in helium intensity and a corresponding decrease in carbon intensity. A comparison of the flat-bottom to the flat-top intensities indicates that the transmission to flat-top is reduced

* matthias.kausel@medaustron.at

[1] Note that uncaptured ions may slightly interfere with RF-based measurements at flat-bottom. This effect has not been investigated yet.

Content from this work may be used under the terms of the CC BY 4.0 licence (© 2026). Any distribution of this work must maintain attribution to the author(s), title of the work, publisher, and DOI.

ISBN: 978-3-95450-252-3 ISSN: 2673-5350 doi: 10.18429/JACoW-IPAC2026-TUP8007

COMMISIONING OF A NEW BEAMLINE FOR MEDICAL RESEARCH AND RADIATION HARDNESS TESTING

J. Bundesmann†, A. Denker, A. Dittwald, T. Fanselow, I. Ja, M. Kang, G. Kourkafas, R. Mendes, N. Noltemeyer, Helmholtz-Zentrum Berlin für Materialien und Energie, Berlin, Germany
J. Reindl, A. Roussetti, Universität der Bundeswehr München, Munich, Germany

Content from this work may be used under the terms of the CC BY 4.0 licence (© 2026). Any distribution of this work must maintain attribution to the author(s), title of the work, publisher, and DOI.

Abstract

The HZB cyclotron accelerator complex provides 68 MeV protons for therapy and related research. The main accelerator is an isochronous sector cyclotron served by two injectors. The treatment room is fixed according to the regulatory agencies and the adjoining experimental station is often overbooked with users for radiation hardness test and dosimetry. To widen the irradiation possibilities, we built up a new beamline for medical research with minibeams and a second target station is prepared for radiation hardness experiments. The setup, possibilities and commissioning for these stations will be presented.

INTRODUCTION

The HZB cyclotron is an isochronous sector cyclotron served by two injectors: a 6 MV single-ended Van-de-Graaff or a 2 MV Tandetron [1,2]. The Tandetron is the standard injector for proton therapy of ocular tumours while the Van-de-Graaff provides also other ion species and permits more sophisticated time structures. The accelerator is available for experiments for three days per month. Until recently, only one experimental station just beside the treatment room was available (Fig. 1).

The increased variety of the experiments lead to beamtime losses due to the necessary changes in the experimental set-up and its proximity to the treatment/patient room in terms of radiation safety. Hence, it became essential to install new target stations. According to the users request, two different target stations were planned:

MiniBEE

This beamline is dedicated for Spatial Fractionated Proton Beam Therapy and will be equipped with a SARRP (small animal radiation research platform) [3,4]. This is a joint project between the HZB and the Universität der Bundeswehr München. The goal are proton beams of different energies with a FWHM of 100 µm and an intensity between 1 pA to 1 nA.

InOperando

This target station will be used for irradiation of solar cells with up to 10^{12} protons/(cm^{2}s). The solar cells will be under operation with parallel illumination of a sun simulator. The sun simulator will provide a spectrum which is typical for space (AM0). For this, a dedicated target station is required which permits a homogeneous irradiation of the solar cells with protons and a parallel irradiation with a sun simulator without with a calibrated AM-0 spectrum.

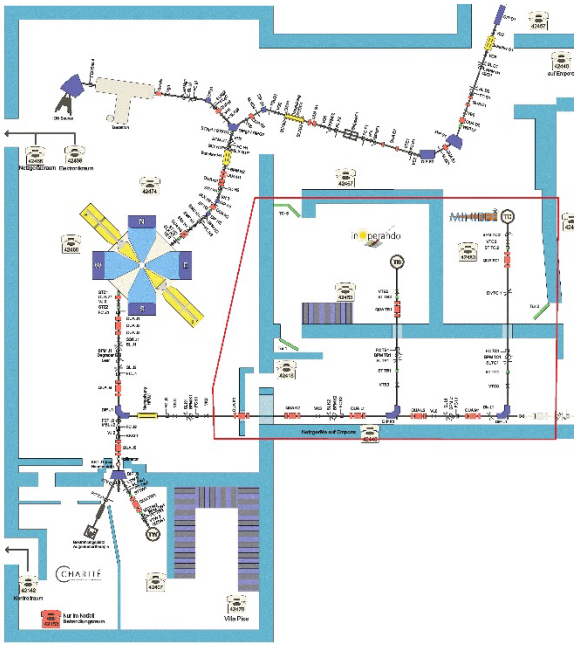

Figure 1: Layout of the HZB cyclotron with Tandetron injector, the Van-de-Graff being not shown here. The treatment room with the adjoining experimental station is at the bottom left. The red line marks the installation of the new beamlines.

BEAMLINES



Figure 2: Optical alignment of the dipoles and triplets using theodolites.

†bundesmann@helmholtz-berlin.de

ISBN: 978-3-95450-252-3 ISSN: 2673-5350 doi: 10.18429/JACoW-IPAC2026-TUP8008

ULTRA-HIGH DOSE-RATE IRRADIATION EXPERIMENTS AT FLUTE

M. J. Nasse*, M. Brosi, J. Pehlivan, S. Goldbach, S. M. Treffert, A. Malygin, E. Bründermann, V. Orian-Rousseau, A.-S. Müller, Karlsruhe Institute of Technology, Karlsruhe, Germany

Abstract

The linac-based test facility FLUTE at the Karlsruhe Institute of Technology (KIT) can be operated with a wide range of beam parameters, such as bunch charge, bunch length, and repetition rate. This flexibility makes FLUTE an interesting test-bed for studies of accelerator-based ultra-high dose-rate irradiation with electron beams. Based on the time structure of the produced electron pulses, the instantaneous dose rate can be tuned to exceed 10^{11} Gy/s with an average dose rate exceeding 40 Gy/s. At the same time, FLUTE can also provide average dose-rates closer to conventional rates in the order of 0.1 Gy/s.

INTRODUCTION

The linear accelerator FLUTE (Ferninfrarot Linac- Und Test-Experiment) at KIT has been designed as a dedicated test facility for accelerator physics and technology, as well as a broadband, short-pulse source for intense THz radiation [1,2]. One goal is, for instance, to test and develop novel diagnostics systems for ultra-short bunches like the compact transverse deflecting experiment based on THz-streaking using a split-ring resonator for the longitudinal bunch charge profile measurement [3,4].

The electron bunches can also be used *directly* in an in-air section of the accelerator to test and characterize diagnostics [5, 6] or to irradiate samples, for instance biological cell cultures. The versatility of FLUTE allows tuning not only the energy, but also the charge and the bunch length over a wide range up to Ultra-High Dose Rates (UHDR). In this paper, we shortly summarize the main characteristics of FLUTE and then present the experiment beamline and in-air section we have developed recently.

FLUTE OVERVIEW

FLUTE consists of several main sections, each followed by a diagnostics section: photoinjector electron source, linac module, bunch compressor, experiment area with the in-air section and dump, see Fig. 1. Picosecond infrared laser pulses from a titanium sapphire laser are frequency tripled and then sent onto a copper cathode, where they generate the electron bunches with a repetition rate of 1–50 Hz. They are accelerated in the photoinjector powered by a 11 MW klystron to an energy of around 5–6 MeV. After passing the diagnostics section I they enter a linac module fed by a 37 MW klystron. A recent complete upgrade of the radio frequency system [7], including both klystrons, the photoinjector electron source, and the linac module of the FLUTE accelerator, resulted in significantly improved stability and reproducibility compared to the previous system. The electron bunches then traverse the diagnostics section II and go through a D-shaped chicane consisting of four dipoles. The chicane serves as a bunch compressor, allowing the adjustment of the bunch length down to the femtosecond regime. After the chicane, a thin aluminum foil can be moved into the electron beam at a 45° angle for THz experiments. When a bunch passes through the foil, transition radiation in the THz range is generated. It is emitted at 90° with respect to the electron beam, where it can be measured and used as a diagnostics, for instance as a bunch compression monitor [2]. After further diagnostics, the electron bunch leaves the ultra-high vacuum beam pipe by passing through a thin metal foil to enter the in-air section. Finally, the beam is stopped in a lead dump.

As a dedicated test facility for accelerator physics and technology, FLUTE has been designed to cover a broad range of parameters such as energy (~6–90 MeV), charge (~70 fC – 800 pC), and bunch length (ps down to a few fs).

IN-AIR SECTION

An in-air section is very useful for a large variety of experiments, for example in the domain of diagnostics or sensor R&D, because it dramatically reduces prototyping and development cycle times since the vacuum does not need to be broken. Small changes or modifications can be applied immediately, several prototypes can be tested within the same beamtime etc. For instance, we recently demonstrated first near-field-sensitive electro-optical measurements of electron-bunch-induced transient signals in the FLUTE in-air section using a photonic-integrated Mach-Zehnder interferometer sensor [5]. Another example in this field is the development of ultra-fast planar pickups for electro-optical beam arrival monitors used at the European XFEL and other free-electron laser (FEL) facilities, where different designs can be quickly and easily tested in series in-air [8].

Another very important field, where an in-air section is indispensable, is the irradiation of biological cell cultures, most notably in the context of radiotherapy studies. Here, we are currently interested in studying the so-called FLASH effect [9,10]. This phenomenon describes the observation that radiotherapy at ultra-high dose rates, typically >40 Gy/s, can significantly reduce damage to healthy tissue while maintaining a comparable effectiveness against cancer cells relative to conventional dose rates (~0.1 Gy/s). This effect is still poorly understood today. Compared to clinical machines, research accelerators such as FLUTE provide a much higher degree of flexibility, allowing both the dose rate and the temporal pulse structure to be varied over a wide range, from conventional to ultra-high dose rates [11].

* michael.nasse@kit.edu

Content from this work may be used under the terms of the CC BY 4.0 licence (© 2026). Any distribution of this work must maintain attribution to the author(s), title of the work, publisher, and DOI.

ISBN: 978-3-95450-252-3 ISSN: 2673-5350 doi: 10.18429/JACoW-IPAC2026-TUP8009

ADVANCEMENTS AND DOSIMETRY OF A SINGLE-TURN EXTRACTION FOR FLASH RADIOTHERAPY STUDIES AT ELSA

L. Thome*, K. Desch, D. Proft, A. Stähler, M. Switka
University of Bonn, Bonn, Germany

Abstract

Ultra-high-energy electrons are used to investigate their effects on cell samples in nanosecond to microsecond pulses at the electron accelerator facility ELSA. This may allow highly efficient treatment of deep-seated tumors through the FLASH effect. Previous studies at ELSA using an initial extraction mode with 250 ns long pulses from the 1.2 GeV booster synchrotron demonstrated the suitability for FLASH radiotherapy studies. A newly developed single-turn extraction scheme from the stretcher ring now enables access to beam energies of up to 3.2 GeV with pulse lengths of approximately 330 ns and improved beam stability. In preparation for upcoming cell irradiation studies with this new extraction mode, precise dose determination is carried out by combining radiochromic film measurements with Geant4 simulations over the full energy range from 1.2 GeV to 3.2 GeV. Depth-dose curves from the previous and current operation modes are compared. Additionally, studies of Cherenkov radiation are performed to evaluate its potential for beam characterization.

FLASH@ELSA

FLASH@ELSA is an experiment investigating the FLASH effect [1] at the electron accelerator facility ELSA located at the University of Bonn. ELSA consists of three acceleration stages. Electrons from either a thermionic or polarized source are first pre-accelerated to 26 MeV with a linear accelerator (linac). They are then accelerated by the booster synchrotron up to typ. 1.2 GeV. Afterwards the electrons are injected with a rate of up to 50 Hz into the stretcher ring, where energies of up to 3.2 GeV can be reached.

FLASH Operation Modes

To provide ultra high dose rates (UHDR) of $\geq 40\,\mathrm{Gy\,s^{-1}}$, which defines the FLASH regime [1], suitable extraction modes to provide short pulse durations are essential. Two operation modes have been developed for FLASH@ELSA to deliver ultra-high dose rates (UHDR) for irradiation studies at different beam energies.

Booster Extraction Mode: For this mode the beam is directly extracted from the booster synchrotron and guided to the experimental site. Part of the stretcher ring functions as a transfer beamline towards the irradiation site. This extraction method provides electron pulses with a pulse length of around 250 ns and charges of up to 2.5 nC at a beam energy of 1.2 GeV.

* l.thome@uni-bonn.de

Single-Turn Stretcher Extraction: This extraction mode features a full beam extraction within one turn from the stretcher ring, capable of storing up to 200 mA of current at low energies. Therein, injection kicker magnets are repurposed for extraction into the external beamline [2]. Figure 1 highlights the locations of the kickers, extraction septa and irradiation site. The single-turn extraction delivers electron pulses with a length around 330 ns. Pulse charges exceeding 2.5 nC are achievable within the investigated energy range from 1.2 GeV to 3.2 GeV, with a estimated limit of 9.5 nC at 2.5 GeV.

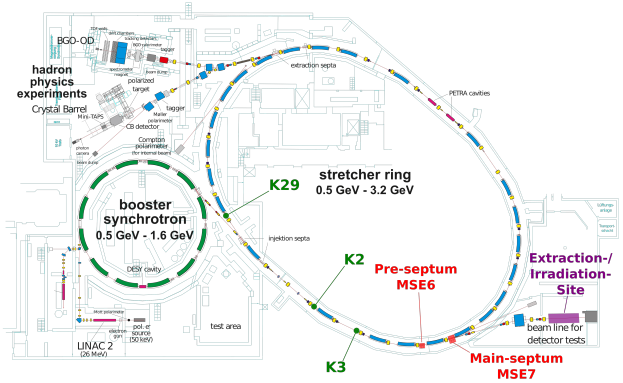

Figure 1: Accelerator facility ELSA with the marked locations of the injection kickers in green, pre- and main-septum in red and the FLASH experimental site in purple.

Irradiation Site

The electron pulses pass several detectors (Fig. 2) before reaching a water phantom for irradiation. After exiting the beam pipe through a thin kapton foil, the pulse charge is measured by an integrating current transformer (ICT). Afterwards the transverse beam profile and position is measured with a luminesce screen (Chromox). The image is analyzed by an in-house developed image analysis software package [3]. Samples and detectors are irradiated within a water phantom, simulating the interaction with the human body. To quantify the applied dose for irradiation studies, radiochromic films (GafChromic™-EBT3) are placed inside the water phantom. Overall, the setup provides comprehensive shot-by-shot information on the beam profile, position and dose distribution. This enables controlled irradiation with knowledge of the applied dose, independent of varying beam positions and profiles.

Content from this work may be used under the terms of the CC BY 4.0 licence (© 2026). Any distribution of this work must maintain attribution to the author(s), title of the work, publisher, and DOI.

ISBN: 978-3-95450-252-3 ISSN: 2673-5350 doi: 10.18429/JACoW-IPAC2026-TUP8013

EVALUATION OF CLOSED ORBIT CORRECTION METHODS FOR THE HELIUM LIGHT ION COMPACT SYNCHROTRON HELICS

H. Huttunen*[1], F. Asvesta, European Organization for Nuclear Research, Geneva, Switzerland
E. Benedetto, Tera-Care, Geneva, Switzerland
[1] also at University of Helsinki, Helsinki, Finland

Content from this work may be used under the terms of the CC BY 4.0 licence (© 2026). Any distribution of this work must maintain attribution to the author(s), title of the work, publisher, and DOI.

Abstract

Within the framework of the Next Ion Medical Machine Study (NIMMS) collaboration at CERN, closed orbit correction schemes are developed for the Helium Light Ion Compact Synchrotron (HeLICS) - a novel synchrotron design in development for cancer treatment. Different options for closed orbit correction are presented, including the possibility of applying beam-based quadrupole alignment without dedicated corrector magnets. The limitations and advantages of the different closed orbit correction methods are evaluated against each other in order to determine the best scheme for HeLICS.

INTRODUCTION

HeLICS is a compact synchrotron currently under design within the NIMMS collaboration — an initiative focused on developing next-generation accelerator technologies for ion therapy with reduced size and cost [1–4]. Its compact design imposes tight constraints on the lattice layout and available space for beam instrumentation [5, 6].

Closed-orbit distortions arising from magnet misalignments can significantly increase the transverse excursion of the beam trajectory, particularly at low injection energies where the beam size is inherently larger. To evaluate the operational robustness of HeLICS under realistic conditions, it is essential to evaluate both the impact of such misalignments on the closed orbit and the effectiveness of available correction strategies. Here, corrector-based schemes are investigated, considering various configurations in terms of the number and placement of correctors. Subsequently, orbit correction using beam-based quadrupole alignment is examined as a more space-efficient alternative to conventional corrector magnets.

HELICS SYNCHROTRON

The triangular HeLICS lattice, with a circumference of 35 m, consists of three 120° bending sections with normal-conducting 60° dipole magnets connected by longer dispersion free straight sections accommodating quadrupoles for tune control, injection and extraction septa, an RF cavity and beam instrumentation [5]. Due to space constraints, the plan for HeLICS is to place Beam Position Monitors (BPMs) inside some of the quadrupoles in the lattice, while orbit corrector magnets would be integrated into the sextupoles [6].

HeLICS employs three sextupoles for chromaticity control, each positioned in one of the bending sections. On top of these sextupoles, at least one additional sextupole is required for slow extraction. The potential locations for the additional sextupoles were determined based on the available space in the ring, taking into account which sextupole combinations are capable of producing the desired resonance excitation for slow extraction [7]. Due to space constraints of the lattice and the flexibility required for operation, a single extraction sextupole cannot be positioned at a favorable phase advance relative to the electrostatic septum for the formation of this excitation. Instead, a virtual sextupole with a specific strength and phase advance is required. The functional sextupole combinations are identified based on their relative phase advance. Following this, the sextupole strengths are determined by first generating a transfer matrix with MADX, and then performing a least-squares optimisation in Python to obtain the required strengths, similar to the approach described in [8]. Finally, the results are verified using MADX.

Three sextupole schemes are identified. Scheme A introduces two dedicated extraction sextupoles in the dispersion-free straight sections. Scheme B also employs two dedicated extraction sextupoles, but places one in a dispersive bending section, thereby affecting the chromaticity unfavorably. Scheme C uses one additional sextupole in a dispersion-free straight section in combination with the three chromaticity sextupoles to provide both chromaticity correction and the desired resonance excitation. These preliminary sextupole schemes set the basis for the potential locations of the orbit corrector magnets, but still require final confirmation from slow extraction studies.

CORRECTOR BASED ORBIT CORRECTION SCHEMES

The primary operational limit caused by alignment errors arises from perturbations on the beam dynamics such as closed orbit distortions [9]. In HeLICS, the tolerances for closed orbit distortions have been determined as $CO_x = \pm 10$ mm in the horizontal plane and $CO_y = \pm 7.5$ mm in the vertical plane [6]. The misalignments are evaluated at the injection working point $(Q_x, Q_y) = (2.4, 1.15)$, where the aperture is most critical due to the low beam energy.

Previous studies have shown that the vertical plane requires orbit correction, while the horizontal plane remains relatively robust due to the choice of the working point [6]. This is attributed to the choice of the working point: the

* heli.huttunen@cern.ch

ISBN: 978-3-95450-252-3 ISSN: 2673-5350 doi: 10.18429/JACoW-IPAC2026-TUP8014

ATSOA AT CERN: A HANDS ON ACCELERATOR COURSE IN THE EURO-LABS FRAMEWORK*

F. Asvesta†, T. Argyropoulos, R. Corsini, I. Efthymiopoulos, W. Farabolini, D. Gamba, M. J. G. Borge, M. Jebramcik, P. Korysko, M. Lozano, A. Malyzhenkov[1], L. Ponce, T. Prebibaj, A. Rodriguez Rodriguez, M. Slupecki[2], CERN, Geneva, Switzerland
[1]also at Swiss International Institute Lausanne, Prilly, Switzerland
[2]also at Department of Communications and Computer Engineering, University of Malta, Msida MSD, Malta

Abstract

Beyond providing Transnational Access to major Research Infrastructures (RIs) across Europe, the European Laboratories for Accelerator Sciences (EURO-LABS) programme supports advanced training activities. Within this framework, an Advanced Training School on the Operation of Accelerators (ATSOA) is organised at CERN. The school targets students, young researchers, and professionals in the field of accelerator science, offering them a unique opportunity to participate in a week of hands-on training. Five CERN facilities — CLEAR, AD/ELENA, ISOLDE, PSB and LEIR — are involved in the training, allowing participants to familiarise themselves with different accelerator types and particle species. Under the guidance of experienced instructors, they carry out dedicated experiments designed to illustrate key physics concepts and operational principles that can be applied in their own work. This contribution gives an overview of the past schools and an outlook for future courses.

INTRODUCTION

The European Laboratories for Accelerator Sciences (EURO-LABS) is a network of 33 research and academic institutions across 18 countries, bringing together the communities of nuclear physics, accelerator science, and detector technology for high-energy physics under a single collaborative framework [1]. One of the key pillars of the EURO-LABS mission, beyond providing "Transnational Access to Research Infrastructures", is the support of advanced training activities for the next generation of accelerator scientists.

Within this framework, the Advanced Training School on the Operation of Accelerators (ATSOA) was established and has been held annually at CERN since 2024. The school targets students, early-career researchers, and young professionals in accelerator science, offering a unique week of immersive, hands-on training in a world-class research environment. Selected participants have their travel, accommodation, and subsistence costs fully covered by EURO-LABS.

The first edition, ATSOA 2024 (Fig. 1, left), took place at CERN in June 2024 [2]. Eighteen selected trainees participated in measurement campaigns at three CERN facilities: the Proton Synchrotron Booster (PSB) [3], the Isotope Separator OnLine DEtector (ISOLDE) [4], and the CERN Linear Electron Accelerator for Research (CLEAR) [5]. Topics included accelerator complex operation, control systems, beam characterisation, superconducting cavity phasing, and steering algorithms.

Building on this success, ATSOA 2025 (Fig. 1, middle), was held at CERN in May 2025 [6], expanding the participating facilities to include the Antiproton Decelerator/Extra Low ENergy Antiproton (AD/ELENA) complex [7]. This enabled additional advanced topics such as electron cooling, as well as increasing the number of participants to 22. The programme was further refined based on feedback from the first editions, with an increased hands-on component.

The third edition, ATSOA 2026 (Fig. 1, right), took place at CERN in April 2026 [8]. Due to ongoing upgrades of ISOLDE aimed at improving future operation [9], it was replaced by the Low Energy Ion Ring (LEIR) [10], allowing participants to work with a accelerator Pb ions.

In all editions, the school typically hosted 18–22 participants per year, with approximately four participants per facility, a limitation driven by the available control room space and the hands-on nature of the training. A summary of the demographics of the participant, including age and gender distribution as well as educational background and nationality, is provided in Fig. 2. During the three editions, a steady increase in interest has been observed, reflected both in the growing number of applications and in the overall quality of applicants. This trend highlights the strong demand for hands-on accelerator training within the community, the unique attractiveness of CERN facilities, and further supports the objectives of the EURO-LABS programme in fostering practical, facility-based education.

In the following sections, an overview of the three schools held to date is provided, focusing on the training format and key content highlights. Future prospects for the school are briefly addressed in the final section.

ATSOA SCIENTIFIC PROGRAMME

The ATSOA scientific programme is structured around a combination of common introductory courses and dedicated hands-on training sessions. At the opening of each edition, participants receive an introduction to the CERN

* EURO-LABS has received funding under the EU Horizon Europe Research & Innovation program, Grant Agreement 101057511
† foteini.asvesta@cern.ch

Content from this work may be used under the terms of the CC BY 4.0 licence (© 2026). Any distribution of this work must maintain attribution to the author(s), title of the work, publisher, and DOI.

ISBN: 978-3-95450-252-3 ISSN: 2673-5350 doi: 10.18429/JACoW-IPAC2026-TUP8016

DEVELOPMENT OF VHEE SCATTERING SYSTEMS FOR FLASH RADIOTHERAPY

S. Wang*[1,2], R. Corsini[1], W. Farabolini[1], A. Gilardi[1], A. Latina[1], C. Robertson[3,4], M. Dosanjh[2]
[1]CERN, Geneva, Switzerland
[2]John Adams Institute, University of Oxford, Oxford, UK
[3]Newcastle upon Tyne Hospitals NHS Foundation Trust, Newcastle upon Tyne, UK
[4]Newcastle University, Newcastle upon Tyne, UK

Content from this work may be used under the terms of the CC BY 4.0 licence (© 2026). Any distribution of this work must maintain attribution to the author(s), title of the work, publisher, and DOI.

Abstract

Very High Energy Electrons (VHEE) are an emerging modality for FLASH radiotherapy, offering deep penetration and magnetic beam control in potentially compact systems. However, achieving transversely uniform dose distributions at ultra-high dose rates remains challenging, as current magnet technology cannot provide sufficiently fast beam scanning. Conventional dual-scattering systems can produce uniform beams but introduce significant bremsstrahlung photon contamination in the VHEE regime, requiring impractically long beamlines to mitigate.

This work investigates replacing the first scatterer with a quadrupole lattice to magnetically enlarge the beam prior to flattening. Simulations using RF-Track and TOPAS show that the optimised quadrupole–scatterer system achieves a uniform beam with uniform radius ≈ 75 mm while reducing photon contamination by 94.5% compared to the conventional approach. These results demonstrate that magnetic beam expansion in addition to a Gaussian scattering foil is a promising solution for FLASH-compatible VHEE delivery, improving dose uniformity while minimising secondary particle production.

INTRODUCTION

Radiotherapy (RT) would benefit approximately half of cancer-patients in approximately half of cancer treatments [1]. While photon therapy dominates clinical practice, its depth-dose profile leads to unavoidable irradiation of healthy tissue [2]. In contrast, hadron therapy provides superior dose conformality through the Bragg peak, but requires large and costly accelerator systems [3].

Very High Energy Electrons (VHEE, 50 MeV to 250 MeV) offer a potential alternative, combining deep penetration with magnetic steerability in more compact systems [4]. VHEE beams are promising for FLASH radiotherapy, where ultra-high dose rates (UHDR) ($\gtrsim 40\,\mathrm{Gy/s}$) reduce normal tissue toxicity while maintaining tumour control [5, 6]. The potential benefits of the FLASH effect could simplify radiotherapy by reducing the need for complex gantry systems and multi-angle irradiation.

In VHEE therapy, achieving transversely uniform dose distributions at these dose rates remains a key challenge. Conventional pencil beam scanning [3] is impractical at UHDR due to limitations in magnet speed [7], motivating alternative beam-shaping approaches.

In the previously studied solution by Robertson *et al*, with dual-scattering system, a first scatterer (S1) broadens the beam and a second, shaped scatterer (S2) flattens the transverse profile by preferentially scattering the central component of the beam with higher intensity [8]. This is the clinical method currently used for low-energy electrons [9]. While effective at producing uniform beams, this approach introduces significant bremsstrahlung photon contamination in the VHEE regime. Reducing this contamination requires increased drift space, leading to beamline lengths incompatible with clinical constraints [10].

To address these limitations, this work investigates replacing the first scatterer with magnetic beam expansion using a quadrupole lattice. By magnifying the beam prior to flattening, the total mass thickness of scattering material can be reduced, thereby minimising secondary photon production while maintaining dose uniformity. The proposed quadrupole–scatterer system is studied using RF-Track and TOPAS simulations, and its performance is compared with a conventional dual-scattering configuration. This paper also touches upon the optimisation of the quadrupole settings to improve the efficiency of the CLEAR dual-scattering foil.

THEORY

Scattering Effects

The Gaussian approximation to Moliere's fundamental theory of multiple Coulomb scattering describes the scattering effect of charged particles in matter [11]. In the VHEE regime, the electrons interact with the scatterers and produce photons mainly from bremsstrahlung [12]. These photons may constitute a large proportion to the measured dose downstream, and do not necessarily have a transversely uniform dose distribution even if the electron beam is flattened; this is due to the differences in scattering mechanisms.

Beam Conformality

Super-Gaussian Fit A super-Gaussian fit is used to parameterise the flattened transverse beam profiles:

$$f(x) = A \exp\left[-\left(\frac{(x-\mu)^2}{2\sigma^2}\right)^P\right], \quad (1)$$

where A is the amplitude, μ the mean of the particle distribution in x, and σ the standard deviation. The parameter

* sabrina.wang@cern.ch

ISBN: 978-3-95450-252-3 ISSN: 2673-5350 doi: 10.18429/JACoW-IPAC2026-TUP8018

A STATUS UPDATE OF LHARA, AN ACCELERATOR-DRIVEN RADIOBIOLOGY RESEARCH INITIATIVE

W. Shields*[1], M. Pereira[1], Royal Holloway University of London, UK
N. Dover, C. Dyson, T.-J. Kuo, K. Long, J. Pasternak, Imperial College London, UK
W. Bertsche[2], University of Manchester, UK
C. Whyte[2], R. Wilson[2], University of Strathclyde, UK
M. Charlton, S. Eriksson, C. A. Isaac, P. Ruksaskchai, D. P. van der Werf, Swansea University, UK
H. Owen[2], UKRI-STFC Daresbury Laboratory, UK
[1]also at John Adams Institute, UK
[2]also at Cockcroft Institute, UK

Abstract

LhARA is a multidisciplinary collaboration that aims to use laser-driven ions, in a hybrid acceleration scheme with a fixed-field alternating-gradient (FFA) accelerator, to deliver a systematic radiation biology programme and help lay the technological foundations for the transformation of proton and ion beam therapy. LhARA is in an R&D phase developing a number of accelerator technologies, and is conducting experiments through the Proof-of-Principle for LhARA and Radiobiology (PoPLaR) programme to examine the effect of laser-driven ions on biological tissue samples. Here, we present a summary of the most recent updates from the LhARA collaboration, including Gabor plasma lenses for beam capture and focusing, magnetic beam delivery schemes for variably-sized, transversely uniform beam profiles, the FFA in LhARA's second stage to reach clinically relevant ion energies, and an overview of the PoPLaR experiment.

THE LHARA/ITRF CONCEPTUAL DESIGN REPORT

LhARA is a proposed facility to deliver protons and ions to enable future ultra-high dose rate particle radiotherapy (including FLASH dose rates above 40 Gy/s and novel spatial fractionation beam delivery) through generation of ultra-short plasma-accelerated ions. This facility is part of the LhARA collaboration's efforts to contribute novel technologies to the future of cancer therapy.

In LhARA, a lower-energy 10/100 Hz source based on target-normal sheath acceleration (TNSA) that produces protons nominally at 15 MeV will be coupled to an FFA (fixed-field alternating-gradient) accelerator that retains the short bunch time structures (10s of ns) up to a maximum proton energy of 127 MeV. A primary application is as part of a UK Ion Therapy Research Facility (ITRF) to conduct radiobiological research. A recently-completed Conceptual Design Report [1] augments previous developments, and a proof-of-principle beamline (PoPLAR) has been constructed and commissioned at the University of Strathclyde's SCAPA plasma-acceleration facility, with first radiobiological irradiations underway.

PHASE 1 DEVELOPMENT

Recently, improvements have been made to the SCAPA 350 TW laser platform that is being used as the LhARA testbed. Pre-pulses have been removed, resulting in improved proton energy and flux, giving reliable 1 Hz production of > 15 MeV protons (> 10^9 at 10 MeV), calibrated via radiochromic film (RCF).

Particle Tracking

The LhARA TNSA source inherently produces a broad exponential-like proton fluence spectrum with a cutoff; we have chosen to select a band somewhat below the cutoff, nominally at 15 MeV ±2%. Selection is achieved via the strong chromatic effect of beam focusing with the Gabor lens lattice [2] and a series of round collimators; tracking of a simulated TNSA source spectrum from 1 to 27 MeV [3] through this lattice is essential to assess energy selection and beam losses. Three energy bands are simultaneously focused at the first collimator (7 m from the source, see Fig. 1) corresponding to the first three Gabor lenses. To avoid these three energy bands being further transmitted, we are considering the use of a tapered collimator since each band has a different transverse extent.

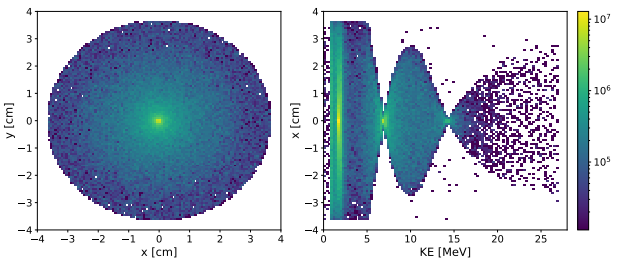

Figure 1: Beam distributions at the energy selection collimator for a 1–27 MeV TNSA spectrum of 10^9 protons. Left: transverse (X–Y) distribution. Right: X–kinetic energy phase space. Three chromatic focal bands are visible, arising from successive Gabor lenses, with symmetry reflecting the cylindrical focusing of the system.

* william.shields@rhul.ac.uk

Content from this work may be used under the terms of the CC BY 4.0 licence (© 2026). Any distribution of this work must maintain attribution to the author(s), title of the work, publisher, and DOI.

ISBN: 978-3-95450-252-3 ISSN: 2673-5350 doi: 10.18429/JACoW-IPAC2026-TUP8027

ESTIMATION OF RADIATION FIELD FOR BDF/SHIP AT CERN

D. O. Wasik*, C. Ahdida, R. Cala', J. A. Coleman-Smith, L. S. Esposito, M. Ferro-Luzzi, M. Fraser, R. Franqueira Ximenes, G. Frisella, J.-L. Grenard, G. Humphreys, R. Jacobsson, G. Lerner, M. Parkin, O. Pinto, P. Santos Diaz, CERN, Geneva, Switzerland

Content from this work may be used under the terms of the CC BY 4.0 licence (© 2026). Any distribution of this work must maintain attribution to the author(s), title of the work, publisher, and DOI.

Abstract

The Beam Dump Facility (BDF) will host the Search for Hidden Particles (SHiP) experiment at CERN's Super Proton Synchrotron. BDF/SHiP is designed to search for feebly interacting particles in a region of mass and coupling accessible only with a dedicated beam-dump configuration. With a beam intensity of 4×10^{19} protons on target (POT) per year at 400 GeV/c, the High-Intensity ECN3 (HI-ECN3) Project will enable this search, while the radiation field is envisaged to be used for parasitic programmes in nuclear astrophysics, materials science, and radiation-to-electronics research. High-momentum protons impinging on a tungsten target generate an intense radiation field, leading to, among other features, cumulative and single-event effects to nearby equipment. In this work, the radiation environment and its impact on electronics of the detectors and associated infrastructure were evaluated through simulations performed with FLUKA Monte Carlo code. The results show that proposed optimisation solutions for shielding reduce radiation levels, keeping most effects within acceptable limits. It is also observed that modifications made to the magnetic field and geometry of the muon shield, which controls the deflection of muons produced in the beam dump to reduce flux reaching the detector, influence muon and neutrino backgrounds.

INTRODUCTION

The Search for Hidden Particles (SHiP) experiment, dedicated to exploring physics beyond the Standard Model, will be hosted by the Beam Dump Facility (BDF) at CERN's Super Proton Synchrotron [1, 2]. The High-Intensity ECN3 (HI-ECN3) Project [3] will operate under the beam conditions summarised in Table 1 (in which POT stands for protons on target), establishing one of the most intense proton-driven beam-dump environments at CERN. The tungsten target is optimized to enhance interactions of beam protons, while promoting the re-absorption of pions and kaons and thereby minimizing the resulting muon and neutrino backgrounds [1].

The simulation study of the radiation environment at BDF/SHiP and its implications for electronics reliability was performed using the FLUKA Monte Carlo code [4–6]. Results from the previous BDF/SHiP design study [7] indicated that the recommended radiation to electronics (R2E) limits could be exceeded in several locations within the ECN3 cavern, mainly in the compressors and superconducting magnet (SM) cryocoolers areas, see Figure 1. In particular, the thermal neutron equivalent fluence was found to exceed recommended thresholds in all assessed locations, highlighting the need for dedicated neutron shielding using borated shielding materials [8]. The updated BDF/SHiP model, shown in Figure 1, features several design elements aimed at reducing radiation exposure in critical areas and improving the confinement of secondary particles: (1) a new muon shield (MS) design, featuring a geometry with twice the volume, and an updated magnetic field map; (2) the addition of 5 cm of 30% borated polyethylene into the confinement walls around the target complex composed of 2 cm of steel, covering the entire TCC8 cross-section; (3) the addition of concrete shielding around Magnetized Hadron Stopper (MHS); (4) a target diameter of 25 cm. In addition, the effect of a vacuum window located approximately 10 m upstream of the target, as well that of an optional mask installed in the beam pipe upstream of the target, is assessed. The implications of these changes are evaluated in terms of their impact on particle transport downstream of the shielding structures and background to the experiment.

Table 1: Beam Parameters for the BDF/SHiP [1]

Parameter	Value	Unit
Proton momentum	400	GeV/c
Nominal beam intensity	4×10^{13}	POT/spill
Integrated extracted intensity	4×10^{19}	POT/year
Total cycle length	7.2	s
Spill duration	1.0	s
Circular dilution radius	50	mm
Beam sigma (H,V)	16, 16	mm

RADIATION TO ELECTRONICS

Protons with a momentum of 400 GeV/c impinging on a 150 cm-long tungsten target generate a strong radiation field. This leads to cumulative effects, i.e. deterministic damage caused by ionising dose and displacement damage, quantified in this study by the total ionising dose (TID) and the silicon 1-MeV neutron equivalent fluence (Si1MeVNE). It also induces Single Event Effects (SEE), i.e. stochastic effects that may be destructive or non-destructive, characterised by the high energy hadron equivalent fluence (HEHeq) and the thermal neutron equivalent fluence (ThNeq) [9, 10]. The objective of this study was to assess the risk that the installation of BDF/SHiP in TCC8 and ECN3 may require, either: (i) placing non-radiation tolerant commercial electronics in designated R2E-safe areas; or (ii) using radiation-tolerant equipment. To this end, the quantities reported in Table 2 are used to define the general requirements for classifying a given zone as an R2E-safe area.

* dominika.oliwia.wasik@cern.ch

ISBN: 978-3-95450-252-3 ISSN: 2673-5350 doi: 10.18429/JACoW-IPAC2026-TUP8029

THE TIARA COLLABORATION: SHAPING TWO DECADES OF EU SUPPORT FOR COORDINATED ACCELERATOR R&D

J.M. Perez[1, †], A. Lucotte[2], T. Torims[3], M. Vretenar[3]
[1, †] CIEMAT, Dept of Technology, Madrid, Spain
[2] IN2P3 (CNRS) Accélérateurs, Détecteurs & Technologie, Paris, France
[3] European Organization for Nuclear Research (CERN), Geneva, Switzerland

Content from this work may be used under the terms of the CC BY 4.0 licence (© 2026). Any distribution of this work must maintain attribution to the author(s), title of the work, publisher, and DOI.

Abstract

European accelerator research involves over 150 institutions –research and technology infrastructures, universities and industry– making impactful R&D reliant on large, well-structured collaborations among all innovation actors. The European Commission's framework programmes can play a strategic role in enabling these collaborations, but their effectiveness requires a coherent organization at the community level.

Founded in 2002 as ESGARD, the TIARA – Test Infrastructure and Accelerator Research Area – collaboration was established to foster and coordinate participation in European Commission calls. To date, TIARA has supported over 25 projects, ranging from design studies for new infrastructures to ESFRI-linked initiatives, securing €180 million in EC funding over 21 years, supplemented by over €245 million in contributions from partners.

INTRODUCTION

Particle accelerators are central to Europe's scientific and industrial leadership, but their full potential depends on a cohesive, strategic approach to technology development. TIARA plays a pivotal role by orchestrating collaboration among Europe's accelerator communities, ensuring advancements are both cutting-edge and aligned with shared priorities. Its mission is twofold: to unite stakeholders, research institutions, and industry, and to streamline responses to European calls, thereby reinforcing Europe's sovereignty in this critical domain. In an era where technological autonomy and collective excellence are paramount, TIARA is crucial to maintaining Europe's competitive edge in accelerator science.

THE TIARA CONSORTIUM

ESGARD

The seed for TIARA was the European Steering Group for Accelerator R&D (ESGARD), established in 2002 by R. Aleksan of CEA, following a recommendation by ECFA, to improve education in accelerator science and to increase support for coordinated accelerator R&D activities in Europe. Its immediate goal was the preparation of a coherent set of proposals European Commission funding within its 6th Framework Programme for research and innovation. This effort led to the highly successful CARE (Coordinated Accelerator Research in Europe) Integrating Activity, approved in 2003, which implemented a strong accelerator R&D programme from 2004 to 2009.

The TIARA-PP Project

The success of CARE and the need for a more structured framework for accelerator R&D in Europe with EC support led to the launch in 2011 of the TIARA Preparatory Phase. This was an EU project dedicated to the definition and preparation of a permanent coordinated European framework for coordination of accelerator R&D initiatives, benefiting scientific fields reliant on advanced accelerators or related technologies. Its purpose was to foster joint projects, share expertise in cutting-edge accelerator technologies, and ensure pan-European coordination to secure Europe's leadership in accelerator science while promoting balanced scientific and technological progress.

The project's ultimate goal of integrating national and international accelerator R&D infrastructures into a single distributed European facility proved overly ambitious, but TIARA-PP succeeded in delivering high-level analyses, including: establishing an advisory mechanism and organizational framework for accelerator technology developers, identifying potential collaborators, surveying Europe's infrastructure needs, developing funding models, formulating recommendations to advance accelerator science and technology, estimating operational and investment costs, and defining Key Accelerator Research Areas along with their critical requirements. TIARA-PP hence delivered one of Europe's most comprehensive analyses of accelerator R&D infrastructures and technologies.

The TIARA Implementation

In TIARA-PP, the optimal collaboration structure for sustainability was explored, leading to the proposal of a consortium based on a Memorandum of Understanding (MoU). The TIARA Collaboration Consortium was officially established in June 2015 following the MoU's signature. The MoU aimed to create a Consortium of European Research Institutions managing major R&D infrastructures in the European Particle Accelerator Research Area. Its purpose was to foster expertise exchange and support joint R&D programs, as well as education and training in Accelerator Science and Technology across Europe.

Since 2015, TIARA has operated with its Collaboration Council convening three times annually. Over time, the consortium's objectives have adapted to the evolving needs of research and technological infrastructures. Its primary focus has been to ensure a coherent and relevant community response to EU calls for various work programs by supporting and advising proposals. TIARA has also served as the unified voice of the accelerator developer

ISBN: 978-3-95450-252-3 ISSN: 2673-5350 doi: 10.18429/JACoW-IPAC2026-TUP8031

JOINT DEVELOPMENT OF SUPERFERRIC CORRECTOR MAGNETS FOR HL-LHC

G. Vandoni†, A. Musso, E. Todesco, CERN, Geneva, Switzerland
F. Gangini, P. Manini, SAES Group, Lainate, Italy
M. Sorbi, M. Statera, Laboratory of Acceleration and Applied Superconductivity, National Institute for Nuclear Physics (INFN), Milano, Italy

Abstract

The HL-LHC project is a major upgrade of CERN's LHC, aiming to enhance the collider's integrated luminosity by a factor of ten within ten operational years. Endorsed as top priority for the European Strategy for Particle Physics in 2013, the project was formally approved by CERN's Council in 2016. To achieve its performance goal, HL-LHC relies on several technology drivers. Among the new magnets for the interaction regions, the superferric – named so, because they combine superconducting NbTi coils with iron pole pieces to enhance the magnetic field near the aperture – high-order mode correctors are key in ensuring beam quality and stability, correcting field errors and compensating non-linearities in the magnet lattice. These magnets were the object of a collaboration between CERN and INFN-LASA Milan, first joint project to deliver its full scope to HL-LHC. INFN-LASA was tasked with design, prototyping, and industrialization. Key to the delivery of 54 correctors by 2023 was the early initiation via the INFN MAGIX project, followed by two agreements for prototyping and series production. The collaboration spanned over a decade and benefited from the early involvement of the industrial partner SAES-RIAL. The paper reviews the collaboration, detailing cost structure, schedule adherence, and industrialization process. Focus is on key factors that contributed to the success of the collaboration and lessons applicable to large-scale partnerships for future accelerator projects.

INTRODUCTION

The High-Luminosity LHC project (HL-LHC) aims to increase the collider's integrated luminosity by a factor of ten beyond its original design, in 10 years of operation. The project was endorsed as top-priority at the 2013 update of the ESPP, paving the way for the project's TDR approval by CERN's Council in June 2016. The upgraded LHC was initially scheduled to deliver first beams around 2026, after a 2-year installation shutdown.

A defining feature of the HL-LHC project is its collaborative model: about 10% of the project's core value is delivered through in-kind contributions. These collaborations are essential not only for CERN budget, infrastructure and expertise leverage, but also to enlarge the know-how and production and testing capabilities in the accelerators community and the industrial partners. To avoid disparity in the Member's States contributions, the deliverables from institutes amongst CERN Member States are co-financed by CERN to 50%.

To achieve its performance goals, the HL-LHC relies on several accelerator technology drivers, including superconducting magnets in Nb_3Sn, superconducting crab cavities, high-current power transmission link based on MgB_2 and low-impedance collimators. Among the new magnets for the interaction regions, the superferric multi-pole corrector magnets ensure beam quality and stability, correcting field errors and compensating non-linearities in the magnet lattice. These superconducting magnets are called superferric, because they combine superconducting NbTi coils with iron pole pieces, enhancing the magnetic field near the aperture. Together with one nested orbit corrector, the multi-pole correctors are integrated in the so-called Corrector Package cryoassembly.

The superferric high-order mode correctors (quadrupole to dodecapole, see Fig. 1) for the HL-LHC work-package WP3 were the object of a collaboration between CERN and INFN-LASA Milan, Italy, the first collaborative sub-project to deliver its full scope to HL-LHC. This partnership, seeded by the INFN MAGIX project and formalized in the KE2291 (for prototypes) and KE3085 (for the series magnets) agreements, spanned over eight years and involved R&D, prototyping and series production, together with the industrial partner SAES-RIAL. The delivery of 54 corrector magnets was completed in November 2021 and fully validated at CERN in 2022.

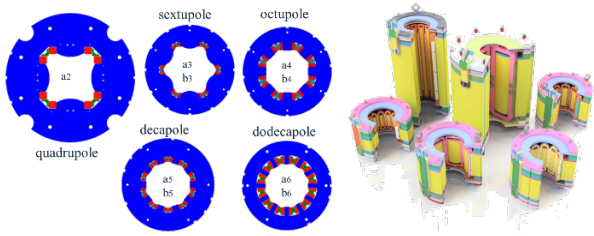

Figure 1: The high order correctors of HL-LHC.

This paper reviews the CERN-INFN collaboration, focusing on the industrialization process, cost structure, schedule adherence. It aims to identify the key factors that contributed to the success of the project and to extract lessons applicable to future large-scale scientific collaborations.

PRECURSORS

In the framework of FP7, grant agreement 284404, the EU commission financed 4.9 M€ of the 21 M€ of the Design study for HL-LHC from 2011 to 2016, when the

†giovanna.vandoni@cern.ch

Content from this work may be used under the terms of the CC BY 4.0 licence (© 2026). Any distribution of this work must maintain attribution to the author(s), title of the work, publisher, and DOI.

ISBN: 978-3-95450-252-3 ISSN: 2673-5350 doi: 10.18429/JACoW-IPAC2026-TUP8032

TOWARDS A COMMUNITY OF PRACTICE IN PROJECT MANAGEMENT OF PARTICLE ACCELERATOR AND BIG-SCIENCE PROJECTS: THE ACCELERTATEPM INITIATIVE

G. Vandoni, M. Battistin, CERN, Geneva, Switzerland
A. Kimber, ESS, Lund, Sweden
E. Rosi, N. Winters, GSI Helmholtz Centre for Heavy Ion Research, Darmstadt, Germany
E. Barbero Soto, Fusion for Energy, Barcelona, Spain
A. Variola, INFN, Rome, Italy
S. Klumpp, DESY, Hamburg, Germany

Abstract

Across Europe, several large-scale particle accelerator and big-science projects — each exceeding hundreds of millions of euros and extending over a decade — are under design or construction, with comparable initiatives underway in the US and China. Despite remarkable scientific achievements, many of them face cost and schedule drift, even when scientific performance targets haven't been scaled down to maintain cost and timeline. Managing these complex, R&D-driven scientific facility projects require approaches distinct from even the largest conventional infrastructure undertakings. Recognizing this need, a group of project management (PM) professionals active in particle accelerator initiatives has launched AcceleratePM, the first international workshop dedicated to PM for accelerator and big-science projects. The first workshop, held at CERN in January 2026, gathered all major laboratories and projects to exchange methods, identify common challenges, and define best practices. This contribution presents the workshop scheme, themes, key-findings and outcomes, showcasing the largest recent projects – amongst which HL-LHC, ESS, FAIR, F4E – and aiming at informing the management of next-generation initiatives such as the Future Circular Collider (FCC). By building on common issues and most effective solutions, AcceleratePM intends to establish a lasting community of practice, shaping how large scientific projects are conceived, planned, and delivered.

INTRODUCTION

Several large-scale scientific projects around the world are currently in preparation, underway, or recently completed. Despite their diversity, they share key features: ambitious scientific goals with never reached performance, interlinked international scientific collaborations with in-kind contributions and personnel exchange, long-term anticipatory R&D programs, and the adoption of cutting edge, innovative technologies.

Project management for these first-of-a-kind, highly R&D-intensive initiatives in scinetific setting cannot follow the same approaches used for conventional infrastructure projects [1]. The AcceleratePM network was founded to create a community of practice in project management (PM) for big science projects. This paper summarizes the outcomes of the first AcceleratePM workshop, held at CERN from 26 to 28 January 2026 [2]. The event gathered more than 100 project managers and scientists representing major international projects – including CERN, FAIR, ESS, EuPRAXIA, the Einstein Telescope, EuXFEL, ITER, and the EIC – from over 20 laboratories and institutions worldwide. The program, constructed following a project's lifecycle, from initiation, through execution and monitoring, to closing, featured 25 presentations and 15 posters, and was interleaved with Q&A sessions and visits to CERN test facilities. Table 1 shows the 2026 consolidated budget of some large projects and time from groundbreaking to first beam.

Table 1: Large Projects Comparative Table

Project	Budget	Timeline
ITER	20 B€	14 yrs
FCC	15 B€	15 yrs
FAIR	3.3 B€	15 yrs
EIC	< 2.8 B$	12 yrs
HLLHC	1.2 B€	14 yrs
ESS	2.4 B€	11 yrs
EuXFEL	1.2 B€	10 yrs
ET	~2.3 B€	7 yrs

A WALK THROUGH THE CONFERENCE

Figure 1 shows a group picture of the participants to the workshop. The EIC at BNL advances through DoE critical decision gates each defining requirements, cost ranges, and performance baselines. To align with annual funding release and enable early physics delivery, the project is split into five independently baselined subprojects. A central integration office ensures overall coherence. CERN has completed the FCC-ee feasibility study amid mixed stakeholder support, aiming for project approval in 2028 for first collisions in 2048. The study provides cost estimates using standardized uncertainty classes and challenges bottom-up estimates with parametric models. Long term technical expertise must be secured along the 14 years of construction. A central Project Office will oversee cost, risk, and procurement across the over 100 contributors. The project's

Content from this work may be used under the terms of the CC BY 4.0 licence (© 2026). Any distribution of this work must maintain attribution to the author(s), title of the work, publisher, and DOI.

ISBN: 978-3-95450-252-3 ISSN: 2673-5350 doi: 10.18429/JACoW-IPAC2026-TUP8033

FAIR PROJECT MANAGEMENT

E. Rosi[1, 2], N. Winters[1, 2]
[1] GSI Helmholtz Centre for Heavy Ion Research, Darmstadt, Germany
[2] Facility for Antiproton and Ion Research in Europe, Darmstadt, Germany

Abstract

The Facility for Antiproton and Ion Research (FAIR), currently under construction in Darmstadt, Germany, is among the most complex international research infrastructure projects currently being realized in Europe. The project combines large-scale civil construction, accelerator systems, scientific installations, and a broad range of international in-kind contributions within one highly interconnected project environment.

The experience gained during the FAIR project has shown that technical expertise alone is not sufficient to manage projects of this scale and complexity. Increasing interdependencies between construction, procurement, installation, commissioning, financing, and international collaboration required the establishment of highly integrated project management structures.

Over the course of the project, the FAIR Project Management Office (PMO) evolved from a mainly reporting-oriented organization into a central coordination and integration structure. Planning, risk and cost management, procurement and in-kind coordination, quality assurance, and configuration management were gradually connected within one integrated management framework.

Particular attention is given to the combination of technical planning, forecasting, and risk assessment methods. Schedule progress, delivery status, technical maturity, resource availability, and risk developments are continuously evaluated together in order to support management decisions and identify critical developments at an early stage.

This paper presents the FAIR project management approach and describes the role of the PMO in coordinating multidisciplinary activities across the FAIR and GSI campus environment.

INTRODUCTION:

International research infrastructure projects differ in many ways from conventional industrial or construction projects. This is especially true for FAIR [1][2], where highly complex technical systems, international supply chains, numerous in-kind contributions, and parallel construction, installation, and commissioning activities must be coordinated within one common project environment [3].

Even small delays in individual systems can directly affect infrastructure availability, installation sequences, or downstream commissioning activities. At the same time, technical conditions, delivery schedules, and project priorities continuously evolve throughout the project lifecycle.

The FAIR experience clearly shows that local optimization of individual technical areas does not automatically lead to stable overall execution. Without central project coordination, projects typically face inconsistent planning assumptions, incomplete interface definitions, competing priorities, and delayed escalation of critical risks.

Professional project management therefore does not serve only an administrative function. Instead, it acts as the organizational integration structure between engineering, procurement, construction, installation [4], quality assurance, finance, and management decision-making.

As project complexity increased, the FAIR Project Management Office (PMO) gradually evolved into an integrated coordination and steering organization. Planning, risk and cost management, quality management, supplier coordination, in-kind coordination, and configuration management were not treated as isolated disciplines, but were closely linked within one common project management framework.

Integrated schedule and resource planning form the central basis for project steering. In addition, risk analyses, cost monitoring, delivery status, technical maturity, and quality and configuration information are continuously consolidated and evaluated together.

Risk management plays a particularly important role. Due to the large number of system interdependencies, deterministic planning methods alone are not sufficient to identify critical developments and support essential decisions on the project. For this reason, FAIR also uses probabilistic risk and forecasting methods, allowing a more realistic assessment of schedule uncertainties and cost at completion situation.

The FAIR experience also demonstrates that professional risk management does not depend only on methods or software tools. Practical experience of the involved project managers is equally important. Only through long-term project experience is it possible to realistically assess complex interactions, critical interfaces, and to trigger efficiently escalation mechanisms.

In large international projects, risks rarely appear as isolated events. More often, they develop from the combination of many initially small and seemingly unrelated problems. Early identification of such developments therefore requires not only structured methods, but also experienced project management organizations with a broad technical and organizational understanding.

Content from this work may be used under the terms of the CC BY 4.0 licence (© 2026). Any distribution of this work must maintain attribution to the author(s), title of the work, publisher, and DOI.

ISBN: 978-3-95450-252-3 ISSN: 2673-5350 doi: 10.18429/JACoW-IPAC2026-TUP8035

accelECR: THE EARLY CAREER RESEARCHER NETWORK IN ACCELERATOR SCIENCE AND TECHNOLOGY

L. Wroe, L. Valle*, P. Desiré Valdor[1], P. Martinez Reviriego, R. Taylor, I. Valencia Ruiz [2]
CERN – European Organization for Nuclear Research, Geneva, Switzerland
[1]also at PARTREC, UMCG, University of Groningen, Groningen, The Netherlands
[2]also at Université Paris-Saclay, Paris, France

Abstract

Early-career researchers (ECRs) are central to the advancement of accelerator science and technology, contributing across all areas - from R&D, theory, and design to experiment, commissioning, and operation - at all scales, from small medical accelerators to large colliders. While accelerator projects are often high-cost, long-timescale, and resource-intensive, ECR perspectives are underrepresented in strategic planning and decision-making. Following the example of particle physics (ECFA ECR) and nuclear physics (NuFFER), the accelerator science and technology community now has its own ECR network: accelECR. Through regular seminars and community-driven events, accelECR fosters knowledge exchange, promotes inclusivity, and improves skill transferability across the field. It also serves as a collective platform through which accelerator ECRs can engage with high-level strategy and decision-making in the field. The motivation, organization, and framework of accelECR are presented in this contribution.

MOTIVATION

Early-career researchers (ECRs) have historically been excluded from institutional, national, and international strategic decision-making. One study, for example, highlights that ECRs hold fewer than 2% of leadership positions across 20 scientific societies in the UK and US [1]. This is despite the critical role of ECRs as future leaders, a source of diverse perspectives and fresh approaches, hands-on contributors, and representatives of the majority of the workforce [2].

Such under-representation is particularly resonant in the field of particle accelerators, where projects can cost several billion US dollars, require more than a decade to construct, and involve thousands of scientists and technicians [3]. The FCC-ee, CERN's preferred option for its next large-scale collider [4], illustrates this starkly: with commissioning proposed for 2045 and an experimental run of 15 years, the project would span the majority of a current ECR's entire career [5].

Neighboring communities have already recognized this need for ECR representation and coordination. For example, the ECFA Early-Career Researcher Panel [6] was established in July 2020 to represent particle physicists (experimentalists, theorists, and phenomenologists) across Europe within the ECFA framework, while NuFFER was formed in October 2024 to serve the European nuclear physics ECR community within the framework of NuPECC [7]. Early-career structures are also maintained within individual collaborations, for example: the ATLAS Early Career Scientist Board [8], CMS Young Scientist Committee [9], Young DUNE [10], and the FCC Early Career Forum [11]. The accelerator science and technology community, however, has lacked a project-agnostic equivalent.

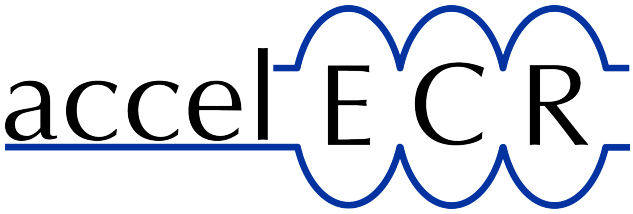

Figure 1: The accelECR logo.

This contribution introduces accelECR (Fig. 1), a project-agnostic ECR[1] network for accelerator science and technology. The network has two aims: first, to build community by fostering knowledge exchange, promoting inclusivity, enhancing skill transferability, and expanding professional networks; and second, to act as a collective platform through which accelerator ECRs can engage with high-level decision-making, strategy, and leadership.

GOALS AND ORGANIZATION

The idea for accelECR was conceived following discussions around the *Early Career Researcher Input to the European Strategy for Particle Physics Update: White Paper*, released in March 2025 [12]. This paper analyzes survey responses from 804 European ECRs with a stake in the 2026 update of the European Strategy for Particle Physics (ESPPU) [13]. Of these, only 62 responses were obtained from those working in accelerator science and technology — a significant underrepresentation of the accelerator ECR community and too small a sample to draw any meaningful conclusions. This highlighted a real missed opportunity to incorporate accelerator ECR perspectives into strategic decision-making.

The goals and organization of accelECR were subsequently developed throughout 2025, with the network for-

* accelECR-organizers@cern.ch

[1] While there is no universal definition of an ECR, accelECR defines an ECR as a researcher working on their Bachelor's, Master's, or PhD thesis, or within 10 years of completing their most recent degree in accelerator science and technology (excluding parental leave or other personal breaks from the 10-year limit).

Content from this work may be used under the terms of the CC BY 4.0 licence (© 2026). Any distribution of this work must maintain attribution to the author(s), title of the work, publisher, and DOI.

ISBN: 978-3-95450-252-3 ISSN: 2673-5350 doi: 10.18429/JACoW-IPAC2026-TUP8037

STATUS OF THE SAFEST PROJECT: THE SAPIENZA LINAC PROTOTYPE FOR VHEE FLASH RADIOTHERAPY

L. Giuliano, S. Akbar, R. Boldrini, E. Chiadroni, M. Coppola,A. Curcio, S. Farina, G. Franciosini, M. Magi,A. Mostacci, M. Migliorati, L. Palumbo, V. Patera, R. Remetti, A. Sarti,
Sapienza University of Rome & INFN – Rome, Rome, Italy
L. Ficcadenti, E. Lalli,
INFN – Rome, Rome, Italy
D. Alesini, F. Cardelli, R. Di Raddo, L. Faillace, G. Franzini, A. Gallo, L. Piersanti, S. Pioli, B. Spataro, A. Vannozzi,
INFN-LNF, Frascati, Italy
G. Cuttone, G. S. Mauro, G. Sorbello, G. Torrisi,
INFN-LNS, Catania, Italy
A. Bilancia, G. Felici, M. Di Francesco, V. Galasso, J. Pensavalle,
S.I.T. Sordina IORT Technologies S.p.A., Aprilia, Italy
A. Battisti, R. Clementi*

Content from this work may be used under the terms of the CC BY 4.0 licence (© 2026). Any distribution of this work must maintain attribution to the author(s), title of the work, publisher, and DOI.

Abstract

Delivered at Ultra-High Dose Rates (UHDR), in the so-called FLASH regime, electron irradiation has shown the remarkable ability to spare healthy tissues while preserving tumor control, opening new perspectives for next-generation cancer treatments. The advancement of high-gradient accelerating structures has enabled the development of compact and cost-effective linear accelerators suitable for clinical environments. Within this framework, we present the electromagnetic design and testing results of the C-band RF prototypes for a 24 MeV Linac being installed at Sapienza University. The linac is composed of a standing-wave and a traveling-wave section. The standing-wave structure has been designed, manufactured, and tuned in collaboration with SIT Company, while the traveling-wave structure has been entirely developed in-house, including full fabrication and tuning, in collaboration with INFN. These prototypes represent a key step toward the realization of an advanced FLASH VHEE source for future clinical applications.

INTRODUCTION

FLASH radiotherapy (FLASH-RT) has recently emerged as one of the most promising innovations in radiation oncology due to its potential to enhance the therapeutic ratio by preserving healthy tissues while maintaining tumor control. Preclinical studies have shown that the delivery of electron beams within extremely short irradiation times ($< 100ms$) and at ultra-high dose rates ($> 10^6$ Gy/s instantaneous dose rate) can significantly reduce radiation-induced toxicity in normal tissues without compromising antitumor efficacy.

The first evidence of the so-called "FLASH effect" was reported in 2014 by Favaudon et al. at Institut Curie [1]. Nevertheless, several aspects of the underlying mechanisms, technological implementation, and clinical applicability remain under active investigation, motivating the development of dedicated accelerator facilities capable of delivering stable and reproducible FLASH beams.

In this context, La Sapienza University of Rome, in collaboration with INFN, is developing a demonstrator of a Very High Energy Electron (VHEE) FLASH linear accelerator aimed at producing electron beams up to 24 MeV for both in vivo and in vitro irradiation studies [2]. The accelerator layout is based on a hybrid C-band architecture operating at 5.712 GHz. The injector section consists of a compact bi-periodic Standing Wave (SW) structure working in $\pi/2$ mode, while the downstream accelerating sections are based on high-gradient Traveling Wave (TW) cavities with a phase advance of $2/3\pi$ per cell. This configuration is designed to provide high accelerating gradients and efficient beam acceleration toward energies suitable for future VHEE FLASH applications (Fig. 1).

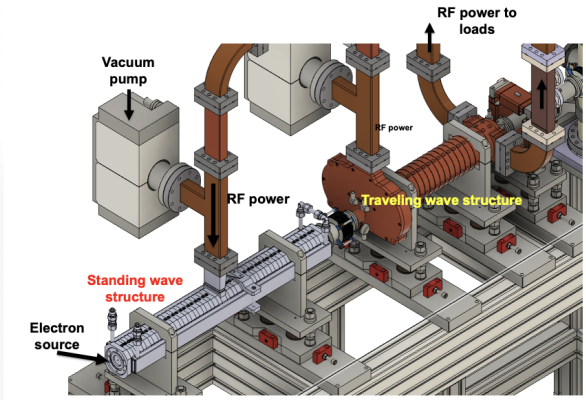

Figure 1: CAD models of the C-band accelerating structures developed for the VHEE FLASH linac demonstrator: Standing Wave (SW) bi-periodic cavity operating in $\pi/2$ mode at 5.712 GHz; (b) Traveling Wave (TW) high-gradient structure with $2/3\pi$ phase advance per cell.

This paper presents the electromagnetic design, fabrication, and experimental validation of the C-band SW and TW

* contracted by Sapienza University of Rome

ISBN: 978-3-95450-252-3 ISSN: 2673-5350 doi: 10.18429/JACoW-IPAC2026-TUP8304

INTEGRATED SUTAINMENT STRATEGY THROUGH A UNIFIED ACCELERATOR SYSTEMS DEFINITON*

M. Pieck†, G. E. Dale, M. S. Gulley, E. L. Kerstiens, C. T. Kelsey, A. C. Koppi, C. Lindenbaum, M. J. McMillen, W. J. Peck, Los Alamos National Laboratory, Los Alamos, NM, USA

Abstract

The sustained reliability and availability of the LANSCE accelerator depend on a clearly defined and integrated "systems" framework. This foundation links five core sustainment strategies: Asset Management, Risk Management, Conduct of Engineering, Training & Qualification, and Data Collection & Analysis. Unifying these under a common structure enables consistent decision-making, coordinated resource use, prioritized maintenance, and system-level performance tracking. It breaks down silos, improves efficiency, and supports targeted workforce development while reinforcing clarity in roles, responsibilities, authority, and accountability. Realizing this vision requires deliberate planning, early stakeholder engagement, and a robust change management strategy to navigate organizational and cultural shifts. This unified framework bridges short-term needs with long-term goals, positioning LANSCE to sustain mission-critical operations through 2050 and beyond. The paper explores this integrated approach as a scalable model for other aging accelerator facilities seeking sustainment without compromising mission continuity.

INTRODUCTION

The Los Alamos Neutron Science Center (LANSCE) is a national user facility supporting materials science, nuclear science, isotope production, and national security missions. Commissioned over 50 years ago, it now operates as a mature accelerator facility where aging infrastructure, evolving mission needs, and constrained resources create growing sustainment challenges [1, 2].

Historically LANSCE has implemented accelerator sustainment through partially independent efforts. Equipment assessments, risk management, workforce qualification, and engineering governance often evolved in response to specific institutional, operational, or funding drivers. While effective within their respective domains, these programs have become organizationally siloed, limiting system-level optimization and obscuring interdependencies between equipment condition, operational risk, engineering rigor, configuration management, and workforce capability, among other things [3].

To address these challenges, LANSCE has initiated the development of a Unified Accelerator Systems Definition (UASD) that was born out of an asset management program initiative. The UASD establishes a structured, accelerator-wide (asset) hierarchy that clearly defines how the accelerator is organized by systems and subsystems. It allows the identification of systems required within each geographic area and therefore clarifies how they collectively support overall accelerator function for an area (e.g. H-Minus Injector). The current level of detail represents a foundational framework, intended to evolve into a more comprehensive and refined structure over time.

At present, the UASD is primarily accelerator (programmatic) centric. However, long-term plans strive ideally for the integration of conventional facility systems—such as facility power, facility chilled water, and other infrastructure, to ensure a fully unified sustainment model.

In plain terms, the UASD shall serve as a common blueprint for understanding the accelerator—not as a collection of individual equipment records, but as an interconnected, mission-driven system.

As for now the UASD:

- Defines the accelerator by systems and subsystems down to the component level
- Clarifies boundaries between systems
- Provides a consistent structure for asset management, risk assessment, engineering standards, training, and data analysis
- Establishes clear roles, responsibilities, authority, and accountability aligned to that structure

Instead of having asset databases, risk models, maintenance plans, and training programs operating in parallel, a UASD creates a single structural backbone that all sustainment functions reference.

The result is:

- Better system-level decision-making
- Risk-informed prioritization
- Consistent engineering rigor
- Clearer workforce alignment
- Improved long-term reliability and availability

For a mature facility like LANSCE, a UASD shifts the focus from managing equipment to managing mission-critical systems over decades, enabling sustainment through 2050 and beyond.

MOTIVATION FOR UNIFIED SYSTEM FRAMEWORK

Aging Infrastructure and Mission Expansion

LANSCE's infrastructure includes legacy systems operating alongside modern upgrades. Components may exceed their original design lifetimes, replacement parts may

* This work was supported by the U.S. Department of Energy through the Los Alamos National Laboratory. Los Alamos National Laboratory is operated by Triad National Security, LLC, for the National Nuclear Security Administration of U.S. Department of Energy (Contract No. 89233218CNA000001). † pieck@lanl.gov, LA-UR-26-23551

Content from this work may be used under the terms of the CC BY 4.0 licence (© 2026). Any distribution of this work must maintain attribution to the author(s), title of the work, publisher, and DOI.

ISBN: 978-3-95450-252-3 ISSN: 2673-5350 doi: 10.18429/JACoW-IPAC2026-TUV2601

COMMISSIONING AND INITIAL OPERATION OF A COMPACT FEL-THz FACILITY AT IUAC, NEW DELHI*

B. K. Sahu †[1], P. Patra[1], J. Karmakar[1], B. Karmakar[1], Madhuri[1], A. Sharma[1], A. Aryshev[2], P. K.Mukhopadhyay[3], Markus Tischer[4], T. Rao[5], S. Ghosh[1], A. C. Pandey[1]
[1]Inter University Accelerator Centre, New Delhi, India
[2]High Energy Accelerator Research Organization, KEK, Tsukuba, Japan
[3]Raja Ramanna Centre of Advanced Technology, Indore, India
[4]Deutsches Elektronen-Synchrotron DESY, Hamburg, Germany
[5]Brookhaven National Laboratory, Upton, NY, USA

Abstract

A compact THz facility, based on Free Electron Laser (FEL) system has been commissioned at Inter University Accelerator Centre (IUAC), New Delhi. The design of the facility is based on pre-bunched FEL where a train of electron micro-bunches having maximum energy of 8 MeV are intended to be injected into a short undulator to produce the THz radiation in the range of 0.18 THz–3.0 THz. The electron micro bunches are produced from the photocathode by striking with the ultra-short laser pulses generated from an advanced Fibre laser system. These electron microbunches are being injected in to the undulator to produce the THz radiation and the electron beam along with the THz radiation are co-propagating through the undulator. At the exit of the undulator, a thin Titanium foil is kept through which the electron beam passes through and the THz radiation gets reflected, subsequently detected by the Schottky Barrier Diode detector. The commissioning details and the initial operation of the of the various sub-systems of the compact FEL-THz facility e.g. high-power RF systems, electron gun, fibre laser system, state of the art photocathode deposition system, undulator, various beam transport and beam diagnostic systems, etc. are being presented in this paper.

INTRODUCTION

Accelerator-based THz radiation sources are the most intense, narrow band and tunable among all known THz sources. These sources offer high peak power, tunability, and narrow radiation bandwidth [1, 2]. Undulator radiation is a well-established mechanism for generating narrowband electromagnetic radiation from relativistic electron beams, and it can be extended into the THz regime using low-energy electron beams and long-period undulators. A key challenge in undulator-based THz generation is to achieve a sufficiently high radiation intensity at longer wavelengths. One effective strategy is to exploit coherent radiation, in which the longitudinal structure of the electron beam leads to constructive interference of the emitted radiation. When electron beams exhibit a periodic longitudinal density modulation, radiation emitted by successive microbunches can interfere constructively, leading to coherent enhancement at frequencies corresponding to the microbunch repetition rate [3]. Although most FEL based THz sources are oscillator type, several pre-bunched FEL facilities either operational or under construction are increasingly gaining prominence. The Compact Free Electron Laser facility known as Delhi Light Source (DLS) [4, 5] at IUAC, New Delhi is a pre-bunched undulator based THz facility for the generation of THz radiation from an undulator driven by multi-microbunch electron beams produced using a normal conducting RF photocathode gun. RF photocathode guns provide a direct and flexible means of generating such structured beams by imprinting the temporal structure of a drive laser pulse train onto the emitted electrons that has recently generated first signature of THz radiation.

DLS Pre-Bunched FEL Facility

The main concept of pre-bunched FEL facilities, as shown in Fig. 1, is the enhancement of the radiation intensity due to super-radiance which is achieved when the bunch length of electron beam is small compared to radiation wavelength so that the contribution from the individual electrons from the same micrbunch adds up in phase and enhance the coherence. Additionally, if there are multiple bunches separated by the radiation wavelength the intensity gets further enhanced by the superposition of the photons in phases from the trailing micobunches of the electrons. The intensity is given as

$$I(\omega) = I_1(\omega)\left[N + N(N-1)|b(\omega)|^2\right], \qquad (1)$$

where,

$$b(\omega) = \frac{1}{N}\sum_{j=1}^{N} e^{i\omega t_j} \qquad (2)$$

is the bunching factor at frequency ω, N is the number of electrons and $I_1(\omega)$ is the spectral intensity of a single electron.

The DLS user facility is designed for THz frequencies in the range 0.18 –3.0 THz using the range of beam energies 4 –8 MeV and the magnetic field of the undulator 0.61 –0.12 T respectively. Electrons are generated from a 2.6 cell copper RF photocathode gun operating at 2860 MHz, by injecting pulsed UV lasers at the proper RF phase. An emittance compensation solenoid is used to focus the beam

* Work supported by BRNS and IUAC, New Delhi
† bhuban@iuac.res.in

Content from this work may be used under the terms of the CC BY 4.0 licence (© 2026). Any distribution of this work must maintain attribution to the author(s), title of the work, publisher, and DOI.

ISBN: 978-3-95450-252-3 ISSN: 2673-5350 doi: 10.18429/JACoW-IPAC2026-TUV3301

DEVELOPING A HYBRID ACCELERATING STRUCTURE BASED ON SHORT-PULSE STRUCTURE WAKEFIELD ACCELERATION *

G. Chen†, P. Piot, J. Power,
Argonne National Laboratory, Lemont, IL, USA
C. Jing[1], Euclid Techlabs LLC, Bolingbrook, IL, USA
[1] also at Argonne National Laboratory, Lemont, IL, USA

Abstract

Accelerating structures powered by ultra-short RF pulses (~10 ns) at the Argonne Wakefield Accelerator (AWA) has demonstrated effective suppression of RF breakdowns and achieved gradients exceeding 400 MV/m at X-band frequencies. To fully exploit the benefits of this short RF pulse operation, an accelerating structure must simultaneously achieve two goals: high group velocity (v_g) to ensure rapid RF filling, and simultaneously maintain high shunt impedance (r) for efficient beam energy gain. Conventional accelerating structures involve inherent tradeoffs between these parameters, and limit their effectiveness in the short-pulse regime. To this end, we developed a hybrid structure composed of two co-optimized traveling wave (TW) sub-structures fed by one coupler at the middle: one backward wave (BW) filling and one forward wave (FW) filling sub-sections. This design not only preserves the short-pulse advantage, but also boosts the beam's energy gain by effectively doubling the acceleration length without requiring extended RF pulse duration. In this work, we present the RF design of the X-band (11.7 GHz) hybrid BW-FW structure in detail.

INTRODUCTION

Short-pulse RF operation has recently gained increasing attention as a promising path toward high-gradient acceleration, with effective suppression of RF breakdown and demonstrated gradients exceeding 400 MV/m at X-band frequencies. At AWA, the short RF pulses is generated in a structure wakefield acceleration (SWFA) scheme through two-beam acceleration (TBA) technique, where a high-charge drive beam passes through a power extraction and transfer structure (PETS) to produce RF pulses with pulse lengths at the level of ~10 ns [1]. This short-pulse regime, however, introduces new challenges for the accelerating structure design. The structure must provide sufficient active acceleration length for meaningful energy gain while still being filled within the short RF duration (~ 10 ns), which requires a high group velocity (v_g). At the same time, a high shunt impedance (r) is also needed to achieve high beam energy gain for a given input power.

However, conventional metallic disk-loaded TW structures present an inherent trade-off between r and v_g: while reducing iris size increases r but weakens cell-to-cell coupling and lowers v_g, thus resulting in longer filling time that conflicts with the short (ns-scale) RF pulse operation. This trade-off has driven the exploration of novel structure designs that can achieve high v_g while preserving high r. A few promising design concepts include: 1) introducing magnetic coupling slots between cells in the conventional metallic structure to increase v_g [2]; 2) parallel filling structures that distribute RF power to each cell along the full accelerating structure, effectively reducing filling time while maintaining r [3,4]; 3) dielectric disk-loaded structures that employ high-permittivity, RF-transparent materials to enhance both r and v_g, though require careful tuning of the dielectric constant, since the RF properties are greatly correlated to the intrinsic material properties [5].

Beyond improving v_g and r within a single structure, in this work, we propose a novel architecture-level design: a hybrid TW structure composed of two halves, one backward-wave (BW) filling sub-section and one forward-wave (FW) filling sub-section, fed by a middle coupler, with each sub-section optimized for both high r and v_g. By filling the two sub-sections simultaneously, the structure further doubles the active acceleration length and energy gain without increasing the RF pulse duration. The RF design is presented in the following section.

STRUCTURE RF DESIGN

Figure 1 shows the design overview of the proposed hybrid BW-FW structure, including the major RF components involved in the optimization and design. The BW and FW single-cell designs are the core of the RF optimization, as they together set the overall performance of the full structure, including its operating frequency, v_g, r, and maximum achievable structure length. The BW half adopts the magnetic-coupling slot design, while the FW half adopts the parallel-filling concept to achieve high v_g. The remaining components such as the matching cells/slots, rectangular-to-circular waveguide adapter, and H-/E-plane power dividers, shown in insets (c)-(e) of Fig. 1 are then designed subsequently based on the optimized BW and FW geometries.

From a system-level perspective, our design prioritizes structures with high v_g. Since the attenuation parameter of a TW structure is given by $\alpha = \omega/(2v_gQ)$, a higher v_g reduces the attenuation per unit length and enables faster RF energy propagation. This relaxes the need for complex constant-gradient geometries, in which the cell dimensions are tapered

* This work is supported by the Physical Sciences and Engineering (PSE) Early Investigator Named Award (EINA) program at Argonne National Laboratory, under contract DE-AC02-06CH11357.

† b288079@anl.gov

Content from this work may be used under the terms of the CC BY 4.0 licence (© 2026). Any distribution of this work must maintain attribution to the author(s), title of the work, publisher, and DOI.

ISBN: 978-3-95450-252-3 ISSN: 2673-5350 doi: 10.18429/JACoW-IPAC2026-TUV7301

THE FIRST BEAM PRODUCED BY A CONDUCTION COOLED SRF PHOTOGUN*

C. Jing†, R. Kostin‡, Y. Zhao, E. Knight, Euclid Beamlabs LLC, Bolingbrook, USA
S. Posen, G. Eremeev, T. Khabiboulline, D. Bice, A. Netepenko, Fermilab, Batavia, USA
G. Chen, W. Liu, E. Wisniewski, S. Doran, A. Ody, J. Power, M. Kelly
Argonne National Laboratory, Lemont, USA

Content from this work may be used under the terms of the CC BY 4.0 licence (© 2026). Any distribution of this work must maintain attribution to the author(s), title of the work, publisher, and DOI.

Abstract

We report on the first beam produced by the world's first conduction cooled SRF photogun. Over the past five years, Euclid, working in collaboration with Fermilab and Argonne National Laboratory, has been developing a continuous-wave (CW), 1.5-cell, MeV-scale, conduction-cooled SRF photogun operating at 1.3 GHz. The primary objective of this effort is to demonstrate ultra-stable electron beams for UEM/UED applications, enabled by the exceptional shot-to-shot stability achievable with SRF technology compared to room-temperature RF photoguns. Although SRF systems were historically too costly for industrial deployment, two recent advancements: Nb_3Sn coatings and conduction cooling, have dramatically reduced system complexity and operating costs. This SRF photogun can deliver true CW operation while dissipating only ~2 W of RF power, eliminating the need for a high-power RF system and significantly reducing facility footprint. This SRF photogun is also featured with a raised Nb3Sn backwall serving as the photocathode, removing the need for an external cathode insert. In this paper, we present the first beam results from this system along with its cooldown performance, Q-slope behavior, synchronization characteristics, and initial beam parameters.

INTRODUCTION

Ultrafast electron diffraction and microscopy place stringent demands on electron source stability, beam throughput, bunch length, and energy spread. Superconducting RF (SRF) photoinjectors operating in continuous-wave (CW) mode offer orders-of-magnitude improvements in bunch repetition rate (laser-limited), as well as superior amplitude and phase stability compared to normal-conducting RF photoguns. However, conventional SRF implementations rely on liquid-helium cryogenic systems, which constrain their deployment to large-scale accelerator facilities only.

Over the past seven years, Euclid has led the development of the world's first conduction-cooled Nb_3Sn SRF photogun, targeting applications in MeV ultrafast electron microscopy. Owing to the significant technical challenges associated with this novel concept, multiple cavity tests were conducted at different stages of development to identify and mitigate unforeseen issues. A record-high gradient of 22 MV/m (equivalent to 44 MV/m at the cathode) was achieved (single opening cavity) during the second vertical test of the Nb cavity (prior to Sn coating), along with a peak quality factor of $Q_0 = 1.2 \times 10^{10}$ at 2 K [1]. In contrast, the second vertical test of the Nb_3Sn-coated cavity reached only 7 MV/m. The low-field quality factor was also reduced, with $Q_0 = 7 \times 10^9$ and noticeable degradation beyond 6 MV/m. Due to resource constraints, a third Nb_3Sn coating iteration was deferred, and the effort proceeded directly to conduction-cooled cryomodule testing. These results were reported in Proc. IPAC2024 [2].

Although the achieved gradient of the Nb_3Sn cavity fell short of the design target, primarily due to the later identified Sn contamination in the coating furnace, the prior work established the feasibility of operating a photogun-class SRF cavity using a commercial cryocooler without liquid helium. Figure 1 presents the integrated cryomodule and its control system.

In this paper, we report subsequent progress, focusing on continued system development, beamline preparation, and the first beam generation experiment.

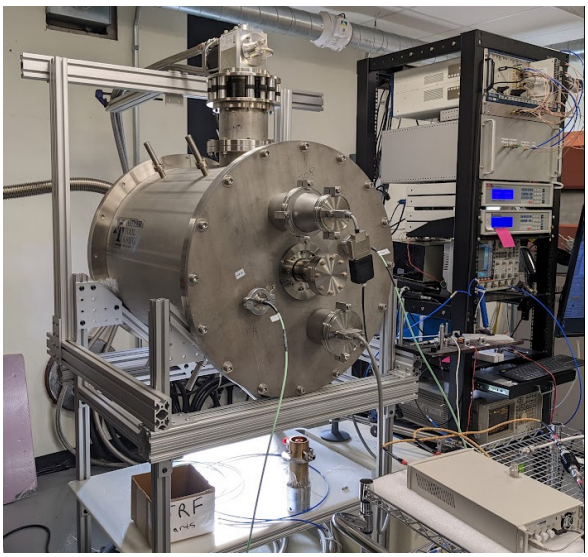

Figure 1: The cavity loaded conduction cooled cryomodule along with LLRF control rack and electronics at Euclid.

BEAMLINE PREPARATION

The beam generation experiment for the conduction-cooled Nb_3Sn SRF photogun was ultimately carried out at the Argonne Wakefield Accelerator (AWA) facility, selected for its proximity to the development site and availability of a 300 *fs* high-power UV laser. A dedicated beamline was designed (see Fig. 2) and installed in the AWA bunker, with supporting infrastructure prepared in advance. Beam dynamics simulations indicated reduced

* Work supported by DoE SBIR Grant # DE-SC0018621.
† c.jing@euclidtechlabs.com
‡ Now with Lam Research Co.

ISBN: 978-3-95450-252-3 ISSN: 2673-5350 doi: 10.18429/JACoW-IPAC2026-TUV7601

HIGH RELIABILITY DIGITAL CONTROL MAGNET POWER SUPPLY SYSTEM FOR SPring-8-II

C. Kondo[†1,2], T. Masuda[1], T. Taniuchi[1], T. Fujita[1], T. Aoki[1], S. Matsubara[1], M. Tajima[1], H. Yamaguchi[1], S. Nakazawa[3], K. Fukami[1,2], T. Watanabe[1,2]
[1]Japan Synchrotron Radiation Research Institute, Hyogo, Japan
[2]RIKEN SPring-8 Center, Hyogo, Japan
[3]SPring-8 Service Co., Ltd., Hyogo, Japan

Abstract

We have developed a new magnet power supply (PS) system for the forthcoming light-source facility, SPring-8-II. Aiming for highly reliable and energy-efficient accelerator operations, various PSs have been designed to meet diverse output current and voltage requirements. Key features of this system include: (i) the integration of Silicon Carbide (SiC) switching devices in PSs for multipole magnets, aimed at enhancing power conversion efficiency; (ii) the implementation of a fully digital control system across all PSs, enabling versatile parameter configuration; and (iii) a series-connected configuration for the main PSs driving multipole magnets to minimize the frequency of PS failures. Auxiliary PSs will be provided for individual magnets where necessary to enable independent current control for betatron beating correction and other purposes. Bipolar PSs for steering magnets have been designed to provide a stable output across the entire current range, including the low-current region, by optimizing the pulse width modulation (PWM) control scheme. Additionally, we propose a cost-effective alternative utilizing shunt resistors for individual current adjustment. Furthermore, a fast PS switcher that can quickly replace a failed PS with a backup PS without beam loss is currently under development.

INTRODUCTION

The SPring-8-II upgrade project has been launched at SPring-8, with the primary goals of achieving a low emittance and establishing a green light-source facility [1, 2]. This upgrade entails the complete replacement of all magnets and the adoption of a 5-bend achromat lattice, aiming for a beam emittance of less than 100 pm·rad. To significantly reduce power consumption, permanent magnets will be employed for the bending magnets [3]. Conversely, to prioritize magnetic field tunability, electromagnets will continue to be utilized for multipole magnets (such as quadrupole, sextupole, and octupole magnets) and steering magnets [4]. Following the removal of the existing power supplies (PSs), new PSs will be custom-designed and manufactured to optimally excite these magnets. To stabilize the electron beam trajectory, these PSs aim for an output current stability on the order of 10 ppm. And, the power conversion efficiency has been designed to be as high as possible to minimize the overall energy consumption of the facility. Additionally, busbar-type PS switchers will be integrated to enable quick replacement of the PS in the event of failures, for reducing the recovery time.

Furthermore, looking toward future implementation, a fast PS switcher for a hot-swap is currently under development for improving the machine reliability of the SPring-8-II storage ring. This device is designed to rapidly substitute a failed PS with a backup one without inducing beam loss by maintaining the magnet excitation current.

This PS upgrade project originated in 2017 with the development of a high-precision, digitally controlled PS [5]. This technology has been successfully applied to magnet PSs at NanoTerasu [6] and pattern-excited magnet PSs at SACLA [7]. Based on these experiences, we optimized the final design for SPring-8-II and commenced mass production in 2025, anticipating the launch of SPring-8-II in 2029. SPring-8 is scheduled to shut down in the summer of 2027; during a period of just over a year, all existing PSs will be replaced, cables will be rewired, and comprehensive operational testing will be conducted.

This paper overviews our design of the electromagnet PS system developed for SPring-8-II and current status of the development.

POWER SUPPLY SYSTEM

The SPring-8-II storage ring comprises groups of magnets arranged in 48 cells. The overall layout is shown in Fig. 1. These 48 cells are categorized into four types: 34 normal section (NS) cells, 2 injection section (INJ) cells, 8 matching section (MS) cells, and 4 long straight

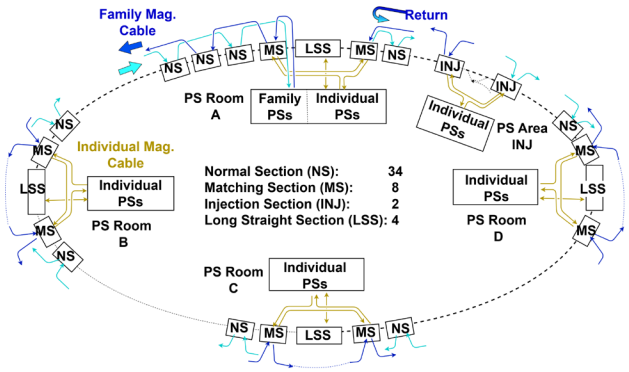

Figure 1: Overall layout of the family and individual magnets in the SPring-8-II storage ring.

†ckondo@spring8.or.jp

Content from this work may be used under the terms of the CC BY 4.0 licence (© 2026). Any distribution of this work must maintain attribution to the author(s), title of the work, publisher, and DOI.

ISBN: 978-3-95450-252-3 ISSN: 2673-5350 doi: 10.18429/JACoW-IPAC2026-TUV8001

COMMERCIAL ACCELERATORS FOR PROTON THERAPY - AN OVERVIEW

A. Peters†, Heidelberg Ionenstrahl-Therapie Centrum, Heidelberg, Germany

Abstract

There are different accelerator types used for proton therapy of diverse tumours. In use are mostly classical cyclotrons, synchrocyclotrons and synchrotrons. In addition, linear accelerators were or are under development. This paper will give an overview on commercially available systems. Not only technical aspects are discussed, but also new developments in treatment methods like ARC and FLASH therapy as well as irradiations in upright position and the backlash on the used accelerator types. Furthermore, practical issues like certification and embedding those systems in a hospital environment will be described and evaluated.

HISTORY

Two discoveries in physics laid the basis for radiotherapy: 1895 Wilhelm Conrad Roentgen found the X-Rays [1] and in 1904 William Henry Bragg published his measurements of energy loss of low-energetic α-particles in air, showing a maximum at end called “Bragg peak” [2], see Fig. 1 for high-energetic particles.

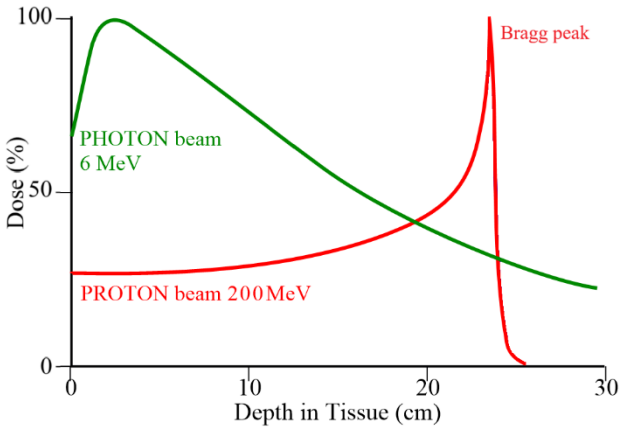

Figure 1: Dose-depth curves of high energetic X-Ray photons and protons in tissue [3].

Whereas X-Rays were used for diagnostics and radiation therapy very soon, becoming the main treatment option in oncology in the following decades, high energetic proton beams were not available before Ernest O. Lawrence and M. Stanley Livingston invented the cyclotron in 1930 [4] and further developments resulted in powerful systems around twenty years later. In 1946 R.R. Wilson first outlined the advantages of radiotherapy with protons [5], pointing to the finite range and Bragg peak for treating deep-seated tumours.

First biological studies started in the early 1950s at LBL, Berkeley and first proton treatments of patients followed in the next years. Later on, other institutes worldwide succeeded, still on an experimental basis at research laboratories and with relatively small patient groups in the beginning. First proton treatment installations at hospitals started in the 1990ies and commercially available systems were offered as from around 2000.

† andreas.peters@med.uni-heidelberg.de

USED ACCELERATOR TYPES

Different accelerator types are used for proton therapy, mostly classical cyclotrons, synchrocyclotrons and synchrotrons [6]. In addition, linear accelerators were or are under development and are described here shortly. Exotic developments like FFAGs, Dielectric Wall or Laser-Driven Accelerators may be options for the future, but are not relevant nowadays and are not scope of this paper.

Cyclotrons

Isochronous cyclotrons used today for proton therapy consist of the following main components [7]:

1. Proton source: Usually Penning effect sources (H_2 gas ionization by energetic electrons in an electrical discharge) are positioned in the middle of the cyclotron.
2. Magnet, resistive or super-conducting: The isochronous cyclotron employs an azimuthally varying field (AVF) to enable isochronism and vertical focusing.
3. RF: The isochronous cyclotron is based on a fixed radio frequency (RF) during acceleration, usually with frequencies between 60 and 90 MHz and 100– 200 kW power is needed. Thus, a c.w. beam is the result.
4. Extraction system: A thin vertical blade acts as the septum and the electrical field of some ten kV deflects the beam out of the cyclotron.



Figure 2: IBA 230 MeV resistive isochronous cyclotron [7].

Following the cyclotron, see Fig. 2, a passive energy variation system is needed, a variable thick target wheel or a wedge-like overlapping slit system, both called degraders. From this point on all beam parameters for tumour

Content from this work may be used under the terms of the CC BY 4.0 licence (© 2026). Any distribution of this work must maintain attribution to the author(s), title of the work, publisher, and DOI.

ISBN: 978-3-95450-252-3 ISSN: 2673-5350 doi: 10.18429/JACoW-IPAC2026-TUV8003

CERN INNOVATION PROGRAMME ON ENVIRONMENTAL APPLICATIONS (CIPEA): LEVERAGING ACCELERATOR TECHNOLOGIES FOR ENVIRONMENTAL IMPACT

E. Chesta†, A. Andersen, A. Ballarino, L. Bottura, M. Calviani, A. Diez Fernandez, S. Doebert, J. Ferreira Somoza, J.-C. Gayde, A. Moros, T. Rimbot, S. Sgobba, S. Stapnes, L. Wroe
CERN – European Organization for Nuclear Research, Geneva, Switzerland

Abstract

The CERN Innovation Programme on Environmental Applications (CIPEA) was launched in 2022 as a call for ideas to stimulate novel environmental applications based on CERN's technologies, scientific expertise and unique research infrastructure. CIPEA has since evolved into an integrated framework encompassing many CERN initiatives aimed at generating environmental impact beyond the Organization's own operational footprint. More than 25 projects are currently being developed with external partners, primarily from industry, drawing on competences integral to accelerator science, including superconductivity, high-field magnets, materials, cryogenics, vacuum systems, radiofrequency technologies, cooling and ventilation, and laser beams. Activities are structured around four key application areas: renewable and low-carbon energy; clean transportation and future mobility; climate-change mitigation and pollution control; and sustainability and green science. CIPEA is largely externally funded, with over 80% of its resources contributed by partner organizations. This paper outlines the programme's overall strategy, describes the priority development axes within each application area, provides an overview of ongoing efforts and highlights selected flagship projects exemplifying CIPEA's innovation potential.

INTRODUCTION

Environmental challenges on a global scale can only be addressed through a combination of efforts: increased efficiency measures with immediate effects, incremental technological developments delivering mid-term benefits, and disruptive innovation aimed at long-term solutions.

CERN's environmental commitment spans all these dimensions. Alongside efforts to reduce its own carbon footprint, CERN supports technological development and breakthrough innovation through CIPEA, a programme designed to harness accelerator, detector and computing technologies for high-impact environmental applications [1].

As CERN's technical expertise must remain primarily focused on high-energy physics priorities and thus cannot be extensively dedicated to societal applications, the most effective way for CERN to achieve broader impact is to build on developments driven by its scientific programme and provide targeted, high-value contributions to large-scale initiatives led by external partners. This approach is aligned with the priorities of CERN's Member States and reinforced by central coordination of an internal strategy aimed at optimising resources and maximising impact. CIPEA relies on the unique expertise of CERN's technical departments, internal support instruments like the KT Fund, and a broad network of external collaborations.

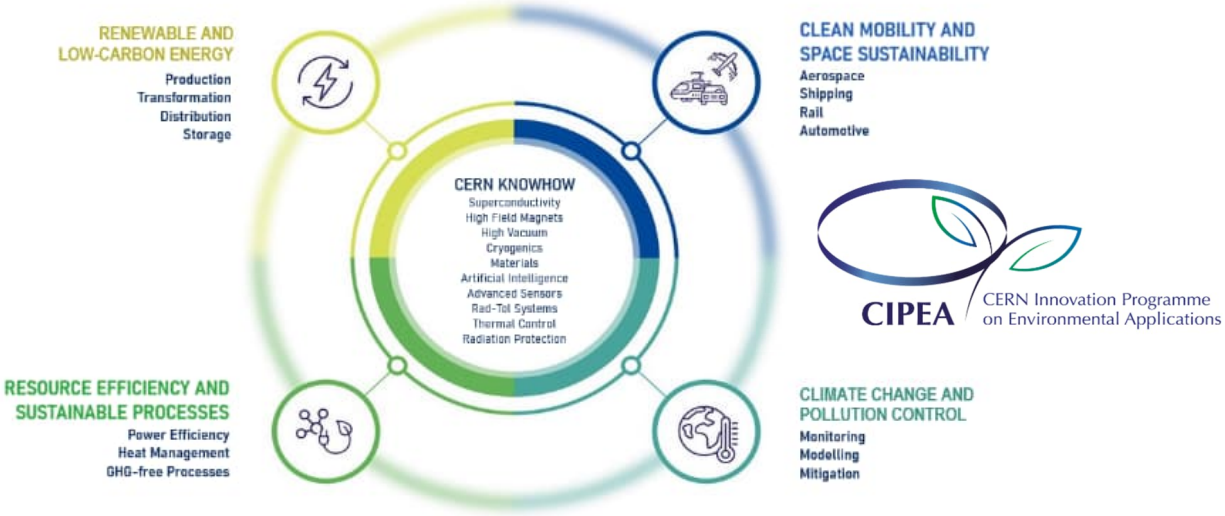

Figure 1: CIPEA strategy - main pillars and knowhow base.

Content from this work may be used under the terms of the CC BY 4.0 licence (© 2026). Any distribution of this work must maintain attribution to the author(s), title of the work, publisher, and DOI.

†enrico.chesta@cern.ch

ISBN: 978-3-95450-252-3 ISSN: 2673-5350 doi: 10.18429/JACoW-IPAC2026-WEO1T01

FIRST SYNCHROTRON INJECTION ATTEMPT INTO THE SuperKEKB HER

N. Iida*, Y. Funakoshi, H. Kaji, T. Kamitani, M. Kikuchi, K. Kodama, H. Koiso, T. Mimashi, G. Mitsuka, T. Mori, Y. Ohnishi, Y. Seimiya, K. Shibata, H. Sugimoto, M. Tawada, T. Ueda, R. Ueki, T. Yoshimoto, High Energy Accelerator Research Organization, Tsukuba, Japan
M. Li, Chinese Academy of Sciences, Beijing, China
K. Oide, European Organization for Nuclear Research, Geneva, Switzerland

Abstract

A synchrotron injection scheme for the SuperKEKB electron high-energy ring (HER) was implemented and experimentally evaluated as the first attempt with a top-up injection during beam collisions. The lattice at the HER injection point was configured to provide a large horizontal dispersion of –1.6 m, and the injection beam energy was accordingly set to +0.6% above the ring energy. Since the beam extraction system is located near the injection point, the optics design was constrained to ensure compatibility with its requirements. Optics solutions were developed and optimized using the ring sextupoles to enlarge the dynamic aperture for β_y^* values of 81 mm, 8 mm, 3 mm, and 1 mm at the IP. A systematic tuning procedure of the injection parameters has been established with turn-by-turn BPMs(TbT-BPMs) in the ring, by which the betatron amplitude of the injected beam was successfully removed. Using those optimized optics, synchrotron injection into the HER was successfully demonstrated, followed by the establishment of stable collisions and the production of luminosity. These experimental results and some remaining issues will be reported.

INTRODUCTION

The peak luminosity of SuperKEKB [1, 2] is currently $5.24\times10^{34}/\mathrm{cm}^2\mathrm{s}$ [3], while the next target is $1\times10^{35}/\mathrm{cm}^2\mathrm{s}$. To achieve this target, it is essential to increase the injection rate for both electrons and positrons. However, at present, improving the injection efficiency remains challenging in both rings [4, 5]. There are at least two primary reasons for this. The first is the growth of the injected beam emittance through the transport line. For both beams, the transverse emittance increases along the downstream beam transport line of the injector by factors of 2 to 5. The second is the beam loss occurring after injection in the storage ring. This loss has several contributing factors, one of which is the horizontal injection oscillation. The current injection scheme of SuperKEKB employs on-momentum, off-axis injection, called "betatron injection"(BI). In this scheme, the injected beam undergoes large horizontal oscillations in the ring, leading to various disadvantages. However, by adopting off-momentum, on-axis injection, so-called "synchrotron injection"(SI) [6–8], these issues can be mitigated, as described below.

* naoko.iida@kek.jp

Horizontal Injection Oscillation

In general, when the injected beam undergoes horizontal oscillations during top-up injection, it becomes susceptible to beam–beam kicks from the opposing beam during collisions, which can lead to beam blowup and tail formation. This is true even for head-on collisions; however, as SuperKEKB employs the nano-beam scheme [9] for collisions, where beams collide with a large horizontal crossing angle. As a result, if the injected beam has a large horizontal amplitude, it collides at a *s*-shifted location where the vertical beta function is large, and the resulting kick may induce beam loss. In SI, the injected beam does not have horizontal oscillations, and therefore such beam loss does not occur. In fact, this scheme had already been considered during the design stage of SuperKEKB [10].

Narrow Dynamic Aperture of the HER

In the HER, the injection efficiency (survival ratio) does not exceed ~ 80 % even 100 turns after injection. One of the causes is believed to be that the injected electron beam, having a large vertical emittance and a large horizontal injection oscillation, exceeds beyond the dynamical aperture of the HER. Furthermore, the dynamical aperture has been reduced due to "mis-wiring" [2, 11] of the cancel coils in the superconducting final focus magnet (QCS) during construction, making it even more restrictive for injected beams undergoing large horizontal oscillations. In SI, however, the injected beam no longer exhibits horizontal oscillations, and therefore an improvement in injection efficiency is expected. Although the injection oscillation is transformed from horizontal to longitudinal plane, simulations described later indicate that the associated disadvantages are much smaller, since the dispersions at the interaction point(IP) is suppressed.

Synchrotron Radiation from Injection Beam

In the case of BI, the injected beam undergoes horizontal oscillations, and synchrotron radiation generated by kicks from the high-field QCS magnets can hit the beam pipe near the IP, potentially contributing to background in the Belle II detector.

Damping Time

Since the longitudinal damping time in the HER, 2900 turns, is a half of that in the transverse plane, the background

Content from this work may be used under the terms of the CC BY 4.0 licence (© 2026). Any distribution of this work must maintain attribution to the author(s), title of the work, publisher, and DOI.

ISBN: 978-3-95450-252-3 ISSN: 2673-5350 doi: 10.18429/JACoW-IPAC2026-WEO1T02

PERFORMANCE STRATEGY FOR THE FIRST YEARS OF THE EIC SCIENCE PROGRAM*

A. Blednykh†, E. Aschenauer, W. Bergan, M. Blaskiewicz,
L. Lari, C. Montag, S. Nagaitsev, V. Ptitsyn, Q. Wu
Brookhaven National Laboratory, Upton, New York, USA

Abstract

The Electron-Ion Collider (EIC) will begin science operations with a staged machine configuration that imposes well-defined accelerator-physics constraints on achievable luminosity and beam parameters. This paper presents the performance strategy that supports the first 3 years of the EIC Science Program. We outline the accelerator-physics activities required to deliver high-repetition-rate electron beams, heavy-ion beams, deuterium, polarized protons, and ^{3}He, together with the performance evolution of electron and hadron polarization systems, spin rotators, bunch patterns, and longitudinal emittance control. The paper highlights the year-by-year integration of new machine capabilities, including progressive increases in beam intensity and average luminosity required to meet evolving science objectives. This framework defines the accelerator-physics roadmap for performance delivery and sustained operation of the EIC Science Program

INTRODUCTION

The Electron-Ion Collider (EIC) is a next-generation accelerator facility under construction at Brookhaven National Laboratory, designed to collide polarized electrons with polarized protons and heavy ions at high luminosity and variable center-of-mass energies [1,2]. The EIC complex (Fig. 1) consists of a DC photoelectron gun, a 750 MeV S-band LINAC, the Beam Accumulator Ring (BAR, 750 MeV), the Rapid Cycling Synchrotron (RCS, 0.750→9 GeV) and two high-energy storage rings: the Electron Storage Ring (ESR) and the Hadron Storage Ring (HSR). Electrons are accelerated in the RCS from 0.750 GeV to 5 and 9 GeV, with provision for acceleration up to 18 GeV following project completion, and subsequently injected into the ESR at the corresponding energy, with 18 GeV operation foreseen as a near-term upgrade. Hadrons are injected from the existing RHIC injector complex into the HSR at 23.8 GeV and ramped to final energies ranging from 41 to 275 GeV, depending on the species, including protons (p), ions, or He³. The 41 GeV energy bypass (Fig. 1, shown in blue) is part of the EIC baseline design. However, its construction and installation are deferred beyond the initial project scope and are planned for implementation during the early years of EIC operations.

The goal of the EIC is to deliver a design luminosity of up to 10^{33}-10^{34} cm^{-2}s^{-1}, enabled by advanced features such as beam cooling systems, a 25 mrad crab crossing angle, high beam currents - up to I_{av}=2.5 A with M=1160 bunches of σ_s~7 mm length in the ESR, and up to 0.7 A / 1 A with M=290 and M=1160 bunches of σ_s~60 mm in the HSR during storage. At injection energy, the bunch length in the HSR is expected to be significantly longer, around σ_s~1.5 m.

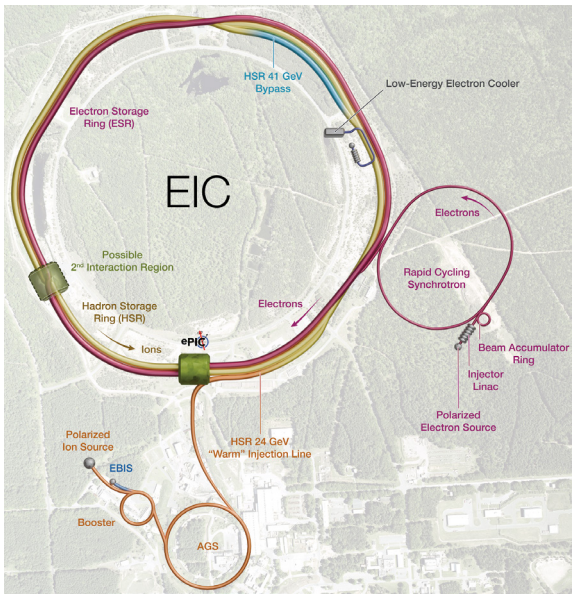

Figure 1: Top view schematic of the Electron-Ion Collider (EIC) accelerator complex, including the electron and hadron injector chains, the Beam Accumulator Ring (BAR), the Rapid Cycling Synchrotron (RCS), and the Electron and Hadron Storage Rings (ESR and HSR).

HSR

Different hadron species are foreseen to collide with the electron beam. Depending on the species, the beam is accelerated to the required operational energy. As an example, the sequence for proton beam injection into the HSR is outlined below; this sequence may be further refined during commissioning.

Since the EIC utilizes RF systems inherited from RHIC, the following steps are performed. The proton beam is injected into HSR at 23.8 GeV in a single-bunch mode, with injection cycle of ~3 s per bunch, accumulating up to 290 bunches using the 24.6 MHz RF system (h=315). The beam is then accelerated to the operational energy (e.g., 275 GeV), after which the spin rotators and snakes are ramped to their operating currents (~10 min). The bunch structure is subsequently formed through a sequence of bunch splitting and longitudinal RF gymnastics, from 290

* Work supported by Brookhaven Science Associates, LLC under Contract No. DE-SC0012704 and DE-AC02-06CH11357 with the U.S. Department of Energy.
† blednykh@bnl.gov

Content from this work may be used under the terms of the CC BY 4.0 licence (© 2026). Any distribution of this work must maintain attribution to the author(s), title of the work, publisher, and DOI.

ISBN: 978-3-95450-252-3 ISSN: 2673-5350 doi: 10.18429/JACoW-IPAC2026-WEO1T03

NEAR RESONANCE POLARIZATION MODULATION (NRPM), A NOVEL METHOD FOR HIGH PRECISION BEAM ENERGY MEASUREMENT IN STORAGE RINGS*

Yi Wu†, T. Pieloni, École Polytechnique Fédérale de Lausanne, Lausanne, Switzerland
Z. Duan, Institute of High Energy Physics, Beijing, China
L. van Riesen-Haupt, Old Dominion University, Norfolk, VA, United States
J. Wenninger, European Organization for Nuclear Research, Geneva, Switzerland
D.P. Barber, University of New Mexico, Albuquerque, NM, United States
A. Blondel, University of Geneva, Geneva, Switzerland
M. Seidel, PSI Centre for Accelerator Science and Technology, Villigen, Switzerland

Content from this work may be used under the terms of the CC BY 4.0 licence (© 2026). Any distribution of this work must maintain attribution to the author(s), title of the work, publisher, and DOI.

Abstract

We propose Near Resonance Polarization Modulation (NRPM), a novel method for high-precision beam energy measurement in storage rings. In this technique, a constant-frequency AC dipole is applied near the spin precession frequency, driving the beam spins coherently. The spin tune can be reliably extracted from the time-dependent polarization signal, enabling a very high-precision determination of the beam energy. Its performance has been demonstrated using the Future Circular Collider e+e- (FCC-ee) Z-pole lattice, exploring a range of configurations including AC dipole strengths and initial polarization levels. The method exhibits robustness against lattice imperfections. Compared to the traditional resonant depolarization (RDP) technique, NRPM offers significantly improved precision, greater tolerance to systematic uncertainties, and simplified operational procedures. Beyond the FCC-ee case study, NRPM is broadly applicable to high-precision energy determination in modern storage rings. The superior precision offered by this technique will significantly advance the state-of-the-art in beam energy measurement, with critical applications in high-energy physics and the measurement of fundamental constants.

INTRODUCTION

Accurate measurement of beam energy in storage rings constitutes an essential requirement in contemporary high-energy physics, providing the foundation for high-precision determinations of elementary particle masses and widths. For storage rings operating with polarized beams, the beam energy (E) is conventionally extracted from the measured closed-orbit spin tune (ν_0), defined as the number of spin precessions per turn for particles on the closed orbit. In an ideal, perfectly aligned lattice, ν_0 is related to the average beam energy along the closed orbit by $\nu_0 = a\langle E\rangle/(mc^2)$, where a is the gyromagnetic anomaly and m the particle mass. In the presence of machine imperfections, the closed-orbit spin tune deviates slightly from this simple relation. Equivalently, ν_0 corresponds to the spin precession frequency $\nu_0\, f_{\mathrm{rev}}$, with f_{rev} the revolution frequency. The center-of-mass energy is subsequently derived from this average energy.

Resonant depolarization (RDP) has long been regarded as the gold standard for high-precision beam energy measurements, with notable implementations at large colliders such as the Large Electron-Positron collider (LEP) [1], at smaller colliders like VEPP-4M [2], and at light sources including the Swiss Light Source (SLS) [3]. The technique operates by sweeping the frequency of an external radio-frequency (RF) field across the spin precession frequency of the beam, the frequency at which depolarization occurs reveals the spin tune and thereby the beam energy. The ultimate precision of RDP is fundamentally limited by kinematic broadening arising from the finite beam energy spread, which smears the resonance onset. In addition, premature depolarization occurring prior to reaching the true resonance condition distorts the fitted line shape and constitutes the dominant source of systematic uncertainty in this method.

The physics program of the Future Circular Collider electron-positron (FCC-ee), particularly at the Z pole and the W-pair threshold, demands an energy calibration with systematic uncertainties substantially smaller than those attained at LEP. The current estimate of the systematic uncertainty at the Z pole is 100 keV [4,5], with the ultimate aim of reducing it to the level of the statistical error of 4 keV. This stringent precision goal motivates a thorough examination and validation of existing energy measurement techniques, as well as the exploration of strategies to further enhance their accuracy.

In this paper, we propose a novel energy measurement technique termed Near Resonance Polarization Modulation (NRPM). In contrast to RDP, which drives the system through the spin resonance, NRPM operates in an off-resonance regime and thereby preserves the bulk polarization of the beam. By applying an external RF field at a fixed frequency in the neighborhood of the spin resonance, a coherent modulation of the spin motion is induced, producing a measurable response whose frequency is directly linked to, and exhibits high sensitivity to, the spin tune. This scheme has the potential to surpass current precision and offers a

* Work supported by the Swiss Accelerator Research and Technology (CHART)
† yi.wu@epfl.ch

ISBN: 978-3-95450-252-3 ISSN: 2673-5350 doi: 10.18429/JACoW-IPAC2026-WEO4M02

BEAM TESTS OF A PERMANENT MAGNET MEDICAL ACCELERATOR ARC FROM 10–250 MeV*

S. Brooks†, G. Mahler, D. Trbojevic, Brookhaven National Laboratory, Upton, NY, USA

Abstract

The FLASH hadron therapy accelerator proposed by Trbojevic uses permanent magnets with nonlinear fields to allow rapid cycling from 10 to 250 MeV while keeping the ring tune constant. A test beamline of four cells from this ring (22.5 degree angle) was built at BNL and tested at the NSRL facility with protons and at the Tandem Van de Graaff with deuterons. The magnets consist of 24 neodymium-iron-boron (NdFeB) wedges magnetised in different directions and arranged to produce the required nonlinear field profile across the oval aperture for the beam movement, with fields of up to 1.85 Tesla. Beams were transmitted at all rigidities tested over a 5.3× momentum ratio, with output location moving systematically with energy as required.

HADRON THERAPY FACILITY

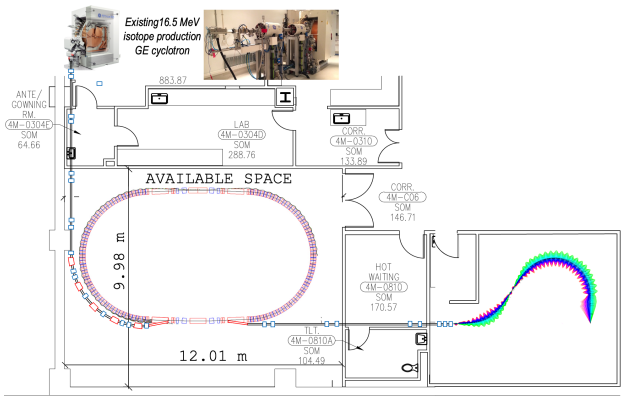

Figure 1: Hadron therapy facility plan view.

A collaboration between BNL and Stony Brook Radiation Oncology has designed a hadron therapy facility capable of ultra-high dose rates (UHDR or FLASH therapy) and rapid energy scanning [1,2]. The facility (Fig. 1) consists of a commercially-available cyclotron injector, followed by a permanent magnet fixed-field accelerator (FFA) ring and a low-dispersion gantry to transport the beam to the patient regardless of the extraction energy.

The wide range of extracted kinetic energies (E_k) shown in Table 1 allows selection of depth within the patient, while the rapid machine cycle rate makes irradiation of the different depths nearly simultaneous. The full treatment charge occurring within a fraction of a second reduces patient motion during the irradiation period and can also provide conditions for the hypothesised FLASH effect that spares healthy tissue.

The optics design of the FFA follows work by Trbojevic who first proposed a non-scaling FFA for medical use [3] and then found adjustments to make the ring tune fixed across the energy range [4]. The team then found systematic ways of generating fixed-tune designs for different applications [5] and better ways of defining the nonlinear magnet fields [6].

Table 1: Hadron Therapy Facility Parameters

Injection E_k	10–30	MeV
Extraction E_k range	65–250	MeV
Arc radius	3.5	m
Machine cycle rate	500–800	Hz
Energy gain per turn	30–45	kV
Treatment charge	60	nC
Treatment time	75–250	ms

FOUR CELL TEST BEAMLINE

A full-scale, full-field prototype of one eighth of the FFA ring arc was built with unit cell given in Table 2. The beamline is four cells long but the cell starts half-way through the F magnet to make the initial and final beam angles zero by symmetry for every energy (Fig. 2).

Table 2: Test Beamline Lattice Cell

Element	**Length (m)**	**Angle (°)**
F	0.18	3.335
O	0.02	0
D	0.123612	2.290
O	0.02	0
Total	0.343612	$5.625 = \frac{360}{64}$
HF	0.09	1.667

Table 3: Orbit Ranges and Peak Fields

Parameter	**F magnet**	**D magnet**	**Unit**
x_{min}	-14.306	-11.148	mm
x_{max}	38.392	24.891	mm
$B_y(0)$	-0.5344	-0.6263	T
$\lvert B_y \rvert_{max}$	1.8462	1.8631	T

The horizontal orbit range and peak fields are given in Table 3. The cell tunes are $Q_x = 0.1608 \pm 0.0004$ and $Q_y = 0.0738 \pm 0.0011$, as plotted in Fig. 3. The beamline before vacuum chamber installation is shown in Fig. 4.

PERMANENT MAGNETS

The field functions of the two magnets are defined by the Fourier coefficients in Table 4 and the formula

$$B_y(x) = c_0 + \sum_{n=1}^{8} s_n \sin(nkx) + c_n \cos(nkx),$$

* Work supported by Brookhaven Science Associates, LLC under Contract No. DE-SC0012704 with the U.S. Department of Energy.

† sbrooks@bnl.gov

Content from this work may be used under the terms of the CC BY 4.0 licence (© 2026). Any distribution of this work must maintain attribution to the author(s), title of the work, publisher, and DOI.

ISBN: 978-3-95450-252-3 ISSN: 2673-5350 doi: 10.18429/JACoW-IPAC2026-WEO3T02

SHORT-PULSE DRIVEN PHOTOGUN FOR VERY HARD X-RAY FREE-ELECTRON LASER

W. H. Tan*, A. Dhar, C. Gunter, J. E. Hernandez Jr., E. Nanni, R. Robles
SLAC National Accelerator Laboratory, Menlo Park, CA, USA

Abstract

X-ray free-electron-laser (FEL) has numerous applications in a wide range of disciplines, such as biology, chemistry and material science. Recently there have been studies on using very hard x-ray FEL to study material properties under extreme conditions. These scientific use cases require FEL photon energies beyond the current state-of-the-art FEL facilities. One pathway of enabling very hard x-ray FEL is to use high gradient radio frequency (rf) driven photogun to deliver bright electron beams. Numerous efforts have been made to push for even higher field gradient while suppressing rf breakdowns. We propose the Compressed Ultrashort Pulse Injector Demonstrator, a 1.6 cell photogun driven by nanosecond high power rf pulses to achieve high gradients with low breakdown rate. This photogun is powered by ultrashort pulses from a rf pulse compressor and a high power klystron. We first show the design of CUPID photogun, followed by its capability of bright beam generation when forming a photoinjector with a superconducting solenoid and downstream linacs. We then use Ming-Xie parameterization to compare FEL performance of CUPID and LCLS nominal injector to demonstrate its improvement in delivering hard x-rays.

INTRODUCTION

The growing interest on very hard x-ray FEL stemmed from the need to understand the mesoscale science, the ability to probe defects of multigranular material and how they behave in extreme conditions [1–6]. Understanding mesoscale science requires x-ray FEL to deliver photon energies at 40 keV and above. One pathway to meet this requirement is use high gradient rf photogun to deliver bright electron beams for FEL [3,4,7]. Pushing for higher gradient photogun has been an important topic for bright electron beam generation as the six-dimensional brightness is proportional to the square of the photogun's gradient, where $\mathcal{B}_{6D} = 2I/\varepsilon_n^2\sigma_\gamma \propto E^2$, where I, ε_n, σ_γ and E are the beam current, transverse emittance, normalized rms energy spread and photogun's gradient respectively [8]. We present Compressed Ultrashort Pulse Injector Demonstrator (CUPID), a 1.6 cell photogun that can achieve high gradient with ultrashort high power rf pulses generated by a novel ultra-high power rf pulse compressor, followed the successful demonstration of high gradient short pulse photogun driven by two-beam acceleration method at the Argonne Wakefield Accelerator (AWA) facility [9]. This photogun operates at 11.424 GHz to utilize an available X-band klystron of the same frequency and rf pulse compressor recently commissioned at SLAC [10].

PHOTOGUN DESIGN

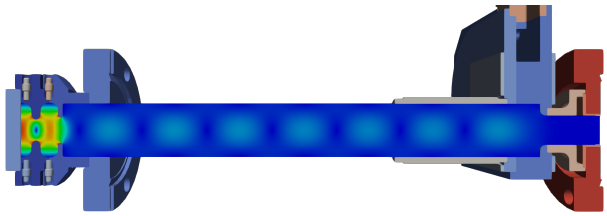

Figure 1: Cut-away view of the relative spacing between the CUPID photogun, the connecting waveguide, and the TM_{10} mode launcher, with superimposed π-mode field map. The relatively long waveguide connecting both components is a design choice to accommodate the physical size of a solenoid designed for bright beam generation. Extended waveguide and solenoid are not shown in this view.

Figure 1 shows the cut-away view of our CUPID photogun, the connecting waveguide and the TM01 mode launcher, with superimposed π-mode field map. The relatively long waveguide connecting both components is a design choice to accommodate the physical size of a solenoid designed to achieve bright electron beams. CUPID photogun achieves high gradient with short rf pulses by having a very short filling time t_{fill}, where it is related to the designed loaded Q-factor, $Q_{\text{load}} = \pi f t_{\text{fill}}$, where f is the operating frequency. Table 1 shows design parameters of CUPID photogun.

Table 1: Design Parameters of CUPID Photogun

Parameter	Value	Unit
Frequency	11.424	GHz
Q_{load}	215	-
S_{11}	–0.59	dB
Field gradient at cathode	500	MV/m
Peak input power	275	MW

BEAM DYNAMICS

Photoinjector Design

In this section we present beam dynamics studies of CUPID photoinjector, it consists of CUPID photogun, enclosed by a superconducting solenoid and connected to downstream S-band linacs. The superconducting solenoid is paired with a bucking solenoid at the back to achieve zero-magnetic field at the cathode to prevent the generation of magnetized beam.

* whtan@slac.stanford.edu

Content from this work may be used under the terms of the CC BY 4.0 licence (© 2026). Any distribution of this work must maintain attribution to the author(s), title of the work, publisher, and DOI.

ISBN: 978-3-95450-252-3 ISSN: 2673-5350 doi: 10.18429/JACoW-IPAC2026-WEO3T03

A PORTABLE MUON SOURCE FOR ARTIFICIAL MUON MUOGRAPHY

L. Guo, M. Kuriki*, Z. Liptak, Hiroshima University, Hiroshima, Japan

Content from this work may be used under the terms of the CC BY 4.0 licence (© 2026). Any distribution of this work must maintain attribution to the author(s), title of the work, publisher, and DOI.

Abstract

Muography is a useful technology for non-destructive inspection of a large-scale structure. Muography with cosmic ray muons has limitations such as low rates, particularly low muon rates in the horizontal direction, and energy spreading, which require long observation times and limit its resolution. Worldwide, large structures such as bridges built during the economic development period of the 1950s-1960s have reached the end of their useful life, and the principle of preventive maintenance is being applied to save the resources, by understanding their interiors and renewing them with priority given to structures that have deteriorated. At this time, a technology of non-destructive inspection applicable to such large structures is required, and Muography using a portable artificial muons source is a promising candidate for this purpose. In this presentation, the results of the investigation of the portable artificial muon source will be presented.

INTRODUCTION

Muons are elementary particles classified as leptons, similar to electrons but with approximately 200 times greater mass. They are generated when high-energy cosmic rays—mainly protons from outer space-collide with atomic nuclei in the Earth's atmosphere. These collisions produce showers of secondary particles, among which muons are the most penetrating. At sea level, roughly one muon per square centimeter per minute reaches the Earth's surface. Muons are naturally occurring and are continuously available as a source of radiation.

Muography [1] leverages the penetrating nature of muons to visualize and analyze the internal structure of large objects without causing any damage. As muons pass through matter, they lose energy and may scatter, depending on the density and atomic number (Z) of the material.

The biggest issue of Muography with the natural muons is the long observation time due to the limited flux of the natural muons. In particular, the rate of muons flying horizontally over the earth's surface is low, making it difficult to ensure sufficient statistical quantities and limited accuracy. Muons falling from the sky have relatively high rates, in which case the detector needs to be placed underground in the object being measured, which is generally difficult to install. We consider a portable muon source to solve these issues. The portable muon source generates a high-rate and mono-energy muon beam which improves the spatial resolution and the observation time. The mono-chromatic muon beam dramatically simplify the kinematics by the fixed initial state, the position and the momentum. The muon firing direction is controllable and muons can be fired at a high rate in the horizontal direction for easy detector installation, which is expected to reduce measurement time and improve resolution.

The high throughput non-destructive measurement by the portable muon source has a high social demand as we already discussed in Ref. [2]. From the 1950s to 1960s, social infrastructures such as roads and railroads were rapidly developed along with economic development in the world. These social infrastructures are now reaching the stage of renewal due to the end of their useful lives. The amount of resources required for the maintenance and renewal of social infrastructures is enormous, and it is desirable to reduce the amount of resources required without compromising safety. The Ministry of Land, Infrastructure, Transport and Tourism in Japan (MLIT) forecasts that maintenance and renewal costs for roads and other social infrastructure will be 5.2 trillion yen in 2018 and 5.9 trillion yen to 6.5 trillion yen by 2048. The cost of highway maintenance and management is 1.5 trillion. The same scale is assumed for railroad and electric power companies. Overall, infrastructure maintenance and management costs in the mid-21st century will be more than 10.4 trillion JPY/year. MILT advocate a policy of preventive maintenance. Those in good condition will have their operational life extended, and those in severely deteriorated condition will be replaced first. The evaluation requires a non-destructive inspection which is applicable to a large structure, such as large bridges and elevated road and rail structures. The needs for nondestructive testing using portable muon sources are high. MILT estimates that preventive maintenance will reduce maintenance costs by 30 % to 50 %. Assuming that 5 % of maintenance costs are inspection costs, the market size is 500 billion JPY/year.

Muography, has emerged as a revolutionary tool for the non-destructive evaluation (NDE) of historical monuments and large-scale artworks. The primary significance of muography lies in its ability to scan massive structures without causing any physical damage or requiring radioactive sources. Currently, muography mostly relies on natural cosmic rays, which requires long exposure times (weeks to months) and specific detector placement (usually underneath or beside the target). The development of portable artificial muon sources would represent a paradigm shift in the field. While cosmic-ray muography is slow due to the low flux of natural muons, an artificial source can provide a high-intensity, controlled beam. This would reduce inspection times from months to hours, enabling rapid assessment of structural integrity after earthquakes or before restoration projects. Artificial sources allow for energy tuning. By controlling the momentum of the produced muons, researchers could distinguish between materials with similar densities (e.g., different types of stone or metal alloys), providing high-definition internal imaging of smaller artifacts like bronze

* mkuriki@hiroshima-u.ac.jp

ISBN: 978-3-95450-252-3 ISSN: 2673-5350 doi: 10.18429/JACoW-IPAC2026-WEO3T04

PROGRESS TOWARDS HIGH-REPETITION-RATE PLASMA WAKEFIELD ACCELERATION AT FLASHFORWARD

J. Beinortaitė*[,1], L. Bishop[1,2], J. Björklund Svensson[1,3], L. Boulton[1], G. Boyle[1,4], P. Burghart[1,5], Y. Chen[1], J. Cowley[6,7], R. D'Arcy[1,6,7], J. P. Díaz[1,5], Á. Ferran Pousa[1], B. Foster[1,6,7], M. Hohmann[1], M. Huck[1], H. Jones[1], A. Kanekar[1,5], A. Křivková[1], C. A. Lindstrøm[1], G. Loisch[1], T. Long[1], A. Maier[1], M. Mewes[1], L. Müller[1], I. Najmudin[6,7], J. Osterhoff[1], T. Parikh[1], F. Peña[1,5], J. Rönsch Schulenburg[1], D. Samoilenko[1], L. Schaper[1], E. Schneidmiller[1], S. Schröder[1], M. Thévenet[1], S. Wesch[1], M. Wing[1,2], I. Zagorodnov[1], J. Wood[1]

[1]Deutsches Elektronen-Synchrotron DESY, Hamburg, Germany

[2]University College London, London, UK

[3]Lund University, Lund, Sweden

[4]James Cook University, Townsville, Australia

[5]Universität Hamburg, Hamburg, Germany

[6]John Adams Institute for Accelerator Science, Oxford, UK

[7]University of Oxford, Oxford, UK

Abstract

Radiofrequency linacs accelerate thousands of bunches per second, which should be matched by beam-driven plasma wakefield accelerators (PWFAs) if their benefits as high-acceleration-gradient energy boosters are to be fully exploited. However, demonstrations to date have accelerated only ~ 10 bunches per second. At FLASHForward, key issues are being solved to bridge this gap. Analytic models have been developed to show how to generate bunch pairs from the photocathode with the longitudinal shape optimised for plasma acceleration, thus reducing stray radiation compared to a collimator system. To deal with large energy depositions from rapid plasma creation and acceleration events, benchmarked models have been built to determine the heating of the plasma source at kHz repetition rates, so that remedial measures can be developed. Furthermore, we have seen that ionisation induced by the wakefield-perturbed plasma can limit the maximum repetition rate. Finally, PWFAs must produce large energy gains for photon science or particle physics applications. We recently demonstrated acceleration of bunches from 1.2 to > 1.7 GeV over 0.5 m of plasma, with < 2% energy spread.

INTRODUCTION

A GeV-per-metre acceleration gradient, surpassing radiofrequency (RF) technology by at least an order of magnitude, can be achieved in plasma-wakefield accelerators (PWFAs) by using an electron bunch to drive a plasma wave, in whose wakefield a trailing electron bunch can be accelerated [1–3]. Such acceleration in plasma can be utilised to shrink the size of future particle linear colliders or increase the photon energy reach of free-electron lasers, provided that other accelerated bunch parameters are preserved. These include the accelerated bunch brightness, energy spread, and repetition rate, which contribute to collider luminosity or average free electron laser (FEL) brightness. The energy transfer efficiency of the acceleration process is a vital consideration to further reduce the environmental impact of future facilities. To prove its applicability, plasma acceleration must either match the burst-mode MHz acceleration of superconducting machines such as FLASH, EuXFEL or ILC [4–6], or GHz acceleration of CLIC [7]. Alternatively, it could be operated continuously at multi-kHz repetition rate to match the average output of these facilities. However, to date, most demonstrations have been performed at 10 Hz or less. High-repetition-rate, high-average-power PWFA stages with high energy gains are also central components of proposals for future compact colliders such as HALHF [8,9], or free-electron lasers such as EuPRAXIA@SPARC_LAB [10], and thus require significant further research.

FLASHForward is a plasma-wakefield acceleration experiment at DESY, focussing on demonstrating the applicability of PWFA for future accelerator facilities by researching the GeV/m acceleration of FEL-quality electron bunches [11,12]. FLASHForward is driven by bunches from the FLASH linac, which are normally used to produce extreme UV and soft x-ray FEL radiation down to 3.2 nm in the fundamental for user experiments. The electron bunches have charges up to 1 nC, energies up to 1.35 GeV and typical emittances of approx. 1 µm [4, 13]. Due to the superconducting radiofrequency architecture of the FLASH linac, the electron bunches arrive in trains of up to 800 bunches with, typically, 1 µs spacing. The trains repeat at 10 Hz. To date, driver-trailing bunch pairs at FLASHForward have been generated with an energy collimator system in a dispersive part of the beamline [14]. Typically the driver has 300-500 pC of charge and a peak current of 1 kA, while the trailing bunch, the front of which trails the centre of the driver by ~ 600 fs, has tens of pC of charge and 0.3-0.5 kA peak current. The bunches are focussed to a β-function of 10-20 mm into discharge-generated plasmas with densities of order 1×10^{16} cm^{-3} to generate the wakefield [15].

* judita.beinortaite@desy.de

Content from this work may be used under the terms of the CC BY 4.0 licence (© 2026). Any distribution of this work must maintain attribution to the author(s), title of the work, publisher, and DOI.

ISBN: 978-3-95450-252-3 ISSN: 2673-5350 doi: 10.18429/JACoW-IPAC2026-WEO5M03

ON THE OPTIMIZATION OF THE NON-LINEAR PERFORMANCE OF 4th-GENERATION LIGHT SOURCES *

B. Kuske†, B. Alberdi-Esuain, Helmholtz-Zentrum Berlin, Berlin, Germany

Abstract

The successful non-linear performance of 4th-generation light sources can be supported through a proper design of the linear lattice. However, important quantities like the injection efficiency and the beam lifetime depend on the optimization of non-linear magnetic fields in the lattice like sextupoles and octupoles, and therefore on numerical optimization. The underlying quantities to be maximized are the limits of stable particle motion in the injection plane, the horizontal dynamic aperture, and the Touschek lifetime, i.e. the momentum acceptance of the ring. Commonly, multi-objective genetic algorithms are used for the direct optimization of the dynamic aperture and momentum acceptance. Alternatively, the resonance driving terms can be minimized. Both approaches need to take the uncertainties introduced by manufacturing tolerances and misalignment in the real machine into account. Using the parameters of the BESSY III storage ring project at HZB, Berlin, this paper compares both approaches and tries to develop an efficient optimization strategy for the upcoming technical design phase of BESSY III.

INTRODUCTION

HZB is preparing to build a 2.5 GeV storage ring as a replacement for BESSY II in the mid 2030s. BESSY III will utilize a multi-bend achromat (MBA) lattice (Fig. 1) to reach an emittance of 100 pm rad to satisfy the users demand for diffraction limited light at 1 keV. Much care has been taken to prepare a promising non-linear performance already in the development of the linear lattice [1]. Phase advances between sextupoles have been set to cancel the resonance driving terms (RDTs) and realise a higher-order achromat (HOA) lattice [2, 3]. The magnetic arrangement was chosen such, that the sextupole strength necessary to compensate for the natural chromaticity is minimal. Small emittance is reached by an optimal use of reverse bends, rather than by strong focusing. Nevertheless, the non-linear performance depends not only on the suppression of resonances, but also on confining the detuning, i.e. the tune's motion for large amplitudes and momentum offsets. This can be achieved by splitting up the initial two chromatic sextupole families into individual circuits and numerically finding an optimum between the robust performance of an HOA lattice with its reduced dependency on tolerances and sufficient momentum acceptance (MA) and dynamic aperture (DA). The MA is of paramount importance for BESSY III, to reach a long Touschek lifetime, important for operational flexibility across various user modes. The DA has to provide a sufficiently large area for injection. This paper investigates how the simultaneous reduction of the RDTs and the detuning terms can be used to define a promising sextupole scheme.

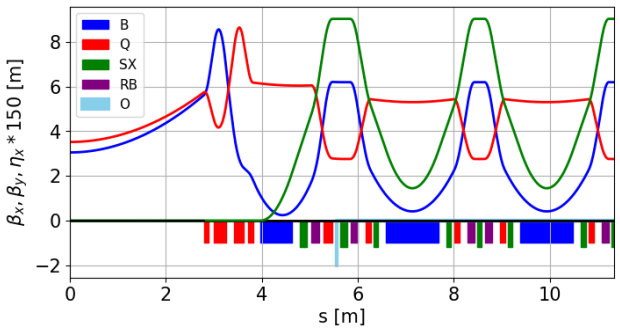

Figure 1: Half of a super period of the BESSY III lattice: $\beta_{x,y}$: blue, red, η_x: green. There is one chromatic octupole (light blue) and no harmonic multipole so far.

The results are compared to those found by multi-objective genetic optimization (MOGA).

SHORT INTRODUCTION TO DRIVING TERMS

The idea to place sextupoles with a certain phase advance between them to cancel non-linear effects originates in the 1970's, one early paper being [4], where transport matrices were used. A general treatment based on Hamiltonian formalism was derived in [5]. Based on [6], a closed form for RDTs applicable to storage rings was developed in [3], and is widely used today.

Following [7], let Eq. (1) be the Hamiltonian of the particle motion in an accelerator,

$$H(x,p_x,y,p_y;s) = \frac{p_x^2+p_y^2}{2(1+\delta)} - \frac{x\,\delta}{\rho} - \frac{x^2}{2\rho^2} + \mathrm{Re}\sum_{n=1}^{M}\frac{k_n+ij_n}{(n+1)!}(x+iy)^{n+1}, \quad (1)$$

with x, y the transverse particle positions, p_x, p_y canonical momentum conjugate to x and y, δ the relative momentum deviation, ρ the bending radius of the reference trajectory, and k_n and j_n the normal and skew multipole strengths of order n. The first three terms describe the solvable linear part of the system and the real part of the complex sum describes the perturbative part due to the non-linear elements in the ring. It is common to change to normalised coordinates and then to a resonance basis: $z^{\pm} = \sqrt{2J_z}\,e^{\pm i\phi_z} = z \mp ip_z$, with $z = x, y$, and ϕ_z the phase advance. Using this basis, and summing up over all elements in the ring, the nth order

* Work supported by German Bundesministerium für Forschung, Technologie und Raumfahrt, Land Berlin, and grants of Helmholtz Association
† bettina.kuske@helmholtz-berlin.de

Content from this work may be used under the terms of the CC BY 4.0 licence (© 2026). Any distribution of this work must maintain attribution to the author(s), title of the work, publisher, and DOI.

ISBN: 978-3-95450-252-3 ISSN: 2673-5350 doi: 10.18429/JACoW-IPAC2026-WEI5M03

REALIZATION OF HIGH-INTENSITY BEAMS WITH SMALLER EMITTANCE WITHOUT A TRANSVERSE FEEDBACK SYSTEM

Y. Shobuda*,1,2, P. Saha[1], T. Toyama[3], I. Yamada[2], N. Yoshimura[4]
[1]Japan Proton Accelerator Research Complex, Tōkai Mura, Japan
[2]Japan Atomic Energy Agency, Tōkai Mura, Japan
[3]High Energy Accelerator Research Organization, Tsukuba, Japan
[4]Toshiba, Kanagawa, Japan

Abstract

The RCS at J-PARC is a kicker-impedance-dominant machine, which exceeds the impedance budget from a classical viewpoint. However, we have achieved a 1-MW beam without any transverse feedback by fully utilizing the indirect space charge effect (due to chamber walls) to suppress beam instabilities. Although the indirect space charge effect is beneficial, the beam instability can still occur in a high-intensity beam with a smaller transverse emittance. To address this, we installed diode stacks and resistors at the ends of the four kicker power cables and have successfully conducted routine operations. This approach theoretically opens the door to achieving high-quality, higher-intensity beams, including a 2-MW beam, as no transverse feedback is required.

INTRODUCTION

The 3-GeV RCS [1] at J-PARC [2] is a proton accelerator to achieve a one megawatt beam by accelerating two bunches containing $N_b = 4.15 \times 10^{13}$ particles per bunch from 400 MeV to 3 GeV in 20 ms with a repetition rate of 25 Hz [3], without any transverse feedback system.

The RCS provides proton beams downstream to both the Material and Life Science Facilities (MLF) and the Main Ring (MR) by accumulating the injection beams from LINAC, following a painting scheme [4]. The standard unnormalized transverse painting emittance, the unnormalized value of the entire painting area, for the MLF is relatively large (e. g., 200 π·mm·mrad). However, the smaller emittance would be better (typically ~50 π·mm·mrad) for the MR, because the beams extracted from the RCS are delivered to the MR through the beam extraction line with a small mechanical aperture, exciting a large residual dose.

In the case of a smaller-emittance beam, special care must be taken regarding space-charge effects. This is because the smaller emittance beam increases the tune spread, expanding the probability of resonance crossing of particles, which restricts the available operational tune on the tune diagram because of the beam losses.

On the other hand, the beam coupling impedances [5] can drive the beam instabilities [5], which may be mitigated by selecting the other tunes.

However, both desirable tune regions for avoiding the resonance crossing and for suppressing the beam instabilities may compete with each other, thereby limiting the overall tunability of machine operation, urging the reduction of the impedance causing the beam instability.

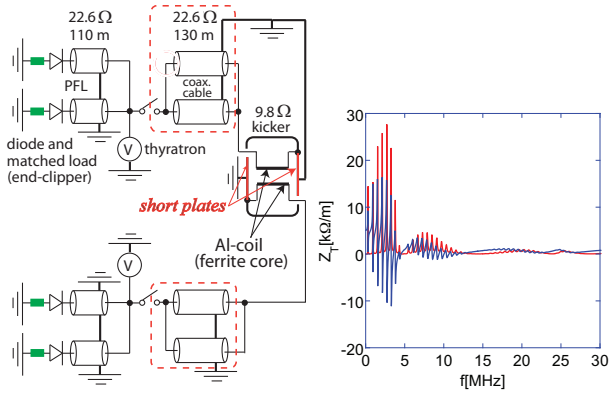

Figure 1: kicker (left); horizontal impedance Z_T (right) with the real part in red and the imaginary part in blue [8].

BEAM-INSTABILITIES AT THE RCS

Historically, the 3-GeV RCS at J-PARC was designed below the impedance budget, except for the kicker impedance from a classical viewpoint [6]. The horizontal impedance $Z_T(\omega)$ at Lorentz-$\beta_s = 1$ for one kicker is shown in the right panel of Fig. 1. Eight kickers (specified by Kicker Nos.1-8) whose impedance is around ten times higher than SNS kicker impedance [7] were installed into the RCS.

The enhancement of the kicker impedance is closely related to the merit of the power-saving of the kicker magnet. As shown in the left panel of Fig. 1, the kicker at the RCS is a transmission line type embedding two ferrite cores. The kicker has four terminals: two connected to the power supply through 130-m-long coaxial cables, and the other two terminated in a short circuit [9]. Shorting the kicker terminals benefits beam extractions by doubling the excitation currents, leading to power savings. Meanwhile, the impedance is enhanced during the acceleration period because the beam-induced current created by the beam passing through the kicker coil is accumulated and retained on the kicker cable owing to the absence of any resistors [10].

Because of the spike structure of the impedance shown in Fig. 1 originating from the kicker cable with open terminal, the beam growth rate critically depends on the operational tune [8]. The left panel of Fig. 2 shows the measured horizontal beam positions for a beam with $N_b = 3.15 \times 10^{13}$ particles per bunch (0.76-MW beam), color-coded accord-

* yoshihiro.shobuda@j-parc.jp

Content from this work may be used under the terms of the CC BY 4.0 licence (© 2026). Any distribution of this work must maintain attribution to the author(s), title of the work, publisher, and DOI.

ISBN: 978-3-95450-252-3 ISSN: 2673-5350 doi: 10.18429/JACoW-IPAC2026-WEO5M04

OPTICS CORRECTION FOR FOURTH-GENERATION LIGHT SOURCES AND FUTURE COLLIDERS

E. Musa*, I. Agapov, K. Paraschou, J. Keil,
Deutsches Elektronen-Synchrotron DESY, Hamburg, Germany
S. M. Liuzzo, S. White, European Synchrotron Radiation Facility, Grenoble, France
S. Habet, Synchrotron SOLEIL, Gif-sur-Yvette, France

Abstract

Accurate lattice-optics correction is essential for achieving the design performance of modern light sources and future circular colliders targeting ultra-low emittances. Such machines rely on strong magnets that are highly sensitive to field and alignment errors. In this work, we investigate approaches for the correction of the linear optics of several accelerators. The study includes selecting appropriate correction steps, defining the fitted parameters, and designing optics correction schemes tailored to the characteristics of each accelerator. Experimental tests were performed at ESRF-EBS, while the simulation studies for PETRA IV, FCC-ee and SOLEIL II investigate the achievable performance of future machines.

CHALLENGES IN LOW-EMITTANCE STORAGE RINGS

The pursuit of developing modern fourth-generation light sources and future circular colliders presents significant challenges. In synchrotron light sources, the performance is characterized by the brilliance [1] of the emitted radiation, which scales inversely with the transverse beam emittances. Similarly, future circular colliders aim to maximize luminosity [2], requiring extremely small beam sizes at the interaction points. Strong focusing and sextupoles required for ultra-low emittance increase the sensitivity to alignment and field errors. In particular, strong sextupoles introduce feed-down effects that further complicate the control of the linear optics under tight alignment tolerances, ultimately impacting the overall machine performance.

Figure 1 illustrates the sensitivity of the FCC-ee at Z energy lattice to unrealistically small transverse alignment errors in both the arc and Interaction Region (IR). For an alignment error of 1 µm, the vertical RMS beta-beating increases significantly to approximately 30% in the IR, demonstrating the high sensitivity of the optics to small misalignments.

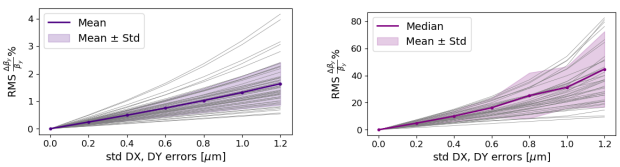

Figure 1: Optics sensitivity to transverse alignment errors for the FCC-ee Z-energy lattice [3].

* elaf.musa@desy.de

OPTICS CORRECTION METHODS

A number of optics correction algorithms and techniques have been developed, including K-modulation, Turn-by-Turn (TbT) beam excitation measurements, and Orbit Response Matrix (ORM)-based methods such as LOCO [4]. Although successfully applied in several accelerators, the K-modulation [5] method can become time consuming for HMBA lattices due to the large number of quadrupoles requiring individual variation.

Optics correction techniques based on TbT beam centroid measurements are widely used, particularly in circular colliders [6]. However the experimental test of these approach in light sources might be limited by hardware problems [7].

LOCO has become a standard tool for optics correction, particularly in synchrotron light sources [8–10]. For machines with strong focusing and complex lattice structures, such as Hybrid Multi-Bend Achromats (HMBA), the correction problem becomes increasingly challenging due to parameter degeneracy and strong correlations between lattice elements.

A comprehensive review of optics correction techniques and their evolution is presented in Ref. [11].

LOCO solves a non-linear least-squares problem by iteratively updating lattice parameters using ORM measurement together with Singular Value Decomposition (SVD) technique as described in Ref. [4]. Strong quadrupole correlations can lead to non-physical solutions.

To mitigate this degeneracy, additional constraints are introduced to regularize the solution. The modified χ^2 function is given by (see Ref. [12] for details):

$$\chi^2 = \sum_{i,j} \frac{\left(C_{\mathrm{mod},ij} - C_{\mathrm{meas},ij}\right)^2}{\sigma_i^2} + \frac{1}{\sigma_{\Delta K}^2} \sum_k w_k^2 \left(\Delta K_k\right)^2, \quad (1)$$

where the second term penalizes large variations of selected quadrupole strengths. The weights w_k allow targeted regularization. Within the Levenberg–Marquardt [13] framework, the parameter update formula becomes:

$$\left(J^T W J + \lambda I + G^T G\right) \Delta \mathbf{p} = J^T W \left(C_{\mathrm{meas}} - C_{\mathrm{mod}}\right), \quad (2)$$

where J is the Jacobian matrix, and W includes the BPMs noise, and G is the constraint matrix defined as

$$G = \mathrm{diag}\left(\frac{w_k}{\sigma_{\Delta K}}\right). \quad (3)$$

Content from this work may be used under the terms of the CC BY 4.0 licence (© 2026). Any distribution of this work must maintain attribution to the author(s), title of the work, publisher, and DOI.

ISBN: 978-3-95450-252-3 ISSN: 2673-5350 doi: 10.18429/JACoW-IPAC2026-WEO5M05

LOW-EMITTANCE, LOW-CHARGE OPTIMIZATION OF THE ARGONNE WAKEFIELD ACCELERATOR FOR THE NANOPATTERNED MICROBUNCHING EXPERIMENT*

R. Margraf-O'Neal†, A. Ody, J. Power, Argonne National Laboratory, Lemont, United States
J. Maxson, Cornell University, Ithaca, United States
R. Ryne, Lawrence Berkeley National Laboratory, Berkeley, United States
H. Xu, N. Yampolsky, Los Alamos National Laboratory, Los Alamos, United States
G. Ha, B. N. Temizel Ozdemir, Northern Illinois University, DeKalb, United States
A. Halavanau, N. Majernik, SLAC National Accelerator Laboratory, Menlo Park, United States
G. Andonian, J. Phillips, J. Rosenzweig
University of California, Los Angeles, Los Angeles, United States
D. Abell, University of Maryland, College Park, College Park, United States

Content from this work may be used under the terms of the CC BY 4.0 licence (© 2026). Any distribution of this work must maintain attribution to the author(s), title of the work, publisher, and DOI.

Abstract

Low-emittance microbunched electron beams are a key ingredient in free-electron lasers (FELs), facilitating gain and coherence in radiation production. It has been proposed, such as by the Compact X-ray FEL (CXFEL) group at Arizona State University, that nano-scale microbunching could be produced by rotating transverse beamlets into the longitudinal plane. Such a technique could make short-wavelength FELs much more compact, reducing cost. Thus, a collaboration has been formed to test this principle using the emittance exchange (EEX) beamline of the Argonne Wakefield Accelerator (AWA). This experiment will take micro-scale transverse modulations on a TEM grid and produce mico-to-nano scale microbunches. Performing this with AWA's 40 MeV electron beam will require low normalized emittance ($\approx$50 nm $\cdot$ rad), and low charge ($\approx$1pC) electron bunches that are not commonly produced at AWA. These proceedings will detail our work to produce and characterize this low emittance in the AWA beamline.

INTRODUCTION

The nanopatterned microbunching experiment [1, 2], to take place in 2027-2028, is sketched in Fig. 1. 44 MeV electrons are scattered by a 12.5 µm TEM grid, creating transverse beamlets that are then demagnified with beamline of five quadrupoles [3] to 3 µm, and converted through emittance exchange to 800 nm microbunching.

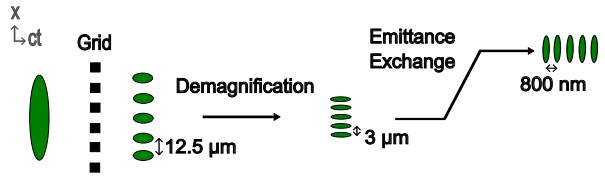

Figure 1: Nanopatterned microbunching experiment.

The nanopatterned microbunching experiment has several requirements on the AWA facility that are outside of its normal operating range. AWA is tuneable within a large charge range (1 pC - 400 nC), but optimized for high charge (100s of nC) bunch trains to drive structure wakefield acceleration [4, 5]. However, to mitigate collective effects, the nanopatterned microbunching experiment must operate at low charge (2-6 pC incident on the TEM grid). Low normalized emittance (50 nm $\cdot$ rad) must be achieved at this charge to preserve the closely spaced transverse beamlets. Our previous measurements in this range, however, found micron-scale normalized emittance at 1 pC [2]. This proceedings will document our progress to push this emittance lower in our development of this low-charge, low-emittance mode for the nanopatterned microbunching experiment.

Two beamtimes, in July 2025 and April 2026, are described in this proceedings. Between these two beamtimes, the AWA gun was replaced and upgraded to a symmetrized design, and the gun solenoids and Ce_2Te photocathode were also replaced. Thus, this proceedings also documents how the AWA gun upgrade changed our measured emittance.

METHODS

High-Resolution Transverse Diagnostics

We installed a Blackfly camera (BFLY-PGE-23S6M-C) with a Nikon AF FX 200 mm f/4D IF-ED Lens and 381 mm (for knife scan) or 62 mm (for quad scan) extension tube. This was focused on a 100 µm thick YAG:Ce screen after a 45° mirror reflection. The light path distance from the YAG to the vacuum chamber window was 165 mm, and the working distance from the end of the camera lens to the YAG was 178 mm or 210 mm respectively.

This set-up resulted in a 1.30 µm and 3.60 µm pixel size. Using a US Air Force target in the installed system, the camera resolution was measured to be 6.2 µm and 7.0 µm for each configuration.

Studying this system [2, 6] indicated that our high-resolution imaging system, with its thick, 100 µm YAG:Ce screen, can only resolve electron beams down to σ = 40-50 µm. In future upgrades, we plan to replace the

* This work is supported by the U. S. Department of Energy, under contract No. DE-AC02-06CH11357.
† rachel4iam@gmail.com

ISBN: 978-3-95450-252-3 ISSN: 2673-5350 doi: 10.18429/JACoW-IPAC2026-WEO6M01

AI AND MACHINE LEARNING TECHNIQUES FOR LNL ACCELERATORS

Y.K. Ong*[1,2], L. Bellan[1], D. Bortolato[1], M. Comunian[1], E. Fagotti[1], M. Giacchini[1], F. Grespan[1], M. Montis[1], A. Pisent[1]
[1]INFN-LNL, Legnaro, Italy
[2]Sapienza University of Rome, Rome, Italy

Abstract

The application of Artificial Intelligence (AI) and Machine Learning (ML) to particle accelerator systems has emerged as an effective strategy for managing complex operations and enhancing performance. At INFN-Legnaro National Laboratories (INFN-LNL), both offline and online AI/ML-driven approaches have been developed to improve beam dynamics, reduce setup times, and increase overall accelerator efficiency.

Offline efforts focus on surrogate modeling of complex facilities such as ANTHEM BNCT, as well as on virtual diagnostics implemented using supervised neural operators. By combining these tools with AI/ML optimization algorithms, new design and commissioning strategies are being explored to further enhance beam quality and operational performance.

In parallel, online real-time optimization strategies based on Bayesian Optimization (BO) has delivered promising results. Notably, at the PIAVE-ALPI superconducting accelerator, the application of BO improved beam transmission up to 85%, a significant increase compared to the typical operational average of 35%. These advances demonstrate the growing impact and future potential of AI/ML technologies in accelerator science and operations.

INTRODUCTION

Future accelerator facilities for particle, nuclear, and photon science will operate at increasingly higher beam energies and intensities, which in turn leads to more demanding operational and design requirements [1–3]. Meeting these goals requires dealing with stronger nonlinear effects, stricter beam quality requirements, improved reproducibility, and greater operational flexibility for a wide range of user applications. The complexity of such designs, driven by the need to meet performance targets within practical and economic constraints, results in significantly higher computational costs during the design phase.

These challenges are closely linked to the need for efficient parameter optimization, which include tuning control parameters during operation to maximize performance (online optimization) and determining optimal configurations during the design phase (offline simulation-based optimization) [4].

Recent advances in optimization algorithms and artificial intelligence have enabled the exploration of increasingly complex and high-dimensional parameter spaces. In parallel, surrogate models have emerged as powerful tools for reducing computational costs by providing fast approximations of high-fidelity simulations, thereby enabling more efficient exploration of both design and operational parameter spaces. Together, these approaches contribute to significant improvements in accelerator performance and operational capabilities.

In this work, we present AI/ML-based techniques and strategies applied to LNL accelerators. The systems considered include the ANTHEM BNCT MEBT line and the PIAVE-ALPI accelerator complex, where both offline and online optimization approaches, combined with surrogate models, have been developed and tested.

ACCELERATOR SYSTEMS AND CHALLENGES

Anthem BNCT Mebt Line

The ANTHEM BNCT facility is a cancer therapy installation currently under construction in Caserta, Italy [5]. It employs an accelerator-based neutron source to deliver epithermal neutrons to patients injected with a tumor-targeting drug containing Boron-10 (^{10}B). This process induces neutron capture, converting ^{10}B into an excited ^{11}B state, which subsequently decays into an alpha particle and ^{7}Li. These reaction products selectively destroy cancer cells while sparing surrounding healthy tissue.

The medium energy beam transport (MEBT) line (see Fig. 1) is located downstream of the TRASCO radio-frequency quadrupole (RFQ) [6]. Its role is to transport and shape the high-intensity proton beam (5 MeV, 30 mA, 150 kW) onto a specially designed beryllium target.

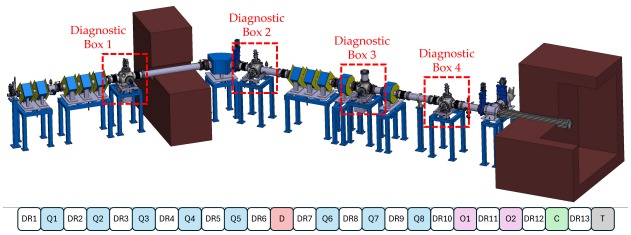

Figure 1: 3D rendering of the ANTHEM MEBT line with beamline elements (DR: drift, Q: quadrupoles, D: dipole, O: octupole, C: collimator, T: target) and diagnostic sections (red dashed boxes) highlighted.

The main challenge of this beamline is to exploit nonlinear effects arising from both the high-intensity beam and the octupole magnets to shape the beam distribution. The objective is to deliver approximately 1 kW/cm^2 of beam power onto a 12 cm × 12 cm target while maintaining high transmission efficiency.

* ysaong@lnl.infn.it

Content from this work may be used under the terms of the CC BY 4.0 licence (© 2026). Any distribution of this work must maintain attribution to the author(s), title of the work, publisher, and DOI.

ISBN: 978-3-95450-252-3 ISSN: 2673-5350 doi: 10.18429/JACoW-IPAC2026-WEP1001

RF CAVITIES AND BEAM LOADING IN THE MUON COLLIDER RECTILINEAR COOLING CHANNEL*

C. Barbagallo*, A. Grudiev, CERN, Geneva, Switzerland
D. Merenich, X. Lu[1], Northern Illinois University, DeKalb, Illinois, USA
T. Luo, Lawrence Berkeley National Laboratory, Berkeley, California, USA
[1]also at Argonne National Laboratory, Lemont, Illinois, USA

Abstract

The rectilinear cooling channel of a muon collider requires high-gradient normal-conducting RF cavities to enable ionization cooling, which is essential to achieve high luminosity. Reaching this performance demands bunches containing $\sim 10^{12}$ or even more muons in the cooling channel. At these intensities, beam-induced wakefields can cause significant beam loading, reducing the accelerating gradient and affecting beam stability. This paper presents the conceptual RF design and analysis of beam-induced effects in copper cavities designed to meet the beam dynamics requirements of the muon cooling channel. Cavities are optimized and compared in terms of RF performance and power requirements. Wakefields and beam loading are analyzed, and a compensation strategy for beam loading is proposed.

INTRODUCTION

The muon collider is a compact high-energy lepton accelerator concept aimed at advancing the frontiers of particle physics [1, 2], with a reference design targeting 10 TeV center-of-mass energy and 10 ab^{-1} integrated luminosity [3]. This requires rapid six-dimensional (6D) ionization cooling to reduce the large muon beam emittance before muon decay [4]. The International Muon Collider Collaboration (IMCC) team recently optimized the cooling lattice [5], a rectilinear channel based on the MAP concept [6] with pre-merging (Rectilinear A) and post-merging (Rectilinear B) sections, each comprising multiple identical cooling cells with absorbers, RF cavities, solenoids, and dipole magnets. The channel includes ~3,660 pillbox RF cavities operating in the TM_{010} fundamental mode (FM) at frequencies f_0 = 352–704 MHz inside multi-Tesla solenoids, and closed with beryllium (Be) windows to enhance the achievable gradient and beam transmission [7, 8]. Muon bunches of $\sim 10^{12}$ particles induce wakefields in the RF cavities, causing beam loading and a reduction of the accelerating gradient.

Guided by the latest lattice and previous Muon Ionisation Cooling Experiment (MICE) cavity designs [9–11], we designed and optimized elliptical copper (Cu) RF cavities with Be-windowed irises for each stage of the cooling channel. RF figures of merit, space-charge and resonant wakefields, and beam loading were simulated in CST Studio Suite® [12] for RF cavities with Be windows to evaluate their impact on cavity performance across the 6D cooling channel.

RF CAVITY DESIGN

The RF cavity design, first presented in [13], follows the elliptical cavity parametrization of [14] (see Fig. 1). It operates in pulsed mode at 5 Hz with a duty factor of $\sim 10^{-4}$.

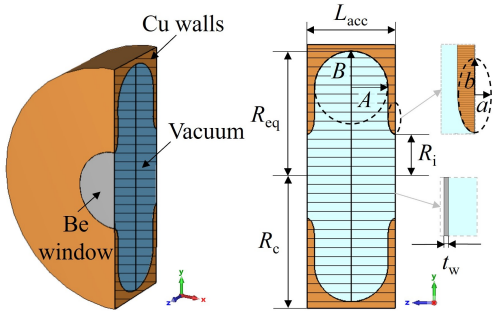

Figure 1: Single-cell RF cavity design for muon cooling [13].

Beam dynamics specifications for each stage of the cooling channel define the accelerating length L_{acc}, the nominal gradient $E_{nom} = TTF\, E_{acc}$, where E_{acc} is the accelerating gradient and TTF the transit time factor, the window radius R_i and thickness t_w (~10 µm to 120 µm depending on the stage), which are used as input for the RF cavity design. The geometrical parameters $A = B$ and the iris ellipse dimensions a and b, were optimized to minimize the peak surface electric field E_{peak} to prevent RF breakdown, while maximizing the FM shunt impedance $(R/Q) \cdot Q_0$ to reduce the surface power losses P_{diss} and the peak power $P_g = P_{diss}\beta_c$, with coupling factor $\beta_c = 1.2$. The equator radius R_{eq} tunes the cell frequency and the cavity radius is $R_c = R_{eq} + a$.

Table 1 reports the main beam dynamics inputs, the geometrical parameters, and the RF figures of merit for the single-cell cavities in the cooling channel. The geometrical shunt impedance (R/Q) is relatively stable across the different stages. The peak surface electric fields E_{peak} are below 40 MV/m, owing to an optimal E_{peak}/E_{acc} of 1.2–1.3, depending on the stage, due to the presence of the windows. Removing the windows, e.g., in the stage-B5 cavity, nearly doubles the losses and brings the E_{peak} close to 50 MV/m. The plug power of the RF system, $P_{plug,tot} = P_{g,avg,tot}/(\eta_g\, \eta_m)$, for a generator duty factor $\sim 10^{-4}$, generator efficiency $\eta_g = 0.7$, and modulator efficiency $\eta_m = 0.9$, remains within acceptable limits for pulsed normal-conducting operation.

* work endorsed by the IMCC
* carmelo.barbagallo@cern.ch

Content from this work may be used under the terms of the CC BY 4.0 licence (© 2026). Any distribution of this work must maintain attribution to the author(s), title of the work, publisher, and DOI.

ISBN: 978-3-95450-252-3 ISSN: 2673-5350 doi: 10.18429/JACoW-IPAC2026-WEP1003

BEAM LOSS DYNAMICS FROM SPURIOUS CLIQ DISCHARGES IN HL-LHC INNER TRIPLET MAGNETS

C. Lannoy*, C. Hernalsteens, D. Pracht, E. Ravaioli, J. Uythoven, D. Wollmann
European Organization for Nuclear Research, Geneva, Switzerland

Abstract

The High-Luminosity Large Hadron Collider (HL-LHC) will increase the nominal LHC integrated luminosity by a factor of 10 and operate with proton beams storing up to 700 MJ of energy per beam. In this upgraded machine, a new quench protection system, the Coupling-Loss Induced Quench (CLIQ) system, will be installed in combination with conventional quench heaters to protect the Nb_3Sn inner triplet superconducting magnets. A spurious CLIQ discharge with circulating beams represents the most critical beam-loss-related failure scenario in the HL-LHC era due to the rapid electromagnetic field perturbations it induces. Simulations combining dynamic electromagnetic field maps from a spurious CLIQ discharge with `Xsuite` beam tracking show that the entire beam can be lost within 4 ms, with critical loss levels, defined as losses sufficient to pose a risk of damage to accelerator components, reached within only a few turns. Both double-Gaussian and q-Gaussian halo profiles are studied, revealing significant sensitivity of beam losses to the tail population distribution. The influence of machine optics is also examined, showing that the baseline round optics provide sufficient safety margin, whereas for the flat optics option this becomes significantly more critical.

INTRODUCTION

The High-Luminosity upgrade of the LHC (HL-LHC) will rely on new Nb_3Sn inner triplet quadrupoles installed around the interaction points IP1 and IP5, hosting the high luminosity experiments ATLAS and CMS, to focus proton beams storing up to 700 MJ per beam [1]. To protect these magnets in case of a quench, the conventional quench-heater system is complemented by the Coupling-Loss Induced Quench (CLIQ) system [2]. CLIQ induces, through a capacitive discharge into the coil of the magnet, an oscillation of the transport current, producing intense coupling losses that heat the conductor internally and quench a large volume of the coil without relying on heat diffusion from external heaters.

While the quench protection logic guarantees that a beam dump is requested before any standard CLIQ discharge is triggered, a spurious CLIQ discharge with circulating beams cannot be excluded and constitutes one of the most critical beam-loss-related failure scenarios of the HL-LHC era. The very fast electromagnetic transient generated by the discharge produces strong perturbations of the magnetic field experienced by the beam in the inner triplet, leading to large losses on the primary collimators (TCPs) within only a few turns. Protection against this failure relies on a dedicated fast interlock [3] requesting beam extraction; the question addressed here is whether the beam can be safely extracted before the losses reach the critical loss level of 1 MJ in the collimation region. This value corresponds to the energy deposition above which permanent damage to the LHC primary-collimator jaws cannot be excluded [4].

This contribution updates previous studies [5,6] of a spurious CLIQ failure, with time-dependent magnetic field maps extending up to 50 ms after the discharge and the use of q-Gaussian transverse beam halo profiles in addition to the conventionally used double-Gaussian.

SIMULATION SETUP

The beam dynamics is simulated with `Xsuite` [7] using the HL-LHC v1.6 optics, with both the round optics baseline ($\beta^* = 15$ cm) and the flat optics option ($\beta^*_{x/y} = 7.5\,\text{cm}/18\,\text{cm}$). The main beam and machine parameters are summarised in Table 1. The TCPs are set to their nominal 6.7 σ retraction. Relaxed collimator settings at 8.5 σ would likely increase the available margin and are therefore conservatively not considered in this paper.

Table 1: Main Beam and Machine Parameters

Parameter	Value
Beam energy	7 TeV
Stored beam energy	700 MJ
Bunch intensity*	2.2×10^{11} p$^+$/bunch
Normalised emittance	2.5 µm
Half crossing angle (IP1/5)	250 µrad
TCP retraction	6.7 σ
β^* (round)	15 cm
$\beta^*_{x/y}$ (flat)	7.5 cm / 18 cm

* Nominal bunch intensity at flat top, relevant for this failure case (compared to 2.3×10^{11} p$^+$/bunch at injection).

The Q2b Nb_3Sn inner triplet superconducting quadruopole magnet on the right side of IP5 [4] was identified as the most critical case for Beam 1, leading to the fastest and largest beam losses [5]. The electromagnetic perturbation produced by a spurious CLIQ discharge in this magnet is computed with COMSOL Multiphysics 5.3a [8] up to 50 ms after the trigger using a 2D-magnet model. The resulting Cartesian field maps are expanded into multipolar components by fitting along the x and y axes. Of all the components extracted, only the normal quadrupole and the skew octupole reach non-negligible amplitudes on the relevant time scale of about 1 ms and are illustrated in Fig. 1. The corresponding time-dependent strengths are used as inputs to the `Xsuite` tracking simulations. The COMSOL model can also include the mitigating effects of the beam

* christophe.lannoy@cern.ch

Content from this work may be used under the terms of the CC BY 4.0 licence (© 2026). Any distribution of this work must maintain attribution to the author(s), title of the work, publisher, and DOI.

ISBN: 978-3-95450-252-3 ISSN: 2673-5350 doi: 10.18429/JACoW-IPAC2026-WEP1004

OVERCOMING RF POWER LIMITATIONS FOR THE HL-LHC ERA*

B. E. Karlsen-Baeck†[1], X. Buffat, A. Butterworth, R. Calaga, S. Kostoglou, C. Marrelli, D. Mirarchi, S. Morales Vigo, B. Salvachua, H. Timko, K. Turaj, D. Valuch, M. Zampetakis
CERN, Meyrin, Switzerland
[1]also at the Department of Physics, Sapienza Università di Roma, Rome, Italy

Abstract

Limitations in RF power at the injection plateau of the Large Hadron Collider (LHC) have been a major concern for the High-Luminosity (HL) LHC era. The increased bunch charge requires more RF power to compensate beam loading. A higher RF voltage at the injection plateau is moreover vital for both the RF capture and to counteract particle leakage from the buckets. The projected RF power with HL-LHC parameters is beyond what the currently installed klystrons can provide. Consequently, an unacceptable amount of particles lost at the start of acceleration is expected. These limitations have now been overcome, thanks to a combination of several mitigations. More power from high-efficiency klystrons will be complemented by an evolved optimization of the RF system parameters in terms of tuning and quality factor. This contribution will give an overview on the operational improvements and mitigation measures that are currently being put in place to handle the HL-LHC beams. Essential studies in the framework of the LHC high-intensity tests in 2026 are outlined.

INTRODUCTION

The Large Hadron Collider (LHC) will undergo a high-luminosity (HL) upgrade for the next physics run starting in 2030 [1, 2]. A large portion of the luminosity increase will come from doubling the design bunch intensity from 1.15×10^{11} protons per bunch (p/b) to 2.3×10^{11} p/b at injection. The higher bunch intensity will significantly increase the power demand of the LHC RF system, due to stronger beam loading effects. In addition, increased RF voltage is required to maintain an acceptable amount of beam losses at the start of the acceleration ramp.

The start-of-ramp losses have two main sources. Uncaptured beam is generated at the bunch-to-bucket transfer when particles from the Super Proton Synchrotron (SPS) arrive outside the RF buckets in the LHC. The momentum spread of the HL-LHC bunches is expected to be larger, requiring a higher RF capture voltage to maintain the current amount of uncaptured particles. The other source is particles leaking from the RF buckets. Filling the two LHC rings with beam at the injection plateau takes on the order of 30 min to 60 min depending on the number of injections. During this time the circulating bunches slowly lengthen due to intra-beam scattering (IBS) and noise from the RF system [3]. Both these effects will cause particles to diffuse out of the RF buckets and circulate asynchronously with respect to the RF system. In particular, IBS-driven bunch lengthening will become stronger with HL-LHC bunch intensities for which a higher RF voltage will be the main cure. Both the uncaptured beam and the particles diffusing out of the RF buckets will keep circulating outside the RF buckets until they are either removed by the abort-gap cleaning using the transverse damper [4] or are lost at the start of the ramp. By design, the start-of-ramp beam losses originating from the off-momentum particles will mainly be intercepted on the collimators in interaction region (IR) 3 [5, 6].

Beam loss monitors (BLMs) are placed all along the LHC ring to track particle losses over 12 running sums. Each running sum of each BLM has a threshold beyond which the BLM will trigger the beam to be sent to the beam dump [7]. Hence, if the capture voltage is insufficient, the amount of off-momentum particles will increase, leading to frequent beam dumps.

There are two ways to overcome these losses. One way is to accept more losses. This can be attained by, for instance, increasing the threshold of the BLM system in IR 3, provided that the equipment can accept more losses. Moreover, by removing additional off-momentum particles with the transverse damper prior to the ramp, a portion of the losses can be moved to the pre-ramp phase. However, the preferred way is to limit the generation of unbunched particles in the first place, which can be done by increasing the RF voltage. For HL-LHC, it is estimated that a total RF voltage of 7.9 MV is required to maintain the current amount of beam losses. This would require a peak RF power beyond the 300 kW available from the LHC klystrons by design [8]. The acceleration of beams during the HL-LHC era will therefore require a combination of both optimizing the RF system to maximize the RF voltage and accepting more start-of-ramp losses.

OPERATIONAL OPTIMIZATION OF THE LHC RF SYSTEM

Studies were conducted on multiple fronts during the current run (2022-2026) to optimize the operation of the RF system in the LHC. One of the conclusions from the last run (2018) was the importance of frequent energy matching between the SPS and LHC [9]. Above a certain offset in energy between the two accelerators, the amount of uncaptured particles would increase significantly, adding to the beam losses at the start of the ramp. These offsets were as high as 200 ppm, corresponding to 90 MeV. After more regular corrections of the SPS-LHC energy matching during the current run, the standard deviation of the offsets for operational fills was reduced to 30 MeV [10].

* Research supported by the HL-LHC project
† birk.beck@cern.ch

Content from this work may be used under the terms of the CC BY 4.0 licence (© 2026). Any distribution of this work must maintain attribution to the author(s), title of the work, publisher, and DOI.

ISBN: 978-3-95450-252-3 ISSN: 2673-5350 doi: 10.18429/JACoW-IPAC2026-WEP1008

MODELING LONGITUDINAL BEAM PARAMETER SPREADS FOR THE HL-LHC ERA*

B. E. Karlsen-Baeck†[1], C. Becker, R. Calaga, I. Karpov, S. Kostoglou, H. Timko, M. Zampetakis,
CERN, Meyrin, Switzerland
[1]also at Sapienza Università di Roma, Rome, Italy

Abstract

Roughly 2500 bunches are accelerated to collision energy during physics production in the Large Hadron Collider (LHC). Due to the beam production scheme in the injector chain, a certain spread in bunch length and intensity at injection into the LHC is unavoidable. The variation in these parameters has implications for RF capture, leakage of particles from the buckets at flat-bottom, and therefore the losses at the start of acceleration. Moreover, bunches with particularly high intensity or short length can become unstable. With the doubling of the nominal bunch charge in the High-Luminosity (HL) LHC era, these variations will become increasingly important. Beam tests have been carried out over the past few years in the LHC with beam intensities up to the HL baseline. Based on data from these studies, projections of longitudinal parameter spreads can be made for the HL-LHC era. In this contribution, the parameters of the beams injected into the LHC are examined in detail. These results are discussed within the context of beam stability and the generation of off-momentum particles at injection energy in the HL-LHC.

INTRODUCTION

The nominal bunch intensity injected into the Large Hadron Collider (LHC) will be increased from 1.8×10^{11} protons per bunch (p/b) during the present run to 2.3×10^{11} p/b for the High-Luminosity (HL-)LHC era [1, 2], which comes with a number of challenges. Due to the limitations of the power available in the LHC radio frequency (RF) system, the beam losses at the start of the energy ramp are expected to increase [3, 4]. Furthermore, recent theoretical studies have shown that the HL-LHC beams could be near the limit of stability in the longitudinal plane [5]. Both of these challenges are strongly influenced by the exact charge and distribution of the beams that will be delivered to the HL-LHC.

Beams with the HL-LHC specifications have already been injected into the LHC during machine development (MD) sessions performed in 2024 and 2025. The bunch parameters like the bunch length and bunch intensity were measured during these sessions. In the following, the analysis of longitudinal beam parameters from these first high-intensity MD sessions are presented. The consequences for the operation of the HL-LHC in terms of beam losses and beam stability are also briefly discussed.

* Research supported by the HL-LHC project
† birk.beck@cern.ch

BUNCH LENGTH AND INTENSITIES DURING HIGH-INTENSITY TESTS

During MD sessions in 2024 and 2025, the LHC captured trains with bunch intensities close to the HL-LHC baseline from its injector, the Super Proton Synchrotron (SPS). In addition to the standard beam for HL-LHC, these bunch intensities have been probed with the two other foreseen beam types as well: The batch compression merging and splitting (BCMS) beam, which has lower transverse emittances, and the 8 bunches 4 empty buckets (8b4e) beam type, which is an alternative to mitigate electron cloud build up, if needed [6].

The bunch length and intensity of the three different beam types for HL-LHC are represented in Fig. 1. The bunch intensity was measured using the fast beam current transformer (FBCT) in the SPS at top energy before extraction. The bunch length was found using the SPS beam quality monitor (BQM), which retrieves the linear charge density of the beam measured by a wide-band longitudinal pick-up [7]. By convention in the SPS and LHC, the bunch length is defined to be the 4σ-equivalent to the estimated full-width at half-maximum (FWHM) of the bunch. The BQM therefore extracts the bunch length by finding the FWHM of the line-density, τ_{FWHM}, and then scales it by $2/\sqrt{2\ln 2}$ to obtain the 4σ-equivalent, $\tau_{4\sigma}$. The 4σ-equivalent bunch length was used to calculate the longitudinal emittance at extraction assuming steady-state conditions. Finally, the LHC bunch length was calculated from the emittance and assuming an RF voltage of 7.9 MV, which is the baseline capture voltage in the LHC during the HL-LHC era.

The LHC Injectors Upgrade (LIU) beam parameter specifications along with their spreads are represented by the shaded areas in the plots in Fig. 1 [8]. For all three beam types, the bunch length is on the lower side of the specifications. During the high-intensity measurements, the main RF voltage at SPS extraction was limited to 8.5 MV for the standard and BCMS beams and 8.0 MV for the 8b4e trains while the LIU baseline is 10 MV. This was caused by limitations in RF power in the SPS. The longitudinal emittance was therefore lower in the MD sessions compared to the baseline for HL-LHC, even though the SPS bunch length was very close to the specified 1.65 ns. The bunch intensity, on the other hand, is within the LIU specifications with a peak-to-peak spread of 2.0×10^{11} p/b to 2.6×10^{11} p/b.

The bunch intensity threshold for longitudinal instabilities increases with the bunch length [9, 10]. How these parameters correlate with each other from the injectors could therefore become important for beam stability in the LHC.

Content from this work may be used under the terms of the CC BY 4.0 licence (© 2026). Any distribution of this work must maintain attribution to the author(s), title of the work, publisher, and DOI.

ISBN: 978-3-95450-252-3 ISSN: 2673-5350 doi: 10.18429/JACoW-IPAC2026-WEP1009

INTERLOCKING OF LATTICE SKEW QUADRUPOLE CIRCUITS IN THE LHC

C. Lannoy*, C. Hernalsteens, S. Kostoglou, J. Uythoven, D. Wollmann
European Organization for Nuclear Research, Geneva, Switzerland

Abstract

The Large Hadron Collider operates with 24 power converter circuits supplying the lattice skew quadrupole magnets for coupling correction. These circuits are currently not interlocked via the Powering Interlock Controller. Recent operational experience shows that a trip of one of these circuits can cause beam losses that can lead to beam dumps via beam loss monitors. This study employs Xsuite beam tracking simulations to assess the impact of individual skew quadrupole circuit failures on beam losses under realistic LHC Run 3 operating conditions. The simulations identify the circuits that were subsequently connected to the beam interlocking system during the 2025 Year-End Technical Stop.

INTRODUCTION

The Large Hadron Collider (LHC) uses 24 lattice skew quadrupole circuits (RQS), 12 per beam, to correct the linear coupling between the horizontal and vertical planes [1]. The circuits are split into two families: eight 4-magnet circuits (4 per beam, named "RQS.A[1–8][1–8].{B1/B2}"), with magnets (MQS) distributed across an arc between two insertion regions and equipped with Energy Extraction (EE) systems, and sixteen 2-magnet circuits (8 per beam, named "RQS.{R/L}[1–8].{B1/B2}"), with magnets on one side of an insertion region, without EE. For identical orbit offsets and currents, the 4-magnet circuits produce a larger integrated kick upon a sudden current decay and are therefore expected to have a larger impact on the beam. Figure 1 shows the position of the Beam 1 RQS magnets around the ring together with the measured orbit (horizontal and vertical) from the Beam Position Monitors (BPM) and the theoretical closed orbit defined by the optics. The orbit at the RQS magnet locations is highlighted.

The RQS circuits are currently not connected to the Powering Interlock Controller (PIC). A trip therefore does not trigger a pre-emptive beam dump request via the Beam Interlock System (BIS): the beam is only extracted reactively if the beam losses exceed the Beam Loss Monitor (BLM) dump thresholds. During LHC Run 3, 36 RQS trip events were recorded [2], of which 17 occurred without beam, 10 were simultaneous with other circuit trips (e.g. electrical grid perturbations), 5 occurred at top energy with visible losses but with the beam surviving, and 4 triggered a beam dump via BLMs due to high losses. All four BLM-triggered dumps took place in 2025 at top energy, caused by circuits RQS.A81B1, RQS.A67B1 (twice) and RQS.L7B2. The latter is a 2-magnet circuit, which shows that the magnet count alone is not sufficient to predict criticality. A previous analysis of RQS circuit trips before 2017 is given in Ref. [3].

This paper summarises Xsuite [4] beam tracking simulations used to assess the impact of individual RQS circuit failures on beam losses under realistic Run 3 conditions, and derives a prioritisation for PIC interlocking of a subset of circuits, deployed during the 2025 Year-End Technical Stop (YETS).

FAILURE SIMULATIONS

Single RQS circuit failures are simulated with Xsuite using the Run 3 LHC lattice at 6.8 TeV in the 2025 pp end-of-levelling configuration ($\beta^* = 18$ cm in IR1/IR5, crossing angle 160 µrad) with the nominal collimator settings. The failure is modelled by ramping one RQS circuit at a time from 0 A to 200 A, the approximate maximum operational current reached during Run 3. The MQS magnets are designed for a nominal current of 550 A, corresponding to a skew-quadrupolar gradient of 120 T/m [1]. The operational currents during Run 3 therefore remain well below the design limit.

A single particle initialised on the unperturbed closed orbit is tracked turn by turn. At each turn, the particle coordinates at the primary collimator (TCP) in IR7 are converted to normalised coordinates and actions J_x, J_y using the unperturbed Twiss parameters. The actions quantify the orbit shift induced by the failure at the TCP location. The transverse beam distribution in each plane ($u = x$ or y) is modelled as a static, conservative double Gaussian,

$$\rho_u(u) = 0.65\,\mathcal{G}(0,1) + 0.35\,\mathcal{G}(0,2), \qquad (1)$$

with $\mathcal{G}(\mu,\sigma)$ a normalised Gaussian. The TCP is treated as a black absorber, meaning that all particles of the static distribution whose action is large enough for their amplitude to exceed the TCP half-gap are considered lost instantaneously. The loss fractions in x and y are computed independently and added, and the cumulative maximum over turns is taken to enforce monotonically increasing losses. The resulting total is converted to MJ via the nominal stored beam energy. This procedure only concentrates on the fast turn-by-turn orbit excursion driven by the dipolar feed-down, which is the fastest failure mode and relevant for machine protection. Long-term effects such as emittance growth or luminosity performance are outside the scope of this study.

Figure 2 summarises the results for Beam 1 with the accumulated loss, the peak orbit change at the TCP, and the sum of the initial orbit offset $\Sigma|x| + \Sigma|y|$ at the magnets of the failing circuit prior to the failure. The circuits showing

* christophe.lannoy@cern.ch

Content from this work may be used under the terms of the CC BY 4.0 licence (© 2026). Any distribution of this work must maintain attribution to the author(s), title of the work, publisher, and DOI.

ISBN: 978-3-95450-252-3 ISSN: 2673-5350 doi: 10.18429/JACoW-IPAC2026-WEP1010

PRELIMINARY ENGINEERING DESIGN OF THE COOLING CELL FOR THE MUON COLLIDER COOLING DEMONSTRATOR*

L. Rossi[1,2] , G. Scarantino[1,3], M. Castoldi[1], D. Giove[1],
C. Barbagallo[4], R. Losito[4], C. Rogers[5], M. Statera[1]

[1]INFN-Milan, LASA laboratory, Milan, Italy, [2]University of Milan, Milan, Italy,
[3]University of Rome La Sapienza, Rome, Italy,
[4]CERN, Geneva, Switzerland, [5]Science and Technology Facilities Council, Swindon, UK

Abstract

The rectilinear 6D cooling channel is a key element of the Muon Collider baseline, enabling the large emittance reduction required before acceleration. The Muon Collider Cooling Demonstrator aims to validate, at engineering scale and in relevant conditions, the integration of a single B5-like cooling cell. This paper presents the preliminary design of the Cooling Cell, developed within the MuCol and IMCC collaborations, and based on a high-field HTS solenoid pair, a low-Z absorber, and a 3-cell 704-MHz normal-conducting RF structure. A key point of the design effort is the introduction of the Inter-Cell Cryostat, a compact architecture that closes the magnetic forces inside the cold mass while decoupling the RF and absorber assemblies at room temperature. This solution enables a feasible mechanical integration, compliant with lattice length constraints, and provides sufficient space for waveguides and diagnostics. However, it requires a remote-handling connection between each cell. The final cell layout incorporates the MAG2.4 HTS solenoids operating at 20 K, an updated RF cavity with thin Al foils, a LiH absorber module, cryogenic and thermal-shield structures, and pillow-seal vacuum interfaces designed for remote-handling assembly. The configuration that we present is a step toward demonstrating the feasibility of the cooling channel of the Muon Collider.

INTRODUCTION

The Muon Collider (MC) baseline cooling concept relies on repeated passage through low-Z absorbers, followed by re-acceleration in RF cavities to restore only the longitudinal momentum, in the presence of alternating solenoidal focusing and dipole fields [1-3].

The rectilinear cooling channel is composed of repeated cells approximately 1 m long, each one integrating a high-field superconducting magnet system, a high-gradient normal-conducting RF cavity, and a low-Z absorber. The cooling cell combines several technologies operating close to their present limits: large bore HTS magnets with peak fields approaching 14 T on the conductor, RF cavities operating at gradients near 30 MV/m in strong magnetic fields, thin metallic windows, compact cryogenic systems, and highly constrained mechanical interfaces [4].

The Muon Collider Cooling Demonstrator has been conceived to address this challenge by proving that a representative cooling cell can be constructed, assembled, cooled down, energized, and operated safely with all major subsystems integrated at full engineering scale. The demonstrator, developed within the MuCol and IMCC collaborations, focuses on a B5-like cooling cell, derived from the baseline B5 cell of the MC cooling section [5, 6].

COOLING CELL ARCHITECTURE

The reference cooling cell is based on three principal subsystems: (i) a pair of high-temperature superconducting solenoids generating the required focusing, (ii) a 704 MHz three-cell normal-conducting copper RF cavity, and (iii) a liquid hydrogen (baseline for MC) or lithium hydride (considered for the demonstrator) absorber located in the beam pipe between RF structures. Additional systems include a low field dipole to generate dispersion over the absorber, vacuum vessels, thermal shields, cryocoolers, support structures, instrumentation, and remote-handling interfaces.

The design follows the one-meter lattice period adopted in the beam dynamics model [7]. This geometric constraint is particularly demanding because the RF cavity, absorber, and magnet system must coexist within a very limited longitudinal space while preserving access for RF waveguides, vacuum pumping, diagnostics, cryogenic services, and alignment systems.

A major breakthrough in the integration effort was the introduction of the Inter-Cell Cryostat. In this architecture (see Fig. 1) the superconducting coils and their mechanical support form a compact self-contained cold mass located between adjacent room-temperature RF structures. The large axial magnetic forces generated by the coils are reacted internally within the cryostat, rather than through the RF cavity or beam-pipe assemblies. This substantially simplifies the integration and allows the RF system and absorber to be supported independently at room temperature.

The Inter-Cell Cryostat offers several advantages. First, it decouples the magnetic and RF systems, enabling parallel development and testing. Second, it provides the radial space required for the RF power coupler and associated waveguide. Third, it reduces thermal bridges between warm and cold components. Finally, it permits modular assembly of the cooling channel from repeated standardized

* Partially funded by the European Union (EU). Views and opinions expressed are however those of the author only and do not necessarily reflect those of the EU or European Research Executive Agency (REA). Neither the EU nor the REA can be held responsible for them. Endorsed by the IMCC (International Muon Collider Collaboration).

Content from this work may be used under the terms of the CC BY 4.0 licence (© 2026). Any distribution of this work must maintain attribution to the author(s), title of the work, publisher, and DOI.

ISBN: 978-3-95450-252-3 ISSN: 2673-5350 doi: 10.18429/JACoW-IPAC2026-WEP1012

FLUKA STUDIES OF SPENT BEAM EXTRACTION IN THE MUON COLLIDER TARGET SYSTEM*

J. Mańczak†, L. Bottura, M. Calviani, D. Calzolari, S. Candido, R. Franqueira Ximenes, H. Guérin, A. Lechner, G. Lerner, CERN, Geneva, Switzerland
C. Rogers, Science and Technology Facilities Council, Swindon, United Kingdom
A. Portone, Fusion for Energy, Barcelona, Spain

Abstract

A multi-TeV muon collider relies on a particle source based on a megawatt-scale proton beam impinging on a target immersed in a magnetic field generated by solenoid magnets, with an initial 20T field that decreases along a downstream tapering region followed by a chicane. The magnets downstream of the target are heavily shielded to protect them from radiation. A specific challenge arises from beam particles that traverse the target without undergoing inelastic collisions, resulting in a collimated, high-power, and nearly monoenergetic spent proton beam that requires a dedicated extraction scheme. Within the International Muon Collider Collaboration, simulations have been performed with the FLUKA Monte Carlo code to evaluate potential extraction strategies in both the target region and the downstream chicane. These studies assess power deposition, dose, and atomic displacements in the target and downstream areas and analyse shielding options to protect sensitive elements. The work defines the main radiation-driven constraints and compares the main benefits and shortcomings of each option.

INTRODUCTION

The International Muon Collider Collaboration (IMCC) is studying the feasibility of a multi-TeV muon collider facility [1–7]. A key challenge lies in the muon production stage, for which the IMCC is developing an integrated front-end concept aimed at delivering a high-intensity, high-brightness muon beam within realistic engineering constraints. The front-end design foresees a high-power proton beam impinging on a target to generate secondary pions that are captured by high-field solenoids and subsequently decay into muons.

Two proton beam parameter options are currently considered for the muon production stage [7]: a proton energy of 10 GeV with a total beam power of 4 MW and a baseline case with 5 GeV protons and 2 MW total power (see Table 1). Both proton beam configurations have previously been studied in terms of radiation loads on the high-temperature superconducting (HTS) magnets surrounding the target, as well as the resulting pion and muon yields [8,9]. The baseline target assembly consists of an 80 cm long isostatic graphite rod (density 1.7 g/cm³, 30 mm diameter) enclosed in a titanium vessel filled with helium gas [10]. For the higher-power configuration (4 MW beam), the design foresees forced helium convection to enhance heat removal and prevent excessive temperatures in the target. Alternative target concepts have also been investigated, including options based on a liquid lead proton target [11], yet this paper focuses solely on the graphite target. For target lengths that maximise the pion yield, a fraction of the primary protons is expected to traverse the target without undergoing inelastic interactions. These protons carry a significant fraction of the beam power within a narrow phase space and must therefore be safely extracted and transported to a dedicated beam dump to avoid excessive radiation loads and power densities in the front-end components. One possible solution consists of a dedicated extraction channel carved inside the shielding mass upstream of the momentum-selection chicane. The feasibility of such an approach depends on the magnetic rigidity of the surviving primary protons and therefore on the proton beam energy. The other option is to incorporate an extraction aperture within the chicane by changing its diameter at the inflection point.

Table 1: Proton Driver Beam Parameters [7]

Beam power [MW]	2/4	Pulse frequency [Hz]	5
Beam energy [GeV]	5/10	Beam size $\sigma_{x,y}$ [mm]	5
Protons per pulse		$5 \cdot 10^{14}$	

In this work, the conceptual feasibility of these two extraction schemes is investigated for the two proton beam power scenarios under consideration. All simulations were conducted using the FLUKA Monte Carlo code [12–14].

EARLY EXTRACTION

In order to extract the spent protons upstream of the chicane, the original front-end magnet configuration presented in [9] must be modified in order to enable tilting the beam and the target with respect to the axis of the solenoids. An extraction channel must then be created through the shielding in the tapering region, where the field decreases from 20 T at the target centre to a baseline of about 1.5 T, which is reached roughly 10 m downstream of the target and is maintained throughout the momentum-selection chicane. From a magnet perspective, it is desirable to limit the radii of the coils that generate the highest field close to the target, favouring design options where the extraction occurs further downstream. However, a closer extraction to the target would require modifying fewer coils and would reduce the fraction of primary beam power transported to the chicane.

* Funded by the European Union (EU). Views and opinions expressed are however those of the author(s) only and do not necessarily reflect those of the EU or European Research Executive Agency (REA). Neither the EU nor the REA can be held responsible for them. Endorsed by the IMCC.

† jerzy.mikolaj.manczak@cern.ch

Content from this work may be used under the terms of the CC BY 4.0 licence (© 2026). Any distribution of this work must maintain attribution to the author(s), title of the work, publisher, and DOI.

ISBN: 978-3-95450-252-3 ISSN: 2673-5350 doi: 10.18429/JACoW-IPAC2026-WEP1014

AN UPDATED ASSESSMENT OF THE ELECTRON CLOUD EFFECTS IN THE DAMPING RING OF THE FCC-ee INJECTOR COMPLEX

O. Etisken*, Kirikkale University, Kirikkale, Türkiye
C. Bayar, Roketsan Inc., Ankara, Türkiye
H. Bartosik, L. Mether, L. Sabato, F. Zimmermann, CERN, Geneva, Switzerland
C. Milardi, M. Zobov, INFN Laboratori Nazionali di Frascati, Frascati (Roma), Italy
T. Pieloni, École Polytechnique Fédérale de Lausanne, Lausanne, Switzerland

Abstract

The new FCC-ee injector complex design, as outlined in the feasibility report, consists of an electron source, two separate linacs for electron and positron beams to accelerate beams up to 2.86 GeV, a positron production target, a damping ring at 2.86 GeV energy for emittance cooling, a bunch compressor, a high energy linac to accelerate the beam up to 20 GeV, and an energy compressor. The primary function of the damping ring design is to accept the 2.86 GeV positron and electron beams coming from the electron linacs, reduce their beam emittances, and deliver the required beam quality for injection into the subsequent high-energy linac. It is essential for decreasing the emittance of the incoming positron beam from 2.36×10^{-6} m·rad to about 1.8×10^{-9} m·rad. Among the collective effects that may limit the performance of the positron rings, the electron cloud (e-cloud) effect remains one of the most significant challenges. This paper presents the results of updated studies of the e-cloud impact on various damping ring design options for the FCC-ee, including the latest version.

INTRODUCTION

The Future Circular Collider e^+e^- (FCC-ee) is a proposed high-luminosity precision frontier collider aiming to perform detailed studies of the Higgs boson, the electroweak sector through precision measurements of the W and Z bosons, and the top quark. The FCC-ee injector complex relies on a 2.86 GeV damping ring (DR) to achieve the low beam emittances required prior to acceleration in the high-energy linac and booster synchrotron, in order to satisfy the stringent luminosity requirements of the collider ring. Several DR lattice configurations have been investigated during the FCC conceptual design and feasibility study phases of the project [1–7].

The e-cloud effects constitute one of the major collective limitations in high-intensity positron storage rings. Electrons present in the vacuum pipe can be trapped by the fields of the positively charged circulating particles. When free electrons in the vacuum chamber get accelerated in the electromagnetic field of the beam and hit the chamber walls, electron amplification can occur through the multipacting effect. In this context, analytical threshold estimations, build-up simulations, and heat-load calculations have been carried out for the considered DR design options [8–12].

* ozgur.etisken@cern.ch, ozguretisken@kku.edu.tr

Two alternative DR designs are considered: six-fold symmetry featuring a circumference of 373.78 m (baseline option) and three-fold symmetry (alternative option) with 384.87 m circumference. The beam parameters used in the analytical and numerical calculations for the DR design options are summarized in Table 1. The e-cloud formation depends on beam and machine parameters. Among these, the Secondary Electron Yield (SEY) of the vacuum chamber surface constitutes one of the most critical inputs for e-cloud simulations. The SEY is defined as the ratio between the emitted and impacted electron current as a function of the energy of the impacting electrons. Since the vacuum chamber material and surface treatment have not yet been finalized, a range of SEY values has been considered in the simulations.

Table 1: Beam Parameters for Both Damping Ring Options: Six-fold and Three-fold Symmetry

Parameter	Six-fold	Three-fold
Circumference [m]	373.78	384.87
Beam energy [GeV]	2.86	2.86
Eq. hor. emit. [nm·rad]	3.37	1.76
Damping time (hor.) [ms]	6.0	6.46
Mom. compaction fac. (10^{-2})	0.16	0.17
Eq. bunch length [mm]	6.83	8.26
Energy spread (10^{-2})	0.08	0.08
Energy loss/turn [MeV]	1.18	1.13
Harmonic number	499	513
Number of bunches	20 (or 28)	20 (or 28)
Beam current [mA]	83.83	78.57
Bunch spacing [ns]	25	25
Bunch intensity (10^{10})	3.15	3.15
Bending magnet field in the arc [T]	0.98	0.94
Assumed chamber radius (x/y) [mm]	25/9	25/9

ELECTRON CLOUD CALCULATIONS

Analytical Estimates

The electron build-up saturates when the attractive beam field is compensated by the field of the electrons, at a neutralization density, given by [11]:

$$\rho_{\mathrm{neutr}} = \frac{N_b}{L_{\mathrm{sep}} \pi b_x b_y}, \tag{1}$$

where L_{sep} [m] is the bunch spacing, N_b is the bunch intensity, $b_{x/y}$ are the horizontal and vertical vacuum chamber radii, respectively. The single bunch e-cloud instability (ECI) occurs above the electron density threshold estimated by [11,

Content from this work may be used under the terms of the CC BY 4.0 licence (© 2026). Any distribution of this work must maintain attribution to the author(s), title of the work, publisher, and DOI.

ISBN: 978-3-95450-252-3 ISSN: 2673-5350 doi: 10.18429/JACoW-IPAC2026-WEP1016

UPDATE ON THE ITN COORDINATED EFFORT FOR ILC TECHNOLOGY DEVELOPMENT IN EUROPE*

L. Monaco†, D. Sertore, Istituto Nazionale di Fisica Nucleare, Laboratori Acceleratori e Superconduttività Applicata, Segrate, Italy
E. Cenni, CEA Université Paris-Saclay, Gif-sur-Yvette, France
A. Yamamoto, High Energy Accelerator Research Organization, Tsukuba, Japan
T. Dohmae, S. Michizono, T. Saeki, H. Sakai, K. Umemori, Y. Yamamoto, High Energy Accelerator Research Organization, Tsukuba, Japan and The Graduate University for Advanced Studies, SOKENDAI, Kanagawa, Japan
K.-M. Schirm, S. Stapnes, European Organization for Nuclear Research, Geneva, Switzerland

Abstract

The ITN-EU consortium, coordinated by CERN with the support of CEA-Saclay and INFN-LASA, is advancing Europe's contribution to the International Linear Collider (ILC) through the development and validation of high-performance superconducting radiofrequency (SRF) cavities. Activities focus on establishing an optimized production chain, from single-cell R&D to the industrialization of 9- cell cavities. Material procurement and quality control have been completed, and prototype single cells are fabricated, and they will be used to assess advanced surface treatment strategies. EU partners are also preparing technical specifications and harmonizing production with Japanese High Pressure Gas Safety requirements. Europe will provide two fully prepared 9-cell cavities for installation in an ILC-type cryomodule assembled and tested at KEK, demonstrating Europe's integrated and strategic role in the global SRF program.

INTRODUCTION

Superconducting radiofrequency (SRF) technology has reached a high level of maturity through large-scale accelerator projects such as European XFEL and LCLS-II and, continues to evolve toward higher performance and cost-effective production. In this context, the realization of the International Linear Collider relies on the development of advanced SRF cavities and an industrially viable production chain. To address these challenges, the ILC Technology Network (ITN) was established in 2023 within the International Development Team framework, bringing together international partners around key accelerator technologies [1, 2].

Europe contributes strong expertise to the ITN through its experience with major SRF projects such as European XFEL and European Spallation Source. Within this framework, the ITN-EU consortium, coordinated by CERN with the support of CEA Saclay and INFN LASA, works in close collaboration with KEK to develop and validate high-gradient SRF cavity production for the ILC. Activities include material qualification, single-cell R&D, industrialization of 9-cell cavities, and preparation for the assembly and testing of an ILC-type cryomodule at KEK, demonstrating Europe's strategic contribution to the global SRF program [3].

MATERIALS AND QUALITY CONTROL

Materials for the single-cell and 9-cell cavities were procured by KEK and delivered to CERN, which coordinates the ITN-EU activities. The technical specifications were defined to comply with Japanese High Pressure Gas Safety (HPGS) requirements. All cavities are fabricated from fine-grain (FG) niobium supplied by Tokyo Denkai, except one single-cell cavity that uses medium-grain (MG) niobium from ATI for cost-reduction studies. Additional spare components were also procured for R&D on surface treatments and for mechanical and welding qualification studies related to HPGS compliance and future large-scale production. To ensure the stringent performance requirements of the 1.3 GHz cavities, quality control was performed on all fine-grain and medium-grain niobium sheets using Eddy Current Scanning (ECS). In 2024, DESY carried out the ECS measurements as a contribution to ITN, confirming that all sheets satisfied the specification requirements and showed no critical foreign material contamination [4].

SINGLE-CELL ACTIVITIES

The strategy we developed focuses on High Gradient (HG) toward High-Q (HQ) cavity performance, since ILC needs to reach 35 MV/m, $Q_0 \geq 1 \cdot 10^{10}$. The optimized procedure developed on single-cell cavities will then be transferred to multicell structures toward cavity industrialization, as described below:

- **High-Q/High-Gradient process development** on two single-cell cavities, beginning with a baseline EuXFEL-like treatment (150 μm bulk EP, 900 °C annealing, 10-20 μm final cold EP, 120 °C baking), and evolving with advanced techniques such as mid-temperature baking (mid-T) and two-step baking. Performance validation will occur in different partner labs (LASA, CEA, DESY, KEK) to enable cross-comparison.
- **Technology transfer to multicell structures**, using two 9-cell cavities to test the industrialization process,

* This work was partially supported by the European Union's Horizon Europe Marie Sklodowska-Curie Staff Exchanges programme under EAJADE (Europe-America-Japan Accelerator Development Exchange) grant agreement no. 101086276
† laura.monaco@mi.infn.it

Content from this work may be used under the terms of the CC BY 4.0 licence (© 2026). Any distribution of this work must maintain attribution to the author(s), title of the work, publisher, and DOI.

ISBN: 978-3-95450-252-3 ISSN: 2673-5350 doi: 10.18429/JACoW-IPAC2026-WEP1017

DESIGN REFINEMENTS AND PROTOTYPING OF LEAD SHIELDING FOR THE FCC-ee ARC DIPOLES

R. Cowan*, G. Banks, B. Humann, A. Lechner, L. Jorat, K. Guergar, A. Romero Francia, R. Seidenbinder, A. Perillo Marcone, M. Calviani, J. Roaldsoy, M. Simoes, S. Sgobba, M. Morrone, V. Giovinco, A. Piccini, M. Timmins, J. Bauche, F. Carra, J. M. Madsen
CERN, Geneva, Switzerland

Abstract

In the Future Circular Collider (FCC-ee) at CERN, lead shielding will be required on the collider arc dipoles around synchrotron radiation (SR) absorber locations to reduce radiation levels in the tunnel and protect sensitive components. The shielding assemblies will be mounted around the yokes, where scattered SR photons are expected to deposit 10-15 MW of power in total (across all absorber locations combined over the entire collider) at the $t\bar{t}$ operating point. Between the yokes and the shielding, a water-cooling system will be integrated to cool both the shielding and the magnet. Recent design studies have focused on refining the geometry and cooling layout to simplify manufacturing, control costs and maintain shielding performance. A shielding prototype is planned to inform design choices and further improvements. This contribution presents the design evolution, plans for a prototype, and cooling system optimisations.

INTRODUCTION

The FCC-ee is presently envisioned as the next large scale collider to be built by CERN, as part of the larger FCC project. This lepton machine would collide electrons and positrons at up to 182.5 GeV in a 91 km tunnel under Switzerland and France [1]. The powerful synchrotron radiation (SR), 50 MW per beam, will be absorbed by approximately 26000 Synchrotron Radiation Absorbers (SRAs) distributed around the arcs [2]. These localise SR losses in an actively cooled copper absorber block within the vacuum chamber. At the highest energies foreseen, these SRAs do not completely shield the tunnel and surrounding environment from scattered radiation, so further shielding will be performed by lead blocks positioned around the SRAs. The blocks will be sufficiently thick to absorb the remaining ~10 MW of radiated power and reduce the dose in the tunnel upper cable trays from >100 kGy to <10 kGy at $t\bar{t}$ [3]. The mass of lead is estimated to be around 800 kg per unit and around 13000 units (one unit per two SRAs) will be needed in the arcs alone, totalling over 10000 tonnes of lead.

LEAD SHIELDING REFINEMENT

The lead shielding has been refined from the previous work [4] to be comprised of large cuboidal blocks, with the intention of reducing production costs. The lead insert, visible in Fig. 1, has been improved to better fit around the vacuum chamber. The sides and insert are extended to reduce shine paths forward and backwards. Additional design improvements being considered for implementation include a cut out in the region with highest power deposition to improve cooling, further integration refinements around the vacuum chamber, and custom geometries to minimise lead use.

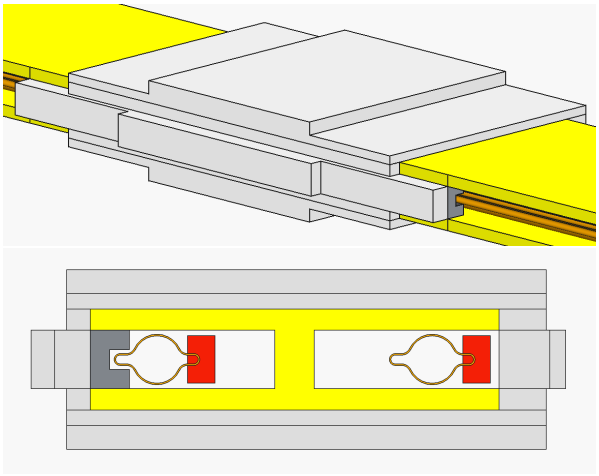

Figure 1: New design of lead shielding. Yoke - Yellow; Lead - Grey; Lead Insert - Dark grey; Vacuum chamber - Orange; SRAs (approx. position) - Red. The insert is the only piece of lead inside the aperture of the magnet yoke, and receives the highest energy deposition of all the lead, due to its proximity to the SRA.

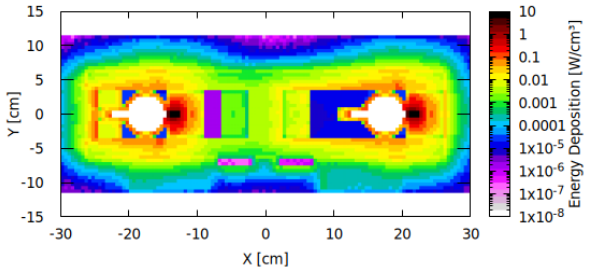

Figure 2: Power deposition in cross section of dipole and shielding, averaged over 1.3 m of shielding.

COOLING SYSTEM DESIGN

The lead, along with the steel yoke, together absorb a maximum of around 750 W per shielding unit [5] at $t\bar{t}$ for the LCC optics [6] (the yoke absorbs about 75% of this, for comparison, the two SRAs themselves absorb ~3.5 kW each). The distribution of the heating is shown in Fig. 2, generated using the FLUKA code [7–10].

* r.cowan@cern.ch

Content from this work may be used under the terms of the CC BY 4.0 licence (© 2026). Any distribution of this work must maintain attribution to the author(s), title of the work, publisher, and DOI.

ISBN: 978-3-95450-252-3 ISSN: 2673-5350 doi: 10.18429/JACoW-IPAC2026-WEP1301

RHIC Au-Au OPERATION AT 100 GeV IN RUN 25

T. Shrey†, G. Atoian, S. Binello, K. Drees, R. Feder, W. Fischer, K. Hock, H. Huang, R. Hulsart
K. Hughes, D Lederle, B. Lepore, C. Liu, G. Marr, K. Mernick, C. Mi, R. Michnoff, M. Minty
J. Morris, D. Raparia, G. Robert-Demolaize, J. Sandberg, M. Sangroula, F. Severino, Y. Than
V. Schoefer, D. Weiss, K. Yip, A. Zaltsman, K. Zeno
Brookhaven National Laboratory, Upton, NY, USA

Abstract

The Relativistic Heavy Ion Collider (RHIC) Run 25 operations consisted of collisions of 100 GeV/u Au beams for the STAR and sPHENIX experiments. A 6-week 100 GeV polarized proton run for sPHENIX and an additional week of fixed target for STAR at 3 energies was added. Finally, a 7-day 100 GeV/u O run was added. A magnet wiring short resulting from the Run 23 failure repair resulted in a 2-month delay to the start of the run. Machine optimizations produced the highest efficiency in the history of the complex, but the run was interrupted by a pair of two-week failure periods. This paper will discuss the progress made by each experiment and the failures and successes of the final year of operation of the RHIC accelerators.

INTRODUCTION

The RHIC program in Run 25 called for 28 weeks of colliding beam operations with 100 GeV Au beams at two interaction points (IP), IP 6 and 8. IP 6 contains the STAR detector; the experimental plan called for a mix of high luminosity at a zero crossing angle for the first 4 hours of a store and then a 1 mrad crossing angle with luminosity levelling at 15kHz for the remainder. IP 8 contains the sPHENIX experiment with plans to run a 1.5 mrad crossing angle for stores. A mid-run Program Advisory Committee meeting resulted in a change of plans to add a 6-week 100 GeV polarized proton run for sPHENIX and a 1-week fixed target run for STAR at 3 energies. Finally, an additional six-day 100 GeV/u Oxygen run was added for the last week of operations.

WIRING FAILURE

After the initial cryogenic cooldown of the blue ring to 4k it was found that the blue main dipole buss would not pass the required high potential test. A week of troubleshooting resulted in narrowing down a possible short location and the decision was made to warm the rings back up and start opening cryostats for investigation. Ultimately the short was found to be the result of a poorly insulated wiring splice in one side of the DX magnet that was replaced after the run-ending failure in Run 23. Cryostats, vacuum chambers and shields were all welded and the run began roughly 2 months late.

GOLD RUN

Removal of a legacy beam collimator upstream of IP8 and a switch to triggered mode allowed the mVTX detector at sPHENIX to operate without the background problems that were discovered in Run 23 and 24 [1]. Constant and meticulous tuning of the ramp and store conditions produced the highest efficiency in RHIC's 25-year history as shown in Fig. 1. Delivered luminosity to the experiments is in Fig. 2.

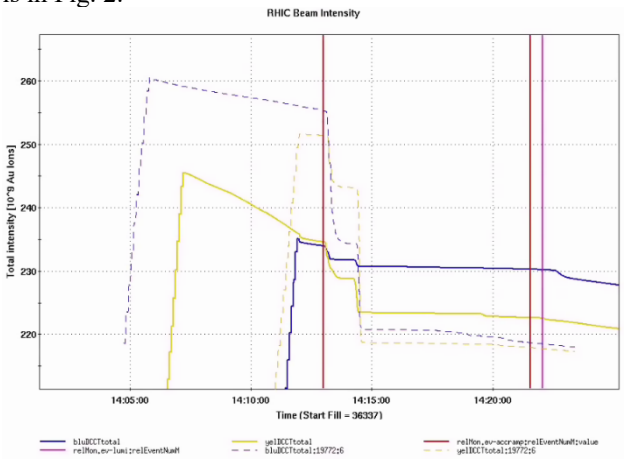

Figure 1: A comparison of Au energy ramps from Run16 (dashed lines) and Run25. In Run16 blue and yellow ramp efficiencies were 92% and 95% compared to Run25 which achieved 99% and 98% at equal or greater intensities.

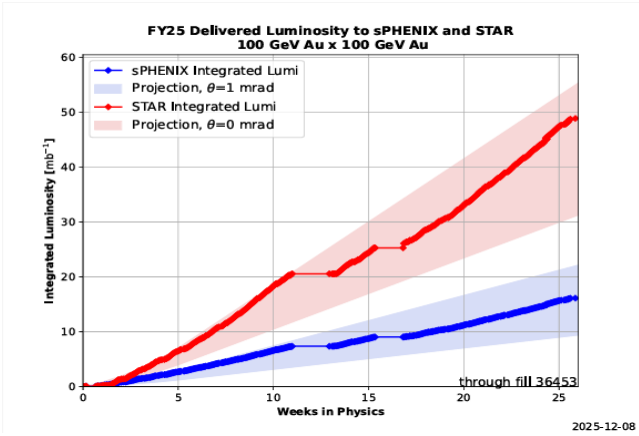

Figure 2: STAR/sPHENIX luminosity plot

Attempts were made through the early part of the run to bring the 56 MHz SRF cavity into operation. While the

Content from this work may be used under the terms of the CC BY 4.0 licence (© 2026). Any distribution of this work must maintain attribution to the author(s), title of the work, publisher, and DOI.

ISBN: 978-3-95450-252-3 ISSN: 2673-5350 doi: 10.18429/JACoW-IPAC2026-WEP1303

HIC SUPERCONDUCTING CIRCUIT FAILURE DURING RUN 23*

F. Micolon†, J. Escallier, R. Feder, W. Fisher, G. Heppner, C. Mi, M. Minty, R. Michnoff, T. Samms, J. Sandberg, S. Seberg, R. Than, J. Tuozzolo
BNL, Upton, New York, USA

Abstract

A failure of the RHIC superconducting circuit occurred at the end of Run 23 and led to an unplanned shutdown and extensive work to replace a damaged superconducting dipole magnet. After an in-depth investigation, the failure was found to originate from an electrical arc within a superconducting current lead. The arc led to large spilling of current through auxiliary superconducting circuits with limited quench stabilization, which resulted in a superconducting splice burning out. This paper will summarize our understanding of the series of events leading to the superconducting circuit damage, describe the repair work undertaken for the remaining RHIC runs and discuss some lessons learned in view of EIC operation.

FAILURE SYMPTOMS

On August 1st 2023 at 12:31pm a magnet quench link interlock (QLI) occurred during high-energy collision operation at 200 GeV with Au ions [1]. The beam was nominally dumped, but shortly after all 12x blue ring DX magnet quench heater were unexpectedly triggered. A few minutes later, a large helium release was observed outside of the Interaction Region 4 (IR4) cryogenic valvebox (Fig. 1), both from the pressure release duct and the vacuum seal at the valvebox bottom flange which gives access to the leadpot, the helium-filled vessel where superconducting current leads are located.

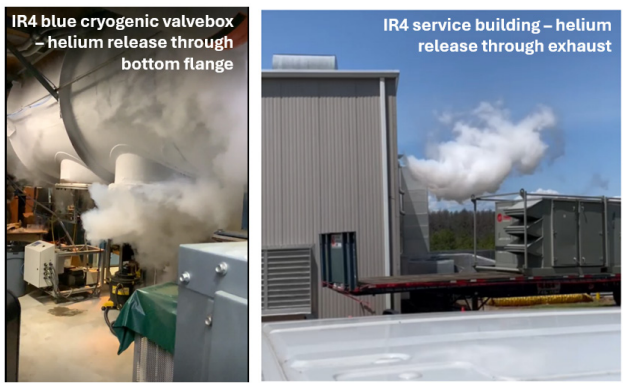

Figure 1: Aug 1st 2023 - Helium release through (left) the blue IR4 valvebox (right) the service building exhaust.

Subsequent electrical diagnostics revealed that the main dipole and quadrupole superconducting (SC) buses were shorted together and to ground, making the collider SC circuits unusable. This concluded the physics Run 23 and led to an early shutdown seven weeks ahead of schedule.

* Work supported by Brookhaven Science Associates, LLC under Contract No. DE-SC0012704 with the U.S. Department of Energy.
† fmicolon@bnl.gov

RHIC SUPERCONDUCTING CIRCUITS

RHIC has two parallel counter-rotating storage rings, the "blue" and "yellow" rings. For each ring, the RHIC SC system is composed of two independent SC circuits, the quadrupole and dipole circuits. The quadrupole circuit is wired symmetrically around the ring from the power supply (PS) located at IR4 and it loops back at IR10 to feed all the SC quadrupole in series (Fig. 2).

On Fig. 2, the outer legs feed all the vertically focusing quadrupoles (Qv) from IR4, the circuits loop back at IR10 and the inner legs feed the horizontally focusing quadrupoles (Qh) with an auxiliary shunt circuit used to trim the Qv/Qh current to adjust the accelerator optics. Two dump resistors are located at IR4.

Both the dipole and quadrupole circuits have a variety of so-called "shunts" auxiliary SC circuits to adjust current locally around each of the six IRs. For example, the final focusing quadrupoles are principally powered through the main Qv/Qh circuits, but adjustment of the magnet current can be done by a "shunt" circuit connected in-parallel at the SC magnet leads inside the helium vessel.

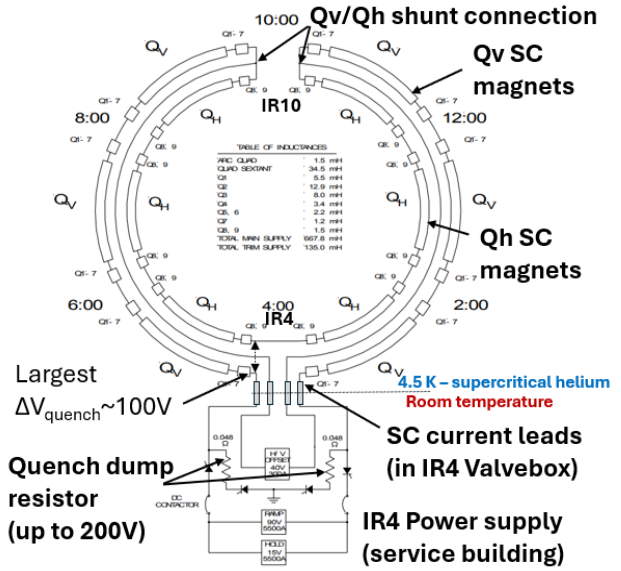

Figure 2: Sketch of the RHIC quadrupole SC circuit [2].

During a quench, the quadrupole circuit voltage goes up to ~200V at the dump resistor, driven by the inductance of the large number of SC magnet wired in series during the current decay.

Any two points of the circuit will see a different voltage-to-ground depending on how many SC magnets separate them. The highest wire-to-wire voltage difference will reach ~100V (~50% of the total dump resistor voltage) at IR4 between the Qh/Qv legs. (see Fig. 2).

Content from this work may be used under the terms of the CC BY 4.0 licence (© 2026). Any distribution of this work must maintain attribution to the author(s), title of the work, publisher, and DOI.

ISBN: 978-3-95450-252-3 ISSN: 2673-5350 doi: 10.18429/JACoW-IPAC2026-WEP1304

INJECTING AND RAMPING TRAPPED BEAM IN HADRON ACCELERATOR*

H. Lovelace III†, S. Brooks, K. Drees, B. Lepore, S. Peggs, G. Robert-Demolaize
Brookhaven National Laboratory, Upton, United States
R. Seviour
University of Huddersfield, Huddersfield, United Kingdom

Abstract

In developing an alternative method of jumping transition in the Electron Ion Collider Hadron Storage Ring, simulations have been performed to show feasibility. Many challenges occur while ramping trapped beam. The effect of snapback on the superconducting magnets, longitudinal oscillations, and evolution of the island tune will be presented.

INTRODUCTION

The Electron Ion Collider (EIC) Hadron Storage Ring (HSR) will collide 110 GeV Au^{+79} with ~10 GeV electrons to provide asymmetric collisions within the electron/Proton Ion Collider (ePIC) detector [1]. The HSR accelerates all species, except protons, through the lattice transition. The higher momentum particles traverse a longer path in the dipoles, but at transition energy, their increased velocity exactly compensates for this path length, causing the revolution period to become momentum-independent. During this time, the beam may suffer from a number of instabilities [2]. The HSR reuses the Relativistic Heavy Ion Collider (RHIC) arc magnets with modified straight sections. A new state of the art interaction region with a 25 mrad crossing angle is where the ePIC detector resides surrounded by crabbing cavities [3, 4]. The method of crossing transition in RHIC is based on the First Order Matched (FOM) scheme discussed in Ref. [5] and commissioned [6] in the early years of RHIC. Ideally, with the reuse of the RHIC arcs and the minimum redesign of all but one straight section, the interaction region where the detector is located, the FOM will continue to be effective in crossing transition [7].

The current HSR contains 24 jump quadrupoles in the arcs that directly effect γ-transition, γ_T, by distorting the lattice dispersion, and 20 jump quadrupoles in the straight sections to mitigate the dispersion and betatron wave that is generated by the excitation of the jump quadrupoles. With cooling, the number of jump quadrupoles is reduced by 4 from the modifications needed in the electron cooling straight section. The FOM becomes less effective with inclusion of a second detector in the HSR due to the need for increased quadrupole strength outside the current power supply limits for sufficient change in the γ_T of the lattice. With this concern, alternative methods of crossing transition must be explored to provide stable operations through future HSR upgrades. The method of crossing transition through the usage of resonance islands was first proposed by M. Giovannozzi [8] and further explored by S. Peggs [9]. The principal premise of the Resonance Island Jump (RIJ) scheme is to inject the beam on-axis or into the island [10] where the γ_T of the island differs from the on-axis γ_T, ramp the beam to transition, and nonadiabatically kick the beam over a single turn to a lower γ_T whether the beam is displaced onto the central axis or into the island. Figure 1 is a schematic of the placement of the beam for the HSR where γ_T of the island is higher than the on-axis γ_T.

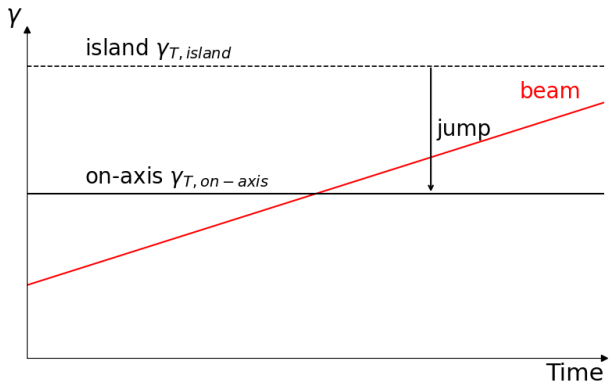

Figure 1: The γ_T of the island is higher than the on-axis γ_T for the HSR. The jump in the HSR case will be from the resonance island to the on-axis with a single turn kick.

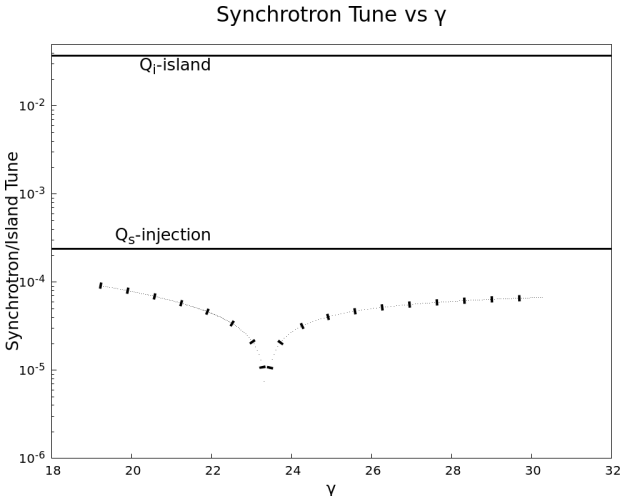

Figure 2: Shown is island tune , Q_I, synchrotron tune, Q_s, and the change in the synchrotron tune during the ramp. The injection Q_s does not cross the Q_I. The dashed marks show the decrease in the Q_s transition is crossed.

* Work supported by Brookhaven Science Associates, LLC under Contract No. DE-SC0012704 with the U.S. Department of Energy.
† hlovelace@bnl.gov

Content from this work may be used under the terms of the CC BY 4.0 licence (© 2026). Any distribution of this work must maintain attribution to the author(s), title of the work, publisher, and DOI.

ISBN: 978-3-95450-252-3 ISSN: 2673-5350 doi: 10.18429/JACoW-IPAC2026-WEP1307

HADRON STORAGE RING SPIN ROTATORS & SPIN TUNE COMPENSATION

K. Hock, J.S. Berg, H. Huang, V. Ptitsyn
Brookhaven National Laboratory, Upton, New York

Abstract

The Electron Ion Collider (EIC) calls for collisions of longitudinally polarized protons and helium-3 on polarized electrons. The polarized hadron beams will be accelerated and stored in the Hadron Storage Ring (HSR). To achieve longitudinal polarization at the interaction point (IP), spin rotators are placed on either side of the IP at 35.28 and -61.35 mrad. Due to the asymmetry of the rotator placement, their ramping and use at store will result in a shift of ν_s from 1/2. The HSR has six snakes that can be used to compensate for the $\Delta\nu_s$. The planned storage energies for protons are 41, 100, and 275 GeV, and for helium-3 are 41, 100, and 183 GeV/u. The updated rotator currents at each of these energies is provided, in addition to the $\Delta\nu_s$ and the compensation requirements of the snakes.

INTRODUCTION

The EIC HSR will be primarily constructed using existing components from the Relativistic Heavy Ion Collider (RHIC). The HSR will have rotator magnets outside of the interaction regions to facilitate longitudinal polarization at the interaction point (IP). The helical dipoles have a period λ=2.4 m. The magnet period is defined as [1]

$$k = H\frac{2\pi}{\lambda} \tag{1}$$

with H being the helicity. The magnet coils have either left-handed (LH, H=-1) or right-handed (RH, H=+1) helicities. The spin rotation from one coil is,

$$\phi = 2\pi\sqrt{1+\chi^2} \tag{2}$$

and

$$\chi = (G+1/\gamma)\frac{qB_o}{m\beta c|k|} \tag{3}$$

where G is the anomalous gyromagnetic g-factor, γ is the Lorentz factor, q and m are the charge and mass, βc is the velocity, and B_o is the magnetic field. The maximum B_o = 4 T which corresponds to a power supply current of 322 A. The relevant parameters for protons and helions are found in Tab. 1.

Table 1: Relevant parameters for polarized protons and polarized helions.

	G	q	m (GeV/c^2)
proton	1.7928474	1	0.93827209
helion	-4.1841536	2	2.80839148

The rotation from a single helix occurs in the laboratory frame about the precession axis defined as,

$$u = \Big[-\frac{\chi}{\sqrt{1+\chi^2}}, -\frac{H}{\sqrt{1+\chi^2}}, 0\Big]. \tag{4}$$

The full rotator assembly consists of four helical dipoles. After transiting the full rotator assembly, the spin been rotated into the horizontal plane. The residual angle from the horizontal plane is $\theta_y = 0$. After the spin is placed in the horizontal plane, it will precess by an amount θ_s, defined as

$$\theta_s = G\gamma\theta_R \tag{5}$$

where θ_R is the bend angle from the IP to the rotator.

The existing RHIC rotators have a helicity pattern of RLRL. These magnets are powered similar to the snakes where the inner and outer coils are powered independently with current I_{in} and I_{out}, but all coils have the same sign for current, such as R+L+R+L+ [2]. The RHIC rotators are placed symmetrically on either side of the IP with an angle of $\theta_R = \pm 3.675$ mrad from the IP. These rotator assemblies will be used for the HSR.

In the HSR, the beam circulates in the counter-clockwise direction, equivalent to the yellow RHIC ring. Thus, the sector 6 rotator is to be the V2H (vertical to horizontal) rotator, and the sector 5 rotator is the H2V (horizontal to vertical). The V2H rotator is located at $\theta_R = -61.35$ mrad from the IP, and the H2V rotator is at $\theta_R = 35.28$ mrad from the IP. This report builds on previously reported results from [3,4]. The outer and inner currents that satisfy longitudinal polarization at the IP is found in Tab. 2.

Table 2: Summary of rotator currents for protons at 41, 100, and 275 GeV, and one set of solutions for helions at 41, 100, and 183 GeV/u.

	protons			helions		
E (GeV/u)	41	100	275	41	100	183
$I_{out,H2V}$ (A)	104	-90	-184	75	174	174
$I_{in,H2V}$ (A)	246	-259	-198	150	221	192
$I_{out,V2H}$ (A)	264	235	75	171	47	174
$I_{in,V2H}$ (A)	215	185	282	160	181	225

ROTATOR RAMP

To satisfy $\nu_s = \frac{1}{2}$, the six snakes will nominally be at $\pm 45°$. That is in a synchrotron with n snakes, ν_s follows

$$\nu_s = \frac{1}{\pi}\sum_{k=1}^{n}(-1)^k\theta_{s,x} \tag{6}$$

Content from this work may be used under the terms of the CC BY 4.0 licence (© 2026). Any distribution of this work must maintain attribution to the author(s), title of the work, publisher, and DOI.

ISBN: 978-3-95450-252-3 ISSN: 2673-5350 doi: 10.18429/JACoW-IPAC2026-WEP1308

DETERMINATION OF THE SPHENIX BACKGROUND SOURCE WITH TRACKING

K. Hock, A. Drees, H. Huang, B. Lepore, K. Mernick,
G. Robert-Demolaize, V. Schoefer, T. Shrey, E. Skordis
Brookhaven National Laboratory, Upton, NY, USA

Content from this work may be used under the terms of the CC BY 4.0 licence (© 2026). Any distribution of this work must maintain attribution to the author(s), title of the work, publisher, and DOI.

Abstract

During the Relativistic Heavy Ion Collider (RHIC) Run24 operations with 100 GeV/u Au beams, significant backgrounds were observed at the sPHENIX MAPS-based VerTeX (MVTX) detector. Extensive studies were performed during RHIC operation to diagnose the source of the background. Through tracking simulations, the primary source of the backgrounds was found and removed prior to beam operations for Run25. The removal of the obstruction resulted in a reduction of backgrounds by an order of magnitude, similar to the best mitigation found during Run24. The tracking simulations that showed the location of the obstruction and the resulting background reduction following its removal are shown.

INTRODUCTION

The MVTX detector is sPHENIX's innermost detector system. It consists of 48 staves that are 0.47 m long and arranged around the beampipe as seen in Fig. 1. During the three week 100 GeV/u Au operation in Run24, significant backgrounds were observed on the sPHENIX MVTX detector. It was determined that the backgrounds were the result of high amplitude particles striking the upstream beampipe taper, where the aperture is reduced from 4 cm to 2.4 cm. This resulted in a highly charged shower of particles transiting longitudinally across the length of the MVTX [1]. This large charge deposited across the length of the staves would cause their electronics to overload, resulting in a reboot sequence known as auto-recovery. The MVTX auto-recovery process takes approximately 20 s to reboot during which the affected staves are no longer collecting data. This reduced the overall acceptance of the detector. There is a maximum of 3 auto-recoveries per minute, and the average auto-recovery rate of all staves, ⟨ARR⟩, is used to generalize the backgrounds. The auto-recovery display of the MVTX detector is seen in Fig. 1 where the red triangles corresponds to the MVTX staves that are in auto-recovery.

Simulations during Run24 showed that a single Au^{79+} ion transiting the 47 cm length of an MVTX stave was sufficient for triggering the auto-recovery sequence. The source of these high amplitude particles prompted many studies during Run24, in preparation for the planned Au Operation in Run25 [2]. Ahead of Run25, there were extensive simulations to diagnose and mitigate the backgrounds. The staves of the MVTX detector and their readout is equivalent to the Inner Tracking System (ITS2) at the ALICE detector, which had a similar background issue during the LHC run 3 with Pb beams [3].

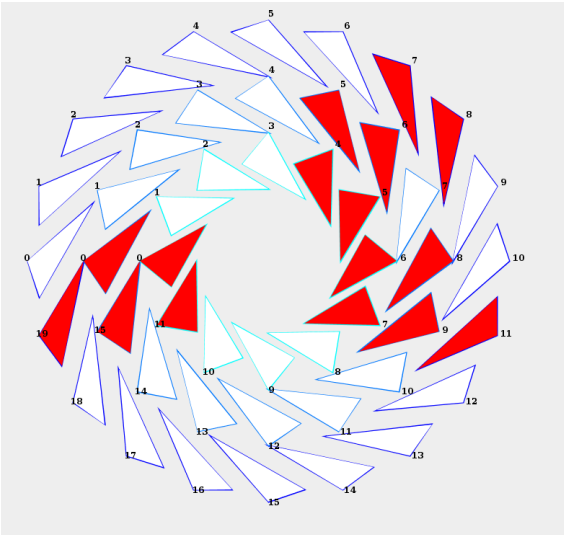

Figure 1: Example MVTX staves where red denotes a stave being in auto-recovery.

TRACKING RESULTS

A particle tracking campaign followed Run24 to determine potential sources of the backgrounds and methods to mitigate what was found ahead of Run25. Both forward tracking toward the MVTX beampipe taper, and reverse tracking with particles originating at the taper, were used to isolate the source of the backgrounds. The tracking was performed using Zgoubi [4] where a lattice has a reference rigidity with a corresponding reference momentum of P_o with a particle's momentum defined as

$$P = 1 + \frac{dP}{P_o}. \quad (1)$$

A particle can be given an initial momentum that differs significantly from P_o, given as dP/P_o. Apertures are coded in Zgoubi with zero length and are inserted into the lattice whenever the real lattice changes diameter and at every quadrupole, regardless of whether the aperture changes there. In cases where there is a large angle of the trajectory, it may miss one aperture but is lost at the next downstream aperture.

Backward Tracking from the MVTX Taper

The initial distribution of particles used for backtracking from the taper is seen in Fig. 2, which also shows the misalignment of the sPHENIX beampipe, centered at 0.8627 cm

ISBN: 978-3-95450-252-3 ISSN: 2673-5350 doi: 10.18429/JACoW-IPAC2026-WEP1311

INVESTIGATIONS OF NON-LINEAR OPTICS CONTROL KNOBS FOR THE FCC-ee

P. Hunchak*, M. Boland, University of Saskatchewan, Saskatoon, Canada
J. Keintzel, CERN, Geneva, Switzerland

Abstract

The non-linear effects that arise from misalignment and field errors have been shown to degrade both the dynamic aperture (DA) and (MA) in simulation of the Future electron-positron Circular Collider machine (FCC-ee). This study focuses on using multipoles, such as sextupoles or octupoles, to control amplitude detuning and higher-order chromaticity as well as investigation of dedicated non-linear correctors. These non-linear parameters are often coupled and the relative strength with which lattice elements act on each non-linearity depends on the local optical parameters. Studies are performed on the placement and strength of non-linear lattice elements to contribute to developing orthogonal correction knobs and first attempts at higher-order corrections to recover the reduced DA and MA are explored.

INTRODUCTION

The Future electron-positron Circular Collider (FCC-ee) is an about 91 km storage ring with thousands of magnetic elements, and will operate at energies ranging from 45.6 GeV to 182.5 GeV per beam [1–3]. The unprecedented size and number of elements leads to extreme importance of tuning systems to address any misalignments and field errors that arise in the construction of such an accelerator. Current magnet estimates state that the arc dipoles will have 10 units of error in normal dipole and quadrupole fields (b_1 and b_2 errors) and 0.5 units of normal sextupole and octupole fields (b_3 and b_4 errors) [4]. One unit is a multipole component of 10^{-4} of the lowest order magnetic field, at a reference radius 0.01 m [5].

It has been found that even when the linear optics are well corrected in the presence of misalignments and field errors, that the momentum acceptance (MA) and dynamic aperture (DA) are still reduced [6–8]. This suggests that non-linear correction schemes will be important to ensure performance reach of the FCC-ee. The effects of b_3 and b_4 errors on the MA and initial corrections of each are discussed in the following. Other tuning studies are ongoing in parallel, see e.g. [9–12].

ARC BEND b_3 ERROR AND CORRECTION

To first order, b_3 errors introduce additional linear chromaticity. Amplitude detuning is also impacted as a second order effect.

The magnet estimates for both random and systematic b_3 errors are 0.5 units. Effects of these errors on the FCC-ee lattice version LCC 106.2.1 [13–15] for the Z energy (45.6 GeV) are explored with simulation using Xsuite and MAD-NG [16, 17]. Tracking of particles to determine MA is performed in Xsuite while MAD-NG is used to calculate high-order optics parameters and Resonance Driving Terms (RDTs). First, the sextupole (b_3) errors are applied to all arc dipoles, and particles are tracked in Xsuite at various momentum offsets ($\Delta p/p = \delta$) and amplitudes for 2500 turns using Synchrotron Radiation (SR) with Quantum Fluctuation (QF). In these scans the particles are initialized with an equal number of horizontal and vertical sigmas amplitude, $N_{\sigma_x} = N_{\sigma_y}$. For each error scenario 10 seeds for the QF are averaged.

As a figure of merit, we consider the area of stable initial conditions for DA and MA, seen in Fig. 1. While applying random b_3 errors does not reduce the MA, systematic b_3 errors reduce this quantity in δ-amplitude space by $\approx 60\%$. The strengths of the four arc sextupole families, two focusing and two defocusing, are adjusted with four 'knobs' to restore the MA. Changing the sextupole strengths, K_2, gives control of the horizontal ($\partial Q_x/\partial J_x$) and cross-term ($\partial Q_{x,y}/\partial J_{y,x}$) amplitude detuning and linear chromaticity ($Q'_{x,y} \equiv dQ_{x,y}/d\delta$). When these amplitude detuning terms and the linear chromaticity are restored to their design values the MA is fully recovered, as seen in Fig. 1.

These corrections result in an absolute change in the sextupole strength of a maximum of -0.013 m^{-3} for one of the defocusing families, sd2a, corresponding to roughly 7 % relative to the nominal setting. For the other three families the change is less than 5 %. For increasing systematic b_3 a linear relationship to the required change in sextupole strengths is found, shown in Fig. 2. While this correction is feasible in the Z lattice, for the 182.5 GeV $t\bar{t}$ lattice the arc sextupoles are near their strength limitation by design, so a similar level of correction could require lengthening the sextupoles.

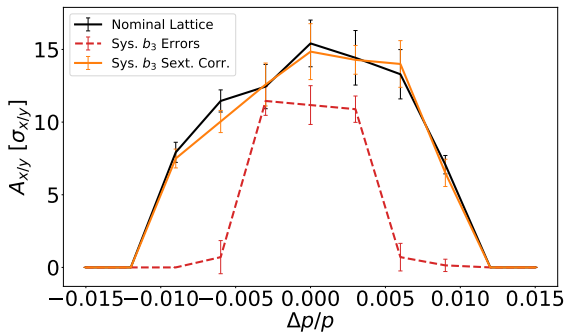

Figure 1: MA of the nominal lattice (black), with systematic b_3 errors (red), and with additional sextupole correction (orange).

* patrick.hunchak@usask.ca

Content from this work may be used under the terms of the CC BY 4.0 licence (© 2026). Any distribution of this work must maintain attribution to the author(s), title of the work, publisher, and DOI.

ISBN: 978-3-95450-252-3 ISSN: 2673-5350 doi: 10.18429/JACoW-IPAC2026-WEP1313

CHROMATICITY COMPENSATION OF A GHOST COLLIDER*

B. R. Gamage†, A. Hutton, Jefferson Lab, Newport News, VA, USA
Peter Williams, STFC Daresbury Laboratory / Cockcroft Institute, Daresbury, UK

Abstract

The GHOST collider final focus system is a pure quadrupole-drift beamline targeting $\beta^* = 2$ mm at four serial interaction points, with peak β-functions reaching ~65 km in the final triplet. Beam tracking simulations reveal that a nominal bunch develops a pronounced C-shape in longitudinal phase space at IP1, with σ_z growing from 0.15 mm to ~2.3 mm — a factor of ~15× increase that directly reduces luminosity. The mechanism is identified as *chromatically amplified betatron path length*: off-momentum particles acquire enlarged betatron amplitudes in the high-β final triplet, generating excess path length via the geometric $\Delta z = -\frac{1}{2}\int (x'^2 + y'^2)\, ds$ integral. Within the monoenergetic Balandin framework, $\epsilon^2\xi^2$ with $\xi = -\frac{1}{2}\int \gamma\, ds$ dominates $\epsilon^2 W^2$ by over four million times; the full beam σ_z is a further factor of ~27 larger, driven by σ_δ-induced chromatic amplitude growth. Phase-advance scans confirm that σ_z is insensitive to the apochromatic ($W \approx 0$) condition. When combined with the geometric hourglass effect, this distortion poses a challenge to maximizing luminosity within the current lattice design.

INTRODUCTION

The GHOST collider [1, 2] final-focus system is a pure quadrupole-drift beamline designed to achieve $\beta^* = 2$ mm at four serial interaction points (IPs) without the use of dipole magnets. The absence of dipoles eliminates synchrotron radiation in the final focus — a significant advantage at high beam energy — but also removes dispersion, precluding conventional sextupole-based chromatic correction. Instead, chromatic correction is performed via phase advance tuning through a matching section, minimizing the Montague W-function [3] at each IP to make them apochromatic [4]. The extreme demagnification required to achieve $\beta^* = 2$ mm produces peak β-functions of order 65 km in the final triplet quadrupoles immediately upstream of each IP.

During beam tracking studies of IP1, a striking C-shaped distortion was observed in the longitudinal phase space: a bunch initialized with nominal parameters develops a non-Gaussian distribution by the time it reaches the IP, with the bunch length growing by a factor of ~15. With $\sigma_z \approx 2.3$ mm comparable to $\beta^* = 2$ mm, this has direct implications for luminosity through bunch lengthening, a non-Gaussian profile, and a significant geometric hourglass effect even when beam-beam effects are neglected.

This paper identifies the mechanism driving the C-shape, quantifies it using the Balandin framework [5], and demonstrates that it is governed by a quantity distinct from the W-function. The nominal beam parameters are given in Table 1.

Table 1: Nominal GHOST Beam Parameters at IP1

Parameter	Symbol	Value
Beam energy	E	275 GeV
Geometric emittance	$\epsilon_{x,y}$	4×10^{-9} m rad
RMS energy spread	σ_δ	2.9×10^{-4}
Initial bunch length	σ_z	0.15 mm
IP beta function	β^*	2 mm
Peak beta in final triplet	$\beta_{\max}$	~65,000 m
Hourglass parameter	σ_z/β^*	~1.15

THE GHOST LATTICE

The lattice consists of four symmetric half-IP sections repeated serially, each de-magnifying from a starting waist down to $\beta^* = 2$ mm at the IP through an upstream and downstream final-focus triplet. The matching section between cells provides sufficient degrees of freedom to control the phase advance independently in both transverse planes. This is used to set $W_a \approx 10$, $W_b \approx 6$ at IP1 in closed geometry — nearly apochromatic — through destructive interference of the ~25,000 peaks of W generated in the upstream and downstream triplets. Figure 1 shows β and W along the beamline to IP1.

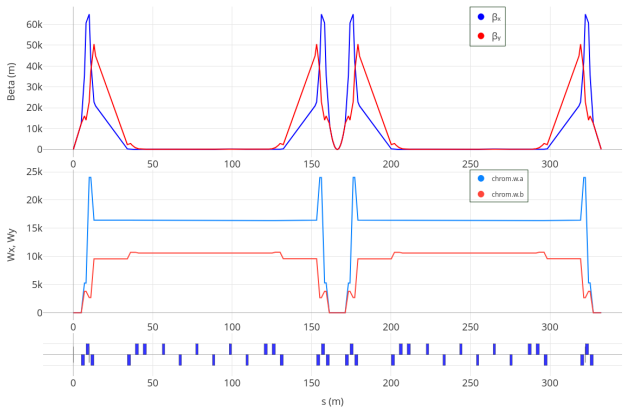

Figure 1: β_x, β_y (top) and Montague W-function (bottom) along the GHOST beamline to IP1. Peak $\beta \approx 65$ km in the final triplet. $W \approx 10$ at IP1 (dotted line) confirms near-apochromatic conditions.

* Work supported by Jefferson Science Associates, LLC under U.S. DOE Contract DE-AC05-06OR23177
† randika@jlab.org

Content from this work may be used under the terms of the CC BY 4.0 licence (© 2026). Any distribution of this work must maintain attribution to the author(s), title of the work, publisher, and DOI.

ISBN: 978-3-95450-252-3 ISSN: 2673-5350 doi: 10.18429/JACoW-IPAC2026-WEP1314

DUAL-RF PHASE CONTROL FOR ADIABATIC ENERGY RAMPING IN THE EIC RAPID CYCLING SYNCHROTRON*

R. Gamage†, T. Satogata, N. Sereno
Thomas Jefferson National Accelerator Facility, Newport News, VA, USA
A. Blednykh, V. Ranjbar, Brookhaven National Laboratory, Upton, NY, USA

Abstract

The Electron-Ion Collider (EIC) Rapid Cycling Synchrotron (RCS) accelerates electrons from 750 MeV to 10 GeV over approximately 64.7 ms. The baseline design ramps both the RF voltage and phase simultaneously to maintain the synchronous phase and synchrotron tune throughout the ramp. This paper presents an alternative approach in which the RF cavities are divided into two groups, each operating at a fixed voltage of 6.5 MV, with the effective voltage synthesised entirely through phase control. Two implementations are studied: a symmetric scheme (Option A) in which both groups vary symmetrically about the synchronous phase, providing exact matching of both the energy gain and synchrotron tune; and an asymmetric scheme (Option B) in which one group is pinned at the final operating phase while the other varies to supply the required energy gain. The adiabaticity of the resulting synchrotron tune evolution is used as the acceptance criterion for Option B. Ramp profiles, phase trajectories, and adiabaticity metrics are presented for both schemes.

INTRODUCTION

The EIC RCS is a key component of the EIC accelerator complex at Brookhaven National Laboratory [1] with on-axis injection into ESR up to 28 nC. During each injection cycle, electrons injected at 750 MeV from the linac are accelerated to a top energy between 5 GeV and 18 GeV, with the nominal operating point at 10 GeV [2]. The RF system consists of eight 591 MHz SRF cavities [3]. The ring operates above the transition energy throughout ($\eta > 0$, $\beta \approx 1$), with a circumference of 1507.015 m, harmonic number $h = 2970$, and momentum compaction factor $\alpha_c = 6.458 \times 10^{-4}$.

The baseline RF ramp simultaneously adjusts the cavity voltage $V_{\mathrm{rf}}(t)$ from 1.12 MV to 13.0 MV and the synchronous phase $\phi_s(t)$ from $\approx 180^\circ$ to $\approx 131^\circ$ to maintain synchronism as synchrotron radiation losses increase with energy [4]. While this approach is well understood, it requires full dynamic range voltage control of all eight cavities throughout the ramp.

A natural question is whether the voltage ramping requirement can be eliminated entirely, replacing it with pure phase control. This paper investigates such a scheme, in which the cavities are split into two independently phased groups, each held at a constant voltage equal to half the peak design voltage. The phasor combination approach used here is analogous to azimuthal combination techniques used in proton synchrotrons [4, 5].

SINGLE-RF BASELINE

In the baseline single-RF system all eight cavities operate at the same phase and voltage. The synchronous phase above transition satisfies

$$\phi_s(t) = \pi - \arcsin\left(\frac{U_0(t)}{V_{\mathrm{rf}}(t)}\right), \tag{1}$$

where $U_0(t) \propto E(t)^4$ is the synchrotron radiation energy loss per turn. The energy gain per turn is $\Delta E = V_{\mathrm{rf}} \sin\phi_s$, and the small-oscillation synchrotron tune is

$$Q_s = \sqrt{\frac{h\,\alpha_c\,V_{\mathrm{rf}}|\cos\phi_s|}{2\pi E}}. \tag{2}$$

The adiabaticity of the ramp is characterised by the fractional change in Q_s per synchrotron period [6, 7],

$$\mathcal{A}(t) = \frac{1}{Q_s^2 f_0}\left|\frac{dQ_s}{dt}\right| \times 100\,\%. \tag{3}$$

Key parameters at injection and top energy are summarised in Table 1.

Table 1: Single-RF Ramp Parameters at Injection and Top Energy

Quantity	Injection	Top energy
Energy	750 MeV	10 GeV
V_{rf}	1.12 MV	13.0 MV
ϕ_s	179.98°	130.87°
Q_s	0.01741	0.03310
U_0	0.30 keV	18.5 keV

DUAL-RF PHASE CONTROL CONCEPT

The dual-RF scheme divides the eight cavities into two groups of four. Each group operates at a fixed voltage

$$V_{\mathrm{fixed}} = \frac{V_{\mathrm{rf,max}}}{2} = 6.5\,\mathrm{MV}, \tag{4}$$

which is the minimum value that keeps the scheme feasible at all times (see Option B). The combined kick seen by the beam is

$$F = V_{\mathrm{fixed}} \sin\phi_a + V_{\mathrm{fixed}} \sin\phi_b, \tag{5}$$

* Work supported by Jefferson Science Associates, LLC under U.S. DOE Contract DE-AC05-06OR23177 and Brookhaven Science Associates, LLC, Contract DE-SC0012704

† randika@jlab.org

Content from this work may be used under the terms of the CC BY 4.0 licence (© 2026). Any distribution of this work must maintain attribution to the author(s), title of the work, publisher, and DOI.

ISBN: 978-3-95450-252-3 ISSN: 2673-5350 doi: 10.18429/JACoW-IPAC2026-WEP1318

PROGRESS OF RF SYSTEMS FOR THE ELECTRON-ION COLLIDER*

S. Verdú-Andrés†, P. Berrutti, M. Blaskiewicz, J. C. Brutus, M. Esposito, K. A. Fahey, J. Fite, L. Guo, D. Holmes, G. Li, D. Lukach, S. Mai, P. D. Malendele, K. Mernick, G. Narayan, J. Rose, F. Severino, A. Singh, K. Smith‡, E. Wang, Q. Wu, B. Xiao, W. Xu, and A. Zaltsman,
Brookhaven National Laboratory, Upton, NY, USA
Z. Conway§, C. Andhare, J. Armstrong, S. Bira, J. Buttles, P. Carriere, A. Castilla, G. Cheng, J. Cox, S. DeHart, P. Denny, P. Dhakal, E. Drachuk, G. Grose, J. Guo, N. Huque, T. Keenan, S. Kuzikov, M. Marchlik, J. Matalevich, P. Minter, M. Oast, A. O'Brien, C. Paul, D. Rath, N. Raut, R. Rimmer, D. Savransky, E. Senecal, S. Shanmuggasundaram, H. Wang, and K. M. Wilson,
Thomas Jefferson National Accelerator Facility, Newport News, VA, USA
S. De Silva, and J. Delayen, Old Dominion University, Norfolk, VA, USA
T. Mastoridis, California Polytechnic State University, San Luis Obispo, CA, USA

Abstract

The Electron-Ion Collider (EIC) under construction at Brookhaven National Laboratory (BNL) is being developed in partnership with DOE's Thomas Jefferson National Accelerator Facility (TJNAF). The EIC will deliver high-luminosity, variable center-of-mass energy collisions of highly polarized electron beams with highly polarized proton beams and ion beams. The EIC RF Systems provide a variety of functions and operate across a wide range of frequencies, utilizing multiple cavity types and technologies. We discuss challenges and proposed solutions for the EIC RF systems, provide high-level system parameters and main design choices, and review progress and plans for the RF Systems of the EIC Storage Rings.

THE ELECTRON-ION COLLIDER

The EIC will provide high-luminosity collisions of polarized electrons with polarized protons and light ions as well as with heavier stable nuclei in a center-of-mass energy range from 20 to 140 GeV. The EIC will reuse the hadron injection system, some components and infrastructure from the Relativistic Heavy-Ion Collider (RHIC) for the Hadron Storage Ring (HSR). The RHIC tunnel will host the HSR and a new Electron-Storage Ring (ESR). The electron injection system will consist of a preinjector (PRB), a Beam Accumulator Ring (BAR), and a Rapid Cycling Synchrotron (RCS). The collider will also have a Low Energy Cooler (LEC) in the RHIC tunnel. A sketch of the EIC accelerator complex is shown in Fig. 1 [1].

The HSR will host up to 1160 bunches, up to 1 A beam current of proton and ion beams, with an energy range from 40 to 275 GeV. A different beam scenario consists of 290 bunches, 0.69 A beam current of proton beams and presents the largest charge per bunch. The HSR is equipped with five different RF Systems to support injection, capture, acceleration, 4-way bunch splitting, compression, and store. For ion beams, the RF systems shall additionally enable transition crossing. The HSR will be a versatile machine as RHIC was, although operating with shorter bunches and higher current beams.

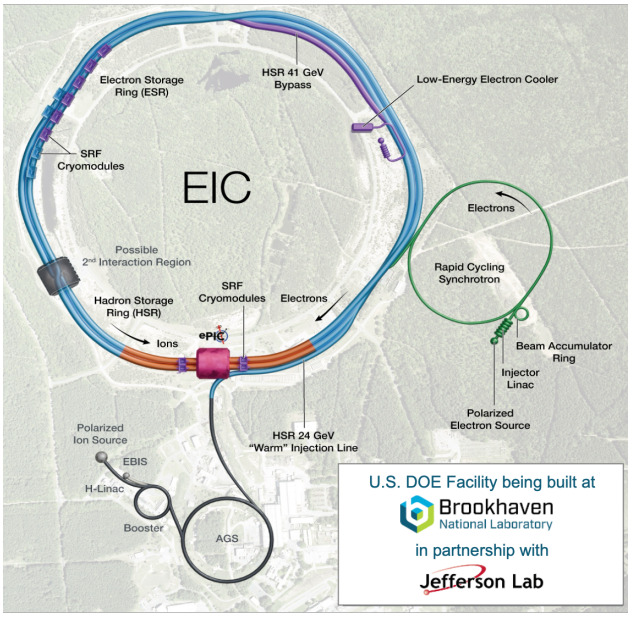

Figure 1: The EIC accelerator complex at BNL.

The ESR will store up to 1160 bunches with beam currents up to 2.5 A over an energy range of 5 to 18 GeV. Operation at the maximum energy of 18 GeV will be limited to 0.227 A to keep synchrotron radiation power within practical limits. The 9 GeV operating point will support the highest current, up to 2.5 A. The ESR employs a 591 MHz RF system to restore the energy lost to the beam.

To preserve polarization rates at collision, the electron injector system will deliver a fresh single bunch of up to 28 nC into the ESR every second at store energy. Highly polarized, 1 nC bunches at a 30 Hz repetition rate will be accelerated in the preinjector and accumulated in a single bunch of 750 MeV at BAR to deliver up to 28 nC bunches to the RCS at 1 Hz. The RCS will provide then fast acceleration to the different ESR store energies. The ramp to 18 GeV is only 120 ms.

* Work supported by Brookhaven Science Associates, LLC under U.S. Contract No. DE-SC0012704 and by Jefferson Science Associates, LLC under U.S. DOE Contracts No. DE-AC05-06OR23177 and DE-SC-0019287.
† Corresponding author: sverdu@bnl.gov
‡ Now at xLight Inc., Palo Alto, CA, USA
§ Now at Subcritical Systems Inc., Austin, TX, USA

Content from this work may be used under the terms of the CC BY 4.0 licence (© 2026). Any distribution of this work must maintain attribution to the author(s), title of the work, publisher, and DOI.

ISBN: 978-3-95450-252-3 ISSN: 2673-5350 doi: 10.18429/JACoW-IPAC2026-WEP1324

HIGH-INTENSITY BEAM ACCUMULATOR RING FOR ELECTRON-ION COLLIDER

H. Dave, F. DePaola, L. Doom, J. Escallier, R. Faussete, G. Fries, G. Ganetis, F. Gao, J. Gosman, A. Khan, Y. Li, I. Lobach, C. Marques, P. N'Gotta, D. Padrazo, J. Rose, T. Shaftan, S. Sharma, V. Smaluk*, C. Stelmach, Y. Tian, R. Todd, X. Yang,
Brookhaven National Laboratory, Upton, United States

Abstract

The Beam Accumulator Ring (BAR) is part of the Electron-Ion Collider (EIC) injector complex at Brookhaven National Laboratory. It is designed to accumulate a polarized 750 MeV electron beam up to a single-bunch charge of 28 nC for injection into the Rapid Cycling Synchrotron (RCS). A compact double-bend achromat lattice is based on the NSLS VUV ring. The BAR design incorporates well-proven magnet, vacuum, RF, beam diagnostics, and control technologies. Comprehensive studies of injection and extraction schemes, error correction, and collective effects demonstrate robust beam accumulation. With the bunch shortening by RF modulation to mitigate the bunch lengthening caused by the microwave instability, all beam parameters at extraction meet the specifications. The preliminary design validates BAR performance goals and establishes readiness for integration into the EIC injector chain.

INTRODUCTION

The Beam Accumulator Ring (BAR) is a part of the Electron-Ion Collider (EIC) injector chain. It is located between the 750 MeV linac-injector and the full-energy (5-18 GeV) Rapid Cycling Synchrotron (RCS), as shown in Fig. 1

The functional role of BAR is the accumulation of charge injected from the linac to reach the high intensity of the polarized electron beam required by the specifications of the Electron Storage Ring (ESR) injection. This function will be realized via successive 30 injections of 1.1 nC bunch at a repetition rate of 30 Hz. Once 28 nC of charge in a single bunch is achieved, the former gets extracted from BAR and injected into RCS. The required beam parameters are collected in Table 1.

Table 1: Specification of Beam Parameters

	At injection	At extraction
Energy	750 MeV	750 MeV
Charge	1.1 nC	28 nC*
Horizontal Emittance	45 nm	< 170 nm
Vertical Emittance	30 nm	< 65 nm
Energy spread	4.5×10^{-3}	$0.5–5\times10^{-3}$
Bunch length	0.7 mm	20–70 mm
Repetition rates	30 Hz	1 Hz

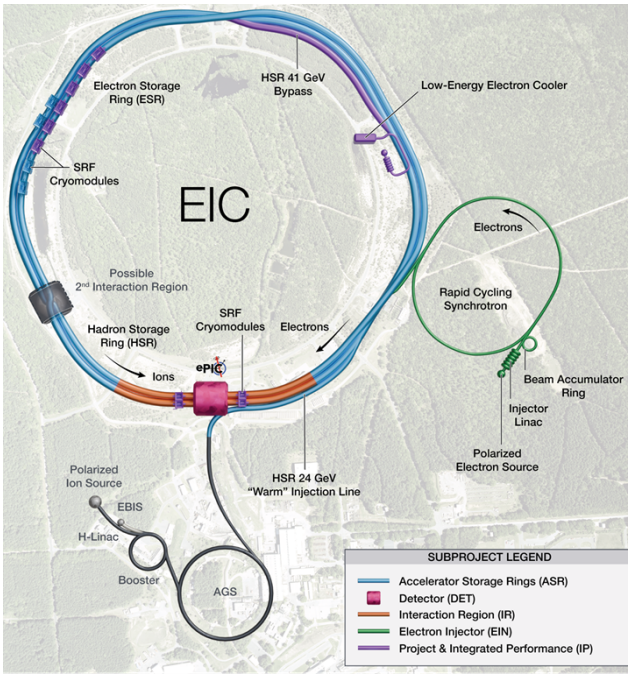

Figure 1: Schenatic layout of the EIC accelerators.

Note, a maximum charge of 32 nC is assumed in BAR in order to provide 28 nC to the RCS with a margin for particle losses along the acceleration and extraction processes.

As the repetition rate of the ESR injector is chosen as 1 Hz, the working cycle for BAR will be 1 second, with about 966 ms for accumulation and 34 ms for extraction. We also consider an option with 1.5-nC injected bunches, allowing extra time for the longitudinal phase space manipulation using RF modulation techniques to provide the bunch length and energy spread required for the injection into RCS. Two beamlines connecting the Linac to BAR and BAR to RCS are being designed to enable lossless beam transport between the accelerators.

DESIGN OPTIMIZATION FOR COST EFFICIENCY

The main goals of the BAR design are a low technical risk and a high reliability. Originally, the BAR lattice design was based on the NSLS VUV ring [1], which met all the requirements listed in Table 1. The maximum single-bunch charge accumulatied in the NSLS VUV ring was about a factor 2 higher than the BAR maximum charge of 32 nC [2]. However, the bunch length measured at NSLS VUV showed that the microwave instability threshold is much lower than

* smaluk@bnl.gov

Content from this work may be used under the terms of the CC BY 4.0 licence (© 2026). Any distribution of this work must maintain attribution to the author(s), title of the work, publisher, and DOI.

ISBN: 978-3-95450-252-3 ISSN: 2673-5350 doi: 10.18429/JACoW-IPAC2026-WEP1325

IMPEDANCE BUDGET FOR EIC BEAM ACCUMULATOR RING

A. Khan*, V. Smaluk, R. Todd, M. Seegitz
NSLS-II, BNL, Upton, NY, USA

Abstract

The Beam Accumulator Ring (BAR) in the Electron–Ion Collider (EIC) injector chain is designed to accumulate charge from multiple linac pulses to produce a high-intensity polarized electron beam for injection into the Electron Storage Ring. At the design single-bunch charge, beam–impedance effects become an important factor for beam stability and component heating. In this work, we develop a longitudinal impedance model of the BAR, combining electromagnetic simulations of the main vacuum components with analytical estimates of the resistive-wall contribution. The total impedance is evaluated by combining all contributions, and key parameters relevant for beam dynamics are extracted. The results provide a consistent basis for assessing collective effects and guiding further optimization of the vacuum chamber design.

INTRODUCTION

The Electron-Ion Collider (EIC) project is under development at Brookhaven National Laboratory to explore the fundamental structure of matter [1]. The Beam Accumulator Ring (BAR) is part of the EIC injector chain [2]. Located between the 750 MeV linac and the 5–18 GeV Rapid Cycling Synchrotron, BAR accumulates charge from multiple linac pulses to provide the high-intensity polarized electron beam required for downstream acceleration and injection into the Electron Storage Ring (ESR).

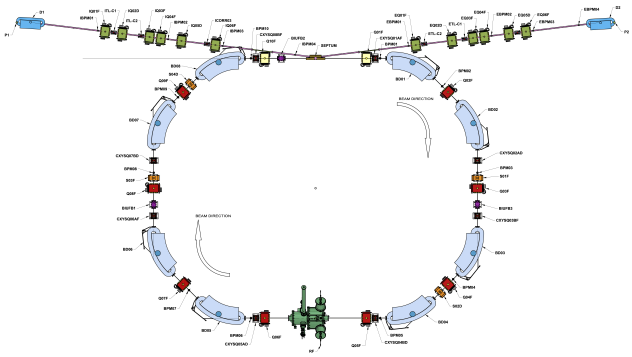

Figure 1: Layout of the Beam Accumulator Ring with injection and extraction transfer lines.

Figure 1 shows the layout of the Beam Accumulator Ring (BAR), including its lattice components such as dipoles, quadrupoles, sextupoles, RF cavities, injection, and extraction systems. The beam is injected from the 750 MeV linac into BAR at a repetition rate of 30 Hz with an initial charge of about 1.1 nC per bunch. Once the single-bunch charge reaches 28 nC (with design margin up to 32 nC), the beam is extracted and transferred to the Rapid Cycling Synchrotron for further acceleration before injection into the ESR.

Achieving this high single-bunch charge presents a major challenge for the BAR design. The interaction of such an intense beam with the vacuum chamber impedance can drive instabilities and cause local overheating of components if the impedance is not carefully controlled. A realistic ring-wide impedance budget is therefore essential for evaluating performance and stability limits.

The present BAR design is based on the NSLS VUV ring lattice and vacuum chamber concept. We have modified and optimized it to satisfy the specific requirements of the EIC injector, including high bunch charge, polarization preservation, and interfaces with the injection/extraction transport lines.

In the original NSLS VUV ring, the bellows contributed the largest share of the geometric impedance [3]. For the BAR design, RF-shielded bellows have been implemented to mitigate this effect. Figure 2 shows the geometries of the unshielded and RF-shielded bellows used in the simulations.

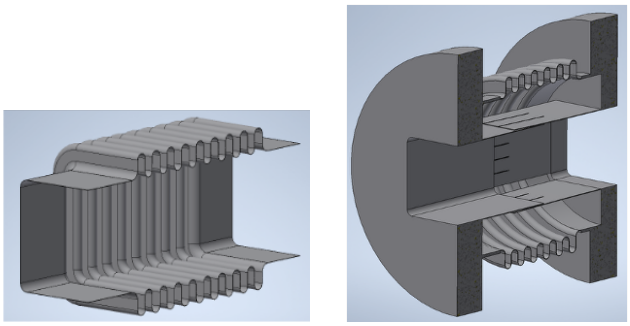

Figure 2: Schematic views of the bellows geometry used in the impedance simulations: (left) unshielded bellows and (right) RF-shielded bellows design with cross-section of 80 mm × 40 mm.

The longitudinal impedance of the bellows was evaluated for both configurations. As shown in Fig. 3, the unshielded bellows exhibit a significantly larger impedance over a broad frequency range, while the RF-shielded design strongly suppresses both the real and imaginary parts of the impedance.

This reduction is also reflected in the loss factor k_{loss}, which quantifies the energy loss per unit charge due to wake-fields. For the present bunch length $\sigma_s = 61.5\,\mathrm{mm}$, the loss factor decreases from 0.31 mV/pC for the unshielded case to 7×10^{-4} mV/pC with RF shielding, corresponding to a reduction by more than two orders of magnitude. This demonstrates that RF-shielded bellows are essential for achieving a low overall impedance budget in the BAR, as reflected in the total impedance model discussed below.

* akhan1@bnl.gov

Content from this work may be used under the terms of the CC BY 4.0 licence (© 2026). Any distribution of this work must maintain attribution to the author(s), title of the work, publisher, and DOI.

ISBN: 978-3-95450-252-3 ISSN: 2673-5350 doi: 10.18429/JACoW-IPAC2026-WEP1326

ANALYTICAL ESTIMATES OF BEAM INTENSITY LIMITATIONS IN THE EIC BEAM ACCUMULATOR RING

A. Khan, V. Smaluk*, Brookhaven National Laboratory, Upton, NY, USA

Abstract

We have done analytical estimates of beam intensity limitations in the Beam Accumulator Ring (BAR), a part of the Electron-Ion Collider injector complex under development at Brookhaven National Laboratory. Analytical models of longitudinal and transverse collective effects are developed using a broadband impedance model calibrated with the beam-based measurement results from NSLS VUV. The study evaluates the impact of resistive-wall and geometric impedances, assessing microwave and transverse mode coupling instabilities, bunch lengthening, and beam-induced heating.

INTRODUCTION

The Electron-Ion Collider (EIC) project is under development at Brookhaven National Laboratory to explore the fundamental structure of matter. The Beam Accumulator Ring (BAR) [1] is a part of the EIC injector. It is dedicated to accumulating a polarized electron beam with the high single-bunch intensity required by the Electron Storage Ring (ESR). The beam with a charge of about 1 nC is injected from the linac into BAR with a repetition rate of 30 Hz. Once the single-bunch charge of 28 nC is achieved, the beam is extracted from the BAR and injected into the Rapid Cycling Synchrotron (RCS), where it is accelerated up to the full energy of 5 to 18 GeV for injection into the ESR.

To provide a cost-efficient solution, the ring circumference was reduced from 50 m of the National Synchrotron Light Source Vacuum Ultraviolet (NSLS VUV) ring to 36 m, and the lattice design evolved from four Double-Bend Achromat cells to two Four-Bend Achromat cells. The BAR beam parameters related to the collective effects are summarized in Table 1, its schematic layout is shown in Fig. 1.

IMPEDANCE MODEL

To estimate the collective effects of beam dynamics, we assume a vacuum chamber with a rectangular cross-section 80 mm × 40 mm (Fig. 2) made of aluminum as a basic option and also consider a 316L stainless steel as a cost-saving option.

The resistive-wall impedance is calculated by analytical equations for a rectangular vacuum chamber [2]. The geometric impedance is approximated by an equivalent broadband resonator (BBR) model, which is adequate to estimate single-bunch effects of low-frequency beam-impedance interaction, such as bunch lengthening and transverse head-tail mode coupling. To determine the resonance frequency and shunt impedance of the BBR model, we fit the intensity-dependent bunch lengthening with experimental data [3] measured at the NSLS VUV. The total longitudinal impedance consisting of the BBR and resistive-wall parts is shown in Fig. 3, assuming the aluminum chamber.

The transverse resistive-wall impedance is also calculated by the analytical equations [2], and the transverse geometric impedance is modeled by an equivalent broadband resonator with the same resonance frequency and quality factor as

Table 1: Lattice and Beam Parameters

Parameter	Value
Energy (GeV)	0.75
Circumference (m)	36.52
Hor. tune	2.42
Ver. tune	1.46
Natural hor. chromaticity	-3.8
Natural ver. chromaticity	-1.6
Momentum compaction	0.084
Hor. damping time (s)	0.0073
Ver. damping time (s)	0.012
Long. damping time (s)	0.0096
Energy spread	5.78×10^{-4}
Energy loss per turn (keV)	14.66
Revolution frequency (MHz)	8.2089
Aver. hor. beta (m)	7.2
Aver. ver. beta (m)	4.7
Aver. hor. dispersion (m)	0.72
RF voltage (kV)	100
RF frequency (MHz)	98.5062
RF harmonic	12
Synchrotron tune	0.0046
Bunch length (mm)	61.5
RF acceptance	0.008

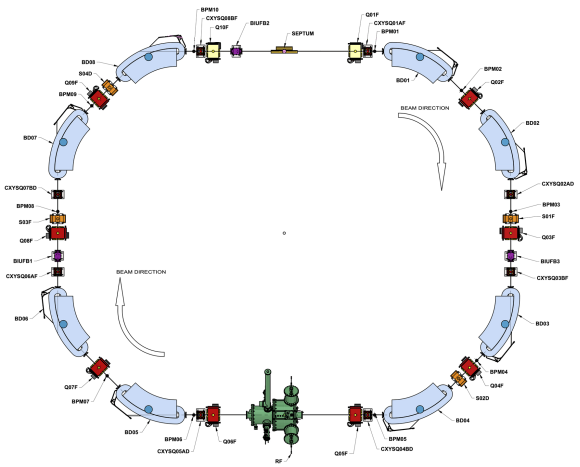

Figure 1: BAR layout.

* smaluk@bnl.gov

Content from this work may be used under the terms of the CC BY 4.0 licence (© 2026). Any distribution of this work must maintain attribution to the author(s), title of the work, publisher, and DOI.

ISBN: 978-3-95450-252-3 ISSN: 2673-5350 doi: 10.18429/JACoW-IPAC2026-WEP1327

BUNCH SHORTENING SIMULATIONS BY RF MODULATION IN THE EIC BEAM ACCUMULATOR RING

A. Khan*, V. Smaluk, J. Rose, C. Marques
NSLS-II, BNL, Upton, NY, USA

Abstract

The Beam Accumulator Ring (BAR) of the Electron–Ion Collider (EIC) injector chain accumulates polarized electron bunches of up to 32 nC before extraction into the Rapid Cycling Synchrotron (RCS). The large momentum compaction of the compact BAR lattice, combined with impedance-driven bunch lengthening, yields an equilibrium rms bunch length that lies at or above the upper edge of the RCS injection specifications. Using a geometric and resistive-wall impedance model together with multi-particle tracking in ELEGANT, we study bunch shortening by RF voltage modulation, in which an abrupt reduction of the RF amplitude induces a quarter-synchrotron-period rotation in longitudinal phase space so that the beam is extracted at its shortest projection. The simulations show that, for both 49 MHz and 98 MHz RF options under consideration, RF voltage modulation compresses the bunch into the required length and energy-spread window with operational margin.

INTRODUCTION

The Electron–Ion Collider (EIC) is under construction at Brookhaven National Laboratory to explore the fundamental structure of matter [1]. The Beam Accumulator Ring (BAR) is a 36.5 m circumference electron accumulator in the EIC polarized-electron injector chain, located between the 750 MeV linac and the 5 GeV to 18 GeV Rapid Cycling Synchrotron (RCS). The main beam specifications at injection and extraction are summarized in Table 1.

Table 1: BAR beam specifications at injection and extraction

Parameter	Injected beam	Extracted beam
Energy	750 MeV	750 MeV
Charge	1.1 nC	28 nC*
Geometric emitt.	hor: 45 nm rad	hor: < 170 nm rad rms
	ver: 30 nm rad	ver: < 65 nm rad rms
Energy spread	0.45 %	0.05 % to 0.5 %
Bunch length	0.7 mm	20 mm to 70 mm
Repetition rate	30 Hz	1 Hz

*Maximum charge of 32 nC in the BAR is assumed to provide margin for possible particle loss.

The functional role of the BAR is to accumulate, over approximately 30 linac pulses at 30 Hz, a single polarized electron bunch for injection into the RCS. The nominal extracted bunch charge is 28 nC, while accumulation up to 32 nC provides margin for losses during extraction and transfer. The design is derived from the NSLS VUV ring lattice and vacuum chamber concept [2], modified to meet EIC injector requirements of high bunch charge, polarization preservation, and matching to the injection and extraction transport lines.

The high single-bunch charge places demanding constraints on the longitudinal dynamics. The rms bunch length at extraction must lie in the 20 mm to 70 mm window set by the RCS RF bucket and downstream machine protection. With the nominal accumulator RF voltage of 100 kV, the equilibrium bunch length is close to the upper edge of this window, and impedance-driven potential-well distortion can push it outside specification. In this study, we summarize the impedance-limited bunch length of the latest BAR lattice, present the RF voltage modulation scheme proposed for bunch shortening before extraction, and show ELEGANT [3] tracking results including the full impedance budget.

BAR Parameters

Key parameters of the current BAR lattice are listed in Table 2. Two RF options are being considered: the baseline 49 MHz system ($h = 6$) inherited from the NSLS VUV RF design [4], and a candidate 98 MHz system ($h = 12$) that offers a shorter natural bunch and eases synchronization with the 591 MHz RCS [5]. Both options use the same 100 kV nominal RF voltage.

The large momentum compaction ($\alpha_c = 0.084$) inherited from the compact VUV-class lattice, combined with the modest RF voltage available in an accumulator, results in a long natural bunch even at zero current. For the 49 MHz option the natural bunch length already exceeds the 70 mm upper limit of the extraction specification; for the 98 MHz option the natural bunch sits just inside the window with negligible margin.

Table 2: BAR Lattice and RF Parameters

Parameter	Value	
Energy	0.75 GeV	
Circumference	36.52 m	
Horizontal emittance	114 nm	
Momentum compaction α_c	0.0843	
Natural energy spread	5.8×10^{-4}	
Energy loss per turn	14.66 keV	
Long. damping time	9.6 ms	
Accumulated single-bunch charge	32 nC	
RF option	49 MHz	98 MHz
Harmonic number h	6	12
RF voltage (nominal)	100 kV	100 kV
Synchrotron tune ν_s	0.0033	0.0046
Natural rms bunch length	87 mm	61.5 mm

* akhan1@bnl.gov

Content from this work may be used under the terms of the CC BY 4.0 licence (© 2026). Any distribution of this work must maintain attribution to the author(s), title of the work, publisher, and DOI.

ISBN: 978-3-95450-252-3 ISSN: 2673-5350 doi: 10.18429/JACoW-IPAC2026-WEP1332

DESIGN AND RECENT DEVELOPMENTS OF THE ELECTRON STORAGE RING FOR THE ELECTRON-ION COLLIDER*

D. Marx†, J.S. Berg, B. Bhandari, D. Holmes, C. Montag, S. Nagaitsev, A. Natochii, S. Tepikian
Brookhaven National Laboratory, Upton, NY, USA
V. Morozov, Oak Ridge National Laboratory, Oak Ridge, TN, USA
K. Deitrick, N. Sereno, Thomas Jefferson National Accelerator Facility, Newport News, VA, USA

Abstract

The Electron-Ion Collider (EIC), which is currently being designed for construction at Brookhaven National Laboratory, will collide polarized electron beams (5-18 GeV) with polarized hadron beams (41-275 GeV for protons) at luminosities up to $10^{34}\text{cm}^{-2}\text{s}^{-1}$ in a 3.8-kilometer ring. The EIC will be the only lepton-hadron collider since HERA at DESY and, in contrast to that earlier machine, will feature high polarization of both electrons and protons, a wide range of center-of-mass collision energies, a wide range of ion species, and much higher luminosities. These properties will make it an ideal machine for exploring the mass and spin dynamics of nucleons. The Electron Storage Ring (ESR) will be built in the existing 3.8-kilometer RHIC tunnel using normal-conducting magnets and a few superconducting magnets for the final-focus quadrupoles and spin-rotator solenoids. The wide range of energies, high polarization, high current, large beam-beam parameters, and stringent geometric constraints make the ESR a particularly challenging machine. Lately, the design of the ESR has advanced considerably with design alternatives and upgrade paths being considered to align with the key deliverables and funding profile of the project. This contribution highlights some of the important recent developments and design studies.

INTRODUCTION

The Electron-Ion Collider (EIC) [1] will collide spin-polarized electron beams with hadron beams (polarized protons and helium nuclei, as well as a broad range of unpolarized heavier atomic nuclei). Its scientific mission is to provide data from collisions that will support the exploration of the mass and spin dynamics of nucleons. The EIC will be built at Brookhaven National Laboratory, leveraging existing infrastructure from the Relativistic Heavy Ion Collider (RHIC) [2–4], including the 3.8-kilometer circular tunnel. One of the two existing RHIC hadron rings will be transformed into a new hadron storage ring (HSR) for the EIC, and a new electron storage ring (ESR) [5–8] will also be built in this tunnel for circulating electron beams for collisions. The electron and hadron beams will be brought into collision in the ePIC detector; a second interaction region and detector may be included in a future upgrade. The existing RHIC injector complex, including the 0.8-kilometer Alternating Gradient Synchrotron (AGS), will serve as the hadron injector for the EIC. A new electron-injector complex is being designed, including a polarized photoinjector, a Beam Accumulator Ring (BAR), and a 1.5-kilometer Rapid Cycling Synchrotron (RCS). Figure 1 shows a schematic of the EIC.

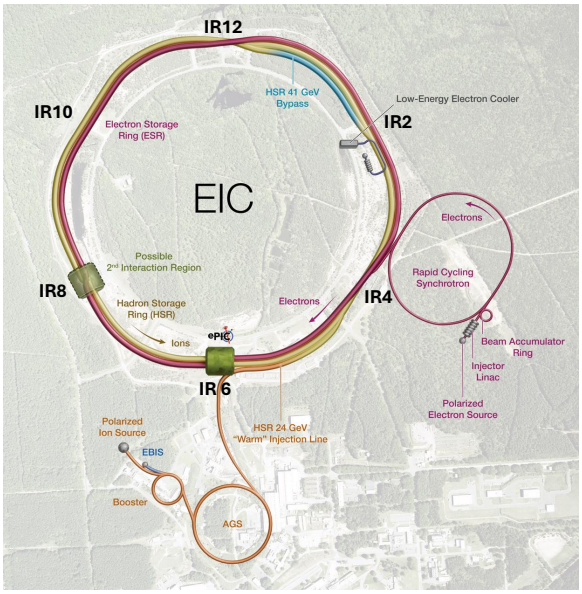

Figure 1: Schematic of EIC (not to scale).

The EIC will be the first collider to collide beams of electrons and ions, as well as the first collider to collide spin-polarized beams of electrons and protons. In contrast to the earlier collider HERA, which operated at DESY, Germany, the EIC will not only collide beams of protons but also a wide range of ion species, such as gold or uranium nuclei. The EIC will collide particles over a very wide range of center-of-mass energies, ranging from about 20 GeV to 100 GeV for electron-proton collisions initially, with a final planned energy of 140 GeV. High polarization and high luminosity are vital for the experimental program. The EIC will be able to produce beams of electrons, protons, and helium nuclei with polarization greater than 70% at collision, and the luminosity will extend to $10^{34}\ \text{cm}^{-2}\text{s}^{-1}$ for certain working points.

The wide beam-energy range, high polarization, large beam-beam parameters, tight bunch spacing, and high beam current together make the ESR a challenging and unique storage ring. Novel solutions have been developed to fulfill these conditions, such as using super-bend triplets in the arc

* Work supported by Brookhaven Science Associates, LLC under Contract No. DE-SC0012704, by Jefferson Science Associates, LLC under Contract No. DE-AC05-06OR23177, and by UT-Battelle, LLC under Contract No. DE-AC05-00OR22725 with the U.S. Department of Energy.
† dmarx@bnl.gov

Content from this work may be used under the terms of the CC BY 4.0 licence (© 2026). Any distribution of this work must maintain attribution to the author(s), title of the work, publisher, and DOI.

ISBN: 978-3-95450-252-3 ISSN: 2673-5350 doi: 10.18429/JACoW-IPAC2026-WEP1333

NICKEL-ZINC FERRITE FAST TUNER OF 24.6 MHZ ACCELERATING CAVITY FOR TRANSITION CROSSING

Guangjiang Li†, Kathryn Chen, Silvia Verdu-Andres
Binping Xiao, Wencan Xu, Alexander Zaltsman

Brookhaven National Laboratory, Upton, USA

Abstract

To keep beam longitudinal stability during transition crossing, the phase of the cavity accelerating voltage needs to change by 180 degrees within sub-milliseconds to complete the gamma jump. Due to the higher beam current in the hadron storage ring (HSR) of the Electron-Ion Collider (EIC) compared with that in the Relativistic Heavy Ion Collider (RHIC), the beam-loading-induced frequency detuning will also increase proportionally. Hence, a fast tuner range of 20 kHz is required for the 24.6 MHz accelerating cavity. The existing ferrite tuner in the 28 MHz cavity in RHIC has a tuning range of 4 kHz with a DC bias current from ~ 5 to 55 A and power dissipation up to 2 kW. We plan to use four such ferrite tuners for each 24.6 MHz cavity to achieve a 20 kHz tuning range. In an effort to understand if the tuning performance could be improved for EIC applications, we characterized the permeability and loss tangent of the M4C21 nickel-zinc ferrite. A full RF simulation of the cavity coupled with the tuner was also performed.

INTRODUCTION

Each RHIC 28 MHz cavity has only one ferrite tuner installed on the long outer conductor with a loop coupler, while one symmetric port remains unused. For the EIC 24.6 MHz cavity, 4 ferrite tuners will be installed, two ports on the long outer conductor and two additional ports located on the endplate [1, 2, 3]. Each ferrite tuner contains eight ferrite toroids with dimensions of 5-inch inner diameter, 8-inch outer diameter, and 1-inch thickness (Fig. 1). Copper plates with water cooling are inserted between each ferrite. The DC power supply Kepco ATE 6-100M provides up to 600 W with an output voltage range of 0–6 V and a current range of 0–100 A. It usually operates from 5 A to 55 A during RHIC experiments. The ferrite material, originally procured by Fermi National Accelerator Laboratory (Fermilab) from Toshiba, has a relative permittivity of approximately 13 and an initial permeability of about 50 [4, 5]. We will adopt the original ferrite tuner RF design. A total of 96 additional ferrite toroids is required for the four 24.6 MHz RF systems (24 toroids per system). Sufficient ferrite material is currently available at our lab, supplied by collaborators at Fermilab.

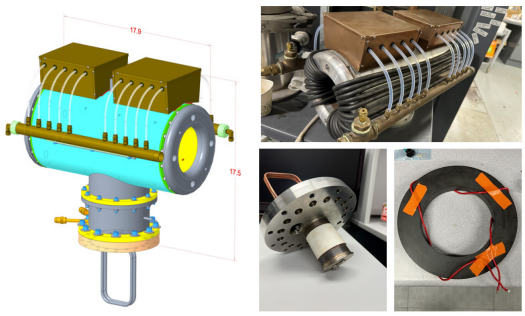

Figure 1: (1) Ferrite tuner model; (2) photos of ferrite tuner, RF window with the loop coupler and ferrite toroid.

Requirement for EIC

The synchrotron frequency describes how fast particles oscillate around the synchronous particle:

$$\omega_s^2 = \frac{heV}{2\pi\beta^2 E}\eta cos\phi_s$$

The slip factor is given by

$$\eta = \frac{1}{\gamma^2} - \frac{1}{\gamma_t^2}$$

where γ is the relativistic Lorentz factor and γ_t is the transition gamma. The slip factor satisfies $\eta = 0$ at the transition energy, where the beam becomes unstable. Below transition, $\eta > 0$, while above transition, $\eta < 0$. The condition for longitudinal beam stability is $\eta\cos\phi_s > 0$. During transition crossing, the RF cavity phase must change such that $\cos\phi_s$ switches from negative to positive. This corresponds to shifting the synchronous phase from ϕ_s to $\pi - \phi_s$ on a millisecond timescale [6].

Besides, the fast tuner also actively in compensating for detuning due to cavity temperaure change and the beam loading. The cavity detuning induced by beam loading is given by:

$$\frac{\omega_g - \omega_0}{\omega_0} = \frac{I_0 R_a sin\phi_s}{2Q_0 V_c}$$

where ω_g is the generator frequency, ω_0 is the cavity resonance frequency, I_0 is the average beam current, R_a is the shunt impedance, ϕ_s is the synchronous phase, Q_0 is the unloaded quality factor, and V_c is the cavity voltage. The equation shows that the frequency detuning is appropotioinal to the average beam current. In Table 1, for heavy-ion operation in the EIC, the average beam current is 0.54 A, which is three times as in RHIC. All above results in a tuning range of 20 kHz for EIC 24.6 MHz system. Each cavity needs four of these tuners, and the total power dissipation must not exceed 3.2 kW per cavity.

*Work supported by Brookhaven Science Associates, LLC under Contract No. DE-SC0012704 with the U.S. DOE.
† Email: gli3@bnl.gov

Content from this work may be used under the terms of the CC BY 4.0 licence (© 2026). Any distribution of this work must maintain attribution to the author(s), title of the work, publisher, and DOI.

ISBN: 978-3-95450-252-3 ISSN: 2673-5350 doi: 10.18429/JACoW-IPAC2026-WEP1340

ORBIT CORRECTION STUDIES ON THE ELECTRON TRANSPORT LINE FROM RCS TO ESR *

I. Neththikumara†,[1], K. Deitrick[1], N. Sereno[1], S. Setiniyaz[1], T. Satogata[1], W. Bergan[2], V. Ranjbar[2]
[1]Thomas Jefferson National Accelerator Facility, Newport News, VA, USA
[2]Brookhaven National Laboratory, Upton, NY, USA

Abstract

A dedicated electron transfer line from Rapid Cycling Synchrotron (RCS) to Electron Storage Ring (ESR), referred to as the RTE line has been designed for the Electron-Ion Collider (EIC). The beamline follows a straight-line geometry, with a length of 133 m, and is consists with two matching sections and a FODO section for beam diagnostics. Imperfections with magnet alignments introduce orbit distortions, making orbit correction scheme a critical component in the design. To facilitate orbit correction, each quadrupole magnet is equipped with a pair of beam position monitors (BPMs) and kickers. The Singular Value Decomposition (SVD) algorithm is used for orbit correction and tolerance studies. This paper presents the ongoing progress in the optics design and error correction scheme of the RTE line.

INTRODUCTION

The U.S. Electron-Ion Collider (EIC) is being designed to be build at Brookhaven National Lab as a collaborative effort between Jefferson Lab and and Brookhaven National Lab. The new electron injector system for the EIC consists of electron linac, Beam Accumulator Ring (BAR), Rapid Cycling Synchrotron (RCS), and Electron Storage Ring (ESR). In the RCS, electrons get accelerated to three different energies; 5 GeV, 10 GeV and 18 GeV [1]. Accelerated electrons will then be transported to ESR using a dedicated transport line referred to as RTE line.

The RTE line extracts electrons using three pulsed kicker magnets and two septum magnets, making 3° extraction angle. A FODO section consists with 9 compact quadrupole magnets reusing 30 cm MIT-Bates quadrupole magnets [2]. Two matching sections are at the ends of FODO section to match Twiss functions from RCS extraction and to ESR injection points. The ESR injection is designed with a 6° or 9° injection angle, using two or three 3° DC septum magnets along with 14 fast-pulsed kickers. More details on the ERS injection is found in [3].

TRAJECTORY CORRECTION WITH SVD

The design of the RTE line evolved to accommodate the changes and requirements of the RCS and ESR ring designs. For this study an RTE line design with 9° ESR injection angle is used. The lattice layout of this line is illustrated in Fig. 1.

* This work is supported by Jefferson Science Associates, LLC., under U.S. DOE Contract DE-AC05-06OR23177 and Brookhaven Science Associates, LLC, Contract DESC0012704

† isurunh@jlab.org

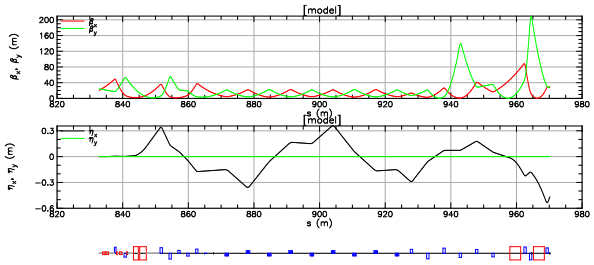

Figure 1: Beta functions, dispersion and the magnet layout of the RTE line with 9° ESR injection

Singular Value Decomposition

The transfer matrix R between two positions in a beamline is,

$$R_{1,2} = \begin{pmatrix} R_{11} & R_{12} \\ R_{21} & R_{22} \end{pmatrix} \tag{1}$$

For a perturbed orbit due to an applied kick ($\Delta x_1'$) at point 1 is measured with a BPM at the point 2. The beam position at point 2 can be described as;

$$\Delta x_2 = R_{12}\Delta x_1' \tag{2}$$

Similarly, for a series of "M" BPMs and "N" kicker magnets, deviated orbit at j^{th} BPM is,

$$\Delta x^j = \Sigma_{i=1}^{N} (R_{12})_{ji}\Delta x_i' \tag{3}$$

Two set of vectors are then created using the beam obit position (X) and the kicks (X'), which the used in the Singular Value Decomposition (SVD) algorithm.

$$X = \begin{pmatrix} \Delta x^1 \\ . \\ . \\ . \\ \Delta x^M \end{pmatrix} \quad , \quad X' = \begin{pmatrix} \Delta x'^1 \\ . \\ . \\ . \\ \Delta x'^N \end{pmatrix}$$

These two vectors are then written as;

$$X = AX' \tag{4}$$

Where, A is a N x M matrix know as the response matrix.

In SVD, this matrix A is decomposed into 3 matrices, U, V and Σ, where U and V are orthogonal and Σ is a rectangular diagonal matrix containing singular values $\sigma_{ii} = \Sigma_{ii}$. One can easily remove the singular vectors with small singular values to increase the robustness of the trajectory correction. After singular vector removal the "pseudo inverse" of A is obtained as $A^{-1} = V\Sigma^{-1}U^T$. The required corrector kicks are then determined by, [4, 5]

$$X' = A^{-1}X \tag{5}$$

Content from this work may be used under the terms of the CC BY 4.0 licence (© 2026). Any distribution of this work must maintain attribution to the author(s), title of the work, publisher, and DOI.

ISBN: 978-3-95450-252-3 ISSN: 2673-5350 doi: 10.18429/JACoW-IPAC2026-WEP1342

DAMPING HIGHER ORDER MODES FOR THE COOL COPPER COLLIDER

S. Morton*, D. Bizzozero, L. Ge, Z. Li, E. Nanni, W. H. Tan
SLAC National Accelerator Laboratory, Menlo Park, CA, USA

Abstract

For next generation particle collider designs, such as the Cool Copper Collider, small beam sizes, short bunch spacing, and beam stability are required to reach the luminosities desired to search for new physics. One challenge to overcome is suppressing the long-range wakefields from higher order modes inside accelerating cavities. Multiple bunches are required to meet the target luminosity, but these wakefields deflect neighboring bunches and lead to emittance growth, hence they must be suppressed to preserve the beam quality. The solution is the addition of damping slots on the accelerator cavities that can couple to these higher order modes and suppress them in the central part of the cavity that the beam passes through to reduce the kick factor of the mode. Additionally, these damping slots can lower the Q value for these modes, causing the excitation to die out between bunches because the mode cannot resonate in the cavity for as long. In this study, we optimize the damping slot geometry to remove higher order modes from the accelerating cavity while preserving the fundamental accelerating mode.

INTRODUCTION

Accelerating cavities can be represented as microwave resonators, which have infinite eigenvalue solutions. The fundamental mode, TM_{010}, acts as the accelerating mode, with an axially symmetric longitudinal electric field along the beam axis and azimuthal magnetic field around the axis. The higher order modes (HOMs) can interact with the beam and have accelerating modes off axis as shown in Fig. 1 that deflect the beam non-uniformly, leading to an increase in beam emittance.

To optimize the radiofrequency (RF) accelerating cavity design for the Cool Copper Collider (C3) [1], careful attention must be paid to retaining the accelerating mode and suppressing the HOMs that spoil beam emittance. The figures of merit for this optimization are the kick factor and Q, which must be minimized for each HOM.

The kick factor is a measure of how much deflecting field the beam experiences for a given small offset from the beam axis along the length of the cavity, normalized to the beam charge. In other words, how much will the beam be deflected or 'kicked' in the cavity?

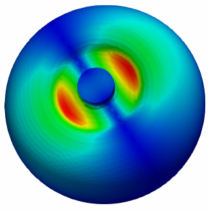

Figure 1: The accelerating cavity without slots as created in Cubit and rendered in Paraview. The second order/dipole mode is shown. Note that the mesh does not need to be very fine for this geometry because there are not any small features and the geometry is simple.

This transverse kick factor (K_n) can be calculated for the nth mode, where $\omega_n/2\pi$ is the frequency of the mode,

$$K_n = \frac{\left|\int_L E_z \exp(j\omega_n s/c)\, dz\right|^2}{4\frac{\omega_n a_n^2}{c} U_n L \left(1 - \frac{v_{gn}}{c}\right)}. \quad (1)$$

Here a_n is the radius of the iris, L the cavity length, E_z is the on-axis electric field, and U_n is the energy stored in the cavity [2]. There is also a dependence on group velocity v_{gn} to correct for the temporal overlap between the mode and the beam, but for cells with π phase advance, as is the case here, this correction can be neglected.

Alternatively, the kick factor can be thought of as the overlap between the wakefield in the cavity W and the bunch distribution $\lambda(s)$ integrated over the length of the cavity

$$k_\perp = \langle W \rangle = \int_L W(s)\,\lambda(s)\, ds \quad (2)$$

for each mode [3].

The other important factor is the quality factor (Q), which determines how long the mode is excited in the cavity. If the mode has a small Q and resonates for a short time, it will be gone before the next bunch is seen. High Q modes will still be in the cavity by the time of the next bunch crossing. Because the structure is cold copper, the walls have low losses and the cavity has large Q factors.

METHODS

In this work, we optimize over the length and width of the damping slots. The slot width, as shown in Fig. 2, is varied from 150 µm to 300 µm and tapers down to a width of 100 µm. The slot length is capped at the cavity radius length due to machining and material constraints.

The final design has a taper down to ~100 µm (a reduction of 7 µm on each slot wall is considered for the addition of lossy Nickel-Chromium (NiCr) on the damping slot walls).

* phia@slac.stanford.edu

Content from this work may be used under the terms of the CC BY 4.0 licence (© 2026). Any distribution of this work must maintain attribution to the author(s), title of the work, publisher, and DOI.

ISBN: 978-3-95450-252-3 ISSN: 2673-5350 doi: 10.18429/JACoW-IPAC2026-WEP1345

DISPERSION SUPPRESSION FOR WEDGE-BASED FINAL COOLING AT A 10 TeV MUON COLLIDER*

I. Karaaslan†, K. DiPetrillo, University of Chicago, Chicago, IL, USA
D. Neuffer, D. Stratakis, K. Yonehara, Fermi National Accelerator Laboratory, Batavia, IL, USA

Abstract

Achieving a luminosity of $10^{34}\,\mathrm{cm}^{-2}\,\mathrm{s}^{-1}$ in a 10 TeV Muon Collider, given the short lifetime of a muon, requires reducing the 6D emittance of the muon beam through a process known as ionization cooling. In the final stage of this cooling process, the transverse emittance must be reduced to ~ 22 µm, typically by allowing longitudinal emittance growth up to downstream acceptance limits. While the current International Muon Collider Collaboration designs involve 40 T solenoids to reach the transverse emittance target, such high-field solenoids come with several disadvantages, including mechanical stress management, quench protection, and potential limitations in relying on High Temperature Superconductor technology. Designed as an alternative to using such solenoids while simultaneously reaching target transverse emittance, the previously proposed wedge-based, reverse emittance-exchange cooling scheme requires excellent dispersion suppression. In this study, we design and simulate a dispersion suppressor channel for the wedge-based final cooling design that reduces dispersion in the target direction to a target value of $D_x = 0.0036$ m.

INTRODUCTION

In the realm of planned next-generation facilities following the completion of the High Luminosity Large Hadron Collider (HL-LHC) at CERN, a circular muon collider stands out from others due to its potential to reach a multi-TeV center of mass energy with greater energy and power efficiency. For a feasible realization of the International Muon Collider Collaboration (IMCC) 10 TeV muon collider design, obtaining luminosities of ~ $10^{34}\,\mathrm{cm}^{-2}\,\mathrm{s}^{-1}$ at the interaction point through emittance reduction at the cooling stage of the collider is crucial [1, 2]. Figure 1 shows the evolution of the muon beam's transverse and longitudinal emittance throughout all cooling stages. The IMCC baseline Final Cooling design features LH_2 absorbers and RF cavities within high-field matching solenoids. In more recent designs, the field strength of these solenoids gets up to ≥ 40 T [3].

Creating and maintaining this ultra-high field regime is one of the major challenges of the design, as such magnets introduce large electromagnetic stresses, the need for quench protection and thermal management (a summary of further progress and challenges can be found in [4]). In this paper, we outline a previously proposed alternative final cooling concept that doesn't rely on high-field solenoids, discuss the requirements for the realization of the full design with a focus on dispersion suppression, and finally demonstrate dispersion suppression with our design.

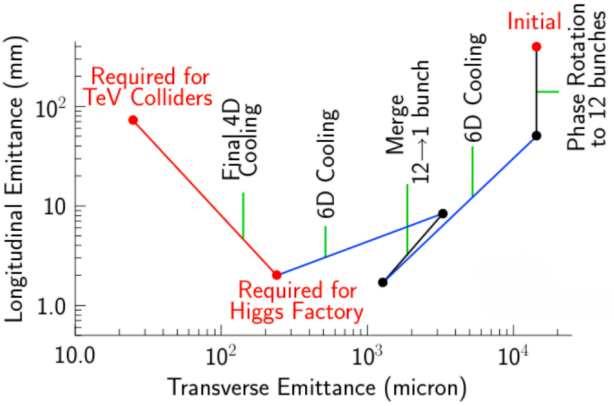

Figure 1: Fernow-Neuffer plot of the muon cooling process [5, 6]. The Final 4D Cooling stage investigated in this study is shown in a red line.

WEDGE-BASED FINAL COOLING DESIGN OVERVIEW

The optimized wedge-based final cooling design is based on the concept outlined in [7]. A diagram of the updated design can be found in Fig. 2. We consider a starting distribution of 145 m transverse emittance with a momentum spread of $\sigma_p = 1.0\,\mathrm{MeV/c}$, corresponding to stage B10 of rectilinear 6D ionization cooling design [8]. The muon beam is initialized with a mean momentum of $p_\mu = 100\,\mathrm{MeV/c}$ where a large reverse-emittance exchange can be realized through a single wedge-shaped solid "dense carbon" diamond material [9] (referred to as just "wedge" hereafter). Dispersion is introduced in the wedge through the wedge's position-dependent non-uniform thickness, exploiting existing momentum-position correlation to preferentially reduce the longitudinal emittance while increasing transverse emittance, achieving reverse-emittance exchange.

The magnets in the dispersion suppression section succeeding the first wedge are positioned to primarily mitigate the dispersion in the x direction. This dispersion correction section design is composed of elements whose fields are linear in transverse coordinates, i.e., dipoles and quadrupoles, which also focus off-momentum particles to the centerline, thereby reducing the beam size and transverse emittance. Prior to this study, the effects of this dispersion section for the final cooling channel have been shown only through manual subtraction of the dispersion from the post-wedge particle distribution.

* Endorsed by the International Muon Collider Collaboration.
† inci@uchicago.edu

Content from this work may be used under the terms of the CC BY 4.0 licence (© 2026). Any distribution of this work must maintain attribution to the author(s), title of the work, publisher, and DOI.

ISBN: 978-3-95450-252-3 ISSN: 2673-5350 doi: 10.18429/JACoW-IPAC2026-WEP1347

FLUKA-BASED OPTIMIZATION OF PION PRODUCTION FOR A MUON COLLIDER DEMONSTRATOR

R. Alharthy*[1], S. Dasu[1], Ch.-H. Nee[1], P. Rao[1], C. Vuosalo[1],
J. Eldred[2], M. Hedges[2], S. Jindariani[2], D. Stratakis[2], K. Yonehara[2]
[1]University of Wisconsin–Madison, Madison, WI, USA
[2]Fermi National Accelerator Laboratory, Batavia, IL, USA

Abstract

This study uses FLUKA simulations to investigate pion production from proton interactions with a graphite target for muon collider applications. A 40 cm target is struck with 0.8 GeV and 8 GeV/c proton beams, and pion yields are evaluated in terms of angular and energy distributions. The dependence of pion yield on target length is also examined, showing saturation near one interaction length for the 0.8 GeV beam, and saturation near two interaction lengths for the 8 GeV/c beam. In addition to total production, a subset of "acceptable" pions is defined based on capture constraints (kinetic energy <400 MeV, forward-going, and escaping the target). The results show that while the 8 GeV/c beam produces higher overall yields, the 0.8 GeV beam provides a larger fraction of pions within the desired constraints. Charge asymmetry is also observed in pion production.

INTRODUCTION

The development of a future muon collider represents a promising path toward probing physics at the energy frontier. A central challenge in realizing such a facility lies in the efficient production of high-intensity muon beams. Since muons are obtained from the decay of charged pions $\pi^{\pm} \rightarrow \mu^{\pm} + \nu$, optimizing pion production at the target station is a critical component of the collider design.

A demonstrator of a muon production system from target to final cooling is needed to make a convincing case for committing to build a muon collider. We investigate the design challenges and site specific optimization of the target system for a demonstrator at FNAL. Pion production is governed by the interaction of a high-energy proton beam with a dense target material, typically via inelastic proton–nucleus collisions. The resulting pion yield depends on several competing factors, including the incident proton beam energy, target material, and geometric parameters such as target length and radius. In addition to total yield, analyzing the energy spectrum and angular distribution of pions plays a crucial role in determining downstream design and efficiency of the capture and transport system.

A key consideration in target optimization is the proton beam energy. Higher energies increase the inelastic proton–nucleus cross section, producing higher pion multiplicities with a stronger forward boost, improving capture efficiency. Beam energies around 8 GeV are therefore commonly used as a reference for both demonstrator and collider-scale studies [1], and are broadly comparable to the 5 GeV-10 GeV proton driver scenarios considered in the Muon Collider 2026 European Strategy update [2].

Lower-energy beams, however, are particularly relevant for a muon ionization cooling demonstrator. Proton energies near 0.8 GeV, such as those foreseen in [3], are not intended for a collider but offer a practical and cost-effective option for a near-term demonstrator [1]. Leveraging existing or planned high-intensity proton infrastructure at Fermilab [4] could further reduce the need for a dedicated high-energy driver.

In this work, we compare pion production from 0.8 GeV and 8 GeV/c proton beams on candidate targets using FLUKA simulations [5, 6]. The 8 GeV/c case represents both demonstrator and collider scenarios, while 0.8 GeV is primarily motivated by demonstrator studies. We evaluate total pion yields and the kinematic distributions relevant for capture, assessing whether lower-energy, high-intensity beams can provide a viable front-end for a muon collider demonstrator.

SIMULATION SETUP

The simulation geometry consists of a graphite target aligned along the beam axis. The target has a length of 40 cm (approximately one interaction length for graphite) and a radius of 0.15 cm. The relatively small radius is chosen to reduce reabsorption and secondary interactions of produced pions, thereby improving pion yield for the demonstrator. A proton beam containing 100,000 primaries is initialized 20 cm upstream of the target, propagating in vacuum.

The primary objective of this study is to characterize pion production within the target for proton beams of different energies. One key observable is the angular distribution of the produced pions. To preserve the intrinsic production kinematics, no magnetic field is included in the simulation.

In selected studies, a comparison is made between pions produced within the target and those that escape it. Escaping pions are recorded by tracking particles crossing the target–vacuum boundary. A custom user routine was developed to register only the first occurrence of each particle. This approach enables the extraction of pion production distributions within the target.

* ralharthy@wisc.edu

Content from this work may be used under the terms of the CC BY 4.0 licence (© 2026). Any distribution of this work must maintain attribution to the author(s), title of the work, publisher, and DOI.

ISBN: 978-3-95450-252-3 ISSN: 2673-5350 doi: 10.18429/JACoW-IPAC2026-WEP1349

DESIGN AND OPTIMIZATION OF A HORN FOCUSING SYSTEM FOR EFFICIENT PION CAPTURE IN A MUON COLLIDER DEMONSTRATOR

P. Rao*, S. Dasu, C.-H. Nee, R. Alharthy, M. Hedges, C. Vuosalo
University of Wisconsin–Madison, Madison, WI, USA
P.-B. Jurj, R. Kamath, Imperial College London, London, UK
K. Yonehara, D. Stratakis, S. Jindariani, J. Eldred
Fermi National Accelerator Laboratory, Batavia, IL, USA

Abstract

This study investigates magnetic horn focusing as a lower-cost alternative to superconducting solenoids for the Muon Collider Demonstrator. We optimized a single horn for pion capture in the 100 MeV/c to 400 MeV/c range using a Bayesian pipeline with a Tree-structured Parzen Estimator. The optimized structure is benchmarked against IMCC baselines and the solenoid channel using FLUKA 2025.1.1 and GEANT4 (geant4-v11.3.2) simulations, providing a quantitative assessment of the horn/solenoid trade-off.

INTRODUCTION

Muon colliders are a compelling option for future high-energy lepton collisions, but their realization depends on efficient muon production and cooling. The conventional approach to pion capture in the muon-production front end relies on superconducting solenoids, which are technically challenging and costly. Magnetic horns, routinely used in neutrino experiments, offer a cost-effective alternative: they focus charged pions of one sign using a pulsed toroidal magnetic field, requiring no superconducting technology.

This paper reports on the design and Bayesian optimization of a single horn for the Muon Collider Demonstrator [3]. The objective is to maximize π^+/μ^+ with $0.2 \le E \le 0.5$ GeV inside a 4D acceptance ellipse, providing the first step toward a complete double-horn design. We describe the target/horn geometry, simulation framework, results, and the exact physics model used by the optimizer.

HORN DESIGN AND SETUP

Beam and Target

An 8 GeV proton beam with Gaussian transverse profile ($\sigma = 4.71$ mm) strikes a tungsten target (radius 6 mm, length 10 cm, $\rho = 19.3\,\mathrm{g/cm^3}$) centered at $z \approx 26$ cm. Earlier studies used a graphite target; the switch to tungsten improves pion production rate per unit length owing to the higher nuclear interaction cross-section [2].

Horn Geometry

The focusing system, illustrated in Fig. 1, consists of three coaxial regions:

- *Neck* ($z = 20$–45 cm): aluminum tube with $r_0 = 2.0$ cm and a 2 mm wall.

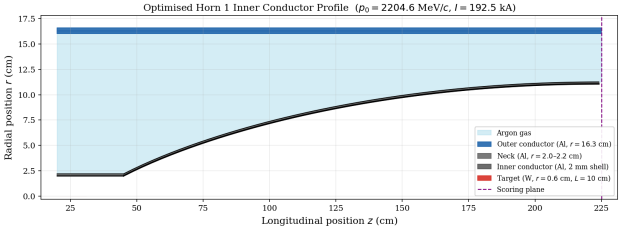

Figure 1: Optimized Horn 1 profile. The inner conductor expands from $r_0 = 2.0$ cm to $r_f = 11.06$ cm; the dashed line marks the scoring plane at $z = 224.0$ cm.

Table 1: Best-Performance Design Parameters

Parameter	Value
Horn length	179.0 cm
Bore radius r_0	2.0 cm
Final inner radius r_f	11.06 cm
Outer conductor radius	16.3 cm
Horn current I	192.5 kA
Twiss (α_x, β_x)	$(-0.24,\ 55.1$ cm)
Twiss (α_y, β_y)	$(-0.25,\ 54.6$ cm)

- *Inner conductor* ($z = 45$–224 cm): 2 mm aluminum shell expanding to $r_f = 11.06$ cm in 50 TRC segments.
- *Outer conductor*: straight aluminum cylinder with $r = 16.3$ cm; argon fills the gap.

From the outside the horn appears as a coaxial cylinder ≈ 2.2 m long and 33 cm in outer diameter with pulsed power feedthroughs at each end. Key optimized parameters are listed in Table 1.

Magnetic Focusing Principle

Current I flows in the $+z$ direction through the inner conductor, producing $B_\phi = \mu_0 I/(2\pi r)$ in the gap. The field focuses π^+ inward and defocuses π^-, making the horn sign-selective. The goal is to redirect large-angle pions so they exit with $p_r \approx 0$; overly strong focusing sends small-radius pions into the conductor wall and is penalized by the optimizer.

SIMULATION RESULTS

Horn results use FLUKA 2025.1.1 [4,5] with 10^5 primary 8 GeV protons; solenoid comparisons use GEANT4 (geant4-v11.3.2). A custom `MGDRAW` routine records particle type, phase-space coordinates, momentum, and arrival time at

* pprao@wisc.edu

Content from this work may be used under the terms of the CC BY 4.0 licence (© 2026). Any distribution of this work must maintain attribution to the author(s), title of the work, publisher, and DOI.

ISBN: 978-3-95450-252-3 ISSN: 2673-5350 doi: 10.18429/JACoW-IPAC2026-WEP1352

HIGH-AVERAGE-CURRENT, HIGH-BRIGHTNESS HVDC ELECTRON GUN DEVELOPMENT FOR EIC HADRON COOLING*

E. Wang†, J. Biswas, M. Gaowei, P. Inacker, R. Lambiase, M. Paniccia, O. Rahman, J. Skaritka, S. S. Kantamneni, K. P. Mondal, Y. Yang
Brookhaven National Laboratory, Upton, United States

Content from this work may be used under the terms of the CC BY 4.0 licence (© 2026). Any distribution of this work must maintain attribution to the author(s), title of the work, publisher, and DOI.

Abstract

The hadron cooler is an essential system for achieving high luminosity in the Electron-Ion Collider (EIC). The required electron source parameters exceed the current state of the art. We are conducting an electron-source R&D program aimed at producing an average current above 75 mA with bunch charges of 1 nC to 3 nC. This proceeding outlines the high-voltage design of a DC gun operating at 500 kV, with conditioning capability up to 600 kV. The design incorporates several unique features, including an inverted ceramic insulator at this voltage level, active cathode cooling, and large single-crystal multi-alkali photocathodes grown on silicon carbide substrates. We are developing the AI conditioning based on the convolution neutroal network. This paper presents recent progress on gun construction, AI conditioning development and preliminary major components test results.

INTRODUCTION

To achieve and sustain the high-luminosity target of $1 \times 10^{34}\,\mathrm{s^{-1}\,cm^{-2}}$, the Electron-Ion Collider (EIC) requires advanced hadron-cooling capabilities. A high-energy cooler for collision energies was designed between 2020 and 2024, but that project was terminated because the high-risk items could not be retired within the EIC project schedule [1]. A low-energy cooler is therefore being designed to cool hadrons at the injection energy of 24.5 GeV. Building on the successful polarized-gun R&D at the EIC [2], we are developing an HVDC gun to serve as the electron source for the hadron cooler. This gun is designed to deliver up to 98.5 mA of average current at voltages exceeding 500 kV to meet the requirements of various hadron cooling schemes for the EIC [3]. The design incorporates several advanced features, including an inverted feedthrough structure and an upgraded active cathode-cooling system using Fluorinert (FC72). To achieve high brightness, the gun will use novel large-crystal K_2CsSb photocathodes grown on 4H-SiC substrates. The design and analysis of the HVDC gun have been completed, and the gun assembly is currently underway. We are aiming for gun conditioning and beam tests in the next few years. In this paper, we discuss the HVDC gun design concepts, key considerations, and novel features. In addition, the major components of the HVDC gun are described in detail, and the AI-driven gun-conditioning approach is presented.

* This work was supported by Brookhaven Science Associates, LLC under Grant No. DE-SC0012704 with the U.S. Department of Energy.

† wange@bnl.gov

HVDC GUN DEVELOPMENT

Electron Source Requirements

The hadron cooler requires an electron source with high brightness, high average current, and high bunch charge. The electron-source requirements for several cooler schemes are listed in Table 1.

Table 1: Comparison of various hadron-cooling electron-source requirements.

Parameter	Precooler	SHC-CeC	HEC-Rec.
I_{ave} [mA]	> 70	90 to 100	60 to 100
ϵ_n [mm mrad]	1.5	3	2
C [nC]	1.2	1	4
Lifetime	1 week	> 3 days	> 3 days

The HVDC gun R&D is guided by the following requirements:

- Development of an electron source capable of delivering a 98 mA beam with a single operational lifetime charge of 60 000 C.
- Operation at voltages exceeding 500 kV with an electric-field gradient on the cathode surface of more than $5\,\mathrm{MV\,m^{-1}}$.

The primary challenges of this R&D effort include developing an efficient cathode-cooling mechanism, achieving long-term stable operation at high voltage, reducing emittance,develop advanced AI enhanced control system, and generating high-bunch-charge beams [4].

Gun Geometry

The inverted structure of the HVDC gun is more compact because both sides of the ceramic are enclosed and are not exposed to either the atmosphere or SF_6 [5]. This design allows for a shorter ceramic feedthrough. A polarized gun using this configuration achieved 350 kV after only 20 h of conditioning [2]. However, scaling this design to higher voltages, such as 500 kV, remains challenging because the potential distribution along the ceramic is difficult to control. The Pierce-shaped cathode and anode system were optimized to minimize emittance and maximize the laser spot size. Applying 550 kV to the electrode results in a cathode-surface gradient of $5.4\,\mathrm{MV\,m^{-1}}$, while all other surfaces maintain gradients below $10\,\mathrm{MV\,m^{-1}}$.With a well-polished surface, field emission can be effectively mitigated. The optimized normalized emittance is 1.02 mm mrad for a bunch length of 250 ps. The field gradient along the electrodes and on axis

ISBN: 978-3-95450-252-3 ISSN: 2673-5350 doi: 10.18429/JACoW-IPAC2026-WEP1353

SPACE CHARGE EFFECTS ON SPIN POLARIZATION IN A HIGH-INTENSITY PREINJECTOR*

E. Wang†, J. Biswas, Brookhaven National Laboratory, Upton, NY, USA

Abstract

We are designing a high-charge, high-polarization preinjector for the EIC. Placing a Wien filter immediately after the gun as the spin rotator offers several advantages over the traditional dipole–solenoid spin rotator located after the linac. However, this is the first attempt to operate a Wien filter in a strong space-charge environment, where the energy spread and self-fields may influence spin dynamics. In this paper, we analytically study space-charge effects on electron-beam polarization in the low-energy region, from the polarized electron gun to the linac entrance. We evaluate spin degradation in the drift from the gun to the Wien filter, inside the Wien filter, and in the bunching section. A comprehensive assessment of polarization-degradation mechanisms under space-charge conditions is presented. We also perform spin tracking through the full low-energy beamline with the General Particle Tracer (GPT) code, including space charge, to benchmark the analytical model and capture higher-order effects.

INTRODUCTION

In the Electron-Ion Collider (EIC), we propose using two Wien filters as a spin rotator to transform the electron spin orientation from longitudinal to vertical in the 300–320 keV energy range [1]. Although Wien filters have been widely used in hadron and electron machines for velocity selection and spin rotation, their application to high-intensity bunches in a space-charge-dominated region is new [2–4]. Existing Wien filters typically operate at pico- or sub-picocoulomb bunch charge, where space-charge effects can be neglected. We previously studied the spin dynamics with the Zgoubi code, which does not include space charge [5]. Those studies therefore did not address the challenges associated with the intense beams required for the EIC.

The particle spin evolution is described by the Thomas–BMT equation [6].

$$\frac{d\vec{P}}{dt} = \vec{\Omega}_0 \times \vec{P} \tag{1}$$

$$\vec{\Omega}_0 = -\frac{Ze}{m\gamma}[(1+G\gamma)\vec{B}_\perp + (1+G)\vec{B}_\parallel + (G\gamma + \frac{\gamma}{1+\gamma})\frac{\vec{E}\times\vec{v}}{c^2}] \tag{2}$$

Here, $\vec{P}$ is defined in the particle rest frame, while $\vec{E}$ and $\vec{B}$ are defined in the laboratory frame. In addition, $\vec{B} = \vec{B}_\perp + \vec{B}_\parallel, \vec{B}_\parallel = (\vec{v}\cdot\vec{B})\vec{v}/v^2$ where $\vec{B}_\parallel$ is parallel to the beam velocity, and $G = \frac{g-2}{2}$ is the anomalous magnetic moment. For electrons, $G = 0.001159$.

* This work was supported by Brookhaven Science Associates, LLC under Grant No. DE-SC0012704 with the U.S. Department of Energy.

† wange@bnl.gov

SPACE CHARGE FORCES

The transverse space-charge fields E_r and B_φ contribute to the variation of the spin vector $\vec{P}$ through Eq. 2. Although the longitudinal space-charge term satisfies $\vec{E}_z \times \vec{v} = 0$, it generates an energy spread that affects the spin polarization. In the following, we discuss two contributions: (i) transverse space charge and (ii) longitudinal space charge. The detailed derivations can be found in [7].

Transverse Space Charge

The transverse space-charge fields can be derived from Gauss's law and Ampere's law:

$$\int_S \vec{E}\cdot\hat{n}dS = \frac{q}{\varepsilon_0} \tag{3}$$

$$\oint_l \vec{B}\cdot\vec{l} = \mu_0 I \tag{4}$$

The beam from the gun initially follows a truncated Gaussian distribution with a one-sigma cutoff, which approximates a uniform distribution. As the beam propagates toward the Wien filter, transverse space charge causes the transverse distribution to evolve toward a Gaussian profile. Therefore, we evaluate the electric and magnetic fields for both uniform and Gaussian distributions.

For a uniform distribution, the transverse electric field is

$$E_r = \frac{IZ_0}{2\pi\beta}\frac{r}{a^2} \tag{5}$$

where $Z_0 = \sqrt{\frac{\mu_0}{\varepsilon_0}} = \frac{1}{c\varepsilon_0} = 377(\Omega)$

The corresponding transverse magnetic field is

$$B_\varphi = \frac{Z_0 I}{2\pi c}\frac{r}{a^2} \tag{6}$$

Equations 5 and 6 give the transverse electric and magnetic fields for the uniform distribution.

For a Gaussian distribution, the transverse electric field is

$$E_r = \frac{I_{pk}Z_0}{2\pi\beta r}e^{-\frac{z^2}{2\sigma_z^2}}(1-e^{-\frac{r^2}{2\sigma_r^2}}) \tag{7}$$

Similarly, the transverse magnetic field for a Gaussian distribution is

$$B_\varphi = \frac{I_{pk}Z_0}{2\pi cr}e^{-\frac{z^2}{2\sigma_z^2}}(1-e^{-\frac{r^2}{2\sigma_r^2}}) \tag{8}$$

Longitudinal Space Charge

The beam energy at the gun exit is 320 keV [8]. The bunch experiences longitudinal space-charge effects that increase the energy spread before entering the Wien filter. Because

Content from this work may be used under the terms of the CC BY 4.0 licence (© 2026). Any distribution of this work must maintain attribution to the author(s), title of the work, publisher, and DOI.

ISBN: 978-3-95450-252-3 ISSN: 2673-5350 doi: 10.18429/JACoW-IPAC2026-WEP1354

PREINJECTOR DESIGN UPDATE FOR THE EIC*

E. Wang†, J. Biswas, Q. Wu, Brookhaven National Laboratory, Upton, NY, United States

Abstract

To mitigate beam instabilities associated with low magnetic fields, the Rapid Cycling Synchrotron (RCS) for EIC has been redesigned to operate with a higher injection energy of 750 MeV, accepting only one bunch at a time and accelerating it immediately to collision energy. As a result, the electron preinjector must also be updated to supply an appropriately matched beam. In the latest concept, the extraction energy has been increased to meet the new RCS requirement, and a dedicated Beam Accumulator Ring (BAR) has been added to provide the required bunch merging. To maintain comparable cost while meeting performance goals, the preinjector design adopts Wien filters for spin rotation, an L-band capture linac to preserve polarization, a reduced bunch charge that eliminates the need for a stretch section, and a high-gradient S-band linac. This paper presents the updated EIC preinjector concept together with supporting design studies and simulation results.

INTRODUCTION

The EIC injector requires a polarized electron bunch at 750 MeV for single-bunch injection into the RCS. The new BAR takes over the bunch-merging function upstream of the ring. Compared with the earlier high-charge concept, this relaxes the preinjector bunch-charge requirement, removes the need for RF-based bunch merging in the preinjector, and allows the design to be optimized for robustness and spin preservation [1]. In the present study, the nominal preinjector bunch charge is 1.2 nC, with operation over about 1 nC to 1.7 nC; this keeps margin above the 1 nC requirement while significantly reducing wakefield and beam-loss risk relative to the previous multi-nC concept. Polarized-source R&D and related cathode development supporting this updated operating point were reported in Refs. [2, 3].

The choice of the main linac is now largely cost-driven. Once the BAR is included, a mature S-band solution becomes attractive because the required charge is modest, the achievable gradient is high, and the hardware can be procured from existing vendors. The spin constraint, however, remains stringent. The polarized source delivers longitudinal spin, whereas the transfer line and ring require vertical spin. The front-end accelerator design is therefore organized around one central rule: after the low-energy spin-rotation section, the beam spin direction should remain vertical throughout the preinjector.

Table 1: Updated preinjector requirements and representative design values.

Parameter	Required	Designed
Bunch charge [nC]	1.0	1.7 (up to 2.0)
RMS energy spread [%]	< 0.45	0.30
Polarization [%]	> 85	85
Norm. emit. [mm mrad]	< 95	80/50 (x/y)
Energy [MeV]	750	750
Spin direction	Vertical	Vertical
Rep. rate [Hz]	30	30 (20 also possible)

SPIN CONSIDERATIONS IN THE PREINJECTOR

Spin transport is one of the main design drivers of the preinjector design. From the Thomas–BMT equation,

$$\frac{d\vec{P}}{dt} = \vec{\Omega}_0 \times \vec{P},$$
$$\vec{\Omega}_0 = -\frac{Ze}{m\gamma}\left[(1+G\gamma)\vec{B}_\perp + (1+G)\vec{B}_\parallel + \left(G\gamma + \frac{\gamma}{1+\gamma}\right)\frac{\vec{E}\times\vec{v}}{c^2}\right], \quad (1)$$

Keeping the required spin orientation through a long solenoidal capture channel becomes difficult once the solenoidal field overlaps the accelerating field, because the beam energy increases continuously inside the RF structure. For an ideal solenoidal section, the condition for zero net spin rotation can be written approximately as

$$\int_S \frac{B_\parallel}{\gamma}\, ds = 0. \quad (2)$$

However, in an accelerating RF structure with strong space-charge effects, both γ and the effective overlap between the longitudinal magnetic field and the RF fields vary continuously along the beam path and from one tuning state to another [4]. In a conventional S-band front end, the taper cavity and the first accelerating section are often embedded in a solenoidal channel to control the beam size in the small aperture. For polarized operation, this is unattractive: the same solenoidal field that provides transverse matching also generates spin rotation, and the zero-net-rotation condition is therefore difficult to maintain during tuning and commissioning because small changes in RF phase, amplitude, launch phase, or solenoid settings alter the energy profile and hence the cancellation of the integrated spin precession.

Another possible approach is to allow the spin direction to deviate from vertical in the linac and then use a solenoid to restore the required orientation between the linac exit and

* This work was supported by Brookhaven Science Associates, LLC under Grant No. DE-SC0012704 with the U.S. Department of Energy.

† wange@bnl.gov

Content from this work may be used under the terms of the CC BY 4.0 licence (© 2026). Any distribution of this work must maintain attribution to the author(s), title of the work, publisher, and DOI.

ISBN: 978-3-95450-252-3 ISSN: 2673-5350 doi: 10.18429/JACoW-IPAC2026-WEP1357

INJECTION REQUIREMENTS FOR ELECTRON SWAP-OUT IN THE EIC-ESR*

Derong Xu†, William Bergan, Yi-Kai Kan, Yun Luo, Christoph Montag, Andrii Natochii, Vahid Ranjbar, Manfred Wendt, Qiong Wu, Brookhaven National Laboratory, Upton, NY, USA

Abstract

The Electron–Ion Collider (EIC) will be the first collider to use electron swap-out injection to maintain high bunch polarization during operation. Meeting the EIC performance goals places stringent requirements on the Electron Storage Ring (ESR) injection process: the injected bunch must be introduced with minimal disturbance to the hadron beam, and electron losses must remain negligible to avoid detector background. This work summarizes the key ESR injection requirements, including orbit accuracy, injected emittance, and fast kicker requirements needed to meet the overall EIC performance requirements.

INTRODUCTION

The Electron-Ion Collider (EIC) is a next-generation nuclear physics facility designed to explore the structure of nucleons and nuclei with unprecedented precision [1]. It will deliver collisions of highly polarized electron and ion beams over a wide range of center-of-mass energies, with key performance parameters including electron average polarization of about 70 % and luminosities of 10^{33-34} cm^{-2}s^{-1} [2].

To meet these performance goals, the Electron Storage Ring (ESR) must be provided with electron bunches of high charge and high polarization over a broad energy range. This is achieved through a dedicated electron injector chain, as shown in Fig. 1, consisting of a polarized electron source and linac, a Beam Accumulator Ring (BAR), and a Rapid Cycling Synchrotron (RCS). The BAR accumulates bunch charge up to 28 nC, and the RCS accelerates the beam while preserving polarization.

Once stored in the ESR, the electron beam polarization decays over time. Maintaining a high average polarization therefore requires frequent replacement of electron bunches, and the EIC adopts a single-bunch swap-out injection scheme for bunch-by-bunch polarization management. To sustain high luminosity, injection into the ESR must take place during ongoing collisions with the hadron beam. The hadron beam has no effective cooling, so any emittance growth accumulates. In a charge accumulation scheme, sufficient separation between the stored and injected electron bunches is required, which introduces transient perturbations to the hadron beam and leads to emittance growth [3]. In contrast, in the ideal limit where each stored electron bunch is directly replaced by a fresh one without mismatch or errors, the swap-out process provides an intrinsically transparent environment for the hadron beam [4].

* Work supported by Brookhaven Science Associates, LLC under Contract No. DE-SC0012704 with the U.S. Department of Energy

† dxu@bnl.gov

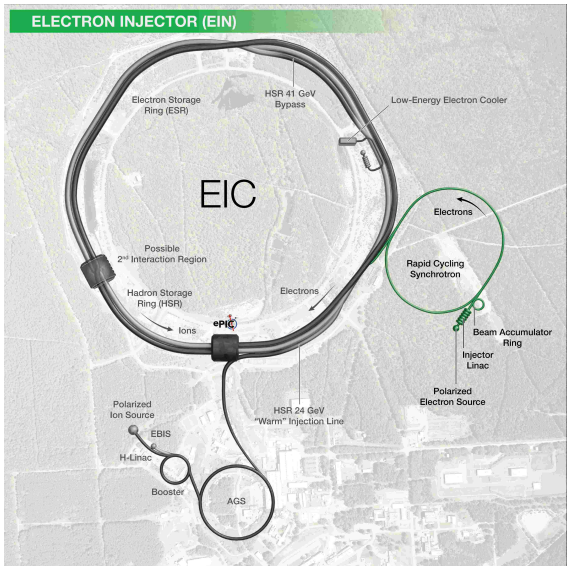

Figure 1: Overview of the EIC facility. The electron injector chain (colored) includes the polarized electron source and linac, BAR, and RCS, delivering electron bunches to the ESR (black).

However, injection errors are unavoidable in practice, and the acceptable hadron beam emittance growth defines the tolerances on injection imperfections. Swap-out injection has been established in modern storage rings such as the APS-U [5], demonstrating the feasibility of high-charge swap-out operation. The focus of this work is to quantify these tolerances for the EIC ESR under its unique operating conditions involving simultaneous injection and collision.

ESR DESIGN CONSTRAINTS

The ESR is designed to operate at multiple energies [6], specifically 5 GeV and 10 GeV, with upgrade capability to 18 GeV, to satisfy the center-of-mass energy requirements.

The physics program requires simultaneous storage of both spin states in the ESR, with a random spin pattern. Due to the Sokolov–Ternov effect, the spin component aligned with the magnetic field in the arcs exhibits a faster polarization decay. Table 1 lists the corresponding constraints for different energies and spin states.

The most stringent requirement arises at 18 GeV, where the shortest replacement interval in Table 1 sets the timescale for bunch replacement and determines the required injection frequency. In addition, to avoid significant loss of integrated luminosity, the initial fill should be completed within 20 min for all electron bunches. Considering both constraints, an injection frequency of 1 Hz is chosen.

Content from this work may be used under the terms of the CC BY 4.0 licence (© 2026). Any distribution of this work must maintain attribution to the author(s), title of the work, publisher, and DOI.

ISBN: 978-3-95450-252-3 ISSN: 2673-5350 doi: 10.18429/JACoW-IPAC2026-WEP1374

EXTRACTION AND INJECTION IN THE ELECTRON INJECTOR FOR THE ELECTRON-ION COLLIDER*

K. E. Deitrick†[1], D. Marx[2], C. Montag[2], I. Neththikumara[1], V. Ranjbar[2], T. Satogata[1], N. Sereno[1], M. Wendt[2]
[1]Thomas Jefferson National Accelerator Facility, Newport News, VA, USA
[2]Brookhaven National Laboratory, Upton, NY, USA

Abstract

The electron injector for the Electron-Ion Collider (EIC) consists of a linear accelerator, a beam accumulation ring, and the Rapid Cycling Synchrotron (RCS) before the electrons are injected into the Electron Storage Ring (ESR) and collided. Extraction from the RCS is complicated by limited space and the nominal beam pipe aperture, while injection into the ESR is complicated due to the limitation of kicker strength, so that the kickers will not impact the proton beam in the adjacent Hadron Storage Ring (HSR); additionally, the ESR kickers must also provide enough kick to the stored bunch for the swap-out scheme. This paper covers the injection into and extraction from the RCS, as well as injection into the ESR, detailing layout, optics, and anticipated parameters of the septa and different kickers.

INTRODUCTION

The Electron-Ion Collider (EIC) is a partnership project between Brookhaven National Lab (BNL) and Thomas Jefferson National Accelerator Facility (TJNAF) to be constructed at BNL, using much of the existing infrastructure of the Relativistic Heavy Ion Collider (RHIC). Collisions occur between the hadrons in the Hadron Storage Ring (HSR) and the electrons supplied by the Electron Storage Ring (ESR); to maintain a high average polarization of the ESR, bunches are frequently replaced using the Rapid Cycling Synchrotron (RCS). The EIC Project construction scope includes one interaction region (IR), sited at the current IR6 of RHIC with a top energy of 9 GeV; however, the results presented here are based on an older version of the design, with a top energy of 18 GeV, which needs to be considered now to allow for a more simple pathway for an energy upgrade in the future [1].

GENERAL APPROACH

As a concept without constraints or complications, injection is relatively simple – the injected bunch exits a septum magnet with some offset and angle relative to the nominal circulating orbit, before a kicker downstream allows for the injected bunch to achieve the nominal circulating orbit. Similarly for extraction, a kicker gives the extracted bunch some angle relative to the nominal circulating orbit, which after some distance translates into an offset from the nominal orbit. The extracted bunch enters the downstream septum magnet with some offset and angle relative to the nominal orbit and is bent into the transfer line.

However, as restrictions and requirements are added, the situation becomes more complex. There is a limit to how strong septa or kickers can be built, magnets between the kicker and septum magnet alter the trajectory of the bunch, and if the bunch orbit or size is too large, the bunch is either scraping through the magnet or a special large-bore magnet is required. While reducing the circulating aperture in the septum region does help in reducing kicker and septum strength, this has consequences for the impedance budget and dynamic aperture of the ring. So while simple in theory, in practice injection and extraction are often a compromise between conflicting requirements.

One of the more easily given criteria is the required offset at the face of the septum magnet within the ring. The minimum offset is the required circulating aperture plus the beam pipe and septum wall thickness plus the injection/extraction aperture. The circulating aperture can either be the nominal inner radius or can be reduced to some factor of the largest circulating beam size (i.e., 7σ to give an envelope for the circulating aperture). Similarly, the injection/extraction aperture is some factor of the largest beam size. Specifying "largest" is important for cases where the geometric emittance changes with energy and the goal is for the layout to remain fixed for different energy configurations.

EIC PARAMETERS

The specific parameters for the injections and extraction scenarios in the electron chain of the EIC are given in Table 1. RCS injection and extraction is for a single bunch up to 28 nC at 1 Hz, while ESR injection is single-bunch swap-out. The reason that the envelope for circulation is left blank for RCS injection is because the circulating aperture is not being reduced, so that requirement is not necessary. Otherwise, these numbers in combination with the horizontal beta values at the face of the septum magnet give the appropriate offset values for each case. A diagram demonstrating how the parameters given dictate the offset at the septum is shown for ESR injection in Fig. 1.

RCS INJECTION

Injection into the RCS is the simplest case – one kicker, one septum magnet, and only one quadrupole separating the two. The injection line from the linac and the beam accumulator ring makes a 9 degree angle with respect to the RCS straight. The layout of the injection chicane is

* Work supported by Jefferson Science Associates, LLC under U.S. DOE Contract DE-AC05-06OR23177 and Brookhaven Science Associates, LLC, Contract DE-SC0012704.

† kirstend@jlab.org

Content from this work may be used under the terms of the CC BY 4.0 licence (© 2026). Any distribution of this work must maintain attribution to the author(s), title of the work, publisher, and DOI.

ISBN: 978-3-95450-252-3 ISSN: 2673-5350 doi: 10.18429/JACoW-IPAC2026-WEP1375

NSLS-II STORAGE RING AUXILIARY DIPOLE POWER SUPPLY

H. Dave†, C. Atariguana, D. Bergman, C. Birla, S. Buda, A. Castiblanco, M. Charumaneeroj, T. Chiesa, R. Edwards, J. Escallier, E. Gomez, J. Gosman, S. Klare, J. Mead, E. Orr, J. Rose, A. Sauerwald, Y. Tian

Brookhaven National Laboratory, Upton, New York, USA

Abstract

The National Synchrotron Light Source II (NSLS-II) storage ring requires a high-current (400 A), high-voltage (1 kV) dipole power supply system to maintain stable beam in the Storage Ring. To reduce downtime of beam resulting from a failure of the dipole power supply, an Accelerator Improvement Project was undertaken to develop a redundant backup power supply system. This paper presents the design and implementation of an in-house developed auxiliary dipole power supply built to serve as a standby system for the main dipole power supply. The auxiliary system utilizes a modular architecture with N+2 redundancy and high-frequency switched-mode power converters with active power factor correction. This design eliminates large 60 Hz transformers, reducing the system footprint to 20% of the original installation while enabling hot-swappable servicing. A transfer switch ensures a rapid transition from primary to backup systems in under 20 minutes. To maintain stringent orbit stability, the system incorporates a custom DC EMI filter and a series-pass linear amplifier, achieving a measured current stability of better than 1 part in 10^5 (10 ppm). This paper presents results demonstrating the system's effectiveness in reducing recovery time and enhancing the overall reliability of NSLS-II beam operations.

INTRODUCTION

The National Synchrotron Light Source II (NSLS-II) is one of the most advanced synchrotron light sources in the world. The facility enables scientists from academia and industry to tackle the most important challenges in quantum materials, energy storage and conversion, condensed matter and materials physics, chemistry, life sciences, and more by offering extremely bright light, ranging from infrared light to x-rays.

To create its intense ultrabright light, NSLS-II has an advanced particle accelerator complex that spins electrons around its half mile long ring at nearly the speed of light. NSLS-II's accelerators are comprised of many complex engineering systems. Running this intense, stable electron beam for 5000 hours every year, with no interruptions, requires constant attention to every integral component [1].

One of those systems that needs to operate reliably is the Dipole Power Supply System (DPSS). This system must meet the 5000 hours of operation requirement without any interruptions. Despite the high reliability of the primary system, a 2022 failure event resulted in over 20 hours of beam downtime, highlighting the necessity for secondary backup DPSS. To that end a decision was made to build an auxiliary DPSS capable of providing reliable power to dipole magnets in case of failure of the main DPSS. After research and careful consideration of multiple different topologies, a compact modular solution was most viable when considering MTTR (Mean Time to Repair), performance and reliability are the main criteria.

PRIMARY NSLS-II STORAGE RING DPSS

Table 1 lists the important parameters from the original Dipole Power Supply System. The new DPSS has same or better performance rating.

Table 1: Dipole Power Supply System Requirements

Parameter	Specification	Unit
Output voltage	822	Volts
Output current	400	Amps
Accuracy	±25	ppm
Ripple current	<10	ppm



Figure 1: Primary Storage Ring DPSS

The Primary DPSS is divided into two banks positive bank and negative bank with center point grounded (Fig. 1). Each bank can provide 600Vdc-max at 400A maximum current making total DPSS output 1200Vmax at 400A. Each bank includes a large 3-phase 60Hz transformer for isolation and SCRs for rectification. A large capacitor bank is used for hold-up during AC line interruptions. Followed by parallel interleaved H-bridges, series pass regulator and LC filter. The H-bridge's effective switching frequency is 30kHz. The control cabinet provides accurate regulation to less than 10ppm.

AUXILIARY NSLS-II STORAGE RING DPSS

To support the rigorous operational demands of the NSLS-II, the dipole power supply system is engineered for both high capacity and extreme stability. The Auxiliary DPSS is designed with similar specifications in mind but with latest technology to achieve greater compactness. Like the primary system, Auxiliary DPSS futures positive

Content from this work may be used under the terms of the CC BY 4.0 licence (© 2026). Any distribution of this work must maintain attribution to the author(s), title of the work, publisher, and DOI.

ISBN: 978-3-95450-252-3 ISSN: 2673-5350 doi: 10.18429/JACoW-IPAC2026-WEP1601

NONLINEAR CHROMATICITY CORRECTION FOR THE INTERACTION REGION OF SUPER TAU-CHARM FACILITY

Linhao Zhang†, Ye Zou, Tao Liu, Jingyu Tang
School of Nuclear Science and Technology, University of Science and Technology of China, Hefei, Anhui, China

Content from this work may be used under the terms of the CC BY 4.0 licence (© 2026). Any distribution of this work must maintain attribution to the author(s), title of the work, publisher, and DOI.

Abstract

The Super Tau-Charm Facility is a new-generation electron-positron collider in the beam energy range of 1-3.5 GeV, with a target luminosity exceeding 5×10^{34} cm^{-2}s^{-1} at 2 GeV using a large Piwinski angle and crab-waist collision scheme. However, the required sub-millimeter vertical beta function ($\beta_y^* < 1$ mm) induce strong nonlinear chromaticity, which severely limits the momentum aperture of the collider rings and leads to a very short Touschek lifetime. To achieve the necessary 1.5% momentum aperture, local correction of the nonlinear chromaticity from the final-focus quadrupoles is essential. In this paper, we derive the theoretical origin of the nonlinear chromaticity and demonstrate dedicated measures to systematically mitigate these nonlinearities order by order. Specifically, we present an updated modular linear lattice for the interaction region to facilitate nonlinear chromaticity optimization. The second-order dispersion at the crab sextupoles is also reduced to nearly zero. By implementing a local chromaticity correction scheme up to the third order, we obtain a momentum aperture of 2% for the interaction region.

INTRODUCTION

The Super Tau-Charm Facility (STCF), proposed in China, is a new-generation high-luminosity electron-positron collider operating in the low-energy range of 1-3.5 GeV [1]. To achieve the target luminosity exceeding 5×10^{34} cm^{-2}s^{-1}, a collision scheme combining a large Piwinski angle and crab-waist correction is adopted. However, the required high beam current, low emittance, and an extremely low vertical beta function ($\beta_y^* < 1$ mm) lead to a very short Touschek lifetime. In particular, the strong nonlinear chromaticity induced by the sub-millimeter β_y^* constitutes a major limitation on the momentum aperture of the collider rings. To improve the Touschek lifetime, a momentum aperture of 1.5% is essential.

A dedicated design of the crab-waist interaction region (IR) for the STCF has been presented [2] and integrated into the collider rings [3], yielding a momentum apperture of approximately ±1.5% and a Touschek lifetime exceeding 300 s at the luminosity of 0.94×10^{35} cm^{-2}s^{-1} and beam energy of 2 GeV. However, residual vertical second-order and horizontal third-order chromaticity originating in the IR, as well as the leakage of second-order dispersion from the IR into the arcs, remain the main factors limiting the momentum aperture. In this paper, we first analyze the chromaticity in a single-pass transport line and identify local correction measures for the IR nonlinear chromaticity. We then update the IR optics design to improve the nonlinear chromaticity correction and reduce the leakage of second-order dispersion from the IR.

CHROMATICITY IN A SINGLE-PASS TRANSPORT LINE

In a single-pass transport line (e. g., one half of the IR), chromaticity is defined as the rate of change of the particle betatron oscillation phase advance with respect to the relative momentum deviation δ. The dependence of the focusing gradient of all magnetic elements on δ is the fundamental cause of chromatic effects. Following Anton's derivation of high-order chromaticity for a ring [4], when considering an off-momentum particle with momentum deviation δ in a transport line, the first- to third-order derivatives of the betatron phase advance μ_z can be expressed as:

$$\frac{\mathrm{d}\mu_z(\mathrm{s})}{\mathrm{d}\delta} = \mp\frac{1}{2}\int_0^s \beta_z(K_1 - K_2D_0)\,\mathrm{d}s' - \frac{a_{1,z}(s)}{2}, \quad (1)$$

$$\frac{\mathrm{d}^2\mu_z(\mathrm{s})}{\mathrm{d}\delta^2} = -2\frac{\mathrm{d}\mu_z(\mathrm{s})}{\mathrm{d}\delta} + \int_0^s \frac{b_{1,z}^2 - a_{1,z}^2}{\beta_z}\mathrm{d}s' \pm \int_0^s \beta_z\left(K_2D_1 + K_3\frac{D_0^2}{2}\right)\mathrm{d}s' \mp \int_0^s \beta_z b_{1,z}(K_1 - K_2D_0)\,\mathrm{d}s' - \frac{a_{2,z}(s)}{2}, \quad (2)$$

$$\frac{\mathrm{d}^3\mu_z(\mathrm{s})}{\mathrm{d}\delta^3} = 6\frac{\mathrm{d}\mu_z(\mathrm{s})}{\mathrm{d}\delta} + \int_0^s\left(-\frac{3a_{1,z}a_{2,z}}{\beta_z} + \frac{3a_{1,z}^2b_{1,z}}{\beta_z} - \frac{3b_{1,z}^3}{\beta_z} + \frac{3b_{1,z}b_{2,z}}{\beta_z}\right)\mathrm{d}s' \mp 3\int_0^s \beta_z\left[-\frac{K_4D_0^3}{6} + K_3\left(\frac{D_0^2}{2} - D_0D_1\right) + K_2(D_1 - D_2)\right]\mathrm{d}s' \mp \frac{3}{2}\int_0^s \beta_z b_{2,z}(K_1 - K_2D_0)\,\mathrm{d}s' - \frac{a_{3,z}(s)}{2}, \quad (3)$$

where z denotes the horizontal or vertical (i.e., x or y) plane, D_0, D_1, D_2 are the first-, second-, third-order dispersion functions respectively (satisfying $D_x(\delta)=D_0+D_1\delta+D_2\delta^2$), and $a_{n,z}$ and $b_{n,z}$ are chromatic Montague functions [5] extended to high order, defined as:

$$b_{n,z} = \frac{1}{\beta_z}\frac{\mathrm{d}^n\beta_z}{\mathrm{d}\delta^n}\Big|_{\delta=0}, a_{n,z} = \left(\frac{\mathrm{d}^n\alpha_z}{\mathrm{d}\delta^n} - \frac{\alpha_z}{\beta_z}\frac{\mathrm{d}^n\beta_z}{\mathrm{d}\delta^n}\right)\Big|_{\delta=0}. \quad (4)$$

Note that apart from the additional term of $-a_{n,z}/2$ appearing in Eqs. (1)-(3) for the single-pass system, all other terms are exactly equivalent to the high-order chromaticity expressions of a ring under periodic boundary conditions. In particular, Eq. (1) has also been given in Ref. [6].

Equations. (1-3) clearly indicates how different orders of chromaticity are generated and how they can be controlled and mitigated:

† zhanglinhao@ustc.edu.cn

ISBN: 978-3-95450-252-3 ISSN: 2673-5350 doi: 10.18429/JACoW-IPAC2026-WEP1603

AN UPDATED PHYSICAL DESIGN FOR THE STCF COLLIDER RINGS

Y. Zou*, L.H. Zhang, T. Liu, P.H. Yang, T.L. He, W.W. Li, H.Z. Li, S.Y. Li, Q. Luo, J.Y. Tang,
University of Science and Technology of China, Hefei, China
D. Zhou, KEK, Oho, Tsukuba, Japan
Y.J. Yuan, L. Wang, Institute of Modern Physics, Chinese Academy of Sciences, Lanzhou, China

Content from this work may be used under the terms of the CC BY 4.0 licence (© 2026). Any distribution of this work must maintain attribution to the author(s), title of the work, publisher, and DOI.

Abstract

The Super Tau-Charm Facility (STCF), proposed by the University of Science and Technology of China, is a next-generation electron-positron collider designed to achieve a luminosity exceeding 5×10^{34} $cm^{-2}s^{-1}$, approximately two orders of magnitude greater than that of BEPCII. Large Piwinski angle with the crab waist collision scheme is applied. However, the extremely small β_y^* (<1 mm) generates very large nature chromaticity. Local chromaticity corrections for both horizontal and vertical planes have been proposed. Touschek lifetime is very challenging due to its low-energy, low-emittance, and high-current. A two-folded lattice has been proposed for the collider rings, with the iterations of version 5. Nonlinear optimization has been carried out with Multi-Objective Genetic Algorithm (MOGA) to maximise the dynamic aperture and momentum acceptance, considering fringe fields and misalignment errors. This paper introduces the updated physical design of the STCF collider rings.

INTRODUCTION

The Super Tau-Charm Facility (STCF), proposed by USTC in China, represents the next generation of electron-positron colliders [1, 2]. It operates over a wide collision energy range of 2 to 7 GeV, with symmetric electron and positron beam energies spanning 1 to 3.5 GeV. The design targets luminosities exceeding 5×1034 cm-2s-1 at the optimal beam energy of 2 GeV and 5×1033 cm-2s-1 at both lowest and highest energies. To achieve these high luminosities, STCF employs a large crossing angle of 60 mrad combined with the Crab-Waist collision scheme [3-5]. The large crossing angle reduces the effective beam length at the interaction point (IP), enabling β_y^* to be compressed below 1 mm. The crab waist scheme effectively mitigates the strong transversal coupling induced by the large crossing angle.

However, the intense focusing at the IP brings very strong nonlinear effects, resulting in significantly reduced dynamic and momentum apertures in the collider rings. These small apertures, combining high beam current and low beam emittance, leading to a very short Touschek lifetime, far shorter than that of other ring-based electron accelerators. This short Touschek lifetime poses challenges for injector design and construction, requiring a substantially higher injection repetition frequency. Balancing these beam dynamics, lifetime, and stability issues [6] with the goal of high-luminosity collisions is a central challenge in the physical design of the STCF collider rings. The design must optimize these critical parameters to meet its performance objectives. Table 1 summarizes the main parameters of the STCF collider rings at the optimal energy.

Table 1: Main Parameters of the STCF Collider Ring

Parameter	Value
Beam energy (GeV)	2.0
Beam current (A)	2.0
Circumference (m)	825.524
β_x^*/β_y^* (mm)	40/0.8
Coupling, $\varepsilon_y/\varepsilon_x$ (%)	1
Hor./Ver. betatron tune	28.545/31.58
Emittance (SR/DW+IBS) (nm)	8.83/3.93
Momentum compact factor (10^{-3})	1.41
Energy spread (DW+IBS) (10^{-4})	8.1
SR power per beam (MW)	1.245
RF voltage (MV)	2.5
Synchrotron tune	0.0193
Energy acceptance (%)	1.62
Bunch length, nature/IBS (mm)	7.55/9.0
Beam-beam parameter, ξ_x/ξ_y	0.003/0.1
Luminosity ($cm^{-2}s^{-1}$)	1.02×10^{35}

OPTICS DESIGN

The STCF collider features a double-ring configuration consisting of an electron ring and a positron ring, both situated in the same horizontal plane. The circumference of each ring is 825.524 m in the lattice of version 5, about 35 m shorter than version 4 [7]. These rings intersect at two points: the collision point within the collision region and another intersection point diametrically opposite to it. To accommodate the intersecting configuration, the drift lengths in the arc sections differ slightly on either side of each ring, creating distinct inner and outer rings separated by approximately 2 meters. Each ring is composed of: one interaction region, four major arc sections (60 degrees for each), and two minor arc sections (30 degrees for each), one intersection region and multiple straight sections. The straight sections serve various functions, including: injection and extraction, collimation, damping wigglers, RF, and tuning sections. Space is also reserved on both sides of the collision region for the installation of Spin Rotators, in preparation for future project upgrades involving beam polarization. Figure 1 shows the new layout and optics function of the STCF collider rings.

* zouye@ustc.edu.cn

ISBN: 978-3-95450-252-3 ISSN: 2673-5350 doi: 10.18429/JACoW-IPAC2026-WEP1604

REDUCTION OF SUDDEN BEAM LOSS IN SUPERKEKB

H. Ikeda†, T. Ishibashi, S. Terui, H. Fukuma, T. Mitsuhashi, K. Shibata, M. Tobiyama, M. L. Yao,
High Energy Accelerator Research Organization, Tsukuba, Japan

Content from this work may be used under the terms of the CC BY 4.0 licence (© 2026). Any distribution of this work must maintain attribution to the author(s), title of the work, publisher, and DOI.

Abstract

Sudden beam loss (SBL) is one of the major problems facing SuperKEKB, and various efforts have been made to solve it. SBL is a beam loss event in which a significant percentage of the beam current is lost in an instant. Beam loss begins within 10 microseconds, the equivalent of one revolution, and as a result, tens of percent of the total charge is lost in a few revolutions before the beam is aborted. In order to solve the problem, various monitors are being analyzed and new beam instrumentation devices are developed. Various circumstantial evidence suggests that removing the black stains caused by the vacuum sealant inside the vacuum chamber is likely to be effective in resolving the SBL. This paper explains, using various measurement results, how much SBL was reduced by cleaning the chamber as much as possible. We also report measurement results that may lead to the identification of the cause of SBL, though it has not been completely solved.

INTRODUCTION

SuperKEKB is a circular collider with the circumference of about 3 km. It consists of the 7GeV electron ring(HER) and the 4GeV positron ring(LER)[1]. SuperKEKB continues to hold the world record for luminosity, with the current record being 5.244 x 10^{34}cm^{-2}s^{-1} set on March 19, 2026. Further improvement in peak luminosity and accumulation of integrated luminosity are challenges for the SuperKEKB accelerator and the Belle II detector. Reducing sudden beam loss (SBL) will help to overcome the challenges. SBL became noticeable after the start of luminosity runs. It is a phenomenon in which a significant percentage of the beam current is suddenly lost in a few turns before the abort [2]. SBL causes damage to accelerator components, quenches of final focusing superconducting magnets (QCS) [3], and large background noise to the Belle-II detector. The total number of SBLs is overwhelmingly high in the LER, and the QCS quenches occur almost at the LER. Figure 1 shows an example of SBL event.

REDUCTION OF SBL

Since SBLs in the LER occur with vacuum pressure bursts and increase in beam size, we suspected an interaction between the dust and the beam [4]. Accordingly, we conducted a knocker study in which dusts were experimentally knocked down by striking the beam duct with a knocker. Since SBLs occurred when knocking on beam pipes with clearing electrodes installed on the upper wall of the chamber, and the number of SBLs decreased after many knocks, some beam pipes with electrodes suspected to be the source of the dusts were flipped. But the effect of flipping the beam pipe was inconclusive.

Subsequently, observation of the inside the beam pipes, where large number of vacuum pressure bursts occurred, revealed the presence of the black stains which were thought to be caused by vacuum sealant. After cleaning the stains, the number of SBLs decreased. Laboratory investigations revealed that the MO-type flanges used in SuperKEKB likely allowed the vacuum sealant to enter the beam pipe in case of an air leak. As a result, we speculate the SBL is generated by beam-dust interaction, and one of the dust sources is the vacuum sealant [5-7]. Since it was confirmed that the vacuum sealant, which had entered the beam pipe, was one of the main causes of SBL in the 2024 operation, during the 2025 shutdown vacuum team opened and cleaned all accessible beam pipes where the vacuum sealant was suspected to have been used. Figure 2 shows the inside the beam pipe where the black stains were found.

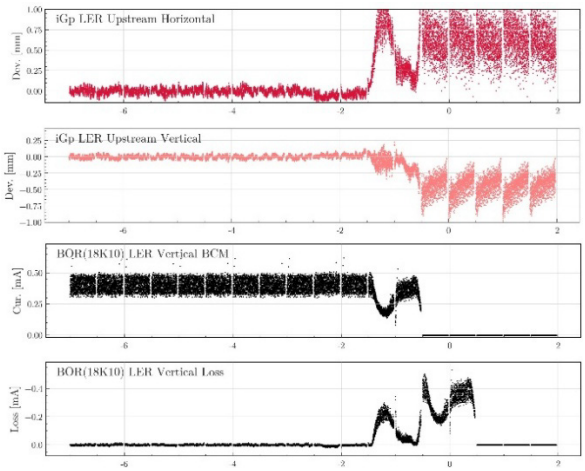

Figure 1: From top to bottom: Horizontal orbit, Vertical orbit, bunch current, and beam loss compared to the previous turn at the SBL abort.

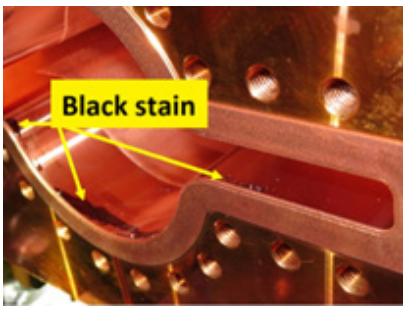

Figure 2: Black stains were observed inside the beam pipe.

†hitomi.ikeda@kek.jp

ISBN: 978-3-95450-252-3 ISSN: 2673-5350 doi: 10.18429/JACoW-IPAC2026-WEP1605

BOOTSTRAPPING INJECTION CONDITIONING STUDY FOR FCC-EE COLLIDER

T. Mori*, High Energy Accelerator Research Organization, Tsukuba, Japan
K. Oide, F. Zimmermann, European Organization for Nuclear Research, Geneva, Switzerland

Abstract

Because of the strong beam–beam force at the interaction points in the FCC-*ee* collider, maintaining the charge balance between the two opposing beams is crucial. Injection of a high-charge beam introduces temporary imbalance, which can lead to beam instability. To mitigate this, bootstrapping injection has been adopted for FCC-*ee*. In this work, the conditioning of bootstrapping injection is studied using a quasi-strong-strong beam–beam scheme implemented in the SAD code. The charge threshold of injected beams for different collision modes is evaluated, and the impact of beam–beam dynamics on injection stability is discussed.

INTRODUCTION

The FCC-*ee* collider is designed to operate in a strong beam–beam regime [1]. In such conditions, the injection process becomes sensitive to nonlinear beam–beam dynamics.

During injection, an imbalance between the two colliding beams leads to asymmetric beam–beam forces, which may induce emittance growth and particle loss. Understanding and controlling this imbalance is therefore essential.

In the present study, a simplified configuration with one bunch per beam is considered. Although the FCC-*ee* design includes four interaction points, collisions occur at two interaction points in the present simulations. Injection dynamics are investigated using a quasi-strong-strong (QSS) simulation scheme.

QUASI-STRONG-STRONG SCHEME

The quasi-strong-strong (QSS) scheme provides an efficient framework for simulating beam–beam interaction with partial self-consistency. The beam–beam force is evaluated interaction point by interaction point along the ring, allowing the effect of individual collisions to be incorporated sequentially within a single turn, while maintaining a weak–strong tracking structure. For this evaluation, the beam parameters immediately upstream of each interaction point are used, lattice effects are naturally incorporated. The QSS scheme provides a partially self-consistent beam–beam interaction by sequentially updating the beam–beam lens using the instantaneous beam moments at each interaction point (Fig. 1).

The simulation is performed using the SAD code [2], enabling the study of injection dynamics in a realistic lattice environment with manageable computational cost.

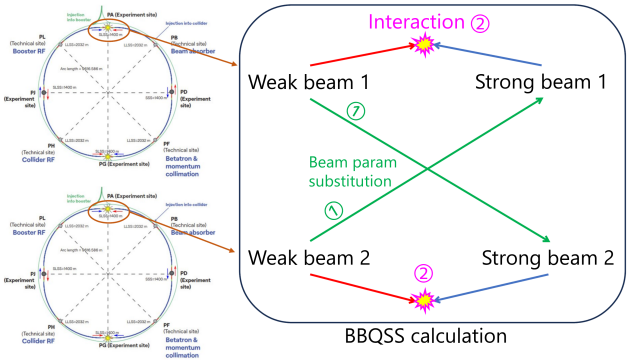

Figure 1: Schematic illustration of the quasi-strong-strong (QSS) beam–beam calculation and bootstrapping injection model. Beam–beam interactions are evaluated interaction point by interaction point within a single turn. In the present study, collisions occur at two interaction points (corresponding to IPA and IPG), although the FCC-*ee* design includes four interaction points. The effective bunch population is increased by injection, while macroparticles are not replenished and are only removed through beam loss during tracking.

Implementation Concept

In the present implementation, QSS is realized by coupling two weak–strong beam–beam simulations that represent the two counter-rotating beams. At each interaction point, the parameters of the opposing strong beam are substituted using the moments evaluated from the corresponding weak-beam tracking immediately before the collision. This substitution is performed at every interaction point, thereby updating the beam–beam elements sequentially along the ring while avoiding the computational cost of full strong–strong tracking.

The updated strong-beam parameters include the beam centroid coordinates and second moments relevant to transverse–longitudinal coupling (e.g. $(x, y, x', y', z, \delta)$, $(\beta_{x,y}, \varepsilon_{x,y})$, $(\sigma_{z,\delta})$, and selected cross-moments such as xz, $x'z$, yz and $y'z$), enabling the study of multi-dimensional effects within the full-lattice framework. Here, standard accelerator coordinates and beam moments are used, following conventional definitions in accelerator physics.

INJECTION MODEL

The injection process is modeled by increasing the effective bunch population,

$$r = \frac{N}{N_{\mathrm{nom}}}, \tag{1}$$

in discrete increments Δr_I.

* takashi.mori@kek.jp

Content from this work may be used under the terms of the CC BY 4.0 licence (© 2026). Any distribution of this work must maintain attribution to the author(s), title of the work, publisher, and DOI.

ISBN: 978-3-95450-252-3 ISSN: 2673-5350 doi: 10.18429/JACoW-IPAC2026-WEP1606

COMMISSIONING OF BEPCII UPGRADE

H. P. Geng[1]*,Y. Zhang[1], Y. R. Wei, J. Xing, H.S. Xu, C. H. Yu[1]
Key Laboratory of Particle Acceleration Physics and Technology,
Institute of High Energy Physics, Chinese Academy of Sciences, Beijing, China
[1]also at University of Chinese Academy of Sciences, Beijing, China

Abstract

The upgrade of Beijing Electron and Positron Collider-II (BEPCII) has begun since the shutdown of BEPCII on July 1st in 2024. The hardware replacement and upgrade has been finished by the end of the year 2024, and the machine commissioning of BEPCII Upgrade project has started since May 2025 after recovery from the cryogenic system fault. The designed luminosity of 1.1×10^{33} cm^{-2}s^{-1} has been achieved on April 28th, 2026. In this paper, we will show the commissioning results of the BEPCII uprade project.

INTRODUCTION

The Beijing Electron Positron Collider II (BEPCII) [1] is a two-ring eletron positron collider running in the tau-charm energy region. The design luminosity of BEPCII has been acheived in 2016 [2] at commissioning mode. Daily operation at designed luminosity has been achieved since Jan. 2023 [3]. The collision energy and data acquisition efficiency upgrade project of BEPCII has been studied since 2019 [4–6], and has begun hardware replacement since July 2024.

BEPCII upgrade is based on the current BEPCII machine, maintaining the existing small Piwinski angle collision scheme unchanged. It increases the collision luminosity at high energies by means of enhancing the beam current and raising the cavity voltage [7–9]. The main logic for parameter selection is to take the synchrotron radiation power of a single beam as the constraint (250 kW) and 120 bunches as the upper limit. At the same cavity voltage, the single-bunch current is kept as low as possible to reduce bunch length stretching and provide the possibility of compressing the vertical β_y^* at the collision point. After selecting β_y^* according to the bunch length, the emittance coupling is determined by the nominal beam-beam parameter $\xi_{y,0}$. The design beam parameters of the upgrade is shown in Table 1.

BEPCII is an operational large scientific facility, and the core purpose of its upgrade is to improve the efficiency of collision, especially in the high-energy region, while attempting and testing the latest accelerator technologies. It can be seen from Table 1 that, the optimized beam energy for the upgrade is 2.35 GeV, and the maximum collision beam energy is extended to 2.8 GeV. The luminosity performance achieved by BEPCII at different energies during its years of operation and the the target luminosity after the upgrade is compared in Fig. 1.

It can be seen that the upgrade will enhance the collision luminosity at beam energies above 2.0 GeV and increase the collision energy up to 2.8 GeV. The luminosity at the optimized beam energy 2.35 GeV can be tripled from 3.5×10^{33} cm^{-2}s^{-1} to 11.0×10^{33} cm^{-2}s^{-1} before and after the upgrade. With this upgrade, the BESIII detector can acquire higher-statistics experimental data in this energy region [10], thereby enabling in-depth exploration of the nature of strong interactions and the origin of hadron masses.

The hardware installation and commissioning of the upgrade project were fully completed in December 2024, followed by a period of cryogenic system failure. After the cryogenic system recovered from the fault, the upgrade project officially entered the beam commissioning phase. This paper provides a comprehensive introduction to the beam commissioning work for the upgrade. The results show that the

Table 1: Comparison of the design parameters of BEPCII upgrade and the running parameters of BEPCII in collision mode.

Parameters	BEPCII	BEPCII upgrade	
Energy [GeV]	2.35	2.35	2.8
RF voltage [MV]	1.6	1.65× 2	1.65× 2
SR power [kW]	110	250	250
Damping time [ms]	12.6	12.6	7.5
Bunch number	56	120	36
Bunch current [mA]	7.1	7.5	12.5
β_x^*/β_y^* [m]	1.0/0.015	1.0/0.0135	1.0/0.03
Emittance [nm·rad]	147	152	200
Coupling [%]	0.53	0.35	0.5
$\xi_{y,lum}$	0.029	0.033	0.043
ν_s	0.027	0.04	0.035
Bucket height	0.0069	0.011	0.009
$\sigma_{z,0}$ [cm]	1.54	1.01	1.40
σ_z [cm]	1.69	1.22	1.60
Peak luminosity 10^{32}cm^{-2}s^{-1}	3.5	11	3.7

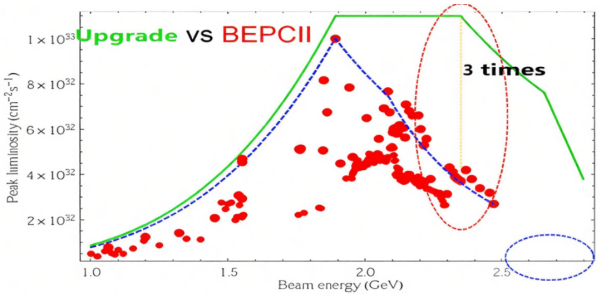

Figure 1: comparison of the luminosity performance achieved by BEPCII at different energies during its operational years and the target luminosity after the upgrade..

* genghp@ihep.ac.cn

Content from this work may be used under the terms of the CC BY 4.0 licence (© 2026). Any distribution of this work must maintain attribution to the author(s), title of the work, publisher, and DOI.

ISBN: 978-3-95450-252-3 ISSN: 2673-5350 doi: 10.18429/JACoW-IPAC2026-WEP1611

THEORY OF THE WAVEGUIDE VARIABLE POWER DIVIDER AND COMBINER

X. He†, Z. Duan, J. D. Liu, J. Y. Li, X. P. Li, H. Shi
Institute of High Energy Physics, Chinese Academy of Sciences, Beijing, China

Abstract

Theoretically, a 180 ° or 90 ° hybrid bridge can serve as a variable power divider and combiner. This study focuses on related theoretical research, selecting the Magic Tee and 3 dB bridge as the required 180 ° and 90 ° hybrid bridges. Based on the scattering matrix of the four-port microwave network, the relationships between input and output amplitude and phase, the phase difference of the two output signals, and the influence of input amplitude or phase error on the output signals are theoretically deduced. Simulations are conducted, and the results match the theory, validating its correctness. The variable power divider and combiner have wide applications and are worthy of study.

INTRODUCTION

Waveguides are the primary choice for transmitting high-power microwaves due to their high power capacity and low transmission loss. The Waveguide Distribution System (WDS) is widely used in areas like accelerators [1] for the transmission, allocation, monitoring, and absorption of high-power microwaves. The Variable Power Divider (VPD) and Combiner (VPC) are convenient for matching different power allocation schemes without altering the WDS layout [2], thus being widely adopted in high-power WDS and worth researching.

The Magic Tee and 3dB bridge are commonly selected as the 180 ° and 90 ° hybrid bridges to achieve VPD and VPC functions. This paper details the theory regarding the relationships between input and output amplitude and phase, the phase difference of the two output signals, and the influence of input amplitude or phase error on the output signals.

THEORY OF THE MAGIC-TEE-BASED VPD AND VPC

The Magic Tee is shown in Fig. 1, it is a four-port 180 ° hybrid bridge with the following scattering matrix

$$S = \frac{1}{\sqrt{2}}\begin{bmatrix} 0 & 0 & 1 & 1 \\ 0 & 0 & 1 & -1 \\ 1 & -1 & 0 & 0 \\ 1 & 1 & 0 & 0 \end{bmatrix} \quad . \qquad (1)$$

Theory of the VPD

Define port 3 and port 4 as input ports with signals $E_3 \times \sin\varphi_3$ and $E_4 \times \sin\varphi_4$. Let E and φ be the amplitude and phase of the input signal respectively. Assume $E_3 = \alpha \times E_4$, $E_4 = 1$, $\alpha \in [0, +\infty)$ and $\varphi_3 = \varphi_4 + \theta$, where α and θ are the magnitude ratio and phase difference of the two input signals at port 3 and port 4. Substituting these conditions into Eq. (1), the output signals of port 1 and port 2 are

$$P_{1out} = \frac{\alpha\cos\theta+1}{\sqrt{2}}\sin\varphi_4 + \frac{\alpha\sin\theta}{\sqrt{2}}\cos\varphi_4 \quad . \qquad (2)$$

$$P_{2out} = \frac{\alpha\cos\theta-1}{\sqrt{2}}\sin\varphi_4 + \frac{\alpha\sin\theta}{\sqrt{2}}\cos\varphi_4 \quad . \qquad (3)$$

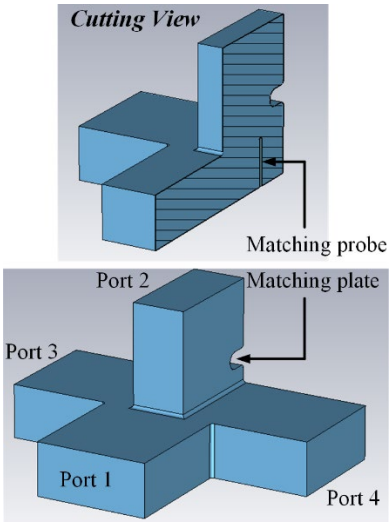

Figure 1: Structure and port definition of the Magic Tee.

So, the output magnitude ratio is

$$\frac{|P_{1out}|}{|P_{2out}|} = \sqrt{\frac{\alpha^2+2\alpha\cos\theta+1}{\alpha^2-2\alpha\cos\theta+1}} \quad . \qquad (4)$$

If $\alpha = 1$, then

$$\frac{|P_{1out}|}{|P_{total-out}|} = \frac{\sqrt{1+\cos\theta}}{\sqrt{1+\cos\theta}+\sqrt{1-\cos\theta}} \quad . \qquad (5)$$

If $\theta \in [0, \pi]$, the value of Eq. (5) varies between [1,0]. This means that if one input signal is equally divided and the two output signals are fed into port 3 and port 4 of the Magic Tee after adjusting their phase difference from 0 to π, output signals of any magnitude ratio can be obtained at ports 1 and port 2, realizing the VPD function.

Influence of the Input Amplitude Error In practice, it is difficult to achieve an ideal 1:1 magnitude ratio of the two input signals at port 3 and port 4. Define the error of deviation from a 1:1 ratio as δ, which can be positive or negative, corresponding to a ratio larger or smaller than 1:1. Replacing the input magnitude ratio with 1 + δ in Eq. (4) gives

$$\frac{|P_{1out}|}{|P_{2out}|} = \sqrt{\frac{\delta^2+2\times(1+\cos\theta)\times\delta+2\times(1+\cos\theta)}{\delta^2+2\times(1-\cos\theta)\times\delta+2\times(1-\cos\theta)}} \quad . \qquad (6)$$

†hexiang@ihep.ac.cn

Content from this work may be used under the terms of the CC BY 4.0 licence (© 2026). Any distribution of this work must maintain attribution to the author(s), title of the work, publisher, and DOI.

ISBN: 978-3-95450-252-3 ISSN: 2673-5350 doi: 10.18429/JACoW-IPAC2026-WEP1613

DEVELOPMENT OF STCF HIGH-EFFICIENCY POSITRON CAPTURE TRAVELING WAVE ACCELERATING STRUCTURES*

Z. Wang, J. Pang†, S. Ma, Q. Jin, A. Zhang, X. Xu
University of Science and Technology of China, Hefei, China
G. Pei, Institute of High Energy Physics, Beijing, China

Abstract

The Super Tau-Charm Facility (STCF) is a next-generation electron-positron collider under development, with a designed center-of-mass energy of 2 GeV to 7 GeV. Positrons generated by a high-energy electron beam striking a target are captured and accelerated to 200 MeV using large-aperture traveling-wave accelerating structures to reduce beam loss. A constant-aperture cavity geometry, in which the group velocity is controlled by the nose-cone length, is proposed to simplify fabrication while maintaining a high accelerating gradient. A pulse compressor is incorporated into the RF system to further enhance the effective RF power. This paper presents the RF design and optimization of 2 m and 3 m large-aperture accelerating structures, both achieving gradients above 15 MV/m.

INTRODUCTION

The Super Tau-Charm Facility (STCF) is a next-generation electron–positron collider designed for ultra-high luminosity operation, featuring high beam current, low emittance, and short beam lifetime. These characteristics impose stringent requirements on the injector and beam injection system.

STCF adopts a full-energy injection scheme, in which both electron and positron beams are accelerated by the linac to the storage-ring injection energy over the range of 1 GeV to 3.5 GeV. The facility operates in top-up mode, requiring continuous injection of high-charge, low-emittance beams at the specified repetition rate [1].

The positron beam is generated by a high-energy electron beam striking a target. Due to the large energy spread and poor beam quality of low-energy secondary positrons, conventional small-aperture structures provide low capture efficiency. To reduce beam loss and improve positron transmission efficiency, large-aperture traveling-wave accelerating structures are adopted.

Unlike conventional disk-loaded structures, the positron capture section employs constant-aperture accelerating structures with lengths of 2 m, 2 m, and 3 m, operating at gradients above 15 MV/m. This paper presents the RF design and optimization of these structures, including the RF system, operating mode, aperture, and cavity geometry.

* This work is supported by the National Key R&D Program of China under Contract No. 2022YFA1602201. We also thank the Hefei Comprehensive National Science Center for their strong support on the STCF key technology research project.

† jpang@ustc.edu.cn

RF SYSTEM

STCF operates primarily in single-pulse mode. Therefore, room-temperature traveling-wave accelerating structures with pulse compressors are adopted in the RF system [1]. To satisfy the high bunch-charge requirement, the linac operates at an S-band frequency of 2998.2 MHz.

A spherical pulse compressor with a dual-polarization-mode coupler is employed [2]. For a square input power envelope, the compressed output waveform exhibits exponential decay. Therefore, a shorter filling time results in a higher average accelerating gradient.

The pulse-compressor gain factor [3], defined as the ratio of the output voltage amplitude to the input voltage amplitude, is expressed as

$$M = \gamma e^{-T_a/T_c} \frac{1-(1-g)^{1+\nu}}{1+\nu} - (\alpha - 1) \qquad (1)$$

where T_a and T_c are the filling times of the accelerating structure and pulse-compressor cavity, respectively; g is the ratio of the residual output power to the input power of the accelerating structure and is related to the attenuation constant; and α is determined by the coupling of the pulse-compressor storage cavity.

Microwave power is supplied by a single 40 MW klystron feeding two accelerating structures, with an estimated waveguide loss of 0.6 dB. The effective RF power is calculated using the pulse-compressor gain factor by Eq. 1.

RF DESIGN OF LARGE-APERTURE LINAC STRUCTURE

Mode Selection and Aperture Optimization

Compared with conventional disk-loaded waveguide structures, the proposed large-aperture accelerating structure adopts a constant-aperture geometry with chamfers on both sides of the iris. The group velocity and related RF parameters are controlled by varying the nose-cone length. A higher group velocity reduces the achievable accelerating field for a given input power, but shortens the filling time and increases the pulse-compressor gain. Therefore, the group velocity must be optimized to maximize the effective accelerating gradient.

Since both the operating mode and iris aperture affect the group velocity and RF performance, these parameters are optimized simultaneously. Four iris apertures, $2a$ = 30 mm, 40 mm, 50 mm and 60 mm, together with three operating modes, $2\pi/3$, $3\pi/4$, and $4\pi/5$, are investigated.

Content from this work may be used under the terms of the CC BY 4.0 licence (© 2026). Any distribution of this work must maintain attribution to the author(s), title of the work, publisher, and DOI.

ISBN: 978-3-95450-252-3 ISSN: 2673-5350 doi: 10.18429/JACoW-IPAC2026-WEP1614

DEVELOPMENT OF STCF S-BAND HIGH-GRADIENT TRAVELING WAVE ACCELERATING STRUCTURES*

S. Ma, J. Pang†, Z. Wang, Q. Jin, University of Science and Technology of China, Hefei, China
G. Pei, Institute of High Energy Physics, Beijing, China

Abstract

The Super Tau-Charm Facility (STCF) is a next-generation electron-positron collider project proposed in China, designed to explore frontier physics in the tau-charm energy region. The facility's accelerator is required to provide electron and positron beams with tunable energies ranging from 1.0 to 3.5 GeV. This study presents the design of a traveling-wave accelerating structure for the STCF. By optimizing the regular-cell configuration, a high shunt impedance is achieved. The peak electric field in accelerating structure is reduced by adjusting the accelerating gradient profile, and an under-coupled output coupler design is adopted to enhance the performance of the accelerating structure. The objective is to achieve an accelerating gradient of 22.5 MV/m with an input power of 45.3 MW, and to further increase the power in pursuit of high-gradient operation in the S-band.

INTRODUCTION

The Super Tau-Charm Facility (STCF), a next-generation electron-positron collider project actively promoted by the Chinese particle physics community, is designed to conduct cutting-edge scientific research in the tau-Charm energy region. Efforts are currently underway to secure support from the central government of China for its construction during the 15th Five-Year Plan period [1, 2].

The design of the STCF linac is based on single-pulse operation, leading to the choice of room-temperature traveling-wave accelerating structures and a waveguide system that incorporates pulse compressors. More specifically, the main electron linac injector will utilize 50 of these accelerating structures, each 3 meters long. They will operate at 2998.2 MHz, which corresponds to the sixth harmonic of the collider ring's frequency of 499.7 MHz.

Multipole components in couplers can lead to degradation of beam emittance, making it essential to select an appropriate coupler design that minimizes these effects [3, 4]. In this study, various coupler configurations were compared to evaluate their multipole characteristics and associated impacts. Within the context of STCF, dual-feed racetrack-shaped couplers were ultimately chosen due to their enhanced capability to suppress multipole components, thereby more effectively reducing multipole-induced effects.

* This work is supported by the National Key R&D Program of China under Contract No. 2022YFA1602201. We also thank the Hefei Comprehensive National Science Center for their strong support on the STCF key technology research project.

† jpang@ustc.edu.cn

Constant-impedance and constant-gradient traveling-wave accelerating structures are widely used in large-scale scientific facilities and industrial applications. However, achieving high gradients in the S-band is often limited by breakdown in individual cells. To address this, a design approach based on peak-field-balanced regular cells is proposed. By tailoring the gradient distribution along the structure, the peak electric field in each cell is equalized. This enables an average gradient of 22.5 MV/m to be achieved in the S-band with an input power of 45.3 MW, while also offering the potential for further enhancement to higher gradient levels.

This paper describes the design of a 3-meter traveling wave accelerating structure for STCF and presents its corresponding parameters. A brief comparison of multipole components arising from different coupler designs is provided, along with an overview of the cooling scheme considerations for the STCF traveling wave structure.

STRUCTURE DESIGN

To accelerate the electron beam to the design energy, the S-band traveling wave accelerating structure operating in the $2\pi/3$ mode at a frequency of 2998.2 MHz will be employed. The operating temperature of the structure is set to 30°C. Dual-feed racetrack-shaped couplers are adopted, along with a regular cell design featuring a modified gradient distribution.

Multipole Components

For the STCF accelerating structure, three typical coupler designs were developed to investigate the impact of multipole components. These include a dual-feed racetrack coupler, a dual-feed coupler, and a single-feed coupler, each optimized as illustrated in Fig. 1. The dual-feed racetrack coupler features a cavity geometry formed by two circles with offset centers, creating a racetrack-like shape. This configuration

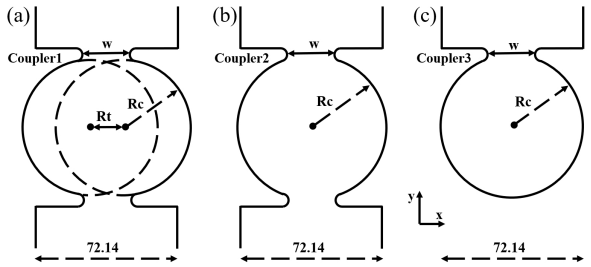

Figure 1: Schematic diagrams of three typical coupler designs.

Content from this work may be used under the terms of the CC BY 4.0 licence (© 2026). Any distribution of this work must maintain attribution to the author(s), title of the work, publisher, and DOI.

ISBN: 978-3-95450-252-3 ISSN: 2673-5350 doi: 10.18429/JACoW-IPAC2026-WEP1615

BEAM ADJUSTMENT BASED ON THE GRADIENT BOOSTING DECISION TREE ANALYSIS IN THE KEK ELECTRON/POSITRON INJECTOR LINAC

T. Sakai*[1], H. Ego[1], S. Shitara[1], S. Ushimoto[2], T. Abe[1], T. Higo[1], Y.Higashi[1]
[1]High Energy Accelerator Research Organization (KEK), Tsukuba, Japan
[2]Mitsubishi Electric System & Service Co., Ltd, Tokyo, Japan

Abstract

KEK-LINAC is an electron/positron linear accelerator used as the injector for the synchrotron radiation facilities (PF ring and PF-AR) and SuperKEKB. The stable operation of experiments at these facilities requires reliable beam supply from the LINAC. We have newly introduced an analytical method based on gradient boosting decision tree (GBDT) to further enhance our beam adjustment capability. GBDT is one of the machine learning methods and has been used as an exceptionally effective model for tabular data. The GBDT analysis handling hundreds of LINAC operating parameters accurately predicted beam-charge and position in the LINAC. Furthermore, by performing SHAP analysis, we have identified key parameters for the beam adjustment and correlations between the parameters. This provided a better understanding of the linac parameters that had previously been difficult to interpret.

INTRODUCTION

KEK-LINAC is a 700-meter S-band (2856 MHz) linear accelerator that generates multi-quality electron and positron beams. This accelerator consists of various components, and the beam conditions can be adjusted by changing the parameters of these components. However, it is difficult to tune all of the hundreds of parameters, and furthermore, it is unclear which parameters are effective for improving the beam quality; as a result, beam tuning relies on the intuition and experience of skilled operators. In this study, we trained a gradient-boosted decision tree (GBDT) [1, 2] using linac parameter data and performed a SHAP analysis to quantitatively evaluate which parameters contribute to the model prediction and how they affect the predicted beam behavior.

ANALYSIS WITH GBDT

Assuming that beam charge and beam size are determined by factors such as the klystron phase, pulse magnet current, ambient temperature, etc., and that time-dependent variations are negligible, the linac operating parameter can be treated as tabular data. In tabular data analysis, gradient-boosted decision trees(GBDT) [1, 2] is one of the most suitable methods and has been in use for a long time [3]. Furthermore, GBDT is a computationally efficient method. In this study, we employed XGBoost, one of the GBDT models [2]. XGBoost is particularly suitable for SHAP-based [4] interpretation, because TreeSHAP [5] provides an exact and efficient algorithm for computing SHAP values for tree ensemble models.

The input data for this study comprised phase and power readings at the klystron output, the current in the pulsed magnets, and the device and ambient temperatures. The input vector comprised approximately 200 parameters. The dataset contains about 100,000 records. The target variable for the machine learning model was the beam charge or the beam size downstream of the linac, or an objective function derived from these quantities.

In this study, the adjustable parameters were actively manipulated to investigate their effects on beam size and charge. For each parameter, a range was defined within the limits of previous operating data, and values were randomly sampled from a uniform distribution within that range.

Figures 1 and 2 compare the true and predicted values of the objective function derived from the beam charge and beam size downstream of the linac. These figures were generated using test data that was not used for training. The objective function J is defined as follows, with the first and second terms representing the beam size and charge terms, respectively:

$$J = \frac{\text{beamsize}}{3} + \left(\frac{1.95}{\text{charge} + \epsilon}\right)^3.$$

Since beam tuning aims to increase the charge and reduce the beam size, a smaller value of this function is considered preferable. The value 1.95 in the second term of J represents the target charge. This term is cubed in order to impose a strong penalty on charge loss. J is preliminary and may be refined or replaced by a more appropriate objective function in future work. As shown in Fig. 2, several data points exhibit inaccurate predictions. This discrepancy is partly attributable to the limited accuracy of the machine learning model, it is also likely affected by the uncertainty in the beam size data itself. The beam size is obtained by fitting the screen image; however, because a Gaussian function is used to fit beam profiles that are not necessarily Gaussian, the fitted values may deviate from the actual beam size.

SHAP ANALYSIS

SHAP analysis was performed to interpret the trained machine learning model and to identify the parameters that strongly contributed to the prediction. SHAP, which is based on Shapley values from game theory, quantifies the contribution of each feature to the model prediction and provides a measure of the feature importance. Here, the term "feature" has the same meaning as "parameter". Since the term

* sakai520@post.kek.jp

Content from this work may be used under the terms of the CC BY 4.0 licence (© 2026). Any distribution of this work must maintain attribution to the author(s), title of the work, publisher, and DOI.

ISBN: 978-3-95450-252-3 ISSN: 2673-5350 doi: 10.18429/JACoW-IPAC2026-WEP1617

REINSTALLATION OF HEAVY CRYOMODULE FOR SCL3 BEAMLINE MAINTENANCE

Yang-Ho Lee, Hyeong-Joo Son
Institute for Rare Isotope Science (IRIS), Institute for Basic Science (IBS), Daejeon, Korea

Abstract

This paper presents a case study on the reinstallation of heavy weight cryomodule (HWR-B #11, HWR-A #9 & #13) for the SCL3 beamline maintenance. Our RAON accelerator, HWR-B combines a cryomodule with a warm section assembled with a quadrupole magnet and a vacuum chamber, with a total weight exceeding 12.5 tons (HWR-A is approximately 7.0 tons). After each annual beam commissioning, some low-efficiency modules were identified to require inspection and repair during maintenance for the following year's beam operation. In particular, the processes of disassembling a large HWR-B or HWR-A cryomodule from the beamline and moving it out of the underground accelerator tunnel needs very strict safety requirements and detailed planning and coordination among related systems and teams. During the first stage of the maintenance procedure, the HWR-B #11, HWR-A #9 & #13 cryomodules was safely removed from the SCL3 beamline using a specially designed moving wheel and then delivered to the contractor for overhaul. After maintenance and testing were completed, the HWR-B #11 cryomodule was reinstalled at its original position on the SCL3 beamline. (However, as HWR-A #9 and #13 required long-term repairs, only the warm sections were reinstalled.) At this time, These tasks required significant effort to prevent steel frame overlap, quadrupole magnet balancing, pipe collisions, and cable breakage in the very narrow space between the HWR cryogenic modules on the beamline. This first in-house beamline maintenance experience provided valuable insight and expertise for the ongoing operation of an accelerator beamline.

SCL3 MAINTENANCE PLAN

During the 1st cool-down and beam commissioning of the SCL3, a low-energy accelerator section, several device repairs and system improvements were required, so beamline maintenance was carried out to improve the cold leak of the several superconducting cavities & modules, stabilize the RF system, add a beam diagnostic device, repair the vacuum TMP, and repair the electromagnet power supply. Through this improvement work, we aimed to contribute to continuously providing stable beams to accelerator experiment users from 2024 to the present [1].

In the case of the HWR-B #11 Crymodule(CM), rather than a simple on-site repair to improve the cold-leak, a precise Overhaul through the manufacturer was decided. Accordingly, beamline disassembly (relevant module), repair and performance inspection & test, and reinstallation were required. In the case of HWR-A #09, #13 CM requiring long-term overhaul and inspection, only the warm section was separated and reinstalled on the beamline for improved beam operation.

HWR-B #11 Maintenance Scope

The main tasks of SCL3 beamline maintenance involve cutting the helium supply pipes of the cryogenic valve boxes connected to each cryomodule, dismantling the work platform, disconnecting the RF rigid coaxial pipes and DC bias, dismantling the module beamlines, disconnecting Warm section, moving to the SRF facility, performing cryomodule repairs and performance tests, and finally completing on-site reinstallation and beamline connection. Figure 1 shows the configuration of the HWR-B cryomodule of the SCL3 beamline, and shows the HWR-#11 configuration and maintenance schedule of the SCL3 beamline [2].

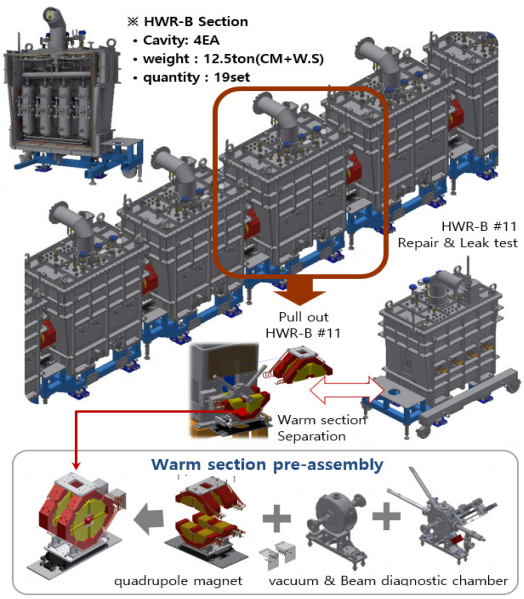

Task	date	Assignment	Remark
• Module Beamline Gate Valve closing	6.5	M.S Kim, Y.J Choi	B#10(R), B#11(F,R), B#12(F)
• SCL3 Warm up	6.12~6.30	T.K Ki 外 Cryogenic team	
• RF Rigid Coaxial Line & DC bias disassembly	6.21~6.23	O.R Choi, J.W Choi	#10, #11, #12 remove(6.22, 7.14)
• Signal & Control & Power cable line separation(String vacuum)	6.26~6.30	M.S Kim, J.W Choi, Y.J Choi, J.S Kang	CM, W.S(6.27), String Vacuum(7.18)
• Cryogenic pipe cutting & Pneumatic line separation	7.3~7.6	J.H Shin(J.M Park), Outsourcing1	7.6(inner pipe separation) 7.13~7.18
• Taking to pieces of cat-walk(only HWR-B#11 area)	~7.6	J.H Shin(J.M Park), Outsourcing1	Front & back CM of HWR-B #11(2set): 7.18
• Quadrupole magnet top-side opening(4set, warm section)	~6.30	J.S Kang, J.W Kwon	Front & back CM of HWR-B #11(2set): 6.28
• Preparation of moving clean booth to HWR #11 area	7.7~7.19	J.W Kwon, E.H Lim, H.J Shon	Front & back CM of HWR-B #11
• Separating Beamline & HWR #11 W.S(Clean booth)	7.7~7.19	J.W Kwon, E.H Lim, H.J Shon	Front & back CM of HWR-B #11
• Separating HWR-B#11 CM & move to ISOL	7.20 & 21	J.W Choi, Y.H Lee(外 7persons)	Preparing to load on a vibration-free truck
• area & leave to SRF building	7.20 & 21	J.W Choi, Y.H Lee(外 7persons)	7.21, 15:00P.M (SRF building)
• Repair and maintenance(Cryogenic inspection)	7.24~11.06	Y.W Jo, J.W Choi, M.K Lee	HWR-B@SRF test facility : 7.24~11.10
- Decomposition & Assembly / 4.5 K cool down test(1st)	~10.13	Y.W Jo, Outsourcing1	
- 4.5K / 2K cool down test(2nd)	10.26~10.31	Y.W Jo, M.S Kim, Outsourcing1	LN2 pre-cooling
- Warm up(HT bunker)	11.01~11.09	Y.W Jo, M.S Kim, Outsourcing1	11.2~11.03 HT finish & delivery preparation
- Delivery to ISOL building & Bring in the basement	~11.10	Y.W Jo, M.S Kim, Outsourcing1	ICABU(11.8~10)
• Putting a warm section on HWR-B#11(alignment)	11.13~14	J.S Kang, J.W Kwon, C.S Seo	SRF → ISOL building, CM+WS Assembly
- Lift & Move HWR-B#11 to SCL3 tunnel	11.13	J.W Choi, Y.H Lee(外 7persons)	Foot Base, spacing between the beam pipes
- Alignment	11.13	C.S Seo, J.H Jo, Outsourcing1(SAE)	(x, y, z) < +- 1 mm, ICABU 2023
- Place HWR-B#11 on the foot-base & bolting	11.14	J.W Choi, Y.H Lee	Caution with VBx pip connections
- Final alignment	11.14	C.S Seo, J.H Jo, Outsourcing1(SAE)	Final beamline alignment
• Clean assembly & Vacuum slow pumping(HWR-B#10-11)	11.15~11.17	J.W Kwon, E.H Lim, H.J Shon	11.16(Assembly), 11.17(Leak test/move)
• Clean assembly & Vacuum slow pumping(HWR-B#11-12)	11.20~11.24	J.W Kwon, E.H Lim, H.J Shon	11.22(Assembly), 11.23(Leak test)
• Assembly cat-walk (B-#11 area)	11.27~	J.H Shin(J.M Park), Outsourcing1	11.24
• Pipe Connection between VBx and HWR-B#11CM	11.27~12.01	J.H Shin(J.M Park), Outsourcing1	welding(11.27), MLI, duct, vacuum, check
• Cryogenic pipe & Pneumatic pipe connection	11.27~12.01	J.H Shin(J.M Park), Outsourcing1	Due date: 7.14~12.11
• Signal & Control & Power cable line connection	12.04~12.08	M.S Kim, Y.J Choi, J.S Kang, J.W Kwon	
• Module & Cavity Vacuum, CM-VBx pre-commissioning	12.04~12.15	J.W Choi, M.K Lee, J.H Shin, M.S Kim	Before cool-down, Vacuum/venting(~12.15)
• RF Rigid Coaxial Line & DC bias assembly	12.11~12.15	O.R Choi	HWR-B #10, #11, #12
• SCL3 beamline Cool down	'24.1.2~	T.K Ki 外 Cryogenic team	Central control system & vacuum check

Figure 1: HWR-B CM configuration & Schedule.

HWR-A #09, #13 Maintenance Scope

The HWR-A CM #09, #13 was removed for long-term repair and performance testing due to reduced efficiency,

Content from this work may be used under the terms of the CC BY 4.0 licence (© 2026). Any distribution of this work must maintain attribution to the author(s), title of the work, publisher, and DOI.

ISBN: 978-3-95450-252-3 ISSN: 2673-5350 doi: 10.18429/JACoW-IPAC2026-WEP1618

MULTIPHYSICS DESIGN AND HIGH-POWER CONDITIONING STAND FOR THE STCF TM020 CAVITY POWER COUPLER*

M. Fan[1,2,3,†] and Y. Wei[1]
[1]National Synchrotron Radiation Laboratory,
University of Science and Technology of China, Hefei, China
[2]Spallation Neutron Source Science Center, Dongguan, China
[3]Institute of High Energy Physics, Chinese Academy of Sciences, Beijing, China

Abstract

For the TM020 cavity used for collider ring beam energy replenishment in the proposed Super Tau-Charm Facility (STCF) project, a waveguide-type power coupler capable of handling CW 300 kW power has been adopted. The power coupler assembly comprises a cavity-welded waveguide coupling port, an online adjustable movable tuner, a 90° waveguide bend, an RF window and a stepped waveguide transition. This paper systematically presents the Multiphysics design of these components. Furthermore, the high-power test configurations for both the RF window and the power coupler are detailed.

INTRODUCTION

The Super Tau-Charm Facility (STCF), which has officially released its Accelerator Conceptual Design Report (CDR), is a proposed next-generation electron-positron collider designed for unprecedented luminosity [1]. To compensate for severe synchrotron radiation losses, several TM020 radio-frequency (RF) cavities are utilized to continuously replenish the storage ring energy. Acting as the critical bridge between the atmospheric power transmission system and the ultra-high vacuum cavity, a high-power waveguide-type coupler has been specifically developed.

Table 1: Parameters of the power coupler

Parameter	Design
Frequency	499.7 MHz
Type	Online adjustable, Waveguide
Number of couplers per cavity	1
Max CW RF power	300 kW
Coupling coefficient	1~6
Tuner insertion depth	0~67 mm
Ultimate vacuum	<5e-7 Pa

* Work supported by the "Hundred Ta\lents Program" of the Chinese Academy of Sciences (No. KJ2310007003), the Fundamental Research Funds for the Central Universities (No. WK2310000114, KY2310000047, KY2310000067), Chinese Academy of Sciences President's International Fellowship Initiative (No. 2025PD0102), Hefei Advanced Light Facility project and STCF key technology research project.
† fanmx@mail.ustc.edu.cn\\\\\\\

The design parameters of the power coupler are shown in Table 1. Since multiphysics design of the waveguide coupling port has been detailed in our previous study [2], this paper mainly focuses on the Multiphysics design of the remaining sub-assemblies and the overall coupler integration. Additionally, the high-power testing setup of the power coupler is designed and performed.

POWER COUPLER DESIGN

To minimize the weight and maintain a compact structure, waveguide size the same as half-height WR1500 waveguide is adopted for the coupler section. Furthermore, given its multifunctional requirements, the coupler is divided into several sub-assemblies to facilitate manufacturing, operation, and maintenance. The specific functions of these components are introduced as follows:

Waveguide Coupling Port Assembly: As the critical component for achieving waveguide-to-cavity coupling, it is welded directly to the cavity to form an integrated unit. Meanwhile, a mounting port is configured on its broad wall to accommodate the movable tuner.

Movable Tuner: This component enables the online adjustment of the coupling coefficient.

90° Waveguide Bend: This assembly provides ports for vacuum pumping and monitoring while simultaneously redirecting the RF power transmission.

RF Window: This is the core component responsible for maintaining vacuum isolation while ensuring reliable high-power transmission.

Stepped Waveguide Transition: This component acts as an adapter, bridging the half-height WR1500 waveguide of the coupler section with the standard WR1800 waveguide utilized in the main transmission system.

The whole assembly of the cavity with power coupler is shown in Figure 1. The commercial software CST and ANSYS are used in the development of the power coupler [3, 4]. As the multiphysics analysis of the Waveguide Coupling Port Assembly have been introduced detailly in ref [2], we will describe the design of the remain components in the follow.

Moveable Tuner

The moveable tuner as shown in Figure 2 employs a choke structure to eliminate direct physical contact between the tuning rod and the external mounting structure. Correspondingly, a mounting port for this movable tuner is configured on the waveguide coupling port assembly.

Content from this work may be used under the terms of the CC BY 4.0 licence (© 2026). Any distribution of this work must maintain attribution to the author(s), title of the work, publisher, and DOI.

ISBN: 978-3-95450-252-3 ISSN: 2673-5350 doi: 10.18429/JACoW-IPAC2026-WEP1619

CONCEPTUAL DESIGN FOR THE COMBINED DAMPING AND ACCUMULATOR RINGS FOR POSITRONS AT STCF

Qihua Zhan[1], Xiaoyu Liu[1*], Mingxuan Chang[2†], Jialian Zhang[3]
[1]University of Science and Technology of China, Hefei, China
[2]Institute of Modern Physics, Chinese Academy of Sciences, Lanzhou, China
[3]Huazhong University of Science and Technology, Wuhan, China

Abstract

The Super Tau-Charm Facility (STCF) is a new generation tau-charm factory designed to collect an enormous and unique dataset in the tau-charm energy region. In order to supply high-quality electron and positron beams to the collider, the STCF injector employs a compatible injector scheme that supports both off-axis and swap-out injection modes. This paper introduces the conceptual design of a combined damping and accumulator rings for positrons at the STCF, aimed at meeting low-emittance beam requirements. The damping ring (DR) and the accumulator ring (AR) share the same lattice, and aligned vertically to reduce construction costs. The detailed lattice design of the DR and AR are presented in this paper.

INTRODUCTION

For the Super Tau-Charm Facility (STCF) [1], to deliver high-quality, full-energy electron and positron beams to the collider rings (CRs), two parallel CR injection schemes are currently under consideration: off-axis injection and swap-out injection. The STCF injector adopts a compatible injector layout scheme, and its layout varies depending on the CR injection mode. For off-axis injection, positron beams are injected into the damping ring (DR), damped, and then extracted to the main Linac. For swap-out injection, positron beams are first damped in the DR, accumulated in the accumulator ring (AR) over three cycles, and finally transported to the ML for acceleration. The AR adopts the same lattice design as the DR. This consistency allows the two rings to be stacked vertically, as shown in Fig. 1. With the exception of the injection sections, all components are aligned vertically one-to-one, enabling both rings to share the same tunnel without a separate enclosure for the AR, thereby significantly reducing construction costs.

In the design of the STCF, the beam energys of positron in both DR and AR are 1.0 GeV. The geometric emittance of the bunch injected into the DR is 1400 nm·rad. According to the design of the STCF CR, the injected positron bunch emittance must be below 6 nm·rad at the nominal energy of 2.0 GeV. This corresponds to a maximum emittance of 12 nm·rad at 1.0 GeV. To meet the injection requirements of the STCF CRs and account for emittance growth during transport, the geometric emittance of the extracted bunch must be less than 11 nm·rad for the off-axis injection scheme with a repetition rate of 30 Hz, and be less than 30 nm·rad for the swap-out injection scheme with a repetition rate of 90 Hz. Main parameter requirements of the two injection schemes are shown in Table. 1.

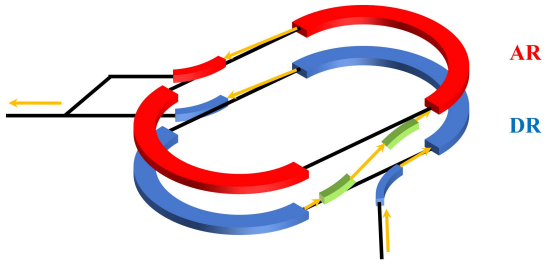

Figure 1: Layout of the DR and the AR. Two rings are stacked vertically, sharing the same lattice and the extraction transport line.

This paper presents the detailed lattice designs of the STCF DR and AR. Since the lattices of the DR and AR are identical, they are collectively referred to as the STCF DR lattice in the following text. The lattice design was carried out using the MAD-X [2] and OPA [3] codes.

LINEAR OPTICS

To reduce the extraction emittance below 11 nm·rad, the beam must be stored in the DR for at least three damping times, and the natural emittance must be less than 10 nm·rad. To reduce the tunnel construction cost, the STCF DR lattice requires a small ring circumference. The current STCF DR meets these goals with a total circumference of 152.4 m, comprising two large arc sections and two long straight sections. The natural emittance of the DR is 9.64 nm·rad. At a repetition rate of 30 Hz, the DR is designed to store either 6 or 12 bunches, thereby satisfying the design specifications. The 6-bunch mode corresponds to an off-axis injection scheme, while the 12-bunch mode is intended for a swap-out injection scheme. Two long straight sections are used for injection and extraction, respectively.

The STCF DR lattice adopts the arc-section FODO design with reverse bends, as used in the SuperKEKB DR [4] and the CEPC DR [5]. Each large arc section consists of 18 FODO cells. Each FODO cell has a length of 2.74 m, a phase advance of 90° / 90° (horizontal / vertical), and a total bending angle of 9°. The ratio of the reverse bending angle to the forward bending angle is set to 0.3. The forward bend

* liuxy@ustc.edu.cn
† changmx@impcas.ac.cn

Content from this work may be used under the terms of the CC BY 4.0 licence (© 2026). Any distribution of this work must maintain attribution to the author(s), title of the work, publisher, and DOI.

ISBN: 978-3-95450-252-3 ISSN: 2673-5350 doi: 10.18429/JACoW-IPAC2026-WEP1621

STATUS OF THE COMPTON POLARIMETER PROJECT AT BEPCII

M. Y. Su, Z. Duan*, J. Gao, Q. F. Han, D. H. Ji, D. Z. Li, Q. Li, X. D. Li, Y. C. Li, G. Lei, Z. J. Liang, G. Lei, Z. H. Ma, L. L. Men X. J. Sun, G. Y. Tang, H. Wang, J. L. Wang, L. Wang, Q. Yang, C. H. Yu, L. D. Yu, W. Zhang, Y. D. Zhang, Y. L. Zhang, N. C. Zhou, D. C. Zhu,
Institute of High Energy Physics, CAS, Beijing, China
A. Martens, J. Tamazirt, F. Zomer, Université Paris-Saclay, CNRS/IN2P3, IJCLab, Orsay, France

Abstract

A laser Compton polarimeter is being developed at the Beijing Electron Positron Collider (BEPCII) for non-destructive diagnostics of transverse electron beam polarization. The project reuses a dismantled wiggler beamline and experimental hutch to transport a circularly polarized 532 nm pulsed laser beam to the electron ring and to guide the backscattered photons to a detector in the hutch. This paper summarizes the present project status, including beamline and optical system upgrades, detection of Compton backscattered photon signals, and recent commissioning with the TaichuPix-3 pixel detector.

INTRODUCTION

Polarized lepton beams are an important ingredient of the physics program of future circular and linear colliders [1–4]. Transverse polarization enables precision beam-energy calibration through resonant depolarization [5, 6], while longitudinally polarized beams can enhance the sensitivity of electroweak and beyond-standard-model measurements. These applications require a reliable, non-destructive beam-polarization diagnostic. Compton polarimetry is therefore widely used because it can measure the helicity-dependent asymmetry of photons or electrons produced by Compton scattering between a polarized laser and a high-energy lepton beam [7–11].

BEPCII provides a useful test bench for developing Compton polarimetry for future colliders. The electron-positron double-ring collider operates in the tau-charm energy range and is being upgraded for higher luminosity and a beam energy reach of up to about 2.8 GeV [12]. At a beam energy of 2.35 GeV, the Sokolov–Ternov polarization build-up time is expected to be on the order of 70 min for the electron storage ring, making transverse self-polarization potentially measurable in routine operation. A Compton polarimeter at BEPCII would support resonant-depolarization studies, beam-energy calibration R&D, and polarized-beam studies relevant to future Z-, W- and Higgs factories [13].

This paper summarizes the implemented Compton polarimeter layout, the first observation of laser-electron Compton signals using a scintillator detector [14, 15], and recent work toward a pixel-detector-based transverse polarization measurement.

* duanz@ihep.ac.cn

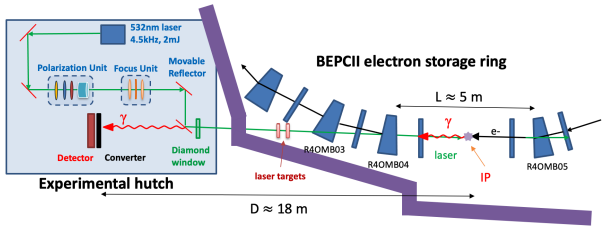

Figure 1: Schematic layout of the BEPCII Compton polarimeter at the 4W2 beamline.

POLARIMETER LAYOUT

The polarimeter is installed at the 4W2 beamline, which originally served a wiggler source and has since been repurposed for the transport of the laser and backscattered photon beams. A circularly polarized laser beam is generated in the experimental hutch, transported through the photon beamline, and brought into collision with the electron beam in a straight section of the electron storage ring. The backscattered photons then propagate through the same beamline and are detected in the hutch. The distance from the nominal interaction point to the detector location is approximately 18 m [15].

The spin-dependent part of the Compton cross section contains a term proportional to the product of the laser circular polarization and the electron polarization. For transverse-polarization measurements, the relevant information is contained in the azimuthal distribution of the scattered particles. A vertically segmented or pixelated detector is therefore required. The TaichuPix-3 CMOS pixel sensor, developed as a CEPC vertex detector prototype, provides a sensitive area of approximately 25.7×15.9 mm^2 and a pixel pitch of 25×25 m^2 [16], in addition to a time resolution of 50 ns. In the BEPCII polarimeter, a high-Z converter is placed upstream of the sensor to convert backscattered photons into charged particles and enhance the detection efficiency.

The laser system is based on a 532 nm pulsed laser with a repetition rate of approximately 4.5 kHz and a maximum pulse energy of 2 mJ. A polarization unit consisting of a linear polarizer, wave plates and a Pockels cell is used to generate switchable circular laser helicity. A three-lens focusing unit transports the laser to the interaction point. In the design estimate, an RMS laser spot size of about 0.5 mm at the interaction point is sufficient for a useful Compton rate, while remaining compatible with the beamline aperture.

Content from this work may be used under the terms of the CC BY 4.0 licence (© 2026). Any distribution of this work must maintain attribution to the author(s), title of the work, publisher, and DOI.

ISBN: 978-3-95450-252-3 ISSN: 2673-5350 doi: 10.18429/JACoW-IPAC2026-WEP1622

BEAM-INDUCED HEATING ANALYSIS AND OPTIMIZATION OF THE STRIPLINE KICKER FOR THE STCF*

B. Zhu, Y. Liu, X. Li, Y. Wang, J. Yang†, K. Fan‡, State Key Laboratory of Advanced Electromagnetic Technology (Huazhong University of Science and Technology), Wuhan, China

Content from this work may be used under the terms of the CC BY 4.0 licence (© 2026). Any distribution of this work must maintain attribution to the author(s), title of the work, publisher, and DOI.

Abstract

The Super Tau-Charm Facility (STCF) is a high-luminosity electron–positron collider currently under design, featuring a single-bunch charge of up to 8 nC and an average beam current as high as 2 A. The swap-out injection scheme imposes stringent requirements on the stripline kicker (SLK), particularly regarding beam-induced heating effects under high-current operation. In this work, the design and optimization of the STCF SLK are presented, with special emphasis on impedance reduction and thermal-effect mitigation. Based on theoretical analysis and CST simulations, the loss factor, total parasitic power loss, and electrode power dissipation are systematically evaluated. The optimized structure with tapered transitions reduces the loss factor and electrode thermal power deposition significantly. Further thermal and mechanical analyses show that the maximum electrode temperature and thermal deformation remain within acceptable limits, while their influence on the electromagnetic field distribution is negligible. The results demonstrate that the optimized SLK satisfies the operational requirements of the STCF under high beam current conditions.

INTRODUCTION

The Super Tau-Charm Facility (STCF) is a next-generation high-luminosity electron–positron collider with beam energies ranging from 1 to 3.5 GeV and a stored beam current of up to 2 A. Owing to the limited dynamic aperture of the storage ring, both off-axis and swap-out injection schemes are under consideration. In particular, swap-out injection requires the kicker system to achieve high injection efficiency while minimizing perturbation to the stored beam and preserving collider luminosity. This operating mode requires the stripline kicker (SLK) to handle a single-bunch charge of 8.34 nC with a bunch spacing of only 4 ns, imposing stringent requirements on the pulse response, electromagnetic stability, and thermal reliability of the kicker system.

At such high beam current, beam–structure interactions can generate substantial beam coupling impedance, resulting in significant parasitic power deposition on the kicker electrodes. The associated temperature rise and thermal deformation of the kicker electrodes may distort the electromagnetic field distribution, degrade kicker performance, and compromise long-term operational stability. Consequently, suppression of beam-induced heating and optimization of impedance characteristics are critical challenges in the SLK design for STCF.

This work presents the design and optimization of the STCF stripline kicker with focus on impedance reduction and thermal-effect suppression. Electromagnetic properties, beam-induced loss, thermal behavior, and thermomechanical deformation are analyzed using theory and CST simulations, and the impact of thermal deformation on electromagnetic performance is evaluated.

DESIGN OF STCF STRIPLINE KICKER

Structural Design

The swap-out injection scheme for the STCF collider ring is currently under preliminary design and optimization. The present configuration adopts five SLKs, each with an effective length of 0.3 m, to provide a total deflection of 2.5 mrad for 3.5 GeV electron and positron beams, corresponding to 0.5 mrad per SLK [1]. The principal design parameters of the STCF SLK are summarized in Table 1.

Table 1: Main Parameters of the STCF Stripline Kicker

Parameter	Value
Injection Energy E [GeV]	3.5
Total Deflection Angle [mrad]	2.5
Number of Kicker	5
Effective Length of per Kicker [m]	0.3
Peak Pulsed Voltage [kV]	17.5
Odd-mode Impedance [Ω]	50
Even-mode Impedance [Ω]	<65
Pulse Rise/Fall Time [ns]	≤2
Pulse Flat-top Time [ns]	≥2
Total Pulse Width [ns]	≤6

The SLK uses an elliptical vacuum chamber with "fender" structures to improve even-mode impedance matching [2]. D-shaped electrodes enhance field uniformity, and tapered transitions at both ends reduce beam-induced heating and impedance discontinuities. The cross-section and prototype are shown in Fig. 1.

*Work supported by National key research and development program of China 2022YFA1602202

† jyang@hust.edu.cn
‡ kjfan@hust.edu.cn

ISBN: 978-3-95450-252-3 ISSN: 2673-5350 doi: 10.18429/JACoW-IPAC2026-WEP1623

LOW EMITTANCE BEAM TRANSPORT SYSTEM OF THE POSITION DAMPING RING FOR THE SUPER TAU CHARM FACILITY*

Xu Yang[1], Ruixuan Huang†,[1], Binghao Zhang[1], Zhouyu Zhao[1], Jingyu Tang[1], Youjin Yuan[2]
[1]University of Science and Technology of China, Hefei, China
[2]Institute of Modern Physics, Chinese Academy of Sciences, Lanzhou, China

Abstract

The Super Tau-Charm Facility is a high-luminosity electron–positron collider operating at a center-of-mass energy range of 2–7 GeV. The stringent requirements for beam brightness and stability pose significant challenges to the injector transport system, especially the positron transport lines of the damping ring. Beam transverse emittance is one of the primary parameters, which is influenced by a mass of components in the lattice design. In this study, a newly developed multistage optimization method is employed to optimize multiple sets of quadrupole strengths along the transport line. The optimized results effectively suppress the emittance growth and maintain compliance of other parameters with damping ring requirements. These results provide a practical reference for the optical design of high-brightness transport systems in next-generation electron–positron colliders.

INTRODUCTION

The Super Tau-Charm Facility (STCF), a next-generation high-luminosity electron–positron collider, is designed to achieve a peak luminosity of 5×10^{34} cm^{-2} s^{-1} at a center-of-mass energy range of 2-7 GeV [1]. This requires high beam brightness, stability, and injection efficiency, making beam quality preservation in the injector transport system critical for overall performance. The main components of beam transport system includes three parts: injection line from the position linac to the damping ring, extraction line from damping ring to main linac, and injection lines from main linac to the collider rings. A preliminary lattice design for the STCF beam transport system has been developed, where the optics matching and emittance preservation was realized [2]. However, the previous beam dynamics optimization was based on an ideal Gaussian beam model. With a more realistic beam distribution, simulations reveal substantial emittance growth and dispersion distortion, indicating limited robustness of the current optimization method. The inclusion of coherent/incoherent synchrotron radiation effects further complicates the beam dynamics and imposes more stringent requirements on lattice optimization [3]. This issue is of greater concern for the positron beam. In this work, we focus on further optimization of the positron beam, thereby enabling the design of a low-emittance transport line under a non-ideal beam model.

* Work supported by the National Key R&D Program of China under Contract No. 2022YFA1602202, the National Natural Science Foundation of China (No.12341501 and 12175224) and the STCF key technology research and development project.
† rxhuang@ustc.edu.cn

In the injection transport line of the STCF damping ring, it consists of a horizontal bending arc with eight 15° dipoles, a chicane-based energy-spread compression system with four 30° dipoles and one 1.6 m accelerating structure, and a matching section with one 10° dipole. Standard FODO cells (40 quadrupoles in total) are used for beam focusing and optics matching (Fig. 1).

Under a fixed lattice configuration, where component positions are fixed, optimizing quadrupole strengths to suppress emittance growth and enhance beam transport remains extremely challenging. The strongly coupled parameters and reliance on numerical simulations make this a high-dimensional black-box problem, limiting the effectiveness of gradient-based methods and making exhaustive parameter scans computationally expensive.

MULTISTAGE BO-NSGAII OPTIMIZATION METHOD

In this study, the strengths of the 31 quadrupole magnets along the beamline are treated as optimization variables. The corresponding optimization problem is formulated in Eq. (1).

$$x^* = \arg\min_{x \in X} f_i(x), \quad i \in \{1,\ldots,n\}$$
$$\text{s.t.} \quad c_j(x) \le 0, \quad j \in \{1,\ldots,m\} \tag{1}$$

Here, $f_i(x)$ denotes the optimization objectives, $c_j(x)$ represents the constraint conditions, and all variables x are confined within the specified range X.

The objectives considered in this work include the dispersion functions (η_x, η_x'), Twiss parameters (β_x, β_y, α_x, α_y) at the beamline exit, and the transverse emittances (ε_x, ε_y). Constraints are imposed on the global maximum β-function along the transport line to limit beam size growth. β and η are given in meters, while the emittances ε are given in nm·rad. To lower the complexity of the optimization, objectives of the same category are combined, as shown in Eq. (2). The initial transverse emittances at the starting point are $\varepsilon_{x0} = 466.31$ nm·rad and $\varepsilon_{y0} = 663.12$ nm·rad. The final target values for the beta functions at the exit were set to $\beta_{x_target} = 9.61$ m and $\beta_{y_target} = 3.98$ m.

$$f_1 = \Delta\varepsilon = \frac{\varepsilon_x - \varepsilon_{x0}}{\varepsilon_{x0}} + \frac{\varepsilon_y - \varepsilon_{y0}}{\varepsilon_{y0}}$$
$$f_2 = |\eta_x| + |\eta_x'|$$
$$f_3 = \Delta\beta = |\beta_x - \beta_{x_target}| + |\beta_y - \beta_{y_target}|$$
$$f_4 = \alpha = |\alpha_x| + |\alpha_y|$$
$$c = \max(\beta) < 100 \tag{2}$$

A multistage optimization framework integrating Bayesian Optimization (BO) [4-6] and the Non-dominated Sorting Genetic Algorithm II (NSGA-II) [7-8] is developed to optimize a non-ideal beam in a fixed lattice. Starting from

Content from this work may be used under the terms of the CC BY 4.0 licence (© 2026). Any distribution of this work must maintain attribution to the author(s), title of the work, publisher, and DOI.

ISBN: 978-3-95450-252-3 ISSN: 2673-5350 doi: 10.18429/JACoW-IPAC2026-WEP2001

RF RECOMMISSIONING OF THE EUROPEAN XFEL LINAC AFTER ITS FIRST THERMAL CYCLE

J. Branlard†[1], V. Ayvazyan[1], C. Christou[1], M. Diomede[1], J. Einstein-Curtis[1], S. Göller[1], M. Grecki[1], M. Herrmann[1], K. Kasprzak[1], D. Kostin[1], P. Nonn[1], B. Richter[1], H. Schlarb[1], C. Schmidt[1], N. Walker[1], M. Wiencek[1], L. Yang[2],
[1] Deutsches Elektronen-Synchrotron DESY, Hamburg, Germany,
[2] Chinese Academy of Science, Institute of Modern Physics, Lanzhou, China

Content from this work may be used under the terms of the CC BY 4.0 licence (© 2026). Any distribution of this work must maintain attribution to the author(s), title of the work, publisher, and DOI.

Abstract

The superconducting linac at the European X-ray Free-Electron Laser (EuXFEL) in Hamburg Germany has been operating at 2 K since its initial cool-down in 2016. After nearly ten years of user operation at cryogenic temperature, the linac was warmed up for the first time in summer 2025 for its first long maintenance period and successfully cooled down again in December 2025. This marks the first complete thermal cycle of all superconducting RF cavities since the start of linac operation in 2017. To avoid mechanical stress on the SRF cavities, frequency detuning before warm-up and retuning after cool-down were required. This contribution describes the approach taken for detuning and retuning all 784 cavities, statistics about the subsequent reconditioning effort, and the RF recommissioning of the SRF linac.

DETUNING AND RETUNING

To allow installation of redundant cryo-valves and avoid thermal cycling the linac for future cryo-safety tests, a six-month long intervention and maintenance period (LIMP) was scheduled from June 2025 till January 2026. In preparation of this first warm up since beginning of operation in 2017, all 776 1.3 GHz and eight 3.9 GHz superconducting cavities were detuned, retuned and subsequently conditioned for the RF startup after the LIMP.

Cavity Detuning

Cavities were not detuned to their warm-tuner position (also known as parking position) but rather to an intermediate detuning, referred to as *safe* position defined as a detuning large enough to avoid unrecoverable plastic deformation due to a thermal cycle. The safe positions were set to either 100 or 200 kHz below the 1.3 GHz resonant frequency, depending if the detuning when the cavity is warm is less or larger than 300 kHz. The motivation to detune "only" to safe is to minimize tuner motor movement to optimize their life expectancy. The detuning operation was done in a semi-automated way, using an emergency software tool developed and used during the covid pandemic, called ED2S (emergency-detune-to-safe) [1]. This one-button tool drives all selected motors to a pre-defined motor position, without actually checking if the cavities are being detuned. Since the pre-LIMP detuning was not an emergency, it was decided to perform the operation with RF on, so that the resonant frequencies could be tracked as cavities were being detuned. The procedure consisted of driving all cavities at a moderate gradient, disabling all feedback and automation algorithms, set the target detuning to safe and launch the ED2S tool. The total detuning took 40 minutes, followed by a systematic check (and adjustment when needed) of the final frequency (FFT of the cavity probe signal). During the process, two motor drivers (4%) failed (one blown fuse and one power supply failure). 47 cavities (6%) were masked from ED2S, mostly out of precaution and were detuned manually. Overall, the entire process could be successfully completed within an eight-hour shift for a crew of eight people, including a 2.5-hour tunnel access to repair the two tuner drivers. Three cavities needed special care: one cavity required an unusually high number of motor steps to reach its destination. The problem was later identified as slippage in the stepper motor rotor and could be addressed by increasing the driver current. The other two cavities stopped at a detuning closer to 100 kHz rather than the targeted 200 kHz due to a software error, which turned out to be a non-issue.

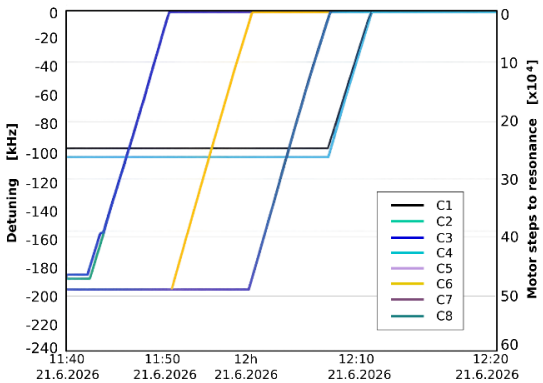

Figure 1: Resonant frequency tracking during retuning of station A11, module 4, cavities 1 to 8.

Tracking the cavity frequency during detuning and retuning allowed to measure the motor sensitivities. We found the behaviour to be very linear over the detuning range, with an average of -0.466±0.0098 Hz/motor step for cavity 1 of every cryomodule and -0.443±0.0061 Hz/motor step for all other cavities (C2-C8). A plausible explanation comes from cryomodule design, since the tuner is assembled differently for cavity 1 due to the presence of a gate valve at the beginning of the cavity string.

†julien.branlard@desy.de

ISBN: 978-3-95450-252-3 ISSN: 2673-5350 doi: 10.18429/JACoW-IPAC2026-WEP2601

HIGHER-ORDER ANALYSIS FOR THE WAKEFIELDS OF A SINGLE-PLATE CORRUGATED STRUCTURE*

Weilun Qin†[1,2], Cheng-Ying Tsai‡[3]
[1]Institute of High Energy Physics, Chinese Academy of Sciences, Beijing, China
[2]Spallation Neutron Source Science Center, Dongguan, China
[3]Huazhong University of Science and Technology, Wuhan, China

Abstract

Single-plate corrugated structures are widely used in x-ray free-electron laser facilities. Accurately modeling the corrugated structure wakefields is of prime importance for correctly simulating their dynamics. In this contribution, we propose a third-order Taylor expansion method for analysing and simulating the single-plate corrugated structures. Our findings indicate that for a small distance and a large transverse beam extension, expansion of the longitudinal wake up to the third order is necessary.

INTRODUCTION

X-ray free-electron lasers (XFELs) offer widely tunable x-ray pulses with unprecedented brightness, driving cutting-edge experiments in a broad spectrum of sciences. Tailoring the temporal and spectral properties of the XFEL pulses often requires manipulation of the electron beam phase space through multiple means. Corrugated wakefield structures [1] are a particular type of passive device used at XFELs for beam manipulation [2–7] as well as diagnostics [8–10]. Such devices utilize the interaction of the electron beam with the surrounding metallic corrugations to passively alter the electron beam phase space. Among them, single-plate corrugated structures [11] are usually used to induce time-dependent slice offset of the electron phase space, aiming for short pulse generation or longitudinal phase space diagnostics.

The modeling of the beam dynamics in the wakefield structures relies on the calculation of the point charge wake functions of the structure. For the single-plate structure, analytical forms of the point charge wake functions were given up to the zeroth-order and first-order approximations [11, 12]. In most of the beam dynamics codes like ELEGANT, assumptions are often made as follows: the longitudinal component is transversely uniform, the transverse component can be decomposed into a uniform term plus one dipole/quadrupole term that scales linearly with the position of the drive/test particle.

When the transverse extension of the electron beam is small and the beam distribution is symmetric, the above assumptions are rather accurate. While in some special cases, higher-order analysis is needed. For example, when the energy spread increase induced by the structure is of interest, the dependency of the longitudinal wake function on transverse coordinates should be included. Another example is when there is a large transverse beam tilt, the linear assumption of transverse wake functions should be examined.

In this paper, we present a general higher-order analysis method for the wakefields and apply it to a single-plate corrugated structure. The method is based on the Taylor expansion of the exact longitudinal wake function [13], which can be obtained analytically or numerically. Our method extends the expansion of Ref. [13] to the third order. Transverse components are connected via the Panofsky-Wenzel Theorem [14]. Taking the exact analytical form of wake functions for the single-plate structure obtained in Ref. [12], we were able to identify the contribution of higher-order terms. The results indicate higher order terms should be properly accounted for in beam dynamics tracking.

This paper is organized as follows: we first introduce the Taylor expansion method, then we calculate all expansion coefficients for the single-plate structure, followed by the analysis of higher-order contributions. Finally, we briefly discuss our findings and conclude this paper.

EXPANSION OF POINT CHARGE WAKE

Consider the two-particle model in the Cartesian coordinate system, where the wakefields are excited by the drive particle located at (x_0, y_0) and probed by the test particle located at (x, y). We expand the longitudinal wake function $w_z(x_0, y_0, x, y, s)$ is known around the beam position $(\bar{x}, \bar{y})$ up to the third-order as

$$w_z(x_0,y_0,x,y,s) \approx h_{00} + \sum_{i=1}^{4} h_{0i}\,\Delta_i + \sum_{i=1}^{4}\sum_{j=1}^{4} h_{ij}\,\Delta_i\Delta_j + \sum_{i=1}^{4}\sum_{j=1}^{4}\sum_{k=1}^{4} h_{ijk}\,\Delta_i\Delta_j\Delta_k, \quad (1)$$

where $\Delta_1 = x_0 - \bar{x}$, $\Delta_2 = y_0 - \bar{y}$, $\Delta_3 = x - \bar{x}$, $\Delta_4 = y - \bar{y}$, the coefficients are given by

$$h_{00}(s) = w_z(\bar{x},\bar{y},\bar{x},\bar{y},s), \quad (2)$$

$$h_{0i}(s) = \frac{\partial w_z}{\partial r_i}(\bar{x},\bar{y},\bar{x},\bar{y},s), \quad (3)$$

$$h_{ij}(s) = \frac{1}{2}\frac{\partial^2 w_z}{\partial r_i \partial r_j}(\bar{x},\bar{y},\bar{x},\bar{y},s), \quad (4)$$

$$h_{ijk}(s) = \frac{1}{6}\frac{\partial^3 w_z}{\partial r_i \partial r_j \partial r_k}(\bar{x},\bar{y},\bar{x},\bar{y},s), \quad (5)$$

* This work was supported by the Department of Science and Technology of Guangdong Province (No.2024QN11X220).

† qinwl@ihep.ac.cn
‡ jcytsai@hust.edu.cn

Content from this work may be used under the terms of the CC BY 4.0 licence (© 2026). Any distribution of this work must maintain attribution to the author(s), title of the work, publisher, and DOI.

ISBN: 978-3-95450-252-3 ISSN: 2673-5350 doi: 10.18429/JACoW-IPAC2026-WEP4302

THE AGS WITH TWO COLD SNAKES

K. Hock*[1], H. Huang[1], V. Schoefer[1]
[1]Brookhaven National Laboratory, Upton, NY, USA

Abstract

To preserve polarization in the Alternating Gradient Synchrotron (AGS), two partial snakes are used to avoid both imperfection resonances and vertical intrinsic resonances. One of these partial snakes is superconducting and the other is normal conducting, the so-called cold and warm partial snakes. Simulations show that adding an additional cold partial snake improves polarization transmission for both polarized protons and polarized helions. In this configuration, the spin-tune gap for protons is large enough to accommodate both Q_x and Q_y. For polarized helions, the spin tune gap is large enough for both Q_x and Q_y to be well separated but the additional cold-snake provides lossless transmission across the very strong $G\gamma = 60 - \nu_y$. This paper serves as an investigation into extraction of polarized helions above 15 GeV/u which is needed to support all snake precession axes of polarized helions in the Hadron Storage Ring.

INTRODUCTION

The Electron Ion Collider (EIC) calls for collisions of highly polarized and high intensity proton and helion beams on polarized electron beams [1]. The target polarization at injection is 75% to support a store average polarization of 70%, with an injected intensity of protons and helions of 3.2×10^{11} and 1.3×10^{11} ions per bunch (ipb), respectively. The beams are polarized at the source and polarization transmission is optimized through acceleration at the Hadron Injector Complex (HIC) and Hadron Storage Ring (HSR) to minimize polarization loss. The HIC consists of the Alternating Gradient Synchrotron (AGS) and the AGS Booster synchrotron. Polarized protons are produced at the Optically Pumped Polarized Ion Source (OPPIS) with a polarization of 80-85% and an intensity up to 8×10^{11} ipb. During normal operations, the proton bunch is shaped via scraping to reach the desired intensity and emittances for optimal polarization transmission. Polarized protons have been operated at the Booster and AGS for RHIC operations with polarization in AGS at extraction energy at 65% and 3.2×10^{11} ipb [2]. Nominal energy ranges correspond to $G\gamma = 2.18$ to 4.5 in the Booster, and $G\gamma = 4.5$ to 45.5 in the AGS. In the Booster, there are two imperfection resonances that do not result in polarization loss. The AGS has two partial snakes, one superconducting and one normal conducting, the so-called cold and warm snakes. These snakes are located a third of the ring apart. The transfer between accelerators at the half integer is due to n_o being nearest vertical when [3]

$$|G\gamma| = 3n + 1.5 \quad (1)$$

where n is an integer. The rotation from the cold and warm partial snakes corresponds to χ_c=10% and χ_w=6% of a 180° rotation, where χ_c and χ_w correspond to the rotation from the cold and warm snakes. In the AGS, the ν_y is set to be inside the spin-tune gap generated by the two partial snakes. Due to the relatively low strength of the partial snakes, both ν_x and ν_y cannot fit in the gap resulting in many horizontal resonances being crossed. These horizontal resonances have been compensated for by a weak tune jump [3], and most recently direct correction of the resonance driving terms generated by the snakes using skew quadrupoles [4]. The weak tune jump leads to modest emittance growth and cannot provide further improvements on polarization transmission. The skew quadrupole system relaxed the stringent timing requirements of the tune jump system and is still being commissioned. Polarized helions have yet to be commissioned, with the upgrade to the Electron Beam Ion Source to provide them scheduled for the 2026 summer shutdown. The source is expected to provide polarization up to 85% with an intensity of 2.5×10^{11} ipb. The intended energy range in Booster corresponds to $|G\gamma|$ = 4.19 to 7.5 or 10.5, and $|G\gamma|$ =7.5 or 10.5 to 49.5 in AGS. In the Booster there are three or six imperfection resonances, and zero or two intrinsic resonances, dependent on the extraction energy. In the AGS, the snakes rotate the spin of helions more than protons due to the higher G, producing a large spin-tune gap that can accommodate both ν_x and ν_y. The rotation of helions with the nominal proton snake strengths corresponds to χ_c=15% and χ_w = 9%. Extraction of helions at $|G\gamma| = 49.5$ corresponds to $B\rho$ = 55.2 Tm, however the design AGS to HSR transfer energy is approximately 80 Tm. This lower energy transfer avoids crossing the $|G\gamma| = 60 - \nu_y$ resonance in the AGS. The highest supported transfer energy for helions that has spin matched from AGS to HSR, consistent with Eq. 1, corresponds to $|G\gamma| = 70.5$ ($B\rho$ = 78.8 Tm). To satisfy $\nu_s = 1/2$ in the HSR there will be six full snakes (180° rotation), with the nominal configuration of these snakes alternating precession axis of ±45°. An alternate configuration is alternating 0° and 90° [5]. However, 90° has a large orbit excursion in the snake aperture and a large matching requirement with the accelerator. The snake aperture has a radius of 4 cm, and the entrance and exit have a reduced vertical aperture to 2.4 cm to accommodate the actively cooled beam screens. At the intended injection energy of $|G\gamma| = 49.5$ and β_y=30 m and ϵ_y = 1.5 μm, there is insufficient aperture as seen in Fig. 1. The minimum supported injection energy for this configuration is 15 GeV. The orbit matching requirement for the accelerator with the snake (y_{match}), the associated maximum orbit excursion in the snake (y_{mas}), and the clearance through the snake are summarized in Table 1.

* khock@bnl.gov

Content from this work may be used under the terms of the CC BY 4.0 licence (© 2026). Any distribution of this work must maintain attribution to the author(s), title of the work, publisher, and DOI.

ISBN: 978-3-95450-252-3 ISSN: 2673-5350 doi: 10.18429/JACoW-IPAC2026-WEP4306

ACCELERATOR UPGRADES REQUIRED FOR BEAM OPERATION AT FERMILAB IN THE PIP-II/DUNE ERA*

S. Krishnagopal†, M. Convery, J. Dey, Fermi National Accelerator Laboratory, Batavia, United States

Content from this work may be used under the terms of the CC BY 4.0 licence (© 2026). Any distribution of this work must maintain attribution to the author(s), title of the work, publisher, and DOI.

Abstract

The Proton Improvement Plan - II (PIP-II) injector linac is an 800 MeV superconducting H^- linac, christened Linac2, that will replace the existing 400 MeV injector to the accelerator complex at Fermilab. The higher energy, intensity and repetition rate require various upgrades to the existing accelerator complex consisting of the Booster, the Recycler Ring and the Main Injector, in order to be able to accept and accelerate beam from PIP-II. In this paper we discuss various upgrades that are required and steps being taken to implement them.

INTRODUCTION

The Proton Improvement Plan-II (PIP-II) [1] will deliver an 800 MeV superconducting H^- linac, Linac2, that will replace the existing 400 MeV normal-conducting injector. PIP-II/Linac2 is an essential upgrade of the existing Fermilab Accelerator Complex that will provide a 1.2 MW proton beam for the Long-Baseline Neutrino Facility and the Deep Underground Neutrino Experiment (LBNF/DUNE) [2].

The higher injection energy, repetition rate and beam intensity provided by Linac2 necessitate a number of changes and upgrades to the rest of the Accelerator Complex comprising three synchrotrons – the Booster, the Recycler Ring (RR) and the Main Injector (MI). Other upgrades are also necessitated by reliability and end-of-life issues of various components, given the vintage of the synchrotrons (between 30 and 50 years). These have been the subject of considerable study over the years by the Accelerator Complex Studies Task Force, and the main conclusions were summarized in the 2024 AD Preparation for the DUNE-PIP-II Era Workshop [3]. In this paper we summarize the drivers of change, and describe the scope of the changes that are addressed by just two complementary efforts: the Accelerator Upgrades sub-project of PIP-II, and Accelerator Complex Evolution (ACE) – PIP-II Integration (P2I) program, that together ensure a smooth transition of the Accelerator Complex into the DUNE/PIP-II era.

DRIVERS OF CHANGE

The key Linac2 beam parameters that drive upgrades across the existing Accelerator Complex are summarized in Table 1. The injection energy doubles from 400 to 800 MeV, the beam intensity rises from 4.5×10^{12} to 6.7×10^{12} protons/pulse, the repetition rate increases from 15 to 20 Hz, and the injected pulse length grows from 30 μs to 550 μs. In addition, beam will be injected into a new section of the Booster – period 11 instead of period 1.

Table 1: Key Parameters of Existing Linac & Linac2

Parameter	Existing linac	Linac2
Beam injection energy (MeV)	400	800
Beam intensity (protons/pulse)	4.5×10^{12}	6.7×10^{12}
Repetition rate (Hz)	15	20
Injection pulse length (μs)	30	550
Booster injection area	L1	L11

Clearly these parameters will drive a large number of changes and upgrades, not all of which can be discussed in this paper. Here, as an example, are a few of the impacts; greater details can be found in Ref. 3.

(1) Injection:
- (a) Shorter combined function magnets (CFM) to make space for injection.
- (b) New ORBUMP and painting magnets for the actual injection.

(2) Repetition rate:
- (a) All CFM girder capacitors changed for 20 Hz frequency.
- (b) Much of the electronics (BPMs, etc.) upgraded for 20 Hz operation.
- (c) More heating of components, requiring more cooling (water and air).

(3) Intensity:
- (a) Need more RF voltage in the Booster and more RF power in MI.
- (b) New transverse and longitudinal dampers to address intensity-driven instabilities.
- (c) New Gamma-T jump system for the MI.
- (d) New Gamma-T jump system for the Booster.

From this example, 1, 2(a) and 3(a-c) are addressed by the PIP-II project, while 2(b) and 3(d) are addressed by ACE-P2I, which also addresses some spares and end-of-life issues. Item 2(c), and other infrastructure related impacts, are addressed by the Accelerator Infrastructure Readiness (AIR) component of ACE, which is beyond the scope of this paper.

* This work was produced by FermiForward Discovery Group, LLC under Contract No. 89243024CSC000002 with the U.S. Department of Energy, Office of Science, Office of High Energy Physics.

†skrishna@fnal.gov

ISBN: 978-3-95450-252-3 ISSN: 2673-5350 doi: 10.18429/JACoW-IPAC2026-WEP4311

PROGRESS ON IMPLEMENTATION OF A VARIABLE WEDGE FOR FRIB ARIS*

Z. Wu†,1,2, X. Rao[1], M. Hausmann[1], B.M. Sherrill[1,3], P. Nariyoshi[1]
[1] Facility for Rare Isotope Beams, East Lansing, MI, USA
[2] Department of Mechanical Engineering, Michigan State University, East Lansing, MI, USA
[3] Department of Physics and Astronomy, Michigan State University, East Lansing, MI, USA

Abstract

A variable wedge system is being developed for the Facility for Rare Isotope Beams (FRIB)-Advanced Rare Isotope Separator (ARIS) facility to provide flexible control of beam energy loss through independently adjustable wedge angle and center thickness. This research evaluates two parallel strategies: a multi-material six-piece solid wedge system and a liquid-filled wedge system. For the solid wedge, the control model and optimization algorithms have been developed and verified, with systematic testing confirming automated control across a 1–20 mrad range. Current efforts focus on exploring sub-mrad regimes (<1 mrad). To address fabrication limitations associated with very thin wedges, a multi-material method was developed in which materials with different densities are selected while maintaining constant areal density. This approach scales the effective thickness range by the density ratio, improving achievable thickness resolution and reducing deviations between calculated and experimentally achievable equivalent wedge configurations. Computational efficiency was further improved by using an L_∞-based trajectory solver to minimize the maximum coordinated actuator displacement. This framework is currently being integrated into the fragment separator simulation code LISE++. In parallel, a liquid-filled wedge model was developed, utilizing bellows-integrated cylindrical housing to enable continuous density tuning alongside adjustable wedge geometry. Together, these developments provide a robust basis for enhancing rare isotope beam delivery at FRIB.

INTRODUCTION

The Advanced Rare Isotope Separator (ARIS) at FRIB utilizes wedge-shaped degraders to provide momentum-dependent energy loss for beam purification [1]. Modern experiments increasingly demand real-time adjustments of wedge angle and thickness [2]. The core design challenge lies in achieving a target areal density ($\rho \cdot t$) that depends on beam transverse position, where ρ is the material density and t is the path length.

A major limitation of conventional single-material wedge systems appears in the small-angle regime, where fabrication and positioning constraints reduce achievable thickness resolution. Another consideration is that each experiment requires a different central thickness and angle. Currently, each wedge set is fabricated separately, leading to discrete jumps in beam parameters rather than continuous tuning.

To address these limitations, this work investigates two parallel strategies:

Multi-material Six-piece Solid Wedge: A multi-material approach is explored to improve achievable thickness resolution in the small-angle regime while maintaining the required areal density.

Liquid-filled Wedge: A bellows-integrated liquid wedge concept is investigated as a continuously tunable alternative to conventional solid wedge systems.

Both systems incorporate L_∞ trajectory optimization to manage vacuum thermal loads. The corresponding control framework is being integrated into the LISE++ framework [3] to provide a standardized utility for the global research community.

MULTI-MATERIAL SIX-PIECE SOLID WEDGE

Mechanical Architecture and Material Strategy

The six-piece variable wedge consists of three independently movable wedge pairs that combine to generate an effective linear thickness gradient along the beam axis [4]. Two quadratic-profile wedge pairs (200 mm long) are used for angle generation, while a complementary linear-profile pair (300 mm long) provides independent center-thickness compensation.

To improve achievable resolution in the small-angle regime, a multi-material strategy is employed. The quadratic wedge pairs are fabricated from materials with distinct densities, typically Al6061 (UNS A96061) and epoxy, allowing the system to optimize angular resolution for different experimental conditions.

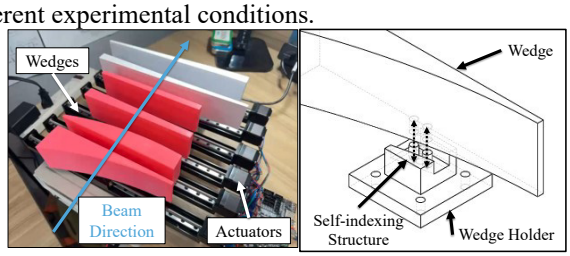

Figure 1: (a) 3D-printed prototype of the six-piece variable wedge system and (b) SolidWorks model of the self-indexing wedge-holder interface.

The mechanical design incorporates a simplified self-indexing interface between the wedge holders and wedge

* Work supported by the U.S. Department of Energy, Office of Science, Office of Nuclear Physics and used resources of the Facility for Rare Isotope Beams (FRIB) Operations, which is a DOE Office of Science User Facility under Award Number DE-SC0023633.
† Email Address: wuz@frib.msu.edu

Content from this work may be used under the terms of the CC BY 4.0 licence (© 2026). Any distribution of this work must maintain attribution to the author(s), title of the work, publisher, and DOI.

ISBN: 978-3-95450-252-3 ISSN: 2673-5350 doi: 10.18429/JACoW-IPAC2026-WEP4313

EXPLORING COUPLED-CAVITY LINAC UPGRADE WITH DISTRIBUTED-DRIVE LINAC AT LANSCE*

H. Xu†, M. Sanchez Barrueta, K. A. Shipman, J. T. M. Lyles, M. Kaemingk, B. Sims, J. T. Yoskowitz, L. D. Duffy, J. W. Lewellen, B. E. Carlsten, E.-C. Huang, B. Comiskey, T. W. Hall, J. A. Vega, Los Alamos National Laboratory, Los Alamos, United States

Abstract

The Distributed-Drive Linac (DDL) concept allows independent control of the radiofrequency (RF) power and phase of each accelerator cell, realized by an RF power system consisting of discrete solid-state amplifier (SSA) units. The DDL concept is under investigation at Los Alamos Neutron Science Center (LANSCE) as a candidate for the future upgrade of the 805-MHz Coupled-Cavity Linac. Independently adjustable RF power and phase of each DDL accelerator cell allows using the same DDL architecture to provide a much higher beam energy at the linac exit, such as 2–3 GeV, for proton radiography (pRad). The DDL architecture would require significant upgrade of the RF infrastructure at LANSCE, including implementing a great number of coaxial transmission lines for 3000–5000 individual DDL accelerator cells. For the pRad operation mode, compact RF pulse compressors are also under investigation.

FROM CCL TO DDL

The 805-MHz Coupled-Cavity Linac (CCL) at Los Alamos Neutron Science Center (LANSCE) has been in operation since 1972, when it was commissioned as part of the Los Alamos Meson Physics Facility (LAMPF). Today, the CCL accelerates negative hydrogen ion (H^-) beams from 100 MeV to 800 MeV over approximately 700 m [1]. The CCL comprises 44 linear modules, each draws 0.6–1.0 MW from one klystron capable of producing up to 1.25 MW peak power. Each CCL module contains several linear multi-cell tanks. In recent years, operation of the LANSCE CCL has become increasingly sensitive to the condition of the aging klystrons.

A team at LANSCE is investigating a new-concept linac architecture, the Distributed-Drive Linac (DDL), as one candidate option for upgrading the CCL. The 805-MHz DDL concept uses independently controlled radiofrequency (RF) power source for each accelerator cell, operating with adjustable power and phase. The RF source under consideration is a unit of solid-state amplifiers (SSAs) with combined power output. The DDL will be able to operate with continuously adjustable output beam energy without compromising the beam-RF synchronization; the DDL will be able to provide beams with kinetic energy beyond 800 MeV, should mission needs arise; in the event of a faulty RF source unit, advanced control algorithms can be used to adjust the RF amplitude and phase of neighboring cells to compensate for the missing acceleration in the affected cell. Meanwhile, the spare management of the RF sources is expected to be significantly less challenging, compared to that of CCL.

When the DDL is implemented to replace the CCL at LANSCE, it is envisioned that each of the 3000–5000 accelerator cells will be powered individually from RF sources located on the second level of the accelerator building, currently used as the klystron gallery. Individual RF power transmission can be accomplished using Electronic Industries Association (EIA) standard 1-5/8-inch coaxial transmission lines.

The work presented in this paper benefits from the synergy with the ongoing Solid-State Power Amplifier (SSPA) effort at LANSCE investigating a multi-stage solid-state RF amplifier architecture with combined RF power output as a potential replacement for a single CCL klystron station [2–5].

DDL CELL OPTIMIZATION

Each individual cell in the DDL operates with a variable transit time of the beam; the RF source for each cell adjusts the initial RF phase that the beam witnesses as it enters the cell to maximize the energy gain. In other words, the phase advance per cell in the DDL is no longer a constant. In comparison, the side-coupled CCL operates in the $\pi/2$ mode, with adjacent accelerating cells operating with a constant, π phase advance.

We are currently optimizing the DDL cell profile for its Tank 1. To optimize the DDL Tank 1 shunt impedance, we performed individual-cell profile optimization using a Multi-Objective Genetic Algorithm (MOGA) on the High-Performance Computing (HPC) clusters at Los Alamos National Laboratory (LANL) [6]. Figure 1 shows a comparison of MOGA-generated designs; Fig. 1a used the existing CCL Module 5 Tank 1 (M5T1, first CCL tank) cell length, with similar shunt impedance but approximately half the peak electric field, compared to the CCL M5T1 cell design; Fig. 1b shows one of the initial attempts applying the DDL concept, exploring using the gap of the re-entrant features to match to the beam transit time over half an RF cycle. The optimization of the cell profile for the DDL concept is underway.

DDL BEAM DYNAMICS

We are currently performing DDL beam simulations to maximize the energy gain of the input, 100-MeV H^- beam through the DDL Tank 1, which has identical length to that of the CCL M5T1 [7]. The optimization takes care of Twiss

* Work supported by U.S. Department of Energy through the Laboratory Directed Research and Development program of Los Alamos National Laboratory, under project number 20260114ER.

† haoranxu@lanl.gov

Content from this work may be used under the terms of the CC BY 4.0 licence (© 2026). Any distribution of this work must maintain attribution to the author(s), title of the work, publisher, and DOI.

ISBN: 978-3-95450-252-3 ISSN: 2673-5350 doi: 10.18429/JACoW-IPAC2026-WEP4314

PLANS FOR CRYOGENIC C-BAND PROTOTYPE TESTS FOR LANL PRAD BOOSTER LINAC*

H. Xu†, M. Kaemingk, E. I. Simakov, E. Olivas, Y. K. Batygin, W. Choi, W. B. Haynes, V. Pavlenko, T. Tajima, S. S. Kurennoy
Los Alamos National Laboratory, Los Alamos, NM, United States

Abstract

We report the plans for testing a four-cell C-band (5.712 GHz) normal conducting radiofrequency (RF) accelerator cavity at liquid-nitrogen temperature under high accelerating gradient, being prototyped and proposed for the booster linear accelerator (linac) upgrade for the Proton Radiography (pRad) facility at Los Alamos National Laboratory. Operating RF structures at cryogenic temperature enhances copper conductivity, enabling higher accelerating gradients and greater RF-to-beam power efficiency. The prototype cavity will be housed inside a cryo-module with foam insulation for both low-power and high-power tests. Pulsed RF power up to 12 MW will be available for the high-power experiment. We also report the engineering and mechanical design of the prototype cavity.

INTRODUCTION

A Laboratory Directed Research and Development (LDRD) Directed Research (DR) project was funded at Los Alamos National Laboratory (LANL) to theoretically and experimentally research on using a high-gradient radiofrequency (RF) accelerator operating at liquid-nitrogen temperature (77 K) for building an energy booster linear accelerator (linac) [1], accelerating the negative hydrogen ion (H^-) beam from 800 MeV to 3–5 GeV, for the upgrade of the Proton Radiography (pRad) facility at Los Alamos Neutron Science Center (LANSCE) [2].

The fundamental RF frequency of LANSCE accelerator complex is 201.25 MHz. Downstream of the LANSCE Coupled-Cavity Linac (CCL), the H^- beam enters the energy booster linac with a kinetic energy of 800 MeV. The beam undergoes bunching and acceleration through L- (1408.75 MHz), S- (2817.50 MHz), and C-band (5635.00 MHz) structures in series, reaching 3–5 GeV before entering the imaging system [3]. In this project, we are designing, fabricating, and testing one S-band (2856.00 MHz) and one C-band (5712.00 MHz) prototype structure, respectively. Both cavities will comprise four cells using distributed coupling. The tests will include low-power characterization at both room temperature and cryogenic temperature, and high-power RF test. The cavity operating frequencies differ from their nominal values due to the unavailability of RF sources at the nominal frequencies.

* Work supported by U.S. Department of Energy through the Laboratory Directed Research and Development program of Los Alamos National Laboratory, under project number 20260012DR.

† haoranxu@lanl.gov

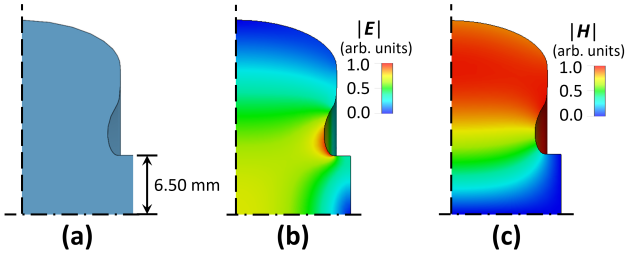

Figure 1: Optimized C-band cell design, with (a) cell profile, (b) normalized E-field distribution, and (c) normalized H-field distribution.

The C-band structure will be tested at LANL, whereas the S-band structure will be fabricated and tested at RadiaBeam Technologies, LLC.

C-BAND CELL DESIGN

The individual cell design for the C-band four-cell cavity was optimized in the code Superfish [4], driven by a Multi-Objective Genetic Algorithm (MOGA) implemented on LANL High-Performance Computing (HPC) clusters [5]. A quarter longitudinal cross section view of the optimized cell design is shown in Fig. 1. The Superfish results were validated in the CST Eigenmode Solver [6], and a summary is provided in Table 1. The cell length, $L_{cell} = 24.38$ mm, is matched to the H^- beam propagation distance over half an RF cycle at 5.712 GHz, at a kinetic energy of 1.6 GeV; the beam aperture radius, $a = 6.50$ mm, was determined taking into account the beam halo.

In the chart, $Z_0 = 120\ \Omega$ is the impedance of free space, and E_{acc} is accelerating gradient. We performed iterative MOGA evaluations and converged to a set of criteria of $E_{pk}/E_{acc} \leq 2.50$, $H_{pk} \cdot Z_0/E_{acc} \leq 1.20$, $\max\{|\mathbf{E}| \cdot |\mathbf{H} \cdot Z_0|/E_{acc}^2\} \leq 2.00$, while maximizing the shunt impedance. In this paper, shunt impedance takes into account particle transit time.

Table 1: Optimized C-band cell eigenmode simulation results in Superfish and CST. Room-temperature (293 K) copper electrical conductivity, 5.8×10^7 S/m, was assumed.

Parameter	Superfish	CST
Resonant frequency [MHz]	5712.44	5710.40
Shunt impedance [MΩ]	1.75	1.74
Unloaded quality factor	12599	12554
E_{pk}/E_{acc}	2.50	2.49
$H_{pk} \cdot Z_0/E_{acc}$	1.16	1.18
$\max\{\lvert\mathbf{E}\rvert \cdot \lvert\mathbf{H} \cdot Z_0\rvert/E_{acc}^2\}$	1.99	1.93

Content from this work may be used under the terms of the CC BY 4.0 licence (© 2026). Any distribution of this work must maintain attribution to the author(s), title of the work, publisher, and DOI.

ISBN: 978-3-95450-252-3 ISSN: 2673-5350 doi: 10.18429/JACoW-IPAC2026-WEP4315

APPLYING MACHINE LEARNING TO LONGITUDINAL PHASE SPACE RECONSTRUCTION IN THE LANSCE CCL*

M. J. Kay†, P. M. Anisimov, C. A. Leon
Los Alamos National Laboratory, Los Alamos, United States

Abstract

Traditional phase scans at LANSCE are useful for tuning longitudinal capture but provide only indirect information about the bunch distribution. This work extends a deep neural network-based reconstruction method to the first two modules of the side-coupled cavity linac. Simulated two-dimensional phase scans were generated with HPSim by varying the RF phases of Modules 5 and 6 and recording the transmitted current after the absorber/collector diagnostic. A retrained network reconstructed correlated Gaussian longitudinal phase space distributions from these scans, recovering their approximate size, orientation, and centroid. These results support further development using realistic distributions and measured CCL phase scans.

INTRODUCTION

The Los Alamos Neutron Science Center (LANSCE) linear accelerator accelerates an H^- beam from 750 keV to 100 MeV in a 201.25-MHz drift tube linac (DTL), and then from 100 MeV to 800 MeV in an 805-MHz side-coupled cavity linac (CCL). Tuning each section of the linac traditionally relies on analyzing empirical observables derived from a sequence of phase scan measurements to verify proper longitudinal capture [1,2]. Although these scans are effective for minimizing beam loss, they provide only indirect information about the longitudinal beam distribution and may obscure features such as distorted bunch shapes or multiple beam cores. To address this limitation, a new method of extracting the longitudinal beam distribution from phase scans has been proposed. This method uses a deep neural network (DNN) to reconstruct the beam distribution from a two-dimensional phase scan (TDPS). This approach was recently demonstrated for the LANSCE DTL using training data generated with the High-Performance Simulator (HPSim) [3,4], where the input beam distribution at the entrance to DTL Module 1 was reconstructed from TDPS data for Modules 1 and 2 [5].

This paper applies the same approach to the first two modules of the LANSCE CCL, Modules 5 and 6. These modules are equipped with an absorber/collector diagnostic similar to that used for DTL phase scans, simplifying the translation of the method to the CCL. As an initial validation, HPSim was used to generate TDPS data for correlated Gaussian input distributions, and a DNN was retrained to reconstruct the longitudinal phase space at the entrance to Module 5. This paper introduces the CCL TDPS, describes its interpretation in terms of longitudinal acceptance, and presents preliminary reconstruction results using synthetic data.

TWO-DIMENSIONAL PHASE SCANS FOR CCL MODULES 5 AND 6

A TDPS is performed by varying the RF phases of two consecutive linac modules while measuring the transmitted beam current at the output. For CCL Modules 5 and 6, this measurement uses the absorber/collector diagnostic located downstream of Module 6. The absorber acts as an energy filter, stopping H^- ions below 121 MeV (96% of the design energy after Module 6), while ions above this threshold are stopped in the collector. The current read from the collector is proportional to the number of H^- ions stopped in the collector and is therefore used as the transmission signal.

By scanning the phases of Modules 5 and 6, the longitudinal acceptance of the CCL is systematically modified. The TDPS produces a map of collector current as a function of the Module 5 phase, ϕ_5, and the relative phase between Modules 6 and 5, $\phi_{65} = \phi_6 - \phi_5$. Figure 1 shows the result of a TDPS simulated in HPSim, in which both ϕ_5 and ϕ_{65} were scanned over 360°. The broad high-current region indicates there is a range of phase settings that provide efficient longitudinal capture. In this simulation, the maximum transmission occurs at $\phi_5 = -137°$ and $\phi_{65} = 90°$.

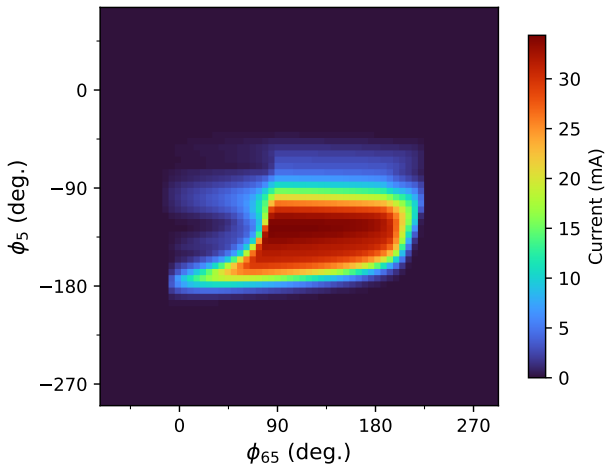

Figure 1: Simulated TDPS for CCL Modules 5 and 6.

The collector current gives a scalar measure of how well the longitudinal acceptance function overlaps with the bunch in phase space. For each phase setting $j = (\phi_5, \phi_{65})$, the CCL and absorber/collector system define an effective longitudinal acceptance function $A_j(\phi, w)$. The collector current

* The research presented in this article was supported by the Laboratory Directed Research and Development program of Los Alamos National Laboratory under project number 20250783MFR.
† mkay@lanl.gov

Content from this work may be used under the terms of the CC BY 4.0 licence (© 2026). Any distribution of this work must maintain attribution to the author(s), title of the work, publisher, and DOI.

ISBN: 978-3-95450-252-3 ISSN: 2673-5350 doi: 10.18429/JACoW-IPAC2026-WEP4317

OVERVIEW OF THE LAMP CONCEPTUAL DESIGN*

K. Bishofberger†, S. Sosa Guitron‡, A. Alexander, A. Braido, G. Dale, D. A. Dimitrov, J. Duran, H. Gaus, D. Gorelov, T. Grumstrup, M. Holloway, S. Kurennoy, J. Lewellen, J. Medina, J. Montross, S. Mosby, C. Rohde, L. Rybarcyk, D. Spernjak, S. Swickley, R. T. Thornton, J. Upadhyay, H. Xu, Los Alamos National Laboratory, Los Alamos, NM, USA

Abstract

The Los Alamos Neutron Science Center (LANSCE) Accelerator Modernization Project (LAMP) will replace the front-end of the aging LANSCE accelerator, specifically to maintain beam delivery to all user stations while improving beam availability and reliability. We present an overview of the LAMP beamline design, including beam physics results, design decisions, and key component capabilities.

PERFORMANCE SUMMARY

Los Alamos Neutron Science Center (LANSCE) is a production accelerator facility, providing both H+ and H– to multiple experimental facilities. Over its 54-year lifetime, reliability has degraded, such as the original Cockroft-Walton injectors and the drift-tube-linac (DTL) tanks.

The LANSCE Moderization Project, LAMP, is a major overhaul of the LANSCE front-end leveraging modern beamline technologies, with reliability and operability as the overarching goals. The project adopts established source technologies, radio-frequency quadrupole (RFQ) acceleration, robust beamline optics, and improved diagnostics [1].

This report summarizes the different beamline sections ('subsystems'), including references to more detailed discussions. Table 1 captures a high-level view of simulation performance, demonstrating that they meet project requirements [2]. Table 1 lists three different beam 'flavors':

- H^+ (IPF): low charge for Isotope Production Facility;
- H^- (Lujan): medium charge mostly for Lujan Center;
- H^- (WNR): high charge for Weapons Research Center.

Other experimental facilities leverage the above flavors with unique timing requirements. For each of these flavors, Table 1 presents the maximum charge Q (in [nC]) per 4.96-nsec window exiting each subsystem. Below this charge is the microbunch's rms normalized transverse emittance (in [μm]). Table 1 quantifies the losses and emittance growth from source to DTL exit in the current design (which has evolved and improved since prior reports [1, 3]).

The final column of Table 1 shows the beam-physics requirement of each flavor. These numbers reflect the amount and quality of each flavor to match current end-station operations. In each case, the LAMP simulations indicate superior charge and emittances. Simulations using lower currents (matching the required charge values exactly) shows even better transmission and emittance.

Table 1: Performance Parameters of Conceptual Design

	Exit of:	Source	LEBT	RFQ	MEBT	DTL	Req
H^+ IPF	Q^*	60	60	59	55	55	25
	ϵ^N_{rms}	0.031	0.039	0.18	0.21	0.29	0.93
H^- Lujan	Q	79	78	77	76	76	53
	ϵ^N_{rms}	0.14	0.24	0.30	0.36	0.44	0.93
H^- WNR	Q	273	254	220	214	213	128
	ϵ^N_{rms}	0.19	0.40	0.45	0.51	0.68	0.93

*units: Q=[nC]; ϵ^N=[μm]

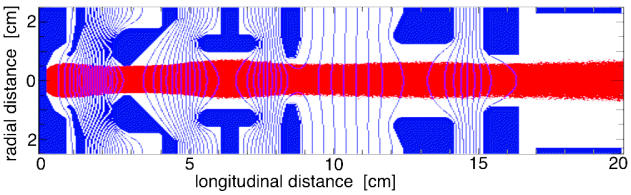

Figure 1: LAMP H^- source electrode geometry and WNR propagation. Lujan is notably different, utilizing different electrode voltages.

SOURCES

LAMP is studying modern source technologies, focusing specifically on technologies that have high reliability given LANSCE's uniquely high 12% duty factor during operation [4]. For H^-, LAMP is considering modeling its source after SNS's highly reliable multi-cusp approach. For H^+, both a duoplasmatron and ECR technologies are being investigated [5].

Independent of the technology, beam simulations launch a beam from a meniscus (using Warp and IBSimu). Figure 1 presents the design's H^- injector, similar to SNS's layout [6], including the high-current WNR beam profile. Lujan beam has different space charge, and thus utilizes different electrode voltages [7].

LOW-ENERGY BEAM TRANSPORT

LAMP's low-energy beam transport (LEBT) is shown in Fig. 2 and discussed in detail elsewhere [7]. The LEBT transports and matches the beam from the sources through multiple choppers, merges the different flavors, enables diagnostics and safety systems, and matches into the RFQ. LAMP requires multiple species and multiple currents, which puts more constraints on the design.

* Work was performed under the auspices of the US Department of Energy by Triad National Security under contract 89233218CNA000001.

† kbish@lanl.gov
‡ salvador@lanl.gov

Content from this work may be used under the terms of the CC BY 4.0 licence (© 2026). Any distribution of this work must maintain attribution to the author(s), title of the work, publisher, and DOI.

ISBN: 978-3-95450-252-3 ISSN: 2673-5350 doi: 10.18429/JACoW-IPAC2026-WEP4318

LAT: A 9-MeV PROTOTYPE "FRONT-END" FOR THE LANSCE ACCELERATOR MODERNIZATION PROJECT

R.T. Thornton*, A. Alexander, K. Bishofberger, C. Buechler, G. Dale, D. Dimitrov, E. Espinoza, H. Gaus, T. W. Hall, M. Halloway, C. Hatch, J. Lewellen, J. T. M. Lyles, J. Medina, M. Sanchez Barrueta, D. Spernjak, S. Swickley, P. Torrez
Los Alamos National Laboratory, Los Alamos, NM, USA

Abstract

The LANSCE Accelerator Modernization Project (LAMP) is designing a modernized front-end, up to 100-MeV, for the LANSCE accelerator. The LAMP front-end will replace the two Cockcroft-Waltons injectors with a single Radiofrequency Quadrupole and replace the Drift Tube Linac (DTL) with a modernized version. As part of the Technical Readiness Evaluation there are Critical Technology Elements (CTEs) that need to be addressed for the project to achieve Critical Decision 3. To address these CTEs and as risk mitigation for an accelerator that is in current operation, we plan to assemble LAMP from ion sources through the first DTL Tank, approximately 9 MeV, in an adjacent facility. This paper discusses the current status and future work of this plan: LAT.

INTRODUCTION

The LANSCE Accelerator Modernization Project (LAMP) is a major initiative managed by Triad National Security, LLC, for the U.S. Department of Energy's National Nuclear Security Administration (NNSA). The project aims to modernize the front end of the LANSCE accelerator complex up to 100 MeV by replacing aging equipment with state-of-the-art components. Key upgrades include replacing two Cockcroft-Walton accelerators with a single modern Radiofrequency Quadrupole (RFQ) and replacing the aging the Drift Tube Linac (DTL).

A distinguishing feature of LANSCE is its capability to simultaneously accelerate and transport two oppositely-charged ion species while supporting five user facilities. Each user facility requires a different beam timing structure. These unique operational requirements present special technical challenges that must be addressed during the modernization effort. To validate critical design elements and reduce technical risk, the LAMP in ADEF Tunnel (LAT) prototype accelerator is being constructed in the Accelerator Development and Engineering Facility (ADEF) to serve as a 9 MeV full-scale prototype and testing platform.

LAMP BASELINE DESIGN VERSION 2

The LAMP baseline design (version 2) [1–7], as seen in Fig. 1 encompasses a comprehensive front-end replacement that fits within the existing LANSCE infrastructure space constraints. The design leverages proven technologies while incorporating innovations necessary for dual-species operation.

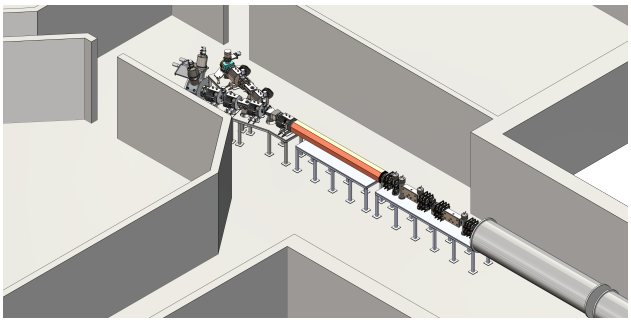

(a) LAMP "front-end" showing RFQ and first DTL cavity.

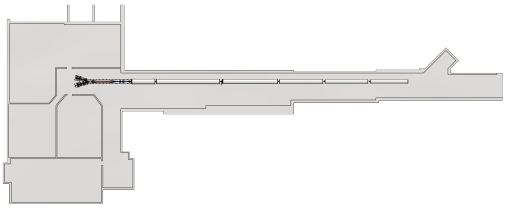

(b) Entire LAMP layout in the LANSCE tunnel.

Figure 1: LAMP baseline v2 front end (a) zoomed in and (b) layout through the DTL tanks in the LANSCE tunnel.

The design extracts the H^+ and H^- beams to 65 keV and merges them together in the Low Energy Beam Transport (LEBT) region before using a single RFQ to accelerate both beams to 2.1 MeV. The beams are then transported through a Medium Energy Beam Transport (MEBT) region before capture in the DTL which accelerates the beams to 100 MeV.

CRITICAL TECHNOLOGY ELEMENTS

Four Critical Technology Elements (CTEs) have been identified that require maturation from Technical Readiness Level (TRL)-5 to TRL-7 to ensure LAMP project success and meet Department of Energy requirements to achieve Critical Decision 3. These elements, MEBT chopper, simultaneous dual-beam acceleration of opposite charged beams in an RFQ, transport of dual beams through a single MEBT post RFQ, and pulsed focusing electrodes, address the unique operational requirements of LANSCE. The following is a summary of Ref. [8].

* rtthorn@lanl.gov

Content from this work may be used under the terms of the CC BY 4.0 licence (© 2026). Any distribution of this work must maintain attribution to the author(s), title of the work, publisher, and DOI.

ISBN: 978-3-95450-252-3 ISSN: 2673-5350 doi: 10.18429/JACoW-IPAC2026-WEP4319

PERFORMANCE BOUNDARIES IN THE NOVEL MULTI-BEAM LANSCE FRONT END

Y. Batygin, H. Salazar, T. Tajima, Los Alamos National Laboratory, Los Alamos, NM, USA

Content from this work may be used under the terms of the CC BY 4.0 licence (© 2026). Any distribution of this work must maintain attribution to the author(s), title of the work, publisher, and DOI.

Abstract

The proposed 100 MeV injector is designed to renovate LANSCE accelerator facility by replacing the 750-keV Cockcroft-Walton injectors, supporting its unique function of delivering multiple, simultaneous beam flavors to several targets. Accelerating multiple beam types in a single RFQ at LANSCE restricts the ability to tune acceleration optimally and focusing due to inherent differences in beam properties (current, charge per bunch, emittance). Strong beam space charge forces induce coupling between degrees of freedom, leading to an unavoidable mismatch in the Front End that necessitates careful six-dimensional matching with accelerator structures. Unavoidable transients of beam chopping in Low Energy Beam Transport result in the development of satellite bunches after the 3-MeV RFQ accelerator and force the removal of these using a sophisticated chopper system after the RFQ. The paper addresses critical challenges within the proposed Front End and advances solutions for their mitigation.

INTRODUCTION

LANSCE linear accelerator consists of a 201.25 MHz Drift Tube Linac (DTL) accelerating particles from 0.75 MeV to 100 MeV and an 805 MHz Coupled-Coupled Linac (CCL), accelerating particles from 100 MeV to 800 MeV [1]. This facility employs multi-pass, high-duty-cycle operation to deliver varied particle beams simultaneously to multiple experimental stations. A 100 MeV proton beam is delivered to the Isotope Production Facility (IPF), while 800 MeV H^- beams are distributed to four experimental areas: the Lujan Neutron Scattering Center, the Weapons Neutron Research facility (WNR), the Proton Radiography facility (pRad), and the Ultra-Cold Neutron facility (UCN). Time structures of the beam are presented in [2]. To mitigate long-term operational risks and achieve future performance goals for laboratory missions, a novel Front End featuring a high-brightness RFQ-based injector was developed, see Fig. 1. The detailed description of the proposed Front End is given in Refs. [2-4].

SUPPRESSION OF SPACE CHARGE NEUTRALIZATION IN LEBT

The novel Front End differs primarily from the existing one by featuring space charge-dominated beam dynamics within the Low Energy Beam Transport (LEBT). A key challenge in this new injector design is managing the distinct space charge neutralization of the low-energy beams. The estimated time for a 100 keV beam to ionize the residual gas at the given pressure of 10^{-6} Torr is 56 μs [5]. With a pulse duration of 625 μs, the Lujan beam achieves full space charge neutralization. Because the WNR beam consists of short, single bunches separated by long 1.8 μs intervals, it will not undergo space charge neutralization. To minimize beam dynamics variations in the LEBT across different beam types, space charge neutralization must be eliminated. Maintaining a deep vacuum of at least 10^{-8} Torr achieves this.

Figure 2 illustrates a simulation of deep vacuum conditions in LEBT using the Molflow code [6]. Pumping is performed at the six pump-out ports with a 1000 L/s pump on each port. Within a beamline of diameter 8 cm, and an outgassing rate of $7{\cdot}10^{-11}$ mbar·L/s·cm^{-2}, which is a typical outgassing rate after pumping down a stainless steel beamline for ~33 hours [7], the achieved vacuum pressure is between $1.4{\cdot}10^{-8}$ Torr and $2.2{\cdot}10^{-8}$ Torr.

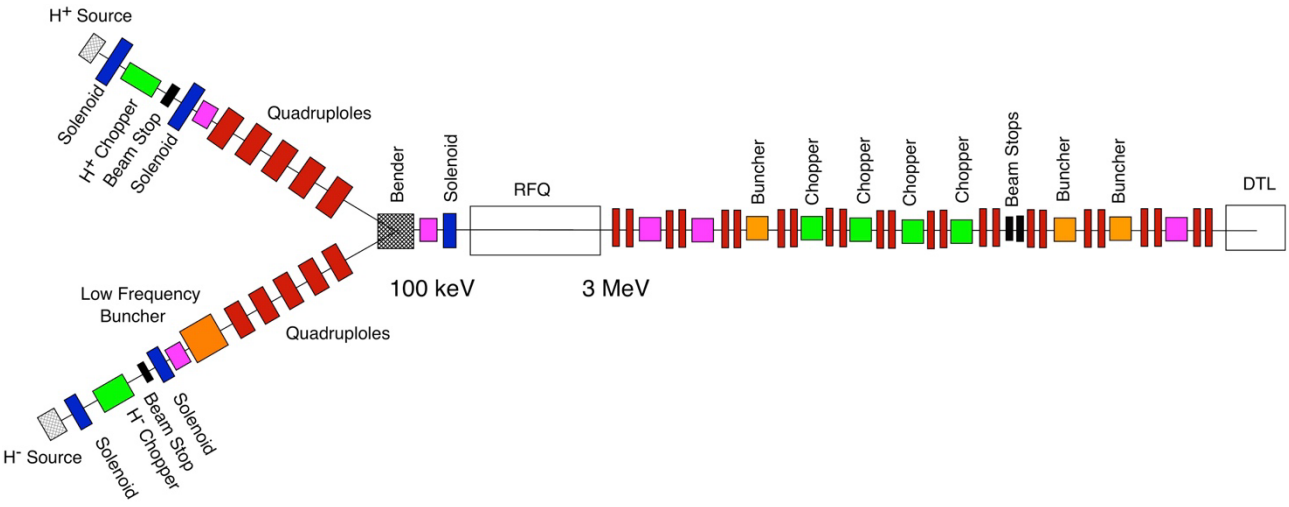

Figure 1: Layout of the proposed LANSCE Front End with distributed beam chopping.

ISBN: 978-3-95450-252-3 ISSN: 2673-5350 doi: 10.18429/JACoW-IPAC2026-WEP4320

HIGH-GRADIENT BOOSTER LINAC FOR MULTI-GeV PROTON RADIOGRAPHY AT LANSCE

S. S. Kurennoy, Y. K. Batygin, H. Xu
Los Alamos National Laboratory, Los Alamos, NM, USA

Abstract

Increasing energy of proton beam at the Los Alamos Neutron Science Center (LANSCE) from 800 MeV to 3-5 GeV will improve radiography resolution ten-fold. This energy boost can be achieved with a compact cost-effective linac based on normal-conducting high-gradient (HG) RF accelerating structures operating at liquid nitrogen temperatures (cryo-cooled). Such an HG booster is feasible for proton radiography (pRad), which requires short beam pulses at very low duty. The pRad booster starts with a short L-band section to capture and compress the 800-MeV proton beam from the existing linac. The main HG linac will be based on S- and C-band cavities. An L-band debuncher at the booster end can reduce the beam energy spread if needed for pRad experiments. We are developing proton cryo-cooled HG standing-wave structures with distributed RF coupling for the booster. Prototype cavity structures at S- and C-band are designed and will be tested cryo-cooled to measure breakdowns at high gradients. The booster linac beam dynamics design is also discussed.

INTRODUCTION

Proton radiography (pRad) was invented at LANL in the 1990s. It employs high-energy proton beams to image material behavior under extreme conditions. Since then, the pRad program at the Los Alamos Neutron Science Center (LANSCE) has performed hundreds of successful experiments, both static and dynamic. The LANSCE pRad now uses 800-MeV H^- beam. For dynamic experiments, multiple pulses from the linac produce movies up to a few tens of frames. Each short pRad beam pulse consists of several successive bunches from the linac, which follow at the linac DTL repetition rate of 201.25 MHz, to multiply the pulse total intensity. This is because the H^- bunch current at 800 MeV is limited to ~10 mA, mainly by the ion source, but also by losses in the linac. On the other hand, the pRad pulses are restricted to 80 ns in length, i.e., contain no more than 16 linac bunches following with 201.25-MHz repetition frequency, to prevent image blur, e.g., see Ref. [1].

Increasing the beam energy for pRad at LANSCE from present 800 MeV to 3-5 GeV would provide significant improvements: for thin objects, the radiography resolution will increase about 10 times, and much thicker objects can be also imaged. We aim to develop the most efficient way to provide proton beams at energies of 3-5 GeV for enhanced proton radiography at LANSCE. A high-gradient (HG) proton booster linac after the existing LANSCE linac offers a viable cost-efficient solution [2]. Its potential location is shown in Fig. 1; the booster (red line) will be much shorter than the existing linac. The booster linac will be based on normal-conducting RF accelerating structures operating cryo-cooled at liquid-nitrogen (LN2) temperature, 77K, at very low duty required for pRad.

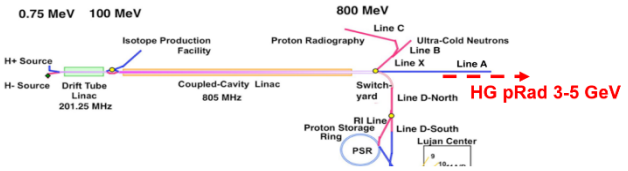

Figure 1: Location of the pRad booster linac (red dashed line) at LANSCE. The existing linac is on the left.

The Laboratory Directed Research and Development (LDRD) program at LANL supported our work on the HG pRad booster as an Exploratory Research (ER) project in 2021-2023. The ER results were presented in [2-4] and summarized in [5]. A larger LDRD Directed Research (DR) project started in Oct. 2025 with the main goal to develop accelerator technology of cryo-cooled HG structures for protons applicable to the pRad booster at LANSCE.

HIGH-GRADIENT PRAD BOOSTER

Requirements for pRad Booster

High-gradient structures for relativistic electrons with velocity $\beta = v/c = 1$ demonstrated accelerating gradients $E_{acc} = E_0 T$ up to 150 MV/m in X-band copper cavities at room temperature [6]. Here E_0 means the average on-axis electric field in the structure cell and T is transit-time factor. When such cavities are operated at cryogenic temperatures (cryo-cooled), gradients up to 250 MV/m were achieved. HG C-band cavities at room temperature provide gradients 50-60 MV/m, but at LN2 temperature one can expect gradients two times higher. 800-MeV protons at the exit of the LANSCE linac have velocity $\beta = 0.84$; at 5 GeV $\beta = 0.987$. Therefore, HG cavities must be modified for protons to cover this velocity range. HG structures for pRad booster must accept the large proton bunches out of the existing linac both longitudinally – this limits RF frequency from above – and transversely, which limits the cavity aperture from below. High accelerating gradients lead to beam defocusing by RF fields, so strong focusing is required. For good quality radiographs, it is important to control the relative momentum spread of the beam. It is $\Delta p/p = 10^{-3}$ at the exit of our 800-MeV linac, and in [2] the beam dynamics design reduced it as $1/p$, i.e., to $3.3 \cdot 10^{-4}$ at 3 GeV. However, this requirement depends on specific pRad experiment.

Operating the HG pRad booster at 77K makes structures more efficient and reduces the required RF power by a factor of 2-3. In addition, it is expected that the RF breakdown rates are reduced in cryo-cooled cavities, though the data for C- and S-band is insufficient. One of our goals is to get

Content from this work may be used under the terms of the CC BY 4.0 licence (© 2026). Any distribution of this work must maintain attribution to the author(s), title of the work, publisher, and DOI.

ISBN: 978-3-95450-252-3 ISSN: 2673-5350 doi: 10.18429/JACoW-IPAC2026-WEP4322

PERSPECTIVE ON PROCUREMENTS OF MAJOR COMPONENTS FOR THE LANSCE ACCELERATOR MODERNIZATION PROJECT (LAMP)

D. A. Dimitrov*, R. Lujan, H. Xu, D. Gorelov, T. Grumstrup, R. Roquemore, T. Hartzell, L. Rybarcyk, S. Kurennoy, D. Dominguez, J. Montross, J. Medina, J. Lyles, M. Barrueta, M. Gulley, M. Pieck, M. Holloway, M. Johnson, M. Bowman, R. Thornton, S. Herrera, W. Hall, S. Swickley, J. Lewellen, G. Dale
Los Alamos National Laboratory, Los Alamos, New Mexico, USA

Abstract

The Los Alamos Neutron Science Center (LANSCE) accelerator delivers different beams to multiple experimental stations simultaneously. These beams have different intensity and time structure. The LANSCE Accelerator Modernization Project (LAMP) seeks to upgrade the technology in the front-end while preserving the unique capabilities of LANSCE. LAMP seeks to replace the two 750-keV Cockroft-Waltons with a single Radio Frequency Quadrupole (RFQ), and a new 100-MeV Drift Tank Linac (DTL). Procurements represent a significant portion of the project's funding and drive schedule decisions. We discuss the process to procure major accelerator components for LAMP with our initial focus on the acquisition of the RFQ and the first tank of the DTL.

INTRODUCTION

The accelerator complex now known as the Los Alamos Neutron Science Center (LANSCE) began operation in 1972 as LAMPF, the Los Alamos Meson Production Facility. In the intervening 53 years, the complex has been expanded in capability several times, both in terms of its accelerator performance and the user facilities it supports.

Today, the LANSCE accelerator is unique in the world both for its ability to concurrently accelerate two beam species, H^+ and H^-, and to support simultaneous user operations at five separate facilities [1]: the Isotope Production Facility, the Lujan Neutron Scattering Center, the Weapons Neutron Research facility, Proton Radiography, and the Ultracold Neutron source. LANSCE also supports specific run modes enabling direct access to the 800 MeV proton beam for diagnostic development, space-radiation testing, and other applications. The LANSCE complex supports a wide variety research critical to the US national security, the broader neutron-based research community, and the national medical isotope program.

Although various aspects of the LANSCE accelerator complex have been upgraded and enhanced over the preceding five decades, the linear accelerator structures themselves are essentially unchanged from their initial installations. In recent years, it has become apparent that the 750 keV Cockcroft-Walton (C-W) based injectors and 100 MeV drift-tube linac (DTL), in particular, have reached the end of their service lives.

The LANSCE Accelerator Modernization Project (LAMP) will replace the "front end" of the LANSCE accelerator, from the ion sources [2] through the end of the DTL, to ensure operation of the facility through at least 2050.

The LAMP conceptual design [3] is based on the use of modern accelerator design approaches and structures, many of which have evolved considerably since the inception of LAMPF. The LAMP DTL, for instance, will incorporate permanent-magnet quadrupole focusing and in-tank diagnostics such as beam current and position monitors. A radio frequency quadrupole (RFQ) accelerator will be used to accelerate the beams from the ion sources for injection into the DTL.

The project has a strategy for efficient execution reflected in its schedule shown in Fig. 1. We have developed an approach for phased early procurements timed to coincide with design maturity, prototyping, removal and installation to meet the schedule. The critical path, shown with red line segments in Fig. 1, indicates the essential role of procurements, in particular large and long-lead ones, to meet the schedule.

Technology development represents one of the two main thrusts of the project. The project has performed an initial internal assessment of Critical Technology Elements (CTEs) and is planning appropriate technology maturation efforts. Technology maturation areas include high-performance beam chopper development, the RFQ Test Stand (RFQTS), and the LAMP in the ADEF (Accelerator Development and Engineering Facility) Tunnel (LAT) demonstration accelerator.

For LAT, we will construct through the first DTL tank in the ADEF tunnel for CTE demonstration and pre-commissioning activities. The LAT test stand effectively represents the new LANSCE front end up to the first DTL tank. A three-dimensional (3D) solid model of the LAMP beam line conceptual design up to (a portion) of the first DTL tank is shown in Fig. 2.

Here, we discuss our approach to procure major accelerator components for LAT and focus on the RFQ and the DTL first tank procurements.

WE USE A TEAM APPROACH TO PROCUREMENTS

At the Los Alamos National Laboratory (LANL), LAMP is an institutional priority and is supported as such by

* dandd@lanl.gov

Content from this work may be used under the terms of the CC BY 4.0 licence (© 2026). Any distribution of this work must maintain attribution to the author(s), title of the work, publisher, and DOI.

ISBN: 978-3-95450-252-3 ISSN: 2673-5350 doi: 10.18429/JACoW-IPAC2026-WEP4324

MATCHING OF CRYSTALLINE BEAMS INTO THE BNL BOOSTER*

S.J. Brooks†
Brookhaven National Laboratory, Upton, NY, USA

Abstract

A method has been developed to match large three-dimensional Coulomb crystals into existing accelerators. Simulations show bunch temperatures below 1 Kelvin persisting for thousands of turns in the BNL Booster and for tens of thousands of turns in an idealised ring (both with no cooling). Focussing forces balance space charge to give zero net phase advance and the crystal structure can be preserved for tens of milliseconds. Magnetic focussing confines all three dimensions of the bunch without RF, since the bunch rotation in the ring plane is not at the ring revolution frequency. A zero temperature, uniformly-filled ellipsoid of charge gives a 15-parameter model that can be used for matching and linear stability analysis.

BOOSTER FIELD MODEL

The calculations that follow require a 3D Maxwellian field model of the booster that is free from discontinuities near the beam orbit. The basic superperiod lattice from [1] was implemented, which contains identical bending dipoles 2.4 m long and F and D quadrupoles 0.50375 m long.

In a local coordinate frame where (0,0,0) is the centre of the dipole arc, z is the beam direction and y is vertical, the dipole field is given by calculating

$$\begin{aligned} t_y &= \tan(y/f) \\ t_{z\pm} &= \tanh((\pm z\cos\tfrac{\theta}{2} + (\tfrac{L}{\theta} - x)\sin\tfrac{\theta}{2})/f) \\ t_{r\pm} &= \tfrac{1}{2}t_{z\pm}(1+t_y^2)/(1+t_y^2t_{z\pm}^2) \\ t_{i\pm} &= \tfrac{1}{2}t_y(1-t_{z\pm}^2)/(1+t_y^2t_{z\pm}^2) \\ \mathbf{B}_1 &= (-(t_{i+}+t_{i-})\sin\tfrac{\theta}{2}, t_{r+}+t_{r-}, (t_{i+}-t_{i-})\cos\tfrac{\theta}{2}), \end{aligned}$$

where L, θ are the dipole length and angle and f=0.15 m determines the fringe field length. The fringe field is shaped like $\frac{1}{2} + \frac{1}{2}\tanh(z/f)$ and the formulae for $t_{r,i\pm}$ come from the complex components of $\tanh(z+iy)$. $\mathbf{B}_1$ is the field of a unit strength dipole, in general it is scaled to $\mathbf{B} = B_{\text{dip}}\mathbf{B}_1$.

A quadrupole with soft ends does not have an analytic formula, so the series expansion in [2] is used with a fringe field function again shaped like $\frac{1}{2} + \frac{1}{2}\tanh(z/f)$. For the quadrupoles, f=0.05 m and the series is calculated up to and including the r^{10} term.

Placing these field models and adding them together, with appropriate transverse extent limits that the beam does not encounter, gives the field illustrated in Fig. 1.

* Work supported by Brookhaven Science Associates, LLC under Contract No. DE-SC0012704 with the U.S. Department of Energy.
† sbrooks@bnl.gov

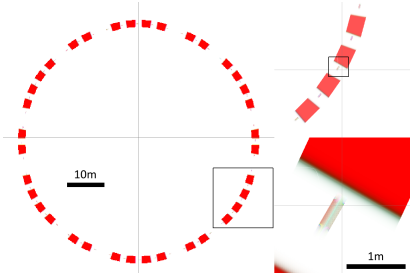

Figure 1: Booster field map with successive zooms (top, bottom right), the small magnet is a quadrupole.

MATCHING METHOD

Repulsive space charge forces dominate the dynamics of Coulomb crystals, while velocity spread and emittance are near zero. Thus, the bunch is modelled as a uniform ellipsoid of charge with zero temperature, parametrised as shown in Fig. 2. The ellipsoid is defined by its centroid $\mathbf{s} = \langle(\mathbf{x}, \mathbf{v})\rangle$, covariance matrix $C = \langle\delta\mathbf{x}\delta\mathbf{x}^T\rangle$ and velocity distribution V where $\delta\mathbf{v} = V\delta\mathbf{x}$. Space charge forces are linear within a uniform charged ellipsoid [3–5], so this form is preserved if external forces are also linear. The centroid $\mathbf{s}$ evolves as a single particle while the 15 parameters (C, V) have time derivatives calculated in [6]. This model does not capture higher-order vibrational motion or phonons.

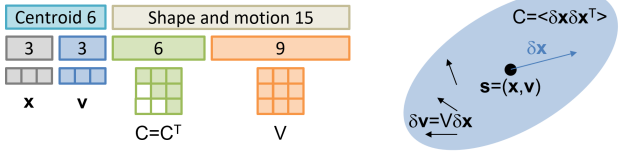

Figure 2: Parameters of the ellipsoid bunch model.

A matched solution for a ring would have $(\mathbf{s}, C, V)_{\text{in}} = (\mathbf{s}, C, V)_{\text{out}}$ over a single turn. In this paper $(\mathbf{s}, C, V)$ are integrated with 4th order Runge–Kutta steps and $\delta t = (8\,\text{mm})/v_{\text{bunch}}$. The centroid dynamics are independent, so the closed orbit with $\mathbf{s}_{\text{in}} = \mathbf{s}_{\text{out}}$ can be found fairly standardly using multi-variable Newton iteration, taking care to find t_{out} that stops the particle exactly at the end of the turn. A similar iteration with 15 variables can also solve $(C, V)_{\text{in}} = (C, V)_{\text{out}}$ and the first derivatives of the mapping are used to obtain an eigenvalue stability analysis [7]. There are, however, some computational and physics issues. If numerical derivatives are used, step sizes in each variable must be chosen carefully as C and V have different units. A slightly enhanced Newton's method [8,9] is used here, which also evaluates the mean square error, so units for the parameter and goal vectors are chosen to make C and V similar magnitude. A second issue is that for some lattices, V tends to infinity after a few cells because one of the ellipsoid's axes tries to invert. Unintuitively, the model passes through

Content from this work may be used under the terms of the CC BY 4.0 licence (© 2026). Any distribution of this work must maintain attribution to the author(s), title of the work, publisher, and DOI.

ISBN: 978-3-95450-252-3 ISSN: 2673-5350 doi: 10.18429/JACoW-IPAC2026-WEP4329

REQUIREMENTS EVOLUTION FOR THE LANSCE ACCELERATOR MODERNIZATION PROJECT (LAMP)*

J. Lewellen†, A. Alexander, K. Bishofberger, G. Dale, D. Dimitrov, H. Gaus, M. Holloway, J. Medina, S. Mosby, D. Spernjak, S. Swickley, R. Thornton,
Los Alamos National Laboratory, Los Alamos, United States

Abstract

The Los Alamos Neutron Science Center (LANSCE) consists of an 800 MeV dual-species (H+ and H-) accelerator serving five separate user facilities, each of which can concurrently receive unique beam delivery patterns tailored for their specific requirements. The LANSCE Accelerator Modernization Project (LAMP) will replace the front-end of the 50-year-old LANSCE accelerator, from ion sources through the end of the 100 MeV drift-tube linac, with the goals of maintaining beam delivery capabilities to all user stations while improving reliability and supporting increased operating hours. These goals drive requirements for the LAMP upgrade project as a whole, and flow down into performance specifications for individual subsystems down to the component level.

INTRODUCTION

In recent years a number of large accelerator user facilities have undertaken significant upgrades and modifications to their facilities. The LANSCE facility is among them: the LANSCE Accelerator Modernization Project (LAMP) [1] will replace the current "front end" of the LANSCE accelerator, ion sources through the end of the 100-MeV drift tube linac.

There are several differences between LAMP and most other projects of similar scale, both in terms of overall scope and of intent. First, LAMP is, as the name indicates, a modernization, not an upgrade. The difference is that LAMP's requirements do not generally incorporate a significant increase in beam delivery performance to the LANSCE user stations. LAMP must, however, maintain existing beam delivery performance to all LANSCE user facilities – concurrent delivery of specifically tailored beam formats to five separate facilities.

Second, LAMP's scope encompasses only a fraction of the LANSCE accelerator complex, specifically the sources through the drift-tube linac (see Fig. 1). It does not include the cavity-coupled linac, downstream beam transport lines,

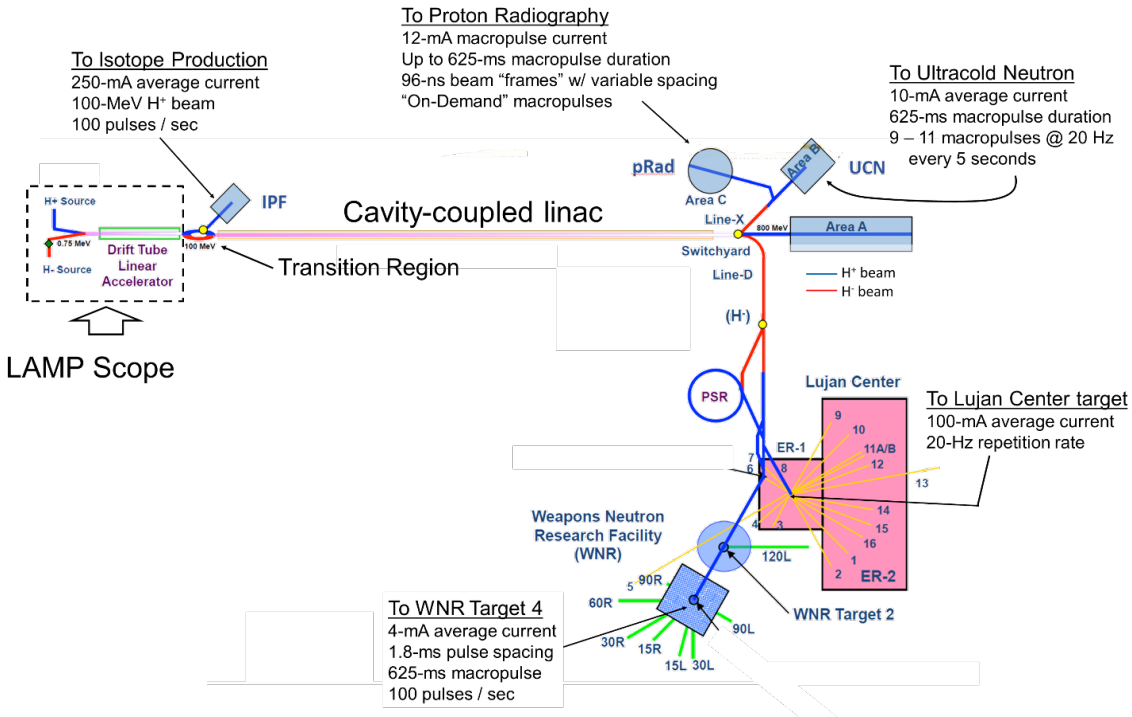

Figure 1: Overview of the LANSCE user facilities, example beam delivery requirements, and LAMP scope.

* Work was performed under the auspices of the US Department of Energy by Triad National Security under contract 89233218CNA000001 LA-UR-26-23706

† jwlewellen@lanl.gov

Content from this work may be used under the terms of the CC BY 4.0 licence (© 2026). Any distribution of this work must maintain attribution to the author(s), title of the work, publisher, and DOI.

ISBN: 978-3-95450-252-3 ISSN: 2673-5350 doi: 10.18429/JACoW-IPAC2026-WEP4331

ERROR AND SENSITIVITY STUDIES FOR LANSCE ACCELERATOR MODERNIZATION PROJECT*

S. Sosa Guitron, K. Bishofberger, G. Dale, D. Dimitrov, B. Garnett, D. Gorelov, S. Kurennoy, J. Lewellen, L. Rybarcyk, J. Upadhyay, H. Xu, LANL, Los Alamos, USA

Abstract

The LANSCE Accelerator Modernization Project (LAMP) aims to modernize the existing LANSCE front-end technologies. Two existing 750 keV Cockcroft Waltons are planned to be replaced by a single radio-frequency quadrupole (RFQ), and a new 100 MeV DTL will be installed. The new LAMP front-end is required to deliver beams with similar timing patterns to what is currently delivered to the experimental stations. Using the physics model of the LAMP front-end, we evaluate errors and sensitivities of multiple transport components and study the effect on the beam intensity and timing.

INTRODUCTION

The LANSCE accelerator facility at LANL has delivered high-power beams to multiple experimental facilities for over 50 years. Critical components in the facility front-end like the Cockcroft Walton (CW) generators are difficult to service or have already required major repairs like the Drift Tube Linac (DTL). To keep the unique beam capabilities that LANSCE provides in years to come, the LANSCE Accelerator Modernization Project (LAMP) [1] plans to replace the two 750 kV CWs with a single RFQ and to install a new 100 MeV DTL. The new front-end will match into existing facilities at the end of the DTL. With these configuration changes, the new injectors, low-energy beam transport (LEBT), and medium-energy beam transport (MEBT) lines need to produce the same beam patterns that LANSCE can currently deliver. We have developed a physics design concept for the front-end that meets the LAMP project requirements [2]. We are now studying the errors and tolerances to evaluate the feasibility of the ideal design under more realistic conditions. In this paper we describe our approach at studying errors and tolerances in the LAMP front-end and discuss preliminary results on applying errors to the LEBT.

Low Energy Beam Transport

The 65 keV LEBT transports both H^+ and H^- beams from the injectors to the RFQ and consists of two independent beam lines that merge at a 30° included angle for injection into the RFQ. The LEBT has solenoids for transverse beam focusing and beam choppers to produce the different temporal structures required by the experimental stations. Figure 1 shows a preliminary mechanical layout of the LAMP LEBT concept and Fig. 2 shows the rms envelope of the Lujan beam in the H^- LEBT using the LANL particle code PARMILA [3]. The Lujan beam is the beam to the Lujan Neutron Science Center target that is accumulated in the Proton Storage Ring.

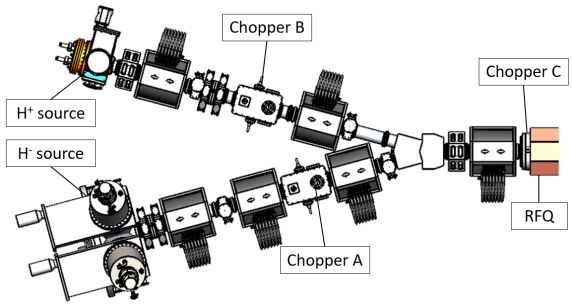

Figure 1: Preliminary mechanical layout of the 65-keV low energy beam transport concept for LAMP.

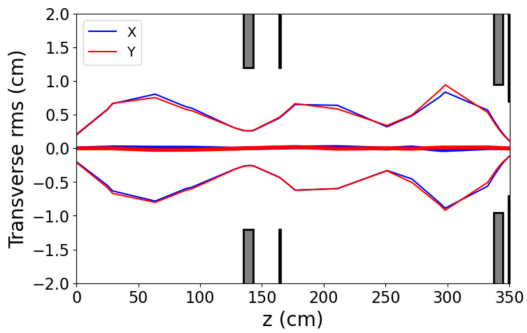

Figure 2: Transverse rms envelopes of the Lujan beam in the LAMP LEBT using PARMILA.

ERROR STUDIES

The purpose of the error studies is to determine tolerances on manufacturing, alignment and field errors in accelerator facilities [4]. This quantifies the average magnitude of error or a given type that can be tolerated before beam quality or other performance metric is unacceptably degraded. For LAMP, we plan to first study the effect of errors applied to individual sections: sources, LEBT, RFQ, MEBT and DTL. Integrated studies using the per-section error thresholds will then be conducted via start-to-end simulations. Ultimately, because the LAMP front-end matches into the 800 MeV cavity coupled linac, the tolerance on errors in all the sections should produce a beam within the acceptance of the LANSCE Linac [5]. Here we are starting to investigate static errors in the LEBT, mainly mechanical alignment and displacements, roll angle and errors in the magnetic field amplitudes. One potential consequence of degraded beam quality is an increase of beam loss, which can damage the accelerators and transport lines, as well as radioactivation concerns at high

* This work benefitted from the use of the LANSCE accelerator facility. Work was performed under the auspices of the US Department of Energy by Triad National Security under contract 89233218CNA000001.

Content from this work may be used under the terms of the CC BY 4.0 licence (© 2026). Any distribution of this work must maintain attribution to the author(s), title of the work, publisher, and DOI.

ISBN: 978-3-95450-252-3 ISSN: 2673-5350 doi: 10.18429/JACoW-IPAC2026-WEP4332

THE LANSCE ACCELERATOR MODERNIZATION PROJECT FRONT-END PHYSICS DESIGN AND MODEL*

S. Sosa Guitron, K. Bishofberger, G. Dale, D. Gorelov, J. Lewellen, J. Montross, L. Rybarcyk, R. Thornton, J. Upadhyay, H. Xu, Los Alamos National Laboratory, Los Alamos, United States

Content from this work may be used under the terms of the CC BY 4.0 licence (© 2026). Any distribution of this work must maintain attribution to the author(s), title of the work, publisher, and DOI.

Abstract

The Los Alamos Neutron Science Center (LANSCE) accelerator at Los Alamos National Laboratory (LANL) delivers different beams to multiple experimental stations simultaneously. These beams have different intensity and time structure. The LANSCE Accelerator Modernization Project (LAMP) seeks to upgrade the technology in the front-end while preserving the unique capabilities of LANSCE. LAMP seeks to replace the two 750 keV Cockcroft-Waltons with a single RFQ, and a new 100 MeV DTL. New low-energy and medium-energy beam transport lines are necessary to produce the required LANSCE beam patterns. This contribution describes design process and the current state of the LAMP front-end physics model.

INTRODUCTION

The LANSCE accelerator facility at LANL is a pulsed radiofrequency accelerator that can produce and deliver multiple beam "flavors" with different intensity and temporal structure, simultaneously, to five different experimental facilities [1]:

- Isotope Production Facility (IPF) target receives 250 μA of H^+ beam at 100 Hz.
- Lujan Neutron Science Center (Lujan) target receives a 625 μs macro-pulse that is accumulated in the Proton Storage Ring (PSR) into a 290 ns pulse. The beam repetition rate is 20 Hz.
- Two other experimental stations receive the Lujan macro-pulse without accumulation in the ring, with different bunch train patterns and on a single-shot mode.
- Target 4 receives a single H^-, 1 ns high-intensity bunch every 1.8 μs for the duration of a 625 μs macro-pulse, the repetition rate is 100 Hz and travels in the same machine cycle as the H^+ beam through 100-MeV.

The existing 750 keV LEBT takes two beam species: H^+ and H^-, out of the 750 kV Cockcroft Walton (CW) generators and uses a combination of a beam chopper and radiofrequency cavities to produce this diverse set of beams. Two 201.25 MHz buncher cavities help accumulate dc beam into the phase acceptance of the DTL, and a 16.77 MHz cavity helps create the high-intensity pulse for Target 4. LANSCE has been in operations since 1972 and critical components are aging systems that are becoming hard to maintain due to lost expertise or simply lack of spares that are no longer fabricated. To maintain the unique capabilities of LANSCE in years to come, the LANSCE Accelerator Modernization Project (LAMP) plans to modernize the facility critical components [2]: replacing the two CWs with a single RFQ, the new standard for ion beam facilities, and installing a new 100 MeV DTL. The new front-end must match into the existing facilities at the end of the DTL. With these configuration changes, the new LAMP front-end is required to produce each of the beams that are currently delivered to target areas. This paper describes the state of the physics design and model of the LAMP front-end and how it meets some of the most critical beam parameters at the end of the front-end concept.

PHYSICS MODEL

To model the new LAMP front-end, we have adopted a suite of accelerator codes that have been widely benchmarked by the community. Individual codes are selected to better capture the dynamics of individual sections of the front-end, but the same particle distributions are propagated through all the codes. In the design phase, we use the envelope codes Trace2D [3] and Trace3D [4] to design the low-energy beam transport (LEBT) and medium-energy beam transport (MEBT) lines. PARMTEQ-m [5] is used to design the RFQ, and PAR-MILA [6] is used to design the DTL, all LANL codes. Trace has proven to be particularly useful in finding compromised solutions to magnet settings that enable the transport of multiple beams.

For simulations with particles, the H^+ and H^- ion injectors are modelled in Warp [7] using available mechanical drawings. The LEBT simulation is done in Impact-t [8] and PARMILA, where Impact-t was first used to determine the required pulse length that preserves the high-current at the center of the pulse when producing the Target 4 beam, and then PARMILA calculates the dynamics at the center of the pulse. The RFQ vein geometry is exported to CST Particle Studio [9] for PIC simulations. The MEBT and DTL are also modelled in PARMILA. Multiple handovers of particle distributions are required when interfacing different codes, these are handled via Python scripts. Below we will describe each section of the front-end using the Target 4 beam as an example.

Injector Systems

The LAMP front-end assumes two 65 keV ion sources: one for H^+ beam and one for H^- beam. The beam physics modelling of the H^+ extraction electrodes is based on the LEDA injector that was in operation at LANL [10]. The H^- ion source is based on the SNS H^- source [11], with modifications to the electrostatic LEBT. This change is motivated by the extraction of dual H^- beam currents out of the

* This work benefitted from the use of the LANSCE accelerator facility. Work was performed under the auspices of the US Department of Energy by Triad National Security under contract 89233218CNA000001.

ISBN: 978-3-95450-252-3 ISSN: 2673-5350 doi: 10.18429/JACoW-IPAC2026-WEP4333

ACCELERATING THROUGH PARTIAL SNAKE RESONANCES WITH BETATRON COUPLING SPIN RESONANCE COMPENSATION

V. Schoefer*, L. Hajdu, K. Hock, H. Huang, J. Laster, W. Lin, K. Zeno
Brookhaven National Laboratory, Upton,NY, USA
E. Hamwi, Cornell University (CLASSE), Ithaca, NY, USA

Abstract

Partial Siberian snakes are used at the Brookhaven Alternating Gradient Synchrotron (AGS) to avoid strong vertical spin resonances during acceleration of polarized proton beam from 2.5 to 23 GeV. An unfortunate side effect is that these snake magnets excite numerous weak resonances associated with the horizontal betatron motion. We present experimental demonstration and operational experience of the compensation of these resonances during acceleration by exciting betatron coupling with a set of 15 pulsed skew quadrupoles.

POLARIZED BEAM ACCELERATION IN AGS

The AGS at Brookhaven National Laboratory served as the injector for the Relativistic Heavy Ion Collider (RHIC) for the entirety of the RHIC physics program, which recently concluded in February 2026 [1]. It will continue to be the injector for the planned Electron Ion Collider for all hadron species including polarized protons and helium-3.

Polarization of proton beam is preserved in the AGS mainly by use of a pair of helical dipole partial snakes, separated by 1/3 of the ring circumference, that rotate the proton spin about the longitudinal direction by 18°and 10.8°, respectively. These magnets allow avoidance of the strongest depolarizing resonances associated with the vertical beam motion. In the presence of horizontal betatron motion, however, partial snakes can themselves drive numerous weak horizontal intrinsic resonances which collectively can lead to substantial polarization loss. Polarized protons are accelerated in the AGS from $G\gamma = 4.5$ to 45.5 which requires passing through 82 horizontal intrinsic resonances where $G\gamma = N \pm \nu_x$ (G is the anomalous gyromagnetic ratio, γ the relativistic factor and N is an integer). Left uncorrected, the horizontal resonances in the AGS result in a 15-20% relative loss in proton beam polarization [2].

Since 2011, a fast tune jump has been used to increase the resonance crossing rate, but this only prevents about half the polarization loss, leaving an 8–10% drop [3–5]. Instead of jumping through the resonances and incurring residual polarization loss, these resonance can instead be compensated and reduced to zero strength via additional betatron coupling. A set of 15 fast ramping thin skew quadrupoles has been installed in the AGS lattice and deployed operationally to individually compensate each of the 82 resonances. The report the correction mechanism and our operational experience.

* schoefer@bnl.gov

Horizontal Resonances

The primary purpose of the AGS partial snakes is to manipulate the spin tune in such a way as to allow avoidance of strong vertical intrinsic resonances and to produce dominating imperfection resonance terms to allow for total spin flips instead of polarization loss at imperfection resonance [6]. A particle executing horizontal betatron oscillations will experience an additional resonance term with frequency at the horizontal betatron tune, ν_x. In the spinor formalism, we can model the spin motion as

$$\frac{d\Psi}{d\theta} = -\frac{i}{2}\begin{pmatrix} F & -\xi \\ -\xi^* & -F \end{pmatrix}\Psi \tag{1}$$

with

$$\xi = iX_s\delta(\theta - \theta_s) + \epsilon_x e^{i\nu_x\theta}$$
$$F = G\gamma - (1 + G\gamma)x''(\theta)\rho$$

where $x(\theta)$ is the particle position relative to the reference orbit, X_s is the angle of rotation produced by the snake, δ is the periodic Dirac delta, θ_s the azimuthal position of the snake and ρ is the bend radius of the local reference orbit. Prime denotes differentiation with respect to the azimuthal angle. A particle on the design orbit has $x = 0$, $\epsilon_x = 0$, so only the intended precessional and snake drive term remain. The term proportional to ϵ_x is an additional resonant term excited at the ν_x by, for example, betatron coupling.

It can be shown that this motion results in a net resonance term given by [7]

$$\epsilon = \frac{1}{2\pi}\int \delta_n(\theta - \theta_s)e^{-iG\gamma\theta + iK\theta} \times \left[1 - \left(\tilde{x}'\frac{(1 + G\gamma)}{2} + \epsilon_x\right)e^{\pm i\nu_x\theta}\right]d\theta\,. \tag{2}$$

The unity term in square brackets is just the snake imperfection. The term proportional to $\tilde{x}'$ is a driving term that appears due to the modulation of the spin phase that occurs, turn by turn, due to betatron motion at the entrance to the snake. One can see that by exciting a particular coupling resonance it is possible to reduce this intrinsic term to zero.

RESONANCE COMPENSATION

For a typical horizontal tune near 8.72 and the standard ramp rate ($dG\gamma/d\theta = 4.7 \times 10^{-5}$), the horizontal resonance crossings are separated in time by 4-5 ms. Between injection and extraction energy ($G\gamma = 4.5 - 45.5$) eighty-two of these resonances are crossed. The main difficulty in designing a compensation system is that the relative phasing of a resonance term driven by a skew quad and that of the

Content from this work may be used under the terms of the CC BY 4.0 licence (© 2026). Any distribution of this work must maintain attribution to the author(s), title of the work, publisher, and DOI.

ISBN: 978-3-95450-252-3 ISSN: 2673-5350 doi: 10.18429/JACoW-IPAC2026-WEP4334

INVESTIGATIONS OF BETATRON COUPLING AND HORIZONTAL PARTIAL SNAKE RESONANCES AT LOW ENERGIES IN THE AGS

V. Schoefer*, W. Lin, Brookhaven National Laboratory, Upton, NY, USA
E. Hamwi, Cornell University (CLASSE), Ithaca, NY, USA

Content from this work may be used under the terms of the CC BY 4.0 licence (© 2026). Any distribution of this work must maintain attribution to the author(s), title of the work, publisher, and DOI.

Abstract

Compensation of depolarizing partial snake resonances using betatron coupling has been demonstrated at the Brookhaven AGS. At the nominal acceleration rate, the depolarization of the proton beam from any one of the 82 resonances is too small to optimize the compensation each individual resonance empirically. The compensation therefore requires accurate modeling of the accelerator lattice and accounting of both known sources of such resonances (the helical dipole and applied skew quadrupole fields) and unknown sources (e.g. sextupole feed-down effects). At low energies in the AGS these efforts are complicated by the large optical effects of the helical dipoles and the near-integer vertical tune required to avoid strong vertical spin resonances. Individual resonances can be investigated by crossing the resonance more slowly, in this case at fixed energies with a slow tune ramp. We report here on progress in both the modeling and experimental investigations into these depolarizing mechanisms.

HORIZONTAL RESONANCES

Helical dipole partial snake magnets are used to avoid strong vertical depolarizing spin resonances in the AGS. These magnets help avoid depolarization from strong imperfection and intrinsic resonances associated with the vertical betatron motion. The 'partial' nature of the snakes (less than full spin flip in one transit) causes an interaction between the spin motion and the horizontal spin motion that excites weak resonance at energies corresponding to $G\gamma = N \pm \nu_x$, where G is the anomalous gyromagnetic ratio, γ the relativistic factor, ν_x the horizontal tune and N any integer. These resonances are weak, but many (82 in the AGS energy range) and result in polarization loss [1]. Since these resonances occur at the same frequencies as spin resonances from betatron coupling, they can be corrected by a set of skew quadrupoles. The design and operational experience with such a system are described in [2, 3]. The resonance compensation from the additional skew quadrupoles relies on the resulting betatron coupling producing motion in the rest of the accelerator lattice, such that the extra spin precessions exactly cancel those introduced by the snake resonances. The correction therefore relies on accurate knowledge of the lattice optics for two different reasons. First, the resulting spin resonance depends on the beta functions and phase advances around the ring and second, because unknown sources of coupling (e.g. from magnet misalignment) produce unknown drive terms that compete with the correction and reduce its efficacy.

* schoefer@bnl.gov

SINGLE RESONANCE CROSSINGS

Initial commissioning of the skew quadrupole resonance compensation system was done by correcting only resonance at relatively high energy (above $\gamma \approx 8.5$). This was done to avoid complications of the optical effects of the helical dipoles and large closed orbit kicks from the skew quads interacting with relatively large horizontal closed orbit offsets at low energy in the AGS. It was noticed that as low energy resonances were gradually added to the correction, the polarization improvement was actually reduced, instead of increased, implying that there were large errors in the calculated corrections. Since the effects of any individual resonance are too small to measure ($\approx 0.1\%$ loss per resonance), investigation of individual resonances requires specialized setups.

The normal acceleration ramp is truncated and a flattop of constant energy is held near the desired resonance. In this case we chose the resonance at $G\gamma = 7.24$. This is low enough that the optical errors are still important, but far enough from injection ($G\gamma = 4.5$) to avoid interference with injection processes. The horizontal tune is set near the resonance condition ($\nu_x \approx 8.76$) and slowly varied, to reduce the resonance crossing rate and exaggerate the polarization loss. For a tune change of $\Delta\nu_x = 0.08$ over 200 ms, the resonance crossing rate $dG\gamma/d\theta = \alpha = 1.7 \times 10^{-7}$, a reduction in crossing rate by a factor of over 250 compared to crossings at the nominal AGS acceleration rate ($\alpha = 4.7 \times 10^{-5}$) (Fig. 1a). Here θ is the ring azimuth. At this rate, relative polarization losses of up to 20 % can be achieved which are easily measurable. The resonance crossing condition is determined by pausing the tune ramp for 50 ms at tunes

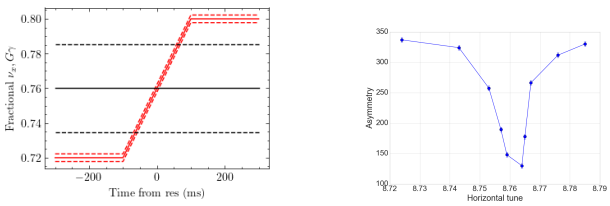

(a) (b)

Figure 1: (a) Schematic of nominal resonance crossing. Horizontal betatron tune is in red, energy in units of $G\gamma$ is in black. Dashed lines indicate the 4σ spread of the quantities due to the beam momentum spread (rms $dp/p = 0.001$. (b) The resonance tune is determined by pausing the tune ramp at various values for ± 25 ms around the expected resonance time. Polarization is lowest when paused exactly on resonance.

ISBN: 978-3-95450-252-3 ISSN: 2673-5350 doi: 10.18429/JACoW-IPAC2026-WEP4339

THE LAMP RFQTS: STATUS, CAPABILITIES AND PLANS

A. Alexander*, W. Choi, J. Duran, T. Grumstrup, M.A. Holloway, M.R. Howard, J.T.M. Lyles, K. Shipman, Y. Shimabukuro, B. Sims, A. Smith, S.I. Sosa-Guitron, C. Taylor, R.T. Thornton,
Los Alamos National Laboratory, Los Alamos, United States

Abstract

The LANSCE Accelerator Modernization Project (LAMP) will replace the front-end of the existing LANSCE accelerator, from ion sources through the end of the 100-MeV drift-tube linac. The RFQ test stand (RFQTS) currently consists of an H^+ ion source, LEBT, and RFQ, but will be expanded to add an H^- ion source and LEBT. It is intended as a flexible testing platform for technology maturation and workforce development. This paper will describe the status of the RFQTS, its current and future capabilities and planned experiments for technology maturation and other applications.

INTRODUCTION

The LANSCE accelerator produces 100 MeV and 800 MeV H- ion beams, which are delivered to 5 user end stations and used for a variety of nuclear, materials, medical and other applications. LAMP will modernize and replace the first 100 MeV of LANSCE, from the ion sources to the drift tube linac [1]. The LAMP project is currently in the preliminary design phase. As part of this process, a variety of technologies must be experimentally demonstrated before the final design can be approved [2]. The RFQ Test Stand is a flexible test stand that repurposes an existing RFQ for technology demonstration and maturation for the LAMP project. A schematic and image of the RFQTS is shown in Figure 1.

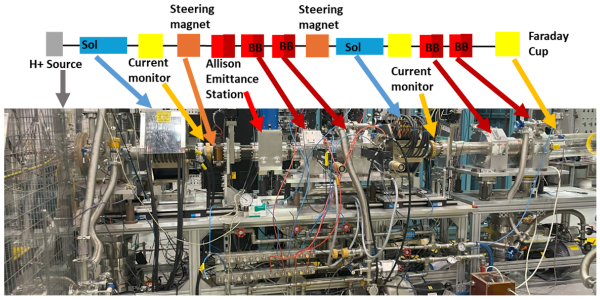

Figure 1: Schematic and photo of the RFQTS H+ beamline.

Comparison to LAMP

The RFQTS beamlines will share the same key components needed for technology maturation. However, because it uses a pre-existing RFQ, both the input and output energy of the RFQ are different from the LAMP design. The input energy of the RFQ (and thus the ion source injector and LEBT energy) is 35 keV, while the RFQ output energy is 750 keV. This is in contrast to the 65 keV LEBT/ RFQ input energy and 2.1 MeV RFQ output energy planned for LAMP [3].

H+ BEAMLINE

The H+ beamline is shown in Fig. 1. The beamline consists of a (LANSCE style) duoplasmatron H+ ion source (shown in Fig. 2), a 35 keV DC injector, and a variety of beamline diagnostics.

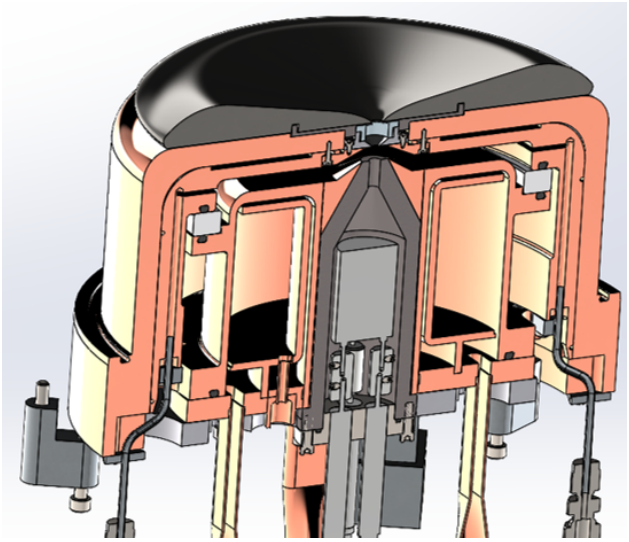

Figure 2: Schematic of the H+ duoplasmatron ion source used at the RFQTS.

The goal of the beamline in this configuration is to experimentally demonstrate a beam that will have a high acceptance into the RFQ. This is done through the slit and collector emittance stations in the second beam box. This is where the front of the RFQ will be placed when it is installed. Another key goal of the RFQTS is to demonstrate diagnostics that will be used for LAMP. LANSCE uses a slit and collector configuration to measure transverse emittance for the ion source transport lines an LEBT (i.e. energies less than or equal to 750 keV), shown in Figure 3.

This style of measurement typically has better resolution than Allison emittance scanners. However, this difference is reduced at lower beam energies. Further, Allison emittance scanners can typically measure higher peak and average power beams. This is important, as the LANSCE style slit and collector emittance scanners are permanently damaged when exposed to the beam unless the duty factor is drastically reduced. As a result, several emittance scanners are typically damaged each year due to user error. Further, there are underlying questions about measurement accuracy if the emittance scanner is needed very close to the ion source, before any choppers. In this case, the plasma pulsing must

* aalexander@lanl.gov

Content from this work may be used under the terms of the CC BY 4.0 licence (© 2026). Any distribution of this work must maintain attribution to the author(s), title of the work, publisher, and DOI.

ISBN: 978-3-95450-252-3 ISSN: 2673-5350 doi: 10.18429/JACoW-IPAC2026-WEP4340

MODELING OF SPACE CHARGE COMPENSATION IN THE RFQTS LEBT

Y. Shimabukuro* A. Alexander†, W. Choi, A. Smith, T. Grumstrup, M. Howard, B. Sims, R. Thornton, Los Alamos National Laboratory, Los Alamos, NM, USA

Abstract

A gas pressure- and gas species- dependent space charge compensation (SCC) model was developed in IBSimu for the RFQ Test Stand (RFQTS) to support the LANSCE Accelerator Modernization Project (LAMP). In LAMP, H^+ and H^- beams must be transported over an extended LEBT before RFQ injection, making SCC a key factor for beam emittance. The present work focuses on positive ion transport in the RFQTS and uses a steady-state approximation for direct comparison with beam measurements. For a 35 keV, 14 mA mixed beam condition, simulations show that a neutralization degree above 80% is required to suppress emittance growth during transport. Parameter scans indicate that the SCC-sensitive region is around 10^{-5}–10^{-6} Torr in Ar. These results define the operating window for upcoming RFQTS SCC experiments and provide input to LAMP front-end engineering design.

INTRODUCTION

The LANSCE Accelerator Modernization Project (LAMP) is replacing the front-end of the existing LANSCE accelerator, from the ion sources through the end of the 100-MeV drift tube linac (DTL) [1–3]. In the current LANSCE configuration, positive and negative hydrogen ions are independently accelerated to 750 keV immediately after extraction using separate Cockcroft-Walton (C-W) power supplies. This direct electrostatic acceleration up to 750 keV is advantageous because it mitigates beam blow-up caused by space charge effects [4]. In LAMP, however, the large C-W systems will be replaced by a single radio-frequency quadrupole (RFQ) capable of accelerating both positive and negative hydrogen beams from 65 keV to 2.1 MeV [5]. Unlike the existing configuration, LAMP requires transport of both beam polarities at 65 keV from the ion sources to the RFQ entrance. Because dual-polarity beams must be merged into a single beamline, the total beamline length reaches about 4 m. This is also the case for the RFQ test stand (RFQTS), a test stand associated with LAMP that is being used for technical maturation [6]. The RFQTS has a 35 keV low-energy beam transport (LEBT) and a 35 keV to 750 keV RFQ. Therefore, beam divergence and emittance growth during LEBT may be non-negligible.

In this study, we investigate the influence of space-charge effects on the RFQTS LEBT beam parameters. As an initial step, the effect of space-charge compensation (SCC) on the positive ion beam is investigated through both experiments and simulations. This paper reports the simulation work carried out to design the RFQTS experimental campaign.

* shimabukuro@lanl.gov
† aalexander@lanl.gov

EXPERIMENTAL APPARATUS

Figure 1 shows a sectional view of the Phase 1 configuration of the RFQTS. Positive hydrogen ion beams are generated by the LANSCE duoplasmatron ion source [7]. A coated nickel-strip filament emits thermionic electrons, which are focused downstream by a solenoid-based magnetic circuit. An arc plasma is formed by the characteristic double-sheath arc discharge and expanded into a boron-nitride plasma expansion cup through a 2.8 mm diameter anode aperture. This cools the plasma and improves its uniformity, resulting in lower emittance growth.

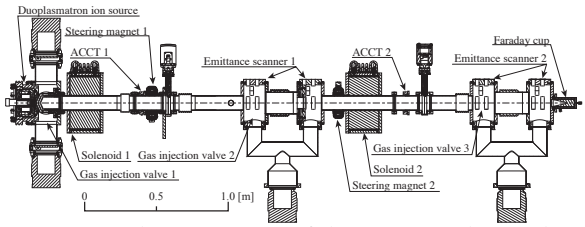

Figure 1: A schematic view of the RFQTS Phase 1 beamline, showing ion optics, diagnostics, vacuum pumps and neutralizer gas injection ports for SCC studies.

As shown in Fig. 2, positive ions are extracted through a 4.92 mm diameter aperture in the Pierce electrode (PE) by the extraction field between the PE and extraction electrode (EE) and are then accelerated to 35 keV using a conventional four-electrode system. A variety of ions are produced, with historical studies suggesting a fraction of 75% H^+, 20% H_2^+ and 5% H_3^+. The third electrode, a Repeller electrode (RE) biased at −2 kV, suppresses back-streaming low-energy electrons from the beam plasma formed downstream of the fourth grounded electrode (GE). Typical operating voltages are 22.6 kV for extraction and 12.4 kV for acceleration, resulting in a 35 keV beam. Although this potential distribution provides limited focusing at the EE exit, this extraction-dominant regime is selected to maximize extractable current while maintaining a low extractor aspect ratio and a broad perveance acceptance.

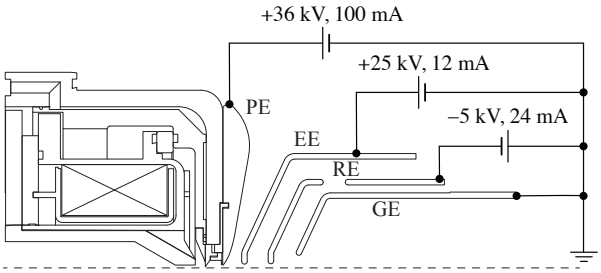

Figure 2: Electrode geometry for the RFQTS.

Content from this work may be used under the terms of the CC BY 4.0 licence (© 2026). Any distribution of this work must maintain attribution to the author(s), title of the work, publisher, and DOI.

ISBN: 978-3-95450-252-3 ISSN: 2673-5350 doi: 10.18429/JACoW-IPAC2026-WEP4346

CST MODELING OF TRAVELING-WAVE CHOPPER STRUCTURES FOR LANSCE AND LAMP*

S. S. Kurennoy†
Los Alamos National Laboratory, Los Alamos, NM, USA

Abstract

The Los Alamos Neutron Science Center (LANSCE) accelerator complex delivers both protons and negative hydrogen ions with various beam time patterns simultaneously to multiple users. An upgrade of its front end to a modern, RFQ-based version – a part of the LANSCE Accelerator Modernization Project (LAMP) – is now in the conceptual design stage. The LAMP will need fast beam choppers both in the low-energy transport (LEBT, 100 keV) before RFQ, and in the medium-energy transport (MEBT, 3 MeV) after RFQ. We use CST to model the existing LANSCE plate-coax helix chopper at 750 keV and to develop fast traveling-wave current structures for LAMP MEBT and LEBT beam choppers. A few structure types: plate-coax helix, meander-folded stripline on high-dielectric-constant substrate, and double-helix like at FNAL – are considered and compared. The structures must provide short rise/fall times of the deflecting electric field (1-ns class in MEBT), while still making it possible for the chopper pulse generators to deliver the required voltages at high repetition rates.

INTRODUCTION

Electromagnetic fast beam chopper systems consist of a deflecting structure, where the beam-deflecting fields are created, and a pulse generator (pulser) that feeds the structure with voltage pulses having a needed time pattern. Required fast switching on/off of the chopper deflecting fields can be achieved in traveling slow-wave chopper structures – two plates with voltage pulses of equal amplitude but opposite sign – where the deflecting field pulse propagates along the structure with the same velocity as the beam.

If a beam travels at velocity βc along the z-axis, and its deflection is in the y-direction (transverse to the structure plates), the deflecting Lorentz force per unit charge is $F_y / q = E_y + \beta Z_0 H_x$, where $Z_0 = \sqrt{\mu_0 / \varepsilon_0} = 120\pi\ \Omega$. The maximal deflecting electric field is $E_{max} = V/h$, where $\pm V$ are potentials applied to two plates and $2h$ is the distance between them. Normalizing the deflection force to E_{max}, we define the chopper deflection efficiency $\eta = \eta_e - \eta_m$, where $\eta_e = E_y/E_{max}$ is the electric efficiency and $\eta_m = -\beta Z_0 H_x/E_{max}$ is the magnetic reduction [1, 2].

The main chopper parameters – length L and aperture $a = 2h$, plus required voltage from pulse generator V – are defined by beam dynamics design. The beam deflection angle α is related to these parameters as follows:

$$\alpha \cong \frac{q}{mc^2\beta^2\gamma}\frac{\eta \Delta V L}{a} \cong \frac{q}{2W}\frac{V_{eff} L}{a}, \qquad (1)$$

where q and m are the charge and mass of beam particles (protons or H^-), $\gamma = (1-\beta^2)^{-1/2}$, η is the structure efficiency defined above, $\Delta V = 2V$ is the voltage between two plates, and effective voltage is $V_{eff} = \eta V$.

The chopper system rise and fall times depend on both system elements – structure and voltage pulse generator. If these elements have the rise/fall times t_s and t_p, correspondingly, the chopper rise/fall times can be estimated as $t_c = (t_s^2 + t_p^2)^{1/2}$. One more effect influences the chopper structure rise/fall time. Even if the voltage on chopper plates is turned on instantaneously, in the regions near the plate ends the fields vary from zero to maximal value – the edge effect. If a beam travels at velocity βc through these edge regions in the structure with aperture a, it effectively experiences field change that is equivalent to rise/fall time $t_e \approx a/\beta c$ [2]. This effect can be noticeable in LEBT, where the beam size is large while the velocity is low.

The traveling-wave chopper at LANSCE was designed for the proton beam at the energy of 750 keV and operates since the 1980s [3]. It is based on plate-coax (or strip-coax) helical slow-wave structure described in the next section.

The LAMP conceptual design continues to evolve. Unlike the description in the abstract, the LEBT chopper in the present version [4] was replaced by an electrostatic device, and the beam energy in the MEBT became 2.1 MeV ($\beta = 0.067$). CST models of the MEBT traveling-wave current structure were adjusted correspondingly.

LANSCE CHOPPER

The slow-wave structure – a helical delay line formed by parallel short sections of a metal stripline connected in series by semi-rigid 50-Ω coaxial cables (UT250A) under the ground plate – was developed at LANSCE in the 1980s [3] to chop a continuous 750-keV beam ($\beta = 0.04$); see Fig. 1.



Figure 1: LANSCE chopper: two plates are tapered out downstream. Coaxial cables are visible on the top plate; the strips can be seen at the bottom one.

There are 97 periods of length 1.016 cm along the beamline; the strip length is 8.407 cm, width 0.7925 cm. The beam aperture is large, with half-gap h = 18 mm, but the deflecting efficiency is high, η = 0.96. The rise/fall times of the structure itself are about 2 ns; the existing pulser at 700 V is much slower, with voltage rise and fall ~7-10 ns.

* Work supported by the US Department of Energy.
† kurennoy@lanl.gov

Content from this work may be used under the terms of the CC BY 4.0 licence (© 2026). Any distribution of this work must maintain attribution to the author(s), title of the work, publisher, and DOI.

ISBN: 978-3-95450-252-3 ISSN: 2673-5350 doi: 10.18429/JACoW-IPAC2026-WEP4347

THE HCHC-XX FAMILY OF HIGH-CURRENT COMPACT CYCLOTRONS: DESIGN, SIMULATION, TESTS

D. Winklehner[1]
[1]Massachusetts Institute of Technology, Cambridge, MA, USA
On behalf of the IsoDAR Collaboration

Abstract

The High-Current H_2^+ Cyclotrons (HCHC) were originally conceived for the IsoDAR experiment, which would place an intense accelerator-driven electron-antineutrino source near a high-resolution underground scintillator detector to enable precision beyond-standard-model searches (e.g., sterile neutrino oscillations). The HCHC design accelerates 5 mA of H_2^+ in a compact cyclotron, exploiting vortex motion–a multiparticle collective effect that can stabilize the radial beam size–to reach proton-equivalent currents roughly an order of magnitude beyond commercial cyclotrons. The beam is efficiently bunched by a Radio-Frequency Quadrupole (RFQ) axially embedded in the cyclotron yoke, placing the RFQ exit within 25 cm of the cyclotron median plane. Upon stripping the single binding electron of the H_2^+ (during or after extraction), 10 mA of protons are delivered on target. Because the novel aspects of this design are confined to the first six turns, the concept can be readily adapted to energies from 1.5 to 80 MeV/amu (HCHC-XX, where XX denotes the energy in MeV/amu). We present the latest HCHC-XX family designs, high-fidelity IBSimu/WARP/OPAL simulations incorporating space charge and conducting boundary conditions, and the fabrication status of a 1.5 MeV/amu prototype.

INTRODUCTION

The High-Current H_2^+ Cyclotrons (HCHC)-XX was originally conceived to drive IsoDAR (Isotope Decay-At-Rest), a decisive search for sterile neutrinos and other beyond-Standard-Model physics [1–4]. The confined underground environment of this experiment necessitates a compact solution while statistics requirements call for a high beam current.

Compact high-current cyclotrons sit at the intersection of fundamental research, medical isotope production, and accelerator-driven applications, and the field has matured rapidly over the past decade. The current benchmark is PSI's separated-sector Injector 2, which routinely delivers 2.2–2.4 mA of 72 MeV protons by exploiting space-charge-dominated "vortex" operation [5] and feeds a 590 MeV Ring cyclotron at world-record beam powers above 1.3 MW with relative losses at the 10^{-4} level [6]. Among compact machines, IBA's Cyclone 70 family–installed at ARRONAX, Zevacor, Moscow, and Arizona–delivers up to 750 µA of 30–70 MeV protons with deuteron and α capability through dual extraction ports [7], while the upgraded Cyclone 30HC reaches ~100 kW of beam power for industrial isotope production [8]. Smaller AVF machines for ^{99m}Tc and FDG production continue to proliferate, with new builds such as Indonesia's DECY-13 illustrating the global push toward in-house radiopharmaceutical drivers [9]. Against this landscape, the HCHC-XX targets a regime that exceeds today's commercial machines by roughly an order of magnitude in current (10 mA of protons after stripping) and matches or surpasses the best research cyclotrons, while remaining compact and mass-manufacturable.

APPLICATIONS OF THE HCHC-XX

In IsoDAR [1–4], paired with a ^{8}Be/^{7}Li target in a low-background underground site [10], an HCHC-60 produces three well-characterized fluxes–an intense $\bar{\nu}_e$ source, monoenergetic photons from nuclear excitations, and neutrons from spallation — enabling sensitive probes of sterile-neutrino oscillations, light "X" particles, axion-like particles, dark-sector n→n′ →n signals, and a world-leading low-Q measurement of the weak mixing angle [2, 11–13].

Beyond particle physics, the same platform serves three high-impact applied missions. In medical isotope production, an HCHC variant accelerating deuterons (an "HCDC") generates secondary neutron fluxes that open domestic, non-HEU pathways to ^{99}Mo/^{99m}Tc generators, ^{225}Ac for targeted alpha therapy, and other therapeutic radioisotopes–addressing supply-chain and regulatory bottlenecks in a growing market [15–18]. For nuclear waste transmutation, an HCHC can be the injector to a ring cyclotron driving a sub-critical reactor, converting long-lived actinides and fission products into shorter-lived species [19]. For fusion

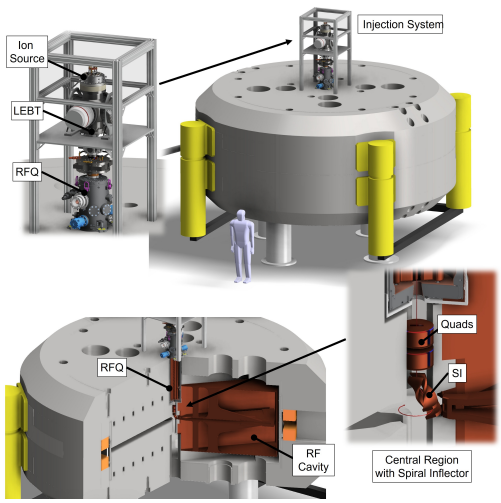

Figure 1: A CAD rendered overview of the HCHC-60 cyclotron design and its main components. We show only one of the four RF cavities for improved visibility. From [14].

Content from this work may be used under the terms of the CC BY 4.0 licence (© 2026). Any distribution of this work must maintain attribution to the author(s), title of the work, publisher, and DOI.

ISBN: 978-3-95450-252-3 ISSN: 2673-5350 doi: 10.18429/JACoW-IPAC2026-WEP4348

USING NORMALIZING FLOWS IN NORMAL-FORM SPACE TO MODEL INTRA-BEAM STRIPPING*

S. Kakkar†, L. Lee, University of Tennessee at Knoxville, Knoxville, TN, United States
N. Evans, A. Hoover, V. Morozov, Oak Ridge National Laboratory, Oak Ridge, TN, United States

Content from this work may be used under the terms of the CC BY 4.0 licence (© 2026). Any distribution of this work must maintain attribution to the author(s), title of the work, publisher, and DOI.

Abstract

Intra-beam stripping (IBSt) is a critical beam-loss mechanism in high-intensity H- linacs and presents a significant limitation to increasing beam power. This work presents a computational framework to evaluate IBSt-induced beam losses along the Spallation Neutron Source (SNS) linac for arbitrary bunch distributions. The calculation is based on evaluating the IBSt loss integral using a probability density function (PDF) trained on discrete-particle bunch distributions with normalizing flows. The input distribution is transformed to scaled normal-form coordinates, which improves both normalizing-flow training and Monte Carlo (MC) sampling. The method is benchmarked against simplified analytically solvable Gaussian bunches and then applied to canonical-angular-momentum-dominated (CAM-dominated) beam distributions, which contain strong inter-plane correlations. The results show that the normal-form-coordinate approach improves MC sampling stability and enables efficient IBSt loss calculations for correlated beam distributions.

INTRODUCTION

High-intensity H^- linacs require careful control of beam loss to support reliable operation and future power upgrades. At the Spallation Neutron Source (SNS), Intra-beam stripping (IBSt) is one mechanism that can contribute to beam loss when particles within the bunch interact and strip the weakly bound electron from H^- ions. Accurate prediction of IBSt loss requires knowledge of the six-dimensional beam phase-space distribution, since the loss rate depends on both the relative velocity of interacting particles and their spatial overlap. For realistic or correlated beams, this distribution is generally not known analytically, making direct evaluation of the IBSt loss integral challenging.

Previous work developed a Monte Carlo framework for evaluating IBSt losses using analytic Gaussian distributions and machine-learned probability density function (PDF)s trained on PyORBIT tracked phase-space data [1, 2]. In this work, we extend that framework by reformulating both normalizing-flow training and MC sampling in scaled normal-form coordinates. The lab coordinates are transformed to normal-form coordinates, where they are uncorrelated in the rms sense, and then scaled so that each of the transformed coordinates has a dimensionless unit rms spread. This improves the overlap between the sampling distribution and the high-density region of the bunch PDF.

* This manuscript has been authored by UT-Battelle, LLC, under contract DE-AC05-00OR22725 with the US Department of Energy (DOE).
† nlns1@ornl.gov

To demonstrate the efficiency of the updated algorithm, we apply it to the challenging case of canonical-angular-momentum-dominated (CAM-dominated) beams. These beams contain strong inter-plane correlations, such as x-y' and y-x', which may make conventional MC sampling in the lab frame inefficient. Therefore, they provide a useful test of the normal-form-coordinate method presented in this paper.

IBST LOSS RATE FORMALISM

We begin with an analytic expression for the IBSt loss rate specified in the bunch rest frame [3]. In this frame, the stripping cross section σ_H describing the interaction probability depends on the magnitude of the relative velocity $\mathbf{u} = \mathbf{v}_1 - \mathbf{v}_2$ between the two interacting particles. The total loss rate can be written as

$$\frac{dN}{dt_{\text{rest}}} = \frac{N^2}{2} \int |\mathbf{u}| \sigma_H(|\mathbf{u}|) f(\mathbf{v}_1, \mathbf{r}_1) f(\mathbf{v}_2, \mathbf{r}_2) \times \delta(\mathbf{r}_1 - \mathbf{r}_2)\, d\Gamma_1\, d\Gamma_2 \tag{1}$$

where f is the phase-space probability density, which is a function of the six phase-space coordinates. The delta function accounts for the fact that IBSt occurs locally, so only particle pairs that overlap at the same position in the bunch contribute to the loss rate.

We convert beam loss per unit time in the rest frame to beam loss per unit length along the linac in the lab frame by means of the following substitutions $dt_{\text{lab}} = \gamma\, dt_{\text{rest}}$ and $ds = \beta c\, dt_{\text{lab}}$ arriving at

$$\frac{dN}{ds} = \frac{1}{\gamma \beta c} \frac{dN}{dt_{\text{rest}}} \tag{2}$$

In the results below, we report the normalized particle number loss rate $(1/N)dN/ds$ as a function of the longitudinal position s along the linac.

NORMAL-FORM-COORDINATE MONTE CARLO METHOD

Coordinate Transformation

In the previous implementation [2], Monte Carlo integration points were sampled directly in the scaled lab-coordinates. This becomes inefficient if the beam distribution is stretched, or strongly correlated. In such cases, a fixed sampling region can include many points where the beam density is low.

The new calculation uses a sequence of coordinate transformations. The integrand functions in Eq. (1) are expressed in terms of the rest-frame coordinates. They are first converted to the lab-frame coordinates. We next apply a transformation to the normal-form coordinates and finally scale them

ISBN: 978-3-95450-252-3 ISSN: 2673-5350 doi: 10.18429/JACoW-IPAC2026-WEP4349

RECENT DEVELOPMENTS IN DTL DESIGN FOR LAMP PROJECT AT LANL *

D. V. Gorelov†, K. A. Bishofberger, D. A. Dimitrov, S. S. Kurennoy, J. W. Lewellen, S. I. Sosa Guitron, Los Alamos National Laboratory, Los Alamos, NM, USA

Abstract

The LANSCE Accelerator Modernization Project (LAMP) at Los Alamos National Laboratory is under way. One of the significant parts of this project is replacement of the existing 50-years old Drift Tubes Linac (DTL). The LAMP DTL will accommodate the existing LANSCE DTL species, namely protons and H- ions, as well as frequency 201.25 MHz and output energy 100 MeV. The input energy of the DTL determined by the optimization of radio frequency quadrupole (RFQ) and medium energy beam transport (MEBT) is 2.1 MeV. This paper is focused on the most significant details of the modeling and simulation of the proposed DTL.

INTRODUCTION

The LANSCE accelerator modernization project (LAMP) is the first stage of the upgrade of the linear accelerator facility at Los Alamos National Laboratory (LANL). This project proposes replacement of the existing CW ion sources for protons and H- with new ion sources and Low Energy Beam Transport (LEBT) at 65 keV, a new RFQ accelerator, and Medium Energy Beam Transport (MEBT) at 2.1 MeV. A new DTL will be designed to accelerate beams up to 100 MeV.

DTL DESIGN PRINCIPLES

The main limitations of the DTL design are the existing RF power amplifier systems at frequency 201.25 MHz and maximum power ~2 MW each. Hence we are planning to have 6 DTL tanks with rf power requirements below 2 MW each.

The other hard limitation is the existing LANSCE tunnel. The total length of the tunnel and the available RF power dictate the range of the accelerating gradient, that can be used in the new DTL.

We are planning to use Permanent Magnet Quadrupoles (PMQs) embedded in the DTL drift tubes for transverse focusing, since their performance give us the desired results without the drawbacks of the electromagnets, as are used in the LANSCE DTL.

One of the important methodological principles of the DTL design is the tunability of the accelerating gradient along the DTL tanks. According to [1], the post couplers used for fine-tuning the accelerating field magnitude, dictate the tank diameter be approximately λ/4 at the fundamental frequency. Other parameters (e.g. drift tube outer diameter, gaps between drift tubes and post-couplers, etc) must be chosen accordingly. This requirement led us to the choice of having tanks 1 and 2 to have diameter of 0.997 m, and tanks 3, 4, 5, and 6 – 0.9375 m.

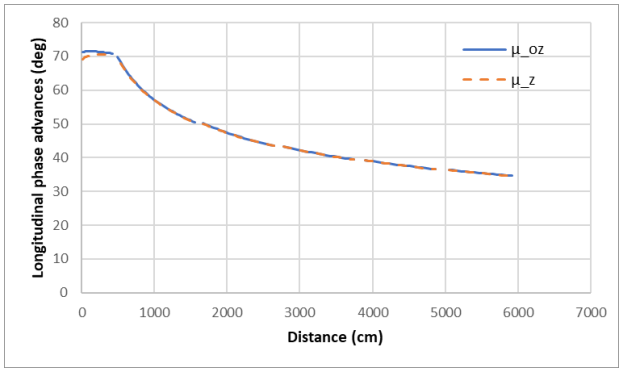

Figure 1: Synchrotron oscillations phase advance per focusing period for negligible beam current and for the design beam current of 35 mA.

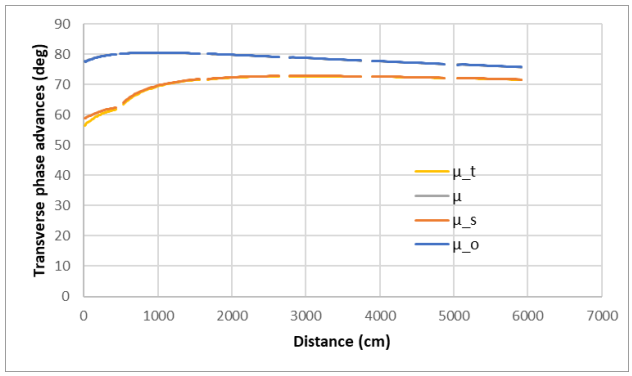

Figure 2: Betatron oscillations phase advance per focusing period for negligible beam current and for the design beam current of 35 mA.

We start the design process with choosing of the suitable synchrotron and betatron oscillation frequencies along the DTL by finding adequate transverse focusing period length and PMQs strength, that can be achieved in practice. The focusing lattice F0D0 was found to satisfy our requirements for the beam dynamics, where "0" represent empty drift tubes, and "F" and "D" – focusing and defocusing quadrupole in horizontal transverse plane respectively. The result of our choice is presented in Fig. 1 and 2. The nomenclature of the variables correspond to Refs. [2, 3].

The presented combination of the phase advances avoids the dangerous parametric resonance anywhere along the DTL, as well as stay below 90º, which is the limit of stable region for beam with high current [4]. Sufficient adiabatic continuity of the oscillation frequencies was preserved and should not cause significant emittance growth in the DTL.

* This work benefited from the use of the LANSCE accelerator facility. Work was performed under the auspices of the US Department of Energy by Triad National Security under contract 89233218CNA000001.
† gorelov@lanl.gov

Content from this work may be used under the terms of the CC BY 4.0 licence (© 2026). Any distribution of this work must maintain attribution to the author(s), title of the work, publisher, and DOI.

ISBN: 978-3-95450-252-3 ISSN: 2673-5350 doi: 10.18429/JACoW-IPAC2026-WEP4602

A BAYESIAN OPTIMIZATION STUDY OF THE LONGITUDINAL LOCALIZED EXCITATION SLOW EXTRACTION FOR THE XIPAF-UPGRADING SYNCHROTRON*

C. H. Li[1, 2, 3], H. J. Yao[1, 2, 3], Y. Xiong[1, 2, 3], S. X. Zheng†, [1, 2, 3]
[1]Key Laboratory of Particle & Radiation Imaging (Tsinghua University), Ministry of Education,Beijing, China
[2]Laboratory for Advanced Radiation Sources and Application, Tsinghua University, Beijing, China
[3]Department of Engineering Physics, Tsinghua University, Beijing, China

Abstract

The longitudinal localized excitation slow extraction method reduces the energy spread of the extracted beam by applying transverse excitation exclusively within specific phase intervals at the edges of the longitudinal phase space of the bunch. For localized square-wave excitation, conventional amplitude modulation formula struggles to achieve uniform beam spill, while the temporal uniformity of the extracted beam is crucial in radiotherapy and related physics experiments. The XiPAF-Upgrading Synchrotron (with a circumference of 39.96 m), developed from Xi'an 200 MeV Proton Application Facility, serves as a dedicated platform for the study and evaluation of single-event effects on core electronics for astronautics. We simulated the localized square-wave excitation slow extraction process using the SynTrack particle tracking code based on the XiPAF-Upgrading Synchrotron's parameters to extract low energy spread beam. Furthermore, a Bayesian optimization method was employed to refine the amplitude modulation curve of the excitation signa, thereby achieving highly uniform beam spill under low-energy slow extraction conditions.

INTRODUCTION

RF-Knockout (RF-KO) serves as a key technique for realizing continuous and stable extracted beam in synchrotrons slow extraction. In recent years, with the advancement of application scenarios including proton FLASH radiotherapy and space radiation environment simulation, stricter demands have been imposed on extracted beam parameters such as energy spread, intensity, spill fluctuation and so on. To address these challenges, we proposed the longitudinal localized excitation slow extraction method [1]. In contrast to the RF-KO approach, this method only applies transverse excitation signal at the edge of the longitudinal phase space, not only reducing the energy spread of the extracted beam but also mitigating both strong space charge effects and spill fluctuation. The feasibility of this method has been preliminarily verified [1] [2].

The temporal uniformity of the extracted beam is a critical metric in slow extraction. Researchers at HIMAC derived the required amplitude modulation function based on the phase space evolution during RF-KO extraction [3] [4]. However, in the proposed longitudinal localized excitation slow extraction method, the localized excitation signal exhibits localization in both time and longitudinal phase space, rendering the conventional RF-KO amplitude modulation formula inapplicable. Bayesian optimization (BO), with its sample efficiency, robustness to noise, and superior global optimization capability, is particularly well-suited for scenarios involving costly objective function evaluations and complex system behavior. Xu et al. [5] applied BO to optimize the injection process at the KARA storage ring, significantly improving injection efficiency in a nine-dimensional parameter space. Wang [6] applied BO to optimize the total extraction efficiency for 10 MeV slow extraction below third-order resonance line, identifying multiple high-efficiency settings within tens of evaluations.

In this study, based on the parameters of the XiPAF-upgrading Synchrotron, we employ Bayesian optimization to modulate the amplitude of the square-wave signal used in longitudinal localized excitation slow extraction.

LONGITUDINAL LOCALIZED EXCITATION SLOW EXTRACTION BASED ON SQUARE WAVE

The longitudinal localized excitation slow extraction method applies transverse excitation precisely to the longitudinal low-density edge region (Fig. 1), effectively reducing energy spread and spill fluctuation of extracted beam while mitigating strong space charge effects. Further details of this method can be found in the Reference [1].

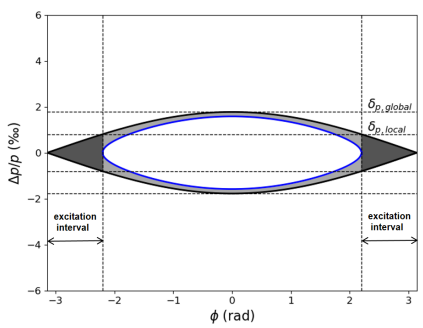

Figure 1: Diagram of longitudinal localized excitation slow extraction method.

* Work supported by the National Natural Science Foundation of China (No. 12075131)
† zhengsx@tsinghua.edu.cn

Content from this work may be used under the terms of the CC BY 4.0 licence (© 2026). Any distribution of this work must maintain attribution to the author(s), title of the work, publisher, and DOI.

ISBN: 978-3-95450-252-3 ISSN: 2673-5350 doi: 10.18429/JACoW-IPAC2026-WEP4604

COMPENSATION OF SECOND-ORDER RANDOM RESONANCES IN THE J-PARC RCS

K. Kojima*, H. Harada, M. Chimura, P. K. Saha
Japan Atomic Energy Agency, JAEA, Tokai, Japan

Abstract

In the Japan Proton Accelerator Research Complex (J-PARC) 3-GeV rapid cycling synchrotron, the shift in the operating point to a higher tune side leads to an increase in the beam loss due to several random resonances excited by the lattice imperfections. To mitigate the resonance-induced beam loss and further enhance the tunability of the operating point, we studied compensating for horizontal half-integer resonance just above the current operating point. A precise half-integer resonance compensation was achieved at the early stage of acceleration by adding trim quadrupole magnets in previous studies. However, the time-dependent component of the lattice imperfections, which is assumed to mainly come from the error field of the main quadrupole magnets, was not evaluated and should deteriorate the resonance compensation during the latter part of the acceleration. We developed a new method for controlling the timing at which the beam approaches the resonance by adjusting the momentum offset and chromaticity-induced tune shift, and experimentally determined the time-dependent component of the lattice imperfections. An analysis based on the resonance driving terms was used to evaluate the optimal resonance compensation for the entire acceleration period.

INTRODUCTION

Figure 1 shows a schematic layout of a 3 GeV rapid cycling synchrotron (RCS) of the Japan Proton Accelerator Research Complex (J-PARC) [1]. The RCS has a three-fold symmetric lattice comprising arc and dispersion-free straight sections. Six trim quadrupole magnets named QDTs are equipped with the RCS at both ends of the straight sections and can be excited individually. The RCS serves as the driver for a material and life science facilities (MLF) as well as the injector for a main ring synchrotron (MR) and provides a 3 GeV proton beam at a repetition ratio of 25 Hz.

In the early stage of acceleration, the space charge force plays a crucial role and pushes the beam toward the lower tune region, as shown in Fig. 2. Although RCS delivers 1 MW beam with a very fractional beam loss, the beam power ramp-up aiming at over 1.5 MW output beam power definitely enhances the space charge force and leads to overlapping of the beam with the structure resonances $\nu_x = 6$ and $\nu_y = 6$ [2–5]. To avoid a beam overlap on the structure resonance, we attempted to compensate for the half-integer resonance $2\nu_x = 13$ located just above the current operating point $(\nu_x, \nu_y) = (6.46, 6.36)$. In previous studies, we successfully demonstrated the half-integer resonance compensation using an additional field generated by the QDTs

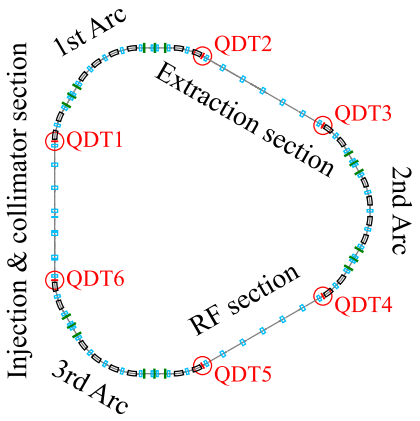

Figure 1: Schematic layout of the RCS. The positions of 6 trim quadrupole magnets named QDT are indicated with red circles.

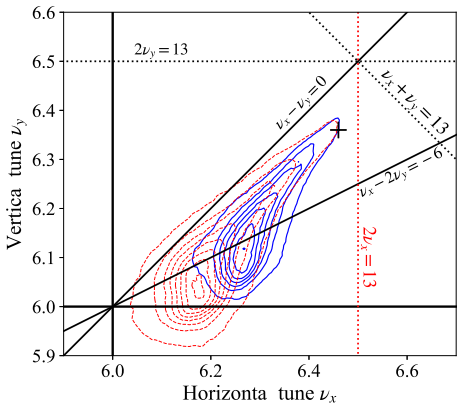

Figure 2: Red curve and blue curve represent the tune footprints of the beam for MLF immediately after injection, corresponding to the output beam powers of 1.5 MW and 1.0 MW, respectively. Structure and random resonances are indicated with solid and dotted lines, respectively. Cross indicates the current operating point.

immediately after injection [6]. On the other hand, the lattice imperfections driving the half-integer resonance are assumed to have two components, namely, the time-dependent component ramping with the magnetic rigidity, which is supposed to mainly originate from the error field of main quadrupole magnets, and the time-independent component having a constant magnetic field. Thus, the perfect resonance compensation over the entire acceleration period of 20 ms is not achieved unless the time-dependent component of the lattice imperfections is taken into account.

To investigate the time-dependent component of the lattice imperfections, the resonance compensation during the later

* kunihiro.kojima@j-parc.jp

Content from this work may be used under the terms of the CC BY 4.0 licence (© 2026). Any distribution of this work must maintain attribution to the author(s), title of the work, publisher, and DOI.

ISBN: 978-3-95450-252-3 ISSN: 2673-5350 doi: 10.18429/JACoW-IPAC2026-WEP4606

COHERENT OSCILLATION SIMULATIONS OF BEAM INSTABILITY GENERATED DURING DEBUNCHING FOR J-PARC SLOW EXTRACTION

M. Tomizawa*, T. Asami, A. Kobayashi, R. Muto, Y. Sato, K. Seiya, Y. Sugiyama, T. Toyama
High Energy Accelerator Research Organization, Tsukuba, Japan
F. Tamura, Japan Atomic Energy Agency, Tōkai Mura, Japan
K. Itahashi, The Graduate University for Advanced Studies, SOKENDAI, Hayama, Japan

Abstract

The J-PARC Main Ring (MR) has achieved a high extraction efficiency above 99.6% during 30 GeV slow extraction at the current beam power of 95 kW (8.4×10^{13} ppp). We have observed ring-wide beam loss due to transverse beam instability associated with vacuum pressure rise and electron cloud, believed to be triggered by longitudinal microwave structure in the beam. To achieve stable operation, we have implemented novel RF manipulations at the injection and for the debunching. The generation of the longitudinal microwave structure and coherent transverse oscillation by the electron cloud during debunching has been investigated using newly developed simulation codes.

INTRODUCTION

The J-PARC Main Ring (MR) has achieved a high extraction efficiency above 99.6% during 30 GeV slow extraction at the current beam power of 95 kW (8.4×10^{13} ppp). However, at beam powers above 30 kW, we observed ring-wide beam loss due to transverse beam instability associated with vacuum pressure rise and electron cloud (EC), believed to be triggered by longitudinal microwave structure in the beam [1]. To achieve stable operation, we implemented phase offset injection into RF buckets [1] and a two-step RF voltage reduction technique for debunching, in addition to chromaticity control [2]. The longitudinal microwave structure generation by the longitudinal impedances [3], electron cloud generation, and coherent transverse oscillation by the electron cloud during debunching have been investigated using newly developed simulation codes. The codes model the electron cloud–beam interaction as a transverse wake (impedance) derived from an EC oscillation defined by neutralization factor and EC-beam distributions. Through this study, we will explore further instability mitigation strategies toward higher beam intensity operations planned for the future.

BEAM INSTABILITY AND MITIGATIONS

The beam debunching for slow extraction was originally conducted by turning off the RF voltage at the flat-top start timing P3 called 1-step debunch, which is shown in Fig. 1 left. The RF voltage during a linear acceleration is set to 400 kV at 4.24 s cycle and adiabatically reduced to 256 kV during 0.1 s parabolic acceleration to a flat top to suppress the beam wake in the RF cavities during debunching. A new

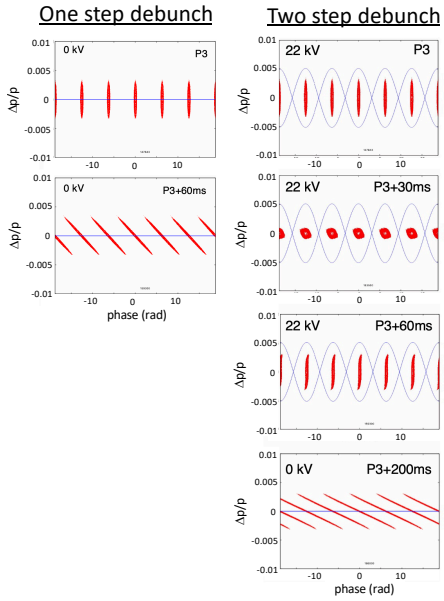

Figure 1: Beam distributions by two debunching manipulations.

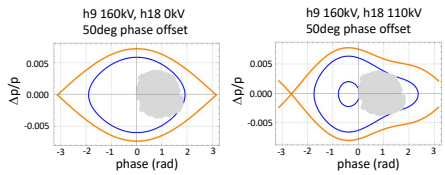

Figure 2: Separatrices and injected beam w/o and w/ 2nd harmonic RF.

RF manipulation technique called 2-step debunching was introduced [2] (see Fig. 1 right). The RF voltage was non-adiabatically reduced from 256 kV to 22 kV and turned off after a half synchrotron period (~60 ms). On the other hand, in order to enlarge the longitudinal beam emittance, 3 GeV beam from the RCS was injected into the MR fundamental RF buckets with a phase offset of typically ~50 deg as shown in Fig. 2 left [1]. In April 2025, a 110 kV second harmonic RF system was implemented with the 160 kV fundamental RF during the flat bottom energy [4]. As shown in Fig. 2 right, the beam is injected with a phase offset of ~50 deg for the fundamental RF bucket center. The second harmonic RF phase center is set at the same phase offset (~50 deg from fundamental RF phase center) [5]. This manipulation reduced the beam loss at the injection energy and the beginning of the acceleration by bunching factor improvement, and also suppressed the instability during debunching. The beam power has reached 92 kW (~8×10^{13} ppp) in physics

* masahito.tomizawa@kek.jp

Content from this work may be used under the terms of the CC BY 4.0 licence (© 2026). Any distribution of this work must maintain attribution to the author(s), title of the work, publisher, and DOI.

ISBN: 978-3-95450-252-3 ISSN: 2673-5350 doi: 10.18429/JACoW-IPAC2026-WEP4608

SCENARIO OF BEAM-BASED ALIGNMENT WITH NEW BPM SYSTEM FOR FUTURE BEAM COMMISSIONING OF 1.3-MW OPERATION AT THE J-PARC MAIN RING

Y. Saito*, The Graduate University for Advanced Studies, SOKENDAI, Hayama, Japan
Y. Sato, J. Takano, Japan Proton Accelerator Research Complex, Tōkai Mura, Japan
T. Asami, N. Kamikubota, K. Niki, M. Okada, K. Satou, K. Seiya, Y. Sugiyama, T. Toyama, T. Yasui
High Energy Accelerator Research Organization, Tsukuba, Japan
S. Hatakeyama, Mitsubishi Electric System & Service Co., Ltd, tsukuba, Japan

Content from this work may be used under the terms of the CC BY 4.0 licence (© 2026). Any distribution of this work must maintain attribution to the author(s), title of the work, publisher, and DOI.

Abstract

In the main ring (MR) at the Japan proton accelerator research complex (J-PARC), beam-based alignment (BBA) is essential for precise calibration of beam position monitors relative to quadrupole magnet centers. With the upgrade of the beam position monitor (BPM) system for better precision scheduled in this summer, frequent and accurate BBA will become increasingly important to optics and orbit correction for realizing less beam loss and stable operation. In this study, a fast BBA method is experimentally investigated and compared with conventional approaches. The fast method uses orbit modulation within a single measurement to efficiently extract offset information. Experimental results show that the fast approach achieves alignment accuracy comparable to the conventional method while significantly reducing the required measurement time. These results demonstrate the feasibility of regular beam-based alignment measurements and provide a path toward more precise optics correction in the MR.

INTRODUCTION

Since new physics research requires a large number of particles, the MR at J-PARC aims to increase its beam intensity from the current value of 0.9 MW to 1.3 MW by JFY 2028 [1]. To achieve this goal, there is a strict limit of a particle loss rate of 1 % or less to suppress radiation. Previous researches have improved the 3-fold symmetry of optics parameters in MR with correction of the current to magnets, which is effective for decreasing the beam loss [2–4]. The observed residue error of the magnetic quadrupole field around 0.1 % has possibility to be caused by an orbit offset from the centers of sextupole magnets, which induces an effective quadrupole field error. After an ongoing upgrade of the beam position monitor (BPM) system, we will pursue further measurements of closed orbit distortion (COD) and correct the orbit error.

To fully utilize the upgraded BPM system whose accuracy is 10 μm [1] in the diameter of 130 mm, the relative positions of the magnetic centers of quadrupole and sextupole magnets with respect to the BPM electrical centers must be accurately determined. This calibration is performed by beam-based alignment (BBA), which evaluates the offset between the BPM origin and the magnet center using beam response measurements. In order to achieve and maintain the accuracy, the BBA procedure needs to be applied repeatedly. Therefore, reducing the measurement time while preserving the required accuracy is essential, and in this study we focus on experimental investigation toward faster BBA implementation for the quadrupole magnets.

* yoshist@post.kek.jp

OVERVIEW OF BEAM BASED ALIGNMENT

The goal of the BBA is to calibrate the BPM origin to the center of the BPM's adjacent quadrupole magnet(Q). The difference between the BPM electrode center and the Q center comes from those misalignment and the differences of the signal transmission gains. In this paper, y_{target} is defined as the BBA's target BPM value, y_i is defined as the value of another BPM i, and I_Q is defined as the current to the trim coil, attached on Q for correction.

The main idea of the BBA is that, if a closed orbit passes through a Q center, $y_{\mathrm{target}} = y_0$, then changing I_Q does not change the orbit y_i. Therefore, in the BBA, linear fit searches the value of y_{target} where $dy_i/dI_Q(y_{\mathrm{target}}) = 0$, which is why the BBA needs to change the orbit y_{target} and the value of I_Q. The change in the orbit y_i as a function of I_Q can be obtained from each available BPM i in the ring. Therefore, we obtain as many BBA results y_{0i} where $dy_i/dI_Q(y_{\mathrm{target}} = y_{i0}) = 0$ as there are BPMs. You can apply statistical analysis to produce the result of y_0.

In the previous method [5], for each BPM, all combinations of the values of y_{target}, which was shifted by local bump, and I_Q were measured one by one. As a result, measurements for all 186 BPMs required a total of approximately 90 hours. Since the BBA is time-consuming, it had not been performed again after around 2014 until starting our study in 2025. The main limitation in speeding up the previous BBA procedure is that, within one cycle from injection and extraction, data were taken only at a single setting of y_{target}. If multiple y_{target} conditions are measured within one cycle, the total measurement time will be reduced.

This limitation is addressed by the Fast BBA method [6]. By modulating the orbit using an AC excitation of a correction magnet within a single cycle, the BBA measurement can be performed faster. In the Fast BBA, the 2-D graph of y_{target} and y_i is used. The line on the graph depends on I_Q, but there should be a fixed point crossing all the lines, which

ISBN: 978-3-95450-252-3 ISSN: 2673-5350 doi: 10.18429/JACoW-IPAC2026-WEP4609

ESTIMATION OF THE REQUIRED DIPOLE CORRECTOR MAGNETIC FIELD FOR PIP-II INJECTION BASED ON BEAM STUDIES*

K. Seiya†, D. Barak, E. Barlas-Yucel, C. Bhat, S. Chaurize, T. M. Omark,
J. -F. Ostiguy, H. Pfeffer, A. K. Triplett, B. Vaughn
Fermi National Accelerator Laboratory, Batavia, USA

Abstract

The Fermilab Booster will accept a 550 µs beam pulse from the new superconducting Linac for PIP-II operations. The Booster is a rapid-cycling synchrotron that uses a resonant magnet circuit ramping at 15 Hz. For PIP-II, the cycle rate will increase to 20 Hz, and the injection pulse length will expand from 40 µs to 550 µs due to the lower output current from the new Linac. Because the Booster main bending field follows a sinusoidal waveform, the magnetic field is not constant during the extended injection window. The longer pulse length and higher repetition rate modify the beam orbit and can lead to increased beam losses.

The Booster contains 48 dipole-corrector packages distributed across its 24 periods. Each package includes horizontal and vertical dipoles, quadrupole, sextupole, skew-quadrupole, and skew-sextupole elements. By driving the dipole correctors with an appropriately shaped sinusoidal waveform during injection, we can compensate the changing average main field and create an effectively flat bending field—referred to as *flat injection*.

Over the past several years, machine studies have been performed to characterize the required correction fields and to determine the corresponding power supply specifications needed for PIP-II operation. In this presentation, we will summarize the study results and discuss the estimated magnetic field requirements and power supply parameters for achieving flat injection in the Booster.

REQUIRED CORRECTOR FIELD BASED ON BEAM MEASUREMENTS

The goal of this work is to compensate the average bending field during injection so that it is effectively flat over an 800 μs interval along the sinusoidal ramp, using dipole corrector magnets. Before estimating the required compensation field for PIP-II operation at 20 Hz and an injection energy of 800 MeV, beam studies were performed under the current operating conditions of 400 MeV injection energy and a 15 Hz ramp [1, 2].

The bending field at injection was inferred from beam orbit measurements. The power supply currents required to generate the corresponding magnetic fields in the dipole corrector magnets were determined through offline test bench measurements. This approach established an indirect relationship between beam orbit displacement and corrector power supply current, and the observed beam response was verified to be consistent with the expected dipole corrector field behavior.

Main Bending Magnet Field vs Beam Orbit

The Booster uses 96 combined function magnets to provide the main bending field [3]. Using the Booster circumference and assuming an injection energy of 400 MeV, the average bending field was calculated.

The injection magnetic field was evaluated by measuring the beam orbit at $\pm$0.5 ms relative to the field minimum, as shown in Fig. 1 (bottom). Beam orbit measurements were performed with the RF feedback loops turned off for different power supply current. The orbit was reconstructed using the averaged signals from 48 beam position monitors (BPMs) located under the corrector packages and distributed in the short and long straight sections over 24 periods. The beam orbit shifted by approximately 2 mm when the main magnet power supply current was changed by 0.1 A.

Figure 1 (top) shows the calculated beam orbits when the bending magnet power supply current was scanned +/- 0.2 A by assuming that magnetic field is ideal sinusoidal curve. The calculation agrees with the measurements, which conclude that the main bending field follows a sinusoidal curve, as expected.

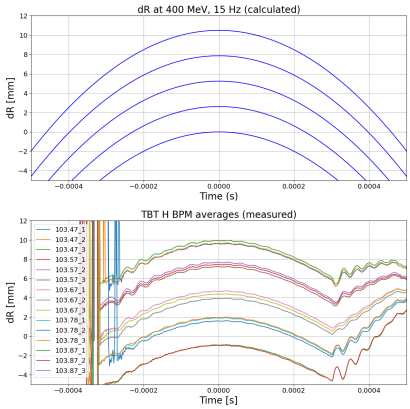

Figure 1: Calculated beam orbit for a change in magnet power-supply current from 103.47 to 103.87 A (top) and the corresponding measured beam orbit (bottom).

Dipole Corrector Magnet Field vs Beam Orbit

The dipole corrector magnetic field was measured and documented in a technical note [4], which reports an integrated field of 0.009 T·m at a current of 24.4 A.

A DC current ranging from −3.4 to +3.4 A was applied to 48 horizontal dipole correction magnet, and the resulting

* This manuscript has been authored by Fermi Forward Discovery Group, LLC under Contract No. 89243024CSC000002 with the U.S. Department of Energy, Office of Science, Office of High Energy Physics.

† kiyomi@fnal.gov

Content from this work may be used under the terms of the CC BY 4.0 licence (© 2026). Any distribution of this work must maintain attribution to the author(s), title of the work, publisher, and DOI.

ISBN: 978-3-95450-252-3 ISSN: 2673-5350 doi: 10.18429/JACoW-IPAC2026-WEP4611

STUDY OF ENERGY JITTER AND ENERGY SPREAD COMPRESSION FOR THE CSNS-II LINAC*

Y. Han † [1,2], M. Huang[1,2], A. Li[1,2], Z. Li[1,2], J. Peng[1,2]
[1]Institute of High Energy Physics, CAS, Beijing, China
[2]Spallation Neutron Source Science Center, Dongguan, China

Abstract

The China Spallation Neutron Source (CSNS) is currently undergoing an upgrade to increase its beam power from 100 kW to 500 kW. As part of this enhancement, the linear accelerator's beam energy will be boosted from 80 MeV to 300 MeV, and the beam current will be raised from 10 mA to 40 mA. To achieve the higher beam energy, 52 superconducting cavities will be added following the drift tube linac. However, these new cavities are expected to increase both energy jitter and energy spread, potentially leading to significant beam loss during injection into the RCS ring. Therefore, it is crucial to carefully manage the energy jitter and energy spread. This paper first presents simulations of the beam energy jitter and energy spread at the end of the superconducting section with dynamic beam and cavities errors. Subsequently, it introduces a comparison of various compression schemes aimed at reducing energy jitter and energy spread.

INTRODUCTION

The China Spallation Neutron Source (CSNS) is an accelerator-based neutron source located in Guangdong Province, China. Commissioning of CSNS began in 2017, and its design beam power of 100 kW was achieved in 2020. The accelerator complex consists of a linear accelerator providing a beam energy of 80 MeV and a Rapid Cycling Synchrotron (RCS) that accelerates the beam energy to 1.6 GeV [1, 2].

Since 2024, the CSNS-II upgrade project has been launched. The beam power will be increased to 500 kW, and two new application beamlines will be constructed. The main parameters of CSNS-II are listed in Table 1. To achieve a beam power of 500 kW, the beam current from the linac will be raised from 10 mA to 50 mA. Meanwhile, the beam energy at the linac exit will be increased to 300 MeV to mitigate the space-charge effect during injection into the RCS. The mitigation of instability has also been probably considered [3, 4].

Two types of superconducting cavities will be installed: spoke cavities and elliptical cavities, as illustrated in Fig. 1. The spoke cavities will accelerate the beam from 80 MeV to 165 MeV, with a total of 20 cavities arranged two per cryomodule. The elliptical cavities will boost the beam energy from 165 MeV to 300 MeV, with 24 cavities grouped three per cryomodule. Each cavity will be powered by an independent RF source, resulting in a total of 44 power sources for the superconducting cavities. Significant jitter in beam energy and energy spread can be anticipated in such a linac system, which must be suitably compressed.

Table 1: The Main Parameters Of The CSNS-II

Project Phase	CSNS	CSNS-II
Beam Power [kW]	100	500
Energy [GeV]	1.6	1.6
Avg. Current [μA]	62.5	312.5
Peak Current at Linac [mA]	10	50
Pulse length [μs]	500	500
Duty Factor at Linac	1.25%	1.25%
RF Cavities at Linac	DTL	+Spoke+Ellip.
Number of Target	1	1
No. of Spectrometers	3	20

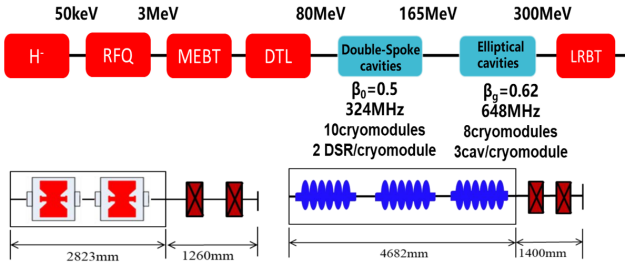

Figure 1: The layout of linac for the CSNS-II.

THE REQUIREMENT FROM THE RCS

The long bunch pulse from the linac will be injected and accumulated into two bunches in the RCS, where constraints on beam energy and energy spread are imposed to improve injection efficiency. Simulations indicate that the momentum jitter $\Delta p/p_0$ should be less than 0.2‰, and the energy spread jitter should be smaller than 1.0‰. For the 300 MeV beam delivered by the linac, this implies that the energy jitter must be controlled within 105 keV, and the energy spread must be limited to 527 keV.

THE ERROR ANALYSIS FOR THE LINAC

The 44 accelerating cavities in the superconducting linac, together with the DTL, will inevitably introduce amplitude and phase errors and jitters, leading to fluctuations in both beam energy and energy spread at the exit of the superconducting section.

* Work supported by by the Open Fund of the China Spallation Neutron Source Songshan Lake Science City (Grant No. KFKT2023A01)T & IHEP talent foundation E15156U110.

† ylhan@ihep.ac.cn

Content from this work may be used under the terms of the CC BY 4.0 licence (© 2026). Any distribution of this work must maintain attribution to the author(s), title of the work, publisher, and DOI.

ISBN: 978-3-95450-252-3 ISSN: 2673-5350 doi: 10.18429/JACoW-IPAC2026-WEP4616

DESIGN OF A COMPACT 8-MeV PROTON LINAC FOR MEDICAL APPLICATION

Yixing Lu, Yusen Guo, Ping Wang†, Xiaoxia Huang, Ruichuang Qin, Yifan Lan, Cheng Wang, Wencheng Fang‡, Zhentang Zhao
Shanghai Synchrotron Radiation Facility, Shanghai, China

Content from this work may be used under the terms of the CC BY 4.0 licence (© 2026). Any distribution of this work must maintain attribution to the author(s), title of the work, publisher, and DOI.

Abstract

The compact accelerator is a great trend in accelerator field, which is able to reduce the scale of the facilities based on accelerators, and meanwhile is attractive to medical devices. A compact 8-MeV proton linac was designed, aiming for medical applications like proton therapy. The linac operates at 714 MHz, comprising an electron-cyclotron-resonance ion source (ECRIS), a radio frequency quadrupole (RFQ), a matching section and an interdigital H-mode drift tube linac (IH-DTL). A 35-keV proton beam with the peak current of 6 mA was injected from the ECRIS into the RFQ. A new beam dynamics design of the RFQ ensures the high transmission of the linac, which is over 59%. The linac has the potential of being more compact because the flexible design of the matching section. The manufacturing of the linac is ongoing, which is proposed to complete by the end of this month. The commissioning of the linac is planned to operate in the near future.

INTRODUCTION

Shanghai Synchrotron Radiation Facility (SSRF) has been dedicated to researches on and development of proton therapy technology for more than ten years. The compact proton therapy accelerator [1], proton computer tomography [2-3] and ultra-high dose rate radiotherapy (FLASH-RT) [4], are undergoing research at SSRF for future advanced proton therapy. As a fundamental component of these facilities, a well-performed proton linac is essential to provide a high-quality proton beam. A compact proton linac was proposed to satisfy both demands of high-quality beam and compactness from medical facilities, which should be able to supply beams with a peak current of over 3-mA in order to support proton synchrotrons.

The compact linac consists of an ECRIS, a low-energy beam transport (LEBT), an RFQ, a matching section and an IH-DTL mainly, as shown in Figure 1. A new beam dynamics design was introduced to the RFQ, which ensures the high transmission of the linac. The matching section includes three electromagnetic quadrupoles and a buncher for beam focusing and rebunching respectively. The IH-DTL is designed with a synchronous phase of 0 degree, which becomes the Kombinierte Null Grad Struktur (KONUS) -like structure assembling with the matching section; meanwhile, it keeps the possibility of direct connection between the RFQ and the IH-DTL. This flexible design is likely to make the linac even more compact in the future.

The pulse length and repetition of the linac are 0.2 ms and 100 Hz respectively. The input beam of the linac is 35-keV, with a peak current of 6 mA. The initial RMS emittance is 0.15 $mm \cdot mrad$. At the exit of the 2-meter RFQ, the beam is accelerated to 4 MeV and the transmission is 59% benefitting from a new beam dynamics design. The IH-DTL has 22 acceleration gaps, accelerating the beam to 8 MeV with the synchronous phase of 0 degree. The transmission in the IH-DTL is about 99%. The length of the RFQ is 2 meters and that of the IH-DTL is 0.51 meter, resulting in the total length of the linac from RFQ to IH-DTL being 3.5 meters. The RMS energy spread at the exit of the IH-DTL is 93 keV, meanwhile the RMS beam length is 11 degrees. These parameters meet the requirements of both higher-frequency linacs and synchrotrons to inject.

RFQ DESIGN

RFQs have a strong focusing effect and are able to focus and accelerate proton beams against the high space charge effect. Therefore, RFQs are utilized broadly in low-energy proton accelerators. The frequency of the linac is 714 MHz, where the four-vane type RFQ is suitable. In order to get a high-transmission and short RFQ, the NFSP (New Four-Section Procedure) beam dynamics design is introduced to the RFQ, where an RFQ is divided into four sections as MS (Maximum-Separatrix), MB (Main Bunching), MBA (Mixed Bunching-Accelerating) and MA (Main Accelerating) [5]. This design allows non-constant average vane aperture so that the focusing strength of the RFQ can vary along the beam axis, hence the focusing strength can be higher along with a lower acceleration efficiency when the energy of the beam is low, meanwhile the acceleration efficiency can be higher along with a lower focusing strength when the energy of the beam is high. As a result, the RFQ can be shorter and the transmission can be higher.

The input beam emittance is $0.15\,\pi \cdot mm \cdot mrad$ and its energy is 35 keV. The peak current injected into the RFQ is 6 mA. The vane voltage of the RFQ is 67 kV and the peak surface field is 47.38 MV/m, which is around 1.9 times as high as the Kilpatrick limit. The minimum aperture radius is 0.91 mm. Smaller minimum aperture can strengthen the focusing effect of the RFQ and improve

† Email address: wangping@sari.ac.cn.
‡ Email address: fangwc@sari.ac.cn

ISBN: 978-3-95450-252-3 ISSN: 2673-5350 doi: 10.18429/JACoW-IPAC2026-WEP4619

SURFACE TREATMENT OF THE PROTOTYPE SPOKE CAVITY FOR THE JAEA-ADS LINAC*

J. Tamura†,1, T. Dohmae[2], Y. Fuwa[1], E. Kako[2], J. Kamiya[1], Y. Kondo[1], S. Kurosawa[1], F. Maekawa[1], S. Meigo[1], H. Sakai[2], K. Umemori[2], I. Yamada[1], B. Yee-Rendon[1]
[1]J-PARC, JAEA, Ibaraki, Japan
[2]iCASA, KEK, Ibaraki, Japan

Abstract

Japan Atomic Energy Agency (JAEA) has been proposing an accelerator-driven nuclear transmutation system (ADS). As a first step toward the practical design of the JAEA-ADS linac, we have been prototyping a low-β ($\approx$0.2) single-spoke cavity. Fabrication of the prototype spoke cavity was finally completed in FY2024. We are currently working on surface preparation for a high-field cavity testing at liquid helium temperature. In FY2025, we performed chemical polishing on the inner surface of the fabricated cavity, and subsequently proceeded to vacuum heat treatment. Although a uniform removal of the surface layer could not be achieved as initially anticipated, there were no defects observed on the inner surface. Hydrogen content of the chemically polished cavity was reduced through the furnace baking at J-PARC.

INTRODUCTION

JAEA has been proposing an ADS as a future nuclear system to efficiently reduce high-level radioactive waste generated in nuclear power plants. In the JAEA-ADS, a high-power proton beam of 30 MW with a final energy of 1.5 GeV is required with high reliability. The latest design of the JAEA-ADS linac is reported in Refs. [1,2]. As shown in Fig. 1, the proposed linac consists of a radio-frequency quadrupole (RFQ), half-wave resonator (HWR), low-β and high-β single-spoke resonators (SSR1 and SSR2, respectively), and low-β and high-β elliptical cavities (ELL1 and ELL2, respectively).

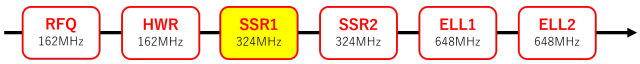

Figure 1: Proposed acceleration structure of the JAEA-ADS linac.

As a first step toward the practical design of the JAEA-ADS linac, we have been prototyping the low-β ($\approx$0.2) single-spoke cavity. The prototype spoke cavity with an operating frequency of 324 MHz was designed by electromagnetic simulation [3], and its dimensional parameters were optimized for higher cavity performance [4, 5]. Figure 2 shows the cross-sectional views of the designed cavity with surface electric and magnetic field distributions. The cavity's design parameters are listed in Table 1.

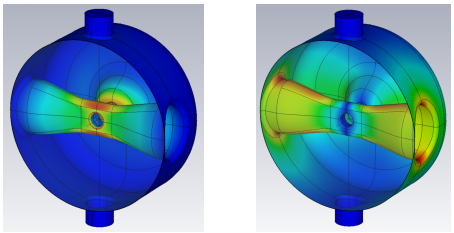

Figure 2: Cross-sectional views of the designed cavity with surface electric (left) and magnetic (right) field distributions.

Table 1: Design Parameters of the Prototype Spoke Cavity

Parameter	Value
f_0	324 MHz
β_g	0.188
β_{opt}	0.24
Beam aperture	40 mm
Cavity diameter	498 mm
Cavity length	300 mm
$L_{eff} = \beta_{opt}\lambda$	222 mm
$G = Q_0 R_s$	90 Ω
$T(\beta_{opt}) = V_{acc}/V_0$	0.81
$r/Q = V_{acc}^2/\omega U$	240 Ω
E_{peak}/E_{acc}	4.1
B_{peak}/E_{acc}	7.1 mT/(MV/m)

The actual cavity fabrication started in FY2020 and continued through the end of FY2024 [6–10]. The prototype spoke cavity is made of pure niobium (Nb), except for the niobium-titanium alloy (Nb-Ti) flanges for the RF ports and beam ports. The major parts were press-formed from 3.5 mm-thick Nb sheets. The nose-shaped end drift-tubes and the port flanges were machined from Nb and Nb-Ti cylindrical blocks, respectively. The shaped cavity parts were joined together by electron-beam welding (EBW), and the EBW assembly of the cavity without helium jacket was finally completed in FY2024.

We are currently proceeding with surface preparation for a high-field cavity testing at liquid helium temperature. In this paper, surface treatment processed to the prototype spoke cavity in FY2025 is presented.

CHEMICAL POLISHING

The inner surface of the fabricated spoke cavity was chemically polished with buffered chemical polishing (BCP) process so that the cavity may achieve sufficiently high field gradient. The BCP acid mixture of nitric acid (67.5 %), hy-

* This work was supported by JSPS KAKENHI Grant Number JP24H00235.
† jtamura@post.j-parc.jp

Content from this work may be used under the terms of the CC BY 4.0 licence (© 2026). Any distribution of this work must maintain attribution to the author(s), title of the work, publisher, and DOI.

ISBN: 978-3-95450-252-3 ISSN: 2673-5350 doi: 10.18429/JACoW-IPAC2026-WEP4621

A SYSTEMATIC ANALYSIS OF CAVITY COMPENSATIONS IN THE JAEA-ADS LINAC UTILIZING THE LIGHTWIN TOOL

B. Yee-Rendon*, Y. Kondo, J. Tamura, S. Meigo, and F. Maekawa,
Japan Atomic Energy Agency, Tokai Mura, Japan
A. Plaçais, F. Bouly, Univ. Grenoble Alpes, CNRS, Grenoble INP, LPSC-IN2P3, Grenoble, France

Abstract

The Japan Atomic Energy Agency (JAEA) is designing a 30-MW linear proton accelerator (linac) for the Accelerator-Driven Systems (ADS) to address the nuclear waste storage challenges. For Accelerator-Driven Systems (ADS) technology to be viable, it is necessary to minimize both the number of beam trips and their duration, thereby exceeding the performance of current linacs. JAEA is focused on implementing fast cavity compensation to minimize beam downtime caused by cavity failures. This approach makes rapid cavity retuning that enables a fast beam restoration with an acceptable quality. Beam dynamics studies for the JAEA-ADS linac have shown that it is possible to achieve a proper beam operation even when multiple cavity failures occur. As the JAEA-ADS linac consists of 293 superconducting cavities, it requires a rapid, automated, and systematic approach to determine the optimal readjustment settings for all cavities. To achieve this, we are utilizing the LightWin tool. This software has been developed for ADS linacs and was successfully applied to ADS MINERVA/MYRRHA linac. It has undergone testing and enhancements to improve SPIRAL2 operation. This study analyzes cavity compensation in the JAEA-ADS superconducting linac using the LightWin tool and compares the results with previous research.

INTRODUCTION

As part of the research and development activities for Accelerator-Driven System (ADS) in the Japan Atomic Energy Agency (JAEA), we are doing R&D on superconducting linear accelerator (linac) to accelerate a 30-MW proton beam to generate spallation neutrons for an 800-MW thermal power subcritical reactor [1]. Table 1 presents the main characteristics of the JAEA-ADS linac [2].

Table 1: Main Parameters for the JAEA-ADS linac

Parameter	Value
Beam current [mA]	20
Proton beam energy [GeV]	1.5
Duty factor (%)	100 (cw)
Beam loss [W/m]	<1

Figure 1 shows the scheme of the JAEA-ADS linac. The JAEA-ADS linac adopts a hot standby scheme in the low-energy section and fast element compensation in the high-energy section to meet stringent reliability and availability requirements for ADS [3]. Previous studies [4–6] have shown that cavity compensation can be implemented with acceptable beam quality in the JAEA-ADS linac. However, those studies focused on the most challenging scenarios, leaving the analysis of all cavities in the high-energy section pending. Additionally, the configuration schemes differ across cavity sections, making it difficult to prepare suitable compensation schemes for all the cavities and complicating its implementation in real-world operations [7]. This study aims to address these challenges by applying cavity compensation throughout the entire high-energy section and identifying a general cavity compensation configuration that could be effective for most of the cases.

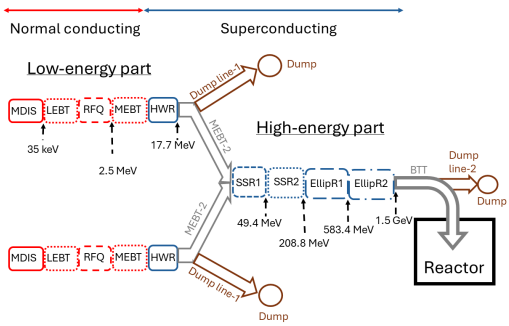

Figure 1: Layout of the JAEA-ADS linac.

JAEA-ADS LINAC: HIGH-ENERGY PART

The high-energy section accelerates a 20-mA proton beam from an initial energy of 17.7 MeV to a final energy of 1.5 GeV. This region includes four cavity sections: two single-spoke resonators sections operating at 324 MHz (SSR1 and SSR2) and two five-cell elliptical cavities operating at 648 MHz (EllipR1 and EllipR2). A summary of the relevant parameters is shown in Table 2. The total number of cavities is 268.

Table 2: Cavity parameters for the high-energy part of the JAEA-ADS linac

Section	SSR1	SSR2	EllipR1	EllipR2
Final energy (MeV)	49.4	208.8	583.4	1500
Frequency (MHz)	324	324	648	648
β_g	0.16	0.43	0.68	0.89
# of cell	2	2	5	5
Cavities per cryomodule	2	3	3	5
# of cavities	66	72	60	70

The Accelerating gradient (E_{acc}) and the synchronous phase (ϕ_s) were tuning to ensure enough longitudinal acceptance for cavity compensation (Fig. 2).

* byee@post.j-parc.jp

This is a preprint - the final version is published with IOP

Content from this work may be used under the terms of the CC BY 4.0 licence (© 2026). Any distribution of this work must maintain attribution to the author(s), title of the work, publisher, and DOI.

ISBN: 978-3-95450-252-3 ISSN: 2673-5350 doi: 10.18429/JACoW-IPAC2026-WEP4622

RECENT ACTIVITIES AT THE J-PARC RFQ-TS*

R. Kitamura, M. Chimura, Y. Fuwa, K. Hirano, M. Ishikawa, Y. Kondo,
T. Kosugiyama, T. Morishita, K. Moriya, H. Nakano, K. Ohkoshi, K. Okabe,
K. Shinto, H. Takahashi, and R. Tasaki, JAEA/J-PARC, Tokai, Japan
T. Miyao, S. Mizobata, K. Nanmo, Y. Sato, and T. Shibata, KEK/J-PARC, Tsukuba, Japan

Abstract

The Japan Proton Accelerator Complex (J-PARC) linac delivers the negative hydrogen (H^-) ion beam with a peak current of 50 mA to the Material and Life science experimental Facility (MLF) and the Main Ring synchrotron (MR) through the Rapid Cycling Synchrotron (RCS). The Radio-Frequency Quadrupole linac Test Stand (RFQ-TS) in the J-PARC linac building is utilized for the evaluation of the beam quality and the tests of apparatuses by the 3-MeV H^- ion beam. Some studies were carried out in the RFQ-TS such as the low-level RF system, the novel magnet, and the beam monitors. Recently, the performance estimation of the some linac apparatuses was carried out with a higher repetition than normal operation. In this sense, the points of the improvement were checked for the ion source, magnets, cavities the RF source, beam monitors, and the control in the RFQ-TS. The results of the beam test were reported in the RFQ-TS.

INTRODUCTION

The Japan Proton Accelerator Research Complex (J-PARC) linac [1] accelerates the negative hydrogen (H^-) ion beam with a peak current of 50 mA to the subsequent synchrotron, which is the Rapid Cycling Synchrotron (RCS) for the Material and Life science experimental Facility (MLF) and the Main Ring synchrotron (MR).

The Radio-Frequency Quadrupole linac Test Stand (RFQ-TS) in the J-PARC linac building is mainly utilized to prepare the spare equipment and investigate the performance of the instrumentation and the beam quality of the front-end for the accelerator science. Some studies are carried out in the RFQ-TS, such as the low-level RF (LLRF) system [2], the novel magnet [3], the laser instrumentation [4], and the beam monitors [5, 6].

The beam repetition is 25 Hz in the current normal operation of the J-PARC linac, Recently, as one of the performance estimation of the linac apparatuses, some apparatuses were operated with a repetition of the 50 Hz, which is twice the normal repetition, in the RFQ-TS, to use the additional 25 Hz for the plan of the proton irradiation facility at the J-PARC [7]. The results of the preliminary beam test were reported in this presentation.

EXPERIMENTAL SETUP

Figures 1, 2, and 3 show the experimental setups of the RFQ-TS, which are the overall view of the RFQ-TS, the H^- ion source (IS), the Low-Energy Beam Transport (LEBT), and the Medium-Energy Beam Transport (MEBT), respectively. The H^- ion source [8] produces the pulsed H^- ion beam accelerated to 50 keV with a peak current of 60 mA and a repetition of 25 Hz in the normal operation. The 50-keV H^- ion beam is transported with the LEBT including two solenoids into the RFQ. Subsequently, the H^- ion beam is accelerated to 3 MeV with the RFQ [9, 10]. The 3-MeV H^- ion beam is transported with the MEBT into the Faraday cup as the beam dump. The MEBT contains the many components such as the three quadrupole magnets, the bending magnet, and the beam instrumentation. The typical peak current at the MEBT was 54 mA.

50-HZ BEAM TEST

In this time, as one of the performance estimation of the linac apparatuses, the 3-MeV H^- ion beam is accelerated with a repetition of the 50 Hz. Since the normal repetition of the apparatuses is 25 Hz, the points of the improvement were checked for them. The 50-Hz beam test was carried out including the performance estimation of the particle counter system and the measurement of the gamma ray and neutron around the RFQ-TS to confirm the operation environment.

Ion Source, Magnets, and Beam Monitors

As for the 50-Hz beam test, the ion source can be operate with a repetition of 50 Hz [8]. The static solenoid and quadrupole magnets work without any problem under the 50-Hz operation. The beam monitor system is also capable of operating without issues at the 50 Hz.

Cavity and RF

Table 1 shows the RF gate width and the typical RF power of the RFQ for the 25-Hz and 50-Hz operation. The RFQ is driven by a 324-MHz Klystron and the dedicated LLRF system [2], which are capable of operating with 50 Hz when provided with the 50-Hz trigger signal. Considering the heat loading of increasing the repetition, the RF gate width in the 50-Hz operation was set to slightly shorter than the half of the 25-Hz operation.

Figure 4 shows the typical waveform of the RFQ in the 50-Hz operation. No frequency shift affected the RFQ operation. Figure 5 shows the typical waveform of the trigger signal, the RFQ and the SCT signal in the 50-Hz operation. The beam was successfully accelerated with a repetition of 50 Hz in the RFQ-TS.

* rkita@post.j-parc.jp

Content from this work may be used under the terms of the CC BY 4.0 licence (© 2026). Any distribution of this work must maintain attribution to the author(s), title of the work, publisher, and DOI.

ISBN: 978-3-95450-252-3 ISSN: 2673-5350 doi: 10.18429/JACoW-IPAC2026-WEP4625

BEAM TUNING STUDIES FOR THE RAON LINEAR ACCELERATOR*

Dong-O Jeon†, Ji-Ho Jang, Yujung Ahn, Institute for Basic Science, Daejeon, South Korea

Abstract

Various studies have been conducted and validated to tune the RAON linear accelerator. The RF set-points of the superconducting cavities and buncher cavities are determined with phase scan technique with 2 BPMs. With the BPM calibration, the beam energy is quite accurately determined with accuracy of tens of keV/u. We check the beam energy from phase scan with dipole scan method. With measured beam parameters, transverse optics can be controlled routinely and matching between sections of the linac is done.

INTRODUCTION

The RAON facility consists of the injector and superconducting linac SCL3 [1]. Beam commissioning of the RAON injector section started since August 2021 with various ion beams, including proton, helium, oxygen, neon, and argon. The low-energy beam transport (LEBT) delivers the beam from the ion source to the RFQ. Various diagnostics are installed for machine tuning and operation. Figure 1 shows the layout of the injector and the first QWR cryomodule along with beam diagnostics.

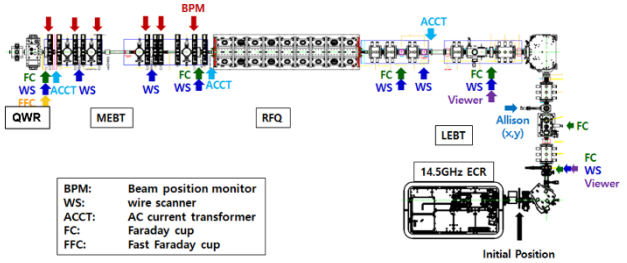

Figure 1: Layout of the injector and the first QWR cryomodule along with beam diagnostics.

Beam accelerated by the RFQ is transported to the superconducting linac through the medium-energy beam transport (MEBT), which provides transverse matching using magnetic quadrupoles and longitudinal matching using four buncher cavities.

In the QWR section, one cavity is installed in each cryomodule, whereas in the HWR section, two cavities are installed in each HWR-A module and four in each HWR-B module. Quadrupole doublets installed in the warm sections provide beam focusing. In addition, beam diagnostics such as beam position monitors (BPMs) and wire scanners are placed in the warm sections. To date, three beam-commissioning campaigns of the superconducting linac SCL3 have been conducted using argon and neon beams, starting with $^{40}Ar^{9+}$ beam followed by two subsequent campaigns of $^{40}Ar^{8+}$ beam and $^{22}Ne^{6+}$ beam.

This paper reports the beam tuning study results of the RAON injector and the superconducting linac. The injector commissioning results are presented primarily for $^{40}Ar^{8+}$ beam, with results from other ion species included as necessary, while the superconducting linac commissioning results are reported for $^{40}Ar^{8+}$ beam.

BEAM TUNING STUDIES

In operating an accelerator, various beam tuning measurements are needed to set the accelerator to the design state: RF set-points of cavities, beam profile measurements for tuning the proper optics, beam current measurements for transmission, orbit correction, etc.

With measured rms beam sizes, beam parameters such as rms emittance, Courant-Snyder parameters are determined. Utilizing these, the beam can be adjusted for better beam transmission and better matching to the downstream accelerator.

RF Set-Points

RF cavities of the RAON are superconducting cavities (QWR and HWR) and normal conducting buncher cavities. Their RF set-points are determined by using the phase scan technique with two downstream BPMs, and a physics application called CAPS has been developed and routinely used. Phase scan can determine the cavity RF set-point and the input beam energy pretty accurately to the accuracy of tens of keV/u. Figure 2 illustrates a typical phase scan result displaying the difference of two BPM phases.

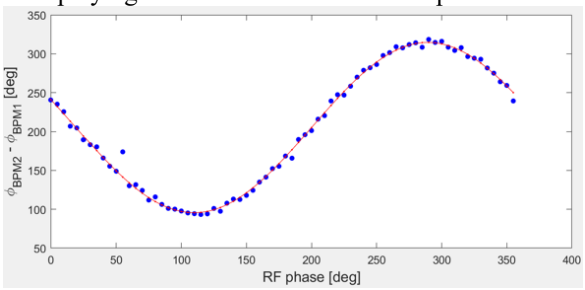

Figure 2: Plot of phase scan with two BPMs.

BPMs had been calibrated, and the beam energy obtained from phase scan has become quite accurate. Beam energy is also checked against beam energy obtained from dipole scan. For instance, $^{40}Ar^{9+}$ beam energy from phase scan (dipole scan) is 21.01 (20.92) MeV/u, and $^{22}Ne^{6+}$ beam energy from phase scan (dipole scan) is 24.50 (24.47) MeV/u. Figure 3 depicts $^{40}Ar^{8+}$ beam energy of the linac obtained from phase scans and TRACK code simulation for $^{40}Ar^{8+}$ beam. They show good agreement.

There are about ten cavities which are turned off for various reasons and rephasing nearby cavities are done to compensate their mismatch effect. Transmission of linac is

* supported by the Institute for Basic Science (IBS-I001-D1)
† jeond@ibs.re.kr

Content from this work may be used under the terms of the CC BY 4.0 licence (© 2026). Any distribution of this work must maintain attribution to the author(s), title of the work, publisher, and DOI.

ISBN: 978-3-95450-252-3 ISSN: 2673-5350 doi: 10.18429/JACoW-IPAC2026-WEP4626

TRANSVERSE PHASE SPACE TOMOGRAPHY AND COMPARISON WITH ALLISON SCANNER DATA IN THE RAON HEAVY ION ACCELERATOR*

D. O. Jeon†, J-H. Jang, Institute for Basic Science, Daejeon, South Korea
J-B. Lallement, European Organization for Nuclear Research, Geneva, Switzerland
V. Dimov, Advanced Oncotherapy / Applications of Detectors and Accelerators to Medicine, Meyrin, Switzerland

Abstract

Tomographic phase space reconstruction method based on the beam dynamics code Travel is applied to the RAON linear accelerator in the LEBT and in the MEBT. Due to the low beam energy and the two dipoles in the LEBT, it matters to include the space charge effect and the second-order effects of dipoles. When compared with the Allison scanner emittance data in the LEBT, the phase space tomography demonstrates a very good agreement even though the actual beam is far from Gaussian. The method of fitting rms beam sizes of wire scanners is also compared with the phase space tomography method. The method of fitting rms beam sizes produces a very good agreement when the actual beam is close to Gaussian, because the beam size fitting method uses Gaussian input beam in the simulation.

INTRODUCTION

The usual phase space tomography is based on linear mapping of several measured beam profiles onto the initial phase space to reconstruct the particle distribution at the reconstruction place. However, the emittance reconstruction methods using linear transfer matrices are reliable only when space charge force or nonlinear effects are negligible and the emittance is conserved. For instance, in the longitudinal plane, the motion is nonlinear even if the space-charge force is ignored. To overcome the limitation under space-charge force and nonlinear effects, a hybrid phase space tomography method was developed at CERN [1] which combines tomography with multi-particle tracking including space-charge effect utilizing the beam dynamics code Travel [2]. This method has been tested and validated theoretically and experimentally using the LINAC4 [3]. This method is applied to the RAON LEBT and MEBT and the results are presented in this paper, which is a summary of Ref. [4].

TRANSVERSE PHASE SPACE TOMOGRAPHY

Tomography in the MEBT

The phase space tomography method is applied to obtain the MEBT input beam transverse distribution using four wire scanners in the SCL (Superconducting Linac) which are marked by the arrows in Fig. 1 for the tomographic reconstruction. Figure 1 displays the layout of the RFQ, the MEBT and the SCL. These four wire scanners are located at periodic locations of the lattice. This is a favourable configuration because the phase advances between the two adjacent wire scanners range from 87° to 80°. The beam dynamics simulation shows that the RFQ output beam is close to Gaussian. For the beam dynamics simulation, the beam distribution obtained from the Allison emittance data is used as the initial beam distribution and is tracked to the RFQ exit.

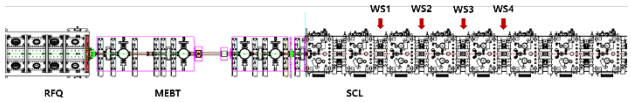

Figure 1: Layout of the RFQ, the MEBT and the SCL. Locations of the wire scanners are marked by the arrows placed between cryomodules. [Courtesy of Ref. [4]]

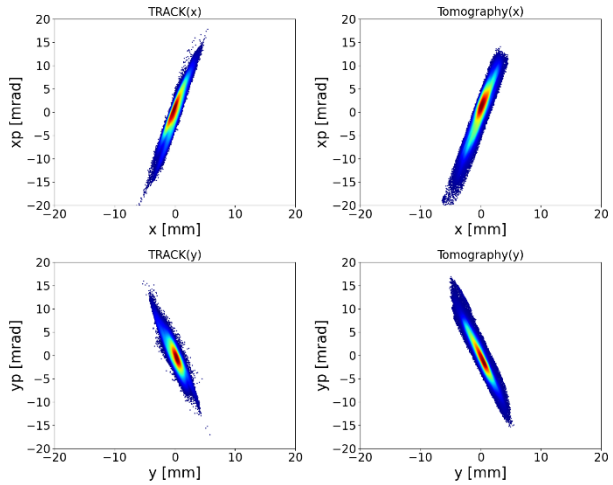

Figure 2: Plots of reconstructed beam distribution by the tomography method on the right and those from TRACK code simulation on the left. The distribution by the tomography method has more low intensity tails contributing to the rms emittances. [Courtesy of Ref. [4]]

Figure 2 shows the reconstructed beam distribution plots at the MEBT entrance by the tomography method, which reveals a Gaussian-like core and very low intensity non-Gaussian beam tails in the plots on the right. Tomography reconstruction produces very similar results to those obtained by the TRACK code. Beam parameters are then extracted from the reconstructed beam distribution which are listed in Table 1. The emittance and lattice functions are obtained from the beam distributions obtained from the TRACK simulation and from the tomography method. They are rms quantities of the beam distribution. For the TRACK code simulation, the beam distribution obtained from the Allison emittance data is used as the initial beam

* supported by the Institute for Basic Science (IBS-I001-D1)
†jeond@ibs.re.kr

Content from this work may be used under the terms of the CC BY 4.0 licence (© 2026). Any distribution of this work must maintain attribution to the author(s), title of the work, publisher, and DOI.

ISBN: 978-3-95450-252-3 ISSN: 2673-5350 doi: 10.18429/JACoW-IPAC2026-WEP4631

LOW-POWER TEST OF BRIDGE COUPLER CONNECTED TO TANK IN DISK-AND-WASHER STRUCTURE FOR MUON ACCELERATION

A. Kondo*, T. Iijima, K. Sumi, Y. Takeuchi, Nagoya University, Nagoya, Japan
E. Cicek, H. Ego, K. Futatsukawa, T. Mibe, Y. Nakazawa, M. Otani, M. Yoshida
High Energy Accelerator Research Organization, Tsukuba, Japan
Y. Kondo, M. Takatoshi, Japan Atomic Energy Agency, Tōkai Mura, Japan
Y. Iwashita, The University of Osaka, Osaka, Japan

Abstract

A muon linear accelerator is under development at the Japan Proton Accelerator Research Complex (J-PARC) for precise measurement of the muon anomalous magnetic moment ($g-2$) and search for the electric dipole moment (EDM). The disk-and-washer (DAW) structure is employed to accelerate muons from 30 % of the speed of light (kinetic energy = 4 MeV) to 70 % (40 MeV) at 1296 MHz. The muon DAW consists of tanks accelerating the muons and bridge couplers that couple the tanks and focus the beam using an internal quadrupole doublet. A bridge coupler prototype was fabricated and tested at low power. This low-power test focused on measuring resonant frequencies, Q-value, and electric field distribution. Furthermore, the bridge coupler prototype was connected to a tank prototype and tested at low power to understand the effects of the connection. This paper summarizes these results and discusses the prospects for actual machine production.

INTRODUCTION

The muon anomalous magnetic moment ($g-2$) and the electric dipole moment (EDM) are highly sensitive probes for physics beyond the Standard Model. Regarding the $g-2$, while recent lattice QCD calculations improve agreement with experimental results, a tension remains between lattice QCD-based and data-driven evaluations, requiring further investigation [1–3]. Furthermore, the observation of an EDM provides a stringent test for time-reversal symmetry violation [4].

At the Japan Proton Accelerator Research Complex (J-PARC), an experiment is being prepared to measure the muon $g-2$ and search for the EDM using novel methods. One of the novel methods is accelerating muons by a linear accelerator (linac). The muon linac consists of four stages. A disk-and-washer (DAW) structure is employed as the third stage of the muon linac, designed to accelerate muons from 30 % of the speed of light (kinetic energy = 4 MeV) to 70 %(40 MeV) at 1296 MHz [5]. A DAW structure cavity is a type of coupled cavity linac (CCL) which consists of disks, washers, and supporting stems. It was first proposed in the 1970s [6] and later used for a proton accelerator [7]. It has a high shunt impedance for middle β and high electric field stability due to high coupling between accelerating cells and coupling cells.

The muon DAW consists of alternating accelerating tanks and bridge couplers. The bridge couplers electromagnetically couple the tanks and provide space for beam focusing using an internal quadrupole doublet. Figure 1 shows an overview of the muon DAW. For the bridge coupler, a coaxial-type one was selected to take full advantage of the high coupling of the DAW structure. Figure 2 illustrates the configurations of the tank-bridge coupler.

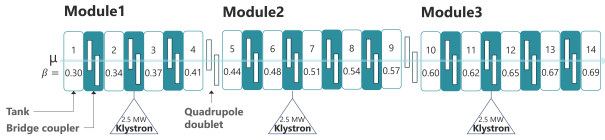

Figure 1: An overview of the muon DAW. The β shown in the figure represents the structure β (β_s) of each tank. The cell length within each tank is fixed according to its β_s.

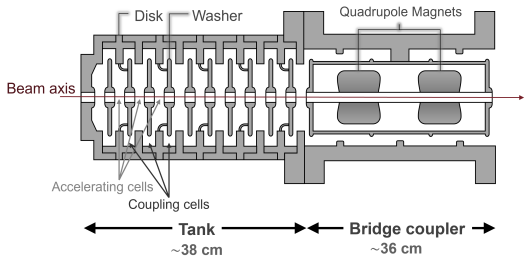

Figure 2: Cross-sectional view of the initial part of the muon DAW, cut vertically along the beam axis.

The development of the muon DAW began with the prototype fabrication of the first tank and bridge coupler. Because this initial section corresponds to the lowest particle velocity, it requires the narrowest accelerating gaps, presenting the most stringent fabrication challenges. A previous study reported the fabrication and performance evaluation of a tank prototype [8]. Also, a bridge coupler prototype was designed, fabricated, and was under evaluation [9]. This paper presents the low-power test results of this bridge coupler prototype, both individually and when connected to the tank prototype. The tests focused on measuring the resonant frequencies, Q-values, and electric field distributions.

DESIGN

The design of the bridge coupler prototype is shown in Fig. 3 and Table 1. This design satisfies all RF require-

* akondo@hepl.phys.nagoya-u.ac.jp

Content from this work may be used under the terms of the CC BY 4.0 licence (© 2026). Any distribution of this work must maintain attribution to the author(s), title of the work, publisher, and DOI.

ISBN: 978-3-95450-252-3 ISSN: 2673-5350 doi: 10.18429/JACoW-IPAC2026-WEP4633

DESIGN OF A DUAL EXTRACTION SYSTEM FOR THE ULTRA-COMPACT MULTIFUNCTIONAL CYCLOTRON CYCIAE-36A

W. Fu, Y. Chai, P. Li, C. Wang, T. Zhang, Z. Liu, L. Qin, L. Xia
China Institute of Atomic Energy, Beijing, China

Abstract

The growing demand for medical isotopes and mobile neutron sources has motivated the development of compact and multifunctional accelerators. China Institute of Atomic Energy (CIAE) has developed an ultra-compact superconducting cyclotron, CYCIAE-36A, capable of accelerating H_2^+ and α particles and delivering proton and α beams for applications including ^{211}At production, PET isotope supply, α-irradiation studies, and neutron imaging. The highly compact layout leads significant challenges for beam extraction. A dual extraction system combining electrostatic deflection and carbon-foil stripping is proposed under the constraints of superconducting magnets, RF cavities, and limited space. In this scheme, α particles are extracted using an electrostatic deflector, while H_2^+ ions are extracted by stripping, enabling variable-energy proton beams in the opposite direction. Phase width control is critical for extraction efficiency. Particle tracking simulations starting from the central region assume phase widths of 20° for α particles and 40° for H_2^+ ions, yielding extraction efficiencies of 85% and 99%, respectively. In addition, the effects of 1st and 2nd harmonic magnetic field components introduced by the magnetic channels during precession extraction were analysed, and corresponding compensation methods were developed to mitigate their impact on beam dynamics.

INTRODUCTION

The strong demands for α particles and high-intensity proton beams in novel α -emitting radionuclide R&D, mobile neutron imaging, solid-target radionuclide production, industrial irradiation have made multi-purpose accelerators an increasingly active area of research. It directly supports national imperatives for comprehensive research platforms and medical-engineering applications. Globally, cyclotrons delivering high-energy α particles are costly and massive, and primarily devoted to basic research (e.g., Russia's Dubna U-200/U-400 [1], Italy's INFN-LNS K800 [2], and South Africa's iThemba K200 [3]).

In the 1960s and 1970s, a few commercial cyclotron manufacturers developed a limited number of normal-conducting heavy-ion cyclotron models to meet the needs of that era, capable of accelerating H^+, H^-, and α particles. With the subsequent rise of the medical radioisotope market, these accelerators have been used mainly for accelerating H^- ions to produce common medical isotopes.

CIAE proposed an ultra-compact superconducting cyclotron. Characterized by its highly compact structure, low cost, and low power consumption, it provides a flexible scientific solution for the aforementioned applications. By utilizing low-temperature superconducting (LTS) technology, external dual beam injection, and bidirectional extraction, it simultaneously accelerates and extracts both α particles and H_2^+ ions, achieving a "five-in-one" multi-purpose functionality.

The overall schematic of CYCIAE-36A and principal parameters are presented in Figure 1 and Table 1, respectively.

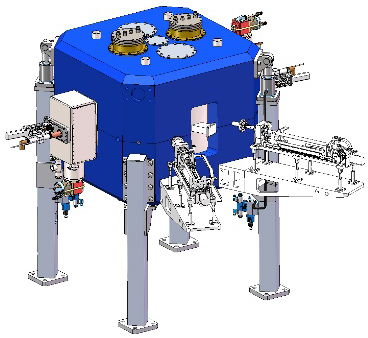

Figure 1: Schematic diagram of CYCIAE-36A.

Table 1: Main Parameters of CYCIAE-36A

Parameters	Value
Sector number	4
Pole radius [cm]	45
Angle of Pole [deg]	42.3
Central field [T]	2.138
RF frequency [MHz]	65.5/65.27
Dee voltage [kV]	50
Weight of Magnet [t]	12.6

EXTRACTION METHOD

The ultra-compact architecture of the CYCIAE-36A imposes strict constraints on the space available for the extraction system. Accommodating the extraction elements for two distinct particle types in a conventional, unidirectional layout is physically infeasible. To address this fundamental spatial constraint, a bidirectional extraction system is proposed.

Because α and H_2^+ possess fundamentally different physical characteristics, their extraction mechanisms must be tailored accordingly. By separating the two extraction paths to opposite sides of the machine, the extraction system optimally utilizes the limited valley space.

†fuwei@ciae.ac.cn

This work was supported by the National Natural Science Foundation of China under Grant of 12427810.

Content from this work may be used under the terms of the CC BY 4.0 licence (© 2026). Any distribution of this work must maintain attribution to the author(s), title of the work, publisher, and DOI.

ISBN: 978-3-95450-252-3 ISSN: 2673-5350 doi: 10.18429/JACoW-IPAC2026-WEP4638

FRINGE FIELD INTERFERENCE AND COMPENSATION OF QUADRUPOLES IN THE CSNS RCS

Y. Li*[1,2], Y.W. An[1,2], C.D. Deng[1,2], J.L. Chen[1,2], Z.P. Li[1,2]
[1]Institute of High Energy Physics, Chinese Academy of Sciences, Beijing, China
[2]Spallation Neutron Source Science Center, Dongguan, China

Abstract

During the beam power upgrade of the Rapid Cycling Synchrotron (RCS) at the China Spallation Neutron Source (CSNS), 16 newly installed trim quadrupoles (QT) cause fringe field interference with adjacent main quadrupoles, distorting lattice parameters and increasing beam loss. Using OPERA, MAD-X, and PyORBIT, it is found that QT reduces QD's integrated field by 0.77%, leading to significant tune shifts and over 10% beta-beat, with beam transmission dropping from 99.76% to 82.74% at the operation tunes. Orbit response matrix measurement confirms a 0.7% field reduction, matching simulations. A compensation scheme successfully reduces beam loss, supporting the beam power upgrade.

INTRODUCTION

As the performance requirements of modern accelerators continue to increase, magnet layouts are becoming increasingly compact. Constrained by physical design considerations and tunnel space limitations, the distance between adjacent magnets is continuously reduced, causing the iron cores of magnets to inevitably extend into each other's fringe field regions. This alteration of fringe field distribution due to the presence of adjacent iron cores, along with its corresponding impact on beam dynamics, is referred to as the fringe field interference effect. This effect induces variations in the integrated magnetic field [1], subsequently leading to issues such as tune shifts and optical parameter distortion. In high-intensity accelerators, it may even cause catastrophic beam loss, severely limiting performance enhancement.

Multiple laboratories worldwide have conducted systematic research on fringe field interference effects. For instance, the Beijing Electron-Positron Collider II (BEPC-II) pioneered the use of 3D multipole expansion techniques to investigate such fringe field interference effects in quadrupole-sextupole combined magnets, achieving an excellent agreement between simulations and experimental results [2]. At the Spallation Neutron Source (SNS) storage ring in the United States, closely packed large-aperture quadrupole magnets in the straight sections were found to exhibit an integrated gradient reduction of more than 1% due to fringe field interference [3]. For the CSNS RCS, the compact layout between large-aperture quadrupoles and adjacent sextupoles has been shown to cause a 2.3% reduction in the integrated gradient of the quadrupoles, leading to significant tune shifts and optical distortions [4]. However, the interference effect between the newly added trim quadrupole magnets (QT), installed for subsequent beam power upgrades, and the main quadrupole magnets has not yet been systematically evaluated. Building upon previous work [4], this paper focuses on investigating the interference effect between the additionally installed trim quadrupoles and the adjacent main quadrupoles in CSNS RCS.

CSNS OVERVIEW

The CSNS RCS [5] has a circumference of 227.92 m and adopts a four-fold symmetric lattice based on triplet focusing structures. A total of 48 main quadrupole magnets are installed in the RCS, which are divided into five families with each powered by a common resonant power supply. To address challenges including optical parameter correction and space charge compensation for high-intensity beams, 24 positions for trim quadrupole magnets were reserved in the initial design of the CSNS RCS [6]. Operational experience has shown that when the beam power exceeds 100 kW, relying solely on the main quadrupoles is insufficient to meet the requirements for optical parameter adjustment [7]. Consequently, 16 programmable trim quadrupoles were additionally installed in the RCS.

Figure 1 shows the actual installation layout of a QT magnet in the accelerator tunnel. As shown, the QT is installed at one end of a main quadrupole (QD), with both magnets sharing a ceramic vacuum chamber with an inner diameter of 272 mm. Constrained by the tunnel installation space, the maximum allowable longitudinal installation length is only 200 mm. Through optimized design, the final iron core length of the QT magnet was determined to be 150 mm. In this extremely compact configuration, the magnetic fields of the QD and QT inevitably extend into each other's fringe field regions, resulting in a significant fringe field interference effect.

3D ELECTROMAGNETIC SIMULATION

To quantitatively evaluate the fringe field interference effect between the QT and QD magnets, a high-precision magnetic field model was first established via the 3D electromagnetic field simulation software OPERA/TOSCA for the systematic analysis of their mutual magnetic influence. Figure 2 shows the 3D simulation model constructed in OPERA/TOSCA, which strictly follows the actual dimensions and end-chamfering angles of the QD and QT magnets. For the accurate simulation of magnetic field distribution, mesh refinement was implemented in the magnet gap and fringe field regions, with a minimum mesh size of 2 mm to

* liyong@ihep.ac.cn

Content from this work may be used under the terms of the CC BY 4.0 licence (© 2026). Any distribution of this work must maintain attribution to the author(s), title of the work, publisher, and DOI.

ISBN: 978-3-95450-252-3 ISSN: 2673-5350 doi: 10.18429/JACoW-IPAC2026-WEP4639

COMMISSIONING AT THE TUNES BELOW HALF-INTEGER FOR CSNS RCS*

J.L. Chen[1], Y.W. An[1], Y. Li[1], H.Y. Liu[1], J.J. Tan[1], L.S. Huang[1], M.Y. Huang[†,1] ,
Institute of High Energy Physics, Chinese Academy of Sciences, Beijing, China
[1]also at Spallation Neutron Source Science Center, Dongguan, China

Abstract

Based on the beam commissioning of CSNS-I RCS, the current tune above half-integer exhibits extremely small parameter margins and severe instabilities. Therefore, to further increase beam power in Phase II, significant optimization of the tune is required. Through extensive simulations, we identified that the tunes below half-integer (near 4.3/5.3) show no instabilities, which is crucial for power enhancement in Phase II. To verify stable operation at the tunes of this region in the actual machine, we conducted a series of machine studies. The results demonstrate that the tunes below half-integer is instability-free and can achieve stable beam supply at 140 kW (corresponding to 700 kW in Phase II under equivalent tune shift due to space charge).

INTRODUCTION

The China Spallation Neutron Source (CSNS) [1, 2] is a high-intensity proton accelerator-based facility serving as a neutron source. Its accelerator complex comprises two main components: an H^- linac and a Rapid Cycling Synchrotron (RCS). The RCS accumulates a beam with an energy of 80 MeV through a multi-turn charge-exchange scheme and accelerates the beam to 1.6 GeV at a repetition rate of 25 Hz. The target beam power for CSNS is specified at 100 kW with a total proton of $N_p = 1.56 \times 10^{13}$. The approval of CSNS Phase II (CSNS-II) [3] aims to enhance the beam power to 500 kW by increasing the linac beam energy to 300 MeV, thereby reducing space charge effects at low energy and improving current intensity in the RCS, corresponding to a total particle of $N_p = 7.8 \times 10^{13}$. Additionally, trim quadrupoles will be adopted in Phase II. A comparison of the parameters between Phase I and Phase II is shown in Table 1.

Table 1: CSNS RCS design parameters

Parameter (Unit)	Phase I	Phase II
Extraction Beam Power (kW)	100	500
Injection Beam Power (MeV)	80	300
Extraction Beam Energy (MeV)	1600	1600
Repetition Rate (Hz)	25	25
Space Charge Tune Shift	0.28	0.19
Beam Average Current (μA)	62.5	312.5
Number of Dipoles	24	24
Number of Main Quadrupoles	48	48
Number of Trim Quadrupoles	/	16

* Work supported by National Natural Science Foundation of China (No. 12405175 and No.12405170)

† huangmy@ihep.ac.cn

For the RCS, betatron tunes are of critical importance. Drawing on the beam commissioning experience of Phase-I, the presently adopted tune setting provides only marginal parameter margins and induces severe beam instabilities [4]. Accordingly, substantial tune optimization is indispensable in Phase-II to accommodate elevated beam power. Extensive numerical simulations have therefore been performed. Simulation results indicate that tune values below the half-integer resonance avoid instability issues entirely while maintaining high beam transmission under higher-power operating conditions. To validate the simulation predictions, dedicated machine studies were conducted under the Phase-I beam configuration. Current experimental results confirm that tunes below the half-integer remain free of instabilities and enable stable beam delivery at 140 kW, which is equivalent to a 700 kW beam performance in Phase-II when accounting for identical space-charge tune shift conditions. This strongly demonstrates that the optimized tune scheme can support reliable and stable 700 kW beam operation in future Phase-II commissioning.

SIMULATION

To address the transverse coupled-bunch instability (TCBI) effectively, it is beneficial to optimize the tune, shifting the betatron oscillation frequency away from the resonance of ceramic chamber, with an ideal target of between 0 and 0.5 [5]. So, we simulated the range for selecting tunes: 4.35-4.45 in x plane and 5.25-5.45 in y plane (below half-integer resonances).

For 100 kW, the transmission rate reached above 99% and there is no beam instabilities, as shown in Fig. 1. However, for 140 kW, under the same conditions, the beam transmission rate is only approximately 97.2%, as shown in Fig. 2. With the help of the Trim Quadrupoles (QTs) [6], the vertical emittance is reduced, thereby optimizing the transmission rate to over 99%, as shown in Fig. 3.

BEAM COMMISSIONING

The space charge effect of 100kW-160kW (Phase I) is equivalent to that of 500kW-800kW at an injection energy of 300MeV(Phase II).

100 kW

At the beginning of beam commissioning, the beam loss in the injection region has decreased significantly and the transmission rate of the RCS was very low (<97%).

We adopted the following optimization methods:

Content from this work may be used under the terms of the CC BY 4.0 licence (© 2026). Any distribution of this work must maintain attribution to the author(s), title of the work, publisher, and DOI.

ISBN: 978-3-95450-252-3 ISSN: 2673-5350 doi: 10.18429/JACoW-IPAC2026-WEP4644

LONGITUDINAL BEAM DYNAMICS SIMULATION FOR GOLD ION ACCELERATION IN THE J-PARC MR

Yasuyuki Sugiyama*, Fumihiko Tamura, Kyosuke Adachi, Hidefumi Okita, Kiyomi Seiya, Masahito Yoshii, Chihiro Ohmori, Keigo Hara, Katsushi Hasegawa, Masahiro Nomura, Masanobu Yamamoto, Taihei Shimada
KEK and JAEA J-PARC, Tokai, Ibaraki, Japan

Content from this work may be used under the terms of the CC BY 4.0 licence (© 2026). Any distribution of this work must maintain attribution to the author(s), title of the work, publisher, and DOI.

Abstract

The J-PARC Main Ring (MR) is a high-intensity proton synchrotron, which accelerates protons from 3 GeV to 30 GeV. In addition to protons, we are considering accelerating heavy ions to GeV/u energies in the MR as part of the J-PARC heavy-ion program (J-PARC HI). The heavy ions will be injected from the new heavy-ion injector into the J-PARC Rapid Cycling Synchrotron (RCS) and delivered to the MR. As the first stage of the program, Au ions are considered the ion species to accelerate. A full stripping beam of Au ions ($^{197}Au^{79+}$) with an energy of 500 MeV/u is injected from the RCS to the MR. Au ions are accelerated up to 11.5 GeV/u and delivered to the hadron experimental facility. Since the change in revolution frequency during acceleration of Au ions is larger than that for protons, additional cavities dedicated to ion acceleration or modifications to the existing RF cavity will be needed to cover a wider frequency range. To estimate the RF system requirements for accelerating Au ions in the MR, we conducted a longitudinal beam dynamics simulation. In this paper, we present the simulation results with various harmonic numbers and acceleration times.

INTRODUCTION

The Main Ring synchrotron (MR) [1] in the Japan Proton Accelerator Research Complex (J-PARC) [2] is a high-intensity proton synchrotron which accelerates protons from 3 GeV to 30 GeV. The beam injection starts at t = 10 ms from the cycle start. The acceleration starts at t = 140 ms and finishes at t = 790 ms. J-PARC MR has two operation modes with different extraction schemes. The fast extraction (FX) mode is used for the beam delivery to the neutrino experiment. In the FX mode, the beam is extracted using the extraction kickers in one turn. The other operation mode is the slow extraction (SX) mode for the hadron experiment. Since the hadron experiments require a smooth time structure for a long duration (~2s), the beam is extracted slowly after the debunching process by turning the RF off. MR delivered 900 kW (2.40×10^{14} protons at 1.28 s cycle, FX) to the neutrino experiment and 96 kW (8.48×10^{13} protons at 4.24 s cycle, SX) to the hadron experiment in April 2026 [3].

In addition to protons, we are considering accelerating heavy ions to GeV/u energies in the MR as part of the J-PARC heavy-ion program (J-PARC HI) [4–7]. The heavy ions will be injected from the new heavy-ion injector into the J-PARC Rapid Cycling Synchrotron (RCS) and delivered to the MR. Ions accelerated in the MR are delivered to the hadron experimental facility by a slow extraction process. As the first stage of the program, Au ions with low intensity (~ 1.0×10^8 particles per pulse) are considered the ion species to be accelerated in the MR.

Because the charge and mass of Au ions differ significantly from those of protons, estimating the RF frequency and voltage patterns is essential to determining RF system requirements for Au-ion acceleration in the MR. In this paper, we present the calculation and simulation results with various harmonic numbers and acceleration times.

ION INJECTION TO MR

In the J-PARC HI program, ions are accelerated in the new injector and delivered to the RCS. The new heavy-ion injector consists of an ion source, a superconducting linear accelerator, and a booster synchrotron. In the RCS, single-bunched ions are accelerated in the ring at a repetition rate of 25 Hz. After acceleration in the RCS, ions are fully stripped in the beam transport line and injected into the MR. In the same way as in the case of protons, ions are injected from the RCS to the MR four times. As a result, four bunches of ions are injected into the MR and accelerated in total.

As the first stage of the program, the acceleration of Au^{56+} and Au^{79+} is considered in the RCS and MR, respectively. The energy of the ions extracted from the RCS is 500.4 MeV/u.

FREQUENCY PATTERN

The revolution frequency pattern can be calculated from the magnetic field pattern of the bending magnet and the MR circumference (1567.5 m). For the protons acceleration from 3 GeV to 30 GeV, the magnetic field strength ranges from 0.143 T to 1.15 T, corresponding to a magnetic rigidity of 12.8 Tm to 103 Tm. The lower minimum magnetic field of 0.101 T is required to have a magnetic rigidity of 9.03 Tm for the Au^{79+} ions with energy of 500.4 MeV/u from the RCS. The maximum energy of Au^{79+} ions after the acceleration in the MR is 11.5 GeV/u.

Since the charge-to-mass ratio of Au^{79+} ions is larger than that of protons, the change in revolution frequency during acceleration of Au ions is larger than that for protons. The revolution frequency changes from 144 kHz to 190 kHz for Au^{79+} ions, while it ranges from 185 kHz to 191 kHz for protons.

* yasuyuki.sugiyama@kek.jp

ISBN: 978-3-95450-252-3 ISSN: 2673-5350 doi: 10.18429/JACoW-IPAC2026-WEP4646

CONCEPTUAL DESIGN OF A 2.45 GHz ECR ION SOURCE FOR PROTON THERAPY

R.C.Qin[1,2], X.X.Huang*[3], C.Yu[3], P.Wang[3], Y.X.Lu[3], Y.S.Guo[3], Y.F.Lan[1,2], D.H.Su[1,2], W.C.Fang†[3], Z.T.Zhao[3]
[1]Shanghai Institute of Applied Physics,Shanghai, China
[2]University of Chinese Academy of Sciences, Beijing, China
[3]Shanghai Advanced Research Institute, Shanghai, China

Abstract

Proton therapy has attracted increasing attention because of its favorable dose distribution enabled by its Bragg-peak behavior. Motivated by the proton therapy facility project at Shanghai Synchrotron Radiation Facility (SSRF), a 2.45 GHz ECR ion source has been designed. This paper presents the conceptual design of the prototype, together with simulation results of the magnetic field configuration, the ridged waveguide and the beam extraction.

INTRODUCTION

Ion therapy has received growing attention in recent years as an advanced radiotherapy modality. Owing to the Bragg-peak behavior, ion therapy enables highly conformal tumor irradiation while reducing the dose to surrounding healthy tissues [1]. Protons and carbon ions are the two most commonly used particles in ion therapy, while helium ions have recently attracted renewed interests as a promising intermediate option between protons and carbon ions [2]. Compared with carbon-ion therapy, proton therapy offers lower biological uncertainty and reduced nuclear fragmentation tails, making it especially suitable for pediatric treatment [3]. In addition, proton therapy facilities are more mature and cost-effective. These advantages of proton therapy motivate the development of compact and cost-effective proton therapy facilities, in which a reliable high-current proton source is an essential front-end component.

Electron cyclotron resonance ion source (ECRIS) is a type of cathode-free plasma source in which electrons are resonantly heated by microwaves under a suitable magnetic field configuration. The heated electrons subsequently ionize the working gas, producing a magnetically confined plasma from which ions could be extracted. ECR ion sources offer the advantages of long lifetime, high reliability and long-time stable operation. ECR ion sources are commonly identified by their microwave frequency. Among them, 2.45 GHz ECR ion sources have been widely used for the production of high-current singly charged ion beams, especially protons [4]. Benefiting from the mature technology, a simple structure, a low cost and high stability, 2.45 GHz ECR ion sources are well suited for the front ends of medical proton accelerator systems.

* huangxx@sari.ac.cn
† fangwc@sari.ac.cn

At Shanghai Synchrotron Radiation Facility (SSRF), a full-linac proton therapy facility has been proposed as a compact and cost-effective solution for future FLASH treatment [5]. As a key component of the injector, the RFQ has been designed and an aluminium-prototype validation have been completed [6]. Under the framework of the SSRF proton therapy facility project, a 2.45 GHz ECR proton source has been designed. This paper presents the conceptual design of the ion source.

DESIGN CONSIDERATIONS AND DESIGN RESULTS

A three-dimensional engineering layout of the 2.45 GHz ECR proton source is shown in Fig. 1. The source mainly consists of the magnetic confinement system, the microwave system, the discharge chamber, and the beam extraction system. Based on this configuration, the following sections describe the detailed design of the magnetic confinement system, the microwave system and the beam extraction system.

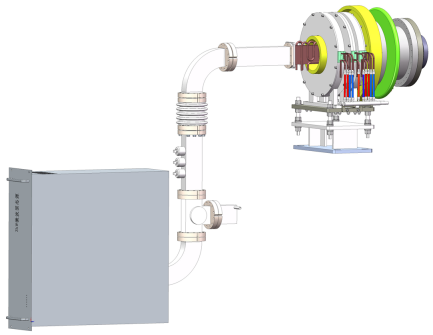

Figure 1: Layout of the 2.45 GHz ECR proton source.

Magnetic Confinement System

In this prototype, electromagnets were adopted instead of permanent magnets to realize flexible adjustment of the magnetic field and to investigate the beam performance under different magnetic field configurations. For a microwave frequency of 2.45 GHz, the corresponding ECR magnetic field is calculated as:

$$B_{ECR} = \frac{2\pi m_e}{e} f \approx \frac{f}{2.8}[kG/GHz] = 875G. \quad (1)$$

The magnetic field is generated by three solenoids, with the central solenoid carrying current in the opposite direc-

Content from this work may be used under the terms of the CC BY 4.0 licence (© 2026). Any distribution of this work must maintain attribution to the author(s), title of the work, publisher, and DOI.

ISBN: 978-3-95450-252-3 ISSN: 2673-5350 doi: 10.18429/JACoW-IPAC2026-WEP4647

DEVELOPMENT OF A GAS-TARGET LASER ION SOURCE TEST SYSTEM FOR THE LAPRIS CONCEPT

S. Matsui†, T. Yorita, Y. Matsuda, H. Kanda, M. Fukuda, T. Tsujisaka, Y. Iwashita
The University of Osaka, Osaka, Japan
T. Nakamura, High Energy Accelerator Research Organization
R. Hajima, K. Kawase, National Institutes for Quantum Science and Technology, Kizugawa, Japan
Y. Fuwa, Y. Kuriyama, Japan Atomic Energy Agency, Tokai Mura, Japan

Abstract

LaPRIS (Laser Plasma RF Ion Source) is a pulsed ion source concept for generating high-quality ion beams using a gas jet, an RF field, and an ultrashort-pulse laser. To investigate laser-induced ion extraction relevant to LaPRIS, we constructed a test system using DC high-voltage extraction and performed preliminary measurements of ions generated by strong-field ionization in a gas target. Time-of-flight measurements using an MCP detector showed laser-correlated ion signals and their dependence on the extraction voltage. These results provide a preliminary demonstration of laser-induced ion extraction relevant to future LaPRIS development.

INTRODUCTION

In high-resolution nuclear physics experiments, the quality of the ion beam injected into the accelerator strongly affects the experimental performance. Experiments using the AVF cyclotron and the ring cyclotron at RCNP require particularly high energy resolution.

At RCNP, a continuous beam generated by an ECR ion source is injected into the accelerator and collimated by slits installed along the beam transport line to achieve high beam resolution. While the transverse emittance can be improved by beam slits, improvement of the longitudinal beam quality requires the phase slit of the cyclotron. To obtain high energy resolution, the injected beam must be confined within a narrow RF phase width. However, since the ECR ion source produces a continuous beam, a buncher is required to compress the beam in the longitudinal direction. Although the present buncher can increase the beam density, it cannot form a sufficiently short bunch. Therefore, phase slit collimation is still required, making it difficult to obtain a high-quality beam with high efficiency.

To address this limitation, we propose a new ion source called LaPRIS (Laser Plasma RF Ion Source) [1]. LaPRIS is a pulsed ion source that generates localized plasma in a gas jet using a focused ultrashort-pulse laser and extracts ions by an RF electric field. Since the laser pulse duration is on the sub-picosecond scale, the generated ion bunch is expected to have an intrinsically ultrashort bunch duration. Therefore, LaPRIS may significantly improve the bunching efficiency compared with conventional methods. In addition, since ionization occurs only in a localized region near the laser focus, the generation of a low-emittance beam is also expected.

H_2 is considered a future target gas for LaPRIS because it can be used as a source gas for proton beam generation in precision nuclear physics experiments. Fig. 1 shows the tunneling ionization yields of N_2 and H_2 calculated using the MO-ADK model [2,3]. At the peak intensity of 1×10^{14} W/cm² used in this experiment, the ionization yields are estimated to be about 50 ions/shot for N_2 and about 10 ions/shot for H_2.

As a step toward the development of LaPRIS for practical application in precision nuclear physics experiments, we constructed a laser-induced ion extraction test system using DC high voltage instead of RF extraction and performed initial measurements of ion signals and their dependence on the extraction voltage.

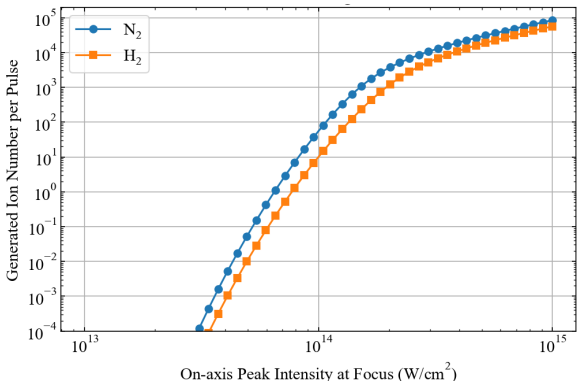

Figure 1: Estimated ionization yield calculated using the MO-ADK model.

EXPERIMENTAL SETUP

Figure 2 shows a photograph of the DC laser-induced ion extraction test system used in this experiment. The system consists of a gas target, DC extraction electrodes, and an MCP detector installed in a vacuum chamber. The chamber pressure was 5×10^{-4} Pa without gas injection and 1×10^{-2} Pa during pulsed gas injection with an average flow rate of 1 sccm.

For gas injection, we used the same piezoelectric pulsed gas valve as in the previous LaPRIS study [1]. The valve was operated with a pulse width of 1 ms and a repetition rate of 10 Hz. For timing control, leakage light from the compressor was detected by a photodiode and used as the

†smatsui@rcnp.osaka-u.ac.jp

Content from this work may be used under the terms of the CC BY 4.0 licence (© 2026). Any distribution of this work must maintain attribution to the author(s), title of the work, publisher, and DOI.

ISBN: 978-3-95450-252-3 ISSN: 2673-5350 doi: 10.18429/JACoW-IPAC2026-WEP4648

EMPIRICAL ORBIT CORRECTION FOR 3-GeV PROTON BEAM TRANSPORT IN FRINGE FIELD FROM FRONT SOLENOID OF SECONDARY BEAMLINE

Y. Yamaguchi*, S. Meigo, Japan Atomic Energy Agency, Tokai, Japan
T. Yamazaki, High Energy Accelerator Research Organization, Tsukuba, Japan

Content from this work may be used under the terms of the CC BY 4.0 licence (© 2026). Any distribution of this work must maintain attribution to the author(s), title of the work, publisher, and DOI.

Abstract

A 3-GeV proton beam from a rapid cycling synchrotron (RCS) is provided to muon and neutron production targets at Materials and Life Science Experimental Facility by a 3-GeV RCS to Neutron facility Beam Transport (3NBT) line in J-PARC. In the 3NBT line, the 3-GeV proton beam is deflected in the vertical direction due to fringe field of a large aperture solenoid for capturing secondary particles from the muon production target located approximately 30 m upstream of the neutron production target. For correcting the orbit deflection and eventually the vertical beam position on the neutron production target, the beam position was measured as function of excitation currents for the coils of the solenoid. In this paper, we report results of the measurement analysis and the orbit correction based on the empirical analysis.

INTRODUCTION

The 3-GeV proton beam transport from a rapid cycling synchrotron (RCS) to a neutron productn target of Materials and Life Science Experimental Facility (MLF) in J-PARC has been stably operated through a 3-GeV RCS to Neutron facility Beam Transport (3NBT) line [1, 2]. The 3NBT line has a muon production target in the most downstream region. As shown in Fig. 1, the muon production target is placed approximately 30 m upstream of the neutron production target and is surrounded by four muon beamlines of D-, U-, S-, and H-lines [3].

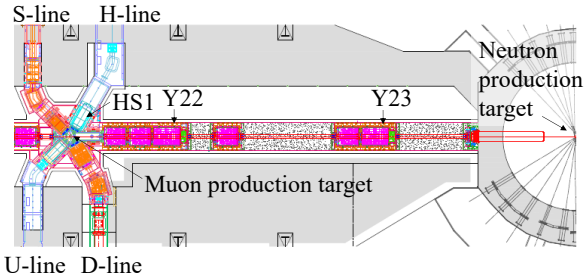

Figure 1: Plan view of 3NBT line between targets. The proton beam comes from the left side of the figure and penetrates the muon production target. The four beamlines surrounding the target extend to experimental areas. At the front of the H-line, a large-aperture capture solenoid HS1 is placed. Between the targets, two vertical steering magnets Y22 and Y23 are placed.

The H-line designed for providing a high-intensity and momentum-tunable muon beam has a large-aperture solenoid HS1 at the front of the beamline for capturing secondary particles, including muons [4]. The front solenoid HS1 comprises three different shaped coils HS1-1, HS1-2, and HS1-3 in order from upstream. These coils can be excited independently for efficiently providing muon beams with a wide range of momenta. The first beam to the H-line was extracted in 2022 [5].

After the H-line operation was started, a proton beam position change in vertical direction was observed at the most downstream profile monitor placed 2 m upstream of the neutron target. The beam position change from the center position resulted from a 3-GeV proton beam orbit change due to a fringe field of the HS1. The fringe field of the HS1 varies because the excitation currents are changed depending on conditions of H-line commissioning or user experiments. This varies the beam position, which reaches over the allowable limit of 3 mm depending on the condition. Thus, active auto-correction of the beam orbit in the 3NBT line is required for the stable operation.

The proton beam orbit can be corrected using two vertical steering magnets Y22 and Y23 shown in Fig. 1. Excitation currents of the Y22 and Y23 are tuned based on orbit calculation using stragetic accelerator design (SAD) code shown in Fig. 2 and excitation currents of the HS1-1, HS1-2, and HS1-3. In the previous correction method, Y22 and Y23 currents were determined on the assumption that a deflection angle due to the fringe field from each coil is proportional to each coil current and is linearly summed in multiple-coil operation. However, the previous method failed to correct in single operation of the HS1-1 or multiple-coil operation. For accurate orbit correction, validity of the assumption above has to be investigated.

In the present study, we have investigated the validity by a comprehensive measurement of the proton beam position at the profile monitor over the entire coil current range and coil combination. The purpose of the present study is to reveal the relation between the beam position change and the coil currents. We present the relation and results of empirical orbit correction based on the relation.

INVESTIGATION OF RELATION BETWEEN BEAM POSITION AND COIL CURRENTS

The measurement of the proton beam position was performed over the entire range of HS1 operation. The HS1 was operated at 125 operation points in the measurement by independent excitation of the three coils at five operation

* yuji.yamaguchi@j-parc.jp

ISBN: 978-3-95450-252-3 ISSN: 2673-5350 doi: 10.18429/JACoW-IPAC2026-WEP4649

SIMULATION-BASED OPTIMIZATION OF A BENT SILICON CRYSTAL FOR BEAM LOSS REDUCTION IN THE J-PARC MAIN RING SLOW EXTRACTION

R. Muto*, T. Asami, T. Kimura, A. Matsumura, S. Murasugi, K. Numai, K. Okamura, Y. Shirakabe, M. Tomizawa, E. Yanaoka
High Energy Accelerator Research Organization, Tsukuba, Japan
K. Itahashi, Y. Saito
The Graduate University for Advanced Studies, SOKENDAI, Hayama, Japan

Content from this work may be used under the terms of the CC BY 4.0 licence (© 2026). Any distribution of this work must maintain attribution to the author(s), title of the work, publisher, and DOI.

Abstract

To achieve a beam power exceeding 150 kW in the J-PARC Main Ring slow extraction, reducing beam loss at the electrostatic septum (ESS) is critical. As a mitigation strategy, we are optimizing the design of a bent silicon crystal to be installed upstream of the ESS. This paper presents FLUKA simulation studies aimed at maximizing the beam loss reduction effect. We demonstrate that volume reflection is preferable to channeling for our operational conditions; its larger angular acceptance accommodates the substantial vertical beam size and relaxes tight crystal torsion constraints. Furthermore, we evaluated the impact of anticlastic deformation on deflection efficiency for both the (110) and (111) crystallographic planes. Although the (111) plane is more susceptible to performance degradation from anticlastic deformation, introducing a downstream beam diffuser narrows the perfomance gap between the (110) and (111) plans, reducing the overall beam loss to ~ 30% of the unmitigated case. Based on these results and the practical material availability, we have selected the (111) plane for volume reflection and are proceeding with crystal fabrication for installation during the next maintenance period.

INTRODUCTION

At the J-PARC Main Ring (MR) [1], 30 GeV protons are slowly extracted using a third-order resonance to the Hadron Experimental Facility [2]. Protons accelerated to 30 GeV are extracted over a period of ~2 seconds. The most critical beam qualities required for this slow extraction beam are high beam intensity and temporal flatness during the extraction period.

The performance of the slow extraction at the J-PARC MR has gradually improved since the start of operations in 2009. Figure 1 shows the trend plots of the beam power and spill duty factor for the J-PARC MR slow extraction. In the operation of April 2026, we achieved a intensity of 8.9×10^{13} protons per pulse. With the current repetition cycle of 4.24 s, this particle number corresponds to a beam power of 101 kW with a high extraction efficiency of 99.6%. Although this beam power has almost reached the acceptable limit of the secondary particle production target currently used in the Hadron Experimental Facility, a new rotating target for accepting over 150 kW beam power is under development,

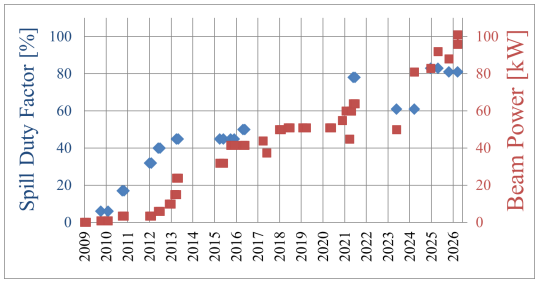

Figure 1: Trend plots of the beam power and spill duty factor for the J-PARC MR slow extraction.

and there is a strong demand from physics experiments for a further increase in beam power. One of the challenges that must be overcome to achieve this beam power upgrade is the further reduction of beam loss during the slow extraction. Therefore, we plan to install a bent silicon crystal upstream of the electrostatic septum. A bent silicon crystal is a silicon crystal that has been mechanically and elastically deformed, and it is known to deflect the trajectory of charged particles. Bent silicon crystals have already been put into practical use for beam collimation at the LHC and for beam loss reduction in the slow extraction of 400 GeV protons at the CERN SPS [3, 4]. In this paper, the beam loss reduction effect of a bent silicon crystal for the case of 30 GeV protons in the J-PARC MR was investigated through simulations using FLUKA [5].

BEAM DEFLECTION EFFECT OF THE BENT CRYSTAL

A bent crystal deflects positively charged particles primarily through two mechanisms: channeling (CH) and volume reflection (VR). In channeling, charged particles are confined within the planar potential created by the crystal planes and deflected along the bent shape of the crystal. While the deflection angle can be controlled by the shape of the crystal, the disadvantage is its small angular acceptance of around ~30 µrad for 30 GeV protons. On the other hand, volume reflection is a phenomenon in which particles outside the channeling acceptance are reflected in the direction opposite to the crystal's bending direction. The deflection angle takes a unique value determined by the crystal structure and cannot be varied; however, since the angular acceptance of VR is determined by the bending angle of the crystal, a larger acceptance can be obtained compared to channeling. Fig-

* ryotaro.muto@kek.jp

ISBN: 978-3-95450-252-3 ISSN: 2673-5350 doi: 10.18429/JACoW-IPAC2026-WEP4652

OPERATIONAL STATUS AND LIFETIME-EXTENSION EFFORTS OF CHARGE-EXCHANGE FOILS IN THE J-PARC 3 GeV SYNCHROTRON

T. Nakanoya†, M. Yoshimoto, P. Saha, R. Saeki, O. Takeda,
Japan Atomic Energy Agency, Tōkai Mura, Japan

Abstract

At the J-PARC 3 GeV Rapid Cycling Synchrotron (RCS), a 400 MeV negative hydrogen (H^-) beam from the linac is converted to proton (H^+) using a charge-exchange foil and then accelerated to 3 GeV. As the output beam power has increased toward the design value of 1 MW, foil deformation and breakage of the SiC support fibers caused by beam irradiation have become major issues, leading to beam dump temperature rises that obstruct stable operation. To improve the reliability of the charge-exchange foil under high power conditions, a stepwise development has been carried out. First, a pure carbon foil was developed to suppress irradiation induced deformation. Beam operation showed reduced deformation compared with previously used hybrid boron-mixed carbon (HBC) foil and graphene thin film (GTF), and beam dump temperature rises were not observed. Next, the arc deposition parameters were optimized by increasing the anode diameter, resulting in further reduction of deformation in beam operation. Finally, carbon nanotube (CNT) wires were adopted as support material instead of SiC fibers. The CNT-supported foil was successfully operated up to 940 kW-equivalent beam power for over 1 month without support failure and beam dump temperature rises. These results demonstrate improved durability of the charge-exchange foil and support stable RCS operation toward 1 MW beam power.

INTRODUCTION

Until now, charge-exchange foils for the RCS have been fabricated in-house at Japan Atomic Energy Agency (JAEA) [1] as HBC foil [2] or have been produced using commercially available GTF [3]. For maintaining stable foil geometry, the foil is supported by a mesh of single-filament SiC fiber from both sides [4], as shown in Fig. 1(a).

In the RCS, to achieve the design beam power of 1 MW, the beam intensity has been increased incrementally [5, 6]. However, the lifetime of the charge-exchange foil has emerged as a critical issue as the beam intensity rises. When the incident particle flux from the linac exceeds 4.5×10^{18} particles per hour (equivalent to output beam power of 600 kW), beam-irradiation-induced damage has emerged prominently as breakage of the SiC fiber and deformation of the foil such as shrinkage and curling. Fig. 1(b) shows a photograph of a foil supported by SiC fiber after beam operation. Multiple SiC fibers near the foil tip where the beam was irradiated, were broken and the foil was visibly deformed. Once the supporting fibers break, the foil can no longer be restrained, and deformation becomes severe at the edges. As this deformation progresses, part of the injected beam no longer hits the foil, leading to a decrease in the charge-exchange efficiency. The injection beam that fails to charge-exchange is discarded in the beam dump. Therefore, increases in beam dump temperature occurred frequently as the beam power increased. When the temperature of the beam dump reaches its upper limit, beam operation must be stopped to protect the beam dump equipment, which constitutes a serious impediment to stable operation.

To address these issues, a stepwise development has been carried out. First, a pure carbon foil was developed to suppress irradiation-induced deformation. Next, the deposition conditions were optimized to further improve the foil durability. Finally, CNT wires were adopted to enhance the radiation resistance of the support structure. The performance of these developments has been evaluated in beam operation at the RCS.

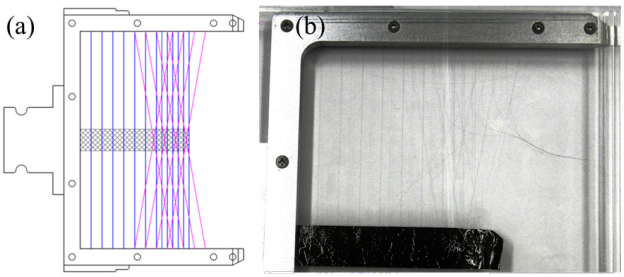

Figure 1: Schematic image of the SiC support fiber pattern (a) and Photograph of the used foil with broken SiC fiber and deformed foil (b).

RESULTS IN BEAM OPERATION

Development of Pure Carbon-based Foil

Figure 2 presents the history of beam power, beam dump temperature, and the type of charge-exchange foils used during the 2022–2023 period. During the period when HBC foil and GTF were used (November 2022 to February 2023), frequent increases in beam dump temperature occurred. Therefore, the foil position was adjusted so that the entire injection beam passed through the foil, ensuring the dump temperature did not exceed 70°C. The point at which position adjustment can no longer suppress the rise in beam dump temperature is the effective lifetime of the foil. Figure 3 shows photographs of an HBC foil taken before and after beam operation. This foil was used under beam operation conditions of 770 kW-eq, and the total number of injected H^- ions reached 2.42×10^{21}. Significant deformation can be observed near the tip where the beam is irradiated.

The deformation observed in HBC foil is considered to arise from irradiation-induced crystallization, in which

†nakanoya@post.j-parc.jp

Content from this work may be used under the terms of the CC BY 4.0 licence (© 2026). Any distribution of this work must maintain attribution to the author(s), title of the work, publisher, and DOI.

ISBN: 978-3-95450-252-3 ISSN: 2673-5350 doi: 10.18429/JACoW-IPAC2026-WEP4654

SYNCHRONIZATION OF LONGITUDINAL HOLLOW ELECTRON BEAM AND ION BEAM IN A STORAGE RING*

X. D. Yang†, Institute of Modern Physics, CAS, Lanzhou, China

Content from this work may be used under the terms of the CC BY 4.0 licence (© 2026). Any distribution of this work must maintain attribution to the author(s), title of the work, publisher, and DOI.

Abstract

In the cooling storage ring, a low-temperature electron beam from the electron cooling device overlaps with a high-temperature ion beam in the storage ring. The overlap occurs at the same average velocity for a certain distance. Through Coulomb interaction, electrons absorb excess energy from ions. This reduces the transverse emittance and longitudinal momentum spread of the ion beam, and increases its phase space density. When cooling a Gaussian-distributed pulsed ion beam with a longitudinal hollow electron beam, the pulses must align at the longitudinal center. This article introduces a synchronization scheme for longitudinal hollow electron beams and ion beams. The scheme includes pulse measurement, triggering delay, synchronization monitoring, and future feedback for automatic correction. This ensures the pulses are always synchronized. The scheme will be used in longitudinal hollow electron beam cooling experiments and will support future investigations into the cooling process.

INTRODUCTION

Electron cooling can improve the quality of ion beams in storage rings by reducing their transverse emittance and longitudinal momentum spread, increasing the phase space density of the ion beams, and thus enhancing collision luminosity.

The basic principle of electron cooling involves overlapping an ion beam with an electron beam moving at the same average velocity. Through Coulomb interactions, the hotter ion beam transfers excess energy to the cooler electron beam, thereby reducing the transverse emittance and longitudinal momentum spread of the ion beam and achieving a higher phase space density.

The electron cooling force is proportional to the electron density, and the cooling force presents a nonlinear distribution. Within a certain range, the cooling force is linearly related to the relative velocity difference between the ion and electron [1].

A direct current electron beam was used in the traditional low-energy electron cooling, which is continuous and generated by an electrostatic high-voltage accelerator with a uniform longitudinal distribution [2].

At higher energy levels, the electron beam is generated by a radio-frequency accelerator, and it consists of a series of short pulses with a uniform distribution of electron beam intensity in the longitudinal direction [3-5].

The ion beam in the storage ring presents a Gaussian distribution in the longitudinal direction. Under continuous electron cooling, the ion beam distribution deviates from the Gaussian distribution, forming a dense core in the central region and a tail in the edge region [6].

A novel solution was proposed in the reference [7]. A longitudinal hollow electron beam was proposed. The traditional DC electron beam in the electron cooler was modulated into an electron bunch with different longitudinal distributions. The stronger cooling was expected in the tail of the ion beam, and the weaker cooling was performed in the tail of the ion beam. The particle on the outside will experience stronger cooling and will be driven back into the center of the ion beam.

The longitudinal hollow electron beam is expected to obtain benefits in the following aspects.

- Suppress intra-beam scattering.
- Control the longitudinal distribution of the ion beam.
- Make the beam bunch contain as many particles as possible.
- Increase the lifetime of ion beams in the storage ring.

The basic requirement for electron cooling is that the electron beam can completely envelop the ion beam. Therefore, it is required that the center of the ion beam pulse and the electron beam pulse remain consistent in the longitudinal direction.

The ion beam pulse rotates in the storage ring with a bunch length of approximately 400 nanoseconds before electron cooling. It presents a Gaussian distribution in the longitudinal direction.

The electron beam is generated by an electron gun, which is a capacitive structure. The voltage applied to the control electrode of the electron gun determines the electron beam intensity. If a pulse cosine waveform voltage is applied to this electrode, a cosine waveform electron beam pulse will be obtained. The pulse length is approximately 500 nanoseconds. The frequency of the electron beam pulse output is exactly the same as the revolution frequency of the ion beam in the storage ring.

In order to ensure that the electron beam and ion beam pulses are always synchronized, the generation time of the electron pulse needs to be adjusted to ensure the centers of the two pulses overlap, and the synchronization is less than 1 nanosecond.

Some primary investigations have been performed in some references, such as the formation of a bunched electron beam at the electron cooler of CSRm [8], double-bunch of electrons [9], and a longitudinal multi-bunch chain of electrons [10]. Some electron cooling experiments using a bunched electron beam have been completed in the CSRm storage ring, in collaboration with the team from Jefferson Lab [11-16].

* Work supported by NSFC No. 12275325, 12275323, 12205346.
† yangxd@impcas.ac.cn.

ISBN: 978-3-95450-252-3 ISSN: 2673-5350 doi: 10.18429/JACoW-IPAC2026-WEP4655

UPDATED DESIGNS OF 6D AND FINAL COOLING CHANNELS FOR A MUON COLLIDER

R. Zhu[1]*, J. Yang[1]
Institute of Modern Physics, Chinese Academy of Sciences, Lanzhou, China
[1]also at University of Chinese Academy of Sciences, Beijing, China
C. Rogers, Rutherford Appleton Laboratory, Didcot, United Kingdom

Abstract

The muon collider is regarded as a strong candidate for probing physics beyond the current energy frontier, combining the advantages of lepton collisions with the potential to reach multi-TeV center-of-mass energies. To obtain the required luminosity, the six-dimensional (6D) emittance of the muon beam must be reduced by several orders of magnitude within the short muon lifetime. This reduction relies on ionization cooling and is realized through two major stages: 6D cooling and final transverse cooling. In this work, we present updated lattice designs for both the rectilinear 6D cooling channel and the final cooling channel. The new design achieves a twofold decrease in the final transverse emittance, representing a significant step toward satisfying the beam-quality demands of a future muon collider.

INTRODUCTION

Electron–positron colliders are attractive because they provide clean collision environments, making events simpler to analyze than those produced in hadron machines. A major limitation for circular electron–positron colliders at high energy is synchrotron radiation, which is already significant for multi-GeV electron beams and becomes increasingly severe toward the multi-TeV regime because of the low electron mass. Muons, by contrast, are much heavier and therefore suffer far less from synchrotron radiation, while still remaining elementary leptons. For this reason, muon colliders are considered a promising option for future high-energy physics research [1]. A central challenge for the entire muon-collider complex is the short muon lifetime, which places stringent constraints on beam production, cooling, acceleration, and collision. In addition, muon beams generated from pion decay have emittances far larger than the acceptance of downstream acceleration systems. As a result, dedicated cooling is required before acceleration. The full cooling channel contains two parts: 6D cooling and final cooling. The 6D cooling system itself is divided into a pre-merge section, which reduces the emittance to the level required for bunch merging [2] ($\varepsilon_T \leq 1.3$ mm, $\varepsilon_L \leq 1.7$ mm), and a post-merge section, which cools the beam again after the emittance growth introduced by bunch merging and further reduces it to ease the demands on final cooling. The final cooling channel must then decrease the transverse emittance to 22.5 μm [3] in order to meet the luminosity target. In this paper, we report updated designs for both the 6D and final cooling channels. Relative to earlier studies [4, 5], G4beamline v3.08 simulations [6] show that the revised designs reduce the output transverse emittance by about a factor of two, while the longitudinal emittance at the end of final cooling remains below the target value of 64 mm [3].

* zhuruihu@impcas.ac.cn

PRINCIPLE OF MUON COOLING

Because the muon lifetime is only 2.2 μs in its rest frame, ionization cooling is the only practical cooling approach for muon beams. In an ionization-cooling channel, muons lose both transverse and longitudinal momentum while passing through an absorber via ionization energy loss. The lost longitudinal momentum is then restored by RF cavities, while the lattice is arranged so that the transverse momentum is not restored, resulting in a net decrease of the transverse emittance. The evolution of the normalized transverse emittance is given by [7]:

$$\frac{d\varepsilon_T}{ds} = -\frac{1}{\beta^2}\frac{dE_\mu}{ds}\frac{\varepsilon_T}{E_\mu} + \frac{1}{\beta^3}\frac{\beta_T E_s^2}{2E_\mu m_\mu c^2 L_R}. \quad (1)$$

where ε_T denotes the normalized transverse emittance, E_μ is the muon energy in GeV, m_μ is the muon mass, β is the particle velocity normalized to the speed of light c, β_T is the transverse beta function, dE_μ/ds is the energy loss per unit length, E_s is the characteristic scattering energy, and L_R is the radiation length of the absorber. The first term describes cooling, while the second represents heating caused by multiple scattering.

To achieve longitudinal cooling, dispersion must be introduced at the absorber location, typically by using a wedge absorber. Under dispersion, particles with higher momentum pass through a thicker region of the wedge and therefore lose more energy, which reduces the longitudinal emittance. In this situation, the equilibrium transverse and longitudinal emittances can be written as [7]:

$$\varepsilon_T^{eq} = \frac{\beta_T E_s^2}{2\left|\frac{dE_\mu}{ds}\right|\beta g_T m_\mu c^2 L_R}. \quad (2)$$

$$\varepsilon_L^{eq} = \frac{\beta_L m_e c^2 \gamma^2 (1-\frac{\beta^2}{2})}{2g_L \beta m_\mu c^2 [\frac{\ln(K\gamma^2\beta^2)}{\beta^2} - 1]}. \quad (3)$$

where g_T and g_L are the transverse and longitudinal partition numbers, respectively, defined as

Content from this work may be used under the terms of the CC BY 4.0 licence (© 2026). Any distribution of this work must maintain attribution to the author(s), title of the work, publisher, and DOI.

ISBN: 978-3-95450-252-3 ISSN: 2673-5350 doi: 10.18429/JACoW-IPAC2026-WEP4658

OPERATIONAL EXPERIENCES AND UPGRADE OF CSNS ION SOURCE

S. Liu†,1,2, H. Li1,2, W. Chen1,2, X. Cao1,2,Y. Xiao1,2, H. Liao1,2, Y. Lv1,2
K. Xue1,2, Z. Lin1,2, S.M. Liu1,2, F. Li1,2
[1]Institute of High Energy Physics, Chinese Academy of Sciences, Beijing, China
[2] Spallation Neutron Source Science Center, Dongguan, China

Abstract

The CSNS ion source has been in operation over 10 years since 2015. It has provided a stable beam current, progressing from an initial beam commissioning power of 10 kW to the current 180 kW. The CSNS ion source is responsible for delivering 30-40 mA H^- at 50 kV. During CSNS phase I, a Penning surface negative ion source was used, based on the ISIS ion source prototype. It met the operational requirement of 100 kW beam power of CSNS phase I. However, due to its short lifetime, typically requiring replacement every month, and its relatively large emittance, it faced significant challenges as the beam power for CSNS phase II is raised to 500 kW. To address this, an RF ion source was proposed and its development began in 2016. This volume ion source has been successful used in SNS and JPAC and offer some advantages such as a longer lifetime, lower emittance, lower cesium consumption. Unlike the internal antenna design used by SNS and JPAC, an external antenna RF ion source was successful developed and put into operation in September 2021. This paper will discuss the extensive operational experience and upgrade of CSNS ion source.

INTRODUCTION

The China Spallation Neutron Source (CSNS) is an accelerator-based high power project with multipurpose currently under operation with an on-target beam power of 100 kW[1,2]. The accelerator complex consists of an 80 MeV H− linear accelerator as the injector and a 1.6 GeV rapid cycling proton synchrotron (RCS). The linear accelerator consists of a 50 keV H− Penning surface plasma ion source (IS), a low energy beam transport line (LEBT), a 3.0 MeV RFQ accelerator, a medium energy beam transport line (MEBT), an 80 MeV drift tube linear accelerator (DTL) and a high energy beam transport line (HEBT). The beam power is 100 kW. For the CSNS upgrade (CSNS-II), the injection energy is increased from 80 MeV to 300 MeV . The beam power is increased up to 500 kW. Since the operation of CSNS, the performance of the ion source has been critically important, as it directly affects the beam condition of the RCS. Even minor fluctuations may lead to an increase in beam loss in the RCS ring. For CSNS phase I, the front end should provide a stable H− beam with energy of 3.0 MeV, a maximum pulsed current up to 15 mA, at a repetition of 25 Hz and beam pulse width of 400 ms before chopping. For CSNS phase II, beam power is up to 500 kW and H− bema current with 40 mA at the RFQ exit before chopping is required. Therefore, higher beam current intensity and lower beam emittance are required from ion source.

PENNING ION SOURCE

The installation of CSNS front end was completed in 2015. A Penning surface plasma source is used to serve CSNS, which is also applied to ISIS [3]. This ion source is characterized by its high emission current density, simple operation, rapid replacement and relatively low cost. The ion source consists of a discharge chamber, an extraction electrode, an analyzing magnet, a -50 kV isolation ceramic insulator, an accelerating electrode and a large vacuum chamber with two turbo molecular pumps [2]. Cesium is used to increase the H^- ion production efficiency. The discharge chamber consists of a molybdenum anode, cathode and aperture plate, where the plasms arc is confined. A transverse magnetic Penning field is applied across the discharge chamber. Hydrogen and cesium are fed into the discharge chamber via holes in the anode. The detail design and operational parameters find reference [4,5].

The CSNS beam supply efficiency is shown in Fig. 1. Starting from 2018, beam commissioning of the accelerator was carried out, and the designed target of 100 kW was achieved in 2019. Penning ion source was installed in 2015, and replaced by RF ion source in 2021. For the discharge chamber of a Penning ion source, its service life is typically one month.

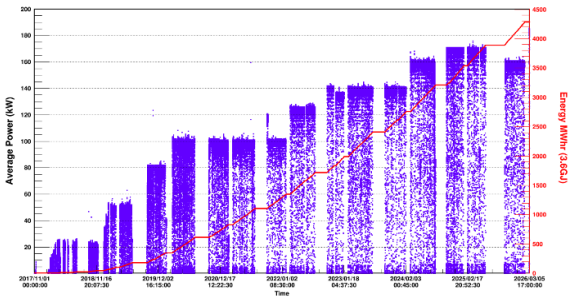

Figure 1: Beam Power from 2018 to 2026.

In general, for each set of discharge chamber, the ion source can produce up to 40 mA H^- ion beam with a beam duty factor about 1.25% (500 μs and 25 Hz) and a normalized rms emittance about 0.8 πmm.mrad. Although the emittance is much larger than the acceptance of RFQ (0.2 πmm.mrad), the H^- ion beam current is still larger than 20 mA within the acceptance of RFQ, which satisfies the current requirement of CSNS phase I. For 100 kW beam power operation, a routine beam current from ion source of about 30 mA is enough. The average expected lifetime of CSNS Penning ion source, mainly limited by the discharge chamber, is about 1 month. The instability of ion source

† liusj@ihep.ac.cn

Content from this work may be used under the terms of the CC BY 4.0 licence (© 2026). Any distribution of this work must maintain attribution to the author(s), title of the work, publisher, and DOI.

ISBN: 978-3-95450-252-3 ISSN: 2673-5350 doi: 10.18429/JACoW-IPAC2026-WEP5003

BENCHMARKING THE XSUITE CODE WITH BEAM POLARIZATION DATA OF THE LARGE ELECTRON POSITRON COLLIDER

G. Iadarola, J. Wenninger*
European Organization for Nuclear Research (CERN), Geneva, Switzerland

Abstract

The 26.7 km long Large Electron Positron collider (LEP) was operated at CERN between 1989 and 2000. The most precise measurements of the Z boson mass and width were made possible thanks to high precision energy calibration of the LEP beams with resonant depolarization. Transversely polarized beams had to be established at LEP to achieve this goal, providing a rich legacy of data on polarized beams at beam energies around 45 GeV. The beam dynamics simulation package Xsuite was recently enhanced to track polarized beams and to evaluate the equilibrium polarization of beams and related quantities. Xsuite code benchmarking with LEP results on transverse polarization and resonant depolarization will be presented in this contribution.

INTRODUCTION

High precision measurements of the Z boson mass and width and of the W boson mass are important pieces of the 91 km circumference Future Circular Collider (FCC-ee) physics program. The goal of this program is to reduce by at least a factor of ten the uncertainties in the beam energy compared to the LEP results [1]. The precision measurement of the beam energies at FCC-ee will rely on resonant depolarization of transversely polarized beams, based on the LEP experience [2, 3].

The Xsuite accelerator simulation framework [4] was enhanced with spin modeling capabilities [5], allowing six-dimensional tracking of particle trajectories together with their spin motion. The module includes integration of the Thomas–BMT equation and a linearized computation of the invariant spin field (ISF). Radiative spin effects are incorporated through the Sokolov–Ternov mechanism and its generalizations, allowing the evaluation of equilibrium polarization and of its buildup times.

This contribution complements the benchmarking of the Xsuite polarization module with LEP polarization and resonant depolarization data collected during the years of LEP operation around the Z boson resonance, mainly in the beam energy range of 44.5 to 46.5 GeV.

SOLENOID COMPENSATION

Each of the four large LEP detectors had solenoids with integrated fields ranging from 2.6 Tm to 10.08 Tm. The betatron coupling induced by those solenoids was compensated by skew-quadrupoles installed in the long straight sections. The spin resonances introduced by the solenoids were not compensated for by this scheme, leading to very low or no transverse polarization at all. The spin correction schema relied instead on orbit bumps installed in the arcs around each experimental IP [6]. The correction relied on vertical double pi-bumps in the arc on either side of every solenoid to minimize the spurious dispersion generated by the large bumps, with peak amplitudes of ≈ 6 mm for the ALEPH solenoid as shown in Fig. 1. The evolution of the polarization vector through this bump is shown in Fig. 2.

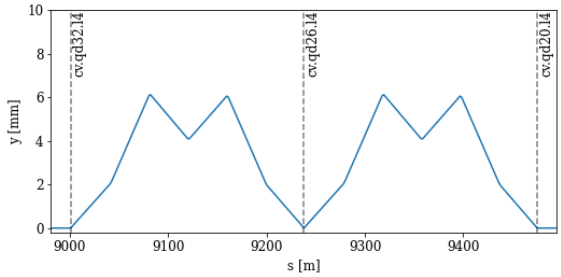

Figure 1: Double pi-bump used to compensate the solenoid of the ALEPH detector. This bump is placed on the left side of the IP, a symmetric bump is placed on the right side.

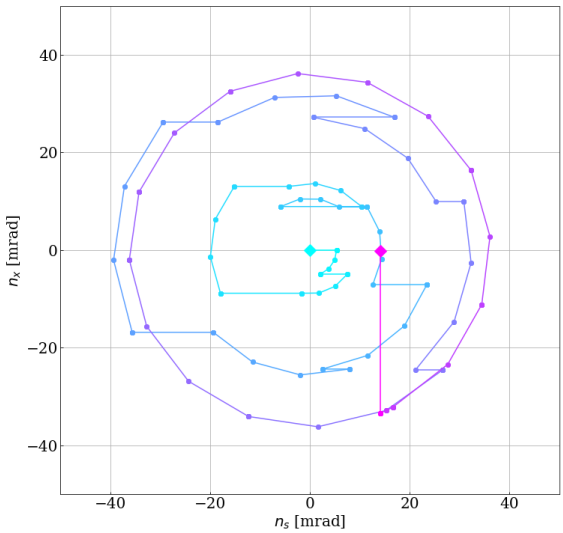

Figure 2: Evolution of the polarization vector projection in the horizontal plane (s-x) through the bump shown in Fig. 1 and half of a solenoid. The polarization vector is initially vertical (cyan rectangle at (0,0)), it ends at the purple rectangle.

The predicted equilibrium vertical polarization with and without solenoid compensation is shown in Fig. 3, in good agreement with the LEP results [2]. With solenoids switched on, the transverse polarization never exceeded a few percent in the absence of the compensation bumps.

* jorg.wenninger@cern.ch

Content from this work may be used under the terms of the CC BY 4.0 licence (© 2026). Any distribution of this work must maintain attribution to the author(s), title of the work, publisher, and DOI.

ISBN: 978-3-95450-252-3 ISSN: 2673-5350 doi: 10.18429/JACoW-IPAC2026-WEP5004

BEAMLINE EXTENSION CONSIDERATIONS FOR AREAL-50 ACCELERATOR

A. Grigoryan[1], A. Asoyan, A. Vardanyan, M.Yazichyan, A. Hovakimyan, M. Ivanyan, G. Amatuni, B. Grigoryan, Center for the Advancement of Natural Discoveries using Light Emission (CANDLE SRI), Yerevan, Armenia [1]also at Yerevan State University, YSU Yerevan, Armenia

Abstract

AREAL linear accelerator, presently operating at CANDLE SRI generates 5-MeV ultrashort electron beams for a wide range of applications. The planned upgrade program aims to increase the beam energy up to 50 MeV in order to expand experimental capabilities and enable the generation of THz radiation. For this purpose, two 1.6-m-long accelerating structures are foreseen to be installed. To ensure optimal beam parameters for efficient acceleration and high-quality beam delivery, existing magnetic and diagnostic systems must be modified and supplemented. In this paper, several aspects of the new beamline design are examined, and the corresponding beam dynamics studies for the proposed layout are presented.

INTRODUCTION

The Advanced Research Electron Accelerator Laboratory (AREAL), operated at the CANDLE Synchrotron Research Institute in Yerevan, is a compact linear accelerator generating ultrashort electron beams with energies up to 5 MeV and sub-picosecond bunch durations [1,2]. The facility supports a broad range of scientific experiments, including advanced accelerator and radiation studies, as well as research in materials and life sciences [3]. AREAL is based on a laser-driven RF gun with a 1.5-cell accelerating system operating at a peak gradient of 110 MV/m, providing high-brightness electron beams.

A key objective of the AREAL upgrade program is the increase of the beam energy up to the 20–50 MeV range, enabling the development of an undulator-based THz radiation source and significantly expanding the experimental capabilities of the facility [4,5]. The upgrade foresees the installation of two traveling-wave accelerating structures, each 1.6 m in length, designed for an average accelerating gradient of 15 MV/m [6]. In this context, strict constraints are imposed on the electron beam dynamics, particularly to ensure effective bunch length compression and preservation of low transverse emittance throughout transport.

To meet the beam quality requirements at the entrance of the accelerating structures, the implementation of an optimized magnetic lattice is essential. The present concept includes solenoid-based emittance compensation complemented by quadrupole doublet configurations for transverse matching of the Twiss parameters.

This paper presents a transverse beam dynamics study focusing on the optimal longitudinal placement of the accelerating structures and the corresponding magnetic configuration required for beam matching and emittance preservation. Attention is devoted to the evolution of the transverse emittance and the Twiss parameter α under the influence of space-charge effects in the low-energy section. The study aims to identify an optimal 'trade-off' between low α values and minimal emittance growth through appropriate adjustment of the magnetic optics configuration, including solenoid-based emittance compensation and quadrupole doublet matching.

BEAM MATCHING FOR THE ACCELERATING SECTION

The extension of the AREAL linear accelerator from its current 5 MeV energy to the 20–50 MeV regime requires careful optimization of the transverse beam dynamics. In the low-energy section, the dynamics are dominated by space-charge effects, which critically influence both longitudinal and transverse phase-space evolution. Simulations performed with the ASTRA tracking program show that an initially short laser pulse ($\approx 0.2ps$) generates an electron beam that experiences significant longitudinal broadening, reaching approximately $0.8\,ps$ after $1.5\,m$ of transport through the accelerating lattice.

The transverse beam evolution is described by the RMS envelope equation, accounting for the space-charge-dominated regime [7]:

$$\frac{d^2\sigma}{dz^2} + k(z)\sigma - \frac{\varepsilon_n^2}{\beta^2\gamma^2\sigma^3} - \frac{K}{\sigma} = 0$$

where σ is the RMS beam size, $k(z)$ is the external focusing strength, ε_n is the emittance, and $K = \frac{2I}{I_A\beta^3\gamma^3}$ is the generalized perveance, where I the peak beam current and $I_A = 17\,kA$ the Alfvén current. The gun section includes a solenoid magnet located downstream of the RF gun for emittance compensation. In the current setup, the solenoid is positioned at 0.565m. In the proposed configuration, the solenoid is moved closer to the cathode—placed approximately 4 cm downstream—and is mounted directly onto the accelerating structure to achieve more effective emittance compensation (Fig. 1).

The evolution of the transverse emittance along the beamline is characterized by the emittance compensation process induced by the gun solenoid. Analysis indicates that the transverse emittance minimum—reaching a value of $\varepsilon = 1.5\,\pi\,mm\,mrad$—occurs at $z = 1.72\,m$ downstream of the photocathode with the solenoid field $B = 0.423T$. This longitudinal position is critical, as it defines the optimal location for the entrance of the accelerating

Content from this work may be used under the terms of the CC BY 4.0 licence (© 2026). Any distribution of this work must maintain attribution to the author(s), title of the work, publisher, and DOI.

ISBN: 978-3-95450-252-3 ISSN: 2673-5350 doi: 10.18429/JACoW-IPAC2026-WEP5005

EXPERIMENTAL CAVITY COMPENSATION IN SPIRAL2 SC LINAC

A. Leduc*, M. Di Giacomo, J-M. Lagniel, G. Normand, A. K. Orduz
Grand Accélérateur National d'Ions Lourds (GANIL), Caen, France
F. Bouly, A. Plaçais
Univ. Grenoble Alpes, CNRS, Grenoble IN2P3, LPSC-INP Grenoble, France

Abstract

During the years of operation of the GANIL SPIRAL2 SC LINAC (Caen, France), issues affecting amplifiers and cavities have preventing the LINAC operation. To maintain the overall accelerator availability, cavity failure compensation studies have been started for D^+ beam, with nominal energy recover and transmission as main goals.

LINAC setting with one failing cavity is calculated for D^+ beam transported in order to reach 40 MeV and keep losses as low as possible. The method for calculating compensation is discussed, cavity compensation simulations and the associated experimental measurements are presented.

INTRODUCTION

To ensure high LINAC reliability, a single cavity failure compensation studies were started. To compensate a cavity failure, it is necessary to readjust the phase and voltage of some cavities downstream, and few upstream. Simulations were performed to determine new LINAC settings with one cavity out of order, with the objective of transmitting the different SPIRAL2 beams through the LINAC with minimal losses while maintaining the highest possible beam energy at the LINAC exit. Similar studies were done mainly on cavities with high beta [1–4]. For the SPIRAL2 LINAC [5], there are two families of cavities, with $\beta = 0.07$ or $\beta = 0.12$. This LINAC has been designed to accelerate a large variety of beams, with different A/Q (from protons $A/Q = 1$ to heavy ions $A/Q = 3$) [6].

In the nominal case, in SPIRAL2, the D^+ beam has a final energy of 40 MeV [7], and a maximum current of 5 mA. Due to the "low" energy of the particles and the high current, the space charge leads to a more complex cavity compensation. In this framework, it has been decided to study the possibility to operate the SPIRAL2 LINAC with one cavity out of order.

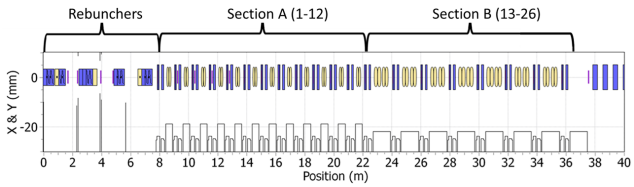

Figure 1: Layout of the SPIRAL2 MEBT and LINAC. Quadrupoles are in blue, cavities and rebunchers in yellow.

The simulations track particles in the MEBT and the LINAC, composed of three rebunchers and 26 cavities. The 12 first cavities ($\beta = 0.07$) compose the section A (1 to 12). The section B ($\beta = 0.12$) is composed of the 14 next cavities (13 to 26) Figure 1.

Simulations are performed using TraceWin [8], with the following parameters for the D^+ beam: initial energy 1.46 MeV, beam current 5 mA at the LINAC entrance, $\varepsilon_{xx'} = 0.20\,\pi$ mm mrad, $\varepsilon_{yy'} = 0.20\,\pi$ mm mrad, and $\varepsilon_{zz'} = 0.30\,\pi$ mm mrad. The nominal energy at the exit of the LINAC is 40 MeV [7]. Calculations are done for a continuous beam with a final beam power of 200 kW. The majority of experiments on SPIRAL2 require D^+ beams, with beam power lower than 2 kW.

NOMINAL LINAC SETTING

The LINAC parameter settings in 2024, with all 26 cavities operational, are used for an initial simulation. Figure 2 shows the phase and radial particles distribution (MEBT and LINAC) for a D^+ beam.

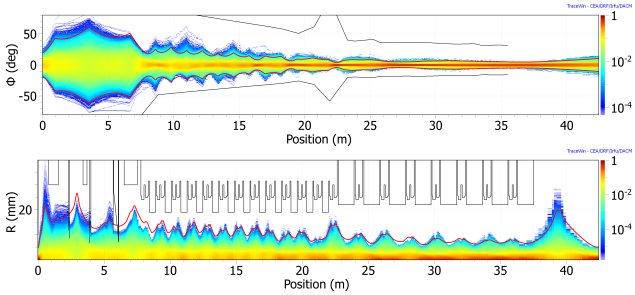

Figure 2: Particles density according to the phase and to the radial position, for the nominal setting (2024).

Beam losses are mainly monitored by BLMs located along the LINAC and the HEBT. Vacuum pressure variation can be also used as a diagnostic [9]. In the case of D^+ beam, only BLMs are used.

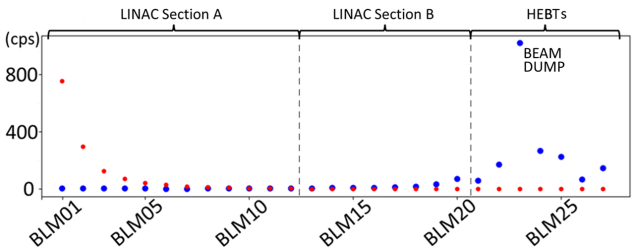

Figure 3: BLMs measurements along the LINAC and the HEBT: for nominal tuning (blue dots) and without beam in the LINAC (red dots). The BLM23 detects back-scatter emissions from beam dump.

Figure 3 shows BLMs measurements along the LINAC. The blue dots correspond to measurement with beam in the LINAC, and in red without beam. BLMs signals will be divided by the final beam power. The signal will be in count per second per watt (cpspW).

Content from this work may be used under the terms of the CC BY 4.0 licence (© 2026). Any distribution of this work must maintain attribution to the author(s), title of the work, publisher, and DOI.

ISBN: 978-3-95450-252-3 ISSN: 2673-5350 doi: 10.18429/JACoW-IPAC2026-WEP5007

ACCUMULATOR-TO-TARGET BEAM TRANSFER LINE FOR ESSνSB+

E. Bouquerel†, M. Dracos, Institut Pluridisciplinaire Hubert Curien, Strasbourg, France
M. Olvegård, Uppsala University, Uppsala, Sweden
On behalf of the ESSνSB+ collaboration

Abstract

The ESSnuSB project aims to generate an intense neutrino beam and the associated muon flux, using a 5 MW high-power proton driver, requiring precise and reliable transport of the accumulated beam to the target station. To achieve this, a dedicated transfer line, named R2T, guides the extracted protons from the accumulator toward the neutrino beam direction while meeting strict geometric constraints. The beam transfer line accommodates horizontal and vertical angular offsets of 16.8° and 1.14° using a compact sequence of horizontal and vertical dipoles, with quadrupoles ensuring controlled beam size and minimal losses. Simulations show that a lattice just over one hundred meters long successfully preserves beam quality and aligns the beam with the required neutrino direction. This guarantees stable, low-loss delivery of the beam to the downstream target system.

THE ESS NEUTRINO SUPER BEAM PROJECT

Understanding the origin of the matter-antimatter asymmetry in the Universe remains one of the most fundamental open questions in modern physics. A compelling explanation requires physics beyond the Standard Model, in particular the existence of Charge-Parity Violation (CPV) in the leptonic sector. The experimental discovery and precise measurement of leptonic CPV would have profound implications for particle physics and cosmology. However, such measurements are extremely challenging due to the weak interaction of neutrinos with matter, which necessitates the use of very intense neutrino beams and large-scale detectors.

The ESSνSB (European Spallation Source neutrino Super Beam) project has been proposed to address this challenge by exploiting the unique capabilities of the European Spallation Source (ESS) linear accelerator [1]. The ESS linac, currently under construction, will deliver a 5 MW proton beam at 2 GeV for neutron production [2]. ESSνSB proposes to upgrade this facility to simultaneously generate an intense neutrino beam by increasing the duty cycle from 4% to 8%, achieved through a doubling of the pulse repetition rate. The concept further relies on the acceleration of H^- ions and the use of an accumulator ring to compress the proton pulse length from 3 ms to 1.2 μs, making it compatible with the operation of a magnetic horn system.

To address the extreme thermal and mechanical stresses induced by such high power and short pulses on the neutrino production target, the beam is distributed over four sequential targets, each equipped with a focusing horn. The facility design also includes a near detector for precise characterization of the neutrino beam and a far Water Cherenkov detector located at a baseline optimized for oscillation studies.

The Conceptual Design Report of ESSνSB has demonstrated the feasibility of the proposed facility and its outstanding physics potential [1]. In particular, the experiment is designed to operate at the second oscillation maximum, where sensitivity to CP violation is significantly enhanced compared to the first maximum. This approach allows for a substantial reduction in the impact of systematic uncertainties, especially those related to neutrino–nucleus cross-sections, which currently represent a major limitation due to the scarcity of data in the relevant energy range (0.2-0.6 GeV).

Based on these results, the ESSνSB+ Design Study aims to further develop and consolidate the project in preparation for submission to the ESFRI roadmap. This extended program includes civil engineering and site studies, as well as the development of complementary facilities for precise cross-section measurements and sterile neutrino searches, and a monitored neutrino beam inspired by the ENUBET concept [3]. These additional infrastructures will play a crucial role in reducing systematic uncertainties and broadening the scientific reach of the project.

Beyond its primary scientific goals, ESSνSB represents a major opportunity to extend the use of a leading European research infrastructure into the domain of fundamental physics. The project is expected to drive technological innovation, stimulate industrial development, and strengthen Europe's position at the forefront of neutrino research.

MAIN COMPONENTS OF THE FACILITY

The ESSνSB facility is based on four main components: the proton driver, an accumulator ring, the neutrino target station, and the near and far detectors (Fig.1).

Proton Driver (ESS Linac): The ESS linac will accelerate protons to 2 GeV in 3 ms pulses at 62.5 mA and 14 Hz for neutron production. Its low duty cycle (4%) allows interleaved H^- pulses, which are used to generate a high-intensity neutrino beam.

Accumulator Ring: To efficiently operate the hadronic focusing system, it is necessary to deliver extremely short and intense proton pulses. The 3 ms pulses from the linac must therefore be compressed by approximately three orders of magnitude. This is achieved using an accumulator ring with a circumference of about 400 m, where the beam is accumulated and rapidly extracted, resulting in pulse lengths of the order of 1 μs.

†elian.bouquerel@iphc.cnrs.fr

Content from this work may be used under the terms of the CC BY 4.0 licence (© 2026). Any distribution of this work must maintain attribution to the author(s), title of the work, publisher, and DOI.

ISBN: 978-3-95450-252-3 ISSN: 2673-5350 doi: 10.18429/JACoW-IPAC2026-WEP5008

INJECTION LOSSES IN THE SOLEIL II STORAGE RING: SENSITIVITY TO BOOSTER AND TRANSFER LINE ERRORS

S. Habet*, A. Loulergue, L. S. Nadolski, M.-A. Tordeux
Synchrotron SOLEIL, Saint-Aubin, France

Abstract

Injection losses are a key challenge for SOLEIL II commissioning because the reduced storage-ring acceptance makes off-axis injection highly sensitive to transport and optics errors. We use multiparticle tracking with a corrected lattice model including realistic static and jitter errors in the booster and Transfer Line 2 (TL2). The results show that losses are primarily governed by the injected phase-space distribution at the Multipole Injection Kickers (MIK). Most particles are intercepted at the septum and at Straight Section 7 (SDM07), while the injection acceptance window sets the efficiency for all studied error scenarios. Emittance exchange improves the horizontal footprint only if the final TL2 focusing errors remain at the percent level; otherwise, the enlarged vertical beam size samples the non-linear MIK field and generates large horizontal over-kicks. These results provide practical tolerances and tuning priorities for top-up commissioning.

INTRODUCTION

The upgrade of the SOLEIL synchrotron to the 4th-generation light source SOLEIL II relies on a Multi-Bend Achromat lattice to reach ultra-low emittance and high photon brightness. This strong focusing, however, reduces the dynamic aperture and momentum acceptance of the Storage Ring (SR), making high-efficiency top-up injection one of the main challenges for commissioning and routine operation [1].

In the baseline scheme, beam injection is performed with an array of five Multipole Injection Kickers (MIKs) [2, 4, 6]. The beam extracted from the booster, with nominal emittances of 5 nm rad horizontally and 0.5 nm rad vertically, is transported through the TL2 and must be injected within the narrow SR acceptance. In practice, static and systematic errors in the booster and transfer line distort the beam phase space and can drive the injected distribution outside the accepted region, leading to localized losses. This paper presents multiparticle tracking simulations used to identify and quantify these loss mechanisms.

INJECTION SCHEME AND ERROR MODELING

To simulate the injection process under realistic machine conditions, a multiparticle tracking approach was employed, including realistic static and dynamic (jitter) errors in the booster and TL2, as summarized in Table 1.

Table 1: Static and dynamic errors in the booster and TL2. Inj.: injection; Extr.: extraction; PS: power supply.

Type	Source	RMS	Comment
Static	TL2 final triplet focusing	1%	Predominant error.
	Pulsed magnet field (LPM)	4.7×10^{-4}	LPM train length effect.
	TL2 quadrupole roll	0.2 mrad	Isolates coupling sources.
	Inj./extr. magnet roll	0.05 mrad	Residual orbit imperfections.
Jitter	Pulsed magnet amplitude	2×10^{-4}	Pessimistic worst-case.
	Booster extracted beam	H: 20 μm, 2.5 μrad V: 2 μm, 1 μrad	Booster PS tracking error (5×10^{-5}).

MULTIPARTICLE TRACKING AND PHASE-SPACE ANALYSIS

To model the beam dynamics, multiparticle tracking simulations were performed using the Accelerator Toolbox (AT) [7] framework. After tracking the distributions through the TL2, they are injected at the middle of the storage ring straight injection section. The storage ring lattice model includes realistic alignment offsets and multipole errors, quantitatively detailed in Ref. [3], which have been virtually corrected using standard operational procedures (orbit correction, BBA, and LOCO).

To fully assess the injection efficiency and complement the global commissioning start-to-end simulations reported in Ref. [3], the particles are tracked over 1000 turns. This tracking duration covers about 2.1 synchrotron periods ($Q_s \approx 0.00209$), which is sufficient to probe the dominant early losses associated with longitudinal mismatch and transverse acceptance limitations, and to estimate the injection capture rate. During the first turn, the MIK field is turned on to simulate the off-axis injection kick. For all subsequent turns, the MIK is turned off and becomes transparent. To accurately reproduce the complex non-linear dynamics induced by the MIK, a thick-lens tracking approach is implemented. The MIK is sliced into small longitudinal steps ds. At each step, the 2D magnetic field maps $B_y(x, y)$ and $B_x(x, y)$—normalized per kiloampere—are interpolated at the exact transverse coordinates of each macro-particle. The

* sami.habet@synchrotron-soleil.fr

Content from this work may be used under the terms of the CC BY 4.0 licence (© 2026). Any distribution of this work must maintain attribution to the author(s), title of the work, publisher, and DOI.

ISBN: 978-3-95450-252-3 ISSN: 2673-5350 doi: 10.18429/JACoW-IPAC2026-WEP5009

UPDATE ON SOLEIL II BOOSTER

V. Kubytskyi*, P. Alexandre, E. Kravishvili, A. Loulergue, M.-A. Tordeux,
Synchrotron SOLEIL, Saint-Aubin, France

Abstract

SOLEIL II is a synchrotron light source aiming to deliver extremely high-brightness beams in the soft-tender X-ray range [1]. The storage ring will operate with an electron beam emittance below 100 pm·rad. To ensure efficient injection into the storage ring, the emittance of the electron beam extracted from the booster must be in the few-nm·rad range (5.2 nm·rad compared to 140 nm·rad for the present booster). To achieve these beam parameters, the booster injection energy is increased from 110 MeV to 150 MeV, and a new booster with a modified 16BA lattice has been designed [2, 3]. We show that the booster design has now converged towards its final configuration: the main dipoles of the 14BA arcs and 2BA matching sections are defined, the booster circumference is fixed, and the beam dynamics along the energy ramp has been studied including both systematic and random multipolar components.

INTRODUCTION

We report on the recent progress and studies for the new Booster of the SOLEIL II project. A completely new booster will be constructed, with a low natural beam emittance of 5.2 nm rad at the extraction energy of 2.75 GeV, compared with 140 nm rad delivered by the present booster. The new booster will occupy the location of the current booster, keeping the racetrack geometry and requiring only minor adaptations to the injection and extraction geometry. Booster operation should remain stable and reliable. The increase of the injection energy to 150 MeV is favourable for the new booster in terms of stability and injection efficiency, remanent fields in booster magnets, reduction of geometrical emittance, sensitivity to linac jitter, beam-gas lifetime and space-charge effects. We use two existing acceleration sections, for the linac energy upgrade which will be performed summer 2026. Injection into the present booster and operation at 150 MeV will take place once authorisation from the French Nuclear Safety Authority is received. The main parameters of the new booster are given in Table 1.

The booster lattice is based on a 16BA higher-order achromat superperiod, composed of 14BA optics in the arcs and 2BA optics in the matching sections. The arc unit cell, shown in Fig. 1, consists of a defocusing dipole D2, two defocusing sextupoles, two focusing quadrupoles and one focusing sextupole. The lattice design was discussed in detail in Ref. [2].

The procurement of assembled girders, including measured and aligned magnets, UHV-clean vacuum chambers and BPMs, is planned for 2027. The booster arc design is being developed toward an integrated implementation of magnets, supports, vacuum chambers and diagnostics.

* viacheslav.kubytskyi@synchrotron-soleil.fr

Table 1: Booster Main Parameters

Parameter	Unit	Present booster	Upgrade booster
Energy range	GeV	0.11–2.75	0.15–2.75
Circumference	m	156.6	156.569
Natural emittance	nm rad	140	5.2
Betatron tunes (H/V)	–	6.65/4.58	13.18/4.195
Natural chromaticities	–	−7.3/ − 5.8	−27/ − 12
Momentum compaction factor	–	2.8×10^{-2}	3.3×10^{-3}
Damping partitions	–	1.0/1.0/2.0	1.6/1.0/1.4
Natural damping times	ms	6.3/5.7/2.7	3.3/5.2/3.7
Energy loss per turn	keV	409	554
Natural energy spread	–	0.66×10^{-3}	0.93×10^{-3}
RMS bunch length	ps	50 at 3.6 MV	25 at 3 MV

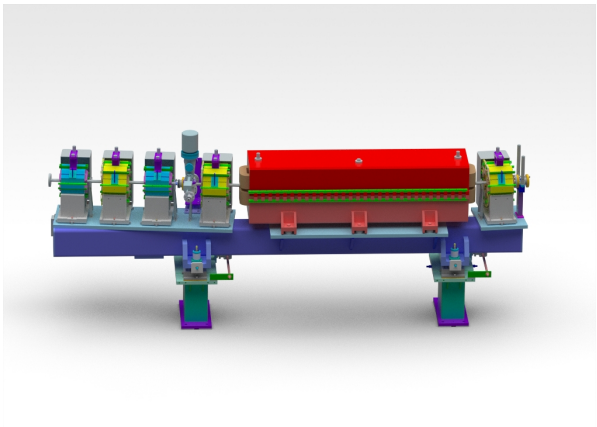

Figure 1: Arc girder with magnetic elements placed.

Several items of equipment have been identified as reusable or adaptable for the new booster: RF cavities, DCCT/FCT, striplines for tune measurement, beam-position screens, injection pulsed magnets and quadrupole power supplies. Some of this equipment belongs to the present storage ring. This strategy reduces the total cost of the booster upgrade while keeping well-known and reliable equipment.

In terms of booster diagnostics, eight BPMs are located in the straight matching sections, and each arc unit cell is equipped with a BPM situated at the end of the girder. This design choice facilitates the installation and alignment of the girders. A dedicated study was performed to optimise the girder placement in terms of orbit-correction performance. The robustness of the booster lattice design with respect to realistic misalignments and calibration errors was presented in detail in Ref. [3].

Content from this work may be used under the terms of the CC BY 4.0 licence (© 2026). Any distribution of this work must maintain attribution to the author(s), title of the work, publisher, and DOI.

ISBN: 978-3-95450-252-3 ISSN: 2673-5350 doi: 10.18429/JACoW-IPAC2026-WEP5018

ULTRALOW-ALPHA OPERATION WITH THREE FAMILIES OF SEXTUPOLES AT THE KARA RING

J. L. Steinmann*, E. Blomley, E. Bründermann, A. Mochihashi, A.-S. Müller,
A. Papash, P. Schreiber, M. Schuh
Karlsruhe Institute of Technology, Karlsruhe, Germany

Abstract

For more than two decades, the Karlsruhe Research Accelerator (KARA) — KIT's synchrotron radiation source and accelerator test facility — has been routinely operated in short-pulse mode, which involves reducing the momentum compaction factor [1]. Recent advances, such as enhanced stability provided by new magnet power supplies [2], have enabled us to surpass previous limitations in achieving extremely small momentum compaction factors. Based on lattice simulations and the introduction of a single additional sextupole magnet we successfully suppressed the longitudinal chromaticity, allowing the "zero-current" bunch length at KARA to be reduced from the previous 2 ps to below 1 ps. We also report on the measurements of the characterization of this improved operating mode.

INTRODUCTION

The steady-state zero-current bunch-length ($\sigma_{z,0}$) in a storage ring is, in first order and ultra-relativistic approximation, given by [3]

$$\sigma_{z,0} = L_0 \delta_p \sqrt{\frac{E_0 \alpha_0}{2\pi \cdot h \cdot e\hat{U}_{\mathrm{RF}}(-\cos\phi_s)}} \tag{1}$$

with the orbit length L_0, energy E_0 of the synchronous particle, the relative momentum spread δ_p, the harmonic number h and the particles charge e. The RF field amplitude $\hat{U}_{\mathrm{RF}}$ and the phase of the synchronous particle ϕ_s define the effective RF voltage. The bunch length for a given energy is therefore proportional to

$$\sigma_{z,0} \propto \sqrt{\frac{\alpha_0}{\hat{U}_{\mathrm{RF}}}}. \tag{2}$$

The RF voltage is an easy parameter to control, but increasing it by several orders of magnitude reaches technical limits and is very energy-intensive. One option for achieving shorter bunch lengths would be to use higher frequencies to get a steeper slope while maintaining the acceleration voltage, but this too is currently limited by technical constraints: Cavities for much higher frequencies become smaller than the beam pipe and the creation and synchronization of high CW power is non-trivial and cost intensive. To achieve greater bunch compression, the primary method used is therefore to reduce the momentum compaction factor in so-called "low-α optics" [4]. Essentially, α_0 is reduced by making the dispersion outside the achromats of the double bend achromat lattice negative by scaling the quadrupole strengths. The dispersion is stretched such that positive and negative contributions in the dipoles cancel each other and the integral reduces to very low values.

The path length variation of beam orbit in a ring can be split into two parts: one independent of momentum deviation (χ) and the other dependent on linear and high order terms of the momentum offset δ: $\frac{\Delta L}{L_0} = \alpha(\delta) \cdot \delta + \chi$. ($\chi$) encompasses both the amplitude-dependent change in path length due to betatron oscillations and the increase in path length caused by the misalignment of the magnetic elements. The momentum compaction factor is up to the second order of energy deviation δ defined by $\alpha(\delta) = \alpha_0 + \alpha_1\delta + \alpha_2\delta^2$ [5]. The linear and higher-order components of the momentum compaction factor depend on the linear and higher-order terms of the dispersion function, as well as on the slope of the dispersion function, which is limited to the second order of the Taylor expansion around the energy deviation in a beam [6]

$$\alpha_0 = \frac{1}{L_0} \oint \left(\frac{D_0}{\rho} \mathrm{d}s \right) \tag{3}$$

$$\alpha_1 = \frac{1}{L_0} \left[\oint \left(\frac{D_0^2}{2\rho^2} + \frac{D_1}{\rho} + \frac{D\prime_0^2}{2} \right) \mathrm{d}s \right] \tag{4}$$

$$\alpha_2 = \frac{1}{L_0} \left[\oint \left(\frac{D_0 D_1}{\rho^2} + \frac{D_2}{2\rho} + D\prime_0 D\prime_1 \right) \mathrm{d}s \right]. \tag{5}$$

The first term of the momentum compaction factor (α_0) is the integral of linear dispersion $D_0(s)$ inside the dipoles of bending radius ρ. The second term (α_1) defines the slope and the third term (α_2) the curvature of the compaction factor as a function of the energy offset [6, 7].

While the higher orders of the momentum compaction factor can be neglected for standard optics, taking them into account is crucial for beam dynamics during operation with a low momentum compaction factor because the momentum acceptance can be drastically reduced [8, 9].

Short bunches start to emit synchrotron radiation coherently at wavelengths comparable to the bunch length. When bent in the dipole magnets, self-interaction of the emitted coherent synchrotron radiation with the bunch leads to the microbunching/microwave instability and bunch lengthening [10]. The emission of additional coherent radiation also increases the energy spread of the bunch which can lead to reduced lifetime if the momentum acceptance is reduced due to the higher orders of the momentum compaction [11].

While α_0 depends on linear optics, α_1 and α_2 depend on the settings of sextupoles and octupoles, respectively [12].

* johannes.steinmann@kit.edu

Content from this work may be used under the terms of the CC BY 4.0 licence (© 2026). Any distribution of this work must maintain attribution to the author(s), title of the work, publisher, and DOI.

ISBN: 978-3-95450-252-3 ISSN: 2673-5350 doi: 10.18429/JACoW-IPAC2026-WEP5019

BEAM-BASED MISALIGNMENT STUDIES FOR PHYSICAL REALIGNMENT OPTIONS AT cSTART

P. Schreiber*, A.-S. Müller, A. Papash, R. Ruprecht
Karlsruhe Institute of Technology, Karlsruhe, Germany

Abstract

One of the objectives of the cSTART project (compact STorage ring for Accelerator Research and Technology) is the injection and storage of ultra-short electron bunches into a storage ring. With a planned storage time of 100 ms and a beam energy between 41 and 90 MeV, the beam will not reach equilibrium conditions. KIT plans injection from two sources, a laser-plasma accelerator and the linac-based FLUTE accelerator. Precise magnet positioning will be important for keeping the intended ultra-short bunch lengths. The initial laser-tracker-based alignments may not be sufficient to meet the requirements for such bunch lengths, resulting in the need for additional realignment options. This contribution presents the first studies of methods for beam-based misalignment measurements at cSTART targeted at the possibility to physically realign the magnets for improved alignment accuracy.

INTRODUCTION

The cSTART project [1] contains the VLA-cSR, the Very Large Acceptance compact Storage Ring for electrons. It is a storage ring with a circumference of 43.2m and a fourfold double bend achromat lattice. The standard optics [2] that will be used for commissioning is shown in Fig. 1. It will operate at an injection rate of 10 Hz resulting in a storage time of less than 100 ms. Due to the long damping time, the beam will therefore never reach equilibrium. The storage ring will be built in about 3.3m height above one of its injectors, FLUTE (Ferninfrarot Linac und Test Experiment). To achieve this, a steel construction will be built inside the FLUTE experimental hall. Due to these circumstances the alignment procedure of magnets is expected to be challenging. The planned alignment procedure consists of a rough element alignment on each girder followed by finer magnet alignments using laser trackers after girder installation. The alignment accuracy of the laser tracker depends on the distance to the components and will be limited to approximately 120 µm peak-to-peak. Following that, a beam-based determination of magnet offsets is foreseen. This determination requires methods and algorithms that need to be developed. Depending on the outcome of these determined offsets, a physical realignment of the main magnets is planned. For this, magnet positioning units (MPU) will be installed for each magnet enabling fine adjustments of the alignment of each magnet with 6 degrees of freedom (3 translations and 3 rotations). To simulate the beam dynamics for the VLA-cSR the accelerator toolbox (AT) [3] is used. Random errors are applied by simulated commissioning (SC) [4]. Since the distribution of errors is created as random distributions, the algorithms for correction, beam-based alignment (BBA) etc. require statistics. As compromise between good statistics and practical computation times, a number of 250 random error configurations have been generated and simulated.

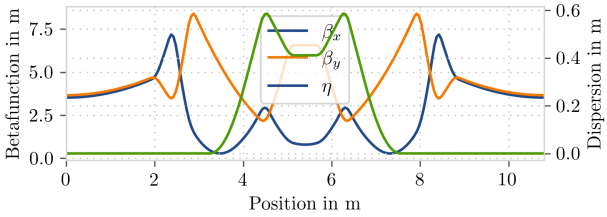

Figure 1: Optics functions for the initial optics used for commissioning of cSTART.

BEAM-BASED ALIGNMENT

A beam-based alignment will be performed to compensate the rough alignment of beam position monitors (BPMs). Being a non-equilibrium machine, the VLA-cSR will never reach closed orbit and thus, methods based on variations of the closed orbit cannot be used. A strategy based on single turn measurements should be employed and such a beam-based alignment procedure has been implemented in simulations. The strategy tries to minimize the effect of a change of quadrupole strength on the beam positions of downstream BPMs closely following the idea behind classical BBA algorithms. Due to the lower number of correctors in relation to the number of quadrupole magnets, it is not possible to build clean orbit bumps. Therefore, the first corrector upstream of the quadrupole magnet is used to distort the orbit and a single turn measurement is done. This also corresponds to the requirement of single or low number of orbits for the measurements due to the non-equilibrium nature of the VLA-cSR. A single turn is tracked using AT, starting at a random injection position. After recording the readings of the first downstream BPM (BPM_D) along with the overall closest BPM (BPM_C) to the quadrupole, the quadrupole magnet strength is changed and the change in position seen by the downstream BPM is taken. Then, the strength of corrector magnet in front of the quadrupole is changed and the procedure repeats. This is done for multiple corrector magnet strengths allowing to fit the reading of BPM_C and extract the reading for minimal disturbance caused by the change to the quadrupole strength. These readings then form the new beam-based alignment orbit that is used for subsequent orbit corrections.Due to the distance between BPMs and quadrupoles, their distribution and the level or misalign-

* patrick.schreiber@kit.edu

Content from this work may be used under the terms of the CC BY 4.0 licence (© 2026). Any distribution of this work must maintain attribution to the author(s), title of the work, publisher, and DOI.

ISBN: 978-3-95450-252-3 ISSN: 2673-5350 doi: 10.18429/JACoW-IPAC2026-WEP5020

MODELING OF MULTITURN INJECTION AT SIS-18 FOR A TRAIN OF UNILAC MICROBUNCHES

A. Lauterbach[1], G. Franchetti[2,3]
[1]Goethe University, Frankfurt, Germany
[2]GSI Helmholtzzentrum für Schwerionenforschung GmbH, Darmstadt, Germany
[3] Helmholtz Research Academy Hesse for FAIR (HFHF), Frankfurt, Germany

Content from this work may be used under the terms of the CC BY 4.0 licence (© 2026). Any distribution of this work must maintain attribution to the author(s), title of the work, publisher, and DOI.

Abstract

Multiturn Injection is an essential tool for achieving high beam intensities in synchrotrons. At SIS-18, a significant increase in the intensity of the uranium beam is foreseen, by several orders of magnitude, up to 1.5×10^{15} ions per injection cycle, prior to acceleration and extraction to SIS-100. Under these conditions, any beam losses during injection become critical, both in terms of beam lifetime and the risk of damaging injection system components, in particular the electrostatic septum. Usually, the optimization of the multiturn injection is carried out considering only the process of injecting one transverse slice of UNILAC macroparticles per turn. We present here a three-dimensional modeling of the injection process, which takes into account the longitudinal structure of the injected beam, namely the train of microbunches, and evaluates differences from previous approaches.

ONE- AND TWO-PLANE MULTITURN INJECTION

In this study, we focus on the well implemented process of multiturn injection in one transverse plane, which has been subject of extensive research in the past [1–3], as well as the process of two-plane multiturn injection, which optimizes the painting of the phase space in both transverse planes and is subject of recent studies [4, 5]. In both cases, the transverse trajectory of the closed orbit center is excited via four steerer magnets, performing a local orbit bump, which enables collecting the beamlets injected outside of the electrostatic septum (ES). This accumulation process is also referred to as phase space painting.

Local Orbit Bump Decrease Functions

The bump amplitude is shaped by an initial maximum $u_{B,\max}$ and a decrease rate per turn, given by a decrease function f. For this work a linear decrease function f_1 is chosen for the one-plane MTI, based on the real bump decrease curve of the SIS18, and an exponential decrease function f_2 for the two-plane MTI, based on the current benchmark of two-plane multiturn injection studies at GSI [4], with $f_1 = u_B(i_t) = u_{B,\max}(1 - \frac{i_t - 1}{j})$, with u being the generalized transverse coordinate standing for x or y correspondingly, i_t the turn number and j being the number of turns until the orbit has decreased back to zero amplitude. For the purpose of this work we set j to the number of injection turns i_{inj}. For the two-plane MTI the decrease function is $f_2 = u_B(i_t) = b_u + (u_{B,\max} - b_u)\frac{1-e^{\tau_u(N_u - i_t)}}{1-e^{\tau_u N_u}}$ with b_u the plateau value the function approaches after N_u turns and τ_u is the exponential decay coefficient defining the shape and steepness of the curve.

Simulation Prerequisites

The injection coordinates of the bunches are set by $X'(s_{\text{inj}}) = X(s_{\text{inj}})[-\alpha_x(s_{\text{inj}})/\beta_x(s_{\text{inj}})]$, where $\alpha(s_{\text{inj}})$ and $\beta(s_{\text{inj}})$ are the Twiss parameters at the longitudinal injection location s_{inj}. For the purpose of this work we implemented a one-plane MTI simulation code in Fortran 2018, utilizing the MICROMAP library for beam initialization and tracking. The SIS18 lattice was used as a representative synchrotron lattice. The code initializes a beamlet at the longitudinal injection point at each turn and performs the corresponding local orbit bump. The particle coordinates are tracked throughout the injection process. Losses are checked at every calculation step, also for $i_t > i_{\text{inj}}$ to check for after-injection losses with $i_{t,1\text{P}} = 100$ and $i_{t,2\text{P}} = 30$. The fixed simulation settings are shown in Table 1. Simulations are performed for two different tune sets "Q1" (Qx=4.238, Qy=3.422) and "Q2" (Qx=4.290, Qy=3.290).

Table 1: Shared simulation settings for multiturn injection in this work for SIS18-lattice with U^{238}_{28+} ions. *)$\Delta p/p$ value is scaled by a Gaussian random value, range [-1, 1].

Parameter	Value	Unit	Description
N_p	100	[1]	Particles per beamlet
i_{inj}	22	[1]	injected beamlets
ϵ_x (injection)	6	[mm-mrad]	Emittance, x-plane
ϵ_y (injection)	6	[mm-mrad]	Emittance, y-plane
Distribution	Gauss(3σ)	[-]	Beam-Distribution
$\Delta p/p*$	$2.5 \cdot 10^{-3}$	[-]	Momentum Spread
E_{nuc}	11.4	[MeV/u]	Energy per nucleon
$\alpha_x(s_{Septum})$	-1.3862	[rad]	Twiss α, x-plane
$\beta_x(s_{Septum})$	14.919	[m]	Twiss β, x-plane
For 2-Plane MTI:			
θ	45	[deg]	Septum tilt angle
$\alpha_y(s_{Septum})$	-0.66484	[rad]	Twiss α, y-plane
$\beta_y(s_{Septum})$	10.517	[m]	Twiss β, y-plane

ISBN: 978-3-95450-252-3 ISSN: 2673-5350 doi: 10.18429/JACoW-IPAC2026-WEP5021

EFFECT OF INTERPLANE CORRELATION ON THE TWO-PLANE MULTITURN INJECTION EFFICIENCY

A. Lauterbach, G. Franchetti[1,2], Institute for Applied Physics, Goethe University, Frankfurt, Germany
[1]GSI Helmholtzzentrum für Schwerionenforschung GmbH, Darmstadt, Germany
[2] Helmholtz Research Academy Hesse for FAIR (HFHF), Frankfurt, Germany

Content from this work may be used under the terms of the CC BY 4.0 licence (© 2026). Any distribution of this work must maintain attribution to the author(s), title of the work, publisher, and DOI.

Abstract

Beamlets provided by LINACs for injection into ring accelerators are subject to interplane correlation effects. Preliminary studies have shown that these correlations negatively affect the efficiency of one-plane multiturn injection. This study shows the effect of different grades of correlation between the transverse planes of the injected beamlets on the injection efficiency of two-plane multiturn injection at the simulation example of SIS-18.

2-PLANE MULTITURN INJECTION

Within the well-known process of multiturn injection (MTI), which has been subject to many studies in the past [1–3], particle beamlets are accumulated turn by turn to fill the available phase space as well as possible while keeping the overall beam emittance low. This process is also called phase space painting. The parameters to be optimized originate from different aspects of the machine and injection setup, for example the tune of the machine, the beta functions of the machine at the entry point of the beamlets, the injection emittance of the beamlets and many others. The overall goal is to inject as many particles into phase space as possible, obeying Liouville's law and avoiding emittance blow-up. More recently, there have been dedicated studies for two-plane MTI [4, 5]. Two-plane MTI extends this optimization process to both transverse planes, x and y, which enables the vertical transverse phase space to be painted as well. This injection method requires different physical machine configurations, such as a tilted electrostatic septum (ES), to allow the entry of the beam with angles y' different from zero. As for conventional one-plane MTI, the injection scheme is designed with a local orbit bump, which is performed by four steerer magnets each in x and y independently. The decrease in steerer strength is defined separately for the x- and y-plane by decrease functions f_x and f_y which can follow different kinds of curves, for example linear or exponential.

BEAM CORRELATION

The correlation between the x- and y-plane of a beam is described by the second order beam moments matrix or covariance matrix C [6]:

$$C = \begin{pmatrix} \langle xx \rangle & \langle xx' \rangle & \langle xy \rangle & \langle xy' \rangle \\ \langle x'x \rangle & \langle x'x' \rangle & \langle x'y \rangle & \langle x'y' \rangle \\ \langle yx \rangle & \langle yx' \rangle & \langle yy \rangle & \langle yy' \rangle \\ \langle y'x \rangle & \langle y'x' \rangle & \langle y'y \rangle & \langle y'y' \rangle \end{pmatrix}. \tag{1}$$

This matrix provides information on how certain phase space coordinates of the beam are correlated with each other. Generally, all elements of the machine lattice that act on the cross-plane elements of C are potential coupling sources. In the ideal case of a decoupled beamline the cross-plane terms of C are zero, but experimental observations have shown measurable coupling effects originating from the linear accelerator section and/or the transfer channel [6]. In this work, we model the interplane correlations caused by an unidentified coupling element. In practical beamlines, such coupling effects may arise from skew quadrupole fields or imperfections in beamline alignment and optics. To simulate the coupling, we introduce two parameterized 4×4 transformation matrices M_1, M_2 of the form:

$$M_1 = \frac{1}{\sqrt{1+\kappa^2}} \begin{pmatrix} 1 & 0 & \kappa & 0 \\ 0 & 1 & 0 & \kappa \\ -\kappa & 0 & 1 & 0 \\ 0 & -\kappa & 0 & 1 \end{pmatrix} \tag{2}$$

with $\kappa \in \mathbb{R}$ and

$$M_2 = e^G = \begin{pmatrix} \cos\lambda\, I & \tilde{\lambda}\, K \\ -\tilde{\lambda}\, K & \cos\lambda\, I \end{pmatrix} \tag{3}$$

with

$$K = \begin{pmatrix} \ell & k \\ k & \ell \end{pmatrix}, \qquad G = \begin{pmatrix} 0 & K \\ -K & 0 \end{pmatrix}, \qquad \tilde{\lambda} = \frac{\sin\lambda}{\lambda} \tag{4}$$

with $k, \ell, \lambda \in \mathbb{R}$.

The matrix M_1 represents an idealized direct mixing between transverse planes and fulfills the symplectic condition [7], when a pre-factor of $1/\sqrt{1+\kappa^2}$ is applied, ensuring that the transformation is physically consistent. Matrix M_2 is built from a generator G with $M_2 = e^G$ and corresponds to a symplectic transformation that resembles a smoother rotational coupling in four-dimensional phase space. The parameterized forms of M_1 and M_2 allow changes in the injection efficiency to be traced back to a single coupling parameter while keeping all other simulation parameters constant. Since multi-turn injection is performed via a closed orbit bump, it is crucial to apply the coupling transformation only to the incoming beam, not to the reference closed orbit. To achieve this, the closed orbit coordinates $\vec{X}_{CO}$ must be explicitly accounted for. While the beam coordinates $\vec{X}$

ISBN: 978-3-95450-252-3 ISSN: 2673-5350 doi: 10.18429/JACoW-IPAC2026-WEP5023

IMPROVING ENERGY SPREAD OF MESA BEAM IN ERL OPERATION*

E. Khidr[1†], F. Hug[1], F. Schliessmann[2]
[1]Johannes Gutenberg-Universität Mainz, Institut für Kernphysik, Mainz, Germany
[2]Technische Universität Darmstadt, Institut für Kernphysik, Darmstadt, Germany

Abstract

MESA, the Mainz Energy-Recovery Superconducting Accelerator, currently under commissioning at Johannes Gutenberg University Mainz, is designed to operate in two modes: external beam (EB) mode, with 150 µA polarized electrons at 155 MeV serving the P2 experiment, and energy-recovery linac (ERL) mode, with an unpolarized beam of 1 mA to 10 mA at up to 105 MeV for the Mainz Gas Injection eXperiment (MAGIX) setup. The latter requires precise control of the energy spread and the bunch length across the beam energies of 30, 55, 80, and 105 MeV. Comprehensive simulations were conducted using the tracking code ELEGANT. Starting with a 4-ps bunch length, the full acceleration and deceleration process in ERL mode was modeled by optimizing the RF phase, and the accelerating gradient fields in off-crest operation, resulting in the desired energy gain in each linac section. To reach the lowest energy spread, an appropriately selected longitudinal dispersion in the recirculation arcs is required. Consequently, the injection arc lattice is optimized by adjusting the arc's longitudinal dispersion R_{56} as the primary tuning parameter. The realization of a chirp together with the tuning of R_{56} enhances the overall beam quality.

INTRODUCTION

MESA is a double-sided superconducting recirculating linear electron accelerator designed to operate at different beam energies for nuclear and particle physics experiments [1]. The overall layout of the MESA is shown in Fig. 1. In ERL mode [2], the MAGIX experiment [3] requires a range of beam energies to perform precision electron scattering measurements, including studies related to dark-photon searches and proton-radius measurements. The MAGIX experimental setup relies on high-resolution magnetic spectrometers, where the combined contributions of the spectrometer optics and the beam energy spread determine the achievable energy resolution. To fully exploit the experimental capabilities, the relative beam energy spread at MAGIX must be in the order of 10^{-4} [4]. While ERL operation enables high current, it entails complex longitudinal beam dynamics that can degrade the energy spread at intermediate energies. This work focuses on the analysis and optimization of the longitudinal phase space in the MESA ERL, with particular emphasis on meeting the stringent energy-spread requirements of the MAGIX experiment.

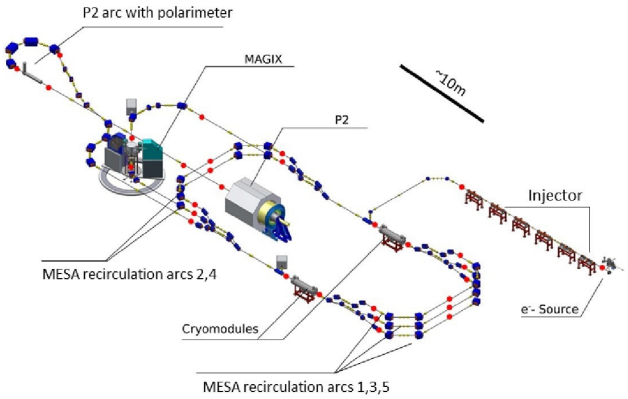

Figure 1: Layout of the MESA facility, starting from the electron source and injector on the right, which provides the low-energy beam guided to the main linac. Downstream of the injector, the beam is accelerated in the first cryomodule located at the central straight section, after which the beam is redirected through arcs 1–5 for acceleration in the first passes and deceleration in the return passes. The MAGIX experiment is located on the upper straight section, while the P2 beamline, with its polarimeter branches off downstream.

LONGITUDINAL PARAMETER OPTIMIZATION

In the ERL operation mode, MESA functions as a multi-turn recirculating linac, in which the electron beam passes twice through the cryomodules, housing two superconducting TESLA-type RF cavities [5], that provide an energy gain of 12.5 MeV per cavity (25 MeV total per pass) before being decelerated to recover the beam energy. Here, the goal is to achieve the correct design energy after each linac pass for proper beam transport, as well as achieving a small energy spread at the MAGIX interaction point. To achieve this, beam-dynamics simulations were performed to identify an optimum working point for the machine. The optimization procedure follows the method successfully used at the Darmstadt multi-turn ERL S-DALINAC [6], adapted here to MESA.

The study focuses on interdependent longitudinal degrees of freedom that manipulate the longitudinal phase space:

The phase-dependent energy gain imparted to each particle as a function of its arrival time is expressed as:

$$\Delta E = qV_{\mathrm{peak},j}\sin(\omega t + \phi_j), \tag{1}$$

where q is the particle charge, ω is the RF angular frequency, t is the particle arrival time, and $V_{\mathrm{peak},j}$ and ϕ_j are the voltage and RF phase of cavity j, respectively.

* Work supported by DFG (GRK 2128).
† ekhidr@uni-mainz.de

Content from this work may be used under the terms of the CC BY 4.0 licence (© 2026). Any distribution of this work must maintain attribution to the author(s), title of the work, publisher, and DOI.

ISBN: 978-3-95450-252-3 ISSN: 2673-5350 doi: 10.18429/JACoW-IPAC2026-WEP5026

TRACKING-BASED LINEAR SYMPLECTIC PARAMETERIZATION OF INSERTION DEVICES*

I. Morozov†, B. Diviacco, S. Krecic, K. Manukyan, S. Dastan, E. Karantzoulis
Elettra-Sincrotrone Trieste S.C.p.A., Trieste, Italy

Abstract

Accurate linear models of insertion devices (IDs) are essential for optics correction, coupling control, and feed-forward strategies in modern light sources. We present a systematic framework that builds a linear transverse symplectic parameterization, including leading-order chromatic effects, directly from Radia's Runge–Kutta (RK) particle tracking. We compare the resulting matrices with those obtained using the standard kick-maps approach for planar and elliptic IDs. The resulting parameterized symplectic models are well suited for constructing feed-forward tables across ID operating ranges.

INTRODUCTION

IDs can have a significant impact on both linear and nonlinear beam dynamics in modern light sources, depending on the accelerator lattice and operating energy. In particular, correction of linear ID effects during changes of ID parameters is a routine operation performed through feed-forward tables. This ensures stable tunes and preserves beam sizes at other beamlines.

The magnetic fields in IDs can be accurately modeled, including realistic geometries and materials, using specialized software, e.g. Radia [1, 2]. Linear effects can be modeled based on a special potential constructed from magnetic field over one ID period [3]. However, this approach relies on several assumptions and does not account for matching sections. To assess the importance of realistic geometries and magnetic fields, a linear-model construction method based on Radia's RK integrator was developed [4]. Different linear models for Elettra 2.0 [5] are compared with respect to their impact on beam optics for both linearly polarized undulators (LPUs) and elliptically polarized ones (EPUs). The EU100 EPU (APPLE-II), with period length $\ell_p = 100\,\mathrm{mm}$, total number of periods $n_p = 40$, and $(k_x, k_y) = (3.9, 6.6)$ with 31 mm gap (see Ref. [6] for details), is used to compare the models and to illustrate the effects on beam optics.

ID TRANSPORT MODELING

Most of the Elettra 2.0 IDs have detailed Radia models that allow accurate magnetic field computation and have been validated previously [7, 8]. Given the magnetic field, the standard procedure is to construct a special potential [3] used to express the transverse angle kicks over one ID period, describing both linear and nonlinear motion. An ID can be modeled by a single thin kick, or a more accurate one-kick-per-period computation can be performed.

* This work is funded by the Elettra 2.0 project
† ivan.morozov@elettra.eu

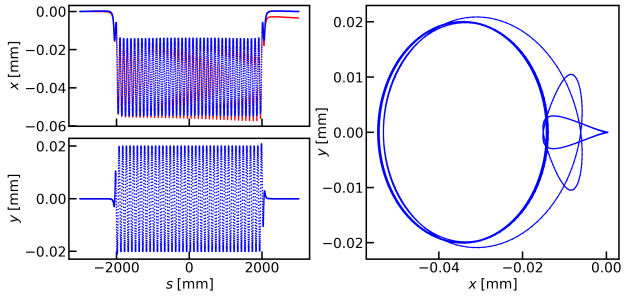

Figure 1: Particle trajectory in the EU100 (APPLE-II) insertion device for unmatched (red) and matched (blue) orbits.

Direct trajectory integration using initial conditions close to the reference trajectory (see Figure 1) can also be used to construct a linear transport matrix in the form of a thin-lens insertion. Other approaches, primarily aimed at nonlinear dynamics, can be constructed by employing parametric field models or by fitting basis functions to field data [9–11].

Elleaume's Potential and Transverse Kicks

Under the assumption that the first-order field integrals vanish, the leading angular kick appears at second order and can be derived from the following potential function:

$$\Phi(x,y,s) = \left(\int_{-\infty}^{s} B_x(x,y,s')\,ds'\right)^2 + \left(\int_{-\infty}^{s} B_y(x,y,s')\,ds'\right)^2,$$

where (B_x, B_y, B_z) are the magnetic field components generated by the ID and available for evaluation at any point in space.

For a periodic ID, the one-period potential is

$$U(x,y) = \oint \Phi(x,y,s)\,ds,$$

and the changes in the transverse slopes $x' = dx/ds$ and $y' = dy/ds$ over one period are

$$\Delta x' = -\frac{\alpha^2}{2}\frac{\partial U(x,y)}{\partial x}, \qquad \Delta y' = -\frac{\alpha^2}{2}\frac{\partial U(x,y)}{\partial y},$$

where $\alpha = e/\gamma mc$.

In practice, instead of evaluating the integral for $U(x,y)$ directly, a truncated Fourier representation of the periodic magnetic field is used. For a fixed transverse position, one or more harmonics of the field components are computed over one period from numerical field samples. The one-period potential is then approximated from the amplitudes of these harmonics.

Content from this work may be used under the terms of the CC BY 4.0 licence (© 2026). Any distribution of this work must maintain attribution to the author(s), title of the work, publisher, and DOI.

ISBN: 978-3-95450-252-3 ISSN: 2673-5350 doi: 10.18429/JACoW-IPAC2026-WEP5027

APPLICATIONS OF HIGH-DIMENSIONAL TIME-DELAY EMBEDDING FOR TIME SERIES COMPLEXITY ESTIMATION

I. Morozov *†, Elettra-Sincrotrone Trieste S.C.p.A., Trieste, Italy
Yu. Maltseva Novosibirsk State Technical University, Novosibirsk, Russia

Content from this work may be used under the terms of the CC BY 4.0 licence (© 2026). Any distribution of this work must maintain attribution to the author(s), title of the work, publisher, and DOI.

Abstract

Turn-by-turn (TbT) data are readily available in modern circular accelerators and are widely used to infer machine parameters in both simulations and experiments. In experiments, TbT data record transverse beam-centroid positions from beam position monitors (BPMs) and therefore include measurement noise. We construct high-dimensional time-delay embeddings of TbT time series, yielding matrix representations of transverse oscillation signals. Since the signals considered are typically near-quasiperiodic and dominated by harmonics of the fundamental betatron frequencies, the embedded matrices are expected to have low effective rank. We leverage this rank structure to define a complexity indicator based on singular-value spectra, which are related to the underlying quasiperiodic structure of the TbT signals. The proposed framework provides a simple, data-driven diagnostic for complexity estimation directly from TbT records and is compatible with experimental datasets.

INTRODUCTION

Modern circular particle accelerators are among the applications in which Hamiltonian, or symplectic, formalisms are successfully employed to model the experimentally observed dynamical behavior. During both the design stage and operation, significant effort is devoted to optimizing the dynamic aperture (DA) of a circular accelerator. The DA is a finite-time stability region in phase space, surrounding an elliptic fixed point, whose initial conditions remain bounded over a prescribed number of revolutions [1]. While the DA is a nontrivial object linked to the celebrated KAM [2] and Nekhoroshev [3] theorems, as well as Arnold diffusion [4], it is also of great practical importance for efficient beam injection and beam-lifetime optimization [5, 6].

The most reliable way to characterize the DA in simulations is the direct tracking of initial conditions within the domain of interest [7]. Together with DA scaling laws [8–11], direct computation makes it possible to extrapolate the DA size to long time scales for which direct numerical tracking is not feasible. Robust and computationally efficient methods for DA size and shape characterization can also be constructed using information from full unstable orbits [12, 13]. While these methods characterize the DA boundary, its internal structure remains unexplored. To characterize this structure, chaos indicators can be employed to determine whether a given initial condition is regular or chaotic. A family of chaos indicators can be constructed using information from tangent dynamics, such as the FLI [14] and GALI [15] indicators. The REM indicator [16] is instead based on the reversibility error obtained from the mismatch between forward and inverse iterations of a map. These methods are well suited for characterizing the internal structure of the DA [17]. FMA [18] is one of the most widely used chaos indicators in accelerator physics. It is based on the invariance of frequencies over time and also benefit from accelerated convergence using Birkhoff averages [19]. In contrast to many other indicators, FMA is based on TbT time-series analysis and can therefore be adapted to experimental data [20]. However, it is not necessarily ideal for the classification of initial conditions [21]. In practice, TbT signals represent beam-centroid transverse oscillations and are affected by measurement noise and beam decoherence.

In this contribution, we present a method for time-series complexity characterization based on the entropy of the SVD spectrum of high-dimensional time-delay embeddings of TbT signals [22]. Time-delay embedding represents a time series in a high-dimensional space of delayed coordinates [23], with Takens' theorem showing that such a representation preserves the geometrical structures relevant to the underlying dynamical system [24]. The singular-value spectrum of this representation can be used to characterize time-series complexity [25, 26] by means of Shannon entropy [27]. Data analysis based on this approach has been successfully applied in different fields, including finance [28] and biomedicine [29]. Motivated by the fast decay of harmonic content in regular quasiperiodic signals, we apply this method to the complexity characterization of TbT time series. The resulting indicator distinguishes structured regular signals, which have low effective complexity, from chaotic signals, which carry richer spectral information. We compare this method with several commonly used chaos indicators and study the effect of measurement noise.

HIGH-DIMENSIONAL EMBEDDING

The transverse dynamics in a circular accelerator can be modeled by the following 4D symplectic Hénon map:

$$
\begin{aligned}
q_x &\to \cos(\mu_x)\, q_x + \sin(\mu_x)\left(p_x + q_x^2 - q_y^2\right), \\
q_y &\to \cos(\mu_y)\, q_y + \sin(\mu_y)\left(p_y - 2q_x q_y\right), \\
p_x &\to \cos(\mu_x)\left(p_x + q_x^2 - q_y^2\right) - \sin(\mu_x)\, q_x, \\
p_y &\to \cos(\mu_y)\left(p_y - 2q_x q_y\right) - \sin(\mu_y)\, q_y,
\end{aligned}
$$

where (q_x, q_y, p_x, p_y) are the normalized transverse phase-space coordinates. In experimental measurements, only the transverse position coordinates q_x and q_y are available. The phase advances are given by $(\mu_x, \mu_y) = (2\pi\nu_x, 2\pi\nu_y)$, with betatron tunes $\nu_x = 0.168$ and $\nu_y = 0.201$.

* ivan.morozov@elettra.eu

† I.M. acknowledges support from the Elettra 2.0 project.

ISBN: 978-3-95450-252-3 ISSN: 2673-5350 doi: 10.18429/JACoW-IPAC2026-WEP5028

ESTIMATING THE STABILITY DOMAIN OF SYMPLECTIC MAPS: A ROBUST METHOD VIA A BOUNDING-SET OF UNSTABLE INITIAL CONDITIONS

I. Morozov * †, Elettra-Sincrotrone Trieste S.C.p.A., Trieste, Italy
M. Giovannozzi ‡, CERN, Geneva, Switzerland

Abstract

Estimating the stability domain in view of its characterisation and optimisation is one of the primary topics of single-particle non-linear beam dynamics. The boundary of the stability domain, the dynamic aperture (DA), has a complicated fractal structure that cannot be reliably estimated by analytical means. Instead, numerical methods are used to estimate the DA, with the additional constraint of identifying only the domain that is simply connected around the origin. The most common case of a DA estimate for 4D systems can be reduced to a lower-dimensional angular scan, thus lowering the computational burden. Here we present a new robust method of DA characterisation based on constructing a cloud of escaping initial conditions that bounds the stable domain and has a significantly lower computational complexity than a direct scan of phase-space variables. The proposed method is applied to a non-linear 4D symplectic map, and the results are compared with those obtained using standard methods, both in terms of accuracy and CPU time.

INTRODUCTION

The DA remains one of the main concepts characterising non-linear performance in currently operating and proposed circular charged-particle accelerators such as the CERN LHC [1] and FCC [2, 3]. Relevant effects include the impact of DA on injection efficiency and beam lifetime. Although strict stability would require initial conditions to remain within the DA region indefinitely, in practice, DA is commonly defined as a finite-time simply connected stable region around the origin [4]. Accurate computation of DA requires repeated iterations of the map representing one-turn propagation in the ring. The number of iterations per initial condition can range from the order of 10^3 for electron light sources, corresponding to a characteristic time scale over which synchrotron radiation produces sufficient damping [5], to 10^7 for proton machines, where synchrotron radiation has a negligible effect [6], considering that ultimately the timescale is also dependent on the duration of the process under consideration, e.g. collisions in the LHC, which is of the order of several hours, corresponding to about several 10^8 iterations. As a result, direct DA computation is a computationally demanding task.

The standard approach to DA estimation is based on iterating initial conditions along rays starting from the origin, which is assumed to be an elliptic fixed point [7]. This provides a significant computational gain compared with scanning a full rectangular grid of initial conditions and directly targets the main central stable region. This method assumes that the DA region has a sphere-like shape, or more generally, that it is star-shaped, and computes the DA volume using a structured grid of angular variables in polar coordinates together with the corresponding equivalent hypersphere radius as the main DA characterisation parameter. In addition to ray-based DA computation, modern algorithms [8], as well as machine learning methods [9–13], are actively being developed to reduce the computational complexity of DA.

Because the DA boundary has a complicated fractal structure, it cannot generally be reliably estimated analytically. Analytical methods work best when the DA boundary is dominated by a single strong resonance. In this case, single-resonance normal forms can be used [14], or a more general map-based computation can be employed [15]. Apart from DA size, typically represented by its equivalent radius, its shape and internal structure are also of interest, especially for studies of the long-term behaviour, when the required number of one-turn map iterations becomes computationally infeasible, and in the context of probing the robustness of accelerator lattice to magnetic field errors. While in 2D phase space the DA boundary is determined by homoclinic or heteroclinic tangles composed of stable and unstable manifolds of hyperbolic fixed points [16–19], in higher dimensions there is no natural boundary enclosing the orbits, and transport from small amplitudes is possible due to Arnold diffusion [20]. The internal DA structure provides information about dominant resonances and is commonly explored using chaos indicators (see, e.g. [21] and references therein), while symmetry lines also allow exploration of the DA shape [22].

In this contribution, we present a new approach to DA estimation based on a bounding set of unstable initial conditions [23]. The method provides a robust estimate of the central stable region by enclosing it with a shell of unstable points. It can be used both to characterise the DA through an equivalent radius and to explore the detailed structure of the stable domain, since full unstable orbits are used in the construction of the bounding set. We present the steps required to construct the bounding set, and we study its computational complexity and the scaling laws of the enclosed stable region [24–28]. The constructed domain is not in one-to-one correspondence with that obtained using standard ray-based DA computation, and it should be understood as a related but *distinct object*, representing the region enclosed by a cloud of unstable initial conditions.

* ivan.morozov@elettra.eu
† I.M. acknowledges support from the Elettra 2.0 project.
‡ massimo.giovannozzi@cern.ch

Content from this work may be used under the terms of the CC BY 4.0 licence (© 2026). Any distribution of this work must maintain attribution to the author(s), title of the work, publisher, and DOI.

ISBN: 978-3-95450-252-3 ISSN: 2673-5350 doi: 10.18429/JACoW-IPAC2026-WEP5034

STATUS OF LATTICE STUDIES FOR ALBA-II

G. Benedetti, O. R. Blanco-García, M. Carlà, Z. Martí, F. Pérez
ALBA Synchrotron, Cerdanyola del Vallès, Barcelona, Spain

Abstract

A 5BA lattice with an emittance of 206 pm·rad at 3 GeV and a circumference of 268.8 m is under design for ALBA-II. The injection is performed off-axis in a straight section only 4.7 m long with a single non-linear kicker needing a horizontal dynamic aperture larger than 6 mm. An optics of the injection section with asymmetric waists of the beta functions, low horizontal beta at the septum location and high beta at the kicker, has proved to perform better than a high beta section. This arrangement in the injection sections allows tuning equal phase advances and chromatic functions in all the cells and recover a pseudo 16-fold symmetric ring both on- and off-energy. The robustness of this solution in presence of errors has improved the injection efficiency with errors from 90% to 100%, keeping the dynamic aperture larger than 7 mm and the same Touschek lifetime longer than 6 hours. The magnetic design along with the performances of the lattice with errors and the injection process are presented in this paper.

INTRODUCTION

The ALBA-II storage ring consists of 16 cells that have the same arc but three different straight section lengths matched by quadrupole triplets. The main aspects of the cell architecture were already presented in [1]. In the last version of the lattice [2], high beta functions were employed in the injection straight section, to achieve the necessary horizontal dynamic aperture (DA) larger than -5 mm, and in three more symmetric straight sections. The best performances of that 4-fold lattice, evaluated with all the effects of errors and corrections, achieved an injection efficiency of 93% on average (more than 50% of the error seeds). Besides this, we realized that due to the large tune shift with energy, Touschek particles within the energy acceptance were crossing the resonance $Q_x = 0.5$ making necessary some evaluations in order to guarantee a reliable estimate of the lifetime. The work of the last year has been dedicated from one side to improve the lattice performances by refining the model and the optimization technique, and on the other side to develop a new optics of the injection section with asymmetric waists that allowed to recover a pseudo 16-fold symmetry with matched phase advances and chromatic amplitude function W_x in all the straight sections. The main benefit of this change in the lattice is its robustness to errors rendering 100% of injection efficiency for more than 90% of the simulated error seeds.

NEW INJECTION SECTION

A new optics for the injection section with low β_x at the septum and high β_x at the double-dipole kicker (DDK, [3, 4]) was implemented adding a quadrupole in the middle of the straight section (Fig. 1). This optics of the injection section allows using the matching quadrupole triplets to make the phase advance of all the straight sections equal, hence recovering a 16-fold symmetry on-energy, while off-energy periodicity 16 is obtained by matching the horizontal chromatic amplitude function W_x at the end of each arc. This configuration renders both large horizontal dynamic aperture at the DDK and good momentum aperture for Touschek lifetime. As additional benefit, the low β_x at the injection point allows the thin-septum blade being positioned closer to the stored beam. Consequently the thin-septum magnet can be shifted towards the DDK leaving more room for the thick-

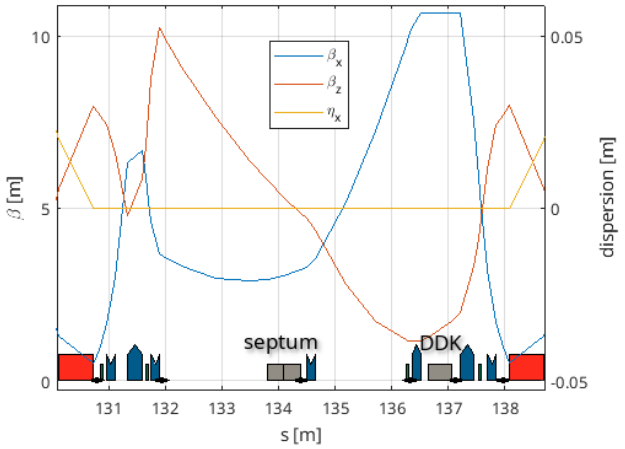

Figure 1: The new optics of the injection section with asymmetric waists to produce low β_x at the thin-septum position and high β_x at the kicker (DDK).

Table 1: Main Parameters of the 5BA Baseline Lattice

Energy	3	GeV
Circumference	268.8	m
Natural emittance	206	pm·rad
Emit. 50% coupling & IDs	158, 79	pm·rad
Betatron tunes	38.17, 13.28	
Natural chromaticity	-95, -34	
Momentum compact. factor	$1.1{\cdot}10^{-4}$	
Energy spread	$1.2{\cdot}10^{-3}$	
Energy loss per turn	910	keV
Damping times	2.7, 5.8, 6.9	ms
Main RF voltage	2.4	MV
Harmonic Number	448	
Bunch length w/o HC	9.0	ps
Total beam current	300	mA
Lifetime 50% coupling & HC	6	h
Straight lengths	4.7, 3.5, 4.4	m
β_x at straight centers	3.4, 2.5, 3.1	m
β_y at straight centers	1.9, 1.7, 1.9	m

Content from this work may be used under the terms of the CC BY 4.0 licence (© 2026). Any distribution of this work must maintain attribution to the author(s), title of the work, publisher, and DOI.

ISBN: 978-3-95450-252-3 ISSN: 2673-5350 doi: 10.18429/JACoW-IPAC2026-WEP5035

FIRST PARALLEL ARC QUADRUPOLE BEAM-BASED ALIGNMENT USING K-MODULATION AT LHC

C. Goffing*[1,2], M. Hostettler[1], J. Keintzel[1], A.-S. Müller[2], J. Wenninger[1]
[1]CERN, Geneva, Switzerland
[2] Karlsruhe Institute of Technology, Karlsruhe, Germany

Abstract

The Large Hadron Collider (LHC) is a circular hadron collider for high-energy particle physics. Off-centre beam passage through quadrupoles results in additional deflection, which needs to be compensated by corrector magnets. Beam-based alignment is an option to reduce the beam offset in the quadrupoles by using an estimate for the Beam Position Monitor (BPM) to magnet offset as reference for the orbit feedback. The in-series powered LHC arc quadrupoles do not allow the variation of the quadrupole strength of individual magnets, this requires a parallel approach for the beam-based alignment. Various approaches based on k-modulation for parallel beam-based alignment are considered.

INTRODUCTION

Beams passing multipole magnets off-centre experience additional field components with lower orders than the misaligned magnets, introducing deflections and leading to orbit and optics deviations. Beam Based Alignment (BBA) is used to reduce the beam offset in the magnet by using orbit correctors to steer the beam towards the magnetic centre of the magnets [1–3]. Transversely misaligned quadrupoles introduce additional dipole fields due to feed-down, leading to closed orbit, dispersion and tune errors, among other effects, compared to a perfectly aligned machine. Traditionally, a BBA is performed on individual magnets [4] using static changes of magnet strength or on multiple magnets using periodic changes with different frequencies, for example at LEP [5]. This requires the ability to vary the strength of individual quadrupoles, which is not feasible for the in-series powered arc quadrupoles of the Large Hadron Collider (LHC) [6] at CERN. Therefore, parallel BBA techniques are required, which have already been investigated for various machines including EBS at ESRF [7] and SPEAR3 at SLAC [8]. This aims to reduce the offset of the beam relative to the magnetic centre of several elements simultaneously. Since the time required scales linearly with the number of quadrupoles in a storage ring, individual BBA becomes a very time-consuming procedure for large machines such as the Future Circular electron-positron Collider (FCC-ee) [9–11], a proposed successor of the High-Luminosity LHC [12], and hence, a fast and precise BBA is necessary [13,14]. With its FODO structure and high number of quadrupoles in the arcs, the LHC is well suited to test parallel BBA experiments for FCC-ee.

* christian.goffing@cern.ch

MEASUREMENT SETUP

The LHC features two separate vacuum chambers, designed for proton-proton collisions with beam energies of up to 7 TeV [6]. The measurements are performed at the injection energy of 450 GeV with one pilot bunch having a population of $\approx 10^{10}$ protons per beam. For the presented beam test arc 56 is chosen, a decisive factor being that all BPMs are functional. For the BBA, all horizontally focusing and defocusing quadrupoles with a strength of $\pm 8.7 \times 10^{-3}\,\mathrm{m}^{-2}$ and length of 3.1 m, distributed over 23.5 FODO cells, each 106.9 m long, are used. In each circuit, 47 in-series powered magnets are varied simultaneously, 23 in beam 1 and 24 in beam 2, or vice versa, depending on the magnet family. The horizontal correctors are located next to the focusing quadrupoles, while the vertical correctors are located next to the defocusing quadrupoles. In arc 56, beam 1 misses 2 correctors, namely MCBV.26R5.B1 and MCBV.28L6.B1.

BBA TECHNIQUES

BBA methods use the orbit changes due to the dipole component of a misaligned quadrupole either directly or through the corrector strength required to keep the orbit constant.

Parallel Quadrupole Modulation Scheme

For the parallel Quadrupole Modulation Scheme (pQMS), the strength of magnets powered in series are modulated simultaneously by up to ±0.36%, while two different orbit bumps are applied with a 12 mm peak-to-peak amplitude with a periodicity of 4 FODO cells.

The orbit response matrix $R_{i,j}$ describes at first order the relationship between a change of the strength $\triangle k_j$ of quadrupole j with beam to magnet offset $\triangle x_{\mathrm{mag},j}$ and the closed-orbit change $\triangle x_{\mathrm{beam},i}$ at BPM i [15, 16]. $R_{i,j}$ is obtained from simulations performed in Xsuite [17] using:

$$R_{i,j} = \frac{\triangle x_{\mathrm{beam},i}}{\triangle k_j \cdot l_{\mathrm{quad},j} \cdot \triangle x_{\mathrm{mag},j}}.$$

The dipolar kick from the modulated off-centre quadrupole with beam offset $\vec{x}_{\mathrm{beam}}$ is obtained by inverting the matrix using the Moore-Penrose inverse or pseudo-inverse [18]

$$\vec{\theta} = R^{+} \cdot \vec{x}_{\mathrm{beam}}.$$

The BPM to quadrupole offset corresponds to the BPM reading at which the reconstructed kick strength vanishes. The beam position at which the kick strength disappears is

Content from this work may be used under the terms of the CC BY 4.0 licence (© 2026). Any distribution of this work must maintain attribution to the author(s), title of the work, publisher, and DOI.

ISBN: 978-3-95450-252-3 ISSN: 2673-5350 doi: 10.18429/JACoW-IPAC2026-WEP5036

SEXTUPOLE BEAM-BASED ALIGNMENT FOR FCC-ee

C. Goffing*[1,2], J. Keintzel[1], A.-S. Müller[2], F. Zimmermann[1]
[1]CERN, Geneva, Switzerland
[2]Karlsruhe Institute of Technology, Karlsruhe, Germany

Abstract

Designed to succeed the High-Luminosity Large Hadron Collider (HL-LHC), the Future electron-positron Circular Collider (FCC-ee) is a proposed next-generation collider focused on lepton collisions for high-energy physics experiments. Achieving ambitious design goals requires excellent control of the orbit and optics. Off-centre beam passage through the sextupoles results in additional focusing and defocusing, together with coupling due to feed-down effects. The sextupole beam-based alignment (BBA) is considered as an addendum to the quadrupole BBA because it reduces both the dipole kicks in the magnet and the optics perturbations from feed-down effects by reducing the beam offset in the sextupole. Various approaches for the individual and parallel sextupole BBA are considered and compared.

INTRODUCTION

In 2020, the European Strategy for Particle Physics Update (ESPPU) [1] identified an Electroweak and Higgs-factory as the highest priority next collider following the High Luminosity Large Hadron Collider (HL-LHC) [2]. One option is the Future electron-positron Circular Collider (FCC-ee) [3–5]. To achieve the high luminosity value of 1.44×10^{36} cm^{-2} s^{-1} at 45.6 GeV [6], excellent orbit and optics control are required, and therefore, implying strict boundaries on the accelerator optics and, thus, on the alignment tolerances of all lattice elements. In particular, the transverse offsets of beam-position monitor (BPM) readings with respect to the centre of adjacent quadrupole and sextupole magnets should be below 20 µm after Beam-Based Alignment (BBA) [6, 7]. Based on the measured offset between magnet and BPM, the beam is centred in the magnets using orbit correctors reducing the effective misalignment.

Misaligned sextupoles change the optics directly through focusing and introduction of coupling. For FCC-ee, sextupoles and quadrupoles are planned to be placed side by side with orbit and optics correctors and beam position monitors (BPMs) in the arc sections, which cover about 85 % of the circumference [6, 8, 9]. Beam-based alignment for FCC-ee is planned for the quadrupoles [10–12]. Sextupole BBA [10] is a possible complementary procedure in the arc sections and a necessary step for the interaction regions. Perturbations caused by sextupole magnets for which the beam is not well centred are compensated by steering magnets along with, normal or skew quadrupole correctors for correction of tune shifts and coupling. In the following, we present an overview of the approaches studied for an individual and parallel sextupole BBA in the arcs.

* christian.goffing@cern.ch

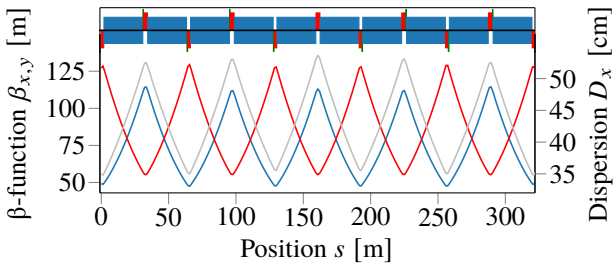

Figure 1: Shown are an LCC arc lattice cell (upper lattice diagram) as well as the horizontal (blue) and vertical (red) β-functions and dispersion D_x (grey).

Table 1: Magnet Strength and Lengths of the Different Arc Sextupole Families for LCC Lattice at Z

Sextupole family	Strength [T m^{-2}]	Length [cm]	Number of sextupoles
SD1A	−39.07	52	408
SD2A	−25.87	52	408
SF1A	46.29	30	408
SF2A	33.41	30	408

ARC LATTICES

For this paper, the Local Chromaticity Correction (LCC) lattice version 105 for Z energy is considered [13]. The lattice is based on a uniform arc layout and a hybrid focusing defocusing (HFD) lattice. Every ten quadrupole magnets, divided into 4 families, form a unit cell [9]. Next to 8 of these 10 quadrupoles a sextupole magnet is located. The arc sextupoles are divided into four families and arranged in an interleaved scheme. Two sextupoles of the SD2A family form the innermost pair, followed outwards by the SF1A and SD1A families, with the SF2A sextupoles being the last and outermost. The phase advance is 51.4° (44.7°) in the horizontal (vertical) plane between two consecutive (de)focusing quadrupoles. Each of the eight arc sections consists of 27 cells. The magnet layout and optics functions are shown in Fig. 1, and the parameters for the arc sextupoles are given in Table 1. Skew quadrupoles are planned to be integrated into the sextupoles in the form of trim windings [14–16].

SIMULATION SETTINGS

In our simulations, the BPMs and vertical orbit correctors are attached at the end of each quadrupole, close to the sextupoles. The horizontal correctors are attached to the end of the dipoles, next to the quadrupole. The nominal collision optics at Z energy is used for the simulations, although the BBA is intended to be part of the accelerator commissioning [6, 7], where a series of different optics

Content from this work may be used under the terms of the CC BY 4.0 licence (© 2026). Any distribution of this work must maintain attribution to the author(s), title of the work, publisher, and DOI.

ISBN: 978-3-95450-252-3 ISSN: 2673-5350 doi: 10.18429/JACoW-IPAC2026-WEP5037

PARALLEL QUADRUPOLE BEAM-BASED ALIGNMENT FOR FCC-ee

C. Goffing*[1,2], J. Keintzel[1], A.-S. Müller[2], F. Zimmermann[1]
[1]CERN, Geneva, Switzerland
[2]Karlsruhe Institute of Technology, Karlsruhe, Germany

Abstract

The Future electron-positron Circular Collider (FCC-ee) is a proposed lepton collider for high-energy particle physics succeeding the High-Luminosity Large Hadron Collider (HL-LHC). Its ambitious design goals demand excellent orbit and optics control and, therefore, set strict limits on alignment tolerances. Beam-based alignment (BBA) is used to relax the mechanical alignment tolerances by determining the offset between the magnet and the measured beam position. Orbit correctors steer the particle beam towards the determined magnetic centre and thus reduce the effective quadrupole misalignment. A parallel BBA technique is compared for the Global Hybrid chromaticity Correction (GHC) and Local Chromaticity Correction (LCC) lattices for FCC-ee using Xsuite simulations.

INTRODUCTION

The Future electron-positron Circular Collider (FCC-ee) [1–3] is a proposed electroweak and Higgs factory succeeding the High-Luminosity Large Hadron Collider (HL-LHC) [4]. The centre-of-mass energy in the range from 91.2 GeV to 365 GeV allows the production of Z, W, Higgs bosons and top-antitop pairs [3]. Two conceptually different lattices have been developed, the so-called Global Hybrid chromaticity Correction (GHC) [5] and Local Chromaticity Correction (LCC) [6] lattices.

The ambitious luminosity target of 1.44×10^{36} cm^{-2} s^{-1} at 45.6 GeV [7], requires excellent orbit and optics control and implies strict boundaries on the accelerator optics and thus on alignment tolerances of all lattice elements. In particular, tight constraints apply for the maximum magnet misalignments and for the transverse offset of nearby beam-position monitor (BPM) readings from the centre of quadrupole and sextupole magnets in the range from 10 µm to 20 µm [7, 8]. With knowledge of the BPM reading corresponding to the magnetic centre, obtained through Beam-Based Alignment (BBA), the beam can be steered using orbit correctors to reduce the effective magnet misalignment.

The FCC-ee arcs contain about 85 % of the quadrupoles in the two lattices, arranged in magnet families to be powered in series. Due to the large number of magnets in the FCC-ee, not only a precise but also a fast method is required. A parallel BBA approach, which has been developed in recent years [9, 10] and simulated for earlier FCC-ee lattice versions [11, 12], is particularly suitable for this purpose. Similar schemes have been tested or used in various machines, including EBS at ESRF [13], SPEAR3 at SLAC [9], NSLS-II at BNL [14], KARA at KIT [15] and LHC at CERN [16].

* christian.goffing@cern.ch

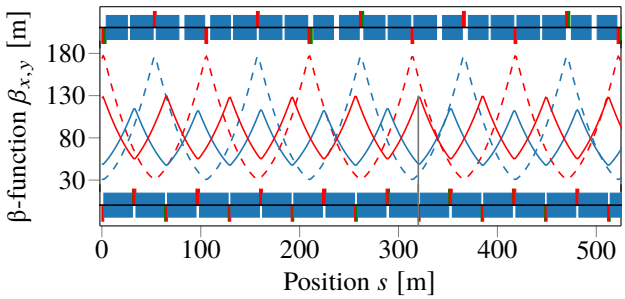

Figure 1: Arc lattice for GHC (upper lattice diagram, one supercell) and LCC (lower lattice diagram, first 320 m are one cell) as well as the horizontal (blue) and vertical (red) β-functions for GHC (dashed) and LCC (solid).

Table 1: Magnet Strength and Lengths of the Different Arc Quadrupole Families for the GHC and LCC Optics at Z

Quad family		Strength [T m^{-1}]		Length [m]	
GHC	LCC	GHC	LCC	GHC	LCC
QD1	QD1A	−1.56	−2.08	2.70	1.86
QF2	QF2A	1.56	1.41	2.70	2.89
QD3	QF3A	−1.56	1.43	2.70	2.89
QF4	QD1AM	1.56	−2.08	2.70	1.86

This paper compares a parallel BBA approach for the arc quadrupoles in the GHC and LCC optics at 45.6 GeV.

ARC LATTICES

For the comparison, the lattice versions 25.3 for GHC and 105 for LCC are considered [17]. In the arc sections, GHC features a FODO lattice with nearly identical quadrupole strengths and a phase advance of 90° per cell. Two different arc sections are used in the lattice, one comprising 89 FODO cells with the quadrupole families QD1 and QF2 and the other comprising 86 FODO cells with the quadrupole families QD3 and QF4. A supercell of the GHC lattice is made out of 10 quadrupole magnets or 5 FODO cells. LCC, on the other hand, is based on a uniform arc layout and a hybrid focusing defocusing (HFD) lattice. Ten quadrupole magnets, divided into 4 families, form a unit cell. The phase advance is significantly lower with 50° (44°) in the horizontal (vertical) plane between two consecutive (de)focusing quadrupoles. Each of the eight arc sections consists of 27 cells. The magnet layout and beta functions are shown in Fig. 1, and the parameters for the arc quadrupoles in Table 1.

BBA TECHNIQUES

A centred beam experiences only the desired focusing upon its passage through an ideal quadrupole. However, if

Content from this work may be used under the terms of the CC BY 4.0 licence (© 2026). Any distribution of this work must maintain attribution to the author(s), title of the work, publisher, and DOI.

ISBN: 978-3-95450-252-3 ISSN: 2673-5350 doi: 10.18429/JACoW-IPAC2026-WEP5038

MODELING AND FIELD ANALYSIS OF THE LEIR BENDING MAGNETS AND OPTICS INTEGRATION

H. Deveci, M. A. Jebramcik
1211 CERN, Geneva, Switzerland

Abstract

This contribution presents the modelling of the dipole magnets of the Low-Energy Ion Ring (LEIR) at CERN. The LEIR dipoles are iron-dominated C-type 90° sector magnets. Each LEIR dipole consists of six blocks of roughly 1 m-long laminated steel yoke with copper coils. The main challenges of the design stem from the axial air gaps and the varying angles between the blocks, which cause unwanted harmonics in the magnetic field. These aspects lead to mismatches between measured and predicted linear optics parameters in LEIR. Due to the unconventional magnet design, efforts are made to obtain three-dimensional field maps and multipole field components with high accuracy. The study began with 2D Finite Element Analysis (FEA) in different cross sections and continued with 3D FEA for the examination of the integrated field and the multipole components. The FEA is computed using different programs for cross-comparison and to increase the model accuracy by fine-tuning. Finally, the results have been integrated into optics codes, and the linear optics is compared with linear optics measurements.

INTRODUCTION

The Low Energy Ion Ring (LEIR) [1] is a key element of the heavy-ion injector chain at CERN. It receives long pulses of lead ions from Linear Accelerator 3 (Linac 3) and converts them into short, high-intensity bunches suitable for further acceleration toward the Large Hadron Collider (LHC). After the RF capture, the bunches are accelerated from an energy of 4.2 MeV per nucleon up to 72 MeV per nucleon over a cycle time of 3.6 s. At extraction, the beam energy is appropriate for transfer to the Proton Synchrotron (PS), where the ions are accumulated and further accelerated.

LEIR was proposed in 1993 as a conversion of the existing Low Energy Antiproton Ring (LEAR) [2]. Optics measurements have historically indicated a mismatch between assumed (model) beam optics and actual beam optics in LEIR [3]. It has been the subject of speculation whether the potential cause for the mismatch between the measured and model beam optics is caused by an incorrect modeling of the bending magnets within the used tracking codes. For these reasons, efforts are being made to obtain exact field maps of the bending magnets to enable a more accurate implementation into tracking codes. The geometry of the bending magnets is characterized by multiple air gaps between magnetic blocks, non-uniform edge orientations, and a gap width that varies along the magnet length. These features significantly increase the complexity of both field computation and accurate numerical modeling [3]. In the context of LEIR, there are additional challenges, such as limited availability of detailed documentation and validated legacy models that are needed for the modeling of magnets using state-of-the-art simulation software.

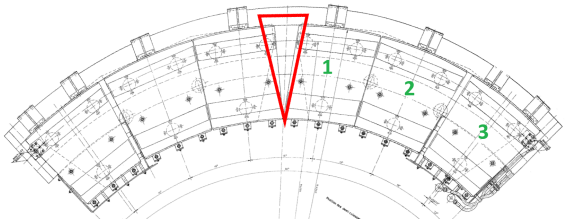

Figure 1: Top view of the LEIR dipole [4].

The LEIR dipole is an iron-dominated, water-cooled resistive magnet. Its mechanical structure is composed of six independent yoke blocks and a single curved bedstead coil extending over the full magnet length. In addition to the main coil, the two outermost blocks also include pole-face windings and back-leg windings. This configuration provides additional degrees of freedom for field shaping and correction, but further increases the complexity of the electromagnetic modeling. Figure 1 is an assembly drawing showing the top view of the magnet, including the yoke blocks, main winding, and the auxiliary equipment. The air gap in the middle is highlighted, as it is critically important for the harmonic content. The yoke blocks are numbered from the centre outward.

Another feature of the outermost yoke blocks is that they have a slightly larger aperture than the remaining yokes, resulting in a lower central magnetic field. Table 1 lists the main parameters of the LEIR dipoles.

Table 1: Parameters of the LEIR Dipole

Parameter	Units	Value
Current at injection / extraction	A	770 / 3290
Resistance at 20 °C	mΩ	6
Inductance	mH	25
Pole gap of central / lateral blocks	mm	80 / 88
Total length	mm	6378
Turns main / back-leg winding		12 / 10

MODELLING AND FEA

A comparative analysis has been performed using parametric models developed in Ansys Maxwell and OPERA. The modelling studies began with 2D and continued with 3D magnetostatic analyses. The pole-face windings and the back-leg windings have not been included in the initial sim-

Content from this work may be used under the terms of the CC BY 4.0 licence (© 2026). Any distribution of this work must maintain attribution to the author(s), title of the work, publisher, and DOI.

ISBN: 978-3-95450-252-3 ISSN: 2673-5350 doi: 10.18429/JACoW-IPAC2026-WEP5039

OPTICS CHARACTERIZATION AND RESONANCE DRIVING TERM STUDIES FOR THE SPS CRAB CAVITY TESTS IN 2025

P. Zisopoulos*, E. MacLean, M. Stefanelli, CERN, Geneva, Switzerland

Abstract

To prepare for the High Luminosity LHC, the crab cavities to be used in the upgrade have been tested in the CERN Super Proton Synchrotron (SPS). Machine studies have been carried out to investigate optics perturbations introduced by the crab cavities and their relation to resonance driving terms. Particular emphasis was placed on identifying possible sextupolar components and assessing their impact on the betatron tune. Measurements using controlled orbit bumps were performed to isolate the cavity contribution and to benchmark model predictions. The results provide valuable input for the interpretation of beam dynamics observations during the tests and for the refinement of the SPS optics model in view of future crab cavity studies.

INTRODUCTION

The crab cavity (CC) studies at CERN aim to validate CC technology for the High-Luminosity LHC (HL-LHC), which requires transverse RF deflection to restore head-on bunch crossing at the interaction points [1]. A CC test module has been installed in the SPS in Long Straight Section 6 (LSS6) [2] to characterise CC operation with proton beams.

Due to the lack of azimuthal symmetry, higher-order RF multipole components arise [3–5]. With the CC module oriented for horizontal crabbing, the dominant component is the normal sextupolar term b_3, which excites resonance driving terms (RDTs) and causes feed-down tune shifts at non-zero orbit offset. For the Radio-Frequency Deflector (RFD) design (currently installed), $K_3L \approx 0.012\,\mathrm{m}^{-2}$ [3].

In parallel with the CC beam tests, short dedicated studies used the SPS extraction sextupole LSE.20602 to emulate the expected CC sextupolar component and validate the measurement technique. The SPS features 215 beam position monitors (BPMs) [6] that provide turn-by-turn (TbT) data, enabling optics measurements via the Optics Measurement and Correction (OMC) tool [7]. The AC dipole excitation scheme implemented in the SPS [8], using the Base-Band Tune (BBQ) system [9] and the transverse damper (ADT), was used for the RDT measurements.

This paper reports results from studies in 2025 covering feed-down tune shifts and optics model characterisation, and a follow-up study in 2026 for AC-dipole RDT measurements.

EXPERIMENTAL MEASUREMENTS

Set-up

All measurements used the SPS LHC injection (Q20) optics at working point $Q_x/Q_y = 20.13/20.18$. The SPS extraction sextupoles (LSE) can be powered individually to generate controlled feed-down via orbit bumps. LSE.10602 was initially tried but abandoned as a chromatic LSF sextupole within the bump produced a spurious shift; LSE.20602 was used instead. A three-corrector orbit bump produced a closed horizontal displacement at LSE.20602, where the Q20 optics give $\beta_x \approx 97\,\mathrm{m}$, $\beta_y \approx 35\,\mathrm{m}$. Table 1 lists key optics parameters at both locations; the β-function ratio between the two locations sets the K_3L scaling required to recover the expected tune shift at the CC.

Table 1: Nominal Q20 Optics Parameters at the Two Key Locations

Element	s [m]	β_x [m]	β_y [m]	D_x [m]
LSE.20602	1341	97	35	1.13
CC (ACFCAN 61738)	6313	41.3	84.1	−0.59

The bump produced closed displacements of $x_+ = +30\,\mathrm{mm}$ and $x_- = -20\,\mathrm{mm}$ on successive plateaux within the same injection cycle. The sextupole strength $K_3L = 0.0125\,\mathrm{m}^{-2}$ (as set in LSA [10]) matches the estimated CC integrated strength.

Two measurement modes were employed: the BBQ system for continuous tune monitoring during the bump (no kicker needed), and single-kick TbT BPM data for optics measurements (phase advance, beta beating) with the OMC tool. Single kicks were applied inside both bump plateaux; Fig. 1 shows the recorded BPM excitation. The beam was a single pilot bunch ($\sim 10^{10}$ protons) for the 2025 sessions.

Optics Measurements

In 2025, a significant mismatch in the cumulative betatron phase advance was found between the best-knowledge model (quadrupole strengths from LSA) and a model matched to the measured tunes. As shown in Fig. 2, the best-knowledge model reaches a phase error of up to $0.4 \times 2\pi$. Matching to the measured tunes requires the defocusing quadrupole strengths to be ~1% larger than the LSA settings; this matched model reproduces the BPM phases closely. This mismatch is currently under investigation, as an accurate optics model is important for both CC beam dynamics interpretation and SPS operation. The horizontal phase advance could not be determined with confidence due to the fast horizontal decoherence.

Figure 3 shows fractional tunes from a 60-turn sliding-window analysis [11] of the single-kick TbT data, with the bare SPS machine. The horizontal coherent motion decays significantly faster than the vertical, limiting the useful signal length. Slow tune modulations from 50 Hz mains ripple of the main magnet converters (~900 turn period) and faster modulations at 600 Hz from 12-pulse rectification are also visible.

* panagiotis.zisopoulos@cern.ch

Content from this work may be used under the terms of the CC BY 4.0 licence (© 2026). Any distribution of this work must maintain attribution to the author(s), title of the work, publisher, and DOI.

ISBN: 978-3-95450-252-3 ISSN: 2673-5350 doi: 10.18429/JACoW-IPAC2026-WEP5040

EFFECT OF BROKEN SUPERPERIODICITY ON HALF INTEGER RESONANCE AND POSSIBLE COMPENSATION*

H. Bartosik and F. Zimmermann†, CERN, Geneva, Switzerland
G. Franchetti‡, GSI, Darmstadt, HFHF and Goethe Universität, Frankfurt, Germany

Abstract

With a perfect two-fold superperiodicity in a storage ring, the half integer resonance is not excited and can be overlapped by the beam tune spread induced, e.g., by beam-beam collisions in a collider, space charge in a hadron storage ring, or energy spread and chromaticity, without detrimental effect on the beam. If the superperiodicity of the quadrupolar lattice is broken, either by design or due to machine imperfections, a resonance stopband is created, which may lead to unstable particle motion. Guided by historical literature, analytical calculations, and toy simulations, we explore the relation between single-particle motion and optics near the resonance. We discuss possible mitigation approaches and the construction of tuning knobs or modified lattices which can reduce the resonance strength. Our discussion here focuses on the linear transverse optics and extends to chromatic resonance effects and linearized space charge forces.

INTRODUCTION

In a storage ring, the equation for the transverse motion of a single particle satisfies the linear Hill's equation [1], also known as the Ermakov-Pinney equation [2–4]:

$$y'' + k(s)y = 0, \ , \tag{1}$$

with $'$ denoting the derivative with respect to the distance along the reference path s, and k a periodic focusing function, $k(s) = k(s + C)$, with C equal the ring circumference.

Considering a pattern of quadrupole focusing errors (Δk), in second order perturbation theory, Courant and Snyder derived the width of the stopband near a half integer resonance $Q \approx n/2$, due to these errors, as [1]

$$\delta Q_n \approx \frac{1}{2\pi} \left| \int_0^C \beta(s)\, \Delta k(s)\, e^{i2\mu(s)}\, ds \right|, \tag{2}$$

and the maximum beta beating as [1]

$$\left(\frac{\Delta\beta}{\beta}\right)_{\max} \approx \frac{|\delta Q_n|}{2|Q - n/2|}\,, \tag{3}$$

where μ is the betatron phase.

In general, however, it is not obvious how to distinguish quadrupole errors $\Delta K = \int \Delta k ds$ from the design values of the integrated quadrupole strengths K, especially if the design focusing structure is not (super)periodic. In addition, the second-order approximations in Eqs. (2) and (3) should break down close to the half-integer resonance.

SINGLE GRADIENT ERRORS

Consider a single gradient error of integrated strength ΔK at $s = 0$. According to Eq. (2) the width of the stopband is

$$\delta Q_n \approx \frac{1}{2\pi}\, \beta(0)\, \Delta K\,. \tag{4}$$

For example, with $\Delta K = 0.01$ m^{-2} and $\beta(0) = 10$ m, the stop band is expected to be $\delta Q_n \approx 0.1/(2\pi) \approx 0.0159$.

Consider the 2×2 transport matrix

$$\mathbf{M}(\mu) = \begin{pmatrix} \cos\mu & \beta \sin\mu \\ -(1/\beta)\sin\mu & \cos\mu \end{pmatrix} \tag{5}$$

and add a thin-lens quadrupole with integrated strength K described by

$$\mathbf{M}_{\mathrm{q}}(K) = \begin{pmatrix} 1 & 0 \\ -K & 1 \end{pmatrix}, \tag{6}$$

so that the product matrix becomes $\mathbf{M}_{\mathrm{tot}} = \mathbf{M}(\mu) \cdot \mathbf{M}_{\mathrm{q}}(K)$. The tune Q of $\mathbf{M}_{\mathrm{tot}}$ can be obtained as

$$Q = \mathrm{Im}\left[\frac{\mathrm{arccosh}\,(\mathrm{Tr}(\mathbf{M}_{\mathrm{tot}})/2)}{2\pi}\right] \tag{7}$$

and, in case of unstable motion, the exponential increment per turn, λ, in units of 2π, by the real part of the square brackets of Eq. (7). The dependence of Q and λ on the base tune $\mu/(2\pi)$ is illustrated in Fig. 1. The stop band is clearly visible, characterized by a constant tune Q and nonzero growth rate λ. The total extent of the stopband is close to the expected width $\delta Q_n \approx 0.016$ from Eq. (4).

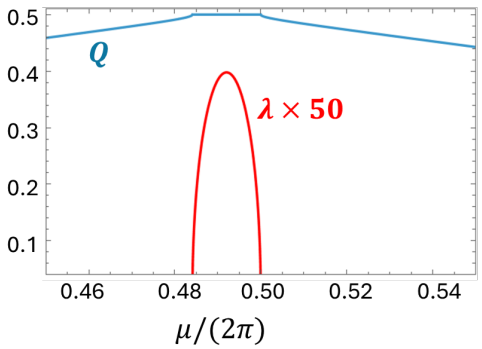

Figure 1: Tune Q and growth rate λ (amplified by a factor 50) as a function of the base tune $\mu/(2\pi)$, with $\beta = 10$ m, and for a single additional quadrupole of strength $K = 0.01$ m^{-1}.

* Work supported, in parts, by the European Union's Horizon Europe programme under grant agreement no. 101290927 (EPITA).

† frank.zimmermann@cern.ch
‡ g.franchetti@gsi.de

Content from this work may be used under the terms of the CC BY 4.0 licence (© 2026). Any distribution of this work must maintain attribution to the author(s), title of the work, publisher, and DOI.

ISBN: 978-3-95450-252-3 ISSN: 2673-5350 doi: 10.18429/JACoW-IPAC2026-WEP5041

UNDERSTANDING ENERGY-INDUCED OPTICS DISTORTIONS IN THE LHC

J. Gray*, C. Caliari, F. Carlier, J. Dilly, S. Horney, J. Keintzel, E. Maclean, K. Sabin, K. Skoufaris, F. Soubelet, M. Stefanelli, R. Tomás, W. Van Goethem,
European Organization for Nuclear Research, Geneva, Switzerland
Y. Angelis, Aristotle University of Thessaloniki, Thessaloniki, Greece
A. Oeftiger, John Adams Institute, University of Oxford, Oxford, United Kingdom

Content from this work may be used under the terms of the CC BY 4.0 licence (© 2026). Any distribution of this work must maintain attribution to the author(s), title of the work, publisher, and DOI.

Abstract

Small momentum offsets in the LHC can generate significant optics distortions, particularly at low β^*. The beam energy carries a relative uncertainty of approximately 10^{-3}, which is insufficient for precise optics control. To better understand the energy contribution to optics measurements, two beam-based techniques have been explored. The first applies a global linear response matrix between BPM phase advances and relative energy offset, denoted as $\Delta p/p$. While effective in simulation, this method is sensitive to phase errors and tends to underestimate the energy shift. We introduce a new approach based on the principle of Deep Lie Map Networks (DLMN), which fits a differentiable tracking model to measured turn-by-turn BPM trajectories. Using the symplectic single-pass forward differentiation capability of MAD-NG, we can fit our simulation to the optimum $\Delta p/p$ that matches the measurement. The results reveal arc-by-arc variations consistent with varying dipolar errors from arc to arc, providing insight into orbit behaviour around the ring. The measured response also agrees well with intentional energy shifts, demonstrating that the DLMN offers a promising new method for analysing the effect of energy on the optics of the LHC.

INTRODUCTION

Small energy offsets in the LHC have been observed to induce measurable optics distortions that become increasingly important as the machine operates at lower β^*. For example, a relative energy change on the order of 10^{-4} was linked to an observed ∼10% increase in beta beating over a two-week period [1]. If the energy shift is left uncorrected, such drifts force repeated optics corrections, unnecessarily increasing time spent commissioning the machine.

The dominant contributors to these energy-dependent optics shifts are the strongest focusing elements in the lattice: the inner triplet quadrupoles surrounding the major interaction points (ATLAS and CMS). With the HL-LHC upgrade and a design β^* of 15 cm, simulations indicate an even greater sensitivity: a relative energy change of 2×10^{-4} can produce up to 50% beta beating [2].

The root cause of energy drifts in the machine has been attributed to changes in the average orbit corrector kicks over time [1]. The RF system maintains path length and so the average corrector strength directly changes the beam energy [1]. Understanding and tracking these energy-induced optics changes is therefore essential to minimise time spent on optics correction and maximise time spent delivering luminosity for physics.

This paper compares two independent beam-based techniques for estimating momentum offsets. The first is a response matrix approach that relates changes in phase advances between BPMs to a change in $\Delta p/p$ [3, 4]. The second is the Deep Lie Map Network (DLMN) method that fits a differentiable symplectic tracking model to turn-by-turn data and extracts arc-level momentum deviations [5, 6].

GLOBAL RESPONSE MATRIX

The first method explored to determine the effect of energy on the optics assumes a linear relationship between changes in momentum offset and changes in observable quantities [3]:

$$\vec{M}(\delta + \Delta p/p) \approx \vec{M}(\delta) + \mathbf{R}(\delta)\Delta p/p \ , \qquad (1)$$

where $\vec{M}(\delta)$ represents the model prediction for an observable vector at a given momentum deviation δ, $\Delta p/p$ is the relative momentum offset from this δ, and $\mathbf{R}(\delta)$ is the response matrix at this point [3]. By comparing measurements to model predictions, a correction can be determined [3]:

$$\vec{M}(\delta)+\mathbf{R}(\delta)\Delta p/p \approx \vec{O} \implies \Delta p/p \approx \mathbf{R}^{+}(\delta)\left(\vec{O} - \vec{M}(\delta)\right) \ , \qquad (2)$$

where $\vec{O}$ is the stacked measured observable vector at multiple locations along the ring and $\mathbf{R}^{+}$ is the SVD-based pseudo-inverse of the response matrix. For this application, the horizontal and vertical phase advances between BPMs are used as the observable vectors, as they are sensitive to momentum offset, mainly due to the triplets.

From simulation in a lattice without errors, we find that this method has only a few percent error in the calculated relative momentum offset over the range of -3×10^{-4} to 3×10^{-4}, as can be seen in Fig. 1.

DEEP LIE MAP NETWORKS

The second method, based on Deep Lie Map Networks (DLMN) [5], uses derivatives of (x, y) with respect to $\Delta p/p$ to converge to an optimal value, where $\Delta p/p$ is the only free parameter in each fit. This approach requires reconstructing

* joshua.mark.gray@cern.ch

ISBN: 978-3-95450-252-3 ISSN: 2673-5350 doi: 10.18429/JACoW-IPAC2026-WEP5042

DEEP LIE MAP NETWORKS FROM SINGLE-PASS FORWARD DIFFERENTIATION

J. Gray*, C. Caliari, F. Carlier, L. Deniau, K. Skoufaris
European Organization for Nuclear Research, Geneva, Switzerland
A. Oeftiger, John Adams Institute, University of Oxford, Oxford, United Kingdom

Content from this work may be used under the terms of the CC BY 4.0 licence (© 2026). Any distribution of this work must maintain attribution to the author(s), title of the work, publisher, and DOI.

Abstract

A new implementation of Deep Lie Map Networks (DLMNs) based on the single-pass forward-differentiation capability of MAD-NG is presented. DLMNs were introduced in earlier work as an optics-modelling framework in which lattice parameters are fitted directly to measured BPM trajectories. In the present implementation, exact derivatives of particle coordinates with respect to lattice parameters are computed during tracking. Rather than relying on backpropagation or finite differences, gradients are evaluated on the fly during tracking, so intermediate states do not need to be stored. This reduces memory use and computation time while preserving precision. The result is a scalable tool for data-driven optics reconstruction that is well suited to larger multi-turn data sets and, ultimately, to digital-twin applications in which model parameters are inferred continuously from live measurements.

INTRODUCTION

Achieving and maintaining good performance in synchrotrons relies on accurate knowledge of the underlying lattice optics [1, 2]. Magnet strength errors, misalignments, and higher-order field components all lead to optics distortions that can degrade beam quality and reduce dynamic aperture, beam lifetime, and machine performance [1, 2]. Identifying and correcting these errors is therefore critical.

Awidely used method for linear optics correction is Linear Optics from Closed Orbits (LOCO), originally introduced in [3]. LOCO determines lattice errors by fitting a model orbit response matrix to measured data, enabling the extraction of quadrupole strength errors and beam position monitor (BPM) calibration factors [3, 4]. This method can be slow and cumbersome for large machines, may fail to converge, and remains sensitive to noise and systematic errors [1, 5]; moreover, typically it is limited to only linear optics, although there exists extensions to nonlinear optics from off-energy closed orbits (NOECO) [6, 7]. On the other hand, methods widely used for example at the Large Hadron Collider (LHC), rely on optics measurements of AC-dipole-driven turn-by-turn data; however, these approaches typically target a specific machine state and do not inherently provide a simulation model applicable to all or even any machine state.

Deep Lie Map Networks (DLMNs), introduced in [8], offer a framework in which an accelerator lattice is treated as a parametrised model whose parameters are optimised directly against measurements. The first implementation of this approach was developed in Julia, using backpropagation techniques from the machine-learning community. In that work, a custom tracking code was implemented to optimise quadrupole and sextupole strengths against measured data [6].

In this work, we present a new DLMN implementation based on the forward-differentiation capabilities of Methodical Accelerator Design – Next Generation (MAD-NG) [9]. By exploiting its truncated power series algebra (TPSA) framework, derivatives of particle coordinates with respect to arbitrary lattice parameters can be computed exactly during tracking. This enables step-by-step gradient evaluation without finite differences or backpropagation, improving efficiency, numerical stability, and memory usage. In contrast to LOCO, which relies on dedicated and expensive beam-time-intensive measurements and structured orbit-response data, DLMN can make use of more routine machine data. The approach has already been applied to LHC measurements to identify beam-energy offsets [10].

DLMN DESIGN

The parametrised lattice model can be interpreted as a machine-learning network in which magnet parameters, such as strengths or misalignments, are optimised to reproduce measured beam positions [6]. The optimisation aims to reduce the loss function using stochastic gradient descent, $\mathscr{L}$, defined as

$$\mathscr{L} = \frac{1}{2} \sum_i \left[(x_{s,i} - x_{m,i})^2 + (y_{s,i} - y_{m,i})^2 \right], \qquad (1)$$

which quantifies the discrepancy between the measured and simulated beam position monitor (BPM) coordinates, $(x_{m,i}, y_{m,i})$ and $(x_{s,i}, y_{s,i})$, respectively. The index i spans all BPMs, turns, and initial conditions. To optimise a parameter k, the derivative of the loss with respect to k is required. Applying the chain rule gives

$$\frac{\mathrm{d}\mathscr{L}}{\mathrm{d}k} = \sum_i \left(\frac{\partial \mathscr{L}}{\partial x_{s,i}} \frac{\mathrm{d}x_{s,i}}{\mathrm{d}k} + \frac{\partial \mathscr{L}}{\partial y_{s,i}} \frac{\mathrm{d}y_{s,i}}{\mathrm{d}k} \right). \qquad (2)$$

Substituting Eq. (1) into Eq. (2) gives

$$\frac{\mathrm{d}\mathscr{L}}{\mathrm{d}k} = \sum_i \left[(x_{s,i} - x_{m,i}) \frac{\mathrm{d}x_{s,i}}{\mathrm{d}k} + (y_{s,i} - y_{m,i}) \frac{\mathrm{d}y_{s,i}}{\mathrm{d}k} \right]. \qquad (3)$$

The remaining task is therefore to obtain $\mathrm{d}x_{s,i}/\mathrm{d}k$ and $\mathrm{d}y_{s,i}/\mathrm{d}k$, either by automatic differentiation or by finite differences.

* joshua.mark.gray@cern.ch

ISBN: 978-3-95450-252-3 ISSN: 2673-5350 doi: 10.18429/JACoW-IPAC2026-WEP5043

CLEANING TURN-BY-TURN DATA FROM THE LHC WITH AUTOENCODERS

J. Gray*, F. Carlier, K. Skoufaris, European Organization for Nuclear Research, Geneva, Switzerland

Abstract

Turn-by-turn (TbT) BPM data in the LHC is often affected by noise, limiting the extraction of resonant driving terms (RDTs) and reducing the precision of nonlinear optics studies. We developed a denoising autoencoder trained on simulated tracking data to reconstruct clean transverse oscillations and suppress noise directly in the time domain. The method produces cleaner frequency spectra and significantly improves RDT visibility compared to established methods such as singular value decomposition, even when trained on fewer turns. In its current form, the autoencoder performs well on data that resemble the training set. However, when applied to new conditions such as different noise levels, excitation amplitudes, tunes, or beam configurations, its ability to generalise decreases. These results demonstrate that autoencoders can substantially improve TbT data quality in specific conditions. Establishing broader and more diverse training datasets is a promising next step toward applying this technique to real LHC measurements.

INTRODUCTION

During LHC commissioning, linear and nonlinear corrections are required to maximise beam lifetime and luminosity [1]. Resonances from horizontal and vertical tune combinations, $(j-k)Q_x + (l-m)Q_y$, are characterised by resonant driving terms (RDTs) f_{jklm}, making RDTs useful diagnostics for nonlinear errors [2–4]. They are inferred from AC-dipole-excited turn-by-turn (TbT) beam position monitor (BPM) data, so reconstruction quality depends directly on the TbT signal quality.

The standard cleaning strategy is singular value decomposition (SVD) [5]. SVD is attractive because it is computationally efficient and effective at removing uncorrelated noise, as demonstrated in [6]. However, it can also suppress important spectral content across all BPMs, which limits RDT reconstruction precision [7].

Autoencoders are widely used for dimensionality reduction and denoising [8], similar to SVD. By learning a compact latent representation and reconstructing the input, they can capture underlying structure while filtering noise. For TbT data, this could improve weak spectral-line visibility for RDT analysis.

We first demonstrate how SVD can remove spatial RDT information in simulated LHC TbT data, then present the convolutional autoencoder and compare both methods in terms of spectral visibility, RDT reconstruction, and generalisation.

* joshua.mark.gray@cern.ch

SVD EFFECT ON RDT RECONSTRUCTION

LHC simulation data are generated by tracking with Xsuite [9] for 1000 turns, then artificial Gaussian noise is added. For frequency analysis, the TbT matrix is decomposed with SVD and the first 12 singular values are retained, a common choice for LHC TbT data [10]. An RFFT is then applied to the cleaned data [10]. From the resulting spectral amplitudes and phases, RDTs are reconstructed [3].

To reduce complexity, the simulation used fixed initial coordinates rather than an AC dipole, giving a maximum physical peak-to-peak amplitude of 2 mm.

The chosen scenario is the LHC ring at 6800 GeV, with tunes $Q_x = 0.28$ and $Q_y = 0.31$, and $\beta^* = 0.3$ m. Although typical LHC BPM noise is around 100 μm, we use 500 μm for an oscillation spanning about -1 mm to 1 mm to highlight the negative impacts of SVD cleaning. The analysis is therefore framed by spectral signal-to-noise ratio (SNR), the usual figure of merit for RDT reconstruction quality [11].

The RDTs f_{3000} and f_{0111} were selected because they are the dominant RDTs in this scenario for their respective planes. Figure 1 shows that these frequencies remain clearly visible after SVD cleaning in the spectrum. However, the reconstructed RDTs along the ring in Fig. 2 show that local RDT information is almost entirely lost. Instead, the signal is driven toward the ring-average RDT value. This removes local diagnostic information, although the average RDT value is still recovered. Consequently, analyses that rely only on ring-averaged RDT values are much less affected by SVD cleaning [4, 11].

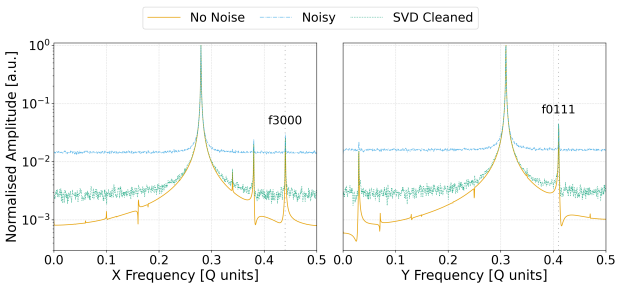

Figure 1: Effect of SVD cleaning on spectral content. Average frequency spectra: raw noisy signal, SVD-cleaned signal, and the no-noise reference.

This loss of local RDT information limits nonlinear-error localisation and motivates denoising methods that preserve local spectral structure.

AUTOENCODER METHOD

Model Architecture and Training

To address this limitation, we use a convolutional autoencoder family implemented in PyTorch and PyTorch Light-

Content from this work may be used under the terms of the CC BY 4.0 licence (© 2026). Any distribution of this work must maintain attribution to the author(s), title of the work, publisher, and DOI.

ISBN: 978-3-95450-252-3 ISSN: 2673-5350 doi: 10.18429/JACoW-IPAC2026-WEP5044

MODELLING LINEAR COUPLING FOR FCC-ee IN XSUITE

V. Gawas*[1], F. Zimmermann, X. Buffat, R. Tomás Garcia
CERN, European Organization for Nuclear Research, Geneva, Switzerland
[1]University of Geneva, Geneva, Switzerland †

Abstract

Accurate control of transverse linear coupling is important for achieving the target luminosity in FCC-ee. We have implemented a simplified FCC-ee coupling model in Xsuite based on linear maps and the Edwards-Teng formalism. This approach is benchmarked against the full FCC-ee optics model, showing good agreement in betatron tunes, beta functions, and coupling-related quantities. The coupling matrix elements are derived as a function of resonance driving terms (RDTs) and validated against analytical calculations of f_{1001} and f_{1010}. The coupled model is then used in strong-strong beam-beam simulations to study the impact of controlled RDT excitations on luminosity, beam size, emittance, and beamstrahlung power at the ZH and $t\bar{t}$ operating points. This work presents a practical framework for coupling studies and provides a basis for developing FCC-ee coupling tolerances and luminosity tuning procedures.

INTRODUCTION

Linear coupling between the horizontal and vertical betatron motion plays a critical role in determining the achievable beam sizes and luminosity in the FCC-ee collider [1]. In the interaction regions (IRs), coupling arises primarily from detector solenoids, anti- and shielding solenoids, quadrupole magnet roll errors, and sextupole magnet misalignments. Even weak coupling can lead to vertical emittance growth, tune splitting, and beam-size blow-up at the interaction point (IP), thereby degrading luminosity and changing beamstrahlung emission.

Beam-beam simulations carried out for assessing the luminosity performance often rely on simplified lattice models, in which the detailed machine optics is replaced by compact linear transport maps combined with a beam-beam element at the interaction point (IP) [2]. For accurately capturing the impact of coupling in such models, a consistent representation of linear coupling is required. To accomplish this, we have implemented a coupled linear transport model in the code Xsuite [3]. Our model is based on the Edwards-Teng formalism [4], which expresses the coupled betatron motion in terms of two normal modes. The transport from the crab sextupoles to the IP is represented by a factorized map consisting of uncoupled normal-mode motion and local coupling matrices at the start and end points.

The model parameters are extracted from a Twiss analysis of the full FCC-ee lattice, including possible skew quadrupole excitations. The complete lattice based on linear transport maps is validated against the full nonlinear lattice of the FCC-ee by comparing linear optics observables such as tunes and IP β-functions.

Our ring model with a single IP comprises an upstream crab sextupole, a coupled transport matrix to that IP, a beam-beam element, the inverse transport to the downstream crab sextupole, and an arc section including radiation damping and quantum excitation. This model can be used combined with strong-strong beam-beam simulations at the IP, to explore the impact of deliberately introduced local IP coupling on luminosity, beam sizes, emittance, and beamstrahlung at different operating energies of the collider.

COUPLED TRANSPORT IN XSUITE

The 4×4 coupled transport between two locations can be written in the Edwards-Teng form as [4]

$$M_{12} = V_{s2} \begin{pmatrix} A_{12} & 0 \\ 0 & B_{12} \end{pmatrix} V_{s1}^{-1} ,$$

where A_{12} and B_{12} are the Courant-Snyder matrices describing uncoupled motion of the two normal modes, and V_{s1}, V_{s2} contain the coupling information. The normal modes are obtained by diagonalizing the full coupled one-turn matrix. In the uncoupled normal-mode coordinates, the dynamics reduces to two independent harmonic oscillators with eigentunes Q_1 and Q_2.

Normal-Mode Optics Parameters

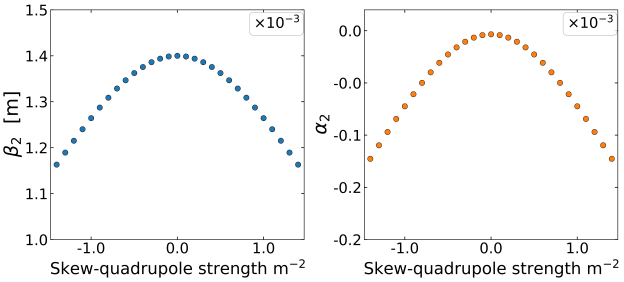

Figure 1: The IP normal mode functions β_2 and α_2 versus the strength of two skew quadrupoles (of opposite sign) inserted in the full lattice after the crab sextupoles on either side of the IP, in the absence of any beam-beam element.

The normal-mode Courant–Snyder matrices are fully determined by the Twiss parameters $\beta_{1,2}$, $\alpha_{1,2}$ and the phase advances of the two eigenmodes. In FCC-ee, the beams are extremely flat and the design tunes are not close to a linear coupling resonance, and after optics corrections the linear coupling is weak, so that the normal-mode optics functions remain close to those of the uncoupled optics. This simplifies the parameter extraction from a Twiss analysis of the

* vaibhavi.gawas@cern.ch
† This work was supported by the Swiss CHART programme.

Content from this work may be used under the terms of the CC BY 4.0 licence (© 2026). Any distribution of this work must maintain attribution to the author(s), title of the work, publisher, and DOI.

ISBN: 978-3-95450-252-3 ISSN: 2673-5350 doi: 10.18429/JACoW-IPAC2026-WEP5046

BEAMSTRAHLUNG AND PAIR PRODUCTION UNDER IP ABERRATIONS AT THE FCC-ee*

V. Gawas†[1], F. Zimmermann, J. P. T. Salvesen, CERN, Geneva, Switzerland
[1] also at University of Geneva, Geneva, Switzerland

Content from this work may be used under the terms of the CC BY 4.0 licence (© 2026). Any distribution of this work must maintain attribution to the author(s), title of the work, publisher, and DOI.

Abstract

Beamstrahlung and secondary pair production are relevant sources of backgrounds but can also be exploited as potential tuning signals at the FCC-ee. They depend on possible interaction point (IP) optics errors and on general beam–beam conditions. Using GUINEA-PIG, we simulate beamstrahlung photons, and pair production through Breit–Wheeler, Bethe–Heitler, and Landau–Lifshitz processes and analyse the spectra, emitted power, and pair count for different sets of IP aberrations, including waist shift, vertical dispersion, and transverse coupling. The resulting photon and pair energy–angle distributions are examined, where comparisons with analytical expectations allow for consistency checks. We also compare GUINEA-PIG beamstrahlung predictions with multi-turn results delivered by the newly adopted code Xsuite, for a further benchmarking of Xsuite's beam-beam simulation package. Our study sheds light on possible beamstrahlung-related signals at the FCC-ee, including electron-positron pair production, and their dependence on the quality of the IP optics tuning.

INTRODUCTION

At future high-luminosity electron–positron colliders such as the FCC-ee, beam–beam collisions at the interaction point (IP) give rise to intense electromagnetic fields that significantly affect the properties of the colliding beams. One of the most prominent consequences is beamstrahlung, namely the emission of synchrotron-like radiation by beam particles in the field of the opposing bunch [1,2]. Together with beamstrahlung, the strong beam-beam fields also lead to the generation of secondary particles through incoherent processes such as Breit–Wheeler, Bethe–Heitler, and Landau–Lifshitz pair production [3, 4]. While these effects constitute important sources of detector background [5], they also carry detailed information on the beam–beam configuration and on the quality of the IP optics.

Beamstrahlung emission and incoherent pair production are sensitive to the local beam sizes and overlap conditions at the IP, especially with FCC-ee's flat beams. Consequently, residual optics aberrations resulting in luminosity degradation, such as waist shifts, vertical dispersion, and transverse coupling can induce measurable variations in the photon emission rates, their energy spectra, and angular distributions, as well as in the production of secondary electron–positron pairs [6–9]. This sensitivity makes beamstrahlung-related observables promising candidates for non-invasive beam diagnostics and for luminosity optimisation strategies at the FCC-ee.

Table 1: Key FCC-ee Beam Parameters for Z and $t\bar{t}$ Energies.

Parameter	Z	$t\bar{t}$
Number of bunches n_b	11200	64
Bunch intensity N	2.16×10^{11}	1.48×10^{11}
Horiz. emittance ε_x [nm]	0.70	1.51
Vert. emittance ε_y [pm]	1.9	1.36
β_x^* [m]	0.11	0.90
β_y^* [mm]	0.7	1.4
Bunch length σ_z [mm]	5.57	1.91
BS bunch length $\sigma_{z,\mathrm{BS}}$ [mm]	15.6	2.32
BS Energy spread σ_δ	1.16×10^{-3}	1.92×10^{-3}
Half-crossing angle ϕ [mrad]	15	15

However, a systematic comparison of the relative impact of different IP aberrations on both beamstrahlung emission and incoherent pair production, as well as their potential use as tuning observables, remains limited. While centroid offsets also constitute IP aberrations, their impact is treated separately [10]. In this study, we investigate the impact of selected IP aberrations on beamstrahlung and incoherent pair production using GUINEA-PIG [11–13], a well-established beam–beam simulation code. We focus on vertical waist shifts and dispersion, which are among the dominant contributors to luminosity degradation and are relevant for operation with low vertical emittance [14]. Transverse coupling, which requires multiturn simulations is not studied here, but is addressed in a complementary study based on Xsuite [14], which also includes beamstrahlung, but not yet any pair production.

Simulations are performed with GUINEA-PIG [13] using 10^6 macroparticles per beam and the beamstrahlung-broadened bunch length $\sigma_{z,\mathrm{BS}}$ as input. We study two FCC-ee working points: the Z pole ($E_{\mathrm{beam}} = 45.6\,\mathrm{GeV}$) and the $t\bar{t}$ threshold ($E_{\mathrm{beam}} = 182.5\,\mathrm{GeV}$). The key parameters for both working points are listed in Table 1 [7].

Only one IP aberration is applied at a time, while all other parameters are kept at their nominal values. The vertical waist shift Δs is scanned over the range $[-1000, +1000]$ µm, and the vertical dispersion D_y^* over $[-100, +100]$ µm. The beamstrahlung power is evaluated independently for each beam every second.

BEAMSTRAHLUNG SCANS

Beamstrahlung provides a direct probe of the electromagnetic fields generated during the beam-beam collision

* This work was supported by the Swiss CHART programme.
† vaibhavi.gawas@cern.ch

ISBN: 978-3-95450-252-3 ISSN: 2673-5350 doi: 10.18429/JACoW-IPAC2026-WEP5047

FINAL FOCUS SYSTEMS AT 550 AND 1500 GEV

L. Kennedy*,[1,2], C. Caliari[2], R. Tomás[2], P. N. Burrows[1]
[1]John Adams Institute, University of Oxford, Oxford, United Kingdom
[2]European Organization for Nuclear Research (CERN), Meyrin, Switzerland

Abstract

The Final Focus System (FFS) results for CLIC at 1.5 TeV have thus far been estimated using a 3 TeV system operated at reduced energy. Here, we present a dedicated design for the 1.5 TeV stage, where we exploit reduced radiation effects to allow stronger dispersion and weaker chromaticity-correcting sextupoles, thereby mitigating beam transport nonlinearities. The resulting design is 220 m shorter and offers a 50% luminosity gain. The performance of both normal-conducting and superconducting beams at 550 GeV are evaluated using the CLIC FFS, addressing the goals defined by the CLIC and Linear Collider Facility at CERN inputs to the European Strategy for Particle Physics Update.

CLIC 1.5 TeV FINAL FOCUS

The 1.5 TeV Final Focus System (FFS) baseline reported in the CLIC Readiness Report (CRR) [1] offers an estimated total luminosity of $3.7{\times}10^{34}\,\mathrm{cm}^{-2}s^{-1}$, based on the transport of a 1.5 TeV beam in a lattice designed for 3 TeV [2, 3]. At 3 TeV, synchrotron radiation induced beam size growth is more significant and must be mitigated by reducing the average dispersion in the system. The resulting reduction in dispersion requires stronger sextupole magnets for chromaticity correction, thereby introducing strong chromatic aberrations and luminosity loss. At 1.5 TeV, we can afford to adopt a more compact FFS featuring shorter and stronger bending dipoles, allowing increased dispersion and weaker sextupoles to reduce chromatic and geometric aberrations. Figure 1 demonstrates the reduction in sextupole strengths k_2 with the increase in average horizontal dispersion η_x and the subsequent improvement in total luminosity $\mathscr{L}_{Tot}$. The resulting lattice features 78% increased dispersion and provides a 220 m shorter FFS relative to the CRR design.

Using MADX [4], the linear optics in the FFS were matched and scanned to find the horizontal and vertical IP beta functions, β_x^* and β_y^*, which best minimise the beam size. The beam is then tracked using PLACET [5, 6] and the luminosity is computed using GUINEA-PIG [7]. Figure 2 shows the total and peak luminosity vs β_y^* and the corresponding higher-order beam sizes computed semi-analytically in MAPCLASS [8, 9].

Including radiation effects generated by the dipoles, quadrupoles and higher-order multipoles, a total luminosity of $5.5{\times}10^{34}\,\mathrm{cm}^{-2}s^{-1}$ is found when $\beta_x^*/\beta_y^* = 5/0.07$ mm. In this configuration, 10% of the luminosity is lost to synchrotron radiation while 33% of the luminosity resides in the 1% peak of the beam energy distribution. Reducing β_x^* from 6 mm (as in the CRR) to 5 mm improves the total luminosity by approximately 10%, while the absolute peak luminosity remains constant. However, the ratio of the total and peak luminosities, $\mathscr{L}_{1\%}/\mathscr{L}_{Tot}$ is reduced by approximately 3% due to enhanced disruption at lower β_x^*, leading to increased background. At $\beta_y^* < 0.07$ mm, we see a decrease in luminosity dominated by an increase in aberrations, along with a more pronounced hourglass effect as we approach $\beta_y^*/\sigma_z < 1$ [10]. Figure 3 shows the resulting linear optics with final drift length $L^* = 6$ m [11].

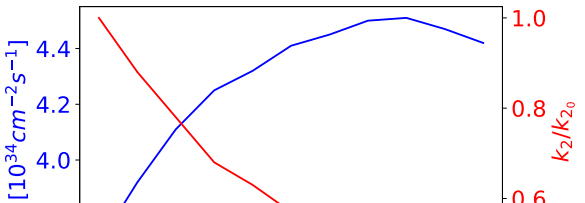

Figure 1: Blue: total luminosity of the 1.5 TeV final focus as a function of average dispersion, η_x. Red: the reduction in sextupole strengths, k_2, as bending angles are increased.

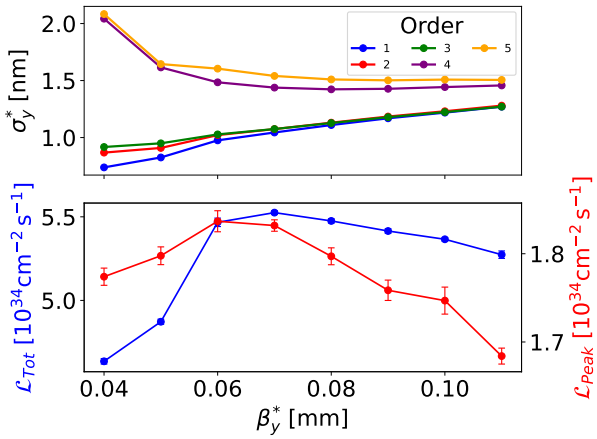

Figure 2: Bottom: total luminosity vs the vertical IP beta function, β_y^*, computed in GUINEA-PIG for a CLIC-type beam at 1.5 TeV. Top: higher-order analytic beam sizes computed using MAPCLASS as a function of β_y^*.

In addition to scaling sextupole strengths with the inverse of the dipole bending angles, MAPCLASS was used to optimise the sextupole, octupole and decapole strengths, targeting further reduction of the higher-order aberrations. In a recent study at 7 TeV [12], we demonstrated that the Gaussian core of the beam is strongly correlated with the lumi-

* lewis.kennedy@cern.ch

Content from this work may be used under the terms of the CC BY 4.0 licence (© 2026). Any distribution of this work must maintain attribution to the author(s), title of the work, publisher, and DOI.

ISBN: 978-3-95450-252-3 ISSN: 2673-5350 doi: 10.18429/JACoW-IPAC2026-WEP5050

OPTIMISATION OF THE TRANSITION ENERGY CROSSING OPTICS IN THE CERN PROTON SYNCHROTRON

M. Bozatzis*,[1], F. Asvesta, H. Bartosik, A. Huschauer, N. Mounet, CERN, Geneva, Switzerland
[1]also at Goethe University Frankfurt, Frankfurt am Main, Germany

Abstract

In view of optimising the performance for the fixed-target experiments in the CERN accelerator complex, studies aimed at increasing intensity in the Proton Synchrotron (PS) are currently taking place. Measurements have revealed losses along the PS cycle for the high intensity beams destined for the nTOF facility, with the majority originating from the transition energy crossing. As well as beam intensity, the transverse beam characteristics were also identified to have an impact on the magnitude of losses, hinting to possible aperture limitations due to the optics perturbations of the transition energy crossing γ_t-jump scheme. The possibility to modify the existing γ_t-jump quadrupole position along the PS ring is examined, in an attempt to optimise the crossing in terms of losses and transverse parameter evolution.

INTRODUCTION

Within the scope of the Physics Beyond Colliders (PBC) study [1], increasing demand for high-intensity beams from fixed-target experiments such as nTOF [2] (neutron time-of-flight) has highlighted the need to address potential operational limitations of the CERN PS. Measurements along the PS cycle for such beams have revealed losses, as shown in Fig. 1. These losses become more pronounced at higher intensities: at the operational intensity of $I_0 \approx 8.4 \times 10^{12}$ ppb, the relative loss is $\Delta I/I_0 \approx -0.8\%$, whereas at $I_0 \approx 9.2 \times 10^{12}$ ppb it increases to $\Delta I/I_0 \approx -1.3\%$. The losses occur predominantly during transition energy crossing, which has been identified as the principal bottleneck for further intensity increases.

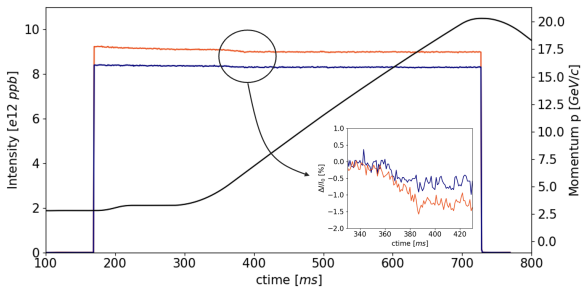

Figure 1: Beam intensity along the PS cycle for $I_0 \approx 8.4 \times 10^{12}$ ppb (blue) and $I_0 \approx 9.2 \times 10^{12}$ ppb (orange), for the nTOF type beam. The proton momentum (black) is shown on a secondary axis. The transmission $\Delta I/I_0$ during transition energy crossing (crossing time: 381 ms) is shown in the inset.

One of the manipulations taking place at the PS transition energy crossing is the γ_t-jump scheme. This procedure increases the transition-crossing speed and is essential for the stable operation of high-intensity beams [3, 4]. Nevertheless, this scheme perturbs the optics, introducing large beta-beating around transition [5, 6], especially in the horizontal plane. These perturbations lead to an increase in the transverse beam size at transition, representing one of the potential loss mechanisms for high-intensity and high-emittance beams, such as those directed to nTOF

One of the parameters influencing the γ_t-jump is the physical positioning of the quadrupoles used in the scheme. In this work, the impact of quadrupole placement on beam losses and transverse beam properties is investigated, with the goal of identifying a more optimal configuration.

GAMMA JUMP SCHEME IMPLICATIONS

In the CERN PS, the implementation of the γ_t-jump scheme relies on powering sets of quadrupoles arranged in doublet and triplet configurations with appropriately defined current functions. This procedure induces a modulation of the horizontal dispersion function D_x along the ring, thereby modifying the value of γ_t and enabling a faster transition crossing [3]. Concurrently, other optical functions are also perturbed, with the horizontal beta function β_x exhibiting the most significant variations [6].

The resulting beta-beating evolves throughout the jump, modulating the beam size, which reaches its maximum shortly before the crossing. The horizontal beam size is expressed as $\sigma_x = \sqrt{N^2_{\sigma,x}\varepsilon_x\beta_x + (N_{\sigma,l}D_x\Delta p/p)^2}$, with β_x, D_x the horizontal beta and dispersion functions and $\varepsilon_x, \Delta p/p$ the measured horizontal emittance and calculated momentum deviation, and $N_{\sigma,x}, N_{\sigma,l}$ the number of horizontal and longitudinal sigmas selected. The alteration of σ_x at ≈ 1 ms before transition is displayed in Fig. 2.

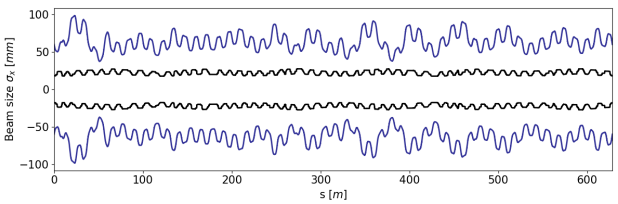

Figure 2: Horizontal beam envelope $\pm\sigma_x$ along the PS ring. The unperturbed beam envelope is shown with the black line and the altered with the blue. The perturbed optics functions are calculated at ≈1 ms before transition, ε_x =12.5 µm and $\Delta p/p = 3 \cdot 10^{-3}$. The number of horizontal and longitudinal sigmas selected is $N_{\sigma,x} = 4$ & $N_{\sigma,l} = 2$.

* miltiadis.bozatzis@cern.ch

Content from this work may be used under the terms of the CC BY 4.0 licence (© 2026). Any distribution of this work must maintain attribution to the author(s), title of the work, publisher, and DOI.

ISBN: 978-3-95450-252-3 ISSN: 2673-5350 doi: 10.18429/JACoW-IPAC2026-WEP5051

BETA FUNCTION MEASUREMENTS USING QUADRUPOLE VARIATION IN SLS 2.0

J. Avila Pulido*[1], J. Kallestrup
PSI Center for Accelerator Science and Engineering, Villigen PSI, Switzerland
[1] also at EPFL Laboratory of Particle Accelerator Physics, Lausanne, Switzerland

Abstract

The Swiss Light Source upgrade, SLS 2.0, is a fourth generation storage ring based on a seven-bend achromat design and is currently under commissioning. Precise knowledge and control of the linear optics are essential for optimal machine performance. This contribution presents measurements of the beta function using the quadrupole variation method at 264 locations around the ring. The corresponding tune shifts were determined with high resolution via the mixed BPM technique combined with Numerical Analysis of Fundamental Frequencies (NAFF).

INTRODUCTION

The Swiss Light Source upgrade, SLS 2.0, features a seven-bend achromat lattice incorporating novel technologies such as longitudinal gradient bends and reverse bending magnets [1]. It has a circumference of 288 meters, operates with a stored beam current of 400 mA, and an electron beam energy of 2.7 GeV. The upgrade results in a more than 40-fold reduction in horizontal emittance compared to the previous storage ring.

With the commissioning phase of SLS 2.0 now in an advanced stage, it is essential to verify that the machine performs as designed [2]. This requires accurate measurement of the linear optics, and comparison with the modeled values.

SLS 2.0 is equipped with 264 octupoles, each featuring auxiliary windings that can be activated to generate normal- and skew-quadrupolar fields. In the following, these windings are referred to as quadrupoles for simplicity. By varying their integrated strength (ΔK) and measuring the resulting tune shift ($\Delta Q_{x,y}$), the average local beta function at the location of a quadrupole can be determined using the expression given in [3]:

$$\beta_{x,y} = \pm\frac{2}{\Delta K}\Big\{\cot(2\pi Q_{x,y})[1-\cos(2\pi\Delta Q_{x,y})] + \sin(2\pi\Delta Q_{x,y})\Big\}. \quad (1)$$

The positive and negative signs correspond to the horizontal (x) and vertical (y) planes, respectively. This technique is commonly referred to as *quadrupole variation* (QV) or *K-modulation*.

Several alternative techniques exist for linear optics measurements; a comprehensive review can be found in [4]. Many of these methods rely on beam position monitor (BPM) data. Since SLS 2.0 is equipped with 115 BPMs, the QV method provides a significantly denser sampling of the lattice functions and therefore serves as a valuable complement to BPM-based measurements.

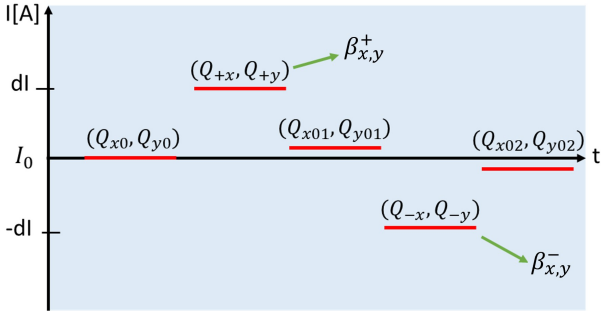

Figure 1: Measurement procedure. First, the initial tune is measured. For each quadrupole, the current is varied by $\pm dI$, and the tune is measured after each change. Using Eq. (1), the beta functions $\beta^{\pm}_{x,y}$ are obtained. After each variation, the current is restored to its initial value and hysteresis is corrected. The procedure is repeated for all quadrupoles.

The main challenges associated with this measurement are tune measurement resolution, hysteresis effects following quadrupole excitation, orbit perturbations induced by quadrupole feed-down, and accurate knowledge of the magnet transfer functions. In this contribution, the first three aspects are addressed.

BETA FUNCTION MEASUREMENT

Measurement Procedure

The basic layout of the measurement technique is sketched in Fig. 1.

Several comments are in order. First, to mitigate the effect of tune jitter, each tune measurement was repeated five times. Second, the excitation current was set to 1 A (corresponding to $\Delta K \approx 0.0072$ m^{-1}, depending on the specific magnet). This value was chosen to be sufficiently large to exceed the tune jitter level while remaining small enough to avoid significant optics perturbations. This choice was based on previous experimental runs in which both higher and lower excitation currents were tested. The selected current produced tune shifts ranging from 6.6×10^{-4} to 6.72×10^{-3} in the horizontal plane and from 6.5×10^{-4} to 3.70×10^{-3} in the vertical plane.

The quadrupole current is changed in both positive and negative directions to compensate for the optics perturbations induced by the quadrupole strength variation.

* jesus.avila-pulido@psi.ch

Content from this work may be used under the terms of the CC BY 4.0 licence (© 2026). Any distribution of this work must maintain attribution to the author(s), title of the work, publisher, and DOI.

ISBN: 978-3-95450-252-3 ISSN: 2673-5350 doi: 10.18429/JACoW-IPAC2026-WEP5052

CONTROL OF NONLINEAR TUNE SHIFTS IN SLS 2.0

J. Avila Pulido*,[1], J. Kallestrup
PSI Center for Accelerator Science and Engineering, Villigen PSI, Switzerland
[1]also at EPFL Laboratory of Particle Accelerator Physics, Lausanne, Switzerland

Abstract

The Swiss Light Source upgrade, SLS 2.0, is a next-generation storage ring featuring an ultra-low-emittance lattice based on a seven-bend achromat design. Achieving such low emittance requires strong focusing, which in turn generates large negative chromaticities. These are corrected using powerful sextupole magnets, introducing nonlinear effects in the beam dynamics. In particular, amplitude-dependent tune shifts (ADTS) and chromatic tune shifts (CTS) play a significant role. This contribution presents measurements of ADTS and CTS performed using high-precision tune measurements. Furthermore, since SLS 2.0 comprises 12 sectors equipped with 22 octupoles each, the control of ADTS and CTS through the use of octupoles is demonstrated.

INTRODUCTION

Ultra-low emittance lattices, such as the Swiss Light Source upgrade, SLS 2.0 [1], require strong focusing to achieve low emittance. However, this results in large negative natural chromaticities, which cause beam instabilities and beam loss. To compensate, strong sextupole magnets are used, but these introduce nonlinear beam motion, which can potentially reduce the dynamic aperture and beam lifetime. In particular, second-order effects such as amplitude-dependent tune shifts (ADTS) and second-order chromaticities become relevant. The ADTS (α_{ik}) and second-order chromaticities ($\xi_m^{(2)}$) are defined as

$$\alpha_{ik} = \frac{\partial Q_k}{\partial J_i}, \qquad \xi_m^{(2)} = \frac{\partial^2 Q_m}{\partial \delta^2}$$

with $i, k = x, y$ denote the horizontal and vertical planes, respectively, $Q_{x,y}$ the tunes, $J_{x,y}$ the actions. Also, $\alpha_{xy} = \alpha_{yx}$. δ denotes the energy deviation and $m = x, y$.

Each of the 12 arcs constituting the SLS 2.0 storage ring is equipped with 24 sextupoles and 22 octupoles used to control the nonlinear dynamics with the goal of maximizing dynamic aperture (DA) and Touschek lifetime (TL). Octupoles allow the control of ADTS and second-order chromaticities at first order [2], and therefore serve as efficient knobs for shaping the tune foot print to avoid resonance crossing [3–5]. Additionally, control of ADTS can be used in the context of round-beam operation while operating on the linear difference resonance, where horizontal off-axis injection will generally lead to unwanted vertical oscillations and occasionally beam losses. By tailoring the ADTS, it is possible to detune the injected beam away from the coupling resonance thereby avoiding losses [6–8].

Following [5], the knobs are defined in the following way,

$$\vec{A} = \mathbf{B}\vec{b}_4, \tag{1}$$

with $\vec{A} = (\alpha_{xx}, \alpha_{xy}, \alpha_{yy}, \xi_x^{(2)}, \xi_y^{(2)})^T$ and

$$\mathbf{B} = \begin{pmatrix} (\beta_x^2)_1 & \cdots & (\beta_x^2)_{N_{\mathrm{oct}}} \\ -2(\beta_x\beta_y)_1 & \cdots & -2(\beta_x\beta_y)_{N_{\mathrm{oct}}} \\ (\beta_y^2)_1 & \cdots & (\beta_y^2)_{N_{\mathrm{oct}}} \\ 4(\eta^2\beta_x)_1 & \cdots & 4(\eta^2\beta_x)_{N_{\mathrm{oct}}} \\ -4(\eta^2\beta_y)_1 & \cdots & -4(\eta^2\beta_y)_{N_{\mathrm{oct}}} \end{pmatrix}, \tag{2}$$

with $\vec{b}_4$ containing the strengths of the N_{oct} octupoles. **B** is a $5 \times N_{\mathrm{oct}}$ matrix with the values of the optical functions evaluated at the octupole locations.

In SLS 2.0, all 264 octupoles are independently powered. However, since measuring the changes in the second-order chromaticity and ADTS generated by individual octupoles is challenging, they were grouped into eight "families" according to the values of the optical functions at their locations: OXX, OXY and OYY (harmonic octupoles), and OCXM, OCY2, OCX2, OCY1, and OCX1 (chromatic octupoles). The current of each family can be varied independently in the range from -5 to 5 A, the equivalence in integrated octupole strength depends on the specific family.

It is worth noting that the optical functions are not exactly identical for all magnets within a given family in SLS 2.0. However, this approximation does not significantly affect the results. The maximum relative difference in the coefficients of Eq. (2), computed using the optical functions at each octupole instead of assigning the same optical functions values to all magnets within a family, is 0.11%.

SECOND-ORDER CHROMATICITY

To measure the second-order chromaticity, frequency shifts from -500 to 500 Hz in steps of 250 Hz were applied to the RF cavities. These shifts corresponds to energy deviations ranging from -1% to 1%. The tune in both planes was measured for each octupole setpoint using the mixed-BPM method with the Numerical Analysis of Fundamental Frequencies (NAFF) [9–11]. From the induced energy deviation, a second-order polynomial fit of Q as a function of δ was performed. The second-order chromaticity was extracted from this fit.

The measured second-order chromaticities in the horizontal and vertical planes are 4.21 ± 0.29 and 27.22 ± 0.28, respectively.

This procedure was repeated changing the strength of all octupoles in a given family in steps of 76 m^{-3} (approximately 1 A), in order to compare with the last two rows of Eq. (2).

* jesus.avila-pulido@psi.ch

Content from this work may be used under the terms of the CC BY 4.0 licence (© 2026). Any distribution of this work must maintain attribution to the author(s), title of the work, publisher, and DOI.

ISBN: 978-3-95450-252-3 ISSN: 2673-5350 doi: 10.18429/JACoW-IPAC2026-WEP5056

ANALYSIS AND COMPENSATION OF CROSSTALK EFFECTS FOR THE DIAMOND-II BENDING MAGNETS

I. P. S. Martin*, R. Ahamad, C. P. Bailey, Diamond Light Source, Oxfordshire, UK

Abstract

The close proximity of the magnets on the Diamond-II girders leads to significant crosstalk effects. This is of particular concern for the dipole component of the bending magnets, as the truncation of the fringe fields reduces the integrated strength and distorts the closed orbit. Tuning of the field amplitude and accurate alignment of the magnets is required to recover the target bend angles. A similar effect is seen on the quadrupole fields, and adjustment of the nominal gradients is required to restore the design optics. In this paper we present an overview of the modelling methods and latest results from these studies.

INTRODUCTION

In the latest generation of electron storage rings, crosstalk between magnets can be significant and must be considered during the design, construction and commissioning phases [1–3]. Compact layouts mean that magnet spacing is frequently below 100 mm, and despite having relatively small bore radii, fringe fields can overlap with the adjacent yokes. This causes a reduction in the integrated strengths and introduces unwanted multipole components.

In the case of Diamond-II [4], the minimum distance between the hard-edge magnet models has been set to 75 mm. At this level, it is anticipated that crosstalk effects will need to be compensated by adjusting target field strengths and realigning the magnets to recover the design parameters. The storage ring contains three families of bending magnet; two types of permanent magnet (PM) longitudinal gradient bends (DL dipoles) and one type of electromagnet (EM) transverse gradient bend (DQ dipoles). Here we present crosstalk studies for these dipoles. Four combinations are considered, namely:

1) Q2L-DL-Q3L: type 1 DL dipoles on girders adjacent to long straights
2) Q2N-DL-Q3N: type 1 DL dipoles on girders adjacent to standard straights
3) Q4N-DL-S5X: type 2 DL dipoles in the centre of each girder
4) Q5N-DQ-Q6N: DQ dipoles adjacent to the mid-straights

OPERA FIELD MAPS

The first stage of the analysis is carried out in OPERA. For each magnet combination, a model is constructed consisting of a dipole in the centre and two quadrupoles (or quadrupole and sextupole) located on either side. All magnets are set to the nominal integrated field strengths. A particle is then tracked through the resulting field map, starting on the design trajectory at a point where the field strength is negligible. The dipole position and strength are then adjusted until the final particle coordinates match the target values, again at a point where the field has dropped to negligible levels. Once the real trajectory is known, the multipole components can be extracted along this path using spherical harmonics.

An example of the dipole component with and without crosstalk effects is shown in Fig. 1 for case 3). As can be seen, the main impact of the crosstalk is to reduce the magnetic length, which in turn reduces the bend angle for the reference particle. This can be compensated by increasing the field strengths of all modules by 0.55 %, 0.49 % and 0.43 % for cases 1-3 respectively, and shifting all type 1 DL dipoles by 0.5 mm longitudinally. For case 4), the DQ dipole needed to be shifted outboard by 80 µm. Table 1 summarises the impact of crosstalk on the dipole magnetic lengths, after the corrections have been applied.

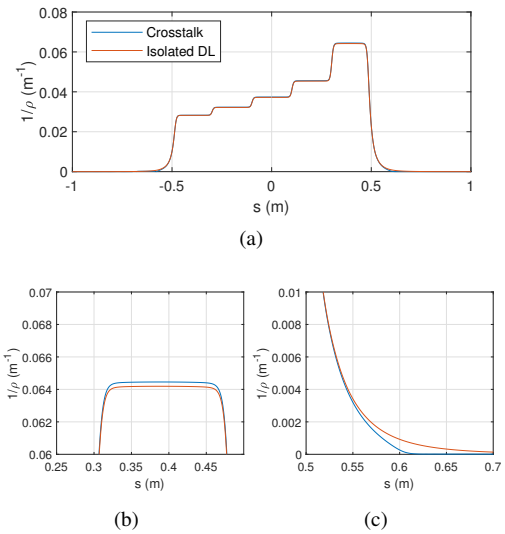

Figure 1: Comparison of dipole bend radius with and without crosstalk. (a): full magnet. (b): peak field. (c): falling edge.

Table 1: Impact of Crosstalk on Magnetic Lengths

Combination	Hard Edge	Without Crosstalk	With Crosstalk
Case 1)	1.153 m	1.157 m	1.150 m
Case 2)	1.153 m	1.155 m	1.150 m
Case 3)	1.116 m	1.114 m	1.110 m
Case 4)	0.870 m	0.870 m	0.867 m

The differences between the design and tracked trajectories are shown in Fig. 2 for case 3). Excluding crosstalk, the soft fringes of the DL dipole bend the beam trajectory

* ian.martin@diamond.ac.uk

Content from this work may be used under the terms of the CC BY 4.0 licence (© 2026). Any distribution of this work must maintain attribution to the author(s), title of the work, publisher, and DOI.

ISBN: 978-3-95450-252-3 ISSN: 2673-5350 doi: 10.18429/JACoW-IPAC2026-WEP5058

BENCHMARKING THE LINEAR LATTICE OF THE ISIS RCS AS A FOUNDATION FOR FUTURE MODEL-BASED OPTIMISATION

H. Rafique[1*], D. J. Adams[1], E. Ahmadi[1], J. Appleby[1,2], H. V. Cavanagh[1], C. Jolly[1], S. Karbassi[1], D. J. Kelliher[1], B. Kyle[1], J.-B. Lagrange[1], S. Machida[1], A. Oeftiger[2], D. W. Posthuma de Boer[1], C. Rogers[1], R. Simpson[2], J. Thompson[1], C. M. Warsop[1], R. E. Williamson[1]
[1]ISIS Neutron and Muon Source, RAL, UK
[2]John Adams Institute, University of Oxford, UK

Abstract

ISIS operates an 800 MeV Rapid Cycling Synchrotron (RCS) delivering protons to neutron and muon targets with a beam power of 0.2 MW. A reliable lattice description is essential for advancing low-loss, high-intensity operation and supports emerging model-driven optimisation enabled by forthcoming Python-accessible controls. A new consolidated low-intensity linear optics model of the ISIS RCS, developed through a continuous programme of systematic measurement-based benchmarking, is presented.

Using enhanced analysis of low-intensity turn-by-turn BPM data, multiple optics measurements have been integrated into a single self-consistent lattice representation. This lattice represents a significant advance over earlier design-only or partially benchmarked descriptions, enabling clearer identification of optics discrepancies and guiding targeted correction measures, including improvements to magnet survey and alignment.

The resulting reference lattice, implemented in MAD-X/cpymad and cross-checked with PTC-PyORBIT, reproduces low-intensity optics with improved predictive performance, particularly for orbit response and optics control. Benchmarks of the consolidated model, resulting improvements, and planned implementation in model-based optimisation of ISIS RCS operation are presented.

MEASUREMENT FRAMEWORK

The ISIS 800 MeV Rapid Cycling Synchrotron (RCS), operational since 1984, has relied on measurement-based validation of its transverse lattice to support high-intensity operation. A defining feature of this programme is the use of low-intensity "chopped" (from 200 µs to 600 ns) diagnostic beams, generated by electrostatic chopping of the ~70 MeV linac beam prior to injection. These short pulses limit space-charge and collective effects, enabling clean observation of coherent transverse motion and providing a reproducible reference state representing the "bare" linear lattice: the machine with AC-powered main magnets and no contribution from programmable dipole and quadrupole correctors.

Early studies used such low-intensity pulses to measure injection oscillations and machine tune without intensity-driven distortions [1, 2]. With the introduction of turn-by-turn BPM diagnostics, lattice parameters could be extracted through tune shifts, relative betatron amplitudes, and

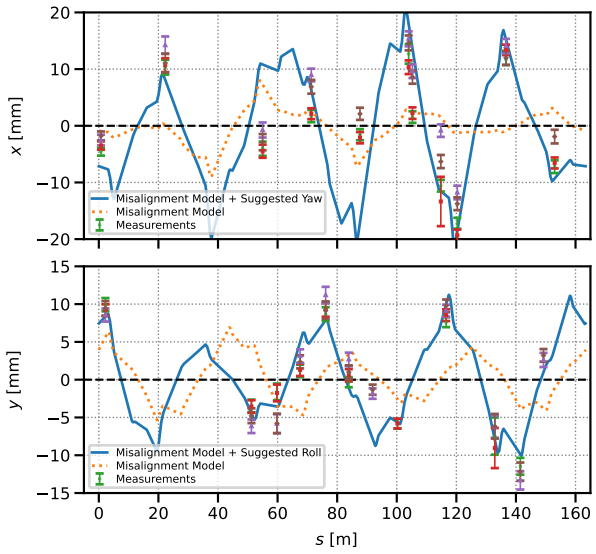

Figure 1: Comparison of measured bare orbit with survey-based misalignment model predictions used to infer main dipole errors.

$\Delta Q/\Delta I$ measurements [3–5]. More recently, these methods have been extended to orbit response, resonance studies, and alignment modelling [6–8].

Turn-by-turn BPM signals are processed to extract coherent oscillation amplitudes, phase, and tune directly from measured data following established methodology [4, 5]. All observables are derived without model preconditioning, ensuring that subsequent comparisons remain measurement-led.

The present work builds on this approach through a set of measurement-driven benchmarking campaigns, culminating in a unified linear lattice model of the ISIS RCS and forming the foundation for model-based operational optimisation.

BENCHMARKING CAMPAIGNS

Orbit Benchmarking and Magnet Alignment

Closed orbit measurements under low-intensity "bare" machine conditions are combined with main magnet survey data to benchmark the lattice at first order. Survey measurements are converted to model-consistent co-ordinates and implemented as misalignments in the lattice [8].

The survey-informed model captures the dominant orbit structure, while residuals provide a model-guided indication

* haroon.rafique@stfc.ac.uk

Content from this work may be used under the terms of the CC BY 4.0 licence (© 2026). Any distribution of this work must maintain attribution to the author(s), title of the work, publisher, and DOI.

ISBN: 978-3-95450-252-3 ISSN: 2673-5350 doi: 10.18429/JACoW-IPAC2026-WEP5069

HL-LHC MAGNETS FIELD QUALITY: CURRENT SITUATION, STRATEGIES AND MITIGATION MEASURES*

A. Fornara†, R. De Maria, L. Fiscarelli, G. Iadarola, M. Giovannozzi, S. Izquierdo Bermudez, E. H. Maclean, K. Skoufaris, G. Sterbini, R. Tomás García, CERN, Meyrin, Switzerland

Abstract

The production of the new superconducting magnets for the luminosity upgrade of the LHC is in full swing. The performance of the magnets is probed by means of detailed magnetic measurements of the transfer function and field quality of the various families of magnets, i.e. triplet quadrupoles and separation and recombination dipoles. In this paper, the current situation in terms of magnetic properties is presented and reviewed in detail. Furthermore, dedicated beam dynamics simulations to address the possible issues for the various families of magnets are presented.

INTRODUCTION

The luminosity upgrade of the CERN Large Hadron Collider (HL-LHC) [1, 2] involves, among other changes, a complete revision of the layout of the interaction regions (IR) for the ATLAS and CMS experiments. The inner triplet quadrupoles, separation, and recombination dipoles will be replaced by new hardware, and crab cavities (CC) will be added. A construction programme, shared among the collaborating institutes, is in full swing, and the production of the new devices is progressing well. An ambitious programme of magnetic measurements is also underway with the goal of providing detailed information about the performance of the magnets and their field quality (FQ). The large volume of data obtained from the magnetic measurements is impressive and, beyond offering an early indication of magnet performance, it can also be used to optimise the installation sequence by enabling the sorting of the magnets. This approach has been explored in the design phase of various modern accelerators (see, e.g. Refs. [3–13]) and has been implemented with success in the CERN LHC [14–16].

Similarly to LHC, sorting is foreseen for the new insertion magnets of HL-LHC and preliminary studies were carried out considering the many possible permutations of triplet quadrupoles [17]. Ideally, a sorting scheme relies on a large pool of magnets, from which subsets are selected and optimally assigned to the most suitable positions in the ring. Unlike LHC, the magnet families for HL-LHC comprise a small number of magnets, which is certainly suboptimal for any sorting approach. Furthermore, severe hardware and scheduling constraints need to be taken into account. The most recent results for the sorting options for the Q2 triplet quadrupole, including currently known constraints, can be found in Ref. [18]. Here, we focus on the current status of magnetic measurements for the Q1/Q3 triplet quadrupoles and the D2 recombination dipoles. These data were then used to devise the optimal allocation of the currently available magnets, and the recommended positions are presented and discussed in detail in this paper.

As a last point, we recall that a sorting algorithm relies on a physical observable that is used as a figure of merit of a given sequence of magnets with a certain FQ. For the case of the Q2, which are split into two cryo-assembly (CA) powered in series, the criterion has been to pair CAs for similar transfer functions to minimise beta-beating. As an additional observable, the amplitude detuning has been considered and minimised, in view of easing the initial beam commissioning. Each Q1 or Q3 CA is made of two magnets, but each CA is independently powered. Hence, beta-beating is not an issue, and the amplitude detuning has been the physical observable to guide the sorting strategy. As far as the D2 dipoles are concerned, the skew-quadrupole component turned out to be the property to be controlled and the observables related with linear coupling have been used for assessing the best slot for the D2s. It is worth noting that the case of the D1 separation dipoles will be considered next, but the presence of a corrector package, housing several linear and non-linear corrector magnets, installed next to the D1 provides an effective means to control the FQ of the D1s. Hence, sorting might be of limited use in that case.

MAGNETIC MEASUREMENTS FOR HL-LHC MAGNETS

The magnetic characterisation of the HL-LHC IR magnets (see Fig. 2 of Chapter 5 in Ref. [2]) is performed during and after production and assembly, at ambient temperature (warm) and at 1.9 K (cold). The results of cold measurements are from the magnet in the vertical test stand or, when available, on the final CA in horizontal configuration, and the latter is taken as the reference whenever it exists. In the absence of cold measurements, the field quality is extrapolated from warm measurements. The measured field harmonics are used as input for beam simulations and form the basis of the sorting strategies discussed in the following sections (see also Ref. [18]). Multipoles are expressed in the magnet reference frame (looking at the magnet from the connection side) and are quoted in units, where one unit is 10^{-4} of the main field at the reference radius R_{ref}, which is taken as 1/3 of the cold-bore aperture. The status of the measurement campaign for each family is summarised in Table 1 and the FQ plots referenced in the table show the integral harmonics at nominal current.

The Q1 and Q3 quadrupoles CA [19, 20] are made of two MQXFA magnets each, first tested individually in the vertical stand and then re-tested once integrated (see

* Work supported by the HL-LHC project

† andrea.fornara@cern.ch

Content from this work may be used under the terms of the CC BY 4.0 licence (© 2026). Any distribution of this work must maintain attribution to the author(s), title of the work, publisher, and DOI.

ISBN: 978-3-95450-252-3 ISSN: 2673-5350 doi: 10.18429/JACoW-IPAC2026-WEP5071

MEASUREMENT OF LOCAL CHROMATICITY IN THE LHC

M. Stefanelli*†, E. Maclean, European Organization for Nuclear Research, Geneva, Switzerland

Abstract

Local chromaticity is defined as the local variation of the total betatron phase advance with momentum deviation δ, and it can be interpreted as a measurement of the chromaticity generated over a limited segment of the lattice, rather than for the entire ring. It can be a useful tool to understand various insights of the beam operation, in particular how the phase is locally modulated by beam energy and how the overall chromaticity builds up along the lattice. The local chromaticity was first evaluated in the Large Hadron Collider (LHC) during the Run 3 commissioning in 2025, when a large RF frequency scan was performed, revealing a very large discrepancy with respect to the LHC optics model. This paper presents the methods and the results of the analysis.

INTRODUCTION

Chromaticity is defined as the variation of the betatron tune with energy. In the LHC, it is typically measured by modulating the beam energy while simultaneously acquiring the tune [1]. This approach is robust and widely adopted for characterizing the effect of energy on the betatron phase. However, chromaticity alone provides no information on how the local chromatic betatron phase varies around the ring. Local chromaticity is thus defined as the chromaticity of a limited segment of the lattice,

$$Q'_{x,y}(s) = \frac{1}{2\pi} \left. \frac{\partial \Delta\phi_{x,y}(s,\delta)}{\partial \delta} \right|_{\delta=0} . \quad (1)$$

When s is equal to the ring length, the local chromaticity reduces to the conventional chromaticity. The phase advance $\Delta\phi_{x,y}(s,\delta)$ can be expressed as the Taylor expansion around the on-momentum value. The expansion is carried out to second-order, proved to be sufficient (see below). The resulting coefficients define the first- and second-order local chromaticity. To evaluate these coefficients, the total betatron phase advance is measured at each BPM for several momentum deviations. Turn-by-Turn (TbT) data were acquired via forced oscillations induced with an AC dipole [2,3]. The induced excitation remains coherent over the 6600 turns of the acquisition window, ensuring high-quality spectral analysis. A correction is applied to compensate for the phase error induced by the AC dipole [4]. A zero-padded FFT (HARPY) [5] was subsequently applied to the acquired data to retrieve the frequency spectrum from which the phase advance is computed. The measured phase advances are then fitted with a second-order polynomial function to extract the local chromaticity coefficients, as shown for an arbitrary BPM, in Fig. 1.

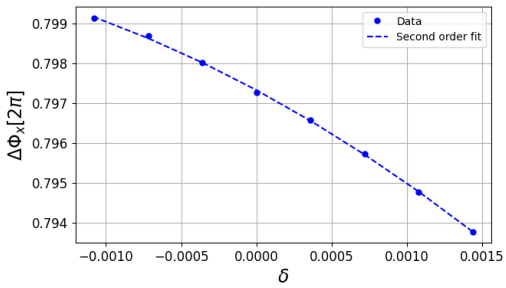

Figure 1: Horizontal phase advance vs δ at BPM.32R3.B1.

MEASUREMENTS – LHC

The local chromaticity was first evaluated in the LHC during Run 3 injection commissioning in 2025. The chromaticity was corrected to approximately 3 units in each plane with the main sextupole magnets (MS). The RF frequency was modulated from −350 Hz to +350 Hz in steps of 50 Hz, which corresponds to a relative momentum deviation δ ranging between $\pm$ 0.0025. The original goal of this measurement was the study of chromatic Resonance Driving Terms (RDTs) [6]. Therefore the machine tune feedback system (QFB) [7] was kept on during the measurement to ensure a constant AC dipole frequency offset. The QFB acts on the trim quadrupoles (MQTs) correcting the tunes to their on-momentum values. For the injection optics, these are $Q_x = 62.28$ and $Q_y = 60.31$. With the corrected chromaticity $Q' = 3.0$, the maximum tune shift being compensated is approximately $\pm$ 0.0075, a small fraction of the nominal tune. As described before, the phase advance is evaluated at each BPM from the initial BPM taken as the reference start of the lattice. In Fig. 2, the difference between the measured and the on-momentum model phase advance is shown for LHC Beam 1 (B1), for both planes, for the tested momentum deviations. A localized spread in the horizontal phase advance at different momenta is immediately visible in the vicinity of IP4 and IP8 for B1, around 6000 and 20000 m. Similar results were obtained for LHC Beam 2 (B2). This behavior is most evident in the horizontal plane, while in the vertical plane the phase advance remains coherent along the ring. As described before, the local chromaticity is extracted from the TbT data. The measured linear local chromaticity for both planes is shown in Fig. 3 for B1, and in Fig. 4 for B2, only for the horizontal plane. The vertical plane results for B2 are similar to those for B1. The second-order local chromaticity for B1 is presented in Fig. 5; again similar results were observed for B2. The second-order local chromaticity is small compared to the linear term. At the maximum tested δ, a direct comparison of the two terms in the Taylor expansion reveals that the second-order contribution is on average one order of magnitude smaller than the linear term. In the vertical plane, the linear local chromaticity is locally compensated, exhibiting oscillations around zero. In

* mattia.stefanelli@cern.ch

Content from this work may be used under the terms of the CC BY 4.0 licence (© 2026). Any distribution of this work must maintain attribution to the author(s), title of the work, publisher, and DOI.

ISBN: 978-3-95450-252-3 ISSN: 2673-5350 doi: 10.18429/JACoW-IPAC2026-WEP5072

EXTRAPOLATED OPTICS MEASUREMENT FROM BPM TO INSTRUMENTATION IN LHC COMMISSIONING

M. Stefanelli*†, J. Dilly, J. Gray, E. Maclean, F. Soubelet, Y. Angelis
European Organization for Nuclear Research, Geneva, Switzerland

Abstract

The Segment-by-Segment (SbS) analysis is a technique employed in particle accelerators to identify lattice errors and determine corrections, by identifying deviations between optics functions propagated through a modeled lattice segment and measured values. At the Large Hadron Collider (LHC), this method is routinely applied during optics commissioning to compensate for strong local errors arising in the experimental insertions and arcs. Beyond error correction, the SbS approach is also of interest for propagating optics functions measured at the BPMs to key instrumentation in other locations in the ring, for example to improve emittance measurements by providing more accurate estimates of the optics functions at relevant devices. In this paper, the analysis methods and results from the recent LHC commissioning are presented.

INTRODUCTION

The segment-by-segment (SbS) technique was developed at the CERN LHC to identify and correct local lattice errors [1, 2]. Since 2008, it has been successfully employed during LHC commissioning and operation [3]. The underlying principle is to split the machine into a series of segments, each treated as a transfer line [2]. The measured optics parameters at the Beam Position Monitors (BPMs) are used as initial conditions and are propagated through the corresponding segment of the machine model. The propagated optics are then compared with the measured data over the selected segment; discrepancies between the two can reveal the presence of local lattice errors. Beyond error identification, the SbS method can also be used to propagate optics measurements from the BPMs to other instrumentation in the ring. The goal of this work is to simplify the application of the technique to estimate optics functions at key instrumentation, enabling its routine use.

METHODS

A GUI has been developed to run the SbS-to-element propagation; an example is shown in Fig. 1. The user selects the target element from the model, then provides a nominal optics model and the corresponding measurement. A range of BPMs on either side of the target instrument must be chosen; the propagation is then performed over a collection of segments defined between the selected BPMs. The number of BPMs included around the target device is a crucial parameter for the reliability of the method. Including more BPMs increases the statistical significance of the result, whereas extending the propagation over longer segments may increase the error on the result due to the accumulated lattice errors along the path. Currently, several optics parameters have been included as propagable quantities: vertical and horizontal phase advance, alpha functions, beta functions, dispersions, momentum dispersions, and the coupling Resonance Driving Terms (RDTs), f_{1001}, f_{1010} (amplitude, phase, real part and imaginary part). The measured quantities at the BPMs are propagated through the segments in both directions — forwards from upstream BPMs and backwards from downstream BPMs. The optics parameters are evaluated at the device location for each segment, together with the propagated uncertainty. A cleaning step removes outliers using two criteria: a standard range filter to remove statistical outliers, and a filter on large relative errors. However, this type of analysis is highly case-specific, and experience has shown that it is preferable for the user to inspect the raw results and make their own selection. The final estimate and its corresponding error are obtained through a weighted average of the filtered results, using the propagated uncertainty at the target device as the weighting factor.

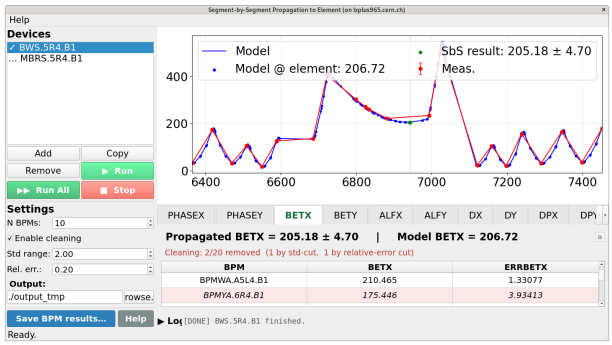

Figure 1: GUI for the SbS-to-element.

Error Propagation

The error propagation for β and α functions and RDTs follows the formalism described in Ref. [4]. For the phase uncertainty, the following expression is used,

$$\sigma^2_{\phi_s} = \left\{\frac{1}{2}\left([\cos(2\phi)-1]\frac{\alpha_0}{\beta_0} - \sin(2\phi)\frac{1}{\beta_0}\right)\right\}^2 \sigma^2_{\beta_0} + \left\{\frac{1}{2}[\cos(2\phi)-1]\right\}^2 \sigma^2_{\alpha_0}, \quad (1)$$

which introduces a sign correction with respect to Ref. [4]. The corrected formula was derived analytically and validated through a series of MAD-X simulations, as described in Ref. [5]. Here, ϕ denotes the phase advance from the initial position to the observation point, in units of radian.

* mattia.stefanelli@cern.ch

Content from this work may be used under the terms of the CC BY 4.0 licence (© 2026). Any distribution of this work must maintain attribution to the author(s), title of the work, publisher, and DOI.

ISBN: 978-3-95450-252-3 ISSN: 2673-5350 doi: 10.18429/JACoW-IPAC2026-WEP5073

MEASUREMENT OF CHROMATIC RESONANCE DRIVING TERMS IN THE LHC

M. Stefanelli*[1], E. Maclean, European Organization for Nuclear Research, Geneva, Switzerland
[1]also at National Institute for Subatomic Physics, Amsterdam, Netherlands

Abstract

The $3Q_y$ resonance is of particular concern at LHC injection given its potential to degrade the lifetime and the machine dynamic aperture. During measurements of the chromatic linear optics for the 2025 LHC commissioning, a large variation of the $3Q_y$ resonance strength across different momentum deviations δ was observed. Further studies were performed to assess the contribution to this variation from higher order multipoles, in particular from octupole and decapole fields. Benchmarking has been performed to the LHC magnetic model revealing that skew-octupole (a_4) errors in the main dipoles alone cannot explain the observed skew-octupole field sources at injection. Methods and results of this analysis are presented in this report.

INTRODUCTION

Resonances $(j-k)Q_x + (l-m)Q_y$ are characterized by the strength of their respective resonance driving terms (RDT), f_{jklm}. Of particular interest for LHC is the $3Q_y$ resonance that has been shown to degrade beam lifetime at 450 GeV [1] and to contribute to collimator hierarchy breakage [2]. For these reasons, this resonance was closely monitored during LHC commissioning in 2025. Of particular note was the large variation in the $3Q_y$ resonance amplitude across different momentum deviations δ. On-momentum, the $3Q_y$ resonance is driven by skew-sextupolar magnetic fields. Correction schemes have been implemented in the LHC to correct the on-momentum $3Q_y$ resonance at injection energy [3]. However, when a particle is off-momentum in a dispersive region, effective skew-sextupole components can be generated through feed-down from higher-order fields. This study focuses on characterizing the impact of skew-octupole and skew-decapole magnetic fields, present in the machine as magnetic imperfections. The Hamiltonians for skew-octupole and skew-decapole magnets follow,

$$S_4(x,y) = -\frac{1}{24}J_4\left(4x^3y - 4xy^3\right), \tag{1a}$$

$$S_5(x,y) = -\frac{1}{120}J_5\left(5x^4y - 10x^2y^3 + y^5\right), \tag{1b}$$

where J_n is the normalized strength of the skew multipole of order n. If a particle has a relative momentum deviation $\delta \neq 0$, its transverse position is shifted in dispersive regions according to $x \rightarrow x + D_x\delta$. Substituting this into the Hamiltonians above introduces new terms proportional to powers of δ. Of particular interest are those terms that feed-down to an effective skew-sextupole term, as these directly drive the $3Q_y$ resonance. The skew-octupole expanded Hamiltonian is given by

$$S_4(x,y,\delta) = -\frac{1}{24}J_4\left(4x^3y - 4xy^3\right) - \frac{D_x\delta J_4}{6}\left(3x^2y - y^3\right) - \frac{D_x^2\delta^2 J_4}{2}(xy) + \frac{D_x^3\delta^3 J_4}{6}(-y), \tag{2}$$

where the arising skew-sextupole terms $\left(3x^2y - y^3\right)$, multiplied by $D_x\delta$, can be identified directly. In the case of the skew-decapole feed-down, the same terms appear multiplied by $D_x^2\delta^2$ instead. It follows directly that a linear dependence of the skew-sextupole Hamiltonian on δ indicates feed-down from skew-octupole components J_4, while a quadratic dependence indicates feed-down from skew-decapole components J_5. Note that Eq. (2) accounts only for the pure skew-octupole contribution; other sources, such as normal-octupole fields in the presence of coupling, and feed-up from lower-order fields with or without coupling, also contribute to the total effective skew-octupole field. Analyzing the momentum dependence of the $3Q_y$ RDT therefore serves two purposes: it directly characterizes how the resonance strength varies with momentum, and it provides an indirect means of probing higher-order multipole fields that cannot otherwise be directly measured.

MEASUREMENTS

The results presented here were obtained during LHC Run 3 commissioning in 2025. The original goal of the shift was to fully commission the injection optics at 450 GeV. The chromaticity was corrected to approximately 3 units in each plane with the main sextupole magnets (MS). The RF frequency was varied by scanning values from −350 Hz to 350 Hz in steps of 50 Hz. This corresponds to a relative momentum deviation δ ranging between ±0.0025. Turn-by-Turn (TbT) data were acquired via forced oscillations induced with an AC dipole [4, 5]. The machine tune feedback system (QFB) [6] was kept on during the entire measurement time to ensure a constant natural tune and AC dipole frequency offset [7], avoiding bias in the forced RDT measurement due to moving closer to or further from the resonance, as δ was varied [8]. The QFB varies the tuning quadrupoles (MQT) powering, keeping the tunes constant while minimally perturbing the optics. The nominal on-momentum tunes for the injection optics are $Q_x = 62.28$ and $Q_y = 60.31$. With the corrected chromaticity $Q' = 3.0$, the maximum tune shift being compensated is approximately ±0.0075, a small fraction of the nominal tune. The AC dipole frequency offsets in tune units were equal to $\Delta Q_x = -0.010$ and $\Delta Q_y = 0.012$. Typically, large AC

* mattia.stefanelli@cern.ch

Content from this work may be used under the terms of the CC BY 4.0 licence (© 2026). Any distribution of this work must maintain attribution to the author(s), title of the work, publisher, and DOI.

ISBN: 978-3-95450-252-3 ISSN: 2673-5350 doi: 10.18429/JACoW-IPAC2026-WEP5074

ADVANCED LINEAR AND NONLINEAR OPTICS STUDIES USING MAD-NG'S PARAMETRIC DIFFERENTIAL ALGEBRA

L. Deniau, European Organization for Nuclear Research, Geneva, Switzerland

Content from this work may be used under the terms of the CC BY 4.0 licence (© 2026). Any distribution of this work must maintain attribution to the author(s), title of the work, publisher, and DOI.

Abstract

Advanced linear and non-linear optics studies require accurate and efficient tools for high-order beam dynamics computations. MAD-NG provides a unique framework combining linear and nonlinear optics modelling, high-order parametric differential map computation through precise automatic differentiation, and Lie-algebraic operations central to nonlinear normal form analysis, all within a unified environment based on the Generalised Truncated Power Series Algebra (GTPSA). These capabilities enable an accurate evaluation of optical functions, chromatic effects, and nonlinear Hamiltonian dynamics. MAD-NG embeds LuaJIT, a high-performance scripting engine, offering automated workflows, symbolic dependencies, and deferred evaluations for efficient lattice design and parametric optimisation. It has been used successfully to improve the LHC beam lifetime at injection (2023) and during collisions (2025) by minimising resonant driving terms. Applied to major projects such as the LHC, HL-LHC, and FCC-ee, MAD-NG demonstrates reliability, scalability, and accuracy for large-scale optics and sensitivity studies while providing a flexible, reproducible, and high-performance environment for modern accelerator modelling and advanced beam dynamics research.

INTRODUCTION

Modern accelerator studies require a consistent description of beam dynamics across linear optics, chromatic effects, and nonlinear dynamics, often under variations of many parameters such as magnet strengths, alignment errors, and RF settings. In practice, this means computing not only optical functions, tunes, and chromaticities, but also their sensitivities and the resonance structure governing beam stability.

Existing tools typically separate these aspects. Tracking codes such as XSuite [1] provide high physical fidelity but limited direct access to sensitivities and high-order structures. Optics codes such as MAD-X [2] manipulate differential maps for analysis and optimisation, but usually through low-order approximations or specialised formalisms that are difficult to extend consistently to high order and large parameter spaces.

MAD-NG [3] addresses this limitation by providing a unified framework in which linear and nonlinear optics, high-order beam dynamics, and parametric studies are described within a single coherent formalism based on differential algebra and the Generalised Truncated Power Series Algebra (GTPSA) [4]. The central object is a parametric differential map from which linear optics, chromatic effects, and nonlinear quantities are obtained consistently. This provides direct access to high-order effects and sensitivities while avoiding repeated perturbations of the lattice and the associated risk of approaching unstable regimes.

PARAMETRIC DIFFERENTIAL MAP FRAMEWORK

In MAD-NG, the central object of the tracking engine is the phase-space propagator

$$z(s) = \mathscr{M}(z_0; \mathbf{p}), \tag{1}$$

where z denotes the phase-space variables and $\mathbf{p}$ a set of machine parameters. The map $\mathscr{M}$ is not constructed as an expanded matrix or tensor a priori, but results from applying the beam-physics functions of the lattice elements to a phase-space DA map, i.e. a set of truncated multivariate Taylor polynomials in the initial variables and selected parameters.

The dynamics is therefore obtained by successive functional application of the element transformations, applied either analytically or, for general elements, through exact element-wise operations and symplectic integration of the Hamiltonian flow. The only approximation is the user-controlled truncation of the GTPSA representation. This allows high-order maps to be computed with the full functional dependence of the physics retained throughout the lattice.

This framework naturally supports parametric studies. Quantities such as strengths, lengths, or misalignments are promoted to DA parameters, so that a single computation provides the local dependence of the optics on these quantities around a chosen reference configuration. The sensitivities and mixed derivatives are then read directly from the coefficients of the same map, without finite differences, repeated tracking, or lattice perturbation.

The same map can also be constructed through Lie-algebraic methods [5]. For instance, for a sextupole,

$$H = H_{\text{drift}} + \frac{k_2}{6}(x^3 - 3xy^2), \tag{2}$$

$$z(s; k_2) = e^{\{\cdot, lH\}}\, z(s_0; k_2), \tag{3}$$

with k_2 treated as a DA parameter. The corresponding map is $\mathscr{M}(\cdot; k_2) = e^{\{\cdot, lH\}}$, implemented in MAD-NG through `exppb`. Tracking and Lie integration thus provide two consistent constructions of the same parametric map.

LINEAR OPTICS AND CHROMATIC SENSITIVITIES

Linear optics quantities are obtained directly from the first-order part of the parametric one-turn map. Twiss parameters, phase advances, and dispersion functions are extracted from the linear normal form of the transfer matrix, while their

ISBN: 978-3-95450-252-3 ISSN: 2673-5350 doi: 10.18429/JACoW-IPAC2026-WEP5075

OPTIMIZATION WITH THE PETRA IV LATTICE SEXTUPOLES FOR THE MITIGATION OF MAGNETIC FIELD IMPERFECTIONS

K. Paraschou*, I. Agapov, A. Aloev, R. Bartolini, E. Musa
Deutsches Elektronen-Synchrotron DESY, Hamburg, Germany

Abstract

As is typical for the design of a fourth-generation light source, PETRA IV includes strong quadrupolar and sextupolar magnets, making the beam dynamics of the storage ring sensitive to magnetic field imperfections. In particular, we show that field imperfections in the quadrupoles can drive nonlinear resonances which can limit the efficiency of the top-up injection scheme in PETRA IV through a reduction of dynamic aperture. This work explores different operational strategies for modifying the strengths of the sextupolar magnets to recover a potential loss in the dynamic aperture and injection efficiency.

INTRODUCTION

The PETRA IV storage ring [1–3] is planned to operate continuously with off-axis top-up injection to recover the charge lost in the beam. It is therefore crucial to have sufficient dynamic aperture in order not to degrade injection efficiency. In PETRA IV, the dynamic aperture is significantly affected by betatron resonances. In particular, the half-integer resonance is known to strongly reduce the dynamic aperture in the horizontal plane with realistic residual linear optics errors.

Normal sextupolar errors, either due to multipolar imperfections in the quadrupole magnets or due to field errors in the sextupole magnets, can excite the third-order resonances $3Q_x, Q_x - 2Q_y$. Correction of such errors in simulations is the subject of this contribution. These errors are expected to arise from the finite precision in aligning the magnet poles. Errors under realistic alignment tolerances are enough to excite the aforementioned third-order resonances and degrade the dynamic aperture down to 5 mm. The dynamic aperture for 100 random realizations of the lattice with residual linear optics errors is visible in Fig. 1. The dynamic aperture after introducing normal sextupole errors (10 b_3 units) is shown in Fig. 2. From the comparison of the two, the dynamic aperture can go from 7-10 mm down to 5 mm. It is clear that with errors of this magnitude, the injection efficiency will get strongly affected as the injected beam (dashed line) overlaps the dynamic aperture.

It is important to note that the quality of the PETRA IV quadrupoles to be procured must meet stricter specifications in order to minimize the risk of operating with suboptimal injection efficiency. Nevertheless, mitigation measures are presented here to alleviate the effects of possible unaccounted b_3 errors. All presented correction strategies use all of the 432 individually powered sextupoles in the PETRA IV lattice.

* konstantinos.paraschou@desy.de

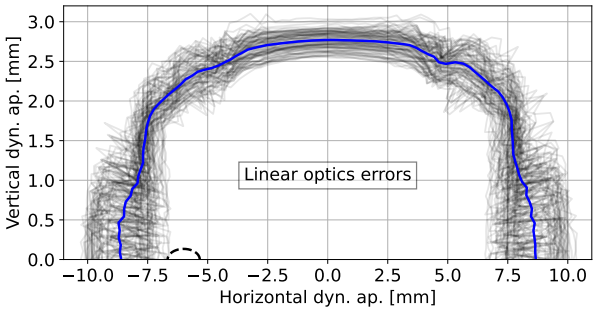

Figure 1: Dynamic aperture with simplified linear optics errors in the PETRA IV lattice, evaluated over 100 error seeds. The dashed line depicts the position and r.m.s. beam size of the injected beam.

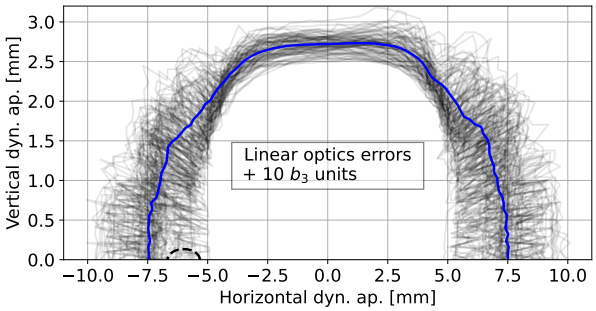

Figure 2: Dynamic aperture with simplified linear optics and b_3 errors in the PETRA IV lattice, evaluated over 100 error seeds. The dashed line depicts the position and r.m.s. beam size of the injected beam.

For this contribution, a simplified scenario is considered where approximately 3 % r.m.s. beta-beating is introduced by assigning a 0.05 % relative field error on all quadrupoles. The dynamic aperture of the 100 random seeds of the lattice is shown in Fig. 1. The dynamic aperture throughout the study is evaluated at the injection point with the Accelerator Toolbox [4,5] tracking code, including the model of physical apertures in the simulation. In this study, it is assumed that the DESY IV booster will serve as the injector of PETRA IV. The r.m.s. beam size contour is drawn in Fig. 1. For the optimization studies, the injected beam is assumed to be injected close to the dynamic aperture with a −6 mm offset with respect to the stored beam, instead of assuming a more optimal injection offset in terms of injection efficiency. The b_3 imperfection (normal sextupole) of a quadrupole is sampled from a random normal distribution with a standard deviation equal to 10 "magnet units" (at a reference radius of 6.5 mm) [6].

Content from this work may be used under the terms of the CC BY 4.0 licence (© 2026). Any distribution of this work must maintain attribution to the author(s), title of the work, publisher, and DOI.

ISBN: 978-3-95450-252-3 ISSN: 2673-5350 doi: 10.18429/JACoW-IPAC2026-WEP5076

TESTS OF COMMISSIONING SIMULATION TOOLS IN OPERATION OF STORAGE RING LIGHT SOURCES

K. Paraschou*, I. Agapov, E. Musa, Deutsches Elektronen-Synchrotron DESY, Hamburg, Germany
T. Hellert, Lawrence Berkeley National Laboratory, Berkeley, CA, USA
N. Carmignani, L. Carver, S. Liuzzo, J.-L. Pons, S. White
European Synchrotron Radiation Facility, Grenoble, France

Abstract

The design of 4th-generation synchrotron light sources employs such strong quadrupolar and sextupolar magnets that the motion of electrons in the storage ring is extremely sensitive to the misalignment and the field imperfections of magnets. As a result, it has become common practice to simulate the steps followed during the commissioning of a light source to compare the sensitivity to different types of lattice errors from a beam dynamics point of view and inform the design of the light source. Although there is significant overlap in the algorithms used to commission and to simulate the commissioning of a light source, they typically consist of separate implementations. This work describes the latest developments in the pySC software for commissioning simulations to allow the use of its tools in a real control system environment for storage rings. Finally, it reports on tests done at the European Synchrotron Radiation Facility Extremely Brilliant Source (ESRF-EBS) to apply these tools to tune the storage ring.

INTRODUCTION

To achieve small emittances, 4th-generation storage-ring light sources need strong quadrupole magnets to focus the particle beams to the needed level. This in turn implies that strong sextupole magnets are needed to correct the natural chromaticity that is generated by the quadrupole magnets. The realistic alignment of such magnets will result in strong feed-down effects, and the calibration errors, either in magnets or diagnostic devices, will make a "perfect" correction impossible. It is therefore an important part during the lattice design process to perform commissioning simulations under realistic errors. This can inform the design in the form of what commissioning procedures are required, how strict the specifications must be in terms of alignment, field calibration, field imperfections, beam position monitor specifications, and others. One of the first examples of such studies can be found in Ref. [1].

The Toolkit for Simulated Commissioning was developed as a tool to model lattices with realistic errors and a set of commissioning algorithms that can be used to simulate the commissioning process [2, 3]. It is written in the MATLAB language and uses Accelerator Toolbox (AT) [4, 5] as its particle tracking engine. pySC is a Python implementation and extension of this idea [6], able to use either Accelerator Toolbox (AT) or Xsuite [7] as its tracking engine. The recent development of pySC was motivated by commissioning studies for PETRA IV [8–10], but the same tools are intended to be useful in the control room. This paper describes the recent reorganization of pySC around reusable tuning applications and reports first tests of these applications at the European Synchrotron Radiation Facility Extremely Brilliant Source (ESRF-EBS) [11, 12].

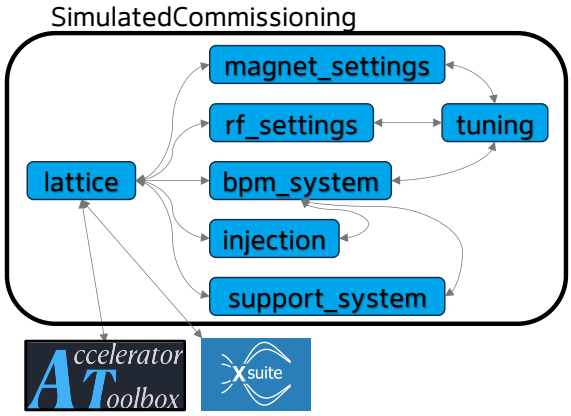

Figure 1: Diagram of the SimulatedCommissioning object.

RECENT pySC DEVELOPMENTS

Earlier pySC development focused on reproducing the simulated commissioning functionality of the original Toolkit for Simulated Commissioning in Python. In the recent development the focus shifted to reorganizing the tuning applications so that they can be reused in real accelerator environments. The reason for this is first and foremost for testing of the algorithms, but also for potential use in operation or in interfacing with other software, such as the Python Accelerator Middle Layer [13]. In order to do that, the pySC software is reorganized to provide a user interface closer to a real control system.

The *SimulatedCommissioning* object is the central state container of a pySC simulation. It is now re-implemented as a structured model that groups the lattice, active and design set-points, support and diagnostic systems, RF and injection state, and the tuning namespace. During initialization, references between these subsystems are propagated, random-number generation is seeded and the stored set-points are sent to the simulated lattice. The same object can also be serialized to JSON, copied, and exposed through a lightweight server. The main objects that make up the SC structure are described below and visualized in Fig. 1. They expose the

* konstantinos.paraschou@desy.de

Content from this work may be used under the terms of the CC BY 4.0 licence (© 2026). Any distribution of this work must maintain attribution to the author(s), title of the work, publisher, and DOI.

ISBN: 978-3-95450-252-3 ISSN: 2673-5350 doi: 10.18429/JACoW-IPAC2026-WEP5077

IMPACT OF A QUASI-RESONANT AC DIPOLE EXCITATION ON TRANSVERSE BEAM SPLITTING

O. Naumenko *, M. Giovannozzi, A. Huschauer, M. Schenk, CERN, Geneva, Switzerland
W. Hillert, Institute of Experimental Physics, Universität Hamburg, Germany

Abstract

To perform Multi-Turn Extraction at the CERN Proton Synchrotron, the beam is transversely split into five separate beamlets, consisting of the core and four islands. It has been shown that an AC dipole excitation effectively controls the characteristics of these beamlets. For this purpose, the AC dipole is set in resonance with the horizontal betatron tune, while the horizontal tune crosses the fourth-order resonance, creating a double-resonance condition, i.e. the simultaneous resonance condition of the horizontal tune and between the horizontal tune and the AC dipole excitation frequency. This increases the fraction of particles that are moved from the core to the islands. Further studies have revealed that slight adjustment of the AC dipole, thereby breaking the double-resonance condition, distributes the beam more evenly across the beamlets. This paper examines this phenomenon by establishing a Hamiltonian model for a system with such a quasi-resonant AC dipole and studying it with numerical simulations.

INTRODUCTION

Since September 2015, the CERN Proton Synchrotron (PS) has routinely delivered high-intensity proton beams to the Super Proton Synchrotron (SPS) using Multi-Turn Extraction (MTE). These beams are used for fixed-target physics at the SPS and generated by utilizing transverse beam splitting, obtained by crossing the horizontal 4th-order resonance [1–4].

The MTE aims to share the beam intensity equally among the five beamlets generated by transverse splitting. Initial experimental studies indicated that the core had higher intensity than the four islands. This was empirically resolved by using the transverse feedback system (TFB) as an AC dipole to excite the beam in the horizontal plane during the resonance crossing process, resulting in an increased beam intensity in the islands.

The impact of this addition has been extensively studied using Hamiltonian models [5, 6], and is currently under further experimental studies to improve the quality of the beam delivered [7, 8]. The results of these studies have revealed features that need to be further investigated theoretically. They point towards a need to better understand the splitting process when the double-resonance condition is broken, specifically when the AC dipole tune is non-resonant.

This work aims to extend previous Hamiltonian models to include this quasi-resonant case and uses detailed numerical simulations to provide an interpretation of the experimental studies that are on-going at the PS [8, 9].

* oleksandr.naumenko@cern.ch

THE DOUBLE-RESONANCE REGIME

A 1-dimensional Hamiltonian system may be used to model MTE splitting. Let the fractional part of the betatron tune be denoted ν_0, and define $\omega_0 = 2\pi\nu_0$. Furthermore, let the fractional part of the tune of the AC dipole be ν_{AC}, with $\omega_{\text{AC}} = 2\pi\nu_{\text{AC}}$. Based on [6], in a double-resonance condition, i.e. for $\omega_0 \approx \omega_{\text{r}}$ and $\omega_{\text{AC}} = \omega_{\text{r}}$ with $\omega_{\text{r}} = \pi/2$, the Hamiltonian in action-angle coordinates (θ, J) reads

$$H^{\text{dr}}(\theta, J) = \Delta\omega_0 J + \frac{\Omega_2}{2}J^2 + GJ^2\cos(4\theta) + \frac{k_{\text{AC}}}{2}\sqrt{2J}\cos\theta, \tag{1}$$

where $\Delta\omega_0 = \omega_0 - \omega_{\text{r}}$ is proportional to the tune in the chosen frame, which itself co-rotates at ω_{r}. $G \geq 0$ represents the strength of the 4th-order resonance, Ω_2 the detuning, and k_{AC} the strength of the AC dipole. This Hamiltonian admits up to 9 fixed points, up to 5 of which are stable, forming the core and islands shown in Fig. 1, where Cartesian coordinates, $(X, Y) = (\sqrt{2J}\cos\theta, \sqrt{2J}\sin\theta)$, are used.

The solutions of the fixed-point equations are analogous to those of the AC dipole Hamiltonian studied in [5, 10]. Using $\Omega_{2,0} = \Omega_2 + 2G$, $a_0 = \frac{3}{2}^{3/2}\frac{k_{\text{AC}}}{2\Delta\omega_0}\sqrt{-\frac{\Omega_{2,0}}{\Delta\omega_0}}$, and $\Omega_{2,j} = \Omega_2 - 2G$, $a_j = \frac{3}{2}^{3/2}\frac{k_{\text{AC}}(1+\Omega_{2,j}/8G)}{4\Delta\omega_0}\sqrt{-\frac{\Omega_{2,j}}{\Delta\omega_0}}$, they are

$$\begin{aligned} Y_{k,0} &= 0,\ Y_{k,j} = \pm\sqrt{\frac{(X_{k,j}^2(2G - \Omega_{2,j}/2) - \Delta\omega_0}{2G + \Omega_{2,j}/2}} \\ \frac{X_{k,0}}{2} &= \sqrt{-\frac{2\Delta\omega_0}{3\Omega_{2,0}}}\cos\left(\frac{\arccos a_0 - 2\pi k}{3}\right), k = 0, 1, 2, \\ \frac{X_{k,j}}{2} &= \sqrt{-\frac{2\Delta\omega_0}{3\Omega_{2,j}}}\cos\left(\frac{\arccos a_j - 2\pi k}{3}\right), j = 1, 2. \end{aligned} \tag{2}$$

The position of the islands is proportional to powers of $\Delta\omega_0$, i.e. the islands move as the resonance is crossed by varying ν_0 linearly from ν_0^{start} to ν_0^{end}. Additionally, $\Omega_{2,0}\Delta\omega_0 < 0$ and $\Omega_{2,j}\Delta\omega_0 < 0$ are necessary conditions for the fixed points to be real and hence for the islands to form.

Now, let the splitting efficiency be $\eta = \sum_{i=1}^{4} N_i/(4N)$, where $N_i, 1 \leq i \leq 4$ is the number of particles in each of the 4 islands, and $N = \sum_{i=0}^{6} N_i$ is the total number of particles (see Fig. 1 for the definition of phase-space regions).

As in the operational case, assume that the islands form for $\Delta\omega_0 \geq 0$, i.e. $\Omega_{2,j}, \Omega_{2,0} < 0$. In this case, the stable fixed-points corresponding to the islands form as soon as $\nu_0 = 0.25$, and their actions then increase as ν_0 increases. Hence, if the starting betatron tune $\nu_0^{\text{start}} > 0.25$, the islands

Content from this work may be used under the terms of the CC BY 4.0 licence (© 2026). Any distribution of this work must maintain attribution to the author(s), title of the work, publisher, and DOI.

ISBN: 978-3-95450-252-3 ISSN: 2673-5350 doi: 10.18429/JACoW-IPAC2026-WEP5078

LONG TERM TRACKING OF HIGH INTENSITY BUNCHED BEAMS WITH COLLISIONALITY

A. Engeda*, Goethe University Frankfurt, Frankfurt am Main, Germany
G. Franchetti, GSI Helmholtz Centre for Heavy Ion Research, Darmstadt, Germany

Content from this work may be used under the terms of the CC BY 4.0 licence (© 2026). Any distribution of this work must maintain attribution to the author(s), title of the work, publisher, and DOI.

Abstract

Modeling binary Coulomb collisions directly in particle-in-cell (PIC) simulations is computationally demanding. For long-term studies of intrabeam scattering (IBS), simulations must be both efficient and physically accurate, which requires careful numerical treatment of the statistical representation of the real beam. To address these challenges, a PIC solver with a Monte-Carlo-based Coulomb collision model (PIC–MCC) has been developed within the MICROMAP library written in gfortran for multi passing (MPI/OPENMP) computation. It combines a fully three-dimensional spectral Poisson solver for space–charge computations with established binary Coulomb collision algorithms to model Coulomb scattering (Takizuka and Abe algorithm) [1]. The objective is to obtain reliable predictions of IBS driven influence on the emittance growth and beam lifetime. For validation, MICROMAP also has implemented analytical IBS models such as the Bjorken–Mtingwa (BM) and the Martini formalisms [2–6]. Long-term PIC simulations are compared with analytical predictions to provide a consistent benchmark for assessing the accuracy of the collision models.

INTRODUCTION

Scattering caused by binary elastic interactions between two charged particles through their electromagnetic fields is referred to as a Coulomb collision. Intrabeam scattering (IBS) arises from the cumulative effect of many small-angle Coulomb encounters between particles in high-intensity beams which leads to growth of transverse emittance [2–4]. In kinetic theory, IBS corresponds to collisional relaxation governed by the Fokker–Planck–Landau collision operator [7, 8]. Analytical growth rates widely used in accelerator physics are derived from the formalisms of A. Piwinski [2,3] and Bjorken–Mtingwa [4]. These theories typically assume Gaussian phase-space distributions, smooth focusing approximation, and weak collective perturbations. This framework allows for the simultaneous treatment of collective space–charge forces and stochastic Coulomb scattering within a particle beam. These assumptions limit the applicability of analytical models in strongly nonlinear or non-Gaussian regimes, where PIC simulations provide a more general description.

Comparison of Analytical IBS Model with PIC-MCC

To validate the binary collision model implemented, the numerical results are compared with analytical IBS growth rates obtained from the extended Conte–Martini (CM) model presented in [5, 6] with more advanced analytical models where the non-ultrarelativistic corrections and the effect of vertical dispersion are incorporated [9].

The comparison is performed using identical beam parameters in both approaches in order to establish a consistent benchmark between the particle-based simulation and the theory. The analytical model assumes a Gaussian beam distribution and neglects collective effects such as space–charge.

The IBS growth rates in the analytical model are determined from the evolution of the beam parameters according to

$$\frac{1}{\tau_i} = \frac{1}{\epsilon_d}\frac{d\epsilon_d}{dt}, \quad d \in \{x, y, s\}, \tag{1}$$

where ϵ_d denotes the emittance in the respective plane.

In particle simulation, each particle undergoing a collision is scattered according to the Monte Carlo collision (MCC) model based on the Takizuka–Abe (TA) algorithm [1]. The ion–ion angular collision frequency ν_{ii} provides a measure of the rate of cumulative small-angle Coulomb scattering in the beam frame and is given with

$$\nu_{ii} = \frac{nq^4 \ln\Lambda}{\epsilon_0^2 m_i^2 v_{eff}^3}, \tag{2}$$

where n is the beam density, q the particle charge, m_i the ion mass, v_{eff} effective thermal velocity and $\ln\Lambda$ the Coulomb logarithm. Why this is nessesary to know will be shown in the section of the "Numerical Tests".

MODELING COLLISIONAL PARTICLE TRACKING

The evolution of the particle distribution function $f(\mathbf{x}, \mathbf{v}, t)$, including binary collisions, is described by the Fokker–Planck–Landau equation [7],

$$\frac{\partial f_i}{\partial t} + \mathbf{v}_i \cdot \nabla_x f_i + \frac{q_i}{m_i}\mathbf{E} \cdot \nabla_v f_i = C[f_i, f_j], \tag{3}$$

where $C[f_i, f_j]$ denotes the Landau collision operator describing binary interactions between ions i and j. In its Boltzmann form, the collision operator can be written as

$$C[f_i, f_j] = \int_{\mathbb{R}^3} d\mathbf{v}_j \int_{S^2} d\Omega \left(\frac{d\sigma}{d\Omega}\right) |\mathbf{u}| \left(f_i' f_j' - f_j f_i\right), \tag{4}$$

where $\mathbf{u} = \mathbf{v}_i - \mathbf{v}_j$ is the relative velocity and (f_i', f_j') denote the post-collision distribution functions. The differential scattering cross section for Coulomb interactions is given

* engeda@iap.uni-frankfurt.de

ISBN: 978-3-95450-252-3 ISSN: 2673-5350 doi: 10.18429/JACoW-IPAC2026-WEP5079

MITIGATING THE PERIODIC RESONANCE CROSSING IN HIGH-INTENSITY BUNCHES BY MULTI-RF

G. Franchetti[1,2,3], S. Albright[4], F. Asvesta[4], H. Bartosik[4], T. Prebibaj[4]
[1]GSI Helmholtzzentrum für Schwerionenforschung GmbH, Darmstadt, Germany
[2]Goethe University Frankfurt, Frankfurt, Germany
[3]Helmholtz Research Academy Hesse for FAIR, Frankfurt, Germany
[4]CERN, Geneva, Switzerland

Content from this work may be used under the terms of the CC BY 4.0 licence (© 2026). Any distribution of this work must maintain attribution to the author(s), title of the work, publisher, and DOI.

Abstract

Periodic resonance crossing driven by space charge in bunched beams leads to slow diffusion over hundreds of synchrotron oscillations, making emittance growth and beam loss difficult to control and hard to describe theoretically. Its pseudo-stochastic nature means reliable predictions typically require full simulations. Mitigation methods such as resonance compensation or space-charge compensation are complex and highly dependent on detailed machine conditions. Here, an alternative approach is proposed: shaping the longitudinal bunch profile using a suitable combination of RF harmonics to reduce the effectiveness of periodic crossings. First experimental studies at the CERN PS Booster show promising results, suggesting this as a viable new direction.

PERIODIC RESONANCE CROSSING IN HIGH INTENSITY BUNCHES

The rise of new operational regimes in particle accelerators has introduced significant challenges for recent projects [1, 2]. For example, the FAIR project [1] involves long-term storage of high-intensity bunched beams over hundreds of synchrotron oscillations. During this time, particles repeatedly traverse regions of varying longitudinal density, coupling the transverse space-charge tune shift to their longitudinal motion. This becomes critical when the tune spread overlaps a lattice resonance, causing resonance islands to vary with longitudinal position and move in the transverse plane. As particles cross these moving islands, their invariant $J_{x/y} = 2\epsilon_{x/y}$ can change: fast crossings produce random-like kicks (scattering), while slow crossings may trap particles. This leads to transverse diffusion, halo formation, and eventual beam loss if the halo exceeds machine acceptance. Experiments at GSI (SIS18) [3] and CERN (PS, SPS) [4, 5] confirm this mechanism. Modeling this process is challenging because the scattering is pseudo-random [6] and nonlinear, leading to diffusion that depends on resonance properties, additional nonlinearities (e.g., amplitude-dependent detuning), and the synchrotron motion speed.

Mitigation Approaches

The impact of resonance islands on particle dynamics depends on resonance strength. Weak resonances cause weaker scattering during periodic crossings, leading to slower halo formation and beam loss—making mitigation more feasible. This was demonstrated at SIS18 [7], where partial compensation of a third-order resonance reduced emittance growth and losses. However, resonance compensation is challenging. It is typically based on single-particle estimates of resonant driving terms [8], whereas in reality the optics are modified by space charge [9, 10]. As a result, compensation varies along the bunch and may become less effective, especially when multiple resonances overlap with the incoherent tune spread. An alternative approach targets the space-charge effect directly using electron lenses, which generate opposing fields to compensate amplitude-dependent detuning. This replaces the continuous space-charge force with localized, longitudinally modulated lenses matched to the bunch profile [11, 12]. Multiple lenses help avoid introducing additional resonances or perturbing the optics. Another strategy, explored at IOTA (FNAL) [13], uses integrable optics based on the McMillan concept [14, 15]. Here, specially designed magnetic fields intrinsically mitigate space-charge effects and stabilize beam dynamics. Ongoing experiments are investigating its effectiveness for periodic resonance crossing in intense proton beams.

NOVEL APPROACH

Here, a different mitigation strategy is proposed: instead of targeting the resonance itself (as in resonance compensation), the detuning (e-lenses), or resonance formation (integrable optics), the goal is to reduce the scattering process directly. This is done by controlling the speed at which instantaneous resonance islands cross particle orbits. If the crossing is slow—so the phase advance in the frame island is many multiples of 2π during one synchrotron oscillation—particles can become trapped. If the crossing is fast, the interaction is much weaker. The next discussion focuses on a 1D resonance of the form $n_x Q_x = N$. The speed of an island crossing is the composition of the speed of the longitudinal motion $\Delta z/\Delta n$, with n the turn number, with the dependence of the instantaneous fixed point $(x_{\mathrm{fp}}, x'_{\mathrm{fp}})$ on the longitudinal position of the particle z. For an axi-symmetric transverse Gaussian distribution, considering a particle with $\epsilon_y = 0$, the dependence of the incoherent space charge tuneshift is $\Delta Q_{x,\mathrm{sc}}(\epsilon_x, z) \simeq \Delta Q_{x0,\mathrm{sc}}(z)/[1 + \epsilon_x/(4E_x)]$, with E_x the horizontal rms emittance, and $\Delta Q_{x0,\mathrm{sc}}(z)$ the maximum transverse incoherent space charge tuneshift at location z (where the particle we consider is). The location of the fixed points is approximately determined by the resonance condition $\Delta Q_{x,\mathrm{sc}}(\epsilon_{x,\mathrm{fp}}, z) \simeq Q_{x,r} - Q_{x0}$, with $Q_{x,r}$ the

ISBN: 978-3-95450-252-3 ISSN: 2673-5350 doi: 10.18429/JACoW-IPAC2026-WEP5080

COMPUTING COHERENT SYNCHROTRON RADIATION FROM LIÉNARD-WIECHERT POTENTIALS

M. Schwarz*, A. Bernhard, M. Brosi, J. Schäfer, A.-S. Müller
Karlsruhe Institute of Technology, Karlsruhe, Germany

Content from this work may be used under the terms of the CC BY 4.0 licence (© 2026). Any distribution of this work must maintain attribution to the author(s), title of the work, publisher, and DOI.

Abstract

The linac-based test accelerator FLUTE contains a bunch compressor to create few-fs scale bunches that generate coherent radiation in the THz regime. The form and spectrum of the THz pulse strongly depend on the evolution of the bunch along the bunch compressor, and hence on the paths of the particles. From a given path of a charged particle, one can compute the emitted radiation by means of the Liénard-Wiechert potentials. A problem with this approach is that one needs to solve an implicit equation for the retarded time. Here, we instead compute the retarded time from the particle time and observer position. Furthermore, the Liénard-Wiechert potentials depend on the acceleration, while macro-particle tracking only yields the particle positions and momenta at fixed times. To compute the acceleration, we interpolate the data using twice differentiable functions. We compare the numerical results to the analytical benchmark case of synchrotron radiation. Finally, we compute the coherent radiation emitted by a simulated bunch during compression.

INTRODUCTION

The electric field of a point particle of charge q, moving on a path $\boldsymbol{r}(t)$ is given by the Liénard-Wiechert field [1]. Since we are interested in the emitted radiation, we neglect the Coulomb term, and focus on the radiation term:

$$\boldsymbol{E}_{\mathrm{rad}}(t_{\mathrm{obs}}, \boldsymbol{r}_{\mathrm{obs}}) = \frac{q\,Z_0}{4\pi} \left. \frac{\boldsymbol{n} \times \left[(\boldsymbol{n} - \boldsymbol{\beta}) \times \dot{\boldsymbol{\beta}}\right]}{(1 - \boldsymbol{\beta} \cdot \boldsymbol{n})^3\, R} \right|_{\mathrm{ret}} . \quad (1)$$

Here, $\boldsymbol{\beta} = \dot{\boldsymbol{r}}/c$ and $\dot{\boldsymbol{\beta}}$ denote the scaled velocity and acceleration of the particle. The observer is located at the spatial position $\boldsymbol{r}_{\mathrm{obs}}$ and receives the field at the time t_{obs}. The unit vector $\boldsymbol{n}$ points from the particle to the observer. Due to the finite speed of light c, a given observer time t_{obs} is related to the retarded time by

$$t_r = t_{\mathrm{obs}} - R(t_r)/c \,, \quad (2)$$

where $R(t_r) = |\boldsymbol{r}_{\mathrm{obs}} - \boldsymbol{r}(t_r)|$ is the distance from the particle to the observer. The field in Eq. (1) have to be evaluated at t_r.

To calculate the field at the observer position and time one needs to know the particle state at the earlier time when the radiation was emitted such that it reaches the observer at $(t_{\mathrm{obs}}, \boldsymbol{r}_{\mathrm{obs}})$. The problem is that Eq. (2) is an implicit equation for $t_r(t_{\mathrm{obs}})$, which is difficult to solve even for simple analytic cases. One solution is to compute the fields in the frequency domain by a Fourier transform. One can then perform a substitution of variables and work directly with t_r. This approach is used on programs such as `SRW` [2] and `spectra` [3]. It works well in the paraxial approximation, but this approximation breaks down for THz frequencies. Another solution is to work in the time domain and solve Eq. (2) by a root-finding algorithm [4]. However, the root-finding needs to work to high precision, since t_r is often in the ns-scale while t_{obs} is in the fs-scale.

In this paper, we work in the time domain, but instead of trying to compute $t_r(t_{\mathrm{obs}})$, we compute the observer time from the particle path $\boldsymbol{r}(t_p)$ as

$$t_{\mathrm{obs}}(t_p) = t_p + R(t_p)/c \,, \quad (3)$$

which is straightforward for a given particle path $\boldsymbol{r}(t_p)$. The time t_p that parametrizes the particle path equals the retarded time. First the r.h.s. of Eq. (1) is evaluated for t_p, yielding $\boldsymbol{E}_{\mathrm{rad}}(t_p, \boldsymbol{r}_{\mathrm{obs}})$. Then we use Eq. (3) to obtain $\boldsymbol{E}_{\mathrm{rad}}(t_{\mathrm{obs}}(t_p), \boldsymbol{r}_{\mathrm{obs}})$. From this point of view, Eq. (3) is just a non-linear rescaling of the time axes.

Given the electric field in the time domain, one can compute the spectrum of the emitted radiation by

$$\left.\frac{\mathrm{d}^2 I}{\mathrm{d}\Omega\,\mathrm{d}\omega}\right|_1 = 2\sqrt{\frac{\epsilon_0}{\mu_0}}\,|\mathrm{FT}\{R\,\boldsymbol{E}, \omega\}|^2 \,, \quad (4)$$

where FT denotes the Fourier transform. Notice that the Fourier transform has to be done w.r.t. the observer time t_{obs}. The index 1 indicates that it is the spectrum of a single particle. To obtain the spectrum emitted by N particles, one first has to sum the electric fields of the particles and then take the modulus. For analytical results, the sum over particles is replaced by an integration over a charge density [5], which results in

$$\left.\frac{\mathrm{d}^2 I}{\mathrm{d}\Omega \mathrm{d}\omega}\right|_N = \left[N + N^2 F(\omega)\right] \left.\frac{\mathrm{d}^2 I}{\mathrm{d}\Omega \mathrm{d}\omega}\right|_1 . \quad (5)$$

Here, F denotes the form factor, which is the squared modulus of the Fourier-transformed line density. It measures the "degree of coherence" of the radiation at (angular) frequency ω, with 1 meaning fully coherent and 0 meaning incoherent. Notice that the coherent radiation scales with the number of particles squared.

SOLVER ALGORITHM

Typically, tracking codes provide 6D phase space coordinates $(\boldsymbol{r}_j, \boldsymbol{p}_j)$ of the macro-particles at positions s_j or times $t_{p,j}$. While it is straightforward to compute the velocities $\boldsymbol{\beta}_j$ from the momenta $\boldsymbol{p}_j$, the acceleration $\dot{\boldsymbol{\beta}}_j$ is usually not

* Markus.Schwarz@kit.edu

ISBN: 978-3-95450-252-3 ISSN: 2673-5350 doi: 10.18429/JACoW-IPAC2026-WEP5081

MODELING OF THE HB^{2}TF INJECTOR IN COMSOL WITH BENCHMARKING USING ASTRA AND RF-TRACK

I. Drebot*, A. Bacci, D. Giove, M. Rossetti Conti, L. Serafini, D. Sertore
INFN, Milano, Italy
A. Olivieri, UNICAL, Cosenza, Italy

Abstract

A comprehensive electromagnetic and beam-dynamics model of the High Brightness Beam Test Facility (HB^{2}TF) electron injector under development at INFN-LASA has been implemented using COMSOL Multiphysics. The model incorporates the DC photocathode gun and the low-energy transport line. Three-dimensional electric and magnetic field distributions were computed and employed for particle tracking within COMSOL, enabling analysis of field effects, mesh resolution impacts, and space-charge contributions. The resulting field maps were exported and imported into ASTRA and RF-Track simulation codes to perform cross-validation of beam dynamics. Comparative studies focus on transverse emittance, bunch length, energy spread, and sensitivity to field map resolution. This work establishes a validated modeling workflow for the HB^{2}TF injector and provides crucial input for its optimization and future commissioning.

INTRODUCTION

The High Brightness Beam Test Facility (HB^{2}TF) [1], currently under development at the INFN-LASA laboratory in Segrate, Italy, is designed to support research and development activities in advanced electron injectors and continuous-wave (CW) high-brightness beam generation. The facility consists of a laser-driven DC photocathode gun followed by a normal-conducting RF bunching and acceleration section, delivering electron beams with energies up to approximately 0.8 MeV and average currents up to 2.5 mA.

HB^{2}TF represents the first stage of the broader BriXSinO injector concept [2], which foresees the integration of an additional bunching section and a superconducting booster linac capable of increasing the beam energy to the 4–10 MeV range while preserving high beam brightness and CW operation [3]. In a later stage, a superconducting energy-recovery linac (ERL) is planned to accelerate the beam up to about 45 MeV.

One of the main objectives of HB^{2}TF is the experimental demonstration of stable high-brightness beam production at repetition rates on the order of 100 MHz. Achieving these operating conditions requires accurate modeling of both the electromagnetic fields and the low-energy beam dynamics, where space-charge effects play a dominant role. For this reason, reliable simulation workflows and cross-validation between different numerical tools are essential for the optimization and future commissioning of the injector.

In this work, a detailed COMSOL Multiphysics [4] model of the DC photocathode gun and the focusing solenoid has been developed, including three-dimensional electromagnetic field calculations and particle tracking through the low-energy beamline. COMSOL Multiphysics was selected due to its capability to provide both direct three-dimensional geometry modeling and self-consistent calculations of electric and magnetic fields, together with integrated particle-tracking simulations within the same computational framework. The generated field maps were exported to ASTRA [5] and RF-Track [6], where dedicated particle-tracking simulations were performed for benchmarking and cross-validation studies.

The DC gun adopts the "inverted insulator" scheme originally developed at Jefferson Lab [7], providing a robust and reliable solution for high-repetition-rate operation while ensuring improved electric-field symmetry, enhanced vacuum performance through the combination of NEG and NexTorr technologies, and compatibility with the INFN photocathode handling system.

MODEL

The initial attempt to import the original CAD model of the DC gun into COMSOL significantly increased the complexity of the simulation due to the presence of numerous small mechanical details that do not affect either the electromagnetic field calculations or the particle dynamics. Therefore, a simplified geometry model was developed based on the original CAD Fig. 1 design in order to improve computational efficiency while preserving the relevant physical features of the system. In the Fig. 2 presented simplified model we can see Spherical cathode with installed photocathode molybdenum plug, anode with hole and solenoid.

By applying a potential of -300 kV to the cathode while grounding the anode and the vacuum chamber, the electric field distribution inside the DC gun can be calculated. Both the electric and magnetic field simulations were performed in full-3D in order to enable future studies of effects related to laser misalignment on the photocathode and their impact on beam quality. In the present work, however, only the axially symmetric configuration is considered. Figure 3 shows the normalized electric field distribution inside the gun structure.

The solenoid was modeled as a coil consisting of 1000 turns of copper wire enclosed within a steel yoke used for magnetic-field concentration and improved thermal management. For the simulations presented in this work, the coil current was set to 3.5 A in order to obtain a visible focusing

* illya.drebot@mi.infn.it

Content from this work may be used under the terms of the CC BY 4.0 licence (© 2026). Any distribution of this work must maintain attribution to the author(s), title of the work, publisher, and DOI.

ISBN: 978-3-95450-252-3 ISSN: 2673-5350 doi: 10.18429/JACoW-IPAC2026-WEP5083

ASSESSMENT OF FABRICATION AND ASSEMBLY TOLERANCES IN AN IH-DTL CAVITY THROUGH ELECTROMAGNETIC AND BEAM DYNAMICS SIMULATIONS

P. Calvo*[1], D. Gavela[1], M. López[2], J. M. Gómez[1], G. Moreno[1], C. Oliver[1], A. Tato[2]
[1]Centro de Investigaciones Energéticas, Medioambientales y Tecnológicas, Madrid, Spain
[2]Added Value Solutions, Elgoibar, Spain

Abstract

This work presents a comprehensive study of manufacturing and assembly errors in a 750 MHz Interdigital H-mode Drift Tube Linac (IH-DTL) cavity designed for a compact and efficient ion beam inyector. Operating at such a high RF frequency significantly reduces the cavity dimensions but it also increases the sensitivity to geometric imperfections, posing a substantial technological challenge for manufacturing and assembly. In this study, realistic machining deviations — including drift-tube misalignments, stem eccentricity, profile machining errors, and end-cell distortions — are introduced within typical fabrication tolerances. Three-dimensional electromagnetic simulations quantify the resulting perturbations in the resonant frequency, accelerating fields, and power efficiency. First, the most critical geometric perturbations were identified by means of a single cavity cell model. Then, those errors were implemented in a complete cavity, applied to all cells. The resulting field maps were subsequently imported into multi-particle beam dynamics simulations to evaluate their impact on beam quality, transmission, and emittance growth. The study provides experimental tolerance thresholds and offers guidance for cavity fabrication, quality control, and commissioning strategies for IH-DTL structures.

INTRODUCTION

H-mode interdigital radiofrequency (IH) cavities are a type of accelerating cavity well known for their high efficiency at low velocities, rendering them particularly suitable for the initial stages of linear accelerators. This type of structure is characterized by high shunt impedance and compact geometry, making it an attractive option for linear accelerators with space constraints and high-intensity requirements [1, 2].

This technological framework is of particular importance in the context of hadron therapy, where compact and efficient accelerators are required to meet demanding clinical specifications. As part of the latest advances, CIEMAT, in collaboration with its industrial partner Added Value Solutions (AVS), is making progress on the design of a high-frequency linear injector intended for radiobiology studies [3], which will serve as a demonstrator for a future linac-based ion therapy facility. This injector is intended to accelerate $^{12}C^{6+}$ and $^{1}H^{+}$ ions up to 10 MeV/u in pulses of 5 µs. IH-DTL structures, designed to operate at 750 MHz, are currently actively being developed [4].

The application of structures operating at frequencies higher than usual entails certain additional constraints in RF design and cavity fabrication, as there is a high sensitivity to geometric deviations, whether in the positioning of the drift tubes, the eccentricity of the rods, machining tolerances, or overall alignment errors. Although these geometric aberrations may be of small magnitude, numerous studies [5, 6] have shown that even small deviations can significantly alter the spatial distribution of the fields [7], causing shifts in the resonance frequency and undesirable variations in the impedance. Furthermore, these alterations not only affect the electromagnetic performance of the cavity, but also have direct consequences on the beam dynamics, including increased emittance, distortion of the longitudinal matching, and cumulative effects in acceleration schemes.

In this context, the study of tolerances in manufacturing is of crucial importance. Therefore, the objective of this report is to assess how geometric errors affect the performance of the first IH-DTL. By means of electromagnetic simulations, statistical analysis of geometric variations, and multiparametric beam tracking, we evaluate representative scenarios of machining errors, misalignments, and dimensional disturbances in order to quantify their impact on the field and beam dynamics, establishing verifiable manufacturing tolerances and acceptance criteria.

IH cavity

The IH cavity, which serves as the basis for the current analysis, is the first of a set of three [8]. It operates in TE110 mode, accelerating the beam from 5 MeV/u to 6.2 MeV/u over the course of 30 cells. The main RF and geometric parameters are specified in Table 1.

Table 1: Main Parameters of the IH-Cavity

Parameter	Value
Design average voltage (kV)	125
Energy gain (MeV/u)	1.23
Frequency (MHz)	749.48
Number of cells	30
Inner aperture (mm)	6
Length (m)	0.65
Power loss (kW)	69.9
ZTT (MΩ/m)	289.3

* pedro.calvo@ciemat.es

Content from this work may be used under the terms of the CC BY 4.0 licence (© 2026). Any distribution of this work must maintain attribution to the author(s), title of the work, publisher, and DOI.

ISBN: 978-3-95450-252-3 ISSN: 2673-5350 doi: 10.18429/JACoW-IPAC2026-WEP5084

A GENERALIZED ANALYTICAL POTENTIAL FOR FAST RFQ BEAM DYNAMICS MODELING

E. Laface*, European Spallation Source ERIC, Lund, Sweden

Abstract

Radio Frequency Quadrupoles (RFQs) are widely used at the front end of linear accelerators to focus, bunch, and accelerate low-energy ion beams. Their electromagnetic field is commonly evaluated with full three-dimensional numerical solvers, which provide accurate field maps but are computationally expensive for fast beam dynamics studies and online applications. The classical Kapchinsky–Teplyakov two-term potential is compact, but its truncated form may not fully reproduce realistic modulated vane fields. In this paper, a generalized analytical RFQ potential is derived from Maxwell's equations in the quasi-static regime relevant to the beam aperture. The scalar potential is obtained as a regular solution of Laplace's equation in cylindrical coordinates and expanded in angular and longitudinal harmonics. The classical two-term approximation is recovered as the lowest-order truncation, while equipotential boundary conditions on the modulated vane surface define a finite matrix problem for the modal coefficients. A framework is also introduced to quantify the accuracy of truncated expansions versus retained terms and transverse radius.

INTRODUCTION

The Radio Frequency Quadrupole (RFQ) is a resonant accelerating structure used at the low-energy front end of ion linacs, where it simultaneously provides transverse focusing, adiabatic bunching, and longitudinal acceleration [1,2]. This is enabled by a four-vane geometry that generates a transverse quadrupole electric field together with a longitudinal component arising from periodic vane modulation.

In RFQ beam dynamics studies, the electromagnetic field is often reconstructed with numerical solvers and then imported into particle tracking codes. Although accurate, this approach can become computationally expensive when repeated field evaluations are required in parameter scans, tuning studies, model-based control, or online applications. For such cases, analytical field representations remain attractive.

The standard analytical description is the two-term potential introduced by Kapchinsky and Teplyakov [1], widely used in RFQ design and simulation codes [3,4]. Because it retains only the lowest-order contributions, it may become insufficient for strongly modulated vanes, for apertures not small compared with the modulation wavelength, or whenever improved field fidelity is required [5].

This work develops a generalized analytical RFQ potential that extends the classical two-term model while preserving computational efficiency. Starting from Maxwell's equations, it derives the scalar potential in cylindrical coordinates and examines how truncation order affects the reconstructed field.

* emanuele.laface@ess.eu

ELECTROMAGNETIC FORMULATION

In vacuum, Maxwell's equations are $\nabla \cdot \vec{E} = 0$, $\nabla \cdot \vec{B} = 0$, $\nabla \times \vec{E} = -\partial \vec{B}/\partial t$, and $\nabla \times \vec{B} = \mu_0 \varepsilon_0 \, \partial \vec{E}/\partial t$. The RFQ is an RF structure, so the full electromagnetic field is time dependent. However, in the beam aperture the transverse dimensions are much smaller than the RF wavelength, and the electric field can be treated to leading order as quasi-electrostatic with harmonic time dependence. We therefore write $\Phi(r,\theta,z,t) = U(r,\theta,z)\cos(\omega t + \phi_s)$, where $U(r,\theta,z)$ is the spatial potential amplitude, $\omega = 2\pi f$ is the RF angular frequency, and ϕ_s is an arbitrary reference phase. To leading order, $\vec{E}(r,\theta,z,t) \simeq -\nabla U(r,\theta,z)\cos(\omega t + \phi_s)$, so the spatial potential satisfies $\nabla^2 U = 0$.

This is the starting point for the analytical RFQ field model considered here.

MODAL EXPANSION IN CYLINDRICAL COORDINATES

The Laplace equation is solved in cylindrical coordinates by separation of variables. We seek solutions of the form $U(r,\theta,z) = R(r)\Theta(\theta)Z(z)$. Using $\nabla^2 = \partial_r^2 + r^{-1}\partial_r + r^{-2}\partial_\theta^2 + \partial_z^2$, substitution into $\nabla^2 U = 0$ gives $\frac{R''}{R} + \frac{1}{r}\frac{R'}{R} + \frac{1}{r^2}\frac{\Theta''}{\Theta} + \frac{Z''}{Z} = 0$.

Angular and Longitudinal Dependence

The angular component must be 2π-periodic. For an RFQ with four-vane symmetry, the natural basis is given by even multipoles, $\Theta_m(\theta) = \cos(2m\theta)$ with $m = 0, 1, 2, \ldots$, and angular eigenvalue $(2m)^2$.

The vane modulation is periodic along the beam axis with fundamental period $\beta\lambda$, where $\beta = v/c$ refers to the synchronous particle and $\lambda = c/f$ is the RF wavelength. The corresponding longitudinal wave number is $k = 2\pi/(\beta\lambda)$, and a convenient basis is $Z_n(z) = \cos(nkz)$, $n = 0, 1, 2, \ldots$, where a sine representation would be equivalent up to a longitudinal phase shift.

Radial Dependence

For a mode indexed by (m,n), the radial equation becomes

$$r^2R'' + rR' - \left[(nk)^2r^2 + (2m)^2\right]R = 0. \qquad (1)$$

For $n \geq 1$, Eq. (1) is the modified Bessel equation of order $2m$, with regular solution

$$R_{mn}(r) = A_{mn}I_{2m}(nkr), \qquad n \geq 1, \qquad (2)$$

Content from this work may be used under the terms of the CC BY 4.0 licence (© 2026). Any distribution of this work must maintain attribution to the author(s), title of the work, publisher, and DOI.

ISBN: 978-3-95450-252-3 ISSN: 2673-5350 doi: 10.18429/JACoW-IPAC2026-WEP5086

ANALYTICAL SOLUTIONS FOR PARTICLE TRACKING IN PLANAR CRYSTAL CHANNELLING

A. Iliopoulou*[1,2], B. Lindström[1,3], S. Van der Schueren[1,4], F. F. Van der Veken[1], D. Veres[1,5]
[1]CERN, Meyrin, Switzerland, [2]University of Macedonia, Thessaloniki, Greece
[3]John Adams Institute at Royal Holloway, University of London, Egham, UK
[4]Sapienza University, Rome, Italy, [5]Goethe University, Frankfurt am Main, Germany

Abstract

Planar particle channelling describes the motion of high-energy particles trapped in the potential well formed by crystal lattice planes, allowing their trajectories to be deflected in a controlled manner. Within the Molière approximation, which incorporates atomic screening and thermal vibrations, this motion is typically either approximated by a harmonic potential or evaluated numerically. Here, we propose a simplified Molière model that yields closed-form analytical solutions expressed through Jacobi elliptic functions. To extend the treatment to bent crystals, symplectic integrators are applied to the equations of motion, ensuring accuracy and long-term stability through symplecticity. This semi-analytical approach to evaluate bent channelling has been benchmarked against existing numerical methods, and the optimal configuration will be integrated into Xsuite's Xcoll package.

INTRODUCTION

Crystals are used in the CERN accelerator complex for a series of applications, including beam extraction [1–3], crystal collimation [4–7], and exotic particle measurements [8–14]. Their significant advantages include a strong beam-bending capability while requiring no additional space due to their small size[1]. Compared to magnets, which inevitably affect the entire beam, crystals influence only the intercepted particles, leaving the rest of the beam untouched [15].

The implementation of crystals into simulations requires studying the underlying particle–matter interactions, such as channelling, dechannelling, volume capture, and volume reflection [16]. Here we focus on the channelling process.

Thus far, existing simulation tools employ either the harmonic approximation of the potential [16, 17], which lacks sufficient accuracy, or a stepwise numerical solution to the Molière model [18], which is computationally expensive.

This paper introduces a new model, based on a simplified Molière potential, which aims to combine adequate accuracy with computational efficiency and is intended for implementation in Xcoll [19, 20], the collimation module of the Xsuite simulation library [21, 22].

MODEL DESCRIPTION

Our model is derived from the Molière potential for a "warm" atomic plane [16], approximating the sum of exponentials by a single exponential, leading to the relation below:

$$U(x) = U_{\mathrm{N}} \left(\cosh \frac{\beta_{\mathrm{i}}}{a_{\mathrm{TF}}} x - 1 \right), \tag{1}$$

$$U_{\mathrm{N}} = 2U_{\max} \frac{\alpha_{\mathrm{i}}}{\beta_{\mathrm{i}}} \, \mathrm{e}^{-\frac{\beta_{\mathrm{i}}}{a_{\mathrm{TF}}} \frac{d_{\mathrm{P}}}{2}}, \tag{2}$$

where[2] $a_{\mathrm{TF}} = 0.4683\, Z^{-1/3}$Å is the so-called screening distance, d_{P} is the planar spacing, and $U_{\max} = 2\pi N Z_{\mathrm{i}} Z e^2 d_{\mathrm{P}}\, a_{\mathrm{TF}}$. For the ^{28}Si (110) plane, we have $U_{\max} = 23.9037$ eV, $d_{\mathrm{P}} = 1.92$ Å, and $a_{\mathrm{TF}} = 0.194$ Å. The parameters $\alpha_{\mathrm{i}} = 0.722452$ and $\beta_{\mathrm{i}} = 0.573481$ are determined empirically to reproduce the original Molière potential with an observed accuracy up to 0.068 eV over the interval $[-x_{\mathrm{c}}, x_{\mathrm{c}}]$, where x_{c} is the maximum amplitude allowed for the particle oscillation.[3]

CHANNELLING EQUATION

Under the continuum approximation, assuming a classical particle trajectory with small angles relative to the crystal lattice planes ($\theta \approx \tan\theta = \frac{p_{\mathrm{x}}}{p_{\mathrm{z}}}$), adiabatic invariance (no energy losses), and a thermally averaged crystal, the particle transverse energy is considered a constant of motion:

$$E_{\mathrm{T}} = \frac{1}{2}\beta p c \theta^2 + U(x) = \text{constant}.$$

The channelling equation is then reduced to a one-dimensional differential equation [23]:

$$\beta p c x''(s) + \partial_x U(x) = 0, \tag{3}$$

where s is the direction of motion along the (potentially curved) path and x is the transverse coordinate along which the oscillation occurs.

Straight Crystal

For a straight crystal, one can substitute Eq. (1) into Eq. (3), leading to analytical solutions expressed in terms of Jacobi elliptic functions [24] as follows:

$$x(z) = 2\mathrm{i}\frac{a_{\mathrm{TF}}}{\beta_{\mathrm{i}}} \, \mathrm{am}\left(\mathrm{i}(\nu z + \phi) \, , \, -2\frac{U_{\mathrm{N}}}{E_{\mathrm{T}}} \right),$$

$$\theta(z) = -2\frac{a_{\mathrm{TF}}}{\beta_{\mathrm{i}}} \nu \, \mathrm{dn}\left(\mathrm{i}(\nu z + \phi) \, , \, -2\frac{U_{\mathrm{N}}}{E_{\mathrm{T}}} \right),$$

* anastasia.iliopoulou@cern.ch

[1] Typically on the mm–cm scale.

[2] N denotes the atomic density of the crystal, Z the atomic number of the lattice atoms, Z_{i} the charge number of the incident particle and e the elementary charge, as explained in Ref. [16].

[3] Based on measurements, we typically use $x_{\mathrm{c}} = \sqrt{0.9}\,\frac{d_{\mathrm{P}}}{2}$ but this can be optimised.

Content from this work may be used under the terms of the CC BY 4.0 licence (© 2026). Any distribution of this work must maintain attribution to the author(s), title of the work, publisher, and DOI.

ISBN: 978-3-95450-252-3 ISSN: 2673-5350 doi: 10.18429/JACoW-IPAC2026-WEP5087

LINEAR AND NONLINEAR EFFECTS OF FRINGE FIELDS ON THE SINGLE-PARTICLE DYNAMICS IN THE HELIUM LIGHT ION COMPACT SYNCHROTRON

S. Van der Schueren*, R. De Maria, H. Huttunen, European Organization for Nuclear Research, Geneva, Switzerland
M. Migliorati, Istituto Nazionale di Fisica Nucleare, Rome, Italy
V. Korchevnyuk, École Polytechnique Fédérale de Lausanne, Lausanne, Switzerland

Abstract

The Helium Light-Ion Compact Synchrotron (HeLICS) [1] is a proposed cancer treatment facility developed within the Next Ion Medical Machine Study (NIMMS) at CERN, designed both for clinical treatment with protons and research with helium ions. Consisting of a triangular lattice with six 60° combined-function magnets with 30° edge angles, this machine challenges the current treatment of fringe fields in beam dynamics simulations. At present, accurate maps for the fringe fields of curved combined-function magnets with edge angles are not available in the literature. In this work we investigate the linear and non-linear effects of these fringe fields through the framework of resonance driving terms, providing an alternative approach to quantify their influence on single-particle dynamics.

INTRODUCTION

The current design of the HeLICS ring is a triangular lattice with a circumference of 35 m, designed to accelerate alpha particles from 5 MeV/u to 220 MeV/u [2, 3]. In machines of this scale, fringe fields can have a significant impact on the beam optics, while the effects are often only taken into account in a late stage of the design of the machine when a magnetic fieldmap is available. Our goal is to develop methods to study the impact of existing combined-function magnets, but also produce field-quality specifications for magnets to be designed, therefore accounting for fringe field effects earlier in the ring design process.

THE HELICS SYNCHROTRON

The HeLICS optics [4], computed with Xsuite [5] and shown in Fig. 1, contains six combined-function dipole-quadrupole magnets with design parameters given in Tab. 1. Since the machine is still in the design phase, a final design and three-dimensional fieldmap of the dipoles are not available.

Fieldmap of the HeLICS dipole

At the present design stage, there is not yet a magnet design that satisfies the most recent optics requirements. To obtain first field maps for the bends, one can use a general

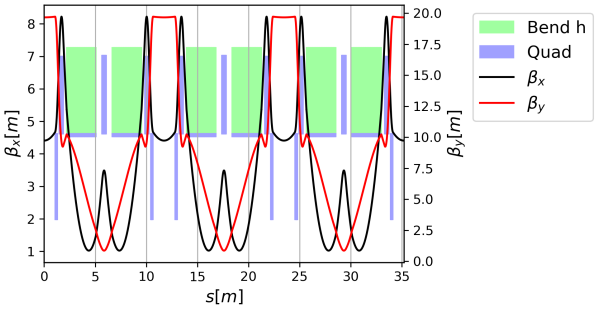

Figure 1: HeLICS optics with $Q_x = 2.39, Q_y = 1.21$.

Table 1: Design Parameters for the Combined-Function Dipoles in the Current Design of the HeLICS Ring

Parameter	Design value
bending radius	2.74 m
bending angle	60 degrees
edge angle	30 degrees
(curved) magnetic length	2.87 m
dipole strength	1.65 T
quadrupole strength	-0.50 T/m

magnetic field expansion in Frenet-Serret coordinates [6],

$$\vec{R}(x, y, s) = \vec{R}_0(s) + x\hat{x}(s) + y\hat{y}(s) \quad (1)$$

$$\frac{d}{ds}\vec{R}_0(s) = \hat{s}(s) \,, \quad (2)$$

with $\vec{R}$ the position of the particle, $\vec{R}_0$ the reference trajectory, and $\hat{x}$ and $\hat{y}$ the horizontal and vertical unit vectors of a coordinate system anchored to the reference trajectory. We have that $\hat{s} = \vec{R}_0'(s), \hat{x}'(s) = h(s)\hat{s}(s)$ and $\hat{y}(s) = -\hat{x}(s)\times\hat{s}(s)$ and $h(s) = 1/\rho(s)$ is the local curvature, see Fig. 2.

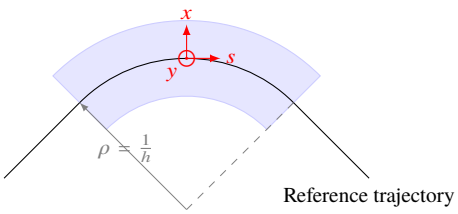

Figure 2: The Frenet-Serret reference frame to describe the combined-function dipole is straight outside of the magnetic length, and bent with bending radius $\rho = \frac{1}{h}$ inside the magnetic length.

* silke.van.der.schueren@cern.ch

Content from this work may be used under the terms of the CC BY 4.0 licence (© 2026). Any distribution of this work must maintain attribution to the author(s), title of the work, publisher, and DOI.

ISBN: 978-3-95450-252-3 ISSN: 2673-5350 doi: 10.18429/JACoW-IPAC2026-WEP5089

HOM STUDY OF THE PERLE'S BOOSTER CAVITY

R. Roux†, Université Paris-Saclay, CNRS/IN2P3, IJCLab, Orsay, France
on behalf of the PERLE collaboration

Abstract

The injector for the PERLE ERL in construction at IJCLab is based on a booster containing 4 superconducting cavities to reach 7 MeV for 20 mA of cw current. The cavities are single cell at 801.58 MHz. Due to the high average current, issues of beam break-up and power dissipation induced by the higher order modes of the cavities are a matter of concern. In this paper, we will report on the systematic survey of the HOM thanks to CST simulations up to 8 GHz. An analysis of their harmfulness as a function of the current spectrum will be shown.

INTRODUCTION

This work takes place in the framework of the design and construction of the PERLE accelerator [1] near Paris in France. PERLE is an Energy Recovery Linac (ERL) aiming to reach 5 MW of electron beam power thanks to a high current, 20 mA and an energy of 250 MeV. For this accelerator, an injector [2] providing such current but with an energy of 7 MeV is required where the main acceleration is given by a booster composed of four single cell superconducting cavities.

A critical issue for superconducting cavities is the potential excitation of high-order modes (HOMs). HOMs correspond to cavity electromagnetic modes at frequencies higher than the fundamental accelerating mode and can be excited when their frequencies coincide with harmonics of the beam repetition rate, which is 40 MHz. The beam consists of a train of electron bunches with a temporal length of 10 ps. Given this short bunch length, the corresponding frequency spectrum is broad, with a rms width of approximately 16 GHz, as determined by the Fourier transform of the bunch temporal profile. The spectrum therefore consists of 40 MHz harmonics modulated by this Gaussian envelope. HOMs can interact with the beam either transversely or longitudinally. Transverse electric (TEmnp) modes can impart transverse kicks to the beam, potentially leading to beam break-up (BBU) instabilities and degradation of the transverse emittance. Longitudinal (TMmnp) modes, on the other hand, can perturb the accelerating field, causing a reduction in beam energy and/or deterioration of the energy spread and bunch length. Because the field decay times of the cavity are long compared to the bunch spacing, these effects can accumulate over successive bunches, making the control of HOM excitation essential for stable beam operation.

In this paper we will give the exhaustive list of all HOM found with CST microwave studio below 8 GHz and we will show their impact on the beam stability does not worth to use complex and expensive countermeasures as HOM extracting couplers or absorbers.

†raphael.roux@ijclab.in2p3.fr

This work received government funding managed by the Agence Nationale de la Recheche (ANR) in the France 2030 framework - reference ANR-24-RRII-0001

RF SIMULATIONS UP TO 8 GHZ

First, using CST Microwave studio, we scanned resonant modes up to 8 GHz for our model of the RF cavity and identified a total of 2290 modes. The relevant parameters for HOM analysis are the mode frequency and its detuning relative to the nearest beam harmonic, the external quality factor Q_{ext}, the longitudinal shunt impedance over quality factor R/Q (R/Q)l and the transversal shunt impedance over quality factor R/Q $(R/Q)^{\perp}$. While the Microwave studio does not directly provide the transversal shunt R/Q $(R/Q)^{\perp}$, it can be computed using the Panofsky-Wenzel theorem [3] as expressed in equation 1.

$$(R/Q)^{\perp} \approx \frac{|V_{\parallel,n}(x_0,0)-V_{\parallel,n}(0,0)|^2}{k_n^2 x_0^2 \omega_n U_n} \quad \frac{|V_{\parallel,n}(0,y_0)-V_{\parallel,n}(0,0)|^2}{k_n^2 y_0^2 \omega_n U_n} \qquad (1)$$

where V(x,y) is the voltage, k, the wave number, ω, the pulsation and U the stored energy equal to one in the simulation. The transverse $R/Q^{\perp}$ was evaluated at an offset position of $x_0 = y_0 = 3$ mm from the cavity axis. Plots of these quantities are shown in Fig. 1 and Fig. 2.

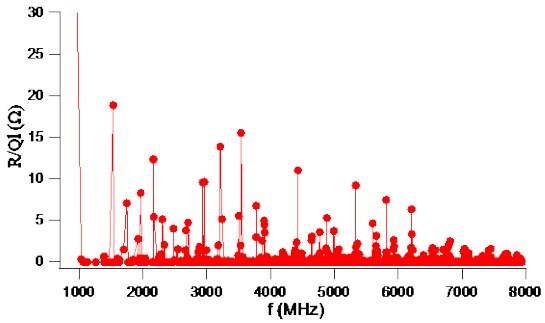

Figure 1: longitudinal R/Ql as a function of frequency.

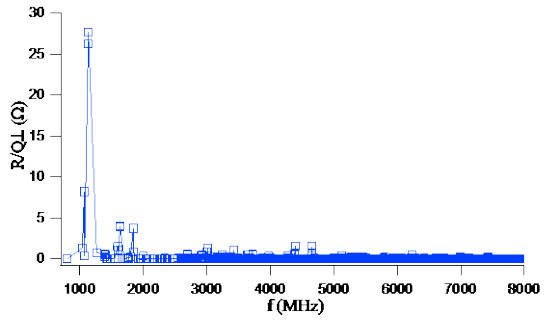

Figure 2: the transversal $R/Q^{\perp}$ as a function of frequency.

We now focus on the modes with a transverse or longitudinal magnitude larger than one in order to assess their potential impact on the beam. The results are summarized in Table 1 and Table 2 for the transverse modes and longitudinal modes, respectively including Δf which denotes the

Content from this work may be used under the terms of the CC BY 4.0 licence (© 2026). Any distribution of this work must maintain attribution to the author(s), title of the work, publisher, and DOI.

ISBN: 978-3-95450-252-3 ISSN: 2673-5350 doi: 10.18429/JACoW-IPAC2026-WEP5090

STATUS OF THE PERLE'S INJECTOR*

R. Roux†, R. Abukeshek, M. Ben Abdillah, E. Bourdelas, S. Brault, S. Chance, O. Dalifard, M. De Vos, J. Demailly, P. Duchesne, P. Duthil, A. Fomin, C. Joly, W. Kaabi, S. Marchal, B. Mercier, J. Michaud, E. Mistretta, L. Perrot, F. Razafimamonji, D. Reynet, G. Sattonnay, H. Saugnac, D. Till, S. Wallon, S. Wurth, J.-F. Yaniche, G. Olry
Université Paris-Saclay, CNRS/IN2P3, IJCLab, Orsay, France
H. Abualrob, An-Najah National University, Nablus, Palestinian Territories
C. Monaghan, University of Liverpool, Liverpool, United Kingdom
I. Bustinduy, J.-L. Munoz, ESS Bilbao, Derio, Spain
J. Angot, M. Baylac, F. Bouly, Y. Gómez Martínez, E. Labussiere, A. Plaçais, Laboratoire de Physique Subatomique et de Cosmologie, Grenoble, France

On behalf of the PERLE collaboration

Content from this work may be used under the terms of the CC BY 4.0 licence (© 2026). Any distribution of this work must maintain attribution to the author(s), title of the work, publisher, and DOI.

Abstract

PERLE is an Energy Revovery Linac (ERL) accelerator for electrons which aims to reach 250 MeV 20 mA cw. First brick of this accelerator is the injector, its main components are the DC photo-injector and a booster holding 4 superconducting cavities. This paper will give an overview of the injector's design, technical details about major components and the schedule of the construction.

OVERALL DESCRIPTION

PERLE [1] is under construction on the campus of the university Paris-Saclay. It aims to demonstrate the feasibility of ERLs at high power, namely 5 MW. It requires an injector which must fulfil specifications shown in Table 1.

Table 1: PERLE Injector Specifications

E (MeV)	7
Q (nC)	0.5
F_{rep} (MHz)	40
I (mA)	20
F_{RF} (MHz)	801.58
σ_z (mm)	3
ε_n (mm.mrad)	< 6

Two main components are indispensable to reach these requirements. First one is the electron source; to provide an electron bunch of 0.5 nC with an emittance lower than 6 mmmrad, a photo-injector is required, since the other classical source -a thermionic gun- cannot reach a such low emittance. In addition, the electron beam is continuously pulsed (CW) at 40 MHz therefore it excludes room temperature radiofrequency (RF) photo-injectors as several hundred of kW of RF power would be dissipated into the walls of cavity and would be very difficult to evacuate. Hence, the source of electrons must be a DC high voltage photo-injector. This critical system was obtained during our design studies through a collaboration with Research Industry [2]. It comprises a photo-injector, a photocathode preparation chamber, and a small beamline.

Downstream of the gun, a room temperature RF cavity (buncher) compresses the bunch to the specified value at the entrance of the main accelerating module.

The second key component is the accelerating module or booster. Superconducting technology was chosen over room temperature RF cavities to limit RF power requirements and thermal losses. Design of the cryomodule is largely inspired from the ESS one, with descriptions and 3D renderings provided, while fabrication drawings are still in progress. A conceptual drawing of the injector is shown in Fig. 1.

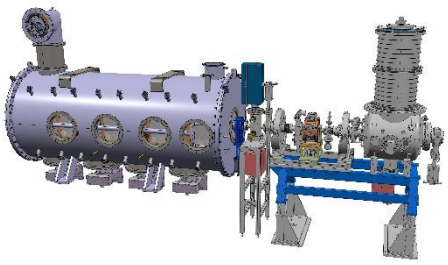

Figure 1: 3D drawing of the PERLE's injector. From right to left the gun vacuum chamber with its insulation ceramic, steerer, solenoid, laser introduction chamber, buncher, screen chamber, solenoid, valve, Faraday cup, valve and the cryomodule containing four superconducting cavities.

Details of these three main components of the injector will be explained in the following sections.

THE DC GUN

Within to a collaboration agreement between IJCLab and Research Instruments (RI) GmbH, the DC photogun as well as a Photocathode Preparation Facility (PPF) [3] were transferred from RI to IJCLab. The latter allows us to prepare materials for the photocathode such as antimonide, potassium and caesium in a glovebox under an argon atmosphere. The photocathode is obtained by deposition on a substrate and transported under vacuum thanks to a load-

†raphael.roux@ijclab.in2p3.fr

This work received government funding managed by the Agence Nationale de la Recheche (ANR) in the France 2030 framework - reference ANR-24-RRII-0001

ISBN: 978-3-95450-252-3 ISSN: 2673-5350 doi: 10.18429/JACoW-IPAC2026-WEP5091

IMPROVED RESISTIVE WALL EFFECTIVE RADIUS TAKING INTO ACCOUNT YOKOYA FACTORS

A. Gamelin*, V. Gubaidulin, Synchrotron SOLEIL, Saint-Aubin, France
S. Thakur, Deutsches Elektronen-Synchrotron DESY, Hamburg, Germany

Abstract

When computing the resistive wall impedance, one must account for variations in beam pipe aperture, conductivity, and beta function. This can be done by either summing individual contributions or using an "effective radius" in an analytic formula. However, the standard "effective radius" formula has limitations: it ignores cross-plane influences and lacks formulas for quadrupolar or monopolar wakes. This paper introduces an improved "effective radius" definition using Yokoya factors, addressing these limitations. This updated formula was used to develop SOLEIL's new impedance model, significantly improving the agreement between simulated and measured instability thresholds.

INTRODUCTION

The resistive wall impedance, describing the way the beam interacts with the resistive part of the beam pipe walls, is a key component present in all impedance models made to study collective effects in synchrotrons. Most of the time, the resistive wall impedance is computed using various analytic expressions, either simple ones like the thick wall formula [1] or more complex ones like the multi-layered cylindrical formula implemented in codes like IW2D [2].

Because of its distributed nature over the full synchrotron circumference, the variation of beam pipe aperture, conductivity, and beta function along the accelerator must be taken into account. It can be achieved by splitting the synchrotron in different sections with the same properties and then summing the different contributions. Another way is to compute an "effective radius" [3], which can then be used in analytic expressions to get the resistive wall impedance for the full accelerator.

RESISTIVE WALL EFFECTIVE RADIUS

The resistive wall effect can be split into its short-range part (single bunch effect) and long-range part (multi-bunch and multi-turn effect). The short-range and long-range parts exhibit different scaling with respect to beam pipe radius a [3]. In the longitudinal plane, the resistive wall wake function is inversely proportional to a^2 for short-range and to a for the long-range regime. In the transverse plane, it is inversely proportional to a^4 for short-range and to a^3 for the long-range regime.

The resistive wall effective radius $a_{\text{eff}}^{(n)}$ for power n [3, Eq. (27)], is defined as:

$$a_{\text{eff}}^{(n)} = \left(\frac{\sqrt{\sigma^*}}{L\beta^*} \sum_i \frac{l_i \beta_i}{a_i^n \sqrt{\sigma_i}} \right)^{-1/n} \tag{1}$$

where the summation on the index i corresponds to the different beam pipe components in the ring, l_i is the component length, a_i its aperture, β_i the beta function at its location, σ_i its conductivity and $L = \sum l_i$ is the total length. The average beta β^* and average conductivity σ^* are defined by:

$$\beta^* = \frac{1}{L} \sum_i l_i \beta_i \quad \text{and} \quad \sigma^* = \frac{1}{L} \sum_i l_i \sigma_i \tag{2}$$

This formula can be applied to either horizontal or vertical planes using a_i as the corresponding aperture and different power of n to get effective radius for long and short range regimes.

Nevertheless, there are several issues with the present definition. It does not clearly define how the longitudinal effective radius should be computed. More generally, both for the longitudinal and transverse effective radius, the influence of one dimension on the other is neglected (for example the impact of the horizontal aperture on the effective vertical radius). Finally, the present definition does not take into account quadrupolar or monopolar wakes.

MODIFIED FORMULA USING YOKOYA FACTORS

We propose a new definition of the effective radius aiming to solve the issues raised above. The idea of the modified effective radius formula is that, to define each section of the accelerator, instead of using the horizontal or vertical aperture only, the smallest dimension $r_{\min}$ (e.g. semi-minor axis for an elliptical pipe) is used in addition to Yokoya factors ($Y_{\text{long}}, Y_{\text{xdip}}, Y_{\text{ydip}}, Y_{\text{xquad}}, Y_{\text{yquad}}$) [4].

For the longitudinal effective radius, it is defined as:

$$r_{\text{long}}^{(n)} = \left(\frac{\sqrt{\sigma^*}}{L} \sum_i Y_{\text{long}} \frac{l_i}{r_{\min i}^n \sqrt{\sigma_i}} \right)^{-1/n} \tag{3}$$

Where $n = 1$ for long range and $n = 2$ for short range regime. For the horizontal and vertical dipolar effective radius, it is defined as:

$$r_{\text{xdip}}^{(n)} = \left(\frac{\sqrt{\sigma^*}}{L\beta_x^*} \sum_i Y_{\text{xdip},i} \frac{l_i \beta_{xi}}{r_{\min i}^n \sqrt{\sigma_i}} \right)^{-1/n} \tag{4}$$

* alexis.gamelin@synchrotron-soleil.fr

Content from this work may be used under the terms of the CC BY 4.0 licence (© 2026). Any distribution of this work must maintain attribution to the author(s), title of the work, publisher, and DOI.

ISBN: 978-3-95450-252-3 ISSN: 2673-5350 doi: 10.18429/JACoW-IPAC2026-WEP5092

DOUBLE RF SYSTEM DESIGN USING NORMAL CONDUCTING PASSIVE HARMONIC CAVITY FOR SOLEIL II

A. Gamelin*, M. Diop, V. Gubaidulin, P. Marchand, R. Nagaoka, F. Ribeiro, L. Zhao
Synchrotron SOLEIL, Saint-Aubin, France

Abstract

Double rf systems are critical for achieving the parameters of fourth-generation synchroton light sources. These systems relax stochastic collective effects but also introduce instabilities, such as Robinson and periodic transient beam loading (PTBL) instabilities, which depend heavily on the cavity parameters. In the framework of the SOLEIL II project, we demonstrate how we can use semianalytical algorithms to predict and analyze these instabilities, in conjunction with multibunch tracking simulations, to optimize rf cavity parameters in high-dimensional parameter spaces, thereby maximizing the Touschek lifetime. Finally, the expected performances of the double rf system, using the optimized normal conducting passive harmonic cavity parameters, are presented.

INTRODUCTION

SOLEIL II [1–3], is a 4th-generation synchrotron light source (4GLS) presently in construction phase. Like most 4GLS, it will rely on a double rf system, composed of main rf cavities (MC) and harmonic rf cavities (HC), to mitigate the intra-beam scattering (IBS) and Touschek effects.

During the design of the accelerator, different HC types were considered: superconducting (SC) passive of the 3rd or 4th harmonic [4, 5], normal conducting (NC) active [6] and passive [7]. Best performances were expected from the SC passive solution, but overall almost similar to what can be expected from an optimized NC HC at a fraction of the cost. The final choice settled on 4th harmonic passive NC cavities, based on a custom design made in the framework of a collaboration with the ESRF [8, 9], which operates on the TM_{020} mode, to achieve low R/Q and large damping of lower and higher order modes (LOM and HOM). These cavities are equipped with a coupling port, which will be used for the rf conditioning before the installation in SOLEIL II, and may be used for powering the cavities in the future if needed.

The present article details the beam dynamics of the double rf system, how the choice of HC parameter was made and the expected performance of the system. The main SOLEIL II parameters relevant to the results shown here are presented in Table 1.

Table 1: SOLEIL II Storage Ring Parameters

Parameter	Value
Electron beam energy E_0	2.75 GeV
Natural emittance	84 pm
Circumference L	353.97 m
Revolution frequency f_0	846.9 kHz
Rf frequency f_{rf}	352.3 MHz
Harmonic number h	416
Momentum compaction factor α_c	1.057×10^{-4}
Energy loss per turn (w/o IDs) U_0	469 keV
Longitudinal damping time τ_L	11.64 ms
Relative energy spread σ_δ	9.06×10^{-4}
Natural bunch length σ_τ	8.9 ps
Main rf voltage V_1	1.7 MV
Main cavity (total) shunt impedance R_{s_1}	20 MΩ
Main cavity quality factor Q_{0_1}	35.7×10^3
Main cavity loaded quality factor Q_{L_1}	6×10^3
Harmonic cavity $(R/Q)_2$ (per cavity)	30 Ω
Harmonic cavity quality factor Q_{0_2}	31×10^3

BEAM DYNAMICS IN DOUBLE RF SYSTEMS

The beam dynamics of the double rf system is investigated by using two distinct approaches. The first is multibunch tracking simulation using `mbtrack2` [10,11], and the second is a set of semianalytical methods used to predict and analyze instabilities, which is implemented in `ALBuMS` [7, 12]. `ALBuMS` solves a system of coupled Haïssinski equations [13] and checks whether the resulting equilibrium is stable or not for various instabilities.

Figure 1 shows the predicted instabilities for SOLEIL II storage ring with 2 passive HC. For each pair of beam current I_0 and HC tuning angle ψ_2 in the plot, either the `ALBuMS` algorithm (left) or `mbtrack2` tracking (right) is used to compute the beam stability at that point. If the corresponding point is unstable, a marker related to the instability is shown. The instability map is superimposed with ξ isolines, the ratio of the harmonic to main cavity "force" [7, Eq. (A4)], showing how far that point is from the "near flat potential conditions".

Several instabilities are predicted in Fig. 1. A longitudinal coupled bunch instability (CBI) driven by a HOM of the MC is shown in purple. The fast mode coupling instability (FMCI) [14], corresponding to the coupling between the dipole ($m = 1$) and quadrupole ($m = 2$) azimuthal modes, is shown in red. Both the periodic transient beam loading (PTBL) instability [15, 16] and pure CBI of coupled-bunch mode number $l = 1$ are shown in green. Overall, the agreement between the predicted instability using the semi-analytical algorithm and what is observed in tracking is excellent.

For the SOLEIL II operation, both the CBI and the FMCI shown in Fig. 1 should not be an issue. The FMCI can be

* alexis.gamelin@synchrotron-soleil.fr

Content from this work may be used under the terms of the CC BY 4.0 licence (© 2026). Any distribution of this work must maintain attribution to the author(s), title of the work, publisher, and DOI.

ISBN: 978-3-95450-252-3 ISSN: 2673-5350 doi: 10.18429/JACoW-IPAC2026-WEP5095

UPDATING THE IMPEDANCE BUDGET FOR ELETTRA 2.0

S. Dastan*, S. Cleva , E. Karantzoulis, S. Krecic, K. Manukyan
Elettra-Sincrotrone Trieste S.C.p.A., Trieste, Italy

Abstract

Elettra 2.0 is a diffraction-limited upgrade of the Elettra storage ring, where beam stability requires an accurate evaluation of the machine impedance. In this work, an updated impedance budget is presented including key vacuum chamber components such as flanges, beam position monitors (BPMs), the scraper system, and resistive wall (RW) effects. Numerical simulations performed with CST Studio Suite and WAKIS are benchmarked against analytical and semi-analytical models. Good agreement is found among the different approaches, providing increased confidence in the updated impedance model and supporting ongoing beam dynamics studies for Elettra 2.0.

INTRODUCTION

The upgrade of Elettra to a diffraction-limited storage ring, described in the Elettra 2.0 Technical Design Report (TDR) [1] and related design studies [2], imposes stringent requirements on beam stability and collective effects. This work presents an updated impedance budget based on detailed numerical simulations and analytical models for selected vacuum chamber components. All calculations assume a Gaussian bunch with rms length σ_z = 4–4.5 mm, corresponding to operation with the third-harmonic cavity (3HC).

SCRAPER IMPEDANCE STUDY

The scraper system considered in this study consists of two cylindrical rods mounted symmetrically with respect to the beam axis inside a rhomboidal vacuum chamber, as shown in Fig. 1. Previous measurements performed on the Elettra scraper system already indicated that the scraper can represent a significant localized impedance source [3], motivating the more detailed analysis presented here. The reference scraper assembly has a total longitudinal length of 93 mm, with the rods positioned at the longitudinal center of the structure and aligned parallel to the beam direction. The surrounding vacuum chamber has a rhomboidal cross section with full horizontal and vertical dimensions of 27 mm and 17 mm, respectively.

In the baseline configuration adopted for the Elettra 2.0 scraper, the rod diameter is D = 13 mm, and the rods can be inserted symmetrically down to a minimum full gap of g = 3 mm. A parametric study was carried out to evaluate the influence of the rod diameter on the longitudinal loss factor. For the Elettra 2.0 geometry, D [Fig. 1(a)] was varied in the range 1–15 mm. The results showed a non-monotonic behavior, with the loss factor increasing up to about D = 5 mm and decreasing for larger diameters, indicating that reducing the rod diameter does not necessarily lead to lower impedance. This behavior suggests that, in addition to the rod diameter, other geometric features—such as the transition between the rods and the vacuum chamber (step) and the overall asymmetry of the structure—also play a significant role in determining the impedance.

Based on these considerations and technical constraints, a rod diameter of D = 13 mm was selected for the final Elettra 2.0 scraper design. The figure provides a schematic view of the main geometric parameters, while the electromagnetic simulations are performed using the full CAD model imported via STL files in order to reproduce the real mechanical design as accurately as possible.

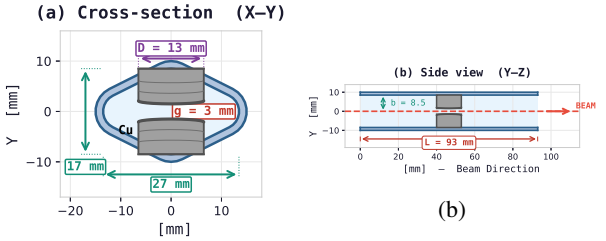

(a) (b)

Figure 1: Schematic geometry of the Elettra 2.0 scraper: (a) transverse cross-section showing the rhomboidal vacuum chamber and cylindrical rods, and (b) longitudinal view along the beam direction. The main geometric parameters are indicated, including the scraper gap g, chamber dimensions, and rod diameter D.

In addition to the geometrical considerations, the numerical results are compared with analytical expressions for short iris-like aperture transitions in the optical regime [4]. In the optical regime, the longitudinal impedance for a rectangular geometry can be expressed as:

$$Z_{\parallel}^{\mathrm{rect}} = \frac{8}{c}\int_0^{\infty} \frac{\sin(\pi a)\cosh(\pi x)}{\cos(2\pi a)-\cosh(2\pi x)} \times \ln\left(\frac{\cosh(\pi x)-\cos(\pi a)}{\cosh(\pi x)+\cos(\pi a)}\right) dx \tag{1}$$

where $a = g/b$ is the ratio between the scraper half-gap and the chamber half-aperture. The corresponding longitudinal loss factor for a Gaussian bunch of rms length σ_z is given by [5]

$$k_{\parallel} = \frac{c}{2\sqrt{\pi}\sigma_z} Z_{\parallel}. \tag{2}$$

The analytical expressions are derived in Gaussian units and are converted to MKS units by multiplying by the factor $cZ_0/(4\pi)$. Using these expressions, the analytical loss

* sara.dastan@elettra.eu

Content from this work may be used under the terms of the CC BY 4.0 licence (© 2026). Any distribution of this work must maintain attribution to the author(s), title of the work, publisher, and DOI.

ISBN: 978-3-95450-252-3 ISSN: 2673-5350 doi: 10.18429/JACoW-IPAC2026-WEP5096

MULTI-BUNCH LONGITUDINAL BEAM DYNAMICS IN THE ELETTRA 2.0 STORAGE RING WITH A DOUBLE-RF SYSTEM

S. Dastan*, S. Di Mitri, E. Karantzoulis, S. Krecic, M. Lonza, K. Manukyan
Elettra-Sincrotrone Trieste S.C.p.A., Trieste, Italy

Abstract

We present a systematic multi-bunch longitudinal beam dynamics study for the Elettra 2.0 storage ring equipped with a double RF system (main RF cavity plus passive third-harmonic cavity). The higher-order modes (HOMs) of the main RF cavity, obtained from 3D eigenmode simulations, are used as input to coupled-bunch instability models. For these HOMs, we compute growth rates using a simple harmonic-oscillator (SHO) model and an extended model including the nonlinear double-RF potential and Landau damping (HHC), and determine the HOM detuning required to bring all growth rates below the damping capability of the longitudinal feedback. The analytical predictions are benchmarked against multi-bunch tracking in Elegant. In parallel, we optimise the double-RF parameters for both uniform and non-uniform fillings using mbtrack2 tracking with the ALBuMS (Algorithm for Longitudinal Multibunch Beam Stability) algorithm. For the operational main-cavity detuning, we identify narrow third-harmonic cavity detuning windows that avoid Robinson-type and periodic transient beam loading (PTBL) instabilities while providing near-flat RF potentials, bunch-lengthening factors up to 4.4 and lifetime improvements up to 3–4. These results define a robust working point for the Elettra 2.0 double-RF system.

INTRODUCTION

In this work, the longitudinal stability problem is studied through two complementary groups of instabilities. The first group consists of HOM-driven coupled-bunch instabilities. These are driven by higher-order modes of the main RF cavity and are analyzed using HOM parameters obtained from electromagnetic simulations. This framework is particularly relevant for bunch-lengthened beams in nonlinear or near-quartic longitudinal potentials, where the instability growth rate and Landau damping must be treated self-consistently. The second group consists of instabilities intrinsic to the double RF system itself. These include Robinson instabilities (dipole/AC, quadrupole, and zero-frequency/DC), fast mode-coupling instability, and periodic transient beam loading (PTBL). In the terminology of the semianalytical ALBuMS [1] framework, the first two correspond to coupled-bunch mode $l = 0$, while PTBL corresponds to $l = 1$. These mechanisms can dominate different regions of parameter space and strongly constrain the accessible harmonic-cavity operating window. The purpose of this paper is therefore to combine these two levels of analysis: first, the study of HOM-driven coupled-bunch growth rates and their reduction via Landau damping in the double-RF potential; second, the global exploration of the harmonic-cavity operating region to identify stable windows that avoid Robinson-type and PTBL instabilities while preserving near-flat-potential conditions, bunch lengthening, and lifetime improvement.

HOM-DRIVEN COUPLED-BUNCH INSTABILITIES

Modes Above Instability Threshold

The higher-order modes (HOMs) of the main RF cavity are obtained from electromagnetic simulations up to 7 GHz [2], which corresponds to the first cutoff frequency for Elettra 2.0 [3]. To identify the modes that can drive longitudinal coupled-bunch instabilities, a rough impedance threshold criterion is applied [4]:

$$Z_{\parallel}^{\text{thresh}} = \frac{1}{N_c} \cdot \frac{1}{f_{\text{HOM}}} \cdot \frac{2E_0 Q_s}{I_0 \tau_s} \tag{1}$$

Here, N_c is the number of cavities, f_{HOM} is the HOM frequency, E_0 is the beam energy, Q_s is the synchrotron tune, I_0 is the total beam current, and τ_s is the longitudinal damping time.

For Elettra 2.0, $Q_s = 2.6 \times 10^{-3}$ without the 3HC and $Q_s \approx 1.0 \times 10^{-3}$ with the 3HC at a detuning of $\sim$ 80 kHz. From this analysis, 78 HOMs are found that exceed the instability threshold in the presence of the third-harmonic cavity (3HC), as shown in Fig. 1. A filtering procedure is applied based on the separation of frequency scales [5], $\omega_s \ll \omega_{\text{HOM}}/(2Q_{HOM}) \ll \omega_0$, where ω_s, ω_{HOM}, ω_0, and Q_{HOM} denote the synchrotron frequency, HOM frequency, revolution frequency, and HOM quality factor, respectively. This ensures that each HOM effectively couples to a single revolution harmonic, with the strongest instability near $f_{\text{HOM}} \approx N f_{\text{rev}}$. After filtering, 69 HOMs are retained.

Growth Rate Analysis

The growth rates of the filtered HOMs are evaluated using two approaches.

SHO model: The simple harmonic oscillator (SHO) model assumes a rigid bunch without Landau damping. In this case, 28 modes exhibit growth rates exceeding the longitudinal feedback capability of Elettra 2.0, which can damp instabilities with growth rates below 1000 s^{-1}, as shown in Fig. 2. To reduce all growth rates below this threshold, a maximum HOMs detuning of $\pm$69 kHz is required. The SHO model shows symmetric behavior around resonance.

HHC model: The higher-harmonic cavity (HHC) [5] model includes Landau damping arising from the nonlinear

* sara.dastan@elettra.eu

Content from this work may be used under the terms of the CC BY 4.0 licence (© 2026). Any distribution of this work must maintain attribution to the author(s), title of the work, publisher, and DOI.

ISBN: 978-3-95450-252-3 ISSN: 2673-5350 doi: 10.18429/JACoW-IPAC2026-WEP5098

RECENT PROGRESS IN IMPEDANCE MITIGATION FOR HL-LHC BEAM INSTRUMENTATION

M. Neroni*, W. Andreazza, R. Calaga, W. Hofle, I. Karpov, G. Khatri, M. Krupa, L. Margerison, M. McLean, C. Pasquino, H. Pommerenke, J. Storey, C. Vollinger
CERN, Geneva, Switzerland

Abstract

In the High-Luminosity LHC (HL-LHC) era, increased beam intensities and brightness impose stringent requirements on the beam-coupling impedance of accelerator components. This contribution summarizes recent studies on impedance mitigation for several new devices to be installed in the framework of the HL-LHC upgrades, illustrating design optimizations based on results from electromagnetic simulation solvers. Examples include the optimized design for crab cavity pick-ups and beam gas ionization profile monitors. These developments contribute to a consistent impedance mitigation strategy that reduces beam-induced heating at high intensities, maintaining device functionality and beam stability in the HL-LHC era.

INTRODUCTION

In preparation for the High-Luminosity LHC (HL-LHC) upgrade, the request for increased beam intensities, while maintaining beam quality poses stringent constrains on the overall beam coupling impedance. Minimising beam-induced heating is essential to preserve device integrity and performance, and it can be achieved by reducing the real part of the impedance. The total power loss is related to the beam intensity and beam coupling impedance through the following formula [1]:

$$P_{\text{loss}} = (f_{\text{rev}} e N_{\text{beam}})^2 \sum_{l=-\infty}^{\infty} |\Lambda(l\omega_{\text{rev}})|^2 \,\text{Re}[Z(l\omega_{\text{rev}})], \quad (1)$$

where f_{rev} is the revolution frequency and the total beam intensity is included in the term eN_{beam}, with e particle charge and N_{beam} accounting for the total number of bunches. The Fourier transform of the total beam distribution is the normalized beam spectrum, $\Lambda(\omega_{\text{rev}})$.

At the same time, it must be ensured that any additional source of beam coupling impedance does not significantly impact the beam stability threshold. In the longitudinal plane, it was observed that broadband impedance sources can reduce the coupled-bunch instability threshold below the one of loss of Landau-damping (LLD) [2]. The LLD threshold is inversely proportional to $\text{Im}(Z/n)$, with $n = f/f_{\text{rev}}$, ratio between the resonant and the revolution frequency. Therefore, keeping these contributions to a minimum is essential to avoid lowering the instability threshold.

Beam coupling impedance studies involve electromagnetic (EM) characterization of devices from the design phase prior to installation. Two mitigation examples are presented: the assessment of beam-induced heating in a beam gas ionization (BGI) profile monitor, and the impedance reduction for high-bandwidth beam position monitors (BPMs) as part of the HL-LHC crab cavities upgrade.

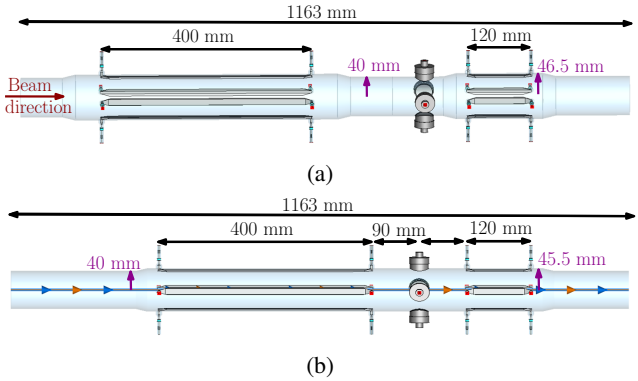

Figure 1: Initial (a) and final (b) geometry of high-bandwidth pick-ups used for intra-bunch measurements and for the crab cavity noise feedback and low-level RF system.

HIGH-BANDWIDTH BEAM POSITION MONITORS

In the framework of the HL-LHC project, combined-function BPMs (pick-ups) were developed to integrate a noise feedback system for the crab cavities and to provide head-tail beam diagnostics. The geometry (Fig. 1a) consists of 400 mm long striplines for intra-bunch measurements [3], followed by button pick-ups and 120 mm long striplines dedicated to the low-level RF system crab cavity noise feedback [4]. The inner surface of the stainless-steel beam pipe has a 10 μm copper coating to reduce resistive wall impedance. Below 50 MHz, even with the copper coating becoming transparent and the response being dominated by the conductivity of stainless steel, the impact on the overall beam coupling impedance remains negligible.

The pick-ups will be installed upstream and downstream of each crab cavity in IP1 and IP5, resulting in a total of four devices per beam. A beam coupling impedance assessment was performed prior to finalizing the design.

Longitudinal impedance simulations were performed with the CST wakefield solver [5]. All electrode feedthroughs were assumed to be impedance matched, as in the real system, to prevent undesired reflections within the structure. Figure 2 shows the resulting longitudinal impedance for the configuration illustrated in Fig. 1a. An oscillatory behaviour is observed up to 2 GHz, associated with the stripline length

* michela.neroni@cern.ch

Content from this work may be used under the terms of the CC BY 4.0 licence (© 2026). Any distribution of this work must maintain attribution to the author(s), title of the work, publisher, and DOI.

ISBN: 978-3-95450-252-3 ISSN: 2673-5350 doi: 10.18429/JACoW-IPAC2026-WEP5101

ADVANCED BEAM COUPLING IMPEDANCE MODELING FOR LHC AND HL-LHC APPLICATIONS*

C. Zannini†, C. Antuono, E. de la Fuente Garcia, G. Rumolo, B. Salvant, L. Sito, J. Sonpar
CERN, Geneva, Switzerland

Abstract

Accurate beam coupling impedance modeling is essential for predicting collective effects and ensuring stable high-intensity operation in the LHC and its High-Luminosity upgrade. Operational experience has shown that even small mechanical details can have a significant impact on the impedance of accelerator components, potentially leading to performance degradation or hardware failure. In addition, impedance sources are not static: beam-induced heating and the resulting mechanical stresses can drive gradual geometric changes, such as loss of electrical contact or deformation of shielding elements, thus modifying the impedance during operation. In this work, we present recent advancements in high-fidelity impedance modeling and demonstrate their relevance through representative case studies in the LHC. These examples show how improved modeling, combined with beam-based diagnostics, provides critical input for operational strategies and supports informed design and optimization of components in view of the challenging HL-LHC requirements.

INTRODUCTION

Accurate impedance modeling is a key ingredient for understanding beam stability and power deposition in the LHC and HL-LHC. Experience from operation has demonstrated that seemingly minor mechanical details, such as RF fingers or spring contacts, can significantly impact impedance and lead to measurable beam-induced heating.

Moreover, impedance is not a static property. Thermal loads and mechanical stresses can induce progressive geometric changes, such as loss of electrical contact or deformation of shielding structures, leading to a dynamic evolution of the impedance during operation.

These observations motivate the development of high-fidelity modeling approaches capable of capturing both detailed geometrical features and their evolution under realistic conditions.

Small-scale geometric features can significantly influence the impedance response and local power deposition, as demonstrated by the failure of an LHC warm vacuum module. This failure occurred in 2023 [1] and was attributed to localized heating of a tension spring used to ensure electrical contact between the fingers and the transition tube (see Fig. 1).

Advanced electromagnetic modeling enabled a detailed understanding of the impedance mechanism responsible for the failure. Beam-induced localized power deposition on the spring was identified, arising from beam offset and the asymmetric distribution of the fingers, which led to the observed localized heating. The estimated power levels were found to be consistent with the observed failure in the presence of degraded finger contact, explaining why the issue occurred only in a limited number of modules. Figure 2 illustrates the localized heating predicted by electromagnetic simulations, in agreement with the spring damage observed in 2023 [1]. This example highlights how geometric details can lead to strong field concentration and significant power deposition. Such effects are often not captured by simplified models, yet they are critical for understanding failure mechanisms.

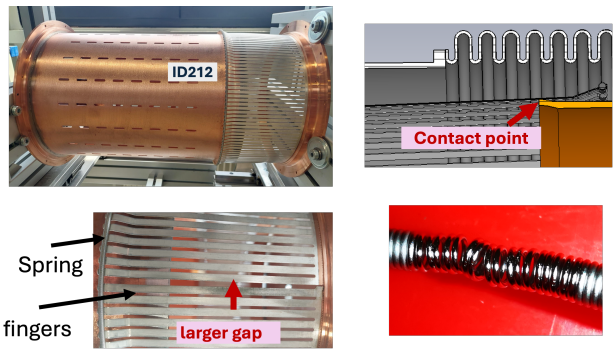

Figure 1: Example of spring contact geometry used in impedance simulations for an ID212 mm module. The top-left picture shows the transition tube, contact fingers, and the spring ensuring electrical contact between them. The top-right picture presents a detailed 3D view of the region between the transition tube and the fingers, which provides impedance shielding of the bellows (shown in gray). The bottom-left picture highlights the non-uniform finger spacing, while the bottom-right picture shows a locally burnt section of the spring.

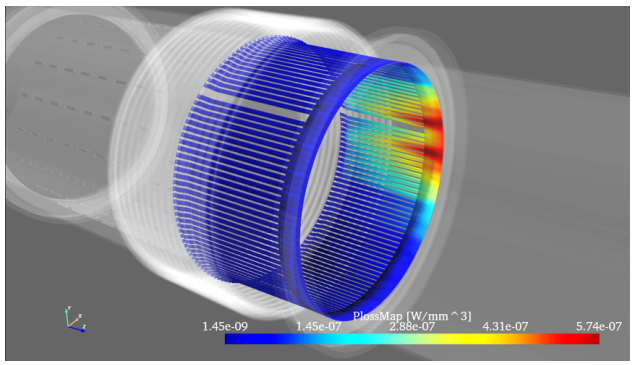

Figure 2: Beam induced power deposition on the ID212 module, highlighting localized heating regions.

* Research supported by the HL-LHC project
† carlo.zannini@cern.ch

Content from this work may be used under the terms of the CC BY 4.0 licence (© 2026). Any distribution of this work must maintain attribution to the author(s), title of the work, publisher, and DOI.

ISBN: 978-3-95450-252-3 ISSN: 2673-5350 doi: 10.18429/JACoW-IPAC2026-WEP5102

CHALLENGES IN BEAM COUPLING IMPEDANCE FOR FCC-ee

C. Zannini*, C. Antuono, E. de la Fuente Garcia, D. Gibellieri[1], E. Macchia, I. Mases Sole, G. Rumolo, L. Sito, CERN, Geneva, Switzerland
A. Ghribi [1], GANIL, Caen, France
M. Zobov, INFN - LNF, Frascati, Rome, Italy
M. Migliorati, University of Rome La Sapienza and INFN, Rome, Italy
[1]also at University of Caen Normandy, Caen, France

Abstract

A comprehensive impedance model is required to ensure beam stability and optimize performance in the FCC-ee main rings. The model integrates contributions from a wide range of components, accounting for both resistive-wall and geometric effects. In this paper, we discuss the main challenges introduced by the peculiar FCC-ee parameter regime. A first difficulty arises from the combination of large beam-pipe dimensions and very short bunch lengths, which drives wakefield simulations into an extremely demanding computational regime, where very fine spatial resolution is necessary to accurately capture the beam–environment interaction. In addition, the beam-pipe cut-off lies within the frequency range excited by the FCC-ee beam. As a consequence, several higher-order modes may propagate over long distances, leading to non-local impedance effects and possible cross-talk between different accelerator elements. This means that the impedance environment cannot be treated as purely local, but requires a distributed description and an assessment of how propagating power is transported and potentially absorbed within the machine.

INTRODUCTION

A reliable impedance model is essential to ensure beam stability in FCC-ee. Compared to previous machines, FCC-ee operates in a regime that uniquely combines ultra-short bunch lengths with relatively large beam-pipe apertures. This configuration pushes a significant fraction of the beam-induced electromagnetic spectrum beyond the cut-off frequency of the vacuum chamber. Consequently, a non-negligible portion of the excited fields is no longer evanescent but can propagate over long distances along the machine. This feature is not marginal but intrinsic to the FCC-ee operating regime. The beam spectrum significantly overlaps with the beam-pipe cut-off frequency, as illustrated in Fig. 1. In contrast to the LHC, where most of the spectral content remains below cut-off, FCC-ee exhibits a substantial fraction of power above cut-off. As a result, higher-order modes can propagate along the vacuum chamber, making propagation effects an inherent characteristic of the FCC-ee impedance environment.

This propagation fundamentally alters the physical picture of impedance modeling. In conventional accelerators, impedance is typically treated as a local property, attributed to individual components whose electromagnetic interaction with the beam decays rapidly with distance. In FCC-ee, however, the presence of propagating modes introduces a non-local coupling between elements: a given structure can influence, and be influenced by, components located far upstream or downstream. As a result, the machine behaves less like a collection of independent devices and more like a distributed electromagnetic system, where interference, reflections, and modal conversion effects play a significant role.

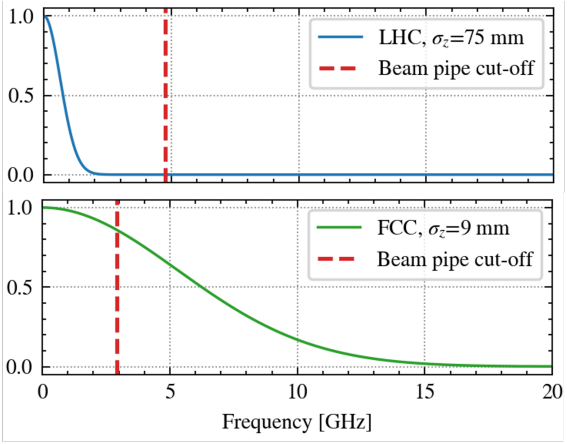

Figure 1: Comparison between beam spectrum and beam pipe cut-off frequency for FCC-ee and LHC. FCC-ee exhibits a substantial fraction of spectral content above beam pipe cut-off.

Such a regime brings new challenges for both simulation and interpretation. Numerical results become intrinsically sensitive to boundary conditions, domain truncation, and the treatment of absorbing boundaries, as these can artificially suppress or enhance propagating content. The very definition of impedance becomes less straightforward, as separating localized contributions from global, propagating effects is no longer trivial. This raises important questions about how to construct a meaningful and robust impedance budget for the machine. Moreover, the presence of propagating power is not only a conceptual challenge for modeling, but also a practical concern for operation. Electromagnetic energy transported over long distances can couple into beam diagnostics, which may therefore respond not only to the local passage of the beam but also to fields generated elsewhere in the ring. This non-local sensitivity complicates the interpretation of measurements and can potentially lead to malfunctions. Altogether, FCC-ee operates in a regime

* carlo.zannini@cern.ch

Content from this work may be used under the terms of the CC BY 4.0 licence (© 2026). Any distribution of this work must maintain attribution to the author(s), title of the work, publisher, and DOI.

ISBN: 978-3-95450-252-3 ISSN: 2673-5350 doi: 10.18429/JACoW-IPAC2026-WEP5104

COLLECTIVE EFFECTS AND IMPEDANCE UPDATE FOR THE DIAMOND-II STORAGE RING

R. Fielder*, N. Blaskovic Kraljevic, D. Rabusov,
Diamond Light Source, Oxfordshire, United Kingdom

Abstract

Impedance and collective effects are significant concerns for the design of modern accelerators. During development of the Diamond-II storage ring, effort was initially focussed on design for the arcs containing the majority of magnets, and geometric impedance was focussed on single bunch effects. We now present updates to the Diamond-II impedance database and the impact on collective effects including additional detail in straights, including injection, insertion devices and RF elements, as well as inclusion of long-range impedance for more elements for multibunch dynamics.

INTRODUCTION

Diamond-II [1] is the upcoming upgrade to the Diamond synchrotron light source. Collective effects are a major consideration for modern accelerators, given the combination of lower beam emittance with generally smaller diameter beam pipes. Ensuring instabilities will not interfere with operations by minimising beam impedance during the design stage is necessary. Diamond-II will have sixfold symmetry, with an alternating series of 48 straights and arcs. Initial design work focussed mainly on the arcs, containing the majority of magnets and responsible for many of the engineering and vacuum constraints. As this work has been completed and orders have been placed with manufacturers, design effort has progressed to the remaining components, including injection elements, insertion devices (IDs), and radio frequency (RF) systems. In this paper we present an update to the Diamond-II storage ring (SR) impedance, highlighting significant changes to both geometric and resistive wall impedance since this was last reported in 2024 [2].

RESISTIVE WALL IMPEDANCE

Resistive wall (RW) impedance for Diamond-II is calculated from an impedance database [3] containing the apertures (horizontal and vertical) and materials for the whole SR. The impedance of each component is then calculated analytically using the ImpedanceWake2D [4] code. This is split into two parts for each component, with one part containing low frequency in the longitudinal plane, while the second part goes to higher frequencies with a larger step size, as described in [2]. The total impedance is summed, including weighting with beta function in the transverse, and tracking performed in Elegant [5]. In order to simplify engineering design and manufacture, all narrow-gap vessels for out-of-vacuum IDs will now use a NEG-coated copper chamber with the same 20 × 8 mm full gap elliptical profile in all locations. While the increased conductivity of copper compared to aluminium should reduce impedance, reducing the vertical aperture in some straights to 8 mm will largely offset this. The only exception to this is in the I06 straight, which will use a stainless steel chamber with the same dimensions to allow fast polarity switching of an electromagnetic/permanent magnet hybrid undulator (EMPHU). It has been determined that Diamond-II requires a dedicated beam abort system [6] which will use a series of fast kicker magnets to kick the stored beam into a beam dump. Again to ease design and manufacturing, these will use identical titanium-coated ceramic vessels to the injection kickers. Additional ceramic vessels have been included in the database for a pair of diagnostics pinger magnets, however, a final decision on whether these additional vessels are required has yet to be made. This results in a significant increase in the total length of ceramic vessels and a corresponding increase in impedance. The total lengths of different materials used is shown in Table 1, although apertures will vary within materials.

Table 1: Summary Of Resistive Wall Parameters In Diamond-II. Multi-Layer Materials Show Values For The Coating Followed By The Underlying Bulk Material

Material	Conductivity [S/m]	Length [m]
Copper	5.96×10^7	48.9
NEG-coated Cu	1.00×10^5, 5.96×10^7	443.4
Ti-coated alumina	2.38×10^6, 0.00	5.0
Stainless steel	1.35×10^6	58.7
NEG-coated steel	1.00×10^5, 1.35×10^6	4.5
Total	–	560.56

Figure 1 shows the long-range resistive wall impedance of the updated impedance model.

GEOMETRIC IMPEDANCE

Geometric impedance is calculated using the wakefield solver in CST Studio [7]. Short range wakes are calculated using a $\sigma = 0.5$ mm drive bunch length and 300 mm wake length, which have been determined to give convergence in Elegant while allowing reasonable simulation times. Some larger models, such as dipole vessels, instead use a $\sigma =$ 1.0 mm drive bunch to reduce the number of mesh cells required. Dipolar wakes have been calculated for all components, while quadrupolar and monopolar wakes are calculated for components with significant asymmetry, and are being added for all other components as computing resources allow. Short range impedance is calculated using all perfect conductor (PEC) material, except in some cases containing

* richard.fielder@diamond.ac.uk

Content from this work may be used under the terms of the CC BY 4.0 licence (© 2026). Any distribution of this work must maintain attribution to the author(s), title of the work, publisher, and DOI.

ISBN: 978-3-95450-252-3 ISSN: 2673-5350 doi: 10.18429/JACoW-IPAC2026-WEP5105

MICROWAVE INSTABILITY MODELLING FOR SOLEIL II

V. Gubaidulin*, A. Gamelin
Synchrotron SOLEIL, Saint-Aubin, France

Abstract

There are two main sources of high-frequency longitudinal impedance: coherent synchrotron radiation (CSR) and high-frequency NEG-coated resistive wall impedance. They can drive microbunching instability, which is a potential risk to maintaining stable and low energy spread beam. To address this, these effects are now integrated into the particle tracking code `mbtrack2`. This paper examines their impact on beam stability in the SOLEIL II storage ring, considering the combined influence of intrabeam scattering, low-frequency longitudinal impedance, and a harmonic cavity.

INTRODUCTION

SOLEIL II [1, 2], a 2.75 GeV fourth-generation light source upgrade with a design horizontal emittance of $\varepsilon_x <$ 100 pm rad (< 60 pm rad with full betatron coupling) is presently in the construction phase. Two operation modes are planned: 416 bunches with 1.2 mA per bunch; 32 bunches with 6.25 mA per bunch. In our previous paper [3], we addressed microwave instability (MWI) arising from broadband longitudinal impedance up to 100 GHz in the presence of intrabeam scattering and harmonic cavity bunch lengthening. At least two potentially important contributions were not included, namely, coherent synchrotron radiation (CSR) [4–7] in dipole magnets and the high-frequency part (< 5 THz) of the impedance of NEG-coated vacuum chamber [8–10].

SIMULATION AND IMPLEMENTATION DETAILS

Impedance Model

Details of the broadband SOLEIL II impedance model (< 100 GHz) can be found in [11]. It consists of two components: resistive wall contribution (computed with `IW2D`) and geometric contribution (computed with `CST Studio`, `GdfidL` and `ECHO3D`). Table 1 shows the dipole magnet parameters relevant to CSR impedance and wakepotential computation. SOLEIL II design includes 178 reverse bends with

Table 1: SOLEIL II Dipole Magnet Parameters Relevant to CSR

Dipole type	Number	L_{dipole}	R_{bending}	h_{halfgap}
short dipole	40	0.44 m	10.74 m	8 mm
long dipole	64	0.88 m	12.80 m	8 mm
superbend	12	0.87 m	12.68 m	4 mm

a bending radius of > 40 m, length < 0.15 m and shielding half-gap of 6 mm. Due to the large bending radius and short length, reverse bends contribute only a negligible amount to CSR impedance and, thus, are ignored.

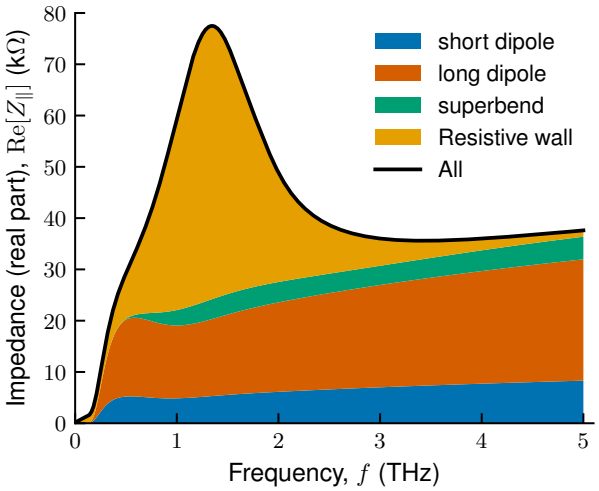

Figure 1: Total impedance (free space and shielding contribution from CSR and NEG-coated resistive wall (RW) impedance), real part (a), imaginary part (b).

Figure 1 displays the extension of the resistive wall component to higher frequencies (< 5 THz) and the contribution of CSR to the impedance (only the real part is shown in the plot). In SOLEIL II, we are expecting CuCrZr vacuum chamber ($\rho_{\text{CuCrZr}} = 2.08 \times 10^{-8}\,\Omega\,\text{m}$) with an effective radius [12] of $r_{\text{eff}} = 5.83$ mm for closed gaps of insertion devices. NEG-coating with 0.5 µm thickness and resistivity of $\rho_{\text{NEG}} = 1.25 \times 10^{-6}\,\Omega\,\text{m}$ is expected. Variation of thickness along the vacuum chamber does not change the impedance significantly for our value of resistivity, contrary to [9, 10], where the resistivity value is higher, and the THz peak is narrower and higher.

First estimation of CSR-driven MWI can be given analytically based on the dipole magnet parameters [7, 13], assuming

$$I_{\text{th}} = I_A \frac{\alpha_c \gamma \sigma_\delta^2 \sigma_s^{1/3}}{R_{\text{bending}}^{1/3}} \left(0.5 + 0.12 \sigma_s \sqrt{\frac{R_{\text{bending}}}{h_{\text{halfgap}}^3}} \right),$$

where $I_A \approx 17$ kA is the Alfven current, α_c is the momentum compaction, γ is the Lorentz gamma, σ_s is the rms bunch length, σ_δ is the rms energy spread.

With this formula for worst case dipole parameters of SOLEIL II, the threshold estimation is $I_{\text{th}} = 1.6$ mA for $\sigma_s = 15$ ps and $\sigma_\delta = 8.547 \times 10^{-4}$. For SOLEIL nominal parameters, we would obtain a larger value $I_{\text{th}} = 5.3$ mA mainly because the momentum compaction factor is four-five times smaller for SOLEIL II. This implies that CSR is more

* vadim.gubaidulin@synchrotron-soleil.fr

Content from this work may be used under the terms of the CC BY 4.0 licence (© 2026). Any distribution of this work must maintain attribution to the author(s), title of the work, publisher, and DOI.

ISBN: 978-3-95450-252-3 ISSN: 2673-5350 doi: 10.18429/JACoW-IPAC2026-WEP5106

BEAM-BASED INSTABILITY AND BUNCH-BY-BUNCH FEEDBACK CHARACTERIZATION AT SOLEIL

V. Gubaidulin*,[1], M. El Ajjouri[1], A. Gamelin[1], R. Sreedharan[1], S. Thakur[1,2]
[1]Synchrotron SOLEIL, Saint-Aubin, France
[2]Deutsches Elektronen Synchrotron DESY, Hamburg, Germany

Abstract

In the context of the ongoing SOLEIL II upgrade, a measurement campaign was conducted to characterize and understand the behaviour of single- and coupled-bunch instabilities, and the performance of transverse bunch-by-bunch feedback system at the present SOLEIL storage ring. This paper presents the keys results of beam current thresholds measurements; growth-damp measurements with resistive feedback. The most recent results constitute a snapshot of instabilities and bunch-by-bunch feedback performance at SOLEIL. These results are compared with an updated impedance model and past measurements. Our results provide guidance in designing the bunch-by-bunch feedback system for SOLEIL II.

INTRODUCTION

Synchrotron SOLEIL [1] is using a transverse feedback system based on that of the Spring-8 [2–4] for the storage ring. It was previously described [5, 6], notably in relation to characterisation and suppression of beam-ion instability [7–9]. Currently, SOLEIL is undergoing an upgrade towards a 4th-generation light source SOLEIL II [10–12], where a transverse feedback system will be required [13, 14]. We need to understand the capabilities of the current feedback system to guide the requirements and design of the future feedback system for instability mitigation in fourth-generation light sources [15].

Beam-based validation of impedance, instability and feedback modelling is a task relevant to many accelerator facilities [16–18]. The impedance model of the SOLEIL storage ring was recently updated [19] using an impedance modelling approach identical to the one for SOLEIL II [13, 20, 21].

Single- and multibunch operation modes of SOLEIL are described in Table 1.

Table 1: SOLEIL Operation Modes

Mode	N_{bunches}	I_{bunch} (mA)	Q_{bunch} (nC)
Uniform	416	1.2	1.4
Hybrid	312+1	1.4+5	1.7+6
8-bunch	8	12.5	14.8
Single-bunch	1	20	23.6

Experimental Setup

The feedback consists of dedicated BPMs, stiplines, RF frontends, a digital signal processor, and power amplifiers. It is set up every few months (after every machine restart) for a single-bunch regime, as it was identified in the past that this is the most demanding mode. After the set-up is verified by achieving the maximal required current in single- (20 mA) and multibunch regimes (500 mA) with open insertion device gaps (IDs). In all measurements, for feedback, a 5-tap FIR filter is applied to a signal with a phase corresponding to purely resistive feedback. All multibunch measurements were made with every rf bucket filled.

Threshold Measurements Beam or bunch current threshold is one of the most basic measures of the effective impedance of an accelerator. In a synchrotron light source, any instability will have a certain threshold current, where the growth time of the instability is slightly shorter than the damping time due to synchrotron radiation damping.

To measure the threshold current, we are gradually increasing the beam current until it is no longer possible to inject or until we start seeing an increase in beam emittance (measured with a pinhole camera). To avoid any instability triggered by an injection event, we inject with bunch-by-bunch feedback turned on and switch it off after the injection. This measurement is useful primarily for the operation team to know the current limits without bunch-by-bunch feedback. Thresholds can also be compared with analytical formulae or with tracking simulations.

Growth-damp measurement is more complex, and it allows for measuring the growth rate of an instability at a certain beam current (above the threshold) by switching the bunch-by-bunch feedback off for a short time window. After the feedback is switched back on, one can measure the damping rate provided by the feedback. All of these actions are done inside the acquisition window, where bunch-by-bunch data is recorded. This allows us to characterise the instability (measure the growth rate of each bunch, analyse the spectrum of bunch-by-bunch data), and measure the strength of the feedback system.

All measurements are automated using `Python` scripts.

RESULTS

Single-Bunch Case

Threshold Measurement Figure 1 demonstrates horizontal (left) and vertical (right) single-bunch instability thresholds measured at SOLEIL in different years. Simulation results were obtained with our code `mbtrack2` [22, 23]. More measurements were done in the vertical plane because the thresholds are lower and determine the feedback requirements. Transverse mode-coupling (TMCI) thresholds

* vadim.gubaidulin@synchrotron-soleil.fr

Content from this work may be used under the terms of the CC BY 4.0 licence (© 2026). Any distribution of this work must maintain attribution to the author(s), title of the work, publisher, and DOI.

ISBN: 978-3-95450-252-3 ISSN: 2673-5350 doi: 10.18429/JACoW-IPAC2026-WEP5107

COUPLED-BUNCH INSTABILITIES WITH A DEFOCUSING HIGHER-HARMONIC RF SYSTEM

R. Heine*, W. Keusgen, Technische Universität Berlin, Berlin, Germany
L. Intelisano, I. Karpov, European Organization for Nuclear Research, Geneva, Switzerland

Abstract

Longitudinal coupled-bunch instabilities limit the beam intensity in many synchrotrons. They can be mitigated by adding a higher-harmonic radiofrequency (RF) system, which modifies the potential well. Of particular interest is the bunch lengthening mode (BLM), in which the higher-harmonic voltage produces a defocusing effect at the bunch centre. Decreasing the peak line density is beneficial, for example, to reduce space-charge and intrabeam scattering. This study investigates the impact of a higher-harmonic RF system in BLM on the intensity threshold and growth rate of coupled-bunch instabilities. The influence of beam parameters such as the bucket filling factor, narrowband impedance properties, and RF system configuration is highlighted. Regimes in which BLM is advantageous or disadvantageous are compared to the ones for a single-harmonic RF (SRF) system. The results are based on semi-analytical solutions of the Vlasov equation as well as macro-particle simulations using the BLonD simulation code.

INTRODUCTION

Coupled-bunch instabilities (CBI) are driven by long-range wakefields, which are produced by a narrowband (NB) impedance source and link the bunches in a synchrotron. If the CBI intensity threshold is exceeded, the affected bunches become unstable, resulting in coherent oscillations in the longitudinal plane. This leads to beam quality degradation and, in the worst case, to beam loss. To lift the intensity limitations due to CBI, double-harmonic RF systems (DRF) have been implemented in several synchrotrons [1, 2]. Although the impact of DRF systems on CBI is well understood and discussed in the literature [3, 4], the interplay among different beam parameters, impedance, and RF systems has not yet been fully disentangled.

Since the BLM offers many benefits for lepton and hadron rings by reducing peak line density, we will investigate how different parameters affect the CBI threshold in BLM. For this purpose, we will utilise the stability diagram (SD) method introduced in [5]. Since we will only use normalised parameters for an analytical equation, the results can be applied to any synchrotron and reflect general properties of CBI. In addition, macro-particle simulations validate the stability diagram method and shed light on the growth rate behaviour for different RF settings.

* ruben.nicholas.heine@cern.ch

MAIN EQUATIONS AND DEFINITIONS

To simplify the calculation, we move from conjugate coordinates particle energy, ΔE, and RF phase deviation, ϕ, of the conventional equations of motion to energy, $\mathscr{E}$, and phase, ψ, of the synchrotron oscillation defined as

$$\mathscr{E} = \frac{\dot{\phi}^2}{2\omega_{s0}^2} + U_t(\phi) \text{ and} \tag{1}$$

$$\psi = \operatorname{sgn}(\eta \Delta E)\frac{\omega_s(\mathscr{E})}{\sqrt{2}\omega_{s0}}\int_{\phi_{\max}}^{\phi}\frac{1}{\sqrt{\mathscr{E} - U_t(\phi')}}d\phi', \tag{2}$$

where U_t is the total potential, ω_s the angular synchrotron frequency, ω_{s0} the angular frequency of small-amplitude synchrotron oscillations in the SRF system, h the harmonic number, and η the slip factor [6, 7].

We assume stationary bunches with a binomial distribution function, $\mathscr{F}$, independent of ψ:

$$\mathscr{F}(\mathscr{E}) = \frac{1}{2\pi\omega_{s0}A_N}\left(1 - \frac{\mathscr{E}}{\mathscr{E}_{\max}}\right)^{\mu}, \tag{3}$$

where μ is the form factor, and A_N is a normalisation factor.

A small perturbation function $\tilde{\mathscr{F}}$ is added to this stationary distribution, which is periodic in ψ and satisfies the linearised Vlasov equation [6].

The perturbation's phase advance from bunch to bunch is $2\pi l/M$, where M is the number of equidistant bunches, and l is the coupled-bunch mode. The Lebedev equation provides the following set of solutions [8, 9]:

$$\tilde{\lambda}_p^l(\Omega) = \frac{\zeta M}{h}\sum_{k=-\infty}^{\infty} G_{pk}(\Omega)\frac{Z_k(\Omega)}{k}\tilde{\lambda}_k^l(\Omega), \tag{4}$$

with the frequency, Ω, which defines the location in the synchrotron side bands, the intensity parameter

$$\zeta = \frac{-qN_p h^2\omega_0}{V_0\cos\phi_{s0}} \tag{5}$$

and the matrix elements G_{pk} coupling the different harmonics (p and k) of the line density perturbation $\tilde{\lambda}^l$:

$$G_{pk}(\Omega) = -i\omega_{s0}^2\sum_{m=1}^{\infty}\int_0^{\mathscr{E}_{\max}}\frac{d\mathscr{F}(\mathscr{E})}{d\mathscr{E}}\frac{I_{mp}(\mathscr{E})I_{mk}^*(\mathscr{E})\omega_s(\mathscr{E})}{\Omega^2/m^2 - \omega_s^2(\mathscr{E})}d\mathscr{E}. \tag{6}$$

where m is the mode number and I_{mp} and I_{mk} are the wave integrals defined in [9].

Content from this work may be used under the terms of the CC BY 4.0 licence (© 2026). Any distribution of this work must maintain attribution to the author(s), title of the work, publisher, and DOI.

ISBN: 978-3-95450-252-3 ISSN: 2673-5350 doi: 10.18429/JACoW-IPAC2026-WEP5109

LONGITUDINAL BEAM STABILITY IN HL-LHC*

I. Karpov†, R. Calaga, B. E. Karlsen-Bæck, H. Timko, and M. Zampetakis,
European Organization for Nuclear Research, Geneva, Switzerland

Abstract

Recent studies showed that the broadband impedance in synchrotrons can significantly alter the longitudinal multi-bunch instability threshold. The results of the beam-based impedance measurement campaign in the Large Hadron Collider (LHC) reveal a discrepancy with predictions based on the present impedance model. A larger imaginary impedance with a lower roll-off frequency would reproduce the observations. Since the impedance will be impacted by the High-Luminosity (HL) LHC upgrades, longitudinal beam stability needs to be carefully re-evaluated. This contribution discusses the outcome of the semi-analytical analysis for the HL-LHC parameters together with the updated broadband impedance model. Future benchmark measurements are proposed to probe the multi-bunch instability threshold driven by the partially compensated main RF cavity impedance. Finally, possible mitigation measures to increase the instability threshold are discussed.

INTRODUCTION

Interaction of a charged particle beam with the beam-coupling impedance of a synchrotron can lead to undamped or exponentially growing coherent oscillations. The instability threshold of a multi-bunched beam in the longitudinal plane was recently revisited, and a generalised approximation for the combination of narrow- and broadband impedances was proposed [1]:

$$1/N_{\mathrm{th}} \approx 1/N_{\mathrm{th}}^{\mathrm{nb}} + 1/N_{\mathrm{th}}^{\mathrm{bb}}. \quad (1)$$

Here, $N_{\mathrm{th}}^{\mathrm{nb}}$ is the intensity threshold of a coupled-bunch instability (CBI) driven by a narrow-band (NB) impedance source, and $N_{\mathrm{th}}^{\mathrm{bb}}$ is the loss of Landau damping (LLD) threshold defined by the broad-band (BB) impedance, both evaluated separately. In the Large Hadron Collider (LHC), LLD was observed since 2010 [2], cured by applying the controlled longitudinal emittance blow-up during acceleration [3]. The longitudinal CBIs were measured only in dedicated machine development (MD) studies [4, 5]. The instability was driven by the fundamental impedance of the 400 MHz radio-frequency (RF) acceleration system after careful adjustments of the feedback RF system. Longitudinal CBI driven by other higher-order modes (HOM) was not yet observed in LHC [6].

The LHC impedance was initially estimated [7], then summarised in the form of a model in the technical design report [8], and later became available for detailed beam dynamics studies [9]. Macro-particle simulations in the longitudinal plane using this model consistently agreed with measurements [10]. However, recent beam-based evaluations with two different techniques indicated about 70% higher $\mathrm{Im}Z/k$ and a lower resonant frequency of the corresponding effective BB resonator impedance [11, 12]. The High-Luminosity (HL) LHC upgrade requires modifying existing and installing new equipment, thereby affecting the overall accelerator impedance. The latest longitudinal beam stability assessment based on the updated impedance model will be described below.

HL-LHC STABILITY PREDICTION

The (HL-)LHC cycle can be divided into three distinct phases critical for the longitudinal stability: (i) beam accumulation at 450 GeV, (ii) energy ramp, and (iii) beam storage at 7 TeV. During the accumulation process, the mismatch between the longitudinal phase-space distribution of the injected beam and the LHC RF bucket leads to oscillations of bunch phase and length. These oscillations vary from bunch to bunch due to the bunch parameter spread defined by the injector complex. The injected bunch train, moreover, affects the circulating beam due to the action of the beam-based feedback loops. In addition, uncontrolled longitudinal emittance blow-up is caused by Intra-Beam Scattering (IBS) and RF noise [13]. Later in the cycle, the controlled emittance blow-up is applied during the energy ramp, resulting in about 1.2 ns-long bunches at the arrival to the flat top. In collision at the maximum beam energy, the bunch length decrease due to the synchrotron radiation is counteracted by periodic single-tone phase excitation [14, 15].

Ideally, macro-particle simulations are needed to include all these effects simultaneously. However, they are not feasible in the LHC scenario with up to ~3000 circulating bunches. Therefore, a semi-analytical analysis at injection and collision energies was performed based on solving the linearised Vlasov equation with the numerical code MELODY [16]. It computes the growth rates of the uniformly filled ring for a combination of resonator-like impedance sources defined by:

$$Z(\omega, R, Q, \omega_r) = \frac{R}{1 + iQ\left(\omega/\omega_r - \omega_r/\omega\right)}, \quad (2)$$

where R is the shunt impedance, Q is the quality factor, and f_r is the resonant frequency. The present LHC impedance model is approximated by a single BB resonator with $Q_{\mathrm{bb}} = 1$, $f_{r,\mathrm{bb}} = 5$ GHz, and $R_{\mathrm{bb}} = 38$ kΩ. The assumption is based on the concept of the effective BB impedance [17, 18]. Recent measurement results suggest using $f_{r,\mathrm{bb}} = 3.4$ GHz, and $R_{\mathrm{bb}} = 44$ kΩ [11, 12]. The lowest threshold of longitudinal CBI is expected to be defined by HOMs of the Double Quarter Wave (DQW) crab cavities [19], which will be installed during the Long Shutdown 3 (LS3). In the

* Research supported by the HL-LHC project
† ivan.karpov@cern.ch

Content from this work may be used under the terms of the CC BY 4.0 licence (© 2026). Any distribution of this work must maintain attribution to the author(s), title of the work, publisher, and DOI.

ISBN: 978-3-95450-252-3 ISSN: 2673-5350 doi: 10.18429/JACoW-IPAC2026-WEP5110

STUDIES OF COUPLED-BUNCH INSTABILITY IN THE HL-LHC*

C. C. Becker† [1], R. Calaga, B. E. Karlsen-Baeck, I. Karpov, H. Timko
CERN, Geneva, Switzerland
[1]also at TU Wien, Vienna, Austria

Abstract

Beam dynamics studies, and in particular detailed macroparticle simulations, are challenging for high-energy hadron synchrotrons due to the large number of circulating bunches. The High-Luminosity Large Hadron Collider (HL-LHC) will accelerate beams with about twice the initial LHC design intensity. It will also feature additional installations such as the crab cavities, which increase the total impedance of the accelerator. In the longitudinal plane, the baseline HL-LHC scenario will push the beam parameters close to the stability limit. It is therefore of interest to study the impact of the crab cavity higher-order-mode impedances, which could lead to coupled-bunch instabilities (CBI), on the beam stability. This is particularly important in the presence of a broad-band impedance, which was predicted to lower the CBI threshold. In this contribution, particle-tracking simulation setups for instabilities, driven by either broad- or narrow-band impedances, are investigated. This paves the way for CBI simulations that take into account both impedance sources, to study the longitudinal stability limits at injection.

INTRODUCTION

Both narrow-band (NB) as well as broad-band (BB) impedances, or equivalently, long-range and short-range wake fields, can drive beam instabilities in accelerators. NB impedances arise typically from resonant modes in cavity-like structures and can drive coupled-bunch instabilities (CBI). BB impedances originate, for instance, from geometric discontinuities, resistive-wall effects, or non-ideal devices within the accelerator and are responsible for single-bunch effects such as the loss of Landau damping (LLD). In previous theoretical work [1], it was shown that the longitudinal thresholds for CBI and LLD are closely linked and that, especially when operating close to the LLD threshold, the BB impedance can reduce the CBI threshold. As part of the upgrade to HL-LHC, crab cavities are going to be installed to help increase the luminosity. Their higher-order modes (HOM) potentially drive CBI and thereby limit the performance [2]. The beam parameters after the upgrade are expected to be close to the LLD threshold. Consequently, to accurately investigate the longitudinal beam stability, both impedance sources must be considered.

To predict the behaviour of the beam after injection into the LHC, macroparticle simulations with the BLonD [3] simulation suite are performed. However, the macroparticle analysis of BB and HOM effects each come with their challenges. Whilst the analysis of single-bunch LLD requires high time resolution, and thereby a large number of macroparticles per bunch, CBI studies require the tracking of hundreds of bunches. This work examines the macroparticle simulation requirements associated with LLD, and CBI induced by the crab-cavity HOMs, defining the requirements for simulations that incorporate both mechanisms.

Table 1 summarises the parameters for the LHC ring, the main accelerating system, and the beam at injection, which were used as an input for the simulations. The parameters represent the baseline scenario for proton operation at injection into the HL-LHC [4].

Table 1: HL-LHC Accelerator, RF and Beam Parameters at Injection

Parameter	Unit	Value
Circumference, C	m	26 658.86
Harmonic number, h		35 640
Beam energy, E	GeV	450
Transition gamma, γ_{tr}		53.8
RF frequency, f_{RF}	MHz	400.788
RF voltage, V_0	MV	8
Bunch intensity, N_{p}	p/b	2.3×10^{11}

Both NB and BB impedances $Z(\omega)$ can be represented by a resonator model, described by an equivalent RCL circuit with a shunt impedance R_{sh}, a resonant angular frequency ω_r and a quality factor Q according to

$$Z(\omega) = \frac{R_{\mathrm{sh}}}{1 + iQ\left(\frac{\omega}{\omega_{\mathrm{r}}} - \frac{\omega_{\mathrm{r}}}{\omega}\right)} \quad . \tag{1}$$

LOSS OF LANDAU DAMPING

To describe the BB part of the longitudinal impedance, a resonator with $Q = 1$, a cut-off frequency of $f_{\mathrm{c}} = f_r = 5\,\mathrm{GHz}$ and an effective imaginary impedance $(\mathrm{Im}Z/k)_{\mathrm{eff}} = 0.07\,\Omega$ (LHC) or $0.075\,\Omega$ (HL-LHC) is well suited [5]. Following Eq. 1, the shunt resistance can be expressed as $R_{\mathrm{sh}} = (\mathrm{Im}Z/k)_{\mathrm{eff}} \times Q \times (f_{\mathrm{r}}/f_{\mathrm{rev}})$. The bunch shape is best described by a binomial distribution function, which, neglecting intensity effects, is given by the line density function

$$\lambda(t) = \lambda_0 \left(1 - \frac{\sin^2\frac{\Delta t}{2}}{\sin^2\frac{\tau_{\mathrm{full}}}{2}}\right)^{\mu+0.5} \quad , \tag{2}$$

with the binomial exponent μ, the normalisation constant λ_0, Δt is the time coordinate with respect to the reference particle and τ_{full} the full bunch length. The bunches at injection in the LHC were observed to have an exponent

* Research supported by the HL-LHC project
† clara.charlotte.becker@cern.ch

Content from this work may be used under the terms of the CC BY 4.0 licence (© 2026). Any distribution of this work must maintain attribution to the author(s), title of the work, publisher, and DOI.

ISBN: 978-3-95450-252-3 ISSN: 2673-5350 doi: 10.18429/JACoW-IPAC2026-WEP5111

LONGITUDINAL MICROWAVE INSTABILITY STUDY AT TRANSITION CROSSING IN THE CERN PS

J. Salinas, J. Flowerdew, A. Lasheen*, M. Neroni,
European Organization for Nuclear Research (CERN), Geneva, Switzerland

Abstract

The beam quality of high-intensity proton and ion bunches in the CERN Proton Synchrotron (PS) is limited by a longitudinal microwave instability at transition crossing. This single-bunch instability manifests itself as a rapid longitudinal emittance blow-up and impacts, for instance, the intensity and bunch length to the AWAKE experiment. In this contribution, results of complete parameter scans are presented to experimentally establish the beam stability limits. These are compared to detailed tracking simulations with the BLonD code, including collective effects with the longitudinal impedance model, beam feedback loops, and the gamma transition jump. Remarkable agreement with measurements is obtained for the instability thresholds and micro-bunch structures. Nonetheless, the characteristics of the simulated instability strongly depend on the modelling of longitudinal space charge, which focuses the micro-bunches but also introduces significant numerical noise. The results improve the understanding of performance limitations due to transition crossing and guide future mitigation strategies.

INTRODUCTION

The longitudinal microwave instability has been observed for decades at transition crossing in the CERN Proton Synchrotron (PS) [1]. This instability, manifesting itself as high-frequency density modulations along the bunch, leads to a rapid and uncontrolled longitudinal emittance blow-up. The modulation is driven by high-frequency impedance sources satisfying $f_r \tau_\ell \gg 1$ (where f_r is the resonance frequency and τ_ℓ is the bunch length). For typical PS bunches with lengths on the nanosecond scale at transition, this points to resonant frequencies above 1 GHz.

More recently, the instability was observed with various ion species [2], and its observation, along with proton beams, is presented in this paper. An example acquisition at the onset of the instability close to transition crossing is given in Fig. 1. The AWAKE experiment [3] at CERN requires short, intense single proton bunches ($N_b = 30 \times 10^{10}$ p+) from the Super Proton Synchrotron (SPS), the downstream accelerator of the PS. The beam parameters are set close to the stability limit in the PS and the instability is presently mitigated by applying a controlled longitudinal emittance blow-up with a dedicated 200 MHz RF system before transition [4]. While this preserves global beam quality and reproducibility compared to the turbulent microwave instability regime, the enlarged emittance imposes a minimum on the smallest achievable bunch length for AWAKE. Moreover, following the impedance reduction campaign in the SPS [5, 6], the microwave instability is now one of the main limitations in providing shorter bunches to the AWAKE experiment [7].

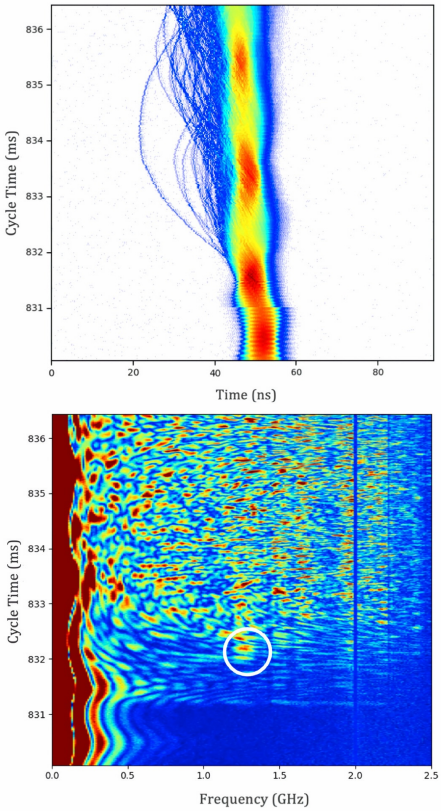

Figure 1: Measured evidence of a 1.3 GHz modulation in a single proton bunch. Evolution of the line density as a waterfall plot (top) and corresponding spectrum obtained from the FFT of each frame (bottom). The effective transition crossing timing happens at a cycle time (c-time) of 831 ms. The colour scale increases from blue to red.

Extensive studies have been conducted since 2017 to identify the source of beam-coupling impedance causing the instability. In particular, an analysis of the spectral components of the modulated bunch profiles was performed both at transition crossing and from dedicated measurements using long bunches with small momentum spread [8, 9]. These provided a more precise measurement of the modulation, 1.3 GHz, compatible with the resonant frequency of the numerous unshielded pumping manifolds located at the downstream end of the main magnet units in the PS [10]. In this paper, a new set of measurements with single proton bunches is presented and compared to tracking simulations using the BLonD simulation code [11], the influence of the pumping manifold impedance as well as space charge is then analysed.

* alexandre.lasheen@cern.ch

Content from this work may be used under the terms of the CC BY 4.0 licence (© 2026). Any distribution of this work must maintain attribution to the author(s), title of the work, publisher, and DOI.

ISBN: 978-3-95450-252-3 ISSN: 2673-5350 doi: 10.18429/JACoW-IPAC2026-WEP5112

BEAM-LOADING COMPENSATION AT TRANSITION CROSSING FOR MIXED INTENSITY BUNCHES

O. Smedt[1,2], A. Lasheen*[1], H. Damerau[1]
[1]European Organization for Nuclear Research, Geneva, Switzerland
[2]École Polytechnique Fédérale de Lausanne, Lausanne, Switzerland

Abstract

To produce beam for the nTOF and East Area experimental facilities at CERN, the Proton Synchrotron (PS) simultaneously accelerates two bunches with very different intensities. This combined acceleration cycle gains time and flexibility for beam sharing across the accelerator complex. However, to fulfil the demanding beam requests for future facilities like the Search for Hidden Particles (SHiP) experiment, a higher bunch intensity delivered to nTOF is essential to maintain the average flux at a reduced repetition rate. This further increases the intensity difference with respect to the low-intensity bunch for the East Area. In this contribution, longitudinal dipole oscillations triggered by the intensity-dependent phase jump at transition crossing are exposed. A mitigation technique is derived analytically and demonstrated in beam tests, by tuning one cavity of the main RF system to a separate harmonic of the revolution frequency. This allowed the elimination of dipole oscillations at transition crossing and the preservation of beam quality, even with a significant increase of the nTOF bunch intensity.

INTRODUCTION

For the beam delivery to the East area experimental facility [1], a particle bunch of 2.2 to 8×10^{11} protons per bunch (p/b) is accelerated in the PS ('EAST bunch'). To run the PS more efficiently, a second bunch can be simultaneously accelerated for the nTOF facility [2]. This parasitic bunch has an intensity of up to 6×10^{12} p/b ('parasitic TOF bunch'). When a cycle is dedicated to the nTOF facility the equivalent bunch ('dedicated TOF bunch') has a higher intensity of 8.4×10^{12} p/b.

The SHiP experiment in the North Area of the SPS will require around two million cycles from the PS per year [3], equivalent to 28 days of dedicated operation of the PS. Servicing SHiP should ideally not affect the average proton flux to other facilities. This is partly achieved by raising the parasitic TOF intensity to the same intensity as on the dedicated cycle. The 40 % intensity increase would allow one dedicated TOF cycle to be removed for every four EAST cycles, without affecting the average proton flux to the nTOF facility. During typical operation of the PS, this change could shorten the supercycle by 5 %.

The parasitic TOF intensity is currently limited by dipole oscillations at transition crossing, induced by the difference in beam loading between the TOF and EAST bunches. These dipole oscillations cannot be mitigated by the beam phase loop, as they only occur for the less intense EAST bunch. The dipole oscillations decohere, resulting in emittance dilution. A mountain range plot of the EAST bunch at transition crossing is shown in Fig. 1. After transition crossing, the inter-bunch distance oscillates with an initial amplitude of 37 ns. The longitudinal RMS emittance is 0.38 eVs 170 ms after these oscillations begin.

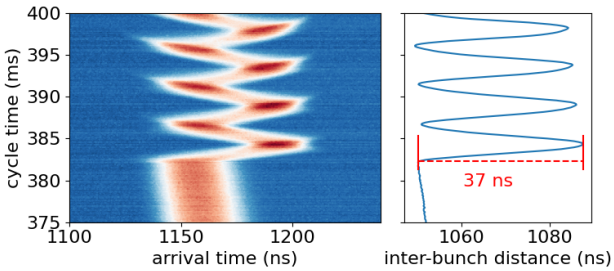

Figure 1: Mountain range plot of an EAST bunch (left) when a parasitic TOF bunch is present in the cycle. Transition crossing occurs at 382 ms with respect to the cycle start. The inter-bunch distance (right) is measured between the centres of two Gaussian profiles, fitted to each bunch. The measurement was performed with an EAST intensity of 2.2×10^{11} p/b and TOF intensity of 6×10^{12} p/b.

In this contribution we analyse the dipole oscillations, and develop a procedure to predict their amplitude. A method for their compensation is proposed and validated with beam tests, making use of existing RF hardware and leveraging the beam induced voltage. The implication of these optimizations on beam extraction is discussed.

DERIVATION OF DIPOLE OSCILLATION AMPLITUDE

The dipole oscillations are caused by the intensity dependent synchronous phase shift which is different for the EAST and TOF bunches. Through energy conservation the synchronous phase, ϕ_s, is known to satisfy

$$V_{\mathrm{ind}}(\phi_s) + V_{\mathrm{RF}}(\phi_s) = \frac{\delta E_s}{e}, \tag{1}$$

where δE_s is the energy gain per turn of the synchronous particle, e is the elementary charge, $V_{\mathrm{ind}}(\phi)$ is the beam induced voltage, and $V_{\mathrm{RF}}(\phi)$ is the voltage of the RF system without beam. The phase ϕ is with respect to the principle harmonic of the RF system, h. With knowledge of the beam induced voltage, this equation can be solved for the buckets of the TOF and EAST bunches to obtain $\phi_{s,\mathrm{TOF}}$ and $\phi_{s,\mathrm{EAST}}$.

* alexandre.lasheen@cern.ch

Content from this work may be used under the terms of the CC BY 4.0 licence (© 2026). Any distribution of this work must maintain attribution to the author(s), title of the work, publisher, and DOI.

ISBN: 978-3-95450-252-3 ISSN: 2673-5350 doi: 10.18429/JACoW-IPAC2026-WEP5114

CHARACTERIZATION OF LONGITUDINAL ELECTRON BEAM QUALITY AT THE SOFT X-RAY BEAMLINE OF SwissFEL

R. Provvedi*, E. Prat, S. Reiche
PSI Center for Accelerator Science and Engineering, Villigen, Switzerland

Abstract

Longitudinal electron beam quality is key at X-ray free-electron lasers (FELs), where electron beams with small slice energy spread and a well-preserved current profile are required to ensure optimal, stable performance. Collective effects such as microbunching instability (MBI) and intrabeam scattering (IBS) can significantly degrade the longitudinal phase-space of the electron beam during multi-stage compression and are therefore a concern across FEL facilities. In this contribution, we will present systematic characterization studies of these mechanisms at the SwissFEL soft X-ray beamline Athos. We will show longitudinal phase-space measurements using radiofrequency transverse-deflecting structures for different accelerator and compression conditions. These characterization studies represent a first step towards the optimization of multi-stage compression schemes aimed at mitigating MBI and IBS effects.

INTRODUCTION

X-ray free-electron lasers (XFELs) are powerful light sources delivering ultrashort, high-brilliance X-ray pulses with atomic-scale spatial and femtosecond temporal resolution [1]. The performance of the FEL amplification process is critically dependent on the quality of the driving electron beam, in particular on its longitudinal phase space (LPS). To achieve the high peak currents required for efficient FEL operation, electron bunches undergo multiple stages of longitudinal compression along the accelerator lattice. While this process is essential for maximizing FEL gain, it concurrently enhances collective effects that can severely degrade the beam quality, thereby limiting the achievable gain and spectral purity, particularly in seeded FEL configurations. Among the effects arising from beam self-interactions, intrabeam scattering (IBS), i.e., multiple Coulomb scattering events, leads to a growth of the uncorrelated energy spread. In contrast to storage rings, the beam in a linear accelerator is not in thermal equilibrium and typically exhibits a higher effective transverse than longitudinal temperature. As a consequence, IBS drives a redistribution of the phase-space density with a net transfer of momentum from the transverse to the longitudinal degrees of freedom, resulting in an energy spread growth [2]. Microbunching instability (MBI), in contrast, is characterized by the amplification of the initial density and energy modulations over a broad wavelength spectrum, primarily driven by longitudinal space-charge (LSC) forces and coherent synchrotron radiation (CSR), during bunch compression and dispersive transport [3, 4].

The SwissFEL facility [5, 6] at the Paul Scherrer Institute (PSI) in Villigen, Switzerland, delivers X-ray radiation through two beamlines, namely Aramis, serving the hard X-ray regime, and Athos, dedicated to soft X-ray production. The latter operates over a wavelength range of 0.65–5.0 nm and is tailored for flexible operating modes, polarization control, and advanced seeding schemes, thereby placing stringent requirements on the longitudinal beam quality. A characterization of the LPS evolution along the accelerator is therefore needed to understand and control the impact of collective effects. In this work, experimental studies of the longitudinal beam quality at SwissFEL Athos are presented, combining high-resolution measurements with ongoing simulation studies. Emphasis is placed on different bunch compression schemes to investigate how IBS- and MBI-driven effects manifest under varying compression and to distinguish the corresponding operational regimes.

LPS DIAGNOSTICS

Measurements

The longitudinal phase space (LPS) of the electron beam at SwissFEL is experimentally characterized using radiofrequency (RF) transverse deflecting structures (TDS) in combination with a two-dimensional profile monitor located in a downstream dispersive section. The TDS imparts a time-dependent transverse kick to the electron bunch, mapping the longitudinal coordinate onto one transverse screen axis, while the relative energy deviation is encoded along the orthogonal axis via the local dispersion. The temporal coordinate is calibrated using the applied TDS voltage and phase, whereas the energy scale is determined from the dispersion at the observation screen. SwissFEL is equipped with multiple TDS systems with different frequencies and resolutions: an S-band TDS (3 GHz, ~10 fs resolution) at the injector, a C-band TDS (5.7 GHz, ~1 fs) downstream of Linac 3 and an X-band TDS (12 GHz, <1 fs) installed after the Athos undulator. A schematic layout of the SwissFEL accelerator lattice, including the relevant diagnostic, is shown in Fig. 1.

This diagnostic setup enables direct, single-shot LPS measurements with femtosecond temporal resolution. From the LPS distributions, several key parameters can be extracted, namely the current profile, energy centroid and slice energy spread (SES) as function of the longitudinal coordinate, as well as the energy chirp along the bunch. To ensure a systematic and reproducible analysis of the measured data, a dedicated analysis framework (MBI Analyzer Tool) has been developed. It processes LPS images acquired from the diagnostic screens and reconstructs slice-resolved beam properties along the bunch. Noise reduction is performed using

* roberta.provvedi@psi.ch

Content from this work may be used under the terms of the CC BY 4.0 licence (© 2026). Any distribution of this work must maintain attribution to the author(s), title of the work, publisher, and DOI.

ISBN: 978-3-95450-252-3 ISSN: 2673-5350 doi: 10.18429/JACoW-IPAC2026-WEP5115

COHERENT TRANSVERSE INSTABILITIES ON THE ISIS PROTON SYNCHROTRON AT INJECTION ENERGY

D. W. Posthuma de Boer*,[1,2], C. M. Warsop[1], R. E. Williamson[1], A. Oeftiger[2]
[1]ISIS Neutron and Muon Source, Didcot, United Kingdom
[2]University of Oxford, Oxford, United Kingdom

Abstract

ISIS is the short-pulsed spallation neutron and muon source at the Rutherford Appleton Laboratory in the UK. Its rapid-cycling synchrotron accelerates up to 3×10^{13} protons-per-pulse from 70 to 800 MeV at 50 Hz, delivering them to fixed targets for neutron and muon production. As a beam-loss limited facility, increasing operational intensity necessitates the reduction of beam losses. Although largely mitigated, a coherent vertical instability continues to drive losses at high intensities and remains an active area of research.

Having recently identified a likely source of the instability's driving impedance, we re-examine observations of instabilities on ISIS when operating as a storage ring at its injection energy. We present the updated vertical driving impedance model, compute analytical predictions of instability growth rates excluding space-charge effects with the PyTMCI Vlasov solver, and compare these with experimental observations across a range of vertical tune settings. We also outline future development plans.

INTRODUCTION

ISIS is the world's longest serving, short-pulsed, spallation neutron and muon source. Based in the UK, its rapid cycling synchrotron (RCS) accelerates intense beams of up to 3×10^{13} protons from 70 MeV to 800 MeV, with a 50 Hz repetition rate. Key RCS parameters are listed in Table 1.

Table 1: Key ISIS Synchrotron Parameters

Property	Value
Average Extracted Beam Power	0.2 MW
Number of Bunches (M)	2
Average Radius (R)	26 m
No. of Superperiods	10
Gamma Transition	5.034
Nominal Tunes (Q_x, Q_y)	4.31, 3.83 (variable)
Peak Incoherent Tune Shift	~ -0.5 [1]
Chromaticity (ξ_x, ξ_y)	-1.1, -1.1 [2]

ISIS is a beam-loss limited facility, so minimising beam-loss is a primary objective of R&D efforts. A vertical head-tail instability was first observed during commissioning [3, 4] and remains a major source of beam-loss around 2 ms through its RCS cycle. This is despite mitigation techniques developed to minimise beam-loss. The instability was thought to be driven by resistive wall, but it grew an order of magnitude faster than analytical predictions, and its dipole moment distribution was also not well predicted.

The dynamics of the 2 ms instability are very complex, making studies challenging with operational beams. Bunched Storage Ring Mode (BSRM) was developed as a way to operate the ISIS synchrotron for instability studies, in a regime more consistent with analytical models [5]. Studies in this mode identified a narrowband vertical impedance centred at ~ 85 kHz. Although its frequency was found to be incompatible with the 2 ms instability seen in RCS mode, its discovery motivated efforts to develop a new low-frequency driving impedance model of the synchrotron from equipment properties [6, 7] and follow-up studies [8, 9]. This paper will present a new analysis of data acquired in earlier studies, briefly introduce the new impedance model, then use it as an input to the PyTMCI Vlasov solver [10]. Its predictions will be compared with experiments and the source of the 85 kHz instability will be identified.

EXPERIMENTAL RESULTS

Experimental Set-up

The injection and accumulation procedures of BSRM are similar to RCS mode, but the injected beams are stored with primary bending and focusing magnets operating with DC. Beams are not extracted, so 100 % beam-loss occurs in the synchrotron hall. To mitigate equipment damage, the repetition rate is reduced from 50 to ~ 1 Hz and beam intensity is reduced by a factor of ~ 10. This also reduces the ratio of the peak incoherent space-charge (SC) tune-shift to synchrotron tune (the SC parameter) to < 10, where coherent modes are less affected by direct SC, and theory without SC is more applicable than for an operational beam [5, 11].

For this experiment, the second-harmonic RF system was disabled whilst the total fundamental RF voltage was ramped from ~ 1 kV to 10.8 kV between 0 and 1 ms. Intensity was reduced to 1.68×10^{12} protons-per-bunch with two bunches circulating at a revolution frequency of ~ 675 kHz. Horizontal tune was constant, whilst vertical tune was varied between injected pulses. Measurements were performed with fast acquisition of vertical beam position monitor (BPM) signals.

With certain tune settings the bunches were observed to oscillate coherently, as can be seen in Fig. 1a; a comparison with the orange sum signal shows that only a portion of the bunch was oscillating coherently. Instability growth rates were obtained from the increasing amplitude of BPM difference signals, which were analysed for time windows with low beam-loss to avoid systematic errors. These windows were identified from intensity monitor signals by eye for each tune setting; one example is shown in Fig. 1b with the window indicated by a shaded region.

* david.posthuma-de-boer@stfc.ac.uk

Content from this work may be used under the terms of the CC BY 4.0 licence (© 2026). Any distribution of this work must maintain attribution to the author(s), title of the work, publisher, and DOI.

ISBN: 978-3-95450-252-3 ISSN: 2673-5350 doi: 10.18429/JACoW-IPAC2026-WEP5117

IMPACT OF LANDAU OCTUPOLES ON THE TRANSVERSE BEAM HALO DISTRIBUTION IN THE LHC*

P. Hermes†, C. Maccani, D. Veres,
European Organization for Nuclear Research, Geneva, Switzerland
M. Rakic, École Polytechnique Fédérale de Lausanne, Lausanne, Switzerland

Abstract

The distribution of beam halo particles in the Large Hadron Collider (LHC) is affected by non-linear fields, in particular by the Landau octupoles used to provide tune spread for beam stabilization. These elements introduce amplitude-dependent tune shifts that deform the transverse phase-space and may alter the steady-state halo population. In this study, tracking simulations are performed to quantify the change of particle amplitude for different octupole settings, without beam-beam interactions, and to investigate whether such non-linear effects could contribute to the variations observed in different measurements. The analysis provides a first assessment of the impact of non-linearities on the observed beam halo characteristics in the LHC. The results indicate that particle amplitudes can be significantly enhanced by non-linearities, with consequences on the halo measured in collimator scrapings.

INTRODUCTION

The transverse beam halo in the LHC is routinely characterized through collimator scraping measurements, in which a collimator jaw is moved transversely into the beam and the resulting particle losses are recorded as a function of jaw position. For a Gaussian beam, the cumulative halo content removed by scraping to a jaw position of a_{cut} (in units of the beam size $\sigma = \sqrt{\varepsilon\beta}$) should follow the Rayleigh distribution, predicting approximately 1.1% for $a_{\mathrm{cut}} = 3$. Scraping measurements in the LHC consistently reveal populations exceeding this expectation [1–4], with strong variations across measurements whose origin is not fully understood.

In the LHC, sextupolar fields can drive third-order resonances, while the Landau octupoles introduce amplitude-dependent tune shifts [5]; in the vicinity of a resonance, these effects result in the distortion of the phase space structure. Collimator jaws intercept particles based on their physical transverse displacement at the collimator location, thus the measured halo population depends on the maximum displacement a particle can reach. In a nonlinear lattice, the latter can differ substantially from the linear expectation.

In this contribution, we develop a method to quantify this non-linear amplitude excursion in simulations and apply it to the 2025 LHC configuration. Results are presented for the horizontal plane of LHC Beam 1 (circulating clockwise), though the same methodology can be applied to all other planes. The results show a significant amplitude excursion, in particular for halo particles, with a strong asymmetry between the two collimator jaws.

THE NONLINEAR AMPLITUDE EXCURSION MAP

Let us define the generalized horizontal amplitude of a particle as $\mathscr{R}_x(\psi_x) = \sqrt{X^2 + P_X^2}$, where $X = x/\sqrt{\beta_x}$ and $P_X = (\alpha_x x + \beta_x x')/\sqrt{\beta_x}$ are the Courant-Snyder normalized coordinates, and $\psi_x = -\arctan(P_X/X)$ is the betatron phase. In the following, all quantities refer to the horizontal plane; the plane index is omitted except where needed for clarity.

In a linear machine, $\mathscr{R} = \sqrt{2J}$ is a constant of motion, where J is the linear betatron action. In a nonlinear lattice, $\mathscr{R}(\psi)$ varies with phase: a particle inserted into a lattice at $(X_0, P_{X,0})$, with initial amplitude $\mathscr{R}_i = \sqrt{X_0^2 + P_{X,0}^2}$, can have a different generalized amplitude as it moves along the ring. We express amplitudes in units of beam sigma via $a(\psi) = \mathscr{R}(\psi)/\sqrt{\varepsilon}$, with $a_i = \mathscr{R}_i/\sqrt{\varepsilon}$ the initial amplitude.

A collimator jaw intercepts particles whose transverse displacement X at the collimator location exceeds the jaw edge position a_{cut}. In a linear machine, the maximum displacement is $X_{\max} = a_i$, reached at $\psi = 0$ ($\psi = \pi$) for the left (right) jaw. In a nonlinear lattice, the maximum displacement depends on the full initial condition $(X_0, P_{X,0})$, not only on $\mathscr{R}_i$. Nonlinearities can therefore drive a particle into the jaw even if $a_i < a_{\mathrm{cut}}$. We quantify this effect through the amplitude enhancement $\Delta a^{\pm}$, defined as

$$\Delta a^{\pm}(X_0, P_{X,0}, Y_0, P_{Y,0}, \Delta p/p, s) = \frac{\sup_{n\geq 1}(\pm X^{(n)})}{\sqrt{\varepsilon}} - a_i, \tag{1}$$

where $X^{(n)}$ is the horizontal normalized coordinate on turn n, and + (−) corresponds to the left (right) side in the moving right-handed coordinate system. In a linear machine, the quantity $\Delta a^{\pm}$ always equals 0. In a nonlinear lattice, phase space distortion shifts the phase at which the maximum displacement occurs, and $\Delta a^{\pm}$ can differ substantially from zero.

For a given direction ($\pm$), fixed vertical conditions $(Y_0, P_{Y,0})$, constant $\Delta p/p$, and lattice position s, $\Delta a^{\pm}$ reduces to a two-dimensional scalar field over $(X_0, P_{X,0})$, referred to as the *Nonlinear Amplitude Enhancement Map* (NAEM). Regions of positive $\Delta a^{\pm}$ indicate trajectories that carry the particle beyond its linear amplitude boundary. The spatial structure of the NAEM is a direct fingerprint of the nonlinear response of the accelerator lattice. Note that the NAEM is defined with respect to a reference emittance but

* Research supported by the HL-LHC project
† pascal.hermes@cern.ch

Content from this work may be used under the terms of the CC BY 4.0 licence (© 2026). Any distribution of this work must maintain attribution to the author(s), title of the work, publisher, and DOI.

ISBN: 978-3-95450-252-3 ISSN: 2673-5350 doi: 10.18429/JACoW-IPAC2026-WEP5118

EFFECT ON 7 TEV PROTON BEAMS FROM THE RESIDUAL MULTIPOLAR FIELDS IN THE HL-LHC HOLLOW ELECTRON LENS*

D. Veres†, P. Geissler, P. Hermes, C. Maccani, S. Redaelli, A. Rossi, CERN, Geneva, Switzerland
G. Stancari, Fermi National Accelerator Laboratory, Batavia, Illinois, USA

Abstract

Hollow electron lenses are a promising tool for controlling beam halo at high-intensity colliders like the HL-LHC. A perfect lens can efficiently deplete particles above the inner radius of the electron beam while leaving the core – which travels through a nominally zero-field region – unaffected. However, residual multipolar fields in the electron beam and non-ideal compensations of entry and exit regions of the electron beam can lead to emittance growth and other undesired effects on the circulating-beam core. This is a particular concern for the operation with pulsed electron beam currents that ensures the fasted depletion rates. In this study, updated two-dimensional field maps from recent studies at CERN's hollow electron beam test stand are used to quantify these effects under HL-LHC conditions. Beam-dynamics simulations are performed to evaluate the emittance evolution and identify the dominant field components contributing to core degradation. The analysis also considers compensation of the dipolar component using nearby electric kicker magnets.

INTRODUCTION

The High-Luminosity LHC (HL-LHC) [1], currently planned to start operation in 2030, will run with an unprecedent stored beam energy of up to 680 MJ. LHC measurements have shown that the beam halo is generally overpopulated [2, 3]. Most recent conservative estimates based on scaling from these measurements show that up to 24 MJ could be stored in the halo above 3σ amplitude in the HL-LHC [3]. Combined with fast failure scenarios [4], such as spurious firing of beam-loss protection systems or crab cavity phase slips, that can cause sudden orbit shifts of up to 2σ, this can result in damage to the collimation system that could be mitigated by active beam halo depletion. The Hollow Electron Lens (HEL) [5, 6] was added to the original HL-LHC baseline [7] for this purpose. While removed from the latest baseline, HEL studies continued at CERN's hollow Electron Beam Test Stand (EBTS). This contribution presents beam dynamics simulations using updated two-dimensional field maps from recent EBTS measurements and simulations.

HOLLOW ELECTRON LENSES FOR BEAM HALO CLEANING IN THE HL-LHC

The HEL produces a low-energy, hollow electron beam using an annular thermionic cathode that runs coaxially to the circulating proton beam over a few meters. The electron beam is characterized by an inner and outer radius r_1 and r_2, respectively. If the electron beam is perfectly cylindrically symmetric, protons below the inner radius experience no net effect from the electrons, as the electric and magnetic fields generated by the electron current are zero. Protons at an amplitude exceeding the inner radius are subject to the electromagnetic field of the electron beam and receive a transverse kick $\theta(r)$ that depends on the protons' amplitude $r = \sqrt{x^2 + y^2}$ in the transverse plane and can be calculated for an electron beam moving in the opposite direction to the proton beam as:

$$\theta(r) = -\frac{1}{2\pi\epsilon_0}\frac{I_t L(1+\beta_e\beta_p)}{\beta_e\beta_p c^2 (B\rho)_p} f(r). \tag{1}$$

Here L is the active length of the HEL, I_t is the total electron-beam current, β_e and β_p are relativistic β-factors of the electrons and protons, respectively, $(B\rho)_p$ is the magnetic rigidity of the proton beam, and $f(r)$ is an amplitude-dependent function given by

$$f(r) = \begin{cases} 0, & \text{for } r < r_1 \\ \frac{1}{r}\frac{r^2 - r_1^2}{r_2^2 - r_1^2}, & \text{for } r_1 \le r < r_2 \\ \frac{1}{r}, & \text{for } r_2 \le r \end{cases} \tag{2}$$

The relevant parameters of the HEL are listed in Table 1.

Table 1: HL-LHC HEL Parameters.

Parameter	Value
Min. inner radius (r_1)	1.1 mm or 3.6σ
Min. outer radius (r_2)	2.2 mm or 7.2σ
Effective length (L)	3 m
Total electron current (I_t)	5 A
Relativistic β_e	0.24

The above description holds for a perfectly cylindrically symmetric, hard-edged electron beam. In practice, non-ideal compensations of the entry and exit bends of the electron beam trajectory, as well as axial asymmetries, lead to residual fields in the $r < r_1$ region. The resulting non-zero transverse kicks on the proton beam core that together with a random pulsing can cause emittance growth and core losses. The HEL can be operated in continuous, deterministic, or random pulsing modes [7]. In the random mode, the HEL is switched on and off each turn with probability p and $1 - p$, respectively. This mode offers the best halo depletion efficiency [7, 8], but has also been identified as the most critical for core emittance growth in the presence of residual fields [9] and is therefore the focus of this paper.

* Research supported by the HL-LHC project.
† dora.erzsebet.veres@cern.ch

Content from this work may be used under the terms of the CC BY 4.0 licence (© 2026). Any distribution of this work must maintain attribution to the author(s), title of the work, publisher, and DOI.

ISBN: 978-3-95450-252-3 ISSN: 2673-5350 doi: 10.18429/JACoW-IPAC2026-WEP5119

REAL-TIME RECONSTRUCTION OF LONGITUDINAL PHASE-SPACE DISTRIBUTION IN HADRON BEAMLINES AND SYNCHROTRONS

S. Sherstiuk*, O. Boine-Frankenheim, Technical University of Darmstadt, Darmstadt, Germany
V. Kornilov, GSI Helmholtz Centre for Heavy Ion Research, Darmstadt, Germany

Abstract

Real-time measurement and control of the longitudinal momentum spread during the beam transfer from the transfer channel (TK) into the SIS18 synchrotron is needed for the low-loss high-intensity operation. For this purpose, two Feschenko-type beam shape monitors (BSM) will be installed in TK. This will enable the single-pass measurements and real-time reconstruction. Simulations using a differentiable tracking scheme will be applied. The underlying beam dynamics model is simplified for computational efficiency, but retaining the key aspects of space-charge and beam loading effects, while providing a sufficient reconstruction accuracy.

INTRODUCTION

Knowledge of longitudinal phase space distribution properties allows operators to control particle losses and to optimize overall machine performance.

For the GSI SIS18 synchrotron [1] it is required to monitor and control the longitudinal momentum spread at injection during regular operation. Additionally, real-time control of the momentum spread should be used as a target function for automatic optimization.

The transfer channel (TK) leads the ion beams from the linear accelerator UNILAC [2] to the synchrotron SIS18. The UNILAC accelerates ions from hydrogen to uranium, in this study we consider U^{28+} ions with the reference kinetic energy 11.4 MeV/u.

TK is a 160-meter long beamline with two buncher cavities, one with a frequency of 108 MHz at the TK's beginning and the second one 57 meters further with a frequency of 36 MHz. For diagnostic purposes two beam shape monitors (BSMs) are going to be installed: one right before the first cavity ($s_0 = 0$ m) and the other one 150 meters further ($s_1 = 150$ m). A key feature of beam dynamics in this beamline is beam elongation in presence of space charge forces. Figure 1 illustrates beam rms length $\tilde{z}$ to transverse size a aspect ratio along the TK. For aspect ratios $\tilde{z}/a \gtrsim 10$ bunches can be modeled as long bunches in a conducting pipe (using the well known g-factor). In the beginning of the TK this criterion is not satisfied and therefore another approximation is needed. Vertical dashed lines mark positions of buncher cavities (green) and BSMs (red). Horizontal dashed line marks the boundary between transition and long bunch regimes.

The phase space reconstruction problem for the TK beam line at GSI can be approached as a constrained optimization problem, described by Eq. (1). The goal is to minimize the difference between bunch profile measurements and their

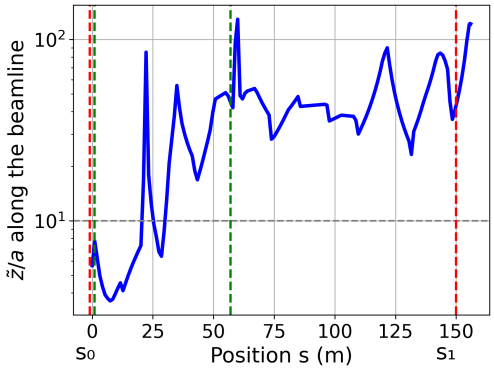

Figure 1: Longitudinal-to-transverse beam aspect ratio along the TK beamline. Vertical dashed lines mark positions of buncher cavities (green) and BSMs (red). Horizontal line marks a boundary for a long-bunch space charge regime.

counterparts from a simulation model at measurement location s_1 in the TK.

We chose the longitudinal envelope equation as a simulation model. It describes evolution of the rms bunch lengths $\tilde{z}(s) = \sqrt{\langle z^2(s)\rangle}$ where $\langle\cdot\rangle$ implies the integration over the distribution functions. Relative momentum spread $\tilde{\delta}(s_0)$ and emittance $\tilde{\varepsilon}$ are simulation parameters that have to be optimized for minimal difference between simulated length $\tilde{z}(s_1)$ and measured length $\tilde{\tilde{z}}(s)$. Length measured by the first BSM $\tilde{z}(s_0)$ is taken as a boundary condition.

The objective function is defined as a normalized squared difference between simulations $\tilde{z}(s_1)$ and measurements $\tilde{\tilde{z}}(s_1)$:

$$\min\left[\frac{1}{M}\sum_{m=1}^{M}\left(\frac{\tilde{z}_m(s_1)-\tilde{\tilde{z}}_m(s_1)}{\tilde{\tilde{z}}_m(s_1)}\right)^2\right] \tag{1}$$

where M is the number of measurements.

Search of optimal values of $\tilde{\delta}(s_0), \tilde{\varepsilon}$ is done by the gradient descent algorithm. Thus the simulation model has to support the calculation of derivatives with respect to the parameters $\tilde{\delta}(s_0), \tilde{\varepsilon}$. Another requirement is the time performance: SIS18 has a ramp-up frequency of 1 Hz and the reconstruction should be done on the same timescale in order to be used in the control room environment.

LONGITUDINAL ENVELOPE EQUATION

It was shown [3, 4] that for a group of particles and under an assumption of emittance conservation $\tilde{\varepsilon} = \sqrt{\langle z^2\rangle\langle\delta^2\rangle - \langle z\delta\rangle^2}$, rms coordinate offset $\tilde{z}$ follows the envelope equation:

* sergei.sherstiuk@tu-darmstadt.de

Content from this work may be used under the terms of the CC BY 4.0 licence (© 2026). Any distribution of this work must maintain attribution to the author(s), title of the work, publisher, and DOI.

ISBN: 978-3-95450-252-3 ISSN: 2673-5350 doi: 10.18429/JACoW-IPAC2026-WEP5120

BEAM DYNAMICS STUDY FOR AN UPGRADED LOW-EMITTANCE RF GUN

A. Asoyan[1], A. Grigoryan[1,2], B. Grigoryan[1], M. Ivanyan[1], E. I. Iiguen[3], B. Zeitler[3], K. Floettmann[3]
[1]Center for the Advancement of Natural Discoveries using Light Emission (CANDLE SRI), Yerevan, Armenia [2]Yerevan State University (YSU), Yerevan, Armenia [3]Deutsches Elektronen-Synchrotron DESY, Hamburg, Germany

Content from this work may be used under the terms of the CC BY 4.0 licence (© 2026). Any distribution of this work must maintain attribution to the author(s), title of the work, publisher, and DOI.

Abstract

High-brightness and low-emittance beams generated in RF gun based accelerators are essential for a number of applications, such as Free-Electron Lasers (FELs), Ultrafast Electron Diffraction (UED) facilities and THz radiation sources. In these accelerators, the final beam characteristics are determined both, by the properties of the electron gun and by the influence of the electromagnetic system along the beamline. To meet the requirements imposed on the beam characteristics, it is essential to identify the optimal parameters of the RF gun and the magnetic system. In this paper, beam dynamics studies of a modified RF gun for the AREAL and the REGAE accelerators are presented, with emphasis on transverse emittance compensation. Simulations were conducted by adjusting the parameters of the focusing and RF systems to identify the optimal configuration of the modified RF gun geometry.

INTRODUCTION

Advanced accelerator-based light sources such as Free Electron Lasers (FEL), THz radiation sources, and Ultrafast Electron Diffraction (UED) systems require electron beams with high brightness and low emittance [1-3]. The most effective way to generate such high-quality electron beams is by using RF-based photocathode guns [4]. In this type of electron source, a high current density beam is generated at the cathode by means of photoemission, which is then immediately accelerated in a high gradient accelerating RF field. The high accelerating field, reachable in an RF cavity allows, on the one hand, to extract a beam with a high phase space density from the cathode, because it compensates the space charge induce retraction field during emission. The rapid acceleration to near relativistic energies, on the other hand, reduces space charge induced emittance growth in the acceleration process and the following beam transport.

In addition, the use of laser pulses allows better control of beam parameters such as charge, transverse and longitudinal bunch sizes, and their distributions. All these factors strongly influence the desired final beam parameters.

Therefore, the development and optimization of photoinjectors is one of the key directions for producing electron beams with improved characteristics in linear accelerators. Efficient operation of an RF gun requires optimization from both the technical and beam dynamics perspectives. From the technical side, this includes an efficient cavity cooling, general RF parameters and the adaptation to geometrical constrains, e.g. for the integration of the solenoid magnet. Concerning the beam dynamics aspects the optimization of the focusing parameters and the length of the half-cell in dependence on the targeted beam parameters are of relevance. Optimization of all parameters within the technical constrains enables an efficient emittance compensation and a precise beam envelope control.

Currently, the AREAL linear accelerator at CANDLE and the REGAE linear accelerator at DESY are operated with the same S-band RF gun design. However, for electron diffraction used in pump-probe experiments and imaging applications at REGAE, and for low energy applications as the planned THz FEL at AREAL, an improved beam quality is required, particularly in terms of emittance compensation and beam envelope control. To overcome these challenges and to extend the application range, an upgraded RF gun is being developed for both facilities. In this design, the focusing solenoid magnet is integrated directly with the gun, and the RF cavity half-cell length is optimized. In addition, the cavity cooling will be upgraded. The aim is to achieve lower emittance beams and increase the repetition rate to the kHz range [5], thereby enhancing the average beam current.

This paper concentrates on the optimization of the half-cell length and studies emittance compensation for ~250 pC electron beams generated at AREAL, with an RF gun half-cell length reduced from 0.57 to 0.45 times half the RF wavelength λ_{RF}.

RF GUN DESIGN OF AREAL AND REGAE

Currently, the RF guns of the AREAL and REGAE accelerators consist of a 1.57 cell resonator operating at 3 GHz (S-band) (Fig. 1). The maximum accelerating gradient reaches 110 MV/m, and electron beams with energies up to 5 MeV [6, 7] are generated.

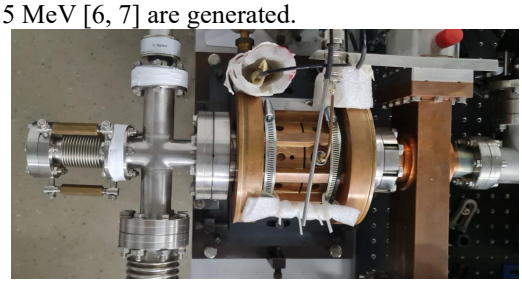

Figure 1: The S-band RF gun installed at the AREAL accelerator. A polished copper cathode is installed in the half-cell of the gun. Left of the copper body an in-vacuum spring mechanism to hold the cathode in place is visible, while on the right side the coaxial RF coupler can be seen.

ISBN: 978-3-95450-252-3 ISSN: 2673-5350 doi: 10.18429/JACoW-IPAC2026-WEP5124

MODELING OF RADIATION WAKEFIELDS USING A SCATTERED-FIELD FORMULATION

J. Christ*, E. Gjonaj
Technical University of Darmstadt, Darmstadt, Germany

Content from this work may be used under the terms of the CC BY 4.0 licence (© 2026). Any distribution of this work must maintain attribution to the author(s), title of the work, publisher, and DOI.

Abstract

Predicting Coherent Synchrotron Radiation (CSR) generated by bent trajectories in electron accelerators imposes significant challenges for analytical modeling and numerical simulations. We present a modeling approach targeting indirect CSR effects created by reflections at chamber walls. Unlike conventional CSR models, the method accounts for arbitrary geometries and bunch dynamics, including dispersion and compression. Computational efficiency is maintained through a scattered-field formulation, which permits the simulation of reflected CSR wakes directly without resolving the internal bunch structure in the same grid. To smooth the radiated field of the particles, point particles are distributed along their trajectory using a temporal variant of the continuous-charge approach. We demonstrate the method for the BC0 bunch compressor of the European XFEL.

INTRODUCTION

The generation of Coherent Synchrotron Radiation (CSR) by electrons undergoing acceleration remains a major source of beam quality degradation in accelerator sections [1]. Especially for electron bunches moving on curved trajectories, CSR can cause energy modulation, emittance growth and microbunching. However, prediction of beam dynamics under the influence of CSR effects remains a challenging task for both analytical and numerical approaches [2].

Analytical CSR models often start from steady-state motion, i.e., a rigid bunch on a circular path. The models are refined for some pre-defined trajectories, with the straight-bent-straight path caused by a finite-length dipole being the most prominent example [3, 4]. To additionally account for shielding effects caused by surrounding geometry, extensions have been developed for parallel plates and, with additional restrictions, for rectangular chambers [4–6]. Numerical approaches using a particle-in-cell (PIC) method are, despite their generality, infeasible for most cases of interest due to the required fine resolution in both space and time. Hence, CSR effects are often accounted for by incorporating (semi-)analytical models in particle tracking codes, inheriting their underlying assumptions [3, 7]. For such models, satisfying agreement between measurements and simulations was achieved [1]. In contrast, some codes solve the Liénard-Wiechert (LW) potentials directly to simulate arbitrary ensembles and trajectories in free space. However, even with advanced schemes and high-performance computing, the computational effort remains high due to the required particle number and the single-particle based evaluation [8, 9]. These numerical approaches focus on the direct part of the CSR field, with the effect of surrounding geometry included in a simplified manner, if at all. In contrast, a mesh-based full-wave electro-magnetic field solver can account for arbitrary geometry but models the electron bunch as current excitation, which neglects e.g. compression [10].

To close this gap, particularly for low- to mid energy sections, we present a method to simulate the indirect (scattered) part of the CSR fields while allowing for arbitrary beam trajectories and geometries. We extend our previous approach [11] by retardation and radiation effects in combination with a variant of the continuous-charge approach by Dohlus [12] to smooth the particle far field.

METHODOLOGY

Scattered-Field Formulation

We briefly summarize the scattered-field formulation developed for the coupled simulation of wakefield and space charge problems [11]. Maxwell's wave equations govern this problem, subject to perfectly electrically conducting (PEC) boundary conditions at the interface Γ and driven by the particle beam current density $\boldsymbol{J}$,

$$\partial_t \boldsymbol{D} - \nabla \times \boldsymbol{H} = -\boldsymbol{J}, \tag{1a}$$

$$\partial_t \boldsymbol{B} + \nabla \times \boldsymbol{E} = 0, \tag{1b}$$

$$\boldsymbol{n} \times \boldsymbol{E}|_\Gamma = 0 \tag{1c}$$

with electric and magnetic field strengths, $\boldsymbol{E}$ and $\boldsymbol{H}$, as well as their corresponding flux densities, $\boldsymbol{D}$ and $\boldsymbol{B}$. These are related by the constitutive relations in vacuum, $\boldsymbol{D} = \epsilon_0 \boldsymbol{E}$ and $\boldsymbol{B} = \mu_0 \boldsymbol{H}$. The normal vector to Γ is denoted $\boldsymbol{n}$. The scattered-field formulation decomposes this *total* field $\boldsymbol{E}$ into an *incident* $\boldsymbol{E}_\mathrm{i}$ and a *scattered* $\boldsymbol{E}_\mathrm{s}$ component. The incident field fulfills (1a) and (1b), however with free-space boundary conditions instead of (1c). The scattered field, on the other hand, fulfills (1b) and the homogeneous version of (1a), with its excitation arising solely from correcting the unphysical incident field at the PEC boundary. In summary, the scattered-field formulation reads

$$\boldsymbol{E} = \boldsymbol{E}_\mathrm{i} + \boldsymbol{E}_\mathrm{s} \tag{2a}$$

$$\boldsymbol{n} \times \boldsymbol{E}_\mathrm{s}|_\Gamma = -\boldsymbol{n} \times \boldsymbol{E}_\mathrm{i}|_\Gamma \,. \tag{2b}$$

This decomposition allows to separate scales and effects, and to use different methods for the respective fields, at the cost of a new boundary condition for the scattered field. Hence, we realize the scattered-field formulation (2) by coupling our in-house space-charge solver REPTIL [13] for the incident field with our wakefield solver PBCI [14] for the scattered

* jonas.christ@tu-darmstadt.de

ISBN: 978-3-95450-252-3 ISSN: 2673-5350 doi: 10.18429/JACoW-IPAC2026-WEP5125

DEVELOPING A PHYSICS-INFORMED GAUSSIAN PROCESS MODEL TO CONSTRUCT AN UNCERTAINTY-QUANTIFIED MACHINE MODEL USING BAYESIAN OPTIMIZATION

V. Isensee*, O. Boine-Frankenheim[1], TEMF, Technical University Darmstadt, Darmstadt, Germany
A. Oeftiger, John Adams Institute for Accelerator Science, University of Oxford, Oxford, UK
E. Kazantseva, GSI Helmholtz Centre for Heavy Ion Research, Darmstadt, Germany
[1]also at GSI Helmholtz Centre for Heavy Ion Research

Abstract

For maintaining the designed optical performance of machines like the GSI heavy-ion synchrotron SIS18 or the FAIR fragment separator SFRS, accurate knowledge of magnetic field and element alignment is crucial. A Gaussian Process model with a physics-informed kernel based on a stochastic ensemble of lattices is proposed. Key advantages compared to Linear Optics from Closed Orbits (LOCO) include (1.) fitting of Gaussian probability distributions for parameters, which inherently model uncertainty, (2.) incorporation of measurement uncertainty from BPM noise, (3.) uncertainty-enabled orbit prediction between BPMs, and (4.) an active-learning strategy for greater sample efficiency than measuring an orbit response matrix. Applied in a simulation of SIS18, the method constructs an effective machine model with minimal orbit uncertainty around the ring, enabling orbit correction with uncertainty-quantified minimal deviation at any location. The SFRS is identified as a compelling target for future application, where sparse instrumentation and complex optics make uncertainty-aware modeling particularly valuable. This physics-informed GP framework provides uncertainty-enabled modeling for rings and beamlines, with potential applications extending to broader optics-correction and beam-tuning tasks.

INTRODUCTION

Accurate knowledge of element alignment and magnetic field errors is a prerequisite for maintaining the designed optical performance of modern accelerator facilities. Conventional methods such as Linear Optics from Closed Orbits (LOCO) [1] reconstruct optics from orbit response matrix (ORM) measurements but return a single best-fit solution without any quantification of residual uncertainty. For facilities operating at the edge of their dynamic range – such as during slow extraction in SIS18, or when commissioning the complex optics of the SFRS [2] – knowing not just the most probable orbit but also the confidence in that prediction is essential.

SIS18 is the heavy-ion synchrotron at GSI in Darmstadt, Germany: a 216 m-circumference ring of 12 identical sections, each with two dipoles and three quadrupoles, equipped with 12 BPMs [3]. The SFRS is the superconducting fragment separator under construction at FAIR, designed to separate exotic rare isotopes produced by projectile fragmentation or fission [4].

Building on the physics-informed Gaussian Process (GP) framework introduced in [5], we present an extended framework with adaptive steerer selection. The core idea is to represent machine variability through a stochastic ensemble of accelerator lattices (generated with MAD-X [6]; alternative simulation codes are equally applicable). The physical correlations are encoded into the GP kernel empirically, following the approach of [7]. The resulting model provides probabilistic orbit predictions at arbitrary positions along the ring or beamline and supports parameter inference via Bayesian optimization [8]. The active-learning component is extended with a physics-informed steerer selection strategy: a phase advance prefilter eliminates geometrically blind steerers, and a submodular batch-selection criterion greedily assembles complementary measurements to reduce posterior uncertainty efficiently.

EXTENDED FRAMEWORK

Adaptive Steerer Selection

In [5], the active learning loop selected steerer settings based on a scalar acquisition function applied to the full GP posterior. A limitation of that approach is that it does not account for the betatron phase advance between a steerer and the quadrupole whose misalignment is to be inferred. The phase advance prefilter is based on the closed-orbit response of a steerer s at quadrupole location p. For a ring, the differential closed orbit at position p due to a kick θ at steerer s is

$$\Delta x_{sp} = \frac{\sqrt{\beta_s \beta_p}}{2\sin(\pi q)} \cos\big(\Delta\phi_{sp} - \pi q\big) \cdot \theta, \tag{1}$$

where β_s and β_p are the Courant–Snyder β-functions at the steerer and quadrupole locations, respectively. $\Delta\phi_{sp}$ is the betatron phase advance from steerer to quadrupole, and q is the fractional tune [9]. The sensitivity of this response to the phase advance is entirely encoded in the cosine factor, and a steerer is therefore discarded if

$$\big|\cos\big(\Delta\phi_{sp} - \pi q\big)\big| < \varepsilon. \tag{2}$$

We choose $\varepsilon = 0.1$. This criterion is dimensionless and lattice-independent: a steerer is retained only if its betatron phase advance places it in a regime where it can produce

* victoria.isensee@tu-darmstadt.de

Content from this work may be used under the terms of the CC BY 4.0 licence (© 2026). Any distribution of this work must maintain attribution to the author(s), title of the work, publisher, and DOI.

ISBN: 978-3-95450-252-3 ISSN: 2673-5350 doi: 10.18429/JACoW-IPAC2026-WEP5127

HIGH-LEVEL APPLICATIONS FOR LINAC COMMISSIONING AT ELI-NP*

A.-C. Cană[1,2], G.-L. Chen[†1], A.-D. Iancu[1,2], R.-D. Pătrășcoiu[1,2], H. Schubert[1], P. Tracz[1], R. Kraus[1], C.-D. Cirdei[1,2], C. Matei[1,2]
[1]ELI-NP/IFIN-HH, Măgurele, Romania
[2]Faculty of Applied Sciences, Politehnica Bucharest, Bucharest, Romania

Abstract

The ELI-NP (Extreme Light Infrastructure – Nuclear Physics) Gamma-ray Beam System (ELI-GBS), currently under construction, employs an 800 MeV linear accelerator (LINAC) to generate high-brightness gamma rays through laser–electron interactions. Its control system is designed as a distributed, EPICS-based architecture, where engineering-level control is provided for devices such as LLRF, modulators, magnets, profile monitors, and current monitors. A set of high-level application tools is required for LINAC beam commissioning, tuning, and the measurement of key accelerator parameters. To meet the beam diagnostic capabilities and performance requirements of the commissioning process, we have developed Python-based high-level application software to support essential commissioning tasks, including gun phase scans, emittance measurements, and beam energy measurements. The software uses the pyepics package to interface with engineering-level device IOCs. To support visualization and offline simulation, a set of Python soft IOCs has also been implemented, enabling realistic emulation of device behavior and data acquisition workflows. The online measurement capabilities of the system will be validated during the upcoming RF Gun commissioning and the subsequent LINAC commissioning phases.

INTRODUCTION

The Gamma-ray Beam System (GBS) at Extreme Light Infrastructure - Nuclear Physics (ELI-NP) is designed to deliver gamma-ray beams via inverse Compton scattering, employing an 800 MeV linear accelerator (LINAC) and a high-finesse optical cavity at the interaction point [1,2]. The LINAC consists of five acceleration modules, each capable of up to 160 MeV, with quadrupole magnets for beam focusing and beam position monitors for orbit diagnostics. The layout of the LINAC and the interaction section are shown in Figs. 1, 2, and 3. The control system is based on EPICS (Experimental Physics and Industrial Control System), which provides distributed process variables (PVs) for device control and monitoring. A similar EPICS-based control and archiving system has been successfully implemented for the gamma beam profile station at ELI-NP [3]. For LINAC commissioning and operation, high-level applications are essential to perform beam physics calculations and measure key accelerator parameters. In this paper, we present Python-based high-level applications developed for LINAC commissioning at ELI-NP. These tools address essential diagnostic tasks, including gun phase scans, emittance measurements, and beam energy measurements. The applications interface with EPICS via pyepics and leverage simulated soft IOCs for offline validation. The implementation details and simulation results are discussed in the following sections.

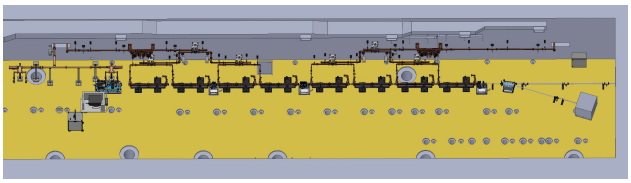

Figure 1: The first half of the ELI-NP linac.

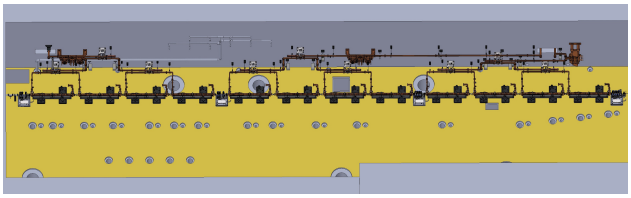

Figure 2: The second half of the ELI-NP linac.

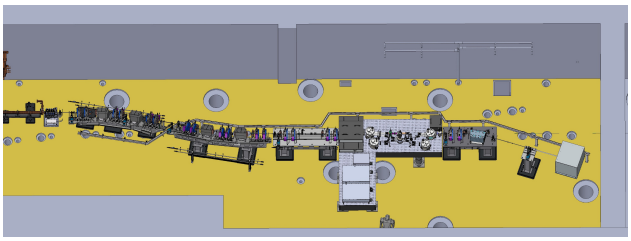

Figure 3: The transport line and the interaction section of the ELI-NP GBS.

IMPLEMENTED HIGH-LEVEL APPLICATIONS

The overall EPICS-based control architecture for the GBS LINAC is shown in Fig. 4. The system consists of device-level IOCs (Input/Output Controllers) that interface with hardware, a centralized archiver for data logging, and an alarm system for monitoring operational status. High-level applications interact with these components via Channel Access (CA) or PVAccess protocols. To achieve the goals of the commissioning process, we have developed Python-based high-level application software to support essential commissioning tasks, including gun phase scans, emittance measurements, beam energy measurements, and beam trajectory correction. The applications utilize key packages such as pyepics and matplotlib, and interface with soft IOCs

* This work is carried out under the contract PN 23 21 01 06 sponsored by the Romanian Ministry of Research, Innovation and Digitalization.
† guangling.chen@eli-np.ro

Content from this work may be used under the terms of the CC BY 4.0 licence (© 2026). Any distribution of this work must maintain attribution to the author(s), title of the work, publisher, and DOI.

ISBN: 978-3-95450-252-3 ISSN: 2673-5350 doi: 10.18429/JACoW-IPAC2026-WEP5128

ION TRANSPORT OPTIMISATION AT THE LOW ENERGY BRANCH

Z. Brencic* [1,2], M. Skobe[1], M. Kelemen[1], S. Sirca[2]
[1]Jožef Stefan Institute, Ljubljana, Slovenia
[2]University of Ljubljana, Ljubljana, Slovenia

Abstract

In majority of the accelerator beamlines, the goal is to achieve the highest possible desired beam throughput. When the beamline consists of only a few optical elements, beam transport optimisation can be achieved by adjusting a few knobs by an experienced operator. But when the beamline operates in a variety of regimes spanning the entire periodic table at various ion energies, the versatility makes beam transport optimisation challenging even for experienced operators. In this proceeding, we present the scaling formulas for optimizing ion transport through the Low Energy Branch (LEB) based on first-order transfer matrix formalisem and describe how we determine the optimal settings for the LEB optical elements.

INTRODUCTION

The Low Energy Branch (LEB) [1] at the Micro Analytical Center (MIC) [2] supplies a variety of high current (up to 50 µA) ion beams, ranging from light (e.g. H, He, C, B, ^{15}N), mid-mass (e.g. Si) to heavy (Ag, W, Pb, Bi) ion beams in the energy range of 100 eV up to 30 keV to different experimental stations.

The LEB consists of electrostatics steerers to correct for beamline misalignment in the $x-y$ plane and move the beam to desired location on the target, the dipole magnet to select the desired m/q ratio, and Einzel lens for focusing the beam. To verify ion transport three Faraday Cup (FC) detectors are used. For full layout of the ion optical components see Fig. 1.

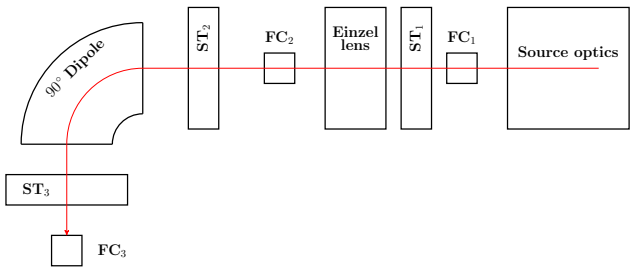

Figure 1: Beam optics elements of the LEB, ST stands for electrostatic $x-y$ steerer.

TRANSPORT OPTIMISATION

When optimising transport through an ion beamline we need to go through several levels of optimisation:

I. Choose the optical elements needed for beam manipulation given desired energy range, mass range and beam currents.

II. Determine the dimensions of optical elements.

III. After the assembly determine the beam element misalignment, imperfections, power supply instabilities.

IV. Determine the parameter ranges that the optical elements will operate in.

V. Maximise the beam current through the beamline by taking into account the beam phase space and all points above.

Steps I and II were performed and completed during the design phase of the LEB. In step II we relied on phase space measurements of the beam exiting the accelerator sources to constrain the design parameters of the optical elements in the LEB. Step III is still underway.

In the upcoming chapters, we cover the optimisation steps IV and V. We use ^{4}He$^+$ beam as a tool for calibration of optics, determination of misalignment and optics scaling factors.

LEVEL IV. OPTIMISATION

At this stage of optimisation we want to determine in what parameter ranges we will operate the components, starting with the dipole magnet.

90-degree Dipole Magnet

LEB has a Danfysik 90-degree dipole magnet with bending radius of $\rho = 240$ mm, exit and entrance angles of 26.6°, and a pole gap of 25 mm. The magnet can operate with coil currents of up to 52 A, but is operated with currents of up to 50 A to avoid overheating.

The current needed to bend the ion of interest (m, q) with specific energy kinetic energy E_k is given by:

$$I_{\text{dipole}} = \frac{D}{\rho}\sqrt{\frac{m * E_k}{q^2}}. \quad (1)$$

The scaling constant D was obtained via calibration using pure ^{4}He$^+$ beam at 20 keV, for which the dipole had to be set to $I_{\text{dipole}} = 9.2$ A, giving us $D = 257.148$ A mm $e_0/\sqrt{\text{keV amu}}$.

For the operation of the beamline we are interested in the maximal kinetic energy that can be bent with the dipole for different ion beams of interest: ^{4}He$^+$ = 590.73 keV, ^{14}N$^+$ = 168.78 keV, ^{28}Si$^+$ = 84.39 keV, ^{120}Sn$^+$ = 19.69 keV and ^{208}Pb$^+$ = 11.36 keV. The dipole coil current constrains the maximal energy of ions we can transport for masses above 110 amu to 20 keV or below, despite the fact

* ziga.brencic@ijs.si

Content from this work may be used under the terms of the CC BY 4.0 licence (© 2026). Any distribution of this work must maintain attribution to the author(s), title of the work, publisher, and DOI.

ISBN: 978-3-95450-252-3 ISSN: 2673-5350 doi: 10.18429/JACoW-IPAC2026-WEP5129

BENCHMARKING OF THE PENELOPE/PENH AND PHITS CODES FOR CALCULATION OF BEAM QUALITY CORRECTION FACTORS IN THERAPEUTIC PROTON BEAMS

Y. Kubyshin*, E. Marin, J. Sempau, Universitat Politècnica de Catalunya, Barcelona, Spain

Abstract

This work benchmarks the PENELOPE/PENH (2021 version) and PHITS Monte Carlo codes to calculate the beam quality correction factor (k_Q) in therapeutic proton beams. The latest PENH extension to PENELOPE enables proton transport simulation, including an approximate description of nuclear reactions and neutron production. PHITS, conversely, is an established multi-particle transport code covering protons, neutrons, and electron-gamma showers. The study compares simulated absorbed doses and k_Q factors by modeling two configurations: a thin reference water cavity and a plane-parallel air cavity representing a typical ionization chamber. To determine the k_Q factors, simulations involve a 1.25 MeV photon reference beam (Cobalt-60) and a 150 MeV monoenergetic proton beam. This comparison assesses the suitability and consistency of the PENELOPE/PENH and PHITS codes for accurate clinical proton beam dosimetry.

INTRODUCTION

The radiation therapy dosimetry protocols (see for example [1]) are based on absorbed dose in photon or proton beams to water in reference conditions. It is determined by measurements with air-filled ionization chambers and using the so-called beam quality correction factor k_Q which takes into account the difference between the reference beam quality Q_0 used for chamber calibration (e.g. MV photons) and the user beam quality (e.g. high-energy protons).

Following the approach introduced in Ref. [2] we consider beam quality correction factor defined as

$$k_Q = \frac{f_Q}{f_{Q_0}} \frac{W_{air,Q}}{W_{air,Q_0}} \,. \tag{1}$$

Here $W_{air,Q}$ and W_{air,Q_0} are the mean energies required to create an ion pair in air for the beam qualities Q and Q_0, respectively. The factor f_Q is calculated as the ratio

$$f_Q = \frac{D_{w,Q}}{D_{a,Q}} \,, \tag{2}$$

where $D_{w,Q}$ is the absorbed dose to water in a water-filled reference volume and $D_{a,Q}$ is the absorbed dose to air in an air-filled volume representing the cavity of an ionization chamber.

The direct way to determine k_Q factors is to measure them with one of ionization chambers for a user beam quality Q. However, this method requires quite complicated laboratory equipment, especially in the case of proton and ion beams, which is not available for most of the laboratories.

An efficient alternative is to perform Monte Carlo (MC) simulations using one of the existing codes, such as PENELOPE/PENH/penEASY or PHITS. There are numerous publications on this approach, see, for example, [3] and references therein.

In article [4] the beam quality correction factors in monoenergetic proton beams were calculated by detailed MC simulation of ionization chambers. In the present paper the absorbed doses and f_{Q_0} and f_Q ratios are calculated for simplified beam settings and simplified geometry representing the cavity of an ionization chamber.

The ratio of W_{air,Q_0} and $W_{air,Q}$ is determined experimentally, as described in the ICRU report 90 [5]. Here we will use the values $W_{air,Q_0} = 34.44$ eV, $W_{air,Q} = 33.97$ eV and $W_{air,Q}/W_{air,Q0} = 1.014(4)$ reported in Ref [4].

The aim of the paper is to benchmark the latest version of the MC code PENELOPE/PENH/penEASY [6, 7] that includes electromagnetic interactions, as an extension of the PENELOPE [8], and also nuclear reactions and neutron production. The penEASY (2024 version) provides a convenient interface to launch simulations.

The benchmark will be done by comparing results of simulations of absorbed doses to the reference water volume and an air-filled volume for two beam qualities, a photon beam and a proton beam, with the PENH and PHITS codes. PHITS [9–11] is a general purpose MC code that allows to simulate the transport of all main particles and nucleus over a wide energy ranges using several nuclear reaction models and nuclear data libraries.

We would like to mention a study that includes MC simulations of the absorbed doses and f_Q/f_{Q_0} ratios using several codes, namely the first version of PENH, FLUKA and GEANT4/TOPAS, and comparison of the obtained results [3]. Here we complete this work with the values obtained with the latest version of PENH and PHITS.

BEAM SETTINGS AND GEOMETRIES

The simulations of absorbed dose to water-filled and air-filled volumes were performed with the MC codes PENH and PHITS in the geometries and beam settings described in this section.

The beams are of square cross section of 10×10 cm^2 impinging on a surface of a water phantom. The photon beam is of energy 1.25 MeV modeling a ^{60}Co source, and the 150 MeV proton beam represents a radiotherapeutic irradiation. Both beams are monoenergetic, monodirectional and perpendicular to the water phantom surface.

* iouri.koubychine@upc.edu

Content from this work may be used under the terms of the CC BY 4.0 licence (© 2026). Any distribution of this work must maintain attribution to the author(s), title of the work, publisher, and DOI.

ISBN: 978-3-95450-252-3 ISSN: 2673-5350 doi: 10.18429/JACoW-IPAC2026-WEP5130

BENCHMARKING THE PENH MONTE CARLO CODE AGAINST PHITS: ASSESSMENT OF PROTON DEPTH-DOSE

Y. Kubyshin*, E. Marin†, J. Sempau‡, Universitat Politècnica de Catalunya, Barcelona, Spain

Abstract

This study provides a benchmark of the PENELOPE/PENH/PenEasy (2021 version) Monte Carlo code for proton transport using reference results from the established PHITS code. The comparison focuses on absorbed-dose distributions generated by a finite-spot proton pencil beam. Integrated depth-dose curves were simulated for energetic beams of 100 MeV and 226 MeV incident on a semi-infinite water phantom. The degree of agreement between PENH and PHITS is quantitatively assessed regarding the depth-dose behavior. The results evaluate PENH's accuracy and establish its suitability for general proton transport applications.

INTRODUCTION

Unlike conventional photon-based radiation therapy, proton radiotherapy offers a more pronounced dose profile characterized by the Bragg peak and a sharp distal dose falloff. These physical properties allow for highly conformal dose delivery to the tumor while minimizing damage to adjacent healthy tissue. However, because of this steep dose gradient, the precision of proton beam delivery is paramount in a clinical setting.

Monte Carlo (MC) simulations have been conducted by using the general-purpose radiation transport codes PENELOPE/PENH/PenEasy [1–4] (from now on PENH) and PHITS [5], which complements the benchmarking between PENH and PHITS conducted in [6].

This study follows a similar structure as Ref. [7], to benchmark various radiation transport codes, being PHITS among them.

PENH

The PENELOPE/PENH/PENEASY code represents a significant evolution in the Monte Carlo (MC) simulation code of radiation transport. The 2024 version of PENELOPE (PENetration and Energy Loss of Positrons and Electrons) has been extended to include proton interactions via the PENH library (2021 version). PENH introduces the necessary physics to model proton-matter interactions, including elastic scattering, electronic stopping, and nuclear reactions. This upgrade maintains the robust "mixed" simulation algorithm of its predecessor, combining hard events with multiple-scattering approximations to ensure both computational efficiency and high spatial accuracy. By integrating proton transport into the existing geometry and material handling systems of PENELOPE, PENH provides a versatile tool for applications in medical physics, such as proton therapy and space radiation protection. This unified approach allows for the simultaneous tracking of primary protons and their secondary electromagnetic cascades within complex geometries. Finally PENEASY (2024 version) provides the interface to launch the simulations.

PHITS

The PHITS code version 3.35, was employed for the inter-code comparison. Nucleon-induced nuclear reactions were modeled by the INCL4.6 model [8]. For neutron energies below 20 MeV, the transport is based on the cross section data library, JENDL-5.0 [9]. Photon and electron transports were calculated by the PHITS built-in EGS5 [10] algorithm.

OBJECTIVES

The main goal is to validate the suitability of PENH to transport protons against the well established by the scientific community radiation transport code, PHITS. The study focuses on the absorbed-dose distributions in a water phantom for two scenarios, regarding the energy of the incident proton beam. The results obtained by PENH and PHITS for each scenario are presented and discussed.

SIMULATION FRAMEWORK

The simulated scenarios, the beam definition and the parameters of the Monte-Carlo simulation for both codes are presented below.

Scenarios

The Integrated Depth Dose Curves (IDDCs) of a pencil proton beam of two energies are considered in this study:

1. 100 MeV (Scenario-1) and,
2. 226 MeV (Scenario-2).

In both scenarios, a mono-energetic and mono-directional proton pencil beam enters a semi-infinite lateral extent water phantom. The depths of the water phantom for scenarios 1 and 2 are 10 cm and 40 cm, respectively, to capture the Bragg peak location.

The absorbed doses were scored by disks of 5 cm radius and 1 mm depth, distributed along the beam direction. The disk radius of 5 cm is chosen to capture all energy deposition. Figure 1 shows the dose obtained at the Bragg peak (blue data) as a function of the radius. Fitting a Gaussian curve to that profile leads to a 1-σ equal to (0.67 cm) which is almost a factor of 10 larger than the considered disks.

* iouri.koubychine@upc.edu
† eduard.marin.lacoma@upc.edu
‡ josep.sempau@upc.edu

Content from this work may be used under the terms of the CC BY 4.0 licence (© 2026). Any distribution of this work must maintain attribution to the author(s), title of the work, publisher, and DOI.

ISBN: 978-3-95450-252-3 ISSN: 2673-5350 doi: 10.18429/JACoW-IPAC2026-WEP5132

FAST AND ACCURATE ACCELERATOR MODELLING WITH FLUKA CAD GEOMETRY WORKFLOW

V. Rodin*[1,2], F. Cerutti[1], L. S. Esposito[1], H. Guerin[1], G. Hugo[1], A. Lechner[1], C. Theis[1], V. Vlachoudis[1]
[1]CERN, Geneva, Switzerland
[2]Jean Monnet University, Saint-Étienne, France

Abstract

Accurate geometric representation is essential in accelerator beam-matter interaction Monte-Carlo simulations, yet conventional Constructive Solid Geometry (CSG) modeling of beamline elements or tunnels remains time-consuming and error-prone. Recent FLUKA developments [1–3] offer a robust alternative to manual CSG implementation by introducing a CAD-based (Computer Aided Design) workflow. The new approach supports CAE (Computer Aided Engineering) volumetric meshes and the direct import of meshes generated in Gmsh, Ansys, or Abaqus [4–6]. This workflow is expected to accelerate model development, particularly for complex geometries. Benchmark comparisons will be presented between FLUKA conventional CSG geometries, FLUKA CAE-mesh geometries, and an independent development carried out in Geant4 to support CAD surface meshes [7]: the results demonstrate that while CAE meshes introduce a modest performance penalty, they provide substantial gains in accuracy, maintainability, and interoperability across design and simulation environments.

INTRODUCTION

In high-energy particle experiments, nuclear physics, and accelerator science, the fidelity of Monte Carlo simulations is fundamentally limited by the accuracy of the underlying geometric model. As modern accelerator designs evolve toward increasingly complex and large configurations, manual Combinatorial Solid Geometry descriptions have become both time-consuming and prone to systematic errors. Consequently, the field is undergoing a necessary transition toward automated, high-fidelity geometry workflows based on CAD and CAE methodologies.

This shift reflects not only the growing geometric complexity of modern accelerator infrastructure but also the practical need to maintain consistency between simulation models and rapidly evolving hardware prototypes. In this context, geometry handling is no longer a purely technical step but a critical component of simulation reliability. At the core of this transition lies the FLUKA geometry kernel, which must efficiently answer two basic queries: the identification of the volume containing each particle, as well as the subsequent volume along its trajectory. The computational speed and precision of these operations are directly determined by the chosen geometric representation. While CSG provides a mathematically well-defined and historically robust framework, its scalability becomes increasingly limited for complex accelerator components.

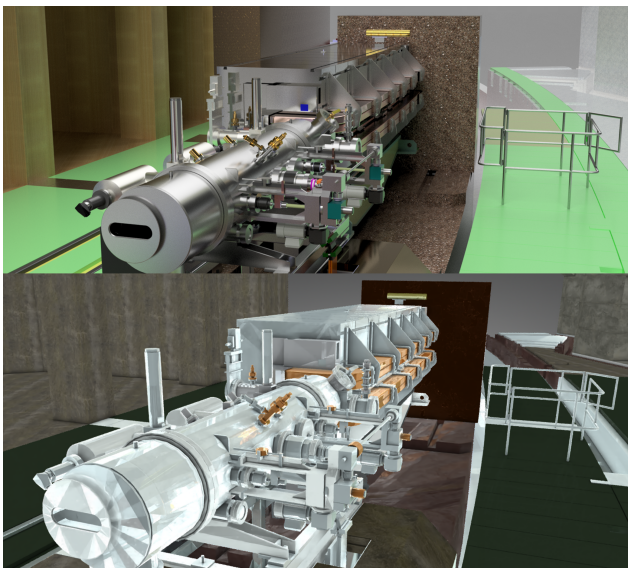

Figure 1: Example of PS geometry implementation for an extraction septa, a dipole magnet, a beam loss monitor, shielding and tunnel infrastructure. (Top) CAD model rendering with Autodesk Fusion 360 [8]. (Bottom) Imported geometry rendering in Flair [9] using the FARM4 path-tracing engine. Various materials were assigned for visual clarity.

In contrast, mesh-based representations introduce a fundamentally different approach. Tessellated surface meshes, typically obtained either directly (e.g., STL, 3MF) or through the discretisation of CAD boundary representations such as STEP, consist of polygonal facets approximating the geometry in a more precise way. Unlike CSG these meshes are not guaranteed to be strictly watertight or manifold, and may contain gaps or inconsistencies that lead to ambiguities in particle tracking.

The introduction of a CAD-to-CAE workflow since FLUKA v4-5.0 represents a significant advancement in this context. Multiple unstructured mesh geometries can be directly imported using standard formats (TetGen, Abaqus, ANSYS and Nastran), with all elements internally mapped to first-order tetrahedra to ensure consistency in tracking. To enable this capability, the core geometry construction, tracking, and scoring algorithms in FLUKA have been extended to support unstructured meshes. On the user side, CAD geometries can be converted using either commercial tools such as ANSYS [5] or open-source solutions like Gmsh [4]. In this context, a complementary meshing script is provided to FLUKA users [10], which leverages open-source tools,

* volodymyr.rodin@cern.ch

Content from this work may be used under the terms of the CC BY 4.0 licence (© 2026). Any distribution of this work must maintain attribution to the author(s), title of the work, publisher, and DOI.

ISBN: 978-3-95450-252-3 ISSN: 2673-5350 doi: 10.18429/JACoW-IPAC2026-WEP5134

A SPATIAL BORIS-LIKE SCHEME FOR PARTICLE TRACKING IN MAGNETOSTATIC FIELDS: IMPLEMENTATION AND PROPERTIES

G. Iadarola[1], S. Buijsman[1,2], R. De Maria[1]
[1]CERN, Geneva, Switzerland
[2]EPFL, Lausanne, Switzerland

Abstract

Accurate and stable integration of charged-particle motion in complex magnetic fields is essential for beam-dynamics simulations in accelerators and beam lines. For the Xsuite simulation framework we have recently developed a spatially discretized Boris-like algorithm that advances particle coordinates using the longitudinal position as the independent variable. The scheme retains the symmetric kick–rotate–kick structure of the standard time-based Boris pusher, ensuring exact preservation of the total momentum magnitude and of the phase-space volume. We derive its formal properties using operator-splitting and backward-error analysis, showing that it is second-order accurate, and that the symplectic error scales quadratically with the integration step. Such properties are also verified by numerical tests on a representative field distribution.

INTRODUCTION

The Boris algorithm [1] is widely used for charged-particle tracking because it is explicit, second-order accurate, volume preserving, and robust over long integrations [2, 3]. In accelerator and beam-line simulations, however, the natural independent variable is often the longitudinal coordinate rather than time. Spatial Boris variants have therefore been considered for beam applications [4, 5].

We have developed a spatial Boris-like integrator for tracking in arbitrary magnetostatic field distributions within the Xsuite simulation framework [6, 7]. The method advances particles using the longitudinal coordinate z as independent variable, while retaining a symmetric drift–kick–rotate–kick–drift structure. This paper summarizes the algorithm, the main preservation and accuracy properties, and numerical checks performed with a solenoid field including fringe terms; full derivations are given in Ref. [8].

SPATIAL FORM OF THE EQUATIONS

For a particle of charge q and momentum P in a magnetostatic field, we can write:

$$\frac{dP}{dt} = qv \times B, \qquad v = \frac{P}{\gamma m}. \tag{1}$$

The total momentum $P = |P|$ is constant. Assuming that the longitudinal component of the momentum P_z does not vanish, the equations can be rewritten using z as independent variable:

$$\frac{dP}{dz} = \frac{q}{P_z} P \times B, \qquad \frac{dr}{dz} = \frac{P}{P_z}. \tag{2}$$

If the magnitude of the momentum is known, the longitudinal component can be obtained from the transverse components as

$$P_z = \sqrt{P^2 - P_x^2 - P_y^2} > 0. \tag{3}$$

In accelerator variables the elapsed time satisfies

$$\frac{dt}{dz} = \frac{\gamma m}{P_z}. \tag{4}$$

BORIS-LIKE SPATIAL STEP

Let $h = \Delta z$ be the step size. The Boris-like step is built as a symmetric drift–kick–rotate–kick–drift composition, defined by the following steps.

Step 1: first half drift

Starting from (x, y, z, P_x, P_y), compute P_z from Eq. (3) and drift the transverse coordinates by half a longitudinal step:

$$x_h = x + \frac{h}{2}\frac{P_x}{P_z}, \qquad y_h = y + \frac{h}{2}\frac{P_y}{P_z}, \qquad z_h = z + \frac{h}{2}. \tag{5}$$

Step 2: field evaluation

The magnetic field $B = (B_x, B_y, B_z)$ is evaluated at (x_h, y_h, z_h).

Step 3: first half kick

The transverse field components B_x and B_y give the first half kick:

$$P_x^- = P_x - \frac{qh}{2} B_y, \qquad P_y^- = P_y + \frac{qh}{2} B_x, \tag{6}$$

Step 4: midpoint longitudinal momentum

The longitudinal momentum used in the central rotation is reconstructed after the first half kick:

$$P_{z,\mathrm{mid}} = \sqrt{P^2 - (P_x^-)^2 - (P_y^-)^2}. \tag{7}$$

Step 5: Boris rotation

The longitudinal field component B_z generates a rotation in the transverse momentum plane. The exact frozen-field rotation angle is approximated with an $O(h^3)$ error, using the following rational coefficients:

$$T = \frac{qB_z h}{2P_{z,\mathrm{mid}}}, \qquad S = \frac{2T}{1+T^2}, \qquad C = \frac{1-T^2}{1+T^2}. \tag{8}$$

Content from this work may be used under the terms of the CC BY 4.0 licence (© 2026). Any distribution of this work must maintain attribution to the author(s), title of the work, publisher, and DOI.

ISBN: 978-3-95450-252-3 ISSN: 2673-5350 doi: 10.18429/JACoW-IPAC2026-WEP5137

XBOINC: A FRAMEWORK FOR VOLUNTEER-BASED BEAM DYNAMICS SIMULATIONS USING XSUITE

C.E. Montanari[1*], D. Di Croce, M. Giovannozzi, S. Redaelli,
F. Van Der Veken, CERN, Geneva, Switzerland
T. Pieloni, EPFL, Lausanne, Switzerland
[1]also at University of Manchester, Manchester, United Kingdom

Abstract

The Xboinc Python package extends the LHC@Home volunteer computing project by integrating the Xsuite simulation toolkit within the BOINC platform. Designed to be the successor to SixTrack's BOINC implementation, the Xboinc framework enables large-scale single-particle tracking based on the novel simulation package Xsuite. Using the computational power of global volunteer computing, Xboinc on LHC@Home provides scalable resources for advanced accelerator physics simulations, such as dynamic aperture studies. The previous functionalities were extended, notably by enabling collimation performance and loss map simulations thanks to the new Xcoll implementation in Xsuite. The synergy between distributed computing and public engagement ensures the continuity of volunteer contributions to particle accelerator research and paves the way for present and future large-scale simulation campaigns.

INTRODUCTION

Since its launch in 2004, the LHC@Home project [1] has used and contributed to the Berkeley Open Infrastructure for Network Computing (BOINC) [2] to harness the idle computing power of volunteers around the world. Volunteer computing provides large scalable computational resources that are particularly well suited for large-scale simulations with modest data transfer per job. For the accelerator physics community, this distributed computing model has historically provided a sustained computational capacity comparable to large Tier-2 Grid sites and making extremely demanding numerical studies more viable [3, 4].

For nearly two decades, LHC@Home has hosted an accelerator physics-oriented project based on SixTrack, the well-established Fortran-based single-particle tracking code [5]. SixTrack leveraged this global volunteer network to conduct large-scale tracking campaigns. These extensive simulations were critical for evaluating the Dynamic Aperture (DA) [6–8], the region in phase space where particle motion remains stable, for the Large Hadron Collider (LHC) [9], considering particle trajectories for up to $10^5 - 10^6$ turns.

Despite SixTrack's historic success, modern scientific computing increasingly relies on flexible, modular setups that can easily interface with general-purpose libraries. To address this, the Xsuite project was launched in 2021 [10,11], combining the capabilities of legacy tools like SixTrack into a single, modern Python-based framework designed for conventional CPUs and GPU computing.

To succeed SixTrack's legacy on volunteer networks, the Xboinc Python package has been developed [12]. Xboinc seamlessly integrates the Xsuite simulation toolkit within the BOINC platform, ensuring the continuity of large-scale single-particle tracking by the volunteer community. Furthermore, transitioning to Xsuite greatly expands the physics functionalities available on LHC@Home. Notably, using Xsuite's Xcoll module [13], Xboinc enables complex particle-matter interaction simulations, allowing for advanced collimation performance evaluations and loss map simulations directly on volunteer machines, a feature that was not available in the previous SixTrack implementation. In this paper, we present an overview of the implementation of the Xboinc framework, detailing its current applications, computational advantages, and technical boundaries. Finally, we outline future development strategies to support volunteer computing for present and future particle colliders.

THE XBOINC PACKAGE

The central challenge of deploying Xsuite on BOINC stems from its architecture: Xsuite is a Python framework that generates and compiles C kernels at runtime, making it impossible to distribute as a frozen executable, as was done for SixTrack. Moreover, the majority of the volunteer machines run native Windows, further complicating the deployment. Xboinc addresses this by exploiting a key property of Xsuite: when simulating beam lines without collective effects, the computationally intensive tracking stage executes entirely in compiled C/C++ code. By leveraging Xobjects and pre-compiled kernels tied to a fixed Xsuite version, it is possible to build a universal C/C++ tracker that covers a broad set of tracking use cases while remaining fully BOINC-compatible.

The Xboinc framework produces two artefacts from this approach: a cross-platform binary executable implementing the tracker and a Python package that manages job submission and results. The binary implements a fixed *input* → *tracking* → *output* pipeline: it receives a serialised beam line and particle ensemble together with tracking parameters (e.g. number of turns), performs tracking, and returns the tracked particles. The binary is compiled for multiple platforms using a CMake + VCPKG build system, currently targeting Linux (64-bit and 32-bit) and native Windows (64-bit and 32-bit), covering the large majority of volunteer machines.

* carlo.emilio.montanari@cern.ch

Content from this work may be used under the terms of the CC BY 4.0 licence (© 2026). Any distribution of this work must maintain attribution to the author(s), title of the work, publisher, and DOI.

ISBN: 978-3-95450-252-3 ISSN: 2673-5350 doi: 10.18429/JACoW-IPAC2026-WEP5138

PROGRESS AND DEVELOPMENTS OF BEAM DELIVERY SIMULATION (BDSIM)

S. Alden[1], W. Shields [1], A. Keyken[1], M. Pereira[1], N. Nishi[1],
Royal Holloway University of London, United Kingdom
S. Boogert[2], M. Deniaud[2], D. Christie[2], J. Burvill[3], P. Mooney[3],
University of Manchester, Manchester, United Kingdom
M. Mannie-Corbisier, Université Libre de Bruxelles, Brussels
B. Lindstrom, L. Nevay, R. Kieffer,
European Organization for Nuclear Research (CERN), Geneva, Switzerland
P. Jurj, R. Kamath, Imperial College London, London, United Kingdom
C. Rogers, Science and Technology Facilities Council, Swindon, United Kingdom
[1] also at The John Adams Institute for Accelerator Science, London, United Kingdom
[2] also at Cockcroft Institute, Daresbury, United Kingdom
[3] also at European Organization for Nuclear Research (CERN), Geneva, Switzerland

Abstract

Beam Delivery Simulation (BDSIM) is a Monte Carlo program (written in C++) that creates a 3D radiation transport model designed for the simulation of accelerators and beamline modelling. BDSIM uses Geant4 for precise particle-matter interactions combined with particle-tracking through 3D geometries of accelerators and their environments. All particle species are tracked, allowing for studies for collimation, beam losses, secondary radiation generation, and dosimetry. BDSIM allows for detailed customisation, with numerous applications in the design of high-energy physics facilities, medical beamlines, particle detection experiments, and novel acceleration experiments. Recent developments to BDSIM are presented, including; coupling between BDSIM and external tracking codes, updates to the muon cooling modelling, updates to DICOM file handling, applications of BDSIM for FCC-ee, scintillation and synchrotron radiation options for secondary control, and general updates.

INTRODUCTION AND GENERAL UPDATES

BDSIM is a Monte Carlo particle-tracking code that uses the Geant4 toolkit to construct 3D models of accelerator and their environment. It is capable of modelling particle-matter interactions and is suited for studies in a wide range of accelerator applications [1, 2]. BDSIM is well supported on multiple platforms, including Conda, Docker, Apptainer, and compilation from source on all common operating systems. BDSIM developers welcome any interested users and contributors who will be supported by the BDSIM community [3].

Sparse Histogram Storage

In BDSIM, output histograms are stored on a per-event basis in a dense format, where the values of all bins are recorded even if they are zero. For situations where there is a low occupancy of the histogram at each event, this can be a source of significant inefficiency in both memory and storage as many zeroes are unnecessarily stored. An option has been developed to instead use sparse histograms which only store the positions of *filled* bins as a vector. This reduces the memory and storage requirements of, for example, scoring meshes and energy loss histograms. A comparison of the size of ROOT files storing per-event histograms is shown in Figure 1, where a significant difference is visible between the storage methods at low occupancies.

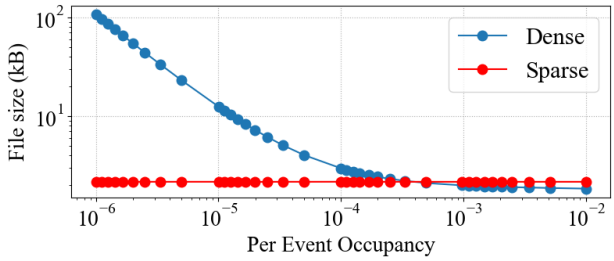

Figure 1: Per-event size of ROOT files output by BDSIM against the occupancy of the stored histograms, comparing between dense and sparse methods of storage.

Sub-Element Scoring

To score a volume in BDSIM, a scoring mesh, limited to a box or cylinder, is typically overlayed across an element within the model. Most elements, however, are composed of multiple volumes and can therefore be decomposed into sub-elements, representing the finest level of 3D geometry. A method of scoring across these specific sub-elements, using their volume as the scoring volume, is being implemented. Each physical volume is registered at construction to an integer identifier and each energy deposit is attributed to a sub element via this identifier. The total energy deposited in each sub-element can then be aggregated. An example model FCC-ee Beamstrahlung dump, shown in Figure 2,

Content from this work may be used under the terms of the CC BY 4.0 licence (© 2026). Any distribution of this work must maintain attribution to the author(s), title of the work, publisher, and DOI.

ISBN: 978-3-95450-252-3 ISSN: 2673-5350 doi: 10.18429/JACoW-IPAC2026-WEP5140

THE 3D-PIC SIMULATION OF THE BEAM-PLASMA INTERACTION INSIDE OF GABOR LENSES*

M. Droba†, [1], O. Meusel[1], H. Podlech[1, 2], K. I. Thoma[1],
[1]Goethe University Frankfurt am Main, Germany
[2]HFHF - Helmholtz Research Academy Hesse for FAIR GSI
Helmholtzzentrum für Schwerionenforschung, Campus Frankfurt , Germany
K. Schulte-Urlichs, GSI Helmholtz Centre for Heavy Ion Research, Darmstadt, Germany

Abstract

Experimental results of the beam transport through a Gabor lens system were not fully understood in the past. The measurement campaign presented at IPAC2013 will be considered as an example with an alternative explanation. Simulation results done by the TraceWin code will be presented and beam impact on the electron column discussed. Especially production of secondary electrons by an ion impact can have massive influence on plasma state and creating waves and instabilities. Additionally, a large scale multi-particles 3D Monte-Carlo-PIC (particle-in-cell) simulations with electrons and ions were carried out. Goal was to understand collective phenomena in non-neutral plasma generated by passing beam in various scenarios. Up to 10^7 macroparticles were implemented in parallel processing on 50 processors of the FUCHS Cluster. Possible influence on the focusing properties and imaging quality will be evaluated and the dependence on time scale and ion beam energy discussed. Simulation results will be presented with an impact on future designs.

INTRODUCTION

Gabor-lens(GL) [1-3] is a cylindrical trap for creation and confinement of rotating electron column in static magnetic and electric fields. Stable and homogenous electron clouds of sufficient densities ($n \sim 10^{14}$ m^{-3}) can be created at specific conditions inside of the lens. Many different types of GL devices were built and studied in Frankfurt University in recent years. Their main application in accelerator physics are space charge compensation and hadron beam focusing from keV up to GeV range. Dynamic processes and waves in an electron column can be generated and applied for hadron beam handling and collimations. The progress in vacuum level control and diagnostics improve reproducibility and stability of the working points. Understanding of diffusion processes across the electric and magnetic fields was important for evaluation of the electron losses and overall efficiency of a production process. The last point also raises questions about possible acting of the GL as a reservoir for the space charge compensation both beam upstream and downstream in a connection with low energy beam lines. That lead also for some reconsideration of the experiments done in the past. Palkovic[4-6] studied focusing properties of the GL placed direct after a duo-plasmatron source in late 80´s. The about 50 mA proton beam was focused at 44 keV kinetic energy and angle acceptance of the ±40 mrad. The measured large emittance growth of the factor 4 was explained as explosive growth due to the space charge explosion direct after the source in a few cm distance in front of a GL.Schulte [7,8] tested 3 mA, 50 keV He^+ and 35 mA, 124 keV Ar^+ beam focusing with a GL at the GSI High Current Test Injector (HOSTI) in mid-2012. The beam phase space distributions were measured with and without GL potential at the end of the beam-line. Because of lost (GL off) and captured (GL on) beam particles overall efficiency was hard to evaluate exactly. Simulations started with back-tracing of the measured distribution at GL off, thus this calculated distribution was used as a starting distribution in all further simulations at various conditions. However, this approach ignored losses along the beam path and underestimated starting emittance. Reversely, emittance growth was overestimated. Assumption of the hollow electron column at low magnetic field levels was another fact needed for the explanations and comparison between simulations and measurements. However, this contradicts experiences from the electron density measurements. In the following, we present different approach, based on the knowledge of the S-shaped initial distribution, similar to that measured at the HOSTI direct behind ion source downstream in 2009 [9].

LEBT SIMULATION

The numerical simulations were carried out with TraceWin code and all geometry data can be found in [8,9]. Initial beam parameters were set I_b=3 mA, W=50 keV He^+ in a distance of 210 mm (Fig. 6.8 in [8]) in front of the GL. GL itself was implemented as modelled cylindrical field map with linear radial electric field. Initial particle distribution was chosen to be of a Gaussian-type with a modified S-shape contour, as seen in Fig. 1 (left).

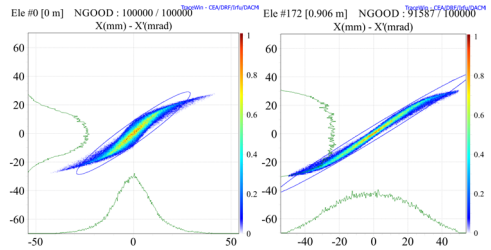

Figure 1: Input(left) and output(right) particle distribution. GL was off and overall transmission achieves 91,6% level.

†droba@iap.uni-frankfurt.de

Content from this work may be used under the terms of the CC BY 4.0 licence (© 2026). Any distribution of this work must maintain attribution to the author(s), title of the work, publisher, and DOI.

ISBN: 978-3-95450-252-3 ISSN: 2673-5350 doi: 10.18429/JACoW-IPAC2026-WEP5144

ION TRAPPING STUDIES AND MITIGATION STRATEGIES FOR THE EIC ERL-BASED STRONG HADRON COOLER

R. Bi*, R. Apsimon, Lancaster University, Lancaster, UK
N. Sereno, S. Setiniyaz, K. Deitrick
Thomas Jefferson National Accelerator Facility, Newport News, VA, USA

Abstract

An Energy Recovery Linac based strong hadron cooler was previously considered for the Electron-Ion Collider. The required electron beam parameters for variable-energy strong hadron cooling place significant constraints on ion trapping and collective effects. This paper presents initial studies of these constraints through a combination of analytical modelling and numerical simulations of ion production, trapping behaviour, and mitigation strategies. A multi-bunch tracking framework based on `ELEGANT` with the `ionEffects` module is used to simulate machine operation over millisecond time scales, corresponding to more than 3×10^5 electron bunches. The simulations include modelling of ionisation processes together with transverse electron–ion dynamics, allowing the evolution and accumulation of ions to be investigated. Analytical expressions based on Gaussian beam distributions are used to estimate ion trapping conditions and benchmark the simulation results. A bi-periodic bunch spacing scheme is also investigated as a possible mitigation method by detuning the ion oscillation frequency. These studies provide an initial assessment of ion trapping in the strong hadron cooler and demonstrate possible approaches for reducing beam–ion effects.

INTRODUCTION

The Electron-Ion Collider (EIC) requires efficient beam cooling to achieve high luminosity. An Energy Recovery Linac (ERL)-based strong hadron cooler is a promising option because it can sustain high average current and continuous operation. However, the high repetition rate and bunch charge also introduce significant beam–ion collective effects. Residual-gas ionisation produces ions that can accumulate and become trapped in the electron beam potential, resulting in emittance growth and particle loss.

This is particularly important in ERL systems, where millisecond-scale operation corresponds to hundreds of thousands of bunch passages, enabling a cumulative build-up of ions within the beam potential. As a result, beam–ion interactions can progressively intensify, leading to significant ion accumulation and eventual particle loss if no mitigation is applied. These considerations motivate a detailed study of ion trapping and its mitigation in ERL-based coolers.

ION TRAPPING CRITERION

Ion trapping is analysed using a linear kick–drift model, in which each bunch passage provides a transverse focusing kick followed by a drift over the bunch spacing S. The corresponding kick and drift transfer matrices are

$$K(a) = \begin{pmatrix} 1 & 0 \\ -a & 1 \end{pmatrix}, \qquad D(S) = \begin{pmatrix} 1 & S \\ 0 & 1 \end{pmatrix}, \tag{1}$$

where $K(a)$ represents the transverse focusing kick with effective focusing strength a, and $D(S)$ represents the drift over the bunch spacing S. The analysis applies independently to the horizontal and vertical planes, with focusing strengths

$$a_{x,y} = \frac{2N_e r_p Q}{A_{\text{ion}}\,\sigma_{x,y}(\sigma_x + \sigma_y)}, \tag{2}$$

as given in [1], where N_e is the bunch population, r_p the classical proton radius, σ_x and σ_y the transverse beam sizes, Q the ion charge state, and A_{ion} the ion mass number.

For a uniformly spaced bunch train, the one-period transfer matrix becomes

$$M = K(a)D(S) = \begin{pmatrix} 1 & S \\ -a & 1 - aS \end{pmatrix}. \tag{3}$$

Stable ion motion requires $|\mathrm{Tr}(M)| \le 2$ [2], leading to

$$0 \le aS \le 4. \tag{4}$$

Ions are trapped when this condition is satisfied, allowing stable confinement within the beam potential over many bunch passages. Since ion accumulation is undesirable, the unstable regime

$$aS > 4, \tag{5}$$

is preferred for ion clearing. The corresponding critical ion mass can be written as [1, 3]

$$A_{x,y} = \frac{N_e r_p S Q}{2\,\sigma_{x,y}(\sigma_x + \sigma_y)}, \tag{6}$$

with the instability condition

$$A < A_{\text{crit}} = \min(A_x, A_y), \tag{7}$$

indicating that lighter ions are more likely to escape the beam potential.

Figure 1 shows the transverse RMS beam sizes along the ERL beamline obtained from the BMAD lattice model. The beam sizes vary significantly along the lattice and directly affect the local trapping condition. The resulting critical mass A_{crit} is shown in Fig. 2. It can be seen that A_{crit} remains below the mass of H_2 over most of the lattice, indicating that even the lightest ions are trapped over a large fraction of the beamline. Only a short region of approximately 0.17 m exhibits $A_{\text{crit}} > A_{H_2}$, where H_2^+ ions are not trapped.

* r.bi@lancaster.ac.uk

Content from this work may be used under the terms of the CC BY 4.0 licence (© 2026). Any distribution of this work must maintain attribution to the author(s), title of the work, publisher, and DOI.

ISBN: 978-3-95450-252-3 ISSN: 2673-5350 doi: 10.18429/JACoW-IPAC2026-WEP5145

RECIRCULATION MODELLING FOR ENERGY-RECOVERY LINACS*

L. Vanhecke† [1], A. Latina[2], T. Pieloni[1], M. Seidel[1,3]
[1]École Polytechnique Fédérale de Lausanne (EPFL), Lausanne, Switzerland
[2]CERN, Geneva, Switzerland
[3]Paul Scherrer Institute, Villigen PSI, Switzerland

Abstract

A flexible simulation scheme has been developed as a high-level `Python` wrapper around `RF-Track` to enable fully self-consistent simulations of recirculating and energy-recovery linear accelerators (ERLs). This framework dynamically routes multi-bunch beams through multiple beamlines based on their evolving phase-space parameters and is integrated directly into the `RF-Track` tracking workflow. Within this scheme, a wakefield model has been implemented that enables higher-order modes to be self-consistently excited and evaluated over successive recirculation passes. This approach enables realistic modelling of multi-pass beam dynamics, including the accumulation of wakefields from previously transported bunches. Two independent benchmarking campaigns have been carried out. The recirculation scheme has been benchmarked against `MAD-X` and `Bmad/Tao`, demonstrating consistent beam transport and routing behaviour across multiple passes. Separately, the wakefield model was validated against `Xwakes`, showing close agreement and confirming the correct implementation of wakefield effects. These results demonstrate the robustness of the approach and provide a pathway toward comprehensive start-to-end simulations of ERL operation.

INTRODUCTION

Energy-recovery linear accelerators (ERLs) [1, 2] represent an important advancement in modern accelerator physics, offering high beam power and excellent beam quality while significantly reducing overall power consumption. Simulating these machines presents unique computational challenges, as the beam is recirculated through the same Radio-Frequency (RF) structures over multiple passes to enable energy recovery, thereby coupling the dynamics of accelerating and decelerating bunches. To fully capture these complex interactions, a modern and flexible computational approach is required to simulate recirculating lattices effectively. The primary motivation for this work is to develop a highly adaptable tool for seamless start-to-end simulations of recirculating accelerators, enabling advanced beam dynamics studies and providing a flexible platform for the design and optimisation of future ERLs.

* Work supported by the Innovate for Sustainable Accelerating Systems (iSAS) and the European Union via its program HORIZON-INFRA-2023-TECH-01-01 under GA No. 101131435
† lode.vanhecke@epfl.ch

MODELLING METHODS

Recirculation Model

A flexible recirculation scheme has been developed and integrated as an extension of `RF-Track` [3], introducing a high-level machine controller that enables self-consistent tracking of recirculating beams through arbitrary lattice configurations. The core of the method is a dynamic routing and tracking algorithm that operates on individual bunches while preserving full six-dimensional phase space information and allowing collective effects such as wakefields to accumulate across multiple passes.

The machine is initialised from a user-defined beam distribution and a lattice description, provided as a structured configuration of seperate beamlines. During initialisation, this description is parsed and converted into `RF-Track`-compatible tracking objects, with each element mapped to its corresponding representation, including RF cavities, drifts, and multipole magnets. RF cavities are constructed from either analytical models or external electromagnetic field maps, with automatic scaling to match the desired accelerating voltage and phase.

A routing table defines the connectivity between beamlines, specifying the next beamline to be traversed after each pass of an individual bunch. This routing can be static or conditional. In the latter case, it selects beamlines dynamically based on desired bunch properties such as average beam energy, enabling energy-dependent routing that is essential for multi-pass recirculating lattices common in ERLs.

The framework additionally supports the generation and transport of arbitrary bunch trains, where individual bunch properties such as charge, timing, phase-space coordinates, and initial offsets can be independently specified. This allows realistic modelling of non-uniform filling patterns and injection scenarios.

Tracking is performed using an event-driven queue. Each bunch is associated with a global time coordinate and is inserted into a priority queue that ensures chronological processing. At each step, the earliest bunch is extracted, tracked through the current beamline, and then reinserted into the queue with an updated global time coordinate and phase-space. The simulation proceeds until all bunches have exited the machine or no further routing is defined (Fig. 1).

The final output is assembled as a combination of all individual tracking steps. In addition, the complete traversal history of each bunch is retained, enabling detailed diagnostics, beam evolution studies, and analysis of recirculation dynamics.

Content from this work may be used under the terms of the CC BY 4.0 licence (© 2026). Any distribution of this work must maintain attribution to the author(s), title of the work, publisher, and DOI.

ISBN: 978-3-95450-252-3 ISSN: 2673-5350 doi: 10.18429/JACoW-IPAC2026-WEP5146

PHASE SPACE TOMOGRAPHY CONSTRAINED BY THE VLASOV–FOKKER–PLANCK EQUATION USING EOSD DIAGNOSTICS AT KARA

F. Donoso*, M. Brosi, E. Bründermann, M. Frank, S. Funkner, J. Gethmann, A.-S. Müller, G. Niehues, M. Reissig, P. Schreiber
Karlsruhe Institute of Technology, Karlsruhe, Germany

Abstract

This study presents the first experimental application of longitudinal phase space tomography constrained by the Vlasov–Fokker–Planck equation (VFPE) using electro-optical spectral decoding (EOSD) diagnostics at the Karlsruhe Research Accelerator (KARA). The EOSD measurements are modeled as the convolution of the system's impulse response with the charge density profile at the time of acquisition. Combining this model with the VFPE we formulate a partial differential equation-constrained optimization framework for the inverse tomography.

Using this framework, we successfully reconstruct the longitudinal phase space of the electron bunch across different dynamical regimes, ranging from the stable state to the onset of micro-bunching. From the reconstructed phase space, we derive macroscopic beam observables including the longitudinal bunch length, energy-spread related horizontal bunch size, and coherent synchrotron radiation (CSR) power. The reconstructed observables are validated against synchronized measurements from three independent diagnostics. Overall, the results demonstrate that the VFPE-constrained approach, combined with a detailed EOSD forward model, provides a physically consistent reconstruction of the phase space density dynamics from EOSD measurements.

INTRODUCTION

Following our previous work [1,2], we applied the longitudinal phase space reconstruction algorithm to electro-optical spectral decoding (EOSD) measurements acquired at the Karlsruhe Research Accelerator (KARA). This partial differential equation-constrained framework enforces physical consistency between the reconstructed initial density and its turn-by-turn evolution. As the EOSD modulation encodes the electric field induced by the bunch within the crystal rather than the direct charge profile, our forward model explicitly incorporates this interaction [3, 4]. The resulting continuous space-time formulation of the reconstruction problem is presented in Eq. (1).

This formulation seeks to reconstruct the complete phase space trajectory, generated from the initial phase space density ψ^*, that best fits the measured EOSD signals. The optimization minimizes the error between the computed phase retardations, $\Gamma(t_n)$, obtained from this trajectory at time, t_n, and the measured signals, $\bar{\Gamma}_n$ for $n = 1, \ldots, m$. The regularization term, $\lambda R(\psi)$, is incorporated to mitigate challenges such as noise in the measurement data and the ill-posed nature of the inverse problem. The temporal evolution of the phase space density, ψ, is strictly constrained by the Vlasov–Fokker–Planck equation (VFPE), where H represents the Hamiltonian of the system , q and p denote the canonical position and momentum coordinates, respectively, and β_d and D correspond to the damping and diffusion parameters [5]. Furthermore, $\rho(q,t)$ defines the bunch profile, which is determined by projecting the phase space density along the position axis. Finally, G maps the bunch profile to the expected phase retardation, modeling the EOSD response [3, 4].

$$\begin{aligned} \min_{\psi^* \geq 0} \quad & \sum_{n=1}^{m} \|\Gamma(t_n) - \bar{\Gamma}_n\|^2 + \lambda R(\psi^*) \\ \text{s.t.} \quad & \frac{\partial \psi}{\partial t} + \frac{\partial H}{\partial p}\frac{\partial \psi}{\partial q} - \frac{\partial H}{\partial q}\frac{\partial \psi}{\partial p} = \beta_d \frac{\partial}{\partial p}(p\psi) + D\frac{\partial^2 \psi}{\partial p^2}, \\ & \rho(q,t) = \int \psi(q,p,t)\mathrm{d}p, \\ & \Gamma(t_n) = G\left(\rho(q,t_n)\right), \\ & \psi^* = \psi(q,p,t_1). \end{aligned} \tag{1}$$

To solve Equation (1), the continuous variables are discretized. This is achieved by solving the VFPE through operator splitting on a discrete spatial grid, where time steps t_n correspond to single-turn revolutions of the electron bunch in the storage ring. The continuous two-dimensional phase space is transformed into a one-dimensional vector, indexed by s, allowing the differential operators to be linearized into transfer matrices. To integrate the diagnostic, the EOSD diagnostic is modeled as a linear time-invariant (LTI) system to allow the measurement process to be formulated computationally as a matrix-vector product, directly representing the convolution of the bunch profile with the system's impulse response. By combining these discrete dynamic and measurement operators, the continuous problem in Equation (1) is recast into the matrix-based optimization problem [2] shown in Eq. (2).

$$\begin{aligned} \min_{\psi^*} \quad & \|\tilde{\mathrm{G}}\psi - \boldsymbol{\Gamma}\|^2 + \lambda R(\psi) \\ \text{s.t.} \quad & \mathrm{M}(\psi(s,t_n)) = \mathrm{D}\cdot\mathrm{R_K}\cdot\mathrm{R_D}\cdot\mathrm{K}(\psi(s,t_n)), \\ & \tilde{\mathrm{G}} = \begin{pmatrix} \mathrm{G}\cdot\mathrm{W} \\ \mathrm{G}\cdot\mathrm{W}\cdot\mathrm{M}(\psi(s,t_1)) \\ \vdots \\ \mathrm{G}\cdot\mathrm{W}\cdot\prod_{n=1}^{m-1}\mathrm{M}(\psi(s,t_n)) \end{pmatrix} \end{aligned} \tag{2}$$

* felipe.donoso@kit.edu

Content from this work may be used under the terms of the CC BY 4.0 licence (© 2026). Any distribution of this work must maintain attribution to the author(s), title of the work, publisher, and DOI.

ISBN: 978-3-95450-252-3 ISSN: 2673-5350 doi: 10.18429/JACoW-IPAC2026-WEP5303

DATA-DRIVEN RECONSTRUCTION OF ACCELERATOR LATTICE ERRORS USING THREE BEAM POSITION MONITORS*

Y. Hidaka†, G. Wang, Brookhaven National Laboratory, Upton, NY, United States

Abstract

There are numerous experimental techniques to quantify errors in a particle accelerator so that they can be corrected to improve the performance of the accelerator. However, these techniques are often limited in scope, for example, identifying only the errors in quadrupole strengths, sextupole strengths, or the centers of these magnets. In this paper, we propose a data-driven method that can estimate many parameters of lattice elements, including those mentioned above, based solely on many sets of transverse position readings in a section that spans three beam position monitors. Preliminary simulation results will be reported.

INTRODUCTION

Accurate identification and correction of lattice errors are essential for achieving optimal performance in particle accelerators. Over the years, a wide range of beam-based techniques have been developed to infer lattice imperfections using beam position monitor (BPM) data. These include methods based on orbit response matrices, turn-by-turn oscillation analysis, and phase-advance measurements, which have demonstrated high precision in determining linear optics parameters such as beta functions and coupling [1]. However, most of these techniques are inherently limited in scope, typically focusing on specific classes of errors, such as quadrupole gradients, sextupole strengths, or BPM calibration factors.

More recently, data-driven approaches based on local reconstruction of phase-space quantities from BPM measurements have been proposed. In particular, Maltseva *et al.* [2] introduced a method that utilizes generating functions to reconstruct transverse momenta from BPM triplets and to compare adjacent lattice sections for error localization. This approach demonstrated that inconsistencies between reconstructed momenta can be used to identify magnetic errors within a bounded region. These methods highlight a key principle: in the absence of errors, phase-space quantities reconstructed from overlapping BPM triplets must be self-consistent, and deviations from this consistency reveal localized lattice imperfections.

In parallel, orbit-based diagnostics such as the reference-subtracted dynamically-bounded orbit (RSDBO) have proven to be powerful tools for isolating local perturbations [3, 4]. By defining a dynamically constrained orbit within a bounded region, RSDBO suppresses the influence of external disturbances and enables robust identification of transverse kicks originating inside that region. However, this technique is fundamentally limited to perturbations that are independent of the transverse beam position, and therefore cannot be directly applied to higher-order elements such as quadrupoles or sextupoles.

Motivated by these complementary developments, we revisit the triplet-based phase-space reconstruction framework and formulate it in a unified and more practical form. It is noted that the basic concept of comparing reconstructed phase-space quantities across BPM triplets is equivalent to the approach introduced by [2], and our initial formulation follows the same underlying principle.

In this work, we extend this framework by introducing an alternative discrepancy evaluation model and a more computationally efficient phase space reconstruction method. These modifications improve the scalability and practical applicability of the method. We collectively denote this generalized framework as PIGLLET (Parameter Identification of General and Local Lattice Elements from Trajectories).

METHOD

PIGLLET is applied to a lattice section bounded by three BPMs, denoted as P1, P2, and P3. The upstream (US) and downstream (DS) sections refer to the subsection between P1 and P2, and to the subsection between P2 and P3, respectively.

The method combines an Iterative INcoming (or INitial) Angle Predictor (IINAP) with parameter fitting. For a given trajectory and assumed lattice model, IINAP estimates the entrance angles (x_i', y_i') from the measured entrance and exit positions (x_i, y_i, x_f, y_f). Once these angles are known, the corresponding exit angles are obtained by a forward pass through the same model. If the assumed element parameters are correct, these reconstructed phase-space coordinates are self-consistent for all trajectories; otherwise, discrepancies remain and can be minimized by fitting the parameter errors.

Two discrepancy models are considered. In P2 angle matching (P2AM), originally proposed in [2], IINAP is applied separately to the US and DS sections. The US estimate gives P1 angles $\tilde{x}_1'$ and $\tilde{y}_1'$ from (x_1, y_1, x_2, y_2), which are propagated to P2 as $\tilde{x}_{2,\mathrm{US}}'$ and $\tilde{y}_{2,\mathrm{US}}'$. The DS estimate gives $\tilde{x}_{2,\mathrm{DS}}'$ and $\tilde{y}_{2,\mathrm{DS}}'$ from (x_2, y_2, x_3, y_3). Correct parameter values should therefore satisfy $\tilde{x}_{2,\mathrm{US}}' = \tilde{x}_{2,\mathrm{DS}}'$ and $\tilde{y}_{2,\mathrm{US}}' = \tilde{y}_{2,\mathrm{DS}}'$ for all trajectories. In P3 position matching (P3PM), used below, IINAP is applied only to the US data; the resulting P1 phase-space coordinates are then tracked through both sections and compared with the observed P3 positions, requiring $\tilde{x}_{3,\mathrm{US}} = x_3$ and $\tilde{y}_{3,\mathrm{US}} = y_3$.

P3PM avoids IINAP evaluation in the DS section, replacing it with a single forward-tracking pass. This is advantageous when the DS section has more parameters or is otherwise more expensive, because IINAP cost grows with

* Work supported by U.S. DOE under Contract No. DE-SC0012704.

† yhidaka@bnl.gov

Content from this work may be used under the terms of the CC BY 4.0 licence (© 2026). Any distribution of this work must maintain attribution to the author(s), title of the work, publisher, and DOI.

ISBN: 978-3-95450-252-3 ISSN: 2673-5350 doi: 10.18429/JACoW-IPAC2026-WEP5304

ADJOINT SENSITIVITY ANALYSIS FOR DESIGN AND OPTIMIZATION*

D. T. Abell†, V. B. Tembo, I. Haber, T. M. Antonsen, University of Maryland, College Park, USA

Abstract

The design of accelerator lattices involves evaluating and optimizing Figures of Merit (FoMs) that characterize a beam's properties. These properties—hence the FoMs—depend on the many parameters that describe a lattice, including the strengths, locations, and possible misalignments of focusing elements. Often what is required is the gradient of the FoM with respect to each of the parameters. For systems that require numerical simulation, a naïve computation of a gradient requires one simulation for the "base case", plus one additional simulation for each parameter of interest—a daunting effort in the case of computationally demanding simulations with many parameters. Adjoint techniques allow one to extract gradient information from one base-case simulation plus an additional one or two carefully prepared simulations [1]. We demonstrate these techniques using the accelerator simulation code WARP, and we present our proof-of-concept results using several different FoMs as the basis for adjoint analyses of a simple beamline with multiple parameters.

INTRODUCTION

The design of all accelerator systems today uses sophisticated, computationally intensive, numerical models. An essential element of the design process is a determination of how various performance metrics vary with respect to the many parameters that define an accelerator lattice. A determination of this dependence has at least two benefits: (i) It establishes the gradient of a given metric in parameter space, which facilitates design optimization using steepest descent. (ii) It yields the sensitivity of a particular design to errors in the lattice, and hence enables designers to set construction tolerances.

Adjoint methods provide a dramatically more efficient way to calculate parameter dependencies than straightforward parameter differencing, which requires a separate simulation run for each adjustable parameter. As an indication of the power of adjoint methods, we point out that adjoint techniques are used in the engineering community in a variety of contexts to compute sensitivities and gradients. The adjoint approach has previously been applied in circuit theory [2], electromagnetics [3], aerodynamics [4], plasma confinement [5–7], as well as in many other fields. They have been used to optimize the design of three-dimensional magnetohydrodynamic equilibria in stellarators [6, 7]. In the context of accelerators, we have recently deployed adjoint methods to optimize electrostatic [8] and magnetostatic [9] focusing systems, as well as to optimize the combination of quadrupole and solenoid magnetic fields needed to transform—in the presence of strong space charge—a flat beam to a round, angular-momentum-dominated beam [1].

* This work supported in part by the US Department of Energy, Office of Science, Office of High Energy Physics, under Grant #DE-SC-0025277.

† dabell@umd.edu

A HAMILTONIAN ADJOINT RELATION

Lots of analysis and algebra (as sketched in the appendix) leads to the following *adjoint relation*, which involves two types of perturbations—true and adjoint, denoted respectively by superscripts (T) and (A):

$$\sum_j \frac{I_j}{I}\left(\delta p_j^{(T)}\cdot\delta x_j^{(A)} - \delta p_j^{(A)}\cdot\delta x_j^{(T)}\right)\Big|_0^L = \int_0^L \mathrm{d}z\,\frac{q}{I}\int \mathrm{d}^2x_\perp \Big\{ \left[-\delta\rho^{(A)}\,\delta\phi^{(T)} + \delta J^{(A)}\cdot\delta A^{(T)}\right] - \left[A \leftrightarrow T\right]\Big\}, \quad (1)$$

where $[A \leftrightarrow T]$ denotes the previous expression in square brackets with the superscripts (T) and (A) interchanged. On the left-hand side (LHS), we have a net change in the symplectic area separating the trajectories of two different perturbed solutions. On the right-hand side (RHS), we see a space-time integral over mixed—(A) and (T)—products of charge and current density perturbations with, respectively, scalar and vector potential perturbations. The utility of the adjoint relation derives from the freedom we have to assign the adjoint perturbations on the LHS: We shall assign them so as to make the LHS proportional to the change in some relevant FoM. This constitutes the *difficult-to-compute* quantity of interest. The RHS—which we can evaluate using a base-case simulation together with an additional pair of carefully instrumented simulations—constitutes the *easy-to-compute* quantity that yields the change we seek to determine in the FoM of interest. Moreover, we can use the linearity of integration to accumulate individual contributions to the RHS, and compute thus the FoM *gradient* with respect to as many parameters as we deem relevant.

We focus on FoMs F that measure some aspect(s) of the particle phase-space distribution at the exit plane $z = L$. See, for example, the FoMs discussed in [1]. We write our F in the generic form

$$F = \sum_j \frac{I_j}{I} f(x_{\perp j}, p_{\perp j})\Big|_{z=L}. \quad (2)$$

To make the LHS of (1) look like a change in the FoM, we assume the True solution has no perturbations to the particle phase-space coördinates at the lattice entrance, $z = 0$, and we assume the Adjoint solution has particle perturbations at the lattice exit, $z = L$, given by the rules

$$\delta x_j^{(A)} = \frac{\partial f}{\partial p_j}\Delta, \quad \delta p_j^{(A)} = -\frac{\partial f}{\partial x_j}\Delta, \quad (3a)$$

where we define the *perturbation scale parameter*

$$\Delta = \Delta(\varepsilon) = \frac{x_{\text{typical}}\,p_{\text{typical}}}{F_{\text{typical}}}\varepsilon \quad (3b)$$

Content from this work may be used under the terms of the CC BY 4.0 licence (© 2026). Any distribution of this work must maintain attribution to the author(s), title of the work, publisher, and DOI.

ISBN: 978-3-95450-252-3 ISSN: 2673-5350 doi: 10.18429/JACoW-IPAC2026-WEP5601

STUDY OF BEAM COUPLING IMPEDANCE AND INSTABILITIES FOR THE SUPER TAU-CHARM FACILITY*

T. He†, W. Li, W. Liang, Z. Meng, Y. Zou, J. Tang, USTC, Hefei, China
D. Zhou, KEK, 1-1 Oho, Tsukuba 305-0801, Ibaraki, Japan

Abstract

The Super Tau-Charm Facility (STCF), a next-generation electron-positron collider in China, is designed to achieve a peak luminosity above 0.5×10^{35} cm^{-2}s^{-1} at 4 GeV in the center-of-mass frame. This paper investigates beam instability issues for the STCF, with the aim of identifying and mitigating risks from beam coupling impedance. Our work analyzes key contributors such as coherent synchrotron radiation, resistive-wall, and geometric impedances, and evaluates their role in driving both single-bunch and multi-bunch instabilities.

INTRODUCTION

The Super Tau-Charm Facility (STCF) is a proposed new-generation electron-positron collider in China, operating at center-of-mass energies from 2 to 7 GeV, with a target peak luminosity exceeding 5×10^{34} cm^{-2}s^{-1} at 4 GeV center-of-mass energy [1]. To achieve this high luminosity, the STCF requires high beam currents and low emittance, making collective effects a critical challenge. The main parameters for the collider rings at three representative beam energies (1 GeV, 2 GeV and 3.5 GeV) are summarized in Table 1.

This paper presents a preliminary study of beam coupling impedances and associated instabilities for the STCF collider rings. Key impedance sources, including coherent synchrotron radiation (CSR), coherent wiggler radiation (CWR), resistive-wall (RW), and geometric (Geo.) impedances, are modeled. The longitudinal impedance model includes CSR from dipoles, CWR from wigglers, RW with NEG coating, and geometric contributions from collimators, BPMs, bellows, etc. Since detailed geometric models for the STCF are currently unavailable, the geometric impedance is estimated by scaling existing impedance budgets from HALF, FCC-ee [2], and SuperKEKB [3], based on the beam pipe aperture of STCF.

The vacuum chamber cross-sectional dimensions are required for the CSR, CWR and RW calculations. The STCF vacuum chamber is divided into three typical sections: the arc, the wiggler section, and the interaction region. Their cross-sectional geometries are shown in Fig. 1. All chambers are assumed to be coated with a 1 μm-thick NEG film. For CSR, the impedance from the dipoles is calculated using the parallel-plate shielding model [4]. For CWR, the impedance from the wigglers is evaluated using the PP-TR model [5]. For RW, the impedance is evaluated using the IW2D code, considering NEG coating with conductivities of 10^5 and 10^6 S/m [6].

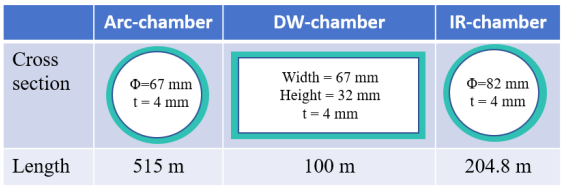

Figure 1: Typical vacuum chamber cross sections for the arc, wiggler, and interaction region.

Table 1: Key Parameters of the STCF Collider Rings for the Lattice V5 Design

Parameters	**1 GeV**	**2 GeV**	**3.5 GeV**
Circumference [m]	825.524	825.524	825.524
Beam current I_0 [A]	0.8	2.0	2.0
Mom. factor α_c [10^{-4}]	13.4	14.1	14.3
Energy spread [10^{-4}]	7.16	8.12	10.02
τ_z [ms]	21.9	8.9	6.45
$\tau_{x,y}$ [ms]	43.79	17.69	12.90
Harmonic number	1376	1376	1376
U_0 (total) [keV]	125.8	622.6	1494
RF voltage [MV]	0.75	2.5	6.0
Synchrotron tune (ν_s)	0.0147	0.0193	0.0228
Betatron tune (ν_x/ν_y)	28.55/33.58	28.55/31.58	28.55/30.58

IMPEDANCE MODELING

Longitudinal Impedance

Based on the modeling methods described above, the longitudinal impedance contributions from CSR, CWR, RW, and geometric sources are evaluated. Figure 2 shows the longitudinal short-range wake potential for a bunch length of 0.5 mm. The geometric wake potential is obtained via scaling, while the CSR, CWR and RW wakes are derived from their respective impedance models up to 2 THz and then Fourier transformed to the time domain. As observed from the wake potential, CSR and CWR dominate the short-range wake potential at low energies (1–1.5 GeV), highlighting their critical role in single-bunch dynamics.

Transverse Impedance

Figure 3 presents the transverse short-range wake potentials for a 0.5 mm bunch. The corresponding kick factors are listed in Table 2. Transverse impedance is dominated by geometric components, especially in the vertical plane. The geometric kick factors are significantly larger than the RW contribution at both 1 GeV and 2 GeV.

* Work supported by the Fundamental Research Funds for the Central Universities (No. WK2310000127) and the National Natural Science Foundation of China (Grants No. 12375324 and No. 12105284).

† htlong@ustc.edu.cn

Content from this work may be used under the terms of the CC BY 4.0 licence (© 2026). Any distribution of this work must maintain attribution to the author(s), title of the work, publisher, and DOI.

ISBN: 978-3-95450-252-3 ISSN: 2673-5350 doi: 10.18429/JACoW-IPAC2026-WEP5602

A REALISTIC PROPORTIONAL-INTEGRAL RF FEEDBACK MODEL FOR LONGITUDINAL BEAM DYNAMICS SIMULATION

T. He*, W. Liang, J. Xiao, X. Huang, University of Science and Technology of China, Hefei, China

Abstract

Modern fourth-generation storage ring light sources predominantly utilize digital I/Q-based proportional-integral (PI) feedback for their radio-frequency (RF) systems. This paper introduces a dedicated PI feedback model implemented in the STABLE tracking code to enable accurate and fast longitudinal beam dynamics simulations. The model's key innovation lies in its treatment of the continuous generator current, which is discretized into electron-bunch-like charge pulses, while the cavity voltage is refreshed on an RF-cycle basis. This methodology offers a more physically accurate model of the beam-cavity-feedback coupling, providing a versatile tool for precise longitudinal beam dynamics studies in single- and multi-RF configurations.

INTRODUCTION

Achieving precise regulation of radio-frequency (RF) cavities is fundamental to the performance of modern storage ring light sources, a task predominantly accomplished by digital I/Q-based proportional-integral (PI) feedback systems. Accurate simulation of the coupled beam-cavity-feedback dynamics is therefore essential, especially for applications like bunch lengthening with harmonic cavities. Existing multi-particle tracking codes provide various approaches to this problem. The ELEGANT code, for example, incorporates an RF feedback model originally designed for analog amplitude/phase systems [1], requiring the conversion of PI parameters into equivalent filter coefficients for simulation [2]. Other codes, such as MBTRACK2, directly implement a PI controller framework to model the cavity response [3,4]. While these tools can model the fundamental cavity dynamics accurately, systematic scans over PI gains, loop delays, and operating conditions in modern digital feedback systems still demand substantial computational effort.

This paper presents a refined, physics-based RF feedback model implemented within the GPU-accelerated STABLE tracking code [5]. The model is natively designed for digital I/Q PI feedback systems and introduces two key advances. First, it employs a high-fidelity cavity model where the continuous generator current is discretized into equivalent charge pulses, and thus the cavity voltage is updated iteratively on an RF-cycle basis, ensuring an accurate representation of transient beam-cavity-feedback coupling interactions. Second, and distinctively, STABLE leverages NVIDIA CUDA for massive parallelization on GPUs. Compared to CPU-parallelized frameworks, this architecture provides a substantial increase in computational throughput for large-scale parameter scans at a lower hardware cost. This combination of physical fidelity and computational power makes STABLE a practical and efficient tool for investigating longitudinal beam instability in the context of modern feedback systems and challenging scenarios like bunch-lengthening harmonic cavity operation.

DISCRETIZATION OF THE GENERATOR CURRENT

To facilitate the numerical calculation of the generator voltage phasor, it is advantageous to discretize the continuous cosine generator current into pulsed charges with the same period. As illustrated in Fig. 1, we demonstrate that the charge of each pulse equals $\frac{1}{2}I_gT$, where I_g and T are the amplitude and period of the generator current, respectively.

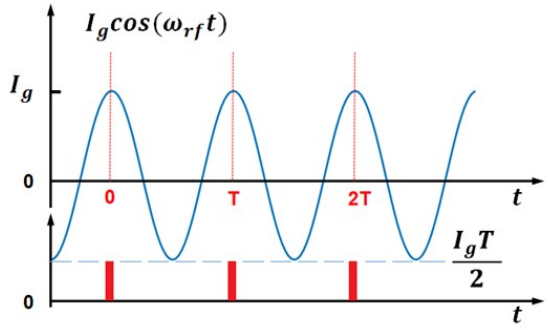

Figure 1: Discretization of a cosine generator current into equivalent pulsed charges.

Analogous to representing a longitudinally distributed bunch charge by an equivalent point charge with a form factor, the equivalent pulse charge for a cosine generator current can be obtained by:

$$Q_g = \int_{-T/2}^{T/2} I_g \cos(\omega_{\mathrm{rf}} t) e^{-j\omega_r t}\, dt = \frac{1}{2} I_g T, \qquad (1)$$

where the approximation $\omega_r \approx \omega_{\mathrm{rf}}$ is used to compute the integral.

It is convenient to represent RF signals (voltages and currents) as complex phasors. In a counterclockwise rotating reference frame with frequency ω_{rf}, we denote the generator current phasor and the equivalent pulse charge phasor as $\tilde{I}_g$ and $\tilde{Q}_g$, respectively. For a pulsed charge excitation at time zero, the resulting cavity voltage phasor is:

$$\tilde{V}_g = \frac{\tilde{Q}_g \omega_r R_L}{Q_L}. \qquad (2)$$

Here, ω_r, R_L, and Q_L are the angular resonant frequency, loaded shunt impedance, and loaded quality factor of the cavity, respectively. Substituting Eq. (1) into Eq. (2) and

* htlong@ustc.edu.cn

Content from this work may be used under the terms of the CC BY 4.0 licence (© 2026). Any distribution of this work must maintain attribution to the author(s), title of the work, publisher, and DOI.

ISBN: 978-3-95450-252-3 ISSN: 2673-5350 doi: 10.18429/JACoW-IPAC2026-WEP6002

TRANSFER LEARNING FOR GENERALIZING A HYBRID AUTOENCODER-ISOLATION FOREST MODEL FOR TIME SERIES ANOMALY DETECTION IN ARRONAX CYCLOTRON OPERATIONAL DATA*

F. Basbous†,[1,2], F. Poirier[1,3], F. Haddad[1,2,3], D. Mateus[4]
IP ARRONAX, Saint-Herblain, France
[2]Nantes Université, Nantes, France
[3]Centre National de la Recherche Scientifique, Paris, France
[4]Nantes University, École Centrale Nantes, LS2N, UMR 6004, Nantes, France

Abstract

In the context of the operational monitoring of the ARRONAX C70XP cyclotron, our previous work addressed the limitations of the Isolation Forest (IF) algorithm in detecting local anomalies, particularly those occurring near the mean of normal data, due to its reliance on axis-parallel splits. To overcome this issue, we developed and validated a hybrid model combining an autoencoder and IF, using time series data from the proton beam intensity on target. This approach significantly improved the detection of both global and local anomalies, with no false alarms observed during evaluation. Building on these results, the present study investigates the use of transfer learning to generalize the hybrid model to other process variables originating from different subsystems, including the source, injector, and cyclotron core. Results suggest that the model can effectively label large volumes of multivariate operational data, supporting the development of a more scalable and integrated anomaly detection framework for the C70XP.

INTRODUCTION

Particle accelerators are safety-critical systems composed of complex and interconnected components and subsystems. Therefore, anomaly detection has become an important research area, as deviations from normal operational behavior can indicate potential faults and help prevent failures, irreversible damage, and costly repairs [1-4],

In our previous work [5], we proposed a hybrid Autoencoder-Isolation Forest (AE-IF) framework for anomaly detection in time-series operational data from the ARRONAX C70XP cyclotron. The approach relies on an autoencoder (AE) trained to learn a compact latent representation of normal operational behavior. The reconstruction errors produced by the AE are then used as input features for the Isolation Forest (IF) algorithm. Trained and validated on proton beam intensity on target time-series data, the model enables the detection of both global anomalies and subtle local anomalies occurring near the mean of normal data. The proposed approach was shown to outperform two alternative IF-based methods applied directly to the raw signal and to the PCA-transformed intensity space.

Despite these promising results, extending this approach to multiple process variables (PVs) remains challenging. The monitoring system involves numerous PVs originating from different subsystems, each exhibiting distinct dynamics and statistical distributions. Training a dedicated anomaly detection model from scratch for each variable requires significant computational effort and optimization time.

One of the techniques proposed to address the challenge of model adaptation is transfer learning (TL), which enables the reuse of knowledge learned from a source dataset when training models for related target datasets [6].

TL has demonstrated significant benefits in anomaly detection tasks, particularly in industrial time-series applications where labelled data are limited, enhancing detection robustness while reducing false positives [6,7]. It has also been successfully applied in Internet of Things monitoring and energy consumption analysis, where it improves detection accuracy while mitigating sensitivity to noise and overfitting [8,9]. For anomaly detection in detector monitoring systems, such as the Compact Muon Solenoid hadron calorimeter spatio-temporal data quality monitoring framework, TL has been shown to enable knowledge transfer across detector subsystems and improve model robustness [10]. However, to the best of our knowledge, the application of TL to anomaly detection in accelerator operational time-series data remains limited.

TL can be categorized according to the similarity of tasks and domains between the source and target problems. In general, TL is divided into inductive, transductive, and unsupervised paradigms [6,10]. Inductive TL is applied when the source and target tasks differ while labelled data are available for the target task. Transductive TL is used when the task remains the same but the source and target domains differ, typically with labelled data available only in the source domain. Unsupervised TL addresses scenarios where both the source and target tasks differ and the data are unlabeled.

Among these categories, transductive TL is particularly relevant to our study since the anomaly detection task remains unchanged while the data originate from different sensors. In this work, we propose a TL framework that reuses the latent representation learned from normal proton

*The Arronax cyclotron is supported by the CNRS, Inserm, INCa, Nantes Université, the Regional Council of Pays de la Loire, local authorities, the French government, and the European Union. This work has been supported in part by the French National Research Agency (ANR) "France 2030 investment plan" under the references I-SITE NExT (ANR-16-IDEX-0007), and Labex DHOLMEN, by financial support from the Pays de la Loire Region and by a grant from INCa-DGOS-INSERM-ITMO Cancer_18011 (SIRIC ILIAD).
†basbous@arronax-nantes.fr

Content from this work may be used under the terms of the CC BY 4.0 licence (© 2026). Any distribution of this work must maintain attribution to the author(s), title of the work, publisher, and DOI.

ISBN: 978-3-95450-252-3 ISSN: 2673-5350 doi: 10.18429/JACoW-IPAC2026-WEP6003

ANOMALY DETECTION AND DENOISING OF NON-GAUSSIAN BEAMS USING 2D IMAGE RECONSTRUCTION TECHNIQUES BASED ON DEEP LEARNING

F.R. Osswald[1†], M. Chahbaoui[2], X. Liang[3]

[1]IPHC, CNRS Nucléaire et Particules, Université de Strasbourg, 67000, Strasbourg, France
[2]Université de Strasbourg, 67000, Strasbourg, France
[3]Sorbonne Université, 75006 Paris, France

Abstract

Automatic image reconstruction tools are essential in fields such as physics, astronomy, and biology. In particle accelerators like CERN's LHC, they are particularly important for evaluating beam quality through beam position, profile, and emittance measurement. Traditional analysis tools no longer meet the accuracy and efficiency demands of future facilities. A new AI-based digital tool is used for 2D transverse phase-space distributions denoising improving the accuracy of RMS emittance measurements. Our focus was to enhance beam halo characterization, ultimately contributing to reduce transport losses, and enabling more sustainable accelerator operations. Challenges are related to noisy experimental data, lack of ground-truth reference images, noise model, and limited training datasets. Our unsupervised deep convolutional neural network (DCNN) can denoise a single image using only itself as input thus greatly improving the accuracy of emittance measurement.

INTRODUCTION

Accelerator facilities increasingly depends on advanced beam-diagnostics capable of supporting stringent performance, and reliability requirements. As beam intensities and stored energies rise, precise control of beam losses becomes essential for machine protection, operational efficiency, activation reduction, and long-term environmental sustainability. These goals require high-accuracy, high-dynamic-range measurements of beam position, profiles, and phase-space distributions. In particular, resolving low-intensity beam halos often five orders of magnitude below the core remains a major challenge due to sensitivity limits, and background suppression. Similar to trends in medical imaging, or Earth-observation systems, accelerator diagnostics demand sophisticated data-processing methods. Traditional analysis techniques appear insufficient for the needs of modern machines [1-2]. AI-based approaches offer promising capabilities for denoising, feature extraction, and multidimensional parameter inference. This paper reviews the state of the art in image-based beam-diagnostic analysis and presents a new method using convolutional filters and NN architectures to enhance measurement fidelity and robustness for future accelerator operation.

BEAM DISTRIBUTIONS

Among the usual beam quality diagnostics, the transverse profile, position, and emittance play a key role in the control of the accelerators and the definition of their luminosity and brightness [3-9]. Beam halo depends on the tails in transverse distribution produced by optics mismatch, field and beam dynamics nonlinearities. The halo is characterized by a variable particle density, which follows a distribution often likened to a Gaussian, which extends well beyond the core of the beam [10-13], but due to the number and complexity of interactions between it and its environment, can take on very different appearances. Emittance growth due to tail increase feeds beam losses and requires six-dimensional beam matching between the different sections of the accelerating structure. This optimization process allows a smaller volume in the 6D phase space, thus increasing beam brightness and reduction of losses [14-15]. These malfunctions induce cascading effects such as quench of SRF cavities, overheating of beam transport equipment, melting, sputtering, activation, etc. The measurement of the halo distribution requires the detection of electric charges over a wide dynamic range up to six orders of magnitude. One of the fundamental challenges lies in distinguishing noise from the true signal in the absence of prior knowledge of the noise distribution. This difficulty is exacerbated by variable experimental conditions and fluctuating background noise, which hinder the development of universally applicable denoising strategies. Classical statistical methods are still widely employed across operational particle accelerator facilities to extract information from beam diagnostics data. However, these approaches encounter significant limitations when confronted with noisy signals, irregularly shaped beam cross-sections, non-elliptical or non-Gaussian phase-space distributions, non-uniform densities, or parasitic contaminating beams [16-18]. The most common approach for RMS emittance determination relies on applying an arbitrary threshold to separate useful signal from background noise. However, even modest noise levels or the absence of minimal halo signals below 10^{-4} of the total beam intensity can introduce substantial bias, with RMS errors exceeding 100% in extreme cases [19-21].

† francis.osswald@iphc.cnrs.fr

Content from this work may be used under the terms of the CC BY 4.0 licence (© 2026). Any distribution of this work must maintain attribution to the author(s), title of the work, publisher, and DOI.

ISBN: 978-3-95450-252-3 ISSN: 2673-5350 doi: 10.18429/JACoW-IPAC2026-WEP6006

GRADIENT-BASED LASER CONTROL FOR END-TO-END PHOTOINJECTOR EMITTANCE OPTIMIZATION AT EUXFEL

D. Ilia[1,2*] A. Aksoy[3], Z. Amirkhanyan[3], F. Brinker[1], M. Cai[1,2], M. E. Castro Carballo[1], Y. Chen[1], J. Good[1], M. Gross[1], U. Große-Wortmann[1], M. Guetg[1], I. Hartl[1], W. Hillert[2], Y. Jiang[1], M. Kerstan[1], A. Klemps[4], M. Krasilnikov[1], J. Kwasniok[1], C. Li[1], X. Li[1], C. Mahnke[1], C. Mohr[1], C. Mustapha[3], A. Oppelt[1], S. Pakluea[3], H. Panuganti[1], F. Pressacco[1], C. Richard[1], F. Stephan[1], A. Tavakol[1], H. Tünnermann[1], G. Vashchenko[3], D. Villani[3], D. Xu[1], S. Zeeshan[1]
[1]Deutsches Elektronen-Synchrotron DESY, Hamburg, Germany
[2]Universität Hamburg, Hamburg, Germany
[3]Deutsches Elektronen-Synchrotron DESY, Zeuthen, Germany
[4]Hamburg University of Technology, Hamburg, Germany

Abstract

Achieving low emittance at the photoinjector is essential for meeting the performance targets of the European XFEL, particularly for high photon energies and future high-duty-cycle operation. Both the temporal structure of the drive-laser pulse and the RF-gun settings contribute significantly to the final beam quality, yet their optimization is complicated by strong nonlinearities in the laser system and complex gun response. We have developed a differentiable, physics-based model of NEPAL, the photoinjector laser of EuXFEL, that enables gradient-driven optimization of the temporal UV pulse shape. The model captures the relevant nonlinearities of the optical chain and allows direct optimization of spectral amplitude and phase to obtain target UV profiles at the photocathode. In parallel, a machine-learning surrogate model is being implemented to optimize the RF-gun operating parameters. Together, these tools provide an end-to-end control framework for emittance reduction at EuXFEL. Initial results demonstrate that the differentiable model enables accurate temporal UV pulse shaping at EuXFEL. Work is ongoing to integrate this approach with ML-assisted gun optimization within the proposed end-to-end control framework.

INTRODUCTION

The performance of X-ray free-electron lasers (XFELs) depends critically on the quality of the electron beam, with the transverse emittance being a key figure of merit. At EuXFEL, reducing the transverse emittance is a primary focus of ongoing development, as it enables operation at higher photon energies [1] and will support the future transition to high-duty-cycle operation. Alongside thermal emittance, space charge is one of the dominant contributions to the bunch emittance, and it can be mitigated by shaping in space and time the photoinjector laser pulses to control the initial electron bunch distribution. In previous work [2, 3], we reported on NEPAL, the photoinjector laser serving EuXFEL, FLASH, and PITZ, which supports both temporal and spatial shaping. In particular, we demonstrated UV flat-top pulse shaping via spectral amplitude and phase control with a spatial light modulator (SLM) in the laser IR front-end. The shaping was achieved through an iterative procedure combining simulation and experimental feedback, and once transferred to the electron beam it produced a measurable impact on the slice emittance. This scheme is, however, entirely manual and heuristic, making the outcome operator-dependent and difficult to reproduce. The underlying difficulty is the optical chain mapping SLM settings to the UV profile, which contains several strongly nonlinear stages and admits no direct analytical inversion. As a result, the manual scheme is too slow and irreproducible to support systematic emittance studies, let alone end-to-end optimization of the gun parameters. In this paper we address this by introducing an automated, gradient-based shaping algorithm that removes the operator dependence and allows for arbitrary shaping, bringing us one step closer to end-to-end optimization of the emittance. We demonstrate accurate temporal UV pulse shaping at EuXFEL, which has already been used operationally for twin-bunch FEL operation. We further deploy the method at PITZ to study the dependence of the emittance on the pulse profile, showing how temporal shaping can now be exploited for systematic exploration and integration with optimization methods targeting the gun parameters.

PHOTOCATHODE LASER TEMPORAL SHAPING

NEPAL delivers picosecond deep-UV pulses at 257 nm to the photocathode through a chirped-pulse amplification (CPA) scheme followed by two stages of frequency conversion (Fig. 1(a), top). Temporal pulse shaping is enabled by a fiber-coupled spatial light modulator (SLM) in the IR front-end, which provides both amplitude and phase control in the spectral domain. The temporal profile impressed at this stage is, however, distorted as the pulse undergoes amplification and propagates through the two nonlinear conversion stages. Moreover, these coupled nonlinear effects preclude a direct, analytical mapping from front-end settings to the UV profile. We therefore formulate the shaping task as an optimization problem: find the spectral filter $u(\nu)$ such that the resulting intensity profile $I_{\text{laser}}(t)$ matches a given

* denis.ilia@desy.de

Content from this work may be used under the terms of the CC BY 4.0 licence (© 2026). Any distribution of this work must maintain attribution to the author(s), title of the work, publisher, and DOI.

ISBN: 978-3-95450-252-3 ISSN: 2673-5350 doi: 10.18429/JACoW-IPAC2026-WEP6007

ACCELERATOR OPTIMIZATION FOR LARGE PARAMETER NUMBERS EMBEDDED IN THE NATIVE FAIR CONTROL SYSTEM ENVIRONMENT

W. Geithner*[1], M. Boschert[2],
Z. Andelkovic[1], F. Herfurth[1], N. Kehl[1], J. Koedel[3],
A. Müller[2], N. Stallkamp[1], S. Trotsenko[1], D. Zisis[3]
[1]GSI Helmholtzentrum für Schwerionenforschung, Darmstadt, Germany
[2]Hochschule Darmstadt, Fachbereich Informatik, Darmstadt, Germany
[3]Technische Universität Darmstadt, Fachbereich Physik, Darmstadt, Germany

Abstract

We report on the latest developments of our end-user application "Device-Automator" for use in the main control room of GSI/FAIR. Recent progress includes a Bayesian optimizer engine ported from Python to Java in addition to the genetic algorithm engine we applied in earlier work. The engines were tested on the HITRAP beamline with up to 58 control parameters and the CRYRING@ESR injection system.

INTRODUCTION

Particle accelerator operation is subject to continuous improvement in efficiency and effectiveness, with the goal of providing beam according to experimental requirements. While *technical* performance is advanced through new physical and technical concepts, machine *operation* must be improved by optimizing the beam provisioning processes.

Accelerator models are one important tool for minimizing setup times if these models are well-developed and matured. However, situations exist where well-established models are not available (new machines, parameter drifts over time, complex and hard-to-model subsystems. etc.) and "manual" tuning of the numerous accelerator parameters such as beam orbit, tune, transport beamline elements, injection systems, etc. – becomes one key aspect of machine operation binding significant personnel resources. Software tools assisting operators are therefore highly desirable. Ideally, such tools should (a) reduce time for machine setup and tuning, (b) reduce operator workload, and (c) achieve beam performance at least comparable to experienced human operators. The implementation of such tools has been facilitated by recent advances in computer science making available ready-to-use optimization libraries, and tailored implementations have been used successfully for optimizing particle beams and related sub-systems; see [1] for an overview.

This has to be framed within GSI Helmholtzentrum für Schwerionenforschung (GSI) and its extension, the Facility for Antiproton and Ion Research (FAIR) [2], currently under construction [3]. While GSI currently operates "only" 5 machines, FAIR will comprise several ion sources, 10 accelerators or decelerators, 2 fragment separators, and numerous experimental sites, operated as injectors to each other or in parallel. Typical experiments last a few days and often require entirely different setups regarding ion species and beam energy. For this future, it can be anticipated that operation will become more challenging and labor-intensive, increasing personnel workload. In addition to that, the FAIR complex must be commissioned before operation which will be a very time-consuming process.

The FAIR Control System (CS) built upon the CERN control system stack, offers two approaches for setting control parameters: device level parameters (magnet currents, voltages, etc.) can be set via the so-called JAPC API [4]. Physics-level parameters (kick angles, tunes, beam energies, etc.) are modeled in the so-called "LSA layer" providing a high-level API [5]. Ideally, applications should integrate as tightly as possible into this given environment.

In the context of this work, CRYRING@ESR and HITRAP are two FAIR-associated machines already in productive or commissioning states [6, 7], are serving as test environments for new concepts such as optimizer tools presented here.

DEVICE-AUTOMATOR APPLICATION

In the context of GSI/FAIR, a series of machine studies employing software optimizers based on the programming language Python showed very promising results [8–10]. To provide an end-user application, the beam automation tool GeOFF, as well implemented in Python, was migrated from CERN to the FAIR control system stack [11].

The FAIR/GSI control system software stack is implemented in C++ and Java [12]. We therefore develop and maintain an application, named "Device-Automator", designed for use in the main control room by operators and accelerator physicists. Device-Automator incorporates optimization tools natively in Java – FAIR CS' native language – enabling direct integration without additional interfaces bridging Java and Python. One key challenge in this approach is the lack of ready-to-use optimization libraries in Java, which are abundant in Python. To address this, we implemented a Bayesian optimizer, and integrated the Jenetics genetic algorithm library [13] and the BOBYQA optimizer available in the Apache math3 library [14].

The GUI of Device-Automator is implemented in JavaFX 21 [15] following the standard technology stack used for FAIR control room applications. This design choice ensures seamless integration with existing tools and a consistent user experience for personnel already trained using other

* w.geithner@gsi.de

Content from this work may be used under the terms of the CC BY 4.0 licence (© 2026). Any distribution of this work must maintain attribution to the author(s), title of the work, publisher, and DOI.

ISBN: 978-3-95450-252-3 ISSN: 2673-5350 doi: 10.18429/JACoW-IPAC2026-WEP6009

EXPLORING CONVOLUTIONAL NEURAL NETWORKS TRAINING STRATEGIES FOR PILE UP CORRECTION IN SINGLE PARTICLE COUNTING

M. Hamdan*, Unaffiliated Researcher, Frankfurt, Germany
T. Habermann, Fulda University of Applied Sciences, Fulda, Germany

Abstract

This work investigates the effect of different training strategies on the performance of convolutional neural networks (CNNs) for real-time pile-up identification and correction in single particle counters at the GSI Helmholtz Centre for Heavy Ion Research. Building on a previously developed CNN capable of detecting particle pulses without domain-specific knowledge, we examine the influence of different loss functions and their hyperparameters on the network's ability to accurately localize overlapping events. We also propose new metrics for particle counting and show how to adapt common metrics for precision and recall to allow a user-defined localization tolerance. Using a dataset of approximately 26,000 manually labeled pulses, we analyze how these training choices impact particle counting and localization performance. The findings provide insights for developing particle counting systems suitable for real-time applications, including potential implementation on FPGA hardware.

INTRODUCTION

Accurate particle counting and precise arrival time determination are fundamental requirements in experimental nuclear and particle physics, as well as in accelerator beam diagnostics. In high-rate environments such as those encountered at the GSI Helmholtz Centre for Heavy Ion Research, scintillator-based single particle counters frequently suffer from pile-up events, where multiple particles arrive within short time intervals and produce superimposed pulse shapes at the detector output. Typically, the number of pile-ups in extracted beams from particle accelerators is much more than one expects from a random discrete process or Poisson process [1, 2].

Previous work [3] demonstrated how convolutional neural networks (CNNs) can be used for pile-up correction in single particle counting and outperform traditional thresholding and local maxima methods without relying on domain-specific knowledge or explicit analytical pulse models. Tested on a dataset of approximately 26,000 manually labeled events, the proposed architecture achieved accurate particle counting and was designed with real-time FPGA implementation in mind. These results established the feasibility of machine-learning-based pile-up correction for accelerator applications.

However, while the network architecture was optimized for deployment constraints, the influence of the training strategy on detection behavior was not systematically investigated. In particular, because particle counting involves sparse event localization in highly imbalanced time-series data, the loss function must address this class imbalance and prioritize particle counting. In [3], the focal loss function [4] was chosen as it is a well-known and widely used loss function for tasks with class imbalance. But a proper investigation into loss functions is still missing.

In this work, we therefore investigate the impact of different loss functions and hyperparameter settings on CNN performance for real-time pile-up identification. The results provide practical guidance for the development of reliable particle counting systems and show how to improve the approach for localization and particle counting.

BACKGROUND

The CNN model presented in [3] is processing windows of data in sequential order. Each window of data contains 256 data points. Figure 1 shows a window of data together with the predicted peak positions shown as black dots. The correct peak positions (ground truth) are marked with dotted green lines.

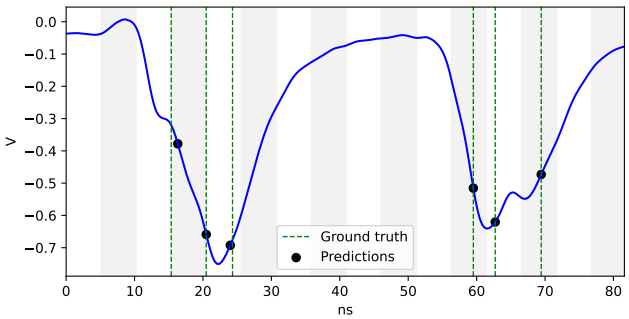

Figure 1: An example containing 6 pulses with all true peak locations and predicted locations shown in the figure. Also, each cell is highlighted.

The CNN model itself splits each window into cells containing 16 data points each. The gray and white background in Fig. 1 is used to highlight each cell. Each cell can predict up to m peaks, and each peak prediction is composed of two features, which are the confidence score and the relative position in the cell. Both features are normalized between zero and one using a sigmoid activation function. A peak is predicted when the confidence score is higher than 0.5. This concept is similar to YOLO [5] box detection models. The CNN model architecture from [3] is a simple CNN with just 6 layers. The architecture is shown in Table 1, where it

* Mahdie.Hamdan@outlook.com

Content from this work may be used under the terms of the CC BY 4.0 licence (© 2026). Any distribution of this work must maintain attribution to the author(s), title of the work, publisher, and DOI.

ISBN: 978-3-95450-252-3 ISSN: 2673-5350 doi: 10.18429/JACoW-IPAC2026-WEP6012

PHOTOINJECTOR EMITTANCE OPTIMIZATION USING LATENT LASER PULSE REPRESENTATIONS

A. Klemps*[1], N. Ay[1], P. K. Banerjee[1], Y. Chen[2], I. Hartl[2], D. Ilia[2], J. Kwasniok[2], H. Tünnermann[2]
[1]Hamburg University of Technology, Hamburg, Germany
[2]Deutsches Elektron-Synchrotron (DESY), Hamburg, Germany

Abstract

We present a beam dynamics study aimed at optimizing the transverse emittance of electron bunches in a photoinjector, motivated by the performance requirements of Free-Electron Lasers. The study is conducted using the accelerator configuration of the Photo Injector Test Facility at DESY in Zeuthen (PITZ), with the overarching goal of developing emittance optimization strategies for the European XFEL photoinjector. To this end, we perform large-scale beam dynamics simulations using the simulation code ASTRA, systematically sampling from a low-dimensional latent representation of temporal laser pulse profiles. This latent space is learned from a broad set of physically plausible pulses using a Wasserstein Autoencoder (WAE), enabling compact and structured exploration of pulse shape variations. The ability to efficiently sample from this representation supports targeted emittance studies that would be computationally prohibitive in the original high-dimensional shaping parameter space. For each simulation, beam quality metrics such as normalized projected emittance and slice mismatches are recorded. The study reveals meaningful correlations between latent coordinates and beam quality, demonstrating the utility of WAE-based representations in guiding laser pulse design. We briefly outline future directions involving neural surrogate models to accelerate beam emittance optimization.

INTRODUCTION

The performance of photoinjectors for Free-Electron Lasers (FELs) critically depends on the generation of electron beams with low transverse emittance. With the commissioning of the photocathode laser system NEPAL [1] at the European XFEL and PITZ, advanced temporal pulse shaping capabilities have become available, enabling the generation of laser pulses with diverse temporal profiles via precise control [2, 3] and opening up targeted emittance optimization studies at EuXFEL [4].

However, the underlying shaping process is governed by a high-dimensional parameter space with several thousand tunable degrees of freedom, making systematic exploration through beam dynamics simulations computationally prohibitive. At the same time, the relationship between temporal pulse shape and resulting transverse emittance remains difficult to characterize due to nonlinear space charge effects.

To this end, machine learning methods have recently been successfully applied to the modeling, control, and optimization of particle accelerators, enabling data-driven representations and predictions of complex beam dynamics such as space charge effects [5, 6].

In this work, we employ latent representations of temporal pulse shapes learned with Wasserstein Auto-Encoders [7], providing a compact, low-dimensional parametrization of physically admissible profiles. Based on samples from this latent space, we perform beam dynamics simulations of the PITZ injector and analyze the impact of longitudinal pulse shaping on transverse emittance.

LATENT PULSE REPRESENTATIONS

WAEs are a class of generative models with a training objective derived from optimal transport theory, enabling well-regularized latent representations and accurate reconstruction of input data. In prior work [8], we trained a convolutional WAE on simulated laser pulse data [9], representing physically admissible temporal profiles generated by the NEPAL pulse-shaping system. The trained model maps each pulse shape given in time domain to a low-dimensional latent representation $\xi \in \mathbb{R}^{32}$, providing a compact alternative to the approximately 6 000 tunable parameters of the spatial light modulator (SLM) used for pulse shaping. This dimensionality reduction enables an efficient parametrization of the pulse space while retaining physically relevant pulse structure.

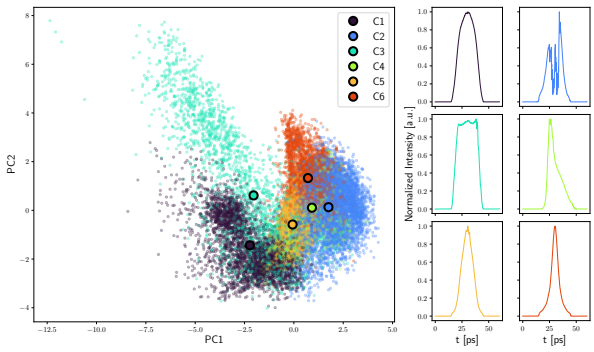

Figure 1: PCA projection of the WAE latent space with Gaussian mixture clustering. Circles denote component means; right panels show decoded mean pulse shapes.

The learned latent space is smooth and structured, clustering pulse shape families (Fig. 1) and enabling physically plausible interpolations. In contrast, the original shaping parameter space is governed by a complex nonlinear optical process not directly accessible in beam dynamics studies. The latent variables therefore provide an efficient interface

* alexander.klemps@tuhh.de

Content from this work may be used under the terms of the CC BY 4.0 licence (© 2026). Any distribution of this work must maintain attribution to the author(s), title of the work, publisher, and DOI.

ISBN: 978-3-95450-252-3 ISSN: 2673-5350 doi: 10.18429/JACoW-IPAC2026-WEP6014

FEL POWER PROFILE PREDICTIONS WITH IMAGE-BASED MACHINE LEARNING AT FLASH

J. Lundquist*, S. Werin and F. Curbis, Dept. of Physics, Lund University, Lund, Sweden
E. Mansten, MAX IV Laboratory, Lund, Sweden
G. Goetzke, Deutsches Elektronen-Synchrotron DESY, Hamburg, Germany

Abstract

Accelerator operators and beamline users can highly benefit from accurate and efficient measurements of FEL (free-electron laser) pulse power profiles. The use of machine learning to predict such profiles is an area of rapid development in the field. This work presents recent measurements and tests at the FLASH FEL at DESY of an image-based machine learning application developed to facilitate online FEL power profile reconstruction. The reconstruction has been performed using machine learning predictions of the longitudinal phase-space (LPS) of electron beams unaffected by the FEL process, originally measured using a transverse deflecting structure. The predictions were used in combination with longitudinal measurements of the LPS of the electron beam after lasing, which does not interfere with delivery to users, to reconstruct the FEL pulse. The results of the reconstruction process have been validated by comparison with a reference method which does not rely on machine learning.

INTRODUCTION

Free-electron lasers (FELs) provide ultrashort, high-brightness photon pulses that enable a wide range of scientific experiments. The temporal profile of these pulses, or the *FEL power profile*, is a key parameter for experiments using FEL light [1]. Direct measurements of single shot FEL power profiles remains a challenging task, often requiring invasive diagnostics and extensive use of dedicated machine time. Applications more suited to routine operations and online monitoring are in high demand [2].

When using the electron beam for FEL power profile measurements, one requires full longitudinal phase space (LPS) measurements, which is done at FLASH using a transverse deflecting structure (TDS) [3, 4]. TDS measurements can be performed either on electron beams that generate FEL radiation (*lasing*) or those that do not (*non-lasing*). The FEL power profile can then be reconstructed from the differences between these two cases. Directly measuring FEL power profiles remains challenging since autocorrelation techniques, normally used for temporal characterization, lack sufficient nonlinear materials with high cross sections for XUV or X-ray photon energies. Methods that can deliver non-destructive, single-shot profiles, such as THz [5] or angular streaking [6], can be considered experiments themselves and often require extensive use of dedicated machine time.

* johan.lundquist@maxiv.lu.se

There is a high demand for applications more suited to routine operations and online monitoring. Advancements in machine learning integration with electron diagnostics has opened up new possibilities for FEL power profile reconstruction. In particular, virtual diagnostics (VDs) focused on LPS predictions can be used in place of TDS measurements [7]. Such an approach can enable real-time estimation of FEL properties, and an application based on electron power profiles has been tested at FLASH, DESY [2].

In this work, also carried out at FLASH, we investigate a different approach. Rather than working only with power profile, we implement an image-based virtual diagnostic to predict the beam's full LPS distribution, before comparing with measurements during lasing for FEL power profile reconstruction. This is also compared directly with a non-machine learning reference method for reconstructing the power profiles.

EXPERIMENTAL SETUP

FLASH2 LPS Measurements

The FLASH FEL at DESY is driven by a superconducting linac with two stages of bunch compression, utilizing two stages of bunch compression in magnetic chicanes, resulting in kA-level peak currents. During the data acquisition, the electron beam was setup with a final energy of 920 MeV in the FLASH2 beamline and an RMS bunch length of approximately 180 fs. The linac was set up to produce a short bunch train of only two bunches in each shot, with a repetition rate of 10 Hz.

The FLASH2 TDS setup uses a X-band PolariX deflecting structure for beam streaking [8, 9]. The 0.8 m PolariX structure is set up 2 m after the last FLASH2 undulator. After the RF streaking, the electron beam is diverted from the photon beam path by a 3.5°-bend magnet and during normal delivery, one bunch in the bunch train is deflected to a scintillating screen for imaging. For the experiments presented here, an on-axis screen was used, as a shortened bunch train was accelerated which would not damage the screen. The TDS setup was calibrated using scans of both the RF phase in the TDS and the current in the dipole deflecting onto the screen. For the data acquisition these procedures returned $0.89\ \frac{\text{fs}}{\text{px}}$ and 0.096 m for the shear parameter and dispersion on the screen respectively.

The data used in this study consisted of 5919 images collected without the beam lasing and 3146 images collected during lasing, all collected at a nominal setpoint for the FLASH accelerator. Lasing was controlled with a horizontal

Content from this work may be used under the terms of the CC BY 4.0 licence (© 2026). Any distribution of this work must maintain attribution to the author(s), title of the work, publisher, and DOI.

ISBN: 978-3-95450-252-3 ISSN: 2673-5350 doi: 10.18429/JACoW-IPAC2026-WEP6015

BAYESIAN OPTIMIZATION OF LONGITUDINAL PHASE SPACE IN THE MAX IV LINAC

J. Lundquist*, J. Björklund Svensson, S. Werin and F. Curbis
Lund University, Lund, Sweden
E. Mansten, MAX IV Laboratory, Lund, Sweden

Abstract

Reaching design performance in modern particle accelerators is a challenge involving many tasks which are time-consuming and difficult to perform. It is always an advantage to be able to simplify high-level operational tasks and measurements through the assistance of optimization techniques. In this work we applied Bayesian optimization via the XOpt framework with the aim to simplify and enhance the operations in the MAX IV linac. The focus of this work has been longitudinal phase-space optimization using signals from a transverse deflector system. Further, a new approach in the optimization of longitudinal phase-space parameters with the use of virtual diagnostics has been developed and implemented.

INTRODUCTION

Within modern accelerators there is a growing need for precise control of both transverse and longitudinal beam parameters. With linear electron accelerators providing beam for light sources requiring femtosecond resolution, the longitudinal phase space (LPS) of the generated beams is of particular importance, as it directly influences the brightness and stability of the resulting photon beams [1]. Achieving and maintaining the key parameters in the LPS of the electron beam is a key issue in such instances.

At MAX IV the linac serves as a full energy injector to two storage rings, at 1.5 and 3 GeV, and also delivers beam for a short pulse facility (SPF) when not injecting to the rings [2]. The SPF houses two separate beamlines, one experimental beamline for light production, and a diagnostic beamline with a transverse deflecting structure (TDS) setup for measuring the beam LPS [3]. The complexity and practicalities of operating the TDS, along with the coupled parameter space and non-linear controls, can make manual tuning of the beam LPS both time-consuming and intrusive to user activities in the experimental beamline. Automated optimization could alleviate many of these issues and enable more efficient, simplified operation of the linac as a whole. In this work we have implemented and tested Bayesian optimization techniques for LPS control in the MAX IV linac, both with integration in the TDS diagnostic system and using a virtual diagnostic as an alternative, non-invasive evaluator of the beam LPS [4–6].

* johan.lundquist@maxiv.lu.se

MAX IV Longitudinal Phase Space Control and Diagnostics

The longitudinal phase space of the beam is defined as its extent in the (t, δ) space, with $\delta = \frac{\Delta p}{p}$ being the relative deviation in energy. Direct measurement of the LPS at MAX IV is performed using the TDS system installed at the end of the linac [3]. The key components of the diagnostic system are two 3 m radio-frequency (RF) structures set up to deflect the beam onto a scintillating YAG screen 20 m downstream. This screen is set up in a dispersive region, thus also enabling the extraction of the beam distribution in δ. While this diagnostic system provides detailed LPS information for automatic optimization, it is also invasive and difficult to operate, providing a use case for the virtual diagnostic covered in a later section.

LPS control in the MAX IV linac is achieved with two separate stages of bunch compression, using an arc-like bunch compression scheme [7]. The principal controlling beam parameter of the compression is the energy chirp of the incoming beam, i.e. the linear correlation between the relative energy deviation and the longitudinal position within the electron bunch. The energy chirp results in longitudinal compression when moving through the bunch compressor arc as the transfer elements of R_{56} and T_{566} result in an energy dependent shift in the longitudinal positions. The energy chirp in the incoming beam is controlled using the off-crest phase of the accelerating RF fields experienced by the beam. This phase is in turn controlled through the filltime in the SLED units providing RF to the accelerating structures, as a feedback system acting on the RF phase will maintain the design energy for the bunch compressors [8]. To control beam compression, one provides a new setpoint in SLED filltime, and as the RF phase is changed by the feedback, the beam will enter the compressor with a different energy chirp.

Bayesian Optimization

Bayesian optimization (BO) is an efficient and effective way of optimizing environments which are expensive to quarry and have noisy or difficult objectives [9]. BO relies on a live probabilistic modeling of the environment, allowing it to set up an approximate model of the system's response to parameter changes. To tune the response model an acquisition function decides the selection of new evaluation points and the model is recalculated with these new points added. In order to thoroughly optimize the environment, it is key that the acquisition function achieves a balance between exploration of unexplored areas and exploitation of

Content from this work may be used under the terms of the CC BY 4.0 licence (© 2026). Any distribution of this work must maintain attribution to the author(s), title of the work, publisher, and DOI.

ISBN: 978-3-95450-252-3 ISSN: 2673-5350 doi: 10.18429/JACoW-IPAC2026-WEP6016

DATA-DRIVEN OPTIMIZATION OF OPEN-LOOP CONTROL FUNCTIONS AT THE CERN SUPER PROTON SYNCHROTRON

A. Menor de Oñate*, M. Schenk, V. Kain, T. Prebibaj, I. Mases Sole, B. Rodriguez Mateos
CERN, Geneva, Switzerland

Abstract

To minimize beam intensity loss during a cycle in the CERN Super Proton Synchrotron (SPS), several machine parameters must be adjusted as functions of cycle time, spanning injection, injection plateau, acceleration, and extraction plateau. Today, these functions are typically tuned manually – a cumbersome procedure that can require hours of operator effort. This paper presents the progress towards automatically tuning time-dependent parameter functions. Using Bayesian optimization (BO), we aim to minimize intensity loss throughout the cycle with intensity measurements as the primary feedback signal. We report results from applying this method to an intentionally detuned machine development beam in the SPS, as a step towards deployment on the operational fixed-target beams. The approach is generic and applicable to time-dependent parameter optimization problems in other machines.

INTRODUCTION

The Super Proton Synchrotron (SPS) provides beams to a range of users, including the LHC and several fixed-target and beam-physics facilities. Each beam is delivered through a "cycle", in which the beam is first injected from the Proton Synchrotron (PS) – possibly over several injections – onto the SPS injection plateau ("flat bottom"). The beam is then accelerated to its target energy and extracted to its destination. An example cycle for a slow-extracted beam is shown in Figure 1, displaying the total beam intensity and momentum alongside three parameter functions targeted by the optimization: the horizontal (Q_{H}) and vertical (Q_{V}) betatron tunes and the total RF voltage (V_{RF}).

Throughout the cycle, the beam is subject to a variety of processes and beam-dynamics phenomena: injection, RF capture, intensity-dependent tune shifts that increase stepwise with each injection, decaying eddy currents compensated by adjustments of the momentum, tune, and chromaticity functions on the flat bottom, and transition crossing during acceleration. This requires multiple machine parameters to be adjusted as functions of cycle time to minimize intensity loss. These parameter functions must be defined before the cycle is executed and are applied open-loop: they cannot be modified during a cycle, only between cycles.

Moreover, the optimal settings depend on the requested beam intensity, which is adjusted several times per year as experimental needs vary, making manual retuning a recurring operational burden. This is particularly relevant for the future Search for Hidden Particles (SHiP) [1] experiment at the SPS, which will ultimately be a high-intensity operational beam delivered at high repetition rate, making the minimization of transmission losses crucial to keep activation of SPS beam equipment at acceptable levels.

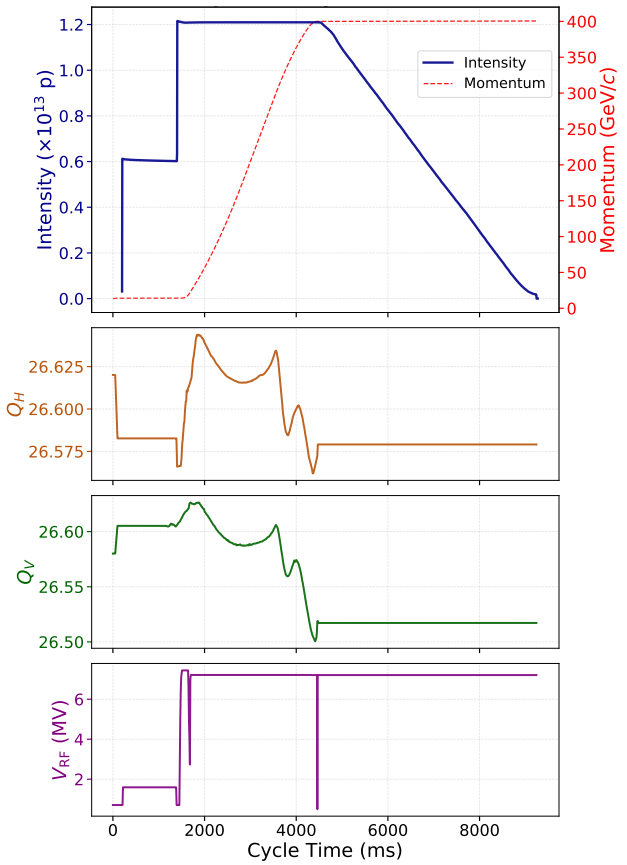

Figure 1: Example SPS cycle for a slow-extracted beam, showing two injections on the injection plateau, acceleration from 14 GeV/c to 400 GeV/c and extraction (top panel). Horizontal (Q_{H}) and vertical (Q_{V}) betatron tunes and RF voltage (V_{RF}) functions are also shown (bottom panels).

Among the parameter functions, the betatron tunes and RF voltage have the largest impact on intensity loss (or equivalently, beam transmission) for the fixed-target beams under study here and are the primary focus of this work. Other parameter functions, such as the chromaticities, will be addressed in future studies. From an operations perspective, optimizing these parameters manually is time-consuming and becomes increasingly difficult at high intensities, where key observables such as tune measurements are unreliable or unavailable, leaving intensity measurements as the primary feedback. This further motivates the use of automated, data-driven optimization, an approach recently applied to related problems at CERN, including Multi-Turn Extraction tuning at the PS [2] and hysteresis compensation in the SPS

* adrian.menor.de.onate@cern.ch

Content from this work may be used under the terms of the CC BY 4.0 licence (© 2026). Any distribution of this work must maintain attribution to the author(s), title of the work, publisher, and DOI.

ISBN: 978-3-95450-252-3 ISSN: 2673-5350 doi: 10.18429/JACoW-IPAC2026-WEP6017

TOWARDS FULLY AUTOMATED TRANSFER LINE COMMISSIONING AT THE CERN SUPER PROTON SYNCHROTRON

A. Menor de Oñate*, M. Schenk, V. Kain, B. Rodriguez Mateos, G. Dal Maso, N. Charitonidis
CERN, Geneva, Switzerland

Abstract

Beam commissioning of slow extracted beams from the CERN Super Proton Synchrotron (SPS) to the North Area experimental targets requires trajectory control through multiple transfer lines using corrector magnets—a process that traditionally demands significant expert intervention. Previous work demonstrated the feasibility of applying reinforcement learning (RL) for automated trajectory correction based on secondary emission monitor (SEM) split-foil intensity measurements, successfully centering the beam on target under nominal conditions [1]. However, this approach fails when the beam is lost or its position exceeds the SEM's active surface, and when the corrector magnets' polarities are not known; common sources of uncertainty during commissioning.

We present an extended multi-stage optimization scheme that addresses these critical limitations by automating beam threading when the trajectory exceeds the SEMs' acceptance, systematically identifying corrector magnet polarity configurations, and optimizing the impact angle to maximize beam intensity at the fixed-target stations, measured by scintillators arranged around the target. The threading algorithm employs quasi-random search combined with Bayesian optimization (BO) to center the beam in the SEMs, before handing over to the RL controller. The automated polarity determination uses online system identification to resolve sign ambiguities in the correctors, eliminating a common source of commissioning delays when using RL or other dedicated steering algorithms. Finally, BO is used to optimize the position of the movable SEM monitors at the targets' locations, maximizing target intensity.

INTRODUCTION

The CERN Super Proton Synchrotron (SPS) sends DC proton and heavy ion beams to the North Area (NA) experimental targets through a number of transfer lines. During commissioning, the beams need to be steered through the lines, and the yield of the NA targets needs to be maximized. The steering actions are done using dipole magnets (correctors), while the beam trajectory along the line is monitored using secondary emission monitors (SEMs), as conventional beam position monitors are not available in the line. SEMs have two foils (either aligned horizontally or vertically) that each measure beam intensity [2]. If the beam hits both foils, position can be inferred by using the intensity difference between foils and by fitting a Gaussian beam profile assuming known emittance and nominal optics. However, when the beam falls on one foil only, the position cannot be inferred. In this scenario, classical steering algorithms that rely on beam position measurements fail. Previous work demonstrated that reinforcement learning (RL) controllers can steer the line in such cases [1].

While this is a step forward, if the beam is completely off the foils, or the magnet polarities are changed from the previous commissioning, the RL agent described in [1] can no longer steer the line, as it relies on valid SEM readings and known corrector polarities. Therefore, an additional automated procedure is needed to optimize the beam intensity at the targets.

With this in mind, the following sequential automated procedures have been tested during commissioning in the horizontal plane of the line: first, steering from severe beam trajectory offsets using Bayesian optimization (BO); second, estimating corrector polarities with kick response measurements that are compared against a model of the transfer line; third, steering the beam to a high symmetry S (done with RL [1] or MICADO [3]) in the SEMs (see Equation 1, where I_1 and I_2 are the intensities on foil 1 and 2 in the SEM), and finally optimizing the intensity at the fixed targets.

$$S = \sqrt{1 - \frac{|I_1 - I_2|}{I_1 + I_2}} \tag{1}$$

STEERING FROM SEVERE BEAM TRAJECTORY OFFSETS (THREADING)

At the beginning of commissioning, the beam may be lost along the transfer line, or its position may fall outside the active surface of the SEMs. In order to bring the beam back to an acceptable symmetry (here targeted at 0.6), the transfer line is divided into segments mapping one or more corrector magnets to the downstream SEM(s), located before the next corrector. Each of these segments is sequentially steered by first taking quasi-random actions that explore the action space of the magnet, generating space-filling samples to maximize exploration. Once the beam is detected in any of the SEMs in the segment, BO guides the steering process. This sequential optimization is referred to as "threading".

When inspecting the optimization landscape (in simulation) of a given segment of the transfer line that needs to be optimized (see left plot in Figure 1, showing the action spaces of two corrector magnets, and the resulting objective value), we observe that a ridge-like solution is present when using two magnets or more, corresponding to the magnet combinations that result in a good objective value:

$$\text{Objective} = \sum_{j=1}^{N_{\text{SEM}}} \begin{cases} S_j^2 & \text{if } I_j^{\text{tot}} \geq I_{\text{min}}, \\ 0 & \text{otherwise.} \end{cases} \tag{2}$$

* adrian.menor.de.onate@cern.ch

Content from this work may be used under the terms of the CC BY 4.0 licence (© 2026). Any distribution of this work must maintain attribution to the author(s), title of the work, publisher, and DOI.

ISBN: 978-3-95450-252-3 ISSN: 2673-5350 doi: 10.18429/JACoW-IPAC2026-WEP6018

HIGH-DIMENSIONAL BAYESIAN OPTIMIZATION FOR SPARSE OBJECTIVES: AN APPLICATION FOR AUTOMATED BEAM COMMISSIONING IN THE LOW ENERGY ION RING AT CERN

B. Rodriguez Mateos*, T. Argyropoulos, V. Kain,
M. Schenk, M. Slupecki†, European Organization for Nuclear Research, Geneva, Switzerland

Abstract

Recent advances in high-dimensional Bayesian Optimization have opened the door to new tools for beam commissioning. At the CERN Low Energy Ion Ring (LEIR), several tuning challenges arise from the complex parameter space governing beam transfer and accumulation dynamics. In this paper we benchmark several state-of-the-art High Dimensional Bayesian Optimization methods to optimize the transfer from Linac3 to LEIR and maximize the accumulated beam inside the ring. We evaluate algorithms based on different strategies: trust region approaches (TuRBO), sparse axis-aligned subspace priors (SAASBO), nested embeddings for mixed spaces (Bounce), and length-scale-adapted priors in regular Bayesian Optimization. Our results demonstrate the relative strengths of each method in the context of particle accelerator optimization, where sample efficiency is critical, the objective function exhibits sparsity in relevant dimensions, and the parameter space contains both local and global structures. The benchmarking provides practical insights for selecting appropriate algorithms for beam commissioning tasks, considering factors such as convergence speed, computational overhead, and robustness to noisy observations.

INTRODUCTION

Modern particle accelerators are complex systems with a large number of tunable parameters that must be carefully adjusted to achieve optimal beam performance. Beam commissioning often requires the simultaneous tuning of tens of parameters spanning transfer lines, injection elements, radio-frequency (RF) systems, and correction magnets, a task traditionally performed manually by expert operators through iterative adjustments. As facilities become increasingly complex and demand ever-higher performance, there is a growing need for automated tuning procedures that can reliably navigate these high-dimensional parameter spaces [1].

Among data-driven approaches, Bayesian Optimization (BO) has demonstrated particular success in a wide range of accelerator physics applications [2], including injection efficiency tuning [3, 4], Free Electron Laser (FEL) performance optimization [5], and trajectory correction [6]. BO treats the objective as a black-box, handles noisy measurements gracefully, and is sample-efficient, a critical feature when each evaluation corresponds to a machine cycle [7]. However, the performance of standard BO with Gaussian Process (GP) surrogates is known to degrade rapidly as the dimensionality of the search space grows: distances between candidate points become increasingly similar, reducing the ability of the GP kernel to distinguish nearby from distant points [8, 9].

Several high-dimensional Bayesian Optimization (HDBO) algorithms have been developed to address this limitation, each with a different inductive bias. Trust-region approaches such as TuRBO [10] restrict the optimization to local hyper-rectangular regions. Sparse-axis-aligned methods such as SAASBO [11] impose a hierarchical sparsity prior on the kernel lengthscales, assuming only a small subset of dimensions is relevant. Nested embedding methods such as Bounce [12] progressively build low-dimensional embeddings, originally designed for combinatorial and mixed spaces but adaptable to continuous problems. Recent work [13] has also shown that standard BO can be made competitive in high-dimensional spaces by rescaling the lengthscale prior with the dimensionality. For comparison, we include CMA-ES [14], a derivative-free evolutionary optimizer widely used as a baseline to probabilistic approaches [15].

The CERN Low Energy Ion Ring (LEIR) provides an ideal testbed for benchmarking these algorithms. LEIR accumulates up to eight multi-turn injections of Pb^{54+} ions from Linac3 through phase-space painting combined with electron cooling, before RF capture and extraction to the Proton Synchrotron [16]. Its high repetition rate, low beam energy, and the regular need for re-tuning due to Linac3 stripper foil aging [17] make it a practical platform for developing and validating data-driven tuning strategies. Previous work at LEIR demonstrated that standard BO with Upper Confidence Bound (UCB) and Log Noisy Expected Improvement (LogNEI) acquisition functions can outperform operational tuning for both injection efficiency and RF capture losses when the number of dimensions is moderate [4]. Extending this to full beam commissioning, however, requires simultaneously tuning on the order of 40 parameters without operational priors, pushing the problem firmly into the high-dimensional regime.

In this paper, we benchmark a representative set of state of the art HDBO algorithms on the task of commissioning the Linac3-to-LEIR transfer and injection starting from an unoptimized initial configuration and without prior knowledge. We consider two operationally relevant beam types, the NOMINAL cycle with 43 tunable parameters and the EARLY cycle with 38, both optimized with respect to the accumulated beam intensity before RF capture, measured with

* borja.rodriguez.mateos@cern.ch
† also at Department of Communications and Computer Engineering, University of Malta

Content from this work may be used under the terms of the CC BY 4.0 licence (© 2026). Any distribution of this work must maintain attribution to the author(s), title of the work, publisher, and DOI.

ISBN: 978-3-95450-252-3 ISSN: 2673-5350 doi: 10.18429/JACoW-IPAC2026-WEP6021

ONLINE REINFORCEMENT LEARNING FOR STRIPPER FOIL AGING COMPENSATION AT THE CERN LOW ENERGY ION RING

B. Rodriguez Mateos*, T. Argyropoulos, V. Kain, A. Lu, A. Menor de Onate, M. Schenk, M. Slupecki†, European Organization for Nuclear Research, Geneva, Switzerland

Abstract

Stripper foil degradation at the CERN Low Energy Ion Ring (LEIR) poses a significant challenge for beam operations. As the heavy ion beam passes through the stripper foil at the end of the injecting linac, the foil degrades over time, altering the beam energy distribution and reducing the achievable accumulated intensity in the ring. Addressing this operational limitation using traditional control approaches is challenging due to the complex, multi-dimensional nature of the multi-turn injection process. This paper presents a reinforcement learning-based controller to compensate for foil degradation and maintain ring performance. The controller observes longitudinal Schottky spectra encodings and time-of-flight measurements from the linac to adjust the ramping and debunching cavity phases, and electron cooler gun and orbit bump in real time. We demonstrate that pre-training the agent in a data driven surrogate model significantly improves both controller performance and sample efficiency during deployment.

INTRODUCTION

The Low Energy Ion Ring (LEIR) at CERN accumulates lead-ion beams for the Large Hadron Collider (LHC) and fixed target experiments by stacking up to eight consecutive multi-turn injections from Linac3. Each 200 µs-pulse is injected at 200 ms intervals through a six dimensional phase-space painting scheme combining a collapsing horizontal orbit bump with a linearly ramped mean momentum in a high-dispersion region. Between injections, electron cooling compresses and drags the circulating beam longitudinally to free momentum space for the next pulse. After accumulation, the coasting beam is captured into bunches and accelerated to 72 MeV/u for extraction toward the Proton Synchrotron. The quality of this process depends critically on the precise matching between the energy distribution delivered by Linac3 and the LEIR electron-cooler parameters.

A well-known operational limitation is the progressive degradation of the carbon stripper foil, installed at the end of Linac3, used to strip Pb^{29+} ions to Pb^{54+}. As the foil ages under beam bombardment, it causes a gradual shift in the injected momentum distribution, with drift rates in the order of 0.06 ‰ per day [1]. Because electron cooling is energy dependent, even small shifts reduce injection efficiency; in extreme cases, accumulated intensity drops by more than a factor of two, requiring foil replacement approximately every two weeks [1]. Historically, these drifts have been corrected manually by adjusting the last Linac3 accelerating tank and retuning the ramping and debunching RF cavities, a procedure that is time consuming, reactive, and dependent on operator availability. Together, these two latter cavities respectively control the mean energy and the shape of its spread along the 200 µs-pulse.

To move toward automated compensation, Madysa *et al.* [2] constructed a data-driven surrogate model of the LEIR injection dynamics: a β-variational autoencoder (β-VAE) compressed the high-dimensional Schottky spectra into a compact latent representation, while multi-layer perceptrons learned both an intensity model and a dynamics model predicting state transitions as a function of parameter changes. Several RL algorithms were trained offline on this surrogate and shown to recover nominal intensity in fewer than 20 steps when the machine was moderately detuned, establishing the feasibility of RL-based optimization for LEIR. However, limited surrogate generalization prevented online deployment.

Building on this, we presented the first operational results of ML-based beam intensity optimization at LEIR [3], deploying Bayesian Optimization with Upper Confidence Bound (UCB) and Log-Noisy Expected Improvement (Log-NEI) acquisition functions to maximize injection efficiency and minimize RF capture losses, consistently exceeding average operational performance. In parallel, the data-driven surrogate model was improved through an enhanced transition model loss incorporating symmetry and fixed-point constraints to enforce physical consistency and mitigate error accumulation during multi-step rollouts. The offline-trained RL agents reached near-target injection efficiency in approximately three cycles, though performance did not yet meet the operational threshold. In this paper, we present the online deployment of an RL agent that autonomously compensates for stripper-foil aging in Linac3 to maintain optimal injection efficiency into LEIR with close to the full operational range of control parameters, and demonstrate that automated RL-based compensation can sustain beam intensity at nominal levels over extended periods without manual intervention.

PROBLEM FORMULATION

Observation Space

The design of an informative and compact observation space is central to RL agent performance. The observation must capture sufficient information about the machine state to allow the agent to infer corrective actions, while remaining low-dimensional enough for efficient training on limited operational data. The primary diagnostic for the longitudinal beam dynamics during the LEIR injection process is the lon-

* borja.rodriguez.mateos@cern.ch
† also at Department of Communications and Computer Engineering, University of Malta

Content from this work may be used under the terms of the CC BY 4.0 licence (© 2026). Any distribution of this work must maintain attribution to the author(s), title of the work, publisher, and DOI.

ISBN: 978-3-95450-252-3 ISSN: 2673-5350 doi: 10.18429/JACoW-IPAC2026-WEP6022

AUTOENCODER ARCHITECTURES FOR BEAM ANOMALY DETECTION AND STATISTICAL DISTRIBUTION CHARACTERIZATION

J. Szumega*[1,2], L. Bougueroua[3], B. Gkotse[1,4], P. Jouvelot[2], N. Minafra[1,5], F. Ravotti[1]
[1]European Organization for Nuclear Research, Geneva, Switzerland
[2]Mines Paris, PSL University, Paris, France
[3]Efrei Research Lab - Université Paris Panthéon Assas, Villejuif, France
[4]University of Wisconsin–Madison, Madison, United States
[5]University College of Dublin, Ireland

Abstract

In accelerator facilities, beam delivery control and assessment require capable monitoring systems, including both hardware and software components. In most accelerator beamlines, precise measurements and reliable beam delivery are critical factors in their operation. At the CERN IRRAD facility, the transverse beam profile contains essential information on the beam properties relevant to the irradiation of materials and components. Building upon the existing Beam Profile Monitor instrument at the CERN IRRAD Facility (IRRAD-BPM), we explore the possibilities of using Machine Learning techniques, with special focus on Autoencoder (AE) architectures. Dealing with a critical system that involves high-energy protons and extreme radiation conditions, we developed an AE-based anomaly-detection system. Its architecture, based on multiple parameters, is a result of hyperparameter optimisation aiming for the highest separation of anomalous samples. Additionally, to mitigate the existing limited IRRAD-BPM coverage that cannot capture the full extent of the beam tails, we perform a statistical inference using this AE architecture. Moreover, by using a Multi-Wire Proportional Chamber (MWPC) device also present on the IRRAD beamline, we improve the beam profile modeling within a data-fusion-like approach.

INTRODUCTION

Experimental irradiation facilities must ensure the delivery of beams with the required characteristics and quality. As such, accurate assessment requires a reliable monitoring system capable of detecting unwanted deviations. During facility operation, deviation events can occur due to glitches during beam production, extraction or transport to the experimental facilities. Consequently, a highly precise anomaly detection needs to be an integral part of a monitoring system. This finally impacts all categories of experiments performed at IRRAD, from detector development and radiation-hardness assessment of electronic components, including both proton [1, 2] and heavy-ion [3] irradiation for space applications where the transverse beam profile properties need to be particularly precise.

The IRRAD facility at CERN uses four IRRAD-BPM sensors [4] to monitor the quality of the PS-extracted (Proton Synchrotron) 24 GeV/c proton beam. This is a grid of 39 metallic pads, 4x4 mm^2 each with 0.5 mm separation, resulting in a total effective coverage of ~6 cm^2 in the dense, central region or a total span of ~12 cm^2. In addition, nearby downstream the IRRAD-BPM on the T8 beamline of the experimental East Area, a Multi-Wire Proportional Chamber (MWPC) is also installed to monitor both proton and heavy-ion beams. It is equipped with 32 wires, with 6 mm separation, for each horizontal and vertical profile measurement. This device can cover a larger beam area of ~345 cm^2. The comparison between the acceptance of these two devices is presented in Fig. 1.

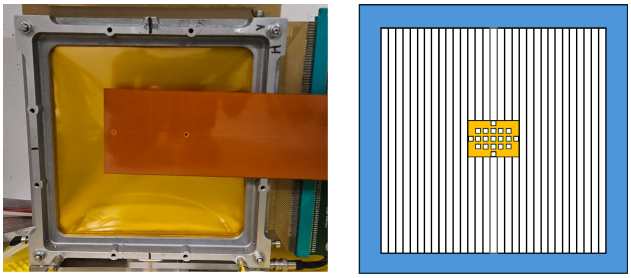

Figure 1: Comparison of the detector dimensions between the Multi-Wire Proportional Chamber (larger detector) and the Beam Profile Monitor. Figure a) shows both encased in protective coating so their internal structure remains hidden. Figure b) is a schema showing an in-scale comparison. While the coverage of the MWPC significantly exceeds that of the BPM, the latter provides better resolution in the beam center.

These two detectors differ in their construction and capabilities for measuring transverse profiles. One is an array of pixel-like pads, capable of 2D profile measurements, but on a narrow surface. The other offers more extensive coverage but reads two 1D profiles only - vertical and horizontal.

By studying autoencoder architectures and heterogeneous data from these detectors, their respective advantages are leveraged to support and improve the beam monitoring capabilities during irradiation experiments.

RELATED WORK

Various neural network architectures are used to detect anomalies. At the Spallation Neutron Source Accelerator (SNS), a machine-learning-based infrastructure has been designed to predict errant beam and detect anomalies in

* jaroslaw.szumega@cern.ch

Content from this work may be used under the terms of the CC BY 4.0 licence (© 2026). Any distribution of this work must maintain attribution to the author(s), title of the work, publisher, and DOI.

ISBN: 978-3-95450-252-3 ISSN: 2673-5350 doi: 10.18429/JACoW-IPAC2026-WEP6023

VIRTUAL BEAM POSITION MONITOR FOR PARTICLE DRIVEN PLASMA WAKEFIELD ACCELERATORS

J. Wolfenden[1]*, C. Welsch[1], University of Liverpool, Liverpool, United Kingdom
E. Belli[2], C. Pakuza, M. Turner
European Organization for Nuclear Research (CERN), Geneva, Switzerland
[1]Cockcroft Institute, Daresbury, United Kingdom
[2]University of Oxford, Oxford, United Kingdom

Abstract

Beam parameters at the interaction point (IP) of a particle driven wakefield accelerator (PWFA) are carefully controlled to optimise the output energy and beam quality of the accelerated witness beam. However, regardless of the parameters achieved, misalignments of beams at a PWFA IP have been shown to produce significant detrimental effects to the witness beam output energy and quality. Online monitoring of pointing stability, or beam jitter, at the IP is therefore essential to discern between beam quality optimisation needs and misalignment issues. However, it is not possible to use standard beam position monitors (BPMs) at these locations. Presented in this contribution is the demonstration of a proposed virtual beam position monitor (vBPM), applied to the IP of the AWAKE experiment at CERN that uses proton bunches as the driver. Upstream BPMs on the proton transfer line are used to infer the transverse position at the IP. A simulation study has been conducted to train a convolutional neural network (CNN) model to perform this inference. Dominant BPMs are highlighted, pointing towards areas of future optimisation to improve the proton beam jitter. An application to recent data collected at AWAKE is also presented, demonstrating the online reconstruction potential for future AWAKE runs.

INTRODUCTION

The alignment of a beam to an interaction point (IP) is often critical to the performance of the interaction. A clear example is the injection point in particle driven wakefield acceleration (PWFA), where incoming beam misalignment can significantly affect the acceleration process and the accelerated witness beam that is produced. This can include a drop in output energy [1], witness beam emittance growth [2], and hosing experienced by the driver [3]. Alignment is required both spatially and temporally, although this contribution focuses solely on transverse spatial alignment.

When the PWFA output beam is sub-optimal, transverse spatial misalignment is only one of several possible contributing factors, since the accelerated beam quality also depends on injection phase, beam loading, plasma-density evolution, beam matching and incoming beam conditions [4, 5]. However, it is often not possible to monitor transverse alignment directly at the PWFA injection point, since beam position monitors (BPMs) and screens cannot be placed there without interfering with operation. Therefore, this contribution develops a new non-invasive method to measure beam-IP alignment: a virtual beam position monitor (vBPM).

VBPM MODEL DESIGN

A vBPM is a new virtual diagnostic (VD) [6, 7], whose inputs are upstream BPM readings, which are used to infer the transverse arrival position of the beam at the IP, operating completely non-invasively. A test case of the proton beam driver at the Advanced Wakefield Experiment (AWAKE) at CERN was selected to efficiently develop this model and methodology. At AWAKE, a 400 GeV SPS proton bunch propagates through a rubidium plasma, where it undergoes seeded self-modulation into a train of microbunches [8, 9]. These microbunches resonantly drive wakefields that have been used to accelerate externally injected witness electrons to GeV energies [5, 10]. The transport line delivering the 400 GeV proton beam from the SPS to AWAKE is by far the largest source of arrival position jitter at the injection point, with uncertainties, such as magnet power supplies, playing a large factor. In this initial proof of concept, all BPM readings along the transport line were included, enabling later permutation analysis to identify which BPMs have the largest effect on the output.

The model architecture chosen was a 1D convolutional neural network (CNN), as shown in Fig. 1. This was selected because it preserves the ordered sequence of the upstream BPM readings along the beamline, allowing the convolutional layers to learn local correlations between neighbouring BPM signals. The model takes the 18 pairs of upstream BPM readings, and passes these through three residual convolution blocks, which systematically increase the number of feature channels from 2 to 128. A residual convolutional block differs from a standard convolutional block by using a skip connection to combine the transformed block input with the output of the convolutional layers. This was used to help preserve information from the original BPM signals while allowing the network to learn deeper, higher-level feature transformations, reducing the risk of useful positional information being degraded through successive convolutional layers. The feature representation is then pooled and then passed through fully connected layers to infer the downstream transverse position, given by the output (X, Y) coordinates.

* joseph.wolfenden@cockcroft.ac.uk

Content from this work may be used under the terms of the CC BY 4.0 licence (© 2026). Any distribution of this work must maintain attribution to the author(s), title of the work, publisher, and DOI.

ISBN: 978-3-95450-252-3 ISSN: 2673-5350 doi: 10.18429/JACoW-IPAC2026-WEP6024

LOCALIZED RESPONSE BASIS FOR DATA-EFFICIENT TRANSVERSE BEAM DISTRIBUTION RECONSTRUCTION USING A MULTIMODE FIBER RELAY

Q. Xu* [1,2], G. Trad[2], S. Burger[2], A. Gilardi[2], M. Bergamaschi[2], F. Roncarolo[2], H. D. Zhang[1], A. Hill[1], C. P. Welsch[1]
[1] University of Liverpool, Liverpool, UK; Cockcroft Institute, Daresbury, UK
[2] CERN, Geneva, Switzerland

Abstract

Transverse beam imaging in radiation areas can be supported by relaying scintillation light through a multimode fiber (MMF) to a camera placed in a shielded area. However, the MMF scrambles the input, so a trained model is required to recover the beam distribution. This work studies a data efficient calibration method in which measured input and MMF output basis pairs are used as building blocks to synthesize training data for the reconstruction model. After an initial digital micromirror device based validation, the method was assessed using real beam data from CERN CLEAR, where data synthesized from a raster scan basis were used to train a Convolutional Autoencoder. The best model using this strategy achieved 7.37% mean normalized root mean square error (RMSE) across four transverse beam parameters, compared with 6.02% for a random scan reference model using roughly twice as many fully paired random scan samples. These results suggest that basis-based synthesis training, when combined with suitable beam image priors, can reduce reliance on large random scan MMF calibration datasets by replacing part of the calibration with a controlled scan of fixed size.

INTRODUCTION

In high radiation accelerator areas, transverse beam imaging can be limited by radiation damage to cameras and associated electronics [1]. One possible mitigation is to relay light from a scintillating screen through a large-core multimode fiber (MMF) to a camera placed in a low radiation area [2, 3]. However, modal mixing in the MMF scrambles the spatial intensity distribution, so the fiber output is not directly interpretable. An inverse reconstruction model is therefore required. Previous work has shown that Convolutional Autoencoder (CAE) models can reconstruct transverse beam distributions from MMF output images [4]. A practical challenge remains the amount and coverage of paired calibration data required for training. In particular, acquiring large paired random scan datasets can be time consuming and may not be convenient for recalibration.

This work investigates whether a measured MMF input-output basis can be used as a compact calibration source for synthetic training data. The approach is motivated by the approximate linearity of the measured intensity mapping under fixed alignment and acquisition conditions [5, 6]. A set of measured input patterns and corresponding MMF output images is used as the basis, and new paired training samples are generated by linearly combining this basis with different coefficient maps. The method is first tested using a controlled digital micromirror device (DMD) source under LED illumination, where a position basis is used to validate the synthesis procedure. It is then assessed using data from the CERN CLEAR facility, where a raster scan basis is used for calibration and independent beam images are used for evaluation.

DMD-SOURCE VALIDATION

MMF Intensity Basis

Light transport through a multimode fiber is often described by a transmission matrix (TM), which maps an input optical field to an output optical field. In optics laboratory systems, such a matrix can be calibrated using an orthogonal basis, such as a Hadamard basis [7]. For accelerator beam imaging context, the input is instead an intensity distribution formed on a screen, so arbitrary optical patterns are not the most suitable calibration target. We therefore use a simple position basis, where the transverse distribution is represented by square blocks on a finite grid. This basis resembles a raster scan and is more directly connected to beam based calibration. After background subtraction and within the linear camera signal range, the MMF relay is treated as a fixed intensity mapping. The synthetic input and output images are written as

$$\begin{aligned} I_{\mathrm{in}}^{\mathrm{syn}}(x,y) &= \sum_{i,j} a_{ij} B_{ij}^{\mathrm{in}}(x,y), \\ I_{\mathrm{out}}^{\mathrm{syn}}(u,v) &= \sum_{i,j} a_{ij} B_{ij}^{\mathrm{out}}(u,v). \end{aligned} \tag{1}$$

Here B_{ij}^{in} is the input square block at grid position (i,j), B_{ij}^{out} is the MMF output image measured for that block, and a_{ij} is the shared intensity coefficient. The same coefficient map is used to synthesize both input and output images. An $n_x \times n_y$ position basis requires $n_x n_y$ measured basis pairs.

DMD Setup and Data Synthesis

To validate the position basis method under controlled conditions, an optical setup based on a DMD was used before the beamline assessment. The setup follows the same MMF relay concept shown in Fig. 1, with the scintillating screen replaced by a DMD. A 680 nm peak emission LED

* qiyuan.xu@liverpool.ac.uk

Content from this work may be used under the terms of the CC BY 4.0 licence (© 2026). Any distribution of this work must maintain attribution to the author(s), title of the work, publisher, and DOI.

ISBN: 978-3-95450-252-3 ISSN: 2673-5350 doi: 10.18429/JACoW-IPAC2026-WEP6027

IMPROVING PEAK PREDICTION IN MEBT SURROGATE MODELS USING FOURIER FEATURE MAPPING*

J. Cha† [1], X. Liu[1], J. Thiyagalingam[1], K. Baker[2]
[1]STFC, Swindon, United Kingdom
[2]ISIS Neutron and Muon Source, Didcot, United Kingdom

Abstract

Accurate prediction of localised beam features such as peak loss and rapid envelope oscillations is essential for reliable operation of the Medium Energy Beam Transport (MEBT) at ISIS. Standard neural network surrogate models often struggle to capture these effects due to spectral bias, favouring smooth variations over sharp changes. In this work, we investigate the use of Fourier feature mapping to improve surrogate model performance on high-frequency beam behaviour. The method projects spatial inputs into a sinusoidal basis, enabling the network to represent high-frequency variations more effectively. We train two surrogate models on MEBT simulation data, one using Fourier feature mapping and the other without, and compare their performance in capturing peak regions. Results show that Fourier feature mapping significantly improves peak prediction accuracy while maintaining comparable performance on global beam trends. This demonstrates a straightforward and computationally efficient approach for enhancing surrogate modelling of beam dynamics in low-energy transport systems.

INTRODUCTION

Particle accelerators, including light sources and neutron facilities, aim to deliver a high-quality and reliable beam to experimental beamlines. This requires tuning machine parameters such as radio-frequency (RF) cavities and magnetic elements based on available diagnostics and operational experience. While particle tracking simulations provide accurate predictions during the design phase, their computational cost limits their use in real-time operation, where beam characterisation is further constrained by limited and often disruptive diagnostics.

Beam loss is a key operational diagnostic, providing an indication of beam degradation and playing a critical role in machine protection. Its spatial distribution is particularly important, but limited diagnostic coverage makes detailed beam behaviour difficult to infer, motivating the use of fast predictive models.

Particle tracking codes such as PARMELA [1], BMAD [2], elegant [3], and ASTRA [4] provide high-fidelity simulations of beam dynamics, but their computational expense prevents their use in time-sensitive applications such as online optimisation and control. Neural network-based surrogate models have therefore been adopted to approximate these simulations with reduced computational cost [5, 6].

Despite their success as universal function approximators, neural networks exhibit spectral bias, favouring low-frequency components and struggling to represent high-frequency variations [7,8]. This limits their ability to capture localised features such as sharp beam loss peaks, where inaccuracies can significantly affect cumulative quantities.

In this work, we investigate Fourier feature mapping to improve the representation of high-frequency beam behaviour in surrogate models. The method augments the input with sinusoidal basis functions, enabling improved capture of rapid spatial variations. It is evaluated on a surrogate model of the Medium Energy Beam Transport (MEBT) at the ISIS Neutron and Muon Source [9], demonstrating improved peak prediction accuracy while maintaining performance on global beam trends.

MEBT MODEL

To investigate the impact of Fourier feature mapping on high-frequency beam prediction, we consider a surrogate model of the planned Medium Energy Beam Transport (MEBT) at the ISIS Neutron and Muon Source.

In the current ISIS configuration, a significant fraction of the beam from the ion source is lost before entering the synchrotron due to transport inefficiencies [10]. The MEBT is designed to improve matching between the radio-frequency quadrupole (RFQ) and the first drift tube linac (DTL) tank, increasing transmission efficiency from approximately 70 % to 96 %.

The MEBT consists of eight quadrupoles for transverse focusing and four rebunching cavities for longitudinal control. The beam dynamics depend on the field strengths of these elements and the incoming beam conditions, including beam size, position, and current.

Beam transport is simulated using the ASTRA particle tracking code [4], implemented via LUME [11]. Simulations track particles along the 2.04 m beamline and evaluate beam properties at 200 points, including beam size, emittance, energy, bunch length, and particle loss.

The local beam loss profile exhibits sparse, high-frequency behaviour with sharp peaks, while cumulative loss forms a step-like function. Accurate prediction of these peaks is critical, as errors can propagate and affect cumulative quantities relevant for machine protection and optimisation. As the MEBT is not yet operational, simulation-based modelling provides the only means to study this behaviour, motivating the development of fast surrogate models.

* This work was supported by the STFC Facilities Fund through the Ada Lovelace Centre.
† jaehoon.cha@stfc.ac.uk

Content from this work may be used under the terms of the CC BY 4.0 licence (© 2026). Any distribution of this work must maintain attribution to the author(s), title of the work, publisher, and DOI.

ISBN: 978-3-95450-252-3 ISSN: 2673-5350 doi: 10.18429/JACoW-IPAC2026-WEP6030

RATE CAPABILITIES OF RADIATION MONITORS BASED ON DIAMOND DETECTORS*

J. Melbinger, M. Bacak, D. Divya, D. Hainz, E. Jericha, TU Wien, Vienna, Austria
T. Fragner, E. Griesmayer, C. Weiss, CIVIDEC Instrumentation, Vienna, Austria
H. Frais-Koelbl, Fachhochschule Wiener Neustadt, Wiener Neustadt, Austria

Abstract

Diamond detectors are widely used in harsh radiation environments due to their intrinsic radiation hardness. At high particle fluxes, single-particle measurements in counting mode are challenging, requiring a transition to current measurement. In this study, a 500 MBq ^{90}Sr beta source was used to investigate the limitations of the counting mode and the transition to current mode. A dedicated readout was implemented using a CIVIDEC ROSY® data acquisition system, with a concurrent counting and current mode. Low-noise CIVIDEC charge-sensitive spectroscopic amplifiers with FWHM of 10 ns, 30 ns, 50 ns and 180 ns were compared. The correlation between count rates and the measured current was studied.

INTRODUCTION

This work presents concurrent counting (AC) and current (DC) measurements for a diamond detector with a 500 MBq ^{90}Sr β-source. In counting mode the amplifiers are counting individual particles. With increasing count rate, pile-up events become more frequent and the AC count rate becomes less reliable as measure for the particle flux. Instead the average ionisation current of the detector is measured with a current amplifier. The count rate for the switch from an AC to a DC measurement depends on the AC output pulse base width (PBW) and the nature of the particle flux, meaning if its deterministic with constant Δt in-between consecutive pulses, or stochastic with Δt following a Poisson distribution.

MEASUREMENT SETUP

The measurement was conducted at the TRIGA Center of TU Wien located at the Atominstitut in Vienna, Austria [1]. A CIVIDEC B1-HV Diamond Beam Loss Detector [2] was used, housing a 4 mm × 4 mm single-crystal chemical vapour deposition (sCVD) diamond sensor with 500 µm thickness. The bias voltage was −400 V, equivalent to an electric field of −0.8 V/µm. The CIVIDEC ROSY® [3], a 14-bit Data Acquisition System (DAQ) with simultaneous AC and DC mode, was used. The data was analysed in real-time in the embedded FPGA of ROSY®, providing the current over time for the DC mode and the count rate and spectrum for the AC mode. Complementary to the real-time data, time windows of 100 ms were recorded in the oscilloscope mode to check for the occurrence of pile-up events. A schematic of the setup and read-out diagram is shown in Fig. 1.

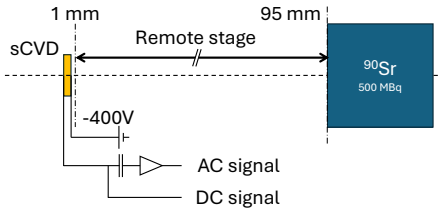

Figure 1: Schematic of the measurement setup with the AC and DC path shown.

The 500 MBq ^{90}Sr source has a diameter of 10 mm and was moved using a remotely controlled linear translation stage. The ^{90}Sr emits electrons with a kinetic energy of up to 546 keV. The resulting ^{90}Y emits electrons with a kinetic energy of up to 2.28 MeV [4]. The low-energy electrons can not reach the detector depending on the distance between source and detector, due to their energy loss in air. The alignment after each amplifier exchange was done visually with a source placeholder. Figure 2 shows the alignment of the placeholder in the front with the diamond detector in the back.

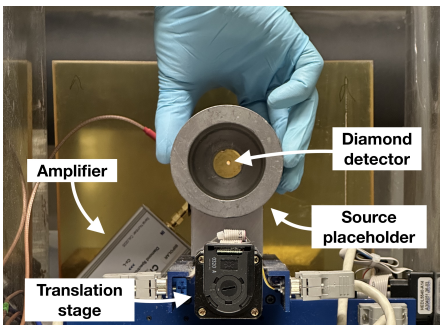

Figure 2: Alignment of the source placeholder with the center of the diamond detector in the background.

The distance between the source and the detector was stepwise varied from d = 1 mm to 95 mm, with 30 s AC and DC measurements at each position.

AC Coupled Amplifiers

Four different capacitative coupled charge sensitive amplifiers from CIVIDEC were used for the AC measurements. The included shaping stage provides a rate optimized gaussian output pulse with a FWHM between 10 ns and 180 ns. The amplifiers in use were the C6-10 Fast Charge Amplifier [5], and different versions of the CxL Spectroscopic Amplifier, namely CxL-30, CxL-50 and CxL-180 [6].

The AC coupling of the amplifier in combination with the internal shaping causes an undershoot. The used ampli-

* julian.melbinger@cividec.at

Content from this work may be used under the terms of the CC BY 4.0 licence (© 2026). Any distribution of this work must maintain attribution to the author(s), title of the work, publisher, and DOI.

ISBN: 978-3-95450-252-3 ISSN: 2673-5350 doi: 10.18429/JACoW-IPAC2026-WEP6031

EXPERIMENTAL EVALUATION OF A DIGITIZER DESIGNED FOR ACCT BEAM CURRENT TRANSFORMERS

D. Coves†, F. Stulle, E. Touzain, Bergoz Instrumentation, Saint-Genis-Pouilly, France
P. Peier, F. Frei, METAS, Wabern bei Bern, Switzerland
L. Soutter, C. Bailat, CHUV, Lausanne, Switzerland

Abstract

To integrate the signals of beam current transformers into accelerator control systems, particle accelerators require high-performance digitizers with optimized bandwidth, sampling rate, and dynamic range. They must be accurate and reliable. And they should be easy to deploy and operate.

A specialized digitizer was developed to interface the Bergoz Instrumentation ACCT sensor and its analog front-end electronics to an accelerator control system. It allows waveform acquisitions preserving the quality of the analog signal. Additionally, it allows controlling the ACCT configuration. Communication is implemented over Ethernet through a simple command protocol and an EPICS soft IOC is provided.

The digitizer was tested with two ACCTs installed at the CHUV Oriatron Linac and a third ACCT at the METAS electron beamline. Results demonstrate improved signal-to-noise ratio, adaptability to multiple beam types, and simplified deployment compared to general-purpose digitizers.

INTRODUCTION

The ACCT from Bergoz Instrumentation is an evolution of the active beam current transformer (BCT) described by Hereward in 1960 [1], which has a lower cutoff frequency compared to conventional BCTs. It is available in a single-range version or with three digitally selectable measurement ranges. The current waveform is provided as an analog output signal.

Various electronics standards are used for acquisition and control across particle accelerators, including VME-bus, CompactPCI, and MicroTCA, each providing high performance but often at the cost of increased integration complexity and required expertise [2].

To address these challenges, a dedicated digitizer was developed to interface ACCT analog signals with accelerator control systems using standard Gigabit Ethernet communication over RJ-45. This approach enables straightforward integration while remaining compatible with existing infrastructures through widely available network interfaces.

Beyond waveform acquisition, the system integrates ACCT electronics range control and on-board data processing, including real-time conversion of voltage waveforms into beam current and pulse charge. This consolidates functionalities typically distributed across multiple hardware modules into a single device.

† dorian@bergoz.com

Modular Digital Solution

The Modular Digital Solution for ACCT (MDS-ACCT) (Fig. 1) is a dedicated digitizer developed by Bergoz Instrumentation. Its design was guided by three main objectives: preserving the integrity of the analog signal during digitization, ensuring long-term sustainability through the use of high-performance and widely available components, and providing an easy-to-use and quick-to-set-up solution that can adapt to different beam types.



Figure 1: MDS-ACCT in its tabletop chassis.

The MDS-ACCT is based on a 16-bit analog-to-digital converter (ADC) operating at 160 MS/s. The digitized samples are streamed to the programmable logic (PL) of a Zynq UltraScale+ system-on-chip (SoC), where they are processed and stored in multiple circular buffers. Upon trigger detection, after a configurable delay, the acquisition is halted, a trigger counter is incremented, and a local timestamp is recorded.

The processing system (PS) of the SoC performs additional operations on the acquired data, such as the computation of the current waveform and the pulse charge. The processed data is packaged into UDP/IP packets, including both waveform data and associated metadata (timestamp, trigger number...), which are transmitted over Gigabit Ethernet.

In addition, long-term sustainability is enhanced by the ability to update both the PL and the PS, as the firmware is stored on a MicroSD card that can be replaced on-site. This therefore allows for the future implementation of additional functionalities.

CHUV Oriatron Linac

The Oriatron eRT6 Linac from PMB-Alcen is a pulsed electron beam accelerator delivering ~5.4 MeV electrons. The grid tension (100 – 300 V), number of pulses, pulse width (0.05 – 4 µs) and pulse repetition frequency (5 – 250 Hz) can be modified [3]. To assess the dose delivered

Content from this work may be used under the terms of the CC BY 4.0 licence (© 2026). Any distribution of this work must maintain attribution to the author(s), title of the work, publisher, and DOI.

ISBN: 978-3-95450-252-3 ISSN: 2673-5350 doi: 10.18429/JACoW-IPAC2026-WEP6032

STUDY OF ION SOURCES USING OPTICAL EMISSION SPECTROSCOPY FOR BEAM MONITORING

A. Ribet†, M. Dubois, L. Gouleuf, F. Lemagnen, V. Metayer, B. Osmond
Grand Accélérateur National d'Ions Lourds, Caen, France

Abstract

Non-interceptive online diagnostics are essential for monitoring ion sources, particularly during physics experiments. Optical Emission Spectroscopy (OES), already used in other laboratories, has been tested at GANIL. The light emitted by the plasma is captured by a CCD camera placed behind a glass window aligned with the ion source and by an optical fiber connected to an optical spectrometer (350-1000 nm). Initial tests were carried out with Ar + He plasma, with an intensity of 80 µAe of $^{40}Ar^{9+}$ measured after the mass separator. Additional studies were performed online in 2025 with a $^{70}Zn^{14+}$ metal beam. Optical measurements made it possible to track changes in the light intensity of the identified wavelengths over time. The use of this technique also provided access to new information (effect of temperature variation, presence of pollution within the plasma, evaluation of the metal ion population) and helped to better identify the needs for optimizing the source settings. These various measures demonstrate the value of developing a dedicated diagnostic tool to continuously monitor beam stability and assist operators during experiments. To this end, initial work has been carried out on automating the analysis of measured optical spectra (definition of baselines, detection and identification of peaks, etc.). This represents the first step towards ultimately achieving complete automation of source adjustments.

MANUSCRIPTS

Introduction

Optical Emission Spectroscopy (OES) is used to monitor the source stability during operation. It is a simple *in situ* diagnostic technique that does not perturb plasma properties. It enables the estimation of key plasma parameters, such as instabilities, the quantity of elements injected into the source, the presence of impurities, and the oven temperature. This technique has been tested and employed in several laboratories, including GSI Helmholtz Centre for Heavy Ion Research, over the past few years [1, 2]. In 2025, initial tests were carried out at GANIL [3].

The diagnostic setup is aligned with the source, downstream of the first mass-separation dipole. Light emitted by the source (from both the plasma and the oven) is collected and focused using a telescope. The signal is then split by a beam splitter, directing 50% of the light to a CCD camera and the remaining 50% into an optical fibre via a collimator. The fibre is connected to the optical spectrometer (Ocean Optics Flame model) for measuring spectral line intensities. The detection system was calibrated over the wavelength range 350–1000 nm.

†alexis.ribet@ganil.fr

Results

The OceanView software (basic software supplied with the device) enables the observation of spectral line intensities over the selected wavelength range and allows monitoring of peak intensity evolution as a function of time. A typical emission spectrum for a $^{70}Zn^{14+}$ beam using N_2 as support gas is shown in Fig. 1. The measurement was performed with a High Frequency (HF) power and an oven power of 152 W and 0.37 W respectively (operating conditions).

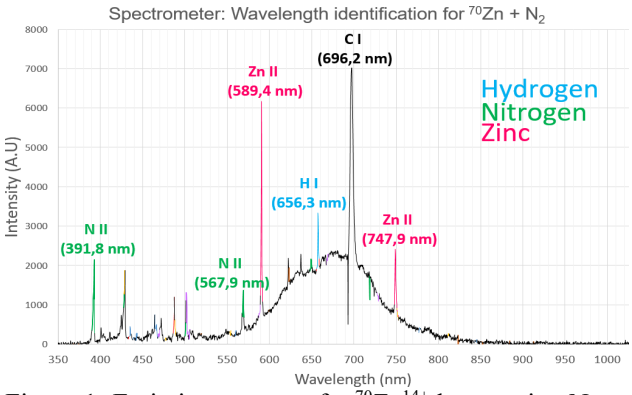

Figure 1: Emission spectra of a $^{70}Zn^{14+}$ beam using N_2 as support gas (P_{HF} = 152 W, P_{oven} = 0.37 W).

The analysis of selected spectral features [4] reveals the presence of two nitrogen emission lines (N II at 391.8 and 567.9 nm), two zinc lines (Zn II at 589.4 and 747.9 nm), one hydrogen line (H I at 656.3 nm), and one carbon line (C I at 696.2 nm). The detection of carbon and hydrogen species in the plasma is likely attributable to the degradation of source and oven components under operating conditions. An overall increase in emission intensity is observed across the 550–850 nm spectral range, suggesting a broadband contribution correlated with the thermal state of the source, and in particular the oven temperature, despite the low power applied. In addition, monitoring the Zn emission lines provides a reliable indicator for tracking real-time variations in the beam current delivered by the source.

Figure 2 displays the temporal evolution over 12 days of operation of key source parameters, including the zinc beam current and injection pressure, together with the intensities of selected emission lines: Zn II at 589.4 nm and N II at 391.8 nm. In addition, CCD camera images acquired

Content from this work may be used under the terms of the CC BY 4.0 licence (© 2026). Any distribution of this work must maintain attribution to the author(s), title of the work, publisher, and DOI.

ISBN: 978-3-95450-252-3 ISSN: 2673-5350 doi: 10.18429/JACoW-IPAC2026-WEP6035

OVERVIEW OF BEAM DIAGNOSTICS FOR PERLE*

M. Ben Abdillah†, S. Brault, A. Fomin, J. Michaud, R. Roux, Université Paris-Saclay, CNRS/IN2P3, IJCLab, Orsay, France
on behalf of PERLE collaboration
J. Wolfenden, Cockcroft Institute, Daresbury, United Kingdom

Abstract

PERLE is an Energy Recovery Linac (ERL) that will be built at the IJCLab in Orsay. It will be the first multiturn ERL with the ambition to reach a beam power of 5 MW. Diagnostics are a key element for the functioning of PERLE, an overview of these diagnostics is discussed. The article focuses on the design and the operation of the diagnostics for PERLE injector. Finally, the article presents challenging diagnostics to monitor beam parameters in PERLE SRF LINAC and PERLE recirculation arcs.

INTRODUCTION

PERLE facility is a new generation energy recovery machine covering the 5 MW power regime with 20 mA beam current and 250 MeV beam energy [1]. It is a compact multiple pass ERL based on SRF technology, to serve as testbed for the validation of a broad range of accelerator phenomena and technical choices for future projects.

An overview of PERLE is sketched in Figure 1. The photocathode gun is on the far right with the injector section immediately following. In this configuration, the peak beam energy is 250 MeV. This is achieved by passing three times through a SRF LINAC .

Starting from a 7 MeV injector, the beam gains 82 MeV per turn, reaching successively 89 MeV, 171 MeV and a final energy of 250 MeV after 3 recirculation passes. After a path length shift of exactly half of RF period, it is then decelerated through the same linac structure to recover the beam energy up to the final dump at 7 MeV, thereby demonstrating full multi-pass energy recovery at high current.

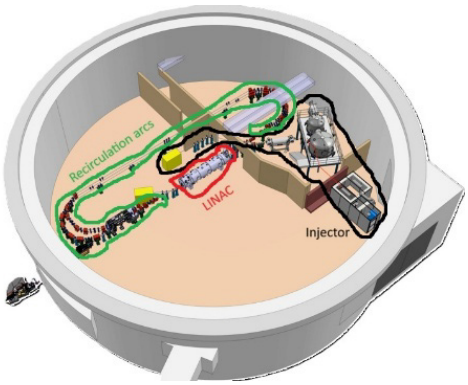

Figure 1: Overview of PERLE in Orsay.

* This work received government funding managed by the Agence Nationale de la Recheche (ANR) in the France 2030 framework - reference ANR-24-RRII-0001
†sidi-mohammed.ben-abdillah@ijclab.in2p3.fr

PERLE diagnostics should monitor specific beam properties at different locations. The following list outlines the diagnostic requirements for PERLE:

- Comprehensive beam measurements at the output of the injector to obtain a precise characterization of the beam at the entrance of the SRF LINAC.
- Calibration of the LINAC cavity phases to optimize the operation of the LINAC.
- Beam path monitoring for each recirculation arc to precisely adjust the length of the path of each beam in the recirculation arcs.
- Monitoring of several beams: measurement of the position of each beam individually.
- Measurement of beams properties in the recirculation arcs for machine protection and optimization of its operation.

Some of these measurements are particularly challenging due the large dynamic ranges over which the beam might operate:

- Beam type: pulsed to cw
- Charge: 10 pC to 500 pC
- Energy: 350 keV to 250 MeV
- Current: 100 µA to 20 mA
- Longitudinal length: 3mm or 10 ps

This article focuses on diagnostics for PERLE injector and details other diagnostics with challenging issues.

DIAGNOSTICS FOR THE INJECTOR

PERLE is currently under construction in the IGLOO building at the IJCLab in Orsay, France. The project is progressing in successive phases, each designed to validate a key step toward the full ERL operation. The first phase, scheduled for late 2028, focuses on realization and the commissioning of the injector sketched in Figure 2.

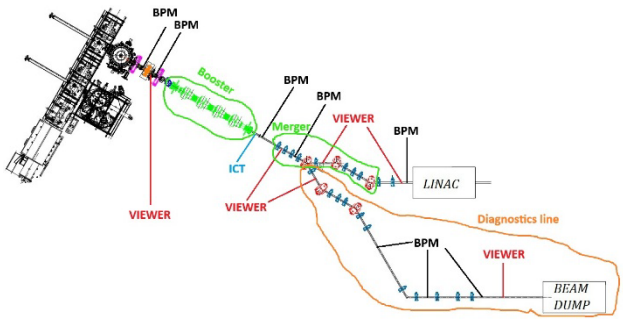

Figure 2: PERLE injector overview with diagnostics.

This includes testing the high current electron gun, aiming to deliver up to 20 mA and 350 keV electron bunches at a repetition rate of 40.079 MHz, as well as the

Content from this work may be used under the terms of the CC BY 4.0 licence (© 2026). Any distribution of this work must maintain attribution to the author(s), title of the work, publisher, and DOI.

ISBN: 978-3-95450-252-3 ISSN: 2673-5350 doi: 10.18429/JACoW-IPAC2026-WEP6036

BEAM POSITIONS MONITORS FOR PERLE INJECTOR*

M. Ben Abdillah†, S. Brault, A. Fomin, F. Fournier
Université Paris-Saclay, CNRS/IN2P3, IJCLab, Orsay, France
on behalf of PERLE collaboration

Abstract

PERLE is an Energy-Recovery Linac (ERL) to be constructed at IJCLab in Orsay. It will be the First ever multi-turn ERL with superconducting RF (SRF) acceleration, and the first ERL with the ambition to reach 5 MW beam operation. Diagnostics are a key element for PERLE operation and among diagnostics, Beam position monitors (BPMs) cover a wide range of applications. This document reports BPM goals for a proper operation of PERLE, it also details the design of BPM detectors and eludes the steps for their realization. it finally discusses the design of BPM electronics to match the presence of multiple beams which need to be individually diagnosed and controlled.

INTRODUCTION

PERLE facility is a new generation energy recovery machine covering the 5 MW power regime with 20 mA beam current and 250 MeV beam energy [1]. It is a compact multiple pass ERL to serve as testbench for the validation of various accelerator phenomena and technical choices for future projects.

An overview of PERLE is sketched in Fig. 1. The photocathode gun is on the far right with the injector section immediately following. In this configuration, the peak beam energy is 250 MeV. This is achieved by passing three times through a SRF LINAC .

Starting from a 7 MeV injector, the beam gains 82 MeV per turn, reaching successively 89 MeV, 171 MeV and a final energy of 250 MeV after 3 recirculation passes. After a path length shift of exactly half of RF period, it is then decelerated through the same linac structure to recover the beam energy up to the final dump at 7 MeV.

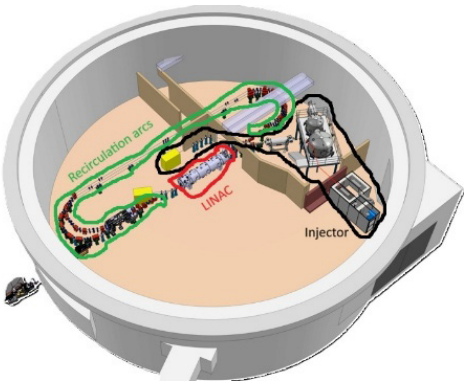

Figure 1: Overview of PERLE in Orsay.

PERLE diagnostics should monitor specific beam properties at different locations. The following list outlines the diagnostic requirements for PERLE BPMs:

- Orbit, charge, and longitudinal length measurements at the output of the injector.
- Calibration of the LINAC cavity phases to optimize the operation of the LINAC [2].
- Beam path monitoring for each recirculation arc to precisely adjust the length of the path of each beam in the recirculation arcs.
- Monitoring of several beams: measurement of the position of each beam individually.

Some of these measurements are particularly challenging due the large dynamic ranges over which the beam might operate:

- Beam type: pulsed to cw
- Charge: 10 pC to 500 pC
- Energy: 350 keV to 250 MeV
- Current: 100 µA to 20 mA
- Longitudinal length: 3mm or 10 ps

This article first details the BPMs for the gun, then it focuses on the realisation steps for the other BPMs. Finally, it discusses solutions for BPM acquisition electronics.

BPMS FOR THE INJECTOR

PERLE is currently under construction in the IGLOO building at the IJCLab in Orsay, France. The project is progressing in successive phases, each designed to validate a key step toward the full ERL operation. The first phase, scheduled for late 2028, focuses on realization and the commissioning of the injector sketched in Fig. 2.

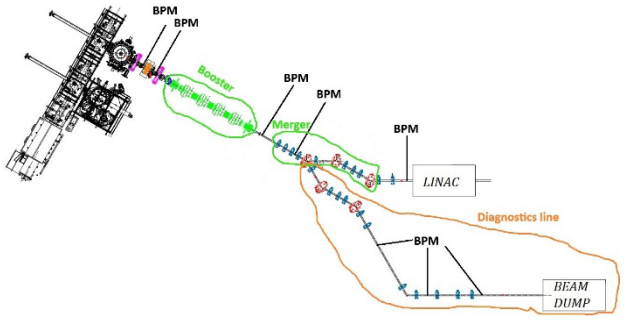

Figure 2: PERLE injector overview with BPMs locations.

Both commissioning and routine operation of the injector look for orbit measurement and correction capabilities with a precision of 100 µm. Although this requirement is stringent, it remains achievable based on the performance levels demonstrated in recent accelerators. Button BPMs are adequate regarding the bunch properties. Eight BPMs are needed in the injector. 2 button BPMs were already purchased with PERLE Gun: the BPM internal diameter is

* This work received government funding managed by the Agence Nationale de la Recheche (ANR) in the France 2030 framework - reference ANR-24-RRII-0001
† sidi-mohammed.ben-abdillah@ijclab.in2p3.fr

Content from this work may be used under the terms of the CC BY 4.0 licence (© 2026). Any distribution of this work must maintain attribution to the author(s), title of the work, publisher, and DOI.

ISBN: 978-3-95450-252-3 ISSN: 2673-5350 doi: 10.18429/JACoW-IPAC2026-WEP6038

SDR BASED MULTIBAND PROCESSING FOR PICKUP SIGNALS IN SYNCHROTRONS

T. Hinderman*, P. Niedermayer, R. Singh
GSI Helmholtz Centre for Heavy Ion Research, Darmstadt, Germany

Abstract

A proof of principle implementation in software-defined radio (SDR) for signal processing at multiple harmonics of the revolution frequency for intensity measurement applications is presented. Two off-the-shelf SDR frontends, USRP X310 and ADALM2000, are combined with the GNU Radio framework to provide real-time signal filtering. A maximum signal processing rate of 5 MSa/s is achieved, and the challenges of real-time processing in these devices are discussed. Beam measurements validating the implemented signal flowgraphs are shown.

INTRODUCTION

Software-defined radio (SDR) technology is recently being adopted for beam operations and diagnostics in accelerators. Applications such as beam excitation [1], signal digitization [2], and a spill optimization system [3] have been successfully commmissioned at the GSI SIS-18 synchrotron using the GNU Radio software. The goal of this work is to expand the application of SDRs to achieve further processing capabilities, namely for multi-band signal processing for synchrotrons.

Particles stored in a synchrotron perform multiple passes at a measurement pick-up location, producing multi-band signals at harmonics of revolution frequency; this is typically referred to as longitudinal Schottky signals. Each of these bands maintains the same integrated power while their heights and widths scale with the harmonics. The longitudinal Schottky signals can be used for non-destructive measurements of beam parameters, such as stored beam charge or current and momentum spread [4, 5]. Since each band encodes the same information distributed over a different number of frequency bins, acquiring many harmonic bands improves the signal-to-noise ratio (SNR) for the measurement. Processing Schottky signals requires the use of external low-noise-amplifiers (LNAs) to ensure that the low signal amplitudes can be detected by the acquisition system. At the same time, these low signals are susceptible to external interferences picked up or introduced by amplifiers and analog-to-digital converters (ADCs) in sampling hardware, which can significantly distort the measurement readings. Thus, Schottky band signals must be isolated from interference peaks using narrow-band filtering to ensure a correct beam measurement.

In this paper, we explore the application of SDR for processing and filtering Schottky bands to address these challenges with beam intensity measurements using the longitudinal Schottky signal.

* tamarahinderman@alum.mit.edu

SYSTEM DESIGN

The SDR processing schema presented in Fig. 1 is designed for live capture and processing of multiple signal bands at frequencies between 16 kHz and 2.5 MHz. Once the multi-band signals are picked-up by capacitive sensors and amplified with LNAs, they are sampled by the ADC in the SDR frontend. The samples are then streamed to the host PC and processed by GNU Radio. The user can set the revolution frequency, harmonic channels, filter bandwidth, and filter decimation in a custom GUI. The end result is an RMS measurement used to calculate the beam intensity.

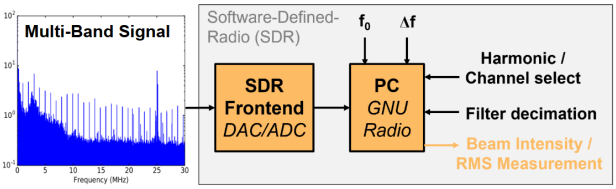

Figure 1: SDR multi-band signal acquisition and processing. Analog processing chain not depicted for brevity.

Frontend Hardware

Four frontend candidates were tested for signal acquisition: the USRP X310, ADALM2000, LimeSDR, and the Red Pitaya SDR-Lab. Based on their ADC rate and compatible frequency range (see Table 1), both the USRP X310 and ADALM2000 were selected for implementation as SDR frontends.

Table 1: SDR Frontend Candidates

Specifications	USRP X310	ADALM2000
ADC Rate	200 MSa/s	100 MSa/s
Streaming Rate	5 MSa/s	4.8 MSa/s
Frequency Range	0 to 30 MHz	0 to 2.5 MHz
Streaming Interface	1-10 GB Eth	USB2.0

Since the USRP is being used for other applications at GSI [1, 3], it was already optimized for data streaming in GNU Radio. Optimizing the ADALM in this processing schema proved challenging. The main parameters of the ADALM devices can be adjusted with the Analog Devices *gr-m2k* block library in GNU Radio. Unfortunately, the ADALM's internal hardware limits sampling rates to 1 , 10 , and 100 MSa/s. For capturing signal bands at higher harmonics and revolution frequencies, a minimum of 3 – 10 MSa/s is required. However, the ADALM could initially only reach 2.5 MSa/s due to the USB2.0 interface limiting

Content from this work may be used under the terms of the CC BY 4.0 licence (© 2026). Any distribution of this work must maintain attribution to the author(s), title of the work, publisher, and DOI.

ISBN: 978-3-95450-252-3 ISSN: 2673-5350 doi: 10.18429/JACoW-IPAC2026-WEP6039

EFFICIENT PARAMETER RECONSTRUCTION FROM GAUSSIAN PULSES USING A GPU

M. Krausewitz*, E. Bründermann, M. Caselle†, J. Gethmann, M. Noll, J. L. Steinmann, A. Streit, A.-S. Müller, Karlsruhe Institute of Technology, Karlsruhe, Germany

Abstract

Pulse parameters such as height, width and peak time provide valuable information about the source. However, real-time evaluation is currently hardly possible for high repetition rates such as those found in a synchrotron. In this contribution, we record the summed signal from beam position monitors at the Karlsruhe Research Accelerator (KARA) with the FPGA-based pulse digitizer KAPTURE-2 and demonstrate the efficient evaluation of Gaussian pulses. To enable real-time analysis of the acquired signals, these must be processed quickly and efficiently. Therefore, the computational workload is accelerated using a GPU, leveraging its parallel processing capabilities. In addition, an approach for parallelization on the CPU is evaluated to determine its effectiveness compared to GPU acceleration. This comparison also evaluates two methods for bunch reconstruction - QR decomposition and gradient-based least-squares minimization.

INTRODUCTION

The Karlsruher Research Accelerator (KARA) has been in operation since 1999; serving as a test facility for accelerator technologies and as a source of synchrotron radiation. Electrons are accelerated in three stages: the electron gun and microtron, the booster synchrotron, and the storage ring.

The booster has a circumference of approximately 26 m and accelerates electrons from 53 MeV to 500 MeV once per second before extracting them into the storage ring. 44 electron bunches are accelerated by a cavity operating at approximately 500 MHz, resulting in a pulse every 2 ns at a fixed point in the lab frame, with a pulse width of at most 1 ns. One turn refers to all 44 bunches passing a given point, occurring at a revolution frequency of 11.36 MHz. The booster ramp is shown in Fig. 1.

These bunches produce pulse-shaped periodic signals whose analysis allows conclusions about accelerator operation. Diagnostics are increasingly moving towards turn-by-turn and bunch-by-bunch measurements. Oscilloscopes are poorly suited for this, as they also record background noise between pulses, wasting storage and bandwidth.

To address this limitation, KIT developed a specialized digitizer, KAPTURE-2 [1], which is specifically tailored to the requirements of high-repetition, MHz-rate sources such as synchrotrons and like KARA. It enables continuous pulse digitization by capturing eight points (settable with 3 ps accuracy) across a pulse at the bunch repetition rate of 500 MHz.

* ujqlg@student.kit.edu
† Now at University of Foggia, Italy

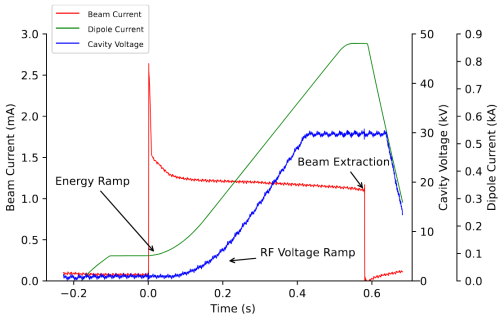

Figure 1: Sequence of a booster synchrotron cycle; injection and extraction can be clearly identified, lasting 600 ms [2].

Previous work has investigated the pulse reconstruction of KAPTURE-2 data from THz pulses, which were analyzed offline after the experiment [3]. Here, the next step will be taken to enable quasi-real-time data analysis in the KARA booster synchrotron. The pulses from beam position monitors shall be examined to extract arrival time (synchronous phase), bunch length, and charge on a bunch-by-bunch and turn-by-turn basis. Later, this information might be used by machine learning based feedback.

Beam position monitors (BPMs) are a key diagnostic instrument, consisting of four electrodes arranged around the beam pipe. The transverse beam position is derived from the relative button signals; for longitudinal diagnostics, a sum signal is formed via an RF combiner.

Over one booster ramp, approximately 300 million pulses are generated over 600 ms at a rate of 500 MHz, with 400 ms remaining until the next recording. Ideally, computations finish within this window, though concurrent computation during recording is also possible.

Mathematical Fundamentals

In this work, the recorded pulses are to be reconstructed and their parameters determined — that is, the width, arrival time, and amplitude of the pulse. For this purpose, they are approximated using Gaussian fits.

A classical Gaussian function is considered first [4]:

$$f(x, \sigma, \mu, A) = A e^{-\frac{(x-\mu)^2}{2\sigma^2}}$$

To convert this into a linear system of equations (LSE), the function is transformed using the natural logarithm:

$$\ln(f) = \underbrace{-\frac{1}{2\sigma^2}}_{a} x^2 + \underbrace{\frac{\mu}{\sigma^2}}_{b} x + \underbrace{\ln A - \frac{\mu^2}{2\sigma^2}}_{c}$$

$$\Rightarrow \vec{y} = \mathbf{X}\vec{\beta}$$

Content from this work may be used under the terms of the CC BY 4.0 licence (© 2026). Any distribution of this work must maintain attribution to the author(s), title of the work, publisher, and DOI.

ISBN: 978-3-95450-252-3 ISSN: 2673-5350 doi: 10.18429/JACoW-IPAC2026-WEP6040

DETERMINING THE INFLUENCE OF TRANSVERSAL BEAM EXCITATION ON BEAM SIZE AND DYNAMICS AT KARA

S. Braner*, E. Blomley, E. Bründermann, M. Caselle‡, J. Gethmann, E. Huttel, M. Noll, J. L. Steinmann, A.-S. Müller
Karlsruhe Institute of Technology, Karlsruhe, Germany

Abstract

Significant beam dynamics parameters, such as energy spread or transversal beam size, can be calculated from the transversal bunch profile. At the Karlsruhe Research Accelerator (KARA), located at the Karlsruhe Institute of Technology (KIT), the beam size in the storage ring is being investigated using the KArlsruhe Linear arraY detector for MHz rePetition rate SpectrOscopy (KALYPSO), a line array that examines the synchrotron radiation emitted at a five-degree port of a dipole magnet. Trench-Isolated Low-Gain Avalanche Diode (TI-LGAD) technology provides superior sensitivity compared to conventional silicon detectors, thereby facilitating the study of low-charge bunches. As the KALYPSO system can be triggered at several megahertz, turn-by-turn analysis can be performed at KARA, which has a revolution frequency of 2.7 MHz. In addition to the study of the energy spread, the analysis of beam size and position modulations can be performed. These can either occur naturally or be induced by a white noise signal on a strip line. In this contribution, the influence of transversal beam excitation on beam size and time-resolved dynamics at KARA is investigated.

INTRODUCTION

To investigate the influence of beam excitation on the machine dynamics of the research accelerator, the vertical beam size is monitored. However, direct imaging of the synchrotron radiation is insufficient, since the measurement is limited by the diffraction limit due to the crotch absorber. Therefore, an interferometric setup is used at the Synchrotron-Light-Monitor-2 (SLM-2) station at KARA to overcome this limitation. In conventional interferometric setups, the interference pattern is typically recorded using an industrial CMOS camera. Such a setup was implemented by Michael Holz [1, 2]. However, the temporal resolution was limited to the millisecond range by the integration time of the CMOS cameras, preventing the observation of fast beam dynamics during excitation. To enable a higher temporal resolution of up to turn-by-turn measurements, the fast line-array detector KALYPSO [3] is used instead. The setup was recently significantly improved by replacing a damaged mirror and a deteriorated vacuum window. This substantially increased the detectable light intensity and enabled single-bunch, single-turn measurements. In addition, a new remotely adjustable mounting system enables rapid alignment in all three spatial dimensions, allowing optimized focusing onto the detector. The use of a macro lens further broadened the interference pattern on the detector, increasing the number of usable pixels and improving the quality of the beam size reconstruction.

BEAM SIZE MEASUREMENT

The intensity observed in a double slit interferometry experiment can be described as a sinc^2 envelope [4].

$$I(x) = (I_1 + I_2)\ \mathrm{sinc}^2\left(\frac{\pi a}{\lambda f}\,x\right)\left[1 + V\cos\left(\frac{2\pi d}{\lambda f}\,x + \psi\right)\right]. \tag{1}$$

Here I_1 and I_2 are the intensities of the synchrotron radiation at the slits, a is the single slit width, d the slit distance, x the position at the detector, f the distance between the lens and the detector screen, ψ is the phase difference between the light arriving from the two slits, λ is the wavelength and V denotes the visibility. The relationship between the complex coherence factor γ and visibility V is given by:

$$V = \frac{I_{\max} - I_{\min}}{I_{\max} + I_{\min}} = \frac{2\sqrt{I_1 I_2}}{I_1 + I_2}|\gamma|. \tag{2}$$

In this case $I_{\max}$ and $I_{\min}$ denote the local maximum and minimum intensities of the interference pattern, respectively. With evenly lit slits, V and $|\gamma|$ are identical.
According to the van Cittert–Zernike theorem, the complex coherence factor γ is given by the Fourier transform of the spatial light-source distribution:

$$\gamma = \int f(x)\ \exp\left(-i\,\frac{2\pi d}{\lambda L}\,x\right)\,\mathrm{d}x. \tag{3}$$

where L denotes the distance between the source point and the double slit [5]. Assuming a Gaussian beam profile results in:

$$V = |\gamma| = \exp\left[-2\left(\frac{\pi w d}{\lambda L}\right)^2\right]. \tag{4}$$

Solving for the beam size w leads to:

$$w = \frac{\lambda L}{\pi d}\sqrt{\frac{1}{2}\ln\left(\frac{1}{V}\right)}. \tag{5}$$

The visibility is reconstructed by fitting

$$y(x) = \alpha_0 \cdot \mathrm{sinc}^2\left((x - b_1)\alpha_1\right)\left[1 + \mathrm{V}\cos\left((x + b_2)\,\alpha_2.\right)\right]. \tag{6}$$

* simon.braner@student.kit.edu
‡ Now at University of Foggia, Italy

Content from this work may be used under the terms of the CC BY 4.0 licence (© 2026). Any distribution of this work must maintain attribution to the author(s), title of the work, publisher, and DOI.

ISBN: 978-3-95450-252-3 ISSN: 2673-5350 doi: 10.18429/JACoW-IPAC2026-WEP6041

CURRENT PROFILE RECONSTRUCTION BY PASSIVE STREAKING OF LOW CHARGE, LOW ENERGY ELECTRON BUNCHES IN DIELECTRIC LOADED WAVEGUIDES

M. Kellermeier*[1], T. Vinatier[1], H. Dinter[1], S. Jaster-Merz[1],
W. Kuropka[1], F. Mayet[1], B. Stacey[1], F. Burkart[1]
[1]Deutsches Elektronen-Synchrotron DESY, Hamburg, Germany

Abstract

Advanced accelerating techniques are evolving rapidly, enabling high energetic electron beams with significantly decreasing footprint. While the accelerating structures shrink impressively, longitudinal diagnostic components with femtosecond resolution like transverse deflecting structures still demand a significant amount of space and complex infrastructure, are costly and require precise synchronization of their power source with the arriving electron bunch. The TWAC project aims for a fully-integrated compact accelerator, delivering ultrashort bunches (≈ 10s of fs) at low charge and energy (10 pC, 10 MeV/c), requiring corresponding small footprint, cost-efficient longitudinal diagnostics. Here, the retained method is passive streaking in dielectric loaded waveguides in which the self-excited transverse wakefields are imposing a varying kick dependent on the intra-bunch longitudinal position. The new parameter regime is investigated at the ARES linac, firstly at medium energy (≈60 MeV/c). A novel forward propagation reconstruction algorithm has been developed, based on a waveguide mode expansion with more than 100 modes to properly model the excited wake.

INTRODUCTION

Diagnosing the longitudinal bunch profile with ultra-high resolution is pivotal for the optimization of linear electron accelerators demanding high peak current, for studying physical effects in extreme compression and space-charge conditions, and for the understanding of potentially undesired phase space correlations, or tailored longitudinal phase-space distributions [1–9]. High-dimensional detailed phase space projections of ultra-short bunches are measurable [10] with a polarizable X-Band transverse deflecting structure (TDS) [11, 12]. However, those structures demand high operational costs, precise RF-beam synchronization and a large footprint, limiting its applicability on compact machines. The TWAC project [13] aims at accelerating and compressing a low-energy beam (≈ 10 MeV/c) in a THz-driven structure to achieve high peak current, cost-effectively diagnosed within a compact, meter-scale footprint. In the past decade, passive streaking [14–18] has evolved into an established, cost-effective alternative for longitudinal bunch profile diagnostics, significantly reducing the costs and operational requirements due to being self-synchronized. Further, the method promises a small footprint at low beam energy. However, assumptions made within the wake model and experimental constraints limit the extendability to ultra-short, low charge, low energy bunches. In this work, a new reconstruction algorithm is outlined which enables the current profile characterization of low charge bunches at low energy from passive streaking in a dielectric loaded waveguide. The algorithm extends previous approaches [15] beyond the linear quadrupole wake in the streaking plane. As the bunch carries less charge it has to be moved closer to the wake-exciting wall, potentially exceeding the limits of validity for the linear approximation of the wake around the centroid. The parameter range targeted by TWAC is currently under study on the ARES linac (Accelerator Research Experiment at SINBAD) at DESY [19, 20]. Here, we report the first results for a low charge (6.9 pC) and medium momentum (63 MeV/c) working point.

WAKE MODEL AND RECONSTRUCTION ALGORITHM

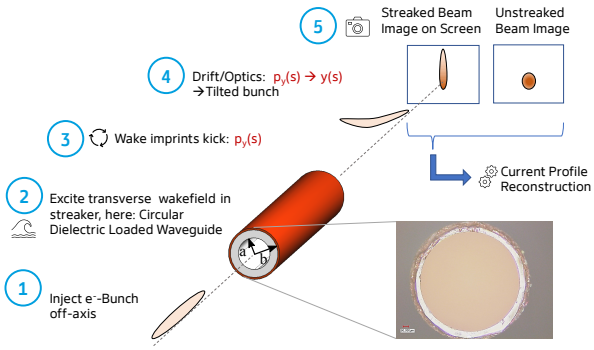

Figure 1: Schematic of the passive streaking principle in a dielectric loaded waveguide.

When an electron bunch gets close to the wall of the surrounding structures, the excited short-range wakefield can act back on the driving bunch, depending on the structure geometry, the bunch current profile, and the involved media of the structure. Fig. 1 outlines the principle of passive streaking in a dielectric loaded waveguide (DLW). This geometry is employed as wakefield structure due to its simplicity and advantageous cylindrical symmetry in contrast to corrugated metallic plates which have been utilized recently [17, 18]. Cylindrical corrugated structures are technologically doable but significantly more demanding and costly. By injecting the beam off-axis, the excited transverse wakefield imprints a kick p_y which varies along the intra-bunch longitudinal position s. The transport downstream of

* max.kellermeier@desy.de, orcid:0000-0002-8840-782X

Content from this work may be used under the terms of the CC BY 4.0 licence (© 2026). Any distribution of this work must maintain attribution to the author(s), title of the work, publisher, and DOI.

ISBN: 978-3-95450-252-3 ISSN: 2673-5350 doi: 10.18429/JACoW-IPAC2026-WEP6046

UPGRADE OF THE BEAM LOSS MONITORING SYSTEM FOR THE UNILAC HEAVY ION LINEAR ACCELERATOR AT GSI

M. Dziewiecki*, L. Braisz, K. Laihem, M. Loy, S. Rauch, A. Russo, M. Witthaus
GSI Helmholtz Centre for Heavy Ion Research, Darmstadt, Germany

Abstract

The beam-loss monitoring system of the UNILAC heavy-ion linear accelerator is based on measuring the beam current at multiple locations along the beamline. Signals from beam–current transformers are amplified, converted into pulse trains and counted within a defined time window. The system has proven to be robust and operationally safe.

The ongoing upgrade aims to replace the current-to-frequency converters and the entire digital subsystem while preserving the established operational principle and the analog front-end. Most important reasons are aging of the electronics, the need for improved scalability, flexibility and safety, and last but not least, alignment with the new GSI/FAIR controls architecture.

The new system operates under the supervision of a System Control Unit (SCU), the standard front-end platform of the GSI/FAIR control system. It is controlled by the Front-End Software Architecture (FESA) and White Rabbit. Once configured, the FPGA-based hardware operates autonomously to ensure high reliability and fail-safe behaviour.

Here we describe the system architecture, its modular hardware, firmware architecture and the software interface.

INTRODUCTION

The beam loss monitoring (BLM) system was introduced to the UNILAC accelerator as part of the upgrade programme for high-current operation of the accelerator by late 1990s [1]. The system uses multiple beam-current transformers at various locations along the accelerator [2]. Transformer signals are amplified by calibrated front-end amplifiers, and the resulting voltages are converted to pulse trains using voltage-to-frequency (V→f) converters. These signals are fed to differential integrators based on digital up/down counters as shown in Fig. 1. If the resulting count within a single beam pulse exceeds a prescribed threshold, the BLM triggers the chopper control circuitry to truncate the beam pulse.

The operation of amplifiers and counters is subject to gate signals to eliminate interferences outside the beam pulse window. A special version of the integrator with only a single, up-counting input is used to control overall beam charge for profile harp protection.

With the concept of *virtual accelerators* at UNILAC [3], various species can be accelerated in adjacent 20 ms-long cycles. To accommodate the required threshold changes, the threshold registers are reloaded at the beginning of each cycle.

* m.dziewiecki@gsi.de

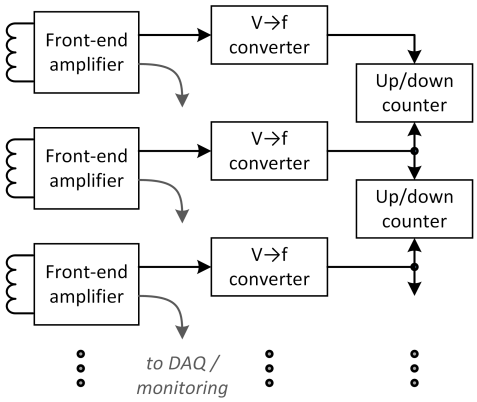

Figure 1: Simplified signal processing flow.

The original BLM system demonstrated robust operation for over 25 years. However, further maintenance and system extensions became impossible due to its ageing design and the lack of legacy electronic components. This factor, coupled with a growing need for a direct, modern interface to the new control system, necessitated a major upgrade.

SCOPE OF THE UPGRADE

The upgrade includes the replacement of the V→f converter electronics, the entire digital section and the control software. The overall principle of operation, the beam transformers and the proven front-end amplifiers remain unchanged.

The hardware changes affect the resolution and range of the system as shown in Table 1.

Table 1: BLM Parameters Before and After Upgrade

Parameter	Original	Upgraded
Resolution	2.2 nC	0.7 nC
Max. pulse frequency	8 MHz	24 MHz
Counter depth [bits]	13 + sign	31 + sign
Counting range	±18.022 µC	±1.5 C [1]

The functions of the V→f converter and the counter, originally implemented in a single device, have been split into separate hardware crates.

The *V→f converter crates* contain custom modules designed specifically for the BLM. The *counter crates* are built from standard hardware components used at the GSI control system, avoiding dedicated hardware development.

The upgraded system is largely scalable and imposes no inherent limits on the number of input signals.

[1] Practical range is limited to <100 µC by max. pulse frequency and beam pulse duration.

Content from this work may be used under the terms of the CC BY 4.0 licence (© 2026). Any distribution of this work must maintain attribution to the author(s), title of the work, publisher, and DOI.

ISBN: 978-3-95450-252-3 ISSN: 2673-5350 doi: 10.18429/JACoW-IPAC2026-WEP6047

CNN-BASED ARRIVAL TIME DETERMINATION IN PILED-UP PARTICLE COUNTER SIGNALS

R. Singh*, P. Boutachkov, GSI, Darmstadt, Germany
T. Habermann†, M. Kumm, Fulda University of Applied Sciences, Fulda, Germany

Abstract

Pulse pile-up limits the count rate, timing precision, and energy resolution of radiation detection systems in accelerator beam instrumentation and downstream experiments. We present the project status of a machine-learning based pile-up recovery system designed for real-time particle counting and time of arrival determination at pulse rates exceeding 10^7 particles/s. The convolutional neural network (CNN) architecture utilized in this project is trained on labelled scintillator data to identify pulses in the piled-up waveforms. This development is primarily aimed at beam spill characterization at GSI/FAIR using plastic scintillators, however the concept presented is general-purpose and could be applicable to any radiation detector. First model implementation is performed on the FPGA onboard a commercial digitizer and its performance is compared against the single threshold leading-edge discriminator.

INTRODUCTION

Radiation or particle detectors communicate the information of the species, charge, energy, arrival time of the detected particles via the electronic pulses produced at its output. Pulse pile-up is defined as the temporal overlap of these electronic pulses/signals when successive radiation events arrive within the resolving time of the detection system. A pulse pile-up arises whenever the mean interval between successive events approaches the characteristic response time of the detector-electronics chain. For radioactive sources, event inter-arrival times are exponentially distributed and intensity fluctuations scale as $\sqrt{N}$. The probability of k events within a resolving time τ at mean rate r is $P(k) = (r\tau)^k e^{-r\tau}/k!$. Poisson process discussed above is statistically the most favorable case for pile-ups, while in slowly extracted beam from synchrotrons, the situation can be significantly worse. The synchrotron beams typically exhibit intensity fluctuations far exceeding the Poisson limit, driven by power supply ripples and the nonlinear dynamics of the resonant extraction process; measured duty factors at GSI SIS-18 are typically 30–70% of the Poisson limit, meaning instantaneous rates regularly exceed several times the mean rate on microsecond timescales [1, 2]. The consequences of spill fluctuation-induced pile-up propagate directly into the physics experiments downstream. The HADES dilepton spectrometer [3], operating at GSI reported occupancy-related pile-up at its interaction rate of ~20 kHz due to substantial aforementioned beam fluctuations on $\approx 10 - 100$ µs timescales that degrade tracking efficiency. The ability to precisely count and timestamp individual beam particles from piled-up signals with sub-nanosecond timing using any of the available counting detectors would simultaneously enable improved spill quality characterization, facilitating faster feedback for extraction optimization [4], and extended operating range in particle rates for the physics detectors downstream.

Pile up Handling Approaches

Initial pile-up handling was focussed on identifying and rejecting piled-up pulses [5, 6], and this evolved into pile-up avoidance using either analog pulse shaping methods [7,8] or more trivially, by detector segmentation dividing the pulses into multiple channels. With the advent of digital processing, conceptual change from pile-up avoidance to pile-up recovery emerged [9]. Most of these "new" recovery methods posed the problem of pile-up as a linear superposition of independent pulses (modelled as analytical functions) whose amplitude and time of arrival had to be determined via various methods. Notable among these de-convolution type methods are template matching [10, 11], maximum likelihood estimation (MLE) [12, 13], and high-yield-pile-up-event-recovery (HYPER) [14]. HYPER is based on W-SUM method which deconvolves a single exponential decay into step function. A systematic comparison between these methods is shown in [13,15]. Arguably the most general classical approach is MLE, however it requires iterative nonlinear optimization for each waveform segment resulting in variable and unbounded computation time, making it a challenge for real-time FPGA implementation at the throughputs required at our targeted rates.

More recently, deep learning approaches have been widely applied to the pile-up correction problem across multiple domains. Primary motivation is to overcome the assumptions in classical methods, e.g. pulses superimpose linearly and follow a known analytical shape. In addition, real detector pulses vary due to detector imperfections, gain drifts, saturation effects which are typically not captured by a pulse template. Deep neural networks trained on real labeled data can potentially learn all these effects often with a risk of model overfitting and improper generalization. A comparison of template matching and CNN in context of particle counting application can be found [16]. Although deep learning approaches appear very different from classical methods, it is helpful to understand them as a form of amortized inference [17], a trained neural network learns the approximate mapping from observed waveform to underlying parameters (peak times, amplitudes, count) that MLE would compute iteratively, but produces it in a single, fixed-time pass. The cost of the iterative optimization is during training, rather

* r.singh@gsi.de
† The work was partially funded by the German Federal Ministry of Research, Technology and Space, Germany under Grant 05K25REA

Content from this work may be used under the terms of the CC BY 4.0 licence (© 2026). Any distribution of this work must maintain attribution to the author(s), title of the work, publisher, and DOI.

ISBN: 978-3-95450-252-3 ISSN: 2673-5350 doi: 10.18429/JACoW-IPAC2026-WEP6048

CONTINUOUS OPERATION OF CRYOGENIC CURRENT COMPARATORS AT FAIR*

T. Sieber†, M. Schwickert, GSI, Darmstadt, Germany
S. Shinde[1], F. Schmidl, Friedrich-Schiller-University Jena, Jena, Germany
T. Stoehlker[1, 2], V. Tympel[1], Helmholtz Institute Jena, Jena, Germany
T. Koettig, CERN European Organization for Nuclear Research, Geneva, Switzerland
[1]also at GSI Helmholtz Centre for Heavy Ion Research, Darmstadt, Germany
[2]also at Institute for Optics and Quantum Electronics, Jena, Germany

Content from this work may be used under the terms of the CC BY 4.0 licence (© 2026). Any distribution of this work must maintain attribution to the author(s), title of the work, publisher, and DOI.

Abstract

Cryogenic Current Comparators (CCC) are superconducting devices for beam current monitoring, based on azimuthal magnetic field (fT range) measurement with ultrasensitive SQUID magnetometers. They are able to provide a calibrated non-destructive measurement of beam current with a resolution of 10 nA or better, independent from ion species and without tedious calibrations procedure.

We have developed the CCC over the last ten years in an international collaboration with the goal of a highly sensitive and continuous current measurement in the transfer lines and rings at FAIR and CERN machines. Besides the efforts to improve the robustness and current resolution of the device, investigations have been performed on the cryogenic support system, which has to provide stand-alone operation in HEBT tunnels without He supply. So far, we have achieved standing times in the range of 6 - 9 months after liquid He filling, recently we have demonstrated stand-alone He liquefaction from gas bottles within ~ 4 weeks, which would avoid He filling in the tunnels. In this contribution we present the status and results of our current work with focus on the cryogenics aspects.

INTRODUCTION

The Cryogenic Current Comparator basically consists of a pickup coil, a SQUID- (Superconducting Quantum Interference Device) magnetometer and a superconducting shielding, which provides an attenuation of non-azimuthal external fields in the range -70 dB to -140 dB, depending on the shield geometry (see below). The shielding guides the superconducting Meissner-Current to the internal pickup loop, which is basically a one- winding coil around a high permeability ring core, acting as a flux concentrator. The latter is used in the 'classical' CCC, shown in Fig. 1, to ensure efficient coupling of the beam to the SQUID circuit. Just like in regular, normal conducting beam transformers, the arrangement can be regarded as a transformer with the particle beam being the primary and the pickup coil being the secondary winding. The signal from the pickup coil is fed to a DC SQUID, which is operated in a compensation circuit, using a so-called Flux Locked Loop (FLL) electronics [1]. Figure 1 shows the original arrangement, developed at PTB (Physikalisch-Technische Bundesanstalt) for electron beam measurement [2], which was later adapted to the heavy ion accelerator application at GSI [3].

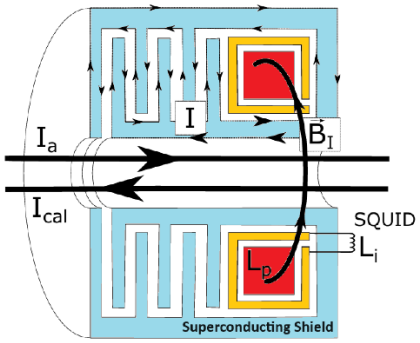

Figure 1: Classical current comparator, shield geometry with radial meanders and high permeability ring core (red) surrounded by the pickup loop (yellow), which is again connected to the SQUID coupling loop. In our case the reference current is not used, Ia is the beam current. Bi = azimuthal field, Li = coupling inductance to squid circuit. The small arrows indicate the Meissner current along the shielding.

The detector development for FAIR started with the classical shielding, like shown in Fig.1. The next step was a shielding with axial meander geometry and without ring core [4], called the 'coreless' or 'axial' CCC. This new design promised some advantages, like reduced magnetic noise and baseline drift (both mainly caused by the toroidal core), reduced costs and weight due to better mechanical stability (which allows for lead as shielding material). However, the axial CCC could not be operated inside the FAIR cryostat due to its sensitivity to external noise and in general its weak coupling to beam (resp. calibration-) current [5]. Consequently, a third CCC type, which combines the axial meander geometry with a twofold classical toroidal core pickup was developed [6] and successfully tested with beam at GSI [7]. It achieved - besides excellent magnetic shielding - a current resolution equal or better than the classical CCC type. This version is called the 'dual

* supported by BMBF under contracts 05P18SJRB1 and 05K25SJA
†T.Sieber@gsi.de

ISBN: 978-3-95450-252-3 ISSN: 2673-5350 doi: 10.18429/JACoW-IPAC2026-WEP6049

FIRST MEASUREMENTS OF THE TRANSIENT ELECTRICAL NEAR-FIELD OF ELECTRON BUNCHES IN THE FLUTE IN-AIR SECTION

S. Funkner*, G. Niehues, E. Bründermann, F. Donoso, A. Malygin, A.-S. Müller,
M. J. Nasse, M. Reissig, R. Ruprecht, J. L. Steinmann
Karlsruhe Institute of Technology, Karlsruhe, Germany
P. Rabiei, S. Toroghi, Partow Technologies LLC, Carlsbad, CA, USA
I. Wilke, Rensselaer Polytechnic Institute, Troy, NY, USA

Abstract

The Ferninfrarot Linac- und Test-Experiment (FLUTE) at the Karlsruhe Institute of Technology (KIT) is a compact linac test facility providing sub-picosecond to femtosecond short electron bunches with energies up to several tens of MeV. The transient electric near-field of such bunches is relevant for understanding coherent THz emission and for developing compact field-sensitive beam diagnostics. Here, we present first electro-optical measurements of bunch-induced near-field signals in the FLUTE in-air section using a photonic-integrated Mach-Zehnder-interferometer sensor placed close to the beam axis. The measured delay-dependent response shows features consistent with electro-optical detection of the transient electric near field of the bunch. Our results establish a basis for future spatially resolved measurements with varying accelerator parameters.

INTRODUCTION

The FLUTE compact linac test facility at KIT provides access to short relativistic electron bunches and to their strong transient electric fields. In particular, the generation of intense THz radiation at FLUTE is closely linked to the temporal and spatial structure of the bunch-induced near field, making field-sensitive diagnostics relevant both for accelerator development and for beam studies.

Electro-optical (EO) sampling is a well-established method for time-resolved measurements of electric fields in the THz frequency band and has been applied to the diagnostics of relativistic electron bunches previously. For example, single-shot EO techniques have enabled sub-picosecond measurements of electron-bunch lengths by encoding the longitudinal bunch profile onto synchronized optical probe pulses [1]. More recently, near-field EO spectral decoding has also been used for high-throughput measurements of individual longitudinal bunch profiles in a storage ring environment at the Karlsruhe Research Accelerator (KARA) [2].

In conventional EO and THz measurements, the field is often sampled at a fixed position while the temporal waveform is reconstructed from the probe delay. Recent EO sampling experiments have demonstrated access to spatiotemporal electric-field profiles around relativistic electron beams [3]. The FLUTE in-air section [4] provides access to the region outside the vacuum tube where the bunch-induced field evolves in space and time after the bunch exits into the air. This makes the setup attractive not only for temporal sampling, but also for future spatially resolved studies of the transient near field.

At the same time, measurements close to the beam axis place strong constraints on detector size, access, and alignment. Conventional EO arrangements based on free-space optics can be comparatively bulky for such a geometry and are not always ideal for fast exploratory scans. A promising alternative is provided by compact photonic-integrated EO sensors based on thin-film lithium niobate. In particular, Mach–Zehnder interferometer (MZI) sensors with oppositely poled lithium-niobate waveguide arms have recently been demonstrated for time-domain detection of freely propagating THz fields [5, 6] and later used at KIT for measurements of coherent synchrotron radiation of electron bunches at KARA [7]. Here, the present work investigates a first application of such an integrated EO sensor to bunch-induced electric near field signals in the FLUTE in-air section.

In the following, we provide a brief overview of the general experimental setup, document the realized geometry, experimental parameters, and provide qualitative simulation results to visualize the expected evolution of the transient electrical fields in the in air-section. We then define the extraction metrics used for evaluation and show the resulting THz time-domain traces. We argue that these first results are consistent with near-field-sensitive detection of the electron bunch while detailed interpretations related to precise timing reconstruction remain part of an ongoing analysis.

EXPERIMENTAL SETUP

During the experiments, electron bunches with an energy of 30 MeV and a charge of (273 ± 5) pC were generated at a repetition rate of 10 Hz. Details about the FLUTE accelerator can be found elsewhere [8, 9].

In brief, FLUTE comprises an RF photoinjector, a traveling-wave linac, a magnetic bunch compressor, and finally the in-air experiment section. Electron bunches are generated by illuminating a copper photocathode with ultraviolet pulses derived from a Ti:sapphire laser system via third-harmonic generation. The bunches are then further accelerated to their final energy in a 3 GHz traveling-wave linac and subsequently transported through a four-dipole magnetic chicane for optional longitudinal bunch compression. During the experiments, the beam exited the vacuum system through a thin metal foil into an in-air section at the end of the beamline.

* stefan.funkner@kit.edu

Content from this work may be used under the terms of the CC BY 4.0 licence (© 2026). Any distribution of this work must maintain attribution to the author(s), title of the work, publisher, and DOI.

ISBN: 978-3-95450-252-3 ISSN: 2673-5350 doi: 10.18429/JACoW-IPAC2026-WEP6050

MEASUREMENTS OF CSR RADIATION AT KARA USING NOVEL THIN-FILM LITHIUM NIOBATE ELECTRO-OPTICAL SENSORS

G. Niehues*, E. Bründermann, S. Funkner, M. Noll, J. L. Steinmann, A.-S. Müller,
Karlsruhe Institute of Technology, Karlsruhe, Germany
P. Rabiei, S. Toroghi, Partow Technologies LLC, Carlsbad, CA, United States
I. Wilke, Rensselaer Polytechnic Institute, Troy, NY, United States

Content from this work may be used under the terms of the CC BY 4.0 licence (© 2026). Any distribution of this work must maintain attribution to the author(s), title of the work, publisher, and DOI.

Abstract

Electro-optical detection provides a powerful method for characterizing the electric fields of relativistic electron beams and their emitted radiation. We report on the use of novel thin-film lithium niobate electro-optical sensors for the detection of freely propagating terahertz (THz) pulses and, for the first time, measurements of coherent synchrotron radiation (CSR) at the Karlsruhe Research Accelerator (KARA). The thin-film lithium niobate sensors, implemented as integrated Mach–Zehnder interferometers, combine a strong electro-optical response with engineered velocity matching and a compact device geometry, enabling sensitive detection of transient THz fields. Using these Mach–Zehnder interferometer waveguide structures, we demonstrate efficient coupling of CSR to the sensors and present first measurement results.

INTRODUCTION

Electro-optical (EO) detection is a well established tool for measuring pulsed THz electromagnetic radiation e.g. [1–3]. Regarding electron accelerators, EO detection has become an established diagnostic method for probing the longitudinal electric fields, and thus the longitudinal beam profiles, of electron bunches e.g. [4, 5], as well as for measuring the radiation emitted by relativistic electron beams e.g. [6]. In both cases the transient field induces a Pockels effect and thus a change in polarization on a synchronized optical probe laser beam, enabling single shot measurements of the pulse shape [7–9]. Recent studies include tomographic reconstruction of the full phase space distribution of electron bunches [10] and far-field EO detection of emitted radiation [11], underscoring the expanding role of EO techniques in electron accelerators.

While bulk EO crystals have traditionally been employed, integrated photonic sensors can simplify the detection chain, reduce the need for bulky free space optics, and improve system robustness. The EO sensor used for the present measurements consists of a photonic-integrated Mach–Zehnder interferometer with an arm length of 600 µm, fabricated in thin film lithium niobate (TFLN) [12]. The waveguide geometry is engineered for velocity matching between the THz wave and the laser probe. The optical probe beam is coupled to the chip via fibers and grating couplers (included in the packaged sensor), while free space coupling of the THz field enables a compact setup at the beamline. First measurements with high-intensity THz radiation pulses generated by optical rectification of femtosecond laser pulses on an organic crystal have been reported [13].

In this study, we present the first coherent synchrotron radiation (CSR) measurements obtained with the TFLN EO sensor at the Karlsruhe Research Accelerator (KARA). The TFLN EO sensor was positioned at the Infrared2 (IR2) beamline with the CSR radiation focused onto the sensor. A femtosecond probe laser was coupled to the EO sensor, and the CSR induced phase modulation converted into an intensity modulation was recorded. The results demonstrate efficient CSR coupling and sensitivity and validate measurements with the TFLN EO sensor as a diagnostic tool for CSR detection.

EXPERIMENTAL SETUP

The experiment was carried out at KARA operating in short-bunch mode (momentum compaction $\alpha_c = 2.6\times10^{-4}$) with two subsequently injected bunches separated by 2 ns, as required by another experiment conducted at the same time. The revolution frequency was 2.72 MHz and the beam energy 1.3 GeV. Measurements were performed with a total beam current of 0.36 mA, corresponding to a combined charge of 133 pC. The bunch-by-bunch system reported a ratio of 0.53 : 0.47 for the two bunches, which results in ≈71 pC for the first bunch, which was measured by the TFLN EO sensor.

Coherent synchrotron radiation (CSR) at the diagnostic port of the IR2 beamline was focused with a single off-axis parabolic mirror onto the TFLN EO sensor (see Fig. 1). A detailed description of the sensor concept can be found in [12, 13]. The sensor is pumped by a fiber coupled femtosecond laser (90 fs, 1560 nm central wavelength) running at 62.47 MHz and phase locked to KARA's 499.76 MHz master clock, allowing controlled frequency detuning and programmable phase shifts of the laser probe pulses (schematic illustration of the components and synchronization can be found in Fig. 2). Only every 23rd laser pulse is modulated because the laser pulses at a repetition rate of 62.47 MHz sampled the CSR at the much lower revolution frequency of 2.72 MHz. Although the filling pattern included two bunches, the laser pulse spacing of about 16 ns samples only one bunch.

A small aperture in the parabolic mirror diverts a fraction of the beam to an optical photodiode that serves as a timing reference. Measurements of the free space CSR beam, cable lengths, and fiber lengths enabled a rough estimate of the tim-

* gudrun.niehues@kit.edu

ISBN: 978-3-95450-252-3 ISSN: 2673-5350 doi: 10.18429/JACoW-IPAC2026-WEP6052

USING A Timepix3 PIXEL DETECTOR FOR A COMPTON BACKSCATTERING POLARIMETER

T. Schiffer*, M. Switka†, K. Desch, D. Proft, University of Bonn, Bonn, Germany

Abstract

The Electron Stretcher Facility (ELSA) in Bonn has the capability to accelerate and extract spin-polarized electrons. A Compton backscattering polarimeter located in the storage ring allows for in situ measurements of the beam polarization degree. Here, a circularly polarized 20 W cw-laser beam is scattering off the stored electron beam. The backscattered photons reach energies of up to some hundred MeV and the photon beam's center of gravity undergoes a polarization dependent vertical shift. Currently an in-house developed silicon strip sensor is used for profile analysis from which the spin-polarization degree is determined. For modernization of the detector assembly, the Timepix3 ASIC pixel detector with 55 µm pitch and a 500 µm thick silicon sensor is a suitable candidate. It allows to obtaining 2D beam information with an excellent time resolution (25 ns), enabling for parallel time resolved horizontal and vertical profile measurements. An in-house developed readout infrastructure allows for high flexibility and adaptability. The detector concept as well as first measurements of the vertical and horizontal profiles from polarized beams under varying conditions are presented.

INTRODUCTION

The electron stretcher facility (ELSA) is a three staged accelerator operated by the University of Bonn. Thermal or spin-polarized electrons are injected into a 26 MeV Linac and accelerated in a fast ramping booster synchrotron to typically 1.2 GeV to fill the ELSA storage ring. Therein, post acceleration occurs up to 3.2 GeV, where several depolarizing resonances have to be crossed. While in the booster synchrotron the crossing of those resonances has negligible impact on the beam polarization, additional precautions have to be taken in the stretcher ring. This is realized by fast ramping tune-jump quadrupole magnets and harmonic orbit correction schemes. For proper setup and fine adjustment of such countermeasures, non-destructive monitoring of the beam polarization is advantageously. To achieve this a laser Compton backscattering polarimeter was set up at the storage ring [1]. The polarimeter uses the spin-dependent angular difference of the backscattered photons to measure the electron beam's polarization degree with a silicon microstrip detector [2]. Since the detector shows signs of aging a new detector system based on a Timepix3 pixel chip detector is in development. First tests with this new detector showed promising results [3].

* schiffer@physik.uni-bonn.de
† switka@uni-bonn.de

COMPTON BACKSCATTERING POLARIMETRY AT ELSA

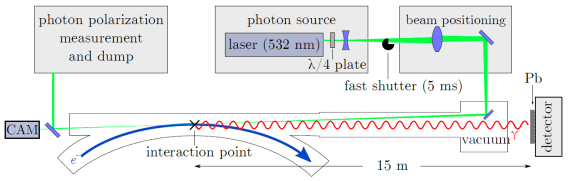

Figure 1: Principle setup of the Compton backscattering polarimeter at ELSA [4].

The Compton backscattering polarimeter [4] uses a 20 W 532 nm continuous-wave laser beam scattering off the stored electron beam (Fig. 1). From the Klein-Nishina scattering cross section [5]

$$\frac{\mathrm{d}\sigma_c}{\mathrm{d}\Omega}\left(\vec{S},\vec{P}\right) = \Phi_0 + \Phi_1(S_1) + \Phi_2(S_3,\vec{P}) \qquad (1)$$

a dependency on the polarization of the laser photons and the polarization of the electrons follows. This leads to a vertical shift Δz of the backscattered beam's center-of-gravity if the helicity (S_3) of the laser beam is altered when a vertically orientated electron polarization (P_z) is given:

$$\Delta z = z_R - z_L = \mathcal{D} P_z S_3 \,. \qquad (2)$$

Here $z_{R,L}$ denotes the mean position of the backscattering profile for left or right circular polarized laser light and $\mathcal{D}$ is the analyzing power of the polarimeter, which is approximately 70 µm/100 %.

Since the energy of the backscattered photons is boosted to energies up to some hundred MeV, a conversion target is beneficial to increase the signal yield. For this a 11.2 mm ($2X_0$) lead converter target is used in front of the silicon microstrip detector. The microstrip detector has 768 vertically

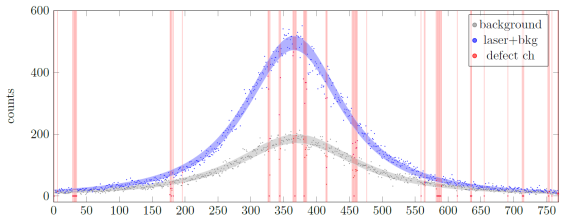

Figure 2: Exemplary vertical backscattering profiles measured with the silicon microstrip detector. Insufficiently operating channels are marked in red [4].

oriented strips of 38.4 mm length at 50 µm pitch. Thus, the active area of the sensor is 38.4 × 38.4 mm^2.

During a measurement, the circular polarization of the laser photons is altered by a rotating $\lambda/4$-plate. During the

Content from this work may be used under the terms of the CC BY 4.0 licence (© 2026). Any distribution of this work must maintain attribution to the author(s), title of the work, publisher, and DOI.

ISBN: 978-3-95450-252-3 ISSN: 2673-5350 doi: 10.18429/JACoW-IPAC2026-WEP6053

ENHANCING BEAM TIME AVAILABILITY BY A FACTOR OF TWO: SIMULTANEOUS OPERATION OF HADRON PHYSICS AND DETECTOR TEST BEAM LINES AT ELSA

D. Proft*, M. Ammann, K. Desch, M. Switka, University of Bonn, Bonn, Germany

Abstract

The electron accelerator facility ELSA houses two external high-energy beam lines. These deliver primary electron beams with energies between 0.8 and 3.2 GeV, extracted via slow resonant extraction from a synchrotron to a total of three different experimental sites. One beam line hosts two hadron physics experiments, while the second, located on the opposite side of the synchrotron, is used for detector tests and medical physics experiments.

Recently a new operation mode has been developed to serve both external beam lines with an extracted electron beam simultaneously. This enables running detector test experiments at low rates (tens of kHz) alongside high-rate hadron-physics experiments at GHz extraction rates, significantly increasing beam time availability.

We present properties and underlying beam dynamics of this operation mode, with particular emphasis on advanced methods for rate control at the second beam line.

ELECTRON STRETCHER FACILITY

At the Electron Stretcher Facility ELSA (see Fig. 1) polarized or unpolarized electrons are accelerated to energies of up to 3.2 GeV within a three-staged accelerator scheme including a Linac, the Booster Synchrotron and the ELSA stretcher ring [1]. A source for polarized electrons or a thermionic gun, operated at 50 kV and a traveling wave Linac are available as pre-injector. The following Booster Synchrotron further accelerates the electrons and transfers them to the main storage ring at an energy of typically 1.2 GeV.

After accumulating typically 30 mA in the stretcher ring, the electrons are accelerated up to 3.2 GeV and are then slowly extracted to one of the experimental sites. The first external beamline splits up and serves two hadron physics experimental sites E1 and E2. The second beamline delivers electrons to the third experimental site E3 utilized for detector testing [2], irradiation experiments and medical physics [3].

Resonant Extraction

The electron beam is extracted from the main storage ring and delivered to the experiments. This is realized via resonant extraction at a third integer betatron resonance in the horizontal plane. This resonance is driven by dedicated sextupole magnets in the dispersion free straights of the storage ring.

During the extraction, the betatron tune in the horizontal plane is shifted towards $Q_x = 4\frac{2}{3}$ by four dedicated fast

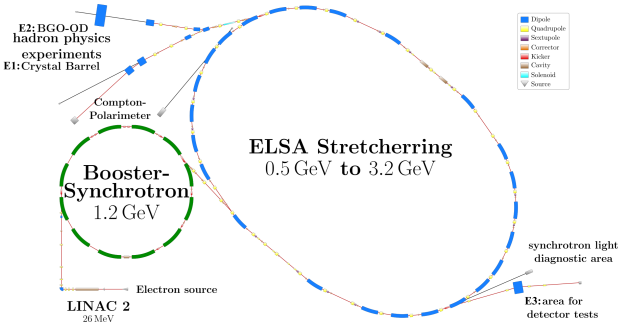

Figure 1: Electron Stretcher Facility ELSA.

ramping air core quadrupole magnets. For each external beamline separate pre- and main septum magnets are installed, guiding a portion of the beam to the external beam lines. Due to a superperiodicity of 2, the Twiss parameters at both extractions points are identical.

In vicinity of the resonance, a separatrix is formed in phase space, indicating the stable region inside (compare simulation in Fig. 2). By the introduced tune shift towards the resonance, the separatrix shrinks in size and more particles become unstable. The rate of unstable particles, and thus, the rate of extracted electrons is then stabilized and controlled by a software PID controller with the air core quadrupole current as control value.

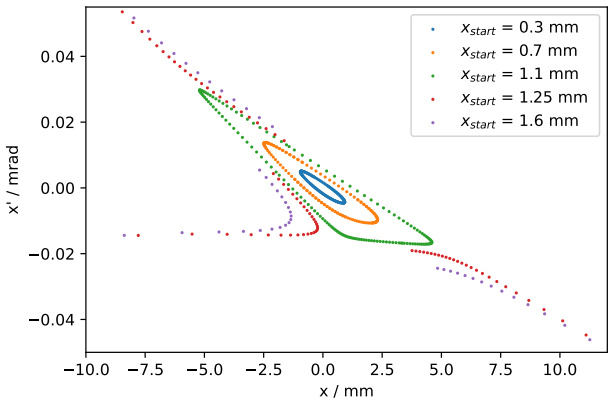

Figure 2: Xsuite [4] simulation of 5 electrons with different start amplitudes for 150 revolutions indicating stable and unstable phase space regions. Extraction sextupole strength was set to $m_{ex} = 1.2\,m^{-3}$. Simulated in vicinity of third integer betatron resonance.

Simultaneous Resonant Extraction Due to the aforementioned superperiodicity of $P = 2$, simultaneous extraction at the first and second beamline is, in principle, naturally possible. The betatron phase advance between the two locations is $\Delta\Psi = 4\frac{2}{3}\pi$. Consequently, an identical separatrix

* proft@physik.uni-bonn.de

Content from this work may be used under the terms of the CC BY 4.0 licence (© 2026). Any distribution of this work must maintain attribution to the author(s), title of the work, publisher, and DOI.

ISBN: 978-3-95450-252-3 ISSN: 2673-5350 doi: 10.18429/JACoW-IPAC2026-WEP6054

DEVELOPMENT OF THE 2 MeV PROTON BEAM DIAGNOSTICS SECTION IN PREPARATION FOR NEUTRON PRODUCTION AT FRANZ

A. Ateş *, L. Bauer, H. Hähnel, P. Müller, R. Tiede, J. Traios, C. Wagner
Institute of Applied Physics, Goethe University Frankfurt, Frankfurt am Main, Germany

Abstract

The Frankfurt Neutron Source (FRANZ) at the Institute of Applied Physics in Frankfurt (IAP) is advancing toward the commissioning of proton beams up to 2 MeV. To support beam tuning behind the RFQ–IH-DTL acceleration chain, a dedicated diagnostics section is being installed downstream of the IH-DTL cavity. The setup focuses on transverse beam characterization using scintillation screens combined with radiation-tolerant camera systems, enabling multi-angle (two-view) imaging of the proton beam under various beam-current and RF settings. Additional instruments include phase probes for energy and RF-phase monitoring, as well as a Faraday cup for current measurements. The camera-based diagnostics are designed to provide reliable visual feedback during early commissioning, particularly in an environment with limited access and the radiation levels typical for this region of the accelerator. This contribution presents the concept, implementation approach, and intended diagnostic capabilities of the camera-driven setup as FRANZ prepares for subsequent steps toward routine 2 MeV operation and the following delivery of the proton beam onto the lithium target for the first neutron production campaigns.

INTRODUCTION

The Frankfurt Neutron Source (FRANZ) is a compact accelerator-driven facility at the Institute for Applied Physics (IAP) at Goethe University Frankfurt, designed to produce neutrons via the $^7\mathrm{Li}(p,n)^7\mathrm{Be}$ reaction with a 2 MeV proton beam [1]. The driver linac consists of a CHORDIS ion source, a 60 keV electrostatic post-accelerator, a Low Energy Beam Transport (LEBT) line, and a coupled RFQ–IH-DTL cavity that accelerates the beam from 60 keV to 2 MeV [2]. Following successful commissioning of the 700 keV RFQ beam with 10 mA peak current [3], the coupled RFQ–IH-DTL has been conditioned and first 1.9 MeV beam was delivered to the diagnostics section [4]. The beam is pulsed at a repetition rate of 10 Hz with a macro-pulse length of 2 ms, resulting in a duty cycle of 2 % and a peak current of up to 6 mA. To support beam tuning behind the RFQ–IH-DTL acceleration chain, a dedicated diagnostics section has been installed downstream of the IH-DTL cavity. This contribution presents the design and first results of this diagnostics section, with particular emphasis on the multi-camera system for non-invasive transverse beam profile measurements using Beam Induced Fluorescence (BIF) in residual gas.

DIAGNOSTICS SECTION LAYOUT

The diagnostics section is installed directly downstream of the IH-DTL exit flange (see Fig. 1). An external quadrupole triplet, positioned immediately behind the IH-DTL, complements the internal IH-DTL quadrupole triplet lens. Together, these two triplets allow matching of the beam envelope throughout the drift section. The beamline is constructed from standard CF cross-pieces equipped with vacuum viewports, providing optical access for the camera systems. The section houses the following instruments:

- A movable scintillation screen mounted opposite the first camera, allowing the operator to switch between interceptive screen imaging and non-invasive BIF observation.
- Two capacitive phase probes separated by a known drift distance for beam energy determination via the Time-of-Flight (ToF) method.
- A Faraday cup at the end of the beamline for absolute beam current measurement.
- Multiple vacuum viewports for external camera installations enabling non-invasive BIF profile monitoring from two orthogonal viewing angles.

By varying the quadrupole field strengths, the beam focus can be adjusted on the scintillation screen or, alternatively, the transverse beam envelope along the drift section can be studied through BIF imaging at different magnet settings.

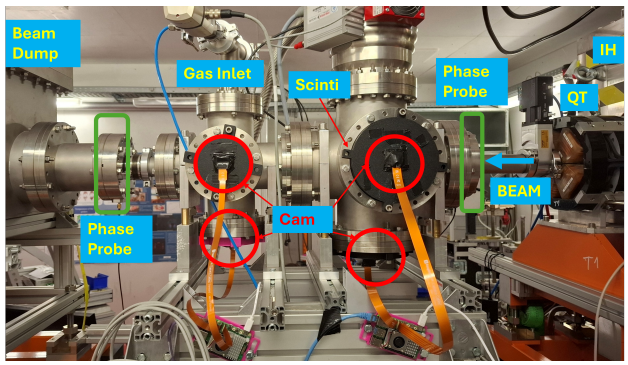

Figure 1: Layout of the diagnostics section downstream of the IH-structure, showing the quadrupole triplet, cross-piece arrangement with vacuum viewports, phase probes, and Faraday cup.

* ates@iap.uni-frankfurt.de

Content from this work may be used under the terms of the CC BY 4.0 licence (© 2026). Any distribution of this work must maintain attribution to the author(s), title of the work, publisher, and DOI.

ISBN: 978-3-95450-252-3 ISSN: 2673-5350 doi: 10.18429/JACoW-IPAC2026-WEP6055

CMOS CAMERA-BASED OBSERVATION AND CHARACTERIZATION OF MULTIPACTING DURING CAVITY CONDITIONING

L. Bauer*[1,2], A. Ateş[1], J. Kaiser[1,2], P. Müller[1], U. Ratzinger[1,2], H. Hähnel[1,2]
[1]Institute of Applied Physics, Goethe University Frankfurt, Frankfurt am Main, Germany
[2]Helmholtz Forschungsakademie Hessen für FAIR (HFHF), Frankfurt am Main, Germany

Abstract

Raspberry Pi cameras (single board CMOS cameras) have already been successfully implemented for ion beam characterization at IAP Frankfurt and are now also being used to investigate multipacting during cavity conditioning. Multipacting appears caused by resonant secondary electron emission. For the standalone RF conditioning of the FRANZ (Frankfurt Neutron Source) RFQ (Radio-Frequency Quadrupole) and the IH-DTL (Interdigital H-mode Drift-Tube-Linac), these cameras were installed both inside and outside the vacuum to detect multipacting and other cavity glowing effects. The occurrence of multipacting at specific power levels within the cavities can be confirmed by simulations. In addition, the observed multipacting is characterized through spectrometer measurements.

INTRODUCTION

At the Institute of Applied Physics (IAP) in Frankfurt, CMOS cameras combined with single-board computers (Raspberry Pi) have been successfully used for ion beam diagnostics [1, 2] and are now applied for the visualization and analysis of multipacting and other optical effects within cavities. This contribution reports results from the standalone conditioning of the RFQ and the IH-DTL at power levels up to 70 kW and 5 kW, respectively. Both cavities are components of the FRANZ project [3] and are finally operated as one cavity .Based on the optical observations of the positions within the cavities where multipacting appears, calculations based on CST simulations have been performed to confirm the appearance of multipacting at specific power levels [4].In addition to the optical analysis of multipacting, further characterization was done by performing mass spectrometer measurements at the RFQ during conditioning.

CAVITY CONDITIONING AND MULTIPACTING

Conditioning describes the gradual increase in RF power coupled into a cavity to achieve stable high-power operation. The FRANZ cavities are conditioned at low RF levels with duty cycles of 90 % to 100 % to ensure an optimal preparation for operation, whereas duty cycles of 1 % to 2 % are applied during beam operation.

A primary challenge addressed during this phase is multipacting, a resonant electron multiplication phenomenon. This process is initiated by free electrons gaining kinetic energy from the oscillating RF field and colliding with e.g. the cavity walls [5].If these remain in phase with the RF field, an exponential electron avalanche can develop within a few RF cycles, potentially degrading cavity performance [6].To identify multipacting regions computationally, a plane-parallel surface approximation is used, with multipacting predicted on paths with a length of x_0 in voltage ranges

$$V_{\min} = \frac{m_e \omega^2 x_0^2}{2e\sqrt{4 + (2n+1)^2 \pi^2}}. \quad (1)$$

and

$$V_{\max} = \frac{m_e \omega^2 x_0^2}{2e}. \quad (2)$$

where n is an integer describing the order of the multipacting. The frequency f is set to 175 MHz for the given cavities. V_{max} represents the limit beyond which multipacting is not longer possible [7].

MEASUREMENT POSITIONS

Single-board CMOS cameras (Raspberry Pi module V3 and module V3 wide) were used to monitor optical emissions caused by multipacting and other optical phenomena in the RFQ and the IH-DTL during conditioning. The analog gain, white balance (AWB), and focal length were fixed after calibration. Additional to the cameras a mass spectrometer and an optical spectrometer were installed at the RFQ. In Fig. 1 the positions of the installed cameras (also the corresponding field of view (FoV)), mass spectrometer and optical spectrometer at the RFQ to characterize multipacting are shown. Camera RFQ-2 provides a direct view of a stem and a small section of the electrodes, while camera RFQ-1 offers a broader view including a stem, its neighboring stems, a larger section of the electrodes, and the RFQ exit. To improve the image quality of camera RFQ-1, which is affected by radiation-induced pixel artifacts, a 3D-printed PETG-Tungsten shielding is currently under investigation [8].
Figure 2 illustrates the position of both outside the cavity installed cameras and their FoVs. Due to its small FoV camera IH-1 will not be further considered here. Camera IH-2 offers a direct view through a grid on the drifttubes and on the tuner nearby the exit of the cavity.

MULTIPACTING CHARACTERIZATION DURING CONDITIONING

Optical multipacting effects were reproducibly observed at the specific positions in defined power level ranges within the FoVs. Figure 3 shows multipacting events in the RFQ acquired with camera RFQ-1 (left) and camera RFQ-2

* l.bauer@physik.uni-frankfurt.de

Content from this work may be used under the terms of the CC BY 4.0 licence (© 2026). Any distribution of this work must maintain attribution to the author(s), title of the work, publisher, and DOI.

ISBN: 978-3-95450-252-3 ISSN: 2673-5350 doi: 10.18429/JACoW-IPAC2026-WEP6056

NOVEL TIME-OF-FLIGHT MEASUREMENT ON A SHORT BASE

Z. Kormány
HUN-REN Institute for Nuclear Research, Debrecen, Hungary

Content from this work may be used under the terms of the CC BY 4.0 licence (© 2026). Any distribution of this work must maintain attribution to the author(s), title of the work, publisher, and DOI.

Abstract

Time-of-flight (TOF) measurements are superior to other methods of measuring beam energy, since the quantity being measured is directly related to the velocity, and therefore the kinetic energy, of the particles. Conventional TOF systems use independent sensors in the beam transport system, each with a separate signal path to the measuring electronics. The unknown difference in signal delay between the paths introduces an absolute error in the measured time. Increasing the flight time can help to reduce the impact of this error. For this reason, a flight path length of several metres is usually applied between the sensors.

A novel method and device have been developed for accurate TOF measurements on a base as short as 20 cm. Two capacitive pickups in a common mechanical structure with an additional electrode are used. The signals from the probes are combined within the vacuum chamber, resulting in a single signal path from the sensor unit to the measuring electronics. Digital signal processing (DSP) is used to determine the distance between the pulses generated by a beam bunch on the probes. The signal processing hardware and software were tested using pulses from a high-precision signal generator. Time measurements with an absolute error of less than 1 ps were achieved. The accuracy of the complete system with beams from a cyclotron was investigated using neutron threshold reactions. The measurement accuracy was found to be at least one order of magnitude better than the accuracy of the energy value calculated from the cyclotron parameter settings.

The prototype unit was developed for the cyclotron at the HUN-REN Institute for Nuclear Research (ATOMKI). Installed in its main beamline, it can continuously monitor the beam energy independently from the beamline in use.

INTRODUCTION

Unlike DC accelerators, the beam energy of cyclic accelerators cannot be determined from the accelerating voltage. When calculating from the machine parameters, values that are not accurately known must also be applied. For circular machines, for example, the radius of the final orbit is required in the formula. Cyclotrons are the worst-case scenario, as this value cannot be determined exactly. Therefore, the nominal extraction radius is used instead, which can lead to significant errors, particularly with multi-particle and variable-energy machines. Therefore, proton therapy cyclotrons, for example, are built as fixed-energy machines, which allow the extracted beam energy to be determined and repeated accurately. The beam is always accelerated to this maximum energy in the cyclotron, and if lower energy is required for treatment, the surplus beam energy is dissipated by a degrader. This has two disadvantages: unwanted extra activation of machine parts and significant electrical energy waste during operation.

At variable-energy machines accurate beam energy is determined by measuring the kinetic energy of the extracted beam in the beam transport system. Of the various measurement methods and systems that have been developed, Time-of-flight (TOF) measurements [1, 2] offer many advantages, including a direct relationship with the energy value, possible non-destructive measurement and low operating costs. However, its large spatial requirement between the probes means it can only be used in dedicated, long beamlines, preventing its use at any accelerator.

At first glance, the flight path length can only be short if the delay difference between the signal paths is extremely small. For instance, the time-of-flight value for a 230 MeV proton beam over 20 cm is approximately 1.12 ns. This means that, to achieve an energy value accuracy of 1×10^{-3}, the absolute time error caused by the delay difference of the signal paths must be smaller than 0.56 ps. Equalising cable and amplifier delays with such accuracy is technically not feasible. However, it is not necessary to equalise the signal path delays perfectly. It is sufficient to know the exact value of the existing difference. The novel device and method ensure that this value is measured with the required accuracy, enabling beam energy measurement on a short base.

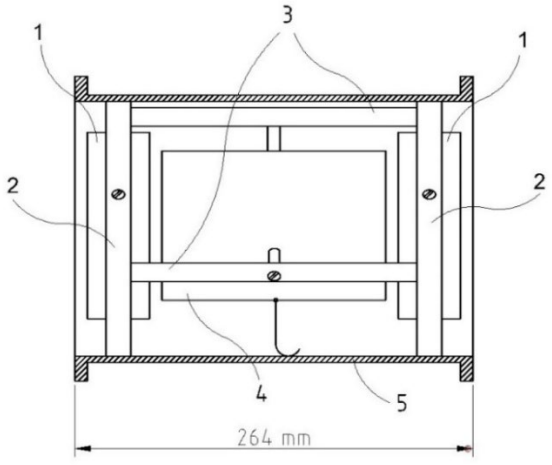

Figure 1: Conceptual structure of the new sensor unit: 1 – capacitive probe, 2 – centring insulator, 3 – spacer, 4 – grounded electrode and 5 – vacuum chamber.

THE NEW DESIGN

Unlike conventional time-of-flight systems, which have two or three probes built independently into the beam transport system at different locations, the novel device uses a special sensor unit comprising two probes and an

ISBN: 978-3-95450-252-3 ISSN: 2673-5350 doi: 10.18429/JACoW-IPAC2026-WEP6062

ELECTROMAGNETIC TEST-BENCH EVALUATION OF PICKUP PROTOTYPES FOR THE ELETTRA 2.0 BUTTON-TYPE BEAM POSITION MONITORS

S. Cleva*, M. Barnaba, S. Bassanese, G. Brajnik, R. De Monte, D. Pozzecco, R. Sergo
Elettra-Sincrotrone Trieste S.C.p.A., Trieste, Italy
A. Passarelli, Istituto Nazionale di Fisica Nucleare, Napoli, Italy
M. Comisso, University of Trieste, Trieste, Italy

Abstract

To reliably and repeatably validate the electromagnetic behavior of the pickup prototypes designed for the Elettra 2.0 button-type beam position monitors, two different radio-frequency test fixtures have been developed. The first test fixture, based on a coaxial-line design that emulates the TEM excitation generated by a relativistic beam, allows to measure the transmission performance of the pickups up to 16 GHz. The second test fixture, employing an antenna-launcher design, extends the measurement range up to 40 GHz. This paper presents a comparison between measured and simulated data, with particular focus on the electromagnetic validation of the first 16 prototypes manufactured using glass as the dielectric material.

INTRODUCTION

Figure 1 shows the reference design for the Elettra 2.0 [1] button-type pickups, together with the SMK connector (pin contact, according to MIL-STD-348B [2]) embedded in the pickup body. Such device is manufactured press fitting the collar C (that implements the reference plane of the SMK connector) on the pickup body B. The insulator collar, indicated in green, fulfils two functions: it provides mechanical support for the central pin P and it ensures vacuum sealing. The pickup is basically a 50 Ω coaxial line from the SMK connector reference plane up to the insulator, which terminates in the conical button that couples with the EM field of the beam. In normal operation, the electromagnetic (EM) energy captured by the gap around the button (the beam port), propagates along the pickup coaxial structure and is delivered to the position detection equipment through the SMK connector (the radio frequency (RF) port).

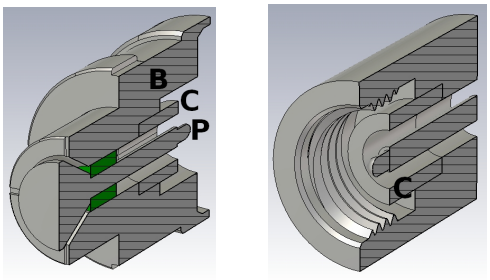

Figure 1: Reference design for the Elettra 2.0 pickups and embedded SMK connector cross sections.

RF CHARACTERIZATION OF PICKUPS

The behavior of any kind of button-type pickup can be fully characterized by reflection and transmission measurements performed under test reference conditions, using time domain (TD) or frequency domain (FD) signal processing methods [3]. Transmission measurements can not be directly executed because the beam port of the pickup is not intended to be directly connected to measuring devices. For this reason a dedicated adapter is required to create a completely closed propagation path that, starting from the RF port of the pickup, passes through the beam port and terminates on one or more 50 Ohm matched test connectors. Once such propagation path has been physically realized, transmission measurements are executed injecting a test signal in the pickup through its coaxial connector and measuring the amplitude and phase (FD) or amplitude and time of arrival (TD) of the signals detected on the adapter's connectors.

TEST FIXTURES

To get a reliable and repeatable EM characterization comparable with simulation, each pickup is mounted on dedicated metallic mechanical supports made of aluminum, named test fixtures, that host RF connectors to perform both reflection and transmission measurements under closed environment test reference conditions. The dielectric material inside the test fixtures is air. Injecting the test signal through a test fixture port the flow of the EM energy that propagates through the pickup can be reversed, allowing bi-directional transmission measurements. In order to define complete self consistent EM test environments, a reference wire pickup has been manufactured using a uniform wire suspended in air as central pin. For the experimental measurements, a Teledyne LeCroy WavePulser 40iX (TDRMI) was employed for time-domain analysis (transmission and reflection up to 40 GHz). For frequency-domain characterization up to 26.5 GHz, a Keysight PNA network analyser (VNAMI) was used.

Two Ports Test Fixture General Description

The simplest type of test fixture, indicated as "2PTF", is based on a two ports, single SMK connector configuration, see Fig. 2 (left). A short wire antenna, that couples with the beam port of the pickup, is directly mounted on the central conductor of the test fixture's SMK connector (plug type). This antenna is aligned along the rotational symmetry axis

* stefano.cleva@elettra.eu

Content from this work may be used under the terms of the CC BY 4.0 licence (© 2026). Any distribution of this work must maintain attribution to the author(s), title of the work, publisher, and DOI.

ISBN: 978-3-95450-252-3 ISSN: 2673-5350 doi: 10.18429/JACoW-IPAC2026-WEP6068

CAPABILITIES AND LIMITATIONS OF NON-REDUNDANT APERTURE INTERFEROMETRY FOR BEAM SIZE MEASUREMENTS

U. Iriso, L. Torino*, A. Turull Barot†, ALBA Synchrotron (Spain), Cerdanyola del Vallès, Spain
B. Nikolic, Cavendish Laboratory, Cambridge, United Kingdom
N. Thyagarajan, Commonwealth Scientific and Industrial Research Organisation, Canberra, Australia
C. Carilli, National Radio Astronomy Observatory, Socorro, NM, United States

Abstract

Non-Redundant Aperture Interferometry (NRAI) is a beam characterization technique developed at ALBA in collaboration with radio-astronomy institutes. It enables the single-acquisition measurement of the full 2D transverse profile of the electron beam using visible synchrotron radiation. To better understand the technique limitations and performance, we performed extensive SRW simulations and compare them with experimental data. This paper presents the results of these studies, which define the capabilities and limits of NRAI applied to the current ALBA machine.

INTRODUCTION

The characterization of transverse beam dimensions is a key aspect in accelerators, as it provides a measurement of beam emittance. These measurements are usually performed using synchrotron radiation at light sources. The most common techniques used are either the X-ray pinhole [1] or synchrotron radiation interferometry (SRI) [2], if visible light is preferred. In the latter case, the measurement is typically unidimensional (two-aperture interferometry) and does not allow for full beam shape reconstruction in a single shot [3].

By using Non-Redundant Aperture Interferometry (NRAI), a technique widely used in astronomy, we have developed a method to acquire all transverse beam dimensions in real time with only one acquisition using visible light [4, 5].

The main idea is to acquire the interference pattern and analyze it in the Fourier domain where, due to the non-redundancy, each pair of pinholes interferes at a specific spatial frequency, allowing us to see distinct peaks. By calculating the visibility or the correlation—summing the intensity within these peaks and identifying the combinations that cause each peak while using the illumination as a free parameter—we can reconstruct the beam profile with a 2D Gaussian and obtain the beam parameters to convert them into laboratory coordinates.

This report describes the results of the NRAI method through Synchrotron Radiation Workshop (SRW) simulations to model the interferometer and the synchrotron radiation in a controlled environment, followed by the experimental validation at the Xanadu beamline [6].

* ltorino@cells.es
† alba2.turull@gmail.com

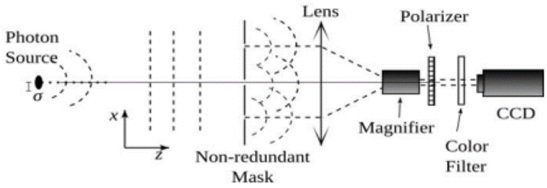

Figure 1: Experimental setup.

EXPERIMENTAL SETUP

The experimental setup (Fig. 1) selects only the visible light of the synchrotron radiation using a half-mirror located upwards with respect to the beam axis. The light then propagates through the Non-Redundant Mask (NRM).

Assuming the source is in the far-field limit, we can model the synchrotron radiation as plane waves passing through the NRM. These masks consist of a combination of pinholes—in our case, 5, 7, or 9—placed in a geometry where each baseline (the vector connecting two apertures) is unique. This ensures that each pinhole pair interferes at a unique spatial frequency in a given orientation, which reduces the risk of incoherence due to turbulence and non-uniformity in the radiation path. The 9-hole NRA mask used in this study is presented in Fig. 2, while the 5 and 7-hole configurations are described in Ref. [5]. As shown in Fig. 1, the light then passes through a lens, a magnifier, a polarizer, and a color filter to select the desired polarization and wavelength, typically horizontal polarization and 400 nm. Finally, the interference pattern is captured by a CCD camera.

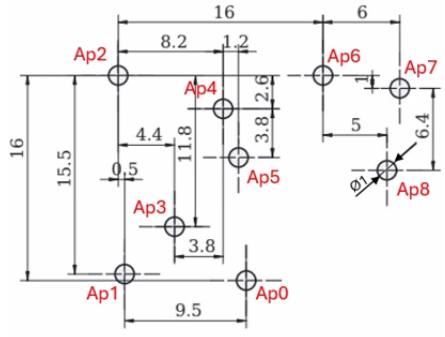

Figure 2: Schematic of the 9-hole NRA mask used at ALBA with the distances in mm.

RESULTS

In this section, the capabilities and limitations of this technique are discussed. To evaluate the performance of the NRAI, simulations were performed with SRW to establish

Content from this work may be used under the terms of the CC BY 4.0 licence (© 2026). Any distribution of this work must maintain attribution to the author(s), title of the work, publisher, and DOI.

ISBN: 978-3-95450-252-3 ISSN: 2673-5350 doi: 10.18429/JACoW-IPAC2026-WEP6069

BUNCH-BY-BUNCH CHARGE, POSITION, AND PHASE DIAGNOSTICS USING AN OSCILLOSCOPE-BASED ANALYSIS FOR ALBA

J. Bañuelos*, U. Iriso, ALBA Synchrotron, Cerdanyola del Vallès, Spain

Abstract

The ALBA synchrotron is preparing its upgrade to ALBA II, a fourth-generation storage ring that will require improved bunch by bunch beam diagnostics in order to fully characterize the beam. To meet these requirements and based on the analysis developed using the HOTCAP code [1], we are integrating an oscilloscope-based analysis tool that processes BPM signals to extract bunch-by-bunch charge, transverse position, and relative measurement of the longitudinal phase. This report summarizes how the tool has been adapted for ALBA. We show results using this method and compare them with other techniques.

INTRODUCTION

ALBA is currently going to an upgrade called ALBA-II [2], where the beam energy is kept at 3 GeV, but the emittance is reduced to 200 pm. The machine upgrade has to comply with several constraints imposed by the decision of maintaining the same circumference (269m), The RF system will be preserved, retaining the six 500 MHz cavities and adding a new third-harmonic cavity (3HC) to lengthen the bunch and improve lifetime [3]. ALBA-II imposes certain performing challenges, which would highly benefit from a bunch-by-bunch diagnostics systems. These effects can be both in the transverse plane (like ion trapping or couple bunch instabilities) and longitudinal plane (like transient beam loading). This report shows an oscilloscope-based acquisition of BPM signals [4], providing a flexible approach for this fast diagnostics and allowing a direct digitization with high bandwidth and sampling rate without dedicated hardware. For a 500 MHz RF system, this requires GHz-class bandwidth and multi-GS s^{-1} to resolve sub-nanosecond BPM signals. We show how this method is implemented at ALBA to extract bunch-by-bunch charge, transverse position, and longitudinal phase from BPM signals. The method is first validated under nominal operating conditions and then used for beam-dynamics studies including tune measurements, beam-loading effects, and RF transients.

MEASUREMENT SYSTEM

The experimental setup relies on commercial instrumentation and is shown in Fig. 1. It consists of a BPM pickup connected through coaxial cables to a high-bandwidth scope (6 GHz, 16 GS s^{-1}), where the four button signals are directly digitized. The acquired waveforms are then transferred to a computer for offline processing and parameter extraction. In this case, the scope is the 4 channels 6 GHz Keysight scope (MXR604B). Precise matching between cables is performed in this process, so there is no need for dedicated hardware synchronization. At ALBA, the revolution period is 896 ns. Acquisitions are typically performed over time windows in the range of 2–10 ms at a sampling rate of 16 GS s^{-1}, corresponding to several thousand turns per acquisition. This results in waveform sizes of hundreds of mega-samples and therefore large datasets, for which the data processing becomes computationally demanding.

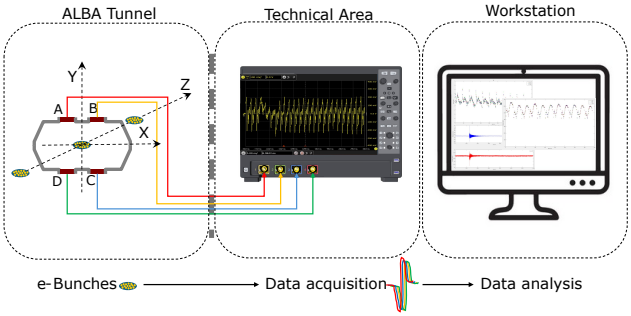

Figure 1: Schematic of the BPM-based acquisition system. The four button signals are directly digitized by the scope and processed offline.

METHOD VALIDATION

The method is thoroughly described in [4]. Briefly, the four signals from the BPM electrodes are acquired using a broadband oscilloscope during *sim*thousands of turns. From multiple turns, a response function (look-up table, LUT) is reconstructed for each bunch and electrode, achieving an equivalent resolution of 0.1 ps. Figure 2 shows a typical response function for one bunch of the LUT using this 3DBPM method, compared with the 6 GS/s raw signal obtained from the fast scope.

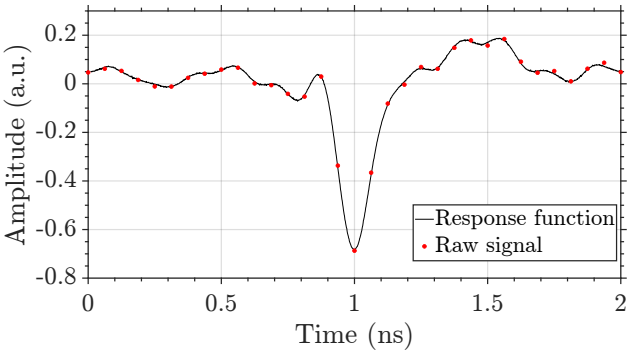

Figure 2: Response function of a bunch passing trough the electrode (bipolar pulse,2 ns duration) reconstructed from multiturn data. Compared with the raw signal (normalized) of the same bunch.

For each of the four BPM channels, the peak-to-peak amplitude of the reconstructed bunch response function is

* jbanuelos@cells.es

Content from this work may be used under the terms of the CC BY 4.0 licence (© 2026). Any distribution of this work must maintain attribution to the author(s), title of the work, publisher, and DOI.

ISBN: 978-3-95450-252-3 ISSN: 2673-5350 doi: 10.18429/JACoW-IPAC2026-WEP6071

MULTI-HARMONIC BUNCHER EXPERIMENT OVERVIEW FOR THE ISOLDE SUPERCONDUCTING RECOIL SEPARATOR PROJECT

I. Bustinduy*, K. Altenmüller, I. de los Bueis, D. Fernandez-Cañoto, P. González, R. González, G. Harper, J. Martín, R. Miracoli, J. Muñoz, S. Varnasseri, A. Zugazaga
ESS Bilbao, Zamudio, Spain

Abstract

The ISOLDE Superconducting Recoil Separator (ISRS) at CERN is a rotatable high-resolution spectrometer able to separate reaction fragments induced by HIE-ISOLDE beams, from the lightest to the heavies nuclear species, at collision energies up to 10 MeV/u. The injection of the ISOLDE beam into this ring requires a more compact bunch structure, so a Multi-Harmonic Buncher (MHB) device was designed for this task. The MHB will operate at a frequency of 10.128 MHz, which is a 10 % of the linac frequency, and would be installed before the RFQ. The MHB was designed as a two electrodes system, and the RF signal composed for the first four harmonics of the fundamental frequency, is fed into the electrodes. The system was first tested in the laboratory upto the nominal power conditions. Prior to delivery of MHB to its final location in ISOLDE, it will be tested with ion source beam at ESS-Bilbao with a β equal to 0.00328. In order to measure the functionality and characteristics of the produced bunches, a set of diagnostics were foreseen. To evaluate beam transmission a set ACCTs and a Faraday Cup were employed, a Wien filter (WF) to measure energy, and a Fast Faraday Cup (FFC) for bunch length measurement. The preparation of the experiment along with the results are presented in this contribution.

INTRODUCTION

The ISOLDE Superconducting Recoil Separator (ISRS) [1] requires a longer bunch spacing than that delivered by the HIE-ISOLDE linac. To meet this need, the ISRS programmeat ESS-Bilbao is developing a multi-harmonic buncher (MHB) operating at 10.128 MHz, one tenth of the linac frequency, so that the beam can be rebunched while remaining synchronized with the downstream accelerator. The package delivered by ESS-Bilbao combines the buncher cavity, the RF generation and control chain, and a dedicated set of beam diagnostics. The MHB design evolved from early concepts [2] toward a wedge-electrode geometry optimized for the ISOLDE beam conditions [3]. On the RF side, the required sawtooth-like waveform is synthesized from the first four harmonics and stabilized with a digital low-level RF control system. The experimental line also includes ACCT current transformers, a Faraday cup, a Wien filter (WF), and a fast Faraday cup (FFC) for future bunch-length measurements [4]. To prepare beam commissioning, the ESS-Bilbao injector was configured to reproduce the reduced velocity required for the ISOLDE case, $\beta = 0.00328$. For this reason, in Bilbao, 10.094 keV $H_2^+$was selected as the commissioning species to adjust the parameters to the intended ISOLDE application.

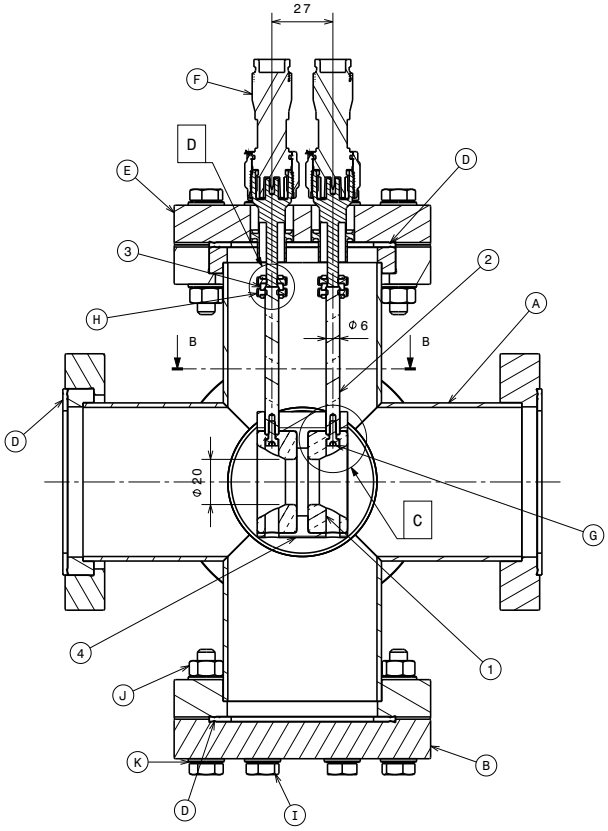

Figure 1: MHB Technical drawing: (1) MHB electrode, (2) Electrode support guide, (3) MHB electrode contact barrel, (4) MHB electrode spacer, (F) HN type male connector, (E) Forethought.

MHB MANUFACTURING

Due to the intended final location of the MHB in the ISOLDE linac, before the REX RFQ, a standard 4 way CF63 vessel has been chosen. One of the critical elements is the required feed-through for the electrodes. We have chosen a tailor made double CF63 HN connector based on the VACOM W-HN50-GS-SE-CE-NI model. This model can work up to 7 GHz and up to 7 kV DC voltage. Among the many studied models, the version 4 (see Fig. 1) is the preferred solution due to its versatility. The maximum field at the required power is monitored by means of electromagnetic simulations to ensure Kilpatrick limit is not reached, currently this value is < 0.85 MV/m (Kilpatrick 5.4 MV/m).

* ibustinduy@essbilbao.org

Content from this work may be used under the terms of the CC BY 4.0 licence (© 2026). Any distribution of this work must maintain attribution to the author(s), title of the work, publisher, and DOI.

ISBN: 978-3-95450-252-3 ISSN: 2673-5350 doi: 10.18429/JACoW-IPAC2026-WEP6074

IFMIF-DONES BEAM ON TARGET DIAGNOSTICS BASED ON OPTICAL METHODS: OTR AND FLUORESCENCE*

J. Herranz-Feito, A. Ortega Moral, I. Podadera, M. Weber, IFMIF-DONES España, Granada, Spain
D. Jiménez-Rey, C. Oliver, CIEMAT, Madrid, Spain
J. Valenzuela-Valdés, UGR, Granada, Spain

Content from this work may be used under the terms of the CC BY 4.0 licence (© 2026). Any distribution of this work must maintain attribution to the author(s), title of the work, publisher, and DOI.

Abstract

The IFMIF-DONES facility located at Escúzar in Spain will consist of an accelerator delivering 125 mA of 40 MeV deuterons onto a liquid lithium target. The beam profile at the target will have a rectangular with two side peaks footprint to meet the irradiation requirements of the facility. The environment conditions are characterised by a high radiation background, an atmosphere of lithium vapor, deuteron scattering with the residual gas and secondary electrons production. To measure the footprint under these conditions optical methods are designed based either on measuring Optical Transition Radiation (OTR) of the beam passing through the liquid lithium or on the Beam Induced Fluorescence (BIF) of the residual gas in the proximity of the liquid lithium. Both alternatives have its advantages and drawbacks. In this paper the study of the pros and cons of both alternatives is presented. Furthermore, an experiment to better characterise the OTR response in liquid lithium is also presented.

INTRODUCTION

The objective of IFMIF-DONES [1] is to test materials under a neutron flux of 10^{15} n·cm^{-2}·s^{-1} which generate a damage similar to the ones expected in a fusion reactor. This neutron flux is produced by the reaction of 40 MeV deuterons with liquid lithium at 300 ºC. An accurate measurement of the beam is essential to properly control the material irradiation.

The nominal beam profile at the target simulated in TraceWin is shown in Fig. 1 [2]. It is characterised by a rectangular shape that it can be controlled from 10 to 20 cm as explained in [3]. To measure deviations of this beam profile and send a fast MPS interlock in case of anomalies, an RF pickup based on eight electrodes is under study [4]. However, to have an accurate measurement of the profile for CODAC monitoring, optical methods are considered based on OTR or BIF.

Optical methods are selected because their components and associated electronics can be located far from the target. This is important because the Target Vacuum Chamber Cell (TVC), the beam lithium interaction region, is characterized by a harsh environment of high irradiation [5] and lithium vapour [6]. To minimise these problems, it is proposed to locate the radiation-sensitive components in the Target Interface Room (TIR), guide the image using an image fiber an locate the diagnostic camera and electronics in a safe environment, as shown in Fig. 2. Under vacuum, a mirror is used to avoid direct irradiation of optical components such as viewports and lenses. Both, OTR and BIF would share the same setup and the observation of one or another depends on the filters used. The pros and cons of both techniques, based on the light yields and spatial profiles are discussed.

* This work has been carried out partly within the framework of the EUROfusion Consortium (Grant Agreement No 101052200 — EUROfusion), funded by the European Union via the Euratom Research and Training Programme, and also by the Regional Andalousian Government under the project TECHAC (ProyExcel_00989).

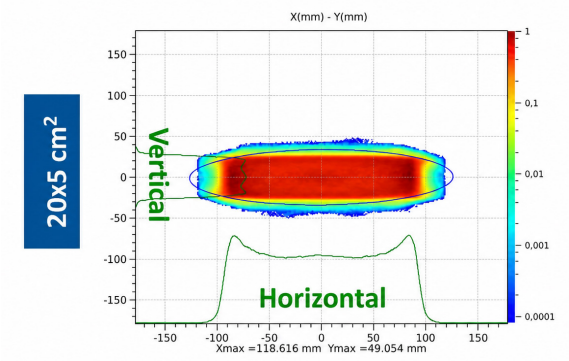

Figure 1: IFMIF-DONES Beam on target profile [2].

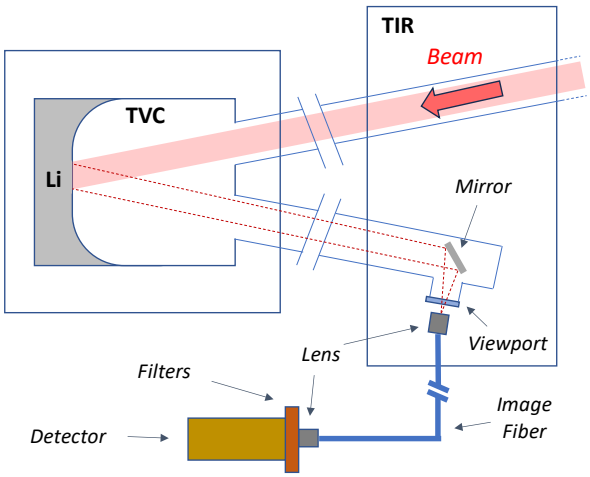

Figure 2: Setup for the Beam on Target diagnostic based on optical methods.

LIGHT YIELDS

The different light yields produced at the TVC have been calculated [7]. The results are shown in Fig. 3. The studied sources are: 1) BIF of deuterons with residual gases, 2) Fluorescence of secondary electrons (SE) with residual gases, 3) OTR of deuterons impinging on the lithium curtain, 4) Thermal radiation and 5) Bremsstrahlung.

ISBN: 978-3-95450-252-3 ISSN: 2673-5350 doi: 10.18429/JACoW-IPAC2026-WEP6075

THE QUADRUPOLAR COMPONENT OF THE ESS LINAC PROTON BEAM

B. Bolling*, N. Milas, European Spallation Source, Lund, Sweden
J. Cederkäll, B. Meirose, Department of Physics, Lund University, Lund, Sweden

Abstract

Beam Position and Phase Monitors (BPMs) are used as part of normal routines to measure the dipole component of a charged particle beam in order to determine its transverse position. However, BPMs are also sensitive to higher-order moments of the beam charge distribution, including the quadrupolar component, which provides access to the difference in horizontal and vertical beam RMS sizes. This work investigates the feasibility of extracting the quadrupolar component of the proton beam of the ESS superconducting linac (SCL) through the BPMs. The theoretical framework for quadrupolar signal formation is reviewed, with emphasis on the relation between pickup sensitivities and beam parameters, and a calibration strategy based on measuring the quadrupolar signal sensitivity with respect to the beam centroid position.

INTRODUCTION

BPMs constitute a fundamental diagnostic tool in particle accelerators, providing information on the dipole component of the beam to determine its horizontal and vertical positions, including at ESS [1]. Beyond position, BPMs are sensitive to higher-order moments of the beam charge distribution, including the quadrupolar component, which encodes information about the difference in horizontal and vertical beam sizes. Access to this information enables non-invasive monitoring of beam shape asymmetries and contributes to improved optics matching and beam quality control.

The ESS superconducting linac (SCL) provides a unique opportunity to exploit quadrupolar BPM signals for high-power proton beams. This paper develops the theoretical basis for quadrupolar signal formation, proposes a methodology for calibration and validation, and outlines a measurement strategy at ESS using BPMs. Figure 1 illustrates the design of the BPMs in the Spoke (SPK) section of the ESS SCL and the rest of the ESS SCL (MBL, HBL and HEBT sections, also referred to as elliptical sections) with the following differences between BPM aperture diameters:

- SPK section BPMs: $d = 57.1$ mm
- Elliptical sections BPMs: $d = 100$ mm

The BPMs in the ESS SCL are located in so-called Linac Warm-Units (LWUs), each typically including a focusing (QH) and defocusing (QV) quadrupole magnet pair, and a BPM and a combined corrector magnet in-between the quadrupole doublet.

The quadrupolar component is defined as

$$\Xi = \sigma_x^2 - \sigma_y^2 + \bar{x}^2 - \bar{y}^2, \tag{1}$$

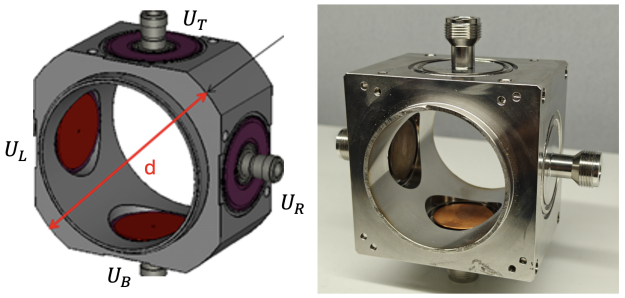

Figure 1: SPK and elliptical (MBL, HBL, HEBT) LWU sections' BPM design (left) and a SPK BPM photograph (right).

where σ_x and σ_y are the rms beam sizes in the two transverse planes, and $(\bar{x}, \bar{y})$ are the beam centroid position offsets relative to the BPM electrical center.

Following the formalism of [2,3], the voltages, U, induced in the four BPM electrodes (R, L, T, B) contain both dipole and quadrupolar terms which in normalized form yields the quadrupolar BPM signal by

$$\Xi_{\Delta/\Sigma} = \frac{U_L + U_R - U_T - U_B}{U_L + U_R + U_T + U_B} = S_Q \left(\sigma_x^2 - \sigma_y^2 + \bar{x}^2 - \bar{y}^2\right) \tag{2}$$

where S_Q is the quadrupolar sensitivity, dependent on the BPM aperture and electrode geometry. Beam centroid positions are obtained from the dipole terms:

$$\Delta_x = \frac{U_L - U_R}{U_L + U_R}, \qquad \Delta_y = \frac{U_T - U_B}{U_T + U_B}. \tag{3}$$

Due to the unavailability during the time of study of beam invasive diagnostic instruments to directly measure the beam profile at given locations, the sensitivities S_Q were calculated based on BPM design parameters and through calibration.

CALIBRATION AND DATA ANALYSIS

The characterization of the quadrupolar response across the ESS SCL was performed by scanning the beam centroid using corrector magnets upstreams the BPMs used for measurements. To extract the sensitivity S_Q, the experimental data were fitted to eq. (2) which can be directly identified from the curvature coefficient $a \equiv S_Q$. This calibration is inherently independent of the beam intensity, relying solely on the transverse distribution of charged particles in the beam.

Operational constraints during the beam studies occasionally resulted in scans performed with a non-zero offset in the non-scanning plane (e.g., a vertical offset $\bar{y}_0$ during a horizontal scan). This offset introduces a parasitic shift in the signal baseline. To recover the real geometric response, a correction protocol was implemented to "align" the data

* benjamin.bolling@ess.eu

Content from this work may be used under the terms of the CC BY 4.0 licence (© 2026). Any distribution of this work must maintain attribution to the author(s), title of the work, publisher, and DOI.

ISBN: 978-3-95450-252-3 ISSN: 2673-5350 doi: 10.18429/JACoW-IPAC2026-WEP6076

OFF-RESONANCE LANDAU CAVITY FIELD PROBE CALIBRATION

D. K. Olsson*, Å. Andersson, MAX IV Laboratory, Lund, Sweden

Content from this work may be used under the terms of the CC BY 4.0 licence (© 2026). Any distribution of this work must maintain attribution to the author(s), title of the work, publisher, and DOI.

Abstract

Higher harmonic RF cavities are used by synchrotron light sources for lengthening the bunches in order to improve Touschek lifetime and increase incoherent synchrotron tune spread. The MAX IV 1.5 GeV storage ring passive Landau cavities are used for this purpose. These cavities are fitted with probe loops which monitor the amplitude of the fields. In order to have an accurate reading of the field amplitude experienced by the beam, each probe loop requires a calibration factor. This calibration factor is usually found using an on-resonance calibration method, which relies on a model cavity shunt impedance. In this paper, an alternative off-resonance calibration method is presented. This method is less dependent on the accuracy of the model shunt impedance.

THE MAX IV 1.5 GEV STORAGE RING

The MAX IV laboratory houses two electron storage rings, the 1.5 GeV storage ring, and the 3 GeV storage ring. This paper will only treat the 1.5 GeV ring. Relevant parameters for this ring can be found in Tab. 1. The ring has two nominally identical passive Landau cavities, which will be referred to as Cavity A and Cavity B.

Table 1: Cavity Parameters of the MAX IV 1.5 GeV Storage Ring

Main cavity frequency	f_0	100 MHz
Beam energy	E_0	1.5 GeV
Main cavity voltage	V_{MC0}	519 kV
Harmonic number	h	32
Energy loss per turn	U_0	114 kV
Landau cavity shunt impedance	R_s	5.55 MΩ
Landau cavity higher harmonic	N	3

ON-RESONANCE CALIBRATION

The field in a passive cavity operating on resonance is given by [1]

$$V_{HC} = |\tilde{F}| I R_s, \tag{1}$$

where $\tilde{F}$ is the complex bunch form factor [2], I is the beam current, and R_s is the cavity shunt impedance.

The probe loop calibration of the cavity can be found by recording the probe loop voltage at a number of currents and fitting a linear function to the probe loop voltage vs. beam current. In the case of the passive Landau cavities at MAX IV, R_s/Q is found using Superfish [3], from which R_s is obtained by multiplying by a measured Q [4]. However, this procedure may give up to 10% error in R_s, which will propagate linearly to the probe loop calibration factor. Previous measurements of the bunch profiles of the 1.5 GeV storage ring have indicated an error of the probe loop calibration of the order of 7 %. This could be partially explained by a similarly sized error in the model shunt impedance used for the calibration [5].

OFF-RESONANCE CALIBRATION

An alternative to the on-resonance probe loop calibration is the off-resonance calibration. This method relies on approximating the total harmonic cavity field as a small perturbation to the main cavity accelerating voltage and calculating the effect this perturbation has on the synchrotron frequency. This method has the benefit of not being as dependent on the accuracy of the modelled R_s.

Self-Consistent Form Factor

The total energy loss per turn for an electron circulating in a storage ring equipped with n passive harmonic cavities is given by

$$U_{total} = U_0 + U_{HC0} = U_0 + e\sum_n V_{HC0,n}\cos(\psi_{HC,n}), \tag{2}$$

where U_0 is the energy loss per turn for a machine without passive harmonic cavities, and $\psi_{HC,n}$ is the tuning angle of the nth harmonic cavity, given by

$$\psi_{HC,n} = \arccos\left(\frac{V_{HC0,n}}{I R_{s,n}|\tilde{F}|}\right), \tag{3}$$

The total RF voltage of a ring with active main cavities and n passive harmonic cavities is

$$V_{RF}(\varphi) = V_{MC}(\varphi) + \sum_n V_{HC,n}(\varphi). \tag{4}$$

The main cavity voltage is given by

$$V_{MC}(\varphi) = V_{MC0}\sin(\varphi + \varphi_s), \tag{5}$$

where φ_s is the synchronous phase, given by

$$\varphi_s = \pi - \arcsin\left(\frac{U_{total}}{eV_{MC0}}\right). \tag{6}$$

Similarly, the harmonic cavity voltage is given by [2]

$$V_{HC,n}(\varphi) = V_{HC0,n}\sin(N\varphi + \varphi_{HCs,n}), \tag{7}$$

where the synchronous phase of the harmonic cavities, $\varphi_{HCs,n}$, is given by

$$\varphi_{HCs,n} = \psi_{HC,n} - \pi/2 - \varphi_{FF}, \tag{8}$$

where φ_{FF} is the form factor phase [2].

The complex form factor is given by the Fourier transform of the density distribution of the electron bunch, ρ, at the Nth

* david_k.olsson@maxiv.lu.se

ISBN: 978-3-95450-252-3 ISSN: 2673-5350 doi: 10.18429/JACoW-IPAC2026-WEP6077

CONTINUOUS AND AUTOMATED MONITORING OF THE HEALTH AND PERFORMANCE OF THE LHC BEAM POSITION MONITOR SYSTEM

J. Martínez Samblas, A. Boccardi, M. Gonzalez-Berges, M. Krupa, CERN, Geneva, Switzerland

Content from this work may be used under the terms of the CC BY 4.0 licence (© 2026). Any distribution of this work must maintain attribution to the author(s), title of the work, publisher, and DOI.

Abstract

We have developed a new automated system to continuously monitor the health and performance of the LHC Beam Position Monitors (BPMs) at CERN. We preprocess turn-by-turn and bunch-by-bunch data through denoising and normalisation before analysing it using a combination of rule-based quality checks and anomaly detection algorithms. All real-time acquisitions are processed on a dedicated Python node, with results stored in HDF5 format and aggregated via the Offline Analysis Framework, which also provides visualisation and reporting. Our system provides robust diagnostics, daily summaries, and dashboards to ensure BPM reliability and maintain high data quality throughout LHC operations.

INTRODUCTION

The Large Hadron Collider (LHC) Beam Position Monitor (BPM) system comprises more than one thousand BPMs organised in 67 Front-End Software Architecture (FESA) devices around the machine [1–3]. It provides turn-by-turn (TBT) and bunch-by-bunch (BBB) measurements that are essential for orbit control, beam diagnostics, machine studies, and routine LHC operation.

Because of its operational importance, we must continuously ensure the quality and availability of BPM data. In practice, acquisitions can be affected by corrupted or incomplete data, inconsistent metadata, missing bunch information, all-zero signals, and waveform distortions such as clipping or saturation. In a system of this scale, manual inspection alone is not sufficient to provide systematic and timely diagnostics.

To address this, we have developed an autonomous monitoring framework combining quality checks, preprocessing, and anomaly detection, with structured outputs for diagnostics, daily summaries, and dashboards.

DATA AND PREPROCESSING

The data used by the monitoring pipeline are obtained in parallel with the standard LHC BPM acquisition channels. They are independent copies of the operational data streams and therefore do not affect the data delivered to operators or orbit feedback.

Input Data

Our framework processes waveform acquisitions produced by the LHC BPM FESA devices. For each acquisition, we retrieve the horizontal and vertical beam position measurements together with the metadata required for their interpretation, such as BPM identifiers, bunch IDs, acquisition dimensions, and timing-related information.

Quality Gates

We apply rule-based quality gates immediately after acquisition to exclude corrupted data, inconsistent metadata, and acquisition failures from anomaly detection. These cases are tracked separately to avoid false positives, for example after missed injections.

The first checks verify the structural integrity of the data. The measured arrays must match the expected dimensions for the corresponding acquisition mode, and the horizontal and vertical planes must have compatible shapes. In addition, the bunch IDs must be consistent across both planes, since any mismatch usually indicates a problem in the acquisition chain or in the associated metadata.

Further checks target clearly non-physical signals. We reject acquisitions containing only zero values, as they correspond to fully invalid measurements. Another validation step enforces that the first sample is equal to zero, which is a safety condition inherited from the LHC BPM FESA system. These gates veto unusable captures before advanced analysis proceeds.

Signal Preparation

After validation, we convert the accepted data into a form suitable for automated analysis. For each transverse plane, we arrange the BPM signals into a matrix M in which each row corresponds to one BPM and each column to one turn, using the turn-by-turn averaged signal as the main input representation. This matrix-based view provides a compact and generic format that we can use with different anomaly detection algorithms without method-specific preprocessing.

An optional denoising step is then applied using singular value decomposition (SVD) [4, 5],

$$M = U\Sigma V^T, \tag{1}$$

where U contains spatial patterns across BPMs, V the corresponding temporal patterns, and Σ the singular values that rank their importance. For denoising, we reconstruct the matrix using only the first r most energetic modes, typically $r = 4$, which capture the dominant correlated content, while weaker modes are discarded as mostly incoherent noise. Figure 1 shows that these first four modes already explain more than 99% of the variance in a representative acquisition, with only marginal gains from additional modes.

ANOMALY DETECTION

We apply anomaly detection independently to the horizontal and vertical planes using zero-value checks, spike detection, SVD-based mode-dominance analysis, Isolation Forest, and tune-based frequency analysis.

ISBN: 978-3-95450-252-3 ISSN: 2673-5350 doi: 10.18429/JACoW-IPAC2026-WEP6078

BEAM INSTRUMENTATION FOR AWAKE FROM RUN 2B TO RUN 2C

C. Pakuza*, E. Belli[1], M. Bergamaschi, S. Burger, S. Doebert, M. Gasior, E. Gschwendtner, M. Krupa, T. Lefevre, T. Levens, B. Moser, A. Topaloudis, M. Turner, CERN, Geneva, Switzerland
P. Muggli[2], Max Planck Institute for Physics, Munich, Germany
L. Stant, Diamond Light Source, Didcot, UK
[1]also at John Adams Institute for Accelerator Science, Oxford, UK
[2]also at CERN, Geneva, Switzerland

Abstract

The AWAKE experiment at CERN is a proof-of-principle facility that uses proton-driven plasma wakefields to accelerate externally injected electrons. Since initial operations in 2016, multiple experimental phases have been completed, with the most recent being Run 2b. Beam diagnostics played a crucial role during this phase, enabling reliable operation and characterisation of the particle beams. The next phase, Run 2c, planned to begin in 2029, will introduce a second electron beamline delivering 150 MeV, 200 fs (RMS)-long electron bunches together with a second plasma. The increased experimental scale and the new measurement requirements impose new demands on beam instrumentation, requiring upgrades to existing systems and the development of new, specialised diagnostics. This contribution presents a non-exhaustive overview of the diagnostic systems used during Run 2b, describes the planned upgrades and developments for Run 2c, and discusses the associated integration challenges.

INTRODUCTION

Following the successful completion of Run 2b in 2025 [1] [2] [3], the AWAKE facility at CERN is undergoing a major upgrade to enable the next stage of proton-driven plasma wakefield acceleration studies. The experiment was originally installed in the TCC4 experimental area in front of the former CERN Neutrinos to Gran Sasso (CNGS) target wall [4]. To accommodate the expanded beamline configuration required for the upcoming phase, the facility is being relocated downstream by ~40 m. This relocation necessitates dismantling of the former CNGS infrastructure, after which the upgraded experiment will be installed in stages, with commissioning planned for 2028 and first proton beam operations expected in 2029 [5].

The next operational phase, Run 2c, will involve a two-plasma configuration, as shown schematically in Fig. 1. A second electron beamline [6] will be added, delivering higher-energy and shorter electron bunches (150 MeV, 200 fs RMS) compared to the existing 18 MeV injector (1–4 ps RMS). In the Run 2c baseline configuration, self-modulation (SM) of the SPS proton bunch will continue to be seeded using the relativistic ionisation front (RIF) of the ionising laser pulse, as successfully demonstrated in previous runs [7]. The lower-energy electron beam will continue to support studies of electron-beam seeding [8] and alignment tolerances, while the higher-energy beam will serve as the witness beam for acceleration studies in the second plasma.

The expanded experimental layout, together with the introduction of additional beamlines and plasma sources, significantly increases the demands placed on beam instrumentation. During Run 2b, beam diagnostics played a central role in enabling reliable operation and detailed characterisation of beam parameters, including transverse beam profile measurements using screen-based diagnostics. For Run 2c, these systems must be extended, upgraded, and complemented with specialised diagnostics capable of, for example, resolving ultrashort electron bunches and supporting precise alignment of the laser and multiple particle beams, the parameters of which are detailed in Table 1, across a larger experimental footprint.

Table 1: Beam parameters at injection for AWAKE Run 2c.

Parameter	Nominal	Range
Proton Beam		
Energy	400 GeV	390–410 GeV
Bunch length (RMS)	85 ps	80–340 ps
Beam radius at waist (RMS)	200 µm	150–220 µm
Charge per bunch	48 nC	8–64 nC
18 MeV Electron Beam		
Energy	18 MeV	–
Energy spread (RMS)	0.2%	–
Bunch length (RMS)	2.1 ps	1–4 ps
Beam radius at waist (RMS)	200 µm	150–220 µm
Normalised emittance	2 mm mrad	–
Charge per bunch	–	100–600 pC
150 MeV Electron Beam		
Energy	150 MeV	–
Energy spread (RMS)	0.2%	–
Bunch length (RMS)	200 fs	200–300 fs
Beam radius at waist (RMS)	5.75 µm	5–10 µm
Normalised emittance	2 mm mrad	–
Charge per bunch	100 pC	100–400 pC

BEAM POSITION MEASUREMENTS

During Run 2b, proton beam position measurements were performed using 21 dual-plane button beam position monitors (BPMs) distributed along the ~800 m-long TT41 transfer line between SPS extraction and the AWAKE experimental area. These BPMs have a 60 mm aperture, matching

* collette.pakuza@cern.ch

Content from this work may be used under the terms of the CC BY 4.0 licence (© 2026). Any distribution of this work must maintain attribution to the author(s), title of the work, publisher, and DOI.

ISBN: 978-3-95450-252-3 ISSN: 2673-5350 doi: 10.18429/JACoW-IPAC2026-WEP6079

A NEW ANALOGUE ACQUISITION FOR THE BPM OF CERN PS

M. Bozzolan, European Organization for Nuclear Research, Geneva, Switzerland

Content from this work may be used under the terms of the CC BY 4.0 licence (© 2026). Any distribution of this work must maintain attribution to the author(s), title of the work, publisher, and DOI.

Abstract

The bunch-by-bunch and turn-by-turn beam trajectory measurement system of the CERN PS accelerator has been in operation for several years. To ensure long-term reliability, the consolidation of the analogue acquisition chain is foreseen during the upcoming LS3 long shutdown including a new architecture with improved performance, which is currently under test in the PS accelerator for final validation. The key element is a custom-designed high impedance head amplifier, replacing the 50Ω amplifier used by the current system, with the advantage of improving, at the same time, bandwidth, dynamic range and noise level. Increased dynamic range opens the possibility of measuring longer acceleration periods without gain switching and better resolution. Increased bandwidth allows the measurement of more beam configuration, in particular with shorter bunch to bunch distance. However, improved performances come at the expense of placing active electronics close to the beamline, in locations with significant radiation exposure, therefore requiring radiation-tolerant electronics. An overview of the PS trajectory system is presented, with the focus on the design of the new analogue acquisition, along with the preliminary bench and beam measurement results.

INTRODUCTION

The CERN PS accelerates either protons from 1.4GeV or ions from 48MeV/u eventually delivered to the downstream accelerators (SPS and AD) and to experimental areas [1]. The bunch intensity range is from $5 \cdot 10^9$ to $\sim 10^{13}$ charges per bunch with a minimum bunch to bunch spacing of 25ns. A versatile RF system allows complex bunch manipulations like merging, compression, splitting and rotation.

For the observation of the beam position 43 electrostatic type pickups, commissioned in the '90s, are installed in the straight sections along the machine. The shape of the four electrodes (Fig. 1) gives a linear, compact (166x80mm aperture, 62mm lenght) and dual-plane position detector [2].

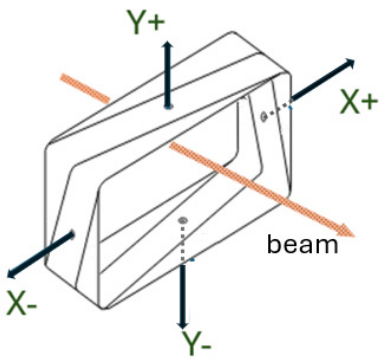

Figure 1: Pickup electrodes.

Each electrode forms a capacitive device with the grounded but not shown surrounding chamber, developing a signal with amplitude proportional to the centre of charge position [2].

Ideally the BPM system should measure the beam position of the individual bunches turn by turn, on every beam configuration and along all the beam cycle from injection to extraction, following the RF beam manipulations. This specification leads to challenging requirements on the acquisition system because of the variety of beam conditions present in the PS. The analogue acquisition's first requirement is a bandwidth wide, flat and extended also at low frequency. This condition is necessary to limit distortion of the time domain response with the consequent possible overlap of signals belonging to different bunches. The second important requirement is a wide dynamic range, ideally allowing the acquisition of the full accelerating cycle without using gain switching that may cause the loss of bunch synchronization.

The system in use can operate without gain switching on regions of the accelerating cycle (i.e. injection, extraction, etc.) but with limited performance if setup to acquire the full cycle. Moreover, bandwidth limitation on both analogue and digital acquisition hinders position measurement when bunch spacing is less than 100ns.

ACQUISITION ARCHITECTURES

The analogue acquisition of an electrostatic pickup can be classified depending on the impedance loading of the electrodes. Depending on this characteristic there are several consequences on both the design of the acquisition and the system performances [3].

Low Impedance (Low-Z) Architecture[1]

In the low impedance case (below ~1kΩ loading impedance), like the PS BPM system in operation (Fig. 2) with 200Ω loading impedance, the main advantage is a relative freedom in the location of the amplifier (e.g. low/free radiation zone), provided that the amplifier input is well matched to the connection line.

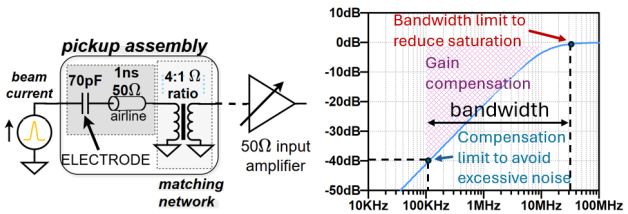

Figure 2: Simplified PS low impedance configuration and frequency response before gain compensation.

[1] 0Ω impedance (i.e. charge amplifier) is a separate case that is more like the high impedance case in terms of positioning constrains and features

ISBN: 978-3-95450-252-3 ISSN: 2673-5350 doi: 10.18429/JACoW-IPAC2026-WEP6080

NEW FINDINGS ON BPM CALIBRATION IN THE LHC

J. Keintzel*, M. Krupa, Y. Angelis, J. Dilly, V. Ferrentino, M. Le Garrec,
J. Gray, D. Jacquet, K. Skoufaris, R. Tomás, J. Wenninger
CERN, Geneva, Switzerland

Abstract

Accurate Beam-Position Monitor (BPM) calibration is essential for high-quality optics measurements and reliable beam-based diagnostics in the Large Hadron Collider. Recent in-depth analyses combining advanced optics-measurement techniques, including measurements of a novel 60° optics, with cross-checks from complementary beam instrumentation have revealed the presence of a previously unnoticed systematic calibration bias of approximately 3 % in arc BPMs. This correction has been implemented at the start of 2025, leading to improved consistency. Despite these improvements, not all aspects of the discrepancy have yet been fully understood. This contribution presents the investigations that enabled the identification of the bias, open questions, and implications for future operation.

INTRODUCTION

The Large Hadron Collider (LHC) [1] at CERN with approximately 27 km circumference is currently in his last year of operation for Run 3 and achieves beam energies of up to 6.8 TeV for two colliding proton beams at a maximum instantaneous luminosity above 2×10^{34} cm^{-2}s^{-1}. Its upgrade, the High Luminosity LHC (HL-LHC) [2], aims at increasing this value to at least 5×10^{34} cm^{-2}s^{-1}, which demands an improved understanding of the existing magnetic lattice and installed beam instrumentation.

Previous studies have used Turn-by-Turn (TbT) data acquired at Beam Position Monitors (BPMs) to measure the momentum compaction factor, α_c, of various optics at injection and top energy of, respectively 450 GeV and up to 6.8 TeV, taken between 2016 and 2022, with α_c, between 3.2×10^{-4} and 3.5×10^{-4} [3, 4]. Additionally, in 2022 a novel optics with a transverse phase advance of 60° in the arc FODO cells, 30 % lower compared to the nominal LHC optics which features roughly 90°, and has hence, a factor 2 larger α_c of approximately 7×10^{-4} has been carefully measured, and analysed [5]. All measurements show consistently a 3 % lower α_c, attributed to an orbit measurement calibration error. We note, that in 2022 only Beam 1 has been measured due to time constraints.

In 2024 a 60° arc cell phase advance optics has been measured for the first time for both beams with one of the goals being to verify 3 % orbit measurement error. In parallel, BPM polynomials, previously derived in 2014 have been re-analysed in early 2025. Consequently novel polynomials have been applied at the start of 2025. With these new settings optics measurements are acquired in 2025 and 2026, at various configurations. Main findings are reported here.

* jacqueline.keintzel@cern.ch

60° OPTICS MEASUREMENTS IN 2024

A 60° optics has been designed and measured in 2024, with one of the goals being helping to conclude on the average arc BPM calibration in both beams. Similar to first measurements of a 60° optics [5], one pilot bunch per beam with up to 5×10^9 protons each is injected and propagated sector-wise with orbit corrections in each step. After a closed-orbit is established a working point of 0.28, 0.31 is established, followed by linear chromaticity and coupling correction.

Optics measurements are performed using AC-dipoles with a $\Delta Q_{x,y}$ of $-0.012, 0.010$ and 6600 turns. Analysis is performed using omc3 [6]. For off-momentum optics measurements, RF-frequency shifts of ±50 Hz, ±100 Hz, and ±150 Hz are applied. Global optics corrections are based on a response matrices including horizontal and vertical tunes, phase advances and normalized horizontal dispersion, and all available quadrupole circuits [1]. Corrections are stepwise applied until the full corrector value is achieved. Linear coupling is corrected to a $|C^-|$ of 0.005 for both beams. TbT data is acquired before and after global corrections are applied. Global corrections reduce the rms β-beating from roughly 18 % to approximately 5 % in both planes and beams as shown respectively in Figs. 1 and 2.

For dispersion measurements, the relative momentum offset at each frequency shift is obtained using $\delta = \langle D_{x,i}\, CO_{x,i}\rangle / \langle D_{x,i}\rangle$ with the model horizontal dispersion D_x and the measured closed orbit CO_x at arc BPM i. After applying global corrections, the rms horizontal dispersion deviation is reduced from 64 cm to 16 cm for beam 1 and from 66 cm to 30 cm for beam 2. Vertically the rms dispersion is roughly 0.2 m. This optics is hence considered to be sufficiency well corrected to analyse α_c and hence BPM calibration.

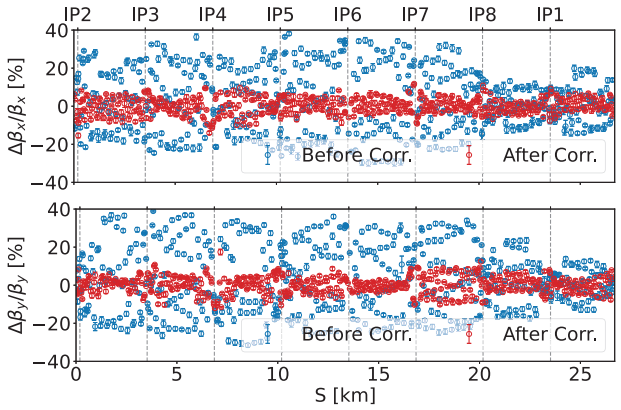

Figure 1: Beam 1 horizontal (top) and vertical (bottom) β-beating before and after applying global corrections.

Content from this work may be used under the terms of the CC BY 4.0 licence (© 2026). Any distribution of this work must maintain attribution to the author(s), title of the work, publisher, and DOI.

ISBN: 978-3-95450-252-3 ISSN: 2673-5350 doi: 10.18429/JACoW-IPAC2026-WEP6081

ADVANCING BEAM QUALITY CONTROL IN THE CERN PROTON SYNCHROTRON

M. Coly, A. Akroh, Z. Ansari, A. Beeckman, D. Cotte, J. Flowerdew, G. Imesch, A. Huschauer, A. Lasheen, R. Maillet, J. Mccarthy, K. Sabin, S. Sainz Pérez, M. Schenk, Y. Wu
CERN, Geneva, Switzerland

Content from this work may be used under the terms of the CC BY 4.0 licence (© 2026). Any distribution of this work must maintain attribution to the author(s), title of the work, publisher, and DOI.

Abstract

Over the past years, the beam quality delivered by the CERN Proton Synchrotron (PS) has significantly improved, driven by major upgrades to both the accelerator and its controls infrastructure. As a result, user requirements have become increasingly demanding, particularly for high-brightness beams for the LHC, but also for fixed-target beams. The PS, known for its versatility in supplying beams with widely varying characteristics to multiple facilities, must now meet tighter performance specifications while maintaining reliability and operational efficiency.

To address these challenges, a new beam quality monitoring framework has been developed, building on recent enhancements in data acquisition and online analysis capabilities. The system defines key beam quality metrics in real time, enabling early detection of drifts, root-cause fault analysis, and provides the foundation for automated corrections and machine learning-based optimisation. Complementing this analytical layer, a dedicated graphical interface provides operators with live observability of key parameters and short-term trends, facilitating rapid decision-making in the control room.

This new approach represents a step change in the way beam quality is monitored and maintained in the PS, from reactive diagnostics to proactive control, supporting both operational stability and the increasingly stringent demands of CERN's experimental program.

INTRODUCTION

The CERN Proton Synchrotron (PS) is part of the CERN injector chain providing beams both for fixed-target experiments and for downstream accelerators such as the Super Proton Synchrotron (SPS) and the Large Hadron Collider (LHC). The PS must deliver beams with a wide range of intensities, bunch structures, and emittances.

With ever-higher performance targets, maintaining beam quality throughout the PS cycle becomes increasingly important. Small deviations in beam parameters can propagate through the injector chain and affect downstream machine performance.

To improve observability of beam conditions during operation, a Beam Quality Monitoring (BQM) framework has been developed. The system combines beam instrumentation data with online analysis algorithms to derive quantitative indicators of beam quality.

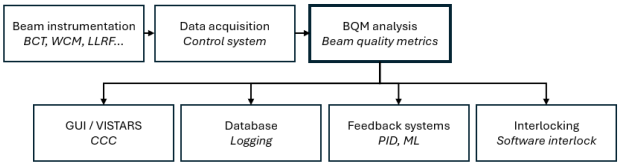

Figure 1: Conceptual architecture of the BQM framework. Signals from beam instrumentation, notably Beam Current Transformers (BCT), Wall Current Monitors (WCM), and Low-Level Radio Frequency (LLRF) systems, are processed online to derive beam quality metrics for several operational purposes.

BEAM QUALITY MONITORING FRAMEWORK

The BQM framework combines beam diagnostics acquisition, online analysis, and data visualisation for operations. Instrumentation data is acquired through the accelerator control system and processed in real time to extract beam quality observables serving as inputs to operational data displays.

These observables are transformed into beam quality metrics describing beam stability and reproducibility throughout the PS beam production processes. Figure 1 shows that the resulting metrics are displayed in operational interfaces used in the CERN Control Centre (CCC) supporting both routine operation and machine development studies.

BQM USE CASES IN PS OPERATION

To help the operations team, BQM metrics are exposed in different ways, depending on operational needs and use cases. The following subsections present representative examples.

Machine-Learning Tools: MTE Efficiency

The BQM framework provides observables to evaluate the efficiency of the Multi-Turn Extraction (MTE) process for the SPS fixed-target experiments, in which the beam is split into five beamlets in the horizontal phase space before extraction [1].

MTE is a resonance-based technique whose performance is determined by the uniformity of the intensity distribution across the beamlets, namely four islands and one core, as illustrated in Fig. 2. The BQM observable, named MTE splitting efficiency, is defined as the average intensity in the islands divided by the total intensity:

$$\eta_{\mathrm{MTE}} = \langle I_{\mathrm{islands}} \rangle / I_{\mathrm{total}}. \quad (1)$$

In case of quality drifts, the operations team can use a machine-learning-based optimisation algorithm to adjust PS

ISBN: 978-3-95450-252-3 ISSN: 2673-5350 doi: 10.18429/JACoW-IPAC2026-WEP6082

A NOVEL APPROACH FOR TRANSVERSE INSTABILITY DETECTION IN THE CERN PROTON SYNCHROTRON

A. Beeckman*, M. Coly, C. Hernalsteens, A. Huschauer, A. Lasheen, T. Levens, S. Sainz Perez,
European Organization for Nuclear Research, Geneva, Switzerland
N. Pauly, Université Libre de Bruxelles, Brussels, Belgium

Content from this work may be used under the terms of the CC BY 4.0 licence (© 2026). Any distribution of this work must maintain attribution to the author(s), title of the work, publisher, and DOI.

Abstract

The CERN Proton Synchrotron faces increasingly demanding requirements from its user community, driven by the need for higher-intensity beams that push the machine to the limits of beam stability. Transverse instabilities, such as head-tail and transverse-mode-coupling instabilities, can arise at specific stages of the machine cycles, depending on the beam parameters. This work introduces a real-time, bunch-by-bunch transverse instability diagnostic system based on wide-band beam position monitor signals. Building on recent developments in longitudinal beam observation, the system extends the software layers to measure beam profiles in both longitudinal and transverse planes. A key feature is its ability to capture multiple time windows within a single cycle, offering a complete view of beam dynamics. Real-time analysis of the transverse beam envelope evolution is performed on the acquired data to detect and characterize performance-limiting phenomena, such as transverse instabilities. The system is fully integrated into operation, allowing simultaneous beam monitoring and optimization across multiple beam types.

INTRODUCTION

The CERN Proton Synchrotron (PS) delivers a wide variety of beams to the Super Proton Synchrotron (SPS) and several dedicated experimental areas. To meet diverse physics requirements, the machine must alternate between distinct settings to deliver beams with different energies, intensities, and time structures. The recent LHC Injectors Upgrade (LIU) project aimed to double the beam intensity at increased brightness of LHC-type beams to meet the performance goals of the High-Luminosity LHC [1]. However, as intensity increases, collective effects become the dominant performance limit [2]. These collective effects are driven by the interaction between the beam and the machine impedance.

This paper addresses measurements of transverse collective instabilities, namely the head-tail instability and the Transverse Mode Coupling Instability (TMCI) in the PS. In head–tail instabilities, transverse wakefields couple the motion of particles within the bunch, potentially leading to coherent oscillations with growing amplitude. Operational stability relies on sextupole magnets to control chromaticity and an active feedback system to damp coherent oscillations, with linear coupling correction improving transverse feedback performance. While these instabilities are theoretically well understood [2–5] and reproduced by high-fidelity simulation tools [6], their real-time identification remains a challenge. Transverse signals are measured with a wide-band beam position monitor, and analog signals are fed into a digitizer to record them in the vertical and horizontal planes.

While transverse beam diagnostics exist, they typically lack continuous, cycle-by-cycle acquisition capabilities. Recent developments in longitudinal beam observation (LBO) [7] have enabled continuous monitoring and optimization of longitudinal beam profiles across multiple time windows within the beam cycle, as well as permanent cycle-by-cycle analysis. Earlier systems, such as OASIS [8], were not designed for continuous raw data acquisition, limiting persistent monitoring and flexible cycle-by-cycle configuration of beam diagnostics.

The present work extends the LBO framework to the measurement and analysis of transverse beam signals in the PS. Originally designed for longitudinal single-channel acquisition, the approach presented here introduces multi-channel acquisition of wide-band beam position monitor signals, enabling the observation of horizontal and vertical beam motion. In addition, a dedicated real-time processing pipeline has been developed to extract transverse activity indicators on a bunch-by-bunch basis, including instability metrics and head–tail mode identification. These additions extend the LBO system, creating a more advanced beam-observation system capable of monitoring both longitudinal and transverse beam quality throughout the machine cycle.

RAW DATA ACQUISITION SYSTEM

The acquisition system is developed in the Front-End Software Architecture (FESA) [9] framework. FESA is a CERN framework for building and deploying real-time control software that interfaces directly with accelerator hardware. The raw data acquisition system design is very similar to that described in [7]. The measuring system is synchronized to each machine cycle via central timing events. The digitizer receives the analog signals from the wide-band beam position monitor and acquires profiles according to trigger signals from a trigger card. The trigger card is synchronized with the beam revolution period, provided by the radio-frequency (RF) systems. Once the acquisition is complete, the data are sent over the network to downstream clients. The start of a new cycle timing event triggers the loading of settings into the digitizer memory, after which incoming triggers initiate profile recording. Once the acquisition completes, data is retrieved from memory and post-processed.

The main difference arises from the multiple channels available from the wide-band beam position monitors (hori-

* amaury.beeckman@cern.ch

ISBN: 978-3-95450-252-3 ISSN: 2673-5350 doi: 10.18429/JACoW-IPAC2026-WEP6084

A VISIBLE-LIGHT MONITOR FOR TRANSVERSE BEAM PROFILE DIAGNOSTICS IN THE SLS BOOSTER

M. P. Rey Barrera*, J. Kallestrup, R. Ischebeck, M. Seidel, L. Zimmermann
PSI Center for Accelerator Science and Engineering, Villigen, Switzerland

Abstract

A visible-light 2D imaging monitor was developed and commissioned in the Swiss Light Source (SLS) 2.0 booster ring to characterize transverse beam behavior during the energy ramp. Installed downstream of a bending magnet, it extracts visible synchrotron radiation via an in-vacuum gold-coated mirror and uses a CMOS camera with motorized optics and filters. The setup accommodates the evolving synchrotron spectrum, with the critical photon energy increasing from 0.2 eV at 100 MeV electron beam energy to approximately 3.9 keV at 2.7 GeV. Long exposures, integrating over hundreds of turns matched to the roughly 1 µs revolution time, enabled measurements of adiabatic damping due to synchrotron radiation emission. In addition, the system provides sufficient sensitivity to image single-bunch charges down to approximately 20 pC, while operating over a broad charge range up to 300 pC. Using short exposures over only a few tens of turns enabled the observation of fast beam size evolution during emittance exchange driven by coupling resonance crossing, a technique first implemented in an electron ring at the SLS. This high-speed acquisition confirmed the optimal extraction timing, corresponding to the minimum horizontal beam size. The monitor provides non-invasive diagnostics for tracking beam stability and optimizing injection into the storage ring.

INTRODUCTION

Injection into fourth-generation synchrotron light sources is challenging due to the reduced dynamic aperture of the storage ring. To ensure efficient injection, the injector must deliver a beam with well-controlled transverse properties and sufficiently small emittance. For SLS 2.0, the injector is a low-emittance booster synchrotron [1], which accelerates the beam to the nominal storage-ring injection energy of 2.7 GeV. In addition, transverse emittance exchange during coupling resonance crossing is implemented near the end of the booster ramp to further reduce the horizontal beam size before extraction [2, 3].

Knowledge of the transverse beam properties throughout the ramp is therefore essential to verify the beam quality delivered by the booster. This is particularly important during the short emittance-exchange process, where the transverse beam sizes evolve rapidly over only a few milliseconds. A non-invasive diagnostic capable of resolving the beam profile at different times during the ramp is therefore required both for commissioning and for routine optimization of the injected beam.

* maria.rey-barrera@psi.ch

The most practical, non-destructive method to measure emittance is through synchrotron radiation (SR). From measurements of the beam profile, parameters like emittance and energy spread can be inferred. In order to measure the beam size evolution during the ramp and the emittance exchange process, we generally require fast acquisition, variable trigger timing, and the ability to handle large intensity variations. Synchrotron light from the booster has previously been used for beam diagnostics at other facilities, such as for transverse beam shape at the ESRF [4], bunch duration monitors at the APS [5], SOLEIL [6], and ELSA [7].

Table 1: Twiss parameters at the extraction point of the bend magnet.

Parameter	Value
β_x [m]	1.9950
β_y [m]	11.1432
α_x	–0.3494
α_y	–0.2005
η_x [m]	0.1864
η'_x	0.0044

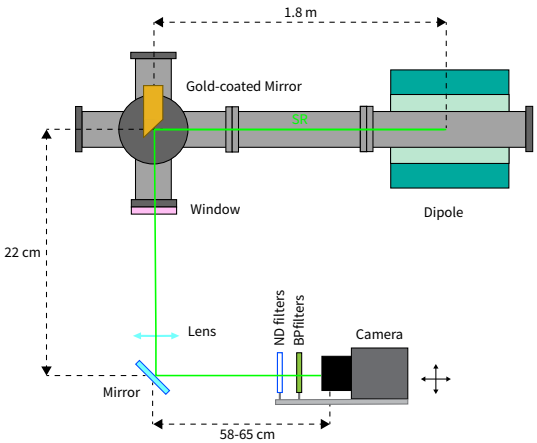

Figure 1: Schematic of the optical system, showing the SR propagating from the in-vacuum gold-coated mirror, to the lens, bandpass (BP) and ND filters, and camera.

EXPERIMENTAL SETUP

The diagnostic system is installed inside the booster tunnel, downstream of a 1.26 m dipole magnet with bend radius of 11.21 m, operating from 0.03 to 0.803 T at 100 MeV and 2.7 GeV electron beam energies respectively during ramp up. It is located 19.5 m before the entrance of the injection septum. The source point is located at the middle of the dipole magnet, where the Twiss parameters are those found in Table 1, and the vertical dispersion is negligible.

Content from this work may be used under the terms of the CC BY 4.0 licence (© 2026). Any distribution of this work must maintain attribution to the author(s), title of the work, publisher, and DOI.

ISBN: 978-3-95450-252-3 ISSN: 2673-5350 doi: 10.18429/JACoW-IPAC2026-WEP6087

STUDYING COHERENT TRANSITION RADIATION SPATIAL IMAGE FEATURES FOR BUNCH LENGTH DIAGNOSTICS

A. Guisao-Betancur*[1,2], C. P. Welsch[1,2], J. Wolfenden†[1,2]
[1]University of Liverpool, Liverpool, UK
[2]Cockcroft Institute, Daresbury, UK

Abstract

Coherent transition radiation (CTR) has been widely used for developing diagnostics of particle beams due to its broadband spectrum, which provides information on the particle distribution, and its relatively simple experimental setup compared to other sources of coherent radiation. For short and ultrashort electron bunches, ps- to fs-long, methods such as CTR spectrometry and interferometry have been used. Recently, an alternative method using point-to-point spatial imaging of the transition radiation source plane has been studied, showing promising results in which image features, such as the image width, can be tied to the bunch length. However, a more in-depth image analysis is required. In this work, an attempt is made to model some of the bunch profile features from the CTR spatial images using conventional image and data analysis techniques. The CTR spatial images are simulated in Ansys Zemax OpticStudio for a broad range of bunch profiles, from single-Gaussian to multi-Gaussian distributions that emulate more realistic bunches. The results form the basis for the next stage of analysis of experimental CTR images for retrieving the longitudinal bunch profile.

INTRODUCTION

Diagnostics for ultrashort electron bunches pose challenges in plasma wakefield accelerators, as well as in short-pulse accelerators in general.

Time-domain methods, such as transverse deflecting structures, are the gold standard for longitudinal measurements down to the required sub-fs range in plasma accelerators [1], but they can be costly and may represent a significant footprint for future accelerators like EuPRAXIA or other plasma-based facilities, where size is an important factor. Transverse deflecting structures, however, are an intercepting diagnostic, which can make this method impractical for monitoring the bunch length at different positions along the beamline; thus, there is a need to develop alternative diagnostics that could potentially be compact and cost-efficient while achieving a similar resolution.

Instead of a time-domain technique, this study focuses on a monitor using polarization radiation [2], specifically coherent transition radiation (CTR). While other works have shown its use in characterizing ultrashort electron bunches via spectroscopy [3–5], the monitor studied in the present work uses point-to-point spatial imaging of the CTR source to determine longitudinal features of the bunch profile [6–8].

* A.M.Guisao-Betancur@liverpool.ac.uk
† joseph.wolfenden@cockcroft.ac.uk

CTR SPATIAL IMAGING

When assuming full transverse coherence of the bunch, that is, its rms transverse size $\sigma_r << \gamma\lambda/2\pi$ [5], the coherent power spectrum of the transition radiation will be given by:

$$S_{\mathrm{CTR}}(\rho(z),\omega) = S_p(\omega)N^2F_z(\rho(z),\omega)\,, \qquad (1)$$

where $S_p(\omega)$ is the spectrum of a single-particle, N is the number of particles in the bunch, and $F_z(\rho(z),\omega)$ is the longitudinal form factor [9].

The particle distribution $\rho(z)$ (or the bunch profile) is contained in the longitudinal form factor, according to:

$$F_z(\rho(z),\omega) = \left|\int_{-\infty}^{\infty}\rho(z)e^{-i\frac{\omega}{c}z}dz\right|^2 . \qquad (2)$$

The bunch profile $\rho(z)$ can be determined by measuring the spectrum and applying iterative phase methods [3–5]. But with CTR in particular, the focus of this work, there is another option to study the particle distribution by analyzing the image distribution for the particle bunch dI^i_{bunch}/dr [6,7]. This image corresponds to a point-to-point spatial image of the CTR source, and it is described, for a given bandwidth $\Delta\omega$, by:

$$\frac{dI^i_{\mathrm{bunch}}}{dr} \approx N_e^2\int_{\Delta\omega}\frac{d^2I^i_e}{d\omega dr}F_z(\rho(z),\omega)D(\omega)T(\omega)d\omega\,, \qquad (3)$$

where N_e is the number of particles in the bunch, $d^2I^i_e/d\omega dr$ is the image distribution for a single electron, $\Delta\omega$ is the bandwidth, $T(\omega)$ is the added transmittance/reflectance of the optical elements and propagation, and $D(\omega)$ is the detector response.

Figure 1 presents the schematic of the monitor prototype. Two off-axis parabolic mirrors (OAPs) are used to image

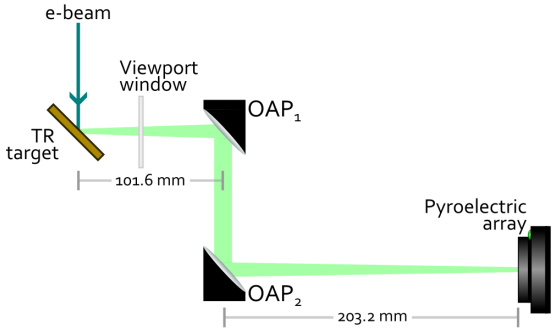

Figure 1: CTR imaging system layout.

the source of the CTR distribution by placing OAP_1 at the reflected focal length (RFL = 101.6 mm) of the center of the

Content from this work may be used under the terms of the CC BY 4.0 licence (© 2026). Any distribution of this work must maintain attribution to the author(s), title of the work, publisher, and DOI.

ISBN: 978-3-95450-252-3 ISSN: 2673-5350 doi: 10.18429/JACoW-IPAC2026-WEP6089

FEASIBILITY OF NON-INVASIVE OSR DIAGNOSTICS IN THE AWAKE RUN-2C INJECTION REGION

D. Ghosal[1,2,*], J. Wolfenden[1,2], M. Turner[3], C. P. Welsch[1,2], AWAKE Collaboration
[1]Department of Physics, University of Liverpool, Liverpool, UK
[2]Cockcroft Institute, Warrington, UK
[3]European Organization for Nuclear Research, Geneva, Switzerland

Abstract

AWAKE experiment at CERN is currently advancing toward Run-2c to demonstrate the higher energy acceleration of electrons while maintaining the beam quality. A second electron beam (of 150 MeV energy) will be injected and accelerated to several GeVs while aiming to keep good emittance. Diagnostics are being upgraded for this geometrically constrained injection-region to enable single-shot characterization of that beam, among which this contribution evaluates the feasibility of optical synchrotron radiation as a non-invasive real-time mean. It can provide shot-by-shot transverse position and profile information without disrupting beam delivery, critical for benchmarking beam-alignment and quality check. The prompt, non-invasive nature also makes it a candidate for future virtual diagnostic implementations, where online beam profiles could inform predictive models or feedback correction schemes. For performance optimizations the expected photon flux, photon statistics, projected image quality are computed with realistic imaging optics and detector quantum efficiency. Results demonstrate that sufficient signal can be extracted through this compact optical chain to achieve the target.

INTRODUCTION

Plasma wakefield acceleration (PWFA) has emerged as a promising route toward compact, high-gradient particle accelerators, achieving accelerating gradients orders of magnitude beyond conventional RF technology [1, 2]. However, the extreme field strengths and complex beam-plasma dynamics in PWFA demand advanced diagnostics capable of characterizing beam quality shot-by-shot without disrupting acceleration. AWAKE (Advanced Wakefield Experiment) is CERN's pioneering facility for proton-driven PWFA, exploiting the high energy density of the Super Proton Synchrotron (SPS) beam to drive wakefields in plasma column, depicted in Fig. 1. Over the past years AWAKE successfully demonstrated the self-modulation of the proton driver and the acceleration of externally injected electrons over a 10-meter plasma [3]. These proof-of-principle results established the viability of higher-quality beam acceleration.

The current AWAKE program is advancing towards the third phase of Run-2 [4], which aims to inject and accelerate a witness electron bunch from 150 MeV to multi-GeV energies while maintaining low emittance. However, any injection error in position, angle, or beam size can lead to

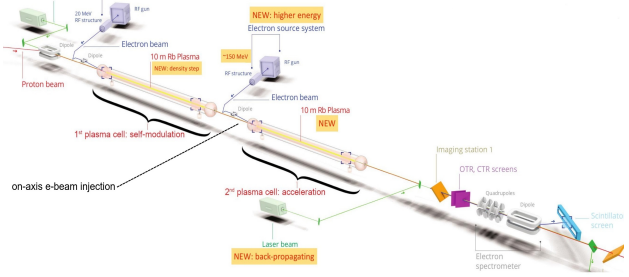

Figure 1: Schematic of AWAKE beamline [3].

emittance growth, reduced acceleration efficiency, or beam loss. As a result, characterizing the witness beam immediately upstream of the second plasma cell entrance is essential for injection alignment verification, shot-to-shot stability monitoring, machine optimization and finally benchmarking simulations. Instead of traditional diagnostics [5, 6] which are not very suitable for online monitoring due to their invasive nature and demand of a multiple measurements, non-invasive real-time beam monitoring are superior for single shot characterization, and critical to understand the initial beam properties entering the plasma, that directly influence acceleration efficiency and overall performance.

Optical synchrotron radiation (OSR), the visible and near-UV portion of the photons spectra (emitted when relativistic electrons traversing in a magnetic field), has emerged as such a powerful non-invasive diagnostic over the years [7, 8]. For AWAKE Run-2c, the dipole in the injection beamline presents an opportunity to extract OSR from the 150 MeV electron beam. However, the region is geometrically constrained by vacuum chambers, limited viewport apertures, and a buffer gas region required for vacuum isolation from the plasma source. The comparatively lower critical photon energy (E_c) at 150 MeV demands careful evaluation of photon yield and detection feasibility. This paper evaluates the physics feasibility of using OSR from the injection dipole for the upcoming the Run-2c as a non-invasive, single shot transverse profile measurement.

EXTRACTION GEOMETRY AND SIMULATION FRAMEWORK

A key parameter E_c dictates approximately half of the total radiated power is emitted above and half below it, with the spectrum extending from the near-IR through the UV. Considering a bending radius of $\rho \sim 1.0$m of the injection

* dghosal@liverpool.ac.uk

Content from this work may be used under the terms of the CC BY 4.0 licence (© 2026). Any distribution of this work must maintain attribution to the author(s), title of the work, publisher, and DOI.

ISBN: 978-3-95450-252-3 ISSN: 2673-5350 doi: 10.18429/JACoW-IPAC2026-WEP6090

STUDIES OF UNUSUAL PICKUP GEOMETRIES FOR THE ARC BEAM POSITION MONITORS OF THE FCC-ee

E. Howling*, P. N. Burrows, John Adams Institute for Accelerator Science, Oxford, UK
M. Gasior, European Organization for Nuclear Research, Geneva, Switzerland

Content from this work may be used under the terms of the CC BY 4.0 licence (© 2026). Any distribution of this work must maintain attribution to the author(s), title of the work, publisher, and DOI.

Abstract

The electron-positron Future Circular Collider (FCC-ee) has challenging requirements for beam instrumentation, including the need for thousands of high-resolution beam position monitors (BPMs) presenting low impedance to the circulating beam. This paper presents studies of different unusual pickup geometries including elliptical, asymmetric and retracted buttons. The impact of the different geometries on the simulated wake impedance and expected voltage signal of the pickups is explored and the potential benefits and disadvantages are described. These studies will inform the design of the FCC-ee arc BPM pickups.

REQUIREMENTS FOR FCC-EE BPMS

The FCC (Future Circular Collider) is a proposed collider project to be built at CERN, with the FCC-ee being the electron-positron machine stage of the project. It would be the largest ever operating accelerator, with high intensity electron beams, and high luminosity goals. Therefore the requirements for the performance of the arc BPMs are stringent, and the conditions they will be operating in are challenging. The resolution requirements are 0.1 µm for orbit, and 1 µm for turn by turn measurements [1].

The FCC-ee will have four different operational modes, each with a different set of beam parameters. The highest beam current will be 1270 mA during the Z mode [1]. To ensure the level of beam heating of the BPM is acceptable, the impedance of the buttons must be very low and the materials used must have suitable thermal properties.

Button BPMs typically have a circular button, but due to the challenging combination of high resolution and low impedance requirements for the FCC-ee arc BPMs, a more unusual geometry may be required.

ELLIPTICAL BUTTONS

Simulation studies using CST showed that elliptical BPM pickups with the longer axis of the ellipse along the z axis of the beam pipe have a smaller wake-loss factor than a round button of the same area [2]. The results suggest that elliptical buttons could be beneficial to reduce the impedance of the FCC-ee arc BPMs, as long as the wake potential ringing is sufficiently low so as not to interfere with the following bunch by an unacceptable amount.

To investigate whether elliptical buttons would be suitable for the FCC-ee arc BPMs, simulations of simplified elliptical buttons of different ratios were run in CST using FCC-ee beam parameters for the $t\bar{t}$ (SR) and Z (BS) operating modes and the FCC-ee beam pipe. The two modes' relevant parameters are summarised in Table 1. SR and BS refer to whether just synchrotron radiation or also Beamstrahlung radiation respectively is taken into account when calculating the bunch length. Of the FCC-ee operating modes, the $t\bar{t}$ mode has the widest beam energy spectrum and the Z (BS) mode has the highest beam intensity during operation, so both are particularly important for resonance and impedance considerations.

Table 1: FCC-ee Beam Mode Parameters Used [1]

Mode	Bunch charge [nC]	Bunch length [mm]
Z (BS)	34.3	15.5
$t\bar{t}$ (SR)	24.8	1.8

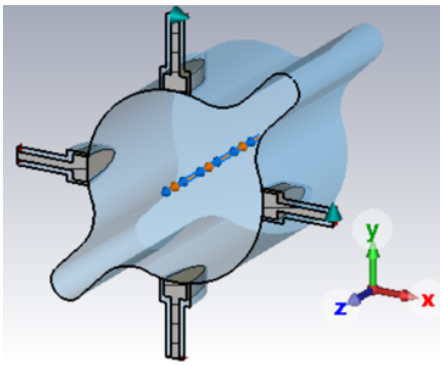

Figure 1: A cross section of the CST model of an elliptical button of ratio 4 in the FCC-ee beam pipe.

The area of the ellipse was kept constant. The 'ratio' refers to the length along the z axis of the button divided by the width along the x or y axis. A CST model of an elliptical pickup with ratio 4 in the FCC-ee beam pipe is shown in Fig. 1. The background is modelled as a perfect electric conductor (PEC) and the vacuum is shown as translucent. The beam pipe winglets are shown skewed, but in reality these would be along the x-axis and the BPMs skewed. However, this setup with the buttons on axis is more compatible with CST.

The CST simulations were run using both the 'direct' and 'indirect interfaces' wake integration settings. Both gave the same trends in results, but with slightly different values. If otherwise unspecified, the 'indirect interfaces' results are shown, as these tend to be more accurate for CST models with waveguide ports. The results for the simulated wake-loss factor for different ellipse ratios using the $t\bar{t}$ (SR) parameters are shown in Fig. 2, with a hyperbolic curve fit to them.

* emily.howling@physics.ox.ac.uk

ISBN: 978-3-95450-252-3 ISSN: 2673-5350 doi: 10.18429/JACoW-IPAC2026-WEP6091

COMMISSIONING THE PASSIVE STRUCTURE WAKEFIELD DECHIRPER ON CLARA*

T.J. Overton†,1,3, B. Higuera Gonzalez[2,3], J.K. Jones[1,3], T.H. Pacey[1,3], Y. Saveliev[1,3]
[1] ASTeC STFC Daresbury Laboratory, Daresbury, UK
[2] The University of Manchester, Manchester, UK
[3] The Cockcroft Institute, Daresbury Laboratory, Daresbury, UK

Abstract

A passive energy dechirper has been installed on CLARA, a 250 MeV electron beam user facility at Daresbury Laboratory. The device, comprising two orthogonal sets of planar dielectric-lined waveguides, is designed to manipulate the longitudinal phase space of the electron bunch, reducing energy spread and thereby delivering higher quality beams for user experiments. We present preliminary results from initial commissioning of the dechirper with the CLARA beam, including measurements of the wakefields excited and changes in longitudinal phase space due to the dechirper. We outline plans for further measurements and discuss how the dechirper will support upcoming user programs.

INTRODUCTION

CLARA is an advanced medium-energy electron test beam facility, capable of delivering electron bunches with up to 250 MeV/c momentum and 250 pC charge for the requirements of individual user experiments in the full-energy beam exploitation (FEBE) hutch [1]. Longitudinal compression is required for the delivery of high current (~kA) and short (~20 fs RMS) bunches. This is achieved at CLARA using a positive energy chirp (high energy tail) and compression through a 4-dipole variable bunch compressor [2].

Passive wakefield structures are increasingly used at accelerator facilities to cancel residual chirp used for compression. These dechirpers work by using the wakefield excited by the bunch itself in corrugated-metallic or dielectric-lined waveguides to decelerate the tail of the bunch such that the energy is more monotonic across the bunch and increase the 6D brightness [3–5]. A passive wakefield dechirper has been designed and installed on CLARA and a simulation campaign conducted before use to evaluate the optimal working parameters with expected beam parameters [6, 7].

CLARA is currently undergoing the final stages of beam commissioning. In these proceedings we will discuss initial commissioning of the passive wakefield dechirper, evaluating the change in energy spread and demonstrating dechirping for an example beam setup.

CLARA PASSIVE WAKEFIELD DECHIRPER

The CLARA beamline is set out as outlined in Fig. 1 and in Ref. [1]. Optics setting sections are arranged after the first, third, and fourth/final linacs, corresponding to approximate beam momenta of 35, 200, and 250 MeV/c respectively. In the section after the third linac, a variable bunch compressor is positioned to allow for varying bunch lengths for the needs of individual experiments [2]. The compression can be measured after the final linac using an S-band transverse deflecting cavity (TDC); the longitudinal profile and/or the longitudinal phase space measured on screens positioned on the CLARA straight and a dispersive section. To achieve compression the bunch is given an energy chirp by accelerating the bunch off-crest in the second and third linacs. To cancel residual chirp, the passive wakefield dechirper is positioned in the final section, after the final linac, before transport to the FEBE arc to the experimental area. Delivery to user experiments in the FEBE chamber is via an arc with non-zero R_{56}, therefore removal of the beam chirp can allow longitudinal diagnostics before the arc to be directly related to beam parameters for user experiments.

The passive dielectric dechirper is designed for controllable longitudinal phase space manipulation whilst maintaining beam quality. The dechirper comprises of two orthogonally orientated planar dielectric lined waveguides (DLWs), as in Fig. 2 and described in detail in Ref. [7]. As in the schematic we will refer to the first horizontally orientated DLW as DCP1 and second vertically orientated DLW as DCP2. Each DLW consists of two parallel 0.2 m long, 2 cm wide, and 200 μm thick quartz plates, providing a 0.4 m total plate length (with a 10 mm gap between the two DLWs). Each plate can be controlled with two actuators along the plate, allowing for gap and tilt control. Together with the controls for the parallel plate it is possible to control the dechirper gap, transverse centre, and tilt. This reduces constraints on beam trajectory into the dechirper. The minimum gap in each DLW is 1.0 mm and the dechirper is considered out of the beam path when set to an 11 mm gap.

Two DLWs are arranged orthogonally to cancel quadrupole-like wakefields excited in each structure. Quadrupole-like wakefields (focusing and defocusing in orthogonal planes) introduce longitudinal variation in the transverse phase space (i.e. longitudinally varying Twiss parameters), increasing the projected emittance. The defocusing/focusing planes switch in orthogonal DLWs so the two DLWs effectively cancel each other and conserve the beam emittance [6].

* Work supported by The Cockcroft Institute and the STFC.
† toby.overton@stfc.ac.uk

Content from this work may be used under the terms of the CC BY 4.0 licence (© 2026). Any distribution of this work must maintain attribution to the author(s), title of the work, publisher, and DOI.

ISBN: 978-3-95450-252-3 ISSN: 2673-5350 doi: 10.18429/JACoW-IPAC2026-WEP6092

TRANSVERSE PHASE SPACE TOMOGRAPHY AT CLARA USING GENERATIVE MACHINE LEARNING

M. A. Johnson*[1,2], A. D. Brynes[1,2], J. K. Jones[1,2], M. King[1,2], A. Wolski[2,3]
[1]ASTeC, STFC Daresbury Laboratory, Sci-Tech Daresbury, Warrington WA4 4AD, UK
[2]The Cockcroft Institute, Sci-Tech Daresbury, Warrington, WA4 4AD, UK
[3]Department of Physics, University of Liverpool, Liverpool, UK

Content from this work may be used under the terms of the CC BY 4.0 licence (© 2026). Any distribution of this work must maintain attribution to the author(s), title of the work, publisher, and DOI.

Abstract

CLARA is a high-brightness electron beam facility at STFC Daresbury Laboratory, aiming to deliver ultra-short electron bunches to a wide range of user experiments. CLARA has recently resumed operations after a major upgrade, and is currently undergoing beam commissioning at its nominal energy (250 MeV) and bunch charge (250 pC). During commissioning, studies of the transverse beam dynamics will be vital for optimizing the accelerator's performance, and for validating the simulation models used during its design. Phase space tomography is a powerful technique for reconstructing a beam's charge distribution in phase space; recent machine learning advances have led to faster, higher-resolution tomographic methods such as generative phase space reconstruction. In this contribution, we present detailed measurements of the 4D transverse phase space at CLARA. We validate the reconstructed phase spaces by using them to accurately predict the appearance of the electron beam for different beam optics configurations. Our results demonstrate methods that are now used for routine characterization of the CLARA beam, and represent the first emittance measurements at the accelerator's design energy.

INTRODUCTION

CLARA at STFC Daresbury Laboratory is a medium energy (250 MeV) linear accelerator that delivers high-brightness, ultra-short electron bunches to a variety of demanding user experiments [1,2]. CLARA is currently undergoing beam commissioning at its maximum bunch charge (250 pC) and repetition rate (100 Hz), after an extended shutdown to allow the installation of a major upgrade. This period saw the addition of a new, high-repetition-rate (up to 400 Hz) electron gun [3]; three additional S-band accelerating linacs; a variable bunch compressor; and an X-band linearizer [4]. During commissioning, detailed measurements of the beam dynamics are essential to optimizing the beam properties ready for user experiments.

Phase space tomography [5–7] is a established method for reconstructing a beam's charge distribution in two or more degrees of freedom. Tomography in two transverse degrees of freedom provides detailed insights into the beam's substructure, and also allows measurement of the betatron coupling. Conventionally, tomography in multiple degrees of freedom has required large data sets and significant computational resources, making it unsuitable for online beam measurements. However, several authors have recently demonstrated new tomographic methods that use machine learning (ML) to quickly reconstruct a beam's charge distribution in unprecedented detail [8, 9]. Experimental studies have shown how these techniques can efficiently reconstruct a beam's full six-dimensional charge distribution, including its time structure and energy spectrum [10, 11].

One aim of CLARA commissioning is to characterize, and ultimately improve, the transverse distribution of the electron beam. Phase space tomography is well-suited to this application, since it can reconstruct an accurate charge distribution that includes the beam's detailed substructure. Previous tomography studies at CLARA [8, 12, 13] have reconstructed the low-energy (35 MeV) beam produced by the accelerator's front end, which was previously operated as a separate user facility between 2018–2022 [14]. However, updated tools have now been developed to characterize the CLARA beam at its design energy of 250 MeV.

These proceedings describe experimental studies aimed at reconstructing the transverse phase space of the high-energy CLARA beam. We use an ML-based method [9, 15] to infer the beam's charge distribution, before using it to accurately predict the beam profile for different quadrupole settings. The method demonstrated here is currently used for routine characterization of the CLARA electron beam, and has already been used in support of several user experiments.

METHOD

Experimental Data

Figure 1 shows the section of CLARA that was used for tomography measurements in this study. The transport and diagnostics section immediately after the final linac includes ten independently-powered quadrupole magnets, and four YAG screens for observing the beam profile. When energized, the first dipole magnet diverts the beam along a spectrometer line, which can be used to measure the beam energy. The second dipole in Fig. 1 directs the beam into a 16-meter-long arc, which delivers electron bunches to the full energy beam exploitation (FEBE) area. The FEBE area is a separately shielded enclosure that includes two large, configurable chambers where the majority of CLARA user experiments take place [16].

Here, we demonstrate the tomography methods used at CLARA by reconstructing the charge distribution of the 250 MeV electron beam for bunch charges up to 250 pC. For the purposes of this study, we made measurements of an

* mark.johnson@stfc.ac.uk

ISBN: 978-3-95450-252-3 ISSN: 2673-5350 doi: 10.18429/JACoW-IPAC2026-WEP6093

SPACE CHARGE COMPENSATION TIME MEASUREMENT FOR A PULSED, HIGH-CURRENT H– ION BEAM

E. L. Flannigan*, R. Abel, D. R. Emerson, D. Faircloth,
B. John, K. Jonathan, D. Morris, O. Tarvainen
Science and Technology Facilities Council, Swindon, United Kingdom

Abstract

Strong space charge effects in pulsed, high-intensity hydrogen ion beams lead to transport losses in the Low Energy Beam Transport (LEBT) of particle accelerators. The space charge compensation (SCC) process lowers the potential of the beam by trapping compensating particles produced by beam-induced ionisation of residual gas. Significant beam losses during compensation build-up necessitate minimising the SCC time. Quantifying the SCC time and determining optimal conditions to reduce it can be done using time-resolved diagnostics. An optical diagnostic based on a Multi-Pixel Photon Counter has been developed at ISIS Neutron and Muon Source to measure the beam-induced light emission during SCC. The transmission through the acceptance-limited RFQ, measured by beam current transformers at the entrance and exit, can also be used to determine SCC time. These two diagnostics have been used at ISIS to measure the SCC time of the 36 keV pulsed H^- beam during parametric sweeps of residual hydrogen gas pressure, beam current and the solenoid magnet current. As predicted by theory, the beam current did not have an effect on the SCC time but the time reduced at higher gas pressures and was altered by the magnetic field.

INTRODUCTION

As pulsed, high-intensity ion beams are transported through the Low Energy Beam Transport (LEBT), space charge forces cause the beam to diverge which can result in beam losses. The space charge of the beam is reduced through the space charge compensation (SCC) process. This process occurs due to ionisation of the background gas in the LEBT, e.g. $H^- + H_2 \rightarrow H^- + H_2^+ + e^-$ for H^- beams. The secondary particles created are either repelled by the beam potential (electrons for H^- beams) or trapped by it (H_2^+ for H^- beams), reducing the local charge density and the electric field inside the beam.

The potential at the centre of the compensated beam, ϕ_c and the uncompensated beam, ϕ_u, may be used to calculate the SCC degree by:

$$\eta = 1 - \frac{\phi_c(z,t)}{\phi_u(z,t)} \tag{1}$$

Significant beam is lost when the SCC degree is low, making the final SCC degree important to beam transport. It is also important to decrease the SCC time, estimated by:

$$\tau = \frac{\eta}{n_g \sigma(E_b) v_b} \tag{2}$$

where n_g is the gas number density, $\sigma(E_b)$ is the energy-dependent beam-induced ionisation cross section, and v_b is the speed of the beam [1]. This equation assumes that only the primary beam ionises the background gas and that all compensating particles created are trapped by the beam potential and non-compensating particles are repelled and removed from the system. As the mobility of the compensating particle is significantly lower for a negative beam, this assumption is more valid for a negative beam.

As the ion beam species and the ion energy in Eq. (2) are set by the design of the system, reducing the SCC time is typically achieved by changing the gas density (gas pressure) or gas species. In the case of negative beams, the pressure range and species are limited, as an increase in the gas density or mass will lead to beam losses through electron detachment. Changes to the focusing fields used in magnetostatic LEBTs may also affect the SCC time, as the magnetic field will affect the dynamics of the secondary particles relevant to the process [2, 3].

As the SCC process is crucial to beam transport in the LEBT, many diagnostic techniques are applied to its study. To measure the SCC degree, time-resolved measurement of the beam potential is required. The SCC time is more easily measured, with multiple time-resolved diagnostics available. While many of the diagnostics used are invasive, experimental measurements and simulation have found that these diagnostics will not only intercept the beam but will also alter the upstream SCC process [3–5]. This, along with the possibility of continued diagnostic measurement during normal accelerator operation, emphasise the advantage of non-invasive diagnostic techniques for studying SCC. This work uses two non-invasive diagnostic techniques, beam current transformers (BCTs) and an optical diagnostic, to estimate the SCC time or equilibration time and to determine the optimal conditions for compensation of a pulsed H^- beam. The optical diagnostic used to measure equilibration time is a novel technique developed at ISIS, with BCT measurements used as validation.

EXPERIMENTAL SETUP

The ISIS Neutron and Muon Source uses a caesiated Penning surface plasma source to generate a pulsed H^- beam [6]. The 36 keV ion beam pulse length is ~200 µs at a repetition rate of 50 Hz. The Penning source routinely produces 50-55 mA, which is injected into the 3-solenoid magnet LEBT. A diagnostic chamber sits between the second and third solenoid magnet. The LEBT transports ~35 mA

* erin.flannigan@stfc.ac.uk

Content from this work may be used under the terms of the CC BY 4.0 licence (© 2026). Any distribution of this work must maintain attribution to the author(s), title of the work, publisher, and DOI.

ISBN: 978-3-95450-252-3 ISSN: 2673-5350 doi: 10.18429/JACoW-IPAC2026-WEP6095

PYTHON BASED CONTROL AND DIAGNOSTIC SYSTEMS FOR AREAL LINEAR ACCELERATOR

G. Amatuni, M. Yazichyan*, A. Grigoryan[1], B. Grigoryan, A. Hovakimyan[1], H. Sargsyan[1], L. Aleksanyan, E. Mnatsakanyan[1], H. Davtyan, A. Otarov, A. Vardanyan grigoryan@asls.candle.am, Center for the Advancement of Natural Discoveries using Light Emission (CANDLE SRI Yerevan, Armenia)

[1]also at Yerevan State University (YSU Yerevan, Armenia)

Content from this work may be used under the terms of the CC BY 4.0 licence (© 2026). Any distribution of this work must maintain attribution to the author(s), title of the work, publisher, and DOI.

Abstract

The AREAL linear accelerator, constructed in Yerevan, Armenia, is designed to generate low-emittance, ultrashort electron beam pulses for advanced research in novel accelerator technologies, coherent radiation sources, and the dynamics of atomic and molecular processes.

This paper presents an overview of the Python-based control system developed for the AREAL accelerator. The system architecture, associated hardware components, and supporting software infrastructure are described in detail. Particular attention is given to the client–server design, database integration, and hardware interfacing solutions. In addition, auxiliary applications that support operation, monitoring, and data management are discussed. Finally, future development directions of the control system, including its adaptation to planned AREAL upgrades, are outlined.

INTRODUCTION

From the control system point of view the AREAL linear accelerator[1-4] components are categorized as follows: vacuum system (ion pumps, vacuum gauges, gate valve and fast closing valve) [5-7], RF system (low-level radio frequency: LLRF) [8, 9], magnet system (solenoid, dipole, corrector and quadrupole magnets) [10, 11], cooling system [12, 13], diagnostic system (CCD cameras for YAG stations, movers and Faraday cups) [14-17], laser system [18], radiation, machine and personal safety systems [19]. The AREAL linear accelerator control system is based on "client/server" model and has three layers of hierarchy. The first layer is an interface to which the devices are connected via RS-232/485, USB and DAQ (Data acquisition), depending on a device type and specifications. The second - middle layer is a MySQL database for parameter and measurement data storage. The third layer is operator interface computers which are located in the control room. The connection between these three layers is performed via TCP/IP protocol [14, 15]. The main programming language for the server and client parts is a Python. The server software allows to get and save the readings of vacuum gauges, ion pumps and dosimeter devices, as well as the last actual positions and values of optical and optoelectronics elements on a laser table in a database. Then they are send to clients for monitoring and also for a reset of positions if necessary.

For implementation of AREAL accelerator control system servers and clients as well as for data analyses and beam parameters measurement tools, Python programming language is selected. Python is an open-source programming language widely used by scientists today. It offers a rich ecosystem of open-source scientific libraries that implement modern algorithms, enabling advanced data analysis, optimization, machine learning, and high-performance computing. In addition, Python provides numerous libraries for interfacing with hardware, managing network communications, and working with databases, including robust support for systems such as MySQL, making it suitable for control and monitoring.

LLRF CONTROL

The LLRF control is performed via LIBERA device which is a digital low level RF stabilization system. The LIBERA device's server part is programmed in a framework of the EPICS control system, so all required IOCs are installed on LIBERA by manufacturers. Channel accesses between IOCs and operator interface software is developed according to RF group requirements. Besides LIBERA device, a Micro Telecommunications Computing Architecture (μTCA) is used for timing stabilization and LLRF control. μTCA is a modular, high-performance hardware platform widely adopted in accelerator control systems, telecommunications, and experimental physics applications [20]. It provides a robust and flexible infrastructure for building scalable and reliable control and data acquisition systems. The key advantages of the μTCA platform include high-speed data transfer through backplane communication, a modular architecture based on Advanced Mezzanine Cards (AMC), deterministic timing and precise synchronization capabilities, and scalability suitable for complex distributed systems. In addition, μTCA systems are designed to meet the reliability requirements of continuous operation environments. It is also valuable with its hot-swap possibility, which allows to replace cards without interrupting device operation. In accelerator applications, μTCA is particularly well suited for LLRF systems, timing distribution, data acquisition and processing, and real-time feedback control. The platform enables tight integration between FPGA-based hardware processing and high-level software control, providing an efficient framework for precise RF signal generation, regulation and monitoring.

Precise timing is a critical requirement in accelerator systems, where RF fields, beam injection, magnet and diagnostic devices operations must be synchronized with nanosecond and, in some cases, picosecond-level accuracy.

ISBN: 978-3-95450-252-3 ISSN: 2673-5350 doi: 10.18429/JACoW-IPAC2026-WEP6099

STATUS OF ACCELERATOR AUTOMATION IN THE COMMUNITY: CLASSIFICATION, SURVEY RESULTS, AND THE ROLE OF AI AND MACHINE LEARNING

S. Reimann*†, GSI Helmholtz Centre for Heavy Ion Research, Darmstadt, Germany
F. Miyahara, High Energy Accelerator Research Organization, Tsukuba, Japan
M. Lafky, Australian Synchrotron, Melbourne, Australia
P. Schuh, SLAC National Accelerator Laboratory, Menlo Park, United States
J. Xing, Institute of High Energy Physics, Beijing, China
G. Johns, Oak Ridge National Laboratory, Oak Ridge, United States
R. Steerenberg, European Organization for Nuclear Research, Geneva, Switzerland
B. Freeman, Thomas Jefferson National Accelerator Facility, Newport News, United States
K. Genge, TRIUMF, Vancouver, Canada
M. Pont, ALBA Synchrotron (Spain), Cerdanyola del Vallès, Spain
G. Marr, Brookhaven National Laboratory, Upton, United States
Y. Iwata
National Institutes for Quantum Science and Technology,
Accelerator and Medical Physics, Inage, Chiba, Japan
L. Hardy, European Synchrotron Radiation Facility, Grenoble, France

Abstract

The increasing complexity of particle accelerators and the growing demand for operational efficiency have intensified the focus on automation in accelerator control systems. However, there is still a lack of a common language to describe and compare the level of automation across different facilities. This article presents a generic classification scheme for accelerator automation, defining five distinct levels ranging from basic operational assistance to full autonomy. To assess the current state of automation in the accelerator community, a structured survey was conducted during the 14th Workshop on Accelerator Operations (WAO 2025). Responses from major laboratories indicate that more than one third of accelerators currently operate at the lowest level 1 (operational assistance), and no facility has yet reached full automation. However, projections show a clear trend toward higher levels within the next decade. Key drivers include optimization algorithms for autotuning, finite-state machines, and closed-loop feedback systems. This study provides both a conceptual framework and a snapshot of current implementation practices, supporting a shared understanding of accelerator automation across the community.

LEVELS OF ACCELERATOR AUTOMATION

The classification introduced in this work is conceptually inspired by SAE J3016 [1], a widely adopted five-level framework for driving automation. Although originally developed for on-road motor vehicles, its structured progression—from full manual control to full autonomy—has proven useful as a generic reference for describing automation maturity. When transferring this concept to accelerator operations, it is adapted to the specific system structure and operational logic of accelerator facilities. Based on this adaptation, we propose the following definition of accelerator automation levels.

Level 0: No Automation

At this level, all control actions are performed manually. Operators directly adjust technical parameters such as currents and voltages without the support of automated systems.

Level 1: Operational Assistance

Initial assistance systems become available to support accelerator operation. These include parameter hierarchy models, beam loss and transmission monitoring, and software-based interlock mechanisms. Importantly, tuning is performed using high-level physics parameters rather than raw hardware settings, thereby reducing operational complexity.

Level 2: Partial Automation

This level introduces true automation into the operational workflow. Parameter-scanning tools and finite-state-machine-based sequencers are used to automate repetitive tasks. In addition, autotuning solutions are available, allowing operators to initiate optimization routines that adjust multiple set values to achieve defined machine objectives.

Level 3: Conditional Automation

The accelerator can operate autonomously under predefined and stable conditions. Once initial configuration is complete, performance is maintained through automatic feedback loops, stabilization routines, and self-correction

* s.reimann@gsi.de

Content from this work may be used under the terms of the CC BY 4.0 licence (© 2026). Any distribution of this work must maintain attribution to the author(s), title of the work, publisher, and DOI.

ISBN: 978-3-95450-252-3 ISSN: 2673-5350 doi: 10.18429/JACoW-IPAC2026-WEP6100

COMMISSIONING OF THE FAIR CONTROL CENTRE

V. Kamerdzhiev*, M. Auel, R. Bär, O. Bertini, K. Grigoryev,
D. Krebs, H. Reuter, C. Schmidt, R.J. Steinhagen, Y. Valdau and S. Reimann
GSI Helmholtz Centre for Heavy Ion Research, Darmstadt, Germany

Content from this work may be used under the terms of the CC BY 4.0 licence (© 2026). Any distribution of this work must maintain attribution to the author(s), title of the work, publisher, and DOI.

Abstract

The FAIR Control Centre (FCC) has been purpose-built on the GSI campus to meet the complex operational demands of the FAIR/GSI large scale accelerator facility. It hosts the Main Control Room (MCR), seminar and meeting rooms of various sizes, offices, and dedicated technical rooms.

The 640 m² MCR is an open, collaborative workspace for accelerator experts, experiment teams, and technical staff. It offers a 24/7 ergonomic environment with advanced acoustic and climate control, height-adjustable consoles, and a water-cooled IT infrastructure. In addition to the console displays, the fully digital MCR features ca. 110 m² of high-resolution LED overview displays for system-level visualization.

Construction of the MCR was completed in November 2025. Console installation began on December 8th, followed by IT installation and commissioning in early 2026. Initial operation of the first consoles was performed in late February, with full MCR operation targeted for June 2026. The GSI accelerators will be controlled from the FCC for the beam time starting in September.

We report on the FCC key features and the project status on its path to completion, with an emphasis on commissioning.

INTRODUCTION

The Facility for Antiproton and Ion Research (FAIR) is one of the most advanced accelerator complexes currently under construction. Multiple accelerators of different types and experimental areas are integrated into a single scientific infrastructure dedicated to nuclear physics and related areas [1,2]. Commissioning of the FAIR Control Centre (FCC) is one of the key activities scheduled for 2026 according to the FAIR&GSI integrated schedule. This follows the start of the cryogenic plant commissioning that started in 2025 and is part of the staged commissioning plan [3]. The increasing scale and complexity of such facilities require equally advanced operational environments [4]. The functional requirements can be summarized in three key dimensions:

- Operational Control: Real-time monitoring and control of accelerator subsystems and beams
- Coordination Platform: Interaction between operators, machine coordinators, experimenters, and technical experts
- Public and Scientific Interface: Representation of FAIR to visitors, stakeholders, and the public

In terms of general use cases the following scenarios are taken into account [5].

- Commissioning and re-commissioning of the FAIR facility after maintenance periods
- Regular operation of GSI/FAIR accelerators
- Machine development
- Operation of machine-based experiments
- Development and testing of control software

The FCC is designed as an integrated environment that combines operational, technical, and collaborative spaces [5]. In addition to the Main Control Room (MCR), it includes meeting and conference rooms, ready rooms for key personnel, IT service areas, and a visitors' gallery. This layout facilitates efficient interaction between operators, machine coordinators, experiment teams, and technical experts. Additionally, MCR personnel have access to lockers conveniently located near the main MCR entrance and to showers located in the basement.

The design follows established best practices from large accelerator laboratories such as CERN, while incorporating specific requirements derived from FAIR's multi-machine operation and high degree of parallelization [6].

The MCR has been designed as the central hub for monitoring, controlling, and coordinating all accelerator operations, experiments, cryogenic and technical infrastructure. It replaces and significantly extends the capabilities GSI's control room infrastructure, addressing both the increased system complexity and the need for improved human-machine interaction [7].

Maintaining operator performance over long shifts is a critical requirement. Acoustic conditions, lighting, and workspace design directly influence efficiency and error rates. The MCR addresses these challenges through a comprehensive ergonomic design, which is validated during commissioning. Among other measures, this is achieved by reducing the number of visitors in the control room through access control to the MCR and a dedicated visitors' gallery. This space is specifically designed to provide insight into operator activities and the current operational status of the GSI/FAIR facilities without requiring direct access to the MCR. The gallery is located on the north side and is directly connected to the MCR via a large window, allowing visitors to observe operators at work. Some synoptic displays are also visible from this area. In addition, the visitors' gallery is equipped with information screens that provide further insight into the accelerator complex. Dedicated exhibits, such as compact magnets or accelerator components, are also foreseen to enhance the visitor experience.

THE MAIN CONTROL ROOM

The MCR is the core element of the FCC. With its surface area of approximately 640 m² it is about twice as large as the former GSI control room. It is designed to host 25

* v.kamerdzhiev@gsi.de

ISBN: 978-3-95450-252-3 ISSN: 2673-5350 doi: 10.18429/JACoW-IPAC2026-WEP6101

EXTENDED MAINTENANCE AND GRADUAL REPLACEMENT OF MIL-1553-BASED FIELD NETWORK AT GSI

V. Kleipa*, R. Baer, M. Dziewiecki, K. Lueghausen, S. Rauch and M. Weiland
GSI Helmholtzzentrum für Schwerionenforschung, Darmstadt, Germany

Abstract

The control system of the GSI accelerator complex dates back to the early 1990s. It is based on a derivative of the MIL-1553 field bus, providing around 1 Mbit/s throughput and deterministic real-time operation. Although a modern control architecture with smart front-ends (System Control Units, SCUs), Ethernet, and White Rabbit is now widely deployed at GSI, several hundred devices still depend on the legacy network and protocols.

The ageing electronics and limited bandwidth provide strong motivation to migrate to the new control system. However, an upgrade is limited by various constraints: strict real-time operation, existing software architecture, physical space and available power sources. Therefore, operation of the legacy interfaces must be ensured for at least another decade while a unified migration strategy is hard to find.

In this contribution, we present a generic approach for extending the lifetime of the existing MIL-1553-based systems and gradual replacement of their components. This includes upgrades of bus controllers, device controllers, the bus itself as well as a new Modbus/TCP-based solution for simple devices.

INTRODUCTION

The GSI's legacy control system is still widely in use at various places in the accelerator complex, including the Unilac linear accelerator and partly the SIS-18 synchrotron and the ESR storage ring.

It uses a custom network solution, the *DeviceBus* [1] for connecting remote devices. DeviceBus is a serial, half-duplex, multipoint interconnect with single master and multiple slaves, net bandwidth of ca. 80 kB/s and range of ca. 200 m. Its physical layer is based on the MIL-Std-1553 bus, however major differences exist between both standards, including different connectors, different data model and lacking redundancy. DeviceBus is a hard real-time standard with short and deterministic latency of ca. 20 µs.

SYSTEM ARCHITECTURE

The concept of the system can be described as *central controllers approach*: relatively few control units (*SE crates*) communicate multiple devices over DeviceBus and *interface adapters* (IFA) as shown in Fig. 1.

The SE crates are quite complex, VME-based systems using multiple Motorola 68000 processors along with a main PowerPC-based computer. They are connected to the accelerator control network and the global timing system, which is another derivative of the MIL-Std-1553. They run the front-end software which communicates to higher control system layers via an in-house developed standard known as *Device Access* [2]. They constitute the boundary between the control software and the real-time hardware.

Interface adapters are in turn rather simple devices which react for incoming instructions on the fly. Therefore, the real-time operation of the system relies on deterministic response time of DeviceBus and interface adapters.

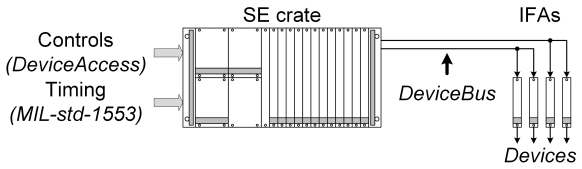

Figure 1: Legacy controls with SE.

This architecture stays in contrast to the new GSI's control hardware with *System Control Units* (SCUs) [3, 4], which can be described as *local controllers*. Here, every device is equipped with a fully-featured controller with access to the control network and timing (WhiteRabbit [5, 6]), and running the front-end software according to the newer FESA standard [7, 8]. There is no intermediate bus, which makes the architecture conceptually simpler — see Fig. 2.

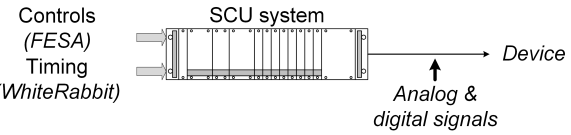

Figure 2: Direct device control with SCU.

UPGRADE STRATEGIES

Continuous upgrade measures tend to replace the legacy controls with SCU-based systems. However, direct replacement of interface adapters with SCUs is hardly ever possible without a deep upgrade to the controlled hardware itself: SCUs are physically larger, draw significantly more power (ca. 35 W vs. 4.5 W) and require better cooling than the interface adapters, and finally they have incompatible backplane interfaces.

Attempts undertaken to find a single replacement architecture for various use cases failed. Therefore, multiple solutions were needed to replace most critical parts of the old architecture, or to extend its lifetime if an upgrade is not viable.

An extensive description of the software upgrade effort can be found in [9]. Here we focus on selected hardware aspects of the upgrade.

* v.kleipa@gsi.de

This is a preprint - the final version is published with IOP

Content from this work may be used under the terms of the CC BY 4.0 licence (© 2026). Any distribution of this work must maintain attribution to the author(s), title of the work, publisher, and DOI.

ISBN: 978-3-95450-252-3 ISSN: 2673-5350 doi: 10.18429/JACoW-IPAC2026-WEP6102

A PYTHON FRAMEWORK FOR INTEGRATION OF MEASUREMENTS INTO THE EPICS CONTROL SYSTEM

P. Schreiber*, E. Blomley, J. Gethmann, M. Schuh, A.-S. Mueller
Karlsruhe Institute of Technology, Karlsruhe, Germany

Content from this work may be used under the terms of the CC BY 4.0 licence (© 2026). Any distribution of this work must maintain attribution to the author(s), title of the work, publisher, and DOI.

Abstract

Many measurements in accelerator physics require dedicated scans of parameters, such as the main frequency of the RF system for chromaticity measurements or a variation of quadrupole strength for beta function measurements, etc. Such measurements cannot be performed by simply reading an instrument, but require a certain measurement procedure. These measurements are typically implemented as scripts, as they are often written by staff or students whose task is the measurement itself. For reusability and maintainability, however, an integration into the EPICS control system is favoured. This has multiple benefits such as the easy archiving of results in the central database or the integration of the measurements into the standard operator panels. To allow non expert staff and students to easily build measurements exposed via the EPICS control system, we built a framework in Python to implement such measurement routines as EPICS input-output-controllers (IOC). This framework allows the author of such measurements to focus on the measurement itself and still benefit from an EPICS integration without the need for extensive knowledge in EPICS IOC development.

INTRODUCTION

Operation of an accelerator facility for user operation as well as experimental science, often requires measurements of certain quantities. Measurements depending on a single device reading are easy to do and reuse, however, once a measurement requires a measurement routine it is more complicated to implement maintainable and reusable routines. While standard measurements, required for every-day operation are usually well integrated in the operation procedures and control systems, more specialised measurements are often developed as scripts, making them sometimes hard to find and reuse.

Integrating measurements into the control system solves this problem. It usually requires a certain understanding of the control system. This requirement is not always fulfilled for students, guest scientists and scientists, therefore, it is difficult for them to implement the integration themselves.

Therefore, the IBPT measurement package implements a framework written in Python [1] to easily write measurements with automatic EPICS [2] integration. It does not require much pre-knowledge and uses pythonic ways to achieve this goal. In addition to the EPICS integration it offers further interfaces as described below.

* patrick.schreiber@kit.edu

MEASUREMENTS

Measurements are intended to be executed multiple times, sometimes within the same process (in the case of IOC integration, as described below). They are implemented by sub-classing a base measurement class that provides the required structures and takes over the integration into the control system. Observables and actuators are implemented as subclasses of the "Monitor" and "Actuator" classes that handle metadata collection and clean-up automatically and are registered to the measurement class. The execution of a measurement is split into three steps:

1. Preparation,
2. Measurement,
3. Post Measurement.

The first step, preparation, allows the code to prepare the measurement each time it is executed. Tasks for this could include gathering general data or setting-up some device. It is not entirely required to implement this, all the steps could be implemented in the second step, but it helps with code maintenance by clearly separating preparation from execution. The second step, the actual measurement, is where the measurement loop should be implemented. It is called right after the preparation step. The loop for executing procedures, e.g. scans, is intentionally left to the user, as having too much forced structure would lower acceptance with newly arriving people. This step can be interrupted in a controlled way when using "break points"[1]. The last step to implement is the post measurement procedure. This is where the analysis of the measured data is happening. The return value of this method must be a dictionary that will be saved to disk.

Preparation

In addition to the usual user implemented preparation, the base measurement will do it's own preparation. All registered monitors and actuators will prepare metadata collection. Actuators will also record the current value and use that for resetting after the measurement is aborted or finished.

Measurement

The measurement method should use the registered actuators to modify the system for the measurement (if required). It should use the "read_data" method to read all the values from actuators and monitors. By using this method, the data, together with metadata is gathered in a data store, that will be saved to disk in any case, even if the measurement fails or

[1] Markers indicating a breakable point, not to be confused with debugging breakpoints

ISBN: 978-3-95450-252-3 ISSN: 2673-5350 doi: 10.18429/JACoW-IPAC2026-WEP6103

IFMIF-DONES CONTROL SYSTEMS AND TESTING PLATFORM

A. Naranjo Jiménez*, C. Carvajal Almendros, M. J. Gutiérrez,
R. Lorenzo Ortega, L. Maindive, I. Podadera, M. Weber
IFMIF-DONES España, Escúzar, Granada, Spain

Content from this work may be used under the terms of the CC BY 4.0 licence (© 2026). Any distribution of this work must maintain attribution to the author(s), title of the work, publisher, and DOI.

Abstract

The IFMIF-DONES neutron source, under construction in Granada, Spain, has high availability targets for its systems. In order to evaluate the architectural and technological choices being made for the control systems, a dedicated testing platform is being developed. Key aspects under evaluation include the EPICS IOC deployment model (container-based) and orchestration solution (currently evaluating Proxmox HA, Docker Swarm and Kubernetes). Integration of existing DONES prototypes into the testing platform is also envisaged. The platform delivers value throughout all the facility's lifecycle. This contribution will report on the design and current progress of the testing platform.

INTRODUCTION

IFMIF-DONES (International Fusion Materials Irradiation Facility - Demo Oriented Neutron Source) [1] is a critical pillar in the global fusion roadmap, designed to test and qualify materials under extreme neutron irradiation. To ensure safe and continous operation of the facility, the Control Systems play a vital role [2]. While manual deployment is beneficial in the early stages, allowing fast development cycles, these methods are inherently prone to human error, lack version control, and often lead to inconsistencies between development, testing, and production environments.

To address these challenges, it was decided to develop CICStest, a Central Instrumentation Control Systems (CICS) [1, 2] test platform. This platform adopts "Control as Code" principles, integrating industrial control standards with modern DevOps practices. Using Infrastructure as Code (IaC) through Ansible, containerization via Docker, and automated orchestration with GitLab CI/CD, CICStest provides a high-fidelity, reproducible environment for validating architectural choices, evaluating different technologies, developing software, human factors evaluation and training.

This paper is organized as follows: First, it presents the hardware infrastructure for CICStest; then, it details the software configuration based on the Phoebus ecosystem; later, it describes on the automated deployment workflow; after that, it presents a Software Development Kit (SDK) developed using the availability of CICStest; and finally, it presents the conclusions and future development lines for CICStest.

HARDWARE CONFIGURATION

The CICStest platform is hosted on a dedicated infrastructure designed to simulate a controlled industrial environment. The core of the system consists of a dedicated Dell PowerEdge R750XS server, which provides the necessary computational resources to achieve virtualization and container orchestration. This setup allows for virtualization and validation of the control environment while the final IFMIF-DONES Control System and networking infrastructure is being developed and constructed. By decoupling the control system development from the physical site availability, the platform ensures that architectural standards and network configurations are pre-defined and tested in advance.

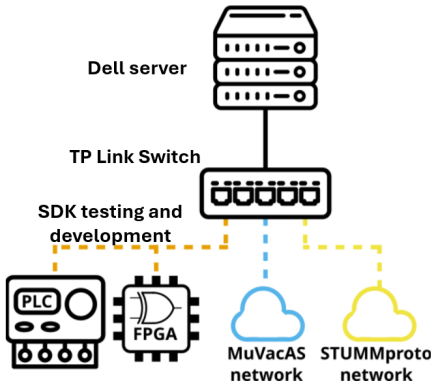

Figure 1: Visual scheme of the hardware configuration of the CICStest server, aiming a future connection to different hardware stations and prototypes.

To manage local traffic and field device communication, the setup includes a TP-Link TL-SG2428P switch, which ensures high-speed data transfer and VLAN segmentation if required. The platform is integrated into the broader infrastructure via a dedicated uplink to the University of Granada (UGR) network, allowing for remote management of different Local Instrumentation and Control Systems (LICS) [2], as shown in Fig. 1.

SOFTWARE CONFIGURATION

The CICStest software ecosystem has a modular, containerized architecture based on the EPICS (Experimental Physics and Industrial Control System) framework. The architecture is divided into three functional layers: Client, Services, and Standard Services [3], represented as three different columns in the mentioned order in Fig. 2.

Client and Control Services

The top layer features Phoebus as the primary integrated control system cockpit, providing a human-machine interface for control, monitoring, and alarm visualization. Supporting this, a suite of dedicated services is deployed:

* naranjo1911@gmail.com

ISBN: 978-3-95450-252-3 ISSN: 2673-5350 doi: 10.18429/JACoW-IPAC2026-WEP6104

RF-API: A MODULAR CONTROL FRAMEWORK IN EPICS FOR RF SYSTEMS AT CLARA*

N. Y. Joshi†,1,2, A. E. Wheelhouse[1,2], J. Wilson[3], W. Edward-Olaniyi[3]
[1]ASTeC, STFC Daresbury Laboratory, Warrington, UK.
[2]The Cockcroft Institute, STFC Daresbury Laboratory, Warrington, UK.
[3]Technology Department, STFC Daresbury Laboratory, Warrington, UK.

Content from this work may be used under the terms of the CC BY 4.0 licence (© 2026). Any distribution of this work must maintain attribution to the author(s), title of the work, publisher, and DOI.

Abstract

The CLARA facility has been upgraded in Phase II to deliver electron bunches up to 250 MeV using a standing wave photo-injector gun, four linac structures and a fourth harmonic lineariser cavity. A transverse deflecting cavity is also employed to measure key bunch parameters. To support reliable and efficient operation, a comprehensive RF Application Programming Interface (RF-API) has been developed within the EPICS control system. This API provides an intuitive interface for operators and serves as a foundation for higher-level machine control applications. It also enhances operational safety by monitoring unintended performance or configuration deviations in the RF systems, automatically alerting RF experts to potential degradation. This paper presents the design, capabilities, and performance of the RF-API and its associated user interface.

INTRODUCTION

The CLARA (Compact Linear Accelerator for Research and Applications) facility is being developed in multiple phases to support the investigation of advanced accelerator technologies relevant to future large-scale facilities [1–3], including the proposed UK XFEL [4, 5]. In addition, CLARA provides electron beams for a wide range of experimental applications, including radiotherapy and plasma-based acceleration studies.

In its Phase II configuration, CLARA employs a normal-conducting S-band standing-wave gun, four travelling-wave linac structures, and an X-band lineariser to accelerate electron bunches to energies up to 250 MeV. Key beam parameters, including bunch length and arrival time, are measured using an S-band RF transverse deflecting cavity (TDC).

Each RF cavity is powered by an independent klystron–modulator system, delivering RF pulse powers in the range of 7–36 MW at the cavity input. The interfaces between RF subsystems are illustrated through a block diagram in Fig. 1. The low-level RF (LLRF) system [6] generates the initial RF signal, which is subsequently amplified through a pre-amplifier and klystron. The amplitude and phase of the RF pulse are primarily controlled via LLRF setpoints, but are also influenced by variations in the high-voltage power supply (HVPS), including cathode voltage and current. Although HVPS parameters are typically adjusted only under specific conditions, thermal drifts within the system can introduce measurable variations in RF output.

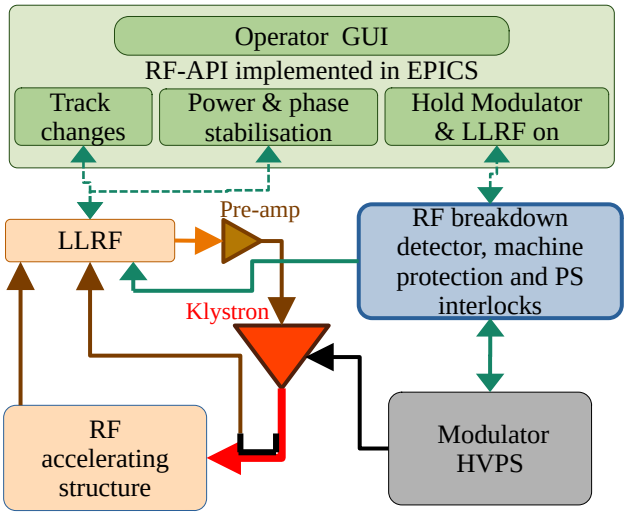

Figure 1: Block diagram of an RF system hardware, protection interlocks and interface with RF-API based control software.

Given the diversity of RF hardware deployed across CLARA, direct low-level control by operators would be impractical and error-prone. To address this, a unified RF Application Programming Interface (RF-API) and graphical user interface (GUI) have been developed using EPICS and Control System Studio (CS-Studio) [7] respectively.

OPERATOR GUI INTERFACE

The operator GUI panels for all seven RF systems are standardised and presented within a single interface to ensure a consistent and efficient user experience, as shown in Fig. 2. The GUI is organised into functional sections, including modulator control, manual override capability, and power and phase adjustment.

Real-time system status is provided through numerical readbacks, status indicators, and colour-coded visual elements, enabling rapid assessment of system status. An interlock tree representation has been implemented to allow operators to efficiently trace the root cause of system trips.

An integrated notification panel displays command status, error messages, and suggested recovery actions via a rolling buffer. In addition, an embedded plotting interface enables short-term monitoring of RF powers, phases, and cavity temperatures.

* This work is funded by STFC-UKRI.
† Nirav.Joshi@stfc.ac.uk

ISBN: 978-3-95450-252-3 ISSN: 2673-5350 doi: 10.18429/JACoW-IPAC2026-WEP6105

VERTICAL EMITTANCE CONTROL USING THE DLS-MBF TUNE PLL EXCITATION AT THE ESRF-EBS

B. Roche*, N. Carmignani, L. Carver, F. Ewald, S. White
European Synchrotron Radiation Facility, Grenoble, France

Abstract

Since the beginning of the ESRF-EBS operation in 2020, the storage ring has been routinely operated with an artificially increased vertical emittance (10 pm, 20 pm, or 40 pm depending on the filling mode) to enhance beam lifetime. Until recently, beam excitation was achieved using pseudo-random noise with a relatively large bandwidth.

We recently have used the "Tune PLL" functionality of the Multi-Bunch Feedback processor, developed at Diamond Light Source (referred to as DLS-MBF), to excite a specific sideband of the transverse betatron resonance with high precision. This technique, initially developed and tested at Diamond Light Source, requires more careful tuning and parameter adjustment but has demonstrated superior performance at the ESRF compared to the previously used white-noise excitation.

In this paper, we describe the implementation of the Tune PLL excitation at the ESRF and present results showing its benefits in terms of beam lifetime improvement, emittance stability, and halo reduction. Using a pinhole emittance measurement, we were able to observe very small emittance fluctuations (down to 50 fm rms) and compare the resulting emittance fluctuations produced by the different blow-up methods.

INTRODUCTION

The ESRF-EBS storage ring, similarly to other fourth-generation light sources (existing or planned), offers an ultra-low horizontal emittance, resulting in a reduced Touschek lifetime. Although the vertical emittance is below 1 pm (after corrections), routine user operation requires an artificial increase to 10 pm, 20 pm, or 40 pm depending on the filling pattern, in order to achieve an optimal compromise between beam lifetime and photon beam quality.

Operation at reduced chromaticity is being considered to enable operation with small in-vacuum undulator gaps [1]. Lowering the chromaticity from the nominal values (10, 8) to (6.3, 4.5) reduces the beam halo, a key limitation for small-gap operation, but degrades the efficiency of the transverse emittance blow-up process [2].

So far, the vertical emittance blow-up has been performed using a magnetic shaker driven by a broadband pseudo-random noise. While robust and simple, this method lacks selectivity and does not optimally transfer excitation into incoherent beam motion. As a result, part of the excitation power drives coherent oscillations of the bunch centroid rather than increasing the occupied phase-space area. To address this limitation, the DLS-MBF Tune PLL method was investigated as a promising alternative excitation technique to improve blow-up efficiency, particularly under low-chromaticity conditions.

In the following, we describe the Tune PLL method and compare the resulting performance with the conventional noise-based excitation, focusing on lifetime and emittance stability. The implementation of this technique at ESRF-EBS was tested during two weeks of user-mode under reduced chromaticity conditions at the end of 2025. The outcome of this test will be discussed.

DIAGNOSTICS

The performance of a blow-up scheme can be assessed through two main criteria: (i) the achievable beam lifetime for a measured vertical emittance, and (ii) the stability of the emittance over a wide range of timescales. Therefore, it is important for this study to have the appropriate diagnostic tools to measure both emittance and the beam lifetime with good accuracy.

The vertical emittance is measured using a pinhole camera system [5]. The system operates at a frame rate of 15 Hz with an exposure time of approximately 10 ms. While absolute calibration remains challenging, the relative measurement stability is excellent, allowing the resolution of very small emittance fluctuations down to about 50 fm rms.

The beam lifetime is obtained from a standard exponential fit of the total beam current. The current is measured either using a Parametric Current Transformer from Bergoz Instrumentation or derived from the sum signal of the BPM electronics, providing consistent and independent measurements.

DIAMOND MULTI-BUNCH FEEDBACK TUNE PLL EXCITATION

The DLS-MBF system, developed at Diamond Light Source in 2017 [6], is a digital bunch-by-bunch feedback processor providing advanced capabilities for transverse beam stabilization and excitation. It was adopted at ESRF soon after [7], replacing a previous in-house system [8], due to its superior performance and flexibility.

In addition to its feedback functionality, the DLS-MBF includes a Tune Phase-Locked Loop (PLL) that enables narrowband excitation by locking onto the phase of the transverse Beam Transfer Function (BTF). This capability is essential for a narrow-band excitation system used for beam emittance blow-up, as it keeps the excitation locked to the resonance frequency. This is important because the betatron tune can drift over time, both slowly and rapidly, due to

* benoit.roche@esrf.fr

Content from this work may be used under the terms of the CC BY 4.0 licence (© 2026). Any distribution of this work must maintain attribution to the author(s), title of the work, publisher, and DOI.

ISBN: 978-3-95450-252-3 ISSN: 2673-5350 doi: 10.18429/JACoW-IPAC2026-WEP6106

UPGRADE PLAN FOR THE ESRF FAST ORBIT FEEDBACK

M. Penot*[1], B. Roche[1]
[1]European Synchrotron Radiation Facility, Grenoble, France

Abstract

The Fast Orbit Feedback (FOFB) at the ESRF was initially developed in 2010. During the upgrade of the storage ring for the Extremely Brilliant Source (EBS) project in 2019, the FOFB architecture was adapted to the new ring, but no significant functional improvements were introduced. The current system is now obsolete in several respects, including the hardware, development tools and practices.

A full refurbishment of the FOFB is now being planned. The main objectives are to enhance system performance through improved correction algorithms and reduced latency, to enable local orbit correction for individual beamlines with the possible integration of X-ray beam position measurements, and to ensure compatibility with future beam position monitors system upgrades. Particular emphasis is placed on long-term maintainability through the adoption of modern software development methodologies and the use of open-source or non-proprietary technologies as much as possible.

INTRODUCTION

The FOFB system plays a crucial role in stabilizing the electron beam by correcting orbit perturbations in real time [1].

In the 32 cells of the storage ring are 320 Beam Position Monitors (BPMs), of which 192 are Libera Birlliance and 128 are Libera Spark. The FOFB currently only uses the Brilliance electronics sampled at 10 kHz, but the Libera Spark BPMs could also be integrated after further validation measurements.

Orbit position data are transmitted via the Diamond Light Source (DLS) Communication Controller. The correction is computed in FPGA-based processing units, and the updated set-points are applied by eight FOFB stations to the steerer power supplies through RS422 serial links [2]. The overall system architecture is illustrated in Fig. 1.

Using a 200 mA storage ring electron beam current, the FOFB efficiently reduces orbit disturbances up to approximately 150 Hz in horizontally and 250 Hz vertically. Above these frequencies, disturbances are amplified up to twice in the 400-500 Hz range as illustrated in Fig. 2. These performance limitations motivate the development of an improved correction loop as part of the ongoing FOFB upgrade. The addition of a phase-lead compensator to the already implemented proportional-integral (PI) corrector will be discussed in the next sections.

* marie.penot@esrf.fr

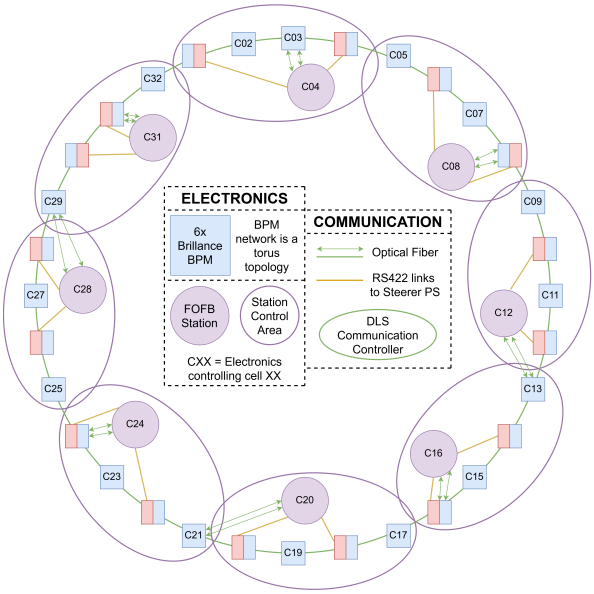

Figure 1: Current topology of ESRF-EBS Fast Orbit Feedback.

CORRECTION LOOP IMPROVEMENT

Theory

PI corrector The ESRF-EBS FOFB correction loop is initially composed of a simple PI corrector in parallel with a 50 Hz notch filter for electrical perturbations.

A PI corrector can be interpreted as a pole (an integrator) at the origin, which guarantees zero steady-state error for step reference inputs, since the integrator accumulates any persistent error until it is eliminated. The absence of the derivative term, as implied previously, reduces the sensitivity to the high-frequency measurement noise.

The exact PI coefficients have been determined experimentally and are indicated in Table 1.

Table 1: Current FOFB PI Parameters

	Horizontal	**Vertical**
K_p [-]	0.26	0.054
K_I [s^{-1}]	1407	1754

As explained in the introduction, the current FOFB achieves effective disturbance rejection up to approximately 250 Hz in the vertical plane and 150 Hz in the horizontal plane. Moreover, a moderate noise amplification above these frequencies is observed but could be further reduced through controller optimization. These frequency ranges can be improved by adding a phase-lead compensator, and tuning the PI corrector parameters to optimize its lower frequencies performance and reduce its effect at higher ones.

Content from this work may be used under the terms of the CC BY 4.0 licence (© 2026). Any distribution of this work must maintain attribution to the author(s), title of the work, publisher, and DOI.

ISBN: 978-3-95450-252-3 ISSN: 2673-5350 doi: 10.18429/JACoW-IPAC2026-WEP6108

STUDIES OF LONGITUDINAL BUNCH-BY-BUNCH FEEDBACK FOR SOLEIL II

E. Kravishvili*,[1,2], Y.-M. Abiven[1], M. El Ajjouri[1], A. Gamelin[1], V. Gubaidulin[1], R. Nagaoka[1], J. Pham[1], L. Zhao[1], R. Sreedharan[1], T. Nakamura[3]
[1]Synchrotron SOLEIL, Saint-Aubin, France
[2]Université Paris-Saclay, Gif-sur-Yvette, France
[3]High Energy Accelerator Research Organization (KEK), Tsukuba, Japan

Abstract

In upgrading the present SOLEIL ring, it has been decided to introduce longitudinal bunch-by-bunch feedback (LFB) in addition to the already existing transverse feedback (TFB), because studies indicate that the new normal conducting fundamental RF cavities may excite longitudinal coupled-bunch instabilities (LCBI) due to their higher-order-modes (HOMs). SOLEIL II also plans to use bunch-lengthening harmonic cavities (HCs) to improve the Touschek lifetime, which may trigger complex LCBIs. The present study aims to develop an LFB system responsible for the longitudinal collective stability of the SOLEIL II beam. The theoretical calculation of the instability growth rate of the HOMs has been carried out, defining the preliminary performance requirements of the LFB. Among the three main parts of the system-detection, signal processing and kicking- the present work focuses on the development of the processing section and the paper also presents some design aspects of the kicker cavity along with a beam-based test converting the currently operating TFB system to LFB by utilizing the stripline as a longitudinal kicker.

INTRODUCTION

The SOLEIL II project aims to reduce the horizontal beam emittance to a value of 85 pm rad, which is almost 50 times smaller than that of the currently operating SOLEIL storage ring (see the related SOLEIL II parameters in Table 1) [1, 2]. Achieving such a low emittance is highly challenging, and beam stability is therefore crucial. As to collective beam stability, at present, SOLEIL operates only with TFB, [3–5] since no LCBI has been observed so far. However, this may not be the case for SOLEIL II. An LFB system may become necessary because studies have shown that the main RF cavity could generate HOMs with a non-negligible risk of driving LCBIs [6, 7]. Since LFB has never been operated at SOLEIL, an experimental study was carried out in the SOLEIL ring in which the existing TFB was converted in the longitudinal plane to gain experience [8]. Details of this experiment are presented in the first part of the paper. The development of an LFB system requires studies in several areas. First, it is necessary to investigate longitudinal coherent beam dynamics in SOLEIL II and identify all possible instabilities. Both theoretical and simulation-based studies must be performed to determine which HOMs are potentially dangerous and to evaluate their corresponding growth rates. These results define the minimum performance requirements for the LFB system. Preliminary results of the beam dynamics studies are presented in the second part of the paper. Once these requirements are established, the development of the LFB system can proceed. The system consists different important components, and two of them are signal processing and kicking [9]. Signal processing is performed using a scheme of Finite Impulse Response (FIR) filter. The development of the FIR filter for SOLEIL II is described in the third part of the paper. In the present study, we shall not describe the digital processors. Finally, one of the key aspects of the system is the stabilization of the beam with the correctly calculated and generated longitudinal kicks. The SOLEIL II longitudinal kicker design is based on the cavity developed at PSI for SLS 2.0 [10], which bases its original concept upon the waveguide overloaded cavity originally developed for DAΦNE [11, 12], along with its unique extensions. Some future perspectives on the longitudinal kicker development for SOLEIL II shall be found at the end of the paper.

Table 1: Some Relevant SOLEIL II Parameters

Energy	2.75 GeV
H-Emittance	85 pm.rad
Circumference	353.96 m
Longitudinal tune (with HC)	0.000 35
Long. radiation damping	12.1 ms

LFB EXPERIMENT

We conducted an LFB experiment primarily to provide the group with practical experience in the longitudinal feedback operation, which is not implemented at our facility. During the experiment, two striplines from the existing TFB system were used. One stripline was employed to longitudinally excite the beam, while the second was used for the feedback operation. For beam detection, sum signals from BPM electrodes was send to developed font-end electronics for the detection of the timing of the bunch. Two important aspects were addressed before the experiment. First, `GdfidL` [13] simulations were performed to determine the frequencies at which the existing striplines could efficiently excite the beam. Second, an FIR filter was configured to provide effective feedback. Each bunch is kicked by a quantity which is obtained by convolving its past longitudinal positions with

* elene.kravishvili@synchrotron-soleil.fr

Content from this work may be used under the terms of the CC BY 4.0 licence (© 2026). Any distribution of this work must maintain attribution to the author(s), title of the work, publisher, and DOI.

ISBN: 978-3-95450-252-3 ISSN: 2673-5350 doi: 10.18429/JACoW-IPAC2026-WEP6109

TEST BENCH DESIGN AND FIRST MEASUREMENT RESULTS FOR THE PETRA IV FOFB ACTUATOR CHAIN

A. Amjad*, H. Schlarb, S. H. Mirza, S. Pfeiffer
Deutsches Elektronen-Synchrotron, Hamburg, Germany
J. M. Christmann, Technical University of Darmstadt, Darmstadt, Germany

Abstract

A fast orbit feedback system is currently being developed for the upcoming PETRA IV at DESY Hamburg. The performance of the FOFB system depends mainly on the frequency response of the subsystems, i.e. the corrector magnets, power supplies, cables and vacuum chambers. A test bench is being developed for measuring the field quality of FOFB corrector magnets and system identification of all integrated subsystems in the kHz range. The first design of the test bench and the initial idea for the different types of measurement methodologies to find the frequency response and magnetic field of corrector magnets are presented below. The subsystems integration and combined frequency response of the FOFB system will be measured in later stage of the project.

INTRODUCTION

The upcoming PETRA IV (a fourth-generation light source) is being designed at DESY. One of the main contributors to the beam quality in PETRA IV will be the Fast Orbit Feedback (FOFB) system [1]. The main purpose of the system is to stabilize the orbit of the beam by applying fast corrections based on the fast input data stream (130 kHz) of the Beam Position Monitors (BPM). The FOFB mainly includes the fast corrector magnets, power supplies, and digital process unit. The overall performance of the FOFB system depends on the frequency responses of the subsystems, such as the corrector magnets, the cables connecting the power supplies to the magnets, and the power supplies themselves, as well as the vacuum chamber under the fast correctors. The most critical subsystem is the corrector magnet in terms of both frequency response and field quality.
A test bench has been developed for the system identification of FOFB subsystems initially for prototypes and later to characterise the series production of the magnets. The following requirements dictate the design of the test bench:

- The fast corrector magnets must be characterised for the position-dependent field quality (DC) as well as the integrated transfer function (frequency sweep) in all three directions. This requires a movable stage to scan the 3D field strength.

- Beyond field quality, the measurement setup should support an integrated field measurement for the system identification of corrector magnets alone and for adding other subsystems in the loop, i.e., vacuum chamber, power amplifiers, and cables. The parasitic capacitance effect of the cables and its effect on the overall signal transfer to the magnet is important to be measured.

- A high-resolution spatial magnetic Hall probe to measure the position-dependent field as well as a search coil for integrated field measurement.

- The setup must also allow investigation of magnetic hysteresis under varying excitation conditions to capture non-linear effects and behaviours crucial to understanding residual fields.

- Frequency sweeps (position-dependent as well as integrated field) with constant amplitude, both with and without DC offset, are also required to evaluate the operating point dependence of transfer functions.

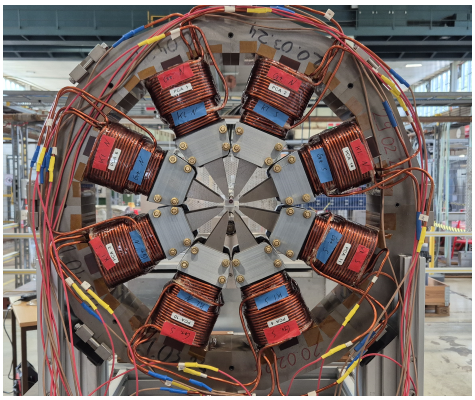

Figure 1: Prototype magnet I.A.

MEASUREMENT SETUP

Prototype Magnet PETRA IV's fast corrector is based on a special 8-pole design for both planes, ensuring better field quality than a dipole geometry per plane, as confirmed by simulations. The first prototype magnet (I.A) is shown in Fig. 1 and differs from the final design in terms of yoke material and lamination thickness; i.e., the yoke (86 mm in length) is made of 1 mm-thick Power-core 1400 AP lamination instead of about 0.3 mm-thick laminations. This first prototype serves as a benchmark for validating the simulations. Coil connections via external bridges allow reconfiguration from dipole to quadrupole mode for magnetic centre measurements. Those external bridges might exhibit greater resistance than direct connections. Lamination misalignments of approximately ±200 µm due to glueing were also observed.

* adeel.amjad@desy.de

Content from this work may be used under the terms of the CC BY 4.0 licence (© 2026). Any distribution of this work must maintain attribution to the author(s), title of the work, publisher, and DOI.

ISBN: 978-3-95450-252-3 ISSN: 2673-5350 doi: 10.18429/JACoW-IPAC2026-WEP6111

HIGHLIGHTS OF SPILL OPTIMIZATION SYSTEM USAGE AT GSI AND PROGRESS OF CONTROLS INTEGRATION

P. Niedermayer*, H. Bräuning, V. Kamerdzhiev, H. Liebermann, T. Milosic, D. Ondreka, R. Singh, J. Stadlmann, M. Traxler, M. Wiebusch, B. Zipfel
GSI Helmholtzzentrum für Schwerionenforschung, Darmstadt, Germany

Content from this work may be used under the terms of the CC BY 4.0 licence (© 2026). Any distribution of this work must maintain attribution to the author(s), title of the work, publisher, and DOI.

Abstract

At the GSI SIS18 synchrotron, the Spill Optimization System (SOS) has been established as a key tool to improve spill quality during resonant slow extraction. During the 2025 beam times, the SOS was routinely used with the radio frequency knock-out (RF-KO) method for several experimental campaigns, enabling improved spill stability and more efficient beam delivery to users under various operational conditions. The experience gained during these runs has also guided the ongoing integration of the SOS into the FAIR control system environment. This integration enables time-multiplexed operation of the system for multiple experiments running in parallel, leading to more efficient operation. It also aims to streamline the setup and monitoring of slow extracted spills through tighter coupling with accelerator controls and unified human and machine interfaces. This contribution summarizes the operational highlights from the 2025 beam times and discusses observed improvements in spill stability and beam usability for the experiments. In addition, the current status and outlook of the full control system integration efforts are presented.

INTRODUCTION

The heavy ion synchrotron SIS18 at GSI provides beams up to uranium to a broad experimental program [1]. Thereby, resonant slow extraction is used to drive particles into the extraction beam lines, either controlled by a quadrupole ramp or by a knock-out excitation (RF-KO). Controlling the temporal structure of the resulting particle spill is crucial to provide high-quality beams to experiments, avoiding pileup and maximizing the experimental yield. In particular, typically observed spill intensity fluctuations and drifts are detrimental to the efficient beam usage.

The Spill Optimization System (SOS) [2–4] was developed to optimize the extraction process using a combination of online feedback and iterative spill-by-spill optimization. Therefore, it digitizes detector signals, determines the average spill rate and the amount of spill intensity fluctuations (spill quality), and produces a tailored multi-band RF signal for the knock-out excitation system [5]. In the case of a quadrupole-driven extraction, it produces a tune ramp with a modulation [6] for the quadrupole power supply. As a result, the system improves the stability and reproducibility of spills, reduces intensity spikes causing pileup, and enables dynamic spill intensity control as required for ion therapy applications. A detailed description of the Spill Optimization System can be found in [2].

* p.niedermayer@gsi.de

OPERATIONAL HIGHLIGHTS

During the 2025 beam times the Spill Optimization System was used as a standalone system for RF-KO extraction. As the control system integration was still ongoing, the system was set up by an expert and operated only for selected experimental campaigns spanning multiple days. In total, the new system was used for 114 shifts, delivering optimized beams to different user communities, including the NUSTAR, R³B and HADES collaborations, bio physics groups and detector research programs [7–11].

HADES FAIR Phase 0 Gold Run

From 26. April through 5. May 2025 the HADES collaboration [12] continued its energy scan of gold collisions for the energy range of $\sqrt{s_{\mathrm{NN}}} = 1.96$ to $2.23\,\mathrm{GeV}$. A beam of $^{197}\mathrm{Au}^{65+}$ ions was delivered from SIS18 using the Spill Optimization System at a spill rate of $3 \cdot 10^6$ ions/s. This corresponds to an event rate recorded by the HADES detector of up to 12 kHz at the energy of $600\,\mathrm{MeV/nucleon}$. Among other factors, the increase compared to previous beam times with only 8 kHz [13] is possible because of the spill quality optimization, which reduces the probability of event pile-up. With the feedback system ensuring the delivery of the desired intensity throughout the full 10 s spill duration and considering 1.4 s spill breaks for injection and acceleration, a duty cycle of 88 % was achieved. Overall, a total of 6 billion events and 260 TB of data were recorded during the 216 hours of the beam time (Fig. 1). The collaboration reports that this is almost the number of anticipated events in the original beam time proposal, even though only about half of the requested beam time was granted.

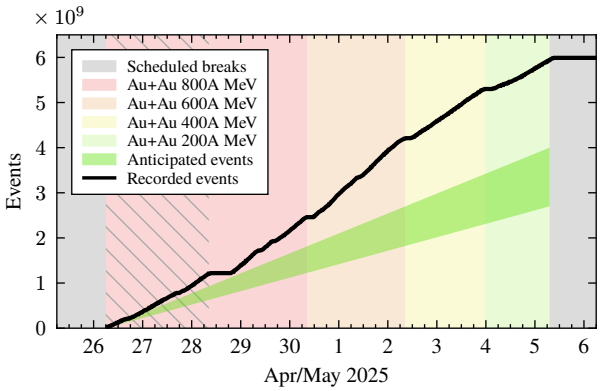

Figure 1: Events recorded by the HADES detector at several energies during the 2025 gold beam time. The hatched area marks the early start on the weekend before the scheduled beam time. The green wedge marks the event rate assumed in the experiment proposal without consideration of the SOS.

ISBN: 978-3-95450-252-3 ISSN: 2673-5350 doi: 10.18429/JACoW-IPAC2026-WEP6113

SYNCHRONIZED DEMULTIPLEXING OF A BEAM CURRENT SIGNAL FOR A BUNCH-BY-BUNCH LONGITUDINAL FEEDBACK SYSTEM

C. Reinwald, H. Klingbeil[1], Technical University of Darmstadt, Darmstadt, Germany
[1]also at GSI Helmholtzzentrum für Schwerionenforschung GmbH, Darmstadt, Germany
K. Groß, M. Hardieck, D. Lens,
GSI Helmholtzzentrum für Schwerionenforschung GmbH, Darmstadt, Germany

Abstract

High-intensity operation of the new SIS100 synchrotron is expected to be sensitive to coupled-bunch and single-bunch instabilities [1]. To counter these effects, a Bunch-By-Bunch Longitudinal Feedback System is currently in development. Operating this feedback system during acceleration and for arbitrary revolution frequencies presents several challenges. Thereby, this article focuses on the timing regarding the processing of a beam current signal provided by a Fast Current Transformer. This signal is utilized as main input for the feedback system in order to detect longitudinal beam oscillations of individual bunches. Therefore, it is demultiplexed into a sequence of segments, each containing the beam current signal of a single bucket. Afterwards, those segments are processed to extract potential oscillation components. The timing of the demultiplexing is controlled via harmonic RF reference signals that must be calibrated. The functionality of this demultiplexing process has been verified through measurements during a machine experiment with beam in July 2025.

INTRODUCTION

In order to counter longitudinal coupled-bunch and single-bunch instabilities during operation of the synchrotron SIS100 currently constructed at the GSI Helmholtz center for heavy-ion research in Germany, a Bunch-By-Bunch Longitudinal Feedback System is in development. A schematic showing the basic topology of the system is provided in Fig. 1.

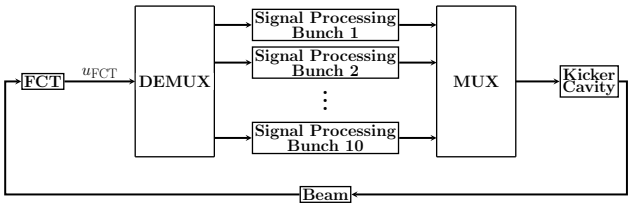

Figure 1: Schematic visualizing the basic topology of the Bunch-By-Bunch Longitudinal Feedback System.

In general, the system utilizes a beam current signal u_{FCT} provided by a Fast Current Transformer (FCT) to detect longitudinal oscillations of individual bunches. An example for u_{FCT} is given on the left-hand side of Fig. 2. This signal is distributed among several, identical signal processing units using a demultiplexer (DEMUX). Thereby, each of these units receives only parts of the FCT signal associated with one specific bunch resulting in signals like $u_{\mathrm{FCT,b1}}$ shown on the right-hand side of Fig. 2. This separation enables an individual monitoring of the single bunches in the ring by their dedicated signal processing units which, in case longitudinal bunch oscillations are detected, generate corresponding feedback signals to damp these oscillations. All feedback signals are combined to one final RF kicker signal by a multiplexer (MUX) which is then applied on the beam through a kicker cavity.

This contribution focuses on the demultiplexing of the beam current signal with a special focus on the synchronization of this process with the synchrotron operation. Thereby, the functionality of this system independent of the current RF frequency is ensured. Further information regarding the working principles of the complete Bunch-by-Bunch Longitudinal Feedback System can be found in [2–4].

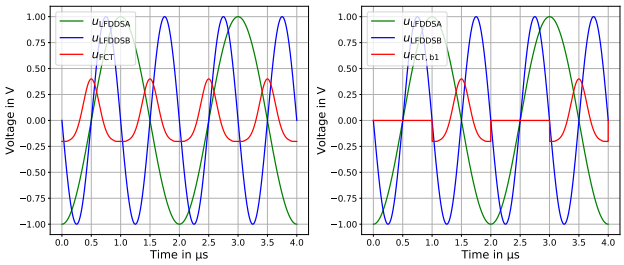

Figure 2: The diagram on the left-hand side shows a schematic of a beam current signal u_{FCT} provided by an FCT and corresponding RF reference signals u_{LFDDSA} and u_{LFDDSB}. Thereby, a harmonic number of $h = 2$ is assumed. The diagram on the right-hand side illustrates a demultiplexed beam current signal $u_{\mathrm{FCT,b1}}$ for bunch one.

SETUP FOR THE DEMULTIPLEXING OF THE BEAM CURRENT SIGNAL

Figure 3 shows a simplified block diagram of the setup used for the demultiplexing of the beam current signal. It includes the DDS modules Longitudinal Feedback DDS A (LFDDSA) and Longitudinal Feedback DDS B (LFDDSB) for the generation of the harmonic reference signals u_{LFDDSA} and u_{LFDDSB} visualized in Fig. 2 using Direct Digital Synthesis (DDS). Additionally, the system includes two Calibration Electronics Modules (CEL) to adjust the phase of the reference signals, a demultiplexer module (DEMUX) to forward the FCT signal to various output ports and, finally, a Trigger Unit to control the switching of the demultiplexer. Various other components like amplifiers, splitters, short coaxial transmission lines, etc. between the main blocks have been omitted for the sake of simplicity.

Content from this work may be used under the terms of the CC BY 4.0 licence (© 2026). Any distribution of this work must maintain attribution to the author(s), title of the work, publisher, and DOI.

ISBN: 978-3-95450-252-3 ISSN: 2673-5350 doi: 10.18429/JACoW-IPAC2026-WEP6114

TOWARDS FAST ORBIT CORRECTION: A MODULAR AND EXTENSIBLE GLOBAL ORBIT FEEDBACK SYSTEM

A. Aljadaa*, A. Ahmad, A. Abbadi, H. Al-Mohammad, M. Attal, S. Kasaei
SESAME Synchrotron, Allan, Jordan

Abstract

At SESAME, orbit correction was previously performed every 5 seconds (0.2 Hz) using MATLAB. However, due to the limited correction speed and MATLAB's unsuitability for production environments, a complete in-house implementation of the system was undertaken using the C programming language. This migration enabled significantly faster correction, a modular architecture to support various control and estimation algorithms, and feedforward control.

INTRODUCTION

At SESAME, the orbit feedback system was redesigned to address the limitations of the previous MATLAB-based implementation, which operated at only 0.2 Hz. The new system, implemented in C, achieves sampling rates up to 10 Hz, enabling correction of higher-frequency disturbances that were previously unaddressable.

The system architecture was designed with modularity as a core principle, facilitating easy modification and integration of different control and estimation algorithms. The complete ecosystem comprises multiple integrated components: C-based core implementation for orbit correction, an EPICS Input/Output Controller (IOC) for process variable management, a Qt-based graphical user interface for system monitoring and control, Python scripts for offline performance evaluation, and MATLAB/Simulink tools for system simulation and controller tuning.

SYSTEM LAYOUT

The orbit feedback system consists of three primary software components that work in concert to achieve orbit correction: a C-based core correction engine, an EPICS IOC, and a Qt-based graphical user interface.

The core correction engine, implemented in C, executes the orbit feedback algorithm at a 10 Hz sampling rate. This component reads slow acquisition (SA) beam position data from the Beam Position Monitors (BPMs) electronics (Libera Brilliance + [1]), applies the selected estimation and control algorithms, and computes the corresponding corrector magnet current setpoints. The modular design allows configurable selection of different controllers and state estimators.

The EPICS IOC [2] serves as the interface layer between the correction engine and the control system infrastructure. It exposes all relevant process variables for both monitoring and configuration, including BPM readings, corrector setpoints, controller gains, and diagnostic signals.

The Qt-based graphical user interface provides operators with comprehensive system visualization and control capabilities. The GUI displays live orbit data in multiple representations: time-domain waveforms for tracking transient behavior, frequency-domain spectra for identifying harmonic disturbances, and spatial orbit distributions for visualizing beam position at all BPM locations. For postmortem analysis, time-resolved plots enable detailed investigation of system behavior following fault conditions. Configuration parameters can also be adjusted through the GUI.

CONTROL SYSTEM DESIGN

The orbit feedback system employs a Singular Value Decomposition (SVD) based correction algorithm [3] to compute optimal corrector magnet current setpoints. This approach decomposes the orbit response matrix into orthogonal eigenmodes, enabling decoupled correction of individual orbit modes while providing inherent numerical stability.

The fundamental correction equation relates the required corrector current changes to the measured orbit deviations:

$$\Delta I = V \cdot S_{\text{inv}} \cdot C_z \cdot U^T \cdot \Delta x,$$

where ΔI is the vector of corrector current changes, Δx represents the orbit error relative to the golden orbit, U and V are the left and right singular vectors of the orbit response matrix, S_{inv} is a diagonal matrix containing the inverse singular values with regularization, and C_z is the controller transfer function in discrete time (z-domain). The SVD formulation allows selective mode correction and natural implementation of Tikhonov regularization [4].

The system incorporates RF frequency adjustment as a primary correction mechanism. Changes in RF frequency modulate beam energy to match the design energy. RF correction is applied first to stabilize beam energy, followed by corrector magnets for fine orbit adjustment. This approach reduces the correction load on the magnets and prevents corrector saturation.

Figure 1 illustrates the control loop architecture. The control system integrates several components: state estimation to filter noisy BPM measurements, feedback control for steady-state and dynamic correction, and feedforward compensation for predictable disturbances. Additionally, regularization techniques are implemented to prevent excessive corrector activity.

Estimator

Raw BPM measurements can contain noise from various sources. To address this, the system implements three selectable state estimation algorithms, each offering different tradeoffs between noise rejection and response time.

* amro.aljadaa@sesame.org.jo

Content from this work may be used under the terms of the CC BY 4.0 licence (© 2026). Any distribution of this work must maintain attribution to the author(s), title of the work, publisher, and DOI.

ISBN: 978-3-95450-252-3 ISSN: 2673-5350 doi: 10.18429/JACoW-IPAC2026-WEP6115

AUTOMATED SOFTWARE WORKFLOW FOR ACCELERATOR CONTROL SYSTEMS USING CONTAINERIZATION

A. Aljadaa*[1], A. Ahmad[1], A. Abbadi[1], M. Alzubi[1,2], R. Khrais[1]
[1]SESAME Synchrotron, Allan, Jordan
[2]Princess Sumaya University for Technology, Amman, Jordan

Abstract

A new software workflow has been developed and deployed at SESAME that solves several issues large facilities may face in their lifecycle. The workflow includes containerizing software in independent units, orchestrating those units from a central manager, managing installation, release, and rollback of deployments, and automating the process through a continuous deployment pipeline. This workflow reduces development and deployment time while eliminating human error.

INTRODUCTION

Managing hundreds of Input/Output Controllers (IOCs) and Graphical User Interfaces (GUIs) in a multi-network facility is challenging due to various sources of failure: hardware failures in servers and networks, operating system issues like high CPU and memory usage, and application issues such as crashes and memory leaks. Traditional manual deployment workflows compound these challenges by introducing human error.

This paper presents an automated workflow implemented at SESAME that containerizes software, orchestrates deployments via Kubernetes, manages releases with Helm, and automates the entire process through continuous deployment. Similar approaches have been successfully implemented at other synchrotron facilities [1]. This approach improves operational efficiency and ensures deployment consistency.

The work focuses on IOCs and GUIs built on the Linux operating system. This paper discusses the following stages: containerization, orchestration with Kubernetes, release management with Helm, and continuous deployment automation.

Figure 1 illustrates the workflow, which is discussed in detail in the following sections.

This workflow has been deployed in production for all machine IOCs at SESAME Synchrotron Light.

CONTAINERIZATION

To address environment inconsistencies between development and production, IOCs and graphical user interfaces are containerized using Docker [2], which was selected for its widespread adoption and robust ecosystem. The containers are configured to run on the host network for direct network access.

All images are stored and versioned in a private Docker registry. Image versioning facilitates rapid rollbacks in case

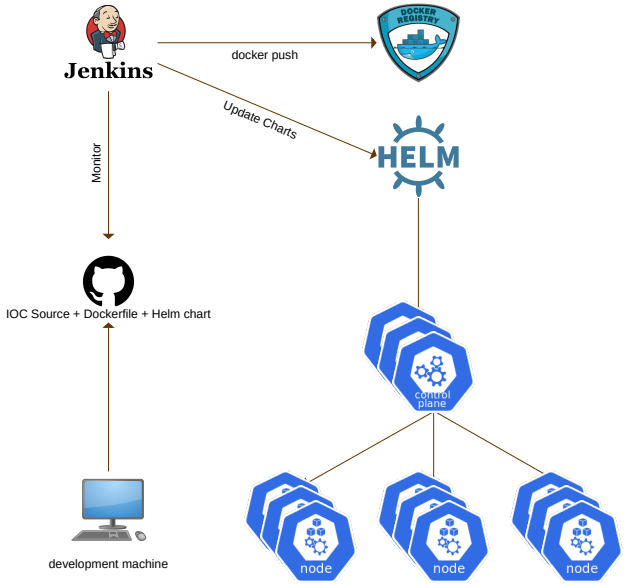

Figure 1: Complete workflow from development to production deployment.

of deployment issues. To optimize these images, a multilayer approach is followed when building Docker images. This modularizes the development process by creating images for common dependencies, thereby reducing development time and standardizing the work. Moreover, this approach reduces the final image size by keeping only the binaries required to run the IOC. The size is reduced to approximately 25 MB instead of several hundred megabytes or even gigabytes.

Figure 2 illustrates the multilayer approach, demonstrating both the modular organization of dependencies and how intermediate build layers are discarded to produce a lightweight Alpine runtime image.

While containerization provides isolation and consistency, centralized management of these containers requires orchestration.

ORCHESTRATION

To manage Docker IOCs from a central node, Kubernetes [3] was selected as the container orchestration tool.

Kubernetes plays a vital role in IOC management, acting as a central manager that provides a global view of the entire system and aggregates logs. Two complementary tools are employed for system management: the Kubernetes dashboard and k9s [4]. The dashboard provides a web-based graphical interface for interactive monitoring and control, while k9s delivers a terminal-based UI with several advantages, including graphics independence that enables

* amro.aljadaa@sesame.org.jo

Content from this work may be used under the terms of the CC BY 4.0 licence (© 2026). Any distribution of this work must maintain attribution to the author(s), title of the work, publisher, and DOI.

ISBN: 978-3-95450-252-3 ISSN: 2673-5350 doi: 10.18429/JACoW-IPAC2026-WEP6116

TUNE COMPENSATION FOR INSERTION DEVICES MOTION AT THE SOLARIS STORAGE RING

M. Ünal†, R. Panas, A.I. Wawrzyniak, W. Wiatrowska
SOLARIS National Synchrotron Radiation Centre, Krakow, Poland

Abstract

Precise control of betatron tune is essential for maintaining beam stability in modern synchrotron light sources. At the SOLARIS storage ring, undulator gap and phase changes present a dominant source of tune perturbations. This study presents a method for local tune compensation during the gap and phase motion of APPLE II type undulator, installed upstream of a dedicated beamline.

The approach, seen in other light sources, employs a tune-feedback system based on two local quadrupoles and two global magnet families driven by a feed-forward table generated from a systematic scan of the undulator parameters (gap, phase) and the corresponding tune shifts. Prior to table generation, the magnets' response matrices for both tune planes were independently obtained.

INTRODUCTION

The SOLARIS synchrotron operates at 1.5 GeV and provides light to seven independent beamlines. Three of them are using APPLE II type undulators for producing linear, circular, or elliptical polarization of high-intensity radiation [1]. Such polarization, particularly that generated via phase shift, induces changes in beam properties, which can affect the stability of experimental conditions. Maintaining small tune variations while preserving other beam parameters is contributing for synchrotron operation.

The current approach is using feed-forward table, for one APPLE II type undulator with the strongest influence on tune [2]. The method includes the betatron tune measurements by exciting coherent transverse oscillations with dipole kicker (horizontal) and pinger (vertical) magnets. Tunes are calculated from turn-by-turn BPM signals using the FFT analysis.

Next, response matrices were measured for the selected global magnet families, including two local quadrupole families positioned around the undulator:

- Defocusing Pole-Face Strips (PFS).
- Focusing quadrupoles (SQFO).

The proposed method ensures effective and reproducible mitigation of tune perturbations during undulator motion, enabling stable machine performance and improved beam quality at SOLARIS. The tune shift was then measured across all undulator gap and phase settings. Finally, using the SVD method, a look-up table was constructed, containing undulators settings and corresponding correcting magnets currents.

†corresponding author: maria.unal@uj.edu.pl

The table was tested in standard operation conditions with both Fast and Slow Orbit Correction Feedback system active. The results and step-by-step procedure are presented in the following sections. Also, a dedicated software was created to coordinate automated scans, response matrix acquisition, and real-time feed-forward correction.

METHODOLOGY

Response Matrices Creation

The response matrix consists of four columns corresponding to two local and two global quadrupole families, and two rows representing horizontal and vertical tune response.

The measurement was performed with the undulator in the open-gap configuration. Quadrupole currents were varied in steps of 0.05 A for focusing quadrupoles and 0.03 A for defocusing magnets, with ±10 steps around the nominal operational value. For each current setting, three tune measurements were recorded, and the median value was used for analysis. The tune was measured by exciting beam oscillations using kicker magnets with an excitation voltage of 60 V. The measurement results are presented in Fig. 1.

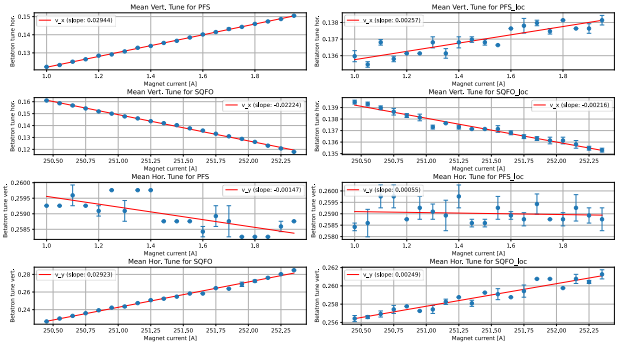

Figure 1: Betatron tune measurements with respect to quadrupole currents. Red line represents the linear fits used to derive response matrix coefficients.

After the measurements, the coefficients a of the linear model was determined from:

$$\nu = a \cdot I + b \, . \tag{1}$$

Where ν denotes fractional tune value and I the quadrupole current. The obtained coefficients are summarized in Table 1. Each measurement was repeated three times per magnet to estimate statistical uncertainty.

Content from this work may be used under the terms of the CC BY 4.0 licence (© 2026). Any distribution of this work must maintain attribution to the author(s), title of the work, publisher, and DOI.

ISBN: 978-3-95450-252-3 ISSN: 2673-5350 doi: 10.18429/JACoW-IPAC2026-WEP6117

BUNCH-BY-BUNCH PHASE PICK-UP SYSTEM IN THE SPS

A. Spierer*, P. Baudrenghien
CERN, Geneva, Switzerland

Abstract

As part of the High-Luminosity LHC (HL-LHC) project, the Super Proton Synchrotron (SPS) Low-Level RF (LLRF) system has undergone a major upgrade during the machine shutdown in 2019-20 to meet the performance requirements of the LHC ion program and high-intensity proton beams. A key development in this context is the implementation of a bunch-by-bunch measurement chain, designed to provide high-resolution diagnostics and bunch-by-bunch phase feedback capability.

This tool is particularly valuable for the ion slip-stacking RF manipulations where precise bunch-masking is required. In addition, it serves as a diagnostic tool to investigate beam loading effects by directly comparing the cavity voltage with the phase evolution of individual bunches. The system is implemented on the MicroTCA platform and employs 5 Gsps digitization of the beam signal from a wall current monitor (WCM).

This paper presents the operational results and commissioning challenges of the new acquisition and phase loop system.

INTRODUCTION

The SPS LLRF upgrade for the HL-LHC era aims to support increasingly demanding beam conditions, including high-intensity proton beams and complex ion manipulation schemes such as slip-stacking. These scenarios impose stringent requirements on longitudinal diagnostics and feedback systems.

The operational narrowband phase measurement system, based on a 200 MHz resonant pick-up and undersampling at 125 Msps, provides averaged phase measurements but lacks the temporal resolution required to resolve individual bunch dynamics.

To address this limitation, a wideband bunch-by-bunch acquisition system has been developed, based on direct digitization at 5 Gsps of a WCM signal that provides the longitudinal bunch profile of the ~3 ns long bunches.

The wideband system overcomes the ~100 ns time constant limitation of the narrowband system, which averages over multiple bunches for 5 ns or 25 ns spacing. However, for low bunch count beams, the absence of resonant averaging reduces phase sensitivity.

It also improves the bunch mask resolution, which is essential for ion slip-stacking operations [1], allowing both phase loops to remain active during ion beams overlap.

Additionally, the system increases the effective bandwidth of the longitudinal damper, now limited primarily by the RF cavity response (~2 MHz).

* arthur.spierer@cern.ch

As a diagnostic tool, it enables:

- Observation of longitudinal instabilities (dipolar and quadrupolar), bunch-by-bunch and turn-by-turn
- Direct comparison of beam phase and cavity voltage
- Improved time-alignment of signals from cavities and pick-up

SYSTEM IMPLEMENTATION

The wideband phase acquisition system is implemented on a MicroTCA platform using an AFCZ board (Ultrascale+™ MPSoC) and Vadatech® FMC217 mezzanine board, synchronized via White Rabbit. The beam signal is acquired from a WCM and digitized at 5 Gsps, with 12 bit resolution. It integrates with the Beam-Control LLRF [2]. The phase and amplitude of the 200 MHz RF component of the individual bunch profiles are transmitted over a 10 Gigabit link, as shown in Fig. 1.

Signal Processing

Phase extraction is performed using a custom FFT algorithm. Only the complex bin corresponding to the RF frequency is computed, equivalent to IQ demodulation but optimized for parallel processing.

The input stream is sliced into 32-sample windows centered on each bunch using a beam-synchronous Numerically Controlled Oscillator (NCO) interpolated to the 5 Gsps data rate. The data is tagged such that the first bunch can be detected and synchronized. For additional details on the signal processing and hardware, refer to [3].

For ion slip-stacking, the processing chain is duplicated to track two RF systems running at different frequencies during a part of the cycle. To merge the two streams, two FIFO interfaces store the samples arriving at different rates, while the read logic waits for data to be available on both channels. A multiplexer selects which RF system a bucket belongs to. The output stream is then used by the two beam-phase loops, which average on their respective bucket ranges. Figure 1 shows the data-flow.

COMMISSIONING CHALLENGES

Calibration and Delay Compensation

The signal propagation delay of 1.4 us between the pick-up and the ADC introduces frequency-dependent phase shift. This must be compensated prior to slicing to maintain alignment with the bunch profile. The phase shift is automatically compensated by the RFNCO, which computes a phase correction in real time using the instantaneous RF frequency.

Content from this work may be used under the terms of the CC BY 4.0 licence (© 2026). Any distribution of this work must maintain attribution to the author(s), title of the work, publisher, and DOI.

ISBN: 978-3-95450-252-3 ISSN: 2673-5350 doi: 10.18429/JACoW-IPAC2026-WEP6118

UPGRADE OF THE LHC LOW-LEVEL RF BEAM-CONTROL FOR THE DIGITAL FREQUENCY DISTRIBUTION OVER WHITE-RABBIT

A. Spierer*, T. Gingold, A. Goujon, G. Hagmann, M. Jaussi, L. Kaffka, H. Timko,
CERN, Geneva, Switzerland

Abstract

In preparation for the High-Luminosity LHC (HL-LHC) era, a significant upgrade to the LHC Low-Level RF (LLRF) Beam-Control system is being implemented. The installation of crab cavities during Long Shutdown 3 (LS3, 2026-29), together with the obsolescence of existing components, necessitates a modernization of the LHC LLRF architecture.

The upgraded Beam-Control system – based on MicroTCA and VME hardware – replaces the frequency program and reconstructs a digital master RF. These frequencies are transmitted over a White-Rabbit (WR) network in the form of Frequency Tuning Words (FTW) to maintain synchronization among the distributed RF devices. This approach enables a scalable RF distribution infrastructure across the accelerator complex and experiments, with improved phase stability and reduced noise.

This paper presents the motivation and design of the upgraded system, including the method used to achieve robust phase synchronization over WR. Finally, it shows results obtained from a dedicated test with beam acceleration in the LHC.

MOTIVATION

In the LHC, LLRF signals are distributed throughout the machine to synchronize equipment with the circulating beam. This equipment includes experiment triggers, beam instrumentation, and RF cavity controllers. For the HL-LHC, crab cavities and their controllers will be installed around the interaction points, several kilometers away from the LLRF Beam Control system located at LHC Point 4.

To support this upgrade, a digital RF distribution over WR has been deployed, based on a first implementation in the SPS [1]. The concept is to send frames containing FTWs, reference phases, and control signals over the WR network. These are received and applied to a Numerically Controlled Oscillator (NCO) in the RF nodes with deterministic latency.

This new distribution is installed in parallel with the existing analog-over-fiber system, allowing performance comparisons prior to LS3. This project involves not only the RF group but also the experiments, controls, and beam instrumentation groups, as they benefit from the improved performance and flexibility of the new system.

This architectural choice offers several advantages: built-in mechanisms to compensate for temperature related phase drifts, cable length compensation, a common infrastructure for RF and machine timing, scalability through Ethernet networking, and progress toward a unified distribution across the accelerator complex. In the case of the LHC, it also provides an opportunity to replace obsolete components.

The main challenges are ensuring a high system availability, phase recovery after power cycles, and preservation of phase noise and latency.

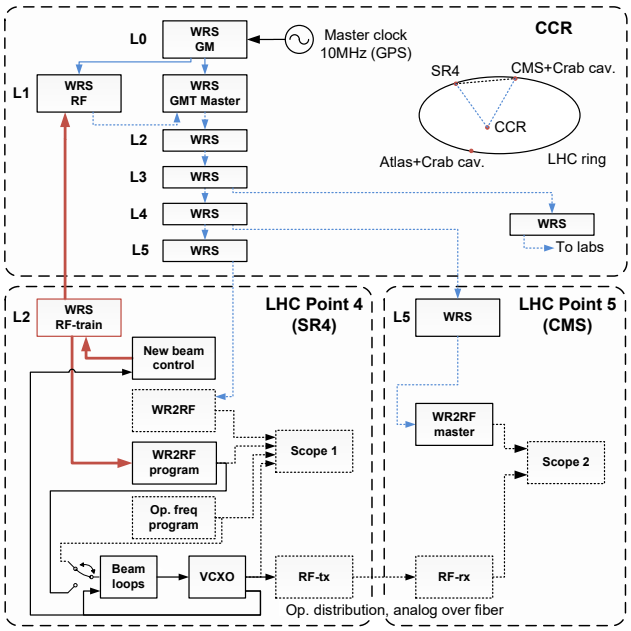

Figure 1: Test setup in the LHC. In red: the latency critical path, in blue: RF distribution over the general timing network. All dashed line equipment will be decommissioned after LS3.

IMPLEMENTATION

Hardware

The Beam-Control upgrade is based on the AFCZ MicroTCA board and WR2RF VME board [2]. They replace several VME-based modules for the function generator (FGC), frequency program, analog and optical distribution.

The function generator is now embedded in the AFCZ FPGA and plays the predefined frequency program of the LHC (around 400 MHz). The frequency is converted to an FTW and transmitted within the WR Ethernet frame (Table 1) once per beam revolution. The RF receivers such as the WR2RF board, reconstruct the analog RF from the received frame.

The master oscillator (VCXO) is locked to the reconstructed analog frequency program via the existing synchro loop and serves as the reference for the accelerating cavities. In the AFCZ, a digital PLL is locked to the VCXO using a 125 MS/s ADC and its frequency correction is used to

* arthur.spierer@cern.ch

Content from this work may be used under the terms of the CC BY 4.0 licence (© 2026). Any distribution of this work must maintain attribution to the author(s), title of the work, publisher, and DOI.

ISBN: 978-3-95450-252-3 ISSN: 2673-5350 doi: 10.18429/JACoW-IPAC2026-WEP6120

AN AUTOMATED PRODUCTION TEST SUITE FOR CAPACITIVE ALIGNMENT SENSOR CONDITIONING ELECTRONICS*

R. Fernandez Bautista†, B. Spoelstra‡, I. Ustenko, J. Kampp, A. Martinez Landete, M. Sosin
European Organization for Nuclear Research (CERN), Geneva, Switzerland

Abstract

The High Luminosity upgrade of the Large Hadron Collider (HL-LHC) at CERN requires exceptional alignment accuracy of accelerator components to reach the luminosity targets and to ensure reliable beam operation. This accuracy is achieved with the help of the Full Remote Alignment System (FRAS), which employs a capacitive Wire Positioning System (WPS) to monitor the position of magnets, RF cavities, and other accelerator components relative to a stretched, conductive, reference wire. Each WPS sensor measures distance offsets with respect to this reference wire with sub-micron-level resolution. The sensors are connected via dedicated cables to specially designed WPS conditioning electronics for signal processing and data acquisition. These modules operate as application specific cards within CERN's Distributed Input/Output Tier (DI/OT), a standardized framework designed for modular electronics operating in radiation-exposed environments.

To support the large-scale production and verification of over 400 WPS conditioning modules, an automated Production Test Suite (PTS) has been developed. The PTS streamlines firmware programming, automates test execution and ensures full traceability through integration with CERN's Enterprise Asset Management (EAM) platform and the Engineering Data Management Service (EDMS). This paper presents the design and validation of the PTS for WPS conditioner electronics, focusing on hardware–software integration and its role to enable reliable production testing for the HL-LHC.

INTRODUCTION

The HL-LHC aims to increase the collider integrated luminosity by roughly one order of magnitude over its operational period, tightening tolerances on the alignment of magnets, crab cavities and other interaction-region components to the sub-100 µm level over several hundred metres [1, 2].

The FRAS achieves this with sensors to monitor and remotely correct these positions from the CERN Control Centre [3]. One of these types of sensor is the WPS sensor which, mounted on to the machine elements, measures the differential capacitance between a ground-referenced conductive wire and four electrodes inside an aluminium housing [4].

The associated WPS Conditioner is a radiation-tolerant DI/OT [5] application card that excites the sensor, performs charge-balancing readout and provides digitised position data to a DI/OT Systemboard [6]. With over 400 of these units to be manufactured and tested, a scalable and reproducible validation process is required, given the complexity of the WPS system.

WPS SYSTEM AND VALIDATION CHALLENGES

WPS Sensor and Conditioner

The WPS system combines capacitive sensors and dedicated conditioner electronics to measure transverse displacements of a reference wire with sub-micron-level precision. The WPS sensor (see Fig. 1a) consists of a split aluminium body with a circular bore and four printed electrodes on flexible PCBs inside the bore [7]. A grounded Carbon–Kevlar wire of 0.8 mm diameter passes through all sensors along each side of the interaction-region.

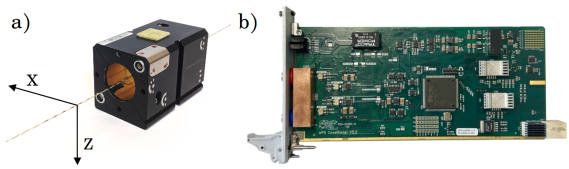

Figure 1: a) WPS sensor with Carbon-Kevlar wire passing through it. b) WPS Conditioner board.

Opposing electrode pairs form two differential channels measuring vertical (Z) and horizontal (X) displacement of the wire relative to the sensor centre. The WPS Conditioner (see Fig. 1b) excites the electrodes with a sinusoidal reference in the 1 kHz to 10 kHz range, drives an active shield on the sensor and cables and uses feedback-controlled charge balancing to obtain a value proportional to the displacement.

Limitations of Manual Validation

Validating the performance of this system currently relies on a dedicated bench (see Fig. 2) using a physical WPS sensor mounted in a mechanical jig with a real wire that can be positioned at five test points by rotating two knobs.

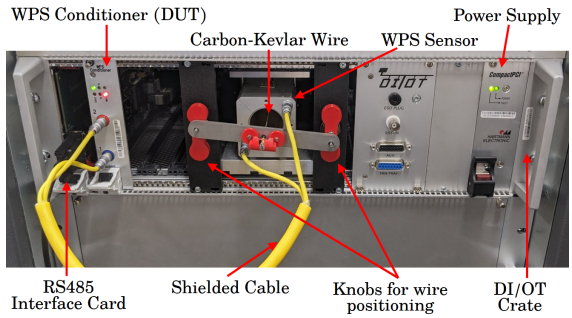

Figure 2: Manual WPS validation bench (to be replaced).

* Work supported by the HL-LHC project at CERN.
† roberto.fernandez@cern.ch
‡ info@baukespoelstra.com

Content from this work may be used under the terms of the CC BY 4.0 licence (© 2026). Any distribution of this work must maintain attribution to the author(s), title of the work, publisher, and DOI.

ISBN: 978-3-95450-252-3 ISSN: 2673-5350 doi: 10.18429/JACoW-IPAC2026-WEP6121

HIGH-PRECISION THREE-AXIS TESLAMETER FOR SUPERCONDUCTING MAGNET ALIGNMENT OF A GYROTRON AT THE SWISS PLASMA CENTER*

D. Popovic Renella, Z. Mitrovic, S. Milosevic, SENIS AG, Baar, Switzerland,
J. Genoud, École Polytechnique Fédérale de Lausanne, Swiss Plasma Center (SPC), Lausanne, Switzerland

Abstract

This paper presents a novel high-precision three-axis Teslameter and its application for magnetic field alignment of a superconducting magnet prior to gyrotron installation, at the Swiss Plasma Center. The instrument integrates an advanced 3-axis Hall sensor with an ultra-compact sensitive volume of 0.10×0.01×0.10 mm³, enabling true point-like vector field measurements. We describe the sensor architecture, Teslameter performance, and calibration procedures, including precise orthogonality characterization. The Teslameter achieves DC accuracy better than 100 ppm and 1 µT resolution. The system was employed to verify and optimize magnetic field alignment for high-power gyrotrons, vacuum electronic devices generating sub-terahertz radiation via the cyclotron maser instability. Efficient operation of these devices requires that the magnetic field axis remain confined within a cylinder of 0.15 mm diameter over a 600 mm length to maintain correct electron–field interaction. Using the Teslameter, the magnetic field was mapped with high accuracy, enabling fine realignment of the superconducting magnet and ensuring the electron beam coincides with the electric field maximum of the transverse electric (TE) mode. This methodology guarantees optimal gyrotron performance, contributing to reliable and efficient operation of Electron Cyclotron Resonance Heating and Current Drive systems in magnetic confinement fusion research.

INTRODUCTION

High-power gyrotrons are critical components in Electron Cyclotron Resonance Heating (ECRH) and Current Drive systems used in magnetic confinement fusion research. Their efficient operation depends on precise alignment of the magnetic field with respect to the electron beam. Even minor deviations can significantly affect device performance and stability. To meet stringent alignment requirements, advanced measurement instrumentation is necessary. This work presents a high-precision three-axis Teslameter developed to perform accurate vector magnetic field measurements and enable fine alignment of superconducting magnets used in gyrotron systems.

*Swiss Plasma Center (SPC): https://www.epfl.ch/research/domains/swiss-plasma-center/

HIGH-PRECISION 3-AXIS TESLAMETER

The 3MH6-E Teslameter (see Fig. 1) combines a highly compact three-axis Hall sensor with advanced analog and digital electronics within a modular measurement platform. The instrument offers four selectable magnetic field ranges: ±100 mT, ±500 mT, ±2 T, and ±20 T. It achieves a DC accuracy better than 100 ppm, while reaching a resolution below 1 ppm in the ±2 T range. The 3MH6-E system features full interchangeability of its Hall probes. Each probe can be connected to any compatible electronics unit without compromising performance, maintaining an overall DC accuracy better than 100 ppm (0.01%). This flexibility is enabled by independent calibration of both the probe and the electronic unit.



Figure 1: 3-axis Teslameter 3MH6-E, reproduced from SENIS website [1].

The signal processing architecture includes low-noise amplification, 24-bit analog-to-digital conversion, and digital correction algorithms addressing linearity, thermal drift, and orthogonality deviations. Integrated temperature sensors continuously monitor both the probe and the electronics, allowing real-time thermal compensation. With sampling rates of up to 7.5 kSPS, the device is also suitable for time-varying magnetic field measurements.

The 3MH6-E is widely adopted in reference laboratories where traceable and absolute magnetic field measurements are required. Typical applications include characterization of magnetic field distributions in undulators, insertion devices, and superconducting magnets. For instance, within the HITRIplus project coordinated by CERN, the

Content from this work may be used under the terms of the CC BY 4.0 licence (© 2026). Any distribution of this work must maintain attribution to the author(s), title of the work, publisher, and DOI.

ISBN: 978-3-95450-252-3 ISSN: 2673-5350 doi: 10.18429/JACoW-IPAC2026-WEP6122

RADIATION SAFETY CHALLENGES ASSOCIATED WITH THE VERY LOW EMITTANCE STORAGE RING UPGRADE OF SYNCHROTRON SOLEIL

J.-B. Pruvost, P. Berkvens, P. Brunelle, F. Marteau, L. S. Nadolski, C. Tournier
Synchrotron SOLEIL, Saint-Aubin, France

Abstract

The SOLEIL II storage ring upgrade project aims at reducing the horizontal emittance of the electron beam from 4 nm.rad for the present ring down to less than 100 pm.rad for the SOLEIL II new 4th generation storage ring. It is based on the replacement of the present double bend achromat by a mixed multi-bend achromat, the so-called 7BA-4BA lattice and a general use of permanent magnets (PMs) for both dipoles and quadrupoles. The corresponding long shutdown is scheduled between October 2028 and October 2030, when user operation will resume. Compared to the present storage ring, SOLEIL II will operate with a slightly reduced beam lifetime and, consequently, with increased beam loss rates. This leads to many challenges in terms of Radiation Safety and Radiation Damage assessments. This paper will present the main characteristics of the SOLEIL II storage ring upgrade and the corresponding main challenges in Radiation Safety to maintain the Experimental Hall as a non-radiation area. A detailed shielding design study is required by the Authority for Nuclear Safety and Radiation Protection (ASNR) as a basis for the authorization request that SOLEIL will submit to recover the ASNR license before restarting the accelerators by the end of 2029. This paper also provides a status update on the shielding design study, mainly driven by extensive use of the FLUKA Monte Carlo code, the remaining radiation safety challenges to be addressed, and the foreseen effects of ionizing radiation exposure of the PMs.

INTRODUCTION

The compact 2.75-GeV, 354-m Storage Ring (SR) will ultimately reach a 50 pm round-beam emittance using an atypical 7BA–4BA lattice [1, 2], extensive use of PM technologies, nearly 100% NEG-coating, 12-mm diameter vacuum chambers, a new in-vacuum nonlinear kicker for transparent top-up operation, new 4th-harmonic cavities, and 10-µm magnet alignment [3]. From a radiation safety point of view, the challenge lies in ensuring that the present SR shielding is as effective as today for the new ring, considering that it will induce more continuous beam losses because of its reduced beam lifetime compared to SOLEIL's.

MATERIALS AND METHODS

To accurately model the behavior of lost beam particles, the loss distribution in the SR is derived from detailed pyAT [4] simulations provided by the Accelerator Physics Group. These calculations include spatial loss probability distributions and the 6D phase-space characteristics of lost electrons. Furthermore, the model accounts for horizontal and vertical physical apertures, including the minimum gaps of in-vacuum insertion devices (IDs), as well as the kinetic energy deviation of the lost beam. All these results are given for electron beam losses arising from the Touschek effect with the best possible error corrections, considering realistic magnetic field errors, alignment errors, and the ID portfolio foreseen ready at the restart of the ring for stage 1 [5]. The corresponding beam lifetime, without harmonic cavity induced bunch lengthening, is 3 hours for a 500-mA stored beam in a uniform-filling pattern. As a conservative assumption, this beam lifetime was retained for all radiation safety calculations and normalization factors. The evaluated gas-scattering beam lifetime being much higher (~60 hours), corresponding beam losses are considered as negligible compared to Touschek's. Except at the septum position in the injection area, beam losses are distributed relatively smoothly along the SR (see Fig. 1), the very narrow beam pipe acting as a distributed collimator. Upon closer examination of the distribution, a few 7BA-4BA cells appeared to accumulate a slightly larger part of the beam losses than the rest of the ring. Four zones were identified, and one was selected for radiation safety simulations as representative of the entire SR. The FLUKA code [6, 7] was chosen for the radiation safety calculations for its ability to simulate, as accurately as possible, high-energy particles transport and interactions in a detailed 3D geometric model that includes magnetic fields characteristics, bill of material, as well as its ability to sample complex beam losses and phase space distributions, thanks to dedicated user routines.

A comprehensive 3D model of two cells of the SR was generated in FLUKA using an advanced version of the vacuum pipe design, permanent and electromagnetic magnets, girders, etc. This was done with the greatest possible accuracy to ensure consistency and to match the magnetic field position and strength that are input in FLUKA's dedicated magnetic field routine. The corresponding tunnel shielding was modeled as built with inner walls and roof blocks cast in ordinary concrete and the port-end and front-end outer walls in haematite heavy concrete. An additional 6-cm thick lead layer covers the entire surface of the front-end wall with an 8 cm thick lead reinforcement centered on the beam plan, +/− 20 cm in height.

NORMAL BEAM LOSSES

The Touschek Beam Losses are simulated for the two cells AN07 and AN08 because of their higher cumulated beam loss probability (12.8% of the total Touschek beam losses in the SR), as shown in Fig. 1. For each lost particle,

Content from this work may be used under the terms of the CC BY 4.0 licence (© 2026). Any distribution of this work must maintain attribution to the author(s), title of the work, publisher, and DOI.

ISBN: 978-3-95450-252-3 ISSN: 2673-5350 doi: 10.18429/JACoW-IPAC2026-WEP6123

BEAM LOSS STUDY FOR THE L-SHAPED CORRUGATED STRUCTURE AT EUROPEAN XFEL

J. Wu*, S. Liu, A. Dehne, N. Walker, Deutsches Elektronen-Synchrotron DESY, Hamburg, Germany
A. Wolski, University of Liverpool, Liverpool, United Kingdom
A. Potter, Diamond Light Source, Didcot, United Kingdom
W. Qin, Institute of High Energy Physics, Beijing, China

Abstract

The European XFEL is a free-electron laser facility based on a superconducting linac with high bunch repetition rates of up to 4.5 MHz. An L-shaped corrugated structure has been installed upstream of the SASE1 undulator for fresh-slice operation and ultrashort-pulse generation. As the electron beam passes through the structure, strong longitudinal and transverse wakefields are excited which induce a correlated energy chirp and transverse kicks along the bunch. Since the distance between the corrugated structure and the beam is typically less than 1 mm, any beam misalignment or tail expansion may result in particles hitting the corrugated surfaces. For the L-shaped geometry this may occur on both the horizontal and vertical surfaces. Such interactions lead to energy deposition and secondary radiation that may cause damage to the downstream undulators. For this reason, studies have been carried out using BDSIM to simulate the losses caused by the L-shaped corrugated structure. Simulation results have been compared with in-situ radiation measurements using an autonomous robot.

INTRODUCTION

The European XFEL employs a superconducting linear accelerator to accelerate electrons to energies of up to 17.5 GeV [1]. It can operate with bunch repetition rates of up to 4.5 MHz within each bunch train. At such high repetition rates, even small beam losses can lead to measurable radiation doses in the downstream beamline, especially in the undulator section [2].

A corrugated structure, also referred to as a dechirper, is a passive device used to manipulate the longitudinal and transverse phase space of an electron bunch through self-induced wakefields. At the European XFEL, an L-shaped corrugated structure [3,4] has been installed upstream of the SASE1 undulator for fresh-slice operation and ultrashort-pulse generation. In operation, the beam is moved towards the inner corner of the structure by local orbit bumps. The L-shaped geometry provides corrugated surfaces in both transverse planes, allowing the structure to generate a correlated energy chirp as well as transverse kicks along the bunch. However, since the typical distance between the beam and the corrugated surfaces is below 1 mm, beam halo, orbit misalignment, or wakefield-driven tail displacement may cause particles to strike the corrugated surfaces, leading to significant downstream losses.

This paper reports work using BDSIM [5] to study particle losses at the L-shaped corrugated structure and the resulting downstream loss pattern. The simulated loss trends are compared with radiation measurements performed with the autonomous MARWIN robot [6]. Experiments were performed to minimize the beam halo population by reducing the apertures of collimators in the dedicated collimation section upstream of the dechirper [7,8]. Under high-repetition-rate operation, the 4 mm aperture setting effectively reduced the measured downstream radiation to a level comparable to the no-bump condition.

BDSIM SIMULATION

Beam loss simulations were carried out using the BDSIM toolkit. The model starts 53 m upstream of the 6 m long corrugated structure and ends at the exit of the SASE1 undulator, as shown in Fig. 1. The model includes the main beamline components, such as quadrupole magnets, undulator modules, radiation absorbers, and the vacuum chamber aperture transitions into the SASE1 undulators.

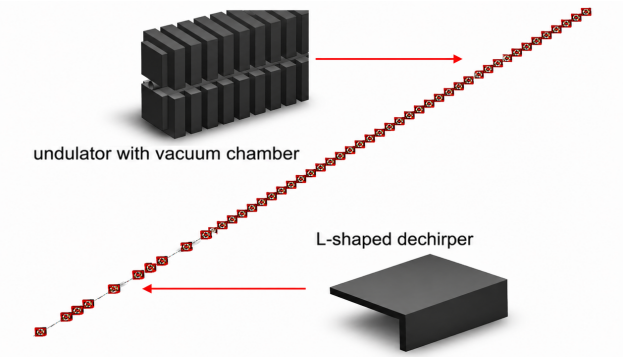

Figure 1: BDSIM model of the L-shaped corrugated structure and the downstream SASE1 undulator line.

A special low-beta optics designed by Qin *et al.* [3] for dechirper operation was used. As shown in Fig. 2, the optics provides small beta functions at the corrugated structure with values of approximately 10 m in both transverse planes. The beta functions shown in the figure were obtained by tracking 1000 Gaussian-distributed particles in BDSIM and are consistent with the designed dechirper optics. This low-beta optics reduces the beam size at the dechirper, allowing controlled orbit bumps that move the beam closer to the corrugated plates.

* jiacheng.wu@desy.de

Content from this work may be used under the terms of the CC BY 4.0 licence (© 2026). Any distribution of this work must maintain attribution to the author(s), title of the work, publisher, and DOI.

ISBN: 978-3-95450-252-3 ISSN: 2673-5350 doi: 10.18429/JACoW-IPAC2026-WEP6124

RADIATION PROTECTION FOR LASER–PLASMA ACCELERATOR FACILITIES AT DESY

S. Zander†, S. Bohlen, M. Kirchen, A. Leuschner, T. T. Liang, A. R. Maier,
A. Martinez de la Ossa, E. Panofski, K. Schubert, M. Thevenet, P. A. Walker, I-L. Yeh
Deutsches Elektronen-Synchrotron DESY, Hamburg, Germany

Abstract

DESY draws on more than six decades of experience in the development, operation, and radiation protection of large-scale user facilities such as PETRA III, FLASH, and the European XFEL. In parallel, the investigation of novel accelerator technologies for future applications has become a key focus. Laser-plasma acceleration (LPA) offers the potential for highly compact, high-gradient sources, as demonstrated by the FLARE, LUX, KALDERA, and VERA facilities at DESY. However, LPA systems introduce new challenges for radiation protection due to broadband emission spectra and the interplay of high-power lasers with plasma-generated secondary radiation fields. This contribution presents the radiation-protection concept for LPA facilities at DESY, covering shielding simulations and designs with a focus on the differences compared to conventional electron accelerators. Finally, operational experience from commissioning the KALDERA LPA and further development stages is discussed, illustrating practical implementation.

INTRODUCTION

Laser-plasma accelerators (LPA) [1], are rapidly evolving from proof-of-principle experiments toward application-oriented user facilities. Their capability to sustain acceleration gradients orders of magnitude higher than conventional radio-frequency (RF) accelerators enables compact machine designs with significant potential for future accelerator technology. At DESY, this development is exemplified by facilities such as FLARE, LUX, KALDERA and VERA.

However, the transition toward higher repetition rates and increased average beam powers of plasma accelerators introduces new challenges for radiation protection. In contrast to conventional accelerators, LPAs generate electron beams with broad energy spectra, significant shot-to-shot fluctuations, and large angular divergence. These characteristics lead to complex radiation fields due to distributed beam losses, in contrast to the point-like source assumptions of conventional shielding, and therefore require adapted radiation protection strategies.

This paper presents radiation protection challenges and mitigation strategies for LPA facilities, with a focus on experimental and simulation studies performed at KALDERA. Particular emphasis is placed on radiation generation close to the laser-plasma source and the contribution of large-angle, low-energy electrons.

RADIATION GENERATION AT ELECTRON ACCELERATORS

Secondary radiation in conventional electron accelerators is primarily generated through the initial process of bremsstrahlung generation when electrons slow down and interact within matter. The resulting bremsstrahlung photon spectrum extends up to the kinetic energy of the electrons. Tertiary processes such as Compton scattering, pair production, and photonuclear interactions contribute additional components, including neutrons, to the mixed radiation field.

As emphasized in established radiation protection literature [2, 3], the relative contributions of the various radiation components depend heavily on the electron energy, the accelerator's beam power, the beam loss geometry, and the surrounding materials.

Even at comparatively low electron energies of a few MeV, significant dose rates can occur. In particular, sideways-emitted bremsstrahlung (90°) reaches a maximum around 10 MeV (Fig.1), and the dose rate scales predominantly with beam power rather than with beam energy. As a result, lower-energy electron accelerators with substantial beam power can be just as relevant for radiation protection as even GeV-range accelerators.

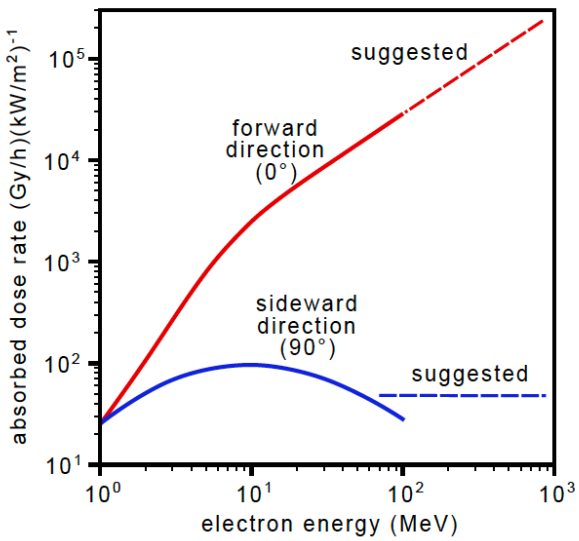

Figure 1: Absorbed dose-equivalent from thick-target bremsstrahlung as a function of electron energy for different emission geometries [2, 4].

† sven.zander@desy.de

Content from this work may be used under the terms of the CC BY 4.0 licence (© 2026). Any distribution of this work must maintain attribution to the author(s), title of the work, publisher, and DOI.

ISBN: 978-3-95450-252-3 ISSN: 2673-5350 doi: 10.18429/JACoW-IPAC2026-WEP6127

GSI OPERATION STATISTICS IN THE FAIR CONSTRUCTION PHASE (2012 – 2025): TRENDS, FAILURES AND LESSONS LEARNED

O. Geithner*,[1], M. Klich[1], M. Vossberg[1], A. Bloch-Spaeth[1], H. Stemmler[1], R. Assmann[1,2], S. Reimann[1]
[1]GSI Helmholtz Centre for Heavy Ion Research, Darmstadt, Germany
[2]JWGU, Frankfurt, Germany

Abstract

We present operational statistics for the GSI accelerator complex during the FAIR construction phase from 2012 to 2025, covering UNILAC, SIS18, ESR, HEST and CRYRING@ESR. The analysis is based on beam-time schedules, availability monitoring, and fault annotations from the Operator Logbook (OLOG). During the last five years, failure entries were systematically reviewed and reclassified to ensure consistent data quality and enable reliable long-term trend evaluation. The main performance indicator discussed is accelerator availability, determined from scheduled operation periods and fault-related downtimes. The evaluated data were used as a quantitative input in the recent POF-5 evaluation process (2028-2034), where they clearly supported refurbishment and consolidation needs at GSI. A technical roadmap was established this year to prioritize these measures according to their impact on stable beam delivery towards FAIR accelerators.

INTRODUCTION

During the FAIR construction phase, the GSI accelerator complex continued operating as a user facility while simultaneously preparing for FAIR integration. This dual role created significant operational challenges.

Many technical systems exceed their original design lifetime, while resources must be shared between maintaining current operation and supporting the FAIR project. Beamtime for experiments must be balanced against shutdown periods required for upgrade [1] and maintenance activities

This paper presents a quantitative analysis of operational statistics from 2012 to 2025 based on beamtime records and operational logbook (OLOG [2]) fault annotations. The goal is to identify key reliability trends and structural limitations during the FAIR transition. The results form the basis for a data-driven prioritization of refurbishment measures summarized in the Technical Roadmap [3].

ACCELERATOR COMPLEX AND DATA SOURCE

The analysis covers the main machines of the GSI accelerator complex that contribute to routine beamtime. The focus is on their role in the beam production chain and correspondent reliability burden.

- UNILAC – linear accelerator forming the backbone of the injector chain.
- SIS18 – main synchrotron providing beam for downstream rings and experiments.
- ESR – experimental storage ring with electron and stochastic beam cooling.
- CRYRING@ESR – low-energy storage ring with electron beam cooling.
- HEST – transfer and extraction beamline systems linking synchrotron, storage rings and experimental caves.

These machines form a strongly coupled production chain; failures in upstream systems frequently propagate downstream, influencing global availability.

DEFINITIONS

The availability calculation is based on operational periods documented in OLOG, which is continuously updated during beamtime. Instead of using the originally scheduled times from long-term planning, the analysis relies on the dynamically adapted beamtime record in OLOG, reflecting the actual operational conditions on daily base. Setup periods include machine preparation, beam tuning and ion source service times. Accelerator availability is defined as the ratio of effective beam-on-target time to the sum of beam-on-target, setup and failure times, summarized over all experiments [4].

LONG – TERM OPERATIONAL TRENDS

Figure 1 shows the evolution of GSI performance between 2012 and 2025. The time values are aggregated over all experiments operated in parallel, which explains the high total number of operation hours per year. The data do not follow a simple linear trend but rather reflect changing operational boundary conditions over time.

The years 2012–2014 represent relatively long beamtime blocks. In 2013, no user beamtime took place due to extensive shutdown activities. During these early FAIR construction years, operation was driven by experimental demand and beamtime scheduling was comparatively continuous.

From 2015 onward, a clear operational shift can be observed. FAIR project activities required longer shutdown periods, infrastructure access, and coordination with civil construction. In addition, personnel resources were increasingly shared between FAIR construction and ongoing GSI

* o.geithner@gsi.de

Content from this work may be used under the terms of the CC BY 4.0 licence (© 2026). Any distribution of this work must maintain attribution to the author(s), title of the work, publisher, and DOI.

ISBN: 978-3-95450-252-3 ISSN: 2673-5350 doi: 10.18429/JACoW-IPAC2026-WEP6130

ASSET MANAGEMENT WORKFLOWS FOR cSTART USING SNIPE-IT

E. Blomley*, J. Gethmann, J. Natal, R. Ruprecht, M. Schuh, J. L. Steinmann, A.-S. Mueller
Karlsruhe Institute of Technology, Karlsruhe, Germany

Abstract

The cSTART project at the Institute for Beam Physics and Technology (IBPT) at the Karlsruhe Institute of Technology (KIT) is introducing a new system to manage all accelerator-related components called Snipe-IT. As the new components arrive, one of the first steps is entering them into the asset database, which creates a unique identifier. This identifier is then also used during the quality inspection process as the main reference. The asset-to-asset associations possible with Snipe-IT provide a simple and efficient method for structuring the components in cabinets and along the storage ring. The flexible custom fields allow to track references to other data sources, which provide the more technical information such as CAD drawings, cable routing, and device documentation. In addition, it also allows to track component specific information. This contribution describes the established workflows, status, and lessons learned using a generic IT asset management system for accelerator component management.

MOTIVATION

Since the commissioning of KARA (Karlsruhe Research Accelerator) at KIT in 2001, the accelerator landscape has expanded to a network of beamlines, laboratories, the linac-based test facility FLUTE (Ferninfrarot Linac und Test Experiment), the upcoming VLA-cSR (Very Large Acceptance - compact Storage Ring) within the cSTART project (compact STorage ring for Accelerator Research and Technology) [1], and a LPA (laser-plasma accelerator) [2] each introducing hundreds of components with distinct life-cycle-demands. Over the years, documentation and tracking have been carried out with heterogeneous tools and inconsistent naming conventions, creating gaps that hinder efficient hardware and software deployment across all IBPT sites. By adopting Snipe-IT [3] — an open-source web-based asset-management system — we can assign a single and persistent identifier to every asset like magnet, power supply, detector module and support device, leverage its extensive feature set and active developer community, and benefit from continuous maintenance, even though the software was not originally designed for particle-accelerator components. The successful use of Snipe-IT on other accelerator facilities [4] motivated our adaptation and guaranteed baseline compatibility with accelerator-related workflows.

FEATURES

Snipe-IT provides a modern and flexible set of features, some make the tool especially interesting for adaptation in this context.

* edmund.blomley@kit.edu

Custom Fields

Custom fields let the database designer create any amount of user-defined data columns, which can be grouped into field-sets, for any asset type, enabling storage of metadata such as serial numbers, calibration dates, as well as device class specific parameters, such as network-related information for network-capable devices or device-specific parameters only relevant for magnets or cameras or motors. These fields are searchable, can be mandatory or optional, and support drop-down lists, numeric values, dates, and free-text entries, making the inventory adaptable to diverse accelerator-instrumentation needs. They can also be made unique or require to adhere to a regex expression which is useful for defining fields related to naming conventions.

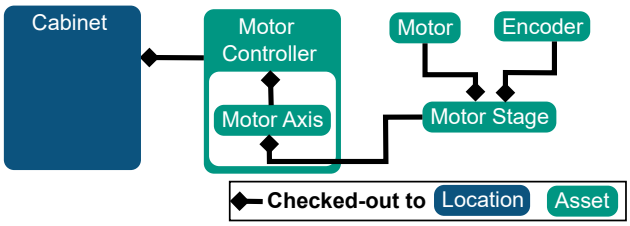

Figure 1: Asset-to-asset-to-location checkout example. Using the built-in checkout system to represent the actual device setup while each component remains a fully fledged asset. In this example the motor axis is considered to be one of multiple axes which can be individually exchanged inside the motor controller crate.



Figure 2: Basic labels. This minimal label is used during the initial registering of new devices based on an already existing generic entries in the database.

Asset Association

In Snipe-IT, assets can be checked out not only to people but also to other assets or to defined locations, enabling the creation of association chains that reflect the physical layout of an accelerator. For example, a motor encoder and motor can be checked out to a motor stage, which in turn is checked out to the motor axis, and finally to the motor controller — each element remains a fully fledged asset with its own custom fields. Cabinets can be represented as locations, allowing a controller to be checked out to a cabinet that belongs to a larger area (see Fig 1).

Content from this work may be used under the terms of the CC BY 4.0 licence (© 2026). Any distribution of this work must maintain attribution to the author(s), title of the work, publisher, and DOI.

ISBN: 978-3-95450-252-3 ISSN: 2673-5350 doi: 10.18429/JACoW-IPAC2026-WEP6131

ON-THE-FLY SCANNING: IMPROVING SCAN TIME OF XAFS AT BM08-XAFS/XRF BEAMLINE

M. Alzubi[1,2], A. Mohammad[1], A. Abbadi[1], N. Al-Bess [2], M. Abugharbiyeh[1], A. Al-Dalleh[1], A. Aljadaa[1], L. U. Khan[1], Y. Momani[1], M. Harfouche[1]
[1]Synchrotron-Light for Experimental Science and Applications in the Middle East (SESAME), Allan, Jordan
[2]Princess Sumaya University for Technology, Amman, Jordan

Abstract

In this work, we present the use of PandABox timing module to implement position-based and time-based on-the-fly scanning to continuously acquire data at the X-ray Absorption Fine Structure (XAFS) and X-ray Fluorescence (XRF) beamline of SESAME synchrotron light source. For position-based scanning, we first developed a module that automatically partitions the user-defined energy and Bragg angle ranges into sub-intervals. Within each sub-interval, the energy-angle mapping is linearly approximated to maintain accuracy within acceptable margins. The method then integrates the position encoding of the Double Crystal Monochromator (DCM) Bragg angle with the synchronous triggering of multiple detectors, including ionization chambers (ICs) and a KETEK SSD detector. For time-based scanning, PandABox is pre-configured to generate triggers at fixed time exposure time intervals. Improvements, performance and comparative results are also discussed in this work.

Keywords: on-the-fly scanning, QEXAFS, DAQ, PandABox, linear fitting, XAFS/XRF

INTRODUCTION

The BM08-XAFS/XRF beamline at SESAME Synchrotron in Jordan serves users who need to measure X-ray Absorption Fine Structure and X-ray Fluorescence spectra [1]. BM08 has traditionally operated in step-scan mode where the DCM moves to an energy point, waits for the mechanics to settle, collects data, then moves on to the next point. This stop-and-go cycle works reliably, but it wastes a lot of time. For a typical XAFS scan spanning hundreds of energy points, the settling delays add up to a significant fraction of the total beamtime time that could otherwise be spent collecting more scans or studying faster sample dynamics.

To enhance system performance, we implemented an on-the-fly scanning mode in which the DCM continuously moves across the user-defined energy range while the detectors are being triggered synchronously at specific pre-calculated energies (angle positions). This eliminates the settling overhead entirely. Similar technique has been adopted at several major facilities worldwide, including the ESRF BM29 beamline [2], the QXAS mode at Diamond B18 [3], the SuperXAS beamline at the SLS [4], and the general XAFS beamline at SSRF [5] in order to reduce acquisition times from tens of minutes to a few seconds while maintaining data quality comparable to step scanning. Continuous on-the-fly scanning can in some few cases be implemented in software (i.e. no need for hardware triggering), as demonstrated at the BEATS beamline [6], our goal is to make it available across all beamlines, on a best-effort basis and whenever applicable as it is already mentioned in our DAQ stander [7, 8]. Currently, we are implementing on-the-fly scanning on HESEB beamline [9].

In this work, we report the implementation of two complementary continuous scanning modes at the BM08 beamline: a *position-based* mode, where triggers are generated at specific encoder positions, and a *time-based* mode, where triggers are generated at fixed time intervals. Both modes rely on a PandABox timing module to synchronize all participating subsystems.

SYSTEM ARCHITECTURE

Beamline Control Infrastructure

The BM08 DAQ system is built on top of the EPICS control system and includes a modular Python-based scanning tool that supports multiple scan modalities and energy calibration. A Qt-based graphical interface, together with epicsQt for live experimental data visualization, allows users to configure and execute scans without interacting directly with low-level control system commands [10]. The detectors connected to the system include ICs for transmission measurements and a KETEK detector for fluorescence measurements.

PandABox Synchronization Module

Continuous scanning is achieved using PandABox, an FPGA-based timing and position-capture module [11]. The module reads the Bragg-angle encoder in real time and continuously tracking of the position during motion. Depending on the selected scan mode, it generates hardware gate signals to trigger all detectors simultaneously, either when the encoder reaches predefined angular positions or at fixed time intervals. As synchronization is handled at the hardware level, the timing remains precise and consistent for every acquired data point.

Architecture and pipeline is described in Figure 1. Also, the internal PandABox block configuration used for this work is shown in Fig. 2.

Content from this work may be used under the terms of the CC BY 4.0 licence (© 2026). Any distribution of this work must maintain attribution to the author(s), title of the work, publisher, and DOI.

ISBN: 978-3-95450-252-3 ISSN: 2673-5350 doi: 10.18429/JACoW-IPAC2026-WEP6132

CHARACTERIZATION OF BEAM LOSS AT MAX IV IN-VACUUM INSERTION DEVICES

M. Muradi*, M. Holz, H. Tarawneh, MAX IV Laboratory, Lund, Sweden

Abstract

Four Libera Beam Loss Monitors (BLMs) were installed downstream of four consecutive in-vacuum undulators (IVU) at the MAX IV 3 GeV storage ring in order to survey beam losses under various operational conditions. The BLMs are operating in counting mode, with the loss-detection threshold defined from measurements taken without a stored beam. The BLMs were configured to provide stable, high-dynamic-range loss detection.

We performed a series of controlled studies to compare the loss signatures produced by different operational events, such as scraping down the beam, sudden beam dumps, full beam injections, and regular top-up cycles. The measurements show that scrape-downs generate the highest localized loss rates, while sudden beam dumps produce almost no detectable signal at the BLM locations. Top-up injections exhibit consistent and repeatable loss patterns, providing a useful benchmark for routine operation. All events were studied with insertion device gaps both closed and open; a significant decrease in detected losses was observed when the gaps were opened.

These results provide a baseline for understanding the local loss behavior downstream of the IVUs and will also provide more refined future operational procedures.

INTRODUCTION

The MAX IV Laboratory in Lund, Sweden, operates the world's first operational multi-bend achromat (MBA) storage ring, providing ultra-low electron beam emittance and extremely high X-ray brilliance [1]. The 3 GeV storage ring hosts ten insertion devices of which six are in-vacuum undulators. These devices provide high photon flux and brightness by operating with very small magnetic gaps down to 4.5 mm (ca. 2.25 mm distance magnet-beam) [2]. The combination of small magnetic gaps and the in-vacuum design means that the undulator magnets are directly exposed to the electron beam and thus are particularly susceptible to localized beam losses that may result in demagnetization or degradation of the magnets.

Understanding beam losses near insertion devices is important for both machine protection and stable operation. Losses may occur during injection, beam dumps, orbit perturbations, or deliberate beam scraping. In IVUs, localized beam losses can deposit energy in the vacuum chamber and magnet structures, potentially leading to heating and partial demagnetization of the permanent magnets. Monitoring these losses therefore provides insight into the behavior of the stored beam and helps ensure safe operation of the insertion devices.

* mostafa.muradi@maxiv.lu.se

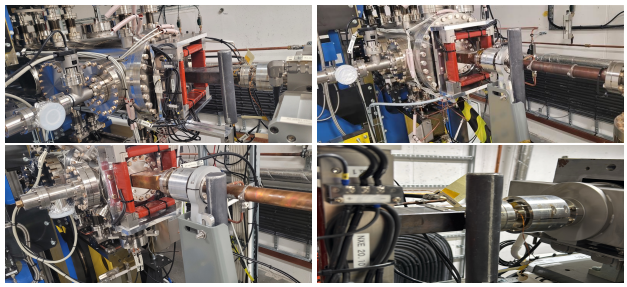

Figure 1: The four Libera BLMs mounted downstream of each observed IVU.

In this work, four beam loss monitors (BLMs) were installed at the exit point of four consecutive IVUs in the MAX IV 3 GeV storage ring. The purpose of the study is to characterize the loss signals produced by different events during operation and to establish a baseline understanding of the local loss behavior near these insertion devices.

Beam Loss Monitors

In our test set-up, we use the Libera BLM system, with detectors based on scintillators coupled to photomultiplier tubes (PMTs). The detectors are positioned close to the vacuum chamber at the insertion device exit points that serve the ForMAX, CoSAXS, BioMAX, and MicroMAX beamlines, see Fig. 1. The PMT output signal consists of unipolar pulses with negative polarity, corresponding to individual loss events [3].

The Libera BLM continuously samples the detector signal with high time resolution (8 ns) and processes it using configurable threshold logic. In counting mode, individual pulses that exceed a predefined threshold are automatically detected and counted, producing a signal in counts per unit time [4], in our set-up counts per second. We determined the thresholds from background measurements taken without a stored beam, ensuring reliable detection of both continuous and transient beam losses.

EXPERIMENTAL RESULTS

A series of experiments were performed to characterize the beam losses under different machine conditions. The study includes full injection, deliberate beam scrape-downs, and routine top-up operation. In addition, dedicated tests were carried out to evaluate the influence of RF and tune variations, as well as the effect of individual insertion device configurations. For all measurements, the BLM signals were analyzed in terms of peak loss rates and, where relevant, accumulated losses over the duration of the event. Throughout all experiments, the detectors have identical configuration settings.

Content from this work may be used under the terms of the CC BY 4.0 licence (© 2026). Any distribution of this work must maintain attribution to the author(s), title of the work, publisher, and DOI.

ISBN: 978-3-95450-252-3 ISSN: 2673-5350 doi: 10.18429/JACoW-IPAC2026-WEP6136

ONLINE PERFORMANCE MONITORING AND EARLY FAULT DETECTION FOR THE B-TRAIN REAL-TIME SYSTEMS AT CERN

K. Diamantis*, M. Bonora-Tam, M. Buzio, V. di Capua, D. Giloteaux, CERN, Geneva, Switzerland

Abstract

At CERN, B-Train systems provide real-time magnetic field information to the RF and other subsystems with high precision and reliability, with less than 3 beam-hours lost per year per machine. Using the Proton Synchrotron Booster (PSB) as a case study, we describe a software performance-monitoring framework, currently in the prototyping phase, aimed at improving the absolute accuracy and trustworthiness of the measurement to help operators to proactively diagnose a variety of beam instabilities. The framework compares measurements with historical data, model-based expectations, and redundant acquisition chains to assess internal errors due e.g. to integrator drift or field marker degradation, apply the necessary corrections, or flag systems for intervention. We expect it to enhance compliance with evolving operational standards and future large-scale applications requiring automated self-diagnostics and remote maintenance.

INTRODUCTION

At CERN, six B-train systems provide real-time magnetic field information based on induction coils that generate a voltage V_c proportional to the derivative of the linked flux, so that by integration we obtain the average bending field $B(t)$:

$$B(t) = B_o + \Delta B(t) = B_o - \frac{1}{A_c}\int_{t_0}^{t} V_c(\tau)\, d\tau, \qquad (1)$$

where A_c is the effective coil area and $B_0 = B(t_0)$ is the magnetic field at the beginning of the integration process, signaled by field markers [1]. These are nuclear magnetic (NMR) or ferrimagnetic (FMR) resonance sensors that trigger on each cycle at a preset value, usually just before injection, to reset the integration and minimize the accumulation of drift due to parasitic currents or localized thermoelectric effects [2]. Each system is composed of a redundant pair of acquisition chains, the operational (OP) and the spare (SP), designed to provide identical results. Each chain includes signal conditioning and custom digital electronics hosted in an industrial Front-End Computer (FEC), and takes inputs from different arrangements of sensors, according to the characteristics of the reference dipoles available in each machine.

The different configurations can be described in a unified way via the concept of *logical magnet gap*, i.e. an abstract source of magnetic field driven by a given current. In the simplest cases, the Proton Synchrotron (PS) and Extra Low ENergy Antiproton (ELENA) rings, this corresponds to the physical gap of a reference magnet hosting sensors for both the OP and SP chains. In the Super Proton Synchrotron (SPS), two dipoles of different types are connected in series and instrumented as a single logical unit. In the Low Energy Ion Ring (LEIR), OP and SP sensors are installed in the fringe field region of two distinct, but nominally identical, bending dipoles in the ring. The Proton Synchrotron Booster (PSB), consisting of four superimposed rings, is the only one where the B-train has two logical gaps, corresponding to the symmetrical pairs of outer (Ring 1 and 4) and inner (Ring 2 and 3) physical gaps, vertically stacked within the same iron yoke. The two outer and the two inner rings are powered in series but independently, to generate identical fields despite different saturation characteristics.

BTRAIN MONITORING FRAMEWORK

The monitoring framework is organized into six hierarchical levels, shown in Fig. 1. Levels 0 to 4 are per-cycle diagnostic signals computed in real-time, generating warnings when issues are detected. Over 120 diagnostics are defined, many of which are iterated over multiple signal paths per chain. The first three levels define quantities related to any OP or SP chain: low- level voltage signal statistics (Level 0), measured field quality indicators (Level 1) and internal consistency metrics based on the comparison of the measured field with the nominal cycle (B_{sim}) and a physical model based on the excitation current (Level 2). Level 3 handles redundancy by evaluating the consistency of OP and SP chains, and Level 4 evaluates consistency across logical magnet gaps. In Level 5 a subset of the computed metrics is stored according to a tiered retention policy for off-line evaluation of historical trends, correlations and discontinuities, either automatically or on-demand, with optional cycle type filtering.

TECHNICAL IMPLEMENTATION

Implementation of the monitoring framework relies on a multi-tier software architecture designed for real-time data acquisition, processing, and visualization.

FESA

Front End Software Architecture (FESA) C++ classes run on FECs and provide the means for gathering and filtering the data from the low level hardware connected to magnetic sensors. FESA ensures hardware integrity and provides Level 0 diagnostics. FESA classes are synchronized with the timing system, which distributes trigger pulses across the accelerator complex [3, 4]. In our implementation, data are gathered for every triggered event and then distributed through CERN's control middleware (CMW).

* konstantinos.diamantis@cern.ch

Content from this work may be used under the terms of the CC BY 4.0 licence (© 2026). Any distribution of this work must maintain attribution to the author(s), title of the work, publisher, and DOI.

ISBN: 978-3-95450-252-3 ISSN: 2673-5350 doi: 10.18429/JACoW-IPAC2026-WEP6138

A BEAM ABORT SYSTEM FOR THE DIAMOND-II STORAGE RING

H. Ghasem,† I.P.S. Martin, A. Potter, Diamond Light Source, Oxfordshire, UK
W. Shields, Royal Holloway, University of London, Egham, UK

Content from this work may be used under the terms of the CC BY 4.0 licence (© 2026). Any distribution of this work must maintain attribution to the author(s), title of the work, publisher, and DOI.

Abstract

Due to the high energy density of the Diamond-II low-emittance electron beam, the risk of damage to storage ring components is considered high. A dedicated beam abort system is one way to safely dump the beam and protect the machine from damage. In this paper, we present the design of a beam abort system for the Diamond-II storage ring. The requirements of the key components will be described, including the kickers and beam dump. Simulations of the effects of beam loss on the beam dump surface and collimator blades will be shown.

INTRODUCTION

The Diamond-II upgrade is a 3.5 GeV light source facility with 162 pm natural emittance and 300 mA average current. It will generate high brightness synchrotron radiation for users across a range of disciplines [1]. Due to the high energy density of the electron beam, a beam abort system has been found to be essential for safely dumping the beam, either intentionally or due to any type of failure mode that might happen. These include:

- fewer than n RF cavities at field, where n is a configurable parameter
- beam excursion outside the ±250 µm EBPM orbit interlock limits
- loss of the Machine Protection or Personnel Safety Systems (MPS or PSS) permit
- manual beam dumps requested over EPICS

The beam abort system will be enabled for stored beam currents above 10 mA. Injection above this current will only be enabled if all beam abort system components indicate they are 'ready to fire'. The need for an additional beam-instability interlock is also under consideration. If a manual beam dump is requested, the multi-bunch feedback system will be set to first increase the beam emittance before dumping the beam.

DIAMOND-II BEAM ABORT SYSTEM

The Diamond-II beam abort system is composed of the following elements:

- two solid beam dumps (BDs)
- horizontal and vertical kicker magnets
- power supplies to power the kickers
- a beam abort controller

The beam dumps and kickers will be located in the K23 and K24 mid straight sections. In the latest design, each of the straights will contain two 200 mm long horizontal kickers and one 400 mm long vertical kicker. The beam dumps are located downstream of the kickers and consist of a main tapered section with a length of 97 cm and a 10 cm flat section at the downstream end. The horizontal gap changes from ±10 mm at the beginning of the main body to ±5 mm at the flat section. The layout for the K23 straight section is shown in Fig. 1. The main parameters for the kickers are given in Table 1.

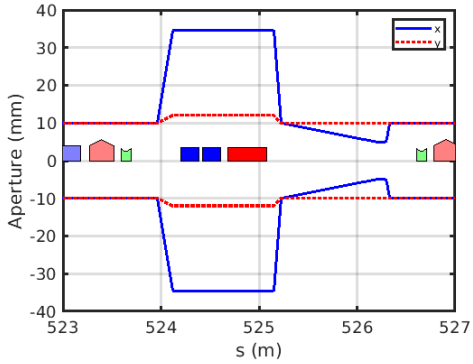

Figure 1: General layout of the beam dump system in K23. The same layout is used for K24.

Table 1: Nominal Parameters for the BD Kickers

Parameter	Hor. kicker	Ver. kicker
Length (mm)	200	400
Kick angle (mrad)	+2.56	-0.35
Pulse shape	Linear rise	Half-sine
Pulse duration (µs)	3.74	1.87
Peak Field (T)	0.15	0.01

Several waveform shapes and kick angles have been investigated for the kickers to spread the individual electron bunches along the length of the BD as evenly as possible. The results of this study indicated that the optimum waveform for the horizontal kickers is a linear rise as a function of time, increasing the kick angle from zero to a maximum value of +2.56 mrad after two turns. This solution is a trade-off between uniformly distributing the bunches and keeping the design of the power supply simple. The peak magnetic field for the kicker is 0.15 T. The optimum waveform for the vertical kicker was found to be a half sine within one turn with the peak value of -350 µrad. The final kick angles as a function of time are displayed in Fig. 2.

TRACKING RESULTS

The Elegant simulation code [2] was used to track all 934 bunches through the Diamond-II storage ring, including the effects of the beam abort system. Each of the tracked bunches contained 400 macroparticles, and the bunch separation was set to 2 ns.

†hossein.ghasem@diamond.ac.uk

ISBN: 978-3-95450-252-3 ISSN: 2673-5350 doi: 10.18429/JACoW-IPAC2026-WEP6140

INTEGRATING FAST BEAM INTERLOCKS INTO AN EVENT-BASED TIMING SYSTEM

L. Perusko†, A. Debenjak, Z. Oven, T. Zagar, Cosylab, Ljubljana, Slovenia
E. J. Harms, L. Szeto, Nusano, Salt Lake City, USA
J. Ringuette*, TerraPower, Bellevue, USA

Content from this work may be used under the terms of the CC BY 4.0 licence (© 2026). Any distribution of this work must maintain attribution to the author(s), title of the work, publisher, and DOI.

Abstract

Accelerators often use separate infrastructures for precise timing and machine protection, which increases cabling, integration complexity and operational overhead. We describe an approach that enhances a standard event-based timing system to provide fast beam interlock functionality on the same platform. Protection logic, flag distribution and rapid reaction paths are implemented directly in the timing firmware, allowing the existing hardware and fiber network used for device triggering to also transport low-latency interlock information. With timing and protection combined, interlock conditions can act immediately on timing outputs while established capabilities such as sequences, delay compensation and timestamping remain fully supported. The system offers flexible configuration of inputs, flags and outputs, and a single operator interface for both timing and protection workflows. Developed by Cosylab in collaboration with Nusano, this solution demonstrates practical architecture for environments where precise timing and fast protection must operate tightly coupled.

EVENT-BASED TIMING SYSTEM

Distributed accelerator control systems require precise orchestration of devices spread across a facility. Timing systems for particle accelerators face particularly demanding requirements: sub-nanosecond synchronization, low jitter and deterministic latency across all endpoints.

An event-based timing system addresses these requirements by distributing a common synchronous clock from a central Event Master (EVM) to a set of Event Receivers (EVRs) over dedicated fiber-optic links. On each clock cycle the EVM may encode an event code into the serial stream; each EVR decodes the stream and reacts to selected event codes according to its individual configuration, generating precisely timed trigger pulses. Despite the differing single-optic cable lengths between the EVM and individual EVRs, triggers issued by different EVRs in response to the same event arrive simultaneously at their respective endpoints as a combined consequence of phase-locking all receivers to the common clock and of the delay compensation subsystem, which corrects for the residual cable-length differences.

MRF timing system

One of the established commercial providers of event-based timing systems is Micro-Research Finland (MRF) [1]. MRF equipment has been deployed at numerous institutes and accelerator facilities over the past two decades. The hardware is available in multiple form factors; the implementation described here uses the mTCA.4 [2] variant, comprising mTCA-EVM-300 event generators and mTCA-EVR-300U event receivers housed in standard mTCA chassis together with system-board computers (SBCs) running the control software.

A key feature of the MRF platform is bidirectional communication: while events flow downstream from the EVM to all EVRs, the data slot of the serial link also supports upstream data transfer from each EVR back towards the EVM. This upstream path, normally used for delay compensation measurements and data buffers, is the foundation on which the interlock extension is built.

For the Nusano linac, the timing system consists of one EVM master and one EVM configured as a fan-out, together serving twelve EVRs distributed across the facility in a two-hop star topology as shown in Fig. 1. The event clock runs at 100 MHz, providing 10 ns resolution on all trigger delays. Timing sequences repeat at up to 400 Hz, with the specific set of triggers within each sequence configured by operations to suit the current machine mode. A GPS synchronized time server provides a PPS signal that synchronizes timestamps across the entire timing system.

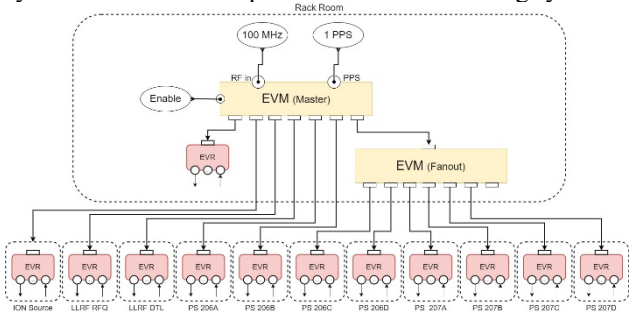

Figure 1: Topology of the Nusano Timing System.

INTERLOCK EXTENSION

Requirements

The Nusano linac requires both a Beam Permit (BP) system, which monitors device readiness and inhibits operation while any subsystem is not ready, and a Fast Beam Interrupt (FBI) system, which responds to sudden faults and latches until explicitly cleared by an operator. Running separate protection hardware would duplicate the fiber infrastructure and create two independent operator interfaces. The chosen approach instead implements BP and FBI

†luka.perusko@cosylab.com
*Current affiliation, was part of Nusano team during the project

ISBN: 978-3-95450-252-3 ISSN: 2673-5350 doi: 10.18429/JACoW-IPAC2026-WEP6144

MODIFICATION OF THE TRANSVERSE ELECTRON BUNCH PROFILE WITH SPATIAL LIGHT MODULATOR AT FLUTE

T. Schmelzer*, M. Brosi, E. Bruendermann, A.-S. Mueller,
Karlsruhe Institute of Technology, Karlsruhe, Germany

Abstract

The linac-based test facility FLUTE (Ferninfrarot Linac-Und Test-Experiment) at the Karlsruhe Institute of Technology (KIT) was designed as a test bench for accelerator technologies with a broad range of beam parameters. The electron bunches are generated in a UV photo-injector, which offers laser pulse shaping as control of the beam parameters. The imprint of a transverse laser profile modulated by a spatial light modulator (SLM) onto the electron bunch was demonstrated at the low energy section of FLUTE. The addition of the linear acceleration structure and bunch compressor section, as well as the upgrade of the RF system, enables experiments with short-pulse electron bunches up to 90 MeV. For this contribution, the SLM was used to recreate the modified electron bunch profile and we present the observed characteristics after passing the traveling-wave RF structure and magnetic chicane.

INTRODUCTION

The electron bunch parameters at modern accelerators are aimed at low emittance and high brightness. In a photo-injector configuration, laser pulse shaping in longitudinal and transverse directions enables direct control over the electron bunch [1]. Combined with machine learning algorithms [2], the laser pulse parameters can be adjusted and long-term effects compensated. Studies indicate that homogeneous ellipsoidal profiles can mitigate space charge effects more effectively than Gaussians [3]. Furthermore, adaptable laser pulse shaping could open the possibility for novel diagnostic approaches with spatial and temporal designs.

In a pixel-based modulation, a liquid crystals SLM allows the influence of intensity and/or phase of the incident laser pulses [4]. The phase of the incident light passing through the liquid crystal pixels is affected, depending on the electrode settings. Each pixel can be modulated independently, resulting in a modulation of the whole laser pulse on the sensor. To generate images in the transverse distribution of the laser pulse, a phase mask known as computer generated hologram (CGH) has to be loaded onto the SLM. An algorithm using inverse Fourier transforms, the Grechberg-Saxton (GS) algorithm can be used for the calculation of the CGH. Spatial light modulators (SLMs) have been used, for instance, at Cornell University [5], DESY [1, 6], and the Daresbury Laboratory [7] to optimize beam homogeneity and reduce emittance.

The modulation of the photo-injector was demonstrated at FLUTE in [8] and [2] where two separated electron bunches were generated simultaneously with the modulated laser pulse. These electron bunches were investigated in the low energy section including one RF structure. Since the first SLM operation at FLUTE, the traveling wave linac and bunch compressor have been added. Furthermore, the laser system was exchanged with a new version, slightly increasing the maximum uncompressed pulse energy to 9 mJ.

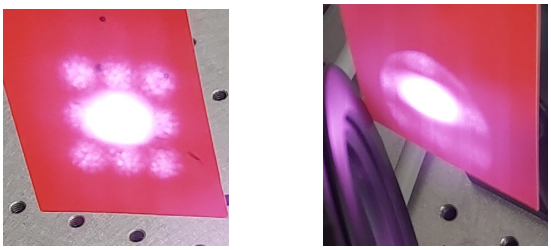

(a) Laser pulse with 3x3 grid modulation 2 m after SLM.

(b) Modulated spots clipping at mirror aperture after 4 m.

Figure 1: Effect of divergence on the spatially modulated laser pulse after the SLM. The high intensity of the non-modulated zero-order is not yet removed.

EXPERIMENTAL SETUP

The experiments were performed at the fully operational test facility FLUTE, where the SLM setup was implemented as selectable addition to the laser pulse transport system. The added flip mirrors allow for simple and reproducible comparison of the laser path with and without the spatial light modulation active.

Transverse Laser Pulse Shaping

At FLUTE the uncompressed laser pulse is transported towards the photo-injector. Next to the start of the accelerator, an optical table for pulse selection, pulse compression and UV-conversion, and a dispersive pulse stretcher is installed. The liquid crystal SLM used for the presented experiments was a commercially available Hamamatsu LCoS-SLM [9], which is optimized for a wavelength range of 800 nm ± 50 nm. In these experiments, the aim was to modulate the transverse laser pulse profile. Therefore, the SLM was installed with a flip mirror setup as a side arm to the main laser path. During installation, it was noticed that the laser beam divergence after the SLM was significantly higher than at normal operation. This led to clipping at the optical components next to the photo-injector. A 1:1 telescope was installed after the SLM, to compensate for the divergence so later optical components could be used without adjustment.

The laser transport from SLM to the optical table next to the photo-injector consists of 2” dielectric mirrors. Especially for holographic images, the divergence of the modu-

* thiemo.schmelzer@kit.edu

Content from this work may be used under the terms of the CC BY 4.0 licence (© 2026). Any distribution of this work must maintain attribution to the author(s), title of the work, publisher, and DOI.

ISBN: 978-3-95450-252-3 ISSN: 2673-5350 doi: 10.18429/JACoW-IPAC2026-WEP6145

THE MYRRHA PHASE 1 MTCA.4-BASED LLRF SYSTEM

A. Bellandi, W. De Cock, F. Frank, J. Geerts, K. Geerts, E. Verhagen
Belgian Nuclear Research Centre, Mol, Belgium

Abstract

The first 100 MeV stage of the MYRRHA superconducting RF linear accelerator is under construction in Mol, Belgium. The machine will produce an instantaneous proton beam current of 4 mA and represents the first step toward the construction of the MYRRHA Accelerator-Driven System (ADS). Such a machine presents several technical challenges for the control of its RF cavities.

First, the required field stability is $\leq 0.1\%$ in amplitude and $\leq 0.1^\circ$ in phase to avoid excessive beam losses. The high loaded quality factor ($Q_L = 2.3 \times 10^6$) and the need to modulate the beam at 250 Hz require sophisticated field- and detuning-control techniques to keep RF power consumption and stability within specifications.

Finally, since the maximum allowed beam-trip duration is less than 3 s, real-time fault detection and recovery techniques must be implemented in the Low-Level RF (LLRF) controller. To meet these stringent requirements, the MTCA.4 standard and the RFSoC-based DAMC-DS5014DR direct-sampling AMC were chosen.

In this proceeding, the LLRF control strategy foreseen for MYRRHA Phase 1 will be presented. The current status of the firmware, software, and analog front-end will also be discussed.

INTRODUCTION

MYRRHA Phase 1 [1] aims to demonstrate the reliability and flexibility required to build an Accelerator-Driven System (ADS). The core of the project is a 4 mA, 70 MeV Continuous-Wave (CW) superconducting proton LINAC, with the option to later extend it to 100 MeV (Fig. 1). Apart from reliability studies, the facility features the Proton Facility (PTF) and Full Power Facility (FPF) to perform nuclear and solid-state physics studies, R&D for fourth-generation nuclear power plants and fusion reactors and enable the production of theranostic radioisotopes. The first part of the accelerator is a 16.6 MeV normal-conducting injector with resonators operating at 176 MHz.

The second part of the accelerator is a superconducting LINAC. The cavities chosen for this section are single-spoke cavities operating at 352.2 MHz. In total, up to 80 resonators will be installed in this phase of the project (see Table 1). The construction of this machine poses unique challenges to the accelerator community: first, the infrastructure targets 40 years of operations. In addition, it requires MTBF values at the same level as nuclear power installations. Finally, contrary to most large-scale high-energy particle accelerators in operation today, MYRRHA Phase 1 is designed to operate with continuously varying beam duty factor. To reach these requirements, the Low-Level RF (LLRF) control system plays a crucial role. To minimize the risks, MYRRHA's ACcelerator Electronics (ACE) group is currently collaborating with Deutsches Elektronen-Synchrotron (DESY). Not only the field controller card, the DAMC-DS5014DR [2], is currently being designed by DESY, but it is planned to reuse several of their firmware and software IPs and packages that are currently deployed in high-reliability superconducting LINACs [3, 4]. Despite the collaboration, several components, such as resonance control, statistics collection, deterministic system reconfiguration, fault detection, post mortem data acquisition, and beam loading compensation techniques, need to be developed to address the unique requirements of MYRRHA.

HARDWARE

The hardware platform chosen for the LLRF system is based on the MTCA.4 standard. The motivation to choose this crate form factor is to achieve high reliability, redundancy and modularity. Each crate will have up to 4 DAMC-5014DR boards to drive an equivalent number of cavities. The synchronization of the boards is orchestrated by a single White Rabbit-capable Advanced Mezzanine Card (AMC) that is interfaced with the DAMC-5014DRs through the MTCA.4 backplane. The timing board is responsible for generating machine triggers and communicate beam parameters and machine configuration data to the controller in real-time. A mCPU AMC, communicating with the RF boards using the PCIe bus of the MTCA.4 crate provides, if needed, additional computing and diagnostic capabilities to the LLRF system.

DAMC-DS5014DR

DAMC-DS5014DR is an RFSoC-based AMC that is optimized for RF-based applications. The board is chosen for several reasons: The use of direct sampling allows using the board for the accelerator frequencies and, possibly, for future 704.4 MHz elliptical cavities foreseen in MYRRHA phase 2. Additionally, using direct sampling simplifies the analog front-end electronics by eliminating the need of additional RF mixers. The ADCs and DACs of the board are driven at 4930.8 MSps and the measured signals are digitally down-converted using an NCO. Then the signals are decimated to 12.327 MSps. The clock frequency of the programmable logic is 123.27 MHz. Apart from the RF converters and programmable logic, the board also features a quad core ARM A53 processor and two ARM Cortex R5 realtime processors. The A53 processor runs the main LLRF EPICS IOC on embedded Linux. This IOC directly communicates with the SoC programmable logic. The custom Real Transition Module (RTM) design in development for MYRRHA, paired with the DAMC-DS5014DR via the MTCA.4 zone-3 connector, provides all the analog signal conditioning fea-

Content from this work may be used under the terms of the CC BY 4.0 licence (© 2026). Any distribution of this work must maintain attribution to the author(s), title of the work, publisher, and DOI.

ISBN: 978-3-95450-252-3 ISSN: 2673-5350 doi: 10.18429/JACoW-IPAC2026-WEP6146

RF SYSTEM STATUS FOR PERLE*

C. Joly†, A. Back, N. Belouchrani‡, S. Berthelot, D. Charlet, P. Gauron, X. Lafay, J.-F. Yaniche
Université Paris-Saclay, CNRS/IN2P3, IJCLab, Orsay, France
F. Bouly, Univ. Grenoble Alpes, CNRS/IN2P3, Grenoble INP, LPSC, Grenoble, France
A. Buthod, Univ. Claude Bernard Lyon 1, CNRS/IN2P3, IP2I Lyon, Villeurbanne, France
on behalf of PERLE collaboration.

Abstract

The PERLE project consists of a 5 MW at 250 MeV Energy Recovery Linac (ERL) demonstrator, with the accelerating cavities operating at 801.58 MHz and 2 K. The superconducting cavities need to be regulated in terms of amplitude, phase and frequency due to perturbations such as microphonics, Lorentz forces and Beam loading. New developments dedicated to PERLE are in progress in order to achieve the performances. Firstly, a Distributed Master Oscillator (DMO), White Rabbit (WR) protocol based allowing to distribute a reference and to generate locally the synchronized RF signals and clocks needed. It is also associated to a timing system using the same WR enhanced hardware (IDROGEN Board) to produce the synchronized timing triggers and gates for all the machine. In addition, a new C&C board of the Frequency tuning system is developing to increase the ecosystem around the IDROGEN board. The LLRF Feedback system is also MTCA based using Off the shelf bards from IOXOS technologies, associated to a RF power Solid state amplifier prototype from JEMA FRANCE upgradeable form 8.8kW to 60kW. An overview and a status of these systems and their implantations will be presented with some outlooks.

INTRODUCTION

The PERLE project aims to build and operate of a 5 MW at 250 MeV Energy Recovery Linac (ERL) demonstrator, with superconducting cavities operating at 801.58 MHz and 2 K with accelerating gradients up to tens of MV/m (cf. Table 1 parameter list). The RF power values are given for a 20 mA beam, without margins.

As shown in Fig. 1, PERLE is composed in a photocathode gun [1] providing 0.3MeV followed by a Low Energy Transport Line allowing to bunch and focus the beam, and measuring some parameters using the beam diagnostics presents on this LEBT. A cryomodule called “Booster” integrating four superconducting mono-cells cavities increase de beam energy to 7 MeV before the injection into the Linac using a merger [2]. In the ERL section a second cryomodule said “Linac cryomodule” is integrated with four superconducting 5-cells elliptic cavities allowing the energy to be increased by 82MeV with each acceleration paths (3-loops planned in the Phase 2 project to achieve ~250 MeV).

Table 1: Elliptic Cavities Parameters

Parameters	Single Cell	Five Cell
Frequency [MHz]	801.58	801.58
Bandwidth [Hz]	471.5	100
G	257.6	274.5
R/Q@β=1 [Ohm]	108.5	523
Lacc=(n.β.λ/2) [m]	0.187	0.935
Q_0	1E+10	3E+10
Q_{ext}	1.7E+6	8E+6
Eacc [MV/m]	9.5	21.9
RF power [kW]	40	25

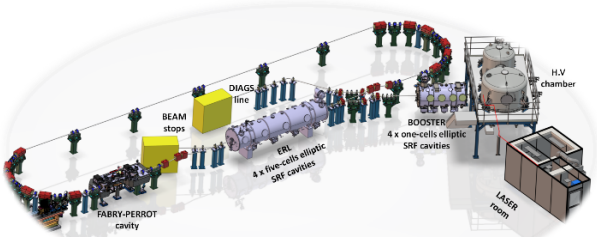

Figure 1: PERLE ERL Phase 1, 1-loop.

Radiofrequency (RF) accelerating cavities and amplitude, phase and frequency control systems require advanced and ongoing R&D due to the ever-increasing performances and accuracy requirements of accelerators to ensure an efficient, reliable and sustainable operation of such high power superconducting accelerators like PERLE.

To limit the joule heating losses and therefore cryogenic consumption, a superconducting cavities quality factor of around 1×10^{10} is required for the Booster, while for the ERL Linac this requirement is set to the challenging value of 3×10^{10}. The external coupling was chosen to minimised the RF power consumption and adds to the operation of some cavities (Linac cryomodule) with a narrow bandwidth (~100 Hz) [3].

In this context, mechanical disturbances such as microphonics caused by the systems surrounding the cavities (e.g., vacuum pumping or helium bath pressure) and radiation pressure can induce a frequency detuning leading to an increase in RF power consumption. To compensate for these variations, which impact beam quality and stability, it is necessary to finely control the accelerating field amplitude (E_{acc}) and phase (φ) as well as the resonance frequency of each cavity, and this in real time by controlling

* The PERLE project is supported by the Agence Nationale de la Recherche via its program ANR-24-RRII-0001 and by the European Union’s program EU HORIZON-INFRA-2023-TECH-01-01 under GA n°101131435.

† Christophe.joly@ijclab.in2p3.fr
‡ Also, at Accelerators & Cryogenic Systems, Orsay

Content from this work may be used under the terms of the CC BY 4.0 licence (© 2026). Any distribution of this work must maintain attribution to the author(s), title of the work, publisher, and DOI.

ISBN: 978-3-95450-252-3 ISSN: 2673-5350 doi: 10.18429/JACoW-IPAC2026-WEP6148

DETUNING ESTIMATION FOR A DOUBLY-FED NORMAL-CONDUCTING GUN

M. Herrmann*, J. Branlard, F. Brinker, M. Hoffmann, V. Katalev, S. Pfeiffer, H. Schlarb, C. Schmidt
Deutsches Elektronen-Synchrotron DESY, Hamburg, Germany

Abstract

At the European Free-Electron Laser (EuXFEL) superconducting linac, a revised normal-conducting gun design with symmetrical feed was successfully installed and tested. Thermal expansion of the solid copper body dominantly affects the detuning transients of this cavity. To improve accuracy, and add time resolution over the duration of a pulse, we implemented and tested an observer that estimates the resonance frequency over time using a parameter-identified white-box model of the RF network. Results were validated against forward and reflected power couplers, cavity voltage, and an algebraic stationary approximation.

INTRODUCTION

On November 2025, a revised gun design [1] has been installed at the EuXFEL (see Fig. 1). From an RF perspective, the main changes in the current revision 5.2 are

- change from single-feed to double-feed with the individual waveguide branches equipped with forward and reflective directional couplers, and
- adding of a (redundant) cavity probe antenna.

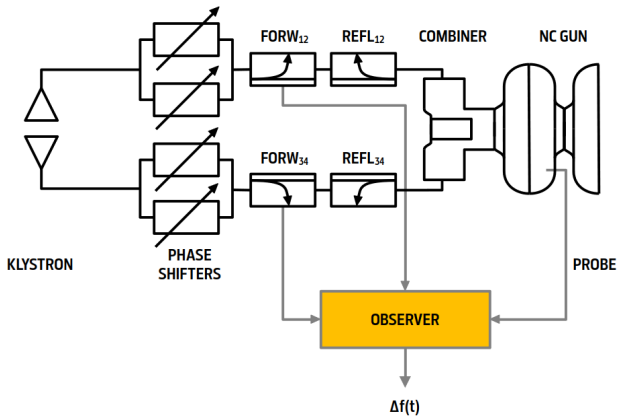

Figure 1: Gun detuning estimation scheme. The observer is a simulation of the gun running in parallel on either a CPU, or an FPGA. The observer is fed by forward voltages of the two respective branches, and the pick-up of the cavity. It serves as a virtual sensor for the unmeasurable detuning Δf.

One of the challenges operating the gun is to keep it on resonance over the course of a pulse where the intra-pulse dynamics are dominated by introduced RF energy, and interpulse dynamics are dominated by convective heat flux to the cooling medium, with the dominating source of detuning being the heat-up of the cavity's inner surface, governing a temperature-to-detuning sensitivity of approx. −21 kHz/K [2].

Since the surface temperature cannot be measured directly, we employ an observer, implemented as an Unscented Kalman filter, which can be considered a virtual (or software) sensor, to estimate time-resolved readings over the length of a pulse, representative for the unmeasurable quantity.

Assuming the estimated surface temperature to be linearly related to detuning, the observer allows for intra-pulse resolved readings of detuning, which potentially enables intra-pulse control actions.

Being an inherently model-based approach, the observer's performance depends on the accuracy of the model, triggering the need for identifying unknown system parameters.

This publication is structured as follows: the modeling section details the ordinary differential equations (odes) representing the coupled RF/detuning dynamics, section parameter identification explains the white-box parameter identification approach, and the observer section gives an outline of the implemented Kalman filter. The paper concludes with a comparison of estimated detuning and its phase-roll approximation, and an outlook for further investigations.

MODEL

By design, the Unscented Kalman filter requires a discrete-time model of the underlying dynamics that propagates the system's states from one sample to the next. In the following, this state transition map is derived from the continuous time description which, in turn, is based on first-order principles.

Continuous Time

Essentially, the gun model consists of a nonlinear 3rd-order odes for coupled RF/detuning of a normal-conducting cavity [3], plus algebraic terms for the lossless combiner [4, 5] with an additional complex parameter ε to account for asymmetry, as detailed in Eqs. (1 – 4).

$$\dot{x} = -\lambda x - yz + bu_x, \tag{1}$$
$$\dot{y} = -\lambda y + xz + bu_y, \tag{2}$$
$$\dot{z} = \rho(z - z_0) + \mu(x^2 + y^2), \tag{3}$$
$$0 = S(\varepsilon)a - a', \tag{4}$$

where x and y are real and imaginary voltage, z is detuning, $b = \frac{2\beta}{\beta+1}\lambda$ is input scalar, λ is half bandwidth, u_x and u_y are real and imaginary forward voltage, z_0 is initial detuning, β

* m.herrmann@desy.de

Content from this work may be used under the terms of the CC BY 4.0 licence (© 2026). Any distribution of this work must maintain attribution to the author(s), title of the work, publisher, and DOI.

ISBN: 978-3-95450-252-3 ISSN: 2673-5350 doi: 10.18429/JACoW-IPAC2026-WEP6149

NARROWBAND ACTIVE NOISE CONTROL FOR CONTINUOUS WAVE OPERATION OF TESLA CAVITIES

B. Richter*[1], J. Branlard, Deutsches Elektronen-Synchrotron DESY, Hamburg, Germany
A. Bellandi, Belgian Nuclear Research Centre SCK-CEN, Mol, Belgium
A. Benwell, J. Diaz-Cruz, S. Hoobler
SLAC National Accelerator Laboratory, Menlo Park, CA, USA
Q. Du, S. Murthy, Lawrence Berkeley National Laboratory, Berkeley, CA, USA
[1]also at Technische Universität Hamburg, Hamburg, Germany

Content from this work may be used under the terms of the CC BY 4.0 licence (© 2026). Any distribution of this work must maintain attribution to the author(s), title of the work, publisher, and DOI.

Abstract

TESLA 9-cell elliptical cavities are used in the accelerators of the European XFEL and LCLS-II. The high duty cycle upgrade study for EuXFEL and the LCLS-II-HE program target loaded quality factors of 6×10^7 and beyond, leading to RF cavity half bandwidths below 11 Hz. Stable operation in these conditions heavily relies on active RF resonance control, since the RF drive power required to maintain amplitude and phase lock would surpass amplifier max ratings if detuning is not compensated. To counteract mechanical vibrations, e.g. introduced by rotational machines in the proximity of the accelerating modules, a dedicated narrowband active noise control algorithm was introduced in previous work. This proceeding presents CPU based implementations and latest test results obtained at the Cryomodule Test Bench (CMTB) at DESY and LCLS-II at SLAC, where the stable operation gradient of a cavity could be increased from 9 to 15 MV/m without violating RF control limits.

INTRODUCTION

Latest XFELs all work towards CW operation of superconducting cavities for electron bunch acceleration. Energy consumption of superconducting cavity operation is mostly determined by required RF power to provide accelerating gradient and by cryogenic load through energy dissipation in cavity walls. The latter is determined by material properties and not changeable after manufacturing of the cavity. However, the required RF power P_f to maintain an accelerating voltage V_c depends on the cavity systems half bandwidth $f_{1/2}$ and detuning Δf

$$P_f = \frac{f_{1/2} V_c^2}{2 \frac{r}{Q} f_0} \left(1 + \left[\frac{\Delta f}{f_{1/2}} \right]^2 \right), \tag{1}$$

where beam loading is neglected [1]. Cavities are operated at $f_0 = 1.3$ GHz is a geometry specific constant. To minimize required amplifier peak power and operational power demand, the $f_{1/2}$ used with TESLA cavities operated in CW is generally chosen as low as possible, while still enabling to fulfill the required RF field stability criteria. However, with lower $f_{1/2}$, detuning effects on power requirement increase, therefore precise resonance control becomes crucial.

* bozo.richter@desy.de

Detuning arises through microscopic mechanical deformation of the cavity geometry. It originates from different sources: the accelerating RF field induces Lorenz force detuning through field interactions with the cavity walls; pressure variations of the liquid helium outside of the cavity leads to deformations; and spatial movements of cavity mounting points lead to deformation by inertia. Through these mounting points, rotational machinery like pumps and ventilators introduce vibrations into the cavity [2].

For active resonance control, TESLA cavities of XFEL, FLASH, and LCLS-II are equipped with piezo tuners allowing to apply unilateral longitudinal force to one of the cavity mounting points. We present practical benefits and implications of employing narrowband active noise control (NANC) to suppress periodic tune disturbances originating from rotational machinery.

NARROWBAND ACTIVE NOISE CONTROL

The NANC algorithm is designed as an adaptive feedforward suppression controller for external harmonic disturbances. The adaption tracks slow disturbance drifts in amplitude, phase, and frequency, including gain and phase effects of the actuator and plant dynamics. It is not suitable to suppress mechanical resonances, which requires dedicated controller design. The notation used in this work is taken from Ref. [3], extended by the frequency adaption given in Ref. [4]. The algorithm is equivalent to that shown in Ref. [5], but different from the active resonance control filter bank of Ref. [6] previously implemented at LCLS-II.

NANC is based on harmonic drive signal components

$$u_m = \mathcal{R}\left(A_m e^{i\omega_m t} \right), \tag{2}$$

defined by a drive vector $A_m \in \mathbb{C}$ and a drive frequency ω_m. The effect of the actuation on the detuning is described by the detuning model

$$\Delta f_m = \mathcal{R}\left(\tau_m A_m e^{i\omega_m t - i\Phi_m} \right), \tag{3}$$

additionally taking into account the forward gain τ_m and phase lag Φ_m of the drive path at the specific ω_m. With this simple model, the measured detuning signal Δf_{meas}, and the external disturbance Δf_{mic}, the partial derivatives of a quadratic cost function

$$J_m = \Delta f_{\text{meas}}^2 = \left(\Delta f_{\text{mic}} + \sum_m \Delta f_m \right)^2, \tag{4}$$

ISBN: 978-3-95450-252-3 ISSN: 2673-5350 doi: 10.18429/JACoW-IPAC2026-WEP6150

DIGITAL LOW LEVEL RF SYSTEM FOR ELETTRA 2.0

C. Pasotti*[1], G. Brajnik[1], M. Cautero[2], M. Colja[1], A. Cuttin[1], A. Pozzer[1], M. Stolfa[1], E. A. Zanin[1]
[1]Elettra - Sincrotrone Trieste S.C.p.A, Trieste, Italy
[2]Department of Physics, University of Trieste, Trieste, Italy

Abstract

The new digital electronics of the four Radio Frequency (RF) plants for Elettra 2.0 (E2.0) is fully designed in house, both hardware and firmware. The Digital Low-Level Radio Frequency (DLLRF) works on a non-IQ sampling technique and it is benefiting from the huge internal development of a System On Chip (SoC) Field Programmable Gate Array (FPGA) boards realized for the electron beam position monitor electronics. Each RF plant will have its own machine protection system based on FPGA board to minimize the interlock intervention time. Initial tests of these new electronics have been carried out during last run of Elettra, however the complete commission is carried out using the RF power plant available in the laboratory. This paper presents the design choices and the performed tests that confirm the achievements of the system's specification.

INTRODUCTION

The Elettra 2.0 storage ring will host four identical 500 MHz Radio Frequency (RF) stations, each comprising a 130 kW continuous-wave solid-state amplifier, the 50 Ω WR1800 waveguide section run, a single-cell normal-conducting cavity, and the necessary electronics for RF power control and interlock [1]. The decommissioned Elettra storage ring relied on analog electronics. Today the Low-Level Radio Frequency (LLRF) is being upgraded with up-to-date digital one thanks to this project. This goal can be achieved choosing between a commercial (turn-key) Digital Low-Level Radio Frequency (DLLRF) system and an internal development effort. Even in the last case, it is essential to balance development costs with the reuse or adaptation of commercially available components and boards.

DIGITAL LOW LEVEL RF SYSTEM

A custom DLLRF system—encompassing both hardware and firmware—has been specifically designed for the E2.0 upgrade. The hardware design prioritized modularity, enabling future modifications to be made with minimal cost and implementation impact. The design also adopted a well established, cost effective technology. The DLLRF is divided into two independent subsystems: the digital RF plant interlock and the digital feedback and control system. This architecture boosts redundancy and reliability while allowing each part to be finely tuned to its specific functions. The RF interlock unit acquires all RF plant signals to execute a rapid RF shutdown in response to any potential warning, and forwards the cumulative RF failure status to the general Machine Protection System (MPS) via optical fiber. On top

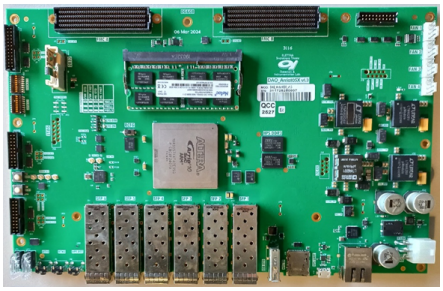

Figure 1: RF Feedback and control mail digital board. Elettra custom development.

of these functions, the RF interlock unit can swiftly shut off the RF for beam dumping, with the operation triggered by an external request. The feedback and control system, in addition to amplitude, phase, and frequency tuning feedback, will carry out the RF power switching on procedure, will follow the proper procedure during externally triggered beam dump, and will record all primary RF signals at the storage ring Turn by Turn (TbT) rate for diagnostics and offline analysis. A pivotal element of this project is the Field Programmable Gate Array (FPGA) based digital board, built around an Altera/Intel Arria 10 and developed in house at Elettra. The board can host two FMC modules, incorporates Double Data Rate (DDR)3 RAM, and offers 10 Gbit/s Ethernet links [2]. It has been further upgraded with a System On Chip (SoC) architecture, as shown in Fig. 1. The board serves as the core of the electron Beam Position Monitor (BPM) diagnostic system; more than one hundred units have been built, and are commissioned and ready for installation in E2.0. Because the entire deployment is well understood and widely distributed, any future issues or bugs can be promptly addressed, and the rapid obsolescence of key components—especially the FPGA and CPU chips—can be managed effectively.

RF INTERLOCK

Handling several kW of RF power requires a reliable and rapid response in the event of any failures. The interlock's electronics feature a robust design based on the Altera Cyclone V GX development board. Additional boards have been designed to condition and monitor more then thirty status signals—water flow rates, temperature, arc detection, amplifier status, and other relevant parameters. Two Analog-to-Digital Converter (ADC) units enable the acquisition of several analog signals, such as cavity vacuum pressure, tuner position and RF drive level. Upon any failure, the digital board actuates a dedicated RF switch to open the RF branch that drives the high power RF amplifier, and simultaneously signals the fault to the MPS via optical fiber. The interlock

* cristina.pasotti@elettra.eu

Content from this work may be used under the terms of the CC BY 4.0 licence (© 2026). Any distribution of this work must maintain attribution to the author(s), title of the work, publisher, and DOI.

ISBN: 978-3-95450-252-3 ISSN: 2673-5350 doi: 10.18429/JACoW-IPAC2026-WEP6153

PLANNED UPGRADE OF THE CERN PROTON SYNCHROTRON BEAM CONTROL SYSTEM

F. J. Diaz Ferreira*, D. Barrientos, Y. Brischetto, T. Gavric, A. Lasheen, B. Woolley
European Organization for Nuclear Research, Geneva, Switzerland

Abstract

The CERN Proton Synchrotron (PS) Low Level RF (LLRF) system is composed of cavity controllers, which regulate the field in the cavities, and a beam control, in charge of maintaining the required longitudinal beam specifications and managing the injection and extraction processes. The current beam control system, implemented using mainly analogue electronics in NIM and VME formats, is set to be replaced by modern digital platforms that have been deployed on other machines in the complex. This upgrade aims for a redesigned, more centralized and standardized system. The new compact digital module will result in significantly reduced hardware requirements and improvement in diagnostics and maintenance. This paper provides an overview of the system's architecture, hardware, firmware, and development plan, focusing on the control loops and the interaction between the module and other components in the system.

MOTIVATION

since 1959, the PS has undergone numerous upgrades to supply proton and heavy ion beams, operating with charges between 10^8 and 4×10^{13} and reaching energies up to 26 GeV. The 628 m circumference ring features 25 RF cavities driven by six distinct RF systems spanning a frequency range of 0.4 to 200 MHz.

The LLRF architecture consists of two primary subsystems: cavity controllers and the beam control. The cavity controllers utilize single and multi-harmonic feedback loops to regulate the phase and amplitude of the RF signals delivered to the cavities. Meanwhile, the beam control subsystem employs radial, phase, and synchronization loops to maintain strict beam parameters and to coordinate injection and extraction timing with adjacent machines.

A renovation of the beam control system is currently underway (Fig. 1). The upgraded architecture utilizes two VMEbus Switched Serial (VXS) crates for the digital demodulation of beam loop inputs, alongside a microTCA crate that processes the beam loops [1]. This hardware selection aligns with CERN's broader strategy to standardize and improve existing accelerator technologies (LHC Injectors Upgrade project). Consequently, the VXS platforms mirror those already deployed in the PSB, AD, ELENA, and LEIR, while the beam loop architecture is based on the modernized systems of the SPS [2] and LHC.

The purpose of this new beam control is to implement the current analogue feedback algorithms as accurately as possible, but improving on diagnostics, operability and maintainability. The possibility of future feature addition is also to be kept in mind.

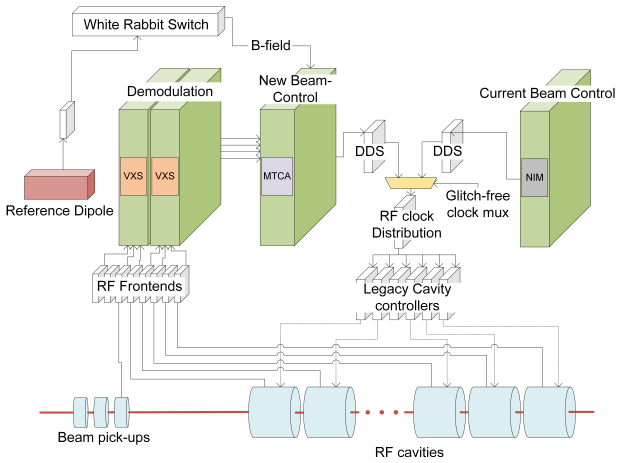

Figure 1: PS LLRF system diagram.

BEAM CONTROL ARCHITECTURE

Following the success in the deployment on the SPS and LHC, the PS Beam Control (Fig. 2) adheres to the same principle for firmware/software boundary definition in the FPGAs.

IP modules developed for other machines will be implemented in hardware for tasks like board housekeeping, White Rabbit (WR) Tx/Rx, generation of local timing from general machine signals, amongst others.

Some firmware modules were also developed for PS specific functions and where interaction with legacy systems was needed, such as the VXS acquisition.

A C++ application is in production for higher-complexity and higher-iteration parts of the beam control, such as calculation of the revolution frequency from the magnetic field [3] and the phase, radial, and synchronization loops.

HARDWARE

One of the main advantages of the new beam control is hardware standarization and condensation. Tens of racks, each having a few NIM crates populated with locally developed analogue electronics, are set to be replaced with two VXS crates and one microTCA crate. Each of the VXS crates contains two VXS switches and four VXS-DSP-FMC carrier boards, each containing two 4-channel 125 MSPS ADC FMCs. The carrier boards contain two FPGAs; one to demodulate and process the signals acquired through the two FMCs ADCs, and the other containg the signal acquisition core, function generators, timings and the so-called

* francisco.javier.diaz.ferreira@cern.ch

Content from this work may be used under the terms of the CC BY 4.0 licence (© 2026). Any distribution of this work must maintain attribution to the author(s), title of the work, publisher, and DOI.

ISBN: 978-3-95450-252-3 ISSN: 2673-5350 doi: 10.18429/JACoW-IPAC2026-WEP6154

BENCHMARKING BEAM DYNAMICS SIMULATIONS FOR THE MYRRHA PHASE 1 ACCELERATOR

L. De Keukeleere†, U. Dorda, J. Hustings, E. Tanke, J. Van De Walle
Belgian Nuclear Research Centre, Mol, Belgium

Abstract

At the Nuclear Research Center SCK CEN in Belgium, the first phase of the MYRRHA project (an accelerator driven system) is under construction. Included in MYRRHA Phase 1 are a 17 MeV normal conducting injector linac (RFQ + CH cavities) and a super-conducting LINAC (60 single-spoke cavities), providing a CW proton beam of 4 mA at 100 MeV. In this contribution, beam dynamics simulations of the MYRRHA Phase 1 accelerator are compared for four different beam dynamics codes: TRACEWIN, PyOrbit3, DYNAC and PyAccel. The beam simulation results for a reference case are compared, as well as the computing times. Furthermore, approximations which can be made to speed up the computation times are discussed. These comparisons are made in view of a future on-line deployment of a simulation tool during beam commissioning.

INTRODUCTION

The last few decades a multitude of beam optics simulation codes were developed within the accelerator community. Despite the many similarities amongst these codes, there are differences in how, for example, space charge and field map tracking are modelled. Furthermore, different software languages or back-ends are deployed, going from Fortran to Python. Hence, the choice does not only depend on the performance, but also on practical considerations like what operating system and software languages will be available in the control room. In this paper four software packages are compared – one of them is tested in two different modes - with respect to beam optics parameters and computing power. All of them are introduced in the next paragraphs.

The first tool considered for developing an online virtual accelerator is *Trace Win* [1], a licensed closed-source software package distributed and maintained by CEA and used as a reference code for projects like IFMIF, ESS and SPIRAL2. It has two tracking 'modes': transfer-matrix tracking and multi-particle tracking. While the former is fast and sufficient for simulating basic beam parameters like envelopes and phase advances, the latter can uncover more detailed behaviour like beam loss and halo formation.

The second tool is the open-source multi-particle tracking code *DYNAC* [2], which contains both a numerical method, capable of simulating single and multi-charge state ion beams in accelerating elements as well as a fast analytical method for single charge state beams. It has been benchmarked against other codes, like TraceWin, as well as against measurements [3, 4]. It is well suited for online modelling and as an aid in view of commissioning [5, 6].

The third tool PyOrbit3, is an open-source Python/C++ implementation of the ORBIT (Objective Ring Beam Injection and Tracking) code [7]. It has multiple space-charge and EM-field tracking models and can be compiled with an MPI for parallel computation. It was already benchmarked and used for large accelerator complexes such as SNS and ESS [8, 9].

The fourth package, *PyAccel,* was developed in-house at SCK CEN and is, like one of the TraceWin modes, a transfer-matrix tracking code, allowing for the fast simulation of collective beam behaviour. It is purely python-based, and the linear space-charge model and EM field dynamics model were adopted from TraceWin. The biggest advantage of having an in-house tool is the level of control and customization.

THE MINERVA ACCELERATOR

The MINERVA accelerator (the layout is shown in Fig. 1) consists of a normal conducting injector followed by a superconducting LINAC. An RFQ installed in the former, bunches a 4mA beam originating from an ECR source at a frequency of 176.1 MHz and accelerates the beam to 1.5 MeV. A sequence of normal-conducting CH cavities then further accelerates the bunched beam to 16.6 MeV. After passing through a matching section, the beam is accelerated to the desired 100 MeV by means of a superconducting LINAC with 60 single spoke cavities pair-wise confined in 30 cryomodules and operating at 352.2 MHz.

In parallel to the requirements tests for MYRRHA [10, 11], two user facilities will be able to receive the beam delivered by High-Energy Beam Transport section (HEBT): The "Proton Target Facility" (PTF) will perform Isotope Separation On-line experiments on non-fissile material targets, while the "Full Power Facility" (FPF) is designed to operate at full CW beam power, i.e. 400 kW, and its main goal is fusion material research [12, 13].

BEAM OPTICS SIMULATIONS

To decide which beam optics codes can be employed to build a virtual accelerator, a comparative study was carried out. The results reported below all correspond to the simulation of one line in the MINERVA accelerator, i.e. going from the exit of the RFQ all the way down to the FPF (see Fig. 1). A qualitative interpretation will be given to the differences amongst the results, as at this point no physical data from beam diagnostics devices are available to compare to.

†lennert.de.keukeleere@sckcen.be

Content from this work may be used under the terms of the CC BY 4.0 licence (© 2026). Any distribution of this work must maintain attribution to the author(s), title of the work, publisher, and DOI.

ISBN: 978-3-95450-252-3 ISSN: 2673-5350 doi: 10.18429/JACoW-IPAC2026-WEP6156

SURROGATE MODELS FOR THE EUROPEAN XFEL OPERATION

B. Veglia*, J. Kaiser, S. Tomin, S. Walker,
Deutsches Elektronen-Synchrotron DESY, Hamburg, Germany

Abstract

Numerical beam dynamics simulation codes are essential for designing and studying particle accelerators, but their computational cost can make them unsuitable for online use and predictions during operations. The use of machine learning-based surrogate models can significantly reduce the required computational time whilst still providing an accurate prediction of the beam properties. In this paper, we present the first results on the training of surrogate models for the prediction of the longitudinal phase space (LPS) at the European XFEL. Finally, we discuss the potential application of such models in the development of a virtual diagnostic tool for use in the European XFEL control room as well as a fast estimator for the final LPS based on the user-provided compression parameters.

INTRODUCTION

The rise of X-ray free-electron lasers (XFELs) over the past decade has provided researchers with ultra-short, coherent X-rays capable of probing matter at the atomic level. At the heart of these facilities is the electron beam; information on its longitudinal phase space (LPS) is vital for achieving the desired lasing performance and developing advanced FEL modes. To monitor this property effectively, scientists rely on longitudinal diagnostics instrumentation. The European XFEL (EuXFEL), schematically shown in Fig. 1, is a 3.4 km hard X-ray FEL in the Hamburg region, Germany. It is equipped with two transverse deflecting structures (TDSs) [1] — one located in the injector diagnostics section and another downstream of the third bunch compressor (BC2) — a coherent radiation intensity spectrometer (CRISP) [2, 3], which reconstructs the current profile, and a single-plate corrugated structure (also referred to as a passive streaker) [4] installed downstream of SASE2. However, all of these diagnostics have important limitations. The TDS downstream of BC2 provides a temporal resolution of only about 10 fs, while the CRISP spectrometer does not measure the phase of the emitted coherent radiation, making the reconstruction ambiguous with respect to the beam orientation and particularly sensitive to noise at low bunch compression. Finally, the analysis of the streaked beam after after interacting with the passive streaker requires a complicated reconstruction [5] making it non-compatible with online tuning.

Ideally, high-resolution TDSs would be situated downstream of the undulator lines in order to directly inspect the LPS in order to directly tune the undulator lasing. However, this is a longer-term goal, likely several years away from completion at the time of writing, and will require considerable investment. Traditional numerical simulations would provide a high-accuracy description of beam dynamics by modeling complex collective effects [6]. However, the substantial computational effort required for these simulations precludes their deployment as live diagnostics for machine operations. To overcome these difficulties, a machine-learning-based surrogate model was developed to provide fast high-fidelity longitudinal phase space predictions.

Virtual Diagnostics

Neural networks for particle accelerator can be used as virtual diagnostics, where learned surrogate models provide information about the state of an accelerator that would otherwise be difficult or even impossible to acquire using a physical diagnostic as in our case. The provided information can give useful data about experiments and help operators tune the accelerator. Previous work has demonstrated the feasibility of using ML models as virtual diagnostics to non-destructively predict the LPS distribution of FACET-II single bunch operation (in simulation) and at LCLS (in experiment) [7, 8]. Neural networks were trained in these studies to create a mapping between non-destructive diagnostic inputs (e.g., linac and e-beam diagnostics that are available on a single shot basis) and the LPS.

In this work, we present the ongoing work into building a ML-based surrogate model for reconstructing the two-dimensional LPS at the EuXFEL from RF settings and the CRISP spectrum. In consideration of the limited amount of LPS measurements available, we decided to base the training of such model on simulated data.

METHODS AND RESULTS

Dataset Generation

In order to effectively train a surrogate model, large scale simulated data is required. For this project, start-to-end simulations were used, tracking the electron beam from the gun down to the end of the collimation section (before the switchyard) including collective effects. For each simulation, the RF parameters for the injector and the first two linacs are randomly selected from a range of values around the working points, as listed in Table 1.

The first three parameters listed in Table 1 are the first-, second-, and third-order coefficient in beam energy profile at the injector exit, which define the detailed compression scenario in the first bunch compressor. The last two parameters, the L1 and L2 chirps, control the compression strengths in the second and third chicane sections. Preliminary studies were conducted in the past [9, 10], where the RF settings where adjusted with relatively small variations based on the nominal design. The aim of this project is to extend

* bianca.veglia@desy.de

Content from this work may be used under the terms of the CC BY 4.0 licence (© 2026). Any distribution of this work must maintain attribution to the author(s), title of the work, publisher, and DOI.

ISBN: 978-3-95450-252-3 ISSN: 2673-5350 doi: 10.18429/JACoW-IPAC2026-WEP6157

GLOBAL START-TO-END OPTIMIZATION WITH BAYESIAN OPTIMIZATION*

B. Veglia†, B. Beutner, S. Tomin, S. D. Walker
Deutsches Elektronen-Synchrotron DESY, Hamburg, Germany

Abstract

Controlling the beam longitudinal phase space (LPS) distribution is crucial for advanced free-electron laser operation modes. At the European XFEL, this task is particularly challenging due to the complex compression scheme, which includes three bunch compressors. We present an approach based on Bayesian optimisation that streamlines the search for compression configurations yielding current profiles with desirable features, such as a flat top or a pronounced spike at either the head or the tail of the bunch. Moreover, this method can also be applied to tune the RF parameters in start-to-end simulations to achieve better agreement with measured longitudinal phase space profiles.

INTRODUCTION

Precise control over the longitudinal phase space (LPS) distribution of electron bunches is fundamental to the operation of modern X-ray free-electron lasers (FELs). At facilities such as the European XFEL (EuXFEL), advanced operating modes—including the generation of attosecond pulses or specific spectral bandwidths—rely on the ability to tailor the bunch current profile with high fidelity. However, achieving this level of control is a significant challenge due to the complex multi-stage compression schemes employed, where nonlinear beam dynamics and collective effects, such as space charge and coherent synchrotron radiation (CSR), play a dominant role.

Consequently, there is a critical need for optimization algorithms that can navigate high-dimensional parameter spaces efficiently, minimizing the number of expensive "black-box" evaluations required to reach an optimal solution. Recent advances in machine learning and global optimization offer a path forward. Bayesian optimization (BO) [1,2] has emerged as a particularly effective tool for accelerator physics [3, 4], characterized by its sample efficiency and ability to handle noisy or uncertain objective functions. By utilizing a surrogate model—typically a Gaussian Process—to map the parameter space, BO can identify promising regions for evaluation without the need for exhaustive grid searches. This approach is equally applicable to online tuning and offline simulation-based optimization, where the goal is to balance the trade-offs between multiple competing beam parameters.

In this work, we demonstrate the application of Bayesian optimization to the EuXFEL compression system, focusing first on the task of model calibration. We show that by automating the tuning of RF parameters within start-to-end simulations, the BO framework can efficiently reconcile physics models with experimental measurements, ensuring that simulation-based predictions accurately reflect observed machine performance. Building on this validated model, we then demonstrate how the algorithm simplifies the search for compression configurations that yield current profiles with specific, user defined features. This includes the generation of distributions such as flat-top profiles or pronounced current spikes at the head or tail of the bunch, which are essential for advanced FEL operations.

MODEL CALIBRATION

A set of measurements was performed at the EuXFEL where the beam compression was varied by scanning the Linac L1 chirp from -12.4 to −4.4 m^{-1} in 9 steps. The chirp is defined as $\frac{-kV\sin\varphi}{E_0+V\cos\varphi}$, where φ and V are the voltage and phase of Linac L1, E_0 = 130 MeV is the initial energy of the beam before L1, and $k = 2\pi f/c, f = 1.3$ GHz. Details about the European XFEL three stage compression system and beam dynamics can be found in [5,6]. The non-invasive CRISP THz spectrometer [7] was used to measure the current profile at each step, obtained from the acquired spectrum through a reconstruction algorithm [8].

Table 1: Optimization Parameters and Their Bounds

Voltage of the first harmonic cavity (inj.)	±	2.5 MeV
Phase of the first harmonic cavity (inj.)	±	0.3 deg
Voltage of the high harmonic cavity (inj.)	±	2 MeV
Phase of the high harmonic cavity (inj.)	±	0.3 deg
Voltage in L1	±	5 MeV
Phase in L1	±	0.3 deg
Voltage in L2	±	15 MeV
Phase in L2	±	0.5 deg

We implemented a BO framework to tune OCELOT simulations [9–11] by identifying the optimal parameters required to reproduce the observed beam characteristics. The optimization parameters included the RF settings for the injector and linacs L1 and L2. The optimizer was implemented using the `scikit-optimize` Python package, utilizing Message Passing Interface (MPI) parallelization on the DESY high-performance computing cluster to accelerate the process by simultaneously evaluating hundreds of simulations.

In each subprocess, the optimizer executes an OCELOT particle tracking simulation and returns a scalar score for minimization. The objective function is defined as the Root Mean Square Error (RMSE) between the reference and simulated current profiles. To ensure a robust comparison, a cross-correlation function aligns the two curves by identifying the temporal shift that maximizes their overlap.

* Work supported by the EuXFEL R&D program.
† bianca.veglia@desy.de

Content from this work may be used under the terms of the CC BY 4.0 licence (© 2026). Any distribution of this work must maintain attribution to the author(s), title of the work, publisher, and DOI.

ISBN: 978-3-95450-252-3 ISSN: 2673-5350 doi: 10.18429/JACoW-IPAC2026-WEP6158

TURNING LOGBOOK DATA INTO OPERATIONAL INSIGHT WITH A NEW STATISTICS SERVICE AT GSI AND FAIR

H. Stemmler*, A. Bloch-Späth, M. Stein, O. Geithner, S. Reimann
GSI Helmholtz Centre for Heavy Ion Research, Darmstadt, Germany

Abstract

It is common practice during accelerator operation to continuously document all relevant machine states and activities. At GSI Helmholtz Centre for Heavy Ion Research (GSI), this is done using an electronic logbook developed in-house and adapted to the specific requirements of accelerator operations, allowing shift crews to record failure events, setup times, and other important information in high detail. A new service, currently under development, aims to simplify the on-demand access to relevant statistics and is being prepared to include data from the Facility of Antiproton and Ion Research (FAIR) as its operations gradually commence in the upcoming beamtimes. This service is built as two layers: a backend layer using the Micronaut framework, which communicates with the database to retrieve logbook entries and calculate statistics, and a frontend layer using the Angular framework, which handles user requests and provides graphical representations of the statistics and their raw data. This paper introduces the new statistics service as an assessment tool based on operational data at GSI and FAIR.

INTRODUCTION

The operational success of large-scale facilities like GSI Helmholtz Centre for Heavy Ion Research (GSI) [1] requires close coordination between multiple departments and technical groups. Precise and continuous documentation ensures that operational data remains accessible and reliable across all teams, which allows for the maintenance of efficient communication between complex, interacting areas such as beam diagnostics and physics, technical infrastructure, and control systems.

At GSI, shift crew operators use OLOG [2], an electronic logbook tool developed in-house to continuously record events that may influence beam delivery or machine performance. These include failure events, machine setups, system adjustments, and unusual operational conditions. By maintaining detailed records of such events, operators, engineers, analysts and coordinators can later revisit any operational period, evaluate performance trends, and identify recurring issues that highlight weaknesses in the facility in need of improvement that might otherwise go unnoticed. A complementary KPI-based approach for quantitative beam-based performance assessment at GSI has recently been introduced in Ref. [3]. Results are presented in Ref. [4].

In addition, documentation becomes increasingly important as facilities expand. With the gradual development of the Facility for Antiproton and Ion Research (FAIR) [5], the complexity and scale of accelerator operations will grow significantly. This increasing operational complexity is also reflected in the FAIR Control Centre concept, which was developed to support the larger and more intricate operational scope of the FAIR/GSI accelerator complex [6, 7].

MOTIVATION

Previous Solution to Generating Statistics

At present, operational documentation at GSI is managed through the OLOG web application (see Fig. 1). This system allows operators to manually record events in an electronic logbook. Up until its last version, the OLOG web application included a feature for generating statistical summaries. Users were able to export tables containing calculated statistics based on the logbook entries stored in the database. These tables would provide information about events as documented by the operators. However, concatenation of statistics over larger time frames had to be done manually, leaving room for error and incorrect conclusions, as previously also highlighted in other institutes [8]. Furthermore, although the system did provide a full event export, an option to export data relevant only to a specific statistic did not exist.

Concept for New Statistics Service

The new statistics service seeks to provide fast and convenient access to accelerator performance data by offering a unified, automated interface for statistical generation. The system is designed to allow users to request specific statistics for a chosen time range and immediately receive both the calculated results and the underlying data.

Once a statistic is selected, the service runs through several steps to first retrieve the necessary entries from the OLOG database. Next, the system processes the data and calculates the requested statistics. Finally, the results are displayed graphically and accompanied by the raw data used in the calculation.

Providing both visualizations and raw data offers several advantages. The automatic graphical representations allow users to quickly use analyses in meetings or presentations, and to visualize the collected data and identify patterns or anomalies in the data, while access to the raw data enables more detailed analyses when needed.

Requirements Aside from ensuring accurate and reliable statistical calculation, the design of the new service is guided by three main objectives.

First, the system must be easy to use. The web interface must remain intuitive and require minimal training, enabling both technical and non-technical users to extract statistics with minimal effort.

* h.stemmler@gsi.de

Content from this work may be used under the terms of the CC BY 4.0 licence (© 2026). Any distribution of this work must maintain attribution to the author(s), title of the work, publisher, and DOI.

ISBN: 978-3-95450-252-3 ISSN: 2673-5350 doi: 10.18429/JACoW-IPAC2026-WEP6163

INOVESALIB: A MODULAR VLASOV-FOKKER-PLANCK SOLVER FRAMEWORK

F. Donoso*, M. Brosi, E. Bründermann, M. Frank, S. Funkner, J. Gethmann,
A.-S. Müller, P. Schreiber,
Karlsruhe Institute of Technology, Karlsruhe, Germany

Abstract

The numerical solution of the Vlasov–Fokker–Planck (VFP) equation is a well-established method to simulate the dynamics of electron bunches in storage rings, including their self-interaction through wake fields. Inovesa is an efficient VFP solver that enables accurate simulations of phase space evolution, capturing phenomena such as coherent synchrotron radiation (CSR) and the micro-bunching instability on standard desktop hardware.

Building on this foundation, we introduce Inovesalib, a redesigned and extensible library version of Inovesa that exposes the core VFP solver as a modular C++ API and provides a Python wrapper for seamless integration into user workflows. Inovesalib decouples the solver core from application logic and offers a plugin architecture that allows users to implement custom algorithms without modifying the underlying solver. The redesigned structure turns Inovesa from a standalone application into a flexible simulation framework, suitable for integration into optimization pipelines, machine learning workflows, and custom tools. We present the library architecture and demonstrate its use in both C++ and Python.

INTRODUCTION

The dynamics of electron bunches in storage rings are governed by complex interactions between the beam and its electromagnetic environment. The phase space density evolution of an electron bunch is of particular relevance for understanding collective effects caused by perturbations through wake fields [1], or equivalently, through the beam coupling impedance. These interactions give rise to phenomena such as coherent synchrotron radiation (CSR) and micro-bunching instabilities, which can significantly degrade beam quality, reduce beam lifetime, and limit the performance of synchrotron radiation facilities [2, 3]. Specifically, the longitudinal dynamics can be described by the Vlasov-Fokker-Planck equation (VFPE), given in Eq. (1), which models the particle density of a bunch in the phase space and in time [3, 4].

$$\frac{\partial\psi}{\partial t} + \frac{\partial H}{\partial p}\frac{\partial\psi}{\partial q} - \frac{\partial H}{\partial q}\frac{\partial\psi}{\partial p} = \beta_d \frac{\partial}{\partial p}(p\psi) + D\frac{\partial^2\psi}{\partial p^2}. \quad (1)$$

Here, ψ denotes the phase space density, H is the Hamiltonian of the system, q and p are the canonical position and momentum coordinates, respectively, and β_d and D represent the damping and diffusion coefficients.

To solve this equation efficiently in practice, Inovesa was developed as a runtime-efficient VFPE solver for desktop-class hardware. The original code base, developed by Schönfeldt at KIT [5], combined a discretized longitudinal phase space model with optimized numerical operators and parallelization, making systematic micro-bunching studies practical on standard workstations within minutes rather than days.

Since its introduction, Inovesa has been applied in a wide range of scientific studies. Steinmann *et al.* [6] used Inovesa to compare time-resolved THz spectroscopic measurements at KARA with VFP simulations, thereby relating measured bursting dynamics to simulated longitudinal substructures and threshold behavior. Schönfeldt *et al.* [7] used Inovesa to investigate how the CSR impedance contributes to the synchronous phase shift at KARA, connecting the solver to an experimentally accessible machine observable. In a related study, Funkner *et al.* [8] developed a non-destructive longitudinal phase space density tomography method, qualitatively validating their reconstructed dynamics against Inovesa simulations driven by KARA machine parameters.

Inovesa has also been used to interpret parameter-dependent instability studies. Brosi *et al.* [9] analyzed the effect of a damping wiggler on the micro-bunching instability at KARA and used Inovesa simulations to study how changes in damping time modify the temporal burst pattern of the emitted CSR. Boltz *et al.* [10] employed Inovesa for passive particle tracking in order to study how CSR wake fields perturb synchrotron motion and may seed micro-structures in longitudinal phase space. Expanding its application, Brosi et al. [11] utilized Inovesa as a primary VFP solver in a cross-code comparison between SOLEIL and KARA. Most recently, Brosi *et al.* [12] applied it at MAX IV to investigate microwave instabilities under varying intra-beam scattering (IBS) conditions, finding good qualitative agreement between simulation and experiment. These studies highlight the role of Inovesa as a reference tool for comparative and interpretive numerical studies, extending its use beyond individual simulation cases.

More recent work used Inovesa for hardware-oriented design, impedance manipulation, and control-oriented machine learning studies. Maier *et al.* [13] simulated the impact of corrugated structures on the longitudinal beam dynamics and emitted CSR power at KARA, and subsequently studied how these effects depend on bunch length conditions in low momentum compaction operation [14]. Wang *et al.* [15] used Inovesa as the CSR simulation environment for accelerated deep reinforcement learning aimed at fast feedback

* felipe.donoso@kit.edu

Content from this work may be used under the terms of the CC BY 4.0 licence (© 2026). Any distribution of this work must maintain attribution to the author(s), title of the work, publisher, and DOI.

ISBN: 978-3-95450-252-3 ISSN: 2673-5350 doi: 10.18429/JACoW-IPAC2026-WEP6164

PROVIDING REPRODUCIBILITY AND ACCESSIBILITY OF RESEARCH SOFTWARE DEVELOPMENT FOR ACCELERATOR PHYSICS AT KARA

F. Donoso*, E. Bründermann, M. Frank, S. Funkner, J. Gethmann,
S. Masoumi, A.-S. Müller
Karlsruhe Institute of Technology, Karlsruhe, Germany

Abstract

Modern accelerator facilities generate heterogeneous data from diagnostics, sensors and simulations, making it difficult to manage, reproduce, and contextualize results as software and models evolve. While FAIR principles (Findable, Accessible, Interoperable, Reusable) are increasingly applied to research data, the iterative development of scientific software, with its rich metadata and benchmarks, rarely follows them. Small changes in compiler flags, dependencies, or hardware can alter outcomes, yet are often undocumented. We address this gap with BenchTune, a telemetry and reporting layer in C++ and Python that interfaces with the Kadi4Mat (Kadi) virtual research environment. BenchTune records metadata for each algorithm run, compiler information, parameters, metrics and stores it in Kadi as portable, traceable research artifacts. A project-view plugin in Kadi visualizes the evolution of a research project, linking code versions, datasets, and benchmark runs into coherent workflows.

As a result, our contribution provides a reproducible framework that supports FAIR principles for research data, enabling sustainable and collaborative research in accelerator physics and beyond.

MOTIVATION

The modern landscape of accelerator physics is increasingly defined by the intersection of high-performance hardware and sophisticated software stacks. At the Institute for Beam Physics and Technology (IBPT), our primary mission is accelerator research at the Karlsruhe Research Accelerator (KARA), using it as a test facility for studies with electron beams, beam diagnostics, and related developments such as magnet systems.

KARA serves as a critical testbed for novel diagnostics, beam dynamics studies, and advanced light source applications, generating large and heterogeneous streams of scientific and technical data even for a medium-sized accelerator. The accelerator infrastructure alone monitors around 30,000 data points across roughly 900 networked devices, with sensors and controllers operating at diverse update rates. The resulting data volume already reaches the order of 100 TB.

In accelerator research, workflows can increasingly be organized from data acquisition through analysis to publication. In our research environment, the provenance of raw and processed data is already treated as a central concern and is addressed according to established FAIR principles [1]. At IBPT, this process has recently been strengthened by the adoption of Kadi4Mat [2] (Kadi), a virtual research environment that supports the structured organization of data, metadata, and links between intermediate and final results within scientific workflows [3].

However, capturing complete algorithm provenance is significantly harder, yet essential for aligning with FAIR for Research Software [4–6] (FAIR4RS). This is particularly true for exploratory research software, which is often developed and executed on personal workstations, local servers, or temporary high-performance computing environments. Although final software versions may eventually be archived in long-term repositories such as Zenodo, the provenance of individual software executions is rarely preserved as a research object in its own right [7]. Such execution-level provenance extends beyond the source code and includes the scientific literature motivating the implementation, metadata describing the execution environment, code variables, runtime parameters, intermediate results, failures, performance measurements, and the configuration and build process of the software artifact. Consequently, important contextual information about how scientific results were actually produced is often lost.

This situation reveals a critical FAIR-gap [4–6] in software driven research. Consider a common scenario: a researcher produces a set of high-quality plots, pushes the code to a Git repository, and archives the dataset on Zenodo. Despite this, a scientist attempting to reproduce the results at a later stage may still fail. The code in the repository may have changed since the plots were originally produced, the exact runtime parameters may never have been documented, and the computation itself may have relied on a specific compiler version, build configuration, dependency stack, or hardware platform that is no longer accessible. Moreover, numerical libraries can exhibit different behavior depending on machine architecture, compilation flags, or backend implementations, leading to different outcomes even when the nominal algorithm remains unchanged. In this sense, access to source code and input data alone is insufficient to guarantee reproducibility, as the metadata describing the software execution, runtime environment, and configuration has not been properly persisted [8].

Software provenance is particularly important in accelerator physics, where many beam properties cannot be measured directly but must be reconstructed from heterogeneous diagnostic data. Many quantities of scientific interest are obtained only through reconstruction processes that combine time-resolved measurements, acquisition systems, physical models, and numerical analysis tools. Because the physics

* felipe.donoso@kit.edu

Content from this work may be used under the terms of the CC BY 4.0 licence (© 2026). Any distribution of this work must maintain attribution to the author(s), title of the work, publisher, and DOI.

ISBN: 978-3-95450-252-3 ISSN: 2673-5350 doi: 10.18429/JACoW-IPAC2026-WEP6165

GENERIC PYTHON ALGORITHM PLUGIN FOR THE EPICS AREA DETECTOR FRAMEWORK

M. Marn*, J. Varlec†, T. Zagar, Cosylab, Ljubljana, Slovenia

Abstract

Area Detector is widely used in accelerator and observatory control systems to build data processing pipelines for images and waveforms, but adding new processing stages normally requires specialized C++ development. This slows prototyping and limits access to modern analysis tools that are predominantly available in Python. We present a new Area Detector plugin that executes user-defined Python algorithms directly on acquired images and their metadata. The plugin integrates advanced scientific libraries and machine learning toolkits, supports GPU acceleration, and enables parallel execution through multi-stage pipelines or Python multiprocessing. Algorithms can be updated without recompiling the IOC, allowing rapid iteration during operations. An automatically generated GUI exposes configurable parameters to operators. The approach is being evaluated on ESA's NEOSTED telescope system, where Python-based routines are used for telescope autofocusing.

INTRODUCTION

Area Detector (AD) [1] is the Experimental Physics and Industrial Control System (EPICS) framework for building image and waveform processing pipelines. At particle accelerators it underpins accelerator diagnostics and beamline instrumentation; at observatories it serves the camera control system. A pipeline is composed as a graph of plugins, each implemented as a C++ class derived from a common base class. Adding a new processing stage therefore requires both C++ and EPICS expertise. This barrier slows prototyping and puts the modern Python scientific computing and machine-learning ecosystem out of reach.

We present `NDPluginPython`, a generic AD plugin that executes user-defined Python algorithms directly on acquired images and their attached metadata. The plugin is being developed in the Telescope On-Site Image Processing (TOSIP) project for the European Space Agency (ESA), with the NEOSTED (Near-Earth Object Survey Telescope Deployment) autofocus use case [2] as its first concrete deployment. While accelerator imaging diagnostics are not the project's first target, the design is fully generic and applies wherever AD is already used.

AREA DETECTOR BACKGROUND

Images travel through an AD pipeline as `NDArray` objects [1]. The `NDArray` is a self-describing container holding pixel data, dimensions, data type, identifier, timestamp, and an extensible list of named attributes (`NDAttribute`). Attributes carry arbitrary named metadata associated with the array. Pipeline elements come in two kinds: drivers, which produce `NDArrays` from a source such as a sensor or a file, and plugins, which consume them through an asynchronous input queue and may produce further `NDArrays`. Both expose parameter records and base operator screens, and connect to one another through named ports that may be reconfigured at run time.

PYTHON PLUGIN ARCHITECTURE

Process Isolation

In current versions of Python's global interpreter lock prevents threads in a single interpreter from running pure Python in parallel [3], which conflicts with the throughput goals of an AD pipeline. Each `NDPluginPython` instance therefore runs the user algorithm in a dedicated child process. The Input/Output Controller (IOC) binary itself is not linked to Python; the child is a separate executable that embeds an interpreter (Fig. 1).

This separation provides two levels of parallelism without changes to the user algorithm. Instantiating the plugin multiple times runs independent interpreters across cores, while the algorithm itself is free to use the standard Python multiprocessing libraries. Graphics processing unit (GPU) acceleration follows naturally: because the child process binds to a user-chosen Python environment, libraries such as CuPy [4], PyTorch [5], or TensorFlow [6] work as they would in a stand-alone script, with no GPU support code required in the IOC. The same isolation contains memory growth and crashes in user code, leaving the IOC unaffected.

Inter-Process Communication

Image data is produced in the parent and consumed in the child. Copying it is costly — the sensors targeted by TOSIP produce frames on the order of 32 MB — so image data and metadata are copied only once, into shared memory, and the algorithm sees the image as a read-only NumPy [7] view backed by that memory. A message-based protocol synchronises parent and child, carrying short events such as image-ready and processing-complete; payloads are written to and read from named locations in the shared segment. The segment is grown on demand to accommodate variable image sizes. A future version will eliminate even this single copy by allocating `NDArrays` directly in the shared memory segment.

Process Lifetime

The plugin spawns and supervises its child. Shutdown follows a graceful-then-forced sequence. Should the parent die unexpectedly, the orphaned child is terminated automatically,

* matic.marn@cosylab.com
† jure.varlec@cosylab.com

Content from this work may be used under the terms of the CC BY 4.0 licence (© 2026). Any distribution of this work must maintain attribution to the author(s), title of the work, publisher, and DOI.

ISBN: 978-3-95450-252-3 ISSN: 2673-5350 doi: 10.18429/JACoW-IPAC2026-WEP6170

PIPELINES: A NODE-BASED EDITOR FOR STREAMLINED OPTIMISATION PROTOTYPING IN THE CONTROL ROOM

S. Preston*[1, 2, 3], I. P. S. Martin[2, 3], P. N. Burrows[3]
[1]Ada Lovelace Centre, Didcot, UK
[2]Diamond Light Source, Didcot, UK
[3]John Adams Institute for Accelerator Science, University of Oxford, Oxford, UK

Content from this work may be used under the terms of the CC BY 4.0 licence (© 2026). Any distribution of this work must maintain attribution to the author(s), title of the work, publisher, and DOI.

Abstract

Development shifts on accelerators are usually time-constrained and infrequent. Meanwhile, control room PCs are not designed for scrappy R&D, and maintaining multiple workflows with python scripts is prone to error. Graphical User Interface (GUI) apps have been successfully deployed and used in the past to perform optimisation at accelerator facilities. However, bookkeeping can become difficult in complex tasks. Furthermore, support is missing for pre-optimisation steps such as response matrix measurements used in slow orbit feedback machine learning algorithms. A PySide node-based visual editor has been developed and tested in the Diamond control room. A logical heirarchy of blocks define processes to perform and an inspector window allows the user to fine-tune blocks to their needs. Separate processes are spawned when compute or time-intensive blocks are run offline, keeping the main UI thread responsive. An optimisation problem is tackled using the app to demonstrate its usefulness.

INTRODUCTION

ML increases the scale of problems that can be confronted but there is a risk that intelligibility is lost as the number of variables invariably increases: it becomes difficult to diagnose why an algorithm failed; it is harder to make changes to an algorithm and keep track of them; it takes more effort to explain how an algorithm works to others. Existing tools either solve a particular problem and must be bespokely built by in-house teams, or they are general purpose but become difficult to monitor when there are many variables and pre-processing steps [1, 2].

Pipelines is a new open-source tool [3] which uses a drag-and-drop Graphical User Interface (GUI) to make it simple to add and remove objects and track how things change. Consider the following example: an optimiser has an objective which is a weighted sum of charges recorded at BPMs in a transfer line but the readings are noisy.

ARCHITECTURE

Upon opening the application, the user is confronted with an editor canvas. This is the space where pipelines are constructed by adding and linking blocks to build the logic required for the specific task. An inspector window appears to the right of the editor and supplies contextual information depending on what is currently happening.

* shaun.preston@physics.ox.ac.uk

Blocks

Nearly everything is a block. A block is a container with a name and other relevant attributes that make it easy to identify. Figure 1 shows a selection of blocks that can be used in the tool.

Each block has one or more sockets from which links can be associated. Incoming sockets sit on the left of a block and outgoing sockets sit on the right. A link is created by left-clicking on an outgoing socket, dragging, and releasing over another ingoing socket. A check is made when blocks are linked to determine if the operation is valid. To illustrate, charge values from BPMs are summed in Figure 2.

Groups

Perhaps the biggest improvement in intelligibility for complex workflows is the ability to group multiple blocks together and add concise labels to those groups. This feature was implemented after it became difficult to interpret pipelines with more than a dozen steerers together with filter blocks. Figure 3 shows how information can be condensed to improve readability.

Inspector

The user interacts with the inspector whenever they select one or more blocks inside the editor. It provides further information that would harm the intelligibility the tool strives towards if it were included alongside the block. Figure 4 shows the information displayed after selecting a hypothetical steerer block.

Hierarchy

The tool offers a level of granularity not seen elsewhere. When an actionable block is run, logic flows right to left, such that downstream blocks trigger upstream blocks until they have all the information they need to update themselves. As a post-processing step, a separate optimiser then searches over coefficients of the smallest singular vectors from the trajectory response matrix to reduce the strengths of correctors that are close to their power supply limits. The response matrix depends on the linear optics which in turn depend on the optimiser. It might be necessary to run several different optimisers with different settings until an optimal solution is found. In this circumstance, the user would prefer to run the optimiser portion of the routine many times first, and this is made possible in the tool. Figure 5 shows a conceptual overview of this.

ISBN: 978-3-95450-252-3 ISSN: 2673-5350 doi: 10.18429/JACoW-IPAC2026-WEP6171

AUTOMATED RF CONDITIONING ON CLARA

Matthew King[1,2], Nasiq Ziyan[1,2], Anthony Gilfellon[1,2], Bradley Wilson[1,2]
[1]ASTeC, STFC, Daresbury Laboratory, Keckwick Lane, Warrington, UK
[2]Cockcroft Institute, Daresbury Laboratory, Keckwick Lane, Warrington, UK

Content from this work may be used under the terms of the CC BY 4.0 licence (© 2026). Any distribution of this work must maintain attribution to the author(s), title of the work, publisher, and DOI.

Abstract

In this paper we present the design and deployment of the software tools used for the automated parallel conditioning of 7 RF cavities on CLARA (Compact Linear Accelerator for Research Applications). The software tools consist of 4 distributed tools with the following responsibilities: Control, Acquisition, Visualisation, and Communication. In combination, these tools enabled the round-the-clock conditioning of all RF cavities with minimal operator intervention, achieving operating parameters for beam commissioning activities.

INTRODUCTION

CLARA is a high-brightness electron beam facility at STFC Daresbury Laboratory, aiming to deliver ultra-short electron bunches to a wide range of user experiments [1]. CLARA has recently resumed operations after a major upgrade, and is currently undergoing beam commissioning [2] at its nominal energy (250 MeV) bunch charge (250 pC) and repetition rate (100 Hz). Prior to beam commissioning, a conditioning programme was conducted on CLARA for its S-Band Photoinjector [3], 4 Linacs, X-Band Linearliser Cavity [4], and Transverse Deflecting Cavity. After the successful proof of automated conditioning using No Operator Automated RF Conditioning (NO-ARC) [5] for the photoinjector [6] at a repetition rate of <50 Hz, it became time to redesign the suite of tools such that the unstaffed conditioning of 7 cavities could happen in parallel at the higher repetition rate of 100 Hz. This would would ultimately allow 24/7 conditioning in a consistent and safe manner and reduce the overall impact of conditioning on the CLARA commissioning schedule.

The primary focus of the redesign was to modularise the codebase into specific services with the following responsibilities: Conditioning, Communication, Data Acquisition, and Visualisation. The previous iteration of NO-ARC had consolidated these responsibilities into a single application which meant that an error in the Operator Interface (Visualisation) could result in the conditioning algorithm being unable to run. These proceedings provide details on the constituent services of the NO-ARC suite and how they were combined to deliver operational cavities to CLARA commissioning activities and experimental users.

CONTROL AND COMMUNICATION

The NO-ARC suite comprises four cooperating applications (see Fig. 1): the conditioning FSM, a central REST API, a data logger, and an operator interface (MetaGUI). One FSM instance and one data logger (DL) instance are deployed per cavity, whilst the API and MetaGUI are shared across all cavities. All inter-application communication is routed through the API, which serves as both a message broker and an in-memory data store. The API is built on `FastAPI` [7], with a `MongoDB` [8] backend providing persistent storage for breakdown and new power data.

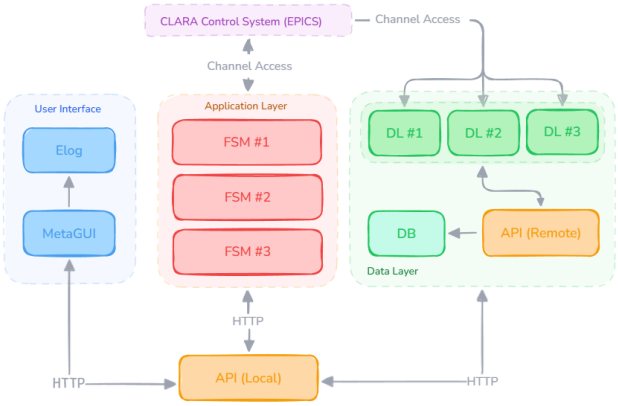

Figure 1: Schematic of NO-ARC suite

State Reporting

Upon initialisation, each FSM instance registers itself as active for the corresponding cavity via the API, and is cleared on shutdown. This mechanism prevents multiple conditioning instances from operating concurrently on the same cavity.

During the runtime of each FSM the current state, previous state, runtime, and conditioning parameters are reported to the API, with additional updates issued upon state transitions. This transient data is stored in memory on the API and shared with the MetaGUI for operator display and for composing automated electronic logbook (elog) entries on state transitions of interest.

Operator Interaction

On startup, any configuration changes are automatically detected and recorded in the elog, ensuring that updates to the conditioning strategy (for example longer soaking periods) are captured without requiring manual intervention.

The MetaGUI provides a graphical interface for monitoring and controlling all active FSM instances, retrieving the latest FSM states via the API to update the display. Operators may terminate conditioning for an individual cavity via the MetaGUI which is sent via the API to the FSM for that cavity. This will result in immediate removal of forward power and transition to a controlled shutdown sequence. Loss of MetaGUI connectivity is treated equivalently and triggers the same shutdown behaviour.

ISBN: 978-3-95450-252-3 ISSN: 2673-5350 doi: 10.18429/JACoW-IPAC2026-WEP6172

DILUTION MONITORING FOR THE BDF/SHiP TARGET

D. Gancarcik*, D. Belohrad, A. Goldblatt, M. A. Fraser, D. Metin, L. J. Nevay, M. M. Nieto, F. Roncarolo, CERN, Geneva, Switzerland

Abstract

The BDF/SHiP experiment requires precise monitoring of the beam dilution pattern on the high-power target absorbing up to 350 kW (avg.). This paper presents the conceptual design of a dedicated Beam Dilution Monitor (BDM), which will enable observation of the circular beam sweep pattern during 400 GeV/c proton operation. The proposed system is based on Secondary-Emission Monitor (SEM) grids comprising 12 µm-thick titanium bands. Detailed simulations were performed to evaluate signal formation, thermal response, secondary-electron collection, and the detectability of dilution magnet failure scenarios. Different detector geometries and interlock strategies were also investigated, demonstrating that the proposed BDM concept can provide sufficiently fast and reliable detection of dilution failures.

INTRODUCTION

The Beam Dump Facility (BDF) is a new, high-intensity facility to be installed in CERN's North Area (NA), developed to receive a high-intensity 400.3 GeV/c proton beam from the Super Proton Synchrotron [1, 2]. The facility will host the Search for Hidden Particles (SHiP) experiment, which aims to explore physics beyond the Standard Model by detecting feebly interacting and long-lived particles produced in proton–target interactions. The BDF relies on directing the proton beam onto a dense target to force interactions. Downstream, an extended hadron absorber and muon shielding system suppress the flux of secondary particles reaching a dedicated low-background decay volume. However, interactions of the primary beam with residual gas and beamline elements upstream of the target can generate a significant muon background that escapes the muon shielding system [3]. Although the beamline will operate under primary vacuum, strict constraints are placed on the amount and location of material introduced along the beamline. In particular, the necessary interceptive beam instrumentation must minimise the material introduced into the beam path and be positioned as close to the target as possible, so any muons created enter the acceptance of the muon shield.

Due to the high beam power on target, transverse dilution is required to limit the peak energy deposition. This is achieved using a system of two horizontal and two vertical magnets installed ~100 m upstream of the target, resulting in a circular sweep with a radius of 50 mm on target and completing four turns during the 1 s-long spill [4]. The nominal beam intensity and RMS beam size at the target is $4 \times 10^{13} p^+$ and 16 mm, respectively. Any deviation from the nominal sweep pattern can lead to a significant increase in local energy deposition, which poses a risk to the target. Leaving the beam undiluted for more than ~100 ms would result in damage to the dump and cause unwanted downtime [5].

A Beam Dilution Monitoring (BDM) system is therefore required to continuously verify the beam trajectory and trigger a beam abort in the event of a malfunction [2]. For machine protection purposes, the system must robustly detect deviations from the nominal sweep pattern with sufficient temporal resolution and low latency to identify dangerous conditions on timescales well below 100 ms. The expected annual operation of 10^6 spills requires high reliability and a very low false-abort rate. The BDM should also provide beam position and size measurements for beam optimisation and to be used by SHiP. Unlike the robust and low-latency machine protection functionality, these diagnostic measurements can rely on more advanced reconstruction and signal processing techniques since they are not part of the primary interlock chain.

BEAM DILUTION MONITOR DESIGN

Two identical BDM units will be produced, each consisting of two orthogonal SEM grids. The upstream and downstream units will be installed at 20 m and 10 m upstream of the target, respectively, corresponding to beam size and sweep radius reduction relative to the target location. To minimise the amount of material permanently present in the beam path, the upstream unit is designed to be retractable, while the same mechanical concept has been adopted for both BDM units for design uniformity. Using two BDM units also allows the beam trajectory angle to be reconstructed and provides redundancy for machine protection.

Several materials have been considered for the BDM bands. A recent beam test conducted in the NA evaluated the performance of different materials for beam profile monitoring under high-intensity conditions [6]. An unbunched 400.3 GeV/c proton beam with intensities of up to several 10^{13} p^+/spill was directed at wires made of various materials, with the beam impacting different transverse positions to assess their response. Among the tested candidates, titanium and tungsten showed good overall performance. However, the higher density of tungsten increases particle shower development, making titanium the selected baseline bans material. This beam test also demonstrated a linear response for approximately 0.05 to 2×10^{10} intercepted protons per band with Signal-to-Noise Ratio (SNR) above 13 using the CERN SEM Digital Acquisition System (DAQ).

The BDM's active area is defined to cover the full transverse beam excursion of ±50 mm, with an additional margin to account for the beam stay-clear region at the extremities of the sweep. The titanium bands, with a thickness of 12 µm

* david.gancarcik@cern.ch

Content from this work may be used under the terms of the CC BY 4.0 licence (© 2026). Any distribution of this work must maintain attribution to the author(s), title of the work, publisher, and DOI.

ISBN: 978-3-95450-252-3 ISSN: 2673-5350 doi: 10.18429/JACoW-IPAC2026-WEP6303

EFFICIENT FIVE-DIMENSIONAL BEAM SIGMA MATRIX DETERMINATION USING DIFFERENTIABLE SIMULATION*

C. Xu†[1], M. Borland[1], L. Emery[1], O. Mohsen[1], Y. Sun[1], K. P. Wootton[1], R. Roussel[2]
[1]Argonne National Laboratory, Lemont, IL, USA
[2]SLAC National Accelerator Laboratory, Menlo Park, CA, USA

Abstract

Precise reconstruction of the beam sigma matrix is critical for transport-line modeling and injection optimization. Our earlier work demonstrated that the differentiable simulation framework Cheetah enables gradient-based recovery of the 5×5 non-temporal sigma matrix at the APS BTS transport line using quadrupole scans. In this paper, we extend the method to improve efficiency and robustness. We introduce a generalized formulation that incorporates multi-screen measurements, providing increased stability in realistic lattice configurations. The differentiable-tracking approach yields physically consistent reconstructions while remaining computationally scalable. These developments form a practical framework for sigma-matrix determination in complex transport lines and support future real-time model calibration and tuning at the APS and similar facilities.

INTRODUCTION

Accurate knowledge of the incoming beam sigma matrix is essential for transport-line modeling, matching, and injection tuning. When performing quadrupole scans in regions with nonzero dispersion, the measured beam moments also contain information about momentum-dependent correlations, allowing reconstruction of the non-temporal 5×5 beam sigma matrix [1]. The downstream beam moments can be determined by linearly solving for the unknown upstream sigma matrix using first-order transport matrices [1, 2]. Despite its efficiency and transparency, this approach's accuracy degrades when the transport line cannot be represented well by a first-order model. Strong chromatic effects, nonlinear fields, and lattice-model errors can produce discrepancies between the measured moments and the linear prediction. These discrepancies may be reduced with subsequent nonlinear fitting or black-box optimization, but the resulting problem is high-dimensional and non-convex, often requiring many tracking evaluations.

Differentiable beam-dynamics simulation provides a practical way to improve the efficiency of general parameter optimization tasks while retaining physics fidelity. Recent codes such as Cheetah [3, 4], Bmad-Julia [5], and JuTrack [6] use auto-differentiation (AD) to propagate derivatives through tracking calculations. This capability has enabled gradient-based high-dimensional beam reconstruction, including generative phase space reconstruction (GPSR) methods for six-dimensional phase-space recovery [7, 8]. In our previous work, we proposed and implemented a Cheetah-based approach for reconstructing the 5 × 5 sigma matrix of the Advanced Photon Source (APS) booster-to-storage-ring (BTS) transport line from quadrupole scan measurements [9]. Although the method showed promising results in simulations and initial measurements, its sensitivity to initial conditions and computational cost limited its application.

In this paper, we extend that method to improve both efficiency and robustness. We formulate the sigma-matrix reconstruction directly in terms of a differentiable, physically constrained covariance parameterization. The method is generalized to include measurements from multiple screens, which adds independent constraints to improve the robustness and reduce the data requirements of real-world measurements. The resulting differentiable-tracking approach preserves physical consistency, remains computationally scalable, and provides a practical path toward online sigma-matrix determination for model calibration and tuning.

GRADIENT-BASED OPTIMIZATION OF BEAM SIGMA MATRIX

We briefly summarize the workflow for reconstructing the incoming beam sigma matrix from quadrupole scan measurements using differentiable simulation. The workflow is outlined in Fig. 1.

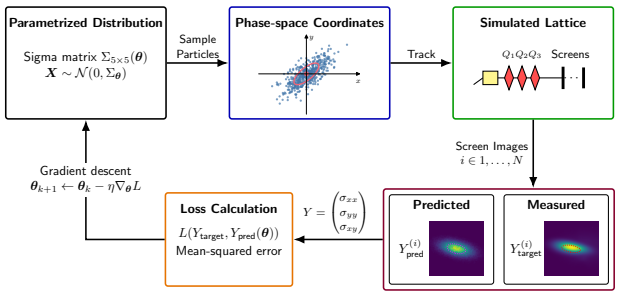

Figure 1: Workflow for the beam sigma matrix reconstruction with differentiable simulation.

The unknown incoming beam distribution is represented by the covariance matrix Σ of the five non-temporal phase-space coordinates (x, p_x, y, p_y, δ). The covariance can be parametrized by a lower-triangular Cholesky factor,

$$\Sigma_{\text{in}}(\boldsymbol{\theta}) = L_{\boldsymbol{\theta}} L_{\boldsymbol{\theta}}^{\top}, \quad \boldsymbol{\theta} \in \mathbb{R}^{15}, \tag{1}$$

which results in 15 degrees of freedom corresponding to the independent elements of the symmetric sigma matrix. The diagonal elements of $L_{\boldsymbol{\theta}}$ are constrained to be positive using

* The work is supported by the U.S. DOE Office of Science-Basic Energy Sciences, under Contract No. DE-AC02-06CH11357.
† chenran.xu@anl.gov

Content from this work may be used under the terms of the CC BY 4.0 licence (© 2026). Any distribution of this work must maintain attribution to the author(s), title of the work, publisher, and DOI.

ISBN: 978-3-95450-252-3 ISSN: 2673-5350 doi: 10.18429/JACoW-IPAC2026-WEP6305

A CONFIGURABLE UNSUPERVISED ANOMALY DETECTION SERVICE FOR THE ADVANCED LIGHT SOURCE

K. Iliev*, T. Hellert, S. C. Leemann, G. Martino, A. Sulc
Lawrence Berkeley National Laboratory, Berkeley, CA, USA

Content from this work may be used under the terms of the CC BY 4.0 licence (© 2026). Any distribution of this work must maintain attribution to the author(s), title of the work, publisher, and DOI.

Abstract

Advanced Light Source (ALS) control systems operate with continuous streams of more than 200 000 EPICS Process Variables (PVs). While most alarms are handled by manually setting a threshold, we present a configurable service that scores live PV streams for anomalies in real time, providing a flexible fault discrimination tool for operators. The service applies a recurrent neural network to capture time-dependent correlations, trained on a given time range using unsupervised one-class loss that requires no labeled fault examples. Furthermore, we embed operationally-aware logic that suppresses false alerts during machine-off periods, ensuring detection quality without manual setpoint tuning per PV. We show the system in operation on live data from the ALS linac modulator capacitor voltage divider channels, and describe its architecture as a configurable, multi-instance service driven by a single JSON specification, enabling straightforward extension to additional PV groups as training data becomes available.

INTRODUCTION

The Advanced Light Source (ALS) [1] at Lawrence Berkeley National Laboratory is a third-generation synchrotron light source currently undergoing a major upgrade (ALS-U). Reliable accelerator operation depends on continuous monitoring of the machine state through the Experimental Physics and Industrial Control System (EPICS) [2], which at ALS exposes more than 200 000 PVs spanning magnets, RF systems, vacuum, diagnostics, and insertion devices.

The conventional approach to fault detection relies on per-channel scalar thresholds: an alarm is raised when a single PV exceeds a manually configured limit. While effective for gross failures, this strategy has well-known limitations. First, setting and maintaining thresholds for a large number of channels is labor-intensive and prone to alarm fatigue. Second, scalar thresholds are blind to *temporal correlations*: a slow drift or an unusual time-dependent pattern across multiple related PVs may indicate an incipient fault long before any individual channel crosses its static limit. Third, machine state transitions, beam dumps, injection pauses, planned shutdowns, routinely drive PV values through alarm regions, generating false positives that erode operator trust.

Machine learning offers a path beyond these limitations [3, 4]. In this paper we present an anomaly detection service that learns the temporal structure of normal PV behavior from unlabeled historical data and produces a single, interpretable anomaly score in real time.

* kirkiliev@lbl.gov

SYSTEM ARCHITECTURE

Design Goals

The service was designed around three requirements: *(i)* zero labeled fault data, *(ii)* real-time operation on live EPICS archiver streams, and *(iii)* straightforward extension to new PV groups without code changes. These goals led to a pipeline architecture with three phases: training, context bootstrapping, and streaming inference, orchestrated by a single JSON configuration file.

Configuration-Driven Multi-Instance Design

Each detection instance is fully defined by an entry in the JSON configuration (Fig. 1). The specification includes the list of PVs to monitor jointly, training data window, time-grid resolution, model hyperparameters, inference polling interval, and anomaly threshold scaling factors. Multiple instances run as independent threads within a single service process, enabling concurrent monitoring of unrelated PV groups.

Adding a new monitored group requires only a new JSON block, a suitable period of historical normal-operation data, and a service restart. The training pipeline then executes automatically, producing a self-contained checkpoint that stores model weights, normalization statistics, and calibrated thresholds.

```
[{
  "instance_name": "LNRF_Modulators",
  "pvs": ["LNRF:MOD1:CapVoltageDivider",
          "LNRF:MOD2:CapVoltageDivider"],
  "training": {
    "start_date": "2025-12-08...", "step_sec": 60,
    "seq_len": 10, "std_clamp": 0.5, "...",
    "model_params": {"latent_dim": 8, "..."}
  },
  "inference": {
    "context_hours": 2, "threshold_scale_warning": 2.0,
    "threshold_scale_anomaly": 3.5, "...",
    "output_pvs": {
      "score": "LNRF:MOD1:CapVoltageDivider:
           AnomalyScore"
    }
  },
  "checkpoint_path": "models/checkpoints/
       lnrf_modulators_v1.pt"
}]
```

Figure 1: Abbreviated JSON configuration.

Pipeline Overview

Figure 2 illustrates the system pipeline. Historical PV data is fetched from the EPICS Archiver Appliance [5], aligned to a uniform time grid, and used to train a one-class Gated Recurrent Unit (GRU) model. The resulting checkpoint is loaded for streaming inference, where new data is continuously merged into a rolling context buffer and scored against the learned normal-behavior manifold.

ISBN: 978-3-95450-252-3 ISSN: 2673-5350 doi: 10.18429/JACoW-IPAC2026-WEP6306

UNSUPERVISED ANOMALY DETECTION AND CHANNEL ATTRIBUTION WITH VARIATIONAL AUTOENCODERS AT THE ADVANCED LIGHT SOURCE

A. Sulc*, T. Hellert, S. C. Leemann, G. Martino, H. Nishimura
Lawrence Berkeley National Laboratory, Berkeley, CA, U.S.A.

Abstract

We present an unsupervised pipeline that learns a compact representation of beam-on machine state at the ALS, detects anomalies preceding beam-loss events, and highlights the responsible channels for operator diagnosis. Archiver data are resampled to a uniform time grid, filtered to beam-on intervals using stored current, and pruned by variability and principal-component analysis. A variational autoencoder with residual encoder-decoder stacks is trained on the standardised PV vectors; the global anomaly score and the per-PV attribution are both derived from per-PV reconstruction z-scores, so the score is an exact decomposition of the channel ranking. We apply the pipeline to 34 beam-loss events from the 2025 ALS user run; in several cases it surfaces early-stage anomalies in the PV subsystems that subsequently led to the beam dump, indicating a framework can act as an early-warning aid for operators.

INTRODUCTION

At third-generation light sources such as the Advanced Light Source (ALS) [1], every unplanned beam dump erodes delivered user beamtime, and recovery hinges on identifying precursors hidden in the minutes before the dump. Those precursors live in a high-dimensional, heterogeneous EPICS [2] stream—magnet power supplies, vacuum gauges, RF cavities, interlocks, cooling circuits—updated continuously and far exceeding what an operator can monitor channel-by-channel in real time.

Supervised classifiers are impractical in this setting: labelled failures are sparse, fault categories evolve, and non-stationary drift across months of operation invalidates static decision boundaries. We instead train a variational autoencoder directly on raw beam-on archiver data, with no external labels and no time axis as a feature: the encoder treats each timestep as an independent PV vector, so what it learns is the hidden cross-channel correlation structure that distinguishes one operating mode from another. Departures from that learned structure both raise a global alarm and surface the responsible channels, while the latent space itself doubles as an differentiable, low-dimensional map of machine state.

Variational autoencoders (VAEs) [3] offer a principled unsupervised alternative. By maximising a tractable evidence lower bound on the log-likelihood of observed proces variable (PV) vectors, the VAE learns a low-dimensional latent manifold of nominal beam-on machine state. Channels whose reconstruction departs from the model's nominal expectation can then be flagged individually. The global anomaly score is built from those same per-channel deviations, so the alarm signal and the per-PV ranking are not separate post-hoc artefacts.

This contribution describes the offline toolchain developed for ALS fault analysis: archiver data alignment and beam-on filtering; channel curation via variability and PCA scoring; the VAE architecture and training protocol; and per-fault anomaly scoring, embedding visualisation, and per-PV reconstruction-residual ranking, all derived from the same per-channel calibration.

DATA PIPELINE

Archiver Retrieval and Time Alignment

The model was trained from manually curated lists of variables. All PVs contributing to a model share a uniform time grid spanning the global data range with configurable step Δt. For training the facility-wide model we use $\Delta t = 1800s$ (30 min), matching the typical PV update cadence of slow diagnostic channels; for per-fault analysis the grid is refined to $\Delta t = 10s$ to resolve faster transients. Values falling within a bin are aggregated by arithmetic mean. For the stored-current PV (`SR:DCCT`) that gates beam-on selection, aggregation uses the bin maximum so that brief excursions above threshold are not missed. Bins without samples are forward-filled (sample-and-hold), consistent with the control-system semantics in which a PV retains its last published value until the next update.

Beam-On Filtering and Channel Smoothing

Training and baseline statistics use only timesteps with `SR:DCCT` above 1 mA (and > 50 mA for fault-window display), excluding injection gaps and empty-ring periods. Near-discrete PVs ($\leq$ 10 unique levels) are label-smoothed to $[\varepsilon, 1-\varepsilon]$ with $\varepsilon = 0.05$ so mean squared error (MSE) gradients remain informative for these channels.

CHANNEL CURATION

Before VAE training, PVs are filtered to retain only informative, non-redundant signals. The curation pipeline ranks channels by variance, range, "active fraction" (fraction of timesteps where $|x - \text{median}| > 0.5\,\sigma$), and coefficient of variation. PVs with fewer than 4096 raw archiver samples or with near-zero variance ($\sigma^2 < 10^{-12}$) are removed unconditionally. An optional bottom-percentile cut on raw variance removes the flattest channels.

* asulc@lbl.gov

Content from this work may be used under the terms of the CC BY 4.0 licence (© 2026). Any distribution of this work must maintain attribution to the author(s), title of the work, publisher, and DOI.

ISBN: 978-3-95450-252-3 ISSN: 2673-5350 doi: 10.18429/JACoW-IPAC2026-WEP6603

LLRF PROTOTYPE DESIGN FOR THE 1.3 GHZ CRYOMODULE OF THE SHENZHEN SUPER-CONDUCTING SOFT X-RAY FEL *

J. Zhu†, Y. Li, W. Li, Z. Zhang, Institute of Advanced Light Source Facilities, Shenzhen, China
H. Ding‡, J. Yang, W. Zhang, Dalian Institute of Chemical Physics, Dalian, China

Abstract

This paper presents the design and preliminary test results of a Low-Level Radio Frequency (LLRF) prototype system developed for the 1.3 GHz standard cryomodule of the Shenzhen Superconducting Soft X-ray Free Electron Laser (S^{3}FEL). The system is implemented within an MTCA.4 platform, integrating eight RF controller boards for superconducting cavity field acquisition and microwave excitation control to stabilize the RF field and ensure steady electron beam acceleration, alongside two tuner controller boards for driving eight coupler motors, eight cavity tuner motors, and sixteen piezoelectric actuators (PZTs). A high-speed peer-to-peer (P2P) backplane bus enables real-time communication between RF and tuner control boards. The report outlines the hardware architecture of this modular LLRF system and discusses initial functional and performance tests, demonstrating its suitability for meeting the precise stability requirements of the S^{3}FEL project.

INTRODUCTION

Free-electron lasers (FELs) are among the most important high-brightness X-ray sources for advanced scientific research. The Shenzhen Superconducting Soft X-ray Free Electron Laser (S^{3}FEL) project adopts a superconducting linear accelerator operating with 1.3 GHz superconducting cavities, targeting an electron beam energy of up to 2.5 GeV and a pulse repetition rate of up to 1 MHz [1]. Such demanding operating conditions impose stringent requirements on the stability of the RF field amplitude and phase within the accelerating cavities.

To maintain stable accelerator operation under high repetition-rate conditions and external perturbations such as microphonics and Lorentz force detuning, a high-performance low-level RF (LLRF) control system is essential. Conventional architectures, such as CompactPCI (CPCI)-based systems, often suffer from limited bandwidth, fixed slot configurations, insufficient scalability, and relatively high latency, making them inadequate for the precision microwave measurement and control requirements of S^{3}FEL.

To address these challenges, this work proposes an MTCA.4-based LLRF prototype system for the S^{3}FEL standard superconducting cavity module. The system is capable of RF field acquisition, microwave drive generation, and cavity resonance tuning through feedback control, thereby meeting the strict stability requirements of the accelerator.

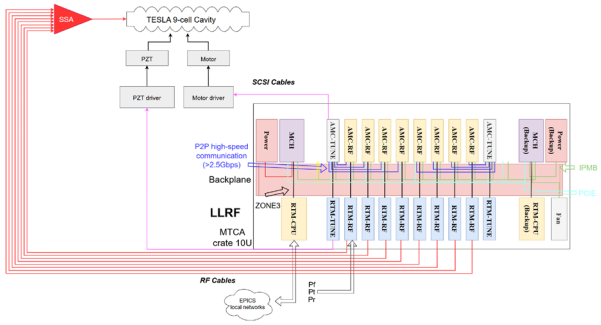

Figure 1: Topology of the MTCA.4-Based LLRF system.

SYSTEM DESIGN AND ARCHITECTURE

The proposed LLRF system is implemented using a standard MTCA.4 chassis, as illustrated in Fig. 1. The prototype microwave measurement and control system for the 1.3 GHz superconducting accelerator module consists of eight RF control boards, two tuning control boards, a power supply module, a MicroTCA Carrier Hub (MCH), and a CPU board. All boards are installed through the MTCA.4 backplane, which provides both power distribution and high-speed signal interconnections.

Each control module consists of an Advanced Mezzanine Card (AMC) and a Rear Transition Module (RTM) [2]. Figure 2 shows the RF control board. The RF AMC card performs microwave drive regulation and digital signal processing, while the RF RTM card is responsible for RF signal acquisition and transmission. The acquired signals include the forward power signal (Pf), reflected power signal (Pr), cavity probe signal (Pt), reference signal (REF), and local oscillator signal (LO). The AMC and RTM communicate through the Zone-3 connector compliant with the MTCA.4 D1.0 specification, jointly enabling RF field stabilization and reliable beam acceleration [3].

Each 1.3 GHz superconducting cavity module contains eight cavities. For each cavity, one slow tuner motor control channel, two piezoelectric actuator (PZT) control channels, and one coupler motor control channel are required [4]. To fulfill these requirements, the system integrates two pairs of MTCA.4 tuning control boards, each consisting of one AMC and one RTM module, with each pair responsible for four cavities. Figure 3 presents the tuning control board.

The tuning AMC card performs signal processing and generates control signals for the motor drivers, while the tuning RTM card outputs control signals for the PZT drivers. Each AMC board provides 16 electrically isolated digital outputs through an FMC expansion module for motor

* Work supported by the National Natural Science Foundation of China (Grant No. 12405221).
† zhujinfu@mail.iasf.ac.cn
‡ dinghongli@dicp.ac.cn

Content from this work may be used under the terms of the CC BY 4.0 licence (© 2026). Any distribution of this work must maintain attribution to the author(s), title of the work, publisher, and DOI.

ISBN: 978-3-95450-252-3 ISSN: 2673-5350 doi: 10.18429/JACoW-IPAC2026-WEP6604

DIGITAL LLRF CONTROL SYSTEM FOR A HIGH-REPETITION-RATE SUPERCONDUCTING LINAC*

Z. Zhang, J. Han, W. Li, J. Zhu†
Institute of Advanced Light Source Facilities Shenzhen, Shenzhen, China
H. Ding‡, J. Yang, W. Zhang, Dalian Institute of Chemical Physics, Dalian, China

Abstract

The development of high-repetition-rate superconducting linear accelerators for advanced light sources imposes stringent demands on the performance of the Low-Level Radio Frequency (LLRF) control system. This report presents the design, implementation, and operational results of a high-precision LLRF system developed for the Dalian Advanced Light Source (DALS) injector—a 1 MHz superconducting linac. The system employs a digital feedback architecture based on a field-programmable gate array (FPGA), enabling high-speed I/Q modulation and demodulation, vector summation, and low-latency feedback control to address the narrow bandwidth challenge posed by superconducting cavities with loaded quality factors up to 4.3×10^7 (half-bandwidth ~15 Hz). High-resolution piezo actuators are integrated for active cavity tuning. During commissioning in August 2025, the system successfully stabilized ten superconducting cavities, supporting beam operation at over 100 MeV, 1 MHz repetition rate, and 0.1 mA current. Closed-loop amplitude and phase stabilities of better than 0.02 % and 0.02 ° were achieved per cavity, with total voltage maintained steadily at 100 MV. The results demonstrate the system's robustness and precision, providing a valuable reference for future LLRF systems in next-generation high-repetition-rate light sources.

INTRODUCTION

The linac section mainly consists of four components: an electron gun [1], a buncher, two 2-cell superconducting cavities, and eight 9-cell superconducting cavities. The electron gun generates electrons, and the buncher captures electrons with different acceleration phases into a smaller phase range to form electron bunches. The 2-cell and 9-cell superconducting cavities then operate at the maximum acceleration phase and constant cavity voltage to increase the electron beam energy. This paper primarily introduces the LLRF control system for narrow-bandwidth 9-cell superconducting cavities under high-repetition-rate beam operation. It covers determining the half-bandwidth of the cavity, the design of the RF control loop and tuning control loop scheme, and the results of high-repetition-rate beam experiments conducted based on this control system. In this experiment, the superconducting cavities have QL = 2×10^7 (half-bandwidth = 32 Hz) and QL = 4.3×10^7 (half-bandwidth = 15 Hz). In subsequent experiments, we will gradually tune all superconducting cavities to QL = 4.3×10^7.

DETERMINING THE HALF-BANDWIDTH OF THE CAVITY

Cavity field buildup consumes energy, and beam passage also requires energy consumption. According to the relevant formula [2], the relationship between beam current, cavity voltage, loaded quality factor (Q_L), and solid-state amplifier (SSA) power P_g can be derived as Eq.(1).

$$P_g = \frac{V_c^2}{\left(\frac{r}{Q}\right)Q_L}\frac{1}{4}\left[\left(1+\frac{\left(\frac{r}{Q}\right)Q_L I_{b0}}{V_c}\right)^2+\left(\frac{2\Delta f Q_L}{f}\right)^2\right] \quad (1)$$

The physical meaning and numerical values of the variables in Eq. (1) are listed in Table 1. We primarily consider two operating conditions: one is the conditioning mode, which is applied after cavity fabrication to remove impurities and burrs; the other is the beam operation mode with an RF frequency of 1.3 GHz.

Table 1: Variables in Eq. (1)

Variables	Physical Meaning	Numerical Values
V_c	Cavity Voltage	12/16/20 MV
r/Q	Shunt Impedance	1036 Ω
I_{b0}	Beam Current	0.1 mA
f	RF Frequency	1.3 GHz
Δf	Detuning	10 Hz

For the first mode, the cavity remains in a resonant state. The relationship between SSA power and cavity voltage as a function of Q_L is shown in Fig. 1. It can be observed that a higher Q_L corresponds to lower power requirements for achieving a given cavity voltage. However, as Q_L increases further, the rate of change of SSA power with respect to Q_L diminishes.

For the second mode, with a cavity detuning frequency of 10 Hz and a beam current of 0.1 mA, the relationship between SSA power and cavity voltage as a function of Q_L is shown in Fig. 2. The results indicate that for

* Work supported by the National Natural Science Foundation of China (Grant No. 12405221).
† zhujinfu@mail.iasf.ac.cn
‡ dinghongli@dicp.ac.cn

Content from this work may be used under the terms of the CC BY 4.0 licence (© 2026). Any distribution of this work must maintain attribution to the author(s), title of the work, publisher, and DOI.

ISBN: 978-3-95450-252-3 ISSN: 2673-5350 doi: 10.18429/JACoW-IPAC2026-WEP6606

DEVELOPMENT OF FAST ORBIT FEEDBACK SYSTEM AT HALF STORAGE RING *

D. Y. Wang†,1, Y. B. Leng[1], Y. M. Deng[1], X. Yang[1], W. Xu[1]
[1]National Synchrotron Radiation Laboratory, USTC, Hefei, China

Abstract

A distributed Fast Orbit FeedBack system (FOFB) is designed at the Hefei Advanced Light Facility (HALF) storage ring. The system controls the beam orbit instability of the storage ring to the submicron level, by BPM, feedback algorithm and actuator to achieve feedback correction of beam orbit. This paper presents the design of the FOFB system of HALF, including open-loop test results.

INTRODUCTION

The Hefei Advanced Light Facility is a fourth-generation storage ring light source. The storage ring has an electron energy of 2.2 GeV, a natural beam emittance of about 86 pm·rad and an operating beam current of 350 mA. The 480 m storage ring is adopted 20 cells of H6BA lattice structure, with 12 BPM and 4 fast corrector magnets in each cell [1]. The closed-loop design bandwidth of FOFB is 500 Hz, and the frequency of FA is 20 kHz.

The fast orbit feedback system includes three subsystems: beam position measurement, feedback controller, and fast correction actuator. Beam position monitors (BPMs) measure the beam-induced voltage signal, and DBPM processors perform high-speed synchronous ADC sampling on the beam signal to extract turn-by-turn (TBT) and FA beam orbit data. The feedback controller collects beam orbit data at different locations in the storage ring and calculates the beam orbit correction values through a feedback algorithm. The fast correction actuator includes fast corrector power supplies, fast corrector magnets, and the vacuum chamber. The beam orbit is stabilized by changing the magnetic field strength through fast corrector magnets.

Table 1: Main parameters of the HALF storage ring

parameter	value
energy	2.2 GeV
circumference	479.86 m
number of cells	20
natural emittance	86.3 pm·rad
transverse tunes (H/V)	48.15/17.15
natural chromaticities (H/V)	−77/−57
energy loss per turn	186.7 keV
momentum compaction factor	9.0×10^{-5}
natural energy spread	0.62×10^{-3}
total absolute bending angle	442.5°
harmonic number (500 MHz RF cavity)	800

II. THE FAST ORBIT FEEDBACK SYSTEM OF HALF

Based on the structural characteristics of the HALF storage ring, 10 beam instrumentation stations are distributed, as shown in Fig. 1. One FOFB processor is installed at each station, connected to 8 local DBPM processors and 16 fast corrector power supplies. Used to process 160 FA data (vertical and horizontal direction for each BPM), and output 160 current setting values corresponding to 80 correction amounts of fast corrector magnets. The FOFB processors are connected via optical fibers to form a bidirectional ring link. The DBPM processors and fast corrector power supplies are connected with local FOFB processor via optical fibers to form a point-to-point link [2].

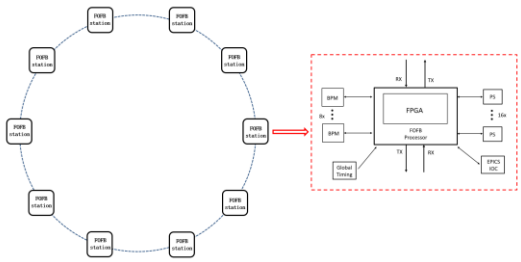

Figure 1: FOFB architecture of HALF.

the HALF fast orbit feedback system adopts an FPGA-based design architecture, as shown in Fig. 2. The fast feedback processor primarily consists of an FPGA chipset, functional components, and external interfaces. The FPGA chipset includes Xilinx Ultrascale+ XVCU9P and Zynq XC7Z020. The former incorporates DSPs for high-performance data and logic operations, with 104 GTY channels for high-speed data transmission; the latter is utilized for system configuration and EPICS software development based on Petalinux. The processor is designed with a 4GB DDR4 data cache space for system state analysis. In terms of external interfaces, it features 10 sets of QSFP connected to FPGA GTY Quad, enabling high-speed optical fiber communication. Additionally, the processor supports external synchronous clock and external trigger signal inputs, as well as Gigabit Ethernet communication.

The processor chassis adopts 1U standard structure and supports FMC expansion interfaces. It can obtain timing information by connecting WR timing sub-board, for generating timestamps of system real-time data.

* This work is supported by the project of Hefei Advanced Light Facility, a major national science and technology infrastructure in China.
† wangdaoyuan@ustc.edu.cn

Content from this work may be used under the terms of the CC BY 4.0 licence (© 2026). Any distribution of this work must maintain attribution to the author(s), title of the work, publisher, and DOI.

ISBN: 978-3-95450-252-3 ISSN: 2673-5350 doi: 10.18429/JACoW-IPAC2026-WEP6607

LONGITUDINAL BEAM DIAGNOSTICS WITH A STREAK CAMERA AT TAIWAN PHOTON SOURCE

C.Y. Liao*, C.Y. Wu, Z.K. Liu, Y.S. Cheng, K.T. Hsu
National Synchrotron Radiation Research Center, Hsinchu, Taiwan, R. O. C.

Abstract

The Taiwan Photon Source (TPS) streak camera system has been used for longitudinal beam studies since the early commissioning stage. This paper first presents a representative high-current instability observation associated with the CU15 insertion device taper and then recent measurements of bunch length and synchronous phase under operation with the superconducting RF (SRF) + passive 3rd harmonic cavity (HC), here abbreviated as SRF HC. The CU15 case shows different instability behaviors along the fill pattern in streak images. The SRF HC measurements provide bunch-by-bunch information under different fill patterns and SRF HC settings for comparison of bunch lengthening and phase shift. Under operation with the passive SRF HC, a phase drift of about 35 ps is observed along the bunch train, consistent with transient beam loading under quasi-uniform filling. These measurements show that the streak camera is useful for longitudinal diagnostics and machine studies at TPS.

INTRODUCTION

The Taiwan Photon Source (TPS), located at the National Synchrotron Radiation Research Center in Hsinchu, Taiwan, is a 3 GeV low-emittance synchrotron light source. Under high-current operation and different fill patterns, longitudinal beam measurements are important for storage ring studies and machine tuning. A streak camera system was introduced at TPS during the early stage of facility development [1]. Subsequent work included early bunch length measurements and longitudinal instability observations at the TPS diagnostic beamline (BL40) [2], ultrashort bunch measurements in low-alpha operation [3], and investigations of impedance effects under single-bunch conditions [4]. Longitudinal instability phenomena under high-current operation have also been reported [5, 6]. As background, Liu *et al.* reported instability in TPS operation with a superconducting RF (SRF) + passive 3rd harmonic cavity (HC), here abbreviated as SRF HC [7–9]. This paper first presents a representative high-current observation associated with the CU15 insertion device taper and then recent streak camera measurements of bunch length and synchronous phase under SRF HC operation.

STREAK CAMERA SYSTEM AT TPS

The TPS streak camera system is installed at the synchrotron radiation diagnostic beamline for measurements of the longitudinal time structure of electron bunches in the storage ring. The block diagram of the streak camera measurement system is shown in Fig. 1. The main instrument is a dual-sweep streak camera, C10910 from Hamamatsu Photonics [10], equipped with one fast sweep unit, one slow sweep unit, and two synchroscan sweep frequencies (125 MHz/250 MHz) for temporal and transverse measurements. The system receives visible light signals emitted from a bending magnet and, after optical transport and focusing, delivers the light to the streak camera, where the temporal distribution is converted into a spatial image. The present measurement modes include synchroscan and dual-sweep operation. The synchroscan mode is mainly used for high-time-resolution measurements of a single bunch and provides bunch length and longitudinal profile information. The streak camera temporal resolution is about 1 ps, as verified with a femtosecond laser source. The dual-sweep mode preserves both fast-sweep and slow-sweep information simultaneously and is therefore suitable for observing the relative behavior of multi-bunch over a period of time. In the present measurements, the dual-sweep mode was used to compare relative bunch phase positions and to observe unstable motion under multi-bunch filling conditions.

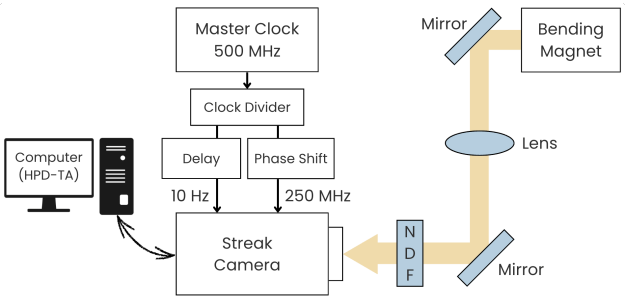

Figure 1: Block diagram of the streak camera measurement system.

LONGITUDINAL BEAM STUDIES

CU15 Taper High Current Observation

In 2019, during TPS operation at 500 mA, deformation of the vacuum chamber taper in the CU15 insertion device at BL19A formed a cavity-like structure, increasing the local impedance and parasitic heat load. Under this condition, the streak camera images provided qualitative evidence of multi-bunch longitudinal instability. As shown in Fig. 2, the bunches in the leading part (a) of the train remained stable in longitudinal position, whereas wave-like oscillation trajectories appeared near the end of the multi-bunch-filled section (b), suggesting longitudinal coupled-bunch motion. The isolated single-bunch region (c) did not exhibit

* liao.cy@nsrrc.org.tw

Content from this work may be used under the terms of the CC BY 4.0 licence (© 2026). Any distribution of this work must maintain attribution to the author(s), title of the work, publisher, and DOI.

ISBN: 978-3-95450-252-3 ISSN: 2673-5350 doi: 10.18429/JACoW-IPAC2026-WEV1001

DEFINING THE NEW FCC-ee BASELINE OPTICS

J. Keintzel*, X. Buffat, C. Carli, M.A. Jebramcik, S. Kostoglou, K. Oide,
P. Raimondi, G. Roy, K. Skoufaris, R. Tomás, F. Zimmermann
CERN, Geneva 23, Switzerland

Content from this work may be used under the terms of the CC BY 4.0 licence (© 2026). Any distribution of this work must maintain attribution to the author(s), title of the work, publisher, and DOI.

Abstract

The Future Circular electron-positron Collider (FCC-ee), with a circumference of approximately 91 km, is being rapidly developed by CERN and its collaborators. Two collider-ring optics proposals have been developed in parallel over recent years. Each proposal features its own strengths and challenges. The Global Hybrid Correction optics (GHC) came first with a ring-distributed correction of the horizontal chromaticity generated in the Interaction Regions (IRs), using many sextupole pairs. A local conventional chromaticity correction section is used in the IR for the vertical plane. The more recent Local Chromaticity Correction (LCC) scheme proposal uses both vertical and horizontal chromatic correction sections in the IRs and keeps a modular design. A comparison process was carried out between late 2025 and early 2026 to prepare for the review process of the FCC-ee baseline magnetic lattice and optics in view of the Technical Design Report. This contribution presents the comparison process of these two optics designs from the perspective of beam dynamics and performance.

INTRODUCTION

Following the recommendation of the European Strategy for Particle Physics (ESPP) in 2013 [1], CERN has launched the conceptual design phase for Future Circular Colliders (FCC) for an electron-positron (FCC-ee) or a hadron-hadron (FCC-hh) synchrotron storage ring at the luminosity and energy frontiers with a circumference of approximately 100 km for the post High Luminosity Large Hadron Collider (HL-LHC) era [2]. Four conceptual design reports (CDRs) have been published in 2019, which also formed the basis for the input to the following ESPP Update (ESPPU) [3–6].

In 2020 the ESPPU recommended, among others, a future hadron collider at CERN with a centre-of-mass energy of 100 TeV with an electro-weak and Higgs-factory as a possible first stage [7]. The so-called integrated FCC program foresees first the construction of the tunnel, associated infrastructures, and the FCC-ee with about 20 years of operation, followed by the FCC-hh, which would provide high energy physics research until the end of the 21st century. The FCC Feasibility Study (FS) has been launched in 2021 to investigate in detail the technical, geological and financial feasibility of the FCC-ee, and concluded in 2025 with the FS report (FSR) in three public volumes, which have been submitted to the ESPPU in 2025 [8–10].

Including various input of the community, e.g. [11–13], in early 2026 the recommendations have been published, with the HL-LHC and the FCC-ee as the, respectively, first and second highest priority for the European community of particle physics [14]. The FCC is currently entering the next phase of the project, the so-called Reference Design Phase, allowing for a possible Council decision in 2028, followed by a Technical Design Report (TDR)-phase currently foreseen to be finished by 2033.

For any present or future collider the accelerator lattice and optics forms the basis for numerous studies and technical designs and must, hence, be designed carefully. The Global Hybrid Correction (GHC) [15] optics has been designed and optimised over more than a decade and represents the baseline presented in the FSR. Over the past three years, the Local Chromaticity Correction (LCC) optics has been developed and investigated in parallel.

To ensure a coherent and cost-effective path towards the TDR a baseline choice between GHC or LCC design must be taken with a first attempt in early 2025 [17]. Therefore, between end of 2025 and beginning of 2026 a detailed comparison between both optics has been performed and summarized in a report. This contribution discusses the path towards the new baseline and focuses on lattice, optics, parameters and performance reach. Technical aspects such as considerations from magnets, power converters, availability, vacuum, or beam instrumentation are not covered, yet further details are provided in the full document [18]. Results described here focus largely on the lowest beam energy of 45.6 GeV per beam corresponding to physics around the Z-pole. Furthermore, first insights on the highest energy of 182.5 GeV, are presented in a separate section.

COMMON OVERALL LAYOUT

Despite several key differences between the GHC and the LCC lattice, both designs respect certain key layout and design principles. The FCC-ee features four experimental Interaction Regions (IRs) and four Long Straight Sections (LSSs). The high energy booster is installed on top of the collider rings, allowing for top-up injection at the collision beam energy. Experimental IRs and LSSs are, respectively, 1400 m and 2032 m long. The LSSs host collimation, RF-cavities for either the FCC-ee or the HEB, injection and extraction, as shown in Fig. 1.

- The overall machine geometry is preserved.
- A circumference is defined by detailed placement and is about 90.6 km.
- Four baseline beam energy stages are considered, namely, 45.6, 80, 120 and 182.5 GeV, corresponding

* jacqueline.keintzel@cern.ch

ISBN: 978-3-95450-252-3 ISSN: 2673-5350 doi: 10.18429/JACoW-IPAC2026-WEV1002

PREPARATION OF THE 2026 LHC HIGH-INTENSITY TESTS IN VIEW OF HL-LHC

S. Kostoglou*, C. Antuono, H. Bartosik, R. Bruce, X. Buffat, I. Efthymiopoulos, M. Hostettler, G. Iadarola, B. E. Karlsen-Baeck, A. Lechner, L. Mether, D. Mirarchi, N. Mounet, Y. Papaphilippou, S. Redaelli, G. Rumolo, B. Salvant, M. Solfaroli, G. Sterbini, H. Timko, R. Tomás, G. Trad, J. Uythoven, D. Valuch, J. Wenninger, C. Wiesner, D. Wollmann, C. Zannini
CERN, Geneva, Switzerland

Content from this work may be used under the terms of the CC BY 4.0 licence (© 2026). Any distribution of this work must maintain attribution to the author(s), title of the work, publisher, and DOI.

Abstract

One of the main drivers of integrated luminosity production in the High-Luminosity LHC (HL-LHC) era is the bunch intensity, expected to reach 2.3×10^{11} protons per bunch at injection compared to the maximum 1.8×10^{11} protons per bunch achieved in Run 3 operation (2022–2026). Such high intensities bring significant challenges, in particular localized beam induced heating due to impedance and the associated risk of equipment damage. In that respect, any issue discovered only in Run 4 (2030-2033), the first run of the HL-LHC era, could lead to significant downtime or intensity limitations until appropriate mitigation measures are put in place. It is therefore essential to identify such potential limitations for elements that will not be upgraded as part of HL-LHC to achieve the target intensity before the end of the presently ongoing Run 3. This paper summarizes the preparation steps and strategy foreseen for dedicated high-intensity tests at the end of the 2026 LHC operation, as a last step before Long Shutdown 3 (LS3). The tests aim at reaching and sustaining HL-LHC beam parameters, in order to probe impedance-related limits and assess equipment non-conformities, as well as potential design issues and unknown limitations in view of reliable HL-LHC operation. Preparation for the high-intensity tests started with dedicated machine development studies in 2025, making significant progress towards HL-LHC beams and identifying critical devices. Key observations and plans for 2026 are presented.

INTRODUCTION

One of the key ingredients required to reach the challenging integrated luminosity targets of the High-Luminosity LHC (HL-LHC) is operation with significantly larger total beam intensity than what is achieved today in routine LHC operation. In the baseline HL-LHC scenario, this corresponds to about 30% higher bunch intensity and 10% more bunches compared to LHC operation in 2026 [1]. At the same time, LHC experience has shown that such an increase in beam intensity can reveal hardware limitations, equipment design weaknesses and previously unknown constraints related to beam impedance-induced heating that are not observed at lower intensities.

Recent examples include failures of warm vacuum modules in 2023 and 2025. In 2023, pressure spikes in sector A4L1 were followed by slow losses and beam dumps. The root cause was traced to beam-induced heating in an RF-finger of a warm vacuum module that damaged the tension spring [2–5]. Because the affected module was installed in a section shared by the two beams circulating in opposite direction, operation was interrupted to replace the faulty module. In 2025, a similar limitation was observed in sector 6L2 [6]. In that case, operation could continue in a degraded mode with asymmetric beam intensities [7]. Since the LHC will enter the Long Shutdown 3 (LS3) after the 2026 run, this is the last opportunity to probe HL-LHC beam conditions, while there is still time to identify and implement mitigations before Run 4. Because most of the installed hardware will remain unchanged after LS3, these tests can already provide meaningful information on HL-LHC readiness.

For this reason, two weeks at the end of the 2026 run will be dedicated to high-intensity tests [8, 9]. Their goal is to demonstrate hardware compatibility with HL-LHC beam conditions or, if that is not achieved, to identify the limiting devices and the corresponding mitigations. Because HL-LHC beam conditions cannot yet be fully achieved before LS3 in a single configuration, the strategy combines different beam types and beam energies. In addition to hardware validation, the campaign will also provide valuable operational experience with HL-type beams in areas such as electron-cloud, beam-beam effects and halo studies.

In this paper, we summarize the target conditions for the 2026 campaign, review the main machine constraints, the lessons learned from the 2025 Machine Development (MD) program and outline the proposed staged strategy to prepare and execute the high-intensity program before LS3.

HL-LHC TARGET CONDITIONS

The purpose of the 2026 high-intensity campaign is to reproduce the HL-LHC operating conditions as closely as possible. In the baseline HL-LHC scenario, the bunch intensity is 2.3×10^{11} ppb at injection and about 2.2×10^{11} ppb at the start of collisions, leaving some margin for losses at the start of the ramp and during the collapse of the separation bumps at top energy when the beams are brought into collision. The reference beam configuration is based on standard 4×72b trains with 2760 bunches, bunch lengths around 1.3 ns, corresponding to an RMS bunch length of 7.61 cm [10], and a collision duration of about 6–7 h [11, 12].

* sofia.kostoglou@cern.ch

ISBN: 978-3-95450-252-3 ISSN: 2673-5350 doi: 10.18429/JACoW-IPAC2026-WEV1301

ACCELERATOR DESIGN EDUCATIONAL PRIMER – CONCEPTUALIZING AND OPTIMIZING THE HYBRID LHEC-LIKE ELECTRON-ION COLLIDER DESIGN*

A. Seryi[1†], A. Formenti[2], A. Huebl[2], R. Lehe[2], C. A. Lindstrøm[3], C. Mitchell[2], T. Pieloni[4], J. Qiang[2], L. van Riesen-Haupt[1], L. Vanhecke[4], J.-L. Vay[2], E. Zoni[2]
[1]Old Dominion University, Norfolk, VA, USA
[2]Lawrence Berkeley National Laboratory, Berkeley, CA, USA
[3]Department of Physics, University of Oslo, Oslo, Norway
[4]École Polytechnique Fédérale de Lausanne, Lausanne, Switzerland

Abstract

The Electron-Ion Collider (EIC) Mission Need requires $\sqrt{s}$ = 20–100 GeV (upgradable to 140 GeV) and luminosity 10^{33}–10^{34} cm^{-2} s^{-1}. The current ring–ring baseline achieves the full scope, including ~10^{34} cm^{-2} s^{-1} across all energies. However, when the design is re-optimized for the lower boundary – accepting 10^{33} cm^{-2} s^{-1} and prioritizing cost – an alternative configuration emerges as more advantageous: a hybrid LHeC-like electron accelerator using multi-pass energy recovery linacs (ERL). This solution reduces electron-beam power by roughly an order of magnitude, yielding nearly a factor of two reduction in total project cost compared with the present baseline while still satisfying the minimum physics requirements. The study performs parametric cost and performance modeling, augmented by AI-driven optimization, to explore this design space. Serving primarily as an educational exercise for the next generation of accelerator experts the paper demonstrates modern design methods: rapid parametric scans, cost-driven optimization, and integration of AI tools. It examines technical feasibility, identifies critical R&D (high-current ERL operation, beam–beam effects, synchronization, etc.), and discusses how such re-optimization studies can be used to train designers in an era when AI dramatically expands exploration of complex accelerator parameter spaces.

PREAMBLE – AI AND EDUCATION

The emergence of AI-assisted coding presents both unique challenges and unprecedented opportunities for accelerator physics education. Institutions like Fermilab and CERN, which host accelerator school USPAS and CAS, need to rapidly adapt their pedagogical approaches, and the Genesis program [1] in the US further encourages AI for accelerated design of particle accelerators. A natural vehicle for developing design skills is the mini-project such as Refs. [2, 3], where students tackle a realistic challenge in a short period. This paper rehearses what such a mini-project looks like when AI tools are available – from parameter optimization and code generation to cost estimation – serving as a draft script for future AI-assisted USPAS or CAS courses.

EIC-LHeC MINI-PROJECT

The mini-project assignment is: *Given the EIC proton beam stored in the RHIC-derived Hadron Storage Ring, design the simplest and most cost-effective electron accelerator complex satisfying the EIC CD0 Mission Need lower boundary – $\sqrt{s} \approx$ 29–100 GeV and $\mathcal{L} \sim 10^{33}$ cm^{-2}s^{-1} – and estimate its cost relative to the ring-ring baseline.*

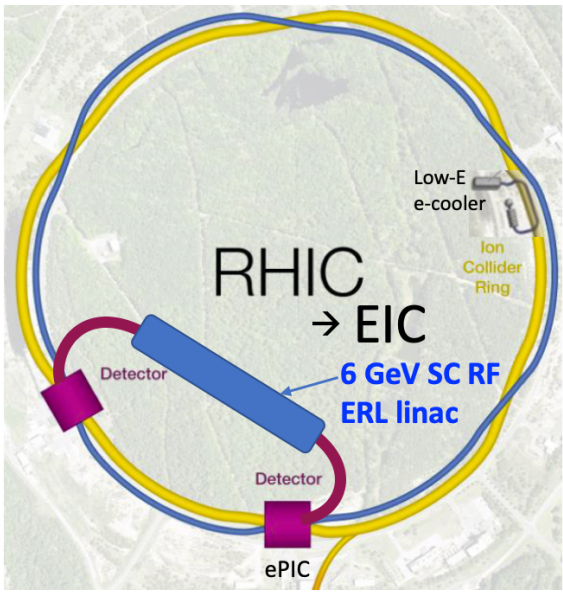

Figure 1: Schematic layout of the EIC built as an LHeC-like hybrid with energy recovery.

The motivation comes from the ESPP Open Symposium [4], where it was argued that inserting a new electron ring into the LHC tunnel for LHeC would be cost-prohibitive and luminosity-limiting [5]. This prompted the question: could replacing the EIC electron storage ring with a superconducting energy-recovery linac (ERL) yield a similar cost-performance advantage? The proposed hybrid keeps the full EIC proton infrastructure intact and replaces the electron ring with a multi-pass ERL: electrons are accelerated in a superconducting radio-frequency (SRF) linac, recirculated through arcs, brought to collision, and then decelerated back through the linac for energy recovery. Key advantages over the ring-ring baseline are: electron beam power reduced by one order of magnitude [each bunch used once, such

* Developed with assistance from AI such as Claude, Gemini, etc.
† aseryi@odu.edu

Content from this work may be used under the terms of the CC BY 4.0 licence (© 2026). Any distribution of this work must maintain attribution to the author(s), title of the work, publisher, and DOI.

ISBN: 978-3-95450-252-3 ISSN: 2673-5350 doi: 10.18429/JACoW-IPAC2026-WEV4301

COMMISSIONING OF THE IOTA PROTON INJECTOR*

A. Romanov†, N. Banerjee, D. Broemmelsiek, K. Carlson, D. Edstrom, J. Jarvis, N. Kuklev, D. MacLean, J. Santucci, T. Thompson, M. Wallbank, J. Wieland, Fermilab, Batavia, IL, USA
B. Simons, Northern Illinois University, DeKalb, IL, USA

Abstract

The IOTA Proton Injector (IPI) at the Fermilab Accelerator Science and Technology facility (FAST) is a machine capable of delivering up to 14 mA pulses of protons at 2.5 MeV to the Integrable Optics Test Accelerator (IOTA) ring. Its construction has been completed in the fall of 2025, followed by a successful commissioning run scheduled to conclude at the end of May 2026. It operates alongside the existing electron injector beamline to facilitate further beam physics research and continued development of novel accelerator technologies at the IOTA ring. This report details the current operational profile, known challenges, and future plans for the proton program development at FAST.

INTRODUCTION

The proton injector for the Integrable Optics Test Accelerator (IOTA) [1], shown in Fig. 1, is an important capability for the research program at FAST/IOTA [2]. IOTA is a research storage ring constructed and operated by Fermilab to study advanced concepts in accelerator physics. During the previous runs the studies at IOTA were performed with electron beams of up to 150 MeV energy, which have negligible space-charge effects. The commissioning of the 2.5 MeV IOTA proton injector with a beam current of 14 mA enabled experiments with intense beams that have strong space-charge tune shifts, constituting 10 – 15 % of the total betatron phase advance in the ring.

PROTON SOURCE

Positive ions with 50 keV kinetic energy are produced in the duoplasmatron ion source (IS) schematically shown in Fig. 2. The resulting beam consists of three different species, p, H_2^+ and H_3^+, and the proportions depend on the exact configuration of the source. This source was previously used as part of the High Intensity Neutrino Source (HINS) experiment [3], and was subsequently adopted by the FAST facility as it fits the desired beam parameters for proton production in the IPI beamline, as shown in Fig. 3. The ion source (IS) was briefly resurrected on site in the HINS enclosure at the Meson Detector Building (MDB) before being fully disassembled and cleaned. During disassembly, it was noted that the 1.25 mm diameter extraction aperture used with HINS was unusually large for a duoplasmatron source, and it has been replaced with a 0.7 mm diameter aperture.

The duoplasmatron uses a filament as a thermionic emitter to excite a DC plasma discharge in the hydrogen gas. Filaments are prepared on-site. The first step is to spot-weld S-shaped mesh to electrodes. It is important to avoid sharp bends and melting through the mesh. The mesh is then gently cleaned with alcohol, and a mixture of barium, calcium, and strontium carbonates is applied. The original recipe involved isoamyl acetate to assist in binding the mixture to the filament and required a lengthy multistep process in a special chamber to avoid contamination of the main vacuum system with hydrocarbon byproducts. In addition, the results were inconsistent in terms of emission efficiency. The final recipe was simplified significantly and consists of the same mix of three carbonates combined with a small amount of isopropyl alcohol to form a paste-like suspension. This paste is then applied to the surface of the nickel mesh with a brush to form a uniform layer that fills the mesh cells. After the alcohol evaporates at room temperature, the activation process can be performed even inside the proton source. There are two outgassing peaks during the process: one corresponds to water evaporation and occurs around 100 °C, and another corresponds to the transformation of carbonates into oxides, which releases carbon dioxide. A filament prepared with this recipe has been in use since spring 2024 and has been

* This work was produced by FermiForward Discovery Group, LLC under Contract No. 89243024CSC000002 with the U.S. Department of Energy, Office of Science, Office of High Energy Physics.

† aromanov@fnal.gov

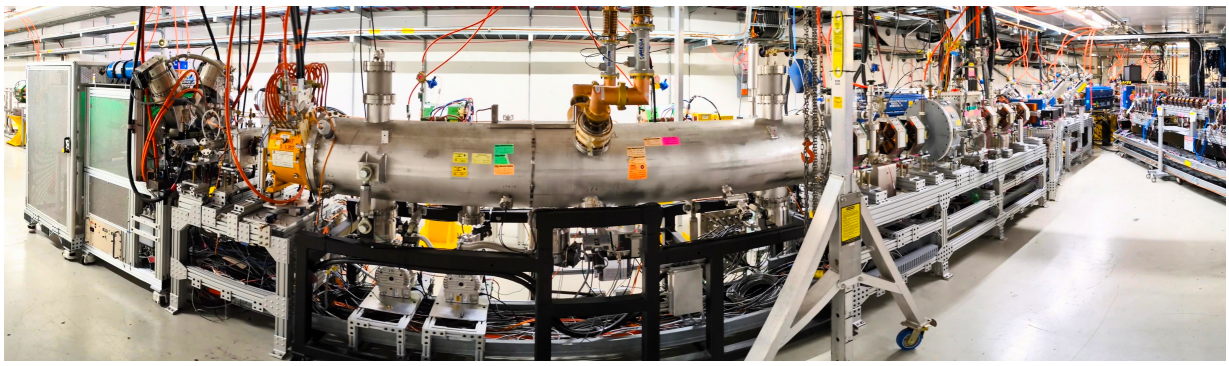

Figure 1: IOTA proton injector.

Content from this work may be used under the terms of the CC BY 4.0 licence (© 2026). Any distribution of this work must maintain attribution to the author(s), title of the work, publisher, and DOI.

ISBN: 978-3-95450-252-3 ISSN: 2673-5350 doi: 10.18429/JACoW-IPAC2026-WEV4302

FIRST EXPERIMENTAL DEMONSTRATION OF USING A CRAB-CROSSING COLLISION SCHEME FOR EFFICIENT LASER-TO-ION BEAM INTERACTION*

A. Aleksandrov†, S. Cousineau, T. Gorlov, Y. Liu, A. Oguz, A. Shishlo, A. Zhukov
Oak Ridge National Laboratory, Oak Ridge, Tennessee, USA

Abstract

Lasers are used in many applications with H^- beams, including laser charge exchange, laser wire scanners, and laser temporal pulse patterning. In these applications, the H^- beams exhibit a wide range of bunch lengths that depend on the focusing by the RF cavities, the energy spread of the beam, and space charge forces. Achieving the required laser pulse length for complete overlap with the H^- beam can be challenging in scenarios where available laser power is constrained. A crab-crossing scheme was proposed to achieve efficient overlap of a short laser pulse with an arbitrarily long H^- beam pulse. This presentation reports the first experimental demonstration of this technique, which increases the efficiency of laser-to-ion beam interaction in a laser charge exchange experiment at SNS

INTRODUCTION

Lasers have recently been used in many applications involving H^-beams, including laser charge exchange, laser wire scanners, and laser temporal pulse patterning [1]. Although the details differ from case to case, all these applications require efficient interaction between ions and photons. The technique described below is being developed for laser-assisted charge injection at SNS, but it can be used for other applications as well.

Charge-exchange injection is used to inject proton beams into circular accelerators. Typically, a thin foil is used to convert accelerated negative hydrogen ions into protons. Passing a high-intensity, high-power beam through the foil leads to foil heating and particle loss due to scattering. Eventually, foil performance and lifetime can become the limiting factors for further increases in injected beam power [2].

An alternative charge-exchange injection scheme, known as laser-assisted charge exchange (LACE), is being developed at the Spallation Neutron Source (SNS) [2]. The scheme uses two magnets to remove the two electrons from the ion. A laser is used to excite the second electron from the ground state to an upper level, thereby reducing the magnetic field strength required in the second magnet. The required laser power is the main limiting factor of this method. Several laser-power-reduction techniques have been proposed, and some have been tested experimentally [3,4].

To mitigate ion-bunch longitudinal expansion in the long beamline between the linac exit and the laser–ion interaction point, we previously proposed a simple crab-crossing collision scheme to improve the temporal overlap between a short laser pulse and a long ion bunch [5]. This paper reports the first experimental demonstration of this technique and its effectiveness in increasing LACE efficiency.

BUNCH SIZE COMPRESSION

The efficiency of the laser–ion interaction scales with the laser power density $\frac{Q}{a_x a_y a_z}$, where Q is the laser pulse energy and a_i are the laser spot size in horizontal, vertical and longitudinal directions. This power density can be increased either by raising Q or by reducing the spot sizes. However, to maintain good overlap, the laser spot cannot be made smaller than the ion bunch in any dimension. In practice, the ion bunch size therefore sets the lower limit on the laser spot size and becomes the primary constraint on achievable power density.

The SNS accelerator layout is shown on Fig.1.

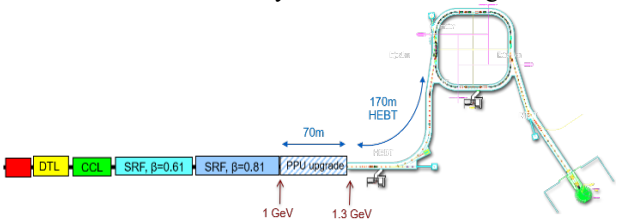

Figure 1: A layout of the SNS accelerator.

The transverse bunch size can be reduced with the quadrupole magnets in the HEBT transport line, down to the limit set by the beam emittance. In contrast, the longitudinal bunch length increases in the ~ 240m drift between the end of the linear accelerator and in the interaction point due to the particle energy spread; for the nominal linac tune, this evolution is shown by the blue curve in Fig. 2. Because the SNS superconducting linac cavities are independently powered and controlled, several cavities near the end of the linac can be re-tuned to provide longitudinal focusing to the laser–ion interaction point, producing the red curve in Fig.2. However, this approach is effective only at low beam current, since space-charge forces prevent the bunch from remaining longitudinally compressed over a long distance. The bunch-length evolution for zero current and for the nominal 30mA beam current is shown in Fig. 3.

We also considered two other approaches for longitudinal bunch compression: (1) beam optics with a negative momentum compaction factor, in which lower-energy particles follow a shorter trajectory; and (2) installing dedicated RF cavities in the beam line closer to the interaction point.

† sasha@ornl.gov.

Content from this work may be used under the terms of the CC BY 4.0 licence (© 2026). Any distribution of this work must maintain attribution to the author(s), title of the work, publisher, and DOI.

ISBN: 978-3-95450-252-3 ISSN: 2673-5350 doi: 10.18429/JACoW-IPAC2026-WEV5002

BUNCH LENGTHENING WITH DOUBLE- AND TRIPLE-RF SYSTEMS FOR MAX 4^U

M. B. Alves*, F. Cullinan, Å. Andersson, P. F. Tavares
MAX IV Laboratory, Lund, Sweden

Abstract

MAX IV is engaged in the design of a major upgrade to its 3 GeV ring, called MAX 4^U . The upgrade aims at an improvement in light source performance to maintain MAX IV's competitive edge beyond the end of this decade. In this contribution, we report on studies of the performance of double- and triple-RF systems for bunch lengthening with MAX 4^U parameters. The stationary bunch profiles and longitudinal instabilities thresholds were evaluated with semi-analytical methods and benchmarked with macroparticle tracking simulations for different settings of the harmonic RF cavities.

INTRODUCTION

MAX IV initiated the conceptual design of MAX 4^U in 2024, aiming to upgrade its present 3 GeV ring, which we will refer to as R3, by reducing its emittance to below 100 pm rad, while preserving the energy at 3 GeV, maintaining the source points, the shielding wall and the injector, all within strict cost and time constraints. In December 2025, the Conceptual Design Report (CDR) was published [1, 2]. Based on these studies, the emittance target for the technical design phase for MAX 4^U has been refined to below 75 pm rad, with all other boundary conditions maintained. The starting lattice for the technical design studies is named TDR-1, which will be the reference lattice throughout this contribution. The relevant parameters for this report are presented in Table 1.

Table 1: MAX 4^U / TDR-1 Lattice Parameters

Parameter	Symbol	Value
Energy	E_0	3 GeV
Natural emittance	ϵ_0	65 pm rad
Circumference	L_0	528 m
Harmonic number	h	176
Momentum compaction	α	5.34×10^{-5}
Energy spread	σ_δ	8.46×10^{-4}
Energy loss per turn (bare)	U_0	474 keV
with IDs		$\approx$ 800 keV
Longitudinal damping time	τ_δ	21.17 ms
Nominal RF voltage	V_{rf}	1.0 MV
Natural bunch length	σ_τ	19 ps
Natural synchrotron frequency	$f_{s,0}$	376 Hz
Design beam current	I_0	500 mA

The MAX 4^U project foresees the reuse of most of the vacuum chambers and vacuum components of R3. This means that, besides the potential addition of new components such as fast stripline kickers for longitudinal injection, the impedance of the ring will be mostly the same. For comparison, the natural bunch length for R3 is around 40 ps, and a lengthening factor between 4 and 5 is obtained with a passive double-RF system, employed for robust operation at high current, raising the Touschek lifetime, avoiding critical heating of machine components, as well as coupled-bunch instabilities driven by higher-order modes (HOMs). The current R3 performance is therefore achieved with bunch lengths in the range of 160 ps to 200 ps. The natural bunch length for TDR-1 is 19 ps, about half of the R3 value. Thus, with the same lengthening factors of a double-RF system, the final bunch lengths would only be half of the values used during operation in R3. To reach the same bunch lengths in the upgrade lattice, a lengthening factor of around 10 is needed. This can be achieved with a triple-RF system.

Additionally, one of the main requirements for bunch lengthening from the TDR-1 lattice design is to alleviate the emittance blow-up from intrabeam scattering (IBS). Considering the Touschek lifetime alone, due to the very low emittance and optimized momentum acceptance, a double-RF system would be sufficient to provide acceptable lifetimes. Nevertheless, the Touschek lifetime is also expected to profit from the longer bunches produced with a triple-RF system.

GENERALIZATION OF FLAT-POTENTIAL

The idea of manipulating the longitudinal dynamics to produce ultralong bunches has been discussed for many years at MAX IV Laboratory, dating back to the conceptual design of R3 [3]. By increasing the number of harmonic cavities, the longitudinal potential can be flattened to an arbitrary order. Here we summarize the formulation used to enforce flat-potential (FP) conditions up to order $2N$ [4], using N harmonic cavities.

Consider a system with N higher harmonic cavities with different RF harmonics, plus the main rf, which defines the set of RF harmonics: $\vec{n} = (n_0, n_1, \ldots, n_N)$, with $n_0 = 1$. The total RF voltage waveform is

$$V_T(\phi) = V_{\mathrm{rf}} \sum_{m=0}^{N} k_m \sin(n_m \phi + \phi_m), \qquad (1)$$

where n_m is the harmonic number for cavity family m, ϕ_m its phase and $k_m = V_m/V_{\mathrm{rf}}$ its fractional voltage. The main cavity voltage is represented by the first term $n_0 = k_0 = 1$, so ϕ_0 is the synchronous phase.

* murilo.barbosa_alves@maxiv.lu.se

Content from this work may be used under the terms of the CC BY 4.0 licence (© 2026). Any distribution of this work must maintain attribution to the author(s), title of the work, publisher, and DOI.

ISBN: 978-3-95450-252-3 ISSN: 2673-5350 doi: 10.18429/JACoW-IPAC2026-WEV6001

OVERVIEW OF THE RF BASED BEAM DIAGNOSTIC MONITORS OF HIPA AT PSI

J. Sun†, P.-A. Duperrex, PSI Center for Accelerator Science and Engineering, Villigen, Switzerland

Abstract

The High Intensity Proton Accelerator (HIPA) at the Paul Scherrer Institute (PSI) delivers a continuous-wave (CW) proton beam at a frequency of 50.63 MHz, with currents up to 2.2 mA and a maximum energy of 590 MeV. The beam is successively directed to two meson production targets before reaching the spallation target. To monitor key beam parameters, various diagnostics based on the RF beam signal detection have been implemented. For beam intensity and energy measurements, resonators tuned at the second harmonic (101.26 MHz) have been deployed on the different beam lines. Capacitive probes in the cyclotrons provide the phase measurements. In addition, a cross-correlation technique applied to phase pick-up signals at the entry and exit of the cyclotron, enables a precise determination of the number of turns completed by the beam. Beam alignment on a rotating target is monitored using a novel fin-and-groove structure engraved on the target surface. The resulting intensity modulation, measured with a downstream beam current monitor, is analysed in the frequency domain to directly infer the beam offset on target. More details are described below.

INTRODUCTION

The HIPA can generate up to 1.4 MW continuous proton beam, the proton beam is accelerated from a Cockcroft-Walton source followed by two cyclotrons: the so-called Injector 2 cyclotron accelerating the beam from 870 keV to 72 MeV and the so-called Ring cyclotron accelerating it to 590 MeV. The beam is then directed through 2 meson graphite targets (Target M and E) to the spallation neutron source SINQ [1]. The Target M has a thickness of 5 mm and absorbs ~1% of the beam. The Target E is 40 mm (alternatively 60 mm) thick and absorbs ~8% (~12%) of protons, layout of the whole facility can be found in Fig. 1. An upgrade project called IMPACT (Isotope and Muon Production using Advanced Cyclotron and Target technologies) is ongoing aiming to renew the Target M and related muon beam lines and build up an online isotope separation facility [2].

Many beam diagnostics monitors that are based on RF signal detection were designed for beam development and operation, a schematic plot can be found in Fig. 2. Resonator type beam current monitor is a key element for beam intensity and transmission measurement, which is also integrated into the interlock system to protect the machine from the abnormal beam jitters or too high beam losses. Inductive pickups are used for bunch phase detection for the two cyclotrons and can be further served as number of turn measurement. For the beam off-axis detection, grooves and bumps are manufactured on the target E, beam intensity then is modulated, and the off-axis information can be derived from the amplitude difference between the specific modulated signals of the downstream current monitor.

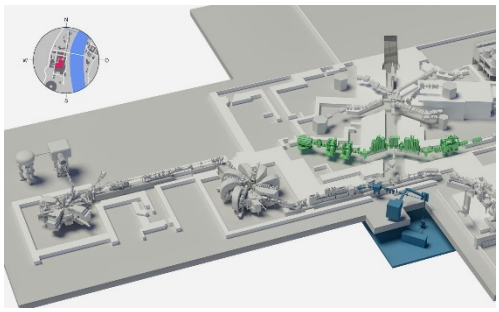

Figure 1: Layout of HIPA with upgrade project IMPACT.

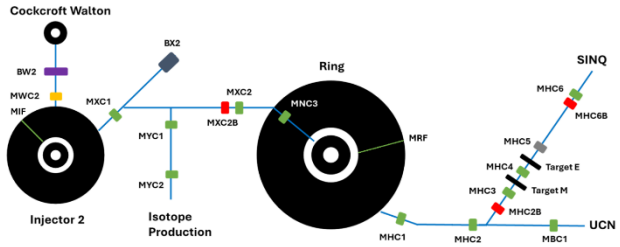

Figure 2: Schematic of the RF based monitors of HIPA, M*F indicates the phase monitors and M*C indicates the current monitors.

RESONATORS

Coaxial resonator (reentrant cavity) [3] can be tuned to a specific resonance frequency by modifying the dimension of the capacitance gap and the inductance wall, see Fig. 3 left. A wall current with the same time structure as the beam bunch will be induced when the bunch passes through the cavity. The amplitude of the magnetic field, as shown in Fig. 3 right, in the resonator is directly proportional to the beam current, a measurement of this field provides a measure of the beam intensity.

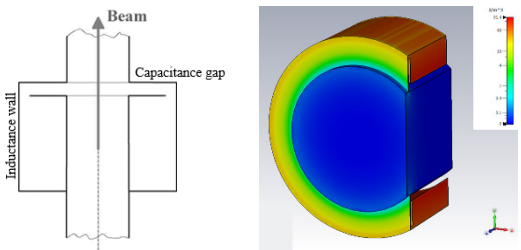

Figure 3: Principle sketch of the cavity type monitor (left); Magnetic field distribution in the cavity (Right).

† jilei.sun@psi.ch

Content from this work may be used under the terms of the CC BY 4.0 licence (© 2026). Any distribution of this work must maintain attribution to the author(s), title of the work, publisher, and DOI.

ISBN: 978-3-95450-252-3 ISSN: 2673-5350 doi: 10.18429/JACoW-IPAC2026-WEV6003

MOONLIGHT ON THE SERENGETI: CASTING (DIGITAL) SHADOWS WITH SIMBA, PUMBA, LAURA AND FRIENDS

J. Jones*, A. Brynes, M. Johnson, M. King, N. Ziyan
ASTeC STFC Daresbury Laboratory, Daresbury, UK and The Cockcroft Institute, Daresbury, UK

Abstract

Digital shadows offer a methodology for bridging physical particle accelerators with their virtual counterparts, enabling predictive modelling, automated control, and improvements in facility design and implementation. A digital shadow for the CLARA accelerator is being developed, integrating two complementary tools: LAURA, an ontology-driven description language for particle accelerator lattices; and SIMBA, a simulation framework that utilises LAURA-defined models to perform start-to-end particle tracking using multiple tracking codes. Together, LAURA and SIMBA form the simulation backbone of a digital shadow, providing a consistent and extensible representation of the accelerator. This architecture is further augmented by pyCATAP, a controls middle layer that interfaces with accelerator control systems, PUMBA, a procedural automation framework for running complex operational tasks and standardising I/O data structures, and SARABI, a framework for generating soft EPICS IOCs from a LAURA lattice.

INTRODUCTION

The increasing complexity of modern accelerators demands more sophisticated tools for facility design, commissioning, operation and user exploitation. Operators must simultaneously manage hundreds of hardware components, diagnose machine faults, and optimise beam parameters. Computational models have historically been maintained as offline artefacts, somewhat decoupled from the live machine. The digital shadow offers a more tightly integrated approach: a continuously updated virtual representation of the physical accelerator that reflects its current state and can be used to support real-time decision-making whilst providing both real and hidden parameters and diagnostics.

A digital shadow differs from a digital twin in the information flow: a shadow allows only a information flow from the machine to the model; a twin implies a bidirectional coupling with the virtual model not only reflecting the physical system but also issuing commands that directly actuate it. In both cases the ultimate goal is for the model to faithfully track the machine state. For CLARA [1], the development of a digital shadow provides a flexible foundation that can evolve towards fuller twinning as confidence in the underlying tools and models develops.

Realising a digital shadow requires solving several interdependent problems: a lattice must be described in a machine-readable, physics-aware format; simulations must be executable against that description; the live hardware state must be accessible programmatically; and operational procedures must be expressible in a way that can exploit all of the above. We present a suite of complementary, interoperable software packages that addresses each of these requirements.

- **LAURA** (Lattice Architecture for a Unified Representation of Accelerators) provides an ontology-driven description language for particle accelerator lattices, encoding elements, sections, and layouts in human-readable YAML that maps directly to typed Python objects via a Pydantic-based data model [2].
- **SIMBA** (Simulations for Integrated Modelling of Beams in Accelerators) is a simulation framework that uses LAURA-defined lattice models to perform start-to-end particle tracking across multiple simulation codes, enabling rapid propagation of beam distributions through the full machine [2].
- **pyCATAP** (Python Controls Abstraction Towards Accelerator Physics) provides hardware interfacing, and acts as a controls middle layer that abstracts EPICS channel access into high-level Python objects, allowing live machine states to be read and written using the same element vocabulary defined in LAURA [3].
- **PUMBA** (Procedures and Utilities for Measurements on Beam-lines and Accelerators) handles procedural automation, and is a framework for encoding complex operational tasks as composable, reusable procedures that can invoke simulations, acquire measurements, and respond to machine conditions.
- **SARABI** (Soft Architecture for Rendering Automated Back-end IOCs) provides a mechanism for generating soft EPICS Input/Output Controllers (IOCs) directly from a LAURA lattice, enabling virtual signals to be published onto the controls network, alongside real hardware signals, closing the loop between the digital shadow and the broader control-room ecosystem.

Together, these tools form a layered architecture in which a single, ontological lattice description drives both simulation and hardware access, while a common data model ensures that experimental measurements, simulation results, and machine set-points are represented consistently. To this end, we also introduce the CLARA integrated model (see Fig.1), a digital shadow, that acts as a stepping stone towards digital twinning. The integrated model codebase has been built to work on a wide variety of facilities, but the focus for this paper is on CLARA.

In this paper we describe the design of each component, the integration between them, and the current capabilities of the individual components and the digital shadow as a whole [4].

* james.jones@stfc.ac.uk

Content from this work may be used under the terms of the CC BY 4.0 licence (© 2026). Any distribution of this work must maintain attribution to the author(s), title of the work, publisher, and DOI.

ISBN: 978-3-95450-252-3 ISSN: 2673-5350 doi: 10.18429/JACoW-IPAC2026-THI2M01

MAX 4^U, AN UPGRADE OF THE MAX IV 3 GeV RING*

E. Al-Dmour†, M. B. Alves, Å. Andersson, M. Apollonio, J. Bengtsson, F. Cullinan, H. O. C. Duarte, M. Grabski, O. Karis, R. Lindvall, E. Mansten, S. Molloy, A. Robert, J. Schnadt, A. Sharma, M. Sjöström, H. Tarawneh, P. Tavares, S. Thorin, K. Åhnberg
MAX IV Laboratory, Lund, Sweden

Abstract

The MAX IV 3 GeV storage ring in Lund, Sweden, was the first implementation of a multibend achromat (MBA) lattice fourth-generation light source. Since it started delivery of light in 2016, several succeeding MBA-based rings and variants have come on-line and many others are being planned, designed, built or commissioned. All of these capitalise on the MBA concept and expand it to push the brightness and coherence performance even further. In order to continue to offer competitive tools to the Swedish and international scientific communities beyond the end of this decade, MAX IV Laboratory launched in 2024 the conceptual design work of MAX 4^U, an upgrade of its 3 GeV storage ring with the goal of an emittance below 100 pm rad. This performance boost is to be achieved through a minimum-interference upgrade in which localised interventions in selected subsystems and components are carefully chosen to provide the maximum performance increase with minimum cost and, equally important, minimum dark time for the MAX IV user community. In 2025, the conceptual design report (CDR) was completed, and the focus in 2026 is to elaborate on the solutions identified for this upgrade through the Technical Design Report (TDR), to be completed by the end of 2028. This contribution describes the latest developments in accelerator physics and engineering aspects of the MAX 4^U design.

INTRODUCTION

MAX IV Laboratory is a Swedish national synchrotron laboratory located in Lund, Sweden. MAX IV Laboratory consists of a 3 GeV and a 1.5 GeV storage ring and a linear accelerator that serves as an injector to both rings as well as a driver for our Short Pulse Facility (SPF). The existing 3 GeV storage ring (R3), the first fourth-generation storage ring in the world, employs a multibend achromat (MBA) lattice enabling a bare lattice emittance of 328 pm rad [1]. Since the MAX IV inauguration in 2016, the storage ring landscape has changed, with several multibend-achromat facilities with reduced emittance now operating worldwide and more underway. Furthermore, the next phase of beamlines that are part of the MAX IV roadmap foresees up to five new beamlines, which are critically dependent on brightness and coherence, which in turn depend on reducing the electron beam emittance. To meet this challenge, MAX IV initiated the conceptual design studies for MAX 4^U in 2024, aiming to upgrade the 3 GeV ring by reducing its emittance to below 100 pm rad, while preserving the energy at 3 GeV, maintaining the source points, the shielding wall and the injector, all within strict cost and time constraints. In December 2025, the Conceptual Design Report (CDR) was completed [2–4]. The main conclusion was to bring the emittance target for the technical design phase for MAX 4^U from 100 pm rad down to 75 pm rad, with all other boundary conditions maintained. The following sections describe the present status of the project focusing on the lattice design that is the basis for the TDR work.

BEAM DYNAMICS

Lattice Design

As the TDR phase of MAX 4^U began at the start of 2026, the lattice design work narrowed to a single lattice candidate named TDR-1, which is an evolution of the CDR lattices. Consequently, as for the latter, the emittance decrease relative to R3 has been achieved primarily by the introduction of reverse bends as illustrated in Fig. 1. The overall structure

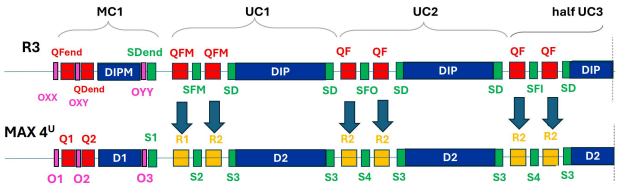

Figure 1: Layout of half an achromat for R3 and MAX 4^U. The different magnets are color-coded: quadrupoles (red), combined-function dipoles (blue), reverse bends (orange), sextupoles (green), and octupoles (magenta).

is retained in order to preserve beamline source points and reuse as much of the existing installation and equipment as possible. Thus, the TDR-1 lattice remains a 7-bend achromat lattice with a periodicity of 20.

That stated, designing an accelerator lattice is always an exercise in multi-objective optimisation. For the TDR-1, these objectives include the usual lattice performance parameters such as emittance, insertion device (ID) straight section beta functions, lifetime and injection efficiency. It should be noted that the intended use of an off-phase/on-axis injection method shifts the relative weights put on the dynamic aperture and the momentum and phase acceptance. The optimisation objectives also include certain engineering parameter thresholds beyond which cost and/or complexity for the upgrade is significantly affected. An example of

* We acknowledge funding from The Crafoord Foundation (Crafoordska stiftelsen) (Grant 20250007).
† eshraq.al-dmour@maxiv.lu.se

Content from this work may be used under the terms of the CC BY 4.0 licence (© 2026). Any distribution of this work must maintain attribution to the author(s), title of the work, publisher, and DOI.

ISBN: 978-3-95450-252-3 ISSN: 2673-5350 doi: 10.18429/JACoW-IPAC2026-THO2M02

RESULTS OF THE FIRST INTERFEROMETRIC MEASUREMENTS OF UNDULATOR RADIATION FROM SINGLE ELECTRONS*

G. Stancari†, J. Jarvis, A. Romanov, A. Shemyakin, A. Valishev
Fermi National Accelerator Laboratory, Batavia, IL, United States
I. Lobach, S. Nagaitsev, Brookhaven National Laboratory, Upton, NY, United States

Abstract

The aims of the CLARA experiment at the Fermilab Integrable Optics Test Accelerator (IOTA) were to directly measure the coherence length of undulator radiation emitted by a single electron and to test whether the radiation is in a pure classical Glauber coherent state or in a quantum mixture of coherent and Fock states. We used a Mach-Zehnder interferometer (MZI) to study visible radiation generated by 150-MeV electrons circulating in the ring. The relative delay between the two arms of the MZI was adjusted by varying the length of one of them with a resolution of 10 nm. The intensity of the circulating beam spanned several orders of magnitude, down to single electrons. A pair of single-photon avalanche diodes (SPADs) was placed at the output of the MZI arms to detect photocounts with high efficiency and timing resolution. We describe the observed interference patterns and photocount rates as a function of interferometer delay. The arrival time distributions of photocounts of undulator radiation, lasers and chaotic light are compared. The implications for the quantum-optical nature of the radiation are discussed. To our knowledge, these are the first direct measurements of this kind.

INTRODUCTION

Synchrotron-radiation sources have had an immense impact on many scientific fields. The same is true for sources of well-defined quantum states of radiation [1, 2]. At Fermilab, using the Integrable Optics Test Accelerator (IOTA) [3], we are carrying out an experimental program to study the classical and quantum properties of undulator radiation from electron bunches and from individual electrons [4]. We are addressing the following scientific questions: What are the properties of radiation from single electrons? Can one directly observe the classical or quantum nature of undulator radiation? We are also interested in new ways to generate quantum states of light and in novel applications of the experimental techniques of quantum optics in accelerator physics and beam diagnostics.

Classical electrodynamics explains a wide range of phenomena: reflection and refraction, interference, diffraction, synchrotron radiation, etc. The theory of quantum optics [5–12] offers a deeper understanding of the nature of radiation and is necessary to explain physical observations such as spontaneous emission, the Lamb shift and the Hong-Ou-Mandel effect [13], for instance. In quantum optics, physical systems are described by different quantum states of radiation. Classical waves, such as those generated by dipole antennas or lasers, are represented by Glauber coherent states. Radiation from individual atoms, parametric down-conversion or quantum dots, on the other hand, corresponds to Fock number states. The properties of thermal or chaotic sources of light, such as light bulbs, black bodies or stars, are represented by incoherent mixtures of states via the density-matrix formalism. Experimentally, states can be identified by observing the statistics of photocounts, such as intensity fluctuations or arrival-time distributions. With multiple photodetectors, one can also study coincidence rates. For instance, Hong, Ou and Mandel observed that when radiation is in a 2-photon number state, coincidences are suppressed [13]. When the energy of the radiation (~eV) is small compared to the energy of the radiating particle (150-MeV electrons, in our case), radiation is expected to be in a coherent state, behaving like a classical wave even when it is emitted by a single electron [14].

It is interesting to note that testing the coherent-state description of a radiation field may in the future be related to the experimental investigation of quantum gravity, following the suggestion that graviton detection sensitivity may be reached with quantum sensors [15, 16].

Radiation from single electrons has been studied in the past [17–19]. Recently, for instance, the techniques of quantum optics were applied to the study of radiation in a tandem undulator [20] and a free-electron laser [21].

In previous experiments [22–25], we verified that intensity fluctuations in undulator radiation contain, in addition to a Poissonian term, a calculable term which depends on beam sizes. Beam emittances can therefore be inferred from intensity fluctuations. With a single photodetector, we observed that photocount statistics was consistent with a coherent state of radiation. Arrival-time distributions were used to measure jitter in the radiofrequency accelerating cavities and to estimate bunch lengths at the smallest beam intensities. The CLARA experiment in IOTA Run 4 (2022–2023) [26] used a Mach-Zehnder interferometer (MZI) to directly measure the coherence length of undulator radiation from single electrons and to study photocount statistics. Preliminary results were presented in Ref. [27]. Here, we present the interferometry results on coherence length measurements and discuss some of the observations of photocount statistics.

* This manuscript has been authored by Fermi Forward Discovery Group, LLC under Contract No. 89243024CSC000002 with the U.S. Department of Energy, Office of Science, Office of High Energy Physics. Work partially supported by the University of Chicago Consortium for Advanced Science and Engineering (CASE). Report No. FERMILAB-CONF-26-0126-AD.

† stancari@fnal.gov

Content from this work may be used under the terms of the CC BY 4.0 licence (© 2026). Any distribution of this work must maintain attribution to the author(s), title of the work, publisher, and DOI.

ISBN: 978-3-95450-252-3 ISSN: 2673-5350 doi: 10.18429/JACoW-IPAC2026-THO3T02

TERAHERTZ TECHNIQUES IN THE ADVANCED ACCELERATOR LANDSCAPE

M.T. Hibberd*[1,2], R. Appleby[1,2], J. Bradbury[1,2], G. Burt[1,3], D.M. Graham[1,2], B. Higuera Gonzalez[1,2], S. Jamison[1,3], J. Jones[1,4], D. Lake[1,3], C. Mosley[1,3], L. Nix[1,3], T. Pacey[1,4], C. Shaw[1,3], S. Siaber[1,3], D. Walsh[1,4]
[1]Cockcroft Institute, Daresbury, UK; [2]The University of Manchester, Manchester, UK;
[3]Lancaster University, Lancaster, UK; [4]Accelerator Science and Technology Centre, Daresbury, UK.

Abstract

Terahertz (THz)-frequency particle acceleration provides a natural "bridge" between conventional electronic-based (radio-frequency RF) and novel photonic-based (laser plasma wakefields LWFA) drivers, offering stable, high-frequency, high-gradient fields for compact interactions, coupled with direct femtosecond-scale synchronization to the THz drive laser. These unique properties ideally position THz technologies to enhance the capabilities of existing RF infrastructure, while also solving key challenges to help drive the transition towards compact high-gradient laser-based accelerator applications.

As a key example, we present our latest experimental results and simulations demonstrating efficient THz-driven chirping and energy modulation of relativistic electron bunches, enabling the compression of ultrashort bunches and picosecond-spaced bunch trains with femtosecond-scale "temporal-locking" to the THz drive laser. These results unlock a potential array of advanced electron-laser applications requiring precise synchronization at the shortest timescales, of which includes solving the external injection challenge that has long-hindered LWFA progress. We will discuss our work towards achieving this goal, in addition to highlighting the other unique roles THz technologies can play in the future advanced accelerator landscape.

INTRODUCTION

The delivery of high-energy, high-charge electron bunches (and bunch trains) with femtosecond-scale bunch length and arrival timing directly synchronized to an external laser promises to open up an array of novel laser-based accelerator applications. These include direct probing of strong-field quantum electrodynamics through relativistic electron-laser collisions [1], free-electron laser (FEL) pump-probe experiments [2], single-shot ultrafast electron diffraction [3], and controlled external electron injection to enable high-quality laser-plasma wakefield acceleration [4]. Amongst others, these examples highlight an exciting transition towards a new accelerator landscape operating at the boundaries of photon science and accelerator physics.

Simultaneously achieving these critical bunch parameters remains out of reach for existing radio-frequency (RF) infrastructure alone, which is ultimately limited by unavoidable sources of jitter stemming from the use of multiple RF systems (e.g. electron gun, linear accelerating cavities) required for high-energy beams and the complex interplay between the inherent energy and timing fluctuations. Laser-generated terahertz (THz) pulses provide a route to overcome these limitations, underpinned by the significant progress in THz-driven acceleration and manipulation of electron beams achieved within the last decade. Proof-of-principle demonstrations with relativistic beams include the first scalable THz linac [5], staged acceleration [6, 7] and novel self-injection schemes [8]. Furthermore, for electron beams with MeV-scale energy and fC-level charge, THz streaking for femtosecond longitudinal diagnostics [9] and THz-driven compression with arrival-time jitter suppression [10, 11] have both been achieved.

Despite these breakthroughs, to facilitate the next-generation of advanced electron-laser applications, femtosecond-scale control of electron bunches at higher energies and charge is critical and has remained a major hurdle to overcome. Here we present a concept and experimental groundwork to achieve this [12], exploiting the phase-velocity matched interaction of laser-generated multi-cycle THz pulses with 35.5 MeV, 30 pC electron bunches in a dielectric-lined waveguide structure. We experimentally demonstrate THz-frequency energy modulation capable of compression into ultrashort picosecond-spaced bunch trains or single bunches as short as 15 fs. Crucially, we also show that the THz interaction simultaneously induces "temporal locking" of the compressed electron bunch (or bunch trains) to the THz drive laser with electron-to-laser arrival-time jitter suppressed down to 25 fs, independent of the as-measured 200 fs laser timing jitter. With optimized THz and electron bunch parameters, our results demonstrate that bunch compression and temporal-locking at the femtosecond level is within reach, entering a new regime exploiting hybrid THz-RF techniques.

CONCEPT AND EXPERIMENT

Standard RF compression techniques utilize off-crest or zero-crossing phase to imprint an energy chirp on the electron bunch, with higher energy at the bunch tail compared to the head, resulting in longitudinal bunch compression after subsequent drift (velocity-bunching) or dispersion (magnetic chicane). We adapt this technique for THz fields with 2-3 orders-of-magnitude higher frequency, enabling efficient chirping of short sub-picosecond input bunches for ultra-short single-bunch compression. Furthermore, injection of

* morgan.hibberd@manchester.ac.uk

Content from this work may be used under the terms of the CC BY 4.0 licence (© 2026). Any distribution of this work must maintain attribution to the author(s), title of the work, publisher, and DOI.

ISBN: 978-3-95450-252-3 ISSN: 2673-5350 doi: 10.18429/JACoW-IPAC2026-THO4M01

UPDATE ON THE FAIR MACHINE INSTALLATION STATUS

J. S. Schmidt†, M. Bepler, J. Bittner, B. Bohlender, R. Cannas, M. Draisbach, H. Hagelskamp, K. Knie, J. Kollarczyk, M. Kranz, H. Leykauf, O. Rodriguez, T. Ziglasch,
Facility for Antiproton and Ion Research, Darmstadt, Germany
H. Albers, M. Bevcic, M. Braun, D. Ph. Brenner, P. Gasik, D. Grünberg, F. Hagenbuck, P. Hofmann, K. Höhne, M. Kis, H. Marcocelli, N. Pyka, H. Simon, M.-M. Schmidt, P. Spiller, F. Tüy, H. Welker, N. Winters,
GSI Helmholtz Centre for Heavy Ion Research, Darmstadt, Germany
M. Sienkiewicz, J. Swierblewski,
Institute of Nuclear Physics, Polish Academy of Sciences, Krakow, Poland

Abstract

The accelerator complex for the Facility for Antiproton and Ion Research (FAIR) is currently being built in Darmstadt, Germany. After the arrival of the cold box for the central cryogenic facility (CRYO2) in winter 2023, the installation of the accelerator components in the machine and supply tunnels started early 2024. Meanwhile the installation has moved forward. CRYO2 has been handed over to the commissioning team and the commissioning is in progress. The accelerator installation is ongoing in all parts of the beamlines of the High Energy Beam Transfer Lines (HEBT), the Super Fragment Separator (SFRS) and the Heavy Ion Synchrotron (SIS100). In parallel, the installation plans for the experiments (NUSTAR and CBM) are being developed and installation preparations are taking place. In this paper the status and challenges of the machine installation in those areas are presented and an outlook for the next steps towards realisation of the project phases for Early and First Science is given.

THE FAIR ACCELERATOR COMPLEX

The new Facility for Antiproton and Ion Research (FAIR) will consist of five main machines, the fast ramping heavy ion synchrotron SIS100 and the Super Fragment Seperator (SFRS), which are both designed based on superconducting magnets, and two storage rings, the collector ring (CR) and the high energy storage ring (HESR). The beam transfer between each of those machines is realised with a complex of normal conducting lines, the high energy beam transfer system (HEBT). The excisting accelerators from the GSI Helmholtz Centre for Heavy Ion Research (GSI) will serve as the injector for FAIR. In addition, a new high intensity proton linear accelerator is planned for injection into the GSI synchrotron SIS18.

Based on the beam from GSI and the five new machines, FAIR will allow researchers to perform a program of experiments with a unique range of ion types, extraction cycles and intensities. The main user collaborations with long term experimental installations at FAIR are NUSTAR, CBM, APPA and PANDA. Their research program as well as the key parameter of the FAIR machines are presented in [1] and [2].

† ja.schmidt@gsi.de

The realisation of the FAIR complex has been split into several stages, which are highlighted in Fig. 1. The building construction for the first stage First Science + is completed already, technical infrastructure installation is ongoing.

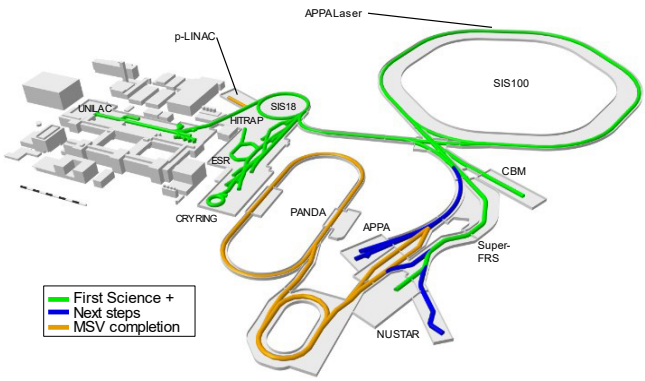

Figure 1: The GSI and FAIR facility with its stages of realisation [3].

MACHINE INSTALLATION AT FAIR

The machine installation activities are part of the FAIR sub-project “Site Management” (SMG) as shown in Fig. 2.

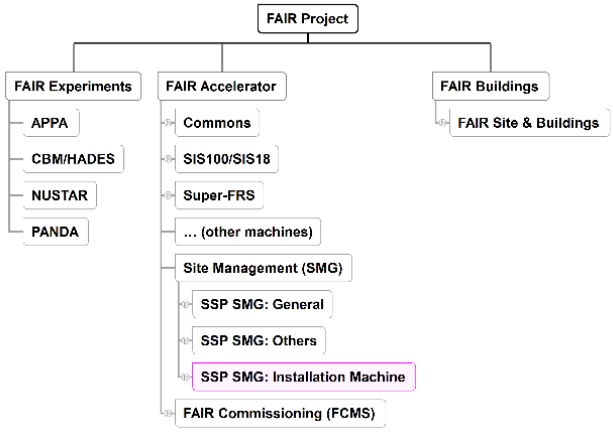

Figure 2: The machine installation within the FAIR project structure.

Content from this work may be used under the terms of the CC BY 4.0 licence (© 2026). Any distribution of this work must maintain attribution to the author(s), title of the work, publisher, and DOI.

ISBN: 978-3-95450-252-3 ISSN: 2673-5350 doi: 10.18429/JACoW-IPAC2026-THO4M02

BEAM COMMISSIONING AND UPGRADE PROGRESS FOR THE CSNS-II RCS*

M. Y. Huang†, [1, 2, 3], X. Li[1, 2], H. C. Liu[1, 2], X. Qi[1, 2], Y. L. Zhang[1, 2], S. Y. Xu[1, 2], X. H. Lu[1, 2]
L. S. Huang[1, 2], H. Y. Liu[1, 2], J. L. Chen[1, 2], Y. W. An[1, 2], K. Zhou[1, 2], Y. Li[1, 2], J. J. Tan[1, 2], J. Peng[1, 2]
Z. P. Li[1, 2], Y. L. Han[1, 2], B. Z. Chen[1, 2], S. Wang[1, 2, 3]
[1]Institute of High Energy Physics, Chinese Academy of Sciences, Beijing 100049, China
[2]Spallation Neutron Source Science Center, Dongguan 523808, China
[3]University of Chinese Academy of Sciences, Beijing 100049, China

Content from this work may be used under the terms of the CC BY 4.0 licence (© 2026). Any distribution of this work must maintain attribution to the author(s), title of the work, publisher, and DOI.

Abstract

For the China Spallation Neutron Source (CSNS), the rapid cycling synchrotron (RCS) accumulates and accelerates the injection beam to the design energy of 1.6 GeV and then extracts the high energy beam to the target. In this paper, firstly, the beam commissioning of the RCS has been comprehensively studied. In order to meet the requirements of beam power increase and stable operation of the CSNS accelerator, the RCS beam losses and radiation dose from different sources are studied and optimized. Secondly, as the second phase of the CSNS, CSNS-II will achieve a beam power on the target of 500 kW. The injection energy of the CSNS-II will be increased from 80 MeV to 300 MeV and the injection beam power will be increased about 20 times. The upgrade of the RCS will be studied in detail, including new injection system, longitudinal dynamics, closed orbit correction, transverse collimators and so on. Based on the detailed simulation and beam experimental results, the upgrade schemes of the critical systems for the CSNS-II RCS have been proven feasible.

INTRODUCTION

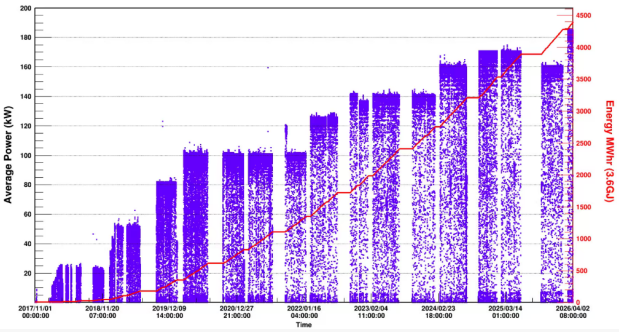

Figure 1: CSNS beam power increase history.

The China Spallation Neutron Source (CSNS) is a multidisciplinary platform [1, 2] and its accelerator consists of an 80 MeV H^- Linac and a 1.6 GeV rapid cycling synchrotron (RCS) with a repetition rate of 25 Hz [3, 4]. Through some hardware optimizations and innovative beam commissioning methods, the CSNS beam power has been increased to 185 kW, exceeding the design target by 85%. Figure 1 shows the CSNS beam power increase history.

Table 1: RCS Main Parameters

Parameters	CSNS	CSNS-II
Output beam power [kW]	100	500
Injection energy [MeV]	80	300
Extraction energy [GeV]	1.6	1.6
Pulse repetition rate [Hz]	25	25
Acceleration time [ms]	20	20
Extraction average current intensity [μA]	62.5	312.5
Circumference [m]	227.92	227.92
Number of dipoles	24	24
Number of quadrupoles	48	48
Number of QTs	0	16
Lattice structure	Triplet	Triplet
Nominal betatron tune [H]	4.86	4.86
Nominal betatron tune [V]	4.78	4.78
Acceptance [pi-mm-mrad]	540	540
Harmonic number	2	2
Particles per pulse [10^{13}]	1.56	7.8
Space-charge tune shift	0.28	0.19

As the second phase, the CSNS-II will improve the beam power on the target from 100 kW to 500 kW. Then, the ac-

† Email address: huangmy@ihep.ac.cn
* Work supported by the Guangdong Basic and Applied Basic Research Foundation (No. 2021B1515120021) and Guangdong Special Support Program (No. 2024TQ08A570)

ISBN: 978-3-95450-252-3 ISSN: 2673-5350 doi: 10.18429/JACoW-IPAC2026-TUI4M00

ACCELERATOR RESEARCH FOR PROTON THERAPY

A. Denker, G. Kourkafas, Helmholtz-Zentrum Berlin für Materialien und Energie, Berlin, Germany
J. Heufelder, A. Weber, Charité – Universitätsmedizin Berlin, Germany
J. Reindl, Universität der Bundeswehr München, Neubiberg, Germany

Content from this work may be used under the terms of the CC BY 4.0 licence (© 2026). Any distribution of this work must maintain attribution to the author(s), title of the work, publisher, and DOI.

Abstract

Proton therapy is a powerful tool in the fight against cancer. The number of accelerators has increased tremendously over the last years. Patients are treated now at over 125 facilities world-wide, which is an excellent example of an extremely successful technology transfer from fundamental research to healthcare. Depending on the tumour species, local tumour control can reach very high levels, e.g. more than 96% for uveal melanoma. To minimize side effects and maintain tumour control, new treatment modalities like FLASH or minibeams are investigated. For FLASH, dose rates should be higher than 40 Gy/s with treatment times below 0.5 s. Minibeams aim for spatial fractionation of the beam. Experiments on cells, organoids and animals have been promising. These new irradiation forms create challenges for the existing and future accelerators: Developments in beam delivery, beam adaptation, and dosimetry are necessary. This paper describes changes on control system, beam shutters, and beam scattering systems which allow now irradiation times of 10 ms with a precision in dosimetry of better than 3% for a Spread-Out Bragg Peak at HZB. The set-up of a target station for minibeams will be presented.

INTRODUCTION

80 years ago, R.R. Wilson described the radiobiological use of fast protons for tumour treatment [1]. From today's point of view the first patients were treated very shortly after. Groundbreaking work was performed at Lawrence Berkeley Laboratory [2]. In the beginning, patients were treated at accelerators originally built for nuclear and particle physics [3]. Since 1985 the Particle Therapy Co-Operative Group (PTCOG) fosters the development of particle therapy [4]. In 1990 the first hospital-based accelerator was installed at Loma Linda [5]. Research comprised, among others, the development of more compact accelerators and the development of new beam delivery techniques, e.g. pencil beam scanning [6]. The field then evolved rapidly, with dedicated and commercial accelerators taking over (Fig. 1) [7].

Proton therapy is now a mature technique, with turnkey solutions available on the market, which broadens its use. However, the number of patients treated with protons is still very small compared to the number of patients treated with electron linacs. These ready-to-use solutions fulfil the requirements of the medical device regulations or comply with FDA, an intricate set of rules and regulations which became more complex over the years. Now it is more difficult to implement modifications as companies prefer their standardized, certified products.

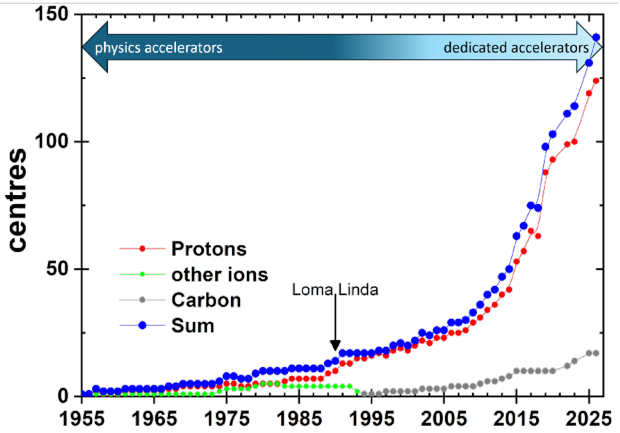

Figure 1: Centres world-wide performing particle therapy. Since installation of the first hospital-based accelerator in 1990 (Loma Linda), the number of facilities increased exponentially [3].

Albeit for some types of tumours like uveal melanomas very high local tumour control rates of more than 95% can be achieved [8], there is still room for improvement. The wish is to maintain the tumour control while reducing the side effects. Two potential techniques are discussed in the community: FLASH beam delivery, which is defined as high dose rates of at least 40 Gy/s in less than 0.5 s. The other technique is the spatial fractionation, where instead of a homogenous field a set of tiny needle beams is applied.

ACCELERATORS

About 50% of the accelerators used for clinical particle therapy as listed by the PTCoG [3] are cyclotrons, 21% synchrocyclotrons and 29% synchrotrons. Cyclotrons – and even more so synchrocyclotrons – are far more compact than synchrotrons. However, they both provide protons with a fixed energy. An interesting new design is an energy variable cyclotron without the magnetic iron [9]. The average beam intensity of synchrotrons is lower than with cyclotrons and synchrocyclotrons, which may present special challenges when considering FLASH irradiations. On the other hand, they often provide both proton and carbon therapy, and permit energy changes without large beam losses.

Besides these well-established accelerator types, there are further developments. A cyclotron is under construction in Caen, France, which shall provide protons, helium and carbon ions [10-12]. Several projects involve the use of proton linacs [13-16] or FFAGs [17-19]. Albeit these projects are very interesting from the viewpoint of an accelerator physicist, none of them treats patients up to now. The

ISBN: 978-3-95450-252-3 ISSN: 2673-5350 doi: 10.18429/JACoW-IPAC2026-THI6T01

OVERVIEW OF THE BEAM POSITION MONITORS DEVELOPMENT FOR THE NEXT GENERATION LIGHT SOURCES

L. Torino*, U. Iriso, ALBA Synchrotron (Spain), Cerdanyola del Vallès, Spain
G. Kube, D. Lipka, S. Vilcins, Deutsches Elektronen-Synchrotron DESY, Hamburg, Germany

Abstract

The development of Beam Position Monitors (BPMs), and particularly the design of the button pickup, is critically important with the new generation of Synchrotron Light Sources. Specifically, the miniaturization of the vacuum pipe and the broadening of the beam spectrum present special challenges for the button's design to meet the superior stability requirements demanded by new feedback systems. This paper will address trends and challenges in BPM design for new light sources, covering material compatibility, precision manufacturing challenges, and the importance of prototyping and testing.

INTRODUCTION

With the rise of fourth-generation light sources (4GLS), new trends have emerged in the design of Beam Position Monitor (BPM) button pickups. These evolutions have been introduced to address the challenges that upgraded machines carry with them, in particular:

- *Miniaturization:* A denser lattice means less space for diagnostics and instrumentation, including BPMs. As these devices are essential to operate the machine, they must be integrated into increasingly tight spaces;
- *Smaller vacuum chamber:* To increase the integrated field of magnets, the transverse dimensions of the vacuum pipe have been reduced. The pickups are now positioned closer to the beam, which improves signal strength but increases challenges regarding impedance;
- *Shorter bunch length:* Furthermore, the bunch lengths of these new machines are shorter, meaning the frequency spectrum excitation is much wider and can intercept higher resonance frequencies. While this is partially mitigated by the use of third-harmonic cavities, it must be taken into account when designing instrumentation that has to operate across a wide range of conditions.

Starting from these considerations, in this paper we will present the solutions adopted by the community and discuss the manufacturing capabilities required for the latest generation of BPM pickups.

PICKUP DESIGN

The design of BPM buttons requires meticulous optimization due to the intrinsic electromagnetic characteristics of the pickup. The gap separating each button from the vacuum chamber effectively acts as a resonant cavity [1]. If the frequencies of the modes trapped within this gap coincide with the bunch excitation spectrum, significant overheating can occur. The frequencies of these trapped modes can be shifted by carefully optimizing the geometric shape of the BPM pickup. Furthermore, while the strength of these modes is influenced by the proximity of the pickup to the beam, the resulting effects can be mitigated through strategic material selection. Following these analytical considerations, electromagnetic simulation tools such as CST are often used to define and validate the final BPM design [2].

Button Shape

The easiest way to shift trapped mode frequencies toward the higher end of the spectrum is to reduce the button radius r [1]. This is because the fundamental resonance in a cylindrical BPM is closely related to the cutoff frequency of the coaxial-like structure formed by the button and its housing. The resonant frequency f_{res} can be approximated by:

$$f_{\mathrm{res}} \approx \frac{c}{2\pi \bar{r}\sqrt{\varepsilon_r}} \tag{1}$$

where c is the speed of light and $\bar{r}$ is the mean radius of the vacuum gap. Since this frequency is inversely proportional to the pickup dimensions, a smaller button inherently pushes the resonances to higher frequencies, potentially moving them outside the bunch excitation spectrum.

Specifically, the voltage amplitude V induced on the button is proportional to the area of the electrode ($V \propto r^2$). Fortunately, in 4GLS where vacuum pipe apertures are significantly reduced (typically $b \simeq 10$ mm), the increased proximity of the pickup to the beam partially compensates for this signal loss, as the sensitivity scales with $1/b$. However, while this proximity is beneficial for signal strength, it is detrimental from an impedance perspective. As the pickup moves closer to the beam, the beam-to-electrode coupling increases the longitudinal and transverse impedances, leading to higher wakefield losses and potential beam instabilities that must be carefully managed in the design phase.

While one could adopt alternative shapes—such as spherical or bell-shaped geometries—to further improve this frequency shift and modify the cutoff characteristics [3], such designs often introduce significant manufacturing challenges. A common trade-off is the use of a conical shape, which pushes the resonant frequencies higher due to the tapering that reduces the volume where modes can be trapped. This design has been selected by several 4GLS [4–6]. Although manufacturing is complex due to the difficulty in maintaining concentricity between the tapered button and its housing,

* ltorino@cells.es

Content from this work may be used under the terms of the CC BY 4.0 licence (© 2026). Any distribution of this work must maintain attribution to the author(s), title of the work, publisher, and DOI.

ISBN: 978-3-95450-252-3 ISSN: 2673-5350 doi: 10.18429/JACoW-IPAC2026-THO6T01

EMITTANCE MEASUREMENT OF THE CERN ANTIMATTER BEAM WITH THE GBAR EXPERIMENT

S. Geffroy*, CNRS/IN2P3, IJCLab, Orsay (France) and the GBAR Collaboration†

Abstract

Emittance measurements were performed for the antiproton and H^- beams delivered by the AD/ELENA facility at CERN, with and without the deceleration stage of the GBAR experiment. The measurements rely on a quadrupole-scan technique using a cylindrically symmetric Einzel lens, with beam-spot imaging on a microchannel plate coupled to a phosphor screen. Transport coefficients are obtained from SIMION particle tracking simulations. For the 100 keV H^- beam, the normalized emittance is found to increase with bunch intensity, ranging from 0.025 to 0.039 mm·mrad in the vertical plane and 0.035 to 0.052 mm·mrad in the horizontal plane. After deceleration to 6 keV, a significant growth of the projected normalized emittance is observed, substantially exceeding the values predicted by SIMION simulations accounting for energy dispersion alone. RF-Track simulations indicate that this growth results from non-linear aberrations induced by the Einzel lens, amplified by space-charge effects. These results provide updated beam models that better match the measured transport efficiencies through GBAR.

INTRODUCTION

The GBAR (Gravitational Behaviour of Antihydrogen at Rest) experiment [1] is located at the CERN Antimatter Factory [2]. Its goal is to measure the free fall of ultra-cold antihydrogen atoms in the Earth's gravitational field. Unlike other antihydrogen experiments, GBAR will produce antihydrogen *ions* ($\overline{H}^+$), which can be sympathetically cooled to the microkelvin range. The production of $\overline{H}^+$ requires two successive charge-exchange reactions occurring within a small interaction region where an antiproton beam overlaps with a positronium (Ps) cloud:

$$\bar{p} + \mathrm{Ps} \rightarrow \overline{H} + e^-, \quad (1)$$

$$\overline{H} + \mathrm{Ps} \rightarrow \overline{H}^+ + e^-. \quad (2)$$

Part of the AD complex at CERN, the Extra-Low Energy Antiproton (ELENA) ring delivers antiproton bunches with a kinetic energy of 100 keV every two minutes and 100 keV H^- bunches every 15 seconds.

The optimal antiproton energy for the double charge-exchange reaction with ground-state positronium is 6 keV [3]. The antiproton beam is therefore decelerated from 100 keV to 6 keV using a 450 mm long drift tube held at -94 kV and pulsed to ground while the beam bunch is inside [4]. While the normalized emittance $\varepsilon_n = \beta\gamma\,\varepsilon_{\mathrm{geo}}$ remains conserved under deceleration, the geometric emittance $\varepsilon_{\mathrm{geo}}$ increases by a factor $\sqrt{100/6} \simeq 4$.

In 2022, the GBAR experiment observed the first production of antihydrogen atoms via the first charge-exchange reaction [1]. However, the measured production rate was limited by both the positronium density and the fraction of antiprotons delivered within the interaction region. To increase this rate, two upgrades were implemented. First, a positronium production cavity was installed, providing a significantly higher positronium density within the interaction volume. Second, a Penning–Malmberg trap was installed on the antiproton beam line upstream of the interaction region [5]. Antiprotons are accumulated and cooled in this trap through Coulomb interactions with a cold electron plasma, reducing the transverse emittance of the $\bar{p}$ beam before extraction and reacceleration to 6 keV for transport through the Ps cavity. The optics for injecting the decelerated antiproton beam into the trap were designed taking into account the expected emittance growth from deceleration. However, experimental measurements yield an injection efficiency of only about 70%. To understand this discrepancy, a measurement of the emittance of both the non-decelerated and decelerated beams was performed.

METHOD

We used the classical quadrupole-scan method [6] with a cylindrically symmetric uni-potential lens, measuring the beam-spot size with a standard microchannel-plate/phosphor-screen imaging system. An example is shown in Fig. 1. The transverse beam sizes are extracted from MCP images by analyzing the intensity distribution on the phosphor screen. A dark image is subtracted to remove background, and a fixed region of interest centered on the MCP is selected.

The transport coefficients necessary for determining the emittance are obtained using the electromagnetic modeling and charged particle tracking software SIMION. Figure 2 illustrates a SIMION model of the electrostatic beam elements used in this study. For each Einzel lens voltage, the linear transport coefficients M_{11} and M_{12} between the reconstruction point and the MCP are determined by tracking test particles with controlled initial conditions. A particle

* sarah.geffroy@ijclab.in2p3.fr

† GBAR Collaboration: P. Adrich (NCBJ), I. Belosevic (IRFU), M. Chung (POSTECH), P. Cladé (LKB), P. Comini (IRFU), D. Cotte (IRFU), P. Crivelli (ETHZ), P. Debu (IRFU), A. Douillet (LKB), S. Geffroy (U. Paris-Saclay), S. Guellati (LKB), P.-A. Hervieux (ICPMS), L. Hilico (LKB), P. Indelicato (LKB), S. Jonsell (Stockholm U.), J-P. Karr (LKB), B. Kim (IBS), S. Kim (SNU), E-S. Kim (Korea U.), N. Kuroda (U. Tokyo), B. Lee (SNU), L. Liszkay (IRFU), D. Lunney (CNRS-IN2P3), G. Manfredi (ICPMS), B. Mansoulié (IRFU), M. Matusiak (NCBJ), V. Nesvizhevsky (ILL), F. Nez (LKB), K. Park (SNU), E. Perez (CERN), P. Pérez (IRFU), C. Regenfus (ETHZ), J-Y. Roussé (IRFU), F. Schmidt-Kaler (Uni-Mainz), K. Szymczyk (NCBJ), F. Tano (U. Tokyo), B. Tuchming (IRFU), D.-P. van der Werf (Swansea U.), D. Won (SNU), S. Wronka (NCBJ), K-H. Yoo (POSTECH), P. Yzombard (LKB)

Content from this work may be used under the terms of the CC BY 4.0 licence (© 2026). Any distribution of this work must maintain attribution to the author(s), title of the work, publisher, and DOI.

ISBN: 978-3-95450-252-3 ISSN: 2673-5350 doi: 10.18429/JACoW-IPAC2026-THO6T02

DEVELOPMENT OF A NEW ULTRASLOW MUON BEAM DIAGNOSTIC SYSTEM FOR THE J-PARC MUON g – 2 / EDM EXPERIMENT

M. Wada*,[1], K. Ishida[2], K. Suzuki[3], M. Kimura[1], M. Lyu[1], S. Kamioka[2], T. Mibe[1,2]
[1]The University of Tokyo, Tokyo, Japan
[2]High Energy Accelerator Research Organization, Ibaraki, Japan
[3]Nagoya University, Aichi, Japan

Abstract

Realization of a low-emittance muon beam requires injection of a phase-space-matched keV-scale muon (ultraslow muon) beam into an accelerator, since beam mismatch leads to emittance growth and reduced acceleration efficiency. In the J-PARC muon acceleration scheme, both invasive and conventional non-destructive diagnostics of such a beam are challenging because of its low energy and low intensity. Here we develop an ultraslow muon diagnostic system compatible with the accelerator under construction at J-PARC. The system is designed to evaluate beam conditions so that the beam can be precisely tuned for acceleration. Commissioning with ultraslow muon sources demonstrates the system's capability as a practical online diagnostic system for beam matching.

INTRODUCTION

Development of a low-emittance muon beam is an important step toward next-generation muon science. Such a beam enables high-precision measurements of fundamental physics parameters, such as the muon magnetic dipole moment, and the search for the electric dipole moment [1]. It is also expected to play key roles in future applications including muon microscopy for probing internal structures of materials [2] and muon colliders for searches beyond the Standard Model [3]. Realization of these studies requires the stable production of a low-emittance muon beam. Conventional high-intensity muon beams are predominantly produced from pion decay in proton-irradiated targets. Such a muon beam is a tertiary beam and has a large phase space volume ($\mathcal{O}(10^3)$ π mm $\cdot$ mrad), which leads to poor matching to the acceptance of the accelerator ($\mathcal{O}(1)$ π mm$\cdot$mrad) and consequently low acceleration efficiency. One promising approach is the acceleration of ultraslow muons produced via laser ionization of muoniums [4, 5]. In this scheme, surface muons stop in a silica aerogel target [6], form thermalized muonium atoms, and are subsequently ionized and accelerated toward a radio-frequency quadrupole (RFQ). The intensity of the ultraslow muon beam is on the order of fC.

Efficient RF acceleration requires accurate matching of the beam parameters to the RFQ acceptance. Accurate determination of the beam emittance and Twiss parameters at the RFQ entrance is therefore essential for beam matching. However, conventional diagnostic techniques [7] are difficult to apply because the beam is both low-energy and low-intensity, while background particles from the upstream beamline further complicate signal identification.

In this work, we develop a diagnostic system to accurately evaluate the parameters of the low-energy and low-intensity ultraslow muon beam while separating the signal from the background and maintaining compatibility with accelerator operation. The system was installed between the muon source and the RFQ and is designed for flexible switching between acceleration and diagnostic modes. Its performance is then demonstrated through beam-based measurements. The experiments were carried out at Materials and Life Science Experimental Facility (MLF) of the Japan Proton Accelerator Research Complex (J-PARC).

DIAGNOSTIC SYSTEM DESIGN

The requirements of the diagnostic system are determined by the limited available space and the beam-matching conditions at the RFQ. To limit emittance growth in the RFQ to within 10 %, accurate beam-parameter measurements are required. The main requirements for the diagnostic system are compactness, flexible mode switching, background suppression, and measurement of beam parameters with an accuracy of approximately 10 %.

Figure 1 shows the schematic of the beamline including the diagnostic system. The upstream section consists of components for muon production, beam transport, and beam steering toward the RFQ. Because of its small momentum, the ultraslow muon beam is highly sensitive to ambient magnetic fields. To maintain the beam trajectory, the ambient magnetic field around the target is monitored using field probes and compensated using cancellation coils. Remaining beam shift is corrected using electrostatic deflectors. Downstream of the electrostatic deflectors, an electrostatic mirror (EM) [8] is used to vertically deflect the beam toward the diagnostic section. The EM, used for energy selection, can be retracted from the beam path by a retraction mechanism so that the beam passes to the downstream accelerator. The EM consists of a positively biased flat backplate and a grounded mesh electrode facing each other, separated by 20 mm and tilted by 45° with respect to the beam axis. A bias voltage of 5.7 kV, corresponding to the extraction energy of the muon beam, is applied to the backplate. A dipole magnet (bending magnet, BM) located downstream and used for momentum selection further deflects the beam by 90°. The magnet has a bending radius of 150 mm, is air-cooled, and operates at a central magnetic field of 2.63×10^{-2} T. The combination of EM and BM suppress background parti-

* mayuwada2001@g.ecc.u-tokyo.ac.jp

Content from this work may be used under the terms of the CC BY 4.0 licence (© 2026). Any distribution of this work must maintain attribution to the author(s), title of the work, publisher, and DOI.

ISBN: 978-3-95450-252-3 ISSN: 2673-5350 doi: 10.18429/JACoW-IPAC2026-THP2006

REALISATION OF THE 1.5 GHz SINGLE-MODE-CAVITY FOR PETRA IV

M. Bousonville†, H. Bienert, P. Drebenstedt, P. Hülsmann, S. Karau, M. Röhling, M. Pröll, M. Lemke, C. Christou, Deutsches Elektronen-Synchrotron DESY, Hamburg, Germany

Content from this work may be used under the terms of the CC BY 4.0 licence (© 2026). Any distribution of this work must maintain attribution to the author(s), title of the work, publisher, and DOI.

Abstract

A third harmonic system is planned for PETRA IV. One possible option for the third harmonic cavity is a novel single-mode cavity based on the choke-mode principle. The DESY device developed on this basis offers the following advantages over alternative designs: a) Very strong suppression of all unwanted modes. b) Coupling factor adjustable during operation. c) The wall currents induced by the fundamental mode are not disturbed by weld seams. This has a favourable effect on the shunt impedance and quality factor. d) The simple geometry of the cavity results in the smallest possible number of independent cooling circuits. The paper describes the development work, introduces the design and highlights some of the cavity's outstanding features. It also discusses the current construction of the cavity.

THE RF SYSTEM FOR PETRA IV

A third-harmonic system is planned for the RF system. This will be used to lengthen the electron bunches in thus increasing their lifetime in the PETRA IV accelerator [1]. 24 cavities are planned for both the 500 MHz (fundamental) and 1.5 GHz (3rd harmonic) systems. The 500 MHz system will utilise EU-HOM cavities [2]. The baseline design for the PETRA IV harmonic cavity is a scaled version of the 500 MHz cavity [3]. However, there are a number of good reasons – which will be discussed later – for using a different design. The choice fell on a single-mode cavity based on the choke-mode principle [4].

DEVELOPMENT

Once the project idea had been conceived, a development concept was drawn up and a project team was put together.

Project Team

The project team consists of a project manager, a physicist, an RF engineer, a mechanical engineer, a product designer and a production planner.

Concept

Care was taken to ensure that the RF and mechanical engineering experts developed the cavity together from the outset. This prevented the RF design from heading in a direction that was mechanically unfeasible. Even the initial designs for the resonator, in various configurations, were discussed with the mechanical engineers. Designs that were difficult or impossible to implement were discarded. Conversely, mechanical requirements were integrated into the CST model and their effects on the RF were investigated. In this way, the RF design and the mechanical design were harmonised.

Review

Once the design had reached a stage of maturity where discussions about production could be held with manufacturers, a review was carried out with a recognised expert [5]. The expert was given access to the comprehensive project documentation. The review concluded that the design was highly likely to work in practice. Practical advice on manufacturing was also provided.

THE CAVITY

The basic principle of the choke-mode cavity is that the choke (Fig. 1) reflects and thus maintains the fundamental mode TM-010, whilst the excitation of all higher-order modes (HOM) is suppressed by the absorber. In theory, this means that, in our case, only 1.5 GHz thereof can be excited by the electron beam. In practice, this is not quite so perfect, but it does result in very strong HOM suppression [6, 7].

Absorber

The absorber is ring-shaped and made of silicon carbide (SiC). In the simulations, we have assumed a dielectric constant $\underline{\varepsilon_r} = 20 - j5$. The SiC ring is held in position by a spring [8]. This has two key advantages.

The spring makes contact with the ring and the cavity only over very small areas. This results in very low thermal conductivity through the material. Consequently, heat is dissipated mainly via thermal radiation. This prevents a hotspot forming in the adjacent copper. The heat from the absorber ring is dissipated over a large area via thermal radiation to the surrounding copper and heats the cavity very evenly, as simulations have shown. The spring and SiC ring can be operated at very high temperatures. The spring is made of Hastelloy and was heated to 900°C. After cooling, no change in the mechanical properties was observed. The SiC ring can withstand even higher temperatures [9]. The thermal simulations showed that the absorber ring does not exceed 300°C in the PETRA IV operational mode with cavity voltage around 100 kV.

The second advantage is that the mechanical stress on the cavity body generated by expansion of the absorber material is greatly reduced by the spring, which can easily cope with this. If the absorber material were soldered in place, the different coefficients of thermal expansion of SiC and copper would lead to significant mechanical stresses in both the ring and the cavity body.

† michael.bousonville@desy.de

ISBN: 978-3-95450-252-3 ISSN: 2673-5350 doi: 10.18429/JACoW-IPAC2026-THP2009

ALBA II ACCELERATOR UPGRADE PROJECT STATUS*

F. Pérez†, ALBA Synchrotron-CELLS, Barcelona, Spain
on behalf of the ALBA II team

Abstract

ALBA is working on the upgrade project that shall transform the actual storage ring, in operation since 2012, into a 4th generation light source, in which the soft X-rays part of the spectrum shall be diffraction limited. The project was launched in 2021 with an R&D budget to build prototypes of the more critical components. The storage ring upgrade is based on a MBA lattice which has to comply with several constraints imposed by the decision of maintaining the same circumference (269 m), the same number of cells (16), the same beam energy (3 GeV), and as many of the source points as possible unperturbed. At present, the lattice optimization, iterating with the technical constraints of space and performance, is ongoing. This paper presents the situation of the project, with the present proposed lattice and equipment design; the status of the prototyping of magnets, pulsed elements. vacuum chambers, buttons BPMs, and girders; the proposed RF system with fundamental and harmonics cavities; and the general context of the upgrade.

INTRODUCTION

The main goal of the accelerator upgrade is the transformation of ALBA into a diffraction limited storage ring, which implies the reduction of the emittance by at least a factor of twenty. The upgrade has been conceived as a cost and time effective process, to be realized by the end of the decade and profiting at maximum from the existing infrastructures.

It has been decided that the storage ring (SR) upgrade shall be done without any major modification of the shielding tunnel, and that the Insertion Devices (IDs) will remain at their present position. The beamlines will be upgraded to profit from the new lattice, though there will be minor changes on the ID light sources.

The beam energy will be maintained at 3 GeV, after having considered several factors, among them, that increasing the energy of the SR would require replacing the whole booster, increasing the cost of the project and lengthening its realization.

The circumference of the upgraded SR is constrained to be the same length as in the present SR in order to reuse the tunnel; and since we want to preserve also the IDs position, a sixteen-cell 4-fold symmetry, as the actual Storage Ring, is imposed, which implies a very compact cell. Details on the layout considerations can be found at [1].

Withing the program "Enabling Technologies for ALBA II", the design and prototyping of the different components for ALBA II is under progress.

LATTICE

Since the last lattice proposal presented in 2025, where octupoles were introduced in the 5 BA cells, the work of the last year has been dedicated from one side to improve the lattice performances by refining the model and the optimization technique, and on the other side to develop a new optics of the injection section with asymmetric waist that allowed to recover a pseudo-16-fold symmetry with matched phase advances and chromatic function W_x in all the straight sections. In Fig. 1 is shown the 16-cells lattice, where the injection section is located in the middle.

The main benefit of this change in the lattice is its robustness to errors rendering 100% of injection efficiency for more than 90% of the simulated error seeds.

Detailed information about the new lattice can be found at [2].

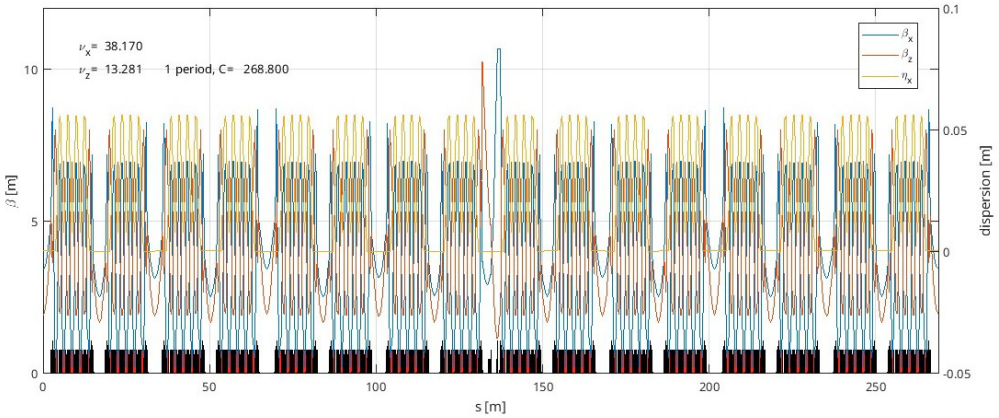

Figure 1: Optical functions of the pseudo-16-fold 5BA lattice proposed for ALBA II.

* Work supported by the Spanish and Catalan Governments, and co-funded by the European Union – NextGenerationEU project Ref. ICTS-MRR-2021-02-CELLS from the Recovery and Resilience Mechanism.
† francis@cells.es

Content from this work may be used under the terms of the CC BY 4.0 licence (© 2026). Any distribution of this work must maintain attribution to the author(s), title of the work, publisher, and DOI.

ISBN: 978-3-95450-252-3 ISSN: 2673-5350 doi: 10.18429/JACoW-IPAC2026-THP2010

RADIATION-INCLUSIVE KICKMAP ANALYSIS OF INSERTION DEVICES AND MITIGATION STRATEGIES FOR MAX4U

G. Pérez Segurana*, M. Apollonio, J. Bengtsson, M. Muradi, M. Sjöström, H. Tarawneh, P. Tavares, S. Thorin, MAX IV Laboratory, Lund, Sweden

Content from this work may be used under the terms of the CC BY 4.0 licence (© 2026). Any distribution of this work must maintain attribution to the author(s), title of the work, publisher, and DOI.

Abstract

Multi-bend achromat lattices allow for the design of extremely low-emittance electron storage rings and are a cornerstone of the performance of storage-ring-based synchrotron light sources. As part of the proposed MAX IV upgrade, MAX4U, we revise the impact of the insertion devices (IDs) on the beam. We extend the kickmap-based tracking analysis by including the effects of radiation and quantify the resilience of the proposed achromats to the different ID settings and configurations. Finally, we present mitigation strategies, both local to each ID and global, that may be tested experimentally in the current MAX IV 3 GeV ring.

INTRODUCTION

The MAX IV 3 GeV storage ring has demonstrated the performance potential of multi-bend achromat (MBA) optics for diffraction-limited synchrotron light sources and provides the operational basis for the MAX 4^{U} upgrade programme [1–5]. The MAX 4^{U} project aims to further improve brightness and coherence while preserving robust operation under a broad range of user configurations, including challenging insertion-device (ID) settings [6]. In this context, a realistic and self-consistent assessment of ID integration is essential, since they can significantly affect the non-linear dynamics.

Previous optics studies for MAX 4^{U} have established linear and non-linear performance trends for candidate achromats and correction strategies [6]. Building on that work, we revisit ID effects using kickmap-based tracking framework [7] extended with $B_{\perp}^{2}$ as developed for the NSLS-II PDR [8,9] to include the radiation effects. The motivation is twofold: (1) to quantify how synchrotron-radiation damping and quantum excitation modify the dynamic response of the lattice; and (2) to compare mitigation options that can be translated into machine-development tests in the present MAX IV ring.

We evaluate local optics re-matching and global tune correction under multi-ID scenarios, with emphasis on operationally realistic constraints on available quadrupole strengths and optics knobs. An overview of the achromat optics, layout and resulting parameters is shown in Fig. 1 and Table 1.

INSERTION DEVICES

Insertion devices constitute a source of optics perturbations. This section summarizes the IDs considered in this work, table 2, and the beam-dynamics mechanisms retained

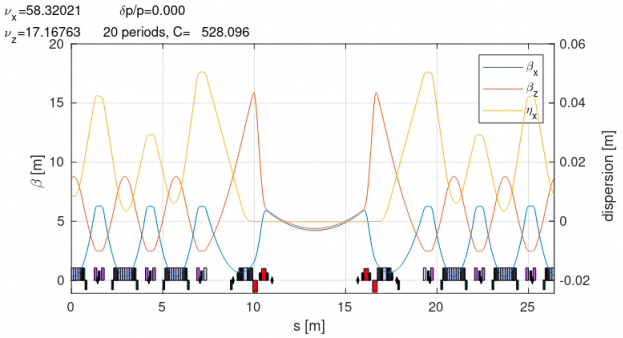

Figure 1: Linear optics of the MAX 4^{U} baseline lattice for one full superperiod shown centered around a long straight. Horizontal beta function β_x (blue), vertical beta function β_y (orange), and horizontal dispersion η_x (yellow) are shown.

Table 1: Key parameters of the MAX 4^{U} baseline lattice used in this study.

Parameter	Symbol	Value
Energy	E	3 GeV
Circumference	C	528 m
Natural emittance	ε_0	65 pm rad
Betatron tunes	Q_x/Q_y	58.32 / 17.17
Chromaticities (corrected)	ξ_x/ξ_y	2 / 2

in the tracking model. A broader overview of planned devices is given in Ref. [10]. The Hamiltonian of a planar insertion device can be written as shown in Eq. (1) [8,11]:

$$\langle H\rangle_{\lambda_u} \approx \frac{p_x^2+p_y^2}{2(1+\delta)} - \frac{y^2}{4\rho_u^2(1+\delta)} + \frac{k_z^2 y^4}{12\rho_u^2(1+\delta)} - \delta + O(p_{x,y}^4)\,, \quad (1)$$

where λ_u is the ID period, ρ_u is the bending radius associated with the peak field, and $k_z = 2\pi/\lambda_u$. The first term corresponds to the linear vertical focusing, while the second represents higher-order component driving the $4\nu_y$ resonance and vertical amplitude dependent tune shift. For elliptically-polarising undulators (EPUs), skew terms introducing coupling are also present. The linear focusing leads to tune shifts and beta-beating, while the non-linear terms can drive resonances and reduce dynamic aperture. These effects are analysed both per device and in combined configurations. The correction strategy developed in the next section therefore separates local restoration around each straight section from global retuning of lattice functions.

* gustavo.perez_segurana@maxiv.lu.se

[1] The TomoWISE beamline is not currently present in the MAX IV ring, but will be present at the time of the upgrade to MAX 4^{U}

ISBN: 978-3-95450-252-3 ISSN: 2673-5350 doi: 10.18429/JACoW-IPAC2026-THP2011

VERTICAL ALIGNMENT OF THE SLS 2.0 STORAGE RING

M. Böge*, M. Aiba, F. Armborst, M. Brinkmann, K. Dreyer,
T. Hoewler, F. Maier, J. Kallestrup,M. Wurm
PSI Center for Accelerator Science and Engineering, Villigen, Switzerland

Abstract

The alignment of girders and individual magnetic elements according to the tight design specifications is of paramount importance for achieving the ultimate performance of the SLS 2.0 storage ring (SR) which is consisting of a large number of SR optics defining permanent magnets. As a result, alignment errors can easily overstrain the very limited capabilities of the electromagnetic dipole corrector magnets. In order to enable a fast realignment during commissioning the girders are vertically remotely adjustable allowing for a realignment within ±0.5 mm (backed by simulations) with stored beam and running fast orbit feedback based on previously taken survey data (Beam-Assisted Girder Alignment). A linear encoder based vertical positioning system monitors the relative girder-to-girder motion. In addition, the orbit correction system helps to identify errors of individual magnets on the girders.

INTRODUCTION

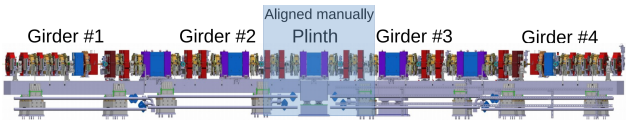

Figure 1: Layout of one arc consisting of 4 girders with vertical remote control and a central plinth with manual magnet alignment capability only.

Between September 2023 and December 2024 the old SLS storage ring was exchanged by the new SLS 2.0 ring [1] which provides a much lower emittance of 150 pm at 2.7 GeV and is installed in the existing tunnel [2]. The combination of lower emittance and higher beam energy provides a factor 60 increase of hard X-ray brightness (>10 keV), which will be further enhanced by means of new undulators of shorter period. The range of radiation sources from period elliptic undulators to superconducting superbends of up to 5 T peak field will support experiments spanning photon energy ranges from 6 eV to 80 keV.

At the beginning of 2025 SLS 2.0 underwent successful commissioning [3] followed by first user operation at the design current of 400 mA at the end of the same year [4] [5].

The improvements in lattice performance also require a very precise alignment of the ≈1000 magnet components, which are distributed over the 288 m circumference on 60 support structures (48 girders and 12 plinths) forming 12 nearly identical arcs (see Figure 1) and 12 straight sections of 3 different lengths. The alignment tolerances are determined by the correctability of the imperfect lattice established by simulations [1]: girder absolute 60 μm RMS, girder-to-girder 20 μm RMS, element-to-element 30 μm RMS, Component roll 300 μrad RMS with a 2σ cut.

INITIAL ALIGNMENT

The alignment process was distributed over multiple stages of the upgrade. The starting point was a solid reference network established for SLS 1.0 in 1999 which was constantly maintained and updated for >20 years to keep measurements around the ring as precise as possible. This network consists of 100 wall references and 53 floor references. In January 2025, the survey network for the final alignment was measured with 55 laser tracker positions and then calculated to get an up-to-date reference for the final alignment campaign [6].

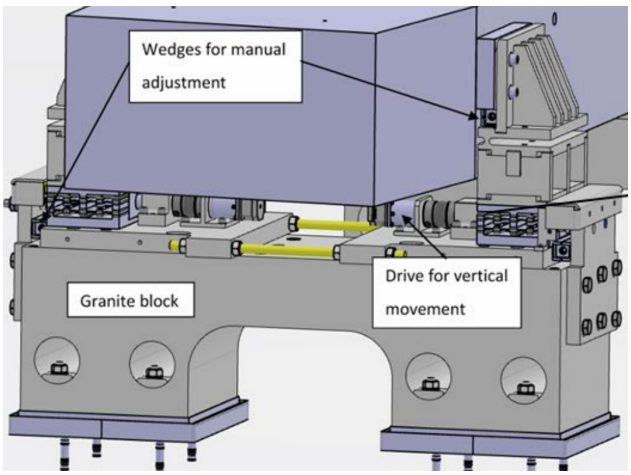

Figure 2: Girder alignment mechanism with remote controlled satellite roller screws with vertical adjustment steps of 1 nm and wedges for manual adjustments [6].

All magnets were measured on measurement benches with vibrating and moving wires defining every magnetic centre with a precision of <30 μm RMS to its fiducials. For some delicate magnet assemblies like the sextupole-quadrupole corrector combinations used for BBA [7] or some delicate permanent magnet combinations the allowed tolerance went down to <10 μm.

After the assembly in the pre-assembly hall with temperature variations <5°C daily, the first step of the initial alignment was the positioning of 23 magnets on the ≈4 m long girders in a temperature controlled environment at 25±0.5°C. The pre-aligned girders were then installed in the tunnel on pre-levelled floor plates providing ±0.5 mm global level precision in order to minimize the successive vertical adjustment with the dedicated wedges depicted in Figure 2.

* Michael.Boege@psi.ch

Content from this work may be used under the terms of the CC BY 4.0 licence (© 2026). Any distribution of this work must maintain attribution to the author(s), title of the work, publisher, and DOI.

ISBN: 978-3-95450-252-3 ISSN: 2673-5350 doi: 10.18429/JACoW-IPAC2026-THP2013

ACCELERATOR FAULT HANDLING AT SLS 2.0

F. Armborst*, M. Aiba, M. Boege, M. Gasche, F. Hämmerli, I. J. Johnson,
J. Kallestrup, R. Kalt, M. Paraliev, V. Schlott, L. Stingelin
PSI Center for Accelerator Science and Engineering, Villigen, Switzerland

Abstract

With the transition from machine commissioning to beamline commissioning and user operation, long-term reliability and high availability of the Swiss light source (SLS) 2.0 accelerator complex at the paul scherrer institute (PSI) have become critical. Rapid, systematic fault handling is essential to minimize downtime and protect the accelerator. This contribution presents the architecture and implementation of key systems developed for fault management at SLS 2.0, including the post-mortem framework, Injection Guard, and controlled emergency beam-dump procedure. The post-mortem system captures and logs comprehensive fault data to support root-cause identification, confirmation of a successful emergency beam dump and continuous improvement. The Injection Guard ensures safe and reliable injection by monitoring critical parameters and preventing injection when safety thresholds are violated. For severe fault scenarios, a controlled emergency beam dump using a fast beam dump controller (BDC), a fast beam dump magnet and a dedicated beam dump protects sensitive components such as the vacuum chamber. Together, these measures form an integrated approach to fault handling that enhances operational robustness and user reliability. Initial experience during early user operation demonstrates their effectiveness and lays the foundation for further optimization and long-term reliability.

INTRODUCTION

The SLS 2.0 design [1] introduced two new key aspects for the machine protection in comparison to SLS-1: the risk of permanent magnet demagnetization from accumulated radiation dose [2] and the risk of machine damage from uncontrolled beam losses. The latter became clear during the project phase of SLS 2.0 when simulations of the loss distribution for coasting beams indicated highly localized energy deposition at devices such as an in-vacuum insertion device (ID) and a superconducting superbend. In addition, following uncontrolled beam losses, the risk of vacuum leaks due to the increased energy density of the low-emittance beam and the thin 1 mm copper vacuum chamber [3] and even thinner 0.5 mm steel vacuum chamber for the corrector magnets is significant. Especially in light of experience from other facilities [4–6] these circumstances gave the necessary motivation to develop a dedicated beam abort system enabling fast and controlled beam energy deposition for minimized risk. The SLS-1 RF phase inversion beam abort technique was no longer viable. The key ingredients for the new beam abort system are the fast BDC, a dedicated beam dump kicker (BDK) and a dedicated beam dump [7]. An overview of the SLS 2.0 machine protection system and initial commissioning [8, 9] experience was presented in [10]. This contribution focuses on the fault handling aspects and further gained experience with the SLS 2.0 machine protection system.

INJECTION GUARD

The injection guard is the initial machine protection layer with the goal of preventing misinjected beams and defusing critical situations that could potentially lead to beam aborts. In contrast to the alarm handler which requires the operator to take action, the injection guard directly enforces a safe machine state by itself. It inhibits the distribution of injection triggers by the timing master and thus the injection of additional charge or dangerous misfiring of the pulsed magnets (e.g., one of the kickers out of the 4-kicker bump fails). The injection guard is a high level application implemented in python and running as a systemd process on a dedicated high level application server. The injection guard monitors the state of critical accelerator subsystems and beam parameters. Monitored systems include vacuum pressure (static limits, detection of abrupt pressure increase), pulsed magnets (status ok and setpoint within nominal operating range), magnets, beam abort system, machine interlock system (MIS), vacuum control system (VCS), radio frequency (RF) and ID gaps. Monitored beam parameters include lifetime, transmission, orbit, tune, total and single bunch charge. The interlock thresholds must be lower than the corresponding beam abort thresholds since many of the monitored systems such as the beam position monitor (BPM) [11] system or the filling pattern feedback (FPFB) [12] will directly request a beam abort when their respective thresholds are surpassed.

BEAM ABORT SYSTEM

When critical machine thresholds are surpassed and risk to the machine is imminent, the beam abort system is activated: When one of the systems connected to the in-house developed compactPCI serial (CPCI-S) [13] based fast BDC [10] hardware detects one of its monitored signals leaving the safe operating range it requests a beam abort. Within less than 1 µs, the fast BDC triggers the distribution of post-mortem and beam dump events to enable other accelerator systems to trigger the acquisition of post-mortem data or enter a safe state for the imminent beam abort, i.e., the main RF [3, 14] prepares for the fast increase of reflected power by reducing forward power and the 4-kicker-bump is inhibited to avoid overlap with the opposing deflection from the BDK. A recent feature upgrade of the BDC has been the addition of a new feature on the firmare (FW) level: synchronization of

* felix.armborst@psi.ch

Content from this work may be used under the terms of the CC BY 4.0 licence (© 2026). Any distribution of this work must maintain attribution to the author(s), title of the work, publisher, and DOI.

ISBN: 978-3-95450-252-3 ISSN: 2673-5350 doi: 10.18429/JACoW-IPAC2026-THP2014

INITIAL USER OPERATION OF SLS 2.0

F. Armborst, M. Aiba, S. Bettoni, M. Boege, H. H. Braun, M. Brinkmann, R. Ganter,
J. Kallestrup and V. Schlott on behalf of the SLS 2.0 Team,
PSI Center for Accelerator Science and Engineering, Villigen, Switzerland

Abstract

The year 2025 marked the transition from installation to commissioning and the beginning of first user operation of the Swiss light source (SLS) upgrade, the SLS 2.0. This contribution reports on the achieved storage-ring performance and operational stability. Storage-ring optics were tuned near design, achieving beta beating within a few percent and optimized dispersion. Sub-micron orbit stability was achieved through fast-orbit feedback supported by the in-house DBPM 3 system, permanent magnets, stable power supplies, and improved environmental control. The injector chain delivered highly reproducible bunch charge, stable energy and optics matching, and transmission exceeding requirements. User operation started with a stable baseline filling pattern and regular top-up injection under defined current-stability conditions. Beamline commissioning progressed in parallel with accelerator-performance optimization, and by the end of 2025 overall 2 diagnostic- and 12 experiment-beamlines were taking light. The achieved machine availability is comparable to the final years of SLS. Operational statistics confirm that SLS 2.0 has rapidly reached a robust operational regime, paving the way for continued performance optimization and full scientific exploitation.

INTRODUCTION

After the completion of the installation phase of the SLS upgrade, the SLS 2.0, and the successful recommissioning of the linac and booster in late 2024, efforts in early 2025 focused on commissioning of the new fourth-generation storage ring [1, 2]. The ring commissioning succeeded rapidly with first electrons injected on the 14th of January, first stored beam on the 23rd of January and design beam current achieved on the 3rd of April. Reaching this milestone ahead of schedule allowed fast beam-dose accumulation for vacuum scrubbing and created favourable conditions for further optimization of injection, orbit feedback, and beamline commissioning at full beam current. After the successful machine commissioning to nominal beam operation parameters within 50 days the focus was shifted to beamline commissioning and user operation. The overview of the beam current development during 2025 given in Fig. 1 nicely shows the rapid progression to stable operation.

BEAMLINE COMMISSIONING

Following the achievement of nominal beam parameters, beamline commissioning focused on the rapid delivery of first light and safe operation permits for user beamlines. It commenced with the permanent magnet superbend beamlines, Debye [3] and PXIII [4], opening their shutters on the 10th of April for first light after 2 days of shutdown for preparing their front-ends (FEs) and personnel safety system (PSYS). Front-end installation was not fully completed during the darktime. It was split into multiple phases [5] which are ongoing in parallel with machine commissioning and operation [6]. For first light the machine started at 60 mA enabling the beamlines Debye [3] and PXIII [4] to open their FE-shutters with little risk and align their beamline elements to get the beam safely to the photon shutter at the end of their optics hutches. Then the beam current was ramped up to the nominal 400 mA. In parallel the radiation protection officers measured the radiation around the optics hutch to ensure that the thresholds are not exceeded and confirm correct function of the implemented radiation shielding. In the next step the photon shutters at the end of the optics hutch were opened bringing synchrotron radiation into the experimental hutch towards the end station. Radiation surveys were then performed around the experimental hutch.

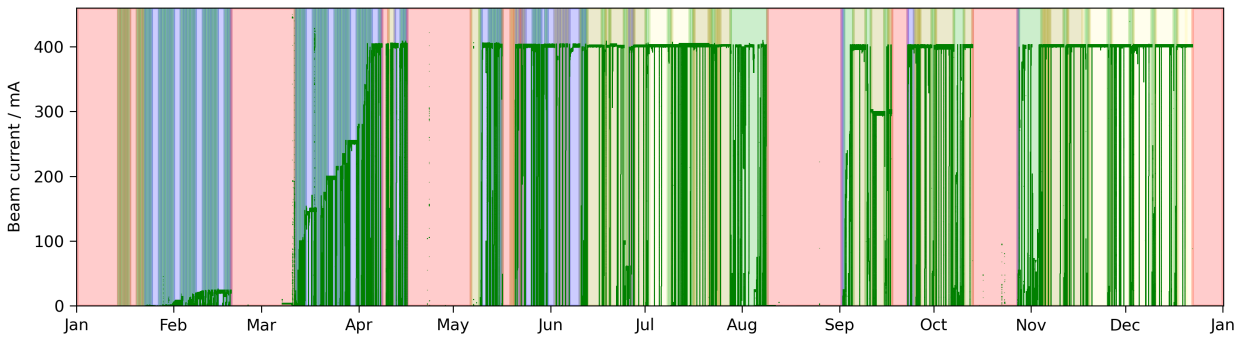

Figure 1: The SLS 2.0 beam current over the entire year 2025. The background colour indicates the scheduled operation mode, i.e., shutdown (red), machine commissioning/development (green), vacuum scrubbing (blue), beamline commissioning/development (olive) and user operation (light yellow).

Content from this work may be used under the terms of the CC BY 4.0 licence (© 2026). Any distribution of this work must maintain attribution to the author(s), title of the work, publisher, and DOI.

ISBN: 978-3-95450-252-3 ISSN: 2673-5350 doi: 10.18429/JACoW-IPAC2026-THP2016

INITIAL COMMISSIONING SIMULATIONS FOR THE DIAMOND-II BOOSTER

D. Rabusov*, I. P. S. Martin, Diamond Light Source, Oxfordshire, UK

Abstract

The Diamond-II booster ring is designed to reduce the emittance and the bunch length for efficient injection into the storage ring. Non-optimal commissioning of the injector might increase the dark-time period and the impact on the existing scientific program. This work explores the strategies for booster commissioning to predict and resolve possible issues. The results include tracking simulations with realistic errors such as alignment of magnets and precision of beam diagnostic devices, errors in the magnet gradients, eddy-current effects, measured multipole errors in magnets, and pulsed-magnet time jitter.

INTRODUCTION

Efficient injection into the Diamond-II storage ring requires the upgrade of the existing booster [1]. This work analyses the performance of the booster during the energy ramp in terms of its robustness to errors such as misalignments, field errors, eddy currents and undesirable multipoles in the magnets. Previously, the initial steps towards setting up the commissioning simulations for the Diamond-II booster ring were carried out in *ELEGANT* [2]. This work demonstrates the progress towards the transition to *AT2* [3] to match with the storage ring studies and simplify the development and testing of online Matlab commissioning tools.

ANALYSIS OF BOOSTER MAGNET DATA

Measured multipole components in the pre-series booster quadrupole and sextupole magnets were provided by the Supplier, Danfysik. The datasets include the measurements performed before and after the reassembly of magnets. In this work, we follow the same procedure as described in Ref. [1] to characterise the dynamic aperture at a fixed energy. However, the main B-field as well as the reference gradients in the booster magnets follow the energy-ramp waveform, and the higher-order multipoles scale accordingly. To take this into account, the pre-series measured data has been extrapolated to match the reference gradients of the quadrupoles and sextupoles at any given energy point. Another obstacle is that the available pre-series data contains only one example magnet for each magnet type. The errors have been added to the model as systematic or random. The model setup includes single-particle tracking for 256 turns and averaging over 20 error seeds. The results below include multipole errors in quadrupoles and sextupoles up to the 17-th order.

The results of the dynamic-aperture characterisation from particle tracking are summarised in Fig. 1, in this case, multipole errors are considered to be systematic. The four panels show the dynamic aperture at fixed energies during the ramp, the energy points are chosen as the injection energy 100 MeV, the point at which the trim sextupole gradient b_3 correcting for eddy currents is the strongest $E = 200$ MeV, then $E = 2.16$ GeV when $b_3 B \rho$ in the trim sextupoles is largest; and the extraction energy 3.5 GeV. The black, blue and red curves correspond to the dynamic apertures without multipole errors, with errors measured before the magnet reassembly, and with the errors measured after the magnet reassembly respectively. The orange curve indicates the physical aperture corresponding to the vacuum chamber.

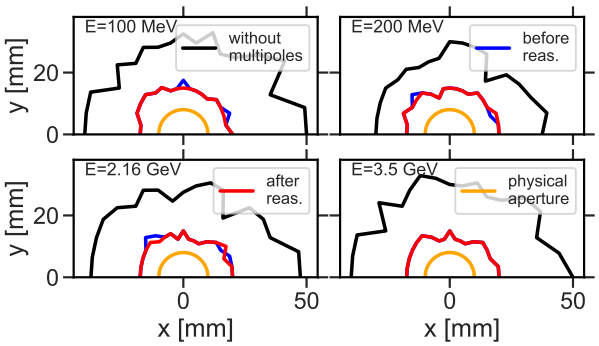

Figure 1: Dynamic aperture throughout the energy ramp. Multipole errors in quadrupoles and sextupoles added as a systematic error.

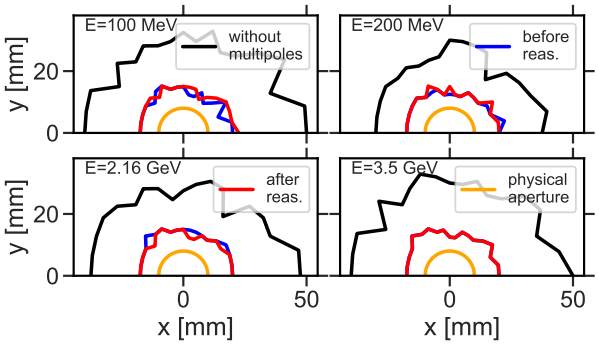

Figure 2: Dynamic aperture throughout the energy ramp. Multipole errors in quadrupoles and sextupoles added as a random error.

Similarly to Fig. 1, the black, blue and red curves in Fig. 2 represent the dynamic apertures without and with the multipoles before and after magnet reassembly. In this case, the errors are added as random components with the measured values being taken as one sigma of a normal distribution truncated at two sigmas. The results of Figs. 1 and 2 suggest that the dynamic aperture reduces when the model includes multipole errors in quadrupoles and sextupoles. However, the dynamic aperture remains larger than the physical aperture

* dmitrii.rabusov@diamond.ac.uk

Content from this work may be used under the terms of the CC BY 4.0 licence (© 2026). Any distribution of this work must maintain attribution to the author(s), title of the work, publisher, and DOI.

ISBN: 978-3-95450-252-3 ISSN: 2673-5350 doi: 10.18429/JACoW-IPAC2026-THP2017

COMPARISON OF NUMERICAL METHODS TO DETERMINE QUADRUPOLE CENTRES FOR BEAM BASED ALIGNMENT

H.-C. Chao*, R. Fielder, I. P. S. Martin, Diamond Light Source, Didcot, United Kingdom

Abstract

A beam-based alignment procedure is used to realign the beam to the centres of the quadrupoles, enabling calibration of BPM offsets. Accurately determining these quadrupole centres is an important step that requires analyzing BPM data collected while modulating the nearby quadrupole and one or more corrector magnets in the ring. In this paper, several numerical methods to extract the quadrupole centres, with or without error analysis, are presented and their results are compared. This study is based on online experiments performed at Diamond.

INTRODUCTION

During the course of a beam-based alignment (BBA) procedure in a modern circular accelerator with many BPMs, the quadrupole centre with respect to a nearby BPM (x_c) can be extracted from the orbit variations when the quadrupole strength and one or more correct magnets (CMs) are modulated. To demonstrate the principle of BBA the acquired BPM data, in the simplest form, are arranged as depicted in Figure 1.

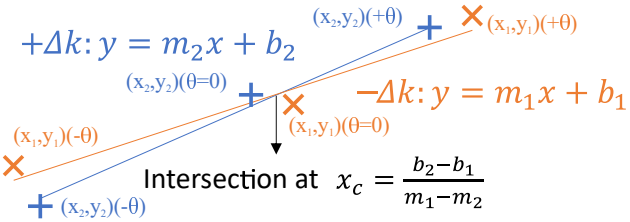

Figure 1: Schematic plot for the principle of BBA. The amplitudes of modulations of the quadrupole and CM are Δk and θ. The subscript 1 is for quadrupole modulation $-\Delta k$ and 2 for $+\Delta k$. The horizontal coordinate is the readout of the target BPM, and the vertical coordinate stands for the readout from one of the other BPMs.

The quadrupole centre with respect to the target BPM seen by the other BPM is given by the intersection coordinate, which can be calculated by the ratio of the difference of two linear fitting coefficients $x_c = (b_2 - b_1)/(m_1 - m_2)$. The absolute uncertainty is defined $u_c \equiv \delta x_c = |x_c| \cdot ru_c$, where the relative uncertainty can be derived by propagating the uncertainties from linear fitting.

$$ru_c \equiv \sqrt{\left(\frac{\delta x_c}{x_c}\right)^2} = \sqrt{\frac{\delta b_1^2 + \delta b_2^2}{(b_2 - b_1)^2} + \frac{\delta m_1^2 + \delta m_2^2}{(m_1 - m_2)^2}}$$

* hung-chun.chao@diamond.ac.uk

FINDING QUADRUPOLE CENTRE

A global quantity can be extracted to represent the ensemble quadrupole centre from information of all BPM data, as each BPM observes the quadrupole centre differently (x_{ci}) with its own uncertainty (u_{ci}). The index i goes through all the BPMs except the target BPM. When more than one CM are varied [1], another index j which stands for the index of modulating CM is added. In this section we will review the legacy methods which are normally used in our current control room and present several alternative approaches.

Legacy Method

In the legacy method only one CM is varied. The approximated location of quadrupole centre $\bar{x}_{ci}$ is the x-intercept of the linear fitting lines of $y_2 - y_1$ vs. $(x_1 + x_2)/2$. The following series of data processes are then applied before taking average of $\bar{x}_{ci}$ as the quadrupole centre.

1. Remove those $\bar{x}_{ci}$ where the fitting residual falls outside of 20 times of the BPM resolution.
2. Remove those $\bar{x}_{ci}$ where the fitting slope is smaller than 0.25 times the max fitting slope.
3. From the remaining $\bar{x}_{ci}$ remove outliers which falls outside of 1 standard deviation range.

The parameters used in these filtering criteria are empirical and not always universal. An alternative legacy method [2] is to find the waist from a quadratic fit of a global merit function $\sum_{BPM}(y_2 - y_1)^2$ vs. $(x_1 + x_2)/2$.

Figure 2 shows an example of the raw data from all BPMs from a BBA measurement, in which the most effective for the target BPM is varied. In this example a strong nonlinear response in the horizontal axis is observed when varying the quadrupole. This nonlinearity may systematically degrade the accuracy of the approximated solution $\bar{x}_{ci}$. Therefore, the direct solution x_{ci} should be used instead.

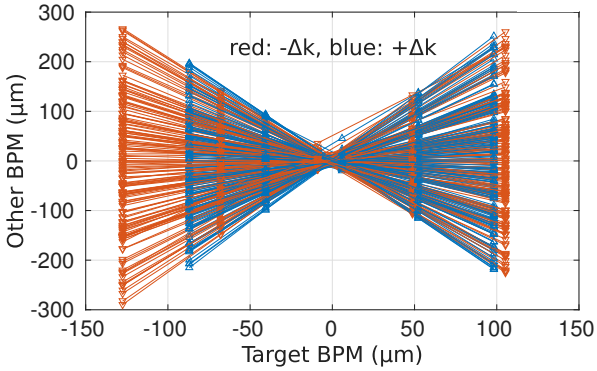

Figure 2: Raw data for the BBA. This measurement is taken from a horizontal BBA on Quadrupole (2, 2) at Diamond.

Content from this work may be used under the terms of the CC BY 4.0 licence (© 2026). Any distribution of this work must maintain attribution to the author(s), title of the work, publisher, and DOI.

ISBN: 978-3-95450-252-3 ISSN: 2673-5350 doi: 10.18429/JACoW-IPAC2026-THP2018

PERIODIC TRANSIENT BEAM LOADING INSTABILITY IN DIAMOND-II

D. Rabusov*, I. P. S. Martin, N. Blaskovic Kraljevic, R. T. Fielder
Diamond Light Source, Oxfordshire, UK

Abstract

This work demonstrates that periodic transient beam loading can affect bunch lengthening throughout the fill patterns as well as cause its time-dependent variation over dozens of synchrotron periods in Diamond-II. The instability can be eliminated by increasing the detuning of the harmonic cavity. The results suggest that introducing longer gaps in the filling pattern might eliminate the instability, but this will reduce the effectiveness of the passive harmonic cavity. Next, this study explores the option of creating a charge variation within the train of the hybrid-fill pattern. This technique can help to flatten the bunch-length variation as well as increase the bunch length in the timing bunch. Finally, the bunch-compression regime was explored using the standard-fill pattern without collective effects. It was found that the harmonic cavity can be detuned such that it shortens bunches instead of elongating them.

INTRODUCTION

As shown in Ref. [1], the periodic transient beam-loading (PTBL) instability might occur when R/Q of the harmonic cavity is not small enough or when the tuning angle is not optimal. Since the harmonic cavity for Diamond-II has been chosen to be superconducting [2], the Q-factor is relatively high (2e8) providing Robinson stability. However, efforts to maximise bunch lengthening increase the risk of the periodic transient beam-loading instability.

The simulation model is implemented in Elegant including the one-turn map, two *RFMODE* elements representing the main and harmonic cavities, and synchrotron radiation. Higher-order modes from the main cavity and longitudinal long-range wakes (both resistive wall and geometric components) are used as the impedance sources in the model. In most of the cases, a beam with 1000 particles per bunch is used. In this work, the case of insertion devices with minimum gaps (IDs closed) was chosen as the reference.

STANDARD-FILL PATTERN

In Diamond-II, the standard-fill pattern is composed of 5 trains, the first four consist of 180 bunches and the last one consists of 179 bunches. The bunch trains are separated by 7-bucket gaps. The nominal bunch length in the case of the standard-fill pattern at 300 mA is $\langle \sigma_t \rangle \approx 45$ ps. A developing PTBL in the standard-fill pattern can be observed in Fig. 1, which shows a snapshot of the bunch length throughout the beam distribution at the last turn of the simulation. Blue and red dots show the bunch length at the nominal 300 mA and when the beam current is increased up to 350 mA respectively. A strong asymmetry in the fill pattern indicates an onset of the instability at 350 mA. However, PTBL is a dynamic effect, thus this snapshot is not enough to characterise the instability.

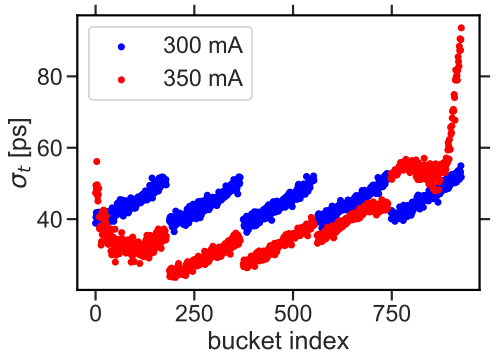

Figure 1: The bunch length throughout the standard-fill pattern at the 50000-th turn at the nominal parameters of the harmonic cavity.

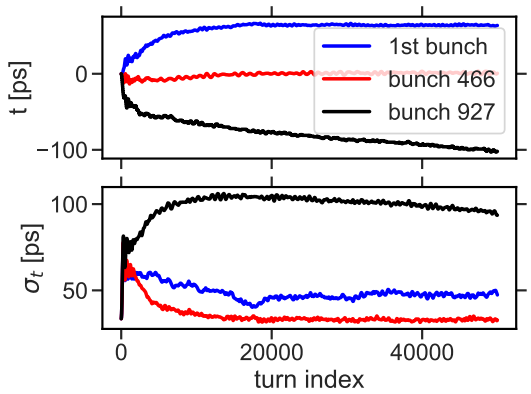

Figure 2: Synchronous time and bunch length of three selected bunches in the standard pattern at 350 mA.

Figure 2 demonstrates how the synchronous time and the bunch lengths vary from their nominal values, indicating that the beam is longitudinally unstable at 350 mA. The results were compared to the simulations with the uniform-fill pattern which was found to be stable at 300 mA and unstable at 350 mA. The results suggest that introducing relatively short gaps in the fill pattern is not sufficient to eliminate the PTBL instability.

Though the nominal current of Diamond-II is 300 mA, it is beneficial to provide strategies to increase the beam-loading safety margin by ensuring stability at 350 mA. Since the shunt impedance and the quality factor of the harmonic cavity are fixed, the only adjustable parameter is the tuning angle. The nominal value of the harmonic-cavity detuning is 57 kHz. PTBL is a dynamic effect, therefore the metric

* dmitrii.rabusov@diamond.ac.uk

Content from this work may be used under the terms of the CC BY 4.0 licence (© 2026). Any distribution of this work must maintain attribution to the author(s), title of the work, publisher, and DOI.

ISBN: 978-3-95450-252-3 ISSN: 2673-5350 doi: 10.18429/JACoW-IPAC2026-THP2019

TESTING OF A PROTOTYPE STRIPLINE KICKER FOR DIAMOND-II

R. Fielder*, A. Amiri, I. Martin, A. Morgan, D. Rabusov, N. Vitoratou
Diamond Light Source, Oxfordshire, UK

Abstract

Diamond-II will use fast stripline kickers for transparent single bunch injection during top-up operations. A prototype stripline and pulser have been developed and have undergone evaluation in the existing Diamond accelerator. Two types of feedthrough connector have been tested, and suitable cables and attenuators have been identified. We present results from an array of checks for the stripline assembly both in isolation and installed in the accelerator with beam. This includes impedance analysis and other effects on electron beam dynamics, as well as analysis of kick strength and timing.

INTRODUCTION

Diamond-II [1] is the upcoming upgrade to the Diamond synchrotron light source. Diamond currently uses a standard four kicker bump for injection, including in top-up mode during user operations, but despite effort to reduce disturbance to the stored beam [2] there is significant impact visible to some beamlines. Diamond-II will instead use six fast stripline kickers [3] to kick only a single bunch during top-up operation. The kick-and-cancel injection scheme [4] uses two kicks spaced a few turns apart to kick the injected bunch inside the dynamic aperture while putting the stored beam back on axis. This significantly reduces the impact of collective effects as well as further reducing the effect on brightness for beamlines compared to aperture-sharing.

A prototype stripline and pulser have been tested at Diamond to prove the feasibility of this kick-and-cancel scheme. The stripline was first connected to a test bench for electrical testing, and then to a pulser providing lower voltage (5.3 kV) than the final design (21 kV). It was then installed in the booster-to-storage (BTS) transfer line using the same pulser for testing with single-pass beam. Finally, the stripline was installed in the storage ring with a fully capable pulser to test the effectiveness of the kick-and-cancel scheme, as well as for investigations into impedance and beam heating effects.

Due to the smaller apertures required for Diamond-II compared to the existing storage ring, the prototype stripline was installed in a vertical orientation and designed with a slightly larger aperture than the Diamond-II striplines to avoid interfering with injection.

INITIAL HARDWARE TESTS

S-parameter measurements were taken, comparing output signal from the four ports for a given input signal at one port. Figure 1 shows simulated and measured reflections back to the input port. The simulation uses a model with no cables and perfect 50 Ω matching, while measurements are shown for the prototype including feedthroughs, and with long cables in addition. There is generally a good match between model and measurement, with the larger amplitude of the dip around 0.9 GHz likely due to the feedthroughs not being perfectly matched. The cables introduce additional noise, especially around the 1 GHz region.

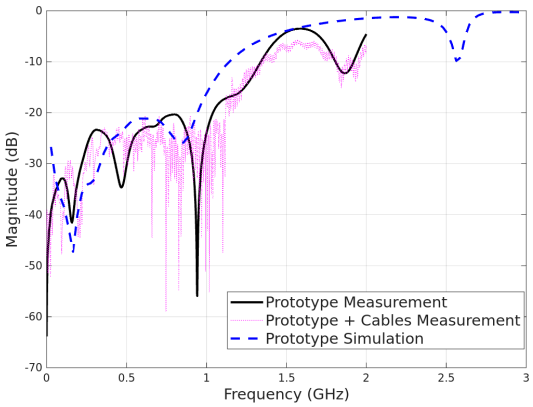

Figure 1: Comparison of simulated and measured reflections in the prototype stripline.

TESTING WITH BEAM IN TRANSFER LINE

The stripline was installed near the beginning of the BTS transfer line in March 2025, as shown in Fig. 2. The pulser and cabling were inside the tunnel nearby to the stripline. An OTR fluorescent screen just under 3 m downstream was used to measure the position of the beam. Since the kick is intended to affect only a single bunch, the injector was operated in single bunch mode for these tests, since a multibunch train of 120 bunches would drown out the target signal. Timing was scanned to obtain the maximum deflection to the bunch. A kick of 65 μrad vertical kick was found, compared to 54 μrad predicted using a simple parallel-plate model.

TESTING IN STORAGE RING

Beam Induced Heating

The stripline was moved to straight 19 of the storage ring in June 2025, upstream of the insertion device (ID) already installed. Cables about 20 m long were run outside the tunnel to avoid radiation damage to the pulser and electronics. Initially the pulser was not connected and all four ports were connected to 100 W attenuators. Thermocouples were attached at various positions externally to monitor temperatures, including on the ports and flanges. Stored current was gradually increased in 75 mA steps and temperatures left to stabilise for about 1.5 hours at each step. Temperature at the

* richard.fielder@diamond.ac.uk

Content from this work may be used under the terms of the CC BY 4.0 licence (© 2026). Any distribution of this work must maintain attribution to the author(s), title of the work, publisher, and DOI.

ISBN: 978-3-95450-252-3 ISSN: 2673-5350 doi: 10.18429/JACoW-IPAC2026-THP2020

OPERATION AND DEVELOPMENTS AT THE ESRF-EBS LIGHT SOURCE

J. L. Revol, K. Andre, C. Benabderrahmane, O. Benezech, P. Borowiec, L. Bortot, N. Carmignani, L. Carver, A. D'Elia, M.Dubrulle, F. Ewald, P Falaise, L. Hardy, G. Le Bec, B. Joly, I Leconte, S. M. Liuzzo, M. Morati, M. Penot, T. Perron, Q. Qin, Z. Qiu, B. Roche, A. Sauret, K. B. Scheidt, V. Serrière, R. Versteegen, J Wade, S. White,
European Synchrotron Radiation Facility, Grenoble, France

Abstract

The European Synchrotron Radiation Facility – Extremely Brilliant Source (ESRF-EBS) represents a major upgrade that enables the scientific community to benefit from the first high-energy fourth-generation storage-ring light source. In December 2018, following three decades of operation, user activities were suspended for a 12-month shutdown to allow the installation of a completely new storage ring. On 25 August 2020, the user program resumed with beam parameters close to nominal values. Since then, the facility has returned to full operational performance, demonstrating excellent reliability.

This paper presents the operational performance of the source over the past year, with particular emphasis on ongoing and planned developments. Current projects aimed at upgrading the injector are also described, including the proposal of a full-energy linear accelerator.

INTRODUCTION

The European Synchrotron Radiation Facility (ESRF), located in Grenoble, France, is a research infrastructure supported by a consortium of 19 partner countries. Since the start of user operation in 1994 [1-3], the facility has provided approximately 5,500 hours of beam time annually from up to 49 beamlines. The accelerator complex comprises a 200 MeV linear accelerator (linac), a 4 Hz full-energy booster synchrotron, and a 6 GeV storage ring (SR) with a circumference of 844 m. The ESRF upgrade programme (2015–2022) involved the design and installation of a new storage ring based on a hybrid multi-bend achromat (HMBA) lattice, replacing the former double-bend achromat configuration [4-9]. This upgrade reduced the horizontal emittance from 4 nm.rad to 133 pm.rad (see Table 1), resulting in a dramatic increase in beam brilliance and transverse coherence.

A wide range of insertion devices —including in-air, in-vacuum, and cryogenic in-vacuum undulators, and wigglers [10] —are installed along the 28 available straight sections (33 beamlines). In addition, radiation from bending magnets, now generated by short bending-magnets and wigglers, serves 16 beamlines.

Started in 2015, the project was conducted in four years with one year downtime for installation. The beam has been back for the users since August 2020 at full operation with an excellent reliability [11-13]. The renewal of the infrastructure and the construction of the new storage ring provided the opportunity to significantly reduce the energy consumption [14].

Table 1: Main Parameters of the Old and New SR

	Units	ESRF	ESRF-EBS
Energy	GeV	6	6
Circumference	m	844.4	844
Lattice		DBA	HMBA
Current	mA	200	200
Lifetime	h	50	23
Emittance H	pm.rad	4000	133
Emittance V	pm.rad	4	10*

(*) Vertical emittance increased from 1 to 10 pm.rad

USER-MODE OPERATION

The reliability of the new accelerator complex is comparable to that of the previous machine in 2018 (see Table 2). In 2025, a total of 5431 hours of beam were delivered to users out of 5489 hours initially scheduled, corresponding to an availability of 98.95% (Fig. 1). Notably, the operational period included eleven one-week intervals without any recorded failures.

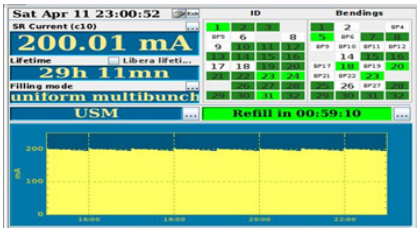

Figure 1: Delivery in April 2026.

Two significant events occurred in 2025. In February, one of the two dipole power supplies of the ramped injector power supply of the booster magnets was damaged and subsequently replaced with a spare unit. During the intervention, the impact on users remained minimal, as the beam current decayed smoothly over a period of 30 hours without any failures. The repair of the H-bridge cabinet took five months before full operational status was restored. On 3 September, a power outage led to an abrupt shutdown of most of the machine's equipment, with full restoration achieved after 12 hours. The root cause was identified as an animal coming into contact with the high-voltage capacitor bank of the high quality power supply system. This rare event has occurred twice in 33 years.

In addition to these events, six beam interruptions were attributed to blocked water flowmeters. These failures

Content from this work may be used under the terms of the CC BY 4.0 licence (© 2026). Any distribution of this work must maintain attribution to the author(s), title of the work, publisher, and DOI.

ISBN: 978-3-95450-252-3 ISSN: 2673-5350 doi: 10.18429/JACoW-IPAC2026-THP2023

THE COOL COPPER OPERATION LINAC DEMONSTRATOR PROJECT

S.M.Liuzzo*, C. Benabderrahmane, N. Benoist, P. Berkvens, P. Borowiec, R. Bourtembourg, T. Brochard, N. Carmignani, T. Perron, L. Carver, K. Andre, P. Colomp, A. D'Elia, M. Dubrulle, F. Ewald, L. Eybert, P. Falaise, D. Frichet, G. Giraud, C. Gonzalez Torres, G. Gatta, G. Chamblas, C. Lefevre, Y. Gouez, B. Joly, G. Le Bec, C. Maccarrone, D. Martin, M. Morati, H. Pedroso Marques, B. Pelissier, J.-L. Pons, Q. Qin, J.-L. Revol, B. Roche, T. Rozier, A. Sauret, K. Scheidt, V. Serriere, S. White, ESRF, Grenoble, France
G. Aymar, A. Dhar, A. Haase, Z. Li, S. Morton E. A. Nanni, W. H. Tan, SLAC, CA, USA
A. Latina, CERN, Geneva, Switzerland
D. Alesini, F. Cardelli, A. Giribono, C. Vaccarezza, G. J. Silvi, LNF, Frascati, Italy
M. Andorf, J. Maxson, Cornell University, Ithaca, NY, USA
P. Craievich, R. Zennaro
PSI Center for Accelerator Science and Engineering, Villigen, Switzerland

Abstract

The ESRF long term strategy for the injectors upgrade includes the possibility of a full energy 6 GeV linac. This linac is required to fit on the ESRF site leading to a maximum footprint of ~ 145 m. High gradient accelerating structure technology from SLAC was selected as the enabling technology to realize such a compact injector linac. The use of a photo electron gun will result in a small 6D beam phase space at extraction and the use of a pulse compression scheme to power SLAC structures will give a sensible cost reduction. The paper will introduce the Cool copper Operation Linac Demonstrator (COLD) project that has started at ESRF with the objective to realize a pre-injector linac and test all the enabling technologies for a high gradient cost effective, 6 GeV linac.

INTRODUCTION

The ESRF is presently considering a complete upgrade of the injectors to a full energy 6 GeV linac. This option is constrained by the limited space available (145 m). High gradient accelerating structure technologies are the only possible candidates to match this constraint. A linac injector would bring several advantages as detailed in Ref. [1]. The present ESRF storage ring (SR) injection efficiency in operation is in the range of 60-75 % depending on the filling mode (80 % is the best achieved). With the linac injector it would reach 100 % and would be transparent to users (no injection oscillations). In addition to this, the very small emittance will open the possibility of further upgrades of the EBS storage ring.

Since the ESRF does not pursue FEL applications, a full energy injector linac can profit from many simplifications, starting from the reduced repetition rate (4-10 Hz) and required beam properties (normalized emittance $\epsilon <$ 12 mm mrad). Stringent requirements are set instead on reliability and maintainability of the injector.

The full energy linac parameters are within the limits of tested or available technology. The selected charge per bunch of 0.7 nC is at the limit of Cu photo-cathode. This value is required to limit the time needed for refills starting from zero current. A smaller charge per bunch could be acceptable if a higher repetition rate is chosen (uniform filling of 992 bunches would require 30 minutes, compared to 25 minutes needed to refill the most frequent mode 7/8+1). Else, the use of higher quantum efficiency cathode (e.g., Cs_2Te) will be possible, thanks to the brazing free technology adopted for the photogun [2].

THE COLD PROJECT

The COLD project will be the first validation at full scale (high power, 2 x 1m long structures) of the high gradient structures designed by SLAC [3] operated at cryogenic temperature enabling a compact linac design. COLD will be composed of an S-band photogun and two cryomodules each hosting two SLAC C-band distributed coupling accelerating structures. The first cryomodule and structures are provided by SLAC. The second cryomodule and accelerating structures will be designed specifically for the ESRF injector purpose. The schematic layout of the installation is shown in Fig. 1. COLD will be built in the next 4-5 years with the objective of validating the key technology for a high availability user facility. In particular, the experimental goals for the demonstrator will include:

- C-band 77 K high gradient technology:
  1. Reproduce expected accelerating gradient
  2. Evaluate performance degradation and failures in the presence of breakdowns. In the case of a distributed coupling accelerating structure, previous experiments and simulations indicate that the breakdowns are limited to only one cell (over 40 in a structure). This would lead to 4 MeV less energy in case of a breakdown rather than 80 MeV.
  3. Measure dark currents [4–8] to assess radiation hazards of a full energy installation.

* simone.liuzzo@esrf.fr

Content from this work may be used under the terms of the CC BY 4.0 licence (© 2026). Any distribution of this work must maintain attribution to the author(s), title of the work, publisher, and DOI.

ISBN: 978-3-95450-252-3 ISSN: 2673-5350 doi: 10.18429/JACoW-IPAC2026-THP2024

DESIGN OF A NON-LINEAR KICKER INJECTION SCHEME FOR THE EUROPEAN SYNCHROTRON RADIATION FACILITY EXTREMELY BRILLIANT SOURCE

S. White, C. Benabderrahmane, D. Baboulin, T. Brochard, P. Brumund, L. Carver, M. Dubrulle, G. Le Bec, C. Maccarrone, M. Morati, B. Ogier, H. Pedroso Marques, A. Sauret, European Synchrotron Radiation Facility, Grenoble, France

Abstract

The European Synchrotron Radiation Facility Extremely Brilliant Source (ESRF-EBS) injection scheme consists in a classical four kickers off-axis injection. During injections, beam lines are perturbed and have to stop data acquisition. A new injection scheme using non-linear kickers was designed. The storage ring and transfer line optics and layout had to be modified to integrate the non-linear kickers in the injection cells and preserve injection efficiency in the presence of strong non-linear fields. This paper reports on the status and advancement of the project.

INTRODUCTION

The standard four kicker bump injection scheme used on the previous machine [1, 2] was adopted for the ESRF-EBS as a low risk solution for the commissioning of the new machine. This option also allowed to recuperate existing hardware from the previous machine such as the septum magnets or the kickers power supplies. 80 % injection efficiency could be achieved in user service mode (USM) with this scheme [3]. Nevertheless, the normalized residual injection perturbations are approximately an order of magnitude larger than for the previous machine due to the beam size reduction. Even though new slow kicker power supplies combined with feed-forward corrections [4] allowed for a major reduction, experiments with beam lines indicated that significant reduction would still be required to achieve transparency [5]. The present systems are now showing their limits to achieve the ultimate goal of transparent injection and alternative schemes have to be considered. Preliminary studies [6] have shown that the non-linear kicker (NLK) injection scheme [7] would provide full transparency while maintaining injection efficiency. The project is now fully integrated in the ESRF long term scientific plan (LTSP).

STORAGE RING LATTICE

In order to facilitate the design of the NLK it is desirable to increase as much as possible the horizontal acceptance at the injection point. The acceptance theoretically scales with $\sqrt{\beta}$, increasing the β-function at the injection point is therefore a natural way of increasing the horizontal acceptance. For the ESRF-EBS storage ring this is easily achieved by reducing the distance between the last 2 focusing quadrupoles on either side of the injection point. While leaving sufficient space between those 2 quadrupoles to insert the NLKs in the injection straight it was possible to increase the horizontal

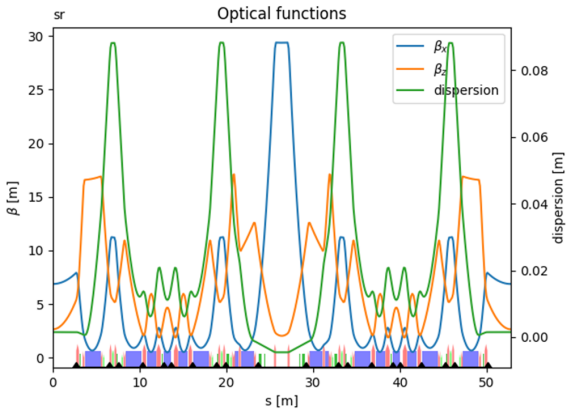

Figure 1: Optics functions of the NLK optics injections cells. The center of the straight is the injection point.

β-function from 18.6 m to 29.0 m. In order to preserve non-linear dynamics, additional constraints on the cell phase advance and twiss parameters at the sextupoles were included in the optics matching. Figure 1 shows the optics function for the 2 injection cells of the NLK lattice. The horizontal β-function reaches a maximum of 29 m at the center of the injection straight which corresponds to the injection point where the NLKs will be inserted.

Table 1 summarizes the lifetime and dynamics aperture calculations with the standard lattice and the NLK lattice. A degradation of lifetime is observed. However, non-linear optimization were not performed prior these calculations and with a transparent injection scheme lower lifetime is acceptable since more frequent injection would be feasible to maintain current stability without affecting beamlines operation. Finally, it is planned to install a fourth harmonic cavity system for bunch lengthening at the ESRF-EBS which is expected to increase the lifetime by a factor of at least 2-3 [8]. The dynamic aperture on the other hand is significantly increased as expected and should allow for a horizontal offset of the injected beam of 8 mm. This corresponds to the distance for the NLK field to reach its peak and is achievable using standard manufacturing processes as described in the following section.

NON-LINEAR KICKER AND POWER SUPPLY

The ESRF NLK design, described in Ref. [9] is based on the approach proposed in Ref. [10]. It consists of a ~30 cm ceramic body where a total of 8 copper wires a glued to form the desired field shape. The conductors are placed such that

Content from this work may be used under the terms of the CC BY 4.0 licence (© 2026). Any distribution of this work must maintain attribution to the author(s), title of the work, publisher, and DOI.

ISBN: 978-3-95450-252-3 ISSN: 2673-5350 doi: 10.18429/JACoW-IPAC2026-THP2026

HARMONIC CAVITY SIMULATIONS FOR THE ESRF

L. R. Carver*, P. Borowiec, A. D'Elia, V. Serriere, S. White,
European Synchrotron Radiation Facility, Grenoble, France

Abstract

The ESRF foresees the installation of a 4th harmonic cavity system to provide bunch lengthening in both multi-bunch filling modes and high bunch current timing modes. Here we will present simulation results of the expected machine performance.

INTRODUCTION

The ESRF-EBS is a 4th generation light source that has been in operation since 2019 with a horizontal equilibrium emittance of $\epsilon_H = 137\,\text{pm}$ [1–3]. The EBS delivers beam in a variety of different filling patterns, splitting the user service mode (USM) between high brilliance filling patterns at a total current of 200 mA (uniform or 7/8+1) or timing modes (4 bunches of 10 mA each, or 16 bunches with 92 mA total). Due to the increased charge density, the lifetime during timing mode operation is significantly reduced. This necessitates an increased vertical emittance, which reduces the transverse coherence. Uniform mode is run with $\epsilon_V = 10\,\text{pm}$ at 25 hours lifetime, 16 bunch mode has $\epsilon_V = 20\,\text{pm}$ for 4.4 hours of lifetime, and 4 bunch mode has $\epsilon_V = 40\,\text{pm}$ for 4.2 hours of lifetime. Table 1 shows the machine parameters for the EBS [4].

Table 1: EBS Machine Parameters

	Units	Value
Energy E_0	GeV	6
Circumference C	m	843.977
Harmonic Number h		992
Revolution Time T_0	μs	2.815
Max. Total Current	mA	200
Max. Single Bunch Current	mA	10
Mom. Compaction Factor α	10^{-5}	8.512
Energy Spread σ_e (@0 mA)	10^{-3}	0.9356
Bunch Length σ_z (@0 mA)	mm	2.921
Sync. Freq f_s (@0 mA)	Hz	1300.58
Energy loss per turn U_0	MeV/turn	2.5325

Harmonic cavity systems are proposed for all 4th generation light sources as a way to alleviate the reduced Touschek lifetime. The harmonic cavities are often operated as either superconducting passive cavities, or normal conducting active cavities [5, 6], although some cases of normal conducting passive cavities can be found [7]. The harmonic system will provide an additional RF voltage which will cancel the first and second derivatives of the main RF voltage at the synchronous phase, flattening the potential and elongating the bunch [8]. However, due to the reduction of the synchrotron tune that follows, beam stability issues are expected (as have been observed and simulated at other facilities) [9]. Dedicated simulations must be performed prior to the installation of a harmonic system in order to prove its feasibility.

These proceedings will first introduce the existing and planned rf installations at the ESRF, before comparing theoretical estimates with beam dynamics simulations for uniform filling mode. Finally, some simulation results in 16-bunch mode will be shown.

ESRF RF SYSTEMS

The ESRF-EBS currently operates with 13 single cell cavities at an RF frequency of 352 MHz. 3 of these cavities are powered by Solid State Amplifiers (SSA) with a maximum forward power of 150 kW, whereas the other 10 cavities are powered by a klystron. Each cavity is designed to deliver 500 kV. It is foreseen that the transmitter will be replaced by a further 10 SSAs, each one providing around 110 kW per cavity.

Table 2: Parameter list for the main and foreseen harmonic systems at the EBS. FP stands for Flat Potential.

	Units	Main	Harmonic
β		2.8	0.5-2.0
$R_{s,u}$ (total)	MΩ	70.6875	6.923
Q_0		37500	35054
N_{cav}		13	3
V_c (total)	MV	6.5	1.48 (FP)

The active harmonic cavity will operate at the 4th harmonic of the RF frequency (1.44 GHz). The cavity design itself is a single cell TM020 with both Higher and Lower Order Mode damping(HOM and LOM). The cavity is still in the design phase, with possible modifications still being possible based on the results of beam dynamics simulations and manufacturing requirements. Figure 1 shows a cutaway model of one cell of the harmonic cavity. Table 2 shows the parameters of the main and harmonic RF systems that are relevant for beam dynamics simulations.

UNIFORM MODE

In order to understand the machine performance in uniform mode, Algorithms for Longitudinal Multibunch Beam Stability (ALBuMS) [10] was used to compute growth rates of different types of instabilities for any different parameter set of main and harmonic cavities. This allowed an easy first probe into the stability region to see which types of instability will be the main limitation for the ESRF case.

* lee.carver@esrf.fr

Content from this work may be used under the terms of the CC BY 4.0 licence (© 2026). Any distribution of this work must maintain attribution to the author(s), title of the work, publisher, and DOI.

ISBN: 978-3-95450-252-3 ISSN: 2673-5350 doi: 10.18429/JACoW-IPAC2026-THP2028

SOLEIL 2025 OPERATIONAL STATUS

L. S. Nadolski*, G. Abeillé, Y.-M. Abiven, P. Alexandre, N. Béchu, F. Bouvet, T. Brioult, P. Brunelle, M.-E. Couprie, X. Delétoille, M. Diop, S. Ducourtieux, S. Duigou, A. Gamelin, V. Gubaidulin, C. Herbeaux, N. Hubert, V. Kubytskyi, M. Labat, R. Lopes, V. Le Roux, A. Loulergue, O. Marcouillé, A. Moutardier, A. Nadji, R. Nagaoka, M. Nouna, J.-B. Pruvost, F. Ribeiro, G. Schaguène, K. Tavakoli, M.-A. Tordeux, Synchrotron SOLEIL, Saint-Aubin, France

Abstract

SOLEIL, the French 2.75 GeV third-generation synchrotron light source, continues to operate as a high-performance research infrastructure serving both academic and industrial communities. This contribution reviews 2025 operational achievements, with an emphasis on accelerator stability, availability, and reliable photon-beam delivery to 29 beamlines. Key performance indicators and operational trends are presented, together with an analysis of major events and mitigation strategies implemented to improve machine robustness. Significant progress in addressing component obsolescence is reported, including advances in BPM electronics, RF systems, and the global control-system upgrade. Updates on the LINAC's modernization program are provided, along with the use of the SOLEIL accelerator as an integrated testbed to validate critical technologies for the forthcoming facility upgrade. Preparatory activities for SOLEIL II are outlined, including progress on the bunch-by-bunch transverse feedback system; development and preparation for qualification of new 352 MHz low-HOM RF cavities; the 1.4 GeV fourth-harmonic system; and upgraded control architectures, highlighting technical readiness for the next-generation machine.

SOLEIL ACCELERATOR PERFORMANCE

SOLEIL is the French third-generation synchrotron light source that has provided highly stable, brilliant photon beams to external users since 2008 (see the main parameters in Table 1 [1]). Its injector complex is based on a 110 MeV LINAC and a full-energy 3 Hz booster ring.

Table 1: Basic Parameters of the SOLEIL Storage Ring

Parameter	Value
Circumference	354.097 m
Energy	2.75 GeV
Nominal Tunes (H/V)	18.146 / 10.216
Natural Chromaticities (H/V)	−53 / −19
Operation Chromaticities (H/V)	1.0 / 2.5
Momentum Compaction	4.18×10^{-4}
RF Voltage	2.6 MV
RF Frequency	352.198 MHz
Harmonic Number	416
V/H Emittance Ratio	1 %
Total Lifetime (500 mA)	10 h

In 2025, the 19th year of accelerator operation, 4873 hours of photon beams were delivered to SOLEIL's 29 beamlines out of 4947 scheduled hours, over 34 weeks. Four top-up filling patterns were used: uniform (71 %), hybrid (23.2 %), 1 bunch (2.9 %), and 8 bunches (2.9 %). Photon-beam availability reached 98.51 % over the year, with 20 weeks above 99 % and 9 weeks at 100 %. The mean time between failures was 97 h, while the mean time to recover was 1 h 26 min (Fig. 1). Despite this strong performance, operating the SOLEIL accelerator complex remains challenging, and failures (Fig. 2) inevitably affect operation; several are summarized below.

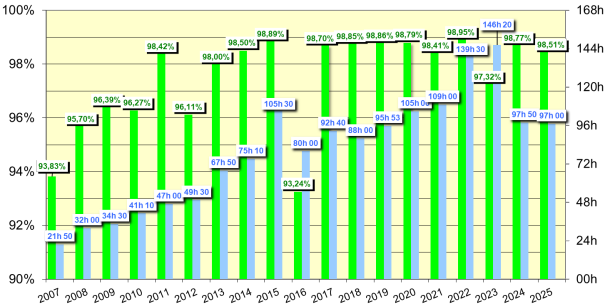

Figure 1: Beam availability (green) and mean time between failures (blue) over the years.

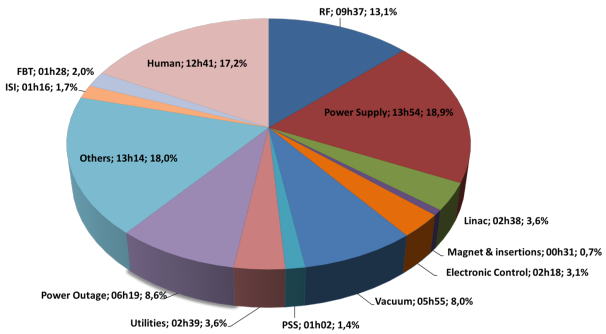

Figure 2: Distribution of beam failures per origin.

Major Incidents

During the first run of 2025, operation was severely challenged by strong degassing in the newly installed CPMU18 undulator, which led to electron-beam excitation driven by local pressure spikes. While a temporary working point was identified to maintain a maximum current of 500 mA, it required numerous titanium sublimation pump firings to lower

* laurent.nadolski@synchrotron-soleil.fr

Content from this work may be used under the terms of the CC BY 4.0 licence (© 2026). Any distribution of this work must maintain attribution to the author(s), title of the work, publisher, and DOI.

ISBN: 978-3-95450-252-3 ISSN: 2673-5350 doi: 10.18429/JACoW-IPAC2026-THP2029

TOWARDS NONLINEAR MODELING OF THE COMBINED SEXTUPOLE-CORRECTOR MAGNETS AT SOLEIL II

Z. Zhang*, A. Loulergue, F. Marteau, T. Mutin, L. S. Nadolski, V. Pinty
Synchrotron SOLEIL, Saint-Aubin, France

Abstract

The SOLEIL II sextupoles are equipped with additional windings to provide normal and skew dipole corrections. Accurate modeling of these combined-function sextupole magnets are particularly challenging due to magnetic saturation, hysteresis, and internal cross-talk between channels. Based on 3D magnetic simulations, polynomial, interpolation-based, and neural-network models were developed to reproduce the saturation and cross-talk effects. These nonlinear models were validated on the first prototype magnet, providing preliminary confirmation of their reliability and demonstrating the feasibility of implementing sextupole-corrector magnets in the SOLEIL II storage ring.

INTRODUCTION

The SOLEIL II project is an upgrade of the SOLEIL synchrotron light source based on the design of a new storage ring with compact, high-gradient magnetic elements [1–7]. In this context, sextupoles are equipped with additional windings for orbit correction. These magnets feature three independent control channels, corresponding to the main sextupole current I_{sx}, the horizontal corrector current I_{ch}, and the vertical corrector current I_{cv}. Their combination enables the generation of specific multipole components, namely a skew dipole a_1, a normal dipole b_1, and a normal sextupole b_3.

Accurate nonlinear modeling of these magnets is essential for the reliable control of both the main and corrector power supplies in storage ring operation. To define the required modeling precision, the impact of sextupole field errors on the dynamic aperture (DA) and the Touschek lifetime was evaluated using random field perturbations applied to all sextupoles in the SOLEIL II lattice. Based on the results summarized in Table 1, a preliminary target relative error (RE) for the sextupole field is set to within ±0.1 %. In addition, considering the impact of corrector errors on the orbit feedback system, the allowable absolute error (AE) of the corrector kick is typically limited to 1 µrad.

Table 1: Sextupole Field Error Impact

SX Strength max. RE	**±0.1 %**	**±0.5 %**
Relative DA impact	Marginal	Weak
Relative Touschek lifetime drop	~−4 %	~−20 %

Twelve types of combined-function sextupole magnets have been designed for SOLEIL II [8, 9]. Nonlinear modeling was first performed on a standard sextupole (length: 90 mm, diameter: 16 mm, gap: 6.2 mm). Based on 3D magnetic simulations using Opera/Tosca [10], the magnetic saturation becomes evident when the main current exceeds 40 A, as shown in Fig. 1. Furthermore, due to internal cross-talk with the dipole correction channels, the integrated sextupole strength at maximum current (50 A) is reduced by approximately 5 %, as illustrated in Fig. 2.

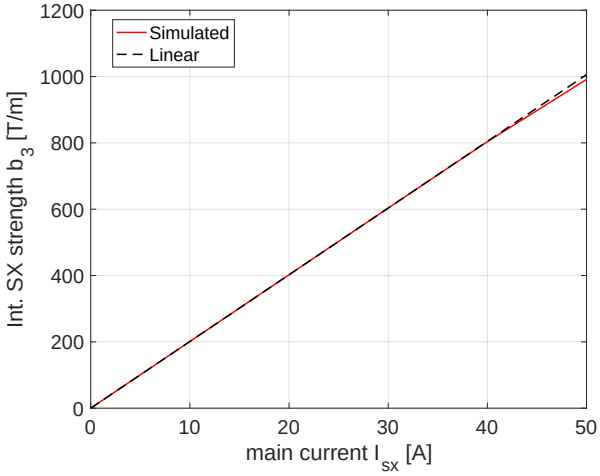

Figure 1: Integrated sextupole strength versus main current, with horizontal and vertical corrector currents set to zero.

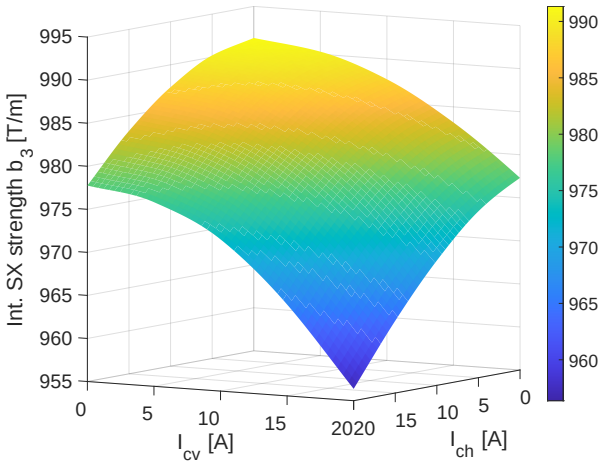

Figure 2: Integrated sextupole strength at a main current of 50 A versus horizontal and vertical corrector currents.

At this preliminary stage, hysteresis effects are not yet considered. The nonlinear modeling of saturation and cross-talk effects in the combined sextupole-corrector magnets is performed using three types of models: polynomial, interpolation-based, and neural-network models. These models are described and compared in this paper, followed by validation against measurements on the first prototype.

* zhandong.zhang@synchrotron-soleil.fr

Content from this work may be used under the terms of the CC BY 4.0 licence (© 2026). Any distribution of this work must maintain attribution to the author(s), title of the work, publisher, and DOI.

ISBN: 978-3-95450-252-3 ISSN: 2673-5350 doi: 10.18429/JACoW-IPAC2026-THP2030

PRELIMINARY STUDIES ON THE INSERTION DEVICE COMPENSATION SCHEME FOR SOLEIL II

Z. Zhang*, P. Brunelle, V. Gubaidulin, S. Habet, Y. Huang[1], A. Loulergue, O. Marcouillé, L. S. Nadolski, M. Valléau, Synchrotron SOLEIL, Saint-Aubin, France
[1]also at University of Science and Technology of China, Hefei, China

Abstract

A substantial fraction of the insertion devices (IDs) installed in SOLEIL will remain in operation during the first phase of the SOLEIL II project. Studies of their impact on the upgraded lattice have been initiated in order to define the preliminary technical requirements for compensation. In this paper, the ID-induced focusing and coupling effects are characterized, followed by investigations of both Linear Optics from Closed Orbit (LOCO) and local feedforward correction schemes. Closed-orbit correction studies are performed based on measurements of the distortions generated by existing IDs on the SOLEIL storage ring and their transfer to the SOLEIL II lattice.

INTRODUCTION

SOLEIL is the French third-generation synchrotron light source, routinely operated for external users since 2008 with twenty ID beamlines [1]. The storage ring of its upgrade project, SOLEIL II, features a lattice composed of alternating 7BA and 4BA high-order achromat cells, providing an ultra-low natural horizontal emittance of about 90 pm rad at a beam energy of 2.75 GeV [2–7]. Such performance is achieved through strong transverse focusing and large bending radii in the dipole magnets, which help suppress dispersion in the arcs. As a consequence, the nonlinear beam dynamics becomes more sensitive to ID perturbations. Therefore, in addition to the closed-orbit feedforward compensation already implemented at SOLEIL [8], dedicated compensation schemes for ID-induced focusing and coupling effects will also be required for SOLEIL II, as already investigated at several other facilities [9–11].

The main parameters of the SOLEIL II bare lattice are summarized in Table 1. The Touschek lifetime was calculated for a total beam current of 500 mA distributed over 416 bunches, assuming a zero-current bunch length of 2.71 mm and an emittance ratio of 30 % [12,13]. The lattice accommodates nineteen IDs foreseen for the first and second phases of SOLEIL II [14,15]. The Phase 1 IDs include six In-Vacuum Undulators (IVUs), one In-Vacuum Wiggler (IVW), three Cryogenic Permanent Magnet Undulators (CPMUs), eight Elliptically Polarized Undulators (EPUs), generically referred to as Helical Undulators (HUs) of APPLE-II type, and one long Adjustable Phase Undulator (APU). Sixteen of these devices are currently operated in SOLEIL and are expected to operate at smaller minimum gaps in SOLEIL II.

Table 1: Main Parameters of the SOLEIL II Bare Lattice

Parameter	Value
Beam energy [GeV]	2.75
Circumference [m]	353.98
Natural emittance [pm rad]	90.5
Betatron tune ν_x / ν_y	54.2016 / 18.3011
Chromaticity Q'_x / Q'_y	1.8 / 1.4
Bunch length [mm][a]	2.71
ID capacity	19
Touschek lifetime [h][b]	3.5

[a] at zero current
[b] calculated without bunch lengthening

To define the technical requirements for ID compensation of SOLEIL II, preliminary studies of ID effects on the upgraded lattice have been initiated. Second-order kick maps of the IDs were calculated using the code `RADIA` [16] and then implemented into the bare lattice to evaluate their linear and nonlinear effects with the `Accelerator Toolbox (AT)` [17–19]. The impact on the on-momentum dynamic aperture was found to remain acceptable, whereas the Touschek lifetime was significantly reduced [5]. As a first step, the LOCO algorithm [20] was applied to assess the potential recovery of the Touschek lifetime in the presence of IDs. This paper presents updated ID-induced focusing and coupling effects and their global LOCO correction based on the latest version of the SOLEIL II lattice, together with a local correction scheme considered more practical for feedforward compensation. Closed-orbit distortions induced by the IDs are also investigated, starting from measurements performed on the existing SOLEIL storage ring and followed by an analysis of their impact on the SOLEIL II lattice.

FOCUSING AND COUPLING EFFECTS

Characteristics of Phase 1 IDs

At the current stage, among the three IDs whose designs differ from those of SOLEIL, only the kick map of the newly designed 5-meter-long APU (APU250) has been updated in the simulations. The kick maps of all other IDs are still based on existing SOLEIL devices, but with smaller minimum gaps to better reproduce the expected operating conditions of Phase 1 of SOLEIL II. For each helical-type undulator, four polarization modes are investigated, namely linear tilted (LT), linear horizontal (LH), linear vertical (LV), and circular (CR) modes.

Assuming a worst-case scenario in which all IDs operate at their minimum gaps and all helical-type undulators are

* zhandong.zhang@synchrotron-soleil.fr

Content from this work may be used under the terms of the CC BY 4.0 licence (© 2026). Any distribution of this work must maintain attribution to the author(s), title of the work, publisher, and DOI.

ISBN: 978-3-95450-252-3 ISSN: 2673-5350 doi: 10.18429/JACoW-IPAC2026-THP2033

DESIGNING RADIATION PROTECTION FOR PETRA IV: CONCEPTS AND CHALLENGES

E. Panofski*, W. Clement, A. Leuschner, T. T. Liang, S. Zander,
Deutsches Elektronen-Synchrotron DESY, Hamburg, Germany

Abstract

DESY, an international accelerator research center, builds on over six decades of experience in the design, construction, and operation of world-class user facilities. The upcoming PETRA IV project represents a major upgrade from PETRA III into a 4th generation light source, involving a complete rebuild of the accelerator and a full redesign of its radiation-protection systems. This upgrade requires advanced shielding calculations and designs for both the accelerator and new buildings, in particular the new user hall, a state-of-the-art personnel safety system, and safety processes fully aligned with current laws and standards. In addition, advanced radiation-detection systems are being developed to ensure continuous monitoring of beam operation. This contribution provides an overview of the initial concepts for PETRA IV's radiation-protection strategy, highlighting key design challenges, safety innovations, and implementation considerations for a modern, high-performance synchrotron facility.

PETRA IV UPGRADE OVERVIEW

The PETRA IV project at DESY represents the upgrade of the existing PETRA III storage ring into a fourth-generation, ultra-low-emittance synchrotron light source based on a multi-bend achromat lattice, aiming at a substantial increase in brilliance and coherence of the photon beam [1]. The upgrade involves the complete replacement of the storage ring, while large parts of the existing tunnel infrastructure and experimental areas are retained (see Fig. 1). The new machine is designed to deliver up to three orders of magnitude higher photon beam brilliance (see Fig. 2), enabling advanced applications such as high-resolution and time-resolved X-ray microscopy [2].

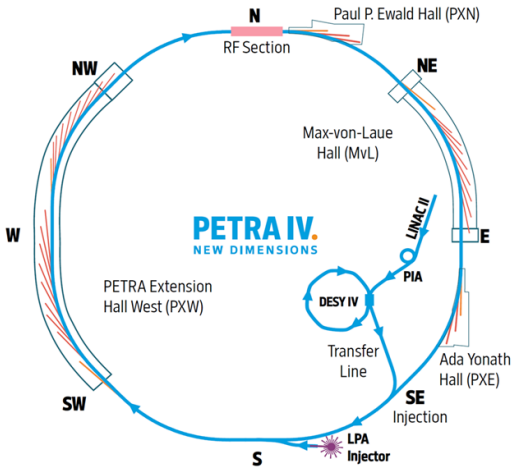

Figure 1: Layout of the future PETRA IV facility.

This performance increase is achieved, among other factors, through a significantly revised magnet lattice, including the use of several thousand permanent bending dipole magnets, allowing for a more compact and stable beam optics. As a result, the emitted X-ray radiation is substantially more focused and coherent compared to PETRA III. However, the changes in beam dynamics also result in a reduction in the beam life-time and a corresponding increase in beam losses during operation.

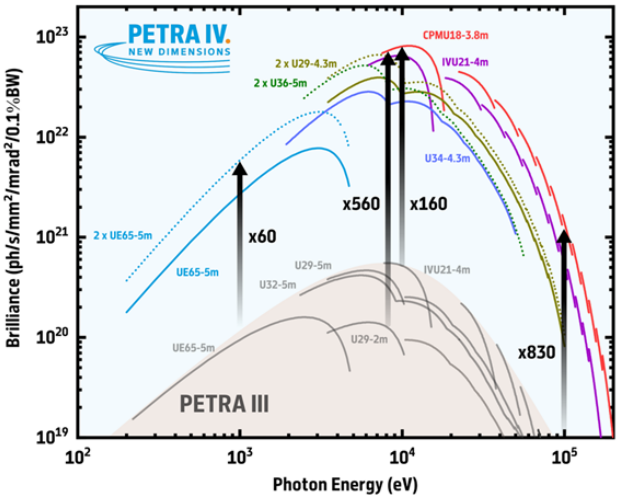

Figure 2: Spectral brightness for PETRA IV in comparison with PETRA III depending on the undulator type.

The configuration of the injector chain is currently subject to ongoing design studies. Established pre-accelerator systems, such as LINAC II and a booster synchrotron DESY IV, are considered as baseline options with largely unchanged primary operating parameters. In addition, an advanced injector concept, i.e. laser-plasma acceleration, are being evaluated as a potential future alternative.

In addition to the accelerator upgrade, a new experimental hall (PETRA West, PXW) will be constructed to host a large number of beamlines and experimental stations. The hall extends over a length of approximately 600 m and will accommodate 18 additional beamlines with roughly 40 experimental and optics hutches. It is partially located underground and extends into areas with public access above ground, imposing strict constraints on radiation shielding design.

Consequently, the radiation-protection concept for PETRA IV must combine advanced shielding methodologies, modern safety system architectures, and full compliance with current regulatory requirements.

* eva.panofski@desy.de

Content from this work may be used under the terms of the CC BY 4.0 licence (© 2026). Any distribution of this work must maintain attribution to the author(s), title of the work, publisher, and DOI.

ISBN: 978-3-95450-252-3 ISSN: 2673-5350 doi: 10.18429/JACoW-IPAC2026-THP2035

SIMULATED COMMISSIONING AND LATTICE ROBUSTNESS STUDIES FOR BESSY III*

B. Alberdi-Esuain†, M. Abo-Bakr, P. Goslawski, S. Joly, J. Voelker
Helmholtz-Zentrum Berlin für Materialien und Energie, Berlin, Germany

Abstract

BESSY III will be a fourth-generation synchrotron light source that aims to deliver diffraction-limited, extremely brilliant soft X-rays, with the goal of becoming a key instrument for discoveries in materials and energy research. During the current design phase, extensive simulation studies are being performed to evaluate and improve the robustness and reliability of the candidate storage ring lattice.

The robustness analysis allows a direct comparison of the expected lattice performance and sensitivity with that of other fourth-generation facilities under realistic error conditions. Building on this, the simulated commissioning process aims to recover optimal machine performance by mitigating the impact of imperfections originating from magnet misalignments and magnetic field errors. This work quantifies the achievable performance of the machine by simulating the full commissioning sequence, including beam-transmission optimisation, sextupole ramp-up, RF-cavity correction, beam-based alignment (BBA), orbit correction, and LOCO-based optics correction. After carrying out the lattice correction, the off-axis injection possibility and the Touschek lifetime are evaluated.

Although the preliminary results provide essential feedback for defining the commissioning strategy and enhancing the overall resilience of the BESSY III lattice design, they do not yet include the complete error set.

INTRODUCTION

BESSY III will be a fourth-generation light source (4GLS) storage ring. It is currently being designed at Helmholtz-Zentrum Berlin. Like other ultralow-emittance rings, its strong focusing optics make it inherently sensitive to magnetic misalignments and field errors, making a detailed commissioning simulation essential during the design phase. This work builds on methods developed for similar facilities [1–4], extending them to the specific BESSY III lattice and error model.

The design energy of the storage ring is 2.5 GeV, with a target emittance of 98 pm-rad. The ring consists of 16 periodic arcs and an injection straight section. It contains 192 BPMs, 144 units of each vertical and horizontal corrector magnets, and skew quadrupole components added to selected sextupoles for coupling correction. The linear optics and the lattice layout for one of the 16 identical arcs of the BESSY III lattice can be seen in Fig. 1.

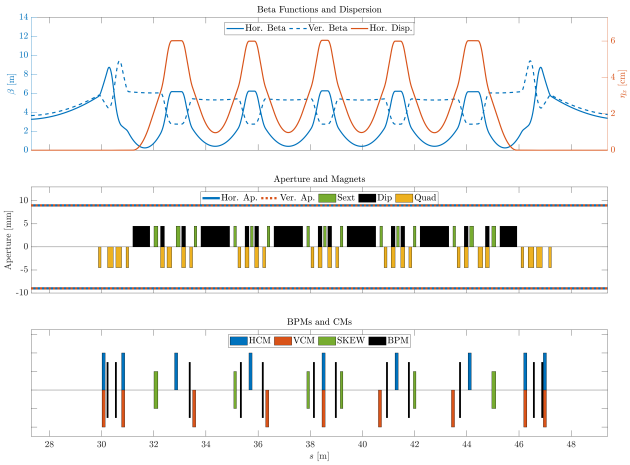

Figure 1: Optics and lattice layout of a BESSY III arc.

ERROR MODEL

The tolerance set employed in this study is divided into four groups: magnet errors, BPM diagnostic errors, RF cavity errors, and injection errors. Key RMS values are listed in Tables 1, 2, and 3.

Table 1: Magnet errors.

Error type	RMS value
Offset (x, y, z)	30 µm
Roll for long bends	180 µrad (z), 60 µrad (x,y)
Roll for short magnets	180 µrad (z), 400 µrad (x,y)
Calibration (steering magnets)	5%
Calibration (all other magnets)	0.1‰

Table 2: BPM and RF cavity errors.

Error type	RMS value	Error type	RMS value
BPM offset	500 µm	BPM noise (CO)	1 µm
BPM roll	180 µrad	RF frequency error	100 Hz
BPM calibration	5%	RF voltage error	5 kV
BPM noise (TbT)	10 µm	RF phase error	90°

Table 3: Injection errors.

Coordinate	x	x'	y	y'	δp	Phase
Units	µm	µrad	µm	µrad	‰	°
Systematic	100	10	100	10	1	0
Random	0	10	0	0	0.1	0.1

All the errors in this study have been truncated at 2σ. Girder and support structure errors are not included because the final girder layout has not been decided yet. Therefore, misalignment errors for both magnets and BPMs are referred

* Yes
† benat.alberdi_esuain@helmholtz-berlin.de

Content from this work may be used under the terms of the CC BY 4.0 licence (© 2026). Any distribution of this work must maintain attribution to the author(s), title of the work, publisher, and DOI.

ISBN: 978-3-95450-252-3 ISSN: 2673-5350 doi: 10.18429/JACoW-IPAC2026-THP2036

ECHO-ENABLED HARMONIC GENERATION AT ELECTRON STORAGE RINGS*

S. Khan†, B. Büsing, C. Mai, A. Radha Krishnan, Z. Usfoor, V. Vijayan
Department of Physics and Center for Synchrotron Radiation (DELTA),
TU Dortmund University, Dortmund, Germany
W. Salah, Department of Physics, The Hashemite University, Zarqa, Jordan

Abstract

Echo-enabled harmonic generation (EEHG) has been proposed as a seeding method for free-electron lasers but can also be employed to generate ultrashort radiation pulses at electron storage rings. Due to the interaction of electrons with femtosecond laser pulses in two undulators (”modulators”), each followed by a magnetic chicane, a longitudinal phase space structure with high harmonic content is produced, which gives rise to coherent emission of radiation at harmonics of the laser wavelength. The length of the coherently emitted pulses in a third undulator (”radiator”) is given by the laser pulse duration. Thus, EEHG pulses can be three orders of magnitude shorter but still more intense than conventional synchrotron light pulses. The latest results of the worldwide first EEHG demonstration experiment at a storage ring (DELTA at the TU Dortmund University) are presented.

INTRODUCTION

Electron storage rings producing synchrotron radiation (SR) in the ultraviolet to X-ray range are standard tools in physics, materials research, chemistry, and biology to study the structure of matter on the atomic scale [1]. Significant progress has recently been made in reducing the beam emittance. The pulse duration, however, is still several tens of picoseconds, while dynamical changes of atoms and molecules such as phase transitions, chemical reactions, lattice vibrations etc. are on the sub-picosecond scale. Femtosecond time resolution at small wavelengths is obtained by laser-based plasma sources and high-harmonic generation, and more recently by high-gain free-electron lasers (FELs) [2]. While around 10 FELs worldwide serve one user at a time with the bunch rate of a linear accelerator, there are about 50 SR sources [3] supplying multiple beamlines simultaneously with stable and tunable radiation at a rate of up to 500 MHz. It is therefore worthwhile to consider methods to improve the time resolution for experiments at storage rings.

Instead of shortening the electron bunches in SR facilities, a pulse duration below 100 fs may be obtained from a ”slice” within a long bunch interacting with a femtosecond laser pulse in an undulator (”modulator”) and causing a periodic modulation of the electron energy. When off-energy electrons are transversely displaced by dispersion, their SR from a second undulator (”radiator”) can be extracted using an aperture [4–6]. The ratio of electrons in the slice and the bunch is $\approx 10^{-3}$, and the fraction of incoherent SR in the short pulse is even lower.

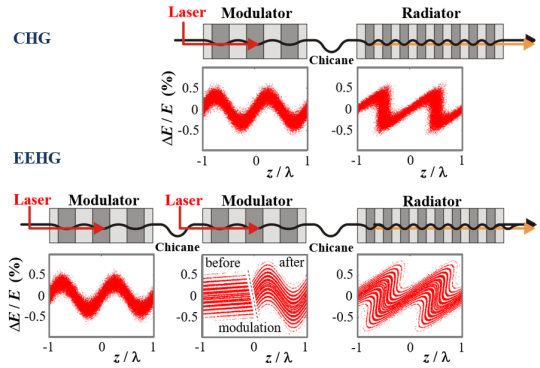

Figure 1: Layout of the CHG and EEHG setup and respective distributions of electrons in phase space (relative energy offset $\Delta E/E$ versus longitudinal position z in units of λ_L).

Coherent emission at harmonics of the laser wavelength λ_L is obtained when the laser-induced energy modulation is converted to a periodic density pattern by a dispersive section (”chicane”). The SR intensity from the short slice is then proportional to the square of the number of electrons and the squared bunching factor b_h^2. Thus, radiation at a laser harmonic h (wavelength λ_L/h) can exceed the incoherently emitted radiation from the whole bunch by an order of magnitude or more. In this scheme, known as coherent harmonic generation (CHG, Fig. 1, top) [7], the storage ring equivalent to high-gain harmonic generation (HGHG) in seeded FELs [8], the bunching factor decreases as $b_h \sim \exp(-h^2)$.

Echo-enabled harmonic generation (EEHG, Fig. 1, bottom) was proposed as an FEL seeding scheme to reach higher harmonics [9]. Here, a twofold laser-electron interaction leads to a more complex density modulation with the bunching factor decreasing as $b_h \sim h^{-1/3}$. EEHG was demonstrated at linear accelerators [10–13] and was implemented for user operation at FERMI (Trieste, Italy) [14].

For short-pulse generation at SR sources, different EEHG setups were proposed with all undulators and chicanes in one long [15] or in two consecutive straight sections [16–18], or even using the whole storage ring as a chicane [19]. As a worldwide first implementation at a storage ring, a demonstration experiment was realized in a single 5 m long straight section of the 1.5-GeV SR source DELTA [20] operated by the TU Dortmund University in Germany.

* Work supported by DFG (contract INST212/236-1), BMBF (contracts 05K22PE1 and 05K22PE4), and by the Federal State NRW.
† shaukat.khan@tu-dortmund.de

Content from this work may be used under the terms of the CC BY 4.0 licence (© 2026). Any distribution of this work must maintain attribution to the author(s), title of the work, publisher, and DOI.

ISBN: 978-3-95450-252-3 ISSN: 2673-5350 doi: 10.18429/JACoW-IPAC2026-THP2037

SPACE-CHARGE-ENHANCED ENERGY MODULATION AT FERMI*

S. Khan†, Center for Synchrotron Radiation, TU Dortmund University, Dortmund, Germany
P. R. Ribič, C. Spezzani, S. Spampinati, E. Allaria, A. Brynes, G. Penco,
M. Trovò, L. Giannessi[2], G. De Ninno[3], Elettra-Sincrotrone Trieste SCpA, Basovizza, Italy
[1] also at Università degli Studi di Trieste, Trieste, Italy
[2] also at Laboratori Nazionali di Frascati, INFN, Frascati, Italy
[3] also at University of Nova Gorica, Nova Gorica, Slovenia

Abstract

High-gain harmonic generation (HGHG) is a seeding scheme for free-electron lasers (FELs), which improves the longitudinal coherence of the radiation output and reduces fluctuations of pulse energy, arrival time, and central wavelength compared to self-amplified spontaneous emission. In the HGHG scheme, a laser-induced energy modulation is followed by a dispersive section, where part of the electrons form density maxima ("microbunches") with the periodicity of the laser wavelength. The electrons between the microbunches have an energy spread correlated with the longitudinal coordinate. Longitudinal space charge (LSC) in a drift section tends to dilute the microbunches, while the correlated energy spread is flattened and can even change its sign. In this case, a second dispersive section can be used to form new density maxima from the electrons between the initial microbunches, and the resulting energy modulation amplitude may be significantly larger than the initial one. Results from experimental demonstrations of this novel LSC-enhanced modulation scheme at FERMI, a seeded FEL user facility in Trieste, Italy, are presented.

INTRODUCTION

The FERMI [1] user facility at the Elettra laboratory in Trieste, Italy, provides powerful radiation in the wavelength range from 100 to 4 nm with two free-electron laser (FEL) lines, FEL-1 [2] and FEL-2 [3]. Both rely on seeding schemes with an external laser, which improve the longitudinal coherence of the radiation output and reduce fluctuations of pulse energy, arrival time, and central wavelength compared to self-amplified spontaneous emission (SASE) [4]. In the high-gain harmonic generation (HGHG) scheme [5, 6], the interaction with a seed laser pulse in a short undulator ("modulator") leads to a sinusoidal modulation of the electron energy. In a subsequent dispersive section ("chicane"), part of the electrons form density maxima ("microbunches") with the periodicity of the laser wavelength, while the electrons between the microbunches have an energy spread correlated with the longitudinal coordinate as shown in Fig. 1(a). FEL amplification and coherent emission take place in a long undulator ("radiator") tuned to a harmonic of the seed wavelength. In order to extend the spectral range compared to the standard HGHG scheme, FEL-2 is based on two successive modulator-radiator stages [3], while FEL-1 was recently upgraded [7, 8] from HGHG to echo-enabled harmonic generation (EEHG) [9, 10], a seeding scheme involving two modulators and a radiator.

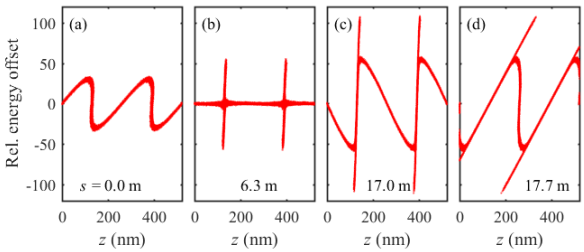

Figure 1: Distribution of electrons in longitudinal phase space, i.e., energy offset versus longitudinal position, (a) following a laser-induced energy modulation and a dispersive section, (b,c) after two different drift lengths s under the influence of LSC, and (d) after a second dispersive section.

Experimental investigations to study the effect of longitudinal space charge (LSC) on density-modulated electron bunches in drift sections were conducted at FEL-1 and FEL-2 [11–14]. LSC accelerates electrons ahead of each density maximum while trailing electrons are decelerated. This tends to broaden the microbunches and thus to reduce their bunching factor while the correlated energy spread between the microbunches is flattened as shown in Fig. 1(b), which may be advantageous for harmonic generation [15]. If the drift section is long enough, the correlated energy spread rises again with opposite sign opening the possibility to enhance an initially small laser-induced energy modulation as proposed in Ref. [13]. When the electron distribution of Fig. 1(c) passes another dispersive section, new microbunches are formed from the electrons between the initial density maxima as shown in Fig. 1(d). In the following, simulations and first experimental results of this LSC-enhanced modulation scheme are presented.

NUMERICAL SIMULATIONS

One-dimensional simulations are based on the coupled equations describing the motion of electrons in longitudinal phase space

$$\frac{dp_i}{d\tau} = \frac{2}{\alpha}\sum_{h=1}^{\infty} b_h \frac{\sin h\theta_i}{h} \quad \text{and} \quad \frac{d\theta_i}{d\tau} = \alpha\, p_i, \quad (1)$$

* Work supported by Heinrich-Hertz-Stiftung, MKW NRW, and by the Bundesministerium für Forschung, Technologie und Raumfahrt (05K22PE1, 05K22PE4).

† shaukat.khan@tu-dortmund.de

Content from this work may be used under the terms of the CC BY 4.0 licence (© 2026). Any distribution of this work must maintain attribution to the author(s), title of the work, publisher, and DOI.

ISBN: 978-3-95450-252-3 ISSN: 2673-5350 doi: 10.18429/JACoW-IPAC2026-THP2038

UNDULATOR RADIATION FROM A SINGLE ELECTRON IN A STORAGE RING*

S. Khan†[1], Y. Asai‡[2,3], Z. Usfoor[1], T. Kaneyasu[3], C. Mai[1,7], H. Miyauchi[4,5], Y. Okano[3], A. Radha Krishnan[1], W. Salah[6], M. Shimada[4,5], V. Vijayan[1], M. Katoh[2,3,4]
[1]Center for Synch. Radiation and Dep. of Physics, TU Dortmund University, Dortmund, Germany
[2]Grad. School of Adv. Science and Engineering, Hiroshima University, Higashi-Hiroshima, Japan
[3]UVSOR Synch. Facility, Institute for Molecular Science, Okazaki, Japan
[4]Research Institute for Synch. Radiation Science, Hiroshima University, Higashi-Hiroshima, Japan
[5]High Energy Accelerator Research Organization, KEK, Tsukuba, Japan
[6]Department of Physics, The Hashemite University, Zarqa, Jordan
[7]Helmholtz-Zentrum Berlin (HZB), Berlin, Germany

Abstract

Low-intensity interference experiments in the time domain have been undertaken by measuring the spectral distribution of synchrotron light from a single relativistic electron in a storage ring. In an undulator, an electron emits light from different magnetic poles leading to a spectral interference pattern - in close analogy to the angular distribution of light behind spatially separated slits. Experiments at the electron storage rings DELTA in Dortmund, Germany, and UVSOR-III in Okazaki, Japan, show directly that the spectral distribution of accumulated synchrotron light from a single electron is essentially the same as the spectrum from a beam of many electrons. While the latter is usually explained by interference between light waves emitted at different undulator poles, the single-electron experiments demonstrate that the photon source point is delocalized over several meters.

INTRODUCTION

Single-electron operation of storage rings has been performed at several facilities in the past. Already in the 1960s, visitors of AdA in Frascati, Italy, the world's first e^+e^- collider, were shown synchrotron light from one electron, which was visible to the naked eye [1]. The stochastic nature of photons from a single electron was studied at VEPP-2 and VEPP-3 in Novosibirsk, Russia [2]. At BESSY and MLS in Berlin, Germany, radiation from a single electron is routinely used by the Physikalisch-Technische Bundesanstalt (PTB) for metrology purposes [3]. The motion of single electrons was tracked at the experimental storage ring IOTA of Fermilab in Batavia, USA [4].

Compared to traditional accelerator physics studies, single-electron operation opens up new opportunities in beam diagnostics and to study the quantum nature of synchrotron light. The knowledge of beam properties, such as the beam size or energy distribution, is usually deduced from the assumed dynamics of single particles under the influence of electromagnetic fields in a storage ring as well as the interaction of these particles with the residual gas and among themselves. These assumptions are rarely tested by observing a single particle directly. While a non-invasive study of single hadrons would be difficult, photons emitted by electrons in a dipole magnet or undulator can be easily detected using, e.g., a photomultiplier tube (PMT).

Classical electrodynamics describes synchrotron radiation with a high degree of precision as an electromagnetic wave [5], but does not explain the stochastic emission of quanta by individual electrons. Thus, the statistical properties of photons provide additional information beyond the classical treatment. A conceptional difficulty arises when a single electron emits only one photon after passing an undulator $\sim$ 100 times. Radiation from a particular magnetic pole would result in a broad spectrum, while a source point delocalized over the whole undulator would lead to a spectrum described by $\sin^2 x/x^2$, a squared sinc function with $x \equiv \pi N_\mathrm{U}(\lambda_0/\lambda - 1)$, where λ_0/λ is ratio of central undulator wavelength and observed wavelength, and N_U is the number of undulator periods [6, 7]. The latter case is a temporal analogy to a photon passing multiple spatial slits with interfering probability amplitudes. To make the analogy to a classical double-slit experiment [8] even more apparent, consider two undulators in an optical-klystron configuration, i.e., tuned to the same wavelength λ_0 with a magnetic chicane between them [9, 10]. Here, two consecutive radiation pulses with longitudinal separation $R_{56}/2$ are produced, and their spectrum with interference fringes reads

$$P_\mathrm{OK}(\lambda) = 2P_1(\lambda)\left\{1 + f\cos\left[2\pi\left(N_\mathrm{U} + N_\mathrm{D}\right)\frac{\lambda_0}{\lambda}\right]\right\}, \quad (1)$$

where $P_1(\lambda)$ is the power spectrum of a single undulator, $N_\mathrm{D} = R_{56}/(2\lambda)$, and a factor $f < 1$ reduces the fringe visibility due to nonzero electron energy spread and emittance.

This paper presents results from two synchrotron light sources, UVSOR in Okazaki, Japan [11], and DELTA in Dortmund, Germany [12], where spectral information from single electrons was obtained using two different methods.

* Work supported by BMFTR (grant 05K22PE4), by the German Federal State NRW, by JSPS KAKENHI (grants 22K18705 and 25H00623) and by IMS, Okazaki, Japan (grants 22IMS6868, 23IMS6610, and 24IMS6809).
† shaukat.khan@tu-dortmund.de
‡ asaiyuya0705@hiroshima-u.ac.jp

Content from this work may be used under the terms of the CC BY 4.0 licence (© 2026). Any distribution of this work must maintain attribution to the author(s), title of the work, publisher, and DOI.

ISBN: 978-3-95450-252-3 ISSN: 2673-5350 doi: 10.18429/JACoW-IPAC2026-THP2039

ELETTRA 2.0 - THE NEW FRONTIER OF SYNCHROTRON RADIATION

E. Karantzoulis†, S. Dastan, S. Di Mitri, A. Fabris, S. Krecic, K. Manukyan, M. Modica, I. Morozov, N. Shafqat, Elettra-Sincrotrone Trieste S.C.p.A., Trieste, Italy

Abstract

With the definitive shutdown of Elettra on July 2, 2025, a new chapter opens for scientific and technological research in Trieste. After thirty-two years of activity with excellent results, Elettra, Italy's 3rd generation light source is handing over the baton to Elettra 2.0, a fourth-generation light source based on an ultra-low emittance and high transverse coherence storage ring, designed to address the challenges of contemporary science. From advanced materials science to biology and medical applications, the new facility will provide researchers with access to vastly enhanced high-resolution three-dimensional imaging, ultra-high-resolution spectroscopies (such as XAS, XPS, and RIXS) and time-resolved techniques on the picosecond scale. In the paper the project is presented including information on the old machine removal, the present installation progress as well as the future plans on short pulses and energy sustainability.

INTRODUCTION AND OVERVIEW

Elettra 2.0 features several critical technological advancements that distinguish it from its predecessor:

1. Storage Ring Upgrade: The core of the Elettra 2.0 project is the replacement of the existing storage ring with a new low-emittance ring [1-7]. This will significantly reduce the present beam emittance by a factor of 50, resulting in a photon source with much higher brilliance and coherence. The storage ring will also include initially one (with the possibility of another one later), superconducting dipole [8] with 6 T peak field for hard X-ray imaging for the new SYRMEP-LS beamline (life and material science enabling in vitro imaging for high resolution morphological studies and clinical application to humans) giving $2x10^{13}$ ph/s at 60 keV and extending the photon energy to 140 keV at lower flux, about 10^{11} ph/s.

The design is compatible with providing in the future simultaneously short pulses as short as 0.5 ps (FWHM) using superconducting deflecting RF cavities for time-resolved experiments requiring high repetition rate and standard single bunch charge, while preserving the transverse coherence

2. Beamline Enhancements: Elettra 2.0 will introduce 10 new beamlines to fully exploit the features of the upgraded storage ring and upgrade many of the existing ones while 8 old ones are removed. The total number of the beamlines are increased to 32 (from 28 of the old machine) whereas a clear shift towards tender and hard x-rays has been decided. New beamlines will include several ones specifically designed for enhanced capabilities in X-ray absorption spectroscopy, photoemission spectroscopy, high-resolution diffraction, coherent diffraction imaging and time-resolved experiments resulting in an enhanced ability to capture ultrafast processes opening thus new possibilities in studying dynamic systems such as chemical reactions and phase transitions in materials.

The new capabilities of Elettra 2.0 will enable research in several scientific and industrial fields like nanotechnology and materials science, quantum materials and pharmaceuticals and health sciences.

The Elettra 2.0 upgrade follows a well-defined project schedule, with several major milestones:

Decommissioning of the old storage ring and installation of the New Storage Ring [9]: This phase began in July 2025 and completed in January 2026 including the complete removal of the old machine that has been stored in a dedicated prefabricate building for radioprotection measurements. The tunnel and service area are refurbished to be ready for the new machine installation. The decommissioning did not include the injectors (100 MeV linac and 2.5 GeV booster and transfer lines) that are refurbished and will be reused. The new storage ring installation started in April 2026, with completion expected by December 2026.

Beam Commissioning and User-mode Operations: Commissioning with beam is scheduled to start in January 2027. In the first trimester of 2027, the new ring and an initial set of 15 beamlines are programmed to be operational and available to researchers whereas all 32 beam lines will be gradually available until the end of the project in 2029.

The project also includes many infrastructural works like renewing the air-condition and cooling systems as well as the electricity plant on site and other, mainly maintenance, works.

MACHINE DESCRIPTION

The enhanced symmetric six bend achromat (S6BA-E) lattice (Fig. 1) has been uniquely designed to meet all experiment / user requirements. The new ring has the same circumference as before, i.e. 259.2 m and consists of 24 symmetric arcs rendering a 12-fold symmetry, producing 12 long straights and 12 short straights sections. Each arc consists of 3-unit cells of the TME (theoretical minimum emittance) type i.e. :

- 3 dipoles, of which one at 0.8 T with vertical field gradient and two with combined transverse (< 22 T/m), and longitudinal gradient (1 and 1.46 T)
- 7 quadrupoles (< 50 T/m) four of which are shifted at 5.16 mm to give the required reverse-bend angle of - 0.4 deg each
- 10 combined sextupoles (< 4500 T/m^2) (4 with correctors, 2 harmonic with correctors and 2 with skew quadrupole coils)

†emanuel.karantzoulis@elettra.eu

Content from this work may be used under the terms of the CC BY 4.0 licence (© 2026). Any distribution of this work must maintain attribution to the author(s), title of the work, publisher, and DOI.

ISBN: 978-3-95450-252-3 ISSN: 2673-5350 doi: 10.18429/JACoW-IPAC2026-THP2041

CHICANE-FREE LASER HEATER SYSTEM FOR MITIGATION OF MICROBUNCHING INSTABILITY IN LINAC-FELS

F. Elisii[1], S. Di Mitri[2,*], G. Perosa[3]
[1] University of Trieste, Trieste, Italy
[2] Elettra Sincrotrone Trieste, Trieste, Italy
[3] European XFEL GmbH, Schenefeld, Germany

Abstract

We introduce a closed-form, verified through numerical integration, of the beam energy spread induced by oblique electron-laser interaction in a short undulator, so-called chicane-free laser heater. This scheme is relevant for high repetition rate free-electron lasers, space constrained, or subject to microbunching instability induced by a standard laser heater chicane. A calculation of the instability gain with the proposed scheme is presented to demonstrate its feasibility [1].

INTRODUCTION

In single pass or recirculating electron linear accelerators (linacs), microbunching instability (MBI) is the beam collective effect causing disruption or dilution of the longitudinal phase space by the amplification of energy and density modulations in succession [2]. The instability is seeded by the granularity of the electron distribution (shot noise), possibly in combination with narrowband phase space structures originated in radiofrequency (RF) photo-injectors [3,4]. The nature of the initial modulations, in combination with some damping mechanisms, commonly bounds the instability to final wavelengths in the range ~0.1–10's μm, hence the naming. Longitudinal damping of the instability is in most cases implemented through a laser heater system [5] in the low energy region of the linac, well before the instability builds up. In this case, the enlargement of the beam longitudinal emittance imposes a tradeoff between FEL spectral purity and intensity [6, 7].

At least three semi-analytical approaches to model MBI have been developed in the last two decades, which can be shortly referred to as, respectively, integral linearized Vlasov-Maxwell equation [8], matrix multiplication [9], and linearized Vlasov-Poisson equation in a plasma [10, 11]. We have recently upgraded the first two models [1], and translated them into Matlab scripts [12], finding excellent agreement in a wide variety of linac-FEL configurations and range of parameters. Here, we use one of the two to study beam heating in parallel *versus* oblique electron-laser interaction, the latter configuration being potentially relevant for very high repetition rate FELs, space constrained, or subject to instability development through the laser heater chicane.

Strictly speaking, the electron-laser interaction in the laser heater undulator does not require *per sé* a chicane, and the laser-induced energy modulation, in the range ~0.5–1 μm, can be translated into uncorrelated energy spread by smearing through the downstream magnetic bunch compressor. To the best of our knowledge, laser heater system at FLASH (Germany) is the only one implementing such scheme [13, 14]. However, a mini-chicane is still present upstream the undulator to inject the laser collinear to the electrons.

In the following, we evaluate the increase in laser peak power required by any pre-determined induced energy spread, in the presence of an oblique superposition (*e.g.*, in the horizontal plane) of laser and electrons. It is evident that the proposed scheme can, on the one hand, save several meters of space that would otherwise be occupied by the laser heater chicane. Moreover, it can offer a more efficient laser-electron interaction, thus a reduced laser power per induced energy spread, by virtue of smaller electron and laser beam spot size, owing to the absence of dispersive electron motion. On the other hand, the increase of peak power due to the larger effective interaction area has to remain compatible with the available average laser power, such as at superconducting linac-FELs requiring beam heating up to MHz repetition rate.

BACKGROUND

The energy modulation amplitude of an electron bunch induced by an external laser at an angle of interaction θ was derived in [15]. Equations 21–23 describing the induced energy modulation amplitude in that paper are recast here for the reader's convenience:

$$\Delta\gamma_{LH}(\theta) = \left(\frac{eE_0N_u\lambda_u}{m_ec^2}\right)\sqrt{I_x(L_u)I_y(L_u)}\cdot$$
$$\cdot\langle sin\left(-\varsigma + a\sin(2\varsigma) + d\cos(\varsigma)\right)\cdot\left(o + p\sin(\varsigma) + q\cos(2\varsigma)\right)\rangle_\varsigma \equiv$$
$$\equiv \left(\frac{eE_0N_u\lambda_u}{m_ec^2}\right)\Sigma_{JJ}(\theta) \quad (1)$$

The following quantities have been introduced:

$$\begin{aligned}
\varsigma &= k_u z \\
a &= \frac{K^2}{4 + 2K^2 + 4\gamma^2\theta^2} \\
d &= \frac{k_s K sin\theta}{k_u\gamma} \\
o &= \left[\frac{1}{2\gamma^2}\left(1 + \frac{K^2}{2}\right) - 1\right] sin\theta \\
p &= -\frac{K cos\theta}{\gamma} \\
q &= -\frac{K^2}{4\gamma^2} sin\theta
\end{aligned} \quad (2)$$

*simone.dimitri@elettra.eu

Content from this work may be used under the terms of the CC BY 4.0 licence (© 2026). Any distribution of this work must maintain attribution to the author(s), title of the work, publisher, and DOI.

ISBN: 978-3-95450-252-3 ISSN: 2673-5350 doi: 10.18429/JACoW-IPAC2026-THP2043

NUMERICAL AND EXPERIMENTAL BENCHMARKING OF MICROBUNCHING INSTABILITY WITH INTRABEAM SCATTERING IN LINAC-FELS

S. Di Mitri[1,2,*], G. Campri[1], F. Elisii[2], G. Perosa[3], S. Spampinati[1]
[1] Elettra Sincrotrone Trieste, I-34149 Basovizza, Trieste
[2] University of Trieste, Dept. Physics, V. A. Valerio I-34100 Trieste
[3] European XFEL GmbH, Holzkoppel 4, G-22869, Schenefeld

Abstract

The benchmark of a semi-analytical model of microbunching instability affecting electron beams in single pass or recirculating linear accelerators with experimental data published in the literature is reported. The model is comprehensive of numerous features of the instability, such as low and high gain contributions, either linearized or at second order, coherent synchrotron and edge radiation, Landau damping by transverse emittance and laser heater, for single and double magnetic bunch length compression. The model is enriched by three different expressions to calculate intrabeam scattering. The inclusion of this effect allows the recovery of agreement with published experimental observations, to date either in disagreement with theory, or in partial agreement by virtue of blind fitting of parameters.

INTRODUCTION

In single pass or recirculating electron linear accelerators (linacs), microbunching instability (MBI) is the beam collective effect causing dilution of the longitudinal phase space by the amplification of energy and density modulations in succession [1]. The instability is one of the potential show-stoppers to longitudinal coherence at the Fourier limit level of linac-driven XUV free-electron lasers (FELs). In particular, it has been recognized at the origin of radiation pedestal and power reduction in X-ray self-seeded FELs [2], and of sidebands in externally-seeded EUV FELs [3,4]. In general, the instability determines FEL bandwidth enlargement and reduction of the spectral flux, in proportion to the harmonic jump of lasing.

The instability is seeded by the granularity of the electron distribution, possibly in combination with narrowband phase space structures originated in radiofrequency (RF) photo-injectors [5,6]. The nature of the initial modulations, in combination with some damping mechanisms, commonly bounds the instability to final wavelengths in the range ~0.1–10's μm, hence the naming.

The spread of particles' path length in dispersive regions, due to either chromatic or betatron motion, washes out modulations at the shortest wavelengths of the broadband instability spectrum, in fact putting in place longitudinal and transverse Landau damping [7]. Transverse damping can be enhanced by optics tuning for an enlarged curl-H_x function [8], while the betatron emittance is preserved. Longitudinal damping is usually more effective than the transverse. It is more effective for larger beam uncorrelated energy spread, and this is in most cases increased by a laser heater system [9] in the low energy region of the linac, well before the instability builds up. In this case, however, the enlargement of the beam longitudinal emittance imposes a tradeoff between FEL spectral purity and intensity [10,11]. Additional damping mechanisms have been identified in the folding of phase space at high energy (phase mixing) [12] and, recently first observed in an electron linac, intrabeam scattering (Landau damping) [13].

At least three semi-analytical approaches to model MBI have been developed in the last two decades, which can be shortly referred to as, respectively, integral linearized Vlasov-Maxwell equation [14], matrix multiplication [15], and linearized Vlasov-Poisson equation in a plasma [16,17]. In the following, we will adopt the first one; for the sake of brevity, we will name it Huang-Kim (HK), with reference to the authors who, after the conceptualization by Saldin *et al.* in [9], first introduced the formalisms with prescriptions for a numerical implementation. The model is basically time-independent (it describes the bunch core slice dynamics), valid in ultra-relativistic regime. The use of effective transverse beam sizes in the calculation of Coulomb interactions justifies 1.5-D approximations to some extent [18].

The Reader is kindly sent to [19] for a systematic report on the numerical benchmark of the Huang-Kim and the Bosch-Kleman-Wu (BKW) semi-analytical models of MBI. Here, we show that the inclusion of intrabeam scattering (IBS) is essential to the recovery of agreement with published experimental observations, to date either in disagreement with theory, or in partial agreement by virtue of blind fitting of parameters.

BENCHMARK OF MEASUREMENTS

FERMI High Charge

The HK formalism was successfully applied in [13] to explain the observed ~100 keV slice energy spread at the end of the FERMI linac in a low charge regime (100 pC), for which IBS was shown to play a critical role in limiting the MBI gain. The exercise is repeated here for the slice energy spread measured at the same facility in high charge regime (600 pC), and reported in Fig.2 of [20].

†simone.dimitri@eletra.eu

Content from this work may be used under the terms of the CC BY 4.0 licence (© 2026). Any distribution of this work must maintain attribution to the author(s), title of the work, publisher, and DOI.

ISBN: 978-3-95450-252-3 ISSN: 2673-5350 doi: 10.18429/JACoW-IPAC2026-THP2044

OPERATIONAL ASPECTS OF CRAB CAVITIES AT THE ELETTRA 2.0 STORAGE RING LIGHT SOURCE

N. Shafqat*, S. Di Mitri[1], S. Cleva[1], S. Dastan[1], K. Manukyan[1], M. Modica[1], A. Fabris[1], E. Karantzoulis[1], A. Grudiev[2], R. Calaga[2], F. Gerigk[2]
[1]Elettra Sincrotrone Trieste, Elettra, Trieste, Italy
[2]European Organization for Nuclear Research, CERN, Geneva, Switzerland

Abstract

We report here the Same-Order Modes (SOMs) and Higher-Order Modes (HOMs) analysis of the superconducting "crab cavity" module designed for the production of picosecond-long X-ray pulses at Elettra 2.0 storage ring light source. The module consists of three radiofrequency (RF) transverse deflecting cavities operating at 3.0 and 3.25 GHz, corresponding to the 6th and 6.5th harmonic of the fundamental frequency of Elettra 2.0. The design is based on the Quasi-waveguide Multicell Resonator (QMiR), firstly developed for the Advanced Photon Source. SOMs/HOMs analysis is performed for the entire module, including tapers to connect it with the Elettra 2.0 ring. CST frequency domain solver (Eigen mode solver) is used for calculation of the impedances of SOMs and HOMs from 2.5 GHz to 7.0 GHz, which are the cut-off frequencies of the Elettra 2.0 rhomboidal vacuum chamber. The results are verified using the time domain solver, wake solver of CST, for the entire range, and even with HFSS for the selected group of SOMs/HOMs.

INTRODUCTION

Elettra Sincrotrone Trieste Italy, is implementing a comprehensive storage-ring upgrade program, Elettra 2.0, aiming at a substantial reduction of the electron beam emittance, increasing thus the photon brilliance and coherence by at least two orders of magnitude. To achieve that, the 12-fold symmetric double bend achromat of the old lattice is replaced by a 12-fold symmetric enhanced six bend achromat (S6BA-E), whereby combined dipoles are used with transverse and longitudinal focusing as well as reverse bend quadrupoles [1]. Crab cavities would be installed to produce extreme ultraviolet and X-ray pulses with durations between 0.5 and 5 ps (FWHM) from the insertion devices, at repetition rates reaching up to 1 MHz. Two superconducting RF cavities operating at the 6th (3 GHz) and 6.5th (3.25 GHz) harmonics of the main ring RF generate a stationary regime in which the electron bunches acquire a vertical tilt that evolves along the storage-ring circumference. Under these conditions, the beam distribution stabilizes in the full six-dimensional phase space [2, 3].

THE ELETTRA 2.0 CRAB MODULE

The Elettra 2.0 crab module is based on quasi-waveguide Multicell Resonator (QMiR) deflecting cavities which were originally developed for the ANL APS upgrade project [4]. The crab module shown in Fig. 1 consists of three individual crab cavities and tapers to connect to the Elettra 2.0 ring. Two side cavities (cav1) would operate at 3.0 GHz, providing a collective transverse peak voltage up to 1.5 MV, while the central cavity (cav2) would operate at 3.25 GHz and would provide a transverse peak voltage up to 1.2 MV. The impedance budget of the crab cavity module is given in Table 1. The crab module would be connected with the Elettra 2.0 ring with tapers and would be installed in one long straight section, 2.0 m in length. Individual crab cavities would be made of Niobium operating at 4 K while the tapers would be fabricated with Stainless Steel and cooled with Helium return gas from the bath to minimize the thermal input from the room-temperature chamber.

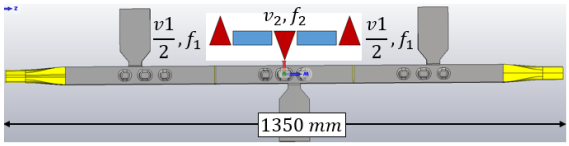

Figure 1: Proposed crabbing scheme for Elettra 2.0.

Table 1: Shunt Impedance Budget for the Crab Cavity Module

Quantity	Value	Unit
R_x	< 4.5	MΩ/m
R_y	< 1.5	MΩ/m
R_z	< 5.0	MΩ GHz

RF design

The initial RF design of individual crab cavities (cav1 and cav2) reported in [5] included circular transitions, which are eliminated in the new design due to space constraints. The new geometry shown in Fig. 2 has the same dimensions of the square waveguides for both cavities, while the distance and spacing between the stubs are used to adjust the frequency. The RF parameters of two crab cavities are listed in Table 2. The superconducting crab module would be connected to the normal-conducting Elettra 2.0 ring using Stainless Steel tapers. As shown in Fig. 3 taper on one side would have a rhomboidal profile, while the other side would have an elliptical profile. The copper rings are introduced between the individual crab cavities. The distance between the individual crab cavities was selected to ensure that there is no coupling of the operating mode, as can be seen from

* nuaman.shafqat@elettra.eu

Content from this work may be used under the terms of the CC BY 4.0 licence (© 2026). Any distribution of this work must maintain attribution to the author(s), title of the work, publisher, and DOI.

ISBN: 978-3-95450-252-3 ISSN: 2673-5350 doi: 10.18429/JACoW-IPAC2026-THP2045

PRELIMINARY THERMAL LOAD CALCULATIONS OF SUPERCONDUCTING DEFLECTING CAVITIES FOR ELETTRA 2.0

M. Modica[1], N. Shafqat[1], S.Di Mitri[2], K.Manukyan[1], S.Cleva[1], S.Dastan, A.Fabris[1], E.Karantzoulis[1]
[1]Elettra-Sincrotrone Trieste S.C.p.A, 3149, Trieste, Italy
[2] University of Trieste, Dept. Physics, 34100, Trieste, Italy

Abstract

Picosecond-long X-ray pulses of moderate intensity and high repetition rate are highly sought after by the light source community, especially for time-resolved fine spectroscopic analysis of matter in the linear response regime. We investigate the upgrade of the Elettra 2.0 diffraction-limited storage ring light source to superconducting radiofrequency transverse deflecting cavities generating a steady-state vertical deflection of selected electron bunches. In this paper, a preliminary design of the cryomodule of the deflecting cavities is reported; both static and dynamic thermal loads are calculated using an analytical approach. The dynamic loads are calculated assuming both bulk Nb and Nb3Sn thin film cavities. The two different solutions involve different cryogenic plants, which will be discussed

SYSTEM OPERATING PRINIPLE

Two superconducting (SC) RF cavities, operating at 6-fold (3 GHz) and 6.5-fold (3.25 GHz) harmonics of the main RF system of the Elettra 2.0 storage ring, establish a steady-state configuration of vertically tilted bunches, with a tilt varying along the ring circumference [1]. Under these conditions, the charge distribution reaches equilibrium in the six-dimensional phase space [2].

The photon beam emitted by tilted bunches exhibits a longitudinal–vertical (t, y) correlation. A vertical slit placed at a given distance from the insertion device (ID) samples the central portion of the elongated photon pulse, thus selecting a shorter time slice at the expense of reduced photon flux. The RF design of the crab cavities is based on the Quasi-waveguide Multicell Resonator (QMiR) concept [3], which exploits a trapped dipole mode to provide transverse deflection of the electron bunch.

CRAB CAVITY RF DESIGN AND LAYOUT

A prototype QMiR cavity was fabricated and successfully tested in a vertical cryostat at 2 K, demonstrating a record transverse kick of 2.6 MV [4]. The crabbing scheme for Elettra 2.0 is illustrated in Fig. 1, while the geometry and main dimensions of a single crab cavity are reported in Fig. 2 [5].

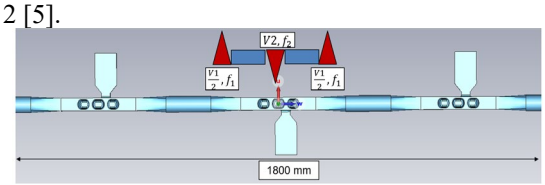

Figure 1: Crabbing scheme for Elettra 2.0.

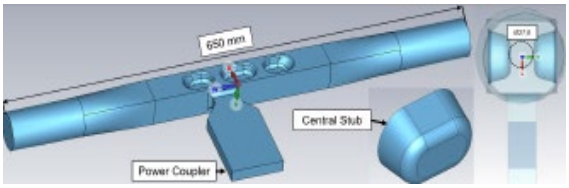

Figure 2: The stub shape for the crab cavities.

RF LOSSES AND THERMAL LOAD IN A PURE NIOBIUM CAVITIES AT 4 K

The effective deflecting voltage determines the dynamic thermal load of the superconducting device. For temperatures below half of the critical temperature (T < Tc/2), where Tc is the critical temperature, the BCS contribution dominates the surface resistance. The geometry factor G=Q0Rsf is a characteristic parameter of the cavity, depending only on its geometry and on the operating temperature.

$$G = Q_0 R_{sf} = Q_0 \omega^2 \lambda_L^3 \mu_0^2 \sigma(T) \exp\left(-\frac{\Delta}{K_B T}\right)$$

where λ_L is the characteristic penetration depth of a static or microwave magnetic field in a superconductor such as niobium, and Δ is the superconducting gap, or binding energy of Cooper pairs.

For the equilibrium temperature $T < T_c/2$, R_{sf} of pure niobium can be expressed in practical units:

$$R_{sf}[\Omega] \approx \alpha \times 10^{-4} \frac{(f[\mathrm{GHz}])^2}{T} \exp\left(-\frac{17.67}{T}\right)$$

where usually $\alpha \approx 1.25$ for $T \approx 2 - 5$ K.

The power dissipated on the internal surface of a tuned superconducting (SC) RF deflecting cavity made of pure niobium, i.e. the dynamic thermal load, can be estimated from the RF surface current losses per period:

$$P_{th} = \frac{\omega_0 U_0 R_{sf}}{G} d_f \equiv \frac{\Delta V_\perp^2}{2R_{sh}} d_f$$

For a pure Nb deflecting cavities system as needed in the Elettra 2.0 light source, as reported in Table 1:

Table 1: Pure Nb features

Feature	Value
$Q_0(T)$	2.2×10^{-7}
Surface resistance [μΩ]	5
Thermal load bare cavity s[W]	177

Content from this work may be used under the terms of the CC BY 4.0 licence (© 2026). Any distribution of this work must maintain attribution to the author(s), title of the work, publisher, and DOI.

ISBN: 978-3-95450-252-3 ISSN: 2673-5350 doi: 10.18429/JACoW-IPAC2026-THP2048

DISMANTLE, ASSEMBLY AND INSTALLATION PLANS FOR THE ALBA II UPGRADE

F. Fernández, J. Boyer, L. Fuentes, R. Monge, M. Pont, Ll. Ribó
ALBA Synchrotron, CELLS, Barcelona, Spain

Content from this work may be used under the terms of the CC BY 4.0 licence (© 2026). Any distribution of this work must maintain attribution to the author(s), title of the work, publisher, and DOI.

Abstract

The 3.0 GeV ALBA Synchrotron Light Source, in user operation since 2012, is preparing for a major upgrade aimed at increasing the brightness and coherence of the delivered X-ray beam. The Storage Ring (SR) will be completely renewed while preserving the Insertion Device (ID) source points, the orbit length and the electron beam energy; the current injector will remain in use. A two-year "dark period" is foreseen for 2030–2031.

This paper presents the Implementation Program developed to prepare and execute the removal and installation of the upgraded SR. The program covers storage and logistics of equipment, preparation of testing and assembly areas, recycling and decommissioning of dismantled components, and the coordination of removal, installation and testing activities in both the tunnel and the Service Area (SA). The program structure, work packages and main implementation strategies are presented.

INTRODUCTION

The ALBA Synchrotron Light Source has been operating with users since 2012, delivering synchrotron radiation from infrared to hard X-rays. An upgrade project, ALBA II, has been launched to transform the facility into a diffraction-limited Storage Ring (SR), significantly enhancing beam brightness and coherence [1]. The upgrade does not only affect the accelerators; it also comprises the construction of two new long beamlines (~200 m), that extend beyond the actual plot, and increasing the capabilities of the data acquisition and processing systems for the future high demanding beamlines.

The SR upgrade maintains several key constraints to ensure cost effectiveness and minimize impact on beamlines: preservation of the 3.0 GeV beam energy, orbit length, injector, Insertion Device (ID) source points and shielding tunnel [2]. The SR will nevertheless be fully renewed (Fig. 1), requiring a carefully planned removal and installation process during a limited two-year dark period in 2030–2031, including both the renewal and the commissioning of the new accelerator and beamlines.



Figure 1: 3D model of one of the 16 ALBA II SR cells.

Given the scale and complexity of the upgrade, ALBA II has been organized under a program-oriented structure that groups the activities into five main programs, each one addressing a major domain of the project while maintaining strong interfaces with the others. The Experiments Program (PG01) covers both, the upgrade of existing beamlines and the construction of the new long beamlines. The Accelerator Program (PG02) is responsible for the design, procurement, integration and commissioning of the upgraded SR [3]. The Computing and Data Program (PG03) addresses the evolution of computing infrastructure, controls, data acquisition and data management required to support both accelerator and user operations. The Infrastructure Program (PG04) encompasses new buildings, modifications to existing facilities, temporary structures and general site works required to host the upgraded accelerator and beamlines.

The focus of this paper is the Implementation Program (PG05), which provides the transversal framework required to physically achieve the upgrade in a safe, coordinated and time-efficient manner. This program is responsible for the preparation and allocation of storage spaces, the logistics and tooling to handle all the equipment, its tracking along all the process, the establishment of testing and assembly areas, the recycling and decommissioning of dismantled hardware, and the coordination of all removal, installation and test activities in the tunnel and Service Area (SA). Acting as the operational interface between the technical programs, the Implementation Program is a key enabler to ensure that the ALBA II upgrade can be executed within the limited dark period while minimising technical risks and impact on the facility schedule.

IMPLEMENTATION PROGRAM

The Implementation Program is structured into six WPs.

WP00 – Program Management

Overall coordination of the program, definition of responsibilities and interfaces between WPs, budget management for external resources, and integration of safety roles within the program.

WP01 – Storage and Logistics

Procurement and assignment of storage areas and handling tools for both, the new ALBA II components and existing ALBA equipment. This WP defines storage requirements, lifting and transport needs, and is responsible for tooling, cranes and logistics.

The different needs along the process and the present available areas to store equipment have been identified. A new temporary building (600~800 m^2) will be built on the ALBA site (Fig. 2). In it, we will store the girders [4] and magnets [5] prior to their characterization and assembly; and later, the girders with assembled and aligned magnets.

Regarding the tooling and besides all the standard logistics equipment, a special device (Fig. 3) is being designed to transport the assembled girders with magnets to/from the assembly zone to the temporary storage building and to the

ISBN: 978-3-95450-252-3 ISSN: 2673-5350 doi: 10.18429/JACoW-IPAC2026-THP2049

OFF-PHASE INJECTION SIMULATIONS FOR MAX 4^{U}

A. Dixon*, M. Apollonio, S. Thorin, F. Lindau, R. Lindvall, E. Mansten, M. Sjöström, and P.F. Tavares, MAX IV Laboratory, Lund, Sweden

Abstract

The MAX IV injector, including a full energy linac and a photo gun, offers a unique capability to deliver low-emittance, well-timed electron pulses suitable for injection. This makes on-axis, off-phase, on-energy injection an attractive option for future operation of the upgraded 3 GeV storage ring, MAX 4^{U}, where stronger focusing, reduced magnet apertures, and narrow-gap undulators all limit the transverse acceptance and challenge the present off-axis MIK scheme. Additionally, the significantly reduced emittance makes injected beam perturbations less transparent to the beamlines. In this work, we investigate off-phase injection for the technical design lattice candidate (TDR-1) and show through simulations that stable capture is achievable despite the reduced dynamic aperture. We also evaluate how the characteristics of the photo gun beam support the longitudinal phase-space requirements of on-axis, off-phase, on-energy injection. These results indicate that the combination of a full energy linac, photo gun-based injector and off-phase injection provide a promising path forward for injection into a low-emittance storage ring at MAX IV.

INTRODUCTION

In order to remain at the forefront of storage ring light sources an upgrade of the 3 GeV ring at MAX IV has been proposed, referred to as MAX 4^{U} [1]. The technical design aims to reduce the emittance from 328 pm rad to below 75 pm rad. An integral aspect of the design is to enable regular transparent top-up injections to ensure stable operation and near-constant current.

The significant emittance reduction of the upgraded lattice means that transverse perturbations of the injected beam become more apparent due to the larger relative difference between source size and the oscillation amplitude. As such, off-axis injection with a multipole injection kicker [2] is less transparent to the beamlines. Additionally, the proposed lattice leads to a reduction in dynamic aperture (compared to the present ring) due to stronger focusing and allows for smaller horizontal aperture undulators. The reduced horizontal acceptance places further demands on the required multipole kicker, where the kicker would need to provide a strong kick at distances closer to the stored beam. As such, an alternative method must be explored for MAX 4^{U}. The proposed scheme must be also transparent and compatible with regular top-up injections.

An injection scheme that meets these requirements is on-axis, off-phase, on-energy injection, based on the method proposed in Ref. [3]. In a longitudinal injection scheme, the electron beam is injected into the longitudinal acceptance of the storage ring [4], and pulsed kickers are used to bring the beam on-axis in the transverse planes.

In this paper, we investigate an on-axis, off-phase, on-energy injection scheme for MAX 4^{U}, a proposed upgrade to the 3 GeV storage ring. We show that the photocathode gun and full energy injector at MAX IV enable this method of injection.

FULL ENERGY INJECTOR

At MAX IV laboratory, a normal conducting S-band linear accelerator (linac) is used to inject at full energy into both 1.5 GeV and 3 GeV storage rings. The linac is also used to deliver bunches to a spontaneous undulator radiation beamline, i.e. the Short Pulse Facility (SPF) [5].

The linac can be operated with two different electron sources: thermionic gun (TG) [6, 7] and photocathode gun (PG) [8]. The former is typically used inject into the storage rings. The latter is used to drive the SPF, however injection with the PG is currently under development. When operating with the TG a chopper system is used to produce bunch trains with 10 ns time separation to match the time separation of RF buckets in the storage rings [7]. In comparison to the electron bunches from the TG, the electron bunches from the PG have lower emittance, energy spread and bunch length. The injector parameters are summarised in Table 1.

Table 1: Electron bunch properties and injection parameters for injection with: thermionic gun (TG) and photocathode gun (PG).

	TG	**PG**
Energy [GeV]	1.5/3.0	1.5/3.0
Repetition rate [Hz]	10	10
Charge/shot [pC]	200-500	200
Bunch length [ns]	1.5-70.0	0.005
Emittance [mm mrad]	10	2-3
Energy spread [%]	<0.25	<0.1
Full fill time [min]	10	10

As the photocathode gun and storage ring frequencies are not at multiples of each other, a new system for synchronising the PG and the RF buckets has been developed. A coincidence system is used to synchronise the electron bunch from the photocathode gun and an RF bucket in the ring. The timing of RF buckets is monitored, and injection shots are triggered when RF bucket coincides with the gun pulse. The coincidence system allows a single RF bucket to be targeted for injection, which could be used for various filling patterns.

* adam.dixon.7536@maxiv.lu.se

Content from this work may be used under the terms of the CC BY 4.0 licence (© 2026). Any distribution of this work must maintain attribution to the author(s), title of the work, publisher, and DOI.

ISBN: 978-3-95450-252-3 ISSN: 2673-5350 doi: 10.18429/JACoW-IPAC2026-THP2050

A COMPARISON BETWEEN ARC-LIKE AND CHICANE-LIKE BUNCH COMPRESSION FOR X-RAY FREE-ELECTRON LASERS*

A. Dixon† and S. Thorin, MAX IV Laboratory, Lund, Sweden
P. Williams[1], STFC Daresbury Laboratory, Daresbury, United Kingdom
A. Wolski[1], University of Liverpool, Liverpool, United Kingdom
A. Brynes[1], STFC Daresbury Laboratory, Daresbury, United Kingdom
T. Charles, ANSTO - Australian Synchrotron, Melbourne, Australia
I. Bailey[1], Lancaster University, Lancaster, United Kingdom
[1]also at the Cockcroft Institute, Warrington, United Kingdom

Abstract

The spectral brightness of a free-electron laser (FEL) is strongly dependent on the properties of the electron beam used to generate the radiation. Bunches used to drive FELs must have high currents, which are produced through longitudinal bunch compression. However, collective effects (such as coherent synchrotron radiation) degrade the emittance and energy spread during the bunch compression process, which in turn reduces the spectral brightness. A compression scheme for an FEL must be designed to reduce the impact of collective effects on the electron distribution in order to generate high spectral brightness FEL pulses. In this paper we compare commonly used four-dipole chicanes to two alternative bunch compressor configurations that are designed to mitigate coherent synchrotron radiation. We show that compression can be achieved with much reduced emittance degradation compared to four-dipole chicanes in two cases: arc compression of positively chirped bunches, and five-dipole compression of negatively chirped bunches. Each is suited to different FEL schemes.

INTRODUCTION

Spectral brightness, which describes the photon density of a radiation source, is a key figure of merit for the performance of light sources, such as FELs. To produce high spectral brightness in an FEL, electron bunches in the undulators must have low transverse emittance, small energy spread and high peak current (i.e. high 6D brightness).

Preserving the 6D brightness of an electron bunch as it is accelerated and compressed from the injector to the undulators is essential for the performance of an FEL. Collective effects, such as coherent synchrotron radiation (CSR) and micro-bunching instability (MBI), that occur in magnetic bunch compressors can significantly degrade the emittance and energy spread of an electron beam [1–6].

A range of strategies have been proposed to mitigate CSR and MBI effects in magnetic bunch compressors, including: minimised β-function in the dipoles of a chicane to reduce CSR-induced emittance growth [7]; asymmetric chicanes that achieve CSR kick cancellation and reduce emittance growth [8–10]; optics balance to achieve CSR kick cancellation between dipoles or achromats [11, 12]; laser heaters to increase the energy spread of electron bunches to limit MBI gain [13]; transverse Landau damping to mitigate MBI gain [14].

In light of these strategies aimed at mitigating CSR and MBI effects in bunch compressors, we compare three bunch compressors for use in a potential future UK X-ray Free Electron Laser (UK-XFEL) facility [15,16]. The comparison aims to understand how the choice of bunch compressors affects the electron bunch properties and the FEL output.

UK-XFEL

The UK-XFEL is proposed to be a next-generation FEL facility. A conceptual design and options analysis has recently been completed, which outlines a facility based on a high-repetition rate, super-conducting linac to drive multiple beamlines and experiments simultaneously [15]. Each beamline will operate at different photon energies and using different FEL techniques, requiring bunch-by-bunch variations in longitudinal electron beam properties. Additionally, low emittance beams will be required for each beamline, so emittance preservation is essential as these bunches are transported from the injector to each FEL.

BUNCH COMPRESSOR OPTIONS

The three bunch compressors that are being considered for UK-XFEL are: four-dipole/symmetric C-chicane (SC), five-dipole/asymmetric S-chicane (C5), and arc bunch compressors. Layouts are shown in Fig. 1.

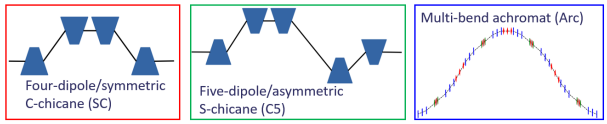

Figure 1: Layout of three types of bunch compressor: four-dipole/symmetric C-chicane, five-dipole chicane, and arc bunch compressors.

Four-dipole chicanes use a C-shaped magnetic layout with four equally powered dipoles of equal length to generate a path-length variation with energy, i.e. longitudinal dispersion R_{56}. Harmonic radio-frequency (RF) cavities would be

* This work was supported by the Science and Technology Facilities Council, U.K., through a grant to the Cockcroft Institute.
† adam.dixon.7536@maxiv.lu.se

Content from this work may be used under the terms of the CC BY 4.0 licence (© 2026). Any distribution of this work must maintain attribution to the author(s), title of the work, publisher, and DOI.

ISBN: 978-3-95450-252-3 ISSN: 2673-5350 doi: 10.18429/JACoW-IPAC2026-THP2051

INSERTION DEVICES CHARACTERIZATION AT THE SLS 2.0

S. Bettoni*,[1], M. Aiba[1], F. Armborst[1], M. Calvi[2], J. Kallestrup[1], D. Zimoch[1]
[1]PSI Center for Accelerator Science and Engineering, Villigen, Switzerland
[2]PSI Center for Photon Science, Villigen, Switzerland

Abstract

Accurate measurement of high-order multipoles in insertion devices is crucial for meeting the beam-dynamics requirements of Swiss Light Source 2.0 (SLS 2.0). A beam-based method using transverse tune-shift measurements can effectively identify sextupole, octupole, and higher-order magnetic components under normal operating conditions, avoiding the need for dedicated magnetic tests. Among the upgraded insertion devices – planar, in-vacuum, and knot-type – only the knot-type device shows significant multipole components beyond sextupole, reaching octupole order. This study focuses on the knot-type device, which is expected to be used in SLS 2.0 and in other modern synchrotron facilities, presenting measurements and comparisons with simulation results.

THE INSERTION DEVICES AT SLS 2.0

The Swiss Light Source 2.0 (SLS 2.0) is a 2.7 GeV fourth generation synchrotron light source currently being commissioned at the Paul Scherrer Institute [1]. The machine lattice is based on a seven-bend achromat scheme including both longitudinal and reverse bends to achieve a very low emittance. The storage ring hosts various insertion devices (IDs), some reused and others newly developed, including in-vacuum planar IDs and advanced APPLE-X knot IDs. Hard X-ray performance is improved with shorter period, more powerful in-house-built in-vacuum undulators. Soft X-ray beamlines now use APPLE-X-knot undulators [2] – based on the design from the SwissFEL Athos beamline [3] – which allow full polarization control and reduce the central heat load. Their advanced "knot" magnetic structure [4–6] also suppresses unwanted higher-order harmonics, improving optical performance and energy resolution. The IDs may introduce higher-order multipole field components affecting the optics, dynamic aperture [7], and beam lifetime. A careful evaluation and correction of these effects is essential to optimize the performance of the machine. In SLS 2.0, the highest multipole order magnet installed and which can be used to control the non-linear optics of the machine is the octupole. Consequently, compensating multipole components beyond the octupole order in the undulators is not straightforward. This is the first time that this kind of ID is installed in a synchrotron, where high resolution beam-based measurements are possible, using the fact that the beam passes through the ID many thousands of times, allowing for a more precise determination of the higher-order multipoles compared to what is possible in a single-pass machine. Beam-based measurements in 2025 showed all IDs have multipoles no higher than sextupole, except the UE36 knot-type (Apple-X) device, which exhibits more significant higher-order complexity.

MODELING

We generated a high-resolution 3D magnetic field map using RADIA [8] with longitudinal step size of 0.5 mm along the longitudinal z-axis, and transverse steps of 20 µm spanning from -2 mm to +2 mm and from -0.2 mm to +0.2 mm in the horizontal (x) and vertical (y) direction, respectively. The asymmetry of the grid range in the transverse plane is due to the fact that we restrict ourselves to the analysis of the normal multipoles in this proceeding. Since the multipoles have to be computed around the reference trajectory at the location $(z, x_{\mathrm{TR}}, y_{\mathrm{TR}})$, the first step of the analysis is the determination of such a trajectory. The transverse particle motion is obtained through a stepwise integration of the field along z. At each step, the transverse angles x' and y' are updated using the local magnetic field components according to:

$$x_i' = x_{i-1}' + \frac{1}{B_\rho} B_y \, \Delta z, \qquad y_i' = y_{i-1}' + \frac{1}{B_\rho} B_x \, \Delta z, \quad (1)$$

where B_ρ is the magnetic rigidity, and B_x, B_y are the transverse magnetic field components evaluated at the particle location at the preceding step. The transverse positions are subsequently updated using the angles:

$$x_i = x_{i-1} + x_i' \, \Delta z, \qquad y_i = y_{i-1} + y_i' \, \Delta z \quad (2)$$

assuming that the angle is sufficiently small to approximate its tangent with itself. Since the field map does not include corrections of the first and second field integrals, appropriate initial conditions in both position and angle must be determined. These are obtained by minimizing the trajectory deviations. Figure 1 shows a comparison between the uncorrected trajectory in the mid-plane and the optimized trajectory obtained by adjusting the initial conditions at the entrance of the ID. In the machine, this procedure corresponds to locally tuning the beam orbit in the ID region using dedicated orbit correctors. The situation is significantly less critical in the vertical plane, where the maximum beam excursion remains below 5 µm.

Following the procedure described in [9] and [10], we expand the vertical component of the magnetic field at longitudinal position z in a reference frame co-propagating with the beam as:

$$\begin{aligned} B_y(x,s) &= \sum_{n=0}^{\infty} \frac{1}{n!} \left. \frac{\partial^n B_y(x,s)}{\partial x^n} \right|_{x=x_{\mathrm{tr}}} (x - x_{\mathrm{tr}})^n \\ &\equiv \sum_{n=0}^{\infty} b_n^T (x - x_{\mathrm{tr}})^n \end{aligned} \quad (3)$$

* simona.bettoni@psi.ch

Content from this work may be used under the terms of the CC BY 4.0 licence (© 2026). Any distribution of this work must maintain attribution to the author(s), title of the work, publisher, and DOI.

ISBN: 978-3-95450-252-3 ISSN: 2673-5350 doi: 10.18429/JACoW-IPAC2026-THP2053

STATUS OF HIGH BRIGHTNESS OPTICS FOR THE DIAMOND-II STORAGE RING UPGRADE

B. Singh, N. Blaskovic Kraljevic, H. Ghasem, I. Martin, Diamond Light Source, Oxfordshire, UK

Content from this work may be used under the terms of the CC BY 4.0 licence (© 2026). Any distribution of this work must maintain attribution to the author(s), title of the work, publisher, and DOI.

Abstract

We report the status of the high-brightness, low-beta optics for the Diamond-II storage ring upgrade. Investigations of lifetime and injection efficiency will be presented. MOGA optimisation studies have been conducted to improve the nonlinear performance, including by increasing the number of sextupole families and varying the octupoles strengths. We present complementary methods to improve the nonlinear dynamics by optimizing sextupoles, octupoles strengths and linear tunes. Finally, we report the impact of insertion devices on lifetime and dynamic aperture and so on injection efficiency.

INTRODUCTION

To further increase the brightness of the Diamond-II storage ring, separate investigations into reducing either the emittance or the beta-functions at the IDs have been carried out for the Diamond-II TDR lattice [1-3]. Latest results for the lattice solution with low beta functions in the insertion straights will be presented in this paper.

The initial tuning of the low beta lattice suffered from low lifetime and small dynamic aperture (DA) leading to poor injection efficiency (IE) at -3 mm offset. Further studies outlined in this paper were successful at improving the Touschek lifetime (TL) to ~1.4h and the dynamic aperture to around 4 mm. This would allow beam to be injected at -3 mm using either the standard 4 kicker bump injection scheme or the transparent kick and cancel injection scheme planned for top-up operation [4].

The linear and nonlinear optimization was initially carried out using OPA. This was sufficient to develop a solid baseline solution. Following this, a Multi-Objective Genetic Algorithm MOGA [5] was used for optimization of the TL and IE and good progress was made. This MOGA optimized optics will be presented in this paper. One important change for the MOGA-optimised optics was to split the six families of sextupoles into ten families according to the local beta functions. These MOGA optimized sextupole families were obtained first for the nominal optics and resulted in significant improvement in TL [5]. The same method has been applied for the low beta optics optimization, resulting in significantly higher TL, IE and DA (both on and off momentum).

LOW BETA OPTICS

The optical functions and main parameters of the low-beta lattice are presented in Fig. 1 and compared to the nominal lattice in Table 1. The strengths of the sextupoles and octupoles obtained from the OPA optimisation were used as the starting point for these studies.

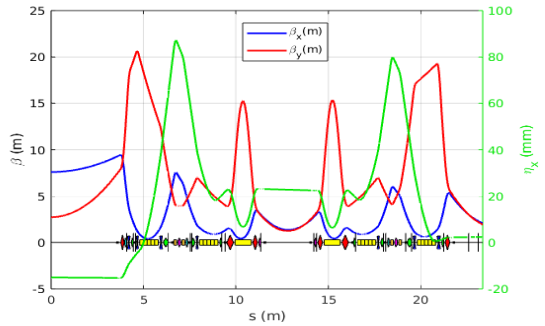

Figure 1: Optical functions in cell 1 for the low-beta optics.

Table 1: Parameters for Nominal and Low Beta Optics

Parameter		Nominal	Low Beta
Q_x		54.14	58.12
Q_y		20.24	21.28
$[\xi_{x0}, \xi_{y0}]$		[-68, -89]	[-72, -101]
ε_x (no IDs) (pm)		162	139
ε_x (all IDs) (pm)		121	127
σ_E (no IDs) (%)		0.094	0.096
σ_E (all IDs) (%)		0.110	0.110
α_C (10^{-4})		1.03	1.10
$\beta_{x/y}$ (m)	Long	8.4/3.4	7.6/2.7
	Standard	5.7/2.3	1.8/1.6
	Mid	2.3/1.7	1.4/1.2
η_x (mm)	Long	5.6	-15.2
	Standard	0.6	2.5
	Mid	22.1	22.0

MOGA OPTIMIZATION

MOGA was used to improve the beam lifetime (TL) and injection efficiency (IE). The variables being adjusted were the horizontal and vertical tunes, the strengths of the ten families of sextupoles and both families of octupoles. Five machine error seeds were used for each possible lattice solution, and the mean TL and IE were used as inputs to the optimiser, to find a solution robust against any specific set of machine errors. Further details of the optimisation method and parameters are given in [5].

A series of three successive optimisation runs were performed, taking the optimum from one run as the input to the following one. The search space was constrained with

ISBN: 978-3-95450-252-3 ISSN: 2673-5350 doi: 10.18429/JACoW-IPAC2026-THP2054

TOP-UP SAFETY SIMULATIONS FOR THE DIAMOND-II STORAGE RING UPGRADE

A. Potter*, S. Birkett, J. Kallikadan, C. Lane, X. Liu, I. Martin, J. Toop-Rose,
Diamond Light Source, Oxfordshire, United Kingdom

Content from this work may be used under the terms of the CC BY 4.0 licence (© 2026). Any distribution of this work must maintain attribution to the author(s), title of the work, publisher, and DOI.

Abstract

Top-up operation at the Diamond-II storage ring will involve injecting bunches of electrons into the ring whilst the photon beamlines are in use. It is important, for the safety of the users, that electrons from the newly injected bunches cannot travel down the photon beampipe to the front end. For a representative beamline, all possible trajectories through the ID straight were identified and tracked through the machine to determine if any combinations of magnet settings exist that would simultaneously allow for stored beam and for electrons to be extracted through the front end. The full range of strengths for all the magnets were considered to account for any magnet power supply failures or different operating modes. Here we present the method used to track the electrons, summarise the results for one beamline and describe the interlocks required to ensure safe operation.

INTRODUCTION

The kick-and-cancel injection scheme will be used during top-up operation at Diamond-II. During top-up, the newly injected bunch will travel around the storage ring off axis until radiation damping causes them to merge with the stored bunches [1]. There is also a risk that a pulsed magnet may fire at the wrong time, for example the beam dump or injection kickers, causing stored bunches to travel through the machine off axis. A bunch will be steered by multipole magnets when passing through them off axis. It is important that the bunches do not recieve a combination of steers from these magnets, that will result in them traveling through the front end beampipe where they could potentially result in an unacceptably high radiation dose

This study continued previous studies done at Diamond [2], and other facilities [3–6] to investigate whether such a combination of steers was possible for each of the front ends.

The method was then extended to investigate the effect that the strengths of certain magnets had, on the possibility of electrons reaching the front end. The results of the simulations were then used to find appropriate interlocks that restrict the range of magnet strengths such that the front ends are safe from electrons.

ACCEPTANCE OF THE FRONT ENDS

The front ends following standard straight sections were investigated first, the locations of the standard straights within the Diamond-II superperiod can be seen in Fig. 1. The acceptance of each front end was calculated as the total phase space area that can pass through the two limiting apertures within the front end. It was found that I15 has a large acceptance when compared to other standard straight front ends. Therefore, the initial studies of top-up safety were done by tracking all of the possible particle paths through the I15 standard straight and SM girder and comparing this with the acceptance of the front end.

Additionally, the I15 front end will contain a beam splitter meaning that there are three distinct paths that electrons could travel through the I15 front end. The straight ahead line (I15), a line angled inboard (I15.1), and a line angled outboard (I15.2).

SIMULATION PROCEDURE

The initial distribution of electrons was generated by calculating the maximum phase space area (in the horizontal plane) that can travel through the insertion device (ID) straight. This included the effects of any chicane magnets and trim coil correctors. The vertical phase space was initially set to zero. All electrons were given the same energy offset which was chosen manually at the start of each simulation.

The SM girder contains six quadrupoles, six sextupoles, one octupole, two anti-bends (offset quadrupoles), two permanent magnet dipoles and one combined function dipole-quadrupole (DQ). For all magnets except dipoles, it was assumed that they could be set to any value between the minimum and maximum strength. This was to account for magnet failures, tuning ranges, and future operation modes. It was assumed that the strength of the DQ could only vary between ± 10 % of its nominal strength without losing stored beam. The strengths of the permanent magnets were not varied throughout the study.

The field strength of each magnet, as a function of the electron coordinates, was calculated using a magnetic field map. This was because the possible paths to the front end involves passing through magnets far off-axis, where it is no longer appropriate to use an ideal field. The tracking through each magnetic element was done by splitting the element into slices, and then using a drift-kick-drift model. Some magnets also contain trim coils used for steering. Two additional field maps where defined for these magnets with the trim coils providing a positive and negative steer.

When the distribution was tracked through a magnet, it was tracked through the magnet multiple times at different strengths, equally spaced between the maximum and minimum possible strengths for that magnet. For the magnets containing trim coils, the distribution was tracked through the magnet three different times for every magnet strength

* andrew.potter@diamond.ac.uk

ISBN: 978-3-95450-252-3 ISSN: 2673-5350 doi: 10.18429/JACoW-IPAC2026-THP2055

DESIGN AND OPTIMISATION OF THE LATTICE FOR THE UK-XFEL SPREADER

A. Potter*, P. Williams, Cockcroft Institute, Daresbury, United Kingdom
A. Wolski, University of Liverpool, Liverpool, United Kingdom
A. Brynes, F. Jackson, Science and Technology Facilities Council, Swindon, United Kingdom

Abstract

The UK-XFEL spreader will distribute 1 MHz bunches between ten undulator beamlines. Each of the different paths through the spreader must transport an electron bunch to the undulator with minimal increase in the emittance and energy spread, whilst also conforming to various geometry constraints. To minimise the energy spread/emittance growth, the design was optimised to mitigate the effect of coherent synchrotron radiation (CSR). This was done by control of the phase advance between repeated sections, and by cancelling CSR kicks using a single kick CSR model. Due to the number of constraints that needed to be adhered to, an optimisation tool was developed to aid in the design of the optics. This paper will give an overview of the optimisation tool, show the design of different sections of the spreader, and then show the results of beam tracking.

UK-XFEL SPREADER LAYOUT

The UK-XFEL spreader will distribute electron bunches between 10 undulator lines [1–3]. FEL 2-6 can be seen in Fig. 1. Only half of design is seen in the figure, the design will be mirrored over x=0. The spacing between two adjacent lines is 8 m. The photon optics will distribute the FEL pulses from each undulator line to numerous end stations, therefore, it was decided that 8 m of space would be needed between the lines so that there would be enough space to fit the end stations.

The straight ahead line (FEL-1) is not included in the spreader design, but is reserved for matter under extreme conditions (MEC) experiments that require high charge bunches. It was decided to put the MEC line on the straight ahead line so that the high charge bunches would not pass through the arc sections where they would be affected by CSR.

FEL-2 is made up of two undulator lines (FEL-2 and FEL-2s) separated by 3 m. This is for two colour pump-probe operation with pulse widely separated in both energy and time. There is a variable path length adjuster (VPLA) chicane along FEL-2s, this allows control over the pump probe separation.

BEAM DYNAMICS AND CSR CANCELLATION

The design of the UK-XFEL spreader was separated into subsections. The separation of the lattice into subsections allowed for the beamline to be optimised in parts, which where then connected together to form a full line using the matching sections. Using subsections simplified the design due to the repeated patterns within the lattice. FEL's 3-6 all follow the same design, just with an additional straight subsection per line along the main diagonal. The subsections are all isochronous and the dispersion is cancelled. The maximum value of the beta function in each subsection was kept as low as possible without interfering with any other constraints. The lengths of the drift sections were set so that the spacing between adjacent lines was 8 m. The linear optics was also designed in way so that the effects of CSR were mitigated.

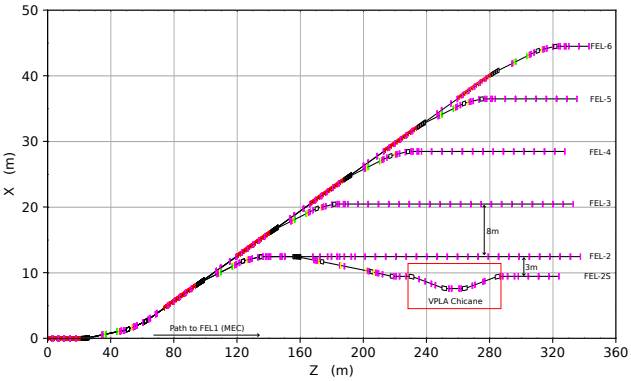

Figure 1: Layout of the beam spreader of the UK XFEL.

CSR Mitigation Within a Subsection

CSR occurs when the bunch is transported through a dipole magnet. The radiation emitted by the electrons at the back of the bunch interacts with the electrons at the front of the bunch. This causes energy loss, and as a result, the bunch is steered too much by the dipole. Therefore, the bunch exits the dipole with a kick in both x and p_x. Due to the horizontal offset when leaving the dipole, the bunch is kicked further by any subsequent quadrupoles it passes through. The kicks from all of the elements add up over the length of a subsection, causing the beam to become deformed and an increase in emittance.

To mitigate the kicks caused by CSR over the length of a subsection, the strengths of the quadrupoles were tuned so that the horizontal kick was cancelled at the exit of the last dipole within the subsection. This was done using a simplified model of the CSR, where the energy loss is applied to the bunch as a single kick at the center of the dipole. The resulting kick in x and p_x, through the second half of the dipole and any subsequent quadrupoles, was calculated using transport matrices.

The energy loss was initially estimated using analytical formula, which can be found in [4], but it was found that

* andrew.potter@diamond.ac.uk

Content from this work may be used under the terms of the CC BY 4.0 licence (© 2026). Any distribution of this work must maintain attribution to the author(s), title of the work, publisher, and DOI.

ISBN: 978-3-95450-252-3 ISSN: 2673-5350 doi: 10.18429/JACoW-IPAC2026-THP2056

LINEAR AND NON-LINEAR OPTICS OPTIMISATION FOR THE DIAMOND-II STORAGE RING

N. Blaskovic Kraljevic*, H. Ghasem, I.P.S. Martin, B. Singh,
Diamond Light Source, Oxfordshire, UK

Abstract

The design performance of the 3.5 GeV Diamond-II low-emittance electron storage ring has been studied as a function of the linear and non-linear lattice tuning parameters. A Multi-Objective Genetic Algorithm (MOGA) has been implemented and refined to optimise both the beam lifetime and the injection efficiency for off-axis injection. The sextupole magnets have been further split into ten families, according to their local linear optics, with each family varied independently as part of the MOGA optimisation; if necessary, the resulting chromaticity is corrected with a subset of the sextupoles to be within an operational range. In addition, the tune and the strengths of the two families of octupoles have been varied as part of the MOGA search. The simulations have been run on 5 machine error seeds, including misalignment, field strength and multipole errors, to obtain a solution which is robust against machine imperfections. The results of the optimisation are presented alongside a comparison of the baseline performance.

INTRODUCTION

The beam lifetime and injection efficiency (IE) of the Diamond-II storage ring [1] has been further optimised by varying the sextupole and octupole strengths. The work presented here builds on the Multi-Objective Genetic Algorithm (MOGA) implemented previously [2], but on this occasion the sextupole families have been subdivided according to their local linear optics. No hardware change is required as each sextupole will be on an individual power supply.

The Diamond-II storage ring design consists of six identical super-periods, with adjacent super-periods separated by a long (L) straight. Each super-period consists of four cells, with adjacent cells within a super-period separated by a standard (S) straight. Each cell also contains a mid (M) straight at its centre [1].

As the linear optics is different according to if the end of the cell is adjacent to a long or standard straight (Fig. 1), the four families of sextupoles S1 to S4 have been subdivided with those closest to a long straight renamed as SnL (with $n = 1, 2, 3, 4$). The remaining sextupoles preserve the existing naming convention where SnA (with $n = 2, 3, 4$) are chromatic sextupoles at high dispersion locations, used primarily to correct chromaticity, and SnX (with $n = 1, 5, 6$) are harmonic sextupoles, used to maximise the dynamic aperture (Fig. 1).

SIMULATION

The Diamond-II storage ring lattice in Accelerator Toolbox (AT2) [3] was used, including apertures for closed collimators and insertion devices (IDs). A radiofrequency (RF) voltage of 1.42 MV was used in the first instance, without a harmonic cavity. Random errors were applied to each of five machine seeds consisting of Δx, Δy transverse misalignment errors, roll errors and fractional strength errors; the 'reduced' errors used [4] replicate the final, corrected machine performance after all optics corrections steps have been applied, without needing to conduct the lengthy and time-consuming commissioning procedure [1]. In addition, random and systematic multipole errors were added to quadrupoles and sextupoles.

The simulation procedure [2] includes orbit, tune and chromaticity correction. For each possible lattice solution, the tune was corrected to the nominal value of $(\nu_x, \nu_y) = (54.14, 20.24)$ using five families of quadrupoles located in dispersion-free regions at the ends of the standard and long straights (Q1N, Q2N, Q0L, Q1L and Q2L). The chromaticity was corrected using all families of chromatic sextupoles only if the chromaticity was either below 2 (in which case it was corrected to 2) or above 5 (in which case it was corrected to 5), to ensure that the chromaticity is large enough to mitigate transverse instabilities [5] and that it is small enough for an optimum efficacy of the transverse multi-bunch feedback.

* neven.blaskovic-kraljevic@diamond.ac.uk

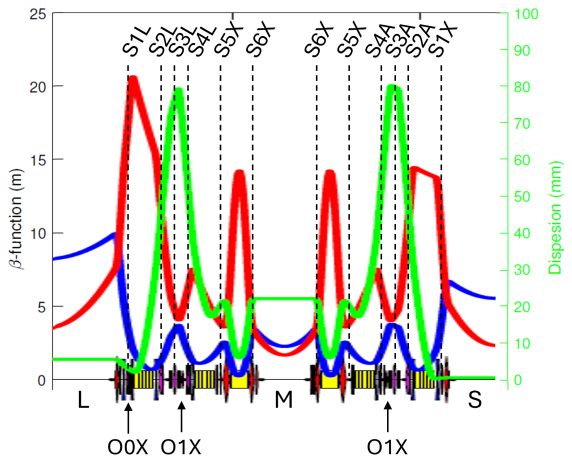

Figure 1: Horizontal (blue) and vertical (red) β functions and dispersion in the first cell between a long (L) and standard (S) straight [1], indicating the location of the sextupoles and octupoles.

Content from this work may be used under the terms of the CC BY 4.0 licence (© 2026). Any distribution of this work must maintain attribution to the author(s), title of the work, publisher, and DOI.

ISBN: 978-3-95450-252-3 ISSN: 2673-5350 doi: 10.18429/JACoW-IPAC2026-THP2057

CHARACTERISATION AND OPTIMISATION OF THE DIAMOND LINAC IN PREPARATION FOR THE DIAMOND-II UPGRADE

N. Blaskovic Kraljevic*, R. Fielder, A. Gracey, A. Potter, A. Tropp, N. Vitoratou,
Diamond Light Source, Oxfordshire, United Kingdom

Abstract

The existing 100 MeV linac at the Diamond Light Source will be used as the pre-injector into the upgraded Diamond-II booster ring for injection into the new 3.5 GeV storage ring. In preparation for the upcoming upgrade, we have characterised the linac beam properties, to provide an input for beam tracking simulations and to optimise the linac beam dynamics. We present the latest linac performance results, the optimisation of the linac and linac-to-booster beam transport and the injection efficiency into the current Diamond booster ring.

INTRODUCTION

Diamond Light Source makes use of a 100 MeV electron linac pre-injector containing two identical 5.2 m-long accelerating structures, together with a three-stage bunching section and a 90 keV thermionic electron gun [1, 2]. The existing linac will continue to be used as a pre-injector into the upgraded Diamond-II booster ring for injection into the new 3.5 GeV storage ring [3]. In preparation for the Diamond-II upgrade, the beam dynamics in the linac and in the first section of the linac-to-booster (LTB) transfer line has been studied to develop the tools to achieve and maintain a high injection efficiency into the booster ring.

SUB-HAMONIC PRE-BUNCHER

The master oscillator frequency at Diamond is 500 MHz, which is the operating frequency of the radiofrequency (RF) cavities in the booster and storage rings. The linac gun and the sub-harmonic pre-buncher (SPB) that follows it are also operated at 500 MHz to produce either a singe bunch or a train of bunches to be injected into the booster and then storage ring [4]. The remaining RF structures in the linac, comprising two bunching units followed by two accelerating structures, are operated at 3 GHz.

Operation of the SPB is not essential to inject beam into the booster; however, operating without the SPB results in the acceleration of around three 3 GHz 'bunchlets' along the linac for each 500 MHz pulse from the gun (Fig. 1a). These bunchlets can have different beam trajectories and energy at the end of the linac, as can be seen on the beam charge distribution observed on screens in the LTB. For measurements involving the analysis of beam screen images (for example, for the emittance measurement described below), the SPB was turned on, and its power and phase was adjusted to obtain a single bunchlet (Fig. 1b).

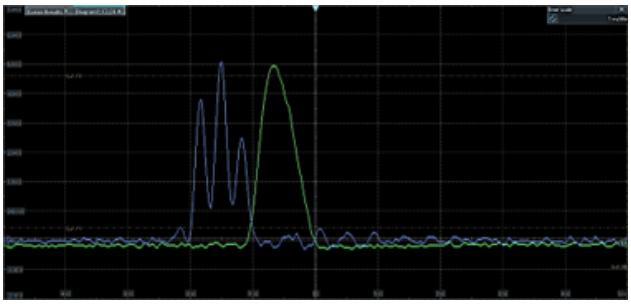

(a)

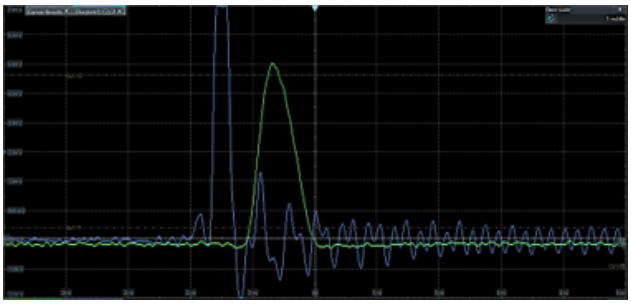

(b)

Figure 1: Wall current monitor oscilloscope traces showing bunch charge as a function of time with (a) SPB off and (b) SPB on, as measured upstream of the SPB (green) and at the end of the linac (blue).

HYSTERESIS CHARACTERISATION

Hysteresis is a known feature of the Diamond magnets due to their iron yokes. The established procedure is to cycle the magnets before setting the desired current. As the corrector magnets and quadrupoles in the LTB (Fig. 2) are on bipolar power supplies operated in the range of −5 A to 5 A, the cycling consists in following the sequence of magnet currents: 5 A → −5 A → 4 A → −3 A → 2 A → −1 A → 0 A. With a wait time of up to 15 s at each setting, the cycling takes close to 2 minutes.

We investigated if a reproducible magnetic field could be obtained for the first horizontal and vertical corrector (STR-01) and the first two quadrupoles (QUAD-01, QUAD-02) in the LTB without performing a full cycling procedure, by performing a beam-based measurement using a downstream beam position monitor (BPM). A step change in corrector or quadrupole setting from 5 A to −5 A results in a significant change in beam position at BPM-02; it was found that it takes ∼1.4 s for the BPM reading to settle on its new value suggesting that a wait time of 2 s is sufficient for both correctors and quadrupoles in the LTB.

The hysteresis loop of STR-01 was mapped out by first fully cycling the corrector to 0 A and then varying the current

* neven.blaskovic-kraljevic@diamond.ac.uk

Content from this work may be used under the terms of the CC BY 4.0 licence (© 2026). Any distribution of this work must maintain attribution to the author(s), title of the work, publisher, and DOI.

ISBN: 978-3-95450-252-3 ISSN: 2673-5350 doi: 10.18429/JACoW-IPAC2026-THP2058

IMPACT OF INJECTION ERROR ON EUV FEL PERFORMANCE IN AN APL-BASED BEAMLINE

M. Miceski*[1,2], M. Matys[1], A. Whitehead[1,2], P. V. Sasorov[1], X. Wu[3], J. Vieira[3], A. Jancarek[1,2], A. Molodozhentsev[1]
[1]The Extreme Light Infrastructure ERIC, Dolní Břežany, Czech Republic
[2]Czech Technical University in Prague, FNSPE, Prague, Czech Republic
[3] Instituto Superior Técnico, Lisbon, Portugal

Abstract

Recent advances in laser-plasma accelerators (LPA**s**) have generated high-quality electron beams characterized by high peak currents and low emittance, making them suitable for compact, next-generation free-electron lasers (FEL**s**). However, variations in laser performance from shot to shot cause mismatches in position and angle at the injection point, complicating efficient beam transport and stable FEL operation. To preserve the electron bunch quality during beam propagation through the transport system, an active plasma lens (APL) can be used as part of the capture mechanism. This report investigates how injection errors influence electron beam properties along the beamline and their subsequent effect on FEL radiation in the extreme-ultraviolet (EUV) range. The results demonstrate an acceptable range of injection errors and emphasize the strengths and limitations of APL as capture system for optimal FEL performance. This work emphasizes the potential of APL technology to develop compact FELs and improve LPA beam applications. Such progress is vital for future FEL facilities at ELI ERIC in the Czech Republic and for the EuPRAXIA project.

INTRODUCTION

Laser–plasma accelerators provide accelerating gradients that are orders of magnitude higher than those achievable with conventional RF linacs, allowing much more compact configurations for generating high-energy electron beams. These beams are attractive candidates for driving next-generation free-electron lasers, capable of delivering ultrashort, high-brightness X-ray pulses. Such radiation sources open new opportunities for femtosecond-scale studies in physics, chemistry, biology, and materials science, as well as for applications in medicine and industry [1].

However, the intrinsically large energy spread and divergence of LPA-based beams present significant challenges for applications such as FELs. Active plasma lens provides an effective and compact solution, offering strong, azimuthally symmetric focusing with high field gradients that significantly reduce chromatic emittance growth. When operated in the linear regime, APL preserve beam emittance [2], making them particularly well suited for high-brightness applications. Their integration into the beamline is therefore a key step toward achieving efficient and reliable LPA-driven FEL operation. Laser pointing stability limits stable FEL operation. These fluctuations translate into transverse and angular offsets of the electron beam, leading to charge loss at beamline apertures. This work presents a tolerance analysis of injection error and determines the threshold values required to keep saturation within the undulator.

FEL FRAMEWORK

Undulator Configuration

The undulator section under consideration consists of two consecutive SwissFEL-type U19 modules [3], each with an undulator period of 19 mm and a length of 2 m, resulting in a total interaction length of 4 m. The beam is matched at the entrance of the undulator such that a beam waist is formed at the center of the 4 m section, minimizing the average transverse beam size throughout the undulator section. This matching condition is essential for maintaining strong FEL coupling and efficient radiation gain. The undulator parameter, K_u, is a tunable quantity and can be adjusted in the range 1.2 to 1.9 by varying the size of the gap.

Electron Beam

The objective is to achieve saturation with the undulator section. To meet this requirement, the electron beam at the undulator entrance must satisfy specific conditions. For an electron beam of 300 MeV, these include an RMS slice normalized emittance below 0.4 mm mrad in both transverse planes, an RMS relative slice energy spread below 0.25% and a peak current of approximately 2.6 kA.

Laser–plasma accelerator technology has recently achieved significant advances that enable stable operation and the generation of high-quality electron beams. In this study, an electron beam of about 300 MeV is used, obtained with the shock-front injection method, as experimentally demonstrated [4, 5]. The initial electron beam is obtained using the OSIRIS PIC code [6]. Its projected parameters are as follows: the RMS divergence is 0.55 mrad (horizontal) and 0.71 mrad (vertical), and the RMS normalized emittance is 0.23 mm mrad (horizontal) and 0.37 mm mrad (vertical). The larger values in the vertical plane are because of the vertical laser polarization. The bunch charge is 24.71 pC, with a bunch length of 0.48 μm. These parameters indicate a high-quality electron beam for a beam obtained from laser–plasma acceleration.

* mihail.miceski@eli-beams.eu

Content from this work may be used under the terms of the CC BY 4.0 licence (© 2026). Any distribution of this work must maintain attribution to the author(s), title of the work, publisher, and DOI.

ISBN: 978-3-95450-252-3 ISSN: 2673-5350 doi: 10.18429/JACoW-IPAC2026-THP2065

EXPERIMENTAL STUDY OF REVERSE TAPERING AND RESONANCE DETUNING IN A SEEDED X-RAY FEL

L. Cao*, S. Liu, T. Long, E. Schneidmiller, J. Wu,
Deutsches Elektronen-Synchrotron DESY, Hamburg, Germany
G. Geloni, G. Perosa, European X-Ray Free-Electron Laser, Schenefeld, Germany

Content from this work may be used under the terms of the CC BY 4.0 licence (© 2026). Any distribution of this work must maintain attribution to the author(s), title of the work, publisher, and DOI.

Abstract

Reverse tapering can suppress the FEL field while preserving electron microbunching for downstream radiators over an appropriate range of taper strength. In a monochromatically seeded FEL, one-dimensional small-signal theory suggests that the response to reverse tapering can be compared with the response to an accumulated resonance detuning. Here, we report on an experimental investigation of the relationship between undulator reverse tapering and resonance detuning in a seeded hard X-ray FEL, where the fixed seed frequency eliminates the influence of SASE photon-energy jitter. A modulator-radiator configuration was used in which U19 to U24 were scanned either by changing the resonance setting or by applying reverse tapering, while U25 was kept as the downstream radiator. The scans were performed with U25 active, to characterize the bunching-driven radiator signal, and with U25 off, to characterize residual upstream radiation. The U25-active spectra comparison shows a good agreement between reverse tapering and resonance detuning. The U25-off spectra show a stronger reduction of residual upstream radiation on the negative-detuning side than the U25-active radiator signal, indicating that the radiation field is suppressed more efficiently than the bunching-related signal, as expected for reverse-taper operation.

INTRODUCTION

High-purity circular polarization in X-ray FELs can be obtained by combining a planar main undulator with a short helical afterburner, provided that the linearly polarized background from the main undulator is sufficiently suppressed and the electron density modulation is preserved. Reverse tapering was proposed for this purpose and was shown to reduce the FEL field by orders of magnitude while maintaining substantial bunching over an appropriate taper range [1–3].

Both reverse tapering and resonance detuning modify the local resonance condition of the beam. However, their relationship is not obvious because reverse tapering produces an accumulated detuning, whereas a resonance-detuning scan applies a direct offset to the whole scanned section. Establishing how these two controls are related is important for understanding reverse-taper operation and for optimizing afterburner schemes. In SASE reverse-taper operation, although the amplified radiation frequency remains close to the resonance condition near the entrance of the tapered section, it is not fixed because of the intrinsic shot noise. In a monochromatically self-seeded FEL, by contrast, the reference frequency is fixed by the narrow-band seed. This allows the same downstream undulator section to be scanned in two controlled and comparable ways: by imposing a direct resonance offset relative to the seed frequency, or by applying a reverse taper.

In addition to the overall scale between taper strength and resonance detuning, the sign of the equivalent detuning is also expected to matter. One-dimensional small-signal theory suggests an asymmetric response with respect to the detuning sign. In the theory, the radiation field amplitude $\tilde{E}$ obeys a third-order linear differential equation. With the trial solution $\tilde{E} \propto \exp(\Lambda\hat{z})$, the corresponding dispersion relation can be written as [4]

$$\Lambda\left[(\Lambda + iC)^2 + \hat{\Lambda}_p^2\right] = i, \tag{1}$$

where C is the detuning parameter and $\hat{\Lambda}_p$ is the normalized coupling parameter. This dispersion relation is not invariant under C to $-C$, and therefore the eigenvalues and the linear propagation matrix of the seeded FEL amplifier are different for the two detuning signs. Since the density modulation, or bunching, is related to the field derivative $\tilde{E}'$, the bunching at the radiator entrance is not expected to satisfy $b(C) = b(-C)$.

Here, we compare reverse tapering and resonance detuning in the linear-gain regime of hard X-ray self-seeding (HXRSS) operation [5, 6] at the European XFEL [7]. The goal is to determine whether the reverse-taper response can be represented by an equivalent detuning offset and to compare the behavior of the bunching-driven radiator signal with the residual upstream radiation.

EXPERIMENTAL METHOD AND SCALING

As shown in Fig. 1, the measurement was performed in SASE2 of the European XFEL after optimizing HXRSS performance. Upstream undulator cells are used to generate SASE radiation, which is filtered by the forward Bragg diffraction crystal to produce the monochromatic seed wake. The weak chicane can be used to delay the electron bunch to overlap with the seed and wash out upstream microbunching.

A gain curve scan, in which the last active downstream cell was removed one by one, was used to choose a modulator-radiator configuration with the radiator placed before saturation. As shown in Table 1, the seeded signal changes weakly up to cell 21, grows rapidly from cell 22 to cell 25, and starts to level off by cell 26. Therefore, U19 to U24 were used as the scanned section and U25 setting was fixed to be used as

* l.cao@desy.de

ISBN: 978-3-95450-252-3 ISSN: 2673-5350 doi: 10.18429/JACoW-IPAC2026-THP2067

INVESTIGATION OF THERMAL DEGRADATION AND STABILITY IN MULTI-ALKALI ANTIMONIDE PHOTOCATHODES: NaKSb(Cs) vs KCsSb

S.K. Mohanty*[1,2], A. Oppelt[1], D. Sertore[2], F. Stephan[1], L. Monaco[2], M. Krasilnikov[1]
[1]DESY, Zeuthen, Germany
[2]Istituto Nazionale di Fisica Nucleare - LASA, Segrate, Italy

Abstract

Multi-alkali antimonide photocathodes have emerged as promising photoemissive materials for electron sources in high-repetition-rate free-electron laser (FEL) applications due to their low thermal emittance and high quantum efficiency in the green wavelength region. To evaluate their feasibility for operation in high-gradient RF guns, a collaborative effort between DESY-PITZ and INFN-LASA was initiated to develop and characterize multi-alkali photocathode materials under operative condition. As part of this effort, a NaKSb(Cs) photocathode belonging to the multi-alkali antimonide family was grown on a molybdenum substrate using a sequential deposition method in the new preparation system at INFN-LASA. A thermal degradation study of this photocathode was conducted, and its behavior was compared with a KCsSb film. This contribution presents the experimental results of the NaKSb(Cs) photocathode, focusing on its thermal degradation behavior and comparative analysis with the KCsSb photocathode.

INTRODUCTION

Alkali-based photocathodes with high quantum efficiency (QE) in the visible spectrum are attractive candidates for producing high-quality electron beams, making them well suited for applications in X-ray free-electron lasers (XFELs) and energy-recovery linacs (ERLs) [1]. However, despite their favorable photoemission properties, these materials are known to experience rapid QE degradation during operation in RF guns. Several studies, including our own operational experience, have reported a relatively short operational lifetime of these photocathodes [2–4]. Multiple factors contribute to this degradation, including chemical poisoning from residual gases, ion back-bombardment, laser-induced heating, and thermal decomposition of the photocathode material. Among these, thermal decomposition, driven by the photocathode operating temperature, may play a significant role in determining the photocathode's operational lifetime. During RF gun operation, the RF power dissipated in the cavity walls leads to heating of the gun structure and cathode region. Even with an efficient water-cooling system, the temperature may rise by tens of degrees Celsius above room temperature [5]. Therefore, investigating the performance and stability of alkali antimonide photocathodes at elevated temperatures is essential for understanding their degradation mechanisms and estimating their operational lifetime in RF gun environments.

Within the alkali antimonide family, two photocathodes—NaKSb(Cs) and KCsSb—were selected to investigate their degradation behavior at elevated temperatures, as they represent widely studied and comparatively robust members of the alkali antimonide photocathode family. The following section presents the growth recipe of the NaKSb(Cs) photocathode and discusses its thermal degradation characteristics, along with a comparison to the KCsSb photocathode.

PHOTOCATHODE PREPARATION

As reported in previous papers, a reproducible recipe for NaKSb(Cs) photocathodes has been established in our R&D preparation system at INFN LASA [6]. Encouraged by these positive results, we recently produced a NaKSb(Cs) photocathode using INFN-designed Mo plugs in a newly developed production chamber. A detailed description of the new production system can be found in references [2, 6–8].

One Mo plug was polished to a mirror-like finish (reflectivity > 54% at 543 nm, compared to the theoretical value of 57% [9]) to enable reflectivity measurements during and after the photocathode growth process. The sample was ultrasonically cleaned before being loaded into the UHV system. Prior to deposition, the cathode plug was heated to 450 °C for at least two to three hours to remove residual contaminants from the surface.

To better investigate the real-time photoemissive and optical properties during film deposition, a multi-wavelength diagnostic setup was implemented. This setup mainly consists of a Laser-Driven Light Source (LDLS) system and a motorized filter wheel. The filter wheel can accommodate up to eight different optical filters (254, 297, 365, 488, 515, 540, 632, and 690 nm) and rotates in a programmed sequence during deposition, enabling real-time monitoring of the photocurrent and reflectivity of the deposited films [7, 8]. For post-production optical characterization, a monochromator in combination with the LDLS light source is used.

RESULTS AND DISCUSSIONS

For the NaKSb(Cs)-1 cathode, the growth process was initiated by depositing a 5 nm thick Sb layer at 90 °C, followed by K and Na deposition at 110 °C until the photocurrent reached its maximum value. Subsequently, to enhance the final QE, Sb and Cs were further deposited in a yo-yo deposition sequence at 110 °C until the photocurrent approached saturation. All thicknesses mentioned above were measured using a Quartz Crystal Microbalance (QCM). The QE at 515 nm was recorded as 3.7% immediately after production. After deposition, the spectral response was measured and

* sandeep.mohanty@desy.de

Content from this work may be used under the terms of the CC BY 4.0 licence (© 2026). Any distribution of this work must maintain attribution to the author(s), title of the work, publisher, and DOI.

ISBN: 978-3-95450-252-3 ISSN: 2673-5350 doi: 10.18429/JACoW-IPAC2026-THP2069

COMPENSATING THE EFFECT OF ASYMMETRICALLY PLACED UNDULATORS IN FODO LATTICES

J. Zemella*, P. Niknejadi, M. Vogt, Deutsches Elektronen-Synchrotron DESY, Hamburg, Germany
Z. Chen, B. Faatz, Shanghai Advanced Research Institute, Pudong, China

Abstract

The dynamical focusing of FEL undulators with variable gap in FODO lattices with varying but overall low energy is detrimental to the FODO optics. In the absence of compensation by adjusting the FODO quadrupole strengths it may drive the cell unstable. Typical examples of FELs in the critical regime are FLASH at DESY and the SXFEL-SBP at the Shanghai Synchrotron Radiation Facility. Before, in our contributions to FEL 2024 and IPAC 2025 we have extensively discussed the case where the undulators are centered inside the FODO drift of a Lattice with symmetric FODO cells. Here we treat the fairly common case where the drifts on each side of the undulator are unequal, which has significant impact on the compensation strategy and stability issues.

INTRODUCTION

In Ref. [1] we have discussed the effect of the transverse focusing of undulator insertions on the electron optics of FODO structures designed to stabilize the beam transport through the long undulator sections of Free Electron Lasers (FELs). At low beam energy in particular, the pre-matched optics (e.g. for open gaps / vanishing undulator strength) may become unstable. The Shanghai Soft X-Ray Free Electron Laser Facility (SXFEL) [2, 3] at the Shanghai Synchrotron Radiation Facility (SSRF), and the Free electron LASer in Hamburg (FLASH) [4–6] at DESY – also in its upgraded form [7–9] – can operate in this potentially unstable regime. The topic has been treated before by various groups [10–12], but not at this generality. Following Refs. [1, 13], we refer to FODO cells with undulators inserted into the "O"-drifts as "FUDU" cells. In Ref. [1] we presented stability criteria and a numerical scheme to maintain an initially matched optics under variation of the undulator strengths. In Ref. [13] we derived a quasi-analytical match-preservation scheme for exactly mirror-symmetric "fUDUf" cells[1], i.e. cells with two identical undulators and identical up- and downstream drifts surrounding each undulator. There, the match-preservation conditions reduce to the real zeros of a polynomial of order of 4 in θ_f .

In most FUDU designs, however, the up- and downstream drifts surrounding each undulator are not identical, breaking the mirror symmetry of the individual insertion. In the present contribution we generalize the scheme of Ref. [13] to this practically relevant asymmetric case. Figure 1 gives a sketch of our our asymmetric fUDUf scheme, and illustrates

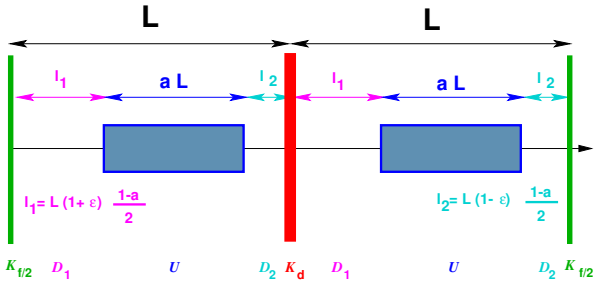

Figure 1: Schematic drawing of an asymmetric fUDUf cell, illustrating our notation.

the meaning of the half-cell length L, as well the filling factor a and the asymmetry parameter ϵ. The match-preservation conditions now yield a polynomial of order of 8 in θ_f, whose roots can be computed easily numerically.

STABILITY ASPECTS OF THE PLANAR ($\theta_{Ux} \equiv 0$) FUDUF

In their 2012 paper [11] Quattromini et al. proposed that undulator focusing should drive the optics of the underlying focusing structure unstable for undulator strengths in certain bands. Here we adopt the cell normal form coordinates and the dimensionless scaled kick strengths $\theta_n := \kappa_n L := k_n l_n L$ ($n = f, d, Ux, Uy$) of Refs. [1, 13], with the k_n, l_n being the "conventional" focusing strengths, and the element lengths respectively, and use throughout the dimensionless β-functions $\bar{\beta}_i := \beta_i / L$ ($i = x, y$), with L the half length of the FODO cell. Moreover, we re-use the notations for matrices representing the thin lens quadrupoles $\underline{K}_f$, $\underline{K}_d$, the drifts $\underline{D}_{l/L}$ of length l, and the (thick lens, planar horizontally wiggeling) undulator $\underline{U}_{a,\theta_{Ux},\theta_{Uy}}$ of length aL, and independent scaled focusing kicks θ_{Ux} and θ_{Uy} (here: $\theta_{Ux} \equiv 0$).

Two of us [12] have analyzed the assertion of Ref. [11] by introducing a parametrization of the half-cell maps using two functions $A_{a,\epsilon}(\theta_{Uy})$, and $B_{a,\epsilon}(\theta_{Uy})$.[2] This parametrization, which factors out the scaled quadrupole kick strengths θ_f and θ_d, enables certain conclusions on the stability of the full fUDUf map $\underline{C}^*$. In particular, it turns out that trace $\underline{C}^*$ is independent of θ_f and θ_d, whenever $A_{a,\epsilon}(\theta_{Uy}) = 0$. Moreover $|\text{trace}\, \underline{C}^*| \leq 2$ then requires that $|B_{a,\epsilon}(\theta_i)| \leq 1$ for the zeros θ_i of $A_{a,\epsilon}$. As usual, the case $|\text{trace}\, \underline{C}^*| = 2$ (here $|B_{a,\epsilon}(\theta_i)| = 1$) must be treated with some extra care. See e.g. Ref. [1]. When $a = 1$, $\underline{C}^*$ is independent of ϵ and we choose $\epsilon = 0$. Then $A_{1,0}$ has zeros at $\theta_n = n^2\pi^2$, $n \in \mathbb{N}_*$. These θ_n are at the same time maxima of $B_{1,0}$ with $B_{1,0}(\theta_n) = 1$. Numerical studies indicate that $\underline{C}^*(a = 1, \theta_{Uy}; \theta_f, \theta_d)$ has a

* johann.zemella@desy.de

[1] We restrict ourselves to fUDUf cells for brevity, but it is clear that analogue results can be derived for dUFUd cells.

[2] In the original paper A and B are functions of $\xi := \sqrt{\theta}$.

Content from this work may be used under the terms of the CC BY 4.0 licence (© 2026). Any distribution of this work must maintain attribution to the author(s), title of the work, publisher, and DOI.

ISBN: 978-3-95450-252-3 ISSN: 2673-5350 doi: 10.18429/JACoW-IPAC2026-THP2070

SIMULATION STUDIES OF SRF CW PHOTOINJECTOR BRIGHTNESS OPTIMIZATION FOR DIFFERENT RF GUN GRADIENTS AND PHOTOCATHODE LASER PULSE SHAPES*

S. Zeeshan†, M. Krasilnikov, X. Li, Deutsches Elektronen Synchrotron DESY, Zeuthen, Germany

D. Bazyl, I. Zagorodnov, Deutsches Elektronen Synchrotron DESY, Hamburg, Germany

Abstract

Developments of a superconducting radiofrequency (SRF) photoinjector for future continuous-wave (CW) operation of the European XFEL are currently underway at DESY. A superconducting L-band 1.6-cell cavity is considered as a high brightness electron source capable of supporting CW operation and meeting the stringent beam quality requirements of cutting edge XFEL facilities. Given the limitations on the attainable gradient in the superconducting gun, photocathode laser pulse shaping provides an effective means of mitigating space charge driven emittance growth. In this study, 4D integral brightness; combining emittance and current profile is used as the main optimization objective. Multiobjective optimization using ASTRA has been performed to minimize the electron beam emittance and maximize its brightness for various temporal and transverse profiles of the photocathode laser pulse in the European XFEL SRF photo injector. Photocathode laser temporal and transverse distributions are compared in terms of achievable 4D beam brightness and their dependence on the attainable RF gradient in the SRF gun. The optimized photo injector working points are propagated through start-to-end simulations to evaluate brightness preservation up to the undulator entrance.

INTRODUCTION

The short wavelength FELs (European XFEL and FLASH) generate high brilliance coherent laser light and require high brightness electron beams [1][2]. To increase the average brilliance even further, the CW operation of photoinjector of the FELs is desired. For the EuXFEL the CW operation is under considerations since many years [3]. The proposed injector for the CW operation will use superconducting L-band 1.6 cell cavity [4]. The injector has been studied in detail including start-to-end simulation calculations for the beam transport to the undulators and FEL simulations on the X-ray intensities for the attainable photon energies [5]. The CW photoinjector layout has been modified later in terms of position of solenoid and the first accelerating cryomodule (A1) guided by the optimization of the photoinjector for the temporal flattop profile of the photocathode laser pulse.

The performance of the SRF photoinjector critically determines the XFEL beam quality and can put constraint in gaining the expected XFEL performance. Advanced shaping of the photocathode laser pulses, both temporaly and transversely, is essential to minimize emittance and maximize brightness, especially given the limited gun gradient and solenoid separation. The longitudinal Gaussian (G) with transverse radial uniform (RU) serves as a basic reference case. This is compared with more advance shapes like longitudinal flattop (FT) with transverse truncated Gaussian (TG) (1σ) which is identified as the most promising candidate for low emittance performance. The longitudinal FT with transverse RU represents a reasonable startup scenario while longitudinal Inverted parabolic (IP) with transverse TG can be considered as a feasible alternative to FTTG. In this study, these laser distributions and RF gradients in the SRF gun are systematically studied to identify optimal operating conditions and to evaluate the tolerance to parameter variations required to achieve the desired beam emittance and brightness. A similar study, covering a broader set of operating scenarios, has been reported for the CW photoinjector of LCLS-II [6].

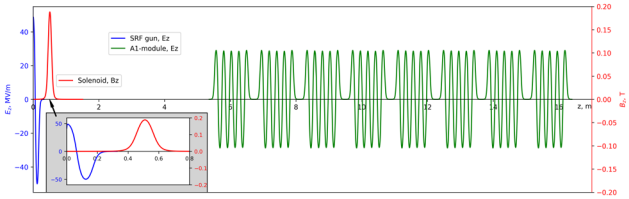

Figure 1: Electromagnetic field distribution along the SC photo injector.

Beam Dynamic Optimization in Injector

To evaluate the performance of the SC photo injector for future CW operation of the European XFEL the layout used in simulations is shown in Figure 1. The layout includes an L-band 1.6-cell SC cavity, an SC solenoid at z=0.5m, and, downstream, the first SC accelerating module (A1), whose first TESLA cavity is centered at z=6m; the setup is optimized to minimize emittance growth. The gun cavity peak field of 50 MV/m and a bunch charge of 100 pC were used as a reference, although lower gradients were also simulated to investigate the corresponding dilution of beam brightness. Thermal emittance of 0.5 μm/mm is used as estimate of expected copper cathodes emittance. The A1 module gradient was set to 29 MV/m, and its phase was fixed on-crest for the purpose of optimizing the photoinjector, with the goal of minimizing both projected and slice emittance at z=20 m. For start-to-end simulations, however, the A1 parameters were varied according to the three-stage bunch compression scheme. Considering the RF gradients achieved so far [7] and the separation of the solenoid from the gun cavity (in contrast to conventional normal-conducting photoinjector layouts), photocathode laser

†sumaira.zeeshan@desy.de

Content from this work may be used under the terms of the CC BY 4.0 licence (© 2026). Any distribution of this work must maintain attribution to the author(s), title of the work, publisher, and DOI.

ISBN: 978-3-95450-252-3 ISSN: 2673-5350 doi: 10.18429/JACoW-IPAC2026-THP2071

SUSTAINABLE DATA TRANSFORMATION STRATEGIES FOR PARTICLE AND FIELD MODELING FREE-ELECTRON LASERS

P. Niknejadi*, S. S. Gurdasani, J. L. Prochnow, L. Schaper
Deutsches Elektronen-Synchrotron DESY, Hamburg and Zeuthen, Germany
N. K. Bhalla, V. S. Lang
Albert-Ludwigs-Universität Freiburg, Freiburg, Germany

Content from this work may be used under the terms of the CC BY 4.0 licence (© 2026). Any distribution of this work must maintain attribution to the author(s), title of the work, publisher, and DOI.

Abstract

Scientific data is commonly stored in formats such as CSV for small to medium datasets, HDF5 for complex hierarchical structures, and NetCDF for gridded and temporal variables. These formats provide robust mechanisms for the structured storage of hierarchical or multidimensional data, but they do not, by themselves, produce the task-specific tensors, masks, and metadata needed for efficient machine learning (ML) or GPU-accelerated computation. In practice, workflows built around these formats often incur substantial transformation overhead. Recent studies have demonstrated the promise of tailored data-transformation and encoding approaches in scientific domains. In particular, convolutional autoencoder–based compression of 3D particle-tracking data can achieve significant reductions in post-processing as well as storage requirements while keeping the essential spatial features for downstream workflows. The key bottleneck is not only data volume, but the mismatch between code-specific simulation output and the physically meaningful tensor structures required for ML. Motivated by the need to reduce the carbon footprint of increasingly large-scale simulations, this work proposes a domain-specific encoding perspective for interfacing particle and field data across different simulation tools, aiming to enhance the scalability and integration of scientific data into more sustainable workflows and future machine learning pipelines.

INTRODUCTION

Accelerator and light-source facilities now heavily rely on large-scale simulation, high-performance computing, data-intensive diagnostics, and machine-learning-assisted optimization. These technologies have enabled researchers to investigate complicated beam physics, design upgrades, and develop advanced accelerator control schemes. At the same time, they have placed a heavier computational, storage, and data-management load on scientific workflows. This issue is part of a larger topic: the responsibility of large-scale science toward the planet. Our earlier work on carbon accounting has highlighted how research activities, including experimental operations and facilities, computing, and travel, can account for a sizable share of emissions [1]. This carbon accounting at the per-researcher and per-project level provides a strong motivating factor for sustainability, making the cost of scientific workflows explicit at the level where many day-to-day decisions are made. Computing plays a particularly significant role in the carbon footprint of digitally intensive research, as simulations, processing, and storage all contribute to the total. This issue is also connected to broader community efforts in resource-aware computation, such as minimizing resource consumption for experiments in Universe and Matter research and improving the availability and usability of scientific data [2, 3]. While a great deal of research-sustainability effort has been spent on facility-level initiatives such as infrastructure and lab efficiency, procurement, and travel policy, these efforts don't necessarily inform the impact of individual researchers' workflows. This perspective led to the Precision in Energy-aware AI Research for Low-carbon Solutions (PEARLS) project, which ties carbon accounting together with sustainable scientific machine learning and resource-aware computation. PEARLS considers research emissions to be part of a workflow of interconnected activities. Data encoding is one part of PEARLS' sustainability strategy, which is part of our focus on data transformation discussed here.

DEFINING THE ENCODING GAP

In practice, accelerator-simulation data often undergo repeated conversion from code-specific output to array- or tensor-format structures amenable to analysis, machine learning training, optimization, and GPU-based workflows. The plasma-based accelerator community, motivated in part by the transition from traditional linear accelerators toward more compact accelerator concepts, has developed important infrastructure, such as SIMBA [4], LAURA [5], and OpenPMD [6, 7], to improve simulation interoperability and data representation with strong emphasis on particle-in-cell (PIC) workflows. LAURA, the Lattice Architecture for a Unified Representation of Accelerators, for example, provides a universal machine-description schema that combines physical, mechanical, and control system data. This is valuable since accelerator physicists, operators, and engineers often describe a machine using different variables, coordinate systems, units, and conventions. Similarly, SIMBA (Simulations for Integrated Modeling of Beams in Accelerators) facilitates unified machine description and code coordination for start-to-end simulations, using code-specific input and output files. While these frameworks do not directly address the data transformation, they support emerging ML workflows. However, their approaches are not automatically transferable to modeling Free-electron Lasers (FELs), where typically particle and field inputs/outputs have different structures, physics assumptions, and downstream objectives.

* pardis.niknejadi@desy.de

ISBN: 978-3-95450-252-3 ISSN: 2673-5350 doi: 10.18429/JACoW-IPAC2026-THP2073

UPGRADE OF THE HIGH REPETITION RATE FEL FLASH TO ALLOW SIMULTANEOUS SASE AND EXTERNAL SEEDING OPERATION

K. Honkavaara*, E. Ferrari, C. Gerth, P. Niknejadi, J. Rönsch-Schulenburg, L. Schaper, M. Vogt, J. Zemella, Deutsches Elektronen-Synchrotron DESY, Hamburg, Germany

Abstract

The Free-Electron Laser FLASH at DESY has provided more than 20 years XUV and soft x-ray SASE radiation for user experiments. In order to keep FLASH as a state-of-the-art FEL, the refurbishment and upgrade project FLASH2020+ was launched. The latest upgrade has been a complete replacement of the FLASH1 beamline in a 14 months shutdown in 2024/25. The new external seeded FLASH1 will provide fully coherent radiation at up to MHz bunch repetition rate (burst). Moreover, the new APPLE-III type undulators enable full polarization control. In addition, FLASH1 hosts, as before, a THz source. FLASH2 continues unchanged in SASE operation. The commissioning of the upgraded facility started in August 2025, and since November FLASH2 is back in user operation. Commissioning of seeding at FLASH1 continues in parallel to FLASH2 user experiments.

INTRODUCTION

FLASH [1–5], the XUV and soft x-ray Free-Electron Laser (FEL) user facility at DESY (Hamburg, Germany), has been more than two decades the worldwide pioneering FEL Facility. In early 2000's, SASE (Self Amplified Spontaneous Emission) lasing in the wavelengths from 80 nm to 120 nm [6–8], and its feasibility for photon experiments [9, 10], was demonstrated at the TTF-FEL [11], driven by the TESLA Test Facility (TTF) 250 MeV superconducting linac [12]. Already then an elongation of the superconducting linac (TTF2) was prepared. VUV-FEL at TTF2 [13] was constructed in the first half of 2000's. It started user operation in summer 2005, and was renamed to "FLASH". The design energy of 1 GeV was reached in 2007, allowing lasing down to 6.5 nm [14]. In 2010, an additional (7th) accelerating module was added to the linac to reach beam energy of 1.25 GeV and photon wavelength down to 4.1 nm [15].

To meet the continuously increasing demands of the user experiments on beam parameters and beam time, it was decided to extend the FLASH facility with a second undulator line driven by the same superconducting linac, but located in a separate building with an attached experimental hall. Since summer 2014 two undulator lines (FLASH1 and FLASH2) are operated in parallel, and in April 2016, the user operation started also at FLASH2.

In order to keep FLASH as a state-of-the-art FEL user facility, the next refurbishment and upgrade project FLASH2020+ [16, 17] was launched in 2018. The main goals were to establish a high repetition rate seeding (1 MHz) at FLASH1, and to extend the wavelength range at FLASH2 down to the oxygen K-edge (2.3 nm). The first upgrade shutdown, to increase the electron beam energy up to 1.35 GeV took place from November 2021 to August 2022. An APPLE III undulator operated as a third-harmonic afterburner was installed to FLASH2 in autumn 2023, enabling SASE radiation with variable, in particular circular, polarization. The high repetition rate seeding at FLASH1 has been realized within the second long shutdown from June 2024 to July 2025. This paper reports the status of the FLASH facility after the latest upgrades.

FLASH LAYOUT

FLASH consists of a photoinjector, a superconducting linac, two undulator lines and two experimental halls. A schematic layout of the facility after the 2024/25 shutdown is shown in Fig. 1.

A high quality, bunched electron beam is produced by a normal conducting RF-gun with a Cs_2Te photocathode and UV injector laser system. A new upgraded laser system [18] has been in routine operation since 2024. A laser heater [19], crucial for the seeded operation, was installed during the 2021/22 shutdown. The superconducting linac has seven TESLA type 1.3 GHz accelerator modules with eight 9-cell Niobium cavities each [20]. A third harmonic module (3.9 GHz) downstream of the first accelerating module linearizes the longitudinal phase space. In the 2021/22 shutdown the two oldest modules (ACC2 and ACC3) were replaced by new refurbished XFEL prototype modules [21] to reach the electron beam energy of 1.35 GeV [22]. The use of superconducting RF allows long RF pulses (up to 800 μs) and thus long electron bunch trains. Several discrete bunch spacing between 3 MHz and 50 kHz are possible. The bunch train repetition rate is 10 Hz. Two C-shape bunch compressors are used to compress the electron bunches at the beam energies of 143 MeV and 560 MeV. The second bunch compressor is a new movable 4-dipole chicane [23].

Until June 2024 FLASH was operated with two SASE undulator beamlines. In the shutdown 2024/25 the old FLASH1 beamline was completely dismounted, including the tunnel infrastructure. After the infrastructure refurbishment, a complete new electron beamline designed for external HGHG (High-Gain Harmonic Generation) [24, 25] and EEHG (Echo-Enabled Harmonic Generation) [26, 27] seeding has been installed. The FLASH1 photon diagnostics has been refurbished and upgraded as well. The FLASH1 hosts, as before, also a THz source: an electro-magnetic undulator, in use at FLASH since 2007, producing radiation between 1 and 300 THz. In order to ensure an adequate THz output, a

* katja.honkavaara@desy.de

Content from this work may be used under the terms of the CC BY 4.0 licence (© 2026). Any distribution of this work must maintain attribution to the author(s), title of the work, publisher, and DOI.

ISBN: 978-3-95450-252-3 ISSN: 2673-5350 doi: 10.18429/JACoW-IPAC2026-THP2076

QUASI-STEADY-STATE MICROBUNCHING FROM MULTI-TURN LASER MODULATION AT THE METROLOGY LIGHT SOURCE

A. Kruschinski*, L. Grossman, C. Mai, M. Marongiu, M. Ries,
Helmholtz-Zentrum Berlin, Berlin, Germany
J. Bian, A. Chao, X. Deng†, W. Huang, X. Liu, X. Lu, Ch. Tang, L. Yan, Z. Yang,
Tsinghua University, Beijing, China
A. Hoehl, R. Klein, Physikalisch-Technische Bundesanstalt, Berlin, Germany

Abstract

Steady-state microbunching (SSMB) has been proposed as a scheme to generate high average power coherent synchrotron radiation at short wavelengths from an electron storage ring. To evaluate the feasibility of this scheme, a proof-of-principle experiment is conducted at the Metrology Light Source (MLS) in Berlin, the first phase of which (PoP I) was concluded in 2024. PoP I utilized a single-shot laser system to provide an energy modulation to the electron beam and investigated the fundamental requirements on storage ring dynamics to enable SSMB. Recently, the second phase of the SSMB proof-of-principle experiment (PoP II) has commenced at the MLS, in which a high repetition rate phase-locked laser system provides turn-by-turn energy modulation of the electron beam on consecutive revolutions around the storage ring. The main goal of SSMB PoP II is to show electrons can be confined to individual microbuckets defined by this laser interaction, reaching a quasi-steady state. This paper presents the first results obtained in SSMB PoP II, where coherent synchrotron radiation has been detected following multi-turn laser modulation, and the ongoing systematic studies of the underlying microbunching process.

INTRODUCTION

To fulfil demands for high average power ultraviolet light sources, for applications such as EUV lithography, the idea of steady-state microbunching (SSMB) has been proposed [1, 2]. The goal of SSMB is to continuously store a microbunched electron beam in a storage ring to enable production of coherent short-wavelength radiation while also benefiting from the inherent high repetition rate of a storage ring to yield very high average power radiation. Theoretical design studies for a possible future SSMB storage ring are ongoing [3–7] and a proof-of-principle (PoP) experiment at the Metrology Light Source (MLS) in Berlin is exploring the feasibility of the idea.

Previously, the SSMB PoP experiment utilized a single-shot laser system to imprint a singular energy modulation onto the electron beam. This phase I of the experiment was successful in showing that the full circumference of the MLS storage ring could be used as a dispersive section to create a microbunching structure from this modulation [8, 9], and explored the necessary conditions on the storage ring optics [10, 11]. Since 2025, phase II of the SSMB PoP experiment has commenced at the MLS and aims to reach microbunching in a quasi-steady state by employing turn-by-turn energy modulation of the electron beam for up to 1000 consecutive revolutions around the storage ring, utilizing a high repetition rate phase-locked laser system [12, 13]. The key goal of SSMB PoP phase II will be to show that electrons can be confined to microbuckets defined by the laser field and perform synchrotron oscillations within.

EXPERIMENTAL SETUP

For phase II of the SSMB PoP experiments, the setup is mostly retained from the phase I efforts, most notably the radiation detection setup at the beamline [14], which remains unchanged except for changes to the triggering procedure [15]. Figure 1 shows a basic sketch of the setup: Energy modulation of the electron beam is achieved by co-propagating a laser in an undulator, the beam is microbunched by transport through the suitably tuned quasi-isochronous storage ring optics, and the coherent radiation emitted at the same undulator and at the same wavelength as the modulation laser is detected on following revolutions. For phase II, a high repetition rate laser system for turn-by-turn modulation is available [12, 13], some key parameters are compared to the previous laser system in Table 1.

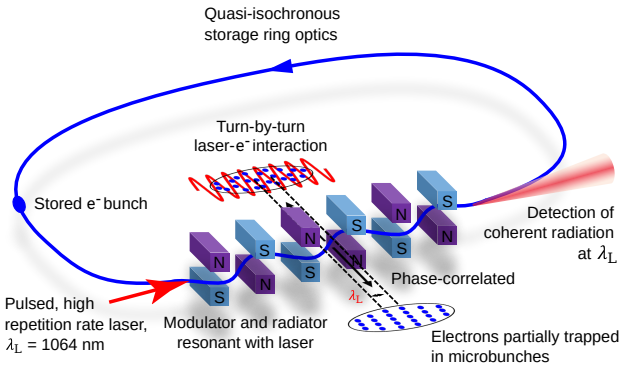

Figure 1: Schematic setup of the SSMB proof-of-principle experiment.

Both laser systems are still available for use with minimum switching effort [15], which is very useful for the setup of the storage ring optics. Because the maximum peak power of the phase II laser is a factor of 1000 weaker than the phase I laser, resulting in an energy modulation depth reduced by a factor of 30, it is significantly more challenging to achieve a reasonable bunching factor in order to be able

* arnold.kruschinski@helmholtz-berlin.de
† dengxiujie@mail.tsinghua.edu.cn

Content from this work may be used under the terms of the CC BY 4.0 licence (© 2026). Any distribution of this work must maintain attribution to the author(s), title of the work, publisher, and DOI.

ISBN: 978-3-95450-252-3 ISSN: 2673-5350 doi: 10.18429/JACoW-IPAC2026-THP2078

THE ATTOSECOND TECHNOLOGY PROGRAM AT THE EUROPEAN XFEL

D.E. Ferreira de Lima[1], G. Geloni *[1], J. Grünert[1], M. Guetg[2], J. Laksman[1], J. Liu[1], A. Madsen[1], L. Mercadier[1], M. Meyer[1], T. Mullins[2,3], A. Scherz[1], S. Serkez[1], J. Yan[2]
[1]European X-Ray Free-Electron Laser, Schenefeld, Germany
[2]Deutsches Elektronen-Synchrotron, Hamburg, Germany
[3]Center for Free-Electron Laser Science, Hamburg, Germany

Content from this work may be used under the terms of the CC BY 4.0 licence (© 2026). Any distribution of this work must maintain attribution to the author(s), title of the work, publisher, and DOI.

Abstract

In this contribution we will discuss the "Attosecond Technology" program at the European XFEL. This strategic program is being launched to cross a new frontier in ultrafast science, enabling experiments that probe and control electron dynamics on their natural timescales. The program is structured into tightly coordinated projects that address the full chain of challenges required for reliable attosecond operation at the European XFEL. These include the following three areas: first, attosecond pulse generation; second, development of next-generation diagnostics, capable of resolving sub-femtosecond temporal structures and, third, dedicated proof-of-principle experiments to validate performance under real experimental conditions and to provide increasing user access to attosecond-class capabilities. These efforts form a roadmap that integrates accelerator physics, FEL science, and experimental methodology. The program aims at delivering reproducible and well-characterized high-power X-ray attosecond pulses in single pulse, X-ray pump/X-ray probe or Optical pump/X-ray probe configuration.

MOTIVATIONS AND STATE OF THE ART

The generation of attosecond pulses in the soft and hard X-ray spectral range allows for imaging and spectroscopy experiments involving ultrafast dynamics in matter, enabling the probing and control of electron dynamics on their natural timescales [1–3]. Over the last twenty years, High Harmonic Generation techniques have been the main route to generating attosecond pulses. However, these techniques are intrinsically limited in spectral reach and pulse power [4–6]. As a consequence, XFEL-based methods are currently the only way to obtain high-power attosecond pulses that allow access to deeper and more complex regimes of matter. For this reason, many XFEL facilities worldwide devote significant effort to attosecond science, among many examples [7–9].

At the European XFEL, important milestones have been recently reached in terms of high-power attosecond pulse generation, diagnostics and usage. In the soft X-ray regime, single-frequency-spike pulses with energies up to the millijoule level have been generated at photon energies in the keV range [10]. Direct temporal measurements based on angular streaking techniques have confirmed pulse durations of a few hundred attoseconds [11]. In addition, two-color pulses with single-frequency-spike spectra and controllable delays have been demonstrated [10], lately also including polarization control of the probe pulse, as well as repeated delivery of short pulses to experiments, see [3] as an example.

In the hard X-ray regime, single-frequency-spike pulses have been generated at photon energies around 9 keV, with pulse energy reaching the hundreds of microjoule level [12]. Direct temporal diagnostics for hard X-ray attosecond pulses are still in an early stage of development. Nevertheless, indirect methods exploiting non-linear effects, together with start-to-end simulations and spectral analyses, consistently indicate pulse durations down to several hundred attoseconds, including moderate stretching due to dispersive transport optics. First demonstrations of two-color schemes and pilot experiments including dedicated diagnostics have also been successfully performed [13].

Despite these significant achievements, the delivery of fully characterized attosecond pulses to users during routine operation is still a very challenging task. Bridging the gap between current R&D stage and reliable user operation is a priority in the competitive research environment, which motivates a dedicated strategy program. Achieving this goal requires coordinating several development directions: standardization and optimization of attosecond pulse generation, acquisition and deployment of advanced diagnostics capable of resolving sub-femtosecond temporal structures, verification of consistent performance under realistic experimental conditions, and the gradual enablement of day-by-day scientific use of attosecond pulses. In parallel, albeit separately from the program itself, a strong users' community must gather around these capabilities.

Given these premises, the Attosecond Technology program is strictly based on attosecond generation methods that have already been experimentally demonstrated. The initial focus is therefore restricted to beamlines where attosecond pulses (single-spike) have been demonstrated, i.e. SASE2 and SASE3. SASE1 will be included in the program once comparable attosecond generation capabilities become available through separate R&D activities developed outside the scope of the program. At the same time, it is recognized that the state of the art in attosecond pulse generation and diagnostics is evolving rapidly. The program will therefore closely follow developments both at the European XFEL and worldwide, maintaining flexibility wherever possible within its phased structure.

* gianluca.geloni@xfel.eu

ISBN: 978-3-95450-252-3 ISSN: 2673-5350 doi: 10.18429/JACoW-IPAC2026-THP2082

STUDY OF BEAM DYNAMICS IN MAGNETIC ELECTRON BUNCHER FOR NOVOSIBIRSK FREE ELECTRON LASER

S. B. Lachynov[†,1,2], N. A. Vinokurov[1,2]
[1]Budker Institute of Nuclear Physics, Novosibirsk, Russia
[2]Novosibirsk State University, Novosibirsk, Russia

Abstract

This paper presents the current state of buncher design for the Novosibirsk Free Electron Laser (FEL) and study of the impact of space charge on transverse dynamics of the bunched beam.

INRODUCTION

Many applications of accelerator technology require electron bunches with length of about 10 ps, the peak current exceeding 100 A and the normalized emittance being less than 100 mm·mrad. To produce such bunches, special electron-optical systems, known as magnetic bunchers, are widely used. Designing a 540° magnetic buncher has started several years ago at Budker INP FEL facility [1]. Such a device enables users to obtain extremely short bunches with large charge. Effective bunching is provided by the particularly strong dependence of the time of flight on the particle energy. In addition, for reduction of the maintenance costs, the whole electron-optical system is based on permanent magnets. The buncher is to be put into operation in the 1.5 MeV electron injection channel of the NovoFel facility.

The following tasks were performed during the development of the buncher.

- Development and optimisation of the electron-optical scheme of the buncher.
- Development and optimisation of the magnetic system elements.
- Study of the influence of the space charge on the electron beam parameters and the corresponding limitations of the minimum electron bunch sizes.

The device consists of two 30-degrees magnets with parallel edges and two magnetic mirrors (see Fig. 1). Radii of the electron trajectories in bending magnets and the distance between magnets are chosen in such a way to ensure the achromatic bend. The calculation of the trajectory, longitudinal dispersion, and the transverse focusing for particles is described in the article [2]. After passing through a 30-degrees magnet with parallel edges, magnetic mirrors, another 30-degrees' magnet with parallel edges and a quadrupole magnetic lens, electron enter a focusing lens with a longitudinal magnetic field with a sharp edge. The latter is necessary to obtain a small transverse size of an electron beam.

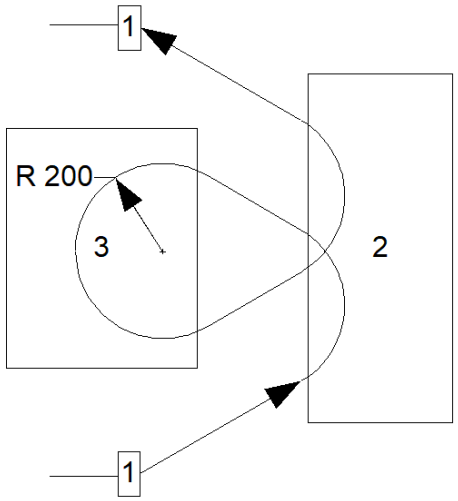

Figure 1: The scheme of the 540-degree bend magnetic electron buncher: 1 - 30-degree magnets, 2 - large magnetic mirror, 3 – small magnetic mirror. The reference trajectory of the electrons is shown by a solid curve.

30-degree magnets and a quadrupole lens already exist. Therefore, this paper presents only the designs and results of calculating the field of magnetic mirrors and an axisymmetric lens with a longitudinal field.

OPTIMIZATION OF THE MAGNETIC SYSTEM ELEMENTS

The process and results of calculation and optimization of magnetic mirrors are described in detail in the article [3]. The schemes of the magnetic mirror and the short-focus lens are shown in Fig. 2 and 3.

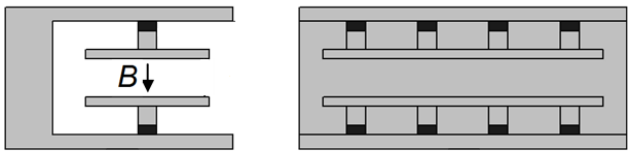

Figure 2: The scheme of a magnetic mirror: left – side view, right – front view. The blocks of the permanent magnet material are shown in black, the iron magnetic cores are shown in grey, and the arrow shows the direction of the field vector in the working gap.

† s.lachynov@gmail.com

Content from this work may be used under the terms of the CC BY 4.0 licence (© 2026). Any distribution of this work must maintain attribution to the author(s), title of the work, publisher, and DOI.

ISBN: 978-3-95450-252-3 ISSN: 2673-5350 doi: 10.18429/JACoW-IPAC2026-THP2084

SwissFEL*plus*: A MID-TERM UPGRADE PLAN FOR THE SWISS FREE-ELECTRON LASER

Thomas Schietinger* on behalf of the SwissFEL team
PSI Center for Accelerator Science and Engineering, Villigen, Switzerland

Abstract

SwissFEL, the free-electron laser facility at the Paul Scherrer Institute (PSI) in Switzerland, is about to complete its first decade of user operation. The experience gained during this period, together with important developments at FEL facilities worldwide, suggests a number of key upgrades to the accelerator and undulator complex that would substantially enhance the scientific capabilities of the two existing SwissFEL beamlines. The SwissFEL*plus* project, planned for 2029–2032, aims to implement these upgrades – including full coherence in the hard- and soft-X-ray regimes via self- and external-laser seeding, as well as preparations for a new beamline – and thereby bring SwissFEL to a new level of scientific excellence ahead of its quantitative expansion with a third beamline. The resulting improvements in beam stability and coherence will benefit applications ranging from atomic physics to biology and will enable new approaches, such as quantum optics for X-rays, with its advantages in the management of radiation damage. This contribution describes the upgrade elements and their expected impact on SwissFEL's photon-science capabilities.

INTRODUCTION

SwissFEL, the Swiss free-electron laser operating at the Paul Scherrer Institute (PSI) in Switzerland, consists of two beamlines: Aramis [1], covering the tender to hard X-ray regime (1.8–12.4 keV), and Athos [2], operating in the soft X-ray range (0.25–1.9 keV). Since the start of user operation, both beamlines have demonstrated reliable performance in self-amplified spontaneous emission (SASE) mode, enabling a broad range of experiments. At the same time, new scientific opportunities have highlighted limitations in the present configuration, particularly with respect to longitudinal coherence, photon energy reach, and polarization control in Aramis. Furthermore, there is an increasing need for experiment synchronization commensurate with the duration of ultrashort FEL pulses.

Proposed for the 2029–2032 funding cycle [3], the SwissFEL*plus* project addresses these limitations through targeted modifications of the accelerator and undulator systems (Fig. 1). The overarching goal is to achieve full spatial and temporal coherence throughout SwissFEL's entire hard and soft X-ray range. Beyond coherence control, the main objectives involve fully exploiting the potential of subfemtosecond pulses, extending the photon energy reach to 18 keV, and expanding the Aramis line's capabilities to include two-color and polarization control (already available in Athos). The following sections briefly summarize the technical implementation proposed to achieve these goals. For more details, we refer to the SwissFEL*plus* Conceptual Design Report [4] published earlier this year.

* thomas.schietinger@psi.ch

COHERENCE CONTROL

External Seeding in Athos

Standard SASE operation results in high transverse coherence but limited longitudinal coherence due to the stochastic start-up of the free-electron laser (FEL) process. For spectroscopy and nonlinear X-ray science, fully coherent pulses are highly desirable.

For the soft X-ray beamline Athos, external seeding based on echo-enabled harmonic generation (EEHG) has been identified as the most promising approach. EEHG allows harmonic upconversion far beyond the reach of conventional high-gain harmonic generation and is capable of covering the Athos wavelength range.

The Athos line is already equipped with the necessary hardware for EEHG, including seed lasers and magnetic chicanes, and initial demonstrations have yielded promising results; however, these same studies reveal that the intrinsic slice energy spread remains a critical limitation for robust operation. Microbunching instabilities and intrabeam scattering, enhanced by the high injector brightness, contribute to an energy spread that must be reduced to below approximately 300 keV for reliable high-harmonic operation.

SwissFEL*plus* therefore encompasses several injector modifications:

- the installation of an additional S-band radio-frequency cavity right after the gun for early energy chirping and ballistic bunching,
- the option to increase the bunch charge to raise peak current with less compression in the linac,
- the relocation of the first bunch compressor upstream to limit the accumulation of microbunching and intrabeam scattering effects, and
- the implementation of a more flexible compression scheme that allows for single- and two-stage compression without affecting the other beamline.

These measures are complemented by additional C-band acceleration sections to compensate for layout changes and to provide an overall energy upgrade.

To facilitate routine EEHG setup via stepwise harmonic upconversion, two additional superconducting undulator modules with large K range will be installed at the Athos line entrance. Improved diagnostics and arrival-time monitoring

Content from this work may be used under the terms of the CC BY 4.0 licence (© 2026). Any distribution of this work must maintain attribution to the author(s), title of the work, publisher, and DOI.

ISBN: 978-3-95450-252-3 ISSN: 2673-5350 doi: 10.18429/JACoW-IPAC2026-THP2086

RF SYSTEM UPGRADE OF ELSA ELECTRON LINAC AT CEA

M. Collet[†, ‡], A.-S. Chauchat[‡], V. Le Flanchec[‡]
CEA DAM Île-de-France, Bruyères-le-Châtel, France
G. Devanz, T. Hamelin, O. Piquet, CEA Paris-Saclay, Gif-sur-Yvette, France

Content from this work may be used under the terms of the CC BY 4.0 licence (© 2026). Any distribution of this work must maintain attribution to the author(s), title of the work, publisher, and DOI.

Abstract

The 19 MeV ELSA electron linear accelerator, operated by CEA DAM for 30 years, is currently undergoing a major upgrade of its RF accelerating structures to boost operational reliability, availability, and performance. The first phase (2022) targeted the second accelerating stage and replaced the 433 MHz klystron modulator. The new modulator, developed by Jema Energy, is based on a high-voltage Marx architecture to enhance pulse stability and overall system maintainability. The second phase (2024) focused on the first accelerating stage, which feeds the 144 MHz photo-injector. The original tetrode-based RF amplifier has been replaced by a high-power solid-state amplifier developed by AMPEGON, capable of delivering up to 1.6 MW peak power. A key challenge of this upgrade was achieving an architecture with a comparable footprint and thermal management constraints to the former tube-based system while preserving RF performance specifications. The upcoming third phase, currently in the design stage, will involve a redesign of the 1.3 GHz RF system, including new accelerating cavities and power sources, to extend beam energy and pulse duration. This contribution provides an overview of the upgrade program, detailing the design considerations, testing, commissioning, and integration activities. It also highlights technological choices, and shares operational lessons learned.

INTRODUCTION

Commissioned in the early 1990s as a high-efficiency IR Free Electron Laser (FEL) [1], the ELSA electron linac at CEA DAM was later repurposed as a user facility, delivering electron and X-ray beams to the scientific community. Its 144 MHz photo-injector, driven by a 72 or 144 MHz Nd:YAG laser interacting with an alkali photocathode, generates low-emittance, high-charge bunches with tunable lengths of 20–100 ps, enabling high-current pulse trains for users [2]. The main accelerator line then includes three 433 MHz cavities. The second stage is constrained by RF source and power supply limitations, restricting operations to 250 µs pulse trains at 10 Hz and capping the maximum linac exit energy at 17 MeV for low beam currents. In 2015, a 1.3 GHz third accelerating stage was added to the X-ray beamline, pushing the beam energy to 30 MeV and enabling higher beam currents, thereby overcoming the second stage's power limitations. The facility features three beamlines: a Bremsstrahlung X-ray line, an Inverse Compton Scattering (ICS) X-ray line and a straight-through electron line. A double-alpha magnet [3] splits and directs the beam into these lines.

However, after more than 30 years of operation, ELSA's original RF systems have reached their limits. Frequent amplifier faults, driven by component obsolescence, have reduced the mean time between failures (MTBF), compromising reliability and increasing downtime. To address these critical issues and meet evolving user demands, we launched a major RF upgrade program. The first phase (2022) replaced the 433 MHz klystron modulator with a high-voltage Marx modulator, improving pulse stability and maintainability. The second phase (2024) substituted the 144 MHz tetrode-based amplifier with a 1.6 MW solid-state power amplifier (SSPA), overcoming footprint and thermal constraints while matching RF specifications [4]. Looking ahead, the third phase will redesign the 1.3 GHz RF system, including new cavities and power sources, to extend beam energy to ~40 MeV and pulse duration to 200 µs. To better understand the motivations behind these upgrades, the following section details the current RF system and its limitations.

RF SYSTEM OVERVIEW

ELSA linac RF system is organized into three distinct accelerating stages, each powered by dedicated RF sources (Fig. 1). This section provides an overview of the original architecture, its operational constraints, and the key limitations that motivated the current upgrade program.

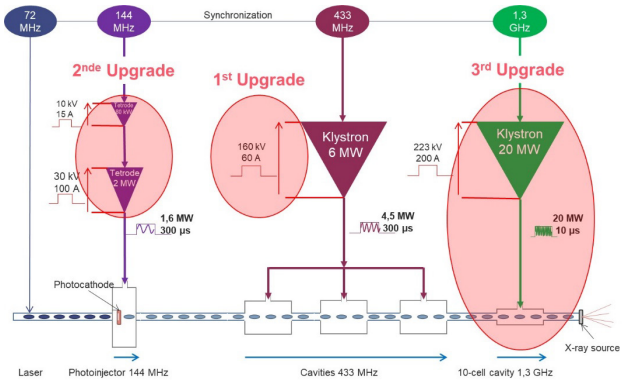

Figure 1: Overview of original ELSA RF system with the three upgrades.

The original RF power sources of ELSA linac relied exclusively on tube-based technologies which, after over 30 years of operation, reached significant performance and maintenance limits (Fig. 2). Specifically, the 144 MHz stage was based on a tetrode-based amplifier paired with high-voltage power supplies, while the 433 MHz and 1.3 GHz stages employed klystrons driven by traditional

†martin.collet@cea.fr
‡Also at Université Paris-Saclay, CEA, Laboratoire Matière en Conditions Extrêmes, Bruyères-le-Châtel, France

ISBN: 978-3-95450-252-3 ISSN: 2673-5350 doi: 10.18429/JACoW-IPAC2026-THP2087

PITZ FACILITY AFTER THE UPGRADE: HIGH BRIGHTNESS BEAMS FOR PHOTO INJECTOR R&D AND FEEDING THz AND RADIATION BIOLOGY EXPERIMENTAL STATIONS

M. Gross†, N. Aftab, A. Aksoy, S. Aminzadeh Gohari, Z. Amirkhanyan, A. Grebinyk, Y. Komar, M. Krasilnikov, B. Li, X. Li, A. Oppelt, S. Pakluea, C. Richard, F. Riemer, E. Tarakci, G. Vashchenko, D. Villani, D. Xu, S. Zeeshan, F. Stephan, Deutsches Elektronen-Synchrotron, Zeuthen, Germany
J. Good, Deutsches Elektronen-Synchrotron DESY, Hamburg, Germany

Abstract

At the Photo Injector Test facility at DESY in Zeuthen (PITZ) 22 MeV, high brightness electron beams are generated to serve mainly as a test facility for the European XFEL. Low emittance beams with bunch charges of less than a pC up to several nC are generated in an L-band photogun, which can provide bunch trains (4.5 MHz bunch repetition rate) of up to 1 ms in length at 10 Hz repetition rate. The three pillars of operation are: 1) R&D on high brightness photoinjectors for European XFEL: Main work topics are photocathodes, laser pulse shaping, machine learning, and operations improvements. 2) THz SASE FEL: Beams with a bunch charge of up to several nC are transported through an undulator to generate THz radiation at wavelengths around 100 µm with pulse energies of more than 100 µJ. Characterization of the THz output includes a FTIR spectrometer, a THz camera and a Michelson interferometer. 3) Radiation biology: In a separated beamline the electron bunches are transported through a thin exit window to an in-air experimental station for *in vitro* and *in vivo* irradiations providing ultra-high dose rates over a worldwide uniquely wide parameter range, with the goal to systematically study the FLASH effect in order to find the underlying principle, which is yet unknown. In addition, the high beam quality and the high bunch repetition rate is used to study spatially fractionated radiation therapy (SFRT) and the combination of SFRT and FLASH radiation therapy FLASH-RT.

INTRODUCTION

The Photo Injector Test facility at DESY in Zeuthen (PITZ) [1] was built as a test facility to develop optimized electron sources for short-wavelength Free Electron Laser (FEL) user facilities like the EuXFEL [2] or FLASH [3] in Hamburg. The main aim is to optimize hardware and operation parameters to minimize the emittance of electron bunches which are typically used in FEL operation. The high brightness beams available at PITZ are also utilized to conduct experiments in various fields. In the past, that were electron diffraction [4] and beam driven plasma acceleration [5, 6]. After a major upgrade of the PITZ facility in the last several years, two experimental end stations are available for investigations into a high-intensity, tunable THz source for pump-probe experiments at FELs and radiation biology at ultra-high dose rates. The current beamline is depicted in Fig. 1. The final beam energy is up to 22 MeV with bunch charges from fC to about 5 nC. Bunch durations are spanning 0.1 ps to 30 ps FWHM with beam sizes available at the experimental stations in the µm to mm range. The available pulse train time structure is governed by the need to drive superconducting linacs with long RF pulses: electron bunch trains consist of up to 4500 bunches within 1 ms with a repetition rate of 10 Hz typically. In the following, the three main PITZ activities are described.

ELECTRON SOURCE DEVELOPMENT

For over 25 years, normal conducting copper L-band (1.3 GHz) guns are developed at PITZ [7]. These are pulsed 1½-cell standing wave cavities with a typical RF power of ~6.5 MW during the RF pulse, an operational cathode gradient of 60 MV/m and an RF pulse length of up to 1 ms at a repetition rate of 10 Hz. This latest generation (Gun5 [7], Fig. 2) features an improved, elliptical cell shape, extended cooling capabilities, and RF pickups for field measurements in the gun cavity, enabling direct feedback.

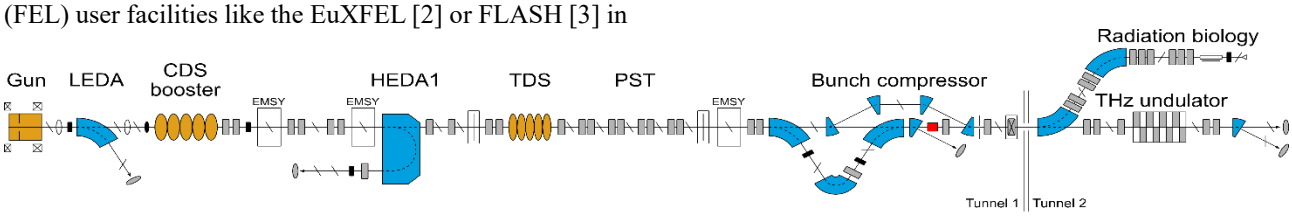

Figure 1: PITZ beamline.

†matthias.gross@desy.de

Content from this work may be used under the terms of the CC BY 4.0 licence (© 2026). Any distribution of this work must maintain attribution to the author(s), title of the work, publisher, and DOI.

ISBN: 978-3-95450-252-3 ISSN: 2673-5350 doi: 10.18429/JACoW-IPAC2026-THP2093

FINDING OPERATION CONDITIONS FOR ULTRA-HIGH DOSE-RATE ELECTRON BEAM DELIVERY AT FLUTE

M. Brosi*, A. Malygin, M. J. Nasse, J. Pehlivan, and A.-S. Müller,
Karlsruhe Institute of Technology, Karlsruhe, Germany

Content from this work may be used under the terms of the CC BY 4.0 licence (© 2026). Any distribution of this work must maintain attribution to the author(s), title of the work, publisher, and DOI.

Abstract

The linac-based test facility FLUTE (Ferninfrarot Linac- und Test-Experiment) at the Karlsruhe Institute of Technology (KIT) was designed to operate over a broad range of beam parameters and to generate ultra-short electron bunches. This versatility enables studies beyond accelerator physics, including applications in medical research. In particular, FLUTE can be used to explore operation modes suitable for investigating the effects of ultra-high dose-rate radiotherapy (FLASH RT) compared to conventional radiotherapy. Achieving the required dose rates for both modalities involved adjusting key beam parameters such as charge, repetition rate, and transverse size. This contribution discusses the strategies used to reach these conditions, the encountered technical challenges, and the results of initial tests on the achievable dose-rate ranges.

INTRODUCTION

With the increase in attention for the FLASH effect caused by ultra-high dose rates (UHDR) in radiotherapy (RT) over the last years, research into the underlying mechanisms and physical requirements has become increasingly important [1]. While it is mostly agreed upon, that the FLASH effect occurs for dose rates above 40 Gy/s, there are other parameters such as pulse length and repetition rate, which affect the average dose rate and the instantaneous dose rate, that depend strongly on the used source of radiation [2].

While clinical linacs operate commonly with pulse duration in the order of microseconds, research accelerators can reach pulse durations in the order of picoseconds. The linac-based test facility FLUTE at KIT is designed to provide electron bunches with bunch lengths down to a few femtoseconds via bunch compression in a magnetic chicane. For experiments towards the FLASH effect, bunch lengths in the order of 1 ps are used. Typical operational parameters are given in Table 1.

Table 1: Operation Parameters for UHDR Experiments

Beam energy	10-30 MeV
Repetition rate	10-50 Hz
Bunch charge	100-350 pC
Bunch length	≈1 ps
Transverse spot size (rms)	≈2-5 mm

For the irradiation experiments, an experimental station was constructed at the end of FLUTE, where the electron beam can be used directly in air before it is absorbed by the beam dump [3]. The exit window from the vacuum section is a 20 µm thick Havar foil.

OPERATION PARAMETERS

The FLASH effect is expected to occur at average dose rates above 40 Gy/s. While clinical linacs provide transverse field sizes of a few centimeters squared, typically up to 20x20 cm, research linacs are typically optimized for small transverse beam sizes in the order of or smaller than 1 mm. To achieve a more homogeneous irradiation of samples, we used the available quadrupoles at FLUTE to widen the transverse beam size at the in-air setup. Transverse beam sizes (1σ rms) up to 5 mm were achieved, while maintaining a mostly symmetric round shape and keeping the measured dose rate above 40 Gy/s at a bunch charge of 300 pC. When going to bigger transverse sizes, the outer parts of the beam start to be scraped off by the vacuum exit window. Therefore, beam sizes between 2 and 5 mm (rms) were typically used.

To allow operation with higher bunch charges in the order of 300 pC, the power density of the UV photo-injector laser pulse on the cathode has to be reduced to avoid damage. This is achieved by defocusing the UV pulses and stretching them in time. The beam optics, e.g., solenoid strength, RF phase in linac, quadrupoles and correctors, was adjusted to ensure that the whole charge per bunch reaches the in-air section at the end of FLUTE. A beam energy of 30 MeV was chosen, as it offers a good compromise of providing enough acceleration in the linac to avoid a strong emittance growth due to space charge also after the linac. At the same time, 30 MeV is still feasibly low to avoid a long penetration depth and therefore the need for some additional build up material in front of the samples. Energies as low as 10 MeV have been demonstrated at FLUTE, although it should be noted that a slightly smaller percentage of the charge could be transported through the machine.

When comparing the beam energy with parameters at more typical clinical linacs, it has to be considered that due to the significantly smaller field size, the percentage depth dose curve is different. For wide field sizes, in the order of several centimeters, the scattering of electrons in the material mainly reduces the density at the edges, while in the middle the number of scattered electrons leaving the volume is balanced by an equal number of electrons scattering into that volume (lateral scatter equilibrium (LSE)) [4]. For smaller field sizes in the millimeter range, scattering reduces the electron density also in the middle and causes a significant widening of the field size, which then changes how the deposited energy is distributed along the penetration depth.

An additional knob to adjust the average dose rate is the repetition rate of the bunches. As FLUTE operates with one

* miriam.brosi@kit.edu

ISBN: 978-3-95450-252-3 ISSN: 2673-5350 doi: 10.18429/JACoW-IPAC2026-THP2094

BEAM DYNAMICS INVESTIGATIONS ACCOMPANYING THE FLUTE FACILITY UPGRADE

M. Brosi*, A. Malygin, R. Ruprecht, J. Schäfer, M. Schuh, A.-S. Müller,
Karlsruhe Institute of Technology, Karlsruhe, Germany

Content from this work may be used under the terms of the CC BY 4.0 licence (© 2026). Any distribution of this work must maintain attribution to the author(s), title of the work, publisher, and DOI.

Abstract

The Ferninfrarot Linac- und Test-Experiment (FLUTE) facility at the Karlsruhe Institute of Technology (KIT) is designed to deliver ultra-short electron bunches offering a broad range of beam parameters for diverse applications and to provide coherent radiation in light pulses spanning the terahertz and far-infrared spectral range. Beyond its current role as a versatile accelerator test facility, FLUTE is intended to become one of the injectors for the Very Large Acceptance-compact Storage Ring (VLA-cSR), presently under construction at KIT within the cSTART project (compact Storage Ring for Accelerator Research and Technology). To fulfill these future roles, FLUTE will undergo a reconstruction and a partial upgrade during the cSTART construction phase. This contribution outlines the planned modifications to the future FLUTE accelerator test facility and presents results from accompanying beam dynamics simulations.

FLUTE FACILITY

FLUTE [1] consists of a low-energy section starting with the photo-injector, which contains a solenoid, diagnostics as well as a spectrometer dipole magnet leading to a side arm with a short beam line and an in-air experimental section. The beam energy here is typically between 5 and 5.5 MeV. The traveling wave linac with a length of 5.3 m is equipped to accelerate the beam up to 90 MeV [2]. The high energy-section contains further diagnostic, a quadrupole triplet and a chicane for longitudinal bunch compression. The high-energy section ends with a second in-air experimental section [3] followed by a Faraday cup and beam dump.

For the construction of the Very Large Acceptance - compact Storage Ring (VLA-cSR) of cSTART on a level 3.3 m above FLUTE [4] in autumn of 2026, FLUTE was temporally deconstructed at the end of March 2026 to protect the components and provide space for construction works in the experimental hall. Reconstruction is planned to start in 2027, as soon as the construction progress at cSTART allows.

For reconstruction, the FLUTE layout is adapted to the additional operation task as an injector for cSTART. The main boundary condition is the transition point to the injection line (FLUTE-IL), which transfers electron bunches into the VLA-cSR. The layout of FLUTE used in this contribution represents the status as of today while the final layout is still under development with some variations in the amount of diagnostics and number of quadrupoles being discussed.

One important change from the previous layout to the new layout is the move of the split-ring resonator (SRR) [5], a THz-streaking longitudinal bunch profile diagnostic, from the low energy section to the high energy section after the bunch compressor. In the course of this, some surrounding valves, one BPM, one corrector and a single quadrupole, currently used to focus the beam into the SRR, will also be removed from the low energy section. This significantly shortens the low energy section and reduces the distance from the electron gun to the linac entrance from 3.2 to ≈1.6 m.

After the linac, the existing quadrupole triplet will be exchanged with two doublets, one after the linac and the other after the chicane to improve the control of the transverse beam properties and match the beam to the FLUTE-IL.

The section after the chicane will continue to contain a chamber for in-vacuum electro-optical spectral decoding [6] as well as a thin aluminum foil for the extraction of transition radiation [7]. Upgraded, the section will also contain two vacuum chambers dedicated to in-vacuum experiments. One will be used for the SRR. The other is intended for the extraction of the THz radiation generated in the superconducting THz-undulator [8] (SCUF) which is delivered and planned to be included. At a distance of 15.95 m from the cathode is the transition point to the FLUTE-IL to cSTART.

Different operation modes are planned to cover the different tasks of FLUTE:

- For the injection of a short bunches into cSTART, FLUTE has to deliver a bunch with the correct longitudinal chirp to the entrance of the FLUTE-IL, in which the bunch will be shortened by the present R_{56} [9, 10].
- For the generation of intense THz radiation [7], FLUTE has to deliver short bunches on the femtosecond scale.
- For ultra-high dose-rate (UHDR) experiments [3, 11, 12] bunch charges in the order of 300 pC are needed.

All operation modes are planned to be usable over the whole range of possible beam energies from approx. 10 MeV up to approx. 90 MeV.

SIMULATIONS

For the different operation modes, tracking simulations with a combination of ASTRA [13] and OCELOT [14] have been conducted. ASTRA is used until after the linac, considering the space charge effect. The tracking through the chicane is done with Ocelot and includes additionally the effects of coherent synchrotron radiation (CSR). For the search for the configurations resulting in the shortest bunch length, an optimization algorithm based on parallel Bayesian optimization [15] was employed. The targeted beam energy was included in the optimization function. The optimizer could vary, within given bounds, the gun RF phase and power, the solenoid strength, the RF phase and power in the linac as well as the strength of the chicane. The transverse optics

* miriam.brosi@kit.edu

ISBN: 978-3-95450-252-3 ISSN: 2673-5350 doi: 10.18429/JACoW-IPAC2026-THP2096

RF PHASING FOR ELI-GBS LINEAR ACCELERATOR*

P. Tracz†[1], H. Schubert[1], N. Militaru[1,2], R. Kraus[1], P. Prelipcean[1], C. Cirdei[1,2], E. Cirstea[1,2], E. Udup[1], C. Matei[1,2]
[1]IFIN-HH / ELI-NP, Magurele-Bucharest, Romania
[2]POLITECHNICA Bucharest, Bucharest, Romania

Abstract

The RF linac for the ELI - Gamma Beam Source (ELI-GBS) is being installed in Bucharest-Magurele (Romania). Traveling wave (TW) accelerating struc tures and SLED cavities are powered by klystrons via waveguide network that includes directional couplers for power monitoring and feedback. Before RF conditioning can begin, the linac must be properly tuned in terms of the RF phase and cavity frequencies. The waveguide system was reviewed with respect to its electrical length to ensure correct RF phase tuning. This work was carried out after installation but prior to connecting the waveguides to the accelerating structures. Fine RF-phase adjustments will be achieved through mechanical deformation of the waveguides. Since each klystron feeds four structures, the waveguides must be tuned so that the RF phase at the entrance of each structure matches its longitudinal position in the accelerator. Considering that only 5-degree deviation in phase can be compensated by mechanical deformation of waveguides, larger discrepancies must be corrected physically by bending existing waveguide components to correct position or even reposition accelerator segments. Therefore precise analysis of the waveguide network was performed using a vector network analyser. This paper reports the results of phase measurements performed on the assembled waveguide system. In addition, directional couplers were individually tested with VNA to verify their performance before integrating them into the system.

INTRODUCTION

The ELI-GBS is based on the RF linac operating in the S-band (2856 MHz). The linac consists of five accelerating modules, each contains one Canon klystron (50 MW peak) that feeds four travelling wave structures with RF power. The TW structures are connected to the SLED system to enlarge peak power. The layout of one linac module is presented in Fig. 1. The ELI-GBS linac design [1] is different from the previous design of the VEGA system from 2020, nevertheless in its initial configuration the accelerating modules are based on the same setup [2].

The beam energy gain per one module is expected to be approx. 160 MeV. The ELI-GBS linac is designed for a top energy of 800 MeV to easily achieve approx. 750 MeV as required by the specification. For optimal operation the accelerating field and electron bunch at the input of each TW structure must be synchronized in such a way

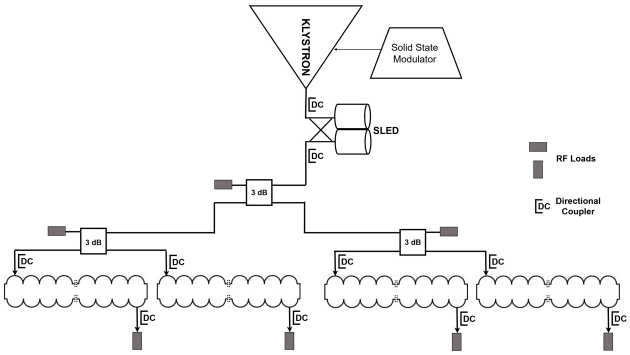

Figure 1: Linac accelerating module.

that the electron bunch travels on the crest (or a predefined phase) of the oscillating RF field. To fulfil that requirement, the distance between the input couplers of two consecutive structures must be an integer of wavelength λ plus the phase shift resulting from the geometry of the waveguide system. Therefore, the geometrical distance between the four accelerating structures in the linac module has to be adjusted in a way that the phase progress in the waveguides connected to each structure has the same phase difference from the RF source to the input coupler plus or minus a correction that comes from the geometrical distance between two consecutive structures, i.e. has to meet a formula: $n \times \lambda \pm \delta$. In a perfect matched and undeformed waveguide system, the phase progress depends only on a geometry of the system's elements, and can be calculated considering the fact that the wavelength of the oscillating RF field confined in the waveguide differs from the wavelength in vacuum. Due to mechanical tolerances the progress of the effective phase can differ from the pre-calculated (designed) one, nevertheless that difference can be measured.

The evaluation and adjustment of the input phases of each TW structure have to be done before performing the RF conditioning. For RF measurements, the vector network analyser was used. The evaluation of the system's geometry was done following the measurements with use of a precise laser tracker.

MEASUREMENT SETUP

The measurement setup is presented in Fig. 2. The RF measurements with use of VNA and phase stable cables were performed to confirm the electrical phase length from the input port i.e., before the 3 dB coupler (φ_0) through the waveguide system that connect each TW structures with the RF source. Just one output port (φ_1, φ_2, φ_3, or φ_4) was used at a time for the measurement, and other three ports were

* Work carried out in part under the contract PN 23 21 01 06 sponsored by the Romanian Ministry of Research, Innovation and Digitization.
† piotr.tracz@eli-np.ro

Content from this work may be used under the terms of the CC BY 4.0 licence (© 2026). Any distribution of this work must maintain attribution to the author(s), title of the work, publisher, and DOI.

ISBN: 978-3-95450-252-3 ISSN: 2673-5350 doi: 10.18429/JACoW-IPAC2026-THP2100

COMPRESSION AND LINEARISATION STUDIES ON CLARA

J. Jones* , M. Johnson , T. Overton , T. Pacey , Y. Saveliev
ASTeC, STFC Daresbury Laboratory, Daresbury, UK and The Cockcroft Institute, Daresbury, UK

Abstract

CLARA is a 250 MeV/c electron beam user facility currently undergoing final beam commissioning at Daresbury Laboratory, in the UK. CLARA features a 4-dipole variable bunch compressor, allowing a wide range of R_{56} values up to 60 mm, coupled with an X-band fourth harmonic cavity (4HC) for longitudinal harmonic correction of the S-band main linacs. An S-band transverse deflecting cavity (TDC) situated in a diagnostic straight following the bunch compressor, coupled with a high-resolution spectrometer beamline, enables full transverse and longitudinal reconstruction of the beam phase space. The FEBE arc, which delivers beam to a dedicated user area, can also act as an additional variable longitudinal compressor, with R_{56} variation of ±50 mm possible with limited dispersion leakage, and with 2 sextupole families for T_{566} correction. A coherent transition radiation (CTR) target is situated at the exit of the arc and can be used for longitudinal tuning. Commissioning of the various longitudinal compression and linearisation systems has recently taken place, to facilitate a first tranche of "friendly" user experiments, several with demanding requirements on the bunch length.

INTRODUCTION

CLARA is an advanced medium-energy accelerator user facility in the north-west of England, UK [1]. Originally envisaged as a free-electron laser test facility, CLARA was designed to explore novel beam dynamics modalities with flexibility in the transverse and longitudinal planes, along with extensive diagnostics capabilities to analyse the resulting beam distributions. As CLARA has transitioned away from FEL science, and towards a user facility for novel acceleration, Very High Electron Energy (VHEE) radiotherapy studies, and advanced diagnostics, it has retained the longitudinal flexibility that is required for these varied application paradigms.

Novel acceleration studies and FELs both benefit from ultra-short electron bunches (<100 fs rms.), and CLARA was designed to achieve ultra-short bunches through a combination of a 4-dipole variable bunch compressor (VBC) with an X-band fourth-harmonic cavity (11.994 GHz) for linearisation (see Fig. 1). The introduction of the FEBE (Full Energy Beam Exploitation) [2] experimental area and its accompanying 4-dipole s-shaped arc added a positive-R_{56}-like compression structure to the system, increasing flexibility. Longitudinal diagnostics in CLARA are concentrated on the transverse-deflecting cavity placed after the final accelerating structure but, for historical reasons, before the FEBE arc. An additional, relative, bunch length measurement is possible after the arc using a coherent transition radiation (CTR) target. Longitudinal timing diagnostics include up to three Beam Arrival Monitors (BAMs) placed either side of the VBC, and at the exit of the FEBE arc.

CLARA is currently undergoing a second round of beam commissioning after a recent, successful, friendly user run [3] involving both VHEE and plasma studies, alongside advanced diagnostics experiments. At this time, the 4HC lineariser and the BAM diagnostics have yet to be fully commissioned with beam. A further run of longitudinal compression studies is expected to be performed once these elements are commissioned.

BEAM TRANSPORT AND COMPRESSION

Compressive Elements

CLARA contains a series of elements to manipulate the longitudinal phase space (LPS) as shown in Fig. 1, including the 4HC for linearisation and the VBC for compression.

A positively chirped LPS (with the bunch head at lower energy than tail) without non-linear components increases compression achievable through the VBC. The VBC comprises a dipole chicane mounted upon a moveable translation stage, which moves out with the dipole current (up to 300 mm of transverse displacement), providing a tuneable negative R_{56} (up to 60 mm).

A passive wakefield dechirper is positioned subsequent to the final linear accelerator and prior to the FEBE arc. Within the two dielectric-lined waveguides (each 0.2 m long), electron bunches generate longitudinal wakefields dependent on the bunch current profile and structure gap. These wakefields effectively reduce energy spread for a positive bunch chirp. The dechirper has recently been commissioned on CLARA, details of which can be found in [4].

Transport to the FEBE hutch, where user experiments are conducted, is via the FEBE arc. The R_{56} component through the arc is non-zero, positive, and tuneable with a nominal value of +7.7 mm [2]. Given the positive R_{56} contribution, the FEBE arc compresses the bunch in the opposite direction to the VBC. Consequently, maximum effective compression within the FEBE hutch necessitates over-compression with the VBC for the beam exiting the CLARA straight section, upstream of the FEBE arc.

CLARA Longitudinal Diagnostics

Diagnostics are positioned in CLARA for measurements of longitudinal and energy profiles as well as the full LPS. An S-band TDC is positioned after the final linac for longitudinal profile measurements. Dispersive sections are positioned along CLARA (Fig. 1) for measurements of the energy spec-

* james.jones@stfc.ac.uk

Content from this work may be used under the terms of the CC BY 4.0 licence (© 2026). Any distribution of this work must maintain attribution to the author(s), title of the work, publisher, and DOI.

ISBN: 978-3-95450-252-3 ISSN: 2673-5350 doi: 10.18429/JACoW-IPAC2026-THP2101

A SEMI-ANALYTIC, MATRIX-BASED MODEL FOR THE BEAM ARRIVAL TIME JITTER

M.A. Johnson*[1,2], P.H. Williams[1,2]
[1]ASTeC, STFC Daresbury Laboratory, Sci-Tech Daresbury, Warrington WA4 4AD, UK
[2]The Cockcroft Institute, Sci-Tech Daresbury, Warrington, WA4 4AD, UK

Abstract

The beam arrival time jitter is an important parameter for many advanced electron accelerators, including next-generation XFEL drivers. Accurate jitter modelling is particularly important during the design of a new facility, where it is often used to determine the tolerances of the RF sources and photoinjector laser. Conventionally, jitter is modeled using computationally intensive start-to-end simulations; in this approach, the entire accelerator is simulated many times, while the parameter associated with each jitter source is varied within its expected tolerance. This approach is time-consuming and scales poorly with the size and complexity of the accelerator. Semi-analytic jitter models therefore have significant advantages, owing to their speed and greater insight into the underlying physics. In this contribution, we propose a simple matrix-based model for the arrival time jitter in a linear accelerator with an arbitrary layout. We validate the model against simulations of CLARA at Daresbury Laboratory, and use it to explore the jitter tolerances of different operating modes.

INTRODUCTION

Many advanced electron accelerators require tight control of the beam arrival time to achieve their maximum performance. For instance, plasma wakefield acceleration (PWFA) schemes using external injection typically require synchronization of the electron beam to within a few femtoseconds, to keep the beam energy jitter within tolerable limits [1, 2]. Likewise, next-generation X-ray free electron laser (XFEL) concepts are likely to place stringent limits on the synchronization of the electron beam, potentially requiring sub-femtosecond timing jitter.

In recent years, several accelerator facilities have targeted state-of-the-art synchronization using a variety of schemes. For example, SwissFEL [3] has achieved an RMS arrival time jitter (ATJ) of ∼10 fs by optimizing the performance of their RF systems to meet demanding stability requirements [4]. The ARES linac at DESY [5] aims to generate extremely short (sub-fs) electron bunches with an ATJ of $\lesssim$10 fs using a variety of bunch compression schemes [6, 7].

Understanding how the ATJ develops along an accelerator is particularly important during the design of a new facility. Accurate jitter modelling can provide insights into how different design choices will affect the stability requirements of the accelerator subsystems, including the RF sources and photoinjector laser. For example, accelerators that use arcs for bunch compression may benefit from a reduced ATJ due to the so-called 'magic angle' effect [8, 9].

Detailed studies of the ATJ often rely on start-to-end accelerator simulations, which can require significant computational resources [10, 11]. Conventionally, the ATJ is evaluated by considering an ensemble of simulations, where the parameter representing each jitter source has been randomly varied within its expected tolerance. While this approach is straightforward, it is often time-consuming and quickly becomes impractical for larger, more complex accelerators.

Considerable insight into the ATJ can be obtained using simple semi-analytic models, which can be orders of magnitude faster while offering a deeper understanding of the underlying physics. These models can quickly estimate the ATJ for different accelerator operating points, making them useful during both the design and operation of a facility. In recent years, several models have been proposed for the ATJ in linear electron accelerators [12–15]. However, these models are often only valid for a specific accelerator layout, or a particular type of bunch compression scheme.

In this paper, we propose a semi-analytic jitter model that is valid for any linear electron accelerator with an arbitrary layout. The model is derived by considering the joint statistical distribution of the beam's arrival time jitter and energy jitter. Lattice elements that affect the beam's jitter distribution are represented as matrix transformations, providing a simple way to propagate different jitter sources along an accelerator. Our model combines physics insights from a number of recent studies [8, 9, 15] and defines a single, self-consistent framework for estimating the ATJ.

SEMI-ANALYTIC MODEL

Photoinjector

The coupled equations for the longitudinal dynamics in a standing wave RF cavity can be written as [15, 16]

$$\frac{\mathrm{d}\gamma}{\mathrm{d}z} = 2\alpha k\, \varepsilon_z\,(z) \cos\left(\phi + kz\right) \tag{1}$$

and

$$\frac{\mathrm{d}\phi}{\mathrm{d}z} = k\left(\frac{\gamma}{\sqrt{\gamma^2 - 1}} - 1\right), \tag{2}$$

where γ is the Lorentz factor of the beam, k is the RF wavenumber, and z denotes longitudinal distance along the axis of the cavity. The function $\varepsilon_z\,(z) \approx \cos\left(kz\right)$ is the dimensionless, normalized field profile of the cavity. The parameter $\alpha = qE_0/2kmc^2$ is the normalized RF gradient, where E_0 is the peak electric field inside the cavity, and q

* mark.johnson@stfc.ac.uk

Content from this work may be used under the terms of the CC BY 4.0 licence (© 2026). Any distribution of this work must maintain attribution to the author(s), title of the work, publisher, and DOI.

ISBN: 978-3-95450-252-3 ISSN: 2673-5350 doi: 10.18429/JACoW-IPAC2026-THP2102

HIGH QUANTUM EFFICIENCY ALKALI-ANTIMONIDE PHOTOCATHODES FOR PERLE HIGH CURRENT DC GUN*

M. De Vos†, S. Brault, J. Demailly, O. Frossard, T. Gerardin, W. Kaabi, B. Mercier, E. Mistretta, D. Reynet, J. Yemane, G. Sattonnay, Université Paris-Saclay, CNRS/IN2P3, IJCLab, Orsay, France
M. Baylac, Laboratoire de Physique Subatomique et de Cosmologie, Grenoble, France

M. Faye, Grand Accélérateur National d'Ions Lourds, Caen, France
On behalf of the PERLE collaboration

M. Hoffmann B. Keune, V. Kuemper, C. Quitmann, RI Research Instruments GmbH, Bergisch Gladbach, Germany

Abstract

Modern particle accelerators, while enabling cutting-edge research, face major challenges in energy efficiency and beam intensity. The PERLE (Powerful Energy Recovery Linac for Experiments) project, developed at IJCLab/CNRS, aims to demonstrate a high-current energy recovery linac (ERL) using superconducting RF technology. By recovering the beam energy after use, PERLE drastically reduces RF power consumption, paving the way for sustainable, high-performance accelerators. A key element is the development of alkali-antimonide photocathodes, combining high quantum efficiency and low thermal emittance. CsK_2Sb photocathodes, in particular, show excellent response to visible light, enabling operation with lower laser power and improved beam quality. Their fabrication relies on a unique deposition system equipped with a dedicated transfer line that links the glove box—where precursors are prepared—to the molecular beam epitaxy (MBE) chamber for growth, and ultimately to the electron gun for installation. First tests at IJCLab achieved a quantum efficiency of 7 %, validating this integrated approach for high-current ERLs such as PERLE.

INTRODUCTION

High-performance electron sources are essential for modern accelerator facilities such as energy recovery linacs (ERLs) and X-ray free-electron lasers (XFELs). These applications require photocathodes capable of delivering high brightness beam at fast time response, low thermal emittance and stable operation [1]. For that, alkali antimonide photocathodes, in particular CsK_2Sb, are widely considered promising candidates due to their high quantum efficiency (QE) in the visible range and their compatibility with high-current operation [2].

However, the performance and lifetime of these photocathodes are strongly influenced by vacuum conditions during growth and operation. Residual gases, such as O_2 and CO_2, can affect the formation of the photocathode, its stoichiometry and contribute to rapid degradation of the quantum efficiency [3,4]. While optimized growth procedures have been widely studied, including sequential and co-evaporation techniques [5,6], the impact of non-ideal vacuum conditions remains a critical practical issue for photocathode preparation systems.

In this paper, we present a comparative study of two CsK_2Sb photocathodes prepared under different vacuum conditions. The results highlight the sensitivity of the growth process and the resulting photoemission properties to vacuum quality, providing insight into the requirements for reliable photocathode production in high-current accelerator environments such as PERLE.

EXPERIMENTAL

Photocathode Preparation Facility (PPF)

The photogun of PERLE is equipped with a Photocathode Preparation Facility (PPF) enabling the transfer of the photocathode under vacuum (Fig. 1) via a trolley. This includes a glovebox, where 2” diameter molybdenum or stainless-steel substrates (pucks) are loaded and where all the chemicals are used. The trolley is then inserted into the transfer line and automatically moved in front of the MBE chamber. One puck at a time can be inserted in the chamber for deposition. After deposition, the puck can be moved to the electron gun via the transfer line.

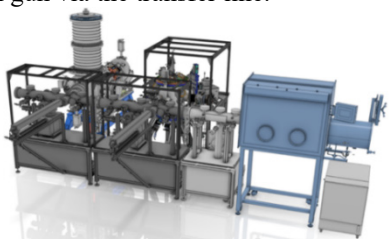

Figure 1: photocathode preparation facility (PPF) with glove box and MBE chamber connected to the photogun.

Precursors Preparation

All precursors were used under argon atmosphere in the glovebox (Ar: 2 bars, O_2 < 5 ppm and H_2O < 1 ppm). Antimony balls (Alfa Aesar, 99.9999 %) were melted in order to remove oxygen contamination inside an alumina crucible, ¼ filled. Potassium (Strem, 99 %) was melted and introduced into a molybdenum crucible. Then, a large excess (10 times) of indium (MaTeck, 99.9999 %) was added

* Work supported by the *Agence Nationale de la Recherche* via its program ANR-24-RRII-0001
†melanie.de-vos@ijclab.in2p3.fr

Content from this work may be used under the terms of the CC BY 4.0 licence (© 2026). Any distribution of this work must maintain attribution to the author(s), title of the work, publisher, and DOI.

ISBN: 978-3-95450-252-3 ISSN: 2673-5350 doi: 10.18429/JACoW-IPAC2026-THP2104

HIGH CURRENT PHOTOGUN FOR THE PERLE ENERGY RECOVERY LINAC*

M. Baylac†, E. Labussière, A. Plaçais,
Laboratoire de Physique Subatomique et de Cosmologie, Grenoble, France
M. Ben Abdillah, E. Bourdelas, S. Brault, O. Dalifard, M. De Vos, J. Demailly, F. Fournier, O. Frossard, T. Gérardin, C. Joly, W. Kaabi, S. Marchal, B. Mercier, E. Mistretta, D. Reynet, R. Roux, G. Sattonnay, A. Segovia-Miranda, M. Vannson, S. Wurth, J.-F. Yaniche, J. Yemane
Laboratoire de Physique des 2 Infinis Irène Joliot-Curie,
Université Paris-Saclay, CNRS/IN2P3, IJCLab, Orsay, France
H. Bzyl, Ingénierie Radioprotection Sureté Démantèlement, iRSD, Orsay, France
M. Faye, Grand Accélérateur National d'Ions Lourds, Caen, France
on behalf of the PERLE collaboration
M. Hoffmann, B. Keune, V. Kuemper, C. Quitmann,
RI Research Instruments GmbH, Bergisch Gladbach, Germany

Abstract

PERLE is a demonstrator intended to investigate multi-turn energy recovery at high-power, under construction in Orsay (France). The electron beam is created by a DC photogun aiming to produce 500 pC bunches at 40.079 MHz to inject the ERL loop. The high intensity electron beam (20 mA) originates from photocathodes of bi-alkali material (CsK_2Sb) optically pumped by visible light. The photocathodes are grown in a preparation facility connected to the gun chamber under vacuum. This paper describes the apparatus and presents the status of its commissioning and the very first beam tests.

INTRODUCTION

Particle accelerators are exceptional instruments widely used for research and society. Progress led to accelerators at increasing energies, which require large electrical power and accelerators must now face the challenge of energy sustainability. Among the options to reduce the energy footprint of accelerators, energy recovery linacs offer an ambitious concept for machines with limited perturbations of the beam at the interaction region such as colliders, free electron lasers or Compton-based sources. In an Energy Recovery Linac (ERL), the beam, after acceleration and interaction, is recirculated and decelerated in the accelerating cavities of the linac. In such a scheme, the power of the beam is recovered to excite the superconducting radiofrequency (SRF) cavities, leading to substantial savings in electrical power to drive the RF power source [1].

PERLE, ENERGY RECOVERY LINAC

PERLE (Power Energy Recovery Linac for Experiments) is a high-power ERL demonstrator in construction in Orsay, aiming to investigate multi-turn energy recovery [2]. The electron beam is recirculated in a superconducting linac, operating at 801.58 MHz, up to three times to a maximum energy of 250 MeV. The high intensity electron beam is created by a photoinjector consisting of a DC gun, a RF buncher at room temperature and a SRF booster (7 MeV) (Fig. 1) [3]. The photogun continuously produces electron bunches at 40.079 MHz, the 20th harmonic of the RF frequency, for continuous injection into the ERL. Bunches at different energies continuously circulate in the loop before being dumped at injector energy [4].

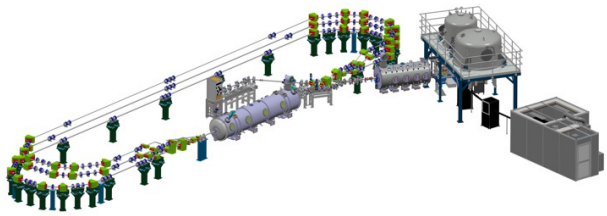

Figure 1: Layout of the PERLE energy recovery linac including injector, merger and spreader region, linac and beam dump in the 3-loop configuration.

PHOTOGUN

The electron source must provide a beam ensuring the high bunch charge and the low emittance required for injection into the ERL loop. Its main requirements are:

- high charge per bunch (500 pC) at 40.079 MHz,
- low emittance (<6 mm.mrad),
- long-term operation and reliability.

Electrons are generated by optical pumping from a photocathode illuminated by an external laser. In a DC photogun, electrons are accelerated and the beam is shaped by a strong static electric field in the gap between the cathode and a pierced anode. The gun voltage reflects a trade-off between a higher bunch charge, favouring stronger electric fields, and the risk of electrical breakdown. The gun is based on the design of the Cornell CBETA photogun [5]. It was produced, along with the photocathode preparation facility, by RI *Research Instruments GmbH* [6] and

* Supported by ANR via *France 2030* (ANR-24-RRII-0001) and the EU's program HORIZON-INFRA-2023-TECH-01-01 (GA n°101131435)
†baylac@lpsc.in2p3.fr

Content from this work may be used under the terms of the CC BY 4.0 licence (© 2026). Any distribution of this work must maintain attribution to the author(s), title of the work, publisher, and DOI.

ISBN: 978-3-95450-252-3 ISSN: 2673-5350 doi: 10.18429/JACoW-IPAC2026-THP2106

THE COMPTON BACKSCATTERING SOURCE COBRA AT THE S-DALINAC*

L. B. Dingeldein†, M. Arnold, R. Grewe, J. Hauf, M. Herbert, K. E. Ide, L. Jürgensen, M. Meier, C. M. Nickel, N. Pietralla, V. Pruy, D. Schneider
Technische Universität Darmstadt, Department of Physics,
Institute for Nuclear Physics, Darmstadt, Germany

Content from this work may be used under the terms of the CC BY 4.0 licence (© 2026). Any distribution of this work must maintain attribution to the author(s), title of the work, publisher, and DOI.

Abstract

The COBRA (Compton Backscattering at a Recirculating Accelerator) source utilizes a 100 W Yb:YAG laser that is synchronized with the electron beam of the superconducting Darmstadt linear accelerator S-DALINAC for head-on collisions. The backscattered photons in the X-ray energy range can be collimated into a quasi-monochromatic beam for electron beam diagnostics and as a technology demonstrator. The first collision of the electron and laser beam is planned within the upcoming beamtime with multi-turn recirculation. During operation, COBRA will utilize stabilization systems for both beams. Later, COBRA is foreseen to be operated during energy recovery mode, serving as a demonstrator for future Compton scattering light sources. This contribution provides an overview of the COBRA source, highlighting recent upgrades to the detector setup and developments of the laser beamline.

INTRODUCTION

Intense photon beams are used in several fields of scientific and commercial applications [1, 2]. There is a need for photon beams at X-ray to γ-ray energies with small bandwidth and a high flux. Prominent examples of light sources emit synchrotron radiation through the bending of the electron beam. The energy of the photon beam is dependent on the energy of the electron beam and therefore limited by the state of magnet technology and the size of the facilities. Alternatively, the photons can be produced by **L**aser-**C**ompton **B**ackscattering (LCB), which describes the process of a relativistic electron transferring its energy onto an incoming photon. Maximum energies for the backscattered photons are reached through head-on collisions. By colliding an initial photon beam with an accelerated electron beam, the backscattered photons with an opening angle of $1/\gamma$ possess a maximum energy of $E_p^{'} \approx 4\gamma^2 E_p$, where γ is the Lorentz factor of the electron beam, E_p is the laser photon energy and $E_p^{'}$ is the backscattered photon energy. There have been multiple approaches to LCB setups: The initial photon beam can be produced by an undulator in an optical cavity like at the **H**igh **I**ntensity γ-ray **S**ource (HIγS) [3]. Another possibility is an external laser system [4, 5]. The highest possible luminosity requires high currents of the electron beam at minimum emittance. **LIN**ear **AC**celerators (LINACs) offer lower emittances than competing facilities like storage rings. **E**nergy **R**ecovery **L**INACs (ERLs) [6] provide comparably high beam currents while simultaneously keeping the beam load for external power supplies minimal, if the ERL is superconducting. The electron energies can be increased with multi-turn superconducting ERLs, which can be built in a compact design and are more energy efficient [7]. The **S**uperconducting **Da**rmstadt electron **LI**near **AC**celerator (S-DALINAC) is the first superconducting multi-turn ERL in the world for which the energy recovery was demonstrated and quantified [8]. We have made steps toward preparing the infrastructure at TU Darmstadt for the world's first demonstration of a fourth-generation photon source, i.e., production of a photon beam from LCB on the electron beam of a superconducting multi-turn ERL.

THE S-DALINAC – A MULTI-TURN ERL

The S-DALINAC (Fig. 1) is TU Darmstadt's major research instrument for nuclear spectroscopy and accelerator science [9]. It can deliver electron beams with energies up to 130 MeV and beam currents up to 60 µA at its 10 MeV injector. The electron beam is bunched at a repetition rate of 3 GHz. The S-DALINAC is a three-time recirculating LINAC, which enables its operation as a multi-turn ERL. A twice-recirculating ERL has been demonstrated with a maximum initial beam current of approximately 7 µA [8]. The lattice of the third recirculation of the S-DALINAC has been upgraded for usage in a thrice-recirculating ERL mode [10] while its feasibility has been studied via beam-dynamics simulations [11].

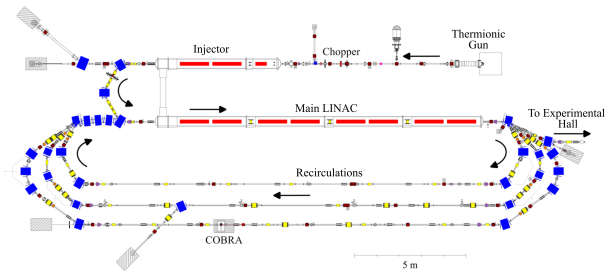

Figure 1: Floorplan of the S-DALINAC. The electron beam produced by a thermionic gun is first accelerated by the injector section and can be accelerated in the main LINAC up to four times due to the three recirculations. The COBRA setup is located in the third recirculation.

* This work is supported by the Deutsche Forschungsgemeinschaft (DFG, German Research Foundation) - Project-ID 499256822 - GRK 2891 'Nuclear Photonics'.

† ldingeldein@ikp.tu-darmstadt.de

ISBN: 978-3-95450-252-3 ISSN: 2673-5350 doi: 10.18429/JACoW-IPAC2026-THP2107

INSTALLATION AND FIRST TESTS OF A HIGH BRIGHTNESS BEAM TEST FACILITY FOR ERL APPLICATIONS AT INFN-LASA *

D. A. Giove†, [1], A. Bacci[1], M. Bertucci[1], A. Bosotti[1], S. Cialdi[1], I. Drebot[1], E. del Core[1], L. Faillace[2], L. Foggetta[1], L. Monaco[1], A. Olivieri[3], R. Paparella[1], M. Rossetti Conti[1], A. R. Rossi[1], V. Petrillo[4], S. Samsam[1], L. Serafini[1], D. Sertore[1], E. Viscione[1]
[1]INFN Milano - LASA, Segrate, Italy; [2]INFN LNF, Frascati, Italy; [3]UNICAL, Cosenza, Italy; [4] UNIMI, Milano, Italy

Abstract

A High Brightness Beams Test Facility (HB^{2}TF) has been funded in 2023 at the INFN-LASA laboratory in Segrate (Italy). The Test Facility will allow us to perform developments in ERL design and to carry out experiments with a high current CW electron beam in frontier areas of accelerator physics.

In this paper we will report on the status of the project and discuss the first tests underway on the main elements involved and available.

INTRODUCTION

The High Brightness Beams Test Facility (HB^{2}TF) at the INFN-LASA laboratory, in Segrate (Milan, Italy) will allow to perform developments in the injector field and to carry out experiments with a high current CW electron beam in frontier areas of accelerator physics. The Test Facility setup comprises a high-performance laser driven DC Gun followed by a normal conducting RF buncher acceleration section to provide 0.8 MeV, 2.5 mA CW electron beam. The facility has been conceived as the first stage of a more complex ERL Linac injector design, named BriXSinO [1], that foresees a second buncher and a SC booster linac able to increase the electron energies up to 4-10 MeV, maintaining beam current up to 2.5 mA, followed by a SC accelerating linac (the ERL) which will allow to reach up to 45 MeV.

The HB^{2}TF goals will provide experimental confirmation of the capability to generate high brightness beams at very high repetition rate (about 100 MHz). The beam dynamics studies that will be applied in HB2TF aim to verify the possibility to inject such a beam in a further stage of acceleration suitable for an ERL advanced experiment. The availability of a Test Facility which would be able to operate for long periods to test all the novelties in this design will be a relevant event in the technological and scientific panorama of the area.

The following section will summarize the characteristics of the main components currently undergoing commissioning, highlighting their specific features and the related design choices.

MAIN PARAMETERS

The design of the first section of the HB^{2}TF facility follows a classic approach to electron beam injectors intended for use in an ERL facility. Essentially, it is based on a DC gun, which utilizes a photocathode excited by a UV laser. The goal is to generate electron bunches of charge up to 100 pC, which, after emission, enter a solenoid to focus them, compensating for natural beam divergence and "space charge" effects in this low-energy region. Because electrons are still at a relatively low energy—a few hundred keV—immediately after emission from the cathode, they spread out quickly; the solenoid provides axisymmetric magnetic focusing to counteract this expansion and tune the emittance oscillations following emittance compensation scheme [2].

Two normal-conducting sub-harmonic bunchers, following a novel layout, have been planned to shape the beam in a suitable way for entry into a superconducting booster.

The frequency of 1.3 GHz is adopted for the SC linac booster, while for BD motivation [3] the frequency of the bunchers is set to 650 MHz, i.e. a sub-harmonic.

Due to budget constraints, the facility currently under construction will be completed up to the first buncher, even though the design of the subsequent elements—both in terms of beam dynamics and technology— of the second section are already included.

BEAM PHYSICS

The HB^{2}TF beamline follows a new design for an ERL injector (or merger) capable of providing high-brightness beams at a relatively low energy of about 4.5 MeV. This machine is designed to work with different starting parameters; however, considering a maximum average current of 2.5 mA, the following simulation has been performed with a bunch charge of 100 pC, which corresponds to a repetition rate of 25 MHz. Although this machine can reach a maximum repetition rate of 100 MHz, we have opted for a single-bunch reference simulation where space charge plays a main role. This choice is conservative and addresses one of the key points in ERL injector optimization, i.e., coping with high-brightness beams still dominated by space charge at the ERL–linac injection, thus representing a challenging optimization.

This design is innovative because it uses two bunchers at the sub-harmonic frequency of 650 MHz to gently compress the beam while accelerating it in a distributed beam gymnastics scheme [3]. The choice of a longer RF bucket allows the trapping of longer, cigar-like electron bunches with lower charge density, resulting in lower final emittances. Additionally, the use of two bunchers provides

† dario.giove@mi.infn.it * work supported by INFN CSN5 committee

Content from this work may be used under the terms of the CC BY 4.0 licence (© 2026). Any distribution of this work must maintain attribution to the author(s), title of the work, publisher, and DOI.

ISBN: 978-3-95450-252-3 ISSN: 2673-5350 doi: 10.18429/JACoW-IPAC2026-THP2111

REDUCED VERTICAL BETA FUNCTION IN KARA'S SHORT STRAIGHT SECTIONS FOR FUTURE R&D

P. Schreiber*, A. Papash, J. L. Steinmann, A.-S. Müller
Karlsruhe Institute of Technology, Karlsruhe, Germany

Content from this work may be used under the terms of the CC BY 4.0 licence (© 2026). Any distribution of this work must maintain attribution to the author(s), title of the work, publisher, and DOI.

Abstract

The KARA storage ring is operated as an accelerator test facility for research and development. It consists of four long and four short straight sections and presently operates five insertion devices (IDs). Four IDs are placed in the long straights with low vertical beta functions and one wiggler resides in a short straight section with a high vertical beta function. For future research and development experiments, a short straight with a lower vertical beta function is desired. Therefore, a new optics has been designed with a lower vertical beta function in the short straights. This new optics has been established in simulations and has recently been commissioned in the machine. Efforts are ongoing to push the vertical beta function even lower. This contribution will report on the ongoing efforts in establishing this new optics.

INTRODUCTION

The KARA storage ring is an accelerator test facility for research and development. In the acceleration chain, electrons are pre-accelerated to 500 MeV by a chain of accelerators ending in a booster synchrotron. They are then injected into the main storage ring, where they are accumulated and subsequently ramped in energy up to a maximum of 2.5 GeV depending on operation mode.

The lattice of KARA has a four-fold symmetry resulting in four long and four short straight sections. The nominal user optics is shown in Fig. 1 and the basic parameters of the lattice and for this optics, are shown in Table 1.

As it was designed as a synchrotron light source KARA includes five insertion devices. Four of which are in long straight sections where the optics was tuned for a low vertical beta function [1]. The fifth insertion device, CatAct [2], is in a short straight section with a higher vertical beta function as a result of the reduced beta function in the long straight sections. With the comparably high vertical beta function, CatAct produces a significant vertical tune shift [3] when powered. Therefore, two vertically focussing quadrupoles surrounding the ID are reduced in power synchronously to powering up the ID, leading to a local compensation of the vertical over-focusing generated by the ID, restoring the vertical tune to the nominal value.

For future research and development activities it might be of interest to install an insertion device at the CatAct position with a significantly reduced vertical gap. With the present optics, however, the lifetime due to gas scattering would be severely reduced. Therefore, a new optics with a reduced vertical beta function in the short straight sections has been investigated and implemented.

* patrick.schreiber@kit.edu

Table 1: Basic Parameters for the User Optics at KARA

Parameter	Value	Unit
Energy range	0.5-2.5	GeV
Circumference	110.4	m
Horizontal Tune	6.71	
Vertical Tune	2.80	
RF frequency	500	MHz
Harmonic number	184	
Momentum compaction factor	9.7×10^{-3}	

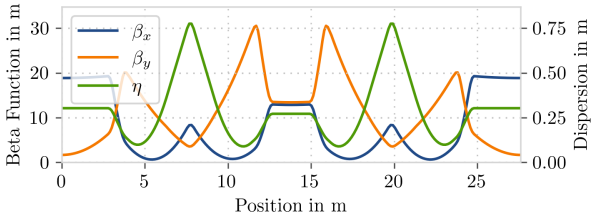

Figure 1: Nominal optics of one cell for the KARA storage ring.

LOW-BETA OPTICS

The reduction in vertical beta function in the short straights is achieved by increasing the vertical tune from 2.8 to 3.57. The new optics, as simulated, is shown in Fig. 2. For the initial development and simulation of the new optics, the simulation code OPA [4] was used. Further simulations including the shown results were performed using pyAT [5].

With a ramping machine such as KARA, there are generally two possible approaches to implement new optics/operating points. One can either use the established injection optics and ramping curves (curves of power supply currents for the energy ramp) and modify the optics with stored beam or implement the new optics already for injection, generate the correct ramping curves and stay with this optics from injection to final energy.

As the low-beta optics required an integer change to the vertical tune, the second approach was required for the implementation of this new optics at KARA. Since this approach requires injection into the new optics, some injection efficiency adjustments were made and the actual implemented optics is slightly different to the planned optics. By converting the actual used quadrupole magnet currents to quadrupole strength, using a polynomial conversion based on magnetic measurements [6], the implemented optics, called '*converted optics*' from now on, was simulated and is shown in Fig. 3. The vertical betatron tune is the same for both model and converted optics, but the value of the vertical

ISBN: 978-3-95450-252-3 ISSN: 2673-5350 doi: 10.18429/JACoW-IPAC2026-THP2114

LAYOUT OF ALBA II ACCELERATOR

L. Ribó*, N. González, F. Fernández, J. C. Giraldo, P. Salmerón, J. Boyer, R. Parise, F. Pérez
ALBA Synchrotron Light Source, Cerdanyola del Vallès, Spain

Abstract

ALBA Synchrotron Light Source will be upgraded into a diffraction limited machine by the replacement of the storage ring, which implies the reduction of the emittance by at least a factor of twenty. Compactness ratio of the magnetic elements has increased by a factor of 2. The new lattice has been designed with two big constrains. Firstly, keeping the same orbit length allows us to preserve the actual injector. Secondly, the medium and short straights will be collinear with respect to ALBA current layout to avoid moving the present Insertion Devices Beamlines. The bending magnet beamlines must be repositioned on the new machine. Magnetic array, vacuum chambers and girders are positioned with respect to the main orbit under tight clearances, that's why envelope studies of those clearances will have to be performed for the 3 subsystems. Easiness of assembling and installation of the different subsystems of the machine has to be considered also as a design requirement, in order to minimize the installation time. A mock-up of one sector is being prepared for this reason. The upgrade will be executed before the end of the decade and will be profiting at maximum all existing ALBA infrastructures, in particular the building.

INTRODUCTION AND GEOMETRICAL CONSTRAINTS

Low Emittance Alba II storage ring is composed by about 720 magnets distributed in 16 arcs. As a first constraint, it is requested the orbit length to be the same as it is in the actual ALBA machine [1], this means 268.800 mm. Apart from that, the straight sections between the arcs where the insertion device (ID) beamlines are already located have to be colinear with the actual orbit, in order to keep these beamlines position as they are now. With respect to the accelerator, linac and booster are not upgraded, but the booster to storage ring transfer line will be redefined.

Another geometrical constraint for fitting the new storage ring is the existing infrastructure. Tunnel walls, roof and the primary cooling circuits will be the same.

The position of the ID front ends centrelines is kept but for two bending magnet actual beamlines a new optimal extraction point has to be found in a way that the optical layout of the beamlines changes minimally.

The full storage ring is composed by 4 quarters, each quarter composed by 4 arcs, and 5 straights, two long, two short and one medium. Medium and short straights are collinear with the ALBA storage ring, not as the long straight which will offset radially with respect the actual beam path.

* lribo@cells.es

LATTICE CELL

The lattice cell is under optimization. At the moment, is composed by 3 dipoles, 2 permanent magnet dipoles. 8 anti-bending quadrupoles, 6 pure quadrupoles, 11 sextupoles, 11 octupoles and 4 correctors fitted in an arc length of 12.800 mm. Additionally, each arc will have 8 to 10 beam position monitors. The tolerances for positioning the magnets and the girder will need to be tighter corresponding to a low emittance new machine, where the emittance is reduced by a factor of 20 [2]. The arc is represented in the next picture (Fig. 1) as a simplified scheme, where the dipoles and the 8 anti-bending quadrupoles are represented. The sextupoles, pure quadrupoles, octupoles and correctors are not represented on the figure but they are distributed evenly between the magnets.

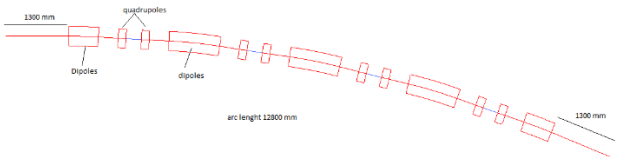

Figure 1: Schematic representation of the lattice arc.

MECHANICAL DESIGN OF THE CELL

Optimization of the lattice is being nowadays a continuous task, that is already converging into the most optimal solution in terms of emittance and beam life time. Due to the project planning, mechanical design cannot wait until the lattice distribution is frozen, that's why an updateable 3D model has been created to implement all the modifications in the most optimal way. Basically, the storage ring arcs are modeled in 4 subassemblies, where magnetic array, vacuum system, girders, Insertion devices, diagnostics and RF systems as others are restricted with respect to a fixed wireframe that follows the beam. This beam wireframe is the master reference for the remaining components of the storage ring, and it is built having the lattice geometrical model as an input. In this way, each time there is a lattice upgrade, the wireframe can be updated and all the components are automatically repositioned

Figure 2 shows an example of the wireframe beam path where all the coordinate axis are located to be the reference when positioning the magnets. After that, the girders and vacuum system are added, as can be seen in Fig. 3, where the compactness of the system can be appreciated

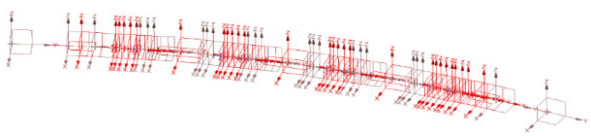

Figure 2: Wireframe beam path with magnets references.

Content from this work may be used under the terms of the CC BY 4.0 licence (© 2026). Any distribution of this work must maintain attribution to the author(s), title of the work, publisher, and DOI.

ISBN: 978-3-95450-252-3 ISSN: 2673-5350 doi: 10.18429/JACoW-IPAC2026-THP2115

BEAM DYNAMICS STUDIES FOR THE MAX 4^{U} LATTICES

M. Apollonio*, E. Al-Dmour, Å. Andersson, J. Bengtsson, A. Dixon, P. Fernandes Tavares, G. Pérez Segurana, M. Sjöström, S. Thorin, MAX IV Laboratory, Lund, Sweden
S. K. Jena, Raja Ramanna Centre for Advanced Technology, Indore, India

Abstract

MAX 4^{U} is an upgrade of the 3 GeV storage ring at MAX IV Laboratory, meant to considerably reduce the emittance of the present machine (328 pm rad), limiting changes to the present infrastructure, keeping the same beamline source points and minimizing costs and dark time for the MAX IV user community. The paper reports on the beam dynamics studies performed during the conceptual design stage resulting in two lattice candidates at 95 and 65 pm rad, showing pros and cons for an informed choice of the final lattice, presently aiming at less than 75 pm rad.

INTRODUCTION

The global quest for reduced emittance machines is the main drive at the core of the MAX 4^{U} project. At the beginning of 2024, as part of the Conceptual Design Report (CDR) [1], we started a thorough study of the possible candidates for an upgraded machine, initially aiming at a lattice delivering less than 100 pm rad with minimal impact on the present infrastructure, a process often described as a *surgical intervention* [2]. These starting goals rapidly produced two lines of investigation: a more conservative one, with reduced intervention on the machine aiming at the control of costs, and a more aggressive path, where the economic factor was relaxed to gain a smaller emittance in return. The two cases, named Absolute Requirement (AR) and Stretch-Goal (SG), are examined in this paper, showing the main differences and weighing pros and cons.

Both the designs stem from the 3 GeV ring of MAX IV [3], a 7BA machine (Fig. 1) and both make use of reverse bends to effectively push emittance reduction [4]. In the AR design these new magnets are located in the central unit cell (UC3), whereas in the SR lattice reverse bends are distributed over five of the seven achromat cells. Another key difference is the introduction of a new combined function dipole family for AR, needed to compensate for the flanking reverse bends, for a total of three bending dipole types (D1, D2 and D3), whereas the SR is based upon two dipole families (D1 and D2). In both architectures, the D1s belong to the matching sections of the achromat. In the next sections, we detail the main traits of the two designs.

Absolute Requirement Lattice

Figure 1 illustrates the transformation from the current 3 GeV lattice to the new designs. One of the main guidelines in its realisation is the preservation of the vacuum system with limited modifications of the magnets whose positions are kept. For AR there is a new sextupole family (S6), while the QF quadrupoles turn into the R1 reverse bends. Sextupoles S1, S3, and S6 have also a quadrupolar component. As said in the previous paragraph, the central dipole in UC3 is modified to compensate for the anti-bending effect, which causes a local change in orbit, confined around the cell. Conversely, the orbit outside the reverse bend region is unchanged, in particular in the matching cell area, where it is important to limit the entry angle at D1 (currently 1.5°) to avoid an excessive power deposition. The Twiss parameters for this lattice are summarized in Fig. 2 (top), whereas a comprehensive collection of parameters is given in Table 1.

In the optimisation process of the lattice, attention was paid to the phase advance between the unit cells, following the robust design philosophy based on the suppression of the resonance driving terms (RDT). In the AR case this approach is highly relaxed due to the non-symmetric nature of the lattice. The RDT cancellation happening every four achromats still results in a machine exhibiting good performance parameters as reported in the relevant section.

Stretch-Goal Lattice

With respect to the AR case, the SG lattice presents distributed reverse bends, which is key to push the emittance down to 65 pm rad. The total orbit variation is therefore more pronounced than in the AR case, although spread over the whole achromat (see Fig. 3). The new orbit entails a reduced entry angle at D1 (1.3°) which could require the replacement of vacuum chambers in this region. The issue is presently tackled both from the engineering perspective and via an optimisation of the original SG design. This lattice considers an achromat-wise RDT cancellation, resulting in a highly-symmetric layout (see Twiss parameters in Fig. 2) with a large robustness in the key performance parameters discussed in the next section.

Performance Comparison

The key parameters utilized to benchmark the performance of the two lattices are the Dynamic Aperture (DA) and the Local Momentum Aperture (LMA). The latter comes also with a determination of the Touschek Lifetime (TLT). In the design process, we also control the amplitude and momentum dependent tune shifts (Fig. 4), which is key to avoid potentially dangerous drifts of the working point towards resonance bands. Figure 5 shows the on-energy DA calculated at the mid-point of straight 1, for the AR (red) and the SG (blue) cases. Individual mis-alignments and gradient errors are introduced, the orbit is corrected and tunes are set to the nominal working points for every error seed. This set of simplified error is a proxy for a more thorough treatment which includes an optics fitting of the machine, presently

* marco.apollonio@maxiv.lu.se

Content from this work may be used under the terms of the CC BY 4.0 licence (© 2026). Any distribution of this work must maintain attribution to the author(s), title of the work, publisher, and DOI.

ISBN: 978-3-95450-252-3 ISSN: 2673-5350 doi: 10.18429/JACoW-IPAC2026-THP2116

SUPERRADIANT TERAHERTZ RADIATION GENERATION AT EUXFEL: FROM DESIGN TO INSTALLATION

K. Peetermans*, F. Giesteira, V. Kalender, L. Müller, B. Steffen, J. Wernsmann,
T. Wohlenberg, F. Lemery, Deutsches Elektronen-Synchrotron DESY, Hamburg, Germany

Abstract

Accelerator-based THz sources offer high energy and repetition rates, making them attractive for pump-probe experiments at X-ray free-electron lasers. The superradiant terahertz radiation generation (STERN) experimental chamber was recently successfully integrated into the European XFEL electron beamline during its long installation and maintenance period. The setup incorporates Cherenkov wakefield structures and a diffraction radiation screen to generate superradiant terahertz (THz) pulses from the electron beam, covering a combined spectral range between 0.3–30 THz. This work describes the design and installation of the experimental hardware, with emphasis on the THz generation and transport components. It reports on the wakefield structure assembly, the 10 m transport line and the laser-based alignment of the elements inside the chamber.

INTRODUCTION

Pump-probe experiments at the European X-ray free-electron laser (EuXFEL) increasingly demand synchronised, high-field THz pump sources that match the repetition rate of the X-rays [1, 2]. The EuXFEL injector accelerates trains of up to 2700 bunches in a 10 Hz burst mode, with a repetition rate inside the train of up to 4.5 MHz [3]. External laser-based THz sources face synchronisation challenges at the few-femtosecond level and cannot reach the high repetition rates of the modern XFELs with sufficiently high pulse energies. Accelerator-based sources are able to operate at the machine repetition rate and exhibit intrinsic timing stability, since both the THz and X-ray pulses derive from the same underlying RF reference and photocathode laser.

The superradiant terahertz radiation generation (STERN) experiment is an R&D project to investigate accelerator-based THz generation at EuXFEL. Two complementary radiation mechanisms are employed: Cherenkov wakefields in dielectric-lined waveguides (DLW) and diffraction radiation (DR) from an aluminum screen [4–10]. A combined spectral range of 300 GHz–30 THz is targeted. The generated pulses are transported via a mirror-based transport line to a dedicated THz diagnostics laboratory, where spectral diagnostics and an electro-optical sampling setup will be installed.

The design of the experimental chamber and THz transport line was described in earlier work [11]. The present contribution reports on the transition from design to installation: DLW production and installation, chamber and beamline assembly and optical alignment of the transport line. An image of the finished installation is shown in Fig. 1.



Figure 1: The STERN experimental chamber installed in the EuXFEL tunnel.

EXPERIMENTAL SETUP

STERN Chamber

The STERN experimental chamber is installed in the EuXFEL tunnel, downstream of the SASE2 undulator section. The chamber houses two types of THz sources sharing a common electron beam axis. The DLW assembly generates narrowband Cherenkov wakefield radiation, while an aluminum screen with 2 and 4 mm diameter holes produces broadband DR. Both sources produce radially polarised fields with an intensity profile that resembles a Laguerre-Gaussian L_0^1 mode in the far field. Figure 2 shows the design of the experimental chamber and the THz transport line. The middle mirror just below the experimental chamber is retracteable to allow either DR or DLW radiation to pass through the line.

The ELPHI Waveguide Block

The DLW assembly, referred to as ELPHI, is a precision-machined aluminium block designed to house several dielectric-lined waveguides. The block and the dielectric materials used are shown in Fig. 3. Stepper motors attached to ELPHI provide six mechanical degrees of freedom: transverse positioning and yaw rotation using small stages directly under the block, longitudinal travel on a rail system, and height, pitch and roll adjustment through three out-of-vacuum actuators.

ELPHI houses 43 cylindrical DLWs spanning inner diameters from 140 m to 4 mm and lengths from 4 cm to 15 cm. The dielectric materials featured in the first experimental run are quartz, aluminum oxide, PEEK and PI Mikro. An exact overview of the waveguide selection will be presented in a forthcoming publication [12]. The estimated radiated energy and frequency coverage is shown in Fig. 4. The block also houses anti-resonant fibers (ARF) cut at different lengths and

* karel.peetermans@desy.de

Content from this work may be used under the terms of the CC BY 4.0 licence (© 2026). Any distribution of this work must maintain attribution to the author(s), title of the work, publisher, and DOI.

ISBN: 978-3-95450-252-3 ISSN: 2673-5350 doi: 10.18429/JACoW-IPAC2026-THP2118

SUPERRADIANT THz GENERATION AND BUNCH COMPRESSION AT DALI

A. Delan*[1,2], U. Lehnert[1], A. Meseck[2], R. Niemczyk[1], A. Wagner[1]
[1]Helmholtz-Zentrum Dresden-Rossendorf, Dresden, Germany
[2]Johannes Gutenberg University Mainz, Mainz, Germany

Abstract

The Dresden Advanced Light Infrastructure (DALI), a 50 MeV superconducting linac currently under development at Helmholtz-Zentrum Dresden-Rossendorf, aims to deliver from one of its sources high-brightness, few cycle THz radiation through superradiant emission in a dedicated undulator. Efficient superradiant generation requires electron bunches with a form factor matched to the desired wavelengths between 0.1 and 3 THz. Achieving such short bunches at the design charge of 1 nC, however, is constrained by space charge forces and coherent synchrotron radiation in the magnetic chicane used for compression. This work discusses the design of the superradiant THz beamline with emphasis on the attainable compression performance and the resulting impact on the THz output. Quantitative tradeoffs between compression strength, bunch quality, and expected radiation yield are discussed to guide the optimization of the DALI THz source.

INTRODUCTION

The superradiant terahertz (THz) source at the Dresden Advanced Light Infrastructure (DALI) [1] will produce THz radiation from 0.3 to 3 THz through the magnetic compression of electron bunches. For higher frequencies from 3 to 30 THz an optical klystron is planned [2]. Details on the progress of the ultrafast electron diffraction setup are given in [3].

This paper outlines two magnetic chicanes for achieving the necessary compression and the resulting radiation of the THz source. Highly intense, few cycle radiation pulses in the range from 0.3 to 30 THz at high repetition rates are of great value in driving and understanding low (meV) energy excitations and fast processes in matter. To achieve significant superradiant emission a form factor above ~0.7 is needed, therefore the bunch length has to be reduced to $\lambda/4$ or less, which corresponds to a minimum required bunch length of 25 µm for emission at 3 THz. Given the initial bunch length of 1 mm a compression factor of up to 40 has to be reached.

INITIAL BEAM

As this work is part the larger DALI project, the particle distribution aims to be as close as possible to that produced by the operating parameters of the linac described in the DALI CDR where further details are given [1]. Simulation of the emission of 1 nC bunches in the gun at repetition rates up to 1 MHz, ballistic bunching, acceleration to 50 MeV in the continuous wave superconducting linac and transport to the expected location of the compressor result in the distribution shown in Fig. 1.

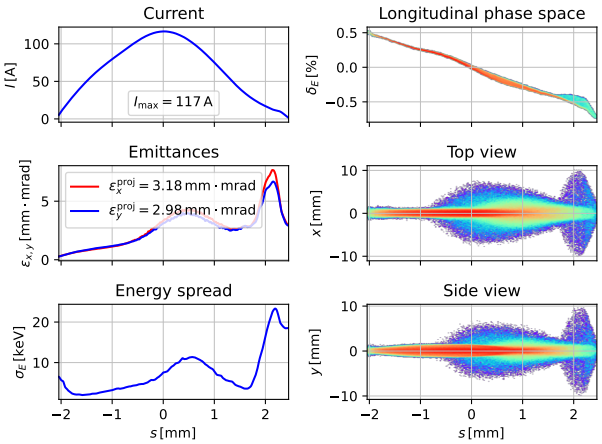

Figure 1: Overview of the bunch properties expected at the entrance of the compressor.

The longitudinal emittance of the electron beam at the compressor entrance is expected to be ~40 keV ps, degraded from originally 20 keV ps at the exit of the first linac cavity. Assuming no residual correlation between energy and longitudinal position, a bunch length of 25 µm forces the energy spread to be at least 1.1 % at 40 keV ps, limiting the usable number of undulator periods. The transverse emittances are of the order of 3 µm rad and the bunch length is 940 µm RMS, see Table 1. The resulting instantaneous current is in excess of 100 A before compression and 4 kA afterwards.

BEAM TRANSPORT

The following transport simulations were done using Ocelot [4] with an electron distribution shown in Fig. 1, comprised of 10^6 macroparticles with second order matrix transport, coherent synchrotron radiation and space charge enabled through the magnet arrangements shown in Fig. 2.

Compressor Layouts

The chicane architectures currently under investigation for compression by up to a factor of 40 are a dogleg-shaped antisymmetric two-cell achromat inspired by the bunch compressor 1 at Max IV [5] and a C chicane, shown in Fig. 2. This choice is motivated by their dissimilar complexity and the expectation of emittance degradation due to non-linear optics, space charge and coherent synchrotron radiation being limiting to the compression. Since the desired compres-

* a.delan@hzdr.de

Content from this work may be used under the terms of the CC BY 4.0 licence (© 2026). Any distribution of this work must maintain attribution to the author(s), title of the work, publisher, and DOI.

ISBN: 978-3-95450-252-3 ISSN: 2673-5350 doi: 10.18429/JACoW-IPAC2026-THP2119

CHARACTERIZATION OF THz RADIATION AT FLUTE

J. Schaefer*, M. Brosi, E. Bründermann, A. Malygin, A.-S. Müller, M. J. Nasse,
R. Ruprecht, M. Schuh, M. Schwarz, N. Smale, J. L. Steinmann
Karlsruhe Institute of Technology (KIT), Karlsruhe, Germany

Content from this work may be used under the terms of the CC BY 4.0 licence (© 2026). Any distribution of this work must maintain attribution to the author(s), title of the work, publisher, and DOI.

Abstract

FLUTE, the Ferninfrarot Linac- und Test-Experiment at KIT, is a compact linac-based accelerator test facility and provides electron bunch energies up to several tens of MeV with a wide range of charges. A bunch compressor allows tuning the bunch length from picoseconds down to the femtosecond-scale. FLUTE can therefore generate short, intense THz radiation for a wide variety of applications. In this contribution, we report on the characterization measurements of THz radiation generated after the bunch compressor.

SETUP

In this paper, we present first THz measurements generated by the FLUTE high-energy section and attempts to separate synchrotron radiation, edge radiation, and transition radiation. First THz emission using the FLUTE low-energy section was measurement last year [1]. At FLUTE [2] electrons are generated and pre-accelerated to 5 MeV in the low-energy section and then brought to 42 MeV by an S-band linac. A four-dipole bunch compressor (BC) allows compressing the bunch longitudinally. We used a quadrupole triplet between linac and BC to focus the beam transversely at the plane of an aluminum foil. The foil is installed at 45° to the beam axis and reflects radiation by 90° toward an extraction window and detector.

The measured radiation can be a combination from three different sources: Synchrotron radiation (SR) is emitted as the beam traverses the dipole bends, and edge radiation (ER) arises from the region of a sharp change in magnetic field at the entrance and exit faces of the rectangular dipole poles. Both SR and ER are reflected off the foil toward the detector. For geometric reasons, the strongest ER reaching the detector is mainly emitted from the last dipole exit face, other edges contribute partially, depending on the set BC deflection angle. The beam also produces transition radiation (TR) upon interaction with the foil, which is directed toward the same detector.

The detector, shown in Fig. 1, consists of four Schottky barrier diode detectors with horn antennas, sensitive at center frequencies of 272, 412, 625 and 925 GHz (± 20 % bandwidth each), referred to as M1–M4. The sensors are mounted on a *yz*-translation stage and arranged with a minimum spacing of 22 mm. This is a common bunch compression monitoring diagnostic, presented for instance in [3]. This arrangement allows for simultaneous coarse measurement of the radiation spectrum with all four diodes without repositioning the detectors. The diodes are linearly polarized; adjacent diodes have orthogonal polarization axes, an unavoidable consequence of the compact geometry, as visible in Fig. 1. The complete assembly can rotate to 0°, 45° and 90° about the center point of the four sensors to probe different polarization projections. Each diode is connected directly to an oscilloscope channel (2 GHz bandwidth, 12-bit native resolution). For each bunch passage, the oscilloscope extracts the extreme value in the time domain per diode channel. The Schottky type diodes yield negative signals when excited, thus the data shown are given as negative voltages. Absolute signal amplitudes between diodes are not directly compared as the individual diode scaling factors are not calibrated.

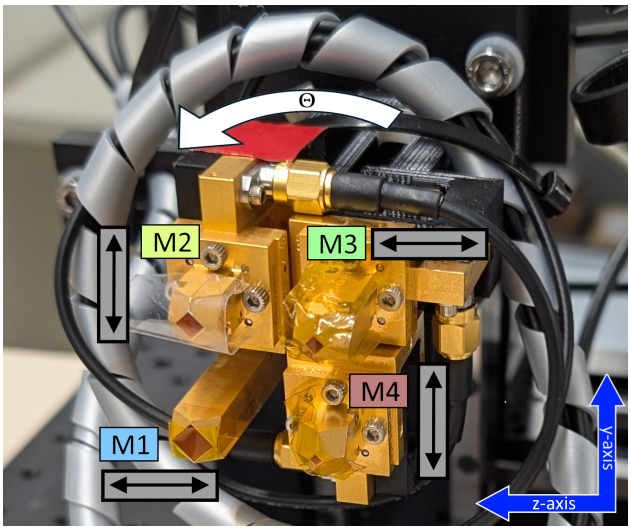

Figure 1: Photograph of the four-diode THz detector assembly. Sensors M1–M4 are arranged with minimal spacing; adjacent diodes have alternating linear polarization axes, as indicated by the gray arrows. The detector can rotate about the center point by Θ and translates in the two transverse directions of the radiation axis *y* and *z*. The photo was taken at Θ = 0°. The tape on-top of the diodes antennas serve as dust protection and is transparent to the measured radiation.

EXPECTED RADIATION SPECTRA

The intensity per frequency f and solid angle Ω interval emitted by a bunch of N electrons is [4]

$$\frac{\mathrm{d}^2 I_i}{\mathrm{d}f\,\mathrm{d}\Omega} = \left[N + N^2\,|F(f)|^2\right] \cdot SPE_i(f,\Omega)\ , \qquad (1)$$

where SPE_i is the single-particle emission spectrum for the individual radiation type $i \in \{\mathrm{ER}, \mathrm{SR}, \mathrm{TR}\}$. For FLUTE, the SPE for ER and SR are discussed in detail in [5] and for TR in [6]. Because the three types have distinct polarisation and angular emission patterns, the linearly polarised diodes

* jens.schaefer2@kit.edu

ISBN: 978-3-95450-252-3 ISSN: 2673-5350 doi: 10.18429/JACoW-IPAC2026-THP2124

ELI-NP GAMMA-RAY BEAM SYSTEM - STATUS UPDATE AND FUTURE

C. Matei*[1,2], A. Boianu[1], G. Chen[1], C.D. Cirdei[1,2], D.G. Ghita[1], A. Ionescu[1,2], N. Militaru[1,2], L. Neagu[1], H. Schubert[1], G. Suliman[1,2], L. Teodorescu[1,2], P. Tracz[1], E. Udup[1]
[1] ELI-NP / IFIN-HH, Magurele, Romania
[2] POLITEHNICA Bucharest, Bucharest, Romania

Abstract

The high brilliance ELI Gamma-ray Beam System (ELI-GBS) is under implementation at the Extreme Light Infrastructure - Nuclear Physics (ELI-NP) in Romania. The system uses an 800 MeV S-band accelerator driver as an Inverse Compton Scattering (ICS) source coupled to an interaction laser and in the future to a high-finesse optical cavity. The γ-ray beam will be available with energies up to 19.5 MeV to drive an ambitious scientific program which requires high spectral density (larger than 5×10^3 photons/s/eV), narrow bandwidth of 0.5%, and linear polarization higher than 95%. The ELI-GBS is foreseen to be finalized in an initial configuration in 2026. Details of the status of the LINAC commissioning, electron - laser interaction system design, and challenges for completing the system are presented.

INTRODUCTION

The ELI-GBS consists of all components necessary to create, accelerate and inject bunches of electrons into an interaction point (IP) for the collision with photon pulses from a dedicated laser system. It consists of six main parts:

- RF electron source
- Linear accelerator (LINAC)
- Electron Transfer Line (ETL)
- Interaction laser system
- Interaction chamber (IC) / optical cavity (OC)
- Electron beam removal and beam dump

The electron bunch is created in the RF electron source shown in the lower right corner in Fig. 2. The bunch is then accelerated in the linear accelerator, transported into the IP where it interacts with laser photons from the interaction laser system. After the electron-photon interaction, γ-ray photons are emitted in the forward direction along with the electrons which are deviated using magnetic fields into a beam dump. The Gamma-ray Beam System design presented in this paper is new and different from previous designs, EuroGammaS design from 2014 [1] and the VEGA design from 2019 [2, 3].

RF ELECTRON SOURCE

The RF electron source is composed of an 1.6-cell RF gun, 11-cell SW booster cavity, solenoid magnets, UV laser, and optical transport assembly. The RF power comes from the 7.5 MW klystron through the waveguide system and enters a 3 dB hybrid, which symmetrically splits the power to the RF gun and the SW booster cavity. The entire system was designed to produce low emittance (ϵ_{xy}< 5 µm), synchronized electron pulses at pulse repetition rates up to 50 Hz with an energy of 13 MeV at the exit of the booster cavity.

Electron bunches are generated in the RF electron source by illuminating the photocathode by ultraviolet picosecond pulses from the injector laser. The injector laser is a commercial industrial class laser system called PHAROS, produced by Light Conversion, comprised of oscillator, pulse stretcher, regenerative amplifier, pulse compressor, and nonlinear harmonic generation stages. Both oscillator and regenerative amplifier are based on Yb:KGW crystals that are pumped by diodes with 980 nm wavelength . UV pulses will be delivered to the photocathode via the UV transport system which directs the beam towards a pair of steering mirrors mounted near the vacuum window.

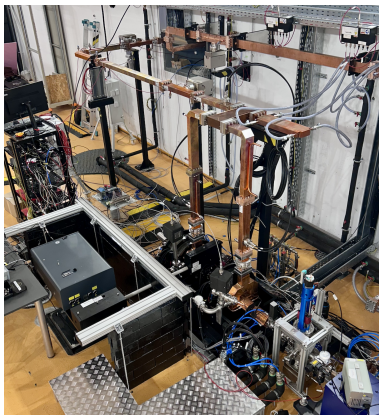

Figure 1: View of the RF electron source, waveguide system, and injector laser on position at ELI-NP.

The RF electron source is fully installed as shown in Fig. 1, connected to the klystron, and receiving RF power for ongoing RF conditioning as of April 2026. The system is under UHV of a few times 10^{-9} mbar. The UV laser and optical transport assembly are fully commissioned. Laser - RF synchronization is achieved by using a commercially available PhaseLock device from TEM Messtechnick.

LINEAR ACCELERATOR

The LINAC consists of five accelerating modules, each with four accelerating structures, with two beam diagnostics stations for beam commissioning and tune up. The main electron beam parameters are summarized in Table 1.

Accelerator Modules

High-power RF pulses are generated by Canon klystrons with a nominal rating of 50 MW, each powered by a solid-

* catalin.matei@eli-np.ro

Content from this work may be used under the terms of the CC BY 4.0 licence (© 2026). Any distribution of this work must maintain attribution to the author(s), title of the work, publisher, and DOI.

ISBN: 978-3-95450-252-3 ISSN: 2673-5350 doi: 10.18429/JACoW-IPAC2026-THP2125

FIRST DEMONSTRATION OF MeV ELECTRON DIFFRACTION USING THE SUPERCONDUCTING RF PHOTOINJECTOR AT THE HELMHOLTZ-ZENTRUM DRESDEN-ROSSENDORF

R. Niemczyk*[1], L. Stein[1,2], A. Arnold[1], J. M. Klopf[1], U. Lehnert[1], S. F. Maehrlein[1,2], A. Ryzhov[1], J. Teichert[1], E. Uykur[1], A. Wagner[1], S. Winnerl[1], R. Xiang[1]
[1]Helmholtz-Zentrum Dresden-Rossendorf, Dresden, Germany
[2]Technische Universität Dresden, Dresden, Germany

Abstract

Ultrafast electron diffraction (UED) allows for the characterization of structural and electronic dynamics in samples with sub-picosecond resolution. Utilizing a continuous wave photoinjector gives rise to MeV UED at MHz repetition rates, which has the benefits of better temporal resolution, higher beam coherence, higher resolution, and high repetition rates than conventional keV sources. A superconducting radiofrequency (SRF) photoinjector is part of the existing ELBE user facility at the Helmholtz-Zentrum Dresden-Rossendorf (HZDR), delivering electron beams in user operation since 2010. The HZDR is currently planning the Dresden Advanced Light Infrastructure (DALI), a source of THz and IR radiation and positrons. One of DALI's end stations will consist of an MeV UED facility, allowing for pump with IR and THz excitation, and probing with an electron beam, generated by an HZDR-type SRF photoinjector. In this proceeding, we present the first MeV electron diffraction results using the HZDR-type SRF photoinjector at ELBE.

INTRODUCTION

Knowledge of structural and reaction dynamics of matter are key in the fields of biology, chemistry, physics, and material science [1, 2]. Ultrafast electron diffraction (UED) allows to obtain both the structural and electronic dynamics in thin samples with time resolution of a few tens of femtoseconds [3]. When employing a photoinjector as an electron source, UED can be carried out at MeV energies – which comes with the benefits of better time and atomic resolution, and higher coherence. Moreover, if a continuous wave injector is used, a higher bunch repetition rate can be reached.

Helmholtz-Zentrum Dresden-Rossendorf (HZDR) operates the Center for High-Power Radiation Sources ELBE [4]. Here, a superconducting radio-frequency (SRF) linear accelerator accelerates electrons to energies of up to almost 40 MeV. The electron beam drives one of several secondary radiation sources in user operation, among them the infrared free-electron laser (FEL) oscillator FELBE, the superradiant THz source TELBE, or the positron source PELBE. ELBE accommodates a thermionic injector, as well as an SRF photoinjector. Depending on the beam requirements of the secondary radiation source, either the thermionic or the SRF injector is used as the electron source. Here, the thermionic injector is installed in line with the linear accelerator, while the SRF gun is next to it, and connected to the linear accelerator via a transfer dogleg.

As ELBE is in operation for now more than 25 years, HZDR is planning its successor facility: the Dresden Advanced Light Infrastructure DALI [5]. DALI will consist of an SRF linear accelerator driving an IR FEL oscillator, while a second SRF linear accelerator will drive a positron source, a superradiant THz source, and another THz source in an optical klystron scheme, all three in parallel [5]. The IR beam from the FEL oscillator will serve as a seed signal for the optical klystron. DALI will also host an MeV UED facility, with an HZDR-type SRF gun serving as the electron source for the UED instrument. Use of an SRF gun for MeV electron diffraction was first reported in Ref. [6].

This contribution reports the first demonstration of MeV electron diffraction using the SRF gun installed at ELBE. This static experiment allows for gaining hands-on experience with this technique, testing instrumentation and diagnostics, and later benchmark experimental results with simulations [7].

SRF PHOTOINJECTOR

A schematic of the SRF gun-II, which is currently installed at ELBE, is depicted in Fig. 1. The SRF gun consists of a 3.5-cell niobium cavity, which is operating at an RF resonance frequency of 1.3 GHz [8]. The cavity is located in a liquid helium bath to establish superconduction for its op-

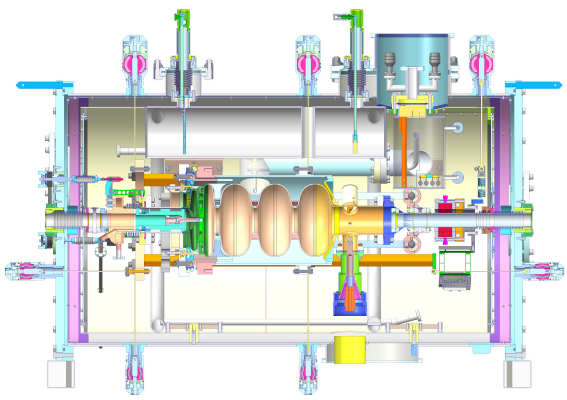

Figure 1: Cross-sectional schematic of the SRF gun-II. The cathode is inserted from the left, where electrons are accelerated within the 3.5-cell cavity and subsequently exit the gun on the right.

* r.niemczyk@hzdr.de

Content from this work may be used under the terms of the CC BY 4.0 licence (© 2026). Any distribution of this work must maintain attribution to the author(s), title of the work, publisher, and DOI.

ISBN: 978-3-95450-252-3 ISSN: 2673-5350 doi: 10.18429/JACoW-IPAC2026-THP2126

A COMMERCIAL MeV-UED INSTRUMENT BASED ON A 2.5 CELL RF-PHOTOGUN*

J. Kraemer, V. Kuemper†, C. Quitmann, A. Ufer,
RI Research Instruments GmbH, Bergisch Gladbach, Germany
M. Pfeiffer, RWTH Aachen University, Aachen, Germany

Abstract

Current research in quantum, nano, and energy materials requires information about material structure on the atomic scale in space and time. These materials show a variety of ultra-fast phenomena such as light absorption, structural changes, phase transitions, thermal or non-thermal melting, all of which happen on the ps or sub-ps scale and involve position changes on the Ångström scale. In this contribution we present the conceptual design for the RI-Bornite instrument, which allows ultra-fast electron diffraction using Mega-electron-volt electron beams (MeV-UED). For this instrument we use a warm (copper) 2.5-cell RF-photogun with a replaceable Cu photocathode. A single Ti:Sa fs-laser system drives both the pump beam (266 nm, ca. 1 µJ/pulse) and the probe beam (800 nm, several mJ/pulse). The system is designed to reliably reach 100 fs temporal resolution. The current sample chamber is optimized for solid-state samples and includes the option for sample cooling and a load-lock. Future versions will allow experiments on liquid or gaseous samples. We present the main design considerations, electron beam dynamics simulations, and the engineering design.

INTRODUCTION

MeV ultra-fast electron diffraction (MeV-UED) is a powerful technique in the field of material science, chemistry, biology, physics and related fields. It provides deeper insights into processes on the atomic scale which happen on ultra-short time scales (fs) like phase transitions, light absorption or structural changes in quantum, nano and energy materials.

We present the conceptual design study for the first commercial MeV-UED system.

A MODULAR ROBUST INSTRUMENT

Our design focusses on a robust design reliably achieving sub 100 fs temporal resolution and allowing future upgrades. The electron beam is created in a 2.5 cell RF-electron gun by a UV laser pulse (50 fs, 256 nm). The electron beam is focused using a single solenoid and an aperture allows reduction of dark current. In this paper we show the sample chamber for solid samples which includes the beam path for the IR pump laser and mechanical stages for sample positioning. Two detectors are located in the far-field with an adjustable distance up to 5 m. We are considering a hybrid pixel detector (PSI, Jungfrau) and a scintillation detector based on an electron-multiplied CCD camera.

The instrument includes the RF-klystron and low-level RF (LLRF) system as well as the fs laser system and an EPICS based control system. This allows controlling the e-beam, the laser beam, the sample and acquiring the data. Data analysis can be done by one of the many open-source codes for diffraction.

The configuration and parameters described in Figure 1 and Table 1 are the design goals for a basic instrument. Optional upgrades which are foreseen in the design include:

- Gaseous or liquid samples
- Optical Parametric Amplifier (OPA)
- Electron pulse compression
- Solenoids for focussing the e-beam at the sample or the detector
- Two separate lasers for pump and probe with delays up to µs and dedicated synchronization

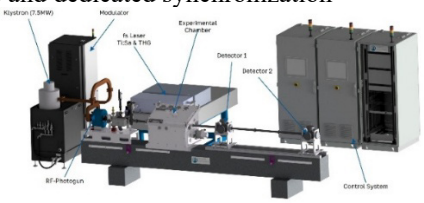

Figure 1: CAD model of the MeV-UED instrument.

Figure 2 shows a schematic overview. The Ti:Sa laser beam is split into the probe beam which is frequency triplet to 257 nm and used to generate the electrons from a Cu-photocathode in the electron gun. The pump beam is guided via a motorized delay line, enters the sample chamber and is directed onto the sample via a mirror.

The sample stage is adjustable in x / y, Rx / Ry.

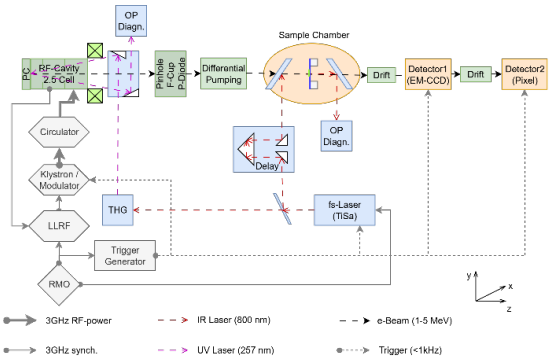

Figure 2: Schematic overview of the MeV-UED System.

†verena.kuemper@research-instruments.de

Content from this work may be used under the terms of the CC BY 4.0 licence (© 2026). Any distribution of this work must maintain attribution to the author(s), title of the work, publisher, and DOI.

ISBN: 978-3-95450-252-3 ISSN: 2673-5350 doi: 10.18429/JACoW-IPAC2026-THP2128

VARIABLE SAMPLE ILLUMINATION AND ANGULAR MAGNIFICATION FOR THE RUEDI ULTRAFAST ELECTRON DIFFRACTION BEAMLINE

S. S. Percival*, A. R. Bainbridge, B. R. Hounsell, J. W. McKenzie
ASTeC and Cockcroft Institute, STFC Daresbury Laboratory, Warrington, UK

Abstract

The RUEDI (Relativistic Ultrafast Electron Diffraction & Imaging) ultrafast electron diffraction (UED) beamline aims to deliver MeV electron bunches for sub-10 fs timescale diffraction experiments. The achievable momentum transfer resolution of the diffraction pattern at the detector is determined by the quality and focusing of the beam at the sample, and the transport of the diffracted beam to the detector. A beamline design is presented which allows for flexible illumination onto the sample and variable angular magnification. The pre-sample electron optics consist of two apertures and two single-solenoid lenses followed by the post-sample optics which consist of two double-solenoid lenses. Simulated results are used to demonstrate the range of capabilities of each system and show that RUEDI will be capable of producing the high-resolution diffraction patterns needed for a world-leading UED machine.

INTRODUCTION

RUEDI is a proposed user facility composed of two beamlines, a single-shot, time-resolved MeV imaging line, and an ultrafast MeV diffraction line with sub-10 fs temporal resolution [1, 2]. The diffraction line will consist of an S-band RF photoinjector [3], a magnetic compression arc and variable electron optics with a large variety of sample pumps and environments available. The design of the electron optics, consisting of a pre-sample condenser system for variable sample illumination and a post-sample projection system for angular magnification onto the detector, are outlined here.

VARIABLE ILLUMINATION

The pre-sample condenser optics allow for the tuning of the bunch charge, spot size and angular convergence onto the sample for different experiments. The condenser section of the beamline, as shown in Fig. 1, consists of two apertures alternating with two single-solenoid lenses. The beam entering the condenser section of the machine is the same for all modes: a 4 MeV, 400 fC bunch undergoing ballistic compression from the magnetic arc which leads to a temporal focus at the sample. This method of temporal compression requires there to be a large energy chirp across the beam, which increases the impact of chromatic aberration effects throughout the beam transport. The two apertures are used to cut the charge of the bunch to a variety of charges from 1.6 fC for stroboscopic experiments up to 160 fC for single-shot experiments.

The different illumination modes provide a trade-off between coherence length, spot size, and the number of electrons hitting the sample. The quality of the bunch at the sample is quantified by its coherence length, L_c, which determines the minimum achievable momentum transfer (Q) resolution, ΔQ_{RMS}, at the detector. The relationship between these two values and their definition with respect to the electron beam properties at the sample are given by

$$\Delta Q_{\mathrm{RMS}} \approx \frac{1}{L_c} = \frac{2\pi\varepsilon_x}{\lambda\sigma_x} = \frac{2\pi\sigma_{x'}}{\lambda}, \tag{1}$$

where ε_x is the geometric transverse emittance, λ is the de Broglie wavelength of the electrons, σ_x is the RMS beam size, and $\sigma_{x'}$ is the RMS uncorrelated divergence of the beam. This assumes that the sample size and energy spread contributions to ΔQ_{RMS} are negligible. Other key parameters include the bunch length which can be affected by strong space charge forces at transverse focuses, and the transverse size of the beam.

The main illumination mode used in diffraction experiments is with the beam focused parallel onto the sample. This improves the Q resolution as the larger beam at the sample reduces the uncorrelated beam divergence and so reduces the contribution of this divergence to the angle of the diffracted beam. This mode gives the best pattern quality and temporal resolution of any mode, but has a limited smallest spot size [4]. Other modes of interest include: a converging illumination mode, which focuses the bunch so it converges onto the sample allowing for higher charge density with minimal focusing, but as this does not have parallel illumination, projector optics are required to focus the resulting diffraction pattern onto the detector; and a small-spot mode which strongly focuses the bunch creating a crossover, allowing for micro-diffraction experiments [5], but with worse temporal resolution due to space charge forces, and detrimental effects on the pattern quality.

Figure 2 shows a comparison of how the beam will be cut and focused by the apertures and solenoids for these three illumination modes. For the parallel and converging modes, the first solenoid lens is used to focus the beam parallel onto the second aperture which cuts the charge. The second solenoid is then used to choose the focus of the beam onto the sample. Cutting the charge in the second aperture removes the outer particles of the bunch as late as possible and so reduces space charge driven emittance growth.

For the small-spot mode, the charge is cut in the first aperture to decouple the charge delivered to the sample from the tuning of the first solenoid. The first solenoid is then used to focus the beam into a transverse crossover such that the beam size at the second solenoid is larger than at the first. The

* suzanna.percival@stfc.ac.uk

Content from this work may be used under the terms of the CC BY 4.0 licence (© 2026). Any distribution of this work must maintain attribution to the author(s), title of the work, publisher, and DOI.

ISBN: 978-3-95450-252-3 ISSN: 2673-5350 doi: 10.18429/JACoW-IPAC2026-THP2129

OPTIONS ANALYSIS OF MHz INJECTORS FOR THE UK XFEL PROJECT

B. R. Hounsell*,1 A. D. Brynes[1], L. S. Cowie[1], J. W. McKenzie[1], B. L. Militsyn[1], S. S. Percival[1], P. H. Williams[1], F. Yaman[1], ASTeC, STFC Daresbury Laboratory, Warrington, UK
C. Davut†,1, O. Apsimon[1], University of Manchester, Manchester, UK
[1]also at Cockcroft Institute, Warrington, UK

Abstract

The UK XFEL conceptual design and options analysis process has recently been completed. The UK XFEL design proposes a superconducting linac operating with up to a 1 MHz repetition rate electron beam and demands beyond state of the art electron beam quality. This leads to strict requirements on the injector. The requirement for MHz repetition rates restricts the electron source technology to a number of options: DC guns, VHF guns, L-band SRF guns, VHF SRF guns and DC-SRF guns. Two of these injector technologies were investigated in detail: a VHF gun and a high field L-band SRF gun. In this proceeding the simulated beam dynamics performance and the technical readiness of the options will be compared and a number of conclusions will be drawn for the UK XFEL project.

INTRODUCTION

The conceptual design and options analysis (CDOA) of the proposed UK XFEL has recently been completed [1]. UK XFEL aims to achieve: near transform limited operation over photon energies from 0.1-20 keV; 6 or more simultaneous FELs at 100 kHz; widely-separated 2-color x-ray pump/x-ray probe. Two parallel injectors will feed a superconducting radio-frequency (SRF) 1.3 GHz L-band linac at bunch repetition rates from 0.1-1 MHz, distributed to the FELs by a spreader. A sketch can be seen in Fig. 1.

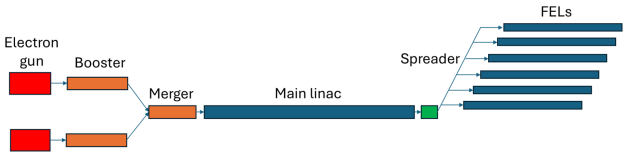

Figure 1: A schematic of UK XFEL showing two injectors and multiple FELs.

The design goals and choices made elsewhere impose requirements on the injector [1]; it must deliver high brightness with a full width (FW) duration <20 ps to match to the L-band main linac at two bunch charges (75 pC and 150 pC) simultaneously for the different FELs with an even spacing of 1 µs, at up to 1 MHz repetition rate. Also, it must be able to deliver two bunches in adjacent main linac buckets for the x-ray pump/x-ray probe mode.

MHz operation implies a limited number of gun options: direct current (DC), normal conducting radio-frequency (NCRF) VHF, SRF L-band, SRF-VHF or combined DC-SRF guns [2]. The choice requires balancing a number of factors: achievable cathode field, exit energy, compatibility with photocathode materials, beam dynamics complexity, and technical readiness. DC guns are the most technically mature option, having been used at several ERLs: JLAB FELs [3], CBETA [4], cERL [5] and ALICE [6]. However, they offer lower cathode fields (few MV/m) and exit beam energies (<500 keV); they have not been chosen for other XFEL facilities. NCRF VHF [7] is the next most mature, with higher cathode fields (< 27 MV/m) and exit energies (around 750 keV); LCLS-II [8] and SHINE [9] are both NCRF-VHF. EuXFEL is investigating a high-field L-band SRF gun with a field up to 50 MV/m [10] and LCLS-II HE an SRF-VHF gun with an exit energy of 1.6 MeV [11]. An SRF VHF gun/injector with parameters appropriate for an XFEL is also being investigated at BNL [12].

An analysis of existing injector designs, balancing technical risk against potential performance, led to these options being studied:

- Design-I: VHF gun with RF + magnetic compression
- Design-II: VHF gun with two-stage RF compression
- Design-III: L-band SRF gun without compression

Achieving low emittance from an injector requires balancing several factors including: cathode emittance; geometric and chromatic aberrations; and linear and non-linear space charge. Optimization was done using the genetic algorithm NSGA-II [13]; results are shown for the 150 pC case.

VHF GUN INJECTOR

Designs-I and II use a NCRF VHF gun [14]. The specifically designed 216.67 MHz gun has a 30 MV/m cathode field, a beam exit energy around 1.1 MeV field due to a longer front extrusion than typical, and a Cs_2Te photocathode. The design philosophy is to use the long RF wavelength to emit a long (>100 ps) bunch, allowing a smaller laser spot without space charge limited emission, to reduce the cathode emittance [15]. The bunch is then compressed in two stages. The benefits to the slice emittance can be seen in Fig. 2.

Each design uses a different two-stage compression scheme. Design-I uses an RF compression stage consisting of a NCRF 650 MHz linearizer and a NCRF 216.67 MHz buncher to compress to approximately 40 ps full width (FW); the bunch is then accelerated to the emittance-dominated regime by an SRF 650 MHz subharmonic booster. The second compression stage is a magnetic C-chicane with a

* ben.hounsell@stfc.ac.uk
† Now at Türkiye Enerji Nükleer ve Maden Araştırma Kurumu, Ankara, Türkiye

Content from this work may be used under the terms of the CC BY 4.0 licence (© 2026). Any distribution of this work must maintain attribution to the author(s), title of the work, publisher, and DOI.

ISBN: 978-3-95450-252-3 ISSN: 2673-5350 doi: 10.18429/JACoW-IPAC2026-THP2130

FROM Cs_3Sb TO Cs_2Te PHOTOCATHODES ON ELSA ACCELERATOR AT CEA DAM

A.-S. Chauchat†,[1,2], M. Collet[1,2], J. Houzet[1], V. Jacob[1], V. Le Flanchec[1,2], A. Pires[1,2], R. Rosch[1,2]
[1]CEA DAM Île-de-France, Bruyères-le-Châtel, France
[2]Université Paris-Saclay, CEA, Laboratoire Matière en Conditions Extrêmes, Bruyères-le-Châtel, France

Abstract

The 19 MeV electron linear accelerator ELSA at CEA DAM operated as an IR-FEL in the 1990s is now a user facility that provides pulsed bremsstrahlung and Inverse Compton Scattering (ICS) X-rays. Renovation of the facility is currently under way to improve system reliability. The 144 MHz photo-injector gun is the key element for producing a low-emittance beam for the ICS X-ray source. While the refurbishment of the 144 MHz RF source has increased the photo-injector's reliability, the short lifetime of the photocathodes has become the facility's weak point. A first step toward improved beam availability for users is to replace the Cs_3Sb photocathodes with Cs_2Te, which is known to have a longer lifetime. The drawback of this material is that it requires illumination with UV light, resulting in less laser energy available for photon-to-electron conversion compared with visible-light operation. This paper will present the fabrication process, compare the two materials in terms of quantum efficiency and lifetime, and describe the laser-system upgrades needed to maintain the same electron-beam current.

INTRODUCTION

Following its operation as a free-electron laser in the 1990s [1], the facility has been repurposed as a user facility delivering electron and X-ray beams to the scientific community. A distinguishing feature of this electron accelerator is its capability to generate low-emittance, high-charge bunches, thereby delivering high-current pulse trains to users [2]. The main accelerator line employs a low-frequency (144 MHz) photoinjector designed to extract high-charge bunches from the photocathode. These bunches are produced via the interaction of a 72 or 144 MHz Nd:YAG laser with an alkali photocathode. The resulting bunch lengths are tunable within the range of approximately 20 to 100 ps. This first accelerating stage boosts the beam energy to 2.2 MeV. The second stage comprises three 433 MHz accelerating cavities. Due to limitations in the RF sources and main power supply, the duty cycle is restricted to 250 µs pulse trains at a repetition rate of 5 Hz. Consequently, for low beam currents, the maximum achievable energy at the linac exit is 17 MeV.

The facility comprises three beamlines: one dedicated to bremsstrahlung X-rays, another to Inverse Compton Scattering (ICS) X-rays, and a third, straight-through line for electrons. A double-alpha magnet, described in [3], is employed to split the beam and direct it into the respective lines. In 2015, a third accelerating stage was added to the X-ray beamline to boost the beam energy to 30 MeV and to enable higher beam currents, circumventing the power limitations of the second stage.

Over the past decade, evolving user demands have necessitated the delivery of continuous high-current beams five days a week. This operational mode places stringent requirements on the accelerator's reliability and availability. Consequently, essential renovations are underway to revitalize this 30-year-old facility. The initial phase involved upgrading the power sources for the first two accelerating stages with state-of-the-art high-power transistor technology [4].

Regarding electron production, alkali antimonide photocathodes on Molybdenum substrates (K_2CsSb, Cs_3Sb, K_3Sb, or Na_2KSb) have been utilized or tested for the past 30 years using a frequency-doubled laser [5, 6]. For the last 15 years, however, only Cs_3Sb on Mo substrates have been employed.

Observations indicate that while the initial quantum efficiency (QE) immediately after fabrication has remained relatively stable over the years, the lifetime of the photocathodes has deteriorated significantly due to pressure increase in the fabrication chamber and in the photoinjector. This degradation results in a drastically reduced time-averaged QE. Practically, a photocathode now survives only about 2 days while delivering a high-current electron beam. Consequently, investigating photocathodes with extended lifetimes has become imperative to ensure the reliable delivery of high-current beams to users.

Cs_3Sb PHOTOCATHODES

Mo Substrate

Material deposition on the Molybdenum substrate is performed in an ultra-high vacuum (UHV) chamber. The pressure in this chamber ranges from 2 to 5.10^{-9} mbar and can rise to 2.10^{-8} mbar during material heating. The substrate consists of a Molybdenum cylinder with a polished face exhibiting surface roughness parameters of R_a = 3 nm and R_q = 5 nm. The polished face measures 50 mm in diameter (Fig. 1).

Content from this work may be used under the terms of the CC BY 4.0 licence (© 2026). Any distribution of this work must maintain attribution to the author(s), title of the work, publisher, and DOI.

†anne-sophie.chauchat@cea.fr

ISBN: 978-3-95450-252-3 ISSN: 2673-5350 doi: 10.18429/JACoW-IPAC2026-THP2131

PRODUCTION AND INITIAL TESTING OF A NANOSTRUCTURED COPPER PHOTOCATHODE IN AN S-BAND RF GUN*

D. Bazyl†, K. Flöttmann, H. Achour, M. Barthelmess, A. Dangwal Pandey[1], D. Elinjikkal, M. Hachmann, V. Hennicke, T. F. Keller[1,2], S. Kulkarni[1], M. Lengkeit, L. Lilje, N. Plambeck, E. Vogel, A. Winiarska-Bialk
Deutsches Elektronen-Synchrotron DESY, Hamburg, Germany
[1] also at Centre for X-ray and Nano Science CXNS,
Deutsches Elektronen-Synchrotron DESY, Hamburg, Germany
[2] also at Department of Physics, University of Hamburg, Hamburg, Germany

Abstract

A copper photocathode based on bulk Cu(100) substrate with a 50 µm-diameter nanostructured region was fabricated and integrated into an S-band radio-frequency gun. We report the procedure for production and preparation of high-quality copper cathodes with nanostructured area compatible with state-of-the-art S-band RF gun. Experimental results indicate absence of increased dark current up to 70 MV/m at the cathode.

INTRODUCTION

The continuous-wave (CW) superconducting radio-frequency (SRF) photoinjector under development at DESY relies on metal photocathodes, predominantly Cu, due to the chemical robustness required for atmospheric handling and subsequent cavity cleaning with the cathode installed. The relatively low quantum efficiency (QE) of Cu limits the achievable bunch charge in CW operation, especially at high repetition rates relevant for CW free-electron laser applications.

Nanoscale surface structuring has been demonstrated as one of the methods for improving QE through increased optical absorption and local laser intensity enhancement [1–3]. One of the questions for nanostructured photocathodes operated in high-gradient RF guns is whether the nanoscale surface features contribute to dark current. In this work, we describe practical experience with fabrication, preparation and initial RF tests of a Cu photocathode incorporating a 50 µm-diameter nanostructured region optimized for 515 nm excitation in a normal-conducting S-band RF gun. The cathode was conditioned to 70 MV/m, with dark current levels comparable to typical values observed during operation with Cs2Te photocathodes. Quantum efficiency was measured at 257 nm on unpatterned regions to evaluate photoemissive characteristics of Cu treated with BPS172 (Cu oxide passivator) [4].

* Work performed in the framework of R&D for future accelerator operation modes at the European XFEL and financed by the European XFEL GmbH.

† dmitry.bazyl@desy.de

CATHODE FABRICATION AND SURFACE TREATMENT

The pattern was designed using SIMULIA CST Studio® [5] to optimize light absorption at 515 nm and enhance the local laser intensity [6]. The geometry consists of cylindrical holes with radius $r = 188$ nm, pitch $d = 356$ nm, and depth of approximately 200 nm. Angle-resolved reflectivity measurements on similar patterns confirmed excitation of surface cavity modes with characteristic Fano-type signatures arising from plasmon–cavity coupling [7]. The hexagonal pattern was implemented over a circular area of 50 µm diameter matching the typical laser spot size at REGAE facility [8].

Single-crystal Cu(100) was selected as the baseline substrate to provide homogeneous milling response during focused ion beam (FIB) nanopatterning. Initial tests on small-grain polycrystalline Cu produced non-uniform patterns with geometric features clearly separated by grain boundaries, whereas patterns on Cu(100) were clearly homogeneous (see Fig. 1).

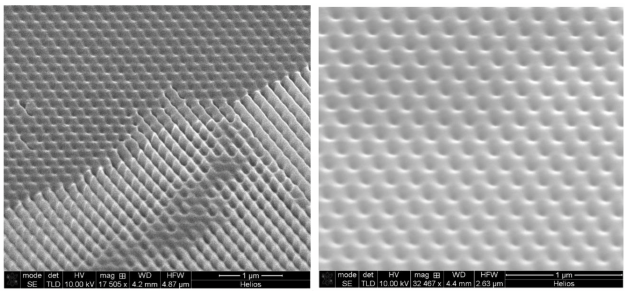

Figure 1: Comparison of nanostructuring on polycrystalline Cu (left) and Cu(100) (right).

A Cu(100) rod of dimensions 20 cm × 2 cm was procured from Surface Preparation Laboratory [9]. Three cathode plugs were fabricated by Edmund Optics son-x GmbH [10] using optical ultra-high-precision diamond turning with an off-center tool trajectory (see Fig. 2). The resulting surfaces had a roughness $S_a < 2$ nm over the emitting area, eliminating the need for polishing. The later is important for cathode geometries with complex mechanical features such as elliptical edges implemented for dark current mitigation. The fabrication sequence is compatible with standard RF guns operated at DESY following adaptions for specific cathode

Content from this work may be used under the terms of the CC BY 4.0 licence (© 2026). Any distribution of this work must maintain attribution to the author(s), title of the work, publisher, and DOI.

ISBN: 978-3-95450-252-3 ISSN: 2673-5350 doi: 10.18429/JACoW-IPAC2026-THP2132

THERMAL STUDY OF A 2 KELVIN COPPER PHOTOCATHODE IN A CW SRF GUN CAVITY *

D. Bazyl†, K. Flöttmann, E. Vogel, I. Zagorodnov
Deutsches Elektronen-Synchrotron DESY, Hamburg, Germany

Abstract

We assess the thermal behavior of a cryogenically cooled copper photocathode integrated into a continuous-wave superconducting radio-frequency injector cavity through direct thermal contact. A coupled three-dimensional thermal-electromagnetic model incorporating both the bulk photocathode and the injector cavity is presented. For the current injector design, the laser heat load is predicted to have a negligible effect on the intrinsic quality factor of the cavity. The cryogenic stability of the copper cathode is identified as the primary operational constraint. To address the associated cooling challenges, we propose a modified cathode plug geometry.

INTRODUCTION

A superconducting radio-frequency (SRF) photoinjector is under development at DESY for continuous wave (CW) operation in a future upgrade of the European X-ray Free-Electron Laser [1, 2]. The cathode is threaded onto the rear wall of the superconducting niobium cavity [3] (Fig. 1, left), an injector design that has reached 50 MV/m in vertical tests [4]. For 100 pC bunches at 1 MHz with a target QE of (1–2.5) × 10^{-4} at 257 nm, the required average UV laser power is 2–5 W (Fig. 1, right), comparable to the ∼1 W RF dissipation on the cavity rear wall at 50 MV/m. This laser heat load must be assessed for both thermal stability and potential quality factor degradation. We invistigate the thermal problem using Comsol Multiphysics® v6.3 [5]. A more detailed description including a two-temperature model for the emitting surface is given in [6].

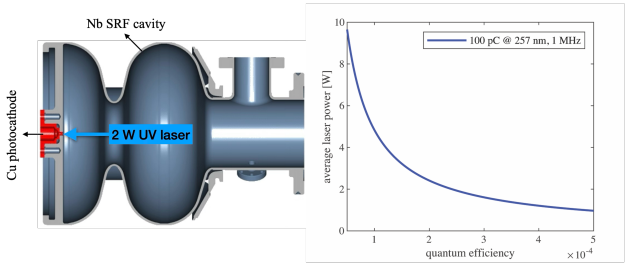

Figure 1: Left: 3D layout of the CW SRF injector cavity with integrated copper photocathode. Right: average laser power required for a Cu photocathode as a function of QE, assuming 1 MHz repetition rate and 100 pC bunch charge (257 nm excitation).

* Work performed in the framework of R&D for future accelerator operation modes at the European XFEL and financed by the European XFEL GmbH.

† dmitry.bazyl@desy.de

THERMAL-ELECTROMAGNETIC MODEL

The laser heat load is applied as a time-averaged inward heat flux boundary condition on the cathode emission surface:

$$-\mathbf{n}\cdot(k\nabla T) = q_{\text{avg}}, \quad q_{\text{avg}} = P_{\text{avg}}(1-R)/A_{\text{spot}}, \quad (1)$$

where P_{avg} is the incident laser power, $R = 0.36$ is the copper reflectivity at 257 nm, and $A_{\text{spot}} = \pi r_{\text{spot}}^2$ is the laser spot area with $r_{\text{spot}} = 430\,\mu\text{m}$. This steady-state approach was validated against a full transient simulation with periodic 1 MHz pulsed heating. At the Cu–In–Nb contact point, the transient solution stabilizes to a mean temperature matching the steady-state result, confirming that the bulk cathode responds to the average power input [6].

The computational model (Fig. 2, left) consists of the copper photocathode plug, the niobium cavity back wall, and the RF vacuum volume. A 1/8th section is simulated due to partial axial symmetry of the back wall. Temperature-dependent thermal conductivities for copper (RRR = 300) [7] and niobium (RRR = 300) [8] are used.

The primary heat transfer path from the cathode to the niobium is the Cu–In–Nb contact, characterized by a thermal contact resistance R_{tc}. Since specific data for this joint are not available, we adopt a conservative estimate $R_{tc} \approx 1.0 \times 10^{-3}\,\text{K}\,\text{m}^2/\text{W}$ at 2 K, extrapolated from measurements on similar Nb–In–Al joints [9] using the T^{-3} scaling consistent with phonon-dominated interfacial transport. This resistance is applied as a boundary condition imposing a temperature discontinuity proportional to the normal heat flux across the interface.

The cooling at the Cu–He II and Nb–He II interfaces is governed by the Kapitza conductance $h_K = aT^3$ [10], with a clean copper surface ($a = 1.0 \times 10^3\,\text{W}\,\text{m}^{-2}\,\text{K}^{-4}$) and BCP cavity-grade niobium ($a = 4.0 \times 10^2\,\text{W}\,\text{m}^{-2}\,\text{K}^{-4}$). The helium bath temperature is $T_{\text{bath}} = 2\,\text{K}$.

The electromagnetic coupling is implemented through a surface impedance boundary condition on the cavity back wall with $Z_s(T) = R_s(T) + iX_s$. The BCS surface resistance at 1.3 GHz is given by:

$$R_s(T) = R_{\text{res}} + \frac{C}{T} f^2 \exp\left(-\frac{\Delta(T)}{k_B T}\right), \quad (2)$$

where the free parameters $R_{\text{res}} = 8.3\,\text{n}\Omega$ and $C = 31182\,\text{n}\Omega\cdot\text{K}/\text{GHz}^2$ were fitted to measurements of the DESY 16G09 cavity.

RESULTS

The analysis of the baseline cathode geometry reveals a potential cooling limitation. For a nominal incident laser

Content from this work may be used under the terms of the CC BY 4.0 licence (© 2026). Any distribution of this work must maintain attribution to the author(s), title of the work, publisher, and DOI.

ISBN: 978-3-95450-252-3 ISSN: 2673-5350 doi: 10.18429/JACoW-IPAC2026-THP2133

DEVELOPMENT OF A PARTICLE-FREE CATHODE LOADLOCK SYSTEM FOR SRF-GUN

R. Xiang†, A. Arnold, S. Gatzmaga, A. Hoffmann, P. Murcek, R. Steinbrück, J. Teichert, Helmholtz-Zentrum Dresden-Rossendorf, Dresden, Germany
C. Adolphsen, J. Maniscalco, J. Smedley, SLAC National Accelerator Laboratory, Menlo Park, CA, USA
W. Hartung, T. Konomi, A. Taylor, B. Tousignant, T. Xu, Z. Yin, Facility for Rare Isotope Beams, East Lansing, MI, USA
J. Lewellen, Los Alamos National Laboratory, Los Alamos, NM, USA

Abstract

A prototype of SRF Gun has been built and successfully tested at MSU for LCLS-II HE project. This gun uses an HZDR-type cathode and required the development and implementation of a special cathode transfer and insertion system to ensure reliable operation. The main objectives were to prevent particle contamination, achieve a transverse alignment accuracy of less than 100 µm over a transfer distance of 1.3 m under ultra-high vacuum conditions (<10^{-9} Torr), and ensure the safe and repeatable insertion of the cathode into the cold cavity of the SRF gun. The cathode suitcase is used to transport a single cathode but can be upgraded in the future to accommodate high quantum efficiency (QE) semiconductor cathodes. To enable robust cathode exchanges, HZDR developed and built a special manipulation mechanism and an automated alignment system. The alignment concept was implemented using a translation rod equipped with contact electrodes and driven by precision stepper motors. Commissioning and final testing were successfully carried out at MSU to validate the transfer process. No change in RF performance was observed after the cathode exchange. The results confirmed that the system meets the design specifications and enables particle-free cathode exchange for the SRF gun at varying temperatures.

INTRODUCTION

Superconducting radio-frequency (SRF) guns are attractive electron sources for next-generation accelerator facilities because they can provide high-brightness electron beams with high repetition rate and low emittance. Compared with normal-conducting RF guns, SRF guns allow continuous-wave (CW) operation with significantly reduced RF power dissipation, making them highly suitable for applications such as energy recovery linacs, free-electron lasers, ultrafast electron diffraction, and compact accelerator-based light sources.

The Quarter-Wave Resonator (QWR) SRF gun developed within the collaboration between SLAC, MSU, HZDR, and ANL is designed as a low-emittance photoinjector capable of stable CW operation at accelerating gradients of 30 MV/m [1]. The gun uses the HZDR-type photocathode concept, which enables cathode replacement without warming up the gun cavity.

One of the major technical challenges in SRF photoinjectors is the implementation of a reliable cathode load-lock system. Particle contamination generated during cathode transport or insertion can significantly degrade SRF cavity performance by increasing field emission or causing cavity quench. At the same time, semiconductor photocathodes require ultra high vacuum to preserve their quantum efficiency and operational lifetime. To address these challenges, a dedicated cathode load-lock system has been developed. The primary goals of the system are to avoid introducing particles into the SRF cavity, ensure accurate cathode positioning during insertion, maintain ultra-high-vacuum conditions during cathode handling, and enable reliable long-term operation.

This paper presents the design, development, and final test result of the particle-free cathode load-lock system developed for the QWR SRF gun project.

SYSTEM DESIGN AND REQUIREMENTS

The load-lock system was developed to support secure cathode exchange while preserving SRF cavity cleanliness. Several design requirements were identified at the beginning of the project. The cathode insertion system had to minimize mechanical contact and keep particle generation less than 10 counts/ft^3 @ 0.3µm, and maintain vacuum levels below 1×10^{-9} Torr during operation. In addition, the cathode position inside the stalk had to be reproducible with transverse alignment accuracy better than 100 µm.

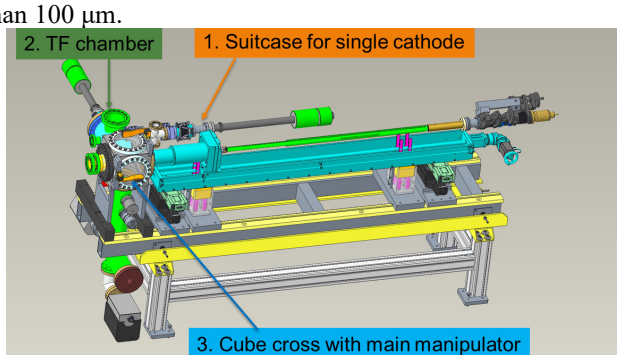

Figure 1: The designed cathode load-lock system with three main vacuum chamber groups.

†r.xiang@hzdr.de

Content from this work may be used under the terms of the CC BY 4.0 licence (© 2026). Any distribution of this work must maintain attribution to the author(s), title of the work, publisher, and DOI.

ISBN: 978-3-95450-252-3 ISSN: 2673-5350 doi: 10.18429/JACoW-IPAC2026-THP2134

PHOTOCATHODE DEVELOPMENT PLAN FOR DALI MULTIFUNCTIONAL FACILITY

R. Xiang†, A. Arnold, S. Gatzmaga, G. Hallilingaiah, A. Hoffmann, P. Murcek, R. Niemczyk, A. Ryzhov, J. Teichert, Helmholtz-Zentrum Dresden-Rossendorf, Dresden, Germany
J. Dube, T. Kamps, J. Kuehn
Helmholtz-Zentrum Berlin für Materialien und Energie, Berlin, Germany

Content from this work may be used under the terms of the CC BY 4.0 licence (© 2026). Any distribution of this work must maintain attribution to the author(s), title of the work, publisher, and DOI.

Abstract

DALI is an accelerator-based terahertz (THz) light source that uses multiple superconducting accelerators to drive CW electron bunches through undulators to emit ultra-intense THz pulses, including two ELBE SRF photo injects as the e- sources for high bunch charge beamline and for the UED, respectively. It requires a versatile portfolio of photocathodes to support diverse electron gun configurations and beam parameters targets. For the SRF gun commissioning, robust polycrystalline copper cathodes and magnesium cathodes will be employed, providing reliable performance and simplified handling during initial RF conditioning. Beam commissioning and routine user operation will firstly rely on the mature Cs_2Te photocathode, chosen for their proven robust, stability and realiable quantum efficiency. To enhance operational flexibility, especially in scenarios where UV laser generation presents challenges for special user appliations, we will consider to apply high-efficiency "green" photocathode optimized for visible-wavelength drive lasers. In parallel, an ultra-low-emittance photocathode in tens of micrometers will be under investigation to meet the stringent beam quality requirements of UED applications. This multi-cathode strategy ensures reliable commissioning, user-friendly operation, and state-of-the-art beam performance across all beamlines of the new accelerator facility.

INTRODUCTION

DALI is planned as a next-generation SRF accelerator facility for multifunctional user applications. The facility aims to deliver high-quality electron beams with flexible beam parameters to support accelerator research, compact THz radiation sources, positron source and ultrafast electron diffraction [1]. Such versatility imposes demanding requirements on the electron sources. Photocathodes are a key component of photoinjectors because they directly determine operational stability and the reachable beam quality. No single photocathode material can simultaneously satisfy all operational requirements of DALI. Therefore, a diversified photocathode strategy is required.

The proposed development plan builds upon more than ten years of operational experience with the ELBE SRF gun-II at HZDR [2], together with recent collaborative developments on new semiconductor photocathodes. The goal is to establish a flexible photocathode platform capable of supporting different operation regimes within DALI.

The photocathode program focuses on three major cathode families. Metallic photocathodes are considered for gun commissioning and ultra-low emittance applications, Cs_2Te photocathodes are intended for reliable high-current operation, and bi-alkali antimonide photocathodes are being developed for high-QE visible-light operation and energy-efficient photoinjectors. In parallel, supporting technologies including cathode preparation systems, UHV transfer systems, surface cleaning techniques, and cathode characterization methods will be discussed as well.

CATHODE PLAN

The DALI facility foresees multiple operational modes requiring substantially different beam characteristics. For high-field THz radiation and compact positron source applications, stable high-bunch-charge and high-average-current operation is essential. On the other hand, UED application requires extremely low transverse emittance and high beam coherence [3].

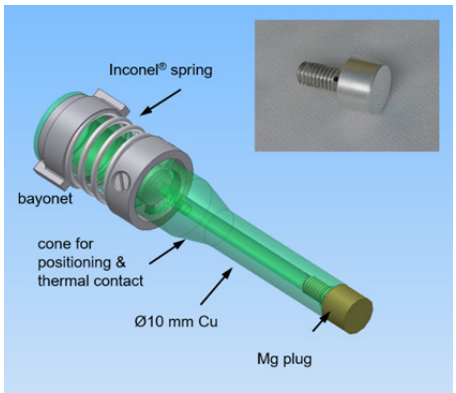

Figure 1: ELBE-style cathode with replaceable plug. The inset photo is a Mg cathode.

To satisfy these requirements, the photocathode system must provide high quantum efficiency (QE), low intrinsic emittance, long operational lifetime, compatibility with SRF environments, low dark current, and fast temporal response while maintaining high operational reproducibility. Experience from the ELBE SRF gun demonstrates the importance of reliable cathode preparation and exchange procedures in long-term SRF operation. Therefore, the DALI photocathode program emphasizes not only cathode performance itself, but also operational robustness and reproducibility.

†r.xiang@hzdr.de

ISBN: 978-3-95450-252-3 ISSN: 2673-5350 doi: 10.18429/JACoW-IPAC2026-THP2135

STATUS OF THE AUTOMATED ACTIVATION OF GaAs PHOTOCATHODES AT PHOTO-CATCH*

Markus Engart †, Joachim Enders, Maximilian Herbert, Robin Petry, Julian Schulze and Vincent Wende, Institut für Kernphysik, Fachbereich Physik, Technische Universität Darmstadt, Darmstadt, Germany

Abstract

Photocathodes based on the III-V seminconductor GaAs are used as photo-electron sources to supply spin-polarized electron beams for accelerator applications. In order to achieve sufficient electron yield, a thin surface layer of cesium combined with an oxidant is applied onto the cathode surface in a process called the cathode activation. It is typically done manually by an experienced operator. This contribution presents the current status in the development and testing of an adaptive algorithm for automated activation at the Photo-CATCH test stand.

INTRODUCTION

Spin-polarized electron beams provide the opportunity to probe a variety of physical systems, from magnetic materials and surfaces to the internal structure of particles and nuclei. These specialized beams can be produced by GaAs semiconductor photocathodes. Following a dedicated activation procedure, which will be addressed later, the GaAs cathodes are irradiated using a polarized laser with a fixed wavelength. Electrons emitted via the photo effect can then be extracted for the desired application.

The main research instrument at the Institue for Nuclear Physics (IKP) of Technische Universität (TU) Darmstadt is the superconducting Darmstadt Linear Accelerator (S-DALINAC) [1]. It is capable of providing both unpolarized and polarized electron beams, depending on the source used. The polarized electrons are created by the Spin Polarized Injector (SPIn) [2]. In order to enable research independent from the schedule of the S-DALINAC, a separate test stand was constructed: Photo-CATCH (Photo-Cathode Activation, Test and Cleaning using atomic Hydrogen) [3]. It features several XHV chambers for the handling of photocathodes, as well as a small beamline with different instruments used for the characterization of the produced electron beam. The photocathodes are prepared in the activaiton chamber, named after the process required for GaAs to achieve negative electron affinity (NEA) [4]. The procedure consists of the application of a thin layer of an alkali metal and an oxidant, in our case cesium (Cs), lithium (Li) and oxygen (O_2). This is typically done manually by an operator, following one of the established recipes, the so-called activation schemes. The quantum efficiency η is an important parameter to compare different activations, it measures the ratio of the outgoing electrons over the incoming photons. However, η shows considerable variation, even when following the same recipe [5]. In an effort to make the activation more reproducible, attempts to automate this process have been made. After a successful proof of principle, an adaptive algorithm was developed, capable of reacting to the different stages of the process [6].

CATHODE ACTIVATION AT PHOTO-CATCH

Photo-CATCH

Of the multiple chambers at Photo-CATCH, only the Cathode Activation Chamber (CAC, Figure 1) is used during the activation procedure. A carousel holds the photocathodes and moves them through the chambers via external manipulators. Small heating coils enable heat cleaning between activations. Cesium (Cs) and lithium (Li) are applied to the cathode with dispenser rods, which release their material in a controlled and reproducible manner. Oxygen flows into the chamber from an external reservoir through a piezo-controlled leak valve, which causes several issues discussed below. A window on the bottom allows the light used for the generation of the photocurrent to enter and hit the cathode surface. The anode ring collects all produced photo electrons using a bias voltage.

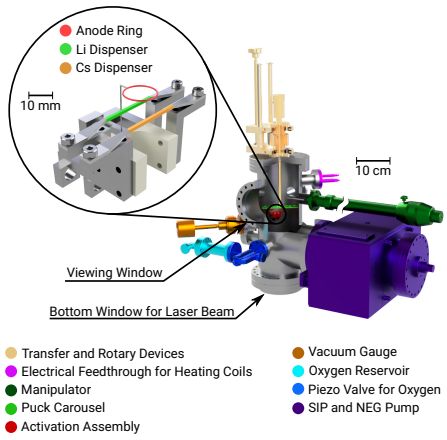

Figure 1: Cathode Activation Chamber (CAC) of Photo-CATCH, used for preparation and characterization of GaAs photocathodes. Figure taken from [7].

The activations discussed here follow the Co-Deposition scheme: Switching on the Cs supply prompts the photo current to rise into a first maximum, the Cs peak. After it has dropped to a specific fraction of the peak value, O_2 is added to cause the second, much higher and longer rise in

* Work supported by DFG (GRK 2128 „AccelencE “, project number 264883531 and Project-ID 499256822 – GRK 2891 ’Nuclear Photonics’)
† mengart@ikp.tu-darmstadt.de

Content from this work may be used under the terms of the CC BY 4.0 licence (© 2026). Any distribution of this work must maintain attribution to the author(s), title of the work, publisher, and DOI.

ISBN: 978-3-95450-252-3 ISSN: 2673-5350 doi: 10.18429/JACoW-IPAC2026-THP2136

PHOTOEMISSION STUDY OF NANOSTRUCTURED PLASMONIC PHOTOCATHODES*

M. Bulgacheva†, E. Gjonaj, Technical University of Darmstadt, Darmstadt, Germany
D. Bazyl, Deutsches Elektronen-Synchrotron DESY, Hamburg, Germany

Abstract

We present a simulation study of a nanostructured plasmonic copper photocathode for use in the new photoinjector that is presently being developed for the high-duty-cycle operation upgrade of the European XFEL. The simulations are based on a spatially resolved photoemission model using the Fowler–DuBridge formalism and including the Schottky effect induced by the accelerating field on the cathode surface. Particle-in-cell simulations are performed to evaluate the phase-space of the beam in the near-cathode region. It is shown that while quantum efficiency is improved, photoemission from the plasmonic cathode leads to a substantially increased transverse emittance and higher energy spread of the beam compared to the case of a flat copper surface. Space-charge effects remain moderate for the operating bunch charge considered in the study.

INTRODUCTION

The future continuous-wave (CW) operation in the high-duty-cycle (HDC) mode of the European XFEL (EuXFEL) requires a robust electron source capable of delivering 100 pC electron bunches at MHz repetition rate [1, 2]. For this purpose, a new SRF L-band electron gun is currently under development at DESY in Hamburg, Germany. The new gun design is foreseen to include a novel nanostructured (NS) copper photocathode [3]. These cathodes offer enhanced quantum efficiency (QE) through improved photon absorption. This allows to reduce the required laser power and, therefore, reduce power losses and potential heating damage in the SRF gun.

Several simulation and experimental studies on NS photocathodes have been reported in recent years [4–8]. However, a self-consistent treatment of plasmonic fields, spatially resolved photoemission, and three-dimensional beam dynamics is still missing. In this paper, we present a complete emission model for NS photocathodes including all these aspects. Furthermore, we present simulation results for a copper photocathode consisting of conical nanoholes and optimized for linear photoemission at 257 nm. The basic simulation methodology was previously shortly mentioned in [3]; here we provide a detailed description of the approach and analyze the results of electromagnetic field and beam dynamics simulations for the considered photocathode.

* Work is funded by the German Ministry of Research (BMBF) under contract 005K2022

† margarita.bulgacheva@tu-darmstadt.de

METHOD

Electromagnetic Field Simulations

Plasmonic photocathodes typically consist of a periodic lattice of sub-wavelength nanoholes that are engraved on a metallic surface as shown in Fig. 1a. Such structures support surface-localized electromagnetic modes known as Surface-Plasmon-Polaritons (SPP) [9]. To increase light absorption, the shape and dimensions of the nanoholes must be optimized for SPP-resonance at the target wavelength [4]. For this purpose, we perform FDTD simulations using CST Studio Suite® [10]. The model consists of a single nanohole with periodic boundary conditions, where a linearly polarized laser is applied from above at normal incidence. We considered various types of structures consisting of conical, square and cylindrical nanoholes. As seen in Fig. 2a, conical nanoholes exhibit approximately half of the peak field strength compared to square and round geometries, while achieving equivalent absorptance. The better field uniformity makes this shape the preferable choice, as it minimizes the risk of optical damage. We therefore consider in the following only conically shaped nanostructures.

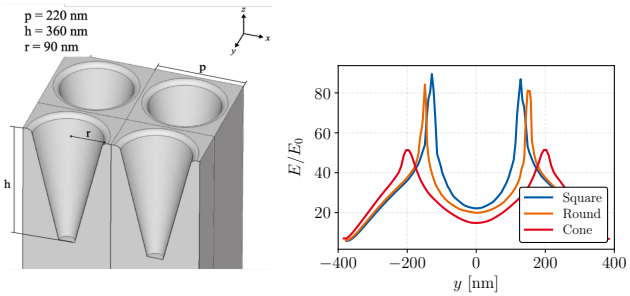

(a) (b)

Figure 1: a) Conical nanohole geometry optimized for a 257 nm laser. b) Field enhancement factor along the surface for square, round, and conical nanohole geometries.

The geometrical parameters including radius, depth and periodicity of the nanoholes are numerically optimized to minimize light reflection at the target wavelength of 257 nm. Figure 1b shows the result of this optimization for the photocathode with conical nanoholes (see also Fig. 1a for the optimal nanohole dimensions). The surface reflectance at 257 nm is reduced from 36% for a flat copper surface to less than 6% for the NS photocathode. This corresponds to an overall photon absorption rate that is ~1.5 times higher than for a flat cathode. However, as shown in Fig. 2b, the power loss density of the plasmonic mode is unevenly distributed on the cathode surface. The light absorption pattern is furthermore anisotropic as it depends on the polarization

Content from this work may be used under the terms of the CC BY 4.0 licence (© 2026). Any distribution of this work must maintain attribution to the author(s), title of the work, publisher, and DOI.

ISBN: 978-3-95450-252-3 ISSN: 2673-5350 doi: 10.18429/JACoW-IPAC2026-THP2137

STATUS OF THE HYBRID ELECTRON GUN DEVELOPMENT AT ELSA

S. Kronenberg*, K. Desch, B. S. Gatzsche, P. Hänisch, J. Orbons, D. Proft, Y. Schober, N. Treska, M. Switka, University of Bonn, Bonn, Germany

Abstract

A redesign of the injector beamline for the S-band linac at ELSA is underway, including the replacement of the existing electron gun by a hybrid gun that combines thermionic emission and thermally assisted photoemission in a single setup. The goal is to offer a new single-bunch injection mode alongside the long pulse mode already provided by the current gun. Measurements have been conducted to verify this emission technique using caesium dispenser cathodes. Another step in the scope of the project is the replacement of the current prebuncher cavity. A new design has been worked on and already undergone different tests of quality factor and bunching capabilities. The development of a dedicated test stand is currently being carried out to facilitate more detailed studies and serve as a prototype for the future injector section. Recent work has concentrated on the lattice and magnet design, as well as on evaluating suitable beam-diagnostic instrumentation.

INTRODUCTION

The ELSA facility (Electron Stretcher Accelerator, located at the University of Bonn) – shown in Fig. 1 – employs a 3 GHz travelling wave linac with both spin-polarised (GaAs photocathode) and non-polarised (thermionic cathode) electron sources, the latter delivers currents of up to 0.5 A. The injector at ELSA, requires modernization due to aging infrastructure, which has resulted in loss of diagnostic capabilities in favor of additional vacuum pumps. Spatial constraints in the injector area complicate replacement planning. Part of the beamline is a 3 GHz prebuncher used for both electron sources. A new dual-mode electron gun is being manufactured to maintain current operational capabilities while enabling single-bunch operation for machine studies in the stretcher ring. The dual mode is realized by using a caesium dispenser cathode, both as thermionic emitter as well as a photoemitter employing thermally assisted photoemission (TAPE).

INFRASTRUCTURE UPGRADES

The ongoing hardware development includes the replacement and modernization of key injector components to improve long-term operational robustness and maintainability. The current work focuses on two main elements of the injector beamline: the electron gun and the prebuncher cavity.

Electron Gun

The design of the gun is realized as a direct replacement of the current electron gun improving maintainability and offering a new mode of operation. The planned gun is employing

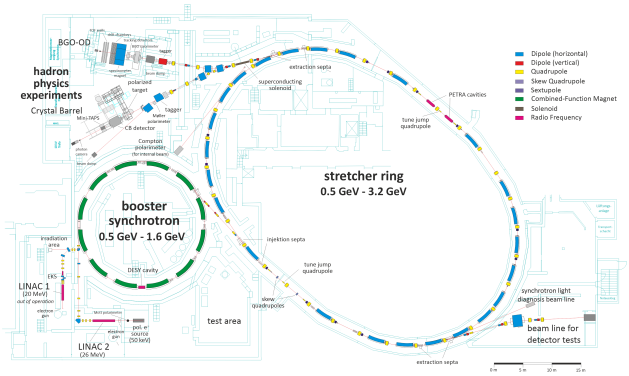

Figure 1: Overview of the ELSA facility.

the Pierce geometry with a 50 keV constant accelerating field. Further details on the gun design are described in [1]. The planned gun design is depicted in Fig. 2. Core of the new design is a gridded caesium dispenser cathode mounted on CF60 vacuum flange. Such cathodes are known to be long lived and operate under vacuum pressures in the range of 10^{-8} mbar to 10^{-9} mbar. During normal operation 1 µs long electron pulses with a charge of 2 µC are produced. The prebuncher compresses the beam longitudinally into multiple short bunches increasing the transfer efficiency through the linac.

In the TAPE mode the heating power is reduced below the emission threshold. The actual emission occurs via laser-induced photoeffect. The heating increases the quantum efficiency (QE) of the cathode. This effect is also known from different kinds of thermionic cathodes. In the case of dispenser cathodes it was observed that a with time decreasing QE can be restored using a heating cycle – rising the surface temperature to the expected values for thermionic operation followed by a reduction back to the TAPE operating temperature. Using the TAPE effect the bunch length can be controlled by the length of the laser pulse. To ensure acceleration of a single bucket within the S-band linac pulse

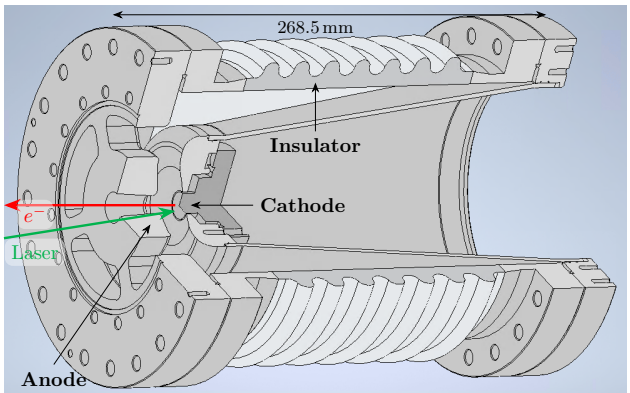

Figure 2: Planned design of new hybrid electron Gun.

* s.kronenberg@uni-bonn.de

Content from this work may be used under the terms of the CC BY 4.0 licence (© 2026). Any distribution of this work must maintain attribution to the author(s), title of the work, publisher, and DOI.

ISBN: 978-3-95450-252-3 ISSN: 2673-5350 doi: 10.18429/JACoW-IPAC2026-THP2139

A TIME-RESOLVED HIGH CHARGE DENSITY ELECTRON PHOTOEMISSION MODEL FOR THE FCC-ee TOP-UP SCHEME

A. Omoumi*, E. Granados, A. Latina, M. Martinez-Calderon
European Organization for Nuclear Research [CERN], Geneva, Switzerland
L. Jones, Science and Technology Facilities Council, Swindon, United Kingdom

Abstract

The generation of ultrabright electron beams relies on photo-injectors, which are influenced by dynamic surface and collective field effects. Predicting the resulting bunch characteristics is complicated due to the superposition of RF field, near cathode image-charge field, and space-charge. These effects are particularly relevant in high charge density photo-injectors operating with sub-ps bunch duration and nC bunch charge. We present an extended Fowler–Dubridge–canonical photoemission model that incorporates self-consistenly the temporal evolution of the aforementioned surface electric fields. We perform this connection by dynamically coupling the resulting fiends and the Schottky barrier. This method links single-particle photoemission physics with collective field effects, enabling the prediction of quantum yield in real time. Our simulations reveal strong spatio-temporal modulation of the photoemissive process, inducing nonlinear collective forces that degrade beam quality through emittance growth and phase-space distortion. The results underscore the important role in shaping the initial laser pulses to tailor the phase space of electron bunches for future colliders.

INTRODUCTION

Top-up injection is a key requirement for FCC-ee to sustain high integrated luminosity and ultimately sets the performance envelope of the machine. For instance, in the $t\bar{t}$ mode at 175 GeV, the nominal beam lifetime of 1 h is already the shortest among the four planned operating points, and in practice is likely to be even lower. Therefore a robust and reliable top-up injection scheme is therefore essential [1].

A first design of the FCC-ee electron gun has been proposed and optimized to meet the specifications of the accelerator complex [2]. The target energy of 200 MeV is achievable while keeping the rms transverse emittance below 4 mm·mrad and the rms bunch length near 1 mm at a peak charge of 5 nC. The high-charge density and ultrafast nature of these bunches induce collective charge fields can reshape the surface potential on femtosecond timescales. The emitted electrons generate a rapidly varying collective field that raise the effective photocathode potential barrier and can partially suppress the photoemission process half way through the laser pulse, distorting the emerging electron bunch phase space [3, 4]. These effects cannot be described in the traditional canonical or analytical simulation frameworks where photoemission is treated as an instantaneous process under quasi-static applied fields.

Particle-in-Cell (PIC) and point-to-point Coulomb solvers treat fields and particle motion self-consistently, accounting for shielding, bunch loading, and geometric field curvature [5–7]. While accurate at the device scale, they require external emission laws, cannot resolve ångström-scale barrier dynamics at practical mesh sizes, and are too computationally intensive for real-time injector optimisation or feedback loops needed in a top-up regime [1, 2].

Canonical photoemission models, including Fowler–DuBridge photoemission, thermal emission, and field emission formulations, provide fast local estimates of current density and incorporate microscopic barrier physics such as Schottky lowering and image potential [8–10]. However, they assume static applied fields and therefore cannot capture the transient collective-field modulation that occurs during high-brightness ultrafast emission.

These limitations motivate the development of a self consistent emission model that bridges microscopic barrier physics with macroscopic collective-field evolution. The model presented here incorporates dynamic modulation of the barrier potential [11, 12]. Its low computational cost makes it suitable for real-time on-demand charge control, aligning directly with the operational requirements of FCC-ee top-up injection scheme.

TIME-RESOLVED PHOTOEMISSION MODEL

A predictive description of photoemission in RF injectors must link microscopic barrier physics with the macroscopic collective fields that evolve during emission. The interplay of the optical laser pulse, photocathode properties, and near-surface charge buildup sets the emission rate (or dynamic quantum yield) and initial phase space, and thus the beam brightness. We introduce here a time-dependent Fowler–DuBridge model that includes dynamic Schottky lowering and self-consistent image- and space-charge feedback.

Because photoemission is confined to the laser spot footprint on the photocathode surface, the emerging charge distribution can be treated as a finite disk rather than the idealized infinite sheet often used in analytic injector models [13]. The infinite-sheet approximation overestimates near-surface screening and artificially clamps the emission current [3, 14, 15].

* anahita.omoumi@cern.ch

Content from this work may be used under the terms of the CC BY 4.0 licence (© 2026). Any distribution of this work must maintain attribution to the author(s), title of the work, publisher, and DOI.

ISBN: 978-3-95450-252-3 ISSN: 2673-5350 doi: 10.18429/JACoW-IPAC2026-THP2141

DESIGN, REALISATION, AND HIGH-POWER OPERATION OF THE FIRST TRAVELLING-WAVE PHOTO-EMISSION ELECTRON GUN

T. G. Lucas*, M. Zykova, C. Beard, H-H. Braun, M. Pedrozzi, M. Dällenbach, N. Kirchgeorg, R. Fortunati, A. Magazinik, A. Ocampo Duque, M. Seidel, R. Zennaro, P. Craievich
Paul Scherrer Institute, Villigen, Switzerland

Abstract

A novel travelling-wave (TW) RF photogun driven by ultra-short RF pulses has been successfully tested, stably reaching cathode fields of 170 MV/m for 100 ns pulses and 190 MV/m for a 10 ns pulse. This cathode surface electric field gradient far surpasses current S-band photoguns and represents a significant step toward increasing the brightness of future XFELs. Here we present an overview of the RF design, its unique tuning-free implementation, and high-power performance, highlighting how TW RF Photogun technology opens new opportunities for advanced electron sources.

INTRODUCTION

Radio-frequency (RF) photoemission electron guns (RF photoguns) are key sources of high-brightness electron beams. High cathode electric fields rapidly accelerate electrons to relativistic energies, reducing space-charge effects and improving beam brightness [1]. The highest brightness electron beams are produced using pulsed S-band room-temperature RF photoguns, which routinely operate at peak cathode fields of 100–120 MV/m, are widely used in X-ray free-electron lasers (XFELs) [2]. Achieving higher cathode fields requires new approaches. Ultra-short RF pulses are promising route to higher gradients because they reduce RF breakdown rates at a given surface electric field, enabling improved high gradient performance [3]. Here, we report the first travelling-wave (TW) RF photogun with a 100 ns filling time. The design supports operation with RF pulses an order of magnitude shorter than typical S-band RF photoguns [2], aiming to extend achievable cathode gradient beyond the current state-of-the-art for next-generation high-brightness electron sources.

REVIEW OF ELECTROMAGNETIC AND MECHANICAL DESIGN

The electromagnetic design of the TW RF photogun is described in detail in [4]; here we provide a brief overview. The design is an 11.5-cell C-band TW RF photogun with coaxially fed input and output couplers. The input coupler uses magnetic coupling slots to feed the cathode cell. This improved mechanical robustness near the region allowing an exchangeable cathode. A long coaxial input line enables integration of the main solenoid and bucking coil around the full structure. The highest electric field within the TW RF photogun occurs at the cathode to support photoemission and subsequent rapid acceleration, while the peak magnetic field is located on the coupling slots of the input coupler.

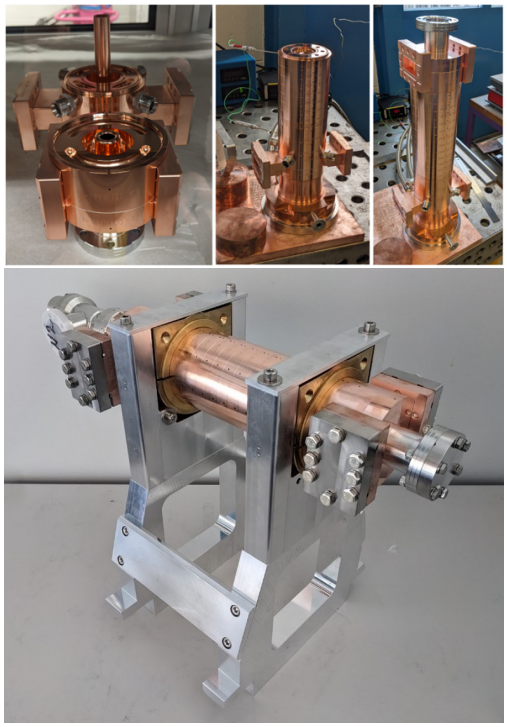

Figure 1: The brazed couplers (top-left); stacking of the cells and couplers (top-middle,top-right); and final realisation of the TW RF photogun (bottom).

REALISATION USING TUNING-FREE TECHNOLOGY

For realisation of the device, the components were machined from oxygen-free high-conductivity (OFHC) copper by VDL ETG Precision with pre-machining followed by high-precision single-point diamond turning and ultra-precision milling. All components were measured with a coordinate measuring machine, cleaned, and inspected before shipment to the Paul Scherrer Institute (PSI) where they underwent assembly and a multi-stage brazing to realise the final device (Figure 1). Final quality assurance of the device included a vacuum leak test, yielding a leak rate of 3.9×10^{-11} mbar·L/s.

LOW-POWER TESTING

Low-power testing of the TW RF photogun was performed in a clean-room environment to minimise contamination.

* thomas.lucas@psi.ch

Content from this work may be used under the terms of the CC BY 4.0 licence (© 2026). Any distribution of this work must maintain attribution to the author(s), title of the work, publisher, and DOI.

ISBN: 978-3-95450-252-3 ISSN: 2673-5350 doi: 10.18429/JACoW-IPAC2026-THP2143

DELIVERY OF CAESIUM TELLURIDE PHOTOCATHODES TO THE CLARA ACCELERATOR AT DARESBURY LABORATORY

H. Churn*,[1], C. Benjamin[1] L.B. Jones[1], K.T. Morrow[1], T.C.Q. Noakes[1],
ASTeC, STFC Daresbury Laboratory, Sci-Tech Daresbury, Warrington, UK
D. Sterland, University of Warwick, Coventry, UK
[1]also at the Cockcroft Institute, Sci-Tech Daresbury, Warrington, UK

Abstract

High performance electron accelerators require high brightness electron beams. To achieve this a photocathode with a high quantum efficiency (QE) and low intrinsic emittance is required while also being robust with a long lifetime and low dark current. Photocathodes based on alkali metals can fulfil these requirements and, as such, are an important area of research for the accelerator physics community.

The Compact Linear Accelerator for Research and Applications (CLARA) at STFC Daresbury Laboratory has recently been upgraded from a copper photocathode to a caesium telluride photocathode. This has enabled a significant increase in bunch charge for a fraction of the laser power. We discuss the process of manufacturing and polishing molybdenum photocathode plugs and the subsequent deposition of caesium telluride thin films. Three photocathodes have been provided to the CLARA facility with consistent and high quantum efficiency. One of these photocathodes has been successfully operating in CLARA since September 2025 with a stable QE of approximately 11 %.

INTRODUCTION

The Compact Linear Accelerator for Research and Applications (CLARA) at Daresbury Laboratory is a state-of-the-art medium energy electron linear accelerator that has recently been commissioned [1, 2]. CLARA has previously been operated using a copper photocathode; however, in order to achieve its intended design specifications of 250 MeV/c 250 pC bunches at 100 Hz repetition rate CLARA has been upgraded to a caesium telluride photocathode.

Caesium telluride has been a photocathode of choice in the accelerator community for many years and is widely used in accelerators across the world [3]. This is due to its high quantum efficiency (QE) and low intrinsic emittance while simultaneously being robust enough the survive the vacuum conditions of a radio frequency (RF) photoinjector, allowing many months, if not years, of operation using one photocathode.

We detail the manufacturing and polishing of three molybdenum plugs and the subsequent deposition of a caesium telluride thin film on each photocathode, before highlighting some key performance data of one of these photocathodes that has been operating in CLARA since September 2025.

* hugh.churn@stfc.ac.uk

PHOTOCATHODE PLUG MANUFACTURE

Machining and Polishing

The CLARA accelerator uses a modified 'INFN-style' photocathode plug similar to those used by many accelerators around the world, including the LCLS-II and the EuXFEL [4, 5]. Two pieces of high-purity sintered molybdenum bar (Mo) were supplied to Abelco GmbH, one from Goodfellow (99.9 % purity) and one from WHS Sondermetalle (99.95 % purity, type 361SR). Abelco manufactured three plugs from each piece of material with initial hand polishing carried out by them using Micromesh abrasive pads from 1500 grade up to 12000 grade.

Fine polishing of the photocathode tips was carried out at DESY Hamburg using the process developed for the EuXFEL photocathodes. This involved an initial IPA clean and vacuum bake for outgassing consisting of a 3 hour controlled ramp to 950 °C, a 3 hour soak at 950 °C and finally an uncontrolled 3 hour cool down to ambient temperature. The baking profile only commenced once the pressure inside the oven had fallen to $< 1 \times 10^{-5}$ mbar. The actual pressure through the soaking and cooling stages was $< 1 \times 10^{-6}$ mbar.

Polishing was carried out with a Streurs TegraPol-21. This has a 6-plug carousel, so was loaded with three blanks to separate the polishing of the different photocathode material batches and avoid any cross-contamination. Polishing was achieved in five steps commencing with Buehler MetaDi Mono Suspension 9 micron polishing grit (coarse) and progressing to a Buehler MetaDi Mono Suspension 0.05 micron (super-fine) grit, with the steps repeated as necessary in order to achieve the required level of surface roughness. The acceptable finish criteria was a reflectance of > 57 % at 532 nm. All 6 of the polished photocathodes attained reflectivity levels of ~63 %, but following careful visual inspection using a x6 magnified eyepiece, 3 were rejected due to the presence of surface defects assumed to be pits linked to the sintered nature of the original source material manufacture. The 3 plugs which were judged to be acceptable for use in the CLARA photoinjector were numbered 033 which originated from the Goodfellow batch, and 034 & 036 which originated from the WHS Sondermetalle batch.

Surface Imaging and Roughness

Upon receipt at Daresbury laboratory, high resolution surface images of the photocathode surfaces were taken using a Keyence VHX-7000 microscope. Figure 1 shows an example image of photocathode 034 at 50x magnification

Content from this work may be used under the terms of the CC BY 4.0 licence (© 2026). Any distribution of this work must maintain attribution to the author(s), title of the work, publisher, and DOI.

ISBN: 978-3-95450-252-3 ISSN: 2673-5350 doi: 10.18429/JACoW-IPAC2026-THP2145

FAST STRIP LINE BASED INJECTION KICKER DEVELOPEMENT AT ESRF

T. Perron*,[1], B. Roche[1], B. Ogier[1], C. Maccarrone[1], S. White[1], L. Carver[1], N. Carmignani[1], S. Liuzzo[1], A. Sauret[1], K. Andre[1], M. Paraliev[2]
[1]ESRF, Grenoble, France
[2]PSI Center for Accelerator Science and Engineering, Villigen, Switzerland

Abstract

This paper reports on the advancement of the design of a fast kicker device at ESRF. The kicker is based on a Strip-Line (SL) device fed by an ultra fast High Voltage (HV) power supply. These fast kickers allow to displace only one bunch instead of the full bunch train, reducing greatly the disturbance observed by users during injection. They are now operated in several institutes and under study in most modern light sources. We will report on the beam dynamics simulations to quantify the expected gain for injection, and describe the advancement of the hardware design and tests.

INTRODUCTION

For the last 15 years, pulsers providing tens of kV over sevral ns are available. The use of fast kickers combining these pulsers with SL is spreading in the accelerator community. The lake of reliability of the power supplies of the early days is now overcome, and some freshly commissioned light sources, like HEPS in China [1], or APS [2] in USA have their injection process relying on these devices. At ESRF, this technology had been tested in 2016 to inject the 200 Mev linac beam into the booster synchrotron. A single RF bucket could be injected in the booster with same efficiency as using the usual injection kicker. Nevertheless, the power supply failed after a few minutes of operation in the tunnel. Interest has risen again these past years even-thought the use of a Non Linear Kicker (NLK) is foreseen to target transparent injection [3, 4], mandatory feature to increase the top-up frequency.

These ultra fast kickers could be a backup solution to the NLK. The "Kick and Cancel" (KC) scheme, proposed for the DIAMOND II light source [5], would indeed be an efficient scheme for accumulation in the main ring. Another interesting feature of the device, combined with the NLK, is its ability to drastically reduce injection losses on vertical low gap ID's, a mandatory condition to close them further.

We will also report on some tests done in 2024, in collaboration with the PSI team, concerning the installation and test of a prototype SL kicker developed by PSI [6], on the ESRF storage ring.

PROTOTYPE DESIGN

The high frequency nature of the pulse traveling through the structure imposes a careful choice of geometry to keep the 50 Ω adaptation. The full setup consists of a HV HF pulser, followed by a low loss HV RF cable connected to the SL kicker. At the other end of the SL, the signal is extracted via another set of cables to an attenuator, in order to be damped and monitored on a scope. The transitions between air and vacuum at the entrance and exit of the SL structure will be ensured by commercial Feed-Throughs (FT). Different type of FT equipped with N and HN connectors will be tested:

- LESKER ref IFTNG012033M
- IFTHG013052
- VACCOM ref CF40R-N50-GS-SE-CE-SS
- CF40R-HN50-GS-SE-CE-NI.

We hope to be able to fully support the blades via their link with the FT, even-thought no solution has been found yet to ensure both, mechanical stiffness and absorption of the heat induced elongation of the blades. The transition between the upstream Vacuum Chamber (VC) profile and the inside of the SL is a complex shape meant to optimise both 50 Ω matching of the structure and beam/VC coupling impedance. We are aiming at making this transition inside of a wide flange, produced via Additive Manufacturing (AM), that will support the FT's flanges. A sketch of a horizontal cut of the flange is shown in Fig. 1 as well as the central section of the kicker showing the blades/VC profile.

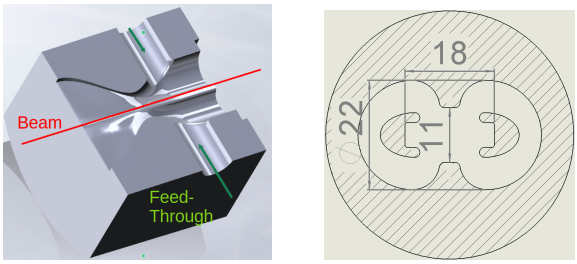

Figure 1: Left: Horizontal cut of the flange showing the complex shape of the transition. Right: Cross section of the central kicker part.

Ultra High Vacuum compatibility (UHV) of samples of three alloys produced via AM are being tested namely, Cu-CrZr, AS7G06, and TA6V grade 5. Some similar tests are reported in [7–9] The central part of the vacuum chamber and the blades will be machined to limit the size of parts produced by AM and optimize the vacuum property of the blades that are expected to reach temperatures above 120 °C. Optimisation of the blade/VC chamber geometry to minimise both coupling impedance and pulse reflection have been performed using the CST code [10]. Present design aims at assembling two devices as shown on Fig. 2. For

* perron@esrf.fr

Content from this work may be used under the terms of the CC BY 4.0 licence (© 2026). Any distribution of this work must maintain attribution to the author(s), title of the work, publisher, and DOI.

ISBN: 978-3-95450-252-3 ISSN: 2673-5350 doi: 10.18429/JACoW-IPAC2026-THP2146

A DEFLECTION ARC FOR A PROPOSED SECOND FAN AT THE EUROPEAN X-RAY FREE ELECTRON LASER

S. D. Walker*, W. Decking, S. Tomin, Deutsches Elektronen-Synchrotron DESY, Hamburg, Germany

Abstract

Transporting low emittance, high current beams like those required for free electron lasers is non-trivial. A deflection arc designed without specific consideration for such high-quality beams may result in degraded performance in the downstream undulators due to non-zero longitudinal dispersion compressing or decompressing the beam, or due to the coherent synchrotron radiation (CSR) increasing both the slice and projected emittances. In this paper we discuss a deflection arc for a proposed second fan at the European X-ray Free Electron Laser and some of the design considerations, particularly in order to assure isochronicity and CSR mitigation.

INTRODUCTION

The European X-Ray Free Electron Laser (EuXFEL) is a 3.4 km-long hard X-ray free electron laser facility in Hamburg, Germany. In order to maximise the number of experimental stations, the accelerator branches at the *switchyard* 2 km from the cathode into two different lines, T1 to the left and T2 directly ahead, housing one and two undulator lines, respectively [1–3]. The installation of additional sets of undulators in these existing tunnel branches is planned. Longer term, however, a whole new tunnel branch is to be dug, requiring a new extraction arc, T20, which will lead to further undulator lines. This extension will be the largest EuXFEL upgrade to date and must be carefully designed in order to maximise the final performance, taking into account both new challenges presented by the geometry as well as findings from operating the EuXFEL hitherto. In this paper particular focus is placed on the extraction arc design from the switchyard. Whereas the total bending angle for the existing T1 arc is 2.3° the total bending angle for the proposed T20 arc will have to be on the order of 7° to fit the tunnel geometry. This, combined with the femtosecond-length bunches characteristic of the EuXFEL, raises concerns regarding impact of coherent synchrotron radiation (CSR) on the beam emittance, a key beam parameter for optimising the final FEL performance.

Although the development of arc-like compressors is an active topic of research [4, 5], in this paper we report the progress in developing a T20 extraction arc design that ought to affect the beam as little as possible. In particular it should be achromatic and isochronous, ideally to high order, and also mitigate the impact of CSR on the beam's phase space.

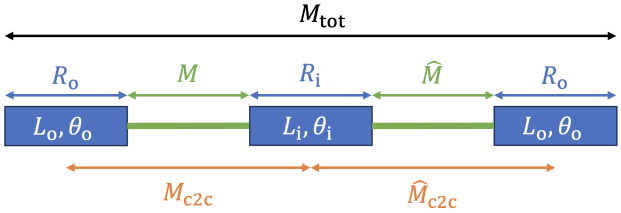

Figure 1: The decomposition of a symmetric TBA with differing inner-dipole length and bending angle into constituent matrices. The $c2c$ subscript denotes the matrix from one dipole's centre to the next dipole's centre.

Coherent Synchrotron Radiation and its Mitigation

Sufficiently short bunches in dipole fields will emit coherent synchrotron radiation that is not blocked by the vacuum chamber. The induced energy spread on a Gaussian beam due to steady-state CSR in a dipole is given by

$$\Delta\sigma_{\mathrm{CSR}} = 0.2459\frac{eQ\mu_0 c^2 L_B}{4\pi\sigma_z^{4/3}\rho^{1/3}} = kL_B, \qquad (1)$$

where Q is the bunch charge, σ_z the bunch length, L_B the dipole length, ρ the dipole bending radius and the remaining variables have their usual meanings [6]. On the right-hand side of Eq. 1 we combine the beam-specific quantities into k, the energy spread growth per unit length. This energy change even within an otherwise-achromatic section will break the achromatic condition and result in a projected emittance growth for the beam at the end of the achromat.

A number of papers have been published on the mitigation of CSR [7–13]. The formalisms and approaches vary but the broad principle is to design the optics in such a way either to mitigate the impact of the CSR on the beam emittance, or to use the CSR in a downstream dipole to cancel the impact of CSR in an upstream one.

The combined impact of CSR and dispersion can be modelled using the so-called *point-kick model* originally described in [11, 13], but the key principle is that dipoles are modelled with 2 × 2 small-angle matrices, which reduce to drifts, with the combined impact of CSR and dispersion treated as a single kick in the centre of the j-th dipole, which is given by

$$K_j = \begin{pmatrix} x_j \\ x_j' \end{pmatrix} = \begin{pmatrix} \rho_j^{4/3} k[\theta_j \cos(\frac{\theta_j}{2}) - 2\sin(\frac{\theta_j}{2})] \\ \sin(\frac{\theta_j}{2})(2\delta_{i<j} + \rho_j^{1/3}\theta_j k) \end{pmatrix} \qquad (2)$$

where k is given in Eq. 1, the subscripts otherwise refer to the angles and bending radii of the j-th dipole, and $\delta_{i<j}$ refers to the energy spread already accrued upstream from before the

* stuart.walker@desy.de

Content from this work may be used under the terms of the CC BY 4.0 licence (© 2026). Any distribution of this work must maintain attribution to the author(s), title of the work, publisher, and DOI.

ISBN: 978-3-95450-252-3 ISSN: 2673-5350 doi: 10.18429/JACoW-IPAC2026-THP2147

THE BESSY III INJECTION SCHEME*

M. Abo-Bakr†, T. Atkinson, P. Goslawski, J. Völker
Helmholtz-Zentrum Berlin (HZB), Berlin, Germany

Abstract

The HZB is presently in the CDR phase for a successor of the storage ring BESSY II, which has been in operation since 1998 in Berlin Adlershof. The lattice of the BESSY III storage ring will be a multi-bend-achromat, enabling a natural emittance of circa 100 pm rad. However, due to the strong multipole magnets needed the dynamic aperture is much smaller compared to earlier generation light sources, complicating the injection significantly. In combination with the demand for a highly efficient, transparent Top-Up injection, this the design of the injection system is challenging for modern light sources.

For BESSY III an Non-Linear-Kicker based injection schemes has been found to the be best suited among the various options and will be introduced in this paper. Necessary adjustments of the optics are presented as well as simulation results of the injection process and hardware requirements for the NLK.

INTRODUCTION

BESSY III [1] is planned as successor of BESSY II [2], a 3rd generation Synchrotron radiation source, operated at HZB since 2000. A CDR is in preparation, presumably completed until the end of this year. BESSY III is planned to operate a high current beam of up to 300 mA at 2.5 GeV electron energy. Like most of the 4th generation light sources, it will be based on a multi-bend-achromat (MBA) lattice to provide high brilliant radiation in the soft to tender X-ray range.

To keep the generated radiation power and with it the heat load on the users beam lines constant, the storage ring (SR) will be operated in Top-Up mode. To minimize radiation safety measures and to enable easy access to the user hall the injection efficiency must be over 90 %, which means that in maximum only a few percent of the accelerated current may be lost at injection into the storage ring. Ideally the injection process should be "transparent", so that distortions of the stored electron beam are minimized and thus the light stability for the users (source point and direction) maximized.

Various options for the injection into light source storage rings have been established over the time, but only few are suited for low emittance storage rings and fulfill the above requirements for BESSY III .

* *Work supported by German Bundesministerium für Bildung und Forschung, Land Berlin, and grants of Helmholtz Association
† Michael.Abo-Bakr@helmholtz-berlin.de

INJECTION OPTIONS FOR BESSY III

4th generation light sources aim for smallest emittances and therefore incorporate complex MBA lattices applying a large number of strong multipole magnets. Compared to previous generation light sources this increased magnet strengths leads to a significant loss of dynamic aperture (DA). For this reason, reaching highest injection efficiencies required for Top-Up operation becomes very challenging.

Four injection schemes were considered to be suitable candidates and have been discussed for BESSY III. Their basic properties are listed in Table 1. All of them require fast pulsed magnets and high quality injectors in the 3rd generation storage ring class, providing low emittance beams with small energy spread and short bunch lengths and high bunch charges.

The most challenging aspects beside an injector with these capabilities are the necessary kick pulse durations down to ns at a very high stability.

In conclusion — also with regard to the extensive experiences at BESSY II — the NLK scheme was decided to be most feasible and it will be used as "standard injection scheme" for BESSY III.

Independent of that choice, for the initial commissioning of the storage ring the injection straight should also host a fast, dipolar kicker for on-axis injection. That will enable first beam threading and achieve a closed orbit. The following orbit and optics corrections will result in a sufficiently large DA allowing the off-axis NLK injection.

NLK INJECTION

Before injection to the storage ring the accelerated beam has to be extracted and transported from the booster synchrotron. This transfer line should be short with a small integrated total angle. To improve the stability, angles from pulsed devices should be kept as small as possible. For that various types of bends with increasing bending angle will be used - pulsed and DC EM magnets and where feasible also permanent dipole magnets. Consequently the injection septum will be split in parts: first a DC septum with a large bending angle and a second pulsed AC septum with a small angle and lower field, so that the thickness of the septum blade can be reduced to circa $1 - 2$ mm.

Integration of Pulsed Injection Elements

Due to large horizontal betatron oscillation amplitudes on the injection path the beam experiences strong non-linear fields, possibly causing beam losses. For that the path from the septum to the NLK should be kept short, ultimately leading to a scheme integrating both components in one "injection section", with the septum placed upstream of the

Content from this work may be used under the terms of the CC BY 4.0 licence (© 2026). Any distribution of this work must maintain attribution to the author(s), title of the work, publisher, and DOI.

ISBN: 978-3-95450-252-3 ISSN: 2673-5350 doi: 10.18429/JACoW-IPAC2026-THP2148

INJECTION STUDIES FOR ELETTRA 2.0

K. Manukyan*, S. Dastan, E. Karantzoulis, S. Krecic,
Elettra-Sincrotrone Trieste S.C.p.A., Trieste, Italy

Abstract

A comprehensive evaluation of injection performance for Elettra 2.0 has been conducted to establish high-efficiency, low-perturbation top-up operation in the upgraded ultralow-emittance storage ring. The baseline four-kicker bump injection scheme, utilizing a 4.3 µs half-sine pulse and a −6 mm stored-beam orbit excursion, achieves injection efficiencies up to 100% under nominal conditions. Beyond the baseline performance characterization, the study examines how machine imperfections and operational parameters influence injection efficiency, including wakefield and third-harmonic cavity effects on the injected bunch. The results establish operational tolerances and highlight optimization strategies that improve injection robustness and long-term stability.

INTRODUCTION

Elettra 2.0 is a 259.2 m long fourth-generation light source that will replace the existing Elettra facility [1, 2]. The new storage ring adopts a specially designed multi-bend achromat (MBA) lattice (so called S6BA-E , Symmetric six Bend achromat and enhanced using reverse bends and dipoles with both transverse and longitudinal gradient) designed to achieve ultralow emittance and to meet al the user requirements. The main design parameters are summarized in Table 1 and the optical functions for a single lattice cell are shown in Fig. 1. The strong focusing required by the MBA design restricts the available dynamic aperture, making efficient injection challenging but essential.

Table 1: Key Parameters of the Elettra 2.0 Storage Ring

Parameter	Value	Unit
Beam Energy	2.4	GeV
Circumference	259.2	m
Harmonic Number	432	
Betatron Tunes (H/V)	32.30 / 9.16	
Natural Emittance	238	pm rad
Energy Spread	9×10^{-4}	

The baseline injection scheme uses a four-kicker bump. Four kicker magnets are powered simultaneously to displace the stored beam by −6 mm horizontally. The injected beam from the booster is guided by three septum magnets to a position of −10 mm. After the bump closes, the injected beam undergoes betatron oscillations until radiation damping merges it into the closed orbit. The schematic layout of the injection bump is shown in Fig. 2.

The kickers are driven by a half-sine pulse of approximately 4.3 µs duration. While tracking simulations for the ideal machine predict high injection efficiency, realistic conditions reduce performance. In-vacuum undulators (IVUs) operating at minimum gap restrict the physical aperture, and magnet misalignments and field errors further reduce transmission. This report evaluates the effect of different booster operating modes on injection efficiency, assesses injection tolerances to realistic machine errors, discusses the mitigation of stored beam distortions driven by bump leakage, and analyzes the effects of wakefields and a third-harmonic cavity (3HC) on injection performance. The `elegant` [3] and AT [4] simulation codes were extensively used for these studies.

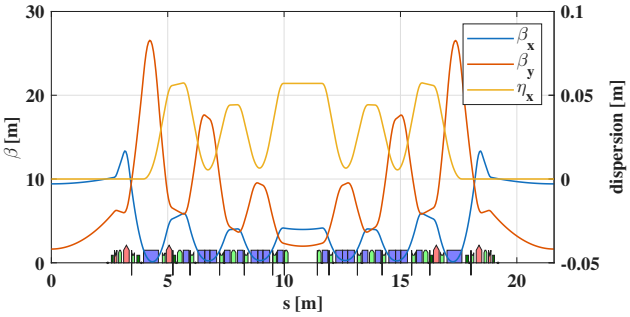

Figure 1: Optical functions (β_x, β_y and dispersion η_x) for one cell of the Elettra 2.0 multi-bend achromat lattice.

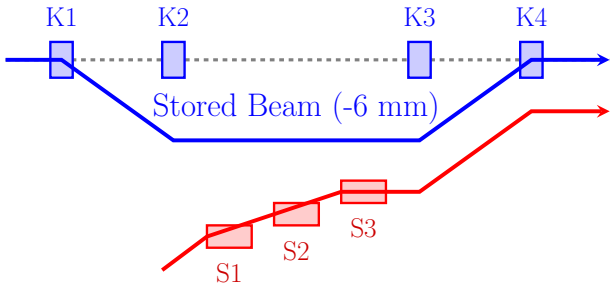

Figure 2: Schematic of the Elettra 2.0 four-kicker injection bump. The stored beam trajectory (blue) is displaced to clear the septum blade, and the injected beam (red) arrives from the booster.

INJECTION TOLERANCES

Achieving high injection efficiency relies not only on the storage ring layout but also on the injected beam properties. While the storage ring undergoes a full upgrade to Elettra 2.0, the existing booster ring has been refurbished [5]. Detailed information on the booster upgrades is available in [6]. Significant effort has been devoted to tuning the booster to meet the requirements of the new storage ring. As a result, the booster emittance has been reduced from 240 nm to 140 nm at 2.4 GeV [7].

* koryun.manukyan@elettra.eu

Content from this work may be used under the terms of the CC BY 4.0 licence (© 2026). Any distribution of this work must maintain attribution to the author(s), title of the work, publisher, and DOI.

ISBN: 978-3-95450-252-3 ISSN: 2673-5350 doi: 10.18429/JACoW-IPAC2026-THP2151

IN-VACUUM AND CRYOGENIC PERMANENT-MAGNET UNDULATORS AT THE ESRF

G. Le Bec*, Ch. Benabderrahmane, Ph. Brumund, R. Versteegen
European Synchrotron Radiation Facility, Grenoble, France

Abstract

The European Synchrotron Radiation Facility (ESRF) operates a large number of in vacuum undulators (IVUs) and cryogenic permanent magnet undulators (CPMUs). Eight IVUs and nine CPMUs are currently in service, and a few more are under construction or planned. CPMU technology is employed for short-period, high-field undulators. These undulators generate intense high-order harmonics and can reach high photon energies up to about 100 keV at the ESRF. A major limitation of this approach is the heat load on the photon front-ends and on the optical elements of the beamlines. This issue can be mitigated by combining a tunable device with a short period, almost monochromatic IVU dedicated to a single photon energy. The various layouts of the ESRF IVU and CPMU straight sections are presented, together with the CPMU operating experience, construction and installation trends.

INTRODUCTION

In-Vacuum Undulators (IVUs) are now standard components of storage-ring-based lightsources and FELs. Because they generate strong magnetic fields at shorter periods than out-of-vacuum devices, they are key elements for improving the source brilliance at high energies. Cryogenic Permanent Magnets Undulators (CPMUs) have been progressively deployed at the ESRF for almost two decades for high photon flux and high-energy beamlines.

The first section focuses on IVUs and CPMUs: after a brief reminder of the main characteristics of these devices, their magnetic gaps and the technologies used at the ESRF are presented. The heat load generated by these undulators on optical components is discussed. The second section gives a brief history of IVU and CPMU installation at the ESRF, and presents the current installation and contruction plans. The third section summarise the operation experience.

IN-VACUUM UNDULATORS

Basics

The peak magnetic field of an undulator varies as

$$B \approx B_0 \exp\left(-\frac{\pi g}{\lambda_0}\right),$$

where g is its magnetic gap and λ_0 its period.

The on-axis wavelength of the emitted radiation is

$$\lambda_R = \frac{\lambda_0}{2\gamma^2 n}\left(1 + \frac{K^2}{2}\right),$$

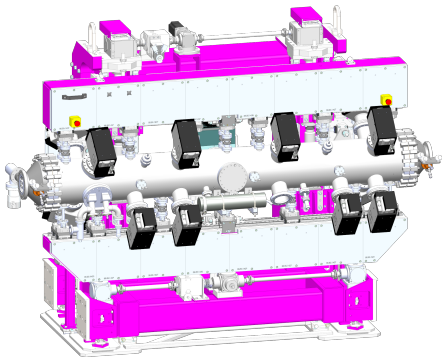

Figure 1: Design view of a cryogenic in-vacuum undulator. The permanent magnets, cooled down by liquid nitrogen, are installed in the cylindrical vacuum chamber visible in the middle.

where γ is the relativistic Lorentz factor, n the harmonic number and K the deflection parameter:

$$K = \frac{e\lambda_0 B}{2\pi mc} \propto \lambda_0 \exp\left(-\frac{\pi g}{\lambda_0}\right).$$

K decreases rapidly with the period λ_0. Short-period undulators typically have a low K value and have a reduced tuning range when the field is varied, unless a high-field technology is used. Finally, the radiated power and power density vary with

$$P \propto B^2$$
$$\frac{dP}{d\Omega} \propto B.$$

It should also be noted that undulators emit mainly first-harmonic radiation for $K < 1$ and high-harmonics for $K > 1$ (see, for instance, reference [3]).

Table 1: Minimum Gaps of Undulators at the ESRF

Out-of-vacuum	11	mm
In-vacuum (side)	6	mm
In-vacuun (middle)	5	mm
In-vacuum (middle, low chroma)	4	mm

Magnetic Gaps

The standard undulator vacuum chambers at the ESRF have a thickness of 10 mm, leading to minimum gaps of about 11 mm for out-of-vacuum undulators. These gaps can be further reduced if the magnets are installed in vacuum [1] [2]. In this case, the magnet arrays are surrounded by a large vacuum chamber (Fig. 1).

* lebec@esrf.fr

Content from this work may be used under the terms of the CC BY 4.0 licence (© 2026). Any distribution of this work must maintain attribution to the author(s), title of the work, publisher, and DOI.

ISBN: 978-3-95450-252-3 ISSN: 2673-5350 doi: 10.18429/JACoW-IPAC2026-THP2152

THE SOLEIL II INSERTION DEVICES

M.-E. Couprie†, R. Baillier, A. Berlioux, Ph. Berteaud, F. Blache, A. Esper, S. Khan, C. Kitégi, A. Lejollec, O. Marcouillé, F. Marteau, A. Mary, T. Mutin, K. Tavakoli, C. Tournier, M. Valléau, J. Vétéran, Synchrotron SOLEIL, Gif-sur-Yvette, France

Abstract

The SOLEIL II Insertion Devices (ID) range from long period Adjustable Phase Undulator, APPLE X, Dual undulators for the intermediate energy spectral range, and in vacuum undulators, cryogenic permanent magnet undulators and wigglers for hard X-rays.

INTRODUCTION

The synchrotron facility SOLEIL (electron beam of 2.75 GeV energy, 500 mA current, 3.9 nm.rad emittance) has been operating since 2006, with a variety of insertion devices enabling to cover five decades in photon energy. On SOLEIL II [1-4], due to the higher number of magnetic elements required to reduce the emittance down to 85 pm.rad, the available length devoted to insertion devices is reduced by 30 %. Choices and technical developments are here reported. SOLEIL II is planned in two stages: construction in stage 1 and towards full performance in stage 2. The evolution of the SOLEIL ID panoply is listed in Table 1.

SOLEIL PRESENT ID PANOPLY

SOLEIL accommodates 12 medium, 8 short and 4 long straight sections with 20 beamlines on insertion devices. In short straight sections are mainly installed planar In Vacuum Undulators (IVU) of period 20 and 24 mm, an In Vacuum Wiggler IVW50 [5] of period 50 mm and three Cryogenic Permanent Magnet Undulator (CPMU) of period 18 mm. The minimum gap of the IVU and CPMU is 5.5 mm gap except 8 mm for IVU24 and 4.5 mm for the IVW50. In the long straight sections, the installed IDs are the two canted CPMU18 [6, 7] and the 10 m long electromagnetic undulator of 640 mm period, HU640. HU640 does not fit in SOLEIL II. In the medium straight sections are installed up to two Elliptically Polarised Undulators (EPU) called generically HU (Helical Undulator) of APPLE II type with a minimum gap of 15.5 mm (except HU36 down to 11.5 mm), or electromagnetic ones HU256, or an out of vacuum wiggler W164, and an Electromagnetic/Permanent Magnet Helical Undulator (EMPHU) of 65 mm period enables fast polarization switching [8].

Table 1: SOLEIL and SOLEIL II (SII) panoply of insertion devices (in italic, to be built). SS for Straight Section. DUAL N for 2 m long DUAL system with new undulator, while DUAL is reusing existing IDs.

Beamline	Present SS	Present ID	SII SS	SII P1	SII P2
LUCIA	SDM16	HU52	SD03C	IVU24	IVU24
PSICHE	SDC03	IVW50	SD04C	IVW50	*CPMW35*
PLEIADES	SDM04	HU80-HU256	SD05MC	HU60	*AX63*
DEIMOS	SDM07	HU52-EMPHU65	SD06L	DUAL HU52-EMPHU65	*Dual HU52-EMPHU65*
PUMA	SDM06	W164	SD07MC	IVU20	*CPMU16*
CRISTAL	SDC06	CPMU18	SD08C	CPMU18	*CPMU15*
GALAXIES	SDC07	IVU20	SD09C	IVU20	*CPMU16*
TEMPO	SDM08	HU80-HU44	SD10ML	DUAL HU44-HU80	*DUALNHU40-HU70*
DESIRS	SDL05	HU640	SD11L	*APU250*	*APU250*
HERMES	SDM10	HU64-HU42	SD12ML	DUAL HU42-HU64	*DUAL HU64-HU42*
PX-ID	SDC10	IVU20-IVU24	SD13C	IVU20	*CPMU16*
SWING	SDC11	IVU20	SD14C	IVU20	*CPMU15*
ANTARES	SDM12	HU60-HU256	SD15MC	HU80	*DUALN HU60-HU90*
ANATOMIX	SDL13	CPMU18	SD16L	CPMU18	CPMU18
NANOSCOPIUM	SDL13	CPMU18	SD16L	CPMU18	CPMU18
SEXTANTS	SDM14	HU80-HU44	SD17MC	CPMU18	*CPMUE38*
SIXS	SDC14	IVU20	SD18C	*AX42*	*CPMU16*
SIRIUS	SDC15	HU36	SD19C	IVU20	*AX38 or CPMU*
CASSIOPEE	SDM15	HU60-HU256	SD20ML	HU36	*DUALN HU44-HU130*
				DUALN HU44-HU130	

†marie-emmanuelle.couprie@synchrotron-soleil.fr

Content from this work may be used under the terms of the CC BY 4.0 licence (© 2026). Any distribution of this work must maintain attribution to the author(s), title of the work, publisher, and DOI.

ISBN: 978-3-95450-252-3 ISSN: 2673-5350 doi: 10.18429/JACoW-IPAC2026-THP2153

WAKEFIELD STUDIES OF IVUE32

P. Volz*, A. Meseck, S. Grimmer,
Helmholtz-Zentrum Berlin für Materialien und Energie, Berlin, Germany

Abstract

The Helmhotz-Zentrum Berlin (HZB) is developing an elliptical in-vacuum undulator, IVUE32, following the APPLE-II design with a magnetic force compensation concept. The undulator will be installed in the BESSY II storage ring. It will feature a 7 mm minimum gap and four magnet rows that can be moved to adjust the polarization of the synchrotron radiation. This shift movement requires a complex taper structure and a longitudinal slit in the shielding foils. Extensive CST wakefield simulations have been conducted to investigate the interaction between the undulator and the beam. The impedance of the device on the beam is studied, as well as the heating of the undulator induced by the beam. The taper structure has to compensate for two axes of motion. The vertical gap movement and the longitudinal shift movement. The shift movement is different for each half of the shielding foil. Previously presented designs used separate foil tensioning systems to independently compensate for the two axes of motion. A length constraint due to the β-function might prohibit the separate compensation. Changing the gap while also compensating for the shift motion introduces an asymmetry in the taper, where the shielding foils have different gradients. Different asymmetric tapers are studied to find the limits for horizontal impedance for the BESSY II beam.

INTRODUCTION

The APPLE II design of IVUE32 [1] as an in vacuum undulator poses several challenges for beam dynamics. Compensation of the two axes of motion requires a complex taper and a longitudinal slit in the shielding foils. These components can cause resonances in impedance, disrupting beam dynamics and heating components. Their impact needs to be investigated before such a device can be installed into the storage ring. We present extensive simulations of possible taper designs and their impact on impedance. As well as studies of possible deviations of shielding foil geometry and the expected heat load.

IVUE32 TAPER SIMULATIONS

Wakefield simulations using the CST Studio Suite Software [2] of the IVUE32 taper structure have been conducted. The taper structure is modeled inside a cylindrical vacuum chamber with a diameter of 40 cm to mimic the vacuum chamber of IVUE32. Earlier design iterations featured an electrical discontinuity in order to preserve vacuum quality. This causes unacceptably high impedance [3], leading to a design with two foil tensioning mechanisms [3]. This design fully separates the gap movement compensation and shift movement compensation, avoiding possible transverse asymmetries due to a compound taper. The detailed simulations of this taper design were not ready for last year's IPAC and are shown in Fig. 1. The longitudinal impedance

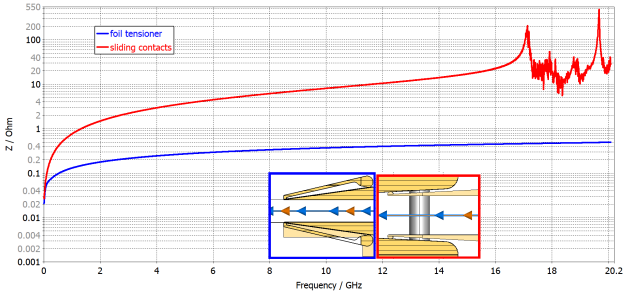

Figure 1: Longitudinal impedance of IVUE32 shift movement compensation at a gap of 7 mm. Sliding contact design (red) compared to foil tensioner design (blue)

of the shift compensation mechanism at a gap of 7 mm is compared to an earlier design with sliding contacts. The foil tensioning mechanism features a very smooth geometry without any significant changes in gap. The sliding contacts of the earlier design cause a 1 mm step in the gap, followed by a small taper. Therefore the foil tensioning design has a lower impedance across the whole spectrum and does not show any resonant frequencies.

The IVUE32 magnet structure will have a length of 2.5 m. The β-function with the current beam optic at the designated straight section can only support the planned minimum gap of 7 mm for about that distance. The foil-tensioner shift-compensation mechanism would maintain the gap of the magnet structure for about 30 cm at either side of the undulator, making it incompatible with the current beam optic. Therefore a compound gap and shift taper that immediately increases the gap from 7.4 mm at the magnet girder to 9 mm is studied. This compound taper introduces transverse asymmetries to the gap geometry that change with the shift state, similar to the case discussed in [3] but with a much lower magnitude. The aim of this simulation study was to find an acceptable compromise between impedance impact and immediate gap increase. Both the gap compensation and shift compensation are modeled as simplified copper foils. Figure 2 shows the compound taper at different shift states from the side with the asymmetry highlighted in red. The vertical axis is exaggerated to better visualize the geometry. The taper connects to the magnet girders at the right with a gap of 7.4 mm. The gap in the shift compensation section increases through various tapers dictated by the foil mounting points and magnet infrastructure to 9 mm. The shielding foil in this section is split longitudinally. This causes a slight asymmetry between the two halves of the foil, highlighted in red, the geometry of which changes with shift movements.

* paul.volz@helmholtz-berlin.de

Content from this work may be used under the terms of the CC BY 4.0 licence (© 2026). Any distribution of this work must maintain attribution to the author(s), title of the work, publisher, and DOI.

ISBN: 978-3-95450-252-3 ISSN: 2673-5350 doi: 10.18429/JACoW-IPAC2026-THP2154

DESIGN, TRAINING AND MAGNETIC FIELD CHARACTERIZATION OF THE SUPERCONDUCTING THz-UNDULATOR COILS FOR FLUTE

A. Grau†, N. Glamann, B. Krasch, D. Saez de Jauregui
Karlsruhe Institute of Technology, Karlsruhe, Germany
T. Gerhard, A. Hobl, H. Wu, W. Walter
Bilfinger Nuclear & Energy Transition GmbH, Würzburg, Germany

Abstract

FLUTE (**F**erninfrarot **L**inac **U**nd **T**est **E**xperiment – far-infrared linac- and test-experiment), a short-pulse linac and short-bunch THz test facility at the Institute for Beam Physics and Technology (IBPT) at the Karlsruhe Institute of Technology (KIT), serves as an accelerator test setup for a variety of accelerator physics studies. In its final stage of expansion, it is foreseen to provide coherent radiation in ultra-short, very intense light pulses in the terahertz and far-infrared spectral range. A superconducting undulator (SCU) at the end of the accelerator structure offers the possibility to generate photon radiation between 4 THz and 12 THz (energies between 16.5 meV and 50 meV) with a high pulse energy. This energy range, for instance, is of interest for studies of water-soluble interactions. The final undulator design was carried out by Bilfinger Nuclear & Energy Transition GmbH (BNET) in close collaboration with the IBPT.

Before assembling the final undulator device, the superconducting coils were trained and magnetically characterized in CASPER II, a magnetic measurement setup which is part of the Magnet and Cryogenics Facilities (MCF) at the IBPT. In this contribution we describe the general SCU layout, present the results of the coil training, the local magnetic field characterization and field integral minimization of the THz-undulator coils.

INTRODUCTION

Solid state physics and biological applications demand an analysis within a wide spectral range from terahertz (THz) to infra-red (IR) whereas the THz frequency range, for instance, is of high interest for interaction and reaction studies of liquids, especially in water, and thus for biological and medical research. To satisfy the increasing interest to use THz radiation, from an accelerator physics point of view, it is necessary to study bunch compression effects, coherent synchrotron radiation, as well as generation mechanisms in theory and experiment. Therefore, during the last years the FLUTE accelerator R&D facility was built at the Institute of Beam Physics and Technology (IBPT) at KIT [1]. In the final state the FLUTE linear accelerator is supposed to serve as an injector for the **C**ompact **ST**orage Ring for **A**ccelerator **R**esearch and **T**echnology (cSTART) [2].

†andreas.grau@kit.edu

In addition to the production of coherent photons in the THz regime at the end of the bunch compressor, an insertion device is foreseen to be installed in an accelerator straight section.

Based on our extensive know-how in magnetic design, magnetic characterization, cryogenics, and to build, in collaboration with our industrial partner BNET, reliable LTS SCUs, we decided to design and built a compact and superconducting THz undulator.

FLUTE ACCELERATOR

The electrons are produced in a photo-injector system, driven by a Ti:Sa laser with 1 kHz repetition rate. The laser pulses are converted at a reduced repetition rate of 10 Hz to 266 nm, to be able to generate electrons from the copper cathode. The 5 MeV electron bunch is focused by a solenoid at the gun exit and subsequently accelerated to 41 MeV by the following linac structure of about 5.2 m length. After additional focussing by quadrupoles, the electrons enter the bunch compressing section, where the chirped pulses are compressed to the bunch length of fs. The accelerated and compressed bunches enter then the insertion device to produce photons between 4 THz and 12 THz, which can be characterized after the device. The FLUTE layout including diagnostics and the insertion device is shown and described in detail in [3] and the main beam parameters of the FLUTE accelerator are given in Table 1.

Table 1: Flute Electron Beam Parameters

Quantity	Value	Unit
Electron energy (E_e)	~41	MeV
Average beam current (I_{AVG})	10^{-6}	mA
Electron bunch length (σ_Z)	1 – 300	fs
	0.3 – 90	µm
Horizontal emittance (ε_x)	1	mm mrad
Vertical emittance (ε_y)	1	mm mrad
Horizontal beta function (β_x)	1.1	m
Vertical beta function (β_y)	1.1	m
Pulse repetition rate	50	Hz

THz-UNDULATOR PARAMETERS

The general goal of the undulator for FLUTE is to produce photons in the low THz regime, i.e. in the range from 4 THz to 12 THz corresponding to photon energies from 16 meV to 50 meV or wave lengths from 75 µm to 2 µm, respectively. The on-axis photon radiation wavelength λ_R emitted by an insertion device such as an undulator

Content from this work may be used under the terms of the CC BY 4.0 licence (© 2026). Any distribution of this work must maintain attribution to the author(s), title of the work, publisher, and DOI.

ISBN: 978-3-95450-252-3 ISSN: 2673-5350 doi: 10.18429/JACoW-IPAC2026-THP2155

UPCOMING INSERTION DEVICES AT MAX IV FACILITY

H. Tarawneh, M. Muradi, M. Holz, MAX IV Laboratory, Lund, Sweden

Abstract

Currently, 17 Insertion Devices (IDs) are in operation at the MAX IV facility. The soft X-ray undulators are based on the 3 APPLE II undulator at the 3 GeV ring, 4 APPLE II and 1 planar undulators at the 1.5 GeV ring, and the hard X-ray IDs are based on room-temperature in-vacuum technology at the 3 GeV ring and the Short Pulse Facility. A recently funded Tomography beamline for materials science at the 3 GeV ring will utilize two sources within the same straight section: a short-period cryogenic permanent magnet undulator (CPMU) with a 14 mm period length for nano-tomography and a 3 T 3-pole wiggler for micro-tomography. Both IDs are currently in production, with installation planned for summer 2027. Further development of a new medical-imaging beamline covering the energy range 15–70 keV at the 3 GeV ring. At the 1.5 GeV ring, a new APPLE II undulator providing polarization control starting at 43 eV photon energy is foreseen to replace an older planar undulator. In this paper, we present the parameters of these upcoming insertion devices and provide estimates of their expected performance.

INTRODUCTION

The MAX IV Laboratory operates a diverse set of insertion devices (IDs) covering a wide range of photon energies and experimental techniques, with ongoing developments aimed at extending performance and functionality. Existing IDs at both the 3 GeV and 1.5 GeV storage rings already provide high-brilliance radiation for a broad range of applications. However, new beamlines and planned upgrades require advanced ID concepts with improved performance, flexibility, and spectral characteristics. This paper presents an overview of upcoming insertion devices at MAX IV, including new installations for the TomoWISE beamline and the future MedMAX beamline, upgrades to the FlexPES insertion device, and modifications to the BALDER wiggler. These developments aim to enhance spectral quality, extend energy coverage, and introduce new operational capabilities such as polarization control and multi-scale imaging.

ID FOR TOMOGRAPHY BEAMLINES

The TomoWISE beamline is a newly funded tomography beamline at the 3 GeV storage ring, designed to cover both nano- and micro-tomography within a single straight section. To achieve this, two complementary insertion devices will be installed.

Cryogenic Permanent Magnet Undulator (CPMU) technology will be used for the first time at the MAX IV 3 GeV ring. The CPMU is a short-period undulator with a period length of 14 mm [1]. The CPMU design is based on using Pr2Fe14B for magnet blocks and Vanadium Permendur for pole material. Operating at cryogenic temperatures, it provides a higher magnetic field strength than room-temperature devices. This allows for higher photon energies and improved brilliance, making it well-suited for high-resolution nano-tomography applications.

The second source is a 3 T, 3-Pole Wiggler (3PW) designed for microtomography. It provides a broad spectrum with high photon flux, enabling fast imaging of larger samples. The combination of CPMU and 3PW enables TomoWISE to span multiple length scales within a single beamline, as shown in the schematic view in Fig. 1.

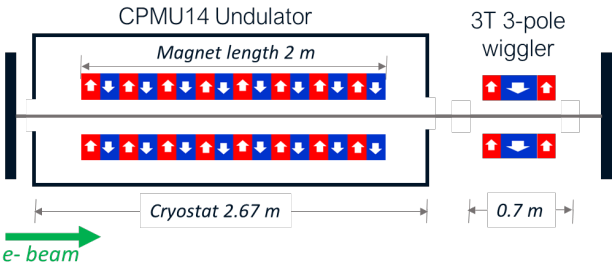

Figure 1: Schematic layout of the two IDs at the 3 GeV ring straight section with available spaces.

The two sources are not allowed to operate simultaneously, and hence, the wiggler gap is movable to allow full neutralization of the wiggler field to operate the CPMU. Both devices are currently in production, with installation planned for summer 2027. Table 1 summarizes the main parameters of the two ID sources. The on-axis field profile along the wiggler is shown in Fig. 2 [2].

Table 1: TomoWISE Insertion Devices Parameters

Parameter	CPMU	3PW
Period length, mm	14	412*
Magnetic gap, mm	3.8	11
Field, T	1.41	3
No. of Periods	143	1 (pole)
Power @500 mA, kW	11.1	1.6
Energy Range, keV	10–65	

(*) Total magnetic length of wiggler

The wiggler vacuum chamber is a NEG-coated chamber with an inner vertical dimension of 8 mm. Fig. 3 shows the CPMU brilliance using the baseline machine parameters of the 3 GeV MAX IV storage ring and the wiggler flux at minimum gap of 11 mm into an aperture of 1×0.1 mrad^2. The CPMU flux estimate at minimum gap into an aperture of 25×25 μrad^2 is shown in Fig. 4.

Content from this work may be used under the terms of the CC BY 4.0 licence (© 2026). Any distribution of this work must maintain attribution to the author(s), title of the work, publisher, and DOI.

ISBN: 978-3-95450-252-3 ISSN: 2673-5350 doi: 10.18429/JACoW-IPAC2026-THP2156

MODELING OF INSERTION DEVICES IN XSUITE

S.F. Buijsman*[1,2], S. Van der Schueren[1,3], R. De Maria[1], G. Iadarola[1], M. Seidel[2]
[1] CERN, Geneva, Switzerland
[2] École Polytechnique Fédérale de Lausanne, Lausanne, Switzerland
[3] Università La Sapienza, Rome, Italy

Abstract

Insertion devices with longitudinally periodic fields—such as undulators, damping wigglers, and polarizing wigglers—play a central role in several stages of the FCC-ee injection chain. Accurate field models and efficient long-term tracking are required, as the strong longitudinal field variation cannot be captured reliably with standard multipole expansions. We introduce in the Xsuite simulation toolkit a general model for such devices based on a Maxwell-consistent series expansion of the magnetic field. The expansion is constructed from the on-axis field and its transverse derivatives and is implemented in BPMETH, which provides a direct interface to Xsuite. Particle tracking is performed using the Boris integrator. We assess the approach by comparing Boris integration with a multipole expansion and compare the convergence of the resulting tracking. This framework enables detailed optics and beam-parameter studies for synchrotron light sources, damping rings, and polarization systems.

INTRODUCTION

Insertion devices such as undulators and wigglers are important components in electron storage rings, such as the damping rings and synchrotron light sources. Their magnetic fields are characterized by significant longitudinal variation of both transverse and longitudinal field components.

Accurate modeling of these devices is challenging. Simplified approaches based on multipole expansions or thin-lens kicks (from hereon referred to as Multipole Kick (MK) models) assume slowly varying fields and typically neglect longitudinal components. As a result, they may fail to capture important effects on both the orbital motion and spin dynamics, especially in devices with complex field structures such as polarizing undulators, which are used, for example, in the SLS2.0.

To address these limitations, we introduce a general field model integrated with the Xsuite simulation toolkit. The method is based on a Maxwell-consistent series expansion constructed from on-axis field data and its transverse derivatives [1]. The resulting field representation is combined with a spatial Boris integrator for particle tracking, enabling efficient and accurate simulation in arbitrary three-dimensional magnetic fields [2]. From hereon, this model will be referred to as the SplineBoris (SB) model.

A key feature of this approach is that it provides a smooth, continuous field description that naturally includes longitudinal components, allowing for consistent tracking of both particle motion and spin, without the need for interpolation at runtime. This makes it particularly well-suited for the study of insertion devices in damping rings and light sources.

Here, we present the SB model, we apply it to an analytical solenoid field map for benchmark purpose and we test it using a field map of a knot undulator that is used in the SLS2.0.

MAGNETIC FIELD MODELING

The magnetic field is modeled using the method outlined in [1]. The magnetic field in a region around the reference axis can be described by the magnetic field components B_x, B_y and B_s and derivatives of transverse components in the mid plane:

$$a_m(z) = \left.\frac{\partial^{m-1}B_x}{\partial x^{m-1}}\right|_{x=y=0} \tag{1}$$

$$b_m(z) = \left.\frac{\partial^{m-1}B_y}{\partial x^{m-1}}\right|_{x=y=0} \tag{2}$$

$$b_s(z) = B_z(0,0,z) \tag{3}$$

Using a recursion relation, the magnetic scalar potential $\Phi(x,y,z)$ can be found from these functions, from which the magnetic field $\vec{B} = -\nabla\Phi$ can be derived. To use equations (1) through (3), we cut the magnetic field map in regions. Each region will have its own set of functions $a_{m,i}(z)$, $b_{m,i}(z)$ and $b_{s,i}(z)$, where i denotes the region.

These functions are modeled as fourth-order polynomials defined as follows. We define:

$$L_i = z_{i+1} - z_i \tag{4}$$

$$t = \frac{z - z_i}{L_i} \tag{5}$$

Here, z_i and z_{i+1} represent the start and end coordinates of region i along the line respectively. This way, $t \in [0,\ 1]$. We introduce five polynomials as

$$f_1(t) = 1 - 18t^2 + 32t^3 - 15t^4 \tag{6}$$

$$f_2(t) = t - 4.5t^2 + 6t^3 - 2.5t^4 \tag{7}$$

$$f_3(t) = -12t^2 + 28t^3 - 15t^4 \tag{8}$$

$$f_4(t) = 1.5t^2 - 4t^3 + 2.5t^4 \tag{9}$$

$$f_5(t) = 30t^2(1-t)^2 \tag{10}$$

We introduce a linear combination $g(t)$ defined as:

$$\begin{aligned} g(t) =& c_1 f_1(t) + c_2 L f_2(t) + c_3 f_3(t) \\ &+ c_4 L f_4(t) + \frac{c_5}{L} f_5(t) \end{aligned} \tag{11}$$

* simon.fanica.buijsman@cern.ch

Content from this work may be used under the terms of the CC BY 4.0 licence (© 2026). Any distribution of this work must maintain attribution to the author(s), title of the work, publisher, and DOI.

ISBN: 978-3-95450-252-3 ISSN: 2673-5350 doi: 10.18429/JACoW-IPAC2026-THP2157

DEMONSTRATION OF A TRANSVERSE GRADIENT UNDULATOR IN AN X-RAY FREE-ELECTRON LASER

C. Kittel*, M. Calvi, E. Prat, Paul Scherrer Insitute, Villigen, Switzerland
N. Sammut[1], University of Malta, Msida, Malta

Abstract

Modern synchrotron light sources employ various types of undulators to generate highly coherent and well collimated X-rays. A large and homogeneous magnetic field around the beam axis is typically the preferred configuration, since it simplifies both alignment and operation. Nevertheless, a nonhomogeneous field, such as that of a transverse gradient undulator (TGU), offers attractive possibilities for advanced operating modes, for example enabling large bandwidth operation in a free electron laser. In this contribution, we present the first beam-based characterization of such a TGU for various magnetic field gradients and X-ray polarization settings, and we compare the experimental results with corresponding simulation data. The measurements were carried out at Athos, the soft x-ray beamline of SwissFEL. This line employs Apple X undulators, whose independent radial and shift motion of all four magnetic arrays makes them uniquely capable of generating the required transverse gradients.

INTRODUCTION

Modern light sources, like free-electron lasers (FEL), employ undulator modules for generating coherent and well-collimated X-rays. The fundamental undulator equation describes the resonance condition, which is used to calculate the photon wavelength (λ) based on the undulator period length (λ_u) and the Lorentz factor (γ) of the electron beam, incorporating the K-value:

$$\lambda = \frac{\lambda_u}{2\gamma^2}\left(1 + \frac{K^2}{2}\right) . \quad (1)$$

Typically, a transversally homogeneous magnetic field around the beam axis is preferred inside the undulator modules, due to its simplicity in alignment and operation. However, certain non-homogeneous magnetic fields, such as those produced by transverse gradient undulators (TGU), offer significant advantages for advanced operating modes.

A TGU is characterized by a gradient in the undulator field strength, known as the K-value, along a specified transverse direction, orthogonal to the electron beam's propagation. Such a design implies that electrons traversing the undulator experience varying K-values depending on their transverse path offset from the central electron trajectory. This contrasts with conventional undulators that aim for a constant magnetic field region to ensure stable photon generation, even if the electron beam trajectory deviates slightly from the magnetic axis.

While TGUs require much more precise alignment compared to their no-gradient counterparts, they offer attractive possibilities for advanced operating modes. These include: (1) Electron Energy Spread Compensation: They can be utilized to compensate for large energy spreads in FEL oscillators [1] and plasma wakefield accelerators [2]. (3) Large Bandwidth Operation: TGUs can enable large bandwidth operation in free-electron lasers (FELs) [3].

The Athos soft X-ray beamline at SwissFEL [4], at PSI in Switzerland, employs 16 APPLE-X undulator modules [5]. They offer full polarization control for the full K-range (0.9 to 3.8) with the exception of reduced K-values around linear polarizations of $\pm 45°$. The undulator modules have four magnetic arrays, each of these are equipped with their own motor for radial and longitudinal movements, which define the undulator strength and polarization, respectively. Additionally, the independent radial movement makes these modules very suitable to create transverse K-gradients of arbitrary strength.

Each of the 12 ton APPLE-X modules is installed on top of a 5-axis remote positioning system, based on motorized camshafts. This is to move the modules to their correct transverse positions, evaluated from dedicated photon-beam-based alignment procedures. Furthermore, the Athos undulator line employs a feedback system to stabilize the electron trajectory passing through it. It uses beam position monitors between each two undulator modules to determine its actual position and sends corrections to the neighbouring corrector dipoles.

MODELLING AND SIMULATIONS

In an APPLE-X undulator module a K-gradient can be achieved by opening two neighbouring arrays radially more ($r + \delta r$) in relation to the remaining two arrays (r). Thus the effective K-value ($\hat{K}$) can be calculated as:

$$\hat{K} = \frac{1}{2}K\,(r) + \frac{1}{2}K\,(r + \delta r) . \quad (2)$$

The TGU model for APPLE undulator devices was described in detail in [6]. From this, we can derive a functional model to describe the K-gradient, also described as α, as:

$$\frac{d\hat{K}}{dx} = \frac{1}{2\sqrt{2}}\left[\frac{dK}{dr}\,(r + \partial r) - \frac{dK}{dr}\,(r)\right] \quad (3)$$

Calculations were done with the RADIA code for circular and linear polarizations. This revealed a very good agreement between the model and simulations in the circular polarization case (see Fig. 1) with differences well below 1%. However, a significant mismatch for the linear case can be observed. For this reason we adapted the model for linear

* christoph.kittel@psi.ch

Content from this work may be used under the terms of the CC BY 4.0 licence (© 2026). Any distribution of this work must maintain attribution to the author(s), title of the work, publisher, and DOI.

ISBN: 978-3-95450-252-3 ISSN: 2673-5350 doi: 10.18429/JACoW-IPAC2026-THP2158

THE FIRST APPLE X KNOT UNDULATORS: MAGNETIC CHARACTERIZATION AND INITIAL PERFORMANCE

S. C. Richter*, A. Kleibert, C. A. F. Vaz, and M. Calvi,
PSI Center for Photon Science, Paul Scherrer Institute, Villigen, Switzerland

Abstract

Concepts for reducing on-axis heat load become essential as photon flux increases in next-generation synchrotrons, especially in the soft X-ray regime. Therefore, APPLE "knot" undulators are promising insertion devices, diverting most energy off-axis without compromising the polarization purity. The first two APPLE X knot undulators, each 2 m long and with a period length of 36 mm, were designed and built at Paul Scherrer Institute (PSI) and installed into the newly upgraded Swiss Light Source (SLS2.0) electron storage ring. This contribution presents the final magnetic characterization results of both novel undulators and derives photon characteristics, including how effectively the radiation power is expected to be reduced on-axis in contrast to a regular elliptical undulator, especially in linear modes. Further, their initial performance with the beam is demonstrated, providing a glimpse of the ongoing beamline commissioning and future operation.

INTRODUCTION

The latest upgrade of the Swiss Light Source SLS to SLS2.0 increased the electron beam energy from 2.4 GeV to 2.7 GeV and reduced the horizontal emittance to a target value of 157 pm. To exploit the improved beam parameters, most existing insertion devices are replaced by undulators with shorter magnetic periods, enabling significantly higher photon beam brightness. In particular for soft X-ray beamlines, this results in an increased radiation power incident on beamline components, making the reduction of on-axis heat load a critical issue. To address this challenge, a novel APPLE "knot" undulator concept was implemented, based on PSI's mature APPLE X design for SwissFEL's Athos line [1].

The resulting device, a 2 m-long UE36kn, with an undulator period $\lambda_u = 36$ mm, was designed to suppress on-axis radiation power for linearly polarized light, similar to figure-8 undulators, while providing enhanced polarization purity. This was achieved by a dedicated magnetic configuration that shifts the main radiation peak, thus higher harmonics, off-axis [2–5]. The original APPLE knot concept employs eight magnet arrays in an APPLE II–type configuration. For UE36kn, the design is adapted to the existing undulator infrastructure at PSI by merging the eight arrays into four combined arrays, with all magnets having the same remanence field $B_r = 1.31$ T, forming a main undulator period length $\lambda_u = 36$ mm. In addition, the magnetic design is simplified by limiting the number of different magnet types to five. A detailed design overview was given in a previous publication [6]. This paper presents the final results of the magnetic characterization, including derived photon characteristics, and the initial performance with the beam in SLS2.0 at PSI.

MAGNETIC CHARACTERIZATION

A compact measurement system was needed as the fish-like magnets on the four arrays in an APPLE X configuration spare only limited space for measuring at small gaps, as Fig. 1 demonstrates in a close-up. To deal with this constraint, a SAFALI-type system serves as the measurement setup consisting of a 3-axis Hall probe, introduced earlier [7].

After the magnet assembly was completed and before being able to assess the final magnetic field configurations experimentally, each undulator was aligned in two steps: First, the Hall probe's position was corrected for the horizontal and vertical positions, x and y, as well as pitch and yaw, respectively, while the beam is pointing along $\hat{z}$; all with respect to the magnetic field, utilizing a newly defined K parameter for the knot-magnet design. Second, minimizing the relative phase among the four rows by correcting the position of all four arrays to each other, leading to improved polarization settings, especially in linear modes. As a next step, the complete magnetic configuration was optimized by using the flexor/screw system introduced in earlier publications [1, 6]. As commonly done for undulators, the goal of shimming was to smooth the undulator field and reduce kicks as best as possible by minimizing the first and second field integrals and thus the phase error. Yet, the novel APPLE X knot magnet design comes with a challenge linked to the keeper design with respect to the shimming process: A single shimming knob consists of a pack of four magnets, each with a different magnetization direction. With a total of

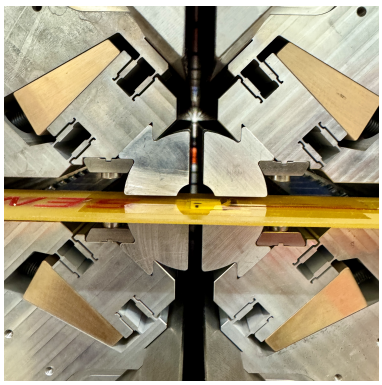

Figure 1: The APPLE X knot UE36kn and its four magnet arrays, including the flexor-based shimming system, during the magnetic characterization at a gap of 13 mm.

* sebastian.richter@psi.ch

Content from this work may be used under the terms of the CC BY 4.0 licence (© 2026). Any distribution of this work must maintain attribution to the author(s), title of the work, publisher, and DOI.

ISBN: 978-3-95450-252-3 ISSN: 2673-5350 doi: 10.18429/JACoW-IPAC2026-THP2601

NUMERICAL SIMULATION OF HELIUM LEAKAGE IN THE EXPERIMENTAL HALL AT TPS

J.C. Chang †, P.J. Wen, S.P. Kao, M.C. Lin
National Synchrotron Radiation Research Center, Hsinchu, Taiwan

Abstract

To utilize helium for experiments efficiently, our beamline people built a helium recovery system at the experimental hall of Taiwan Photon Source (TPS). This system includes four helium recovery balloons, each with a capacity of approximately 13.8 m^3, and is equipped with pressure relief valves. Considering the potential safety hazard of oxygen deficit in the vicinity when helium leak occurs, this study applied numerical simulations to analyse the oxygen content distribution during cases of helium leak.

INTRODUCTION

The National Synchrotron Radiation Research Center (NSRRC) and the Max Planck Institute for Chemical Physics of Solids (MPI CPfS) in Germany jointly constructed the submicron soft X-ray spectroscopic beamline TPS 45, as shown in Fig. 1. Its goal is to utilize various synchrotron radiation spectroscopic techniques to reveal the electronic structure of novel strongly correlated materials. The TPS 45 beamline uses liquid helium to cool the superconductors to conduct experiments at low temperatures. However, to keep precious helium from dissipating into the atmosphere and causing unnecessary waste [1], the volatile gaseous helium produced during the cooling process is recovered and reused through four balloons, as shown in Fig. 2.

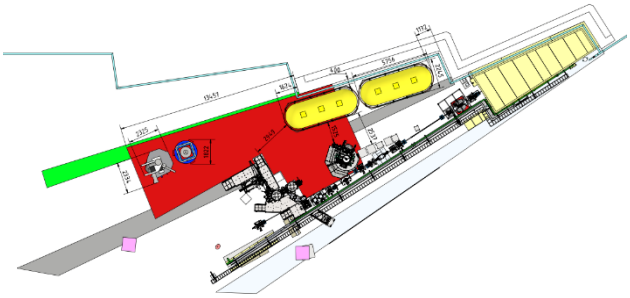

Figure 1. Top view of the TPS45 beamline.

Each experiment requires 50 liters of liquid helium. The volume of each cylindrical balloon with length of 5.5 m and diameter of 1.9 m is 13.8 m^3. However, if helium leaks from the balloons, it may cause oxygen deficiency in the area, posing a hazard to personnel conducting experiments there. Therefore, an oxygen-deficiency assessment is required to ensure personnel safety [2]. As a result, a series of simulations was conducted to estimate oxygen concentration under various helium leakage conditions [3].

The helium recovery system was set up in the TPS experimental hall. The inner and outer ring radii of the experimental hall are 87 m and 104 m, respectively, with a height of 10.5 m.

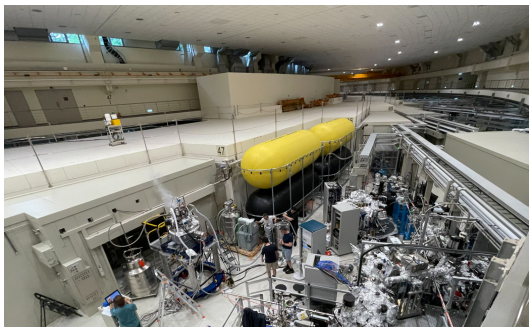

Figure 2. TPS45 helium recovery balloon.

The helium recovery system consists of four helium recovery balloons (as shown in Fig. 1). The pressure relief valve has an inner diameter of 4 cm and a pressure relief range of 20-60 mbar, which is adjustable and currently set at 50 mbar. The balloons can continuously supply pressure up to 500 mbar, and the flow rate is controllable. This study focuses on numerical simulation analysis of helium leakage in this system. To conserve memory, we model a 1/12 segment of the experimental area, within which the helium recovery system is located (as shown in Fig. 3).

NUMERICAL SIMULATION

CFD (Computational Fluid Dynamics) began from the early 30s of the 20th century to solve the linearized potential equations with 2D methods. As rapid development of numerical analysis and computer science, CFD has been widely applied in many fields. In this study, we perform the CFD to simulate helium leakage in the experimental hall of TPS.

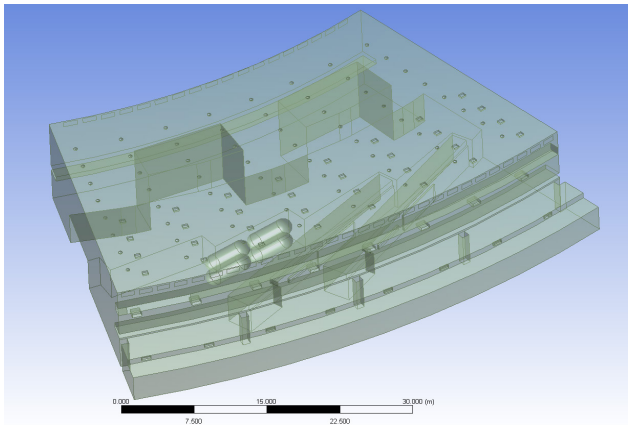

Figure 3: 3D schematic view of one twelfth of the TPS experimental hall.

We performed CFD of 3D numerical simulation using a commercial code Fluent R.16.2. [4]. To save computing

Content from this work may be used under the terms of the CC BY 4.0 licence (© 2026). Any distribution of this work must maintain attribution to the author(s), title of the work, publisher, and DOI.

ISBN: 978-3-95450-252-3 ISSN: 2673-5350 doi: 10.18429/JACoW-IPAC2026-THP3001

A VERSATILE BEAM SPLITTING SYSTEM FOR SIMULTANEOUS DELIVERY OF THREE BEAMS TO INDUSTRIAL APPLICATIONS AT THE GANIL ACCELERATOR

M. Lalande, C. Barthe Dejean, P.-E. Bernaudin, E. Dessay,
J. Djelloul, B. Jacquot, I. Mowgood, M.-H. Stodel
Grand Accélérateur National d'Ions Lourds, Caen, France

Content from this work may be used under the terms of the CC BY 4.0 licence (© 2026). Any distribution of this work must maintain attribution to the author(s), title of the work, publisher, and DOI.

Abstract

The demand for heavy-ion irradiation in space applications has grown significantly in recent years, surpassing the available beam time at GANIL. To address this, we are developing an innovative beam splitting system combining stripper/degrader techniques with two large-aperture DC magnetic septa. The originality of this approach lies in generating and transporting three different charge states obtained through partial stripping (typically from a $^{129}Xe^{48+}$ beam at 50 MeV/u). These charge states are selected, separated from each other by the two septa and directed to three independent beamlines. These lines remain adjustable to accommodate various ion beams and magnetic rigidities. A key challenge is ensuring full operational independence of the beamlines, including control of beam intensity and access to experimental areas, which requires significant reconfiguration of the facility. Unlike time-sharing systems using fast switching magnets, our concept optimizes ion accelerator efficiency through a full parallel operation with a 100% duty cycle. This upgrade will enable simultaneous irradiations in three experimental areas, greatly enhancing GANIL's capacity to support high-demand, long-term irradiation programs. Moreover, this concept could be applied to other accelerator facilities desiring to feed multiple irradiations setup simultaneously without switching magnets.

MANUSCRIPTS

GANIL (Grand Accélérateur National d'Ions Lourds) [1] is one of the world's leading international laboratories dedicated to research using ion beams, ranging from ^{12}C to ^{238}U accelerated from 0.1 and 95 MeV/u. The facility house five cyclotrons and a superconducting LINAC. Equipped with high-performance detection instruments, the facility enables researchers from around the globe to conduct unique experiments across diverse fields, including nuclear physics, atomic physics, condensed matter physics, astrophysics, and radiobiology.

Alongside its scientific mission, GANIL also devotes a portion of its activities to industrial applications. In recent years, there has been a sharp increase in beam demand from the space applications for radiation testing of electronic equipment [2-6]. To meet this growing need and the other various demands of the scientific community, GANIL continually adapts and improves its beam production and guidance capabilities [7].

To significantly expand the beam time allocated to industry from 400 hours in 2023 to approximately 2,000 hours per year by 2030, several projects are being carried out simultaneously. One of these solutions is beam sharing.

Operating a complex accelerator requires substantial resources, including high initial investment, specialized personnel, and significant electricity consumption, all for a limited number of scientific experiments. Beam sharing, a strategy identified early in GANIL's development, aims to maximize the return on investment. The concept of conducting simultaneous experiments to enhance the accelerator's scientific impact has been successfully implemented at GANIL, notably on the medium-energy (SME, 1990) and low-energy (IRRSUD, 2003) beamlines.

Beam sharing has been employed at GANIL for several years by pulsing magnets to alternately direct the beam into two separate experimental caves at a frequency of every 10 seconds [8]. Similar multi-user platforms, relying on pulsed magnets, have also been implemented at other facilities worldwide [9].

To address these challenges, we propose to develop a new multi-users platform (shown on Fig. 1) for industrial applications at GANIL, designed to enable fully simultaneous experiments. Our approach involves splitting the high-energy $^{129}Xe^{48+}$ beam (50 MeV/u) into several distinct charge states via partial stripping. Three charge states are then selected and separated using large-aperture DC magnetic septa, whose design and integration require dedicated studies, and then guided in three different beamlines.

In this paper, we present a detailed design of this beam-splitting system, highlighting its potential to implement multi-user access at GANIL.

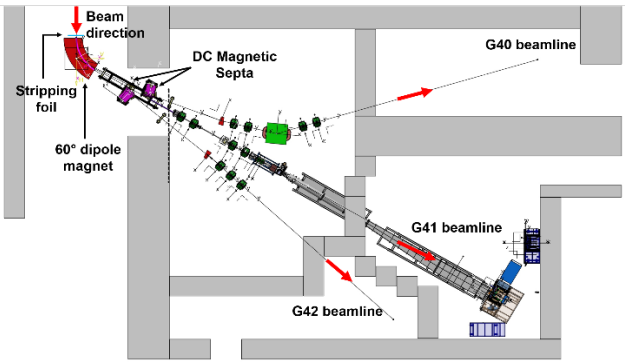

Figure 1: Schematic view of the three beamlines dedicated to the industrial applications at GANIL. The middle beamline is already in use, the others are in study.

ISBN: 978-3-95450-252-3 ISSN: 2673-5350 doi: 10.18429/JACoW-IPAC2026-THP3004

HYBRID OPTIMISATION OF THz-DRIVEN TAPERED WAVEGUIDES FOR SYNCHRONOUS ACCELERATION OF WEAKLY RELATIVISTIC HIGH-QUALITY ELECTRON BUNCHES

F. Peczek*, [1], R. Appleby[1], J. Bradbury[1], G. Burt[2], D. Graham[1], M. Hibberd[1], S. Jamison[2], R. Letizia[2], L. Nix[2]
The Cockcroft Institute, Sci-Tech Daresbury, Daresbury, UK
[1]also at The University of Manchester, Manchester, UK
[2]also at Lancaster University, Lancaster, UK

Abstract

Downscaling particle accelerators is crucial to expanding their range of applications. Dielectric-lined waveguides (DLWs) can support hybrid modes with a strong accelerating component. Excited by terahertz (THz) frequency pulses, DLWs can deliver high accelerating gradients over cm-scale interaction lengths, promising the development of future compact electron accelerators. By precisely tailoring the waveguide geometry, the modal field profile and phase velocities can be tuned to maintain synchronisation between the weakly relativistic bunches and the accelerating mode over extended distances. Here, we design and evaluate THz-driven tapered DLWs delivering high-quality, MeV-level electron bunches in two types of symmetrical DLW waveguides: rectangular and cylindrical. We use analytic models of accelerating modes to simulate transport and acceleration of an externally injected 100-keV electron beam across various DLW geometries. A genetic algorithm is employed to identify Pareto-optimal geometries based on the final bunch characteristics.

INTRODUCTION

The key to more compact and affordable accelerators of the future is to push for higher accelerating gradients and enhanced beam quality. THz structures offer a promising solution that delivers exceptional control over the longitudinal and transverse phase space of sub-picosecond electron bunches. The gradients of $1\,\mathrm{GeV\,m^{-1}}$ have been demonstrated in THz-driven DLW waveguides [1].

Moreover, the last few decades have brought major advances in THz-generation technology, especially laser-driven sources, such as optical rectification in lithium niobate ($LiNbO_3$) [2–4]. To reach longer pulse lengths (satisfying narrowband requirement of accelerating structures), method was developed utilising, instead of a single crystal, stacks of periodically-poled lithium niobate (PPLN) wafers [5, 6].

In the subrelativistic regime, the particle velocity increases significantly throughout the interaction, and it quickly slips out of phase alignment in a constant-phase-velocity structure. Several schemes have been proposed to address this issue, including the use of phase shifters [7], multi-stage acceleration [8], and tapered geometry [9, 10]. By tailoring the cross-sectional geometry of the DLW along its longitudinal direction, the phase velocity of the accelerating waveform can be adjusted to maintain synchronism with the accelerated bunch. Tapered design, however, often requires a slowly varying geometry, which is challenging to manufacture. Here, we address this problem with a stepped geometry solution. We introduce a design process involving optimisation via a genetic algorithm that can be applied to a wide set of operating parameters, tolerance limits and desired bunch qualities.

* filip.peczek@manchester.ac.uk

TAPERED DIELECTRIC-LINED WAVEGUIDES

We consider two types of geometries offering distinctive accelerating modes: LSM_{11} in rectangular DLW and TM_{01} in cylindrical one. In the following, we describe their impact on beam dynamics depending on their transverse and longitudinal position.

Rectangular

Under the assumption that cross-sectional geometry determines the modal wavenumbers (k_x, k_y, k_z) through the dispersion relation and a lossless waveguide, the modal amplitude $A_R(z)$ can be found by considering the conservation of energy flux (power flow) [10]. Therefore, the accelerating LSM_{11} inside the vacuum region of a rectangular DLW, shown in Figure 1, takes form:

$$\begin{aligned}
E_x &= A_R(z) k_x k_{0y} \cos\left(k_x x + \frac{\pi}{2}\right) \cos\left(k_{0y} y\right), \\
E_y &= A_R(z) (k_x^2 + k_z^2) \sin\left(k_x x + \frac{\pi}{2}\right) \sin\left(k_{0y} y\right), \\
E_z &= A_R(z) k_z (-i k_{0y}) \sin\left(k_x x + \frac{\pi}{2}\right) \cos\left(k_{0y} y\right), \\
H_x &= -A_R(z) \omega \varepsilon_0 k_z \sin\left(k_x x + \frac{\pi}{2}\right) \sin\left(k_{0y} y\right), \\
H_y &= 0, \\
H_z &= A_R(z) i \omega \varepsilon_0 k_x \cos\left(k_x x + \frac{\pi}{2}\right) \sin\left(k_{0y} y\right),
\end{aligned} \tag{1}$$

where each term is multiplied by a travelling wave expression with a phase offset ϕ:

$$\exp\left(i\omega t - i\int_0^z k_z(z)\,dz + i\phi\right). \tag{2}$$

The accelerating mode LSM_{11} supported by the rectangular waveguide consists not only of a desired strong longitudinal electric field component but also non-zero transverse

Content from this work may be used under the terms of the CC BY 4.0 licence (© 2026). Any distribution of this work must maintain attribution to the author(s), title of the work, publisher, and DOI.

ISBN: 978-3-95450-252-3 ISSN: 2673-5350 doi: 10.18429/JACoW-IPAC2026-THP3304

STATUS OF 22 GeV CEBAF UPGRADE USING FFA ARCS*

S. Ogur†, R. M. Bodenstein, S. A. Bogacz, K. E. Deitrick, B. R. Gamage, R. Kazimi, D. Khan, E. Nissen, Y. Roblin, R. Ruber, T. Satogata, N. Sereno, A. Seryi,
Thomas Jefferson National Accelerator Facility, Newport News, VA, USA
J. S. Berg, S. J. Brooks, D. Trbojevic, Brookhaven National Laboratory, Upton, NY, USA
G. H. Hoffstaetter, Cornell University, Ithaca, NY, USA
V. Morozov, Oak Ridge National Laboratory, Oak Ridge, TN, USA.

Abstract

Jefferson Lab is exploring an upgrade to extend CEBAF's energy to ~22 GeV within the existing tunnel by incorporating Fixed-Field Alternating-gradient (FFA) arcs. In this scheme, the two lowest-energy electromagnetic arcs—one on each side of the racetrack— are removed, the remaining arcs are reassigned accordingly, and a new pair of high-energy FFA arcs enables six additional recirculations using the existing SRF linacs. The non-scaling FFA lattice employs Halbach-derived permanent magnets with provisions for dipole, quadrupole, and higher-order components, offering large momentum acceptance and reduced operating cost. Implementing this concept requires updated linac optics, modifications to the remaining arcs, and a redesigned electromagnetic switchyard. Ongoing beam-dynamics studies address synchrotron-radiation–induced energy loss and emittance growth, along with strategies for their mitigation.

INTRODUCTION

CEBAF at Jefferson Lab has delivered world-leading nuclear physics results since the 12 GeV upgrade reached full operations in 2016 [1]. A rich approved programme will run for at least the next decade, while the community has identified a compelling scientific case for a further upgrade to ~22 GeV [2]. The higher energy opens three categories of new physics: (i) *unique* measurements accessible only at 22 GeV—near-threshold J/ψ production to probe the proton's gluonic content and charm-containing multiquark spectroscopy; (ii) *enrichment* of existing 12 GeV topics including 3D nucleon tomography and hard-exclusive processes; and (iii) *complementarity* with the future EIC through precision mapping of the nucleon sea at intermediate to high x and identification of short-range correlations. Operating well above EIC luminosities in fixed-target mode, the facility would use existing halls and detectors, minimising cost and technical risk. The upgrade strategy exploits Fixed-Field Alternating-Gradient (FFA) technology demonstrated at the Cornell–BNL ERL Test Accelerator (CBETA), which achieved eight-pass energy-recovery recirculation with a single set of FFA return arcs [3]. A pair of Halbach-derived permanent-magnet FFA arcs, replacing the two highest electromagnetic arcs at CEBAF, can simultaneously transport six beam passes spanning a factor of two in energy, adding up to six new recirculation passes within the existing 80.6 m-radius tunnel. Figure 1 shows the overall upgrade concept.

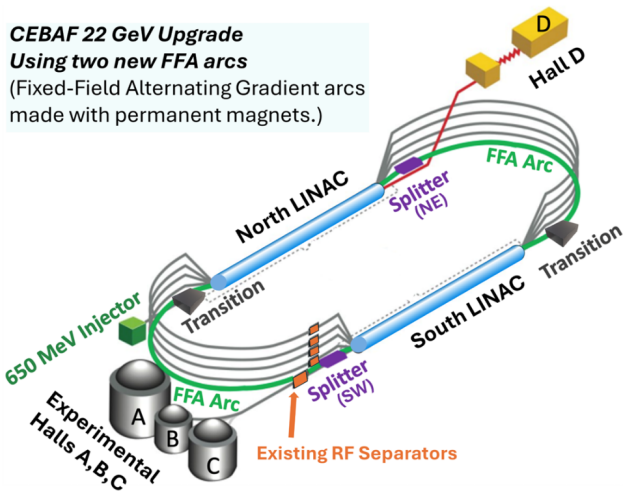

Figure 1: Overview of the FFA@CEBAF 22 GeV upgrade concept. Two new FFA arcs (green) become the highest-energy arcs after removal of the lowest-energy electromagnetic arcs. NE and SW splitter beamlines separate the six FFA passes. The 650 MeV injector is housed in the existing LERF building.

MACHINE LAYOUT AND LINAC OPTICS

The upgrade is staged: an initial configuration reaches ≈20 GeV with five new FFA passes; subsequent cryomodule upgrades (replacing lower-gradient cryomodules with C100 units) raise the linac energy from 1.1 to 1.21 GeV per pass and the top energy to 22 GeV. The existing five-and-a-half-pass racetrack is retained for the first four and half passes.

650 MeV Universal Injector

The existing 123 MeV injector is replaced by a three-pass racetrack in the Low Energy Recirculation Facility (LERF) vault [4]. Three C-75 cryomodules (eight 5-cell, 1497 MHz cavities each, 71.3 MeV energy gain per pass) take an 8 MeV photo-injector beam to 650 MeV in three recirculations. All five 180° arcs use Flexible Momentum Compaction (FMC)

* This material is based upon work supported by the U.S. DOE, Office of Science, Office of Nuclear Physics contract DE-AC05-06OR23177 and authored in part by UT Battelle, LLC, under Contract No. DE-AC05-00OR22725.

† sogur@jlab.org

Content from this work may be used under the terms of the CC BY 4.0 licence (© 2026). Any distribution of this work must maintain attribution to the author(s), title of the work, publisher, and DOI.

ISBN: 978-3-95450-252-3 ISSN: 2673-5350 doi: 10.18429/JACoW-IPAC2026-THP3305

FFA BEAM TRANSPORT DEMONSTRATION DEVELOPMENT FOR THE CEBAF 22 GeV UPGRADE*

S. Ogur†, S. A. Bogacz, E. Nissen,
Thomas Jefferson National Accelerator Facility, Newport News, VA, USA
S. Brooks, D. Trbojevic, Brookhaven National Laboratory, Upton, NY, USA

Abstract

Jefferson Lab is planning an upgrade of the Continuous Electron Beam Accelerator Facility (CEBAF) to deliver highly polarized electron beams up to 22 GeV using Fixed-Field Alternating-gradient (FFA) magnets. As the application of FFA technology in the 10–22 GeV energy range is unprecedented, experimental validation is required prior to full-scale implementation. To support this effort, a dedicated FFA test insert is proposed within the existing CEBAF infrastructure, with candidate locations in the Beam Switchyard (BSY) dump line or the Hall C beamline. The testbed will consist of a half or full FFA cell using combined-function permanent magnets and will enable systematic studies of beam transport, field quality, alignment, and magnet performance under realistic conditions. Operation with polarized beams in the 5–11 GeV range will closely replicate the energy scaling of the full upgrade. This paper presents the current design status and layout options for the proposed FFA beam transport test line.

INTRODUCTION

The 22 GeV CEBAF energy upgrade [1] proposes to install new high-energy FFA return arcs, after removal of the lowest-energy electromagnetic arcs and reassignment of the remaining CEBAF arc stack [2]. Each cell pairs a focusing and a defocusing combined-function magnet that simultaneously provides dipole bending and strong quadrupole gradients, while an open mid-plane geometry suppresses synchrotron radiation emission into the magnet bore. The resulting lattice must simultaneously transport six co-propagating electron beams spanning a 2.2:1 momentum ratio — a configuration with no direct experimental precedent at multi-GeV energies. The proposed design is a *non-scaling* FFA: particles at different momenta follow distinct closed orbits within the shared aperture, with orbit position and betatron tunes varying continuously across the energy range. The momentum-dependent beta functions and dispersion at the cell boundary require optical matching to be satisfied simultaneously for all six beams, while the momentum compaction factor α_c varies across the arc, influencing beam stability and the synchrotron radiation integral. Recent work has explored reducing α_c in single FFA beam arcs to control these effects [3]. Additionally, synchrotron radiation induces energy oscillations that perturb both betatron tunes and spin precession, with the orbit shift coupling radiation excitation directly into the transverse phase space [4]. To de-risk the upgrade program at an early stage, we plan to submit a lab-directed R&D project to deploy a single FFA magnet test insert within the current CEBAF complex in the 5–11 GeV range. The two candidate locations are indicated in Fig. 1. The testbed complements ongoing field-quality and radiation-resilience studies on prototype magnets [5] by providing the first beam-based measurements of multi-energy closed orbits and optical functions through an FFA element.

CANDIDATE TEST SITES

The primary site-selection criteria are: (i) compatibility with CEBAF's current operating energy range up to ~11 GeV, (ii) a momentum ratio close to the 2.2:1 of the upgrade, and (iii) sufficient upstream optics flexibility to match into the FFA periodic boundary conditions across all energies simultaneously.

BSY Dump Line

The BSY dump line is presently unused and could be refurbished as a dedicated high-energy FFA test facility [6], following the precedent of the CBETA fractional-arc test [7]. The line contains three dipoles; in the proposed configuration the first dipole (MBJ4C01) is replaced by the scaled FFA insert, as illustrated in Fig. 2. The remaining two dipoles and the downstream quadrupole triplet provide the necessary optical leverage for matching. Beam orbits through a single magnet or a full half-cell would be measured over the 5–11 GeV range, with the exact longitudinal position of the insert retained as an optimisation parameter. The BSY option offers a clean, unencumbered lattice and the possibility of long uninterrupted machine time without competing with the Hall physics program.

Hall C Beamline

Hall C offers an operational beamline equipped with a comprehensive diagnostic suite developed for nuclear-physics experiments, as shown in Fig. 3. Beyond orbit and optics measurements through a full FFA cell, the Hall C option uniquely enables polarisation transport studies: the existing Møller and Compton polarimeters provide absolute polarisation measurements at one-percent level [8], allowing direct experimental tests of spin-tune predictions [4] across the 5–11 GeV range. This is directly relevant to the high-polarisation goals of the 22 GeV upgrade [1] and cannot be

* This material is based upon work supported by the U.S. DOE, Office of Science, Office of Nuclear Physics contract DE-AC05-06OR23177 and authored in part by UT Battelle, LLC, under Contract No. DE-AC05-00OR22725.

† ogur@jlab.org

Content from this work may be used under the terms of the CC BY 4.0 licence (© 2026). Any distribution of this work must maintain attribution to the author(s), title of the work, publisher, and DOI.

ISBN: 978-3-95450-252-3 ISSN: 2673-5350 doi: 10.18429/JACoW-IPAC2026-THP3308

DESIGN OF A SHORT-PULSE SEPTUM POWER SPLITTER FOR DISTRIBUTED X-BAND HIGH-GRADIENT ACCELERATION

S. Colmekci*,[1], G. Rijal[1], M. Shapiro[1], X. Lu[1,2], S. Doran[2], J. Power[2]
[1]Northern Illinois University, DeKalb, IL, USA
[2]Argonne National Laboratory, Lemont, IL, USA

Abstract

Using short radiofrequency (RF) pulses is a promising method for increasing achievable accelerating gradients while significantly suppressing RF breakdown probability. However, short-pulse operation requires a structure with a commensurately low filling time to ensure efficient gradient buildup. To achieve this, we utilize a distributed power coupling scheme that delivers RF power to each cavity simultaneously through a waveguide array. This parallel feeding mechanism drastically reduces the filling time of the entire accelerating structure compared to traditional series-fed designs. Furthermore, this topology allows for greater flexibility in cavity optimization and yields higher shunt impedance.This work presents the design and simulation of a novel septum power splitter specifically engineered to drive an accelerating structure in this short-pulse regime. The splitter is integrated with a four-cell prototype, enabling each cavity to be powered individually and concurrently. The system is designed for short *X*-band RF pulses with peak powers up to 400 MW at 11.7 GHz. The four-cell structure is over-coupled and maintains a 120° phase advance between adjacent cells. CST simulation results confirm the performance of this design in achieving high accelerating gradients. Finally, we outline the experimental plan for the prototype demonstration at the Argonne Wakefield Accelerator.

INTRODUCTION

Achieving high accelerating gradients is crucial for a wide range of accelerator applications to reduce the overall size and cost. As the attainable gradient is limited by radiofrequency (RF) breakdown [1], short RF pulses have emerged as an effective method for achieving higher gradients. Empirical scaling laws [2] describe the relationship between pulse length and attainable gradient at a constant breakdown rate, suggesting that gradients well beyond conventional limits may be achieved using nanosecond-scale pulses. This regime provides a viable path toward the next generation of ultra-compact accelerator applications.

Accelerating structures driven by short RF pulses require short structure filling times. It is challenging to achieve both a short filling time and a high accelerating gradient in conventional accelerators, as sequential RF power transfer between cells inherently leads to a trade-off between these two requirements. In contrast, distributed power coupling [3, 4] enables efficient RF power delivery to each accelerating cavity driven by short RF pulses, thereby reducing the structure filling time . This approach also provides greater flexibility in the cavity geometry optimization, which can lead to improved shunt impedance [5, 6].

Motivated by the demands of short-pulse operation and distributed power coupling schemes, we previously introduced, fabricated, and low-power tested an *X*-band parallel waveguide power splitter at 11.7 GHz [7]. Power coupling among the four output waveguides is achieved by three triangular septa with optimized dimensions, each placed between two adjacent waveguides. This previously reported splitter [7] equally divides the incident RF power into four output ports with a 90° phase advance between adjacent ports. The low-power measurement results showed good agreement with simulations.

In this work, following the successful validation of the 90° waveguide splitter design, we present a reconfigured septum-based RF power splitter integrated with a four-cell accelerating structure, designed to provide a 120° phase advance between adjacent cavities for short-pulse acceleration. In this architecture, the RF power is delivered simultaneously to each cavity through the waveguide array. To accommodate short-pulse operation, the standing-wave accelerating structure is designed in an over-coupled regime to reduce the filling time and ensure efficient RF power coupling at 11.7 GHz. Simulation results demonstrate that the proposed architecture achieves a high shunt impedance and a high accelerating gradient in the *X*-band under short-pulse operation. The complete structure, comprising the RF power splitter integrated with the four-cell accelerating structure, is currently under fabrication, and high-power tests are planned at the Argonne Wakefield Accelerator (AWA).

WAVEGUIDE ARRAY POWER SPLITTER

We previously designed a prototype of a 1-to-4 power splitter based on a waveguide array for short-pulse operation at *X*-band [7]. Specially designed septums on the

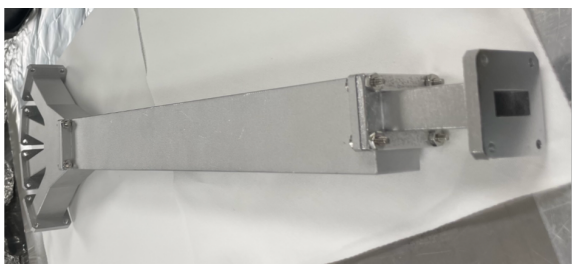

Figure 1: 3D-printed waveguide array prototype used for low-power measurements.

* scolmekci1@niu.edu

Content from this work may be used under the terms of the CC BY 4.0 licence (© 2026). Any distribution of this work must maintain attribution to the author(s), title of the work, publisher, and DOI.

ISBN: 978-3-95450-252-3 ISSN: 2673-5350 doi: 10.18429/JACoW-IPAC2026-THP3309

MODERNIZING THE AWA FACILITY: ENHANCED BEAM QUALITY AND CAPABILITIES FOR HIGH-GRADIENT RF AND BEAM PHYSICS RESEARCH *

J. G. Power†, G. Chen, S. Doran, J. Hlavenka, W. Liu, R. Margraf-O'Neal, A. Ody, P. Piot, E. Wisniewski
Argonne National Laboratory, Lemont, IL, USA

Abstract

The Argonne Wakefield Accelerator (AWA) is a 1300 MHz, 65 MeV normal-conducting photoinjector LINAC supporting a broad research program in high-gradient RF acceleration, beam physics, and AI/ML-based accelerator operations. The facility produces electron bunches spanning 1 pC to 100 nC, including high-charge (~100 nC, ~25 kA), high-brightness (~hundreds nm emittance), and arbitrarily shaped formats, and delivers beam to 5 device-under-test zones along two primary experimental beamlines.

Over the past decade the AWA has undergone extensive modernization, including replacement of the drive gun with an RF-symmetrized photoinjector; upgrade of the drive laser from a 248 nm excimer to a 262 nm Ti:sapphire system; transition to a distributed EPICS-based control system; and deployment of a digital LLRF system developed by the LBNL BACI group. Recent experiments have demonstrated accelerating gradients >300 MV/m in X-band structures, peak cathode fields >400 MV/m, and beam-driven RF power generation >565 MW.

Near-term plans include RF-symmetrized linac cavity replacements and an asymmetric EEX beamline upgrade. A proposed AWA-II upgrade would double the beam energy to ~130 MeV, further expanding the facility's reach for high-gradient RF and beam physics research.

INTRODUCTION

Accelerator test facilities play a critical role in the development of new technologies for future use at major accelerator user facilities. The Argonne Wakefield Accelerator (AWA) facility at Argonne National Laboratory supports a cost-effective accelerator research program spanning high-gradient normal-conducting RF acceleration [1,2], novel electron source development, advanced beam physics and diagnostics, and AI/ML-based accelerator operations.

In recent years, the AWA facility has undergone substantial modernization aimed at improving beam quality, operational reliability, diagnostics capability, and support for AI/ML-based accelerator operation. Major upgrades include deployment of an EPICS control system [3], an RF-symmetrized photocathode gun, digital low-level RF (LLRF) [4], and upgrades to the photocathode drive laser system.

The modernization program also supports the growing role of the AWA as an AI-ready testbed for developing and validating new AI/ML techniques towards autonomous accelerator operations: fast tuning, drift stabilization, virtual diagnostics, and performance optimization [5,6].

This paper summarizes the present status of the AWA facility, recent modernization efforts, current experimental capabilities, and future development directions.

FACILITY OVERVIEW

The AWA facility (Fig. 1) is centered around a normal-conducting, 1300 MHz, 65 MeV photoinjector LINAC. The RF gun uses a Cs2Te photocathode and can produce electron bunches with charges spanning from 1 pC to 100 nC in a single electron bunch and trains of 2–16 bunches with total charge exceeding 500 nC. The facility supports a variety of beam formats including high-charge, high-current beams (~100nC, ~25kAmps) or high-brightness beams (~hundreds nm) or shaped bunches (e.g. flatbeams and/or ramped bunches).

The flexible experimental area includes two primary experimental beamlines: the straightahead beamline and the emittance-exchange (EEX) beamline. Distributed along these beamlines are five experimental device-under-test (DUT) zones supporting high-charge beam physics, high-gradient RF acceleration, 6D phase-space manipulation, coherent synchrotron radiation (CSR) [7], coherent radiation generation, THz-driven acceleration, and advanced longitudinal beam diagnostics. The straightahead beamline primarily feeds Zones 3a, 3b, and 5, while the EEX beamline delivers beam to Zone 4. Zone 2 supports beam preparation and shaping prior to injection into downstream beamlines.

The AWA includes extensive diagnostics and infrastructure. Longitudinal phase-space diagnostics are provided by transverse deflecting cavities located at the end of each beamline, while transverse phase-space diagnostics and YAG:Ce screens are distributed throughout the DUT zones. Additional diagnostics include a 12 GHz oscilloscope for RF measurements. Facility infrastructure includes an EPICS-based control system, five high-power RF systems, and two synchronized laser systems: Ti:Sa-based 262 nm photocathode laser system [8] and a low-power commercial erbium-doped fiber 1550 nm laser system [9] used for laser-electron beam diagnostics.

* Work supported by the U.S. Department of Energy under contract No. DE-AC02-06CH11357.
† jp@anl.gov

Content from this work may be used under the terms of the CC BY 4.0 licence (© 2026). Any distribution of this work must maintain attribution to the author(s), title of the work, publisher, and DOI.

ISBN: 978-3-95450-252-3 ISSN: 2673-5350 doi: 10.18429/JACoW-IPAC2026-THP3311

HOFMANN STABILITY CHARTS REVISITED FOR PIP-II: FROM CLASSICAL THEORY TO ASSUMPTION-FREE AND ML-DRIVEN MAPS

Abhishek Pathak*, Fermi National Accelerator Laboratory, Batavia, IL, USA

Abstract

The Hofmann stability chart remains the standard graphical tool for visualizing parametric resonances in space-charge–dominated linacs, but the published higher-order ($\ell = 3, 4$) dispersion relations are routinely used in the isotropic limit and the chart returns a binary stable/unstable verdict. We revisit the chart for the PIP-II linac along three complementary tracks within the smooth-focused Kapchinskij–Vladimirskij (KV) framework. (1) A validated higher-order anisotropic dispersion solver implements the full S^2 and S^4/S^6 blocks of Hofmann's Eqs. (36) and (41); an internal-consistency audit identifies the $(1 \mp 2\hat{\eta}^2/\alpha)$ factors on the α-coupling terms of the S^4 block of Eq. (36) that are required for the equation to reduce analytically to its own stated isotropic-limit closed form Eq. (37). (2) A probabilistic chart layer with ensemble Monte Carlo uncertainty bands wraps the deterministic solver on top of an engineering jitter budget consistent with the PIP-II Final Design Report. (3) A solver-labelled random-forest surrogate with isotonic post-hoc calibration approximates the deterministic chart with held-out expected calibration error $\leq 1\%$ and sub-millisecond inference. We bound chart-based claims to the perturbative validity domain $S^2 \lesssim 10$; under that bound, seven of 38 perturbative-valid PIP-II periods exhibit nonzero coherent growth, with the dominant new contributions coming from $\ell = 3$ modes lifted by the anisotropic correction. The three non-perturbative periods are deferred to the companion paper's lattice-periodic Floquet treatment [7].

INTRODUCTION

The PIP-II 800-MeV H^- superconducting linac at Fermilab [1, 2], currently under construction as the proton driver for LBNF/DUNE, is the first CW-capable megawatt-class SRF proton linac in the United States. It accelerates a 2-mA average current through 119 individually powered cavities in five families (HWR, SSR1, SSR2, LB650, HB650) over 23 cryomodules and ~186 m. The design adopts a non-equipartitioned trajectory in which $\varepsilon_z/\varepsilon_x$ evolves freely from ~0.9 at injection to ~8.5 in the LB650 section, and the working point traces a path across the Hofmann $(\nu_z/\nu_x, \nu_x/\nu_{0x})$ plane that skirts the standard parametric resonance bands.

The conventional Hofmann analysis [3] addresses such a trajectory under restrictive assumptions: smooth focusing, a KV phase space [4], the $\ell = 2$ collective mode in the isotropic limit, zero incoherent tune spread, and a binary stable/unstable verdict. We address those limitations within the same smooth-focused KV framework along three tracks. Track 1 implements the higher-order anisotropic ($\ell = 2, 3, 4_e$) dispersion relations directly from Hofmann's Eqs. (36) and (41) with full S^4/S^6 blocks rather than their iso-limit reductions, and bounds chart-based claims to the perturbative validity domain $S^2 \lesssim 10$. Track 2 wraps the solver in an ensemble Monte Carlo loop to produce probabilistic margins. Track 3 trains a fast solver-labelled surrogate for online working-point screening. The full anisotropic transcription, derivation of the missing $(1 \mp 2\hat{\eta}^2/\alpha)$ factors, per-period PIP-II application, and the Floquet treatment of the three non-perturbative lattice periods are presented in the companion PRAB submission [7].

METHODOLOGY

Self-Consistent Parametrization

All three tracks share a common mapping from lattice variables (tune ratio $R \equiv \nu_z/\nu_x$; transverse tune depression $\eta \equiv \nu_x/\nu_{0x}$; emittance ratio $\varepsilon_z/\varepsilon_x$) to the Hofmann internal variables. Following Ref. [3],

$$\hat{\eta} = \sqrt{R/(\varepsilon_z/\varepsilon_x)}, \tag{1}$$

with the symmetry flip $\hat{\eta} \to 1/\hat{\eta}$ applied whenever $\hat{\eta} < 1$ to maintain $\hat{\eta} \geq 1$; the post-flip tune ratio is $R_{\text{eff}} = R$ before the flip and $1/R$ after, with $\alpha = 1/R_{\text{eff}}$. The dimensionless space-charge parameter is

$$S^2 = (1 - \eta^2)(1 + \hat{\eta})/(R_{\text{eff}}^2 \eta^2), \tag{2}$$

with $S^2 = 0$ for $\eta \geq 1$. The growth rate in units of the zero-current transverse tune is $\gamma/\nu_{0x} = \sqrt{-s}\, G_{\text{scale}}$ with $G_{\text{scale}} = R\eta$ before the flip and η after, where $s < 0$ is an unstable root of the dispersion relation.

Track 1: Validated Higher-Order Dispersion Solver

For $\ell \geq 3$ the dispersion relation is

$$D_\ell(s) = (1 + \hat{\eta})^\ell + S^2 \sum_{k \in \mathcal{P}_\ell} \frac{N^{(1)}_{\ell k}(\alpha, \hat{\eta})}{d_{\ell k} - s} + S^4 \sum_{(i,j) \in \mathcal{Q}_\ell} \frac{N^{(2)}_{\ell ij}(\alpha, \hat{\eta})}{(d_{\ell i} - s)(d_{\ell j} - s)} + \cdots = 0, \tag{3}$$

with $d_{\ell k}$ the squared pole frequencies and $N^{(1)}_{\ell k}, N^{(2)}_{\ell ij}$ the residues from Hofmann's $\ell = 3, 4$ Eqs. (36), (41), (45). We implement the full anisotropic S^2 block for $\ell = 2, 3, 4_e, 4_o$

* abhishek@fnal.gov

This work was produced by FermiForward Discovery Group, LLC under Contract No. 89243024CSC000002 with the U.S. Department of Energy, Office of Science, Office of High Energy Physics.

Content from this work may be used under the terms of the CC BY 4.0 licence (© 2026). Any distribution of this work must maintain attribution to the author(s), title of the work, publisher, and DOI.

ISBN: 978-3-95450-252-3 ISSN: 2673-5350 doi: 10.18429/JACoW-IPAC2026-THP3314

DESIGN AND OPTIMIZATION OF A 10.0625 MHz LOW-FREQUENCY BUNCHER FOR A 201.25 MHz RFQ ACCELERATOR*

K. Shipman†, A. Alexander, J. Lewellen, S. Sosa Guitron, R. Thornton, H. Xu
Los Alamos National Laboratory, Los Alamos, United States

Abstract

The LANSCE Accelerator Modernization Project (LAMP) will replace the front-end of the existing LANSCE accelerator, from ion sources through the end of the 100-MeV drift-tube linac. The LAMP design includes injecting a bunched beam into an RFQ. The RFQ test stand (RFQTS) will demonstrate this technique using an existing RFQ. This paper discusses the design of the low frequency buncher for the RFQTS. CST simulations were used to study the effects of gap length, bunching voltage, and beam-pipe aperture on the transmission efficiency, transit-time factor, emittance growth, and bunching efficiency. The optimized LFB provides effective pre-bunching, while a downstream solenoid focuses the beam to minimize transverse emittance growth and ensure proper injection into the RFQ.

INTRODUCTION

The Los Alamos Neutron Science Center (LANSCE) accelerator facility uses two Cockcroft-Walton accelerators to produce H^- and H^+ beams for six end-user facilities [1]. The LANSCE Modernization Project (LAMP) plans to replace the aging Cockcroft-Waltons with a single Radio-Frequency Quadrupole (RFQ) [2]. This upgrade requires research and development to maintain the beam timing and parameters required by users.

To support LAMP development, an RFQ Test Stand (RFQTS) is under construction using an existing RFQ with an input energy of 35 keV and output energy of 750 keV [3]. The RFQ is a 4-rod structure manufactured by Kress GmbH [4, 5].

The Weapons Neutron Research (WNR) facility at LANSCE requires high peak-current beam operation. At LANSCE, this is achieved using a Low-Frequency Buncher (LFB) to compress the H^- beam into 5 ns high-current bunches [6]. To reproduce similar beam conditions on the RFQTS, an LFB system is also required for the test stand.

This work presents the design and optimization of a 10.0625 MHz LFB for the RFQTS operating with a 35 keV, 15 mA proton beam. The buncher uses a two-gap beam-pipe structure with a center beam pipe driven by an RF voltage to longitudinally bunch the beam. Electrostatic and particle-in-cell (PIC) simulations were performed using CST Studio Suite [7] to evaluate bunching performance and RFQ transmission.

LEBT OVERVIEW

The low-energy beam transport (LEBT) line for the RFQTS is shown in Fig. 1. For the simulations presented in this work, the ion source is assumed to produce a 35 keV, 15 mA ion beam. A chopper generates 150 ns beam pulses that are transported to the LFB, where the beam is modulated by RF electric fields. Downstream of the LFB, a solenoid with a peak B-field of 0.28 T focuses the beam before injection into the RFQ. The RFQ bunches and accelerates the beam to 750 keV. The component configuration considered in this work is based on continued development of the RFQTS LEBT design presented in [8].

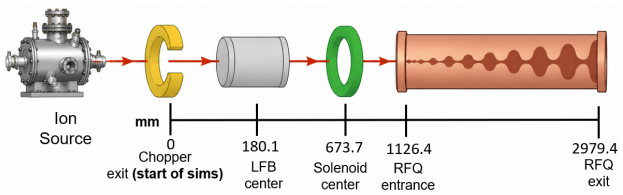

Figure 1: Simplified RFQTS LEBT layout showing the relative spacing of the ion source, chopper, LFB, solenoid, and RFQ.

LFB DESIGN

Figure 2 shows the LFB geometry and dimensions considered in this work. The outer diameter (OD) and gap sizes were varied in the simulations and do not represent final design values. The beam-pipe wall thickness was chosen to be 6.35 mm so the gap edges could be beveled to reduce electric-field enhancement. The structure consists of three beam-pipe sections enclosed by an outer tank, with the center section separated from the two grounded outer sections by two gaps. The center beam pipe is driven by an RF voltage that generates longitudinal electric fields across the gaps to modulate the beam energy.

The RF phase is chosen so the leading portion of the beam is decelerated while the trailing portion is accelerated, producing longitudinal bunching. The second gap reinforces this energy modulation and increases the bunching effect.

The two gaps are separated by a distance of $\beta\lambda/2$ to maintain the correct RF phase relationship. For a 35 keV proton beam operating at 10.0625 MHz, this corresponds to a gap-center spacing of 128.6 mm.

ELECTROSTATIC STUDIES

Electrostatic simulations of the LFB were performed to evaluate the electric-field distribution and transit-time factor (TTF) for varying gap sizes. A 1 kV DC voltage was applied

* LA-UR-26-23555 Approved for public release; distribution is unlimited.
† kshipman@lanl.gov

Content from this work may be used under the terms of the CC BY 4.0 licence (© 2026). Any distribution of this work must maintain attribution to the author(s), title of the work, publisher, and DOI.

ISBN: 978-3-95450-252-3 ISSN: 2673-5350 doi: 10.18429/JACoW-IPAC2026-THP3325

HIGH-GRADIENT RADIOFREQUENCY PHOTOINJECTOR WITH A DETACHABLE CATHODE ASSEMBLY

I. Shalaby*, L. Malin, M. Holl, S. Karkare, S. G. Tantawi
Arizona State University, Tempe, AZ, USA

Abstract

We present an RF photoinjector architecture that utilizes the TM_{02} mode in the first half-cell housing the cathode. Unlike the conventional TM_{01} mode configuration, this design introduces a controlled discontinuity in the surface field, producing a region free of surface currents. This unique topology allows the cathode to be mechanically separated from the gun body without compromising RF performance or requiring precise electrical continuity at the interface. The photoinjector should, in principle, deliver a very high cathode gradient and, consequently, high beam brightness. At the same time, the detachable cathode assembly is compatible with load-lock systems, which can transfer high QE semiconductor cathodes into high-gradient RF photoinjector structures under UHV.

INTRODUCTION

High-energy electron beams have provided an immense utility in various applications in research, such as X-ray generation [1] and ultrafast electron diffraction (UED) [2, 3], and in industrial applications, such as semiconductor metrology [4, 5] and medical treatment [6, 7]. Following electrons creation from a cathode surface through a photoelectric process, electrons are typically accelerated to relativistic energies (tens of MeVs), using high-gradient RF (~120 MV/m) fed into the photoinjector cavities. Acceleration upon creation is critical for minimizing emittance growth and producing high-brightness electron beams, highlighting the vitality of photoinjector assemblies.

TM_{01} VS TM_{02} DESIGNS

While TM_{01} is the minimalist mode of operation for photoinjector cavities design, multiple issues can emerge due to high RF fields on the metallic surface. For instance, imperfect brazing process of the cathode surface can lead to discontinuities and breakdowns, as well as cavity detuning beyond a reasonable range of the mechanical tuning pins. Significant damage to the cathode surface can inevitably leads to disposal of the entire photoinjector assembly. Moreover, the TM_{01}-mode design is inherently incompatible with semiconductor cathodes, which provide high QE, as they require growth and transfer under UHV. In this work, we present an alternative mode of operation, TM_{02}, for the cathode cavity which completely avoid brazing complications by using a braze-free cathode plug. This standalone cathode plug provides a soft tuning knob for the cathode cavity using precise positioning of the cathode plug. The detachable plug can be easily replaced, if damaged, and can also host semiconductor cathodes via a load-lock system.

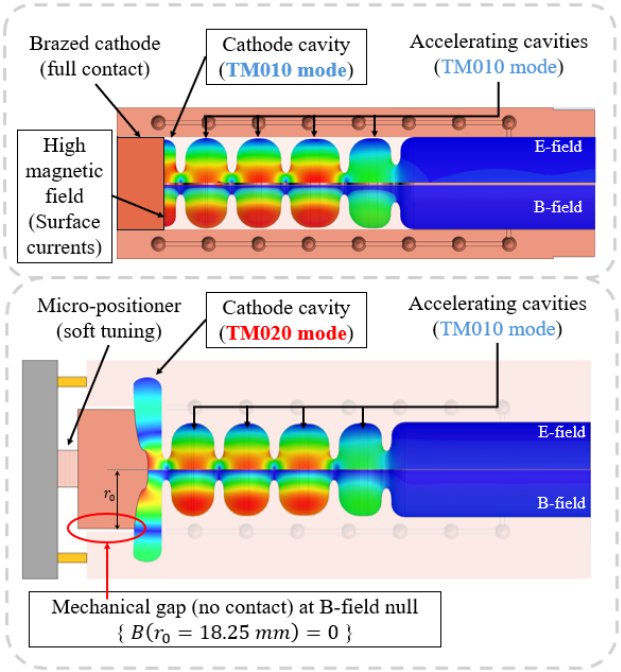

Figure 1: Comparison between TM_{01} amd TM_{02} designs for the first cathode cavity of a photoinjector assembly.

As shown in Fig. 1, designing a standalone cathode plug is feasible, in the TM_{02}-mode, by exploiting a magnetic field null on the metallic surface where surface currents are eliminated and a mechanical gap can be implemented without breakdown risks. This gap allows for a free-standing cathode which can be precisely positioned for tuning, easily replaceable, and can be integrated into a larger vacuum assembly for semiconductor cathodes integration.

CAVITY DESIGN OPTIMIZATION

To reach an optimal cavity design, it is necessary to strike a balance between the acceleration voltage V_{acc} and power losses on the metallic walls P_{loss} due to surface currents. Shunt impedance ($R_{\mathrm{s}} = |V_{\mathrm{acc}}|^2/P_{\mathrm{loss}}$) is the figure of merit used to evaluate and optimize cavity performance. Power loss is calculated using ($P_{\mathrm{loss}} = \frac{1}{2\delta\sigma}\oiint_S |H_{\parallel}|^2\, da$), where $H_{\parallel}$ is the surface magnetic field, δ is the skin depth, and σ is the conductivity. On the other hand, the acceleration voltage is calculated using the on-axis electric field E_z. Since electrons reach relativistic speeds fairly quickly under high gradient RF, a Lagrangian formalism is used for a single electron in a linear electric field E_z. This results in two transcendental equations $\{\partial\gamma/\partial z = (e/m_e c)|E(z)|e^{i(\omega t+\phi)}\ ,\ \partial t/\partial z =$

* isshalab@asu.edu

Content from this work may be used under the terms of the CC BY 4.0 licence (© 2026). Any distribution of this work must maintain attribution to the author(s), title of the work, publisher, and DOI.

ISBN: 978-3-95450-252-3 ISSN: 2673-5350 doi: 10.18429/JACoW-IPAC2026-THP3603

DESIGN OF AN S-BAND CHOKE-MODE TRAVELLING-WAVE ACCELERATING STRUCTURE

Hongbo Yu, Hao Zha*, Jiaru Shi, Huaibi Chen, Jingyuan Zhao
Department of Engineering Physics, Tsinghua University, Beijing, China

Abstract

Charged particle bunches excite wakefields in accelerating cavities, and the transverse components of these wakefields can degrade beam stability. Since these effects are mainly driven by higher-order modes (HOMs), effective HOM suppression is essential for accelerator operation. The choke-mode structure is one of the approaches used for HOM damping.

This study presents the design of a 2856 MHz S-band choke-mode travelling-wave accelerating structure. The fundamental-mode parameters of the single cell and cavity chain are optimized using electromagnetic simulations. HOM characteristics and wakefields are analyzed using HFSS and CST simulations, and a two-step optimization of the choke geometry is performed. The results show a clear reduction in transverse wake impedance, demonstrating effective HOM suppression.

INTRODUCTION

In accelerator structures, wakefield effects arise when a charged bunch travels through the cavity and induces image currents on the cavity wall. The transient currents subsequently excite electromagnetic fields inside the structure, which in turn interact with both the driving bunch itself and the following bunches.

When the wakefield acts on subsequent bunches, it is referred to as the long-range wakefield. In general, long-range wakefields form resonant modes inside the accelerating structure. Among them, dipole modes produce transverse kicks to the beam, leading to beam offset variation and degradation of transverse beam quality. Since the frequencies of dipole modes are always higher than that of the fundamental accelerating mode, accelerating structures with higher-order-mode (HOM) damping capability are essential for suppressing transverse long-range wakefields.

A choke-mode structure introduces a radial choke branch that reflects the accelerating mode back into the cavity, while most HOMs propagate along the radial line and are absorbed by loads located at the end of the branch. The choke-mode structure also provides advantages such as relatively simple fabrication and lower surface magnetic field.

This paper presents the design of an S-band choke-mode accelerating structure, including simulations of the fundamental mode for both single-cell and cavity chain configurations, as well as optimization studies for HOM suppression.

*zha_hao@mail.tsinghua.edu.cn

CAVITY CHAIN DESIGN

A choke-mode travelling-wave linear accelerator operating at 2856 MHz was designed using Ansys [1] softwares. The structure operates in the $3\pi/4$ mode and consists of 20 cells. The detailed design parameters are listed in Table 1. Based on the design specifications, the RF input power was minimized as much as possible.

Table 1: Design Specifications of the Choke-Mode Accelerating Structure

Parameter	Value
Working Frequency	2856MHz
Operating mode	$3\pi/4$
Number of cells	20
Length of the linac	78.6cm
Input RF power	$\leqslant$18MW
Output beam energy	$\geqslant$9MeV
Filling time	$\leqslant$300ns

The typical single-cell geometry of the choke-mode structure used in simulations is shown in Fig. 1. To reduce the computational cost of simulations, only a 5° azimuthal section of the axisymmetric cavity was modeled.

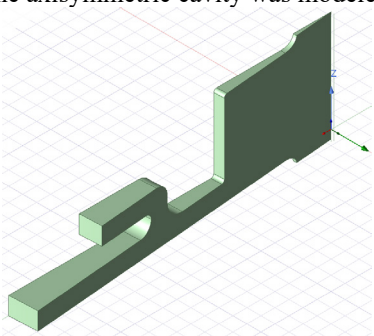

Figure 1: A typical single-cell geometry of the choke-mode structure.

In the simulations, the relationship between the cavity radius (b) and the iris aperture radius (a) was first determined to maintain a constant operating frequency for different iris apertures. Based on these results, the variations of the quality factor (Q), the group velocity (v_g), and (R/Q), as functions of the iris aperture radius were subsequently obtained from the single-cell simulations.

Numerical simulations were performed under the discrete-cell approximation. Assuming that the input power of the n-th cell is P_n, the following recursive relation can be obtained.

Content from this work may be used under the terms of the CC BY 4.0 licence (© 2026). Any distribution of this work must maintain attribution to the author(s), title of the work, publisher, and DOI.

ISBN: 978-3-95450-252-3 ISSN: 2673-5350 doi: 10.18429/JACoW-IPAC2026-THP3604

DUAL-PILLAR DIELECTRIC LASER ACCELERATION STRUCTURE FOR RELATIVISTIC ELECTRONS

Q.X. Chen†,1, S. Maru[1], K. Sakaue[1]
[1] The University of Tokyo, Tokyo, Japan

Abstract

Dielectric laser acceleration (DLA) has the potential to provide accelerating gradients on the order of GV/m and is therefore considered a promising alternative to conventional radio-frequency accelerators. Extending DLA operation to relativistic electrons is still at an early stage and is important for realizing compact accelerator systems. In this study, we perform a systematic parameter scan of a top-illuminated fused silica dual-pillar DLA structure to determine the optimal configuration based on electron energy gain. The resulting energy modulation of a relativistic electron bunch is then evaluated using the optimized structure. The simulation results show clear laser-induced energy modulation with an equivalent accelerating gradient on the order of several hundred MV/m. The planned DLA experimental platform at The University of Tokyo linear electron accelerator is also introduced. These results provide guidance for future DLA experiments with relativistic electron beams.

DLA PRINCIPLE AND DESIGN

A grating-based DLA can be regarded as the inverse process of Smith-Purcell radiation [1], as shown in Fig. 1. In the Smith-Purcell effect, an electron passing near a periodic grating emits radiation. In the inverse process, an incident laser excites an evanescent near field at the grating surface. The grating provides the spatial harmonic required to match the optical phase velocity to the electron velocity, producing a longitudinal electric field that can accelerate or decelerate the electron depending on its optical phase. The synchronicity condition is

$$\lambda_g = n\beta\lambda \qquad (1)$$

Where λ_g is the grating period, λ is the laser wavelength, $\beta = v/c$ is the normalized electron velocity, and n is the spatial harmonic order. For the first harmonic and relativistic electrons, this is approximately $\lambda_g = \lambda$.

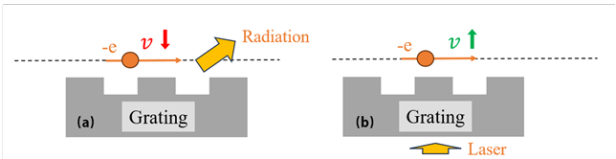

Figure 1: Schematic illustration of the Smith-Purcell effect (a) and inverse Smith-Purcell effect (b).

* Work supported by the MEXT Development of Key Element Technologies to Improve the Performance of Future Accelerators Program, Japan, Grant Number JPMXP1423812204, and JSPS KAKENHI Grant Number 26H02038.
† chenqixin@g.ecc.u-tokyo.ac.jp

Compared with conventional double-grating DLA structures, the dual-pillar geometry offers a simpler and more flexible platform for beam manipulation, while avoiding the mechanical alignment difficulty between two separated gratings [2]. It can also support symmetric optical-field excitation in the channel and can be configured for acceleration, focusing, bunching, or beam steering.

As shown in Fig. 2, three typical illumination schemes can be used for a dual-pillar DLA: double-sided illumination, single-sided illumination with a Bragg reflector, and top illumination. Double-sided illumination can provide the highest field symmetry in the acceleration channel, but it requires precise spatial, temporal, and phase alignment of two incident laser pulses. Single-sided illumination simplifies the optical system by using only one drive laser; however, without perfect compensation from the reflector, the excited field can become asymmetric in the channel, which may introduce unwanted transverse effects. Top illumination further simplifies the optical layout and relaxes the alignment requirements [2, 3]. Although this configuration may provide a slightly lower maximum accelerating field than the other schemes, it offers the best simplicity and feasibility for experimental implementation and future applications, including multi-channel operation and on-chip integration.

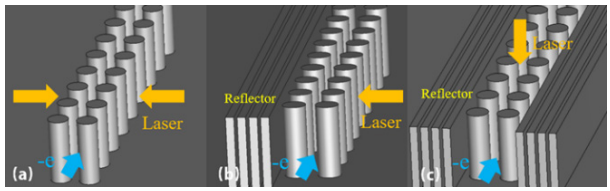

Figure 2: Illumination schemes for a dual-pillar DLA: (a) dual-sided, (b) single-sided with a Bragg reflector, and (c) top illumination.

In this study, a laser wavelength of λ = 1950 nm is used for both simulations and future experiments. Fused silica is selected as the baseline material for the DLA structure because its laser damage threshold is nearly one order of magnitude higher than that of silicon [4, 5]. This allows higher incident laser fields and makes it possible to reach accelerating gradients of several hundred MV/m. Since the interaction length of the proposed structure is limited [6, 7], a high accelerating gradient is required to obtain a measurable energy gain, especially for high-energy electron beams where a clear energy modulation signal is needed.

SIMULATION RESULTS

The geometric parameters of the top-illuminated dual-pillar DLA structure are optimized using CST Studio Suite. The simulation model is shown in Fig. 3. The electron

Content from this work may be used under the terms of the CC BY 4.0 licence (© 2026). Any distribution of this work must maintain attribution to the author(s), title of the work, publisher, and DOI.

ISBN: 978-3-95450-252-3 ISSN: 2673-5350 doi: 10.18429/JACoW-IPAC2026-THP3605

DESIGN OF A DIELECTRIC LASER ACCELERATOR STRUCTURE FOR LOW β CHARGED PARTICLES

S. Maru†, K. Sakaue, The University of Tokyo, Tokyo, Japan
D. Satoh, T. Shibuya, National Institute of Advanced Industrial Science and Technology, Tsukuba, Japan
M. Konrad, J. Litzel, P. Hommelhoff, Friedrich-Alexander-Universität Erlangen-Nürnberg, Erlangen, Germany

Content from this work may be used under the terms of the CC BY 4.0 licence (© 2026). Any distribution of this work must maintain attribution to the author(s), title of the work, publisher, and DOI.

Abstract

Dielectric laser acceleration (DLA) is a novel acceleration scheme using dielectric nanostructures with high damage thresholds for the laser electric field. In DLA, the typical structural period is determined by the product of β, the electron velocity normalized to the speed of light, and the laser wavelength λ At low β, the structural period becomes extremely small, making fabrication impractical and limiting the range of initial energies that can be accelerated. In fact, DLA has so far been demonstrated only for initial energies above approximately 10 keV. We design DLA structures that extend the range of initial kinetic energy that can be accelerated to lower energies. By setting the structural period to an odd multiple of $\beta\lambda$ and specifically employing a $3\beta\lambda$ structure in this work, the fabrication constraints associated with low initial energies can be improved. As a result, acceleration is driven by enhanced third-order Fourier components of the laser field generated during transmission through the pillars, rather than by the original incident laser component. In this paper, we will report on a pillar cross-sectional design capable of accelerating low-energy electrons (5 keV) based on acceleration simulations.

INTRODUCTION

Dielectric laser acceleration (DLA) is a method for accelerating charged particles using laser near-fields when dielectric microstructures are irradiated with laser pulses. Since visible and near-infrared lasers are employed as the driving source, the operating frequency is more than four orders of magnitude higher than those of conventional radio-frequency accelerators. In addition, the achievable accelerating gradient is determined by the damage threshold of the dielectric material and can reach the GV/m scale, e.g., 1.8 GV/m for SiO_2 [1]. Therefore, DLA enables compact accelerators with high accelerating gradients.

A schematic illustration of DLA is shown in Fig. 1. To maintain phase-synchronism between the laser field and electrons, the accelerating structure is designed as a dielectric periodic structure with a period L determined by the following condition:

$$L = m\beta\lambda \quad (1)$$

, where m is the spatial harmonic order of the diffraction modes generated by the laser field, β is the electron velocity normalized to the speed of light, and λ is the laser wavelength. The channel width is determined by the decay length of the laser near-field used for acceleration [2]. For visible and near-infrared (NIR) lasers, the channel width is typically on the order of several hundred nanometers.

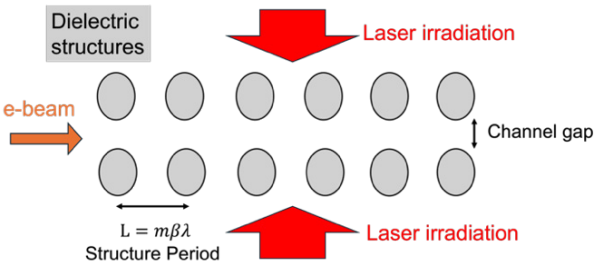

Figure 1: Schematic of dielectric laser acceleration.

On the other hand, one of the major challenges in DLA is the acceleration of electrons with very low initial energies, for which the fabrication of the accelerating structure becomes extremely difficult. This originates from the phase-matching condition for low-energy, non-relativistic electrons, which requires an excessively small structural period, thereby imposing a lower limit on the electron energy that can be accelerated. To address this issue, acceleration schemes based not on the incident laser field itself but on higher spatial harmonics of the laser field generated as the electrons pass through the pillar structure have been proposed, which have also been experimentally demonstrated using grating structures [3].

We aim to develop an ultra-compact accelerator based on DLA. To realize such a system, direct DLA of low-energy electrons without a pre-acceleration stage is required. Therefore, we investigate accelerating structures that enhance higher-order spatial harmonic components and design structures capable of accelerating electrons at lower energies.

DESIGN OF PILLAR STRUCTURES

In this study, the accelerating structure was designed to utilize the third spatial harmonic component, with the structural period set to $3\beta\lambda$. The $3\beta\lambda$ dual-pillar structure enables fabrication-compatible DLA structures for very low-energy electrons by avoiding the extremely small periods required in conventional $\beta\lambda$ -period structures.

Conventional dielectric laser accelerators generally utilize optical near-fields formed by the interference of laser fields irradiated onto both sides of the structure. However,

†senamaru@g.ecc.u-tokyo.ac.jp

ISBN: 978-3-95450-252-3 ISSN: 2673-5350 doi: 10.18429/JACoW-IPAC2026-THP3613

PRELIMINARY DESIGN OF AN RF-FOCUSED INTERDIGITAL DRIFT TUBE LINAC

Q. Kong*[1], H. Liu[1,2], A. Li[1,2], S. Liu[1,2], Y. Yang[1,2],
Spallation Neutron Source Science Center, Dongguan, China
[1]also at Institute of High Energy Physics, Beijing, China
[2]also at University of Chinese Academy of Sciences, Beijing, China

Abstract

The development of compact and efficient low-energy linear accelerators is crucial for advanced scientific and medical applications. While H-mode Drift Tube Linacs (DTL) offer superior shunt impedance compared to conventional Alvarez structures, they traditionally suffer from transverse defocusing and longitudinal instability when operating at a 0° synchronous phase. This paper presents the comprehensive design and beam dynamics study of a Radio-Frequency Focused Interdigital (RFI) H-mode DTL. By modifying the drift tubes to include internal pole tips, transverse quadrupole focusing is achieved directly via the RF fields, eliminating the need for internal magnetic lenses. We evaluate three transverse focusing lattices (FDFD, FFDD, and FFFDDD) using TraceWin, determining the optimal balance between beam transmission and required focusing voltage. Furthermore, a single cell optimization was performed and a high effective shunt impedance of 259 MΩ/m has been achieved.

INTRODUCTION

In the low-to-medium β(0.05< β <0.2), the Alvarez-type Drift Tube Linac (DTL) [1] operating in the TM010 mode served as the standard architecture for ion acceleration. However, the Alvarez-DTL suffers from a sharp decline in effective shunt impedance due to the insert of quadrupoles in drift tubes, which presents significant drawbacks in terms of power consumption and facility footprint. In contrast, H-mode linacs, which operate in the TE110 (Interdigital H-mode, IH) [2] or TE210 (Cross-bar H-mode, CH) modes, provide exceptionally high shunt impedance and highly compact structural dimensions within this low-β range.

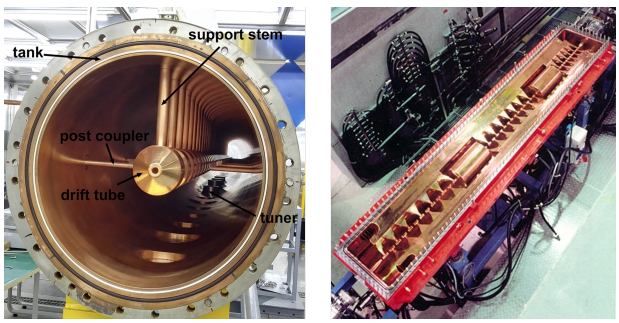

Figure 1: Alvarez-DTL structure for CSNS and IH-DTL structure for GSI HLI project.

Despite their superior RF efficiency, conventional H-mode accelerators encounter severe beam dynamics bottlenecks. The fundamental challenge arises from the strong transverse RF defocusing forces inherent in the acceleration gaps. To mitigate this without employing lenses in every drift tube, designers typically adopt the KONUS (Kombinierte Null-Grad Struktur) beam dynamics concept [3], where the beam is accelerated at a 0° synchronous phase. Over multi-gap sections, this lack of longitudinal confinement inevitably leads to beam filamentation, substantial longitudinal emittance growth. Furthermore, to periodically refocus the beam, external magnetic lenses such as Permanent Magnet Quadrupoles (PMQs) or Electromagnetic Quadrupoles (EMQs) must be inserted into specific drift tubes. Integrating these magnets into the heavily space-constrained vacuum environment—while simultaneously managing precision alignment and complex water-cooling systems—drastically escalates manufacturing complexity and overall construction costs.

To overcome these physics and engineering limitations, the Radio-Frequency Integrated (RFI) focusing H-mode DTL is proposed. By redesigning the geometry of the drift tubes to include internal electrode extensions, this structure generates a transverse electrostatic-like quadrupole field directly derived from the accelerating RF power. This innovation not only eliminates the need for internal magnetic lenses but also permits operation at negative synchronous phases, thereby restoring deep longitudinal stability. This paper systematically explores the realization of this structure, detailing the comparative selection of transverse focusing lattices, and the 3D electromagnetic optimization of the combined drift tube.

OPERATIONAL PRINCIPLE OF THE RFI H-MODE DTL

The innovation of the RFI H-Mode DTL lies in the geometry of its combined drift tubes. Conventional cylindrical drift tubes are replaced by an integrated structure featuring four internal electrode extensions (pole tips), as shown in Fig. 2. As the cavity is excited in the TE110 mode, these internal tips are alternately charged by the RF field, effectively generating a time-varying RF quadrupole field inside the drift tube.

Because transverse focusing directly generated from the RF field, the linac is no longer restricted to the 0° synchronous phase required by KONUS dynamics. Instead, it can stably operate at a negative synchronous phase, as shown in Fig. 2, thereby providing a stable longitudinal bucket to

* kongqy@ihep.ac.cn

Content from this work may be used under the terms of the CC BY 4.0 licence (© 2026). Any distribution of this work must maintain attribution to the author(s), title of the work, publisher, and DOI.

ISBN: 978-3-95450-252-3 ISSN: 2673-5350 doi: 10.18429/JACoW-IPAC2026-THP3614

DEVELOPMENT AND CHARACTERIZATION OF A FEBIAD ION SOURCE FOR RI BEAM PRODUCTION AT THE RAON ISOL SYSTEM

Je Hwan Han[1,2*], Yeong Heum Yeon[1†], Hyung Joo Woo[1], Kyounghun Yoo[1], Wonjoo Hwang[1], Hee Joong Yim[1], Ha-Na Kim[1], Dong Joon Park[1], Jae-Won Jeong[1], Jae Hong Kim[1], JunYoung Moon[1], SeongJin Heo[1], Takashi Hasimoto[1], Hyoun Woo Jung[1], Young Jae Lee[1], Jin Ho Lee[1], Moses Chung[3‡]

[1]Institute for Rare Isotope Science, Daejeon, Korea

[2]Department of Physics, Ulsan National Institute of Science and Technology, Ulsan, Korea

[3]Pohang University of Science and Technology, Pohang, Gyeongbuk, Korea

Abstract

RAON is a heavy-ion accelerator facility in Korea that uniquely combines Isotope Separation On-Line (ISOL) and In-Flight (IF) techniques to produce a wide range of Rare Isotope (RI) beams. In the ISOL system, ion sources are continuously being developed to expand RI beam production capabilities. Among them, the Forced Electron Beam Induced Arc Discharge (FEBIAD) ion source is a promising candidate for efficient RI beam generation.

A prototype FEBIAD ion source was evaluated at the offline facility, where successful Ar, Kr, and Xe isotope beam extraction demonstrated its operational feasibility. Since the FEBIAD ion source operates at elevated temperatures, structural deformation due to thermal expansion can occur. In particular, bending and variations in the gap between the anode grid and cathode have been identified as critical issues.

To mitigate these effects, a new FEBIAD ion source design was developed and fabricated to ensure structural stability under high-temperature conditions by adding a heating strap and allowing the body to slide. The Sliding-type FEBIAD successfully achieved Kr isotope beam separation in offline tests. Subsequent online experiments confirmed stable operation of the source under ISOL conditions, demonstrating its suitability for reliable RI beam production. Future work will involve RI beam extraction experiments using various targets within the RAON ISOL system.

INTRODUCTION

The ISOL (Isotope Separation On-Line) system at RAON consists of a cyclotron, Target Ion Source (TIS) module, pre-mass separator, radio-frequency quadrupole (RFQ) cooler-buncher, electron beam ion source (EBIS) charge breeder, and A/Q separator [1]. Three types of ion sources — surface, laser, and plasma — are planned for operation. Currently, the surface and laser ion sources are in operation, while the plasma ion source is under development and testing. An offline test facility has been established at RAON for the development and performance evaluation of ion sources. The facility consists of a TIS chamber, X–Y steerers, electrostatic quadrupole triplet (EQT), dipole magnet, and beam diagnostics. The layout of the RAON offline test facility is shown in Fig. 1.

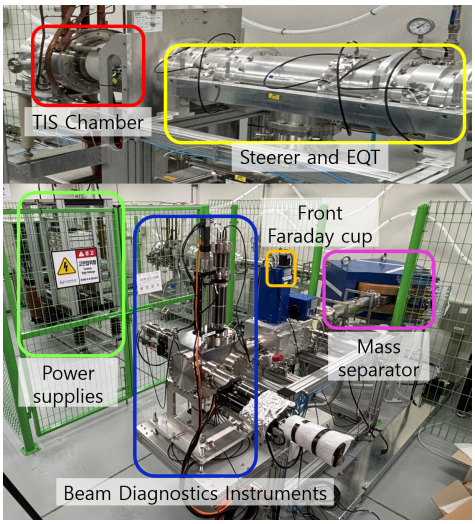

Figure 1: RAON ISOL Offline Test Facility

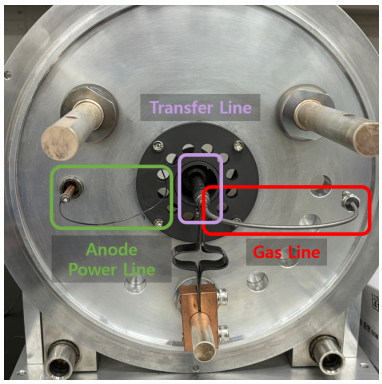

Figure 2: Prototype FEBIAD ion source installed in the TIS chamber.

The prototype FEBIAD ion source was fabricated based on the MK5 structure developed at CERN ISOLDE [2], as shown in Fig. 2. Its operational characteristics were evaluated at the RAON offline test facility. The FEBIAD adopts an electron impact ionization scheme in which electrons

* jwksmin@ibs.re.kr
† Corresponding author: yhyeon@ibs.re.kr
‡ Corresponding author: moses@postech.ac.kr

Content from this work may be used under the terms of the CC BY 4.0 licence (© 2026). Any distribution of this work must maintain attribution to the author(s), title of the work, publisher, and DOI.

ISBN: 978-3-95450-252-3 ISSN: 2673-5350 doi: 10.18429/JACoW-IPAC2026-THP3616

CAVITY GEOMETRY OPTIMIZATION FOR MULTIPACTOR SUPPRESSION IN A VHF CW ELECTRON GUN*

Yitong Duan[1,2], Lianmin Zheng[†1,2], Yingchao Du[1,2]
[1]the Department of Engineering Physics, Tsinghua University, Beijing, China
[2]the Key Laboratory of Particle and Radiation Imaging, Tsinghua University, Ministry of Education, Beijing, China

Abstract

VHF CW photocathode electron guns suffer from severe multipactor effects that significantly degrade their operational performance. In this work, the RF cavity geometry was optimized via CST simulations to suppress multipactor, employing a three-phase strategy with fixed key structural parameters. Compared with the SHINE gun baseline, the optimized cavity achieves a much lower multipactor growth rate α while preserving excellent high-performance RF characteristics. This demonstrates that geometry optimization is an effective approach to mitigate multipactor in VHF CW photocathode electron guns.

INTRODUCTION

VHF photocathode electron gun [1] is a CW-mode resonant cavity that produces high-quality electron bunches at MHz-class repetition rates for applications including high-repetition-rate free-electron lasers and ultrafast electron diffraction. Developed by Tsinghua University, this VHF gun has been successfully applied to the SHINE facility [2] and Dalian Advanced Light Source Test Facility. Operating at 216.667 MHz, it has achieved a cathode gradient of 27 MV/m and a voltage of 780 kV under 75 kW RF power during high-power conditioning [1], which currently represents the highest cathode gradient among room-temperature CW electron guns.

In the SHINE gun, multipactor occurs below 16 MV/m and is suppressed above this threshold. During startup, the power ramp-up from 0 to 75 kW passes through the multipactor-prone region, requiring pulsed operation before CW mode. Power reflection anomalies can also induce multipactor, which degrades vacuum, shortens cathode lifetime, and risks ceramic window damage, thus threatening the long-term reliability of the VHF gun.

SIMULATION

Multipactor simulations were performed in CST Studio Suite [3], utilizing CST Microwave Studio for rf field simulations and CST Particle Studio for particle dynamics simulations.

Fig. 1 presents the optimized cavity profile together with the corresponding distributions of electric and magnetic field strengths.

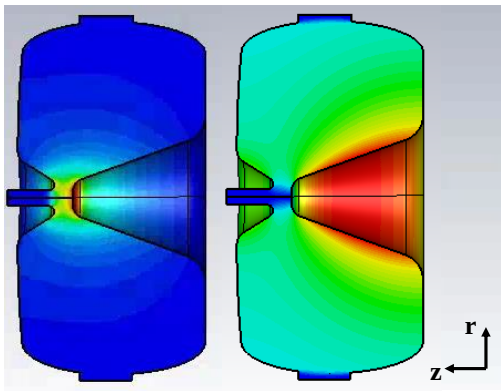

Figure 1: Distribution of the amplitude of electric (left) and magnetic (right) fields in the cavity.

The Furman model [4] decomposes SEY into three components: true secondary, rediffused, and elastically backscattered electrons (sum of these yields total SEY). As shown in Fig. 2 [5], secondary electron generation involves three physical processes: (a) elastic surface collisions producing elastically backscattered electrons; (b) incident electron penetration/scattering generating rediffused electrons; (c) energy transfer to bound electrons, followed by surface transport and emission as true secondary electrons.

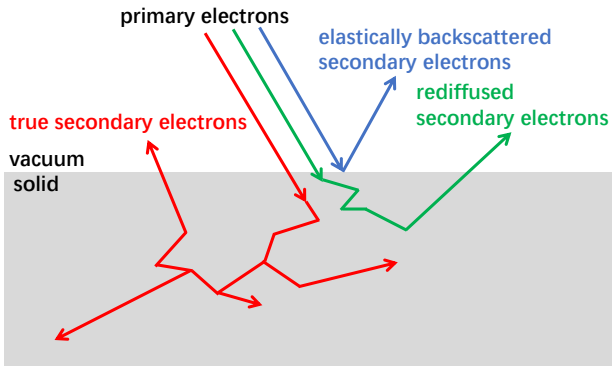

Figure 2: Three types of secondary electrons in Furman's model.

The temporal evolution of particle populations at four cathode gradients is presented in Figure 3. After 60 ns, the particle number varies linearly with time on a logarithmic scale, indicating exponential growth and thus multipactor onset. For quantitative analysis, the region of clear exponential growth in Fig. 3 was fitted by

$$N_e(t) = N_0\, e^{\alpha t} \quad (1)$$

* Work supported by the National Natural Science Foundation of China (NSFC) under Grant No. 12275149.
† email: zhenglm2019@mail.tsinghua.edu.cn

Content from this work may be used under the terms of the CC BY 4.0 licence (© 2026). Any distribution of this work must maintain attribution to the author(s), title of the work, publisher, and DOI.

ISBN: 978-3-95450-252-3 ISSN: 2673-5350 doi: 10.18429/JACoW-IPAC2026-THP3617

INITIAL BEAM CHARACTERIZATION FROM A COLD FIELD EMITTER IN A VHF ELECTRON GUN

Y. Qin, Y. Wang, B. Song, R. Zou, L. Zheng, R. Li, Y. Du*
Department of Engineering Physics, Tsinghua University, Beijing, China

Content from this work may be used under the terms of the CC BY 4.0 licence (© 2026). Any distribution of this work must maintain attribution to the author(s), title of the work, publisher, and DOI.

Abstract

High-quality electron beams are critical for imaging experiments that provide detailed microscopic structural insights into materials. The Very-High-Frequency electron gun, capable of operating in continuous and pulsed modes, is a preferable option. In this paper, we employ a tungsten tip with an apex radius of curvature approximately 100 nm as a cold field emission cathode in the VHF gun and measure the beam charge, transverse emittance, and energy spread to characterize the beam quality. In preliminary experiments, we have achieved a normalized transverse emittance of 54.01 nm·rad. With an electron gun power of 37 kW, we obtained a strong beam current of approximately 6 μA, which remained stable and continuous for several hours in a single experiment. By using an aperture to block electrons with large divergence angles and adjusting the solenoid's focusing strength, we propose to converge the target-energy electron beam onto the aperture, increasing its transmission rate and optimizing the energy spread. Prior to optimization, the energy spread was approximately 3.57 % at 536 keV when using a 20 μm diameter aperture.

INTRODUCTION

The Very-High-Frequency (VHF) electron gun is capable of operating in both pulsed and continuous wave modes at room temperature, providing a high-quality electron source for large-scale facilities such as ultrafast electron diffraction (UED) platforms and X-ray free electron laser (XFEL). The VHF electron gun at Tsinghua University is integrated with a loadlock and utilizes a replaceable plug, allowing different types of cathodes to be used to meet various experimental requirements. Currently, commonly used cathode types include photocathodes, thermionic cathodes, and field emission cathodes. Among these, photocathodes are limited by quantum efficiency and laser repetition frequency, resulting in relatively low average current density. While semiconductor photocathodes can achieve quantum efficiencies $1 \times 10^{-3} - 2 \times 10^{-1}$ [1], higher than those of metal photocathodes, but they also suffer from disadvantages such as short lifespan, high fabrication costs, and strict operational environment requirements.

Although thermionic cathodes offer the advantage of higher average current density, they have a broad emission phase and carry the risk of electron back-bombardment [2]. The principle of field emission is based on the Fowler-Nordheim equation (Eq. (1)) [3], the characteristic of current density varying approximately exponentially with electric field strength gives it the advantages of a narrow emission phase and high average current density, without the need for heating or reliance on complex and expensive laser systems. Current research demonstrates that a small single diamond pyramid with a 20 μm base can emit a current of 10 μA; experiments have yielded a normalized transverse emittance of 0.689 μm·rad [4], further demonstrating the potential of field emission cathodes:

$$J_0 = \frac{AE_s^2}{\phi} \exp\left[\frac{B\phi^{3/2}}{E_s}\theta(C\frac{\sqrt{E_s}}{\phi})\right] \quad (1)$$

We employed a modified conventional replaceable plug combined with a sharp tip emitter to create a cold field emission cathode, which was assembled into a VHF gun for beam experiments. We confirmed that the current signal could be generated continuously and stably for several hours in a single experiment. The beam charge, transverse emittance, and energy spread are measured to characterize the beam quality.

PLUG DESIGN AND OPTIMIZATION

We employ a replaceable cathode plug, which is inserted into the electron gun via a loadlock while maintaining a high vacuum (as low as $1 \times 10^{-9} Pa$) throughout the process. In previous attempts, we tried drilling small holes directly into the flat surface of the plug to allow the emitter to protrude. However, during experiments, stray dark current frequently appeared on the detection screen, causing it to mix with the desired field emission current signal and making it impossible to separate them. These spurious signals likely originate from intense field enhancement caused by uncontrollable microstructures at the sharp, vertical edges of the holes, even though the plug's surface has undergone precise mirror polishing.

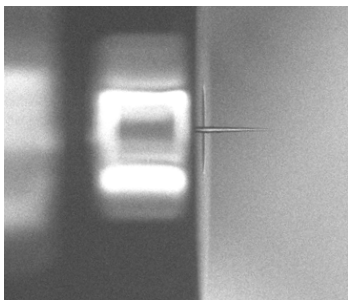

Figure 1: Tungsten tip protruding from the plug center.

In these experiments, the upper surface of the plug was machined with a dimple 1 mm deep and 2 mm in diameter, and the hole was drilled at the center of the dimple. The recessed structure suppresses the electric field, thus decreasing the

* dych@tsinghua.edu.cn

ISBN: 978-3-95450-252-3 ISSN: 2673-5350 doi: 10.18429/JACoW-IPAC2026-THP3620

PHOTOCATHODE PREPARATION STUDIES BASED ON A PHOTOCATHODE IN-SITU RESEARCH APPARATUS*

X. D. Li†,1, Z. G. Jiang[1], Q. Gu[1], H. Meng[1], Q. Zhou[2], M. Zhang[1], D. Gu[1], T. Hou[1], Z. H. Tong[1], W. J. Fan[2], C. Wang[2], Z. P. Liu[2], G. Shu[2], H. J. Qian[2], C. C. Xing[2]
[1] Shanghai Advanced Research Institute, Chinese Academy of Sciences, Shanghai, China
[2] Zhangjiang Laboratory, Shanghai, China

Abstract

The photocathode in-situ research apparatus integrates preparation, characterization, and environmental control under ultra-high vacuum to prevent surface contamination, establishing a real-time "preparation-monitoring-regulation" closed-loop for high-performance photocathodes such as Cs_2Te. Following comprehensive commissioning, which is utilized for Cs_2Te photocathode preparation, CsBr protective layer deposition, and temperature-dependent performance measurements. In-situ grazing-incidence wide-angle X-ray scattering (GIWAXS) characterization at the Shanghai Synchrotron Radiation Facility (SSRF) revealed that the crystal structure of sequentially deposited Cs_2Te photocathode changes synchronously with the quantum efficiency (QE) improvement, validating the apparatus for studying high QE photocathodes.

INTRODUTION

We have prepared high QE Cs_2Te photocathodes with internationally leading performance that have been successfully applied in the SHINE (Shanghai High repetition rate XFEL and Extreme light facility) commissioning [1], demonstrating excellent long-term stability. An innovative intermittent Te and continuous Cs deposition eliminates QE fluctuations caused by equipment and operator variations [2]. A dedicated in-situ research apparatus was designed, assembled, and commissioned to systematically study the intrinsic mechanisms behind the high QE and long lifetime of Cs_2Te, guiding further optimization.

This paper consists of three sections: the first introduces the photocathode in-situ research apparatus, the second details the Cs_2Te photocathode preparation based on the apparatus, and the third describes the GIXWAS characterization applied during the preparation process.

I. APPARATUS AND ITS FUNCTIONS

The photocathode in-situ research apparatus integrates four functions: preparation, testing (characterization), environmental control, and data integration, with detailed as follows:

- Preparation: Photocathode deposition equipment, such as PVD.
- Testing: QE measurement and in-situ characterization (e.g., GIWAXS).
- Environmental Control: UHV (10^{-8} Pa) environment with temperature control (-100 °C to 450 °C).
- Data Integration: Software control of all subsystems, real-time collection and analysis of preparation parameters and performance data.

The photocathode in-situ research apparatus based on synchrotron radiation beamlines integrates material synthesis and real-time characterization, utilizing high-brightness synchrotron X-rays (5–150 keV) to enable in-situ preparation, characterization, and performance testing of photocathodes under controlled conditions (Fig. 1). It mainly consists of the following components:

- Vacuum Chamber: A spherical SS 316L UHV chamber, equipped with ion pumps, NEG pumps, and vacuum gauges, ensures high-performance photocathode preparation and minimizes degradation during testing.
- Evaporation Source Unit: Evaporation sources (SAES alkali metal dispensers and slitted 304 SS capillaries containing Sb, Te, CsBr, etc.) with high-precision DC power supplies for controlled deposition. A film thickness meter (FTM) with temperature-controlled chiller to measure the deposition thickness and rate on the substrate.
- Performance Testing Module: A temperature control module for substrate heating/cooling, a drive light system with real-time optical power measurement (incident and reflected), and a photocurrent collection system (cathode-chamber/anode-mask) for photocathode QE and stability evaluation.
- Synchrotron Radiation Coupling Interface: Beryllium windows (CF63 for X-ray entrance, CF35 for fluorescence exit, and a square window for reflected/diffracted signals) maintain UHV while enabling real-time monitoring of photocathode crystallinity (via GIWAXS) and elemental composition (via XRF).

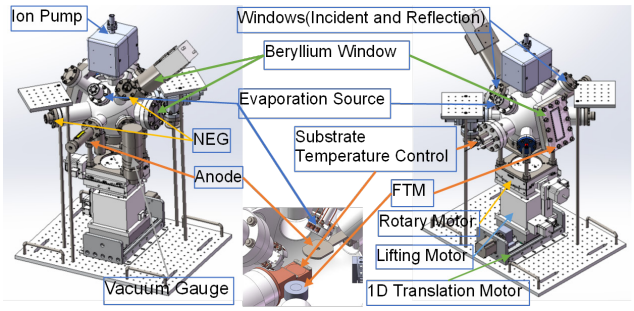

Figure 1: Schematic of the photocathode in-situ research apparatus.

* Work supported by National Natural Science Foundation of China (No.11405251, No. 11905276, No. 12075302) and the BL16B1 beamline of Shanghai Synchrotron Radiation Facility (SSRF).
† lixudong@sari.ac.cn

Content from this work may be used under the terms of the CC BY 4.0 licence (© 2026). Any distribution of this work must maintain attribution to the author(s), title of the work, publisher, and DOI.

ISBN: 978-3-95450-252-3 ISSN: 2673-5350 doi: 10.18429/JACoW-IPAC2026-THP3621

4K SUPERCONDUCTING RF ELECTRON GUN

L. Guo, M. Kuriki*, Z. Liptak, Hiroshima University, Hiroshima, Japan
T. Konomi, Facility for Rare Isotope Beams, East Lansing, United States
A. Arnold, J. Teichert, R. Xiang, Helmholtz-Zentrum Dresden-Rossendorf, Dresden, Germany
H. Hayano, High Energy Accelerator Research Organization, Tsukuba, Japan

Abstract

A superconducting accelerator is an excellent technology that can efficiently accelerate high-current beams and is being applied to free electron lasers and next-generation linear electron-positron colliders such as ILC. Not only for the fundamental science, but also the high current electron beam plays a rather important role in industrial and medical applications. This is because the demand for high-current beams is also strong in these applications. While superconducting accelerators are becoming more widely used, there are not many examples in practical use of the superconducting RF gun, such as the ELBE RF Gun in HZDR. The entire accelerator should be superconducting for its energy efficiency and technical compatibility. To bridge this technical gap, we propose a superconducting RF gun utilizing the latest 4K superconducting technology, which can generate continuous, high-brightness beams. As the cathode, we study both the photo and thermionic cathodes.

INTRODUCTION

Recent technological demands have intensified interest in CW Relativistic Electron Beam (CWREB). Their unique properties make them indispensable in diverse applications such as CW free-electron lasers (CW FELs), sterilization of medical, medicine, and food packaging, RI production, and inspection of large-scale infrastructure etc. As a result of the development of the superconducting accelerator technology especially by TESLA project followed by ILC project, this technology has been well matured and the superconducting accelerator is now widely used in many advanced accelerator project, XFEL [1], ELBE [2], LCLS-II [3], SHINE [4], and expected to be used in ILC [5]. However, the electron source for these projects are DC biased electron guns or Normal conducting RF gun. One of the exception is ELBE in HZDR which employs SRF Gun operated at 13 MHz CW up to 1-mA beam current [[6, 7]]. This is only one demonstrated example for CWREB.

On the other hand, there are strong demands for the CWREB source from not only the scientific facilities like FELs and colliders, but also from industrial and medial applications. Sterilization technology has become an important infrastructure for modern medicine. One of the biggest issue is the high price of existing electron beam sterilizers. Currently widely used sterilization methods are displayed on a cost (horizontal axis) and safety and risk (vertical axis) plane in Fig. 1.

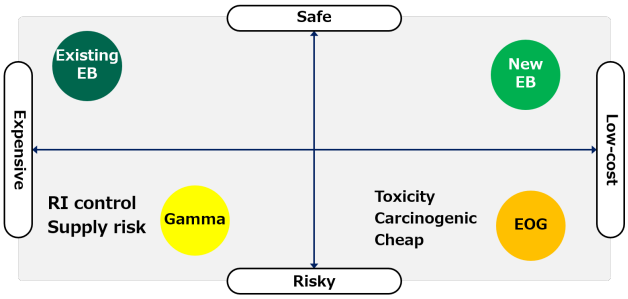

Figure 1: Currently widely used sterilisation methods are displayed on a cost (horizontal axis) and safety and risk (vertical axis) plane.

While electron beam sterilization (EB) is safe, risk-free and stable in its supply, its cost is very high compared to other methods. EOG (Ethylene Oxide Gas) sterilization is inexpensive and there is no concern about supply, but health hazards due to gas residues have been raised and it is also known to be carcinogenic. Public health authorities such as the Japanese Ministry of Health, Labour and Welfare and the US FDA have stated that EOG sterilization is an undesirable method and is only allowed to be used when no other suitable alternative method applicable.

Gamma sterilization requires large quantities of radioactive isotopes that emit gamma rays, such as Co, but the nuclear reactors used for RI production are aging and there are global supply concerns. CWREB SRF Gun is a good candidate to solve these issues. EB sterilization needs typically ~5-MeV electron beam. CWREB SRF Gun can generate the required beam of energy on its own, enabling compact and inexpensive electron beam sterilizers.

Targeted alpha therapy (TAT) using Actinium-225 (^{225}Ac) is an emerging and highly promising approach for treating certain types of cancer [8]. It combines the high-energy, short-range cytotoxicity of alpha particles with the specificity of molecular targeting, enabling selective destruction of tumor cells while sparing surrounding healthy tissue. ^{225}Ac is a radioactive isotope that emits alpha particles during its decay chain which is suitable for TAT. High purity is required when producing isotopes for use in radio pharmaceuticals.

Figure 2 shows cross-section of the photo nuclear reaction of $^{226}\mathrm{Ra}(\gamma, n)^{225}\mathrm{Ra}$ peaked at 10–15 MeV [9]. For the RI production, CWREB is useful in energy of 30 MeV or more to generate gamma in the energy region by Bremsstrahlung. The production of radioisotopes via photonic nuclear reactions offers several advantages. The high penetrating power

* mkuriki@hiroshima-u.ac.jp

Content from this work may be used under the terms of the CC BY 4.0 licence (© 2026). Any distribution of this work must maintain attribution to the author(s), title of the work, publisher, and DOI.

ISBN: 978-3-95450-252-3 ISSN: 2673-5350 doi: 10.18429/JACoW-IPAC2026-THP3627

NON-RESONANT MULTIPACTOR MECHANISM AND SEY IMPACT IN A VHF CW ELECTRON GUN*

Yitong Duan, Lianmin Zheng†, Yingchao Du
Department of Engineering Physics, Tsinghua University, Beijing, China and
Key Laboratory of Particle and Radiation Imaging, Tsinghua University,
Ministry of Education, Beijing, China

Abstract

Electron trajectory analysis within the cavity shows that the energy dispersion and angular distribution of secondary electrons strongly influence their dynamic behavior. Despite the overall non-resonant nature of multipactor, multiple resonant modes can still be identified from the statistical distribution of electron flight times. This work investigates the effect of RF cavity geometry on multipactor characteristics, and clarifies the underlying mechanisms via statistical analysis of particle trajectories.

INTRODUCTION

Multipactor [1] is a nonlinear electron multiplication phenomenon induced by high-frequency electromagnetic fields in radio-frequency (rf) devices under vacuum. When primary electrons, accelerated by these electromagnetic fields, impinge on metallic or dielectric surfaces,they generate secondary electrons that further strike the surfaces, triggering an electron avalanche through continuous multiplication. In particle accelerators, multipactor is most likely to occur in resonant cavities operating in long-pulse or continuous-wave (CW) modes. CW resonant cavities are especially prone to this phenomenon, as continuous microwave excitation facilitates the rapid accumulation of secondary electrons.

The very-high-frequency (VHF) photocathode electron gun [2] is a typical resonant cavity working in CW mode. In this study, we verify that the multipactor occurring within the cavity is non-resonant [3], meaning that the motion of electrons is not synchronized with the time-varying electromagnetic field.

SIMULATION SETUP

The Furman model [4] is rooted in a rigorous physical foundation and functions as a phenomenological probabilistic framework. It quantifies the stochasticity of electron–surface collisions by linking microscopic event probabilities to macroscopic measurable parameters. In this model, each electron–surface collision generates n secondary electrons ($n = 0, 1, 2, \ldots$), where P_n denotes the probability of emitting exactly n secondary electrons. For physical consistency, the probabilities satisfy the normalization condition, with P_0 representing the absorption probability of incident electrons (no secondary emission):

$$\sum_{n=0}^{\infty} P_n = 1, \quad P_n \geq 0. \tag{1}$$

The secondary electron yield (SEY) δ is the expectation of secondary electron number n, defined as:

$$\delta = \langle n \rangle = \sum_{n=1}^{\infty} nP_n. \tag{2}$$

The Furman model divides secondary electron yield (SEY) into three components: true secondary, rediffused, and elastically backscattered electrons, which correspond to three distinct physical emission mechanisms. Measured secondary electron yield (SEY) values vary considerably among different research groups, mainly attributed to differences in copper impurity content and surface treatment techniques. To guarantee the conservativeness of simulations, we adopted the Furman model embedded in CST, as illustrated in Fig. 1.

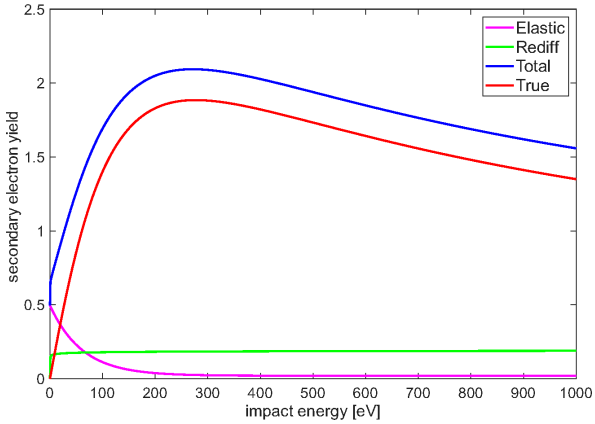

Figure 1: SEY of copper as a function of incident electron energy in CST Furman model.

NON-RESONANT MULTIPACTOR

Previously, multipactor intensity was evaluated by tracking the evolution of particle count. Here, we analyze microscopic electron trajectories to reveal multipactor behavior from the perspective of electron dynamics. Typical trajectories of primary and secondary electrons are shown in Fig. 2.

Under time-varying electromagnetic fields, the primary electron experiences repeated acceleration and deceleration with significant deflection, reaching a peak energy of 400 eV

* Work supported by the National Natural Science Foundation of China (NSFC) under Grant No. 12275149.
† zhenglm2019@mail.tsinghua.edu.cn

Content from this work may be used under the terms of the CC BY 4.0 licence (© 2026). Any distribution of this work must maintain attribution to the author(s), title of the work, publisher, and DOI.

ISBN: 978-3-95450-252-3 ISSN: 2673-5350 doi: 10.18429/JACoW-IPAC2026-THP4001

SIS100 – A NEW AND UNIQUE HEAVY ION SYNCHROTRON UNDER CONSTRUCTION

P. J. Spiller*,[1], S. Bareli[1], P. Aguar Bartolome[1], J. Blaurock[1], A. Bleile[1], L. Bozyk[1], A. Chiuchiolo[2], M. Chorowski[3], O. Ciosk[1], T. Eisel[1], A. Illuk[3], J. Kaether[1], M. Kauschke[1], J. Ketter[1], P. Knoblauch[1], J. Kollarczyk[1], P. Kowina[1], U. Laier[1], D. Lens[1], D. Ondreka[1], I. Petzenhauser[1], V. Plyusnin[1], I. Pongrac[1], N. Pyka[1], P. Rottlaender[1], C. Roux[1], J. Schmidt[1], M. Sienkiewicz[4], P. Streicher[1], S. Sorge[1], K. Sugita[1], A. Szwangruber[1], P. Szwangruber[1], S. Wilfert[1], D. Winters[1], T. Winkler[1]
[1]GSI Helmholtz Centre for Heavy Ion Research, Darmstadt, Germany
[2]INFN, Salerno, Italy
[3]Wroclaw University of Technology, Wroclaw, Poland
[4]Institute of Nuclear Physics IFJ PAN, Cracow, Poland

Abstract

SIS100 is a fast-ramped superconducting heavy-ion synchrotron under construction at GSI, Darmstadt, and will serve as the main accelerator of Facility for Antiproton and Ion Research (FAIR). It is designed to deliver intense beams from protons to uranium, including medium charge state ions such as U^{28+}. A central design goal is stabilization of the dynamic vacuum to minimize charge-exchange-driven beam loss. Key features include a charge-separator lattice, cryogenic ion catchers, cryo-adsorption pumps, a liquid-helium-cooled ultra-high-vacuum system, and rapid acceleration. The concept has been validated in SIS18 and the SIS100 string test. Despite its superconducting technology, SIS100 will provide cycling flexibility comparable to room-temperature machines. Installation in the tunnel began in early 2024, with beam commissioning foreseen for the end of 2028.

INTRODUCTION



Figure 1: Prototype SIS100 quadrupole unit.

SIS100 is the central synchrotron of the FAIR complex [1]. The machine design and principal parameters have been described in detail in Ref. [2]. A major design objective is the stabilization of the dynamic vacuum during operation with medium charge state heavy ions, where charge-exchange processes can lead to significant beam loss. The overall mitigation strategy—including the charge-separator lattice, cryogenic ion catchers, cryo-adsorption pumping, the liquid-helium-cooled ultra-high-vacuum system, and the fast acceleration scheme—has been developed and documented in Refs. [3–5]. Experimental verification of the underlying concepts has been carried out at the existing SIS18 synchrotron and in the SIS100 string test, confirming the effectiveness of the adopted measures in reducing charge-exchange-driven beam loss.

* p.spiller@gsi.de

GENERAL PROJECT STATUS

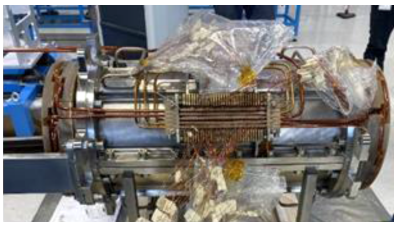

Figure 2: Multipole corrector magnet manufactured in industry.

The procurement of components for the FAIR subproject SIS100 progresses largely according to plan. The production and testing of superconducting quadrupole units, comprising the main s.c. quadrupole magnets, the steerer- and sextupole magnets, including their shipment, continued closely to scheduled. So far, 82 quadrupole units of 166 have been accepted and approved for pairwise integration into quadrupole modules. Following a careful risk assessment and in order to minimize risk for project execution and schedule completion, further 36 quadrupole units have been contracted to industry. In order to prepare the series production in industry, four prototype s.c. quadrupole units and one multipole corrector, comprising three different multipole coils (Figs. 1 and 2) have been manufactured and are presently cold tested.

For qualification of the industry units, dedicated equipment for power tests and magnetic field measurements at cold has to be build-up at GSI. The procurement of the corresponding components, such as testing cryostats, preparation benches and anti-cryostats has been launched. For the development of the required magnetic field measurement equipment consisting of stretched wire systems and rotating coil probes a collaboration with mutual benefit with CERN has been established.

At the beginning of the Ukraine crisis the integration of quadrupole units into quadrupole modules at company BNET had to be interrupted. After catching up the unit production, the module integration process could be fully re-established, and the desired integration rate of two modules per month has almost been achieved. For cold testing, the integrated modules are shipped from company BNET in Germany to the Thor test facility in Salerno, Italy [6]. An updated integration schedule and slightly extended scope

Content from this work may be used under the terms of the CC BY 4.0 licence (© 2026). Any distribution of this work must maintain attribution to the author(s), title of the work, publisher, and DOI.

ISBN: 978-3-95450-252-3 ISSN: 2673-5350 doi: 10.18429/JACoW-IPAC2026-THP4002

NEW CAPABILITIES OF SIS18 AFTER UPGRADE PROGRAM AS FAIR INJECTOR

J. Stadlmann*, D. Lens, H. Liebermann, Ph. Niedermayer, D. Ondreka, A. Pastushenko, P. Spiller
GSI Helmholtz Centre for Heavy Ion Research, Darmstadt, Germany

Abstract

SIS18, the main synchrotron of the present GSI accelerator complex, will serve as booster for the FAIR facility. Several major and minor upgrade programs were realized since 2008 to improve SIS18 for this purpose. We will report on new capabilities of the synchrotron for present and future user operation, which were not directly attributed to FAIR injector operation. Namely, a spill feedback system to control macroscopic spill shape and optimize spill microstructure during slow extraction. The operation of SIS18 with the new FAIR control system in conjunction with the RF upgrades allows beam operation without restrictions at lower injection energies. Acceleration of two beams consisting of ions with different mass to charge ratios at different revolution frequencies during acceleration are now possible and were successfully demonstrated in 2025. Possible users are medical research and plasma physics. As outlook we describe future plans for beam shaping before fast extraction for medical research.

INTRODUCTION

Due to the requirements of both, the FAIR project [1] and the research on the present campus, many upgrades have been done to GSI's accelerator complex [2, 3]. The priorities were mainly on refurbishing the machine for extended operation as FAIR injector and performance enhancing measures to fulfill the design parameters as injector for the future FAIR facility.

Beside the needed hardware upgrades and refurbishment the existing control system and setting generation software was replaced by a modern system. The established homegrown system was based on old hard- and software standards and most experts were retired, making it impossible to maintain. Moreover new hardware devices were increasingly difficult to implement. The new control system software is an LSA based framework developed together with CERN and will be used to operate all FAIR accelerators [4–6]. It was step-wise rolled out on the existing facility's accelerators. It is right now used to fully operate all machines but the injector linac UNILAC, where it is in the final test phase.

One of the hardware systems, which was completely refurbished and expanded is accelerating RF system. In addition to the two existing ferrite-loaded cavities operating at fourth harmonic (h=4) three new MA-loaded cavities operating at (h=2) have been installed to fulfill the future needs of booster operation for FAIR including dual harmonic operation [7]. The complete low level RF system (LLRF) has been renewed [8].

* j.stadlmann@gsi.de

The sum of all upgrades mainly aimed at FAIR operation allows us to develop new modes of operation and capabilities beyond the originally intended reach and already offer them to our users at the present campus for tests and research operation.

NEW CAPABILITIES OF SIS18 WITH MODERN HARD- AND SOFTWARE

In the following we will present examples of new modes and capabilities whose development can be attributed as a trade-off of FAIR related upgrades.

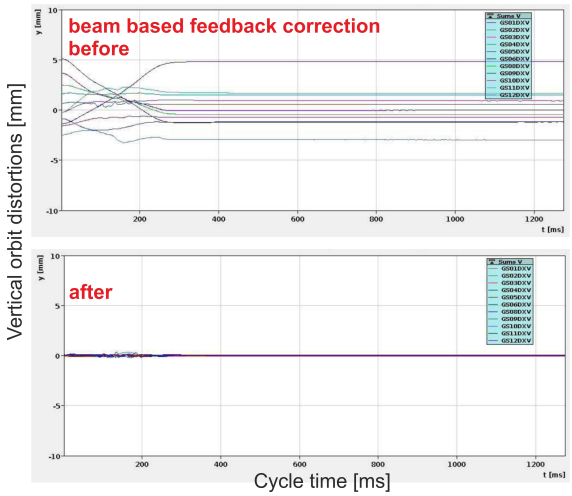

Figure 1: Measurements of the vertical closed orbit distortions (COD) in SIS18 before and after run of the beam based COD feedback prototype presented in Ref. [9]

Beam Based Feedback Systems

The new control software in addition with the refurbishment and upgrades of the existing beam diagnostics systems allows us to integrate beam based feedback systems directly in the control system environment. The main benefit of the new hard- and software are measurement data availability through standard interfaces and constant handling of machine settings over the full accelerator complex. Instead of creating multiple 'black box' feedback system with detector and actor, measurement and feedback can be either fully done in the new environment for slow systems or being integrated, operated and monitored for direct fast feedback systems.

Examples of such systems are presented in Ref. [9, 10]. A result of closed orbit correction prototype is presented in Ref. [9]. Results of a test are shown in Fig. 1. A correction tool for the macro spill structure of a slowly extracted beam has been developed and successfully tested as presented

Content from this work may be used under the terms of the CC BY 4.0 licence (© 2026). Any distribution of this work must maintain attribution to the author(s), title of the work, publisher, and DOI.

ISBN: 978-3-95450-252-3 ISSN: 2673-5350 doi: 10.18429/JACoW-IPAC2026-THP4005

CORRECTION OF LONG-RANGE BEAM-BEAM DRIVEN OPTICS PERTURBATIONS FOR THE LHC

S; Horney*, E. Maclean, T. Persson, R. Tomás, CERN, Meyrin, Switzerland
P. N. Burrows, JAI for Accelerator Science, Oxford, UK

Abstract

Optics measurements in the LHC are usually performed with low-intensity, non-colliding pilot beams in the interest of machine safety. However, long-range beam-beam (LRBB) interactions can drive substantial optics perturbations. In 2024, a weak-strong measurement scheme was developed that probes the weak beam while leaving the strong beam unaffected, and machine tests validated this method. In 2025, a reported luminosity discrepancy between ATLAS and CMS motivated further study of the LRBB-induced β-beat in the new 18 cm flat-optics configuration. A large β-beat was observed, reaching typical LHC machine-protection limits. Correction strategies using magnets in the experimental insertions were demonstrated successfully, and, for the first time, non-linear corrections addressing sextupolar and octupolar resonance driving terms were also successfully demonstrated for example the measurement of the $3Q_y$ correction.

MOTIVATION

Long-range beam-beam (LRBB) interactions impact key performance parameters, including dynamic aperture, beam lifetime, and luminosity, and has been extensively studied in accelerators such as Tevatron [1] and the LHC [2], using a combination of simulations and measurements of some of these observables.

Direct optics measurements including LRBB effects have historically been lacking, primarily due to the difficulty of performing measurements under such conditions. LHC optics commissioning and measurements have typically been conducted using low-intensity, non-colliding bunches. In 2024, a novel method for optics measurements in the presence of LRBB effects was developed [3].

In 2025, a luminosity imbalance between the CMS and ATLAS experiments was reported [4], motivating detailed investigations into its origin. This new approach was exploited to measure the β-beating in the presence of LRBB. The peak β-beat was found to reach approximately 20%, corresponding to the machine-protection limit. The horizontal β-beating for LHCB1, with a β^*=18/60 cm, is shown in Fig. 1. These conditions correspond to a crossing angle of 160 µrad and a strong-beam intensity of 1.5×10^{11} ppb. The usual operational scenario at end-of-squeeze is an intensity of around 1.1×10^{11} ppb but even at those intensities the β-beat would be substantial.

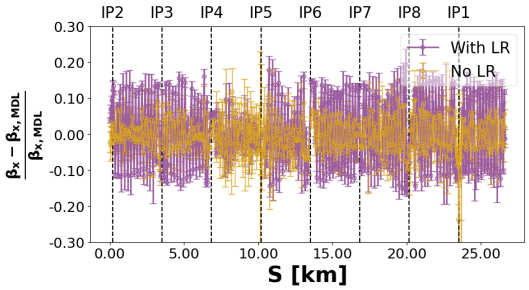

Figure 1: Horizontal β-beating vs s with and without LR effects for LHCB1, crossing angle = 160 µrad.

When the crossing angle was reduced to 120 µrad, the peak β-beating increased further, as shown in Fig. 2.

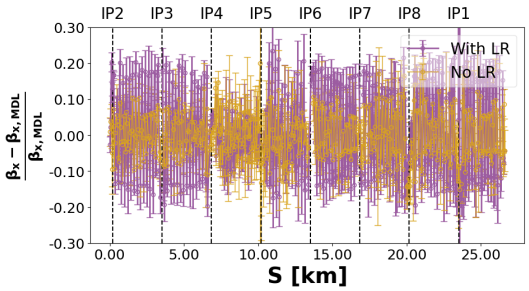

Figure 2: Horizontal β-beating vs s with and without LR effects for LHCB1, crossing angle = 120 µrad.

Maintaining low β-beating is essential to preserve an operational margin against optics drifts, accommodate additional optics trims and corrections [5], and to ensure compliance with machine-protection constraints.

The increase in β-beating between the two crossing angles exhibits a correlation of comparable magnitude with the corresponding increase in luminosity imbalance reported.

To assess whether the observed luminosity imbalance could be reproduced in simulation, an Xsuite model including LRBB effects was employed. The resulting luminosity imbalance, summarised in Table 1, was also found to be consistent with the values reported by the experiments.

Table 1: Simulated luminosity imbalance from LRBB for an intensity of 1.1×10^{11} ppb for each crossing angle.

Crossing angle [µrad]	Luminosity imbalance in favour of CMS [%]
160	4.5
120	7.4

* sasha.jade.horney@cern.ch

Content from this work may be used under the terms of the CC BY 4.0 licence (© 2026). Any distribution of this work must maintain attribution to the author(s), title of the work, publisher, and DOI.

ISBN: 978-3-95450-252-3 ISSN: 2673-5350 doi: 10.18429/JACoW-IPAC2026-THP4006

NON-LINEAR RESONANCE FEED-DOWN - A NEW TECHNIQUE FOR CORRECTING HIGH ORDER ERRORS IN THE LHC

Sasha Horney*[1,2], E. Maclean[1], J. Dilly[1], R. Tomás[1], P. N. Burrows[2]
[1]CERN, Meyrin, Switzerland
[2]JAI for Accelerator Science, Oxford, UK

Abstract

Optics errors from the interaction points (IPs) of the LHC, where β^* is most strongly squeezed, can significantly impact machine performance and protection. In anticipation of the HL-LHC, correction strategies extending up to dodecapole order are being targeted. Direct measurement of high-order resonance driving terms (RDTs) remains challenging, however. Applying crossing angle orbit bumps in the experimental insertions induces feed-down from higher-order errors, increasing the magnitude of lower-order RDTs. Leveraging this effect, a novel correction scheme based on RDT feed-down was implemented for the first time in 2025. Skew-octupole errors were successfully corrected, which enabled optics measurements at the collisions working point, down to an unprecedented level of β^* = 18 cm. Measurements of feed-down from dodecapole errors, to decapole RDTs were also achieved, opening a practical pathway to efficient corrections of very high-order optics errors.

MOTIVATION

Control of non-linear errors in experimental insertions has long been recognised as critical for collider performance. Such effects were already studied for accelerators such as the Tevatron [1], RHIC [2, 3], and SuperKEKB [4–6].

The LHC is especially sensitive to interaction region (IR) optics errors due to the large β-functions in the triplet quadrupoles required to reach low β^* at the IP. This sensitivity will increase in the High-Luminosity LHC (HL-LHC), where further reduction of β^* leads to even larger β-functions in these triplets. As a result, the upgrade targets correction of optics errors up to dodecapolar order [7, 8].

Following the successful application of non-linear forced-RDT measurements with the AC-dipole [9] at both injection [10] and top energy [11], attention has shifted towards extending these techniques to higher-order RDTs in order to correct optics errors originating from the IRs. Direct measurement of such higher-order terms, particularly of decapolar order and above, remains experimentally challenging.

In the LHC, commissioning procedures routinely include corrections for lower-order non-linearities, in particular the sextupolar and normal octupolar components [12], by exploiting their feed-down to tune. This feed-down effect originates from the beam traversing a magnet with a transverse offset, arising from either magnet misalignments or a displaced closed orbit, therefore generating effective lower-order field components from higher-order magnetic fields [13].

This approach was first extended to decapolar and dodecapolar error correction via feed-down to amplitude detuning, demonstrating successful results [14], albeit at the cost of significant machine time.

Building on this, it was proposed that higher-order magnetic errors could be corrected indirectly through their feed-down contributions to lower-order non-linear RDTs, therefore reducing operational time while avoiding the need for direct measurement [15].

CORRECTION PRINCIPLE

The correction procedure is based on performing forced-RDT measurements under identical machine conditions, namely at the same tunes, differing only in the applied crossing angle. This enables the determination of the partial derivative of the RDT with respect to the crossing angle.

In parallel, the simulated RDT response to a variation in crossing angle is evaluated with each corrector of interest powered at equal strength for both crossing angle configurations. The excitation of each corrector is chosen to emulate the targeted non-linear error. From these simulations, the corresponding partial derivatives of the RDT with respect to the crossing angle are obtained.

By matching the simulated derivatives to the measured responses, the optimal strengths of the correctors can be determined, therefore providing the required correction, as illustrated in Fig. 1.

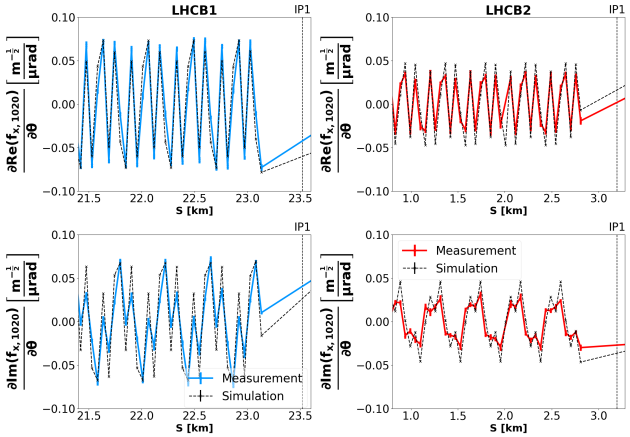

Figure 1: Demonstration of the matching of the partial derivatives in simulation with those in measurement for both beams.

A new GUI was developed to to allow the analysis to be performed online in the CCC during commissioning.

* sasha.jade.horney@cern.ch

Content from this work may be used under the terms of the CC BY 4.0 licence (© 2026). Any distribution of this work must maintain attribution to the author(s), title of the work, publisher, and DOI.

ISBN: 978-3-95450-252-3 ISSN: 2673-5350 doi: 10.18429/JACoW-IPAC2026-THP4008

LONGITUDINAL OPTIMIZATION OF HL-LHC BEAMS IN THE CERN SPS

L. Intelisano*, H. Bartosik, J. Flowerdew, I. Karpov, A. Lasheen, K. Li, I. Mases,
G. Papotti, C. Zannini, European Organization for Nuclear Research, Geneva, Switzerland

Abstract

In the framework of the High-Luminosity (HL) upgrade of the Large Hadron Collider (LHC), the bunch intensity from the injectors must be doubled with respect to the nominal design value. To meet these demands, the Super Proton Synchrotron (SPS) has been upgraded to deliver 2.3×10^{11} protons per bunch in multiple trains of up to 72 bunches. An extensive campaign of beam studies in the SPS has demonstrated that all required parameters in terms of bunch intensity and length, as well as their spreads, are achieved for the relevant production schemes. Fine-tuning of the longitudinal beam properties, including controlled emittance blow-up and optimization of the higher-harmonic RF system, was essential. Sporadic non-rigid dipole oscillations, likely induced during the longitudinal blow-up, have been investigated in detail. Spectral analysis of the measured bunch position reveals prominent lines at multiples of 600 Hz, crossing the frequency band in which the blow-up is active. The impact on beam quality is evaluated, and possible mitigation strategies are discussed.

INTRODUCTION

As part of the LHC Injectors Upgrade (LIU) project [1], the Super Proton Synchrotron (SPS) underwent major upgrades during Long Shutdown 2 (2019-2020) to enable the delivery of high-intensity, high-brightness beams required for the High-Luminosity LHC (HL-LHC) [2–4]. To maintain longitudinal stability, the SPS relies on a sophisticated beam control system [4]. A central component is the beam phase loop, which locks the RF phase of the accelerating voltage to that of the bunches detected by a pickup. Furthermore, the feedback system enables the injection of a controlled phase-noise waveform into the phase loop. This broadens the synchrotron frequency spread, enhancing beam stability via Landau damping [5, 6], and thereby increasing the longitudinal emittance [7].

The HL-LHC beam asks for up to four batches of 72 bunches spaced by 25 ns with 2.3×10^{11} protons per bunch and a bunch length at extraction of 1.65 ns ± 10 % [1]. Despite the RF power limitations [8], the nominal HL-LHC parameters were achieved for the first time in 2024 and successfully reestablished in 2025 [9]. However, bunch quality degradation has been observed, characterized by a cluster of particles performing coherent phase oscillations around the bunch center. A worst-case scenario is depicted in Fig. 1, where the evolution of the bunch density, measured as instantaneous current with a Wall Current Monitor [10], reveals high-density regions oscillating near the synchrotron frequency. These non-rigid dipole oscillations may lead to uncaptured particles when the bunch trains are injected into the LHC.

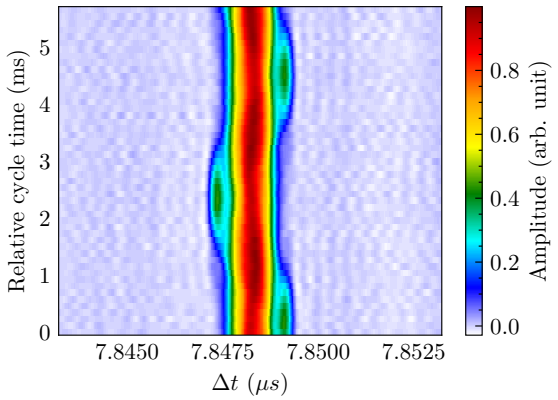

Figure 1: Example of a non-rigid dipole oscillation observed in the SPS before extraction. The color scale indicates the normalized instantaneous current displayed as a function of the longitudinal position.

This contribution analyzes the non-rigid dipole oscillations observed in 2026 following the partial restoration of the full RF power capabilities [11]. It details their mitigation through optimized longitudinal emittance blow-up settings and discusses their potential origin.

MEASUREMENT SETUP AND BUNCH-BY-BUNCH ANALYSIS

To characterize the beam quality of the full bunch train, the bunch profile evolution was measured at three relevant stages of the acceleration cycle (Fig. 2): before the controlled emittance blow-up (green), immediately after (orange), and at top energy before extracting to LHC (blue).

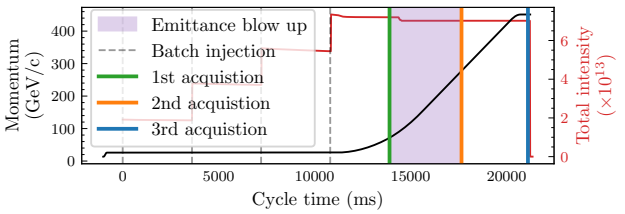

Figure 2: LIU momentum program illustrating three distinct stages in the cycle (vertical lines). Dashed lines indicate the injection of each batch of 72 bunches.

For each set of measured bunch profiles, the core is extracted by computing, at each time sample, the minimum line density value observed across all consecutive acquisitions (hold-minimum), as illustrated in Fig. 3 (left, black dashed curve). This reference core was then subtracted from the corresponding measured profiles to isolate the perturbation component of the longitudinal line density (Fig. 3, right).

* leandro.intelisano@cern.ch

Content from this work may be used under the terms of the CC BY 4.0 licence (© 2026). Any distribution of this work must maintain attribution to the author(s), title of the work, publisher, and DOI.

ISBN: 978-3-95450-252-3 ISSN: 2673-5350 doi: 10.18429/JACoW-IPAC2026-THP4010

SHORT HIGH-INTENSITY BUNCHES FOR THE AWAKE EXPERIMENT

I. Karpov*, S. Albright, H. Damerau, J.A.D. Flowerdew, G. Hagmann,
L. Intelisano, A. Lasheen, G. Papotti, A. Spierer
CERN, Geneva, Switzerland

Abstract

The AWAKE facility utilises high-intensity single bunches to drive resonant wakes in plasma for the acceleration of electrons. Twice shorter bunches are required from the CERN Super Proton Synchrotron (SPS) for the next phase of the experimental programme. In addition, the reproducibility of the bunch distribution and intensity is essential. This contribution summarises the key improvements to approach the new target parameters. An enhanced bunch production scheme was developed in the Proton Synchrotron Booster (PSB). It allows the preservation of the small longitudinal emittance during acceleration in the Proton Synchrotron (PS) without triggering an instability during the transition crossing. In addition, a double-voltage jump bunch rotation scheme has been implemented in the SPS, with radio-frequency (RF) voltage functions synchronised to the variable extraction time. The measurement results confirm the feasibility of achieving the target beam parameters.

INTRODUCTION

The Advanced WAKefield Experiment (AWAKE) [1], aims at demonstrating plasma wakefield acceleration of an electron beam for future high-energy physics applications. It requires as short as possible proton bunches to be extracted from the Super Proton Synchrotron (SPS) with a target intensity of 3×10^{11}. The initial longitudinal emittance is typically determined by the radio-frequency (RF) manipulations in the Proton Synchrotron Booster (PSB) and, then, limited by instabilities during the Proton Synchrotron (PS) transition crossing [2, 3]. The longitudinal beam stability during the SPS energy ramp is maintained by deploying a double-harmonic RF system operating at 200 MHz and 800 MHz. As soon as the synchronisation process is completed at a momentum of 400 GeV/c [4], a two-step bunch compression scheme is applied (Fig. 1): (i) the RF voltage is adiabatically decreased, resulting in bunch lengthening; (ii) a non-adiabatic RF voltage jump is triggered, resulting in a bunch rotation in phase space. After approximately one quarter of a synchrotron oscillation period, the bunch is extracted with about 170 ps rms length. Note that the extraction time, t_{extr}, with respect to the start of the SPS cycle can vary up to 100 ms. In the present system implementation, the voltage jump is initiated by the beam control (BC) module of the SPS low-level RF system [5] once an extraction timing event arrives in the synchronisation module. Since the 800 MHz cavity controller does not directly communicate with the BC module, the 800 MHz RF voltage stay constant during the 200 MHz RF voltage jump. This conventional scheme was in use until the end of 2023.

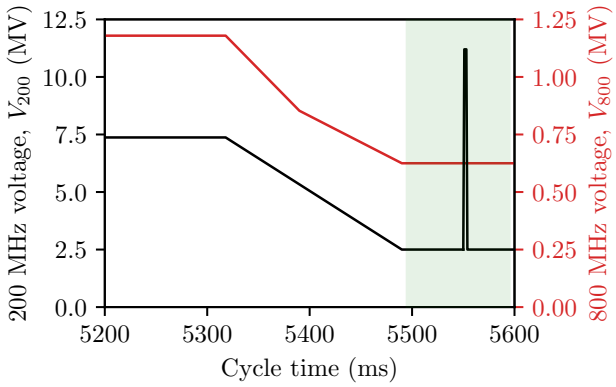

Figure 1: Example of 200 MHz and 800 MHz RF voltage programmes at 400 GeV/c in October 2023. The green area indicates the range of the extraction time variation.

For the next phase, Run 2c [6, 7], bunches twice as short are required based on the latest simulations [8, 9]. Moreover, reproducibility and stability of the proton beam parameters are essential. The following sections describe the necessary advancements to meet the target parameters and prepare for the next data-taking period in 2029.

DOUBLE BUNCH ROTATION IN SPS

The compression factor after a non-adiabatic RF voltage jump depends on the final, V_f, and initial, V_i, RF voltages. In linear approximation, it is equal to $\sqrt{V_f/V_i}$. The RF voltage, V_i, is limited by the initial longitudinal emittance and beam intensity, which define the longitudinal mode-coupling instability threshold. It was studied by comparing the dedicated measurements with macroparticle simulations [10], and more recently also applying the linearised Vlasov equation [11, 12]. Until the end of 2023, achieving the target bunch length at extraction required reducing the RF voltage to a level at which the instability was triggered. In that scenario, the bunch shape changed from cycle to cycle as the beam was extracted at different stages of the instability (Fig. 2).

To avoid this instability, an alternative approach was implemented. The first stage of adiabatic voltage reduction was replaced by an adiabatic voltage increase to guarantee beam stability. Then, the RF voltage is non-adiabatically reduced to a small value, leading to a fast bunch lengthening without instability (see Fig. 3). Finally, the RF voltage is restored non-adiabatically to the initial value, leading to a bunch rotation. A similar, double-bunch rotation scheme was originally proposed in [13] and tested to mitigate an

* ivan.karpov@cern.ch

Content from this work may be used under the terms of the CC BY 4.0 licence (© 2026). Any distribution of this work must maintain attribution to the author(s), title of the work, publisher, and DOI.

ISBN: 978-3-95450-252-3 ISSN: 2673-5350 doi: 10.18429/JACoW-IPAC2026-THP4011

ABSOLUTE ENERGY AND MACHINE LENGTH CALIBRATION IN THE SPS

R. De Maria*, H. Bartosik, S. Cettour Cave, G. Iadarola, F. Murgia, P. Zisopoulos
European Organization for Nuclear Research (CERN), Geneva, Switzerland

Abstract

This contribution presents the results of an absolute-energy and machine-length calibration of the CERN Super Proton Synchrotron (SPS) using two different particle species on the same magnetic cycle. A review of the SPS ring geometry and magnet alignments led to an update of the machine circumference used in the optics models, improving their agreement with the as-built machine. The measurement determines the effective machine circumference from absolute energy calibrations and the revolution period. It repeats a similar calibration performed in the early 2000s, using the magnetic centre of the sextupoles as a reference, and complements it with beam position monitor (BPM) centres. A comparison between new and old measurements and models is presented.

SPS RING GEOMETRY REVIEW

The SPS optics model was updated to better match the as-built machine. The machine survey was compared against the GEODE survey database [1], which represents the current installed state of the machine. All discrepancies between the two data sets were then systematically identified and analysed [2]. Each displacement identified during the comparison was projected onto the reference trajectory in the horizontal and vertical machine planes and evaluated at well-defined locations, such as the entrance or exit of each beamline element.

Bending Magnet and Starting Point Adjustments

An initial analysis, focusing on a simplified model containing only the bending dipole magnets, revealed a discrepancy between the optics model and the as-built machine reference geometry stored in the GEODE survey database. Specifically, the machine diameter in GEODE is larger than expected from the SPS as designed by 4 mm, corresponding to about 14 mm in circumference with respect to the nominal 11/7 circumference ratio to the Proton Synchrotron (PS) [2]. The discrepancy has a limited impact on the absolute beam energy, but more importantly, it makes the as-designed geometry unsuitable as a new reference for alignment. Furthermore, the present reference circumference does not fully close, leaving a gap of approximately 170 µm between the start and end points. The cause of this discrepancy was identified as a difference in the calculation of the beam trajectory path (s), also known as the beam cumulative distance (beam DCUM) [2, 3]. This fundamental difference in reference length leads to a measurable discrepancy in the bending magnet length. The magnetic length of the bending dipole is defined as the face-to-face distance, i.e., the chord length, whereas the optics calculation software defines the magnetic length of a bending magnet based on the arc path.

The difference between the two trajectory definitions (arc and chord) is given by

$$\Delta L_{\text{arc-chord}} = L_{\text{chord}} \left(\frac{\alpha}{2\sin(\alpha/2)} - 1 \right) = 18.603\,\mu\text{m}, \quad (1)$$

where $\alpha = 2\pi/744$ is the bending angle of a single dipole magnet and 744 is the total number of bending dipoles in the SPS. While a single discrepancy of 18.603 µm may appear negligible, its accumulation over all dipoles gives

$$\Delta L_{\text{total}} = 18.603\,\mu\text{m} \times 744 = 13.840\,\text{mm}. \quad (2)$$

This accumulated difference causes the SPS circumference, as recorded in the survey reference geometry, to deviate from the nominal design value, resulting in a non-conforming machine geometry. A further significant correction, which reduced the residual discrepancy, involved adjusting the position and orientation of the starting point of the SPS optics model. The applied orientation corrections were $\Delta\Theta = 0.329\,\mu\text{rad}$ (yaw), $\Delta\Phi = 0.012\,\mu\text{rad}$ (pitch), and $\Delta\Psi = 0.030\,\mu\text{rad}$ (roll). The position corrections were $x_0 = -9.012\,\mu\text{m}$, $y_0 = -3.870\,\mu\text{m}$, and $z_0 = -0.187\,\mu\text{m}$. To fully close the machine ring in the optics model and better match the reference geometry, empirical adjustments were applied: the per-dipole arc-chord correction was increased from 18.603 µm to 19.340 µm, and the distances between elements in the straight sections were fine-tuned.

Following these adjustments, the global discrepancy between the new model and the old reference was reduced to below 10 µm. This allowed the new model to serve as a single source of truth for both alignment and beam operations.

Sextupole Inconsistencies

To make the model better match the as-built machine, all beamline components were analysed. Quadrupoles (QD, QF) and octupoles (LOD, LOE, LOF, LOEN) showed no significant discrepancies. However, for sextupoles (LSF, LSD), a mismatch was identified through a comparison of two historical documents on magnet characteristics [4, 5].

Around 1983, all SPS sextupoles were replaced with new models. Although they retained the same names in the databases, their characteristics differed slightly. While the mechanical lengths of the LSF and LSD were correctly updated in the database, their magnetic lengths remained unchanged from those of the original sextupoles. To ensure consistency with the latest available data [5], the magnetic lengths were updated from 0.423 m to 0.435 m for the LSF, and from 0.420 m to 0.426 m for the LSD.

* riccardo.de.maria@cern.ch

Content from this work may be used under the terms of the CC BY 4.0 licence (© 2026). Any distribution of this work must maintain attribution to the author(s), title of the work, publisher, and DOI.

ISBN: 978-3-95450-252-3 ISSN: 2673-5350 doi: 10.18429/JACoW-IPAC2026-THP4012

BEAM PERFORMANCE REACH AT THE CERN PSB FOR THE ISOLDE FACILITY

F. Asvesta*, S. Albright, C. Bracco, G. P. Di Giovanni, A. Findlay, I. Frank, M.A. Fraser, G. Gnemmi, L. Le, M. Marchi, E. Piselli, T. Prebibaj, A. Rodriguez Rodriguez, S. Rothe, M. Schenk, P. Skowronski, S. Stegemann
CERN, Geneva, Switzerland

Abstract

The Proton Synchrotron Booster (PSB) at CERN is the first synchrotron of the proton accelerator chain and provides beam not only to the LHC and the rest of the injector complex, but also directly serves ISOLDE. This facility is one of the most demanding users in terms of beam intensity, receiving more than 60% of the overall protons produced at CERN. To further optimise beam delivery while accommodating new beam users at CERN, systematic studies are conducted to identify the performance reach. Current efforts focus on maximizing the achievable intensity in the PSB and assessing the impact on the isotope production at the facility.

INTRODUCTION

The Isotope Separator OnLine Detector (ISOLDE) is a radioactive ion beam facility at CERN, exploiting GeV energy protons to access the full range of production mechanisms, spallation, fission, and fragmentation, for the creation of exotic nuclei [**?**]. The facility is hosting up to 60 experiments per year across a broad physics programme spanning nuclear structure, nuclear astrophysics, fundamental interactions, condensed-matter physics, and medical applications. Consequently, ISOLDE places unique and growing demands on the CERN accelerator complex and in particular on the Proton Synchrotron Booster (PSB).

Protons for ISOLDE are delivered by the PSB, the first synchrotron in the CERN injector chain, currently operating at 1.4 GeV and providing intensities of 3.2×10^{13} protons per pulse (ppp), i.e. 0.8×10^{13} protons per ring (ppr) in each of the four rings of the PSB. The average beam current delivered to ISOLDE, and consequently the protons on target (PoT), depends on the intensity per pulse and the number of pulses that PSB can allocate to ISOLDE, while serving the other users of the complex, such as LHC or any of the fixed target experiments. The beam delivery is organized using a supercycle, which is essentially a sequence of beam users linked in all accelerators that define the facilities that are served. During Run 3 (operations from 2021 to 2026), typical operation at 40% occupancy of the supercycle yielded average currents of 1.6 µA to 2.0 µA to ISOLDE.

The beam allocation at CERN, however, is set to face new challenges in Run 4 (operations from 2028 to 2033) with the introduction of the new Beam Dump Facility dedicated to the Search for Hidden Particles (BDF/SHiP) experiment at the Super Proton Synchrotron (SPS) [**?**]. In particular, dedicated beam sharing studies conducted in recent years have shown that accommodating SHiP in the supercycle substantially increases SPS demands, thereby reducing the number of slots available to upstream users, including ISOLDE [**?**]. Depending on the specific supercycle configuration and the proton flux requirements of other facilities such as EAST, n_TOF, and AD, ISOLDE's share of PSB pulses could drop from ~47% to as low as 30-35%, leading to a potential PoT reduction of up to 15-20% relative to Run 3, in the absence of any mitigation measures. One such measure would be an increase in the number of protons delivered per PSB pulse to ISOLDE, partially compensating for the reduced slot occupancy.

In parallel, the ISOLDE improvement programme is preparing a set of infrastructure upgrades during the Long Shutdown 3 (LS3), from 2026 to 2028 for ISOLDE, to extend the facility's capabilities [1]. These include an upgrade of the PSB to ISOLDE transfer line to transport protons at up to 2.0 GeV [2] together with the replacement of beam dumps, ventilation upgrades, and improvements to low-energy beam delivery systems. These upgrades open up the facility to a new regime of exploitation due to the higher beam energy and the option of higher intensities reaching up to 6 µA.

In this context and in order to assess the performance reach and propose suggestions for further improvements, the Injectors Performance for Fixed Target (IP-FiT) study was launched in 2025 [3]. Under the IP-FiT study, the systematic studies of the achievable PSB intensity for ISOLDE are coordinated, serving both as a mitigation strategy for reduced slot availability during BDF/SHiP operation and as input to long-term design choices for the ISOLDE infrastructure. The present contribution reports on the performance reach of the PSB for ISOLDE beam delivery and the implications for isotope production at the facility.

PSB INTENSITY REACH

To assess the intensity reach of the PSB in the LIU era [4, 5], dedicated studies for the ISOLDE user have been conducted since the PSB restart in 2021. In particular, intensities up to 1.6×10^{13} ppr at 1.4 GeV have been demonstrated during dedicated Machine Development (MD) studies at the end of 2023 [6]. Furthermore, higher intensities up to 1.7×10^{13} ppr at 1.4 GeV were achieved in 2024 [7]. Finally, the highest intensities were reached in 2025, exceeding 1.8×10^{13} ppr and 1.45×10^{13} ppr at 1.4 GeV and 2 GeV respectively, as shown in Fig. 1. Note that the reduced inten-

* foteini.asvesta@cern.ch

Content from this work may be used under the terms of the CC BY 4.0 licence (© 2026). Any distribution of this work must maintain attribution to the author(s), title of the work, publisher, and DOI.

ISBN: 978-3-95450-252-3 ISSN: 2673-5350 doi: 10.18429/JACoW-IPAC2026-THP4013

PHASE SPACE MEASUREMENTS ON THE ISIS SYNCHROTRON

S. Karbassi*, H. Cavanagh, B. Kyle, R. Williamson
ISIS Neutron and Muon Source, RAL, United Kingdom

Abstract

The ISIS Neutron and Muon source produces pulsed neutrons and muons for multi-disciplinary scattering and spectrometry experiments. Up to 3×10^{13} protons per pulse are accumulated over a ~200 µs injection period, then accelerated from 70 to 800 MeV in the 50 Hz rapid cycling synchrotron. This beam is then extracted to one of two spallation neutron targets. An electrostatic chopper is installed in the transfer line between the injector linac and the synchrotron, which allows injection of beam pulses between 100 ns – 5 µs, filling a fraction of the machine acceptance of the synchrotron. Beam Position Monitor (BPM) measurements of chopped beams are routinely used to determine synchrotron lattice parameters. As part of ongoing improvements to measurement, modelling and control of ISIS beam dynamics, a new tool has been developed to routinely use these BPM signals to generate phase-space ellipses. Preliminary results from commissioning of this tool are presented, showing good agreement with the linear transverse model of the ISIS RCS.

INTRODUCTION

The ISIS synchrotron accelerates on the rising edge of a 50 Hz sinusoidal field. High intensity proton beams are achieved using charge-exchange injection of H^- ions from the linear accelerator (linac) over 200 µs, corresponding to around 130 beam revolutions. Injection typically begins 0.4 ms before the minimum of the main magnetic field.

To mitigate space-charge effects, transverse phase-space painting is implemented in both planes. In the horizontal plane, the energy mismatch between the fixed linac beam energy and the falling magnetic field of the synchrotron results in a moving dispersive closed orbit. In the vertical plane, a programmable dipole in the injection line is used to vary the injection point vertically throughout the injection period.

The betatron tunes are programmable throughout the acceleration cycle, with the nominal working point set to $(Q_x, Q_y) = (4.31, 3.83)$ [1]. Tune control is achieved using 20 trim quadrupoles, with two installed in each of the ten superperiods. Programmable dipole magnets, seven in each transverse plane, are used to provide orbit correction.

CHOPPED BEAM ELLIPSE RECONSTRUCTION

A diagnostic beam, typically 600 ns, can be produced by the electrostatic chopper located in the transfer line between the linac and the synchrotron. Timing control allows selection throughout the 200 µs injected pulse, enabling the study of time-dependent beam properties. Such beams facilitate detailed measurements of transverse beam dynamics, as the injected beam fills only a limited portion of the machine acceptance.

The synchrotron is equipped with 35 AC-coupled beam position monitors (BPMs), comprising nineteen vertical and sixteen horizontal monitors. For chopped beam measurements, high gain BPM signals are acquired for ~100 µs, allowing turn-by-turn position extraction for 50 turns.

The transverse beam position on the nth turn may be described by the following theoretical expression [2]:

$$y_n = A \exp\left(-\frac{(\pi n \delta Q)^2}{2}\right) \cos\left(2\pi n \left[Q_0 + \frac{n\Delta Q}{2}\right] + 2\pi\phi\right) + n\Delta R + R_0. \quad (1)$$

Here,

y_n : beam position on the nth turn,
A : initial betatron amplitude,
Q_0 : initial betatron tune,
R_0 : initial closed-orbit offset,
δQ : tune spread,
ϕ : initial betatron phase divided by π,
ΔQ : change in tune per turn,
ΔR : change in closed orbit per turn.

A least-squares fit can be applied to the measured beam positions, allowing the extraction of the lattice parameters as well as the reconstruction of the turn-by-turn beam position at each BPM. Key parameter determination from this expression has been employed operationally for many years. However, it is also possible to use these fitted parameters to generate a visualisation of the transverse phase-space ellipse and to derive the corresponding Twiss parameters.

In practice the spread in betatron frequencies in the beam causes decoherence of the oscillations, seen as damping [3]. In order to omit this effect time dependent parameters are excluded from the fit, simplifying Eq. (1) to:

$$y_n = A \cos\left(2\pi n Q_0 + 2\pi\phi\right). \quad (2)$$

Beam position measurements from two consecutive BPMs can be obtained on a turn-by-turn basis. Given a known monitor separation and phase advance between these monitors, the measurements can be combined geometrically to obtain phase-space coordinates and reconstruct the transverse phase-space ellipse.

Based on this approach, a new control-room software tool has been developed to visualise the transverse phase space using the results of chopped beam measurements. In its simplest implementation, the method is applied to two

* sara.karbassi@stfc.ac.uk

Content from this work may be used under the terms of the CC BY 4.0 licence (© 2026). Any distribution of this work must maintain attribution to the author(s), title of the work, publisher, and DOI.

ISBN: 978-3-95450-252-3 ISSN: 2673-5350 doi: 10.18429/JACoW-IPAC2026-THP4014

IMPLEMENTATION UPDATE OF MYRRHA PHASE 1 (MINERVA)

U. Dorda†, A. Fabich, Belgian Nuclear Research Centre, Mol, Belgium

Abstract

This contribution provides an update on the development of the 4 mA, 100 MeV continuous-wave (CW) superconducting proton linac - the first stage of MYRRHA's accelerator-driven system (ADS). We present the improved accelerator layout and beam optics design, outline the key design choices for critical components, and report on the latest manufacturing and civil construction progress.

INTRODUCTION

An accelerator driven system aims to eliminate the issues of current fission reactors: Accumulation of long-lived nuclear waste, operation of a critical system and the need for weapons-grade material. The main objective of MYRRHA [1] is to design, construct and operate an ADS as a technology demonstrator for the transmutation of nuclear waste but also e.g. for the production of medical radio-isotopes material studies. For this purpose SCK CEN, the Belgian nuclear research center SCK CEN, is currently constructing a 100 MeV superconducting RF (SRF) linac as the technology demonstrator for its high reliability beam delivery capabilities and to deliver beam to two user stations. In a later stage it will be extended to 600 MeV and coupled to the subcritical nuclear reactor (see Fig. 2).

ACCELERATOR

The main accelerator parameters are summarized in Table 1.

Table 1: Main Accelerator Parameters

Parameter	Value
Particle type	Protons
Energy	100 MeV
Beam Current	4 mA
RF-operation	CW
Beam operation	Pulsed to CW
Cycle length	4 ms
# Pulses per cycle	max 2

The 100 MeV accelerator which is implemented in the current first implementation stage consists of a

1. normal conducting section to 17 MeV [2]
2. injector switching section
3. superconducting RF section up to 100 MeV
4. HEBT to switch beam delivery between a tuning beam dump (representing the future extension) or two user stations.

Injector Layout Update

For the final 600 MeV configuration, the accelerator will incorporate two independent injectors, enabling seamless switching in the event of a failure in one system. Earlier studies proposed a symmetrical layout, with both injectors featuring a dog-leg to direct the beam to a switching dipole. However, in 2024, the layout was redesigned to enhance reliability and simplify operation: one injector is now aligned in a straight line with the superconducting linac (SC-linac), while the other is offset to the side. Two switching solutions are currently under evaluation:

- A switching dipole configuration with a 1s ramp rate
- A kicker-septum system (Fig. 1), which allows both injectors to deliver beam pulses to the SC-linac e.g., alternating injectors for the two pulses within a single 4 ms cycle. This approach ensures continuous, full validation of both injectors. In the event of a failure in one injector, only the kicker timing sequence requires adjustment.

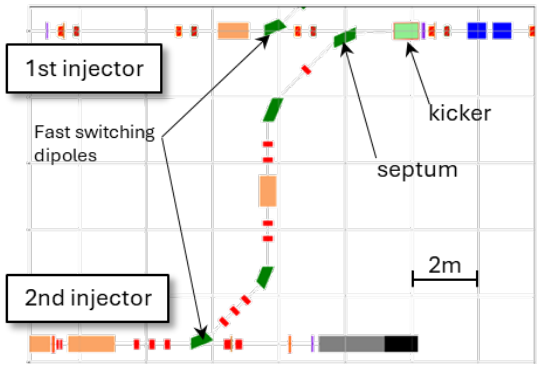

Figure 1: The kicker-septum solution for the 2nd injector.

SC-Linac Update

As an additional benefit, this layout and optics change allowed to significantly improve the longitudinal acceptance of the SC-linac as shown in Fig. 3.

The total number of cryo-modules, 30 for the MYRRHA phase 1 SC-linac, is determined by the following rules for high intensity linacs and specific requirements for the MYRRHA phase 1 SC-linac: a) the longitudinal phase advance remains <90 degrees in 1 lattice period, b) the field in each cavity remains < 7.0 MV/m to allow for fault compensation, c) the synchronous phase in each lattice period (i) evolves as $\varphi_i = \varphi_{i-1}\left(\frac{\beta_{i-1}\gamma_{i-1}}{\beta_i\gamma_i}\right)^{3/2}$ and d) the final energy should be 100 MeV. Details on the longitudinal design are given in [3, 4].

Content from this work may be used under the terms of the CC BY 4.0 licence (© 2026). Any distribution of this work must maintain attribution to the author(s), title of the work, publisher, and DOI.

ISBN: 978-3-95450-252-3 ISSN: 2673-5350 doi: 10.18429/JACoW-IPAC2026-THP4015

CONSTRUCTION AND STATUS OF NEWGAIN RFQ

O. Piquet †, A. Deville, A. Dubois, P. Hamel, V. Hennion, S. Jurié, M. Oublaid, L. Picault, O.Tellier
CEA/IRFU, Université Paris-Saclay, Gif-sur-Yvette, France

Abstract

A new injector called NEWGAIN will be added to the SPIRAL2 Linear Accelerator in parallel with the existing one. It will be mainly composed of an ion source and a Radio Frequency Quadrupole (RFQ) connected to the superconductive LINAC. The RFQ is a standard four-vane bulk copper cavity, composed of 7 segments of about 1m. The new RFQ will accelerate at 88.05 MHz particles with charge-over-mass ratio (Q/A) between 1/3 and 1/7, from 10 keV/u up to 590 keV/u. This paper will present the status of the RFQ section fabrication and its necessary support systems. The fabrication and delivery of these components will lead to its installation, which is a major milestone for the project.

INTRODUCTION

The purpose of the NEWGAIN project [1] is to develop a new injector, consisting of a superconducting electron cyclotron resonance (ECR) ion source and a Radio Frequency Quadrupole (RFQ) (A/q = 7), for the SPIRAL2 LINAC. It will enable GANIL to provide ion beams of worldwide highest intensities (from proton to uranium), thus opening up unprecedented opportunities for nuclear structure and reaction studies at the extremes of the chart of nuclides from N=Z nuclei at the proton dripline to super-heavy species, including the discovery of new elements, and the production of radioisotopes. It also makes it possible to extend the use of SPIRAL2 beams to interdisciplinary research as well as applications.

The NEWGAIN RFQ cavity RF is very close to the SPIRAL2 RFQ cavity, currently operating in GANIL as they both operate at the same frequency. The choice was made to mechanically assemble the cavity with metallic vacuum gasket between copper parts as tube and vanes. The RF design and thermomechanical study of this new RFQ follow the procedure developed at CEA and presented in Refs. [2, 3].

RFQ DESCRIPTION

The RFQ cavity is made of seven sections, each one meter long, directly coupled. Each of these sections results from the assembly of four vanes into a copper tube. The vanes are bolted to the tube with Helicoflex seals. These seven sections are also mechanically joined via metal seals at the copper tubes.

The RFQ cavity in Fig. 1 is also equipped with:

- 56 tuners,
- 4 RF power couplers
- 24 pumping ports (equipped with 12 turbomolecular pumps)
- 18 pick-ups for voltage law control and LLRF
- 580 cooling connectors (on cavity, end flanges, tuners and power couplers).

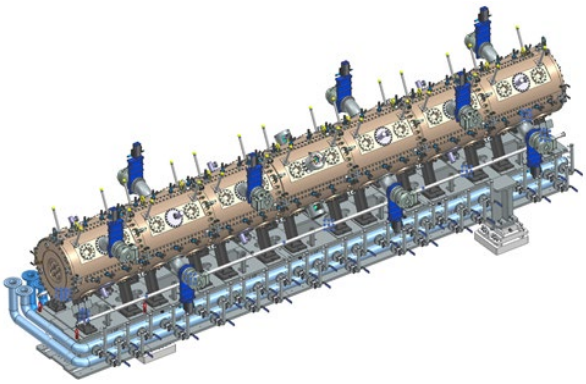

Figure 1: General layout of the NEWGAIN RFQ.

RFQ FABRICATION

Qualification Phase

Since January 24, the RFQ contract was assigned by an international tender to CINEL company. The first part of the contract validated the manufacturing process of an initial vane, realized with a machining tolerance of ±20 µm for the modulations and the vane ends (Fig. 2)



Figure 2: First vane of NEWGAIN RFQ.

This vane was then installed on a copper test piece (Fig. 3) to qualify the assembly process using a large racetrack-shaped Helicoflex® seal (Seals manufactured by Technetics Group). A leak test was then performed.



Figure 3: Assembly test for Helicoflex® seal.

Content from this work may be used under the terms of the CC BY 4.0 licence (© 2026). Any distribution of this work must maintain attribution to the author(s), title of the work, publisher, and DOI.

ISBN: 978-3-95450-252-3 ISSN: 2673-5350 doi: 10.18429/JACoW-IPAC2026-THP4016

STATUS OF THE IH-DTL CAVITIES DESIGN AND PROTOTYPING FOR THE ICONE PROJECT

A. Dia, G. Ferrand†, D. Uriot, O. Piquet, CEA Paris-Saclay, Gif-sur-Yvette, France

Content from this work may be used under the terms of the CC BY 4.0 licence (© 2026). Any distribution of this work must maintain attribution to the author(s), title of the work, publisher, and DOI.

Abstract

CEA is committed to delivering a LINAC in the frame of the ICONE project, in order to accelerate an 80-mA beam of protons up to 25 MeV, with a duty cycle of 6%. The LINAC project is divided into five workpackages: Source and LEBT, RFQ, MEBT, DTL and HEBT. The initial acceleration and bunching will be provided by a 4-vane RFQ cavity. For the DTL part, two solutions with copper cavities were studied from 3.7 MeV to the final energy: an IH-DTL and an Alvarez DTL LINAC. This talk will present the design of the IH-DTL solution at 352 MHz. Prototypes of certain parts, including a small cavity, and a permanent magnet, are tested in 2025/2026. Results of these tests will be presented.

INTRODUCTION

The ICONE project [1] aims to develop a compact high-current proton linac for accelerator-driven neutron source applications within the HICANS framework [2-3]. The accelerator will deliver an 80 mA proton beam accelerated up to 25 MeV with a duty cycle of 6%.

A first global study of the RF components was presented in [4], including the main accelerating structures and the two DTL solutions investigated for the project. The present work focuses on the optimization of the IH-DTL cavities to improve the RF efficiency and reduce power consumption while preserving the required accelerating performance.

An IH-DTL prototype was manufactured and experimentally characterized through low-power RF measurements and Bead-Pull tests. Resonance frequency, quality factors, tuner sensitivity and EM field distribution were measured and compared with simulations, showing good agreement. The prototype is now awaiting authorization for high-power RF tests.

IH-DTL CAVITIES OPTIMIZATION

The IH-DTL cavities geometry definition was updated to improve flexibility and prevent imperfections in the geometry during the design and optimization process, enabling better control of the capacitive loading at the cavity ends and improving the accelerating field distribution. This updated parametrization, that affects more the tilt angle of the end stems, provides an efficient way to adjust the field profile without introducing additional structures such as girders [5], and was applied to the full set of cavities, whose results are presented in Table 1.

Table 1: Results of RF Simulations of the IH-DTL Cavities

Cavity	β	Acc. Gradient	RF losses	Peak E-field	RF acceleration consumption
		[MV/m]	[kW]	[MV/m]	[kW]
1	0.09	1.40	11.6	10.9	28.1
2	0.0963	2.95	52.1	21.0	63.5
3	0.1058	3.50	76.0	24.1	82.7
4	0.1167	3.12	78.2	22.7	104.1
5	0.1289	3.40	100.1	25.0	128.1
6	0.1418	3.40	109.4	24.6	142.3
7	0.1548	3.40	120.2	24.0	156.9
8	0.1679	3.40	132.6	24.4	170.2
9	0.1810	3.40	146.2	23.8	185.2
10	0.1941	3.40	161.3	23.2	202.2
11	0.2073	3.40	178.6	23.4	219.5
12	0.2204	3.40	198.4	24.4	233.4
		Total	1364.7		1716.3

To further reduce RF consumption, a dedicated optimization was performed on representative cavities of the Linac, namely a middle energy cavity and the last cavity. The optimization focused on two main geometrical parameters: the tilt angle of the end stems and the outer radii of the drift tubes. The tilt angle was first adjusted to improve the field distribution along the cavity axis, followed by a refinement of the drift tube radii to reduce RF losses while maintaining acceptable peak electric field levels.

The optimized configurations show a consistent improvement in RF performance as shown in Table 2. For both cavities, the RF power consumption is reduced by 10%, while maintaining the required accelerating conditions. This improvement is accompanied by a moderate increase in peak electric field, which remains within acceptable operational limits. In addition, the optimization leads to a better control of the field distribution along the beam axis as illustrated in Figure 1. This approach can be extended to the remaining cavities if the IH-DTL solution is selected for the project.

Table 2: Results of RF Simulations Before and After Optimization

Cavity	Model	Q_0	V_{acc} @1J	RF losses	Peak E-Field	Kilp
			[MeV]	[kW]	[MV/m]	
6	Initial	11226	2.75	109.4	24.6	1.35
	Optimal	11407	2.89	97.6	26.0	1.43
12	Initial	12724	2.98	198.4	24.4	1.34
	Optimal	13453	3.07	178.1	24.8	1.36

†guillaume.ferrand@cea.fr

ISBN: 978-3-95450-252-3 ISSN: 2673-5350 doi: 10.18429/JACoW-IPAC2026-THP4017

A NEW BEAM DYNAMIC DESIGN PROCEDURE

P. Hamel[1], A. Deville[1], O. Piquet[1], R. Duperrier[1]
[1]CEA-IRFU, Gif-sur-Yvette, France

Content from this work may be used under the terms of the CC BY 4.0 licence (© 2026). Any distribution of this work must maintain attribution to the author(s), title of the work, publisher, and DOI.

Abstract

The beam dynamics design of a Radio Frequency Quadrupole (RFQ) is usually optimized to match the beam parameters at the entrance and exit of the cavity. This design step defines the vane geometry—such as the distance from the vane tips to the beam axis, the vane-tip radius, the modulation type and amplitude, and the modulation length—and also provides the inter-vane voltage for the next stage: the RF design. Based on the inter-vane voltage profile along the cavity, the 2D cross-section is then adjusted to match the local cutoff frequency of the quadrupole mode, typically by modifying the quadrant volume where the magnetic field is dominant. In this paper, we propose a new approach to RFQ beam dynamics design. Instead of considering only the geometry near the beam axis, the full 2D cross-section—including the quadrant region—is integrated directly into the beam dynamics optimization. The resulting inter-vane voltage can then be obtained by preserving the magnetic-field region's area along the cavity, which may simplify the manufacturing process.

INTRODUCTION

At CEA/IRFU, the RFQ design process is divided into several stages [1], including beam dynamics [2], RF design [3], and thermomechanical analysis. Each stage provides inputs to the next, and iterative feedback is often required when the expected specifications are not met, leading to time-consuming optimization loops.

In an RFQ, the transverse geometry of the cavity can be separated into two regions: the vane tips close to the beam axis, which are determined by beam dynamics requirements, and the outer part of the quadrant, which is mainly used to adjust the RF properties of the structure. The RFQ cavity can be modeled as a succession of longitudinally varying waveguide cross-sections, each characterized by a local cutoff frequency. This local cutoff frequency directly governs the intervane voltage distribution along the cavity required for the beam dynamics.

In conventional design approaches, the beam dynamics stage defines only the vane-tip geometry, while the RF design stage adjusts the outer quadrant geometry to achieve the cutoff frequency and voltage profile. This separation introduces a weak coupling between beam dynamics and RF constraints, resulting in iterative design cycles. Additional requirements, such as maintaining a constant cavity volume for mechanical or thermal considerations, further increase the complexity of the optimization.

To address these limitations, this paper proposes a method to derive an analytical approximation of the cutoff frequency as a function of the main geometrical parameters of the RFQ cross-section, within a predefined range of validity. This approach enables the estimation of the local cutoff frequency directly during the beam dynamics design stage, allowing indirect control of the outer geometry and facilitating the enforcement of additional constraints such as constant cavity volume.

In addition, an analytical estimation of the RF power dissipation is introduced, providing a tool for early-stage optimization of the cavity energy efficiency.

The paper first introduces the key geometrical parameters describing the RFQ cross-section, along with the relationship between local cutoff frequency and intervane voltage. Then, the methodology used to construct the analytical approximations for cutoff frequency and power dissipation is presented. Finally, these formulations are integrated into the beam dynamics design process, and a design example satisfying RF and mechanical constraints is obtained.

CELL DESIGN

From a microwave point of view, an RFQ is merely a waveguide-based circuit, consisting of small 3D devices at the end regions, connected by multiple cells of waveguide with constant cross-section. The geometrical parameters for a quarter cell are presented in Fig. 1.

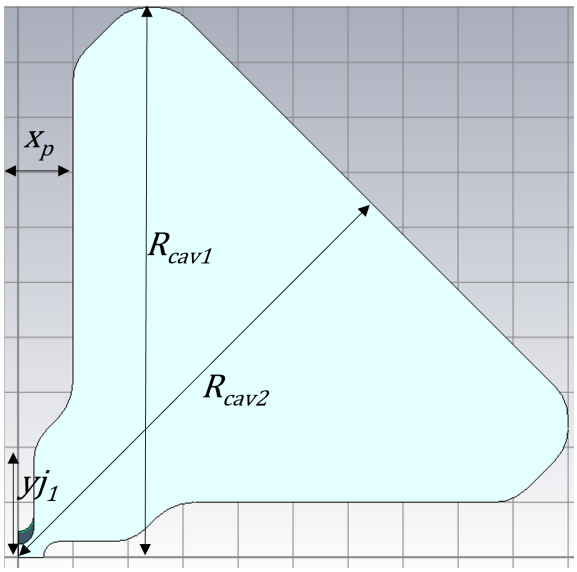

Figure 1: Geometrical parameters of quarter cross section.

Mechanical considerations impose constraints on the vane width x_p: it must be large enough to accommodate cooling channels, while being as small as possible to minimize RF power losses.

The beam dynamics design stage mainly controls the geometrical parameters close to the vane tips. The parameter r_0 represents the average distance from the vane to the beam

ISBN: 978-3-95450-252-3 ISSN: 2673-5350 doi: 10.18429/JACoW-IPAC2026-THP4019

TOWARDS AUTOMATED CAVITY FAILURE COMPENSATION IN THE SPIRAL2 SC LINAC

A. Plaçais*[1], F. Bouly[1], M. Di Giacomo[2], J.-M. Lagniel[2], A. Leduc[2], G. Normand[2], A. Orduz[2], B. Yee-Rendon[3]
[1]Univ. Grenoble Alpes, CNRS, Grenoble INP, LPSC-IN2P3, Grenoble, France
[2]GANIL, CEA/DRF-CNRS/IN2P3, Caen, France
[3]JAEA/J-PARC, Tokai, Japan

Abstract

RF systems in high-power particle accelerators such as SPIRAL2 are susceptible to failures, causing significant beam downtime. Cavity failure compensation can restore nominal beam conditions, but finding optimal settings is a complex challenge. This study adapts LightWin to SPIRAL2, implementing the NSGA-III algorithm for high-dimensional, constrained optimization. We demonstrate successful single-cavity-failure compensation, recovering nominal beam energy without longitudinal losses. These developments advance automation for SPIRAL2, but suboptimal transverse envelopes highlight the need for quadrupole retuning in LightWin.

CAVITY FAILURE COMPENSATION FOR HIGH AVAILABILITY

The SPIRAL2 superconducting (SC) linac is dedicated to accelerating intense ion beams, from protons to ions up to $A/Q = 7$ [1]. In this machine, RF cavity or associated system failures are a major source of beam interruption [2]. In case of RF failure, neighbouring cavities can be retuned to continue operation, sometimes even recovering nominal beam conditions. This cavity failure compensation has demonstrated practical feasibility on SNS [3] and SPIRAL2 [1, 4], and was applied during SPIRAL2 operation [5].

However, manually determining compensation settings is complex, time-consuming, and may be incompatible with operational constraints. To address this, we developed LightWin [6], an open-source tool for automatic cavity failure compensation. Originally designed for ADS linacs, where compensation is facilitated by specific design features, we are adapting LightWin to all linac types. In this study, we present our latest developments, enabling its operation on the SPIRAL2 SC linac, and perform a compensation study on a single cavity failure.

This paper is organized as follows. We first introduce the LightWin code and its parametrization. We then present the latest updates, focusing on optimization algorithms and SPIRAL2-specific challenges. Next, we showcase a compensation scenario and compare it to the settings from Ref. [5].

* placais@lpsc.in2p3.fr

THE LightWin FRAMEWORK

Code Architecture and Features

LightWin [6] is an open-source tool for finding compensation settings, previously detailed in [7]. Written in Python, it provides beam dynamics and optimization tools, and is designed for use with any linac and cavity failure compensation strategy. Its main feature is automatic operation, enabling compensation settings to be found for any number of failure scenarios without intervention. This enables both rapid database creation for compensation settings and systematic comparison of multiple strategies across the same failure set. Its modular structure allows switching between different beam dynamics solvers and optimization algorithms. Here, we use two beam dynamics solvers: `Envelope1D`, an envelope longitudinal solver without space-charge effects, and `TraceWin`, which calls the reference code TraceWin to track the beam in 3D with multiparticle simulations, accounting for space-charge effects. All presented beam dynamics results were calculated with TraceWin, while compensation settings were found using LightWin. In LightWin, compensation is formulated as an optimization problem [8]:

$$\left.\begin{aligned} &\text{Minimize } f_m(\mathbf{x}), && m = 1, 2, \cdots M \\ &\text{subject to } g_j(\mathbf{x}) \geq 0, && j = 0, 1, \cdots J \\ &x_i^{(L)} \leq x_i \leq x_i^{(U)}, && i = 1, 2, \cdots N \end{aligned}\right\} \quad \begin{aligned} &\text{(1a)} \\ &\text{(1b)} \\ &\text{(1c)} \end{aligned}$$

where f_m are the M objective functions, g_j the J inequality constraints, and $\mathbf{x}$ the N-variable vector. Each variable x_i is bounded by $x_i^{(L)}$ and $x_i^{(U)}$. N, $\mathbf{x}^{(L)}$, and $\mathbf{x}^{(U)}$ define the design space. In our case, $N = 2n$, where n is the number of compensating cavities, each contributing two variables: electric field amplitude and phase.

Optimization for ADS Linacs

LightWin has been used for MINERVA [7, 9] and JAEA-ADS [7, 10, 11] SC linacs. These linacs, part of Accelerator-Driven Systems (ADS), cannot tolerate repeated or prolonged beam interruptions [12]. Their features facilitate failure compensation: very high longitudinal acceptance and cavities operable with accelerating fields E_{acc} above baseline [13, 14]. In our studies [7, 9–11], we could compensate single cavity failures with three to five compensating cavities.

We generally used the Downhill Simplex algorithm [15], best suited to single-objective, low-dimensional (*i.e.* few-variable) problems without constraints. The variable vector

Content from this work may be used under the terms of the CC BY 4.0 licence (© 2026). Any distribution of this work must maintain attribution to the author(s), title of the work, publisher, and DOI.

ISBN: 978-3-95450-252-3 ISSN: 2673-5350 doi: 10.18429/JACoW-IPAC2026-THP4020

STATUS OF THE NEW HEAVY ION ALVAREZ-TYPE INJECTOR AT GSI

M. Heilmann*, T. Dettinger, X. Du, L. Groening, M. Kaiser, M. Maier, S. Mickat, A. Rubin, C. Xiao
GSI Helmholtz Centre for Heavy Ion Research, Darmstadt, Germany
L. Ferreira, S. Roupioz
European Organization for Nuclear Research, Geneva, Switzerland

Abstract

The Alvarez-type drift-tube LINAC (DTL) at GSI presented here accelerates intense heavy-ion beams with A/q ≤ 8.5 from 1.4 to 11.4 MeV/u. It replaces a DTL being more than 45 years old in order to satisfy the requirements of future FAIR operation. The 108.408 MHz Alvarez DTL design has been finalized since 2021, and all tanks for the 55 m long post-stripper injector have been manufactured. Advanced copper-plating procedures were developed for the 2 m long and 2 m in diameter tank sections as well as for the drift tubes. These two different plating processes are now successfully applied in series production, ensuring uniform layer quality and low RF-critical surface roughness. The first five of 25 tank sections and over 40 drift tubes have been plated to specification. The all drift tubes with internal pulsed quadrupoles has undergone magnetic acceptance measurements to confirm compliance with the field-quality and gradient requirements. This contribution reports the current project status and highlights the assembly of the drift tubes and the electrical connection of the internal quadrupoles.

INTRODUCTION

The UNIversal Linear ACcelerator UNILAC (Fig. 1) at GSI (Helmholtzzentrum für Schwerionenforschung, Darmstadt, Germany) will serve as main operation injector for the Facility for Antiproton and Ion Research FAIR (Fig. 2) and [1]. The UNILAC is able to deliver ion beams (protons [2] up to uranium with charge state 30+ [3, 4]) for different experiments in parallel (pulse-to-pulse switch mode) with individual ion species and energies. For the upcoming FAIR project an upgrade of the UNILAC in terms of high beam intensities, quality, and high availability is required [5, 6]. The construction of a completely new Alvarez-DTL 2.0 will fulfill these requirements with new beam dynamics [7]. Additionally, an increased shunt impedance per surface field on the drift tubes [8] is essential for the new RF-design (Table 1) [9]. The RF-design study with CST-simulations [10] of the Alvarez 2.0-cavities [11, 12]

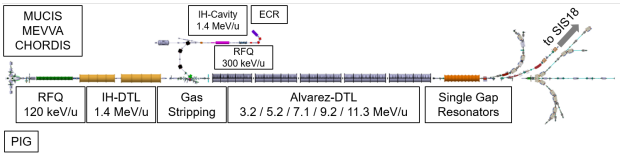

Figure 1: Schematic overview of the upgraded GSI UNILAC with five individual Alvarez-type post-stripper DTLs.

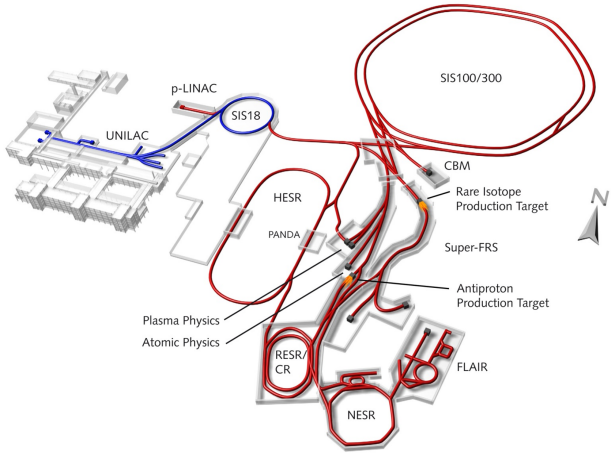

Figure 2: Schematic overview of the current GSI (blue) and the new FAIR complex in the complete expansion stage (red) [1].

Table 1: Parameters for the Upgraded UNILAC.

Parameter	Unit	Value
RF-frequency	MHz	108.408
A/q		≤ 8.5
Electrical beam current	emA	1.76×A/q
Synchronous phase	deg	-30 / -25
Input beam energy	MeV/u	1.358
Output energy	MeV/u	3.212 – 11.318
Beam pulse length	ms	≤ 1.0
Beam repetition rate	Hz	≤ 10
Alvarez-cavities / sections	#	5 / 25
Drift tubes / cavity	#	25 – 52
Drift tube length	mm	109.9 – 327.0
Drift tube diameter	mm	180.0 – 190.3
Aperture diameter	mm	30 / 35
Transverse focusing type		F–D–D–F
Max. RF-power per cavity	MW	1.35
RF-source / cavity	#	1
Total length	m	55.0

was verified with a scaled model [13–15] and the mechanical cavity design [16] ended with an successful high power RF-test of the copper plated FoS-cavity [17].

ALVAREZ 2.0 CAVITY TANK

The five Alvarez 2.0 cavities, each with out of five tank sections (Fig. 3), have been delivered to GSI, with the last tank arriving in December 2025. The cavities are made of stainless steel with a wall thickness of 12 mm; the internal di-

* manuel.heilmann@email.de

Content from this work may be used under the terms of the CC BY 4.0 licence (© 2026). Any distribution of this work must maintain attribution to the author(s), title of the work, publisher, and DOI.

ISBN: 978-3-95450-252-3 ISSN: 2673-5350 doi: 10.18429/JACoW-IPAC2026-THP4021

HEAVY ION FOCUSING USING A GABOR LENS INSIDE A DRIFT TUBE STRUCTURE

M. Heilmann*, GSI Helmholtz Centre for Heavy Ion Research, Darmstadt, Germany
C. Butz, M. Droba, M. Mack, O. Meusel
IAP, Goethe University Frankfurt, Frankfurt am Main, Germany

Abstract

Space-charge lenses based on confined non-neutral plasmas, such as electron clouds, provide strong, axially symmetric focusing for high-intensity ion beams (Table 1) and serve as an alternative to conventional quadrupole magnets. The so-called Mobley drift tube integrates a Gabor Lens (GL) into a drift tube of a linear accelerator, enabling beam focusing within an accelerating RF structure. The confined electron cloud does not come into direct contact with the accelerating field; a re-entrant snout geometry is introduced and optimized to minimize the RF field amplitude in the region where the electron cloud forms. Confinement of sufficiently high electron density is achieved in the beam pipe of the drift tube without any external electron source, relying solely on self-sustained processes. This contribution presents simulations and RF measurements of an RF- and vacuum-compatible prototype Mobley drift tube designed for heavy-ion beams, providing insight into the operational feasibility and focusing performance of Gabor lenses integrated in LINAC drift tubes.

INTRODUCTION

A Gabor-lens [1–3] consists of a positively charged cylindrical electrode, a radial magnetic field and ground electrodes designed to capture and confine the generated, rotating electron clouds that focus and transport the hadron beams [4, 5]. The original concept of the lens envisaged the use of a longitudinal magnetic field generated by a solenoid coil for the radial confinement, in this case a Helmholtz coil configuration is used.

In heavy ion accelerator facilities operating in the low [6] up to high β range [7, 8], various types of focusing elements are used, such as magnetic quadrupoles or solenoids. These magnetic quadrupoles can be positioned inside a drift tube in a linear accelerator or outside the cavity. The alternative is the Mobley drift tube [9], which integrates a Gabor-lens into a drift tube. Drift tubes with internal magnetic focusing elements (single, double or triple quadrupole lenses) are now installed in many different LINACs, but the construction, operation or repair of these internal lenses presents a challenge. In addition to focusing and transporting heavy-ion beams, it is also possible to study the interaction of an electron shower between two drift tubes. The electron shower can be activated with the described Mobley-Gabor lens for detailed experiments involving threshold measurements.

Table 1: Heavy Ion Beam Parameters

Parameter	Unit	Value
Ion		U^{28+}
Max. current	mA	15.0
Input beam energy	MeV/u	1.358
Beam pulse length	ms	≤ 1.0
Beam repetition rate	Hz	≤ 10

MOBLEY-GL AND RF

The Mobley-Gabor lens (see Fig. 1) is an improvement of the Gabor-lens, as it is located in a linear accelerator and within a accelerating RF-field. The electric field in the accelerating gap increases in accordance with the RF period. The field has not yet reached its peak when the particle beam enters the accelerating gap, and by the time it leaves the gap, the field has already begun to decrease again. The end plates of the drift tube are the ground electrodes of the Gabor lens.

The general design of a Gabor lens uses a solenoid to ensure radial confinement via a longitudinal magnetic field. The Mobley drift tube required a design change from the

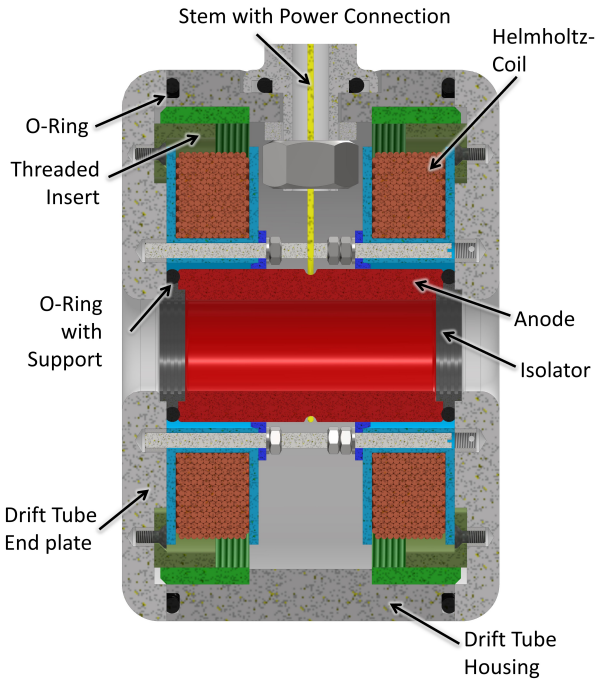

Figure 1: Test setup of a Mobley-drift tube with integrated Gabor lens (anode, isolation, end plate of the drift tube, Helmholtz coil) into a drift tube of a linear accelerator.

* m.heilmann@gsi.de

Content from this work may be used under the terms of the CC BY 4.0 licence (© 2026). Any distribution of this work must maintain attribution to the author(s), title of the work, publisher, and DOI.

ISBN: 978-3-95450-252-3 ISSN: 2673-5350 doi: 10.18429/JACoW-IPAC2026-THP4022

ACCELERATOR DEVELOPMENT FOR THE HIGH BRILLIANCE NEUTRON SOURCE (HBS-I)

A. Lehrach[1]*, T. Gutberlet, U. Rücker, P. Zakalek
Forschungszentrum Jülich, Jülich, Germany
H. Podlech[2], O. Meusel
Johann Wolfgang Goethe-Universität, Frankfurt, Germany
[1]also at III. Physikalisches Institut B, RWTH Aachen University, Aachen, Germany
[2]also at Helmholtz Research Academy Hesse for FAIR (HFHF), Frankfurt, Germany

Abstract

Accelerator-driven neutron sources offer an attractive alternative to reactor- and spallation-based facilities for providing high-quality neutron beams for research and industry. With the availability of high-current proton accelerators, a new class of compact High-Current Accelerator-driven Neutron Sources (HiCANS) has recently become feasible. These facilities combine medium-energy proton beams in the tens-of-MeV range with beam currents up to 100 mA, compact target–moderator systems, and optimized neutron transport to deliver thermal, cold, epithermal, and fast neutrons.

The HBS-I project at Forschungszentrum Jülich is developing such a next-generation neutron source, designed as a flexible and cost-efficient research infrastructure. This paper presents the development and design of the 100 mA, 20 MeV pulsed proton linac, including the front-end, RFQ, CH-DTL, and the High-Energy Beam Transport (HEBT) system. The accelerator is optimized for high reliability, low beam losses, and uniform target irradiation through fast beam scanning, forming the technical foundation for a compact and high-brilliance neutron source.

INTRODUCTION

Neutrons are an essential probe for investigating the structure and dynamics of matter across a wide range of length and time scales, making them indispensable for research in physics, chemistry, biology, and materials science. As capacities at conventional reactor-based neutron sources have declined significantly in recent decades, accelerator-driven neutron sources have emerged as a promising and sustainable alternative. These facilities use high-current pulsed proton beams in the tens-of-MeV range to generate neutrons in compact target–moderator systems, enabling efficient operation with significantly reduced shielding and cooling requirements.

The High Brilliance neutron Source (HBS-I), recently shortlisted by the German Federal Ministry of Research, Technology, and Space, is designed to provide high-quality neutron beams for a broad scientific and industrial user community. HBS-I employs a 100 mA, 20 MeV pulsed proton beam to produce small-diameter neutron beams suitable for experiments requiring high brilliance and small sample volumes. The facility will support research in energy materials, quantum materials, nanoscience, life sciences, and industrial applications.

Developed in collaboration between Forschungszentrum Jülich, Goethe-University Frankfurt, and Helmholtz-Zentrum Hereon, HBS-I represents a major step toward a new national neutron source [1]. Its compact design, modular accelerator concept, and flexible neutron instrumentation offer a forward-looking solution to the challenges currently faced by neutron research in Germany and Europe.

ACCELERATOR DESIGN AND KEY PARAMETERS

The HBS-I linac must provide a highly reliable, efficient and maintainable high-current proton beam for continuous user operation. To achieve this, the accelerator design follows several key principles. First, the choice between superconducting and normal-conducting technology is guided by the top-level beam parameters listed in Table 1, including beam current, duty cycle and final energy. For the required 100 mA, 20 MeV operation with an upgrade option to 30 MeV, a compact normal-conducting solution offers the most robust and cost-effective approach. Reliability and availability are central design drivers. All components are operated well below their technical and physical limits to minimize failure rates and simplify thermal management. A modular layout ensures straightforward access for maintenance and repair, while redundancy in critical subsystems further enhances operational stability. Together, these measures form the basis for a linac optimized for long-term,

Table 1: Top-Level Beam Parameters

Parameter	Specification
Particle type	Protons
Beam current	100 mA
Beam loss limit	1 W/m
Final energy	20 MeV
Upgrade option	30 MeV
Beam duty factor	2 to 4 %, DC
Pulse length	208 µs to 833 µs
Repetitions rate	24 to 96 Hz

* a.lehrach@fz-juelich.de

Content from this work may be used under the terms of the CC BY 4.0 licence (© 2026). Any distribution of this work must maintain attribution to the author(s), title of the work, publisher, and DOI.

ISBN: 978-3-95450-252-3 ISSN: 2673-5350 doi: 10.18429/JACoW-IPAC2026-THP4023

FIRST BEAM TEST OF AN ADDITIVELY MANUFACTURED H-MODE LINAC STRUCTURE MADE FROM PURE COPPER

H. Hähnel[1,*], A. Ateş[1], L. Bauer[1], B. Dedić[1], J. Kaiser[1], P. Müller[1], U. Ratzinger[1], G. Dollinger[2], M. Mayerhofer[2], P. Reichart[2]
[1]Institute of Applied Physics (IAP), Goethe University Frankfurt, Frankfurt am Main, Germany
[2]Institute for Applied Physics and Measurement Technology, University of the Bundeswehr Munich, Neubiberg, Germany

Abstract

We present results from a 1.4 MeV proton beam test of the first IH-Type linac structure additively manufactured (AM) from pure copper. The cavity has been tested up to 25 kW at a duty cycle of 2 %, which corresponds to a cavity voltage of 1 MV with peak fields at the drift tubes reaching up to 68 MV/m without RF breakdown at full power. A 1.4 MeV proton beam from a Van de Graaff accelerator has been accelerated up to 2.2 MeV, demonstrating the effective acceleration voltage of 0.83 MV at full power. These high power beam tests show performance en par with conventionally manufactured H-mode structures, paving the way for future linac structures benefiting from the advantages of additive manufacturing.

INTRODUCTION

Additive manufacturing (AM) especially of metals has become a promising method for the manufacturing of linac cavities. Recent studies on AM copper include a 750 MHz 4-vane RFQ prototype [1,2], S Band and X Band cavities [3–5], as well as the 433 MHz IH-DTL presented in this paper [6,7]. A more detailed description of the beam test presented in this proceeding can be found in [8]. The main benefits of the AM method are in most cases a significant reduction in cost, the fact that almost any internal cooling structure is easy to implement and manufactured along with opening up a new design paradigm for cavity geometries.

Cavity

The 433 MHz IH-DTL cavity was designed as a platform for a proof-of-concept of AM drift tube structures (Fig. 1). Previously tested with copper plated stainless steel AM structures, the cavity is now fitted with pure copper AM parts. The main parameters of the cavity are summarized in Table 1. The on axis field distribution of the cavity as used in the beam test was measured by bead pull, as can be seen in Fig. 2. Cavity vacuum is reliably in the order of 2×10^{-7} mbar to 4×10^{-7} mbar without RF.

Power Tests and Beam Tests

After successful high power RF tests of the cavity in 2024 [9] and 2025 [10], the cavity was used to accelerate a 1.4 MeV proton beam from the Van de Graaff accelerator at the institute of atomic physics in Frankfurt. The beam test setup is depicted in Fig. 3. A Si-PIN diode detector was used to measure the energy spectra of the beam after passing the cavity. The measurement was gated to the RF pulse of the cavity, measuring only particles that passed the cavity while it was active. The expected energy spectrum behind the cavity is basically a high resolution phase scan of the cavity (as can be seen from fieldmap simulations in Figs. 4 and 5). From this measurement, the effective acceleration can be deduced from the high energy peak which corresponds to the particles entering the cavity at the correct synchronous phase and following the intended gap sequence. The details will be discussed in the following.

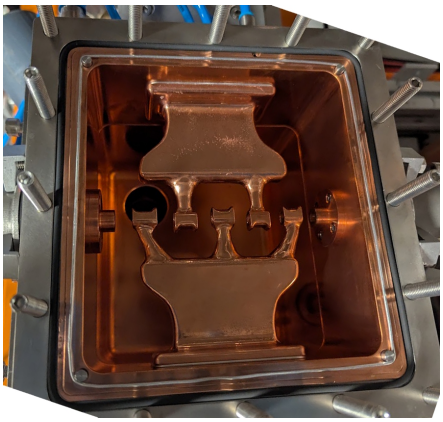

Figure 1: AM IH-DTL with the polished copper AM girders mounted for operation.

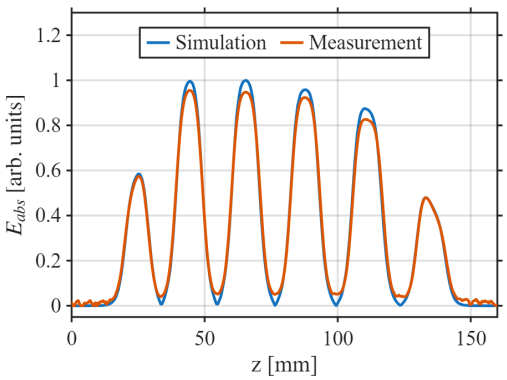

Figure 2: Comparison of the on-axis field distribution simulated with CST Microwave Studio with bead pull measurements of the AM-IH-DTL with the final copper AM girders installed. After baseline correction of the measured data, both curves are normalized to the same total area.

* haehnel@iap.uni-frankfurt.de

Content from this work may be used under the terms of the CC BY 4.0 licence (© 2026). Any distribution of this work must maintain attribution to the author(s), title of the work, publisher, and DOI.

ISBN: 978-3-95450-252-3 ISSN: 2673-5350 doi: 10.18429/JACoW-IPAC2026-THP4026

UPDATE ON ESS MEDIUM BETA CAVITIES AT INFN LASA

D. Sertore*, M. Bertucci, A. Bosotti, E. Del Core, F. Fiorina, L. Monaco,
R. Paparella, P. Spruzzola, B. Vitali[1], C. Pagani[1,2]
[1]INFN Milano - LASA, Segrate, Italy
[2]University of Milan, Segrate, Italy

Abstract

INFN LASA is involved in the delivery of four Medium Beta cavities to ESS ERIC as part of the Italian In-Kind Contribution to the "Operation Phase".

The cavities have been fabricated and tested bare before the integration into the helium vessel. After successful performance verification, the cavities will be integrated and finally validated at DESY AMTF before their delivery to CEA for installation into the cryomodule. We report the results of the fabrication and tests as well as lessons learned so far.

INTRODUCTION

The European Spallation Source (ESS) linear accelerator employs superconducting radio-frequency (SRF) cavities to accelerate the proton beam to its final energy of 2 GeV, corresponding to world record power of 5 MW beam on target [1].

The Medium Beta (β = 0.67) section is based on six-cell elliptical cavities operating at 704.42 MHz and provides acceleration between 256 MeV and 571 MeV. INFN Milano-LASA completed the production of 36 Medium Beta cavities as part of the ESS in-kind contribution program to the "Construction Phase" [2].

Following the completion of the series production and the qualification campaign [3], ESS identified the need for additional qualified cavities to support the assembly of a spare cryomodule and to increase operational flexibility over the machine lifetime. Four additional Medium Beta cavities were therefore requested as part of the Italian contribution to the "Operation Phase" of the ESS accelerator. Beyond addressing this operational requirement, the activity was also intended to confirm the maturity and robustness of the production and surface treatment workflow developed during series production.

This paper presents the status and the results of the first vertical RF tests of these four new cavities, with particular emphasis on RF performance, field emission behavior, and process reproducibility.

CAVITY DESIGN AND PARAMETERS

The cavities adopt the standard ESS Medium Beta elliptical design and are then fully compatible with the existing cryomodule infrastructure. No changes to cavity geometry, RF parameters, or interfaces were introduced with respect to the series production. The main cavity parameters are summarized in Table 1.

Table 1: Main Parameters of the ESS Medium Beta Cavity

Parameter	Value
Frequency	704.42 MHz
Geometry beta	0.67
Number of cells	6
Operating temperature	2 K
Active length	0.855 m
Optimum β, β_{opt}	0.705
Max R/Q at β_{opt}	374 Ω
E_{acc} at β_{opt}	16.7 MV/m
Q_0 at nominal gradient	$\geq 5 \times 10^9$

PRODUCTION AND SURFACE PREPARATION

Niobium Material and Quality Control

High-purity niobium sheets were procured by ESS by Ningxia Orient Tantalum Industry Co., Ltd. (OTIC). Before shipment, we inspected all the sheets at the vendor premises to identify possible visible defects that could be removed before shipment.

Moreover, the Nb sheets underwent Eddy Current Scanning at DESY to identify potential inclusions or subsurface defects not identify by the visual inspection. All Nb sheets satisfied the acceptance criteria and were then released for cavity fabrication, ensuring full traceability throughout the production chain.

Cavity Fabrication

Cavity fabrication was carried out at Zanon Research and Innovation S.r.l (ZRI) following the ESS-qualified manufacturing workflow [4, 5]. The process started with the deep drawing of the half-cells. The measurements done after this stage indicated a problem with the drawing process which resulted in out of shape components. This issue was quickly identified and resolved by the manufacturer, who implemented corrective actions to restore the process control and ensure that the half-cells were within the required dimensional tolerances.

Half-cells were then trimmed, and electron-beam welded into dumbbells. Intermediate RF frequency measurements were performed after each welding step to control cumulative errors. End groups, including the fundamental power coupler and pickup antenna ports, were subsequently welded.

Based on dimensional and RF measurements, we combined the different subcomponents to form the final four

* daniele.sertore@mi.infn.it

Content from this work may be used under the terms of the CC BY 4.0 licence (© 2026). Any distribution of this work must maintain attribution to the author(s), title of the work, publisher, and DOI.

ISBN: 978-3-95450-252-3 ISSN: 2673-5350 doi: 10.18429/JACoW-IPAC2026-THP4027

INFN LASA ACTIVITIES TOWARD PIP-II

R. Paparella†, M. Bertucci, A. Bosotti, E. Del Core, F. Fiorina, L. Monaco, C. Pagani[1], D. Sertore, P. Spruzzola, B. Vitali, Istituto Nazionale di Fisica Nucleare, Laboratori Acceleratori e Superconduttività Applicata, Segrate, Italy
[1] University of Milan, Segrate, Italy
J. Bernardini, V. Chouhan, L. Grassellino, K. McGee, J. Ozelis, Fermi National Accelerator Laboratory, Batavia, United States

Content from this work may be used under the terms of the CC BY 4.0 licence (© 2026). Any distribution of this work must maintain attribution to the author(s), title of the work, publisher, and DOI.

Abstract

INFN LASA is advancing its in-kind contribution to the PIP-II project at Fermilab, with significant progress achieved in both cavity production and testing infrastructures. The main activity is the fabrication of 38 five-cell $\beta = 0.61$ superconducting cavities for the LB650 section of the linac. Manufacturing is well advanced, with mechanical production of the series cavities progressing while the two pre-series ones are being used to validate the complete industrial workflow, including surface processing and final preparation, that is mostly entrusted to industrial partners. To ensure compliance with the stringent performance requirements of PIP-II, all cavities will undergo final qualification through a vertical cold tests facility at DESY AMTF (Germany) that is being finalized and commissioned. Lastly, the cavities will proceed with the delivery to CEA Saclay (France) as fully validated components ready for string assembly. This contribution summarizes the status of these activities, presenting updates from the manufacturing of series cavities, results from pre-series qualification and recent upgrades to both LASA and DESY testing infrastructures.

INTRODUCTION

The Fermilab Proton Improvement Plan II (PIP-II) Linac is designed to deliver a 1.2 MW H^- beam, with future scalability to multi-megawatt operation, in support of the Long-Baseline Neutrino Facility (LBNF) and Deep Underground Neutrino Experiment (DUNE) programs [1].

Once it reached 800 MeV, the beam is transferred to the upgraded Booster Ring and subsequently injected into the Main Injector. The Linac operates with a flexible 0.55 ms, 2 mA beam pulse structure, while its radiofrequency (RF) systems are capable of continuous-wave operation.

A key element of the accelerator is the 650 MHz superconducting low-beta section (LB650), consisting of 36 five-cell elliptical cavities installed in 9 cryomodules and accelerating the beam from 177 MeV to 516 MeV.

The operational target for the LB650 cavities is a quality factor of 2.4×10^{10} at an accelerating gradient of 16.9 MV/m under cryomodule conditions [2], with even higher performance required during vertical cold tests.

THE LB650 CAVITY DESIGN

All 38 superconducting cavities, including 36 series and 2 pre-series units, will be delivered by Istituto Nazionale di Fisica Nucleare (INFN) following successful vertical testing.

The cavities will be fully dressed, equipped, maintained under ultra-high vacuum, and ready for string assembly. INFN LASA developed the electromagnetic and mechanical design of the LB650 resonators [3], including all interfaces with the cryomodule environment, such as ports, flanges, power couplers, tuners, helium vessels, and associated interconnections.

THE LB650 CAVITY SURFACE TREATMENT RECIPE

The cavity surface preparation sequence begins with bulk electro-polishing (EP), providing a total material removal of 140 μm, including a final 20 μm "cold" EP step. Current-voltage measurements are performed during each treatment to ensure process reproducibility and stable reaction conditions throughout production.

Each chemical treatment is followed by ethanol rinsing to remove Sulphur contaminants that could degrade cavity performance and enhance field emission.

A degassing heat treatment is then carried out in vacuum at 900 °C for 3 hours, followed by in-vacuum cooling. This step is combined with frequency and field-flatness tuning, taking advantage of the softened mechanical state of the cavity after high-temperature treatment.

The final surface preparation includes an additional 40 μm electro-polishing, again with the last 20 μm performed in cold conditions, followed by more than 48 hours of exposure to ISO4 clean air to promote complete re-oxidation of the inner surface.

Subsequently, a mid-temperature bake at 350 °C for 3 hours in vacuum furnace is performed to enhance the quality factor at medium and high accelerating gradients. Since this treatment defines the final RF surface properties, it is carried out in a fully qualified furnace capable of guaranteeing state-of-the-art vacuum conditions. The LB650 series will benefit from the significant experience gained in these last few months on executing Mid-T treatment both in a lab environment and in industry [4].

Finally, to preserve the optimized inner surface, cavity tuning and helium-vessel integration are performed in a particle-free argon atmosphere. During the complete integration process, a dedicated flanging and monitoring system derived from the Eu-XFEL Frequency Monitoring System (FMS) [5] is used to continuously control and, if necessary, correct cavity frequency and field flatness.

†rocco.paparella@mi.infn.it

ISBN: 978-3-95450-252-3 ISSN: 2673-5350 doi: 10.18429/JACoW-IPAC2026-THP4030

ARGITU RFQ BEAD-PULL TUNING AND RF TESTS AT ESS-BILBAO

J. L. Muñoz*, I. Bustinduy, D. Fernández-Cañoto , N. Garmendia, P. González, G. Harper, J. Martín
ESS-Bilbao, Zamudio, Spain

Abstract

In this paper we describe the static tuning procedure of the ARGITU/HiCANS-platform RFQ at ESS-Bilbao. The machining and assembly of the RFQ were finished during 2025. The cavity is a 3.1-m-long, four-vane structure operating at 352.2 MHz. It will accelerate a 40 mA (designed up to 65 mA) proton beam from 45 keV to 3.0 MeV. The RFQ will operate at 1 % duty cycle in the first stages of the ARGITU HICANS platform, and later as the injector of the linac at a maximum duty cycle of 5 %. The static tuning of the cavity has been carried out combining bead-pull field-profile measurements with a conventional SVD algorithm and a genetic algorithm, the latter required by the limited tuner range available near the operational frequency. The whole procedure and the results are described in this paper.

INTRODUCTION

The ARGITU RFQ is the first accelerating cavity of the ESS-Bilbao proton linac for the HiCANS platform project of a compact accelerator-driven neutron-source [1–3]. It is a 352.2 MHz, four-vane RFQ designed to accelerate protons from 45 keV to 3.0 MeV in a 3.1 m long copper structure [4–7]. One of the characteristics of ESS-Bilbao RFQ is that no brazing was used for the assembly of the vanes that form each segment.

The RFQ was assembled, and its alignment was verified by using mechanical probes and laser-tracker measurements. The RFQ is designed assuming a uniform inter-vane voltage of 85 kV, so in the ideal assembly the field profile along the RFQ length will be flat, as well as symmetric in the four lobes. The deviations from this ideal behavior are caused by the modulation itself as well as by perturbations caused by the assembly and mechanical deformations of the structure. As a result, the measured field in the four lobes is not flat along the longitudinal coordinate and is not identical in all quadrants. Tuning is therefore required to recover the design longitudinal field profile and to bring the resonant frequency close to the value that will be used in operation.

The RFQ has 64 tuner ports, two of which are occupied by the power-coupler ports in the final configuration. The tuning campaign was carried out with 62 plunger tuners installed. Each plunger tuner is attached to a high-precision manual actuator, with a total tuner range of 25 mm. The RFQ was placed in a laboratory room with controlled temperature, with the bead-pull apparatus attached. Figure 1 shows the RFQ installed in the bead-pull bench.

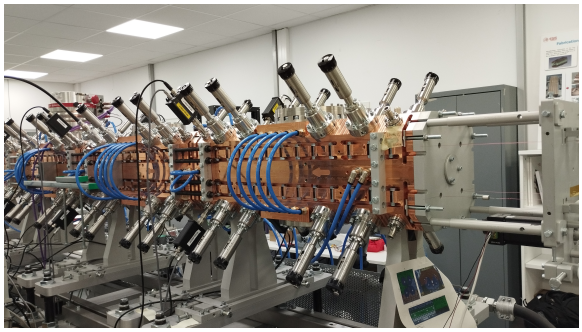

Figure 1: ESS-Bilbao RFQ installed in the bead-pull bench. The tuner actuators, pickup loops and bead-pull apparatus are visible.

BEAD-PULL MEASUREMENTS

The field profile was measured with the bead-pull technique. A small metallic bead was moved through high-magnetic-field lobe regions by the action of a computer controlled motor. The phase perturbation of the transmitted RF signal was recorded with a network analyzer. The bead moves along two of the lobes in the positive direction (beam direction), and along the negative one in the other two, so the data processing software needed to take care of this. The four traces were synchronized in the longitudinal direction using the perturbation caused by the first of the plunger tuners in the measured trace. Traces were then shifted to match this position. Finally, the base-line magnitude of the traces, in positions outside of the RFQ (which should be of zero amplitude) were used for height and drift compensation. The four longitudinal traces, $q_1(z)$ to $q_4(z)$, were assigned signs according to the quadrupolar-mode convention and normalized before being combined into the quantities $Q = \frac{q_1 - q_2 + q_3 - q_4}{4}$, $D_s = \frac{q_1 - q_3}{2}$ and $D_t = \frac{q_2 - q_4}{2}$.

The quadrupolar component Q represents the useful accelerating-field profile and is normalized to an average value of 100 %. The dipolar terms D_s and D_t quantify asymmetries between opposite lobes. The ideal tuning target used in the procedure is therefore a flat $Q(z)$ profile and dipolar components as close as possible to zero.

The initial configuration used for the response characterization had all tuners inserted to the same penetration. The measured profiles, shown in Fig. 2, presented a strong longitudinal slope in Q and large dipolar components. Nineteen longitudinal positions were selected from the traces to form the profile vector used by the tuning algorithms. The selected positions avoided regions where the bead passed too close to tuners, pickups or coupler openings, because such regions can create local distortions that are not representative of the global accelerating profile. Cavity frequency for this configuration was 349.995 MHz.

* jlmunoz@essbilbao.org

Content from this work may be used under the terms of the CC BY 4.0 licence (© 2026). Any distribution of this work must maintain attribution to the author(s), title of the work, publisher, and DOI.

ISBN: 978-3-95450-252-3 ISSN: 2673-5350 doi: 10.18429/JACoW-IPAC2026-THP4031

COOLING SKID, THERMAL CHARACTERIZATION AND SIMULATIONS FOR THE ARGITU RFQ AT ESS-BILBAO

J. L. Muñoz*, I. Bustinduy, D. Fernandez-Cañoto, N. Garmendia, P. González, R. González, G. Harper, S. Masa, ESS-Bilbao, Zamudio, Spain

Abstract

The ARGITU RFQ at ESS-Bilbao is a 352.2 MHz, 4-vane RFQ that will accelerate protons from 45 keV to 3.0 MeV. The RFQ is a 3.1 meters long structure machined in OFHC copper of high purity, and no brazing has been used to assemble the vanes that conform each of the four segments. The cooling of the structure is carried out by cooling channels that runs longitudinally along the vane tips and transversal in the vacuum grid region. In a first stage, the RFQ will operate at a maximum duty cycle of 1 %, and for this stage a first version of the water cooling skid has been designed, built and tested. The vane cooling channels in this setup runs in series from segment to segment allowing a simpler design. A dedicated chiller that provides great stability and control has been integrated in the system, as well as water flow and temperature valves and sensors monitored using IO link technology. The cooling water skid, the tests performed with the RFQ and their correlation with FEM simulations are described in this paper. The dynamic tuning of the RFQ during conditioning and operation are also described.

INTRODUCTION

The ESS-Bilbao RFQ is the first accelerating structure of the ARGITU neutron source and the HiCANS platform project [1–3]. The RFQ is 3.1 m long, machined in OFHC copper. It is and assembly of four segments of approximately 800 mm length, each one assembled using rubber gaskets instead of brazing to facilitate any replacement in case of damage. It will accelerate protons from 45 keV to 3.0 MeV at a frequency of 352.2 MHz [4, 5]. The RFQ has been fabricated, assembled and tested at low RF power. The tuning, including cooling water in the process, has also been finished [6]. The next commissioning stages require conditioning with RF power and beam. The initial configuration for HiCANS platform project first stages will be limited to low duty cycles below approximately 1 %, because power couplers at this stage do not have active cooling [7]. This reduced duty factor relaxes the average thermal load, but it does not remove the need for a stable and well-characterized water-cooling system.

RF power losses produce thermal deformation and therefore a change of resonant frequency and field profile. Conversely, changes in cooling-water temperature or flow modify the temperature field in the vanes and body, and can be used to compensate frequency drift. For this reason, cooling specifications define not only water flow and temperature magnitudes, but also stability requirements. The present work focuses on the cooling implementation for HiCANS-platform specifications, the technology used for this and on the first measurements of RFQ frequency as a function of the water-cooling conditions.

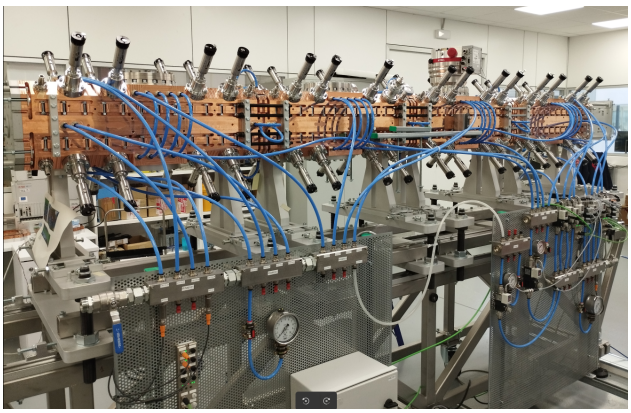

Figure 1: ESS-Bilbao RFQ connected to the cooling skid during the first water-cooling and frequency characterization campaign.

RFQ COOLING SETUP

The RFQ body includes several families of machined cooling channels. Channels type 1 run close to the vane tips and are the most effective ones for frequency control; channels type 2 are placed in the external vane region; and channels type 3 cool the vacuum-grid region. The full RFQ cooling specification gives nominal flow rates of 3.3 l/min per type 1 channel and 6 l/min for type 2 and type 3 channels, with a total RFQ-body flow, excluding tuners, couplers and pickups, of about 437 l/min [4, 5]. In the setup for HiCANS-platform, the cooling skid is simplified with a single chiller and a common inlet water temperature. Type 1 and 2 channels are connected in series, whereas type 3 channels are arranged in parallel between segments to minimize temperature gradients caused by coolant heating. This arrangement reduces the number of independently controlled circuits and is adequate for the low-duty-cycle commissioning phase.

Figure 1 shows the RFQ and the cooling skid. The system includes the SMC chiller, piping, manual flow adjustment elements, SMC PF3W7 flow-temperature sensors and the corresponding EPICS monitoring and control. The sensors validation campaign showed temperature stability below approximately ±0.1 °C at fixed set points and good flow stability for the sensors. The flow and temperature-meter sensors are connected to the control system directly via IO-link technology, without needing a PLC.

* jlmunoz@essbilbao.org

Content from this work may be used under the terms of the CC BY 4.0 licence (© 2026). Any distribution of this work must maintain attribution to the author(s), title of the work, publisher, and DOI.

ISBN: 978-3-95450-252-3 ISSN: 2673-5350 doi: 10.18429/JACoW-IPAC2026-THP4032

RF DESIGN AND BEAM DYNAMICS OF A 3 GHZ SCDTL OPTIMIZED IN TERMS OF $(S_c^{\max}/E_a^2)/ZTT$ FOR CARBON ION ACCELERATION IN A MEDICAL INJECTOR

Eduardo Martinez-Lopez*, Nuria Fuster-Martínez, Marça Boronat, Juan Carlos Fernández-Ortega, Daniel González-Iglesias, Juan Fuster, Benito Gimeno, Daniel Esperante
Instituto de Física Corpuscular, Paterna, Spain
Alexej Grudiev
European Organization for Nuclear Research (CERN), Geneva, Switzerland
Concepción Oliver
Department of Technology, CIEMAT, Avenida Complutense 40, Madrid, 28040, Spain

Abstract

This study presents a comprehensive methodology for the RF design and optimization of a 3 GHz SCDTL structure in terms of the modified Poynting vector S_c and the effective shunt impedance ZTT. By systematically refining the geometry of both accelerating and side-coupling cavities, the design achieves a maximized effective shunt impedance and accelerating gradient while ensuring compliance with breakdown limits based on the modified Poynting vector. The optimized structures are subsequently used to investigate beam dynamics constraints for a representative C^{6+} carbon ion beam, which is pre-accelerated in 750 MHz structures up to 10 MeV/u and then further accelerated in the proposed SCDTL structures from 10 MeV/u to 85 MeV/u.

INTRODUCTION

Hadron therapy is a cancer treatment modality that employs hadrons to irradiate tumors with high precision. To enable such fast and precise energy modulation, LINAC-based systems rely on a sequence of radio-frequency (RF) accelerating cavities, which transfer energy to the particles through oscillating electromagnetic fields. The design of low-energy accelerating structures should be primarily guided by the effective shunt impedance per unit length (ZTT), as it directly determines the energy efficiency of the system:

$$ZTT = \frac{\Delta W^2}{P_d \times L} \tag{1}$$

where ΔW is the energy gain, P_d is the dissipated peak power, and L is the active length of the LINAC.

For compact hadron therapy LINACs, the radio-frequency operating frequency $f_{\mathrm{RF}} = 3$ GHz has been established as the standard for accelerating structures operating above 10 MeV/u. At lower energies, however, a reduced RF frequency is required, with 750 MHz commonly adopted in several LINAC designs [1]. This choice is motivated by beam dynamics considerations: the RF defocusing scales as $\Delta p_{\mathrm{r}} \propto f_{\mathrm{RF}}/\beta^2\gamma^2$, while the longitudinal energy acceptance scales as $\omega_{\max} \propto \sqrt{\beta^3\gamma^3/f_{\mathrm{RF}}}$, where β is the particle velocity normalized to the speed of light and γ is the Lorentz factor [2].

The frequency transition is typically performed around 10 MeV/u [3–5]. The most efficient and widely used structure for this purpose is the 3 GHz SCDTL, which is commonly employed to accelerate ions from 10 to 100 MeV/u [1, 6, 7]. The SCDTL is composed of a series of short accelerating cavities interconnected by side-coupling cavities (SCCs) via coupling slots. The use of short cavities removes the requirement for post-coupler stabilization, thereby simplifying the overall structure [8].

This paper presents the design and optimization of 3 GHz SCDTL structures in terms of the figure of merit $(S_c^{\max}/E_a^2)/ZTT$, where S_c denotes the modified Poynting vector and E_a the effective accelerating gradient. The achievable accelerating gradients are evaluated, and the optimized structures are subsequently employed in beam dynamics studies. Special attention is given to longitudinal capture, particularly to the effects associated with the frequency transition from 750 MHz to 3 GHz.

THE RF CAVITIES

The accelerating and side-coupling cavities were designed separately to resonate at $f_{\mathrm{RF}} = 3$ GHz. The RF design optimization of the cavities was carried out using `SUPERFISH` [9, 10], applying the Slater perturbation method, and subsequently validated using full 3D electromagnetic simulations in `CST Microwave Studio` [11].

The RF Accelerating Cavity

Figure 1 shows the geometry of the accelerating cavity of a SCDTL structure designed to operate in the TM_{01} mode with a zero-mode field configuration and a cell length equal to $\beta\lambda$, where λ is the RF wavelength. The resonant frequency f_{RF} is primarily determined by the cavity diameter D. The inner radius of the drift tubes corresponds to the cavity aperture radius r. The initial and final cells, which contain the noses, have a length of $\beta\lambda/4$ each.

The RF Side-Coupling Cavity

The accelerating cavities are interconnected via side-coupling cavities (SCCs) through coupling slots. The length

* Corresponding author: Eduardo.Martinez@ific.uv.es

Content from this work may be used under the terms of the CC BY 4.0 licence (© 2026). Any distribution of this work must maintain attribution to the author(s), title of the work, publisher, and DOI.

ISBN: 978-3-95450-252-3 ISSN: 2673-5350 doi: 10.18429/JACoW-IPAC2026-THP4033

OUTCOMES OF THE DONES CONSOLIDATION PROJECT ACTIVITIES*

I. Podadera†, J. Aguilar, S. Becerril-Jarque, A. Ibarra, R. Lorenzo, J. Maestre, A. Moreno Cortes, C. Torregrosa-Martín, M. Weber, IFMIF-DONES España, Granada, Spain
M. Kubkowska, IPPLM, Warsaw, Poland
M. Hoic, D. Miler, University of Zagreb, Zagreb, Croatia
B. Brañas, D. Cano-Ott, F. Martín-Fuertes, E. Mendoza, M. Roldán, CIEMAT, Madrid, Spain
W. Królas, A. Maj, IFJ PAN, Krakow, Poland
M. Tarantino, ENEA, Rome, Italy
M. D'Andrea, L. Bellan, F. Grespan, A. Pisent, INFN, Rome, Italy
T. Tadic, RBI, Zagreb, Croatia
D. Radloff, M. Rieth, H.-C. Schneider, KIT, Karlsruhe, Germany
S. Chel, A. Letourneau, Université Paris-Saclay – CEA- IRFU, Gif-sur-Yvette, France

Content from this work may be used under the terms of the CC BY 4.0 licence (© 2026). Any distribution of this work must maintain attribution to the author(s), title of the work, publisher, and DOI.

Abstract

IFMIF-DONES is an ESFRI facility based on a 40 MeV, 5 MW beam power deuteron accelerator and a liquid lithium target currently under construction in Granada (Spain) as part of the European roadmap to fusion electricity. Its main goal is to characterize and qualify materials under a neutron field with an induced damage similar to the one expected in a fusion reactor, developing a material database for the future fusion nuclear power plants. Moreover, a number of medium neutron flux experiments in other irradiation areas for fusion and non-fusion applications have been proposed and are under analysis. Although the construction phase is ramping up, the European EURATOM Project DONES-ConP1 has been directed at the preparation of the key documentation and to consolidate contributions from the parties. In this contribution, the main outcomes of the project, such as the first proposal of the DONES Experimental Programme, consolidation of the DONES users community, users and machine interfaces, the evolution of the ideas for the complementary experiments, organization and project documentation for safety licensing will be presented and described.

INTRODUCTION

The DONES Consolidation Phase 1 Project (DONES-ConP1) [1] was an European Project within the EURATOM Work Programme formed by ten European institutions and observers, key in the area of fusion technology development and interested in the DONES Programme. The main objectives were: 1) Developing an **experimental programme** in fusion and also expanding to non-fusion areas, associated to widen the DONES Users community, 2) Completing the framework of the in-kind and partnership procurements by assessing the **strategy of the in-Kind Contributions** (IKC's) and 3) Updating **key documentation** for policy-makers about financial, legal and organisational project organisation related to the international character of the IFMIF-DONES Facility.

EXPERIMENTAL PROGRAMME

Fusion Programme

The main goal of the facility [2] is the validation of structural materials for fusion reactor in-vessel components. Several critical parameters were identified for study: temperature, displacement damage (2–50 dpa) and transmutation rates (He/H) shall be characterized for the baseline materials EUROFER97, CuCrZr, and tungsten in order to **create the materials properties database under fusion prototypic irradiations**, prioritized by parameters and conditions originating from EU DEMO requirements. A major methodological advance was the proposal of "flip-and-average" approach for High Flux Test Module (HFTM) specimen boxes (Fig. 1), improving dose uniformity to within ±10% and ensuring high-quality experimental data. The proposed programme includes a first campaign in two phases, covering over 85% of priority objectives: 1) verification of 14 MeV neutron energy damage effects, 2) assessment of transmutation phenomena, and 3) characterization of material properties under DEMO-representative conditions. The results detail planned **neutron irradiation campaigns,** covering both structural and functional materials, and specifies the testing methods to be implemented after exposure—such as tensile, fracture, fatigue, creep, and microstructural analyses using small-specimen techniques. It provides a mapping between irradiation modules and their associated Post Irradiation Experiments (PIE) workflows, defining the sequence of activities from sample retrieval to data validation.

Additionally, a catalogue of irradiation modules and their integration with future Test Blanket Module (TBM)

* This work has been carried out within the framework of the DONES-ConP1 Consortium, funded by the European Union via the Euratom Research and Training Programme - Euratom Work Programme 2023-2025 for nuclear research and training under Grant Agreement No 101145952 — DONES-ConP1, and partly co-financed by the Polish Ministry of Science and Higher Education within the programme called 'PMW' for 2023-2025. Views and opinions expressed are however those of the author(s) only and do not necessarily reflect those of the European Union or the European Commission. Neither the European Union nor the European Commission can be held responsible for them.
† ivan.podadera@ifmif-dones.es

ISBN: 978-3-95450-252-3 ISSN: 2673-5350 doi: 10.18429/JACoW-IPAC2026-THP4035

TESTING OF THE QWR SERIES FOR THE NEW ISIS MEBT

I. Rodriguez†, J. Cawley, A. Letchford
ISIS, Rutherford Appleton Laboratory, STFC, Didcot, UK

Abstract

The quarter wave resonator (QWR, a.k.a. λ/4 resonator) for the new ISIS MEBT is a bunching cavity that longitudinally compresses the H^- beam into smaller bunches. It has two gaps with a distance of βλ/2 between mid-gaps, and works in π mode at the resonant frequency of 202.5 MHz, with a phase angle of -90 degrees, and a maximum voltage per gap (E_0L) of 55 kV. The detailed RF and thermal design were developed, followed by the manufacturing and testing of a prototype, all presented elsewhere. Parts for 5 new cavities were later manufactured, whose details were also presented elsewhere. This paper discusses how these new cavities were assembled, tuned and tested. The assembly was done in the metrology lab to ensure the correct alignment of the nose cones to the stem ring, with the subsequent doweling. Unexpected problems were also found, including the installation of the automatic tuner finger-strips, how to achieve the expected quality factor and the conditioning of the cavities to cope with multipacting.

MANUFACTURING, ASSEMBLY AND TUNING

The current ISIS LINAC directly connects the RFQ to the first DTL tank at an energy of 665 keV. A MEBT was designed to improve the beam matching and to add other beam chopping features. The new MEBT consists of four QWRs, a beam chopper and eight quadrupole magnets.

The electromagnetic, thermal and mechanical designs, including the manufacturing, of a first prototype for the new QWR cavity were previously presented [1, 2]. A first prototype was assembled, tuned and successfully tested [3], which led to the manufacturing of the remaining parts for the series production of 5 additional cavities.

All production tanks for the cavities followed the same manufacturing method as in the prototype cavity, which involved machining from a solid billet to minimise welding.

The brazing jig was optimised to improve the disassembly process. Key changes included reducing the contact area for sliding parts and modifying the tapered section to have 3 points of contact rather than a full ring. Pushing screws were added for all parts to aid disassembly.

New stems and lids were ordered after the success of the prototype. The manufacturer proposed to use C110 rather than the specified C103 copper. The grade is a purer grade with better electrical properties, so the material change was agreed after discussing with the brazing company. When brazing the first of the production cavities, the brazing result did not follow the prototype result of the C103 lids and stems, which was identified as a wetting problem with the purer C110 copper when brazed in vacuum. At this point, it was decided to manufacture new C103 lids but continue to use the C110 stems due to cost and complexity of that part. Further to this, it was found that the diameter of the lip at the top of the stainless-steel tanks, which is a location feature for the lid, varied by up to 40 µm between cavities. Each lid needed to be machined to match each cavity.

To check the suitability of C103 lids with C110 stems, several test pieces were brazed which passed visual inspection and leak checks to give confidence. The production brazes were an improvement on the C110 set but did not completely replicate the success of the trial pieces.

In fact, the outcome of different brazes varied significantly between each tank. Examples included excess flow, partial flow and no flow through the joint (Fig. 1), all with the same parameters.

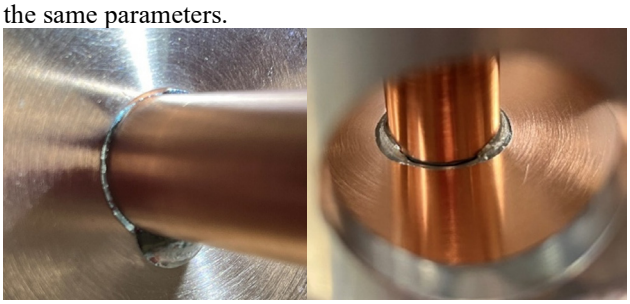

Figure 1: Braze joint problems.

Many of the cavities were brazed multiple times to improve the joint (Fig. 2). Eventually, only 4 out of the 5 cavities passed the vacuum leak test. It was decided to braze the failed one in an air oven rather than a vacuum oven, to allow the use of soldering flux. This was successful, although it needed thorough cleaning to remove the flux and polishing of the tarnished surfaces.

QWR	Lid	Stem	Oven	Braze processes	Joint
1	C103	C103	Vacuum	1) 275ºC, 15 mins, 1 ring solder, Vertical 2) 275ºC, 15 mins (Rerun)	**Top**: Full **Bottom**: Full **Droplet**: None
2	C103	C110	Vacuum	1) 275ºC, 15 mins, 1.75 solder rings, Inverted 2) 300ºC, 15 mins, Inverted 3) 300ºC, 15 mins, +0.3 solder ring, Inverted	**Top**: Full **Bottom**: Partial **Droplet**: None
			Air	4) 240ºC, 90 mins, Inverted, Flux	
3	C103	C110	Vacuum	1) 275ºC, 25 mins, 2 rings solder, Vertical 2) 275ºC, 15 mins (Rerun) 3) 300ºC, 30 mins, +0.5 solder ring, Inverted	**Top**: Full **Bottom**: Partial **Droplet**: Medium
4	C103	C110	Vacuum	1) 275ºC, 15 minutes, 1.75 solder rings, Vertical 2) 275ºC, 15 minutes, +0.4 solder ring (Rerun)	**Top**: Full **Bottom**: Full **Droplet**: Large
5	C103	C110	Vacuum	1) 275ºC, 15 minutes, 1.75 solder rings, Vertical	**Top**: Full **Bottom**: No flow **Droplet**: None

Figure 2: Cavity braze parameters.

The main problem later identified was the reduced silver content of C110 copper and the variability of the outcome due to the low temperature of the braze (275 ºC). The water channel joint, brazed at higher temperature (1000 ºC), produced consistent results each time without any problems.

After brazing, the stem and lids were aligned inside each final tank in metrology, where the cavity and stem offset were measured. They were finally dowelled to allow for repeatable assembly and fix the rotation of the lid.

† iker.rodriguez@stfc.ac.uk

Content from this work may be used under the terms of the CC BY 4.0 licence (© 2026). Any distribution of this work must maintain attribution to the author(s), title of the work, publisher, and DOI.

ISBN: 978-3-95450-252-3 ISSN: 2673-5350 doi: 10.18429/JACoW-IPAC2026-THP4037

FFA MAGNET PROTOTYPE FOR HIGH POWER PULSED PROTON DRIVER

J.-B. Lagrange*, C. Jolly, D. Kelliher, A. Letchford, S. Machida, S. Mohanavelu, C. Prior, I. Rodriguez,C. Rogers, J. Speed, Science and Technology Facilities Council, Swindon, UK
T.-J. Kuo, Imperial College London, London, UK
S. Brooks, Brookhaven National Laboratory, Upton, NY, USA

Abstract

The Fixed Field Alternating Gradient (FFA) accelerator is a natural candidate for a high-power pulsed proton driver, although no high-power FFA has yet been constructed. As a critical component of the accelerator, the main magnets have been the subject of particular study. Operational flexibility, in terms of machine optics, over a large range is an essential feature of such a machine. In order to explore this in more detail a dedicated FFA prototype magnet has been designed and manufactured. This magnet was manufactured and delivered to the Rutherford Appleton Laboratory (RAL) in the UK in 2025, and field measurements are subsequently planned to establish its characteristics. This paper will discuss the design, manufacture, and measurement plans of the prototype magnet.

INTRODUCTION

The Fixed Field Alternating Gradient Accelerator (FFA) is a compelling option for the next-generation high-power proton accelerator, such as the proposed ISIS-II facility at the Rutherford Appleton Laboratory (RAL). Unlike conventional synchrotrons, FFAs use DC magnets to enable high repetition rates and flexible longitudinal dynamics, making them ideal for high power pulsed applications like neutron and muon spallation sources. The FETS-FFA project [1] aims to design and build a 12 MeV proton FFA prototype ring as a proof-of-principle to validate the feasibility of high-intensity beam acceleration in an FFA, addressing key challenges such as beam loss control, machine tuneability and power efficiency. As a critical part of the hardware the main magnets have been designed [1]. Essential features for these magnets include zero-chromaticity during acceleration, dynamic aperture larger than the physical aperture to avoid uncontrolled losses, and flexibility in terms of tune point to allow different operation as a function of beam intensity. Zero-chromaticity is achieved when the magnet follows the scaling field law [2–4] defined by:

$$B = B_0 \left(\frac{r}{r_0}\right)^k \mathscr{F}\left(\theta - \tan\xi \ln\left(\frac{r}{r_0}\right)\right), \qquad (1)$$

where B_0 is the reference field at radius r_0, k the geometrical field index, ξ the spiral angle and $\mathscr{F}$ the arbitrary fringe field function. For the FETS-FFA ring, the field index k ranges from 6 to 9, and the spiral angle is 30 deg. A reverse bend magnet (D-magnet) is included to allow a change in vertical tune by changing the field strength ratio between the F and D magnets, while the k-value must be able to vary to change the horizontal tune.

To balance practical constraints and feasibility, a scaled-down single radial sector magnet was designed instead of a full-scale doublet. The goal for this prototype is to investigate the manufacturing process of such a magnet, to benchmark measurements with the OPERA [5] model, to establish a method to control the magnet, and finally to elaborate and verify correction schemes to locally correct closed orbit distortions (COD) and higher-order errors. The spiral effects of the magnet cannot be investigated with this prototype (i.e. manufacturing process of spiral nested coils, edge correction), and the effects of saturation will be difficult to study under normal current operation. The cross-talk of neighbouring magnets will also not be observed. The manufacturing process of winding spiral coils could be tested by producing a set of nested coils as a separate project, and benchmarking OPERA simulations could provide an insight on the behaviour of the full-scale doublet.

MAGNET PROTOTYPE DESIGN AND MANUFACTURING

Design Specifications

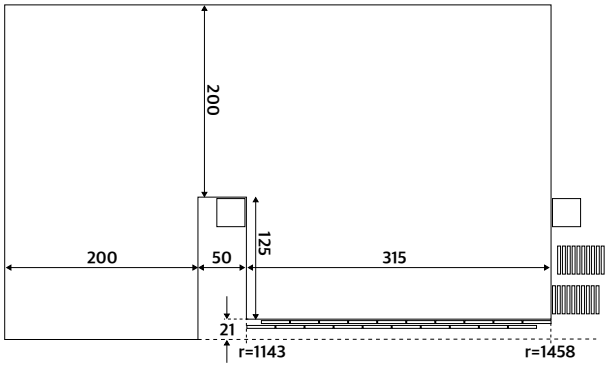

Figure 1: Transverse dimensions in mm of the prototype.

A flat gap with distributed coils was chosen to generate the field gradient, as in the FETS-FFA magnet [1]. Key parameters are summarised in Table 1. The transverse parameters are shown in Fig. 1, and the field errors after optimising the coil currents for the different k-value cases using OPERA 2D are presented in Fig. 2. The main coils are in a pancake shape, while the trim coils are saddled and nested, wound over 2 overlapping layers, and returning over 2 vertical layers.

* jean-baptiste.lagrange@stfc.ac.uk

Content from this work may be used under the terms of the CC BY 4.0 licence (© 2026). Any distribution of this work must maintain attribution to the author(s), title of the work, publisher, and DOI.

ISBN: 978-3-95450-252-3 ISSN: 2673-5350 doi: 10.18429/JACoW-IPAC2026-THP4038

MODELLING OF COUNTER-ROTATING MULTI-TURN WAKEFIELDS IN THE MUON COLLIDER RCS CHAIN

L. S. Thiele*, [1,2], S. Albright[1], R. Calaga[1], H. Damerau[1], A. Grudiev[1], I. Karpov[1], E. Lamb[1], S. Lauber[1], U. van Rienen[2,3], S.-A. Udongwo[2]
[1]CERN, Geneva, Switzerland
[2]Institute of General Electrical Engineering, University of Rostock, Rostock, Germany
[3]Department of Life, Light and Matter, University of Rostock, Rostock, Germany

Abstract

The future multi-TeV muon collider facility will employ a superconducting radiofrequency (RF) system with thousands of cavities in the rapid-cycling synchrotron (RCS) chain. This RF system, shared by both beams, will accelerate two counter-rotating μ^+ and μ^- bunches simultaneously. Due to the high intensity of up to 2.7×10^{12} particles per bunch, the induced voltage in both the fundamental and several higher-order modes is significant. A strong impact on longitudinal beam quality and the luminosity in the collider is expected. Modelling wake potentials in the RF system of the RCS chain is challenging. The long-range wakefields will interact with both the co- and counter-rotating bunches due to the high quality factor and corresponding long decay constants of the fields in the cavities. These two-beam interactions are studied, with particular attention to the specificities caused by the directionality of the induced fields.

INTRODUCTION

The proposed muon collider facility aims to collide two muon bunches at up to 10 TeV centre-of-mass energy, offering a resource-efficient path to highest energy collisions with leptons. Following cooling and pre-acceleration, the complex consists of a chain of four RCSs that sequentially accelerate the bunches from 63 GeV to 5 TeV. The first two accelerators are planned to be located in the same tunnel, while the last two are to be placed in separate tunnels.
Due to the short muon lifetime of $\tau_\mu \approx \gamma \times 2.2\,\mu s$ in the lab frame, the acceleration needs to be performed rapidly but under the stringent constraint of high beam quality in the collider. The relativistic Lorentz factor, γ, increases with energy. If the longitudinal emittance can not be preserved, the available luminosity will be impaired. The rapid acceleration of the bunches requires a large voltage, which is planned to be provided by thousands of 9-cell 1.3 GHz TESLA cavities [1]. An overview of the RF system parameters is given in Table 1.
The RF system is intended to be common to the μ^+ and μ^- bunches to enable a more cost- and energy-efficient acceleration. Both bunches are expected to have the same intensity of 2.7×10^{12} particles per bunch at the injection of RCS1, resulting in a high instantaneous and low average beam current. In combination with the small aperture of TESLA cavities, this will lead to high induced voltages of several megavolts in both the longitudinal and transverse planes, potentially perturbing the beam and causing emittance growth, instabilities, or beam loss. The high quality factor of the superconducting cavities will cause the induced voltages to persist until the passage of the counter-rotating bunch. The co-rotating beam on the next turn will also be affected. The external quality factor of the fundamental mode (FM) is expected to be around 10^6, while the quality factors of the higher-order modes (HOMs) are at least an order of magnitude lower in the strongly damped TESLA cavity.
The high accelerating voltage of several gigavolts per turn, combined with the fast acceleration rate, results in a large phase-advance of the fast synchrotron motion [2]. To reduce the effective synchrotron tune and preserve beam stability,

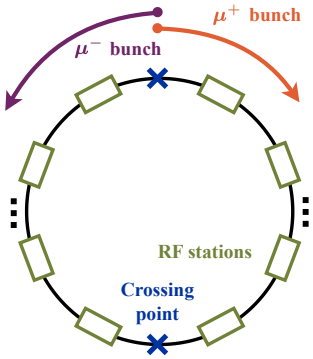

Figure 1: RF system distribution in the muon collider RCS chain. Due to the counter-rotating beams, the time difference between passage of the two bunches will be different in every RF station.

Table 1: Main RF system parameters from the consolidated parameter report of the MuCol project [2]. The stable phase, ϕ_s, is defined from the rising zero-crossing of the sine-wave.

RCS	1	2	3	4
E_{inj} [GeV]	63	313	750	1500
E_{ej} [GeV]	313	750	1500	5000
ϕ_s [°]	148	153	134	118
V_{RF} [GV]	27.6	17.5	15.7	72.7
n_{turns}	18	55	66	55
C [km]	5.99	5.99	10.7	35.0
α_p [10^{-4}]	10.4	9.0	3.2	2.1

* leonard.thiele@uni-rostock.de

Content from this work may be used under the terms of the CC BY 4.0 licence (© 2026). Any distribution of this work must maintain attribution to the author(s), title of the work, publisher, and DOI.

ISBN: 978-3-95450-252-3 ISSN: 2673-5350 doi: 10.18429/JACoW-IPAC2026-THP4039

OVERVIEW OF THE ESS NEUTRINO SUPER BEAM PLUS PROJECT

E. Salehi*, N. Milas, European Spallation Source, Lund, Sweden
on behalf of the ESSνSB+ project

Content from this work may be used under the terms of the CC BY 4.0 licence (© 2026). Any distribution of this work must maintain attribution to the author(s), title of the work, publisher, and DOI.

Abstract

The ESS neutrino Super Beam (ESSνSB) project aims to produce an intense neutrino beam optimized for measurement at the second neutrino oscillation maximum, providing an enhanced capability to discover CP violation in the lepton sector and to measure the CP violating phase with high precision. ESSνSB will be integrated into the ESS accelerator facility, which is originally designed to deliver a 2.0 GeV, 5 MW proton beam for neutron production, and will accelerate the additional pulses required for the neutrino production. By using interleaved pulses in ESS proton linac, the power will be effectively increased from 5 to 10 MW. This project has received funding from EU in the framework of Horizon Europe 2020 (2018-2022) and Horizon Europe (2023-2026) to carry out feasibility studies. Initial design studies- covering all parts from the upgrade of the ESS proton linac up to the location of the neutrino far detector- are documented in the Conceptual Design Report (CDR). A continuation of this work, ESSνSB+, aims to enable neutrino-nucleus cross-section measurements and sterile neutrino searches. It proposes two low-energy facilities; nuSTORM, which produces neutrinos from muons decays in a storage ring, and LEMNB, low energy monitored neutrino beam, which monitors the neutrinos by tagging the muons associated with these neutrinos from the decay of the pions. An updated overview of the project will be given in this work.

INTRODUCTION

Reactor-based neutrino experiments have provided crucial information in the search for the Charge Party (CP) violation in the leptonic sector [1]. In particular, the precise measurement of the third neutrino mixing angle, θ_{13}, opened the possibility of discovering the Dirac CP violating phase, δ_{CP} , requires high-intense neutrino beams.

To achieve high-intense neutrino beam, the European Spallation Source neutrino Super Beam (ESSνSB) project has been proposed to use the powerful 5 MW,2 GeV proton beam of ESS proton linear accelerator, located near Lund in Sweden [2]. In a future upgrade of ESS, the facility could simultaneously deliver protons for both neutron and neutrino production without interfering with main mission of ESS. This would involve doubling the linac power and increasing the linac pulse rate from 14 Hz to 28 Hz. In addition, the background reduction at the far detector requires compressing the proton pulses length from 2.86 ms to 1.2 µs, which can be accomplished by using a proton accumulator ring. Accumulator ring requires that H^- acceleration in the linac and electron stripping at the injection into the ring. To ensure efficient beam accumulation while minimizing beam losses, a design for a laser stripping injection scheme is under study, with this method a much cleaner injection with H^- can be achieved [3]. In parallel, a Liouvillian Injection Optimization method is also being studied to avoid the need of a more complex linac design. This method would allow direct proton injection with 4D multiturn accumulation whiteout H^- stripping. It allows the beam to be distributed in both horizontal and vertical planes using a tilted septum [4]. Finally, a target station design incorporates four targets and four magnetic horns to handle the high-power proton beam and produce neutrinos to the near and far detectors.

The high neutrino beam power enables operation at the second neutrino oscillation maximum, where the sensitivity to CP violation and violating parameter, δ_{CP}, is significantly higher compared to facilities operating at the first oscillation maximum [5, 6]. The ESSνSB has been designed with both near and far detector complexes. The near detector complex, located at ESS site, includes a water Cherenkov detector, a super fine-grained scintillator detector, and an emulsion detector. The far detector complex consists of a large water Cherenkov detector with two 270 ktons tanks, be installed in the Zinkgruvan mine in northern Sweden, approximately 360 km from the source at a depth of about 1 km. [7].

The design study of ESSνSB project has carried out in the framework of the European Union H2020 program to assess the feasibility of integrating a neutrino super beam facility with the ESS neutron source. This study approved and conducted between 2018 and 2022, focused on the precision measurement of the CP violating phase using long-baseline (LBL) neutrino experiments and explored additional physics opportunities enabled by the large neutrino detectors, including supernova explosions, proton decay, and solar neutrino studies. The design study and the physics performance of experiment have been compiled in the Conceptual Design Report published in 2022 [8].

The study demonstrates strong sensitivity to CP violation measurement, as shown in Fig. 1 [8]. The results assume a 5 % normalization uncertainty and a total running of 10 years, divided equally between neutrino and antineutrino modes. The left panel shows the CP violation discovery sensitivity as a function of true value of δ_{CP}, reaching up to about 12 σ for maximal the CP violation ($\delta_{CP} \sim \pm 90°$). The middle panel demonstrates that the ESSνSB will cover more than 70% of the δ_{CP} values with a significance exceeding 5 σ, to reject the no-CPV hypothesis. The right panel shows that the expected precision on the measured value of δ_{CP} will be better than 8° over the full parameter range.

As a second-generation long–baseline neutrino facility, ESSνSB, offers high-precision measurement of CP violation phase, providing valuable constraints for phenomenological models of CP violation. A comparison with DUNE and

* elham.salehi@ess.eu

ISBN: 978-3-95450-252-3 ISSN: 2673-5350 doi: 10.18429/JACoW-IPAC2026-THP4040

SIMULATION OF LIOUVILLIAN MULTI-TURN INJECTION FOR DIRECT PROTON ACCUMULATION

E. Salehi*, N. Milas, M. Eshraqi, European Spallation Source (ESS), Lund, Sweden
M. Olvegård, Uppsala university, Uppsala, Sweden

Content from this work may be used under the terms of the CC BY 4.0 licence (© 2026). Any distribution of this work must maintain attribution to the author(s), title of the work, publisher, and DOI.

Abstract

In the ESS neutrino super beam (ESSnuSB) project, an efficient injection into the accumulator ring is required for minimizing beam loss during injection, reducing capital cost, and simplifying the overall project. To meet these requirements, the Liouvillian Injection Optimization (LIO) method has been developed for direct proton injection into the accumulator using a 4D multi-turn accumulation process without stripping. This method enables to paint both the horizontal and vertical phase-space simultaneously using a tilted septum. In this study, the LIO method has been investigated using the PyOrbit simulation code. The results demonstrate the method's dependency to the lattice tune, the injected beam beta function, the close-orbit route, and space-charge effects, which play a dominant role on the efficiency of the injection process. This work present the optimization of the method considering space charge effects, lattice nonlinearities, and considerations on the its capabilities.

INTRODUCTION

The European Spallation Source neutrino Super Beam (ESSνSB) project has been designed to use the high-power proton beam at the European Spallation Source facility near Lund, Sweden, in order to produce a high-intense neutrino beam for precision measurements of charge–parity (CP) violation in the leptonic sector [1]. The current ESS linac delivers a 5 MW proton beam at 2 GeV. In a future upgrade of ESS, the facility would simultaneously operate for both neutron and neutrino production without interfering with the main neutron program of ESS. Achieving this goal would require a doubling of the linac power, along with increasing the pulse repetition rate from 14 Hz to 28 Hz, corresponding to 10 % duty cycle. Due to the operational constraint of the magnetic horn in the neutrino target station, the proton bunch length must be compressed from 2.86 ms to 1.2 µs. This can be achieved using a proton accumulator ring.

Conventional accumulator ring operates on charge-exchange injection, which requires the acceleration of H- in a linac and stripping its electron at injection. In the ESS case, this approach involves integrating both proton and H^- sources in the front end. However, using H^- ions introduce several challenges, including limited H^- source reliability and lifetime, losses due to H^- stripping in the linac and transfer line to the ring, and a substantial increase in the complexity of the control and safety system. Recently, a promising approach for achieving a cleaner H^- injection and reducing beam losses, called laser stripping injection, has been under study [2].

* elham.salehi@ess.eu

In parallel, in order to avoid the added complexity of the dual source front-end and the challenges associated with H^- stripping in the linac, a Liouvillian Injection Optimization method has been studied in this paper [3]. This method enables direct proton injection into the accumulator ring through a 4D multiturn accumulation process without H^- stripping. This method eases an efficient phase-space painting in both horizontal and vertical planes using a tilted septum, which simplifies the injector design and reduces operational complexity.

LIO METHOD

The developed Liouvillian Injection Optimization (LIO) code is based on a formalism similar to that of MISHIF [4] to minimize the ring acceptance to achieve 100% accumulation efficiency (no beam loss) within the smallest possible emittance. To achieve this goal, a tilted septum is used at an angle θ with respect to the horizontal plane at the injection point. This configuration allows both vertical and horizontal planes to be explored simultaneously, enabling more efficient phase space painting and increasing the number of injected particles at a given turn. At the beginning of the injection process, the local closed-orbit is shifted close to the septum using two groups of bump magnets (horizontal and vertical), enabling the beam to be injected near the center of phase space. As the injection continues, the local closed-orbit gradually shifts back to the center position of orbit, thereby distributing the injected particles toward the outer region of the ring acceptance in both planes. By controlling the closed-orbit shift, circulating particles are effectively prevented from hitting the septum.

In order to achieve optimal phase space painting, some parameters must be properly chosen, including the machine tunes (μ_x and μ_y), the initial injected beam parameters, the initial closed-orbit shift, and the ring optics at the injection point. The painting process can be described by the following equations, which link the injected beam parameters to those of the accumulated beam [3, 4]:

$$\frac{\beta_{r,x}}{\alpha_{r,x}} = \frac{\beta_{i,x}}{\alpha_{i,x}} = \frac{x_i - x_{co}(n)}{x_i' - x_{co}'(n)} \tag{1}$$

$$\frac{\beta_r}{\beta_i} = (\frac{\varepsilon_r}{\varepsilon_i})^{1/3} \tag{2}$$

where the subscripts i and r refer to the injected and accumulated beams, respectively. Similar expressions apply to the vertical plane. The parameters α and β are the Courant-Snyder (C-S) parameters, ε denotes the emittance, (x_i, x_i') represent the position and angle of the injected beam in the

ISBN: 978-3-95450-252-3 ISSN: 2673-5350 doi: 10.18429/JACoW-IPAC2026-THP4042

INVESTIGATIONS OF A NOVEL BUNCH COMPRESSION TECHNIQUE FOR HADRON ACCELERATORS*

J. Holmberg† [1,2], N. Milas[2], F. Curbis[1,3], M. Eshraqi[2]
[1]Department of Physics, Lund University, Lund, Sweden
[2]European Spallation Source, Lund, Sweden
[3]MAX IV laboratory, Lund, Sweden

Abstract

Bunch compression is necessary for many accelerator applications, one of which being the creation of muons for the proposed muon collider. The design of a proton driver to deliver a short and very intense proton pulse to a target for the creation of muons is being developed. Some challenges with the proposed baseline design, notably the ambitious requirements for the radiofrequency system, motivate the investigation of alternative compression methods. A series of chirped bunch trains can be compressed in the same compressor ring as in the baseline design, removing the need for an accumulator ring and radiofrequency cavities in the compressor ring. Such a scheme has been investigated using PyORBIT simulations, where the chirp is created by off-frequency cavities at the end of the linac. The impact of space charge was investigated, and was found to be too detrimental for realising the proposed scheme with the current parameters. However, other use cases are foreseen.

INTRODUCTION

The proposed muon collider [1] has stringent requirements on the proton driver, which serve to ensure that the target produces enough muons in a short enough time to be captured and cooled to create useable bunches for the collider stage. An average power of 2 MW at a repetition rate of 5 Hz is required, which at the proton energy of 5 GeV corresponds to bunches with 5×10^{14} protons. The compression should achieve an RMS bunch length of 2 ns, which with the other parameters represents an unprecedented proton density, even though the baseline design divides the bunch in two [1, 2]. The proposed design which delivers this consists of a high intensity 5 GeV linear accelerator (linac), followed by an accumulator ring and a compressor ring, as shown in Fig. 1.

CHIRP CREATION

As the lattice for the compressor ring is designed to maximise the slippage factor for rapid compression, it can in principle fulfil its function even without radiofrequency (RF) cavities providing synchrotron motion in the bucket. A series of short bunches from the linac, which delivers 2 ps bunches, given an appropriate chirp will eventually stack on top of each other in the compressor ring. To create the required chirp, two cavities can be added at the end of the linac, operating at frequencies slightly shifted from the nominal frequency, $f = f_0 \pm \Delta f$.

The bunches will experience the superposition of the field in the two cavities, which has a beating envelope with the same frequency as the frequency shift Δf. As seen in Fig. 2, the bunches receive different energies and a chirp is created over a train of bunches. Chopping the source pulse from the linac appropriately, a series of such bunch trains with varying amplitude are injected directly into the compressor ring. A frequency shift which is an integer fraction of the revolution frequency in the ring ensures overlapping bunch trains. The bunch trains compress during the injection, but must all reach maximum compression simultaneously. Consequently, the final bunch train receives the largest chirp amplitude, and the others follow a $1/t$ dependence over the injection time t.

TOY MODEL

To identify potential parameters for the compression, a toy model was first developed which treated the compression analytically using the slippage factor from the compressor lattice. A frequency shift corresponding to the revolution frequency of the compressor ring was chosen, 0.94 MHz. Bunches are spaced at a frequency of 352.21 MHz from the linac, meaning around 100 bunches can be placed within the linear region of the envelope, and thus only around a quarter of the pulse can be utilised. The current from the linac is 80 mA, determining the total number of bunches to be 3.5×10^5 in order to reach the required intensity of 5×10^{14} protons. Consequently, the injection takes a total of 4122 turns. Based on the high-β cavities in the ESS linac, the energy gain in the off-frequency cavities was conservatively chosen to 10 MeV [3]. For the slippage factor of $\eta = 0.17$, this amplitude compresses the bunches in 248 turns according to

$$\frac{dT_{\mathrm{rev}}}{T_{\mathrm{rev}}} = \eta \frac{dp}{p}. \tag{1}$$

The amplitude was increased from 0.6 MeV to 10 MeV across the injection, and the bunch trains are all simultaneously compressed after 4370 turns. For the baseline design, the compression in the compressor occurs in ~50 turns. In Table 1, the resulting parameters of the toy model are shown, and the compression after 4370 turns is shown in Fig. 3, where each bunch is treated as a single macroparticle.

Improving the Design

While the toy model parameters indeed achieve the required proton driver parameters, it is clear that collective

* Work supported by the European Union and endorsed by the IMCC
† johanholmberg01@gmail.com

Content from this work may be used under the terms of the CC BY 4.0 licence (© 2026). Any distribution of this work must maintain attribution to the author(s), title of the work, publisher, and DOI.

ISBN: 978-3-95450-252-3 ISSN: 2673-5350 doi: 10.18429/JACoW-IPAC2026-THP4044

CONSOLIDATION OF THE ANTIPROTON DECELERATOR ELECTRON COOLER

A. Rossi*, C. Accettura, W. Andreazza, J. Bauche, J. Cenede, N. S. Chritin, J. Ferreira Somoza, A. Frassier, D. Gamba, G. Khatri, C. Machado, V. Maire, O. Marqversen, A. Sinturel, Y. Thurel, T. Todorcevic, G. A. Tranquille, L. von Freeden
European Organization for Nuclear Research, Geneva, Switzerland

Abstract

A new electron cooler, replacing the 40 year old one, will be installed starting in 2027, during Long Shutdown 3, in the CERN Antiproton Decelerator ring. The new electron cooler aims to improve reliability, cooling time and beam losses. The design of the new electron cooler, very similar in geometry, electron intensity and energies to the present device, will add electron beam magnetic expansion from the gun to the cooling section and enhance the field quality in the cooling section so to reduce electron transverse energy; approach the H/V orbit corrector magnets and improve relative position measurement of the antiproton and electron beams so to better centre the two beams; allow faster switching of the electron beam on/off at the gun so to ease operations. Ultimately, the testing strategy will ensure highly reliable operations. This paper presents an overview of the status of the project.

INTRODUCTION

The new electron cooler [1, 2] for the Antiproton Decelerator (AD) ring, whose 3D assembly rendering is shown in Fig. 1, has been entirely designed at CERN and is currently under production. It is set to replace the existing cooler, illustrated in Fig. 2, which, although only operational in the AD since the year 2000, is over 40 years old, having originally been repurposed from the Low Energy Antiproton Ring (1982–1997) [3, 4]. The new device aims at a high reliability, by design and robustness of the ancillary equipment.

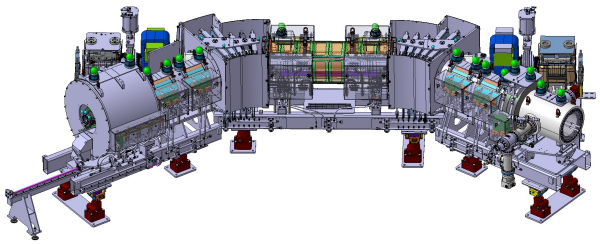

Figure 1: 3D rendering of the new AD electron cooler, with the supporting system, and, from left to right, the expansion solenoid, injection arm solenoid, toroid (pancake), drift solenoid, toroid (pancake), extraction arm, compression (squeeze) coil and collector. Behind the injection and extraction arms the H/V orbit compensators and sector valves.

Moreover, it is expected to have improved performance in terms of time of cooling, mainly obtained by limiting the electron transverse and longitudinal temperature and switching on/off the electron beam during the energy ramps [5], as described in the following. In this paper we give a status of production of the different components, details of the testing strategy and criteria for giving the green-light to deinstall the current device and start installation. A brief overview of planning for installation will also be given.

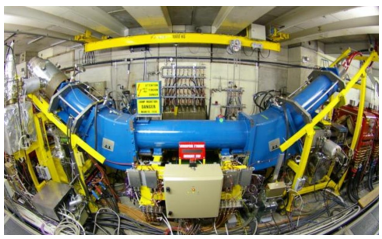

Figure 2: Photo of the 40 year old electron cooler currently installed and operating in the AD ring.

DESCRIPTION OF THE NEW AD ELECTRON COOLER AND COMPARISON WITH WHAT CURRENTLY INSTALLED

The new AD electron cooler design retains the geometry, electron beam intensity (up to 2.4 A), and energy (up to 27 keV) of the current system. Both designs share a drift solenoid length of 1505 mm and a magnetic field intensity of 60 mT [6], enabling electron beam cooling of antiprotons at beam momenta of 300 and 100 MeV/c [7]. The injection/extraction arms also maintain the same field intensity (60 mT) and axis angle (36°) relative to the drift solenoid. Conversely,

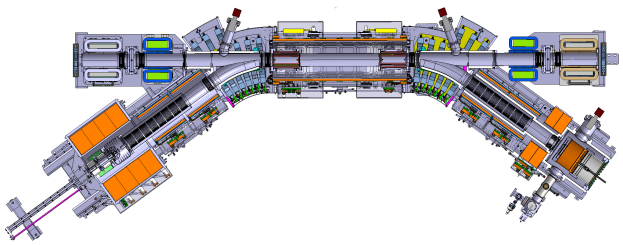

Figure 3: Top view drawing of new AD electron cooler.

compared to the existing electron cooler magnet system, the new magnet system gives a factor five improvement in field quality, $\left|\frac{B_\perp}{B_\parallel}\right|$, in the cooling region [1, 2, 6], thus limiting sources of electron beam heating. Furthermore, the new electron gun is immersed into a strong solenoid (nominal 0.24 T, called 'expansion solenoid') allowing the electron beam to expand transversely along the field line. Assuming adiabatic expansion and conservation of the magnetic mo-

* adriana.rossi@cern.ch

Content from this work may be used under the terms of the CC BY 4.0 licence (© 2026). Any distribution of this work must maintain attribution to the author(s), title of the work, publisher, and DOI.

ISBN: 978-3-95450-252-3 ISSN: 2673-5350 doi: 10.18429/JACoW-IPAC2026-THP4045

PERFORMANCE AND EVOLUTION OF THE STOCHASTIC COOLING SYSTEM IN CERN'S ANTIPROTON DECELERATOR

W. Höfle*[1], D. Gamba[1], L. Ponce[1], S. F. Rey[1], D. Sittard[1,2]
[1]CERN, Geneva, Switzerland
[2]Technical University of Munich, Munich, Germany

Abstract

The Antiproton Decelerator (AD) is part of CERN's Antimatter Factory which decelerates antiprotons from a momentum of 3.57 GeV/c to 100 MeV/c. Stochastic cooling is essential to reduce longitudinal and transverse emittances at the momentum plateaus in the first part of the cycle. The present hardware of the stochastic cooling system is optimized for a momentum of 3.57 GeV/c while it has reduced performance at 2 GeV/c. This work reports on recent performance improvements of the stochastic cooling system which have contributed to the record intensity of 6.3×10^7 antiprotons per cycle, decelerated and extracted from the AD. Possible future consolidation of the system with new kicker and pick-up structures, better adapted to the operation at both momenta, is outlined.

INTRODUCTION

The CERN Antiproton Decelerator (AD) ring [1] started operation in 1999. The decelerator relies on reused stochastic cooling equipment from the CERN Antiproton Collector (AC), the fixed energy collector ring that provided antiprotons at a momentum of 3.57 GeV/c in the 1980's for the SpS collider project. For the design of AD, only the lowest frequency band (900 MHz – 1600 MHz) of the original three bands of AC, was retained [2]. Optimized for a fixed beam momentum of 3.57 GeV/c for AC, operation in AD extended the use of stochastic cooling to a second momentum plateau at 2 GeV/c.

Since the initial design study of the AD with a minimum aim of 1×10^7 antiprotons provided per minute [3], beam parameters have evolved and today a record 6.3×10^7 is every two minutes extracted from AD. A summary of intensity compared to initial AD commissioning [4] and earlier operation is given in [5].

The motivation of the present work is to assess how recent consolidation work, including the replacement of the comb notch filters originally implemented with coaxial cables by optical fiber technology [6, 7], has improved the system performance, notably by increasing the robustness of the cooling system and flattening the frequency response, while also identifying remaining performance limitations in view of possible future upgrades. In this longer-term perspective, the study of pick-ups and kickers is further motivated by the need for spare components, possibly with improved performance, highlighted by a vacuum leak in a kicker tank during start-up in 2021 [8].

* Wolfgang.Hofle@cern.ch

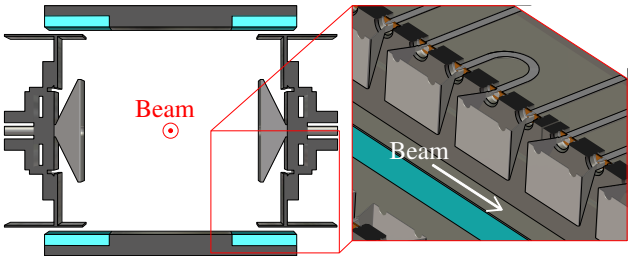

Figure 1: Model of the kickers and pick-ups. View perpendicular to the beam (left) and a side-cut through the double-loop geometry (right). Ferrites are colored in cyan.

KICKERS AND PICK-UPS

Identical electromagnetic structures are used for the kickers and pick-ups. Each kicker / pick-up features an array of 24 so-called double-loop devices [9] [10, p. 398] interacting with the beam. A double-loop device is seen on the right side of Fig. 1 in the center. A double-loop is a series connection of two striplines, powered from the up stream end, with a delay line in between. At the desired frequency, the delay corresponds to half a wavelength which leads to resonant enhancement of the shunt impedance at the expense of reducing the bandwidth by approximately a factor of two.

Figures of Merit

The efficiency of a kicker is determined by how much momentum change it can apply to a beam for a given amount of total RF power P_{incident} incident to its ports. The kickers in the AD stochastic cooling system are excited in longitudinal and transverse modes in order to selectively apply longitudinal or transverse kicks. The longitudinal and transverse kick factors

$$K_{\parallel/\perp} = \frac{V_{\parallel/\perp}}{V_{\text{incident}}}, \tag{1}$$

are a measure of the efficiency of a kicker [11]. The longitudinal and transverse beam voltages $V_{\parallel/\perp}$ are proportional to the longitudinal and transverse momentum changes, respectively. The equivalent incident input voltage V_{incident} is determined by the total incident RF power P_{incident} and the reference impedance Z_0 by $V_{\text{incident}} = \sqrt{2Z_0 P_{\text{incident}}}$.

The efficiency of a pick-up is determined by how much output power it delivers for a given amount of beam current or dipole moment of the beam. The longitudinal transfer impedance

$$Z_{p\parallel} = \frac{V_{\text{out}}}{I_{\text{beam}}}, \tag{2}$$

Content from this work may be used under the terms of the CC BY 4.0 licence (© 2026). Any distribution of this work must maintain attribution to the author(s), title of the work, publisher, and DOI.

ISBN: 978-3-95450-252-3 ISSN: 2673-5350 doi: 10.18429/JACoW-IPAC2026-THP4046

DEVELOPMENT OF AN OPTICAL BEAM PROFILE MONITOR FOR THE HZB CYCLOTRON

A. Denker†, A. Akin, J. Bundesmann, A. Dittwald, T. Fanselow, I. Ja, M. Kang, G. Kourkafas
Helmholtz-Zentrum Berlin für Materialien und Energie, Berlin, Germany

Content from this work may be used under the terms of the CC BY 4.0 licence (© 2026). Any distribution of this work must maintain attribution to the author(s), title of the work, publisher, and DOI.

Abstract

The HZB cyclotron accelerator complex provides 68 MeV protons for proton therapy and related research. The main accelerator is an isochronous sector cyclotron served by two injectors. Originally, the cyclotron was designed for heavy ions. Hence, the beam profile monitors (BPM) on the high energy side are not appropriate for protons at the low intensities used for proton therapy. At the experimental station as well as the treatment station, the profile and shape of the beam is determined via a mirrored image of a scintillator screen in air. For the experimental station, a LabVIEW code has been developed which displays the shape, transverse beam distribution, size and position of the beam. As this tool proved to be very helpful when tuning the beam for experiments, an installation within the beam line in vacuum was designed for several locations where the beam is focused. The design of the new beam profile monitors and their performance will be presented.

INTRODUCTION

The HZB cyclotron can provide both light and heavy ions over a broad energy range [1]. In the past, mainly heavy ions with energies between 1 MeV/u to 10 MeV/u have been used. Only a small amount of beamtime was used for light ions. For this reason, the BPMs in the high-energy beamline of the cyclotron were designed for heavy ions. They consist of a rotating wire which require a certain intensity to provide a good signal. The special development for low intensities [2] proved to be too sensitive for regular operation. Nowadays the main use of the cyclotron is ocular tumour therapy with 68 MeV protons and a typical intensity below 30 nA [3]. At these energies, the thin wires become transparent for the proton beam, and the signal of the BPM is overwhelmed by noise. Based on the excellent experience of the 2D cameras used at the experimental station [4], new optical BPMs have been developed and installed. The need for new BPMs arises due to the installation of two new dedicated beamlines, one for radiation hardness tests and one for minibeam experiments, the project MINIBEE [5,6].

LAYOUT

The camera and the objective of the BPMs are outside the vacuum pipe, looking through a CF35 glass window onto the scintillating material which is tilted 45° versus the beam direction (Fig. 1). The camera lens is held by an adjustable tripod, fixed by a 3D printed holder. The shielding against stray light is also 3D printed. The scintillating material is mounted on a CF16 linear manipulator (Allectra GmbH [7]) which permits placing the BPM in the beam or outside of the beam. Limit switches not only supervise the position of the BPM but are also used for powering/depowering the camera to minimize radiation damages to the camera.

At the bottom is the holder for the scintillating material, tilted at 45° with respect to the beam axis. The size of the scintillator visible by the camera is 20 mm x 20 mm.

The whole system is mounted on a CF100 flange.

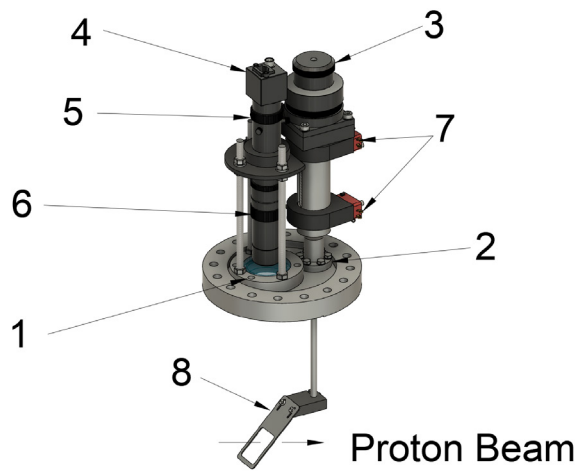

Figure 1: The optical BPM. On the CF100 is mounted the CF35 glass window (1) and the CF16 feedthrough (2) for the manipulator (3). The lens (4) of the camera (5) is shielded against stray light (6). Limit switches (7) control the position of the holder with the scintillating material (8).

CAMERA AND READOUT

The monochrome camera Blackfly S, model BFS-PGE-13Y3M-C (Edmund Optics [8]) was chosen because of a good price/performance ratio. The quantum efficiency of the CMOS sensor is above 50% in the region from 475 nm to 650 nm, providing excellent sensitivity over a broad range of wavelength. The CMOS sensor has 1.3 Megapixels (1280 x 1024) with a pixel size of about 20 µm. The resolution of the on-chip ADC is 10bit. The maximum read-out rate is 85 images per second, well suitable for live observation of the beam spot when tuning the beam. The VZM™ 100i Zoom Imaging Lens [9] was chosen, because it has a field of 26 x 26 mm, a focus distance of 175 mm with a large working tolerance of ±3 mm.

†denker@helmholtz-berlin.de

ISBN: 978-3-95450-252-3 ISSN: 2673-5350 doi: 10.18429/JACoW-IPAC2026-THP4047

AN UPGRADED EXTRACTION SEPTUM AND A NEW DIAGNOSTIC SECTION FOR THE BONN ISOCHRONOUS CYCLOTRON

D. Sauerland*, S. Neubert, University of Bonn, Bonn, Germany

Abstract

The Bonn Isochronous Cyclotron provides light ion beams of a charge-to-mass ratio $Q/A \geq 1/2$ with kinetic energies ranging from 7 MeV to 14 MeV/A to five experimental sites. To improve operation reliability, the cyclotron's electrostatic extraction septum is upgraded using components, manufactured by laser-powder bed fusion (L-PBF). The new copper septum blade holder reduces thermal load on the blade and the integrated cooling system's leak rates to the vacuum. Also, a new beam diagnostic section for the future ion beam analysis setup in Beamline D is under construction, comprising a secondary electron monitor, a Faraday cup (FC) and a beam screen (BS). Both, FC and BS, are made from aluminium using L-PBF and are pneumatically retractable. Cooling is provided through coaxial water tubes, integrated into the pneumatic rods. Here, progress of the septum upgrade will be reported and details of the new diagnostic section will be provided.

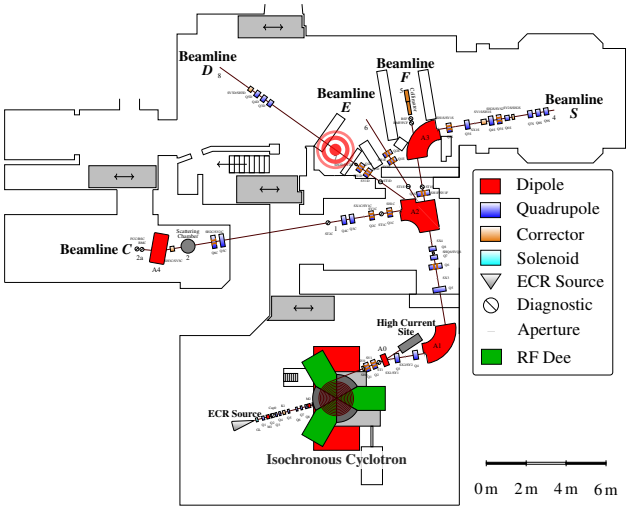

Figure 1: Overview of the accelerator facility with future location of the diagnostic section.

BONN ISOCHRONOUS CYCLOTRON

Figure 1 shows the accelerator facility of the Bonn Isochronous Cyclotron. The cyclotron supplies five experimental sites with proton, deuteron, alpha and other light ion beams of $Q/A \geq 1/2$ at kinetic energies between 7 and 14 MeV/A. 14 MeV protons are used at the high-homogeneity irradiation site. 28 MeV Deuterons are utilized to generate a neutron beam, using a copper/tungsten collimator. This beamline is currently being commissioned. In future, low energetic alphas will be used in an ion beam analysis setup (IBA), comprising Rutherford backscattering and particle-induced X-ray emission.

The ion beam is provided by two external electron cyclotron resonance (ECR) sources located beside and underneath the cyclotron. The generated 2 to 8 keV ions are transported through the low-energy beam line and are injected axially into the cyclotron's magnetic center using an electrostatic hyperboloid inflector.

The Bonn Isochronous Cyclotron [1] is designed as a three-sector isochronous AVF cyclotron featuring a magnetic field distribution with 120° rotational symmetry. For this purpose, the magnet structure is subdivided into three hill and three valley regions without spiral shaping. Each valley accommodates a broadband dual-gap dee resonator capable of providing peak acceleration voltages of up to 40 kV. Routine operation is performed at the third harmonic, where the applied RF frequency amounts to three times the ions' orbital frequency. Accessible Q/A is constrained by the RF frequency range and the maximum average magnetic flux density.

After about 120 turns, the beam is extracted by an electrostatic septum into a field-compensated extraction channel. The extracted particles are subsequently transported either to the high-current site or via the high-energy beam line to five experimental areas.

EXTRACTION SEPTUM UPGRADE

The main component in the cyclotron's extraction is the septum. Once the beam passes a 0.2 mm-thick tungsten septum blade, it is deflected into the extraction channel by static electric fields between blade and antiseptum, biased with up to 40 kV.

As already discussed in Ref. [2], a septum upgrade is in progress. The upgrade includes a redesigned antiseptum with improved operation reliability and a newly developed copper blade holder with integrated water cooling, manufactured utilizing the laser-powder bed fusion technique (L-PBF). Thermal simulations, using `CST Studio`, indicated an enhanced cooling performance and reduced thermal load on the septum blade compared to the previous design.

Testing a First Prototype

One prototype blade holder has been manufactured for test purposes. After copper tubes have been soldered to the cooling channel's in- and outlet, its leak rate has been measured as $6.2(3) \times 10^{-9}$ mbar l s^{-1}, using a helium leak detector. Additionally, the holder with air-filled cooling channel has been integrated into a vacuum recipient and repeatedly evacuated with a turbo molecular pump.

As is shown in Fig. 2, no systematic differences in the pressure evolution during evacuation were observed between

* sauerland@hiskp.uni-bonn.de

Content from this work may be used under the terms of the CC BY 4.0 licence (© 2026). Any distribution of this work must maintain attribution to the author(s), title of the work, publisher, and DOI.

ISBN: 978-3-95450-252-3 ISSN: 2673-5350 doi: 10.18429/JACoW-IPAC2026-THP4048

DESIGN AND OPTIMIZATION OF A FAST ELECTROSTATIC CHOPPER FOR FLASH PROTON THERAPY RADIOBIOLOGY EXPERIMENTS

D. H. Saucedo-Cuberes*, M. C. Jiménez-Ramos†, J. García López
Universidad de Sevilla, Seville, Spain
N. Fuster-Martínez‡, C. Blanch, D. Esperante
Instituto de Física Corpuscular (CSIC-UV), Paterna, Spain
G. Khatri, V. Rodin, European Organization for Nuclear Research, Geneva, Switzerland

Abstract

FLASH proton therapy has shown the potential to reduce normal-tissue toxicity while maintaining tumor control by delivering radiation in ultra-high dose-rate pulses (>40Gy/s). However, more radiobiology experiments are needed to better understand the subjacent mechanism and optimize its application beam parameters. To explore this regime using the Cyclotron at Centro Nacional de Aceleradores in Seville, we have developed a fast electrostatic chopper for beam length structure manipulation in order to be able to produce short and high intensity pulsed beams. In this paper, we present the design and optimization of this device, intended to generate well-defined beam pulses for radiobiology experiments in the FLASH regime. Electromagnetic simulations were performed with CST Particle Studio to define the electrode geometry, determine the required operating voltage, and carry out tolerance studies for the mechanical design. The designed chopper was integrated into a full TOPAS model of the external cyclotron beamline to evaluate the need of additional subsystems such as slits for bema size control at the entrance of the electrostatic chopper and a collimator to absorb the deflected beam. First studies carried out with this model are also presented.

INTRODUCTION

In recent years, FLASH radiotherapy has emerged as a promising technique capable of reducing normal tissue toxicity while preserving tumor control when radiation is delivered at ultra-high dose rates, typically above 40 Gy/s, although the underlying mechanisms remain under investigation [1]. Experimental studies have explored this effect using electron, photon, and proton beams, with proton FLASH therapy attracting particular interest due to its favorable depth-dose distribution and precise tumor targeting capabilities. Several facilities worldwide have adapted cyclotrons and synchrotrons to investigate this regime; however, limitations in beam delivery systems, especially regarding temporal beam structure and dose-rate control, still hinder systematic radiobiological studies.

In this context, this work presents the technological developments carried out to establish a platform for FLASH proton beam studies at the Centro Nacional de Aceleradores (CNA). The facility operates an IBA Cyclone 18/9 cyclotron capable of accelerating protons and deuterons up to 18 MeV and 9 MeV, respectively, and includes an external research beamline for applied beam physics experiments. This work focuses on the electromagnetic (EM) design and installation of a fast electrostatic chopper for temporal beam shaping, adjustable slits for transverse beam control, and initial TOPAS simulations to evaluate and optimize the system performance.

EM AND MECHANICAL DESIGN

Electrostatic choppers are widely used in accelerator to manipulate the temporal structure of charged particle beams using time-dependent electric fields. By applying synchronized voltage pulses to a pair of electrodes, selected portions of the beam can be transmitted or deflected, enabling the generation of short beam pulses with controlled temporal characteristics. Their fast response, precise timing control, and non-interceptive operation make them well suited for applications requiring flexible beam shaping and high temporal resolution [2]. They consists of two parallel electrode plates installed inside an ultra-high-vacuum (UHV) chamber and separated by a fixed gap. The achievable beam deflection, y(V), depends on the applied voltage, beam energy, and electrode geometry according to:

$$y(V) = \frac{q_p \cdot V \cdot L}{d \cdot m_p \cdot v^2} \cdot \left(D + \frac{L}{2}\right) \tag{1}$$

where q_p and m_p are the proton charge and mass, respectively; V is the applied voltage; L is the electrode lenght, d is the inter-electrode gap; D is the distance from the end of the chopper to the observation point; and v is the proton velocity. In addition, the deflection angle induced by the chopper can also be estimated as:

$$\theta(V) = \frac{q_p \cdot V \cdot L}{d \cdot m_p \cdot v^2} \tag{2}$$

To evaluate the feasibility of the proposed system for its implementation at CNA, the beam deflection downstream of the electrostatic chopper was analytically calculated using Eq. 1 for different operating voltages. The study considered an 18 MeV proton beam, a fixed inter-electrode gap d of 24 mm, a distance D of 1.344 m, and electrode lengths of 300 mm and 350 mm. Figure 1 shows the comparison of the deflection obtained for different operating voltages using

* dsaucedo@us.es
† mcyjr@us.es
‡ nuria.fuster@ific.uv.es

Content from this work may be used under the terms of the CC BY 4.0 licence (© 2026). Any distribution of this work must maintain attribution to the author(s), title of the work, publisher, and DOI.

ISBN: 978-3-95450-252-3 ISSN: 2673-5350 doi: 10.18429/JACoW-IPAC2026-THP4049

TRACES OF THE VORTEX EFFECT IN PSI INJECTOR II

C. Baumgarten*, H. Zhang, Paul Scherrer Institute, Villigen, Switzerland

Abstract

Injector II is part of PSI's high intensity proton accelerator (HIPA) facility. It is to date the only cyclotron worldwide that makes use of a space-charge driven effect ("Vortex Effect") which causes bunches not to expand but to "roll up" in the horizontal plane. The effect prevents the cyclotron bunches from expanding longitudinally so that the phase width stays unusually small and the former flat-top resonators could be replaced by normal accelerating resonators. The effect has been simulated in PIC-codes like OPAL and experimentally verified by bunch shape measurements. We present measurements of radial probes which contain residual traces of this effect and we show how it is used to analyze and fit the beam optics in the transfer line between Injector II and the Ring cyclotron.

THE HIGH INTENSITY PROTON ACCELERATOR (HIPA)

The accelerator part of the high intensity proton accelerator facility (HIPA) [1] is shown in Fig. 1. The DC proton beam is generated by an ECR ion source and accelerated by a Cockcroft-Walton to 870 keV. Two bunchers, a first and a third harmonic, enhance the proton density within the phase acceptance of the Injector II cyclotron. After extraction at 72 MeV the beam is guided in the IW2-beamline to the injection of PSI's Ring cyclotron. The Ring cyclotron accelerates the bunches to 590 MeV before two sequential graphite targets are used to generate pions and muons. The re-collimated beam is then transported to the Swiss spallation neutron source SINQ (not shown). If the space charge

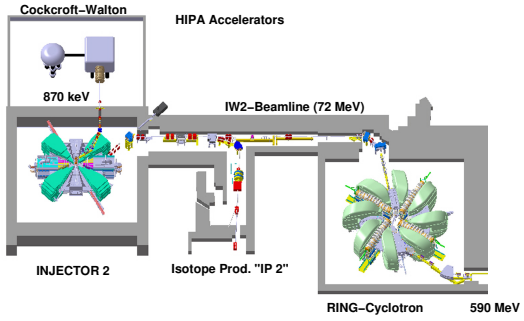

Figure 1: Layout of PSI's High Intensity Proton Accelerators (HIPA). The experimental areas and user facilities are not shown.

self-force of bunches in isochronous cyclotrons is strong enough, then it induces the so-called "Vortex effect", first described by Gordon [2]. The effect can be attributed to the coupling terms between the longitudinal and the transverse-horizontal beam motion [3, 4]. The Vortex effect leads to the formation of almost round bunches with dense cores. Depending on the details of the bunch formation halos in the form of tails or side-bunches are formed, typically in two opposite arms [5]. The Vortex effect prevents bunches from expanding longitudinally which leads to an unusual short phase width. This allows to operate the former flat-topping resonators (third harmonic, 150 MHz) in accelerating phase, thus reducing the number of turns from about 100 [6] to about 83. Furthermore it suggested to upgrade Injector 2 and to replace the low-voltage former flat-tops by high-voltage accelerating resonators operating at the first harmonic of 50 MHz [7]. The upgrade project has been completed, with some delay, in 2025 and enabled to further reduce the number of turns from about 83 to now about 60. This decreased the losses in the Ring cyclotron in 2025 by a factor of 4 compared to 2015.

INJECTOR II: BUNCH CORE

The bunch core can be described by the theory of linear coupled optics. The non-linearity of the space-charge force outside the bunch core leads to self-matching by filamentation and emittance increase. Then the linear theory allows to determine the parameters of matched bunches, provided beam current and emittances are known [4, 8–11]. Figure 2

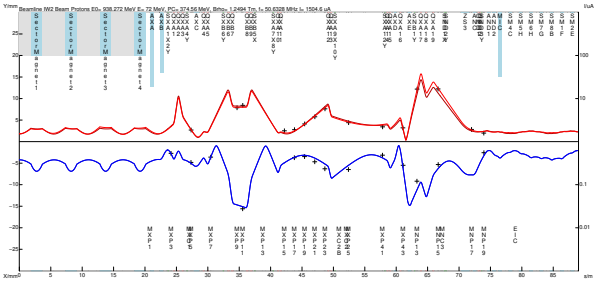

Figure 2: Fitted beam envelopes [10] ("x" in blue, "y" in red) from the last turn of Injector II along the transfer line "IW2", including the first turn of the Ring cyclotron. The crosses indicate the beam size ($2\,\sigma$) as measured by beam profile monitors.

shows a fit of the optics of the beam transfer line based on a matched beam in the last turn of Injector 2, varying only the (eigenvalue-) emittances. A series of these fits for various beam currents allows to obtain the emittance in dependence of beam current (Fig. 3) and to confirm theoretical calculations which suggest that [4]

$$\sigma^4 - K I \sigma - \frac{4\,\varepsilon^2 R^2}{\gamma^2} = 0\,, \qquad (1)$$

where σ is the radius of the (spherical) bunch, ε the (horizontal) emittance, R the radius in the cyclotron and K a perveance:

$$K = \frac{R^2\,q}{5\,\sqrt{5}\,\pi\,\varepsilon_0 f_{rf} m c^2\,\beta^2\,\gamma^4}\,. \qquad (2)$$

* christian.baumgarten@psi.ch

Content from this work may be used under the terms of the CC BY 4.0 licence (© 2026). Any distribution of this work must maintain attribution to the author(s), title of the work, publisher, and DOI.

ISBN: 978-3-95450-252-3 ISSN: 2673-5350 doi: 10.18429/JACoW-IPAC2026-THP4053

E-GUN AND TEST STAND DEVELOPMENT FOR THE PULSED ELECTRON LENS FOR SPACE CHARGE COMPENSATION AT GSI*

K. Schulte-Urlichs†[1], D. Ondreka[1], P. Spiller[1], K. Thoma[1,2]
[1] GSI Helmholtzzentrum für Schwerionenforschung, Darmstadt, Germany
[2] Goethe-University Frankfurt, Frankfurt, Germany

Abstract

At GSI the design of a prototype electron lens to demonstrate space charge compensation in bunched ion beams is being continued. The ultimate goal is to increase the beam intensity for FAIR by compensating for the space charge forces in the synchrotrons operating with high intensity beams by overlapping with a pulsed electron beam in the electron lens. The development of the key components — e-gun and collector — is currently underway with the aim of installing them in the SIS18 e-cooler and demonstrating the concept for the first time.
The conceptual design of the RF-modulated electron gun is completed, construction will start in mid 2026 and delivery is scheduled for autumn 2026. In the meantime, a test stand is being designed and will be set up at GSI to commission the e-gun and subsequently the collector.
In this contribution, an overview of the ongoing activities regarding the details of the gun design, collector and the test stand set-up will be presented.

INTRODUCTION AND OVERVIEW

In many low-energy hadron synchrotrons, the beam intensity is limited by its own space charge. To increase this limit, GSI is developing a prototype pulsed electron lens for space charge compensation. Electron lenses compensate for space charge by overlapping a high-intensity electron beam with a positively charged ion beam. To compensate for a bunched ion beam, the electron beam must be modulated at the RF frequency to follow the bunch profile.

The potential of pulsed electron lenses has been characterized in simulations for the SIS100 synchrotron. Using a low number of symmetrically distributed electron lenses is expected to increase the space charge limit by up to 50%, and using a larger number of lenses is expected to increase it by up to 100% [1]. Realizing such a lens is challenging since it requires very high electron intensities. The objective is to generate, transport, and dissipate beam currents of up to 15 A at a beam energy of 35 keV with a time structure ranging from DC to full modulation at frequencies from 0.4 to 1 MHz.
For this reason, an rf-modulated electron gun and collector have been developed to meet these specific requirements. They are scheduled to undergo testing in the SIS18 electron cooler in the near future.

* The project will partially be supported by EPITA reference GA No. 101290927.
† k.schulte-urlichs@gsi.de

RF-MODULATED E-GUN

The concept of the rf-modulated electron gun, as well as its preliminary technical design, has been developed over the past few years. It has been further optimized in collaboration with the company NTG in recent months and production is set to begin in the coming weeks. Figure 1 represents the preliminary design proposed by GSI and new design that was developed in collaboration with NTG.
For beam modulation, a grid is installed near the cathode

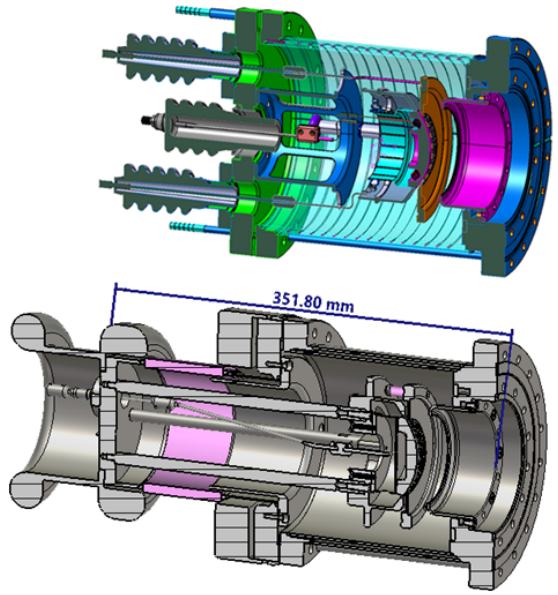

Figure 1: Preliminary design by GSI (top) and optimized design (bottom) during the procurement process of the rf-modulated e-gun.

- for beam extraction the grid will be operated on cathode potential and on -3 kV below the cathode potential to block the beam. As the grid imprints its structure on the electron beam, different kinds of grids were designed and will be tested in order to investigate the impact on the ion beam in the synchrotron. The cathode radius has been set to 30 mm, but the beam can be further expanded in the magnetic field to completely overlay the ion bunch.
A key consideration during the design optimization was the temperature management of the structure in the area around the cathode. Thermomechanical simulations for a cathode temperature of 900 °C were performed to deduce the temperature distribution of the environment and revealed that the e-gun chamber must be cooled. Nevertheless, the main ceramic insulator that isolates the electrode system from ground becomes very hot, still about 300 °C. The experience

Content from this work may be used under the terms of the CC BY 4.0 licence (© 2026). Any distribution of this work must maintain attribution to the author(s), title of the work, publisher, and DOI.

ISBN: 978-3-95450-252-3 ISSN: 2673-5350 doi: 10.18429/JACoW-IPAC2026-THP4055

CONFINEMENT OF ELECTRON CLOUDS IN A BENDING MAGNET

F. Jafari*, O. Meusel, M. Droba, J. Rausch, Goethe University Frankfurt,
Frankfurt am Main, Germany

Abstract

Dipole magnets in linear accelerators or synchrotrons are used to bend ion beams. In case of intense ion beams, space charge compensation is a strategy to overcome intensity limits. So far the reduction of the beams space charge is not investigated in bending magnets by experiments. Therefore, a Gabor-lens was constructed and immersed in a H-type bending magnet to provide a pure electron plasma. Usually, Gabor-lenses are ion optical devices used for focusing and deflecting ion beams. With the setup presented in this paper it will be possible to compare the bending of intense ion beams with and without space charge compensation. Furthermore, the impact of spontaneous built-up of electron clouds observed in synchrotrons can be studied. First experimental results compared with numerical simulations regarding the confinement of electron plasmas within the dipole-Gabor-lens system will be presented. First beam dynamic simulations will show the impact of space charge compensation within bending magnets.

INTRODUCTION

To enhance the performance of linear accelerators and synchrotrons, such as GSI and FAIR facilities, for achieving more accurate experiments, the intensity of ion beams must be increased. However, the space charge generated by heavy-ion beams within the beam pipe counteracts the focusing effect of the enclosing magnets. Consequently, the acceleration of a bunch consisting of a high number of positively charged particles is limited and leads to unstable beam transport. Due to the negative charge of electrons, their corresponding electromagnetic fields can be used to compensate the space charge of high-intensity ion beams [1].

Additionally in high-energy particle accelerators, such as the Large Hadron Collider (LHC) at CERN, the formation of electron clouds (EC), driven by photoemission and secondary electron emission (SEE), causes beam instabilities. These clouds grow exponentially in the presence of positive charged, high-density bunches within the beam pipe [2]. To study these effects under controlled laboratory conditions, a Gabor-lens was developed with an electrode system integrated into a dipole-magnet and oriented orthogonally to the beam axis.

SETUP

The dipole-Gabor-lens (DGL) consists of a H-type dipole-magnet, chosen for its superior mechanical stability and field homogeneity compared to C-type magnets, providing a homogeneous magnetic field B_y. Within the vacuum chamber, a cylindrical copper anode ($R_A = 0.05$ m, $L = 0.1$ m) is immersed vertically, perpendicular to the beam axis and aligned parallel to the magnetic field lines, as illustrated in Figs. 1 and 2. The dual box end caps made of non-magnetizable stainless steel serve as ground electrodes. Additionally these caps enable the investigation of the SEE impact on the plasma properties. Moreover the anode wall incorporates two rectangular apertures (65 mm×25 mm) along the beam path for optical diagnostics, radial diffusion measurements, and future ion beam passage. Furthermore, shortening tubes made of magnetizable iron are mounted to transform the magnetic field distribution along the beam path, facilitating the radial investigation of particles.

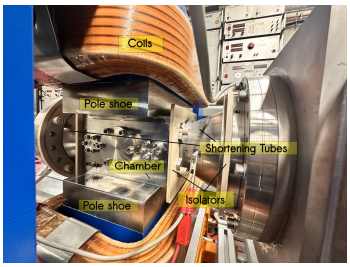

Figure 1: Experimental setup: Axial view along the beam path.

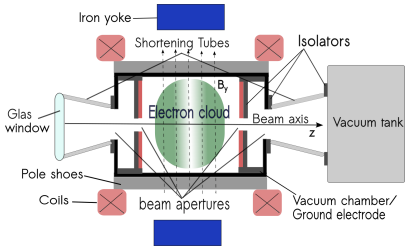

Figure 2: Schematic representation of setup illustrated in the yz-plane.

Electron Confinement

The confinement of charge carriers within the DGL is realized by the superposition of magnetic and electric fields in two directions. For a more accurate description of the dipole-Gabor-lens, the y-axis, which is parallel to the B-field lines, is defined as the symmetry axis of the cylindrical anode.

Longitudinal confinement The electric potential well, generated by the applied potential Φ_A to the anode, confines electron in y-direction, which is reduced by radial space charge potential Φ_r of confined non-neutral plasma. Under full potential depression ($\Phi_A = -\Phi_r$), the maximal axial electron density is proportional to the applied voltage [3].

* s0900530@stud.uni-frankfurt.de

Content from this work may be used under the terms of the CC BY 4.0 licence (© 2026). Any distribution of this work must maintain attribution to the author(s), title of the work, publisher, and DOI.

ISBN: 978-3-95450-252-3 ISSN: 2673-5350 doi: 10.18429/JACoW-IPAC2026-THP4056

MACHINE PHYSICS STUDIES FOR THE MYRRHA PHASE 1 LINAC AT SCK CEN

L. De Keukeleere, J. Van De Walle, U. Dorda, J. Hustings, E. Tanke
Belgian Nuclear Research Centre, Mol, Belgium

Content from this work may be used under the terms of the CC BY 4.0 licence (© 2026). Any distribution of this work must maintain attribution to the author(s), title of the work, publisher, and DOI.

Abstract

At the Nuclear Research Center SCK CEN in Belgium, the first phase of the MYRRHA project (an accelerator driven system) is under construction. Included in MYRRHA Phase 1 are a normal conducting injector linac (RFQ + CH cavities) and a super conducting (SC) linac, providing a CW proton beam of 4 mA and 100 MeV. In this contribution the recent changes to the MYRRHA Phase 1 linac design and the associated machine physics studies are reported. First of all, the layout of the MYRRHA linac was changed from two identical injector linacs each including a dog leg to one straight injector (for the MYRRHA phase 1) and a (future) second injector with a dogleg. The beam dynamics studies of the straight linac and two options for the second injector are presented. Secondly, the impact of a detailed mechanical integration of the beam line elements, which is a compromise between the ideal theoretical layout and a realistic and pragmatic implementation, on the longitudinal and transverse phase space distributions are presented. Finally, the losses along the SC linac are compared for the new and old injector layout.

GENERAL OVERVIEW

The MYRRHA Phase 1 accelerator contains a Low Energy Beam Transfer line (LEBT) which is described in detail in contribution [1]. The main purpose of the LEBT is to match the continuous 4 mA proton beam into the Radio Frequency Quadruple (RFQ) which accelerates the beam from 30 keV to 1.5 MeV.

Following the RFQ, the proton beam is injected into a first matching section (ME1), consisting of 2 normal conducting re-bunching quarter-wave resonators with a quadrupole triplet in between them. Following the ME1 section, the beam is accelerated by 15 normal conducting CH cavities from 1.5 MeV to 16.6 MeV. After the first 7 CH cavities, around 5 MeV, a second matching and diagnostics section is installed with a doublet and 1 re-bunching CH cavity. All components from the source up to this point are referred to as the 'injector'. Selected machine physics details and studies related to the injector are presented in the following paragraph.

Before the beam is injected into the superconducting linac, it passes through another diagnostics section and sections dedicated to fast switching between 2 identical injectors. Different designs for the second injector are presented in the paragraphs below. Note that for MYRRHA Phase 1, only 1 injector will be constructed.

Finally, the beam is injected into a superconducting linac consisting of 30 lattice periods of 3.040 m. Each lattice period consists of a normal conducting quadrupole doublet and 1 cryomodule (QM) containing 2 superconducting single spoke cavities. The superconducting section is referred to as the "Low Beta" (LB) section. Subsequently, the beam is distributed to the user facilities PTF and FPF (see [2]) via the High Energy Beam Transfer Lines (HEBT) or the high energy beam dump.

THE NORMAL CONDUCTING INJECTOR

An Alternative Second Injector

Although a second identical injector will not be constructed during the MYRRHA Phase 1, it was nevertheless decided to change the second injector concept from two symmetric injectors which both inject into the super conducting (SC) linac via a dog-leg (see bottom part in Fig. 1) to a layout where the first injector is 'in-line' with the SC linac (i.e. a straight linac for MYRRHA Phase 1) and the second injector can inject into the SC linac with either a dog-leg or a septum-kicker.

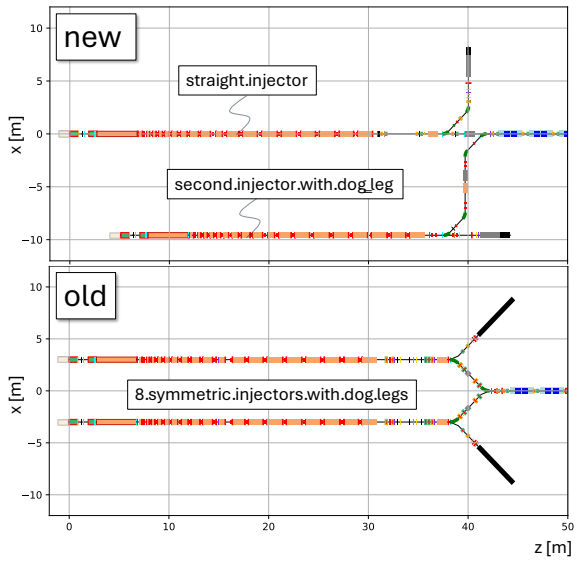

Figure 1: (bottom) The original concept of 2 identical injectors and the (top) the currently implemented solution.

The major benefit of the new injector layout is the improved matching at the entrance of the SC linac. As can be seen from Fig. 2, the longitudinal matching has improved considerably. The 'red' highlighted protons, which are lost at higher energy in the SC linac and are related to longitudinal halo from the injector, have completely disappeared. For the second injector, the beam parameters can be monitored and validated continuously very close to the injection.

ISBN: 978-3-95450-252-3 ISSN: 2673-5350 doi: 10.18429/JACoW-IPAC2026-THP4057

THE LOW ENERGY BEAM TRANSFER (LEBT) LINE AND RFQ FOR THE MYRRHA PHASE 1 FACILITY

L. De Keukeleere, U. Dorda, J. Hustings, E. Tanke, J. Van De Walle, Belgian Nuclear Research Centre, Mol, Belgium

Abstract

At the Nuclear Research Center SCK CEN in Belgium, the first phase of the MYRRHA project (an accelerator driven system) is under construction. Included in MYRRHA Phase 1 are a normal-conducting injector linac followed by a superconducting linac, ultimately providing a CW proton beam of 4 mA and 100 MeV.

In this contribution, ongoing simulations of the Electron Cyclotron Resonance (ECR) ion source and Low Energy Beam Transfer (LEBT) line, which includes 2 solenoids, are described with an emphasis on the effects introduced by space charge and their effect on the performance. Details of the Radio Frequency Quadrupole (RFQ) simulations and benchmarking results as obtained with the codes Toutatis [1] and DYNAC [2] are presented.

INTRODUCTION

The MYRRHA (Multi-purpose hYbrid Research Reactor for High-tech Applications), currently under development at SCK CEN in Belgium, is a pioneering accelerator-driven system (ADS) designed for applications in nuclear waste transmutation, material research, and radioisotope production. A central component of this facility is a high-reliability proton accelerator delivering a continuous wave (CW) beam with strict requirements on beam losses and availability. To validate the accelerator concept and associated technologies, the first implementation phase, referred to as MYRRHA Phase 1, is presently under construction [3, 4].

The normal-conducting injector generates a high-intensity proton beam from an ECR ion source. This beam is subsequently transported through a LEBT line and injected into a Radio Frequency Quadrupole (RFQ), operating at 176.1 MHz. The RFQ bunches and accelerates the beam from 30 keV to 1.5 MeV. A schematic overview of the accelerator layout up to the RFQ is shown in Fig. 1. Downstream, CH cavities and a superconducting linac accelerate the beam to 100 MeV.

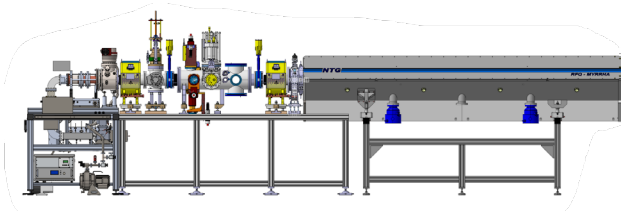

Figure 1: Layout of the injector front-end showing the ion source on the left side, the LEBT and, RFQ tank at a length of 4 m.

INJECTOR FRONT-END

The injector front-end, consisting of the ECR source, LEBT, and RFQ, determines beam quality and transmission. Space-charge effects are significant in the LEBT and require compensation.

Efficient RFQ operation relies on precise matching of the transverse phase space to its acceptance, as well as adequate longitudinal capture during the bunching process. While beam losses this stage should be minimized, accurate matching of the RFQ output is essential, as longitudinal tails may induce losses in the downstream linac.

Beam dynamics simulations are performed using TraceWin and DYNAC. TraceWin supports multi-particle tracking with space-charge modelling through field maps, and is coupled to the Toutatis package for RFQ simulations using time-based integration. DYNAC also provides multi-particle tracking with space-charge modelling, but uses the PARMTEQ/GENRFQ approach [5] for the RFQ. The comparison between these approaches enables benchmarking of the predicted beam dynamics.

RFQ ACCEPTANCE AND LEBT MATCHING

The RFQ acceptance was determined using an iterative method in TraceWin coupled to the Toutatis library. An initially overfilled beam distribution (50k macroparticles, 30 keV, 4 mA) was tracked through the RFQ, and particles reaching the nominal output energy of 1.5 MeV were identified and mapped to their initial coordinates at the RFQ entrance to reconstruct the accepted phase space. The resulting distribution was used to generate refined input beams, and the procedure was repeated until convergence of the Twiss parameters within 3% was achieved.

For an input emittance of $\varepsilon = 0.15$ π·mm·mrad, the matched RFQ entrance parameters were found to be $\alpha = 0.75$ and $\beta = 0.03675$ mm/π·mrad, yielding a transmission of 99.69%, of which less than 0.02% fail to be accelerated.

Following this, the LEBT line was optimized to match the beam to this RFQ acceptance. The simulations start 60 mm downstream of the ion source extraction aperture, where complex ion source-related effects (e.g., residual magnetic fields, stray electric fields, and space-charge build-up) are assumed negligible.

A uniform transverse distribution of 10k macroparticles was generated at the source with the following parameters:

- $\alpha_{xx}' = \alpha_{yy}' = -5.2571$
- $\beta_{xx}' = \beta_{yy}' = 0.529$ mm/π·mrad
- $\varepsilon_{xx}' = \varepsilon_{yy}' = 0.12$ π·mm·mrad
- Beam energy: 30 keV
- Beam current: 4.017 mA

Content from this work may be used under the terms of the CC BY 4.0 licence (© 2026). Any distribution of this work must maintain attribution to the author(s), title of the work, publisher, and DOI.

ISBN: 978-3-95450-252-3 ISSN: 2673-5350 doi: 10.18429/JACoW-IPAC2026-THP4059

STUDIES OF TRANSVERSE EMITTANCE GROWTH OF LHC-TYPE BEAMS ON THE LONG INJECTION PLATEAU OF THE CERN SPS

I. Mases Solé*[1], F. Asvesta, H. Bartosik, K. Li, C. Zannini, P. Zisopoulos
CERN, Geneva, Switzerland
G. Franchetti[1,2], GSI, Darmstadt, Germany
[1]also at Goethe University Frankfurt, Frankfurt, Germany
[2]also at Helmholtz Research Academy Hesse for FAIR (HFHF), Frankfurt, Germany

Abstract

Transverse emittance growth was observed during the long injection plateau for high-intensity multi-bunch LHC-type beams in the CERN SPS, showing a clear dependence on the working point. The working point was adjusted to reduce emittance growth usually observed when the transverse tunes were too close to the integer resonances; however, a residual increase in emittance persists. To characterize this behavior and investigate its possible causes, transverse profile measurements were performed with the SPS wire scanners at several points along the injection plateau. These measurements are used to quantify the evolution of the transverse emittances and to assess the presence and possible generation of overpopulated tails.

INTRODUCTION

Following the implementation of the LHC Injector Upgrade (LIU) project [1] from 2019 to 2021, the intensity of LHC-type beams in the CERN SPS has been progressively increased from 1.3×10^{11} p/b to 2.6×10^{11} p/b. These high-intensity, multi-bunch beams are subject to significant collective effects during the long SPS injection plateau, which is needed for accommodating several batches from the pre-injectors, typically from three to five depending on the LHC filling pattern.

The beams experience transverse tune shifts originating from the SPS beam coupling impedance. These impedance-driven tune shifts accumulate along the bunch trains (the bunches are grouped in a relatively small part of the ring circumference), leading to bunch-to-bunch tune variations [2]. Properly accounting for these variations is essential when setting the machine working point during the injection plateau.

The dependence of the achievable beam brightness on the working point was studied in 2024 and 2025 [3]. For intensities prior to the LIU upgrade (up to 1.3×10^{11} p/b), the operational tune correction approach for LHC beams in the SPS consisted in correcting the coherent tunes of each newly injected batch to $Q_x^{\mathrm{coh}}/Q_y^{\mathrm{coh}} = 20.13/20.18$. This setting provided the best beam transmission and beam quality, consistent with working point studies performed with single bunches in the early days of LHC beam commissioning in the SPS [4]. Since 2021, the intensity per bunch has been gradually increased and the transverse emittances reduced, thanks to improvements in the CERN pre-injectors (PSB and PS) that came with the LIU project. As a result, the LHC-type beams have become significantly brighter and space-charge effects induce very large incoherent tune spreads that depend on the beam variant used. For the so-called Standard beam the maximum incoherent tune shift is approximately $\delta Q_x^{\mathrm{SC}}/\delta Q_y^{\mathrm{SC}} \approx -0.11/-0.18$, while for the BCMS beam (Bunch Compression Merging and Splitting) [5] it can reach values like $\delta Q_x^{\mathrm{SC}}/\delta Q_y^{\mathrm{SC}} \approx -0.14/-0.24$.

Achieving the LIU target beam parameters [6] with the tight budgets on losses and emittance blow-up (in both cases 10% from injection to extraction) has proven to be challenging. In particular, the beam suffers from losses on the injection plateau as well as transverse emittance degradation.

The transverse tunes had to be increased with respect to $Q_x^{\mathrm{coh}}/Q_y^{\mathrm{coh}} = 20.13/20.18$ to avoid emittance blow-up, especially for the BCMS beam [3]. Additionally, the coherent tunes at injection of each train were adjusted such that the incoherent tune shift induced by the quadrupolar impedance is approximately compensated along the cycle. Like that, the tune footprint remains roughly in the same area of the tune diagram and does not approach higher-order resonances such as $Q_x + 3Q_y = 81$ [7], resulting in a reduction of losses and improvement of brightness [3].

After all these optimizations, a residual emittance increase of the order of 8–10% (on average) still persists during the long injection plateau with the Standard LIU beam. This paper presents a series of measurements performed with the Standard LIU beam in October 2025, aimed at characterizing the transverse emittance growth in the SPS, as well as the development of non-Gaussian overpopulated tails.

BEAM PARAMETERS

For the Standard beam, each injection from the Proton Synchrotron (PS) consists of 72 bunches spaced by 25 ns. On the long injection plateau of the SPS, 4 batches from the PS are injected, with 3.6 s between consecutive injections, and 200 ns separation between batches. This results in a train of 4×72 bunches accumulated in the SPS. Table 1 summarizes the main LIU target beam parameters for the Standard beam at SPS injection and extraction. These parameters correspond to the requirements that the SPS needs to achieve for the HL-LHC [8].

The beam parameters used for the measurements were as follows: an intensity per bunch of $N = 2.65 \times 10^{11}$ p/b, and transverse emittances of $\epsilon_x/\epsilon_y = 1.77/1.82\,\mu$m at PS extraction. In 2024 and 2025, some emittance blow-up from

* ingrid.mases.sole@cern.ch

Content from this work may be used under the terms of the CC BY 4.0 licence (© 2026). Any distribution of this work must maintain attribution to the author(s), title of the work, publisher, and DOI.

ISBN: 978-3-95450-252-3 ISSN: 2673-5350 doi: 10.18429/JACoW-IPAC2026-THP4061

THE HIGH INTENSITY ECN3 PROJECT AND THE SPS BEAM DUMP FACILITY AT CERN

M.A. Fraser* and C. Ahdida on behalf of the HI-ECN3 project team
CERN, Geneva, Switzerland

Abstract

The Search for Hidden Particles (SHiP) fixed-target experiment has been approved to lead the search for dark matter at CERN, which has so far evaded discovery at the Large Hadron Collider. To meet SHiP's demanding beam and infrastructure requirements, the High-Intensity ECN3 (HI-ECN3) project has been mandated with upgrading CERN's North Area and equipping its only underground experimental cavern (ECN3) with a new Beam Dump Facility (BDF) capable of exploiting the maximum slow-extracted proton intensity available from the Super Proton Synchrotron (SPS). This contribution summarises the key technical challenges currently being addressed in the HI-ECN3 technical design phase and outlines the schedule, developed in synergy with the ongoing North Area Consolidation project (NA-CONS), to complete the upgrade and deliver first beam to the BDF in 2031, ensuring SHiP data taking before Long Shutdown 4 (LS4).

INTRODUCTION

The HI-ECN3 project will exploit the SPS at its limit and increase the beam intensity transferred to the ECN3 underground cavern by over an order of magnitude. This will allow ECN3 to house a BDF capable of meeting the challenging requirements of the SHiP experiment. The project builds on well over a decade of R&D, including the SPS BDF Comprehensive Design Study [1] published in 2020, iterated further through the recent Physics Beyond Colliders Study Group's effort to assess the Post-LS3 Experimental Options in ECN3 [2, 3]. In March 2024, the CERN management endorsed the physics case presented by the SHiP collaboration [4–9], together with the construction of the HI-ECN3 facility. Following ratification by the CERN Council in June 2024, the HI-ECN3 project was officially approved and mandated to upgrade the necessary accelerator and experimental area infrastructure. This commitment is in addition to the ongoing investment to consolidate the North Area and to secure CERN's long-term future serving the worldwide high-energy fixed-target user community, including experiments, test-beams, and irradiation facilities.

HI-ECN3 PROJECT

The HI-ECN3 project will construct a BDF capable of absorbing a 400 GeV proton beam with an average power of up to 350 kW to deliver 4×10^{19} protons on target per year over 15 years. The publication of the facility Technical Design Report (TDR) is expected this year ahead of a Cost, Scope and Schedule Review (CSSR) that will baseline the project and define its work breakdown structure that is under draft as part of the TDR phase.

RUN 4 TIMELINE

A post-LS3 (Run 4) timeline was expressly requested as part of the project's mandate to reduce the demand on CERN resources during LS3. This was achieved by decoupling ECN3 from the North Area so that works can continue after LS3 and throughout Run 4, in parallel to North Area operation. Ground has already been broken at ECN3 during 2025 to prepare the worksite for the start of the civil engineering works scheduled in LS3. Dismantling of the NA62 experiment and its related beamline infrastructure will start during the SPS ion run in August 2026. The required upgrades to the North Area will be implemented as part of NA-CONS Phase 1 and the renovation of the TCC2 target area in LS3. The project timeline [10] is summarised in Fig. 1 with the aim of commissioning the BDF and SHiP before LS4, and thus have LS4 to complete the detector and take any remedial actions required to achieve the required zero-level background.

SHiP Implementation Strategy

The CERN management have requested a staged approach to the construction and installation of the SHiP detector. The SHiP collaboration has prepared an initial configuration with a simplification of several key subsystems, with the objective of installing the muon shield, decay volume, background taggers and main spectrometer such that commissioning can take place and the background suppression verified ahead of LS4. The SHiP collaboration plans to install the initial configuration of the detector in the years 2029 - 2032, to start the detector commissioning in the second half of 2032 and data taking in 2033. The SPS and PS Experiments Committee (SPSC) supports the staging strategy for the detector presented in BDF/SHiP's annual report [11], which was evaluated by the SPSC as feasible for installation, commissioning and operation before LS4.

TECHNICAL DESIGN HIGHLIGHTS

The design is driven by the need to operate at unprecedented beam intensities while meeting the stringent background requirements of SHiP. Key technical challenges include controlling beam losses during slow extraction and transfer to the BDF, minimising beam-induced backgrounds at SHiP, ensuring safe and reliable target operation, and implementing robust machine protection systems. These

* mfraser@cern.ch

Content from this work may be used under the terms of the CC BY 4.0 licence (© 2026). Any distribution of this work must maintain attribution to the author(s), title of the work, publisher, and DOI.

ISBN: 978-3-95450-252-3 ISSN: 2673-5350 doi: 10.18429/JACoW-IPAC2026-THP4062

COMMISSONING OF THE S^3 SPECTROMETER: ADVANCES, CHALLENGES AND OUTLOOK

F. Lutton, J. Piot, M. Aburas, G. Brunet, M. Cloitre, F. Esnault, M. Faye, S. Ferey, B. Haize, F. Hausknost, A. Lefevre, Th. Lefrou, F. Legruel, S. Lemoal, R. Levallois, J. Livin, C. Meurie, S. Perat, L. Rossard, H. Savajols, F.Salvetti, N. Simon-Baudouin, M-H. Stodel, M. Vabre, G.Voltolini, A. Wagret-Quatromme
Grand Accélérateur National d'Ions Lourds CNRS-IN2P3/CEA-IRFU, Caen, France
A. Sinnana, Commissariat à l'Énergie Atomique et aux Énergies Alternatives / IRFU, Paris, France

Content from this work may be used under the terms of the CC BY 4.0 licence (© 2026). Any distribution of this work must maintain attribution to the author(s), title of the work, publisher, and DOI.

Abstract

The linear accelerator of the SPIRAL2 facility at GANIL delivers both light ions to study nuclear reactions with neutrons in the Neutron for Science (NFS) experimental hall, and heavier ions to produce exotic nuclei, like heavy and super heavy nuclei, in the Super Separator Spectrometer (S^3). By combining electromagnetic components and thanks to their very large aperture, S3 is a powerful tool to purify most of the elements of interest produced in the target from the primary intense ion beam, and retrieving them up to the focal plane to analyse them. The search for very rare events in nuclear reactions requires advanced technics that are not standard in our laboratories, which in S3 are fulfilled by the 7 superconducting multipoles triplets, the large gap of the electric dipole, the high performance movable beam dump and the fully instrumented target station. This poster will generally give an overview of the on-going technical installation and commissioning of this new scientific facility at GANIL.

INTRODUCTION

The Super Separator Spectrometer (S^3) [1, 2] is being installed and commissioned at the SPIRAL2 [3, 4] facility in GANIL. It is designed to isolate and study rare isotopes produced by fusion-evaporation reaction using the high intensity stable beams provided by the LINAC accelerator of SPIRAL2. S^3 will tackle two main scientific cases: the study of superheavy nuclei and N=Z nuclei around 100Sn. Its two stages approach aims at reducing the background from the unreacted beam and light reaction products in the separator (first part) and at identifying the produced fusion-evaporation residues by A/Q in the mass spectrometer (second part). It will allow to access isotopes with production cross-sections down to the femtobarn region thanks to its high rejection and high transmission. In this contribution we report on the status of the installation and tests of the components of S^3.

†franck.lutton@ganil.fr

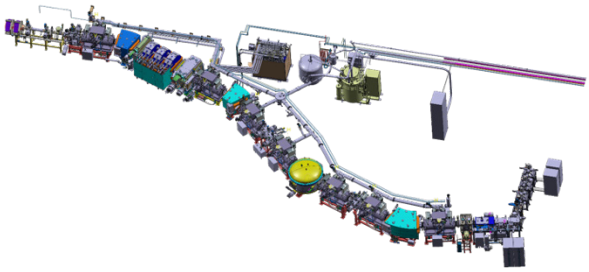

Figure 1: Layout of the Super Separator Spectrometer.

MAGNETS

The two stages of S3 are arranged symmetrically around an intermediate focal plane in order to cancel optical aberrations. The first stage is a momentum achromat composed of two magnetic dipoles (D_M) and four triplets of multipoles (M) in a $MMMD_MMMMMMD_MMMM$ configuration. The second stage is a Mass separator composed of one electric dipole (D_E), a magnetic dipole and four triplets of multipoles in a $MMMD_EMMMMMMDMMMM$ configuration (Fig. 1).

Magnetic Dipoles

Three magnetic dipoles are installed in S^3. They provide a maximal magnetic field of 0.72 T and maximum Bρ of 1.82 Tm, with a bending radius of 4 m and a gap of 230 mm (Fig. 2). The power supply and cooling circuit have been tested in 2026.

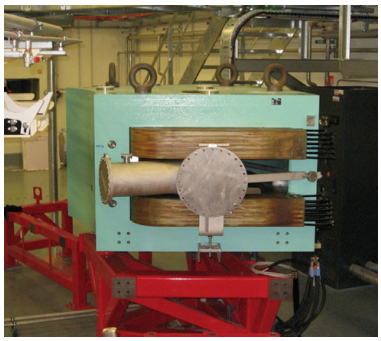

Figure 2: Magnetic dipole of the mass separator.

ISBN: 978-3-95450-252-3 ISSN: 2673-5350 doi: 10.18429/JACoW-IPAC2026-THP4063

UPDATE ON THE BEAMLINES DESIGN FOR THE SPIRAL2-DESIR PROJECT AT GANIL

L. Perrot[1]*, B. Blank[2], J.F. Cam[3], L. Daudin[2], K. Lacombe[2], C. Michel[4], H. Ramarijaona[1], J.C. Thomas[4], F. Varenne[4], V. Watt-Morel[4]
[1]Université Paris-Saclay, CNRS/IN2P3, IJCLab, Orsay, France
[2]Université de Bordeaux, CNRS, LP2I Bordeaux, Gradignan, France
[3]Université Caen Normandie, CNRS/IN2P3 ENSICAEN, LPC, Caen, France
[4]GANIL, CEA/DRF – CNRS/IN2P3, Caen, France

Abstract

The SPIRAL2 facility at GANIL (Caen, France) has been operational since 2019. In 2027, the DESIR facility will begin receiving beams from the SPIRAL1 facility. At a later stage, DESIR will also receive radioactive ion beams from the S3-LEB facility, connected to the S3 separator of SPIRAL2. Construction of the DESIR building was completed in 2025. Many components of the beamline systems have already been manufactured and stored on-site at GANIL. Additionally, several experimental setups are currently under development and in the process of full qualification at partner laboratories, including HRS, GPIB, and PIPERADE at LP2IB, MLLTRAP and LINO at the ALTO-LEB facility (IJCLab, Orsay), and MORA at LPC-Caen. The DESIR facility requires long transfer and distribution beamlines to deliver beams to the experimental setups. Those beams can be passing through many purification devices as high resolution separator and radio-frequency cooler buncher for high selection, emittance reduction and bunching. These lines are designed to transport mono-charged radioactive ion beams with energies up to 60 keV. Since 2012, various electrostatic systems have been developed and thoroughly reviewed as part of the beamline design process. This paper focuses on the already advanced installation of a beamline section and associated utilities and auxiliary systems located in the original GANIL building, which will enable the transfer of beams from the SPIRAL1 facility. It also provides a brief overview of the beam optics for the lines to be installed in the experimental hall, which will serve the experimental setups dedicated to nuclear physics research.

INTRODUCTION

Since the foundation of GANIL-SPIRAL2 in Caen close to 50 years ago, the installation produce heavy ion beams at high intensities and of very exotic nuclides. These beams are produced thanks both by the cyclotrons complex and by the LINAC. The DESIR (Decay, Excitation and Storage of Radioactive Ions) facility [1] will receive beams delivered by the S3-LEB (Low Energy Branch of the new Super Separator Spectrometer) of SPIRAL2 and from the SPIRAL1 cyclotron. Nuclides will be produced in fusion-evaporation, transfer and deep-inelastic reactions, and will notably consist in refractory elements. RIB produced in the fragmentation of high-intensity heavy ions and/or thick targets at the upgraded SPIRAL1 facility will also be available at DESIR. Nuclear physics as well as fundamental weak-interaction physics and astrophysics questions will be addressed by means of laser spectroscopy, decay studies, mass spectrometry and complementary trap-assisted measurements (e.g. Fig. 1).

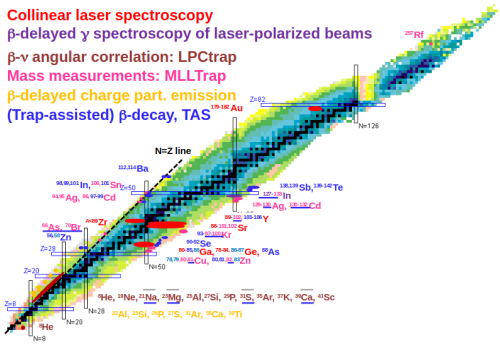

Figure 1: The nuclide chart indicates the nuclei accessible at the DESIR facility once fully operational.

Experience at other ISOL facilities evidences that ion beams with a high degree of purity are required to push experiments towards the limits of nuclear stability [2–4]. Building construction is already finished in 2025. The building was completed in 2025. Process installation began in mid-2025. Nearly 80% of the beamline subsystems have already been manufactured and are stored at GANIL-SPIRAL2.

FEW WORDS ON BEAM LINES

The experimental hall, which will house the experimental set-ups, is 44.5 meters long and 30 meters wide (e.g. Fig. 2).

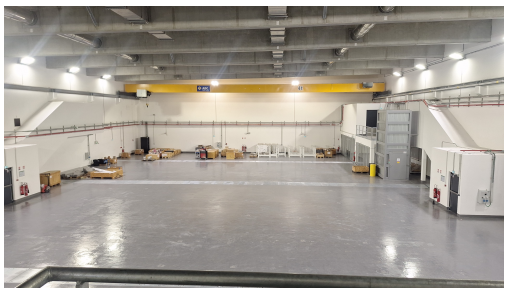

Figure 2: View of the experimental hall of the DESIR facility. The experimental set-ups will be installed step by step.

* luc.perrot@ijclab.in2p3.fr

Content from this work may be used under the terms of the CC BY 4.0 licence (© 2026). Any distribution of this work must maintain attribution to the author(s), title of the work, publisher, and DOI.

ISBN: 978-3-95450-252-3 ISSN: 2673-5350 doi: 10.18429/JACoW-IPAC2026-THP4064

RECENT RESULTS OF BEAM EMITTANCE AND TRANSPORT AT ALTO-LEB PLATFORM IJCLAB

S. Morard*,[1], L. Perrot[1], F. Lemaitre[1]
[1]Université Paris-Saclay, CNRS/IN2P3, IJCLab, Orsay, France

Abstract

The ALTO research platform at the Laboratoire de physique des 2 infinis Irène Joliot Curie (IJCLab) is dedicated to wide-ranging research in nuclear physics, nuclear astrophysics and interdisciplinary activities such as health physics. ALTO-LEB is the low energy beam area of ALTO where neutrons rich exotic nuclei are studied. This paper focuses on the final analysis of beam emittance measurements made at ALTO-LEB dedicated to the characterisation of the ion source. The obtained results were also used to study beam transport along the low-energy beam line, and the outcomes of this study are also presented. Those results are also directly connected to the reliability of ALTO-LEB beam lines initiated at IJCLab in 2018.

EMITTANCE MEASUREMENTS AT ALTO-LEB

A dedicated beam qualification has been done at the ALTO-LEB facility [1] during spring 2023 and 2024. Many results have been already publish [2, 3]. Part of these experimental campaigns were dedicated to beam emittance measurements in order to characterise the beam delivered by the target ion source system. The emittance measurments at ALTO-LEB were performed with an Allison scanner based system [4] developped at the CNRS/IPHC Strasbourg laboratory [5]. Emittance was never measured at ALTO-LEB facility before. This facility was constructed step-by-step during the last 20 years. It was therefore a unique opportunity to have the CNRS/IPHC emittance meter.

During the experimental campaign, emittance has been measured at two location (e.g. Fig. 1). We also measured the beam profile at two locations were EMS beam profilers are available at the installation.

The nominal beam emittance measurement was repeated many time during our campaigns. This measurement was performed approximately 4 meters downstream of the ion production location, as it was not possible to place the device directly in front of the target–ion source system (e.g. Fig. 2).

We present the main result obtain using the new analysis method developed in this context [6, 7] (e.g. Fig. 3).

Horizontal emittance and Twiss parameters are:

- $\epsilon_{rms-x} = 4.2 \pm 2.2\ \pi$.mm.mrad,
- $\alpha_x = -9.7 \pm 5.2\ \pi^{-1}$,
- $\beta_x = 19.2 \pm 10.3$ mm./(π.mrad).

Vertical emittance and Twiss parameters are:

- $\epsilon_{rms-x} = 2.0 \pm 0.3\ \pi$.mm.mrad,
- $\alpha_x = -0.7 \pm 0.1\ \pi^{-1}$,

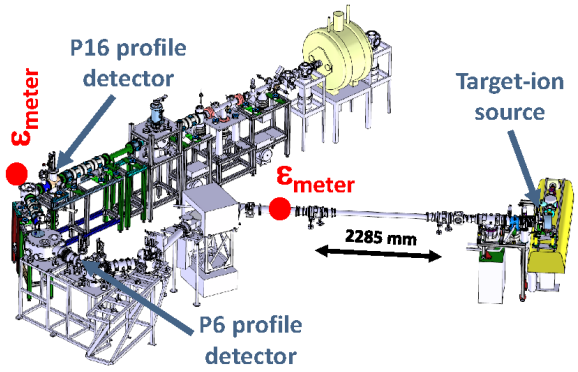

Figure 1: Isometric view of the ALTO-LEB beam lines. Emittance measurements were performed at the locations indicated by red dots. The available beam profilers are labeled P6 and P16. 30 keV and mono-charged ion beam (like stable $^{85}Rb^{1+}$ produced by surface ionisation) is emitted at the target ion source location.

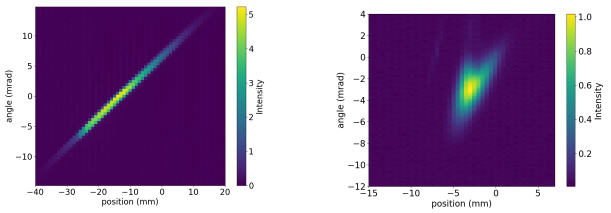

Figure 2: Measured transverse phase-space for the nominal beam at ALTO-LEB. Left: horizontal plane, right: vertical plane.

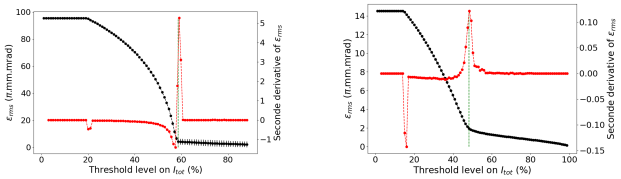

Figure 3: Analysis of the transverse phase-space for the nominal beam at ALTO-LEB. Left: horizontal plane, right: vertical plane.

- $\beta_x = 1.0 \pm 0.1$ mm./(π.mrad).

These measurements were also used to study the beam dynamics in preparation for the commissioning of the new beamline recently developed at ALTO-LEB, which will lead to two new experimental setups.

OPTICAL ELEMENTS STUDIES

The ALTO-LEB beamlines reflect the history of the facility through the changes they have undergone [3]. Optical components were added in stages as new experimental se-

* sophie.morard@cern.ch

Content from this work may be used under the terms of the CC BY 4.0 licence (© 2026). Any distribution of this work must maintain attribution to the author(s), title of the work, publisher, and DOI.

ISBN: 978-3-95450-252-3 ISSN: 2673-5350 doi: 10.18429/JACoW-IPAC2026-THP4065

DEVELOPMENT OF MASS-DEPENDENT FOCUSING TECHNIQUES IN QUADRUPOLE MASS FILTERS

E. Traykov*, T. Adam, E. Bouquerel, C. Maazouzi
Institut Pluridisciplinaire Hubert Curien (IPHC), CNRS-IN2P3, Strasbourg, France

Abstract

A new mass-separation technique based on mass-dependent focusing in radio-frequency (RF) quadrupoles is presented. The focusing effect was originally observed during ion-optical simulations for the definition of the low-energy beamline of the S3 spectrometer and was subsequently developed further during a maturation project funded by SATT Conectus. The novel technique can be combined with the standard operating principle of quadrupole mass filters (QMF), which is based on the stability of ion-motion. The expected gain in performance, in terms of mass resolution and transmission, exceeds an order of magnitude compared to current quadrupole mass filters. Recent simulations have shown that the technique can simultaneously achieve resolving powers above 10000 (FWHM) and transmission efficiencies above 80 % over a broad mass range from 80 u to 2000 u and for ion kinetic energies up to several hundred eV. Experimental verification using a dedicated quadrupole prototype validated the focusing principle and enabled resolving powers of 14300 for Cs^+ ions. The compactness, simplicity, speed, and low cost of quadrupoles, together with the expected performance gains, make the technique particularly attractive for isobaric separation of short-lived exotic nuclei. Several related projects are currently under preparation, including collaborations on short-lived radioactive ion beam identification and implementation of the technique in commercial mass spectrometry (MS) filters and analyzers.

RF QUADRUPOLE OPERATION

Stability-Based Operation

RF quadrupoles have been a cornerstone of mass spectrometry since their introduction in the 1950s, serving both as standalone analyzers and as mass filters in hybrid MS instruments [1, 2]. Their operating principle is based on the stability of motion for ions with specific mass-to-charge ratios, as described by the Mathieu equations and stability diagrams (Fig. 1).

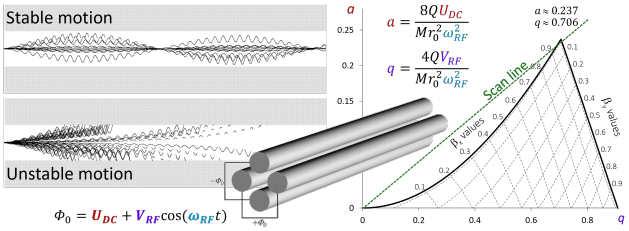

Figure 1: Mathieu equations and motion stability diagrams define standard, stability-based operation of QMF.

In standard operation, the stability range is determined by the intersection of the scan line with the apex of the stability region, which depends on the ratio between the RF and DC potentials. Mass resolution can be increased by operating at higher DC potentials, resulting in a narrower stability overlap and therefore a smaller mass range of ions in stable motion. However, this increase in resolution is associated with reduced ion acceptance and transmission.

Mass-Dependent Focusing

In both transverse planes, the oscillatory motion of ions passing through the QMF can be described by ω_{RF} and secular frequencies ω_0, ω_1, ω_2, etc. [2]:

$$\omega_0 = \frac{\beta}{2}\omega_{RF},\ \omega_1 = \left(1 - \frac{\beta}{2}\right)\omega_{RF},\ \omega_2 = \left(1 + \frac{\beta}{2}\right)\omega_{RF},$$

where β_x and β_y ($0<\beta_x,\beta_y<1$) are the iso-lines passing through the operating point corresponding to a reference ion mass (Fig. 1). Fine tuning of the RF and DC parameters allows an oscillation node (or beat minimum) to be formed at the same longitudinal position in both transverse planes. The focal position can then be further adjusted through the kinetic energy of the ions to match a small exit aperture. Due to the strong mass dependence of the focal position, only a narrow mass range of ions is transmitted (Fig. 2).

EXPERIMENTAL VERIFICATION

Prototype Quadrupole and Experimental Setup

After extensive SIMION [3] simulations for performance optimization and error studies, a high-precision prototype quadrupole was built and installed to verify the focusing technique. The prototype featured exceptional machining precision and custom electronics with improved RF stability. The experimental setup (Fig. 3) consisted of a Cs+ source and a six-element focusing lens for precise injection into the entrance aperture. After selection by the QMF, the ions were detected using a Faraday cup, a two-plate MCP detector with a phosphor screen, and a zoom-lens camera.

Experimental Results

The experimental verification of the focusing technique was achieved by measuring the node-related multi-peak structure during RF scans using single-mass Cs+ ions. This characteristic structure represents a unique mass-dependent fingerprint associated with multiple focusing nodes in both transverse planes (Fig. 4, left panel). A fine multi-parameter sweep was implemented in the system control in order to achieve simultaneous focusing in both planes. This enabled signals as narrow as 20 Hz to be obtained, corresponding to

* emil.traykov@iphc.cnrs.fr

Content from this work may be used under the terms of the CC BY 4.0 licence (© 2026). Any distribution of this work must maintain attribution to the author(s), title of the work, publisher, and DOI.

ISBN: 978-3-95450-252-3 ISSN: 2673-5350 doi: 10.18429/JACoW-IPAC2026-THP4067

SIMULATION BASED MACHINE PROTECTION FOR THE Super-FRS

J. Wirtz*[1,2], A. Ali[1], A. Andres[1], R. Gebel[1], J. Hetzel[1], D. Kallendorf[1,2], E. Kazantseva[1], A. Obertelli[2], S. Pietri[1], H. Simon[1], F. Wamers[1], H. Weick[1], M. Winkler[1]
[1]GSI Helmholtzzentrum für Schwerionenforschung, Darmstadt, Germany
[2]Technische Universität Darmstadt, Darmstadt, Germany

Content from this work may be used under the terms of the CC BY 4.0 licence (© 2026). Any distribution of this work must maintain attribution to the author(s), title of the work, publisher, and DOI.

Abstract

Starting in 2027, the Super-FRS will produce and separate rare isotopes for nuclear physics experiments at the Facility for Antiproton and Ion Research (FAIR). To reach isotopes further toward the nuclear drip line, the separator uses heavy-ion beams of higher energy (>1.5 GeV/u) and intensity ($>3 \cdot 10^{11}$ ^{238}U/s) compared to previous facilities. These primary beams, as well as the secondary fragment beams produced in reaction targets, can damage detectors along the beamline and may cause quenches in the superconducting magnets. To prevent such scenarios, it is essential to ensure that all beams are correctly separated and stopped in dedicated beam dumps. For this purpose, a machine protection system is being developed to verify every new machine setting required during diverse experimental campaigns. To avoid slowing down machine operation, the system simulates, in near real time, all (fragment) beams for different magnet settings, targets, degraders, and detectors throughout the entire separator. The planned capabilities of this machine protection system and the currently achieved prototype are presented.

INTRODUCTION

Exotic nuclei are produced at in-flight fragment separators by the fragmentation and fission of relativistic heavy-ion beams. To meet the demand of nuclear physics research for increasingly rare nuclei, the Super-FRS (Superconducting Fragment Separator) is currently being installed as part of FAIR (Facility for Antiproton and Ion Research) in Darmstadt, Germany [1]. Compared to the previous GSI fragment separator FRS [2], the new separator can handle higher primary beam intensities and has larger momentum- and angular acceptances to catch more fragments. The Super-FRS will receive primary beams from the SIS18 and SIS100 synchrotron, which can accelerate ions ranging from protons to Uranium up to magnetic rigidities of 100 Tm [3]. For the Super-FRS intensities of $5 \cdot 10^{11}$ Uranium ions per cycle of between 0.4 and 2.7 GeV/u are expected. Depending on experimental needs, these ions can be extracted either fast in ~ 70 ns or slow in 1–10 s. In the former case this translates to an instantaneous power shortly exceeding 500 GW and even in the latter case corresponds to more than 20 kW of average beam power.

In the Super-FRS these intense primary beams are used to produce exotic nuclei in a graphite target wheel of up to 8 g/cm^2 thickness. Behind the target, a cocktail beam, consisting of the degraded primary beam and more than 3000 different fragments for the heaviest beams (as simulated in Fig. 1) enters the separator. It is the purpose of the separator to filter for exotic fragments of interest while preventing other, multiple orders of magnitude more intense beam components from overwhelming detector systems. The Super-FRS, presented in Fig. 2, uses a combination of magnets, degraders, and slits to achieve this separation. It will usually be operated as a double stage $B\rho$-ΔE-$B\rho$ separator [7]. In this setting the fragments of interest will be achromatically focused both after the pre- and main-separator, while fragments of different charge or mass number are horizontally separated. For different experiments the main-separator can serve three different branches dedicated to low-energy, high-energy and storage ring experiments.

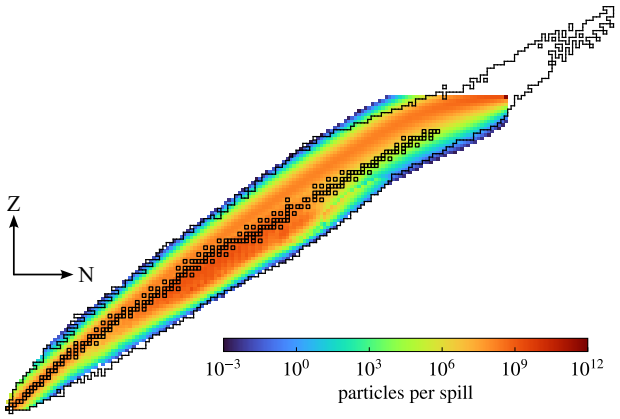

Figure 1: Fragments produced by a 1.5 GeV/u $5 \cdot 10^{11}$ ^{238}U spill on 8 g/cm^2 C simulated with Mocadi [4] and cross sections from [5, 6].

MACHINE RISKS

The target area of the Super-FRS is designed to receive beams of the highest intensities from the accelerator. The first eight magnets after the target are radiation-resistant normal-conducting magnets, unlike the remaining superconducting magnets. Dedicated beam catchers are installed behind the first three dipoles to absorb the most intense beam components. Other sections further downstream of the separator are not designed to handle these high intensities.

Superconducting Magnets

The superconducting NbTi coils in the Super-FRS are cooled to 4.5 K by liquid helium and will quench if they exceed a temperature of about 7 K [8]. A misguided beam locally depositing >1 mJ/g into the coil could induce a quench and a beam depositing >10 W into the 4.5 K cryostat could

* j.wirtz@gsi.de

ISBN: 978-3-95450-252-3 ISSN: 2673-5350 doi: 10.18429/JACoW-IPAC2026-THP4068

NON-LINEAR PHASE SPACE TUNING FOR IN-FLIGHT FRAGMENT SEPARATORS

D. Kallendorf*[1,2], A. Andres[2], S. Appel[2], M. Bajzek[2], J. Hetzel[2], V. Isensee[1,2], E. Kazantseva[2], P. Madysa[2], S. Pietri[2], H. Weick[2], J. Wirtz[2,1]
[1]Technical University of Darmstadt, Darmstadt, Germany
[2]GSI Helmholtz Centre for Heavy Ion Research, Darmstadt, Germany

Abstract

Next generation in-flight fragment separators like the Super-FRS are built with large apertures to accept high momentum spreads. The wide beam and momentum variation gives rise to large aberrations from non-linear effects, if not suppressed precisely. Models and simulations are able to predict most effects, but to achieve the highest performance, fine tuning of the ion optics with beams, based on measured aberrations for the machine is needed.

While the main focal planes provide single particle tracking to measure the phase space, the target area instrumentation can only provide coarse information about the overall distribution of the beam. This poses a challenge, as knowledge about the polynomial order of the phase space distortion (in terms of transfer maps) enables a much faster optimization.

In this setting, we used a normalizing-flow-like approach, to find an invertible symplectic kick-rotation-* map, which transforms the measured data into an initial distribution, to extract a possible transfer-map and determine the distortions by order.

Integrated in the Generic Optimisation Frontend and Framework (Geoff), the method was validated in simulations and with a multiple charge state uranium beam at GSI's fragment separator (FRS), by fine-tuning even significantly detuned optics.

TRANSFER MAPS

The main scope of day-to-day beam-line tuning is alignment and focus of beams by means of dipole and quadrupole magnets. In case of small beam emittances and small apertures, linear optics can be used to describe the transformation of normally distributed beam, whereas the transformations are applied to the stochastic mean and covariance of the beam distribution. While knowledge of these stochastic momenta is still valuable for the fragment separators, the nonlinearities in dipoles and quadrupoles lead to their wrong characterization when linear transformations are used to describe the system, as illustrated in Fig. 1a.

The transfer map description is a powerful tool to describe non-linear effect in accelerators, by expressing the final particle coordinates as polynomial $\mathcal{T}$ of the initial coordinates. The coefficients of the polynomial, called transfer map coefficients can give insight into the beam dynamics and are notated in short-form as $(x_\mathrm{f}^i|x_\mathrm{i}^j)$ for the first order and $(x_\mathrm{f}^i|x_\mathrm{i}^j x_\mathrm{i}^k)$ for the second order, such that final coordinate x_f^i has this coefficient for the respective monomial in the initial coordinates. In the rare case that the full phase space coordinates before and after a section are available, this polynomial can be computed by polynomial regression. More commonly, the distribution of the phase space is available from reconstructive methods [1], but knowledge about the coefficients is still desirable.

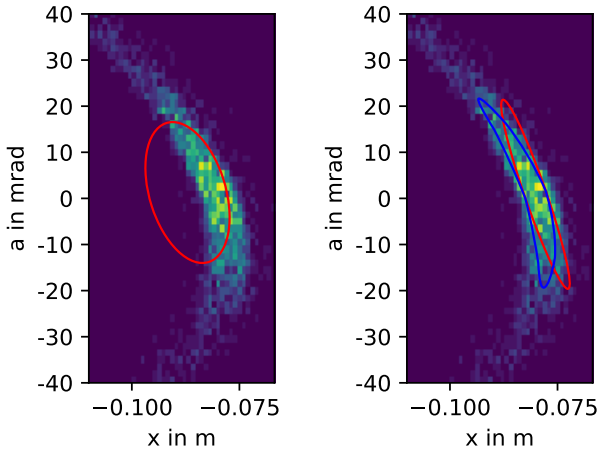

(a) Linear phase space (red) from mean and covariance

(b) Linear (red) and quadratic (blue) phase space from generalized Irwin model.

Figure 1: Determining beam properties from a simulated quadratic distorted phase space.

Alternatively this map can be used to describe a distortion from a desired phase space onto a measured one, to get insight into the distortion.

A Model for Symplectic Transfer Maps

Using the theory of Irwin [2] there is a simple way to parameterize an approximation $\mathcal{T}$ to a symplectic map $\mathcal{M}$. Using a series of kicks $\mathrm{K}_{c_n} := \exp(:g_n:)$, where g_n is a polynomial in x with coefficients c_n of degree P, $:\cdot:$ describes the Lie-operator and rotations R_Δ in the x-a-plane with a fixed angle Δ, the approximation $\mathcal{T}$, called Irwin model and defined as

$$\mathcal{T} := \mathrm{K}_{c_1} \circ \mathrm{R}_\Delta \circ \mathrm{K}_{c_2} \circ \mathrm{R}_\Delta \circ \ldots \circ \mathrm{K}_{c_k} \circ \mathrm{R}_{-\Delta}^k \circ \mathrm{R}_\varphi \approx \mathcal{M}$$

agrees up to order $P-1$ with the original map $\mathcal{M}$.

* d.kallendorf@gsi.de

Content from this work may be used under the terms of the CC BY 4.0 licence (© 2026). Any distribution of this work must maintain attribution to the author(s), title of the work, publisher, and DOI.

ISBN: 978-3-95450-252-3 ISSN: 2673-5350 doi: 10.18429/JACoW-IPAC2026-THP4069

Super-FRS CONTROLS FOR COMMISSIONING

A. Ali*[1], S. Pietri[1], A. Andres[1], R. Gebel[1], J. Hetzel[1], E. Kazantseva[1], H. Simon[1], H. Weick[1], M. Winkler[1], D. Kallendorf[1,2], V. Isensee[1,2], J. Wirtz[1,2]
[1]GSI Helmholtz Centre for Heavy Ion Research, Darmstadt, Germany
[2]Technical University of Darmstadt, Darmstadt, Germany

Abstract

The Super-FRS project is a state-of-the-art spectrometer for nuclear physics studies, currently being built at the Facility for Antiproton and Ion Research (FAIR). The Super-FRS will serve as the workhorse of nuclear physics research, using intense primary beam from the synchrotrons of FAIR to produce, select and identify rare isotopes. In addition to its technical capabilities for the production and separation of nuclei, the Super-FRS will support a wide range of nuclear physics experiments through the integration of dedicated experimental equipment or adaptation of the ion-optical layout. To achieve this flexibility and enable commissioning in 2027, extensive work on controls, data acquisition, and modeling is underway. In order to preserve the versatility of the Super-FRS as a platform for diverse investigations while ensuring full interoperability between the control, experimental data acquisition, standard beam diagnostic components, and analysis systems, the software suite must allow the seamless combination of experimental data with beam-diagnostic information, enabling the use of standard operational tools (operator-driven and automated).

INTRODUCTION

The operation of the Super-FRS [1] demands an advanced control and data acquisition infrastructure capable of managing a vast array of subsystems, including a network of diagnostic and detectors for particle identification, superconducting magnets, and mechanical drives.

This paper details the integrated operational approach that bridges the boundary between online physics analysis and real-time accelerator control. First, the core unified analysis pipeline is described, governed by the S-FRSRoot commissioning framework, which rapidly translates raw detector streams into high-level physical observables. Following this, LSA-centric control hierarchy [2] is outlined, designed to execute high level user parameters and regulate the underlying accelerator hardware.

ANALYSES FRAMEWORK

Unified Commissioning and Analysis Framework (S-FRSRoot Commissioning version)

To guarantee comprehensive data processing from the first day of commissioning, a unified software ecosystem named *S-FRSRoot Commissioning* has been developed. Built upon the FairRoot architecture [3], this framework drives the complete online data pipeline. It acts as the core analytical engine, managing the real-time ingestion and parsing of raw data streams from the DAQ. The framework systematically applies mapping and calibration logic, executes cross-detector reconstruction algorithms, and ultimately extracts the final event-by-event Particle IDentification (PID).

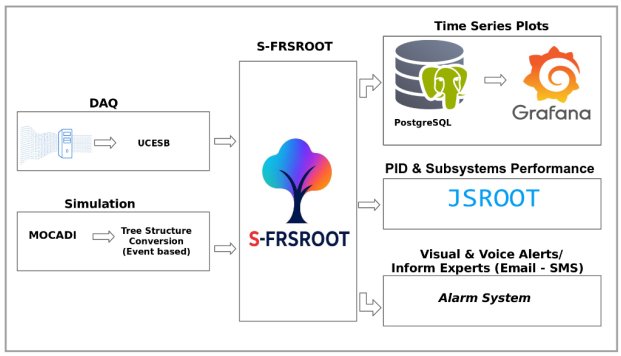

Figure 1: S-FRSRoot Framework Overview.

Currently, the core engine autonomously processes data across multiple PID subsystems, including the tracking system, the Time-of-Flight (ToF), and the Multiple Sampling Ionization Chambers (MUSIC) [4, 5]. To support real-time operation, live data visualization is actively achieved via integrated JSRoot [6] online monitors and PostgreSQL/Grafana dashboards, complete with dedicated GUI gating logic. Consequently, the online monitor is established as a fully "physics-ready" diagnostic tool that remains intrinsically compatible with offline analysis demands.

With the integration of the new Super-FRS PID detectors into the beamline, dedicated software modules have been developed to manage their specific signal processing pipelines. Furthermore, a dual-pipeline architecture has been implemented to cleanly separate the generation of the calibration Look Up Tables (LUT) from the high-level cross-detector reconstruction and analysis tasks. An overview of this ecosystem is illustrated in Fig. 1.

Data Ingestion and Reconstruction

The S-FRSRoot commissioning framework features a multi-stage, modular pipeline that systematically transforms raw electronic signals into high-level physical observables, ensuring full compatibility between online diagnostics and offline analysis.

Stage 1: Raw Data Ingestion and Unpacking

The ingestion layer captures real-time DAQ streams or offline data, utilizing a dedicated unpacker to translate raw hardware binaries into the framework's core structures. This

* a.ali@gsi.de

Content from this work may be used under the terms of the CC BY 4.0 licence (© 2026). Any distribution of this work must maintain attribution to the author(s), title of the work, publisher, and DOI.

ISBN: 978-3-95450-252-3 ISSN: 2673-5350 doi: 10.18429/JACoW-IPAC2026-THP4072

DEVELOPMENT OF A SURROGATE MODEL OF THE T09 BEAMLINE AT THE CERN PS EAST AREA

D. Banerjee*, P. Alexaki, J. Bernhard, N. Charitonidis, G. Dal Maso,
M. van Dijk, S. Esen, A. M. Goillot, F. Metzger, L. J. Nevay,
B. Rae, S. Schuh, F. W. Stummer, CERN, Geneva, Switzerland,
E. Barber, University of Surrey, Surrey, UK
R. Jakob Tietgen, Johannes Gutenberg Universitaet, Mainz, Germany

Abstract

The T09 beamline of the PS East Experimental Area delivers mixed secondary particle beams for diverse experiments and test beams. This requires the possibility of generating flexible beam conditions. Predicting beam parameters at the experimental area, such as particle composition, spatial profiles, and momentum spread, typically demands time-intensive simulations with tools like BDSIM and FLUKA. This work presents the development and first studies of a surrogate model of the T09 beamline that reproduces key beam characteristics with greatly reduced computational cost, making it a promising candidate for future real-time applications. Trained on a database of detailed BDSIM simulations spanning multiple collimator configurations, the model employs machine-learning-based regression to predict beam transmission, spot size, and phase-space parameters. Preliminary validation against full Monte Carlo simulations shows agreement at a level of 15 % for the tested configurations, supporting rapid parameter scans and indicating potential for future real-time beam optimisation. This approach is also scalable for other CERN beamlines.

INTRODUCTION

The East Area at CERN has served the physics community for over 50 years, delivering secondary beams produced from the 24 GeV/c proton beam extracted from the Proton Synchrotron [1]. Following the East Area renovation [2] during Long Shutdown 2, the updated facility began operation in 2021. The T09 beamline accepts secondary particles at a 30 mrad vertical production angle, is approximately 50 m long, and includes three bending dipoles, eight quadrupoles, and three four-jaw collimators, providing a selectable relative momentum spread ($\Delta p/p$) between 0.7 % and 15 %. Each experiment requires flexible operation with regular adjustment of collimator and quadrupole settings to tailor beam flux, momentum spread, spot size, and phase-space properties. Predicting the resulting beam properties requires full Monte Carlo runs with BDSIM [3], which can take hours per configuration due to the low yield of the secondary beam necessitating large event statistics. A fast surrogate model, trained to emulate simulation output, will enable real-time beam property prediction and efficient parameter optimisation. This paper summarises the first studies performed to confirm the efficacy of such a model for the T09 beamline.

* dipanwita.banerjee@cern.ch

SIMULATION CAMPAIGN AND DATASET

In this study, detailed simulations of the beamline were performed using BDSIM [3], a Geant4-based [5] Monte Carlo code tracking particles through the magnetic lattice while modelling various physics processes including particle interactions with matter. The T09 BDSIM model was validated against MAD-X [4] as shown in Fig. 1. Then a split-simulation strategy was employed: a short run to a marker downstream of the T09 target produced a filtered particle distribution, which was reused as input for all full-beamline runs, substantially reducing the per-configuration computational cost.

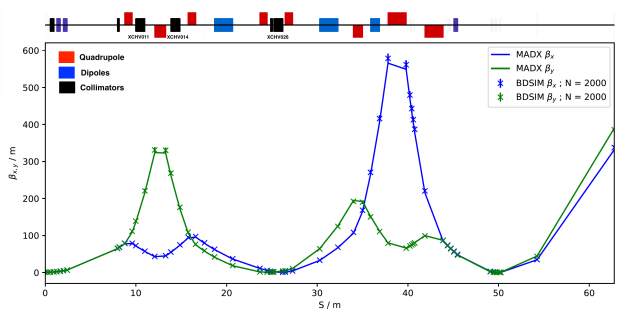

Figure 1: MAD-X vs. BDSIM validation. The optics of the beamline is also shown here with the different elements.

Five diagnostic markers were placed at the end of the beamline (`exp1–exp5`) 1 m apart to record the beam parameters. Only 26 configurations were simulated, defined by six input parameters: the horizontal and vertical half-apertures of collimators XCHV011 and XCHV014, ranging between ±5 mm and ±50 mm, and XCHV026, ranging between ±1.5 mm and ±45 mm. For each configuration, 1×10^9 primary particles on target equivalent of secondary beam were tracked and processed to produce phase-space histograms in Y–X, X'–X, Y'–Y, and p–X at the marker locations. The beamline was simulated with the reference momentum at 15 GeV/c. An 80 %/20 % train–test split yields 21 configurations for training and 5 for evaluation. The training was performed only for the horizontal parameters X, X', and momentum p to validate the approach.

SURROGATE MODEL ARCHITECTURE

Histogram Encoding

Rather than predicting scalar optics parameters, the surrogate model was trained to predict full histogram distri-

Content from this work may be used under the terms of the CC BY 4.0 licence (© 2026). Any distribution of this work must maintain attribution to the author(s), title of the work, publisher, and DOI.

ISBN: 978-3-95450-252-3 ISSN: 2673-5350 doi: 10.18429/JACoW-IPAC2026-THP4078

DEVELOPMENT AND TECHNICAL FEASIBILITY OF THE FIGURE-8 STORAGE RING CONCEPT FOR HIGH CURRENT BEAM STORAGE

S. Schwarz*[1,2], M. Droba[2], O. Meusel[2], H. Podlech[2], K. I. Thoma[2]
[1]FAIR - Facility for Antiproton and Ion Research in Europe GmbH
[2]Goethe-University Frankfurt, Frankfurt am Main, Germany

Abstract

The Figure-8 Storage Ring (F8SR) is an innovative concept for storing low-energy proton and ion beams below 1 MeV in a compact, stellarator-like geometry embedded in magnetic fields of 6 T–7 T. Previous studies established feasibility of the magnetic lattice and indicated the potential for long confinement times at high stored current. This paper concentrates on the mechanical engineering development toward a Technical Design Concept, with emphasis on the ring support structure, magnet-cryostat integration, cryogenic and electrical supply infrastructure, vacuum hardware integration, and installation in a realistic accelerator hall. The assessment indicates that the concept is technically feasible using established accelerator engineering methods, provided that alignment stability, thermal contraction management, well-defined magnetic force load paths, and vibration control are treated as top-level requirements from the earliest design stage.

INTRODUCTION

High-current storage of low-energy proton and ion beams is a key enabling capability for beam–plasma interaction experiments and fusion-relevant beam-driven systems. At energies below 1 MeV, beam lifetime and operational robustness are strongly influenced by space-charge effects, beam–gas interactions, and sensitivity to lattice and alignment errors. These constraints motivate compact ring architectures with strong focusing, good symmetry properties, and ultra-high vacuum (UHV) performance [1–3]. The Figure-8 Storage Ring (F8SR) addresses the requirements for a symmetric figure-eight shape of the central axis embedded in a strong magnetic field environment of approximately 6 T–7 T. In addition to beam-optical advantages, the figure-eight layout imposes distinct mechanical challenges: the machine combines non-trivial three-dimensional geometry with superconducting magnets, cryogenic distribution, high-current power conversion, and UHV beam pipes, all within a limited installation envelope. General layout with the detailed design of the EX-2 section is depicted on Fig. 1.

Earlier work emphasized orbit stability, lattice definition, and diagnostic and vacuum feasibility. The next step is the consolidation of scientific requirements into an integrated Technical Design Concept (TDC) that defines interfaces, assembly sequences, maintainability, and safety provisions. The present paper focuses on the mechanical and infrastructural aspects that dominate technical feasibility: the structural concept of the ring support frame, the integration of superconducting magnet cryostats and vacuum chambers, the routing and isolation of cryogenic and electrical services, and the integration into an accelerator hall including foundations, access, and safety systems.

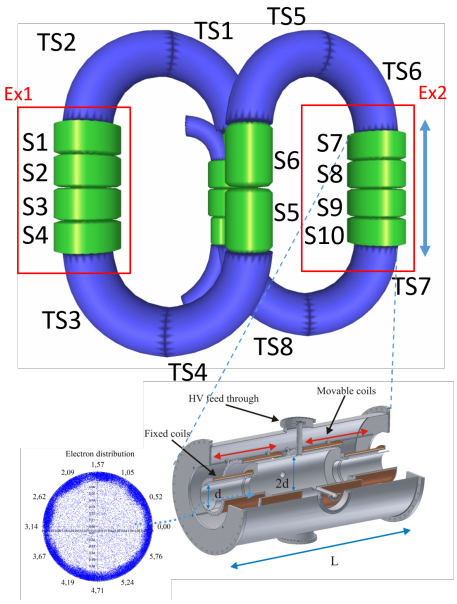

Figure 1: General layout of the F8SR (TS-toroidal sectors, S-solenoidal sectors, EX- Experimental area). Possible electron distribution generated in EX-2 is shown as well (left-down).

INTEGRATION OF SUPERCONDUCTING MAGNETS AND CRYOSTATS

Mechanical Interfaces & Force Management

Magnetic fields in the 6 T–7 T range strongly suggest superconducting coils (e.g., NbTi or Nb_3Sn technology) housed in individual cryostats. The cryostat contains a cold mass (coils and supporting structure), thermal shields, and a vacuum vessel. Mechanically, the principal challenge is to support the cold mass with sufficient stiffness while limiting conductive heat flow to the helium temperature stage. Low-thermal-conductivity suspension elements (such as GFRP or titanium rods) are arranged to carry gravitational loads and anticipated magnetic-force components. Because the ring geometry introduces curvature and potentially non-planar orientations, the suspension system must provide controlled stiffness in the transverse directions to avoid micro-motions that could degrade field reproducibility or trigger quenches.

* S.Schwarz@iap.uni-frankfurt.de

Content from this work may be used under the terms of the CC BY 4.0 licence (© 2026). Any distribution of this work must maintain attribution to the author(s), title of the work, publisher, and DOI.

ISBN: 978-3-95450-252-3 ISSN: 2673-5350 doi: 10.18429/JACoW-IPAC2026-THP4079

RETRIEVING THE LONGITUDINAL NONLINEAR TUNES FROM FCT MEASUREMENTS

J. Rausch*[1], A. Sherjan[1,2], G. Franchetti[1,2,3], B. Lorentz[2]
[1]Goethe University Frankfurt, Frankfurt, Germany
[2]GSI Helmholtz Centre for Heavy Ion Research, Darmstadt, Germany
[3]Helmholtz Forschungsakademie Hessen für FAIR, Frankfurt am Main, Germany

Abstract

In synchrotrons and storage rings, the longitudinal dynamics of bunched beams is crucial in understanding beam loss. A fast current transformer (FCT) can be used to monitor the longitudinal bunch distribution. We use consecutive FCT measurements to analyze the beam's oscillations in the RF bucket at the Experimental Storage Ring (ESR) at GSI. At varying amplitudes of oscillation, the tunes in the non-linear bucket are reconstructed and discussed.

INTRODUCTION

Motivation

During the Machine Development (MD) time 2025 at the ESR, an effort was made to evaluate and improve the optics model of the machine. Beam based optimization studies were undertaken to improve the optics [1] and determine the non-linear components of dispersion [2]. Investigations on the longitudinal dynamics were possible using FCT measurements that were taken during times when the optics of the machine [3] was untouched. The synchrotron tune can be extracted from this measurement data and compared to the expected values given by the optics model and the machine settings during measurements.

Synchrotron Tune

The synchrotron tune in a storage ring is given by the rotation frequency of the beam in the RF-bucket ν_s in relation to the revolution frequency ν_r

$$Q_s = \frac{\nu_s}{\nu_r} , \tag{1}$$

where Q_s is the tune for small oscillation amplitude, for larger phase it has amplitude dependent components. The equations of motion of one particle in the bucket, without acceleration and radiation losses are

$$\dot{\phi} = \frac{2\pi q}{\beta^2 T_r}\left(\alpha_p - \frac{1}{\gamma^2}\right)\frac{\Delta E}{E_0} \tag{2}$$

$$\Delta\dot{E} = -\frac{qV}{T_r}\sin(\phi) \tag{3}$$

with T_r the revolution time of the on-momentum reference particle.

For small values of phase ϕ, Eqs. (2) and (3) can be approximated linearly as the harmonic oscillator. For the storage case without acceleration this results in a synchrotron tune of

$$Q_{s,0} = \sqrt{\frac{qVh}{2\pi\beta^2 E}\left|\left(\alpha_p - \frac{1}{\gamma^2}\right)\right|} , \tag{4}$$

with V the cavity gap voltage, E the beam energy, h the harmonic number, α_p the momentum compaction factor, relativistic β, γ. For phases $\phi \neq 0$ where $Q_s \neq Q_{s,0} = \text{const.}$ the differential equations represent the model of a non-linear pendulum. Its period can be determined exactly by an infinite series [4]. For the non-linear tune this yields

$$Q_s = Q_{s,0}\left(\sum_{n=0}^{\infty}\left(\frac{(2n)!}{(2^n n!)^2}\right)^2 \sin\left(\hat{\phi}/2\right)^{2n}\right)^{-1} . \tag{5}$$

The presented measurements give an approximation of both the zero order synchrotron tune as well as the higher order components in the ESR and are compared to the theoretical model.

MEASUREMENT PROCEDURE

Beam and Machine Setup

The measurements have been made during the Machine Development time at the Experimental Storage Ring (ESR) at GSI. For the MD, $^{40}Ar^{18+}$ beam with an energy of 400 MeV/u was provided by SIS18. The beam was injected into the ESR, bunched and stored at the injection energy. Additionally the beam was cooled with the electron cooler, which could also be switched off during storage. The cavity was used for bunching with a very low RF amplitude of $V = 146.61$ V. The bunching frequency was chosen with harmonic number $h = 1$.

FCT

For retrieving the longitudinal distribution of the stored and bunched beam, the current signal of the beam was measured by a Fast-Current-Transformer (FCT). The longitudinal beam profile of a cooled vs. non-cooled beam is shown in Fig. 1a, where τ is the time window of continuous measurement.

In Fig. 1b many consecutive continuous measurements, as Fig. 1a, are performed automatically at equal times intervals, each identified by the starting time t. All consecutive measurements of Fig. 1b are referred to as one measurement set. With the bunch not centered in the bucket, the expected oscillation can be observed in Fig. 1b.

* rausch@iap.uni-frankfurt.de

Content from this work may be used under the terms of the CC BY 4.0 licence (© 2026). Any distribution of this work must maintain attribution to the author(s), title of the work, publisher, and DOI.

ISBN: 978-3-95450-252-3 ISSN: 2673-5350 doi: 10.18429/JACoW-IPAC2026-THP4080

TOMOGRAPHIC RECONSTRUCTION OF LONGITUDINAL PHASE SPACE FROM FCT MEASUREMENTS

J. Rausch*[1], A. Sherjan[1,2], G. Franchetti[1,2,3]
[1]Goethe University Frankfurt, Frankfurt, Germany
[2]GSI Helmholtz Centre for Heavy Ion Research, Darmstadt, Germany
[3]Helmholtz Forschungsakademie Hessen für FAIR, Frankfurt am Main, Germany

Abstract

For the analysis of longitudinal dynamics in synchrotrons and storage rings, the reconstruction of the beam distribution in longitudinal phase space is of high interest. This study applies a tomographic method to longitudinal beam profiles measured in the ESR to reconstruct longitudinal phase space. We show the limitations of these methods for the nonlinear beam dynamics in an RF bucket.

INTRODUCTION

Tomography provides the reconstruction of an n-dimensional distribution from projections in $(n-1)$-dimensional image-space with a range of projection angles. In case of a beam in longitudinal phase space, the distribution of beam density is measured along the direction of motion s while the beam itself rotates in the RF bucket. Other works on longitudinal phase space tomography typically use an iterative approach [1–3] to ensure small errors of reconstruction despite the typically small numbers of projections and the non-linear character of synchrotron oscillations. A direct reconstruction method, however, is computationally beneficial and therefore desirable for real time diagnostics during machine operation. In this study we apply the direct filtered back projection (FBP) method for reconstruction and analyze the resulting uncertainties of reconstruction for different types of beam distribution. The measurement of these longitudinal beam profiles is performed by a Fast Current Transformer (FCT).

Beam Rotation

Under the influence of the RF cavity, the beam follows trajectories in the bucket, each identified by its maximum phase $\psi_{\max}$. For small $\psi_{\max}$ the beam particles describe an elliptic rotation with constant synchrotron frequency. For large $\psi_{\max}$, both the trajectories are non-elliptic and the rotation frequency is not constant. The synchrotron frequency has the value

$$\omega_s = \omega_{\mathrm{rev}} \sqrt{\frac{qVh}{2\pi\beta^2 E} \left| \left(\alpha_p - \frac{1}{\gamma^2} \right) \right|}, \tag{1}$$

with ω_{rev} the revolution angular frequency, V the cavity gap voltage, E the beam energy, h the harmonic number, α_p the momentum compaction factor, relativistic β, γ.

Reconstruction

To reconstruct the 2D phase space from longitudinal beam profiles, it is assumed that the rotation frequency is constant for all particles of the beam. Under this assumption the measured FCT beam profile shows the 2D phase space distribution projected onto the coordinate s under continuosly changing angles. Since the FCT performs triggered measurements of current over time, the position s is measured as the time τ of arrival of a beam particle in the FCT. The beam and machine parameters, yielding the synchrotron frequency, and the time steps Δt between consecutive profile measurements determine the steps of projection angle

$$\Delta\vartheta = \omega_s \Delta t \ . \tag{2}$$

For the beam phase space reconstruction the FBP method is applied. All measured profiles are first filtered by a high-pass Ram-Lak filter. Then these pre-processed profiles are back projected onto the 2D space. The background that results from the back projection is obtained from the density in the region outside the bucket and is used as a lower cut-off for the resulting distribution. To retrieve the distribution in phase space, the time coordinate τ is renormalized to phase

$$\psi = 2\pi \frac{h\tau}{T_{\mathrm{rev}}} \ , \tag{3}$$

with h the harmonic number and T_{rev} the revolution time of the reference particle. While the rotation used in the tomographic method yields coordinates of ψ in both directions, the energy deviation dE/E can be estimated by the height of the bucket $(dE/E)_{\max}$

$$\frac{dE}{E} = \frac{\psi}{\psi_{\max}} \left(\frac{dE}{E} \right)_{\max} \ . \tag{4}$$

Measurements

The measurements of a stored Ar^{18+} beam were made during machine development (MD) time at the Experimental Storage Ring (ESR) [4] at GSI. The beam was injected, RF bunched and cooled by the electron cooler. During storage at injection energy of 400 MeV/u sets of profile measurements were made with the FCT after varying storage duration. The number of beam profiles in one set was limited to 49 for technical reasons. The time interval between consecutive profiles was chosen so that roughly two periods of oscillation were measured in one set and therefore the oscillation

* rausch@iap.uni-frankfurt.de

Content from this work may be used under the terms of the CC BY 4.0 licence (© 2026). Any distribution of this work must maintain attribution to the author(s), title of the work, publisher, and DOI.

ISBN: 978-3-95450-252-3 ISSN: 2673-5350 doi: 10.18429/JACoW-IPAC2026-THP4081

SPACE CHARGE COMPENSATED ION BEAM EXTRACTION

J. Rausch*,[1], O. Meusel[1], H. Podlech[1,2,3]
[1]Goethe University Frankfurt, Frankfurt, Germany
[2]Helmholtz Research Academy Hesse for FAIR (HFHF), Frankfurt, Germany
[3]GSI Helmholtz Centre for Heavy Ion Research, Darmstadt, Germany

Abstract

The generation of high intensity ion beams requires high density plasma in the ion source. Earlier studies [1] have shown how high plasma densities can be achieved with a combined RF- and arc-discharge without using a filament as an electron emitter. While space charge compensation in the extraction region could benefit the space charge limited extraction of high intensity beam, in conventional extraction systems however the compensating electrons need to be blocked from entering the extraction region by means of a suppression voltage to prevent sparking in the high voltage gap. Therefore we propose the controlled use of a separately produced electron beam to compensate space charge right at the extraction gap. The concept of achieving superposition of electron and ion beam by propagating the e- beam through the plasma generator chamber is evaluated. First beam dynamics simulations for the electron beam as well as extraction studies for the compensated and non-compensated case are presented.

INTRODUCTION

Development of Accelerators in recent years is directed more and more towards reaching higher intensities [2–4]. To reach higher beam intensity, first the necessary beam current has to be provided by an ion source. Previous studies have investigated the concept of a hybrid ion source to reach high density plasma states needed for high current beam extraction. This work focuses on the extraction region, where the ion beam is formed by de-neutralizing the plasma and accelerating the ions in a high potential difference in the extraction gap. We propose a method to overcome the limitations of extracted current density given by the Child-Langmuir law by the use of a spacecharge compensating electron beam. While other work [5] has shown partially beneficial effects using a pulsed electron beam, moving upstream towards the ion source and dumped inside the ion source, we investigate the comoving beam which can be created and dumped independently of the ion source. Simulations of the overlapped beams in the triode extraction are performed to show the possibilities for mitigating the space charge limitations.

MOTIVATION

A measure for the maximum current density J that can be extracted using a potential difference across a gap of two

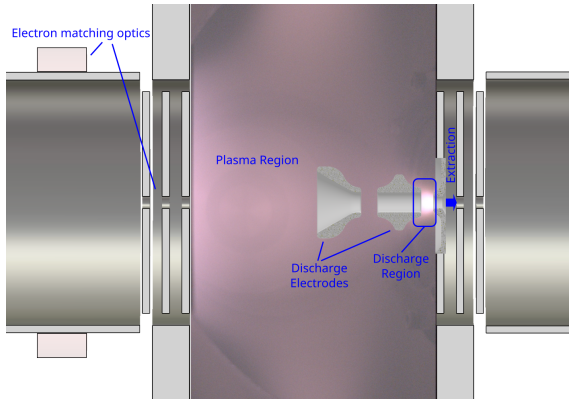

Figure 1: The plasma chamber including hollow discharge electrodes, studied in [1], with the added injection electrodes on the left.

electrodes is the Child-Langmuir law

$$J = \frac{4}{9}\epsilon_0\sqrt{\frac{2q}{m}}\frac{V^{3/2}}{d^2}\,, \tag{1}$$

with q the charge and m the mass of the charged particle, V the accelerating voltage and d the distance between the accelearating electrodes. While originally derived for ion discharge currents [6] and later appplied to electrons beam formation from a hot cathode surface [7], it is commonly applied to the extraction of ion beams [8,9]. The proportionality of

$$J \propto \frac{V^{3/2}}{d^2} \tag{2}$$

limits the extractable absolute current for a given size of aperture. To overcome this limitation we simulate the effects of a high density electron beam overlapping the ion beam extraction which lowers the local current density due to the opposite charge of the comoving electron beam.

SIMULATION

Setup

The setup of the simulated geometry is based on the plasma generator built for the studies of [1]. It is shown in Fig. 1. The used extraction electrodes used are a simplified triode system used for first tests. To reach the extraction region, the electron beam has to propagate through the plasma generator. To match the electron beam into the plasma region, a similar triode system is used as an injection lens at the opposite of the plasma generator. Additionally for the simulation one solenoid, placed 31 mm before these injection electrodes, is used. A very low energy of 6 keV

* rausch@iap.uni-frankfurt.de

Content from this work may be used under the terms of the CC BY 4.0 licence (© 2026). Any distribution of this work must maintain attribution to the author(s), title of the work, publisher, and DOI.

ISBN: 978-3-95450-252-3 ISSN: 2673-5350 doi: 10.18429/JACoW-IPAC2026-THP4083

DEVELOPMENT OF THE SPIN TUNE MODEL FOR EDM INVESTIGATIONS AT STORAGE RINGS

A. Piccoli*, R. Shankar, P. Lenisa, University of Ferrara and INFN–Sezione di Ferrara, Ferrara, Italy
A. Lehrach, RWTH Aachen University, Aachen, Germany and FZ Jülich, Jülich, Germany

Abstract

Electric Dipole Moments (EDMs) are sensitive probes of CP violation and could help address some open questions of the Standard Model. Recent advances in storage ring and polarimetry technologies enabled the development of a new experimental method for EDM investigations. One of the main parameters involved in the EDM studies via storage rings is the Spin Coherence Time (SCT), *i.e.*, the time during which the spins of all particles in a stored beam precess coherently. A long SCT increases the experimental sensitivity and minimises the statistical uncertainties. To identify the optimal working conditions, the single-particle spin tune, defined as the number of spin precessions around the vertical axis per revolution, must be tracked with extremely high precision. A lattice-independent model was developed to accurately track the spin tune of single charged particles in a variety of storage rings, both existing and proposed, and was directly applied to SCT optimisation. In this contribution, the model was tested on the hybrid storage ring, a new-generation device conceived for EDM investigations, which uses electrostatic deflectors for confinement and magnetic quadrupoles for focusing.

INTRODUCTION

Despite its remarkable success, the Standard Model (SM) leaves several fundamental open questions. Among them, the observed matter-antimatter imbalance in the Universe, known as baryon asymmetry, is one of the most compelling [1]. The underlying mechanism, called baryogenesis, is an asymmetric process that requires CP violation [2]. The baryon asymmetry is quantified by the baryon-to-photon density ratio η [3]. While the SM predictions are consistent with $\eta \sim 10^{-18}$ [1], the measurements are of the order of 10^{-10} [4]: this means that the CP violation incorporated in the SM is insufficient to account for the observed baryon asymmetry. Therefore, new sources of CP violation beyond the SM are needed. A powerful probe of CP violation is the Electric Dipole Moment (EDM) [5]. It is an intrinsic fundamental property of particles, defined as the permanent asymmetry in the distribution of electric charges within the particle with respect to the spin orientation. In the SM the EDMs are predicted to be extremely small, but many SM extensions predict significantly larger EDMs that could be within or closer to the reach of current and future experiments [6]. Since direct measurements of the EDM are experimentally challenging because of its tiny magnitude, very high precision techniques are required. One of them involves the use of storage rings [7]. By injecting into a storage ring a longitudinally polarized particle beam under the frozen spin condition, *i.e.*, with all spins remaining aligned with their momenta, the existence of a non-vanishing EDM can be revealed as the build-up of vertical polarization, due to the interaction of the particle EDMs with an external radial electric field. This polarization build-up can be measured using a polarimeter, as shown in Fig. 1. The spin tune and the Spin Coherence Time (SCT) are two fundamental quantities in the EDM investigations using storage rings. The single-particle spin tune is the number of spin precessions around the vertical axis per revolution and is defined as [8]:

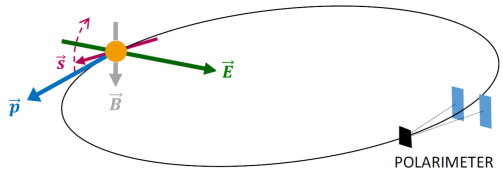

Figure 1: Schematic of the principle of the EDM measurement for a single-particle.

$$\nu_{s,0} = \frac{f_{\text{spin}}}{f_{\text{rev}}}, \tag{1}$$

where f_{spin} is the spin frequency and f_{rev} is the revolution frequency. When a beam is considered, since particles are distributed in phase-space, each of them experiences slightly different fields and has its own spin tune. As a result, there is a distribution of the spin tunes of the individual particles within the beam, called spin tune spread. For a polarized beam, this spread causes spin decoherence and, consequently, depolarization. The SCT is the time over which the beam polarization decreases to 1/e of its initial value [9]. It must be maximised, within the limits set by the beam lifetime and the machine operation, because it determines how long the EDM signal can accumulate. To obtain a long SCT, it is necessary to minimise the spin tune spread and, thus, to accurately track the single-particle spin tune. A lattice-independent model for accurately tracking the spin tune of single charged particles has been developed in a variety of storage rings, both existing and proposed. The single-particle spin tune can be expressed as a sum of contributions arising from synchrotron and betatron motion, as well as from chromaticities. The novelty of this work lies in its direct application in SCT optimisation: it is possible to determine the lattice optical properties which minimise the spin tune spread and, thus, maximise the SCT. In this contribution, the model is applied to the hybrid storage ring, a new-generation device for EDM investigations that combines electrostatic deflectors for confinement and magnetic quadrupoles for focusing.

* apiccoli@fe.infn.it

Content from this work may be used under the terms of the CC BY 4.0 licence (© 2026). Any distribution of this work must maintain attribution to the author(s), title of the work, publisher, and DOI.

ISBN: 978-3-95450-252-3 ISSN: 2673-5350 doi: 10.18429/JACoW-IPAC2026-THP4084

EVALUATION OF LASER-ASSISTED CHARGE-EXCHANGE INJECTION INTO THE ESSNUSB+ PROTON ACCUMULATOR*

A. Opanasenko†,1, N. Milas[2], M. Olvegård[1]
[1]Uppsala University, Uppsala, Sweden
[2]European Spallation Source, Lund, Sweden

Abstract

Laser-based H⁻ charge-exchange injection offers an attractive alternative to conventional carbon-foil stripping for injection into multi-megawatt proton rings. In foil-based systems, foil heating and degradation, radioactivation, and uncontrolled beam losses are factors limiting the achievable average beam power. In this work, we evaluate the feasibility of implementing laser-assisted H⁻ charge-exchange injection into the 5 MW ESSnuSB (European Spallation Source neutrino Super Beam) proton accumulator. The analysis is based on numerical and asymptotic solutions of the Schrödinger equation for a two-level model describing the interaction of a relativistic hydrogen atom with a Gaussian pulsed laser beam.

INTRODUCTION

Laser-based H⁻ charge-exchange injection offers an attractive alternative to conventional carbon-foil stripping for injection into multi-megawatt proton rings. In foil-based systems, foil heating and degradation, radioactivation, uncontrolled beam losses, and transverse emittance growth are factors limiting the achievable average beam power. It motivated to carry out deep investigations for developing the laser assisted methods [1,2]. In this work, we evaluate the feasibility of the tree-step laser-assisted H⁻ charge-exchange injection into the ESSnuSB (European Spallation Source neutrino Super Beam) proton accumulator [3].

A THREE-STEP SCHEME

We consider a three-step laser-assisted H⁻ charge exchange injection into a proton ring without stripping foils [1,2]. The scheme of the beam – laser interaction is shown in Fig.1. It consists of: i) a first magnet-neutralizer of the H⁻ beam using Lorentz stripping, ii) a colliding system of a high power laser and the H^0 beam to excite H^0 atoms to the 3p state using the Rabi oscillation, and iii) a second magnet to strip the $H^0(3p)$ to a proton beam by Lorentz stripping. In this paper, we focus on the second step - excitation of H^0 from the ground state $(1s)$ to the excited $(3p)$. The excitation energy is $\hbar\omega_0$ =12.10 eV in the rest frame of the atom.

Elliptic Gaussian Laser Beam

We consider a linearly polarized elliptical Gaussian laser beam that crosses the H^0 beam axis at an angle α as shown in Fig.1. The interaction point (IP) is located at a distance z_L from the laser waist. The vertical component of the electric field, E_y, in the rest frame K' of an individual atom in the beam is given by

$$E'_y(t') = \mathrm{Re}\left\{\sqrt{\frac{2P}{\pi\sigma_y\sigma_x c\epsilon_0}}\frac{\omega'}{\omega}e^{-\frac{(t')^2}{2{\sigma_{t'}}^2}+i\left(\omega' t'-\frac{\Gamma(t')^2}{2}+\varphi_0\right)}\right\}, \quad (1)$$

where $\sigma_{t'} = \frac{\sigma_x}{c\gamma\beta sin\alpha}$ is the rms interaction time of the atom with the laser; $\Gamma = \sqrt{\frac{1}{2}\left(\frac{\omega}{c}\theta_{0x}\sigma_x\right)^2 - 1}\Big/\sigma_{t'}^2$ is the frequency sweep rate; ω' is the Doppler shift of the laser frequency ω

$$\omega' = \omega\gamma(1+\beta cos\alpha). \quad (2)$$

The following values correspond to the laboratory frame K: γ is the relativistic factor; β is the velocity ratio, α is the angle between the laser and the H^0 beam as shown in Fig.1; $\sigma_{x,y} = \frac{w_{0x,y}}{\sqrt{2}}\sqrt{1+\left(z/z_{0x,y}\right)^2}$ is the transverse size of the laser beam at the IP ($z = z_L$); P is the power of the laser micropulse, $w_{0x,y}$, $z_{0x,y}$, and $\theta_{0x,y}$ is the waist, Rayleigh range, and divergence of the laser beam, corresponding to the x and y directions.

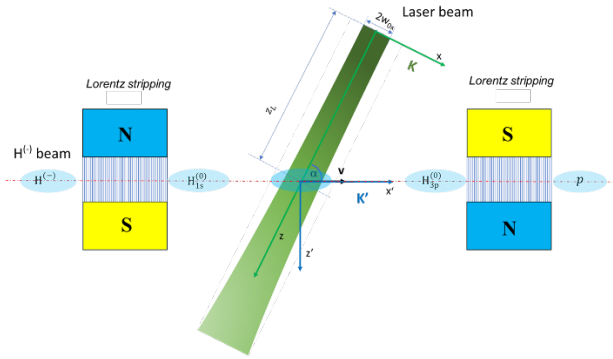

Figure 1: Three-step laser-assisted H⁻ charge exchange injection. K - laboratory frame, K' - rest frame

Doppler Broadening

The relativistic factor γ and angle α of an atom of the bunch with energy spread σ_γ and divergence σ_α in the transfer line between the linac and the IP with the values of dispersion function D_x and derivative D'_x, can be expressed in terms of the deviations $\Delta\gamma$ and $\Delta\alpha$ (correlated and uncorrelated) from γ_0 and α_0 of the reference particle

$$\gamma = \gamma_0 + \Delta\gamma,\ \alpha = \alpha_0 - D'_x\frac{\Delta\gamma}{{\beta_0}^2\gamma_0} + \Delta\alpha_{uncor}. \quad (3)$$

* Work supported by the European Union, Project 101094628
† anatoliy.opanasenko@physics.uu.se.

Content from this work may be used under the terms of the CC BY 4.0 licence (© 2026). Any distribution of this work must maintain attribution to the author(s), title of the work, publisher, and DOI.

ISBN: 978-3-95450-252-3 ISSN: 2673-5350 doi: 10.18429/JACoW-IPAC2026-THP4087

STATUS OF AISHA ION SOURCE AT CNAO

S. Marangoni[†,1], S. Alpegiani[1], E. Bressi[1], G. Castro[2], L. Celona[2], G. Costanzo[2], L. Falbo[1], S. Gammino[2], L. Lanzavecchia[1], O. Leonardi[2], A. Malinverni[1], M. Manzini[1], P. Meliga[1], R. Monferrato[1], C. Priano[1], F. Russo[2], D. Siliato[2], M. Spairani[1], G. Venchi[1], F. Zanoli[1]
[1]Fondazione CNAO, Pavia, Italy
[2]Istituto Nazionale di Fisica Nucleare – Laboratori Nazionali del Sud, Catania, Italy

Abstract

CNAO is one of the few centres all around the world able to treat patients affected from cancer by proton and carbon ions beams. The clinical beams are produced by a synchrotron equipped with two ECR (Electron Cyclotron Resonance) sources. A third source, based on the AISHa (Advanced Ion Source for Hadron therapy) source of the INFN-LNS laboratory, has been installed in order to produce new species that will be interesting both for clinical and R&D purposes. This paper shows the most important results along with the issues occurred and the solutions found during the first phase of the commissioning of the source with helium ions beams.

INTRODUCTION

Medical application systems installed in hospitals must deliver ions with enough current to keep patient treatment times short, as well as ensure high reliability, stability, and reproducibility of the produced and accelerated beam. Additionally, sources designed for hospital use should be easy to optimize and maintenance should be straightforward and efficient. Fondazione CNAO uses two Supernanogan ECR (Electron Cyclotron Resonance) sources to produce proton and carbon ions for daily treatments. To generate new ion species, a third ion source called AISHa-CNAO has been installed. This system is based on the design developed at INFN-LNS [1-2], but it includes several enhancements intended to allow continuous operation for several months without requiring maintenance stops. The source has been integrated in the whole CNAO layout by a dedicated low energy beam line (LEBT) shown in Fig. 1 and described in [3].

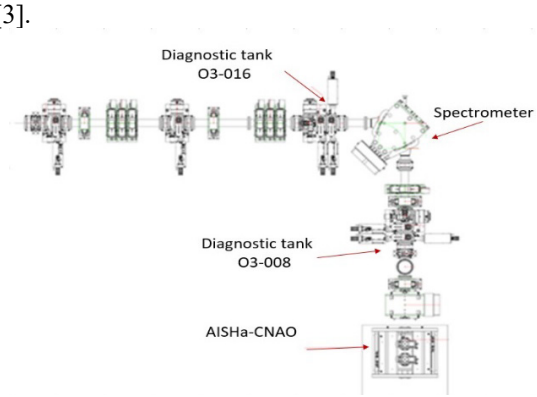

Figure 1: AISHa-CNAO LEBT layout, where magnets and diagnostics tanks are showed.

AISHa has been developed to operate effectively within both clinical environments and nuclear physics laboratories. Its engineering specifically allows it to accommodate an oven for producing metallic ions. CNAO has received approval to generate Helium, Carbon, and Oxygen as gas beams, as well as Lithium and Iron as metallic beams. Since AISHa was installed at CNAO, it has primarily been used to produce Helium—commissioning of which is still underway [4]—so that Helium beams can eventually be used in CNAO's treatment rooms for patient care.

MAINTENANCE AND DC-BIAS UPGRADE

Plasma confinement is realized in AISHa by a permanent hexapole magnet and four superconducting solenoids whose currents are set to proper adjust the longitudinal magnetic field profile. Plasma is generated by radio-frequency (RF) delivered by a klystron with adjustable frequency; the extraction voltage is set to match beam energy to the LINAC acceptance. A negative biased puller electrode is used to protect the plasma lens. A DC-bias electrode is positioned inside the plasma chamber to increase the plasma density and stabilize the beam extracted current. CNAO is the first centre that experienced a long-term operation with AISHa source. For this reason there was not a precise maintenance plan except of the maintenance of standard parts (vacuum components and so on). An accurate supervision of source parameters was needed to understand source behaviour over time.

A particular attention has been paid to monitor the HV power supplies. Since the beginning some discharges have been observed on the repeller electrode. The control system just gives a warning if the puller overcurrent lasts less than 2 seconds, while it gives an interlock and switches off the klystron if the overcurrent lasts for more than 2 seconds. After one month of operations, we observed that the warning occurred more frequently day by day and that sometimes the interlock was triggered. Since it was not possible to service the source we tried a cleaning procedure with a high-pressure oxygen flux, but the problem came back again when raising the microwave power to values higher than 1 kW.

An inspection of the plasma chamber showed that the chamber was dirty and that the effect was due to the erosion of the DC-bias material. Furthermore the extraction insulator had discharge spots caused by the material sputtered from the DC-bias in correspondence of the plasma loss lines. This was a clear evidence that the sputtering of the beam on the bias was excessive for source long-term

† stefano.marangoni@cnao.it

Content from this work may be used under the terms of the CC BY 4.0 licence (© 2026). Any distribution of this work must maintain attribution to the author(s), title of the work, publisher, and DOI.

ISBN: 978-3-95450-252-3 ISSN: 2673-5350 doi: 10.18429/JACoW-IPAC2026-THP4088

RF-KO EXTRACTION AT CNAO FOR CLINICAL BEAMS

S. Marangoni, S. Alpegiani, E. Bressi, G. Debernardi, L. Falbo,
P. Meliga, C. Priano, G. Venchi, F. Zanoli
Fondazione CNAO, Pavia, Italy

Abstract

CNAO is one of the few hadron therapy centres all around the world that produce both proton and carbon ions beams. It is based on a synchrotron in which the beams are extracted by a slow extraction mechanism that uses either a betatron core or an electrostatic exciter referred to as RF-KO (Radio-Frequency Knock Out). The RF-KO extraction method has been commissioned and in May 2024 we started using RF-KO for proton treatments, while in June 2025 we started using RF-KO for carbon treatments. This paper illustrates characteristics of clinical beams and the impact on patient treatment, comparing the results of the present extraction method with the betatron core one.

INTRODUCTION

The National Centre for Oncological Hadrontherapy (CNAO) in Pavia is one of the few centres worldwide that provides clinical treatments for oncological pathologies with both proton and carbon ions beams. The beam particles are accelerated by a 25 m diameter synchrotron up to 400 MeV/u for carbon ions and up to 250 MeV for protons [1]. Alongside with protons and carbon ions, CNAO can provide other ionic species: helium beams are currently under commissioning in treatment and experimental rooms [2] and other species are foreseen in the next future.

In a hadrontherapy synchrotron it is necessary to extract the beam slowly over periods of the order of a few seconds in order to deliver the dose to the patients in a controlled and measurable way. For this purpose a third order resonance excited by a sextupolar field can be used: after acceleration, beam particles are brought out of the stable region, they become unstable in the horizontal transverse phase space until they reach the electrostatic extraction septum.

CNAO was designed to extract particles by the use of a betatron core [3] that accelerates slowly the beam with a DC voltage of few volts: changing the momentum spread with a high horizontal chromaticity allows to change particles tune until they cross the resonance line of Steinbach diagram. The drawback of betatron extraction is that beam must be unbunched during extraction: this creates problem in a multiacceleration regime. Indeed in multiacceleration regimes, after the delivery of beam at a given energy, the remaining beam in the ring is accelerated to a higher energy but the trapping process to pass from coasting to bunched beams is very inefficient. Since CNAO plans to implement multiacceleration, in 2018 an electrostatic RF kicker [4] has been installed to implement RF-KO (Radio-Frequency Knock Out) that allows to extract bunched beams. In the RF-KO extraction the horizontal RF field increases the amplitude of betatron oscillations until the particles cross the Steinbach lines.

Passing from betatron to RF-KO extraction needed great changes in the synchrotron optics in addition to the implementation of strategies to use RF-KO kicker to match CNAO clinical requirements. Since 11th May 2024 proton treatments are performed by RF-KO extraction and since 21st June 2025 also carbon treatments are performed by RF-KO. This paper will summarize CNAO RF-KO characteristics, a part of which have been already presented in [5], and then it will illustrate beam calibrations and optimizations that led to treatments using RF-KO.

CNAO RF-KO DESCRIPTION

In order to have resonant perturbations with RF-KO extraction, the frequency of the RF signal must match the horizontal betatron frequency. Due to the beam momentum spread, the betatron frequency is not unique and therefore a sweep in RF-KO frequency is needed to correctly excite all the particles. In addition to FM modulation, the RF signal must be also AM modulated to match the spread in betatron amplitudes, but a purely analytical approach for the voltage ramp [5] is not sufficient to guarantee a uniform distribution of extracted particles over time.

It has been implemented a feedback system ("Voltage feedback") on the RF-KO voltage: at a rate of 1 kHz the system reads the counts from the dose delivery system (DDS) and change the kicker voltage using a IIR filter to keep the intensity constant.

The frequency sweep amplitude is adjusted roughly to 10 kHz while the maximum frequency is firstly set to one third of the revolution frequency and then it is finely adjusted energy per energy considering extraction efficiency and the maximum power deliverable by RF-KO amplifier (500 W).

The voltage feedback guarantees a perfect control of beam extracted intensity on the time scale of the voltage feedback; however looking at the spill structure at a 10 kHz frequency a ripple appears due to the synchrotron power supplies ripple.

To smooth time spill structure an additional feedback has been implemented using an iron-free quadrupole (air-core) that can provide small but very fast corrections to the machine tune. Every 50 µs, the air-core feedback system computes the derivative of the counts from the dose delivery and uses it to regulate air-core quadrupole current to smooth spill structure.

The implementation of voltage and air-core loops makes the measurement of particles at the dose delivery of fundamental importance for beam extraction. This aspect needed a specific study in using RFKO extraction in real treatments due to the way beam is delivered to the patients in CNAO.

Content from this work may be used under the terms of the CC BY 4.0 licence (© 2026). Any distribution of this work must maintain attribution to the author(s), title of the work, publisher, and DOI.

ISBN: 978-3-95450-252-3 ISSN: 2673-5350 doi: 10.18429/JACoW-IPAC2026-THP4090

IMPLEMENTATION OF MULTI-ENERGY EXTRACTION CONFIGURATIONS AT MEDAUSTRON

K. Holzfeind*, E. Renner, TU Wien, Vienna, Austria
F. Plassard, EBG MedAustron GmbH, Wiener Neustadt, Austria

Abstract

Moving from extracting one single energy per cycle to multiple energies promises improvements in time and power budgets of medical synchrotrons. To ensure reproducible and accurate beams for treatment, hysteresis effects must be considered. To avoid losses during energy changes, the beam has to be moved away from the extraction resonance. Different methods of moving the working point were compared regarding their robustness, adaptability and speed by means of measurements and Xsuite simulations. The measurements were taken at the synchrotron facility MedAustron. The methods are devised for the PIMMS-based lattice with one resonant sextupole and off-momentum operation, and differ in how the working point is shifted during the energy change regarding the timing of element ramps and off-momentum contributions.

INTRODUCTION

The synchrotron-based ion beam treatment and research center MedAustron, based on the Proton Ion Medical Machine Study (PIMMS) [1, 2], provides 62 - 252 MeV proton and 120 - 402 MeV u^{-1} carbon ion beams ($^{12}C^{6+}$) for irradiation of cancer patients. The center further delivers different beam modalities to nonclinical research users. These include the clinical beam modalities as well as low-flux beams, 800 MeV protons and helium ion beams. Ion beam therapy exploits the *Bragg peak* of heavy, charged particles in tissue for highly conformal radiation doses. To modify the penetration depth of the Bragg peak, the energy of the incoming ion beam must be adapted. Nominally, synchrotron operation for patient treatment follows the subsequent workflow: Multiturn injection and acceleration to the energy specified in the treatment plan, followed by betatron core-driven 3rd-order resonant slow extraction [3] until the prescribed dose is delivered. The process concludes with the dumping of any unused beam and conditioning the beamline for the following injection.

In recent years radio frequency knockout (RFKO) [4] has been investigated as alternative slow extraction mechanism at MedAustron [5,6]. RFKO has some advantages compared to betatron core-driven extraction, such as the compatibility with dynamic intensity control [7], and multi-energy extraction (MEE). With MEE the prescribed dose for several energy slices of the treatment plan can be delivered within one cycle of the synchrotron by re-acceleration or deceleration of the beam after each extraction phase. MEE could shorten the duration of patient treatment significantly and reduce power consumption. This proceeding will report on the current progress of first experimental tests of RFKO MEE at MedAustron. The ongoing studies focus on loss mitigation during the energy changes, including ensuring robustness in failure scenarios. In this context, different methods for increasing the stable phase space area during these energy ramps are presented and discussed.

* katrin.holzfeind@tuwien.ac.at

STABLE AREA DURING ENERGY RAMPS

For slow extraction at MedAustron, the $3Q_x = 5$ resonance is excited by powering one resonant sextupole. Its normalized strength

$$S = \frac{1}{2}\beta_x^{3/2} k_2 l \,, \tag{1}$$

depends on the horizontal beta-function at the location of the sextupole β_x, its length l and the normalized sextupole magnet gradient k_2. The resonance separates the phase space in regions, where particle perform stable or unstable motion. The area of the stable region,

$$A = \frac{48\sqrt{3}\pi^2}{S^2}(\delta Q)^2 \,, \tag{2}$$

is directly proportional to the square of tune distance from the resonance, $\delta Q = Q_{\text{particle}} - Q_{\text{resonance}}$, and inversely proportional to the square of the normalized sextupole strength S. In order to avoid losses during the energy change the stable area in the horizontal phase space should increase compared to the beam's emittance.

Methods

There are various ways of how this can be achieved. Firstly one can weaken the resonance by decreasing the normalized sextupole gradient k_2, method (a). For $S \gg 1$, the stable area is can also be effectively increased by changing δQ (method (b) - (d)).

Evidently, the resonance can be excited and diminished by (a) turning the resonance driving sextupole on and off. Up to 50 ms will be added to the energy change duration as they are needed for the full resonant sextupole ramp. However, the resonance can also be weakened instead of completely turned off. An example for one such implementation: When increasing the energy, $\Delta E > 0$, and thus the magnetic rigidity $B\rho$, while delaying the gradient ramp of the resonant sextupole, k_2 decreases (blue line in Fig. 1 (b)).

When focusing on changing the tune distance other methods, such as (b) including dedicated optic magnet ramps to change the tune, (c) ramping the momentum offset via radial loop regulation or (d) addition of a delay to the $B\rho$-ramp

Content from this work may be used under the terms of the CC BY 4.0 licence (© 2026). Any distribution of this work must maintain attribution to the author(s), title of the work, publisher, and DOI.

ISBN: 978-3-95450-252-3 ISSN: 2673-5350 doi: 10.18429/JACoW-IPAC2026-THP4092

INFLUENCE OF SYNCHRO-BETATRON RESONANCE ON SLOW EXTRACTION OF HIGH-FREQUENCY BUNCHED BEAMS AT SIS18*

J. Yang, P. Forck†, K. Groß, T. Milosic, R. Singh, S. Sorge
GSI Helmholtz Centre of Heavy Ion Research GmbH, Darmstadt, Germany

Abstract

Measurements and simulations of the slow extraction of bunched particle beams via tune scan at the GSI heavy ion synchrotron SIS18 were performed to study the temporal structure of the spills. The arrival times of extracted single particles were recorded in relation to the bunch-forming 80 MHz rf signal. It is demonstrated that high-frequency bunching leads to an enlarged synchrotron tune and, hence, to isolated synchro-betatron resonances that are crossed during the tune scan. The resonances affect the temporal structure of the extracted beams on time scales ranging from nanoseconds to seconds.

BUNCHED BEAM SLOW EXTRACTION

Most users of the GSI synchrotron SIS18 demand resonant slow extraction with a typical duration between 1 and 10 s. The tune-scan method is performed by increasing the horizontal tune towards a 3rd integer resonance, i.e., $Q_x \rightarrow 4\frac{1}{3}$. For coasting beam extraction, pronounced fluctuations appear on time scales from 10 µs up to several ms. They are related to the current ripple of the quadrupole magnets [1–3]. These fluctuations are referred to as spill micro-structure. Several schemes for mitigating spill micro-structures on coasting beams were examined at GSI [2–6].

In addition, the spill micro-structure mitigation by creating stationary bunches inside the synchrotron has been investigated at GSI [5, 6] and is adopted in ion synchrotrons for cancer treatment; further literature is compiled in [7]. Commonly, acceleration and bunching are performed with ferrite-loaded cavities that provide a maximum rf of $f_{\mathrm{rf,max}} = 5.5$ MHz, corresponding to an rf harmonic number $h = 4$. The modifications of the spill micro-structure for such conditions were previously investigated through measurements and MAD-X simulations [8]. It was also shown experimentally that the ferrite cavity rf imprints bunch-synchronous time structures on the extracted beam of typically 10 ns duration and separated by the bunch period of 200 to 300 ns. These structures are referred to as spill nano-structures and, unfortunately, limit the applicability of the extracted beams for some fixed-target experiments.

In this work, we describe the temporal structure for high-frequency bunching with $h = 90$ in order to reduce the separation between the extracted bunches. The high harmonic numbers are achieved by installing a pillbox-like rf-cavity in SIS18, which provides a frequency range of 80.2 to 81.6 MHz. Tunability is required to match harmonics for the relevant extraction energies between 0.3 and 2 GeV/u. More cavity parameters are described in [9].

During extraction, the horizontal tune Q_x is scanned, and synchro-betatron resonances (SBR) [10–12] are crossed at the resonance condition

$$nQ_x + mQ_s = p \quad \text{with} \quad n, m, p \in \mathbb{Z} \setminus \{0\} \, . \tag{1}$$

where Q_s is low-amplitude synchrotron tune [10, 13]. SBRs are excited due to the coupling of horizontal and longitudinal particle motions by dispersion at the bunching cavity and sextupole fields, as well as chromaticity. For a circulating beam with velocity βc, mass Am_0c^2, ionic charge qe, and gap voltage U_{gap}, the low-amplitude synchrotron tune Q_s is

$$Q_s = \sqrt{\frac{1}{2\pi} \cdot \frac{qe}{Am_0c^2} \cdot \frac{|\eta|}{\beta^2\gamma} \cdot h \cdot U_{\mathrm{gap}}} \propto \sqrt{h \cdot U_{\mathrm{gap}}} \tag{2}$$

with $\eta = 1/\gamma_{\mathrm{tr}}^2 - 1/\gamma^2$ being the phase slip factor and β, γ being the Lorentz factors; $\gamma_{\mathrm{tr}} = 5.58$ is the transition energy. As the synchrotron tune Q_s increases, the spacing between SBRs becomes larger. For the investigated gap voltages, a fraction of particles is at the periphery or even outside the stationary bucket. Hence, the amplitude-dependent decrease of the synchrotron tune is quite relevant for resonant slow extraction.

MEASUREMENT SETUP AND ANALYSIS

In measurements with high-frequency bunching, a $^{14}N^{7+}$ beam was injected into SIS18 at 11.4 MeV/u via multi-turn injection, filling the horizontal acceptance, and was subsequently accelerated to the extraction energy of $E = 300$ MeV/u by the ferrite-loaded cavity operating at harmonics $h = 4$. After debunching, the beam was adiabatically rebunched in 0.25 s to build bunches at 81.44 MHz ($h = 90$). The gap voltage was varied between $U_{\mathrm{gap}} = 0.5$ and 13 kV; for comparison, a coasting beam was also measured. At $U_{\mathrm{gap}} = 2$ kV, $Q_s = 0.0038$; other values scale according to Eq. (2). An extraction duration of $t_{\mathrm{ex}} = 8$ s using a tune ramp $\Delta Q_x = 0.0061$ was chosen; the average extraction rate was $r_{\mathrm{av}} \approx 10^6$ s^{-1}. The extracted particles were detected using a BC400 plastic scintillator coupled to a photomultiplier. The particles' arrival times were recorded by a TDC (CAEN V1290N) [14]. The system's overall time resolution is better than 0.3 ns. The data are displayed using the extraction rate as a function of extraction time or relative to the zero-crossing of the bunching frequency.

For the micro-structure evaluation, time bins of $\Delta t = 10$ µs are generated and analysed using the average counts $\langle c \rangle^2(t_{\mathrm{ex}}) = \mu_c^2(t_{\mathrm{ex}})$ and the variance $\langle c^2 \rangle(t_{\mathrm{ex}}) = \sigma_c^2(t_{\mathrm{ex}})$

* This project has received funding from the European Union's Horizon 2020 Research and Innovation programme under GA No 101004730.

† p.forck@gsi.de

Content from this work may be used under the terms of the CC BY 4.0 licence (© 2026). Any distribution of this work must maintain attribution to the author(s), title of the work, publisher, and DOI.

ISBN: 978-3-95450-252-3 ISSN: 2673-5350 doi: 10.18429/JACoW-IPAC2026-THP4093

FLAT C/HE SPILLS FOR ONLINE RANGE MONITORING IN PARTICLE THERAPY *

A. Pastushenko†, C. Graeff, B. Gålnander, R. Hetzel, D. Ondreka, J. Stadlmann, L. Volz,
GSI Helmholtz Centre for Heavy Ion Research, Darmstadt, Germany
E. Renner, TU Wien, Vienna, Austria

Abstract

The use of mixed ion beams is a developing approach aimed at improving current carbon-ion therapy by enabling online monitoring of dose deposition. In such a configuration, the main dose is still delivered by carbon ions, while lighter ions traverse the patient with negligible dose contribution and can be used for imaging. The main challenges of this approach include the need to simultaneously accelerate both ion species and to slowly extract them with a stable species ratio, a prerequisite for potential clinical application. At GSI, a mixed beam of $^{12}C^{3+}$ and $^{4}He^{+}$ ions was provided in May 2025 for biophysics experiments. The very small mass-to-charge difference of 0.065 % between these ion species enables simultaneous acceleration in the SIS18 heavy-ion synchrotron. To slowly extract them with transverse RF-knockout, chromaticity in the ring was adjusted, and the spill optimization system was used. These measures enabled a nearly rectangular spill with a constant helium/carbon ratio within the spill, confirmed by ionization-chamber measurements in the medical cave. This contribution presents the experimental results and discusses their implications for mixed-beam operation.

INTRODUCTION

Particle therapy with ions, particularly carbon ions, offers significant advantages over other treatment methods in terms of dose localization. A maximum stopping power is reached near the end of the ion path, forming the so-called Bragg peak, which enables highly localized dose deposition. However, this also poses a challenge, since range uncertainties may cause the Bragg peak to fall outside the targeted tumor area. It is one of the major challenges in ion therapy [1]. One proposed solution is the addition of a small fraction of helium ions to a primary carbon beam [2]. In this approach, the helium ions traverse the patient and enable range monitoring, while the carbon ions deliver the therapeutic dose. Such a scheme was successfully tested at the SIS18 synchrotron at GSI in 2023 [3]. Parallel investigations of the mixed helium/carbon beams are also being carried out at other facilities, in particular at MedAustron [4, 5].

The simultaneous acceleration of carbon and helium ions is possible because the charge states can be chosen such that both ion species have nearly identical mass-to-charge ratios. For the studies presented here, $^{12}C^{3+}$ and $^{4}He^{+}$ were used. The relative difference in mass-to-charge ratio is only 0.065 %, making the two species nearly indistinguishable from the machine point of view. At the same time, the 2023 measurements showed that the slow extraction of the mixed beam is highly sensitive even to this small difference in mass-to-charge ratio. The goal of the experiment in 2025 was to fine-tune the slow extraction in order to achieve a stable helium-to-carbon ratio within the spill. This paper summarizes the mixed beam measurements performed at SIS18 in May 2025.

Table 1: SIS18 Synchrotron Parameters at Extraction Relevant to the May 2025 Mixed-beam run.

Parameter at the extraction	Value
Kinetic energy, E_k	225 and 260 MeV u^{-1}
Working point, Q_x/Q_y	4.33/3.28
Natural chromaticity, ξ_x^N / ξ_y^N	-6.5/4.1
Norm. horizontal emittance, ϵ_x	≈16 µm
Slow extraction scheme	RF-KO
Spill length	2 s

MACHINE AND EXPERIMENT DESCRIPTION

The carbon–helium mixture is produced in the ECR ion source using methane, with helium as a support gas [6]. The injector was tuned to $A/q = 4$, resulting in the extraction of $^{12}C^{3+}$ and $^{4}He^{+}$. This also leads to a small oxygen contamination from $^{16}O^{4+}$. The mixture is accelerated in the UNILAC linear accelerator to the energy of 11.5 MeV u^{-1} and injected into SIS18 over multiple turns. The mixed beam is then accelerated to the desired kinetic energy and slowly extracted towards GSI's medical research room (Cave M). A transverse RF-KO extraction scheme was used to provide a spill length of 2 s. In May 2025, the tests in Cave M were performed at two energies: 225 and 260 MeV u^{-1}. Other extraction parameters relevant to the May 2025 mixed-beam run are listed in Table 1.

The analysis of the extracted beam was performed using the setup installed in Cave M. A schematic representation of the apparatus is shown in Fig. 1. It comprises three ionization chambers (IC), namely IC1, IC2, and IC3 [7]. IC1 is located at the nozzle, while IC2 and IC3 are positioned, by means of range shifters, at the carbon and helium Bragg peaks, respectively. The signal from each ionization chamber is sampled at 50 kHz and can be monitored online for

* This project has received funding from the European Union's Horizon 2020 research and innovation programme under grant agreement No 101124273. Views and opinions expressed are however those of the author(s) only and do not necessarily reflect those of the European Union or the European Research Council Executive Agency. Neither the European Union nor the granting authority can be held responsible for them.

† a.pastushenko@gsi.de

Content from this work may be used under the terms of the CC BY 4.0 licence (© 2026). Any distribution of this work must maintain attribution to the author(s), title of the work, publisher, and DOI.

ISBN: 978-3-95450-252-3 ISSN: 2673-5350 doi: 10.18429/JACoW-IPAC2026-THP4094

MODIFICATIONS OF THE HIGH-ENERGY BEAM TRANSPORT AT GSI AND ITS SUBSYSTEMS FOR FAIR

C. Hessler*, U. Clausen, O. Geithner, F. Hagenbuck, L. Heyl, A. Krämer, A. Krause, B. Mai, S. Reimann, A. Reiter, M. Schwickert, S. Strohmenger, Y. Valdau, B. Walasek-Höhne, H. Welker
GSI Helmholtz Centre for Heavy Ion Research, Darmstadt, Germany

Abstract

The High-Energy Beam Transport at GSI (GSI-HEBT) is a system of transfer lines which delivers heavy ion beams from the SIS18 synchrotron to various experiments, the fragment separator and the storage rings ESR and CRYRING@ESR. The High-Energy Beam Transport for FAIR (FAIR-HEBT) will also branch off from the GSI-HEBT. This connection is currently under construction and requires several modifications in the GSI-HEBT to accommodate FAIR beamline devices within tight space constraints. Furthermore, FAIR will be operated from a new, fully digital control room. Therefore, all remaining analog devices of GSI-HEBT had to be digitized, in particular the cameras of the scintillating screens and the fast current transformers. The power converters for the magnets in GSI-HEBT, which are needed for beam transport to FAIR, are currently being upgraded to FAIR standard. These modifications of GSI-HEBT will be discussed in this paper in detail.

INTRODUCTION

The GSI Helmholtz Centre for Heavy Ion Research in Darmstadt, Germany operates an accelerator complex providing ion beams ranging from protons to uranium. The facility comprises the UNILAC linear accelerator, the SIS18 synchrotron, the fragment separator FRS, and the storage rings ESR and CRYRING@ESR. Experiments can be performed in several experimental areas located at different positions along the accelerator chain. The experimental caves downstream of SIS18, the FRS, and the storage rings are supplied with beam via a complex system of beam transfer lines known as the GSI High-Energy Beam Transport (GSI-HEBT).

The Facility for Antiproton and Ion Research (FAIR) is currently under construction as an extension of the GSI accelerator complex [1,2]. It will use the existing UNILAC and SIS18 of GSI as an injector and will include a new superconducting heavy-ion synchrotron (SIS100), a superconducting fragment separator (SFRS), and several new experimental areas. FAIR will be connected to the GSI-HEBT via the FAIR High-Energy Beam Transport (FAIR-HEBT). For the connection and operation of FAIR, several modifications and upgrades of the GSI-HEBT had to be implemented.

* c.hessler@gsi.de

FAIR CONNECTION

The new beamline towards FAIR (T1S1 line) branches off from the existing beamline serving the target hall and ESR (TE line) at the same location where the beamline to the FRS branches off. Consequently, the installation of the T1S1 line will lead to an extremely dense arrangement of beamline equipment in this area. In preparation for the FAIR connection, the originally installed two-way deflection magnet GTS1MU1 had already been replaced by a new three-way deflection magnet several years ago. Installation of the beamline components of the T1S1 line was scheduled for autumn 2025.

Issues and Collisions

Due to the very tight space constraints, the new beamline could only be designed with minimal mechanical clearances. The first quadrupole and the first main dipole magnet of the T1S1 line must be installed in close proximity to the existing TE line (Fig. 1). To avoid a collision with the beam pipe of the TE line, the first quadrupole had already been designed with a cutout in the iron yoke. The remaining clearance between these magnets and the beam pipe of the TE line was planned to be on the order of only 1 cm.

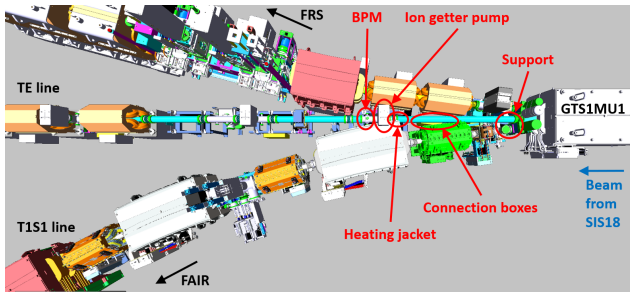

Figure 1: Old (planned) layout of the branching point area showing the existing beamlines to FRS and ESR/target hall (TE line) and the planned T1S1 beamline to FAIR. Collisions are indicated with red circles.

Shortly before the start of installation, however, several collisions between T1S1 beamline components and equipment of the existing TE beamline were identified in the 3D model. In particular, the first main dipole magnet of the T1S1 line interfered with a beam position monitor (BPM), an ion getter pump, and bake-out jackets of the beam pipe of the TE line. Additional conflicts were detected between supports of the T1S1 line and the connection boxes of the bake-out system, as well as with other supports belonging to the existing beamlines (Fig. 1).

Content from this work may be used under the terms of the CC BY 4.0 licence (© 2026). Any distribution of this work must maintain attribution to the author(s), title of the work, publisher, and DOI.

ISBN: 978-3-95450-252-3 ISSN: 2673-5350 doi: 10.18429/JACoW-IPAC2026-THP4095

AUTOMATED MINIMIZATION OF UNCONTROLLED BEAM LOSS FOR SLOW EXTRACTION FROM SIS18

S. Appel, P. Madysa, S. Sorge*, GSI Helmholtz Centre for Heavy Ion Research, Darmstadt, Germany
O. Boine-Frankenheim, O. Kazinova, Technical University of Darmstadt, Darmstadt, Germany

Abstract

The GSI heavy ion synchrotron SIS18 delivers ion beams via slow extraction to various experiments for a wide range of ion species, beam energies, and spill lengths. For the upcoming FAIR Early Science program, extraction intensities of more than 1E9 uranium ions per second are required at energies up to about 1 GeV/u. One of the most important tasks for the slow extraction is limiting uncontrolled particle losses. Limits arise from the requirement to avoid damage of the extraction septa and to minimize the activation of accelerator components. For the highest expected intensities, the limits are a few percent only. That requires a robust optimization of the machine settings. Therefore, automated schemes using numerical optimizers are developed at GSI and tested for quadrupole-driven and RF KO slow extraction, in simulation as in measurements. We will report on first results that demonstrate the fast convergence of the observed transmission toward similar values, both in simulation and in measurements. The validated simulation model allows for important insights into the optimized settings.

INTRODUCTION

The Facility for Antiproton and Ion Research (FAIR) is an international center of heavy-ion accelerators, designed to advance research in heavy-ion and antimatter physics [1]. The facility's complexity demands a high degree of automation for future operations [2]. As part of this effort, we developed a framework called Generic Optimisation Frontend and Framework (*Geoff*) [3], which allows machine experts and operators to solve concrete optimization problems and reuse these solutions in an operational context.

Many present and future experiments at GSI and FAIR use slow-extracted beams from the SIS18/SIS100 synchrotrons [4]. For the upcoming FAIR Early Science program, extraction intensities of more than 10^9 uranium ions per second are required at energies up to about 1 GeV/u from SIS18. A slow-extracted beam is also referred to as *spill*. Critical tasks during the slow extraction of heavy ion beams at SIS18 are to ensure a good spill quality achieved by a low spill structure level according to the requirements of fixed target experiments, and to minimize uncontrolled particle losses in order to avoid component activation and ensure stable operation. The losses are influenced by the tuning of nonlinear lattice elements and orbit parameters. Therefore, automated optimization approaches, as enabled by *Geoff*, provide a promising tool to improve extraction performance and reduce losses in a systematic and reproducible manner.

* s.sorge@gsi.de

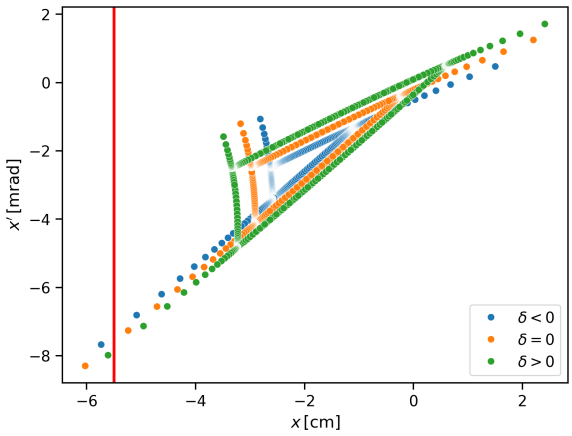

Figure 1: Simulated transverse phase space trajectories (x, x') of particles with different momentum offsets.

SLOW EXTRACTION IN SIS18

Slow extraction from ring accelerators is widely used for delivering hadron beams to fixed-target experiments and for tumor irradiation in hadron cancer therapy. Most schemes rely on the excitation of a third-integer lattice resonance with sextupoles. In SIS18, the resonance condition is given by $13 = 3Q_{x,\mathrm{r}}$, yielding a resonance tune of $Q_{x,\mathrm{r}} = 13/3 = 4.\overline{3}$. This creates a triangular stable phase-space area in the horizontal plane, bounded by separatrices, see Fig. 1. The betatron motion of particles is stable inside this region and unstable outside. The size of the stable phase-space area depends on the distance between particle and resonance tunes and is therefore sensitive to the particle momentum offset via chromatic tune shifts, as shown in Fig. 1. Slow extraction is performed by adiabatically approaching the resonance such that particles gradually become unstable, leave the stable phase-space region, and are extracted when reaching the electrostatic septum. Two standard extraction modes exist in SIS18: quadrupole-driven and RF knockout [5]. The present work focuses on quadrupole-driven extraction, where the tune is swept across the third-integer resonance starting from $Q_{x,\mathrm{start}} < Q_{x,\mathrm{r}}$.

A key challenge in slow extraction is the minimization of uncontrolled particle losses, which cause irradiation, component damage, and increased operational costs. The electrostatic septum (ES) and magnetic septum (MS) are particularly sensitive to such losses and therefore require careful optimization. In general, losses should be kept below 5–10 %. Losses of low-energy particles need to be stronger suppressed, as their impact is greater and is not limited to slow extraction losses. The ES applies a transverse kick required for beam extraction using a high electric field. Its anode consists of an array of wires with a diameter of 100 µm

Content from this work may be used under the terms of the CC BY 4.0 licence (© 2026). Any distribution of this work must maintain attribution to the author(s), title of the work, publisher, and DOI.

ISBN: 978-3-95450-252-3 ISSN: 2673-5350 doi: 10.18429/JACoW-IPAC2026-THP4096

OPTIMIZATION OF ONE AND TWO-PLANE MULTI-TURN INJECTION IN THE SIS18 SYNCHROTRON

S. Appel*, P. Madysa, GSI Helmholtz Centre for Heavy Ion Research, Darmstadt, Germany
H. Alsmeier, O. Boine-Frankenheim, R. Findeisen, S. Hirt, E. Lenz, M. Pfefferkorn, C. Reinwald
Technical University of Darmstadt, Darmstadt, Germany

Abstract

In the SIS18 heavy-ion synchrotron at GSI, loss-induced vacuum degradation and reduced beam lifetime limit high-intensity operation with uranium ions. During multi-turn injection (MTI), even small localized losses can trigger pressure bump instabilities, making optimized injection control essential to reach FAIR intensity goals. We present a comprehensive study on optimizing the MTI process in the SIS18 at GSI, combining experimental measurements and simulations. Online optimization using the derivative-free BOBYQA algorithm enabled direct improvement of machine performance. Multi-objective Bayesian optimization (BO) was applied to reconstruct the Pareto front experimentally between injection efficiency and beam losses, providing insight into the best achievable performance. On this basis, we introduce a multi-fidelity BO framework that integrates prior knowledge from low-fidelity models with high-fidelity experimental measurements, achieving improved sample efficiency. Complementary simulation studies on two-plane injection indicate a further potential for loss reduction. The results demonstrate effective, adaptive MTI optimization and support future autonomous tuning strategies.

INTRODUCTION

The Facility for Antiproton and Ion Research (FAIR) is an international center of heavy-ion accelerators, designed to advance research in heavy-ion and antimatter physics [1]. The facility's complexity demands a high degree of automation for future operations [2]. As part of this effort, we developed a framework called Generic Optimisation Frontend and Framework (*Geoff*) [3], which allows machine experts and operators to solve concrete optimization problems and reuse these solutions in an operational context.

A critical challenge for FAIR is the MTI into SIS18, which serves as a booster for SIS100 synchrotron. The MTI is a major bottleneck for achieving target beam intensities. Losses during injection can degrade the vacuum and limit the intensity of intermediate charge-state beams, and so must be minimized [4–6]. To address this challenge, online optimization campaigns were performed using classical algorithms such as BOBYQA, as well as advanced methods including BO and multi-fidelity BO. These approaches leverage simulations and machine measurements to efficiently reduce beam losses.

MULTI-TURN INJECTION

The MTI of the SIS18 is central for reaching target intensities of FAIR without exceeding acceptable beam losses of a few percent. Individual beamlets are stacked in a horizontal phase space until machine acceptance is reached. A time-dependent closed-orbit bump, generated by four bumper magnets, guides each incoming beamlet into the free phase space near the previous ones, typically using an exponential bump decay. After injection, the beamlets undergo betatron oscillations with horizontal tune Q_x and pass the injection point again after each turn. If the orbit bump decays too slowly, the beamlets may hit the inner septum and be lost; losses can also occur at limited acceptance [7, 8]. The **loss fraction** η quantifies the particles lost during injection:

$$\eta = \frac{N_{\text{lost}}}{N_{\text{inj}}} = \frac{I_{\text{TK}}n - I_{\text{SIS18}}}{I_{\text{TK}}n}, \tag{1}$$

where averaged $I_{\text{TK}}n$ is the ideal injected current and I_{SIS18} is the actual accumulated current. "TK" stands for the injection beamline to the SIS18. Low η indicates a more efficient injection. The effective number of accumulated turns is then $m = n(1 - \eta)$. In [9], the ideal injected current is defined more precisely as the sum of TK pulses per turn, which accounts for fluctuations and local variations. For optimal phase-space filling [10], injected emittances can be mapped to upright ellipses and the lattice functions mismatched so that the curvature of the incoming beamlets matches the acceptance. Previous studies demonstrate that horizontal emittance is a key factor for MTI performance: smaller emittance leads to reduced losses and higher accumulation. Experimental measurements and simulations confirm this trend, increasing confidence in the MTI simulation model implemented in Xsuite [7, 8, 11].

ONLINE OPTIMIZATION

Building on promising optimization results in simulation [7, 12], online MTI optimization campaigns were performed at SIS18 to reduce beam losses, as shown in Fig. 1. In the November 2023 and May 2024 campaigns, five injection parameters[1] and four beamline steerers were optimized using *Geoff* and **classical algorithms**. The parameter values were randomized before each run to avoid bias from favorable initial states. BOBYQA performed robustly when fluctuations were reduced by taking the median of three measurements for each iteration. Losses decreased from approximately 45 % (manual tuning) to 15 % in 2023 and

* s.appel@gsi.de

[1] Orbit bump amplitude and decay, two septum steerers, and a timing offset.

Content from this work may be used under the terms of the CC BY 4.0 licence (© 2026). Any distribution of this work must maintain attribution to the author(s), title of the work, publisher, and DOI.

ISBN: 978-3-95450-252-3 ISSN: 2673-5350 doi: 10.18429/JACoW-IPAC2026-THP4097

ROBUST REAL-TIME OPTIMIZATION OF SIS18 INJECTION USING GAUSSIAN PROCESS MPC*

S. Hirlaender, B. Halilovic, Paris Lodron University, Salzburg, Austria
S. Appel, P. Madysa, GSI Helmholtz Centre for Heavy Ion Research, Darmstadt, Germany

Abstract

We present advancements in the data-driven Model Predictive Control (MPC) framework for optimizing multi-turn injection (MTI) into the SIS18 synchrotron. Building on our prior work on safe, sample-efficient optimization, we systematically investigate the impact of current noise and transverse emittance fluctuations. By incorporating realistic error models derived from dedicated measurements of fluctuations on injected current and emittance into simulations, we demonstrate that the Gaussian Process model effectively filters random uncertainty, maintaining robust operation where standard numerical optimizers degrade.

Furthermore, we report on the successful deployment of the framework during live SIS18 tuning. The controller autonomously adjusted injection parameters, demonstrating reliable convergence, enhanced efficiency, and a substantial reduction in tuning iterations compared to model-free RL methods, which often face challenges in real-world applications. These results establish data-driven MPC as a powerful tool for real-time optimization in noisy, high-stakes accelerator environments, setting the stage for safe learning-based control across FAIR facilities.

INTRODUCTION

Data-driven control and reinforcement learning (RL) offer strong potential for accelerator control problems beyond the scope of classical methods [1,2]. However, RL in accelerator applications is challenged by limited data availability and the trade-off between training stability and data efficiency [3].

Model-based reinforcement learning (MBRL) addresses this issue by using predictive environment models to estimate future states and rewards. This reduces the required interactions with the accelerator [4,5]. Gaussian processes (GPs) provide probabilistic models of the system dynamics and capture uncertainties essential for safe exploration.

GP-MPC [5] trains n independent GPs (one per state dimension) on observed transitions $(s_k, a_k) \to s_{k+1}$, using an ARD-RBF kernel whose lengthscales automatically identify the relevance of each input dimension. At each step the controller propagates uncertainty through a finite planning horizon H via moment matching and minimizes an uncertainty-aware cost using L-BFGS-B. Actions are relative adjustments Δa, so the GP effectively performs derivative-free gradient estimation of the reward landscape through its posterior mean and variance. After each real interaction, the GP dataset grows and hyperparameters are re-optimized, forming an online learning loop.

* simon.hirlaender@plus.ac.at

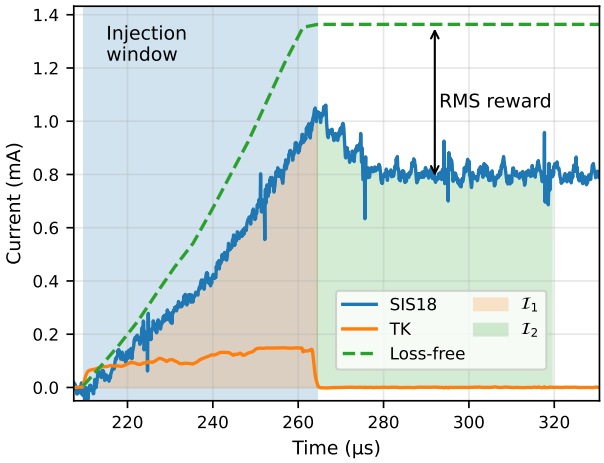

Figure 1: SIS18 injection measurement: stored current (blue), incoming TK beam current (orange) and ideal current (green) during the optimization. The integral values measure, in addition to the septum loss and reward, the states.

This work demonstrates the effectiveness of this approach for the highly non-linear SIS18 injection simulation, achieving reliable performance within a number of interactions compatible with real-machine operation.

MULTI-TURN INJECTION

FAIR, the Facility for Antiproton and Ion Research, will provide antiproton and ion beams of unprecedented intensity and quality [6]. Multi-turn injection (MTI) into SIS18 is a key bottleneck for achieving the FAIR intensity goals. This is particularly important for intermediate charge-state ions, where it is critical to avoid loss-induced vacuum degradation [7,8]. The MTI employs four bumper magnets to create a closed-orbit bump that allows successive beamlets to fill the horizontal phase space in accordance with Liouville's theorem.

After injection, the beamlets undergo betatron oscillations with horizontal tune Q_x and pass the injection point again after each turn. Particle losses occur at the septum and at the machine acceptance and are quantified by the loss fraction η, defined as the ratio of lost to injected particles. Lower η indicates higher injection efficiency, with $\eta = 0$ corresponding to loss-free injection. A more detailed description of the MTI can be found in [9–11]. The validated SIS18 MTI model is implemented in Xsuite and benchmarked against experiments [10–12].

The effect of **injection quality** on the accumulated beam current is shown in Fig. 1. Ideal settings yield a monotonic increase, while mismatched injection leads to losses. The

Content from this work may be used under the terms of the CC BY 4.0 licence (© 2026). Any distribution of this work must maintain attribution to the author(s), title of the work, publisher, and DOI.

ISBN: 978-3-95450-252-3 ISSN: 2673-5350 doi: 10.18429/JACoW-IPAC2026-THP4098

STATUS OF THE FAIR SIS100 KO EXCITER

S. Orth*[1], M. Frey[1], H. Klingbeil[2,1], U. Laier[1], D. Lens[1], N. Shurkhno[1], R. Stassen[3], B. Zipfel[1]
[1]GSI Helmholtzzentrum für Schwerionenforschung, Darmstadt, Germany
[2]Technical University of Darmstadt, Darmstadt, Germany
[3]Forschungszentrum Jülich, Jülich, Germany

Abstract

One of the planned slow extraction options for the SIS100 under construction at FAIR will be the excitation of a 3rd order resonance by means of the radio-frequency knock-out (RF KO) method. The system that is currently in its design phase will consist of two identical RF stations, each capable of providing a voltage amplitude of up to 5 kV between two electrodes (distance: 90 mm, length: 1.5 m) in the frequency range from 100 to 400 kHz. This contribution presents the design of the overall system, highlighting the transformer topology with eight transformers per RF station that are connected in parallel on their primary side and in series on their secondary side. Each primary side will be driven by a semiconductor amplifier via a 230 m long coaxial line. Investigations concerning the magnetic alloy (MA) based ring cores which form the inductance of the transformers and the effects of reflections along the transmission line between the amplifier and the transformer are shown as well as studies on the geometry of the exciter plates. The design presented here fulfills the competing requirements on amplitude, bandwidth, field homogeneity, cooling capacity, and space constraints.

SYSTEM OVERVIEW

The SIS100 KO Exciter will utilize the radio-frequency (RF) knock-out (KO) method, i. e., excitation of a 3rd order resonance to increase the betatron oscillation amplitude. Early studies showed that a stripline design like it is used for the SIS18 KO Exciter at GSI would result in extreme power demands. B. Breitkreutz and colleagues from Forschungszentrum Jülich (FZJ) came up with the current design of a capacitive kicker that is fed by several transformers (winding ratio 1:3) with primary sides connected in parallel and secondary sides connected in series to add the up-transformed voltages [1]. To ease the manufacturing, it was decided to split the available installation space in two parts and build two identical kickers. While this slightly reduces the available length of the electrodes, it also halves the capacitance which the power amplifiers (PA) see, thereby increasing the usable bandwidth (at the cost of a doubled number of PAs, however).

A schematic of the planned layout is shown in Fig. 1. Eight PAs (four for each electrode) will be used for each kicker, and each PA shall deliver up to 1 kW of RF power. Since the Low-Level RF components together with the PAs are located far away from the kickers, approximately 230 m long transmission lines are necessary.

* s.orth@gsi.de

Further electrical and mechanical properties of the SIS100 KO Exciter are summarized in Table 1.

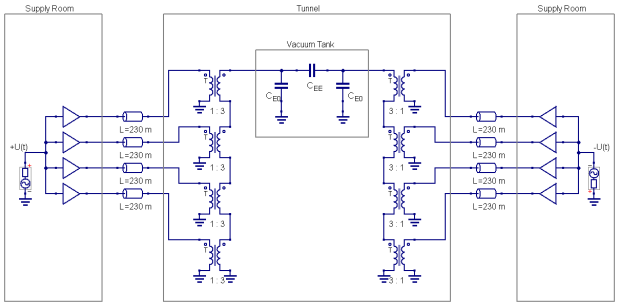

Figure 1: Schematic of the planned SIS100 KO Exciter layout for one of the two identical kickers.

Table 1: Electrical and Mechanical Properties of Each of the Two SIS100 KO Exciters

installation space	1.9175 m
horizontal electrode length (single kicker)	1.5 m
vertical electrode width	60 mm
horizontal electrode spacing	90 mm
vacuum tank diameter	400 mm
frequency range	100 to 400 kHz
voltage amplitude $\hat{U}_B$ (across the electrodes)	5 kV

Excitation Signal

The excitation signal itself and the means of its generation are still being discussed, but one promising option is to use a dedicated spill optimization system similar to the one used at the SIS18 KO Exciter to deliver special excitation signals for increased spill quality [2].

Transformer

To allow for higher harmonics of the 3rd order resonance to be used in the optimized excitation signal, a high bandwidth is desired. This can be achieved by minimizing the capacitance the kicker represents to the PAs. In order to extract as many particles as possible from the synchrotron, the voltage amplitude $\hat{U}_B$ should be as high as possible. This can be achieved by increasing the transformer ratio. However, increasing the transformer ratio also increases the capacitance seen by the PAs and thus limits the bandwidth. While increasing the number of PAs for each electrode would also result in a higher voltage amplitude $\hat{U}_B$, this also increases

Content from this work may be used under the terms of the CC BY 4.0 licence (© 2026). Any distribution of this work must maintain attribution to the author(s), title of the work, publisher, and DOI.

ISBN: 978-3-95450-252-3 ISSN: 2673-5350 doi: 10.18429/JACoW-IPAC2026-THP4100

COMMISSIONING OF HELIUM BEAMS AT CNAO

S. Marangoni†, S. Alpegiani, E. Bressi, L. Falbo, P. Meliga, C. Priano, G. Venchi, F. Zanoli
Fondazione CNAO, Pavia, Italy

Abstract

CNAO (Centro Nazionale di Adroterapia Oncologica) is one of the few hadrontherapy centres all around the world that produce both proton and carbon ions beams.

It is based on a synchrotron in which the beams are extracted by a slow extraction mechanism by means of either a betatron core or an RFKO electrostatic exciter. Recently a third source, AISHa-CNAO (Advanced Ion Source for Hadrontherapy), has been installed to produce new species to be used for clinical or experimental purposes.

In this article, we show the commissioning status of the helium beams generated by the new source.

INTRODUCTION

CNAO center has four beam lines for hadrontherapy treatments and one room (XPR-room) dedicated to experimental activities. Up to now the available species for treatments and experiments are proton and C^{6+} ions: a new low energy beam line [1] with a third source has been recently installed to produce new species with great impacts under the clinical, radiobiological and nuclear physics point of view. The installed source, named AISHa-CNAO, is an improved version of the source AISHa (Advanced Ion Source for Hadron therapy) designed by LNS-INFN [2, 3] to generate high brightness multiple-charged ion beams. After its installation, AISHA-CNAO has been commissioned and set for the production of Helium beams [4] that are particularly interesting for their clinical features. Helium beams are under commissioning in all the treatment rooms and in the experimental room: this paper shows the results and the status of this commissioning.

LEBT COMMISSIONING

CNAO low energy line is shown in Fig. 1, where the part installed for the third source (O3-line) is highlighted by a red shape. The line has been designed considering the space left by the three sources and the original LEBT. The result was a line whose length makes beam transmission difficult considering the low beam energy (the magnetic rigidity is just 0.02577 T·m due to LINAC design) and the number of installed diagnostics monitors. To overcome these difficulties, beam transport was studied dividing LEBT in three parts. Source settings and the magnets between the source and the spectrometer were optimized experimentally to produce the maximum current with the minimum emittance at the first diagnostics tank after the spectrometer. Right after, Twiss parameters obtained by the emittance measurement [4] were used as input for MADX [5] simulations: the two quadrupole triplets were matched to obtain the carbon ions Twiss parameters in the diagnostic tank (O2-023 tank) after carbon source spectrometer. The Twiss parameters obtained by emittance measurement in O2-023 tank were used as input for MADX simulations to compute the right Twiss parameters at the LINAC entrance. The dispersion was found by measuring the horizontal displacement of the beam changing the extraction high voltage of the source.

MADX simulations were just the starting point: optimizations were done changing simultaneously the currents of the quadrupoles of each triplet. The result was a transmission of about 60% along the O3-line and of 90% from the end of O3-line to the LINAC entrance where, at present, about 500 μA can be transported. To improve this scenario the installation of two diagnostic tanks is foreseen in the two-year period 2026-2027.

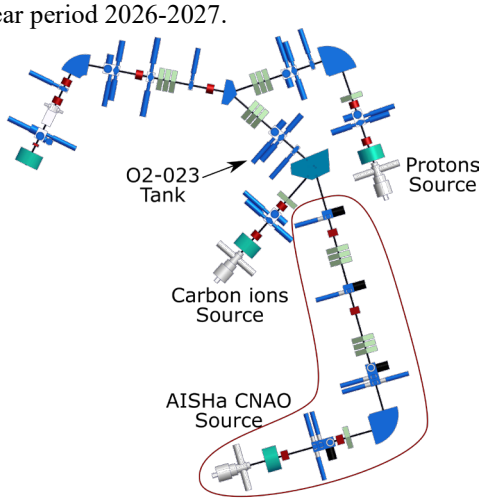

Figure 1: LEBT layout with AISHa-CNAO source. O3-line is high-lighted by a red shape.

LINAC AND MEBT COMMISSIONING

Next step was to accelerate the helium beams to the energy of 7 MeV/u through a LINAC, which at CNAO includes a RFQ (RadioFrequency Quadrupole) cavity and an IH-DTL (Interdigital H-type Drift Tube Linac). The 48 accelerating cells of the last one are divided in four sections among which 5 sections with pulsed magnets (13 quadrupoles and 4 kickers) are present.

Pulsed quadrupole currents have been scaled by the ones used for protons using the magnetic rigidity.

Considering that the power of a cavity is proportional to the square of the accelerating voltage and that the energy gain is proportional both to the voltage and to the ratio between atomic and mass number, the power of the amplifiers for Helium ($^4_2He^{2+}$) was obtained multiplying by 4/9 the power used to accelerate protons (H_3^+).

After a final tuning of these values, an acceleration from 8 keV/u to 7.148 MeV/u has been obtained, as given by a TOF (Time Of Flight) measurement, with a transmission through the LINAC of about 28%, that is similar to LINAC

† stefano.marangoni@cnao.it

Content from this work may be used under the terms of the CC BY 4.0 licence (© 2026). Any distribution of this work must maintain attribution to the author(s), title of the work, publisher, and DOI.

ISBN: 978-3-95450-252-3 ISSN: 2673-5350 doi: 10.18429/JACoW-IPAC2026-THP4103

MODELLING BEAM LOSSES IN CERN'S SUPER PROTON SYNCHROTRON WITH XSUITE

L. Pauwels*[1,2], H. Bartosik[1], G. Iadarola[1], N. Pauly[2], S. Redaelli[1], F.F. Van der Veken[1], D. Veres[1,3]
[1]CERN, Meyrin, Switzerland, [2]Université libre de Bruxelles, Brussels, Belgium,
[3]Goethe University, Frankfurt am Main, Germany

Abstract

Studies are ongoing at CERN's Super Proton Synchrotron (SPS) to understand the origin, distribution, and possible mitigations of observed beam losses. The existing equipment in the machine allows for dedicated measurements to identify bottleneck regions with higher losses. A well-suited and accurate simulation model of the SPS is indispensable to be able to study the impact of underlying beam dynamics on the loss distribution. This paper reviews the current status of the SPS model in Xsuite for loss simulations. The aperture model has recently been improved, and additional features can be enabled on demand, such as collimators and lattice non-linearities. Furthermore, the impact of the beam sagitta in bending magnets can be represented by introducing aperture offsets. This paper presents the results of the current setup, compares them to dedicated measurements, and outlines the next steps for further improvements.

INTRODUCTION

The Super Proton Synchrotron (SPS) at CERN accelerates beams up to 450 GeV. It delivers protons and ions to CERN's North Area for fixed-target experiments, and serves as the last injector for the Large Hadron Collider (LHC) [1]. As such, the reliability and performance of its operation directly impact LHC filling efficiency. Uncontrolled beam losses lead to unnecessary activation of machine elements, potential downtime, and reduced beam availability [2]. Understanding where losses occur and what drives their origin and distribution around the ring is, therefore, an operational challenge, essential both for machine protection and for identifying possible mitigations, including anticipating the radioactive dose on machine components.

Loss maps, where controlled losses are generated at low intensity to assess in a safe way the beam loss distributions around the ring, are a well-established tool widely used in the LHC [3]. In the SPS, dedicated beam intercepting devices are installed but not used in standard operation. Adapting this methodology to the SPS allows identification of aperture bottlenecks, characterisation of the loss distribution, and connection to the underlying beam dynamics.

Producing meaningful loss maps requires a reliable and accurate simulation model of the machine. This paper describes the current state of the SPS model in Xsuite [4] developed for this purpose, reviews its key ingredients, and presents the first results compared to measurements conducted in dedicated machine development (MD) sessions.

* lise.eliane.pauwels@cern.ch

SPS MODEL IN XSUITE

Lattice and Aperture Model

The SPS model in Xsuite is built from two separate MAD-X input files: a lattice sequence and an aperture sequence. The lattice sequence was recently updated as part of the Engineering-to-Alignment (E2A) campaign [5], launched to harmonise the two main CERN accelerator geometry databases (the Layout Database (LDB) and GEODE) after the Long Shutdown 2. In particular, a systematic discrepancy in the SPS dipole lengths–where the magnetic length was treated as an arc length rather than a chord length, accumulating to a 14 mm error around the ring–was identified and corrected, along with several other element length and position inconsistencies [6]. The resulting lattice sequence is used as the basis for the model presented here.

The aperture sequence is also generated from the LDB, which contains position, type, and standardised aperture definitions for every element in the CERN accelerator complex, complemented by technical drawings, design notes and additional references. However, at present, the LDB of the SPS is not complete. Some elements have no aperture definition assigned, some have incorrect apertures due to unreported hardware replacements, and some definitions do not match the referred technical drawings. Manual checking and correction were therefore necessary to produce a usable aperture model. Anomalous loss spikes in simulations proved a useful diagnostic for this process–in one instance, unexpectedly high losses on a specific element were traced back to a chamber replacement not recorded in the LDB. Although in this process we converged to a continuous and realistic model for the full ring, the aperture model is considered a work in progress, and comparison to dedicated measurements remains an essential validation tool.

Beam Sagitta in Bending Magnets

The SPS dipoles are rectangular bending magnets (RBends), rather than sector bends (SBends) like is the case in the LHC; see Fig. 1. In an SBend, the magnet body follows the curved reference frame, such that the physical chamber is always symmetric around the reference trajectory. For an RBend, the vacuum chamber is straight, while the reference particle follows a curved arc inside it. In the present implementation of Xsuite [4], the aperture of an RBend is by default centred on the reference trajectory–a good approximation for tracking purposes, but insufficient in the context of loss studies where the exact position of the physical chamber walls matters. It is therefore necessary to explicitly shift the aperture profiles along the magnet to account for the

Content from this work may be used under the terms of the CC BY 4.0 licence (© 2026). Any distribution of this work must maintain attribution to the author(s), title of the work, publisher, and DOI.

ISBN: 978-3-95450-252-3 ISSN: 2673-5350 doi: 10.18429/JACoW-IPAC2026-THP4104

COLLIMATOR PRE-SERIES PRODUCTION FOR CERN'S HIGH LUMINOSITY LARGE HADRON COLLIDER OPERATION*

T. Parmentier†, O. Aberle, C. Accettura, C. Antuono, F. Bonetti, J. Braken, M. Calviani, F. Carra, G. Cattenoz, J. Daricou, S. Fridstrom, H. Garcia Gavela, L. Gentini, E. Kaijanen, M. Kyprianidis, J. Lendaro, N. Mounet, F.-X. Nuiry, A. Perillo Marcone, C. Piccinni, F. Pirotte, L. Puddu, J. M. Quetsch, S. Redaelli, R. Seidenbinder, R. Viscardi. European Organization for Nuclear Research (CERN), Geneva, Switzerland

Abstract

In the framework of the High Luminosity Large Hadron Collider (HL-LHC) project, the accelerator's collimation system will be upgraded. Thirty-six new collimators of five different designs will be produced, including units of completely new designs, as well as replacements for existing collimators and spare units. The production of these collimators is taking place in two stages: starting with a pre-series of three units (first stage), to validate the subsequent production of the 33 remaining series units (second stage). This paper describes the production and testing process of the three pre-series collimators, from the production of the jaws, through vacuum vessel manufacturing and collimator assembly, to their delivery and acceptance testing at CERN. It details relevant production methods, including electron beam welding, vacuum brazing and bending of cooling pipes. The extensive testing campaign carried out on the pre-series units is described here, including both Quality Assurance (QA) assessments during production as well as the Site Acceptance Test (SAT) campaign upon reception of the collimators. The goal is to validate both the collimator functionality and the production capabilities.

INTRODUCTION

The High Luminosity Large Hadron Collider (HL-LHC) necessitates extensive upgrades of the entire LHC accelerator ring, including its collimation system [1] (Fig. 1). A total of 36 new collimators, including operational and spare units, of 5 different designs will be produced for installation during Long Shutdown 3. The quantities to be produced and attributes for each collimator type are given in Table 1. The production includes two types of the presently installed single-beam collimators: TCSPM and TCTPM [2, 3], as well as devices of three new types: TCLPX, TCTPXV and TCTPXH [3, 4] (Fig. 2). The pre-series include one TCLPX, one TCTPXH and one TCSPM collimator.

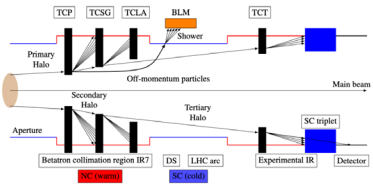

Figure 1: LHC multi-stage collimation schematic.

These new types, also called double-beam collimators, will be installed in the recombination regions near Interaction Points 1 and 5, where the beams approach each other transversally as they get close to the collision point. Both counter-rotating beams share the same vacuum vessel (collimator tank): the un-collimated beam circulates through a drift tube while the collimated beam is centered between the collimator jaws. With this new design, the double-beam collimators can cope with the reduced intra-beam distance, whereas the single-beam collimators, with separate vacuum chambers for both beams, cannot.

Table 1: Collimator Types

Type	Qty	Attributes
TCSPM	12	Single beam secondary collimator with Cu-coated graphite jaws
TCTPM	10	Single-beam tertiary collimator with Tungsten Heavy Alloy (WHA) jaws
TCLPX	5	Double-beam physics debris collimator with WHA jaws
TCTPXV	5	Double-beam tertiary vertical collimator with WHA jaws
TCTPXH	4	Double-beam tertiary horizontal collimator with WHA jaws

Before launching the series production, CERN has prototyped two collimators, a TCTXH and a TCLPX, to validate their new designs, master the production processes, and check their compliance with functional specifications. The pre-series includes a TCLPX, TCTPXH and TCSPM collimator. The production has been set up in a build-to-print fashion according to a Technical Specification [5]. The design of the collimators, production drawings, testing procedures and test-benches are provided before the start of the production. The raw materials and commercial components were thoroughly inspected and validated before assembly. The fabrication and metrology of components, assembly of collimators and execution of tests are defined in the Manufacturing and Inspection Plan [6].



Figure 2: Three pre-series collimators at CERN.

* Work supported by the HL-LHC project, https://hilumilhc.web.cern.ch/
† thibaut.parmentier@cern.ch

Content from this work may be used under the terms of the CC BY 4.0 licence (© 2026). Any distribution of this work must maintain attribution to the author(s), title of the work, publisher, and DOI.

ISBN: 978-3-95450-252-3 ISSN: 2673-5350 doi: 10.18429/JACoW-IPAC2026-THP4105

MITIGATION OF MUON BACKGROUNDS AT LHC FORWARD-PHYSICS EXPERIMENTS THROUGH ORBIT BUMPS*

A. Donadon Servelle†, J. Boyd, R. Bruce, F. Cerutti, M. Hostettler, A. Keyken, S. Ilieva, B. Lindström, S. Redaelli, A.-G. Serban, G. Vasquez, J. Wenninger, CERN, Geneva, Switzerland

Abstract

The Scattering and Neutron Detector at the LHC (SND@LHC) and the Forward Search Experiment (FASER) are located at the CERN Large Hadron Collider, 480 m from the ATLAS experiment on opposite sides. They study high-energy neutrinos and dark matter candidates produced in the proton-proton collisions at ATLAS. A key challenge for both experiments is the muon background, produced in the collisions and by nearby proton losses in the LHC ring. In 2024, a reversal of the magnet polarity of the final-focus system in IR1 caused a substantial increase in muon background at both experiments. Although nominal triplet polarity was restored in 2025, background levels remained significantly higher than in 2023. To mitigate the losses in cell 11, considered the origin of the main contribution to the background, orbit bumps were designed to displace the losses away. The bumps were designed using both conventional techniques and a novel Xsuite-based matching method employing beam losses as the optimisation observable. Experimental tests done in 2025 confirmed a background reduction in SND and FASER when activating the bumps. This study demonstrates that the proposed strategy is a viable operational solution for reducing muon backgrounds in future physics operations.

INTRODUCTION

The production of forward particles in proton-proton collisions at the Large Hadron Collider (LHC) [1] offers a unique opportunity to explore physics processes at energies never seen before. The Scattering and Neutron Detector (SND@LHC) [2] and the Forward Search Experiment (FASER) [3], located on opposite sides of the interaction point 1 (IP1) near ATLAS [4] (see Fig. 1), are dedicated to such studies. Their physics programmes aim to measure high-energy neutrinos and to search for particles potentially linked to dark matter.

A major challenge for SND and FASER operation is the background induced by high-energy muons emerging from the collisions or nearby proton losses on the machine aperture. These muons can penetrate a substantial amount of material and reach the experiments, potentially contaminating the emulsion detectors requiring more frequent replacements, which need to be minimised to limit LHC downtime. Understanding and minimising these backgrounds is therefore crucial for ensuring good performance and smooth operation of both experiments.

During the 2024 LHC operation, an inversion of the inner triplet magnet polarity in insertion region 1 (IR1) modified the secondary particle flux toward FASER and SND, resulting in a significant increase in the observed muon rates. Although the nominal polarity configuration was restored in 2025, background measurements remained noticeably higher than those recorded in 2023 (see Fig. 2 and Table 1). Dedicated FLUKA [5] studies for the radiation transport of the particles coming out of the collisions at IP1, combined with wide-angle tracking detectors data in SND, revealed that collisional proton losses in the dispersion suppressor (DS) region downstream of IP1 (cell 11) constituted the main source of excess background. The increase of losses in cell 11 was shown to be caused by a change of crossing plane from vertical in 2023-2024 to horizontal in 2025.

In this context, operational mitigation strategies were considered necessary to reduce this background. To do so, orbit bumps were developed to locally displace the collisional proton losses away from the cell 11. This article presents the development, including novel matching concepts based on beam losses, as well as the measured background during experimental tests of these bumps in the LHC, which were considered for deployment in the LHC 2026 run.

Table 1: Relative Measured Muon Rates Normalised to 2023 [6]

	2023	2024	2025
FASER	1	1.95	1.11
SND	1	2.07	1.43

LOSS ORIGIN ANALYSIS AND STEERING WITH ORBIT BUMPS

Among the multiple magnet families in the LHC, the orbit corrector dipoles (MCB) enable localised beam steering adjustments without affecting the global machine configuration. To mitigate the cell 11 losses, dedicated strengths were determined for the MCB correctors between IP1 and this cell (~400 m downstream of ATLAS) to produce two different bumps (see Fig. 3): the first approach looks to displace the losses downstream (Bump 1), while the second upstream (Bump 2). Horizontal bumps are most effective in modifying dispersive losses in cell 11, whereas such bumps can be generated using correctors between cell 5 and 17 (mcbch.5/7/9/13/15/17.r1.b1).

To carry out the matching of both bumps, it was first needed to simulate the losses produced from IP1 due to the proton-proton collisions. These particles were produced with the DPMJET-III [7] event generator included in FLUKA [8–10], which has recently been included in

* Research supported by the HL-LHC project.

† andre.donadon.servelle@cern.ch

Content from this work may be used under the terms of the CC BY 4.0 licence (© 2026). Any distribution of this work must maintain attribution to the author(s), title of the work, publisher, and DOI.

ISBN: 978-3-95450-252-3 ISSN: 2673-5350 doi: 10.18429/JACoW-IPAC2026-THP4106

HIGH-LUMINOSITY LHC COLLIMATION PERFORMANCE WITH MACHINE ERRORS AND DURING FAST FAILURES*

A. Donadon Servelle†, R. Bruce, R. Cai, B. Lindström, S. Redaelli
European Organization for Nuclear Research, CERN, Geneva, Switzerland

Abstract

Due to the increase in stored beam energy to almost 700 MJ in the High-Luminosity LHC, the safe handling of any beam losses by the collimation system is more critical than at the LHC, designed for 362 MJ per beam. The cleaning performance of the collimation system could be negatively impacted by imperfections and errors in machine elements. Errors in collimator jaw positions or angles, optics and orbit, and machine aperture imperfections can produce increased losses at sensitive locations. In addition, fast failure scenarios, such as asynchronous beam dumps, could cause large single-turn losses, posing a potential threat to different machine elements, including collimators. In this paper, simulations with Xsuite were performed to assess the performance of the collimation system, comparing results for an ideal machine against scenarios including imperfections, and predicting the resulting beam losses around the ring due to an asynchronous beam dump.

INTRODUCTION

Various imperfections can affect the performance of accelerators. While the design performance of the collimation system in protecting the accelerator from beam losses is initially assessed using simulations in an ideal lattice, it is important to quantify the impact of realistic errors. In this context, understanding how imperfections degrade the cleaning efficiency and affect loss distributions is a key ingredient for a robust machine protection strategy.

Previous studies have highlighted the sensitivity of the LHC collimation system [1–3] to imperfections in both collimator settings and machine aperture [4,5]. Building on these results, the present work focuses on errors in the upgraded High-Luminosity LHC (HL-LHC) [6] on collimator jaw tilts, transverse offsets, and half-gaps, as well as offsets of the magnet apertures. For each collimator jaw and each error source, values are sampled from a normal distribution, with the widths derived from measurements [4]. By repeating the simulations for many random seeds, the variation of the main observables for collimation performance, namely the local cleaning inefficiency and the losses on tertiary collimators (TCTs) have been studied.

In addition, the LHC is exposed to a range of failure scenarios in which beam losses can become critical. Examples include injection and extraction kicker failures, beam instabilities, and failures of magnets or power supplies. Among these, failures of the beam extraction system are particularly critical, as they can generate large single-turn losses that may damage sensitive equipment, e.g. magnet apertures or tungsten-based collimators such as TCLAs (shower absorbers) and TCTs.

During a normal beam extraction, 15 horizontal kicker magnets, called MKDs, rise from zero to full field synchronously during a 3 μs abort gap (about 3% of the revolution period) with no beam passing (see Fig. 1). An asynchronous beam dump (ASDs) occurs when all MKDs fire synchronously outside of the abort gap, hence giving intermediate kicks to passing bunches that risk to be deflected onto sensitive elements. In a single-module pre-fire (SMPF), one of the 15 MKDs fires with beam passing, and the rest of the kickers re-trigger shortly after. This is potentially more critical than an ASD as more bunches can be mis-kicked with the effect depending on which module fires first.

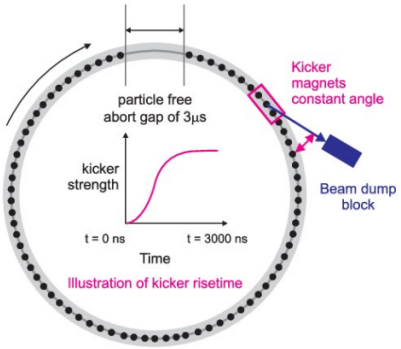

Figure 1: Illustration of ASD.

In the following two sections, these studies are presented in detail and summarised in the HL-LHC context.

MACHINE IMPERFECTIONS

The simulations were performed with Xsuite [7], using its collimation package Xcoll [8] coupled with the default scattering routine *everest* [9]. Xsuite also features coupling to FLUKA [10–12], or Geant4 [13, 14], for collimator simulations, but for this study *everest* was chosen due to its simpler and faster model.

For the simulations, the optics correspond to the HL-LHC round optics configuration v1.6, including a new high-β optics in the collimation insertions (insertion region 3 - IR3, and insertion region 7 - IR7) and $\beta^* = 15$ cm, relaxed collimators settings as defined in [15], and the following rms values for the normal distributions of the error parameters:

- Collimator tilts: 200 μrad
- Collimator offsets: 180 μrad
- Error on collimator centring: 0.17 sigma

* Research supported by the HL-LHC project.
† andre.donadon.servelle@cern.ch

Content from this work may be used under the terms of the CC BY 4.0 licence (© 2026). Any distribution of this work must maintain attribution to the author(s), title of the work, publisher, and DOI.

ISBN: 978-3-95450-252-3 ISSN: 2673-5350 doi: 10.18429/JACoW-IPAC2026-THP4108

TOWARDS A BEAM DUMP DESIGN FOR THE HL-LHC: ANALYSIS OF RUN 3 DUMPS AND ENERGY DEPOSITION STUDIES ON THE HL-LHC TDE ASSEMBLY

H. Guérin*, G. Banks, C. Bracco, Y. Dutheil, A. Lechner, A. Lund,
V. Rodin, N. Solieri, European Organization for Nuclear Research, Geneva, Switzerland

Abstract

In the Large Hadron Collider (LHC), two beam dumps (TDEs) ensure the safe and reliable disposal of the extracted beams. During Run 4, the stored beam energy will increase from 490 MJ achieved so far during Run 3 to a maximum of 710 MJ [1]. A new design, capable of withstanding the increase in dumped energy, is therefore presented for the HL-LHC TDEs. This contribution includes an analysis of the beam energy actually dumped during Run 3, and presents energy deposition studies on the new design of the HL-LHC TDEs. The energy absorption breakdown between the main components of the new TDE is presented, as well as the leakage to the surrounding shielding and cavern. Transverse and longitudinal peak energy densities are also shown, for standard dump events and considering failure scenarios in the beam dilution system.

INTRODUCTION

At the Large Hadron Collider (LHC), the beam dump system [2] ensures the safe and reliable extraction and absorption of the two counter-rotating beams. The extracted beams are separated from the circular orbit and directed towards dedicated caverns that host the Target External beam Dumps (TDEs). To limit the peak energy density in the dump core and windows, dilution kickers sweep the beam in a circular pattern before impact with the dump, transversally spreading its energy density.

In Run 3 (2022-2026), the stored beam energy has reached 490 MJ, with beams accelerated to 6.8 TeV and with up to 4.5×10^{14} circulating protons. In the HL-LHC era, nominal target parameter will lead to a stored beam energy of 710 MJ, with a maximum of 6.0×10^{14} protons circulating at an energy of 7 TeV [1]. New beam dumps dedicated for HL-LHC operation and shown in Fig. 1 have been developed to cope with the increase in stored beam energy.

Measuring close to 8.4 m in length and 720 mm in diameter, the dumps consist of segmented blocks made of graphitic materials contained in a Ti-6Al-4V (Grade F-5 [3]) vessel, enclosed by upstream and downstream titanium windows of the same grade.

Compared to the Run 3 TDE devices [4], the new design features a titanium-alloy vessel, replacing the stainless steel vessel, a feature that allows to minimise the vibrations induced by the beam impact. The segmentation of the core

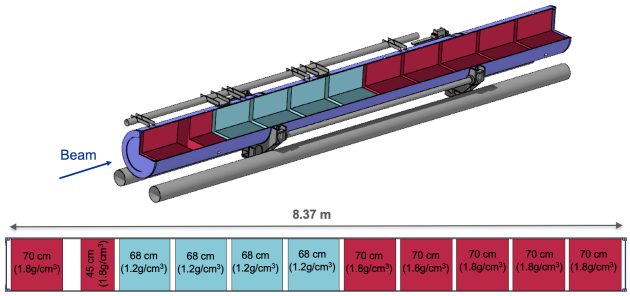

Figure 1: Simplified cut views of the HL-LHC TDE, showing its main components –low (dark red) and high (light blue) density absorbing blocks, vessel and windows– supported by a support cradle and surrounded by air cooling ducts.

is also modified but features the same main segments of varying density:

1. An upstream high density section, aimed at quickly enhancing the longitudinal shower development, constituted by isostatic graphite blocks ($1.7\,\mathrm{g\,cm^{-3}}$);

2. A central lower-density segment, constituted by Carbon Fiber Composite (CFC) plates ($1.2\,\mathrm{g\,cm^{-3}}$), whose reduced density allows for reducing the peak energy density and therefore the temperature reached in the core material;

3. A downstream high density section, ensuring a maximal absorption of the longitudinal shower tails, and consisting of 5 blocks of isostatic graphite.

The core blocks and CFC plates will be shrink-fitted to the vessel, to enhance thermal conduction.

In this contribution, two main topics are addressed. In the first section, the history of beam dumps recorded in Run 3, which occurred at high stored beam energy, is analysed. The results are compared with estimates previously made in the HL-LHC TDE functional specification document. The second part of this paper focuses on energy deposition studies, performed with FLUKA [5, 6] simulations, and assessing its energy absorption capabilities.

RUN 3 DUMPS ANALYSIS

Defined in 2022, not long after the start of Run 3, the functional specifications of the HL-LHC TDE estimated that the LHC dumps should be designed to handle a total of 440 dump events at flat top energy per operational year, at half the maximum beam intensity. The latter corresponded

* Research supported by the HL-LHC project.
Corresponding author: helene.chloe.guerin@cern.ch

Content from this work may be used under the terms of the CC BY 4.0 licence (© 2026). Any distribution of this work must maintain attribution to the author(s), title of the work, publisher, and DOI.

ISBN: 978-3-95450-252-3 ISSN: 2673-5350 doi: 10.18429/JACoW-IPAC2026-THP4110

TOWARDS THE DETAILED DESIGN OF THE HIGH LUMINOSITY LARGE HADRON COLLIDER BEAM DUMPS

A. Lund*, N. Solieri†, G. Banks, D. Grenier, H. Guerin, U. Bagnolo, V. Maire, T. Coiffet, A. Perez-Fontenla, L. Latussek, G. Notarianni, A. Lechner, C. Bracco, E. Sioula, P. Iannotti, A. Perillo Marcone, M. Calviani
The European Organization for Nuclear Research (CERN), Geneva, Switzerland

Abstract

The High Luminosity (HL) upgrade of the Large Hadron Collider (LHC) requires two new beam dumps capable of absorbing up to 710 MJ in 86 µs [1]. This paper presents the key R&D activities supporting the detailed design of the beam dump vessel and carbon-based core.

The dump is an 8.4 m long, 720 mm diameter thin-walled Ti-6Al-4V cylinder with a shrink-fitted carbon core. The vessel is fabricated from Ti-6Al-4V (Grade F-5) seamless blanks joined by circumferential electron-beam welds. Fatigue testing validated the weld integrity under beam-induced vibrational loads.

Candidate core materials were tested in the HiRadMat-65 experiment reproducing HL-LHC nominal and accidental beam-dilution scenarios with no observable damage, confirming their suitability for HL operation.

These results substantiate the final engineering design of the HL-LHC beam dumps. The research was supported by the HL-LHC project.

INTRODUCTION

Two beam dumps are installed in the LHC, one for each counter-rotating beam, to safely absorb the beam energy. The original beam dumps were upgraded during LS2 in preparation for Run 3 [2]. For HL-LHC, new beam dumps will be installed designed to withstand up to 710 MJ.

A cross-sectional view of the HL design is shown in Figure 1. The dump consists of an 8.4 m long, 0.72 m diameter, 12 mm thick Ti-6Al-4V (Grade F-5 [3]) vessel, formed from 12 circumferentially electron-beam welded segments. The shrink-fitted core comprises three sectors: upstream and downstream blocks of high-density (HD) isostatic graphite (IG) with a density of 1.7 g/cm^3, and a central low-density (LD) sector of four stacks of 17 plates of 40 mm thick carbon-fibre-reinforced carbon (CFC) with a density of 1.2 g/cm^3. The lower density of the central sector is selected to reduce the peak energy density from the particle shower. Shrink fitting ensures high thermal contact conductance for heat transfer to the air-cooled vessel. Upstream and downstream Ti-6Al-4V windows enclose a 0.15 bar relative overpressure argon atmosphere inside the device to prevent oxidation of the core materials.

During a beam dump, extraction kicker magnets deflect the beam out of the LHC ring into 600 m long extraction lines [4]. The beam is swept into a spiral pattern with dilution kickers to reduce the deposited energy density. In the event of dilution failures, the energy density in the core increases; the most critical identified scenario is the two-missing-horizontal-kickers (2MKBH) scenario [5].

Upon beam impact, a shower of secondary particles develops longitudinally and radially through the dump core. The resulting energy deposition for HL-LHC beam parameters has been evaluated using FLUKA Monte Carlo simulations [6–8]. At full intensity, 76.5% of the 710 MJ is deposited in the dump core, 2.5% in the vessel, 18.9% in the shielding surrounding the device, and the remainder in the cavern, molasse, and air [9]. Energy deposition constitutes the primary load on the system. The HL design therefore addresses three key aspects: (i) the vessel's dynamic vibrational response, (ii) the ability of the core materials to withstand the induced thermal shock, and (iii) adequate cooling between dumps. This paper discusses the two first aspects whereas details regarding cooling solutions can be found in Ref. [10].

VESSEL

In the vessel, the total energy deposited per full intensity dump within 86 µs is 18 MJ, resulting in an almost instantaneous temperature increase of 112 °C. The thermal field varies through the wall thickness, along the vessel axis, and circumferentially due to the beam sweep pattern.

* asbjoern.lassen.lund@cern.ch
† nicola.solieri@cern.ch

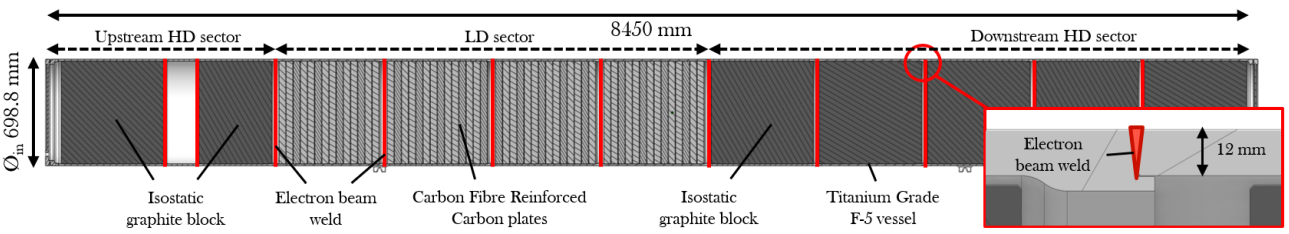

Figure 1: Cross-sectional view of the HL-LHC beam dump design. Ti-6Al-4V vessel segments with shrink-fitted carbon-based core, joined circumferentially by electron-beam welds.

Content from this work may be used under the terms of the CC BY 4.0 licence (© 2026). Any distribution of this work must maintain attribution to the author(s), title of the work, publisher, and DOI.

ISBN: 978-3-95450-252-3 ISSN: 2673-5350 doi: 10.18429/JACoW-IPAC2026-THP4112

HIGH POWER CONDITIONING AND FIRST 2 MEV BEAM RESULTS OF THE COUPLED RFQ-IH-DTL FOR FRANZ

H. Hähnel[1,2,*], A. Ateş[1], L. Bauer[1,2], B. Dedić[1], J. Gröbel[1], J. Kaiser[1], K. Kuempel[1], P. Müller[1], H. Podlech[1,2], U. Ratzinger[1,2], A. Schall[1], R. Tiede[1], J. Traios[1], C. Wagner[1], R. Assmann[1,3], C. Zhang[2,3]

[1]Institute of Applied Physics (IAP), Goethe University Frankfurt, Frankfurt am Main, Germany
[2]Helmholtz Research Academy Hesse for FAIR (HFHF), Frankfurt am Main, Germany
[3]GSI Helmholtz Centre for Heavy Ion Research, Darmstadt, Germany

Abstract

The Frankfurt Neutron Source FRANZ is a compact-accelerator driven neutron source based on the $^7Li(p,n)^7Be$ reaction using a 2 MeV proton beam. Following successful stand-alone RF conditioning of the IH-DTL up to 10 kW cw, the coupled RFQ-IH-DTL cavity was assembled, tuned and conditioned up to 200 kW. First beam experiments have been performed, demonstrating proton acceleration to 2 MeV. We report on the high-power conditioning, coupling and LLRF tuning procedure, as well as initial beam commissioning results.

INTRODUCTION

The Frankfurt Neutron Source (FRANZ) is a compact accelerator driven facility originally initiated in the early 2000s [1–6]. It is designed to provide a 2 MeV proton beam for neutron production via the ^{7}Li$(p,n)^7$Be reaction [7]. The produced neutrons with a kinetic energy around 30 keV can be used for a number of experiments in the fields of applied physics and experimental astrophysics [8].

Beam Commissioning Progress

Significant progress on the driver linac was made in recent years. The commissioning of the new CHORDIS ion source [9, 10] in late 2020 was a first milestone. Since the CHORDIS ion source only provides a 35 keV proton beam, an electrostatic post-accelerator was developed and commissioned at IAP to reach the desired beam energy of 60 keV [11]. After stable operation was confirmed, the Low Energy Beam Transport line (LEBT) was commissioned and the 60 keV beam was transported up to the point of injection into the RFQ in late 2021. Following a redesign of the RFQ electrodes for 60 keV [12,13], new electrodes were delivered and mounted in the RFQ in summer 2023. The RFQ was then tuned, conditioned and commissioned with a 10 mA proton beam until the end of 2023. Emittance measurements and bunch shape measurements of the 700 keV proton beam behind the RFQ followed in 2024, reporting a RFQ transmission of 92.7 % [14, 15]. In 2025, the RFQ and IH-DTL were combined to form a coupled RFQ-IH-DTL cavity. The cavity was commissioned with beam in late 2025 with a measured beam energy of 1.9 MeV. The results of the cavity tuning and beam commissioning are reported here.

* haehnel@iap.uni-frankfurt.de

The Coupled RFQ-IH-DTL

To reduce space requirements and save the need for a second high power amplifier, the FRANZ main accelerator cavity was designed as a coupled RFQ-IH-DTL which consists of a 700 keV four-rod RFQ and a short 1.3 MV IH-DTL with an internal triplet lens [6]. The cavities are coupled inductively by a large coupling flange at the meeting point of the two cavities (see Fig. 1). Due to this fixed coupling, the RF phase between RFQ and IH-DTL is locked and had to be carefully considered during the RFQ beam dynamics design to ensure the correct phase relation between the last cell in the RFQ and the first gap in the IH-DTL. Due to this setup,

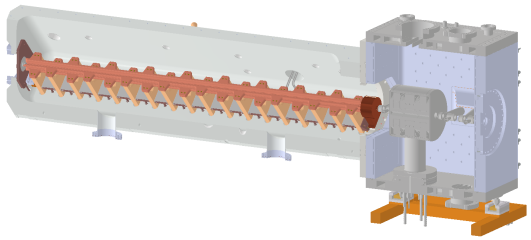

Figure 1: CAD cross-section of the coupled RFQ-IH-DTL cavity. The RFQ is on the left side and the IH-DTL with an internal quadrupole triplet lens is coupled to it on the right.

the voltage ratio between the IH-DTL and the vane-vane voltage of the RFQ is directly dependent on the coupling strength between the two cavities. After the redesign of the RFQ for 60 keV, the ideal ratio was calculated to be

$$\frac{U_{0,IH}}{U_{RFQ}} = \frac{2.06\,\mathrm{MV}}{60\,\mathrm{kV}} = 34.34 \qquad (1)$$

to match the beam dynamics simulated. To reach this ratio, both cavities have to be tuned to a frequency close to the common frequency of 175 MHz so that the correct coupling is achieved [6]. In practice, this tuning was only possible with an extensive bead pull measurement campaign.

BEAD PULL MEASUREMENTS

In contrast to typical bead pull measurements for single cavities, where usually only the relative voltage distribution withing the cavity is of interest, for the coupled RFQ-IH-DTL, two calibrated bead pull measurements are required. The RFQ vane-vane voltage U_{RFQ} is measured perpendicular to the RFQ vanes. To ensure a homogeneous field

Content from this work may be used under the terms of the CC BY 4.0 licence (© 2026). Any distribution of this work must maintain attribution to the author(s), title of the work, publisher, and DOI.

ISBN: 978-3-95450-252-3 ISSN: 2673-5350 doi: 10.18429/JACoW-IPAC2026-THP4113

DEVELOPMENT AND CHARACTERIZATION OF A NEUTRON BEAM AT THE BONN ISOCHRONOUS CYCLOTRON

M. Loepke*, R. Beck, S. Neubert, D. Sauerland, University of Bonn, Bonn, Germany

Abstract

The Bonn Isochronous Cyclotron provides light ion beams with a charge-to-mass ratio Q/A ≥ 1/2 and kinetic energies ranging from 7 to 14 MeV per nucleon to one of five experimental sites. It is planned to extend the facility's irradiation and experimentation capabilities by providing a neutron beam at one of the experimental areas in the near future. The neutrons are produced in a thick carbon converter through the deuteron breakup and proton stripping reactions. Protons are stopped in the converter whereas the neutrons' flux and angular energy distribution is optimized by a subsequent copper/tungsten collimator. `Geant4` simulations were done and benchmarked against literature in preparation. The predicted neutron yield is in the order of 10^7 neutrons/s, the beam profile is a circular flat top beam with a FWHM of approx. 4 cm and energy distribution is centered around 10 MeV. The beam profile was measured by using a 2D-Line-Scan with a scintillator with n-gamma discrimination properties. The energy distribution will be measured with activation foils. This contribution gives an overview of the setup and compares the simulated beam profile with experimental measurements.

BONN ISOCHRONOUS CYCLOTRON

In Fig. 1, the accelerator facility of the Bonn Isochronous Cyclotron [1] is shown. Here, five experimental sites are provided with light ion beams with a charge-to-mass ratio Q/A ≥ 1/2; like protons, deuterons or alpha particles and kinetic energies ranging from 7 to 14 MeV per nucleon.

The ion beam, generated by two electron cyclotron resonance sources is subsequently directed through a low-energy beamline below the cyclotron and then injected vertically into its magnetic center using an electrostatic hyperboloid inflector.

The Bonn Isochronous Cyclotron is an isochronous, three sector, azimuthally varying field cyclotron. It features a 120°-symmetry in its azimuthal magnetic field pattern due to its magnet yoke being separated into three hill and valley sectors with 0° spiral angle. In each valley, a broadband dual-gap dee is located, providing an acceleration voltage of up to 40 kV

The beam is extracted to a field-compensated channel in a single-turn extraction, using an electrostatic septum. The extracted beam can either be guided to the high current site, used to produce induced radioactivity in target material, or it is transported to the experimental sites via the high-energy beamline [2]. The installation of the proton irradiation site for high-uniformity radiation hardness tests of Si detectors at beamline C is now complete. In the future low energetic alphas will be used in an Ion Beam Analysis setup at beamline D, employing Rutherford backscattering spectrometry (RBS) and particle induced X-ray emission (PIXE). At beamline F, deuterons impinging on a carbon target are utilized to generate neutrons. A collimator made of tungsten and copper encased in borated polyethylene (PE) is then used to create a directed beam of neutrons. This beamline is currently being commissioned.

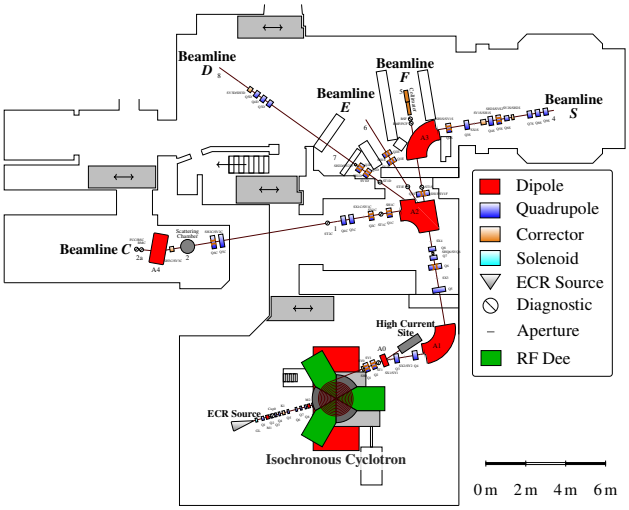

Figure 1: Overview of the accelerator facility.

THE NEUTRON IRRADIATION SITE

The neutron irradation site is located at beamline F. Here, the primary beam is monitored downstream of the A3 magnet with a diagnostic section, consisting of a secondary electron monitor for beam intensity and position monitoring, a pneumatically retractable Faraday cup for its calibration and a pneumatically retractable *Chromox* scintillation screen to monitor the beam profile. The primary beam is then extracted into air through a 30 µm AlMg3 exit Lenard window and onto a neutron production target.

This converter target is thick enough to stop the primary beam. It is mounted at the entrance of a 124 cm long collimator. Figure 2 shows a sketch of the collimator. The inner layer of the collimator consists of tungsten forming an opening cone in the downstream direction. The outer layer is composed of copper acting as a moderator for fast neutrons due to its (n,2n) and (n,3n) cross-sections. The collimator is encased in 30 cm PE, which due to its high hydrogen content further moderates the neutrons' energy through elastic collisions. The PE contains 5% boron, which is a neutron absorber for thermal neutrons due to its (n,α) cross-section.

An enclosure of the irradiation site is neccessary to lower the ambient dose rate in other parts of the facility. Two 50 cm thick concrete walls on the sides of the collimator hold steel

* loepke@hiskp.uni-bonn.de

Content from this work may be used under the terms of the CC BY 4.0 licence (© 2026). Any distribution of this work must maintain attribution to the author(s), title of the work, publisher, and DOI.

ISBN: 978-3-95450-252-3 ISSN: 2673-5350 doi: 10.18429/JACoW-IPAC2026-THP4114

BEAM DYNAMICS OF HICANS PLATFORM: BENCHMARKING RF-TRACK SIMULATIONS OF THE LEBT, RFQ AND TRANSFER LINE

K. Altenmüller*, I. Bustinduy, D. Fernandez-Cañoto, G. Harper, R. Miracoli, J. Munoz, S. Varnasseri
ESS Bilbao, Zamudio, Spain

Abstract

We present beam dynamics studies for the future compact accelerator neutron source HiCANS platform, carried out with the RF-Track code. The simulations were used to optimize the layout and geometry of various components of the beam line. The results are compared to other codes and measurements. The studied beamline consists of the LEBT with two solenoids, an RFQ and a dogleg style transfer line. The RFQ was modeled using fine-grained field maps. The simulations were used to optimize the LEBT geometry for maximum RFQ transmission. To benchmark the LEBT simulations we studied the magnetic focusing of different hydrogen species and compared it to measurements in the existing ESS-Bilbao injector. Furthermore, the transmission in the RFQ and output phase space was simulated for different beam currents, and the results were compared against GPT. The lattice of the transfer line was designed and error studies were performed using RF-Track and validated with TraceWin. We demonstrate how RF-Track serves as fast and convenient tool for extensive optimization processes including full particle tracking and calculation of space charge effects.

INTRODUCTION

HiCANS platform is a high-current accelerator-driven neutron source, currently under development at ESS-Bilbao, Spain [1]. Its ion source provides protons at 45 keV in 1.5 ms-pulses with a frequency of 30 Hz and peak current of 50 mA. A LEBT equipped with two solenoids matches the beam to the next stage, the RFQ (352.21 MHz), which accelerates the beam up to 3 MeV [2, 3]. A dogleg-style transfer line guides the beam to the target and moderator unit, equipped with a lithium spallation neutron source [4]. HiCANS platform is a fully fledged neutron source, but it also serves as demonstrator for a future expansion with a drift-tube LINAC, called Argitu.

Beam dynamics simulations helped to improve the LEBT design, study the RFQ and define the layout of the transfer line. As principal tool the RF-Track code was used [5]. It allows multi-particle tracking in time in a 3D volume with full space charge calculation. An advantage of RF-Track is that the space charge calculation can be performed at a larger step size than the integration, which speeds up the simulation. The space charge effects are calculated by the particle-in-cell method. We integrated RF-Track into a custom Python framework that allows us to quickly create and run modular simulations, which also can be accessed by function calls in optimization processes. A demonstration of this implementation can be found in reference [6].

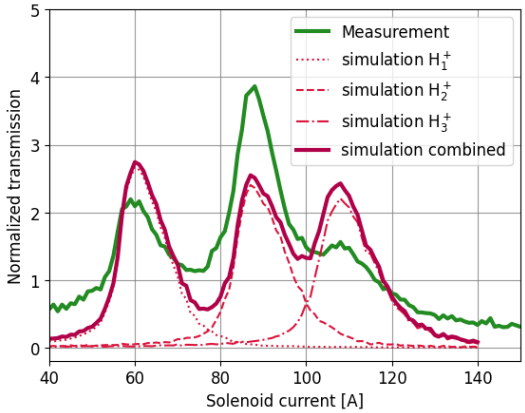

Figure 1: Scan of solenoid focusing: the measured and simulated transmission of different hydrogen species.

SIMULATION VALIDATION

We validate the accuracy of the simulations with measurements and by comparing RF-Track results with other codes. The RF-Track settings itself are optimized by producing a slow, but highly accurate reference simulation, using the 4th-order Runge Kutta method, and then we try to reproduce the results using faster algorithms and larger time steps until convergence is achieved.

Experimentally, we study the magnetic focusing of the hydrogen-species H^+, $H_2{}^+$ and $H_3{}^+$ in the LEBT by measuring the beam current while scanning over the solenoid current. The simulated and measured transmission are shown in figure 1. The peak positions are in good agreement within a few Ampere.

We also compared beam dynamics simulations of the RFQ between RF-Track and GPT 2.8 [7]. The output phase space distributions between both codes show small differences, however, RF-Track provides a more accurate interpolation of the field map next to wall boundaries (note that we used a very old version of GPT).

Finally, we simulated the beam trajectories in the transfer line with RF-Track and TraceWin [8]. The comparison of the beam envelopes is shown in figure 2. On the first meters, the envelopes are in very good agreement. Towards the end of the transfer line, deviations appear, which can be explained by different quadrupole and sector bending magnet models used in each simulation.

* kaltenmueller@essbilbao.org

Content from this work may be used under the terms of the CC BY 4.0 licence (© 2026). Any distribution of this work must maintain attribution to the author(s), title of the work, publisher, and DOI.

ISBN: 978-3-95450-252-3 ISSN: 2673-5350 doi: 10.18429/JACoW-IPAC2026-THP4115

ALTERNATIVE FABRICATION PROCESS FOR CARBON STRIPPER FOILS USED IN PARTICLE ACCELERATORS

A. Batista, B. Bhaskar, P. Costa Pinto, L. Ferreira, E. Mahner, L. Mourier, M. Slupecki, W. Vollenberg, European Organization for Nuclear Research (CERN), Geneva, Switzerland

Content from this work may be used under the terms of the CC BY 4.0 licence (© 2026). Any distribution of this work must maintain attribution to the author(s), title of the work, publisher, and DOI.

Abstract

Carbon foils are widely used in particle accelerators to produce ion beams with high charge states. These stripper foils are primarily deposited on a soluble substrate, (e.g. NaCl or betaine-sucrose) that is subsequently dissolved to provide a free-standing foil. For use in accelerators, the free-standing foils need then to be mounted on a metallic frame, a delicate and time consuming operation. In this paper, we propose an alternative fabrication process, where the foils are deposited directly onto a metallic supporting frame. The process involves the surface preparation of plain copper plates, in-situ Ar-H_2 plasma treatment to enhance adhesion, deposition of the carbon film by magnetron sputtering, and removal of the copper from the central part of the supporting plate by chemical etching, to create an aperture for the passing ion beam. We describe the different fabrication steps, the quality control approach used to assess the carbon areal density, the thermal outgassing rate, and the porosity of the foils. The first beam test results using CERN-produced carbon stripper foils, obtained with Pb54+ ion beams at 4.2 MeV/u at LINAC 3, are presented.

PREPARATION OF THE FOILS

The fabrication process involves three main steps: (1) preparation of the supporting frames, (2) carbon coating, and (3) chemical etching of the copper in the central window of the frame. The areal density of the carbon film is determined by weighing the frame before and after coating. After completion of the etching step, the porosity is evaluated by optical microscopy, and the outgassing rate is measured after 24 h of pump-down. The three steps are detailed in the following subsections.

Preparation of the Supporting Frames

The supporting frames consist of ETP copper rectangles (15.1 × 25.1 × 1 mm), with a central pocket (depth: 0.9 mm, diameter: 25 mm), as shown in Fig. 1. The surfaces of the frames must be free of scratches, as these can act as initiation sites for cracking and subsequent mechanical failure of the foil.

Surface preparation includes degreasing in an ultrasonic bath, followed by chemical etching using a solution of Ammonium persulphate (200 g/mol) and Sulfuric acid (8 ml/l) to remove surface defects and induce controlled roughness (~0. 7 Ra), thereby reducing residual stress in the deposited films (approximately 30 µm of material is removed from the surface. The frames are then passivated in a chromic acid solution and rinsed with demineralized water.

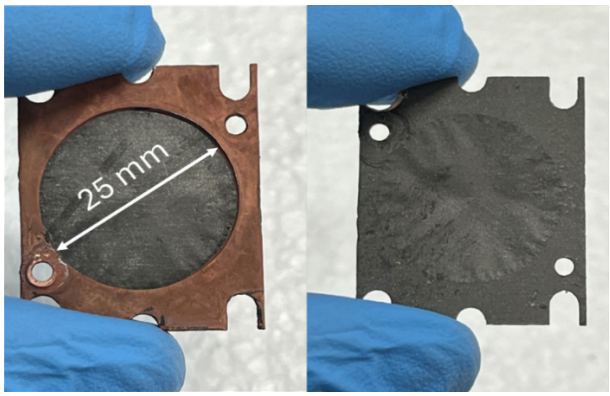

Figure 1: Copper frames with carbon foil.

Coating Process

Four frames are coated simultaneously in each deposition run. Prior to mounting on the sample holder, the mass of each frame (m_0) is measured using a precision balance (Mettler AE240, resolution: 0.01 mg, accuracy ~3%). To minimize contamination-induced defects (porosity), the frames are assembled in an ISO-5 cleanroom environment and transported to the coating system in a hermetically sealed container. During transfer into the vacuum chamber, the frames are exposed to ambient air for approximately 15 minutes before pump-down.

The system is baked at 120 °C for 8 h. The base pressure prior to deposition is in the 10^{-6} mbar range. To enhance adhesion, the copper frames are exposed to an Ar (98%)–H_2 (2%) plasma generated by a remote plasma source (GV10x UHV DS Asher, IBSS Inc., USA), reducing surface oxides. The low ion energy (<45 eV) minimizes sputtering, and the associated mass loss is negligible.

Table 1: Distribution of CERN and GSI (Reference) Samples in the Arms of the LINAC Beam Stripper

Arm-Sample	Foil 1 µg/cm²	Foil 2 µg/cm²	Foil 3 µg/cm²	Foil 4 µg/cm²
1-GSI_150	151	151	151	149
2-GSI_120	120	121	122	149
3-CERN_130	128	131	131	118
4-GSI_100_A	98	98	97	96

High-purity argon (quality 60) is then introduced to a pressure of 8 × 10^{-4} mbar, and carbon deposition is initiated. Carbon is sputtered from a high-purity graphite target using a planar magnetron (Gencoa) operated in DC mode at 160 W (630 V, 0.26 A). The target-to-substrate distance is 185 mm, and the deposition rate is 13 µg/cm²/h. During

ISBN: 978-3-95450-252-3 ISSN: 2673-5350 doi: 10.18429/JACoW-IPAC2026-THP4116

CONCEPTUAL BEAMLINE DESIGN FOR COMPLEMENTARY EXPERIMENTS AT IFMIF-DONES

L. Bellan†, M. D'Andrea, L. Ferrari, F. Grespan, A. Palmieri, A. Pisent, INFN-LNL, Legnaro, Italy

Abstract

A deuteron beam of unprecedented intensity will be used at the International Fusion Materials Irradiation Facility – DEMO Oriented Neutron Source (IFMIF-DONES) to produce a fusion-like neutron flux and characterize the properties of materials in the challenging environment of a fusion reactor. Recently, the possibility of extracting a small fraction of this beam for complementary experiments in a parasitic mode has gained traction within the users community. This paper describes the conceptual design of the extraction system and a proposal for a distribution line capable of serving different experimental stations, without perturbing the main deuteron beam while keeping the same peculiar pulse structure and high peak current.

INTRODUCTION

The International Fusion Materials Irradiation Facility – DEMO Oriented Neutron Source (IFMIF-DONES) [1-3] is a state-of-the-art facility currently under construction in Spain to study the properties of materials in the challenging environment of fusion reactors like DEMO [4]. Material specimens will be irradiated with a fusion-like neutron source produced by the interaction of an intense deuteron beam, accelerated by a superconducting radiofrequency (SRF) linac, with a liquid lithium target. Given the unprecedented deuteron beam parameters, listed in the middle column of Table 1, the potential users community has recently expressed interest in dedicating a fraction of the fully accelerated beam to parasitic experiments. In particular, the extraction of one deuteron bunch every 1000, while keeping the same pulse structure and peak current as the main beam, can be envisaged resulting in the parameters listed in the rightmost column of Table 1.

Table 1: Parameters of the Dones Main and Parasitic Deuteron Beam, Assuming a 1/1000 Extraction Rate

Quantity	Main beam	Extracted beam
Beam energy	40 MeV	40 MeV
Frequency	175 MHz	175 kHz
Average current	125 mA	125 µA
Power on target	5 MW	5 kW
Bunch spacing	5.7 ns	5.7 µs
Bunch length	2 ns	< 10 ns

Proposals for competitive experiments that can exploit the peculiar pulsed time structure of the extracted beam are being investigated [5,6]. A typical application would be a neutron time-of-flight (nTOF) facility to investigate the nuclear cross section of materials relevant for fusion reactors. Direct use for radioactive ion beams production can also be considered, enabling the production of refractory elements.

† luca.bellan@lnl.infn.it

A preliminary design of an extraction and distribution line for the parasitic deuteron beam was developed by the Legnaro National Laboratories (LNL) [7].

BEAM EXTRACTION

As shown in Fig. 1, the parasitic deuteron beam must be directed towards the experimental hall, located in the floor below the linac. An extensive study was carried out using TraceWin [8] to design a suitable extraction line.

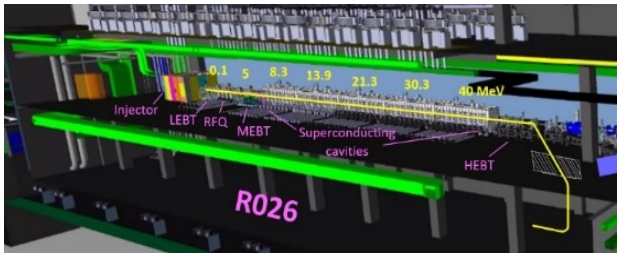

Figure 1: Drawing of the interface between the accelerator floor and the experimental hall R026. The yellow line shows the synchronous particle path.

A travelling-pulse deflector at the beginning of the High Energy Beam Transfer (HEBT) line can be used to apply a kicker field acting on a single bunch while the rest of the beam stays unperturbed. Since the HEBT does not include longitudinal lenses, the deflector must be placed within the first 3.5 m so that the minimum achievable rise/fall time of the kicker pulse, which can be as short as a couple ns [9,10], can still fit within the bunch spacing (see Table 1). At the end of this region, the bunch is about 1.77 ns long, as shown in Fig. 2. Therefore, the kicker field pulse can have the structure represented schematically in Fig. 3.

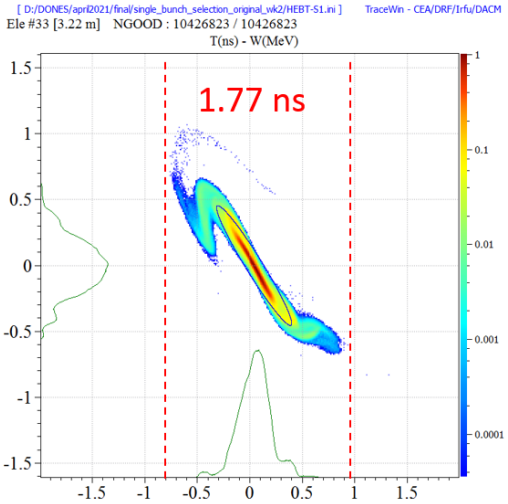

Figure 2: Longitudinal phase-space of the beam at the end of the deflector region. The abscissa reports the energy spread in MeV, while the ordinate reports the time in ns.

Content from this work may be used under the terms of the CC BY 4.0 licence (© 2026). Any distribution of this work must maintain attribution to the author(s), title of the work, publisher, and DOI.

ISBN: 978-3-95450-252-3 ISSN: 2673-5350 doi: 10.18429/JACoW-IPAC2026-THP4117

OPTIMISING THE PROTON AND ELECTRON TRANSFER LINES DESIGN FOR HIGH-QUALITY ELECTRON ACCELERATION IN AWAKE RUN 2C

E. Belli*[1,2], P.N. Burrows[1], Y. Dutheil[2], F.M. Velotti[2]
[1]John Adams Institute for Accelerator Science, Oxford, United Kingdom
[2]CERN, Geneva, Switzerland

Abstract

The Advanced Wakefield Experiment (AWAKE) is developing a novel plasma-based accelerator concept in which self-modulated proton bunches generate wakefields capable of accelerating electrons to energies relevant for particle physics. Completed in 2025, the Run 2b experimental phase aimed to demonstrate wakefield-amplitude stabilisation after saturation of the self-modulation process via a plasma density step while establishing the experimental configuration needed for high-quality electron acceleration in Run 2c. In Run 2c, the goal is to demonstrate acceleration up to about 10 GeV while preserving the quality of the accelerated electron beam. To achieve this, a new configuration of the proton transfer line is under investigation to compensate for the bending introduced by the 150 MeV electron line dipole in the interaction region between the two plasma cells. In parallel, the experimental requirements for the 150 MeV electron line have evolved to minimise the physical gap between the two plasma cells, demanding an optimised focusing scheme to deliver a beam with a transverse size of a few microns into the second plasma section. A new design of the 150 MeV electron transfer line is therefore proposed, including detailed error studies to assess its robustness under realistic operational conditions.

INTRODUCTION

The goal of the upcoming Run 2c phase of the AWAKE experiment [1, 2] is to achieve electron energies up to 10 GeV while preserving the quality of the accelerated electron beam in terms of emittance and energy spread. To achieve this, the proton bunch self-modulation [3,4] and the electron bunch acceleration will be separated into two plasma cells, in order to prevent the emittance growth of the electron bunch which would occur if exposed to the defocusing fields of the unmodulated proton bunch. A schematic of the proposed Run 2c beamline configuration is shown in Fig. 1. An 18 MeV seeding electron beamline [5] will be used to inject electron bunches into the first plasma cell to seed the proton bunch self-modulation. To include a second plasma cell in the new configuration, the first plasma cell will be shifted 40 m downstream, requiring a reconfiguration of the proton beamline [6]. In addition, a new 150 MeV beamline will be installed to inject a witness electron bunch, produced with a 10 Hz frequency, into the second plasma cell, thus probing the proton driven wakefield acceleration. This document focuses on the latest optics design of the 150 MeV electron line and the newly proposed configuration of the proton line.

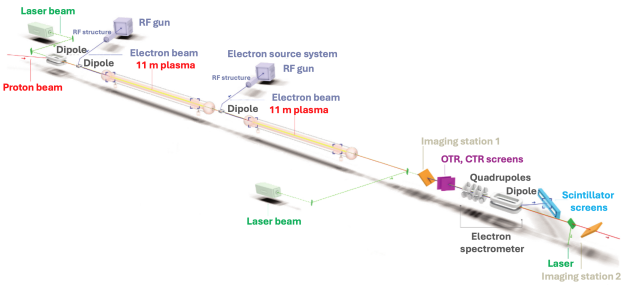

Figure 1: Schematic of the configuration of the seeding and witness electron beamlines and plasma cells in Run2c.

ELECTRON LINE OPTICS DESIGN

A preliminary design of the witness electron transfer line was presented in [7]. To satisfy the spatial constraints imposed by the tunnel geometry, the design of this line was particularly challenging. A dog-leg configuration, consisting of two 15° bending dipoles, was therefore adopted to transport the electron beam from the source to the entrance of the second plasma cell, where it is then injected on the same axis as the proton and laser beams (on-axis injection). Additional complexity arises from the very tight experimental requirements: electrons must be injected into the second plasma stage with micron-level precision in both position and beam size, in order to ensure proper matching to the accelerating and focusing regions of the wakefields. The main beam parameters are summarized in Table 1.

Table 1: Beam parameters for the AWAKE Run 2c electron transfer line.

Parameter	Value
Momentum p	150 MeV/c
Relative energy spread $\Delta p/p$	0.2 %
Normalised emittance $\varepsilon_{x,y}$	2 mm mrad
Beam size $\sigma_{x,y}$ at waist	$\leq 1.5\sigma^*$, $\sigma^* = 5.75$ µm
Bunch length σ_z at waist	60 µm
Dispersion $D_{x,y}$ at waist	0 m

Compared to the initial design presented in [7], the new design described in this paper includes several modifications. The first is the use of existing magnets available from other facilities, which are compatible with a new family of power converters [8], providing the accuracy class required for this line. In addition, from the experimental physics requirements, the gap between the two plasma stages must be

* eleonora.belli@cern.ch

Content from this work may be used under the terms of the CC BY 4.0 licence (© 2026). Any distribution of this work must maintain attribution to the author(s), title of the work, publisher, and DOI.

ISBN: 978-3-95450-252-3 ISSN: 2673-5350 doi: 10.18429/JACoW-IPAC2026-THP4301

FRIB ACCELERATOR IMPROVEMENT PROJECTS TO MITIGATE BEAM LOSSES IN POST-STRIPPER LINAC*

X. Rao†, P. N. Ostroumov, S. Miller, A. S. Plastun, N. Bultman, Q. Zhao, M. Hu
Facility for Rare Isotope Beams, Michigan State University, East Lansing, MI, USA

Abstract

The Facility for Rare Isotope Beams (FRIB) is planning four Accelerator Improvement Projects (AIPs) during a two-month summer shutdown to mitigate beam losses induced by the stripper. The motivation for this project has been described in previous publications. The implementation of these projects is required to accelerate multiple-charge-state heavy-ion beams simultaneously as beam power on target ramps up.

These projects require modification of approximately 30 meters of beamline within the FRIB tunnel and include installing larger-bore magnets and beamline components before and after the liquid lithium stripper, implementing new second-harmonic cavities, replacing the dipole chamber with a high-heat-load-rated version at Folding Segment 1, and installing new quadrupole magnets at Folding Segment 2. Effective integration of design, technical device fabrication, installation, and commissioning within a limited shutdown window requires close coordination among multiple engineering and physics teams. This paper presents the planning methodology, execution strategy, and planned performance outcomes of these upgrades to manage concurrent accelerator improvement projects within a constrained maintenance schedule.

INTRODUCTION

FRIB is currently in user operation, with primary beam power progressively increased from the kilowatt level to beyond 20 kW [1, 2, 3], and with an ultimate design goal of reaching 400 kW on target.

The FRIB accelerator is a state-of-the-art superconducting heavy-ion linear accelerator (linac). A key feature of the FRIB linac is the implementation of a liquid lithium stripper, which enables efficient acceleration at high beam power. In contrast to conventional carbon foil strippers—prone to rapid degradation under high power density—the liquid lithium stripper provides enhanced robustness and operational lifetime.

Despite transverse focusing of the beam onto the stripping medium, intrinsic thickness non-uniformity of the liquid lithium film across the beam spot introduces additional energy spread via spatially dependent energy loss, beyond the baseline contribution from energy straggling.

During routine operation, additional factors such as ion source instability and unintentional beam contamination can further induce beam losses. These losses may lead to vacuum degradation and increased risk of damage to downstream superconducting cavities. To mitigate these effects, four AIPs are being implemented; their design, integration, and impact are presented in this paper.

PROJECT SCOPE

2H Buncher Cavity

Multi-Gap buncher (MGB) cavities (operating at 161 MHz) are currently utilized at Folding Segment 1 (FS1) beamline for longitudinal matching between superconducting linac segments [4]. Beam after MGB1 shows non-linear "tails" in the longitudinal phase space distribution, which may cause beam loss at downstream Linac Segment 2 (LS2) cryomodule.

To mitigate this loss, 2H buncher cavity is designed [5] by linearizing the effective voltage of MGB. Beam dynamic analysis is performed to compare longitudinal acceptance with no 2H cavity, one 2H cavity, or two 2H cavities (one after each MGB cavity). Analysis results show that with two 2H cavities, all particles fit within the longitudinal acceptance of LS2. Figure 1 shows the MGB cavity upstream of the new 2H buncher cavity.

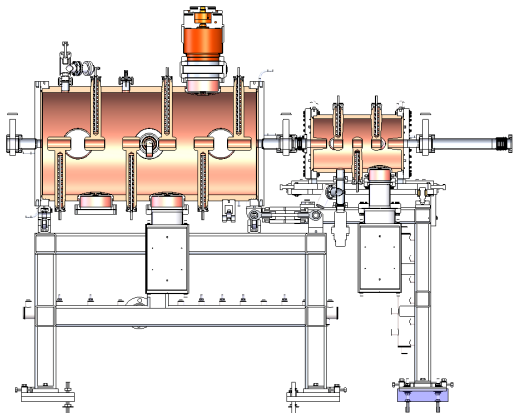

Figure 1: FRIB MGB upstream of 2H buncher cavity.

The 2H cavity operates at 322 MHz, and utilizes existing type of RF amplifier. β number is 0.186, calculated Q_0 value is 1.3×10^4, and the maximum RF power for Uranium beam is 4.6 kW. It has the same 36 mm aperture as MGB. Thanks to the successful fabrication and implementation of FRIB other room temperature cavities [6], the design use similar cavity and cooling design as FRIB MGB, and utilizes other existing systems (tuner, coupler, linear actuator, etc.) to streamline maintenance, repair and spare inventory management.

Larger Bore Beamline Near Stripper

Charge stripping is inherently accompanied by transverse and longitudinal emittance growth due to angular

*This material is based upon work supported by the U.S. Department of Energy, Office of Science, Office of Nuclear Physics and used resources of the Facility for Rare Isotope Beams (FRIB) Operations, which is a DOE Office of Science User Facility under Award Number DE-SC0023633
†rao@frib.msu.edu

Content from this work may be used under the terms of the CC BY 4.0 licence (© 2026). Any distribution of this work must maintain attribution to the author(s), title of the work, publisher, and DOI.

ISBN: 978-3-95450-252-3 ISSN: 2673-5350 doi: 10.18429/JACoW-IPAC2026-THP4303

TECHNOLOGY MATURATION FOR THE LANSCE ACCELERATOR MODERNIZATION PROJECT (LAMP)*

J. Lewellen†, M. Holloway, A. Alexander, K. Bishofberger, G. Dale, D. Dimitrov, R. Garnett, H. Gaus, J. Medina, S. Swickley, R. Thornton, Los Alamos National Laboratory, Los Alamos, United States

Abstract

The LANSCE accelerator is extraordinarily flexible in its ability to simultaneously accelerate both H+ and H- beams, and provide concurrent beam delivery to five independent user stations. LANSCE has been in operation for more than 50 years, and many of the accelerator structures, such as the Cockcroft-Walton injectors and drift-tube linac tanks, are original. To address end-of-life concerns and position the facility for extended operation into the future, the LANSCE Accelerator Modernization Project (LAMP) encompasses replacement of the upstream portions of the LANSCE accelerator, from the H+ and H- ion sources through the end of the drift-tube linac. In order to meet beam delivery requirements with modern equivalent systems, elements of the LAMP design require technical maturation. This paper describes the Critical Technology Elements (CTEs) in the LAMP conceptual design, presents the design elements requiring additional development, and discusses the maturation plan and schedule.

INTRODUCTION

The LANSCE Accelerator Modernization Project (LAMP) [1] will modernize the upstream portion of the LANSCE accelerator, replacing aging 750-keV Cockcroft-Walton injector with modern, 65- keV H^+ and H^- ion sources feeding into a single 201.25-MHz Radio Frequency Quadrupole (RFQ), and replacing the DTL [2].

LAMP's design approach maintains LANSCE's unique dual-beam capability while reducing facility footprint and operational complexity. However, this configuration incorporates design elements requiring technology maturation.

Four Critical Technology Elements (CTEs) have been identified that must achieve Technology Readiness Level (TRL) 7 prior to CD-2 approval: (1) beam choppers; (2) a dual-species RFQ structure; (3) a dual-species MEBT; and (4) dual-current gated H^- ion source. The technology maturation strategy employs two test facilities: the RFQ Test Stand (RFQTS) for initial component validation and the LAMP in ADEF Tunnel (LAT) for integrated system demonstration in a relevant environment.

This paper describes the technical challenges of each CTE, the maturation approach, and progress toward achieving TRL-7 for all critical technologies.

CRITICAL TECHNOLOGY ELEMENTS

The LAMP project has identified three CTEs requiring technology maturation to TRL-7 prior to CD-2 approval. Each addresses unique technical challenges arising from the dual-species capability and modernization requirements.

CTE A: Beam Choppers

The LAMP front-end requires beam choppers at two locations: downstream of the 65-keV ion source in the Low Energy Beam Transport (LEBT) and in the 2.1-MeV MEBT section. These choppers must provide fast rise/fall times (~10 ns in LEBT, ~2-3 ns in MEBT) to generate the disparate LANSCE bunch train patterns, and to provide single high-charge microbunch delivery to the Weapons Neutron Research (WNR) facility [3].

The 65-keV LEBT chopper faces the challenge of operating in a space-charge dominated environment where beam dynamics are highly sensitive to electric field perturbations. The 2.1-MeV MEBT chopper must maintain "clean" chopping performance to minimize activation of downstream accelerator components. Both choppers must achieve >99.9% extinction efficiency to meet stringent "dark current" requirements for WNR.

CTE B: Dual-Species RFQ Structure

Operating at 201.25 MHz, the LAMP RFQ must accelerate both H^+ and H^- beams in the same macropulse from 65 keV to 2.1 MeV while maintaining good beam quality and high transmission for both species.

The RFQ design must also accommodate significant differences in beam current requirements: high peak bunch charge but low average current for the H^- beams to WNR; modest beam current for the concurrently accelerated H^+ beams to the Isotope Production Facility (IPF); and moderate beam current to the remaining LASNCE user facilities [4,5]. Additionally, RF power coupling and thermal management become more complex when optimizing for two distinct beam loading conditions.

CTE C: Dual-Species MEBT

The MEBT transport line between the RFQ and DTL must transport both H^+ and H^- beams using a single set of steering correctors and focusing elements. This seemingly straightforward beamline presents subtle but significant challenges for dual-species operation.

Magnetic focusing and steering elements affect both species, but in opposite directions (steering correctors) or planes (quadrupoles). The LAMP MEBT includes rebuncher cavities to longitudinally match beams into the DTL; these cavities must provide appropriate RF phasing and amplitude for both species despite their different bunch charges exiting the RFQ.

* Work was performed under the auspices of the US Department of Energy by Triad National Security under contract 89233218CNA000001.
† jwlewellen@lanl.gov LA-UR-26-23710

Content from this work may be used under the terms of the CC BY 4.0 licence (© 2026). Any distribution of this work must maintain attribution to the author(s), title of the work, publisher, and DOI.

ISBN: 978-3-95450-252-3 ISSN: 2673-5350 doi: 10.18429/JACoW-IPAC2026-THP4307

COMMISSIONING STATUS OF THE H- ION SOURCE FOR THE LANSCE ACCELERATOR MODERNIZATION PROJECT*

M. R. Howard†, A. Alexander, T. P. Grumstrup, E. Loftin,
J. T. M. Lyles, B. Sims, A. Smith, R. T. Thornton
Los Alamos National Laboratory, Los Alamos, United States

Abstract

The LANSCE Accelerator Modernization Project (LAMP) will replace the front-end of the existing LANSCE accelerator, from ion sources through the end of the 100 MeV drift-tube linac. LAMP requires higher peak H- beam currents, and longer lifetimes, than provided by the existing LANSCE H- ion sources. The project is currently constructing an SNS multicusp cesiated source design with an internal RF antenna. This paper discusses the H- source performance requirements for LAMP, and progress towards assembling, commissioning, and operating an SNS-type source at the LAMP RFQ Test Stand (RFQTS).

INTRODUCTION

The Los Alamos Meson Physics Facility (LAMPF) was originally commissioned in 1972 [1]. Now known as the Los Alamos Neutron Science Center (LANSCE), it is one of the oldest high-average-power accelerators in the United States [2]. LANSCE simultaneously produces high intensity H+ and H- beams and delivers beam to six different end stations. Currently, Cockroft-Walton generators are used to accelerate both ion species to 750 keV. Unfortunately, over recent years there has been a decrease in the reliability of the Cockroft-Walton generators and the Low Energy Beam Transport (LEBT) regions. In addition, the filament based H- ion source used at LANSCE cannot produce sufficient peak current for users while also meeting ion source lifetime requirements. Two of the primary goals of the LANSCE Accelerator Modernization Project (LAMP) include replacing the Cockroft-Walton generators with a dual-beam Radio-Frequency Quadrupole (RFQ) [2–4] and replacing the filament based H- ion source with an RF (2 and 13 MHz) based ion source heavily inspired by SNS. The RFQ Test Stand (RFQTS) was developed to demonstrate simultaneous dual-species propagation through an RFQ [3–5]. The test stand consists of a 35 keV H- beamline and H+ beamline which will merge and inject into an existing 750 keV RFQ. Note that these energies are different from the 65 keV LEBT and RFQ input energy and 2.1 MeV output energy planned for LAMP [6].

The H- beamline will utilize a multicusp, cesiated source design with an RF antenna, modeled after the H- source in use at SNS [7–9]. Initial assembly of the H- source for the RFQTS was completed in late 2025. In this paper, we outline the building and commissioning process.

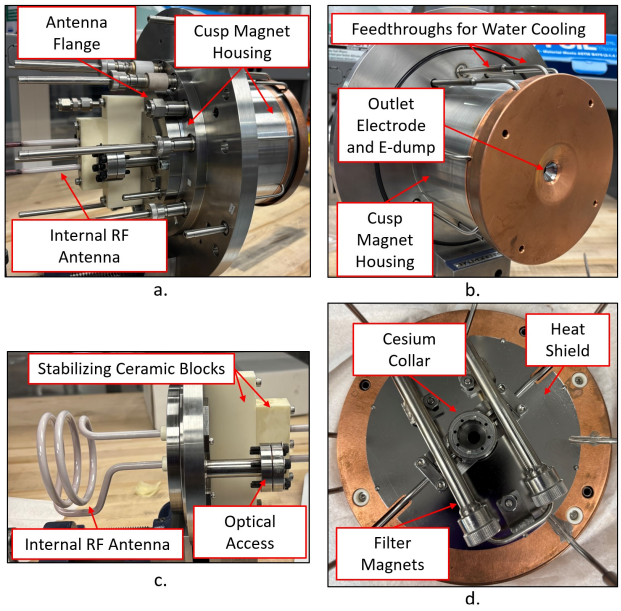

Figure 1: a.) Image of the fully assembled H- source. b.) Downstream view of the H- source showing the outlet electrode and e-dump. c.) Image of the fully assembled antenna flange. d.) Image of the components in the outlet electrode assembly.

SOURCE DESIGN

The SNS internal RF antenna design was selected as the H- source for RFQTS due to its high peak current and long lifetime. This source can produce H- beams with a current of over 100 mA with a lifetime of over 4 months [10]. These current levels far exceed what can be extracted with the present injector at LANSCE (<20 mA) [11] and meet the needs of the LAMP project.

The source body can be separated into three primary parts: the back flange, which contains the plasma chamber and permanent magnets to confine it, the antenna flange, which couples the RF power to the gas to produce the plasma, and the outlet electrode, which contains the cesium converter, Pierce electrode, and electron dump. Each of these sections/parts contain various components critical to plasma formation and H- beam production. Fig. 1 shows various images of the source with relevant components labeled.

The back flange houses 20 NdFeB cusp magnets, each with B_R = 13500 Gauss, that create the magnetic field which contains the plasma generated by the internal RF antenna.

* Work supported by Triad National Security, LLC for the National Nuclear Security Administration of U.S. Department of Energy under contract 89233218CNA000001.

† mrhoward@lanl.gov

Content from this work may be used under the terms of the CC BY 4.0 licence (© 2026). Any distribution of this work must maintain attribution to the author(s), title of the work, publisher, and DOI.

ISBN: 978-3-95450-252-3 ISSN: 2673-5350 doi: 10.18429/JACoW-IPAC2026-THP4310

SLOW EXTRACTION BEAM COMMISSIONING FOR THE Mu2e EXPERIMENT AT Fermilab*

V. Nagaslaev†, G. Annala, J. Berlioz, G. Deinlein, B. Drendel, J. Morgan, A. Narayanan
J. StJohn, D. Still, D. VanderMeulen
Fermi National Accelerator Laboratory, Batavia, IL, USA

Abstract

Following the successful completion of the Muon g-2 experiment run at Fermilab, the Muon Campus facility has been reconfigured from delivering 3 GeV muon beams to the g-2 storage ring to providing slow-extracted 8 GeV proton beam spills for the Mu2e experiment. The first full-scale commissioning run with slow extraction was conducted during the 2025 run, followed by the second run in early 2026. We present the results and current status of this commissioning campaign.

BEAM REQUIREMENTS

The Mu2e experiment [1] requires a slowly extracted 8 kW proton beam delivered in short (<200 ns) pulses separated by ~1.6 μs intervals. To achieve this, beam is slowly extracted from the Delivery Ring (DR), where a single harmonic H = 4 RF bunch circulates with a revolution period of 1.695 μs. The machine cycle begins with two batches of 84 bunches at 53 MHz transferred from the Booster to the Recycler. After fast rebunching to 2.5 MHz in the Recycler, the resulting eight bunches are transferred bucket-to-bucket to the DR, one at a time.

The design parameters are summarized in the Table 1.

Table 1: Original Design Beam Parameters

Beam kinetic energy	8GeV
Beam intensity at injection	1e12
Cycle time	1.4 sec
Spills per cycle	8
Spill length	53ms
Beam power	8kW
Spill Duty Factor	>60%
Extraction efficiency	>98%

While beam intensity and time structure are dictated by experimental requirements, beam loss control is critical for machine operation. Due to radiation constraints, excessive losses may significantly limit the achievable beam power.

DELIVERY RING AND SX

The Delivery Ring is a reconfigured version of the Debuncher ring from the former Fermilab Antiproton Source [2], adapted for the Muon Campus, which serves both the g-2 [3] and Mu2e experiments. Following completion of the g-2 program, a new beamline to the Mu2e experimental hall was constructed and a Slow Extraction (SX) system implemented. The original Antiproton Source optics has been preserved, with modifications to support slow extraction. Figure 1 shows the Delivery Ring lattice functions. The ring circumference is 505 m and consists of three arcs and three straight sections (SS). The lattice follows a regular FODO structure with maximum beta functions of 15 m in both planes. Dispersion reaches up to 2 m in the arcs and is suppressed in the straights using the "missing dipole" scheme

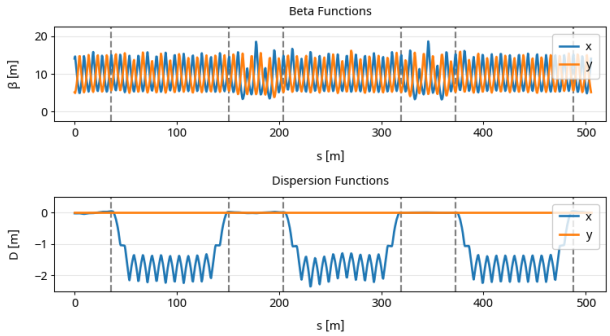

Figure 1 Lattice functions, optimized for SX.

Figure 2 shows the main features of the new machine:

Extraction system: Injection and extraction are both located in SS30. While the injection scheme remains unchanged from g-2 operations, Mu2e employs two electrostatic septa (ESS1 and ESS2) instead of a single-pass kicker.

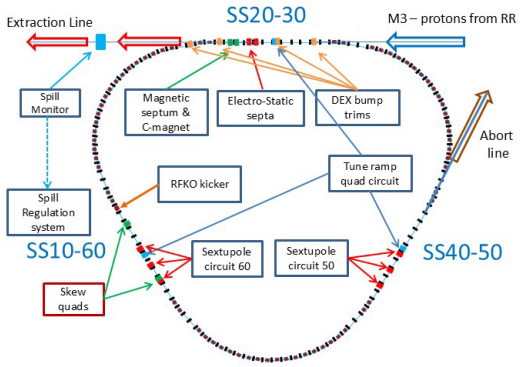

Figure 2 Delivery Ring configuration with SX elements.

The two ESS have 12 mm gap and operate at 86 kV. Together they provide a horizontal deflection of 2 mrad. The septum planes consist of 25 μm thick, 1 mm wide W/Re foils with 2.5 mm spacing. Downstream, two magnetic septa—a Lambertson magnet (ELAM) and a C-magnet (CMAG)—deflect the extracted beam vertically into the

* This work is supported by Fermi Forward Discovery Group, LLC, acting under Contract No. 89243024CSC000002.
†vnagasl@fnal.gov

Content from this work may be used under the terms of the CC BY 4.0 licence (© 2026). Any distribution of this work must maintain attribution to the author(s), title of the work, publisher, and DOI.

ISBN: 978-3-95450-252-3 ISSN: 2673-5350 doi: 10.18429/JACoW-IPAC2026-THP4311

SECOND GENERATION FERMILAB MAIN INJECTOR 8 GEV BEAMLINE COLLIMATION FINAL DESIGN, INSTALLATION AND COMMISSIONING

K. Hazelwood*, P. Adamson, B. Babacan, K. Danison-Fieldhouse, R. Donahue, B. Flanagan, T. Funk, M. Galante, M. Kucera, C. Montiel, D. Morris, R. Neswold, P. Neville, F. Novak, C. Olsen, A. Saewert, M. Stec, A. Watts
Fermi National Accelerator Laboratory†, Batavia, United States

Abstract

A novel transverse beam collimation system has been installed and commissioned in the Fermilab Main Injector 8 GeV beamline. The new collimation system compliments existing collimators and helps ensure the Fermilab Main Injector and Recycler accelerators are capable of handling the increased beam power promised from the Fermilab PIP-II upgrade, currently underway. This paper will present the final design and installation of the collimation system as well as initial results from its commissioning.

INTRODUCTION

The Main Injector 8 GeV Beamline (MI8) allows for beam extracted from the Fermilab Booster to be injected into the Booster Neutrino Beamline (BNB), the Main Injector accelerator (MI), or the Recycler Ring (RR). Due to the limited aperture of the Recycler Ring, it is necessary to collimate transverse beam halo and tails before that beam is lost in an uncontrolled fashion at those aperture restrictions. Transverse beam collimators have been installed in MI8 since 2006; though, they are now undersized for the current beam flux being transmitted through the MI8 beamline [1–5]. A project has been underway since the spring of 2021 to design and install an additional collimator system in the MI8 beamline to better control the beam losses in downstream machines and handle the anticipated increase in beam flux after the PIP-II upgrade is completed [6, 7].

FINAL DESIGN

An extensive alternatives decision process was undertaken to decide on the design for the second generation of MI8 collimators [7]. The final design utilizes two approximately 88 ton collimators each consisting of four jaws, with pairs dedicated to either horizontal or vertical motion [8]. Past collimator designs required moving multi-ton collimator bodies to restrict the beam aperture. This design instead moves approximately 98 lb 304 stainless steel jaws within the vacuum vessel itself. This allows for much smaller motors, faster movement of the jaws, fewer vacuum connections and more steel for radiation shielding. Invar steel plungers and small vacuum bellows connect each jaw to two synchronized stepper motors. Since the jaws are in vacuum, most heat dissipation occurs via conduction; thermal contact with the surrounding vacuum vessel is made with AlBr conduction pads. Opposite the conduction pads are spring loaded roller bearings that ensure the jaw is kept in thermal contact. Each jaw has an aperture equal to $\pm 5\,\sigma$ of 20 π−mm−mrad (95 %, normalized) beam emittance at that location in the beamline lattice. Likewise, each jaw is machined with an upstream taper to match the beamline lattice beta function. Internal upstream and downstream masks provide additional shielding from secondary particle spray. Multiple layers of marble significantly reduce radiation doses to personnel from the activated collimator steel during tunnel accesses.

PROTOTYPE

A one-jaw prototype was constructed to to validate key design assumptions. The prototype consists of one full-size jaw inside a vacuum vessel, two motion motors, a 1 kW heater tape affixed to the inside jaw aperture, and thermocouples both inside and outside the vacuum. A vacuum window on one end enabled direct measurement of jaw position with a ruler during testing (Fig. 1). Tests confirmed repeatable jaw travel, expected thermal expansion, and sufficient heat transfer from the jaw to the vessel exterior. The only design change resulting from the prototype was swapping the jaw thermal-conduction pads from Cu to AlBr, which offers slightly lower thermal conductivity but markedly higher strength and reduced long-term wear [9].

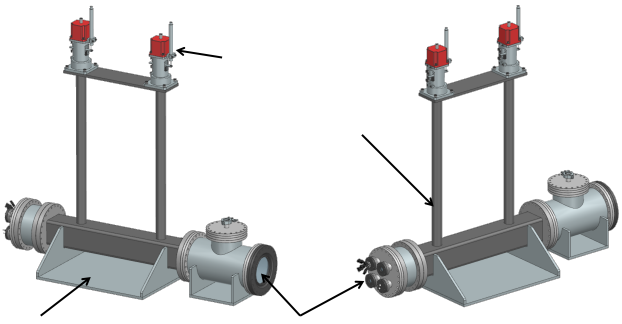

Figure 1: Illustration of the MI8 Collimator prototype test stand.

INSTALLATION

Due to the size and complexity of the new MI8 collimators, the installation was done in stages.

* kjh@fnal.gov

† This manuscript has been authored by Fermi Forward Discovery Group, LLC under Contract No. 89243024CSC000002 with the U.S. Department of Energy, Office of Science, Office of High Energy Physics.

Content from this work may be used under the terms of the CC BY 4.0 licence (© 2026). Any distribution of this work must maintain attribution to the author(s), title of the work, publisher, and DOI.

ISBN: 978-3-95450-252-3 ISSN: 2673-5350 doi: 10.18429/JACoW-IPAC2026-THP5005

RECENT DEVELOPMENTS OF BLOND FOR NEW LARGE SCALE ACCELERATOR FACILITIES

S. Lauber*, S. Albright, C. Becker, H. Damerau, J. Flowerdew, N. Gallou, P. Hickersberger, L. Intelisano, B. E. Karlsen-Bæck, I. Karpov, E. Lamb, A. Lasheen, M. Marchi, O. Smedt, H. Timko, L. Valle, J. Wulff, M. Zampetakis,
European Organization for Nuclear Research, Geneva, Switzerland
M. Schwarz, Karlsruhe Institute of Technology, Karlsruhe, Germany
L. Thiele, University of Rostock, Rostock, Germany
R. Heine, Technische Universität Berlin, Berlin, Germany

Content from this work may be used under the terms of the CC BY 4.0 licence (© 2026). Any distribution of this work must maintain attribution to the author(s), title of the work, publisher, and DOI.

Abstract

The Python-based Beam Longitudinal Dynamics (BLonD) simulation suite is an open-source framework for modelling the motion of charged particles in circular accelerators. BLonD has been in use since 2014 and is utilised successfully at several accelerator facilities such as J-PARC, ISIS, and CERN. Furthermore, BLonD is applied for the design of new synchrotrons such as the Future Circular Collider (FCC) and the Muon Collider. Both projects demand more complex simulations, as effects like strong synchrotron radiation or wake fields due to counter-rotating beams become important. In recent years, the BLonD community has also called for an improved user interface to ease the creation of input files for the simulations. This publication presents the latest software developments for BLonD. A redesigned, highly modular software architecture and improved user interface are currently being implemented, which simplify the creation of complicated relationships between physical phenomena. Preliminary testing and user feedback show improved scalability and flexibility, enabling the efficient development of particle-tracking simulations for next-generation accelerators, while facilitating the analysis of existing synchrotrons.

INTRODUCTION

With over a decade of development, the Beam Longitudinal Dynamics (BLonD) [1, 2] particle-tracking software is used to describe the evolution of a distribution of particles in the longitudinal phase space. BLonD was based on a modular structure to support the operation of existing accelerators, and to perform the longitudinal beam physics and radio frequency (RF) design of future accelerators. Over the years, it developed into a comprehensive software package that accounts for the interaction of the beam with the RF systems, RF noise, beam and cavity feedback, wake fields (in frequency and time domains), as well as synchrotron radiation and quantum excitation. Furthermore, it offers extensive support for generating initial distributions for single- and multi-bunch beams with arbitrary filling patterns and provides numerous implementations to model low-level radio frequency (LLRF) systems. Thanks to these features, BLonD has been employed to study longitudinal beam dynamics in numerous facilities [3–12].

BLonD is being upgraded from version 2 (V2) to version 3 (V3). The primary motivation for rolling out a new major release is the introduction of the so-called *Assembler* that links the various user-side classes into a consistent simulation setup. Consequently, there is an extensive number of Application Programming Interface (API) changes on the user side. To implement this functionality, monolithic classes had to be abandoned and replaced by a hierarchical, object-oriented system, which affects the majority of the code. This substantial reworking also allowed so-called type hints to be integrated into the major revision to simplify development. Furthermore, the ongoing research and development for the Future Circular Collider (FCC) [5, 11, 12] and the Muon Collider [6, 13, 14] required adjustments to the code architecture. This includes features such as counter-rotating beams, fast magnetic ramps, and sub-turn resolution of synchrotron radiation, which were only partially supported in BLonD V2.

CODE STRUCTURE

In its core routines, BLonD tracks the longitudinal macroparticle time offset Δt and energy offset ΔE on a turn-by-turn basis by modeling the user-selected interactions between the beam and the particle accelerator. First, the beam energy is updated according to the kick equation as a function of the longitudinal coordinate $\Delta E_{i+1} = \Delta E_i + f(\Delta t)$. The kick can contain energy changes due to the RF system, induced voltages, synchrotron radiation, etc. Second, the time coordinate is updated by the drift equation, based on the new energy coordinate as $\Delta t_{i+1} = \Delta t_i + g(\Delta E_{i+1})$. In addition, the properties of the accelerator, such as the RF frequency or the reference orbit, can be modified by the interaction with the beam.

The new structure of BLonD V3 can be analysed from various perspectives: the computational backends, the class-based middle layer, the abstract flow graph invoked by user input, and the public API classes. For the computational backends, the interaction between the beam's macroparticle coordinates and the various simulation components is central. For a single computing node Python (+ Numba [15] and Cupy [16]) and C++ (+ OpenMP [17] and CUDA [18])

* simon.fabian.lauber@cern.ch

ISBN: 978-3-95450-252-3 ISSN: 2673-5350 doi: 10.18429/JACoW-IPAC2026-THP5009

IMPACT OF LANDAU DAMPING FROM OCTUPOLES ON INSTABILITY GROWTH RATES MEASURED IN THE LHC*

C. Antuono†, D. Amorim, X. Buffat, N. Mounet, B. Lindström, R. Soòs[1,2]
CERN, Geneva, Switzerland
[1]also at IJCLab, CNRS/IN2P3, Orsay, France
[2]also at Université Paris-Saclay, Orsay, France

Abstract

Dedicated instability studies were performed in the LHC to quantify the impact of Landau octupoles on transverse beam stability. Controlled single-bunch instabilities were intentionally triggered at injection energy, and the corresponding growth rates were measured while systematically varying the Landau octupole knob. A clear correlation between the octupole current and the measured instability growth rate was observed. These measurements are compared with theoretical expectations to improve and benchmark the real part of the LHC impedance model, in particular its broadband component. The results not only provide valuable input for refining the impedance model, but also represent a direct quantitative observation of Landau damping in the LHC.

INTRODUCTION

The beam coupling impedance, which characterizes the electromagnetic interaction between the beam and its surrounding environment, can lead to an exponential growth of coherent oscillations of the beam centroid, potentially resulting in beam degradation or loss [2]. Impedance-driven instabilities therefore represent a potential limitation on the achievable proton bunch intensity in both the Large Hadron Collider (LHC) and its high-luminosity upgrade (HL-LHC), making it essential to accurately estimate, monitor, and control the machine impedance over time.

The machine impedance can be experimentally probed through instability measurements. In particular, the growth rate of transverse instabilities is directly related to the real part of the transverse impedance [2]. The stability of the beam is ensured through a combination of Landau damping, chromaticity, and transverse feedback systems. Landau damping plays a central role in stabilizing the beam by introducing a spread in betatron frequencies, which suppresses the coherent motion. In the most critical phase for stability in the LHC, i.e. at flat top before collisions are established, the tune spread is primarily generated using Landau octupole magnets. By adjusting the octupole current, the strength of the nonlinear detuning, and therefore the amount of Landau damping, can be controlled.

In order to measure instability growth rates in a controlled and quantitative manner, it is necessary to operate in a regime where Landau damping is minimized. In previous measurements, the presence of strong Landau damping prevented the observation of clear exponential growth, limiting the precision of the measurements [1]. Therefore, a dedicated experimental strategy was developed to reduce the stabilizing effect of octupoles while maintaining controlled beam conditions. Because of the operational constraints associated with performing such measurements at top energy, the experiments presented in this work are carried out at injection energy, where rapid cycling and improved reproducibility can be achieved. Although the impedance at injection is dominated by fixed-aperture elements rather than collimators, the latter can be tightened to partially reproduce a configuration closer to that at top energy [1]. This approach enables systematic and repeatable measurements while retaining sensitivity to the dominant impedance contributions, both at top energy (collimators) and at injection (fixed-aperture devices).

In this paper, we present a systematic study of instability growth rates measured under conditions of minimized Landau damping. ensuring controlled instabilities and characterizing them as a function of chromaticity, bunch length, and collimator settings. The results are compared with theoretical predictions, providing valuable input for benchmarking the LHC impedance model.

STRATEGY FOR INSTABILITY MEASUREMENTS

The measurements presented in this study were performed on September 4th, 2025, at injection energy (450 GeV), allowing fast, reproducible instability excitation. Although impedance-driven instabilities are more critical at top energy, their characterization is significantly slower because of the long cycle time required for injection, ramp, and dump. Injection energy offers a practical compromise for controlled experiments.

At injection, the impedance is distributed among several machine components including devices such as beam screens and warm sections. To partially reproduce flat-top-like conditions, the collimator gaps were systematically reduced below their nominal values, allowing the collimators to become a dominant contribution to the transverse impedance even at injection energy. To investigate their impact, the measurements were repeated for different IR7 collimator configurations: nominal (operational) configuration (primaries at 5.7σ, secondaries at 6.7σ, and tertiaries at 10σ), a tighter configuration with reduced gaps (primaries at 3.5σ, secondaries at 4.5σ, and tertiaries at 10σ) to enhance the collimator impedance contribution, and a configuration with

* Research supported by the HL–LHC project
† chiara.antuono@cern.ch

Content from this work may be used under the terms of the CC BY 4.0 licence (© 2026). Any distribution of this work must maintain attribution to the author(s), title of the work, publisher, and DOI.

ISBN: 978-3-95450-252-3 ISSN: 2673-5350 doi: 10.18429/JACoW-IPAC2026-THP5301

SIMULATION OF INTRABEAM SCATTERING WITH NONLINEAR DAMPING AND DIFFUSION IN SCIBMAD

J. P. Devlin*[1], D. T. Abell[2], G. H. Hoffstaetter[1,3], B. Nash[4]
[1]CLASSE, Cornell University, Ithaca, New York, USA
[2]IREAP, University of Maryland, College Park, Maryland, USA
[3]Brookhaven National Laboratory, Upton, New York, USA
[4]Emily Griffith Technical College, Denver, Colorado, USA

Content from this work may be used under the terms of the CC BY 4.0 licence (© 2026). Any distribution of this work must maintain attribution to the author(s), title of the work, publisher, and DOI.

Abstract

In many modern accelerators, intrabeam scattering (IBS) leads to measurable changes in a beam's dimensions during operation. For a Gaussian beam, there are many well-known methods to calculate the growth rates. However, while growth rates are very useful, they generally do not provide insight into how IBS interacts with effects beyond linear dynamics. To avoid this limitation, we apply IBS kicks, with both damping and diffusion components, to macroparticles during element-by-element tracking. These kicks are derived from first principles and are chosen to give the same growth rates as traditional methods for a Gaussian beam, with no special form assumed for the covariance matrix of the distribution. The beam generally becomes non-Gaussian during tracking, but the kick is nevertheless approximated by that of a Gaussian beam with the same covariance matrix. This method of IBS simulation has been implemented in SciBmad, allowing for analysis of IBS effects in beams with nonlinear spin-orbit dynamics, synchrotron radiation, beam-beam interactions, and more. Furthermore, tracking with IBS kicks is parallelized on both the CPU and the GPU.

INTRODUCTION

Intrabeam scattering (IBS) in charged-particle beams is a significant source of beam-size growth in many modern accelerators. The growth rates for a Gaussian beam have been studied extensively and the seminal formulations were introduced by Piwinski in [1] and Bjorken and Mtingwa in [2]. However, analyzing the interaction of IBS with nonlinear dynamics and other collective effects generally requires IBS kicks during macroparticle tracking. The usual approach is to apply a purely diffusive kick which produces the correct growth rates, but this approach neglects a damping component of the kick [3]. Additionally, the phase-space dependence of the kick is usually chosen heuristically, if not eliminated entirely [4]. In this work, the kicks are derived from first principles and the origin of the phase-space dependence is made clear.

* jpd285@cornell.edu

DAMPING AND DIFFUSION COEFFICIENTS

For stochastic kicks $\delta\vec{p}$ distributed according to some function g, the damping and diffusion coefficients are

$$\begin{aligned} b_i(\vec{z}) &= \int \mathrm{d}\Phi\, \dot{n}(\vec{z})\delta p_i(\vec{z},\Phi)g(\Phi), \\ d_{ij}(\vec{z}) &= \int \mathrm{d}\Phi\, \dot{n}(\vec{z})\delta p_i(\vec{z},\Phi)\delta p_j(\vec{z},\Phi)g(\Phi), \end{aligned} \tag{1}$$

where $\vec{z}$ is the six-dimensional phase-space vector and $\dot{n}$ is the number of kicks per unit time [5]. In the case of IBS, Φ is the phase-space coordinate of the other particle involved in a scattering event and g is the beam's phase-space distribution. Therefore, computation of the damping and diffusion coefficients requires knowledge of the kick $\delta\vec{p}$ due to a scattering event and the number of scattering events per unit time $\dot{n}$.

The scattering kick follows from standard results on Coulomb scattering when the motion is nonrelativistic [6]. To transform into a frame where the motion of all particles is approximately nonrelativistic, we apply a Lorentz transformation along the negative longitudinal axis with the reference Lorentz factor γ_0. Assuming the transverse momenta are small and all speeds are near the reference value v_0, this approximation will be good and the resulting transformation is

$$\begin{pmatrix} x \\ y \\ z \\ p_x \\ p_y \\ p_z \end{pmatrix} = \begin{pmatrix} 1 & 0 & 0 & 0 & 0 & 0 \\ 0 & 1 & 0 & 0 & 0 & 0 \\ 0 & 0 & \gamma_0^{-1} & 0 & 0 & 0 \\ 0 & 0 & 0 & p_0^{-1} & 0 & 0 \\ 0 & 0 & 0 & 0 & p_0^{-1} & 0 \\ 0 & 0 & 0 & 0 & 0 & \gamma_0 p_0^{-1} \end{pmatrix} \begin{pmatrix} X \\ Y \\ Z \\ P_X \\ P_Y \\ P_Z \end{pmatrix}, \tag{2}$$

where p_0 is the reference momentum. This new frame will be called the beam frame, in contrast to the lab frame. Capital letters are used to denote beam-frame quantities and, as usual, the lab-frame transverse momenta p_x and p_y are normalized by p_0 (while the beam-frame momenta are not). Additionally, the longitudinal momentum has a different meaning in the two frames: p_z is the usual accelerator variable $(p - p_0)/p_0$, while P_Z is actually the longitudinal component of the momentum vector.

All further calculations will be done in the beam frame. The transformation given by Eq. (2), along with the time-dilation relation $\mathrm{d}T = \mathrm{d}t/\gamma_0$, specifies the transformation be-

ISBN: 978-3-95450-252-3 ISSN: 2673-5350 doi: 10.18429/JACoW-IPAC2026-THP5302

DIFFERENTIABLE, CPU-/GPU-PARALLELIZED, SYMPLECTIC SPIN-ORBIT TRACKING IN SCIBMAD

J. P. Devlin*[1], G. H. Hoffstaetter[1,2], D. Sagan[1], M. G. Signorelli[2]
[1]CLASSE, Cornell University, Ithaca, New York, USA
[2]Brookhaven National Laboratory, Upton, New York, USA

Abstract

SciBmad is a new software library for accelerator simulation and design. Three key pillars which drove the development of SciBmad's tracking code are full differentiability (forwards-, backwards-, and Taylor-mode), high performance, and strict symplecticity. Differentiable integrators enable the trivial extraction of lattice functions and their higher-order generalizations, facilitate the use of machine learning tools, and make optimizations more efficient. The integrators have also been heavily optimized for performance, with SIMD parallelization on the CPU and GPU parallelization for various hardwares. Finally, SciBmad uses Yoshida's symplectic schemes to integrate the fully nonlinear Hamiltonian for magnetic multipoles, RF cavities, and combinations thereof, including implicit symplectic integration where required. All elements allow for spin tracking, which is guaranteed to be orthogonal due to the generality of Yoshida's scheme. Additionally, synchrotron radiation can be turned on in all elements. In this case, the use of a symplectic scheme guarantees that all damping results from the synchrotron radiation and not from numerical errors due to non-symplectic integration.

INTRODUCTION

Tracking simulations are an extremely important tool in accelerator physics as they provide the most accurate probe of nonlinear spin-orbit motion. Many quantities, such as the dynamic aperture and attainable beam polarization, can only be computed reliably through tracking. As these simulations sometimes require hundreds of thousands or even millions of turns, tracking codes must be as efficient as possible. However, accuracy, at least in the qualitative sense, cannot be sacrificed. Some tracking codes are extremely efficient because they use precomputed Taylor expansions of the motion, but it is easy to find examples where these codes produce qualitatively incorrect results. Other codes use numerical schemes like Runge-Kutta to integrate the full equations of motion, but when the number of steps is reduced to achieve reasonable efficiency, these schemes exhibit problems like artificial damping.

Accelerator physicists have realized that the ideal tracking code, which should be both efficient and accurate, must use symplectic integrators [1]. The canonical example of such a code is the polymorphic tracking code (PTC) [2]. As with Runge-Kutta schemes, the accuracy of a symplectic integrator can always be improved by reducing the step size. However, symplectic integrators do not exhibit the artificial damping seen in other schemes because they produce symplectic maps for any step size. Therefore, the tracking code for our new accelerator simulation program SciBmad is based entirely on symplectic integration [3]. The details of its tracking code, along with some examples, are presented in this paper.

HAMILTONIAN MOTION

The motion of charged particles in accelerators is primarily due to external electromagnetic fields. In a canonical coordinate system, this motion can be represented by a Hamiltonian function and is therefore symplectic. The coordinates in SciBmad are the radial offset x, the vertical offset y, and $z = -\beta c(t_0 - t)$. The subscript 0 indicates "reference" quantities (which may be chosen arbitrarily but should be self-consistent) and the reference time is defined by $s = \beta_0 c t_0$, where s is the distance along the reference trajectory. For a particle with momentum $\vec{P} = m\gamma\vec{v} + q\vec{A}$, where $\vec{A}$ is the vector potential, the momenta conjugate to SciBmad's coordinates are $p_x = P_x/P_0$, $p_y = P_y/P_0$, and $p_z = (P - P_0)/P_0$. In this set of coordinates, the Hamiltonian is

$$H_z = -h\sqrt{(1+p_z)^2 - (p_x - a_x)^2 - (p_y - a_y)^2} - a_s + \frac{\sqrt{(1+p_z)^2 + \widetilde{m}^2}}{\beta_0}, \tag{1}$$

where $\widetilde{m} = (\beta_0\gamma_0)^{-1}$ and $h = 1 + gx$ with the horizontal curvature g. The restriction to horizontal curvature is not a problem because the coordinate system can always be rotated to satisfy this constraint.

SYNCHROTRON RADIATION

The motion of ultrarelativistic particles in electromagnetic fields can be damped significantly by synchrotron radiation. The radiation process leaves the slopes (x', y') invariant and changes the particle energy. The resulting equation of motion is

$$\frac{\mathrm{d}p_z}{\mathrm{d}s} = -\sqrt{h^2 + x'^2 + y'^2}\,\frac{2}{3}\,\frac{r_0}{(mc^2)^3}E_0^3(1+p_z)^2 \times \left\| \frac{\vec{\mathscr{E}}_\perp}{c} + \vec{\beta} \times \vec{\mathscr{B}} \right\|^2, \tag{2}$$

where m is the mass and r_0 is the classical particle radius [4, 5]. We have defined the "normalized" fields $(\vec{\mathscr{E}}, \vec{\mathscr{B}}) = (q/P_0)(\vec{E}, \vec{B})$ and $\perp$ indicates the component of

* jpd285@cornell.edu

Content from this work may be used under the terms of the CC BY 4.0 licence (© 2026). Any distribution of this work must maintain attribution to the author(s), title of the work, publisher, and DOI.

ISBN: 978-3-95450-252-3 ISSN: 2673-5350 doi: 10.18429/JACoW-IPAC2026-THP5303

APPLICATION OF THE NONLINEAR OPTICS FROM OFF-ENERGY ORBITS METHOD AT THE SIRIUS STORAGE RING

M. M. S. Velloso*[1], X. R. Resende, F. H. de Sá
Brazilian Synchrotron Light Laboratory, Campinas, Brazil
[1]also at Gleb Wataghin Institute of Physics, University of Campinas, Campinas, Brazil

Content from this work may be used under the terms of the CC BY 4.0 licence (© 2026). Any distribution of this work must maintain attribution to the author(s), title of the work, publisher, and DOI.

Abstract

The applicability of the Nonlinear Optics from Off-Energy Closed Orbits (NOECO) method to the SIRIUS storage ring is investigated. Off-energy orbit response matrices (OEORMs) were measured and used for sextupole strength calibration through a Levenberg-Marquardt (LM) fitting procedure with Tikhonov regularization. The fitted strengths reproduced the measured chromaticities with reasonable accuracy and were consistent with control system estimates. Analysis of the OEORM Jacobian revealed strong correlations among sextupole family signatures, indicating significant quasi-degeneracies in the inverse problem. Machine experiments and model-based simulations showed that localized perturbations are redistributed across correlated families, especially in the presence of small optics mismatches. The results indicate that OEORM-based calibration is feasible at SIRIUS, although its resolving power is fundamentally limited by parameter correlations and model imperfections.

INTRODUCTION

NOECO [1] is a calibration method that fits chromatic sextupole strengths to best reproduce the measured OEORM, in a least-squares sense. The OEORM is defined as the numerical derivative of the orbit response matrix (ORM) with respect to relative energy deviations δ:

$$\mathrm{OEORM} = \frac{\mathrm{ORM}_{+\delta} - \mathrm{ORM}_{-\delta}}{2\delta}, \tag{1}$$

where $\mathrm{ORM}_{\pm\delta}$ corresponds to the ORM measured at energy deviation $\pm\delta$ and ORM elements read

$$\mathrm{ORM}_{ij} = \frac{\Delta u_i}{\Delta \theta_j}, \tag{2}$$

with $\mathbf{u} = \begin{bmatrix}\mathbf{x} & \mathbf{y}\end{bmatrix}^\top$ and $\Delta\theta = \begin{bmatrix}\theta_x & \theta_y\end{bmatrix}^\top$. At SIRIUS, like the ORM, the OEORM is a 320×281 matrix, with the dispersive orbit response as the last column.

Regarding SIRIUS sextupole lattice, there are 6 achromatic sextupole families in the straight sections and 15 chromatic families in the arcs [2]. The NOECO scheme purports to calibrate the chromatic lattice only.

OEORM MEASUREMENTS AT SIRIUS

OEORM measurements at the SIRIUS storage ring are carried out according to the following procedure. Energy deviations of $\delta = \pm 0.5\%, \pm 0.25\%$ are introduced into the beam by adjusting the RF master oscillator frequency around the nominal operating frequency f_0. The required frequency shifts Δf are calculated as $\Delta f = -\alpha f_0 \delta$, where δ is the desired energy shift and $\alpha = 1.636 \times 10^{-4}$ is the lattice momentum compaction factor at $\delta = 0$. At each energy offset, a fast "AC" ORM measurement [3] is performed. Using the ORMs measured over the energy shift range together with the ORM at $\delta = 0$, the data are fitted with a linear model of ORM versus energy deviation. The OEORM corresponds to the angular coefficient of the fit.

THE FITTING SETUP

The objective function to be minimized is

$$\chi^2 = \sum_{ij} \frac{|\mathrm{OEORM}_{ij}^{\mathrm{meas}} - \mathrm{OEORM}_{ij}^{\mathrm{model}}|^2}{w_{ij}^2}, \tag{3}$$

where $\mathrm{OEORM}^{\mathrm{meas}}$ is the measured OEORM and $\mathrm{OEORM}^{\mathrm{model}}$ the model prediction. The weights w_{ij} represent the OEORM experimental noise.

The fitting parameters are the chromatic sextupole strengths (15 knobs) together with calibration gains for BPM readings (320) and calibration gains for corrector strengths (280). The gains enter the minimization as linear transformations applied to the measured OEORM:

$$\mathrm{OEORM}'^{\mathrm{meas}} = G^{\mathrm{BPM}}\, \mathrm{OEORM}^{\mathrm{meas}}\, G^{\mathrm{corr}}. \tag{4}$$

The parameter vector to be calibrated is organized as

$$\mathbf{P} = \begin{bmatrix}\mathbf{S} & \mathbf{G}^{\mathrm{corr}} & \mathbf{G}^{\mathrm{BPM}}\end{bmatrix}^\top,$$

with dimensions $15 + (120 + 160) + (2 \times 160) = 615$. Off-diagonal elements of the OEORM are not considered in the fitting, eliminating the need of couplings among the horizontal and vertical BPMs signals as additional parameters. The vector $\mathbf{P}$ minimizing the least-squares problem is iteratively calculated until convergence as $\mathbf{P}^{(n+1)} \to \mathbf{P}^{(n)} + \Delta\mathbf{P}^{(n)}$, with Levenberg-Macquardt (LM) steps

$$\Delta\mathbf{P}^{(n)} = -\left[J^\top J + \lambda \mathrm{diag}(J^\top J)\right]^{-1} J^\top \mathbf{r}^{(n-1)}, \tag{5}$$

with $\mathbf{r}^{(n)}$ being the residuals vector at the n-th iteration. The residuals elements $r_k = \left(\mathbf{r}^{(n)}\right)_k$ are obtained from the vectorization of the weighted OEORM residue ath the n-th iteration

$$r_k = \frac{\mathrm{OEORM}_{ij}'^{\mathrm{meas}} - \mathrm{OEORM}_{ij}^{\mathrm{model}}}{w_{ij}}, \tag{6}$$

* matheus.velloso@lnls.br

ISBN: 978-3-95450-252-3 ISSN: 2673-5350 doi: 10.18429/JACoW-IPAC2026-THP5305

EMITTANCE MEASUREMENTS IN THE BTS TRANSFER LINE AT THE CANADIAN LIGHT SOURCE

C.-L. M. Randall *, W. A. Wurtz
Canadian Light Source, Saskatoon, Canada

Content from this work may be used under the terms of the CC BY 4.0 licence (© 2026). Any distribution of this work must maintain attribution to the author(s), title of the work, publisher, and DOI.

Abstract

During the injection process at the Canadian Light Source (CLS), approximately one third of the electron beam is lost from the Booster Ring (BR) to the Storage Ring (SR) at controlled locations in the Booster-to-Storage Ring (BTS) transfer line. In 2021, the BTS was upgraded to allow the facility to run in Top-Up mode. Included in this upgrade was the installation of new diagnostic CCD cameras in the transfer line with the intent to use them to measure beam properties and better understand the electron beam extracted from the BR.

This paper presents emittance measurements, using these diagnostic cameras, of the electron beam extracted from the BR. Using two quadrupoles, one focusing and one defocusing, quadrupole scan measurements were performed to measure both the horizontal and vertical emittances in the BTS. An estimated emittance in the BR was also measured using a combination of images of the synchrotron radiation produced by the BR and betatron functions, dispersion, and energy spread values obtained from simulations. These measured emittances were then compared to expected theoretical emittances of the BR from synchrotron radiation integrals.

INTRODUCTION

In 2021, the BTS was upgraded such that Top-Up mode could be run at the CLS. During the upgrade, new diagnostic cameras and screens were installed in the BTS that allowed us to look at the beam in the transfer line. One of these diagnostic setups was placed early in the BTS transfer line after a pair of quadrupoles such that quadrupole scans could be done to measure the horizontal and vertical emittances of the electron beam extracted from the BR.

Emittance is a measure of the beam size in phase space coordinates. It is used as a metric of beam quality where a smaller emittance is typically preferred. If the electron beam extracted from the BR has a much emittance then expected, it could be part of the reason for the losses experienced in the BTS transfer line.

The emittance used in this paper is defined as [1–3]

$$\epsilon^2 = \sigma_{11}\sigma_{22} - \sigma_{12}^2 = \langle x_i^2\rangle\langle x_i'^2\rangle - \langle x_i x_i'\rangle^2, \quad (1)$$

where the σ components come from the σ matrix

$$\sigma = \begin{pmatrix} \sigma_{11} & \sigma_{12} \\ \sigma_{12} & \sigma_{22} \end{pmatrix} = \epsilon \begin{pmatrix} \beta & -\alpha \\ -\alpha & \gamma \end{pmatrix}. \quad (2)$$

The Twiss parameters contained within the σ matrix provide information about the beam, including position and momentum distributions.

QUADRUPOLE SCANS

Quadrupole scans are a common method of measuring beam emittance [1–4]. Using the sigma matrix together with the transport matrices M, the propagation of the beam profile can be described by [1]

$$\sigma(s_1) = M(s_1|s_0)\sigma(s_0)M(s_1|s_0)^\top, \quad (3)$$

which expands into the quadratic equation

$$\sigma_{1,11} = \sigma_{0,11}M_{11}^2 + 2\sigma_{0,12}M_{11}M_{12} + \sigma_{0,22}M_{12}^2. \quad (4)$$

When changing a quadrupole's strength, the beam shape can be seen changing on a view screen. Figure 2 is an example using a focusing quadrupole. These changes in horizontal and vertical beam sizes are then measured by calculating the 1σ of the respective distribution. The relation between quadrupole strength and 1σ beam size squared $\sigma_{1,11}$, (also referred to as variance) is then plotted and the σ matrix values can be obtained by fitting the data to Eq. (4), as shown in Fig. 1. Then the emittance can be calculated using Eq. (1).

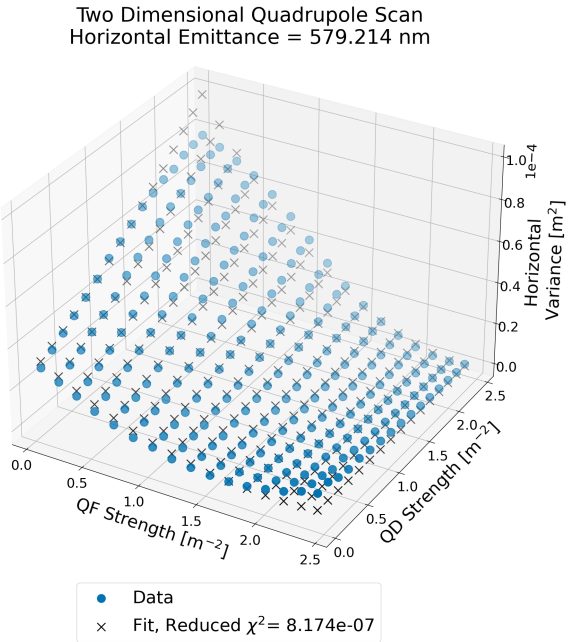

Figure 1: Horizontal variance plotted against focusing quadrupole (QF) strength and defocusing quadrupole (QD) strength, with a fit of the data to calculate horizontal emittance.

* chelsea-lea.randall@lightsource.ca

ISBN: 978-3-95450-252-3 ISSN: 2673-5350 doi: 10.18429/JACoW-IPAC2026-THP5306

MATCHING OF MULTIPLE ENERGY BEAMLINES FOR THE CEBAF ENERGY UPGRADE*

S.J. Brooks†, Brookhaven National Laboratory, Upton, NY, USA

Abstract

It is currently planned to increase the energy of the CEBAF recirculating linear accelerator to 22 GeV by adding two new recirculating arcs that contain multiple new energy passes. These new passes at six different energies must be matched to the existing linac simultaneously, as the beam is continuous (CW), so magnets cannot be ramped. This paper studies propagating several energies in the same beam pipe with a line of quadrupoles acting on all of them simultaneously, with the goal that the combined effect produces a match for each energy. Computer optimisation of the performance this system under various constraints (beamline length, number of magnets) is studied.

MATCHING CONSTRAINTS

The proposed CEBAF upgrade achieves an energy increase by replacing the highest energy arcs of the racetrack by ones that contain up to six energies [1], enabling more passes through the two linacs on the North and South of the facility. The bulk of the 180° angle of each muiti-energy arc is implemented using a fixed-field accelerator (FFA) lattice with permanent magnets [2] and homogenous cells. However, matching these six beams of different rigidities to the linacs is non-trivial. The parameters to be matched for each energy roughly divide into three groups:

1. Orbit position and angle x, x' together with their energy derivatives D_x, D'_x (there is no vertical orbit motion in the FFA arcs);
2. Optical functions $\beta_x, \beta_y, \alpha_x, \alpha_y$;
3. Time of flight Δt and its energy derivative R_{56}.

Matching group 1 for a multi-energy beamline has been experimentally demonstrated at the CBETA FFA [3] using an adiabatic line, with shorter non-adiabatic matches also possible [4] to a reasonable level of accuracy. Group 3 is hardest to match because changing the time of flight separately for each energy usually requires splitting them into lines taking different paths, as was done at CBETA and is planned for the CEBAF upgrade [5]. Once the energies are separated, matching all the parameters is much easier. The disadvantage is that multiple split lines (six in this case) can be large and costly, so reliance on these should be minimised. It is therefore being considered to have split lines only on one side of each linac, to deal with all the time of flight effects, with a merged line on the other side. This merged line would still have to match the group 2 optical parameters with all six energies in the same line.

* Work supported by Brookhaven Science Associates, LLC under Contract No. DE-SC0012704 with the U.S. Department of Energy.

† sbrooks@bnl.gov

Table 1: Matching Conditions Before the Beamline

Beam E_k (GeV)	β_x **(m)**	β_y **(m)**	α_x	α_y
10.55	16.63	19.75	0.14	0.03
12.75	58.31	64.75	0.51	-0.2
14.95	61.5	64.53	-0.29	-0.91
17.15	40.81	39.37	-0.65	-0.88
19.35	21.74	25.17	-0.01	-0.07
21.55	26.72	33.88	0.47	0.36

Table 2: Matching Conditions After the Beamline

Beam E_k (GeV)	β_x **(m)**	β_y **(m)**	α_x	α_y
10.55	4.157	6.515	3.049	-3.19
12.75	2.951	6.477	1.822	-3.037
14.95	2.718	6.995	1.539	-3.206
17.15	2.602	8.035	1.399	-3.636
19.35	2.521	10.132	1.311	-4.549
21.55	2.455	16.84	1.247	-7.524

Previous work on this section [6] had success with group 1 but difficulty with group 2, so here we concentrate on group 2 and assume that group 1 is already matched to zero with a method similar to [4]. This paper studies matching from the optical parameters after the linac (Table 1) to the parameters for entry into the FFA section (Table 2), with all six energies going through the same magnets. The beta functions from the linac are significantly larger than those of the FFA. As the orbit is at $x = y = 0$, only quadrupoles are required.

OPTIMISATION

The optimisation has $6 \times 4 = 24$ constraints and as many variables as there are quadrupole gradients. The lengths are not varied, as this made seemed to make the optimisation more prone to local minima. Even without varying the lengths, getting stuck in a local minimum of the sum-of-squares error was very common. The basic optimisation method is to take the Jacobian response matrix and apply SVD to yield a damped pseudo-inverse equivalent to the Levenberg–Marquardt method [7]. Some higher-order corrections [8] were also added. However, this optimisation was restarted to random points ('basin hopping') multiple times before getting the first 30-magnet solution shown below.

For the shorter beamline with 40 magnets, simulated annealing was applied. In this, random steps are accepted with probability $\min(1, e^{-\Delta E/T})$ where ΔE is the change in sum-of-squares error and T is a 'temperature' parameter, which here decreases by $10^{-4}T$ on every step. The difficult part is generating suitable random steps that are not so large they always get rejected, nor are so small they do not adequately explore the landscape, which is required for annealing to

Content from this work may be used under the terms of the CC BY 4.0 licence (© 2026). Any distribution of this work must maintain attribution to the author(s), title of the work, publisher, and DOI.

ISBN: 978-3-95450-252-3 ISSN: 2673-5350 doi: 10.18429/JACoW-IPAC2026-THP5314

UNIVERSAL INJECTOR AT LERF – BASELINE DESIGN*

S. A. Bogacz†, M. Bruker, J. Grames, J. Gubeli, C. Hernandez-Garcia,
K. Jordan, I. Neththikumara, S. Ogur, T. Satogata, N. Sereno
Thomas Jefferson National Accelerator Facility, Newport News, VA, USA
A. Fomin, Université Paris-Saclay, CNRS/IN2P3, IJCLab, Orsay, France
V. Lizárraga-Rubio, Universidad de Guanajuato, Guanajuato, Mexico

Abstract

A new electron injector complex has been proposed within the Low Energy Recirculating Facility (LERF) vault, which would serve both the 22 GeV CEBAF and the positron programs, while being compatible with the electron source required to produce positrons for Ce$^+$BAF. The baseline design of a 3-pass recirculator features a main linac configured with three cryomodules, five isochronous arcs and three straight sections, allowing electron beam acceleration up to 650 MeV. The injector offers the flexibility to extract 1-pass and 2-pass energy electrons, as needed for positron production, with final reconfiguration to a 3-pass 650 MeV injector for 22 GeV CEBAF. This paper provides an overview of the baseline design of the Universal injector complex, including the 8 MeV injector and the recirculator. A comprehensive suite of beam dynamics studies to validate our design is being launched, starting with start-to-end tracking with Elegant followed by the orbit correction and error mitigation.

LATTICE ARCHITECTURE AND OPTICS

The injector complex [1] is arranged in a racetrack configuration hosting three C-75 cryomodules [2], each containing eight 5-cell cavities operating at 1497 MHz; all three cryomodules are located in a single straight. Starting from an 8 MeV injection energy, the final energy of 650 MeV is reached in three recirculation passes, with each cryo-module providing a 71.3 MeV energy boost. The beam is injected into the racetrack via a three-bend isochronous merger. Five 180° arcs provide recirculation: three on the West side and two on the East side of the racetrack. They are separated vertically by 90 cm (45 cm + 45 cm), with the lowest-energy arcs at the top of the stack. The overall layout is illustrated in Fig. 1. A vertical switch-yard is laid out as a 'three-tier-spreader', initiated by a single vertical bend common to all three passes. The lower-energy spreaders (1st and 2nd pass) are configured as two-step ascents with dispersion suppression in between. The top-energy spreader (3rd pass) features a compact four-point-chicane achromat whose second magnet is shared with the 2nd pass spreader. Recombiners on the East end mirror the spreaders. All arcs employ the Flexible Momentum Compaction (FMC) lattice architecture [3]. The overall optics architecture has been inspired by the PERLE [4, 5] at Orsay.

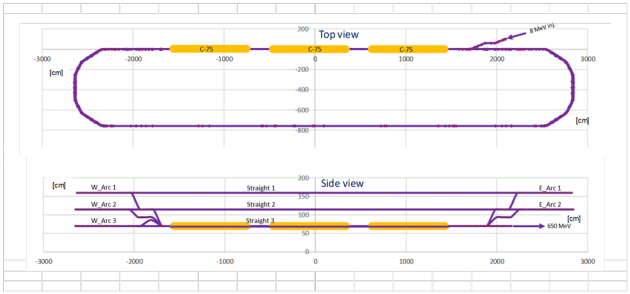

Figure 1: Top and side views of the 3-pass racetrack, featuring vertical stacks of arcs on each side (3 West + 2 East), separated by spreaders and recombiners. The linac, composed of three C-75 cryomodules, achieves a final energy of 650 MeV in three passes.

Merger

Injection at 8 MeV is accomplished through a fixed-field, three-bend merger whose last magnet is placed at the entrance of the linac (Fig. 2). The three-bend configuration and optics architecture, similar to the PERLE [4] design, was chosen for its compactness while maintaining functional modularity. Two quadruplet families flank the merger to provide optimized input/output Twiss functions. The initial quad in the dispersive region, Q1, controls momentum compaction; the subsequent pair Q2 and Q4 closes the achromat; an additional de-focusing quad Q3 at the zero-dispersion crossing balances the beta functions strongly constrained in the horizontal plane. The merger optics (Fig. 3) is tuned to the isochronous condition, yet the architecture also supports non-zero momentum compaction with orthogonal tunability of horizontal dispersion and M_{56}.

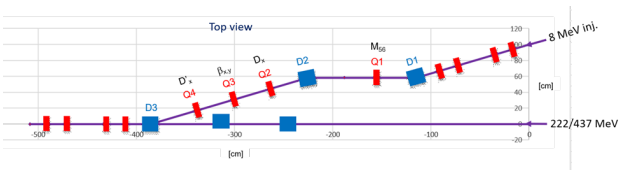

Figure 2: Top view of the 3-bend merger connected to the linac straight, including a re-injection chicane that closes the orbit bump initiated by the last merger bend D3.

Multi-Pass Linac

The last merger bend closes the orbit bump at the lowest injection energy but would deflect higher-pass beams. To suppress the resulting higher-pass bumps, a re-injection chicane is completed by placing two opposing bends upstream

* This material is based upon work supported by the U.S. DOE, Office of Science, Office of Nuclear Physics contract DE-AC05-06OR23177.
† bogacz@jlab.org

Content from this work may be used under the terms of the CC BY 4.0 licence (© 2026). Any distribution of this work must maintain attribution to the author(s), title of the work, publisher, and DOI.

ISBN: 978-3-95450-252-3 ISSN: 2673-5350 doi: 10.18429/JACoW-IPAC2026-THP5316

SIMULATION AND ANALYSIS OF HIGH-ENERGY BEAM TRANSPORT LINES AT LANSCE

C.-M. Alvinerie*, C. E. Taylor
Los Alamos National Laboratory, Los Alamos, NM, USA

Abstract

The Los Alamos Neutron Science Center (LANSCE) target stations require reliable beam quality to carry out experiments under optimal conditions. Maintaining the bunch structure through the beam transport from the 800-MeV Linac to the target stations is crucial. Currently, beam transport tuning is the primary tool to control the beam from the source to end of the linac, but not as readily used for the beams' remaining travel to the target stations. Our legacy models for the high-energy beamlines (HEBT) are simulated with TRANSPORT simulation code. Now, we are exploring newer more accurate accelerator physics codes such as Elegant and MAD-X. These models are continuously improved by incorporating key known beam characteristics and updated lattice elements. They are benchmarked against experimental data where diagnostics are available. We are improving these tools to better understand beam optics and conduct studies aimed at optimizing beam performance. In this paper, we present the latest simulation results supporting more predictive beam transport downstream of the 800-MeV Linac.

INTRODUCTION

The Los Alamos Neutron Science Center provides high-intensity neutron beams over a broad energy range for material research. To meet the diverse experimental requirements, the facility produces two proton beams with distinct energies. The Isotope Production Facility (IPF) utilizes a 100 MeV H^+ beam, whereas four downstream user stations—Proton Radiography (pRad), Ultra-Cold Neutrons (UCN), Lujan Center, and Weapons Neutron Research (WNR)—are supplied with an 800 MeV H^- beam with distinct timing patterns. Both beams have an initial energy of 0.75 MeV and are accelerated to 100 MeV by the 201.25 MHz Drift Tube Linac. Subsequently, the H^- beam is further accelerated to 800 MeV by the 805 MHz Side Coupled-Cavity Linac (CCL) and distributed downstream to the user stations via the High-Energy Beam Transfer (HEBT) lines.

In recent years, efforts have been made to improve the models of the HEBT beamlines, downstream the CCL, delivering beam to several user stations [1], primarily using Elegant [2] and MAD-X [3]. Ultimately, this will improve our understanding of beam transport and enable better control of the beam parameters along the beamlines.

In this paper, we present current efforts to model the beamlines delivering beam to the Weapons Neutron Research. The first section provides an overview of the beamline configuration, followed by the presentation of simulation results.

* calvinerie@lanl.gov

HEBT BEAMLINES CONFIGURATION TO THE WNR TARGET

The Weapons Neutron Research (WNR) facility is a pulsed neutron source used for nuclear science, material studies and detector development. The high- energy neutrons (from 100 keV to 800 MeV) are produced via spallation: the high-energy proton beam, generated at the end of the 805-MHz CCL and transported downstream through 250 m beamline length, strikes a tungsten target. Then, neutrons travel along a flight path that depends on the type of experiment (goals, energy ranges, and resolutions). For more details on the neutron experiments at LANSCE, see Reference [4].

In this paper, we focus on the high-energy beam transport from the end of the 805-MHz CCL to the WNR target. The configuration of these beamlines is presented in Fig. 1.

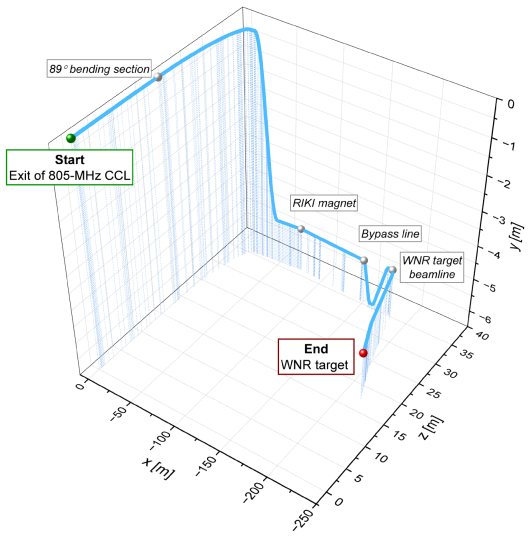

Figure 1: Beamline floor plan (Z–X–Y) from the 805 MHz CCL exit to the WNR target, where z, x and y respectively defined along the beam trajectory from the CCL, the horizontal north–south direction, and the vertical up–down direction. The intermediate markers in gray indicate the entrance of each beamline section.

The Switchyard receives the 800 MeV H^- beam and transports it in a straight section. The beam is focused by two quadrupole doublets, while the final bending magnets deflect the beam by approximately 6° to the right into Line D.

The beam then enters an 89° horizontal bending section composed of four bending magnet triplets that steer the beam south. Achromatic conditions are achieved using quadrupole triplets, ensuring minimization of dispersion. In the vertical bend, the beam is directed downward, producing an elevation

Content from this work may be used under the terms of the CC BY 4.0 licence (© 2026). Any distribution of this work must maintain attribution to the author(s), title of the work, publisher, and DOI.

ISBN: 978-3-95450-252-3 ISSN: 2673-5350 doi: 10.18429/JACoW-IPAC2026-THP5319

BEAM-BASED ALIGNMENT FOR SEXTUPOLES VIA PARALLEL OPTIMIZATION

X. Huang*, SLAC National Accelerator Laboratory, Menlo Park, United States

Abstract

We propose a method to perform beam-based alignment measurement for multiple sextupoles simultaneously by minimizing the induced orbit shifts from sextupole modulation through parallel local orbit optimizations. The parallel optimization is made possible by using local orbit bumps as knobs and separating the induced orbit kicks through model-based response matrices. The approach reduces slow, multi-knob optimization problems into multiple fast, single-knob optimization problems. The method is demonstrated in simulation.

INTRODUCTION

Beam-based alignment (BBA) aims at finding the magnetic centers of magnets which can be used to define the orbit target. BBA is important for accelerator commissioning and operation as there are many benefits when the beam is steered through the magnet centers. Quadrupole BBA is often an important step in the commissioning of new accelerators and a routine task on operating machines. Sextupole BBA is less common presently. However, as misalignments in sextupoles cause linear optics and coupling errors which have big impact on the performance of low emittance storage rings, it may be more important to steer beam through sextupole centers in such machines.

Similar to quadrupole BBA, sextupole BBA can be done through measurements of the induced orbit shifts (IOS) from modulation of the strengths of the magnets. Parallel-BBA (PBBA), a method to simultaneously find the centers of multiple quadrupoles by correcting the induced orbit shifts has been proposed and demonstrated at SPEAR3 [1]. It has also been successfully tested at other facilities [2–4]. Another parallel method for quadrupole BBA, parallel-QMS (P-QMS), scans the orbits at the targeted magnet locations to find the beam orbits with zero induced kicks [5], using the measured IOS and the orbit response matrix to isolate the induced kicks by the magnets.

Both PBBA and P-QMS can be extended to sextupoles. In Ref. [6], the P-QMS method is applied to sextupoles by fitting the induced horizontal kicks to the horizontal or vertical orbits to parabolic curves from which the magnetic field centers can be found. The principle of PBBA is to minimize the IOS with orbit changes at the magnet locations. This method has been tested to sextupoles in experiments [5]. However, convergence can be very slow when applied to multiple sextupoles simultaneously since it becomes a nonlinear multi-dimensional optimization problem, unlike the linear case when PBBA is applied to quadrupoles.

* xiahuang@slac.stanford.edu

In this paper, we propose an approach to divide the nonlinear multi-dimensional problem into multiple 2-dimensional optimization problems that can be optimized on the machine in parallel. This approach can greatly expedite the convergence toward the optimum. We also propose a coding structure for implementing online optimization algorithms which not only facilitates parallelizing multiple instances, but also allows better control of the optimization process.

SEXTUPOLE BBA BY MINIMIZING IOS

The IOS is the orbit change before and after the targeted magnet group changes its strengths. The IOS can be accounted for with the induced kicks at the magnet locations due to the orbit offsets at these magnets,

$$\Delta\mathbf{x} = \mathbf{R}_{x,s}\Delta\boldsymbol{\theta}_{x,s}, \quad \Delta\mathbf{y} = \mathbf{R}_{y,s}\Delta\boldsymbol{\theta}_{y,s}, \tag{1}$$

where $\mathbf{R}_{x/y,s}$ are orbit response matrices from kicks applied at the magnet locations to the BPMs and $\Delta\boldsymbol{\theta}_{x/y,s}$ are such kicks due to modulating the strengths of the magnets. For sextupoles, the induced kicks and the orbit offsets are related through,

$$\Delta\theta_{x,s} = -[\Delta K_2 L]\frac{1}{2}\left((x_s - x_0)^2 - (y_s - y_0)^2\right) \tag{2}$$

$$\Delta\theta_{y,s} = [\Delta K_2 L](x_s - x_0)(y_s - y_0), \tag{3}$$

where $[\Delta K_2 L]$ is the change of integrated strength, (x_0, y_0) represents the sextupole field center and (x_s, y_s) the orbit at the magnet. When the beam passes through the sextupole field center, the induced kicks are zero in both planes.

The magnetic centers can be found by online optimization, using the beam orbits at the magnet as knobs. The objective can be the sum of squares of the IOS on all BPMs in both planes. It is a relatively simple problem if one sextupole is involved at a time (with only 2 knobs). However, for cases with multiple sextupoles powered by a common power supply, it becomes a challenging nonlinear optimization problem (with $2N_s$ knobs for N_s sextupoles). For most optimization algorithms, convergence becomes considerably slower as the dimensionality of the optimization problem increases. The slow convergence could inhibit the use of the method to realistic sextupole BBA problems.

The difficulty of slow convergence can be addressed by dividing the single optimization problem with multiple sextupoles into multiple optimization problems, each targeting one sextupole only, which can be carried out simultaneously in parallel. This is possible because the induced kicks by the different sextupole magnets can be separated out, using

$$\Delta\boldsymbol{\theta}_{x,s} = \left(\mathbf{R}_{x,s}^T\mathbf{R}_{x,s}\right)^{-1}\mathbf{R}_{x,s}^T\Delta\mathbf{x}, \tag{4}$$

Content from this work may be used under the terms of the CC BY 4.0 licence (© 2026). Any distribution of this work must maintain attribution to the author(s), title of the work, publisher, and DOI.

ISBN: 978-3-95450-252-3 ISSN: 2673-5350 doi: 10.18429/JACoW-IPAC2026-THP5320

SYMPLECTIC INTEGRATOR FOR INSERTION DEVICES TRACKING AT SIRIUS

G. R. Ascenção[1*], V. Souza[1], F. H. de Sá, X. R. Resende
Brazilian Synchrotron Light Laboratory (LNLS), Campinas, Brazil
[1]also at Gleb Wataghin Institute of Physics, University of Campinas, Campinas, Brazil

Abstract

This paper describes the development of an explicit symplectic integrator for insertion devices based on the method of Wu, Forest, and Robin, and applies it to the CPMU13, a new SIRIUS insertion device designed for operation in a high-beta straight section with a minimum gap of 4.65 mm. We detail the magnetic field fitting procedure and benchmark particle tracking results against a conventional kickmap approach.

INTRODUCTION

The Brazilian Center for Research in Energy and Materials (CNPEM) is currently developing the ORION project [1], a biosafety level 4 laboratory integrated with three beamlines of the SIRIUS synchrotron light source. One of these beamlines, HIBISCO [2], will be installed in a high-beta straight section ($\beta_x = 17.2\,\mathrm{m}$ and $\beta_y = 3.6\,\mathrm{m}$) and will employ a cryogenic permanent magnet undulator (CPMU) [3] as its photon source.

To meet the beamline requirements, the insertion device (ID) is designed with a period length of 13.6 mm and a total of 147 periods, reaching a peak magnetic field of 1.08 T at a minimum gap of 4.65 mm.

A key concern is the impact of the ID on nonlinear beam dynamics, particularly for particles with large transverse amplitudes, as encountered during injection. This is especially relevant for SIRIUS, where injection is performed off-axis using a nonlinear kicker [4]. Accurate modeling of the ID effects is therefore essential to ensure the robustness of the injection process.

Most tracking codes currently model ID effects using kickmaps [5], a well-established tool in the synchrotron community. However, kickmaps in general are not symplectic, and the impact of this non-symplecticity on long-term particle stability remains insufficiently explored in the literature. In this work, the WFR (Wu–Forest–Robin) [6] integrator is employed as a benchmark against kickmap-based tracking, enabling a more rigorous assessment of the dynamics and ensuring accurate modeling of the new CPMU at SIRIUS.

WFR INTEGRATOR FOR S-DEPENDENT MAGNETIC FIELDS

Under the paraxial approximation, the Hamiltonian describing the motion of a charged particle with charge q in Cartesian coordinates can be written in extended phase space, including (z, p_z), as

$$H(x,p_x,y,p_y,\delta,l;\sigma) = \frac{(p_x-a_x)^2}{2(1+\delta)} + \frac{(p_y-a_y)^2}{2(1+\delta)} + p_z - a_z, \tag{1}$$

where $p_i = P_i/P_0$ denotes the transverse momenta normalized to the reference momentum P_0, δ is the relative momentum deviation, l is the path length, and $a_i = qA_i/(P_0 c)$ is the normalized vector potential. The independent variable is denoted by σ.

The exact Lie map associated with a step $\Delta\sigma$ is given by

$$\mathscr{M}(\Delta\sigma) = \exp\left(-\Delta\sigma : H :\right). \tag{2}$$

In practice, a symplectic integrator is obtained by factorizing this map. Assuming the gauge $a_z = 0$, a second-order approximation of $\mathscr{M}$ can be constructed as

$$\begin{aligned}\mathscr{M}_2(\Delta\sigma) = {} & \exp\left(: -\frac{(p_z-\delta)\Delta\sigma}{2} :\right) \\ & \times \mathscr{A}_y \exp\left(: -\frac{p_y^2\Delta\sigma}{4(1+\delta)} :\right)\mathscr{A}_y^{-1} \\ & \times \mathscr{A}_x \exp\left(: -\frac{p_x^2\Delta\sigma}{2(1+\delta)} :\right)\mathscr{A}_x^{-1} \\ & \times \mathscr{A}_y \exp\left(: -\frac{p_y^2\Delta\sigma}{4(1+\delta)} :\right)\mathscr{A}_y^{-1} \\ & \times \exp\left(: -\frac{(p_z-\delta)\Delta\sigma}{2} :\right),\end{aligned} \tag{3}$$

where the operators $\mathscr{A}_i$ are defined as

$$\mathscr{A}_i = \exp\left(- : \int a_i(x,y,z)\,\mathrm{d}i :\right). \tag{4}$$

The dependence of the vector potential on the longitudinal coordinate z is naturally incorporated through the operators $\mathscr{A}_i$ [6].

GENERAL UNDULATOR MODEL FOR THE WFR INTEGRATOR

To evaluate the operators $\mathscr{A}_i$, an analytical representation of the vector potential components A_i is required. For this purpose, we adopt a Fourier-based model of the 3D static magnetic field of a planar undulator, given by

$$\begin{aligned}B_y &= \sum_{m,n} \cos(mk_x x)\cosh(k_{ymn} y)\,(C_{mn} f_n(z) + D_{mn} g_n(z)) \\ B_x &= \sum_{m,n} \frac{mk_x}{k_{ymn}} \sin(mk_x x)\sinh(k_{ymn} y)\,(C_{mn} f_n(z) + D_{mn} g_n(z)) \\ B_z &= \sum_{m,n} \frac{nk_z}{k_{ymn}} \cos(mk_x x)\sinh(k_{ymn} y)\,(C_{mn} g_n(z) + D_{mn} f_n(z)).\end{aligned} \tag{5}$$

* gabriel.ascencao@lnls.br

Content from this work may be used under the terms of the CC BY 4.0 licence (© 2026). Any distribution of this work must maintain attribution to the author(s), title of the work, publisher, and DOI.

ISBN: 978-3-95450-252-3 ISSN: 2673-5350 doi: 10.18429/JACoW-IPAC2026-THP5321

CORRECTION OF THE PATH-LENGTH COORDINATE IN TRACKCPP FOR ACCURATE LONGITUDINAL TRACKING

V. D. de Souza*[1], F. H. de Sá, M. M. S. Velloso[1], X. R. Resende
Brazilian Synchrotron Light Laboratory, Campinas, Brazil
[1]also at Gleb Wataghin Institute of Physics, University of Campinas, Campinas, Brazil

Abstract

The Trackcpp application, developed by the Accelerator Physics Group at the Brazilian Synchrotron Light Laboratory, models synchrotron accelerators and beam transport lines to perform six-dimensional particle tracking and optics calculations. The path-length, one of the coordinates, measures the difference between a particle's arrival time, in units of length, and the accelerator cumulative length. This variable is therefore fundamental for describing the interaction of radio-frequency cavities and particles. However, the current implementation leads to limitations when simulating the longitudinal motion in accelerators that operate with non-nominal rf-frequency. This work proposes a modification to the path-length variable that enables accurate longitudinal tracking at arbitrary rf-frequencies.

THEORETICAL BACKGROUND

Computational tools for modeling and simulating particle dynamics are essential for the design, optimization, and operation of particle accelerators. At the Brazilian Synchrotron Light Laboratory (LNLS), the Accelerator Physics Group (FAC) has developed a suite of packages for modeling the SIRIUS light source complex [1]. At the core of these tools is Trackcpp [2], a C++ application that simulates particle tracking in a six-dimensional (6D) coordinate system [3] with symplectic transfer maps based on pass-methods from version 1.3 of the *Accelerator Toolbox* [4]. The 6D state of a particle is

$$\mathbf{x} = (x,\ p_x,\ y,\ p_y,\ \delta,\ z)^T, \tag{1}$$

where x and y are the transverse displacements, p_x and p_y are the normalized transverse momenta, $\delta = (E - E_0)/E_0$ is the relative energy deviation, and z is the path-length deviation.

The equations of motion for a charged particle in an accelerator are derived from a Hamiltonian formulation in which the independent variable is the arc length, s, along a reference orbit rather than time t [3, 5–7]. Within this formalism, the path-length deviation is defined via a canonical transformation that replaces the time t and its canonical momentum by the path-length and the energy deviations [5, 6]:

$$F_2(t, \delta) = \left(\frac{s}{\beta_0} - ct\right)\left(\frac{1}{\beta_0} + \delta\right), \tag{2}$$

which yields

$$z = \frac{\partial F_2}{\partial \delta} = \frac{s}{\beta_0} - ct, \tag{3}$$

where $\beta_0 = v_0/c$ is the relativistic velocity factor and c is the speed of light.

This definition works well when the Hamiltonian is time-independent. When time-dependent components are present, such as the rf-cavities, only keeping track of the z coordinate may lead to loss of information. Considering the model of the cavity gap-voltage is $V_g \sin(2\pi f_{\mathrm{rf}} t)$, the phase advance over successive turns in the ring is given by:

$$\phi_n = 2\pi f_{\mathrm{rf}}\,(t_{n+1} - t_n) = 2\pi f_{\mathrm{rf}}\left(\frac{L_0}{\beta_0 c} - \frac{z_{n+1} - z_n}{c}\right) \tag{4}$$

where L_0 is the ring circumference, n is the turn number and we considered $s_{n+1} = s_n + L_0$.

If f_{rf} is equal to the nominal rf-frequency, defined by:

$$f_{\mathrm{rf},0} = \frac{h\,\beta_0\,c}{L_0}, \tag{5}$$

where h is the harmonic number, the first term on the r.h.s. of Eq. (4) reduces to $2\pi h$, which means that the z coordinate can replace t in the argument of the sin function without loss of generality. This is a common approach in modern tracking codes [4, 8]. However, if the accelerator operates at a de-tuned frequency $f_{\mathrm{rf}} = f_{\mathrm{rf},0} + \Delta f$, the phase advance per-turn gains an additional factor, $\Delta\phi$, given by

$$\frac{\Delta\phi}{2\pi} = \Delta f\,\frac{L_0}{\beta_0 c} = -\frac{f_{\mathrm{rf}}}{\beta_0 c}\Lambda, \tag{6}$$

where Λ is the phase slip correction factor in units of traveled distance, given by

$$\Lambda = L_0\left(\frac{f_{\mathrm{rf},0}}{f_{\mathrm{rf}}} - 1\right). \tag{7}$$

This factor has to be taken into account during tracking to correctly reproduce the dynamics.

There are several ways to deal with this issue: one can keep track of the time of flight, as is done in *Elegant* [9], or, as implemented in new versions of the *Accelerator Toolbox* [10], the cavity pass-method can include a turn-dependent phase, $n\Delta\phi_0$. The main drawback of these methods is that the argument of the sin function increases indefinitely with the turn number, which causes loss of precision when tracking for a few thousand turns[1].

* vitor.souza@lnls.br

[1] To avoid this problem, in Elegant is possible to change the the time-of-flight of the particles at the cavity with the lowest rf-frequency, so that the integer part of the phase is subtracted from the particle's variable. See Ref. [11] for more details.

Content from this work may be used under the terms of the CC BY 4.0 licence (© 2026). Any distribution of this work must maintain attribution to the author(s), title of the work, publisher, and DOI.

ISBN: 978-3-95450-252-3 ISSN: 2673-5350 doi: 10.18429/JACoW-IPAC2026-THP5322

EXACT SOLUTION OF DUAL HARMONIC MOTION

S. Koscielniak*, TRIUMF, Vancouver, Canada

Abstract

The pendulum equation is the archetype for longitudinal motion within an RF bucket. The restoring force is sinusoidal. The case that the confining potential is composed of fundamental and second harmonic is called "dual harmonic". The solution to the pendulum equation of motion in terms of Jacobi elliptic functions is well known, for 140 years. The solution to the dual harmonic equation, also in terms of elliptic functions, is almost unknown. Here we present the solutions for confined and unbounded motion, with almost arbitrary ratio of the two harmonics. The oscillation frequency as a function of oscillation amplitude is a collateral prediction.

INTRODUCTION

Let t, x and $p = \dot{x}$ be time, position and momentum; and dots denote time derivatives ($dx/dt \equiv \dot{x}$). This article concerns the motion of a particle having the equation of motion $\ddot{x} + \omega^2 F(x) = 0$. The force law $F(x)$ and potential function $U(x)$, respectively, are

$$\begin{aligned} F(x) &= \sin x + q \sin 2x \\ U(x) &= [1 - \cos x] + (q/2)[1 - \cos 2x]\,. \end{aligned} \tag{1}$$

q is the ratio of harmonic amplitudes. Positive ratio $q > 0$ increases the restoring force yielding the bunch shortening mode. Negative ratio $q < 0$ reduces the restoring force, providing the bunch lengthening mode. Ensembles of particles that homogeneously populate equi-density contours of the corresponding Hamiltonian $H(x, \dot{x})$, constitute bunches. The nature of the fixed points changes abruptly at $|q| = 1/2$. For $|q| < 1/2$, there is a single well with stable fixed point (SFP) at $x = 0$ and unstable fixed points (UFP) at $x = \pm\pi$. For $|q| > 1/2$, a second, local well emerges; and the nature of the fixed points (FPs) change. For the bunch lengthening case, $q = -1$, Shaposhnikova wrote a solution for the motion in the dual-harmonic well and used it as basis for the calculation of the beam transfer function [1]. In Oct/Nov 2023 Koscielniak obtained the solution for $q = +1$, and in Jan/Feb 2024 extended the method to arbitrary q. A comprehensive investigation is reported in Ref. [2].

Basic Properties of Jacobi Elliptic Functions

The elliptic functions may be defined either by differential equations or as the inverse of incomplete integrals. There are four sets of 3 functions, giving a total of twelve. However, the properties of all may be derived from the principal set: cn, sn, dn. Each function has two arguments (z, m); z is the phase in radian, and m is the Jacobi parameter. $k = \sqrt{m}$ is called the elliptic modulus. The Jacobi elliptic functions are solutions of the system of equations and initial conditions

$$\dot{X} = Y\,Z, \qquad \dot{Y} = -Z\,X, \qquad \dot{Z} = -m\,X\,Y\,. \tag{2}$$

$$\mathrm{sn}(0, m) = X(0) = 0, \quad \mathrm{cn}(0, m) = Y(0) = 1 \tag{3}$$

and $\mathrm{dn}(0, m) = Z(0) = 1$.

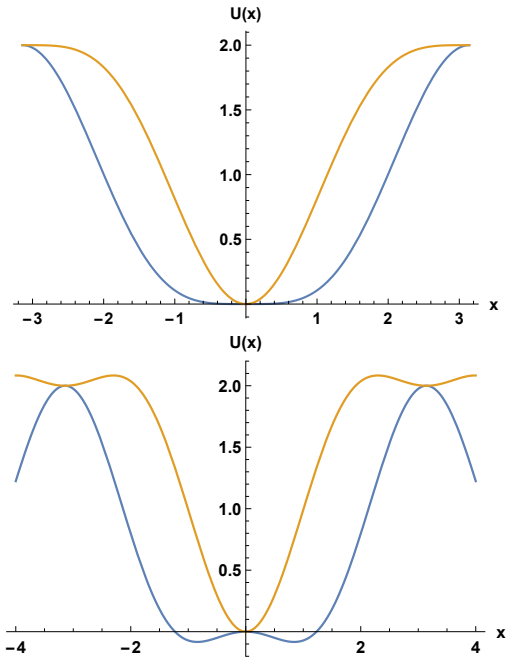

Figure 1: Potential $U(x)$ versus position x. Upper: $|q| = 1/2$. Lower: $|q| = 3/4$. Negative and positive q shown blue and yellow, respectively.

DUAL HARMONIC WELL

We write the potential function in terms of $x/2$; leading to the Hamiltonian:

$$\begin{aligned} 2J\omega^2 &= \omega^2 U(x) + (1/2)(\dot{x})^2 \\ U(x) &= 2[\sin(x/2)]^2 \left\{1 + 2q - 2q[\sin(x/2)]^2\right\}\,. \end{aligned} \tag{4}$$

The solution is of the form:

$$\sin[x(t)/2] = Y(t)/\sqrt{1 - X^2(t)}. \tag{5}$$

Substitution into the Hamiltonian yields: $2J\omega^2 =$

$$2\omega^2 Y^2 \left[\frac{(1+2q)}{B} - 2q\frac{Y^2}{B^2}\right] + 2\frac{[B\dot{Y} + Y\,X\,\dot{X}]^2}{A\,B^2}\,. \tag{6}$$

$$A = (1 - Y^2 - X^2)\,, \quad B = (1 - X^2)\,. \tag{7}$$

We substitute the explicit functions

$$Y = \sqrt{r}\,\mathrm{cn}(at, m) \quad \text{and} \quad X = \sqrt{p}\,\mathrm{sn}(at, m) \tag{8}$$

where a, r, p, m, J are adjustable constants; leading to a cubic equation in powers of $[\mathrm{sn}(at, m)]^2$. The coefficients of

* shane@triumf.ca

Content from this work may be used under the terms of the CC BY 4.0 licence (© 2026). Any distribution of this work must maintain attribution to the author(s), title of the work, publisher, and DOI.

ISBN: 978-3-95450-252-3 ISSN: 2673-5350 doi: 10.18429/JACoW-IPAC2026-THP5325

SCIBMAD: A DIFFERENTIABLE, GPU-PARALLELIZED SOFTWARE LIBRARY FOR PARTICLE ACCELERATOR DESIGN, NONLINEAR ANALYSIS, AND MACHINE LEARNING*

M. G. Signorelli†[1], J. P. Devlin[2], G. H. Hoffstaetter[1,2], D. Sagan[2]
[1]Brookhaven National Laboratory, Upton, NY, USA
[2]CLASSE, Cornell University, Ithaca, NY, USA

Content from this work may be used under the terms of the CC BY 4.0 licence (© 2026). Any distribution of this work must maintain attribution to the author(s), title of the work, publisher, and DOI.

Abstract

We present SciBmad, a new accelerator physics software library developed to meet the needs of all accelerator design, analysis, and virtual modeling. SciBmad consists of a set of modular packages featuring fully differentiable and CPU/GPU-parallelized symplectic integrators, spin tracking and radiation, flexible and differentiable lattice definitions, nonlinear normal form analysis tools with Lie algebraic methods, batch parameter parallelization, and more. It is fully usable in Julia and easily callable from Python, making it easy to integrate it with external optimizers and machine learning frameworks. All releases of SciBmad undergo rigorous, automated testing with maximal code coverage, and all integrators are validated against PTC. With a growing list of features and contributors, SciBmad aims to be a powerful tool for any accelerator physics application.

INTRODUCTION

Since the dawn of the computer, the world has had no shortage of accelerator physics codes: from way back to SYNCH and RACETRACK [1], to the early differentiable codes COSY-INFINITY and the Polymorphic Tracking Code (PTC) [2–4], up to more recent frameworks such as MAD-NG, Xsuite, and Cheetah [5–7]. Many of them, at least implicitly, put some claim to being the "best". In this paper, we will follow this time-honored tradition, and provide the world with yet another accelerator physics code, which we also feel, in our clearly unbiased opinion, is the "best". We leave it up to you, dear reader, to decide.

It goes without saying that all of these softwares have pioneered new and useful features. Many machines have been designed and commissioned using all combinations of them. With 50+ years of codes, accumulated experience, and theory, the needed features of an accelerator physics code are, to a degree, understood now; standing on the shoulders of giants, a wishlist for a "dream" code might be:

- ❏ Natural syntax and easy to use in high-level programming languages (e.g. Python or Julia)
- ❏ Flexible accelerator lattice definitions including arbitrary parameter interdependencies
- ❏ Super fast (CPU/GPU parallelized) 6D symplectic, nonparaxial particle tracking including spin and radiation
- ❏ CPU/GPU parallelization over different lattices
- ❏ Fully forwards-/backwards-/Taylor differentiable to extract gradients w.r.t. anything for optimization/analysis
- ❏ Nonlinear parametric normal form analysis tools
- ❏ Modular and easy to integrate with other programs, optimizers, machine learning frameworks, etc

While many existing accelerator physics codes excel at various subsets of these, to our knowledge none simultaneously satisfy all. With the Electron-Ion Collider (EIC) design at Brookhaven National Laboratory progressing rapidly, the need to do so has only grown. To that end, inspired by all codes past and present, we introduce SciBmad.

SCIBMAD

SciBmad is a new accelerator physics software library that, in the spirit of classical Bmad [8], consists of a set of modular packages currently including:

1. **BeamTracking.jl:** Universally polymorphic/differentiable, parallelized integrators for simulating charged particles on the CPU and various GPUs (NVIDIA CUDA, Apple Metal, Intel oneAPI, and AMD ROCm)
2. **Beamlines.jl:** Fast, differentiable, and fully-featured accelerator lattice definitions and deferred expressions
3. **NonlinearNormalForm.jl:** Perturbation theory of differential-algebraic maps, including spin and damping, using Lie algebraic methods [9, 10]
4. **GTPSA.jl** Fast high-order automatic differentiation using the Generalised Truncated Power Series Algebra (GTPSA) library in MAD-NG [5, 11, 12]
5. **FundamentalFrequencies.jl:** GPU-batchable numerical analysis of fundamental frequencies [13]
6. **AtomicAndPhysicalConstants.jl:** Physical constants and properties for any atomic or subatomic particle

* Work supported by the U.S. Department of Energy under Contracts No. DE-SC0012704 (Brookhaven Science Associates, LLC) and No. 89233218CNA000001 (Office of Science, ARDAP), and by resources of the National Energy Research Scientific Computing Center, a DOE Office of Science User Facility, under award HEP-ERCAP0034811.

† msignorel@bnl.gov

ISBN: 978-3-95450-252-3 ISSN: 2673-5350 doi: 10.18429/JACoW-IPAC2026-THP5327

STUDIES OF MAGNETS MISALIGNMENT IN RING-BASED ELECTRON COOLER

J. Unger*, G. Hoffstaetter, Cornell University (CLASSE), Ithaca, NY, USA
A. Fedotov, J. Kewisch, S. Seletskiy, Brookhaven National Laboratory, Upton, NY, USA

Abstract

Performance of Electron Ion Collider (EIC) will benefit from cooling of protons at the highest collision energy (γ=294). The required cooling can be provided by the Ring Electron Cooler (REC) – a non-magnetized RF-based electron cooler, employing an electron storage ring. The REC is a "racetrack" consisting of a 170 m long cooling section (CS), a wiggler section opposing the CS and containing eighteen 2.4 T damping wigglers with highly nonlinear field profile, and two matching arcs. The REC utilizes an elaborate correction scheme to achieve the target dynamic aperture (DA) in the baseline lattice. Alignment errors in magnet placement will be present in a constructed ring and will disrupt the DA correction scheme. In this paper, we describe studies of alignment errors, their effect on the dynamic aperture, define tolerances to various misalignments and propose a procedure for misalignment correction.

INTRODUCTION

To achieve high luminosity, the Electron-Ion Collider's (EIC) Hadron Storage Ring must mitigate emittance growth driven by intra-beam scattering (IBS). At the highest collision energies ($\gamma \approx 294$ for protons), a proposed solution is the Ring Electron Cooler (REC): a non-magnetized, RF-based electron cooling cooler [1] featuring a dedicated electron storage ring [2]. The REC lattice integrates of a 170 m cooling section, a damping wiggler section containing eighteen 2.4 T wigglers, and two matching arcs. The strong nonlinearities introduced by the wigglers require careful optimization of the dynamic aperture (DA).

Previous studies of the REC lattice demonstrated that the baseline optics and correction schemes are capable of achieving the required DA under ideal conditions [3]. In a realistic machine, however, construction and installation tolerances will introduce magnet misalignments that perturb the closed orbit, modify the optics, and potentially reduce the DA below acceptable levels. In particular, the REC lattice is highly sensitive to orbit distortions in the wiggler section, where increased dispersion and betatron oscillations pose a risk of increasing the electron beam emittance and degrade cooling performance.

In this paper, we study the effects of magnet alignment errors on the REC dynamic aperture and emittance. Translation and tilt errors for all major magnet families are investigated to establish alignment tolerances. Orbit correction schemes utilizing beam position monitors (BPMs) and corrector kickers are then evaluated to determine their effectiveness in restoring acceptable machine performance under realistic error conditions. Finally, the resulting emittance growth, including the effects of IBS and beam-beam scattering (BBS), is examined.

ALIGNMENT ERRORS

Initially, all magnet types were tested for different rms translation errors and rms tilts about the longitudinal axis to meet the criteria of meeting the DA goal in 50% of ran error seeds, with the number of seeds chosen at 1000. No orbit, tune, or other correction was applied at this stage and all combinations of magnet and error type were run individually. Quadrupoles were further split, showing the quadrupoles near the cooling section to be more sensitive than those in the arcs or wiggler section These results are used to inform relative tolerances of magnet types when combined with each other and correction and are shown in Table 1.

Table 1: Tolerances for individual magnet type translations and tilts without orbit correction. Used as baseline for magnet sensitivity to errors.

Magnet type	Translations	Tilts
Wiggler	10 µm	0.5 mrad
Sextupole	100 µm	>25 mrad
Dipole	500 µm	0.5 mrad
Quadrupole	5 µm	1 mrad

ORBIT CORRECTION

Translations and tilts in wigglers and dipoles could largely be corrected by the two sets of BPMs and correctors on either side of each magnet. Quadrupole translation errors have the strictest tolerances of all magnet types, but as mentioned previously, this could be partially mitigated by a determination of which quadrupoles have the largest contribution to the reduction of DA. Sextupole tolerances are large compared to other magnet types and do not present any particular concerns.

The orbit correction scheme chosen for this study, while including translation errors for all magnet types, uses a BPM and a dual-plane corrector kicker at each quadrupole. An RMS BPM error also assumed during orbit correction. The splitting of errors between magnet types after correction are placed in Table 2, and are chosen to keep >90% of runs above 5σ. This was achieved with BPM errors of 5 µm or 10 µm and shown in Figs. 1 and 2.

A potential concern in this orbit correction scheme is the placement of a kicker and BPM at each quadrupole is difficult to obtain in the arcs, where the separation between quadrupole and dipole magnets in the current lattice is 10cm.

* jeu8@cornell.edu

Content from this work may be used under the terms of the CC BY 4.0 licence (© 2026). Any distribution of this work must maintain attribution to the author(s), title of the work, publisher, and DOI.

ISBN: 978-3-95450-252-3 ISSN: 2673-5350 doi: 10.18429/JACoW-IPAC2026-THP5328

SPACE CHARGE DYNAMICS IN RING-BASED ELECTRON COOLER

J. Unger*, G. Hoffstaetter, Cornell University (CLASSE), Ithaca, New York, United States
A. Fedotov, J. Kewisch, S. Seletskiy, Brookhaven National Laboratory, Upton, United States

Abstract

The Ring Electron Cooler (REC) is designed to provide cooling to 275 GeV protons at Electron Ion Collider (EIC). The REC is a non-magnetized RF-based electron cooler employing a 150 MeV electron storage ring. Electron bunches of 21 nC are needed to achieve cooling rates required by EIC. The tune shift in the electron storage ring induced by e-bunch space charge (SC) is ≈0.14 in both planes. This paper investigates the SC-driven beam dynamics in the REC, the resulting emittance growth, and potential beam loss.

INTRODUCTION

The Ring Electron Cooler (REC), is under design as a possible solution to the cooling need for the Electron Ion Collider's (EIC) Hadron Storage Ring (HSR) at its top energy of 275GeV. In the REC, cooling of the protons is accomplished via electron cooling [1] in a 170m long cooling section where the cooling ring and HSR overlap. The electron current in the REC is maintained by top-up injection of a high charge 21nC bunches. This high charge per bunch, means the space charge will be an important addition to the dynamics, shifting the tune and increasing emittance. As damping the growth from beam-beam scattering and intrabeam scattering is accomplished by a section that contains 18 2.4T wigglers each 4.2m long [2], image currents in this section also have the potential to shift the tune.

Previous estimates of the space charge tune shift indicated a substantial shift of ≈0.14 in both planes. This tune shift gives indication that space charge may be important to beam stability and emittance growth. In this paper, we determine the tune shift achieved in the full lattice through tracking using a Bassetti-Erskine approach and determine the severity of space charge on bunch stability and emittance increase.

TRACKING WITH SPACE CHARGE

Initial estimates of the space charge tune shift from direct space charge, used the first term of the formula [3, 4]

$$\Delta Q_{x,y} = -\frac{Nr_0}{4\pi\beta^2\gamma}\left(\left\langle\frac{\beta_{x,y}}{\sigma_{x,y}\left(\sigma_x+\sigma_y\right)}\right\rangle\frac{\varepsilon_0^{x,y}}{\gamma^2 B_f} + \left\langle\beta_{x,y}\right\rangle\frac{\varepsilon_1^{x,y}}{h^2 B_f} + \left\langle\beta_{x,y}\right\rangle\beta^2\frac{\varepsilon_2^{x,y}}{g^2}\right) \quad (1)$$

where N is the number of particles per bunch, β and γ are the relativistic factors, the ε's are the Laslett coefficients, B_f is a bunching factor, h is the height of the vacuum chamber, and g is the pole gap. Initial estimates used a smooth β approximation for a round beam where $\left\langle\beta_{x,y}\right\rangle = L/\left(2\pi Q_{x,y}\right)$, simplifying the equation to be independent of lattice specific optics. Under this approximation, the tune shift estimate was ≈0.14 in both planes. As an optimized lattice now exists, these estimates can be compared against tracking with space charge.

In order to track the number of turns necessary to collect meaningful data of space charge dynamics, a suitable model must first be chosen. The damping time of the ring is 50,000 turns, meaning that effects from space charge on this order could be important. This time scale makes 3D self-consistent models too time intensive to yield results in a reasonable amount of time, so in this study an approximate model is used that neglects longitudinal kicks and gives a transverse kick that is given by the Bassetti-Erskine formula [5] with properly chosen coefficients

$$K_y + iK_x = \frac{r_e N}{\gamma^3\sigma_z}\exp\left[\frac{-z^2}{2\sigma_z^2}\right]\sqrt{\frac{\sigma_x+\sigma_y}{\sigma_x-\sigma_y}}\left\{\operatorname{erf}\left[\frac{x+iy}{\sqrt{2\left(\sigma_x^2-\sigma_y^2\right)}}\right] - \exp\left[-\frac{x^2}{2\sigma_x^2}-\frac{y^2}{2\sigma_y^2}\right]\operatorname{erf}\left[\frac{x\frac{\sigma_y}{\sigma_x}+iy\frac{\sigma_x}{\sigma_y}}{\sqrt{2\left(\sigma_x^2-\sigma_y^2\right)}}\right]\right\} \quad (2)$$

In order to measure the space charge tune shift in the bunch, a 5000 particle bunch was tracked over 2000 turns using Bmad [6], with the tune of the particles determined by a NAFF algorithm of the final 1000 turns. The space charge model was the before mentioned Bassetti-Esrkine with the assumption of the constant emittance. The result of this tracking was the tune footprint in Fig 1, where it can be seen that the highest shifted particles appear near the estimated tune shift. It can additionally be seen that tune shift sits just past a strong sextupole resonance, with many particles sitting along the resonance line.

While using the assumption of a constant emittance is appropriate for determining the initial tune shift, in order to study long term effects, any change in the size of the beam should be accounted for. This was done by updating the emittance used in the Bassetti-Erskine model every 1000 turns, which was small when compared to multiple damping periods. This changes the space charge kick overtime, and, for a beam with presumably increasing emittance, this will lead to a weakening of the space charge tune shift. This can be seen in Fig. 2 where the core tune shift is plotted over the run.

The effect this has on the full bunch is shown in Fig. 3, where it can be seen that the tune footprint begins to shrink, with particles beginning to leave the region of the sextupole resonance. Despite crossing resonances, increased particle losses in tracking are not observed.

* jeu8@cornell.edu

Content from this work may be used under the terms of the CC BY 4.0 licence (© 2026). Any distribution of this work must maintain attribution to the author(s), title of the work, publisher, and DOI.

ISBN: 978-3-95450-252-3 ISSN: 2673-5350 doi: 10.18429/JACoW-IPAC2026-THP5329

DYNAMIC APERTURE OPTIMIZATION FOR THE RING-BASED ELECTRON COOLER

J. Unger*, G. Hoffstaetter, Cornell University (CLASSE), Ithaca, NY, USA
A. Fedotov, J. Kewisch, S. Seletskiy, Brookhaven National Laboratory, Upton, NY, USA

Abstract

Electron Ion Collider (EIC) will benefit from cooling protons at the highest collision energy (γ=294). The required cooling can be provided by the Ring Electron Cooler (REC) - an RF-based non-magnetized electron cooler employing an electron storage ring. As stored electrons cool the EIC protons, their emittance is gradually increased by both the intra-beam and beam-beam scattering. To counteract the heating of electron bunches, eighteen dedicated damping wigglers are utilized. These wigglers require substantially non-linear field with peak value of 2.4 T, occupy a large portion of the electron storage ring, and dominate beam dynamics in the REC. In this paper we describe our approach to maximizing dynamic aperture in the REC, which includes careful optimization of wigglers parameters and development of an elaborate correction scheme for non-linear beam dynamics.

INTRODUCTION

The Ring Electron Cooler (REC), is under design as a possible solution to the cooling need for the Electron Ion Collider's (EIC) Hadron Storage Ring (HSR) at its top energy of 275GeV.

In order to counteract emittance growth in the HSR, the REC design uses electron cooling [1] with a multi-turn ring. The electron bunches will be reused for cooling on many turns. To counteract the growth of electrons emittance and energy spread, caused by intra-beam scattering (IBS) and proton-electron beam-beam scattering, substantial radiation damping is needed. The cooling of electrons through radiation damping is facilitated by dedicated wigglers, with the parameters important for cooling and dynamic aperture shown in Table 1.

The wiggler section contains 18 wigglers alternating with short sections housing quadrupoles and sextupoles. These are arranged in 17 alternating wiggler blocks. Each of these wigglers have a 2.4T main field and are 4.2m long, and are responsible for the majority of the electron damping [2].

Another consideration in a ring based cooler is the need to maintain a dynamic aperture sufficient to obtain the beam lifetime needed for the desired cooling. This was determined to lead to a requirement of 5σ for the transverse and momentum apertures.

LATTICE OVERVIEW

The REC layout is shown in Fig. 1. It has a trapezoidal shape, with the wiggler section opposing the 170-meter-long cooling section (CS). The arcs connecting the CD and wigglers contain 10-meter-long straight sections that house the RF and injection systems.

Table 1: Baseline Parameters

N_e	$1.3{\cdot}10^{11}$
Relativistic γ	293
Total length [m]	426
Cooling section length [m]	170
Cooling section η_x [cm]	100
Cooling section $\beta^*_{x,y}$ [m]	180, 160
Number of wigglers	18
Wiggler length [m]	4.2
Wiggler field [T]	2.4
RF frequency [MHz]	98
RF voltage [kV]	2.1
Emittance (x,y) [nm]	7.8, 7.8
Fractional tune (x,y)	0.16, 0.15
Space charge tune shift (x,y)	0.08, 0.12

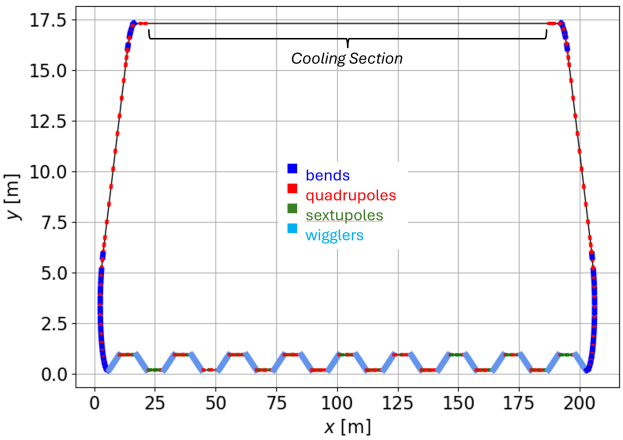

Figure 1: REC floor plan.

In order to reduce emittance growth due to IBS, the $\mathcal{H}$ inside the wiggler must be minimized:

$$\mathcal{H}_x = \gamma_x \eta_x^2 + 2\alpha_x \eta_x \eta_x' + \beta_x \eta_x'^2 \quad (1)$$

Inside the wigglers, the periodic dispersion is small, leading to the first term in $\mathcal{H}_x$ to have small contribution. The derivative of dispersion (η_x') is large in the wigglers, leading to the need to reduce β_x. This is accomplished by adding horizontal focusing in the wigglers, resulting in the optics in Fig. 2. Large β-function is desirable in the cooling section to boost cooling, leading the overall optics in Fig. 3

There are multiple choices of wiggler fields that can achieve similar focusing, however the non-linear effects of these fields on dynamic aperture can vary significantly. The

* jeu8@cornell.edu

Content from this work may be used under the terms of the CC BY 4.0 licence (© 2026). Any distribution of this work must maintain attribution to the author(s), title of the work, publisher, and DOI.

ISBN: 978-3-95450-252-3 ISSN: 2673-5350 doi: 10.18429/JACoW-IPAC2026-THP5333

MULTI-PARAMETER MITIGATION OF CSR-INDUCED EMITTANCE GROWTH IN 3D BEAMS

O. H. Ramachandran[1,2*], G. Ha[1,2], C.-K. Huang[3], X. Lu[1,2], J. Power[2], J. Qiang[4]
[1]Northern Illinois University, DeKalb, IL, USA
[2]Argonne National Laboratory, Lemont, IL, USA
[3]Los Alamos National Laboratory, Los Alamos, NM, USA
[4]Lawrence Berkeley National Laboratory, Berkeley, CA, USA

Abstract

Phase space degradation due to Coherent Synchrotron Radiation (CSR) presents a significant challenge in the generation of high-brightness electron beams. In this work, we use a new 3D CSR code, currently in development, to understand the combined effect of longitudinal profile shaping and shielding in beams of large transverse size. Our results indicate that longitudinal profile shaping alone produces modest improvements in the high-Derbenev regime, while the addition of shielding walls preserves the level of improvement achievable in the 1D limit, even at gap sizes significantly larger than the conventional shielding threshold for a Gaussian beam.

INTRODUCTION

Collective effects such as Coherent Synchrotron Radiation (CSR) within a compressed electron bunch place stringent limits on the achievable beam brightness in X-ray free-electron laser (FEL) facilities and linear colliders. As a short, high-intensity bunch propagates through the bends of a magnetic bunch compressor, the tail-head CSR interaction induces correlated energy changes along the bunch, leading to increased projected transverse emittance [1] and the seeding of microbunching instabilities [2].

Several mitigation strategies have been explored. Shielding the bend magnets with parallel conducting plates reduces the long-range CSR interaction and has been demonstrated experimentally to suppress CSR-induced energy spread [3]. Tuning the optical lattice can cancel the emittance growth through careful design of the dispersion function [4]. Longitudinal profile shaping — preparing the initial current profile so that the integrated CSR wake is uniform along the bunch — was proposed in [5] and demonstrated to reduce emittance growth by more than an order of magnitude in the 1D limit. This result was further updated in [6] through a multi-parameter optimization study that also included shielding walls placed at gap sizes larger than $(R\sigma_z^2)^{1/3}$, the threshold at which shielding can independently mitigate energy spread for a Gaussian bunch.

The accuracy of 1D CSR models depends critically on the Derbenev parameter

$$\kappa = \frac{\sigma_x}{\sigma_z}\left(\frac{\sigma_z}{R}\right)^{1/3}, \tag{1}$$

which characterizes the relative importance of the transverse beam structure on the CSR interaction. For $\kappa \ll 1$ the 1D approximation holds; for $\kappa \gtrsim 1$ the transverse variation of the wake plays a significant role and cannot be compensated by longitudinal shaping alone. As a result, there is a gap in the literature in understanding the effects of profile shaping, particularly in conjunction with shielding for beams of large transverse size. In the rest of this work, we show preliminary profile shaping results for beams of high κ and explore its effectiveness in minimizing CSR induced energy spread.

NUMERICAL FORMULATION

The radiated electric and magnetic fields at any point in space and time are computed following Jefimenko's equations:

$$\mathbf{E}(\mathbf{r},t) = \frac{1}{4\pi\epsilon_0}\int d\mathbf{r}'\left[\frac{\mathbf{R}}{|\mathbf{R}|^3}\rho_r + \frac{\mathbf{R}}{c|\mathbf{R}|^2}\dot{\rho}_r - \frac{\dot{\mathbf{J}}_r}{c^2|\mathbf{R}|}\right], \tag{2}$$

$$\mathbf{B}(\mathbf{r},t) = -\frac{\mu_0}{4\pi}\int d\mathbf{r}'\left[\frac{\mathbf{R}\times\mathbf{J}_r}{|\mathbf{R}|^3} + \frac{\mathbf{R}\times\dot{\mathbf{J}}_r}{c|\mathbf{R}|^2}\right], \tag{3}$$

where $\mathbf{R} = \mathbf{r} - \mathbf{r}'$, subscript r denotes evaluation at the retarded time t_r, and the retardation condition $c(t - t_r) = |\mathbf{R}|$ is solved using the algebraic form derived by Cai and Ding [7]:

$$\xi = \alpha - \frac{\beta}{2}\sqrt{\chi^2 + \zeta^2 + 4(1+\chi)\sin^2\alpha}, \tag{4}$$

with $\chi = x/R$, $\zeta = y/R$, $\xi = -\ell/2R$, and α the retarded half-angle. The resulting longitudinal and transverse wake kernels are integrated over α from the magnet entrance to the observation point. Near $\alpha = 0$ the kernel is singular; this is handled by a change of variables $\rho = \alpha^2$ in a small *bubble* region around the singularity, after which standard Gauss quadrature applies throughout. The fields are computed on a moving mesh that follows the bunch, with the fields interpolated onto the particle coordinates at each step. The charge and current densities entering Jefimenko's equations are represented as sums of smooth 3D Gaussian shape functions (although any smooth function will suffice):

$$\rho(\mathbf{r}',t) = Q_b\sum_i w_i S_i(\mathbf{r}'(t)), \tag{5}$$

$$\mathbf{J}(\mathbf{r}',t) = Q_b\frac{\partial\mathbf{r}'(t)}{\partial t}\sum_i w_i S_i(\mathbf{r}'(t)), \tag{6}$$

* oramachandran@anl.gov

Content from this work may be used under the terms of the CC BY 4.0 licence (© 2026). Any distribution of this work must maintain attribution to the author(s), title of the work, publisher, and DOI.

ISBN: 978-3-95450-252-3 ISSN: 2673-5350 doi: 10.18429/JACoW-IPAC2026-THP5335

MAGNETIC FIELD RECONSTRUCTION FROM SPARSE MEASUREMENTS FOR COMPLEX GEOMETRIES*

J. W. Phillips†, B. Naranjo, J. B. Rosenzweig
University of California Los Angeles, United States
P. Alva Rosa, Augsburg University, Minneapolis, United States
J. A. Phillips, MiraCosta College, Oceanside, United States
D. McCormick, D. Storey, J. M. Cruz Jr.
SLAC National Accelerator Laboratory, Menlo Park United States

Abstract

Precise 3D field measurements of large, complex magnet geometries are time-consuming and error-susceptible. For large magnets, it is common to record Hall probe data on a sparse grid, then use an interpolation algorithm to estimate field values at the remaining points. For common magnet geometries, such as quadrupoles and dipoles, linear interpolation often provides accurate results. However, for complex magnet geometries, this method can yield lower accuracy. In this paper, we present a method based on a locally Maxwell-consistent algorithm for sparse Hall probe measurements. Through the k-nearest neighbors algorithm, we locally fit the magnetic field with Tikhonov regularization. We test this method on a novel Compton spectrometer, capable of measuring single-shot, double-differential, energy-angle gamma spectra, ranging from 180 keV to 28 MeV. Using held-out validation, we demonstrate that we can reconstruct its magnetic fields with higher accuracy than linear interpolation and radial basis function (RBF) interpolation with cubic, thin plate spline, and quintic kernels. We also analyze the dependence of point sparsity on accuracy.

INTRODUCTION

Magnets are ubiquitous in particle accelerators, serving to focus beams, correct aberrations, and analyze particle energies. Precise field characterization is essential for beam-transport simulations and magnet evaluation [1]. Common methods of characterizing magnetic fields are Hall probe and rotating coil measurements [2]. These procedures take long periods of time, limiting grid fineness over large volumes; the magnetic field must then be reconstructed in the regions between the measured points through interpolation. For conventional magnet geometries with dominant multipole fields, there exist analytic models that can be used for a full 3D reconstruction [3]. Achieving an accurate reconstruction through global fitting can be difficult, however, for complex geometries. Alternatively, common interpolation methods like linear and radial basis function (RBF) interpolation can be used; however, they do not automatically enforce Maxwell's equations, resulting in potentially non-physical results. There exist more sophisticated methods that enforce Maxwell's equations, including Gaussian process regression with Maxwell-consistent kernels [4, 5], utilization of a harmonic basis [6–8], and other divergence-free approaches [9–11]. However, each of these methods is limited by computational expense, regular grid requirements, incomplete Maxwell enforcement, or incompatibility with Hall probe measurements.

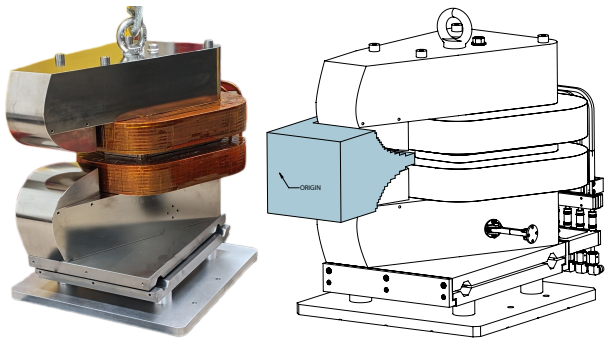

Figure 1: The left image shows CPT, the gamma spectrometer built at UCLA. The filled-in region on the right drawing illustrates the magnetic field measurement volume.

At the University of California, Los Angeles (UCLA), we are building a broadband Compton spectrometer, dubbed CPT, for installation at FACET-II SLAC National Laboratory as shown in Fig. 1 [12–14]. Its complex geometry requires a precise 3D field map, motivating our development of a simple yet accurate method for magnetic field reconstruction that is effective on sparse measurements. We find the nearest k points using a k-nearest neighbors (KNN) search. We then use Tikhonov regularized least squares to locally fit a harmonic polynomial expansion to the measured field values in that neighborhood. Since the harmonic polynomial basis functions are solutions to Laplace's equation by construction, the reconstructed field is locally Maxwell-consistent.

Using held-out validation, we apply this method to Hall probe measurements of CPT. Next, we compare to linear and RBF interpolation with various kernels. We then demonstrate how the interpolation accuracy degrades with sparsity.

A NOVEL COMPTON SPECTROMETER

CPT is a single-shot, double-differential, energy-angle gamma spectrometer capable of measuring energy from 180 keV to 28 MeV. Incident photons Compton scatter off a beryllium wire, resulting in Compton electrons. These elec-

* The authors thank the Tigner Traineeship in Accelerator Science, DOE award DE-SC0024907, and the US Department of Energy, under Contract No. DE-SC0009914.

† jphillips@physics.ucla.edu

Content from this work may be used under the terms of the CC BY 4.0 licence (© 2026). Any distribution of this work must maintain attribution to the author(s), title of the work, publisher, and DOI.

ISBN: 978-3-95450-252-3 ISSN: 2673-5350 doi: 10.18429/JACoW-IPAC2026-THP5337

LCLS-II GUN FPC WINDOW MP ANALYSIS

L. Xiao†, A. Haase, F. Zhou, SLAC National Accelerator Laboratory, Menlo Park, CA, USA
T. Luo, Lawrence Berkeley National Laboratory, Berkeley, CA, USA

Abstract

The RF analysis of the LCLS-II Gun fundamental power coupler (FPC), including the ceramic window, has been analyzed using SLAC-developed 3D parallel finite-element electromagnetic code suite, ACE3P. Comprehensive multipacting (MP) simulations were carried out to investigate potential discharge regions within the FPC coaxial line and window assembly. The results reveal strong two-point MP between the ceramic disk and the window shielding sleeve at specific input power levels. In addition, the studies show that the external magnets mounted on the two FPC arms can only provide localized suppression of MP within regions influenced by their fringe magnetic fields. Therefore, effective MP mitigation in the LCLS-II FPC relies primarily on TiN coatings applied to the coaxial copper surfaces and ceramic disk, which reduce their secondary electron yield (SEY) below unity. Detailed analysis and findings from the LCLS-II Gun FPC MP simulations are presented.

INTRODUCTION

Since 2023, the SLAC Linac Coherent Light Source II (LCLS-II) has been in operation, with its photoinjector delivering a low-emittance beam at a high repetition rate [1]. The LCLS-II photoinjector uses a normal conducting RF gun (Fig. 1) operating at 186 MHz in continuous wave (CW) mode.

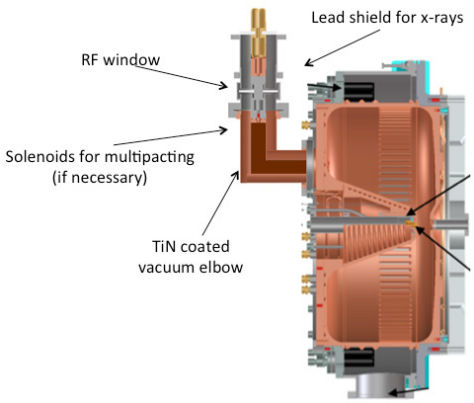

Figure 1: Cross-section of LCLS-II RF gun.

An elbow in the FPC prevents emitted particles from the cavity from reaching and striking the window. The FPC assembly uses the Toshiba Type No. 4278 S coaxial ceramic window, originally designed for the SNS SRF cavity. It transmits up to 1000 kW peak power at 805 MHz and 60 kW average power. Vacuum leaks have occurred in the FPC windows during operation, requiring replacement. The reasons for these failures remain unknown.

This paper uses SLAC's ACE3P code suite [2] to study multipacting (MP) in the LCLS-II RF Gun FPC window. MP happens in the FPC coaxial line, as well as between the ceramic disk and shielding sleeve at specific input powers. Magnets on the FPC elbow arms suppress MP in regions with sufficiently strong magnetic fields. No DC bias or solenoid is present near the FPC window. Consequently, efficient mitigation of MP in the LCLS-II FPC primarily depends on the application of TiN coatings to the coaxial copper surfaces and ceramic disk, which serve to reduce their secondary electron yield (SEY) to below unity. Further details are provided in the following sections.

RF SIMULATIONS

For RF simulation, half of the LCLS-II Gun (Fig. 2) is modelled due to two symmetric coaxial FPC couplers on the cathode plate. Coupling is set by adjusting the antenna loop angle; in this simulation, it is 70 degrees for critical coupling.

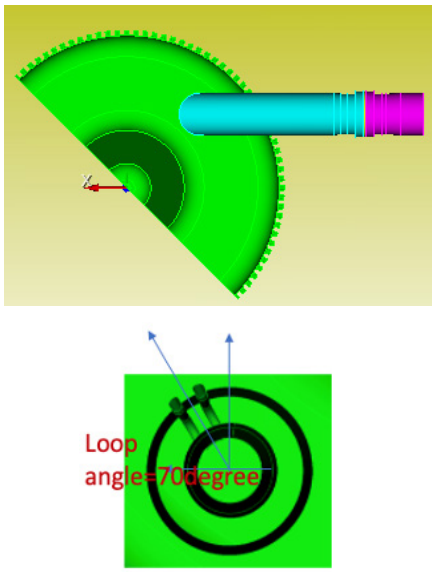

Figure 2: A half of LCLS-II RF gun simulation model (up) and a close-up of the coupling loop geometry (down).

The ACE3P S-Parameters solver, S3P, was utilized to stimulate the operating mode of the LCLS-II RF Gun. Figure 3 presents the reflection coefficient as a function of frequency, alongside the resonant mode electrical fields at 186.603 MHz, based on an input power of 1 W per coupler. The simulated reflection coefficient at resonance is 0.06; this value may be further reduced through optimization of

†liling@slac.stanford.edu

Content from this work may be used under the terms of the CC BY 4.0 licence (© 2026). Any distribution of this work must maintain attribution to the author(s), title of the work, publisher, and DOI.

ISBN: 978-3-95450-252-3 ISSN: 2673-5350 doi: 10.18429/JACoW-IPAC2026-THP5339

IMPEDANCE ANALYSIS OF LONG VACUUM CHAMBERS VIA LONGITUDINALLY REDUCED GEOMETRIES

I. C. de Almeida, A. P. B. Lima, F. H. de Sá
Brazilian Synchrotron Light Laboratory, Campinas, Brazil

Abstract

Beamlines of modern synchrotron light sources demand the installation of long undulators with small gaps in the storage ring. The vacuum chamber of these devices requires time-consuming wakefield simulations for impedance estimation. Furthermore, these structures can exhibit trapped modes, demanding extensive eigenmode simulations for impedance characterization. This paper presents a method to estimate a conservative impedance envelope for trapped modes from a longitudinally reduced geometry, reducing both computational time and numerical artifacts inherent to long simulations. The proposed methodology is validated through the impedance analysis of the APPLE-2 undulator for the SIRIUS IPE beamline.

INTRODUCTION

Modern light sources demand long insertion devices with small gaps to achieve stronger magnetic fields and improved photon beam properties. These chambers might present a large horizontal aperture and a small vertical aperture compared to the standard storage ring vacuum chamber. Such geometries can support beam excited trapped modes below the beam pipe cutoff frequency, requiring extensive wakefield and eigenmode simulations for accurate impedance characterization. For long devices, the large number of trapped modes and the computational burden associated with large meshes become a major challenge. This paper therefore presents a method to estimate a conservative impedance envelope for trapped modes using eigenmode simulations of a longitudinally reduced geometry.

To demonstrate this approach, the impedance analysis of the APPLE-2 undulator for the SIRIUS IPE beamline is used as a case study. As shown in Fig. 1, the 3.774 m aluminum straight section of the APPLE-2 undulator previously used at the Swiss Light Source (SLS) has a horizontal aperture of 57 mm and a vertical aperture of 8.3 mm [1]. The copper transitions from the undulator elliptical chamber to the standard 24 mm inner diameter round vacuum chamber of SIRIUS were developed in-house.

The wakefield simulations of the complete geometry of the undulator with the tapered transitions were performed using ECHO3D [2] with a bunch length of 2.5 mm, a mesh step size of 0.5 mm in all three dimensions and a wakelength of 25 m. Figure 2 shows the real part of the vertical dipolar impedance, where numerous vertical dipolar modes were identified to be trapped below the beam pipe TE_{11} mode cutoff of 7.32 GHz. The characterization of these modes through a reduced geometry is discussed in the following sections.

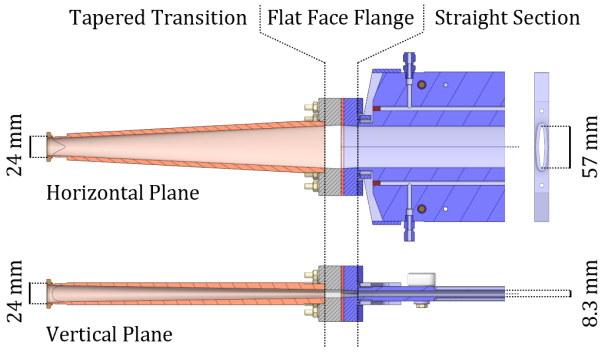

Figure 1: Horizontal and vertical views of a part of the aluminum straight section of the APPLE-2 undulator and one of the copper transitions to the standard 24 mm round vacuum chamber of SIRIUS. The elliptical cross section of the straight section is also shown.

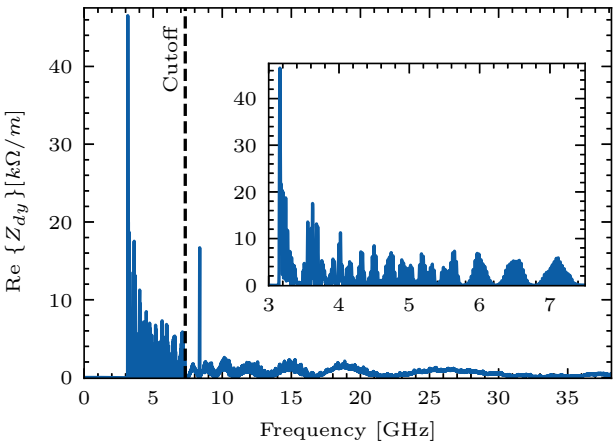

Figure 2: Real part of vertical dipolar impedance obtained from wakefield simulations of the complete undulator chamber. The detail shows the frequency range below the beam pipe cutoff.

EIGENMODE SIMULATIONS

To estimate the vertical dipolar shunt impedance of the trapped modes, the mode frequency, the longitudinal electric field, and the surface integral of the squared magnitude of the tangential magnetic field can be obtained from eigenmode simulations using ANSYS High-Frequency Structure Simulator (HFSS) [3]. Since the transverse electric and magnetic fields are related to the longitudinal electric field through the Panofsky-Wenzel theorem, the vertical dipolar shunt impedance is given by Eq. (1).

Content from this work may be used under the terms of the CC BY 4.0 licence (© 2026). Any distribution of this work must maintain attribution to the author(s), title of the work, publisher, and DOI.

ISBN: 978-3-95450-252-3 ISSN: 2673-5350 doi: 10.18429/JACoW-IPAC2026-THP5344

USING CHROMATICITY TO SUPPRESS INSTABILITIES AT γ_t TRANSITION

M. A. Balcewicz*, J. Eldred, Fermi National Accelerator Laboratory, Batavia, United States

Abstract

For many synchrotrons which cross γ_t transition, a high intensity threshold has been identified beyond which significant beam losses are observed. These losses are due to a high-intensity mode coupling instability, which can be suppressed by adjusting the chromaticity curve to cross zero slightly after γ_t transition.

INTRODUCTION

The Fermilab Booster crosses the transition energy γ_t approximately halfway through the energy ramp. For sufficient bunch intensity when crossing transition large dipole oscillations and losses are observed in the bunch tail. This loss is believed to be due to a beam instability which is excited when synchrotron oscillations slow around γ_t transition. These dipole oscillations are concentrated around the tail of the bunch. Below the loss threshold tail dominated dipole oscillations can be observed using a dipole kicker.

The intensity threshold for losses is above 6.0×10^{12} ppp (particles per pulse, each pulse has 81 bunches). PIP-II and LBNF/DUNE upgrades require 6.7×10^{12} ppp with $\geq 95\%$ of the beam extracted, making it necessary to mitigate this beam instability.

TRANSITION INSTABILITY

The observed high-intensity instability is believed to be a form of Transverse Mode Coupling Instability (TMCI), with the large tail amplitude created by wakes accumulating along the bunch length. This amplitude is partially stabilized by space charge forces. The large tail amplitude is variously understood to be a characteristic of TMCI at very strong space charge [1], the Convective Instability [2], or Beam Break Up [3] occurring much more rapidly than the synchrotron oscillations.

To reach the required intensity it is necessary to minimize growth due to TMCI. At lower intensities, space charge can decouple TMCI modes and stabilize the beam [4]. However, in the limit where $\Delta Q_{sc}/Q_s \rightarrow \infty$, space charge instead makes the instability threshold vanishingly small [1]. Near transition where the synchrotron tune is small, space charge cannot be used to minimize emittance growth. A small nonzero chromaticity can be used to dampen TMCI. However, the beam is unstable to Head-Tail when the effective chromaticity $\xi_{eff} \equiv \xi/\eta < 0$, where ξ is the chromaticity and η is the phase slip factor. Without a γ_t jump system the beam will at least be unstable to TMCI or Head-Tail near transition.

Instabilities do not need to be fully stabilized to avoid particle losses. Instead it is sufficient limit the dipole amplitude such that minimal beam is lost to the aperture. With this objective in mind, the total growth of coherent modes and their respective tail amplification can be optimized and a new working point can be determined for high-intensity operations.

In order to find a new working point, a simulation campaign has been undertaken to better understand the functional dependence of transition crossing instabilities in the Fermilab Booster.

SEMI-ANALYTIC INSTABILITY MODEL

The semi-analytic Multiple Loop Square Well (MLSW) model [5] is used to simulate instabilities over possible transition crossing schemes and determine the coherent modes and growth rates. This model considers linear dynamics with space charge, wakes, synchrotron tune, and chromaticity. Longitudinal coupling is provided by a layered longitudinal phase space within nested square potential wells.

With fully coherent transverse motion, the system determines the tune shift of coherent synchro-betatron modes and their respective dipole amplitudes (the eigenvalues and eigenvectors). By stitching together the solutions at settings across transition it is possible to approximate how coherent modes evolve, but not calculate the relative contribution of each mode.

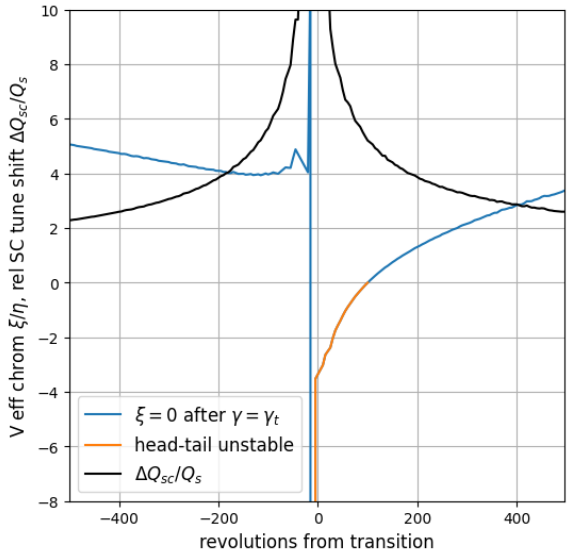

Figure 1: Vertical chromaticity and synchrotron tunes near beam transition. Other parameters can be considered approximately constant within this region. For these settings the vertical chromaticity curve crosses 100 revolutions after transition driving Head-Tail instability.

* balcewic@fnal.gov

Content from this work may be used under the terms of the CC BY 4.0 licence (© 2026). Any distribution of this work must maintain attribution to the author(s), title of the work, publisher, and DOI.

ISBN: 978-3-95450-252-3 ISSN: 2673-5350 doi: 10.18429/JACoW-IPAC2026-THP5349

MODELING AND MEASURING MISMATCHED BEAM TRANSPORT AND HALO FORMATION IN A HIGH-INTENSITY LINAC *

T. E. Thompson†, A. Aleksandrov, K. Ruisard, A. Zhukov, ORNL, Oak Ridge, USA

Content from this work may be used under the terms of the CC BY 4.0 licence (© 2026). Any distribution of this work must maintain attribution to the author(s), title of the work, publisher, and DOI.

Abstract

Ongoing studies at the Spallation Neutron Source (SNS) Beam Test Facility (BTF) seek to characterize halo formation in the early stages of a high-power linac with specific focus on determining the contribution from mismatched beam transport and to replicate halo measurements using well-benchmarked particle-in-cell simulations. The BTF is a 2.5 MeV, 10- meter test beamline equipped with advanced phase space diagnostics allowing detailed characterization of beam distributions. This paper details recent advances in improved transport of mismatched cases in the BTF, and direct measurements of 2D phase space projections with 6 orders of magnitude in dynamic range.

INTRODUCTION

Halo formation and scraping is a significant source of beam loss in modern accelerators. Understanding the mechanisms of its formation will lead to better mitigation strategies and loss reduction. The Beam Test Facility (BTF) is well equipped for halo studies as it is a Front-End replica of the Spallation Neutron Source (SNS) that produces a high-intensity, medium energy (2.5 Mev) H- beam [1]. This beam travels along a ~10 meter beamline that has the diagnostic capability to conduct 6D measurements [2] and 2D high dynamic range (HDR) measurements [3, 4].

The BTF has two diagnostic stations capable of the HDR measurements needed to study halo formation, between them is a 9.5 cell permanent magnet quadrupole (quad) FODO line with sets of electromagnets before and after. This arrangement allows a wide variety of beam transport conditions between measurement stations and importantly provides the ability to match and mismatch into the FODO line, a diagram of the BTF is shown in Fig 1.

Recently, full HDR characterization of halo for a variety of match and mismatch cases was performed at the BTF [5]. This study attempted to analyze the halo formation of a matched case and four increasingly mismatched cases by taking HDR measurements after transport through the FODO line. However, in-depth analysis of halo formation was limited due to scraping.

* This material is based upon work supported by the U.S. Department of Energy, Office of Science, Office of High Energy Physics. This work has been authored by UT-Battelle, LLC under Contract No. DE-AC05-00OR22725 with the U.S. Department of Energy. This research used resources at the Spallation Neutron Source, a DOE Office of Science User Facility operated by the Oak Ridge National Laboratory. The US government retains and the publisher, by accepting the article for publication, acknowledges that the US government retains a nonexclusive, paid-up, irrevocable, worldwide license to publish or reproduce the published form of this manuscript, or allow others to do so, for US government purposes. DOE will provide public access to these results of federally sponsored research in accordance with the DOE Public Access Plan (https://www.energy.gov/doe-public-access-plan)

† thompsonte@ornl.gov

PREVIOUS BEAM HALO STUDY

Halo studies at the BTF categorize optics cases by the mismatch factor M, defined using the offset of input Twiss Parameters from the matched Twiss Parameters, where larger M directly relates to larger mismatch [5]. Currently, these studies are confined to equal mismatch in the x and y planes. The magnet settings for these conditions are created using the particle-in-cell (PIC) code PyORBIT [6], and simulated bunches created from sampling 2D measurements taken at the first diagnostic station before the FODO line. This methodology allows determination of how to manipulate the core of the beam to produce desired beam orientations into the FODO line.

Current optics cases are designed from low dynamic range (LDR) measurements as a full HDR characterization had not been completed until recently. This is sufficient to determine sets of magnet currents that produce the desired orientation of the core of the beam, however, it is insufficient to predict the movement of high amplitude particles that are most likely to be scraped along the beamline. When these cases are implemented in the BTF, with available corrector magnets and transmission quads tuned, beam transmission is less than optimal for all mismatch conditions and becomes markedly worse for high mismatch as reported in Table 1. The transmissions reported are measured by comparing beam currents at the beginning of the BTF using a BCM to the end using a faraday cup.

Table 1: Current Beam Transportation Efficiency

Optics Case	Transmission
Matched	95%
M 0.67	94%
M 1.37	93%
M 1.90	90%
M 2.35	86%

A complete set of HDR 2D measurements were taken for all five mismatch conditions, and observation of halo formation was attempted, though restricted due to scraping [5]. From these measurements new simulation bunches were created allowing more accurate prediction of possible scraping locations. It is the goal of this research to use the improved simulation capability to reduce particle loss and increase transmission allowing for cleaner observations of halo formation.

ISBN: 978-3-95450-252-3 ISSN: 2673-5350 doi: 10.18429/JACoW-IPAC2026-THP5350

SEARCH FOR VLASOV-POISSON EQUILIBRIUM DISTRIBUTIONS USING GENERATIVE MODELS *

Austin Hoover†
Oak Ridge National Laboratory, Oak Ridge, Tennessee, USA

Abstract

This work proposes the use of generative models and differentiable simulations to search for smooth equilibrium phase space distributions in arbitrary external fields. The model parameters are optimized using a two-term loss function: one term suppresses density fluctuations, while a second term pulls the solution toward some target value, for example, to encourage smoothness. As an initial demonstration of this approach, we search for a four-dimensional equilibrium distribution in a linear continuous-focusing lattice.

INTRODUCTION

This work proposes a method to search for equilibrium phase space distributions in periodic focusing channels. Equilibrium distributions are solutions to the Vlasov-Poisson (V-P) system:

$$\frac{\partial f}{\partial t} + \frac{\partial H}{\partial \mathbf{x}'} \cdot \frac{\partial}{\partial \mathbf{x}} - \frac{\partial H}{\partial \mathbf{x}} \cdot \frac{\partial f}{\partial \mathbf{x}'} = 0. \tag{1}$$

$$\frac{\partial}{\partial \mathbf{x}} \cdot \frac{\partial}{\partial \mathbf{x}} \phi(\mathbf{x}, s) = -\frac{q}{\epsilon_0} \int f(\mathbf{x}, \mathbf{x}', s) d\mathbf{x}'. \tag{2}$$

$$H(\mathbf{x}, \mathbf{x}', s) = \frac{1}{2}|\mathbf{x}'|^2 + U(\mathbf{x}, \mathbf{x}', s) + \frac{q}{mc^2\beta^2\gamma^3}\phi(\mathbf{x}, s). \tag{3}$$

Here f is the distribution function, H is the Hamiltonian, U is an external potential, ϕ is the self-generated electric potential, $\mathbf{x}$ is the position, $\mathbf{x}'$ is the momentum, s is the position on the reference trajectory, q is the particle charge, ϵ_0 is the electric constant, m is the particle mass, c is the speed of light, β is the synchronous particle velocity, and γ is the Lorentz factor.

Equilibrium distributions are functions of invariants. In continuous-focusing channels where $U(\mathbf{x}, \mathbf{x}', s) = U(\mathbf{x}, \mathbf{x}')$, the Hamiltonian is an invariant and there are an infinite number of solutions of the form $f = f(H)$. In s-dependent focusing channels, the Hamiltonian is not an invariant and solutions are more difficult to find. The Kurth distribution [1] is a solution for the special case of spherically or axially symmetric linear fields. The only known solution in *arbitrary* linear fields is the Kapchinskij-Vladirskij (K-V) distribution [2], which is a function of the Courant-Snyder invariant. The K-V distribution is unstable over a range of beam and lattice parameters [3] and is generally assumed to be far from real distributions in accelerators. Furthermore, the K-V solution is only valid in two-dimensional focusing fields; it is unknown if there are solutions for (s-dependent) three-dimensional or nonlinear fields.

Lund [4] considered this problem for linear FODO channels with equal phase advances in the two planes of motion. The FODO lattice was mapped to a continuous-focusing (CF) lattice with the same average phase advance. Equilibrium distributions were generated in the CF lattice and then linearly transformed to match the periodic K-V envelope in the FODO lattice. This process generated surprisingly well-matched beam distributions. However, it is unclear how to adapt this method to (i) linearly coupled lattices, (ii) nonlinear lattices, or (iii) six-dimensional phase space distributions.

This work introduces a brute-force optimization to drive the distribution toward equilibrium in arbitrary external fields. The idea is to represent the distribution as a generative model—a neural network (NN) that transforms a simple base distribution to a more complicated distribution [5]—and to optimize the model parameters using gradient-based methods, enabled by differentiable particle-in-cell (PIC) simulations. The rest of this paper will discuss implementations of this approach and demonstrate convergence for a linear two-dimensional continuous-focusing lattice.

PROBLEM SETUP

Consider a periodic lattice of length L, such that $U(\mathbf{z}, s) = U(\mathbf{z}, s+L)$, and write the distribution function after n periods as $f_n(\mathbf{z})$, where $\mathbf{z} = (\mathbf{x}, \mathbf{x}')$ is the phase space vector. Let $\mathscr{M}f$ propagate the distribution function through one period: $f_{n+1} = \mathscr{M}f_n$. We seek a periodic distribution function $f_0 = f_1 = \mathscr{M}f_0$.

We also need to constrain the distribution emittance, since it is always possible to find a solution by scaling the emittance until space charge is negligible. The emittance is defined as $\varepsilon = |\det \Sigma|^{1/2}$, where $\Sigma = \langle \mathbf{z}\mathbf{z}^T \rangle$ is the covariance matrix. The algorithm should enforce $\varepsilon = \tilde{\varepsilon}$ for target emittance $\tilde{\varepsilon}$.

We may also wish to pull the distribution toward some target $\tilde{f}$, either to stabilize training or to select one of multiple solutions; for example, to pull the solution away from the K-V equilibrium in a FODO channel. If there is only one

* This manuscript has been authored by UT-Battelle, LLC, under Contract No. DE-AC05-00OR22725 with the U.S. Department of Energy. The United States Government retains, and the publisher, by accepting the article for publication, acknowledges that the United States Government retains a non-exclusive, paid-up, irrevocable, world-wide license to publish or reproduce the published form of this manuscript, or allow others to do so, for United States Government purposes. The Department of Energy will provide public access to these results of federally sponsored research in accordance with the DOE Public Access Plan (http://energy.gov/downloads/doe-public-access-plan)

† hooveram@ornl.gov

Content from this work may be used under the terms of the CC BY 4.0 licence (© 2026). Any distribution of this work must maintain attribution to the author(s), title of the work, publisher, and DOI.

ISBN: 978-3-95450-252-3 ISSN: 2673-5350 doi: 10.18429/JACoW-IPAC2026-THP5354

ANALYSIS OF EXPERIMENTAL RESULTS INVESTIGATING SHIELDING FOR COHERENT SYNCHROTRON RADIATION MITIGATION

A. Tilton*, G. Ha† and X. Lu, Northern Illinois University, DeKalb, USA
C. Huang, Los Alamos National Laboratory, Los Alamos, USA
J. Qiang, Lawrence Berkeley National Laboratory, Berkeley, USA
J. Power and O. Ramachandran, Argonne National Laboratory, Lemont, USA

Content from this work may be used under the terms of the CC BY 4.0 licence (© 2026). Any distribution of this work must maintain attribution to the author(s), title of the work, publisher, and DOI.

Abstract

An experiment was conducted at Argonne Wakefield Accelerator to evaluate the efficacy of shielding plates with varying gap sizes on the suppression of coherent synchrotron radiation (CSR) effects in a compression environment. The longitudinal phase spaces upstream and downstream of the compression beamline were measured with three different shielding gap sizes. Although the results were broadly consistent with expectations, several issues require further clarification, including beam stability and nonlinear stretch and shortening under strong CSR fields. The analysis was performed using the 1D longitudinal tracking code, BELT, and included both CSR and space-charge effects. We present the analysis results.

INTRODUCTION

Coherent Synchrotron Radiation (CSR) often has adverse effects, inducing nonlinear energy spread and transverse emittance growth. Although CSR effects on the beam depend on various factors, including the bending angle and current profile, previous studies have demonstrated that the vacuum-chamber geometry is also an important factor [1–3]. This effect is often referred to as CSR shielding. To date, studies of CSR shielding have mainly focused on demonstrating the shielding effect itself. Further study in a realistic compression environment is necessary to exploit this mechanism for beam-quality preservation.

To experimentally study CSR shielding in a compression environment, a chicane-like beamline was constructed at the Argonne Wakefield Accelerator (AWA). The first campaign encountered several issues associated with the large R_{56} of the beamline ($\approx$ 0.45 m) and the resulting sensitivity to the α-BBO crystal setup [4]. In the second campaign, we addressed the issues identified during the first run and measured longitudinal phase spaces affected by CSR for various shielding-gap sizes.

The measurement results show the expected shielding-gap-dependent changes in the longitudinal phase spaces. However, clear signs of machine instability prevent us from drawing firm conclusions directly from measurements. To better understand the collected data and prepare the third campaign, we performed an analysis using a one-dimensional tracking code, called BEam Longitudinal Tracking (BELT) [5]. This lightweight code was used to model the chicane-like beamline at the AWA facility.

* z2047997@students.niu.edu
† gha@niu.edu

We first briefly introduce the experiment setup, which was described in our earlier publication [4], and discuss the experiment results. We then present the simulation results from the BELT code and discuss the issues encountered during the analysis.

MEASUREMENT OF CSR EFFECTS ON A BEAM WITH VARIABLE SHIELDING

The experiment was conducted at the AWA facility using a reversed-chicane beamline [4]. As shown in Fig. 1, the beamline consists of two identical doglegs and two quadrupoles that flip the phase space, allowing the two identical doglegs to operate like a chicane. This layout has a large R_{56} of 0.45 m [4]. Each dipole in the reversed chicane is equipped with a tunable parallel-plate shielding gap. Longitudinal phase-space diagnostics are available both upstream and downstream of the reversed chicane, allowing the CSR-induced changes to the beam to be measured across the chicane.

During the experiment, bunches with charges of 1-2 nC and a nominal energy of approximately 44 MeV were prepared. The variable shielding-gap was scanned sequentially from 3 cm to 2 cm and then to 1 cm. The 3 cm gap measurement was repeated to assess measurement consistency. At each gap size, the measurement was repeated with a horizontal slit (50 mm×2 mm) installed upstream of the chicane. This slit reduces the total bunch charge by blocking the beam in the vertical direction while minimally perturbing the horizontal or longitudinal phase spaces. This low-charge case was used as the reference corresponding to the CSR-off case in the simulations. The measured phase space images are displayed in Fig. 2.

From Fig. 2, it is clear that the CSR-induced energy modulation strongly depends on the shielding-gap size. Although the overall structure follows the typical steady-state CSR wake pattern [6], the distance between the energy-loss trough and the trailing energy plateau decreases as the shielding gap is reduced. This behavior is expected from the suppression of low-frequency components of the CSR wake by parallel-plate shielding [1]. In contrast, small energy modulations originating from α-BBO setup errors become more pronounced as the gap is reduced. At this stage, it is unclear whether these modulations originate from laser-system instability or from modulation amplification through a mechanism similar to microbunching instability [7].

Although the results show the expected shielding-gap-dependent changes, they also show clear signs of machine instability. The measurement began with the 3 cm gap, and

ISBN: 978-3-95450-252-3 ISSN: 2673-5350 doi: 10.18429/JACoW-IPAC2026-THP5360

A FLAT-PULSE ANALYTIC FRAMEWORK FOR MODELING INVERSE COMPTON SCATTERING AND PONDEROMOTIVE BROADENING *

E. Breen†[1], E. Rogers[1], G. Krafft[1,2], B. Terzić[1]
[1]Old Dominion University, Norfolk, USA
[2]Jefferson Lab, Newport News, USA

Abstract

We present a new general analytic formula for radiation spectra from inverse Compton scattering with a flat laser pulse at an arbitrary scattering angle. Using the analytic solution for a flat laser pulse, we build an approximation of a Gaussian pulse as a series of flat pulses with varying field strengths. From this description we obtain an expression for the phase modulation between successive flat pulses due to changing field strength, which produces ponderomotive broadening in the scattered spectra.

INTRODUCTION

Inverse Compton scattering (ICS) is a promising mechanism for generating compact, high-brightness x-ray and gamma-ray sources. In ICS, photons from a laser pulse collide with relativistic electrons and are upshifted in frequency through relativistic Doppler effects. Modern ICS systems operate in regimes where nonlinear interactions between the laser field and electron motion become significant, producing harmonic generation and ponderomotive broadening in the scattered spectrum.

Accurate modeling of these spectral effects generally requires detailed numerical calculations of the electron trajectory inside the laser field. While several numerical approaches exist, analytic or semi-analytic methods remain valuable because they provide physical insight into the scattering process and can substantially reduce computational cost.

In this work, we present a new analytic framework that approximates an arbitrary laser pulse envelope as a sequence of flat laser pulses. Exact solutions for radiation generated by flat pulses are then combined coherently with phase corrections between successive pulse segments. This approach reproduces nonlinear spectral broadening while preserving much of the simplicity of the analytic flat-pulse solution.

ANALYTIC SCATTERED SPECTRUM FOR A FLAT LASER PULSE

Calculating the scattered spectrum in inverse Compton scattering requires calculating the effective motion of the electron as it passes through the laser pulse. In the linear and nonlinear regimes, as well as both the Thomson and Compton regimes, this requires computing [1]

$$\begin{aligned} D_1(\omega') &= \frac{1}{\gamma(1-\beta\cdot\hat{k})}\int \tilde{A}(\xi')\, e^{i\Phi(\xi')}d\xi', \\ D_2(\omega') &= \frac{1}{\gamma^2(1-\beta\cdot\hat{k})^2}\int \frac{\tilde{A}^2(\xi')}{2} e^{i\Phi(\xi')}d\xi', \\ \Phi(\xi') &= \frac{\omega'}{c}\left(\begin{array}{c} \xi'\frac{(1-\beta\cdot\hat{k}')}{(1-\beta\cdot\hat{k})} - I_2\int_{-\infty}^{\xi'}\tilde{A}(\xi'')d\xi'' \\ +I_1\int_{-\infty}^{\xi'}\tilde{A}^2(\xi'')d\xi'' \end{array}\right), \end{aligned} \tag{1}$$

$$\begin{aligned} I_1 &= \frac{1-\hat{k}\cdot\hat{k}'}{2\gamma^2(1-\beta\cdot\hat{k})^2}, \\ I_2 &= \left(\frac{\beta\cdot\varepsilon}{(1-\beta\cdot\hat{k})}(1-\hat{k}\cdot\hat{k}') - \hat{k}'\cdot\varepsilon\right)\frac{1}{\gamma(1-\beta\cdot\hat{k})}, \end{aligned} \tag{2}$$

where β is the initial electron velocity vector divided by the speed of light, $\hat{k}$ and $\hat{k}'$ are the unit vector incident and scattered photon directions, ϵ is the polarization of the incident laser, and $\tilde{A}$ its normalized vector potential

$$\tilde{A}(\xi) = a(\xi)\cos\left(\frac{2\pi\xi}{\lambda}\right). \tag{3}$$

The spectrum is then computed from these expressions [2].

For a flat pulse laser envelope with strength a and with N full periods with wavelength λ, $\tilde{A}(\xi) = a[\Theta(\xi + N\lambda/2) - \Theta(\xi - N\lambda/2)]$, these integrals can be evaluated exactly in terms of Bessel functions, just as in case of undulators [3]

$$\begin{aligned} D_1(\omega') = &\frac{ae^{i\frac{\omega'}{c}\Phi_c}}{\gamma(1-\beta\cdot\hat{k})} \\ &\times\sum_{n=0}^{\infty}\frac{\sin((\frac{\omega'}{cQ(a)}-\frac{2\pi n}{\lambda})\frac{N\lambda}{2})}{\frac{\omega'}{cQ(\theta)}-\frac{2\pi n}{\lambda}}G_x^n(\omega'), \end{aligned} \tag{4}$$

$$\begin{aligned} D_2(\omega') = &\frac{a^2e^{i\frac{\omega'}{c}\Phi_c}}{2\gamma^2(1-\beta\cdot\hat{k})^2} \\ &\times\sum_{n=-\infty}^{\infty}\frac{\sin((\frac{\omega'}{cQ(a)}-\frac{2\pi n}{\lambda})\frac{N\lambda}{2})}{\frac{\omega'}{cQ(\theta)}-\frac{2\pi n}{\lambda}}G_z^n(\omega'), \end{aligned} \tag{5}$$

where the phase term, Φ_c, is constant

$$\Phi_c = I_2\frac{a\lambda}{2\pi}\sin(\pi N) + I_1\left(\frac{a^2\lambda}{8\pi}\sin(2\pi N) + \frac{a^2}{4}N\lambda\right). \tag{6}$$

We define expressions for the Bessel function component

* Work supported by the NSF CAREER grant No. 1847771 and the NSF CSSI grant No. 2513760, and by Jefferson Science Associates, LLC under U.S. DOE Contract No. DE-AC05-06OR23177.

† ebree001@odu.edu

Content from this work may be used under the terms of the CC BY 4.0 licence (© 2026). Any distribution of this work must maintain attribution to the author(s), title of the work, publisher, and DOI.

ISBN: 978-3-95450-252-3 ISSN: 2673-5350 doi: 10.18429/JACoW-IPAC2026-THP5361

CASE STUDIES WITH HED-MELT, MODELING HIGH-ENERGY-DENSITY CONDITIONS IN ACCELERATORS *

A. Dick†, A. Dhruv, M. Borland, J. Dooling, A. Grannan, Y. Lee, R. Lindberg, G. Navrotski
Argonne National Laboratory, Lemont, Illinois, U.S.A.
D. Lee, S. Riedel, University of California Santa Cruz, Santa Cruz, California U.S.A.
N. Cook, RadiaSoft, Boulder, Colorado U.S.A.

Abstract

The HED-Melt (**H**igh **E**nergy **D**ensity **M**odeling of **El**ectron Beam Impacts **T**oolkit) software suite was developed for studying the damage resulting from beam impacts in accelerators [1]. We have made additional improvements to the toolkit workflow and physics modeling, and have examined specific loss scenarios matching the operation conditions in the Advanced Photon Source Upgrade (APS-U) storage ring. Losses were observed in two operational modes, high-coupling 48-bunch timing mode (up to 140 mA) and high-coupling 216-bunch "many-bunch mode" (up to 200 mA). Data recorded during these losses and observations of collimator damage are presented and were used to improve the simulation workflow.

INTRODUCTION

The upgraded Advanced Photon Source (APS) storage ring began commissioning in April 2024 and has now been operating for two years. In this time, a significant number of fast beam losses have occurred. Five sectors contain in-board, horizontal collimators, which intercept the beam during these losses, and prevent damage to more sensitive beamline components [2]. The increased brightness of the APS-U lattice gives rise to energy densities intense enough to cause significant damage to collimators and other machine components [3]. While the collimators are designed to absorb beam impacts and can be replaced as needed, it is advantageous to minimize damage. A vertically-deflecting fan-out kicker (FOK) kicks the beam when a fast beam loss is initiated, spreading out the energy density vertically over the face of the collimator. However, we have seen a number of scenarios where steps of the fast beam abort process do not operate as designed. Additionally, we continue to see damage to collimator surfaces, requiring them to be replaced during machine maintenance shutdown periods. The beam losses seen in the upgraded storage ring provide us with the ability to study the damage to collimators as well as the effectiveness of the collimators for machine protection.

The HED-Melt framework [4] was developed to study potential High-energy density (HED) conditions in accelerators [5–8]. While the tool is useful in estimating damage to materials from beam impacts in ideal/nominal cases [1], the operational data often presents edge-cases. Previous simulation results show the benefits and limitations of the current model. We will discuss how the observations of beam losses inform our modeling and will present a method of using turn-by-turn (TBT) beam position monitor (BPM) data, collected during user operations, to simulate specific loss events. This allows HED-Melt to be used in two ways; (i) the design and planning of new machines and machine protection systems, and (ii) understanding and predicting damage in specific operational configurations. Currently, no diagnostics are in place to monitor the health of the collimators installed in the machine. The second prong is, therefore, important in prioritizing collimator access during the limited machine downtime.

APS-U OPERATIONS

The storage ring contains collimators in five non-user-serving sectors around the injection region. Each collimator is positioned near the beam axis in order to intercept the beam during losses while also minimizing the impact on beam lifetime. After a series of lifetime and dynamic aperture studies, the collimator in sector 1 was retracted fully in October 2025. Of the remaining four collimators, impacts are most frequently observed in sector 38 and damage to this collimator is the most severe. Several studies of the FOK indicated the beam was being insufficiently kicked and timing issues were seen in some beam loss events. As a result, the FOK voltage was increased, in October 2025, to provide a larger vertical deflection. To date, seven collimators have been replaced, with sector 38 being replaced between every user run. Figure 1 shows examples of two collimators damaged by beam strikes, both removed in May 2025.

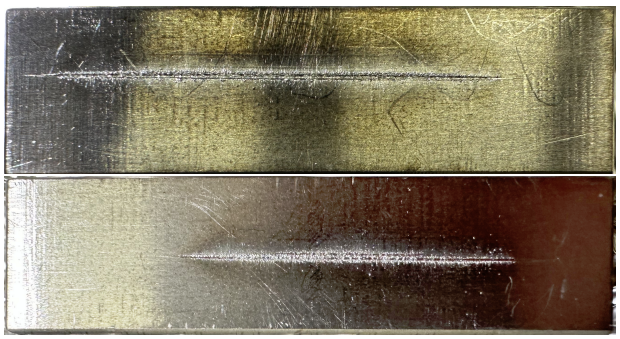

Figure 1: Photos of collimator jaws removed from sector 38 (top) and 1 (bottom) in May 2025, showing damage from beam strikes. The jaw is 14 mm tall (y) and 50 mm in length (z). Upstream is to the left.

As of the first user run of 2026, APS-U has operated in two fill patterns; (i) 216-bunch "many-bunch mode" up to

* Work supported by the U.S. D.O.E.,Office of Science, Office of Basic Energy Sciences, under contract number DE-AC02- 06CH11357.
† ajdick@anl.gov

Content from this work may be used under the terms of the CC BY 4.0 licence (© 2026). Any distribution of this work must maintain attribution to the author(s), title of the work, publisher, and DOI.

ISBN: 978-3-95450-252-3 ISSN: 2673-5350 doi: 10.18429/JACoW-IPAC2026-THP5362

A LEVEL SET BASED IMMERSED BOUNDARY METHOD FOR MODELING PHASE TRANSITION DYNAMICS IN HIGH-ENERGY-DENSITY BEAM SIMULATIONS*

A. Dhruv†, A. J. Dick, J. Dooling, A. Grannan, Y. Lee, R. R. Lindberg, G. Navrotski, K. Weide,
Argonne National Laboratory, Lemont, Illinois, U.S.A.
D. Lee, S. Riedel, University of California, Santa Cruz, California, U.S.A.
N. Cook, RadiaSoft, Boulder, Colorado, U.S.A.

Content from this work may be used under the terms of the CC BY 4.0 licence (© 2026). Any distribution of this work must maintain attribution to the author(s), title of the work, publisher, and DOI.

Abstract

We demonstrate a level-set immersed boundary method for solid-liquid-gas transitions in collimator material under the high-energy-density conditions of fourth-generation storage-ring beam strikes. Two signed-distance functions λ and ϕ track the solid-liquid and liquid-gas interfaces; their zero contours advance under interface-normal velocities derived from the Stefan energy balance, carrying the latent heats of fusion and gasification rather than relying on temperature thresholding. A narrow-band Gaussian envelope localizes the source to a tube around each interface, a defensive phase mask restricts forcing to liquid cells, and Sussman re-initialization restores signed-distance form each cycle. A 2D aluminum beam-strike test validates the kinematic layer in isolation and lays the foundation for a staged path to a coupled interface-aware hydrodynamic capability for fourth-generation collimator damage modeling.

INTRODUCTION

Fourth-generation storage rings, exemplified by APS-U [1] and contemporaries (ESRF-EBS, SLS 2.0, ALS-U), reach unprecedented brightness through ultra-low-emittance lattices. An abnormal whole-beam dump deposits 10 to 100 J mm^{-3} in a sub-millisecond window [2], driving collimator material through solid, liquid, and gas phases within a single revolution. Predictive damage modeling for fourth-generation collimator design therefore requires a faithful three-phase treatment.

The established pipeline couples ELEGANT beam tracking, FLUKA energy deposition, and the FLASH radiation-hydrodynamics solver [3]. Phase is currently assigned per cell by temperature thresholding: a cell is solid, liquid, or gas according to whether $T < T_{\mathrm{melt}}$, $T_{\mathrm{melt}} \le T < T_{\mathrm{gas}}$, or $T \ge T_{\mathrm{gas}}$ [3]. Calibrated against measurements [2], this discrete tag nevertheless resolves interfaces only at the mesh-cell width, omits latent heat from the interface energy balance, applies no physical boundary condition at the melt or gas front, and re-solidifies or re-condenses instantly when the local temperature falls back below T_{melt} or T_{gas}, erasing the prior melt and gas history.

This paper replaces the discrete tag with two signed-distance functions, λ (solid-liquid) and ϕ (liquid-gas), each advanced by a Stefan-derived interface-normal velocity that carries the appropriate latent heat. The demonstration is deliberately narrow: a 2D aluminum beam-strike test in which the level sets are advected passively while the threshold tag still drives density, conductivity, and EOS, so the kinematic layer is validated in isolation before being coupled back into the active physics.

PROBLEM FORMULATION

The canonical test (Fig. 1) is a 2D Cartesian domain $x \in [-0.30, -0.25]$ cm, $y \in [-0.25, 0.25]$ cm on a 20×200 uniform grid ($\Delta x = \Delta y = 25\,\mu$m). A solid aluminum jaw ($\rho_s = 2.70\,\mathrm{g\,cm^{-3}}$, $T_0 = 453\,\mathrm{K}$) occupies $x < x_{\mathrm{edge}} = -0.26$ cm; helium gas ($\rho_g = 10^{-5}\,\mathrm{g\,cm^{-3}}$) fills the remainder, and no liquid is present at $t = 0$. Beam energy is delivered as 100 ps bunches separated by the 3.682 μs revolution period, with cumulative dose calibrated to exhaust the sensible-heat budget to $T_{\mathrm{melt}} = 933\,\mathrm{K}$ within one revolution. The volumetric deposition rate $\dot{q}(x, y)$ is read from a FLUKA-format dose map; here a uniform disk of radius $r_b = 0.02$ cm centered on $(x_{\mathrm{edge}}, 0)$, representative of the secondary-shower footprint from ELEGANT/FLUKA tracking of an APS-U beam-loss scenario [2, 3].

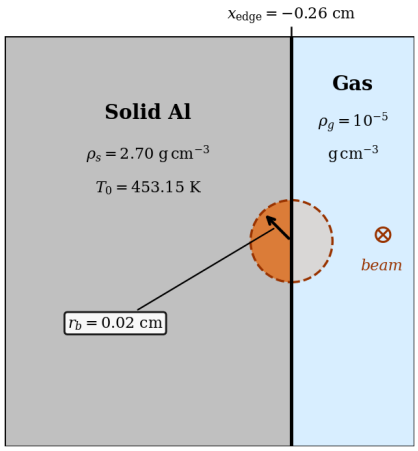

Figure 1: 2D test problem. Solid Al jaw (gray) at $x < x_{\mathrm{edge}}$, helium fill (blue) to the right; shaded disk ($r_b = 0.02$ cm) is the beam footprint. $\lambda > 0$ in the solid, $\phi < 0$ in the gas.

Thermal evolution follows the two-temperature energy equation,

$$\rho c_p\, \partial_t T + \rho c_p\, \mathbf{u}\cdot\nabla T = \nabla\cdot(k\nabla T) + \dot{q_L}, \qquad (1)$$

* Work supported by the U.S. D.O.E.,Office of Science, Office of Basic Energy Sciences, under contract number DE-AC02- 06CH11357.

† adhruv@anl.gov

ISBN: 978-3-95450-252-3 ISSN: 2673-5350 doi: 10.18429/JACoW-IPAC2026-THP5363

AN EFFICIENT SYMPLECTIC MODEL FOR RF CAVITIES INCLUDING TRANSVERSE FOCUSING

D. Sagan, Cornell University, Ithaca, NY, USA *

Abstract

Tracking through RF cavities is complicated due to the presence of time-varying electric and magnetic fields, which are not amenable to algorithms developed for static fields. Many simulation programs use simplified models that neglect transverse focusing even though it can play an important role at low energies. Other programs track using field maps which can be slow and potentially non-Maxwellian (and therefore not symplectic).

To avoid some of these problems, presented here is an RF cavity model which is symplectic and computationally efficient. Spin tracking is included and transfer maps of arbitrary order can be computed. Additionally, DC solenoid and multipole components can easily be included.

This model is an extension of the work of Rosenzweig and Serafini extended to avoid the ultra-relativistic approximation. The model has been incorporated as part of the Bmad and SciBmad ecosystems of libraries and programs.

INTRODUCTION

Accurate simulation of linac beamlines, requires a tracking model for RF accelerating cavities that captures both the longitudinal energy gain and the transverse focusing effects. At one extreme are models that only have a longitudinal kick and ignore transverse focusing entirely. Another approach is to integrate the particle motion. Integration with the electromagnetic field is accurate but can be computationally expensive and non-symplectic if interpolation is needed to calculate the field. Integration using a split Hamiltonian derived from the field (similar to a "kick-drift-kick" model) can be constructed [1] and while this is symplectic, there is the problem that many time steps may be needed to ensure that the transverse kick is accurate. The root of the problem is that, as shown below, the net first order transverse kick in a cylindrically symmetric RF cavity is zero leaving only the second order "pondermotive" force. However, integration using a field based Hamiltonian will only have a zero first order kick in the limit of an infinite number of steps.

The model described here occupies a practical middle ground. It is based on the work of Rosenzweig and Serafini [2] extended to be symplectic at non ultra-relativistic energies where the normalized particle velocity β is significantly less than one. The model uses a kick-drift-kick Hamiltonian for the longitudinal kick and an integrated Hamiltonian for the transverse kick which ensures that the pondermotive force is properly accounted for. Spin tracking is included in the model and, the model allows for DC solenoid and multipole fields to be superimposed on the cavity.

This algorithm has been incorporated into the Bmad [3] and SciBmad [4] ecosystems of libraries and programs.

PHASE-SPACE COORDINATES

The phase space canonical coordinates used in this paper are

$$x, P_x, y, P_y, \tau, E \tag{1}$$

where P_x and P_y are the transverse momenta, E is the energy, and τ is

$$\tau = c(t_{\rm ref} - t) \tag{2}$$

with c being the speed of light, $t_{\rm ref}$ is the reference time, and t is the particle time.

CAVITY MODEL

The cavity structure of length L is modeled as having a number N_c of contiguous cells. Within each cell, the RF is ignored and the particle energy is constant. Kicks are applied at the ends of the cells. The kick points, which are one more than the number of cells, are indexed from zero to N_c. Entrance and exit fringe kicks are applied at the ends of cavity.

EDGE KICKS

At the entrance and exit ends of the cavity, the radial electric fringe field produces a transverse kick. Adapting Rosenzweig and Serafini Eq. (12), the appropriate fringe Hamiltonian H_f is:

$$H_f = \pm\frac{q}{2c}\, G\, \cos(\theta_{\rm rf})\, (x^2 + y^2), \tag{3}$$

where q is the particle charge, G is the voltage gradient, and $\theta_{\rm rf}$ is the RF phase (discussed below). The top (minus) sign applies at the entrance end of the cell and the bottom (plus) sign at the exit end.

This Hamilton gives the fringe kicks

$$\begin{aligned} \Delta P_x &= \mp\frac{q}{c}\, G \cos(\theta_{\rm rf})\, x, \\ \Delta P_y &= \mp\frac{q}{c}\, G \cos(\theta_{\rm rf})\, y, \\ \Delta E &= \mp\frac{\pi f q}{c^2}\, G \sin(\theta_{\rm rf})\, (x^2 + y^2). \end{aligned} \tag{4}$$

The entrance kick will be defocusing and the exit kick will be focusing for accelerated particles.

The spin precession due to the fringe is calculated using the Thomas-BMT equation with the radial electric field integrated over the fringe being

$$\int_{\rm fringe} \mathbf{E} = \pm G\, \cos(\theta_{\rm rf})\, (x, y, 0) \tag{5}$$

* Work supported by DOE grant DE-SC0025351

Content from this work may be used under the terms of the CC BY 4.0 licence (© 2026). Any distribution of this work must maintain attribution to the author(s), title of the work, publisher, and DOI.

ISBN: 978-3-95450-252-3 ISSN: 2673-5350 doi: 10.18429/JACoW-IPAC2026-THP5602

ANALYSIS AND RESEARCH ON MEASUREMENT ERRORS CAUSED BY MAGNET MISALIGNMENT IN ENERGY ANALYSIS SYSTEMS*

Y. Wang, Y.F. Zeng, H. Hu, D.Y. Xiao, D. Lu, K.F. Liu†, T.N. Hu‡,
Huazhong University of Science and Technology, Wuhan, China

Abstract

Accurate evaluation of the beam energy and momentum spread plays a crucial role in the commissioning and operation of electron accelerators. The energy analysis (EA) system, consisting of a dipole with associated upstream and downstream drift sections, is widely applied in accelerator facilities due to its structural simplicity, large measurement range, and high resolution. However, assembly errors are inevitably introduced during engineering implementation. These errors lead to offsets or tilt angles between the input beam and the designed system axis. Such misalignment necessarily affect the accuracy of the measurement results of the EA system, and the impact may be even more significant for low-energy e-beams with the energy of a few MeV. In this paper, based on the low-energy injector experimental platform currently under construction, the misalignment induced errors are analyzed in depth, and potential compensation methods are explored. The results offer critical theoretical and practical guidance for enhancing measurement precision.

INTRODUCTION

With the widespread application of particle accelerators, diagnostic techniques for high-quality electron beams [1, 2] have advanced significantly. The performance of such accelerators is highly dependent on the quality of the electron beam, necessitating precise characterization of the beam energy spectrum.

Energy analysis systems based on magnetic deflection are widely adopted [3–5] due to their stable operation and low cost. A typical system consists of a dipole magnet, an entrance slit, a downstream fluorescent screen, and the drift sections in between. The working principle relies on combining the dispersive properties of sector magnets with beam transport theory [6–8]. The momentum deviation δ is measured via magnetic dispersion, and the corresponding kinetic energy T is determined by the relativistic relation $T = \sqrt{(BRec)^2 + m_0^2c^4} - m_0c^2$, where B is the magnetic field, R the bending radius, c , e and m_0 represents the light speed, the electron charge and mass, respectively. For an electron with initial transverse offset x_0, angular divergence x_0', and momentum deviation δ, after passing through a beamline described by the transfer matrix M, its final horizontal position can be expressed as $x_1 = m_{11}x_0 + m_{12}x_0' + m_{13}\delta$,

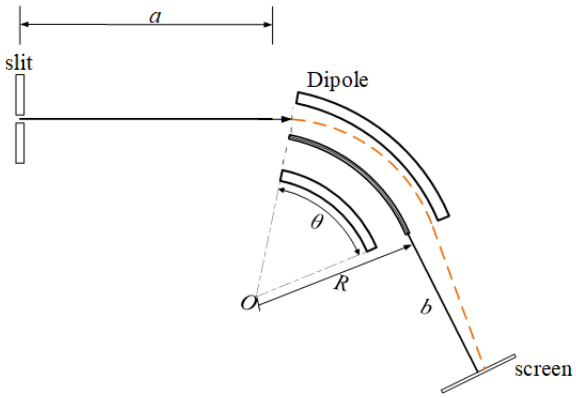

Figure 1: Schematic Diagram of Beam Bunch Deviation from the Center Caused by Magnet Translation and Tilting.

where m_{11}, m_{12}, and m_{13} are the corresponding elements of the transfer matrix M.

However, in practical engineering implementations, installation and alignment errors [9] of magnets are unavoidable. This paper analyzes the particle trajectories to calculate the momentum spread and energy measurement errors caused by dipole magnet translation and tilt. Furthermore, a correction method for the translation-induced energy measurement error is proposed.

ALIGNMENT ERROR IMPACTS ON ENERGY AND MOMENTUM SPREAD MEASUREMENTS

To facilitate analysis, the design parameters of the HuTeX system are adopted as an example, where the bending radius of the dipole magnet is 300 mm and the bending angle is $\pi/3$ radians. The drift lengths a and b are 607 mm and 450 mm, respectively. Given that the vertical alignment errors within the uniform field gap have a negligible impact on the beam trajectory, only errors in the horizontal plane are considered. Furthermore, to simplify the numerical analysis, a one-dimensional (1D) bunch simulation model is employed, where the influence of the initial transverse beam size is neglected.

Under the current engineering accuracy, maximum deviations of ±1 mm for magnet translations and ±1 mrad for tilts are defined based on the practical mechanical alignment tolerances. A schematic of the off-center beam injection caused by magnet translation and tilting is presented in Fig. 1.

For a given energy analysis system, the multi-particle beam may be treated as a single electron when measuring the central energy. The focus is placed on the trajectory of the central-energy electron and its position on the screen. The electron trajectory can be analyzed using a geometric

* Work supported by the National Natural Science Foundation of China (No.12575164 and No.12341501)
† kfliuhust@hust.edu.cn
‡ TongningHu@hust.edu.cn

Content from this work may be used under the terms of the CC BY 4.0 licence (© 2026). Any distribution of this work must maintain attribution to the author(s), title of the work, publisher, and DOI.

ISBN: 978-3-95450-252-3 ISSN: 2673-5350 doi: 10.18429/JACoW-IPAC2026-THP5605

CLOSED ORBIT AND REALIGNMENT IN THE CSNS RCS

Y. Li*,[1,2], J. Liang[1,2], X. H. Lu[1,2], T. Wang[1,2], Y. W. An[1,2]
[1]Institute of High Energy Physics, Chinese Academy of Sciences, Beijing, China
[2]Spallation Neutron Source Science Center, Dongguan, China

Abstract

Closed orbit distortion is one of the key factors affecting the operational performance of accelerators, and realignment is an effective solution to mitigate orbit distortion and reduce beam loss. To address the severe orbit distortion observed in the Rapid Cycling Synchrotron (RCS) of the China Spallation Neutron Source (CSNS), a systematic analysis was performed during the 2025 summer shutdown for the renovation of the injection region. Based on high-precision alignment data, the CSNS magnet orbit smoothing method and the MAD-X program were combined in the analysis, and the transverse adjustment of only four quadrupole magnets was proposed. After realignment, the maximum bare horizontal orbit is reduced from 23.45 mm to 20.7 mm, and the maximum bare vertical orbit is reduced from 9 mm to 7 mm. The results validate that the partial magnet realignment strategy can effectively mitigate orbit distortion, providing a feasible and efficient maintenance approach for high-power proton accelerators with limited alignment resources.

INTRODUCTION

For high-power proton accelerators, extremely high beam orbit stability is required. Factors such as installation errors and ground settlement can lead to beam orbit distortion, subsequently causing beam loss, making components radioactive, and limiting operational power. While orbit correction systems can partially mitigate this issue, realignment is a more fundamental approach.

Similar efforts have been undertaken at several domestic and international facilities. Following the major earthquake in 2011, the J-PARC RCS completed a large-scale realignment in 2013, laying the foundation for a 1 MW power upgrade [1]. The Shanghai Synchrotron Radiation Facility (SSRF) experienced unsatisfactory orbit correction performance due to uneven ground settlement. In 2022, a comprehensive realignment was carried out, reducing the closed orbit distortion from 280 µm 50 µm. At ISIS, after five main dipole magnets were adjusted in early 2025, vertical deviations and beam loss were significantly reduced [2].

Since it officially started operation in 2018, the bare orbit in the CSNS RCS, particularly in the horizontal direction, has exhibited significant distortion, with orbit exceeding 20 mm recorded by some Beam Position Monitors (BPMs). Due to the use of common power supplies, conventional beam-based alignment (BBA) methods are inapplicable, and orbit correction has shown unsatisfactory effectiveness, severely constraining beam commissioning efficiency and operational reliability. As the upcoming CSNS-II upgrade demands higher orbit quality, further mitigation of the orbit distortion is urgently required. To this end, taking advantage of the 2025 summer shutdown window for renovating the injection region, this paper proposes a realignment scheme that adjusts only a small number of magnets based on high-precision alignment measurement data. The effectiveness of the scheme is then validated through numerical simulations and beam experiments.

STATUS OF ORBIT AND ALIGNMENT

The China Spallation Neutron Source [3] is a pulsed neutron source facility driven by a proton accelerator. As the core component of CSNS, the RCS undertakes the critical task of accelerating 80 MeV proton beams injected from the linac to 1.6 GeV, which subsequently strike a tungsten target to produce high-flux neutrons. The design beam power for the CSNS Phase I is 100 kW, while its upgrade project, CSNS-II, aims for 500 kW.

The CSNS RCS has a circumference of 227.92 m and adopts a four-fold symmetric lattice based on triplet focusing structure. Table 1 lists the magnet types and their corresponding number in the RCS ring. For orbit measurement and correction, a total of 32 bidirectional BPMs and 37 dipole correctors are installed around the ring.

Table 1: Summary of Magnets for the CSNS RCS

Magnet Type	Number
Dipole	24
Quadrupole	48
Horizontal Corrector	22
Vertical Corrector	15
Trim Quadrupole	16
Sextupole	16
Octupole	8

High-intensity proton synchrotrons have stringent requirements for beam loss (typically less than 1 W/m). Although the overall requirements are currently satisfied, the relatively large transverse emittance of the beam in the RCS ring, coupled with the significant horizontal orbit distortion, lead to elevated radiation doses in some areas, increasing maintenance challenges. Figure 1 shows the bare orbit of the CSNS RCS before realignment in 2025. The maximum bare horizontal orbit reaches 23.45 mm, while the vertical orbit is close to 10 mm. Even after orbit correction, the horizontal closed orbit still exceeds 10 mm.

To monitor tunnel settlement and component position changes in the CSNS RCS ring, the alignment group has conducted annual alignment measurements since 2018. For

* liyong@ihep.ac.cn

Content from this work may be used under the terms of the CC BY 4.0 licence (© 2026). Any distribution of this work must maintain attribution to the author(s), title of the work, publisher, and DOI.

ISBN: 978-3-95450-252-3 ISSN: 2673-5350 doi: 10.18429/JACoW-IPAC2026-THP5608

STUDY OF RADIATION DAMPING ENHANCED STORAGE RING LATTICE

Shouxu Zhi, Wanbin Li, Bingfeng Wei*, Yuejing Huang, Zhenghe Bai†, Guangyao Feng‡
National Synchrotron Radiation Laboratory, USTC, Hefei, China

Abstract

The reduction of beam emittance from third-generation to fourth-generation storage ring light sources is based on suppression of quantum excitation, while radiation damping becomes weaker. This leads to severe intra-beam scattering effect in fourth-generation light sources. To suppress this effect, this paper proposes a radiation damping enhanced lattice concept, which is numerically studied.

INTRODUCTION

The natural emittance of a storage ring is determined by the balance between quantum excitation and radiation damping. Suppressing quantum excitation or enhancing radiation damping can lower the emittance. Fourth-generation storage ring light sources commonly employ multi-bend achromat (MBA) lattices, where the dispersion function in bends is significantly reduced, thereby effectively suppressing quantum excitation [1]. However, the increased number of bends leads to a weaker average dipole field, which reduces the radiation energy loss. Consequently, the radiation damping becomes weaker and the damping time becomes longer. Table 1 lists the changes in natural damping time for several light sources before and after their upgrades to the fourth generation. The damping time becomes longer after the upgrade. Therefore, in the lattice design of diffraction-limited storage rings (DLSRs), the ultra-low emittance is achieved mainly by suppressing quantum excitation, while the radiation damping is generally not enhanced but rather significantly weakened, resulting in a longer damping time.

Table 1: Natural Damping Time Becomes Longer After Upgrading Third-Generation Storage Ring Light Sources to Fourth-Generation Ones

	Energy	τ_y	τ_y before upgrade
ESRF-EBS	6 GeV	13.0 ms	7.0 ms
Diamond-II	3.5 GeV	18.1 ms	7.2 ms
SOLEIL II	2.75 GeV	14.0 ms	3.3 ms
SLS 2.0	2.7 GeV	7.6 ms	6.1 ms
Elettra 2.0	2.4 GeV	9.2 ms	7.8 ms
ALS-U	2 GeV	14.4 ms	9.1 ms

Note: For ease of comparison, the natural damping times in the table are uniformly taken in the vertical direction, as the damping partition number in this direction is always 1. Meanwhile, for light sources with beam energy changes before and after the upgrade, the damping times before upgrade are converted to correspond to the upgraded energy.

* weibf@ustc.edu.cn
† baizhe@ustc.edu.cn
‡ fenggy@ustc.edu.cn

In DLSRs, especially medium- and low-energy rings, the ultra-low natural emittance and weak radiation damping can cause severe intrabeam scattering (IBS), leading to an increase in the actual equilibrium emittance. In the Hefei Advanced Light Facility (HALF) storage ring, the emittance growth induced by IBS is very severe [2]. Raising the storage ring energy to enhance radiation damping can effectively suppress this emittance growth [3,4], which is also why HALF employs electromagnets to retain the capability for energy increase. Furthermore, as the radiation from bends weakens, the contribution of radiation from insertion devices (IDs) relatively increases, and the emittance fluctuation caused by adjusting the ID gaps becomes more pronounced. which requires compensation wigglers or other means to suppress the emittance variation [5,6]. In addition, the weak radiation damping is also unfavorable for suppressing beam instabilities.

If quantum excitation is suppressed while radiation damping is not weakened but even enhanced in lattice design, the aforementioned problems will be better resolved. This paper proposes a novel wiggler-bend element for the design of radiation damping enhanced lattices.

PRINCIPLE OF RADIATION DAMPING ENHANCED LATTICE

A common solution for enhancing the radiation damping is to place damping wigglers in the dispersion-free straight sections. Damping wigglers can reduce the emittance while significantly enhancing radiation damping. The emittance reduction due to a damping wiggler with N_p periods in a dispersion-free section is [7]:

$$\frac{\epsilon_{xw}}{\epsilon_{x0}} = \frac{1 + \frac{8C_q}{30\pi J_x} N_p \frac{\beta_x}{\epsilon_{x0}\rho_w} \gamma^2 \frac{\rho_0}{\rho_w} \Theta_w^3}{1 + \frac{1}{2} N_p \frac{\rho_0}{\rho_w} \Theta_w}, \quad (1)$$

where ϵ_{x0} is the natural emittance without wiggler and ϵ_{xw} is the emittance with wiggler, Θ_w, ρ_w are wiggler parameters, J_x is the horizontal dampling partition number, C_q is the quantum radiation constant. Therefore, it would be more effective to place the wiggler at low-β_x positions. However, the β_x at straight sections is usually not very small. Taking the HALF storage ring as an example, the straight-section β_x is close to 7 m. We notice that β_x is usually small in bending magnets, and therefore a damping wiggler can be combined with a bending magnet to form wiggler-bends that can effectively enhance radiation damping and reduce emittance.

Content from this work may be used under the terms of the CC BY 4.0 licence (© 2026). Any distribution of this work must maintain attribution to the author(s), title of the work, publisher, and DOI.

ISBN: 978-3-95450-252-3 ISSN: 2673-5350 doi: 10.18429/JACoW-IPAC2026-THP5609

DYNAMIC APERTURE OPTIMIZATION BASED ON THE CONVEXITY OF THIRD-ORDER RESONANCE DRIVING TERM VARIATIONS

Wanbin Li, Zihan Wang, Yuejing Huang, Bingfeng Wei*, Zhenghe Bai†
National Synchrotron Radiation Laboratory, USTC, Hefei, China

Abstract

Reducing the longitudinal variation of third-order resonance driving terms (RDTs) is much more effective in enlarging storage ring dynamic aperture (DA) than minimizing third-order one-turn RDTs. Recently, we proved the convexity of the quantitative expression for third-order RDT variations. Then, an efficient numerical method for DA optimization was developed, where a high-quality initial population for an intelligent algorithm is generated with a Gaussian distribution based on this convexity. In this paper, we study the impact of the variance of the Gaussian distribution on the optimization performance of this method. It is found that the method shows good optimization performance for small variances, and that the performance remains robust even at a very small variance. In addition, different intelligent algorithms perform well with a small Gaussian variance.

INTRODUCTION

Dynamic aperture (DA) is a crucial metric in the design of a storage ring, as it influences beam injection and beam lifetime. In the variable space of sextupole strengths, DA typically exhibits a complex distribution characterized by multiple local optima, making its optimization a non-convex optimization problem. Recently, it was demonstrated that reducing the variation of lower-order resonance driving terms (RDTs) along the longitudinal position of a storage ring effectively reduces higher-order nonlinear terms, thereby improving DA much more effectively than reducing the commonly-used one-turn RDTs [1].

Our recent work [2] further proved that the quantitative expression for the longitudinal variation of third-order RDTs, denoted as $f_{3,\mathrm{rms}}$, is a special convex function whose distribution shows strong consistency with that of DA in the sextupole strength space. Therefore, the non-convex DA optimization problem can be approximately treated as a convex optimization problem. Based on this, an efficient DA optimization method was developed [2], in which a high-quality initial population for an optimization algorithm is generated using a Gaussian-distributed sampling based on the geometric structure of $f_{3,\mathrm{rms}}$. In this paper, we will study the impact of the variance of the Gaussian-distributed initial population on the optimization performance of the proposed method. The effect of different optimization algorithms will also be studied.

* weibf@ustc.edu.cn
† baizhe@ustc.edu.cn

CONVEXITY OF THE LONGITUDINAL VARIATION OF THIRD-ORDER RDTS

In this paper, we quantify the longitudinal variation of third-order RDTs using the expression [3]

$$f_{3,\mathrm{rms}} = \sqrt{\sum_{3=j+k+l+m} \sum_{i=1}^{N} |f_{jklm}(z_i)|^2 / N}, \qquad (1)$$

where $f_{jklm}(z_i)$ represents the geometric RDT at the position of the i-th sextupole, and N is the number of sextupoles in a storage ring lattice. Recently, we proved that $f_{3,\mathrm{rms}}$ is a special convex function whose iso-surfaces form a series of concentric, coaxial ellipsoidal surfaces in the space of the sextupole strengths [2]. When the constraint of chromaticity correction is included, $f_{3,\mathrm{rms}}$ can be expressed as a quadratic convex function defined on $\mathbb{R}^{N-2}$ [2]:

$$f_{3,\mathrm{rms}} = \sqrt{\frac{1}{2}\mathcal{K}^T \mathcal{D} \mathcal{K} + \mathcal{G}^T \mathcal{K} + \mathcal{H}}, \qquad (2)$$

where $\mathcal{K}$ is the variable vector of sextupole strengths, $\mathcal{D}$ is a positive definite matrix, $\mathcal{G}$ is a constant vector, and $\mathcal{H}$ is a constant.

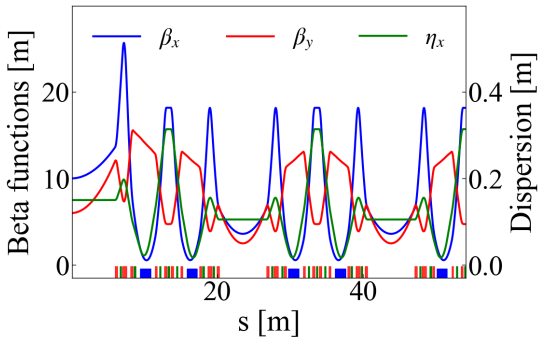

Figure 1: Linear optical functions and magnet layout for half a super-period of the SSRF storage ring lattice.

To illustrate the convexity of $f_{3,\mathrm{rms}}$ and its relationship with DA, the SSRF storage ring lattice [4], shown in Fig. 1, was used for parameter scanning in the sextupole strength space. For each nonlinear solution, $f_{3,\mathrm{rms}}$ was calculated, and DA was tracked through frequency map analysis using the `elegant` code [5]. The total frequency diffusion rate of all surviving particles, denoted as $\sum d_r$, was used to characterize both the DA size and the stability of particle motion. For this scanning case, to reduce computation cost, we regrouped the eight sextupole families into four: two (SF and SD) in the arc sections and the other two (SF1 and SD1) on both sides of the straight sections. In the scanning, the

Content from this work may be used under the terms of the CC BY 4.0 licence (© 2026). Any distribution of this work must maintain attribution to the author(s), title of the work, publisher, and DOI.

ISBN: 978-3-95450-252-3 ISSN: 2673-5350 doi: 10.18429/JACoW-IPAC2026-THP5610

STORAGE RING NONLINEAR OPTICS CORRECTION BASED ON CLOSED ORBIT BUMP

Yuejing Huang*, Bingfeng Wei, Penghui Yang, Guangyao Feng†, Zhenghe Bai‡,
National Synchrotron Radiation Laboratory, USTC, Hefei, China

Abstract

This paper presents a new method for nonlinear optics correction of storage ring lattices, which is based on locally generated orbit bumps and the corresponding response matrices. This method is conceptually similar to nonlinear optics from off-energy closed orbits (NOECO), but can be applied to the situation with harmonic sextupoles. Instead of off-energy closed orbits, it exploits the feed-down effects of sextupoles with generated local bumps to directly probe the sextupole components of a lattice. A second-order bump response matrix is constructed from the difference between orbit response matrices measured with positive and negative local bumps. A least-squares fitting procedure is then applied to minimize the difference between measured and model second-order bump response matrices, from which sextupole strength correction can be obtained. Preliminary simulations on the Hefei Advanced Light Source lattice demonstrate the theoretical viability of the method, though high sensitivity to realistic residual errors poses practical challenges that require further investigation.

INTRODUCTION

The advent of fourth-generation storage rings, characterized by multi-bend achromat (MBA) lattices, has pushed the requirement for precise tuning of nonlinear magnets to unprecedented levels. In these ultra-low emittance machines, strong sextupole and octupole magnets introduce strong nonlinearity and have a significant impact on the injection and beam lifetime [1]. Consequently, establishing an effective and precise correction scheme for nonlinear optics to restore the designed performance is of critical importance.

Currently, several established methods exist for characterizing nonlinear optics. Techniques based on extracting information from turn-by-turn beam position data, such as amplitude-dependent tune shifts, frequency maps, and resonance driving terms, can be powerful but may be limited by beam decoherence when operating at non-zero chromaticity. The LOCO method was successfully used for linear optics correction [2], while an off-energy closed orbit based method named NOECO (Nonlinear Optics from Off-Energy Closed Orbits) was proposed for the nonlinear correction [3, 4] and successfully applied at the MAX IV and NSLS II storage rings [3–5]. NOECO fits a lattice model to a measured off-energy orbit response matrix (OEORM), taking advantage of the chromatic gradient feed-down effect. However, NOECO inherently relies on dispersion to induce off-axis orbits within sextupoles. It is therefore insensitive to harmonic sextupoles located in dispersion-free regions, limiting its universality for lattices that heavily rely on harmonic sextupoles for nonlinear optimization.

Inspired by the methods of LOCO and NOECO, we propose a new nonlinear correction method, i.e., nonlinear optics from closed orbit bump, which utilizes the second-order orbit response matrix with local bumps. By introducing local closed orbit bumps at the locations of sextupoles, the feed-down effects can be exploited to calibrate the sextupole strengths regardless of the local dispersions. In this paper, the idea and framework of the nonlinear correction method are introduced. Preliminary simulations are applied to the Hefei Advanced Light Source (HALF) lattice to demonstrate the procedure, followed by a discussion of the method's limitations in the presence of realistic imperfections.

METHOD

Feed-Down Effect from Orbit Bumps

The proposed method is directly analogous to NOECO but replaces the momentum deviation δ with a spatial displacement generated by a local orbit bump. When the beam closed orbit has a transverse offset Δx from the magnetic center of a sextupole, the beam experiences a feed-down quadrupole gradient given by

$$\Delta k(s) = b_2(s)\Delta x(s), \tag{1}$$

where s is the longitudinal location, $\Delta k(s)$ is the effective quadrupole gradient, and $b_2(s)$ is the sextupole strength. Unlike the off-energy closed orbit shift $\delta x(s) = \eta(s)\delta$, where $\eta(s)$ is the dispersion and δ is the energy deviation, the local closed orbit bump $\Delta x(s)$ can be arbitrarily introduced at any sextupole location based on the orbit response matrix (ORM), granting the ability to be applied to both chromatic and harmonic sextupoles.

Provided that the linear optics has been restored, this feed-down quadrupole field perturbs the linear optics and subsequently the ORM, which can be utilized to probe the strengths of sextupoles.

Construction of Local Bump Orbit Response Matrix

Similar to the OEORM method, a symmetrization with a 2nd order orbit response matrix is utilized to isolate the linear dependence of the ORM on the sextupole strengths. The local bump orbit response matrix (LBORM) is constructed by taking the difference between two ORMs measured at two local closed orbit bumps of equal amplitude but opposite directions.

* pb188560@mail.ustc.edu.cn
† fenggy@ustc.edu.cn
‡ baizhe@ustc.edu.cn

Content from this work may be used under the terms of the CC BY 4.0 licence (© 2026). Any distribution of this work must maintain attribution to the author(s), title of the work, publisher, and DOI.

ISBN: 978-3-95450-252-3 ISSN: 2673-5350 doi: 10.18429/JACoW-IPAC2026-THP5611

LATTICE DESIGN TO ACHIEVE REVERSIBLE MICROBUNCHING IN A STEADY-STATE MICROBUNCHING (SSMB) STORAGE RING

J. Zhao, Z. Pan, X. Deng, A. Chao, C. Tang*, Tsinghua University, Beijing, China

Abstract

Steady-state microbunching (SSMB) has been proposed as a new light source mechanism to generate high average power coherent radiation in electron storage rings. One approach to achieving SSMB is the reversible microbunching scheme, which introduces a laser-based energy modulation to electron bunches in a localized insertion section to form microbunching, and then uses a subsequent energy demodulation to remove the microbunching and restore the bunches to their nominal state in the storage ring. In this paper, we report a modulation–demodulation lattice design for an SSMB storage ring based on the reversible microbunching approach. By self-consistently accounting for non-ideal effects such as intrabeam scattering (IBS) and higher-order nonlinearities, sub-nanometer longitudinal position deviations of the electrons between the laser modulators can be achieved, ensuring precise cancellation of the energy modulation and maintaining the electron bunches in a steady state, thereby ensuring high average radiation power.

INTRODUCTION

High-average-power extreme ultraviolet (EUV) and even soft X-ray sources are in increasing demand for applications in lithography [1] and scientific research [2]. The steady-state microbunching (SSMB) [3,4] light source has been proposed to address this need. By combining the high repetition rate of storage rings with the high peak power of coherent radiation, SSMB implements precise longitudinal dynamics manipulation to enable electron bunches to emit coherent radiation with power proportional to the square of the number of electrons on a turn-by-turn basis. This mechanism can achieve high average radiation power across a spectrum spanning from THz to X-rays. Different spectral ranges necessitate varying degrees of precision in longitudinal dynamics manipulation. For the EUV regime, several scenarios have been proposed, including Longitudinal Weak Focusing (LWF) [5, 6], Longitudinal Strong Focusing (LSF) [7], and Generalized Longitudinal Strong Focusing (GLSF) [8,9]. These schemes utilize the extremely small emittance in a certain dimension of the storage ring to achieve very short bunch lengths. In addition to these longitudinal focusing schemes, another approach to realizing SSMB is the reversible microbunching scheme [10]. To realize SSMB in the EUV regime, we specialize this scheme into the Echo SSMB scheme [10]. This method introduces Echo-Enabled Harmonic Generation (EEHG) [11] in a localized section of the ring to induce microbunching at the radiator for coherent emission. Subsequently, an inverse operation is applied to undo the laser modulation and bunch compression, returning the bunch to its equilibrium state. To maintain the steady state of the storage ring during such reversible operations, the modulation insertion region must be as isochronous as possible. This ensures that the energy spread growth, caused by imperfect modulation cancellation, remains minimal and within the tolerance afforded by radiation damping. In this paper, we present an insertion lattice design with sub-nanometer longitudinal path length deviation precision to meet the requirements of high-average-power EUV radiation in Echo SSMB.

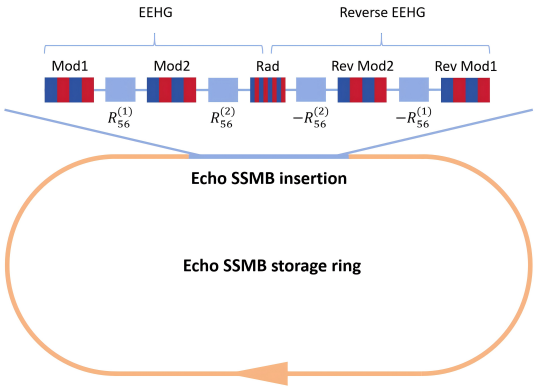

Figure 1: Schematic layout of an Echo SSMB storage ring, highlighting the insertion section encompassing the complete EEHG and reverse EEHG processes.

ECHO SSMB SCHEME

The Echo SSMB storage ring layout is illustrated in Fig. 1. Initially, the modulators Mod1 and Mod2, along with the $R_{56}^{(1)}$ and $R_{56}^{(2)}$ lattices, are configured to generate an optimal bunching factor at the radiator center. To ensure reversibility, a $-R_{56}^{(2)}$ lattice is employed to cancel $R_{56}^{(2)}$, forming an isochronous achromat between Mod2 and Rev Mod2, defined as the inner lattice. Subsequently, the energy modulation from Mod2 is removed by Rev Mod2, and a $-R_{56}^{(1)}$ lattice is introduced to neutralize $R_{56}^{(1)}$, constituting the outer lattice.

The longitudinal dynamics of the insertion are given by

$$\begin{aligned} \delta &= \delta + A_1 \sin(k_L z), \quad z = z + R_{56}^{(1)}\delta; \\ \delta &= \delta + A_2 \sin(k_L z), \quad z = z + R_{56}^{(2)}\delta; \\ z &= z - R_{56}^{(2)}\delta, \quad \delta = \delta - A_2 \sin(k_L z); \\ z &= z - R_{56}^{(1)}\delta, \quad \delta = \delta - A_1 \sin(k_L z), \end{aligned} \tag{1}$$

where A_1 and A_2 are the relative modulation amplitudes. Longitudinal path length deviations between the laser modulators lead to an increase in the energy spread of the storage

* tang.xuh@tsinghua.edu.cn

Content from this work may be used under the terms of the CC BY 4.0 licence (© 2026). Any distribution of this work must maintain attribution to the author(s), title of the work, publisher, and DOI.

ISBN: 978-3-95450-252-3 ISSN: 2673-5350 doi: 10.18429/JACoW-IPAC2026-THP5614

NONLINEAR OPTIMIZATION OF THE HALF STORAGE RING LATTICE

Bingfeng Wei*, Penghui Yang, Yuejing Huang, Guangyao Feng, Zhenghe Bai†
National Synchrotron Radiation Laboratory, USTC, Hefei, China

Content from this work may be used under the terms of the CC BY 4.0 licence (© 2026). Any distribution of this work must maintain attribution to the author(s), title of the work, publisher, and DOI.

Abstract

The Hefei Advanced Light Facility (HALF) is a 4th-generation storage ring light source currently under construction in Hefei, China. Its storage ring utilizes a modified hybrid 6BA lattice. The HALF storage ring employs off-axis injection and is planned to operate in a full-coupling mode, which requires a large dynamic aperture and control of amplitude-dependent tune shifts. This paper presents the optimization of the nonlinear dynamics for the HALF storage ring, introducing a new version of the lattice and an alternative lattice solution featuring a larger dynamic aperture.

INTRODUCTION

The Hefei Advanced Light Facility (HALF), a diffraction-limited storage ring, is currently under construction in Hefei, China. The HALF storage ring consists of 20 modified hybrid six-bend achromat (H6BA) lattice cells, providing 20 long straight sections (LSS) and 20 medium straight sections (MSS) [1, 2]. With a circumference of 479.86 m, the lattice achieves a natural emittance of 85 pm·rad at a beam energy of 2.2 GeV. All magnets in the storage ring are electromagnetic, allowing for flexible adjustment of strengths. This design not only preserves the option to increase the beam energy to 2.5 GeV but also provides considerable flexibility for lattice optimization. Although the main magnet layout and magnet designs have been finalized, the optimization of the linear optics and nonlinear dynamics continues. This paper reports the latest results on nonlinear dynamics optimization for the HALF lattice.

OPTIMIZATION MOTIVATION AND METHOD

The primary motivation for the nonlinear optimization of the HALF lattice is to control the amplitude-dependent tune shifts (ADTS), which are critical for injection. The working point of the HALF storage ring is on the linear difference resonance $\nu_x - \nu_y$, which can enhance the horizontal-vertical coupling, thereby increasing the beam volume and mitigating the intra-beam scattering (IBS) and Touschek scattering. However, this coupling complicates the off-axis injection, where the bunch is injected with a horizontal offset of approximately +6 mm. The large horizontal amplitude can couple into the vertical plane, potentially causing beam loss. Therefore, controlling ADTS is essential to keep the injected beam away from the coupling resonance. Earlier designs provided preliminary ADTS control; however, recent detailed tracking simulations revealed that the injection efficiency remains limited by coupling. Hence, further improvement of the nonlinear dynamics for the HALF lattice is required.

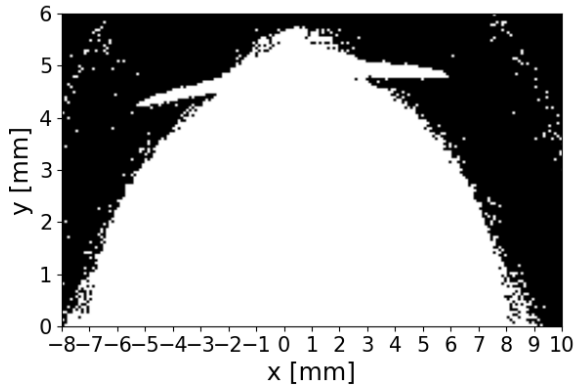

Figure 1: DA of the HALF V2024 lattice. The tracking was performed using Accelerator Toolbox [4] over 1000 turns.

In addition to ADTS control, the dynamic aperture (DA) with RF also requires improvement. Previous result presented a DA of approximately 9 mm for the HALF V2024 lattice [3], yet detailed analysis revealed an unstable region between $x = 8$ and 9 mm where particle survival is scattered. This reduces the usable DA to only about 8 mm, as shown in Fig. 1. Achieving a larger DA is therefore another key optimization goal.

Given that the HALF lattice offers few nonlinear knobs, the nonlinear optimization necessitates including quadrupole strengths as variables. In addition, HALF employs offset quadrupoles for reverse bends (RBs), allowing their quadrupole strengths to be adjusted while maintaining their dipole fields, until the offsets are fixed for installation. Furthermore, since magnet designs are already finalized, all optimizations must respect physical limits on magnet strengths.

To address the requirements above, the optimization was conducted in two stages. The first stage employed an analytical method for DA optimization and ADTS control. Reducing ring-averaged resonance driving terms (RDTs) is very effective in improving DA [5, 6], and the first-order ADTS can also be derived from driving terms. The efficiency of the analytical method enabled rapid optimization and exploration of various constraint settings. Many good solutions were obtained in this stage, with DA exceeding 8 mm and well-controlled ADTS. However, the analytical method provides indirect optimization of the actual tracking performance. In the second stage, where marginal gains in DA become important, a careful balance between DA details, ADTS, and other parameters is required. Therefore, based on the results from the first stage, the second stage performed a tracking-based optimization to enlarge the DA in the injection direction and control the tracked ADTS.

* weibf@ustc.edu.cn
† baizhe@ustc.edu.cn

ISBN: 978-3-95450-252-3 ISSN: 2673-5350 doi: 10.18429/JACoW-IPAC2026-THP5615

A PRELIMINARY STUDY OF FULL-COUPLING OPERATION FOR THE HALF STORAGE RING

P. Yang, X. Liu*, G. Liu, Y. Huang, Z. Bai
National Synchrotron Radiation Laboratory, USTC, Hefei, China

Content from this work may be used under the terms of the CC BY 4.0 licence (© 2026). Any distribution of this work must maintain attribution to the author(s), title of the work, publisher, and DOI.

Abstract

To mitigate the intra-beam scattering effects and improve Touschek lifetime, a full-coupling operation based on the linear difference resonance is preliminarily studied for the Hefei Advanced Light Facility (HALF). The dependence of coupling ratio on skew quadrupole strength and the distance to the difference resonance is analyzed. With a coupling ratio of 90 %, particle tracking simulations confirm that the expected equilibrium emittances are achieved. However, beam loss occurs during the off-axis injection due to the excitation of the vertical motion. Amplitude-dependent tune shifts are tailored by reducing the octupole strengths to shift the injected beam away from the coupling resonance, which suppresses the beam loss effectively. This study demonstrates the feasibility of high-coupling operation in HALF and highlights the importance of optimizing nonlinear detuning for good injection efficiency.

INTRODUCTION

The Hefei Advanced Light Facility (HALF) is a greenfield fourth-generation synchrotron radiation light source proposed by NSRL [1]. It operates at 2.2 GeV with a 480 m circumference comprising 20 hybrid six-bend achromat lattice cells, yielding a natural emittance of 86 pm rad. The relatively low beam energy and ultra-low emittance result in strong intra-beam scattering (IBS) effects in the storage ring, significantly increasing the equilibrium emittance and limiting the Touschek lifetime. To suppress the IBS effects and further improve the beam lifetime, a full-coupling operation (or round beam operation) mode can be adopted, in which the horizontal and vertical beam emittances are made comparable. Simulations for HALF show that, if the transverse coupling ratio is increased from 10 % to 100 %, the horizontal equilibrium emittance with the IBS effect considered can be reduced from 190 pm rad to 88 pm rad, and the Touschek lifetime increases by approximately a factor of two.

Operating the machine on the linear difference resonance with finite coupling is a straightforward way to generate round beams, which has been studied in many storage rings including APS, NSLS-II, ALBA, HEPS, Korea-4GSR, PETRA IV and SLS 2.0 [2–8]. In this scheme, the transverse tunes are adjusted to approach the difference resonance, and then weak skew quadrupoles are used to excite the resonance, thereby causing the exchange between horizontal and vertical motions. Detailed theories on the weak betatron coupling can be found in Ref. [9]. Since strong skew quadrupoles are not needed, the operation remains near a typical decoupled regime, allowing horizontal and vertical optics to be handled independently. In addition, distortions to the closed orbits, linear optics and nonlinear dynamics performance are relatively small. However, for HALF, which adopts an off-axis injection scheme, beam loss at devices with small vertical apertures (the vertical collimator and in-vacuum undulator, etc.) may occur during the injection, due to the excitation of the vertical motion.

In this paper, the full-coupling operation scheme based on the linear difference resonance is preliminarily studied for the HALF Storage. The key factors affecting the coupling ratio are first studied and then the realization of high-coupling beam is verified based on particle tracking. Finally, the issues of beam loss during the beam injection are briefly discussed.

FACTORS AFFECTING THE COUPLING RATIO

Based on the perturbation theory and ignoring the vertical dispersion, the coupling ratio of transverse equilibrium emittance at the coupling resonance can be expressed as

$$\kappa = \frac{\varepsilon_y}{\varepsilon_x} = \frac{|C|^2}{\frac{4}{1+J_x}\Delta^2 + |C|^2}, \quad (1)$$

where J_x is the horizontal damping partition number and $\Delta = \nu_x - \nu_y$ is the difference of the fractional parts of unperturbed betatron tunes. C is the coupling driving term, defined as

$$C = \frac{1}{2\pi} \oint \mathrm{d}s \sqrt{\beta_x \beta_y} K_{sq}(s) e^{i[\phi_x(s) - \phi_y(s) - \frac{2\pi s}{L}\Delta]}, \quad (2)$$

where L is the circumference, K_{sq} the skew quadrupole strength, $\beta_{x,y}$ and $\phi_{x,y}$ the unperturbed beta functions and phases at skew quadrupoles, respectively. From the equation, we see that the coupling ratio is mainly decided by the distance from resonance Δ and the coupling coefficient C, with the later one depending on the layout and the strengths of skew quadrupoles. While for Δ, in a real machine, it cannot be made exactly zero due to the tune spread inside the bunch, power supply noise and so on. APS operation shows that $\Delta \leq 0.005$ is easily reachable [2].

To avoid generating undesired vertical dispersion, 40 skew quadrupoles located in the dispersion-free regions of HALF are used to excite the linear coupling resonance. These quadrupoles currently share the same strength but different polarities to maximize $|C|$ with the smallest possible strength. The dependence of the coupling ratio on skew quadrupole strength is then studied. With Δ tuned to be 0.005, the variations of $|C|$ and κ with skew quadrupole strengths are

* liuxy@ustc.edu.cn

ISBN: 978-3-95450-252-3 ISSN: 2673-5350 doi: 10.18429/JACoW-IPAC2026-THP5616

SIMULATION OF THE MAGNET ERROR CORRECTION FOR THE SUPER TAU-CHARM FACILITY COLLIDER RINGS

J. Bao, P. Yang*, Y. Zou, L. Zhang, T. Liu, J. Tang
University of Science and Technology of China, Hefei, China

Abstract

Due to the complex optics and strong magnets of the Super Tau-Charm Facility (STCF) collider rings, the luminosity and beam dynamics are highly sensitive to magnetic field errors. Based on error sensitivity studies for the STCF and error tolerances adopted in other collider rings, a preliminary error budget has been established. This paper presents error correction results for STCF collider rings with center-of-mass energy of 2 GeV using a systematic correction chain, that includes first-turn trajectory correction, orbit correction via dispersion-free steering method, beta correction via LOCO method, and β_y^* correction with the k-modulation method. Simulation results show that after correction, the global closed orbit, β-beat, dispersion distortion, and coupling ratio are effectively reduced to acceptable levels. Consequently, the impact on nonlinear dynamics and luminosity is greatly suppressed.

INTRODUCTION

Aiming to investigate rich frontier physics in the tau-charm energy range and probe new physics beyond the standard model, the Super Tau-Charm Facility (STCF) [1, 2], proposed by the University of Science and Technology of China, is designed as a new-generation double-ring electron-positron collider. It covers a center-of-mass energy (CME) from 2 GeV to 7 GeV and reaches a high luminosity exceeding 1×10^{35} cm^{-2}s^{-1} at the optimal CME of 4 GeV. Table 1 summarizes the current main design parameters of the STCF collider rings with CME of 2 GeV. The previous magnet layout and linear optics performance of the collider rings (version 4) are presented in [1]. To reach such high luminosity, the collider adopts a large Piwinski angle and crab-waist collision scheme [3], similar to other e^+/e^- colliders including SuperKEKB [4], FCC-ee [5], CEPC [6] and BINP-SCTF [7].

Based on error sensitivity studies for STCF and the error tolerances adopted in other collider rings [8, 9], we have established a preliminary error budget, as summarized in Table 2. All errors are assumed to follow Gaussian distributions truncated at 2.5σ. The RMS horizontal and vertical misalignments of quadrupoles are generally 50 μm, with tighter tolerances of 30 μm applied to the quadrupoles in the final focus telescope section (Q_{FFT}) due to their higher sensitivity. Similarly, the RMS misalignments of sextupoles are 50 μm in the arc sections and 30 μm in the interaction region (IR). In this paper, we present the simulation of error correction for the STCF collider rings at a CME of 2 GeV, based on the version 5 lattice.

* penghui1@ustc.edu.cn

Table 1: Main Design Parameters of STCF Collider Rings at a CME of 2 GeV

Parameter	Value
Beam energy of single ring, E	1 GeV
Circumference, C	825.5 m
Natural emittance, ε_{nat}	3.25 nm
Coupling ratio, κ	1 %
Beta functions at IP, β_x^*/β_y^*	40 mm / 2 mm
Betatron tune, ν_x/ν_y	28.55 / 33.58
Beam current, I	0.8 A
Touschek lifetime τ	267 s
Luminosity, L	7.95×10^{33} cm^{-2}s^{-1}

Table 2: Magnet Error Budget of the STCF Collider Rings

Magnet	Misalignment			Rotation	Main field
	Δx (μm)	Δy (μm)	Δz (μm)	(mrad)	(%)
Dipole	100	100	100	0.1	0.02 %
Quadrupole	50	50	100	0.1	0.02 %
Q_{FFT}	30	30	100	0.1	0.02 %
Arc Sextupole	50	50	100	0.1	0.02 %
IR Sextupole	30	30	100	0.1	0.02 %

CORRECTION METHOD AND RESULTS

Correction System Layout and Correction Flow

Drawing on the experience gained from other collider rings, we outline the correction system layout as follows. Beam position monitors (BPMs) are placed in drifts adjacent to quadrupole magnets to allow beam-based alignment of their magnetic centres. Correctors are placed at locations with large beta functions: horizontally near focusing quadrupoles and vertically near defocusing quadrupoles. Sextupoles, which exhibit strong nonlinear magnetic fields, are equipped with both correctors and skew-quadrupole coils. To suppress the transverse coupling, additional dedicated skew quadrupoles are also installed in the long straight sections. Based on the error budget, 100 random error seeds are generated. To restore the orbits, linear optics, and other performance indicators, the following correction chain is performed for each seed: i) first turn trajectory correction; ii) closed orbit and dispersion correction; iii) linear optics and coupling correction; iv) β_y^* correction.

First-turn Trajectory Correction

The first-turn trajectory correction employs the trajectory response matrix and the singular value decomposition (SVD) method to steer the trajectory within the physical

Content from this work may be used under the terms of the CC BY 4.0 licence (© 2026). Any distribution of this work must maintain attribution to the author(s), title of the work, publisher, and DOI.

ISBN: 978-3-95450-252-3 ISSN: 2673-5350 doi: 10.18429/JACoW-IPAC2026-THP5617

MULTIPARTICLE BEAM DYNAMICS OF ELEBT INTEGRATED WITH UPGRADED RFQ IN LINAC4

N. Jakhar[1]*, C. Thakur[1], S. Kumar[2,3], J. Sharma[4], M. K. Kashyap[1]
[1]Renewable Energy Laboratory, School of Physical Sciences, Jawaharlal Nehru University, New Delhi, India
[2]Department of Physics and Astrophysics, University of Delhi, Delhi, India
[3]Inter-University Accelerator Centre, New Delhi, India
[4]Department of Physics, South Asian University, New Delhi, India

Abstract

Electrostatic low-energy beam transport (ELEBT) section as a part of future upgradation proposal in LINAC4 at CERN, is proposed to handle 45 keV H^- ion beam with 70 mA max beam current. The design allows maximum input rms normalized emittance of 0.5 π mm mrad without significant growth. A dual einzel system is incorporated in the decelerating-accelerating (DA) mode to control beam blow up within 70% of the beam pipe aperture. The ground electrode of these einzel systems also houses radio frequency electrodes for beam chopping. It chops the beam as per the requirement of the upgraded radio frequency quadrupole (RFQ). The transverse and longitudinal beam optics are studied for the full system of ELEBT + RFQ. It is also validated theoretically using multi particle beam analysis. We achieved beam transmission more than 90% with all emittances well in control. The design details with respect to field computation and beam dynamics will be presented.

INTRODUCTION

Linear accelerators (LINACs) are widely used as injectors to big synchrtrons and have wide range of applications in nuclear physics, medical applications, neutron generation, and material science research. The beam quality produced at the low-energy injector stage strongly affects the performance of the complete accelerator system; therefore, efficient beam transport and matching at low energies are essential. LINAC4 [1–4] is a normal conducting H^- linear accelerator developed at CERN as an injector to the Proton Synchrotron Booster (PSB), to support future high luminosity Large Hadron Collider (LHC) upgrades. The accelerator is approximately 86 m long and consists of an H^- ion source, a Low Energy Beam Transport (LEBT) section, a 352 MHz Radio Frequency Quadrupole (RFQ), a chopping line, Drift Tube Linac (DTL), Cell-Coupled Drift Tube Linac (CCDTL), and Pi-Mode Structures (PIMS). The H^- beam extracted at 45 keV is accelerated to 3 MeV by the RFQ and finally up to 160 MeV before injection into the PSB. The use of H^- ions enables efficient charge-exchange injection, reducing beam losses and improving beam brightness for the CERN accelerator chain.

The LEBT section transports the beam from the ion source to the RFQ while preserving beam quality. Conventional magnetostatic LEBT (MLEBT) systems based on solenoids are widely used in facilities such as J-PARC, ESS, IFMIF, and LINAC4. However, MLEBT systems require space charge compensation, which can lead to emittance growth and beam losses. Electrostatic low energy beam transport (ELEBT) systems provide an alternative solution with compact geometry, absence of transverse coupling, and reduced emittance growth for intense low-energy beams. Among the two operating configurations of the einzel lens, the deceleration-acceleration (DA) mode provides higher refractive power than the acceleration-deceleration (AD) mode for the same applied voltage, enabling shorter focal lengths at lower voltages and making it suitable for compact ELEBT designs.

Recently, compact ELEBT systems for LINAC4 [5] have been simulated with 93% beam transport of 70 mA H^- beams at 45 keV and proper matching to the RFQ acceptance. Previously, RFQ design and upgrade studies [6] explored beam dynamics, vane geometries, and other design parameters for compact high-current RFQ systems. Compact RFQ [7] have been studied in terms of maximum energy gains by exploiting the maximum surface fields allowed by vane materials. Furthermore, start-to-end simulation approaches [8] provide a consistent framework for understanding the complete beam transport and acceleration process. Following these studies, the present work simulates the integrated ELEBT and RFQ system for the LINAC4.

DESIGN CRITERIA FOR THE ELEBT AND RFQ

The ELEBT is designed to transport 45 keV H^- beams with minimum emittance growth and beam losses. The simulated beam transmission was optimized for beam currents up to 70 mA while matching the RFQ. A compact dual einzel lens system operating in deceleration–acceleration (DA) mode was adopted for stronger focusing and reduced emittance growth. The RFQ was designed to accelerate the H^- beam from 45 keV to 3 MeV RFQ [6] in LINAC4 RFQ, designed and upgraded with a design normalized rms transverse emittance of 0.5 π mm mrad for high-current operation (70 mA beam). The beam dynamics inside the RFQ are governed by the transverse focusing and longitudinal bunching RF fields. The longitudinal equation of motion of

* plasmaniketan@gmail.com

Content from this work may be used under the terms of the CC BY 4.0 licence (© 2026). Any distribution of this work must maintain attribution to the author(s), title of the work, publisher, and DOI.

ISBN: 978-3-95450-252-3 ISSN: 2673-5350 doi: 10.18429/JACoW-IPAC2026-THP5621

STUDY ON EVALUATION METHOD FOR TRANSIENT RESPONSE OF CONDUCTOR SURFACE TO LARGE PULSE CURRENT*

H. Iinuma†, H. Sato, Ibaraki University, Ibaraki, Japan
T. Takayanagi, Japan Atomic Energy Agency, Tōkai Mura, Japan
Y. Tanaka, Kyokuto Boeki Kaisha LTD, Tokyo, Japan

Abstract

To measure spin precession in ultra-precise magnetic fields, a method for three-dimensional spiral beam injection has been developed. For example, a muon beam with a momentum of 300 MeV/c must be confined within a controlled storage region (radius 33.3 ± 1.5 cm, height ± 5 cm) in a solenoid-type storage magnet (central magnetic flux density 3 T) based on medical MRI technology, with the local magnetic field variation controlled to be less than 0.1 ppm. A vertical kick by magnetic field is required to suppress the motion in the axial direction of the solenoid, and trial calculations have shown that a pulsed magnetic field can be excited by applying a pulsed current with a half-sine waveform (peak current 1 kA, pulse width 120 ns, frequency 25 Hz) to a kicker coil with a radius of 37 cm and a height of 10 cm. Generating a magnetic field using an extremely fast pulsed current requires a calculation method that takes into account the transient response on the conductor surface, with a skin effect of approximately 35 μm. In this presentation, we will apply the OPERA model to the geometry of the current kicker field generating conductor, and discuss the modeling by practicable mesh on the conductor surface and the evaluation of the time-space distribution of the generated kicker field. In addition, we will also discuss the model calculation method including the wall of the vacuum chamber around the kicker device.

INTRODUCTION

In this paper, we focus on the kicker system designed to control the longitudinal motion along the solenoid axis while maintaining a circular orbit with a radius of 0.33 m, and to confine the beam within the effective magnetic field region (weak focusing potential) of the solenoidal magnet. A key feature of the kicker system is that the conductor carrying the pulsed high current covers the entire storage orbit. By placing an axially symmetric kicker coil conductor inside an axially symmetric solenoidal magnetic field, an axisymmetric pulsed magnetic field is generated. This configuration ensures that the beam is naturally confined to an axisymmetric orbit, leading to highly stable beam motion during storage. The overall concept of the three-dimensional spiral injection is shown in Fig. 1 and described in Ref. [1]. Details of superconducting storage magnet design and field calculation method are given in Refs. [2] and [3].

* Work supported by JSPS KAKENHI Grant Nos. 26287055, 19H00673, 22K14061, and 23KJ0590.
† hiromi.iinuma.spin@vc.ibaraki.ac.jp

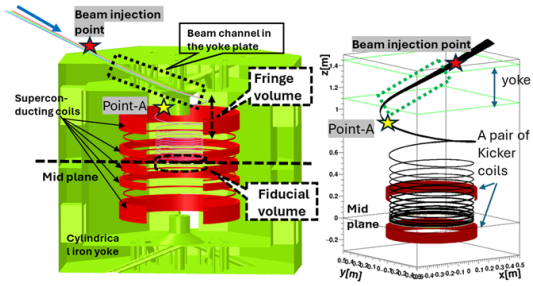

Figure 1: Schematic view of the solenoidal storage magnet and beam injection configuration.

BEAM DYNAMICS DURING THE KICK

Figure 2 shows the longitudinal motion of 1000 particles injected with optimized beam shaping and tracked under the kicker field. The trajectory is sampled every 10 ps (1000 slices correspond to 10 ns). After the kick, 974 particles are confined within $|z| < 0.05$ m, demonstrating efficient longitudinal confinement. Details of phase space matching, so-called a strong X-Y coupling, for the three-dimensional spiral injection is described in Ref. [4].

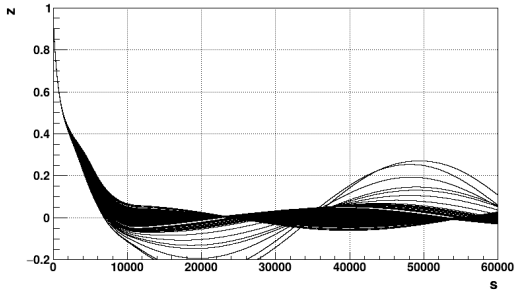

Figure 2: Longitudinal motion of 1000 particles during and after the kicker, showing confinement along the solenoid axis.

Vertical Phase Space

Figure 3 shows the longitudinal phase-space motion along the solenoid axis. The gray curves represent 200 trajectories, and the colored filamentary structures correspond to selected slices of 1000 trajectories. The kink structure around 0.2<z<0.5 m originates from the focusing effect of the kicker field. Since the solenoidal field provides strong radial focusing but weak control in the longitudinal direction, the kicker field is required to suppress the beam spread during injection. This enables efficient capture of the beam into the weak focusing potential, defining the primary role of the kicker system.

Content from this work may be used under the terms of the CC BY 4.0 licence (© 2026). Any distribution of this work must maintain attribution to the author(s), title of the work, publisher, and DOI.

ISBN: 978-3-95450-252-3 ISSN: 2673-5350 doi: 10.18429/JACoW-IPAC2026-THP5623

TOWARD A ROBUST TPS-II 6BA LATTICE

N.-Y. Huang*, F.-H. Tseng, M.-S. Chiu, H.-W. Luo, P.-J. Chou
National Synchrotron Radiation Research Center, Hsinchu, Taiwan
X. Zhang, Australian Nuclear Science and Technology Organisation, Clayton, Australia

Abstract

The Taiwan Photon Source upgrade (TPS-II) study aims to realize an ultralow emittance lattice compatible with the existing TPS tunnel. This work presents an updated 6BA lattice design with a natural emittance of 67 pm−rad at 3 GeV, followed by an preliminary evaluation of its robustness study under machine errors. A key innovation in this design is the strategic integration of sextupole components within the dipole magnets. This approach effectively flattens the amplitude-dependent tune shift (ADTS) and expands the dynamic aperture (DA) while preserving the momentum acceptance (MA). The results establish a feasible and robust path toward the next phase of TPS-II lattice development and engineering integration.

INTRODUCTION

As the TPS approaches its first decade of operation since 2016, a feasibility study for a 4th generation diffraction limited storage ring upgrade, TPS-II, is underway. TPS is a 3 GeV, 518.4 m storage ring housed in a common shielding tunnel with its booster. While the primary objective of the upgrade is to enhance scientific capabilities, energy sustainability is also a key motivation. The new lattice aims to reduce beam emittance at least tenfold from TPS of which the beam emittance is 1.6 nm−rad, resulting to an order-of-magnitude increase in brightness and coherence fraction. Following the successful experiences of 3rd- to 4th-generation storage ring light source upgrades, such as ESRF-EBS [1], APS-U [2], and SLS 2.0 [3], the team evaluated various lattice configurations, balancing the competing demands against scientific, engineering, and facility constraints [4]. To upgrade the TPS, the tangential angle of all beamlines must remain unchanged to preserve the utility of existing experimental hutches. The straight sections must remain longer than 5 m to accommodate current insertion devices and RF modules. While minimizing beamline realignment is desirable, maintaining the storage ring circumference is critical to avoid the consequential RF synchronization risks. Additionally, ensuring feasible magnet strengths is essential for not only the realistic manufacturing but also the reliable operation.

To ensure long term competitiveness and machine robustness while preserving the identical circumference in the constructed tunnel, a 6BA lattice with relaxed constraints on source-point offset has been selected as the primary candidate. A significant advantage of the 6BA lattice is its ability to cancel the nonlinear geometric driving terms between chromatic sextupoles at specified phase conditions without the need for additional harmonic sextupoles. This promising feature not only simplifies the nonlinear optimization but also relaxes the constraints on the quadrupoles adjacent to the straight sections, which are primarily dedicated to tune and phase matching. The potential of 6BA lattice is well recognized, as evidenced by ongoing upgrade studies for BESSY-III and AS-II [5, 6].

LATTICE ARRANGEMENT AND BASIC PERFORMANCE

The TPS-II 6BA lattice plans to adopt permanent combined dipoles in the arcs, which creates essential space for vacuum and diagnostic components and reduces the power consumption correspondingly. To maintain operational flexibility, the quadrupoles adjacent to the straight sections and the multi-function magnets within the arc will remain electromagnets. A multi-function magnet, refers to the SLS 2.0 design philosophy [7], incorporates quadrupole, skew-quadrupole and octupole in a single unit allowing for optics correction and coupling control within the arc. Additionally, to ensure the performance of bending beamlines, longitudinal gradient bends featuring a center field at 1.233 T are incorporated at specified survey angles.

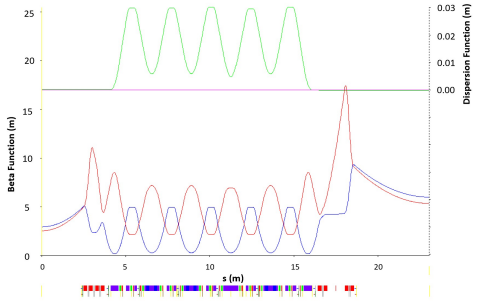

Figure 1: Optics function of the TPS-II 6BA lattice. The arrangement of elements is depicted using different colors: blue for dipoles, purple for combined dipoles, red for quadrupoles, and green for sextupoles.

The linear lattice setup and the analysis of nonlinear dynamics are performed using OPA [8], and the beam performances are verified through ELEGANT tracking [9]. Figure 1 presents the optics functions of the arc connecting the short and long straight sections. The main parameters are summarized in Table 1. The lattice achieves a natural emittance of 67 pm−rad at 3 GeV. With Intra-Beam Scattering (IBS), the horizontal emittance remains around 82 pm−rad at a bunch charge of 1.04 nC and a coupling of 12 %, achieving roughly a 20 fold reduction in emittance compared to the

* huang.ny@nsrrc.org.tw

Content from this work may be used under the terms of the CC BY 4.0 licence (© 2026). Any distribution of this work must maintain attribution to the author(s), title of the work, publisher, and DOI.

ISBN: 978-3-95450-252-3 ISSN: 2673-5350 doi: 10.18429/JACoW-IPAC2026-THP5624

APPLICATION PROGRAM FOR RW IMPEDANCE CALCULATION FOR TPS RINGS

M.-S. Chiu†, P. J. Chou, N.-Y. Huang, H.-W. Luo, F.-H. Tseng
National Synchrotron Radiation Research Center, Hsinchu, Taiwan

Abstract

A Python application program has been developed for resistive-wall (RW) impedance and coupled-bunch instability calculation in the Taiwan Photon Source (TPS) booster ring (BR) and storage ring (SR). The main purpose is to evaluate whether the RW impedance associated with present and future chamber configurations, especially the accumulation of narrow-gap insertion-device (ID) chambers planned for TPS, can become an operational concern. The code combines analytical thick-wall RW formulas with segmented chamber modelling so that each section can be assigned its own length, cross section, aperture, conductivity, and magnetic permeability. For the SR, ID segments can be imported automatically from a workbook to estimate the total RW impedance from all planned IDs and to scan mitigation options such as bunch lengthening with the passive superconducting harmonic cavity, chamber replacement, or material changes. For the BR, the same framework evaluates injection-energy RW behaviour in mixed elliptical and circular chambers. The program reports segment and total transverse RW impedances, dominant coupled-bunch modes, coherent tune shift, growth rate, and growth time through a graphical user interface (GUI) and headless export mode. It also provides a practical computational basis for future TPS upgrade (TPS-II) chamber and ID studies.

INTRODUCTION

Resistive-wall (RW) wake fields arise from the finite conductivity of the vacuum chamber and can drive transverse coupled-bunch instabilities [1]. For the TPS booster ring (BR) [2], this issue is particularly important at 150 MeV injection energy, where synchrotron-radiation damping is weak and narrow stainless-steel chambers can excite fast coherent motion. For the TPS storage ring (SR) [2], the concern is different but equally relevant: standard arc and straight chambers coexist with many insertion-device (ID) vacuum chambers, some with small gaps, so the effective RW impedance depends strongly on the installed machine configuration, bunch length, and fill pattern.

A unified application program is therefore useful for connecting chamber geometry and material choice to instability metrics that can be used in engineering design and operation studies. The present Python program was developed as a general-purpose TPS analysis tool. It sup-ports BR and SR ring presets, segmented chamber descriptions, template-based material selection, and work-book-driven ID configuration for the SR. The practical objective for TPS operation is to import the currently planned future IDs, accumulate their RW contribution together with the stand- ard SR chambers, and determine whether the resulting coupled-bunch growth times remain acceptable or require mitigation. The same software can then be reused to test cures in a controlled way, including bunch lengthening with the harmonic cavity, replacing selected chambers, increasing aperture, or changing conductivity assumptions.

The workflow is intentionally close to how TPS studies are carried out. Users first define ring parameters, then build the segmented chamber model, either manually or by importing ID metadata. The code next evaluates segment-wise RW impedance, sums the total machine impedance, samples the impedance at coupled-bunch spectral lines, and computes coherent tune shift and growth rate. Because the same data structure can be applied to both the present TPS rings and future upgrade scenarios, the program also serves as a screening platform for TPS-II [3], where new arc chambers, long straight sections, and future IDs should be checked early for possible RW-driven instability risks.

GUI AND PYTHON CODE STRUCTURE

The software is organized around ring presets, segment templates, imported ID metadata, and a shared analysis engine. At start-up, the program loads BR and SR default machine parameters, then constructs notebook pages for the visible chamber segments. In SR mode, a workbook loader reads the selected configuration sheet and rebuilds the ID pages dynamically. Each page stores editable fields for cross section, dimensions, length, conductivity, and permeability, while the numerical backend converts these values to a unified segment list before computation. This arrangement allows the user to switch from booster studies to storage-ring future-ID studies without rewriting the underlying algorithm.

The GUI shown in Fig. 1 is split into two functional regions. The left panel contains ring selection, workbook controls, machine parameters, and chamber-segment pages; a vertical splitter and a scrollable input frame keep large SR configurations accessible on a single monitor. The right panel displays segment-wise impedance curves, the full growth-rate distribution, and a zoom around the selected reference mode. A recalculation prompt prevents accidental use of stale results when parameters are changed, while the same backend also supports command-line export in nogui mode. In practice, the code structure follows a clear narrative: parse ring and segment inputs, instantiate material and geometry models, evaluate frequency-dependent RW impedance, assemble the total machine impedance, scan modal growth rates, and finally render plots and export numerical summaries.

This narrative structure was chosen so that the application remains readable for machine-physics users. Instead of

†chiu.ms@nsrrc.org.tw

Content from this work may be used under the terms of the CC BY 4.0 licence (© 2026). Any distribution of this work must maintain attribution to the author(s), title of the work, publisher, and DOI.

ISBN: 978-3-95450-252-3 ISSN: 2673-5350 doi: 10.18429/JACoW-IPAC2026-THP5626

BEAM DYNAMICS STUDIES FOR THE SPS-II 3-GeV BOOSTER SYNCHROTRON WITH 270-MeV LINAC INJECTOR*

S. Jummunt†, T. Yan, P. Boonpornprasert, S. Chunjarean, P. Sunwong, P. Sudmuang, P. Klysubun
Synchrotron Light Research Institute, Nakhon Ratchasima, Thailand

Abstract

The Siam Photon Source II (SPS-II) booster synchrotron plays a crucial role in delivering high-quality electron beams, enabling efficient injection, and ensuring stable and reliable operation of the fourth-generation storage ring. To improve booster performance and operational robustness, the linear accelerator (linac) injection energy has been upgraded to 270 MeV. This work presents comprehensive beam dynamics studies of the SPS-II booster during energy ramping from 270 MeV to 3 GeV. Particle-tracking simulations were performed under realistic operating conditions, including synchrotron radiation effects, multipole field errors, residual closed-orbit distortions, and aperture constraints. The simulation results demonstrate stable beam acceleration and high transmission efficiency throughout the energy ramping cycle.

INTRODUCTION

The Siam Photon Source II (SPS-II) storage ring is based on a double triple-bend achromat (DTBA) lattice designed to achieve a natural emittance below 1 nm·rad while supporting a stored beam current of 300 mA [1]. As the SPS-II design has progressed, several machine parameters have been refined through accelerator physics studies, including an updated RF frequency of 499.654 MHz [2] and an increase in the linac injection energy to 270 MeV.

The SPS-II booster is designed to accelerate the injected beam from the linac to 3 GeV while preserving beam quality for efficient storage-ring injection. To reduce construction costs, the booster adopts a concentric design with a minimized number of magnets and power-supply families. A FODO lattice with combined-function magnets is selected to achieve a low beam emittance of 5.89 nm·rad. In addition, the booster operates at a repetition rate of 2 Hz to support efficient top-up injection and short filling time [3]. The booster lattice and operating conditions have been systematically optimized through beam dynamics simulations under realistic machine conditions, including magnetic field errors, multipole components, magnet misalignments, residual orbit distortions, and aperture limitations [4].

The studies indicate that beam injection and the early stage of energy ramping are the most critical operating conditions affecting beam capture and transmission efficiency. Therefore, this work focuses on the investigation of injection efficiency and beam dynamics performance during energy ramping with 270 MeV injection.

UPGRADE OF LINAC INJECTION ENERGY

The original SPS-II injector design was based on a 150-MeV linac. At this low injection energy, the dipole magnets operate at low excitation current, where magnetic field stability and reproducibility become less reliable. Consequently, the injection process becomes highly sensitive to magnetic imperfections and beam mismatch, leading to orbit distortion, reduced beam capture efficiency, and beam loss during the early stage of energy ramping.

To improve injection efficiency and operational robustness, two approaches were investigated: enlarging the vacuum chamber aperture and increasing the linac injection energy [5]. Although a larger aperture could relax acceptance constraints, it would require larger magnet bores and more complex magnet and power-supply designs. Therefore, increasing the injection energy to 270 MeV was identified as the more practical and effective solution.

The higher injection energy improves magnetic field reproducibility through increased dipole operating current. Together with the enhanced beam quality provided by the upgraded linac, these improvements lead to better injection matching, higher beam capture efficiency, and more robust booster operation. However, only a single bunch with a maximum charge of 0.42 nC is generated by the linac and accelerated through the booster. Therefore, to minimize the injection time and ensure efficient storage-ring filling, the booster design emphasizes low-loss injection, stable energy ramping, and high transmission efficiency during acceleration from 270 MeV to 3 GeV.

SIMULATION MODEL AND MACHINE CONDITIONS

To evaluate booster performance under realistic operating conditions, beam dynamics simulations include magnetic field errors, multipole field components, magnet misalignments, residual closed-orbit distortions, and physical aperture constraints. The simulations were performed using the ELEGANT code [6].

Injected Beam Parameters

The injected linac beam is assumed to have an energy of 270 MeV, with a geometric transverse emittance of 10 nm·rad in both transverse planes and an energy spread of 0.36%. The linac provides a single-bunch charge of 0.42 nC. The beam is transported through the low-energy beam transport (LBT) and matched at the end of the kicker magnet, which is defined as the booster injection point. Detailed linac beam parameters will be reported elsewhere.

* Work supported by Synchrotron Light Research Institute, Thailand
† siriwan@slri.or.th

Content from this work may be used under the terms of the CC BY 4.0 licence (© 2026). Any distribution of this work must maintain attribution to the author(s), title of the work, publisher, and DOI.

ISBN: 978-3-95450-252-3 ISSN: 2673-5350 doi: 10.18429/JACoW-IPAC2026-THP5627

SYMPLECTIC INTEGRATION FOR STORAGE RING BASED FEL IN GENESIS*

Weihang Liu[1,2,3†], Fancong Zeng[1,3], Weilun Qin[1,2,3], Yu Zhao[1,2], Jianliang Chen[1,2]
[1]Institute of High Energy Physics, Chinese Academy of Sciences, Beijing 100049, China
[2]Spallation Neutron Source Science Center, Dongguan 523803, China
[3]University of Chinese Academy of Sciences, Beijing 100049, China

Content from this work may be used under the terms of the CC BY 4.0 licence (© 2026). Any distribution of this work must maintain attribution to the author(s), title of the work, publisher, and DOI.

Abstract

Symplectic integration is essential for simulating the long-term stability of systems such as storage rings. In contrast, it has traditionally been considered unnecessary for single-pass free-electron laser (FEL) simulations. Consequently, standard FEL simulation codes, like Genesis, have not fully incorporated symplectic methods in their treatment of the beam dynamics. However, with the growing interest in storage ring-based FELs, the requirement for symplectic tracking in the FEL dynamics process has emerged. This paper presents a modification of the Genesis code to implement a symplectic algorithm for its dynamical part. A comparative analysis between the symplectic and non-symplectic approaches is conducted. The results demonstrate that the symplectic Genesis preserves the symplecticity of beam dynamics without compromising the accuracy of the radiation simulation, thereby providing a more reliable tool for accurate storage ring FEL modeling.

INTRODUCTION

Symplecticity is a fundamental property of long-term conservative dynamical systems, such as the single-particle dynamics in storage rings. In such systems, symplectic integration schemes are essential for suppressing nonphysical numerical artifacts during long-term tracking. By contrast, symplecticity is usually less critical for short-term dynamical processes, such as single-pass free-electron laser (FEL) amplification, where the electron beam typically experiences the FEL interaction only once and long-term accumulation effects are absent. For this reason, most FEL simulation codes do not explicitly require symplectic integration. A representative example is the widely used GENESIS code [1].

However, with the increasing demands of advanced photon science, the limited temporal resolution and moderate single-pulse photon flux of storage-ring light sources have become bottlenecks for many experiments. FELs can provide high single-pulse flux and temporal resolution down to the attosecond regime [2], but their number of user beamlines and operational stability are still difficult to match those of storage-ring light sources. Combining storage-ring operation with FEL-type radiation processes may therefore provide a promising route toward next-generation light sources [3–6].

* Work supported by National Natural Science Foundation of China (No. 12405176)

† liuwh@ihep.ac.cn

To study the beam dynamics in such hybrid systems, a symplectic treatment of the FEL interaction becomes important. In this work, we present a symplectic improvement of the particle integration scheme based on GENESIS. The details of the proposed modification are described in the next section. Benchmark comparisons between the original and symplectic schemes are presented in Sec. 3. Finally, conclusions are given in the last section.

SYMPLECTIC MODIFICATION

In GENESIS, the FEL interaction is modeled by solving the coupled Maxwell equations and Lorentz force equations [1]. The coupling between the electromagnetic field and the particles is treated using a leapfrog integration scheme, which is symplectic. The equations of motion are separated into transverse and longitudinal parts. The transverse coordinates are advanced by first-order matrix multiplication, which also preserves symplecticity. However, the longitudinal variables, namely the particle energy and longitudinal position, or equivalently the ponderomotive phase, are integrated using a fourth-order Runge–Kutta method. Since the Runge–Kutta scheme is not symplectic in general, this part may break the symplectic structure of the full FEL tracking.

To formulate the entire FEL interaction within a symplectic framework, the Runge–Kutta integrator is replaced by a symplectic scheme. In this work, we adopt the Yoshida integrator [7], which has been widely used in accelerator tracking codes such as AT and ELEGANT [8]. The Yoshida scheme provides fourth-order accuracy by composing several second-order symplectic maps with appropriately chosen coefficients. The corresponding pseudocode is given below.

Algorithm 1 Symplectic Yoshida 4th-order Step

Require: Step size dz
1: $w_1 \leftarrow 1.35120719195966$
2: $w_2 \leftarrow -1.70241438391932$
3: SYMPLECTIC2ORDERSTEP($w_1 \cdot dz$)
4: SYMPLECTIC2ORDERSTEP($w_2 \cdot dz$)
5: SYMPLECTIC2ORDERSTEP($w_1 \cdot dz$)

ISBN: 978-3-95450-252-3 ISSN: 2673-5350 doi: 10.18429/JACoW-IPAC2026-THP5632

THEORETICAL ASSESSMENT OF STEADY-STATE MICROBUNCHING (SSMB) FOR PAL-EUV

Youngmin Park[1*], Jaehyun Kim[2], Moses Chung[1,2†],
[1]Pohang University of Science and Technology (POSTECH), Pohang, Republic of Korea
[2]Pohang Accelerator Laboratory, Pohang, Republic of Korea

Abstract

This study presents a theoretical investigation of steady-state microbunching (SSMB) within the design framework of the PAL-EUV ring. An analytic longitudinal dynamics model that includes laser-induced energy modulation, radiation damping and quantum excitation, and nonlinear momentum compaction is formulated to examine whether the baseline ring parameters can support sustained microbunch formation. Using this framework, we evaluate the required energy-chirp strength, the stability conditions for microbucket formation, and the expected radiation power under laser modulation. The analysis further identifies the conditions under which SSMB can be sustained, and provides key guidance for assessing its applicability to the PAL-EUV. These results establish a foundation for subsequent feasibility studies and future experimental development.

INTRODUCTION

Steady-state microbunching (SSMB) is a storage-ring-based light source concept that aims to generate coherent radiation with high repetition rate and high average power. In SSMB, electrons are microbunched at an optical or shorter wavelength scale so that the radiation is enhanced by longitudinal coherence. Since the original proposal, several theoretical and experimental studies have been carried out to investigate SSMB mechanisms, beam dynamics, and possible radiation applications [1–3].

Among the various schemes for generating microbunching in a storage ring, this work focuses on the feasibility of first-turn SSMB in the PAL-EUV ring. In this scheme, an energy modulation induced by an infrared laser is converted into density microbunching after one revolution in a quasi-isochronous storage ring. To satisfy the required longitudinal condition, the PAL-EUV lattice is first corrected by tuning quadrupole and sextupole families. Macroparticle tracking is then performed using ELEGANT [4], and the radiation from the resulting microbunched beam is calculated using SPECTRA [5].

PAL-EUV RING AND ONE-TURN SSMB

PAL-EUV is a compact 400 MeV electron storage ring being developed for EUV radiation applications. The ring has a circumference of 36 m and adopts a 5-bend achromat lattice to achieve low horizontal emittance and high-brightness radiation. The lattice, consisting of 14 quadrupoles and 16 sextupoles per cell, provides sufficient flexibility not only for linear optics correction but also for the control of nonlinear terms.

The low horizontal emittance of PAL-EUV can provide strong transverse coherence in the EUV wavelength range. However, the radiation from a conventional storage-ring beam is not longitudinally coherent, because the bunch length is much longer than the radiation wavelength. To obtain longitudinal coherence, the electron beam must be microbunched at the radiation wavelength or at a related seed-laser wavelength. Among the various schemes for generating microbunching in a storage ring, this study focuses on evaluating the applicability of first-turn SSMB to the PAL-EUV ring. In this scheme, a laser modulator imposes an energy modulation at the laser wavelength, and the modulation is converted into density microbunching after one revolution through the ring.

A stability conditions for first-turn microbunching is that the longitudinal slippage caused by the uncorrelated energy spread should be sufficiently small compared with the laser wavelength. This condition can be written as

$$|\eta| C_0 \sigma_\delta \lesssim \frac{\lambda_L}{2\pi}, \tag{1}$$

Here, η is the slippage factor, C_0 is the ring circumference, σ_δ is the energy spread, and λ_L is the modulation laser wavelength. Since the slippage factor depends on the relative momentum deviation δ, it can be expanded into the leading term η_0 and higher-order terms such as $\eta_1\delta$ and $\eta_2\delta^2$. Therefore, the PAL-EUV lattice should be tuned close to a quasi-isochronous condition while also controlling the nonlinear slippage terms to suppress phase smearing during one-turn transport.

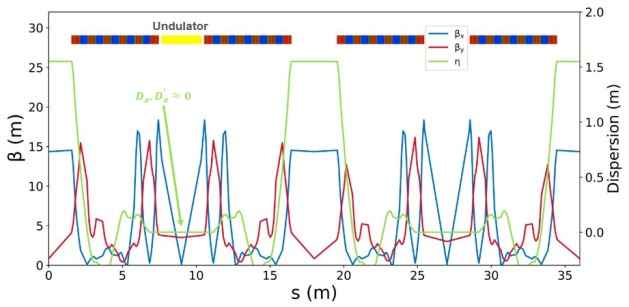

Figure 1: Corrected PAL-EUV lattice and beta functions and horizontal dispersions for the first-turn SSMB study.

* pym102048@postech.ac.kr
† moses@postech.ac.kr

Content from this work may be used under the terms of the CC BY 4.0 licence (© 2026). Any distribution of this work must maintain attribution to the author(s), title of the work, publisher, and DOI.

ISBN: 978-3-95450-252-3 ISSN: 2673-5350 doi: 10.18429/JACoW-IPAC2026-THP5633

OPTIMIZING MOMENTUM APERTURE IN KOREA-4GSR VIA HIGHER-ORDER CHROMATICITY AND W-FUNCTION ANALYSES

Junha Kim*,[1,3], Jaehyun Kim†,[3], Gyeongsu Jang[3], Jimin Seok[3],
Jaeyu Lee[3], Hyunchang Jin[4], Moses Chung‡,[2]
[1]Ulsan National Institute of Science and Technology (UNIST), Ulsan, Republic of Korea
[2]Pohang University of Science and Technology, Pohang, Gyeongbuk, Republic of Korea
[3]Pohang Accelerator Laboratory, POSTECH, Pohang, Gyeongbuk, Republic of Korea
[4]Korea Basic Science Institute, Cheongju, Korea

Content from this work may be used under the terms of the CC BY 4.0 licence (© 2026). Any distribution of this work must maintain attribution to the author(s), title of the work, publisher, and DOI.

Abstract

Diffraction-limited light sources require strong magnets that inevitably induce sever nonlinear effects and limit the Touschek lifetime (TLT). In this study, systematic tune and chromaticity scans were performed for the Korea-4GSR to identify optimal working points and characterize lattice properties under realistic errors. Analyzing momentum-dependent tune shift (MDTS) profiles clarified the physical mechanism behind the error-induced chromaticity preference. Because direct tracking-based lifetime optimization is computationally prohibitive, we propose an efficient indirect optimization method that targets the minimization of chromatic *W*-function fluctuations, effectively bypassing the multi-turn tracking bottleneck.

INTRODUCTION

The Korea-4GSR storage ring utilizes 28 Hybrid 7-Bent Achromat (H7BA) cells to achieve an ultralow emittance, incorporating 26 insertion device straight sections and 2 high-β sections [1]. Although the ring possesses a 2-fold geometric symmetry, it maintains a 28-cell symmetry in terms of on-momentum phase advances [2]. However, the extremely strong quadrupoles and sextupoles required for emittance reduction induce severe nonlinear beam dynamics, restricting the momentum aperture (MA) and limiting the TLT.

To identify the optimal operating working points for maximizing the TLT baseline, systematic chromaticity scans were executed under both ideal and error-affected conditions, revealing a distinct discrepancy in lifetime behavior depending on lattice errors. To navigate this error-induced regime, a direct tracking-based Multi-Objective Genetic Algorithm (MOGA) optimization was first performed to maximize on-momentum dynamic aperture (DA) and tracking-derived TLT.

The optimization results closely matched the scans, and deeper analysis highlighted correlation between suppressed off-momentum chromatic *W*-function fluctuations and enhanced TLT baseline. Guided by this physical relation, an indirect MOGA optimization framework was formulated. Replacing the intensive multi-turn tracking loops with the fast minimization of *W*-function fluctuations eliminated the computational bottleneck, drastically accelerating the optimization speed while securing a robust lattice design.

* joonha9609@postech.ac.kr
† Corresponding author: picoma@postech.ac.kr
‡ Corresponding author: moses@postech.ac.kr

SYSTEMATIC LATTICE SCANS

Systematic 2D chromaticity scans (ξ_x, ξ_y) were performed to explore off-momentum dynamics. As shown in Fig. 1, a striking discrepancy in TLT behavior is observed between the lattices. In the ideal bare lattice (Fig. 1a), the peak lifetime occurs at higher horizontal (ξ_x) and lower vertical chromaticity (ξ_y). Conversely, introducing realistic errors shifts this preference to a low ξ_x and high ξ_y region (Fig. 1b). This occurs because off-momentum particles easily survive integer resonance crossings in the bare lattice where driving terms are weak, whereas errors severely amplify these resonances, triggering premature beam loss as soon as the tunes hit the integer lines.

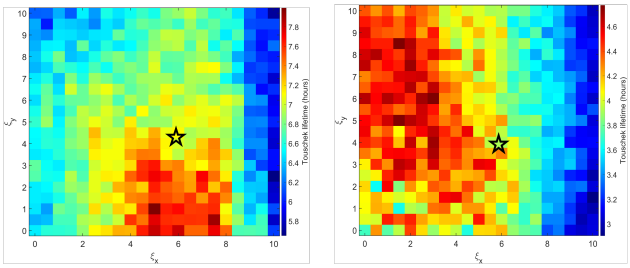

(a) Bare lattice (b) Error lattice

Figure 1: Systematic chromaticity scans (ξ_x, ξ_y) evaluating the Touschek lifetime for (a) the ideal bare lattice and (b) the error lattice with alignment and multipole errors. The color bars indicate the Touschek lifetime in hours. The black stars represent the initial chromaticity configuration.

To clarify this mechanism, the second-order horizontal chromaticity $|C_{x,2}|$ was mapped, revealing a strong inverse correlation with the TLT distribution (Fig. 2). Insufficient lifetime configurations (Min) correspond precisely to regions where $|C_{x,2}|$ is excessively amplified, whereas the optimal configuration (Best: $\xi_x = 1, \xi_y = 6$) minimizes this term. This relationship is confirmed by the MDTS curves evaluated in the dispersion-free region (Fig. 3). Minimizing $|C_{x,2}|$ flattens and broadens the parabolic tune footprint, delaying off-momentum particles from intersecting the destructive integer resonance line ($\nu_x = 69.0$), thereby extending the MA and lifetime.

ISBN: 978-3-95450-252-3 ISSN: 2673-5350 doi: 10.18429/JACoW-IPAC2026-THP5634

OPTIMAL FIELD PROFILE IN LONGITUDINAL-GRADIENT SUPERBEND MAGNETS FOR THE HEFEI ADVANCED LIGHT SOURCE VIA MULTI-OBJECTIVE OPTIMIZATION

J. Xia*, Z. Bai, Ch. Chen, J. Xu, Z. Zhu, J. zhao,
University of Science and Technology of China, Hefei, China

Abstract

The Hefei Advanced Light Source (HALF) covers the VUV to soft X-ray range and plans to replace two conventional 0.9 T B4 dipoles in the storage ring with 6 T superbends to extend the photon-energy reach. Increasing the peak field while keeping the field integral unchanged leads to significant changes in the field profile, which may affect the storage-ring optics and beam parameters. To identify a field profile that preserves machine performance, this work applies a multi-objective genetic algorithm to optimize the longitudinal field distribution of the superbend. The resulting profile reduces the impact of the enhanced peak field on lattice performance and provides guidance for the magnetic design and implementation of the superbend for HALF.

INTRODUCTION

The Hefei Advanced Light Source (HALF) is designed to provide high-brightness synchrotron radiation in the vacuum ultraviolet (VUV) to soft X-ray range. To extend its photon-energy reach, the conventional 0.9 T B4 dipoles in the 5th and 15th cells are planned to be replaced by 6 T superbends, as illustrated in Fig. 1 [1].

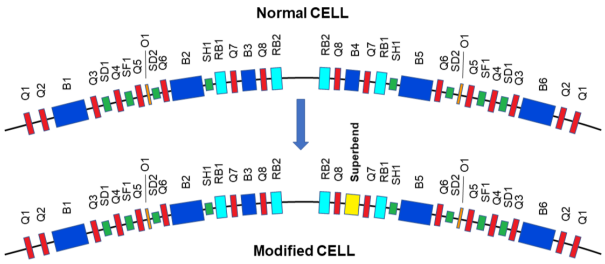

Figure 1: Magnet layout of a normal and modified cell. The LGB and superbend magnets are shown in blue and yellow, respectively.

To preserve the original bending angle, the superbend field integral should remain consistent with that of the conventional B4 dipole. With the peak field increased from 0.9 T to 6 T, the longitudinal field profile must be optimized to enhance the high-energy photon capability while maintaining acceptable lattice performance.

In this work, a multi-objective genetic algorithm is used to optimize the longitudinal field profile of the HALF superbend and provide a target profile for subsequent magnetic design.

* waterx09@gmail.com

SUPERBEND FIELD PROFILE AND OPTIMIZATION PROBLEM

Baseline Dipole and Superbend Requirement

The main B4 dipole parameters and superbend requirements are summarized in Table 1. Fig. 2 compares the B4 field profile with an illustrative superbend profile having the same field integral. Under the fixed field-integral constraint, the 6 T peak field requires a shorter effective high-field region, making the longitudinal field profile a key design variable.

Table 1: Main Parameters of the B4 Didpole and Superbend

Item	Unit	B4	SB
Peak field	T	0.9	6
Field integral	T·m	0.3682	
Bending angle	°	2.87	
Magnetic length	mm	560	< 500
Pole gap	mm	46	> 40
GFR	mm	±8	
$\Delta B/B$ and multipoles	/	$< 5 \times 10^{-4}$	

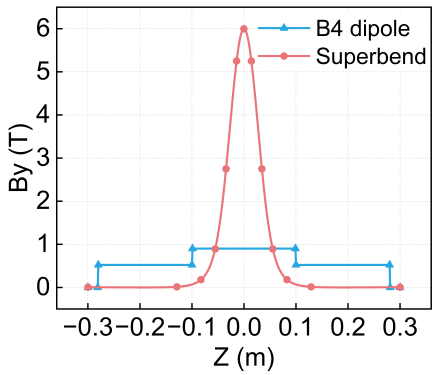

Figure 2: Longitudinal field profiles of the conventional B4 dipole and an illustrative superbend.

Field-Profile Parameterization

Previous studies have shown that hyperbolic profiles can closely approximate optimized longitudinal-gradient bending-magnet fields while maintaining a smooth analytical form [2]. Therefore, a hyperbolic-like function is adopted to parameterize the longitudinal field profile of the superbend.

Assuming symmetry with respect to the magnet center, a relative field distribution is defined as

$$B_{\mathrm{rel}}(z) = \frac{1}{\left[1 + h\left(\frac{|z|}{z_0}\right)\right]^m}, \quad (1)$$

Content from this work may be used under the terms of the CC BY 4.0 licence (© 2026). Any distribution of this work must maintain attribution to the author(s), title of the work, publisher, and DOI.

ISBN: 978-3-95450-252-3 ISSN: 2673-5350 doi: 10.18429/JACoW-IPAC2026-THP5635

CODE BENCHMARKING OF LONG-TERM STORAGE OF HIGH INTENSITY BUNCHED BEAM

A. Engeda*, Goethe University Frankfurt, Frankfurt am Main, Germany
Y. Yuan, Institute of High Energy Physics, Beijing, China
G. Franchetti, GSI Helmholtz Centre for Heavy Ion Research, Darmstadt, Germany

Abstract

Most PIC solvers used in accelerator physics rely on 2D field models, which can limit accuracy for moderate to high intensity beams where space–charge effects dominate. A common approach to compute the self–consistent electric field in particle–based simulation codes is the use of a spectral Poisson solver based on FFT. In the "MICROMAP" library, a fully 3D FFT–based Poisson solver has been implemented. At the China Spallation Neutron Source (CSNS), an alternative technique based on tensor decomposition (TD–based) has been developed "TEST" (Tensor Element Symplectic Track). In this proceeding, we present a benchmark comparing the traditional FFT–based solver implemented in "MICROMAP" and the TD–based method for long–term tracking of high intensity bunched beams at low energy in the 3-dimensional space. We examine the differences in the beam rms dimension tracked over a long term.

INTRODUCTION

Space–charge effects are central in high intensity beam dynamics, significantly affecting the envelope evolution. In particle–in–cell (PIC) simulation, these effects are typically computed by depositing the particle charge onto a mesh, solving Poisson's equation calculating the smoothed electrostatic potential [1–3]. By differentiating the potential, one obtains the electric field. For realistic beam distributions, analytic solutions of Poisson's equation are difficult to determine, so numerical solvers are required. Among the most common approaches are FFT–based solvers and more recent TD–based methods [4, 5].

A benchmark of these two approaches is presented in the context of a PIC code with emphasis on numerical comparability. We compare the two solvers under identical beam and lattice parameters, focusing on long–term rms evolution.

Governing Equations

The electrostatic potential $\phi(\vec{x})$ generated by the beam charge density $\rho(\vec{x})$ satisfies Poisson's equation $\vec{\nabla}^2\phi(\vec{x}) = -\frac{\rho(\vec{x})}{\epsilon_0}$, where ϵ_0 is the vacuum permittivity. Once ϕ is computed, the electric field is obtained by $\vec{E}(\vec{x}) = -\vec{\nabla}\phi(\vec{x})$. In a PIC framework the charge density is represented on a mesh from macro-particles whose charge is deposited onto nearby grid points. Poisson's equation is then solved on that mesh and the resulting electric field is interpolated back into the position of the particles to update their momenta. This sequence is repeated over many time steps, making the Poisson solver one of the dominant components in the computational load.

* engeda@iap.uni-frankfurt.de

THEORETICAL FRAMEWORK

Spectral FFT Method

The classical spectral approach uses the fact that, under suitable boundary conditions, the discrete Laplacian is diagonalized on a Fourier basis. In the simplest free space or periodic setting, the potential can be solved by transforming the charge density into Fourier space, dividing by the wavenumber dependent Laplacian symbol, and transforming back to physical space. This makes FFT-based Poisson solvers particularly attractive because they avoid explicit assembly of large sparse matrices and can be implemented with very low algorithmic complexity per grid point.

For a uniform Cartesian grid, the method can be summarized as follows:

1. Deposit the charge density ρ in the mesh. Transform ρ into Fourier space using FFT.
2. Solve the algebraic relation for each mode, $\tilde{\phi}^{(\vec{k})} = -\frac{\rho(\vec{k})}{\epsilon_0\vec{k}^2}$.
3. Apply inverse FFT to recover the electric potential ϕ.
4. Compute the electric mean field $\vec{E} = -\vec{\nabla}\phi$, in physical space.

The strength of the FFT method is its speed. It is especially effective when the computational domain is rectangular and the boundary conditions are compatible with the transform basis. Its main limitations are reduced flexibility for complex geometries and the need for careful treatment of boundary conditions. In beam dynamics applications, FFT–based solvers are widely used because they provide a good balance of accuracy and computational cost for large scale simulations.

Tensor Decomposition Method

Tensor decomposition methods represent multidimensional arrays and operators in compressed low-rank format [4, 5]. Instead of storing the full 3D grid or operator explicitly, the method approximates them using factors whose size grows much more slowly with dimension. This is especially valuable in 3D Poisson problems, where the full tensor product structure can be expensive in memory and arithmetic cost.

Based on this method, we use tensor decomposition and n-mode product. The algorithm of TDM is following, first we obtain the charge density tensor $\hat{\rho} = K\times_1 U^{(1)}\times_2 U^{(2)}\times_3 U^{(3)}$ with PIC method and suppose the potential tensor $\hat{\varphi} = S \times_1 U^{(1)} \times_2 U^{(2)} \times_3 U^{(3)}$, where the basis $U^{(1)}$, $U^{(2)}$ and

Content from this work may be used under the terms of the CC BY 4.0 licence (© 2026). Any distribution of this work must maintain attribution to the author(s), title of the work, publisher, and DOI.

ISBN: 978-3-95450-252-3 ISSN: 2673-5350 doi: 10.18429/JACoW-IPAC2026-THP5636

BENCHMARKING IMPEDANCE CALCULATIONS FOR TWO TYPES OF TRANSITION STRUCTURES IN HALF: CST VS. ECHO3D

X. Huang, H. Yao, J. Xiao, T. He*, University of Science and Technology of China, Hefei, China

Abstract

Photon masks and tapered transitions in the Hefei Advanced Light Facility (HALF) storage ring are typical transition structures that can make non-negligible contributions to the geometric impedance. In this work, ECHO3D is used to benchmark the CST calculations for these two types of structures. The longitudinal and transverse wake potentials, the corresponding impedance spectra, and the resulting loss factor, kick factor, and effective impedance are analyzed and compared. This study provides a reference for impedance evaluation of these transition structures in HALF.

INTRODUCTION

The Hefei Advanced Light Facility (HALF) is a diffraction-limited storage-ring light source currently under construction [1]. In the storage ring, 11 tapered transitions will be installed in Phase-I to match the small-gap insertion-device chambers to the vacuum pipe with a diameter of 26 mm. In addition, 248 photon masks are installed in the ring to intercept synchrotron radiation and protect sensitive vacuum components. Previous studies have shown that both tapered transitions and photon masks can make non-negligible contributions to the impedance budget of HALF: tapered transitions because of their relatively large single-element impedance, and photon masks because of their large number [2].

Previous results for these two types of structures were obtained using CST Wakefield Solver [3]. To assess their reliability, ECHO3D [4] is used in this work to benchmark the CST calculations. The models of the photon mask and tapered transition are shown in Fig. 1. For benchmarking purposes, the central elliptical pipe section in the tapered-transition model is shortened to 30 mm to reduce the computational cost. In the actual HALF design, this section has two lengths, 1.95 m and 4.56 m. The main parameters of the photon masks and tapered transitions are summarized in Tables 1 and 2, respectively.

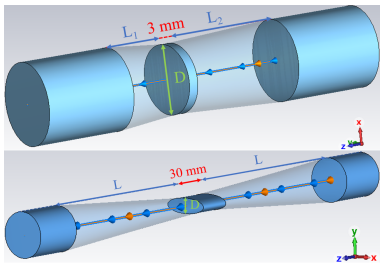

Figure 1: Schematic models of the photon mask (top) and the tapered transition (bottom).

In Table 1, Types 1, 2, and 3 correspond to (L_1, L_2) values of $(37, 20)$, $(32, 20)$, and $(25, 15)$ mm, respectively, and the listed β functions are averages over the corresponding mask locations. For the tapered transitions in Table 2, the average beta functions at the corresponding locations are $\beta_x = 6.99$ m and $\beta_y = 3.12$ m.

Table 1: Summary of Photon-Mask Parameters

Component	D [mm]	Type	β_x [m]	β_y [m]	N_{elem}
Mask 1	22.8	1	5.90	9.04	20
Mask 2	24	1	4.11	6.65	20
Mask 3	23.2	1	2.18	3.71	20
Mask 4	20	2	1.41	5.88	20
Mask 5	22	1	2.97	2.54	20
Mask 6	24	3	2.33	3.78	20
Mask 7	20.4	1	2.59	7.69	20
Mask 8	24	1	7.94	6.96	16
Mask 9	24	1	7.94	6.96	4
Mask 10	24	1	6.24	8.64	2
Mask 11	24	1	6.24	8.64	6
Mask 12	20	1	1.51	14.67	20
Mask 13	20.4	1	3.37	11.71	20
Mask 14	22	2	5.79	7.73	20
Mask 15	20.8	1	7.78	5.22	20

Table 2: Summary of Tapered-Transition Parameters

Component	D [mm]	L [mm]	N_{elem}
Wiggler	8	110	2
HU115	9	110	1
EPU120	12.6	110	1
EPU42/46/63	8	110	3
EPU44A/44B	8	50	2
LPU38A/38B	8	110	2

To resolve the geometric impedance up to 200 GHz and the short-range wakefield details, a Gaussian bunch with an rms length of 0.5 mm is used in both codes. In CST, the wakefield solver with the indirect-interfaces integration method is employed to handle the concave geometries. The longitudinal and transverse mesh sizes in CST are approximately 25 μm and 50 μm, respectively. In ECHO3D, the corresponding mesh sizes are 50 μm and 100 μm, respectively, following Ref. [5]. Test calculations show that the ECHO3D results are essentially converged with respect to the longitudinal mesh, whereas further refinement of the transverse mesh is limited by the available computer memory. The resulting wake potentials and impedance spectra are then used to evaluate the loss factor, effective impedance, and kick factor for the benchmark.

* htlong@ustc.edu.cn

Content from this work may be used under the terms of the CC BY 4.0 licence (© 2026). Any distribution of this work must maintain attribution to the author(s), title of the work, publisher, and DOI.

This is a preprint - the final version is published with IOP

ISBN: 978-3-95450-252-3 ISSN: 2673-5350 doi: 10.18429/JACoW-IPAC2026-THP5638

EXPERIMENTAL DESIGN FOR VALIDATING RELATIVISTIC PONDEROMOTIVE DYNAMICS VIA LASER MODULATION OF MeV ELECTRON BEAMS*

J. Zhang, G. Feng, Z. He†, Y. He, X. Xu, F. Zhang, H. Zhang, J. Chen,
National Synchrotron Radiation Laboratory,
University of Science and Technology of China, Hefei, China

Abstract

We present a design for the experimental validation of relativistic ponderomotive dynamics on a realistic MeV electron-beam platform. The scheme combines an S-band gun with a co-propagating focused laser pulse to induce longitudinal momentum modulation in relativistic electrons. Using a non-paraxial laser-field model and beam-dynamics simulations, we evaluate the expected post-interaction energy signatures and their observability on a practical beamline. Particular attention is given to the dependence of the modulation on laser focusing, beam parameters, and synchronization errors. The analysis identifies the dominant force contributions governing the final energy distribution. These results provide a practical route for translating previously derived relativistic ponderomotive theory into a testable experiment.

INTRODUCTION AND OBJECTIVE

In previous work, relativistic ponderomotive dynamics in focused laser fields were derived analytically [1–3]. The present study addresses the next step required for experimental validation, namely the translation of that theoretical framework into a practical beamline configuration with realistic MeV electron-beam and laser parameters.

The proposed scheme is based on an S-band electron gun and a co-propagating focused laser pulse, with the aim of generating a measurable longitudinal momentum modulation in a relativistic electron bunch. In this context, the relevant question is whether the corresponding post-interaction energy signature can be resolved under realistic operating conditions, including finite emittance, energy spread, focusing constraints [4, 5], as well as laser–electron interaction effects and relativistic ponderomotive response [6, 7].

The objective of this paper is therefore to establish a parameterized validation scheme for relativistic ponderomotive dynamics. A realistic experimental layout is defined, the corresponding observables are identified, and the expected modulation signatures are evaluated by means of field-based beam-dynamics simulations.

THEORETICAL BASIS AND VALIDATION PRINCIPLE

The on-axis longitudinal ponderomotive response in a focused traveling-wave laser field was derived in the laboratory frame as

$$F_{p,z}^{(\mathrm{theory})} \simeq -\frac{q^2}{2m}\left[\frac{1}{\gamma_0(\omega - kv_{0z})^2}\partial_z\langle E_z^2\rangle - \frac{2\langle E_z^2\rangle}{\gamma_0^2(\omega - kv_{0z})^3}\partial_z\Omega_{\mathrm{OC}}\right], \quad (1)$$
$$\Omega_{\mathrm{OC}} = \gamma_0(\omega - kv_{0z}),$$

where $\langle E_z^2\rangle$ is the cycle-averaged squared longitudinal field on axis and Ω_{OC} is the Doppler-shifted carrier frequency in the oscillation-center frame. Eq. (1) is the primary theoretical quantity from which the present validation scheme is constructed [1, 8, 9].

However, the applicability of Eq. (1) is itself conditional, because it relies on the cycle-averaged description of the laser–electron interaction [3, 10]. This validity is governed by the effective number of optical cycles experienced by the electron within the interaction region,

$$N_{\mathrm{eff}} \simeq \frac{|\Delta\Phi|}{2\pi} = \frac{2\pi w_0^2}{\lambda^2}\frac{1 - s\beta_e}{\beta_e} - \frac{1}{4}, \quad (2)$$

where w_0 is the focal waist, λ is the laser wavelength, $\beta_e = v_{0z}/c$, and $s = 1$ and $s = -1$ correspond to co-propagating and counter-propagating geometries, respectively. The condition $N_{\mathrm{eff}} \geq N_{\mathrm{min}}$ then defines a critical beam waist, analogous to phase-slippage and finite-interaction-length effects in laser–electron interactions [11],

$$w_0^{\mathrm{crit}} = \sqrt{\frac{(N_{\mathrm{min}} + 1/4)\lambda^2\beta_e}{2\pi(1 - s\beta_e)}}, \quad (3)$$

which separates the multi-cycle regime, where cycle averaging is reliable, from the near-critical and sub-cycle regimes, where phase-dependent effects become increasingly important [1].

This point determines the validation strategy adopted in the present work. The experiment is not designed merely to detect a nonzero downstream energy change, but to test whether the observed beam response evolves with w_0 in the manner predicted by Eqs. (2) and (3). In other words, the quantity to be validated is not only the longitudinal ponderomotive response itself, but also the transition between interaction regimes controlled by the laser waist. The critical waist therefore becomes the central physical concept linking the theory to the experiment.

The final diagnostic is a downstream magnetic spectrometer, since the force in Eq. (1) cannot be measured directly.

* Work supported by the National Key Research and Development Program of China (Grant No. 2024YFA1612200).

† hezhg@ustc.edu.cn

Content from this work may be used under the terms of the CC BY 4.0 licence (© 2026). Any distribution of this work must maintain attribution to the author(s), title of the work, publisher, and DOI.

ISBN: 978-3-95450-252-3 ISSN: 2673-5350 doi: 10.18429/JACoW-IPAC2026-THP5639

DESIGN CONCEPT OF CERAMIC CHAMBERS AT THE J-PARC RCS: AN ANALYTICAL PERSPECTIVE

Y. Shobuda*, Japan Proton Accelerator Research Complex, Tōkai Mura, Japan
M. Kinsho, Japan Atomic Energy Agency, Tōkai Mura, Japan
T. Toyama, High Energy Accelerator Research Organization, Tsukuba, Japan

Abstract

Ceramic chambers are essential for rapidly accelerating high-intensity beams at the J-PARC RCS, as they mitigate the effects of eddy currents on the chambers. An analytical perspective could provide valuable insight into the design of ceramic chambers, though computer simulations and demanding measurements need to certify the estimates. The identity of bending magnets, including chambers, is a key to reducing beam losses at the injection area of the RCS.

INTRODUCTION

The 3-GeV RCS (rapid cycling synchrotron) [1] at J-PARC [2] is a proton accelerator to achieve a 1-MW beam by accelerating two bunches containing $N_b = 4.15 \times 10^{13}$ particles per bunch (ppb) from 400 MeV to 3 GeV in 20 ms with a repetition rate of 25 Hz [3], without any transverse feedback system [4].

Developed ceramic chambers [5], as shown in Fig. 1 [6], are placed in all magnets at the RCS. The outer surface of the ceramic, with radius a_{II}, is covered with N rectangular copper stripes (RF shields) of horizontal width h_x and radial thickness t, each stripe terminated at one end by capacitors. The inner surface, with radius a_I, is coated with a titanium nitride (TiN) layer of thickness Δ. The ceramic chambers with TiN coating are essential for rapidly accelerating high-intensity beams within 20 ms, as they mitigate the effects of eddy currents in the chamber and suppress secondary electron emission when the halo part of the proton beam collides with the chamber surface, avoiding the electron cloud instability [7].

An analytical analysis could provide valuable insights in designing the ceramic chambers, which may assist the development of ceramic chambers in the next generation, supported by the success of the J-PARC RCS [3].

DESIGN CONCEPT IN TERMS OF BEAM-IMPEDANCES AND CHAMBER HEATING

Determination of the Thickness of RF shields

Since the screening effect of the electromagnetic field is important for designing the RF shields, the thickness t of the RF shields is determined by considering the leakage field from the chamber [8].

For simplicity, let us consider a g long cylindrical metal chamber with conductivity σ_c, where the inner radius and

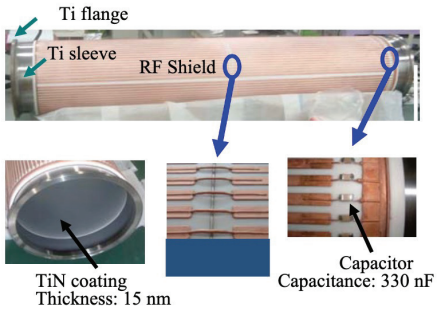

Figure 1: A ceramic chamber covered with RF shields.

the thickness are a_{II} and t, respectively. At this standpoint, it is essential to accelerate 'non-relativistic' beams with Lorentz-β and -γ at the RCS. Finally, the general form of resistive-wall impedance, except for the space charge impedance [9, 10], is simplified as [11],

$$Z_L \simeq \frac{\nu_2 g}{2a_{II}\pi\sigma_c \tanh(\nu_2 t)}, \tag{1}$$

for the non-relativistic beams, in the frequency range of

$$\frac{\frac{c\beta^2\gamma^2}{2\pi t\sigma_c Z_0(a_{II}+t)\left|\Gamma+\log[\frac{(a_{II}+t)}{t^2\beta\gamma Z_0\sigma_c}]\right|}}{\sqrt{[1+\frac{t\beta^2\gamma^2}{(a_{II}+t)(\Gamma+\log[\frac{(a_{II}+t)}{t^2\beta\gamma Z_0\sigma_c}])}]}} \lesssim f < \frac{c}{\pi t^2 Z_0\sigma_c}, \tag{2}$$

with c is light velocity, $k = \omega/c\beta$, $\nu_2 = \sqrt{k^2 + jk\beta Z_0\sigma_c}$, $Z_0 = 120\pi$ [Ω], and $\Gamma = 0.577216$. Notice that Eq. (1) becomes a dc-resistance when the skin depth is larger than t, which means that the wall currents shield the electromagnetic field from the non-relativistic beam.

Figure 2 illustrates the outcomes with the parameters $t = 0.5$ mm, $\sigma_c = 5.9 \times 10^7$ S/m, $a_{II} = 157.7$ mm, $g = 0.86$ m, and $\beta = 0.97$. The red, blue, green, and black lines represent the exact result of the resistive-wall impedance [9, 10], the exact result for infinite t, Eq. (1), and the dc-resistance, respectively. Eq. (1) well reproduces the exact result. When the skin depth exceeds t ($f \lesssim 17$ kHz), the impedance approaches the dc-resistance until the frequency becomes extremely low, around 50 Hz. Ultimately, whether this low-frequency limit is sufficient to shield the electromagnetic fields was validated by measurements [12].

Determination of the Area Ratio Covered by the Stripes

The area ratio $\theta = Nh_x/2\pi a_{II}$ covered by N stripes is determined by referring to the space-charge impedance [13]

* yoshihiro.shobuda@j-parc.jp

Content from this work may be used under the terms of the CC BY 4.0 licence (© 2026). Any distribution of this work must maintain attribution to the author(s), title of the work, publisher, and DOI.

ISBN: 978-3-95450-252-3 ISSN: 2673-5350 doi: 10.18429/JACoW-IPAC2026-THP5642

IMPEDANCE STUDIES ON THE ELECTROSTATIC SEPARATORS

N. Wang*, Y.Z. Liu, Y.D. Liu, S.K. Tian, B. Chen
Institute of High Energy Physics, CAS, Beijing, China
University of Chinese Academy of Sciences, Beijing, China

Abstract

Electrostatic separator is a crucial component required in the future high energy circular electron position colliders to separate electron and positron beams, therefore the two beams can be separated, either to avoid beam collision at certain locations or share the RF cavities at high beam operation energies. The impedance contribution from the component is one of the main concerns during the design of the electrostatic separators. In this paper, the impedance characteristic of the electrostatic separator is investigated systematically. The transverse higher order modes trapped in the component is examined by simulations. The mitigation of the trapped modes is also explored.

INTRODUCTION

Electrostatic separators have been used extensively in the 19th century in electron positron colliders to generate closed orbit displacements of opposite sign depending on the charge of the stored beams. So that parasitic collisions can be avoided outside the experimental detector. This scheme allows multiple bunches of electrons and positrons to be stored when the two beams sharing the vacuum chamber, thereby increasing the luminosity, such as in LEP [1], BEPC [2], and CESR [3], etc. Nowadays, along with the development of the future high energy electron positron colliders, the wide operating beam energy range required quite different RF voltages. In order to save the number of cavities at top energies, the sharing scheme of RF cavities in both rings were proposed in the Circular Electron Positron Collider (CEPC) [4]. The electrostatic separators, combined with dipole magnets are utilized to provide both electric and magnetic fields in order to assure both beams pass through the centre of RF cavities, while avoiding synchrotron light hits the cavities. For the incoming beam, the electric and magnetic forces cancel each other, leaving the beam undeflected. For the outgoing beam, the electric and magnetic forces act in the same direction, yielding a doubled deflecting force. In CEPC, 40 separators are requried and located symmetrically at both ends of the RF regions. During Higgs mode, all RF cavities are shared by the electron and positron beams. For the W and Z modes, the separators in the RF region are turned off so that all bunches can be filled around the entire electron and positron rings.

The electrostatic separators show several impedance effects that may degrade the machine performance. First, the parasitic beam power loss in the components can cause heating of the electrodes, which may further induce increased outgassing and thus provoke a significant rise in pressure [1]. Besides, they have been important contributors to the overall impedance and the RF fields generated during the beam passage can also degrade the high voltage performance. Recent studies in CEPC show that the transverse trapped modes in the component are important contributors to the coupled bunch instabilities at the Z-pole operation mode [5].

In the following, the design features and impedance characteristics of the electrostatic separator are introduced. Then the properties of the transverse trapped modes and their influence to the beam are presented, followed by an investigation of potential mitigation strategies. Finally, conclusions are drawn.

DESIGN FEATURES

The electrostatic separator consists of a pair of Titanium parallel electrodes mounted in a stainless steel vacuum tank [6]. Each electrode is supported by two metal-ceramic supports, which insulate the electrode from the vacuum tank, therefore the electrode can be charged to its desired voltage via high voltage feedthroughs situated at the extremities of the electrode.

Each electrostatic separator has an effective length of 4 m and a design electric field strength of 2 MV/m. The two electrodes are biased with equal magnitude but opposite polarities of high voltage. The separation between the two parallel electrodes is 75 mm. The cross section of the electrodes are optimized with bump edges to improve the field homogeneity. In order to decrease the beam coupling impedance, the ground plates are introduced on the side wall of the vacuum chamber and tapering ends are adopted between the vacuum tank and beam pipe. To further mitigate the thermal effects from the beam parasitic power loss dissipated on the electrodes, cooling loops are adopted on the back of the high voltage electrodes.

The longitudinal cross section of the simplified model used in the wakefield simulations is shown in Fig. 1. The green plates show the two parallel electrodes located vertically. The yellow slot shows one of the two ground plates settled between the electrodes. They are supposed to provide smooth path for the image current and to mitigate the interruption introduced by the electrodes. Taper transitions are designed at both ends of the vacuum tank and the ground plates to provide smooth transition to the nominal beam pipe.

IMPEDANCE CHARACTERISTICS

The longitudinal and transverse impedances are simulated with CST [7] wakefield solver taking a Gaussian excitation beam with rms bunch length of 6 mm. The real and imagi-

* wangn@ihep.ac.cn

Content from this work may be used under the terms of the CC BY 4.0 licence (© 2026). Any distribution of this work must maintain attribution to the author(s), title of the work, publisher, and DOI.

ISBN: 978-3-95450-252-3 ISSN: 2673-5350 doi: 10.18429/JACoW-IPAC2026-THP5645

BEAM COUPLING IMPEDANCE MODELING FOR THE HEFEI ADVANCED LIGHT FACILITY *

T. He†, W. Li, X. Liu, Z. Bai, G. Feng, University of Science and Technology of China, Hefei, China

Abstract

The Hefei Advanced Light Facility (HALF), which is being built as a 4th-generation synchrotron light source, faces performance challenges directly from instabilities associated with beam coupling impedance. This paper presents a systematic impedance modeling study based on two computational campaigns, establishing both narrow-band and broad-band impedance budgets. Key impedance sources are identified and their impacts assessed, informing targeted optimization and mitigation strategies. The resulting model enables a comprehensive analysis of impedance-driven beam dynamics for the HALF storage ring.

INTRODUCTION

Geometric discontinuities in vacuum components generate beam coupling impedance, classified into broad-band and narrow-band types. Broad-band impedance, from rapidly decaying wakefields, affects single-bunch dynamics and sets the single-bunch current threshold. Narrow-band impedance, from slowly decaying trapped-mode wakefields, drives multi-bunch instabilities and limits the total average current. Both effects are critical for the HALF storage ring [1]. For convenience, key vacuum components are grouped into five functional systems: (1) RF system (main and harmonic cavities); (2) insertion devices (IDs): long (4.2 m) and short (1.1 m) in-vacuum undulators (IVUs), plus tapered transitions for out-vacuum undulators (OVUs); (3) vacuum mechanical system: photon masks, gate valves, four RF-shielded bellows; (4) beam diagnostics: 240 BPM-bellow blocks, 7 standalone BPMs, collimators, feedback kickers, tune striplines, current monitor; (5) injection system: non-linear kicker, septum, dual-channel kicker.

Two computational campaigns were performed using the CST Wakefield Solver [2], except for the main and harmonic cavities which were modeled with ECHO2D [3]. The first campaign targeted narrow-band trapped modes. For most components, a bunch length of 5 mm and a wake length of 10 m were used, with a frequency range up to 20 GHz. For large structures such as IVUs, where critical trapped modes lie in the hundred-MHz range, a longer bunch length of 50 mm was adopted, with a frequency range up to 2 GHz. For incompletely decaying wakes, a Particle Swarm Optimization (PSO) fitting method was used to extract trapped-mode parameters, i.e., the resonant frequency f_r, shunt impedance R, and quality factor Q. The second campaign addressed broad-band impedance up to 200 GHz using a bunch length of 0.5 mm and a wake length of 300 mm. The resulting short-range wakes form the basis for the impedance budget and single-bunch instability tracking simulations.

NARROW-BAND IMPEDANCE

Tables 1, 2, and 3 summarize the most significant trapped modes for the longitudinal, horizontal, and vertical planes, respectively. The trapped modes in each table are listed in order of increasing frequency.

In the longitudinal plane (Table 1), the gate valves exhibit the most significant trapped modes, both in terms of total aggregate impedance and per-unit contribution. With 40 units installed throughout the ring, the mode at 7746 MHz alone contributes a total shunt impedance of 114.1 kΩ, an order of magnitude larger than any other component. This is primarily due to the cavity-like geometry of the gate valve structure, which supports high-Q resonances. The BPM-bellow blocks, with 200 units, also contribute substantially through multiple modes across the frequency spectrum. Notably, near 8.7 GHz and 19 GHz, multiple trapped modes with relatively high Q-factors and large cumulative impedances are observed, which can be primarily attributed to the common and similar bellow structures present in these components.

For the horizontal plane (Table 2), the collimators represent the dominant impedance sources. Despite having only two units, the horizontal collimators exhibit very high transverse shunt impedances, with the mode at 4228 MHz reaching $\beta R_t = 6.05\,\mathrm{M\Omega}$. The BPM-bellow blocks, while having lower per-unit impedances, contribute significantly due to their large population of 200 units, particularly the high-Q mode at 13 879 MHz, which accumulates to $\beta R_t = 13.1\,\mathrm{M\Omega}$.

The vertical plane (Table 3) presents the most severe impedance challenges. The long IVU exhibits two ultra-low-frequency modes at approximately 27 MHz and 56 MHz with extremely high transverse shunt impedances, $\beta_y R_t = 257\,\mathrm{M\Omega}$ and 81 MΩ, respectively. The short IVU also contributes two strong modes at 57 MHz and 226 MHz, with $\beta_y R_t = 119\,\mathrm{M\Omega}$ and 23.2 MΩ. These modes arise from the ridge-waveguide-like structure of the IVUs, and their impedance characteristics are highly dependent on the magnetic gap. The NLK contributes a significant mode at 1564 MHz with $\beta_y R_t = 14.3\,\mathrm{M\Omega}$. The BPM-bellow blocks again show a strong cumulative effect, with the high-Q mode at 13 879 MHz accumulating to nearly 20 MΩ. These vertical plane impedances, particularly the IVU modes, are expected to pose the greatest risk for multi-bunch instabilities.

* Work supported by the Fundamental Research Funds for the Central Universities (No. WK2310000127) and the National Natural Science Foundation of China (Grants No. 12375324 and No. 12105284).

† htlong@ustc.edu.cn

Content from this work may be used under the terms of the CC BY 4.0 licence (© 2026). Any distribution of this work must maintain attribution to the author(s), title of the work, publisher, and DOI.

ISBN: 978-3-95450-252-3 ISSN: 2673-5350 doi: 10.18429/JACoW-IPAC2026-THP5646

STUDY ON HIGH ORDER MODES DRIVEN LONGITUDINAL COUPLED-BUNCH INSTABILITIES IN HALF STORAGE RING*

W. Li, T. He†, X. Liu, Z. Bai
National Synchrotron Radiation Lab., University of Science and Technology of China, Hefei, China

Abstract

Longitudinal higher-order modes (HOMs) trapped in vacuum components such as gate valves are a potential source of coupled-bunch instabilities in the HALF storage ring. Using macroparticle tracking simulations, we study these instabilities under bunch lengthening provided by a passive third-harmonic cavity. Two distinct instability types are identified: a centroid-oscillation mode and an energy-spread-growth mode. The former can be suppressed by a longitudinal feedback system, while the latter cannot. Quantitative thresholds as a function of HOM frequency with different bunch distributions are obtained to guide the impedance optimization of HALF vacuum components.

INTRODUCTION

The Hefei Advanced Light Facility (HALF) is a fourth-generation diffraction-limited storage ring currently under construction, with a design target beam current of 350 mA [1]. Designed to deliver ultra-low emittance and high brilliance, HALF operates with a low momentum compaction factor, making it inherently sensitive to collective effects that can limit its performance [2].

Higher-order modes (HOMs) are electromagnetic resonances that can be excited by a particle beam as it interacts with surrounding structures, potentially driving coupled-bunch instabilities and leading to beam loss. In the HALF storage ring, both the main RF cavities (MC) and the passive third-harmonic cavity (HC) are designed as superconducting cavities, whose intrinsic HOMs are expected to be heavily damped through dedicated absorbers. Consequently, the primary concern for HOM-driven instabilities shifts to other vacuum components, most notably the gate valves. A similar situation was encountered at the SIRIUS light source: unanticipated longitudinal coupled-bunch instabilities were observed, and subsequent beam-based measurements combined with impedance modeling identified the HOMs trapped in small cavity-like structures of the vacuum gate valves as the most likely driving source [3].

To address this, we have performed macroparticle tracking simulations to study the longitudinal HOM-driven instabilities in the HALF storage ring. Under the condition of bunch lengthening provided by the HC, the dependence of the instability growth rate on HOM parameters, specifically resonant frequency and shunt impedance is thoroughly examined. The primary goal is to obtain quantitative longitudinal impedance thresholds that can directly guide the design and impedance optimization of vacuum components, ensuring stable high-current operation in HALF.

SIMULATION STUDIES

The main parameters of the HALF storage ring relevant to longitudinal dynamics are summarized in Table 1. Although we plan to adopt uniformly distributed gaps with 90% fill ratio to suppress ion instabilities, for simplicity we consider only the uniform fill case in this study. The short-range wakefield induced bunch profile distortion is also neglected.

Table 1: Main Parameters of the HALF Storage Ring

Parameter	Symbol	s
Circumference	C	479.86 m
Beam energy	E_0	2.2 GeV
Beam current	I_0	350 mA
Harmonic number	h	800
MC voltage	$V_{\rm rf}$	1.2 MV
Energy loss per turn	U_0	380 keV
Momentum compaction	α_p	9.4×10^{-5}
Natural rms bunch length	σ_{t0}	7.16 ps
Natural energy spread	$\sigma_{\delta 0}$	7.44×10^{-4}
HC R/Q	R/Q	40.5 Ω
HC quality factor	$Q_{\rm HC}$	2×10^8
Longitudinal damping time	τ_z	14 ms

Our simulations are carried out using the STABLE code [4], a GPU-accelerated macroparticle tracking framework originally developed for longitudinal beam dynamics studies. For a Gaussian bunch distribution and a uniform fill pattern, the growth rate of the longitudinal coupled-bunch instability driven by a narrow-band HOM can be expressed as [5]

$$\alpha_\ell = \frac{eI_0\alpha_p}{4\pi E_0 \nu_s} \sum_{p=-\infty}^{\infty} \omega_{p,\ell}\, \mathrm{Re}\, Z_\parallel(\omega_{p,\ell})\, e^{-(\omega_{p,\ell}\sigma_t)^2} \quad (1)$$

where $\omega_{p,\ell} = (ph + \ell + \nu_s)\omega_0$, ℓ is the coupled-bunch mode index, ν_s the synchrotron tune, ω_0 the angular revolution frequency, and σ_t the rms bunch length. For a single resonator impedance of the form

$$Z_\parallel(\omega) = \frac{R_s}{1 + iQ\left(\frac{\omega_r}{\omega} - \frac{\omega}{\omega_r}\right)}, \quad (2)$$

the sum is typically dominated by a single revolution harmonic p_0 when the HOM bandwidth is narrow compared to the revolution frequency. The maximum growth rate then occurs near resonance, where $\omega_r \approx (p_0 h + \ell + \nu_s)\omega_0$.

The passive HC controls the bunch length by adjusting its detuning frequency $\Delta f_{r,\rm HC}$. Figure 1 shows the longitudinal

* Work supported by the National Natural Science Foundation of China (No. 12475158, No. 12341501 and No. 12375324).
† htlong@ustc.edu.cn

Content from this work may be used under the terms of the CC BY 4.0 licence (© 2026). Any distribution of this work must maintain attribution to the author(s), title of the work, publisher, and DOI.

ISBN: 978-3-95450-252-3 ISSN: 2673-5350 doi: 10.18429/JACoW-IPAC2026-THP5650

SIMULATION-BASED OPTIMIZATION OF RF CAVITY PI CONTROLLERS FOR BEAM STABILITY IN HIGH-CURRENT STORAGE RINGS*

Wenshu Liang, Tianlong He†, Qing Luo‡, Zhenghe Bai§
National Synchrotron Radiation Laboratory, USTC, Hefei, China

Abstract

In high-current electron storage rings, tuning the radio-frequency (RF) cavity's proportional-integral (PI) controller is crucial for beam stability. Traditional online trial-and-error methods risk beam loss due to improper parameter settings. This paper proposes a pre-commissioning method based on particle-tracking simulations that self-consistently model the coupled beam-cavity-feedback dynamics. The method delineates a theoretically stable operating region for the PI controller, providing reliable guidance for initial online settings. Applied to the Super Tau-Charm Facility (STCF) parameters, it successfully identifies stable operating ranges for the feedback parameters. This simulation-based approach not only promises to guide design and commissioning but also substantially mitigates the risk of beam loss during operation.

INTRODUCTION

In high-current electron storage rings, longitudinal coupled-bunch instability (CBI) driven by the RF cavity accelerating mode can impose stringent limits on the achievable stored beam current. Digital low-level RF (DLLRF) systems employing proportional–integral (PI) controllers are widely used to regulate cavity fields; however, the PI gains together with the total loop delay reshape the closed-loop cavity response and, consequently, the effective impedance seen by the beam. As a result, stability margins can be highly sensitive to controller settings [1].

In practice, PI loop parameters often require optimization via parameter scans during operation [2]. The strong coupling among the beam, cavity, and feedback systems, combined with variations in operating conditions—such as beam current, cavity detuning, and system latency—can alter the optimal PI control parameters. More critically, inappropriate PI parameter settings can induce beam instability or even lead to beam loss [3].

To address these challenges, this paper presents a simulation-based methodology for pre-commissioning PI parameters. The method utilizes the GPU-accelerated particle-tracking code STABLE [4]. By implementing a PI controller model based on I/Q signal processing, we perform systematic parameter scans to identify the boundaries of beam stability. In parallel, the Nyquist criterion is applied to evaluate the intrinsic stability of the feedback loop and to quantify its gain margin. This combined analysis produces a stability map informed by both beam-tracking results and Nyquist analysis. The map provides reliable a priori guidance for the design and commissioning of DLLRF systems, significantly reducing the risk associated with online tuning and helping to prevent instabilities arising from suboptimal parameter choices.

SIMULATION WORKFLOW AND STABILITY ANALYSIS

Figure 1 illustrates the proposed workflow to identify the stable region of PI loop parameters. Based on the coupled beam–cavity–DLLRF model, we construct a stability map by evaluating the growth rate of the fastest-growing coupled-bunch mode. In parallel, we apply a Nyquist-based screening to eliminate parameter points that render the feedback loop intrinsically unstable. The resulting safe operating region for PI tuning is given by the intersection of the beam-stable region and the loop-stable region.

Beam–Cavity–LLRF Interaction Model

The interaction is simulated using the GPU-accelerated code STABLE [4], which implements a digital PI controller with I/Q baseband processing [5]. Dynamics are advanced at the bucket level: cavity voltage is updated per RF bucket using a pulse-discretized generator current, and beam loading is applied according to the bunch filling pattern. Key factors, including FIR filtering and the total loop delay, are explicitly included.

Scan Strategy and Stability Definition

A two-dimensional parameter scan over the proportional gain K_P and the loop delay τ_d is performed, as these parameters significantly affect the closed-loop cavity impedance distribution and the system's stability margins. Given that tracking simulations indicate the integral gain K_I has a relatively minor influence on beam instability, it is fixed at a specified nominal value. To improve computational efficiency, all scan points are initialized using the steady-state solution from a single reference point. For each parameter set, tracking simulations are run for up to 4×10^4 turns; if the beam oscillation amplitude exceeds a preset threshold, the current simulation is terminated early and the computation proceeds to the next parameter point.

The operational stability boundary is determined jointly by beam-dynamical stability and feedback-loop stability.

* Work supported by the Fundamental Research Funds for the Central Universities (No. WK2310000127) and the National Natural Science Foundation of China (Grants No. 12375324 and No. 12105284).

† htlong@ustc.edu.cn
‡ luoqing@ustc.edu.cn
§ baizhe@ustc.edu.cn

Content from this work may be used under the terms of the CC BY 4.0 licence (© 2026). Any distribution of this work must maintain attribution to the author(s), title of the work, publisher, and DOI.

ISBN: 978-3-95450-252-3 ISSN: 2673-5350 doi: 10.18429/JACoW-IPAC2026-THP5652

IMPACT OF INITIAL ENERGY SPREAD ON THE ACCURACY OF ENERGY SPREAD GROWTH FORMULA IN A FREE ELECTRON LASER

W. Huang, C. Tang*, X. Deng, Z. Pan, Tsinghua University, Beijing, China

Abstract

Evaluating the energy spread growth due to radiation is crucial for the design of steady-state microbunching (SSMB) insertion section. This study systematically benchmarks a classical analytical formula against three-dimensional numerical simulations to validate its accuracy under varying initial energy spreads. Our findings reveal that while the formula provides reliable estimations for beams with small initial energy spreads, its predictions deviate significantly as the initial energy spread increases. Such discrepancies arise because larger initial energy spreads amplify three-dimensional effects and nonlinear beam dynamics, which compromise the idealized analytical model. This study shows that comprehensive 3D simulations are indispensable for robust and accurate SSMB insertion section design.

INTRODUCTION

Storage ring-based light sources, such as the proposed SSMB scheme [1–3], have the potential to provide high average power EUV radiation for lithography.

In the design of the insertion section for SSMB storage rings, a crucial requirement is the implementation of reversible laser modulation [4]. Specifically, the laser modulation imparted on the electron beam upstream must be compensated by an inverse modulation downstream, aiming to restore the beam as closely as possible to the steady-state parameters of the storage ring. During this process, the energy spread growth of the electron beam due to radiation is a critical parameter. Excessive energy spread growth will result in incomplete cancellation of the laser modulation, thereby decreasing the radiation power.

In a storage ring FEL, Eq. (1) is commonly used to calculate the energy spread growth of the electron beam in the lasering process [5, 6]:

$$\Delta\sigma_\delta = \sqrt{\frac{2\rho P}{P_{\text{beam}}}}, \tag{1}$$

$$\rho = \left[\frac{1}{8\pi}\frac{I_p}{I_A}\left(\frac{K[JJ]}{1+K^2/2}\right)^2\frac{\gamma\lambda_r^2}{2\pi\sigma_x^2}\right]^{\frac{1}{3}},$$

here P is the radiation power, P_{beam} is the beam power and ρ is the FEL(Pierce) parameter. For an SASE FEL starting up from electron shot noise, the radiation power can be written as $P \approx \frac{1}{9}P_n \exp\left(\frac{z}{L_G}\right)$, where $P_n = \sqrt{2\pi}\frac{\rho^2\gamma mc^3}{\lambda_r}$ is the shot noise power, z is the distance along the undulator, and L_G is the FEL gain length. This equation is valid for the one-dimensional (1D) high-gain FEL regime. To account for 3D FEL processes, the authors in [5, 6] adapted it by setting the power to $P = P_n \exp\left(\frac{z}{L_G^{3D}}\right)$ and substituting the gain length L_G^{3D} with Ming Xie's formula [7].

Nevertheless, the accuracy of this formula in 3D FEL processes has yet to be validated by simulation results, especially in cases with different initial energy spreads. In this study, we focus on comparing the predictions of this formula with simulation results under various initial energy spreads.

METHODOLOGY

To evaluate the applicability of Eq. (1), we perform numerical simulations using the FEL code GENESIS [8].

Simulation Setting

The simulation parameters are mainly chosen from [6], which are listed in Table 1 and the optical functions of one undulator section is shown in Fig. 1.

Table 1: Main Simulation Parameters

Parameters	Value
Beam energy E (MeV)	988
Radiation wavelength λ_r (nm)	13.5
Bunch current I_p (A)	150
Normalized emittance $\gamma\epsilon_{x,y}$ (mm mrad)	1.66
Undulator period λ_u (cm)	2.6
Undulator parameter K	2.4
β-functions in undulator $\beta_{x,y}$ (m)	~2.5
FEL parameter ρ	0.001 29

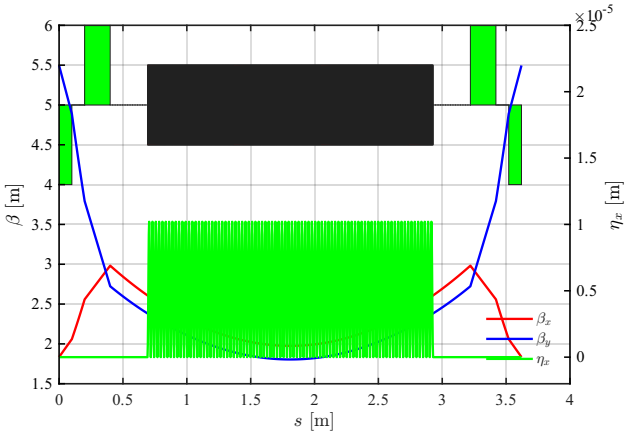

Figure 1: Optical functions of one undulator section.

For simplicity, a longitudinally uniform electron bunch with a length of 100 μm is adopted for the simulation. We conduct 3D FEL simulations with varying initial energy spreads of the electron bunch.

* tang.xuh@tsinghua.edu.cn

Content from this work may be used under the terms of the CC BY 4.0 licence (© 2026). Any distribution of this work must maintain attribution to the author(s), title of the work, publisher, and DOI.

ISBN: 978-3-95450-252-3 ISSN: 2673-5350 doi: 10.18429/JACoW-IPAC2026-THP5653

THE IMPACT OF TRANSVERSE-LONGITUDINAL COUPLING ON LONGITUDINAL MICROWAVE INSTABILITY

J. H. Bian, X. J. Deng, W. H. Huang*, C. X. Tang, Tsinghua University, Beijing, China
A. Kruschinski, C. Mai, M. Ries, Helmholtz-Zentrum Berlin, Berlin, Germany
A. Hoehl, Physikalisch-Technische Bundesanstalt, Berlin, Germany

Content from this work may be used under the terms of the CC BY 4.0 licence (© 2026). Any distribution of this work must maintain attribution to the author(s), title of the work, publisher, and DOI.

Abstract

In a storage ring with an extremely small global phase slippage, the bunch length can vary significantly within one turn due to the partial phase slippage and transverse-longitudinal coupling, which means the adiabatic approximation usually adopted for longitudinal dynamics breaks down. The impact of such a bunch length variation and exchange of the head and tail part of the beam arising from the partial phase slippage on the coherent synchrotron radiation (CSR) induced longitudinal microwave instability (MWI) threshold has recently been theoretically investigated by some of the authors. In this work, we have extended the study to consider the influence of transverse-longitudinal coupling.

INTRODUCTION

Accelerator-based light source is an important direction in the current development of accelerator. At present, there are two main types of these light sources, storage ring-based synchrotron radiation light sources and linear accelerator-based free electron lasers (FELs). They can provide high repetition rate and high peak power radiation, respectively. A novel storage ring-based light source mechanism known as steady-state microbunching (SSMB) is under investigation [1-4], which is promising to combine the advantages of these two sources and generate fully coherent radiation with both high repetition rate and high peak power. Such a SSMB ring exhibits extremely broad prospects in both scientific research and industrial applications.

The classical approach to achieving microbunches in an electron storage ring is to design a quasi-isochronous magnetic lattice with a very small global phase slippage factor η, which is based on the "zero-current" bunch length scaling law $\sigma_z \propto \sqrt{|\eta|}$ given by Sands [5]. However, when the global phase slippage factor becomes extremely small, the scaling law breaks down due to the impact of the partial phase slippage and transverse-longitudinal coupling. A more accurate expression for the bunch length is $\sigma_z = \sqrt{\epsilon_z \beta_z + \epsilon_x H_x}$, where ϵ_z and ϵ_x denote the longitudinal and horizontal emittance, and H_x represents the horizontal chromatic function. Note that under such conditions, the bunch length can vary significantly around the ring and is no longer a constant. A systematic analysis for the single-particle dynamics in this regime can be performed using Chao's SLIM formalism [6].

* huangwh@mail.tsinghua.edu.cn

Coherent synchrotron radiation (CSR) induced longitudinal microwave instability (MWI) is the dominant collective effect limiting the beam current in electron storage rings with short bunches. Bane *et al.* have proposed a threshold formula applicable to conventional storage rings with the assumption that the bunch length remains constant around the ring within one turn [7]. Some of the authors extend the formula to account for the impact of the partial phase slippage, calculating the bunch wake based on the evolution of the bunch in longitudinal phase space over one revolution [8]. However, a more comprehensive analysis needs to consider the influence of transverse-longitudinal coupling. In this work, we therefore generalize the instability study to 4D phase space building on our earlier results. We find that a new dynamical characteristic emerges where particles with different betatron actions no longer behave identically when transverse-longitudinal coupling is taken into account. And we also propose a method for evaluating the threshold of CSR induced longitudinal MWI in this scenario. Although this work focuses on the longitudinal MWI, our results provide useful references for studies of other collective instabilities when there exists coupling between different dimensions.

THEORETICAL STUDY

To focus on the issues we concerned, here we only consider the horizontal and longitudinal dimensions and use the state vector $\mathbf{X} = (x, x', z, \delta)^T$. Under the assumptions that the storage ring is planar x-y uncoupled and the radio frequency (RF) cavities are placed at dispersion-free locations, which is the typical setup for present synchrotron light sources, the longitudinal bunch length can be expressed as $\sigma_z = \sqrt{\epsilon_z \beta_z + \epsilon_x H_x}$. The first term under the square root arises purely from longitudinal dimension, while the second term originates from transverse-longitudinal coupling. In conventional storage rings, the second term is typically much smaller than the first and can be neglected. Meanwhile, since the influence of the partial phase slippage is also insignificant, β_z can be approximated as a constant around the ring, leading to a fixed bunch length. However, when the global phase slippage factor is extremely small, the partial phase slippage factor causes β_z to vary drastically over one turn, and the contribution from transverse-longitudinal coupling is no longer negligible. These two effects together result in a strong variation of the bunch length along the entire ring, which is the scenario considered in this work.

In our previous work [8], we have investigated in detail the impact of the partial phase slippage on CSR induced

ISBN: 978-3-95450-252-3 ISSN: 2673-5350 doi: 10.18429/JACoW-IPAC2026-THP5654

LONGITUDINAL BEAM INSTABILITY IN SSMB LASER MODULATORS: A CAVITY MODE DECOMPOSITION APPROACH

Y. Dai*, T. Li, Z. Liu, X. Deng, L. Yan, Tsinghua University, Beijing, China

Abstract

Steady-state microbunching (SSMB) is a promising mechanism for generating high-average-power coherent radiation by maintaining microbunches in a storage ring. In an SSMB laser modulator (LM), the interaction between electron bunches and the recirculating coherent undulator radiation can drive longitudinal beam instabilities, which may limit the overall performance. In this work, we investigate the longitudinal single-bunch multi-turn instability using a cavity mode decomposition approach. The evolution of the longitudinal wakefield is derived by expanding the radiation into a complete set of cavity eigenmodes, accurately capturing the optical evolution of the field over multiple turns. Based on the derived wakefields, the longitudinal beam dynamics equations are formulated to analyze the instability growth rates. Numerical simulations show excellent agreement with the theoretical model, validating the mode decomposition technique. These findings provide critical insights into the instability characteristics and suggest effective mitigation strategies for the design and operation of SSMB storage rings.

INTRODUCTION

In 2010, Ratner and Chao proposed the concept of steady-state microbunching (SSMB) to generate high-average-power coherent radiation in storage rings [1]. In an SSMB storage ring, the conventional radiofrequency (RF) cavity is replaced by a laser modulator (LM) system, which generally comprises an undulator and a laser cavity, as schematically illustrated in Fig. 1. When the electron beam traverses the undulator, it oscillates and is modulated by the laser field, enabling microbunching at optical wavelengths. However, the emitted undulator radiation will bounce and evolve within the cavity. The interaction between the beam and the radiation may trigger longitudinal beam instabilities, degrading the performance of the storage ring [2–6].

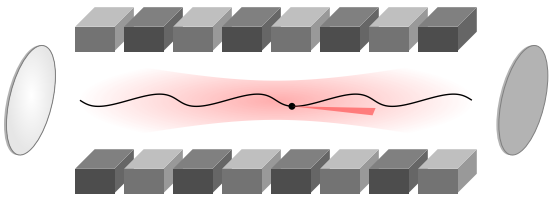

Figure 1: Laser modulator.

To account for the recirculating nature of radiation within the optical cavity, the cavity properties, such as diffraction and mirror-induced focusing, must be considered. In this work we adopt a mode-decomposition approach. By expanding the radiation into a complete set of cavity eigenmodes, we are able to represent the global evolution of the radiation as the sum of individual mode components. This approach provides further insights into the LM instability characteristics of SSMB storage rings. More details of this work can be found in Ref. [7].

CAVITY MODE DECOMPOSITION

Hermite–Gaussian Modes

In the optical cavity, the envelope $u(\boldsymbol{r})$ of a laser field with frequency ω and wavenumber $k = \omega/c$ propagating along the z-axis satisfies the paraxial wave equation. In Cartesian coordinates, the solutions are the Hermite–Gaussian modes [8]:

$$E_{mn} = E_0 \frac{w_0}{w(z)} H_m\left(\frac{\sqrt{2}x}{w(z)}\right) H_n\left(\frac{\sqrt{2}y}{w(z)}\right) \exp\left(-\frac{x^2+y^2}{w^2(z)}\right) \times \exp\left[-\mathrm{i}\frac{k(x^2+y^2)}{2R(z)} + \mathrm{i}(m+n+1)\psi(z) - \mathrm{i}kz\right], \tag{1}$$

where E_0 is the amplitude normalization constant, H_m and H_n are Hermite polynomials, $w(z) = w_0\sqrt{1+(z/z_\mathrm{R})^2}$ is the beam waist, $R(z) = z + z_\mathrm{R}^2/z$ is the radius of curvature of the wavefront, $\psi(z) = \arctan(z/z_\mathrm{R})$ is the Gouy phase, and $z_\mathrm{R} = \pi w_0^2/\lambda$ is the Rayleigh length.

Mode Decomposition of Undulator Radiation

By completeness, any paraxial field can be expanded in terms of Hermite–Gaussian modes:

$$\boldsymbol{E}(\boldsymbol{r}) = \sum_{mn} C_{mn}\boldsymbol{E}_{mn}(\boldsymbol{r}), \tag{2}$$

the excitation of mode coefficient ΔC_{mn} by a moving electron with velocity $\boldsymbol{v}$ is proportional to the work done by the mode field on the electron along its trajectory $\boldsymbol{r}(t)$ [9]. The energy spectrum of the radiation of the mode is given by the Parseval theorem:

$$\frac{\mathrm{d}W_{mn}}{\mathrm{d}\omega} = \frac{e^2}{8\pi P_{mn}}\left|\int_{-\infty}^{+\infty} \boldsymbol{v}\cdot\boldsymbol{E}^*_{mn}(\boldsymbol{r})\,\mathrm{e}^{-\mathrm{i}\omega t}\,\mathrm{d}t\right|^2, \tag{3}$$

where P_{mn} is the power normalization constant of the mode [9, Eq. (4)]. The Hermite–Gaussian mode components of the undulator radiation are shown in Fig. 2 with the parameters in Table 1.

For planar undulators, due to the absence of electron motion along the y-axis, only the even-n modes with x-polarization (σ-mode) and odd-n modes with y-polarization

* dyj24@mails.tsinghua.edu.cn

Content from this work may be used under the terms of the CC BY 4.0 licence (© 2026). Any distribution of this work must maintain attribution to the author(s), title of the work, publisher, and DOI.

ISBN: 978-3-95450-252-3 ISSN: 2673-5350 doi: 10.18429/JACoW-IPAC2026-THP5656

INVESTIGATION AND MODELING OF INTRABEAM SCATTERING EFFECTS IN MICROBUNCHED BEAMS

A. Liu, ShanghaiTech University, Shanghai, China
Ch. Feng, Shanghai Advanced Research Institute, CAS, Shanghai, China
J. Li, Zhangjiang Laboratory, Shanghai, China
W. Wan†, Quantum Science Center of Guangdong-Hong Kong-Macao Greater Bay Area, Shenzhen, China

Abstract

Intrabeam scattering (IBS) increases emittance and energy spread in low-emittance beams. In angular-dispersion-induced microbunching (ADM) beam lines, nanometre-scale density peaks cannot be represented reliably by a single smooth rms bunch length. This work separates the classical local IBS source from the microbunching spectrum: the former supplies the lattice and phase-space scattering kernel, whereas the latter modifies only the local pair-density weight. Rest-frame smoothing and a microbunching-dependent Coulomb-logarithm correction are introduced to exclude density structures below the collision resolution. For a 26.172 m branch line, the model gives single-pass microbunching-induced enhancements of 5.630% in the vertical-emittance source and 8.330% in the energy-spread-variance source. The additional source is concentrated in two intervals where the microbunching weight overlaps the local IBS kernel.

INTRODUCTION

Intrabeam scattering (IBS) is the cumulative effect of small-angle Coulomb scattering between particles in the same bunch. After transformation from the beam rest frame to the laboratory frame, the scattering appears as growth of transverse emittance, momentum spread and bunch length. The effect is distinct from the Touschek effect, in which rare large-angle events dominate particle loss [1].

Classical IBS theories [2-4] usually assume a line density that is smooth on the collision scale. This assumption is not guaranteed in angular-dispersion-induced microbunching (ADM) transport, where laser modulation and dispersive transport can generate 10 to 12 nm density peaks [5-8]. Replacing the distribution by a single rms bunch length can underestimate the local pair density, while counting all high-frequency spectral content without a resolution criterion can overestimate the collision rate.

The model is a local source estimate, not a new Gaussian fit or a full three-dimensional binary-collision simulation. The smooth-beam IBS kernel is kept as the lattice and phase-space weight, and the tracked microbunching spectrum supplies a resolvable density multiplier. Density, Coulomb-logarithm and baseline-kernel assumptions can therefore be tested independently.

DENSITY-WEIGHTED IBS MODEL

Let s be the coordinate along the branch line. For channel i, where i denotes either the vertical-emittance or energy-spread-variance channel, a smooth-beam baseline gives a local source

$$R_i^0(s) = C_i(s)\ln\Lambda_0(s)K_i(s). \quad (1)$$

Here C_i contains common beam factors, ln Lambda_0 is the smooth-beam Coulomb logarithm, and K_i is the local optical kernel that maps rest-frame scattering into the selected beam invariant. The microbunching spectrum is calculated at each WATCH location from the particle distribution. The shot-noise-subtracted harmonic power is

$$B_h(s) = \max(|b_h(s)|^2 - N_m^{-1}, 0). \quad (2)$$

where the maximum operation subtracts the estimated shot-noise floor and clips negative values to zero. The finite-resolution density-squared factor is

$$F_{\mathrm{eff}}(s;H,\alpha) = 1 + 2\sum_{h=1}^{H} B_h(s)W_h(s;\alpha). \quad (3)$$

Here N_m is the number of tracked macroparticles. The smoothing factor suppresses harmonics whose rest-frame wavelength is below the effective collision resolution. In the present calculation the resolution length is taken proportional to the smaller transverse beam size,

$$W_h(s;\alpha) = \exp\left[-\frac{1}{2}\left(\frac{\ell_{\mathrm{res}}}{\lambda_h^{\mathrm{rf}}}\right)^2\right], \quad \lambda_h^{\mathrm{rf}} = \gamma_0\lambda_0/h. \quad (4)$$

The working point H = 30 and alpha = 1 resolves the observed microbunch peak width while suppressing unresolved higher harmonics. The density factor is combined with a microbunching-dependent Coulomb-logarithm correction,

$$M(s) = F_{\mathrm{eff}}(s;H,\alpha)\frac{\ln\Lambda(s)}{\ln\Lambda_0(s)}. \quad (5)$$

The added single-pass source and relative enhancement are then obtained by applying the same local kernel as for the smooth beam,

$$g_i^{\mathrm{add}} = \int [M(s)-1]R_i^0(s)\frac{ds}{\beta_0 c}, \quad \eta_i = \frac{g_i^{\mathrm{add}}}{g_i^0}. \quad (6)$$

The denominator in Eq. (6) is the smooth-beam single-pass source. The same M(s) is used for both channels, but their kernels are integrated separately. Fig. 1 summarizes the branch-line layout and highlights the two high-overlap intervals used in the local-source analysis.

Content from this work may be used under the terms of the CC BY 4.0 licence (© 2026). Any distribution of this work must maintain attribution to the author(s), title of the work, publisher, and DOI.

† wanweishi@quantumsc.cn

ISBN: 978-3-95450-252-3 ISSN: 2673-5350 doi: 10.18429/JACoW-IPAC2026-THP5662

TIME-OF-FLIGHT CONTROL AND PASSIVE COMPRESSION IN AN α-MAGNET BEAMLINE FOR MHZ MEV UED

B. Song*, Y. Yang, P. Lv, Z. Wang, L. Zheng, Y. Du, W. Huang, C. Tang, R. Li
Department of Engineering Physics, Tsinghua University, Beijing, China

Abstract

A passive-compression beamline for high-repetition-rate MeV ultrafast electron diffraction (UED) is studied using a normal-conducting very-high-frequency (VHF) gun and a low-gradient α-magnet. The design uses the negative longitudinal dispersion of the α-magnet to compensate the positive dispersion accumulated in the gun and drift sections, while retaining a small residual total dispersion to reduce the required momentum chirp and suppress nonlinear longitudinal distortion. For near-MeV beams, the velocity-dependent contribution to R_{56}^{α} is included when setting the compression and time-of-flight (TOF) operating point. GPT simulations with CST-calculated field maps and three-dimensional space charge show that a 4.1 fC bunch can be compressed to 4.7 fs RMS at the sample, with a statistical TOF jitter of 1.9 fs RMS and normalized transverse emittances of 5.6 nm·rad and 5.2 nm·rad in the horizontal and vertical planes, respectively. These results identify controlled residual longitudinal dispersion as a practical condition for simultaneously achieving few-femtosecond compression and high timing stability in MHz-class MeV UED.

INTRODUCTION

Ultrafast electron diffraction (UED) is a powerful tool for probing structural dynamics in matter with atomic spatial resolution and femtosecond temporal resolution [1, 2]. Compared with conventional keV UED systems, MeV UED benefits from reduced space-charge broadening, increased penetration depth, and improved diffraction fidelity for thicker samples [3]. These advantages make relativistic UED attractive for experiments requiring both high temporal resolution and sufficient scattering signal.

High repetition rate is also important because it improves accumulated diffraction statistics and enables measurements of weakly scattering, dose-sensitive, or irreversible processes. Normal-conducting very-high-frequency (VHF) guns operated in continuous-wave mode are promising sources for this purpose because they can provide near-MeV electron beams at MHz repetition rates with good stability and compact system integration [4].

To fully exploit such sources, the electron bunch must be compressed to the few-femtosecond regime without degrading transverse beam quality or introducing excessive arrival-time jitter. RF and THz bunchers can provide strong longitudinal phase-space rotation, but they introduce additional synchronization or high-field requirements. Passive magnetic compression avoids an externally phased field and is therefore attractive for high-repetition-rate UED. Its performance, however, is governed by the same longitudinal dispersion that determines the sensitivity of the arrival time to energy fluctuations.

An α-magnet provides a compact source of negative longitudinal dispersion and naturally generates a high-horizontal-dispersion plane that can be used for energy selection. Recent work has shown sub-5-fs compression with a high-gradient α-magnet and a low-jitter photoinjector [5]. In a VHF-gun beamline near the MeV scale, however, the positive drift dispersion and the velocity-dependent contribution inside the α-magnet are both significant. The central design problem is therefore not simply to minimize R_{56}^{tot}, but to choose a residual dispersion that enables compression while maintaining low TOF jitter.

BEAMLINE DESIGN

The proposed beamline is driven by a normal-conducting VHF gun operating at 216.7 MHz. The gun produces near-MeV electron bunches with a nominal kinetic energy of about 784 keV at the sample-side working point. The schematic layout is shown in Fig. 1. After emission from the photocathode, the beam is focused by a solenoid and passes through an upstream collimator before entering the α-magnet.

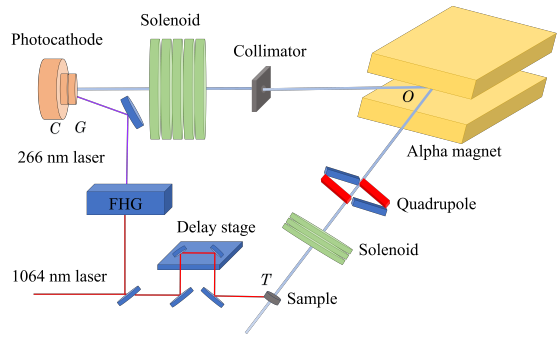

Figure 1: Schematic layout of the proposed MeV UED beamline based on a VHF gun and an α-magnet compressor.

The upstream collimator acts as a first-stage phase-space selection element. It reduces the charge density near the downstream waist, suppresses space-charge-driven nonlinear growth, and removes large-amplitude particles before the dispersive section. This cleaning is important because the following α-magnet couples transverse position, momentum deviation, and path length.

The α-magnet plays two roles. First, it provides the negative longitudinal dispersion required to rotate the longitudinal phase space and compress the bunch. Second, it produces a plane with large horizontal dispersion near the

* sbt24@mails.tsinghua.edu.cn

Content from this work may be used under the terms of the CC BY 4.0 licence (© 2026). Any distribution of this work must maintain attribution to the author(s), title of the work, publisher, and DOI.

ISBN: 978-3-95450-252-3 ISSN: 2673-5350 doi: 10.18429/JACoW-IPAC2026-THP5663

HOLLOW BUNCH METHOD FOR IMPROVED SPOT DOSE ACCURACY IN 3D PBS PROTON FLASH*

Y. Xiong, H. J. Yao, P. Z. Fang, S. X. Zheng†, Tsinghua University, Beijing, China

Abstract

A longitudinal localized kick-driven fast extraction technique has been employed to enable three-dimensional (3D) proton pencil beam scanning (PBS) at ultra-high dose rate (FLASH) for large-volume targets. However, it was observed that the longitudinal line density of the proton bunch significantly influences spot dose accuracy. In this study, a hollow bunch method—implemented by using two harmonic waves to manipulate the longitudinal phase space—is applied to reduce the line density in the extraction region. The RF parameters are carefully chosen so that the evolution of the phase space satisfies the requirements. Simulations conducted with the SynTrack code demonstrate that this method can effectively reduce the line density in the extraction region, thereby offering the potential to improve spot dose accuracy.

INTRODUCTION

Ultra-high dose rate (FLASH) radiotherapy has become a research hotspot [1] in the field since its ability to reduce normal tissue toxicity while maintaining tumor control was first discovered in 2014 [2]. This effect was initially observed in electron beam radiation and later confirmed with X-rays [3] and proton beams [4]. Several approaches exist to realize proton FLASH delivery, among which three-dimensional (3D) proton pencil beam scanning (PBS) with FLASH delivery is considered the most promising.

For large-volume targets, a delivery scheme in which the scanning layer is aligned parallel to the beam direction has been applied to address the timing limitation of approximately 100 ms [5]. A dedicated rapid cycling synchrotron (RCS) was designed to support this approach. For each scanning spot, a longitudinal localized kick-driven fast extraction technique is employed to facilitate rapid beam extraction during acceleration while maintaining precise control of the spot dose [6]. However, it has been identified that the longitudinal beam line density significantly impacts on the spot dose accuracy, and reducing the line density is a crucial means of improving dose accuracy.

In Ref. [6], the line density was reduced by decreasing the total number of particles stored in the synchrotron. This leads to a trade-off between spot dose accuracy and the irradiated volume size. This paper aims to reduce the longitudinal line density in the extraction region while maintaining the total stored particles by using hollow bunch method.

* Work supported by the National Natural Science Foundation of China (No. 12075131).

† zhengsx@mail.tsinghua.edu.cn

HOLLOW BUNCH CREATION

The hollow bunch method was initially proposed by CERN to increase the bunch factor at transfer from the PSB to the PS [7]. Reducing the peak current and direct transverse space charge forces leads to less blow-up and lower losses at low energy in the PS.

The basic principle of this method involves using the $h = 1$ and $h = 2$ RF systems to form longitudinal phase space with buckets shown in Fig. 1. Particles are initially distributed

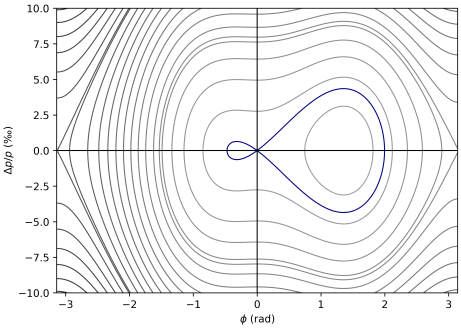

Figure 1: The iso-Hamiltonian map of the longitudinal phase space in hollow bunch method. Particles will move along the iso-Hamiltonian line and the violet contour is the boundary of the stable region (bucket).

inside the large bucket. By manipulating the voltage and phase of the RF system, the large bucket shrinks while the small bucket expands. During this process, particles originally inside the large bucket flow into the newly emerged bucket and the peripheral regions (with lower density) enter the new bucket first, as illustrated in Fig. 2. Consequently,

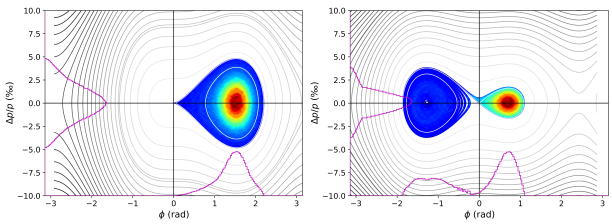

(a) (b)

Figure 2: The evolution of particle distribution in the longitudinal phase space in hollow bunch method. (a) there is only one bucket with the second bucket has not been formed; (b) as the original bucket shrinks, the newly formed bucket become larger and is filled with low density particles.

the new bucket region has a lower longitudinal density and can be used as the extraction region to improve spot dose accuracy.

Content from this work may be used under the terms of the CC BY 4.0 licence (© 2026). Any distribution of this work must maintain attribution to the author(s), title of the work, publisher, and DOI.

ISBN: 978-3-95450-252-3 ISSN: 2673-5350 doi: 10.18429/JACoW-IPAC2026-THP5664

PARAMETER OPTIMIZATION OF A NOVEL EMITTANCE COMPENSATION SCHEME FOR THE HALF STORAGE RING*

Xiaoyu Liu, Zhenghe Bai†, Gangwen Liu, Zhouyu Zhao
National Synchrotron Radiation Laboratory, USTC, Hefei, China

Abstract

The Hefei Advanced Light Facility (HALF) is a diffraction-limited storage ring light source, and the random adjustments in insertion device gaps can result in significant beam emittance variations. In prior work, we introduced a novel emittance compensation scheme based on the quantum excitation effect, utilizing a short variable-gap wiggler and a fixed dispersion. This paper investigates the influence of wiggler parameters on the compensation performance and beam dynamics. With the installation space requirements, the optimal parameters for the compensation wiggler within the HALF storage ring are determined.

INTRODUCTION

Diffraction-limited storage rings (DLSRs) employ multi-bend achromat (MBA) lattices to achieve ultra-low emittances. The average dipole field is reduced compared to third-generation light source storage rings, which makes the the radiation energy from bending magnets has a significant reduction and becomes comparable to that from insertion devices (IDs). As a result, independent adjustment of ID gaps by users will induce random emittance variations. HALF storage ring is a DLSR utilizing a hybrid-MBA lattice, with 20 long dispersion-free straight sections and 20 short dispersive straight sections [1, 2]. The Phase-I IDs of HALF include 10 user undulators and 2 damping wigglers (DWs) [3], the emittance variation induced by independent adjustment of user ID gaps reaches $\pm 7.5\%$, which need to be compensated.

Several methods have been developed to compensate for ID-induced emittance variations in DLSRs [4–7]. These approaches include active compensation using variable-gap wigglers in dispersion-free straight sections to leverage radiation damping, passive compensation via dispersion leakage into ID straight sections to minimize effective emittance variations, and the use of variable dispersion bumps within fixed-gap wigglers. Recently, a novel emittance compensation scheme based on the quantum excitation effect has been proposed for the HALF storage ring, in which a short variable-gap wiggler is installed in a dispersive straight section and the two DWs are fixed at their minimum gaps [8]. This scheme offers multiple advantages compared to the original radiation-damping-based scheme, such as shorter damping times, smaller energy spread variations, two additional wiggler beamlines and weaker attraction force between compensation wiggler poles.

To optimize the compensation wiggler parameters in the quantum-excitation-based scheme, this paper presents an investigation of their interrelations for emittance compensation and their influence on beam dynamics. This paper is organized as follows: Section II introduces the novel emittance compensation scheme and its advantages for the HALF storage ring. Section III investigates the dependence of the wiggler field on the effective length and period length. Section IV examines the linear and nonlinear beam dynamic effect associated with compensation wiggler parameters. Section V addresses the installation space requirements. Section VI presents the conclusions.

NOVEL EMITTANCE COMPENSATION SCHEME

To compensate for emittance variations, the original emittance compensation scheme for HALF is to adjust the gaps of two DWs located in long dispersion-free straight sections, which is the widely used method in other DLSRs. This method works primarily based on the radiation damping effect, the emittance will decrease to the target value when the magnetic fields of two DWs increase. Recently, a novel quantum-excitation-based emittance compensation scheme was proposed for the HALF storage ring. In this scheme, a variable-gap wiggler will be installed in the 20th short straight section of the HALF storage ring, which is currently vacant and unavailable for user beamlines, with two DWs operating at their minimum gaps. The dispersion in the short straight sections of HALF storage ring is relatively large, when the short wiggler field increases, the quantum excitation effect will be enhanced and the emittance will be increased up to the target value. Since the two DWs operate at their mininum gaps to reduce the emittance, the compensated emittance could be the same as the radiation-damping-based scheme.

To compare the performance of the two emittance compensation schemes, a emittance compensation simulation has been conducted for the zero current case. The random adjustment of user ID gaps is shown in panel (a) of Fig. 1, and the emittance and energy spread variations are shown in panel (b) and (c), respectively. The compensated emittance is 72 pm·rad for both schemes, however, the energy spread variations during emittance compensation are significantly different. In the radiation-damping-based scheme, the user ID gap reduction induces a smaller emittance and energy spread, to compensate for emittance variation, the compen-

* Work supported by the Fundamental Research Funds for the Central Universities (No. WK2310250135)

† baizhe@ustc.edu.cn

Content from this work may be used under the terms of the CC BY 4.0 licence (© 2026). Any distribution of this work must maintain attribution to the author(s), title of the work, publisher, and DOI.

ISBN: 978-3-95450-252-3 ISSN: 2673-5350 doi: 10.18429/JACoW-IPAC2026-THP5665

PRELIMINARY STUDY ON BEAM-BEAM INTERACTION WITH MULTI-PHYSICS EFFECTS IN THE SUPER TAU-CHARM FACILITY

S. Li*, Q. Luo†, T. Liu, L. Zhang, Ye Zou
University of Science and Technology of China, Hefei, China
K. Ohmi, High Energy Accelerator Research Organization, Tsukuba, Japan

Abstract

The Super Tau-Charm Facility (STCF) aims to achieve a peak luminosity of 1×10^{35} cm^{-2}s^{-1} utilizing the crab-waist collision scheme. While this configuration permits a high beam-beam parameter ($\xi_y \sim 0.1$), it amplifies the sensitivity of transverse beam dynamics to collective effects. This paper presents a comprehensive multi-physics investigation using a self-consistent, GPU-accelerated strong-strong simulation framework to evaluate the coupled impacts of lattice nonlinearities (LN), 3D wakefields (WK), and space-charge (SC) forces. Results show that inherent LN exacerbates the beam-beam-driven X-Z instability (XZI) via pronounced X-Y coupling. Conversely, the longitudinal wakefield provides a stabilizing effect; the induced potential-well distortion leads to bunch lengthening and synchrotron tune spread, offering Landau damping that mitigates coherent vertical beam size blow-up. Furthermore, transverse wakefields and SC forces induce dynamic tune shifts that systematically redistribute the XZI stopbands. By optimizing the horizontal fractional tune within $\nu_x \in [0.554, 0.560]$, the collider effectively maintains stable collisions against these multi-physics perturbations.

INTRODUCTION

The crab-waist (CW) collision scheme [1] effectively suppresses beam-beam resonances and minimizes the hourglass effect by implementing a large crossing angle and an ultra-low vertical beta function at the interaction point (β_y^*). The proposed STCF relies on this scheme to achieve unprecedented luminosity in the Tau-Charm energy region [2].

However, the extreme beam parameters demanded by the CW scheme push the beam dynamics into a highly sensitive regime. The intense and highly nonlinear beam-beam (BB) force couples strongly with lattice nonlinearities (LN) from the final focus quadrupoles and CW sextupoles, modifying amplitude-dependent tune shifts [3, 4]. Furthermore, collective effects such as wakefields (WK) and space charge (SC) forces, which are pronounced in high-intensity machines, introduce additional dynamic tune shifts and incoherent tune spreads.

A hallmark challenge in such colliders is the coherent X-Z instability (XZI), primarily driven by synchro-betatron resonances (typically satisfying the condition $2\nu_x - m\nu_s = n$) [5]. The presence of LN, WK, and SC actively modulates the topology of these resonance stopbands. Therefore, self-consistent strong-strong simulations that encapsulate these couplings are indispensable.

Building on previous beam-beam studies [6, 7], this paper presents multi-physics simulations based on the STCF V5 lattice. Key machine parameters at the nominal 2 GeV energy are summarized in Table 1 [8]. Utilizing the GPU-accelerated code BBSCL, we systematically evaluate these coupled effects to establish a robust operational working point.

Table 1: Machine Parameters for STCF V5 at 2 GeV

Parameters	Units	Value
C	m	825.524
$2\theta_c$	mrad	60
I_b	mA	3.03
ϵ_x / ϵ_y	nm / pm	8.83 / 88.3
β_x^* / β_y^*	mm	40 / 0.8
σ_{z0}	mm	7.55
ν_x / ν_y / ν_z	-	28.545 / 31.58 / 0.0193
N_b	-	660
ξ_x / ξ_y	-	0.003 / 0.1
L	cm^{-2}s^{-1}	1.02×10^{35}

MULTI-PHYSICS COUPLING

Lattice Nonlinearities and Beam-Beam

The frequency map analysis (FMA) for the STCF V5 lattice at the nominal working point $(\nu_x, \nu_y) = (0.550, 0.580)$ demonstrates that the BB interaction significantly enhances tune diffusion (Fig. 2). This drastic expansion of the tune footprint forces large-amplitude particles to cross dense high-order resonance lines, thereby modulating the stable tune space.

A systematic comparison between the ideal linear lattice (BBSS) and the real nonlinear lattice (BBSCL) in Fig. 1 reveals the shrinking of the stable luminosity window. In the unstable regime ($\nu_x < 0.554$), LN acts as an extreme amplifier for the XZI. While pure XZI primarily excites horizontal and longitudinal oscillations, the severe X-Y coupling inherent in the interaction region's sextupole aberrations channels this horizontal resonance energy directly into the vertical plane. This coupling mechanism leads to a catastrophic growth of the root-mean-square (RMS) vertical beam size σ_y.

Furthermore, a distinct σ_y growth is observed even within the theoretically stable window. Control simulations with a reduced bunch population ($1/10N_p$) confirm that the bare

* lisya@mail.ustc.edu.cn
† luoqing@ustc.edu.cn

Content from this work may be used under the terms of the CC BY 4.0 licence (© 2026). Any distribution of this work must maintain attribution to the author(s), title of the work, publisher, and DOI.

This is a preprint - the final version is published with IOP

ISBN: 978-3-95450-252-3 ISSN: 2673-5350 doi: 10.18429/JACoW-IPAC2026-THP5666

ONE POSSIBLE APPROACH FOR INTRABEAM SCATTERING CALCULATION OF ARBITRARY PHASE SPACE DISTRIBUTIONS

W. Wu, Z. Pan, Ch. Tang, X. Deng, Tsinghua University, Beijing, China

Content from this work may be used under the terms of the CC BY 4.0 licence (© 2026). Any distribution of this work must maintain attribution to the author(s), title of the work, publisher, and DOI.

Abstract

Traditional analytical models for intrabeam scattering (IBS) typically assume a Gaussian beam distribution in phase space. In this paper, we present an extended analytical IBS model that employs Hermite-Gaussian polynomials as basis functions to calculate the IBS diffusion coefficient for arbitrary phase space distributions. The generating function method is adopted to simplify the relevant calculations into a numerically solvable integral form. This approach retains the efficiency inherent to analytical models while ensuring calculation accuracy for non-Gaussian beam distributions.

INTRODUCTION

Advanced accelerator-based light sources demand increasingly high brightness and coherence, requiring smaller emittance and shorter bunch lengths. In this regime, intrabeam scattering effect (IBS) becomes a critical performance-limiting factor.

Traditional IBS analytical models, such as those of Piwinski [1] and Bjorken–Mtingwa [2], assume a Gaussian phase space distribution. However, advanced concepts like steady-state microbunching (SSMB) can lead to significantly non-Gaussian distributions [3]. While Monte Carlo methods can handle such cases [4], they are time-consuming and offer limited theoretical insight for design. This paper presents a more analytical approach for calculating IBS effects for arbitrary phase space distributions.

Diffusion Coefficient Due to IBS Effect

Early IBS studies focused on the growth rate τ, as IBS is a slow, multi-turn process. However, recent research on SSMB storage rings shows that even single-pass IBS kicks on momentum spread can significantly affect performance. Therefore, we extend the IBS description from τ to the diffusion coefficient in Fokker-Planck equation (FPE).

IBS effect corresponds to a diffusion process in 6D phase space, described by the FPE [5]. The diffusion coefficient tensor D_{ij} quantifies this process. From a microscopic perspective, the Langevin equation provides an equivalent description [6], allowing random kicks to be generated according to D_{ij}. This technique is particularly useful when such kicks are critical, such as the SSMB scenario. Thus, adopting the diffusion coefficient is a natural extension.

In general, the diffusion coefficient is a local function of phase space coordinates. To simplify the FPE, it is often averaged over the entire phase space, becoming a constant [6]. This approximation is valid when IBS effect is weak enough compared to the external forces, so that the phase space distribution remains dominated by single-particle motion. Currently, this condition is still valid in most cases.

Under this simplification, D_{ij} is approximated by its average $\langle D_{ij}\rangle$.

$$\langle D_{ij}\rangle = \left\langle \frac{d(\delta p_i \delta p_j)}{dt} \right\rangle, \tag{1}$$

where δp_i refers to the components of momentum change $\delta\mathbf{p}$ in a single collision event.

Following the similar deduction of Bjorken and Mtingwa [2]:

$$\begin{aligned}\langle D_{ij}\rangle = \frac{1}{2N}\iiint \rho_1(\mathbf{x},\mathbf{p}_1)\rho_2(\mathbf{x},\mathbf{p}_2)(q_iq_j)d^3\mathbf{x}d^3\mathbf{p}_1d^3\mathbf{p}_2 \\ \int \frac{md^3\mathbf{p}_1'}{E_1'}\int \frac{md^3\mathbf{p}_2'}{E_2'} \\ |M_c|^2\frac{m^2}{E_1E_2}\frac{\delta^4(p_1'^{\mu}+p_2'^{\mu}-p_1^{\mu}-p_2^{\mu})}{(2\pi)^2}, \\ \mathbf{q} := \mathbf{p}_1' - \mathbf{p}_1 = (q_1,q_2,q_3).\end{aligned} \tag{2}$$

Equation (2) is the general form of the simplified diffusion coefficient. Further simplifications depend on the assumed phase space distribution.

If $\rho(\mathbf{z})$ is Gaussian, Eq. (2) is equivalent to the Bjorken–Mtingwa result. For double- or multi-Gaussian distributions, it yields results from our unpublished work [7]. Next, we present an approach to evaluate $\langle D_{ij}\rangle$ for arbitrary phase space distributions using Hermite–Gaussian polynomials.

Hermite-Gaussian Polynomials

Hermite-Gaussian polynomials are a class of basis functions in $\mathbb{R}^n$ space. Their definition is well-known and has multiple forms. We adopt one common definition. [8, Eqs. (1) and (16)].

$$H_{\mathbf{j}}(\mathbf{z};\Sigma) := \frac{(-1)^{|\mathbf{j}|}}{\phi_{\mathbf{z}}(\mathbf{z};\Sigma)}\left(\frac{\partial}{\partial\mathbf{z}}\right)^{\mathbf{j}}\phi_{\mathbf{z}}(\mathbf{z};\Sigma) \tag{3}$$

$$\phi_{\mathbf{z}}(\mathbf{z};\Sigma) := (2\pi)^{-N/2}(\det\Sigma)^{-1/2}\exp\left(-\frac{1}{2}\mathbf{z}^T\Sigma^{-1}\mathbf{z}\right). \tag{4}$$

$$\mathbf{z} = (x, p_x, y, p_y, z, \delta).$$

The phase space has 6 dimensions, thus $N = 6$ and $\mathbf{j}$ has 6 components. The symbol $\mathbf{j} = (j_1,\ldots,j_6)$ denotes the degree of the multi-variable Hermite-Gaussian polynomial.

This basis is suitable for expanding the beam phase space distribution function ρ. Since the diffusion coefficient $\langle D_{ij}\rangle$ can be viewed as a functional of ρ, it can also be associated with Hermite-Gaussian polynomials.

We could represent our phase space distribution as a series of Hermite-Gaussian polynomials.

$$\rho(\mathbf{z}) = \sum_{\mathbf{n}\in\mathbb{N}^6} a_{\mathbf{n}}H_{\mathbf{n}}(\mathbf{z};\Sigma)\phi_{\mathbf{z}}(\mathbf{z};\Sigma). \tag{5}$$

ISBN: 978-3-95450-252-3 ISSN: 2673-5350 doi: 10.18429/JACoW-IPAC2026-THP5667

PRELIMINARY STUDY ON THE COLLECTIVE EFFECTS IN THE STORAGE RING-BASED COHERENT LIGHT SOURCE*

Y. Wang[1,2], W. Fan[3], Q. Zhang[†4], J. Li[3], Z. Zhao[4]
[1]Shanghai Institute of Applied Physics, Chinese Academy of Sciences, Shanghai, China
[2]University of Chinese Academy of Sciences, Beijing, China
[3]Zhangjiang Laboratory, Shanghai, China
[4]Shanghai Advanced Research Institute, Shanghai, China

Abstract

The storage ring–based coherent light source (SRCLS) operates under extreme conditions: ultra-low emittance, short bunches, high current, and strong damping. In such conditions, collective effects become critically important. This paper presents a preliminary study of the key collective effects in the SRCLS, including the Touschek effect, intra-beam scattering, resistive-wall impedance, and ion effects. Through numerical simulations and theoretical analysis, the impact of these effects on beam dynamics is evaluated. The results demonstrate that stable operation of the SRCLS can be achieved under the designed parameters.

INTRODUCTION

Synchrotron radiation light sources have undergone four generations of development since the early 1970s. The SRCLS combines the advantages of both diffraction-limited light sources and free-electron lasers, and including a high-current, short-bunch storage ring [1,2]. Through the angular dispersion modulation (ADM) scheme, the SRCLS can generate ultra-high-brightness and coherent radiation [3].

However, such a light source must operate under extreme conditions: ultra-low vertical emittance, short bunches, high current, and strong damping. These conditions not only inherit the collective-effect constraints of fourth-generation storage rings, but also introduce more severe challenges [4]. High current and short bunches will significantly enhance collective effects, including the Touschek effect, intra-beam scattering (IBS), resistive impedance, and ion effects, thereby threatening beam stability. A detailed study of these collective effects is therefore essential to ensure stable operation.

This paper focuses on the validation operation of the SRCLS and systematically investigates three main types of beam collective effects: the Touschek effect and intra-beam scattering (IBS) under ultra-low vertical emittance and high bunch density; resistive-wall (RW) impedance and transverse coupled-bunch instabilities (TCBI) induced by small-aperture vacuum chambers; and the effects of residual gas ion trapping and fast ions on beam quality. Finally, a summary of the research results is presented at the conclusion.

* This work is supported by the Shanghai Municipal Science and Technology Major Project.
† zhangql@sari.ac.cn

TOUSCHEK EFFECT AND IBS

The Touschek effect originates from single large-angle Coulomb scattering between electrons inside a bunch, and directly determines the beam lifetime. IBS arises from cumulative multiple small-angle Coulomb scattering. Generally, it manifests as a gradual growth of the beam in its six-dimensional phase space. This leads to simultaneous increases in transverse emittance, bunch length, and energy spread. Consequently, together, these two effects constitute the core physics challenge for maintaining beam quality under ultra-low emittance operation.

Touschek Effect

In this paper, the Piwinski model is adopted to calculate the Touschek lifetime, which is applicable to arbitrary beam energy and transverse momentum distributions [5]. The Touschek lifetime is jointly determined by the local momentum acceptance and the RF cavity momentum acceptance, where the local momentum acceptance is defined by both the physical aperture of the vacuum chamber and the dynamic aperture. The momentum acceptance of the RF cavity can be obtained by Eq. (1) [6],

$$\delta_{\mathrm{RF}} = \sqrt{\frac{2U_0 c}{\pi f_{\mathrm{rf}} E_0 \alpha C}\left(-\cot(\varphi_{\mathrm{s}}) - \varphi_{\mathrm{s}} + \frac{\pi}{2}\right)}, \qquad (1)$$

where U_0 is the energy loss per turn of the storage ring, c is the speed of light, f_{rf} is the radio-frequency frequency, E_0 is the beam energy, α is the momentum compaction factor, C is the circumference of the storage ring, and φ_{s} is the synchronous phase.

The local momentum acceptance can be obtained via multi-turn tracking with Elegant. The RF cavity momentum acceptance and local momentum acceptance of SRCLS are shown in Fig. 1. The results indicate that the Touschek lifetime of the storage ring is mainly limited by the local momentum acceptance. Considering the requirement of the ultra-low vertical emittance for ADM, the calculated Touschek lifetimes with a low coupling factor under 1 A current are shown in Fig. 2. The Touschek lifetime decreases rapidly as the coupling factor is reduced in the low coupling factor region. To meet the requirements, the vertical emittance is adjusted by introducing skew quadrupole components in the sextupoles located in the dispersion-free regions at both ends of the straight sections, while keeping the lattice parameters nearly unchanged. With a vertical emittance of

Content from this work may be used under the terms of the CC BY 4.0 licence (© 2026). Any distribution of this work must maintain attribution to the author(s), title of the work, publisher, and DOI.

ISBN: 978-3-95450-252-3 ISSN: 2673-5350 doi: 10.18429/JACoW-IPAC2026-THP5671

SIMULINK ANALYSIS WITH NEW COUPLING BETA MEASUREMENT FOR VERTICAL TEST AT IRIS*

Juwan Kim†, Heetae Kim
Institute for Rare Isotope Science, Daejeon, South Korea

Abstract

There have been concerns regarding the uncertainties of Q-factor measurements in vertical test system when the coupling beta is too low or too high. Forward and reverse power readings can be affected by cross-contamination in the bidirectional coupler and by re-reflection from the circulator, resulting in increased measurement uncertainty. This uncertainty becomes more significant when the cavity is far from critical coupling, because the dissipated power is determined from the difference between the forward, reverse, and transmitted powers.

To address this issue, we are recently developing a new method for measuring the coupling factor, β, based on the emitted power ratio between the input coupler and the pickup coupler. When the coupler geometry is mechanically fixed, the external quality factors (Q_e, Q_t) of each coupler remains constant. During cavity field decay, the emitted power ratio of the reverse power, P_r, and the pickup power, P_t, remains constant. this emitted power ratio makes it possible to calculate the coupling factors of both couplers with the transfer function.

This method reduces the sensitivity of coupling-factor measurements to RF power measurement errors. Simulink simulations were performed to evaluate the validity and accuracy of the proposed method. The Simulink model provides improved understanding and quantitative evaluation of measurement uncertainties in the vertical test system.

INTRODUCTION

HWR, QWR, SSR1, SSR2 cavities have been tested in vertical test facility at IRIS. HWR and QWR have been installed into the tunnel and are in operation [1]. We are in the second phase of SCL2 line, which is to use SSR1 for the former part of SCL2 line and SSR2 for the latter part. During HWR and QWR vertical tests, variable couplers have been used for the vertical test. It made it easy to do the vertical test. For we could adjust the position of the coupler, we were able to adjust the coupling between the coupler and the cavity well and do the conditioning for the cavity. But because of the complexity of the coupler, the multipacting and the outburst of outgassing took place in many cases. This was suspected to be the cause of the degradation of the performance of the cavity. We have changed the input coupler to the fixed type. The coupling coefficient of the fixed-type coupler had to be adjusted prior to the cleanroom assembly. We measured the external Q of the input coupler and the pickup coupler [2].

* This research was supported by the National Research Foundation of Korea (NRF) funded by the Ministry of Science and ICT (RS-2022-00214790).
† niceneph@ibs.re.kr

We have been using the same Q calculation process as applied in the variable coupler use case for the fixed type coupler [3]. The variable coupler can move the position of the antenna tip freely within the mechanical limit so that we might be able to adjust the coupling to be critical because the reverse power which is composed of the vector sum of the reflected power at the input coupler and the emitted power from the cavity can be minimized, thereby reducing the error in the critical coupling.

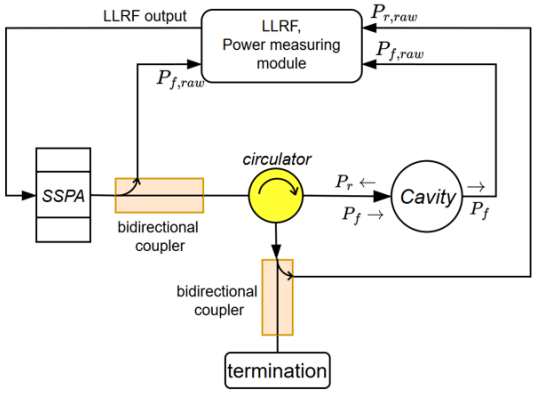

Figure 1: RF Diagram for Vertical Test at IRIS

Figure 1 shows the RF diagram for the vertical test of IRIS. We placed the directional couplers at the input port side of circulator and at the termination side to reduce the error term caused by the re-reflected power from the circulator. All calculations are using three powers, $P_{f,raw}$, $P_{r,raw}$, $P_{t,raw}$ which are each the uncalibrated forward, reverse, pickup power. P_f, P_r, P_t are the calibrated forward, reverse, pickup power at the input and pickup coupler RF plane. The reverse power is the vector sum of the reflected power at the coupler and the emitted power from the cavity [4, 5] and is expressed as:

$$P_r = \left|\sqrt{P_{ref}}e^{i\phi_{ref}} + \sqrt{P_e}e^{i\phi_e}\right|^2 \quad (1)$$

where P_{ref} is the power reflected at the coupler from the forward power and ϕ_{ref} is the phase thereof. If we knew Q_t and β_t. Then, Q_0 can be expressed as:

$$Q_0 = \frac{P_t Q_t}{P_f - P_r - P_t} \quad (2)$$

where $P_f - P_r - P_t$ is the dissipated power at the cavity inner surface. The external Q-factor of a coupler does not change unless the structure of the coupler and the cavity is changed. If we knew β_t in any field level, then we could know Q_0.

Obtaining β_t using the above equation has a limitation that if P_0 approaches zero, in other words, if the coupling is too weak or too strong and the reverse power is increased,

Content from this work may be used under the terms of the CC BY 4.0 licence (© 2026). Any distribution of this work must maintain attribution to the author(s), title of the work, publisher, and DOI.

ISBN: 978-3-95450-252-3 ISSN: 2673-5350 doi: 10.18429/JACoW-IPAC2026-THP5677

PRELIMINARY ANALYSIS OF TRANSIENT BEAM-LOADING EFFECTS IN ELECTRON STORAGE RINGS WITH A 3RD HARMONIC CAVITY

T. Y. Lee*, E.-S. Kim†, Korea University Sejong Campus, Sejong, South Korea
K. H. Kim, Grand Accélérateur National d'Ions Lourds, Caen, France

Abstract

In a 4th generation electron storage ring, harmonic cavities are often employed for increasing bunch length and beam lifetime. Effective bunch lengthening can be achieved when the first derivative of total accelerating voltage is near zero. However, the accelerating voltage fluctuation due to transient beam-loading (TBL) effect can affect the bunch lengthening in the harmonic cavity system. Therefore, we utilize both a Haissinski equation solver and a macroparticle tracking code to predict equilibrium beam distribution under TBL effects. The equilibrium longitudinal beam distributions obtained from both approaches are presented and cross-validated for different fill patterns.

INTRODUCTION

Korea-4GSR, the first fourth-generation electron storage ring project in South Korea, has been planned to be constructed in Ochang [1]. To increase the beam lifetime and the threshold current of longitudinal beam instabilities, third-harmonic cavity (3HC) systems will be adopted in Korea-4GSR project. The additional accelerating voltage provided by 3HC, flattens the longitudinal potential and increases the rms bunch length.

However, when a non-uniform fill pattern is applied, the additional voltage given by 3HC can deviate from the designed value due to beam-cavity interaction. It leads to the bunch-to-bunch variations in the beam induced voltage. Consequently, since the total accelerating voltage is no longer identical across the bunch train, the bunch profile (i.e., the bunch centroid and rms length) also becomes asymmetric. This phenomenon is known as *transient beam loading* (TBL) effects, which is a major concern in the fourth-generation light sources adopting the non-uniform fill pattern.

There are two methods to predict the bunch profile under TBL effects. One is a semi-analytical method, which numerically solves the Haissinski equation. The Haissinski equation describes the equilibrium beam distribution, and a fixed-point iteration method is commonly used to obtain its solution. The other is the macroparticle tracking code method, which requires more computational resources than semi-analytical method. In contrast to semi-analytical method, it can predict not only steady state, also dynamic behavior.

For a cross-validation of two methods, the different fill patterns are considered. The specific configurations of fill pattern are shown in Table 1.

Table 1: Fill Patterns Used for Simulations

	Train	Number of Train
Uniform	1332f	1
Single train	1024f + 308g	1
Multi train	250f + 83g	4
Hybrid	901f + 215g + 1f + 215g	1

The total average beam current I_0 is fixed to 400 mA, is the target nominal current of Korea-4GSR. However, excluding the single train case, these fill patterns are hypothetical and are not currently considered for the Korea-4GSR storage ring.

LONGITUDINAL MOTION WITH 3HC

Equation of Motion w/o Beam Effects

In an electron storage ring, the equation of longitudinal motion with a 3HC can be written as follows:

$$\begin{aligned} \frac{d\tau}{dt} &= \alpha_c \delta \\ \frac{d\delta}{dt} &= \frac{1}{E_0 T_0}\Big(V_1 \sin(h\omega_0\tau + \phi_{s1}) \\ &\quad + V_2 \sin(3h\omega_0\tau + \phi_{s2}) - U_0 \Big) \end{aligned} \tag{1}$$

where α_c is a momentum compaction of a ring, h is RF harmonics, E_0 is a beam energy [eV], $T_0 = 2\pi/\omega_0$ is a revolution period, and U_0 is a radiation loss per turn [eV]. (V_1, ϕ_{s1}) and (V_2, ϕ_{s2}) denote the amplitude and phase of a main RF voltage and a 3rd harmonic RF voltage, respectively.

Flat Potential Condition

The term inside the round bracket in the second expression of Eq. 1 represents a one turn energy gain or *accelerating voltage* $V_{acc}(\tau; V_1, V_2, \phi_{s1}, \phi_{s2})$. For effective bunch lengthening, $V_{acc}(\tau)$ should satisfy the following *flat potential condition* [2]:

$$\begin{aligned} \sin(\phi_{s1}) &= \frac{m^2}{m^2-1}\sin(\phi_{s0}) \quad (\frac{\pi}{2} < \phi_{s1} < \pi) \\ V_2 &= V_1 \sqrt{\frac{1}{m^2} - \frac{1}{m^2-1}\sin^2(\phi_{s0})}, \quad (V_2 > 0) \\ \tan(\phi_{s2}) &= -\frac{m\sin(\phi_{s0})}{\sqrt{(m^2-1)^2 - m^4\sin^2(\phi_{s0})}} \quad (-\frac{\pi}{2} < \phi_{s2} < 0) \end{aligned} \tag{2}$$

where $\sin(\phi_{s0}) = U_0/V_1$, $m = 3$ since a 3HC is considered.

* satori1103@korea.ac.kr
† eskim1@korea.ac.kr

Content from this work may be used under the terms of the CC BY 4.0 licence (© 2026). Any distribution of this work must maintain attribution to the author(s), title of the work, publisher, and DOI.

ISBN: 978-3-95450-252-3 ISSN: 2673-5350 doi: 10.18429/JACoW-IPAC2026-THV4001

SIMULTANEOUS ACCELERATION OF TWO IONS WITH UNEQUAL MASS-TO-CHARGE RATIO IN A SYNCHROTRON

D. Ondreka*, H. Liebermann, A. Pastushenko, P. Spiller
GSI Helmholtz Centre for Heavy Ion Research, Darmstadt, Germany
E. Renner, TU Wien, Vienna, Austria

Abstract

In this contribution, we report on the successful simultaneous acceleration of a beam composed of two different ions with unequal mass-to-charge ratio within the same cycle of the heavy ion synchrotron SIS18 at GSI. While acceleration of multiple charge states of a single ion species has been accomplished in linear accelerators, in a synchrotron this has never been done before to the knowledge of the authors. In a proof-of-principle experiment, low intensities of $^{56}Fe^{25+}$ and $^{209}Bi^{68+}$ were successively injected with horizontal multi-turn injection. Using two RF cavities, each ion species was then independently captured and accelerated in the same magnetic fields at its respective revolution frequency, the bunches of the lighter ion continuously overtaking those of the heavier ion. Such a beam composed of different ions has potential applications in particle therapy, plasma physics, nuclear physics, and materials research. The distinct revolution frequencies make this scheme attractive whenever independent control over the extraction of both ions is desired.

INTRODUCTION

Accelerators are usually designed to deliver one ion species at a time. For many applications, this is sufficient, since fast switching of ion species can be implemented if necessary. However, there are applications where simultaneous acceleration of different ion species is very useful. We focus here on cases where the difference in mass-to-charge ratio prevents simultaneous acceleration when setting up the accelerator for a single ion. For brevity, we denote this scenario *multi-species acceleration* in this contribution.

In linear accelerators, acceleration of several charge states of one isotope has been successfully demonstrated at FRIB [1, 2] and at GSI [3]. There, the goal is to increase beam intensity by reducing losses due to the broad charge state distribution of heavy ions after a stripping stage. In a synchrotron, multi-species acceleration has never been achieved before to the knowledge of the authors. Demonstrating the feasibility is therefore interesting in itself. In addition, there are real applications that would profit from simultaneous delivery of two ion species. For instance, in plasma physics experiments a heavy ion for target heating could be accompanied by a light ion serving to probe the generated plasma. In fact, this idea was brought up at GSI more than two decades ago [4], but not realized at the time.

Recently, the idea got attention in relation to developments of the GSI biophysics group for online range monitoring in particle therapy (PT) [5]. This concept requires, in addition to the main ion used for treatment (usually carbon), simultaneous delivery of a lighter ion with sufficient range to traverse the patient. While a mixture of ^{12}C and ^{4}He can be provided by single-species acceleration [6, 7], dual-species acceleration would allow for more ion combinations and provide additional flexibility through independent control of the two spills using KO extraction in this context.

SIS18 with its injector UNILAC satisfies all prerequisites for dual-species acceleration. It supports fast switching of ion species and has enough RF cavities to enable two independent RF programs. With the advent of the FAIR control system (FAIR-CS) [8], developed over the last years to support complex operation modes of SIS18 and the two storage rings ESR and CRYRING, the implementation of this scheme became possible. We therefore took an experimental approach and programmed the necessary extensions for incorporating a second ion species and and additional RF program into the SIS18 machine model. The scheme was tested when the beam time schedule offered $^{56}Fe^{25+}$ and $^{209}Bi^{68+}$ at once. This combination is by chance similar to $^{3}He^{2+}$ and $^{12}C^{6+}$, which constitutes an attractive choice for online range monitoring in PT.

IMPLEMENTATION

The two ions to be accelerated in SIS18 are characterized by their mass-to-charge ratios $(m/q)_1 < (m/q)_2$. Since UNILAC delivers either ion with the same energy of 11.3 MeV/u, ion 1 is injected first and accelerated to the magnetic rigidity for injection of ion 2. Next, ion 2 is injected and both ion species are accelerated with the same field ramp, each having its own RF program. As SIS18 employs multi-turn injection, horizontal phase space must be shared between the two ions. This requires the amplitude of the time-dependent bump at the injection septum to be reduced for the second injection, much like in the scheme used to create mixed $^{12}C/^{4}He$-beams for research in PT at MedAustron [9].

When implementing this concept, we were able to build on the unified modular settings management system for all circular accelerators integrated into the FAIR-CS. This system has been developed at GSI based on the LSA framework [10, 11] in a collaboration between machine physicists and control system experts. Essentially, it enables machine physicists to program new operation modes by creating new cycle types

* d.ondreka@gsi.de

Content from this work may be used under the terms of the CC BY 4.0 licence (© 2026). Any distribution of this work must maintain attribution to the author(s), title of the work, publisher, and DOI.

ISBN: 978-3-95450-252-3 ISSN: 2673-5350 doi: 10.18429/JACoW-IPAC2026-THV5301

DESIGN OF NSLS-II LATTICE WITH COMPLEX BEND REPLACEMENT

M. Song*, Y. Hidaka, B. Kosciuk, T. Shaftan, G. Wang,
Brookhaven National Laboratory, Upton, United States

Abstract

The demands of a higher-brightness photon beam push the electron beam emittance of storage rings toward a diffraction-limited level. The complex bend lattice offers a new approach to achieve low beam emittance. To pave the way for a full lattice upgrade, NSLS-II is planning to replace two existing dipoles with complex bends as a feasibility demonstration. This paper presents the design of the NSLS-II lattice with high-gradient complex bend replacement. Nonlinear beam dynamics are optimized to provide sufficient dynamic and momentum apertures for off-axis injection and reliable operation. In addition, the robustness of the optimized lattice to realistic errors is also evaluated.

INTRODUCTION

In recent decades, beamline users have demanded brighter synchrotron radiation. To meet this need, storage rings have continued to lower the beam emittance in order to increase the photon beam intensity. Since beam emittance ϵ scales as $\epsilon \propto 1/N_d^3$ [1], increasing the number of dipoles N_d in a storage ring is an effective way to reduce emittance. As a result, fourth-generation storage ring light sources around the world use multi-bend achromat (MBA) lattices [2–6]. In these lattices, the number of bending magnets is higher than in the double-bend achromat (DBA) [7] or triple-bend achromat (TBA) [8] used in third-generation light sources. However, if the goal is to push the emittance even closer to the diffraction limit within the same storage ring tunnel, it becomes more difficult to provide enough space for ring elements and insertion devices (IDs). For example, a lattice option for MAX-IV upgrade uses a 19-BA achromat and can reach 16 pm·rad in a 500-meter ring tunnel [9]. This design offers high performance by reducing the emittance by a factor of 20 compared to the current MAX-IV ring. However, the arrangement of the lattice elements leaves very little space for IDs and other ring equipment.

This example adequately illustrates the limit of the MBA approach in its current form. Therefore, it motivates the search for new accelerator technologies and lattice solutions. One method adopted in next-generation storage ring upgrades is the use of complex bend (CB), a new magnet concept first proposed for the NSLS-II upgrade [10]. The CB has gone through several stages of development. The initial concept consisted of a series of short dipole magnets interleaved with strong quadrupoles [11]. It then evolved into a design in which the quadrupoles were shifted transversely to generate dipole fields [12]. More recently, it has advanced to the current design, which uses permanent-magnet dipole-quadrupole combined-function magnets (PMQs), in either Halbach or hybrid type [13, 14]. Using this latest version of the CB, low-emittance storage ring designs have been developed for the NSLS-II upgrade at beam energies of 3 GeV [15] and 4 GeV [16].

To evaluate the potential limitations and technical challenges introduced by the CB lattice, a new installation project has been initiated at NSLS-II to replace the existing two dipoles with CBs, as shown in Fig. 1. This modification will allow beam dynamics with CBs to be studied during regular machine operation. However, it breaks the symmetry of the current NSLS-II lattice [17]. Relevant simulation and experimental studies of a developed asymmetric NSLS-II lattice are reported in [18]. To reduce the impact on normal operation, the modified asymmetric lattice must preserve high injection efficiency and long beam lifetime. In this work, we developed an NSLS-II lattice with two CB replacements and performed a nonlinear beam dynamics optimization of the modified lattice. The results show that the performance degradation caused by the lattice change can be mitigated through further optimization. In addition, we carried out a comprehensive error analysis to demonstrate the robustness of the developed lattice. These studies provide a basis for the smooth installation of CBs and for a future upgrade of the NSLS-II to a CB-based lattice.

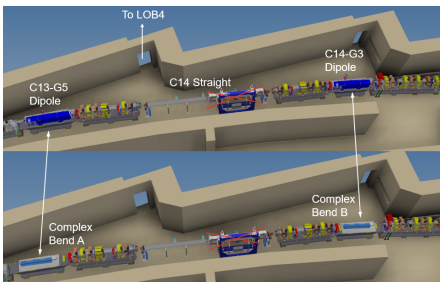

Figure 1: Schematic layout of the dipole replacement with CB magnets in Cells 13 and 14 of the NSLS-II storage ring.

LATTICE WITH COMPLEX BENDS

The NSLS-II storage-ring lattice consists of 30 cells, each based on a DBA structure [17]. The lattice with CB replacements was developed from the NSLS-II operational lattice, specifically the 17-IDs lattice.

To replace a 2.62-meter-long NSLS-II dipole with a bending angle of 6 degrees, a symmetric dipole replacement scheme was used to preserve the overall optics symmetry, with the dipoles on Girder 5 in Cell 13 and Girder 3 in Cell 14 selected for replacement. The CB magnet includes not only focusing PMQ (CB-BQF) and defocusing PMQ (CB-BQD) elements, but also pure dipole (CB-B) elements to provide the required bending angle and to match the floor coordinates. In addition, the CB-BQD and CB-BQF are

* msong1@bnl.gov

Content from this work may be used under the terms of the CC BY 4.0 licence (© 2026). Any distribution of this work must maintain attribution to the author(s), title of the work, publisher, and DOI.

ISBN: 978-3-95450-252-3 ISSN: 2673-5350 doi: 10.18429/JACoW-IPAC2026-THV5302

USING NEURAL-NETWORK ANSATZ FOR THE GENERATING FUNCTION IN THE HAMILTON-JACOBI EQUATION TO OBTAIN SYMPLECTIC TRANSFER MAPS FOR ELEMENTS WITH ANY MAGNETIC FIELD CONFIGURATION*

I. Lobach†, Y. Li
Brookhaven National Laboratory, Upton, NY, USA

Abstract

We present a novel method to generate a symplectic transfer map for any beamline element defined by its magnetic vector potential, even when it is known only on a 3D grid. The method uses a neural network (NN) as an ansatz to solve the Hamilton-Jacobi (HJ) equation for the unknown generating function of the second kind. This generating function is chosen to connect the solution of a simpler system with an exact analytical solution (e.g., an ideal hard-edge quadrupole) to the system with a more complex field configuration (e.g., a quadrupole with an Enge fringe field profile). This design dramatically reduces the learning burden on the NN. The learned generating function defines the trajectories and the element's symplectic transfer map via implicit equations for the particle's position and explicit equations for its momenta. The implicit equations are typically solved to machine precision in a few iterations using Newton's method combined with automatic differentiation capability of the NN. The method's accuracy can be conveniently estimated by how well the NN solution satisfies the original Hamiltonian. We validate the method with 1D and 2D examples for drift space, hard-edge quadrupole, and quadrupole with Enge fringe field profile.

INTRODUCTION

Modern accelerator lattices increasingly rely on magnets with strong gradients, combined-function components, and pronounced 3D end effects, making accurate field modeling a central issue for long-term beam-dynamics studies. This trend is evident in recent and upcoming facilities such as NSLS-IIU [1, 2], APS-U, and ALS-U, where complex magnet geometries with large sagitta and overlapping fringe fields challenge standard fast symplectic methods [3, 4]. At the same time, realistic evaluation of dynamic aperture, beam lifetime, and injection efficiency requires stable long-term tracking with maps that remain symplectic over many turns. Direct trajectory integration through magnetic fields on 3D grids [5] can provide high fidelity, but it is often too computationally expensive for routine optimization and large-scale tracking studies. These considerations motivate the development of efficient, field-based, symplectic models for beamline elements with arbitrary magnetic field configurations. Several approaches for approximating symplectic transfer maps with neural networks have been considered before, such as Henon neural networks, Hamiltonian neural networks, SympNets [6–20]. In this paper, we propose a new generating function-based approach.

METHOD DESCRIPTION

Consider the Hamiltonian system of interest, with canonical coordinates (q, p), where $q = (q_x, q_y)$ and $p = (p_x, p_y)$, and a generally complicated Hamiltonian

$$H = H(s, q, p). \tag{1}$$

Here, we assume the Frenet–Serret coordinate system, s is the reference-particle path length. Further, we introduce a second Hamiltonian system with canonical coordinates (Q, P), where $Q = (Q_x, Q_y)$ and $P = (P_x, P_y)$, and a simpler Hamiltonian

$$K = K(s, Q, P), \tag{2}$$

chosen such that its equations of motion admit an analytical solution. Hereafter, we may also refer to the systems with Hamiltonians H and K as system H and system K, respectively. For example, system K can be a linear hard-edge lattice model, and system H can be a lattice model with nonlinear fringe fields. The goal is to construct a canonical transformation from the simple system K to the more complex system H.

To this end, we postulate the existence of a generating function of the second kind,

$$G = G(s, q, P), \tag{3}$$

which maps (Q, P) to (q, p) via

$$Q = \frac{\partial G}{\partial P}, \tag{4}$$

$$p = \frac{\partial G}{\partial q}. \tag{5}$$

According to Hamiltonian mechanics, the two Hamiltonians are related by

$$\frac{\partial G}{\partial s} + H\left(s, q, \frac{\partial G}{\partial q}\right) = K\left(s, \frac{\partial G}{\partial P}, P\right), \tag{6}$$

where we have already used Eqs. (4),(5). Equation (6) is the Hamilton–Jacobi (HJ) partial differential equation that must be solved to determine $G(s, q, P)$. Note that this is the most general version [21, p. 373], while often only the case of

* Work supported by the U.S. Department of Energy under Contract No. DE-SC0012704, and the Field Work Proposal 2025-BNL-PS040

† ilobach@bnl.gov

Content from this work may be used under the terms of the CC BY 4.0 licence (© 2026). Any distribution of this work must maintain attribution to the author(s), title of the work, publisher, and DOI.

ISBN: 978-3-95450-252-3 ISSN: 2673-5350 doi: 10.18429/JACoW-IPAC2026-THV5303

A HYBRID PHYSICS AND DATA-DRIVEN MODELING FRAMEWORK FOR ACCELERATORS WITH AUTOMATIC DIFFERENTIATION*

Y. Hao†, H. Alamprese, W. Fung, C. Ratcliff, Facility for Rare Isotope Beams, East Lansing, MI, USA
J. Wan, Institute of High Energy Physics, Beijing, China
J. Qiang, Lawrence Berkeley National Laboratory, Berkeley, CA, USA

Abstract

In modern accelerator modeling, many lattice components can be accurately described using established first-principles physics. However, certain intricate effects, such as complex boundary conditions, collective interactions, and self-fields, remain difficult to model reliably and efficiently from theory alone. At the same time, high-resolution beam position and profile measurements provide rich information about these poorly understood dynamics. In this paper, we present a hybrid modeling framework with built-in automatic differentiation, designed to seamlessly integrate physics-based lattice models with data-driven representations of complex effects. This approach improves predictive accuracy, enables gradient-based optimization, and offers a practical path toward more faithful digital twins of accelerator systems.

INTRODUCTION

Accurate modeling of accelerator beam dynamics is essential for optimizing machine performance and enabling reliable operation of modern accelerator facilities. Traditionally, accelerator models are constructed from first-principles beam physics and detailed lattice descriptions, followed by parameter fitting using diagnostic measurements. While this approach has been highly successful, some important effects remain difficult to model accurately due either to incomplete physical understanding or to prohibitive computational cost. Examples include collective effects, complex electromagnetic structures such as undulators, RF cavities, and magnets with sophisticated geometries.

Recently, machine learning (ML) based surrogate models have emerged as a promising approach for improving accelerator modeling. In this framework, difficult-to-model or computationally expensive physical processes are replaced by neural-network (NN) or Gaussian Process trained using either simulation data or experimental measurements.

One recent example is the ML representation of the space-charge Hamiltonian for beam tracking [1], using a kick-drift model, with macroparticles drifting through short beamline segments, followed by space-charge kicks generated from a Hamiltonian map predicted by a NN using the instantaneous beam distribution as input. The Hamiltonian formulation preserves the symplectic structure of the tracking algorithm even when the neural-network approximation does not perfectly reproduce the true self-field Hamiltonian.

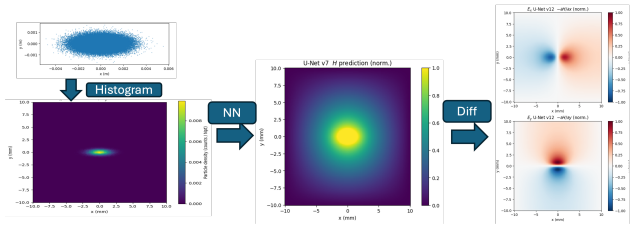

Figure 1: The flow chart of the ML workflow for space charge calculation.

However, the ML-based space-charge models does not naturally work with auto-differentiation package to get the gradients of simulation outputs with respect to the initial beam coordinates or lattice parameters, such as drift lengths or quadrupole strengths. This limitation prevents the direct application of gradient-based optimization and sensitivity analysis in hybrid physics-ML simulations.

In this work, we present an automatic-differentiation-enable implementation of a hybrid accelerator tracking model that combines conventional beam optics with a NN-based space-charge solver. The proposed approach preserves differentiability through both the physics-based tracking and the ML space-charge calculations, enabling gradient evaluation for the beam dynamics studies.

ML SPACE CHARGE MODEL

Following our earlier work [1], we retrained the NN space-charge model using identical computational domains for both the spectral Poisson solver and the grid boundary for the NN model (20 mm×20 mm). The workflow of the ML-based space-charge solver is illustrated in Figure 1. The transverse macroparticle distribution is first converted into a density histogram, which serves as the input to the NN. The NN predicts the space-charge Hamiltonian map, from which the space-charge kicks are obtained by spatial differentiation.

To evaluate the accuracy of surrogate model, we consider a bi-Gaussian transverse beam distribution with $\sigma_x = 3\sigma_y$. Figure 2 compares the electric field predicted by the neural network with the analytical Bassetti–Erskine solution. The surrogate model reproduces the field with better than 10% accuracy while preserving the symplectic structure of the particle tracking.

AD-ENABLED HYBRID MODEL

To demonstrate the automatic-differentiation capability of the NN-based space-charge solver and its integration with

* Work supported by the DOE Office of Science, Office of High Energy Physics, with Award No. DE- SC0024170 and No. DE-SC0023722. The work of J. Q. is also supported by the U.S. Department of Energy under Contract No. DE-AC02-05CH11231.

† haoyue@msu.edu

Content from this work may be used under the terms of the CC BY 4.0 licence (© 2026). Any distribution of this work must maintain attribution to the author(s), title of the work, publisher, and DOI.

ISBN: 978-3-95450-252-3 ISSN: 2673-5350 doi: 10.18429/JACoW-IPAC2026-THV5602

UNIVERSAL REPRESENTATION OF CHROMATIC ABERRATION IN ELECTRON BEAM OPTICS

K. Soutome†,[1,2], T. Hara[1], E. Iwai[1,2], K. Yasutome[1], T. Hiraiwa[1], H. Maesaka[1,2], H. Tanaka[1]
[1]RIKEN SPring-8 Center, Hyogo, Japan
[2]Japan Synchrotron Radiation Research Institute, Hyogo, Japan

Abstract

We present a novel unified approach to the expression and correction of electron beam chromatic aberrations, which comprehensively covers optical systems of both a single-pass beam transport line and a circular accelerator satisfying periodic boundary conditions. In an electron circular accelerator, linear chromaticity has been utilized to express the first-order difference in beam focusing caused by the electron energy deviation, which can be computed by a well-known formula using a beam envelope function. However, this conventional formulation is incompatible with non-periodic beam transport lines, such as XFELs driven by linacs and the final focus system of linear colliders. We address this discrepancy by deriving a generalized formula that seamlessly connects the two different accelerator topologies. Our representation not only reproduces the well-known ring chromaticity but also provides a consistent and practical definition of chromatic aberrations for a single-pass transport line and their correction methods. This presentation outlines one approach to resolving this apparent contradiction and the universal formula to express chromatic effects.

INTRODUCTION

There are two main types of accelerator topologies. One is a "closed" transport system that satisfies periodic boundary conditions, and the other is an "open" transport system without any conditions. A typical example of the former is a storage ring, where machine parameters such as Courant-Snyder or Twiss parameters [1, 2] are automatically determined to satisfy the boundary conditions. An example of the latter is a beam transport line or a single-pass linac such as linear colliders or XFEL linacs, and machine parameters are obtained by tracing the initial values at the entrance to the downstream point. In both "open" and "closed" transport systems, the correction of chromatic aberration is an important topic, and for a better understanding and correction, a general formulation that seamlessly describes the chromatic aberration for the two different accelerator topologies will be helpful.

As for the linear chromaticity in the open transport system, it is calculated as the first-order term of the energy-dependent component of the betatron phase traced from the entrance [3]. In contrast, in the closed transport system such as storage rings, a well-known formula is used for calculating the linear chromaticity [2]. Thus, even when considering the chromaticity alone, it does not appear to be straightforward to describe the two accelerator topologies in a unified manner.

† soutome@spring8.or.jp

In this work, we present a unified formulation for describing the chromatic aberration of both open and closed beam transport systems [4]. Since the betatron motion can be described by the linear equation of motion with quadrupole field strengths multiplied by a factor $1/(1+\delta)$, where δ is the relative momentum deviation, the transfer matrix formalism is applicable [5-8]. With this in mind, we adopt a chromatic aberration-decoupled formalism, which separately treats ideal particle motion with a design momentum ($\delta = 0$) and perturbative motion due to non-zero δ. With this formulation, we treat the betatron motion up to the first order of δ, and we can derive a formula of chromatic aberration seamlessly connecting the two different accelerator topologies. Boundary conditions can also be taken into account easily. As an example of the application of our formulation, we show an efficient correction scheme of the chromatic aberration for a tentative chicane lattice designed for the BL3 beamline of SPring-8 Angstrom Compact free electron LAser (SACLA) [9].

FORMULATION

The betatron motion for off-momentum particles in a beam transport line can be described by the transfer matrix formalism with quadrupole field strengths multiplied by a factor $1/(1+\delta)$, where $\delta \equiv \Delta p/p_0$ is the relative momentum deviation:

$$\begin{pmatrix} x^{[out]} \\ x'^{[out]} \end{pmatrix} = M \begin{pmatrix} x^{[in]} \\ x'^{[in]} \end{pmatrix}. \tag{1}$$

The transfer matrix M is parametrized as

$$M \equiv \begin{pmatrix} m_{11} & m_{12} \\ m_{21} & m_{22} \end{pmatrix} = \begin{pmatrix} \sqrt{\frac{\beta^{[out]}}{\beta^{[in]}}}(\cos\psi + \alpha^{[in]}\sin\psi) & \sqrt{\beta^{[in]}\beta^{[out]}}\sin\psi \\ \frac{\alpha^{[in]}-\alpha^{[out]}}{\sqrt{\beta^{[in]}\beta^{[out]}}}\cos\psi - \frac{1+\alpha^{[in]}\alpha^{[out]}}{\sqrt{\beta^{[in]}\beta^{[out]}}}\sin\psi & \sqrt{\frac{\beta^{[in]}}{\beta^{[out]}}}(\cos\psi - \alpha^{[out]}\sin\psi) \end{pmatrix}, \tag{2}$$

and the Courant-Snyder parameters (β, α, γ) is transformed as

$$\begin{pmatrix} \beta^{[out]} \\ \alpha^{[out]} \\ \gamma^{[out]} \end{pmatrix} = \begin{pmatrix} m_{11}^2 & -2m_{11}m_{12} & m_{12}^2 \\ -m_{11}m_{21} & 1+2m_{12}m_{21} & -m_{12}m_{22} \\ m_{21}^2 & -2m_{21}m_{22} & m_{22}^2 \end{pmatrix} \begin{pmatrix} \beta^{[in]} \\ \alpha^{[in]} \\ \gamma^{[in]} \end{pmatrix}. \tag{3}$$

We now expand M and (β, α, γ) in terms of δ so that we can decouple the terms due to chromatic aberration and

Content from this work may be used under the terms of the CC BY 4.0 licence (© 2026). Any distribution of this work must maintain attribution to the author(s), title of the work, publisher, and DOI.

ISBN: 978-3-95450-252-3 ISSN: 2673-5350 doi: 10.18429/JACoW-IPAC2026-FRI5T01

BEAM DYNAMICS IN THE SNS LINAC AND BEAM TEST FACILITY*

K. Ruisard†, A. Aleksandrov, T. Thompson, A. Wood
Oak Ridge National Laboratory, Knoxville, TN, USA

Abstract

The Spallation Neutron Source linear accelerator is the highest power superconducting hadron linac in the world. Along with this distinction comes the significant complication of deposited power from beam loss, exacerbated by the fact that the linac transports H^-. This paper summarizes our understanding of beam loss in the SNS linac and highlights research being done to improve that understanding. The question of beam loss due to halo has motivated development of a detailed model fidelity project at the SNS Beam Test Facility, which includes unique phase space diagnostics for 4D-6D distributions, and high-dynamic-range 2D distributions.

INTRODUCTION

In the Spallation Neutron Source, beam loss has been a major concern since the early days of operation. During initial commissioning, losses in the superconducting linac (SCL) threatened to limit operation. The source of this loss was eventually determined to be intrabeam stripping of H^- ions [1, 2]. The mitigation was to reduce quadrupole gradients in the SCL to increase average beam size and reduce the probability of H^- collisions. This mitigation was possible due to the generous aperture (8 cm compared to 2–3 cm in the warm linac).

This mitigation of stripping losses is an example of how physical understanding can support large operational shifts. This change to the design optics of the SNS enabled the ramp to 1.4 MW. The SNS linac still operates near this set of optics, with some "drift" in parameters after years of empirical loss tuning.

The question of fully understanding beam loss in a realistic accelerator model is a multi-faceted issue [3], encompassing not only intrabeam stripping but also halo losses, residual gas and field stripping, proton contamination, dark current and other effects. The dominant mechanisms in the SNS linac are understood to be loss from halo scraping and intrabeam stripping. To achieve a subsequent reduction of beam loss that is on order with the intrabeam stripping discovery will require a trusted model of the beam distribution in the linac for a wide range of operating parameters. This would make it possible to redesign the linac optics towards a lower-loss state.

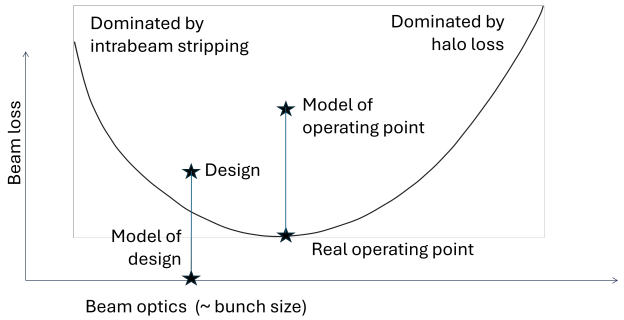

Figure 1: Illustration of beam loss landscape for SNS linac. The linac runs with parameters shifted from design, at an operating point that is understood to balance halo losses with stripping losses. The PIC model for the linac predicts lower losses for design than the best operating point.

BEAM LOSS IN THE SNS LINAC

The current operating point of the linac is understood to be at a local beam loss minimum, depicted in Fig. 1. Loss tuning for the linac is performed by machine specialists within the operations group, who have developed a mental map of the complex cause/effect relationships of the operating parameters and the measured beam loss signals, as well as the relationship of beam loss signals to measured activation. Through joint effort between operations and accelerator physics group, we have developed a reproducible, loss-minimized machine state that can be restored after shutdowns or beamline disruptions (such as detuned superconducting cavities) [4, 5]. At this state, we are below the commonly accepted limit of 1 W/m losses, with "hotspots" in the linac typically not exceeding 0.3 W/m.

The SNS recently completed the Proton Power Upgrade [6], which raised beam energy from 1 GeV to 1.3 GeV. Along with a modest increase in average beam current, this enabled a ramp of the beam power on target to 2.0 MW in April 2026. Following the completion of the Second Target Station, beam power will increase to 2.7 MW. Beam loss in the linac is expected to rise moderately but remain below the 1-W/m limit. After the first few runs since PPU installation, there is an unexpectedly high activation area near the ring injection, but not at any locations in the linac.

While acceptable linac losses are predicted at 2.7 MW, radiation damage to components in the linac tunnels will accrue faster. Improved methods that keep losses at or below

* This material is based upon work supported by the U.S. Department of Energy, Office of Science, Office of High Energy Physics, and has been authored by UT-Battelle, LLC under Contract No. DE-AC05-00OR22725 with the U.S. Department of Energy. This research used resources at the Spallation Neutron Source, a DOE Office of Science User Facility operated by the Oak Ridge National Laboratory. The US government retains and the publisher, by accepting the article for publication, acknowledges that the US government retains a nonexclusive, paid-up, irrevocable, worldwide license to publish or reproduce the published form of this manuscript, or allow others to do so, for US government purposes. DOE will provide public access to these results of federally sponsored research in accordance with the DOE Public Access Plan (https://www.energy.gov/doe-public-access-plan).

† ruisardkj@ornl.gov

Content from this work may be used under the terms of the CC BY 4.0 licence (© 2026). Any distribution of this work must maintain attribution to the author(s), title of the work, publisher, and DOI.

ISBN: 978-3-95450-252-3 ISSN: 2673-5350 doi: 10.18429/JACoW-IPAC2026-FRO5T01

THE DETECTION OF THE FIXED LINES IN FOUR-DIMENSIONAL PHASE SPACE *

H. Bartosik[1], G. Franchetti[2,3,4], F. Schmidt[1]
[1]CERN, Geneva, Switzerland
[2]GSI Helmholtzzentrum für Schwerionenforschung GmbH, Darmstadt, Germany
[3]Goethe University Frankfurt, Frankfurt am Main, Germany
[4]Helmholtz Research Academy Hesse for FAIR, Frankfurt am Main, Germany

Content from this work may be used under the terms of the CC BY 4.0 licence (© 2026). Any distribution of this work must maintain attribution to the author(s), title of the work, publisher, and DOI.

Abstract

One-dimensional resonances create fixed points and islands in the Two-dimensional phase space, which has long been recognized as crucial for the diffusion of particles in high-intensity bunches. Coupled resonances are even more relevant, but their dynamics is more difficult to grasp as it happens in a four-dimensional phase space. Following a conceptual and theoretical investigation, a detailed experimental campaign has been carried out in the CERN SPS to investigate the existence of the four-dimensional fixed lines. The experimental investigation has been exceptional complex as it required an extreme control of all accelerator parameters. We report here the difficulties encountered and the main findings, their impact, and possible applications.

INTRODUCTION

Nonlinear resonances are of concern for high-intensity and high brightness beams, as for the SIS100 in the Facility for Antiproton and Ion Research (FAIR) project at GSI [1], and for the operation of the accelerator chain at CERN after the LHC injectors upgrade (LIU) [2]. Studies performed over the last 15 years on one-dimensional (1D) resonances have shown that space charge induced periodic resonance crossing is a prominent mechanism behind halo formation and associated particle loss for high-intensity bunches.

1D-RESONANCES AND SPACE CHARGE

The presence of nonlinear magnetic elements in a synchrotron excites resonances that modify the topology of the orbits in the Poincaré surface of section. The resulting *resonant dynamics* of one-dimensional resonances (of the form $n_x Q_x = N$ or $n_y Q_y = N$) is characterized by distinctive structures in the Poincaré surface of section, namely fixed points, islands, and separatrices. In this case, the two degrees of freedom are decoupled, and the mixed coordinate planes (x, y) and (x', y') exhibit the characteristic rectangular structure described in Refs. [3, 4]. Islands generated by one-dimensional resonances have been observed in several facilities, including CERN, the Tevatron, and the Indiana University Cyclotron Facility [4–6]. Precise control of these islands is essential for the implementation of novel extraction schemes (see Refs. [7–9]).

* Work supported, in parts, by the European Union's Horizon Europe programme under grant agreement no. 101290927 (EPITA).

In a bunched beam, the slow synchrotron motion drives particles through regions of varying longitudinal bunch density, thereby inducing a nonlinear modulation of the transverse tune due to space charge effects. Because the synchrotron motion is slow, the transverse dynamics operates in the regime of "amplitude modulation," as described in Ref. [10]. In this regime, the transverse motion of a particle experiences a modulation of the amplitude-dependent space-charge tune shift. This effect becomes particularly relevant when a lattice one-dimensional resonance overlaps with the space-charge tune spread of the bunched beam. Under these conditions, periodic resonance crossing can occur, driven by the interplay between transverse incoherent space charge and synchrotron motion. Experiments performed at the CERN-PS [11] and at the SIS18 at GSI [12] have confirmed this mechanism.

2D-RESONANCES AND SPACE CHARGE

For two-dimensional (2D) resonances, the orbits in the Poincaré surface of section evolve in a four-dimensional phase space whose topology may elude direct geometric intuition. When the accelerator tunes are set near the third-order resonance, i.e. when the distance to the resonance satisfies $\Delta_r = Q_x + 2Q_y - N \simeq 0$, the particle dynamics acquire distinctive features due to the presence of nonlinear fields. In particular, the phase advances per turn, $\Delta\phi_x$ and $\Delta\phi_y$, are no longer constant, and the single-particle emittances ϵ_x and ϵ_y, computed from the particle coordinates according to the definition of Courant and Snyder [13], are no longer invariant; we therefore denote them by a_x and a_y. A perturbative analysis of the dynamics shows that a_x and a_y satisfy the relation $2a_x = a_y + C$, where C is a constant determined by the initial conditions. Consequently, the resonance properties can be described using only a_y, together with the phase combination $\Omega = \phi_x + 2\phi_y$. For a fixed value of C, the pair (Ω, a_y) evolves turn by turn in this space. However, there exists a stationary pair of values $(\Omega_{\text{fl}}, a_y)$ [14]. When transformed back to the Courant-Snyder coordinates $(\hat{x}, \hat{p}_x, \hat{y}, \hat{p}_y)$ at a given accelerator location, i.e. on the Poincaré surface of section, this special solution acquires the topology of a one-dimensional closed curve parameterized as follows:

$$\begin{aligned} \hat{x}(t) &= \sqrt{a_x}\cos(-2t - \alpha + \pi M), \\ \hat{y}(t) &= \sqrt{a_y}\cos(t), \\ \hat{p}_x(t) &= -\sqrt{a_x}\sin(-2t - \alpha + \pi M), \\ \hat{p}_y(t) &= -\sqrt{a_y}\sin(t). \end{aligned} \tag{1}$$

ISBN: 978-3-95450-252-3 ISSN: 2673-5350 doi: 10.18429/JACoW-IPAC2026-FRO5T02

APPROXIMATE INVARIANT ANALYSIS – AN EFFICIENT FRAMEWORK FOR NONLINEAR BEAM DYNAMICS

Y. Li*, S. Nagaitsev, D. Xu, Brookhaven National Laboratory, Upton, NY, USA
Y. Hao, Michigan State University, East Lansing, MI, USA
C. Mitchell, Lawrence Berkeley National Laboratory, Berkeley, CA, USA

Abstract

We present an efficient framework for nonlinear beam dynamics, termed Approximate Invariant Analysis (AIA). The framework is based on the construction of approximate invariants [Y. Li, D. Xu, and Y. Hao, *Phys. Rev. Accel. Beams*, vol. 28, pp. 074001, 2025] and on the extraction of the betatron frequency with the geometric foundations of Poincaré rotation number [S. Nagaitsev and T. Zolkin, *Phys. Rev. Accel. Beams*, vol. 23, pp. 054001, 2020]. The method is demonstrated using the National Synchrotron Light Source II (NSLS-II) storage ring as an illustrative example.

INTRODUCTION

In most existing ring-based particle accelerators, the presence of nonlinear magnets renders the machines non-integrable Hamiltonian systems. Consequently, exact analytical solutions for particle motion are generally unattainable because the system lacks a complete set of conserved quantities. A central goal of single-particle beam dynamics is therefore to assess particles' long-term stability.

Traditional nonlinear beam-dynamics analysis is usually rooted in Hamiltonian perturbation theory. The linearized beam motion is first parameterized using Courant-Snyder theory [1]. Once stable linear motion is established, nonlinear contributions are treated as perturbations. Common tools for studying nonlinear dynamics include, though are not limited to: (1) classical Hamiltonian perturbation theory, which employs canonical transformations to systematically average out fast oscillatory terms, thereby simplifying the Hamiltonian and highlighting the essential slow dynamics [2]; and (2) Lie-algebraic methods, which decompose nonlinear perturbations into resonance-driving terms [3]. Such perturbation methods can be extended to high order terms by combining with differential algebra [4] and normal-form [5] techniques.

Kolmogorov-Arnold-Moser (KAM) theory [6–8] proves that long-term stable motion can persist in the presence of nonlinear perturbations, provided they remain sufficiently small. In such regions – referred to as the dynamic aperture in accelerator physics – quasi-periodic trajectories reside on invariant tori, which, although deformed, continue to inhibit chaotic diffusion. Reference [9] presents a method for constructing approximations to the invariant tori using Approximate Invariants (AI), enabling a qualitative assessment of particle stability by examining whether the resulting tori remain closed. Moreover, for a given torus, the associated quasi-constant betatron frequency can be extracted using the Poincaré rotation number (PRN) via a geometric approach [10]. Building on these established foundations, this paper introduces an efficient framework for nonlinear beam dynamics analysis – Approximate Invariant Analysis (AIA) – and demonstrates its application using the National Synchrotron Light Source II (NSLS-II) storage ring [11].

APPROXIMATE INVARIANT

Although the concept of closed orbits is well known, we briefly revisit it for the sake of completeness of the overall framework. In accelerator physics, three types of closed orbits are commonly considered. An ideal transverse closed orbit coincides with the design trajectory, passing through the magnetic centers such that $\mathbf{X}^T = [x, p_x, y, p_y] = [0, 0, 0, 0]$ throughout the entire machine. The construction of approximate invariants (AIs) around the ideal reference orbit has been described in Ref. [9]. In the presence of magnetic imperfections and alignment errors, the actual closed orbit, denoted by $\mathbf{X}_{\mathrm{co}}$, deviates from the design trajectory. Furthermore, for an off-momentum particle, a momentum-dependent dispersive closed orbit is superimposed on this distorted orbit. Thus, a realistic closed orbit reads as

$$\mathbf{X}_{co}(\delta, s) \approx \mathbf{0} + \mathbf{X}_{co}(s) + \sum_{i=1,2,\cdots} \mathbf{D}_i(s)\delta^i, \qquad (1)$$

here $\mathbf{D}_i(s)$ is the ith-order dispersion vector at s, $\delta = \frac{\mathrm{d}P}{P_0}$ is the relative momentum deviation[1]. Dispersive orbits can be obtained through iteration with re-normalized magnet bending or focusing strengths with $P = (1 + \delta)P_0$. If there exist nonlinear magnets, it usually differs from the linear parameterization as shown in the left subplot of Fig. 1. High order dispersions can be obtained by a polynomial fitting as shown in the right subplot, or by implementing a differentiable map tracking.

Once a closed orbit is established, one-turn maps in the form of truncated power series (TPS) [4, 12, 13] can be obtained by tracking particles through the entire ring. Using the method described in Ref. [9], two independent and Poisson-commuting AIs are constructed by computing the eigenvectors of the transpose of the one-turn transfer matrix expressed in square form. These AIs describe a family of (approximately) invariant tori in the transverse phase space (x, p_x, y, p_y). In this paper, we only focus on the AI that predominantly characterizes the horizontal motion in the

* yli@bnl.gov

[1] Strictly speaking, in the presence of an RF cavity system operating at a fixed frequency, variations in the closed-orbit path length lead to small changes in the beam momentum.

Content from this work may be used under the terms of the CC BY 4.0 licence (© 2026). Any distribution of this work must maintain attribution to the author(s), title of the work, publisher, and DOI.

ISBN: 978-3-95450-252-3 ISSN: 2673-5350 doi: 10.18429/JACoW-IPAC2026-FRO5T03

TOPOLOGY AND NON-LINEAR MATCHING: FROM KAM TORI TO BEAM PROFILES

G. Sterbini*, H. Bartosik, A. Fornara, M. Giovannozzi, CERN, Geneva, Switzerland
P. Bélanger, University of British Columbia and TRIUMF, Vancouver, British Columbia

Abstract

In modern circular accelerators, beam mismatch at injection into non-linear lattices can play a crucial role for beam quality degradation. In this work, we explore the process of non-linear matching in the Kolmogorov–Arnold–Moser (KAM) quasi-periodic regime, focusing on how the intrinsic phase-space structure influences the evolution of initial beam distributions. Using a topological approach, we quantify how Gaussian beams can develop non-Gaussian tails when propagated through non-linear focusing elements, as a consequence of the shape of the underlying invariant tori. These results are relevant for the design and operation of high-intensity storage rings and colliders where beam-halo control is critical.

INTRODUCTION

During the injection process between a transfer line and a synchrotron, the problem of beam filamentation and its related beam "emittance dilution" has been systematically studied in the linear approximation (e.g., Refs. [1, 2]).

The aim of this paper is to generalise the problem to the non-linear case. Namely, given

1. a non-linear lattice where we neglect all collective effects (single particle dynamics) and
2. the distribution $f_0(\vec{x},\vec{p})$ at turn $N = 0$ and position s_0,

we aim to find the equilibrium distribution for $N \to \infty$, $f_\infty(\vec{x},\vec{p})$, also referred to as the matched distribution.

Using the progress of modern computing power and tracking codes (see, e.g. Ref. [3]), this problem can be directly addressed, in its most general form, via numerical tracking, e.g. by computing turn-by-turn $f_N(\vec{x},\vec{p})$ and monitoring its evolution from f_N to f_{N+1}.

In non-linear lattices, given the known mechanism of chaotic trajectories and related diffusion, this convergence is ill-posed in a strict mathematical sense. However, in most practical cases, the profile of a mismatched beam converges to a steady state in a fraction of a second.

This is possible because the time constant of the filamentation process, $\tau_{\mathscr{F}}$, is much shorter than that of the diffusive process, $\tau_{\mathscr{D}}$ ($\tau_{\mathscr{F}} \ll \tau_{\mathscr{D}}$). In addition, the extent of possible chaotic layers in quasi-integrable Hamiltonian systems can be neglected for our purpose. In the CERN Large Hadron Collider (LHC), the filamentation process takes a few hundred turns [4], while the diffusive processes (mainly driven by collective effects such as IBS, space charge, electron-cloud, beam-beam, …) have time constants of tens of minutes (see, e.g. Refs. [5–7]).

It is possible to recover the well-posed mathematical meaning of the convergence of f_N to f_{N+1} for $N \to \infty$ by introducing an additional working hypothesis along with the two aforementioned ones, namely $\tau_{\mathscr{D}} \to \infty$. This is equivalent to assuming that all particles of $f_0(\vec{x},\vec{p})$ undergo quasi-periodic motion, i.e., the initial distribution is fully contained in a region where the system is integrable. The existence of such regions follows from the Kolmogorov-Arnold-Moser (KAM) theory, which was developed mainly in the context of the long-term stability of Hamiltonian systems. In fact, it was an essential offspring of perturbation theory, which then enabled important applications to the stability analysis of Hamiltonian systems [8–10]. Here we will focus on its topological implications [11] for the non-linear matching.

In the following, we will comment on the potential and limits of this approach. For clarity, we will remain as close as possible to numerical tracking, maintaining a close connection between simulations, visualisations, and results.

THE 2D HÉNON MAP EXAMPLE

In this section, we show a step-by-step numerical approach, assuming

1. the simplest non-linear map, the 1-degree-of-freedom quadratic Hénon map (see Eq. 5.1.2 of [12])

$$z_{N+1} = e^{i2\pi Q_x}\left[z_N - \frac{i}{4}\left(z_N + z_N^*\right)^2\right], \qquad (1)$$

   where $z_N = x_N - i\,p_{x,N}$ is the phase space position at turn N and Q_x is the map's tune,
2. a uniform beam distribution

$$f_0 = \begin{cases} \dfrac{1}{\pi r^2}, & \text{if } x^2 + p_x^2 < r^2, \\ 0, & \text{otherwise.} \end{cases} \qquad (2)$$

The same approach can be easily applied to different non-linear lattices and distributions. In fact the analysis is performed on the resulting turn-by-turn data and is based on the only assumption of quasi-periodic motion. Without loss of generality, we consider a linearly normalised phase space (thus, the units of x and p_x are expressed in units of $\sqrt{\mathrm{m}}$).

Using the Xsuite tracking code [3], we can compute, for a given set of initial conditions (e.g. linearly distributed in $0 \le x \le 0.5\ \sqrt{\mathrm{m}}$ with $p_x = 0$ and tune $Q = 0.2071$ [12]), their $(x, p_x)|_N$ coordinates for $N_{\max} = 5$ kturns, as in Fig. 1.

If the distribution of Eq. (2) is non-vanishing in the region of resonant stable islands of Fig. 1, the limit distribution $f_\infty(x, p_x)$ will not, in general, converge, i.e., we will observe persisting envelope oscillations in the x-projected profile of f_∞. For simplicity, we will assume that the distribution

* guido.sterbini@cern.ch

Content from this work may be used under the terms of the CC BY 4.0 licence (© 2026). Any distribution of this work must maintain attribution to the author(s), title of the work, publisher, and DOI.

ISBN: 978-3-95450-252-3 ISSN: 2673-5350 doi: 10.18429/JACoW-IPAC2026-FRI6M01

FROM FEMTOSECOND TO ATTOSECOND RF FIELD CONTROL*

F. Ludwig†, B. Boghrati, J. Branlard, M. Fenner, M. Hoffmann, U. Mavric, H. Pryschelski, L. Springer and H. Schlarb, Deutsches Elektronen-Synchrotron DESY, Hamburg, Germany

Content from this work may be used under the terms of the CC BY 4.0 licence (© 2026). Any distribution of this work must maintain attribution to the author(s), title of the work, publisher, and DOI.

Abstract

In the past two decades, radio-frequency (RF) controls have improved by two orders of magnitude achieving meanwhile sub-10 fs phase stabilities and 0.01 % amplitude precision. Analog-to-digital-converters (ADCs) are the main limitation for further increase in detector resolution. Alternative architectures are therefore needed to overcome this limitation. The presented work covers a novel application of the suppressed-carrier detector, which extends conventional heterodyne receivers and improves the residual time jitter of the regulated RF-field in the cavity far below 1 fs. A practical implementation of the proposed principle is presented. The setup was used to drive a superconducting RF cavity at 1.3 GHz frequency at a Cryo-Module Test Bench (CMTB) at a gradient of 8 MV/m. The measured out-of-loop residual time jitter of the RF field was 189 as (10 Hz to 1 MHz). The limiting factors of the setup have been identified by feeding the measurements to a system model. In conclusion, a general discussion about future steps is presented.

RF CONTROLS WITH FS-PRECISION

Pump-and-probe experiments at Free-Electron-Lasers with 10 fs resolution require ultra-short electron beams with excellent longitudinal phase space and time jitter stability. This requires multiple bunch compressor stages, short- and long-term stable RF field in the accelerating modules and a precise reference distribution system.

RF-Controls Noise Contributions

In this section, the main noise contributions caused by the RF-control and their impact on the additional timing jitter are derived. Operating the accelerating structures at frequency f_{rf}, the arrival time jitter after a bunch compressor is given by [1]

$$\sigma_{t,out}^2 \approx \left(\frac{R_{56}}{c_0}\frac{\sigma_A}{A}\right)^2 + \left(\frac{C-1}{C}\right)^2 \left(\frac{\sigma_\varphi}{2\pi f_{rf}}\right)^2 + \left(\frac{1}{C}\right)^2 \sigma_{t,in}^2 \quad (1)$$

with $\sigma_{t,in}$ and $\sigma_{t,out}$ the incoming and outgoing arrival time jitter, σ_A and σ_φ the RF amplitude and phase stability, C the compression factor and R_{56} the momentum compaction factor of the chicane. To achieve a timing jitter in the order of 10 fs, the relative RF amplitude stability and phase stability of the RF-control system with respect to the reference must be typically in the order of 0.01 %, respectively 0.01 deg at 1.3 GHz cavity frequency. Neglecting cavity effects like Lorentz- force detuning and beam-loading, the cavity regulation system can be solved algebraically within a small signal analysis in the Laplace-domain [2] or numerically for amplitude and phase. Considering the dominant phase noise sources in the cavity regulation, namely the field detector $S_{\varphi,DWC}$, actuator chain $S_{\varphi,ACT}$, main reference $S_{\varphi,MO}$, and cavity microphonics $S_{\varphi,MIC}$, the residual phase noise, defined as the difference between the main reference and the cavity field, results in

$$\begin{aligned} S_{\varphi,RES}(f) &= \left|\frac{s}{s+\omega'_{12}}\right|^2 S_{\varphi,MO}(f) \\ &+ \left|\frac{\omega'_{12}}{s+\omega'_{12}}\right|^2 \left(S_{\varphi,DWC}(f) + \frac{1}{g_0^2} S_{\varphi,ACT}(f)\right) \\ &+ \left|\frac{s+\omega_{12}}{s+\omega'_{12}}\right|^2 S_{\varphi,MIC}(f) \end{aligned} \quad (2)$$

with $s = j\omega = j2\pi f$, the closed-loop cavity bandwidth $\omega'_{12} = g_0\omega_{12}$ and proportional controller gain g_0. Here the main reference is high-pass filtered, the field detector is low-pass filtered and microphonics are both high-and low-pass filtered. Assuming 1/f-noise from the main reference $K_{MO}\, f^{-1}$, white noise contributions for the other noise sources, cavity bandwidth f_{12} and the conversion of the frequency detuning to phase noise from an oscillator of quality factor Q_L

$$S_{\varphi,MIC}(f) = \left(\frac{2Q_L}{f_{rf}}\right)^2 S_{\Delta f,MIC}(f) = \left(\frac{1}{f_{12}}\right)^2 S_{\Delta f,MIC}(f), \quad (3)$$

the integrated jitter within the effective noise bandwidth $g_0 f_{12}$ with (9) from [2] leads to

$$\begin{aligned} \sigma_{\varphi,RES}^2 &\approx K_{MO}\ln(2) \\ &+ \left(g_0\, S_{\varphi,DWC} + \frac{1}{g_0}\, S_{\varphi,ACT}\right) \frac{\pi}{2}\, f_{12} \\ &+ \frac{2}{(g_0\, f_{12})^2} S_{\Delta f,MIC}\, \Delta f_{MIC}\,. \end{aligned} \quad (4)$$

Depending on the noise sources Eq. (4) can be minimized by an optimal gain between the field detector and actuator noise and choosing an appropriate cavity bandwidth f_{12}. If the field detector noise is sufficiently low, actuator and microphonic noise can be further reduced by increasing the gain. This highlights the critical need for ultra low-noise field detectors with less than 1 fs within the pulse repetition rate and effective noise bandwidth, typically [10 Hz, 100 kHz].

Field Detectors with sub-10 fs Resolution

The requirements on field detectors in the GHz-range for superconductive cavities with less than 10 fs resolution for amplitude and phase are very demanding [3]. The main features are: 360 deg detection, short-term stability, channel-to-channel isolation, minimal latency and no PM to AM conversion. Today widely used is the non-IQ sampling, which combines the advantages of existing

* Supported by HGF/MT (ARD-ST3)
† frank.ludwig@desy.de

ISBN: 978-3-95450-252-3 ISSN: 2673-5350 doi: 10.18429/JACoW-IPAC2026-FRO6M03

ADVANCING ACCELERATOR SCIENCE THROUGH DATA-INTENSIVE RESEARCH AND TRAINING*

C. P. Welsch†, [1], Cockcroft Institute, Warrington, UK
[1]also at University of Liverpool, Liverpool, UK

Abstract

The Liverpool Centre for Doctoral Training for Innovation in Data Intensive Science (LIV.INNO) continues to make significant progress in developing precision diagnostics for accelerator facilities. This contribution presents recent results from four projects that collectively demonstrate how data-intensive methods, advanced modelling and modern instrumentation can enhance measurements under challenging conditions.

It is shown how detailed studies into detector dead time, after-pulsing and timing for the LHC Longitudinal Density Monitor provide quantified error budgets and mitigation strategies that improve satellite and ghost bunch measurements; how a comprehensive evaluation of multimode-fiber imaging techniques offers practical guidance on model selection, robustness and achievable accuracy for radiation-tolerant transverse profile diagnostics; how measurements of optical transition radiation (OTR) from low-energy electrons can be used to establish clear dependencies on target roughness and incidence angle, and how this allows experiment optimization; how the LHC Beam Gas Curtain has developed into a reliable, minimally invasive beam monitor, used for monitor calibration and machine optimization. In addition, this contribution gives an overview of the comprehensive LIV.INNO training, its recent and forthcoming events, and shows how structured skills development and collaboration across science, healthcare, industry and sustainability drive innovation.

INTRODUCTION

LIV.INNO was established in 2022 to train almost 40 PhD students in data intensive research, stretching across Nuclear, Particle and Astrophysics, as well as Accelerator Science [1]. The center builds on the success of its predecessor, the LIV.DAT Centre for Doctoral Training, which successfully trained another 40 PhD students between 2017 and 2023 [2]. Both centers leverage Liverpool's long-standing leadership in postgraduate training from major training programs, including several Marie Skłodowska-Curie Actions networks [3].

RESEARCH

The research activities within LIV.INNO are unified by a common focus on extracting reliable physical insight from complex, high-volume and often imperfect experimental or simulated datasets. The projects presented in the following sections demonstrate how data-intensive methodologies enable measurements and optimization under conditions where conventional approaches face significant limitations. Common themes include the application of machine learning for reconstruction and inference, Monte Carlo techniques for modelling detector response and uncertainty propagation, statistical analysis of low-signal measurements, and the integration of simulation with experimental data to improve robustness and predictive capability. These approaches are complemented by advanced instrumentation, real-time data acquisition and high-performance computing techniques that together support precision diagnostics for next-generation accelerator facilities.

Longitudinal Density Monitor for the LHC

The Beam Synchrotron Radiation Longitudinal density monitor (BSRL) at the Large Hadron Collider (LHC) provides non-invasive measurements [4, 5] of the longitudinal charge distribution of circulating beams using time-correlated single-photon counting of synchrotron radiation. These measurements are particularly important for quantifying nominally empty low-population ghost and satellite bunches, which can influence machine protection and luminosity calibration. Recent work by Alex Jury has focused on characterizing the full measurement chain, combining historical measurements, dedicated laboratory measurements, cross-comparison with independent diagnostics, and simulation.

Comparison of BSRL bunch-length measurements with independent diagnostics suggested that the use of the Beam Synchronous Timing (BST) reference was consistent with an observed effective Gaussian timing broadening of approximately 300 ps [6]. This was identified as a dominant source of timing uncertainty. Following this analysis, the BSRL timing input was taken directly from the RF system during the 2023-2024 technical stop. Post-intervention data show improved timing consistency and more reliable bucket assignment.

Operational data showed a gradual reduction in detected counts per unit beam charge over the course of Run 3. Additionally, measurements of the optical fiber used to transport the synchrotron radiation to the detector in a radiation shielded area, together with wavelength-dependent transmission behavior and partial recovery during beam-free periods, are consistent with radiation-induced attenuation in the current fiber system [7]. Chromatic dispersion in the transmission line remains a significant contributor to pulse broadening. Current estimates indicate total spreading of approximately 569 ps for Beam 1 and 629 ps for Beam 2. These results motivate fiber replacement or removal.

* This work was supported by the Science and Technology Facilities Council (STFC) under grant agreement ST/W006766/1.
† carsten.welsch@cockcroft.ac.uk

Content from this work may be used under the terms of the CC BY 4.0 licence (© 2026). Any distribution of this work must maintain attribution to the author(s), title of the work, publisher, and DOI.